THE 41ST ASMS CONFERENCE ON MASS SPECTROMETRY & ALLIED TOPICS
May 30 - June 4, 1993

TABLE OF CONTENTS

INTRODUCTION & CITATION NOTICE iv

ASMS BOARD OF DIRECTORS iv

ASMS INTEREST GROUP COORDINATORS v

ASMS COMMITTEES v

ASMS CORPORATE MEMBERS vi

LISTING OF EXTENDED ABSTRACT TITLES BY SESSION viii

ABSTRACTS

Monday Orals
- Spray Ionization 1a
- Fast Chromatography/Mass Spectrometry 13a
- Accelerator Mass Spectrometry 22a
- Distonic Ions 26a

Monday Posters
- Metabolism and Drugs 32a
- Carbohydrates 73a
- Environmental 112a
- Computer Applications 144a
- Ion Molecule Reactions 160a
- Petroleum, Process Monitoring & Misc. 201a
- FAB/SIMS/Plasma Desorption 213a
- Nucleotides 240a

Tuesday Orals
- Biopolymers & Their Ions 263a
- Neutralization-Reionization MS 277a
- LC/MS Determination of Small Molecules 286a
- Metal Ions/Ion Molecule Reactions 298a

Tuesday Posters
- Metabolism of Drugs 310a
- Proteins 347a
- Environmental 388a
- Laser Desorption/Ionization 407a
- Trapped Ions 438a
- Ion Fragmentation & Structure 476a
- Biological Miscellaneous 514a
- Polymers 524a

Wednesday Posters
- Metabolism & Drugs 540a
- Proteins 578a
- Environmental 622a
- Laser Desorption/Ionization 649a
- Trapped Ions 681a
- Elemental Analysis & Isotope Ratios 721a
- Electrospray, API, Supersonic Beams 740a

Thursday Orals
- Laser Desorption/Ionization 773a
- Trapped Ion MS 789a
- Environmental Analysis 803a
- Elemental & Isotope Ratio Analysis 815a

Thursday Posters
- Metabolism & Drugs 831a
- Proteins 867a
- MS/MS 910a
- TOF 940a
- Ion Molecule Reactions 958a
- Ion Fragmentation and Structure 1000a
- Electrospray, API, Supersonic Beams 1040a

Friday Orals
- Immunology 1076a
- Fullerenes & Metal Carbon Clusters 1082a
- Analysis of Surfaces 1087a
- Polymer Analysis 1092a

Plenary Lecture, The Mass-Changing Reaction Between MS and MS, Christie G. Enke and Richard A. Yost 1099a
- Recipients of 1993 Award for Distinguished Contribution in Mass Spectrometry

WORKSHOP AND INTEREST GROUP MEETING REPORTS
- Young Mass Spectrometrists, "Perspectives on Publication from the Inside" 1101a
- Field/Portable Mass Spectrometry 1102a
- Isotopic Applications Interest Group; "Signals and Noise" 1103a
- Laboratory Managers Interest Group; "Automation in the Mass Spectrometry Laboratory" 1104a
  - Matching LC with MS; Current and Future Options 1105a
- Summary of Discussion at the ASMS Meeting 1106a

INDEX OF AUTHORS 1107a

INDEX OF KEY WORDS 1119a

INTRODUCTION

This volume represents the official record of the annual meeting and is designated as the Proceedings of the 41st ASMS Conference on Mass Spectrometry and Allied Topics.

The extended abstracts contained in the Proceedings provide brief descriptions of the research presentations made at the meeting and include both oral and poster contributions. In addition, reports from workshops and interest groups and the ASMS business meeting are included.

Special thanks are given to Chris Enke for overseeing the arrangement of the technical program and Judith A. Sjoberg and her staff of Professional Association Management for coordinating the printing and distribution of the Proceedings.

Alan G. Marshall
Editor and Member-at-Large
ASMS Board of Directors

CITATION NOTICE

This volume contains the extended abstracts of papers presented at the 41st ASMS Conference on Mass Spectrometry and Allied Topics. The material is not copyrighted and appearance of material in this volume does not jeopardize the author's right to publish the information in scientific journals.

Reference to individual abstracts contained in this volume should be cited as follows:

> Author(s); title; Proceedings of the 41st ASMS Conference on Mass Spectrometry and Allied Topics, San Francisco, CA, May 30 - June 4, 1993

ASMS BOARD OF DIRECTORS

President	Henry M. Fales National Institutes of Health Building 10, Room 7N 318 Bethesda, MD 20892
Vice President for Programs	Christie Enke Department of Chemistry Michigan State University East Lansing, MI 48824
Vice President for Arrangements	Sanford P. Markey Nat'l Inst. of Mental Health Building 10, Room 3D40 Bethesda, MD 20892
Secretary	Brian Chait The Rockelfeller University 1230 York Avenue New York, NY 10021
Treasurer	Barbara Larsen E. I. duPont de Nemours E228-120A Post Office Box 80228 Wilmington, DE 19880
Member-at-Large (Proceedings)	Alan G. Marshall The Ohio State University 120 West 18th Avenue Columbus, OH 43210
Member-at-Large (Education)	Kenneth L. Busch Sch. of Chem. & Biochem. Georgia Inst. of Technology Atlanta, GA 30332
Member-at-Large (Measurements and Standards)	Jack D. Henion Coll. of Vet. Med. @ Cornell Diagnostic Laboratory 925 Warren Drive Ithaca, NY 14850
Past President	Robert C. Murphy The National Jewish Center 1400 Jackson Street Denver, CO 80206
Executive Director	Judith A. Sjoberg 815 Don Gaspar Santa Fe, NM 87501 (505) 989-4517

INTEREST GROUP COORDINATORS

Laboratory Managers	Andrew N. Tyler Harvard University (617) 496-3571
Biomedical Applications	Steven A. Carr Smith Kline & French (215) 270-6650
Computer Applications	David E. Smith P-E Sciex (416) 881-4646
Desorption Ionization	Richard Van Breemen North Carolina State Univ. (919) 747-2942
Elemental Analysis	Robert (Sam) Houk Iowa State University (515) 294-9462
Energy & Petrochemicals	Dean V. David Unocal Science & Technology (714) 577-1212
Environmental Applications	M. Judith Charles Univ. of North Carolina (919) 966-3857
Fundamentals	Robert R. Squires Purdue University (317) 494-7322
History of Mass Spectrometry	Lawrence R. Phillips National Cancer Institute (301) 496-5531
Isotopic Applications	James Stoffel(s) Batelle Northwest Laboratories (509) 376-2142
LC/MS & Related Topics	Ross C. Willoughby Extrel Corporation (412) 967-5708
Metal Ion Coordination Chemistry	Julie Leary Univ. of Calif. @ Berkeley (415) 642-0701
Polymeric Materials	George J. Kallos Dow Chemical Company (517) 636-5340
Surface Science	Allen Brown Kratos Analytical (201) 825-7500
Young Mass Spectrometrists	Jon Amster University of Georgia (706) 542-2001

ASMS COMMITTEES

Asilomar Conference	Laszlo Tokes (chair) Syntex Research (415) 855-5713
	Arnie Falick R. Graham Cooks Alan G. Marshall Robert C. Murphy
Audit	Kelsey D. Cook (Chair) University of Tennessee (615) 974-8019
	Frank H. Field Peter J. Todd
Education	Kenneth L. Busch (Chair) Georgia Inst. of Technology (404) 894-4030
	John Chakel James A. Kelley Elizabeth A. Stemmler Alfred Yergey
Measurements & Standards	Jack D. Henion (Chair) Cornell University (607) 255-3235
	John Bartmess Phillip C. Price Sharon Lias Anne Giordani
Nominating	Jean H. Futrell (Chair) University of Delaware (302) 831-1247
	Catherine Fenselau Sharon Lias Michael Story Richard Yost
Sanibel Conference	Jeannette Adams (Chair) Emory University (404) 727-6522
	Edward Chess Jack D. Henion Rebecca O'Malley Vernon Reinhold

ASMS 1993 CORPORATE MEMBERS

ATI-UNICAM
PHONE: (608) 831-5515
Allen Scientific Glass, Inc.
PHONE: (303) 442-2141
Analytica
PHONE: (203) 488-8899
Arthur D Little Inc
PHONE: (617) 864-5770
Balzers
PHONE: (603) 889-6888
Bruker Instruments
PHONE: (508) 667-9580
Cambridge Isotope Laboratories
PHONE: (617) 938-0067
Charles Evans & Associates
PHONE: (415) 369-4567
Comstock, Inc.
PHONE: 615/483-7690
Detector Technology, Inc.
PHONE: (508) 867-5411
ETP Electron Multipliers
PHONE: 61 2 8741155
Elsevier Science Publishers
PHONE: (212) 633-3917
Finnigan MAT
PHONE: (408) 433-4800
Fisons Instruments
PHONE (508) 524-1000
GB Scientific
PHONE: (415) 898-7606
Galileo Electro-Optics
PHONE. (508) 347-9191
Hamamatsu Corporation
PHONE: (908) 231-0960
Hewlett-Packard
PHONE: (415) 857-6028
Hitachi Instruments Inc.
PHONE· (408)432-0520
IBM Adstar Analytical Laboratory
PHONE: (408) 256-5151
Ionspec Corporation
PHONE: (714) 261-7743
Isotec Inc
PHONE. (513) 859-1808
JEOL USA, Inc.
PHONE: (508) 536-2271
K and M Electronics
PHONE: (413) 781-1350

Kratos Analytical
PHONE: (201) 825-7500
LC Packings, Inc.
PHONE: (415) 552-1855
LeCroy Corporation
PHONE: (914) 578-6011
Linden-Chromasspec
PHONE: (609) 737-2859
Los Gatos Circuits (LGC)
PHONE: (408) 456-0969
Mass Evolution, Inc.
PHONE: (713) 875-6219
Mass Spectrometry Svcs. Ltd.
PHONE: 44 61-7898611
Millipore/Extrel Mass Spec
PHONE: (412) 967-5763
NIST
PHONE: (301) 975-2505
Oneida Research
PHONE: (315) 736-3050
PE Sciex
PHONE: (416) 881-4646
Palisade Corporation
PHONE: (607) 277-8000
Phrasor Scientific
PHONE: (818) 357-3201
Research Scientific Services
PHONE. (919) 876-8689
Scientific Glass Engineering
PHONE: (512) 837-7190
Scientific Instrument Services
PHONE: (908) 788-8000
Sciex, Inc.
PHONE: (416) 881-4646
Sensar Corporation
PHONE (801) 561-8679
Shrader Analytical Laboratory
PHONE· (313) 894-4440
TEXMS
PHONE: (713) 447-2474
Teknivent Corporation
PHONE· (314) 994-0500
Teledyne MEC
PHONE: (415) 691-9800
Tracer Technologies
PHONE: (617) 776-6410
Varian Associates
PHONE: (510) 939-2400
Vestec Corporation
PHONE. (713) 796-9677

MONDAY ORALS

Spray Ionization

On the Release of Ions from Charged Droplets in Electrospray Mass Spectrometry 1a

Ethylene Glycol as a Solvent for Electrospray Mass Spectrometry 2a

The Potential of Electrospray Ionization with Ultra-high Resolution Mass Spectrometry for Biopolymer Characterization 3a

A Reflecting Time-of-Flight Spectrometer with Orthogonally Injected Electrospray Ions 4a

Studies of a High Intensity Electrospray Ion Source Connected to a High Mass Post Accerleration Ion Detector 5a

Observation of Noncovalent Complexes by Electrospray Ionization on a Magnetic Sector Mass Spectrometer 6a

Conformation Dependent Copper Binding Ability of an Engineered Protein Assessed by Electrospray mass Spectrometry 7a

The Observation of Biomolecular Ions Beyond m/z 3,000 by Electrospray Ionization Mass Spectrometry 8a

Capillary Electrophoresis/Electrospray Ionization on a Magnetic Sector Mass Spectrometer 9a

Rapid Separation of Enzymatically Digested Proteins Using Packed Capillary Perfusion Column LC/ESI/MS 10a

Technique for the Removal of Buffers and Heart Cutting of Peaks in Gradient Capillary HPLC Prior to Electrospray Mass Spectrometry 11a

A New API Source for Magnetic Sector Instruments 12a

Fast Chromatography/Mass Spectrometry

High Speed GC/MS with Focal-Plane-Ion Detection 13a

Maximizing the Utility of Fast GC Analysis with TOF-MS and Time Array Detection 14a

Orthogonal Acceleration TOFMS for Micro-column Chromatography 15a

A Electrospray Time-of-Flight Mass Spectrometer for Chromatography Applications 16a

Time-of-Flight Technology for High Speed GC/MS 17a

Recent Developments in LC/TOF Mass Spectrometry 18a

Two Approaches to Fast GC/MS for Process Monitoring 19a

Fast GC-MS in Supersonic Molecular Beams 20a

Interfacing High Speed Transfer Line Gas Chromatography to Ion Trap Mass Spectrometry; Advantages and Limitations 21a

Accelerator Mass Spectrometry

Tracing Attomoles of 14C-Labeled Organic Compounds in Natural Systesm 22a

Calcium Kinetic Study in Human by 41Ca Tracing 23a

Advances in the Earth Sciences through Accelerator Mass Spectrometry 24a

The Anlysis of Heavy Elements by AMS; A New Mass Spectrometry 25a

Distonic Ions

Distonic Ions; their Status in Gas Phase Ion Chemistry 26a

Investigation of Distonic Radical Cations by Ion-Surface Collisions 27a

Synthesis and Structural Characterization of Novel Distonic Ions Using Ion-Molecule Reactions 28a

Neutralization-Reionization (NR) Studies on Distonic Radical Cations 29a

The RF-Only Mode Event in FTMS: A Means of Generating and Characterizing Distonic Ions 30a

Ion-Molecule Chemistry of The Methylene Dimethylsulfonium Ion: A Novel Alpha-Distonic Ion 31a

MONDAY POSTERS

Metabolism and Drugs

Electrospray LCMS Analysis of Ganefromycins 32a

Analysis of Flavins by Thermospray HPLC/MS and Electrospray MS 33a

Quantitation of Vecuronium Bromide by Electrospray/Tandem Mass Spectrometry 34a

The Application of Electrospray Ionization in the Analysis of Catecholamines by LC/MS 35a

Electrospray MS and MS/MS for Metabolite Identification in Various Animal and Human Biotransformation Studies 36a

Electrospray Ionization Mass Spectrometry of Glutathione and N-Acetylcysteine Conjugates of Electrophilic Metabolites of Acetaminophen 37a

Identification of Tamoxifen Metabolites in Breast Cancer Patients by Electrospray LC/MS 37c

Determination of Antibiotics by using Ultrasound Nebulization Electrospray Mass Spectrometry 38a

Determination of Cysteinyl Leukotrienes Using Electrospray/Tandem Mass Spectrometry. 39a

Structure Elucidation of Taxanes by ESI-MS and ESI-MS/MS 40a

The Metabolism of Substance P Studied by in vivo Microdialysis and On-Line LC/ESI/MS 41a

Monitoring In-Vitro Enzymatic Reactions Using An Integrated microdialysis/Ionspray Tandem Mass Spectrometry System 42a

Metabolism of Hexamethylene Diisocyanate (HDI) in the Rat Utilizing Ionspray LC-MS/MS Techniques 43a

Identification, and Quantitation of Metabolites of a Novel Non-benzodiazepine Anxiolytic Compound (CL 273,547) by Thermospray LC/MS in Tandem with 14C Detection and an Off-Line Stable Isotope 44a

Determination of Reserpine in Plasma by Ion Spray LC/MS/MS 45a

Determination of Vitamin B12 by Ionspray Liquid Chromatography Mass Spectrometry 46a

Nanoliter Flow, LC-ESI-MS for Analysis of Endogenous Neuropeptides 47a

Characterization of Brimonidine Metabolites by HPLC/Thermospray Mass Spectrometry 48a

Simultaneious HPLC Radioactivity and Mass Spectrometry Monitoring. A Drug Metabolism Application 49a

Investigation of Factors Influencing In Vivo Microdialysis/MS/MS Studies 50a

Analysis of Quaternary Isoquinoline Alkaloids by Ion Spray Ion Trap Mass Spectrometer (IS/ITMS) 51a

Assessment of in-vitro Liver Slice Metabolic Activity Using Microcolumn Separation Systems Coupled with ESI/MS 52a

Quantitative Analysis of the Immunosuppressant FK-506 in Rat Serum by high Performance Liquid Chromatography-Electrospray MS/MS Techniques 53a

Structural Analysis of Rapamycin and Related Compounds Using (M+Li) + Ions Generated by LSIMS 54a

Investigation of Photochemical Reactions via on-line Thermospray Tandem Mass Spectrometry 55a

Comparison of GC/MS and LC/MS Methods for Determining Nicotine Absorption in Tobacco Smokers 56a

Electrochromatography/Mass Spectrometry of Steroids: 57a

Mass Spectrometrically-Guided Development of a Fluorescent Label for Enhanced Detection in HPLC 58a

A Comparison of the Analysis of Gentamicin Sulfate by Thermospray and Electrospray HPLC/MS 59a

Recognition of Quaternary Amines and Ammonium Salts Using Tandem Mass Spectrometry 60a

Analysis of N-acetyl-cysteinyl-ursodeoxycholic Acid in Human Bile by Solid Phase Extraction and HPLC - cf-FAB Detection 61a

Mass Spectral Characteristics and Identification of Metabolites of Mesoridazine and Other Related Piperidine Type Phenothiazines 62a

Automated Interpretation of Biological Fluid Organic Samples by a Benchtop GC-MS 63a

Rapid GC/MS/MS Assay for 5-Methoxyflavone in Plasma 64a

Immunoaffinity Chromatography and GC/MS/MS for the Identification of Cross-reactants with an immunoassay for Benzoylecgonine 65a

Microscale Chemical Reactions to Probe the Structure and Reactivity of Isolated Natural Products 66a

Detection of Vitamin D Metabolites by On-Line Capillary Liquid Chromatography and Fast Atom Bombardment Mass Spectrometry 67a

Determination of Cortisol in Human Plasma by Gas Chromatography/Negative Ion Chemical Ionization/Mass Spectrometry 68a

The Rapid Structure Characterization of Synthetic and Natural Products by FAB-Mass Spectrometry using Na+ and K+ Salts 69a

Characterization of Human Cerebrospinal Fluid (CSF) Phospholipids by Fast Atom Bombardment Mass Spectrometry (FABMS) 70a

Quantitative Determination of Hydroxybutorphanol and Norbutorphanol in Human Plasma by GC/ECCI/MS 71a

The Characterization of Abscisic Acid Metabolites Using Packed Capillary LC/Continuous Flow Secondary Ion MS 72a

Carbohydrates

A Mass Spectrometric Study of Phenolic Glycolipids 73a

The Characterisation of Lipophilic Peroctylated Cyclodextrins by Electrospray Mass Spectrometry 74a

Characterization of Chemically-modified Cyclodextrins and their Host-Guest Complexation with Drugs by Ion Spray Mass Spectrometry 75a

Characterization of Avidin by Electrospray Ionization Mass Spectrometry 76a

Characterization of Oligosaccharides by LC-MS Technologies 77a

A General Approach to Carbohydrate Characterisation of Glycoproteins by Exo-glycosidase Digestion and Matrix Assisted Laser Desorption Mass Spectrometry 78a

Characterization of Permethylated Gangliosides by off-line HPLC, LSIMS, MS/MS and MALDI-TOFMS 79a

Mass Spectrometry of C-Glucosides Containing S-Atom at C-2 80a

Analysis of Heterogeneity of Native -Acid Glycoprotein 81a

Predictability of Fragmentations in Negative Ion FAB MS of Reducitng Oligosaccharides 82a

Does Conformation Play a Role in the Fragmentation Behavior of Oligosaccharides? A Study with Three -D-NeuAc-(2-6)-SS-D-Gal Sialosides and Six Related, Conformationally more Rigid -D- 83a

Comparative Study of Carbohydrate Structrues of Recombinant Human Platelet-Derived Growth Factor Expressed in Chinese Hamster Ovary and in Saccharomyces Cerevisiae 84a

Electrospray Mass Spectrometry of heparin Oligosaccharides 85a

Structure Determination of the Major Sialylated Oligosaccharide Chains of Recombinant-Derived Erythropoietin Expressed in Chinese Hamster Ovary Cells 86a

Structural Characterization of the Carbohydrate Chains of Saponins by FAB-MS/MS 87a

Structural Studies of the Glycosylation of the Gastric H+, K+-ATPase 88a

Structural Determination of the O-linked Oligosaccharides of Recombinant Human Granulocyte-Colony Stimulating Factor 89a

Structural Determination of a Sulphated Tetrasaccharide Ligand for the Cell Adhesion Molecule E-Selectin by LSIMS 90a

Structural Analysis of Glycosylation on the HIV Envelope Glycoprotein gp 120 91a

Structural Elucidation of Branched Oligosaccharides: Isotope Labeling Studies 92a

Detailed Structural Characterization of an Exopolysaccharide from Rhizobium Meliloti by ESI and Low Energy CID 93a

Sequencing of Glycopeptides Using Sequential Digestion Followed by Microbore HPLC/Electrospray Mass Spectrometry 94a

Microcolumn HPLC-CF-LSIMS of UV-absorbing Neoglycolipids Derived from Oligosaccharides 95a

Electrospray Ionization of Divalent Metal Chloride-coordinated Oligosaccharides 96a

An Analysis of Mono- and Oligosaccharides by Electrospray Mass Spectrometry 97a

Use of Matrix-Assisted Laser Desorption Mass Spectrometry for Examination of Oligosaccharide Mixtures 98a

Analysis of Glycoalkaloids in a Crude Mixture by Positive-Ion and Negative-Ion L-SIMS and Four-Sector Tandem Mass Spectrometry 99a

Oligosacharide Profiling by LC-ESI-MS: Focus on Mucins 100a

Glycoform Detection in CHO-derived Interleukin-4 by LC / CID / Electrospray Mass Spectrometry 101a

Enhanced Carbohydrate Detection by Multiple Ion Monitoring (MIM) of HPLC Effluents 102a

Quantitation of D-Glucose and 13C6-(U)-D-Glucose methylboronate Pentafluoropropionates in Human Plasma by Methane NCI GC-MS 103a

Quantization Studies of Polymethylated -cyclodextrins by ESMS 104a

Matrix Additives to Enhance Signal Intensity of Gangliosides in Negative FAB-MS Analysis 105a

The Self-Association of Sialyl Lewis X 106a

Optimisation of Identification of Oligosaccharides by Matrix-assisted Laser Desorption Mass Spectrometry 107a

Matrix-Assisted Laser Desorption of O-Glycopeptides Using Linear and Reflectron Time-of-flight Instruments 108a

The Role of Lipooligosaccharides in Pathogenesis of Haemophilus Species and Possible Strategies for Therapeutic Intervention 109a

Mass Spectrometry of Cyclodextrin Amino Acid Adducts: 110a

An Integrated Mass Spectrometric Approach (PD, FAB, ESI and Low Energy CID) to Characterize the Peptidoglycan of Various Microorganisms 111a

Environmental

Strategies for the Identification of Compounds Causing Odors in Water. A Study of a Creosote Spill 112a

Tandem Mass Spectrometry of Human Skin Emanations for the Determination of Mosquito Attractants 113a

Direct Analysis of Polycyclic Aromatic Hydrocarbons in Airborne Particulate Matter by Laser Time-of-Flight Mass spectrometry 114a

Laser Photoionization Time-of-Flight Mass Spectrometry Applied to Nitrated Polycyclic Aromatic Hydrocarbons and Nitrobenzocoumarin Derivatives 115a

Laser Photoionization Time-of-Flight Mass Spectrometry of Arsenic and Chromium Compounds in Airborne Particulate Matter 116a

Analysis of Sulfonated Azo Dyes by GC/MS of Their tert-Butyldimethylsilyl Derivatives 117a

GC/MS Detection of Thiodiglycol and Thiodiglycol Sulfone in Water and Concrete Using TMS Derivatization 118a

Mass Spectrometric Studies of Tetraphenylborate Hydrolysis Products from a Simulated Feedstock 119a

Real-time Measurement of Reactive and Toxic Hydrocarbons in Auto Exhaust 120a

Thermal Study of Rutin by Thermogravimetry/Gas Chromatography/Mass Spectrometry 121a

Interpretation of the Distribution of Environmental Contaminants in Gulf of Mexico Oysters using Log-Normal Distribution Functions 122a

Supercritical Fluid Extraction in the Analysis of Environmental Organic Pollutants 123a

Selectivity and Sensitivity Enhancements of Halogen Detection Utilizing MIP/CRIMS and Negative Chemical Ionization 124a

Determination of Benzene in Food by Direct Sampling Ion Trap Mass Spectrometry 125a

Development of a Method for the Direct Purge Analysis of Volatile Organics in Water 126a

Multispectral Identification of Chlorine Dioxide Disinfection By-Products in Drinking Water 127a

Identification of PCB Degradation Products in Gamma-Ray Irradiated Solution of PCB's in Isopropanol 128a

The Analysis of TCDD in Human Serum using Very High Resolution SIR 129a

Investigation into Interferences in Dioxin Analysis by HRGC-HRMS 130a

Mass Profile Monitoring in Trace Analysis: Polychlorinated Dibenzo-p-dioxins and Dibenzofurans in Crab Tissues from Raritan/Newark Bay System 131a

Comparison of Pre-operational and Post-operational PCDD/F in Milk Samples Taken from Farms Located Near a New Recovery Incinerator by HRGC/HRMS 132a

Pattern Analysis of Alkyl Aromatic Compounds from Biota Samples Taken After the Exxon Valdex Oil Spill 133a

GC Inlet Modifications Improving the Analysis of Aromatic Hydrocarbon Metabolites in Fish Bile 134a

Comprehensive Analysis of Mississippi River samples by GC/PCI/MS/MS and GC/NCI/MS 135a

Alkylbis(trifluoromethyl)phosphine Sulphide Homologs as Multidetection Retention Index Standard in GC/MS and in GC/MS/MS 136a

Identification and Quantification of 2,4,6-Tribromoaniline in the Color Additive D&C Red No. 22 (Eosin Y) by GC/MS 137a

The Photolytic Degradation of Pentachlorophenol in Organic Solvents 138a

A Sampling/Calibration "Pipeline" for the Analysis of Hazardous Gas Cylinders 139a

MicroVolume Gas Analysis: Design, Construction of Utilization of a Mass Spectrometer System for Analysis of Gases in Semiconductor Packages 140a

FAB MS and HPLC Analysis of Fumonisin B1 and Fumonisin B2 in Food Substrate Cultures 141a

The Use of Internal Standards to Improve Linearity and Reproducibility in the Thermospray LC/MS Analysis of Chlorinated Phenoxyacetic herbicides 142a

Liquid Chromatography/Thermospray Mass Spectrometry for Characterization of Commercial Chlorinated n-paraffin Mixtures 143a

Computer Applications

Chemometric Assessment of GC/MS and GC/MS/MS Data Naphthenic Biomarkers 144a

Computer Program for Interpreting Peptide Mass Spectra Utilizing Hydrogen-Deuterium Exchange Information 145a

Quantitative Aspects of Maximum Entropy Applied to Multiply Charged Electrospray Data 146a

Curve-fitting for Resolution of Overlapping Chromatographic Peaks in High Precision Gas Chromatography-Combustion Isotope Retio Mass Spectrometry (GCC-IRMS) 147a

Analysis of Natural and Adulterated Essential Oils by MDGC/FTIR/MS 148a

The Application of Self-modelling Mixture Analysis to Automated Mass spectrometry 149a

Evolving Factor Analysis and GC/MS - An Ideal Combination 150a

Resolution and Quantization of Geometric Isomers using Solids Probe/Factor Analysis 151a

Improving Performance of Mass Spectral Search Algorithms 152a

The Control of Quality in a Comprehensive Mass Spectral Library 153a

PC-based Modular Data System for Time-of-Flight Mass Spectrometry 154a

Software for Acquisition and Analysis of TPEPICO-TOF-MS 155a

Networking a Laboratory Information Management System (LIMS) with a Mass Spectrometer Data System 156a

An Instructional HyperCard Stack for Users of the Mass Spectrometry Laboratory at the University of Illinois 157a

Ion Optical Study of Low Acceleration Ion Source 158a

Identification of Proteins by their Peptide Masses in DNA Databases 159a

Ion Molecule Reactions

Complexation Selectivity of Metal Cations toward Organic Molecules by FAB Mass Spectrometry 160a

Mechanistic Investigations into the Anionic Oxy-Cope Rearrangement in the Gas-Phase 161a

Complexation of Alkaline Earth and Transition Metal Ions with Polyethers in a Quadrupole Ion Trap 162a

Examination of Hydrogen-Bonding Interactions in Host-Guest Chemistry and Selective Ion-Molecule Reactions in a Quadrupole Ion Trap 163a

Recognition of Chiral Ammonium Salts using Chiral Crown Ether Hosts in the Gas-Phase 164a

Fourier Transform Ion Cyclotron Resonance Mass Spectrometric Investigation of Gas Phase Cryptate Complexes 165a

Influence of Polarizability and Ligand Flexibility on Multidentate Attachment of Alkali Metal Cations: Kinetics and Thermochemistry of Cation Binding by Isomers of Dicyclohexano-18- 166a

Fourier Transform Ion Cyclotron Resonance Mass Spectrometric Investigation of Calixarenes and their Complexes with Alkali Metal and Organic Cations in the Gas Phase 167a

Chiral FAB Mass Spectrometry 168a

Gas Phase Reactions of the Group 11 Ions with Small Alkanes 169a

Transition Metal Ion Reactions with Laser Desorbed Amino Acid and Peptide Neutrals in a Fourier Transform Mass Spectrometer 170a

Chemistry of NO and CO Ligands on MCon+ Clusters (M = Sc, V; n =1, 2) 171a

Formation of Strongly Bound Trasition-Metal Molecular Silane Complexes. n2-Coordination of Si-H 172a

Fe-(L)+(L=c-C5H6, C4H6) Mediated Extrusion of CO from Furan. A Model Study Relevant to Catalytic Hydrodesulfurization 173a

Hydrogenolysis Rates of Group 4 Methyl Metallocenes 174a

The Change in Reactivity of the FeCp+ Ion After Collisional Thermalization Using Quadrupolar Excitation 175a

Gas Phase Ion - Molecule Chemistry of Cyclooctatetraene Iron Tricarbonyl { 4-C8H8Fe(CO)3} by FT-ICR Spectroscopy 176a

Activation of Metal Carbonyls by Charge Transfer Reaction 177a

Gas-Phase Study of RCCo3(CO)9 (R=H, CH3, Ph, Cl) with Selected Organic Neutrals 178a

Reactions of Metal Carbonyl Anions with Methyl Formate in the Gas Phase 179a

Gas-Phase Ion-Molecule Reactions of Cr2(CO)5 - with Ketones and Alkenes 180a

Electron Affinity Measurements of Halogenated Metalloporphyrins 181a

Photoactivated Gas Phase Ligand Switching 182a

Thermoneutral Proton and Ligand Exchange Reaction Rates for Protonated and proton Bound Dimer Dimethyltartrate ions 183a

A Redetermination of the Proton Affinity Scale from Nitrogen to t-Butylamine by Variable Temperature High Pressure Mass Spectrometry 184a

Isomers of CHNO+ and the proton affinity of NCO at N 185a

Role of Reactant Vibrational Excitation and Collision Energy in the Ion-molecule Reaction NH3+ + ND3 186a

Br+ Addition to Gaseous Aromatic Compounds: Mechanism and Linear Free Energy Effects on Reaction Rates 187a

A Study of the Temperature Dependence of the SN2 Reactions of Cl with Methyl Bromide, Ethyl Bromide, iso-Propyl Bromide and n-Butyl Bromide at Atmospheric Pressure Using an Ion Mobility-Mass 188a

Kinetic Isotope Effects for the SN2 Reactions of Solvated Anions with Methyl Halides 189a

Competitive SN2/SNi Reactions Occuring in the Collision Cell of Triple Quadrupole from Low Kinetic Energy MH+ and [M+NH4]+ Ions Prepared from the Disastereomeric 1,2-Indanediols 190a

Guided-Ion Beam Studies of Reactions of Ions with NO 191a

Effects of Kinetic Energy on Both Endothermic and Exothermic Ion-Molecule Reactions in a Quadrupole Ion Trap Mass Spectrometer 192a

H/D Exchange in low Energy Collisions Between Protonated Aromatics and D2) or DC3OD 193a

Target Capture and Ion/Molecule Reactions in High Energy CID of Peptides Ions 194a

Gas Phase Basicities of Guanidine and Urea 195a

Breakdown Curves for the Dissociation of Protonated Peptide Ions Obtained by Laser Desorption/Chemical Ionization 196a

Proton Transfer Rate Constrants Measurements of Amino Acids and Dipeptides in a fourier Transform Mass Spectrometer 197a

Gas-Phase Basicities of Small Carbohydrates 198a

Gas-Phase Basicity Studies of Glycine and Diglycine by Mass Spectrometry and Ab Initio Calculations 199a

The Experimental and Theoretical Gas-Phase Basicity of Linear Oligomeric Peptides - Trends and Sites of Protonation 200a

Petroleum, Process Monitoring & Misc.

Analysis of High Molecular Weight Hydrocarbons by Short Column Gas Chromatography Mass Spectrometry 201a

Characterization of Wax Fractions from Lube oil Basestocks by Thermal Extraction-Gas Chromatography/Mass Spectrometry 202a

The Analysis of a Complex Mixture of Acidic Materials Derived from Petroleum by Capillary Electrophoresis and ESI - MS.: a Preliminary Off-line Investigation 203a

Characterization of Asphalts and Estimation of Bond Strengths Between Organic Components and Aggregates by Probe Microdistillation/Mass Spectrometry 204a

Evaluation of Mass Spectrometric Methods for Determination of Sulfur Types in Petroleum Samples 205a

The Determination of 2-Napthylamine in Petroleum Products by High-Performance Liquid Chromatography and Mass Spectrometry 206a

Geoporphyrin Analysis using Electrospray Ionization-Mass Spectrometry 207a

Using in-situ Mass Spectrometry to Study the Chemistry of a Small Scale Benchtop Minireactor 208a

In-situ Mass Spectrometry for Process Monitoring in a Chemical Plant 209a

Two Improved Probe Designs and a Modified Source for Desorption Chemical Ionization on the HP5989A Mass Spectrometer 210a

The Analysis of Alkylated Diphenyl Amines by High-Performance Liquid Chromatography / Particle-Beam / Mass Spectrometry 211a

Comparison of Field Desorption and Thermospray Mass Spectrometry for the Analysis of Petroleum Residua 212a

FAB/SIMS/Plasma Desorption

Multi-Sample Probe for Fast Atom Bombardment Mass Spectrometry 213a

The Use of a Variable Focus Cesium Ion Source to Facilitate the On-line Generation of FAB Spectra with particle Beam LC/MS 214a

Selective Enhancement of Ions Intensity by Adding Surfactant in Static FAB 215a

FAB MS of Non-Volatile Compounds in the Transition Range between Liquid and Solid 216a

Investigation of [M-H]+ Formation in FAB/LSIMS for a Compound with High Proton Affinity 217a

Improved Dynamic LSIMS (FAB) Sensitivity Using a Cold Finger to Enhance Pumping 218a

The Effects of Analyte and Matrix Properties on the "True" Reduction-Oxidation Extents Observed in FAB/LSIMS Analysis of Peptides 219a

The Effect of Functional Groups on the Reduction Behavior of Phenothiazine-related Dyes in LSIMS/FAB Mass Spectrometry 220a

A Comprehensive Study of Beam-Induced Dehalogenation of Organic Compounds in LSIMS: Effect of Analyte Structure, Halogen Type and Matrix Chemistry 221a

Sample Charge Compensation on a Large Sample Ion Microprobe 222a

Determination of Flux from a Saddle Field Fast Atom Bombardment Gun 223a

Time-of Flight Secondary Ion Mass Spectrometric Analysis and Imaging of Avian Egg Membranes 224a

Liquid Secondary Ion Mass Spectrometry of Hypervalent Siliconates 225a

Massive Cluster Impact (MCI) Mass Spectrometry - Source Design and Performance 226a

A Kinetic Model for Sensitivity Enhancement by Surfactant-analyte Ion Pairing in Liquid Matrix Assisted SIMS 227a

TOF-SIMS Studies of Ion Formation and Fragmentation Mechanisms in Polyglycols 228a

Secondary Ion Mass Spectrometry Depth Profilling of Ti-Implanted AlInAs and InP at Room and at Elevated Temperatures 229a

Measurement of Secondary Emission from Low Work Function Materials: Potential Emission for High mass Analysis by Mass Spectrometry 230a

Characterization of Fingerprint Residues on Surfaces using Neutral-Beam SIMS 231a

Correlation Between Initial Radial kinetic Energies and Chemical Composition of Secondary Ions, Sputtered Electronically from Organic Solids 232a

Comparision of Plasma Desorption- and Thermospray-Mass Spectra of Mercapturic Acids 233a

Applications of PD-MS in the Analysis of the Genetics of Quaternary Ammonium Compound Accumulation in Plants 234a

The Characterization of Tri-Nickel Cluster Compounds using 252cf Plasma Desorption and FAB Mass Spectrometry 235a

LC-MS Analysis of some Photographic Colour-Coupling Compounds Using a Continuous-Flow FAB Interface 236a

Information on the Ionization Processes Involved in FAB/LSIMS through Electrospray Ionization 237a

Formation and Sputtering of Fullerenes by MeV Ion Beams 238a

Identification of Degradation Products of the Antibiotic Laidlomycin Propionate by Mass Spectrometry 239a

Nucleotides

Quantification of Malondialdehyde-deoxyguanosine (M1G-dR) Adduct by GC ECNCI MS 240a

Differentiation of Isomeric C8-Substituted Dinitrotoluene Adducts of Guanine by FAB MS/MS 241a

Distinguishing Isomeric Monomethyl Guanines by FAB Mass Spectrometry Combined with Permethylation 242a

Low Energy Tandem Mass Spectrometry of Diol-Epoxide-Deoxynucleoside Adducts 243a

Characterization of Modified Oligodeoxynucleotides by Electrospray Mass Spectrometry 244a

Computer-Assisted Interpretation of Electrospray-Tandem Mass Spectra of Oligonucleotides 245a

MALDI Mass Spectrometry of Oligonucleotides and Nucleic Acids 246a

Electrospray LC-MS of Modified Oligonucleotides 247a

The Use of On-Line Field Amplification Stacking for the Capillary Electrophoresis-Mass Spectrometric Analysis of DNA Adducts 248a

Experimental Conditions for the Matrix-Assisted Laser Desorption FTMS Analysis of Modified Oligonucleotides 249a

MALD-FTMS for the Characterization of Ultraviolet and X-ray Damage to Nucleic Acid Constituents 250a

7 Day Low Level Dose Response Study of MeIQx in Rats using Accelerator Mass Spectrometry 251a

Analysis of DNA-Carcinogen Adducts by Electrospray CZE-MS 252a

Spatial Distribution of Nucleic Bases Using SIMS 253a

Mass Spectrometric Identification of 2'-Deoxycytidine Adducts from Reactions with Acrolein and 2-Bromoacrolein 254a

Enhanced Sensitivity in the Negative Ion FAB-MS Analyses of Polyanionic Organic Compounds Through the Use of Cationic Additives to the FAB Matrix 255a

Quantitative Fast Atom Bombardment Mass Spectrometry: Estimation of Cyclic nucleotide-Dependent Protein Kinase Activity 256a

Ultra Trace Analysis of Oxidized Nucleosides in Biological Matrices 257a

Use of On-Line Thermal Denaturation to Study the Stability of Quadruple-Stranded Nucleic Acid Structures 258a

Collision-Induced Dissociation of Permethylated Derivatives of Site-Specifically 15N and 18O-Labeled Guanosines 259a

Evaluation of Variable Post-Translational Modification of Histones by Electrospray Ionization Mass Spectrometry and Tandem Mass Spectrometry 260a

Product Ion Scans of the BH2+ Ion: A Tool for Investigating the Structure of Deoxynucleosides Modified by Arylamine and Diol-Epoxide Carcinogens 261a

Studies on the Binding of Actinomycin D to Single-Stranded DNA by Negative Ion Spray Mass Spectrometry 262a

TUESDAY ORALS

Biopolymers & Their Ions

Posttranslational Modifications and Mass Spectrometry: What the Well Dress Protein is Wearing and How to Tell 263a

Mass Spectrometric Based Strategies for the Structural Characterization of Recombinant Human IL-12" 264a

Combination of Mass Spectrometric Methodologies for the Determination of Peptide and Protein Structure 265a

A Strategy for Mass Spectrometric Characterization of Nucleotide-Protein Complexes after UV-induced Cross-linking 266a

Application of Ion Spray Mass Spectrometry in Probing Protein-Protein/Protein-Ligand Intramolecular Interaction 267a

Identification of proteins in One-and Two-Dimensional Gels by Mass Spectrometric Peptide Mapping 268a

Surface Induced Dissociation of Peptides in a Four Sector Mass Spectrometer 269a

Determination of Posttranscriptional Modification in Ribosomal RNA by Mass Spectrometry 270a

The Hows and Whys of Multiply-charged Oligonucleotide Decompositions 271a

Electrospray Ionization of Plasmid DNA and Detection by Mass Spectrometry 272a

Quantification of Apolipoprotein A-1 by Isotope Dilution FAB MS 273a

Detailed Structural Characterization of Carbohydrate and Glycoconjugate oligomers Using Selective Chemical Modification, ES and CID Analysis 274a

MS/MS of Cobalt-coordinated Branched Pentasaccharide Isomers: Linkage Position Determination using Electrospray Ionization 275a

From the Outer Membrane to the GAS Phase: Making Ions of Bacterial Surface Antigens 276a

Neutralization-Reionization MS

Neutralization-Reionization Mass Spectrometry 277a

Neutralized Ion Beam Studies of O2: A New State for an Old Molecule 278a

Collisional Electron Transfer: Where Does the Electron Go? 279a

Investigation of Ion Structures by Neutralization-Reionization Mass Spectrometry Methods 280a

Neutralization-Reionization Mass Spectrometry; what next? 281a

The Quest for the Elusive Iminols with NRMS and Multiple Collision Experiments (MS/MS/MS) 282a

Investigation of Ionized Cyclopropanol. Does it Exist? 283a

Detection and Characterization of Novel [C2H3NO] + Isomers and their Neutral Counterparts 284a

The Characterization of Labile Metallocenes and Their Neutral Counterparts by Tandem Mass Spectrometry 285a

LC/MS Determination of Small Molecules

Current Status and New Leads in the Analysis of Small Molecules by LC-MS 286a

Electrospray Ionization at LC Compatible Flow Rates on a Magnetic Sector Mass Spectrometer 287a

LC/ESMS Characterization of Small Molecule Mixtures in Industry 288a

Liquid Chromatography (LC)/Particle Beam (PB) and Thermospray (TSP)/Mass Spectrometry (MS) in Environmental Analyses 289a

Electrospray LC/MS of Lower Molecular Weight Molecules 290a

New APCI Technology Enhances Pharmacokinetic Studies in Biological Samples 291a

Comparison of Thermospray and Ionspray for the Analysis of Drug Conjugates 292a

Characterization of Low Molecular Weight Thermally Labile Analytes Using Capillary Supercritical Fluid Chromatography/Mass Spectrometry (SFC/MS) 293a

Profilling of Bacterial Metabolites by On-line Capillary LC - Electrospray MS 294a

Plasma Source Atmospheric Pressure Ionization Detection of Liquid Injection Using An Ion Trap Storage/Reflection Time-of-Flight Mass Spectrometer 295a

Structure Elucidation Strategies Applied to Taxol and Taxanes 296a

Petroleum Polars Characterized by Compound Class Separation and On-Line LC/MS 297a

Metal Ions/Ion Molecule Reactions

Bond Energies and Electronic States of Unsaturated Organometallic Complexes 298a

Substituent Effects and Solvation Energetics from Electron-Transfer Equilibirum Studies of Gas-Phase Metal Complexes 299a

Reaction of State Selected V+ with C2H6 and C3H8 300a

Accurate Bond Dissociation Energies from Equilibrium Clustering Measurements: Co+.(H2)1-7, V+.(H2)1-6, Co+.(CH4)1-3 and Co+.(C2H6)1-3 301a

Gas-Phase Ion-Molecule Reactions of Fe+ with Model Peptides: Ground Versus Excited Electronic State Reactions 302a

Isotopic Fractionation in the Formation of He2 303a

Fundamentals of Tandem Mass Spectrometry 304a

Isotopomer Differentiation Using Metal Ion Chemical Ionization 305a

Transition Metal Cluster Anions: Periodic Trends in Oxidation and Chemisorption Reactions 306a

The Negative Chemical Ionization Reactions of the Atomic Oxygen Radical Anion with Selected Alkenes 307a

Antiaromatic Ions: The Formation, Reactivity, and Thermodynamic Properties of a Cyclopropenyl Anion 308a

Ion-Molecule Reactions of Dicoordinated Boron Cations 309a

TUESDAY POSTERS

Metabolism of Drugs

The Structure Elucidation of Taxol Analogs and Impurities Using LC/MS and LC/MS/MS Profiling Protocols 310a

Detection of Alkaloids by Positive Ion Thermospray LC/MS Using a Nonconventional Ion Pairing Agent 311a

Coupling of Capillary High-Performance Liquid Chromatography with Continuous-Flow Liquid Secondary Ion Mass Spectrometry for the Determination of Flavonoid Conjugates 312a

Mass Spectrometry of Three New Toxins Produced by Alternaria Alternata f.sp. lycopersici 313a

Supercritical Fluid Extraction and LC/MS of Thiosulfinates Found in Allium Species 314a

LC/MS Identification and Characterization of Components Isolated from Chaparral 315a

Separation and Identification of Didemnins and Ecteinascidins by On-line Microbore Liquid Chromatography/Continuous Flow Fast Atom Bombardment Mass Spectrometry 316a

Identification of S-linked Conjugates of 2-Chloroethyl Isocyanate as metabolites of N,N-bis(2-Chloroethyl)-N-nigrosourea(BCNU) in the Rat by Ionspray LC-MS/MS 317a

The Utilisation of Modern LC/MS Methods to Study the Phase I and Phase II of Metabolism of Trimetazidine in Human Subjects 318a

Development of a LC/MS/MS assay for FIAU 319a

Particle Beam LC-NCI MS Assay of Kynurenic Acid in the Media of Cultured Cells 320a

Identification of Rat Liver Microsomal Metabolites of Atevirdine Mesylate by Particle Beam LC/MS 321a

Quantitation of Hydroxybenzoates in Biological Fluids as Indices of Hydroxyl Radical Production 322a

Quantitative Determination of Retinoic Acid in Rat Serum and Rabbit Plasma by GC/NCI-MS 323a

Quantitative Determination of Lanosterol and Dihydrolanosterol in Plasma, Serum, and Tissues by GC-MS for Evaluation of Cholesterol Lowering 324a

Quantitative Determination of Butorphanol in Human Plasma by GC/ECCI/MS 325a

Quantitative Determination of the Antipsychotic Agent CP-88,059 in Human Serum by HPLC/MS/MS 326a

A NCI GC/MS Method for Olanzapine in Human Plasma 327a

Analysis of Bile Acids and Sterols in cecum and Colon Contents from the Sprague-Dawley Rat by GC/FID-MS 328a

Quantitative Determination of -Cyclodextrin in Human Urine by Electrospray LC/MS 329a

Quantitative Analysis of GR38032 by Isotope Dilution Partcile Beam-LC/MS using Normal Phase and Reverse Phase HPLC 330a

Quantification of Peptide Isotopomer Abundances and Determination of Protein Turnover Rates by Using Mass Isotopomer Distribution Analysis (MIDA) 331a

Determination of 15N Enrichment of Taurine in Cat Urine by GC/MS 332a

Enantioselective Glucuronidation of the Antipsychotic Agent 5-Fluorophenyl-hydroxbutyl-5-fluoro-phrimidinylplperazine (5F-FHPP) and Related Analogs by Rat Liver UDP-glucuronosyltransferases 333a

Derivatizations for Enhanced Detection of N-linked and O-linked Glucuronide Conjugates by LSIMS 334a

Analysis of Insulin-Acyl Glucuronide Adducts by Electrospray/Mass Spectrometry 335a

Assay of the 13C-enrichment and Concentration of Acetate in Biological Fluids 336a

Applications of GC-CRIMS to the Investigation of Metabolic Disease 337a

A Comparison of Substituted Phenylboronic Acids as Derivatization Reagents for NCI/MS 338a

Quantitative Analysis of Peptido-Leukotrienes in Nasal Secretions by Two-Dimensional Gas Chromatography/Mass Spectrometry 339a

On the Problem of Sensitivity for Detection of LTC4, LTD4, and LTE4 in LC CF-FAB 340a

Continuous Flow Liquid Secondary Ion Mass Spectrometry (CF-LSIMS) Characterization of in vitro and in vivo Metabolism of 5-Lipoxygenase Inhibitor L-702,618 341a

Characterization of Pineal Metabolites by Thermospray LC/MS/MS and GC/MS 342a

Characterization of Synthetic Immunostimulatory Lipoidal Peptides by FAB-, ESI- and MALDI-MS 343a

Enzymatic Conversion of NAAG to NAA in vivo using Microdialysis/Mass Spectrometry 344a

Hydrolysis of Peptide and Protein Drugs by Immobilized Hepatic Proteases Measured Using Continuous-Flow FAB LC-MS and MS-MS 345a

An Essay for Urinary Peptidal Leukotrienes using Immunoaffinity Extraction and Capillary HPLC / CF-LSIMS Detection 346a

Proteins

Association of Peptides with Bovine Serum Albumin (BSA) by Electrospray Ionization Mass Spectrometry 347a

Study of Molecular Association by Electrspray Mass Spectrometry 348a

Structural Characterization of the Lung Surfactant Protein SP-B by Mass Spectrometric Methods 349a

Use of Electrospray MS to Characterize Covalently Modified Proteins: Factors Affecting Resolution and Sensitivity 350a

Structural and Functional Characterization of the Lung Surfactant Protein SP-C -Electrospray Mass Spectrometric Identification of Noncovalent Dimers 351a

Reversibility of Heat Induced Conformational Changes of Proteins Studied by Electrospary Ionization Mass Spectrometry 352a

Determination of Primary Structure and Biological Activity of Different Recombinant Human Epidermal Growth Factor Proteins 353a

Structural Characterization of Cyclic RGD-Containing Peptides by Ionspray Tandem Mass Spectrometry 354a

Application of Electrospray Mass Spectrometry to Structure Studies of Bovine Adenosine Deaminase 355a

Electrospray Mass Spectrometry Characterization of Cathepsin B C-Terminal Processing 356a

Studies of The ras P21-GDP/GTP Noncovalent Complexes by Ion Spray Mass Spectrometry 357a

Comparison of Charged Peptide Derivatives for High Energy CID MS/MS 358a

High Resolution and MS/MS Matrix-assisted Laser Desorption on a fourier Transform Mass Spectrometer 359a

The Analysis of Biomolecules by Electrospray Ionization on a Magnetic Sector Tandem Mass Spectrometer 360a

Analysis of Pyridinoline and its Derivatives by Positive-Ion L-SIMS and four-sector Tandem Mass Spectrometry 361a

HPLC-PB-CI-MS and HPLC-TSP-MS of Linear Peptides (Efrapeptins) and Cyclodepsipeptides (Destruxins) of Fungal Origin 362a

Capillary HPLC/MS Analysis of Hydrophobic Peptides from the 2-Adrenergic Receptor 363a

Electrospray mass Spectrometry Analysis of Opioid Peptide Precursors 364a

Tandem Mass Spectrometric Identification of a Specific Cysteic Acid Residue in Oxidized Low Density Lipoprotein 365a

Structural Determination of a Modified Membrane Lipopeptide from Mycobacterium avium by Using Electrospray, FAB, and Precursor Ion Scanning 366a

Mass Spectral Analysis of Peptide Adducts of the Lipid Peroxidation Product 4-Hydroxy-2-nonenal 367a

Structure Determination of ESI-MS of Putative Locust Diuretic Peptides 368a

Characterization of the Dragline Protein Collected from the Spider Nephilia clavipes 369a

Charting of Pituitary Glycoproteins by Capiliary Liquid Chromatography - Electrospray Mass Spectrometry 370a

Analysis of Abnormal Glycoproteins of Patients with Carbohydrate Deficient Glycoprotein Syndrone 371a

Structure of the Disialylated Transferrin Specifically Found in Carbohydrate-Deficient Glycoprotein Syndrome 372a

HPLC/ESI/MS of Tryptic Digests on Modified Cytochromes 373a

Characterization of Cytochrome P450lin by Mass Spectrometry 374a

Chemical and Mass Spectrometric Characterization of the Heterogeneous N-terminal Lipid Modification of Photoreceptor G-Protein -Subunit 375a

Characterization of Peptides Extracted from the Human Class I MHC Molecule, HLA-B7 376a

Structural Analysis of Peptides Associated with the Class I MHC Molecule HLA-A24.1 377a

Application of Mass Spectrometry in the Determination of the Primary Structure of Interleukin-1 Converting Enzyme (ICE) 378a

Characterisation of Recombinant IL4 379a

Protein Ladder Sequencing in Solid Phase Peptide Synthesis 380a

Technical Improvements Needed to Fully Integrate MS into the Reference Hemoglobinopathy Laboratory 381a

Amino Acid Sequence Determination of Neuropeptides by Using Electrospray Ionization on a Magnetic Deflection Mass Spectrometer 382a

Use of High Resolution MSn Capabilities for Peptide Sequence Determination Using a Quadrupole Ion Trap Mass Spectrometer 383a

A Mass Spectrometric Assay for The Detection of Pyroglutamic Acid in Peptides 384a

Matrix Assisted Laser Desorption/Ionization of RNase Glycation 385a

Automated Peptide Mapping and Sequencing by LC-ESI-MS 386a

Probing Secondary Structures of Proteins by Mass Spectrometry 387a

Environmental

An Atmospheric Pressure Low-Power Microwave Plasma Ionization Source for Liquid Chromatography - Mass Spectrometry (LC-MS) 388a

A Comparison of Analytical Techniques (API/MS, GC/MS and FTiR), for the Measurement of Combustion Products from a Variable-Fuelled Automobile 389a

The Application of HPLC Flow-FAB anmd ESI-MS to the Analysis of Pesticide Transformation Products 390a

A Quantitative Study of Carbamate Pesticides Using Direct Injection/Electrospray Ionization Mass Spectrometry 391a

Sensitivity Enhancement in an Atmospheric Pressure Ionization (API) Source Mass Spectrometer via Gas-Phase Neutral Derivatization 392a

Application of Thermospray LC/MS to the Study of Small Organic Acids in Radioactive Mixed Hazardous Wastes 393a

Capillary Liquid Chromatographic Mass Spectrometric Identification of Arsenic Compounds used as Animal Feed Additives 394a

Short Path Thermal Desorption GC-MS for the Analysis of Sodium Carbonate and Sodium Bicarbonate 395a

Thermospray LC-MS Measurement of Brucine in Serum and Urine 396a

Formation of Dialkyl- and Diaryltin Buffer Adduct Ions Under Electrospray-LC/MS Positive Ionization Conditions 397a

Analysis of Ionic Textile Dyes and Degradation Products Using CE-MS and CE-MS-MS with Ionspray Ionization 398a

Characterization of Maillard Reaction Products by Capillary Electrophoresis-Mass Spectrometry 399a

Capillary Electrophoresis/Electrospray Mass Spectrometry of Some Hazardous Industrial and Agricultural Chemicals. 400a

Determination of Tin Alkylates in Environmental Samples using Thermospray and Electrospray LC/MS 401a

A Study of the Relative Particle Beam Transport Efficiency of Typical Commercial Additives in Common Reverse Phase Solvent Systems 402a

The Identification of Organosulfur Compounds in Produced Water by Mass Spectrometry 403a

Determination of Hydroxyatrazine in Water at Low-ppt Levels by using Carbon Black Cartridge Extraction and High Resolution FAB-MS 404a

Identification of Volatiles and Semi-Volatiles in Honey 405a

Using GC/MS for the identification of Volatile and Semi-Volatile Components in Food 406a

Laser Desorption/Ionization

Photodissociation-Photoionization Mass Spectrometry 407a

Protein Phosphorylation Site Study 408a

Complex Formation Between Macromolecules in Matrix-Assisted Laser Desorption Ionization 409a

Structural Characterization of A Cytosolic Glutathione-s-transferase by Fast Atom Bombardment CAD and Matrix Assisted Laser Desorption Mass Spectrometry 410a

Gas-Phase Ion-Molecule Reactions of Peptide Ions with Small Neutral Molecules 411a

A Comparative Study of Matrices for Matrix-Assisted Laser Desorption/Ionization (MALDI) of Taxol and Various Taxanes 412a

Matrix-assisted Laser Desorption/Ionization by Fourier Transform Mass Spectrometry 413a

Applications of Mass Spectrometry to the Determination of Tertiary and Quaternary Protein Structure 414a

Mass Spectrometric Investigation of Proteins Separated by 2-dimensional Electrophoresis 415a

Matrix-Assisted Laser Desorption/ionization TOF Mass Spectrometry as a Probe of Protein Structure 416a

Evaluation of Phosphorylation-dependent Protein Bioactivity by Matrix-assisted Laser Desorption Time-of-flight Mass Spectrometry 417a

Evaluation of Matrix-Assisted Laser Desorption/Ionization Time-of-Flight Mass Spectrometry for use in Clincial Assays 418a

Real Time Analysis of Single Aerosol Particles 419a

Examination of Native and Degraded IgG Antibodies by Micellar Electrokinetic Capillary Chromatography and Matrix Assisted Laser desorption/Ionization Mass Spectrometry 420a

Carbohydrate-Containing Matrices for MALDI: Applications to Recombinant Protein Digests and in situ Digests of Proteins from Two-Dimensional Gels 421a

An Investigation into the Advantages Offered by an Array Detector on Magnetic Sector Instrumentation for Different Ion Sources 422a

Comparison of Field Desorption and Matrix Assisted Laser Desorption Ionization of An Industrial Oligomeric Additive 423a

Direct MALD-MS Analysis of Protease Digests: Comparative Study of Analysis Parameters 424a

Cleavage of the Asp-Pro Bond of Peptides in MALD-TOF Mass Spectrometry 425a

MALD on a Magnetic-Sector Mass Spectometer equipped with an Integrating Array Detector 426a

An Improved Illumination System for Matrix-Assisted Laser Desorption 427a

Spatial Map of the Polycyclic Aromatic Hydrocarbons (PAHs) in the Allende (CV3) and Bjurbole (L4) Meteorites 428a

Analysis of Polycyclic Aromatic Hydrocarbons (PAHs) in Cosmic Dust 429a

Laser Desorption Studies of Oxidative Decomposition in K3C60 and related Fullerenes 430a

Analysis of Lipid-A from Gram Negative Bacteria Using Matrix-assisted Laser Desorption Time-of-Flight Mass Spectrometry 431a

Matrix-Assisted CO2 LD/FTMS of Peptides 432a

Direct LD/FTMS of Microbial Polyesters 433a

Detection of Large Molecular Ions by Secondary Ion and Electron Emission 434a

Photodissociation of Precursor Ions Produced by MALDI in a Four-Sector Tandem Mass Spectrometer 435a

Matrix-Assisted Laser-Desorption Mass Spectrometric Analysis of Proteins Adsorbed on Nylon Membranes 436a

Time-of-Flight Mass Spectrometry Studies of Laser Desorbed Neutral Gramicidin S Molecules 437a

Trapped Ions

Consideration for the Size and Power Reduction of a Field Transportable Ion Trap Mass Spectrometer 438a

The Next Horizon in Portable GC/MS for Air Monitoring Applications 439a

Larger Cells for ICR Spectrometers with Electromagnets 440a

Laser Desorption Ion Trap Mass Spectrometry of the Polymeric Component of Coal 441a

Isotopic Masses at ppb Precision (!) from FT/ICR Mass Difference Measurements 442a

Applicaton of a Mechanical Shutter for Pressure Control in External Source Electrospray FTICR 443a

A Novel Benchtop Ion Trap Mass Spectrometer for GC/MS/MS 444a

Infrared Multiphoton Dissociation Studies in the Quadrupole Ion Trap using a Multi-Pass Optical Arrangement 445a

Boundary-Activated Dissociation of Mass-Selected Ions in a Quadrupole Ion Trap 446a

Nature and Effect of Non-Linear Resonances in Ion Traps 447a

Quadrupolarized ICR Cubic Ion Trap 448a

Contaminant Analysis Using Novel Sampling Strategies and Laser Desorption Mass Spectrometry 449a

An Improved Calculation of Peak Shape in FTMS 450a

SWIFT Excitation/Ejection of Ion Axial Motion in Quadrupole Ion Trap Mass Spectrometry 451a

Minimization of Radial Electric Field Effects in Open Cell Geometries used for External Source FTICR 452a

New Methods of Operation for the Quadrupole Ion Trap 453a

Time-Dependent Behavior of Multiply Charged Electrosprayed Ions Trapped in a Fourier Transform Ion Cyclotron Resonance Mass Spectrometer 454a

Enhanced Trapping of Laser Desorbed Ions in a Quadrupole Ion Trap by use of a Transient RF Trapping Field 455a

The Reduction of Matrix Effects in a Quadrupole Ion Trap Mass Spectrometer 456a

Protein Structural Elucidation by Electrospray Ionization Tandem Fourier-Transform Mass Spectrometry 457a

Ion Trap Mass Spectrometry Combined with Inductively Coupled Plasma/Mass Spectrometry 458a

Effects of Ion Trap Parameters on Mass Axis Stability: Influence of Manifold Temperature, Pressure, and Axial Modulation Voltage on Mass Spectra of Hydrocarbons 459a

Optimizing Ion Accumulation in External Source Fourier Transform Mass Spectrometry 460a

Electrospray on an Ion Trap Mass Spectrometer: Comparison of Axial vs. Diagonal Injection of Ions into The Trap 461a

Off-Center ICR Cubic Ion Trap: Reduction of Space Charge and Manipulations of Coherent magnetron Motion 462a

Non-Resonance Excitation and Ejection in Ion Trap 463a

A Simple Physical Model for the Origin of the 2 z Resonance in FT-ICR 464a

A Basic Theoretical Approach for the Description of Non-Linear Ion Traps 465a

A New Type of Structures of Linear Quadrupole Mass Filters and Ion Traps with and without FT Techniques 466a

Ion Trajectory Simulations for a Radio Frequency Glow Discharge Fourier Transform Ion Cyclotron Resonance Mass Spectrometer 467a

Selected Ion Storage Target Compound Analysis in Complex Matrices Using Ion Trap GC/MS 468a

Optimization of a New API Ion Trap System for On-Line HPLC and CE Applications 469a

Particle Beam Mass Spectrometry on Ion Trap and Sector Instrumentation for Pharmaceutical Analysis 470a

An Electrostatic Ion Guide Interface for SIMS with an FT/ICR Mass Spectrometer 471a

Determination of Ion Frequencies in an Quadrupole Ion Trap Using a Fast DC Pulse "Pump" and a Laser "Probe" 472a

Evidence for "Black Holes" during EI in a Quadrupole Ion Trap Mass Spectrometer 473a

Ion Isolation and Modulated Ion Excitation for GC-MS/MS In An Ion Trap Mass Spectrometer 474a

Ion Energy-Modulated Stored Waveform Ion Modulation (SWIM) Two-Dimensional FT/ICR MS/MS 475a

Ion Fragmentation & Structure

Activation of Aromatic Rings in Thermal Energy Gas Phase Metal Ion-Molecule Reactions 476a

Intermediacy of Ion-Neutral Complexes in the Dissociation of Protonated Alkyl Ether Ions 477a

On the Role of Ion-Neutral Complexes in the Alkene Loss from the Molecular Ions of Alkyl Phenyl Thioethers 478a

Competitive Fragmentation Pathways for Ion-Neutral Complexes in Metastable Ions from Electron Impact on SS-Fluorophenetole 479a

Structure and Vibrational Frequencies of ionized Ethane: A Fluctional Molecule? 480a

Theoretical Study of the Ring Closure of the 1,7-Octadiyne Cation 481a

Doubly Ionized States of Fluorinated Methanes 482a

Singlet State Energy Levels of C2H4 2+ 483a

An Experimental and Computational Study of Double Ionization of CH2I2, CHI3 and CI4 Molecules 484a

The Relative Migratory Aptitudes of Fluoride and methyl in a Gas Phase Carbocation 485a

A Mechanism of Gas Phase Aldose-ketose Isomerization: A study using Tandem Mass Spectrometry and Theoretical Calculations 486a

Competition Between Dissociation and Bond Formation in CH3CHOH+ and CH2CH3 Formed by Bimolecular Processes 487a

Gas-Phase Radical Cation Rearrangements of 4-Vinylcyclohexene to Bicyclo[3.2.1]-2-Octene 488a

Dynamics of the Unimolecular Dissociation of Dimethylformamide Radical Cation 489a

Fragmentation of Diethyl Dicarboxylates under EI and CI Conditions 490a

A Comparative Study of the Dynamics of Low and Medium Energy Collision-Induced Dissociation of Isomeric Ions 491a

Internal Energy Effects on the Fragmentation of Ions and Neutrals 492a

Decomposition of the Ethyliodonium Ions in the Gas Phase 493a

Dechlorination of PCB's in Electron Capture Negative Ion Chemical Ionization Mass Spectrometry 494a

EI-Linked Scan Studies of Dimethylaminomethylene-O-Trialkylsilyl Nucleosides 495a

The Neutral Products from the Remote Site Fragmentation of Fatty Acid Derivatives 496a

Collisional Dissociation Technique for Assignment of metalloporphyrin Cation Electronic Structure 497a

Ion Molecule Reactions and MS3 Studies on Taxol and Related Natural Products 498a

Investigation of Fluoroformic Acid, Its Radical Cation, and Its Protonated Form by Tandem Mass Spectrometry Techniques 499a

Negative Ion Chemical Ionization/Collisionally Activated Dissociation Studies of Aryl Pentafluorobenzoates 500a

HTeTeH is Stable in the Gas Phase 501a

Organic Sulfur Radicals by Neutralization-Reionization Mass Spectrometry 502a

Neutralization-Reinization Mass Spectrometry (NRMS) Studies of Ethylene Glycol Polymers 503a

Analysis of Triphenylmethane Dyes by Mass Spectrometry 504a

Do Reactivity Probes Reveal Ion Structure? The Case Against Dipole-Stabilized Ions 505a

The Structures of Gas-Phase C7F7+ Ions 506a

Structural Investigation of Impurities in Synthesis of LY225698 507a

Where do Fullerenes Come from, Anyway? 508a

The Resilience of C60 Towards Decomposition and Ionization 509a

Isotope Effects on the Mass Spectral Fragmentation of the Mixed Glycerol-d5-glycerol Clusters 510a

Comparison Between Tandem Mass Spectra of Cyclic Peptides Obtained with a Four-Sector Mass Spectrometer and an External Ion Source FTMS 511a

Mechanisms of Fragmentations of Cationic Peptide Ions: 512a

Elimination of Propene from Metastable n-Propyl- and isopropylammonium Ions 513a

Biological Miscellaneous

Measurement of Long-Chain Fatty Acyl CoA Species by GC/MS 514a

Low-energy Tandem Quadrupole Mass Spectrometry of unsaturated FAME: A Revealing Study of Unique Ion Chemistry 515a

Tandem Mass Spectrometry of Multiunsaturated Triacylglycerides: Problems and Solutions 516a

Characterization of Dairy Triglycerides Isolated Using Supercritical Fluid Fractionation by Field Desorption, Desorption Chemical Ionization, and Tandem Mass Spectrometry 517a

Analysis of Bull Sperm Plasma Membrane Phosphatidylcholines by Negative Ion FAB-CAD-MS/MS 518a

Characterization of Oxidized Phospholipids Using Fast Atom Bombardment Tandem Mass Spectrometry 519a

Thermospray LC/MS Analysis of Phospholipid Molecular Species in Rat Brain Mitochondria 520a

Positive-ion L-SIMS and Four-Sector Tandem Mass Spectrometry of Aminophospholipids Using Scanning-array Detection 521a

Characterisation of Glycolipids and Sphingolipids by Matrix-Assisted Laser Desorption 522a

Examination of Phospholipids by Matrix-Assisted Laser Desorption 523a

Polymers

Comparison of Several Contemporary Ionization/Mass Analyzer Techniques for Large Components of Complex Fossil-Derived Materials 524a

FAB-MS and SIMS Characterization of Polyamic Acid Precursor Formation from BPDA and ODA 525a

Secondary Ion Detection of Polymers in Matrix-Assisted Laser Desorption Mass Spectrometry 526a

Rapid Evaluation of Polymers using Particle Beam/Chemical Ionization Mass Spectrometry 527a

Desorption Chemical Ionization and Liquid Secondary Ion Mass Spectrometry of Dimer and Trimer Fatty Acids 528a

Application of MALDI Mass Spectrometry to Different Classes of Synthetic Polymers 529a

Direct Analysis of Polypropylene Compounds by Thermal Desorption and Pyrolysis Mass Spectrometry 530a

Thermal Decomposition-(Gas Chromatography)-Mass Spectrometry [TD-(GC)-MS] for Thermal Behavior Study of Polymers 531a

A Method for Distinguishing Chlorosulfonated Polyethylene from Chlorinated Polyethylene Using Pyrolysis/GC/MS 532a

GC/MS Determination of Aromatic Isocyanates and Amines as Degradation products in Polyurethane Foams Used in Breast Implants 533a

GPC/MS Using a Particle Beam Interface 534a

Polyamic Acid and Polyimide Characterization Using GC/MS and Particle Beam LC/MS 535a

Direct Chemical Analysis of UV Laser Ablation Products of Organic Polymers Using Reflection Time-of-Flight Mass Spectrometry (Re TOF-MS) and Gas Chromatography/Mass Spectrometry (GC/MS) 536a

Analysis and Quantification of Polymer Additives in Polyolefins by Particle Beam LC/MS 537a

Surface Additives on Bulk PET Studied with High Mass Accuracy ToF-sSIMS 538a

Nonpolar Polymer Analysis by Continuous Flow Fast Atom Bombardment Mass Spectrometry (CF-FAB/MS) 539a

WEDNESDAY POSTERS

Metabolism & Drugs

Analysis of Acycarnitines in Biological Fluids by Electrospray LC/MS: Application to Human Metabolism Studies 540a

Derivatives for Detection of Anabolic Ketosteroids by Positive Electrospray Mass Spectrometry 541a

Determination of 5-HT3 Antagonists in Biological Fluids Using Heated Nebulizer and Electrospray LC/MS and LC/MS/MS 542a

Identification of Xenobiotic Conjugates by Positive and Negative Ion Electrospray Mass Spectrometry 543a

Identification of Metabolites and RG-12915 in Human Urine Using API-LC/MS and LC/MS/MS Techniques 544a

Characterization of Biliary Rapamycin Metabolites by Ionspray Liquid Charomatography/Mass Spectrometry 545a

Saxitoxin Detection in Rat Urine by HPLC and CE-ESIMS 546a

Confirmation of Des-Methyl Danofloxacin Residues in Swine Liver by HPLC/ESI-Tandem Mass Spectrometry 547a

An HPLC/ESI-Tandem Mass Spectrometry Method for the Confirmation of Doramectin Residues in Cattle Liver and Fat 548a

Identification of the Anticonvulsants Felbamate and Phenytoin and their Metabolites by Thermospray Tandem Mass Spectrometry in Clinical Human Urine Samples 549a

Identification of the Felbamate Metabolite 3-Carbamoyloxy-2-Phenylpropionic Acid (W-3049) in Human and Dog Urine by Negative Ion Thermospray Tandem Mass Spectrometry 550a

Analysis of The Squalestatins By On-line Packed Capillary LC-DLSIMS 551a

DCI, TSP and ESI Investigations of SS-carbolines 552a

Identification of Fadrozole (CGS 16949a) Metabolites in Human Urine by Stable Isotope Pattern Recognition Gas Chromatography/Mass Spectrometry 553a

Drug Metabolism Studies Using "Intrinsic" and "Extrinsic" Labels: 15N vs CI In Midazolam 554a

Profiling of Tryptophan Metabolites in Cell Culture by HPLC-CRIMS 555a

The Application of Liquid Chromatography/Chemical Reaction Interface Mass Spectrometry (LC/CRIMS) to Quantitative Studies in Drug metabolism 556a

Analysis of Catecholamine Metabolites by Electron Capture Mass Spectrometry 557a

Studies of nitrogen Metabolism Using CRIMS: Labeled Glutamine in Cell Culture 558a

Hepatic First-Pass Metabolism of Diphenhydramine in Sheep 559a

Characterization of Metabolites of [14C] Cyoctol Excreted in the Urine of Rats by Gas Chromatography-Mass Spectrometry 560a

The Metaboism of Essential Fatty Acids in Humans: Studies on the Effects of Dietary Fats on the Conversion of 2H5-18:3n3 & 2H5-18:2n6 to Long Chain Polyunsaturates 561a

The Metabolism of Fluorinated VPA Analogues 562a

Identification of Glutathione Conjugates of Tris-(2,3-Dibromopropyl)phosphate by Tandem Mass Spectrometry: Applications of Stable Isotopes as Mechanistic Probes 563a

A GC-MS-MS Screening Strategy for the Identification of N-Acetylcysteine Conjugates Derived from Chemically-Reactive Drug Metabolites of Haloalkanes 564a

Applicaiton of Negative Ion Chemical Ionization Isotope Dilution Gas Chromatography/Mass Spectrometry to Pulse Dose Bioavailability Studies of mefloquine 565a

Intensive Hydrogenation: A New Concept for Biological Sample Preparation 566a

In Vitro Pancreatic Lipase hydrolysis of Emulsified Common Fats and Oils by high Temperature Gas Chromatography/Flame Ionization and Mass Spectrometry. 567a

Plasma Testosterone by Negative Chemical Ionization GC/MS 568a

Comparison of Electron Impact, Positive and Negative Chemical Ionization Mass Spectrometry of Benzodiazepines 569a

Characterization of LTD4 Antagonist Metabolic Profiles Using Capillary HPLC / Continuous-Flow Liquid-Secondary-Ion Mass Spectrometry 570a

FAB Accurate Mass Measurements Using a Rotating Probe on the VG ZAB-2SE Mass Spectrometer 571a

Structure Determination and Diagnostic Value of Abnormal Bile Acids in Urine from Patients with Generalized Peroxisomal Disease 572a

The Identification of Ketoconazole Metabolites in the Mouse Liver by liquid SIMS ms/ms 573a

Complete Mass Spectrometric Structure Elucidation of an Unknown Possible Metabolite 574a

Structure Elucidaton of Novel Leukotriene B4 metabolites from Cultured human Keratinocytes 575a

Multiresidue Analysis of Sulfonamide Antibiotics in Milk Using LC-Atmospheric Pressure Chemical Ionisation-MS 576a

Studies of New Secondary Metabolites of Streptomyces Spectabilis by FABMS, FABMS/MS, and LC/FABMS Moving Belt Interface 577a

Proteins

Analysis of Very Hydrophilic Proteins by Electrospray Mass Spectrometry 578a

Mass Spectrometric Characterization of a Family of Hydrophobic Peptides with Antibiotic Properties Containing Both L- and d-Amino Acids 579a

Comparative CID Study of Peptides Using Electrospray Ionization Versus LSIMS as the Primary Ionization Method 580a

Electrospray Ionization Mass Spectrometry of Peptides and Proteins in the Presence of Detergents 581a

Optimization of LCMS Flow Rate for Maximum Mass Spectrometer Detection and Minimum Run Time. 582a

Analysis of Peptides by the Desorption/Ionization Technique K+IDS, K+-Ionization of Desorbed Species 583a

Fast Atom Bombardment Mass Spectra of Peptides Derivatized with 2-Iminothiolane 584a

Chloroformate Derivatization of Peptides for Detection by FAB-MS 585a

Identification of Novel Chemical Modifications in Proteins: gem-Diamino formation and Guanidino N-displacement Product in -Lactamase and Carbonic Anhydrase 586a

The Characterization of Products of Reactions of Hydroxyl radical with Amino Acids and Peptides using GC/MS 587a

ESI/MS Detection and Characterization of Novel Thiohydantoin Amino Acid Derivatives 588a

Synthesis and Mass Spectrometric Characterization of Reference Phosphopeptides 589a

Tandem Mass Spectral Studies of N-Acylated Tetraglycines and Tetraalanines as Models for the Free Oligopeptides 590a

Hydrogen/Deuterium Exchange of Gaseous, Multiply-Charged Protein Ions 591a

Conformation of Proteins Studied by Deuterium Exchange Electrospray Ionization Mass Spectrometry 592a

Protein Backbone Amide Hydrogen Exchange Determined by HPLC FABmS: Applicaton to Rabbit muscle Aldolase 593a

Using AMASS to Determine a Criterion for the Verification of Peptide Structrue 594a

Interpretation of Peptide CID Spectra using Artificial Neural Networks 595a

Rapid Identification of Proteins by Database Matching of Proteolytic Peptide Masses 596a

Molecular Characterization of Surface Topology in Protein Tertiary Structures by Amino-Acylation and Mass Spectrometric Peptide Mapping 597a

Characterisation of the WHO International Reference Standard for Thyroxine Binding Globulin by ESMS 598a

Phosphorylation of Human and Bovine Prothymosin In Vivo 599a

Characterization of the Phosphorylated Ribosomal Protein S7 from Tetrahymena 600a

Mass Spectrometry of Phosphopeptides Isolated by Immobilized Metal-Ion Affinity Chromatography 601a

An Approach to Characterize Phosphorylation Sites in Phosphopeptides and Phosphoproteins by Combining Enzymatic and Chemical Reactions with MALDI-TOF Mass Spectrometry 602a

Analysis of Amylin and Related Peptides from Biological Fluids Using LC/MS/MS 603a

Characterization of SS-Amyloid1-42: A Major Component of Cerebrovascular Amyloid Deposits 604a

ESMS of Human Serum Amyloid P Component: Confirmation of the Structure and Analysis of the Role of the Glycan 605a

Identification of Water Insoluble Human Lens Crystallins by Mass Spectrometry 606a

Elucidation of High-order Structure in Lens -crystallin by Continuous-Flow HPLC FABMS 607a

Analysis of the Bacitracin Complex by LC-Ionspray mS 608a

Post Translational Modifications of Recombinant Barley -amylase 1 Expressed in Yeast, Characterized by Electrospray Mass Spectrometry 609a

Capillary LC - Electrospray - MS Reveals Expression of more than one Rat Proopiomelanocortin 610a

Characterization of Three Isoforms of Soybean Agglutinin by ESI MS 611a

Characterization of Protein Post-Translational Modification by ESI-MS 612a

Primary Structure Characterisation of Legume Lectins; Sequence Assignment and Identification of post-translational Modifications using LC-MS and 1C-MS-MS 613a

Investigations into the Post-Translational Modification and Mechanism of Isopenicillin N: Acyl-coenzyme A Acyltransferase using EIMS 614a

Recombinant Human Neurotrophin-4 (NT-4): Characterization of Protein Folding by Matrix-Assisted Laser Desorption TOF and Electrospray Ionization Mass Spectrometry 615a

Effects of Anions on Electrospray Ionization Mass Spectra of Peptides and Proteins 616a

Analysis of Biliproteins by Electrospray Ionization Mass Spectrometry 617a

Determination of the Disulfide Bonding Pattern of Peptide Toxins from the Spider Agelenopsis Aperta Using Electrospray Ionization Mass Spectrometry 618a

Mass Spectrometric Characterization of the Phosphorylated Proenkephalin A-neuropeptides 619a

Identification of Two Sites of Phosphorylation in Bleached Bovine Rhodopsin by Tandem Mass Spectrometry 620a

Mass Spectrometry of Protein Samples Containing Detergents 621a

Environmental

Predicting Degradation Products of Environmental Contaminants by On-line Electrochemistry/Mass Spectrometry 622a

A Mass Spectrometer Based Diagnostic to Analyze the Hostile, High Enthalpy Exhaust of a Hypersonic Engine 623a

Identification of Polychlorodibenzothiophenes in Crab Tissues from Raritan/Newark Bay 624a

Neutral Precursor Scans 625a

Residual Volatiles Analysis of Deacidification Treatment of Books Using On-Line SFE GC MS 626a

MS/MS Characterization of Phosphate Esters 627a

Extraction of Trace Elements in Coal Fly Ash and Subsequent Determination by Inductively Coupled Plasma Mass Spectrometry (ICP-MS) 628a

Determination of Methanol in Water Samples using a Modified EPA Method 8015, Direct Injection GC/MS, and Purge and Trap GC/MS 629a

Chemical Ionization of Pesticides Using Ion Trap Technology 630a

Low PPB Detection Limits for the Analysis of Atmospheric Contaminants in Ultrapure Inert Gases 631a

Enhancement of Molecular Ion Detection by Variation of Mass Analyzer Thermal Energy for C10-C28 Alkanes by ITD/MS 632a

Survey of Volatile Organic Chemical Emissions from Waste Compsoting Facilities Using Protable Samples and Thermal Desorption Gas Chromatography/Mass Spectrometry 633a

Direct Detection of Tributyl Phosphate Adsorbed on Surfaces of Environmental Interest by Static SIMS 634a

A New Analysis Technique for Environmental Levels of Mercury Using Inductively Coupled Plasma-Mass Spectrometry 635a

Evaluation of Electrospray and FAB for Study of Organometallic Parasiticides 636a

Determination of Acid and Base-Neutral Pesticides in Water by LC-MS with a New Micro Particle Beam Interface 637a

Analysis of Pesticide Residues in Food Using GC/MS/MS with an Ion Trap Mass Spectrometer 638a

Ion Trap GC/MS Analysis of Pesticides Using Chemical Ionization with Selective Ion Ejection 639a

Compositional Analysis of Submicron Particles in Air by Time-of-Flight Mass Spectrometry 640a

Matching Probability of Library Search in Screening Environmental Samples by GC/MS 641a

Identification of Surfactants in Formulated Detergents by using FAB on the AutoSpec-Q Mass Spectrometer 642a

Detection of Metal Complexing Agents on Mineral Surfaces by Static SIMS 643a

Infraret Pyrolysis of Polymers for GCMS Analysis 644a

Modular Inlet Systems and Sampling Devices for Mobile Environmental Mass Spectrometry 645a

Automated Analysis of Selected Organic Compound in Urban Air by a (low cost ?) Isotopic Dilution Criofocussing GC/MS Method. 646a

A Novel High Resolution Mass Spectrometer for Automated Target Compound Analysis 647a

LC/MS Analysis of Mutagenic/Carcinogenic heterocyclic Aromatic Amines in Food Products 648a

Laser Desorption/Ionization

Indirect Measurement of Spatial Spread and Initial Velocity Spread of Ions Produced in MALDI 649a

High Mass Resolving Power for High-Mass Ions in LD FT/ICR/MS: Quadrupolar Axialization and Ion Cooling 650a

MALDI Fourier Transform Mass Spectrometry 651a

Heavy Atom Effects on Matrices for Matrix-Assisted Laser Desorption/Ionization Mass Spectrometry 652a

Direct UV Laser Desorption Ionization of Peptides containing Absorbing Chromophores 653a

Matrix Assisted Laser Desorption Ionization of Hydrophobic Peptides and Proteins 654a

Monitoring Biomolecular Reactions Using Matrix Assisted Laser Desorption Mass Spectrometry 655a

Geometric Signal Averaging Applied to Matrix-Assisted Laser Desorption/Ionization Time-of-Flight Mass Spectrometry 656a

Matrix-Assisted Laser Desorption/Ionization of Oligonucleotides 657a

Ladder Sequencing of Post-translationally Modified Proteins 658a

Matrix-assisted Laser Ablation of Proteins and Oligonucleotides Using Nanosecond pulses of Tunable Mid-ir Radiation 659a

Structural Characterizationof Oligonucleotides by Matrix-Assisted Laser Desorption/Ionization Mass Spectrometry 660a

Collector Studies of Angular Distributions and Fragmentation of Proteins and Oligonucleotides Ablated from Ice and Uv-absorbing Matrices 661a

Effects of Desorption Technique and Post-Ionizing Laser Pulse Width on Molecular Fragmentation 662a

Laser Desorption and High Temperature Methods for Vaporization and Ionization in Particle Beam LC/MS Interfacing 663a

Power-dependent Calibration Shifts in Pulsed Laser Ablation Time-of-flight Mass Spectrometry 664a

Hyperthermal Surface Ionization Mass Spectrometry in Supersonic Molecular Beams 665a

pH Effects and Insulin Cleavage in Matrix Assisted Laser Desorption Mass Spectrometry 666a

Investigating the Ionization Step in MALDI: Matrix-Dependent Formation of [M+H]+ vs. [M+Na]+ Ions of Small Peptides 667a

A Postacceleration Detector for Time-of-flight Mass Spectrometry Utilizing Ion To Photon Conversion 668a

High Mass Resolution and High Mass Accuracy MALD/I Spectra with a Triple Electrostatic Analyzer Time-of-Flight Mass Spectrometer (TOF-MS) 669a

Initial Kinetic Energies of Peptide Ions Formed by MALDI 670a

Design of a New Flow Probe for Continuous-Flow Matrix-Assisted Laser Desorption Ionization 671a

Optimization of Ion Extraction and Ion Detection for Continuous-Flow Matrix-Assisted Laser Desorption Ionization 672a

Basic Matrices for the Matrix Assisted Laser Desorption/Ionization Mass Spectrometry of Proteins and Nucleic Acids 673a

Influence of Amino Acid Gas Phase Proton Affinities on Ion Yield from Matrix Assisted Laser Desorption Ionization (MALDI) 674a

A New Matrix for MALDI Analysis of Water Insoluble Organic Molecules 675a

Studies of Oligonucleotides by matrix-assisted Laser Desorption Time-of-Flight Mass Spectrometry 676a

Cleavage of Interchain Disulfide Bonds Following Matrix-Assisted Laser Desorption 677a

Analysis of Mycotoxins from Amanita Phalloides by Matrix Assisted Laser Desorption Mass Spectrometry 678a

Antisense DNA Therapeutics: Use of Matrix-Assisted Laser Desorption Mass Spectrometry for Complete Sequence Verification of Methylphosphonate Oligonucleotides 679a

Angular- and Time-resolved Intensity Profiles of Ejected MALDI Ions 680a

Trapped Ions

An External Ion Source FTMS for the Analysis of High Molecular Weight Biomolecules 681a

Storage Tandem MS, Nucleophilic Substitutions in the Gas Phase 682a

The Effect of Z-Direction Stretched Geometry on Ion Injection into a Quadrupole Ion Trap Mass Spectrometer 683a

Deflection of Laser-Produced Ions in Laser-Desorption/FTMS 684a

Determination of Relative Dissociation Energies in an Ion Trap Mass Spectrometer 685a

Trajectory Modeling of Electrosprayed Protein Ions in an FT/ICR 686a

Equilibrium Distribution of Space Charge in a Quadrupole Ion Trap 687a

Chemical Ionization in Ion Trap GC-MS Using Selective Ion Ejection Techniques 688a

Numerical Computation of Trapping and Excitation Electric Fields and Ion Trajectory Simulations in an ICR Ion Trap 689a

Non-Linear Resonance Conditions and their Relationships to Higher Multipole Fields in Quadrupole Mass Filters and Non-linear Ion Traps 690a

Electric Trap Fields and High Mass Ions in FTMS: Peak Ratios 691a

Simulation of Excitation Profiles Generated by External Source FTICR Ion Distributions 692a

Experimental Investigation of Ion Secular Frequency During Isolation in a Quadrupole Ion Trap 693a

Optimization of the Simple Open Cylindrical Trapping Geometry for FT/ICR 694a

Determination of Phosphorylation Sites on the Sendai Virus P Protein by MALD-TOF and MALD-ITMS 695a

Mechanistic Study of Saccharide Fragmentations Using Fourier Transform Mass Spectrometry and Semi-empirical Calculations (AM1) 696a

Investigations Into The Factors Which Affect Mass Measurement Accuracies Obtained with the Quadrupole Ion Trap Mass Spectrometer 697a

Uni-Directional Ion Ejection in Ion Trap 698a

Internal Ion Impact Ionization in FT/ICR Mass Spectrometry 699a

Mass-Selective Ion Accumulation in the Ion Trap: Ion Injection Using Filtered-Noise Fields 700a

Self-CI in the Ion Trap 701a

Combined RF and Magnetic Trapping in a High Pressure Fourier Transform Mass Spectrometer 702a

Electron Beam Potential Depression as an Ion Trap in Fourier Transform Ion Cyclotron Resonance Mass Spectrometer 703a

Ion Molecule Reactions and Electron Detachment of O2 - in a Quadrupole Ion Trap Mass Spectrometer 704a

Negative-ion Fragmentation Pathways of Four Isomers of Dinitrotoluene (DNT) 705a

Extended Mass-to-Charge Range Operation of a Non-Linear Quadrupole Ion Trap 706a

Pulse Sequency for the Study of Simultaneously Trapped Positive and Negative ions with ICR 707a

Multiparticle Simulations of Operating Modes of the Quadrupole Ion Trap Mass Spectrometer 708a

New Applications of Ion Tomography 709a

Computer Simulations of Ions in an Electrostatic Ion Guide for FT/ICR Mass Spectrometry 710a

Investigations in Resonance Excitation in the Quadrupole Ion Trap Mass Spectrometer 711a

Characterization of High-Mass Analysis on the Quadrupole Ion Trap Mass Spectrometer 712a

Evaluation of a Low Cost, Low Homogeneity, Vertical Bore 7 T Magnet for FTICR 713a

Matrix-Assisted Laser Desorption/Ionization in the Quadrupole Ion Trap: A New Method for Trapping Energetic Ions Using Controlled Gating of the Trapping Field 714a

The Development of Mass-Selected Automatic Gain Control on a Quadrupole Ion Trap Mass Spectrometer 715a

Gas Chromatography/Ion Trap Mass Spectrometry Using an External Ion Source 716a

A New Model for the Estimation of Ion Kinetic Energy in a Quadrupole Ion Trap 717a

FTMS External Ion Source for Ion-Molecule Reactions 718a

Characteristics of a FT/ICR Mass Spectrometer based on a 0.4 T Permanent Magnet 719a

High-Resolution Fourier-Transform Mass Spectrometry of Large Biomolecules 720a

Elemental Analysis & Isotope Ratios

Experimental and Theoretical Relative Ion Yields for Glow Discharge Mass Spectrometry 721a

Development of a Pulsed-Gas Glow Discharge Ion Source for High mass Resolution on a Fourier Transform Ion Cyclotron Resonance Mass Spectrometer 722a

The Effect of Cryogenic Cooling on the Gaseous Impurity and Analyte Ion Signals in GDMS 723a

Characteristics of a Radio Frequency Powered Glow Discharge Cell for the Analysis of Flat Samples 724a

Analysis of Electrodeposited Metal Ions by Glow Discharge Mass Spectrometry 725a

An Improved Double Quadrupole Mass Spectrometer for Versatile Radio Frequency Glow Discharge Studies 726a

Glow Discharge - Isotope Dilution Mass Spectrometry 727a

Isotopic Analyses by Glow Discharge Mass Spectrometry 728a

Design of an Array - Detector Mattauch - Herzog Mass Spectrometer for Atomic Mass Spectrometry 729a

Optimization of an ICP/High Resolution Mass Spectrometer System for Elemental Analysis 730a

ICP TOFMS System for Use in Elemental Analysis 731a

Elemental IonSpray-Mass Spectrometry: Analysis of Solutions of Metal Salts 732a

Metal Isotope Ratio Determination with Laser Desorption Time-of-Flight Mass Spectrometry 733a

Determination of Subpicogram Quantities of Technetium-99 in Environmental Samples by Positive Thermal Ionization Mass Spectrometry 734a

Simultaneous Observation of UO+ and U+ Ion Ratios via Total Evaporation Thermal Ionization Msss Spectrometry 735a

Lead Analysis by Electron Capture Negative Chemical ionization GC/MS 736a

A Study of Meso-Substituted Zinc Tetrabenzporphyrins by Fast Atom Bombardment Mass Spectrometry (FAB/MS) 737a

Gas Chromatography-Combustion Isotope Ratio Mass Spectrometry (GCC-IRMS) at Femtomole Carbon Levels and High Enrichments (dPDB>100 0/00) 738a

Comparison of Polymer Additives Analysis by High Temperature GC/MS vs. Particle Beam LC/MS 739a

Electrospray, API, Supersonic Beams

The Roles of Solvation, Basicity, and Hydrophobicity in the Electrospray Mass Spectrometry of Amines and Amino Acids 740a

Sensitivity, Dynamic Range and Solvent Effects in Electrospray Ionization 741a

Investigation of Aqueous Solution Chemistry using Electrospray Mass Spectrometry 742a

Peptide Charge State Effects on Electrospray and Capillary Electrophoresis/Electrospray Mass Spectrometry 743a

The Use of Multiple Sprayer System in the Electrospray Mass Spectromety 744a

Characterization of a New Atmospheric Pressure Ionization Interface for Liquid Chromatography-Mass Spectrometry 745a

Fundamental Energy Studies of Electrospray Ions Entrained in a Free Jet Expansion 746a

Application of Orifice Potential Ramping for the Sequence Identification of Phosphorylated Proteins 747a

Capillary LC/MS and LC/MS/MS Analysis of Peptides Using a New Capillary LC/MS Interface and A Redesigned Collision Cell 748a

Combining Capillary Electrophoresis with Electrospray ionization/Ion Trap Mass Spectrometry for Biopolymer Analysis 749a

High Mass Accuracy Electrospray Fourier Transform Ion Cyclotron Resonance Mass Spectrometry 750a

FTICR Characterization of Beam Dynamics and Electrostatic Contributions to Electrospray Ion Kinetic Energy 751a

A Direct Injection Electrospray Source for Fourier Transform Ion Cyclotron Resonance Mass Spectrometry 752a

High Energy CID of Multiply Charged Polypeptides and Polynucleotides Produced by Electrospray 753a

High Flow Electrospray LCMS on a High Performance Magnetic Sector Mass Spectrometer 754a

On-Line Interface of Capillary Electrophoresis with Time-of-Flight Mass Spectrometry 755a

Electrospray Ionization-Collisionally Activiated Dissociation on a Bench-Top Mass Spectrometer 756a

Secondary Electron Resolved Mass and Charge State Spectrometry 757a

The Use of a Fast Scanning Focal Plane Detector in LC-ESI/MS 758a

Quantitative Analysis of Pharmaceutical Target using a CCD Array Detector and Electrospray Mass Spectrometry 759a

Direct Formation of Liquid Ions from Polar Liquid Solutions 760a

Creation of Molecular Beams for Inducing Surface Ionization of Organic Compounds in LC-MS using a Modified Particle-Beam Interface 761a

The Application of Low Flow Techniques to Particle Beam Liquid Chromatography / Mass Spectrometry 762a

Use of Ionspray MS/MS for Verification of Methylphosphonate Oligonucleotide Sequences 763a

The Effect of Physical Parameters on Electrospray Response 764a

Studies of the Physical Processes of Electrospray 765a

Optimization of the Ionspray Mass Spectrometer as an LC Detector 766a

Chemical Derivatization for Electrospray Ionization-Mass Spectrometry 767a

High Resolution Precision Mass Measurements of Noncovalently Bound Protein Aggregates Using Electrospray Ionization Fourier Transform Ion Cyclotron Resonance Mass Spectrometry 768a

Determination of a Hypolipidaemic Agent in Plasma by Liquid Chromatography Tandem Mass Spectrometry using Atmospheric Pressure Chemical Ionization 769a

Photographic Studies of Electrospray Aerosols 770a

Predominance of Solvent Dielectric Constant in Determining Analyte Charge State in Negative Ion Electrospray Mass Spectrometry 771a

Elemental Electrospray Mass Spectrometry 772a

THURSDAY ORALS

Laser Desorption/Ionization

Wavelength Specific Resonance Enhanced Multiphoton Ionization for Isomer Discrimination Via Fragmentation and Metastable Analysis 773a

Application of PSD-MALDI to the Localization of Modification Sites in Peptides 774a

Evaluation of Crystallization Methods for Matrix-Assisted Laser Desorption-Ionization of Proteins 775a

Suppression of Metastable Interference in MALDI Spectra Obtained with a Reflecting Time-of-Flight Mass Spectrometer 776a

Heat Load on Guest Molecules in Matrix Assisted Laser Desorption 777a

Anomalous Ionization in a Laser Time-of-Flight Mass Spectrometer 778a

LDMS of Proteins and Peptides Absorbed on Membranes 779a

Matrix Assisted Laser Desorption Ionization of Aerosols 780a

Solid-phase Reactions of Picomole Quantities of Proteins Monitored by Matrix-assisted Laser Desorption/ionization TOF Mass Spectrometry 781a

REMPI and Mass Spectra of Cold Perfluorinated Polyethers 782a

Hydrocarbon Polymer Analysis by Laser Desorption/Chemical Ionization Fourier Transform Mass Spectrometry (LDCI/FTMS) 783a

MALDI Mass Spectrometry of Gel-electrophoretically Separated Proteins 784a

Laser Desorption/Ionization of Small Biomolecules 785a

Laser Vaporization and REMPI TOF Detection for DNA Sequencing 786a

Matrix-Assisted Laser Desorption Mass Spectrometry of Oligonucleotides 787a

Fragmentation of Small Oligodeoxynucleotides by MALDI/TOF Mass Spectrometry Using 355 nm Radiation 788a

Trapped Ion MS

Ion Trap Mass Spectrometry 789a

Mass Resolution in a Quadrupole Ion Trap 790a

Parallels and Perpendiculars Between Magnetic and non-Magnetic Ion Traps 791a

Penning Traps in Physics Research 792a

Biological Ion Trap Mass Spectrometry 793a

Fundamentals and Recent Applications on an Atmospheric Pressure Ionization Differentially Pumped Benchtop Ion Trap 794a

Estimation of the Polarizability of Gaseous Ions by Ion Trap Mass Measurements 795a

Ion Remeasurement in Fourier Transform Ion Cyclotron Resonance Mass Spectrometry 796a

Characterization of Large Linear Molecules by Tandem Mass Spectrometry 797a

Remeasurement and Collisional Thermalization of Ions by Quadrupolar Excitation in a Fourier Transform mass Spectrometer 798a

Averaging Theory for Ion Motion in a Cubic FT-ICR Cell 799a

Precise Mass Determination of Trapped Microparticles and Macro-ions by Optical Techniques 800a

Non-Linear Resonance Effects During Ion Storage in a Quadrupole Ion Trap 801a

Development of Automated Selected Ion Storage for Quadrupole Ion Trap Mass Spectrometry 802a

Environmental Analysis

Environmental Analysis with Quadrupole Ion Traps: Past, Present, and Future 803a

On-Line Analysis of Single Microparticles by Laser Desorption 804a

High-Speed Two-Dimensional GC and GC/MS for Complex Environmental Samples 805a

Ultratrace Analysis of Organic Compounds in Water 806a

Application of ICP-MS to the Determination of Radioactive and Nonradioactive Trace Constituents in Water from Abandoned Urnium Mines 807a

Detection of Trace Drug and Explosive Evidence by Ion Mobility Spectrometry 808a

Application of Mass Spectrometry in the Studies of Degradation Mechanisms of p-Phenylenediamine in Aquatic Environments 809a

Tandem Mass Spectrometry Study of Cyano Containing Pyrethroid Insecticides: 810a

Discrete Energy Electron Capture Mass Spectrometry with Gas Chromatographic Inlet 811a

Congener Specific Quantitation of Polychlorinated Biphenyls by GC/MS/MS 812a

Reliable Compound Identification at Low Levels in Complex Environmental Samples 813a

Monitoring Life Support Environments via Ion Trap Mass Spectrometry 814a

Elemental & Isotope Ratio Analysis

Trace Element Determination by GC/MS 815a

Radiofrequency Plasma Ionization Time-of-Flight Mass Spectrometry 816a

Multi-Channel He ICP Mass Spectrometer for Elemental Analysis with Transient Signals 817a

Recent Advances in Isotope Ratio Measurement by Inductively Coupled Plasma-Multiple Collector-Mass Spectrometry 818a

Application of ICP-MS to Impurity Analysis of Semiconductors for Room Temperature Radiation Detectors 819a

Sputtered Atom Ionization in a Pulsed Radio Frequency Powered Glow Discharge 820a

Optimization of a Radio Frequency Powered Glow Discharge Mass Spectrometry (rf-GDmS) System 821a

RF Glow Discharge Ionization with FT/ICR/MS Detection 822a

Using Ion-Molecule Reactions to Enhance High Resolution GD/FTICR Mass Spectrometry 823a

Direct Analysis of Soils by Radio-Frequency Powered Glow Discharge Mass Spectrometry 824a

The Application of Glow Discharge-Fourier Transform Ion Cyclotron Resonance (GD-FTICR) Mass Spectrometry to Isotope Ratio Measurements 825a

Imaging Isotope Ratio and Trace Element Analysis of Gold Ore 826a

High Spatial Resolution Isotope Ratio Imaging Using Secondary Ion Mass Spectrometry 827a

High Precision Liquid Chromatography-Combustion Isotope Ratio Mass Spectrometry (LCC-IRMS) 828a

Isotope Chemistry in the Jar: Direct Isotopic Analysis from Head Space Gas Mixtures using a GC-IRMS System 829a

Improvements in Sensitivity and Precision Attained with the Application of Ion Counting Techniques to Isotope Ratio Analysis of Zinc and Iron Using FAB/SIMS 830a

THURSDAY POSTERS

Metabolism & Drugs

Metabolism of 4-VPA to Glutathione Conjugates in the Rat: Identification of Novel Adducts Using Ionspray LC/MS/MS 831a

Quantification of Topiramate, A Novel Anticonvulsant, in Rat Brain Fluid by In-Vivo Microdialysis and Thermospray Liquid Chromatography / Mass Spectrometry 832a

On-Line Capillary Electrophoresis-Tandem Mass Spectrometry of Drug metabolite mixtures 833a

Estradiol and Estradiol Metabolites Analysis by Electrospray Mass Spectrometry 834a

Electrospray Mass Spectrometry Analysis of Isomeric C-Glycosidic Flavonoids 835a

Matrix-Assisted Laser Desorption Mass Spectrometry of Dynorphin A (1-17) Processing in Human Plasma and Rat Brain 836a

Rapid Analysis of Erythromycin A and its Metabolites in Fish Tissue using LC-MS and MS-MS 837a

High Performance Liquid Chromatography - Electrospray MS/MS and MS/MS/MS for Metabolite Identification of a Peptide-Based Renin Inhibitor 838a

Mass Spectrometric Determination of Indole Carbinol, its Glucosinolate, and Analogs in Cruciferous Vegetables 839a

Characterization of Flavonoids by LC/MS/MS 840a

Analysis of Carotenoids in Human Serum by Using Capillary Column Continuous-Flow Fast Atom Bombardment Liquid Chromatography-Mass Spectrometry 841a

Further Developments in Neonatal Screening by Automated Dynamic LSI Tandem Mass Spectrometry 842a

Structure Determination of Metabolites from the Neuroleptic Drug Haloperidol Using Ion Trap MS 843a

Regioselective Analysis of Hydroxyeicosatetraenoate in Phophatidycolines in LSI/MS/MS 844a

EI, CI, and FAB Mass Spectral Characterization and Identification of Noberastine Metabolites 845a

Negative Ion Fast Atom Bombardment / Collision-Induced Dissociation Mass Spectrometry in the Study of Ursodeoxycholic Acid Metabolism in Man. 846a

Charge-Remote Fragmentation of Doubly Conjugated Bile Acids 847a

Mass Spectrometry of Sertraline and Related Compounds 848a

Fast Atom Bombardment Mass Spectrometry Using a Glycerol Matrix Saturated with a 3:1 Mixture of Non-Labelled and Trideuterated Tetramethylammonium Hydroxide to Count the Number of Anionic 849a

GC-MS Analysis of Phenylacetic Acid Conjugates in the Rat Brain 850a

Quantitative Analysis of 11-Hydroxy, 8,9-epoxy-eicosatrienoic Acid from human Umbilical Venous Endothelial Cells (HUVEC) by GC/EC NCI MS 851a

Mass Spectrometry-based Strategy for Checking Originality of Metabolites in Biologically Active Fermentation Broths 852a

Characterization of 20-hydroxyeicosatetraenoic Acid Glucuronide by LSI/MS/MS 853a

A Single Assay for the Determination of Oxalic, Glycolic, Glyceric, Glyoxylic and Hydroxypyruvic Acids in Urine by Positive Ion Chemical Ionization GC/MS 854a

Thermally Induced Fragmentation in the NCI Mass Spectra of Amino Acid n-Propyl Ester, N(O,S)-Heptafluorobutyramide Derivatives (AA-PrHFB) 855a

Interfering Substances in the Gas Chromatographic Analysis of Diamines in Seafood 856a

Trace Analysis of a Lewisite Decomposition Product in Urine and Serum 857a

Collision Induced Intramolecular Claisen Condensation in Triglyceride Negative Ions and Assignment of Positional Isomers 858a

Isolation and Detection of Drugs from Spent Fly Puparia (Phoridae): "Drugs in Bugs" 859a

Characterization of 4-Quinolone Antiobiotics by Chemical Ionization Ion Trap Mass Spectrometry 860a

The Analysis of 1,4-Benzodiazephines by Selective Ion-Molecule Reactions with Dimethyl Ether Ions in a Quadrupole Ion Trap 861a

Partial Identification of Metabolites of a Novel Platelet Activating Factor Antagonist by Mass Spectroscopy 862a

Mechanistic Studies on the Metabolic Oxidation of Terminal Olefins to Carboxylic Acids 863a

Automated Statis Headspace Sampling with Gas Chromatography - Mass Spectrometry for the Identification and Quantitative Analysis of Volatile Organic Impurities in Drugs and 864a

A Comparison of Gas Chromatography-Mass Spectrometry Assays for In Vivo Lipid Peroxidation 865a

Analysis of Polyethylene Glycol with TSP LC-MS 866a

Proteins

Selective Detection of Phosphopeptides by Electrospray LC/MS 867a

Application of Electrospray Mass Spectrometry to the Identification and Quantitation of a Novel Variant in a Dimeric Recombinant Protein 868a

Mass Spectrometry of Non Covalent Complexes 869a

Electrospray Ionization Mass Spectrometry of Hemoglobin Adduct Formation in Rats 870a

An Ion Spray Mass Spectrometric Study of Molecular Recognition between the Vancomycin Family of Antibiotics and a Model Bacterial Cell Wall Mucopeptide Precursor 871a

Mass Spectrometry of Bi-Substrate Inhibitors and Their Targeted Protein Kinases 872a

The Use of Packed Capillary LC/MS to Monitor Phosphokinase Activity in Rat Cardiomyocytes 873a

Probing the Catalytic Domains of Protein Kinases with the Aid of Mass Spectrometry 874a

Analysis of Iron-Sulfur Proteins by Electrospray Mass Spectrometry 875a

Effect of Proline Residue in Transition Metal in Binding in Peptides Studies by 252Cf-PDMS 876a

Studies of Anticancer Drugs Binding with the Metal-Detoxification Protein, Metallothionein II, by Ion Spray Mass Spectrometry 877a

Formation Study of Metal Complexes self-assembly by ESMS 878a

Studies of Metallothionein and Anticancer Alkylating Agent Interactions 879a

Influences of Peptide Side Chains on the Metal Binding Site in Metal Ion-Cationized Peptides: Participation of Aromatic Rings in Metal Chelation 880a

Disulfide Bond Analysis of Recombinant Proteins Using FAB and MALDTOF Mass Spectrometry 881a

Strategy to Determine Disulfide Bridge Arrangements, Selective Reduction of Cystines using TCEP 882a

Use of Mass Spectrometry to Monitor Chemical Reactions in Proteins 883a

Observation of Methionyl and Tryptophyl Oxidation in Electrospray Ionization and its Analytical Application 884a

Gas Phase Reduction-Alkylation for the Identification of Disulfide Bonds at Subnanomole Levels 885a

The Reactive Site of an Enzyme Inhibitor Complex of the Thiol Protease Cruzain Determined by High Energy Tandem Mass Spectrometry 886a

The Determination of the Primary Structure of the Glutaredoxin Isolated from Human Erythrocytes (hErGRx) 887a

The Characterization of Naturally Occurring Complex Peptide Mixtures by ESI-MS and MALDI-TOF-MS 888a

Analysis of Protein Free Sulfhydryl Content by Heavy Atom Labeling and Matrix-Assisted Laser Desorption Ionization Mass Spectrometry 889a

Tertiary Structure Selective Characterization of Protein Thiol Groups by Specific Chemical Modification Reactions Combined with Mass Spectrometric Peptide Mapping 890a

Structures of Recombinant Human Macrophage Colony Stimulating Factor (rhM-CSF) and in vitro Refolded Intermediates: Analysis of the Sulfhydryl Alkylation of Free Cysteinyl Residues Using Fast 891a

Matrix-Assisted Laser Desorption Mass Spectra of POD Derivatives used in an Enzyme Immuno Assay 892a

MALDI Measurements of Intermediate Filament Proteins in Chaotropic Buffers 893a

Quantitation of Protein Multimeric Species Using MALD TOF MS 894a

Characterization of Peptides and Glycoprotein Digests Using Capillary Electrophoresis Combined with Ionspray/Tandem Mass Spectrometry 895a

From Dipeptides to Oligopeptides: Analysis by Capillary Electrophoresis/Electrospray Mass Spectrometry: 896a

Mass Spectrometry of Proteins Isolated from Capillary Gel Electrophoresis 897a

Matrix-Assisted Laser Desorption mass Spectrometric Analysis of a Pegylated Recombinant Protein 898a

ESI- and MALDI-FTMS of Small Peptides for the Identification of Proteins 899a

Matrix-Assisted Laser Desorption Mass Spectrometry in the Determination of Subunit Stoichiometry of Giant (3,900 kDa) Earthworm Hemoglobin 900a

On-Line Magnetic Sector LC-MS-MS analysis of a Tryptic Digest of -Lactoglobulin by CF-LSIMS with Array Detector 901a

Electrospray Ionization of Trypsin Generated a-Lactalbumin Peptides 902a

Development of Methods for Structural Confirmation of Peptides 903a

Non-Covalent Interactions of Crown Ethers with Cytochrome c Using Electrospray Mass Spectrometry 904a

How Big are Gas Phase Proteins? Collision Cross Sections for Multiply Charged Protein Ions 905a

Characterization of Minor Components in Rat Liver Histone H1 by Electrospray Mass Spectrometry Using the Ion Abundance Profiles 906a

Glycopeptide Mapping and Structural Confirmation by Electrospray LC/MS 907a

A Novel, Rapid and Semi-Quantitative Method for the Optimization of Synthetic Peptide Substrates 908a

Sequence Analysis of Bacitracin A and Related Components by Electrospray Mass Spectrometry 909a

MS/MS

Dilithiated Fragments of a Mono-lithiated Ion? Unraveling B/E Linked Scan Spectra Using Labeled Lithium Ions 910a

Charge-Remote Fragmentation of Potential-Sensitive Dyes by FAB Mass Spectrometry and MS/MS 911a

Surface-Induced Dissociation of Fullerenes 912a

Tandem Mass Spectrometry of Fullerene Derivatives: 913a

A Systematic Study of Surface Characteristics Associated with Enhancement of Both Surface-Induced Dissociation (SID) Efficiency and Energy Deposition 914a

A Quadrupole/ToF MS/MS Experiment for Study Effects of Impact of Macromolecular Ions on Surfaces 915a

Separation and Analysis of DNA-PAH Adducts by CE Combined with MS/MS Using an Array Detector 916a

Predicting the Amino Acid Content of Peptides from Immonium Ions in High Energy CID Spectra 917a

Effect of Electrospray Ionization Conditions on Low-energy MS/MS Spectra of Peptides 918a

CAD/MS/CAD/MS of Multiply Charged Peptides with Electrospray Ionization 919a

The Mechanism of Formation of Peptide dn and wn Ions Evaluated by Reaction Intermediate Scanning on a BEqQ Hybrid 920a

Tandem Mass Spectrometry of Highly Basic Peptides - The limitations of Low-Energy MS/MS of Doubly-Protonated Molecules 921a

Liquid Chromatography-Tandem Mass Spectrometry of Maillard Reaction Products and Amadori Compounds 922a

Disastereomers Selectivity Using Metal Complexes: A MIKES Study 923a

Characterization of Lipids in Marine Oils by LSI/MS/MS 924a

A Kinetic Treatment of Resonant Excitation in the Ion Trap Mass Spectrometer 925a

Time Dependant Mass Spectral Fragmentation Pathways of 1,9-Decadiyne, 1,2,9,10-13 C-1, 9-Decadiyne 926a

Unimolecular Kinetics of Neutrals and Ions 927a

A Comparative Study of MS-MS Data Produced by Tandem Magnetic and hybrid MS-MS Instruments and the Implications of the Conclusions on the Design of a Hybrid Magnetic Sector-orthogonal 928a

A Hybrid Tandem Mass Spectrometer 929a

MSn in the Quadrupole Ion Trap Using Filtered Noise Fields 930a

Gas Chromatography-Tandem Mass Spectrometry Implemented on a Bench-Top Quadrupole Ion Trap-Based Instrument using Random Noise to Effect CID 931a

Comparison of a Octopole with a Quadrupole as a Collision Cell in a Hybrid Instrument 932a

Performance Characteristics of a New Hybrid Mass Spectrometer System 933a

Studies on Reducing the Scale of a Double Focusing Mass Spectrometer 934a

Photodissociation of MALDI Generated Proteins via 193 nm and 118 nm Photons in a TOFMS 935a

MS/MS of Multiply Charged Ions: Determination of Charge States by Medium Resolution Linked Scans 936a

Rapid, Continuous Recording of High Energy Collision-Induced Dissociation Spectra Using Charged Coupled Device (CCD) Detection Under Mac 3 Control on a Kratos 4-Sector Concept IIHH: 937a

A Tandem Time-of-Flight Mass Spectrometer Using Photodissociation 938a

The Use of Tandem Mass Spectrometry in the Study of Complex Mixtures 939a

TOF

Using Clusters as a Tool to Probe MALDI Mass Calibration 940a

Post Source Pulse Focusing with Linear Time-of-Flight Mass Spectrometry and Matrix Assisted Laser Desorption / Ionization (MALDI) 941a

The Design of an Ion Trap Storage/Reflectron Time-of-Flight Mass Spectrometer 942a

A Compact, High Performance Time of Flight Mass Spectrometer 943a

Time-of-Flight Mass Spectrometer for On-Line Single Particle Analysis 944a

Tandem Time-of-flight Mass Spectrometry of Organic Molecules by Surface Induced Dissociation 945a

On-line Laser Mass Spectrometrical Analysis of Atmospheric Particles 946a

Accurate Mass Measurement in a MALDI Reflector Instrument Using External Calibration 947a

A Dual Reflectron Tandem Time-of-Flight Mass Spectrometer 948a

Kinetic Energy Measurements of Matrix Assisted Laser Desorption Generated Ions with an Electrostatic Analyzer Based Time-of-Flight Mass Spectrometer 949a

Variable Distance Time-of-Flight Mass Spectrometer 950a

Ion Peak Shape Calculations and Time-of-Flight Mass Spectrometer Instrument Design 951a

Automation of Sample Analysis by Matrix Assisted Laser Desorption Mass Spectrometry 952a

Primary Ion Production from Various Gases for Spontaneous Desorption Mass Spectrometry 953a

Analytical Performance of an Inductively Coupled Plasma-Time-of-Flight Mass Spectrometer (ICP-TOFMS) 954a

Correlation Methods for Obtaining Structural Information on Some Alamethicin Peptides 955a

High-Speed Data Acquisition and Processing System for Time-of-Flight Mass Spectrometry 956a

Sub-PPB Detection of Impurities in High Purity Gases by Atmospheric Pressure Chemical Ionization Time-of-Flight Mass Spectrometry 957a

Ion Molecule Reactions

Competitive Reactivity as a Probe of Reaction Coordinates in Gas-Phase Ion/Molecule Chemistry 958a

By What Mechanisms do Anionic Nucleophiles React with Di-tert-Butyl Peroxide 959a

New Insights into the Gas Phase Anion Chemistry of Nitrous Oxide 960a

Structures of CHS2 - Anions and Reactivities with CS2 Molecules 961a

Gas-Phase Chemistry of Halocarbene Radical Anions: Acidities of Radicals and the Related Molecules 962a

Mechanism of Reaction of Fe+ with organosilanes. Generation and Characterization of Transition-Metal-Silylene and -Silene Cationic Complexes in the Gas Phase 963a

Selective Ion-Molecule Reactions of Lactams with Dimethyl Ether Ions 964a

Application of Site-Selective ion Molecule Reactions to Alkaloids 965a

Ion-Molecule Reactions and Dissociation of Glycols in a Quadrupole Ion Trap: Evidence of Intramolecular Interactions 966a

Isomer Distinction in a Quadrupole Ion Trap: Functional Group Interactions of Dicarboxylic Acids and Esters 967a

Isomer Distinction of Disubstituted Benzenes in a Quadrupole Ion Trap 968a

Characterization of Dissociation Behaviour of Gas Phase Protonated and Alkylated Organophosphorus Compounds by Tandem Mass Spectrometry 969a

Ion-molecule Reactions of Dicoordinated Boron Cations with Organic Alcohols 970a

Two-Center Three Electron Sulfur-Sulfur Bond Energies in Gas-Phase [(Me)2S S(Et)2]+ 971a

Product Formation and Fragmentation Pathway for the Reaction of Benzene Radical Cations and N-methylimidazole 972a

Investigation of Electrophile/Nucleophile Reactions of Polyheteroatomic (e.g. N,S,O) Organic Cations with Allylic Molecules (CH2=CH2-CH-X, X=Cl,Br,I,CNS,OH,OCOCH3) in Q2 of a 973a

An Experimental and Theoretical Study on the Existence of the H3C-S=O+ Ion as a Stable Gas Phase Species 974a

The Rich Gas Phase Ion/Molecule Chemistry of the Distonic Radical Cation CH2-O-CH2+ Revealed by Multiple Stage (MS2 and MS3) Mass Spectrometry Experiments 975a

Gas Phase Addition/Elimination Reactions of Carbanions with Carbonyl Groups Measured on the Quadrupole, Quistor, Quadrupole Tandem Mass Spectrometer 976a

Methane Loss in Dimethyl and Trimethyl Oxonium Ions 977a

Deprotonation of CH2(CH2)nXH2+ Distonic Ions (n=0,1,2; X=O,NH) 978a

Reaction of tert-C4H9+ Cation with Arenes: Intermediacy of - complexes 979a

Selective Identification of Benzyl and p-Tolyl Ions in The Mixture of C7H7+ Ions 980a

Electron Impact Induced Self-Protonation and Self-Condensation of Allenic Ketones 981a

Differentiation of Isomers through Energy-Resolved CID and Ion/Molecule Reactions in an Ion Trap Mass Spectrometer 982a

Further Investigations of Nucleophile/Electrophile Ion/Molecule Reactions in an Ion Trap Mass Spectrometer 983a

Sample Ion/Sample Molecule Reactions in Chemical Ionization Msss Spectrometry 984a

Evaluation of Ion Formation of Carbamate Pesticides in TSP- and ESP MS using Different Eluent Additives and Proton Affinity Calculations 985a

Fate of Selected Negative Ions Following Electron Capture at Atmospheric Pressure 986a

Atmospheric Pressure Chemical Ionization (APCI) using Photoionization 987a

Analyses of Phenol and Chlorophenol Isomers by Atmospheric Pressure Ionization and Mass Spectrometry Techniques 988a

Positive Ion Chemical Ionization of Polycyclic Aromatic hydrocarbons and Related Compounds 989a

NICI of Selected PCB congeners: Moderating Gas, Temperature, and Contaminant Effects 990a

Characterization of Novel Chemical Ionization Reagents by GC / MS and Quadrupole Ion Trap Mass Spectrometry 991a

Fragmentation and Ion-Molecule Reactions of Ethanolamine Using FTmS 992a

The Ion Chemistry of Nitrosamide 993a

Accurate Mass Measurements in Desorption Chemical Ionization (DCI) Mode 994a

Alkali Metal Cationization of Some Pyrrolidine Amides 995a

Cluster Ion Formation in Liquid Secondary ion Mass Spectra of Diquaternary Pyridinium Oxime Salts 996a

Investigation of the Penning Ionization Process using the Rare-Gas Metastable Beam Source 997a

Characterization of Ar/CH4 and Xe/CH4 Glow Discharge Plasmas 998a

Rearrangement of -Silyl-Substituted Carbenium Ions. An Investigation of Relative Migratory Aptitudes 999a

Ion Fragmentation and Structure

An Experimental and Theoretical Study of the Hydrogen-Bridged Radical Cations [CH3C=O...H...O=CH2] and [CH3CH=O...H...O=CH]+ 1000a

Deuterium Exchange Kinetics of Gas Phase Peptides: The Search for Intramolecular Interactions 1001a

Spontaneous Unimolecular Dissociation of Weakly Bound Ionic Clusters Under Low-Pressure Conditions 1002a

Photodissociation and Relaxation of Gas-Phase Aluminum Cluster Ions 1003a

Mass Spectra of Mercury/Alkali and Cadmium/Alkali Clusters and Their Structure 1004a

Positive and Negative LC/MS Analysis of C60, C76 and C84 Fullerenes 1005a

Mass Spectrometric Characterization of Synthetic Derivatives of Buckminsterfullerene 1006a

Generation of Fullerene-Based Compounds and Characterization by FTMS 1007a

Radial Velocity Distribution Measurement of Ions Ejected by Laser Desorption 1008a

Gas-Phase Proton Affinity Modifies Molar Response Factors in Fast Atom Bombardment 1009a

The Formation of Nitric Acid and Nitric Acid Complexes from Gas-Phase Ammonium Nitrate Clusters 1010a

Tetraalkylammonium Cations and Their Neutral Counterparts 1011a

Positive FAB-MS-Spectra of Several Cobalt- and Chromium-SS-diketonates 1012a

Study of Co(III) Clusters Using FAB Mass Spectrometry 1013a

Fragmentation Reactions of Multiply-Protonated Peptides 1014a

Fragmentation Studies of Doubly-Charged Alkali Metal Peptide Ions 1015a

Gas-Phase Fragmentations of Anionic Complexes Between Peptides and Transition Metal Ions: Comparisons with Alkaline Earth Metal Ions: 1016a

Structural Determination of Precursor Ions in the Collision Induced Dissociation of Ca2+ -Specific Peptides by Molecular Modeling 1017a

Collision Induced Dissociations of Deprotonated Proline Peptides 1018a

Fragmentation of Protonated Peptides: Agreement Between Surface-Induced Dissociation Spectra and Quantum Chemical Predictions 1019a

Conformational Studies of Multiply Charged Protein Ions using Collisional Activation and Ion-Molecule Reactions 1020a

Role of Ion Kinetic Energy in Collision-Induced Dissociation Processes: Dissociation of CS2+ 1021a

Fundamental Studies of Molecular Ion-Surface Collisions: Pyridine/Ag(111) 1022a

Surface-Induced Dissociation of Ferrocene at Self-Assembled Monolayer and Single Crystal Surfaces 1023a

Collisions of Perfluoropropylene Ions with Solid Surfaces 1024a

Reactions of Organosilanes with Self-Assembled Monolayer Surfaces 1025a

Reactions of Immonium Ions with Self-assembled Monolayer Films 1026a

Surface-induced Dissociation Spectra of Ketones 1027a

Determination of Bond Energies by Collisional Dissociation of Electrospray Ions in Free jet Expansions 1028a

The Effect of Charge on Ion Stability: A Quantitative Comparison. 1029a

Photodissociation of Solvated Ions 1030a

Infrared Multiple Photon Dissociation Spectra of Solvated Ions 1031a

Obtaining Structural Information on the Aglycones of Macrolide and Azalide Antibiotics by ESI-Tandem Mass Spectrometry of Lithium-Attachment Ions 1032a

A Study of Air Sensitive Compounds Containing Low Coordinate Cationic Phosphenium and Arsenium Centres by Electrospray Mass Spectrometry 1033a

Selective Multiphoton Ionization Studies of Deuterium-Substituted -Fluorophenetoles 1034a

Resonance-Enhanced Multiphoton Ionization Studies of an s-Cis Polyene 1035a

Multiphoton Ionization of Clusters of Biomolecules: Bases and Nucleosides 1036a

Nanosecond and Femtosecond Multiphoton Ionization - Comparison of Fragmentation Behaviour 1037a

(M-2H)+ Formation in the FD-MS Analysis of Hydrocarbons 1038a

Infrared Spectroscopy of Matrix Isolated Products from Electron Impact Ionization of Gas Phase Molecules 1039a

Electrospray, API, Supersonic Beams

Ultra Small Volume and Flow Rate Electrospray ionization Mass Spectrometry with a Sheathless Source 1040a

Optimization and Evaluation of a Capillary Electrophoresis - Electrospray Mass Spectrometry Interface Employing Opposite Polarities at the Injector and Ion Source 1041a

Improved Microbore HPLC Electrospray Mass Spectrometry Interface 1042a

A Performance Evaluation of Several Sample Introduction Techniques Used for Electrospray Ionization 1043a

Negative Ion Formation in Electrospray Mass Spectrometry 1044a

Comparison of Buffer Systems in Capillary Electrophoresis-Electrospray Ionization/Mass Spectrometry 1045a

On-Capillary Isotachophoresis/Capillary Electrophoresis for Sample Cleanup and Loadability Enhancement in Capillary Electrophoresis/Electrospray/Mass Spectrometry 1046a

Design and Construction of a Thermospray-type Interface for On-line Capillary LC/MS 1047a

Design of Electrospray Interfaces for Finnigan-MAT TSQ-70 and VG-ZAB Mass Spectrometers 1048a

Linear Calibration curves using Particle Beam LC/MS 1049a

Hydrogen/Deuterium Exchange in Electrospray Ionization Mass Spectrometry as a Practical Tool for Structure Elucidation 1050a

Ion Source Effects on -Lactam and Macrolide ESI Mass Spectra 1051a

Tyrosinase-catalyzed Hydroxylation of Leucine Enkephalin: Electrospray Ionization Mass Spectrometric Identification of the Reaction Products 1052a

Analysis of Mureidomycin Antibiotics by Ionspray Mass Spectrometry 1053a

The Use of Electrospray-Mass Spectrometry for the Analysis of Pharmaceuticals, Proteins and Peptides 1054a

Use of an On-line Liquid Chromatography Trapping Column for Electrospray Mass Spectrometric Analysis of Cytokine Mediators Involved in Inflammatory Skin Disorders 1055a

Analysis of Synthetic Peptide Impurities Using Capillary Electrophoresis/Electrospray Mass Spectrometry 1056a

Practical Considerations in the Capillary Electrophoresis - Electrospray Mass Spectrometry of Peptides and Proteins 1057a

Effect of Gas-Phase Acid Addition on the Electrospray Mass Spectrum of Myoglobin 1058a

Probing Ketone-protein Adducts by means of Electrospray Mass Spectrometry 1059a

Structural Analysis of Lipids by Negative ESI/MS/MS 1060a

Chemical Properties of Diaryldiazomethane: An Electrospray Ionization Mass Spectrometric Study 1061a

Quantification of a New Aryl Amidine LTB4 Antagonist (CGS 25019C) in Human Plasma Using Electrospray LC/MS 1062a

Evaluation of Tandem MS vs. API Interface Voltage using Ionspray to Distinguish Isomers of Diarrhetic Shellfish Poisoning Toxins 1063a

Characterization of Case-Associated Compounds in Oils Implicated in the Spanish Toxic Oil Syndrome Using Atmospheric Pressure Ionization Mass Spectrometry 1064a

Use of Crown Ethers to Enhance Electrospray Ionization Mass Spectra of Samples Containing Alkali Metal Salts 1065a

On-Line Accurate Mass Analysis of a Pesticide Mixture by APCI LCMS on a Magnetic Sector Instrument 1066a

Analysis of Venoms Used in Pesticide Research by Electrospray Ionization Mass Spectrometry 1067a

Ionization of Aromatic Hydrocarbons in Solution for Analysis by Electrospray Ionization-Mass Spectrometry 1068a

Studies of 1,3-Cycloaddition of Fullerene by Electrospray Ionization Mass Spectrometry 1069a

ESI-MS is a Useful Tool for Studying Fullerene Chemistry 1070a

The Characterisation of Novel Ionic Platinum Complexes by Electrospray Ionisation Mass Spectrometry 1071a

Electrospray Ionization Mass Spectrometry of Metallocenes and Oganometallic Salts 1072a

Electrospray vs. FAB for Organometallic Analyses 1073a

A Heated Capillary Atmospheric Pressure Ionization Source with an Atmospheric Pressure Chemical Ionization Interface 1074a

Development of High Sensitivity Detectors for Mass Spectrometry 1075a

FRIDAY ORALS

Immunology

Id of Disease State Assoc Processed Antigens Presented to the Immune System by Class I MHC Molecules 1076a

Electrospray/capillary Liquid Chromatography (ESI/LC) and Matrix Assisted Laser Desorption (MALD) Mass Spectrometry for the Analysis of Expressed Domains of Carcinoembryonic Antigen (CEA) 1077a

Structural and Mechanistic Studies of Enzymes by Capillary HPLC-MS 1078a

Separation and characterisation of lipopolysaccharides from B. catarrhalis and H. influenzae by CE-MS and CE-mS-MS 1079a

Structural Characterization of the Adjuvant Active Compounds in Quillaja Saponaria Molina Extracts 1080a

The Role of Mass Spectrometry in the Structure Determination of Mucins Expressed by Carcinomas 1081a

Fullerenes & Metal Carbon Clusters

Characterization of Naturally-Occurring and Modified Fullerenes by FTMS 1082a

Analysis of Fullerene Soot Extracts by Liquid Chromatography-Mass Spectrometry Using Atmospheric Pressure Ionization 1083a

Carbon Cluster Anions From C-6 to C-60: The Latest News! 1084a

Mass Spectrometric Study of Unusual Fullerence Coalescence Products 1085a

Laser Desorption Mass Spectrometry of Photopolymerized C60 Films 1086a

Analysis of Surfaces

Dynamic Secondary Ion Mass Spectrometry 1087a

Static SIMS Studies of Alkylmethylphosphonic Acids Adsorbed on Substrates of Environmental Interest 1088a

Biological Sample Preparation for Imaging Organic SIMS 1089a

Surface Characterization by Reactive Collisions of Methyl Halide Ions with Self-Assembled Monolayer Surfaces 1090a

Laser-Induced Thermal Desorption/FTMS of Organic Thin Films on Ti and oxidized Ti Metal Foils 1091a

Polymer Analysis

Modern Analysis as the Catalyst for Today's Evolving Polymer Science 1092a

The Analysis of Polymers by Matrix-Assisted Laser Desorption Ionization/Time-of-Flight Mass Spectrometry 1093a

ToF SIMS Study of Additive Migration on Polymer Surfaces 1094a

Microstructure of Copolymers by Statistical Modeling of their Mass Spectra 1095a

Direct and Matrix-Assisted Laser Desorption Fourier Transform Mass Spectrometry of Polymers 1096a

Pyrolysis Field Ionization Mass Spectrometry (Py-FI-MS) of Polyolefins 1097a

Characterisation of Polyester-based Surface Coatings by Pyrolysis GC/MS and Electrospray MS 1098a

ON THE RELEASE OF IONS FROM CHARGED DROPLETS IN ELECTROSPRAY MASS SPECTROMETRY

F.W. Röllgen, U. Lüttgens, Th. Dülcks and U. Giessmann[1]
Institute of Physical and Theoretical Chemistry, University of Bonn,
Wegelerstr. 12, D-53115 Bonn, FRG
[1]Finnigan MAT, D-28197 Bremen, FRG

In electrospray mass spectrometry (ES MS) charged droplets are formed by electrohydrodynamic disintegration of liquids at atmospheric pressure. Induced by solvent evaporation, ions are released from these droplets and mass analyzed. The mechanism of release of ions from charged droplets is not clear yet. Two basically different mechanisms are currently discussed. In the so-called "ion evaporation model" solvent evaporation leads to a decrease of the radius of charged droplets and an increase of the surface field strength by successive decompositions at the Rayleigh limit, until the critical field strength of ion evaporation is reached for sufficiently small droplets below the Rayleigh limit. In the second model, the electrohydrodynamic decomposition of droplets above the Rayleigh limit is considered to produce small droplets, from which one or several ions are desolvated by solvent evaporation, charge condensation and coulomb repulsion. Both mechanisms require significant solvent evaporation to achieve the required surface field strength for the release of ions by electrohydrodynamic or ion evaporation processes. By raising the electrolyte concentration the solvent evaporation also decreases the Debye length, which provides a measure of the interaction between cations and anions in the desolvation process.

We have measured the intensity ratio Ba^{2+}(solv)/$BaBr^{+}$(solv), obtained from $BaBr_2$ dissolved in a water/methanol solution (vol. ratio 1:1), as a function of concentration (Fig. 1) to investigate the effect of electrolyte concentration on the release of ions from droplets. For a concentration of the initial solution of $c_o=10^{-3}$ M an intensity ratio $Ba^{2+}/BaBr^{+} > 10$ was obtained. The mean size and charge state of the droplets could be estimated from the observed colored sprays (Higher Order Tyndall Spectra), the applied flow rate of 2 µl/min and the measured spray current of ~100 nA. Accordingly, the electrolyte concentration (c_{Ra}) of the droplet reaching the Rayleigh limit was by a factor of about 10^2 higher than the initial concentration. Considering the Debye lengths for the water/methanol solvent of $\lambda(c_o) = 5$ nm and $\lambda(c_{Ra}) < 0.5$ nm for the solution at the Rayleigh limit, the above ion intensity ratio of 10 is hardly compatible with the release of ions from droplets with concentrations of $c > 10^2 c_o$.

This result and results of other ES MS investigations, such as the observed correlations between the kind and abundance of ions in ES spectra and ion concentrations in the applied solution point to the release of ions from solutions with solute concentration not significantly enhanced by solvent evaporation.

Consideration of possible decomposition pathways of charged droplets and the particular conditions of ESI regarding the movement of charged droplets in a dry, frequently heated gas led us to propose a new mechanism of release of ions from charged droplets. In this mechanism the "slow" decomposition of ellipsoidally shaped,

charged droplets, moving in a dry gas, i.e. under conditions of a high rate of solvent evaporation, leads to the repeated release of ions from the tip shaped apex of the droplets.

Ellipsoidal droplets with a sufficiently long main axis decompose below the Rayleigh limit and do not relax into a spherical shape for a charge state of $\beta = N/N_{Ra}$ with $1 > \beta \geq 0.5$, where N is the number of charges of the droplet and N_{Ra} the number of charges at the Rayleigh limit. Such ellipsoidal droplets may be formed by electrohydrodynamic disintegration of the solution at the end of the capillary and by disintegration of droplets at the Rayleigh limit ($\beta = 1$). The change of a spherical to an ellipsoidal shape of moving droplets may be induced by the imposed difference of the external pressure in the direction of the field and/or by a different evaporation rate of the solvent in and perpendicular to the moving direction of the droplets.

The formation of a protrusion at the apex of the ellipsoid and the repeated release of ions from the protrusion is driven by the coulomb repulsion between the excess charges, a decrease of the flow resistance, a high rate of solvent evaporation and a fast charge relaxation in the protrusion compared to the "slow" electrohydrodynamic disintegration of the protrusion.

The release of ions from charged droplets, as proposed by this mechanism, is favored by a low heat of vaporization, a low surface tension of the solvent and a low concentration of the electrolyte. It is compatible with the observed critical dependence of ES ionization on a high rate of solvent evaporation from the droplets, the high ionization efficiency of ES ionization and the rather uncritical dependence of ES mass spectra on the electrospray conditions (axial and rim emission modes, IonSpray conditions etc.).

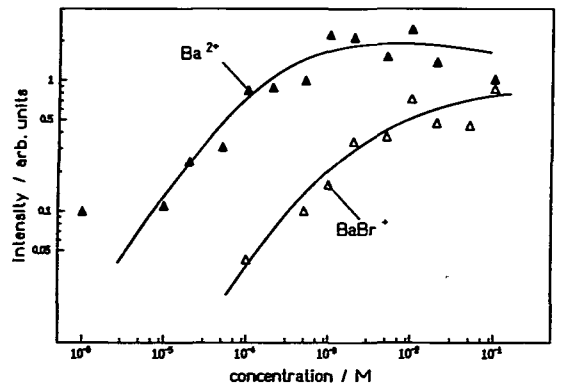

Fig. 1: Intensity of Ba^{2+} and $BaBr^{+}$ signals of ES spectra vs. different concentrations of a solution of $BaBr_2$ in H_2O/MeOH (vol. ratio 1:1); flow rate: 2 µl/min.

ETHYLENE GLYCOL AS A SOLVENT FOR ELECTROSPRAY MASS SPECTROMETRY

K.W.M. Siu, R. Guevremont and J.C.Y. Le Blanc, Institute for Environmental Chemistry, National Research Council of Canada, Montreal Road, Ottawa, Ontario, Canada K1A 0R6

Ethylene glycol solutions of gramicidin s, myoglobin and tetrabutylammonium bromide have been analyzed by means of electrospray mass spectrometry and their spectra compared with those of aqueous solutions. The evaporation of water and ethylene glycol droplets, initially at room or elevated temperatures, in air at room temperature has been modelled. It was found that under conditions where a water droplet's radius would shrink approximately 30%, an ethylene glycol droplet shrinks negligibly. Further, droplets that are initially hot (such as those that are ejected from a heated electrospray needle) cool very rapidly due to evaporation and heat loss to ambient air, and subsequently evaporate much like droplets that are initially at room temperature. Figure 1 shows the evaporation of a water and an ethylene glycol droplet, both initially at 70°C, in air at 25°C. For gramicidin s, the ion abundances in ethylene glycol as solvent (Figure 2b) were approximately 200 times lower than those in water (Figure 2a) under room temperature operating conditions. In experiments where the spray probe was heated to approximately 100°C to reduce the viscosity of ethylene glycol (Figure 2c), the gramicidin response difference between the solvents decreased to about a factor of 40. Similar trends were observed for myoglobin and the tetrabutylammonium ion. The experimental gramicidin responses in ethylene glycol are orders of magnitude larger than the responses expected from the degree of ethylene glycol evaporation. This observation calls the conventional solvent evaporation electrospray mechanism in question. The temperature dependence of the $(M+2H)^{2+}$ ion abundance appears to correlate well with that of ethylene glycol viscosity (Figure 3). It is speculated that reducing solvent viscosity by means of heating the spray probe increases the velocity of ions drifting in ethylene glycol towards the solution/air interface and increases the total number of analyte ions desorbed at the Taylor cone during electrospray.

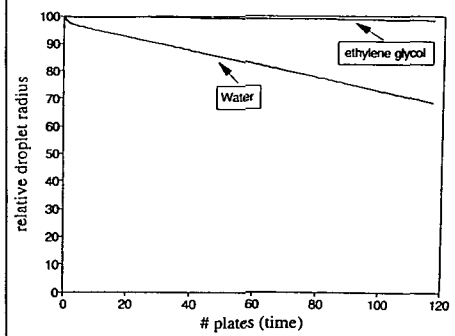

Fig. 1

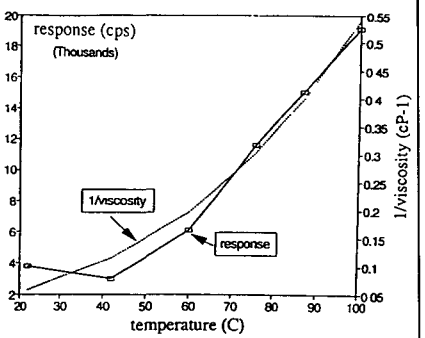

Fig. 3

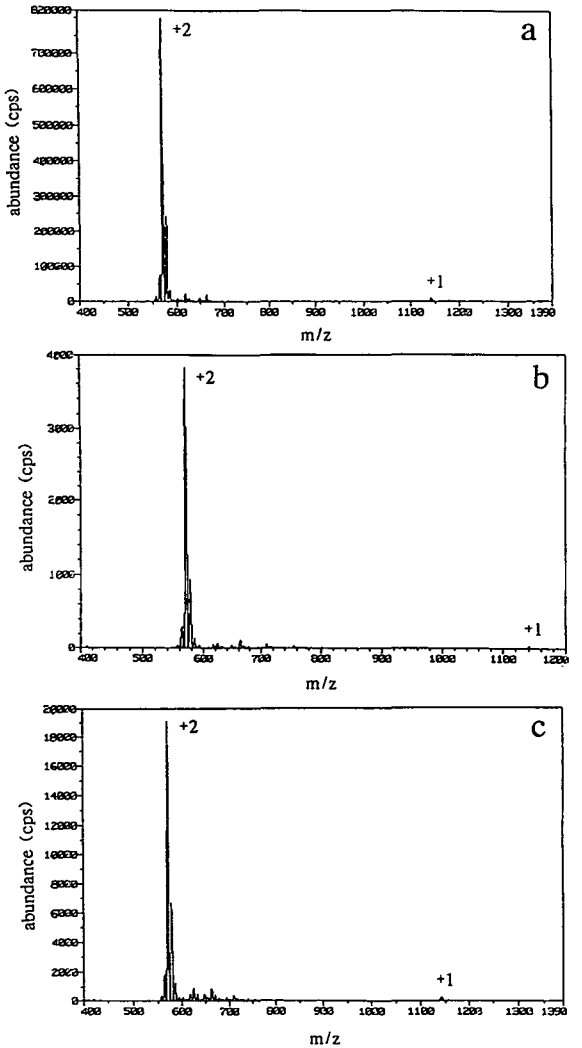

Fig. 2

The Potential of Electrospray Ionization with Ultra-High Resolution Mass Spectrometry for Biopolymer Characterization

Richard D. Smith, Steven A. Hofstadler, James E. Bruce, Brian E. Winger and Alan L. Rockwood

Chemical Sciences Department
Pacific Northwest Laboratory
Richland, WA 99352

Electrospray ionization (ESI) allows a broad range of large biopolymers to be analyzed using mass spectrometry. Given a sufficiently pure sample of a biopolymer, molecular weight measurements of approximately 0.01% accuracy, or better, can generally be made using ESI with quadrupole mass spectrometers operating with a resolving power of approximately 10^3. However, such pure samples are the exception due to the difficulties, costs and losses associated with purification; most biopolymer samples are actually mixtures. In addition to the common heterogeneity of biopolymers, which can arise from an assortment of chemical and biochemical processes, ESI mass spectra can be complicated by adduction of small solution species, residual solvation, dehydration, and (depending upon interface conditions) dissociation products. In these situations, higher resolution mass spectrometric analysis can provide additional information that can greatly assist characterization. Higher precision mass measurements, which generally accompany higher resolution measurements, can aid in the identification of adducting species, biopolymer variants, or components of noncovalent complexes. The use of ESI with high resolution MS for characterization of biopolymers also has a number of other advantages. Resolution of the 1-Da isotopic spacing allows the charge state to be determined, a capability which is particularly useful for interpretation of complex CAD mass spectra.

To realize the benefits of higher resolution measurements for molecular ions of larger biopolymers, a significant gain in resolution is necessary over that generally provided by low resolution mass spectrometers. One typically desires sufficient resolution to resolve the 1 Da differences of the isotopic envelope. Figure 1 shows calculated mass spectra for an equimolar mixture off two adducts of a model ß-chain Hemoglobin in three different resolution regimes. At a resolution of 3000, typically the best obtainable by "low resolution" instrumentation, the isotopic envelope is unresolved and the protein molecular weight is determined from the peak apex or centroid. At high resolution (40,000), as shown in the middle of Figure 1, the isotopic envelope is resolved to nearly baseline. However, at this resolution the small 0.03 Da mass difference between the two adducts is insufficient for their resolution. At extremely high resolution (>5 x 10^5 for the case illustrated), these two species can be resolved. The inset on the right side of Figure 1 shows the isotopic "fine structure" associated with one peak in the isotopic envelope. Two points are noteworthy regarding ultra-high resolution of large biopolymers. First, resolution of the isotopic "fine structure" requires a huge additional increase in resolution (generally to >10^7 for molecules of this size) and would be extremely challenging due to statistical constraints upon abundance measurements. Second, the isotopic "fine structure," if unresolved, ultimately places a limitation upon the application of very high resolution methods as molecular weight increase. However, within these mild constraints, high resolution can in principle provide an effective approach for separating such mixture components and assisting in their identification.

The prospects are excellent for such ultra-high resolution ESI-MS based upon Fourier transform ion cyclotron resonance (FTICR). As shown in Figure 2, high resolution spectra of proteins can be obtained using ESI-FTICR instrumentation being developed at our laboratory. At present, resolving powers of better than 2.5 million and mass measurement accuracies to better than 1 ppm have been obtained.

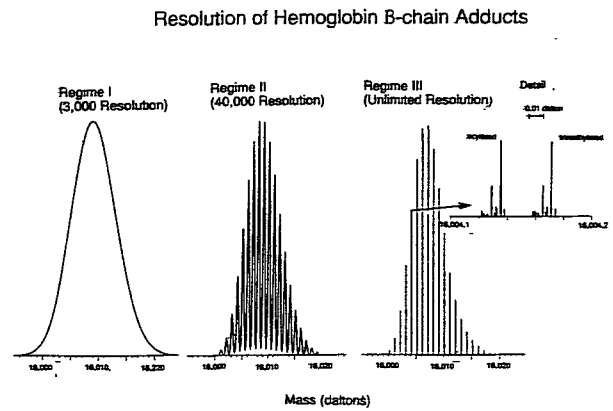

Figure 1 Calculated masses for a equimolar two component mixture of model hemoglobin ß-chain adducts at three resolving powers.

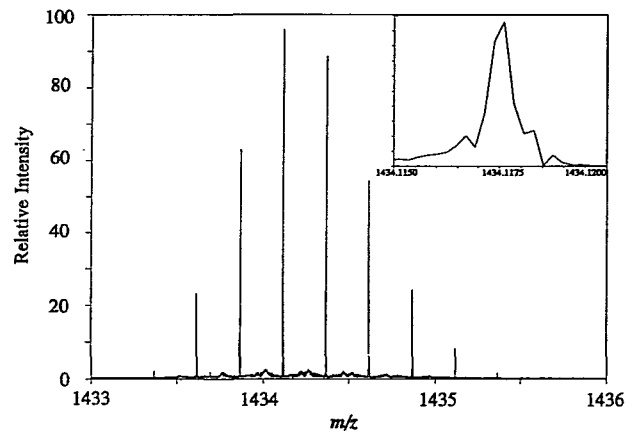

Figure 2 Ultra-high ESI-FTICR mass spectrum for the $(M+4H)^{4+}$ molecular ion of bovine insulin demonstrating a resolving power of 2.5 x 10^6.

This research was supported by internal PNL exploratory research through the U.S. Department of Energy. Pacific Northwest Laboratory is operated by Battelle Memorial Institute for the U.S. Department of Energy, through contract DE-AC06-76RLO 1830.

A Reflecting Time-of-Flight Mass Spectrometer with Orthogonally Injected Electrospray Ions.

A. Verentchikov*, W. Ens and K.G. Standing,
Physics Department, University of Manitoba, Winnipeg, Canada R3T 2N2

An electrospray (ESI) source, similar to the one designed by Aleksandrov et.al. [1], has been coupled to a reflecting time-of-flight mass spectrometer (TOF) [2]. Ions are injected into the instrument perpendicular to the flight path and extracted by pulses applied to a deflection plate using the method introduced by Dodonov *et al* [3]. Signals, observed in either the linear or reflecting mode, were recorded by a time-to-digital converter at a repetition rate of ~5kHz.

The resolution was considerably improved by operation in the reflecting mode giving a value $(M/\Delta M)_{FWHM}$ ~5000 (Fig.1) for melittin (2846u) and the B-chain of Insulin (3496u) comparable to the value observed in SIMS measurements [2]. This resolution enabled assignment of the charge states (1+ to 4+) of the peaks in the spectrum obtained from a tryptic digest of a recombinant protein (28,932u) [4], which was found to have suffered a post-translational modification (loss of ~700u). For peptides heavier than insulin the analytical resolution is defined by the overall width of the isotopic distribution (from 1000 to 1500).

Precision. Though the resolution for peptides of ~30,000u is higher than in MALD, the accuracy of mass determination appears to be similar (~100 ppm).

The sensitivity of the instrument is demonstrated by the spectra in Fig.2, which consumed 50 and 10 fmoles of Cytochrome C (12,361u, 1 pmole/µL solution at flow rate 0.01µL/sec, recorded in 5 and 1 sec). The absence of unimolecular decay and a single ion counting mode for data acquisition produce spectra with a very low background. The sixth isotope of angiotensin (883u) (10^3 times smaller than the first one) is clearly seen after a minute of recording time.

The mass/charge (m/z) range is practically unrestricted on the TOF instrument. This was used to show that the ion formation mechanism in the ESI ion source sometimes provides ions with a high m/z (i.e. with a low charge). Fig.3 shows the upper part of the spectrum of β-Galactosidase (113,600u), containing the second (less charged) part of the envelope in the range 3000<m/z<6000. Spectra of some other peptides- porcine pepsin (in a positive mode) and proteinase-K in a unfolded form- showed peaks beyond the normal m/z range for quadrupole instruments (m/z<2400). A murine anti-(human α1- acid glycoprotein) monoclonal antibody with an average molecular weight of 149,600 u, recorded previously on a quadrupole instrument [5], was observed in ESI/TOF to be mainly concentrated in the region 2500<m/z<3500 (Fig.4). A higher m/z range is often necessary when intact complexes are analyzed under mild conditions (water solution with neutral pH). Figure 5 illustrates two spectra of the enzyme Carbonic Anhydrase, with acidic solution and in pure water. The latter spectrum shows the intact complex of the enzyme with its cofactor Zn, but it appears at much higher m/z.

References

1. M. L. Aleksandrov *et al*, Dokl. Phys. Chem. **277** (1985) 572.
2. X.Tang *et al*, Int. J. Mass Spectrom. Ion Processes, **85** (1988) 43.
3. A.F.Dodonov *et al*, instrument built in 1985; USSR patent SU1681340A1,Feb.1987; 12th Int. Mass Spectrom.Conference.1991, Amsterdam, Extended abstracts p.153.
4. IclR, synthesised by L.Donald and H.Duckworth at Chem.Dept. Univ. of Manitoba.
5. R.Feng and Y.Konishi, Anal.Chem, **65** (1993) 645.

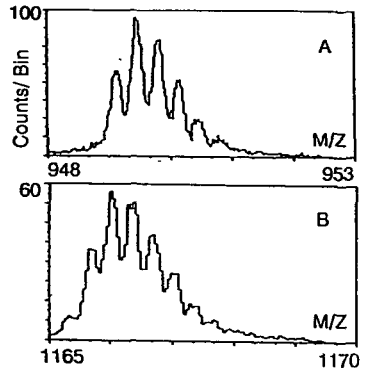

Fig.1 Isotopes of 3+ peaks of
A- melittin (2846u)
B- B-chain of Insulin (3496u)
Resolution on FWHM is ~5,000

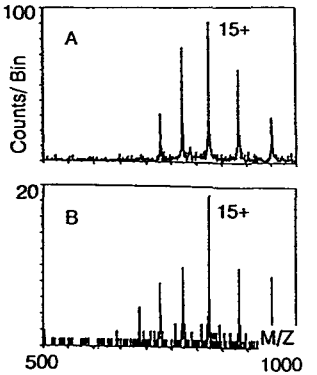

Fig.2 Sensitivity:
Cytochrome-C (12,361u)
A- 50 f mole (5sec recording)
B- 10 f mole (1sec recording)

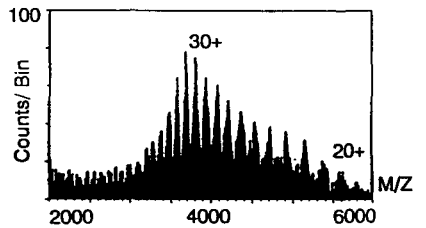

Fig. 3 β-Galactosidase
in water/methanol pH~4
measured M.W. 113,600 +100u

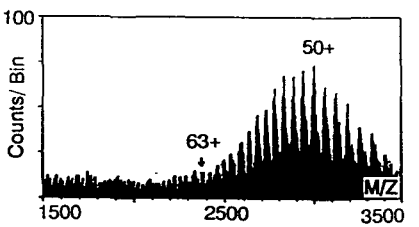

Fig. 4 Glycoprotein antibody
in water with 10% acetic acid
measured M.W. 149,600+100u

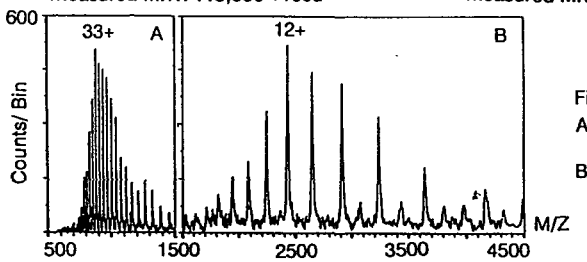

Fig. 5 Carbonic Anhydrase II
A - in water/methanol pH~4
without Zn (29,023u)
B- in pure water with its
cofactor Zn (29,088u)

STUDIES OF A HIGH INTENSITY ELECTROSPRAY ION SOURCE CONNECTED TO A HIGH MASS POST ACCELERATION ION DETECTOR

Y. Xu*, Y. Bae, R.J. Beuhler, and L. Friedman

Chemistry Department
Brookhaven National Laboratory
Upton, N.Y. 11973

Electrospray ionization (ESI) has been shown to generate multi-charged ions which can be identified by determination of mass to charge ratios.(1) Mass or charge determination in electrospray mass spectra requires sufficient resolution to separate ions carrying different charges. With sufficient resolution of very high molecular weight ions, the identification of masses of unknown samples may be difficult or impossible. If ions are subjected to post-acceleration followed by determination of secondary electron pulse spectra,(2) ion masses and charges can be established. Secondary electron pulse spectra are obtained by accelerating electrons generated from a detector dynode and determining the energy deposited by the electron pulse into a solid state detector. Electron pulses measure the electronic excitation deposited in the detector dynode. This excitation is related to the sum of the atomic masses in a molecular ion and its velocity.(3) Ion velocities can be calculated directly from ion mass to charge ratios and ion kinetic energies. Thus secondary electron yields can provide the information necessary for computation of ion masses.

The application of this technique of mass determination to ESI spectra of polyethylene glycols(4) provides evidence of decomposition for polymers with

molecular weights greater than 20,000 amu. The conclusion that PEG polymers with mass 5,000,000 amu can be generated with 4000 charges must be seriously questioned. The possibility that decomposition occurs in the acceleration column after mass analysis was tested by using energy selector plates to filter lower energy ions before impact on the detector dynode. The results of this test indicated decomposition prior to mass analysis.

Secondary electron spectra can reveal the presence of ions with radically different mass or charge in spectra which show unresolved ions with similar or identical mass to charge ratios. The use of secondary electron pulse spectra for mass determination of multi-charged ions will be demonstrated in studies of the monomer and dimer of apoferritin (molecular weights of 480,000 and 960,000 and with m/e values of approximately 13,500 and 19,000 respectively). Multi-charged high molecular weight solvent clusters containing methanol and water were also detected and the charge determined to be 21 on a mass of 294,000 amu. The larger linear PEG polymers were the only cases in a variety of studies where evidence was found for ion decomposition.

This research was carried out at Brookhaven National Laboratory under contract DE-AC02-76CH00016 with the U.S. Department of Energy and supported by its Division of Chemical Sciences, Office of Basic Energy Sciences.

[1] S. F. Wong, C. K. Meng and J. B. Fenn, *J. Phys. Chem.* **92**, 546 (1988).

[2] R. J. Beuhler and L. Friedman, *Int. J. Mass Spectr. Ion Phys.* **23**, 81 (1977).

[3] R. J. Beuhler and L. Friedman, *J. Appl. Phys.* **48**, 3928 (1977).

[4] T. Nohmi and J. B. Fenn, *J. Am. Chem. Soc.* **114**, 3241 (1992).

Observation of Noncovalent Complexes by Electrospray Ionization on a Magnetic Sector Mass Spectrometer

Joseph A. Loo
Parke-Davis Pharmaceutical Research
Division of Warner-Lambert Company
2800 Plymouth Road, Ann Arbor, MI 48105

Noncovalent interactions play many significant roles in biochemistry. Many types of superstrate/substrate binding are examples of intermolecular noncovalent interactions, including antibody-antigen, protein-cofactor, receptor-ligand, and enzyme-substrate pairings. Intermolecular noncovalent interactions are also responsible for aggregation of proteins into multimers (quaternary structure). These weak interactions can be disrupted by a varying solution conditions, such as pH, temperature, and solvent composition.

Electrospray ionization (ESI) has become an almost indispensable method in determination of peptide and protein primary structure. In electrospray, highly charged liquid droplets containing the analyte are formed at atmospheric pressure. By virtue of its ability to form stable gas phase ions with a paucity of fragmentation, ESI has been classified as an "ultrasoft" ionization method. Recently, several groups have shown that ESI-MS has the capability to examine noncovalently-bound systems. Because noncovalent bond energies are about an order of magnitude lower than typical covalent bond strengths, such weakly-bound molecular entities are very susceptible to collisionally activated dissociation. Previous ESI work on noncovalently-bound systems have been performed on quadrupole mass spectrometers. ESI analysis on a double focusing mass spectrometer requires ion acceleration to keV energies. Several noncovalent systems were investigated to test the feasibility of studying such weakly-bound biochemical systems with ESI-magnetic sector MS.

Instrumentation. ESI-MS analyses was performed on a Finnigan MAT 900 mass spectrometer (E-B geometry) equipped with a 20 kV conversion dynode/electron multiplier point detector and an array-type focal plane detector. Analyses were performed at full accelerating voltage (5 kV).

An electrospray ionization interface based a heated glass capillary inlet was used. Droplet desolvation was accomplished by a countercurrent stream of warm nitrogen and by collisional processes in the electrospray interface by adjustment of the voltage difference between the tube lens at the exit of the metalized-end of the glass capillary and the first skimmer element. A stream of SF_6 coaxial to the spray aided in suppression of possible corona discharges, especially important for electrospray of aqueous solutions.

Results and Discussion. Several noncovalent biochemical systems are amenable to ESI with magnetic sector instruments. In general, for studying such weakly-bound systems, the type of mass spectrometer is less important than the type of electrospray interface employed. Energy must be applied to strip away solvent molecules as the analyte travels through the ESI interface. However, applying too much energy to the system may disrupt the weak noncovalent forces holding two/several macromolecules together.

Peptide Heterodimer Interaction. ESI-MS was used to test for noncovalent interactions between human angiotensin II (M_r 1046) and 8 synthetic octapeptides that are considered complementary peptides (encoded by DNA sequences complementary to the DNA sequence that codes for human angiotensin II) or analogues of these antisense peptides. The relative abundance of the doubly-charged heterodimer complex broadly correlates to the trend observed with solution phase studies such as ^1H NMR. Dissociation constants for the reaction in solution is in the high micromolar range.

Heme-Globin Protein Interactions. Myoglobin is composed of a polypeptide chain (16.9 kDa for horse myoglobin) and a heme prosthetic group (Fe-protoporphyrin IX) noncovalently bonded in a hydrophobic crevice. Organic solvents and low pH conditions are known to denature myoglobin, expelling the heme

from the pocket. The mass spectrum of myoglobin taken from solutions of acidic pH reflects a molecular mass for the apo-protein only (and a peak representative of a singly charged ion for the heme). ESI mass spectra taken from pH 6 aqueous solutions shows only ions for the myoglobin protein-heme complex. Increasing the voltage difference between the tube lens and skimmer of the electrospray interface promotes collisional dissociation of the complex. Similarly, hemoglobin (Hb) is a tetrameric complex composed of two α-chains and two ß-chains, each bound to one heme molecule. At physiological pH, the tetramer is in equilibrium with the dimer species (α-heme/ß-heme, not α-heme/α-heme or ß-heme/ß-heme). From an aqueous solution, the α-heme and ß-heme complexes were observed in the mass spectrum, along with the 32.2 kDa α-heme/ß-heme complex.

Protein aggregation. Many protein systems exist as multimeric species or aggregates in solution. Alzheimer's disease is a neurodegenerative disorder characterized by abnormal deposition of protein in the brain. These amyloid deposits are composed of a polypeptide 39-43 residues in length. Amyloid peptides are known to form higher order aggregates in solution. ESI-MS of the ß-amyloid peptide (1-40) in water shows evidence for dimer, trimer, and tetramer formation. The 1-28 peptide did not show this tendency for self-association, consistent with previous literature studies.

Concanavalin A (Con A, 25.6 kDa) is a lectin metalloprotein isolated from jack bean that selectively binds polysaccharides. Con A has been reported to be a dimer at pH 5.5 and a tetramer at pH greater than 7. Abundant multiply-charged dimer species and a weaker set of multiply-charged ions for the tetrameric form was detected by ESI-MS for Con A at pH 6 (Figure below).

Conclusion. Several noncovalent biochemical systems are amenable for study with electrospray ionization and magnetic sector mass spectrometry. The larger *m/z* range of a magnetic sector instrument is an important advantage for studying such systems. Understanding how instrumental parameters affect the observed relative abundance of weakly-bound species is critical for characterizing such systems. Mass spectrometry is a powerful technique for analyzing *gas* phase molecules, but it also may eventually provide insight in the *solution* phase behavior of biological molecules.

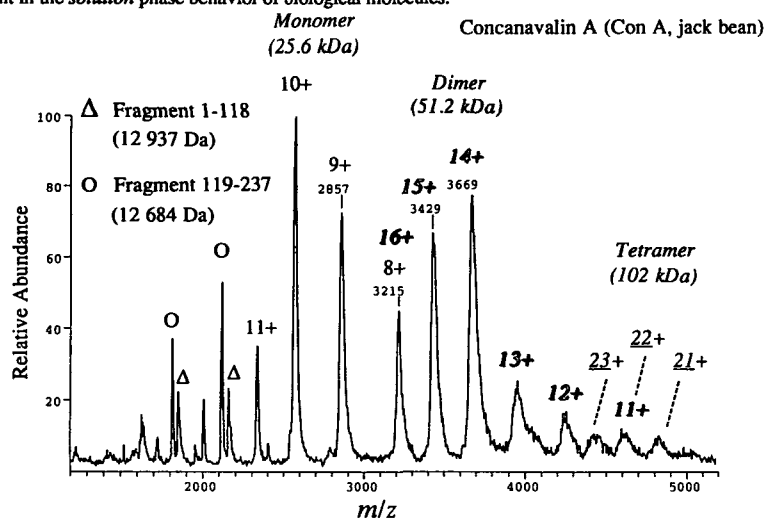

Conformation Dependent Copper Binding Ability of an Engineered Protein Assessed by Electrospray Mass Spectrometry

Gert Talbo, Kenneth Morand, Mark Kelly, Matti Saraste and *Matthias Mann

Protein and Peptide Group,
European Molecular Biology Laboratory,
Heidelberg, Germany

An engineered protein was constructed by introducing a copper binding site (Cu_A-like site) into the previously copper less CyoA subunit of the *E.coli* cytochrome *o* quinol oxidase complex [1]. Cu_A is a unique metal center; it is not known whether it has one or two copper atoms. Work by Allen and Hutchens [2] suggested the possibility of assessing the copper binding ability of the genetically engineered protein by electrospray mass spectrometry (ESMS).

ESMS was first employed in assessing the correctness of a series of mutants used in determining the number of necessary ligands to the copper or coppers in the CuA like site. Subsequent measurements of the wild type protein resulted in the expected molecular weight and also showed two different conformations of the protein when sprayed in 1% aqueous formic acid. The presence of different conformations was indicated two envelopes with different charge states.

Mutants with no ability to bind copper where then analyzed in the presence of 10 and 100 μM $CuCl_2$. At the 100 μmolar level they showed a significant adduction of one and two copper atoms per molecule.

The engineered protein was produced with copper present in the growth medium and ESMS analyzed. The resulting spectra show almost exclusively peaks corresponding to the compact conformation of the protein with two bound copper atoms (Fig 1). These findings - together with spectroscopic and chemical assay data not shown here - strongly support the bi nuclear model of the Cu_A site. Unspecific association of copper - as in the case of non copper binding protein in large access of copper containing solution - would have lead to a distribution of the number of copper atom per molecule.

Engineered protein was also grown in the presence of trace amounts of copper in the growth medium and analyzed while taking care to avoid copper containing solvents as much as possible. It then showed the expected molecular weight and the compact and extended conformation. Additionally, the compact conformation of the engineered protein showed an extra set of peaks corresponding to two bound copper atoms (Fig. 2).

In addition to lending strong support to the bi nuclear Cu_A model, the above findings indicate that ESMS can be used to verify the number of metal ions in redox centers of proteins. Interpretation of the copper adducts as specific protein metal interaction rests on comparisons of wild type and engineered protein, the fact that a discreet +2 Cu state was observed and that the Cu binding occurred only on the "native" conformation under conditions of trace amount of copper during cell growth.

1: John van der Oost *et al. EMBO Journal* **11**, 3209 (1992)
2: M. Allen and T. W. Hutchens *Rapid Commun. Mass Spectrom.* **6** 308 (1992)

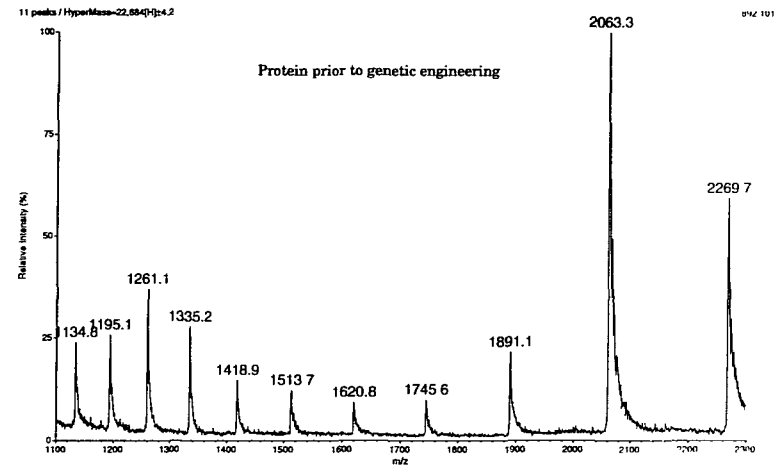

Figure 1. Wild type CyoA subunit of *E coli* cytochrome *o* quinol oxidase complex showing the expected mass and an open and a "native" conformation.

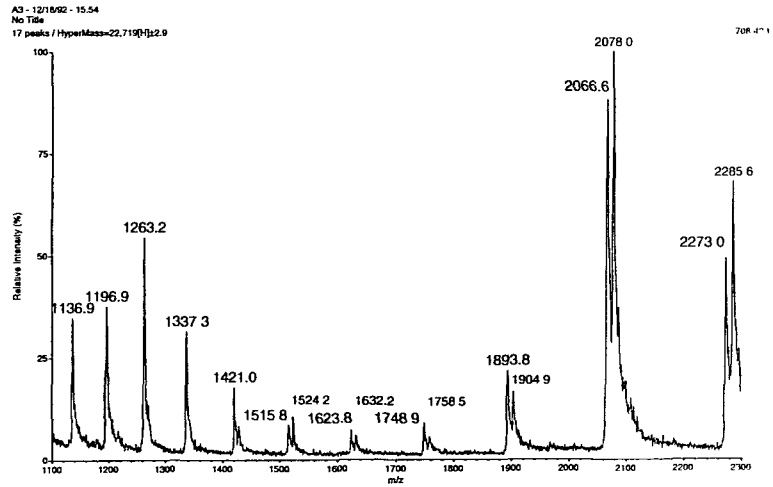

Figure 2. CyoA subunit with a copper binding site reintroduced by site directed mutagenesis Cells were grown in trace amounts of copper Note that the native conformation but not the extended conformation binds two coppers

THE OBSERVATION OF BIOMOLECULAR IONS BEYOND *m/z* 3,000 BY ELECTROSPRAY IONIZATION MASS SPECTROMETRY

Karen J. Light-Wahl, Brian E. Winger and Richard D. Smith, Chemical Sciences Department, Pacific Northwest Laboratory, P.O. Box 999, Richland, WA 99352

The production and detection of multiply-charged molecular ions by electrospray ionization (ESI) of relatively low *m/z* values (< 3,000) with quadrupole mass spectrometers is well established for proteins extending to at least M_r > 200,000. The mechanisms most commonly proposed for ion formation suggest that highly functionalized molecules such as peptides and proteins will generally form molecular ions with sufficiently high charge such that they will be observed below *m/z* 3,000.

An extended *m/z* range low resolution quadrupole mass spectrometer has been developed to investigate the low charge state, high *m/z* ions, that may be produced by ESI. Initial results have shown that ions can be produced and observed by ESI-MS to well beyond *m/z* 3,000 under appropriate solution and interface conditions.[1] For example in the negative ion ESI mass spectrum of bovine cytochrome *c* in 10 mM NH_4OAc, ions are observed with charge states extending to the $(M-H)^-$ ion at *m/z* ~12,400. The negative ESI-MS of porcine pepsin (M_r 34,584) in 1% acetic acid solution has produced the highest *m/z* ion observed to date as a broad peak near the $(M-H)^-$ ion at *m/z* ~ 34,000 (Figure 1).

Perhaps the most important aspect of using an extended *m/z* range quadrupole instrument is the ability to observe ions from solutions that are at near physiological pH. Most ESI-MS experiments of proteins have been carried out in acidic solutions (or alkaline solutions for negative ion formation) to increase the protonation of the molecule. These conditions allow species with lower *m/z* values to be detected within the *m/z* range of most commercial quadrupole mass spectrometers. However, the recent application of ESI-MS to the study of biologically important noncovalent associations[2] and higher order protein structure has brought about the need to use solution conditions more amenable to preserving weak structural associations which often require near neutral pH solutions. Conformational constraints under these solution conditions (i.e. hydrogen bonding, secondary structure) can reduce the number of potential charging sites. In addition, the more compact structures generally existing under these conditions might also be expected to increase Coulombic contributions and tend to decrease charging in the gas phase. Thus, ESI-MS with neutral pH solutions generally benefits from the use of an extended *m/z* range quadrupole instrument.

Concanavalin A (Con A), a lectin composed of four nearly identical 237 amino acid protomers, provides a good example of the importance of an extended *m/z* range instrument when studying noncovalent associations with ESI-MS.[3] At pH >7 this protein is known to exist primarily as a tetramer in solution; whereas, at pH ~ 5 it should be primarily a dimer. No trimer species are known to be present at either solution pH. Figure 2a shows the ESI mass spectrum obtained from Con A in a pH 5.7 solution (10 mM NH_4OAc), where it should exist in solution primarily as a dimer. Ions indicative of the tetramer are observed near *m/z* 5,000 in the positive ion ESI mass spectrum of Con A in aqueous 10 mM NH_4OAc (pH 8.4) and are labeled Q^{20+} to Q^{22+} in Figure 2b. Under appropriate interface conditions, this solution behavior is qualitatively observed by ESI-MS utilizing the extended *m/z* range quadrupole mass spectrometer. These and other results confirm that high *m/z* ions can be formed by ESI and that weak noncovalent associations are most likely to be retained for low charge state species.

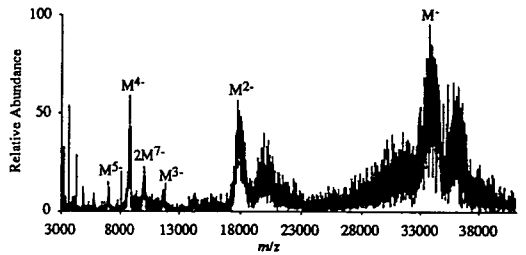

Figure 1. Negative ion ESI mass spectrum of porcine pepsin in 1% HOAc solution.

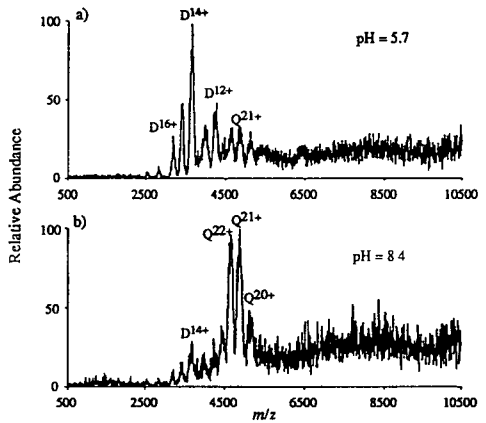

Figure 2. Positive ion ESI mass spectrum of concanavalin A in aqueous 10 mM NH_4OAc with a) pH = 5.7 and b) pH = 8.4. The peaks labeled Q represent the intact tetramer of Con A whereas the peaks labeled D represent the dimer species.

1. B. E. Winger, K. J. Light-Wahl, R. R. Ogorzalek Loo, H. R. Udseth, and R. D. Smith, *J. Amer. Soc. Mass Spectrom.*, in press.
2. K. J. Light-Wahl, D. L. Springer, B. E. Winger, C. G. Edmonds, D. G. Camp, II, B. D. Thrall, and R. D. Smith, *J. Amer. Chem. Soc.*, 115, 803 (1993).
3. K. J. Light-Wahl, B. E. Winger, and R. D. Smith, *J. Amer. Chem. Soc.*, in press.

Pacific Northwest Laboratory is operated for the U.S. Department of Energy by Battelle Memorial Institute under Contract DE-AC06-76RLO 1830.

CAPILLARY ELECTROPHORESIS/ELECTROSPRAY IONIZATION ON A MAGNETIC SECTOR MASS SPECTROMETER

Kenneth B. Tomer[1] and John R. Perkins[2], [1]National Institute of Environmental Health Sciences, PO Box 12233 Research Triangle Park, NC 27709, USA [2]Kratos Analytical, Barton Dock Road Urmston, Manchester M31 2LD UK

Capillary electrophoresis (CE) provides a rapid, highly efficient means of separating complex mixtures with high sensitivity. As part of our interest in coupling nanoscale separation techniques with mass spectrometry, we have interfaced CE with both continuous flow FAB on a magnetic sector instrument (1) and electrospray ionization (ESI) on quadrupole instruments (2,3,4). We have now also interfaced CE with ESI on a magnetic sector mass spectrometer (a Kratos Concept ISQ). In this interface, the standard Kratos probe has been modified to accommodate a sheath flow (Fig. 1). A plexiglass handle has been incorporated to isolate the union between the sheath flow and the CE column.

Figure 1.

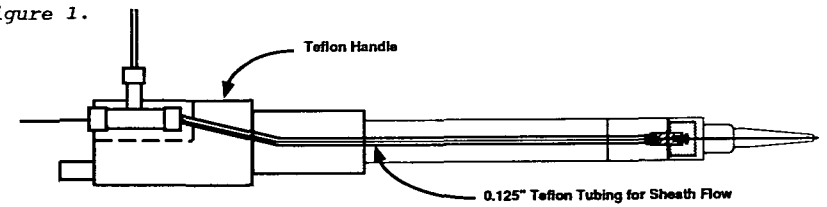

In addition to simple peptide mixtures, we have challenged the combination of techniques using a naturally occurring complex mixture of polypeptides and proteins, namely snake venoms. Although the raw snake venoms have been reported to contain 20 to 30 components, analysis by capillary electrophoresis in combination with mass spectrometry has shown the presence of over 100 components in the venom from *Dendroaspis polylepis* (4). One example which illustrates the necessity of both the separating power of capillary electrophoresis and the mass-resolving capabilities of the MS is in the CE/ESI/MS analysis of the venom of the black and white cobra (*Naja melanoleuca*). Two of the phospholipases, DE-III (M_r = 13346) and DE-IIIA (M_r = 13350.9), which differ in only two out of 120 amino acids, have identical pI's indicating that they would exhibit similar electrophoretic mobilities, and, thus, not be readily separated by CE. One of the major components in the CE/ESI/MS analysis showed $(M + 8H)^+$ and $(M + 7H)^+$ ions at mass 1669.6 and 1908.2, respectively (Fig. 2). Detailed analysis of the data showed that, in fact, each ion was a composite of two components (Fig. 3). M_r values of 13348.9 and 13345.7 were determined for the two components which were within 0.015% of the theoretical values.

References

1. Moseley, et al., *Anal. Chem.*, 63, 109 (1991).
2. Moseley, et al., *J. Am. Soc. Mass Spectrom.*, 3, 289 (1992).
3. Parker, et al., *J. Am. Soc. Mass Spectrom.*, 3, 563 (1992).
4. Perkins, J. R., Tomer, K.B. *Electrophoresis*, in press.

Figure 2.

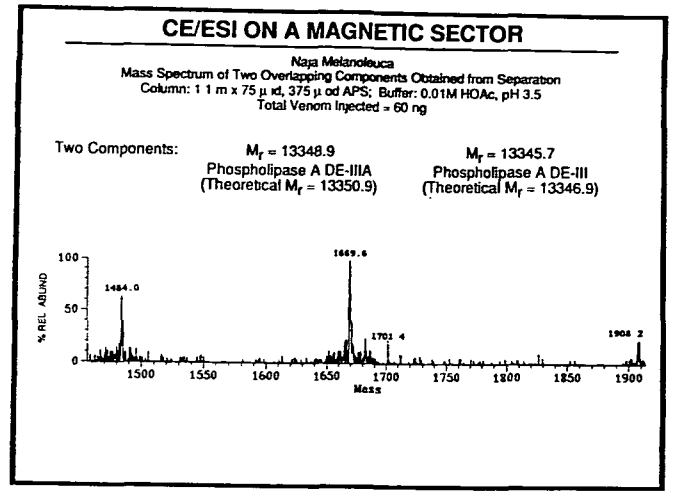

Figure 3.

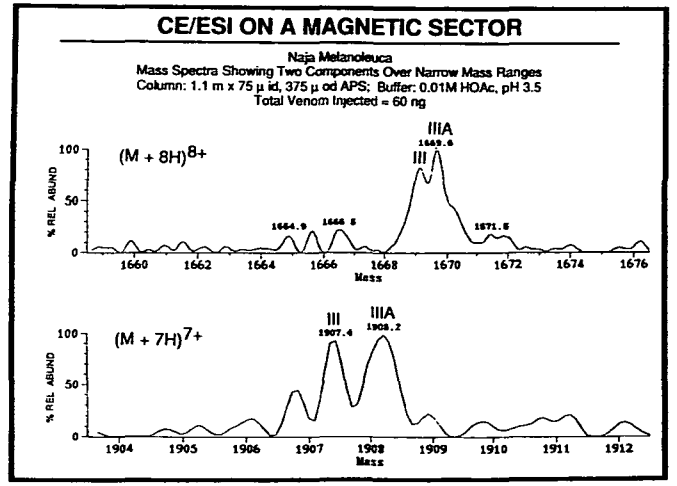

Applications of Packed Capillary Perfusion Column HPLC/MS/MSfor the Rapid Mapping and Sequencing of Enzymatic Digests

D.B. Kassel[1¥], Bori Shushan[2], Takeo Sakuma[2] and Jean-Pierre Salzmann[3]

[1¥]Glaxo Research Institute, 5 Moore Drive, Res. Tri. Park, NC 27709 [2] PE-Sciex, 55 Glen Cameron Rd., Thornhill, Ontario CANADA [3] LC Packings, USA, 80 Carolina St., San Francisco, CA

INTRODUCTION

Perfusion particle chromatography was introduced recently as a novel development in the field of HPLC for the rapid separation of biomolecules. The principal advantage this method affords over conventional reverse phase HPLC is the ability to operate at very high flow rates while maintaining both high sample loading capacity and chromatographic resolution. The principal advantage this technique brings, therefore, is speed, a critical operating parameter for industries in which the major focus is either process development or high throughput applications. Unlike conventional RP-HPLC, in which liquid flows around the particles surface (convection) and diffuses into the particle pores (via molecular diffusion), perfusion column chromatography enables analyte to be transported not only around the particle surface but within the particle as well. This was made possible by the ability to manufacture particles consisting of a complex network of through pores (6000-8000Å) and smaller diffusive pores (300 Å). The potential for exploiting the features of perfusion column chromatography for liquid *chromatography-mass spectrometric applications was achieved recently by members of our laboratory (1). The* optimal flow rates of perfusion columns are, in general, 5-10 times the flow required for reverse phase porous packing materials (*i.e.,* C18, C4). We demonstrated that by packing perfusion material into 320 µm i.d. capillary fused silica, the columns could be operated at flow rates compatible with electrospray ionization while maintaining linear velocities that fell within the perfusive flow regime. Three principal advantages that packed capillary perfusion columns offered for mass spectrometric analysis were; the ability to i) rapidly desalt protein samples, ii) rapidly separate protein and large peptides in 1/10 the time required using capillary C4 columns and iii) recycle rapidly, thereby allowing higher sample throughput.

RESULTS AND DISCUSSION

Packed capillary perfusion columns have now been evaluated for their ability to rapidly separate and sequence enzyme digests by HPLC/MS/MS using electrospray ionization (ESI) and compared directly against packed capillary reverse-phase materials (*e.g.,* Vydac C18, 5 µm, 300 Å particles). The sensitivity of the technique when coupled directly to electrospray ionization was examined against conventional capillary HPLC. Columns were operated under perfusing conditions, using a flow rate of 45 µl/min. In general, chromatographic retention times were reduced by a factor of 4-6 while maintaining comparable resolution to that of capillary C18 180 µm i.d. and 320 µm i.d. columns The feasibility of performing in-line LC/MS/MS for the sequence determination of enzymatic digests using capillary perfusion columns was determined. Tryptic digested src homology (SH2) domain of $pp60^{c\text{-}src}$ was used for this in-line LC/MS/MS study. Using a modified PE-Sciex API III collision cell it was possible to fully sequence several of the tryptic peptides of SH2 from a total sample concentration of 25-50 picomoles The results are shown below.

For these studies, enzyme digests were compared directly using packed capillary C18 (180 µm i.d.) and packed capillary perfusion columns coupled to electrospray ionization mass spectrometry. Total ion current chromatograms generated for 10 picomole and 50 picomole of c-src SH2 tryptic digest injected onto a packed capillary C18 and packed capillary perfusion column were compared, The total analysis time was reduced by a factor of 5 in the case of the perfusion column experiment (data not shown). However, the sensitivity of detection (both UV and mass spectrometric) was approximately 25-fold higher for the capillary C18 analysis The enhanced sensitivity for the capillary C18 analysis could be attributed to the flow rate used in the analysis (*i.e.,* 2 µl/min) relative to the flow rate used in the perfusion analysis.

Even so, the signal-to-noise achieved for the perfusion analysis (at the 50 picomole level) was more than sufficient to generate very interpretable LC/MS/MS spectra at high signal-to-noise. A modified API-III collision cell was evaluated in these studies. The collision cell was modified to provide a multiple collision regime as described elsewhere (PE-Sciex, Thornhill, Ontario, Canada). Shown in Figure 1a and 1b are the LC/MS/MS spectra for m/z 847, the $[M+2H]^{2+}$ ion of one of the SH2 tryptic peptides. The quality of the CID spectra generated by both the capillary C18 and perfusion column LC/MS/MS analyses were excellent. A 21-fold signal enhancement was observed using the Vydac C18 column relative to the perfusion column. Importantly, the signal-to-noise of the perfusion LC/MS/MS CID spectrum at the 50 pmol level for this 13 amino acid peptide compared quite favorably with the Vydac C18 LC/MS/MS CID spectrum. The entire sequence of this peptide was deduced readily from the observed prominent y_n ion series (13). CID spectra of the same quality and signal-to-noise were achieved for all 6 of the peptides characterized by perfusion chromatography/MS/MS in real time.

Capillary perfusion column flow rates used are generally 10-25 times greater than those corresponding to conventional 320 µm i.d. and 180 µm i.d. capillary C18 columns. Consequently, the elution volume of the peptides will be greater and hence the concentration of analyte in the elution volume will be decreased. Peak widths are found to be reduced, typically by a factor of 2-3, when comparing 320 µm i.d. packed capillary perfusion columns with 180 µm i.d. packed capillary C18 columns. This difference, though, is not sufficient enough to overcome entirely the dilution effect to the analyte. One method to overcome this limitation is to pack perfusion material into smaller i.d. capillaries (*e.g.,* 180 µm i.d. or 100 µm i.d. columns). We have now had the opportunity to evaluate chromatographically such column packings. Optimal flow rates for 100 µm i.d. and 180 µm i.d. perfusion columns have been determined to be 4-7 µl/min and 25-30 µl/min, respectively. Figure 2 shows the sensitivity enhancement achieved (using UV detection) for the separation of SH2 tryptic peptides (40 pmol injections) upon going from 320µm to 180 µm to 100µm i.d packed capillary perfusion columns The UV generated data demonstrate that an order of magnitude increase in sensitivity is possible with column packings of 100 µm i.d.and therefore should enhance the sensitivity of detection by MS analysis.

REFERENCES

1. D.B Kassel, M.A. Luther, D.H. Willard, S.P. Fulton and J.-P. Salzmann (1993) *Techniques in Protein Chemistry IV*, R. Hogue-Angeletti, Ed., Academic Press, pp 55-64.

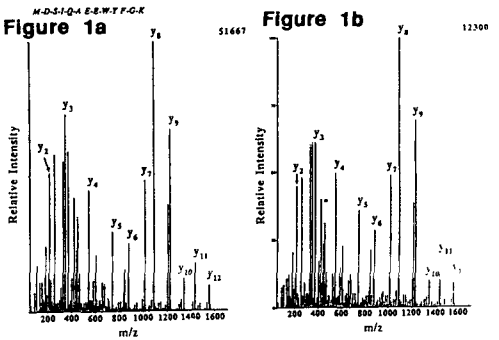

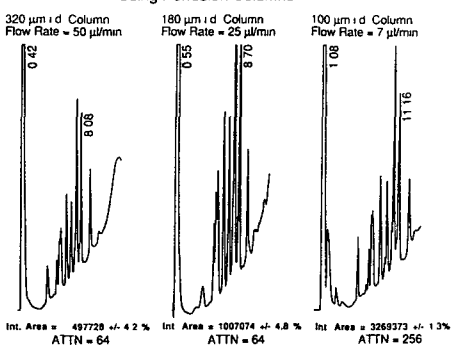

TECHNIQUE FOR THE REMOVAL OF BUFFERS AND HEART CUTTING OF PEAKS IN GRADIENT CAPILLARY HPLC PRIOR TO ELECTROSPRAY MASS SPECTROMETRY.

*John Roboz, Ankuo Meng, and Qitao Yu, Department of Neoplastic Diseases, Mount Sinai School of Medicine, New York, NY, 10029, and Remco van Soest, LC Packings, 1057 HM Amsterdam, The Netherlands.

Objectives: (1) Remove buffers which interfere with electrospray (ESP) analysis of proteins and peptides by source clogging or by suppressing ionization; (2) Facilitate introduction of selected HPLC peaks or peak portions from multicomponent samples to prevent source contamination with unimportant constituents, or remove overwhelming components when trace analytes are poorly resolved.

Principle of Technique: (1) Use mobile phase composition to retain important constituents on top of capillary column; (2) Wash out buffer isocratically, directing effluent to waste; (3) Separate constituents with appropriate HPLC gradient; (4) Introduce selected HPLC peak or parts thereof into ESP source by switching dump valve.

Experimental. Samples: Protein and peptide mixtures were prepared in water, and in two buffers: (1) Phosphate, 0.05 M, pH 7.0; (2) "Tris-Mix": 20 mM tris-acetate, pH 7.5, 20 mM NaCl, 0.1 mM EDTA, and 15 mM 2-mercoptoethanol. HPLC. Capillary columns: 15 cm X 320 um, packing 5 um, 300 A pore; C-18 type for peptides, C-4 for proteins. Mobile phase: A= Acetonitrile-water, 1:9 v/v plus 0.1% TFA, B= same as A but 9:1 v/v. Buffers were washed out with 10% B for 10 min. Separation gradient: 10% B to 90% B in 15 min, isocratic for 10 min. Starting flow rate from conventional HPLC pumps 0.4 mL/min, reduced to 5 µL/min by mixer-splitter before entering the column and subsequently the ESP source. UV detector: µ-flow cell (8 mm path), detection at 220 nm. ESP-MS. Cone voltage (VG Quattro ESP): 70 V; source temp.: 65 C; scan speed: 10 sec/500-1400 mass range.

Results. Features of the system (Fig. 1) include flow reduction from conventional HPLC pumps from mL/min to µL/min with a mixer-splitter, a convenience valve to switch from protein to peptide column, µ-flow cell to increase UV sensitivity, and a proprietary electronic micro-dumping valve to direct flow into the ESP source or to waste.

Fig. 2 shows that the transformed ESP spectra of β-lactoglobulin A and B (from a 10 pmole protein mixture) are identical from samples dissolved in water and in the phosphate and tris-mix buffers after washing; without washing, ESP spectra could not be obtained at all. Similarly, ESP spectra of 6 peptides (oxytocin, met-enkephalin, leu-enkephalin, α-melanocyte stimulating hormone, insulin B, and neurotensin, 10 ng ea) dissolved in phosphate and tris-mix buffer were the same as controls after buffer removal.

Fig. 3a shows HPLC heart cutting with the dumping valve in a mixture containing 50,000 fmole luteinizing hormone releasing hormone, LHRH, and 500 fmole of angiotensin B; as shown in Fig. 3b, intense ion current of the doubly charged ion could be obtained using mass chromatography, while most of the excess LHRH was removed as shown by total ion current (TIC). Significantly lower detection is possible with selected ion monitoring.

Experiments aimed to determine the effects of rapidly switching the dumping valve on the ability to recover and maintain ESP beam stability revealed that switching for as little as 3 sec and scanning for as little as 10 sec would still maintain ion current equilibrium in a gramicidin model for tuning and performance checking.

It is concluded that this simple technique may be widely employed to eliminate problems caused by buffers, and to facilitate easy introduction of individual HPLC peaks or parts of peaks.

Supported by the T. J. Martell Foundation for Leukemia, Cancer and AIDS Research.

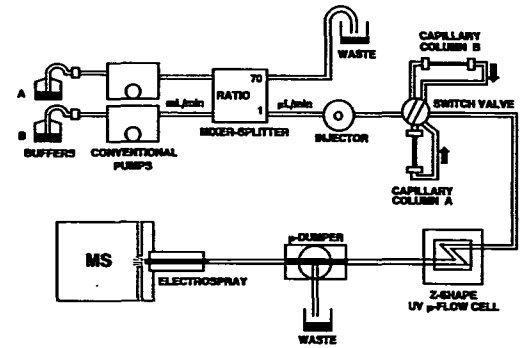

Fig. 1.

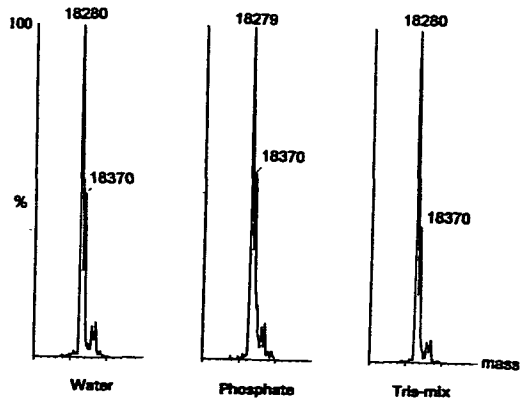

Fig. 2.

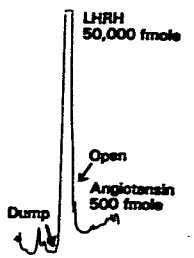

Fig. 3a.

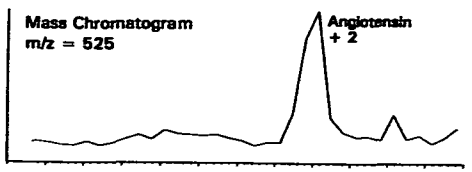

Fig. 3b.

A New API Source for Magnetic Sector Instruments

P. Dobberstein, R. Pesch, and E. Schroeder, Finnigan MAT, Bremen, Germany

The API source from the TSQ 700 quadrupole instrument [1] was adapted to the magnetic sector instruments MAT 95 and MAT 900. The principal components stayed in principle unchanged, as there are the heated metal capillary after B. Chait and coworkers [2], the tube lens, the skimmer, and the rf-only octapole (see **Fig. 1**).

The major modifications are:

1) An additional pumping stage for the octapole compartment, providing a pressure of about 2×10^{-5} Torr in the ion acceleration region.

2) The + /- 5 kV high voltage insulation for the region between the capillary and the lens system.

3) Modification of the supply electronics for operation at +/- 5 kV.

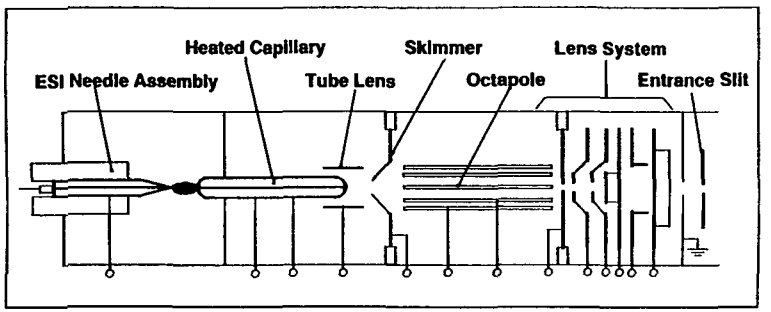

Fig. 1

Both components, the metal capillary and the octapole, which have proven their good performance with respect to reliability and ion transmission already on the TSQ 700, show excellent performance on the sector instruments as well, resulting in high sensitivity and extremely high resolving power.

On a MAT 95 a resolution of **R = 20 000** is obtained easily in ESI operation, allowing baseline resolution of the isotope pattern of multiply charged **Myoglobin** ions.

An **Exact Mass Determination** was performed using the **11+** isotope pattern of **Lysozyme** as the reference and the **13+** isotope pattern of **Myoglobin** as the "unknown".

The raw spectrum obtained by summation of narrow electrical high resolution scans shows

---

[1] I. Mylchreest, M. Hail, M. Uhrich, and I. Jardine, 9th Montreux Symposium, Nov. 4 - 6, 1992 Montreux, Switzerland, P 41.

[2] S. Chowdhury, V. Katta, and B. T. Chait, Rapid Com. Mass Spectrom. , 1990, 4, 81 - 87.

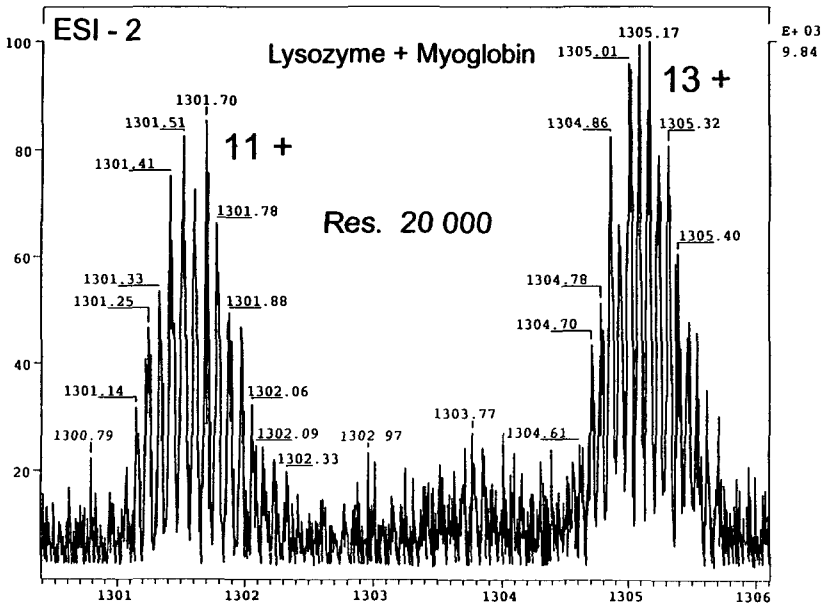

Table 1: Mass Position of Sample Peak

13+ Peak of Myoglobin (horse heart)

Theory: (769c 1212h 218o 210n 2s +13h)/13

No.	%	Theory	Experim.	mmu
6	25.7	1,304.5428	1,304.5483	5.5
7	43.5	1,304.6195	1,304.6226	3.1
8	63 7	1,304 6962	1,304.6971	0.9
9	82.2	1,304.7730	1,304.7761	3.1
10	95.2	1,304.8497	1,304.8551	5.4
11	100 0	1,304.9265	1,304.9248	-1.7
12	96 2	1,305.0031	1,305.0037	0.6
13	85.5	1,305.0798	1,305.0828	3.0
14	70.7	1,305.1564	1,305.1617	5.3
15	54.7	1,305.2332	1,305 2314	-1.8
16	39 7	1,305.3099	1,305.3105	0.6
17	27 3	1,305.3865	1,305.3802	-6.3

baseline resolution on both isotope patterns (**Fig.2**).

For data evaluation the measured spectrum was smoothed and with CMASS recalibrated, using the highest isotope peak in the measured 11+ pattern of Lysozyme as the lock mass and the corresponding peak in the calculated isotope pattern of Lysozyme [613c 915h 185o 193n 10s +11h]/11 as the reference.

The comparison of the calculated isotope pattern of the 13+ peak of Myoglobin with the recalibrated experiment is given on **Table 1.** The average mass deviation of the 12 most intense isotope peaks is:

1.5 mmu at m/z = 1 305 or 1 ppm

HIGH-SPEED GC/MS WITH FOCAL-PLANE ION DETECTION

Piet A. Leclercq and C.A. Cramers
Laboratory of Instrumental Analysis, Department of Chemical Engineering
Eindhoven University of Technology, P.O. Box 513, 5600 MB Eindhoven, The Netherlands

Scanning mass spectrometers, such as quadrupoles or magnetic sector instruments, waste all but a small fraction of the ions leaving the ion source. Due to this inefficiency, detection limits in conventional GC/MS are of the order of 1 ng/s of solute, which is about the maximum sample capacity of narrow-bore (50 μm I.D.) columns.

Each type of mass spectrometer has a maximum scan rate which is determined by fundamental laws that govern the scanning process and the minimum time required to measure the intensity at each mass [1]. A modern quadrupole mass spectrometer may be scanned at a rate of up to 10 - 20 spectra/s [2], whereas magnetic instruments are substantially slower. There are, however, two reasons which demand that at least 5 - 10 spectra per GC-peak width should be acquired. The first is to minimize changes in sample concentration in the ion source during one scan, in order to minimize distortion of relative peak intensities for a given spectrum. The second reason for high scan-repetition rates is to enable the accurate reconstruction of the chromatogram from consecutively recorded mass spectra, and the deconvolution of overlapping GC peaks.

The limitations in sensitivity and spectrum repetition rate of scanning instruments are incompatible with the working range and separation speed of narrow-bore gas chromatography. These limitations can be overcome by applying non-scanning mass spectrometers. By measuring all masses at the same time, the speed for obtaining mass spectra is virtually only limited by state-of-the-art detectors and electronics. Moreover, detection limits are in the sub-picogram range, because this kind of measurement is equivalent to selected ion monitoring at all masses simultaneously.

Three techniques can be used for the detection of an array of masses without scanning [1]. These are *spatial array* detection, applicable with magnetic mass dispersion, *time array* detection in time-of-flight (TOF) mass spectrometry, and *frequency array* detection in FT ion cyclotron resonance mass spectrometry. (The quistor, or ion trap detector (ITD) can detect about half of the ions present by scanning, and might be seen as a time array detector as well). While capillary GC/FTMS is feasible, and GC/ITD has become very popular nowadays, both methods do not fully utilize the sample because ionization is performed in a pulsed mode.

GC/TOFMS with time array detection is being pursued at the Michigan State University, in cooperation with Wollnik *et al.* from the Giessen University in Germany [3]. At the Eindhoven University we opted for the spatial array detection of all ions along the focal plane of a Mattauch-Herzog type double focussing sector analyzer (AMD MMH1). The detector is a microchannel electron multiplier array, also called a microchannel plate (MCP) multiplier. Basically, the MCP can be seen as an "electronic photoplate", which converts the ions into secondary electrons. Our first approach [4], the use of 1000 discrete collector electrodes with 1000 electron counters covering 100 mm of the focal plane (0.6 of a mass decade), turned out to be not practical. The need to still switch electric or magnetic fields in order to acquire a complete spectrum, as well as the very high costs, were prohibiting. Since then we are developing an electro-optical ion detector (EOID) covering 300 mm of the focal plane [5], applying modern optical readout systems used in image processing for office automation (copiers, fax machines). The construction of a MCP with an active length of 300 mm (spanning 1.2 mass decades), by stacking 6 pieces in a row without junction discontinuities, is one of the technological barriers yet to overcome. In this array detector, the electron image from the MCP is converted into photons by a phosphor screen. The light image is transferred via fiber optics ("rod lens array") and detected by a linear CCD array with 4800 photodiodes. The photodiode array can be read out in a few microseconds once every millisecond.

While still developing the detector, Sinha and Gutnikov published the results of a similar approach recently [6]. They used a small Mattauch-Herzog type mass spectrometer with an EOID of 127 mm, covering the mass range of 25 - 500 amu. Applying a 3 m x 50 μm i.d. GC kolom, they could obtain complete mass spectra every 20 ms. The detection limit was found to be 75 fg for benzene, and the linear dynamic range was 10^3.

References

1. J.F. Holland, C.G. Enke, J. Allison, J.T. Stults, J.D. Pinkston, B. Newcome and J.T. Watson, *Anal. Chem.* **55** (1983) 997A.
2. P.A. Leclercq and C.A. Cramers, *J. High Resolut. Chromatogr. Chromatogr. Commun.* **11** (1988) 845.
3. R. Grix, R.E. Tecklenburg, J.T. Watson, J.F. Holland, G.E. Yefchak, B.D. Gardner, J. Allison, C.G. Enke and H. Wollnik, *Proceedings of the 39th ASMS Conference on Mass Spectrometry and Allied Topics*, Nashville, TN, May 1991, p 154.
4. P.A. Leclercq, H.M.J. Snijders, C.A. Cramers, K.H. Maurer and U. Rapp, *J. High Resolut. Chromatogr.* **12** (1989) 652.
5. P.A. Leclercq, H.M.J. Snijders, R. Pesch and K.H. Maurer, *12th International Mass Spectrometry Conference*, Amsterdam, August 1991, Abstracts, p 237.
6. M.P. Sinha and G. Gutnikov, *Anal. Chem.* **63** (1991) 2012.

Maximizing the Utility of Fast GC Analysis with TOF-MS

J.F. Holland, J. Allison, J.T. Watson, R.D. McLane and C.G. Enke
Department of Biochemistry and Chemistry, Michigan State University, East Lansing, MI 48824

The proliferation of chromographic techniques, detection and injection procedures has encouraged the authors to postulate an analytical power factor for chromatography. As shown in Equation 1 this factor is defined empirically as the number of components eluted per second. As shown in Equation 2, a

$$\text{Emperical } P = \frac{\text{Compouds Successfully Analyzed}}{\text{Total Chromatographic Elution Time}} \qquad \text{Equation (1)}$$

$$\text{Theoretical } P = \text{Maximum that can be analyzed per second} \qquad P = f_c \times f_o \times f_d \times f_g \qquad \text{Equation (2)}$$

theoretical factor may be determined by taking into account a chromagraphic separation factor (f_c), that is enhanced by an overlapped peak deconvolution ability factor (f_o), and by a multi-channel detection factor (f_d), all of which are attenuated by Poisson distribution factor (f_g). This theoretical power factor gives the maximum number of compounds that can be resolved chromatographically and detected with a single channel detection and a Poisson factor of one. In fast chromatography, the peak widths at baseline (FWB) are typically from 50 to 200 milliseconds. The minimum number of data points needed for reasonable levels of quantitative accuracy for isolated peaks is approximately 10. The number of points needed for the deconvolution methods would be from 20 to 40 per peak. This implies that for the peak widths commonly experienced in fast chromatography, data collection rates ranging from 50 to 400 per second would be required. These rates are within the realm of a single channel detector system, however, there are problems with fast chromatography, such as the onerous requirements of speed and reproducibility on the injection process; the need for internal standards; the need for reproducible elution profiles on the intensity axis and reproducible behavior on the time axis; the limited effectiveness of deconvolution routines; and the magnitude of problems presented by unknowns. The attempted solution of these problems places stringent requirements on the mechanical and instrumental aspects of this methodology. Clearly, many of these requirements would be ameliorated if more than one channel of detection were employed as in mass spectrometry. Converting the band-pass requirements for the simple case of isolated peaks necessitates spectral generation rates from 50 to 200 per second. Peaks needing deconvolution would require still higher rates.

These spectral generation rates simply cannot be accommodated by modern commercial mass spectrometry. Only an array-detection type mass spectrometer is appropriate to meet these data collection demands with acceptable ion counting statistics. Of the array types, frequency, spatial and temporal, only the spatial array of ion detection or the time-array subsequent to time-of-flight (TOF) extraction appear to be adequate.

Historically, the application of TOF to chromatography has not been successful. The reasons for this have been overcome. The first reason is the data collection methodology. The development

of time-array detection (TAD) using an integrating transient detector wherein all the information within each and every transient wave form is collected and used, increases the efficiency of the information utilization by 10^4 over conventional approaches. The second drawback of the poor resolution with a 3-D ionization volume has been solved by using an ion mirror to reconstruct the space focal plane on the detector surface. The third historical drawback has been the deleterious effect of pressure on the ion source. Smaller columns and flow have abated this problem. The last major drawback was the loss of information suffered by duty cycles. Sources are being designed to store ions between source extractions to recover signal otherwise lost in the duty cycle. All of these advances in TOF have led to the development of an M-TOFMS-TAD with good sensitivity and resolution, and with spectral generation rates up to 300 s^{-1}. This has led to the development time-compressed chromatography (TCC) whereby the chromatographic resolution is intentionally degraded by increased carrier flow to reduce the analysis time. The high-speed M-TOF-TAD spectral files are processed by deconvolution routines to recover the information in 1/10 to 1/100 the time required by convetional analyses. Figure 1 shows a portion of a TCC run in which 22 compounds are analyzed in 14 seconds. Positions of individual detected compounds are revealed by clusters of peak coincidence lines along the abscissa. The empirical power factor for this chromatography would be 1.57 s^{-1}. The theoretical power factor, even when considering the attenuation of the multi-dimensional detector factor due to fragmentation of the various components, still yields a theoretical power factor 100 s^{-1}. Clearly, this potential will carry TCC well into the realm of fast chromatography.

22 COMPOUNDS in 14 SECONDS

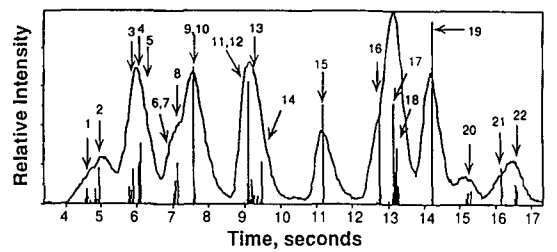

Component	Time (s)	Component	Time (s)	Component	Time (s)
dichloromethane	4 57	carbon tetrachloride	7.60	trans-1,3-dichloropropene	12 70
cis-1,2-dichloroethane	4 90	benzene	7 60	toluene	13 10
bromochloromethane	6 00	1,2-dichloropropane	9 07	1,1,2-trichloroethane	13.20
2,2-dichloropropane	6 03	1,3-dichloropropane	9 07	3,3-dichloro-1-propene	14.10
chloroform	6 07	trichloroethene	9.17	chlorodibromomethane	15.17
1,1,1-trichloroethane	7.00	bromodichloromethane	9.43	1,2-dibromoethane	16.13
1,2-dichloroethane	7.07	cis-1,3-dichloropropene	11 17	tetrachloroethene	16 57
1,1-dichloropropane	7 33				

Figure 1

ORTHOGONAL ACCELERATION TOFMS FOR MICROCOLUMN CHROMATOGRAPHY

Karin E. Markides and Edgar D. Lee
Sensar Corporation, 479 West Universal Circle, Sandy, UT 84070, USA
Milton L. Lee
Department of Chemistry, Brigham Young University, Provo, UT 84602-4672, USA

Desty demonstrated in the early sixties that speed could be significantly increased in capillary column gas chromatography by using short, narrow-bore, capillary columns [1]. Limitations in speed are primarily defined by instrumental factors, one of the most important being detection.

High speed detection has been emphasized by several recent studies involving comprehensive multidimensional separations. A comprehensive two-dimensional GC-GC separation has been demonstrated by Liu and Phillips [2]. In that system, a conventional capillary column (250 μm i.d.) was used in the first dimension and a short, narrow bore column (50 μm i.d.) was used in the second dimension, with a thermal desorption modulator as an interface. The separations on the second column could be generated every 2 s. The peak widths in the high speed chromatograms ranged from 30 to 100 ms. A scan rate of 1.5 to 20 ms was required in order to define such narrow bands. Bushey and Jorgenson recently demonstrated a high speed, comprehensive 2D system using a combination of LC-CE [3] with a switching valve as an interface. A solute eluting in the high speed CE separation in their LC-CE system had a migration time of 55 s, with an eluting band width of less than 1 s. A comprehensive, on-line SFE-GC system has recently been reported [4] in which high speed GC separations were used to monitor the extraction process. The extracted material from an SFE cell was sampled continuously with 10-s time intervals; therefore, a high speed GC chromatogram was generated every 10 s.

The main limitation in coupling mass spectrometry to microcolumn separations is the inherently slow speeds of scanning mass spectrometers. Typically, scan times are greater than 100 milliseconds for quadrupole and sector instruments. Assuming that a minimum of 10 points is required to define a chromatographic peak, these instruments are limited to peaks that are 1 s or greater in width.

Because of its high spectral acquisition rate, time-of-flight mass spectrometry (TOFMS) is the ideal mass spectral detection system for high speed separations. A full spectrum is obtained in less than a millisecond. Recently, a new TOFMS system based on atmospheric pressure ionization (API) was constructed, and preliminary data were reported [5]. This system utilizes a supersonic jet expansion into the vacuum chamber to improve resolution, and off-axis pulsing into the flight tube to increase sensitivity. In this study, preliminary testing of this new API TOFMS system was made, particularly with reference to its possible coupling with the various microcolumn separation techniques. Our initial studies have centered on the coupling of capillary supercritical fluid chromatography to the MS. Figure 1 shows a schematic diagram of the coupled system, and Figure 2 shows averaged full-scan spectra of N-nitrosodiphenylamine obtained by SFC analyses of this thermally labile compound with different interface/ion source temperatures.

REFERENCES

1. D.H. Desty, *Adv. Chromatogr.* **1**, 199 (1965).
2. Z. Liu and J. Phillips, *J. Chromatogr. Sci.* **29**, 227 (1991).
3. M.M. Bushey and J.W. Jorgenson, *Anal. Chem.* **62**, 978 (1990).
4. Z. Liu, P.B. Farnsworth, and M.L. Lee, *J. Microcol. Sep.*, in press.
5. C-H. Sin, E.D. Lee, and M.L. Lee, *Anal. Chem.* **63**, 2897 (1991).

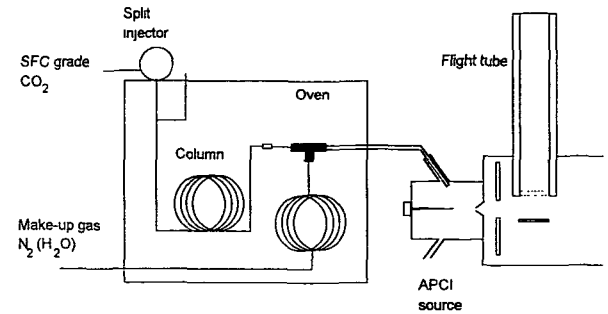

Figure 1. *SFC-TOFMS instrumentation.*

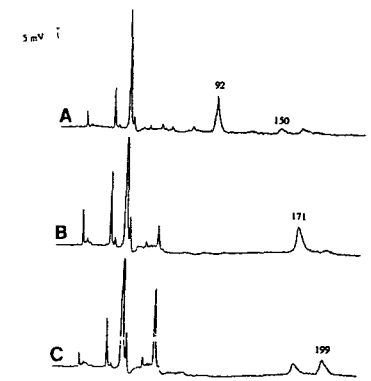

Figure 2. *APCI full scan spectra of N-nitrosodiphenylamine (198 daltons) with (A) oven at 55°C and interface/ion source at 100°C, (B) oven/interface at 55°C and ion source at 100°C, and (C) oven/interface/ion source at 55°C. SFC conditions: CO_2 density program at 0.09 g mL^{-1} min^{-1} from 0.15 g mL^{-1} to 0.85 g mL^{-1} after a 1 min isopycnic period; N-nitrosodiphenylamine retention time was 7.2 min; 4 m x 50 μm i.d. methylpolysiloxane open tubular SFC column. TOFMS conditions: 256 full scan average; discharge at 6.3 μA (3000 V); 12 V nozzle; 4493 V MCP, 2093 V flight tube; N_2 (H_2O saturated) at 5 mL^{-1} min^{-1}; signal optimized for water cluster (37 m/z).*

An Electrospray Time-of-Flight Mass Spectrometer for Chromatography Applications

T. Dresch, E. Gulcicek, J. F. Banks, C. Whitehouse and J. Fenn[a] and J.G. Boyle
Analytica of Branford, Inc., 29 Business Pk Dr, Branford, CT 06405
[a] Dept. of Chem. Eng., Yale University, New Haven, CT 06520

Continuous ionization sources have been coupled to time-of-flight mass spectrometers for many years. Interest has renewed in this practice as researchers seek the benefits of direct MS coupling to separations systems, 'soft' ionization sources which provide sub-picomole sensitivities, unlimited m/z range capability and systems with characteristic scanning speeds capable of analyzing rapidly eluting compounds. A particular configuration of an Electrospray-TOF-MS has been fabricated which meets each of these criteria.

Using a modified Electrospray ion source with excellent parallel focussing optics and well characterized ion energy profiles, TOF mass spectra have been generated in the linear mode using an orthogonal extraction technique for enhanced mass resolving power. A compact, linear geometry instrument has been shown to yield mass resolving powers in excess of 500. Sensitivities for various biomolecules allow full mass spectra to be recorded on the second and sub-second time frames. The instrument is completely free of mass dependent aberrations, allowing detection efficiency to be optimized for all m/z constituents simultaneously. Mass accuracies have been found to quite good (less than 50 ppm) by virtue of the TOF timebase stability. Despite synchronization losses, TOF duty cycle factors associated with the ion source geometry are still greater than dispersive instruments in the scanning mode.

Both pure electrospray and ultrasonically assisted electrospray (Ultraspray) have been interfaced to this system, allowing the use of both low (1-10 $\mu l\ min^{-1}$) and moderate (50 $\mu l/min^{-1}$) flowrates. An LC system (1.0 mm I.D.) with flowrates of ca. 50 $\mu l\ min^{-1}$ has been coupled to the ESI-TOF instrument to generate time resolved mass spectra of compound mixtures. We have found that the optimal acquisition of these data necessitate the use of high speed acquisition hardware with integrating capabilities for enhanced signal to noise ratios.

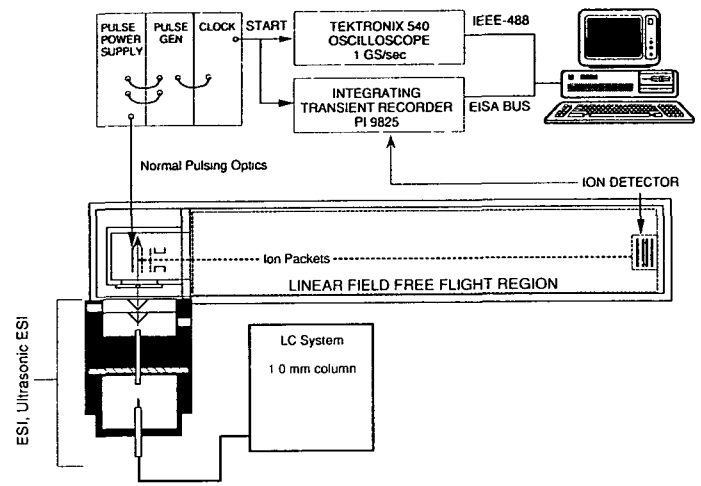

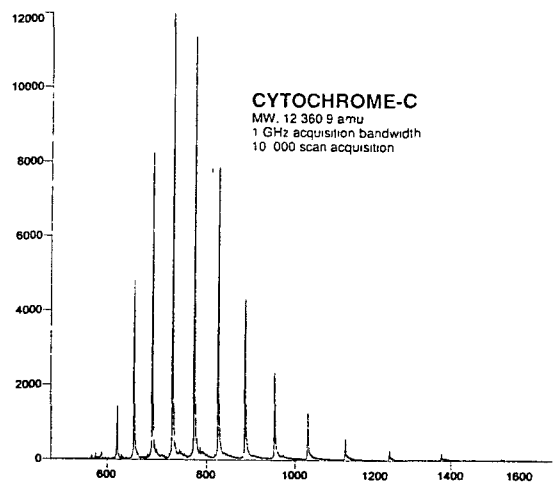

Time-of-Flight Technology for For High Speed GC/MS

J. Coles and M. Guilhaus, Department of Analytical Chemistry,
The University of New South Wales, PO Box 1 Kensington, NSW 2033, AUSTRALIA

Introduction

Most ion sources used in chromatography/mass spectrometry are continuous and involve the ionization of gaseous molecules. The distribution of molecular speeds of ions, time of ionization and their starting positions prior to TOF analysis preclude the attainment of analytically useful mass resolving powers unless steps are taken to correct for these initial dispersions.

A key advantage of TOFMS for chromatography/mass spectrometry is its speed which is limited by the arrival time of the heaviest ion (typically 100μs) and the requirement to obtain adequate statistics (several hundred ions in a spectrum). Adequate statistics can now be achieved with 100 to 1000 duty cycles from an EI source if the TOF duty-cycle efficiency is high. This results in data acquisition rates of 10 to 100 spectra per second which is a significant advance on scan rates on quadrupole and sector mass spectrometers.

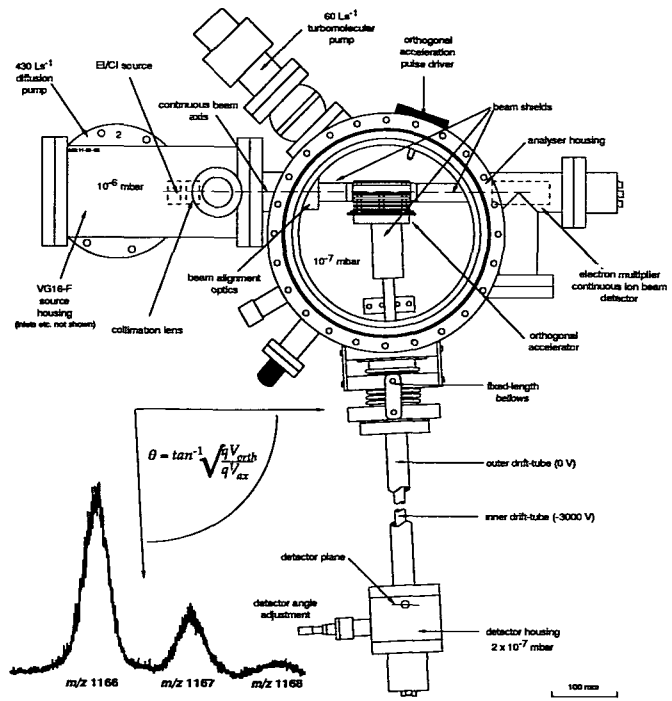

Extraction of ion packets from a low-energy continuous ion beam by application of a pulsed orthogonal field can be an effective way to achieve relatively high duty-cycle efficiencies [1]. Once a section of the beam has been orthogonally extracted and leaves the first mesh delimited accelerating field, the extraction pulse can be relaxed to allow the continuous ion beam to refill the extraction region. With the correct choice of instrumental geometry and ion energies, the time for the heaviest ion to drift to the detector can be made to be about the same as the time for that component of the ion beam to refill the extraction region. Thus the analyzer efficiency increases towards the high mass end of the spectrum where it is usually most needed (opposite to the transmission characteristics of quadrupole mass filters).

If the ions in the continuous ion beam are traveling with minimally divergent trajectories, ion velocity vector components orthogonal to the beam are very small and if the orthogonal direction is chosen for the TOF analysis, conventional spatial focusing methods are able to correct for the spread of ion initial distances from the detector without the complication of a significant initial velocity dispersion. The acceleration pulse can be applied very quickly and reproducibly thus practically eliminating the temporal dispersion.

Our device does not require a reflectron and is designed to conserve the ion velocity components in the direction of the ion beam giving rise to an oblique ion trajectory in contrast to other "orthogonal" instruments which retard the ion-beam velocity with deflection optics [2]. Our investigations show that this steering step perturbs the space-time focusing advantage of the minimized initial orthogonal velocity spread and significantly decreases the resolving power attainable.

Results

Our prototype achieves a resolving power of m/Δm (fwhm) = 4000 at m/z c.1000. At higher mass the resolution approaches 5,000. The duty cycle efficiency leads to a sensitivity advantage over scanning analyzers of in the range of 100-1000 in terms of the number of ions detected or 10-30 in S/N. With suitable detection electronics, data acquisition rates of 50-100 spectra per second will be readily available.

Conclusion

The orthogonal acceleration / beam-velocity-conserved TOFMS geometry offers optimum duty-cycle efficiencies (high sensitivity) high resolving powers without the need for steering plates or ion reflectors. The approach is modular with respect to other continuous ion sources for broader use in chromatography/mass spectrometry. A GC/MS TOF instrument could be compactly designed to provide adequate resolving power (say m/Δm = 1000) with a 0.5m flight tube.

References

1. J.H.J. Dawson and M. Guilhaus, *Rapid Commun Mass Spectrom.*, 3 (1989) 155; J.N. Coles and M Guilhaus, *Trends Anal. Chem.*, 12 (1993) 203; A.F. Dodonov, I.V. Chernushevich and V.V Laiko, Extended Abstract from the *12th International Mass Spectrometry Conference*, Amsterdam, The Netherlands, August 26—30, 1991.
2. G.J. O'Halloran, R.A. Fluegge, J.F. Betts and W.L. Everett, Technical Documentary Report No. ASD-TDR-62-644, Part I & II, prepared under Contracts AF33(616)-8374 and AF33(657)-11018 by The Bendix Corporation Research Laboratories Division, Southfield, Michigan, 1964; Ph. Gerhardt, S. Löffler and K.H. Homann, *Proceedings of the 22nd Symposium (International) on Combustion*, The University of Washington, Seattle, WA, August 14—19, 1988; T. Bergmann, T.P. Martin and H. Schaber, *Rev. Sci. Instrum.*, 61 (1990) 2592; C.H. Sin, E.D. Lee and M.L. Lee, *Anal. Chem.* 63 (1991) 2897; D.P. Myers and G.M. Hieftje, *Proceedings of 40th ASMS Conf. on Mass Spectrom. Allied Topics*, Washington DC, May 31—June 4, 1992, p247; J.G. Boyle and C.M. Whitehouse, *Anal. Chem.*, 64 (1992) 2084.

RECENT DEVELOPMENTS IN LC/TOF MASS SPECTROMETRY

Liang Li
Department of Chemistry, University of Alberta
Edmonton, Alberta T6G 2G2, Canada

We are in the process of developing interfacing techniques for combining solution-based separation methods with time-of-flight MS. Specifically, a pulsed sample introduction (PSI) interface [1] is being developed for combining conventional LC with TOF using laser-induced multiphoton ionization (MPI). In addition, continuous-flow matrix-assisted laser desorption (CF-MALD) [2] is being developed for micro-LC and capillary electrophoresis detection. In this presentation, new results on the performance of these interfaces were highlighted. However, much of the development and improvement in these areas is dependent on the use of a sophisticated data system for recording and storing transient signals and performing postdata analysis. In this report, we briefly describe the data system and illustrate its applications for PSI LC/TOFMS and CF-MALD. To our knowledge, no commercial data system dedicated for chromatography/TOF is currently available. We note that several groups have developed quite sophisticated data acquisition systems for high speed TOF [3-5].

Our data acquisition system is developed for laser ionization TOFMS. It involves the use of a digital oscilloscope (LeCroy 9400A) for mass spectral recording, followed by the transfer and storage of the data to a PC (486DX) via a GPIB. A software based on LabWindows is written to maximize the speed of data transfer and storage. To achieve rapid data storage, software double buffering is used so that the GPIB board can transfer the data from the LeCroy digitizer by direct memory access (DMA) to one buffer, while concurrently the contents of the second buffer is transferred to the disc. Table 1 lists the data recording speed of our system with different record lengths. This table shows that mass spectra can be recorded and stored at a speed ranging from 14 spectra/sec to 50 spectra/sec. This simple and readily adaptable system is found to be adequate and useful for operations in laser work where the use of very high repetition rates possesses no advantages or in the situations where only limited repetition rates can be used. It should be noted that the disk consumption rate is very high with laser ionization LC/TOF. For example, when the laser is operated at 10 Hz and the record length of one mass spectrum is set at 10 k, a 30-min chromatographic run would generate more than 180 Mbytes of data. In our system, the stored data can be transferred to other computers via ethernet. For offline data storage, a Hewlett Packard 35470A SCSI DAT drive is currently used to download the data from the hard disk to a tape. A 90 m tape can store 2 gigabytes of data. The data transfer rate is 10 MBytes/min.

In the past we relied on a boxcar integrator to monitor the ion intensity changes during the elution of samples in PSI LC/TOFMS. With the new data system, both total ion and selective ion chromatograms can be constructed from the mass spectra recorded. Figure 1 shows a comparison between the UV chromatogram of seven PAHs and the total ion chromatogram obtained from LC/TOF with the PSI interface. Figure 1 illustrates that the PSI interface does not degrade the performance of LC separation significantly. The data system also allows us to perform flow injection experiments with CF-MALD. Figure 2 shows the ion profile of five repeat injections of myoglobin obtained by flow injection CF-MALD with a parallel ion extraction configuration which has been described elsewhere [6]. The total amount of sample for each injection is 400 femtomoles. To construct the ion profile (i.e., peak area vs time) shown in Figure 2, the area of the myoglobin peak is calculated by the data system. Then ten peak areas are averaged to generate one time point in Figure 2. Since the mass spectra are recorded at a repetition rate of 10 Hz, one time point represents one second. In addition, 5-point data smoothing was performed to generate Figure 2.

In summary, much of the progress in LC/TOF is dependent on the use of a dedicated data system. We have developed a mass spectral recording and storing system based on GPIB data transfer for laser ionization LC/TOFMS. We have demonstrated that the system is essential and extremely versatile for performing PSI LC/TOF and CF-MALD.

References

1. Wang, A.P.L.; Li, L. *Anal. Chem.* 1992, 64, 769.
2. Li, L.; Wang, A.P.L.; Coulson, L.D. *Anal. Chem.* 1993, 65, 493.
3. Holland, J.F.; Newcombe, B.; Teckenburg, Jr. R. E.; Davenport, M.; Alison, J.; Watson, J.T.; Enke, C.G. *Rev. Sci. Instrum.* 1991, 62, 69.
4. Emary, W.B.; Lys, I.; Cotter, R.J.; Simpson, R.; Hoffman, A. *Anal. Chem.* 1990, 62, 1319.
5. Lincoln, K.A.; Bechtel, R.D.; Mateos, M.A. *Int. J. Mass Spectrom. Ion Processes* 1990, 99, 41.
6. (a) Whittal, R.M.; Nagra, D.S.; Li, L. This volume. (b) Nagra, D.S.; Li, L. This volume.

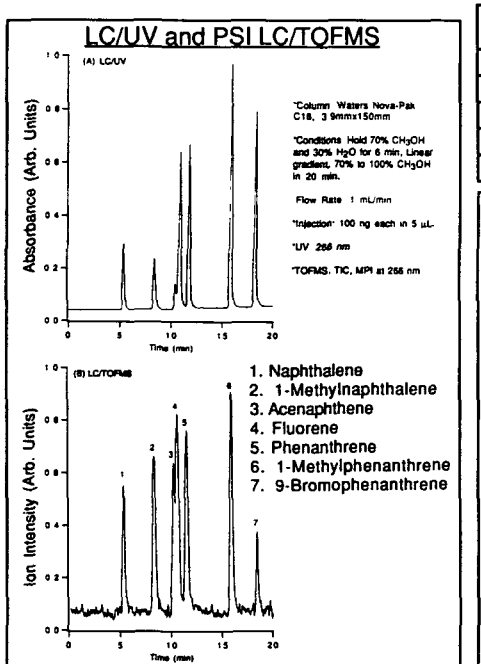

Figure 1

Table 1. Data recording speed.

Record Length (Bytes)	Acquisition Rate (Hz)
1024	50
2048	44
5120	31
10240	22
20480	14

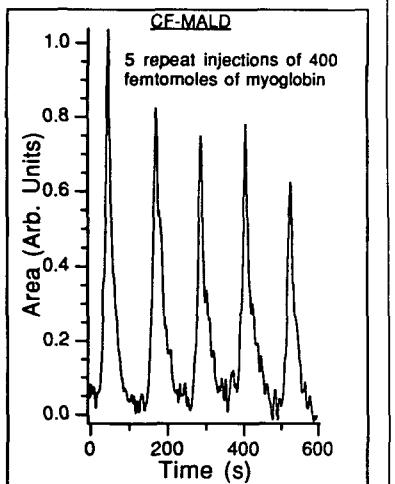

Figure 2

TWO APPROACHES TO FAST GC/MS FOR PROCESS MONITORING

Steve Doherty, Bill Winniford
Dow North America, Western R&D Labs, Pittsburg,CA 94565.

We have investigated two approaches to the coupling of fast GC with a mass spectrometer for rapid analysis of vapor-phase reactors. Fast GC uses narrow I.D. or short capillary columns to reduce the analysis times compared to conventional GC by a factor of 10-100. This work has been directed towards providing an analytical system for unattended operations on processes that may have high variability over time, such as catalyst screening reactors or for fenceline monitoring. Both applications used a Hewlett Packard 5971A mass selective detector (MSD) to perform the mass spectrometry.

The first approach involved modifications to a commercially available fast gas chromatograph, the Microsensor Technologies Inc. (MTI) Model 200D GC. The MTI GC has been used extensively in-house for monitoring reactor eluents and process streams, due to its analytical flexibility and portability. Typical separations take less than two minutes, but the integral thermal conductivity detector (TCD) can not provide any structural information on unknowns. Since the TCD is a non-destructive detector, the GC eluent can be directed through the TCD and into a mass spectrometer for analysis by EI. The modifications required for interfacing the mass spec did not impair the integrity of the chromatographic separation, and provided an additional dimension of information for identifying unknowns.

The second approach employed short lengths (2.5 to 15 feet) of narrow-bore (10-100 micron I.D.) capillary chromatographic column held within a temperature controlled isothermal transfer line. The same length of capillary is used to both provide pressure drop into the mass spec ion source, and effect a separation of the individual components. Injection was made via a Valco 6 port valve with an external sample loop. In these experiments the MSD was the only detector used. **Figures 1** and **2** show typical separations, with baseline resolution in less than 30 seconds in both cases.

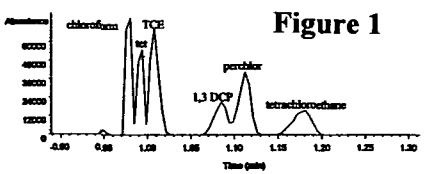

Figure 1

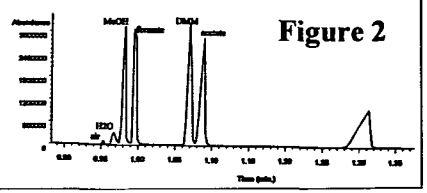

Figure 2

In addition to providing very rapid separations, this method offers a high degree of flexibility. We have used membrane inlets for monitoring organics in water, and with what were far from optimized conditions, we obtained reproducible analyses (RSD's < 5%) on the 30-45 second time scale, as seen in **Figure 3**.

Figure 3

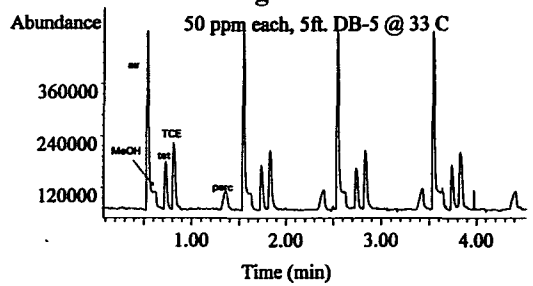

Another interesting application is demonstrated in **Figure 4**. In this analysis, 200 ppm carbon tetrachloride and perchloroethylene were separated in 30 seconds at ambient temperature, using ambient air as the carrier gas. Combined with the fact that the mass spectrometer and valve actuation are easily automated, this provides a flexible GC/MS system that could be used for unattended process monitoring with a lmost no maintenance.

Figure 4

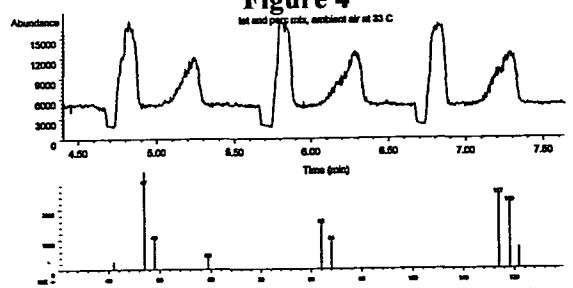

This combination of fast GC and mass spec provides rapid, highly efficient separations and sensitive detection . The molecular specificity of the mass spectrometer has another advantage; by using selected ion monitoring plots, the analyst can even resolve partially overlapping spectra (provided that each analyte has at least one characteristic ion), effectively increasing the resolving power of the combination. The hardware is inexpensive and mechanically simple, and is well-suited to automation. As such, it is ideally suited to process monitoring and environmental assessment applications.

FAST GC-MS IN SUPERSONIC MOLECULAR BEAMS

Aviv Amirav and Shai Dagan

School of Chemistry, Tel Aviv University, Tel Aviv 69978, Israel, Fax 972-3-6409293

A supersonic molecular beam is based on the expansion of the sample molecule seeded in a light carrier gas into the mass spectrometer vacuum system. A short 50 cm long megabore capillary column connects the heated injector-atmospheric pressure inlet and the supersonic nozzle. This column serves as an ultra-fast GC with total analysis time down to one second.

Fast GC-MS in supersonic molecular beams (SMB) is characterized by a very high carrier gas flow rate up to 240 ml/min and a carrier gas linear velocity controlled in the range 40-2000 cm/sec. This high flow rate and the septum free manual injection facilitate a very fast injection response time.

Both fly through electron impact and hyperthermal surface ionization serve as ion sources for the mass spectrometric analysis. The hyperthermal directional molecular kinetic energy serves to discriminate against the vacuum background ionization. Thus only molecules from the fast GC are ionized and mass analyzed (quadrupole) with the resulting ultra-fast ion source response time. In Fig. 1 the one or two seconds single ion monitoring GC-MS of four aromatic molecules is shown. In addition, the vacuum background elimination also result in a tail free fast GC-MS even with relatively non-volatile molecules as shown in Fig. 2.

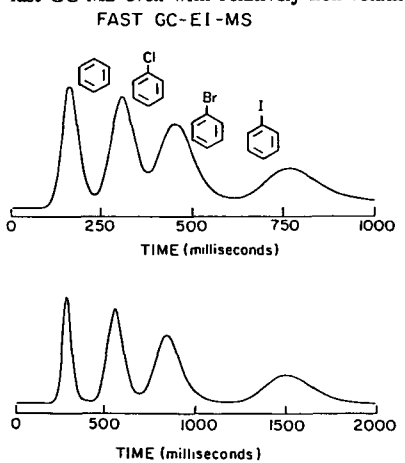

Fig.1 - Fast GC-MS

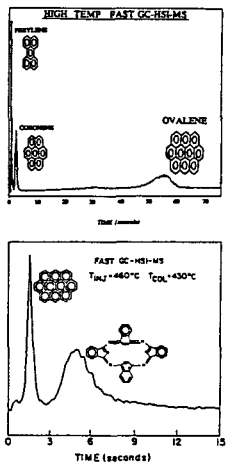

Fig.2 - High Temperature Fast GC-MS

The combination of fast elution time and hyperthermal surface ionization enables minimum detection level of 400 attogram as extrapolated from figure 3 which demonstrate the detection of 100 femtogram perdeuterated anthracene featuring noise free baseline with single ion monitoring quadrupole mass analysis. Fast GC-MS with final elution time constraint will be discussed in terms of optimal column length and carrier gas velocity. The fast analysis of thermolabile molecules and target compounds in complex mixtures such as tetraethyllead in gasoline will be demonstrated and discussed. In figure 4 two seconds GC-MS detection of coffeine in coffee is shown both in regular and decaffeinated brands. The fast GC inlet can also be coupled to a conventional GC with practically unlimited carrier gas flow rate and injected sample size. Over 100 mL splitless injection can be tolerated repeatedly.

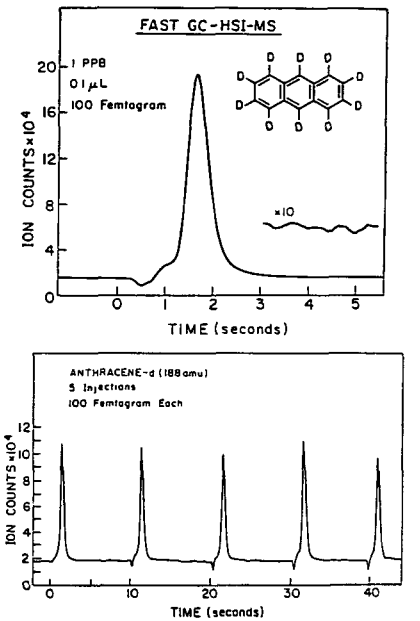

Fig.3 - Ultra Sensitive Fast GC-MS

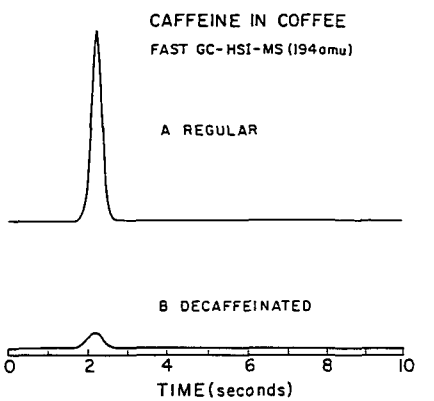

Fig.4 - Fast Caffeine in Coffee GC-MS

Interfacing High Speed Transfer Line Gas Chromatography to Ion Trap Mass Spectrometry; Advantages and Limitations

Neil S. Arnold, William H. McClennen and Henk L.C. Meuzelaar
Center for Micro Analysis & Reaction Chemistry
University of Utah, Salt Lake City, UT 84112

The Ion Trap Detector (ITD, Finnigan-MAT) was originally introduced as a gas chromatography (GC) detector for laboratory benchtop GC/MS analyses. Its introduction coincided with a rising interest in vacuum outlet short column GC/MS [1] for high speed chromatographic separations. Advantages for such short column applications, including high operating pressures (10^{-3} torr) sensitivities (.1 fg/s) and scan speeds (5500 amu/s) relative to conventional quadrupole instruments, have fueled interest in ion trap based instruments for high speed, high resolution GC/MS analyses. Subsequent interest has been fueled by new developments in mobile instruments, high sensitivity MS^n capability, AGC-based dynamic range enhancement, and axial modulation based resolution enhancement.

High performance GC separations, produced in capillary flow restrictors (so-called "transfer line (TL)GC") and utilizing a simple vapor sampling interface [2] have been shown to provide rapid and sensitive atmospheric vapor analyses in GC separations requiring less than 10 s. This interface enables introduction of vapor samples via only deactivated quartz and fused silica surfaces into the transfer line GC column. The use of such sampling systems allows high speed GC/Ion Trap MS to be a near real time technique with low ppb level sensitivities. Figure 1 illustrates a repeated (x 2) selected ion chromatogram of a 4 ppb alkyl benzene mixture demonstrating a 10 to 1 S/N ratio. In Figure 2, the concentration of various substituted benzenes are traced as evolved from a 2 minute rotary kiln combustion experiment. Vapor samples are taken at 10 s intervals allowing the concentrations to effectively be traced in real time.

In Figure 2 GC resolution between peaks is effectively governed by the duration of the sampling pulse. With sufficiently high detector scan rates high GC resolutions may be utilized. Figure 3 illustrates the relationship between various GC parameters in the fixed pressure drop TLGC system (see reference 3). Obtaining theoretical plate values of 1000 to 10,000 plates at few second retention times implies that 10-100 ms wide GC peaks must be resolved to utilize the full potential of the GC separation. Figure 4 illustrates the potential of such separations in SIM traces of m/z 57, obtained from headspace of unleaded gasoline. This sampling rate of 15.6 scans/sec was obtained on a quadrupole instrument (HP 5971A) rather than an ITD instrument, but illustrates the need for higher ion trap scan rates.

Hardware considerations have limited ITD instruments and their successors (e.g., Magnum, Saturn) to an actual scan rate of 5500 amu/s and an effective rate which is over 4 times lower. The demands of interfacing ITD instruments to high speed transfer line GC require extending the limits of the ion trap based system. It should be pointed out that actual scan function durations are approximately 60 ms long (150 amu scan range) in an ITD based system so that internal data processing overhead reduction should allow scan rates up to 16 scans/sec in redesigned hardware systems. More importantly, the combined use of buffer gas and axial modulation have already allowed 2nd generation Ion Trap instruments to obtain peak widths between .1 and .2 amu wide for a 3 to 6 times improvement over unit mass resolution.

Figure 5 illustrates a PFTBA spectrum obtained at 4 x 10^{-4} torr in He at 22000 amu/s on a modified ITMS system. Inset are the actual data system peak profiles for m/z 69 and 502. While the A/D conversion rate is only 1.5 conversions/amu, unit mass resolution was verified by an analog oscilloscope. Actual peak width for m/z 502 is ~.6 amu FWHM and the C_{13} peak is readily resolved in the analog signal. This is 4 times the "normal" scan speed for the Ion Trap system. Theoretical evaluations [4,5] indicate that resolution in a high scan speed limit should decrease inversely with the square root at the scan speed.

If this is the case the prospects of obtaining total scan rate improvements of 10 to 50 times at unit mass resolution seems practical on both theoretical and hardware grounds.

ACKNOWLEDGEMENTS

The work is sponsored by Army Research Office ERDEC, and the Advanced Combustion Engineering Research Center (funded by NSF, State of Utah and 23 industrial participants). The authors wish to acknowledge the technical help and support of G. Hars, W. Du and P. Cole.

1. Trehy, M.L.; Yost, R.A.; Dorsey, J.G., *Anal. Chem.* 58:14-19 (1986).
2. Arnold, N.S.; McClennen, W.H.; Meuzelaar, H.L.C., *Anal. Chem.* 63:299-304 (1991).
3. Arnold, N.S.; Kim, M.G.; McClennen, W.H.; Dworzanski, J.P.; Meuzelaar, H.L.C., *Proc. 1992 Workshop on Ion Mobility Spectrometry*, Mescalaro, NM, June 1992.
4. Goeringer, D.E.; Whitten, W.B.; Ramsey, J.M.; McLuckey, S.A.; Glish, G.L., *Anal. Chem.* 64:1434-1439 (1992).
5. Arnold, N.S.; Hars, G.; Meuzelaar, H.L.C., submitted to *Anal. Chem.* 1993.

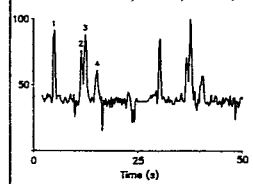

Figure 1. Two repetitive selected ion chromatograms from a 4 ppb alkyl benzene mixture. 1) toluene; 2) m-xylene; 3) p-xylene + ethyl-benzene, 4) o-xylene.

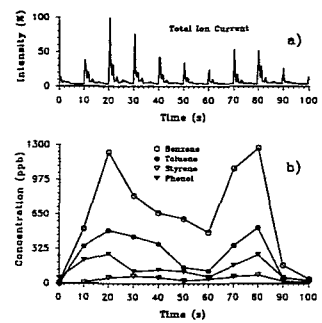

Figure 2. a) Repetitive chromatograms monitoring substituted benzenes from a transient combustion experiment. b) Actual concentration profiles of 4 substituted benzene compounds.

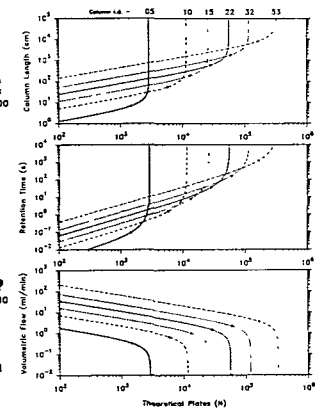

Figure 3. Theoretical prediction of GC characteristics for a fixed pressure drop system. Carrier gas He, inlet pressure 1 atm, viscosity 200 μpoise, diffusivity 0.3 cm^2/s and capacity factor 5.

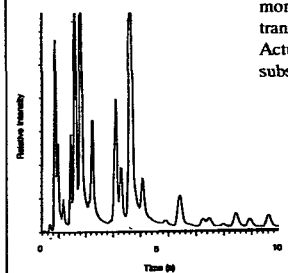

Figure 4. SIM chromatogram (m/z 57) for a gasoline headspace. Peak widths as small as 180 ms have been obtained with 100 ms vapor sample pulse and 15.6 scans/second.

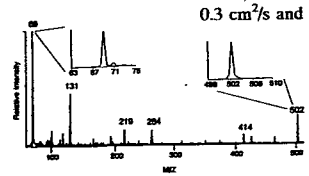

Figure 5. PFTBA spectrum obtained at 22,000 amu/s with unit mass resolution. Insets show actual peak widths. Peaks are under sampled at ~1.5 A/D conversions per amu.

TRACING ATTOMOLES OF ^{14}C-LABELED ORGANIC COMPOUNDS IN NATURAL SYSTEMS

J.S. Vogel[1], K.W. Turteltaub[2], C.E. Frantz[2], M.R. Creek[2], E.D. Fultz[2], K.T. Bogen[3] and G. Keating[3]
[1]Center for Accelerator Mass Spectrometry, [2]Biomedical and Biotechnology Research Program, and [3]Environmental Research Division
University of California, Lawrence Livermore National Laboratory
Livermore, CA 94550

Soon after the discovery of radiocarbon, two distinct applications of the isotope were developed that still predominate present uses: radiocarbon dating for chronometry, and radiocarbon tracing of labeled chemicals, especially in biological research. A primary goal in the development of accelerator mass spectrometry was the enhancement of ^{14}C dating through mass spectrometic detection. Although it was recognized that AMS could also be used for tracing ^{14}C in biomedical applications, no effort was made to develop practical methods for handling enhanced ^{14}C levels with AMS until biomedical researchers joined in forming the Center for AMS at LLNL in 1988.

AMS measures ^{14}C as an isotope ratio from graphite that is compared to that of a standard. Combustion and conversion to graphite of the samples destroy all chemical information. Careful separation and definition of all carbon in the sample before combustion are essential. Small amounts of natural or unlabeled organic materials will not change the isotope ratio appreciably, but attomole amounts of compounds labeled at many mCi/mmol easily contaminate samples. Contamination in laboratories previously used for ^{14}C labeled compounds can only be avoided by the most scrupulous use of disposable containers and processes that protect the sample from contamination through active design.

Living components of the biosphere contain 115 amol of ^{14}C per mg of carbon, or 1.4 parts per trillion. AMS is sensitive to 1 ppq for ^{14}C dating purposes, equivalent to 57,000 years of decay from biosphere levels, or 80 zmol per mg. Precisions of 0.5-2% are readily obtained in AMS measurements, sufficient to measure enhancements of a few amol in contemporary biological tissues. Sample preparation processes developed for biomedical use are not as sensitive as those for dating, but we detect 800 zmol/mg in samples as small as 100 µg. Samples are ideally 1 mg in size for efficient conversion to graphite for use in an AMS cesium sputter source, but the sample may contain a large fraction of ^{14}C-free carbon carrier as a dilutant. Separated samples of DNA or defined proteins may only weigh nanograms or micrograms but ^{14}C is quantified in them to 10 amol precision after dilution to 100-1000 µg. A 100 amol/mg sample produces a count rate of 200-400 cps in AMS, in contrast to it's decay rate of 0.0015 dpm. The upper limit to AMS quantification is set at 10-50 fmol ^{14}C per mg carbon (specific activity ≈20 pCi/mmol) to avoid contaminating the ion source which is also used for ^{14}C chronometry.

The most direct use of ^{14}C-AMS in biomolecular tracing measures the ^{14}C content of tissues or fluids at specific time points after dosing, or after a series of different doses at a

single time in an array of hosts. If the dissection or collection is contamination free, the isotope ratio converts directly to a specific dose per tissue weight for pharmacokinetic studies. For example, maximum levels of 1000 amol/mg-tissue of 2-amino-1-methyl-6-phenylimidazo[4,5-*b*]pyridine (PhIP) are found in organs to a sensitivity of 2 amol/mg less than an hour after a single dose of 41 ng/kg. A chronic daily dosing with 47 ng/kg of 2-amino-3,8-dimethylimidazo[4,5-*f*]quinoxaline (MeIQx) resulted in liver and kidney saturation levels of 470 amol/mg-tissue. Benzene in whole liver tissue was quantified at 6 amol/mg after an acute dose of only 1 ng/kg. Dermal absorption of 5 ppb aquatic solutions of trichloroethylene and chloroform was qauntified at pmol/mg levels after exposures as short as 1 minute from compounds labeled only at the 5-10 µCi/mmol level (0.01% labeled). Such low radioactive and chemical doses could permit realistic human exposures to be tested directly on human subjects.

Pharmacodynamic study of detailed chemical binding with specific biomolecules requires selection and purification of components from bulk tissues. Since contamination is likely from equipment used in previous studies, we use individual and disposable separatory tools for each sample. DNA samples are purified on ion exchange columns designed for PCR analysis. Silica and cellulose TLC plates can be scraped to remove the spot or area containing the desired component. Affinity media, dialysis, precipitation/solubility, and molecular weight separations are performed in disposable plasticware. More complex molecular analysis requires the use of HPLC or electrophoresis. We created the world's largest HPLC by collecting 1 minute elution solutions, diluting a portion of each into carrier carbon, converting these to graphite, and measuring ^{14}C content by AMS. The sensitivity, determined by the baseline of hydrolyzed hepatic DNA from an undosed mouse, is 20 amol/min. Similarly digested DNA from an acutely ^{14}C-MeIQx dosed mouse (30mCi/mmol, 50mg/kg) indicates 65 fmol of MeIQx bound per µg of DNA throughout the rigorous DNA purification. The absolute quantity of the deoxynucleotides injected is determined from the UV trace before eluent collection. Our initial tests of plate gel electrophoresis show that molecular weight markers, even supposedly "unlabeled" ones, may migrate sufficiently across lanes to cause ^{14}C contamination, but that the procedure can detect differential binding of a labeled compound among proteins. The acrylamide gel itself provides the carrier carbon in small plugs excised at developed spots. Capillary zone electrophoresis is also being explored and may prove a more effective method than gel electrophoresis for studying binding of labeled compounds to macromolecules using AMS.

Presently, CAMS/LLNL is the only AMS facility of the 25-30 worldwide that devotes a significant effort to ^{14}C detection for biomedicine. We plan to increase throughput to 500-1000 samples per week by obtaining a dedicated spectrometer. Small spectrometers are being developed for more widespread application of this sensitive technique.

Work performed at Lawrence Livermore National Laboratory under the auspices of the U S. Department of Energy, contract W-7405-ENG-48

Calcium Kinetic Study In Human By ^{41}Ca Tracing.

E. Venczel[b], E. Boaretto[a], Z. Gelbart[b], G. Hollos[c], R. R. Johnson[b], M. Paul[a], J. Prior[d], V. Sossi[b], : (a) Racah Institute of Physics, Hebrew University, Jerusalem, Israel; (b) TRIUMF and University of British Columbia, Vancouver; (c) Accelerator Laboratory, Weizmann, Rehovot, Israel; (d) Vancouver General Hospital, Vancouver, Canada.

^{41}Ca ($T_{\frac{1}{2}} = 1 \times 10^5$ years) is an ideal tracer [1] for long-term studies of calcium kinetics in biological systems for several reasons: (i) due to its long half life it behaves as a stable nuclide for a human time scale causing no collateral radiation effects; (ii) its natural abundance is extremely low (^{41}Ca/^{41}Ca $= 10^{-15}$); (iii) using Accelerator Mass Spectrometry (AMS) ^{41}Ca isotopic concentrations can now be measured to very high sensitivity (typical sensitivity of our system ^{41}Ca/^{41}Ca $< 10^{-13}$).

An experiment was initiated in a human subject by intravenous injection of a 126ng dose of ^{41}Ca on July 18, 1990. The ^{41}Ca concentration and the ^{41}Ca/^{40}Ca isotopic ratios in serum and urine were measured at time points over a 900 day period. The isotopic ratio decreases exponentially with a slope change in the later time period corresponding to the slow release of calcium from the stable bone pool. A three compartmental model analysis indicates that the data are in relative agreement with known (D. Elmore et al, Nucl. Instr. and Meth. B52 (1990) p531) time constants of the different calcium pools (Fig 1).

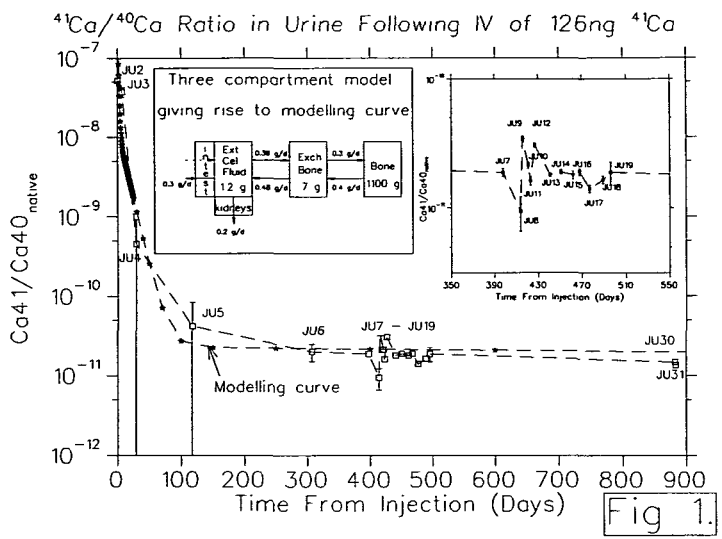

Fig 1.

This information established the steady-state concentration of ^{41}Ca in the subject's skeletal bone pool.

Preparation of samples for analysis by AMS required simple chemistry. With an injected dose of 100ng, required volumes of urine from day1 - day200 fall in the range of 0.1-3.0mL plus an appropriate quantity of carrier ^{40}Ca to attain a ^{41}Ca/^{40}Ca ratio $\sim 10^{-11}$ were needed. From day 201 onward the required sample size typically 1000mL, was large enough to recover 30mg of native calcium so that no additional carrier was necessary. Calcium recovered from the biological samples was prepared as calcium hydride (Fig. 2), the required molecular form of calcium for AMS analysis. The prepared CaH_2 samples were analyzed by AMS on the Pelletron Tandem Accelerator at Weizmann, Rehovot, Israel.

At time points after the establishment of a relative steady-state, fluctuations in the native ^{41}Ca/^{40}Ca ratio were observed (Fig 1). we are developing a more sophisticated compartmental model to take into account these ^{41}Ca/^{40}Ca ratio variations. a relationship between these changes and hormone balance is being explored.

Further studies in women during pre-menopause and after may help to understand the effects of hormonal influences on bone resorption Such studies may also show which subjects may be suffering from the early onset of osteoporosis, indicated by significantly higher native ^{41}Ca/^{40}Ca ratios, due to elevated resorption of bone calcium.

In conclusion we have demonstrated: The ability of monitoring ^{41}Ca levels in biological samples from a human subject over a long time period; life-long observations of bone resorption are feasible with a nominal dose of 100ng of ^{41}Ca (equivalent to 0.01% of background radiation) with no significant radiation effects.

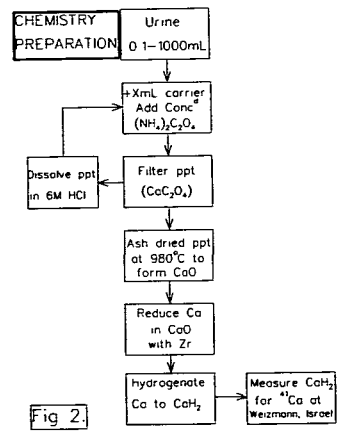

Fig 2.

Advances in the Earth Sciences through Accelerator

Mass Spectrometry

Fred M. Phillips, Geoscience Department, New Mexico Tech, Socorro

Measurement of many naturally-occurring long-lived radionuclides by decay counting is difficult or impossible due to the long counting times or large sample sizes that are required. This impediment has been removed by the application of accelerator mass spectrometry (AMS), which can routinely measure many rare radionuclides on milligram-sized samples at atomic abundance ratios as low as one in 10^{15}. This analytical development has for the first time allowed the application of many cosmogenic and anthopogenic nuclides to problems in the earth sciences. This talk will focus on three applications:

Demonstration of rapid sediment recycling through volcanoes over subduction zones. Berylium-10 produced is by cosmic rays in the atmosphere, but only negligibly in the subsurface. The atmospheric ^{10}Be is deposited in relatively high concentrations in oceanic sediments, since deposition of sediment is low in the open ocean. ^{10}Be has now been measured by AMS in the lava of volcanoes that overlie subduction zones. This proves that subducted ocean crust is indeed recycled through volcanoes. It also shows that the time for recycling is short, since ^{10}Be has only a 1.4 million year half-life.

Dating the formation age of landforms. Most landforms cannot be dated by conventional methods, rendering difficult the development of chronologies for earth-surface processes. This difficulty can now be overcome by using AMS to measure the amounts of cosmogenic radionuclides that have accumulated in surface rocks, and hence inferring the exposure time. Nuclides that are produced by cosmic radiation in rocks include ^{10}Be, ^{26}A1, ^{36}C1, and ^{40}Ca. They can be used to date the exposure time (or to determine the erosion rate) of rocks on time scales from 10^3 to 10^6 years. Applications include dating young lava flows, determining chronologies of glacial advances, dating meteorite impact craters, estimating erosion rates of mountain ranges, and revealing the history of sand dunes.

Reconstruction of variations in cosmic radiation. The intensity of cosmic radiation is thought to have varied in the past due to changes in the terrestrial and solar magnetic fields. It is now possible to test these magnetic field histories by using AMS to measure cosmogeic nuclides in suitable geological repositories. ^{10}Be has been measured in ice cores and shows marked changes in concentration with time. More recently, ^{36}C1 has been measured in fossil urine from pack rat midden collected in the western United States. The ^{36}C1/C1 ratio in this fossil urine has varied by a factor of approximately two over the past 20,000 years.

Presented at the 41st ASMS Conference on Mass Spectrometry

The Analysis of Heavy Elements by AMS; A New Mass Spectrometry?

L.R.Kilius. IsoTrace Lab, University of Toronto, Toronto, Canada, M5S 1A7

Whereas the light isotopes such as ^{10}Be, ^{14}C, ^{26}Al and ^{36}Cl are measured routinely on dedicated Accelerator Mass Spectrometry (AMS) facilities, the measurement of heavy nuclides on similar equipment has not been as widespread. This has been in part due to the more stringent requirements of resolution and bending power for magnetic and electrostatic analyzers in order to separate molecular hydrides and the more abundant atomic beams near the masses of interest.

A successful measurement of heavy elements cannot be performed by a simple scaling of existing AMS systems to accomodate the heavier masses. Backgrounds generated by an extended ion energy distribution from sputter ion sources, small angle scattering within the residual gas, the decay of metastable molecules and other atomic process dominate in the high mass region ($M \gg 40$). The traditional AMS solutions for atomic and molecular isobar separation using nuclear physics detector technology to identify uniquely the atomic number is not possible in this mass region. At best, molecular fragments can be separated on the basis of energy differences, provided they were not originally hydrides. Atomic isobars must be eliminated at the ion source using negative ions or must not be present, as for example, in the measurement of platinum group element abundances.

Generally the lessons learned from conventional mass spectrometry need be applied. Multiple arrays of electric and magnetic analyzers prior to injection into the accelerator and for post acceleration analysis are required. In all cases the resolving power of these devices should exceed the resolution attainable by detector technologies. This includes energy and time of flight detectors. Therefor the accelerator is no longer bound by the requirement to generate ions in an energy range suitable for ion detectors. Instead it serves to decouple the low energy spectrometer system from the high energy spectrometer system by virtue of charge exchange and an energy shift. This has the effect of removing most backgrounds generated by the sputtering process. The higher energy also benefits the reduction of backgrounds created by scattering in the residual gas as ions will tend to lose charge rather than maintain the same charge state at these energies.

At the IsoTrace laboratory, we have successfully extended AMS for the routine measurement of ^{129}I. Figure 1 illustrates the distribution of ^{129}I measured along coastal sites within the northern hydrosphere (Rai). The $^{129}I/^{127}I$ ratios ($x10^{-10}$) range over 4 orders of magnitude and are associated with the massive releases near nuclear fuel reprocessing facilities such as those at Sellafield, UK and Cap la Hague, France. Within the English channel, sample sizes smaller that 3 ml of water were used while ^{129}I in samples as small as 100 ml from the Arctic were measured (Rai). A higher dynamic

range is attainable as the machine background for AMS measurements is consistenly below $2x10^{-14}$.

We have also utilized the heavy element system for the study of negative ions for which little or no previous data were available. Positive identification of the group IIb negative ions(Ca-Ra) have been made in addition to the negative ions of Ce, Pr, Nd, Sm, Eu, Gd, Tb, Dy, Tm, Yb, Lu, Hf, and Pu (Gar). In some cases binding energies have been determined using electric field dissociation and AMS (Nad).

The heavy element program continues to evolve with the addition of high resolution injection systems for the analysis of actinides (Zha) and the development of ion sources with microprobe capabilities for in-situ platinum group element analysis.

(Rai) Raisbeck, G.M. et al. sub. to Geophys. Research Lett. 1992
(Gar) Garwan, M.A. PhD Thesis, University of Toronto, 1993
(Nad) Nadeau, M-J. PhD Thesis, University of Toronto, 1993
(Zha) Zhao, X-L. PhD Thesis, University of Toronto, 1993

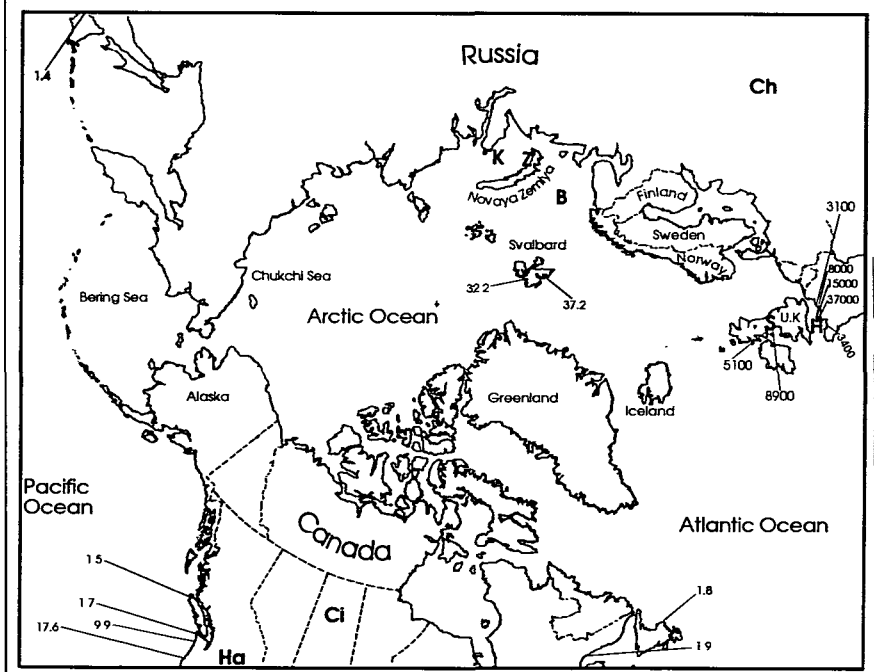

DISTONIC IONS; THEIR STATUS IN GAS PHASE ION CHEMISTRY.

John L. Holmes, Chemistry Department, University of Ottawa, Ottawa, Ontario, Canada K1N

Distonic ions have been a feature of gas phase ion chemistry for about 25 years, but it is only in the past 10 years that methods, both experimental and theoretical, have been developed sufficiently to establish distonic ion structures and energies.

At the same time, parallel and overlapping studies of distonic and ylid ions in matrix-isolated radiolyses and similar experiments, using electron spin resonance spectroscopy, have been conducted with remarkably little contact or even cross-referencing between the two disciplines.

At the present stage of development of the detailed understanding of ion fragmentation mechanism, distonic ions can be introduced with confidence as stable reaction intermediates and/or as alternative configurations for molecular ions. This confidence springs from the relative ease with which the (proposed) distonic ion can often unequivocally be generated via fragmentation reactions of larger ionized molecules. This approach is particularly fruitful when the distonic ion has the structure of a protonated free radical, e.g. is generated by the intramolecular transfer of a proton to a hetero atom within a larger molecular ion, followed by the loss of a small molecule.

In marked contrast the intermediacy of ion-radical complexes in ion fragmentations is much harder to establish by experiment and so rests heavily on ab initio molecular orbital theory calculations.

One of the earliest distonic ions was the intermediate species in the McLafferty rearrangement, e g the ion $HC^+(OH)CH_2CH_2C^{\bullet}H_2$, formed from butanal as the intermediate leading to $HC(OH)CH_2^{+\bullet}$ + C_2H_4. The existence of such an ion as a stable intermediate was long a subject for sharp controversy as "stepwise" or "concerted" was debated for the nature of the γ-hydrogen transfer in the molecular ion, leading to the above products [1]. It is now generally accepted that such ions are stable species in the gas phase, capable of being independently generated and studied.

Perhaps the most thoroughly studied simple distonic ion (experiment and theory) is the ethene-water complex ion $C_2H_4OH_2^{+\bullet}$, discovered by Terlouw et al. in 1981 [2]. The ion cannot rearrange to any isomeric $C_2H_6O^{+\bullet}$ structure and has only one dissociation channel, producing the formal ion-dipole component species, ionized ethene and water [3]. It is also the $C_2H_6O^{+\bullet}$ ion of lowest enthalpy.

Identification of distonic ions is pursued by all the presently available mass spectrometric techniques, $\Delta_fH°$ determinations, measurement of metastable ion (MI) and collision induced dissociation (CID) mass spectra, isotopic labelling and, as has been emphasized recently [4], by reactivity studies. Such work is often greatly aided by high level molecular orbital theory calculations.

Unfortunately, the unequivocal identification of a distonic ion, or even the proof of its participation in a fragmentation mechanism is often no easy task. The presence of a distonic ion will be obscured if it can undergo extensive interconversion with other isomeric forms below the lowest dissociation energy of the ensemble. Thus the existence of the ethene-methanol ion $C^{\bullet}H_2CH_2O^+(H)CH_3$ is very difficult to substantiate because it certainly rearranges, before fragmenting to ionized

cyclopropane and a water molecule. Indeed, the three $C_3H_8O^{+\bullet}$ isomers $^{\bullet}CH_2CH_2O^+(H)\ CH_3$, $^{\bullet}CH_2O^+(H)CH_2CH_3$ and $CH_3CH_2CH_2O^{+\bullet}H$ all fragment via the same distonic species, $^{\bullet}CH_2CH_2CH_2O^+H_2$ [5].

Note that for labelled saturated molecular ions, information on structure and/or fragmentation mechanism assignment may be lost, due to H/D scrambling prior to dissociation. However, H/D mixing in such species must involve the participation of distonic ions.

Finally, the preparation of structurally "pure" distonic ions (e.g. for reactivity studies) may be frustrated if facile rearrangements are possible at energies close to the ground state of the ion.

Many distonic ions, e.g. $^+CH_2OC^{\bullet}H_2$, $^{\bullet}CH_2CH_2OC^+H_2$, $^{\bullet}CH_2CH_2C^+H_2$, correspond to ring opened molecular ions. It is easy to show that the relative $\Delta_fH°$ values only rarely correlate with the potential release of ring strain energy if the distonic ion were produced from the cyclic form.

It has been customary to estimate $\Delta_fH°$ values for distonic ions using the thermochemical cycle:

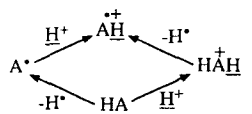

In general the [C-H] bond dissociation energy (BDE) in the neutral HA and its proton affinity (PA) are known or can be estimated. It is then assumed that the BDE in the protonated species $HA^+\underline{H}$ is the same as in HA and that the PA value for $A^{\bullet}$ if the same as that of HA There is no doubt that this approach works well for a wide range of keto/enol type distonic ions [6], but for the simple ions $^{\bullet}CH_2O^+H_2$, $^{\bullet}CH_2CH_2O^+H_2$, $^{\bullet}CH_2Cl^+H$, $^{\bullet}CH_2CH_2CH_2O^+H_2$ the estimated $\Delta_fH°$ values are more than 10 kcal mol^{-1} lower than the best experimental and theoretically derived values from high level ab initio molecular orbital theory calculations. Thus the [C-H] bond energies in e.g. $D[H\text{-}CH_2CH_2O^+H_2]$ are much higher than in their neutral counterparts (e.g. $D[H\text{-}CH_2CH_2OH]$). State-of-the-art theoretical calculations have failed to show any geometrical change in the molecule upon protonation which can readily account for the strong C-H bond [7] and so the explanation lies elsewhere.

[1] M.B. Stringer, D.J. Underwood, J.H. Bowie, C.E. Allison, K.F. Donchi and PJ. Derrick, Org. Mass Spectrom. **27**, 270 (1992), and references therein.

[2] J.K. Terlouw, W. Heerma and G. Dijkstra, Org. Mass Spectrom. **16**, 326 (1981).

[3] P.J. Ruttink, J. Phys. Chem. **91**, 703 (1987).

[4] K.M. Stirk, L.K.M. Kiminkinen and H.I. Kenttamaa, Chem. Rev. **92**, 1649 (1992).

[5] J.R. Cao, M. George and J.L. Holmes, Org. Mass Spectrom. **26**, 481 (1991).

[6] J.L. Holmes and F.P. Lossing, Int. J. Mass Spectrom. Ion Processes **92**, 111 (1989).

[7] L. Radom, private communication, 1993.

Investigation of Distonic Radical Cations by Ion-Surface Collisions J. L. Jones, Á. Somogyi, R.L. Franklin, A. Dongré, M. B. Smith, V.H. Wysocki; Department of Chemistry, Virginia Commonwealth University, Richmond, VA 23284-2006

Experimental. All experiments are performed in an instrument designed for ion-surface collisions.[1] The instrument consists of two quadrupoles arranged at 90°, with a surface placed to intersect the ion optical path of the quadrupoles. The mass-selected incident ion beam collides with the surface at 45° with respect to the surface normal. Surfaces used for this work consist of self-assembled monolayer films of alkanethiols chemisorbed onto vapor-deposited gold ($CF_3(CF_2)_7CH_2CH_2SAu$, $CH_3(CH_2)_{17}SAu$, and $CD_3(CD_2)_{19}SAu$).[2]

Calculations. MNDO and *ab initio* (HF/6-31G**) calculations have also been carried out on several ion structures. MNDO bond orders are also used for the description of ion structures and fragmentation processes.[3]

Results and Discussion. Our investigations of distonic radical ions are based on application of ion-surface collision mass spectrometry and quantum chemical calculations. The ions currently being investigated are listed below along with the reason for investigation:

Ion	Purpose	Ion	Purpose
$CH_2(CH_2)_nOH_2^+$	standards; well-characterized by other techniques, allows evaluation of ion-surface collision behavior (surface-induced dissociation or ion-surface reaction)	$CH_2{=}YH^+ + Z$ ↓ ZCH_2YH^+ or CH_2YHZ^+ Y=heteroatom, Z=surface species	determine whether distonic or conventional ion is produced by reaction of even-electron ions with radicals from surface; compare with theory
$CH_2(CH_2)_nOHX^+$ X=Li, Na	these and related ions are proposed distonic ion products of CAD experiments; attempt to confirm whether distonic	peptide (a+1) and (z+1) ions (precursors to d and w ions, respectively)	determine whether actually distonic, support with model based on MNDO bond order calculations
$RCHS^+(CH_3)_2$ ↓-e $RCHS^+(CH_3)_2$ R=C_6H_5CO	determine whether these solution-stable sulfonium ylidions can be produced by oxidation of the ylide in the ESI source		

For $CH_2(CH_2)_nOH_2^+$ ions (n=0, 1), collisions with the fluorinated organic monolayer surface lead to characteristic dissociation products. Collisions at monolayer surfaces with available H from alkanethiolate surfaces lead to H-addition with subsequent fragmentation of the adduct. A deuterium labeled surface is used to confirm reactions (e.g., $CH_2OH_2^+ + CD_3(CD_2)_{19}SAu \rightarrow CH_2D^+$). Ionized ethanol

$CH_3CH_2OH^+$ appears to be more reactive toward H-addition than does its distonic isomer, $CH_2(CH_2)_nOH_2^+$. This is in line with enthalpy calculations, which show that H addition is more exothermic for the conventional isomer (using C_7H_{16} as a model for the surface chains). Allow H addition is predicted to be exothermic for both isomers and fragmentation of either is endothermic, fragmentation competes favorably with reaction which suggests a fairly high barrier to the entropically less favorable H addition.

Ab initio calculations show that replacement of H^+ with Li^+ or Na^+ leads to structures that are best described as ion-radical complexes with formally separate charge and radical sites. The ion-radical complexes differ from the distonic isomers of small alcohols in that the O-X bond is more ionic in character.

MNDO bond order calculations suggest that the (a+1) and (z+1) distonic peptide ion fragments are reasonable intermediates for formation of side-chain cleavage ions (as proposed by Biemann based on experimental results[4]). Bond order values for the a_2+1 ion shown below (Scheme I) predict easy loss of NH_3, consistent with related experimental observations for the (a_2+1) ion of pentaalanine.[5]

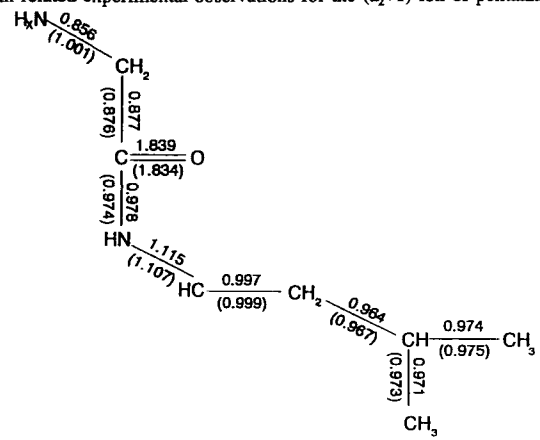

Scheme I. MNDO bond orders for the neutral (x=2) are shown in parentheses. (For (a_2+1) model, x=3.)

References

1 Wysocki, V.H.; Ding J.-M.; Jones, J.L.; Callahan, J.H.; King, F.L. *J. Am. Soc Mass Spectrom.* **1992**, *3*, 27.

2 (a) Winger, B.E.; Julian, R.K., Jr.; Cooks, R.G.; Chidsey, C.E.D. *J. Am. Chem. Soc.* **1991**, *113*, 8967. (b) Morris, M.; Riederer, D.E., Jr.; Winger, B.E.; Cooks, R.G.; Ast, T.; Chidsey, C.E.D. *Int. J Mass Spectrom. Ion Processes* **1992**, *122*, 181. (c) Somogyi, Á.; Kane, T.E.; Ding, J.-M.; Wysocki, V.H. *J. Am. Chem. Soc.*, in press.

3 Császár, A.G.; Somogyi, Á.; Pócsfalvi, G.; Traldi, P. *Org. Mass Spectrom.* **1992**, *27*, 1349, and references therein.

4 Johnson, R.S.; Martin, S.A.; Biemann, K. *Int. J. Mass Spectrom. Ion Processes* **1988**, *86*, 137.

5 Thornburg, K.R.; Schey, K.L.; Knapp, D.R. *J. Am. Soc. Mass Spectrom.* **1993**, *4*, 424.

Synthesis and Structural Characterization of Novel Distonic Ions By Using Ion-Molecule Reactions

Rebecca L. Smith, Krista M. Stirk, Hilkka I. Kenttämaa
Department of Chemistry, Purdue University, West Lafayette, IN 47907.

In recent years, it has become that distonic ions are common and stable gas phase species. The long-lived molecular ions of many common organic compounds spontaneously rearrange to a distonic form. Distonic ions are also formed as intermediates in unimolecular dissociation reactions of gaseous radical cations, including the McLafferty rearrangement. In order to examine the properties of distonic ions, it is necessary to be able to generate a variety of stable distonic ions. Distonic ions are typically made by isomerization or dissociation of conventional radical cations. For example, the α-distonic ion $^{+}CH_2OCH_2^{\cdot}$ is generated by loss of formaldehyde from ionized 1,3-dioxolane. This approach, however, limits the type and size (number of heavy atoms between the charge site and radical site) of distonic ions which can be formed.

Ion-molecule reactions performed in an FT-ICR can be used to synthesize a variety of novel distonic ions. For example, $^{+}CH_2OCH_2^{\cdot}$ can be used to transfer $CH_2^{+\cdot}$ to neutral acetone to produce the α-distonic ion, $(CH_3)_2C^{+}OCH_2^{\cdot}$. Neutral ketene transfers CH_2-groups in consecutive reactions to various radical cations, yielding stable distonic product ions. For example, transfer of a CH_2-group to the distonic ion $^{\cdot}CH_2CH_2CH_2CO^{+}$ generates the first known stable δ-distonic ion: $^{\cdot}CH_2CH_2CH_2CH_2CO^{+}$.

Compared to other types of radical cations, distonic ions demonstrate unique reactivity toward many neutral reagents, such as dimethyl disulfide and cyclohexanone. Distonic ions typically undergo radical type reactions with these reagents while most conventional radical cations react by charge exchange. For example, the ion $^{\cdot}CH_2CH_2CH_2CH_2CO^{+}$ abstracts a thiomethyl group from dimethyl disulfide whereas its conventional isomer, ionized cyclopentanone, as well as numerous other isomeric structures studied, undergo facile charge exchange (Figure 1). Cyclohexanone is another neutral reagent which can be used to distinguish between various radical cations: conventional radical cations typically undergo charge exchange with cyclohexanone, while many distonic ions transfer a radical chain as a radical cation to this molecule.

It appears likely that many distonic ions, such as $^{\cdot}CH_2CH_2CH_2CO^{+}$, react with neutral reagents such as dimethyl disulfide via a charge initiated mechanism. In this mechanism, a covalent bond is initially formed between the charge site of the ion and a sulfur lone pair of electrons. Radical substitution then occurs at one of the sulfur atoms, resulting in a sulfur-sulfur bond cleavage followed by loss of a thiomethyl radical from the collision complex. Support for this mechanism is obtained for example from the fact that thiomethyl abstraction by $^{\cdot}CH_2CH_2CH_2CO^{+}$ involves a six-membered transition state and occurs with 26% efficiency, while the reaction with $^{\cdot}CH_2CH_2CH_2CH_2CO^{+}$ occurs with only 2% efficiency. The latter reaction would involve a seven-membered transition state (Figure 2).

Figure 1

Reaction with Dimethyl Disulfide

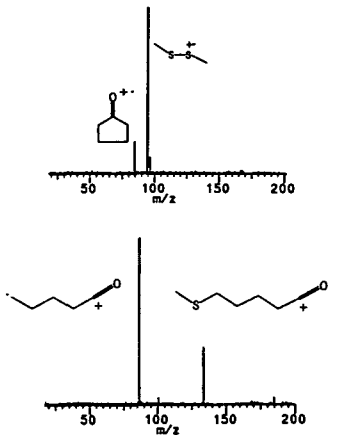

Figure 2

Proposed Mechanism for Reaction of Several Distonic Ions with CH_3SSCH_3

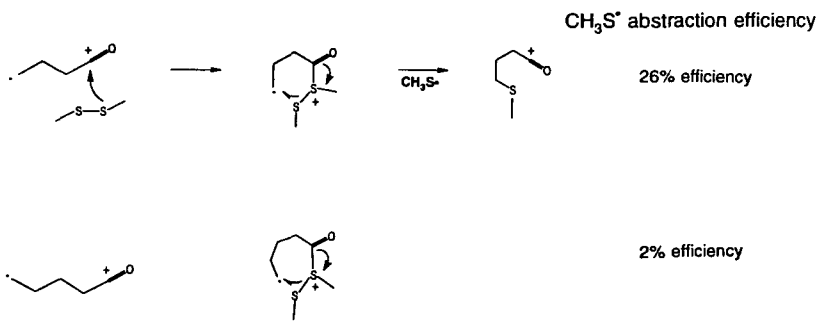

NEUTRALIZATION-REIONIZATION (NR) STUDIES ON DISTONIC RADICAL CATIONS

Chrys Wesdemiotis, Michael J. Polce, Sarka Beranova, and Fred. A. Wiedmann
Department of Chemistry, The University of Akron, Akron OH 44325-3601

Distonic radical cations represent the molecular ions of diradicals, *i.e.* species with two unpaired electrons at non-adjacent atoms. Being extremely reactive, diradicals do not exist freely. In sharp contrast, the corresponding distonic radical ions are usually stable and readily accessible in the mass spectrometer. The tailored preparation of specific distonic ions is possible through known rearrangement fragmentations or ion-molecule reactions. Once formed, these ions can serve as the starting material for the synthesis of gaseous, elusive diradicals in neutralization-reionization mass spectrometry (NRMS) experiments. The incipient diradical formed upon neutralization may survive intact, rearrange, or dissociate. The mass spectrum obtained after reionization of the neutral product(s) can reveal information on the stability and reactivity of the intermediate diradical as well as on the structure of the original distonic ion.

The distonic ion $\cdot CH_2CH_2OCH_2^+$ ($\mathbf{1}^{\cdot+}$), which represents the C-C ring-opened isomer of oxetane ($\mathbf{2}^{\cdot+}$), is formed from the 1,4-dioxane molecular ion by $CH_2{=}O$ loss. In the metastable time window, $\mathbf{1}^{\cdot+}$ and $\mathbf{2}^{\cdot+}$ decompose via complicated rearrangements. Both cations mainly lose $\cdot H$ to yield $CH_3CH_2C{\equiv}O^+$, as established by MS/MS/MS. Cation $\mathbf{1}^{\cdot+}$ also produces $C_2H_6^{\cdot+}$ (CO loss) and $C_2H_3O^+$ ($\cdot CH_3$ loss), whereas for $\mathbf{2}^{\cdot+}$, the elimination of $\cdot CH_3$ is not observed and the loss of CO proceeds to a lesser extent and with a ~5 times smaller kinetic energy release (2.3 vs. 19 meV). Upon CAD, $C_2H_4^{\cdot+}$ which can be formed by direct bond cleavage(s) from both ions becomes the base peak but several rearrangement processes, such as the CO loss, still remain dominant. The CAD spectra of $\mathbf{1}^{\cdot+}$ and $\mathbf{2}^{\cdot+}$ contain diagnostic differences: the abundances of $C_3H_{0\text{-}3}^+$ are substantially higher for $\mathbf{2}^{\cdot+}$ and the CH_2 loss more dominant for $\mathbf{1}^{\cdot+}$, in agreement with the original ion structures. This result is in line with the unique ion-molecule reactions of these two isomers [1].

Neutralization of $\mathbf{1}^{\cdot+}$ gives the diradical **1**, a proposed intermediate in the pyrolysis of oxetane to ethylene (28 Da) and formaldehyde (30 Da). The NR spectra of $\mathbf{1}^{\cdot+}$ (Figure 1a) and d_6-$\mathbf{1}^{\cdot+}$ (Figure 1b) attest that **1** indeed dissociates extensively into $CH_2{=}CH_2 + O{=}CH_2$. In contrast, the NR spectrum of $\mathbf{2}^{\cdot+}$ contains an abundant survival ion (Figure 1c) and is fairly similar to the corresponding CAD spectrum, consistent with the expected stability of **2**. Thus, large differences are observed between the NR spectra of $\mathbf{1}^{\cdot+}$ and $\mathbf{2}^{\cdot+}$ due to the distinct reactivities of the intermediate neutrals. The dissociation products of **1** are also characteristic for the connectivity of the precursor distonic ion.

It is evident from the presence of ions above *m/z* 30 in Figure 1a (above *m/z* 32 in Figure 1b) that **1** does not decay entirely. The small fraction remaining undissociated neither ring-closes to **2** (Figures 1a vs. 1c) nor undergoes 1,4-H migration to the carbene **3** (Figures 1a vs. 1d; $\mathbf{3}^{\cdot+}$ is produced by electron impact of ethyl glyoxylate). This means that the critical energies needed for C-C bond formation (**1** → **2**) and H-atom migration through a five-membered ring (**1** → **3**) must be higher than the energy required to cause C-O bond cleavage in the diradical.

Characterization of a diradical is only possible if the spectra of isomerically pure ions are known. In the above case, the chemistry of **1** could be assessed because isomers $\mathbf{2}^{\cdot+}$ and $\mathbf{3}^{\cdot+}$ yield unique fragments (see Figures 1c and 1d), based on which any isomerization of **1** can be probed. This is not true for other isomers. For example,

the CAD spectrum of the distonic ion $^+CH(CH_3)OCH_2\cdot$ ($\mathbf{4}^{\cdot+}$, from 2-methyl-1,3-dioxolane) is identical within experimental error to the spectra of ionized propylene oxide ($\mathbf{5}^{\cdot+}$) and ionized vinyl methyl ether ($\mathbf{6}^{\cdot+}$). The NR spectra of the first two isomers also are practically indistinguishable, corroborating that ring-opening of $\mathbf{5}^{\cdot+}$ to yield the more stable distonic ion $\mathbf{4}^{\cdot+}$ is facile. However, differences are observed between the NR spectra of $\mathbf{4}^{\cdot+}$ and $\mathbf{6}^{\cdot+}$, suggesting that the resemblance between the CAD spectra of these two isomers is due to collision induced isomerization prior to dissociation. Isomeric ions decomposing via common pathways can still show distinct NR spectra because of different neutralization cross-sections of the precursor ions and/or distinctive reactivities and reionization cross-sections of the intermediate neutrals. Based on absolute abundances (*i.e.*, NR yields), the NR spectrum of the distonic ion $\mathbf{4}^{\cdot+}$ contains ≤30% $\mathbf{6}^{\cdot+}$. Whether the ~30% $\mathbf{6}^{\cdot+}$ result from isomerization (in µsecs) of the original precursor ion $\mathbf{4}^{\cdot+}$ before neutralization and/or from rearrangement of the intermediate diradical **4** to **6**, remains unclear. Ion-molecule reactions have shown that the former does take place in the msec time domain [2].

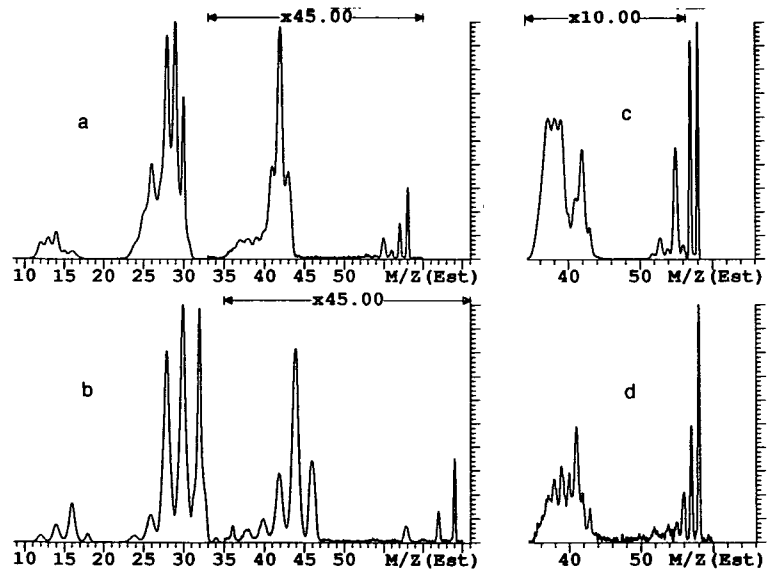

Figure 1. NR Xe/O_2 mass spectra of (a) $\cdot CH_2CH_2OCH_2^+$, $\mathbf{1}^{\cdot+}$ and (b) $\cdot CD_2CD_2OCD_2^+$, d_6-$\mathbf{1}^{\cdot+}$. Partial NR Xe/O_2 spectra of (c) ionized oxetane, $\mathbf{2}^{\cdot+}$ and ethoxy carbene, $\mathbf{3}^{\cdot+}$.

1 Stirk, K. M.; Kiminkinen, L. K. M.; Kenttämaa, H. I. *Chem. Rev.* **1992**, *92*, 1649-1665.
2 Van de Guchte, W. J.; van der Hart, W. J. *Org. Mass Spectrom.* **1990**, *25*, 309-311.

The RF-Only Mode Event in FTMS: A Means of Generatilon and Characterizing Distonic Ions

M.L. Gross, D.L. Rempel, C.L. Holliman, Dept. of Chem., Univ. of Nebraska, Lincoln, NE 68588

For over twenty years, we have been interested in the reactions of radical cations and nucleophiles. One of the earliest reactions we discovered was that of the cyclopropane radical cation and ammonia to give the distonic ion $\bullet CH_2NH_3^+$ [1,2]. Although this bimolecular reaction appeared to provide an interesting route to distonic ions, characterization by using sequential ion-molecule reactions was difficult because the distonic $\bullet CH_2NH_3^+$ is a good gas-phase acid and disappears in rather uninteresting proton-transfer reactions.

Nevertheless, the opportunity of studying bimolecular reactivity of distonic ions remained intriguing. Success would require the design of distonic ions with no acidic protons on the heteroatom. Other workers have shown that suitably configured distonic ions can be used as reagents in bimolecular reactions [3,4].

A potential solution to the problem is to use, in lieu of ammonia, a base with no hydrogens bonded to nitrogen. Pyridine is an obvious choice, and we recently found that the cyclopropane radical cation reacts with pyridine to give $C_5H_5\overset{+}{N}\text{-}CH_2\bullet$ [5].

An interesting question is whether distonic ions, such as $\bullet CH_2NH_3^+$ and $C_5H_5\overset{+}{N}\text{-}CH_2\bullet$, can be used to explore the intrinsic reactivity of gas-phase free radicals. To address this question, we decided to generate the β-distonic ion $C_5H_5\overset{+}{N}CH_2CH_2\bullet$ in which the unpaired electron site is "insulated" from the aromatic ring by a methylene group. We hoped that a distonic ion of this type would react as a primary free radical.

This β-distonic ion can be easily generated in an ionized mixture of pyridine and ethene in a high-pressure (chemical ionization) source. Interfacing the high-pressure source to a tandem mass spectrometer, we were able to study the product ion by obtaining CAD spectrum.

The principal reactions of the putative $C_5H_5\overset{+}{N}CH_2CH_2$ are reversion to the pyridine radical cation, formation of protonated pyridine, and some charge stripping to give the doubly charged version of the distonic ion. Replacing pyridine with C_5D_5N gave a new ion which, when activated, gave return to not only $C_5D_5N^+\cdot$ but also $C_5D_5HN^+\cdot$, $C_5D_3H_2N^+\cdot$, etc. This isotopic "scrambling" is strong evidence that a covalently bonded species had formed.

Although a tandem mass spectrometer outfitted with a high-pressure source is appropriate for demonstrating that the alleged distonic ion can be prepared in the gas phase, it suffers two major drawbacks in a program to characterize the ion in question. The first is that the origin of the ion cannot be easily determined. Is it the C_2H_4 or the C_5H_5N radical cation? The second is that sequential reactions of the adduct ion are difficult to conduct because the residence time of the ions in a CI source is short. Thus, a trapping technique is motivated.

Fourier transform mass spectrometry is one possibility, but the low pressure of FTMS will not support formation of the pyridine/ethene adduct. The energy released as bonding occurs between the two reactants sometimes causes the adduct to revert to starting materials or to produce fragments of the adduct. Although no adduct is seen under normal conditions (i.e., 10^{-6} torr) of FTMS, evidence could be obtained that a short-lived adduct is forming because isotopic exchange occurs, and $C_5D_5N^+\cdot$ becomes $C_5D_4HN^+\cdot$.

To solve problems of this type, an FT mass spectrometer must be modified to operate momentarily as a high-pressure trap. In that way, not only can the advantages of high pressure sources or traps be imported to FTMS but also the usual feature of FTMS (e.g., ion trapping, high resolving power, exact mass measurement, nondestructive detection, and multichannel detection) can be utilized in ion chemistry studies.

D. Rempel [6] recently solved this problem by designing and implementing a high pressure ("ion trap") event for the FTMS event sequence. This strategy allows one to switch rapidly from the usual Penning trap mode of FTMS to the Paul (quistor or quadrupole ion trap) mode so that collisional stabilization of product ions can occur. Following that, the Penning mode can be reestablished for double resonance, collisional activation, or mass analysis. A series of Penning-Paul-Penning sequences can be stitched together so that collisionally stabilized adducts formed in the first Paul mode can be subsequently reacted in a second Paul mode.

When the pyridine radical cation is allowed to react in the presence of ethene during the high-pressure Paul mode, the adduct $C_5H_5\overset{+}{N}CH_2CH_2\bullet$ can be prepared in high yield. The only other product of any significance is protonated pyridine. No adduct is seen if all conditions remain the same except the ethene radical cation replaces the pyridine radical cation, confirming that the latter reacts with neutral ethene to give the pyridine/ethene adduct.

We are now in a position to examine the reactivity of the $C_5H_5\overset{+}{N}CH_2CH_2\bullet$ species. The putative distonic ion can be prepared in high yield and stored in the presence of neutral pyridine and ethene for periods of tens of seconds. The first neutral reagent that was tested was molecular oxygen, a stable diradical. The choice was motivated by the strong prospect that the adduct has an unpaired electron and should react readily with molecular oxygen.

The preferred means of conducting the reaction with oxygen is to add a second rf-only-mode event to follow the isolation of the pyridine/ethene adduct, a process that is readily conducted in the Penning (usual FTMS) mode. High yield of a species, possibly existing as $C_5H_5\overset{+}{N}CH_2CH_2OO\bullet$, was achieved. The reaction is consistent with the proposed β-distonic ion structure.

Semiempirical molecular orbital calculations (AM1) also support the β-distonic ion structure assignment. The ion's calculated heat of formation is 216 kcal whereas those of the conventional ethyl pyridine isomers are in the range of 230-235 kcal, demonstrating the inherent stability of the adduct ion. The calculations were carried out by Professor K. Fountain of N.E. Missouri State University.

Conditions were then worked out so that a survey of bimolecular reactivity could be rapidly conducted. The adduct ion was prepared in the Paul mode at a pressure of He of greater than 0.001 torr. After a return to the Penning mode, unwanted ions such as protonated pyridine were ejected. A return to the Paul mode was then implemented during which a pulse of a neutral reagent accompanies the helium pulse. Mass analysis in the Penning mode completed the event sequence.

Reactive neutrals include a set of molecules containing electron-deficient double bonds: methyl vinyl ether, methyl acrylate, and 1,3-butadiene. Adducts are formed for each neutral, and in some cases, the ethene moiety was replaced by the new olefin. Unreactive neutrals include ethene, propene, 1-butene, acetonitrile, and vinyl chloride. It also was not possible to abstract H from isobutane or a halogen from methylene chloride or methyl bromide. It appears that the distonic ion radical prefers to react with electron-deficient olefins, a preference that points to a nucleophilic nature for the radical ion.

In summary, the new capabilities for FTMS are well-suited for ion chemistry. Specifically, the high pressure mode can be used to prepare and the to react the β-distonic $C_5H_5\overset{+}{N}CH_2CH_2\bullet$. It now appears possible to establish the intrinsic reactivity of free radicals by using mass spectrometric methods to follow the chemistry of distonic ions.

References

1. M.L. Gross and F.W. McLafferty, *J. Am. Chem. Soc., 93,* 1267 (1971).
2. T.M. Sack, R.L. Cerny, and M.L. Gross, *J. Am. Chem. Soc., 107,* 4562 (1985).
3. B.C. Baumann, J. K. MacLeod, L. Radom, *J. Am. Chem. Soc., 102,* 7927 (1980).
4. K.M. Stirk, L.K.M. Kiminkinen, H.I. Kenttamaa, *Chem. Rev., 92,* 1649 (1992).
5. S.J. Yu, M.L. Gross, and K.R. Fountain, *J. Am. Soc. Mass Spectrom., 4,* 117-124 (1993).
6. D. L. Rempel and M. L. Gross, *J. Am. Soc. Mass Spectrom., 3,* 590-594 (1992).

The Use of Distonic Ions to Study Free-Radical Reactions by Mass Spectrometry

Leonard J. Chyall, Rebecca L. Smith, Krista M. Stirk, and Hilkka I. Kenttämaa

Department of Chemistry, Purdue University, West Lafayette, IN 47907-1393

Distonic radical ions have spatially separated radical and charge sites which result in both ionic and radical-type reactions with neutral reagents. Recently, we have been interested in the ion-molecule chemistry of distonic ions which react preferentially at the radical center. The study of these ions offers the possibility of using mass spectrometry to model free-radical processes in the gas phase. In this study, a dual cell Fourier-transform ion cyclotron resonance mass spectrometer was used to examine the radical-type chemistry of two novel distonic ions: the methylene dimethylsulfonium ion (**1**); and the 4-dehydroanilinium ion (**2**).

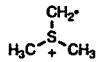

1

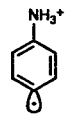

2

Ion **1** (*m/z* 76) was prepared in the source side of the dual cell instrument by a variety of ion-molecule reactions. The reaction between ionized ethylene oxide and dimethyl sulfide provides the most practical synthetic route to **1**.[1] The distonic structure of **1** was established by its reaction with added dimethyl disulfide; transfer of a thiomethyl group took place to give a product ion of *m/z* 123. Thiomethyl abstraction is typically observed when distonic ions react with dimethyl disulfide, while there are no examples of conventional radical cations which react in this manner.[2]

The reactivity of **1** with several types of neutral reagents which are known to be good radical traps was examined. It was found that alkyl iodides cleanly transfer an iodine atom to **1**. The efficiency of this reaction increases with increasing methyl substitution at the carbon of the C-I bond in the neutral reagent. For example, methyl iodide did not react with **1** while *tert*-butyl iodide underwent iodine atom transfer at 24% of the predicted collision rate. The efficiencies for abstraction of an iodine atom from ethyl iodide and isopropyl iodide fell between these two limits. These results are consistent with radical-type behavior for **1**.

The ion-molecule reactions of **1** with hydrogen atom donors was also examined. Hydrogen atom transfer occurs when **1** is allowed to react with thiophenol and benzeneselenol, giving rise to the trimethylsulfonium ion. Reaction of **1** with 1,4-cyclohexadiene provided the trimethylsulfonium ion along with two other product ions which correspond to transfer of ionized methylene, and adduct formation with loss of a methyl radical. Similar products were also observed when **1** was allowed to react with 1,3-cyclohexadiene and cyclohexene. The products which correspond to adduct formation with loss of a methyl radical indicate that the charge site is participating in the reaction.

The proximity of the charge site to the radical site in **1** makes it difficult to determine the role the charge site plays in these reactions. This issue can be addressed by studying the

radical-type reactivity of distonic ions in which a neutral reagent can interact with either the charge site or the radical site, but not with both centers simultaneously. We have synthesized the 4-dehydroanilinium (**2**) which uses the inflexibility of the aromatic ring to inhibit the interaction between the two reactive sites of the molecule. The synthesis of **2** was accomplished by performing collision-induced dissociation (CID) on protonated 4-iodoaniline.

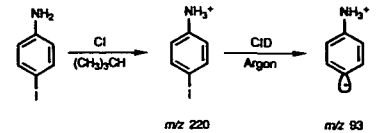

Ion **2** (*m/z* 93) abstracts a thiomethyl group from dimethyl disulfide and an iodine atom from isopropyl iodide. These two reactions clearly demonstrate that the charge site need not participate in the abstraction process.

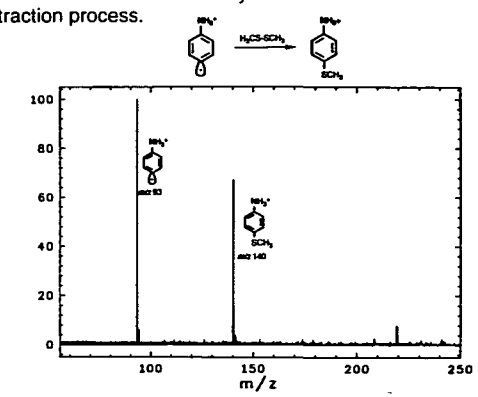

In summary, we have shown that reagents which contain relatively weak bonds will undergo abstraction reactions with **1** and **2**. Ion **2** represents a novel class of distonic ions where the charge and radical sites are separated by a rigid carbon skeleton. The ion-molecule chemistry of these ions is a promising method to examine free-radical chemistry in the gas phase using mass spectrometry.

We are indebted to the National Science Foundation of the United States for their financial contributions to this work.

1. van Amsterdam, M. W.; Zappey, H. W.; Ingemann, S.; Nibbering, N. M.M. *Org. Mass Spectrom.* **1993**, *28*, 30-36.

2. Stirk, K.M.; Orlowski, J. C.; Leeck, D. T.; Kenttämaa, H. I. *J. Am. Chem. Soc.* **1992**, *114*, 8604-8606.

Electrospray LCMS Analysis of Ganefromycins

Mahender R.Alluri*, Guy T. Carter and Donald B. Borders,
American Cyanamid Company, Natural Products Discovery,
Lederle Laboratories, Pearl River, NY 10965.

INTRODUCTION: Ganefromycins (formerly designated LL-E19020 antibiotics) isolated from *Streptomyces lydicus* ssp. *tanzanius*, are a new family of elfamycin antibiotics. Ganefromycin α (1) shows very promising activity as a performance enhancement agent in livestock, while displaying an extremely narrow spectrum of antibacterial activity versus human pathogens including mainly *Streptococci* and several anaerobes. Owing to the thermal lability of ganefromycin, TSP-MS failed to give molecular ions as did EI and CI, and only FAB had been successful in the production of molecular ion species. Our preliminary experiments with electrospray ionization (ESI), however, have shown abundant $[M+Na]^+$ ions can be generated. ESIMS analysis of ganefromycins is fairly sensitive yielding useful spectra with 10 picomoles of sample. In addition to molecular ion species, fragment ions can be produced by varying the repeller voltage in the ESI (Vestec) source. In this report we will discuss the advantages of ESIMS analysis of the ganefromycins in comparison with TSP-MS and present an analysis of the ESI fragmentation.

EXPERIMENTAL: Mass spectra were recorded using a TSP-46 single quadrupole instrument (Finnigan-MAT, San Jose, CA) interfaced with a Vestec ESI source or Finnigan TSP source. ESI spectra were obtained in the positive ion mode whereas TSP spectra were obtained in both positive and negative ion mode. ESI-MS conditions were : electrospray needle voltage 2kV; flow rate 2 µl/min; mass range 200-1700 amu; 5 sec/scan; repeller voltage 20-60 V TSP-MS conditions jet 230 °C; vaporizer temperature 70-85 °C; repeller voltage 1KV; discharge ionization electrode voltage 1 kV; flow rate 1.2 ml/min; mass range 200-1300 amu; 2 sec/scan. The HPLC system consisted of a Waters 600-MS solvent delivery system and WISP 710B autosampler with 990-MS photodiode array detector. The ganefromycins were separated on a C-18 column (5µ, 150 mm x 3.9 mm). The mobile phase was a gradient of CH_3CN in 0.1M NH_4OAc (pH=6.5) buffer at a flow rate of 1.2 ml/min. The detection was by UV absorbance at 230 and 300 nm. Ganefromycins were isolated from culture broths in our laboratory. Samples (1 mg/ml) were dissolved in $CH_3CN/H_2O/HOAc$/0.1 % aq. NaCl (50/50/3/1) for ESI-MS analyses. An artificial mixture (2mg/ml each) of the 3 compounds was separated on the above HPLC system and the corresponding peaks were collected for ESI-MS analysis. The mixture (10 µl) was also subjected to TSP-LC/MS analysis.

RESULTS AND DISCUSSION: Ganefromycins showed abundant $[M+Na]^+$ ions by ESI-MS when the repeller voltage was held between 30-40 V. To achieve maximum sensitivity of 10 pmole as the minimum detectable amount, it was necessary to add Na^+. At higher repeller voltages, eg. 60 V, structure-specific fragment ions were also observed (Figs. 1 & 2). HPLC separation of ganefromycins α, γ and β-methyl ester is shown in Fig. 3. Collection and concentration of these peak fractions provided ample material for ESI-MS analysis. Although TSP-MS was unable to generate molecular ion species for the ganefromycins, the whole molecule was represented by fragment ions. Thus in the positive TSP spectrum, abundant ions derived from the trisaccharide moiety were observed, whereas the negative TSP spectrum contained abundant ions derived from the aglycone.

Figure 1: Structures and Electrospray MS Fragment Ions of Ganefromycins

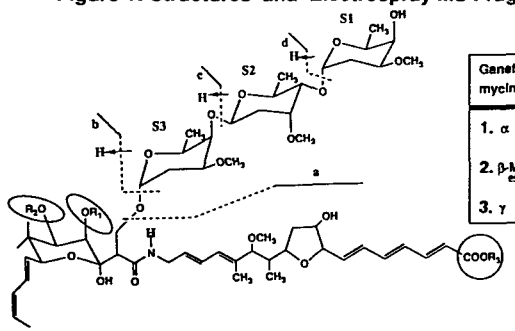

Ganefro-mycins.	$-R_1$	$-R_2$	$-R_3$	ESIMS $[M+Na]^+$
1. α	$C_6H_5CH_2CO$	H	H	1248
2. β-Me ester	H	$C_6H_5CH_2CO$	CH_3	1262
3. γ	$HO-C_6H_4CH_2CO$	H	H	1264

Figure 2. Positive Ion ESIMS of Ganefromycin-α

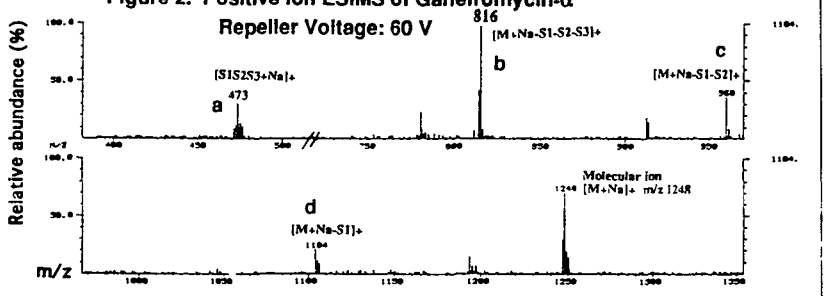

Figure 3: HPLC/UV Analysis of Ganefromycin-α, β-Me and γ mixture

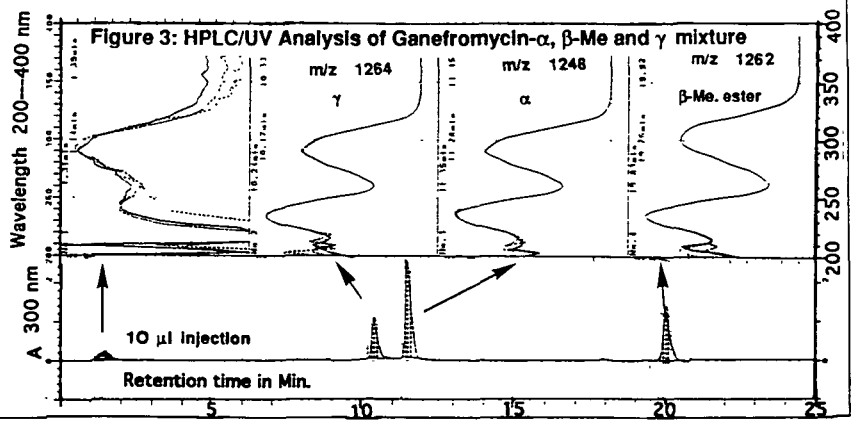

ANALYSIS OF FLAVINS BY THERMOSPRAY HPLC/MS AND ELECTROSPRAY MS.

J.Abián*, F.Sanchez-Baeza[1] and E.Gelpí.
Dept of Neurochemistry and (1) Dept of Biological Organic Chemistry, CID, CSIC
Jordi Girona 18-26, 08034 Barcelona, Spain.
S.Susín and J.Abadia
Dept of Plant Nutrition, Estación Experimental de Aula Dei, CSIC.
P.O.Box 202, 50080 Zaragoza, Spain.

INTRODUCTION

Flavins are redox cofactors in many biological redox systems. Some of these compounds such as flavin-adenine dinucleotide (FAD) or flavin 5´-monophosphate (FMN) can not be submitted to GC/MS analysis due to their lability, high polarity and ionized phosphate moieties.
In this work we report on the analytical conditions for Riboflavine, FAD and FMN characterization by Thermospray (TSP) HPLC/MS and by Electrospray (ESP) MS. These techniques were applied to the characterization of a flavine-like compound detected by HPLC-Vis in extracts from Fe-depleted plants (*Beta vulgaris*). The HPLC fraction containing the unknown was shown to be a mixture of two compounds (X1 and X2) that were isolated and submitted to ESP and TSP analysis (1).

EXPERIMENTAL

Spectrometer: Finnigan TSQ 700 triple quadrupole mass spectrometer
Column: 5 µm (15x0.46 cm) Spherisorb ODS-2 (Phase Separations)
Eluents: A) a 0.05 M ammonium acetate in water (1% formic acid).
B) a 0.05 M ammonium acetate in water/methanol (1:1 v/v, 1% formic acid).
Gradient: From 5% to 40%B in 4 min. Then up to 60% B in 9 min.
Thermospray: Finnigan interface and source
Interface, source and manifold temps.: 105 °C, 250 °C and 70 °C respectively.
Acquisition rate: 0.5 scan/s.
Electrospray: Analytica of Branford interface
Sample flow rate: 1 ul/min. Drying nitrogen flow: 5 ml/min
Electrospray voltage: 3500 V (positive ions) and 2800 V (negative ions)
Scan range: 200-1000 amu; Scan rate: 2 sec.

RESULTS

ESP spectra of flavins afforded mainly molecular weight information with signals due to proton or sodium adducts. In the negative ion mode, FMN and FAD showed intense $[M-2H]^{-2}$ ions, due to the acidic phosphate moieties, that are an indication of the number of acidic places in these molecules. The best responses were obtained for FAD and FMN in the negative ion mode and Rfv in the positive ion mode. Only for FAD in the positive ion mode a molecular ion could not be observed (conc. 10 pmols/µl in MeOH).
TSP HPLC/MS analysis allows the characterization of flavins by means of common and intense fragment ions that contain the flavin ring (Figure 1). Signals corresponding to the $[AH_2]^+$ and $[BH_2]^+$ ions in the positive ion mode and to the A^- and B^- ions in the negative ion mode are observed in all cases. Other intense ions formed by loss of HPO_3 (FMN, fragment R) or to the adenine and

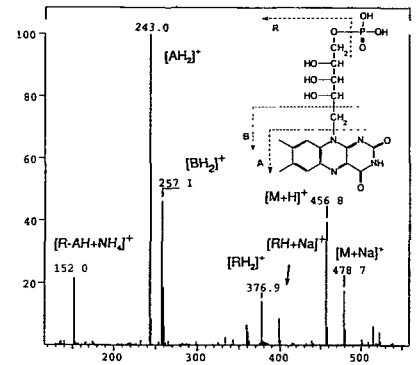

Fig. 1 Thermospray MS of FMN.

adenosine moieties (FAD) affords additional estructural information. Taking into consideration the $[M+H]^+$ and $[M-H]^-$ signals for Rfv and FMN and the $[AdenineH_2]^+$ and $[M-H]^-$ signal of FAD, response follows the order: FAD(+) > Rfv(+) > FMN(+) > Rfv (-) > FMN(-) > FAD(-).

When compounds X1 and X2 isolated from plant extracts were submitted to ESP analysis, both showed identical ESP mass spectra indicating the same molecular weight than FMN (456 u), but differing from the spectrum of the later by the absence of the $[M-2H]^-$ signal. In addition, ^{35}P-NMR indicated the absence of phosphor. These results suggested the presence of sulphur which was confirmed by ICP spectroscopy and tandem MS. Unequivocal characterization of the compounds was completed by H-NMR and shown to be two riboflavin derivatives not previously described in plants: riboflavin 3´-sulphate and riboflavin 5´-sulphate.

Tandem MS of the isobaric $[M-H]^-$ ions of FMN and the sulphate ester isomers (Figure 2) allows a) differenciation of phosphates and sulphates: ion at m/z 79 (PO_3^-), absent in sulphates; weak signal at m/z 80 (SO_3^-) in sulphates; b) differentiation of the position of esterification: Characteristic ions at m/z 139 (**g**) (5'- and 3'-esters) and at m/z 153 (**h**) (only 3'-esters) and intense signal at m/z 241 (**a**) (3'-esters).

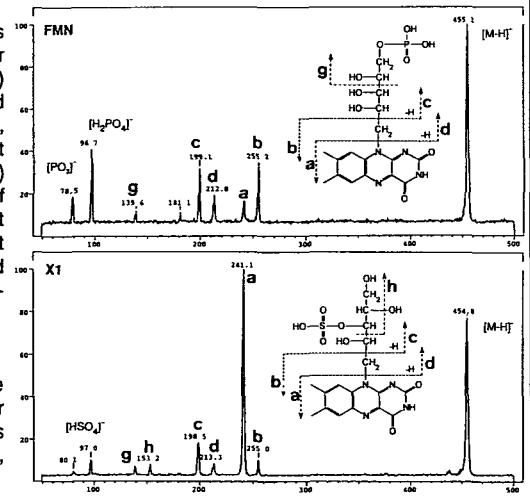

Fig. 2 Daughter ion spectra of the $[M-H]^-$ signal of FMN and riboflavine 3'-sulphate (X1).

Acknowledgements
Authors gratefully acknowledge Montse Carrascal and Aurora Poc for their skillful assistance obtaining mass spectra and growing the plants, respectively.

References

1.- Susín S., Abián J., Sánchez-Baeza F., Peleato M.L., Abadía A., Gelpí E. and Abadía J., (JBC, In Press).

Analysis of Vecuronium Bromide by Electrospray/Tandem Mass Spectrometry of Doubly-Charged Ions

Diane Rindgen[1], Jeevendra A. J. Martyn[2] and Paul Vouros[1], [1]Department of Chemistry and the Barnett Institute, Northeastern University, Boston, MA 02115, [2]Massachusetts General Hospital and Shriners Burns Institute, Boston, MA 02114

Vecuronium bromide is a monoquaternary ammonium steroid in clinical use as a muscle relaxant. The normal scan ESI spectrum of this compound shows a characteristic doubly-charged ion at *m/z* 279.4 as the base peak. This ion forms by loss of the bromide counter-ion and attachment of a proton. We have previously investigated the collision-induced dissociation behavior of this ion and have identified both doubly- and singly-charged fragment ions (1). Critical evaluation of these data indicates ion processes with potential analytical utility. For example, a singly-charged product ion at *m/z* 430.6 results from the combined loss of piperidine and an acetyl group. An analogous transition is observed for hexadeuteriated vecuronium bromide (*m/z* 282.4 ---> *m/z* 433.6). A transition involving formation of a singly-charged product ion from a doubly-charged precursor ion is highly selective in that the fragment ion being detected appears at a higher *m/z* value than the precursor ion. The selective nature of this type of transition can be advantageous when analyzing drugs in complex biological matrices. Toward that end, we have evaluated the suitability of the *m/z* 279.4 ---> *m/z* 430.6 transition for the quantitative determination of vecuronium bromide in plasma.

The MRM and normal scan ESI data were acquired on a VG Quattro triple quadrupole mass spectrometer equipped with a VG electrospray ionization source. The infusion solution consisted of a 50/50, by volume, mixture of HPLC grade acetonitrile/water with 1% glacial acetic acid and was continuously infused using an Isco uLC-500 Micropump operated at a flow rate of 2.5 - 3.0 uL/min. NF grade nitrogen was used as both the nebulizing and bath gas and the flow rates of each were optimized on the day of the analysis. Samples were analyzed in a flow injection mode using a Rheodyne injector equipped with either a 0.5 uL internal sampling loop or a 5 uL external loop. Vecuronium bromide was provided by Organon Laboratories, Ltd. and a standard stock solution was prepared in acetonitrile. Working solutions were made by dilution in the infusion solution. Bis-trideuterioacetyl (d_6) labeled vecuronium was prepared by acetylation of 3,17-deacetylvecuronium using d_6-acetic anhydride. Solid phase extractions were performed using Bond Elut C_1 cartridges from Varian Sample Preparation Products (Harbor City, CA).

Systematic studies were performed to evaluate the effect of different source and instrument parameters on the signal intensity of the *m/z* 279.4 ---> *m/z* 430.6 transition. The results of these studies indicate that the signal response for this transition optimizes at the following settings: source temperature = 60 °C; sampling cone voltage = 60 V; collision energy = 10 V; IE2 = 10 V. Examination of standard samples of vecuronium and the hexadeuteriated internal standard indicates that detection at physiologically significant levels can be realized (Figure 1).

The solid phase extraction procedure used for the isolation of vecuronium bromide and the internal standard, d_6-vecuronium, from plasma was similar to that described in reference 2 with changes made in the compositions of the eluting and reconstitution solutions. The analytes were eluted from Bond Elut C_1 columns as ion pairs using ammonium acetate in methanol. The optimal

concentration of the eluting solution was determined to be 50 mM. Extracts were reconstituted in a 0.01% trifluoroacetic acid/acetonitrile (by volume) solution prior to mass spectrometric analysis.

Preliminary studies of plasma samples show that the signal intensities from this transition are not consistent with those obtained from the pure samples. The recovery data suggest that signal loss may be due to co-extracted plasma constituents causing suppression of ion formation by charge competition or adsorption of the drug on residual matrix components. In either case, further sample cleanup is indicated.

REFERENCES

1. Rindgen, D., and Vouros, P., Investigation of the Fragmentation of Singly- and Doubly-Charged Ions of Neuromuscular Blocking Agents Using Electrospray/Tandem Mass Spectrometry, *Proceedings of the 40th ASMS Conference on Mass Spectrometry and Allied Topics*, Washington, DC, May 31 - June 5, 1992.

2. Ducharme, J., Varin, F., Bevan, D. R., Donati, F., Theoret, Y., *J. Chromatogr.*, **573**, 79 (1992).

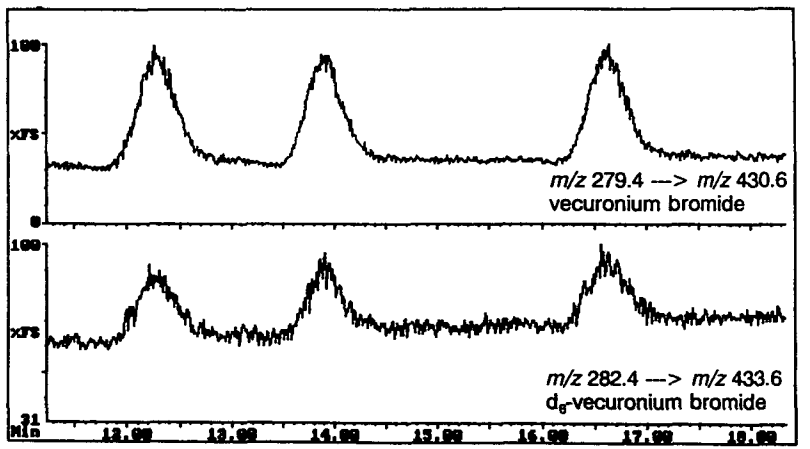

Figure 1 - Replicate injections of 25.1 ng vecuronium and 5.1 ng d_6-vecuronium at a source temperature = 60 °C; sampling cone voltage = 60 V; collision energy = 10 V; IE2 = 10 V.

The Application of Electrospray Ionization in the Analysis of Catecholamines by LC/MS

*Alexander B Schilling, The Hewlett Packard Company, Naperville, IL 60566

Introduction:

Catecholamines are a group of neurotransmitters of interest to workers in biology and medicine. Normally their analysis using liquid chromatography is accomplished with the use of electrochemical or fluorescence detectors because of the high sensitivity achievable (femtomole level) with these detectors Earlier work employing thermospray (TS) LC/MS has demonstrated detection limits on the order of a picomole for this class of compounds. The electrospray ionization (ESI) technique is believed to produce ions via the same ion evaporation mechanism postulated for TS, but with a higher efficiency. As a result, lower detection limits have been reported for a number of biologically active compounds than were possible by employing TS LC/MS. The chromatographic analysis of these compounds requires the use of ion-pairing agents such as octane sulfonic acid to improve the retention and separation of these polar compounds on reverse phase columns. In thermospray LC/MS the concern is that the usual ion pairing agents may lead to clogging of the vaporizer probe. In ESI the concern lies with the effect of buffer modifiers on the ability to form a spray and therefore the ionization process as well as whether any physical obstruction may occur. An earlier evaluation[1] of the compound pentadecafluorooctanoic acid (PDFOA) on thermospray found that it was a good substitute for the sulfonic acids in the analysis of catecholamines It would be of interest therefore, to investigate the effects of using PDFOA in the ESI analysis of these compounds.

Experimental

A mixture of catecholamines including dopamine, epinephrine, norepinephrine, and several metabolites were run on a HP 5989A LC/MS/DS with an Analytica electrospray interface. The source was equipped with a chromatography spray needle and operated under positive ion mode with the CapEx voltage at 90V and either in scan mode (80-220 amu) or SIM mode. A Supelco LC-18-DB column (2.1 x 250 mm 5 u particle) was used on a HP 1090L HPLC equipped with a diode array detector (280 nm) with an isocratic solvent system consisting of 77·23 (0.01 M NH_4Ac pH 4.0 with 0.01 M PDFOA 0.01M NH_4Ac in methanol with 0.05% formic acid and 0 01 M PDFOA) A flow rate of 0.4 mL/min was used and a column temperature of 40 C was maintained The injection volume was 3 uL. The column effluent was combined with a co-organic solvent flow of 0.4 mL consisting of either n-butanol:ACN, isopropanol, or methanol using a valco tee prior to entering an Accurate solvent splitter The splitter has the capability of providing either a 50·1 or 125:1 split ratio resulting in final flow rates of 16 or 6 4 uL/min respectively to the electrospray source

Results and Discussion·

The results indicate that ESI produces the same type of ions observed in the thermospray MS of these compounds In the absence of the ion-pair agent, ESI can exceed the detection limits of thermospray (1 pmole) by an order of magnitude or more (20-100 fmole). Under

[1] Schilling, A.B., The 40th ASMS Conference, Wsahington D.C. 1992

chromatographic conditions using the ion-pair reagent (PDFOA), the detection limit for these compounds is actually less than that of thermospray by almost an order of magnitude. This decrease may be due to a decrease in the efficiency of the spray or ionization process or by physical occlusion of the inlet capillary. The decrease occurs even if the co-organic solvent flow is varied from mixtures less likely to mix readily with the mobile phase (nBu·Acn) to those more likely to mix well (MeOH). Co-organic solvent addition generally facilitates spraying at higher flows in ESI by lowering the surface tension of the effluent and increasing droplet formation. It is unlikely that physical occlusion is occurring as it was possible to restore full sensitivity after discontinuing use of the ion-pair even after large lengths of time spent spraying the reagent into the source This suggests that PDFOA may yet have other applications in ESI as a discharge suppresser in negative ion mode or when trying to chromatograph these or other compounds requiring an ion pair in APCI work, where gas phase ionization predominates. PDFOA does produce an intense ion at 413 amu in the negative ion mode, so SIM mode may be necessary depending on the mass range required. Since only amine containing catecholamines are readily detected in positive ion mode, many deaminated metabolites possessing catechol functional groups that can be detected electrochemically are not amenable to this mode of ESI. It should be mentioned that others have demonstrated that the catecholamines can successfully be chromatographed without ion-pair reagents on the newer polymeric columns and this bypasses the problem of dealing with the ion-pairing agent altogether

Summary of Base Ions Detected for The Catecholamines in ESI vs TS LC/MS (Positive Ion Mode)

Compound	MW	Base Ion (TS)	Base Ion (ESI)
DOPA	197	198	198
GABA	103	104	87
DOPAC	168	123	ND*
HIAA	191	192	192
Norepinephrine	169	152	152
Epinephrine	183	166	166
Homovanillic Acid	182	200	ND
DHBA	139	123	123
Dopamine	153	154	137
Serotonin	176	177	161
Tyramine	137	138	121

*ND- Not Detected

Electrospray MS and MS/MS for Metabolite Identification in Various Animal and Human Biotransformation Studies

T.A. Gillespie, P.L. Bonate, J.D. Cornpropst, A.F. DeLong and L.A. Shipley
Eli Lilly and Company, Lilly Corporate Center, Indianapolis, IN 46285

LY246708/NNC 11-0232 (3 - [4- (hexyloxy) - 1,2,5 - thiadiazol - 3 - yl] - 1,2,5,6 - terahydro - 1- methylpyridine) is a potent and selective muscarinic M_1-agonist. It is currently undergoing clinical investigation for the symptomatic treatment of Alzheimer's disease. Early pharmacokinetic/balance studies conducted in rats and monkeys suggested extensive metabolism of parent compound. A biotransformation study was conducted in human volunteers using ^{14}C-labeled LY246708 at an oral dose of 75 mg (50µCi). The purpose of this work was to identify urinary and plasma metabolites of LY246708 (figure 1) in man.

Sample Preparation

Human urine was pooled (500 mL) from 0 - 24 hr, freeze-dried and reconstituted with 25 mL of MeOH/H_2O (50/50). The samples were then applied to a C18 SPE cartridge , washed and then eluted with MeOH. The urine samples were dried and reconstituted in 250 µL of MeOH/H_2O (50/50). Samples were then injected onto a YMC Basic column (25 cm x 0.46 m) and separated by using a gradient consisting of 20% MeOH/80% 50 mM NH_4OAc for 30 min, then to 100% MeOH over 75 min. Fractions were collected and dried. Human plasma samples were pooled (30 mL) from 1, 1.5, 2 and 4 hr time points. These samples were obtained from a nonradiolabled study conducted in man at an oral dose of 150 mg of LY246708. The plasma samples were applied to a CN/C18 combination SPE ("piggy-backed"), washed and eluted with methanol. The samples were then injected onto a Zorbax RX-C8 column (25 cm x 0.46 mm) and separated using 100% 50 mM NH_4OAC (pH5) for 15 min, followed by a gradient up to 100% MeOH over 60 min. The fractions were then collected and dried for analysis.

Experimental

All experiments were performed on a Finnigan MAT TSQ700 coupled with an Analytica of Branford ES source. The urine samples were injected (100 - 150 µL) onto a short YMC Basic column (5 cm x 0.46 mm) coupled to the ES interface. The isocratic system was ACN/0.2M acetic acid (50/50) at a flow of 1 mL/min. This was then split with a low dead volume tee for infusion into the ES source at 2.5 µL/min. The drying gas (N_2) was 30 mL/min @ 250°C. A voltage of approximately -4200 V was used for ionization. Mass spectral analysis was performed in centroid mode at 1 sec/scan. Plasma samples were direct infused (DI) at a rate of 2 µL/min after reconstitution with 200 µL of MeOH/1% acetic acid (50/50). The drying gas (N_2) for this analysis was 20 mL/min @ 250°C. A voltage of between -3500 to -3800 V was used. Analysis was performed in the profile mode at 1 sec/scan and averaged for 1 min. Daughter (product) ion spectra were obtained using a collision offset voltage of -20 eV and a collision pressure of 2.0 mTorr (argon).

Results and Discussion

Identification of the urinary metabolites of LY246708 in man was accomplished almost immediately after the completion of the ^{14}C-labeled study. The use of a short (5 cm) HPLC column provided sufficient separation, coupled with ES and MS/MS to give positive identification of 8 tentative metabolites of LY246708 in urine. This information confirmed that extensive first pass metabolism was occurring in humans. In addition, utilizing DI/ES, 8 tentative metabolites were identified in human plasma by MS/MS. The hexyl side chain appeared to be the major site of metabolism in that 7 of the 8 metabolites identified in the urine and plasma exhibited some form of oxidation to this side chain. Furthermore, the tetrahydropyridine ring also demonstrated biotransformation in 5 of the metabolites identified in urine and 4 identified in plasma. N-oxidation appeared to be the major metabolism route in the

case of this ring. The CID spectra of the N-oxide metabolites found in both urine and plasma exhibit a base peak at m/z 197 representing the loss of H_2O and subsequent loss of the side chain from the protonated molecular ion (figure 2). In addition, the peak at m/z 60 (addition of oxygen onto the peak a peak at m/z 44 observed for the parent CID spectrum representing the ion $[CH_3NHCH_2]^+$) was used to confirm the site of metabolism as occurring on the tetrahydropyridine ring. The N-oxide was further confirmed through the use of deuterium labeled exchange experiments performed with the ES interface. In addition, a glucuronide has been identified in human urine following oxidation of the side chain. The CID spectrum of the glucuronide metabolite shows a base peak at m/z 298 representing the characteristic loss of 176 daltons from the protonated molecular ion (figure 3). The site of hydroxylation on the side chain is unknown at this time. The thiadiazole nng appears to be metabolically inert in humans. The summary of identified metabolites for LY246708 is shown in figure 4.

Conclusions

ES can be successfully utilized for identification of a variety of metabolites in animal and human biological fluids. Coupled with MS/MS, ES can provide positive, rapid identification of metabolites when biological samples are sufficiently "clean". ES/MS/MS is an extremely valuable tool for the identification of conjugated metabolites found in a variety of biological fluids. Short column (5 cm) LC can be utilized to provide additional clean-up for identification of metabolites in "dirty" biological samples.

Figure 1

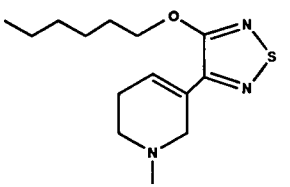

Figure 2

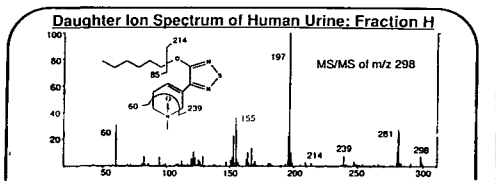

Figure 3

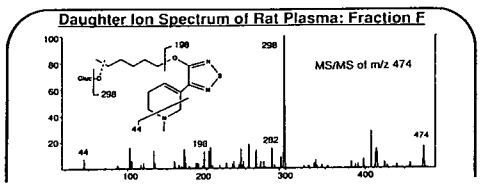

Figure 4

	URINE	PLASMA	ANIMAL
desmethyl O-butyl carboxylic acid	+	+	+
O-butyl carboxylic acid	+	+	+
N-oxide O-butyl carboxylic acid	+	-	+
hydroxyl O-butyl carboxylic acid	-	+	+
hydroxyl	+	+	+
hydroxyl - gluc	+	-	+
dihydroxyl N-oxide	+	-	-
carboxylic acid	-	+	+
ketone N-oxide	+	+	-
hydroxyl N-oxide	-	+	-
N-oxide	+	+	-

+ = was identified
- = has not been identified

ELECTROSPRAY IONIZATION MASS SPECTROMETRY OF GLUTATHIONE AND N-ACETYLCYSTEINE CONJUGATES OF ELECTROPHILIC METABOLITES OF ACETAMINOPHEN

S. Oishi[1], G. E. Bronson[2], L. Baczynskyj[2], and W. J. Adams[2]
[1]Department of Medicinal Chemistry, University of Washington, Seattle WA 98195;
[2]Upjohn Laboratories, The Upjohn Company, Kalamazoo, MI 49001.

Acetaminophen (APAP) has previously been shown to be metabolically activated to form the reactive, electrophilic metabolites N-acetyl-p-benzoquinoneimine (NAPQI) and p-benzoquinone (BZQ) when administered *in vivo* [1]. Both NAPQI and BZQ readily undergo conjugation reactions with glutathione (GSH, γ-glutamylcysteinylglycine) to form glutathion-S-yl conjugates which can then be biotransformed to N-acetylcystein-S-yl (NAC) conjugates and excreted in the urine. The toxicity of APAP, which is observed when high doses of APAP are ingested, has been attributed to NAPQI. However, latent forms of NAPQI that are less powerful oxidizing agents have been proposed to account for the fact that high doses of APAP do not cause oxidant stress *in vivo*[2,3] (e.g., *ipso* GSH conjugate[3]). It has also been reported that the glutathion-S-yl conjugates of p-hydroquinone (HQ) are more nephrotoxic that BZQ itself[4]. These observations suggest that the glutathion-S-yl conjugates and perhaps the N-acetylcystein-S-yl conjugates of APAP may play a role in the toxicity of APAP. We report here an investigation of the *in vitro* reaction of BZQ and NAPQI with GSH or NAC under physiologically relevant conditions; and the utility of electrospray ionization mass spectrometry (ESIMS) for the detection of the GSH and NAC conjugates formed.

EXPERIMENTAL: Synthetic BZQ and NAPQI were added dropwise to a molar excess of GSH or NAC in phosphate buffered saline (pH 7.4) at 37°C under both argon and air at two different concentrations of GSH and NAC (2 mM and 100 mM). Samples were periodically withdrawn from the reaction mixtures and quenched by lowering their pH to ≤ 3.5 by addition of 0.25 M HCl before storage at -20°C. The quenched reaction mixtures were chromatographed on a reversed-phase HPLC column (Vydac C_{18}, 330 A, 4.6 mm i.d. x 25 cm) using water/methanol/acetic acid mobile phases and either isocratic or linear gradient conditions. Column eluate was monitored with a UV detector (254 nm). Chromatographic fractions were collected for direct introduction into the mass spectrometer; or were lyophilized and redissolved in water/methanol/acetic acid solutions before introduction into the mass spectrometer. ESI mass spectra were recorded using a Vestec 201A mass spectrometer equipped with a Vestec ESI source and a Teknivent Vector II data system.

RESULTS AND DISCUSSION: Chromatographic analysis of quenched reaction mixtures indicated that the reaction of BZQ and NAPQI with GSH or NAC under anaerobic or aerobic conditions resulted in the formation of multiple products (e.g., see Figure 1). ESIMS characterization of these products demonstrated that the mono- and di-glutathion-S-yl-hydroquinone conjugates and the mono-, di- and tri-N-acetylcystein-S-yl-hydroquinone conjugates (e.g., see Figure 2) were formed following reaction of GSH or NAC with BZQ; and that the mono- and di-N-acetylcystein-S-yl-acetaminophen conjugates were formed following reaction of NAC with NAPQI. Although we were not able to confirm by ESIMS that the di-glutathion-S-yl-acetaminophen conjugate was formed because of the limited availability of NAPQI (only limited experiments at GSH concentrations of 2 mM were done), it seems probable that the di-glutathion-S-yl-acetaminophen conjugate was formed based on evaluation of the chromatographic data. Differences clearly exist in the reactivity of BZQ and NAPQI under

physiologically relevant conditions. BZQ reacts almost exclusively with GSH and NAC *via* a Michael addition reaction, whereas NAPQI is extensively reduced to APAP in addition to reacting *via* a Michael addition reaction. Since the more highly substituted conjugates were formed under anaerobic conditions in the presence of BZQ or NAPQI and excess nucleophile, it follows that the oxidation potentials of the mono- and di-substituted hydroquinone conjugates and the mono-substituted acetaminophen conjugate are lower than those of p-hydroquinone and acetaminophen, respectively. Comparison of chromatograms of mixtures incubated under anaerobic and aerobic conditions (e.g., compare Figures 1A and 1B) indicated that the glutathion-S-yl- and N-acetylcystein-S-yl-hydroquinone conjugates are susceptible to oxidation by molecular oxygen to reactive quinones, but that the corresponding acetaminophen conjugates are not susceptible to oxidation by molecular oxygen to reactive quinone imines. The results of this study suggest that protein cysteinyl thiols adducted *in vivo* by reaction with BZQ or NAPQI are susceptible to chemical oxidation to the corresponding quinone and quinone imines, respectively, and subsequent protein crosslinking reactions, which may be of toxicologic significance. The utility of ESIMS for the detection of the GSH and NAC conjugates of p-hydroquinone and acetaminophen was demonstrated by this research.

[1]G. A. Pascoe, C. J. Calleman and T. A. Baillie, *Chem.-Biol. Interactions*, *68*, 85-98 (1988); [2]C. V. Smith and J. R. Mitchell, *Biochem. Biophys. Res. Commun.*, *133*, 329-336 (1985); [3]D. B. Axworthy, K.-J. Hoffmann, A. J. Streeter, C. J. Calleman, G. A. Pascoe and T. A. Baillie, *Chem.-Biol. Interactions*, *68*, 99-116 (1988); [4]S. S. Lau, B. A. Hill, R. J. Highet and T. J. Monks, *Mol. Pharmacol.*, *34*, 829-836 (1988).

A; 0 hr post initiation of reaction. B; 2 hr post initiation of reaction

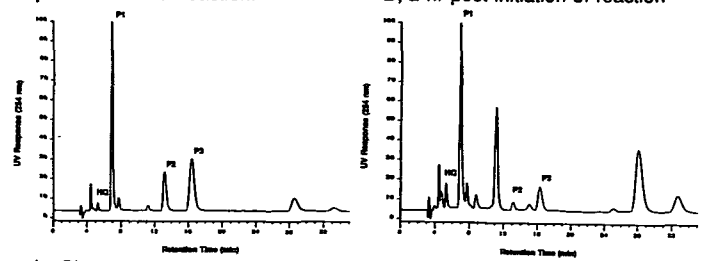

Figure 1. Chromatograms of BZQ and NAC aerobic reaction mixture.

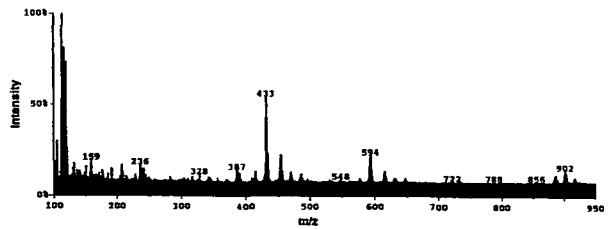

Figure 2. ESI mass spectrum of di-N-acetylcystein-S-yl- and tri-N-acetylcystein-S-yl-hydroquinone conjugates, $[M + H]^+$ = m/z 433 and m/z 594, respectively (peak P3 components, Figure 1A and 1B).

Identification of Tamoxifen Metabolites in Breast Cancer Patients by Electrospray LC/MS

G.K. Poon*[1], Y.C. Chui[2], R. McCague[1], M.G. Rowlands[1], R. Feng[3], P.E. Lønning[4] and M. Jarman[1]

1 Drug Development Section, Institute of Cancer Research, Surrey, UK. 2 CanTest Ltd., Vancouver, B.C., Canada. 3 National Research Council, Montreal, Quebec, Canada. 4 Dept. of Oncology, University of Bergen, Bergen, Norway.

Introduction

The major clinical application of tamoxifen [*trans*-1-(4-[2-dimethylamino)ethoxy]phenyl)-1,2-diphenylbut-1-ene] [1] is in the treatment of breast carcinoma. It is an antiestrogen and inhibits tumor growth by competitively antagonizing the binding of estradiol to estrogen receptors. When the drug is given orally to the patient, it is extensively metabolized. The metabolic profile of tamoxifen in female patients is well documented [see review 2]. In plasma, *N*-desmethyltamoxifen (metabolite X) is the major metabolite; 4-hydroxytamoxifen (metabolite B) is a minor metabolite; *N*-didesmethyl-tamoxifen (metabolite Z) is present in serum when the patients are receiving long term tamoxifen treatment; 4-hydroxy-N-desmethyltamoxifen (metabolite BX) and metabolite B are excreted as conjugates in bile and urine; and finally, metabolite D [3,4-dihydroxytamoxifen] has been tentatively reported in human bile and faeces of animals. In the previous studies, determination of these metabolites relies on off-line liquid chromatographic (LC) separation with mass spectrometric (MS) detection, or LC separation with fluorescence detection, or GC/MS with sample derivatization before the analysis. This study has demonstrated that tamoxifen and its analogues can be easily analyzed in the biological fluid by on-line LC/MS using a pneumatically assisted electrospray interface.

Experimental

Plasma and urine samples were collected from patients who had been given a single dose of tamoxifen. Phase I metabolites were extracted with hexane (containing 2% butanol) and Phase II metabolites were purified using solid phase cartridge. The extracts were applied to a microbore HPLC system using a Suplex pKb-100 column (250 x 1mm) and a linear gradient elution from 20% acetonitrile : 80% buffer to 100% acetonitrile in 20 min at 0.2 ml/min. Identification of the metabolites are achieved by LC/ESI/MS on a Sciex API III triple quadrupole mass spectrometer. Tandem mass spectrometry was performed to provide structural information.

Results

In the plasma sample, the parent drug was detected ($[M+H]^+$ at m/z 372), *N*-desmethyltamoxifen ($[M+H]^+$ at m/z 358) is the major metabolite and tamoxifen *N*-oxide [$(M+H]^+$ at m/z 388) is present in trace amount [Fig. 1 a-c].

In the urine extracts, four glucuronide conjugates of tamoxifen analogues were obtained. These include the glucuronide conjugates of 4-hydroxy-tamoxifen [Fig. 1d], two *N*-desmethyl-hydroxylated tamoxifen and a dihydroxy-tamoxifen.

Conclusion

Glucuronide conjugation is a principle metabolic pathway of tamoxifen. This report describes for the first time direct analysis of tamoxifen metabolites in human urine and plasma samples, the isolation of tamoxifen *N*-oxide in human and the identification of conjugated metabolites as their intact molecules. Some of these metabolites (as aglycone) could make important contributions to the biological actions of tamoxifen in patients.

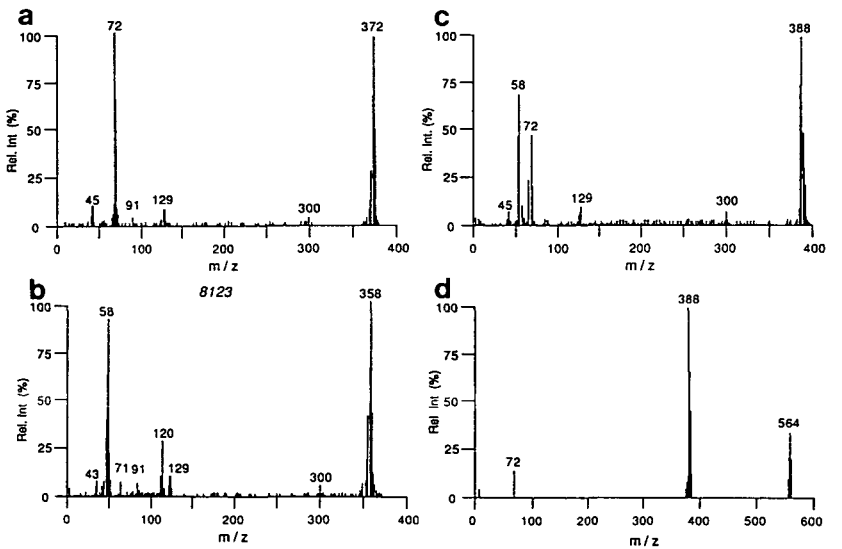

Figure 1. Product ion spectra of (a) the parent drug; (b) the metabolite X; (c) the metabolite tamoxifen *N*-oxide; and (d) the metabolite 4-hydroxy tamoxifen glucuronide.

References

1. B.J.A. Furr & V.C. Jordan, *Pharmacol. Ther.* **25**, 127-205 (1984).
2. P.E. Lonning, E.A. Lien, S. Lundgren & S. Kvinnsland, *Clin. Pharmacokinet.* **22**, 327-358 (1992).

Acknowledgements

This work is supported by Cancer Research Campaign & Medical Research Council, UK.

DETERMINATION OF ANTIBIOTICS USING ULTRASONIC NEBULIZATION ELECTROSPRAY MASS SPECTROMETRY

Robert D. Voyksner, Markus Linder and Rolf Straub,
Analytical and Chemical Sciences, Research Triangle Institute,
P. O. Box 12194, Research Triangle Park, NC 27709

INTRODUCTION

A number of veterinary drugs (β-lactams) are frequently used to prevent infections. These drug residues can contaminate meat and milk products destined for human consumption. In order to insure human food safety, new methods using HPLC/ES-MS were evaluated to monitor these antibiotics. These methods must handle large numbers of samples (fast) and provide the sensitivity and specificity to identify the antibiotics at ppb levels.

Typically the speed of the HPLC/MS analysis has been limited by HPLC retention times. However, the development of perfusion HPLC provides a tremendous speed advantage over conventional packed columns. Unlike conventional packing material, perfusion packing enables transport of molecules through the pores of the packing material. Now flow rates can be increased without large back pressure and diffusional flow can be minimized resulting in high chromatographic resolutions together with short retention times. These higher flow rates (50 μL/min) can be handled by the electrospray interface using a capillary shield to assist in desolvation and ultrasonic nebulization to assist in the initial droplet formation.

This paper presents the development of a perfusion LC/electrospray MS method for β-lactams. Emphasis will be placed on parameters that affect LC resolution and ES sensitivity.

EXPERIMENTAL

Separations were performed on Poros II LC Packing Perfusion column 0.32 x 150 mm, 7-8 μm particles, 4000Å porous. The mobile phase was a gradient from 100% water to 40-60% acetonitrile in water in 4 or 5 minutes. Buffers including formic acid (FOA), heptafluorobutyric acid (HFBA) and trifluoracetic acid (TFA) were added to the mobile phase at 0.1-1% levels up to 25 mM for HFBA). The flow rates for the separation were 40-50 μL/min and injection volume was 0.5 μL.

The electrospray MS system was a HP5989 equipped with a HP electrospray interface with an ultrasound nebulizer (Analytica of Branford). The MS was scanned from 180-550 daltons in 1 s or SIM was used to improve scan speed (necessary for perfusion chromatography due to the 2-4 s peak widths) and sensitivity. For SIM operation the $[M+H]^+$ ion for each β-lactam was monitored for 50 or 100 ms to improve the cycle time to 0.3-0.6 s.

RESULTS AND DISCUSSION

The separation of the β-lactams by perfusion LC was evaluated in six different buffer systems. The ion chromatograms for the $[M+H]^+$ ions for the β-lactams in each mobile phase are presented to evaluate perfusion column resolution and electrospray sensitivity. The optimal solvent for electrospray sensitivity (FOA) was the least desirable for the LC separation of the individual β-lactams. The use of TFA (0.1%) provided slight improvement

in the separation but electrospray responses were from a factor of 4 (cetiofur) to 10 (penicillin G) lower than with formic acid. The addition of HFBA to the formic acid solution as an ion pair reagent improved the separation as the molarity of this reagent was increased from 0.5 mM to 25 mM. On the other hand, the electrospray signal decreased as the molarity of HFBA increased. The mobile phase employing 0.5% FOA and 5 mM HFBA resulted in the best compromise between sensitivity and chromatographic separation.

The electrospray mass spectra recorded for each β-lactam exhibited intense $[M+H]^+$ ions and several key fragment ions necessary for confirmation, at a capillary voltage of 120 V. The on-line LC/MS detection limits for the β-lactams studied ranged form about 30 ng to 200 pg. Cetiofur exhibited the best detection limits (200 pg) followed by cephapirin (600 pg), ampicillin (2 ng), penicillin G (10 ng) and cloxacillin (35 ng). The response of cetiofur and cephapilin was linear over the concentration range of 1-300 ng.

Ultrasonic nebulization aided in handling the higher flow rates, high aqueous mobile phase and buffers such as TFA and HFBA used in the separation of β-lactams. The ultrasonic nebulizer permitted perfusion LC separation at optimal flow rates of 50-60 μL/min. This flow rate resulted in less than 20% loss in signal intensity relative to the electrospray flow rates of 3-5 μL/min. Also, β-lactams eluting at greater than 80% water containing buffers such as 0.1% TFA or 25 mM HFBA could be effectively ionized without significant signal suppression or spike noise. For example, the relative response for cetiofur using ultrasonic vs conventional electrospray needle nebulization is presented in Table 1. The relative response for cetiofur is nearly constant using ultrasonic nebulization while the response using the conventional electrospray needle assembly ranged from 16% to 73% of the ultrasonic generated signal.

CONCLUSIONS

Perfusion LC/electrospray-MS offers the potential to separate and confirm target β-lactams in less than five minutes. The development of the perfusion LC/electrospray-MS conditions resulted in compromises in chromatography and electrospray-MS operation. Some of these compromises such as higher flow rates, high aqueous content and the presence of higher molarity of buffer were minimized by the use of ultrasonic nebulization.

This work was supported by a FDA Cooperative Agreement No. FD-U-000589.

Table 1

Electrospray ion current for the $[M+H]^+$ of cetiofur using conventional and ultrasonic nebulization in 80% water and 20% acetonitrile at 50 μL/min

	Relative Ion Current (%)	
Buffer	Ultrasonic	Conventional Needle Assembly
0.1% TFA	96	16
0.2% FOA, 5 mM HFBA	100	73
0.2% FOA, 25 mM HFBA	88	44

DETERMINATION OF CYSTEINYL LEUKOTRIENES USING ELECTROSPRAY/TANDEM MASS SPECTROMETRY

Ralph Orkiszewski, Ulla Justesen, Hartmut Jaeschke* and Simon J. Gaskell
Center for Experimental Therapeutics, Baylor College of Medicine, Houston, TX 77030, and * Drug Metabolism Research, The Upjohn Company, Kalamazoo, MI 49001

We have previously reported[1] the use of [^{13}C]-isotope dilution and a GC/MS-based procedure (based on the method reported by Balazy and Murphy[2]) for the determination of cysteinyl-leukotrienes (LTC_4 and N-acetyl LTE_4) in rat bile. The procedure involves addition of [$^{13}C_4$]-internal standards (prepared in this laboratory[3]), fractionation of bile by reverse-phase HPLC, and hydrogenation to yield 5-hydroxyeicosanoic acid from each of the cysteinyl leukotrienes. (This approach accordingly requires efficient separation of individual leukotrienes prior to hydrogenation.) The product is converted to the pentafluorobenzyl ester, trimethylsilyl ether for GC-negative ion MS analysis with selected ion monitoring. This method has been applied to the study of endotoxin-induced cysteinyl-leukotriene production in vivo.[1,4] The biliary excretion of LTC_4 and N-acetyl LTE_4 was increased by 190 and 1000%, respectively, following administration of *Salmonella enteritidis* endotoxin. Studies involving the depletion or augmentation of serum complement indicated that complement mediates endotoxin-induced cysteinyl leukotriene formation.[4] In the present work, we have made further use of the GC/MS procedure to compare biliary leukotriene excretion in the rat following administration of endotoxin from two different sources, *S. enteritidis* and *E. coli*. Figure 1 shows the biliary concentrations of N-acetyl LTE_4 as a function of time. In agreement with previous studies,[1,4] administration of *S. enteritidis* endotoxin resulted in a marked elevation of biliary N-acetyl LTE_4. Endotoxin derived from *E. coli*, however, was without effect.

The complexity of the GC/MS-based procedure and the reliance on chromatographic separation for the differentiation of individual cysteinyl leukotrienes has encouraged further effort on the mass spectrometric detection of the intact analytes. In earlier studies,[1] FAB/tandem MS was used to confirm the presence of LTC_4 in rat bile. Additional HPLC fractionation was required before MS analysis, however, and the sensitivity of detection achieved was modest. We have therefore investigated the analysis of cysteinyl-leukotrienes using electrospray MS. Electrospray ionization yielded predominantly singly charged ions; both $[M+H]^+$ and $[M+Na]^+$ ions were observed, with N-acetyl LTE_4 showing a substantially greater propensity than LTC_4 for formation of the sodiated ion. Selected ion monitoring (SIM) analyses (with loop injection of authentic analyte) gave a detection limit for LTC_4 of approximately 100 pg, by monitoring of $[M+H]^+$ ions. This detectability is comparable to that observed in our previous work[1] using continuous-flow FAB; in our hands, however, electrospray MS is a substantially more robust method. Electrospray MS/SIM of N-acetyl LTE_4 $[M+Na]^+$ ions gave a detection limit of approximately 300 pg. Low energy CAD of LTC_4 $[M+H]^+$ yielded m/z 308 (protonated glutathione) as the most prominent product ion; selected reaction monitoring analyses for this fragmentation gave a detection limit of ca. 5 ng. Figure 2 shows a packed capillary LC-electrospray MS analysis of authentic N-acetyl LTE_4, with SIM of both $[M+H]^+$ and $[M+Na]^+$ ions. Satisfactory chromatography is observed and the sensitivity is sufficient to detect the leukotriene in amounts corresponding to those expected in extracts of bile following *S. enteritidis* endotoxin administration. Analyses of bile extracts (obtained by reverse-phase HPLC fractionation) by LC-electrospray MS/SIM, however, were disappointing, the response to the leukotriene components being masked or suppressed by other extract constituents. It is clear that further development of the procedure requires improved complementarity between the initial bile fractionation procedure and the chromatographic separation achieved during LC-MS.

1. Raftery MJ, Justesen U, Jaeschke H, Gaskell SJ. Biol Mass Spectrom 1992; 21: 509.
2. Balazy M, Murphy RC. Anal Chem 1986; 58: 1098.
3. Raftery MJ, Gaskell SJ. J Label Compds Radiopharm 1991; 29: 314.
4. Jaeschke H, Raftery MJ, Justesen U, Gaskell SJ. Am J Physiol 1992; 26: G947.

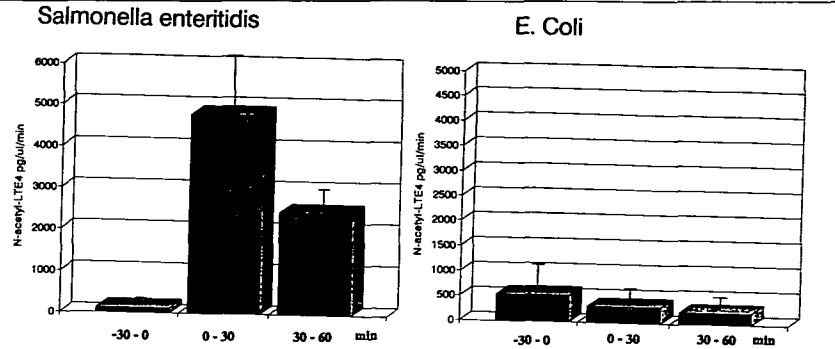

Figure 1. Biliary excretion of N-acetyl LTE_4 following administration of endotoxin from *Salmonella enteritidis* or *Escherichia coli*.

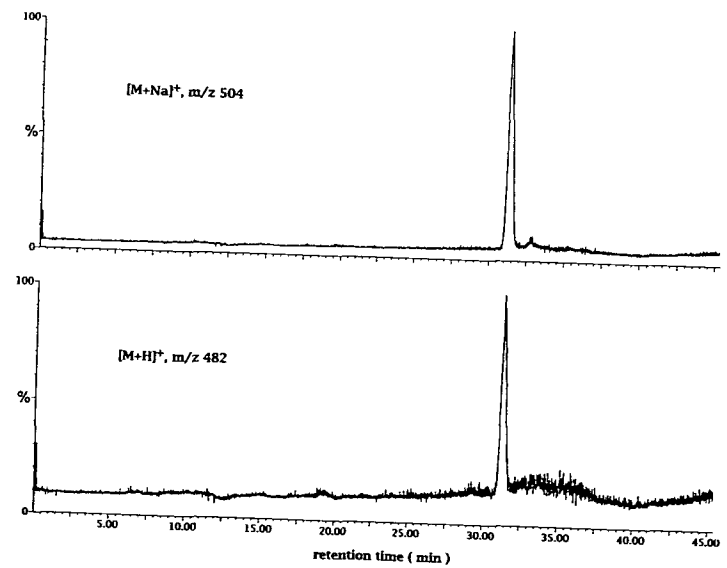

Figure 2. Reverse-phase packed capillary LC-electrospray MS of N-acetyl LTE_4 (50 ng), with SIM of $[M+Na]^+$ and $[M+H]^+$ ions.

Structure Elucidation of Taxanes by ESI-MS and ESI-MS/MS

Francis Bitsch, John Kim, and C.H.L. Shackleton
Children's Hospital Oakland Research Institute, Oakland, CA 94609, USA
Wenwen Ma and Matthew Nieder
ESCAgenetics Corps, San Carlos, CA 94070, USA

Introduction

Taxol, a natural component extracted from the bark of the yew tree (*Taxus* species) has been shown to be an efficient antitumor agent especially in the treatment of ovarian, breast and skin cancer. Until recently, most taxol was obtained by extraction of the bark of the pacific yew tree, *Taxus brevifolia* but the supply is limited because this species is neither abundant nor fast growing. Only about 100mg is obtained from 1kg of dry yew tree bark so it takes approximately three trees to provide enough taxol to treat one patient.

Different sources of taxol were therefore explored. Our studies (ESCAgenetics) have demonstrated the biosynthesis of taxol and taxanes by *Taxus* species cell cultures.

Mass spectrometry of taxol using EI, CI, FAB, electrospray ionization and thermospray ionization has previously been reported. We were interested in the structural characterization of taxanes using microbore HPLC and electrospray ionization mass spectrometry. Collision activated decomposition in the atmosphere-vacuum interface and CID MS/MS were used for the structure elucidation of taxanes with various C-13 side chains.

Results

We were able to detect protonated molecule ions of taxanes at the level of 10 ng in full scan MS and 200 pg using Selective Ion Recording.

Collision Activated Decompositions (CAD) in the atmosphere vacuum interface yielded specific fragments. The fragments observed under low collision energy conditions are similar to those observed in CID MS/MS (**Figure 1**). The main fragmentation occurs at the bond between the taxane ring and the side chain (C-13) and the fragmentation yield at this position is particularly great in the case of 10-deacetyl taxanes.

The fragments observed by CAD in the electrospray interface were used as markers for the location of taxanes in cell culture extracts.

Structure modifications in the side chain are frequently observed among cell culture produced taxanes. We were able to partially elucidate the structure of the side chain of various known and new taxanes by CID tandem mass spectrometry of the side chain fragment obtained by collisional activation in the ES source.

Effectiveness of this technique is demonstated using the well-known taxane compounds cephalomannine and taxol (**Figure 2**).

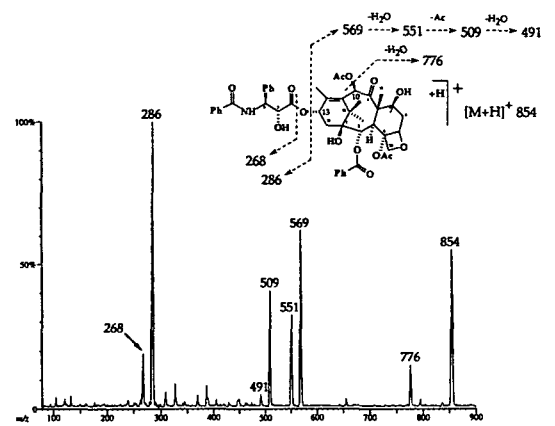

Figure1. CID mass spectrum of $[MH]^+$ 854 from Taxol. Collision energy: 25eV; Collision gas: Ar.

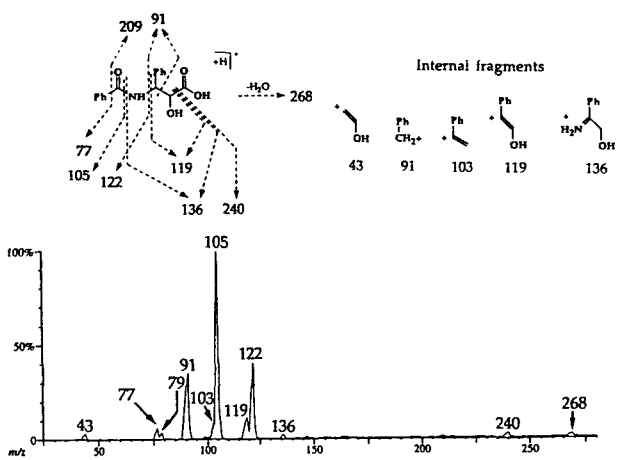

Figure 2. CID mass spectrum of side chain fragment 286 from Taxol. Vnozzle-skimmer: 85 volts, Collision energy: 85eV; Collision gas: Ar.

METABOLISM OF SUBSTANCE P BY *IN VIVO* MICRODIALYSIS AND LC/ESI/MS

P.E. Andrén, M.R. Emmett, B.B. DaGue and R.M Caprioli
The Analytical Chemistry Center and Department of Biochemistry
The University of Texas Medical School, Houston, Texas 77030

INTRODUCTION

Neuropeptides constitute a large and still growing group of putative neurotransmitters or neuromodulators in the nervous system. Little is known about their metabolism and inactivation *in vivo*, although many investigations have been done by *in vitro* techniques. The present studies focus on intracerebral metabolism of exogenous substance P (SP), an eleven amino acid peptide, using microdialysis and nanoscale liquid chromatography electrospray ionization mass spectrometry (LC/ESI/MS).

METHODS AND MATERIAL

Rats (Sprague-Dawley, 250-400 g) were anesthetized with an intraperitoneal injection of pentobarbital 45 mg/kg and a microdialysis probe (CMA/10, 4 mm membrane length) was stereotaxically implanted into the striatum. The probe was perfused at a flow rate of 0.3 μL/min with artificial cerebrospinal fluid (5 mM KCl, 120 mM NaCl, 1.2 mM $MgCl_2$, 1.8 mM $CaCl_2$, 0.15% phosphate buffered saline, pH 7.4). Two hours after probe implantation, a 1, 10, 25 or 50 μM solution of SP in artificial CSF was introduced into the microdialysis probe and infused for several hours. The microdialysis probe was used to both introduce SP1-11 into the brain, as well as collect proteolytic fragments produced by enzymic hydrolysis.

Nanoscale-LC/ESI/MS The recovered dialysis samples were loaded into a 10 μL loop on a 10-port injection valve and injected onto a fused silica capillary column (50 μm i.d. x 10 cm packed with 10 μm spherical C-18 particles) using a syringe pump at 5 μL/min. After washing with 5% methanol/0.25% acetic acid, the peptides were eluted with 50% methanol/0.25% acetic acid at about 800 nl/min in a one-step elution program. The spray nozzle of the ESI source (Vestec Corp) was a fused silica capillary (50 μm i.d. x 280 μm o.d.) which had the tip modified by HF treatment to form a cone about 75 μm o.d. in order to increase the sensitivity (for further technical details, see Emmett and Caprioli). The mass spectrometer (Finnigan TSQ70) was scanned from 200-1000 Da in 4 sec. All data were acquired in the profile mode.

Microbore-HPLC. In addition to nanoscale-LC/ESI/MS, the dialysate of two hours infusion of SP1-11 (1 μM) into the striatum were collected and analyzed and fractionated using microbore-HPLC. Fractions were lyophilized and then analyzed by direct infusion using ESI/MS.

RESULTS

A: IDENTIFICATION OF SP-FRAGMENTS PRODUCED IN VIVO

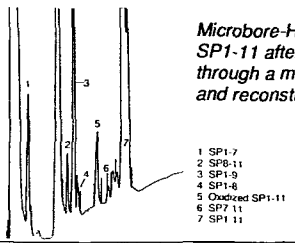

Microbore-HPLC of degradation products (SP fragments), derived from SP1-11 after a two hours infusion of 1 uM SP1-11 into the striatum through a microdialysis probe. Fractions were collected and lyophilized and reconstituted in 4 uL H_2O and analyzed by ESI/MS.

Electrospray mass spectra of SP fragments produced in vivo.

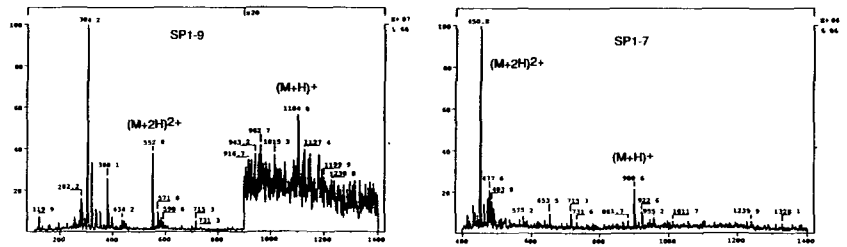

B. FORMATION OF OXIDIZED SP1-11 IN VIVO

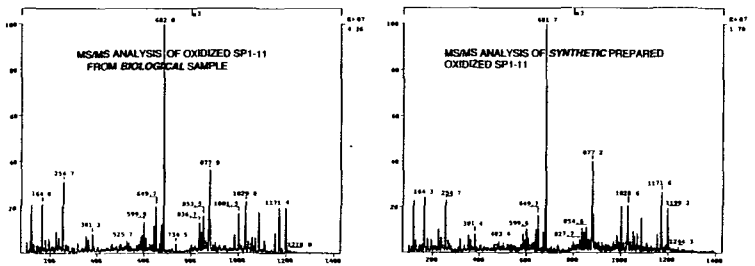

CONCLUSIONS

1. The coupling of high performance fused-silica LC nano-columns with micro-ESI/MS in this study takes advantage of the similar liquid flow requirements of each system, to provide a sensitive and highly specific analytical system.
2. The present data show that *in vivo* microdialysis can be used to study protease activity, and that several SP fragments were identified after exogenous infusion of SP at low *concentrations*.
3. Both N- and C-terminal fragments with partly overlapping sequences were found in the present study, showing the complexity of SP-degradation. The SP-metabolites formed were N-terminal fragments SP1-9, SP1-8, SP1-7 and C-terminal fragments SP5-11, SP6-11, SP7-11, SP8-11 and oxidized SP (SP-O). When deuterated SP, [D_8-phe^8]SP, was infused into the striatum, the corresponding metabolites were formed.
4. The combination of microdialysis and LC/ESI/MS can be used to provide direct monitoring of aqueous biological samples, including *in vivo* intracerebral analysis. Our future plans to further characterize the proteases involved in SP-degradation include the use of several specific enzyme inhibitors.

ACKNOWLEDGMENT

This study was supported by the Swedish MRC Grant #9113, and, in part by NIH Grant #GM 43783.

MONITORING IN-VITRO ENZYMATIC REACTIONS USING AN INTEGRATED MICRODIALYSIS/IONSPRAY TANDEM MASS SPECTROMETRY SYSTEM

Edward H. Kerns, Steven E. Klohr, Kevin J. Volk, and Mike S. Lee
Bristol-Myers Squibb Pharmaceutical Research Institute
Wallingford, Connecticut 06492

Microdialysis is an effective sampling method for obtaining nanogram quantities of analyte from biological systems with a minimum of disruption of the system (1-5). Applications of microdialysis include the intra-cerebral sampling of neurotransmitters, the on-line analysis of drugs in the blood of living systems and the sampling of reaction mixtures. Previous reports have discussed fundamental studies of on-line systems combining microdialysis sampling with mass spectrometers via a continuous flow FAB ion source (3-5), a thermospray ion source (6) and an ionspray ion source (7). Methods of coupling microdialysis sampling probes with ionspray tandem mass spectrometers and applications of this system for monitoring dynamic *in-vitro* biochemical systems have been further investigated using model compounds (buspirone, angiotensin I, and biotin methyl ester). This approach utilizes the mass spectrometer to provide structural and quantitative information for dynamic *in-vitro* biochemical systems in real time.

Microdialysis was performed using model CMA/12 microdialysis probes (20 kD cutoff) and a CMA/100 syringe pump (Bioanalytical Systems). A Sciex API III triple quadrupole mass spectrometer was used with an ionspray interface operated in the positive ion mode. Dialysis fluid was acetic acid (0.05%) for peptide cleavage and buspirone metabolism studies, and 2 mM ammonium acetate (pH 6 9) for avidin binding studies Peptidase reactions were carried out with Carboxypeptidase Y and Angiotensin I (40 ng/µL) with a final volume of 200 µL. Liver metabolism studies utilized approximately 0.1 g of minced rat liver (Hilltop) incubated with 5 µg of buspirone in a 300 µL volume of 2 mM ammonium acetate for approximately 6 hr prior to direct analysis by microdialysis Protein binding studies utilized Avidin, biotin methyl ester (BME), and biocytin (BC). Reactions were caried out at 37 C in a 0.5 mL conical Reactivial (modified to 200 µL) equipped with a stirring bar. Constant stirring provides sample mixing and eliminates dialysis gradient formation in the solution. The vial was placed in a block heater/stirrer for temperature control and mixing The microdialysis probe was coupled directly to the ionspray interface vial a zero dead volume coupling.

Results using these model systems were as follows: Rapid Carboxypeptidase Y cleavage of angiotensin I was monitored using microdialysis/MS. The reaction proceeded rapidly up to residue 4 (proline). The appearance and degradation of each peptide was independently observed, indicating the use of this system for monitoring biochemical reaction products and kinetics. Metabolites of buspirone with a mass 16 Daltons greater than buspirone were observed after incubation of buspirone with liver preparation. One metabolite was determined to be hydroxylated on the pyrimidine ring and the other was determined to be hydroxylated on the azaspirone ring using MS/MS substructural analysis on line with microdialysis sampling. These metabolic products are consistent with previously characterized metabolites of buspirone, indicating the use of this system for monitoring *in-vitro* tissue activity. The binding of biotin methyl ester to avidin was very rapid, as indicated by an immediate quantitative decrease in free BME ligand concentration in the supernatant monitored by microdialysis. The bound avidin-BME complex was excluded from the dialysate by the dialysis membrane, thus providing a differentiation between free and bound components. Competitive binding studies, in which biocytin was added to avidin-BME complex indicated that BME was not competitively released by BC at concentrations twice the BME concentration. Thus, protein-ligand binding may be monitored using microdialysis on-line with mass spectrometry.

The microdialysis membrane permits higher molecular weight components to be excluded from the sample going to the mass spectrometer Thus, only free reactants, products and ligands are monitored and the concentration of protein in the dynamic reacting system is undisturbed. Using this approach biochemical reactions can be monitored and structural information can be obtained in real time without the need for sample storage, time consuming HPLC separations and sample degradation. Thus, the combined MD/MS/MS system may be used for studying in-vitro tissue reactions, enzymatic reactions and protein binding.

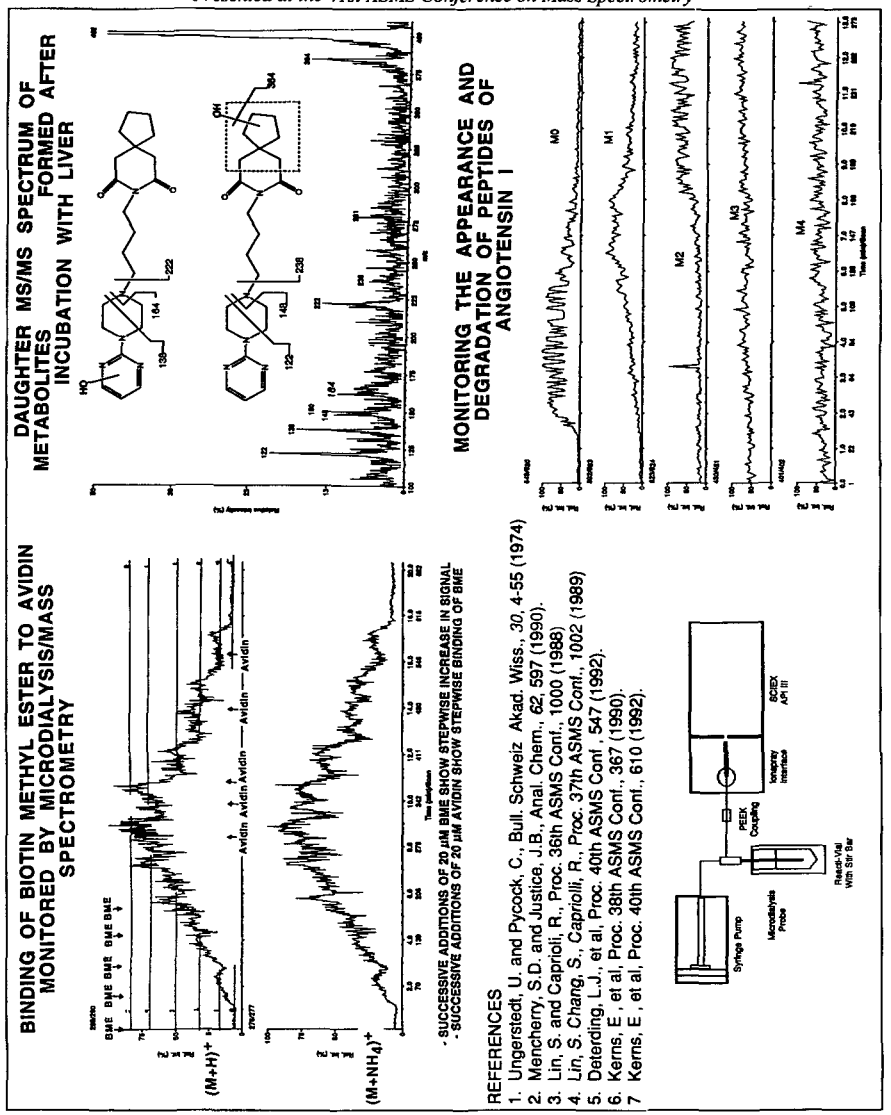

REFERENCES
1. Ungerstedt, U. and Pycock, C., Bull. Schweiz Akad. Wiss., *30*, 4-55 (1974)
2. Mencherry, S.D. and Justice, J.B., Anal. Chem., *62*, 597 (1990).
3. Lin, S. and Caprioli, R., Proc. 36th ASMS Conf., 1000 (1988)
4. Lin, S. Chang, S., Caprioli, R., Proc. 37th ASMS Conf., 1002 (1989)
5. Deterding, L.J., et al, Proc. 40th ASMS Conf., 547 (1992).
6. Kerns, E., et al, Proc. 38th ASMS Conf., 367 (1990).
7. Kerns, E., et al, Proc. 40th ASMS Conf., 610 (1992).

Metabolism of Hexamethylene Diisocyanate (HDI) in the Rat Utilizing Ionspray LC-MS/MS Techniques.

*K.M. Brandt, M.R. Davis and T.A. Baillie

Department of Medicinal Chemistry, School of Pharmacy,
University of Washington, Seattle, WA 98195

1,6-Hexamethylene diisocyanate (HDI) is used as an electrophilic crosslinking agent in the plastics industry. Normally, glutathione (GSH) captures electrophilic xenobiotics to form *S*-linked conjugates which are excreted into bile. However, it has been shown recently with methyl isocyanate (MIC) that conjugation with GSH is reversible under physiological conditions and it has been proposed, therefore, that GSH may serve as a "carrier" of this toxic isocyanate *in vivo*. The focus of the present study was to determine if conjugation with GSH is involved in the metabolism of HDI in the rat.

Ionspray LC-MS/MS techniques were developed using a Perkin-Elmer Sciex API III triple quadrupole mass spectrometer to detect and quantify both the GSH conjugates and the subsequently formed *N*-acetylcysteine (NAC) conjugates of HDI in bile and urine, respectively, of rats dosed with HDI. GSH conjugates were analyzed by constant neutral loss scanning (loss of 129 Da, derived from cleavage of the γ-glutamyl moiety) while NAC conjugates were analyzed by parent ion scanning of *m/z* 143 (protonated 6-aminohexylisocyanate).

Experimental:

Bile from rats given an i.p. dose of HDI (60 μmol) was collected over ascorbic acid for 4 h after dosing and was filtered before analysis. Urine from rats dosed with HDI (60 μmol for the qualitative study and 20 μmol for the quantitative study) was collected over ascorbic acid for 4 h and 24 h after dosing for the qualitative and quantitative experiments, respectively. Urine samples were filtered prior to analysis. Biological samples were analyzed by ionspray LC-MS/MS with Ar as the collision gas.

Results and Discussion:

Figure 1 shows the reconstructed LC-MS/MS chromatograms of the synthetic NAC-HDI conjugates, while Figure 2 shows the reconstructed LC-MS/MS chromatograms obtained from urine of HDI-dosed rats. The quantitative analysis revealed the presence of the NAC conjugates of HDI in urine (1.3 ± 0.9% of dose), but not of the corresponding GSH conjugates in bile. Control experiments indicated that the GSH-HDI adducts are unstable in bile, and decompose to the corresponding diamine, 1,6-hexamethylenediamine. Although the results of this study suggest that conjugation with GSH is not a quantitatively important metabolic pathway of HDI in the rat, this study nevertheless demonstrates the operation of such a process *in vivo*, and raises the possibility that reactive, carbamoylating GSH conjugates of HDI may mediate the toxic effects of this important industrial chemical.

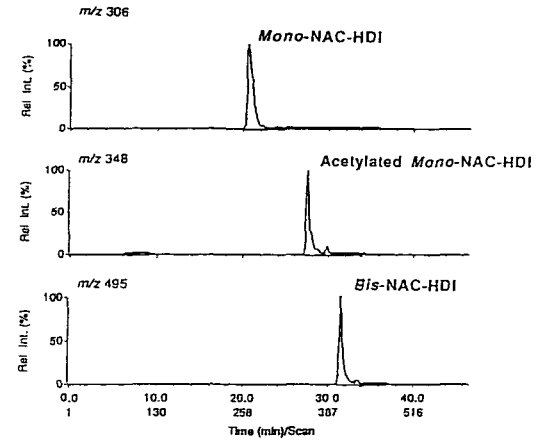

Figure 1. Reconstructed LC-MS/MS Chromatograms of the Synthetic *Mono-*, *Bis-*, and Acetylated *Mono*-NAC Conjugates of HDI. Parent Ion Scanning of *m/z* 143.

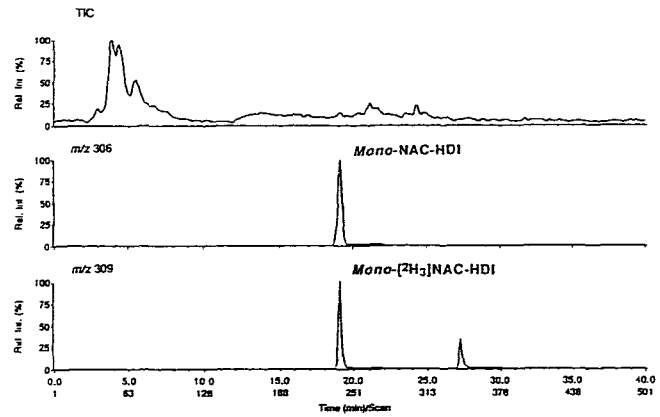

Figure 2. Reconstructed LC-MS/MS Chromatograms of Urine of Rats Dosed with HDI. Parent Ion Scanning of *m/z* 143.

Acknowledgement:

This research was supported by grants from the National Institutes of Health, (ES05500 and RR05543), which are gratefully acknowledged.

Identification and Quantitation of Metabolites of a Novel Nonbenzodiazepine Anxiolytic Compound (CL 273,547) by Thermospray LC/MS in Tandem with ^{14}C Detection and an Off-Line Stable Isotope Recognition Computer Program.

Elizabeth Graham*, D. Cosulich, W. DeMaio, J. Ashraf, G. Morton, I. Zagloul;
American Cyanamid, Metabolism Reseach and Radioisotope Synthesis Dept.
Medical Research Division, Pearl River , NY 10965

Anxiolytic, CL 273,547, a nonsedative, nonbenzodiazepine, is being developed as an anxiolytic agent. This work was performed to elucidate the structures of CL 273,547 metabolites (Figure 1), and to compare human and dog *in vivo* metabolism. CL 273,547 metabolites were isolated from the urine of dogs dosed orally 50 mg/kg (specific activity 0.31 µCi/mg). These metabolites were compared to urine metabolites from humans dosed orally 90 mg (45 mg tetradeuterated CL 273,547 and 45 mg CL 273,547, specific activity of 0.182 µCi/mg).

Experimental

Sample Preparation: Urine samples were lyophilized and extracted into methanol. The methanol was evaporated and the extracts were redissolved into HPLC mobile phase before injection to the HPLC system.

Instrumental: Thermospray (TSP)/MS analysis was performed on a Finnigan MAT TSQ-70 mass spectrometer with a Vestec Model 704A TSP interface. The HPLC system consisted of two LKB 2152 pumps with a gradient controller. UV detection was performed using a Spectroflow 783 Kratos at 230 nm with a 100 µL high pressure cell. ^{14}C detection was performed using a Raytest Ramona LS-4 system with a 100 µL lithium glass scintillator flow cell.

A Waters Model 510 HPLC solvent pump was used for post column addition of mobile phase.

Apparatus:

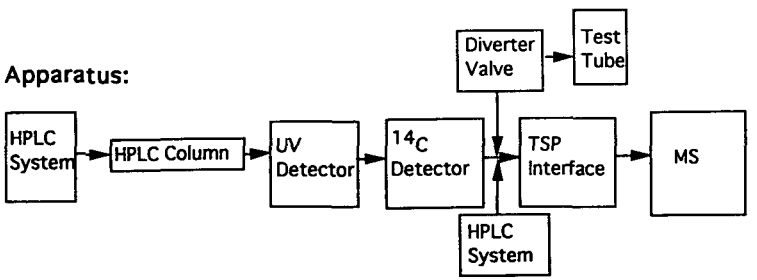

The dog produced M1, M2, M2', M4 and M8. The human produced all of the metabolites shown in Figure 1. In addition, there was significant intrasubject differences both in the metabolite and amount they produced. A typical HPLC ^{14}C profile in man is shown in Figure 2a. The corresponding TSP/MS chromatogram is shown in Figure 2b.

Confirmation of drug related metabolites in humans was achieved by recognition of the D_0-D_4 pattern of the drug, dosed 50% D_4-CL 273,547 and 50% D_0-CL 273,547. A stable isotope recognition program in "C" was written for the Apple Computer to identify this pattern.

Figure 1: Proposed Biotransformation Pathway of CL 273,547 in Man

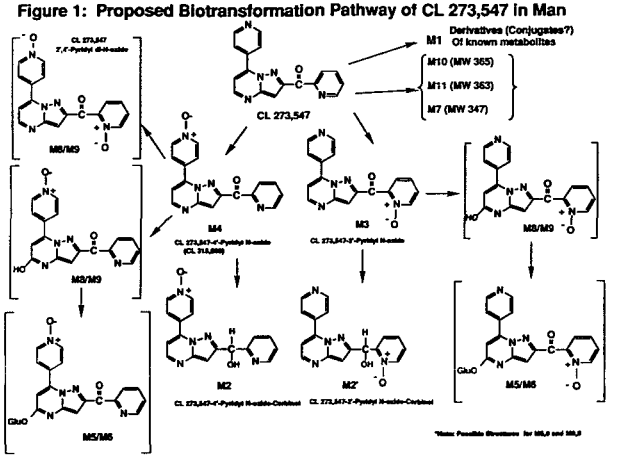

Figure 3a: Anxiolytic Metabolic Profile from Extracted Urine of Subject 6 Following a Single Oral Dose with 90 mg ^{14}C-CL 273,547 HPLC Radiochromatogram

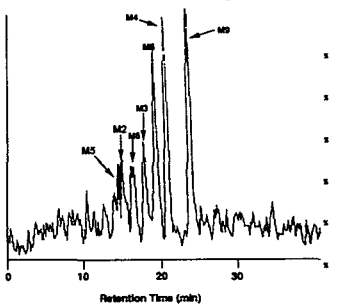

Figure 3b: Metabolite Profiles from Extracted Human Urine from Subject 6 Following a Single Oral 90 mg Dose of Cl 273,547 (50%D_0/50%D_4) HPLC Mass Chromatograms

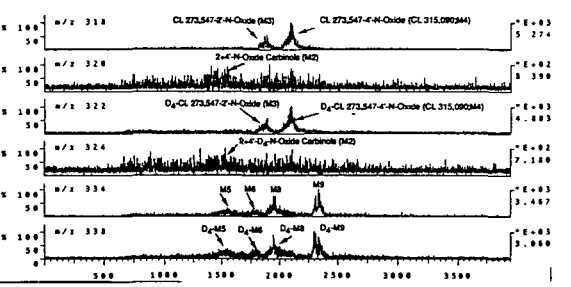

Determination of Reserpine in Plasma by Ion Spray LC/MS/MS, Timothy Wachs and Jack D. Henion, NYS College of Veterinary Medicine, Cornell University, 925 Warren Drive, Ithaca, NY 14850.

Determination of basic drugs such as reserpine and LSD present many analytical challenges by conventional GC/MS techniques. However, the basicity of these drugs makes them ideal candidates for ionization techniques such as ion spray that do not require volatility. Additionally, HPLC, the method of choice for separation of basic drugs, is an ideal way to introduce the analyte into an ion spray or electrospray interface.

Reserpine, which is used as an antihypertensive agent in humans and as a tranquilizer in the horse is administered at dose levels of 1-3 µg/kg of body weight. In order to monitor plasma levels in clinical studies or for forensic determination, detection limits in the low picogram/mL of plasma are required. For clinical analyses where a large number of samples need to be analyzed, rapid methods for sample preparation and analysis are also desirable.

Sample extraction, liquid chromatography, and the mass spectrometer interface and mass spectrometry were investigated separately and together in order to optimize sensitivity and the speed of the analysis. For quantitation, MS/MS selected reaction monitoring was chosen, which also adds a final "clean-up" step in the general separation scheme. Since reserpine (see figure) is a basic drug with low volatility, atmospheric pressure ionization (via ion spray) is a method of choice. Internal standards, which are necessary for quantitative analysis, were compared for suitability. Labeled reserpine was not readily available thus two analogous compounds were chosen, triethoxyreserpine and rescinnamine (see figure).

Ideally, the internal standard should co-elute for API applications since interactions and ion suppression may occur with other co-eluting impurities in the sample. The mass spectral behavior of the internal standard and the analyte should also be similar. Of the two potential internal standards, rescinnamine does co-elute under the HPLC conditions used and was chosen as the internal standard in spite of dissimilar fragmentation behavior. Under the optimal reserpine MS/MS conditions used in this study, rescinnamine fragments to a much greater degree, requiring careful control of MS/MS conditions.

Use of 2 mm id LC columns vs 4.6 mm is advantageous because of the increase in sensitivity of ion spray while still maintaining reasonable (10-20µL) injection volumes. The full 200 µL/min HPLC flow rate was directed to the ion spray interface on a Sciex API instrument. This is possible since the eluent has a high organic content (80% acetonitrile) and the sprayer was carefully positioned with respect to the heated interface plate such that any condensation did not interfere with ion sampling. A 30-40% loss in sensitivity is the price paid for the elimination of a post-column split and its inherent shortcomings.

The goal of very rapid analysis times can be met by combining good sample extraction and clean up with fast liquid chromatography and MS/MS as the final separation step. Isocratic conditions are a must if rapid analysis time is to be achieved without resorting to precise timing of injection sequences. A Keystone Scientific Inertsil ODS2 100 x 2 mm column with 80:20 acetonitrile:water, 5 mM ammonium acetate, provides a retention time of approximately three minutes for reserpine with good separation of residual components from serum extractions. The resultant analyses can be done in five minutes or less.

Two different extraction schemes were investigated in order to provide "clean" extracts. A three step liquid/liquid extraction (1) provides clean extracts and good (~50%) recovery at the low picogram levels. However, the method is tedious and very time consuming but could probably be automated. The recent introduction of several solid phase extraction systems based on a thin disk of fiber glass or Teflon and adsorbent provides promise for the rapid and easy separation of drugs like reserpine from plasma. In order to

develop a method using this technology, a Hewlett-Packard 5985B mass spectrometer equipped with an API heated capillary interface was used to monitor the extraction of rescinnamine from equine and human plasma. Spiked plasma that was diluted 1:1 with n-saline and carbonate buffer was extracted with ToxiLab Spec C8 cartridges. A 20% acetonitrile wash was used for clean up Recovery of the analyte was done with 300µL of methanol. Recovery levels were one half or less than that for the liquid/liquid system but ease of use and the short work-up time of this method warrants further development of the method.

Using liquid/liquid extraction, the limit of determination of reserpine in human plasma was at the 25 pg/mL level with a linear response up to at least 500 pg/mL. Human administrations are usually at the 100 to 500 µg dose level, with plasma levels rarely exceeding the 500pg/mL level. The level of reserpine in human plasma from a 100 µg administration study could be quantified out to 36 hours after administration.

(1) Suckow, R.F.; Cooper, T.B.; Asnis, G.M. *J. Liq. Chromatogr.* **1983**, *6*, 1111-1122.

Structures of Reserpine and Internal Standards Triethoxyreserpine and Rescinnamine

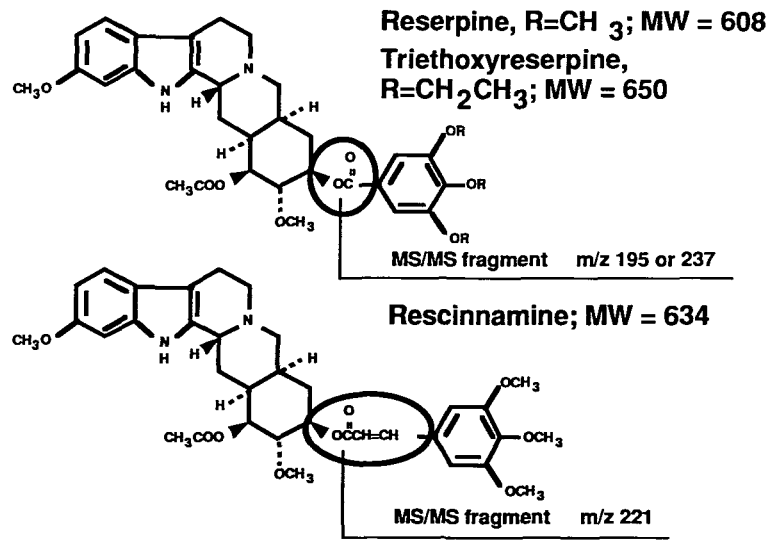

Determination of Vitamin B_{12} by Ionspray Liquid Chromatography Mass Spectrometry

Isamu Matsumoto, Yoshihisa Umeda*, Yasuko Ogawa*, Ikunoshin Kato* and Tomiko Kuhara.

Division of Human Genetics, Medical Research Institute, Kanazawa Medical University, Uchinada, Ishikawa, Japan and *Biotechnology Research Laboratories, Takara Shuzo Co., Ltd., Kusatsu, Japan

Introduction

The vitamin B_{12} dependent reactions can be classified in two groups, on the basis of the cofactor used: methylcobalamin; CH_3Cbl or deoxyadenosylcobalamin; AdoCbl. Only three reactions have so far been discovered in mammals. These reactions are catalysed by methionine synthetase (EC2.1.1.13. CH_3Cbl cofactor), methylmalonyl CoA mutase (EC5.4.99.2. AdoCbl cofactor) and leucine mutase (AdoCbl cofactor). Thus the reduced biosynthetic activity of either CH_3Cbl in the cytosol or AdoCbl in the mitochondoria results in a metabolic disorder of homocystinuria or methylmalonic acidemia. The frequency of the latter diseases is relatively high in all over the world. About half of them are the deficiency of apoenzyme, thus are not responsive to vitamin B_{12} therapy. However, the remaining half are due to the reduced activity of an enzyme of AdoCbl synthesis.

We have attempted to determine CH_3Cbl, AdoCbl and cyanocobalamin in order to understand the above mentioned 2 metabolic disorders more precisely. The principal difficulty of the determination of vitamin B_{12} is that the serum concentration is only in minute (10^{-10}g/ml) amounts and is labile to the heat and light. Thus we have applied ionspray mass spectrometry (ISMS) for the analysis of vitamin B_{12}.

Experimentals

Authentic cyanocobalamin was dissolved in purified water to the final concentrations of 50, 100, 250, 500, and 1000 pg/µl. A 20 µl portion of the solution was applied to the column (Develosil ODS-5, 1.5 x 150 mm, Nomura Chemical Co., Ltd., Nagoya, Japan), and eluted by a linear gradient at a flow rate of 80 µl starting with 100% H_2O followed by increase in the acetonitrile concentration to 40% in 5 minutes; the concentration of TFA was kept at 0.1% (v/v). The Perkin-Elmer Sciex API III triple quadrupole mass spectrometer was used for the quantitation.

We have also determined cyanocobalamin by ^{252}Cf-plasma desorption mass spectrometry, using Biolon TM_{20} Mass Analyzer.

Results and Discussion

In ionspray mass spectrum of cyanocobalamin, singly charged molecular ion was observed at m/z 1356 and doubly charged ion at m/z 679 (Fig. 1). The plot of peak areas of the selected ion monitoring chromatogram (SIM) versus amount of cyanocobalamin in the five injected solutions showed good linearity over the range from 50 pg/µl to 1 ng/µl.

Our LC/SIM method was confirmed to be useful to determine cyanocobalamin in serum by a recovery test; a serum containing 0.4 ng/µl of cyanocobalamin was pretreated with microfilter, and subjected to LC/MS assy resulting in the concentration of 0.34 ng/µl (85% recovery). ^{252}Cf-plasma desorption MS gives almost the same sensitivity as LC/MS assay (Fig. 2). However, the above results obtained with ionspray LC/MS and ^{252}Cf-plasma desorption MS are not satisfactory for the quantitaion of blood level of vitamin B_{12}. Further studies are undertaken.

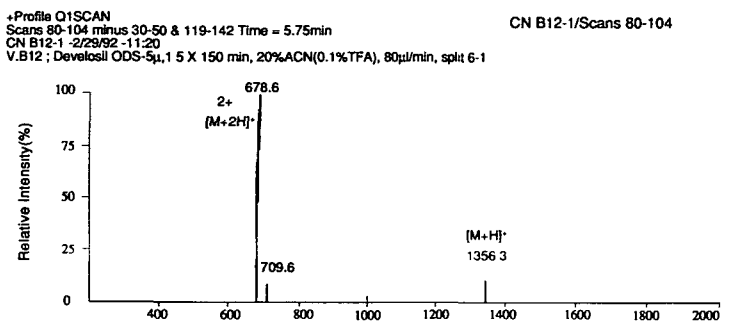

Fig.1 Ionspray Mass Spectrum of Vitamin B_{12}

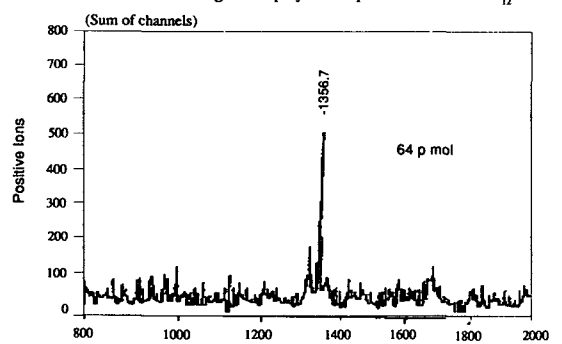

Fig.2 ^{252}Cf-plasma desorption Mass Spectrum of Vitamin B_{12}

NANOLITER FLOW-LC/ES/MS FOR ANALYSIS OF ENDOGENOUS NEUROPEPTIDES

Mark R. Emmett* and Richard M. Caprioli
The Analytical Chemistry Center and the
Department of Biochemistry and Molecular Biology
University of Texas Medical School, Houston, Texas 77225

INTRODUCTION

Electrospray ionization mass spectrometry (ES/MS) has the capabililty to accurately determine mass over a large range. As with other soft-ionization techniques, ES is sensitive to high salt concentrations which severely inhibits sensitivity. By coupling LC to an ES interface, the problem of salt interference can be greatly reduced. High salt concentrations are present in all biological fluids and this along with very dilute analyte concentrations (atto and femtomolar concentrations for many neuroactive substances) have limited the application of MS techniques to the biological sciences. The specificity of MS technology is needed in these areas due to the incontinance of antibodies that are used in radioimmunoassay and radioreceptorassay (1).

In vivo microdialysis is a technique that allows sampling of extracellular fluids from a living animal. Microdialysis eliminates the need to extract substances from post mortem tissue and can be used to monitor the accumulation/release of neuroactive substances in specific brain regions over time in one animal, thus eliminating the sacrifice of several animals to provide a single pharmacological time course. Microdialysis does have the limitation in that samples gathered are very dilute and in high salt biological fluids.

In this report, we discuss the modification of a Vestec ES source to deliver a "microspray" at nanoliter flow rates. These modifications increased the sensitivity by 100 fold along with increased signal stability. By coupling this modified source with nanoflow-LC chromatography (2, 3), we have developed a system that is capable of detecting endogenous release of neuropeptides in the brain collected by in vivo microdialysis.

MATERIALS AND METHODS

ES/MS: ES spectra were generated using a modified Vestec Electrospray Ion Source (4) with a 5 kV dynode.

Microspray: In order to detect the endogenous release of neuropeptides via microdialysis, the sensitivity and stability of the ES/MS had to be greatly increased along with a decrease in the solvent flow rate. These three parameters were achieved with the introduction of the "microspray" needle.

To reduce the flow in our system, a smaller i.d. needle was constructed. Van Berkel (5) described a system in which the HV connection was made through the liquid flow and the sample sprayed from a 100 micron fused silica capillary. We varied the i.d. of the capillary and constructed a cone shape tip for the spray "needle". Microspray "needles" were constructed from fused silica capillary with i.d. ranging from 5 to 250 microns. The polyamide was burned away (approximately 0.5 cm) with a microtorch and the exposed silica tip lowered into a 49% solution of hydrofluoric acid (HF) while distilled H_2O was pumped through the capillary at 500 nl/min. The progress of the etching was monitored with a microscope every 10 min. If the tip was rough after digestion, either digestion was repeated or the tip was carefully ground to a flat end under a stereomicroscope. The breech of the "needle" was attached to a stainless-steel zero dead volume fitting with a 0.02" thru-hole, the high voltage connection was here. Needle voltage varied from 2.0-3.5 kV. Nozzle voltages averaged 200 to 280 V. The repeller voltage was set to 10.

N_2 Carrier Gas: The standard Vestec ES system uses no counterflowing gas, but does allows the entry of ambient air. When maximum sensitivity was needed, the background from ambient air

would sometimes mask the signal of interest. The problem was eliminated by using ultra-pure, dry N_2 at approximately 1 ATM.

Nanoliter Flow Liquid Chromatography: Columns were packed using procedures as described by Mosely et. al. and Kennedy, R.T and Jorgenson, J.W. (2, 3) with modification. Mobile phase varied from 5-50% MEOH with 0.25% HOAC.**Microdialysis:** CMA/10 microdialysis probes (BAS inc.) were used in the in vivo experiments. Probes were stereotaxically implanted into the striatum of male Sprague/Dawley rats under pentobarbital anesthesia. In all experiments, Ringers solution (artificial CSF, 5 mM KCl, 120 mM NaCl, 1.2 mM $MgCl_2$, 1.8 mM $CaCl_2$, 0.15% phosphate buffered saline, pH 7.4) was perfused thru the probe at a rate of 436 nL/min.

RESULTS

Figs. 1 and 2 illustrate the sensitivity of nanoscale LC/Micro-ES/MS, ME at 50 and 10 fm total. Fig. 3 shows the endogenously released ME from rat striatum.

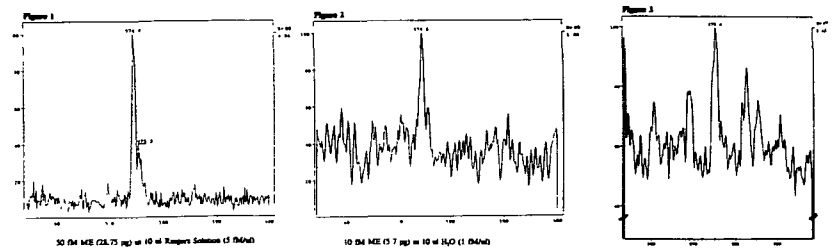

CONCLUSIONS

The development of a Microelectrospray source has provided greatly increased stability and sensitivity for low flow rate applications. This LC/ES/MS interface is now capable of detecting endogenously released neurocompounds from biological microdialysates in physiological salt solutions.

In Summary:

I. The combination of a narrow spray, the close proximity of the "needle" and nozzle and nanoliter flow rates are major contributing factors yielding the enhanced performance shown here.

II. Addition of dry, ultrapure N_2 increases our signal to noise up to 5 fold.

III. The combination microelectrospray with nanoscale LC allows analysis of samples down to 10 fM ME (5.7 pg of ME) in a total volume of 10 ul of biological salt solution obtained from a 50 AMU mass scan.

REFERENCES

1) Dass, C., Kusmierz, J.J., Desiderio, D.M., Jarvis, S.A., and Green, B.N., *J. Am.Soc. Mass Spectrom.* **1991**, 2, 149-156.
2) Kennedy, R.T. and Jorgenson, J.W. *Anal. Chem.* **1989, 61, 1128-1135.**
3) Mosely, M.A., Deterding, L.J., Tomer, K.B. and Jorgenson, J.W. *Anal. Chem.* **1991**, 63, 1467-1473.
4) Allen, M.H. and Hutchens, T.W. *Rapid Commun. Mass Spectrom.* **1992**, 6, 308-312.
5) Van Berkel, G.J., McLuckey, S.A., and Glish, G.L. *Anal. Chem.* **1992**, 1586-1593.

Characterization of Brimonidine Metabolites by HPLC/Thermospray Mass Spectrometry. *Andrew Acheampong, Hai Nguyen, Dale Harcourt, Diane Tang-Liu and Michael Garst. Allergan, Inc. Irvine, CA 92713-9534.

Brimonidine [also known as AGN 190342 and UK-14,304-18) is a potent ocular hypotensive currently being evaluated for the treatment of glaucoma. It is a more selective α2-adrenergic agonist than clonidine which also contains the 2-amino-imidazoline moiety. Following intravenous or oral administration of ^{14}C-brimonidine tartrate to animals and humans, the degree of brimonidine metabolism was investigated by generating plasma and urinary metabolite profiles. Using reverse phase ion-pair HPLC, the in vivo metabolite profiles revealed 9 metabolites (I, IIa, IIb, IIIa, IIIb, IV, V, VI, VII). In this report, we describe the application of HPLC/thermospray (TSP) mass spectrometry to identify metabolites produced in vitro by rat liver 10,000*g* preparations. The identification of metabolites was supported by comparison with synthesized compounds.

Brimonidine and ^{14}C-brimonidine were incubated in rat liver homogenate 10,000*g* fractions prepared using standard procedures. Following incubations and extraction, metabolites were partially separated by HPLC fractionation methods. LC/MS analyses were performed using a Vestec TSP interface with vaporizer at 160-170°C and source block at 260-300°C. A Beckman C18 column (25 cm x 4.6 mm id, 5 µm) was used in ion-pair LC and LC/MS analyses. The mobile phase was either MeOH/NH_4Ac (20:80 v/v) or MeOH/H2O//TEA/AcOH (14:86:0.075:0.1 v/v) pumped at a flow rate of 1ml/min. Reverse phase ion-pair HPLC was employed to compare retention times of metabolites and authentic standards. The ion-pairing reagent was heptanesulfonate.

Analysis of rat liver extracts by ion-pair HPLC with radioisotope detection (Figure 1) showed at least 7 metabolites (I, IIc, IIIa, IV, V, VI, VI and VII). Under positive ion TSP/MS conditions, brimonidine and metabolites produced debrominated-protonated ions, protonated molecular ions, or other diagnostic ions for structural identity of new metabolites of brimonidine (Table I). Like FAB/MS, TSP/MS also showed ions formed by debromination with addition of H. Metabolite VI is the known guanidine derivative formed probably by the N,N dealkylation pathway. Figures 2 and 3 show the TSP mass spectra of metabolites IIIa and MV, respectively. Metabolite IIIa was confirmed as the quinoxalin-2,3-dione derivative (Figure 4). Metabolites IV and V which exhibited characteristic ions at m/z 280, 282 $(MH-CO)^+$ were proposed to be either 2 or 3-quinoxalinone derivative. Preliminary studies suggest that IIIa, IV and V are formed with mammalian liver aldehyde oxidase. MVII was 4',5'-dehydrobrimonidine.

Table I. Thermospray Mass Spectral Data of Metabolites and Reference Compounds

Compound	Characteristic Ions (m/z)
Brimonidine	292, 294 $(MH)^+$; 214 $(MH - Br + H)^+$
Imidazolin-4'-one derivative	228 (MH-Br+H); 306,308 $(MH)^+$; 407,409 $(MH+TEA)^+$
Metabolite IIIa	245 $(MH - Br)^+$; 246 $(MH - Br + H)^+$
Quinoxalin-2,3-dione derivative	324, 326 $((MH)^+$; 245 $(MH-Br)^+$; 296, 298 $(MH-CO)^+$
Metabolite IV	280, 282 $(MH - CO)^+$; 202 $(MH - CO - Br + H)^+$
Metabolite V	308, 310 $(MH)^+$; 280, 282; $(MH - CO)^+$; 202
Metabolite VI	266, 268 $(MH)^+$
Guanidine derivative	266, 268 $(MH)^+$; 188 $(MH - Br + H)^+$
Metabolite VII	290,292 $(MH)^+$; 212 $(MH-Br+H)^+$; 391,393 (MH+TEA)
4',5'-dehydro brimonidine	290, 292 $(MH)^+$; 212 $(MH - Br + H)^+$

The results of this study indicate that LC/MS with TSP ionization was useful for the identification of brimonidine metabolites. The debromination fragmentation ions facilitated the identification of metabolites. Under the TSP conditions used, most of the protonated molecular ions underwent extensive fragmentation and were prominent only at high concentrations of metabolites or reference standards.

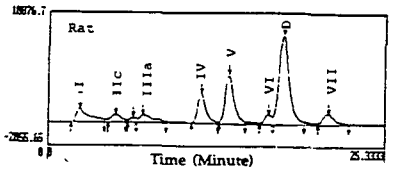

Figure 1. Ion-pair HPLC chromatogram of ^{14}C-metabolites from rat liver extract.

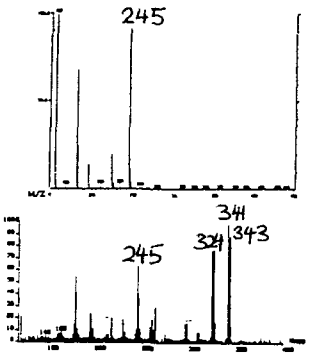

Figure 2. TSP spectrum of MIIIa

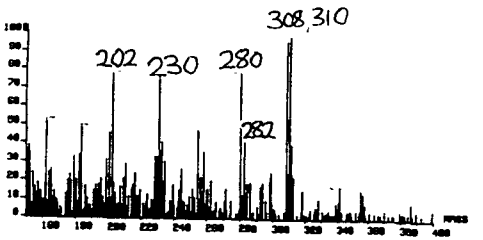

Figure 3. TSP spectrum of MV.

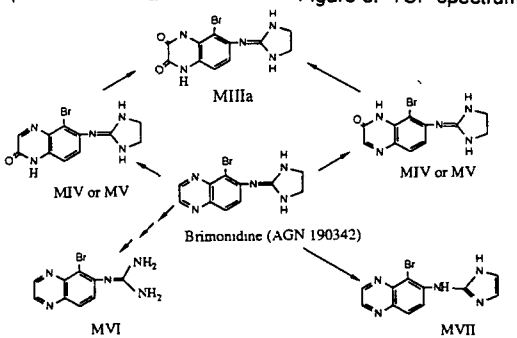

Figure 4. Proposed metabolic pathway of brimonidine

Simultaneous HPLC radioactivity and mass spectrometry monitoring. A drug metabolism application

Hassan G. Fouda, Michael Avery and Kimberly Navetta
Central Research Division, Pfizer INC, Groton, CT 06340

The usefulness of electrospray and atmospheric pressure chemical ionization mass spectrometry for drug metabolism studies is now widely appreciated. Electrospray is particularly indispensable due to its high ionization efficiency and its applicability to labile conjugates and polar metabolites. Indeed, the powerful combination of HPLC - electrospray and collision induced dissociation (CID) was shown in our laboratory to generate substantial information on the metabolism of xenobiotics in various *in vivo* and *in vitro* matrices. However, since the ionization efficiencies of unknown metabolites vary and since their CID daughter spectra are not always predictable, definitive quantitative metabolism information can only be obtained by radiolabeled studies.

We have put together an HPLC system incorporating electrospray ionization, CID mass spectrometry and radioactivity monitoring. Both the radioactivity and the mass spectrometry data are acquired in the same time domain by a single data system, hence facilitating matching the two types of information.

The utility of the system was demonstrated by application to investigatinG the metabolic pathways of tenidap, a new anti-inflammatory agent. The relative abundance and structural information of four metabolites were determined from direct HPLC injection of a crude bile sample from a monkey administered ^{14}C labeled tenidap.

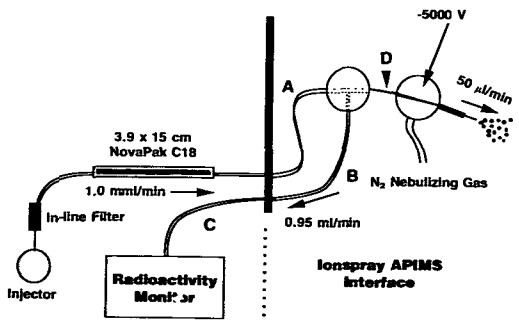

HPLC Radioactivity and Mass Spectrometry Total Ion Current Profiles of a Bile Sample from a Monkey Administered ^{14}C Labeled Tenidap

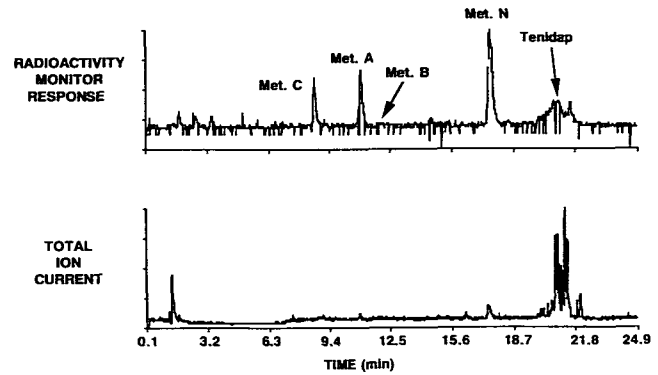

Metabolite N
CID Daughter Ion Spectrum of m/z 415

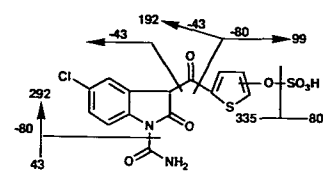

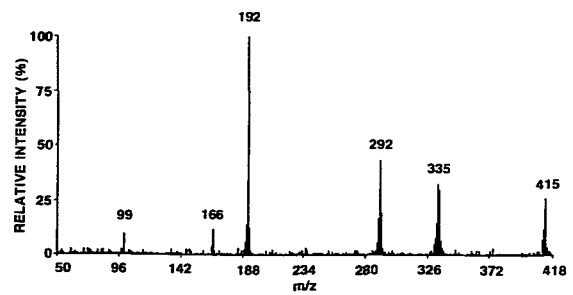

INVESTIGATION OF FACTORS INFLUENCING *IN VIVO* MICRODIALYSIS/MS/MS STUDIES

L.J. Deterding[1], K. Dix[2], L.T. Burka[2], and K.B. Tomer[1]

[1]Laboratory of Molecular Biophysics
[2]Experimental Toxicology Branch
National Institute of Environmental Health Sciences
Research Triangle Park, NC 27709

Microdialysis (MD) has become an important technique for the *in vivo* sampling of extracellular fluid in discrete compartments of living systems. This technique is being widely used in physiological, pharmacological, toxicological, and behavioral studies for the recovery of endogenous or exogenous substances. MD offers several advantages over conventional (CONV) sampling techniques-such as, minimal damage to sampling site, little alteration of fluid balance, ability to simultaneously introduce and collect substances, and ability to continuously sample over a desired length of time. We have recently shown that *in vivo* microdialysis coupled with tandem mass spectrometry (MD/MS/MS) is an effective technique for the real-time analysis of tris(2-chloroethyl) phosphate (TRCP), an organophosphate flame retardant and suspected carcinogen, in biological systems (1). Free TRCP concentration vs time profiles were generated following MD sampling in the blood via the jugular vein of anesthetized animals. CONV studies were also performed in awake animals which involved blood withdrawal followed by sample workup and chromatographic analysis. Free TRCP concentration vs time profiles were generated and compared to those obtained from the MD/MS/MS studies. The most noticeable difference observed was that the initial free TRCP concentrations in plasma in MD/MS/MS studies were much higher (by an order of magnitude) than those observed in the awake animals in the CONV studies. Beyond 10-min post-dosing, similar free TRCP concentrations were observed between MD/MS/MS studies and CONV studies. Several factors may contribute to the observed differences in initial free TRCP concentration, including effect of anesthesia, presence of the indwelling jugular cannula in CONV studies, blood sampling regimen in CONV studies, and the *in vitro* standard calibration curve in plasma for the MD/MS/MS studies.

The above mentioned factors and the possible contribution they may have on the observed differences in the initial TRCP concentrations between MD/MS/MS studies and CONV studies have been investigated. In the CONV studies, the animals were awake, heparinized and dosed via the indwelling jugular cannula whereas in the MD/MS/MS studies, the animals were anesthetized, not heparinized and dosed via the femoral vein. The presence of heparin, anesthesia, and/or the cannula may alter TRCP plasma protein binding, distribution and pharmacokinetics. In addition, the site of i.v. administration may be a contributing factor. CONV studies, therefore, were performed in anesthetized animals to determine what effect the anesthesia had on the initial TRCP concentration. The animals were dosed via the femoral vein and sacrificed 2-4 min post-dosing and blood was removed and analyzed for TRCP concentration. In addition, animals were anesthetized and dosed without the presence of the indwelling jugular cannula to determine if the cannula may alter the TRCP pharmacokinetics in any manner. In CONV studies, blood is removed from the animal at each timepoint, thereby, altering the fluid balance of the animal. Conversely, MD maintains fluid balance as there is not net loss or gain of blood volume. The effect of the withdrawal of blood samples in CONV studies was investigated by anesthetizing animals and implanting them with MD probes which were not connected on-line to the mass spectrometer. The results of these studies are shown in Table 1. These parameters seem to alter the observed initial TRCP concentrations, but

none of these factors are solely responsible for the observed difference in initial TRCP concentration in plasma from animals studied by CONV methods vs the MD/MS/MS method.

Another factor investigated is the validity of the *in vitro* calibration of the microdialysis probes for use in studies *in vivo*. The effects of both biological fluid and temperature were investigated to determine if these parameters effected the *in vitro* calibration of the microdialysis probes. Blood, plasma, and water were used at both 24 °C and 37 °C. The relative recovery of free TRCP concentration varied with the biological fluid used and increased as temperature increased (Figure 1). It, therefore, appears that the method of *in vitro* calibration of the microdialysis probes has a major effect on the MD/MS/MS studies. The reason for this is possibly due to the fact that it is difficult to measure and/or mimic such a dynamic system as the living animal.

Reference:

(1) Deterding, L.J.; Dix, K.; Burka, L.T.; Tomer, K.B. *Anal. Chem.* 64 **1992**, 2636.

Table 1. Observed Initial Free TRCP Concentration in Plasma

Group of Animals	Time Post-Dosing (min)	Free TRCP Conc (mg/L)
MD/MS/MS Studies		
Rat 1	2.17	76.8
Rat 2	3.17	65.9
Rat 3	3.17	95.2
CONV Awake		
Rat 1	2.0	20.3
Rat 2	2.0	18.3
Rat 3	2.0	15.5
Rat 4	2.0	13.4
CONV Anesthetized		
Rat 1	2.1	14.3
Rat 2	2.2	12.7
Rat 3	2.1	13.7
CONV No Cannula		
Rat 1	3.6	10.1
Rat 2	2.7	8.4
Rat 3	2.6	8.6
CONV With MD Probe		
Rat 1	3.2	10.1
Rat 2	2 6	10 5
Rat 3	3.5	11.7

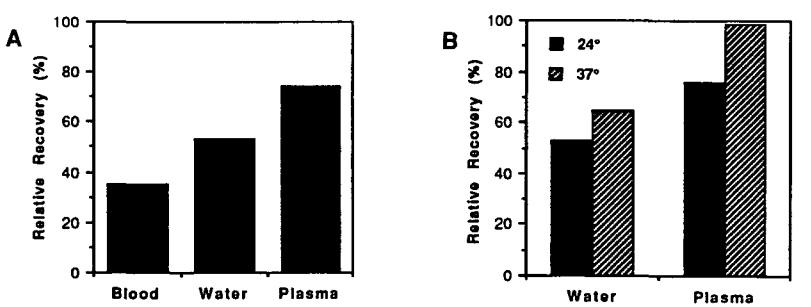

Figure 1. Effect of (A) biological fluid and (B) temperature on the relative recovery of free TRCP *in vitro*.

Determination of Quaternary Isoquinoline Alkaloids by Ion Spray Ion Trap Mass Spectrometer (IS/ITMS).

H. K. Lim[1,3], W-N. Wu [2], A. Mordehai[3] and J.D. Henion[3], [1]Wyeth-Ayerst Research, CN 8000, Princeton, NJ 08543, [2]The R.W. Johnson Pharmaceutical Research Institute, Spring House, PA 19477, and [3]Drug Testing and Toxicology, Cornell University, Ithaca, NY 14850.

Natural products are an important source of novel therapeutic agents in a drug discovery program. For example, the isoquinoline alkaloids isolated from *Berberidaceae*, *Menispermaceae*, *Papaveraceae*, *Rutaceae*, and *Ranunculaceae* families have hypotensive, analgesic, antimicrobial, muscle relaxant and antitumor activities. Previously, structural elucidation of a total of 8 quaternary isoquinoline alkaloids in the bark (280 g) from *Phellodendron wilsonii* involved exhaustive extraction with hot ethanol, liquid-liquid partitioning, column chromatography and finally repeated crystallization prior to mass spectrometric characterization (1). Furthermore, all these quaternary isoquinoline alkaloids have been analyzed by FAB/MS which is an insensitive technique for characterizing these compounds as indicated by typical sample requirements of ≥10 µg (2).

The aim of this study is to investigate the suitability of IS/ITMS for the determination of these quaternary isoquinoline alkaloids. Good quality mass spectra were successfully acquired for 12 protoberberines, 4 aporphines, 2 protopines and 2 bisbenzylisoquinolines isolated from *Rutaceae* and *Ranunculaceae* families by flow injection analysis of 5 ng of each compound in 50% acetonitrile/5 mM NH_4COOH pH 3.5 at a flow of 50 µL/min. Low "up-front" CID (30 V) mass spectra show predominantly molecular (quaternary), doubly charged molecular (bisquaternary) and protonated molecule (tertiary) ions. Increasing the "up-front" CID voltage to 68V resulted in mass spectra with structurally informative fragment ions in addition to molecular weight. The results show that IS/ITMS is a thousand fold more sensitive than FAB/MS for detecting these compounds. Further appreciation of the potential sensitivity of the IS/ITMS is from Figure 1 which shows the limit of detection for berberine corresponding to on-column injection of 6.25 pg under full-scan mode (m/z 150-400) and gave a reasonably good quality background-subtracted mass spectrum (Figure 2).

On-line LC-IS/ITMS was developed for separation and confirmation of a total of 7 and 5 isoquinoline alkaloids in methanolic extracts from bark (*Phellodendron wilsonii* , 5g) and an herbal medicinal tablet (0.3g), respectively. Conclusive identification of each compound was by a combination of co-injection with authentic standard and/or comparison of retention time and mass spectra generated under low and high "up-front" CID conditions. Figure 3 shows the total ion chromatogram from LC-IS/ITMS analysis of a mixture of standards and bark extract. Also, a reasonably good quality high "up-front CID mass spectrum is obtained for a minor component in the extract identified as jatrorrhizine (Figure 4). Other alkaloids that have also been identified include berberine (major component), palmatine, phellodendrine, tetrahydropalmatine, magnoflorine and thalifendine. Also, tentatively identified are some isomeric alkaloids. Therefore, the data obtained clearly indicate that on-line LC-IS/ITMS is a very powerful analytical tool for rapid structural elucidation of constituents in a natural product for drug discovery.

Acknowledgement: We would like to thank Wyeth-Ayerst Research and R.W. Johnson Pharmaceutical Research Institute for their financial support of H.K. Lim and W-N. Wu. We also the Eastman Kodak Co. for financial support of the API/ITMS development.

References

1. W-N Wu, L.A. Mitscher and J.L. Beal, *LLoydia* **39**, 249 (1976).
2. J.A. Massucci, G.W. Caldwell, W-N Wu, R.K. Isensee and J.R.B. Slayback, *Proceedings of 35th ASMS Conference on Mass Spectrometry and Allied Topics* , Denver, CO, p514, 1987.

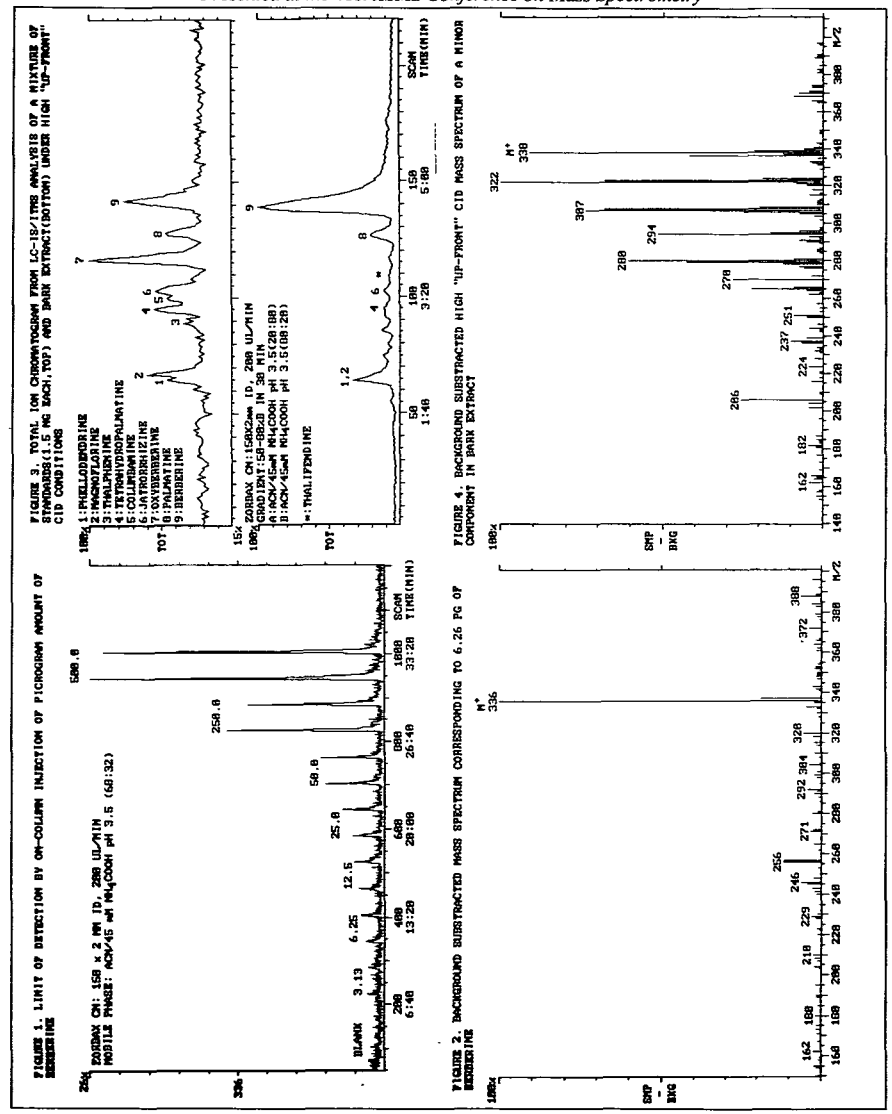

ASSESSMENT OF *IN-VITRO* LIVER SLICE METABOLIC ACTIVITY USING MICROCOLUMN LC/ESI/MS AND LC/ESI/MS/MS,

*M.A. MOSELEY, J.S. WALSH, J.E. PATANELLA, K.A. HALM, AND S.E. UNGER, DEPARTMENT OF DRUG METABOLISM, GLAXO RESEARCH INSTITUTE, RESEARCH TRIANGLE PARK, NC 27709

The combined tools of chromatography and mass spectrometry have proven to be very useful in the profiling of drug metabolites derived from animal toxicology studies and in the identification of metabolites from human clinical trials. The discovery of biologically active human drug metabolites not previously observed in the animal toxicology studies can adversely affect the clinical study, therefore, the ability to identify human metabolites prior to clinical trials is advantageous. Precision cut liver slices have been used as an *in-vitro* model of coupled Phase I and Phase II drug biotransformations (1), and the use of slices of "transplant quality" human livers allows the generation of human drug metabolites prior to clinical trials. This *in-vitro* liver slice approach offers the ability to rapidly and inexpensively generate metabolites from animal and human systems in a relatively clean matrix, and characterization of the resultant samples by LC/MS and LC/MS/MS provides a similarly rapid means of identifying the metabolites. The goal of this work was to demonstrate the utility of the combined techniques of *in-vitro* liver slice metabolism and LC/ESI/MS and LC/ESI/MS/MS identification of human drug metabolites.

This approach requires a method for assessing the viability of the liver slicse, and 7-ethoxycoumarin (7-EC) has proven to be a particularly useful probe of coupled Phase I and Phase II biotransformations (2-3). The metabolic viability of the liver slices was quantitatively determined using a LC/UV assay with authentic standards of 7-EC and its principle metabolites (7-hydroxycoumarin, 7-hydroxycoumarin sulfate, and 7-hydroxycoumarin glucuronide) (4), and LC/ESI/MS was used to confirm the structures of the 7-EC metabolites.

Omeprazole, an inhibitor of gastric acid secretion, was chosen as a test compound to demonstrate the utility of the combined techniques of *in-vitro* liver slice metabolism and LC/ESI/MS/MS identification of the resultant metabolites. Previous MS analysis of *in-vivo* omeprazole metabolites from rat urine (5) had shown this compound generates a number of both Phase I and Phase II metabolites which have proven to be difficult to analyze by either direct probe insertion electron ionization (even with derivatization) or by on-line thermospray LC/MS. While LC/ESI/MS has been applied to characterize omeprazole metabolites in rat urine (5), no LC/MS/MS data on omeprazole metabolites (animal or human) has been reported.

To assist in the data interpretation, constant infusion of a $5x10^{-5}$M solution of omeprazole was used to generate a MS/MS reference spectrum comprised of 12 daughter ions. Use of a high orifice bias voltage (100V) generated the same fragments in the ion source, permitting the acquisition of MS/MS spectra of the eight most abundant ions observed in the MS/MS spectrum of omeprazole, in effect yielding MS/MS/MS spectra of omeprazole.

Human liver slices were incubated with 156 µM omeprazole for 4 hours. Solid phase extraction was used to remove salts and concentrate the drug and its metabolites. Five microliter aliquots of the 10x concentrated samples were injected onto a Hypersil BDS C18 LC column (1 mm i.d., 250 mm long), corresponding to an injection of 12 nmoles or 4 µgrams of omeprazole. The drug and its metabolites were eluted with a gradient elution program of 5% to 80% (over 75 minutes) acetonitrile in 2mM ammonium acetate (pH 6.8), with a mobile phase flow rate of 40 µL/minute. Unmetabolized omeprazole was the major component of the sample, however, numerous metabolites were also observed, including both Phase I and Phase II metabolites. LC/ESI/MS/MS spectra permitted the identification of most metabolites, including the differentiation of isobaric metabolites. For example, the alcohol metabolite (Figure 1) and the sulfone metabolite (Figure 2) are clearly distinguished on the basis of their LC/ESI/MS/MS spectra. While the majority of the previously reported metabolites in rat urine (5) were found in this study to also be *in-vitro* human metabolites, several of the rat urine metabolites were not found, and several of the *in-vitro* human metabolites were not found in the rat urine study. Moreover, this current work identified all of the human metabolites which have been found to be reported in the literature, as well as several additional human metabolites not yet reported.

The microbore LC/ESI/MS and LC/ESI/MS/MS analyses were performed on a Sciex API-3 equipped with an IonSpray™ interface, and the capillary LC/ESI/MS analyses were performed on a Finnigan TSQ-700 with an Analytica of Branford ESI interface.

The high throughput of the combined techniques of *in-vitro* human liver slice metabolism and LC/ESI/MS and LC/ESI/MS/MS identification of human drug metabolites permits the rapid screening of a number of structurally different drug candidates. This approach should prove to be of significant utility to the drug discovery and drug development process.

References

1) P.F. Smith, G. Krack, R.L. McKee, D.G. Johnson, A.J. Gandolfi, V.J. Hruby, C.L. Krumdieck, and K. Brendel, *In-Vitro Cellular & Developmental Biology*, 22(12), 706,1986.
2) J. Barr, A.J. Weir, K. Brendel, and I.G. Sipes, *Xenobiotica*, 21(3), 331, 1991.
3) J. Barr, A.J. Weir, K. Brendel, and I.G. Sipes, *Xenobiotica*, 21(3), 341, 1991.
4) J.S. Walsh, J.E. Patanella, and M.A. Moseley, *Fourth North American ISSX Meeting*, Bal Harbor, Florida, November, 1992.
5) L. Weidolf and T.R. Covey, *Rapid Communications in Mass Spectrometry*, 6,192,1992.

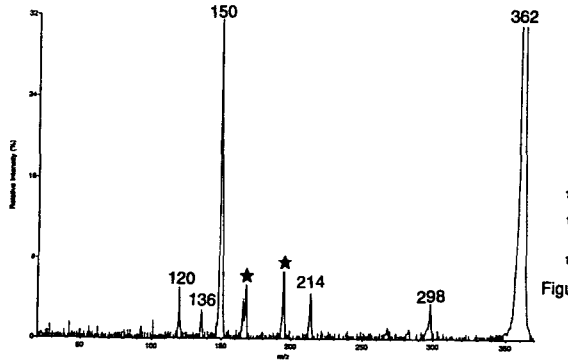

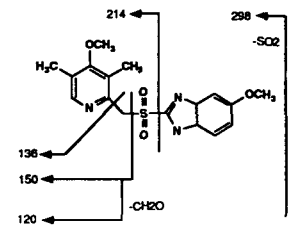

Figure 1) LC/ESI/MS/MS spectrum of the sulfone metabolite of omeprazole

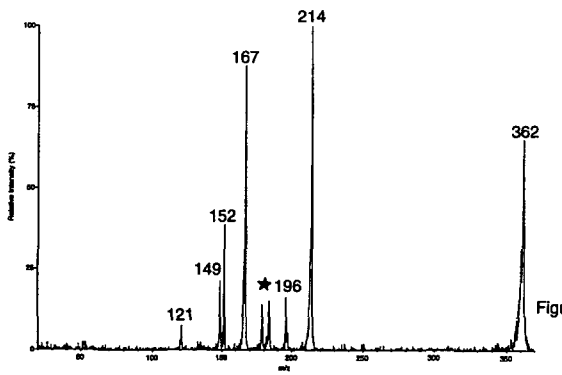

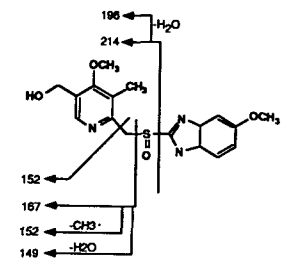

Figure 2) LC/ESI/MS/MS spectrum of an alcohol metabolite of omeprazole.

★) Background dimer ions

Quantitative Analysis of the Immunosuppressant FK-506 in Rat Serum by High Performance Liquid Chromatography-Electrospray MS/MS Techniques.

R. P. Schneider *, M. J. Cole, and H. G. Fouda. Central Research Division, Pfizer Inc, Groton, CT 06340

FK-506 is a macrolide immunosuppressant agent that is currently used in organ transplant patients.[1] Although structurally different from cyclosporin A, FK-506 shares many of the pharmacological effects of cylclosporin A.[2] Published methods of FK-506 quantitation have included enzyme immunoassays [3] and fluorescence derivatization procedures,[4] with minimum detection limits of *ca.* 2 ng/mL.

A specific HPLC/MS/MS assay has been developed for FK-506. The assay utilizes reverse phase microbore HPLC coupled to a pneumatically assisted electrospray (Ionspray) interface of a Sciex API III mass spectrometer. During the assay development, it became apparent that extracted components of the serum matrix were binding to the uncoated fused silica tubing normally used in the electrospray interface. This phenomenum caused poor reproducibility and accuracy for FK-506 quantitation, especially at concentrations less than 0.5 ng/mL. Replacement of the uncoated fused silica tubing with a crosslinked capillary column (DB-5) provided accurate and reproducible results.

Control rat serum was fortified with FK-506 and cyclosporin (the internal standard), followed by extraction at serum pH with methyl t-butyl ether. The organic solvent was recovered and evaporated to dryness. Serum residues were reconstituted in 25 µl of HPLC mobile phase and 5 µl were injected onto the HPLC/MS/MS system. Monitoring the collision induced dissociation product ions of the FK-506 and cyclosporin ammonium adducts provided good sensitivity and specificity. Quantitation of the analyte was accomplished over a linear dynamic range of 100 pg/mL to 20 ng/mL. The intra-assay precision was < 11% (for n=5), and the accuracy of the assay was less than or equal to 8.6% of the fortified concentrations. Instrumental reproducibility for replicate injections of standard solutions was 2.2% when monitoring ratios of drug/internal standard.

1 R. Venkataramanan, A. Jain, V. Warty, et al. *Transplant. Proc'd.*, **23**, 931, (1991).
2 K. Takada, H. Usada, M. Oh-Hashi, et al. *J. Pharmacobio-Dyn.*, **14**, 34, (1991).
3 K. Tamura, M. Kobayashi, K. Hashimoto, et al. *Transplant. Proc'd.*, **19**, 23, (1987).
4 K. Takada, M. Oh-Hashi, H. Yoshikawa, et al. *J. Chromatogr.*, **530**, 212, (1990).

Analysis of Serum Samples Containing Known Amounts of FK-506.

Intra-Assay Parameters: 5 samples were fortified at each concentration (except for those noted by the * where n=2).

Fortified Conc (ng/ml)	*Conc. found (ng/ml) mean ± S.D.*	*% C. V.*	*mean accuracy*
0.10	0.11 0.004	3.8	111
0.20	0.21 0.02	8.6	104
0.50 *	0.52	n/a	103
1.00	1.00 0.04	3.9	100
5.00 *	4.80	n/a	97
10.00	10.2 0.26	2.6	102
20.00	21.6 1.29	6.0	108

Structural Analysis of Rapamycin and Related Compounds Using $(M+Li)^+$ Ions Generated by LSIMS. *J P. Kiplinger, M A. Guadliana; Pfizer, Inc., Groton, CT 06340

Rapamycin (**1**) is an antitumor, antifungal, and immuno-suppressive agent isolated from cultures of *Streptomyces hygroscopicus*[1]. The compound presents a difficult mass spectrometric problem, producing little structural information by positive CI, EI, FAB and Ionspray[2].

Because of its structural homology with FK-506, rapamycin is of interest to a number of pharmaceutical companies as an immunosuppressant[3]. The ability to structurally characterize rapamycin analogues in small amounts by mass spectrometry is of potential value in a search for new drug candidates. It is therefore desirable to develop a mass spectrometric method for rapid screening of novel rapamycin-like molecules which gives useful structural information.

Alkali metal salts are often added to LSIMS matrices in order to cationize samples with alkali metal ions. Rapamycin cationizes poorly with proton, but very well when sodium ions are present in the matrix. Similarly, we have found that lithium ions cationize rapamycin and related molecules, producing strong $(M+Li)^+$ ions and abundant fragment ions, particularly when they are activated collisionally. These fragments have been attributed to their precursors using B/E linked scanning and identified using high-resolution LSIMS. Some of the fragment ions were shown by labeling with $^6Li^+$ ions[5] to be derived from an $(M+2Li-H)^+$ ion, but all other significant fragments were monolithiated.

Structures of the fragment ions of the $(M+Li)^+$ ion of rapamycin were assigned based on reasonable assumptions about fragmentation mechanisms, and by examining spectra of rapamycin analogues. These structures were then confirmed, wherever possible, by peak matching at high resolution to poly(ethylene glycol) standards.

Fragment m/z	Measured mass	Formula	Δ (ppm)
818	818.5047	$C_{46}H_{69}NO_{11}Li$	+1.99
626	626.3480	$C_{33}H_{49}NO_{10}Li$	- 5.83
593	593.4017	$C_{35}H_{54}O_7Li$	- 2.12
591	591.4249	$C_{36}H_{56}O_6Li$	+2.04
443	443.3011	$C_{25}H_{40}O_6Li$	+5.88
329	329.2297	$C_{19}H_{30}O_4Li$	- 2.17

The fragmentation scheme shown is particularly useful in characterizing rapamycin-like molecules that have been modified at one or two sites. Virtually every part of the molecule is present in at least one charged fragment, and is also lost as an uncharged fragment. This means that a modification at one location that produces a change in mass may be localized to a region of the molecule by noting which fragments change in mass relative to rapamycin and which do not. We have examined other analogues of rapamycin, and the changes in masses of the fragment ions make identification of modified structures straightforward.

Since biosynthetic pathways producing rapamycin-like molecules cannot produce random, infinite variations in the compound, it is likely that most analogues will be simply modified in one or two places. Furthermore, these modifications should be consistently found at certain locations within the molecule. In such cases, it should be easy to identify many new structures based entirely on the fragment ion spectra generated from their $(M+Li)^+$ ions.

1) Vezina, C.; Kudelski, A.; Sehgal, S. N.; *J. Antibiot.* 1975, **28**, 721.

2) Cantone, J.; Chan, K.; *Proc. 40th ASMS Conf. on MS and Allied Topics*, Washington, DC, May 31-June 5 1992, p. 1881.
3) Schreiber, S.; *Chem. Eng. News*, Oct. 26, 1992, p. 22.
4) Adams, J.; *Mass Spectrom. Rev.* **9**, 141-186 (1990).
5) Kiplinger, J. *41st ASMS Conference*, San Francisco, ThP 89

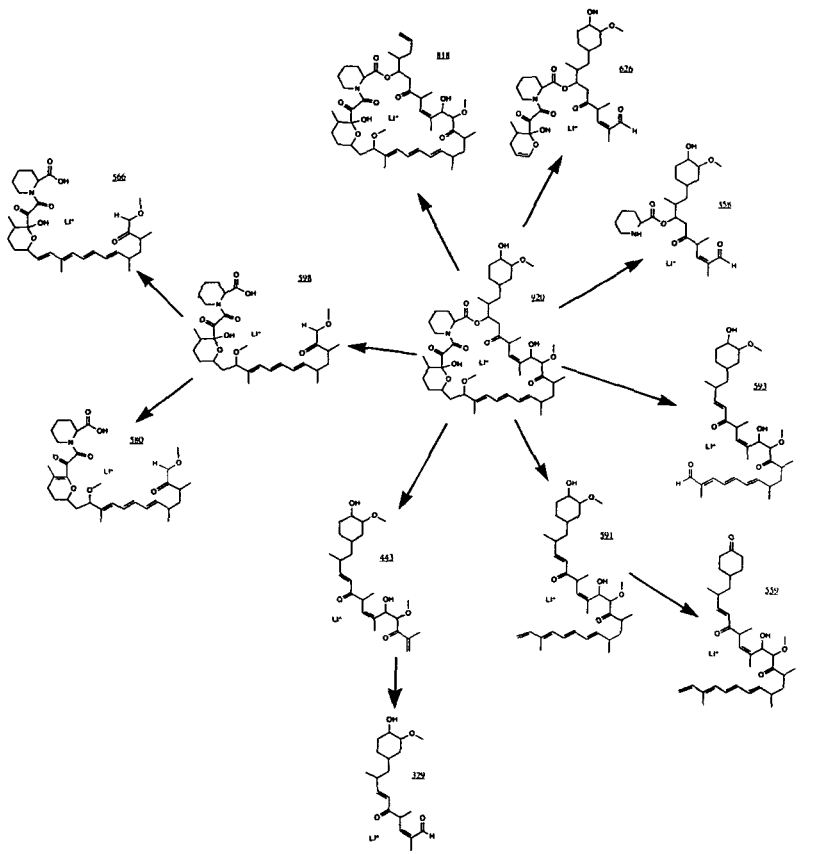

Investigation of Photochemical Reactions via on-line Thermospray Tandem Mass Spectrometry

J. D. Laycock* and R. A. Yost; Dept. of Chemistry, University of Florida, Gainesville, FL 32611
J. Martin E. Quirke; Dept. of Chemistry, Florida International University, Miami, FL 33199

Introduction

Initial results show the feasibility of using photochemistry/TSP/MS/MS to monitor reactions occurring at biologically relevant wavelengths. A high intensity illuminator afforded a high yield of photoproducts and MS/MS data provided information to elucidate possible structures of the products. We will use our instrumentation to investigate the photosensitization reactions of classes of biomolecules such as amino acids, nucleic acids, and short chain peptides. In the preliminary studies reported here, the monitoring of the photosentization of tryptophan (trp) by hematoporphyrin (Hp) has been demonstrated.

Experimental

A schematic of the on-line photolysis system is shown in **Fig. 1**. The setup consists of an Isco LC-2600 syringe pump, a loop injector, a photochemical reactor, a Vestec thermospray probe and ion source, a Finnigan TSQ 45 mass spectrometer, a liquid nitrogen cold trap, and a 300 L/min mechanical pump.

The photochemical reactor was designed in our laboratory and consists of a 300 W xenon arc lamp and a flow cell with an aluminum housing, both of which are contained in a vented, black box. The arc lamp and the cell housing are fan cooled. The box is vented to a hood to remove ozone that is generated by the lamp. Previous photolysis TSP/MS work utilized a PTFE KOTR (knitted open tubular reactor) as the flow cell. Our interest in the investigation of photochemical reactions at visible wavelengths using a high intensity arc source necessitated the development of a new cell. The cell was made from Pyrex 7740 1/4" tubing. In order to withstand the thermospray backpressures, a brace was constructed to hold the swagelock fittings in place.

All data were collected using a Finnigan TSQ 45 with a Vestec thermospray ion source installed. The buffer solution consisted of 0.1 M ammonium acetate solution with the pH adjusted to 10.4 by the addition of ammonia. The flow rate for all experiments was 1.0 mL/min, which corresponds to a residence time of 1.0 min for the cell. The 300 W lamp was operated at 17 A.

All mass spectra were obtained in the filament-off mode with a source temperature of 260 °C and a probe tip temperature of 205 °C. The collision energy was 30 eV with an argon pressure of 1.4 mTorr in Q2.

Results

Fig. 2a shows the normal thermospray mass spectrum of trp (MW 204). The spectrum exhibits almost exclusively the $[M+H]^+$ ion at m/z 205. Low intensity ions at m/z 222 (indicating the $[M+NH_4]^+$ adduct) and m/z 161 (loss of CO_2) were detected. When the same solution of trp was injected with the lamp on (**Fig. 2b**), additional low intensity ions were observed at m/z 145, 177, 201, and 218. The ion at m/z 161 was significantly increased in intensity.

Fig. 3a shows the spectrum for the trp/Hp mixture with the lamp off. The ions at m/z 145, 161, 201, and 218 were detected but were much lower in intensity than in **Fig. 2b**. In **Fig. 3b**, is shown the spectrum for the trp/Hp mixture with lamp on. The ions at m/z 145, 201, and 218 were dramatically increased in intensity with numerous other ions also detected.

In **Fig. 4**, the proposed structure is 4-(2-amino-2 carboxyethyl) quinazoline. The dominant

ion in the daughter spectrum appears at m/z 145 and can be accounted for as the [M+H]+ ion of 4-methyl quinazoline. The ions at m/z 155 and 183 can be attributed to neutral loss NH_3+HCOOH and NH_3+H_2O respectively.

Conclusions

Visible-wavelength photochemistry on-line with TSP/MS/MS for the detection and structure elucidation of tryptophan (trp) photoproducts has been demonstrated. A 300 W arc lamp provided sufficient light intensity to convert approximately 80% of trp to photoproducts in the presence of hematoporphyrin (Hp). Hp was found to increase dramatically the abundance of photoproducts observed. MS/MS data led to the proposal of quinazoline derivatives as the main photoproducts. This is in accordance with previous observations that trp reacts to give quinazolines when photosensitized in the presence of ammonia.

1. Ballard, J. M.; Grinberg, N.; Flow Injection-Thermospray-Mass Spectrometry; Proceedings of the 40th ASMS Conference on Mass Spectrometry and Allied Topics, Washington, DC, May 31-June 5, 1992.

Fig. 1 Schematic Diagram of the Instrumentation

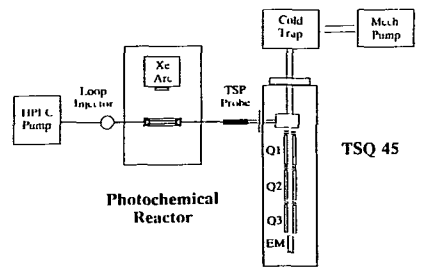

Fig. 3 TSP Spectrum of Trp/Hp mixture

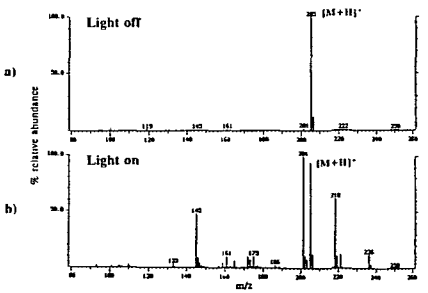

Fig. 2 TSP Spectrum of Trp

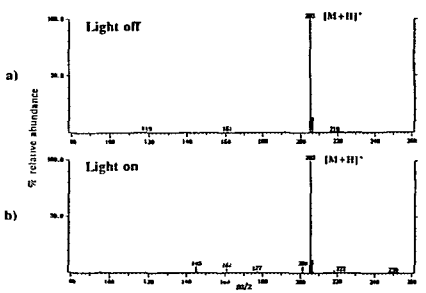

Fig. 4 Daughter Spectrum of Photoproduct at m/z 218

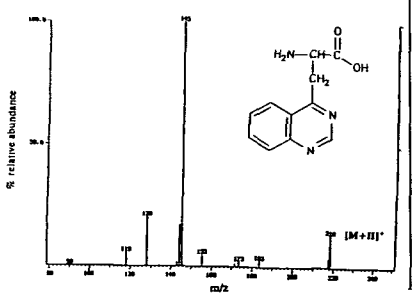

COMPARISON OF GC/MS AND LC/MS METHODS FOR DETERMINING NICOTINE ABSORPTION IN TOBACCO SMOKERS

*G. D. Byrd, Biological Chemistry Laboratory, R. J. Reynolds Tobacco Co.
Winston-Salem, NC 27102.

Studies have shown that more than 80% of nicotine absorbed by humans is excreted in some form in the urine [1,2]. Thus, quantification of nicotine and its metabolites in 24 h urine samples is a viable means for estimating nicotine absorption in smokers. Most absorbed nicotine is excreted as free and conjugated forms of nicotine, cotinine, and 3'-hydroxycotinine. Various analytical methods have been used to determine these analytes in biological matrices. In this study, two methods for the determination of nicotine and its metabolites in smokers' urine were compared. The first method was a thermospray-LC/MS method developed in our laboratory [3] and the other was a modification of a published GC/MS method [4].

As part of our comparison, we prepared a standard smokers' urine by pooling urine from nine smokers and freezing 5 mL aliquots. This standard urine is routinely used for quality control and methods development in our laboratory and for comparative studies with other laboratories. Ten samples of the standard urine were analyzed by each method following beta-glucuronidase treatment to hydrolyze glucuronide conjugates. An immunological assay was also performed on the standard urine using a polyclonal RIA method for both nicotine and cotinine.

According to the GC/MS method of Voncken et al. [4], a saturated potassium carbonate solution was added to urine followed by extraction with n-butylacetate. The organic layer was sampled by injection in the splitless mode onto a DB5 column directly interfaced to a quadrupole mass spectrometer. The method was modified to include labeled analogs of each analyte (methyl-d_3 for nicotine, cotinine, and 3'-hydroxycotinine) as internal standards and by treating the urine with beta-glucuronidase prior to addition of potassium carbonate and extraction. Isotope dilution provided a more accurate and precise quantification and enzyme treatment freed glucuronide conjugates of these analytes to improve total accounting of absorbed nicotine. Although this method does not directly account for nicotine-N'-oxide, this compound decomposes thermally in the GC to nicotine, which adds to the total account of nicotine absorption.

The thermospray LC/MS method [3] used the same internal standards and glucuronidase treatment as the GC/MS method. The treated urine was filtered and injected directly onto the reversed-phase HPLC column for analysis. Samples were also analyzed without enzyme treatment to assess the amount of glucuronide conjugates by differences in the free forms of nicotine, cotinine, and 3'-hydroxycotinine. The LC/MS method provided data on the minor metabolites nicotine-N'-oxide, cotinine-N-oxide, and demethylcotinine.

Analytical results on the standard urine are summarized in Table I below. There was good agreement for major analytes (nicotine, cotinine, and 3'-hydroxycotinine) between the LC/MS and GC/MS methods with differences less than 20%. Total nicotine excretion determined by the two methods showed a difference of less than 5%. For the same set of standards ranging from 0.1 to 23 ug/mL, the GC/MS method had better sensitivity for nicotine (3 times) and 3'-hydroxycotinine (1.5 times) than the LC/MS method. Both methods had similar sensitivity for cotinine. Though limited in number of analytes, the RIA supported data from the chromatographic methods. The polyclonal RIA results agreed well for total cotinine and nicotine.

These results show that both methods are suitable for the determination of total nicotine absorption in smokers. The GC/MS method is more sensitive, easier to operate, and available to more laboratories. However, the LC/MS method provides a better quantitative metabolic profile. Both methods could be expanded to include certain minor metabolites.

References

1. M. Curvall, E. K. Vala, G. Englund, and C. R. Enzell, 43rd Tobacco Chemists' Research Conference, Richmond, VA, 1989.

2. G. A. Kyerematen, M. L. Morgan, B. Chattopadhyay, J. D. deBethizy, and E. S. Vessell, Clin. Pharmacol. Ther., **48**, 641-651, 1991.

3. G. D. Byrd, K.-M. Chang, J. M. Greene, and J. D. deBethizy, Drug Metab. and Dispos., **20**, 192-197 (1992).

4. P. Voncken, G. Schepers, and K.-H. Schafer, J. Chromatogr., **479**, 410-418 (1989).

Table I: Concentrations of nicotine and metabolites in standard smokers' urine as determined by three different methods.

DMC = demethylcotinine, NIC = nicotine, COT = cotinine, NNO = nicotine-N'-oxide, CNO = cotinine-N-oxide, 3HC = *trans*-3'-hydroxycotinine

	Concentrations (ug/mL)						TOTAL
METHOD	NIC	COT	3HC	NNO	CNO	DMC	NIC
GC/MS (Enzyme treated samples)							
AVG	2.64	4.06	6.28				11.69
SD	0.10	0.19	0.90				0.59
%RSD	4%	5%	14%				5%
LC/MS (Enzyme treated samples)							
AVG	2.86	4.23	5.14	0.38	0.54	0.20	12.11
SD	0.23	0.25	0.21	0.07	0.16	0.02	0.58
%RSD	8%	6%	4%	19%	31%	11%	5%
LC/MS							
AVG	2.04	1.59	4.03	1.14	0.55	0.14	
SD	0.28	0.11	0.34	0.08	0.03	0.04	
%RSD	14%	7%	5%	9%	7%	25%	
RIA							
AVG	2.29	4.06					
SD	0.33	1.05					
%RSD	14%	26%					

ELECTROCHROMATOGRAPHY / MASS SPECTROMETRY OF STEROIDS

D. B. Gordon, G. A. Lord, Dept. Biological Sciences, Manchester Metropolitan University.
D. S. Jones, Kratos Analytical, Manchester.
L. W. Tetler, Centre for Mass Spectrometry, UMIST, Manchester, M60 1QD, UK.

INTRODUCTION.

Coupling of HPLC to mass spectrometers has resulted in a synergistic relationship extending the power of both techniques. The direct introduction of HPLC effluent into a FAB source via a fused-silica capillary as reported by Ito et al. [1], offered compatibility with the low flow rates used with packed capillary columns. These columns enable the analysis of extremely small amounts of sample, of particular importance for biological material, and show increased chromatographic performance.

Traditionally, solvent flow through HPLC columns is achieved by hydrodynamic pressure produced by suitable pumps, but as early as 1974, Pretorius [2] demonstrated the phenomenon of electroosmosis, effecting solvent flow through packed fused-silica capillaries, hence the term "Electrochromatography". The method was forgotten until 1981, when it was revived by Jorgenson and Lukacs [3], as an aside to their paper on capillary zone electrophoresis (CZE). However, it was Knox and Grant in 1987 [4] who developed the technique, and led to current interest.

The advantage of electroosmosis is that a flat flow profile is produced, in contrast to the parabolic Poisseuille flow of pressure driven systems, resulting in enhanced chromatographic performance, which can be particularly useful in coupling to mass spectrometry, when narrower chromatographic peaks produce higher mass flux.

EXPERIMENTAL.

Fig. 1 shows a schematic diagram of the system, utilizing a conventional CZE instrument (Isco Model 3140 Electropherograph).

The column consisted of a fused silica capillary 70 cm. x 50 μ i.d., slurry packed to a depth of 35 cm. with 3 μ ODS Hypersil (Shandon, U.K.). The eluent used was 80% acetonitrile 20% sodium tetraborate 4 mM, and a voltage of 30 kV was applied. Electromigration was used to apply samples onto the column, and detection was by UV (200 nm.) through the capillary wall, 50 cm. from the inlet.

Mass spectrometry was carried out on the first two sectors of a Kratos Concept IIHH, in positive mode. Acceleration voltage was 8 kV with 8 keV Xe FAB ionisation, and mass range 230-500 was scanned at 3 s. per decade.

The column was connected to a frit-FAB probe via a tee-piece, at which glycerol was incorporated as a 1% solution in 50% methanol / 50% water, to act as matrix and to make up the flow to approx 5 μl/min.

RESULTS & DISCUSSION.

Fig. 2 shows an off-line separation of aromatic compounds, and demonstrates the high number of theoretical plates achievable, (N~400,000/M. for benzyl alcohol).

Fig. 3 is a mass chromatogram of an on-line separation of three steroids, approximately 10 pmol. of each on-column. Mass spectra are shown in Fig. 4.

The main drawback with the technique, besides the intricacy involved, is disruption of flow due to air bubble formation in the column, presumably resulting from Joule heating and de-gassing of the eluent. When this occurred, it was necessary to use pressure pumping to push solvent through the column and drive out the bubbles in order that electroosmotic flow could be restored.

We are continuing work on this technique, particularly in regard to overcoming some of the problems encountered, such as air bubble formation in the column and extending applicability to a wider range of compounds. We believe the technique offers particular advantages in coupling to MS, especially with the possibility of using sub-micron packings and longer columns, than feasible with conventional HPLC. This may enable separation and determination of previously intractable mixtures, especially in the biological field, and often where amounts only in the femtomole region are available.

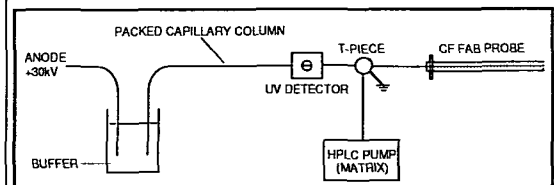

FIGURE 1: SCHEMATIC DIAGRAM OF ELECTROCHROMATOGRAPHY / MS SYSTEM

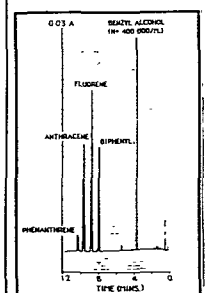

FIGURE 2: SEPARATION OF AROMATICS

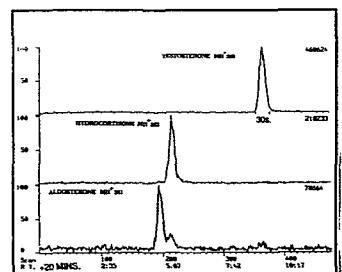

FIGURE 3: STEROID MASS CHROMATOGRAM

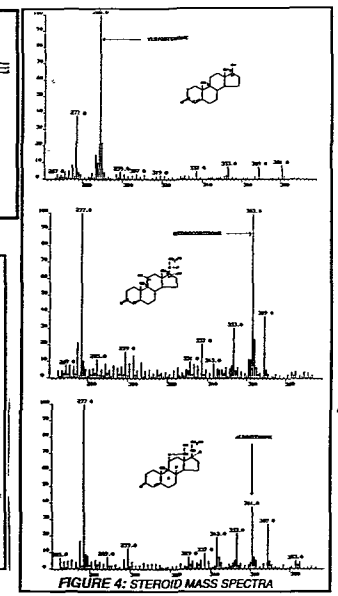

FIGURE 4: STEROID MASS SPECTRA

REFERENCES: [1] Y.Ito, T.Takeuchi, D.Ishi and M.Goto, J.Chromatog., **346,** 161 (1985).
[2] V. Pretorius, B. J. Hopkins, J. D. Schieke, J. Chromatog., **99,** 23 (1974).
[3] J. W. Jorgenson, K. D. Lukacs, J. Chromatog., **218,** 209 (1981).
[4] J.H.Knox, I.H.Grant, Chromatographia, **24,** 135 (1987).

ACKNOWLEDGEMENTS: We thank Jones Chromatography (U.K.) for loan of CZE equipment and ICI (U.K.) for loan of HPLC equipment.

Mass Spectroscopically-Guided Development of a Fluorescent Label for Enhanced Detection in HPLC

Lawrence R. Phillips, Jeffrey G. Supko and Louis Malspeis

Laboratory of Pharmaceutical Chemistry
Developmental Therapeutics Program
Division of Cancer Research
National Cancer Institute
Frederick, Maryland 21702-1201

Summary: *The alkylacylation reagent 7-[(chlorocarbonyl)methoxy]-4-methylcoumarin was synthesized, spectroscopically characterized, and investigated for its potential to give stable, highly fluorescent compounds of primary and secondary alcohols, for enhanced detection in high-performance liquid chromatography (HPLC).*

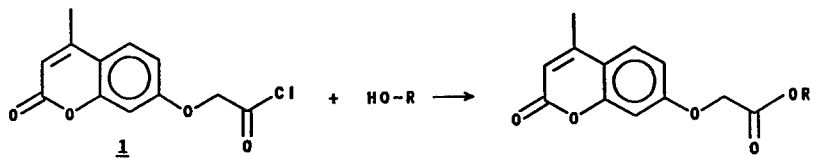

Introduction

7-[(Chlorocarbonyl)methoxy]-4-methylcoumarin 1 (CMMC) has been proposed for fluorescent labeling of primary and secondary hydroxyl groups[1]. We have developed synthetic procedures which allow the gram-scale production of 1 in high purity and we have thoroughly characterized this acid chloride by mass spectrometry and multinuclear and multi-dimensional nuclear magnetic resonance spectroscopy. Reagent 1 reacts smoothly with a variety of primary and secondary hydroxyl compounds to give the corresponding esters.

Methods

Synthesis. CMMC was synthesized from 7-(carboxymethoxy)-4-methylcoumarin by modification of the method proposed by Karlsson, et. al.[1] To 7-(carboxymethoxy)-4-methylcoumarin (100 mg, 0.43 mmol) was added freshly distilled thionyl chloride (1.5 ml, 20.6 mmol). The resulting mixture was stirred and heated to reflux for 1 h. Heating was discontinued and the reaction mixture, a clear, yellow-green solution, was stirred at ambient temperature for an additional 18 h. Hexane (8 ml) was then added to the reaction mixture, and the resulting precipitate was collected on a fritted disc filter. The collected solid was washed with an additional 10 ml of hexane. The slightly bluish-white solid was then freed of solvent *in vacuo*, yielding 96 mg of crystals (0.38 mmol, 88%) mp 126-127°C (uncorrected). ^{1}H-NMR ($CDCl_3$): δ 7.54 (d ($^3J_{HH}$=8.8 Hz),1H), 6.87 (dd,1H), 6.78 (d ($^4J_{HH}$=2.2 Hz),1H), 6.19 (s,1H), 5.00 (s,2H), 2.39 (s,3H). ^{13}C-NMR (^{1}H decoupled; $CDCl_3$): δ 18.67, 72.17, 102.19, 112.07, 113.14, 115.22, 126.08, 152.09, 155.01, 159.38, 160.68, 169.40. Mass spectrum (70 eV): *m/z* 252 ($M^{+\cdot}$, 100), 224 (34), 189 (64), 159 (34), 147 (68). HRMS, *m/z* 252.0180 (calculated for

$C_{12}H_9ClO_4$: 252.0189). For storage, 93 mg of the CMMC was transferred to a 25 ml volumetric flask, dissolved in methylene chloride (final concentration was approximately 14.8 mM), sealed under nitrogen, and stored in the dark at 5°C.

Derivatization Procedure. To a solution of CMMC (0.93 mg, 3.7 µmoles) in 0.25 ml of methylene chloride was added methyl alcohol (10 µl, 7.9 mg, 247 µmoles) and pyridine (5 µl, 4.9 mg, 62 µmoles). The resulting solution was vigorously mixed, allowed to stand for 10 minutes, and then concentrated to dryness under a stream of nitrogen gas at room temperature. The residue was analyzed without further purification.

Results and Discussion

Although ester derivatives of 1 readily elute from reversed-phase HPLC columns, analyses of these compounds by capillary GC/MS were unsuccessful for all but the lowest molecular weight materials due to limited volatility. Although there are reports of the use of CI and FAB MS in the examination of compounds of similar structure, we find that EI (70 eV) MS provides the most extensive indication of chemical structure.

Table. Selected ions from the electron-ionization (70 eV) mass spectra of various esters of 7-(carboxymethoxy)-4-methylcoumarin.

	R-OH	m/z 189 (% rel. abund.)	base peak (m/z)	M^+ m/z(%)
1	Methanol	(16)	147	248(93)
2	Ethanol	(30)	262	262(100)
3	Decanol	(58)	374	374(100)
4	Benzyl alcohol	(20)	91	324(42)
5	2-Propanol	(65)	43	276(73)
6	2-Butanol	(63)	290	290(100)
7	Cyclododecanol	(60)	234	400(59)
8	Cholesterol	(5)	368	602(12)
9	2-Adamantanol	(5)	135	368(20)
10a	1,4-Butanediol	(58)	306	306(100)
10b	1,4-Butanediol	(41)	234	522(20)
11	tert-Butanol	[presence of ester not detected]		

All molecular ions yielded exact mass data consistent with proposed molecular formulae. Derivatization conditions were manipulated to yield either 10a, the monoester, or 10b, the diester.

All derivatives give a distinctive molecular ion (relative abundance (100%-12%), and ions at m/z 189 which are indicative of the 7-carbonylmethoxy-4-methylcoumarin moiety. Loss of CO from the coumarin group occurs unpredictably. For those compounds possessing a suitable structure in the alcohol portion of the ester, the McLafferty rearrangement is seen, leading to a characteristic ion at m/z 234.

References

1. K.-E. Karlsson, D. Wiesler, M. Alasandro, and M. Novotny (1985) *Anal. Chem.* **57**, 229-234.

A Comparison of the Analysis of Gentamicin Sulfate by Thermospray and Electrospray HPLC/MS

T.A. Getek[1] and T.M. Heinze[2]
[1]Forest Laboratories, 300 Prospect Street, Inwood, NY 11696
[2]National Center for Toxicological Research, Jefferson, AR 72079

Overview: Previous work has reported the successful separation of the gentamicin sulfate (GS) complex by HPLC/MS using Thermospray (TS) ionization with a trifluoroacetic acid (TFA) ion pair mobile phase [1] The three major fractions of GS, C_{1a}, C_2, and C_1, were detected via TS ionization, as well as a minor fraction considered to be the C_{2a} component. A comparison was undertaken to determine the advantages of TS ionization versus electrospray (ES) ionization for GS and, in general, for aminoglycoside antibiotics.

Thermospray Ionization: The experimental and chromatographic conditions for the HPLC/MS have been reported [1], and a typical trace can be observed in Figure 1. The mass spectrum for the C_{1a} component of GS is seen in Figure 2. Because of the glycosidic bonds, the components in GS are thermally labile and the predominating mass spectral peaks are the individual sugars that have resulted from the breaking of these bonds. The $[M+H]^+$ peak as noted in Figure 1 is only a few percent relative abundance (%RA). Although not observed in the C_{1a} mass spectrum, a m/z 322 ion is sometimes observed for a disaccharide fragment. For quantitation purposes, the ions in the region of m/z 125 to 165 were utilized for GS.

Electrospray Ionization: ES ionization used a Vestec ES probe and controller interfaced to a Finnigan 4500 quadrupole. The mass spectra displayed were acquired using the infusion techniques at flow rates of 1 to 6 μL/min. Nominal concentrations of GS and other aminoglycosides were 100 μg/ml, and 95/5 water/methanol was the liquid carrier unless noted otherwise. Typical ES settings were 2.5 kV generating approximately 0.15 μA. The repeller was approximately 8 V and the nozzle (flat plate design) ranged from 50 to 200 V. The ES mass spectrum for the GS complex barely produced discernible $[M+H]^+$ ions at high concentrations infused, but did generate the $[M+2H]^{2+}$ ions as the base peaks. In addition, because the sulfate salt was infused, the sulfuric acid adducts of GS were detected as the $[M+2H\ H_2SO_4]^{2+}$ ions. Previously unreported work [2] for the ES ionization of GS gave the $[M+H\ H_2SO_4]^+$ ions as well, which was also noted in earlier FAB studies of GS [3]. In order to verify the ES effects of sulfate salts of gentamicin, a sample of tobramicin (TB) which was the free base was analyzed by ES ionization. The mass spectrum for TB (non-sulfate) can be seen in Figure 3. In this case, a significant singly charged species is observed at m/z 468, as well as the doubly charged molecular ion at m/z 235. On addition of sulfuric acid to TB, followed by infusion and ES ionization, the mass spectrum changed as indicated in Figure 4. With sulfuric acid, the TB singly charged molecular ion has completely vanished and the doubly charged species remained the base peak. An ion at m/z 283 which is representative of the $[M+2H\ H_2SO_4]^{2+}$ ion is now observed with addition of sulfuric acid. This confirmed the effect of sulfate on the appearance of the ES mass spectrum for GS.

Summary: The type of information obtained via TS and ES are unique for the two ionization modes. Although ES ionization via infusion is reported here, it was estimated that the detection limits for GS by HPLC/MS with ES ionization would be approximately 40 ng on-column for the conditions and instrumentation utilized. This is a factor of ten better than reported for TS ionization. The type of ions used for quantitation in the two ionization modes, however, would be different: fragment ions for TS and doubly charged molecular ions for ES. One disconcerting point about ES ionization for GS is that the appearance of the mass spectrum using similar equipment and conditions from several laboratories is quite diverse. This could be a point to consider for potential interlaboratory quantitations for analytes of interest via ES ionization with HPLC/MS.

1 T. Getek, M. Vestal, and T Alexander, J. Chromatogr., 554 (1991) 191.
2 Unpublished data, M Allen, Vestec Corp , Houston, TX
3. T. Getek, W. Korfmacher, and J. Freeman, 36th ASMS Conference, San Francisco, CA, 1988, p 984.

THERMOSPRAY HPLC/MS OF GENTAMICIN

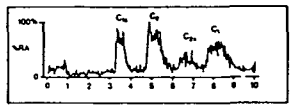

Figure 1 HPLC/MS of gentamicin sulfate by thermospray ionization using TFA containing mobile phase. Percent relative abundance (%RA) was plotted against chromatographic run time.

THERMOSPRAY MASS SPECTRUM OF C1a FRACTION

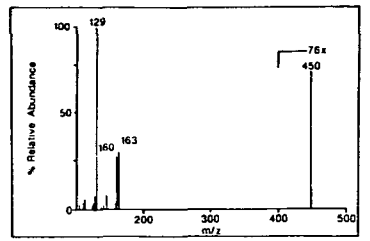

Figure 2. The TS ionization of gentamicin sulfate at the conditions selected produces substantial fragmentation of the compound as exhibited for the C1a fraction. The ions at m/z 129, 160 and 163 represent the individual sugar fragments that constitute the C1a component The $[M+H]^+$ ion is observed at m/z 450. Although not seen in Figure 3, an ion at m/z 322 is sometimes observed and is indicative of a disaccharide fragment

ELECTROSPRAY IONIZATION OF TOBRAMICIN (NON-SULFATE)

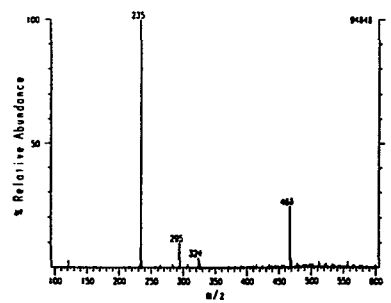

Figure 3. The infusion of tobramicin (non-sulfate) was performed at 5 4 μL/min with 95/5 water/methanol and 1.25% acetic acid added. The doubly charged ion at m/z 235 is observed; however, a significant $[M+H]^+$ ion is detected at m/z 468. When acetic acid was not present in the infusion, a weak but detectable ion was observed at m/z 468 with no ion discernible at m/z 235. The ion at m/z 295 may represent some acetic acid adduct of the doubly charged species.

ELECTROSPRAY IONIZATION OF TOBRAMICIN WITH H_2SO_4 ADDED

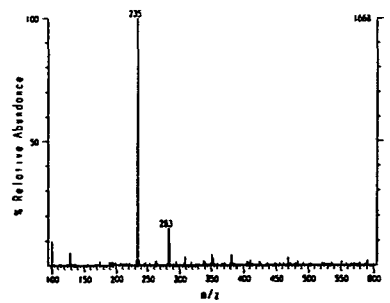

Figure 4. The mass spectrum shows tobramicin with sulfuric acid added. The infusion was 95/5 water/methanol with 0.25% H_2SO_4. It is seen that the singly charged ion at m/z 468 has disappeared and the base peak is the $[M+2H]^{2+}$ ion at m/z 234 The ion at m/z 283 represents the $[M+2H{\cdot}H_2SO_4]^{2+}$ ion.

Recognition of Quaternary Amines and Ammonium Salts Using Tandem Mass Spectrometry;

Daniel L. Norwood, Dixie L. Fisher, James O. Mullis, and M. Arthur Moseley; Glaxo Research Institute, Five Moore Drive, Research Triangle Park, NC 27709.

Introduction:

A problem often encountered in pharmaceutical development projects is the recognition of quaternary amine/ammonium salt drug substance degradation products and impurities. Thermospray (TSP), liquid secondary ion mass spectrometry (LSIMS), and electrospray ionization (ESI), the most commonly used techniques in such studies, do not distinguish $[M+H]^+$ ions of neutral species from the M^+ ions of quaternary amines. In the process of developing enhanced methods for molecular weight confirmation of drug substance related structures, an interesting behavior of quaternary ammonium salts was observed. Precursor scans of quaternary ammonium M^+ ions observed in $LSIMS^+$ exhibited prominent cluster ions of the structure $[xM+(x-1)anion]^+$. This differs from the cluster ions $[xM+H]^+$ commonly observed from neutral species in LSIMS and TSP.

Three classes of quaternary ammonium chlorides (sigma-bonded, conjugated, and sigma-bonded with a single carboxylic acid group) and a series of hydrochloride salts of neutral amines, representative of a range of drug products, were studied with LSIMS, TSP HPLC/MS, and ESI HPLC/MS to investigate cluster ion behavior. Precursor scans of M^+ and $[M+H]^+$ ions ("molecular weight confirmation scans") and full scan spectra (positive and negative ion) were examined to identify ions unique to quaternary ammonium compounds. The utility of a wide range of LSIMS matrix modifiers (positive and negative ionization modes) was investigated, as was TSP mobile phase modification with trifluoroacetic acid.

Experimental:

LSIMS spectra were obtained using VG 70VSEQ (hybrid) and VG Quattro (triple quadrupole) mass spectrometers. All compounds (0.1M, 1 µL) were analyzed in glycerol (neat or 5% aq.), with additives in a 1:1 molar ratio. Matrix additives investigated were: *p*-toluene sulfonic acid, potassium ferricyanide, potassium ferrocyanide, tetrabutylammonium dihydrogen phosphate, trifluoroacetic acid (TFA), sodium chloride, lithium iodide, trichloroacetic acid, and cobalt dichloride.

TSP spectra (positive and negative ion) were obtained using the VG Quattro; full scan and precursor ion spectra were generated from 0.5 mg/mL solutions (40:60 methanol:water, 0.1% TFA), introduced continuously into the ion source at 1 mL/min. Further studies were done, injecting 5 µg aliquots onto a guard column (AdSorbosphere C18, 5 µ particles), eluting with 100% methanol (0.2 mL/min.), makeup flow 0.4 mL/min. 3% TFA (aq.).

ESI^+ spectra (full scan and precursors of M^+ ions) were acquired using a Sciex API III triple quadrupole instrument, orifice voltage 35V and 150V. Samples were introduced via fused capillary, 10 µL/min., $1X10^{-4}$M in methanol.

Results/Discussion:

Full scan mass spectra of quaternary ammonium chlorides consistently exhibited abundant dimeric cluster ions at either $[2M^+$+anion$]^+$ (unique to quaternary ammonium compounds) or $[2M^+-H]^+$ (equivalent in mass to $[2M+H]^+$). These ions can serve as a "tripwire", or indication, that a compound has a quaternary ammonium structure. Precursor ion spectra of M^+ and $[M+H]^+$ ions were generated as "molecular weight confirmation scans", clearly establishing the ion relationships despite, in many cases, a considerable amount of chemical background. Addition of LiI and NaCl

yielded equivalent results, with $[2M+anion]^+$ ions formed only from quaternary amines not containing a carboxylic acid group (see Figure 1) and $[M^+-H+cation]^+$ or $[M+cation]^+$ ions formed from carboxylic acid-containing quaternary ammonium salts or neutral compounds. None of the matrix modifiers examined in $LSIMS^+$ experiments was useful in distinguishing between the carboxylic acid-containing quaternary ammonium compounds and neutral species.

$LSIMS^-$ experiments were needed for definitive distinction between neutral compounds and carboxylic acid-containing quaternary ammonium compounds. The most obvious feature is that none of the quaternary ammonium compounds studied form an ion at equivalent mass to the neutral species' $[M-H]^-$ (not formed by all neutrals). Two acidic protons would need to be present in a quaternary ammonium compound to form an ion at an equivalent mass to $[M-H]^-$. Matrix addition using trifluoroacetic acid gave consistently abundant cluster ions, but spectra were no more definitive than the positive ion experiments. However, addition of LiI showed consistent formation of an abundant $[M^+-H+I+LiI]^-$ for acid-containing quaternaries in approximately a 1:1 ratio with $[M^++2I]^-$, forming a doublet 6 amu apart. Other species showed only the $[M^++2I]^-/[M+I+HI]^-$ ions, and sometimes extremely weak ions at $[M^+-H+I+LiI]^-/[M+I+LiI]^-$.

Thermospray experiments were not promising for quaternary recognition. Precursor cluster ions ($[2M^++Cl]^+$ and $[2M^+-H]^+$) were observed only when extremely high concentrations of sample solution were infused directly into the mass spectrometer. Attempts to generate TFA adduct ions (5 µg/injection, 2% TFA) were not successful

Initial electrospray ionization experiments, which included a single example from each compound class, show promise for quaternary recognition. The two quaternary ammonium compounds studied (no carboxylic acid group) exhibited ions at $[2M^++Cl]^+$. Conversely, spectra of octanoyl carnitine chloride (a carboxylic acid-containing quaternary ammonium salt) exhibited $[2M^+-H]^+$ ions. No dimeric species was observed in ESI spectra of Ranitidine HCl, a neutral amine.

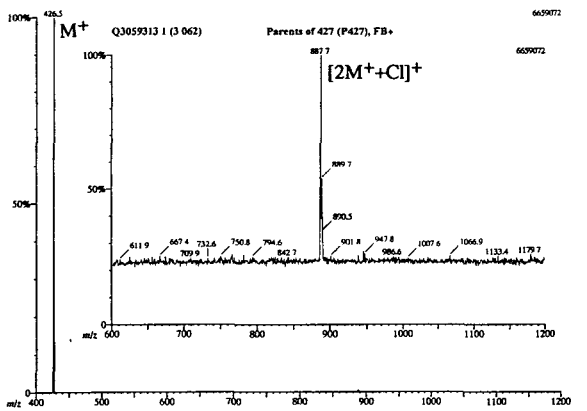

Figure 1. LSIMS+ molecular weight confirmation scan (precursors of M+, m/z 426) of methylbenzethonium chloride in the presence of a 1:1 molar ratio of NaCl.

Analysis of N-acetyl-cysteinyl-ursodeoxycholic acid in human bile by solid phase extraction and HPLC - cf-FAB detection.

R. Bagnati [1], E. Davoli [1], E. Zuccato [1], G. Galliani [2] and R. Fanelli [1].
1 Istituto di Ricerche Farmacologiche "Mario Negri", via Eritrea 62, 20157 Milano, Italy.
2 Farma Resa s.r.l., via Como 5, 22063 Cantù (CO), Italy.

SUMMARY

The new drug N-acetyl-cysteinyl-ursodeoxycholic acid (URSCYS), a bile acid analog, is under investigation for its effectiveness in dissolving gallstones. We present here a preliminary study on the metabolism of this drug in man. For the identification of URSCYS and its metabolites we developed a method involving purification of bile samples by solid phase extraction, and subsequent analysis by HPLC - cf-FAB, with a capillary split interface between the liquid chromatograph and the mass spectrometer. The method was able to identify and quantitate URSCYS, its metabolites glyco-ursodeoxycholic acid and tauro-ursodeoxycholic acid and all the major natural bile acids in their free and conjugated forms.

EXPERIMENTAL

Bile samples were extracted with silica-C_{18} cartridges and with columns packed with 0.5 g of piperidinohydroxy-propyl Sephadex LH-20, according to Goto et al. (Clin. Chim. Acta, **87**:141-7, 1978). This procedure allowed separation of different bile fractions, containing free, glyco and tauro conjugated bile acids. The purified extracts were dried and dissolved in the initial mobile phase for HPLC analysis (solvent A: ammonium acetate 0.01 M + ammonia 0.01 M + glycerol 0.8% / solvent B: methanol + glycerol 0.8%; 50:50, v/v) and separated with a C_{18}-analytical column, using a gradient elution from 50% B to 74% B in 12 minutes (0.4 ml/min flow rate). An UV detector (206 nm) was first connected at the end of the column and then a "capillary split" was used to interface the HPLC with the cf-FAB probe. The "capillary split" was made by using a zero-dead volume T-connector and deactivated fused silica capillaries as tubings. A 150 µm ID capillary (30 cm lenght) was used from the UV detector to the T-connector and a 50 µm ID capillary (240 cm length) was used from the T-connector to the cf-FAB probe. The third capillary connected to the T-interface was a 150 µm ID capillary (50 cm length) and was directed to waste. The split ratio of the T-interface was ca. 1:100, producing a 4 µl/min flow rate in the cf-FAB probe and an excellent stability of the signal. The mass spectrometer was a double focusing (EB optics) instrument, controlled by a Teknivent Vector 2 data system and equipped with a saddle field FAB gun which was operated with xenon at 7 kV and 1.5 mA discharge current. Detection of URSCYS and identification of its metabolites was made using full scan aquisition from m/z=200 to m/z=600.

RESULTS

Standard solutions of URSCYS and other bile acids were injected into the HPLC-cf-FAB system to acquire the relative retention times and FAB mass spectra. The cf-FAB mass spectra of URSCYS and of glyco and tauro conjugated bile acids showed the presence of protonated molecular ions and of other ions corresponding to the addition of NH_4^+, Na^+ or K^+ ions and to the loss of water molecules and of the conjugated aminoacid molecules. The retention times of the substances obtained with cf-FAB detection were about 3 min higher than those obtained with the UV detector. The delay was due to the time necessary for the samples to flow through the capillaries of the cf-FAB interface.

Human bile samples were collected from 1 h to 12 h after administration of a single oral dose of 1.5 g of URSCYS. In all samples the presence of URSCYS and of unconjugated ursodeoxycholic acid was not evidenced. Four natural bile acids (glyco-cholic acid, glyco-chenodeoxycholic acid, tauro-cholic acid and tauro-chenodeoxycholic acid, in their respective SPE fractions) were instead present at constant concentrations in all samples. The presence of two metabolites, identified as glyco-ursodeoxycholic acid and tauro-ursodeoxycholic acid, with increasing concentrations, was evidenced in the bile samples collected starting after 2 h and 30 min from administration (fig. 1). The identification was made by comparison with retention times and cf-FAB mass spectra of authentic standards of the substances (fig. 2).

The quantitation of the substances was made by comparison of the peak areas of the UV traces of samples and standards. Quantitation by cf-FAB mass spectrometry was not accurate because of the lack of a suitable internal standard.

CONCLUSIONS

The method here developed allowed the analysis of several bile acids by HPLC-cf-FAB detection. The operations of the cf-FAB interface and sources were relatively simple, reproducible and reliable. During a working day, after an initial conditioning time (about 1 h), the system did not require cleaning of the FAB probe or substantial re-optimization of the operating conditions.

The use of HPLC-cf-FAB detection with the capillary split connection described may be of great interest for the analysis of several substances difficult to analyze with other methods.

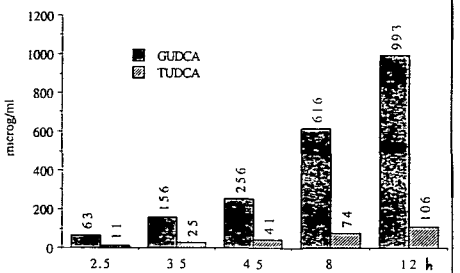

Fig. 1 Concentrations of glyco-ursodeoxycholic acid (GUDCA) and of tauro-ursodeoxycholic acid (TUDCA) in human bile after administration of URSCYS.

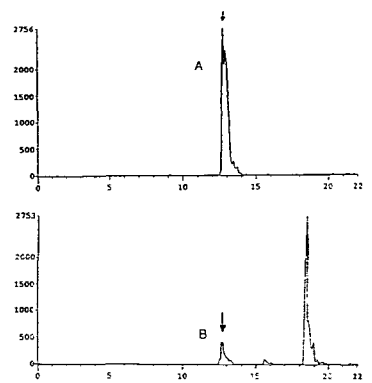

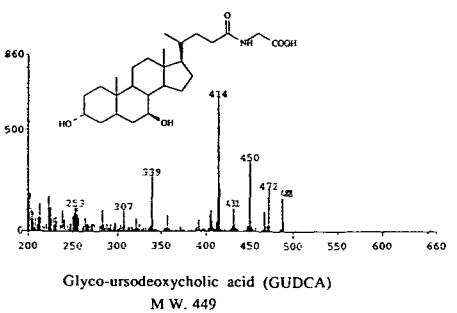

Fig. 2 Reconstructed ion chromatograms (m/z=450) and mass spectrum, obtained by HPLC-cf-FAB, of glyco-ursodeoxycholic acid, one of the metabolites of URSCYS. (A): standard solution; (B): bile sample.

Mass Spectral Characteristics and Identification of Metabolites of Mesoridazine and Other Related Piperidine Type Phenothiazines

Ge Lin, G.McKay, E.M.Hawes and K.K.Midha, College of Pharmacy, University of Saskatchewan, Saskatoon, Saskatchewan, Canada, S7N 0W0.

Mesoridazine (I Fig. 1) is a piperidine-type phenothiazine antipsychotic agent. This drug (2-$SOCH_3$) and two related drugs of this class, namely thioridazine (2-SCH_3) and sulforidazine (2-SO_2CH_3, II Fig. 1) are extensively metabolized and the established metabolic routes include S-oxidation of the ring 2-substituent, aromatic hydroxylation and S-oxidation of the phenothiazine ring. Although metabolic oxidation of the piperidine ring to lactams and N-oxides might be predicted, the literature information concerning such metabolism is lacking.

In view of our recent interest in the lactam formation of piperidine-type phenothiazine antipsychotic agents, the metabolism of mesoridazine in rat after oral administration was investigated by mass spectrometry with various modes of ionization and plasmaspray HPLC-mass spectrometry.

Mesoridazine besylate was a gift from Sandoz Inc. All synthetic reference standards were synthesized in these laboratories. β-glucuronidase enzyme (also containing sulphatase activity) was from Sigma Chemical Company and the silylating reagent, N-methyl-N-(tert.-butyldimethylsilyl)-N-trifluoroacetamide (MTBSTFA) was from Pierce. HPLC grade solvents were from BDH Chemicals Canada Ltd. The metabolic study was carried out in Lewis rat (n=5), dosed orally with mesoridazine 20 mg/kg and the 0-24h urine collected. Organic extracts of urine samples were first chromatographed by HPLC. Fractions corresponding to the observed chromatographic peaks were collected, dried and analyzed by direct probe mass spectrometry using different modes of ionization. The identity of each metabolite was confirmed by comparison of its HPLC and mass spectral behaviour with that of authentic reference standards. Except sulfoxides the positive EI mass spectra of all other metabolites exhibited molecular ions (M^+) with high intensity, while sulfoxides gave very weak molecular ion signals. Other diagnostic fragment ions, such as the ion at m/z 112 corresponding to the piperidinone moiety for lactam metabolites, were also observed in this mode (Table 1). For negative EI mode an appropriate molecular ion (M^-) for each sulfoxide was observed as the base peak (Table 1). Pseudomolecular ions were observed for all compounds including sulfoxides in FAB. The FAB mass spectral profile of each metabolite was similar to that obtained from EI positive mode. PSI mass spectra of all metabolites gave the protonated molecular ions (MH^+) with high intensity but almost no fragment ion information. In the case of lactam metabolites, an adduct ion formed with diethylamine present in the HPLC solvent system formed the base peak (MH^++73) (Table 1).

The urinary extracts were also analyzed by in-line HPLC-MS using a plasmaspray interface. In all cases the identity of metabolites were confirmed by direct comparison of their retention times and mass spectral data with those obtained for synthetic standards (Table 2). The availability of authentic samples of putative metabolites of mesoridazine synthesized in these laboratories (Lin et al. J.Hetero.Chem.,28,215,1991) enabled definitive characterization of the isolated metabolites. The identification of phenolic metabolites were also examined by use of HPLC-MS after derivatization with MTBSTFA. The metabolites identified were sulforidazine (II), mesoridazine ring sulfoxide (III), sulforidazine ring sulfoxide (IV), N-desmethylmesoridazine ring sulfoxide (V), lactam of mesoridazine (VI), lactam of mesoridazine ring sulfoxide (VII), lactam of sulforidazine ring sulfoxide (VIII), hydroxylated sulforidazine (IX), con-jugated hydroxylated sulfo-ridazine (X) and conjugated hydroxylated

mesoridazine (XI). Figure 1 summarizes the metabolic profile proposed for mesoridazine in rat.

Figure 1. Proposed metabolic pathway of mesoridazine in rat urine

* Not detected intermediate

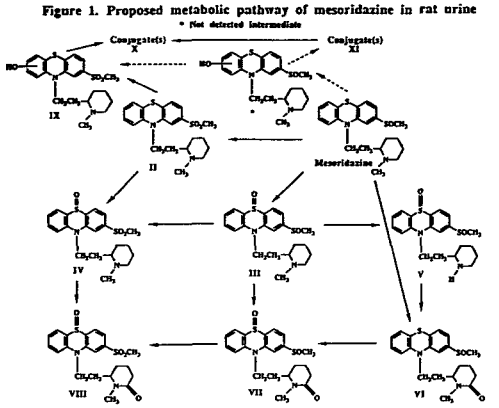

Table 1. Mass spectral data of mesoridazine metabolites analyzed by direct probe sample using various modes of ionization

Compound	No	m/z (% intensity) EI⁺	EI⁻	FAB	PSI
Mesoridazine	I	386(M^+ 17) 385(32) 274(33) 261(7) 260(5) 126(7) 98(100)	386(M^- 29) 385(100)		387(MH^+ 100) 371(6) 356(5)
Sulforidazine	II	402(M^+ 14) 290(4) 277(3) 276(2) 126(19) 98(100)	402(M^- 1) 387(100) 276(9)	403(MH^+25) 402(8) 290(5) 126(8) 98(100)	403(MH^+ 100)
Mesoridazine ring sulfoxide	III	402(M^+ 1) 387(6) 386(16) 274(3) 261(2) 260(3) 126(10) 98(100)	402(M^- 100) 387(35)		403(MH^+ 100) 387(7)
Sulforidazine ring sulfoxide	IV	418(M^+ 1) 402(18) 401(36) 290(34) 277(8) 276(4) 126(10) 98(100)	418(M^- 100) 403(46) 292(5)		419(MH^+ 100)
Lactam of mesoridazine	VI	400 (M^+ 100) 385(36) 384(12) 274(17) 261(15) 260(27) 140(19) 138(4) 126(6) 112(97)	385 (100)	401(MH^+ 42) 385(9) 384(14) 274(10) 261(5) 260(7) 140(9) 126(4) 112(100)	474(MH^++73,100) 401(MH^+ 5)
Lactam of mesoridazine ring sulfoxide	VII	416(M^+ 20) 401(14) 400(37) 274(100) 261(13) 260(19) 140(7) 138(21) 126(3) 112(64)		417(MH^+ 12) 401(45) 385(52) 274(9) 261(6) 260(10) 140(14) 126(12) 112(100)	490(MH^++73,100) 474(23) 417(MH^+ 4)
Lactam of sulforidazine ring sulfoxide	VIII	432(M^+ 6) 417(13) 416(49) 290(53) 277(36) 276(17) 140(19) 138(11) 126(17) 112(100)	432(M^- 100) 417(70) 401(26) 292(37) 138(10) 112(87)	433(MH^+ 100) 417(9) 416(9) 290(30) 277(5) 276(12) 140(9)	506(MH^++73,100) 490(88) 433(MH^+ 6)

Table 2 Comparison of retention time and mass spectral data between isolated metabolites from rat urine and reference standards analyzed by plasmaspray HPLC-MS

Compound	No	Metabolite Rt (min)	Standard Rt (min)	Metabolite m/z (MH^+ %intensity)	Standard m/z (MH^+ %intensity)
Mesoridazine	I	5 7	5 7	387 (100)	387 (100)
Sulforidazine	II	5 1	5 0	403 (100)	403 (100)
Mesoridazine ring sulfoxide	III	7 2	7 2	403 (100)	403 (100)
Sulforidazine ring sulfoxide	IV	5 6	5 5	419 (100)	419 (100)
N Desmethyl mesoridazine ring sulfoxide	V	5 4		389 (88)	
Lactam of mesoridazine	VI	4 6	4 6	401 (100)	401 (100)
Lactam of mesoridazine ring sulfoxide	VII	5 1	5 2	417 (100)	417 (100)
Lactam of sulforidazine ring sulfoxide	VIII	4 7	4 7	433 (100)	433 (100)
Unconjugated hydroxylated sulforidazine[a]	IX	4 7		533 (6)	
Conjugated hydroxylated sulforidazine[b]	X	4 5		533 (35)	
Conjugated hydroxylated mesoridazine[a]	XI	5 1		517 (19)	

[a] Analyzed as a tert.-butyldimethylsilylated derivative
[b] Analyzed as a tert. butyldimethylsilylated derivative of unconjugated form

[The financial support from the MRC of Canada (PG-34) and the University of Saskatchewan (studentship G.L.) are gratefully acknowledged].

AUTOMATED INTERPRETATION OF BIOLOGICAL FLUID ORGANIC SAMPLES BY A BENCHTOP GC-MS.

James D. Shoemaker MD PhD, E.A. Doisy
Department of Biochemistry and Molecular Biology, St. Louis University School of Medicine, St. Louis, MO 63104

Most initial screening of urine samples for inborn errors of metabolism is performed on the isolated acidic fraction of urine by gas chromatography, with or without analysis of amino acids and carbohydrates by other means. We now report our experience with over 1000 samples screened by automated GC-MS. The method of sample preparation [J. Chromatogr., 1991, 562:125-138] allowed quantitation of untargeted and 159 targeted carbohydrates, amino and organic acids in each sample. Software to automate the interpretation of these samples was adapted to a low-cost, benchtop GC-MS.

A DOS-based program was written in the EPAL language supplied with the instrument, a FISONS MD 800. The program elicited entry of patient data and non-targeted library search parameters, and controlled the automatic sampler. During acquisition of data, the program identified TIC peak tops, matched the respective mass spectra against a library of over 1900 spectra of TMS derivatives of biological interest, and entered the name of the best match, the TIC peak area, height and other parameters in a dBASE-compatible data base. Adjacent peaks matching the same library entry were automatically combined. At the end of each run, the program printed a normalized TIC chromatogram, a list of "best matches" (with their fit parameter, area percent and area as a percent of creatinine area), a page for the analyst's interpretation headed by the patient data, and performed a targeted search of 159 peaks from 127 compounds. Concentrations were printed as millimoles analyte per mole creatinine. Creatinine itself was a major constituent of most samples and was itself quantitated in each run by isotope dilution of d_3-creatinine added as an internal standard. Finally, the program automated the transfer of the patient information and concentrations of 127 metabolites to a dBASE database. A menu-driven search program was created to retrieve the excretion rates of compounds according to diet, medications, diagnoses and other patient parameters.

Results from the benchtop instrument were comparable to results from the VG Trio 2 which was used for the initial screening of over 1000 clinical samples for inborn errors of metabolism. The benchtop instrument identified metabolites consistant with diagnoses including: medium chain acyl-CoA dehydrogenase (MCAD) deficiency, lysinuric protein intolerance, glycerol kinase deficiency, ornithine transcarbamylase deficiency (hetero- and homozygotes), homocystinuria, transferase galactosemia, methylmalonic acidemia, renal glycosuria, maple syrup urine disease, sialic acid storage disease, Canavan's disease, aspartylglucosaminuria and others.

The quantitation of amino acids and carbohydrates resulted in useful diagnostic information in about 20% of cases, and essential diagnostic information in about 1%. For example, 306 of 903 samples reviewed contained significant amounts of di- or monosaccharides. In 5% of the 903 samples, disaccharide was accompanied by intermediates such as 3,4-dihydroxybutyric acid (DHB) which may arise from bacterial fermentation of carbohydrate, suggesting inefficient assimilation.

One or more amino acids was abnormally elevated in 251 of 903 samples reviewed. In 58 cases the pattern of amino aciduria supported or suggested the diagnosis of renal or hepatic dysfunction. In 23 cases, kynurenine, formiminoglutamic acid or 3-methylhistidine were increased suggesting pyridoxine deficiency, folate deficiency or negative protein balance, respectively. Very high glutamate and/or glutamine excretion was found to accompany some cases of metabolic acidosis.

Metabolites of medications were found in 282 of 903 samples. The most common in descending order of frequency were: acetaminophen glucuronide, an unknown beta-lactam antibiotic metabolite, valproic acid glucuronide, isomaltose (a contaminant in i.v. dextrose solutions), chloral hydrate glucuronide, vitamins (including ascorbate, pantothenate, niacin, and 4-pyridoxic acid) and carbamazepine diol. Drug metabolites were of diagnostic significance in only one case when aspirin poisoning was the unsuspected cause of metabolic acidosis in a 2-week-old infant.

Very high levels of hexitols, including mannitol, inositol, galactitol and sorbitol were noted in 197 of 903 samples reviewed. Therapeutic use of mannitol or its presence in radiographic materials accounted for a minority of cases of mannitol hyperexcretion. A prospective study in adults has led to the hypothesis that these hexitols are produced as "compatible osmolites" in renal cells during periods of dehydration and hyperosmolarity, then excreted upon rehydration. However, hyperexcretion of hexitols was documented in only 14 of 38 cases where dehydration was part of the presenting complaint. Most samples were collected after fluid resuscitation.

Laboratories which perform organic acid screening for the detection of inborn errors of metabolism may use gas chromatography alone as the initial screening tool. The cost-effectiveness of initial screening by GC-MS rather than GC alone was illustrated by comparing the cost of the automated GC-MS with the cost of a single ICU admission for a hypothetical "near-miss" Sudden Infant Death case due to MCAD deficiency. This diagnosis sometimes depends on detection of low concentration acyl-glycines which may be missed on gas chromatograms.

A Rapid GC/MS/MS Assay for 5-Methoxyflavone in Plasma

Timothy R. Baker*, Linda J. Tulich, Kenneth R. Wehmeyer, and Gary R. Kelm,
The Procter & Gamble Company, Miami Valley Laboratories, Cincinnati, OH, 45239-8707

In the course of drug discovery and development, analytical assays for various pharmaceutical candidates in biological fluids are required. These assays provide input for pharmacokinetic, toxicokinetic, and pharmacodynamic studies. Compounds must be quantitated in a variety of complex matrices such as plasma, urine, and feces. Matrix differences in the biological fluids of different species studied (e.g. rat, dog, human) are also a factor in developing an analytical assay. Often, a limit of quantitation in the low ng/mL range is required for these assays. During the course of the development of a successful drug, analysis of over 10,000 samples could be required.

The drug candidate 5-methoxyflavone (5MFL), currently under investigation, is shown below with its $^{13}C_6$-labeled internal standard (IS). Other analytical techniques like GC/MS or HPLC could be utilized for the analysis of a compound like 5MFL, however, there are a number of compelling reasons for using Gas Chromatography/Tandem Mass Spectrometry (GC/MS/MS). Firstly, the high degree of specificity and sensitivity afforded by MS/MS requires considerably less method modification (retention changes or cleanup) for different matrices. Additionally, distinct compounds of similar volatility can be determined with similar assays by simply modifying the MS/MS transition monitored.The 5MFL assay was quickly developed from GC/MS/MS procedures initially designed for quantitation of another flavone analog. In general, MS/MS detection reduces method development time. Also, a very high sample throughput is possible since significant chromatographic separation is not required. For this assay the GC is primarily an inlet system that separates the analyte from the solvent. Finally, the high degree of specificity reduces interferences and increases the level of confidence in the data.

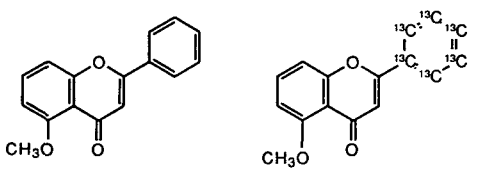

Plasma samples (1.0 mL or 0.1 mL) were prepared using solid phase extraction techniques. GC/MS/MS experiments were conducted on a Finnigan/MAT TSQ700 tandem mass spectrometer, using an Rtx-5 capillary column. Analytes were ionized using standard electron ionization (EI) conditions. Product ions were created via collisionally activated dissociation (-20 eV) with 1.0 torr of argon in the second quadrupole.

The EI mass spectra of 5MFL and its stable isotope labeled analog had base peaks at m/z 252 and m/z 258, respectively. These peaks corresponded to the M+· of each compound. The MS/MS spectra of these precursors (also not shown) were dominated by peaks at m/z 223 and 206 (m/z 212 and 239 for IS). Of particular interest here was the abundant dissociation of the M+· ion to form an ion of m/z 206 (m/z 212 for labeled 5MFL). This

dissociation, or transition, was monitored for the selective detection of the two compounds (i.e., m/z 252 ---> m/z 206 and m/z 258 ---> m/z 212).

The determination of 5MFL (and $^{13}C_6$-5MFL) proceeds as follows. The plasma extract was injected (1 uL) into the gas chromatograph. The analytes eluted in about 4.5 minutes, directly into the ion source of the mass spectrometer and were subjected to electron ionization. Only molecular ions were allowed to pass through Q1. Fragmentation of these ions in Q2 created product ions, but only the product ions of m/z 206 (m/z 212 for IS) were allowed to pass through Q3 and strike the detector (electron multiplier).

The absolute recovery of the solid phase extraction process was validated with ^{14}C-5MFL. These recoveries ranged from 89-102%. The calibration curve used for the samples described here had a percent deviation of 5.05 and a correlation of 1.000 . To validate the method, blank dog plasma was spiked with varying amounts (50 to 1000 ng/mL) of 5MFL. The determined values ranged from 94-99% of the spiked amounts.

The assay has been utilized for several pharmacokinetic studies. Results of one of these is shown below. Previously generated total radiolabel plasma concentration data suggest that 5MFL is well absorbed in the dog and that the terminal elimination half-life of the radiolabeled species is over 200 hours. In contrast, the parent 5MFL plasma concentration data generated by these analyses indicated that the compound was rapidly cleared (extraction ratio greater than 0.9) with a terminal half-life of about 15 minutes. Bioavailability was variable, with values of 72 and 33% for the two dogs. Both of these values were in excess of the amount predicted by the clearance of the drug. One possible explanation is that first-pass metabolism was saturable. This could account for the variability observed in bioavailability.

The short plasma half-life of the compound and its rapid clearance suggests that additional work is needed to ascertain the duration of its pharmacological effects. If the duration of the pharmacological effects are similar to the plasma half-life, synthetic modifications to reduce the clearance of the compound to improve bioavailability and increase its plasma half-life and duration of action may be considered

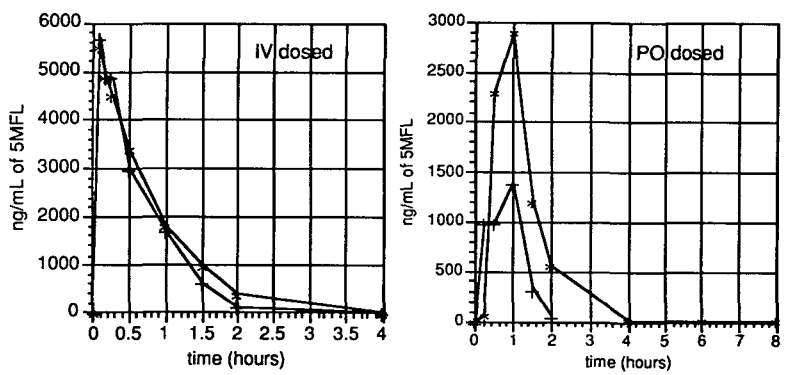

Immunoaffinity Chromatography and GC/MS/MS for the Identification of Cross-reactants with an Immunoassay for Benzoylecgonine

Chad C. Nelson,[1] Jill Visor,[2] and Karen Fogerson[2]
[1] Northwest Toxicology, Salt Lake City, Utah 84124, [2] Syva Co., San Jose, CA 95161

Cocaine is readily metabolized in the human body to an array of products for which metabolic pathways have been extensively studied and reviewed.[1] In addition to cocaine metabolites, however, several cocaine structure-related natural products are commonly found in coca leaf extracts, and synthetic preparations are often characterized by numerous structural and optical isomers of cocaine. Although highly specific, immunoassays for benzoylecgonine, which is the major metabolic product of cocaine, are subject to minor levels of cross-reactivity with compounds structurally similar to benzoylecgonine. Following immunoaffinity chromatography, GC/MS has been previously used to confirm the presence of drugs.[2,3] The present study describes the combination of immunoaffinity chromatography and tandem mass spectrometry to provide a highly specific and selective means to identify and characterize components that exhibit interaction with the antibody of the immunoassay.

Mass spectra were acquired on a Finnigan TSQ-70 mass spectrometer using positive-ion CI with methane reagent gas. CID spectra were obtained using argon collision gas at 30-40% transmission of the incident protonated molecule at a collision energy of 25-40 eV. Immunoaffinity separations were performed using Syva polyclonal antibodies coupled to a CNBr-sepharose column. A urine sample was applied, then the column was washed with 55 mM Tris buffer (pH 8) with 50 mM NaCl. Analytes were eluted with 0.2M acetic acid (pH 2.6).

The Strategy used in the present study for characterizing possible cross-reactants with an immunoassay for benzoylecgonine involved the following: a) determine MS/MS scan functions which target possible structural modifications of benzoylecgonine and identify families of cocaine-related compounds, b) analyze benzoylecgonine-positive urine samples by GC/MS/MS for the presence of cocaine-related components, metabolites, and other natural products, and c) collect immunoaffinity-purified urine samples and analyze by GC/MS/MS to identify those components which specifically interact with the immunoassay antibodies. Initially, dissociation products resulting from collisional activation of protonated molecules of model compounds of benzoylecgonine (Figure 1), cocaine, and ecgonine methylester were studied. Several product ions and neutral eliminations common to the model structures were targeted and used to "screen" urine extracts by GC/MS/MS by utilizing specific parent and neutral-loss scan functions. For example, parent-ion analysis of *m/z* 82 and neutral-loss analysis of 122 u were used to identify components that have structural moieties of N-methylecgonine and benzoate, respectively. Parent-ion analyses of *m/z* 82 and 240 were the most informative experiements. GC/MS/MS analysis of several urine extracts revealed 11 different benzoylecgonine-related compounds and natural products. For example, The CID spectrum of meta-hydroxybenzoylecgonine is shown in Figure 2.

A previously unreported metabolite of cocaine, para-hydroxybenzoylecgonine (Figure 3), was identified in all of the urine samples analyzed and was confirmed by comparison with authentic standard. Meta-hydroxybenzoylecgonine was also present in all of the urine samples examined (Figure 3). Following immunoaffinity separation, parent-ion analysis of *m/z* 82 of the resulting eluent showed the presence of meta and para-hydroxybenzoylecgonines and *cis*-cinnamoylecgonine (a natural product) in all of the urine samples studied, demonstrating some level of cross-reactivity with the immunoassay for these compounds.

References

1. For example, a) Casale, J. F., Waggoner, R. W., Jr., *J. Forensic Sci.* (1991), 1312; b) Lowry, W. T., Lomonte, J. N., Hatchet, D., Garriot, J. C. *J. Anal. Toxicol.* (1979), **3**, 91; c) Smith, R. M. , Poquette, M. A., Smith, P. J. *J. Anal. Toxicol.* (1984), **8**, 29; d) Baugh, L. D., Liu, R. H. *Forensic Sci. Rev.* (1991), **3(2)**, 101.
2. Rule, G., Henion, J. *Proc. 40th ASMS Conf. Mass Spectrom. Allied Topics*, (1992), 1899.
3. Gaskell, S. J. and Brownsey, B. G. *Clin. Chem.* (1983), **29(4)**, 677.

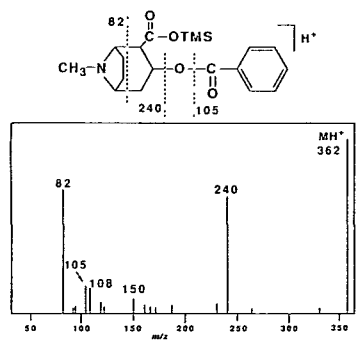

Figure 1. CID mass spectrum of protonated benzoylecgonine.

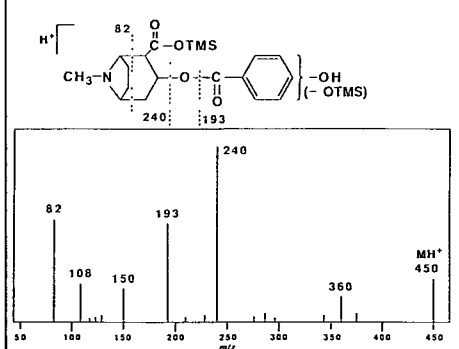

Figure2. CID mass spectrum of protonated m-hydroxybenzoylecgonine.

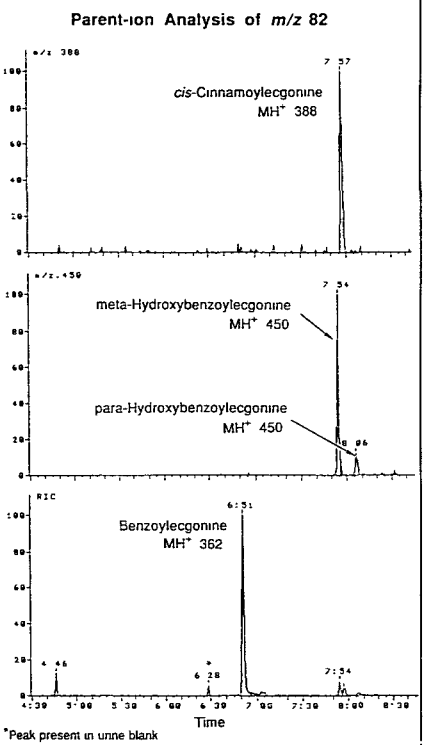

Figure 3. Parent-ion analysis (*m/z* 82) of a urine sample after immunoaffinity chromatography.

Microscale Chemical Reactions to Probe the Structure and Reactivity of Isolated Natural Products

Steven E. Klohr, Kevin J. Volk, Mike S. Lee, and Edward H. Kerns, Bristol-Myers Squibb
Pharmaceutical Research Institute, 5 Research Parkway, Wallingford, CT 06492

The structural diversity of biologically active natural products produced by plants and microorganisms provide challenging structure elucidation targets. This diversity often yields novel classes of compounds which posses a unique mechanism of action, providing important leads in the drug discovery effort. Our initial structure elucidation strategy involves the coordinated use of tandem mass spectrometry (MS/MS) and high resolution mass spectrometry (HRMS) to obtain detailed substructural information.[1,2]

In order to provide additional substructural information, we employ solution phase chemistry prior to mass spectrometric analysis. The insights obtained via MS analysis of various solution phase reactions complement those obtained in the gas phase. The specificity of this method allows for the evaluation of chemical reactivity, functional group identification, and provides detailed structural information that cannot be obtained from the isolated natural product. The sensitivity of mass spectrometric analysis enables these reactions to be performed with a few micrograms of material and characterized with little or no reaction workup. Furthermore, the small quantity of material required enables multiple reaction conditions and reagents to be evaluated early in the elucidation process when only limited quantities of material are available. The coupling of our existing structure elucidation protocols with this novel methodology provides further insights into the molecular structure of unknown natural products.

Here we demonstrate the role of microscale chemical reactions in the structure elucidation of natural products. This methodology is illustrated with the depsipeptides sandramycin and luzopeptin, the antitumor antibiotic kedarcidin and substance P. Our approach utilizes a systematic strategy with MS/MS and HRMS techniques for the substructure analysis of the isolated natural product. Reaction conditions are then selected to probe the structure or reactivity of the natural product with a few micrograms of material Full scan and MS/MS experiments are used to identify modified substructures of the reaction product and compare to the original compound.

Treatment of 5 ug of the depsipeptides luzopeptin and sandramycin with 10 ul of 0.1 M Na_2CO_3 and 10 ul of methanol for 3 hours hydrolyzed the esters linking the two substructures. MS/MS analysis of the protonated molecular ion provided sequence information that was not obtained from the MS/MS analysis of the cyclic parent species (Figure 1). The additional loss of 42 Daltons from the expected molecular weight of the luzopeptin product indicated the type of ester on the nitrogen heterocycle. The oxidation of 5 ug of the model thiol containing compound substance P with m-chloroperbenzoic acid, followed by MS analysis identified the site of oxidation (+16) as the methionine residue.

The reduction of the enediyne antibiotic kedarcidin [3] was performed with 5 ug of the kedarcidin chromophore in 20 ul of methanol for 30 minutes. The solution was evaporated to dryness and extracted with dichloromethane. Full scan Ionspray MS analysis indicated the addition of four hydrogens and MS/MS experiments localized this to the core (Figure 2). The reduction of two additional compounds in the extract indicated that these were also enediynes. Furthermore, the neutral loss of 144 (mycarose) was not apparent in the MS/MS spectrum of the unreduced material.

References

1. Klohr, S.E., Lee, M.S., Rosenberg, I.E., Proc. 39th ASMS Conference, 1059, (1991).
2. Lee, M.S., Klohr, S.E., Rosenberg, I.E., Proc. 39th ASMS Conference, 1061, (1991).
3. Leet, J.L., Schroeder, D.R., Hofstead, S.J., Golik, J., Colson, K.L., Huang, S., Klohr, S.E., Doyle, T.W., Matson, J.A., *J. Am. Chem. Soc.*, **114**, 7946 (1992).

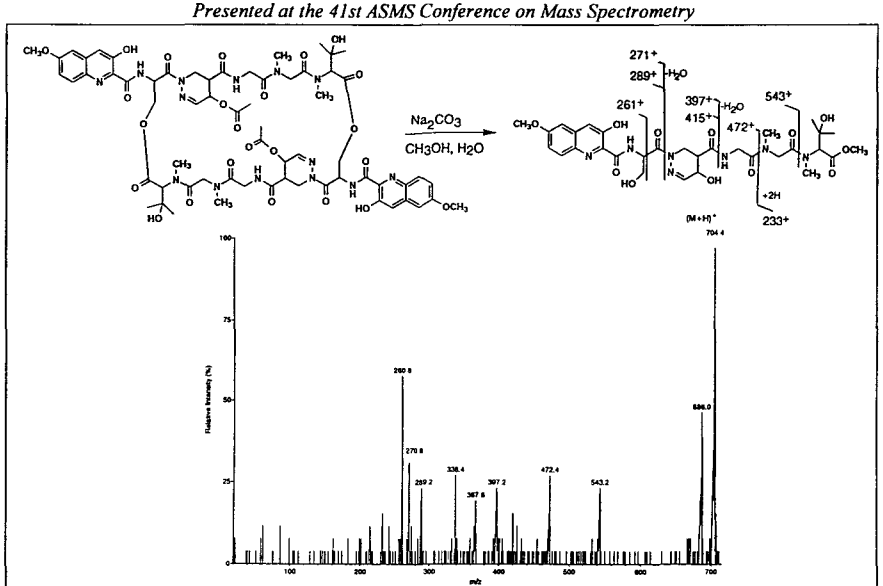

Figure 1. Methanolysis of the Depsipeptide Luzopeptin.

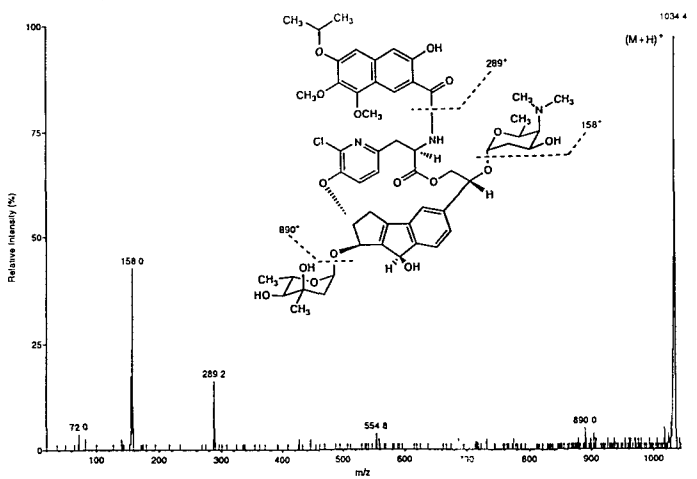

Figure 2. Reduction of the Enediyne Antitumor Antibiotic Kedarcidin.

DETECTION OF VITAMIN D METABOLITES BY ON-LINE CAPILLARY LIQUID CHROMATOGRAPHY AND FAST ATOM BOMBARDMENT MASS SPECTROMETRY

Bernice Yeung* & Paul Vouros
Department of Chemistry & Barnett Institute,
Northeastern University, Boston, MA 02115
G. Satyanaraya Reddy
Women & Infants Hospital and Brown University School of Medicine,
Providence, RI 02905

INTRODUCTION

The derivatization of vitamin D_3 metabolites with 4-phenyl-1,2,4-triazoline-3,5-dione (PTAD) and their subsequent characterization by MS and MS/MS have previously been demonstrated[1]. A sensitive and unique ion transition has been identified and used for detection by multiple reaction monitoring (MRM). The transitions monitored are $MH^+ \rightarrow$ m/z 298 and $MH^+ \rightarrow$ m/z 314 (for A-ring hydroxylated metabolites). In the current work, an on-line capillary LC has been incorporated for sample introduction to the MS. The same ion transitions have been utilized for a variety of vitamin D_3 metabolites, and their detection limits and linearity by this method have been examined. Also, in a separate study, the increase in UV detectability due to the derivatization with PTAD has been investigated quantitatively.

EXPERIMENTAL

Chemicals: Vitamin D_2, D_3 and PTAD were purchased from Aldrich (Milwaukee, WI). All other metabolites were obtained from Hoffmann-LaRoche (Nutley, NJ). [26,27-^{3}H]25(OH)D_3 was purchased from Amersham (Arlington Heights, IL).

MS Conditions: All data were obtained on a VG Quattro triple quadrupole mass spectrometer (VG Biotech, UK). MS/MS was performed with a collision energy of 50eV and attenuation by Ar.

Capillary LC: A Carlo Erba Phoenix 30 capillary LC system (Fisons Instruments, MA) was operated on-line with the MS at 5μL/min in isocratic mode. A C_{18} (320μm I.D.) Fusica column (LC Packings, Switzerland) was used.

Analytical HPLC: A Waters 600E system with a 990 photodiode array detector (Waters Associate, Milford, MA) was employed. A C_8 (4.6mmx15cm) column (Rainin Instruments, Woburn, MA) was used. Wavelengths monitored were 226nm for the PTAD derivatives and 265nm for the metabolites.

RESULTS

(1) Figure 1 shows the MRM detection of 2 of the 4 vitamin D_3-PTAD derivatives examined at amounts near their detection limits (triplicate injections).

(2) Figure 2 demonstrates the specificity of MRM detection for metabolites that normally coelute (Fig. 2a, top: vitamin D_3-PTAD, 94pg; bottom: vitamin D_2-PTAD, 278pg) and/or isobaric (Fig. 2b, top: 24,25$(OH)_2D_3$-PTAD, 6.5ng; bottom: 1,25$(OH)_2D_3$-PTAD, 7.3ng). Triplicate injections were done in both situations.

(3) Figure 3 illustrates the increase in UV sensitivity of 25(OH)D_3 by PTAD derivatization. UV responses of labelled 25(OH)D_3 are compared before and after the reaction with PTAD. For the same amounts of sample, the UV sensitivity has been found to have increased by 5-fold after the derivatization.

CONCLUSIONS

The following has been achieved in our current work with vitamin D:

- The use of PTAD derivatization and capillary LC-MS/MS allows sensitive detection of the metabolites readily in the low to mid pg (mid to high fmol) levels;
- Specificity of MRM permits the distinction of isobaric and/or coeluting metabolites;
- The derivatization increases the UV response of the metabolites by 5-fold;
- The described method is applicable to synthetic metabolites such as Δ^{16}-1,25$(OH)_2D_3$-PTAD for which specific radioreceptor and protein binding assays are not yet available;
- Detection at physiologically relevant level has been achieved for all the test compounds except for 1,25$(OH)_2D_3$.

REFERENCE

1. B. Yeung, G.S. Reddy and P. Vouros, presented at the 40th ASMS Conference, Washington DC, May 31-June 5, 1992.

Figure 1

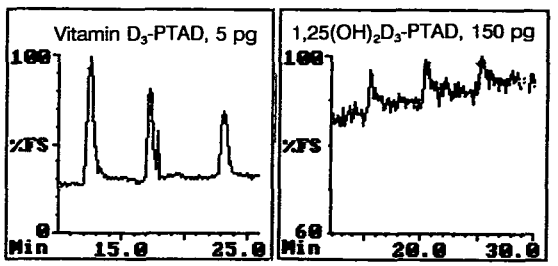

Figure 2a

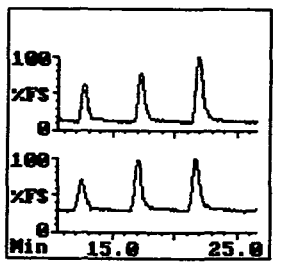

Figure 3

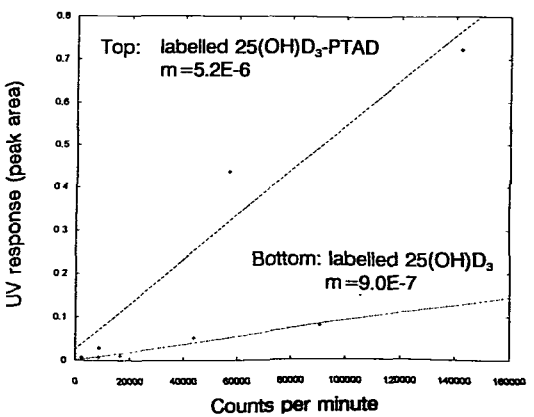

Figure 2b

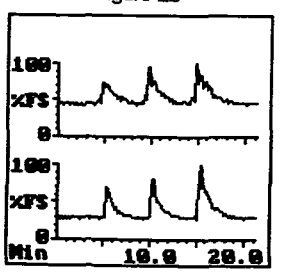

Determination of Cortisol in Human Plasma by Gas Chromatography/Negative Ion Chemical Ionization/Mass Spectrometry

*Fong-Fu Hsu, Liezhen Wang and Dennis M. Bier
Department of Medicine, Washington University School of Medicine
St. Louis, MO 63110

The reported GC/MS methods for the determination of cortisol in humans required complicated derivatization procedures. Moreover, only a limited sensitivity of 2 pmol (s/n = 3) can be achieved [1-2]. Quantification of daily cortisol production rate using thermospray liquid chromatography/mass spectrometry (LC/MS) has also been reported. Nevertheless, the method inherited the instability of a LC/MS, and the detection was limited to 5 pmol (s/n = 5) [3-4].

We developed a simple and sensitive method using negative ion chemical ionization capillary GC/MS detection by selected-ion-monitoring (SIM) of the molecular ion of cortisol-pentafluoropropionic acid ester. This method utilized readily available d_4-cortisol as an internal standard, a simple procedure for sample clean-up, and a single step for sample derivatization. A cortisol amount as low as 0.02 pmol (s/n > 10) can be easily detected. This detection method also allows precise determination at isotope ratio of 1 to 5 %, and therefore it can be potentially used in the quantification of cortisol production in humans, including infants and children where plasma sample volume is limited.

The derivatization of cortisol with HFB/acetonitrile or PFP/acetonitrile (50:50 v/v) at room temperature yields three compounds which can be separated easily and identified by GC/MS The mass spectra of the major component (93 %) and its d_4-labelling counterpart are shown in figure 1 (panel A and B).

Selected-ion-monitoring performed by simultaneous recording of m/z 782 for cortisol-PFP and m/z 786 for d_4-cortisol-PFP (M^- ion for both compounds) prepared from a 0.1 ml plasma (with 10 pmol addition of d_4-cortisol) is shown in figure 2. The linearity of the method can be shown from the area-response ratio of cortisol-d_0/cortisol-d_4 ranged from 0.1-10 pmol of cortisol (figure 3A). The correlation coefficient for the data exceeded 0.98 for five measurements.

Results obtained from different measurements are summarized in table 1. Table 1 also shows the amounts of cortisol added are in agreement with the amounts of cortisol measured. The standard curve plotted for 1 % to 10 % mole ratios of d_4/d_0 cortisol-PFP (n=5) after correction of the M + 4 ion current area contributed by natural isotopic abundance of unlabelled cortisol (0.138 %), is shown in figure 3B. The linearity of the detection method demonstrates that it could be used to quantify cortisol production in humans if d_4-cortisol were used as a tracer and infused intravenously at a constant rate to achieve a circulating isotopic enrichment between 1 and 5 mole % excess d_4-cortisol. Furthermore, the ability to precisely quantify isotope enrichment in plasma samples of 0.1 ml makes the method applicable to infants and children.

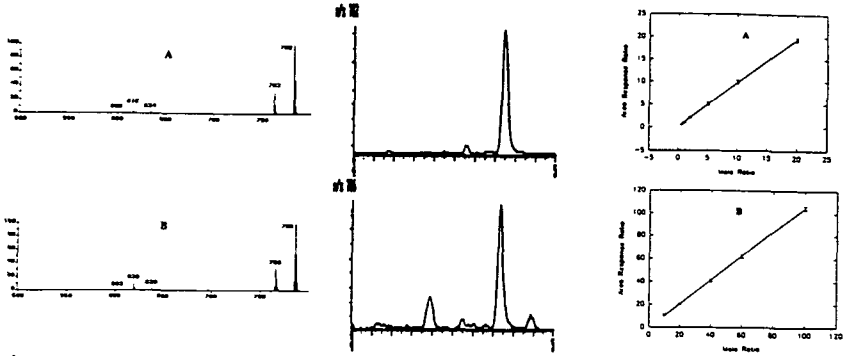

Figure 1. The NCI mass spectra of d_0- (panel A) and 9,11,12,12-d_4- (panel B) 3,11,21-tris(pentafluorobutyryl)-2,4,16-pregnatrien-20-one.

Figure 2. The SIM chromatogram of the PFP derivative prepared from a 0.1 ml plasma sample (with 10 pmol addition of internal standard).

Figure 3. Standard curve obtained by plotting relative area between unllabelled and labelled cortisol-PFP ion vs. the expected ratio. Curve A: plotted from 0.1-10 pmol injection of cortisol with 0.2 pmol of d_4-cortisol; Curve B: plotted from isotope ratio ranged between 1 and 10 mole % excess of d_4-cortisol.

TABLE 1. Accuracy of cortisol measurement in human plasma

Amount added (pmol)	Average amount measured (pmol)		
0.0	*35.6 ± 0.8;	27.1 ± 0.3;	31.6 ± 1.7
10	46.7 ± 0.5;	36.7 ± 1.6;	42.8 ± 0.9
20	55.4 ± 1.4;	45.7 ± 1.5;	54.4 ± 0.3
50	84.6 ± 0.6;	77.9 ± 1.9;	83.9 ± 1.5
100	132.8 ± 1.6;	**	134.7 ± 1.3

Each amount added was extracted in triplicate. The average amounts listed above were expressed in pmol/0.1ml plasma.
* Average amount of four measurements from the plasma pool of three different male subjects. ** not measured.

Acknowledgements
This work was supported by NIH grants RR-00954, RR-06021, HD-20805 and AM-20579.

References

1. Shibasaki, H., Arai, I., Furuta, T., and Kasuya, Y. (1992) *J. Chromatogr.* **576**, 47-52.
2. Shibasaki, H., Furuta, T., and Kasuya, Y. (1992) *J. Chromatogr.* **579**, 193-202.
3. Esteban, N.V., and Yergey, A.L. (1990) *Steroids* **55**, 152-158.
4. Esteban, N.V., Yergey, A.L., Liberato, D.J., Loughlin, T., and Loriaux, D.L. (1988) *Biomed. Environm. Mass Spectrom.* **15**, 603-608.

The Rapid Structure Characterization of Synthetic and Natural Products by FAB-Mass Spectrometry using Na^+ and K^+ Salts

*J.L. Whitney, S.E. Klohr, K.J. Volk, E.H. Kerns, M.S. Lee, Bristol-Myers Squibb Pharmaceutical Research Institute, 5 Research Parkway, Wallingford, CT 06492

The structure characterization of synthetic and natural products by mass spectrometry at Bristol-Myers Squibb typically involves the use of fast atom bombardment (FAB) ionization. Paramount to this characterization effort are the quick and efficient production of abundant molecular ions for molecular weight determination and diagnostic fragment ions for substructural information.

Traditionally, the molecular weight determination of an unknown natural product or unexpected synthetic product involves multiple analyses. Initial analyses often include sample and matrix only to look for potential $[M+H]^+$ ions. Subsequent analyses involve the addition of solid NaI or KI to the sample/matrix solution. Several separate analyses can be time consuming and not reproducible. Furthermore, the addition of salt in this manner does not guarantee an optimal amount present in the solution. Although salts have frequently been used for molecular ion confirmation and enhancement[1,2], their role in substructural characterization has not been commonplace.

We have developed a rapid characterization protocol utilizing a standard methanolic NaI/KI solution which is added to the probe prior to sample and matrix addition. This results in the consistent addition of a reproducible and optimal amount of salt. The optimal amount of salt present enhances molecular adduct ions, avoiding the problem of a "false negative" which can result from compounds which do not form $[M+H]^+$ ions. In addition to ion enhancement, radical ions are distinguished easily from protonated molecular ions when adduct ions are produced.

Structural information can also be obtained by unique functional group identification. Figure 1 illustrates the salt adduct pattern of etopiside phosphate. Notice the observation of all combinations of mono-and di-salt association, indicative of the phosphate group. These ion species and ratios are consistent and quite reproducible for many different classes of compounds containing a phosphate or carboxylic acid moiety.

Substructural characterization is possible since certain, often class specific, diagnostic fragment ions exhibit salt adduct ions. A class specific salt adduct substructural "template" for use in structure elucidation and confirmation can be generated. Figure 2 shows the salt adduct "fingerprint" of taxol. This pattern serves as a "template" by which other related taxane spectra can be compared to elucidate unique substructural fragments. This substructural "template" approach was used to characterize a mixture of two taxanes, 10-desacetyl taxol and taxol (figure 3). Molecular ion and sidechain and core substructural regions were "tracked" by identifying their respective Na^+ and K^+ adduct ions, differing by 16 daltons. The molecular ion region indicates a molecular weight difference of 42 daltons. By examining the core and sidechain fragment regions, the 42 dalton difference is localized to the core region. This is consistent with the expected structures of the two compounds.

The utility of this protocol for the rapid characterization of synthetic and natural products was illustrated with the antitumor compounds 10-desacetyl taxol, taxol and etopiside phosphate. The capability of identifying $[M]^+$ and $[M+H]^+$ formation, unique functional groups and fragmentation patterns was illustrated. A salt adduct substructural "template" approach was introduced and shown to be useful for elucidating unknowns, identifying components in mixtures, and characterizing expected reaction products.

References

1. C. Fenselau and R.J. Cotter, *Chem. Rev.* 87, 501 (1987).
2. B.N. Pramanik, P.R. Das and A.K. Bose, *J. Nat. Prod.* 52, 534 (1989).

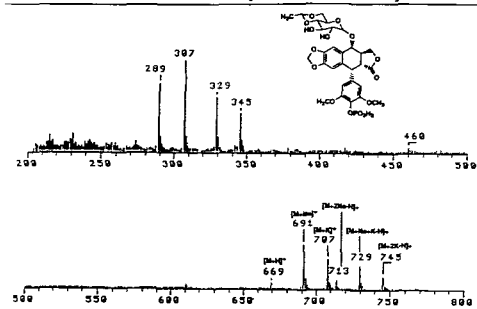

Figure 1. FAB Mass Spectrum Showing Phosphate Salt Adduct Pattern

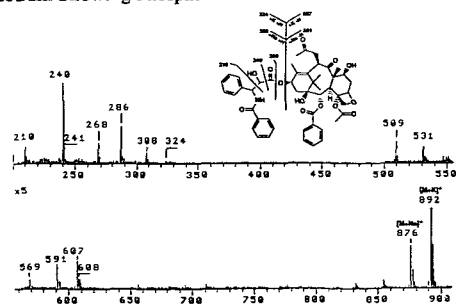

Figure 2. FAB Mass Spectrum Showing Substructural "Template" of Taxol

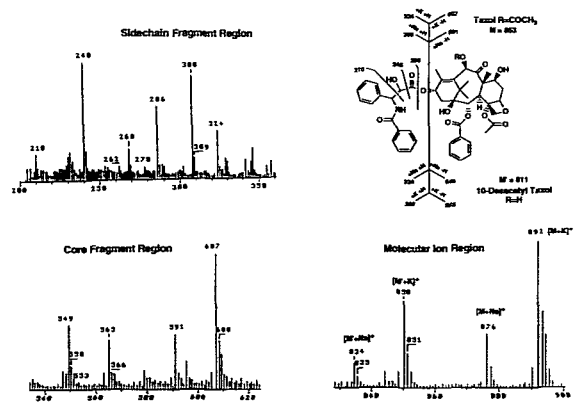

Figure 3. FAB Mass Spectrum Showing Substructural Characterization of a Taxane Mixture

CHARACTERIZATION OF HUMAN CEREBROSPINAL FLUID (CSF) PHOSPHOLIPIDS BY FABMS

Nevena Mollova[1,2], Ida (Ki) Moore[1], John Hutter[3], Petra Miketova[1,2] and Karl H. Schram[2]
Colleges of Nursing[1], Pharmacy[2] and Medicine[3], University of Arizona, Tucson, AZ 85721

INTRODUCTION

Elevated total phospholipid levels in CSF have been found in various diseases of the central nervous system (CNS)[1]. The commonly used method for analysis of CSF phospholipids is normal phase HPLC[2]. Although HPLC provides separation and quantitation of the components, no information is available concerning the number, type or structure of the individual molecular species within the phospholipid classes. Fast atom bombardment mass spectrometry (FABMS) combined with tandem mass spectrometry (FABMS/MS) has proven to be a valuable technique for analysis of phospholipid mixtures[3-5]. In this work, FABMS and FABMS/MS were used for analysis of CSF phospholipids to identify markers of neurotoxicity associated with cancer treatment in children.

METHODS

Sample preparation: The lipids are extracted from 1 ml of CSF and separated by normal phase HPLC[2]. The crude extracts were dried under N_2.

FABMS and FABMS/MS analysis was performed on a four sector instrument of BEBE geometry (AMD Intectra, Harpstedt, Germany) operating at an accelerating voltage of 6 kV in both the positive and negative ion detection modes. Data acquisition and instrument control were accomplished using two SAM 68k computers (KWS Computersysteme, GmbH, Ettlingen, Germany). The mass range was scanned from m/z 90-2000 at 60 sec/decade at resolution 2000. The dried HPLC fractions or crude extracts were dissolved in 5 μl $CHCl_3$ and 1 μl of the solution was mixed with 1 μl of m-nitrobenzylalcohol and placed on the target at 8°C. FABMS/MS spectra were obtained in the following manner: (1) precursor ions were mass selected with MS1 and linked B/E=const scans were performed using MS2. Collision-induced dissociations (CID) occurred in the third FFR with argon at a pressure sufficient to attenuate the precursor ion beam by 50%; (2) precursor ions were selected with B1 and Mass Analyzed Ion Kinetic Energy Spectra (MIKES) were acquired using MS1.

RESULTS

Treatment of childhood leukemia with methotrexate (MTX) may be associated with CNS cell membrane damage which is expected to induce changes in CSF phospholipid composition[6]. To investigate the effect of the MTX treatment on the CNS and to find markers of the cell membrane damage a series of patient CSF samples have been analyzed by normal phase HPLC and FABMS. Positive FABMS and MIKES was used for identification of diacylglycerol (DAG), phosphatidylcholine (PC) (Fig. 1) and lysophosphatidylcholine (LPC) fractions. MIKES of $[M-Me]^-$ for the most abundant PC molecular species (m/z 761, Fig. 1) in negative FAB ion mode was used for characterization of the type and the position of the fatty acid residues (Fig. 2). The presence of DAG and LPC is in agreement with the expected MTX treatment-related increased CNS cell membrane lipolysis, probably a result of activation of the phospholipases A_2 and C.

We analyzed a crude lipid extract of patient CSF using FABMS (Fig. 3). PC and sphingomyelin (SM) are the predominant molecular species possibly a result of the suppression effect under static FAB conditions. Four sector B/E=const linked scans were performed for characterization of the main PC (m/z 761, Fig. 4) and SM molecular species.

CONCLUSIONS

The application of FABMS and FABMS/MS analysis, in combination with normal phase HPLC, of human CSF phospholipids enables: **(1)** identification of the phospholipid classes; **(2)** identification of the various molecular species in the class of phospholipids; **(3)** structural characterization of the individual molecular species; **(4)** investigation of the mechanism of the cancer treatment related neurotoxicity in children.

FABMS and FABMS/MS analysis of total CSF lipid extracts provide characterization of only the major phospoholipid classes.

REFERENCES

1. R. A. Fishman, "CSF in diseases of the nervous system", W. B. Saunders Co, Philadelphia, PA, 1992, pp. 245.
2. S. Chen and P. Chan, J. Chromatogr. **344** 297 (1985).
3. M. Cole and C. Enke, Anal. Chem. **63** 1032 (1991).
4. D. Bryant, R. Orlando, C. Fenselau, et al., Anal. Chem **63** 1110 (1991)
5. S. Chen, et al., Rapid Commun. Mass Spectrom. **6** 454 (1992).
6. I. Moore, et al. Monograph of the First American Cancer Society National Conference on Cancer and Nursing Research, 27-37 (1991).

ACKNOWLEDGEMENTS

This work was supported by grants from National Center for Nursing Research (NR0255703), Arizona Disease Control Research Commission, the Biotechnology Program, and NIH shared Instrumentation Program.

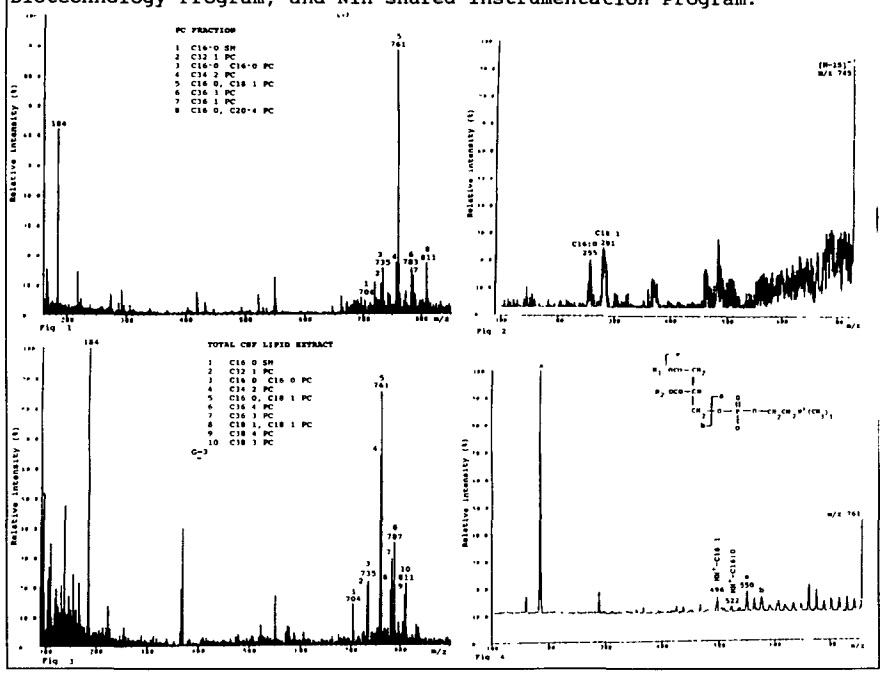

Quantitative Determination of Hydroxybutorphanol and Norbutorphanol in Human Plasma by GC/ECCI/MS

Daniel E. Mulvana
Bristol Myers Squibb, Pharmaceutical Research Institute
Syracuse, NY 13221

Butorphanol (**III**, Figure 1) is a synthetic opioid[1] indicated for the relief of moderate to severe pain. At the low transnasal doses administered (1 mg), the expected plasma Cmax is 1-2 ng/ml. Plasma levels of the metabolites hydroxybutorphanol (**I**, Figure 1)and norbutorphanol (**II**, Figure 1) are expected to be considerably less than this. Thus, a very sensitive assay was needed for the determination of complete plasma pharmacokinetic profiles of the metabolites. An assay method was developed which fulfilled this requirement by incorporating solid phase extraction, derivatization, and separation and detection by capillary gas chromatography-electron capture chemical ionization-mass spectrometry (GC/ECCI/MS). The assay will be used in conjunction with a separate assay for the parent drug.

Plasma samples (0.5 ml) containing butorphanol and the metabolites were diluted with 0.5 ml 10 mM ammonium acetate, pH 6.0. The internal standard (**IV**,Figure 1) was added and the samples were transferred to Bond Elut® CN-N extraction columns. Following two washes with buffer and one wash with 70% acetonitrile in water, the compounds were eluted with 1% triethylamine in acetonitrile with extraction recoveries of 73% for **I** and 64% for **II**. After removal of the elution solvent under nitrogen, the compounds were derivatized in a glove bag under a dry nitrogen atmosphere by adding 100 µl of 5% trifluoroacetic anhydride in ethyl acetate, capping and vortexing the tubes, and allowing them to remain at ambient temperature for 1 hour. The solvent was removed under nitrogen and the sample was reconstituted in 20 µl of toluene.

Separation and detection were accomplished using a Hewlett-Packard 5988A mass spectrometer interfaced to an HP 5890 Series II gas chromatograph. The processed samples (3 µl) were injected in the splitless mode onto a 15m DB-1 (0.25 mm ID, 0.25 µm film thickness) GC column at an injection port temperature of 285 °C. The initial oven temperature was 150 °C and was ramped at 25 °C/min to a final temperature of 310 °C for 2.1 min. The base peak was the trifluoroacetate anion (m/z 113) for all compounds (Figure 2). However, the signals from the molecular anions of both metabolites were sufficient to enable good sensitivity in the selected ion monitoring (SIM) mode. The derivatized compounds were detected by SIM of ions 451.0 for **II**, 631.0 for **I** and 505.0 for the internal standard. The ion source temperature was 120°C and methane was used as the buffer gas at a pressure of 0.75-0.85 Torr.

The assay was linear over the desired concentration range of 20 -1000 pg/ml for **I** and 50-1000 pg/ml for **II**. All standard curves from the validation (n=5) had r^2 values of ≥ 0.991 for **I** and ≥ 0.985 for **II**. The derivatives were stable in the cooled (~10°C) autosampler tray for at least 24 hours. Analysis of replicates (n=5) of plasma quality control (QC) samples at concentrations of 192, 580, and 868 pg/ml over three separate days showed the assay to be precise and accurate. For the hydroxybutorphanol assay, intra- and inter-assay precisions (%RSD) were within 9% and the grand mean predicted concentrations for all QC samples deviated from the nominal by less then 5%. Intra-assay QC deviations were all within 11%. For the norbutorphanol assay, intra- and inter-assay precisions (%RSD) were within 8% and the grand mean predicted concentrations for all QC samples deviated from the nominal by ≤ 6%. Intra-assay QC deviations were all within 13%.

The results show that the assay is sensitive, specific, precise, accurate, and reproducible and is expected to be sufficient for accurate determination of **I** and **II** in human plasma.

1. Monkovic', I., Conway, T.T., Wong, H., Perron, Y.G, Pachter, I.J. and Belleau, B. J. Am. Chem. Soc., **95**, 7910 (1973).

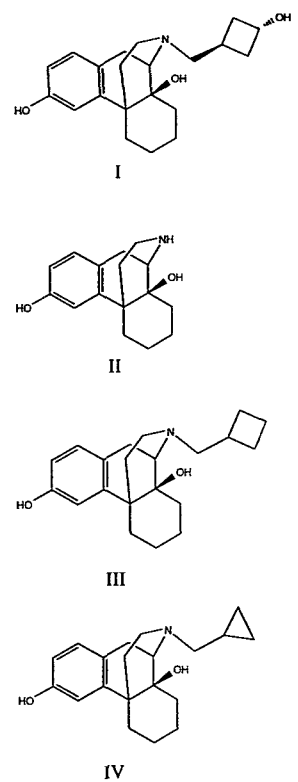

Figure 1.

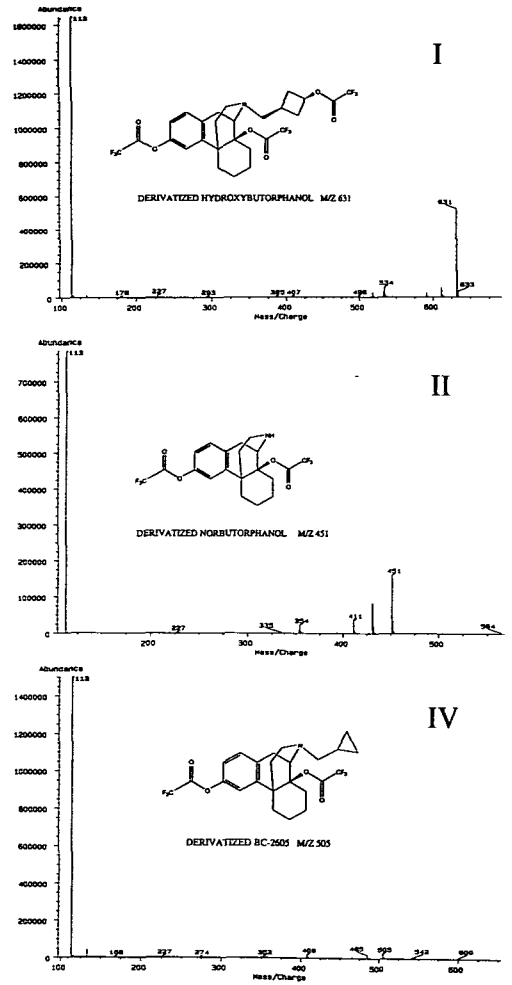

Figure 2. Scan data from processed I , II, and IV.

The Characterization of Abscisic Acid Metabolites Using Packed Fused Silica Capillary Liquid Chromatography/Continuous Flow Secondary Ion Mass spectrometry

L.R. Hogge, D.J.H. Olson, G.D. Abrams, and D.L. Barton, National Research Council of Canada, Plant Biotechnology Institute, Saskatoon, Sask. Canada S7N 0W9

INTRODUCTION:

Oxidation of the plant hormone abscisic acid (ABA) by plants is known to give rise to two isomeric alcohols, 7'-hydroxyabscisic acid (7' OH ABA) and 8'-hydroxyabscisic acid (8' OH ABA), the latter of which readily isomerizes to a third isomeric substance, phaseic acid (PA). A method has recently been developed in our laboratories which generates 8' OH ABA in solution from PA (unpublished), and we have sought an analytical technique for the separation and characterization of mixtures of the three isomeric metabolites that could be applicable to extracts of plant material.

. This report describes methodology developed in this laboratory utilizing packed fused silica capillary LC in conjunction with continuous flow secondary ion mass spectrometry for the separation and characterization of these isomers. The report includes the observed differences in the individual isomers SIMS and CID product ion spectra.

EXPERIMENTAL:

All LC analyses were done using an Applied Biosystems Model 140A solvent delivery syringe pump. Samples (1 microliter made up in 25% acetonitrile in water) were injected through a Rheodyne Model 7520 injector onto a reversed phase spherisorb 3 micron C18 ODS2 packed fused silica capillary column prepared in this laboratory .

The mobile phase used for the LC analyses consisted of the following:

Solvent A 0.1% TFA; 2% glycerol in 80% acetonitrile.

Solvent B 0.1% TFA in 2% glycerol

Elution was achieved by using gradient conditions (described below) at a flow rate of 3 microliters/min. The gradient elution program as follows: 85% B for 3 min, then decreased to 72% B in 15 min, held for 5 min and decreased to 30%B after 40 min

The LC system was interfaced to a VG Analytical 70-250 SEQ hybrid mass spectrometer equipped for continuous flow SIMS analysis. The continuous flow SIMS stainless steel frit probe tip was designed in this laboratory . The probe tip was maintained at 50 degrees C. Spectra were obtained by scanning from m/z 500 to 80 (resolution of 1000 10% valley) at a rate of 3 sec/decade with a 0.5 sec. delay.

Product ion spectra were acquired by scanning from 50 to 500 every 3 sec. Xenon was the collision gas used at a pressure of 8 $X10^{-5}$ Torr. The collision energy was 16 volts (laboratory frame).

RESULTS AND DISCUSSION:

Phaseic acid, 7' OH and 8' OH ABA could not be separated (with this LC hardware) using isocratic LC conditions. However, employing the above gradient elution completely resolved the isomers. Figure 1 shows the chromatogram obtained from the analysis of a synthetic mixture containing the three isomers.

The CF/LC/SIMS spectrum obtained for each isomer is presented in Figure 2. The three spectra are similar, all having intense ions at m/z 373 indicating the glycerol adduct ion, m/z 281, the protonated molecular ion and m/z 263, the protonated molecular ion - H_2O. However, the spectrum of PA contains a fragment ion at m/z 165 that is not observed in the spectra of either 7' OH or the 8' OH ABA. This ion could be formed as a result of the loss of water from the 1' position and a subsequent loss of a rearranged portion of the side chain, resulting from cleavage between carbons 4 and 5. The spectra of 7' OH and 8' OH ABA both contain an ion at m/z 233 which is not observed in the spectrum of PA. This ion is postulated

to be formed as a result of the loss of methanal and water from the protonated molecular ion. In the spectrum of 8' OH ABA, the protonated molecular ion is the base ion while in the 7' OH ABA spectrum the molecular ion - H_2O is the most intense ion.

The collision induced dissociation (CID) product ion spectrum of the protonated molecular ion was also recorded for each isomer. Although the CID spectra, shown in Figure 3, contain many of the same intense ions as the LC/SIMS spectra, such as m/z 263, the protonated molecular ion - H_2O, m/z 165 in the PA spectrum and m/z 233 in the 7' OH and 8' OH ABA spectra, they are distinct from each other.

These mass spectral data along with the retention data allow the analyst to distinquish the isomers from each other. It should be noted that although the CID product ion spectra are somewhat different for each of these isomers, chromatographic separation of isomeric mixtures in conjunction with MS/MS provides much more reliable data.

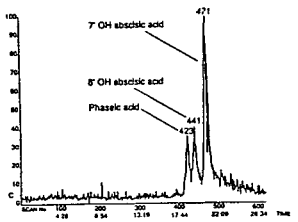

Figure 1

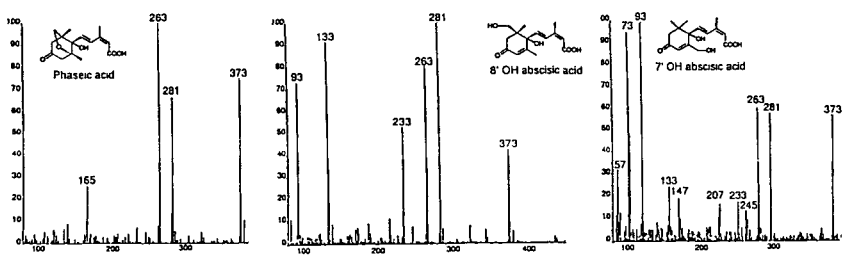

Figure 2

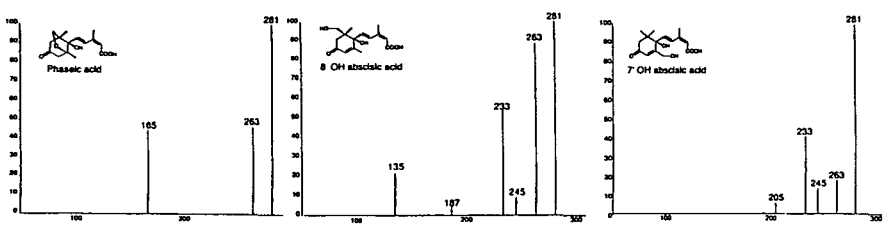

Figure 3

A MASS SPECTROMETRIC STUDY OF PHENOLIC GLYCOLIPIDS

A.I. Mallet[¶], D.E. Minnikin*, S. Hartmann* & M. Riddel[‡]l. St John's Institute of Dermatology[¶], UMDS, University of London, London SE1 7EH, UK, Dept pf Chemistry*, University of Newcastle upon Tyne, NE1 7RY, UK and Dept. of Medical Microbiology[‡], University of Gothenburg, S-41346, Sweden.

INTRODUCTION

Certain mycobacteria synthesise the dimycocerosic acid esters of 1,3 diols, the glycosylphenolphthiocerols, leading to the so-called phenolic glycolipids (PGL). Figure 1 shows the structures of these compounds and, apart from the stereochemical isomerism possible, there are a number of possible components according to the values of chain lengths present (x and y in the structures) and of the number of branched methyl groups on the mycocerosic acid side chains.

FIGURE 1. Phenolic glycolipid.

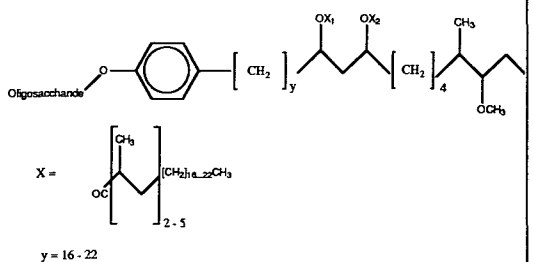

We report here the results of a study using FAB (LSIMS) MS in which we have surveyed families of PGL from a number of species and where we have determined the size of the mycocerosic acid chains. Confirmation of the substitution patterns has been obtained by tandem hybrid MS-MS. We have also investigated the use of MALDI-TOF mass spectrometry for analysis of the molecular species present.

METHODS.

Lipids were extracted by aqueous methanol:petroleum (1) from the dried organisms. Purification was carried out by silica gel chromatography.

Mass Spectrometry was performed on a VG Analytical (Fisons Instruments, UK) VSEQ hybrid tandem mass spectrometer. All spectra were obtained with a Cs gun operated at 30 kV and the sample (approx. 1 µg) was applied to a matrix of m-nitrobenzoic acid/methanol containing 0.1% NaI. MS -MS was carried out using a collision gas pressure of 2×10^{-6} torr (indicated) of Xenon in the Rf-only cell and a 20 ev collision energy (laboratory frame of reference). All spectra were collected in the continuum mode.

RESULTS

The PGL do not give protonated molecular ions by FAB ionisation and it is only by the formation of the sodiated (2) (or other alkali metal ion) species that a quasi-molecular ion can be detected. Clear spectra for mixtures of the molecular species present are obtained and these spectra also contain weak fragment ions corresponding to the successive loss of saccharide and of one mycocerosic acid side chain.

Table 1 summarises the species we have identified in a number of Mycobacteria and the tentative identification of the side chain lengths from the fragment ions present in the spectra.

In the case of *M. tuberculosis* (Canetti) we have been able to correlate the above identifications with the presence in the MS-MS spectra of two or three signals according to the presence of

TABLE 1

Species	M+ + Na	M- - olig	M- - olig - f.a.	C atoms in phenol unit	C atoms in mycocerosate
M. tuberculosis	1905, 1922 1850	1411 1454	952	Y=16	29
M. bovis	1488, 1530 1572	1828 1418	910 952	Y=16	26 29
M. marinum	1572 1586 1602	1418 1440	980	Y=18	29
M. kansasii	2134 2149 2178	1553 1524 1567	-	—	—
M. ulcerans	2105 2049 2079	1524	994 1022 1050	Y=16	30 32 34

a symmetrically or unsymmetrically substituted pattern of the mycocerosic acid side chains -X in Fig. 1- (Figure 2). These results extend the discovery of symmetric patterns of substitution found by PDMS in this organism earlier (3).

Off-line collection of HPLC fractions serves to show the nature of the isomers present with separation of species with differing number of branched chain methyl groups being specially difficult.

Figure 2

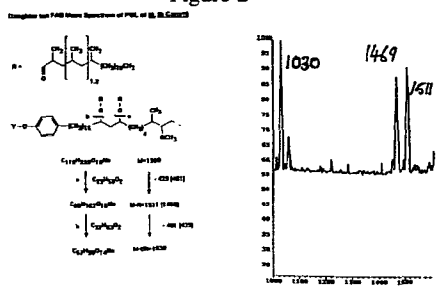

We have also carried out a preliminary study of these PGL mixtures using MALDI-TOF mass spectrometry. In an esculetin matrix clear signals, again from M. tuberculosis (Canetti) are obtained for the molecular ion region (M + Na)+.

DISCUSSION

While we have made advances towards the molecular speciation of this family of compounds three important questions still remain to be answered.

1. What is the precise configuration of attachment of the mycoserosate side chains?
2. Can a distinction be made between the isomeric esters of the trimethyl-branched C_{29} and the tetramethyl-branched C_{30} mycocerosates?
3. Can the stereochemistry be determined?

We are attempting to develop an on-line continuous flow FAB system, using non-aqueous solvent systems, so as to be able to carry out HPLC separation directly linked to the mass spectrometer and in the hope that this will provide a long lasting stable ion beam from which MS-MS measurements can more easily be performed in both positive and negative ion modes.

ACKNOWLEDGEMENTS.

We thank Dr David Harvey for the MALDI-MS spectra.

REFERENCES.

1. Minnikin D M et al Eur J. Clin. Microbiol., (1987) **6** 703-707
2. Marin L.M.L. et al Biochemistry, (1991) **30** 10536 - 10452.
3. Jardine I., et al., Anal. Chem., (1989) **61** 416.

The Characterisation of Lipophilic Peroctylated Cyclodextrins by Electrospray Mass Spectrometry (ESMS).

D. Parker and P.S. Bates, Dept. of Chemistry, University of Durham, South Road, Durham, DH1 3LE, UK. and B.N. Green, Fisons Instruments, VG Biotech, Tudor Road, Altrincham, Cheshire, WA14 5RZ, UK.

Lipophilic per-octyl cyclodextrins (CDs), when incorporated into an electro-active membrane, have been used as ionophores in enantioselective sensors for β-arylamino-alcohols. They contain a cavity which is size-selective for the binding and detection of tetrahedral ammonium ions. Hitherto, these compounds have been characterised by FDMS, but gave variable relative intensities for the various alkylated species. Methods involving NMR and DCI following reductive depolymerisation were reproducible but indirect.

Here we show that per-octyl α-, β- and γ-CDs may be characterised directly by ESMS, and the formation of complexes with various cations demonstrated. Furthermore, the selective binding behaviour of these CDs towards a variety of cations may be observed directly in competitive experiments by analysing them with mixtures of the cations in solution.

The water insoluble CD derivatives were analysed on a VG Quattro-BQ, a quadrupole instrument with a mass range of 4000 for singly charged ions. Of various solvents tested, 2-propanol containing 10 mM NH_4OAc gave intense, stable and reproducible spectra of the NH_4^+ adducts, suitable for characterisation, at concentrations of 20-50 pM/μl. Similar solutions containing various cation mixtures were used to study the competitive complexation phenomena. Mass scale calibration employed the NH_4^+ adducts from PPG3000 (1 μg/μl CH_3CN/H_2O plus 1 mM NH_4OAc). Masses were measured as average values based on the atomic weights of the elements .- C=12 011, H=1.00794, N=14.00674 and O=15.9994.

The α-, β- and γ-CDs contain 6, 7 and 8 glucose units resp. in a ring structure Incomplete octylation of the hydroxyls (3 per glucose), leaves a variable number of residual hydroxyls in the 3-position of the glucose units Methylation of the per-octyl CDs occurs on these residual hydroxyls to give the methyl-capped per-octyl CDs.

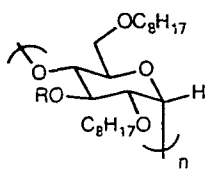

n=6 for α-CD
n=7 for β-CD
n=8 for γ-CD

R=H or C_8H_{17} for per-octyl CDs
R=CH_3 or C_8H_{17} for methyl-capped CDs

In Fig. 1 are spectra which illustrate the characterisation of per-octyl β-CD and methyl-capped per-octyl β-CD. They clearly show the distribution of species due to incomplete octylation of the CD. Good agreement for the mean number of octyls incorporated into all three CDs was obtained between ESMS and the less direct methods involving reductive depolymerisation Finally, Fig. 2 shows the response of per-octyl α-CD in a competitive experiment between a mixture of 0.2 mM ephedrinium trifluoroacetate and 10 mM NH_4OAc in 2-propanol. It shows that the selectivity for binding the ephedrinium ion is about 150 times higher than for the NH_4 ion.

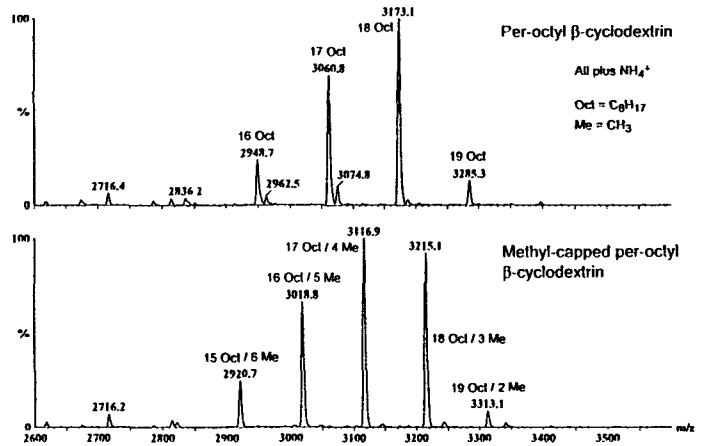

Fig. 1. Characterisation of per-octyl β-CD and methyl-capped per-octyl β-CD.

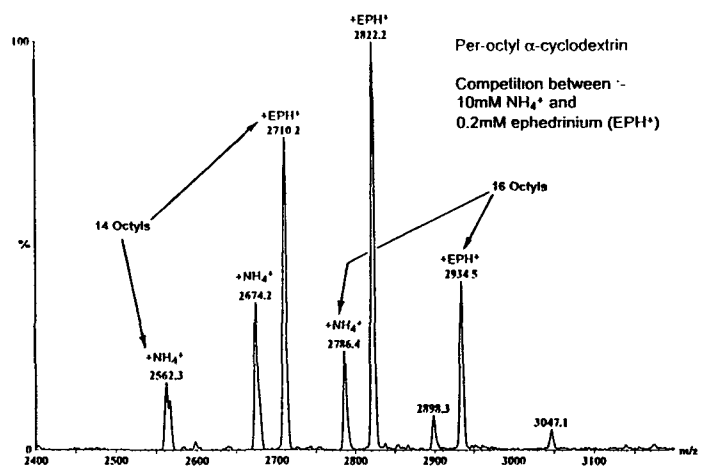

Fig. 2. Competitive binding of ephedrinium$^+$ and NH_4^+ with per-octyl α-CD.

Characterization of chemically-modified Cyclodextrins and their Host-Guest Complexation with Drugs by Ion Spray Mass Spectrometry.

H. K. Lim[1,2], K. Chan[1], M.Y. Zhang[1] and J.D. Henion[2], [1]Wyeth-Ayerst Research, CN 8000, Princeton, NJ 08543 and [2]Drug Testing and Toxicology, Cornell University, Ithaca, NY 14850.

Chemically modified cyclodextrins are cyclic oligosaccharides consisting of 6,7, or 8 α 1,4-linked glucose units which have undergone nonselective hydroxy chemical modifications. As a result, multiple species with various substituents are present which pose tremendous challenge to separation and characterization. These chemically modified cyclodextrins have a wide range of pharmaceutical use including enhancing solubility and separation of chiral drugs. The basis for these properties is related to the ability of these chemically modified cyclodextrins to form host-guest inclusion complexes with drug molecules. Substituents such as 2-hydroxypropyl or sulfate groups in varying numbers have been attached to the cyclodextrin molecules. Although 2-hydroxypropyl-β-cyclodextrin (HP-β-CD) has been characterized by electrospray MS, the number of substituents was not established (1).

We are interested in the full characterization of these modified cyclodextrins and their host-guest inclusion complexes by ion spray MS. The positive ion mass spectra of 2-HP-β-CD and 2-HP-γ-CD obtained at a mild declustering potential of 30V contained predominantly doubly charged ions corresponding to protonation of the cyclodextrins. In each case, the doubly charged ion cluster indicates the presence of 2-11 and 2-12 of 2-hydroxypropyl groups on the 2-HP-β-CD and 2-HP-γ-CD, respectively. Figure 1 is the positive ion mass spectrum of the 2-HP-β-CD containing species with 2-11 of 2-hydroxypropyl groups. The negative ion mass spectra of sulfated α-, β- and γ-cyclodextrins are characterized by three ion clusters with 3-5, 4-6 and 5-7 negative charges, respectively. These ion clusters indicate the presence of 5-11, 6-13 and 10-18 sulfate groups on α-, β- and γ-cyclodextrins, respectively. Figure 2 shows various species (6-13) and charge states (4-6) of sulfated β-CD.

Host-guest inclusion complexes have been observed with either 2-HP-β-CD or 2-HP-γ-CD and amine drugs like isoproterenol and atenolol. The mass spectra of host-guest complexation of either 2-HP-β-CD or 2-HP-γ-CD with isoproterenol or atenolol show the protonated drug molecule and the doubly charged ion clusters from protonation of the cyclodextrins and their respective complexes such as (drug)-cyclodextrin and (drug)$_2$-cyclodextrin. That host-guest inclusion complexes were not artifacts of the ion spray process is suggested by the presence of complexes even after centrifugal filtration with molecular weight cut-off of 1000 (figures 3). Futhermore, that the particular ions are indeed complexes is supported by MS/MS experiments which show the dissociation of the complexes into their respective protonated guest and host (Figure 4).

References

1. L. Prokai, Brewster, M.E. and Bodor, N, Proceedings of the 40th ASMS Conference of Mass Spectrometry and Allied Topics, Washington, DC, May 31- June 5, 1992, p. 18-19.

Acknowledgement: This work is supported in part by Wyeth-Ayerst Research.

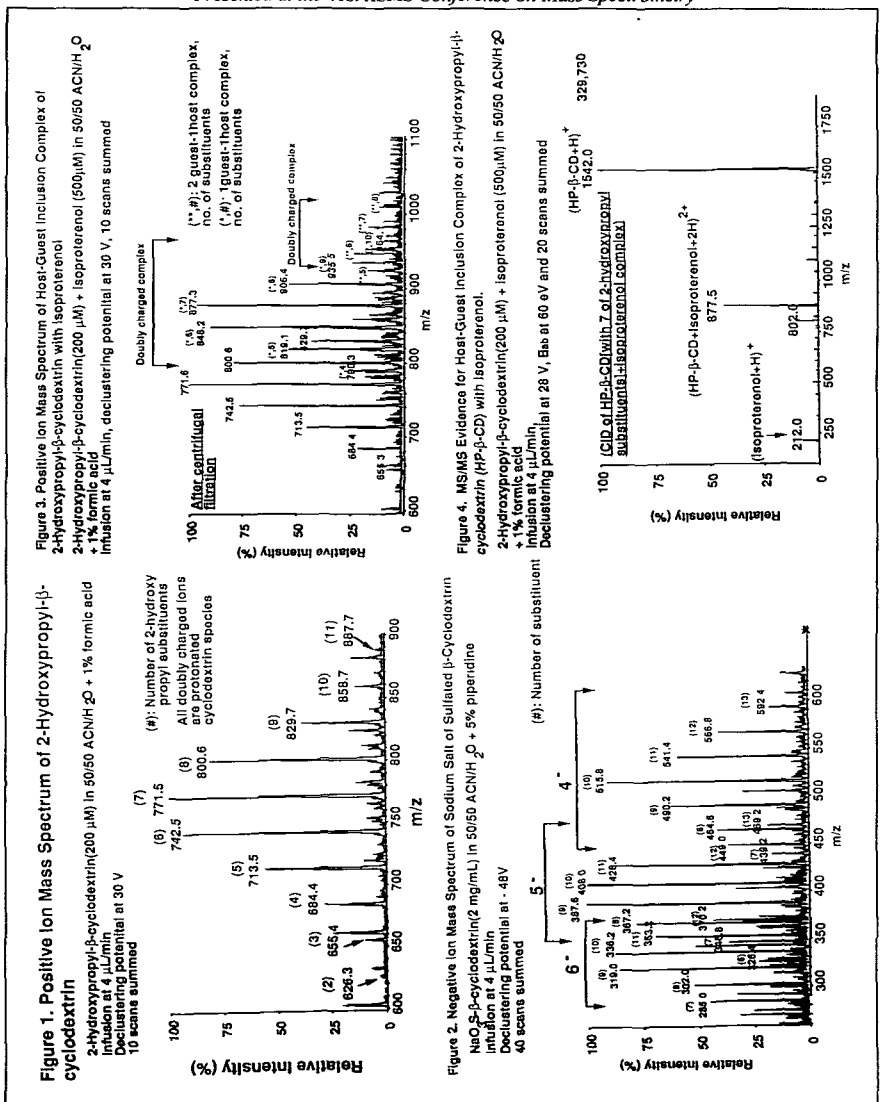

Characterization of Avidin by Electrospray Ionization Mass Spectrometry

Philip B. Smith[1], A. Peter Snyder[2], Tracey A. Simmons[3], and Martha M. Vestling[3].

[1]Geo-Centers, P.O. Box 68, Aberdeen Proving Ground, MD, 21010-0068,
[2]Edgewood R,D & E Center Aberdeen Proving Ground, MD, 21010-5423,
[3]Dept. Chemistry & Biochemistry, University of Maryland Baltimore County, MD 21228.

The application of electrospray ionization mass spectrometric techniques (ESI-MS) for the determination of the primary sequence of proteins has found widespread utility. However, only recently have these techniques been extended to the characterization of the oligosaccharide moiety of glycoproteins. Avidin a commercially available and relatively inexpensive glycoprotein was chosen as a test compound to evaluate the application of ESI-MS techniques to the characterization of glycoproteins.

The active form of Avidin a 60,000 Da. glycoprotein is a tetramer of 4 identical subunits[1]. The 128 residue primary sequence proposed by DeLange and Huang was confirmed by mass mapping and tandem mass spectrometric sequence analysis of proteolytic digests after enzymatic cleavage with endoproteinase Lys-C and removal of the carbohydrate moiety with N-glycosidase F. Comparison of results before and after N-glycosidase F incubation confirmed that the carbohydrate moiety was attached at Asn-17. A minor variant with Thr rather than Ile at position 34 was identified by tandem mass spectrometry as illustrated in Figure 1.

ESI-MS analysis of avidin revealed extensive sample heterogeneity, as illustrated in Figure 2. At least 16 different glycoforms were detected for the avidin subunit ranging in mass from 15,400 to 16,200 Da. Using the incremental masses for hexose and N-acetylhexose, it was possible to characterize the carbohydrate composition for each of the 16 glycoforms. Different distributions of the glycoforms were observed for different avidin preparations, suggesting the utility of ESI-MS for the determination of oligosaccharide heterogeneity in recombinant proteins.

REFERENCE

1. R.J. DeLange and T. Huang, *J. Biol. Chem.* **246**: 698-709 (1971).

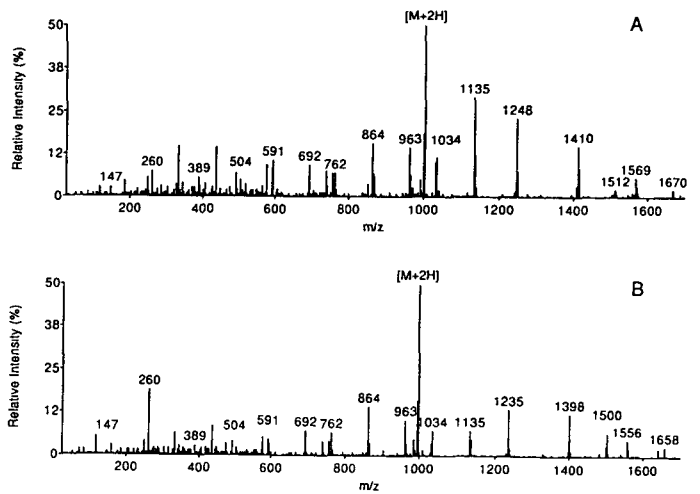

Figure 1. CAD product ion mass spectra of A) GEFTGTYITAVTATSNEIK and B) GEFTGTYTTAVTATSNEIK

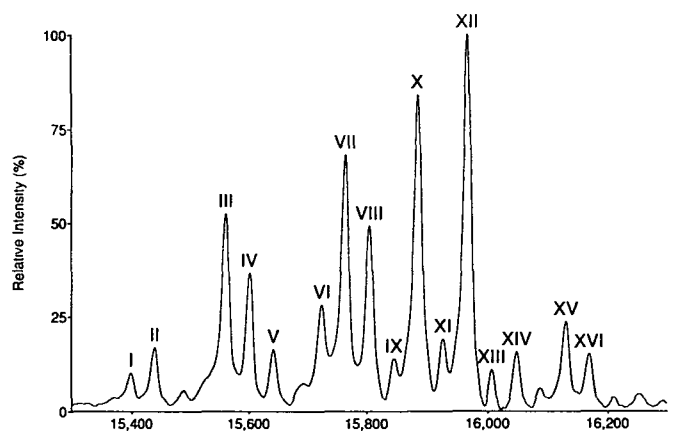

Figure 2. Reconstructed molecular weight plot for avidin

Characterization of Oligosaccharides by LC-MS Technologies.

W.M.A. Niessen[1], R.A.M. van der Hoeven[1], H.A. Schols[2], J. van der Greef[1] and A.G.J. Voragen[2].

1. Division of Analytical Chemistry, Center for Bio-Pharmaceutical Sciences, P.O. Box 9502, 2300 RA Leiden, The Netherlands.
2. Wageningen Agricultural University, Department of Food Science, Bomenweg 2, 6703 HD Wageningen, The Netherlands.

Introduction

In the past few years, considerable progress has been made in the development of methods for characterization of oligosaccharides in complex mixtures, especially with respect to the on-line coupling of high-performance anion-exchange chromatography (HPAEC, the separation method of choice for oligosaccharides) to thermospray and ionspray mass spectrometry. In this presentation, attention is paid to three aspects related to these developments:

- On-line HPAEC thermospray MS analysis of sugar oligomers in complex mixtures.
- Negative-ion thermospray MS of oligosaccharides.
- Structure elucidation by tandem mass spectrometry.

Experimental

A Finnigan MAT TSQ 70 tandem mass spectrometer, equipped with a 20 kV conversion dynode detection system, is used. A thermospray interface, operated at a block temperature of 400°C, a vaporizer temperature of 100°C with discharge and filament off, is applied in combination with HPAEC (performed on a Dionex HPAEC system equipped with a CarboPac PA100 column and a PAD electrochemical detector). An electrospray interface, operated with 3-3.5 kV nebulization potential and optimized tube-lens and nozzle-skimmer potentials is used with constant infusion (1-2 µl/min) via a Harvard Apparatus Model 22 syringe pump.

Rhamnogalacturonan digests

Pectin molecules from apple cell-wall material are considered to contain a galacturonan backbone and so-called "hairy" (ramified) region with a galacturonan backbone rich in rhamnose. Modified hairy regions have been isolated from pectins in apple juice and digested with a new rhamnogalacturonase[5]. HPAEC-MS of these digests confirm previous observations with NMR[6]. The following peaks were detected:

#	m/z	identity
1	685	$(Rha)_2$-$(GalA)_2$
2	847, 435	$(Rha)_2$-$(Gal)_1$-$(GalA)_2$
3	847, 435	$(Rha)_2$-$(Gal)_1$-$(GalA)_2$
4	1009, 516	$(Rha)_2$-$(Gal)_2$-$(GalA)_2$
5	1007, 515	$(Rha)_3$-$(GalA)_3$
6	1331, 677	$(Rha)_3$-$(Gal)_2$-$(GalA)_3$
6'	1331, 677	$(Rha)_3$-$(Gal)_2$-$(GalA)_3$
7	1493, 758	$(Rha)_3$-$(Gal)_3$-$(GalA)_3$

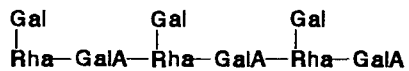

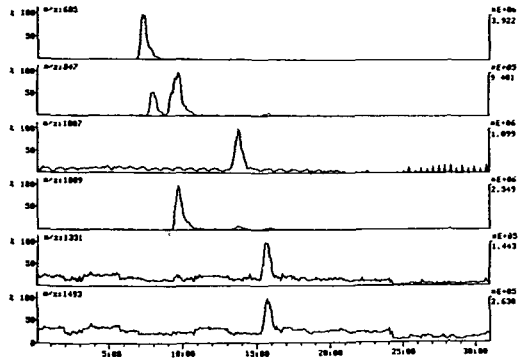

Negative-ion detection in HPAEC-thermospray-MS

Significant improvements in response are achieved in negative-ion mode relative to positive-ion mode. The mass spectra in negative-ion mode are more complex due to the formation of a series of adduct ions, e.g., $[M-H]^-$, $[M+OAc]^-$, $[M+HSO_4]^-$, and $[M+SO_4]^{2-}$. Further studies are needed to investigate negative-ion mode for other sugar types, e.g., glucuronic acid containing oligomers.

Tandem Mass Spectrometry of Oligosaccharides

Under the present ionization conditions, no fragmentation is observed. Fragmentation is required for further characterization of unknown oligosaccharides with respect to type of sugar and linkage and linkage position. Therefore, the use of tandem mass spectrometry was investigated, initially in combination with constant sample infusion in electrospray MS. Preliminary results indicate that differentiation between isomeric oligomers based on type of fragments and/or relative peak intensity is possible. As an example, the typical fragment ions observed in the negative ion MS-MS of two tetraose are given below:

Glc-(α-1,4)-Glc -(α-1,4)-Glc-(α-1,4)-Glc

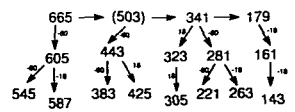

Gal-(α-1,6)-Gal-(α-1,6)-Glc-(α1-β1)-Fruct

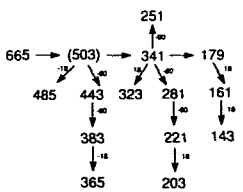

Acknowledgements

Dionex B.V. (Breda) is acknowledged for the loan of a HPAEC system.

Rapid and Sensitive Sequencing of N-Linked Oligosaccharides Using Matrix Assisted Laser Desorption Mass Spectrometry (MALD) and Mixtures of Specific Glycosidases.

*C.W. Sutton, J.A. O'Neill and J.S. Cottrell, Finnigan MAT Ltd., Hemel Hempstead, Herts. HP2 4TG, UK.

As more and more proteins are isolated it becomes apparent that an increasing number are glycosylated. In addition, many of the proteins that are being developed for therapeutic applications are also glycosylated. In the latter case quality control of the product is important for meeting FDA approval. Whereas rapid and sensitive techniques are available for characterisation of the protein component, developments in the analysis of the carbohydrate moiety have been much slower.

Edge et al (1) recently demonstrated the potential of using glycosidases to determine the carbohydrate sequence of free oligosaccharides. Subsequent analysis of the digest products was by the relatively slow and low resolution technique of Bio-Gel P4 gel permeation chromatography. This limited the approach to isolated oligosaccharides cleaved from the protein. MALD, on the other hand, is a high resolution technique with good accuracy (<0.1% error), sensitivity (0.1 to 10 pmol) and rapid analysis time (5 minutes). It has already been well established in the analysis of a wide range of biomolecules including peptides and oligosaccharides. As MALD has a high tolerance to buffers and is economical in sample use it is ideal for monitoring glycosidase digests.

A strategy for the general preparation and preliminary identification of glycopeptides is briefly described. The combination of glycosidase digests and MALD analysis is then used to demonstrate the effective elucidation of oligosaccharide structures. This approach is illustrated with special attention to the detailed characterisation of the two glycosylation sites of Tissue Inhibitor of Metalloproteinases (TIMP 1), Asn_{30} and Asn_{78} using specific glycosidases. Both sites have common features - (i) extensive heterogeneity due not only to varying levels of terminal sialic acid residues, but also in levels of terminal galactose residues, (ii) predominantly fucosylated antennary complex oligosaccharides are present, though Asn_{30} has a higher proportion of tri- and tetra-antennary structures than Asn_{78}. Digests using two different proteases enabled identification of non-glycosylated Asn_{78}-containing peptides indicating that there was only partial site occupancy.

The published specificity of the exoglycosidases had been primarily determined using free oligosaccharides as substrates. Bovine fetuin glycopeptides of known structure are used to demonstrated that the enzymes retained the same cleavage specificity in the presence of the peptide moiety.

In addition, a number of glycopeptides of well characterised glycoproteins - bovine fetuin, human α_1-acid glycoprotein and recombinant human tissue plasminogen activator - have been analysed in analogous digests to assess the potential accuracy of MALD for quantification. Comparison of results from MALD with previously published data, suggest that MALD can be used to determine the proportions of asialo-oligosaccharides on a particular glycosylation site with excellent reproducibility (Table 1).

(1) Proc. Natl. Acad. Sci. USA 89, 6338-6342 (1992) Fast sequencing of oligosaccharides: the reagent array analysis method. Edge, C.E. et al.

Table 1. Quantification - Comparison of Published Results with MALD-MS

Protein	Species	Glycosylation Site	Peptide	Oligosaccharide Published	LDMS % *	Cited %	Method	Reference
tPA	human, rec	N448	aa 441-449	Biantennary, fucosylated	66.7	61 5	HPAEC	3
				Triantennary, fucosylated	24 3	30 3		
				Tetraantennary, fucosylated	9 0	8 2		
fetuin	bovine	N156	aa 144-159	Biantennary	20.9	25.0	FAB-MS	4
				Triantennary	73 0	75 0		
				Triantennary, fucosylated	6 1	0 0		
a1 acid glycoprotein	human	N75	aa 69-83	Biantennary	1.7	0.0	RP-HPLC	5
				Triantennary	27.6	20.9		
				Tetraantennary	69 4	79 1		
		N54**	aa 50-63	Biantennary	9 0	9 0		
				Triantennary	39 1	32 0		
				Tetraantennary	50 7	58 9		
		N54***	aa 49-63	Biantennary	7 5	9 0		
				Triantennary	35 1	32.0		
				Tetraantennary	56 0	58 9		
		N16 ****	aa 1-21	Biantennary	10.9	8 8		
				Triantennary	85 7	91.4		
				Tetraantennary	1 1	0 0		

* In some cases oligosaccharides were observed not belonging to the groups identified in the publications - consequently the LDMS result may be less than 100%

** Joint chymotryptic/tryptic cleavage product, confirmed by Edman degradation sequencing

*** Joint chymotryptic/tryptic cleavage product, confirmed by Edman degradation sequencing

**** Genetic variant, gln21-> arg, confirmed by Edman degradation sequencing

Characterization of derivatized gangliosides by off-line HPLC, LSIMS, MS/MS and MALDI-TOFMS

*H. Perreault and C.E. Costello
Dept. of Chemistry, Massachusetts Institute of Technology, Cambridge, MA 02139

INTRODUCTION Gangliosides are essential membrane-bound glycosphingolipids of all vertebrates occurring in highest concentration in the central nervous system. Most gangliosides contain invariable tetrasaccharide backbones and a variable number of sialic acid residues. Native species are difficult to characterize in positive ion LSIMS and MALDI-TOFMS because the molecular ion-related peaks are relatively small and only little structural information is available. This may become a problem when mixtures are investigated, especially if the contribution from the background is high. Sensitivity and selectivity problems can be addressed by using derivatization, chromatography prior to mass spectral analysis and MS/MS. We report on three derivatization methods that yield more sensitivity and structural information in the positive ion mode and on MS/MS characterization of specific fragments. We also show that chromatographic methods such as HPLC can help to clean up samples in order to facilitate mass spectral analysis.

EXPERIMENTAL LSIMS and MS/MS spectra were recorded with a JEOL HX110/HX110 (E1B1-E2B2) instrument, operated at +10 kV accelerating voltage. The Cs^+ ion gun was operated at 25 kV. High energy collisions were induced at 7 keV in a collision cell (helium) located between MS-1 and MS-2. MALDI-TOFMS experiments were conducted with a modified VT2000 (Vestec Corp.) time-of-flight mass spectrometer. A nitrogen laser source (337 nm) was used. Peracetylated (PAC), permethylated (PME) and perbenzoylated (1) gangliosides derivatives were prepared. The gangliosides studied were obtained from human brain extracts and from commercial sources.

RESULTS For large gangliosides, direct permethylation is not possible because the native species are not soluble in the reaction solvent. Peracetylated derivatives are good intermediates because they are easily dissolved in organic solvents and also easily permethylated in the conditions that are routinely used for native material. The positive ion LSIMS and MALDI-TOFMS spectra of PAC gangliosides indicate that the formation of lactones occurs upon derivatization. These lactones do not interfere with subsequent permethylation, as the products are fully methylated according to the LSIMS and MALDI-TOFMS spectra of PAC-PME compounds. The positive ion LSIMS spectra of the PME derivatives of gangliosides have abundant (relative to the native species) $(M+H)^+$ and/or $(M+Na)^+$ and structure-related fragment ions (2), that include ceramide-related ions. When subjected to high energy collisions, the latter yield CID spectra which can denote heterogeneity in the structure of the ceramide in certain cases.
Mixtures of native gangliosides are conventionally separated by high performance thin layer chromatography (HPTLC) (3). HPLC can be substituted for HPTLC if substantial amounts of native material are available, but the UV detection becomes restricted if only nanomoles of gangliosides are to be analyzed. In the latter case, perbenzoyl derivatives (1) provide a substantial increase in sensitivity since benzoyl groups strongly absorb at 230 nm. Post-derivatization cleanup or separation can be conducted either in normal or reversed phase HPLC; Figure 1 shown the normal phase chromatogram obtained for the cleanup of PBZ GD1b. In our hands, the normal phase method provided no separation between individual species and thus was used as a cleanup

method after the PBZ reaction. The reversed phase HPLC method offered better resolution and individual species were eluted at different times. However, no separation between homologs of the same species was obtained. PBZ gangliosides, like PME species, show a substantial increase in sensitivity in LSIMS relative to the native species. Figure 2 shows the molecular ion region of the LSIMS spectrum obtained for PBZ GD1b. This region shows a high lability of the benzoyl groups as they are ejected from the molecular ion and from the $(W\text{-}NH)^+$ fragment (partial loss of the base chain). The low and middle-mass region of the LSIMS spectra of PBZ derivatives contains abundant ions that CID experiments indicate are related to the sugar and ceramide structures. The assignments of these ions are not yet complete.

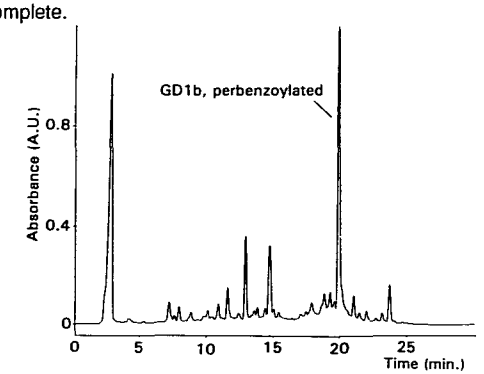

Figure 1: Reversed phase HPLC chromatogram of the reaction mixture of PBZ-GD1b

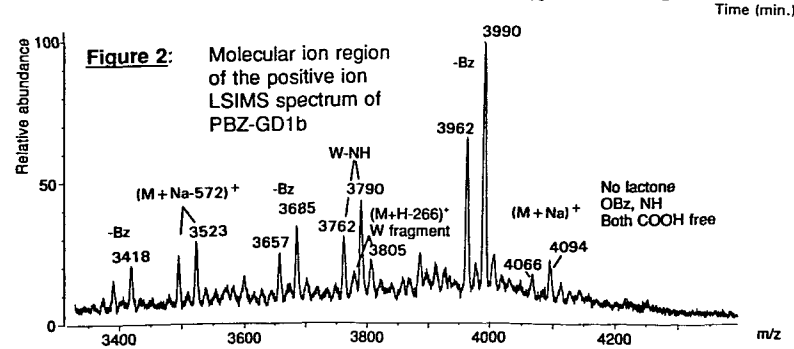

Figure 2: Molecular ion region of the positive ion LSIMS spectrum of PBZ-GD1b

The authors would like to acknowledge L. Svennerholm for kindly providing the GQ1b and GP1b/1c samples and M.D. Ullman for his precious advice on the perbenzoylation of gangliosides. These studies were supported by the NIH Center for Research Resources, Grant No. RR00317, to K. Biemann. H. Perreault is supported by a NSERC fellowship (Canada).

1 M.D. Ullman and R.H. McCluer, *J. Lipid Res.*, **26**, 1985, 501-506.
2. C.E. Costello and J.D. Vath, in *Meth. Enzymol*, Vol. 193, 738-768, J.A. McCloskey Ed., Academic Press, 1990.
3. H. Miller-Podraza, J.E. Månsson and L. Svennerholm, *FEBS Letters*, **288**, 1991, 212-214.

Mass Spectrometry of 3,4,6-Tri-0-Benzyl-C-Glucopyranosides Containing XC_6H_4S Substituents at C-2.

B.V. Rozynov[1], R.J. Liukkonen[2], R.M. Carlson[2], D.W. Kuehl[3]
I.P. Smolikova, R. Caple, W.A. Smit

1. Shemyakin Institute of Bioorganic Chemistry, Moscow, 117871, Russia
2. University of Minnesota-Duluth, Duluth, MN, 55812, USA
3. U.S. EPA, ERLD, Duluth, MN, 55804, USA

Introduction

There has been a growing interest in the synthesis of C-glucopyranosides due to their biological activity and possible use in biochemical, medical, and plant physiological studies. Electron impact (EI) mass spectrometry has been shown to be an efficient method for the structural characterization of acetylated derivatives of C-alkyl and C-aryl glucopyranosides (1,2). Recently we reported the synthesis of several 3,4,6-tri-o-benzyl-c-glucopyranosides modified at the C-2 position with XC_6H_4S, where X=CH_3 or Cl (3). The objective of this study was to access the use of EI and electron attachment negative chemical ionization (NCI) mass spectrometry for the structural characterization of these benzylated 2-thio modified C-glucosides.

Experimental

Low resolution mass spectra were recorded on a Finnigan-MAT model 4500 mass spectrometer using a desorption direct sample introduction probe. EI ionization energy was 70eV. NCI spectra were obtained with Argon at 0.5-1.0 Torr. Elemental composition was determined using a Finnigan-MAT model 95 operating at 7000 resolution.

Results

The benzyl ion (m/z 91) was found to be the base ion for each compound studied by EI. However, the molecular ion was significantly intense to allow molecular weight determination. Fragmentation was interpreted in terms of positive charge localization of the molecular ion (4) and proceeded according to rules for normal carbohydrates (5). The proposed fragmentation pathways are shown in schemes I-IV below. Electron attachment spectra and subsequent disassociation produced molecular anions and fragment anions diagnostic of the thio moiety at C-2.

Conclusion

EI and NCI mass spectra are highly sensitive toward and diagnostic of benzyl derivatives of C-2 thio modified glucopyranosides.

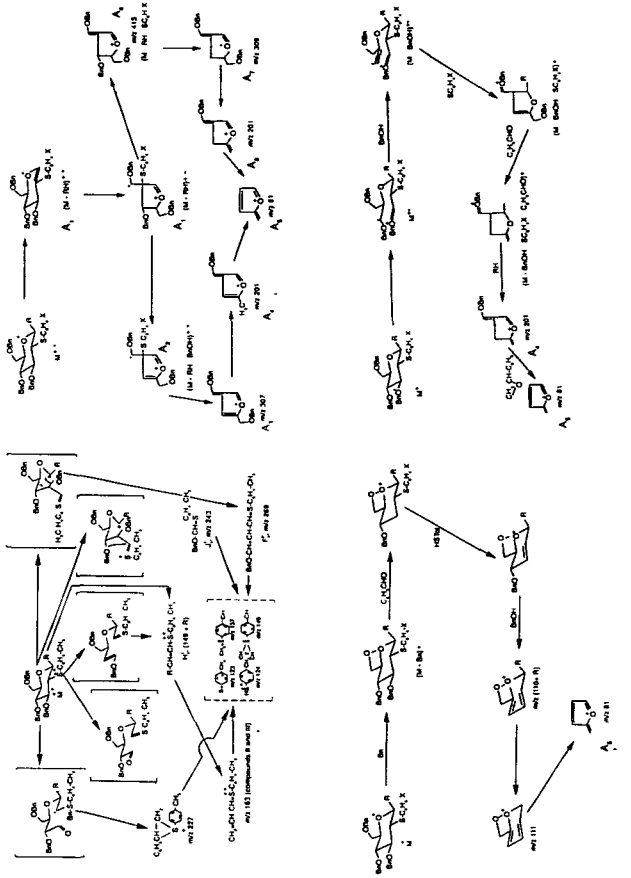

References

1. Rozynov, B.V., et. al. IZV. Akad. Nauk USSR, Sen. Kim. (1976) 5:1157
2. Biaznikova, M.G., et. al. Antibiotiki (1984) 29(12):884
3. Smoliakova, I.P, et. al. Tetrahedron Lett. (1993) 34(19):3047
4. Rozynov, B.V., et. al. Mass Spectral Characterization of 3,4,6-Tio-O-Benzyl-C-Glucopyranosides containing XC_6H_4S Substituents at C-2. (1993) Rapid Communication Mass Spec, submitted
5. Kochetkov, N.K., et. al. Carbohydr. Chem. (1966) 142:39.

Analysis of Heterogeneity of Native α_1-Acid Glycoprotein

Simin D. Maleknia[1], Micheal J. Trueheit[2], James E. Carlson[2], H. Brian Halsall[2] and Catherine E. Costello[1]
Department of Chemistry, Massachusetts Institute of Technology, Cambridge, MA 02139-4307
Department of Chemistry, University of Cincinnati, Cincinnati, OH 45221-0172

Introduction Human α_1-acid glycoprotein (orosomucoid; OMD) is an acute phase reactant present in blood. OMD contains five *N*-asparaginyl-linked glycan chains with variations in the branch numbers and in the sialic acid and/or fucose content.[1-3] The concentrations of the glycoforms differ at each site with disease state.[4] Mapping the sialic content at each site may prove useful to the study of glycosyl transferase activity. An earlier investigation described the glycoform heterogeneity of the glycoprotein after desialylation. This was achieved by analyzing the glycopeptides from a proteolytic digest (*Staph* V-8) using HPLC and affinity chromatography in conjunction with matrix-assisted laser desorption ionization time-of-flight mass spectrometry (MALDI-TOFMS).[2] A similar approach has been applied to analyze the sialic acid content of the individual glycopeptides. An ultimate goal is to differentiate the various isomers (glycomers).

Experimental A Modified VT2000 (VESTEC) linear time-of-flight mass spectrometer was operated at an accelerating voltage of ± 30 kV. The laser source was a nitrogen laser (337 nm) with a 3 ns pulse width. A Lecroy 9540A digitizing oscilloscope with a 400 MHz sampling rate was used. The matrix consisted of the 2:1 mixture of *o*-aminobenzoic acid and nicotinic acid at a concentration of 12 g/l. Total sample applied was in the range of 5 to 10 pmoles.

Results & Discussion The technique of MALDI-TOF has been applied to show the higher order heterogeneity induced by the presence of sialic acids. The sialic acid pattern is unique to the individual sites. The glycoform heterogeneity at site III is indicated in Figure 1A. The maximum number of sialic acids (two through four) is observed for each carbohydrate structure. Separation of tetra-, tri-, di- and mono-sialylated glycoforms was achieved by HPLC purification (column:C_{18}, gradient: 100% H_2O to 60% acetonitrile at 1ml/min.). Glycopeptides with the highest number of sialic acids showed the lowest retention time. The higher order effect of sialic acids was removed by neuraminidase digestion (Figure 1B). At this site, more branching is observed with tetrantennary form predominating. Similarly, tri- and terta-antennary structures are more abundant at sites IV and V. Several glycoforms with an additional *N*-acetyllactosamine are also observed. Additionally, fucosylated glycoforms are detected for tri- and tetra-antennary structures. The relative abundances of glycoforms are presently being compared to chromatographic data. A sialic acid content of 15.0 per mole has been reported for human α_1-acid glycoprotein by acid hydrolysis and high-pH anion exchange chromatography (HPAE).[5] Future goals include complete mapping of the sialic acid content at each site and detailed structural elucidation of glycomers by application of oxidation, reduction and alkylation reactions.

Presented at the 41st ASMS Conference on Mass Spectrometry

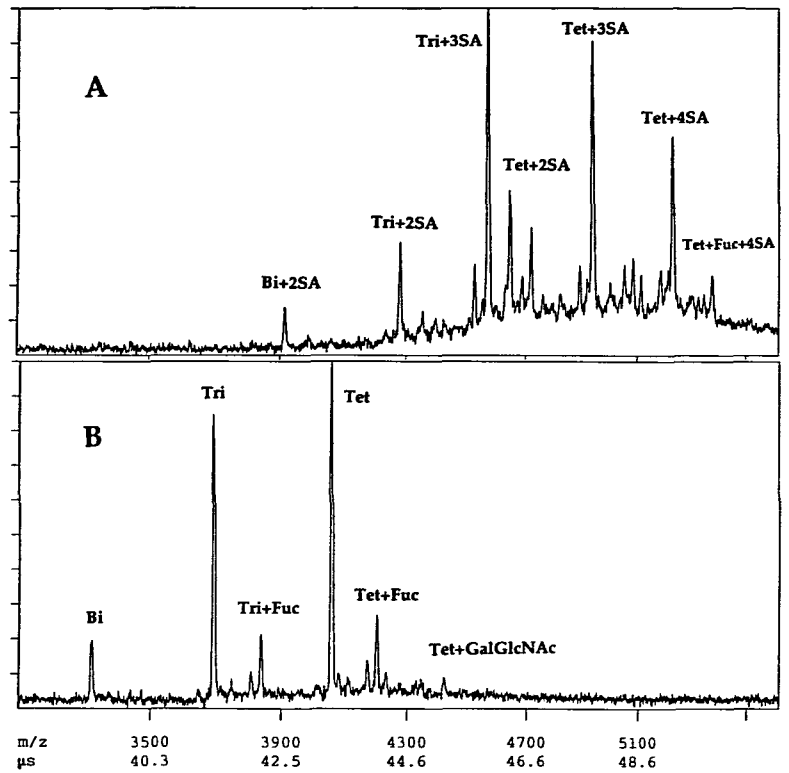

Figure 1: negative ion MALDI-TOF mass spectra of glycopeptides at Site III.
B) after neuraminidase digestion.

1. K. Schmid, R. B. Nimberg, A. Kimura, H. Yamaguchi and P. Binette *Biochim. Biophys. Acta* **1977**, *492*, 291.
2. M. J. Treuheit, C. E. Costello, H. B. Halsall *Biochem. J.* **1992**, *283*, 105.
3. P. Hermentin, R. Witzel, R. Doenges, R. Bauer, H. Haupt, T. Patel, R. B. Parekh and D. Brazel *Anal. Biochem.* **1992**, *206*, 419.
4. M. J. Treuheit and H. B. Halsall *Chromatographia*, in press.
5. P. Hermentin, J. Seidat *Protein Glycosylation: Cellular, Biotechnological and Analytical Aspects*, H. S. Conradt, Ed. **1992**, GBF Monograph 15, 185.

Acknowledgements This work was supported by the NIH Center for Research Resources Grant No. RR00317 awarded to K. Biemann.

Predictability of Fragmentations in Negative ion FAB MS of Reducing Oligosaccharides.

D. Garozzo*, G. Impallomeni, R. Rapisardi, E. Spina, L. Sturiale and E. Vinciguerra.

Istituto per la chimica e la tecnologia dei materiali polimerici del C.N.R.
Viale A. Doria 6, 95125 Catania, Italy

In soft ionization mass spectrometric analysis of underivatized carbohydrates, molecular ions can undergo three kinds of fragmentation: cleavage of the glycosidic bond between two monosaccharide units, breakdown of one of the sugar rings at the extremities of the molecule, and loss of substituents, if any.

Negative Ionization is able to promote sugar ring fragmentation in reducing underivatizated oligosaccharides.

This fragmentation starts from the reducing end producing fragments that are characteristic of the linkage positions present in the oligosaccharide.

In the sugar ring fragmentation, the negative charge is retained on the non-reducing end of the molecule. The peculiarity of negative ionization is supposed to be the selective deprotonation of the anomeric hydroxyl, which is more acidic with respect to the alcoholic groups, with formation of an ion bearing the negative charge on the reducing end. In this way, fragmentation starts from the reducing end, and a progressive erosion of monosaccharide units towards the non reducing end of the oligosaccharide occurs. This "peeling" of monosaccharide units results in the formation of a saccharide containing one sugar unit less then the molecular ion and with the new anomeric hydroxyl negatively charged, thus reproducing the initial situation at the reducing end.

On the other hand, fragmentation of the glycosidic bond can, in some cases, produce ions with retention of the negative charge on the reducing end of the oligosaccharide.

This is the case when a 3-O linkage is present; fragmentations observed in a trisaccharide, b trisaccharide and 3-fucosyllactose are reported in scheme 1a, b and c respectively.

The fragmentation pattern outlined in scheme 1 shows that, after the elimination of the monosaccharide linked at the 3-O position, the reducing sugar ring looses the hydroxyl or the substituent group at the C4 together with an hydrogen atom, as well as the C5-C6 moiety. This allows, in principle, to establish the molecular weight of substituents of the reducing unit not only at the 3-O position but also at the remaining linkage sites using a combination of MS and tandem MS experiments.

Sugar ring fragmentations can be suitable for the differentation of monosaccharides if a substitution at one OH is present (i.e. N-acetamido glucose, deoxyglucose). In Fact, the negative ion FAB mass spectra of three x N-Acetamido x- deoxy glucose (x=2,3,6) permit easily differentiation between the monosaccharides; in fact peak at m/z 119 (loss of C1-C2) is present only in 2 N-Acetamido glucose, peak at m/z 160 (loss of C1-C2) is present only in 6 N-Acetamido glucose, and these peaks are absent in the spectrum of 3 N-Acetamido glucose.

An analog situation is present in 2- and 3-deoxyglucose.

ACKNOWLEDGEMENTS

Partial financial support from the Italian Ministry for University and for Scientific and Technological Research (MURST) and from the National Council of Research (CNR) (Rome), Finalized Project of Fine and Secondary Chemistry, is gratefully acknowledged.

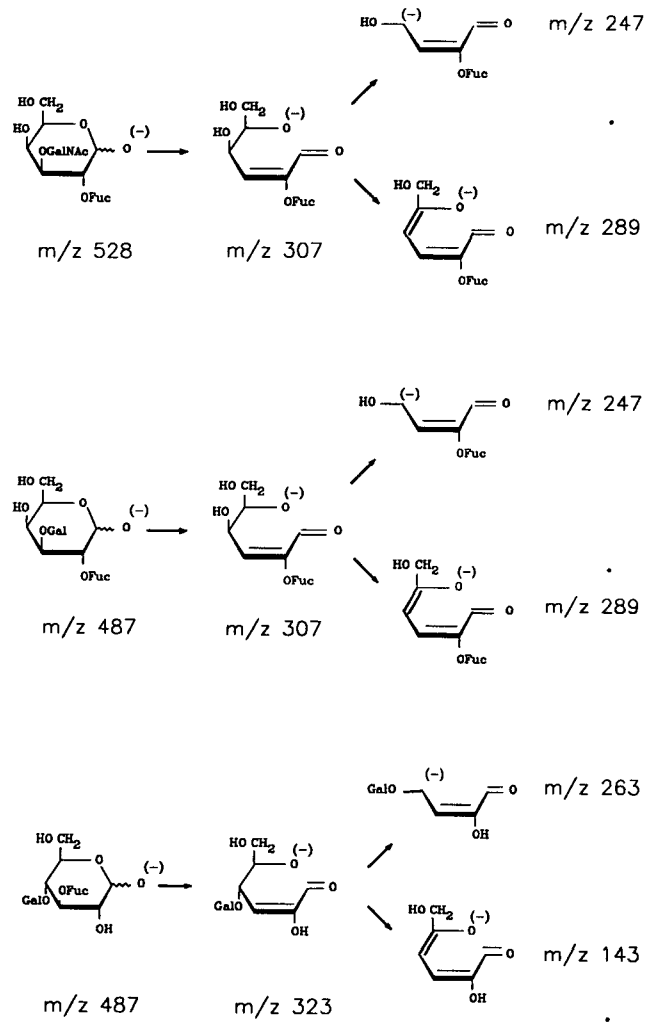

Does conformation play a role in the fragmentation behavior of oligosaccharides? A study with three α-D-NeuAc-(2-6)-β-D-Gal sialosides and six related, conformationally more rigid α-D-NeuAc-(2-6)(6-R,S)(6-Me)-β-D-Gal derivatives.

*Zamas Lam[§], Subramaniam Sabesan[¶] and Barbara Larsen[¶].

The DuPont Company, [§]Haskell Laboratory for Toxicology and Industrial Medicine, Newark, DE 19714. [¶]Central Science & Engineering, Wilmington, DE 19880.

Oligosaccharides in aqueous solution can exist as an equilibrium mixture of conformers, each with a distinct local energy minimum and barrier to interconversion. The desorption process in mass spectrometry supplies excess kinetic energy to the oligosaccharides and as a result, the conversion between various conformers is expected to be more rapid in the gaseous phase as compared to the aqueous phase. In spite of this, we observe a similarity in the gas phase unimolecular decomposition behavior of sialosides that are known to have similar conformational properties in aqueous solution.

The unimolecular decomposition behavior of α-D-NeuAc-(2-6)-β-D-Gal sialoside (1) which represents the terminal units of many glycoproteins and glycolipids was compared to two C-6 methyl analogs which exists as the *gt* (2) and *tg* (4) rotamers. From nmr studies, it has been established that the natural sialoside 1 exists predominantly in the *gt* orientation. In the unimolecular decay of the analogs, the *gt* rotamer has a prominent fragment ion at m/z 558 (loss of ethylene), while the *tg* rotamer does not. The natural sialoside also has a prominent loss of an ethylene unit, which suggests that during the desorption process the *gt* orientation is favored.

To explain the fragmentation behavior, a hydrogen bonded complex and proton migration model is proposed. The protonation of the sialosidic oxygen may take place *via* the carboxylate group. If the C-6 arm of the galactose is maintained in the *gt* rotamer orientation, this proton can then be stablized by three hydrogen bonds involving O-6, O-5, and O-4 of the galactose. This proton is in very close proximity to the trimethyl silyl ethyl aglycone, therefore, it can migrate to the aglycone oxygen and result in the loss of the ethylene unit. For the *tg* rotamer, there can only be weak hydrogen bond stabilization involving O-6 and O-4.

The unimolecular decay of β-D-NeuAc-(2-6)-β-D-Gal sialoside (10) as compared to the methyl C-6 analogs which by design are in the *gt* (11) and *tg* (12) conformation is less conclusive. The natural β-sialoside gave less fragmentation than the natural α-sialoside but more the the *gt* and *tg* β-sialosides.

In the fragmentation of the isopropylidiene derivatives, the *tg* sialoside (8) favored the loss of acetone and the *gt* sialoside (5) produced abundant N-acetylneuraminyl (m/z 292) fragment. The unimolecular decay of the natural sialoside (3) gave a very prominent m/z 292 ion suggesting the *gt* orientation was favored during the desorption process.

The isopropyliediene thio analogs appear to follow a similar fragmentation mechansim as the natural sialoside. The *gt* sialoside (6) favors the formation of the m/z 292 fragments more than the *tg* sialoside (9). The fragmentation of the natural sialoside (3) is simlar to the *tg* sialosides suggesting that 3 is predominantly in the *tg* orientation during the desorption process.

In conclusion, the oligosaccharides appear to maintain their aqueous conformation during the desorption process, the fragmentation process is conformation mediated, and an excess energy are required to overcome interconversion barrier.

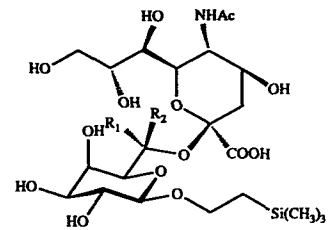

1 $R_1, R_2 = H$
4 $R_1 = CH_3, R_2 = H$
7 $R_1 = H, R_2 = CH_3$

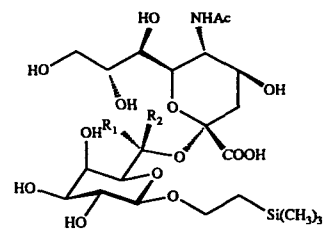

10 $R_1, R_2 = H$
11 $R_1 = CH_3, R_2 = H$
12 $R_1 = H, R_2 = CH_3$

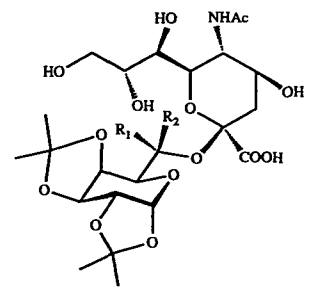

2 $R_1, R_2 = H$
5 $R_1 = CH_3, R_2 = H$
8 $R_1 = H, R_2 = CH_3$

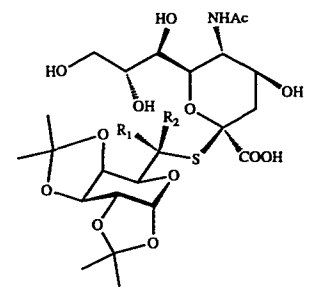

3 $R_1, R_2 = H$
6 $R_1 = CH_3, R_2 = H$
9 $R_1 = H, R_2 = CH_3$

Comparative Study of Carbohydrate Structures of Recombinant Human Platelet Derived Growth Factor Expressed in Chinese Hamster Ovary and in Saccharomyces Cerevisiae

Eric Watson, Anjali Bhide, Bhavanna Shah, William C. Kenney and *Herman van Halbeek.

Amgen Inc., Amgen Center, Thousand Oaks, CA 91320.

*Complex Carbohydrate Research Center and Department of Biochemistry, The University of Georgia, Athens, GA 30602.

Platelet-derived growth factor (PDGF) is a major mitogen in serum for connective tissue and glial cells (1,2). There are two homologuous chains, termed A and B, that are disulfide bonded and as a result three different dimeric forms are present : AA, AB, BB. Recombinant glycoproteins produced by different cell lines and eukaryotic organisms have been the subject of much interest in recent years. Recombinant glycoproteins are most frequently expressed in either Chinese hamster cells or in Saccharomyces cerevisiae as hosts for their biotechnological production on a commercial scale. While both types are capable of producing N-and O-linked glycans, there are structural differences between these glycans. The availability of recombinantly produced PDGF in CHO and yeast cells provided sufficient amounts for characterisation by chemical techniques and allowed us to compare the different glycosylation produced by CHO cells and in yeast.
In this report, glycans of recombinant PDGF-BB produced both in yeast and in CHO cells are described. . Structure determination was

carried out using carbohydrate composition, methylation analysis, MALDI and 500-MHz H-NMR spectroscopy. The carbohydrate structures of rhPDGF expressed in CHO cells comprised O-linked oligosaccharides that were linear tri- and tetra-oligosaccharides with one and two sialic acids respectively. The major N-linked oligosaccharides were complex type di-, tri and tetra-antennary N-acetyllactosamine that contained one, two and three sialic acids. All complex type oligosaccharides contained fucose α(1-6) linked to the proximal N-acetylglucosamine residue. Mature human PDGF-BB does not contain consensus sites for N-linked glycosylation and the presence of N-linked glycosylation as shown here arises from incomplete removal of the precursor sequence.

The presence of several substituted neuraminic acids, NeuGC, Neu5Ac2en, Neu5,9Ac2 and Neu2,7-anhydro5Ac in minor amounts were identified by GC-MS as their trimethylsilyl derivatives under electron impact ionization conditions Figure shows these EI-MS.

The carbohydrate structures in yeast cells were much less diverse and consisted solely of mannose in monosaccharide and dissacharide forms in approximately equal amounts. Both of these are typical yeast O-glycans. There was no evidence from chromatographic separations for other glycans such as trisaccharides being present.

References

(1) Heldin, C.-H., Wasteson,A., and Westermark, B. (1985) Mol. Cell . Endocrinol. 39, 169-187.

(2) Ross,R., Raines, E.W., and Bowen-Pope, D.F. (1986) Cell 46, 155-169.

Electrospray Mass Spectrometry of Heparin Oligosaccharides

*W. Chai[1], B.N. Green[2] and A.M. Lawson[1]

[1]MRC Clinical Research Centre, Watford Road, Harrow, Middlesex HA1 3UJ, UK
and [2]VG Bio Tech, Tudor Road, Altrincham, Cheshire WA14 5RZ, UK

Introduction

Despite the widespread use of heparin in medicine as an anticoagulant, and the increased interest in its possible role in cellular recognition, the assignment of the precise structures of the biologically active regions in the polysaccharide chains of heparin remains a difficult task.

Mass spectrometry, particularly FABMS (and L-SIMS), has been used for analysis of heparin oligosaccharides with either thioglycerol (1) or triethanolamine (2) as matrix. Ion-spray mass spectrometry has been demonstrated for analysis of oligomer fragments of hyaluronic acid and chondroitin 6-sulphate (3), members of the same glycosaminoglycan (GAG) family as heparin, but having none or only one sulphate group per disaccharide repeat unit, respectively. Among the GAGs, heparin is the most heavily sulphated with highly heterogeneous regions which represent a major challenge to structural analysis.

In the present study, five disaccharide fragments derived from heparin and three from chondroitin sulphate were analysed by ESI-MS using a triple-stage quadrupole instrument (VG-Quattro-BQ, VG Biotech, Altrincham, U.K.), in order to assess the sensitivity of the technique and its ability to give structural information on these anionic oligosaccharides.

Results and Discussion

Good quality negative-ion spectra were obtained from all eight GAG-derived disaccharides examined using less than 0.6 nmol of material with low nozzle-skimmer voltage. The nozzle-skimmer voltage has a strong affect on the fragmentation (desulphation) and charge states, and it can be optimized to give essentially no fragmentation in the normal ESI mass spectra. Isomeric structures having the same number of sulphates gave similar ESI spectra. As representative, the spectrum of disaccharide I-S, ΔUA(2S)1-4GlcNS(6S) (MW 577, with 3 sulphates), and the data transformed onto a true molecular mass scale are shown in Fig. 1.

The ESI spectra are dominated by $[M-nH]^{n-}$, where M represents the mass of the free acid and the charge (n) is largely dependent on the number of sulphate groups present. Molecular mass and composition (in terms of uronic acid, hexosamine and sulphate groups) can be easily derived. Although less abundant sodium adduct ions are also present, sulphate loss and other fragmentations were not observed at the low nozzle-skimmer voltage used.

Collision-induced ESI-MS/MS experiments were carried out to determine if more detailed structure could be deduced since, depending on conditions, fragmentation was only either limited or dominated by losses of sulphate substituents in the normal ESI spectra.

In ESI-CID-MS/MS spectra of the singly charged $[M-H]^-$ precursors, both glycosidic and ring fragmentation occurs to give useful information on the glycosidic linkages and sulphate positions. The ESI-CID-MS/MS spectra of heparin disaccharides II-A and III-A (Fig. 2) demonstrate the significant differences in the spectra of isomeric structures which would allow unambiguous differentiation of possible isomers. Interestingly, the four monosulphated disaccharides examined here by low energy argon collisional activation showed very similar fragmentation patterns to those produced by high energy FAB-CID-MIKE (4).

Doubly and triply charged, and sodiated quasi-molecular ions were also selected as precursors, but complicated and less informative daughter-ion spectra were obtained (not shown). Further work is needed to optimize conditions for ESI-MS/MS of multiply sulphated and higher oligomers.

Fig. 1. Negative-ion ESI spectrum of I-S.

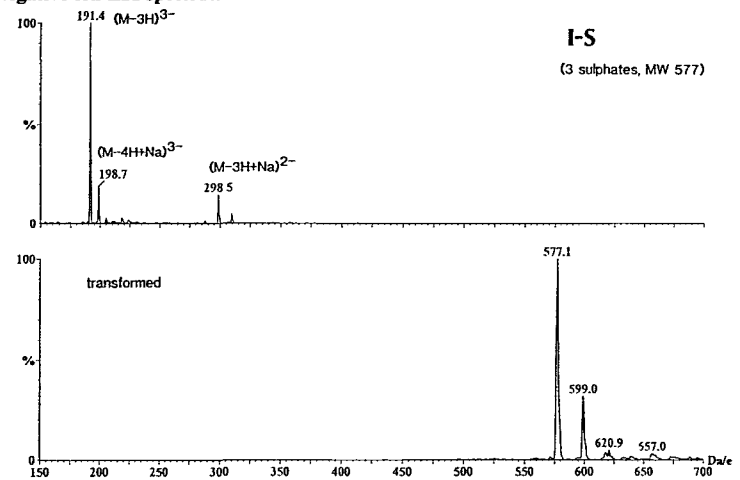

Fig. 2. ESI-CID-MS/MS spectra of II-A and III-A.

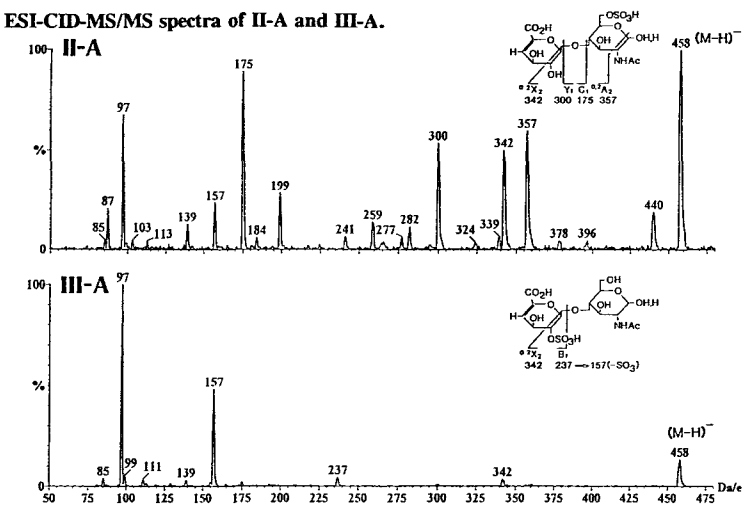

References

(1) V.N. Reinhold, S.A. Carr, B.N. Green, M. Petitou, J. Choay & P. Sinay, *Carbohydr. Res.*, **161**, 305 (1987); (2) L.M. Mallis, H.M. Wang, D. Loganathan & R.J. Linhardt, *Anal. Chem.*, **61**, 1453 (1989); (3) K. Takagaki, K. Kojima, M. Majima, T. Nakamura, I. Kato & M. Endo, *Glycoconjugate J.*, **9**, 174 (1992); (4) D.J. Lamb, H.M. Wang, L.M. Mallis & R.J. Linhardt, *J. Am. Soc. Mass Spectrom.*, **3**, 797 (1992).

Structure determination of the major sialylated oligosaccharide chains of recombinant derived erythropoietin expressed in Chinese hamster ovary cells.

E.Watson, Anjali Bhide and *Herman van Halbeek.

Amgen Inc., Amgen Center, Thousand Oaks, CA 91320

*Complex Carbohydrate Research Center and Department of Biochemistry, The University of Georgia,Athens, GA 30602.

Introduction

Anemia is a major complication arising from chronic renal failure and a reduction in EPO production is the cause for this disease. Studies have since shown that anemia can be corrected following the administration of recombinant EPO (1,2).

Structural characterisation of oligosaccharides in EPO produced in CHO, Baby hamster kidney (BHK) and HeLa cells has been described (3-6). These EPOs have been shown to contain about 40 % N-linked carbohydrates with the major structures being di-,tri-, and tetra-antennary oligosaccharides. O-Linked structures are also present but in much smaller amounts. In only one of these studies was the identity of intact N-linked sialylated oligosaccharides considered (3) where it was shown that one, two and three sialic acids were present on the di-, tri- and tetra-antennary structures respectively.

However comparison of retention times with authentic carbohydrates and carbohydrate composition of the separated oligosaccharides indicated that there was one additional sialic acid present as compared to the results by Sasaki et al(3).

Results and Discussion

Asparagine linked oligosaccharides were released enzymatically with N-glycanase and fractionated by anion-exchange chromatography O-Linked oligosaccharides were released under alkaline borohydride conditions. The primary structures of the major O- and N-linked oligosaccharides were unambiguously established by permethylation analysis, FAB-MS and 500-MHz H-NMR spectroscopy The most abundant N-linked oligosaccharides were diantennary, 2,4-branched tri-antennary, 2,6-branched tri-antennary, and tetra-antennary with the latter having zero, one, two, and three N-acetyllactosamine repeating units. Figure shows FAB-MS of the ABEE derivatives of the major N-linked oligosaccharides. The major di-,tri- and tetra-antennary structures are fully sialylated having two,three and four sialic acids linked exclusively α(2-3) to galactose The majority of N-linked structures (>95%) contain α(1-6) linked fucose at the proximal GlcNAc residue The primary structures of two O-linked oligosaccharides, determined to be mono-and disialyl oligosaccharide alditols, is also reported.

References

(1) Eschbach, J , Egrie, J J , Downing, M , Browne, J Adamson , J.(1987) N.Engl J.Med 316, 73-78.

(2) Sobota, J.(1990) Erythropoietin treatment of end-stage renal disease: in Garnick(ed). Erythropoietin in Clinical Applications: An International Perspective.. 1st ed (Dekker, New York)

(3) Sasaki, H , Bothner, B , Dell, A , and Fukada , M (1987) J Biol Chem ,262,12059-12076

(4) Takeuchi, M , Takasaki,S , Miyazaki, H , Kato,T , Hoshi, S , Kochibe, N,. and Kobata., A.(1988) J. Biol.Chem., 263, 3657-3663.

(5) Tsuda,E., Goto, M., Murakami, A., Akai, K., Ueda,M., Kazwanishi,G., Takahashi, N , Sasaki, R , Chiba, H , Ishihara, H , Mori, M , Tejima, S , Endo, S.,and Arata, Y (1988) Biochemistry, 27, 5646-5654.

(6) Ohashi, H , Miyata, M , Ishii, Y., Takeuchi,M , Takasago,A , Suzuki,T , and Sudo ,T (1989) Trends Anim Cell Culture Technol. 1, 115-120

(7) Lin, F.-K , Suggs, S , Lin, C.-H., Browne, J.K., Smalling, R., Egrie, J.C , Chen, K.K., Fox, G.M , Martin, F , Zutabinsky, Z., Badrawi, S.M., Lai, P.-H and Goldwasser,E (1985) Proc. Natl Acad Sci. USA 82,7480-7485.

Structural Characterization of the Carbohydrate Chains of Saponins by FAB-MS/MS

Douglas M. Sheeley[1], Lewis K. Pannell[2], Henry M. Fales[1],
Marie-Genevieve Dijoux[3], and Georges Massiot[3].

[1]NHLBI, [2]NIDDK, NIH Bethesda, MD 20892, and
[3]Universite de Reims, France

Saponins are a broad class of compounds which are found in a number of plants, most notably alfalfa and many of the legumes. They exhibit a variety of activities, depending upon their specific structure. Many have a strong hemolytic activity, and are extremely toxic to cold blooded animals, with a diminished effect on mammals. These compounds also bind cholesterol and bile acids, and have consequently been examined as possible treatments for hypercholesterolemia. Saponin structures vary widely but share some basic features. All consist of a hydrophobic core made up of a sterol or triterpene, and one or more carbohydrate chains attached to this core structure through a variety of linkages.

In this study, some of the mass spectrometric techniques used in the sequence analysis of a single saponin structure **(Figure 1)** have been summarized. ^{252}Cf PDMS provides molecular weight assignment and several fragment ions indicative of glycan sequence. One ion, however, at mass 489 could be not be assigned unambiguously. It is either a sequence ion from the long chain, or a loss of acetic acid from the 549 ion of the short chain. The mass resolution of the instrument is not adequate to distinguish 487 from 489. For the tetrasaccharide, linear and branched chains cannot be distinguished from this spectrum.

Pyranoxonium fragment ions representing each carbohydrate chain were generated by FAB and subjected to MS/MS by B/E linked scan in order to sequence each chain individually. Results for the **Xyl-Glc-Glc** chain (m/z 835) were consistent with the structure determined earlier by PDMS. Results for the **Xyl-(Ara)-Rha-Ara** chain (m/z 921) were more complex. MS/MS of the 921 ion gives a much broader peak at 489 than would ordinarily be expected **(Figure 2)**. This has been identified as a second field free region metastable ion, whose actual mass is 139 (two acetic acid losses from the very strong 259 ion). This type of metastable ion is detected when a fragment ion generated in the ion source (rather than by collision) is transmitted through the magnetic sector, and undergoes a unimolecular decomposition in the second field free region during a B/E linked scan[1]. The presence of this metastable peak obscures the region around m/z 489. By looking at the MS/MS spectrum of the 705 fragment, this problem was eliminated. The 2nd FFR metastable was detected because the B/E spectrum was acquired in profile mode. If the spectrum had been centroided automatically, this peak could have easily been mistaken for a sequence ion.

MS/MS of the 705 ion from the series 921-->705-->259 shows a strong ion at 259 as expected, with a strong ion at 429, and a weak one at 489. The 429 and 489 ions are due to glycosidic cleavage with charge retention on the reducing end of the molecule (i.e., loss of a terminal xylose), either with or without acetyl transfer. These data are supportive of a branched structure. This assignment could have been altered if a sequence ion at m/z 489 had been assigned. The assignment can be confirmed by methylation analysis, because there is only one deoxyhexose present in the molecule. The alditol acetates of doubly or singly linked rhamnose residues should be easily distinguishable by GC-MS.

(1) R. P. Morgan, C. J. Porter, and J. H. Beynon, Org. Mass Spec. (1977) 12(12):735-738.

I.

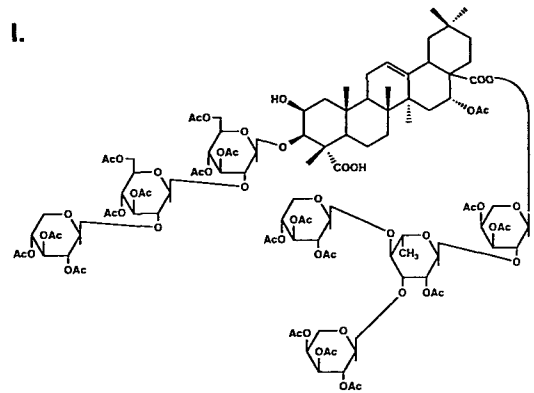

II. **Daughters of m/z 921**

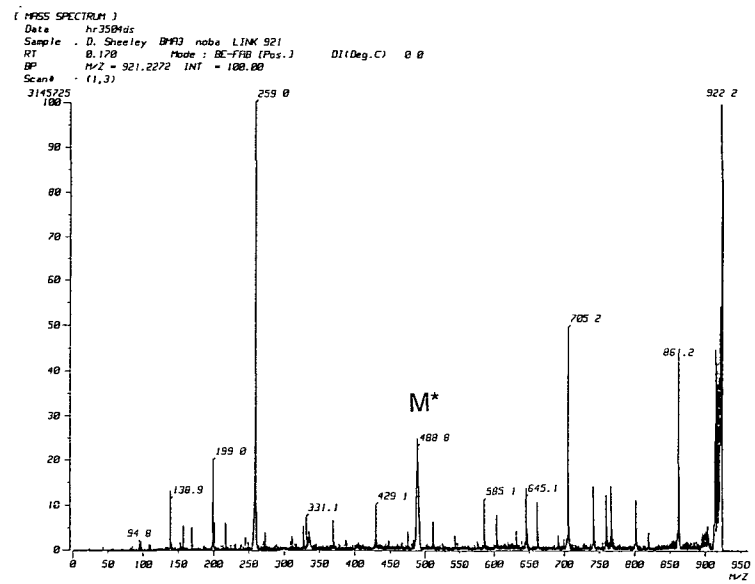

Structural studies on the glycosylation of the rabbit gastric H^+, K^+-ATPase

*P H Lipniunas[1], K Tyagarajan[2], D Chow[2], J G Forte[2] and R R Townsend[1].
[1]*Department of Pharmaceutical Chemistry, University of California, San Francisco, CA 94143-0446.*
[2]*Department of Molecular and Cell Biology, University of California, Berkeley, CA 94720.*

The H^+, K^+-ATPase is the membrane protein which is responsible for the acidity of gastric secretions. The protein is a heterodimer consisting of a catalytic α subunit of 110 kDa and a β subunit which migrates as a broad band at 60-80 kDa on SDS PAGE. Only the β subunit is glycosylated. From the primary peptide sequence the β subunit contains seven potential *N*-glycosylation sites. Both *N*- and *O*-linked oligosaccharides have been found (Weitzhandler et al., *J. Biol. Chem.* (1993) **268**, 5121-5130) and the *N*-linked chains are apparently novel asialo-structures, based on chromatographic studies.

We have begun studies to determine i) which peptide loci are glycosylated ii) the molecular weight profile of oligosaccharides at each glycosylation site and iii) the presence of unique structural features, all using pmol quantities of the H^+, K^+-ATPase β subunit. From HPLC electrospray mass spectrometric analyses (LC-ES-MS), (which utilized 6-8 pmols of a tryptic digest injected into the mass spectrometer), we observed glycopeptides containing five of the seven potential *N*-linked sequons. They were all occupied by asialo-complex structures, some of which were apparently elongated by lactosamine repeats. In addition we observed a series of ions which were consistent with the respective peptides containing *N*-linked polylactosamine structures with 1-3 additional Hex residues. We surmise that these additional Hex residues are terminal non-reducing α-linked Gal. The Asn-99 and/or Asn-103 sites gave ions consistent with fucosylated species. A tryptic glycopeptide containing Asn-222 was consistent with a biantennary series with up to two lactosamine repeats. A tri- or tetra-antennary series with up to five or six lactosamine repeats, respectively, was consistent with the observed ions from the Asn-161 containing glycopeptide. A greater proportion of Hex:HexNAc residues, possibly indicating α-Gal structures, was also observed at this site. The tryptic fragment containing Asn-146 produced ions suggesting tri- or tetra-antennary structures with two or three lactosamine repeats, respectively, and a surfeit of Hex residues. Glycopeptides containing both Asn-99 and Asn-103 produced ions suggesting that only one of these two sites is occupied in the same glycopeptide. A tryptic cleavage at Arg-104, which is adjacent to the Asn-103 glycosylation site supports that Asp-103 is unoccupied. Interestingly, the consensus sequence at Asn-103 in the pig gastric H^+, K^+-ATPase β subunit is missing (Toh et al. *Proc. Natl. Acad. Sci. USA* (1990) 87, 6418-6422). The ions arising from the glycopeptides containing both the Asn-99 and Asn-103 sites indicated fucosylated asialo-complex structures ranging from biantennary to tetraantennary structures which seemed to be capped with Hex residues. Eighty percent of the peptide sequence was identified during analysis of the tryptic peptides by LC-ES-MS.

The average molecular mass of the intact glycosylated β subunit was determined, by Matrix Assisted Laser Desorption Mass Spectrometry, to be 55750 Da. Since the open

reading frame for the full length rabbit cDNA clone predicts that the gastric β subunit contains 291 amino acids giving a molecular weight of 34002 Da, the β subunit is approximately 37 % carbohydrate by weight. Studies are under way to ascertain which other potential *N*-linked sequons are glycosylated and the location(s) of the *O*-linked chains.

This work was supported by NIH grants RR01614 and DK38972, NSF grant DIR 8700766 and the Wenner-Gren Center Foundation.

Structural determination of the O-linked oligosaccharides of recombinant human granulocyte-colony stimulating factor.

E. Watson, T. Arakawa ,W. C. Kenney.and *Herman van Halbeek
Amgen Inc., Amgen Center, Thousand Oaks, CA 91320

*Complex Carbohydrate Research Center and Department of Biochemistry, The University of Georgia,Athens, GA 30602

Colony stimulating factors or haematopoietic hormones comprise a group of growth factors that are responsible for regulating the formation of blood cells in the stem cells of bone marrow. Human granulocyte-colony stimulating factor (G-CSF) is one of a group of glycoproteins that are now known to be responsible for controlling the growth and differentiation of hematopoietic progenitor cells (1-3). G-CSF differs from other members of this family largely as a result of its cellular specificity for neutrophilic granulocytes and their precursors, and also because of its ability to induce terminal differentiation in certain lines of myeloid leukemic cells (4-6).

Carbohydrate structures of human granulocyte-colony stimulating factor (rhG-CSF), expressed in Chinese hamster ovary cells (CHO), have been determined. rhG-CSF was found to contain ~4% carbohydrate by weight, representing two O-linked oligosaccacharides. These structures were released by alkaline borohydride reductive cleavage and separated by ion exchange chromatography into two fractions that were shown to contain one and two sialic acids, respectively. Figure 1.shows the chromatogram of the oligosaccharides released from rhGCSF.

Structure determination was carried out using carbohydrate composition, methylation analysis, fast atom bombardment-mass spectrometry, and 500-MHz ^{1}H-NMR spectroscopy Figure 2 shows the negative ion FAB-MS 0f the isolated oligosaccharides The structures of these oligosaccharides are as follows:

Neu5Acα(2-3)Galβ(1-3)GalNAc-ol

and

Neu5Acα(2-3)Galβ(1-3)
Neu5Acα(2-6) GalNAc-ol

The presence of the substituted sialic acid, N-glycolylneuraminic acid has previously been reported on N-linked oligossacharides obtained from human recombinant glycoproteins that were expressed in Chinese hamster ovary CHO cells (7) We report here that N-glycolylneuraminic acid is also present on O-linked oligosaccharides of thus obtained glycoproteins. HPLC analysis of the sialic acids released from rhG-CSF shows N-acetylneuraminic acid and N-glycolylneuraminic acid present in the ratio of ~96:4. N-glycolylneuraminic acid was unambiguously identified by electron impact mass-spectrometry of its trimethylsilyl derivative

References

(1) D. Metcalf, The Haemopoietic Colony Stimulating Factors (Elsevier,Amsterdam, 1984)

(2) T.R. Bradley and D Metcalf, Aust J Exp Biol Med Sci.44,287-300 (1966)

(3) Y Ichikawa, D.H Pluznik, L Sachs, Proc Natl Acad Sci U.S.A 56,488-495 (1966)

(4) N.A. Nicola et al , J Biol Chem 258,9017-9023 (1983).

(5) A.W Burgess and D. Metcalf, Int.J Cancer 26,647-652 (1980)

(6) D Metcalf and N.A Nicola, Int.J. Cancer30,773-780 (1982)

(7) C.H.Hokke, A.A. Bergwerff, G.W K. van Dedem, J. van Oostrum, J.P. Kamerling and J F.G Vliegenthart FEBS Lett., 275, 9-14. (1990).

Structural Determination of a Sulphated Tetrasaccharide Ligand for the Cell Adhesion Molecule E-Selectin by LSIMS

A.M. Lawson, W. Chai, C.T. Yuen and T. Feizi.

MRC Clinical Research Centre, Watford Road,
Harrow, Middlesex, HA1 3UJ, UK.

Introduction

There has been intense interest in the oligosaccharide structures that interact with selectins, a small class of recently discovered cell adhesion proteins involved in normal and pathological biology of blood cells. One of these proteins, E-selectin which is implicated in the first stage of recruiting neutrophils to sites of inflammation has been shown to recognise oligosaccharides having the 3-sialylated 3'-fucosyl-N-acetyllactosamine sequence of the type found on leucocytes. In the present study by using a TLC plate binding technique with neoglycolipids derived from O-linked acidic oligosaccharides, obtained from a human ovarian cystadenoma glycoprotein preparation, it was shown that a series of neoglycolipid bands were recognised by E-selectin. Among these, a novel class of oligosaccharide ligand was identified by mass spectrometry that is sulphated rather than sialylated (1).

Results and Discussion

A number of active bands were detected from among the neoglycolipids derived from the glycoprotein preparation. Of most interest were structures from the lower molecular weight fractions which might be expected to contain the minimum epitope being bound by E-selectin. The spectrum of a highly active neoglycolipid band showed a $[M-H]^-$ ion at *m/z* 1465 which suggested a dHex.Hex_2.HexNAc composition with an additional 80Da equivalent to a sulphate or phosphate group. Glycosidic fragment ions *m/z* 1365, 1219, 1203 and 854 allowed the sequence to be assigned as (80)-Hex-(dHex)HexNAc-Hex.

The combined positive and negative spectra supported the presence of sulphate and not phosphate. The extent to which neoglycolipid spectra could be used to distinguish these substituents was investigated using neoglycolipids of the model oligosaccharides, HSO_3-GlcNAc-Gal and H_2PO_3-Man_5 (Figs 1 and 2). They show characteristics, particularly in positive mode, which reflect the difference in chemical stability to acid conditions. Proton attachement leads to facile loss of sulphite and gives rise to $[MH-SO_3]^+$ as the most abundant ion and absence of MH^+ in the sulphated disaccharide. Man_5-phosphate in contrast shows only a small ion for HPO_3 loss and an intense MH^+. The negative ion spectra of each are similar although from the sulphated structure sulphite loss is again prominent.

Methylation analysis, to determine linkage positions of the active oligosaccharide required modification to take account of the water solubility of permethylated oligosaccharide sulphates. Purification of the aqueous layer following permethylation by the NaOH/DMSO slurry method (3) can be achieved by AG50WX8 chromatography. The E-selectin saccharide ligand was deduced to be a mixture of the isomeric structures

HSO_3-3Gal1-4/3(Fuc1-3/4)GlcNAc1-3Gal

The permethylated spectrum of this mixture was less useful than its neoglycolipid spectrum. While $[M-H]^-$ is produced no fragmentation of the sulphate occurs and hence no indication of sulphate substitution is given. The positive ion spectrum in contrast shows loss of sulphite (ie $[M-SO_3+Na]^+$) with MH^+ being replaced by intense salt adduct ions which make interpretation of an unknown spectrum difficult. In addition the expected glycosidic fragmentation of normal glycans was absent.

References

(1) Yuen, C.T., Lawson, A.M., Chai, W., Larkin, M., Stoll, M.S. Stuart, A.C., Sullivan, F.X., Ahern, T.J. & Feizi, T. *Biochemistry* **31** (1992) 9126-9131.
(2) Lawson, A.M., Hounsell, E.F., Stoll, M.S. Feeney, J., Chai, W., Rosankiewicz, J.R. & Feizi, T. *Carbohydr. Res.* **221** (1991) 191-208.
(3) Ciucanu, I and Kerek, F. *Carbohydr. Res.* **131** (1984) 209-217

Fig. 1. LSI spectra of HSO_3-6GlcNAcβ1-3Gal

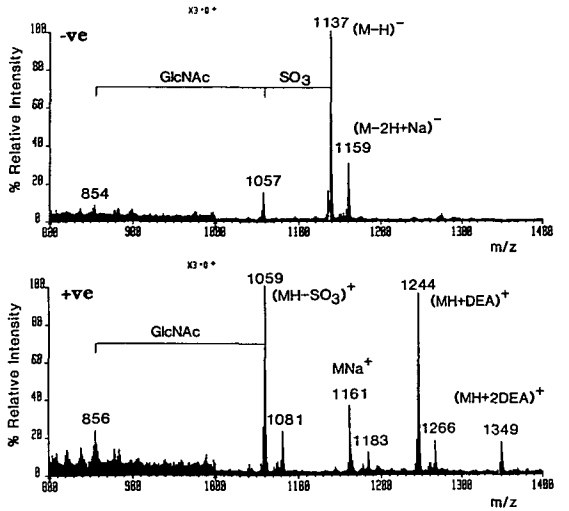

Fig. 2. LSI spectra of H_2PO_3-6Manα1-3Manα1-3Manα1-3Manα1-2Man

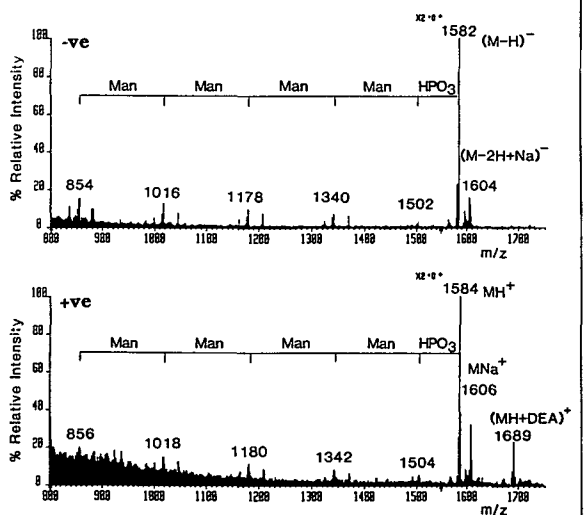

Structural Analysis of Glycosylation on the HIV Envelope Glycoprotein gp120

*John Caesar, Steve Chan, Bruce Reinhold, Tun-Hou Lee and Vernon Reinhold,
Harvard School of Public Health, Boston, MA 02115

The envelope glycoprotein gp120 expressed on the surface of the human immunodeficiency virus (HIV) functions as a ligand for the CD4 receptor glycoprotein on human T cells. Oligosaccharides were implicated in the infectious process by studies utilizing endoglycosidase inhibitors (1) and glycosylation site mutagenesis (2,3). In particular, the inhibitor study implied that high mannose glycosylation on gp120 was sufficient for viral infectivity (1). Efforts to analyze the gp120 glycan structures in greater detail have focused on recombinant material expressed in different cell lines. Insect cell (Sf9)-expressed gp120 was used for the work described in this poster, based on its in vitro biological activity (4).

The glycans from this Sf9-expressed gp120 were profiled by supercritical fluid chromatography (SFC)-negative chemical ionization (NCI)-MS (5). Electrospray ionization (ESI)-MS has been used in the present study to confirm the SFC-MS profile and HPLC-ESI interfacing was developed to continue the preliminary investigation of glycoform distributions at gp120 glycosylation sites.

ESI-MS: We used a Finnigan MAT TSQ700 triple quadrupole mass spectrometer operated either in the direct infusion mode or interfaced with HPLC. For direct infusion, unless otherwise specified, samples were dissolved in 70% methanol/water, 0.5 mM sodium acetate, and pumped into the ESI source at 0.75 µl/min. The operating needle voltage was roughly -4 kV, and nitrogen drying gas flow was maintained at 15 psi and a temperature of 220 degrees C. A nitrogen sheath gas flow was maintained at 25 psi.

HPLC INTERFACING: *The HPLC-MS runs that were done with an acetonitrile/ water/TFA* mobile phase used 2-methoxyethanol as a sheath liquid. However, it became clear that continued use of the methoxyethanol sheath caused a loss of sensitivity, most noticable when operating under infusion conditions. The standard buffer used for the direct liquid infusion of dissolved peptides into the Analytica ESI source is 50% methanol/water with 0.5% acetic acid. Since the infusion conditions required no liquid sheath flow, it seemed plausible that if the HPLC elution was done with a water/ methanol/acetic acid mobile phase, a liquid sheath might be unnecessary.

Glycans were released from gp120 using either hydrazinolysis or N-Glycanase (Genzyme Corp., Cambridge, MA). Glycan hydrazides were first analyzed by ESI-MS as underivatized protonated species. Improved sensitivity and collision (CID) experiments were possible for permethylated samples, analyzed as metal ion adducts (6). Figure 1 shows the ESI spectrum on enzymatically released glycans that were permethylated following periodate oxidation and aldehyde reduction.

Table 1 presents glycoform distributions, calculated from the peak intensities in the mass spectra of the ion chromatogram of a Lys C digest of gp120. The asterisks refer to the HPLC-MS run under sheathless conditions.

The Sf9 cells synthesized gp120 with high mannose glycans ranging in size from M_3GN_2 to M_9GN_2, with at least two isomers each of M_4GN_2, M_5GN_2, M_6GN_2 and M_7GN_2. One fucosylated structure was identified: M_3FucGN_2. Figure 2 shows this glycoform in high abundance on fragment L17. It is probable that the Endo H-resistant glycoforms from the Sf9 cell line were not complex glycans as reported (7), but the branched trimannose structures found in this study, based on the inactivity of Endo-H toward substrates containing the branched trimannose glycan (8).

The glycoform distributions were found to vary dramatically with glycosylation site. In particular, two sites possessed the M_3FucGN_2 in high abundance, and one of these sites was critical for viral infectivity in assays performed on a glycosylation site mutant (3).

References

1. R. Gruters, J. Neefjes, M. Tersmette, R. de Goede, A. Tulp, H. Huisman, F. Miedema, H. Ploegh, *Nature* **330**, 74-77 (1987).
2. W. Lee, W. Syu, B. Du, M. Matsuda, S. Tan, A. Wolf, M. Essex, T. Lee, *Proceedings of the National Academy of Sciences* **89**, 2213-2217 (1992).
3. T.-H. Lee, personal communication (1992).
4. product literature, (1991) Repligen Corp., Cambridge, MA
5. J. P. Caesar, I. Koski, B. Reinhold, V. Reinhold, 40th ASMS Conference on Mass Spectrometry and Allied Topics, Washington, D.C., (1992), pp. 1609-1610.
6. S. H. Chan, B. B. Reinhold, V. N. Reinhold, 40th ASMS Conference on Mass Spectrometry and Allied Topics, Washington, D.C., (1992), pp. 977-978.
7. D. L. Jarvis, M. D. Summers, *Molecular and Cellular Biochemistry* **9**, 214-223 (1989).
8. R. B. Trimble, A. L. Tarentino, *Journal of Biological Chemistry* **266**, 1646-1651 (1991).

FIGURE 1

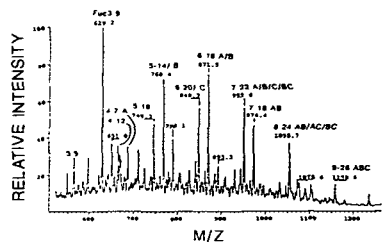

FIGURE 2

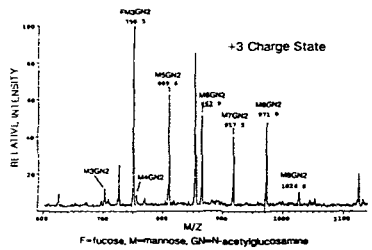

TABLE 1

Lys C Fragment	M9	M8	M7	M6	M5	M4	FM3	M3
L17	6 9	22.6	21 5	19 0	7 3	2 9	16 1	3 8
L17*	2.7	14 8	12.1	15 6	19 4	2 2	31 3	1 9
L26	44 5	34 7	13 6	7 2	0	0	0	0
L27	0	42 8	39 5	13.8	2 9	1 1	0	0
L30	2 4	16.8	27 9	18.7	14 9	5.7	3 1	10 6
L36	3 1	16 0	17 7	12 1	22.7	4 2	17 1	7 1
L36*	3 2	8 8	11.4	7.3	11 4	5 9	30 2	21 7

M=mannose, F=fucose

Structural Elucidation of Branched Oligosaccharides: Isotope Labeling Studies

*Zhongrui Zhou and Julie Leary, University of California, Berkeley, CA 94720

We have previously shown that MS/MS of divalent metal ion coordinated oligosaccharides can be used to determine the linkage position in branched oligosaccharides. To apply the methodology to higher and more complicated oligomers, a clearer understanding on the dissociation process of branched oligosaccharides is required.

In this study, isotope labeling experiments were conducted in order to elucidate detailed fragmentation processes. Branched trisaccharides, 3-fucosyllactose, B-trisaccharide, and the linear isomer 2'-fucosyllactose, were either labeled with ^{18}O at their anomeric positions, or perdeuterated at all their hydroxyl groups. MS/MS of $^{26}MgCl^+$ coordinated precursors, in combination with semiempirical calculations, reveal the origins of ring cleavage neutral losses, thereby allowing us to propose mechanisms for the dissociation processes, and to make unambiguous assignments as to the linkages.

3-Fucosyllactose. By studing the product ion spectrum of 3-fucosyllactose, we are able to make corresponding ion assignments and identify a 1,4 linkage between fucose and glucose rings. Figure 1 shows the product ion spectrum of ^{18}O labeled 3-fucosyllactose. The ions at m/z 453 and 393, which correspond to two and four carbon chain neutral losses from $[M-H+^{26}Mg]^+$ at m/z 515 respectively, involve loss of the ^{18}O-labeled portion of the molecule, thus supporting our reducing ring cleavage assignment. Futhermore, the presence of ion at m/z 453 allows us to assign the two carbon chain neutral loss to C1/C2 position of the reducing ring, therefore eliminationg the possible linkage location for fucose ring at C2 position. The doublet at m/z 307 and 309 clearly suggests the presence of two different reaction pathways, one of which involves the anomeric ^{18}O which is included in the two carbon chain neutral loss from m/z 369. Deuterium labeling study is in agreement with the ^{18}O labeling study. Important information is that the ions at m/z 460 and 399 are due to two and four carbon chain neutral losses from m/z 515, respectively. The 61 AMU difference between two and four carbon chain neutral losses tells us that the second two carbon neutral loss is an aldehyde, and that the only origin of this aldehyde is C5/C6 of the reducing ring. This fact actually eliminates another possible linkage location for fucose ring at C6 of the reducing ring, and leads to the assignment of 1,3 linkage between fucose and glucose ring.

B-trisaccharide. The product ion spectrum of B-trisaccharide shows dramatic differences from that of 3-fucosyllactose. The characteristic three carbon chain neutral loss, which only occurs after fucose ring is cleaved off (it is observed from m/z 367, but not m/z 513), suggests a 1,3 linkage between two galactose rings and a 1,2 linkage between fucose ring and reducing galactose rings. Product ion spectrum of ^{18}O B-trisaccharide (Figure 2) supports the assignments. In contrast to 3-fucosyllactose, the two carbon chain neutral loss from $[M-H+^{26}Mg]^+$ gives rise to an ion at m/z 455, i.e., the ^{18}O labeling on anomeric position retaines, indicating that the loss occurs at C5/C6 posion of the reducing ring. This fact clearly rules out the possibility of 1,6 linkage between galactose and fucose rings. On the other hand, a 1,4 linkage is also not suggested, since we should have seen two carbon unit loss from C1/C2 position based on what we have learned from 3-fucosyllactose. Then the only posibility left is a 1,2 linkage between reducing galactose and fucose rings. The data obtained from deuterium labeling study is also in agreement with the assignments. For example, the two carbon chain

neutral loss from $[M-D+^{26}Mg]^+$ (m/z 522) gives rise to an ion at m/z 461. The 61 AMU difference clearly indicates that the loss is an aldehyde, coming from C5/C6 position of the reducing ring.

2'-Fucosyllactose. It is interesting to consider whether and how there are differences between 2'-fucosyllactose and its branched isomer 3-fucosyllactose. In contrast to 3-fucosyllactose which has fucose ring linked to reducing glucose, 2'-fucosyllactose is a linear trisaccharide and has fucose ring linked to non-reducing galactose via 1,2 linkage. The product ion spectrum of $^{26}MgCl^+$ coordinated 2'-fucosyllactose shows diagnostic ions at m/z 291 and 259, which assign a 1,2 linkage between fucose and non-reducing galactose rings. The ^{18}O and ^{2}H labeling experiments support our assignments, and again, they provide more detailed information on dissociation process.

On the basis of the information described above, in combination with semiempirical data, we have suggested dissociation processes for these $^{26}MgCl^+$ coordinated trisaccharides.

Figure 1. ^{18}O 3-Fucosyllactose

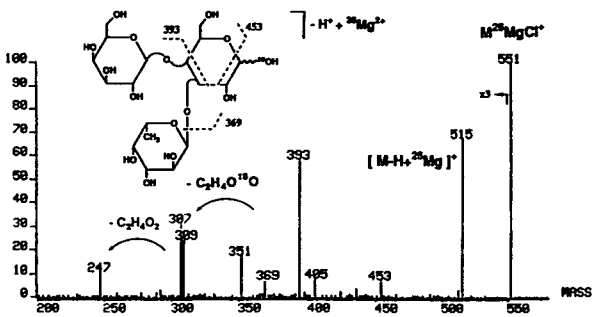

Figure 2. ^{18}O B-trisaccharide

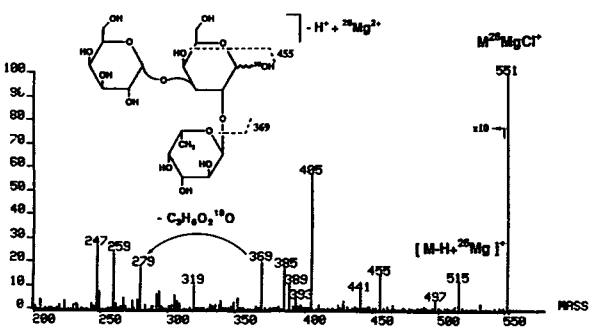

Detailed Structural Characterization of an Exopolysaccharide from Rhizobium Meliloti by ESI and Low Energy CID.

Bruce B. Reinhold, Siu Y. Chan and Vernon N. Reinhold, Harvard University School of Public Health, Boston, MA 02115.

Nitrogen fixing soil bacteria of the genus Rhizobium colonize specific host plants through the induction and invasion of root hair nodules. Successful colonization requires a number of chemical messages to control this complex, multistep process and extracellular polysaccharides are required for these signaling steps. Mutation studies have demonstrated that specific oligosaccharide structural features are necessary. As an example, mutants of *R. meliloti* strain Rm1021 produces an EPS (EPS I) that induces nodule formation 'pseudonodules' but lacks the ability to invade. A spontaneous mutant of the same strain has also been isolated that has the cryptic capacity to synthesize a second exopolysaccharide of considerably different structure (EPS II) which makes and invades nodules, and fixes nitrogen. This mutant was able to overcome the defects of EPS I in alfalfa, but not on four other plants that are normally hosts for Rm1021. The structural features of bacterial exopolysaccharides are thus directly involved in determining host range and have little influence on nodulation since both the succinoglycan producing wildtype strains and galactoglucan producing mutant strains of *R. meliloti* are able to infect their host plant properly

A biotechnology that would extend the range of host species offers great economic potential and consequently this system has been intensively researched in order to elucidate the complex signaling mechanism between the bacterium and plant host. A classic paper (Aman et. al. 1981) has detailed many aspects of the exopolysaccharide structure including the glycosyl composition, linkage and sequence. Proton NMR had revealed the presence of succinate and acetate moieties of the core oligosaccharide, although the location of the residues containing these functional groups and the site of derivatization were not determined. This succinyl moiety was subsequently shown to be essential for functional activity of the exopolysaccharide.

The ability to efficiently ionize and effectively fragment large oligosaccharides in a triple quadrupole with ESI and alkali metal cationization opens new doors in the structural biology of carbohydrates. The simplicity and sensitivity of this technique stands in stark contrast with the labor and material required of previous methodology.

In the current study the residue positions of the acetyl and succinyl groups were determined by a single ESI CID spectrum of the (neutral) permethylated oligosaccharide. Subsequent permethylation under basic conditions replaced the succinyl and acetyl modifications with deuterated methyl groups. The CID spectrum of this molecule verifies the residue locations determined in the previous spectrum, supports much of the backbone linkage assignment of Aman et. al. by specific ring-opening fragmentations, and determines the specific site of the acetyl modification. Location of the succinyl group The site of the succinyl modification was determined by clasical methylation analysis and GC MS of the methylated alditol acetates.

Figure 1 Electrospray MS of extracellular polysaccharide from Rhizobium meliloti. The oligosaccharide was (neutral) permethylated without cleaving the acetyl or succinyl esters. [Carb Res 78, 372-374 (1980) 145, 247-265 (1986)] The intense peak at 955 Th is the molecular ion adducted with two sodium cations and this ion was collided to identify the location of the acetyl and succinyl esters.

Figure 2 Expanded view of part of the CID spectrum of the neutral then base permethylated exopolysaccharide. The precursor was the doubly-natriated molecular ion. The substitution position of the acetyl ester is identified by a 3 Da shift in the ^{3,5}A ring-opening fragment.

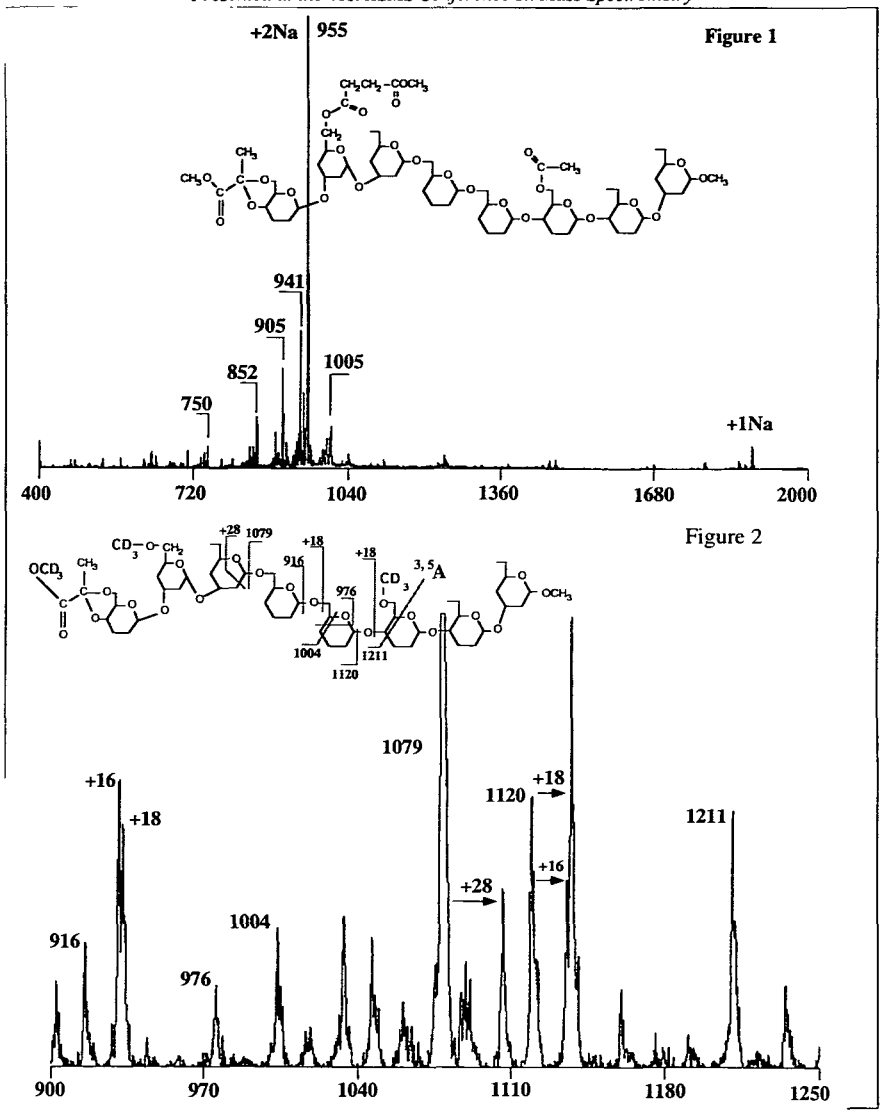

Sequencing of Glycopeptides Using Sequential Digestion Followed by Microbore HPLC/Electrospray Mass Spectrometry

Christine A. Settineri and Alma L. Burlingame
Department of Pharmaceutical Chemistry and Mass Spectrometry Facility
University of California, San Francisco, CA 94143-0446

A method has been developed for sequencing oligosaccharides attached to partially purified glycopeptide mixtures using sequential digestion with highly specific glycolytic enzymes (glycosidases). This method involves digestion of glycopeptides with one to three glycosidases at a time, followed by purification with microbore HPLC coupled directly to an electrospray mass spectrometer for analysis of the products. Less than 5% of the sample injected onto the HPLC enters the mass spectrometer, therefore, approximately 95% of the sample can be recovered and digested with more glycosidase(s). Since different glycosidases require different buffer and pH conditions, this is an ideal method for removing the buffer salts as well as for further purifying the glycopeptides before each subsequent digestion step.

Glycopeptides were isolated by microbore HPLC separation of trypsin and endoproteinase glu-C digests of one nanomole of bovine fetuin and recombinant human nerve growth factor receptor (NGF-R), respectively. *N*-linked glycopeptide-containing fractions were identified in both digests by on-line HPLC/electrospray ionization mass spectrometry (LC-ESIMS). These fractions were isolated and digested with a series of exoglycosidases (shown in Table I) to identify and distinguish the different glycoforms present and where possible, determine the exact linkages between the monosaccharides. The fetuin glycopeptides [residues (54-85) and (127-142)] contain known carbohydrate structures and were used as standards to confirm the expected specificity of the enzymes and optimize reaction conditions. The NGF-R glycopeptide ^{24}GVAQPXGANQTVXEPXLD^{41} was then investigated to determine the sequence and linkages of the glycoforms attached at Asn-32 of this peptide.

Enzymes (in sequencing order)	*Enzyme Source*	*Conc. (U/ml or mU/ml)*	*pH optimum*	*Digestion Buffer*	*Digest Time (hours)*
1a. Sialidase	Newcastle Disease Virus	0.02-0.05	5.0-6.0	A	16-22
b. Sialidase	*Arthrobacter ureafaciens*	0.8-1.0	5.0-5.5	A	16-22
2. β-Galactosidase	*Streptococcus pneumoniae*	0.03-0.07	5.5-6.5	A	16-22
3. β-GlcNAcase	Chicken liver	1.0	4.0	A or B	16-22
4. α-Mannosidase	Jack bean	3.5	4.0-4.5	A + 25 mM $ZnCl_2$	16-22
5. β-Mannosidase	*Helix Pomatia*	2.0-4.0	4.0-4.5	A + 25 mM $ZnCl_2$	15-22
6. GlcNAcase	Chicken liver	2.0	4.0	A or B	12-18
7. α-Fucosidase	Bovine epididymis	0.2	6.0-6.5	C	16

Buffer A - 30 mM Sodium Acetate, pH 5.0
Buffer B - 100 mM Sodium Citrate Phosphate, pH 4.0 w/ 250 mg/ml Bovine Serum Albumin (BSA)
Buffer C - 100 mM Sodium Citrate Phosphate, pH 6.0 w/ 250 mg/ml Bovine Serum Albumin (BSA)

TABLE I - Exoglycosidase reaction mixtures used for sequencing glycopeptides.

The LC-ESIMS spectrum of the undigested NGF-R N-linked glycopeptide mixture showed considerable heterogeneity in the attached oligosaccharides. The molecular ions present in this spectrum correspond to NGF-R residues (24-41) containing fucosylated bi-, tri- and tetraantennary (or polylactosaminyl) complex structures containing zero, one and two sialic acids. This heterogeneity was considerably reduced by treatment with Newcastle disease virus sialidase, which removed all the sialic acid residues. Since this enzyme cleaves only α2-3 and α2-8 linkages, the linkage of the sialic acid to the next monosaccharide, galactose (determined by the next reaction with β-galactosidase), must be α2-3 (as expected with a Chinese hamster ovary cell-derived protein) since galactose contains only six carbons. With the fetuin glycopeptides, the Newcastle disease virus sialidase removed only some of the sialic acids present, as expected, since these bovine-derived glycopeptides are known to contain both α2-3 and α2-6 linked sialic acid residues.

The asialo spectrum showed evidence of a pentaantennary (or polylactosaminyl) oligosaccharide as well. The highly branched structures can be distinguished from less branched polylactosaminyl structures using exoglycosidase sequencing. β-galactosidase treatment of the glycopeptide mixture will only cleave the terminal galactose residues, so treatment of a bi- or triantennary polylactosaminyl structure will result in fewer galactose residues being cleaved than a tetra- or pentaantennary structure of the same mass. In fact, β-galactosidase treatment of the NGF-R glycopeptide resulted in cleavage of a maximum of three galactose residues, indicating the presence of triantennary structures with one and two additional lactosaminyl groups attached at the non-reducing termini. Similar rationale were used to determine the remaining sequence and linkages by combining the specificities of the glycosidases. For example, by combining the specificities of *S. pneumoniae* β-galactosidase and Chicken liver β-N-Acetylhexosaminidase, one can prove that a hexose-N-acetylhexosamine disaccharide unit is Galactose linked β1-4 to N-acetylglucosamine. Not all the glycosidases are specific enough to determine the exact linkage between every monosaccharide in the entire structure, however, they are specific enough that one can determine the exact sequence of specific monosaccharide residues in the carbohydrate structure.

The HPLC separation step with each ESIMS analysis was helpful due to side reactions that can occur from low level contaminants in the glycosidases. For example, the β-galactosidase contains protease activity which caused about 10% of the fetuin glycopeptide (54-85) to be cleaved down to (61-85) in the reaction mixtures which contained this enzyme. The two other glycopeptides were not proteolytically cleaved when using the *same concentration* of the β-galactosidase. However, if a two times greater concentration of the β-galactosidase was used, some protease activity was seen with all three glycopeptides. Therefore, we found it best to always try to use the minimum concentration of glycosidase in the reactions.

In conclusion, sequential exoglycosidase digestion of the NGF-R N-linked glycopeptide ^{24}GVAQPXGANQTVXEPXLD^{41} was used to determine three major carbohydrate glycoforms attached to Asn-32 are the following biantennary structures with the indicated linkages:

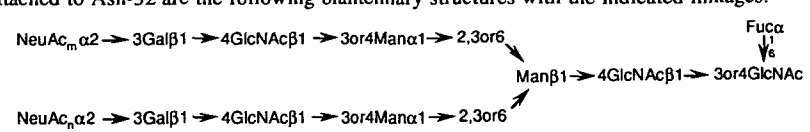

where m + n = 0-2.

In addition, mono- and disialo fucosylated triantennary structures containing 0, 1, and 2 additional polylactosaminyl groups were also found.

This work was supported by NIH grant DRR 01614 and NSF grant DIR 8700766.

Microcolumn HPLC-CF-LSIMS of UV-absorbing Neoglycolipids Derived from Oligosaccharides

P. Verner, W. Chai, J. Rosankiewicz and A. M. Lawson
Medical Research Council, Clinical Research Centre, Harrow, Middlesex, HA1 3UJ, United Kingdom

Dipalmitoyl phosphatidylethanolamine (DPPE) is currently used as a reducing terminal derivatization agent for oligosaccharides and their mass spectrometry (1). The resulting neoglycolipids formed from oligosaccharide and DPPE by reductive amination give particularly abundant molecular ions in liquid secondary ion mass spectrometry (LSIMS) and their fragmentation reflects the composition, sequence and branching of the oligosaccharide moiety. Typically, HPTLC separation of neoglycolipid mixtures is carried out with analysis by LSIMS directly from the plate.

We prepared a range of UV chromophore-containing derivatization agents based on DPPE or 2-dihexadecyl-glycero-3-phosphoethanolamine (DHPE). These reagents are comparatively straightforward to synthesise and their stability is similar to that of DPPE and DHPE.

Two of these derivatives, namely DHPET and DHPEL, were more fully investigated to examine their suitability for HPLC, LSIMS and biological studies.

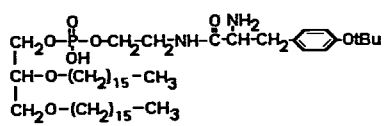

DHPET

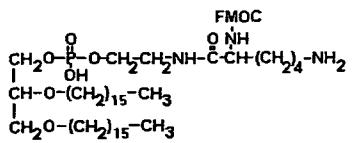

DHPEL

Neoglycolipids were prepared from various oligosaccharides with DHPET and DHPEL. These compounds retained the favourable LSI mass spectral features of DHPE and DPPE based oligosaccharide derivatives [Fig.1].

Analytical and microcolumn HPLC separation of these neoglycolipids was attempted on silica, amino, ODS-silica and ODS-polymer reversed phase columns using various mobile phases and modifiers. An ODS-silica reversed phase column with chloroform-methanol-water-TFA mobile phase was selected for separation of these conjugates prior to introduction to MS. Neoglycolipids separate according to their polarity on this phase with the reagent eluting last [Fig.2].

A coaxial flow interface was constructed for continuous flow LSIMS delivering the HPLC column effluent and the matrix separately to the probe tip. This has permitted different matrix compositions and mobile phase:matrix ratios to be easily tested. A matrix composed of diethanolamine-tetramethylurea-nitrobenzylalcohol added in a ratio of 1:20 to column effluent gave the best signal-to-noise ratio in continuous flow LSIMS experiments. Complete mass spectra were obtained from 2 pmol of neoglycolipid using continuous multichannel analysis mode.

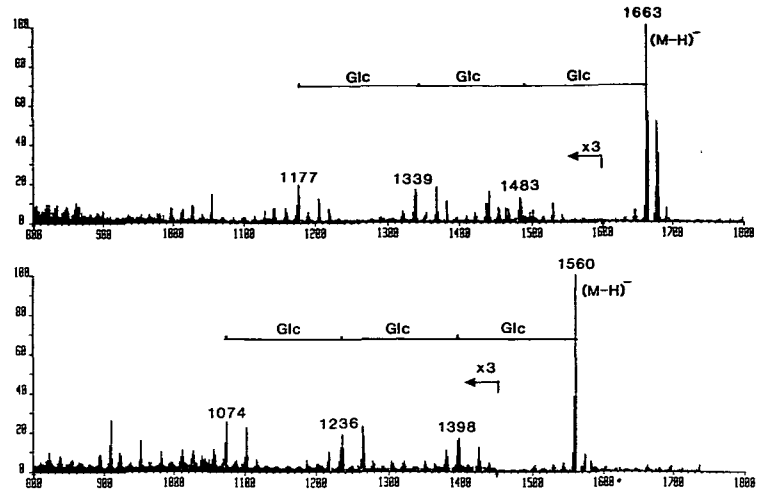

Figure 1. Mass spectra of maltotetraose-DHPEL and maltotetraose-DHPET

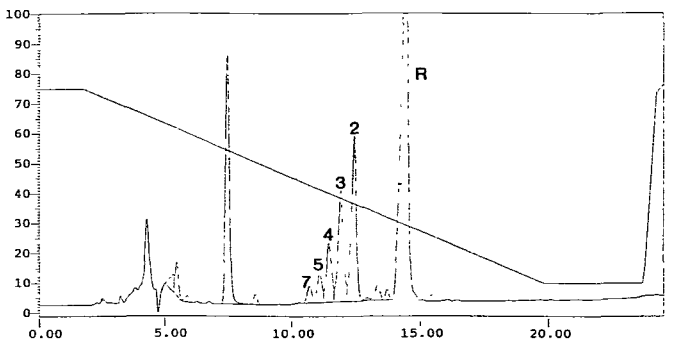

Figure 2. Chromatogram of a mixture of maltoses of polymerization degree 2 - 7 on ODS silica column.

Reference: 1. A. M. Lawson, W. Chai, G. C. Cashmore, M. S. Stoll, E. F. Hounsell and T. Feizi, Carbohydr.Res., **200**, 47 (1990).

Electrospray Ionization of Divalent Metal Chloride Coordinated Oligosaccharides.

Aberra Fura and Julie A. Leary, Department of Chemistry,
University of California, Berkeley CA 94720.

Previous reports[1] indicated that as oligosaccharides becomes larger and more structurally complex, coordination of more lithium ions is necessary for the unambiguous determination of linkage positions. In this study, the analytical usefulness of coordination of divalent metals, calcium and magnesium to three branched trisaccharides, 3-fucosyllactose, B-trisaccharide and 2'-fucosyllactose has been investigated using electrospray ionization (ESI) and tandem mass spectrometry (MS/MS).

The ESI of these trisaccharides, upon coordination with the above divalent metal ions, yielded several cluster ions. The relative abundance of these ions was found to depend on the concentration of the saccharide and the metal, their relative concentration ratio and the skimmer voltage. Thus when the molar concentration of the metal salt was less than that of the saccharide there was a relative increase in the abundance of the ions which represent $[M_n + Metal]^{2+}$ (where n is 1,2,3 etc. and M is the trisaccharide). The opposite trend is observed when the concentration of the metal ion is increased. However, this phenomenon is dependent on the concentration of the oligosaccharide and the coordinating metal. For instance, at the 3-fucosyllactose concentrations of 1500, 100, 50, 12 pmol/µl, the ion at m/z 563, $[M+CaCl]^+$, is maximized at a 1:1, 2:1, 5:1, and 10:1 metal to trisaccharide concentration ratios respectively.

The relative intensity was also observed to depend on the sampling skimmer voltage. Thus at lower skimmer voltages, solvent molecules remain attached to the metal due to lack of complete dissolvation. At higher voltage the spectra were dominated by fragment ions, resulting from the collisional dissociation in the low pressure region of the source.

The singly charged ions, $[M+CaCl]^+$ and $[M+MgCl]^+$, enhanced the sensitivity and led to analytically useful fragmentation upon collisional dissociation. MS/MS and MS/MS/MS of these ions produced ions due to glycosidic cleavages as well as ions resulting from the cleavage of the reducing ring. The MS/MS spectrum of the complex, $[M+CaCl]^+$, (Figure 1A) where M is 3-fucosyllactose showed ions at m/z 527,321,261, in addition to the precursor ion at m/z 563. The ion at m/z 527 is due to the loss of the fucose residue and two consecutive two carbon chain neutral losses at m/z 321 and 261. The first two carbon chain loss comes from C-1 and C-2 of the reducing ring. The ion at m/z 261, which represents a second two carbon chain neutral loss from C-5 and C-6 of m/z 321, as also confirmed by MS/MS/MS indicates that the linkage of the remaining disaccharide portion at m/z 321 must be 1,4, since these kinds of losses are characteristic of this linkage type as observed previously.[1] The C-3 is therefore the only logical place where fucose ring can be attached. The corresponding MS/MS spectrum of $[M+MgCl]^+$ also showed the above dissociation ions. In addition, it also indicated the presence of less abundant ions at m/z 451 and 391, due to the direct loss of two and four carbon chain neutrals along with HCl from the precursor ion at m/z 511. For B-trisaccharide, the corresponding MS/MS spectrum of $[M+CaCl]^+$ (Figure 1B) showed ions at m/z 545, 381, 291 and 261, in addition to the precursor ion at m/z 563. The ion at m/z 545 arise from the loss of H_2O and the ion at m/z 381 is due to the simultaneous loss of HCl and fucose ring. The ion at m/z 291 and 261 represents a three and four carbon chain neutral losses respectively, from the ion at m/z 381 as also confirmed by MS/MS/MS. These losses are specific for 1,3-linkage type in the disaccharide portion of the molecule having free

hydroxyl groups on C-4 and C-6 carbons of the reducing ring. Additionally, no two carbon chain loss is observed, thus narrowing down the possibility of the fucose ring attachment to C-2 of the reducing ring. The MS/MS of the corresponding $[M+MgCl]^+$ was also studied but found to show several more ions produced by more than one dissociation pathways. The MS/MS spectrum of $[M+CaCl]^+$ (Figure 1C) of the third isomer, 2'-fucosyllactose, showed ions at m/z 467 and 407 due to the loss of $C_2H_4O_2$ and $C_4H_8O_4$, respectively, from the precursor with simultaneous loss of fucose moiety indicating that the fucose ring is now attached to the non-reducing ring. However, definite information as to which carbon the fucose ring is bonded to was lacking.

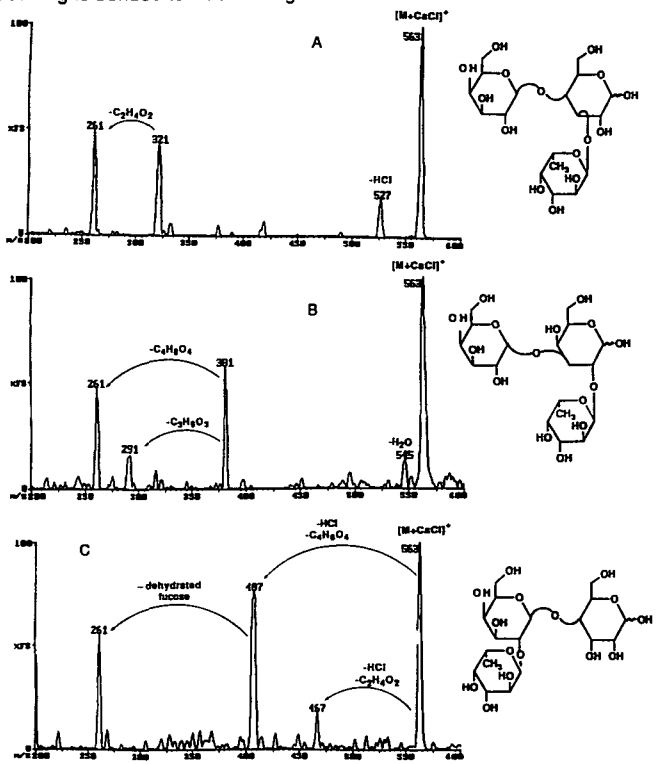

Figure 1. MS/MS spectra of $[M+CaCl]^+$ at 50% transmittance of Argon.

Reference.
1.Staempfli, A.; Zhou, Z.; Leary, J.A. *J. Org. Chem.* **1992**, *57*, 3590.

An Analysis of Mono- and Oligosaccharides by Electrospray Mass Spectrometry

Jennifer M. Duker and Edward W. Sheehan
Millipore/Extrel Mass Spectrometry, 575 Epsilon Drive, Pittsburgh, PA 15238

Simple sugars, or monosaccharides, are single polyhydroxy aldehyde or ketone units that provide the building block foundations for the larger covalently linked oligo- and polysaccharides. As bioorganic molecules, carbohydrates serve important biological functions in both the animal and plant worlds. In the form of sugar and starch they represent a large part of the total caloric intake for animals, while in plants, they are central to metabolism and the utilization of solar energy.

Based on the size of the saccharide of interest, the structural elucidation can often be complex. NMR (nuclear magnetic resonance) is commonly used to analyze sugars, however, in general these results are hindered by the complexity of larger molecular weight compounds. A more definitive means of analysis is provided by mass spectrometry. Mass spectrometry serves as an additional analytical tool for the analysis of carbohydrates and other compounds varying in molecular weight and structural complexity.

A series of mono- and oligosaccharides have been previously evaluated by particle beam LC/MS at various detection limits. This investigation looks at the use of electrospray for the evaluation of these same compounds. Negative electrospray was used to look at these compounds due to the resulting increase in sensitivity and response. In addition, collisonally induced dissociation (CID) was used to partially elucidate the structures of some complex oligosaccharides. This investigation, along with previous EI and CI spectra, allows us to fully characterize the compounds of interest. Further analysis of the data provided response factors at given injection volumes as well as multiple point calibration curves.

EXPERIMENTAL

This study evaluates the feasibility of utilizing a benchtop LC/MS with Particle Beam and Electrospray interfaces for the analysis of simple sugars. The compounds evaluated consist of monosaccharides up to 4 units in length.

MASS SPECTROMETER
- EXTREL benchmark™ mass spectrometer
- ThermaBeam™ Particle Beam interface
- Electrospray interface

LIQUID CHROMATOGRAPHY
- WATERS 600MS LC pump and controller
- Particle Beam
  - Solvents: (A) Methanol (B) H_2O
  - Mobile Phase: 80% A / 20% B
  - Flow Rate: 0.5ml min
- Electrospray
  - Quenching Gases: O_2 and SF_6
  - Solvents: (A) Methanol/Isopropanol (70/30) (B) H2O
  - Mobile Phase: 85% A / 15% B
  - Flow Rate: 0.2ml min, 100:1 split

Calibration Curve for Stachyose
The response is linear, r=0.998

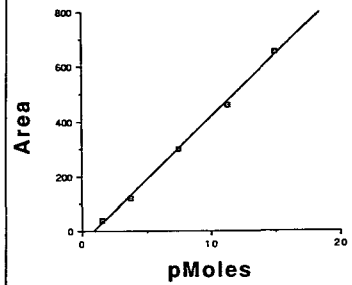

Total Selected Ion Chromatogram of 5 Drug Metabolites by LC/MS

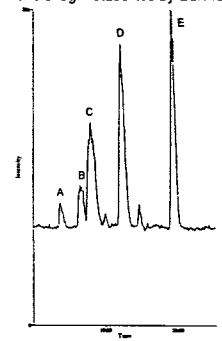

Positive Chemical Impact Stachyose

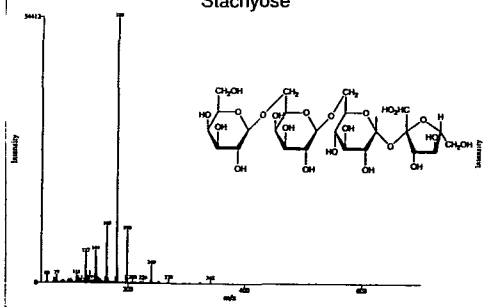

Negative Electrospray Stachyose

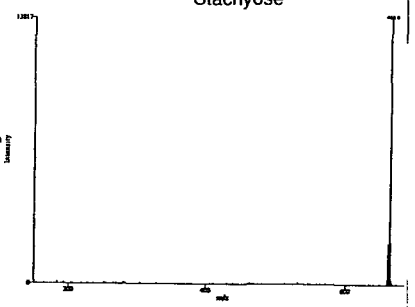

CONCLUSIONS

ThermaBeam™ LC/MS Analysis of Sugars:
- Sugars up to tetrasaccharide's yield the same characteristic EI spectra
- PCI of sugars provides molecular weight information as well as some structural information
- PCI was sensitive to all analyzed sugars
- PCI provided limited quantitative information but extensive qualitative information

Negative Electrospray LC/MS analysis of sugars:
- [M-H]- for some analyzed sugars
- Sensitivity and detection limits for high molecular weight compounds
- Linear calibration and extensive quantitative information

Use of matrix-assisted laser desorption mass spectrometry for examination of oligosaccharide mixtures.

D. J. Harvey

Glycobiology Institute, Department of Biochemistry, University of Oxford, South Parks Road, Oxford, OX1 3QU, UK.

Introduction

Matrix-assisted laser desorption mass spectrometry using substituted benzoic acids as matrices has been shown to produce abundant $[M + Na]^+$ ions from complex oligosaccharides[1,2]. 2,5-Dihydroxybenzoic acid (2,5-DHB) generally gives the strongest signal. This paper examines the use of the technique for examination of *N*-linked oligosaccharides released from glycoproteins.

Experimental

Materials. Reference oligosaccharides and sugar mixtures were obtained from IgG, ovalbumin, transferrin, ribonuclease, thyroglobulin, ovomucoid, fetuin and horseradish peroxidase by hydrazinolysis. 2,5-DHB was obtained from Aldrich Chemical Co. Ltd.,

Sample preparation. The matrix solution was prepared by dissolving 50 µmol (7 mg) of 2,5-DHB in acetonitrile (0.7 ml) and water (0.3 ml). 1.0 µl of this solution was placed on the target followed by about 0.2 µl of the solution of oligosaccharide (containing about 100 pmol of oligosaccharide). These solutions were allowed to mix and evaporate to dryness at room temperature. The deposit was then recrystallised on the target by the addition of about 0.2 µl of ethanol, allowed to dry, and the target was introduced into the mass spectrometer.

Mass Spectrometry. LD spectra were acquired with VG TOFSpec and Finnigan Lasermat TOF mass spectrometers, and with a VG Autospec mass spectrometer fitted with an array detector. All three instruments were fitted with a nitrogen laser operating at 337 nM. Spectra were obtained using multiple laser shots to give a good signal:noise ratio. Oligosaccharide compositions were assigned using a computer program written for the Windows 3.1 environment.

Results and Discussion.

2,5-DHB has been shown to give a concentration-dependent, signal from reference oligosaccharides (1 - 2 KDa range) and this matrix produced good spectra from all oligosaccharide mixtures examined. Representative profiles are shown in Figs 1 - 4. Oligosaccharide profiles could be obtained in less than 5 mins with higher resolution than by the existing method using Bio-Gel P4 chromatography (16 hours). With all of the mixtures examined, the known oligosaccharides were characterised and mass measured, usually to within ± 2 Daltons on the TOF instruments and to 0.5 Daltons on the sector instrument (low resolution mode). This was sufficient, to assign a composition in terms of isobaric sugars. In several cases, particularly with ovalbumin (Fig. 3), a number of unreported oligosaccharides were detected (unfilled peaks).

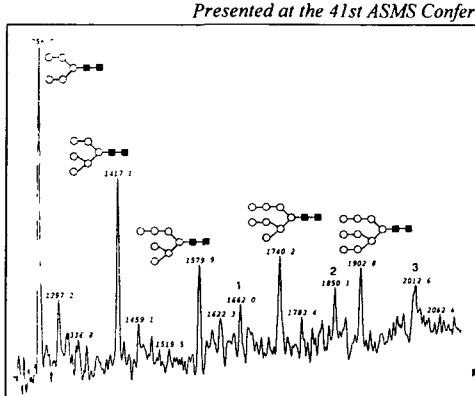

Fig. 1. LDMS of ribonuclease oligosaccharides.

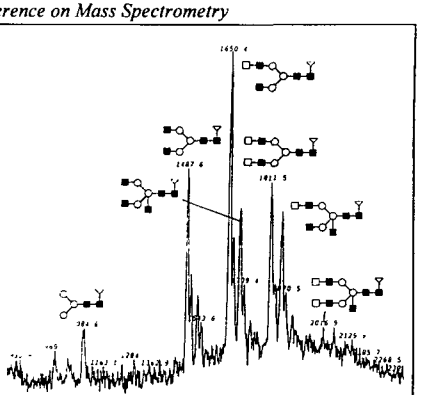

Fig. 2. LDMS of IgG oligosaccharides.

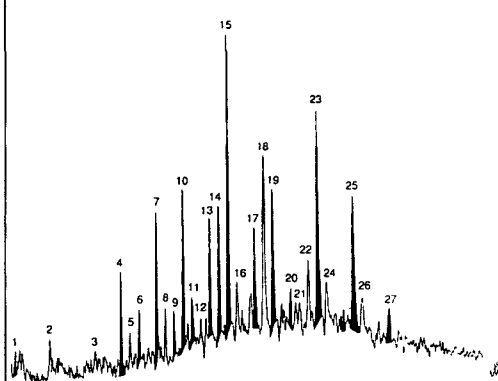

Fig. 3. LDMS of ovalbumin oligosaccharides.

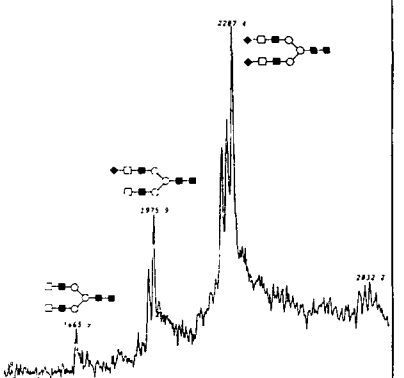

Fig. 4. LDMS of transferrin oligosaccharides.

Transferrin contained predominantly sialylated sugars (Fig. 4); these gave a mixture of ions in the positive ion mode in which each carboxylic acid group could acquire a sodium ion; the fully sodiated form predominated. In the negative ion mode, only one peak was observed suggesting that this is a more appropriate mode for anionic sugars.

References

1. K. K. Mock, M. Davey and J. S. Cottrell, *Biochem. Biophys. Res. Commun.*, **177**, 644 (1991).
2. B. Stahl, M. Steup, M. Karas and F. Hillenkamp, *Anal. Chem.*, **63**, 1463 (1991).

Identification of Glycoalkaloids in A Crude Mixture by Tandem Mass Spectrometry With Scanning-Array Detection

Su Chen[1], Peter J. Derrick[1], Fred A. Mellon[2] and Keith R. Price[2]
[1]Institute of Mass Spectrometry and Department of Chemistry, University of Warwick, Coventry CV4 7AL, and [2]AFRC Institute of Food Research, Norwich Laboratory, Norwich Research Park, Colney, Norwich NR4 7UA, UK

The glycoalkaloids (GA) are a group of nitrogenous, steroidal glycosides found in some common food plants of the *solanum* species, including potatoes, tomatoes and aubergines (eggplant). Although the chemical structures of these biomolecules have been known for years, common procedures for the identification of various aglycones and monosaccharides (mainly L-rhamnose,D-glucose,D-galactose and D-xylose) in the glycoalkaloids are time-consuming and require significant quantities of sample. MS/MS method has been used for analyzing a wide range of GA, including GA crude mixtures (1). In this communication, the identification of GA in a crude mixture by positive ion LSIMS and MS/MS is reported.

Experimental: The potato extract was isolated from etiolated potato shoots and prepared by a previously described method (2). All spectra were obtained on a Kratos CONCEPT II HH four-sector tandem mass spectrometer equipped with a scanning-array detection system (3). The acquisition-time of 10 seconds was made possible by using a charged-coupled device (CCD) to register the signal. Experimental parameters were controlled by a MACH 3 data system which recorded and processed mass spectra in an identical manner to that used with a conventional point detector. CID of precursor ions was conducted in a flexicell which was floated at a potential of 4 kV related to the earth. Helium was used as collision gas and was set to a pressure sufficient to attenuate the precursor ion beam by 60%. The samples were dissolved in a 2:1 mixture of MeOH/TFA and the solution was transferred to the LSIMS probe tip and dried, after which NBA was added. The amount of sample loaded for positive ion analysis was 200 ng for conventional mass spectrometry and 200-2,000 ng for tandem mass spectrometry.

Results: CID MS/MS spectra of the $[M+H]^+$ ions, generated by LSIMS of a crude mixture (fig.1a), induces three major fragmentation processes, Z-, Y- and ^{1,5}X-cleavages, which are structurally informative. Signals resulting from X0-, Y0- and ^{1,5}X0-cleavages provide information on structures of various aglycone moieties in all GA. Linkages and positions of the sugars in trisaccharide- and tetrasaccharide-containing GA can be identified depending on the presence or absence of the ions due to Zα+β- and Yα+β-cleavages and intensity differences of the peaks due to ^{1,5}Xα- and ^{1,5}Xβ-cleavages (fig. 1b and 1c), respectively. The positive ion method has the advantage of i) lower detection limit in the conventional mass spectrometry; ii) numerous and intense fragment ions that are structurally informative; and iii) the capability of analysing minor components (fig. 1b) in crude extracts. Comparable analysis by other analytical means would not have provided the amount of structural information on the compounds of the glycoalkaloid mixture.

References

1) Chen, S., Derrick, P. J., Mellon, F. A. and Price, K. R., Submitted to Anal. Biochem.
2) Coxon, D. T., Price, K. R. and Jones, R. G. (1979) J. Sci. Food Agric. **30**, 1043.
3) Evans, S., Buchanan, R., Hoffman, A., Mellon, F. A., Price, K. R., Walls, F. C., Hall, S., Burlingame, A. L., Chen, S. and Derrick, P. J. (1993) Org. Mass Spectrom., **28**, 289.

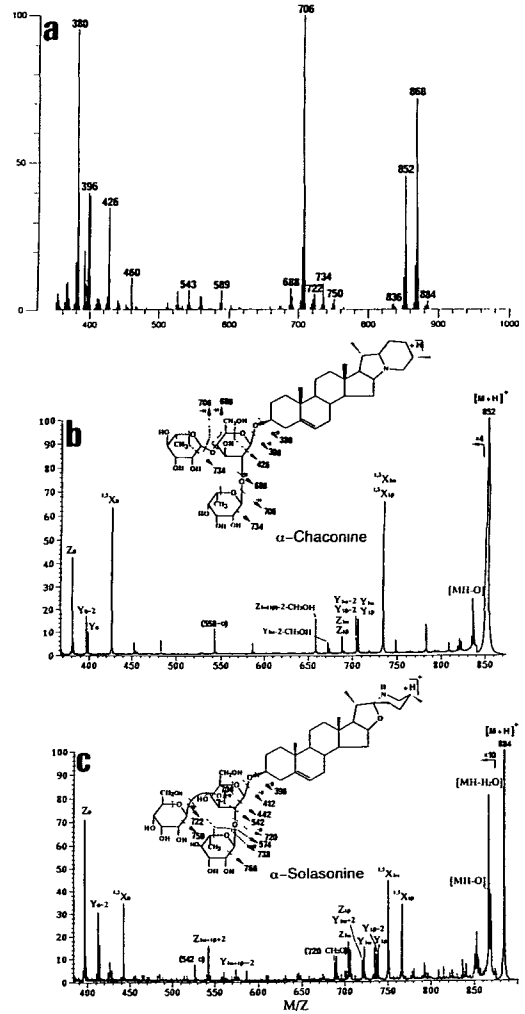

Figure 1a. Positive ion LSI mass spectrum of a GA mixture extracted from potato shoots;
1b. CID MS/MS spectrum of the ion at m/z 852 in figure 1a;
1c. CID MS/MS spectrum of the ion at m/z 884 in figure 1a;

Oligosaccharide Profiling by LC-ESI-MS: Focus on Mucins.

Rene Mora, Jeffrey M. Drazen and Vernon N. Reinhold.
Harvard University School of Public Health,
665 Huntington Avenue, Boston, MA 02115.

Carbohydrates fulfill important structural and functional roles within tracheobronchial mucins, and there is increasing evidence that changes in mucin carbohydrates may have profound pathophysiological consequences. With an eye toward the structural analysis of mucin glycans, we have been investigating methods for the chemical release of O-linked oligosaccharides from mucin glycoproteins, the derivatization and chromatographic separation of these oligosacharides, and the interfacing of such chromatography with electrospray mass spectrometry.

Our results to date indicate the following: (i) O-linked glycans can be released from mucins in intact form and with a yield of greater than 85% by hydrazinolysis at 75C for six hours. The distribution of O-linked glycans found in fetuin as well as in bovine submaxillary mucin by hydrazinolytic release matches closely with those profiles previously obtained by reductive elimination.
(ii) Both N- and O-linked glycans containing a reducing end group, whether released by hydrazinolysis or enzymatic means, may be subjected to end-group labeling by hydrazine and PITC. Such labeling greatly enhances the spectrophotometric detection of these glycans. When combined with the resolving power of normal-phase chromatography of glycans on aminosilica columns, complex mixtures of oligosaccharides present in relatively small amounts may be chromatographically purified as individual species. The chromatogram shown below represents the separation of less than 10 ug of ribonuclease b glycans, and it suggests that there is separation not only on the basis of size but also among different isomers.

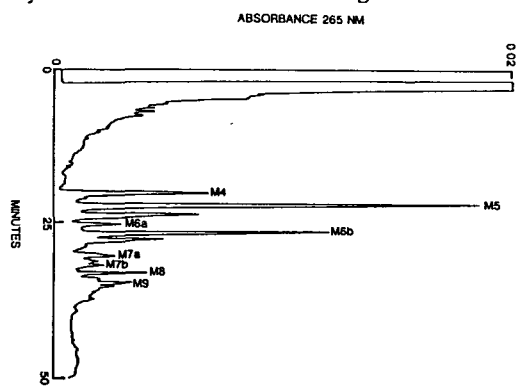

(iii) Such released glycans are amenable to permethylation and mass spectrometric detection by ESI-MS, with sodium adduction. As previously demonstrated, this approach provides sensitivity in the low picomolar range (1). When hydrazino-PITC-labeled glycans are subjected to basic permethylation, there is full derivatization of all glycan hydroxyl groups as well as the amine moieties on the hydrazine and the phenylisothiocyanate. Glycans derivatized in this manner, when subjected to electrospray ionization, may appear either as the protonated or the sodiated species, depending on the solvent conditions . (iv) Complex mixtures of permethylated glycans may be subjected to capillary reverse-phase HPLC separation, coupled with on-line ESI-MS, using water and methanol as the eluants The inclusion of 0.5 mM NaAc in both the iorganic and organic solvents provides the needed alkali metal ion for adduction and electrospray ionization. The chromatogram shown below, generated with 200 ng of ribonuclease b glycans, demonstrates the sensitivity of this technique.

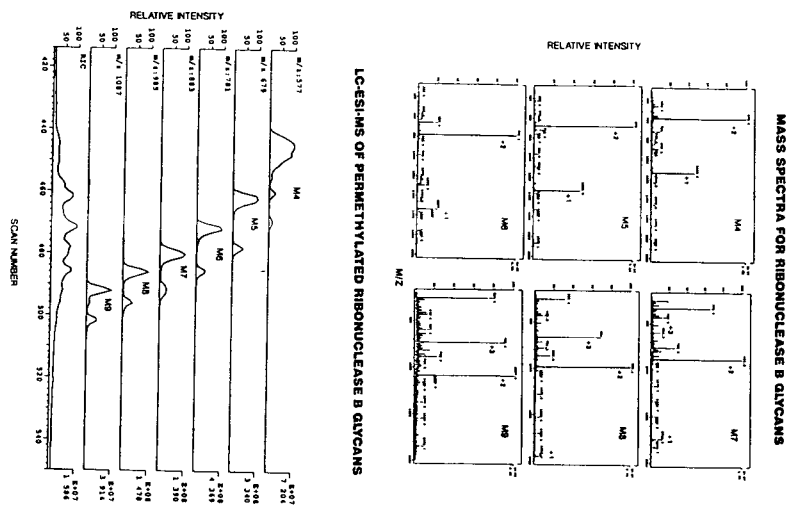

The longer term goal of these efforts is to combine these and other methodologies under development into a general approach to the structural analysis of mucin glycans.

(1) Stephen Chan, et al. Detailed Structural Characterization of Glycoprotein N- and O-linked Glycans by ESI and CID. The 40th Conference on Mass Spectrometry and Allied Topics, May 31-June 5, 1992, Washington, D.C.

GLYCOFORM DETECTION IN CHO - DERIVED INTERLEUKIN-4 BY LC - CID - ELECTROSPRAY MASS SPECTROMETRY.

***A. Tsarbopoulos, B.N. Pramanik, E. Huang and T. Covey[1].**

Schering-Plough Research Institute, Kenilworth, NJ 07033 and [1]Sciex, Thornhill, Ontario L3T 1P2, Canada.

Human interleukin-4 (IL-4), previously known as B-cell stimulatory factor, is a T-cell derived lymphokine which mediates the proliferation and differentiation of B-cells, and also stimulates mature T-cell proliferation. The gene encoding human IL-4 has been cloned and expressed in Chinese Hamster Ovary (CHO) cells. The mature polypeptide sequence is 129 amino acid residue long and contains two asparagine residues in the consensus sequence Asn-X-Ser/Thr which is required for N-linked glycosylation.

Several mass spectrometric (MS) techniques have been recently developed for identifying glycopeptides in chromatographically separated fractions from complex digest mixtures of glycoproteins, mainly by mapping prior to and after enzymatic digestion with peptide:N-glycosidase F (N-Glycanase). In this report, we assess the utility of the electrospray (ES) ionization method in combination with enhanced ion-source fragmentation towards the identification of the glycopeptides in the LC chromatogram and the early indication for the various glycoforms present in the chromatographic fractions.

Analysis of CHO IL-4 by electrospray MS, using a Sciex API III triple quadrupole mass spectrometer, generated three envelopes of multiply charged ions from 8+ to 10+ each comprising several peaks corresponding to the individual glycoforms of the glycoprotein (Fig. 1). Then the CHO IL-4 glycoprotein and its deglycosylated (*E. coli*-derived) counterpart were cleaved enzymatically by either trypsin or V8 protease and the resulting peptide digest mixtures were analyzed by reversed-phase HPLC in conjunction with ES MS. This approach provided information on the glycopeptide fragments along with protein mapping. ES MS analysis of the tryptic digest of CHO IL-4 provided mapping of the protein backbone including confirmation of the existing disulfide pattern in the protein molecule. It should be noted that ES analysis of the *E. coli* IL-4 tryptic digest yielded only signals corresponding to the average mass of the disulfide-paired peptides $T_{1,2}$-T_{22}, T_6-T_{16} and T_4-T_{10}, i.e., 1734.4, 2124.7 and 2943.1 Da, respectively. This is in contrast to the LSI and PD MS analysis, where additional signals corresponding to the cysteine-containing constituent peptides were observed. In the analysis of the CHO IL-4 tryptic digest these disulfide-indicative ES signals were shifted to higher m/z values due to incomplete cleavage at the lysine residues near the glycosylation site, thus resulting to the incorporation of the T_5-CHO glycopeptide on the adjacent disulfide-linked peptides T_4 and T_6.

Comparative LC-ES tryptic mapping of the CHO and *E. coli* IL-4 allowed the identification of peaks 11 and 14 in the total ion chromatogram of CHO IL-4 as the ones containing the glycopeptide fragments (Fig. 2). The ES mass spectrum of the *E. coli* IL-4 peak 11 exhibited multiply charged ions corresponding to the $T_{5,6}$-T_{16} disulfide (Fig. 3), whereas that of CHO IL-4 showed two ion envelopes corresponding to triply and quadruply charged glycopeptides (Fig. 4). The m/z spacing between the peaks in each ion envelope revealed the variations in the NeuAc and Hex-HexNAc content, and the corresponding glycopeptide mass values were 4921, 5286, 5577 and 5868. It should be noted that low mass ions indicative of the carbohydrate units were either very weak or absent in the ES spectrum of Fig. 4. The presence of these sugar-specific ions (m/z 162 for Hex^+, m/z 204 for $HexNAc^+$, m/z 292 and 274 for $NeuAc^+$ and m/z 366 for $Hex\text{-}HexNAc^+$) was enhanced by increasing the orifice (OR) potential, which controls the extent of fragmentation in the declustering region (the region before the first mass filter, Q1) of the API III mass spectrometer (HIGH SOURCE FRAGMENTATION). The ES mass spectrum of peak 11 at elevated OR potential (110 V) is shown in Fig. 5, where all sugar-specific oxonium ions are clearly observed. Moreover, this spectrum shows that the intact glycopeptide signals tend to shift to lower m/z values within the ion envelope of the same charge state, due to the partial loss of carbohydrate units such as the NeuAc end cap units. Although this is only happening to a small extent, it can be eliminated by stepping the OR potential with mass as it was recently shown by Carr et al. (Protein Sci. 1993, 2, 183-196). Even

though this enhanced fragmentation in the ion declustering region lacks mass selectivity, it yields the same structural information as fragmentation in the second quadrupole with much higher sensitivity and product ion resolution. These carbohydrate screening results agreed with those deduced from the PD MS analysis of the isolated and derivatized carbohydrate components (See Proceedings of the 38th ASMS Conference, pp. 1341-2).

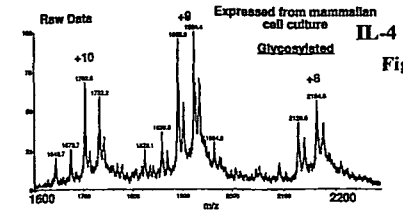

Fig. 1

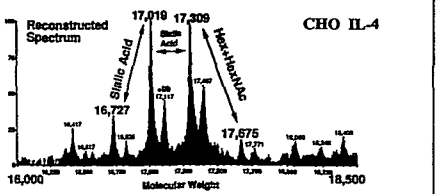

Fig. 2

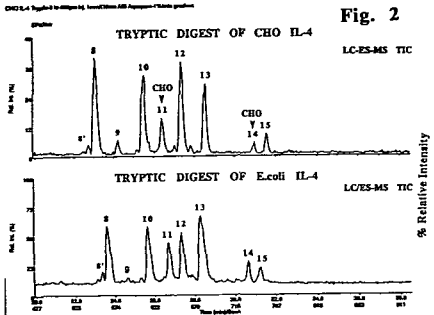

Fig. 3

ES MASS SPECTRUM OF CHO IL-4 TRYPTIC PEAK 11
LOW SOURCE FRAGMENTATION

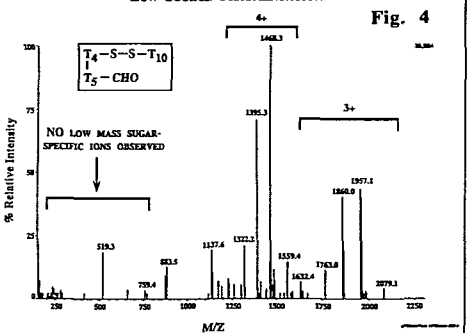

Fig. 4

ES MASS SPECTRUM OF E. coli IL-4 TRYPTIC PEAK 11

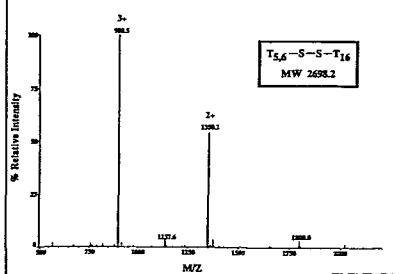

ES MASS SPECTRUM OF CHO IL-4 TRYPTIC PEAK 11
HIGH SOURCE FRAGMENTATION

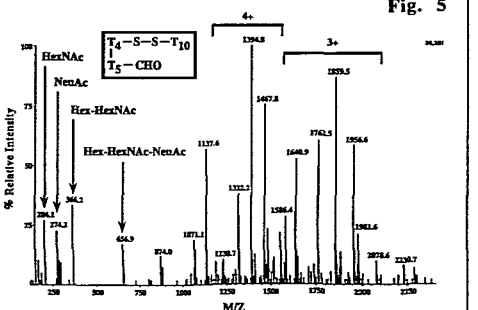

Fig. 5

Enhanced Carbohydrate Detection by Multiple Ion Monitoring (MIM) of HPLC Effluents

Stephen Chan, Bruce Reinhold and Vernon Reinhold
Department of Nutrition, Harvard University School of Public Health, Boston, MA 02115

Understanding the structure-functional relationship of carbohydrates in biological systems has been recognized as a vital aspect in biomedical research. Although the details of carbohydrate structure are still rarely pursued, and only then, when relatively large amounts of sample become available. With new attention to the role carbohydrates play in lymphocyte trafficking, modulation of the immune response, nitrogen fixation and their well established roles in cellular differentiation, a greater effort must be directed to supporting full characterization at the biological amounts frequently available.

Carbohydrates or glycans derived from extracts of biological samples could be in a matrix containing many other species even after extensive sample clean-up. We have demonstrated the utility of the permethylation technique to enhance sample clean-up and improve electrospray ionization (ESI) efficiency [1]. Even so, for analyzing glycans in a complex matrix, separating the glycans from the matrix would enhance not only the ESI efficiency of the glycans, but also produce cleaner and more interpretable mass spectra. In this research, on-line HPLC separation prior to ESI analysis is used to separate glycans from matrixes and, with an appropriate solvent gradient, separate the different glycoforms among the glycans. If the detection of a specific glycoform is the only interest, the sensitivity of the analysis could be greatly improved if only the ions associated with the glycoform are monitored during the HPLC run. The identity of the glycoform would be unambiguous if more than one ion characteristic of the glycoform are monitored. The multiple ion monitoring (MIM) technique is accomplished by collisional induced dissociation (CID) which produces characteristic fragment ions associated with the interested glycoform.

Both high-mannose and complex type glycans were used in this research in order to demonstrate the feasibility of the (MIM) technique. High-mannose glycans were enzymatically released from Ribonuclease B by means of endoglycosidase F. This protein is known to contain a single N-linked site of high-mannose glycans. Complex glycans were enzymatically deglycosylated from recombinant erythropoietin (EPO) using N-glycosidase F. All the released glycans were permethylated prior HPLC injection. This would remove all hydrophilic residues because the last step of permethylation involves several stages of water/ chloroform extraction. The HPLC separations were performed using a C4 capillary column with a pre-column (1: 600) solvent splitting. Effluents eluded from the column were directly infused into an eletrospray ionization source (ESI) at a flow rate of about 1 ul/min. The solvent gradient contains water and methanol with 0.5 mM of sodium acetate. During MS/MS scannings, the collision offset voltage of a Finnigan TSQ-700 triple stage mass spectrometer was maintained at between 27 to 35 V, depending on the type of glycans being monitored. The collision pressure of argon was set at about 3.5 mtorr.

All five known high-mannose glycoforms were separated under our HPLC conditions (Figure 1). Anomers and selected isobers appear to separate well under these conditions. The chromatrograph derived from monitoring a single characteristic ions of Man_9 glycans reveals remarkable improvement in signal to noise ratio. This allows the anomers to be better baseline separated. By monitoring more than one characteristic ions associated with the glycoform, the MIM chromatrograph allow further structure identities of the glycoform to be exposed.

The HPLC conditions used for separating the high-mannose glycoforms did not allows the complex glycan to be well separated. However, the MIM chromatrograph derived from monitoring the loss sialic acids from a tetraantennary complex glycan provides additional identity for the compound with enhanced signal to noise ratio. In case of monitoring a specific structure from a very complex mixture, MIM is needed to reduce ambiguity for the positive identification.

Reference

1. S. H. Stephen Chan, Bruce B. Reinhold and Vernon N. Reinhold; " Detailed Structural Characterization of Glycoprotein N- and O-Linked Glycans by ESI and CID " Proceedings of the 40th ASMS Conference on Mass Spectrometry and Allied Topics. Washington, DC, May 31 - June 5 1992.

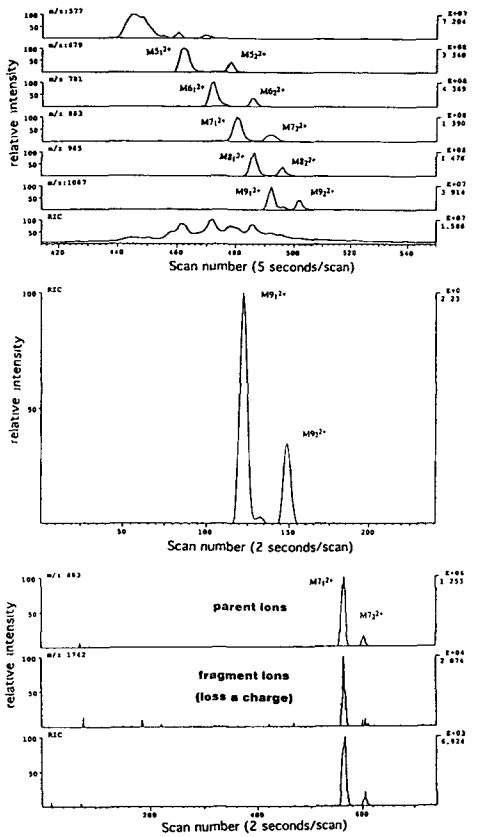

Figure 1. Mass chromatrographs of high-mannose glycans derived from Ribonuclease B. The MS/MS studies based on single ion monitoring (middle) and multiple ion monitoring (bottom) are also shown.

QUANTITATION OF GLUCOSE AND $^{13}C_6$-(U)-D-GLUCOSE METHYLBORONATE PENTAFLUOROPROPIONATES IN HUMAN PLASMA BY METHANE NCI GC-MS.

Jiri Zamecnik, Garry Seabrook, Defence and Civil Institute of Environmental Medicine, Operational Medicine Division, North York, Ontario, M3M 3B9, Canada.

Introduction and Methods

For our study of substrate utilization in humans exposed to cold we needed a method which would allow us to measure both $^{13}C_6$-(U)-D-glucose ($^{13}C_6G$) and D-glucose (G) in a single small volume sample, with a simple sample preparation. We have developed a methane NCI GC-MS method based on cyclic methylboronate-pentafluoropropionate derivatization using $^2H_3$-(5,6,6)-D-glucose (D_3G) as an internal standard (IS). Two calibration curves were produced, one for G was prepared in water in duplicates (500, 1000, 1500 and 2000 µg/mL), the second calibration curve for $^{13}C_6G$ was prepared in duplicates in human plasma (1, 5, 10, 50 and 100 ng/mL of plasma). The samples of heparinized frozen human plasma and control plasma pool samples were allowed to thaw and aliquots of 10 µL undiluted or 100 µL of diluted (1:10) plasma were used. The IS (100 ng/100µL of D_3G in water) was added to all samples and calibrators. All tubes were vortexed and freeze-dried overnight. The freshly prepared solution of methyl boronic acid (MBA - 100 µL of 1 mg/mL solution in dry pyridine) was added to all tubes, heated at 95°C for 1 h, pyridine was then removed under a stream of nitrogen. Pentafluoropropionic anhydride (PFPA, 100 µL) was added and tubes were heated for an additional 45 min at 75 °C; 1 µL aliquots were injected into GC/MS (Finnigan MAT TSQ-70). The samples were stable for up to 5 days. The GC conditions: injector in split mode (1:30) at 280°C, GC oven 160°C to 260°C at 15°C/min; separator 280°C, capillary DB-5 J&W Scientific 30 m column, 0.25 mm I.D. The ion source temperature was 110°C, filament current 200 µA, electron multiplier 1600V, scanning a single quadrupole in a selective ion monitoring mode (SIM) using methane as CI gas in negative mode. Masses 374 m/z (G), 377 m/z (D_3G) and 380 m/z ($^{13}C_6G$) were monitored with a dwell time of 100 µsec. The typical retention time was 3.5 min, with D_3G eluting slightly ahead of the other two glucoses. There were no interfering peaks in all the three monitored channels.

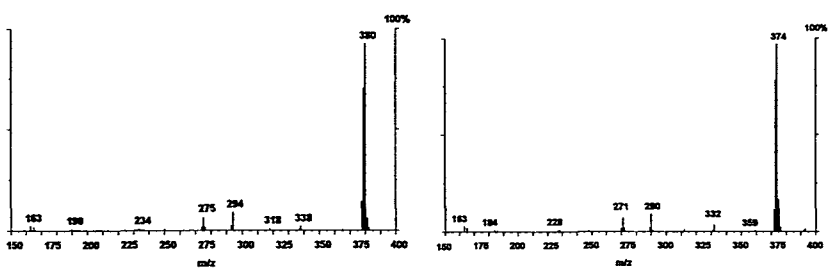

$^{13}C_6$-(U) D-glucose and D-glucose methylboronate-pentafluoropropinates methane NCI

Results and Discussion

We have developed G and $^{13}C_6G$ assays using MBA derivatization because the derivatives had good stability and excellent GLC properties (1-5). To increase the sensitivity we used PFPA and methane NCI. The sample size was typically 1-10 µL of plasma. Small lumps of insoluble material were observed in all sample tubes after the last derivatization step, with the derivatized glucoses remaining dissolved in PFPA. The small sample size, impurity precipitation and use of split injection (1:30) allowed us to skip any pre-purification steps. The crude derivatized plasma extracts were injected directly into the GC-MS. Other hexoses present in human plasma samples eluted from the GLC column at different retention times than glucose. This simple workup allowed us to complete a batch of 60 samples in one and a half days. The contribution of D_3G IS into either of the sample channels (0.351% into 374 and 0.436% into 380 m/z) at 100 ng/tube did not affect the results. The calibration curves were calculated by least square fitting of all points and plotted, as a ratio of areas for (377 m/z and 374 m/z over 380 m/z) against the glucoses plasma concentrations (r>0.998). The precision calculations were done on pooled plasmas used for the quality control (5.1 ng/mL of $^{13}C_6G$ and 750 µg/mL of G). The within assay coefficients of variation (%CV) assays were 3.79% for G and 2.33% for $^{13}C_6G$ (n=10). The between assays %CV were 5.05% and 3.91% (n=10). The limits of detection (3x SD of baseline, 6) were 3.7 pg/mL, the limits of quantitation (10x SD of baseline, 7) were 12.5 pg/mL, for both assays. In conclusion, the method of assaying both glucoses was reliable, fast and proved most applicable to kinetic studies of glucose utilization in humans.

References

1. Pickert A, Overkamp D, Renn W, Liebich H, Eggstein M. *Selected ion monitoring gas chromatography/mass spectrometry using uniformly labelled (^{13}C) glucose for determination of glucose turnover in man.* Biol Mass Spectrom 1991;20:203-9.

2. Eisenberg Jr. F. *Cyclic butaneboronic acid esters: novel derivatives for the rapid separation of carbohydrates by gas-liquid chromatography.* Carbohyd Res 1971;19:135-8.

3. Wood PJ, Siddiqui IR, Weisz J. *The use of butaneboronic esters in the gas-liquid chromatography of some carbohydrates.* Carbohyd Res1975;42:1-13.

4. Kossa WC. *Cyclic boronates as derivatives for gas chromatography-mass spectrometry of bifunctional organic compounds.* In: Chemical Derivatization in Analytical Chemistry, Vol. 1, Chapter 2, R.W. Frei and J.F. Lawrence, Plenum Press, New York, 1981:99-125.

5. Zamecnik J. *Use of cyclic boronates for GC/MS screening and quantitation of Beta-adrenergic blockers and some bronchodilators.* J Anal Toxicol 1990;14:132-6.

6. Long GL, Winefordner JD. *Limits of detection.* Anal Chem 1983;55:712A-9A.

7. Needleman SB, Romberg RW. *Limits of linearity and detection for some drugs of abuse.* J Anal Toxicol 1990;14:34-8.

QUANTIZATION STUDIES OF POLYMETHYLATED β-CYCLODEXTRINS BY ESMS

Leize E.[1], Dupont A.[1], Le Tavernier J.F.[2] and Van Dorsselaer A.[1]
[1]Laboratoire de Spectrométrie de Masse Bio-Organique, URA 31 CNRS-Université Louis Pasteur, 1 rue Blaise Pascal, 67000 Strasbourg. [2] Centre de Recherche en Biotechnologie ORSAN, Courtaboeuf, France.

INTRODUCTION:

β-cyclodextrins present attractive properties: for example, they are good pharmacological carriers and they can be used as stationary phases for liquid chromatography. Unfortunately, β-cyclodextrins are characterized by a low solubility. This drawback is circumvented by using modified β-cyclodextrins (methylated, ethylated and hydroxypropylated) which exhibit the properties of native β-cyclodextrins without their inconveniences. There is an analytical need to determine the degree of alkylation and the purity of these derivatized β-cyclodextrins which are often produced as mixtures of several states of *methylation usually ranging from 13 to 18. Using conventional analytical tools (RP-HPLC, NMR)*, accurate characterization of modified β-cyclodextrins is difficult to achieve.

We have already described the characterization of PolyMethylated β-CycloDextrins (PMCD) by ESMS, using NH_4^+ adducts [1]. This method does not lead to fragmentations and is characterized by an easy preparation of samples, short times of analysis and very high sensitivity (picomole scale). Unfortunately, in this former work, the percentage of each methylation state could not be determined because we had no access to the response factors.

We show here that ESMS can be used for an accurate quantization of the methylation degree in a PMCD mixture. We evaluate also the possibilities of dodecylamine to replace NH_4^+ for ionisation.

RESULTS:

Determination of the best ionization agent:

ESMS Spectra with NH_4^+ (Fig.1): Only molecular ions $[M+NH_4]^+$ were produced for each number of methylations. The presence of small doubly-charged ions $[M+2NH_4]^{2+}$ did not interfere with quantization, as the profiles of the mono-charged and the doubly-charged ions were identical. Therefore, only the mono-charged ions were used for quantization.

ESMS Spectra with dodecylamine (Fig.2): We observed almost exclusively the mono-charged ions [M+dodecylamine]. Comparing to the NH_4^+ spectra, the peaks were more intense and sharper. The doubly-charged ions were smaller than with NH_4^+. Surprisingly, for the same sample of PMCD, the different peaks did not display the same relative intensity with dodecylamine than with NH_4^+. Moreover, the pattern of the mono-charged and that of the doubly-charged ions were very different.

Conclusion: The mono-charged ion profile observed for NH_4^+ and dodecylamine are different. The quantization study have been designed to determine which profile is closer from the actual distribution.

Quantitative study:

In this study, we have used trimethyl β-cyclodextrin as an internal standard.

To prove that the intensities of the peaks corresponding to the different numbers of methylation represent accurately the proportions of the species present in solution, we have to demonstrate the linearity of the response and the equality of the response factors.

Linearity of the response: We have to prove that the experimental values of the relative intensities of the peaks, for each methylation number, can be deduced by calculation from the combination of A and B values.

Identity of the response factors: We have to prove that the sum of the relative intensities of each methylation degree is the same for different PMCD preparation with the same total concentration. For that purpose, we used several PMCD preparations:

- preparation A containing PMCD with 14 to 18 methylations

- preparation B containing PMCD with 13 to 15 methylations

and 3 mixtures of A and B in different ratios: 1/1 (sol.C), 2/1 (sol.D), 1/2 (sol.E).

Conclusion: The results are summarized in table 1:

In the case of NH_4^+: The correlation between experimental and calculated values is well established. This demonstrates the **linearity** of the response.between the concentration and the peak height. Moreover, the sums of the relative intensities are very close; eg. the A/B ratio is about 1.2. Therefore, **quantization** of the PMCD with NH_4^+ as charging salt **is then possible.**

In the case of dodecylamine: The agreement between the calculated values and the experimental ones is poor, and the sums of the relative intensities are quite different between the 5 solutions studied; eg. the A/B ratio is close to 1.6. This two points show that quantization can not be obtained with dodecylamine probably because of the discrimination by the degrees of methylation due to the size of the guest molecule.

CONCLUSION:

ESMS allowed us to determine the relative repartition of methylations with a good accuracy in several mixtures of PMCD, containing from 13 to 18 methylation number, provided that NH_4^+ is used as charging salt. This method is all the more interesting as it is simple, fast and accurate.

REFERENCES:

1. O. Sorokine et al., *Procedings, 40th ASMS*, **1992**, 1645-1646.

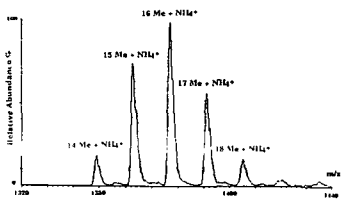

Fig 1: ESMS spectrum with NH_4^+.

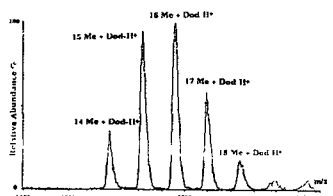

Fig.2: ESMS spectrum with dodecylamine.

	Intensities relative (I) to the internal standard (%)									
Degree of Me	with NH4+					with DODECYLAMINE				
	Sol A Exper	Sol B Exper	Sol C Exper / *Calc.*	Sol D Exper / *Calc.*	Sol E Exper / *Calc.*	Sol A Exper	Sol B Exper	Sol C Exper / *Calc.*	Sol D Exper / *Calc.*	Sol E Exper / *Calc.*
13 Me	0	19.4	9.5 / *9.7*	7.1 / *6.5*	13.5 / *12.9*	0	11.5	7.7 / *5.8*	5.0 / *3.8*	9.3 / *7.7*
14 Me	17.4	100	54.2 / *58.7*	45.7 / *44.9*	71.8 / *72.5*	19.6	100	67.2 / *59.8*	59.9 / *46.4*	81.0 / *73.2*
15 Me	51.3	25.4	39.9 / *38.4*	43.5 / *42.7*	33.4 / *34.0*	74.5	25.3	56.3 / *49.9*	71.8 / *58.1*	48.4 / *41.7*
16 Me	61.4	4.9	35.6 / *33.2*	43.5 / *42.6*	23.3 / *23.7*	81.0	5.7	54.0 / *43.4*	73.4 / *55.9*	40.9 / *30.8*
17 Me	35.7	0	20.6 / *17.9*	28.8 / *23.8*	13.5 / *11.9*	44.7	2.3	27.0 / *23.5*	38.8 / *30.6*	20.6 / *16.4*
18 Me	12.1	0	7.6 / *6.1*	9.8 / *8.1*	5 / *4.0*	15.8	2.3	10.0 / *9.1*	13.5 / *11.3*	7.5 / *6.8*
∑ I	177.9	149.7	167.4	176.4	160.5	235.8	147.1	222.2	282.4	207.6
A/B			1.19					1.60		

Table 1: Summarized results for quantization.

Matrix Additives to Enhance Signal Intensity of Gangliosides in Negative FAB-MS Analysis

Shyong, B. J., Huang, Z. H., Gage, D. A., Hollingsworth,R. I., and Sweeley, C. C.
Michigan State University, East Lansing, MI 48824

In order to characterize low levels of acidic carbohydrates and glycosphingolipids from biological materials by FAB-MS, we have investigated the effect of adding cationic surfactants and crown ethers to the FAB matrix forln order to characterize low levels of acidic carbohydrates the analysis of several standard gangliosides and carbohydrates containing sialic acid. In addition to commercial surfactants, we have synthesized a series of quaternary ammonium-type surfactants for this study.

Our approach for this study was to compare the spectra of analytes in the concentration range 10-100 pmol/ml by negative FAB-MS with standard matrices (TEA or glycerol) with and without the addition of surfactants or additives. With surfactant assistance, the molecular ion intensity of acidic carbohydrates and glycoconjugates was increased up to 10 fold.

Interest in the role of glycosphingolipids (GSLs), gangliosides, and related carbohydrate compounds has increased due to their multiple biological functions. Enzymatic, immunological, and spectroscopic techniques have been developed to structurally characterize these compounds. In practice, mass spectrometry has proven to be one of the most sensitive analytical approach. However, the sensitivity available with standard methods is often insufficient to analyze the quantities of glycoconjugates that can be isolated from biological sources. To characterize picomole levels of gangliosides and acidic carbohydrates from biological materials by FAB/MS, we have evaluated the signal enhancement effect of adding cationic surfactants or crown ethers into the matrix for the analysis of several standard gangliosides and related carbohydrates.

The examined analytes are dissolved in chloroform:methanol (1:2) (1μg/μl) to prepare stock solutions. Serial dilutions were made as needed. The additives (cationic surfactants or crown ethers) were prepared with as aqueous methanolic (1:1) solution (10 μg/μl) to facilitate quantitative handling. The additive solutions were also diluted as needed. Applied matrices (TEA or Gly) were diluted with equal volumes of methanol. Samples were prepared for analysis by loading on the probe tip 1 μl of the diluted analyte solution, 1 μl additive solution, and 1 μl of the matrix solution without mixing.

A JEOL HX-110 double focusing mass spectrometer was utilized for this study and operated in the negative mode at 10-kV accelerating voltage and 1:1000 resolution. Single scans were acquired by scanning the mass range in about 30 seconds. Spectral data were shown from a single scan while the numerical values for the absolute intensities were obtained from an average of three scans.

The results from this study could be concluded as following:

1. The relative intensity of the $[M-H]^-$ signals in the negative FAB spectra of gangliosides and acidic carbohydrates was increased by the addition of surfactants or crown ethers, except for the trisialo compound GT_{1b}.
2. The signal-to-noise ratio in the spectra obtained with surfactant assistance was improved, so that in some cases low abundance fragments were more readily detected.
3. The enhancement was quite specific to the combination of analyte and additive used.
4. Adding surfactants to the matrix increased the persistence of the signal under NI-FAB.

Analyte/matrix	Employed additives	Intensity ± STD (Analyte + matrix)	Gain (fold)
G_{T1b}(46 pmol)/TEA	aza15C5 10 μg	49,591 ± 1,019 (104,830 ± 13,739)	0.47
G_{D1b}(56 pmol)/TEA	PPN-Ac 200 ng	341,456 ± 17,287 (292,883 ± 127,866)	1.2
G_{D1a}(56 pmol)/TEA	aza15C5 10 μg	25,315 ± 10,428 (13,258 ± 11,388)	1.9
G_{M1}(10 pmol)/TEA	HPPBr 200 ng	164,256 ± 48,427 (116,060 ± 68,644)	1.4
G_{M3}(13 pmol)/TEA	aza15C5 10 μg	922,355 ± 439,327 (151,737 ± 183,893)	6.1
Lac-Cer (15 pmol)/TEA	HETPPBr 1 μg	125,166 ± 14,659 (14,717 ± 1,331)	8.5
SA-Lac (158 pmol)/Gly	N-ONBr 500 ng	6,397,243 ± 1,261,704 (508,681 ± 239,900)	12.4
SA (81 pmol)/Gly	BzTC 200 ng	1,113,242 ± 116,963 (117283 ± 29494)	9.5

Table: Surfactant-assisted negative ion FAB-MS of GSLs, gangliosides and related carbohydrate compounds. The intensity of $[M-H]^-$ was an average from the numerical value of three successive scans. Gain was calculated from the ratio between the ion intensity of the $[M-H]^-$ signal with and without added surfactant.

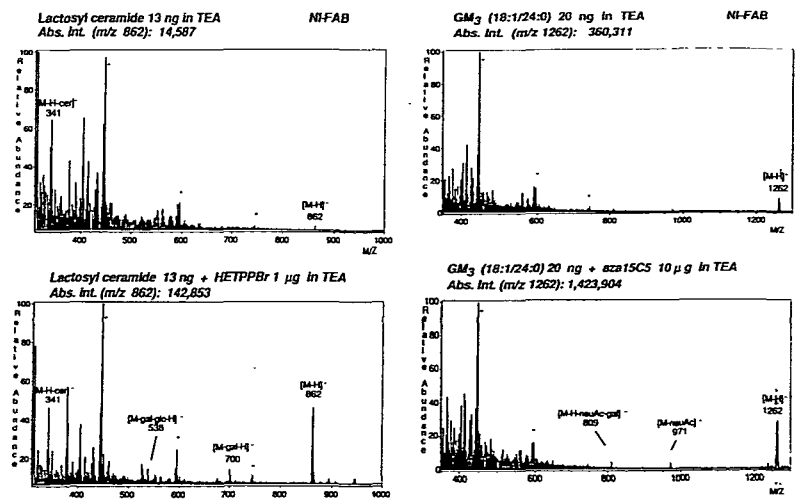

Drug Analysis Using MALD-MS: Application to Influx Kinetics, Multidrug Resistance and Chemical Change *In Vivo*

Gary Siuzdak*
Department of Chemistry

Andrés Bustamante, and Darryl Rideout
Department of Molecular Biology

The Scripps Research Institute, La Jolla, California, 92037

The ability to detect and quantify exogenous drug and toxin molecules introduced into cells and tissues is crucial for drug design, preclinical and clinical pharmacology, and toxicology. Current methods for identification and quantitative analysis of exogenous molecules in cells and tissues include scintillation counting of radiolabelled molecules, fluorimetry, HPLC and secondary ion mass spectrometry (SIMS). However, these methods have considerable limitations including disposal problems associated with radiolabeling and SIMS' requirement that a drug contain an element not present at competing concentrations. Consequently, the application of matrix-assisted laser desorption/ionization mass spectroscopy (MALD-MS) toward the analysis of intracellular drugs may be a viable alternative.

We initially tested the effect of crude mammalian cell lysate on the ability of MALD-MS to quantify aqueous tetraphenylphosphonium (TPP), a molecule that preferentially inhibits the proliferation of carcinoma cells. The TPP cation was readily identified and quantified (using methyl triphenyl phosphonium chloride, MTPP, as an internal stanard) at subpicomole levels in crude lysate, **Figure 1**. A quantitative MALD-MS time course for TPP cation accumulation

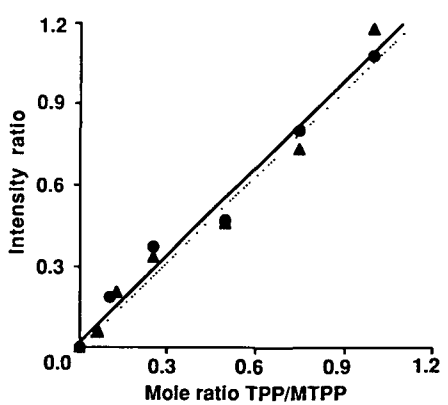

Figure 1. Effect of FaDu carcinoma cell hypotonic lysis on linear correlation between intensity ratio (TPP/MTPP) and the mole ratio (TPP/MTPP), 10.0 μM MTPP internal standard. The points, ● and ▲, represent analyses performed with and without cell lysate present.

into FaDu cells was comparable with a time course using scintillation counting. MALD-MS was also capable of demonstrating the reduced accumulation of the cationic drug rhodamine-123 by Dox^R MCF7, a multiply drug resistant breast adenocarcinoma cell line, relative to the nonresistant parent line MCF7. In addition, MALD-MS was used to follow a chemical reaction inside intact FaDu cells: the formation of a hydrazone, II-51, from benzaldehyde and an acylhydrazide, II-25, **Figure 2**. Cells were exposed to II-25 at 10mM for one hour followed by three washings with cold phosphate buffered saline (PBS).The intact cells were then exposed to benzaldehyde and also washed three times with cold PBS. The peak corresponding to II-51 (m/z=594) was readily observed upon mass analysis of the cell lysate from cells treated with II-25 followed by benzaldehyde (**Fig. 5D**). In control experiments, cells treated with II-25 alone or benzaldehyde alone produced no evidence of the II-51 ion (**Figs. 5A and 5B**). These results suggest that MALD-MS will be useful for the study of other chemical reactions, including the metabolism of cationic drugs and toxins in cells and tissues.

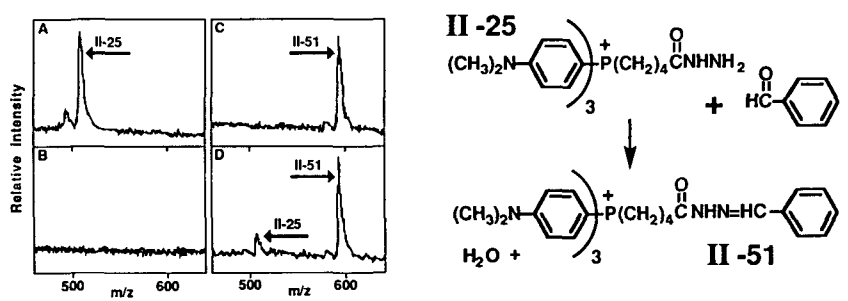

Figure 2. Observing intracell interactions through MALD mass spectra of FaDu cells exposed to: (A) II-25, (B) benzaldehyde, (C) II-51, and (D) II-25 followed by benzaldehyde.

These studies demonstrate the potential applications of MALD-MS for the study of cationic drugs in cultured cells and suggests its prospect for quantification of drugs, toxins, and their metabolites in plasma, tissue biopsies, and other biological matter. MALD-MS is superior to other methods in terms of analytical feasibility and specificity through the ease of sample preparation and the ability to provide molecular weight information. Recent quantitative results with heterogeneous mixtures of uncharged carbohydrates (1) and the ability to observe picomole quantities of anionic molecules (2) suggest that detection of uncharged and anionic drugs and toxins in cells may also be possible with MALD/MS.

1) Harvey, D. Paper presented at the Sanibel Conference on Carbohydrate Mass Spectrometry, sponsored by the American Society for Mass Spectrometry, Sanibel Island, Florida, 23 January 1993.

2) Juhasz, P., Costello, C.E. (1992) *J. Am. Soc. Mass Spectrom.*, 3, 785-796. Keogh, T., Baker, T.R., Dobson, R.L.M., Lacey, M.P., Riley, T.A., Hasselfield, J. A., Hesselberth, P.E. (1991) *Rapid Comm. in Mass Spectrom.*, 7, 195-200.

Optimisation of Identification of Oligosacchardies by Matrix-assisted Laser Desorption Mass Spectrometry

Walter Blackstock, Glaxo Group Research Ltd, Greenford, Middlesex, UK.
Anne Maisey, John Hoyes, VG Analytical, Fisons Instruments, Wythenshawe, Manchester, M23 9LE, UK.

Introduction

Complex oligosaccharides may be linked to proteins via Asparagine (N-linked) or Serine/Threonine (O-linked); the former are known to be implicated in a variety of recognition processes, including host-pathogen interaction, cell-cell adhesion and protein targeting and are now the subject of intense research interest.

The full characterisation of a glycoprotein is complex and the depth of structural determination may ultimately be limited by the small amount of material usually available. Not only does the site of glycosylation have to be determined, but the oligosaccharide portion is invariably heterogeneous and the heterogeneity may depend on the expression vector and its maturity.

Two approaches to characterising N-linked glycoproteins are in use. The first is to cleave off the intact oligosaccharides by hydrazinolysis and to characterise the oligosaccharide pool. As the protein is destroyed, information regarding the sites, and extent of attachment of the oligosaccharide chains can only be surmised. In addition mass spectrometry techniques for characterising underivatised oligosaccharides are not particularly sensitive, when compared to the levels reached for peptides. The second approach, which we favour, is to characterise the glycopeptide pool resulting from standard enzymatic cleavages and to use the specificity of exo-glycosidases to determine the extent and type of glycosylation. In this way, information regarding the site of glycosylation is retained.

Carr (1) and others have convincingly shown that electrospray ionisation is able to locate the glycopeptides in an enzyme digest by scanned orifice LC/MS. As a complement to this approach, we have sought to use matrix assisted laser desorption time of flight mass spectrometry firstly to locate glycosylated peptides in an enzyme digest (2), and secondly, to determine as far as possible the nature of the glycosylation by trimming away the sugars with specific glycosidases (3,4). The emphasis has been to shorten analysis time, and to work with as little material as possible.

Methods

To develop our strategy for dealing with complex glycoproteins, we are working with bovine alpha-1 acid glycoprotein (Sigma). As far as we are able to ascertain, the sequence of this protein is not listed in the protein data bases, but some homology with other well characterised alpha-1 acid glycoproteins may be presumed. Further characterisation is in hand.

Alpha-1 acid glycoprotein was treated with sialidase (C. perfringens) to remove sialic acid, and then reduced and pyridinethylated by standard techniques. Cleavage of the above with Glu-C (Boehringer), and subsequent separation of the digest by reverse phase FPLC (Pharmacia) yielded fractions further analysis. For the present discussion, work on fraction 6 (Fn6), a glycopeptide, is presented.

Matrix assisted laser desorption time-of-flight (MALDI-TOF) mass spectrometry was carried out on a TofSpec (VG Analytical), in linear flight mode. A nitrogen laser operating at 337nm desorbed the ions (and neutrals), from the sample applied to a multi-position stainless steel disposable target. Detection was by dual micro-channel plates. Sampling rate was 500 MHz and data were processed on a VAXstation using Opus software.

The matrix employed was alpha-cyano-4-hydroxy cinnamic acid which yields excellent sensitivity and resolution for 200fmol to 1pmol of sample. Exoglycosidases were purchased from Oxford GlycoSystems and used as directed. For composite digests using the reagent array method of Edge (3), the enzymes were mixed immediately prior to use.

The ease of use of the laser has allowed many enzyme reactions to be followed in 'real-time' and our observation is that, at least for glycopeptides, the seemingly obligatory 24 hour digest times are not required, and that some reactions are complete in 30 minutes! Clearly, this is important, and a complex sequence of digests and their analysis, can often be completed in a day, rather than a week.

Results

Separation of a Glu-C digest of the reduced and pyridinethylated desialylated protein allowed the glycopeptides to be identified by their characteristic pattern. Fig. 1a shows a characteristic example Fn6. The characteristic "fingerprint" may be attributed to mixtures of tri- and tetra-antennary forms admixed with fucosylation. It serves to easily distinguish peptides from glycopeptides.

Treatment of Fn6 with exoglycosidases specifically removes individual sugars, progressively reducing the molecular weight (Figs 1b-d). Indeed the difference in the peak top data corresponds to the loss of multiples of hexose and N-acetylhexose indicated.

Conclusions

Matrix assisted laser desorption time-of-flight mass spectrometry combined with the specificity of enzymes offers a very powerful and rapid way of making inroads into the structure of glycopeptides and thereby glycoproteins. We have observed that many enzyme cleavages are fast and combined with the sensitivity of MALDI-TOF, this makes for fast analysis on small amounts of protein. We find this approach more useful than hydrazinolysis, as the linkage information to the protein is retained. As with most scientific endeavours, no single technique should be pushed to provide all the answers and we suggest that intelligent use of this approach combined with electrospray and gas phase sequencing, is an efficient way of characterising glycoproteins.

References

1. S.A. Carr, M.J. Huddleston, M. Bean in *Protein Science* (1993), **2**, 183-196.
2. M.J. Treuheit, C.E. Costello, B. Halsall in *Biochem J.* (1992), **283**, 105-112.
3. C.J. Edge, T.W. Rademacher, M.R. Wormald, R.B. Parekh, T.D. Butters, D.R. Wing, R.A. Dwek in *Proc. Natl. Acad. Sci. USA*, (1992), **89**, 6338-6342.
4. C.W. Sutton, J.A. O'Neill, J.S. Cottrell, *Sanibel Poster*, 1993.

Fig.1

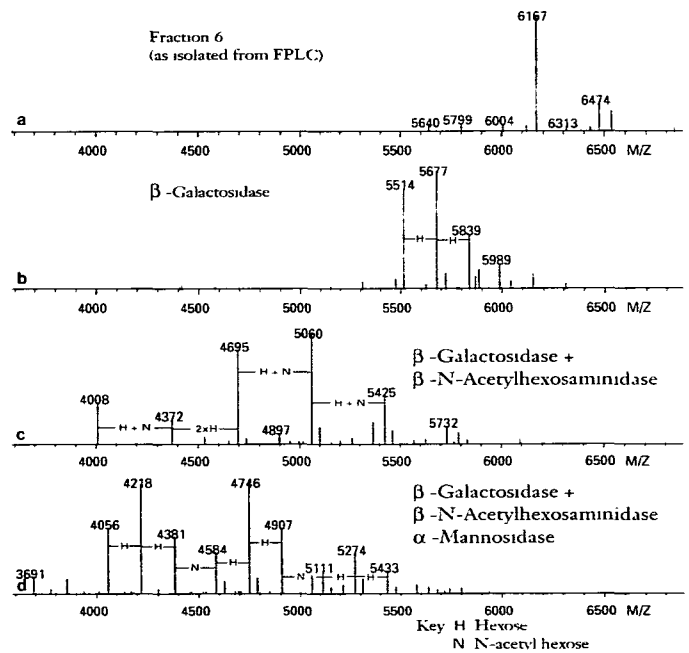

Matrix-Assisted Laser Desorption of O-Glycopeptides Using Linear and Reflectron Time-of-flight Instruments

Marc R. Chevrier* and Robert J. Cotter

Department of Pharmacology and Molecular Sciences
The Johns Hopkins University School of Medicine
Baltimore, MD 21205

INTRODUCTION. The classification of carbohydrates linked to a protein depends on the type of attachment and the structure of the sugar chain. O-linked sugars are linked to the hydroxyl group of serine or threonine. There are three types of O-linkages:

- Ser(Thr)-GalNAc {Labile to mild alkaline treatment}
- Ser-Xyl {Labile to mild alkaline treatment}
- Ser(Thr)-GlcNAc {Very labile to mild alkaline treatment}

O-linked N-acetylglucoseamine [O-GlcNAc] are a particularly interesting type of O-glycosylation. This type of glycosylation occurs intracellularly and as a mono-substituted sugar with no additional branching Analogous to phosphorylation, O-GlcNAc may serve to activate enzymes. It may also function to "cap" phosphorylation sites [1]

In contrast, N-linked sugars are linked to the free amino group of asparagine residues. The linkage [Asn-GlcNAc] is stable to mild alkaline treatment. N-linked sugars are either complex or high-mannose, a classification based on their branching and composition after synthesis and processing in the rough endoplasmic reticulum and Golgi apparatus There are numerous glycosidases and transferases which have been characterized for N-glycans. N-glycans are generally attached to Asn in a well characterized consensus sequence [2]

O-linked carbohydrates are generally more difficult to analyze than N-linked carbohydrates for several reasons:

- O-linked sugars do not have a distinct consensus sequence
- O-specific glycosidases or glycosyltransferases are less available
- O-linked sugars are more labile to basic treatment

We developed techniques using MALDI/MS to allow high sensitivity determination of carbohydrate sites and microheterogeneity for O-glycopeptides. Sialyl glycopeptide A and tryptic glycopeptides from human glycophorins were used to select matrices and crystallization conditions which would result in high sensitivity observation of intact O-linked glycopeptides. We then used these techniques to identify O-GlcNAc sites on simian alpha crystallins and rat neurofilaments The mass spectra were obtained using two instruments, a custom linear TOF described previously[3] and a commercial linear/reflectron TOF [Kratos MALDI III]

EXPERIMENTAL. Sialyl glycopeptide A [SGA], a dipeptide carrying three sugars including a sialic acid, was used to screen matrices for efficacy at 337nm. Five matrices (α-cyano-4-hydroxycinnamic acid, caffeic acid, ferulic acid, gentisic acid, and sinipinic acid) were all utilized to analyze titrations of SGA. In addition, tryptic glycopeptides from human glycophorins were prepared and analyzed by MALDI/MS using the matrices found to be optimal for SGA. In order to reduce the complexity of the digest mixtures, a single dimension of HPLC [Vydac C_{18} / TFA.ACN] was employed. A synthetic peptide YSDSPSTST was glysosylated *in vitro* with β-N-Acetylglucosamnyl transferase. This peptide then served as a substrate in a number of glycosidase and glycosyltransferase experiments prior to MALDI/MS analysis. Using similar methodology, peptides with O-linked GlcNAc from simian crystallins and rat neurofilaments were

subsequently analyzed. Confirmations were provided by chemical deglycosylation[4], specific enzymatic glycosylation[4], and radiolabeling in conjunction with manual Edman microsequencing.[5]

RESULTS AND DISCUSSION. 337 nm MALDI/MS sucessfully analyzed numerous O-linked glycopeptides in femtomolar quantity This additional sensitivity was much higher than afforded by Edman microsequencing and also permitted a reduction in preparative chromatography since unfractionated or partially fractionated digest mixtures could be analyzed directly In our experience, α-cyano-4-hydroxycinnamic acid and gentisic acid yielded the best sensitivities. For glycopeptides with sialic acids, gentisic acid consistently offered higher sensitivities than any other of the five matrices In general, the linear mode of operation offered higher sensitivities, whereas the reflectron mode could offer significantly higher resolutions (circa 2000 versus 450 for glycopeptides < 3 kDa) This additional resolution was exploited to reduce preparative chromatography by analyzing proteolytic digest mixtures which were only partially fractionated.

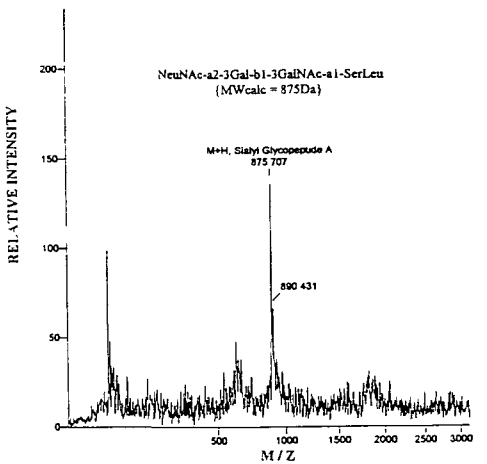

LITERATURE CITED

1 R. S Haltiwanger, W G. Kelly, E P Roquemore, M. A Blomberg, D L Y Dong, L Kreppel, T -Y. Chou, G W Hart, *Biochem Soc Trans* 20, 264-269 (1992)

2 Molecular Biology of the Cell, B Alberts *et al*, Garland Publishing, New York 446-448 (1989)

3 M. R. Chevrier, R. J Cotter, *Rapid Commun Mass Spectrom* 5 611-617 (1991)

4 M. R Chevrier, M. A Blomberg, D L Y Dong, E P Roquemore, G W Hart and R J Cotter, *MALDI/MS Techniques for the Analysis of O-Linked Carbohydrates.* (In preparation)

5 D L Y Dong, Z. -S Xu, M R. Chevrier, D W Cleveland, R J Cotter, G W Hart, *Enzyme* (1993) (In press).

The Role of Lipooligosaccharides in Pathogenesis of *Haemophilus* Species and Possible Strategies for Therapeutic Intervention.

W. Melaugh, N. Phillips, J. Engstrom, M. Tullius and B. W. Gibson.
University of California, San Francisco, CA 94143-0446

Pathogenic *Haemophilus* species, such as *Haemophilus influenzae* which causes pneumonia and meningitis, and *Haemophilus ducreyi* which is responsible for chancroid, display on their outer membranes surface antigens that enable these organisms to adhere to and invade host cells. The focus of our research is investigating the role of lipooligosaccharides (LOS), one of the most abundant and structurally diverse of the surface antigens.

LOS consist of a lipid portion (lipid A) which is embedded in the outer membrane and a carbohydrate region which projects out into the environment of the cell. The amphipathic nature of LOS makes it difficult to directly analyse these molecules by mass spectrometric techniques since they tend to aggregate in solution and exhibit low solubility in most solvents. The traditional approach has been to take advantage of the susceptibility of the ketosidic linkage between the lipid A portion of the molecule and the oligosaccharide moiety to mild acid hydrolysis and to study the two parts separately. Structural studies by liquid secondary ion mass spectrometry and tandem mass spectrometry of the oligosaccharide fraction thus obtained have shown that many *Haemophilus* strains contain epitopes that mimic blood group antigens, allowing these organisms to evade the host immune system.

While such an approach has been useful, the hydrolysis conditions required to rupture the ketosidic bond cause chemical modification of the LOS molecule and critical structural information is lost during the hydrolysis step. For example, a phosphate group on KDO undergoes β-elimination during the mild acid hydrolysis leaving an anhydro KDO species. We have also found using electrospray ionization mass spectrometry (ESI-MS) that many *Haemophilus* strains are sialylated on a terminal lactosamine but the sialic acid is lost during the hydrolysis step. *O*-deacylation of the LOS using mild hydrazine renders the molecule water-soluble and amenable to analysis by ESI-MS. Figure 1 shows the negative-ion ESI-MS of *H. ducreyi* 35000 *O*-deacylated LOS in the triply-charged $[(M-3H)^{3-}]$ molecular ion region from m/z 800-1000, before and after neuraminidase treatment.

The significance of sialic acid is not completely understood, but it is believed to be crucial to the organism's ability to cause disease since it is known that in other bacteria the removal of sialic acid renders the pathogens vulnerable to lysis by serum. We know for example that a mutant strain of *H. ducreyi*, 188-2 which lacks terminal lactosamine and sialolactosamine, shows lower adherence to human cells of the genital epithelia than that of the parent strain. One of our goals is to develop inhibitors to the sialyltransferase since infectious agents lacking this critical sugar may be less virulent. Figure 2 shows on the left a schematic of the outer membrane sialyltransferase adding the activated sugar nucleotide to the lactosamine acceptor of the LOS. On the right is a potential bi-substrate analog which we propose as an inhibitor of this sialyltransferase.

This work was supported by the grants from NIH (RR01614, AI24616), NSF instrumentation program and the UC Universitywide AIDS program.

References

Gibson, B. W., Melaugh, W., Phillips, N. J., Apicella, M. A., Campagnari, A. A., and Griffiss, J. M., *J. Bacteriol.*, **175**, 2702-2712 (1993).
Melaugh, W., Phillips, N. J., Campagnari, A. A., Karalus, R., and Gibson, B. W., *J. Biol. Chem.*, **267**, 13434-13439 (1992).
Phillips, N. J., Apicella, M. A., Griffiss, J. M., and Gibson, B. W., *Biochemistry*, **32**, 2003-2012 (1993).

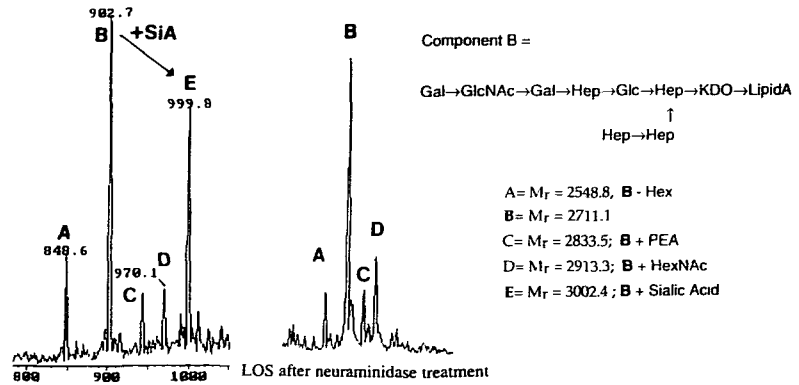

Fig. 1. Negative-ion ESI-MS of the *O*-deacylated LOS from *H. ducreyi* strain 35000 before and after treatment with neuraminidase. The spectral regions shown contain only triply charged ions, $(M-3H)^{3-}$. Following neuraminidase treatment, the sialylated component **E** is converted to the major species, component **B**.

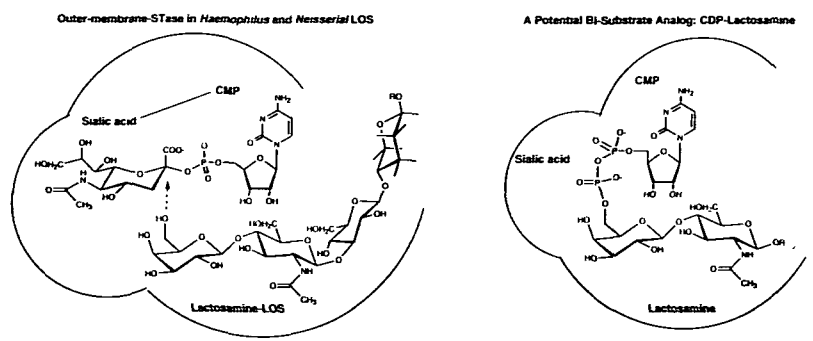

Fig. 2. Schematic representations of the *Haemophilus* silayltransferase, purported to be an outer-membrane enzyme, transferring sialic acid to C-6 of a LOS structure containing terminal lactosamine (left) and binding CDP-lactosamine, a potential bi-substrate analog inhibitor (right).

MASS SPECTROMETRY OF CYCLODEXTRIN AMINO ACID ADDUCTS

Simon N.Davey and Lee W.Tetler
Centre for Mass Spectrometry, UMIST, Manchester, M60 1QD

David A.Leigh, John P. Smart, Ada Truscello
Department of Chemistry, UMIST, Manchester, M60 1QD

Cyclodextrins, readily available degradation products of starch by an amylase of *Bacillus Macerans* [1], have been extensively studied due to their ability to form inclusion complexes with a range of small organic molecules. The three natural cyclodextrins, macrocycles consisting of six (alpha CD), seven (beta CD) or eight (gamma CD) alpha-(1,4)-linked glucose residues, are bucket shaped molecules with a hydrophobic cavity and a hydrophilic exterior which gives rise to their unique binding characteristics. The complexes formed by cyclodextrins have found industrial uses in areas as diverse as pharmaceuticals, agrochemicals and food additives [2].

Since the cyclodextrins are chiral molecules they can exhibit chiral preference when binding, encapsulating one enantiomer of a guest more favourably than the other. This has led to the exploitation of cyclodextrins as stationary phases for chiral HPLC systems [3]. Traditional techniques (e.g. NMR) can be either time consuming or inaccurate so there is a need for facile techniques for assessing both the stoichiometry of binding and the association constant for the complex. Mass spectrometry can play a valuable role in this analysis.

The detection of crown ether alkali metal complexes by fast atom bombardment mass spectrometry (FAB-MS) was first demonstrated by Johnstone and Rose in 1982. More recently Stoddart and others have shown that the mass spectral intensities of the ions corresponding to the cyclodextrin guest complex indicate the amount of species present in each solution.

We demonstrate the potential of FAB-MS as a powerful tool for the detection of enantioselective binding by cyclodextrins of amino acid methyl esters. It is well documented that cyclodextrins preferentially bind the D-enantiomers of amino acids [4] and this is supported by the spectra we have obtained. Accordingly our results show that a 1:1 mixture of phenylalanine and permethylated alpha cyclodextrin will preferentially bind the D-isomer by a factor of eight. This is apparent for all the permethylated cyclodextrins and the same phenomenon is observed with tryptophan. Results to date indicate that this does not occur to the same extent with the perbenzyl cyclodextrin, although the D-isomer preference is still observed, the magnitude of the preference is markedly reduced.

The fragmentation of the species observed in the FAB mass spectrum show losses of methanol from the protonated complex ion and of permethyl from the protonated cyclodextrin ion. Attempts to obtain tandem mass spectra have proved difficult but the data so far suggests that the predominant fragmentation is not the loss of the amino acid species from the complex.

To date we have characterised the complexes of four cyclodextrins with six amino acid isomers. Work is ongoing to obtain MS/MS data for these experiments and also to provide explanations for the complexation of these molecules.

Acknowledgements
The authors would like to acknowledge SERC and Kratos Analytical Ltd for financial assistance to SND and SERC for a studentship to JPS..

References

[1] D. French, *Adv. Carbohydrate Chemistry*, **12**, 189, (1957).
[2] J. Szejtli, *Cyclodextrins and Their Inclusion Complexes*, Akademia Kiado, Budapest, 1972.
[3] D.W.Armstrong, X. Yang, S.M. Han, R. Menges, *Anal Chem*, **59**, 2594, (1987).
[4] K.B. Lipowitz, S. Raghotharma, Jia-an Yang, *J. Am. Chem. Soc.*, **114**, 1554, (1992).

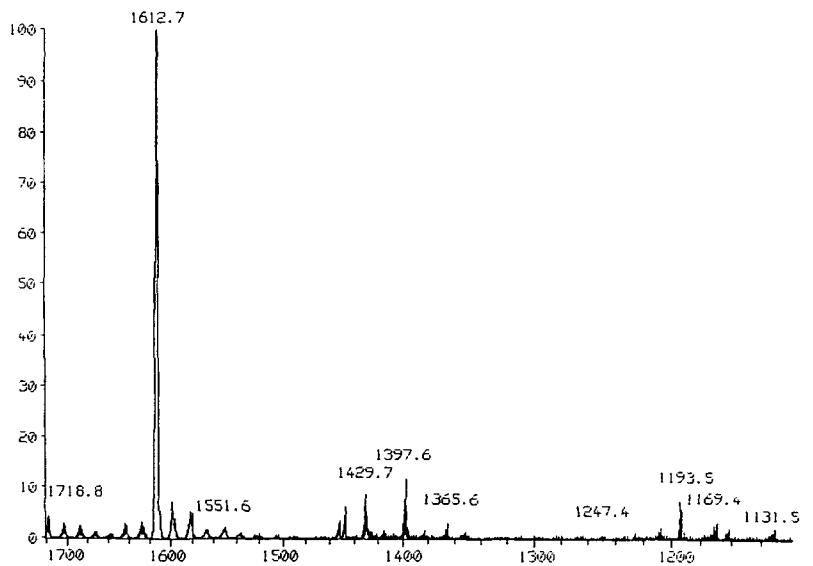

Figure 1. Mass spectrum of Permethyl beta cyclodextrin and D-tryptophan deuterated methyl ester

AN INTEGRATED MASS SPECTROMETRIC APPROACH (Cf-252 PD, FAB, ESI AND LOW ENERGY COLLISION INDUCED DISSOCIATION) TO CHARACTERIZE THE PEPTIDOGLYCAN OF VARIOUS MICROORGANISMS

G. Allmaier, M. Caparros[1], M de Pedro[1], B Pfanzagl[2], W. Loffelhardt[2], E R Schmid and E Pittenauer

Institute for Analytical Chemistry, University of Vienna, Währinger Str 38, A - 1090 Vienna, Austria
[1]Center of Molecular Biology - C S. I. C , University of Madrid, E - 28049 Madrid, Spain
[2]Institute of Biochemistry and Cell Biology, University of Vienna, A - 1030 Vienna, Austria

Peptidoglycan (PG) or murein can be envisaged as a giant macromolecule surrounding the cytoplasmic membrane. PG is a heteropolymer unique to bacterial cell walls that consists of a glycan backbone with short peptide side chains linked via a lactyl moiety to the sugar unit The peptides are cross-linking the glycan chains of various length (up to 200 disaccharide units). This network provides stress-bearing mechanical strength, enormous fexibility and structural dynamics simultaneously Nature has provided numerous subtle variants in the chemical composition of murein among microorganisms. The first molecular target of the still most important group of antibiotics, β-lactams, is a group of unique proteins, called penicillin-binding-proteins (PBP), which are involved in several stages of PG biosynthesis. A complete understanding of the complicated chain of events leading from inhibition of PBPs to bacteriolysis is now accelerated by some recent progress in PG structural analysis based on new chromatographic [1] and mass spectrometric [2 - 4] techniques. The majority of studies aiming at the structural characterization of PGs is based on muramidase digest of the macromolecule, fractionation of the PG fragments by LC and subsequent amino acid / amino sugar analysis. But in more or less all cases the chromatographic separation of the PG fragment mixture turned out to be relative complex. Because of small, but for the understanding of the biosynthesis important variations of the PG fragment pattern it is desirable to monitor complete PG digest profiles, which is a formidable task by classical biochemical techniques in any respect.

Our integrated mass spectrometric approach is based on screening the entire muramidase-cleaved and

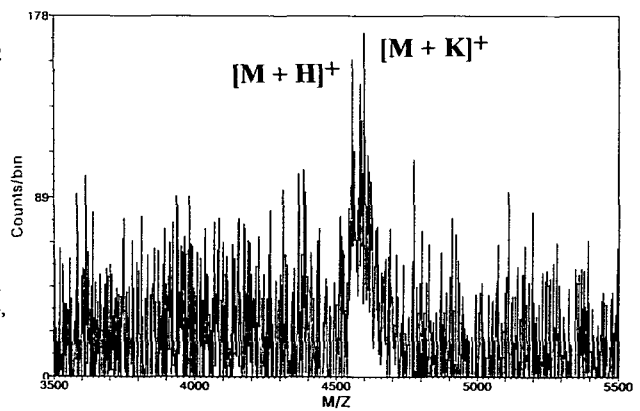

Fig. 1. Positive ion Cf-252 PD mass spectrum of a peptidoglycan pentamer [tetrakis (disaccharide tetrapeptide) disaccharide tripeptide] isolated from *Synecococcus spec.*, showing a protonated and potassiated molecular ion at m/z 4556 2 (calculated 4557.7, Δm = - 1 5 u) and 4597.1 (calculated 4595 8, Δm = + 1.3 u).

$NaBH_4$-reduced PG after RP-18 HPLC separation with a water/acetonitrile/TFA gradient by positive and negative ion PD mass spectrometry [3, 4]. Molecular weight information was obtained for simple PG

monomers to complex PG oligomers (Fig 1) of various origin Based on these values of the individual PG fragments and on determined amino acids and amino sugars in the total hydrolysate of the murein sacculus, the primary structure could be assigned in most cases In case of doubtful or uncorrelated PD mass spectrometric data, an aliquot of the same fraction was analyzed by ESI [4] (Fig 2) or FAB mass spectrometry with analyzer systems exhibiting higher resolving power If the structure can not be determined unequivocally even by these means, tandem mass spectrometry has to be applied. A hybrid instrument (BEqQ) combined with FAB was used to obtain low energy CID spectra which exhibited a high content of structural information [6]. Alternatively, the use of ESI as source for single or double charged precursor ions in combination with a triple quadrupole instrument was evaluated for generating of CID spectra [4] Especially this set-up offers the possibility of on-line LC/MS/MS for screening of complex PG digests Structural modifications (e g , N-acetyl putrescine coupled to D-Glu in *Cyanophora paradoxa* [6] or amino acid exchange in PG by a biosynthetic technique in *E. coli* [5]) and subtle variations (e.g , amidation or linkage inversion) of the PG could be determined by combining various MS techniques and amino acid analysis The outlined strategy was applied for the characterization of PG digests of *E. coli*, *Cyanophora paradoxa*, *Synecoccus spec.*, *Enterococcus faecium* and *Staphylococcus aureus*

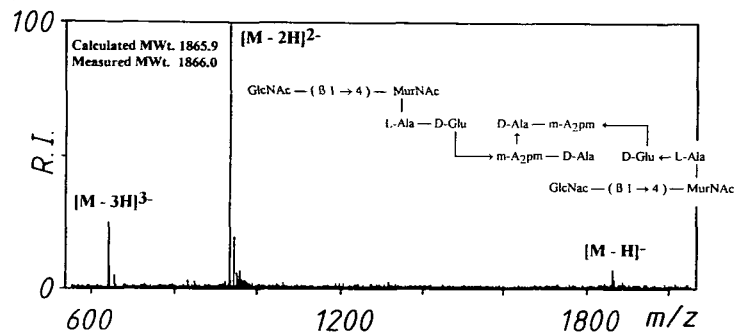

Fig. 2. Negative ion ESI mass spectrum of a PG dimer bis (disaccharide tetrapeptide) with a m-A_2pm - Ala linkage isolated from *E. coli*, exhibiting single and multiple deprotonated molecular ions at m/z 1865.2 (calc. 1864.9, Δm = + 0 3 u), 931.9 (calc 931.9) and 621 0 (calc 620.9, Δm = + 0.1 u).

References

1. B. Glauner and U. Schwarz, in *The Target of Penicillin*, ed. by R. Hackenbeck, J V. Holtje and H. Labischinski, Walter de Gruyter, Berlin, 29 (1983)
2. S. A. Martin et al , J. Biol. Chem. **259**, 12652 (1984).
3. G. Allmaier et al , Rapid. Commun. Mass Spectrom. **6**, 284 (1992)
4. G. Allmaier and E. R. Schmid, in *Bacterial Growth and Lysis: Metabolism and Structure of the Bacterial Sacculus*, ed by M. A. de Pedro, J.- H- Höltje and W. Löffelhardt, Plenum Press, New York, 23 (1993)
5. M. Caparros et al., FEBS Letters **316**, 181 (1993).
6. E. Pittenauer et al , Biolog. Mass Spectrom. **22**, in press (1993).

Acknowledgements

This work was supported by the Hochschuljubiläumsstiftung der Stadt Wien (H - 00155/92 to G. A.). Travel money was made available by grant 01/93 from the Scientific Technical Cooperation Austria - Spain Acciones Integradas. The authors are grateful to U J. Jürgens (Albert-Ludwigs-Universität, Freiburg i. Br., BRD) for the peptidoglycan sample of *Synecococcus spec.* PCC 6714 We are indebted to T. Hutton (Fison, Altrincham, UK) for her assistance to obtain the ESI mass spectra.

STRATEGIES FOR THE IDENTIFICATION OF COMPOUNDS CAUSING ODORS IN WATER. A STUDY OF CREOSOTE SPILLS.

*J. Rivera[1], F. Ventura[2], J. Romero[2], R. Boleda[2], R. Lloret[2], J. Martin[2] and L. Mohedano[1].

1-Mass Spectrometry Lab. CID-CSIC; J. Girona 18. 08034-Barcelona (Spain).
2-Aigües de Barcelona; P. Sant Joan 39. 08009-Barcelona (Spain).

Tastes and odors in water is frequently one of the major complaints of consumers. Volatile organic compounds from both anthropogenic and natural sources are usually associated with these effects. In most cases, routine closed-loop stripping analysis (CLSA) which is suitable for the identification of compounds at trace levels (ppt), gives account of the responsible compounds.

Recently, we were surprised to find high abundance of 2-3 ring PAH in CLSA extracts identified by GC/MS from river water with odor problems. We associated such unexpected results to the presence of creosote, a complex mixture obtained from distillation of coal tar which constituents are 85-90% PAHs. Two creosote wood-preserving factories located in the upper course of the river might be responsible for the spills.

Liquid-liquid-extraction (LLE) and analysis by HPLC using a fluorescence detector (FL), corroborated our suspition after giving close results for river water extracts and creosote from each one of the factories. In addition, the presence of heavier PAH no detected by the CLSA method was observed. This confirmed that creosote was the responsible for the intense odor but no conclusions about which factory dumped it.

The comparison of the GC profiles of the creosotes used by both factories during the first episode, showed similar profiles and only the relationship naphtalene/isoquinoline (N/I) was dramatically different (15.7 and 0.55 respectively) for each creosote. Then, this ratio could be potentially useful in this case for the univocal identification of the responsible of dumping.

However, during the last episode both creosotes showed the same profile. There is only one supplier of creosote in Spain, but depending occasionally on market prices, **B** factory imported it from France.

The two creosotes were spiked in Milli-Q water, extracted by the CLSA and LLE methods and analyzed by GC. The results showed that recoveries of PAH by the CLSA method decreased dramatically for compounds heavier than fluorene, whereas good recoveries were obtained using the LLE method even for the heavier PAH.

Table: Mean recoveries of selected compounds from creosote by CLSA and LLE.

Compound	CLSA	LLE
Naphthalene	91	74
Isoquinoline	0	67
1-methylnaphthalene	91	109
Acenaphthene	54	94
(9H)-Fluorene	25	112
Phenanthrene	3	104
Fluoranthene	0	90
Benzo[*a*]pyrene	0	88

The main disadvantage of CLSA, arises for its unability to recover three or more rings PAH and isoquinoline. Therefore, it was insuitable for tracing which was the origin of the spill. However, the CLSA method is the most useful technique for the identification of creosote spills at the ppt level and particularly suitable when no odor problems are detected by consumers.

On the other hand, LLE and GC/MS is the method of choice for the individual characterization of compounds and in this case to prove which factory dumped into the river. HPLC-FL is useful to determine the level of PAH listed as priority pollutants.

From levels of PAH priority pollutants measured in river water and their chromatographic profiles it can be inferred that **A** factory was responsible for the first creosote spill and **B** for the second.

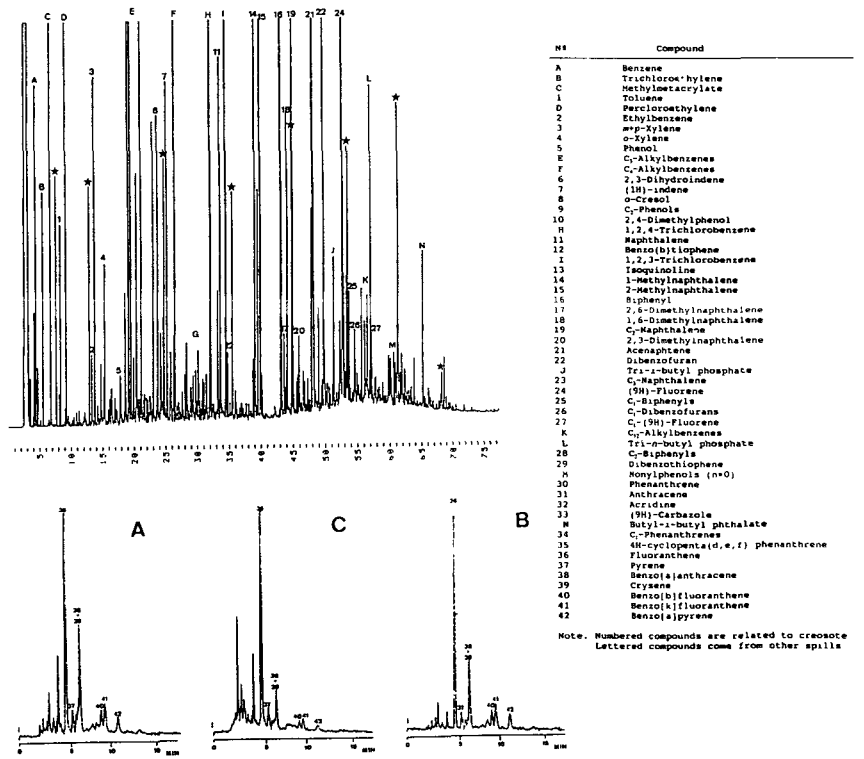

Top: GC profile of raw water polluted by creosote. Bottom: HPLC/Fl profiles of left: creosote A; middle: raw water; right: creosote B.

Tandem Mass Spectrometry of Human Skin Emanations for the Determination of Mosquito Attractants

Ulrich R. Bernier and Richard A. Yost
Department of Chemistry, University of Florida, Gainesville FL 32611
Carl E. Schreck and Don R. Barnard
USDA Medical and Veterinary Entomology Research Laboratory, Gainesville, FL 32604

Introduction

Identification of volatile compounds which emanate from the skin and attract mosquitoes will provide for an understanding of the basis for chemical attraction of mosquitoes to hosts. Additionally, this information may be used to better control these insects, and these attractants may be incorporated into a form of pest control relying on attractants rather than repellents. This work is centered upon the identification of attractants from the human skin; additional compounds are being tested which have not yet been identified as emanating from the skin. Insight into the differences in attractiveness among hosts may be gained by studying factors which change attractiveness. The underlying premise of this work is that sample analysis by mass spectrometry should allow for sample detection in a fashion similar to that which mosquitoes encounter: a volatilized sample in the gas phase.

Experimental

Bio-assays are conducted in an olfactometer which allows quantitation of the proportion of mosquitoes attracted to a (sample) compound. Sample introduction for all mass spectrometric analyses is accomplished via a transfer line with either a deactivated 1 m x 0.10 mm i.d. fused silica open tubular (FSOT) column or a 7 m x 0.18 mm i.d. DB-1 FSOT column fitted directly into the ion source of the Finnigan MAT TSQ70 triple quadrupole mass spectrometer. Human samples are collected by rubbing five 3 mm diameter glass beads for five minutes. The beads are then placed in a 5 cm x 0.25" o.d. glass vial fitted with a 0.25" inch Swagelok cross inside a Varian 3400 GC oven. During analysis, the temperature is typically ramped from 30°C to 210°C over 5 minutes, with the transfer line held at 210°C. Chemical ionization using methane at an indicated source pressure of 1700 mtorr was used in all cases; MS/MS was performed with argon collision gas at an indicated pressure of 1.4-1.5 mtorr. The Q2 collision offset was -15 V for positive ions and +15 V for negative ions.

Results

The most suitable introduction technique is direct thermal desorption of deposited components off of glass beads enclosed in a small vial. Although adequate sensitivity is achieved from sampling 5 beads, temporal resolution is poor. Identification of lower molecular weight components, such as lactic acid, pyruvic acid, and propanoic acid is still straightforward due to the limited number of possible isomers for each molecular weight. *Figure 1* demonstrates the identification of ethylene glycol by comparison of sample and standard daughter spectra of the $[M+H]^+$ ion (m/z 63). Several carboxylic acids have been found to be slightly attractive to mosquitoes; neutral loss scans of 44 u from positive and more so negative ions can be used to screen samples for this class of compounds.

Lactic acid is the only widely-recognized attractant for *Aedes aegypti* [Takken, W., *Insect Sci. Applic.*, 1991, **12**, 287-295]; thus, this compound was used as the model for single compound studies involving altering attraction of mosquitoes to a sample. It should be noted that lactic acid alone is not as attractive to mosquitoes as is a human sample deposited by rubbing glass beads in the palm of the hand. Since lactic acid is a carboxylic acid, its volatility should be susceptible to acid/base effects. The expected result is that at a pH above the pK_a, most of the lactic acid will be dissociated to lactate,

reducing the amount of lactic acid in the gas phase. This agrees with the decreased attractiveness observed for lactic acid at higher pH, as shown in *Figure 2*.

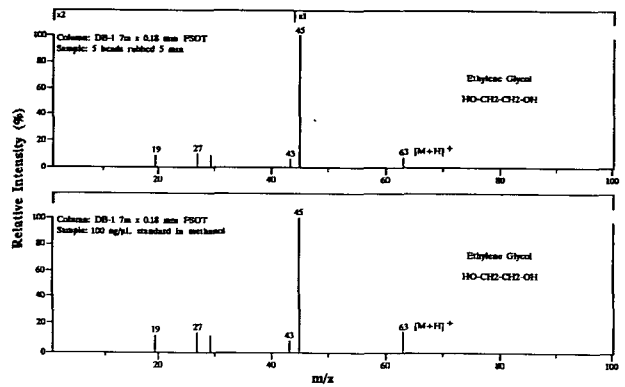

Figure 1. Comparison of Ethylene Glycol Daughter Spectra of Hand Sample (Top) and Standard (Bottom)

Conclusions

Direct thermal desorption of samples deposited on glass beads allows for detection of volatile compounds of interest; however, temporal resolution is poor, therefore cryo-focussing will be used in future work. Neutral loss spectra (such as neutral loss of 44 for carboxylic acids) allow for targeting compound classes of interest. Identification of compounds from MS/MS spectra is possible both by spectral interpretation (for low molecular weight species) and by comparison to standards. Lactic acid is of particular interest since it is the sole compound previously confirmed to be attractive for *Aedes Aegypti*. However, additional acids as well as alcohols have been found to be attractive. Sample matrix conditions (including pH) play a role in attractiveness; future studies will consist of bio-assay and MS/MS studies of the esters of lactic acid as well as studies involving acidified and basicified rubbed glass beads.

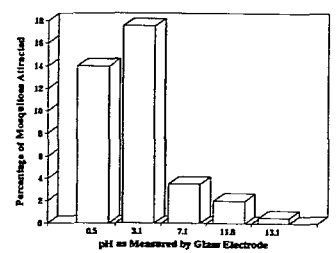

Figure 2. Effect of pH on Attractiveness of a Methanolic 1% L-Lactic Acid Solution

Acknowledgement

Funding for this work supplied by the United States Department of Agriculture Medical and Veterinary Entomology Research Laboratory, Gainesville, FL.

DIRECT SCREENING OF PAHs IN AIRBORNE PARTICULATE MATTER BY LASER TIME-OF-FLIGHT MASS SPECTROMETRY

Catherine H. Smith and Peter B. Kelly, Department of Chemistry;
Daniel P.Y. Chang, Department of Civil Engineering; and
A. Daniel Jones, Facility for Advanced Instrumentation,
University of California, Davis CA 95616.

Polycyclic aromatic hydrocarbons (PAHs) are formed during combustion of organic material and readily condense on particulate matter to become airborne. Current methods for the screening of PAHs in soot and fly-ash samples are labor-intensive and time-consuming. A two-step laser desorption laser photoionization mass spectrometry (LDLPMS) technique has been developed which provides a means for rapidly screening particulate matter samples for PAHs, with no prior extraction or separation steps.

Experimental:

The laser mass spectrometry experiments are performed with a custom-built linear time-of-flight instrument. The particulate sample is mounted on the flattened face of a metal probe tip using double-sided sticky tape. Pulsed IR radiation at 10.6 μ generated by a CO_2 laser is focussed to a 1 mm^2 spot size on the sample. Pulsed UV radiation at 266 nm produced by a Q-switched Nd:YAG laser is focussed into the plume of desorbed neutral molecules to effect resonance enhanced multiphoton ionization of the PAHs.

Results:

The response curves for PAHs doped into silica gel, Figure 1, indicate that the LDLPMS method is semi-quantitative and calibration curves can be constructed over several orders of magnitude. The sensitivity of the technique lies in the 10 ppm range, with an absolute sensitivity on the order of 20 picograms. The best response factors were obtained for phenanthrene and pyrene. The response factors for PAHs in the mass range 228 to 278 were 75% lower. The higher boiling point compounds may not be as efficiently removed from the particulate matter in the thermal desorption step. Only a very small portion of a sample can be analyzed using the LDLPMS method, thus the reproducibility is influenced by sample inhomogeneity. Several samples should be screened to obtain representative values.

The application of the LDLPMS technique to NIST SRM 1650 Diesel Particulate Matter, Figure 2, indicates the presence of PAHs ranging in ring size from two to four. NIST SRM 1650 material contains 71 ppm phenanthrene (m/z 178) and 50 ppm each of fluoranthene and pyrene (m/z 202).

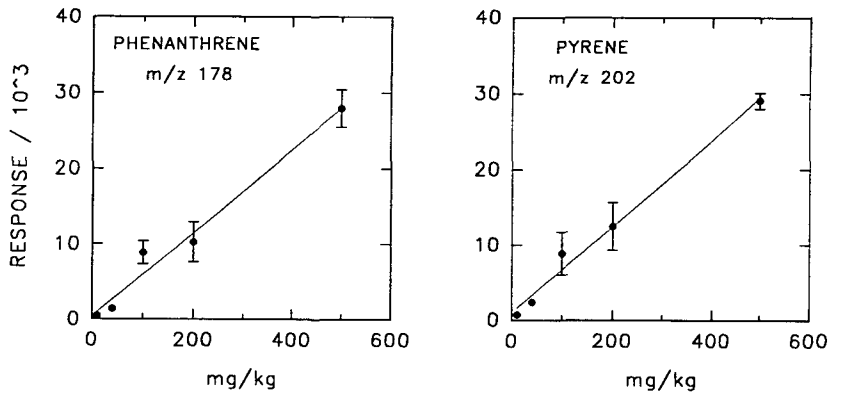

FIGURE 1. Response curves for PAHs doped into silica gel using the LDLPMS method. IR power: 5 MW/cm^2; UV power: 10 μJ/pulse; 500 shots averaged.

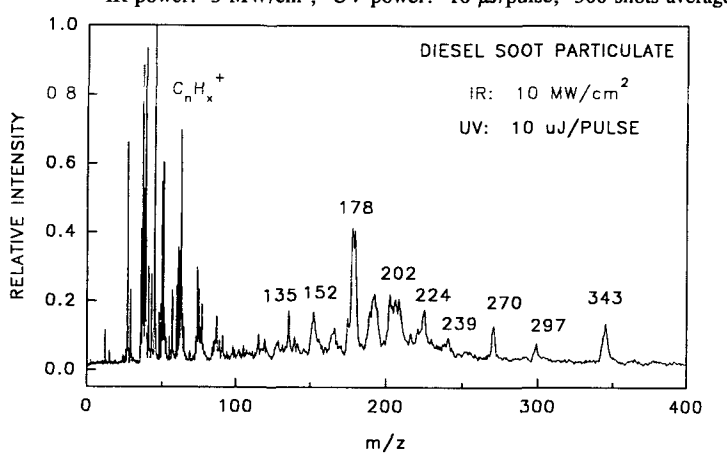

FIGURE 2. Application of the LDLPMS method to NIST SRM 1650.

The support of the National Institutes of Health "Superfund" program (Grant 2-P42-ES04699) and the California Air Resources Board (Grant A9-32-099) is gratefully acknowledged.

LASER PHOTOIONIZATION TIME-OF-FLIGHT MASS SPECTROMETRY APPLIED TO NITRATED POLYCYCLIC AROMATIC HYDROCARBONS AND NITROBENZOCOUMARIN DERIVATIVES

Rae A. Noyes, Catherine H. Smith and Peter B. Kelly, Department of Chemistry;
Daniel P.Y. Chang, Department of Civil Engineering; and
A. Daniel Jones, Facility for Advanced Instrumentation,
University of California, Davis CA 95616.

The analytical chemistry of nitrated polycyclic aromatic hydrocarbons (nitro-PAHs) is of widespread interest due to the highly mutagenic properties of this chemical class and their ubiquitous presence in the environment. Nitro-PAH can readily condense on respirable particulate matter. Nitro-PAH have been identified in diesel particulate, urban and indoor air particulate, wood and cigarette smoke condensates, and many other environmental samples.

In our laboratory, we are studying the application of laser photoionization time-of-flight mass spectrometry (TOF-MS) to the detection and identification of atmospheric pollutants in particulate samples. Laser photoionization mass spectra were obtained using 266 nm and 213 nm irradiation for four nitro-PAH compounds: 9-nitroanthracene, 1-nitropyrene, 2-nitrofluorene, and 2-nitro-9-fluorenone. Two nitrated heterocyclic compounds, 6- and 7-nitrobenzocoumarin, were investigated at 213 nm.

Experimental:

The experiments are performed with a custom-built linear TOF-MS instrument. A sample is typically prepared by depositing a small aliquot of the sample solution on the flattened face of a metal probe tip. The sample is allowed to air-dry, forming a thin solid layer. Pulsed UV radiation is generated by a Q-switched Nd:YAG laser and focussed into the source region perpendicular to the flight tube axis, such that the beam grazes the surface of the sample probe. Spectra are usually obtained with a UV laser energy of 10-20 μJ/pulse.

Results:

Photoionization of nitro-PAHs at 266 nm or 213 nm yields positive molecular ion for each of the standards studied. Characteristic photofragments include $[M\text{-}NO]^+$, $[M\text{-}NO_2]^+$, $[M\text{-}NO\text{-}CO]^+$, and NO^+, as shown in Figure 1. A very strong $[M\text{-}NO]^+$ ion peak was observed in all spectra and was often the base peak. An intense NO^+ ion peak accompanies the $[M\text{-}NO]^+$ peak at 213 nm, but is only weakly present at 266 nm. These observations suggest that the $[M\text{-}NO]^+$ radical is formed via an excited state nitro-nitrite photorearrangement, Figure 2, followed by dissociation to the observed odd-electron ion. The NO fragment is subsequently ionized by a multiphoton ionization process. The photofragmentation of the nitrobenzocoumarins initially follows the same pathway as the nitro-PAHs. These photorearrangement reactions may play a significant role in the atmospheric transformation of nitro-PAHs.

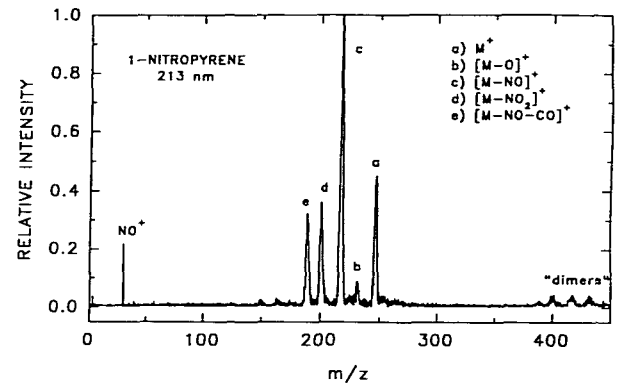

FIGURE 1. Laser photoionization mass spectrum of 1-nitropyrene at 213 nm.

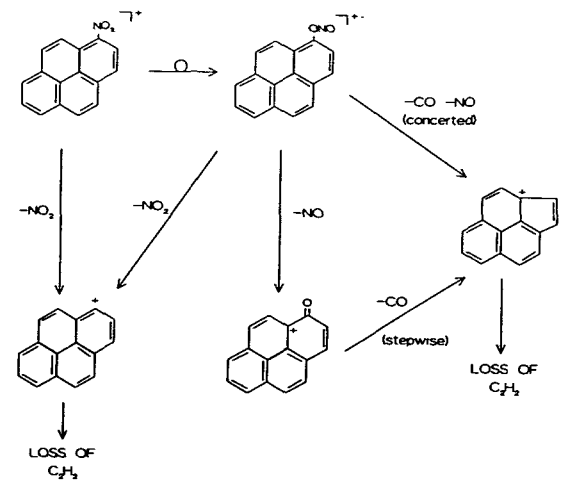

FIGURE 2. Photofragmentation pathways in nitro-PAH.

The support of the National Institutes of Health "Superfund" program (Grant 2-P42-ES04699) and the California Air Resources Board (Grant A9-32-099) is gratefully acknowledged. We also acknowledge the Air Force Institute of Technology and the U.S. Air Force Academy for their funding and sponsorship of Capt. Rae A. Noyes.

LASER PHOTOIONIZATION TIME-OF-FLIGHT MASS SPECTROMETRY OF ARSENIC AND CHROMIUM COMPOUNDS

Catherine H. Smith, Rae A. Noyes and Peter B. Kelly, Department of Chemistry;
Daniel P.Y. Chang, Department of Civil Engineering; and
A. Daniel Jones, Facility for Advanced Instrumentation,
University of California, Davis CA 95616.

The formation of volatile metal compounds during incineration results in atmospheric emission of toxic heavy metals associated with flyash. Analysis of metals present in airborne particulate matter usually involves aqueous extraction, which may alter the oxidation state of some metal species, followed by determination of the total metal content. The toxic properties of a metal may often depend on its oxidation state, e.g. Cr(III) vs. Cr(VI), consequently knowledge of not only the metal content but also the speciation of the metal is essential to assessing the hazards associated with the products of incineration. In our laboratory, we are studying the application of laser photoionization time-of-flight mass spectrometry (TOF-MS) to the detection and identification of atmospheric pollutants in particulate samples. Laser photoionization mass spectra were obtained using 266 nm and 213 nm irradiation for inorganic and organic As(III), As(V), Cr(III), and Cr(VI) compounds.

Experimental:

The experiments are performed with a custom-built linear TOF-MS instrument. A sample is typically prepared by depositing a small aliquot of the sample solution on the flattened face of a metal probe tip. The sample is allowed to air-dry, forming a thin solid layer. Crystalline samples are mounted using sticky tape. Pulsed UV radiation is generated by a Q-switched Nd:YAG laser and focussed into the source region perpendicular to the flight tube axis, such that the beam grazes the surface of the sample probe. Spectra are usually obtained with a UV laser energy of 10-20 μJ/pulse.

Results:

Laser photoionization mass spectrometry of both inorganic and organic arsenic compounds yields structurally significant fragment or cluster ion peaks, as shown in Figure 1. The arsenic ion is only weakly observed at 213 nm and is not observed at 266 nm. The AsO^+ ion is observed in oxygen-containing compounds. The laser photoionization mass spectra of the As(III) and As(V) oxide compounds are significantly different and may allow determination of arsenic speciation in environmental samples.

Photoionization of organic chromium compounds yields intense Cr^+ peaks as well as structurally significant fragment ion peaks. Covalent chromium oxide compounds such as CrO_3 and Cr_2O_3 also yield intense Cr^+ peaks. A wide range of Cr-O cluster ions are observed for CrO_3. The Cr^+ ion is not observed in the photoionization of the ionic compound $K_2Cr_2O_7$, and Cr-O cations are only weakly observed. Certain inorganic chromium compounds may yield more structurally significant fragment ions in negative ion mode.

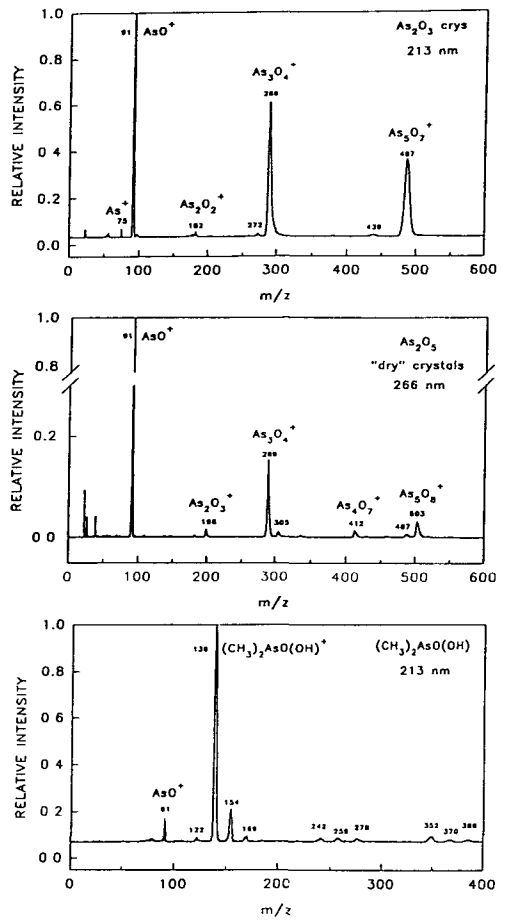

Figure 1. Laser photoionization mass spectra of As(III) and As(V) compounds.

The support of the National Institutes of Health "Superfund" program (Grant 2-P42-ES04699) and the California Air Resources Board (Grant A9-32-099) is gratefully acknowledged. We also acknowledge the Air Force Institute of Technology and the U.S. Air Force Academy for their funding and sponsorship of Capt. Rae A. Noyes.

Analysis of Sulfonated Azo Dyes as Their *tert*-Butyldimethylsilyl Derivatives

Samuel A. Testino, Jr. and Kenneth L. Busch, School of Chemistry and Biochemistry, Georgia Institute of Technology, Atlanta, Georgia 30332-0400

Sulfonated azo dyes are used extensively in the textile industry as pigments and coloring agents. Some of these dyes are discharged into the environment during the manufacturing and applications process. This is of concern because azo dyes and their aromatic amine metabolites have been shown to cause cancer in test studies.

Until now, the involatile nature of sulfonated azo dyes has required them to be analyzed by FAB mass spectrometry[1] and various LC/MS techniques, including thermospray[2] and electrospray.[3] Here, we demonstrate the ability to characterize some sulfonated azo dyes by direct inlet EI and CI and GC/MS of their *tert*-butyldimethylsilyl (tBDMS) derivatives.

Derivatization reactions. A procedure for tBDMS derivatization has been previously described.[4] Sulfonate groups, as well as polar -OH and $-NH_2$ substituents, are derivatized in a single step procedure.

$$RSO_3^- \xrightarrow[\text{tBDMCS}]{\text{MTBSTFA}} RSO_3tBDMS$$

To a solution of 2-3 mg of the sulfonated azo dye in acetonitrile was added 18 mg of *tert*-butyldimethylchlorosilane (tBDMCS) and 100 μL of N-methyl-N-(*tert*-butyldimethylsilyl)-trifluoroacetamide (MTBSTFA). The mixture was then heated at 70°C for 3 hours prior to analysis.

Direct inlet MS. The molecular ion is observed for the tBDMS derivative of each azo dye studied under EI conditions, except for acid orange 10, which required "softer" isobutane CI to keep the molecular ion intact. A spectrum of the tBDMS derivative of acid orange 7 is shown in Figure 1. Characteristic fragments of the tBDMS derivatives include $[M-15]^+$ (loss of methyl) and $[M-57]^+$ (loss of t-butyl) ions, as well as ions resulting from cleavage of the azo linkage.

GC/MS. A typical chromatogram of a tBDMS- derivatized sulfonated azo dye obtained on a DB-5 column is shown in Figure 2. Many of the extraneous peaks in the chromatogram can be attributed to decomposition products formed upon thermolysis of the labile azo linkage in the GC injection port and can be used to help characterize the azo dye being analyzed. The temperature limit of the available DB-5 column (350°C) limited the number of dyes that we could analyze; however, it should be possible to analyze all of the dyes using a specially-coated high temperature column (temp. limit, 400°C).

1. J.J. Monaghan *et al.*, *Org. Mass Spectrom.*, **17**, 569 (1982).
2. M.A. McLean and R.B. Freas, *Anal. Chem.*, **61**, 2054 (1989).
3. A.P. Bruins *et al.*, *Anal. Chem.*, **59**, 2647 (1987).
4. L.-K. Ng and M. Hupé, *J. Chromatogr.*, **513**, 61 (1990).

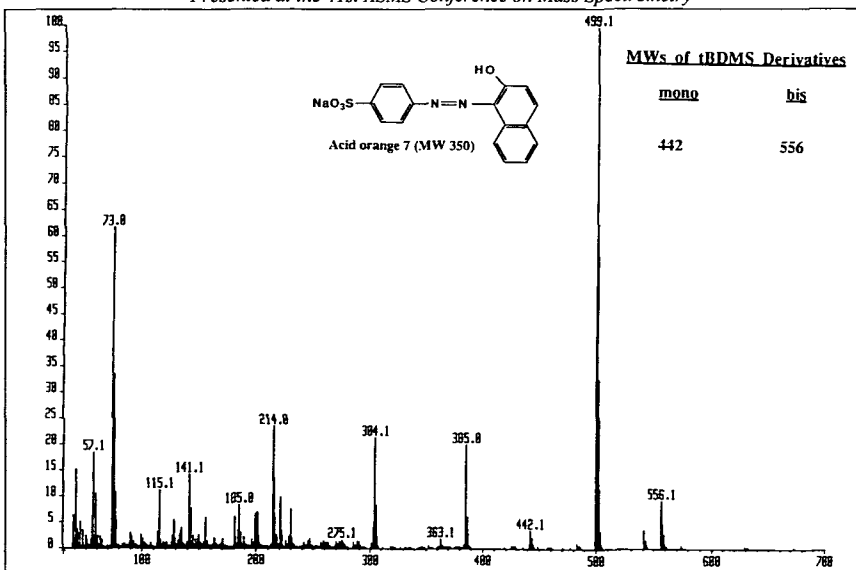

Figure 1. Direct inlet EI of tBDMS derivative of acid orange 7.

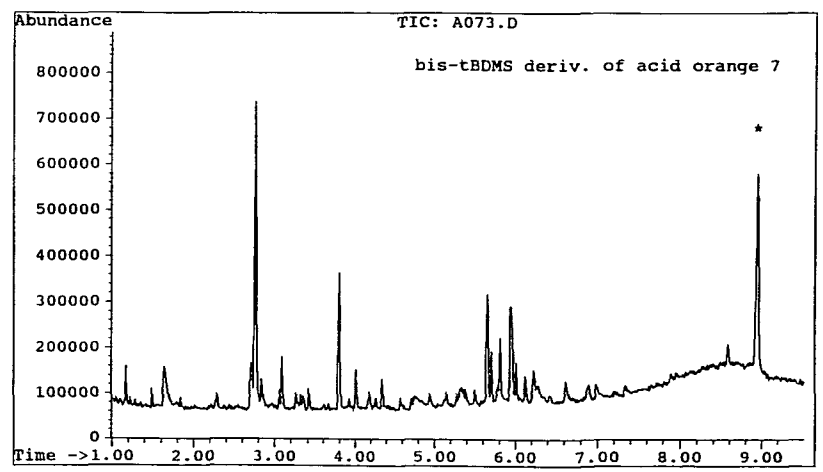

Figure 2. Gas chromatogram of tBDMS derivative of acid orange 7.

GC/MS DETECTION OF THIODIGLYCOL AND THIODIGLYCOL SULFONE USING TRIMETHYLSILYLATION DERIVATIZATION

Dennis K. Rohrbaugh and Stephen G. Pleva
U.S. Army Edgewood RD&E Center, APG, MD 21010-5423

Multinational chemical weapon treaty verification efforts have created renewed interest in the detection of scheduled compounds and their degradation products. Two degradation products of mustard gas, thiodidiglycol (TDG) and thiodiglycol sulfone, are difficult to analyze at low levels in the original state by GC/MS. In this study these compounds were converted to their trimethylsilyl (TMS) derivatives and analyzed by EI and methane CI GC/MS as part of 2 round robin exercises.

TDG and TDG sulfone were derivatized by addition of 300 µl THF and 180 µl N,O-Bis(trimethylsilyl) trifluoroacetamide (BSTFA) to the freeze-dried extract of 25 ml water. EI spectra were obtained on an HP 5970A (30m x .25mm DB-5 column). Methane CI (0.6 Torr) spectra were obtained on a Finnigan 5100 equipped with a 15m x 0.25mm DB-5 column. Injection temp was 200°C and the oven was programmed from 60-260°C at 10°C/min.

The first study was a national round robin exercise consisting of 15 water samples containing TDG, TDG sulfone and 10 other compounds spiked at 20, 90 and 160 ppb. Using BSTFA derivatization, both compounds were reliably detected at the 20 ppb level. Typical full scan chromatograms and CI spectra are shown in Figures 1 and 2. Neither molecular ion was observed under EI conditions. Small amounts of the ion resulting from loss of a methyl group were observed (m/z 251 for TDG and m/z 283 for TDG sulfone). The base peak for TDG sulfone under methane CI conditions was the potonated molecular ion at m/z 299, with the only major ion fragment resulting from loss of a methyl group (m/z 283). No molecular ion was observed for the TMS derivative of TDG but the methane adducts at m/z 295 and 307 were observed. Major fragments are m/z 177 from loss of the OTMS group (base peak) and m/z 251 from loss of a methyl group (40% of base). Selected ion monitoring under methane CI conditions using m/z 177 for TDG and m/z 299 for TDG sulfone can be used to provide increased sensitivity.

The second study involved the detection of schedule 1 compounds and their degradation products in three matrices, concrete, rubber and paint, as part of the third United Nations International Round Robin Exercise. A diesel fuel background was also added to the samples in addition to the spikes. TDG and TDG sulfone were detected in the concrete samples after extraction with water, freeze-drying and BSTFA derivatization. A methane CI total ion chromatogram is shown in Figure 3.

When the above concrete samples were extracted with D_2O (for NMR analysis), it was noted that deuteration of TDG sulfone but not TDG occurred. A comparison of spectra obtained for the TMS derivative of TDG sulfone when using water vs. D_2O is shown in Figure 4. This emphasizes the importance of avoiding deuterated solvents for mass spectral analysis or being aware that deuteration reactions can occur which complicate mass spectral interpretation.

Figure 1

Methane CI Chromatogram of a TMS-Derivatized Water Sample Containing 90ppb TDG and 160ppb TDG Sulfone

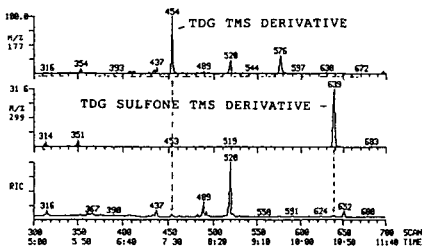

Figure 3

CI Chromatogram of TMS-Derivatized Water Extract From Concrete Containing TDG and TDG Sulfone

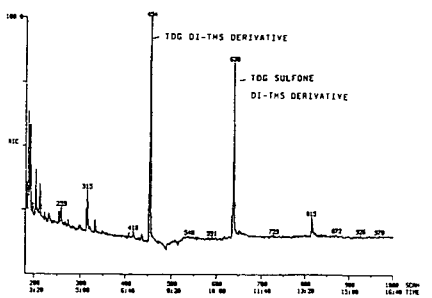

Figure 2

Methane CI Spectra of TDG and TDG Sulfone Di-TMS Derivative

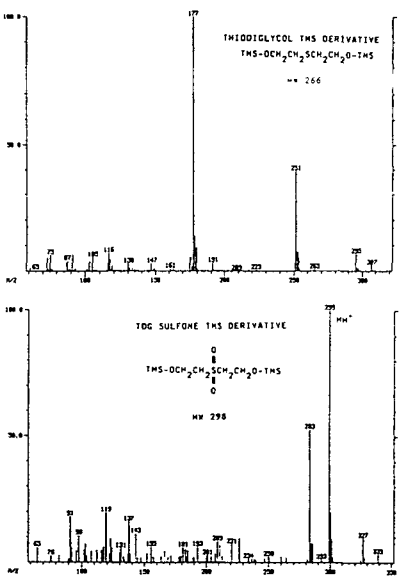

Figure 4

CI Mass Spectra of TDG Sulfone After Extraction With Water Vs. D_2O

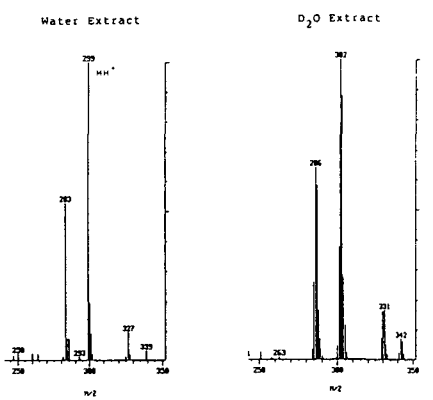

Mass Spectrometric Studies of Tetraphenylborate Hydrolysis Products from a Simulated Feedstock

*G. J. Kunkel, M. G. Bartlett, R. E. Carlson, S. A. Testino, K. L. Busch, S. K. Wallace, J. C. Richardson, and R. F. Browner
School of Chemistry and Biochemistry, Georgia Institute of Technology, Atlanta, Georgia 30332, USA

R. E. Eibling
Westinghouse Savannah River Company, Savannah River Laboratory, Aiken, South Carolina 29808, USA

The Savannah River Site has generated approximately 83 million gallons of high-level radioactive waste. The existing inventory has been reduced to 35 million gallons by evaporation and is stored in underground tanks. The Site is planning to process this highly radioactive liquid waste by concentrating the radioactive species and encapsulating them in a borosilicate glass. The process uses sodium tetraphenylborate and sodium titanate to precipitate the radioactive cesium-137 and absorb the radioactive strontium-90 and most of the plutonium. Any remaining organic compounds in the precipitated aqueous slurry must be removed for compatibility with the borosilicate glass formation. Acid hydrolysis (with a copper (II) catalyst) is used to generate benzene. Unfortunately, during this process, several undesirable byproducts are formed. Identification of the remaining organic and inorganic byproducts in the aqueous slurry and the mechanisms by which they form is desired.

Several analytical methods, including mass spectrometry, are being used to identify organic and inorganic products in a simulated nonradioactive feedstock. We have used GC-MS to identify several organic species in the feedstock including phenol, biphenyl, 2-phenylphenol, 3-phenylphenol, 4-phenylphenol, and some nitrogen-containing compounds (see Figure 1). These identifications have been confirmed using LC - UV/VIS. Cyclohexane was used in initial studies as the solvent against which the basic aqueous extract was partitioned. Use of ethyl acetate provides a more complete extraction that provides evidence for approximately twice the number of organic compounds. Ion chromatography has been used to identify several anionic species in the sample. Figure 2 contains an ion chromatogram with labeled ion peaks for an aliquot of the slurry analyzed directly. The ions identified are consistent with the additives and catalysts known to be present in the mixture.

Capillary electrophoresis, more sophisticated LC separations, and high-resolution Particle Beam LC-MS analysis are currently being used to analyze the simulated feedstock. The LC and CE results indicate the presence of a far greater array of organic compounds than expected. Over 60 individual organic compounds can be identified in individual chromatographic traces. Many of these are present at levels currently too low for positive mass spectral identification. Consequently, new methods of sample collection and concentration are being devised. Since sample is not limited in this case, these methods include solvent/solvent partitioning followed by sample concentration.

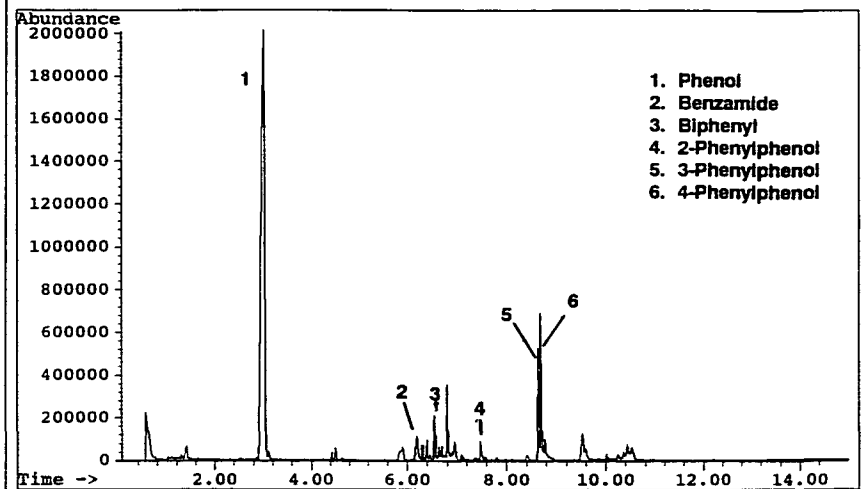

Figure 1. GC-MS TIC Trace of an Ethyl Acetate Extract.

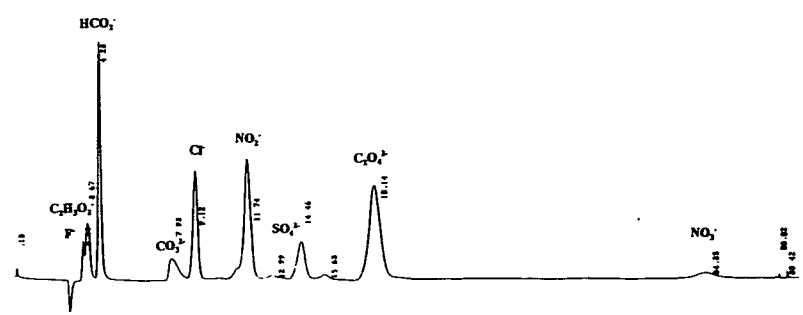

Figure 2. Ion Chromatogram of the Aqueous Slurry.

Real-time Measurement of Reactive and Toxic Hydrocarbons in Auto Exhaust: Methods Development.

Mark A. Dearth and T. J. Korniski, Ford Motor Co., Scientific Laboratory, Maildrop SRL 3061, P.O. Box 2053, Dearborn, MI 48121-2053.

Hydrocarbon analysis in vehicle exhaust becomes ever more difficult as emissions control systems and engines become more efficient. Also, State and Federal regulators are mandating that more chemical information be reported on the composition of these emissions. In an effort to reduce both the instrumentation and the manpower required to meet these testing needs, on-line methods of analysis are actively being sought.

One potential method is based on atmospheric pressure corona discharge ionization (APCDI) and tandem mass spectrometry (MS/MS), and uses nitric oxide (NO) as a reagent gas. Nitric oxide is a proven reagent gas in low pressure CI (1-3), and it was a logical next step to use NO as a reagent gas in APCDI. Nitric oxide is favored because: 1) it has an ionization potential of 9.25 eV; 2) it will not ionize N_2, O_2, CO_2, and small alkanes; 3) it will ionize alkenes, aromatics, and oxygenates.

This report describes some of the various instrumental and sample parameters that effect ionization by NO, and its potential for the real-time analysis of hydrocarbons in auto exhaust.

Experimental

All experiments were conducted using an Sciex API-III tandem mass spectrometer. The ion source region was heated to 100°C and tightly sealed, to reduce interference effects due to extraneous water The glass interface supplied by the manufacturer was modified to allow heating of the sample gases to 350°C. A ceramic sleeve was fitted to the end of the glass interface to contain the sample gases in a narrow region around the discharge needle (data not shown).

Synthetic blends of hydrocarbon gases (Scott Specialty Gases) were diluted to volume with nitrogen. Nitric oxide (9000 ppm; Airco) was diluted with N_2, air (99.999) and with the sample gases. Typical dilutions resulted in a 3000 ppm mixture of nitric oxide and a factor of 200 dilution of the sample gases.

Results

Nitric oxide reacts with various hydrocarbons in the manner previously documented under low pressure CI conditions. Representative parent and daughter ion spectra for various hydrocarbon classes can be seen in Figure 1.

Nitric oxide strongly enhances the ionization of most species, either by adduct formation or charge exchange, as depicted in the plot in Figure 2. The aromatic compounds strongly associate with NO, but can be induced to lose neutral NO by increasing the extraction voltage potential difference between the orifice (OR) and the first quadrupole lens (RO) of the API-III instrument.

The robustness of this ionization process to water, a major component of the exhaust matrix, was a major concern. Even traces of water dramatically reduce the response for all compounds, as shown in Figure 3. Average signals (ion counts per second or ICPS) drop by

almost 90% at 450 ppm water in the sample gas However, the effect of water can be reduced by heating the sample stream. Water at 100 ppm reduces compound responses by 60% at a sample gas temperature of 110°C, but only by 15% with heating (@ 350°C) With water's interference minimized, this real-time method can measure a variety of previously untenable hydrocarbons at the ppb-pptr level While developed for automotive emissions measurement, this technique has equal potential for process or ambient air monitoring applications.

Literature Cited

1 Einolf, N.; Munson, B Int J. Mass Spectrom Ion Phys **1972**, 9, 141
2. Hunt, D. F.; Ryan, J F Chem. Commun. (J Chem. Soc Sect D), **1972**, 620
3 Chai, R., Harrison, A G Anal. Chem., **1983**, 55, 969

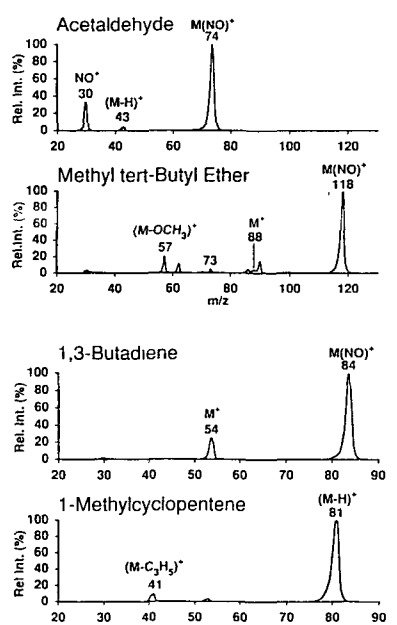

Figure 1

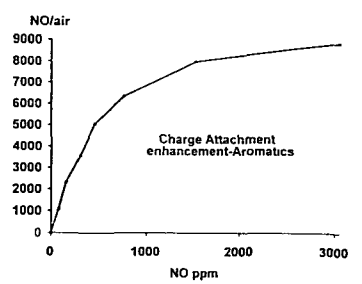

Figure 2

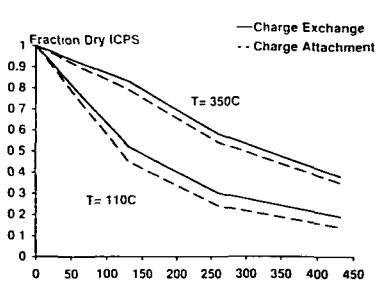

Figure 3

THERMAL STUDY OF RUTIN BY ON-LINE THERMOGRAVIMETRY/ GAS CHROMATOGRAPHY/MASS SPECTROMETRY

Henry L. Chung*, John C. Aldridge, and Jessie M. Rivers

R. J. Reynolds Tobacco Company, Bowman Gray Technical Center, Winston-Salem, NC 27102

Thermal analysis has become an important analytical technique with the introduction of modern thermal analytical instruments. An on-line thermogravimetry/gas chromatography/mass spectrometry (TG/GC/MS) system (1) was used to study the stabilbity, weight loss, and thermal degradation products of rutin. The on-line TG/GC/MS system employed a Du Pont 951 thermogravimetric analyzer equipped with a 9000 thermal analysis system interfaced to a Hewlett-Packard 5890 GC/5970 MSD system. The TG/GC interface consisted of a heated transfer line, an adsorbent trap packed with Tenax and a six-way valve. Rutin was heated and purged with air at a flow rate of 30 ml/min during the heating and purging process. The TG temperature was programed from 30°C to 900°C at 20°C/min. The volatile compounds generated in the TG were swept into an adsorbent trap. The purge gas, after passing through the trap, was vented to the atmosphere. After the heating and purging process, the trap was rapidly heated to 200°C and the volatile compounds in the trap were swept into the GC/MS system by helium at a flow rate of 35 ml/min. The volatile compounds were separated by GC. A 60 m X 0.25 mm ID DB-1701 (0.25 μm film thickness) fused silica capillary column was used for compound separation. The GC injection temperature was 250°C. The column head pressure was 25 psi. The column temperature was held at 35°C for 10 minutes, programmed to 220°C at 3°C/min and held for 48 minutes. An open-split GC/MS interface was used and the temperature was at 275°C. The mass spectrometer was operated at 70 eV in the EI mode. The ion source of the mass spectrometer was maintained at 250°C. The mass range scanned was from 29-500 amu. The volatile compounds were identified by mass spectra. The on-line TG/GC/MS system permits evolution of thermal degradation products of rutin by

TG, separation of the volatile thermal degradation products by GC, and identification by MS. The thermogram of rutin depicts a curve with four plateaus showing sample weight loss as a function of increasing temperature. The first decomposition occurred over a temperature range of 82-159°C with a weight loss of 5%. The second decomposition was between 275-374°C with 29% weight loss. The third decomposition occurred over a temperature range of 374-669°C with 62% weight loss. The fourth decomposition was between 669-900°C, and involved a further 4% weight loss. Thus, a temperature profile of stability and weight loss from rutin was obtained. The total ion chromatogram showed that a number of thermally degraded compounds were formed from rutin under the conditions studied. The volatile compounds were identified by mass spectra. The volatile degradation products were identified as ketones, furan derivatives, benzene derivatives, acids, aldehydes, furanone derivatives, pyranone derivative and phenol derivatives.

(1) H. L. Chung and J. C. Aldridge, "On-Line Thermogravimetry/Gas Chromatography/Mass Spectrometry", Analytical Instrumentation, 20, 123-135 (1992).

Interpretation of the Distribution of Environmental Contaminants in Gulf of Mexico Oysters using Log-Normal Distribution Functions

*T.J. Jackson, T.L. Wade, T.J. McDonald, J.L. Sericano, and J.M. Brooks, Geochemical and Environmental Research Group, College of Geosciences and Maritime Studies, Texas A&M University, College Station, TX 77845

In the National Status and Trends Mussel Watch Program, over 80 sites in the Gulf of Mexico have been sampled for oysters and analyzed for trace organic contaminants during the first seven years of this program. The contaminant concentration found in oysters reflects the current contaminant burden of the ecosystem. The PAHs were analyzed by SIM-GC-MS using a HP5890 GC interfaced to a HP5970MSD, and the organochlorines by GC-ECD.

The cumulative frequency distribution function was used to deconvolute the distribution for contaminant concentrations (PAHs, PCBs, DDTs, Chlordanes and Dieldrin) into two log-normal probability density functions and calculate summary statistics for each population. This approach has the advantage of examining the Gulf of Mexico as a single heterogeneous environmental system and provide information for environmental evaluation. The lower concentration level population (Pop 1) is associated with sites whose source of contaminants is probably due to chronic contamination (i.e., water runoff, atmospheric deposition). The higher level contaminant concentration population (Pop 2) is associated with local point sources of input. The temporal pattern for the mean concentration for some contaminants is consistent with large-scale climatic factors such as the El Niño cycles which affect the precipitation regime

The two log-normal probability density functions are controlled by changing the mean and spread for each population. The probability density functions are then summed using the proportion of each population, which is also a controllable variable. The sum of the probability density functions is then compared to the actual cumulative frequency distribution. The best fit for the modeled cumulative frequency distribution is determined by the minimum in the sum of the absolute deviations between the actual data and the model data (Figure 1).

The model uses a spreadsheet to calculate and compare the data which is generated. The inputs to the model are, a table of log values versus cumulative percent for a particular analyte, the mean value and spread for each population and the percent of the data in population 1, which are used to generate a table for each population, which contains the values for the mean minus 3s to the mean plus 3s versus the value for the gaussian function. The model table compares the analyte data with the model data using the lookup function with the appropriate population table to compute the cumulative distribution from the model data.

The model determines, the median concentration for each population, the percent of the data in Population 1 and the concentration above which Population 2 samples dominate the distribution (Figure 2).

Dieldrin displays a general decrease in concentration with time, as does the Chlordanes concentration. DDTs, PCBs and PAHs display a cyclic distribution which is consistent with large-scale climatic factors such as the El Niño cycle (Figure 3).

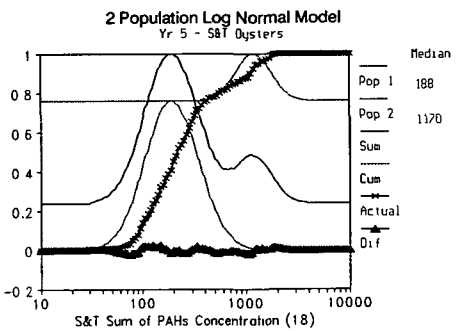

Figure 1

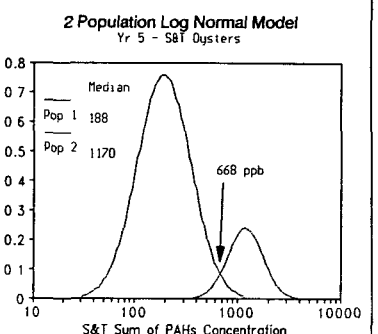

Figure 2

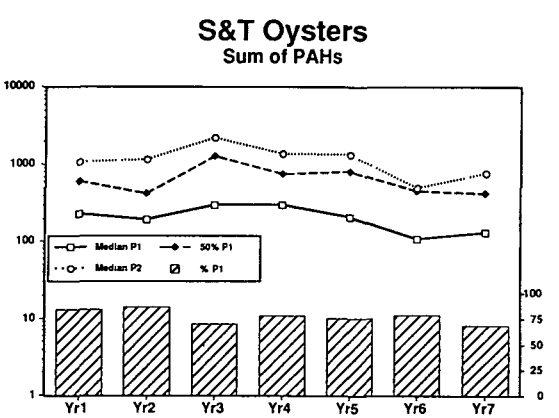

Figure 3

SUPERCRITICAL FLUID EXTRACTION IN THE ANALYSIS OF ENVIRONMENTAL ORGANIC POLLUTANTS

Iddys Figueroa, Arturo Hornedo and Osvaldo Rosario
University of Puerto Rico, Rio Piedras, Puerto Rico, 00931.

It is very important in environmental analysis, to remove the compounds of interest as efficiently as posible from the matrix being studied in such a way that artifacts are minimized and sample integrity is mantained. There are several methods of extraction for non-volatile and semi-volatile organic compounds from liquid and solid matrices. The most comonly used methods of extracting organic compounds from liquids are liquid-liquid extraction, solid-phase extraction and Dean Stark, from solids are Soxhlet extraction and ultrasonic extraction. The use of one technique or another depends on the matrix, the efficiency and the time available to perform the analysis. The majority of these methods require the use of organic solvents that present problems of sample dilution, disposal and toxicity.

Recently, interest has emerged in a relatively new technique of extraction for environmental analysis called Supercritical Fluid Extraction (SFE). A supercritical fluid is a substance that is over its critical temperature and critical pressure. By changing the pressure and temperature of this fluid, its properties change continuously from liquid-like to gas-like and hence its physical properties of viscosity and diffusivity change continuosly between those of a liquid and those of a gas, improving the solvating power of this fluid. The fluid most commonly used is CO_2 which eliminates the use of organic solvents and sample dilution. A modifier can also be added such as methanol to increase the polarity of the fluid.

The purpose of this work is to develop a methodology based on supercritical fluid to exract non-volatile semi-volatile and thermally labile compounds from diverse matrices such as adsorbents, filters, soil and biological matrices. The SFE systems commercially available are made for specific aplications and do not offer sufficient flexibility for changing the working conditions. For this reason a system of extraction was constructed. This SFE system allows changing conditions such as the size of the extraction cell,

collection mode, restrictor type and possibilities of using the system on-line or off-line.

After the equipment was assembled, all the unions, seals and valves were submitted to 10,000 psi of CO_2 and once demonstrated to withstand these pressures, experiments to optimize the extraction conditions were performed. The analytical technique used to monitor the efficiency of the extraction was HPLC with U.V. detector. Previous to the extraction experiments, the chromatographic parameters were optimized for a selection of standards representatives of a broad range of chemical properties as is the case with environmental samples.

Mixtures of the standard compounds were loaded onto a cartridge packed with glass wool and the optimum parameters such as pressure, temperature and volume of CO_2 were determined. The optimum parameters are 500 atm,50°C and 50 mL of CO_2. The same mixture was loaded into a cartridge packed with Tenax adsorbent, already preconditioned, and the extraction was performed using the parameters optimized using the glass wool. The recovery was compared with the injection of the mixture directly in the HPLC and the recovery percent was higher than 85% for most of the standard compounds but for 2,3-dichlorophenoxy acetic acid, 1-(2-chlorophenyl)-2-thiourea, monuron and bromacil.

Selectivity and Sensitivity Enhancements of Halogen Detection Utilizing Microwave-Induced Plasma/Chemical Reaction Interface Mass Spectrometry and Negative Chemical Ionization

Jeffrey T. Morre' and Mehdi Moini*
Department of Chemistry and Biochemistry
The University of Texas at Austin,, Texas 78712

Recently [1,2] we applied the GC-MIP-CRIMS technique to the selective detection of chlorine-containing compounds in complex mixtures utilizing MIP-CRIMS using electron impact ionization. Here we report the MIP-CRIMS detection of chlorinated and brominated compounds in complex mixtures using negative chemical ionization (NCI). The mass spectrometer used was a Finnigan MAT TSQ-70. In this study, SO_2 has been found highly effective as a reaction gas for selective detection of chlorine- and bromine-containing compounds using GC-MIP-CRIMS.

WHY NEGATIVE CHEMICAL IONIZATION

1) Inherent higher sensitivity of NCI for for halogen containing compounds: It has been shown that electron capture chemical ionization (negative chemical ionization) for many halogenated compounds is more sensitive compared to other forms of CI or to EI. This is because for many halogenated compounds electron capture rate constant is greater than, e g., proton transfer rate constant.

2) Less background chemical noise: In the SO_2 containing helium plasma environment, chlorine and bromine of the Cl- and Br-containing compounds predominantly form HCl and HBr, respectively. In EI mode of ionization $H^{35}Cl$ m/z 36 was the most abundant ion that was completely selective for chlorine-containing compounds, i.e., only chlorine-containing compounds produced peaks in the m/z 36 mass chromatogram However, the most sensitive selective mass chromatograms for bromine in the electron impact ionization mode are $(H^{79}Br)^+$ m/z 80 and $(H^{81}Br)^+$ m/z 82, but these channels were saturated because of the $^{32}SO_3$ m/z 80 and $^{34}SO_3$ m/z 82 formation in this plasma Therefore, the second most sensitive bromine mass chromatogram, $S^{79}Br$ m/z 111, has to be used for bromine detection. As a result, the minimum detectable amount of bromine was higher than it would have been if m/z 80 could have been used.

In the negative chemical ionization mode the most sensitive selective mass chromatograms for bromine is $(^{79}Br)^-$ and $(^{81}Br)^-$ that have no interference with $(^{32}SO_3)^-$ m/z 80 and $(^{34}SO_3)^-$ m/z 82 m/z. For this reason, the detection limits of bromine containing compounds improve significantly under NCI condition.

Selectivity and Dynamic Range. The selectivity of the GC-MIP-CRIMS of chlorine-containing compounds in complex mixtures is demonstrated using a mixtures of PCBs (Figure 1), and chlorinated pesticides (Figure 2). M/z 35 represents a selective mass chromatogram

for chlorine, m/z 81 represents a selective bromine mass chromatogram The linear dynamic range is at least three orders of magnitude.

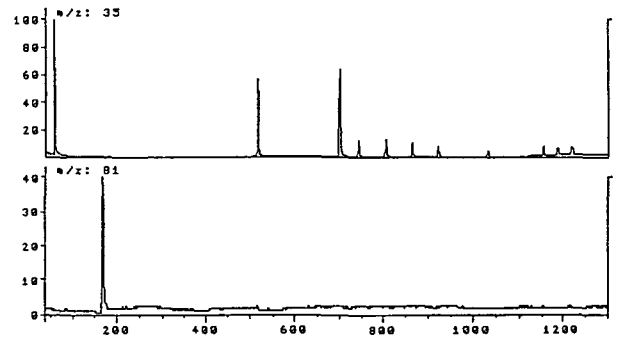

Figure 1. Selectivity of chlorinated compounds for a mixture of PCBs. Cl^- m/z 35 represents the selective mass chromatogram for chlorine-containing compounds. The PCBs concentrations were: 2-chlorobiphenyl (100 μg/mL), 3,3'-dichlorobiphenyl (100 μg/mL), 2,4,5-trichlorobiphenyl (10 μg/mL), 2,2',4,4'-tetrachlorobiphenyl (10 μg/mL), 2,3',4,5',6-pentachlorobiphenyl (10 μg/mL), 2,2',3,3',6,6'-hexachlorobiphenyl (10 μg/mL), 2,2',3,4,5,5',6-heptachlorobiphenyl (5 μg/mL), 2,2',3,3',4,4',5,5'-octachlorobiphenyl (5 μg/mL), 2,2',3,3',4,4',5,5',6-nonachlorobiphenyl (5 μg/mL), 2,2',3,3',4,4',5,5',6,6'-decachlorobiphenyl (5 μg/mL).

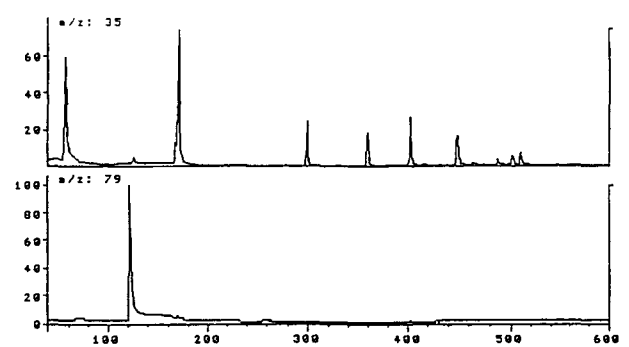

Figure 2. Selective detection of a chlorine-containing pesticide mixture. 500 μg/mL of the following pesticides: Atrazine, Endrin, Heptachlor, Heptachor epoxide, Hexachlorobenzene, hexachlorocyclopentadiene, Methoxychlor. 1 μL injected.

(1) The 39th and 40th annual conferences on Mass Spectrometry and Allied Topics, 1991 and 1992. (2) J. Morre and M. Moini *Bio. Mass Spectrom.* **1992**, *21*, 693.

DETERMINATION OF BENZENE IN FOOD BY DIRECT SAMPLING ION TRAP MASS SPECTROMETRY

S.A. Barshick, S.M. Smith, M.V. Buchanan, and M.R. Guerin, Analytical Chemistry Division, Oak Ridge National Laboratory, Oak Ridge, TN 37831-6120

Two methods, purge & trap GC/MS and Direct Sampling Ion Trap Mass Spectrometry (DSITMS), were developed and evaluated for the determination of benzene in food. DSITMS involves the direct introduction of purged volatile organic compounds (VOCs) into an ion trap mass spectrometer with no trapping or chromatographic separation prior to detection. Compared to a conventional purge & trap GC/MS method (such as EPA method 624), this amounts to a significant reduction in analysis time and cost per sample analysis.

In this work, a purge and trap GC/MS approach was developed based upon EPA method 624 (VOCs in environmental samples) and adapted for the determination of benzene in food. In this approach, volatiles are purged from a sample using a helium purge flow of 40 mL/minute for 11 minutes. The volatiles are trapped on a OV-1/Tenax/silica gel resin trap and then desorbed for 4 minutes at 180°C. The volatile components are then separated on a 30 m, 0.25 mm i.d., 1.0 μm film RTX-5 column that is heated from 25 to 225°C resulting in a total GC/MS analysis time of 35 minutes per sample. The components are ionized using 70 eV electron ionization. Benzene and its internal standard, fluorobenzene are selectively detected using selected ion monitoring. In the DSITMS approach, volatiles are purged directly into the mass spectrometer without trapping or chromatographic separation. A helium purge flow rate of 50 ml/minute is used and data is collected for 3 minutes. Water, introduced in the helium purge gas stream, is used as the chemical ionization reagent to provide proton transfer from H_3O^+ to neutral benzene producing an $(M+H)^+$ ion at m/z 79. Using the unique software capabilities of the ITMS, fullscan and MS/MS data are collected over the same purge profile. This allows the detection of an internal standard and identification of other components in the sample using the fullscan mode and adequate sensitivity and selectivity for the detection of benzene using the MS/MS mode.

Initial studies were performed to determine detection limits for benzene in water by purge & trap GC/MS and DSITMS. Both methods were shown to be linear (correlation coefficents of 0.9977 for DSITMS and 0.9957 for GC/MS) from 0 to 800 ppb benzene in water. Assuming a target concentration between 0 and 25 ppb, EPA method detection limits (MDLs) were less than or equal to the EPA criteria of 5 ppb in drinking water for both methods. Overall, the DSITMS approach has slightly lower detection limits (1.3 ppb) than purge & trap GC/MS (4.9 ppb) for the determination of benzene in water.

Table 1 summarizes the results for the analysis of 3 types of blind QA/QC samples (water, water + VOCs, and milk). Unknown sample concentrations were calculated using the water calibration lines and by single standard addition. For the DSITMS approach, the standard addition calculation had lower percent errors than the calibration plot because the standard addition method takes into account matrix effects. Chemical interferents were not a problem in the GC/MS method because they could be separated chromatographically from benzene. The calculated concentrations of benzene using the linear regression line determined from the water calibration data were low for the milk samples for both instruments. These low results were due to the matrix and the less than 100% purge efficiency of benzene in milk relative to water. The standard addition approach, however, eliminates any matrix effects and the need to run calibration lines for each of the food matrices. Overall, confidence intervals and percent errors using the standard addition approach

were similar for both instruments for all matrix types analyzed and were more accurate than the linear regression method using water calibration data.

A preliminary study was conducted for six targeted foods using the standard addition approach and both instrumental methods. Each food type was analyzed as is (blank) and fortified with two levels of benzene so that a 3 point standard addition line could be plotted. A fortified water sample was also analyzed to determine relative recoveries of benzene from the different food matrices. Benzene recoveries relative to water in all foods except coffee were typically less than 50% and were comparable for both instrumental methods. Using the standard addition plot the amount of benzene in each food was determined. In all six foods, the amounts of benzene found by the purge & trap GC/MS method were below the method detection limits. The amounts of benzene found using the DSITMS approach were also below the method detection limits for all foods except tomatoes and roast chicken. Based on 95% confidence intervals, however, it can be concluded that no significant amount of benzene was found in any of the six foods analyzed by either technique.

In this study, it was shown that comparable results (detection limits, accuracies, and percent recoveries) can be obtained for DSITMS and purge & trap GC/MS. Overall, the DSITMS approach had slightly lower detection limits than purge & trap GC/MS, although comparable results were obtained for the quantification of benzene in blind QA/QC samples (percent errors ranging from 0 to 60% with acceptable errors based on EPA QA acceptance criteria ranging from 37 - 151%). Purge efficiencies and amounts of benzene found for each of the six foods relative to water were also comparable for the two methods. In terms of time and cost-effectiveness, however, the DSITMS method was much faster, requiring only 3 minutes per sample compared to 35 minutes per sample by purge & trap GC/MS.

Table 1: Results for Triplicate Analyses of Benzene in Blind Samples

Target Concentration (Sample)	Method	Mean	95% Confidence Interval
7.2 ppb (water)	GC/MS	4.5	+/- 2.3
7.2 ppb (water)	ITMS	8.3	+/- 4.5
6.3 ppb (VOC mix)	GC/MS	5.3	+/- 2.2
6.3 ppb (VOC mix)	ITMS	6.3	+/- 3.0
201 ppb (milk)	GC/MS	156	+/- 19
402 ppb (milk)	ITMS	332*	+/- 259*

* low concentration and large error reflect the use of non-uniform volatile organic analysis vials that did not seal properly

Research sponsored by the National Cancer Institute under Interagency Agreement DOE No. 0485-0485-A1 under U.S. Department of Energy Contract DE-AC05-84OR21400 with Martin Marietta Energy Systems, Inc.

DEVELOPMENT OF A METHOD FOR THE DIRECT PURGE ANALYSIS OF VOLATILE ORGANICS IN WATER*

M.B. Wise, M.V. Buchanan, M.R. Guerin, R. Merriweather, and C. K. Bayne
Oak Ridge National Laboratory
P.O. Box 2008, MS-6120
Oak Ridge, TN, 37831-6120.

Introduction

Direct Sampling Ion Trap Mass Spectrometry (DSITMS) has been under development in our laboratory for a number of years as a means of rapidly detecting and quantifying volatile organic compounds (VOCs) in environmental samples. Over the past years, efforts have focused primarily on the development and modification of instrumentation for field and laboratory applications of DSITMS. Early data generation efforts were mostly aimed at the acquisition of pilot data which demonstrated the utility of the DSITMS technique. As this technology has started to mature and gain acceptance among other users, it has become necessary to develop concise analytical procedures and generate the validation data to support regulatory acceptance of DSITMS methods.

Method

At this time, a method has been developed for the screening of 34 EPA TCL volatile organics in water samples by direct purge into the ion trap. This method is designed to detect the presence of one or more of the VOCs at or above a threshold level of 5 ppb with a total analysis time of 3 minutes. The method utilizes a helium purge with a flow rate of 100 mL/min. Approximately 1% of the effluent is directed to the ion trap through a capillary restrictor and the remaining 99% is vented to atmosphere or can be collected on a sorbent tube for sample archival purposes. The ion trap is operated over a scan range of 45 to 300 amu using fixed ionization times for improved detection limits. Alternating electron ionization and chemical ionization scans are routinely employed. This provides enhanced compound selectivity for compounds such as alkyl-aromatics and also improves the detection limits for water soluble analytes such as aldehydes and ketones. The CI reagent is water, which is introduced into the ion trap at a constant rate along with the analytes. Quantification is performed by integrating the purge profile area for m/z values corresponding to the target analytes. The objective is to minimize the occurrence of false negatives.

Results

Method detection limits (MDL) and Certified reporting limits (CRL) have been determined for each of the volatile organics based on criteria of EPA and Army Environmental Center, respectively. Standard spectra have been generated under EI and CI conditions and potential interferences have been identified and noted where appropriate. Linearity has been established over a range of at least 1 ppb to 100 ppb and response factors for each compound have been established relative to internal standards. Appropriate QA/QC has been incorporated in the analytical method including steps for mass calibration and detailed instrument performance checks.

Conclusion

A screening method has been successfully developed for VOCs in water based on direct purge into an ion trap mass spectrometer. A draft of this method has been submitted to the Department of Energy and also to the Environmental Protection Agency for consideration for inclusion in the SW-846 manual. As a laboratory or field screening method, it will be possible to process in excess of 100

water samples per day. This high throughput will greatly improve the ability to perform site characterizations in an efficient and timely manner. Furthermore, additional cost savings will be realized by eliminating the non-contaminated samples from the sample load submitted for complete analysis by conventional purge and trap GC/MS.

Example DSITMS Detection Limits for Volatile Organic Compounds in Water

Compound	Ionization Mode[a]	MDL[b] (ng/mL)	CRL[c] (ng/mL)	Quant Mass (m/z)
Acetone	CI	2.3	3.1	59
Benzene	EI	1.7	2.3	79
Bromoform	EI	2.0	2.7	173
Carbon Disulfide	EI	1.5	2.1	76
Carbon Tetrachloride	EI	1.3	1.8	117
Chlorobenzene	EI	0.5	0.6	112
Chloroform	EI	1.5	2.0	83
Chloromethane	EI	4.7	6.3	49
Dibromochloromethane	EI	4.4	5.8	129
1,1-Dichloroethene	EI	2.0	2.6	96
trans-1,2-Dichloroethene	EI	1.7	2.3	96
Dichloromethane	EI	3.0	4.0	49
2-Hexanone	CI	2.1	2.8	101
Methyl Ethyl Ketone	CI	3.2	4.2	73
Tetrachloroethylene	EI	1.3	1.7	166
Toluene	CI	0.5	0.6	93
1,1,1-Trichloroethane	EI	0.6	0.8	97
Trichloroethylene	EI	2.7	3.5	132
Vinyl Acetate	CI	3.3	4.4	75
Vinyl Chloride	EI	1.0	1.3	62
Xylenes	CI	1.9	2.5	107

[a] Ionization mode used for optimum detection of compound

[b] Method Detection Limit as defined by U.S. Environmental Protection Agency

[c] Certified Reporting Limit as defined by U.S. Army Environmental Center

*Research sponsored by the U.S. Army Toxic and Hazardous Materials Agency, Interagency Agreement No. 1769-A073-A1, and the Office of Technology Development, U.S. Department of Energy, under contract DE-AC05-84OR21400 with Martin Marietta Energy Systems, Inc.

Multispectral Identification of Chlorine Dioxide Disinfection By-products in Drinking Water

*Susan D. Richardson, Alfred D. Thruston, Jr., and Timothy W. Collette, U.S. Environmental Protection Agency, Athens, GA 30605-2720.

Kathleen Schenck Patterson and Benjamin W. Lykins, Jr., U.S. Environmental Protection Agency, Cincinnati, Ohio 45268.

Introduction

Due to concern over the presence of trihalomethanes (THMs) and other chlorinated by-products in chlorinated drinking water, alternative disinfection methods are being explored. Chlorine dioxide (ClO_2) has been considered as an alternative to chlorine because it produces fewer THMs than chlorine and has other desirable properties, such as providing excellent disinfection, controlling odor and taste, and removing manganese and iron from water. However, very little is known about the identity of organic disinfection by-products (DBPs) that are produced by chlorine dioxide treatment.

Using multispectral identification techniques (combination of mass spectral and infrared methods), we identified more than 40 DBPs produced by chlorine dioxide treatment at a pilot plant in Evansville, Indiana. This is the first such comprehensive study of chlorine dioxide DBPs. Among the more interesting compounds identified were a series of maleic anhydrides and halopropanones.

Experimental

Multispectral identification techniques included gas chromatography coupled with low and high resolution electron-impact mass spectrometry (GC/EI-MS), low resolution chemical ionization mass spectrometry (GC/CI-MS), and Fourier transform infrared spectroscopy (GC/FT-IR). CI-MS experiments utilized methane gas, and GC/MS analyses were performed on either a VG 70-SEQ high resolution hybrid mass spectrometer or a Finnigan 4500 quadrupole mass spectrometer. GC/FT-IR experiments were performed on a Hewlett Packard Model 5965B IRD. Water samples were collected from a pilot-scale drinking water treatment plant in Evansville, IN, where the following treatment variations were applied: 1) liquid ClO_2, 2) liquid ClO_2 + $FeCl_2$ + Cl_2 + dual media filtration (sand and anthracite), 3) gaseous ClO_2, and 4) gaseous ClO_2 + $FeCl_2$ + Cl_2 + dual media filtration. Water samples (90 L) were concentrated by adsorption on Amberlite XAD resins, and the ethyl acetate eluents were then concentrated to 2 ml by Kuderna-Danish.

Results and Discussion

Rather than attempting to identify a few expected target by-products, our objective was to identify every compound that was detected in the sample extracts. In most cases, the multispectral techniques afforded very precise identifications for the semi-volatile by-products. Of the 40+ DBPs identified, the most unusual compounds were a series of maleic anhydrides, whose structures are shown below. The basic ring structure of these maleic anhydrides is similar to MX, 3-chloro-4-(dichloromethyl)-5-hydroxy-2(5H)-furanone, the controversial mutagenic chlorination by-product. Compound **5**, 2-*tert*-butyl maleic anhydride (which was one of the most concentrated by-products), was particularly difficult to identify, as there was nothing remotely similar in the mass spectral library databases (NIST or Wiley), there were no EI-MS ions characteristic for maleic anhydrides, and there was no molecular ion present in the EI mass

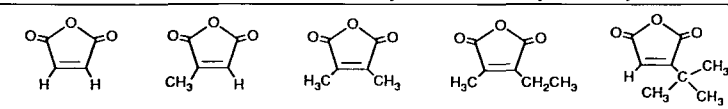

1 **2** **3** **4** **5**

spectrum. Methane CI-MS provided the molecular weight, high resolution EI-MS provided empirical formula information on fragments, and GC/FT-IR provided functional group information. Because the maleic anhydrides exhibit an extremely unusual infrared absorbance characteristic of the furandione functional group present in their structures, GC/FT-IR was key to identifying the maleic anhydrides. The EI mass spectrum and IR spectrum for Compound **5** are shown below.

When DBPs for the different treatment variations were compared, we discovered that the form of ClO_2 used was not important; both liquid and gaseous ClO_2 have the same effect. However, added reducing agent ($FeCl_2$), along with residual chlorine and dual media filtration, do cause a greater variety of by-products to be formed. Finally, although many DBPs were identified, all appear to be of extremely low concentration (1 to 10 ng/L, ppt). These levels are 1000 to 1,000,000X lower than those levels typically found for chlorinated drinking water. Chlorine dioxide appears to be a promising alternative to chlorine for treatment of drinking water, based on the levels of semi-volatile DBPs produced.

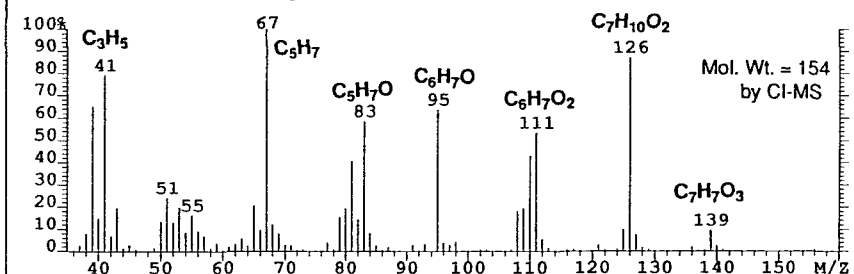

EI mass spectrum of 2-*tert*-butyl maleic anhydride (Compound **5**).

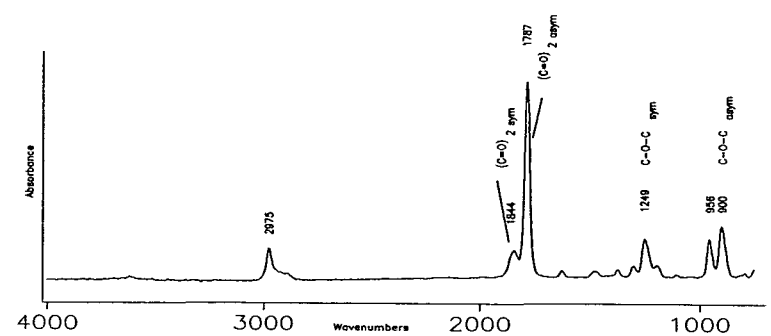

GC/FT-IR spectrum of 2-*tert*-butyl maleic anhydride (Compound **5**).

Identification of PCB Degradation Products in Gamma-Ray Irradiated Solutions of PCB's in Isopropanol. W. B. Knighton and L. J. Sears, Department of Chemistry, Montana State University, Bozeman, Montana 59717. R. E. Arbon, B. J. Mincher and D. H. Meikrantz, EG&G Idaho Inc., Chemical Sciences Group, Idaho National Engineering Laboratory, Idaho Falls, Idaho 83415.

Destruction of polychlorinated biphenyls (PCB's) and other halogenated wastes by incineration is meeting with increasingly stronger public opposition. As a result, significant effort is being directed at the development of alternative disposal methods for the PCB's. Towards this end, we have explored gamma-ray irradiation as a method for detoxifying halogenated wastes. Radiolysis offers numerous advantages over incineration, including minimization of gaseous and particulate effluents and the ability to verify that the hazardous materials have been reduced to acceptable limits prior to being discharged.

We report here the results of gamma radiolysis of octachlorobiphenyl (OCB) in aerated neutral isopropanol solutions. Unlike radiolysis under alkaline conditions, where PCB's undergo stoichiometric dechlorination to free chloride and lower chlorinated biphenyls (1,2), the degradation of OCB in neutral isopropanol produces not only the expected less chlorinated PCB species, but also a series of solvent altered PCB congeners. The identity of these altered PCB compounds is reported and a mechanism is proposed for the radiolytic degradation of OCB in neutral isopropanol.

Samples were gamma irradiated with spent nuclear fuel at the Advanced Test Reactor (EG&G Idaho) as described previously (3) at a dose rate of approximately 1 MRad/hr. Absorbed doses were measured using a FWT-60 radiochromic dye dosimeter (Far West Technology, Goleta, CA). Samples were analyzed by GC/MS (VG 7070-EHF) operated in the EI mode using a J&W 60m DB-1 column.

Figure 1 shows an EI total ion chromatogram for a solution of OCB in neutral isopropanol after receiving a 12 Mrad dose The large envelope of peaks having retention times shorter than that of OCB starting material consists of a series of less chlorinated congeners ranging from trichloro- to heptachlorobiphenyl. The peaks having retention times longer than that of OCB are due to the presence of a series of solvent altered compounds. The mass spectrum of the most predominant member of this series is shown in Figure 2. The proposed structure of this compound is also shown in Figure 2. Chemical derivatization techniques verified that the isopropanol group was bound to the biphenyl ring via a carbon linkage.

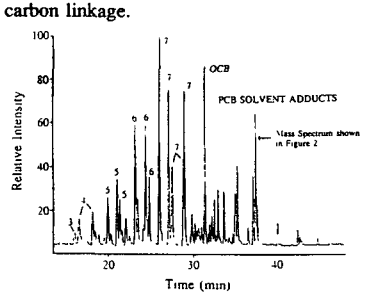

Figure 1 GC/MS EI total ion chromatogram for an octachlorobiphenyl in isopropanol solution after receiving a 12 Mrad dose Peaks are labelled to indicate the level of chlorination on the biphenyl ring

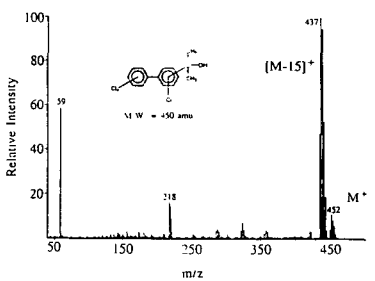

Figure 2. EI mass spectrum for the indicated peak in Figure 1 Insert shows the tentative structure of the isopropanol substituted PCB assigned to this mass spectrum

The following mechanism is proposed for the radiolytic recomposition of OCB.

$$(CH_3)_2CHOH + \gamma \rightarrow [(CH_3)_2CHOH]^* \quad (1)$$
$$[(CH_3)_2CHOH]^* \rightarrow e^- + [(CH_3)_2CHOH]^+ \quad (2)$$
$$[(CH_3)_2CHOH]^+ \rightarrow (CH_3)_2\dot{C}OH + H^+ \quad (3)$$
$$OCB + e^- \rightarrow HCB^\cdot + Cl^- \quad (4)$$
$$HCB^\cdot + (CH_3)_2CHOH \rightarrow HCB + (CH_3)_2\dot{C}OH \quad (5)$$
$$HCB^\cdot + (CH_3)_2\dot{C}OH \rightarrow HCB[(CH_3)_2\dot{C}OH] \quad (6)$$
$$OCB + (CH_3)_2\dot{C}OH \rightarrow HCB^\cdot + (CH_3)_2CO + HCl \quad (7)$$

The first three reactions provide a simplified scheme of the gamma radiolysis of isopropanol. The production of the α-hydroxyisopropanol radical is generalized via Reaction 3. While other solvent radicals are produced, these undergo H abstraction with the solvent and ultimately lead to the formation of the α-hydroxy radical. It is the products of the solvent radiolysis that are thought to be responsible for the radiolytic degradation of OCB. Direct action on OCB by the gamma radiation is not significant.

The presence of substances which are both efficient electron and radical scavengers, CCl_4 or nitrobenzene, in the irradiated solution virtually inhibits the destruction of OCB. This eliminates positive ions as being reactive towards OCB. Irradiation of OCB solutions saturated with SF_6, an efficient electron scavenger, reduces the radiolytic decomposition efficiency about 95%. SF_6 is thought to be unreactive towards the α-hydroxy solvent radical. These results indicate that solvated electrons, Reaction 4, are the primarily responsible for the destruction of OCB, but that reaction with the α-hydroxy solvent radical, Reaction 7, occurs to a measurable extent.

Heptachlorobiphenyl or other less chlorinated PCB's observed in the degradation of OCB are formed via a sequence of reactions starting with Reaction 4 or 7 followed by H abstraction with the solvent, Reaction 5. The production of the isopropanol PCB adduct is thought to be produced via the radical-radical reaction in Reaction 6. However, a series of radical neutral reactions could also lead to the observed product.

References

(1) Singh, A., Kremers, W., Smalley, P., and Bennet, G. S., *Radiat Phys. Chem.* 25, 11 (1985).
(2) Sawai, T., Shimokawa, T., and Shinozaki, Y., *Bull. Chem. Soc. Jpn.* 47, 1889 (1974).
(3) Mincher, B. J., Meikrantz, D. H., Murphy, R. J., Gresham, G. L., and Connoly, M. J., *Int. J. Appl. Radiat. Isot.* 42, 1061 (1991).

The Analysis of TCDD in Human Serum using Very High Resolution SIR

***Jeremy R. Hart[1] and Donald G. Patterson Jr.[2]**
1 – VG Analytical, Fisons Instruments, Manchester, M23 9LE
2 – Centers for Disease Control, Atlanta, GA 30333

INTRODUCTION

The analysis of polychlorinated dibenzo-*p*-dioxin and dibenzo-furans in human serum samples has often presented difficulties due to the limited amount of source material available for adequate clean-up In addition, the need to provide improved statistical information in epidemiological studies of human exposure requires that quality data is obtained from lower sample quantities and on a more cost effective basis.

As part of an evaluation of an experimental clean-up technique[1], 5 samples were prepared for analysis, including one extracted from 2.4 grams of human serum. This paper describes the results obtained from the analysis of TCDD (tetra-chloro-dibenzo-dioxin) using conventional, 10,000 resolution GC–MS and shows the improvements observed at 22,000 resolution.

METHODS

From their final dry state, each sample was re-constituted in a make-up solution containing $^{13}C_6{}^{12}C_6$–1,2,3,4–TCDD as a recovery and resolution check[2] standard in 5µl of toluene

Each sample was analysed using a VG AutoSpec–Ultima mass spectrometer and HP 5890A GC fitted with a J&W 60 metre DB–5MS column. All data was acquired in the SIR mode monitoring 7 ions (including lock mass and check channel).

Due to their low volume, manual injections of 2 µl were used for all samples and an autosampler used for calibration standards.

Data Review and Quality Control

The data from the analyses of TCDD at 10,000 resolution clearly indicated a problem due to chemical interferences. This is marked by the presence of some peaks in only one of the mass channels and an unstable baseline Some peaks of interest were also masked thus preventing accurate quantification

Data from the sample make-up showed a small (<5 fg) 1,2,3,4–TCDD peak only The use of separate syringes for all samples and checks on solvent blanks following a standard's injection confirmed that there was no measurable carry-over.

These and additional performance checks based on the calibration standards, i e isotope ratios, dynamic resolution and the lock-mass-check channel stability, confirmed that the interferences were due to components, present only in the samples, that were unresolved at 10,000 resolution

Sources of Interference and the need for Higher Resolution

There are several polychlorinated-biphenyl and related compounds that are possible sources of interference. The NIST library lists 113 chlorinated compounds that include mass 322 in their spectrum, of these 39 are biphenyls. For example, 4,4'–Biphenyldiol, 3,3'5,5'–tetrachloro–, m/z 321.9122 would require > 18,000 resolution for 10% valley separation Also, at these detection levels, the consideration of abundant sensitivity is important.

As there was only sufficient sample for one further set of analyses, it was decided to perform this with the mass spectrometer tuned to 22,000 resolution.

RESULTS

The resulting data showed that the chemical interferences were largely eliminated (figure 2), *and that high sensitivity was still maintained with a DL < 10 fg The analysis was repeated for* the remaining samples in the series; each showing significant improvement in data quality.

A calibration curve was generated, at 22,000 resolution, using 5 standards to cover the range 10 fg to 200 fg The 20 fg calibration standard has maintained an excellent signal to noise ratio of greater than 20 1 (based on a 4σ noise definition, smoothed data), and an isotope ratio of 0.80

The new data could now be quantified using fully automated procedures, OPUSquan results for the 2.4 gram serum sample are shown here for the confirmed TCDD peaks

Figure 1 Sample 906-29E 10,000 RP

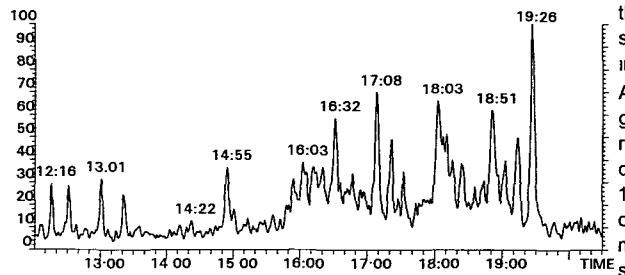

Figure 2 Sample 906-29E 22,000 RP

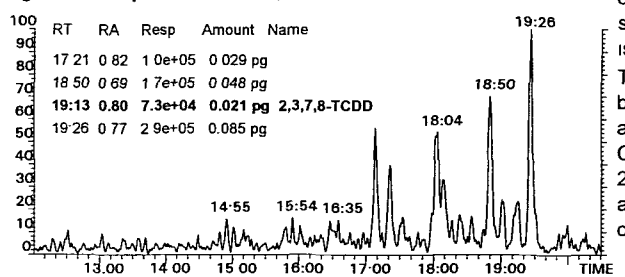

CONCLUSIONS

Without the ability to acquire very high resolution SIR data at this level of sensitivity it would have been necessary to re-extract the samples using an improved method — as in the example illustrated, that possibility does not always exist.

This paper has shown that, with current instrumentation, very high resolution SIR is a practical option where femtogram detection limits are required of samples obtained from serum or other difficult matrices.

References:

1. Turner, W.E , Cash, T.P , Patterson, D.G., Jr. and Shirkhan, H An Evaluation of the FMS Dioxin Prep System for Automated Sample Cleanup Adapted to Human Serum. *Presented at 12th International Meeting on Organohalogen Compounds, Dioxin '92, Finland.*
2. Alexander, L R., et al Performance of the High Sensitivity Ion Source for PCDD/PCDF Analyses in Human Serum and Adipose Tissue. *Chemosphere, Vol. 19, Nos 1–6, pp 241–248, 1989.*

Investigations into Interferences in Dioxin Analysis by HRGC-HRMS

T. Takasuga[1], T. Inoue[1], P. Ireland[2] and C. Moore[2]

[1] Shimadzu Techno Research Inc., Kyoto 604, Japan

[2] Kratos Analytical, Manchester M31 2LD, UK

Introduction

Current methodology for dioxin analysis utilises high resolution capillary gas chromatography coupled with high resolution mass spectrometry (HRGC-HRMS). In order to maintain the highest sensitivity at the same time as increasing the selectivity, the mass spectrometer is operated in the selected ion monitoring (SIM) mode at 10,000 resolution. Additionally, as the samples are often complex matrices containing many potential interferences at much higher levels, an extensive clean-up procedure also precedes the HRGC-HRMS analytical step. Despite this extensive clean-up and the use of HRGC-HRMS, interferences can still occur, especially when a large variety of samples are analysed on a regular basis. Identification of these interferences can yield valuable information on their likely source, and also indicate possible alternative clean-up strategies.

Air Sample - I

The chromatograms of the ions monitored for pentachlorodibenzofurans (PeCDFs) and the $^{13}C_{12}$-labelled internal standards in the standard, peak top SIM analysis of an ambient air sample are shown in Figure 1. A number of components are observed which do not have relative retention times that correspond to PeCDFs, even though the observed isotope ratios are within accepted limits for PeCDFs.

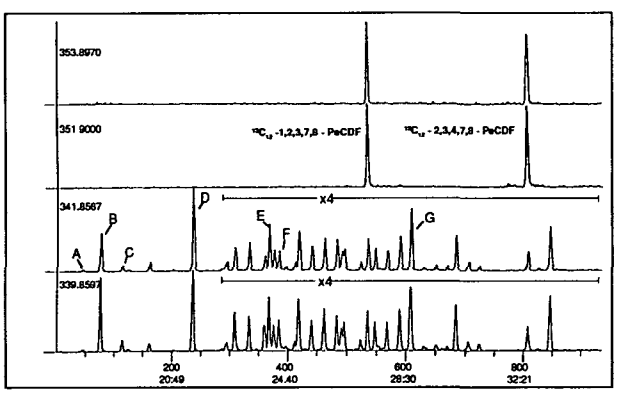

Figure 1: Ion chromatograms for PeCDFs and $^{13}C_{12}$-PeCDFs from a standard, peak top SIM analysis of an ambient air sample. Resolution: 10,000; GC column: SP-2331. A selection of the suspected interferences are labelled A to G

The peak profiles of two of these interferences, together with that of a component presumed to be a PeCDF, can also be seen. Clearly from the accurate masses and isotope ratios the two interferences appear to be different. A standard scanning analysis was also performed on this sample and the spectrum for the component labelled B is shown identifying this compound as chlordane, with the other interferences being related compounds. A scanning analysis of a sample of technical chlordane, coupled with comparison to previously published data,[1] enabled the identification of γ-(*trans*)-chlordane, α-(*cis*)-chlordane, *trans*-nonachlor and octachlordane, as well as dihydroheptachlors.

Air Sample - II

As a consequence of the identification of the interfering species, an additional carbon column chromatography clean-up step was added to the original multilayer silica column chromatography (silica, 10% $AgNO_3$/silica, 22% H_2SO_4/ silica, 2% KOH silica, silica) and alumina column chromatography stages. Interferences due to chlordane and related compounds can also be seen in the ion chromatograms for TCDFs and hexachlorodibenzofurans (HxCDFs) as well as the PeCDFs of this ambient air sample using the original clean-up strategy.

Addition of the extra carbon column clean-up step results in the removal of most of these interfering species as can be seen in the lower chromatogram.

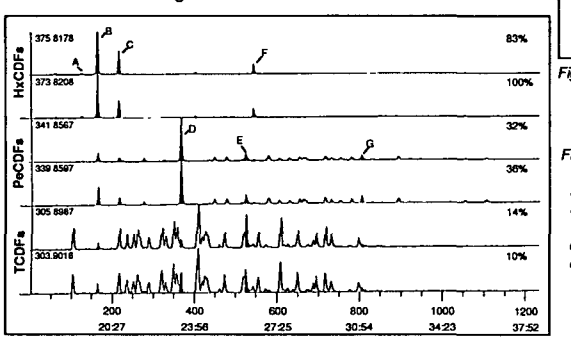

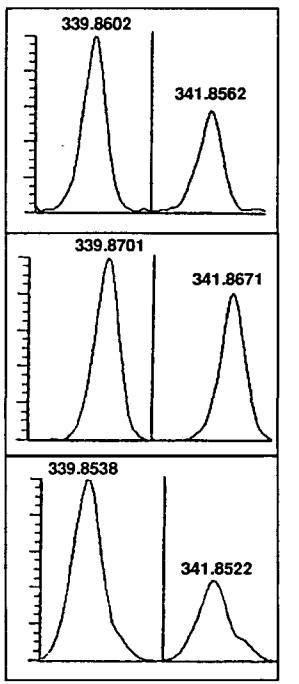

Figure 2: Ion peak profiles of PeCDF (top), interference G (middle) and interference B (bottom)

Figure 4a: Ion chromatograms for TCDFs, PeCDFs and HxCDFs from the standard, peak top SIM analysis of an ambient air sample. Resolution: 10,000; GC column: SP-2331, mixed silica column chromatography and alumina column chromatography clean step.

Interference	*Identity*
A	*trans-nonachlor*
B	*γ-(trans)-chlordane*
C	*α-(cis)-chlordane*
D	*dihydroheptachlor*
E	*dihydroheptachlor*
F	*octachlordane*
G	*dihydroheptachlor*

References

(1) Dearth & Hites, Environ. Sci. Technol. (1991), 25, 245-254

Mass Profile Monitoring in Trace Analysis: Polychlorinated Dibenzo-p-dioxins and Dibenzofurans in Crab Tissues From Raritan/Newark Bay System

Zongwei Cai[1], V. M. S. Ramanujam[1], M. L. Gross[1] and A. Cristini [2] (1) Midwest Center for Mass Spectrometry, Department of Chemistry, University of Nebraska, Lincoln, NE 68588, (2) Biology Department, Ramapo College of New Jersey, Mahwah, NJ 07430.

In 1983, several species of fish from Newark Bay, New Jersey, were reported to contain elevated levels of 2,3,7,8-tetrachlorodibenzo-p-dioxin (TCDD) (1). The data have resulted in the placement of restrictions on the consumption of crustaceans from Newark Bay, Arthur Kill and Kill van Kull, but not those from Raritan Bay. These earlier data, however, suggest that an additional study should be performed to establish further the levels of polychlorinated dibenzo-*p*-dioxins and dibenzofurans (PCDD/Fs) in the tissues of these species of crustaceans from the system.

During September 1991 and June 1992, 30 - 40 adult, legal size blue crabs (Callinectes Sapidus) were collected from each of the following four stations in the Raritan/Newark Bay system: Station 1 - Sandy Hook Bay; Station 2 - East Reach of Raritan Bay; Station 3 - Newark Bay; Station 4 - Wards Point. The crabs were dissected and the tissues from 5 - 7 male and female animals were composited for muscle and pancreas samples, respectively. The samples were analyzed for 17 selected 2,3,7,8-substituted PCDD/Fs.

The sample preparation of the crab muscles and pancreas tissues included basic digestion, liquid-liquid extraction with hexane, acid wash and multiple column chromatographic clean-up. Quantification of PCDD/Fs in the sample extracts was performed by using capillary gas chromatography/high resolution mass spectrometry (GC/HRMS) and selected ion monitoring in the mass profile mode (2).

Application of the mass profile monitoring offers high certainty of identification, especially in trace analysis, because it has high diagnostic capability (2). In addition to the two dimensions of information, chromatographic retention time and intensity of signals obtained from conventional peak top monitoring mode, the mass profile mode provides a third dimension of information - accurate mass measurement. Figure 2 shows mass chromatograms and mass profile data for the analysis of TCDD in a crab pancreas sample collected from station 3. The mass profiles (right side of the figure) were acquired for 2,3,7,8-TCDD (A) by the mass profile technique. The isotope ratio that comes from the peak intensities of the two selected ions (M and M + 2) for TCDD, the accurate masses of the selected ions, and the retention time of the GC peak result in a reliable identification of 2,3,7,8-TCDD. Moreover, analysis of mass profile data for peaks (B) has resulted in the identification of a tetrachlorodibenzothiophene (TCDT), a sulphur analogue of TCDF, because mass profile provides accurate masses for the selected ions of this interesting interference.

The concentration levels of 2,3,7,8-TCDD in pancreas samples are listed in Table 1. 2,3,7,8-TCDD/F were found not only in muscle and pancreas samples collected from station 3 but also in pancreas samples from three other stations. The levels of 2,3,7,8-TCDD in pancreas tissues of the crabs from station 3 (up to 1 ppb) are elevated by a factor of 5 to 10 times those of samples from other stations. Even the muscle samples from animals taken from station 3 have detectable levels of 2,3,7,8-TCDD (less than 50 ppt) whereas those from other stations have "no detectable" levels of 2,3,7,8-TCDD (detection limit 0.5 to 1.0 ppt). Other selected 2,3,7,8-substituted PCDD/Fs were at lower levels (less than 100 ppt) or, for most samples, not detected.

The analytical results support the suggestion that the source of dioxin contamination in the system is a chemical manufacturing plant located on the Passaic River, approximately three kilometers upstream of Newark Bay (3).

(1) Belton, T.J. *etal, A study of 2378-TCDD contamination in selected finfish, crustaceans and sediments of New Jersey waterways,* Office of Science and Research, NJ Department of Environ. Protection, Trenton, NJ.
(2) Tong, H.Y., Giblin, D.L., Lapp, R.L., Monson, S.J., Gross, M.L. *Anal. Chem.* **1991**, *63,* 1772.
(3) Bopp, R.F., Gross, M.L., Tong, H.Y. etal, *Environ. Sci. Technol.* **1991**, *25,* 951.

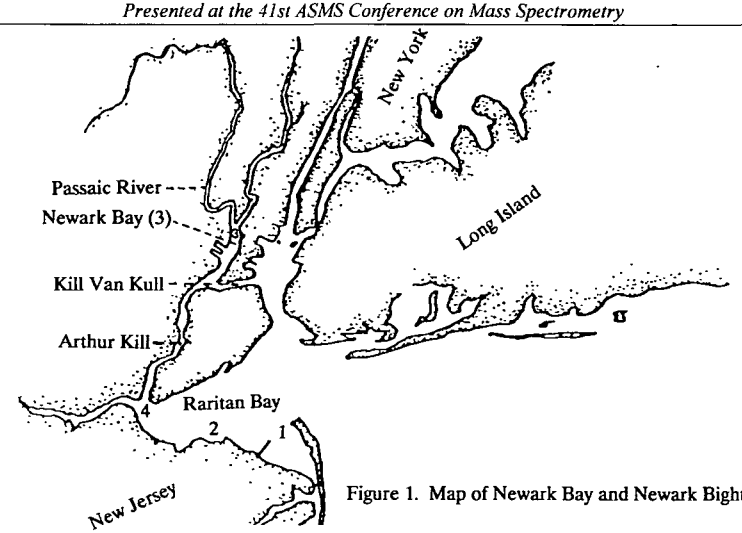

Figure 1. Map of Newark Bay and Newark Bight.

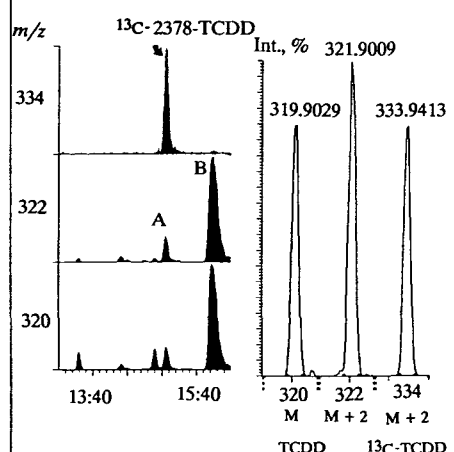

Figure 2. Mass Chromatograms and Mass Profile Spectra of TCDD.

Table 1. Levels (ppt) of 2378-TCDD in Pancreas.

Station	M/F [1]	Date [2]	2378-TCDD
1	M	9/91	50
2	M	9/91	90
3	M	9/91	940
4	M	9/91	210
1	F	9/91	40
2	F	9/91	90
3	F	9/91	690
4	F	9/91	65
1	M	6/91	80
2	M	6/92	70
3	M	6/92	450
4	M	6/92	80
1	F	6/92	n/a
2	F	6/92	55
3	F	6/92	530
4	F	6/92	60

1. M = male, F = female; 2. Collection Date.

Comparison of Pre-operational and Post-operational PCDD/F in Milk Samples Taken from Farms Located Near a New Resource Recovery Incinerator by HRGC/HRMS.

*Brian D. Eitzer and Mary Jane Incorvia Mattina, The Connecticut Agricultural Experiment Station, P. O. Box 1106, New Haven, CT 06504.

It has been well documented that polychlorinated dibenzo-p-dioxins and polychlorinated dibenzofurans (PCDD/F) are produced by the combustion of municipal solid waste (MSW) (1). These highly toxic compounds have been reported in cow's milk, with areas close to incineration sources showing higher concentration levels than more rural areas. It is therefore of interest to examine how the PCDD/F concentrations in cow's milk taken from the same set of farms located a short distance from a newly constructed resource recovery MSW incinerator change over time.

Samples of cow's milk were obtained once a week for three weeks from each of five farms located between two and eight miles from a newly constructed resource recovery incinerator. Two sets of samples were collected, one in November 1991, prior to incinerator start-up, the other in March of 1993, approximately one year after the incinerator went into operation. Portions of five of the pre-operational samples were initially examined by high resolution gas chromatography/high resolution mass spectrometry (HRGC/HRMS). The remainder were frozen at -4°C to be analyzed at the same time as the post-operational samples, reducing errors in the comparison of the sample sets from altered instrumental conditions.

Milk samples were analyzed as follows: 200 mL of raw milk was spiked with a set of 9 C 13 PCDD/F standards and extracted with 900 mL of 2:1 acetone:hexane in a large separatory funnel. The aqueous portion was washed twice with 200 mL of hexane. All hexane fractions were combined and the extracts were passed through sodium sulfate. The combined hexane fractions were reduced in volume to 75 mL, washed with 30 mL of distilled water and slurried for two hours with acid silica (40 g sulfuric acid/60 g neutral silica) The hexane solutions were then subjected to a semi-automated column chromatographic clean-up procedure described elsewhere (1) The extracts were analyzed by HRGC/HRMS on a Kratos Concept 1S. The GC was temperature programmed from 200°C to 330°C with selected ion monitoring of five groups of ten ions (two ions for each homolog) at a resolution of 10,000. Only the 2,3,7,8-substituted PCDD/F congeners were quantified.

The results are summarized in Table I which shows the average value and standard deviation for each of the three groups of data; pre-operational analyzed in 1991, pre-operational analyzed in 1993, and post-operational analyzed in 1993. As can be seen in the table the method is quite sensitive with detection limits at the fg/g concentration level. Although the standard deviations are on the high side, the data are quite acceptable given the ultra-trace levels reported. The results seem to indicate that the incinerator has not caused any significant increase in the concentrations of PCDD/F in the milk samples taken from these farms to date.

1. Ballschmiter, K., Buchert, H., Niemczyk, R., Munder, A., Swerev, M. Chemosphere, 1986, 15(7), pp.901-915.

2.. Eitzer, B D., Huang, L. Q., and Paiva, A. A. Chemosphere, 1992, 25(7-10), pp.1305-1309.

Table I. Average PCDD/F Concentrations in fg/g ± S.D.

Congener	Pre-Operation (Analyzed 1991) (n=5)	Pre-Operation (Analyzed 1993) (n=5)	Post-Operation (Analyzed 1993) (n=6)
2,3,7,8-TCDF	20 ± 17	22 ± 8	22 ± 11
2,3,7,8-TCDD	27 ± 54	42 ± 32	33 ± 36
1,2,3,7,8-PeCDF	16 ± 13	7 ± 3	8 ± 7
2,3,4,7,8-PeCDF	18 ± 8	10 ± 4	16 ± 5
1,2,3,7,8-PeCDD	22 ± 16	17 ± 9	21 ± 17
1,2,3,4,7,8-HxCDF	42 ± 31	13 ± 7	14 ± 8
1,2,3,6,7,8-HxCDF	46 ± 34	9 ± 4	10 ± 8
1,2,3,7,8,9-HxCDF	42 ± 36	10 ± 4	17 ± 14
2,3,4,6,7,8-HxCDF	39 ± 36	5 ± 2	10 ± 9
1,2,3,4,7,8-HxCDD	79 ± 75	61 ± 62	35 ± 44
1,2,3,6,7,8-HxCDD	98 ± 23	38 ± 20	30 ± 12
1,2,3,7,8,9-HxCDD	58 ± 29	19 ± 7	26 ± 20
1,2,3,4,6,7,8-HpCDF	65 ± 58	72 ± 17	62 ± 53
1,2,3,4,7,8,9-HpCDF	40 ± 37	8 ± 4	22 ± 15
1,2,3,4,6,7,8-HpCDD	200 ± 120	260 ± 150	190 ± 130
OCDD	630 ± 850	2160 ± 2400	1440 ± 1700
OCDF	390 ± 550	560 ± 500	260 ± 220

Pattern Analysis of Alkyl Aromatic Compounds from Biota Samples Taken After the Exxon Valdez Oil Spill.

Douglas G. Burrows, L. Scott Ramos* and Donald W. Brown.
Environmental Conservation Division, Northwest Fisheries Science Center,
National Marine Fisheries Service, NOAA. 2725 Montlake Blvd. E., Seattle, WA 98112.
* Infometrix, Inc. 2200 Sixth Ave., Suite 833, Seattle, WA 98121

The *Exxon Valdez* ran aground on Bligh Reef in Alaska's Prince William Sound on March 24, 1989, and spilled ca. 11 million gallons of Prudhoe Bay crude oil. In a survey to determine if the spill had contaminated the fisheries resources used by the natives for subsistence, hundreds of samples of biota were taken from many harvesting locations inside and outside the Sound, and analyzed for aromatic compounds (U. Varanasi, D.W. Brown, T. Hom, D.G. Burrows, C.A. Wigren, L.J. Field, J.E Stein, K.L. Tilbury, J T. Landahl, B.B. McCain, and S-L. Chan. Survey of Alaskan Subsistence Fish, Marine Mammal, and Invertebrate Samples Collected 1989 - 1991 for Exposure to Oil Spilled from the *Exxon Valdez*., in preparation).

The purpose of this paper was to use the GC/MS-derived patterns of aromatic hydrocarbons (AHs) to evaluate the possible sources of the contaminants found in invertebrates and to compare patterns of AHs from different sampling areas. The chemometric tools of Hierarchical Cluster Analysis (HCA) and Principal Component Analysis (PCA) offer an objective approach to characterize the similarities and differences. The results from the PCA and HCA analyses were compared to manually classifying the samples into different groups based on visual analysis of their patterns.

The GC/MS ion peak areas were collected for each compound of interest and were normalized to focus on pattern differences and not concentration differences between samples. For visual comparisons, the pattern graphs were prepared by normalizing the compound peak areas to a particular C_2 phenanthrene that was present in all the samples. These ratios were then plotted as bar graphs with the same vertical scale. The pattern graphs for all the samples were visually divided into groups.

For HCA and PCA analysis, the peak areas normalized by using the sum of the areas of all the compounds measured in a sample, were analyzed using the Pirouette® data analysis software on a PC. HCA analysis divided the samples into groups (Figure 1) based on similarities in their compound profiles. PCA was used to calculate the factors (linear combinations of the compound ratios) which were responsible for the differences between the samples. The first three factors account for more than 80% of the variability between the samples. By plotting these factors on a 3-D scatter graph (Figure 2) it is possible to view the groupings of and linear distances between sample points. Simultaneous examination of the HCA and PCA results helped to achieve an optimal division of samples into groups.

Another result of PCA is a measure of the contribution of each compound to the PCA factors. It is possible to correlate certain sample groups with groups of compounds based on the compound contributions to the PCA scores. For example, the Windy Bay samples (**A**) are distinguishable from other sample groups based on the C_3-dibenzothiophenes, C_3-phenanthrenes/anthracenes and C_1-benzanthracenes/chrysenes (C_1-BAA/CHR), while the oil and fuel samples (group **G**) are distinguishable by the higher peak ratios of C_1-, C_2- and C_3-naphthalenes (recognizing that such comparisons may not include factors such as exposure, metabolic processes, depuration, etc.). The group **E** samples are distinguishable by higher peak ratios of parent PAHs, C_1-fluoranthenes/pyrenes and C_1-BAA/CHR, indicative of combustion products.

The visual analysis of the pattern graphs shows that the *Exxon Valdez* crude oil (EVCO) is characterized by high ratios of alkyl naphthalenes relative to the reference C_2-phenanthrene, and moderate ratios of alkyl dibenzothiophenes, alkyl phenanthrenes, some high molecular weight aromatic compounds (HACs), and low ratios of anthracene. The patterns of the samples from the Kodiak sites and the Old Harbor site (**J**) are a similar to the pattern of weathered EVCO with some parent HACs superimposed on it. The patterns of two samples (**E1-2**) from Tatitlek did not show signs of oil contamination probably because the spilled EVCO flowed away from this area. However, these patterns are similar to that of the urban sediment from Puget Sound (**E3**) which had higher peak ratios of parent AHs relative to alkyl substituted components (typical of combustion products). The Chenega Bay 7 (**E4-5**) site sample patterns show similar high peak ratios of parent hydrocarbons with some oil contamination. The Windy Bay site sample patterns (**A**) resemble that of weathered EVCO, but with some increased HAC ratios. The patterns of the less volatile alkyl phenanthrenes and dibenzothiophenes are similar to those patterns in weathered EVCO from

Snug Harbor 15 months after the spill; however, the patterns of ACs in Windy Bay mussels appear even more weathered, possibly resulting from many variables such as weathering, exposure, depuration, etc.

The visual analysis divided the samples into more groups than PCA and HCA, but there are only a few major differences between the two methods that couldn't be explained by moving the group separation line further down the cluster analysis dendrogram. The HCA-PCA analysis is much faster than visual analysis, gives quantifiable separations and can be easily reapplied to some subset of the data set (i.e., using fewer compounds or only certain compound groups).

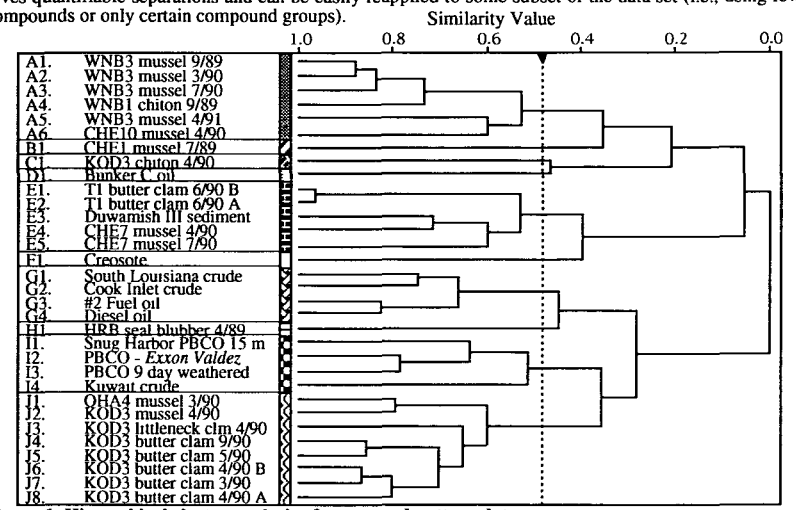

Figure 1. Hierarchical cluster analysis of compound pattern data.

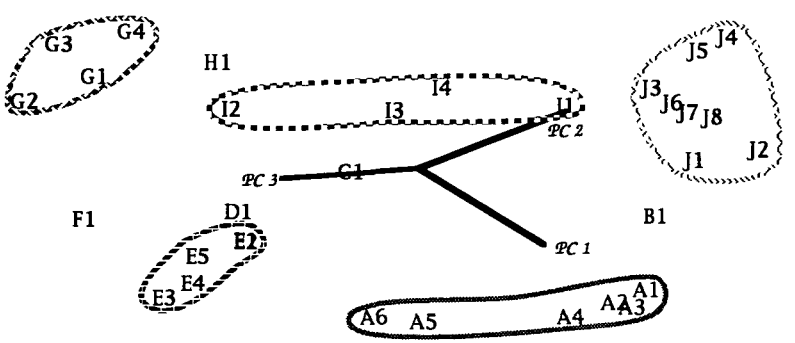

Figure 2. Three-D graph of first three principal component analysis factors of compound pattern data.

GC Inlet Modifications Improving the Analysis of Aromatic Hydrocarbon Metabolites in Fish Bile

Jennie L. Bolton, *Douglas G. Burrows,
Marc Nishimoto, Donald W. Brown

Environmental Conservation Division, Northwest Fisheries Science Center,
National Marine Fisheries Service, NOAA, Seattle, WA 98112

Introduction

Derivatization is often necessary when analyzing polar compounds by GC/MS to insure good chromatographic behavior.[1,2] Studies of metabolites of polycyclic aromatic hydrocarbons (PAHs) from the ß-glucuronidase-hydrolyzed bile of fish exposed to individual PAHs[5], and to extracts of contaminated marine sediments or other complex mixtures[3,4], have shown that many of these polar metabolites could only be analyzed as derivatives. In fish species, for example, the primary metabolite of phenanthrene was shown to be a dihydrodiol[5], however, due to dehydration of this dihydrodiol in the GC inlet, only a mixture of hydroxyphenanthrenes was seen in underivatized samples. We present improvements in GC inlet parameters enabling the direct analysis of a wide range of polar metabolites without prior sample derivatization.

Experimental

Hydrolyzed bile of English sole which had been exposed to a sediment extract from a site highly contaminated by PAHs, was analyzed in full scan mode. Metabolites were identified, and a selected ion monitoring (SIM) method was devised to quantitate compounds of interest. The effects of GC insert material and diameter, insert deactivation, and injector temperature were evaluated in SIM mode. Peak shape and arene-dihydrodiol decomposition were monitored, and relative standard deviations of analyte responses were analyzed for several inlet configurations.

Results and Discussion

Tailing of arenols and breakdown of dihydrodiols was lessened by decreasing the injector temperature from 300°C to 250°C. Use of a 4 mm i.d Vycor® insert, instead of 2 mm i.d. Pyrex® glass, allowed larger injections with improved column loading. When the Vycor® insert and its fused silica wool plug were carefully silanized[6] and kept from air and moisture until placed in the heated block of the GC injector, % RSDs of analyte responses, calculated against an internal standard, were further reduced. In addition, metabolites of 5-ring PAHs were identified,

which was not possible in previous studies without sample derivatization, due to the extreme tailing exhibited by these compounds when GC conditions were not optimized.

Conclusion

GC injector temperature, injection volume, insert diameter and inlet deactivation are variables affecting the analysis of polar compounds such as arenols. When these GC inlet parameters are optimized, many metabolites which previously could only be detected as various derivatives can now be directly, reproducibly quantified in hydrolyzed bile extracts.

Acknowledgement: Financial support to M. Nishimoto was provided by a SETAC New Investigator Award, funded by the Air Force Office of Scientific Research.

References

1. C.J.W. Brooks, W.J. Cole, J.H. Borthwick, and G.M. Brown. *J. Chrom.* 239 (1982) pp191-216
2. W. Jennings. *Gas Chromatography with Glass Capillary Columns, 2nd ed.* 1980 Academic Press pp 203-206
3. M.M. Krahn, D.G. Burrows, G.M. Ylitalo, D.W. Brown, C.A. Wigren, T.K. Collier, S-L. Chan and U. Varanasi. *Environ Sci. Technol.* 26 (1992) pp 116-126
4. M.M. Krahn, D.G. Burrows, W.D. MacLeod, Jr., and D.C. Malins. *Arch. Environ. Contam. Toxicol.* 16 (1987) pp 511-522.
5. J.E. Solbakken and K.H. Palmork. *Comp. Biochem. Physiol.* 70C (1981) pp 21-26
6. D. Rood. *A Practical Guide to the Care, Maintenance, and Troubleshooting of Capillary Glass Chromatography Systems.* 1991 Huthig Buch Verlag GmbH pp 117-119

COMPREHENSIVE ANALYSIS OF MISSISSIPPI RIVER SAMPLES BY GAS CHROMATOGRAPHY/POSITIVE CHEMICAL IONIZATION/ TANDEM MASS SPECTROMETRY AND GAS CHROMATOGRAPHY/ NEGATIVE CHEMICAL IONIZATION/MASS SPECTROMETRY

Colleen E. Rostad and Thomas J. Leiker
U.S. Geological Survey
5293 Ward Road, Mail Stop 408
Arvada, Colorado 80002

Anthropogenic organic compounds in water and suspended sediment phases were identified by mass spectrometry and used as a basis for characterizing the transport and fate of these organic contaminants in a large river system. The samples included suspended sediment and water from sixteen sites on the Mississippi River and some of its major tributaries from above St. Louis, Missouri, to below New Orleans, Louisiana. In addition to the typical GC/electron impact/MS analysis, extracts of the complex sample matrices were analyzed for selected herbicides by gas chromatography/positive chemical ionization/tandem mass spectrometry (GC/PCI/MS/MS) and for halogenated compounds by GC/negative chemical ionization/mass spectrometry (GC/NCI/MS).

Organic compounds present in the aqueous and sediment phases were initially identified by GC/electron impact/MS analysis. The aqueous phase contained some very water-soluble organic compounds which were unique to particular tributaries. The Illinois River uniquely contained tris(2-chloroethyl)phosphate, and three isomers of tris(chloropropyl)phosphate. The Ohio River uniquely contained trimethyltriazinetrione.

A technique was developed to rapidly analyze and quantitate in 20 minutes these specific compounds in the sample extracts by GC/isobutane-PCI/MS/MS. An automatic sampler was used to inject samples continuously to increase efficiency and reproducibility. Terbuthylazine was used as the internal standard. These tributary-specific compounds were found in all samples taken from the tributary, and downstream in the Mississippi River from the source tributary, but not in samples from upstream. Analysis of water samples taken from 15 verticals evenly-spaced across the Mississippi River at sites below tributary confluences indicated that the distributions across the river, of these very water-soluble compounds, were not uniform.

The sample extracts were then reanalyzed for halogenated organic compounds by GC/methane-NCI/MS. Compounds identified to be associated with the sediment included PCBs, chlordane, nonachlor, DCPA (dacthal), pentachlorobenzene, hexachlorobenzene, and trifluralin, among others. Decaflurobiphenyl and 4,4-dibromooctafluorobiphenyl were used for internal standards. Because of their low water solubility and high partition coefficients, few of these compounds were identified in the aqueous phase.

The specificity of the NCI analysis minimized the need for extensive sample cleanup. However, the complex, concentrated sample extracts still entered the ion source, contaminating the ion volume and significantly reducing the life of the filament. NCI requires colder source temperatures, so the ion volume had to be changed often to maintain sensitivity. The removable ion volumes enable quick replacement with very little retuning required. The linear range of the electron multiplier (EM) was less for NCI than for electron impact (EI), because the number of ion counts resulting in EM saturation was much less for NCI than for EI. Whether this was a fault of the conversion dynode electron multiplier is unknown. The EM was changed twice during this study, and the limited range of the EM occurred with new EMs also. Because of the specific response of NCI, the NCI data files required less disk space than EI data files from the same sample. Hence, more samples could be analyzed before the data system disk space approached capacity and required immediate quantitative and archival processing.

The aqueous and sediment extracts were then reanalyzed by GC/isobutane-PCI/MS/MS for water-soluble herbicides. These herbicides included atrazine, simazine, alachlor, metolachlor, and some of their degradation products. Terbuthylazine was used as the internal standard. The analysis took only 12 minutes per sample because the GC was temperature-ramped as rapidly as possible (20 degrees per minute) and simultaneous parent/daughter ion pairs were used. The hydrophilic herbicides were detected in both the water and the suspended sediment phase, which enabled calculation of their sediment-water partition coefficients. Detection of these compounds in the suspended sediment phase in very complex sample extracts required extreme specificity and sensitivity, which was provided by the GC/isobutane-PCI/MS/MS technique. These agricultural herbicides are widely used in the Mississippi River Basin on various crops.

Between each type of analysis, the ion volume was changed, reagent gas stabilized, and the system retuned, while the GC column parameters remained unchanged. The turbomolecular pumps handled the high manifold pressure, resulting from the reagent gas required for chemical ionization and the collision gas required for collision activated decomposition, very well for extensive periods of time. Dual terminal access to the data system, even during complex computer-controlled acquisitions, optimized the efficiency of data processing.

Given a maximum number of samples and minimum time frame, the versatility of the mass spectrometer provided extensive quantitative information on a variety of compound classes. Compounds unique to each river were identified and the data served as a basis for studying the mixing of contaminants at the confluences of the major rivers. The information obtained from the non-standard mass spectrometric techniques provided a technical base for assessing the contaminant transport and fate in the Mississippi River and its tributaries.

ALKYLBIS(TRIFLUOROMETHYL)PHOSPHINE SULPHIDE HOMOLOGUES AS MULTI-DETECTION RETENTION STANDARD IN GC/MS AND GC/MS/MS

Antti Hesso [1,2], Jarkko Tornaeus [1], Heikki Björk [2]
1) Institute of Occupational Health, Topeliuksenkatu 41 aA, SF-00250 Helsinki, Finland
2) University of Helsinki, Dept. of Organic Chemistry, Vuorikatu 20, SF-00100 Helsinki, Finland

INTRODUCTION

The use of relative retention times or retention indices in GC/MS offers an independent identification method by which the reliability of the analyte identification can be improved in complex environmental samples.

METHODS

Alkylbis(trifluoromethyl)phosphine sulphides ($M_3...M_{20}$) meet the demands for good gas chromatographic behaviour and the demand of multidetector detectability in gas chromatography [Scheme 1].

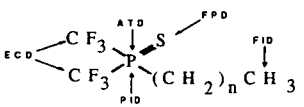

SCHEME 1. M-sesie and sites of interaction with GC-detectors

The chemical structure of alkyl bis(trifluoromethyl)phosphinesulphides (n=3-20) forms homologue serie and possesses functional groups suitable for use flame ionization detection (FID), electron capture detection (ECD), alkaline thermoionization detection (ATD) [N,P], photoionization detection (PID) and flame photometric detection (FPD)[P,S]. The standard solution (2.5 10^{-4}M) including even number homologuos (M3, M4-M20) was obtained from HNU-Nordion, Helsinki, Finland.
GC-MS analysis were performed by VG Autospec Q instrument (VG Analytical, Manchester UK.) interfaced with HP 5890 Series II gas chromatograph. The used fused silica capillary columns were NB-54 and NB-1701 (HNU-Nordion, Helsinki, Finland).

RESULTS

The mass spectrometric behaviour of alkyl bis(trifluoromethyl)phosphine sulphides (M-serie) were characterized by EI, HR-EI, PCI, NCI and by low energy tandem mass spectrometry.
The positive ion chemical ionization shows effective protonation by isobutane and methane (FIG 1. resp. FIG 3.). The formation of $[MH-102]^+$ -ions is significant under CI/CH_4 conditions for all members of the serie.The proton affinity of alkyl bis(trifluoromethyl) phosphine sulphides seems to be too low for effective protonation by ammonia.
M-serie shows excellent sensitivity by NCI (CH_4, NH_3), spectra are shown in FIG 2. resp. FIG 4. The characteristic ions are $[201]^-$, $[101]^-$ and $[M-69]^-$.
Under electron ionization conditions extensive formation of compound and group specific ions are characteristic. Ions at m/z 273^+ and m/z 241^+ are compoud specific for M_{10} corresponding loss of [M-69] and [M-101] respectively from molecular ion . Ions at m/z 147^+, $[C_2H_3F_3PS]$, m/z 202^+ $[C_2F_6PS]$ and m/z 229^+ $[C_4H_5F_6PS]$ are group specific ions for whole M-serie (FIG. 5).
The group specific ion at m/z 201^- formed under NCI conditions fragments extensively under low energy MS/MS analysis giving ion at m/z 132^-.

CONCLUSIONS

according the results, the behaviour of alkylbis(trifluoromethyl)phosphine sulphides under electron ionization and under positive and negative chemical ionization fulfill the characteristics of good retention marker compounds in GC/MS and GC/MS/MS analysis of complex environmental samples. Under ammonia positive ion chemical ionization conditions M-serie will not protonate, but by using pulsed PICI/NICI techniques and combining the retention information from NICI with the environmentally sensitive method of PICI, the full sensitivity of retention markers can br gained.

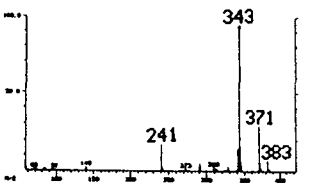

FIG 3.. PI/CI/CH4 -spectrum of M10

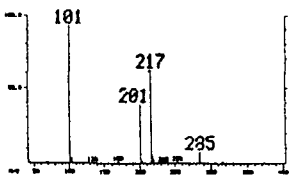

FIG 4. NI/CI/NH3 -spectrum of M8

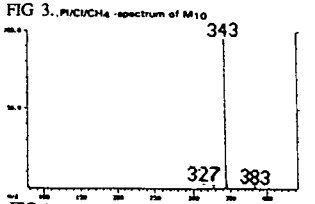

FIG 1. PI/CI/C4H10 -spectrum of M10

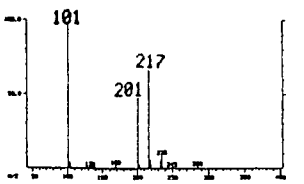

FIG 2.. NI/CI/CH4 -spectrum of M8

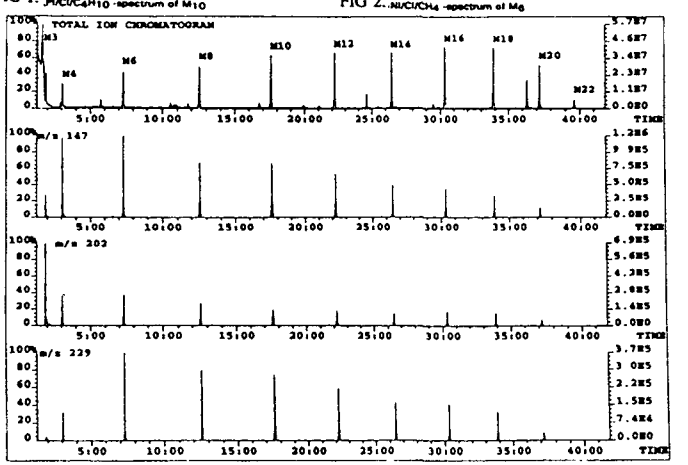

FIG. 5. Total ion current chromatogram of M-serie homologues M3, M4 - M20 and ion chromatograms for the group specific ions

IDENTIFICATION AND QUANTIFICATION OF 2,4,6-TRIBROMOANILINE IN THE COLOR ADDITIVE D&C RED No. 22 (EOSIN Y) BY GC/MS

Adrian Weisz[a] and Denis Andrzejewski[b]

[a]Office of Cosmetics and Colors and [b]Office of Scientific Analysis and Support, U.S. Food and Drug Administration, Washington, D.C. 20204

INTRODUCTION: D&C Red No. 21 (R21, mainly 2',4',5',7'-tetrabromofluorescein, **1**) and its disodium salt, D&C Red No. 22 (R22, Colour Index No. 45380, **2**), are U.S.-certified color additives listed for use in drugs and cosmetics. (R22 has an additional important use as a biological stain, under the name Eosin Y). They are batch certified by the U.S. Food and Drug Administration (FDA) to ensure compliance with specifications described in the Code of Federal Regulations (CFR) [1]. These color additives are synthetically prepared by the bromination of fluorescein. GC/MS analyses of several extracts of D&C Red No. 22 revealed the presence of 2,4,6-tribromoaniline (TBA). Because current regulations for D&C Red No. 22 do not specify a limit for TBA, it was of interest to determine the extent and level of contamination of certified lots of the color.

EXPERIMENTAL: **Identification:** Each test portion (45-61 g) was Soxhlet-extracted with chloroform for approximately 50 h. The solvent was eliminated by rotary evaporation. The residue was redissolved in 1 ml chloroform and 0.5 μl was injected into a Hewlett-Packard 5890 gas chromatograph, which was interfaced with an HP-5971 mass selective detector. Full scan data were acquired. The GC was equipped with a Supelcowax 10 fused silica capillary column, 30 m x 0.25 mm ID and 0.25 μm film thickness. The column temperature was increased from 40 to 100°C at 15°C/min. and from 100 to 250°C at 10°C/min. The total ion chromatogram of an extract of a test portion from sample 4 (Table 1) is shown in Fig. 1.

Quantification: GC/MS quantification of TBA was performed on a 9610 Finnigan Mat gas chromatograph interfaced to a 4023 Finnigan Mat quadrupole mass spectrometer (MS) with an Incos 2300 data system. Electron ionization data were obtained at 70 eV electron energy and 0.25 mA emission current at a source temperature of 240°C. The MS was operated in the selected ion monitoring (SIM) mode. The GC was equipped with a SPB-5 fused silica capillary column, 30 m x 0.25 mm I.D. and 0.25 μm film thickness. GC parameters were: injection port temperature 220°C; transfer line temperature 250°C; initial temperature 40°C (1 min.) ramp to 80°C and increase to 250°C at 10°C/min. Helium was the carrier gas at a linear velocity of 35 cm/sec. TBA was quantified by measuring the ion area ratios of m/z 329 for TBA and m/z 357 for the N,N-dimethyl-TBA that was co-injected as the internal standard. TBA was quantified using a six-point calibration curve based on analyses of standard solutions that contained internal standard and 1, 10, 25, 50, 100 and 200 ng/μl TBA. The instrument response was linear over this range (Fig. 2).

RESULTS AND DISCUSSION: Samples from 22 certified lots of commercial D&C Red Nos. 21 and 22 were analyzed for TBA. These lots represent (5) domestic and (1) foreign manufacturers that requested certification for these color additives in the past 3 years. The study includes a lot of D&C Red No. 21 (sample 1, Table 1) used in the animal feeding studies upon which FDA based its safety evaluation. Recovery of TBA from fortified samples was quantitative. Eight samples (36.4%) have been found to contain TBA (range 0.6-14 ppm, as shown in Table 1). Specifically, all the batches submitted by manufacturer A were found to contain TBA while all those submitted by manufacturer D did not contain TBA.

CONCLUSION: These findings suggest that the presence of 2,4,6-tribromoaniline as an impurity in D&C Red No. 22 may be avoided through modification of the manufacturing process.

1. Code of Federal Regulations (1992) Title 21, Part 74, U.S. Government Printing Office, Washington, D.C.

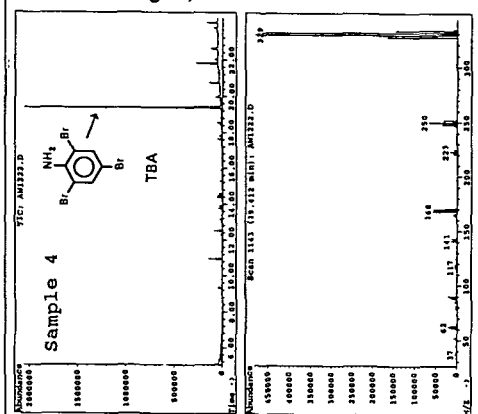

Fig. 1 Identification of TBA in D&C Red No. 22.

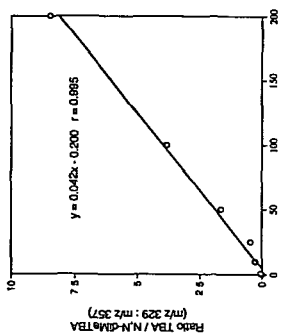

Fig. 2 TBA calibration curve.

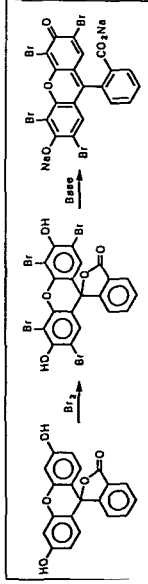

TABLE 1
2,4,6-Tribromoaniline (TBA) found in certified lots of D&C Red Nos. 21 and 22 by GC/MS

Sample	Manufacturer	Color Additive	TBA found, ppm
1[a]	AA-4533	R21	---
2	A	R22	0.6
3	A	R22	7.2
4	A	R22	9.0
5	A	R22	13.6
6	A	R22	0.8
7	B	R22	---
8	B	R22	---
9	B	R22	---
10	B	R22	1.8
11	B	R22	---
12	B	R22	---
13	B	R22	---
14	C	R22	14.0
15	C	R22	---
16	D	R22	2.6
17	D	R22	---
18	D	R22	---
19	D	R22	---
20	D	R22	---
21[b]	E	R21L	---
22[b]	F	R21L	---

[a]From toxicology test batch.
[b]Lakes, R21 precipitated onto an insoluble substratum, e.g. alumina, at 10-40% total color content.

The Photolytic Degradation of Pentachlorophenol in Organic Solvents

Michael T. Walsh and Leonard L. Ingram, Jr.
Mississippi Forest Products Laboratory
Mississippi State, MS 39762

Pentachlorophenol (PCP) is widely used as a wood preservative for the treatment of utility poles, fence posts, lumber and structural wood components of buildings that may be in ground contact. Recent statistics show that in one year 21.6 million pounds of PCP and 29 million gallons of petroleum solvents were used in the wood treating industry.[1] Two major routes of transformation of PCP in the environment are microbial and photolytic degradation. Previous research has been done on the photodegradation rate and photoproducts of PCP in water under different conditions and of PCP in hexane at 254 nm.[2,3,4] Our objectives were to study the rate of photolysis of PCP in different organic solvents at a wavelength simulating sunlight and to identify the products formed.

A 125-Watt medium pressure mercury lamp located in a double-walled immersion well was used to photolyze 100 ppm PCP solutions in selected solvents. The 313 nm line of the lamp was isolated by circulating a solution of potassium chromate and sodium carbonate between the lamp and the samples.[5] A Tracor 560 gas chromatograph was used to determine the amount of PCP remaining in each sample. Identification of photoproducts was accomplished with a Kratos MS80RFA GC/MS system with a J&W DB-5 capillary column (0.625 mm by 30 m).

Pseudo first-order reaction rates were calculated as the slope of the line from the plot of $\ln(C_t/C_0 x100)$ versus photolysis time; where C_t is the concentration of the sample at time t and C_0 is the initial concentration. Figure 1 illustrates the reaction rate for PCP in hexane, cyclohexane, cyclohexene and benzene. The photodegradation rate of PCP in hexane was 4.5 times faster than that of PCP in benzene. The 2,3,4,5- isomer of tetrachlorophenol was the major product formed under these test conditions. Solvent addition products were found in all solvents. Figure 2 shows mass spectra of solvent addition products found in a) hexane and b) benzene. No products were found where two solvent molecules dimerized. The photolysis of PCP in 100% hexane also produced the 3,4,5- isomer of trichlorophenol.

Results from this study showed that the rate of photolysis of PCP was affected by the surrounding medium. Organic solvents tested did not affect the preference for hydrogen substitution on the tetrachlorophenol radical. PCP in the organic solvents tested followed reductive dechlorination at 313 nm with a loss of chlorine from the <u>ortho</u>- position. The major photoproducts under these conditions were 2,3,4,5-tetrachlorophenol, 3,4,5-trichlorophenol and solvent addition products. The pseudo first-order rate constants indicated the presence of different solvents affected the rate of photolysis.

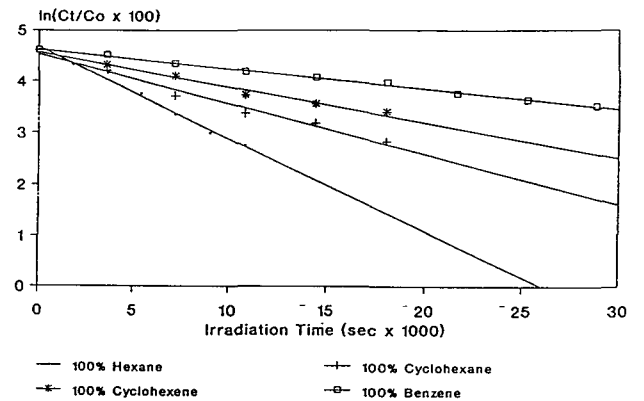

Figure 1 First-order plots for the photodegradation of PCP (100 ppm) in selected solvents

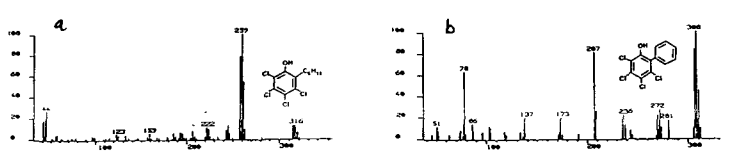

Figure 2. Mass spectra and possible structures of solvent addition products from the photolysis of PCP in a)hexane and b) benzene.

References

1. Micklewright, J.T. 1990. Wood Preservation Statistics, 1988. Proc. American Wood Preservers' Association 86:258-272.

2. Crosby, D.G. and N. Hamadmad. 1971. The Photoreduction of Pentachlorobenzenes. J. Agr. Food Chem. 19:1171-1174.

3. Wong, A.S. and D.G. Crosby. 1978. Photolysis of Pentachlorophenol in Water. Environ. Sci. Rev. 12:19-25.

4. Wong, A.S. and D.G. Crosby. 1981. Photodecomposition of Pentachlorophenol in Water. J. Agr. Food Chem. 29:125-130.

5. Baas, P. and H. Cerfontain. 1979. Photochemistry of α-Oxo-oximes. J. Chem. Soc. Perkin Trans. 2:151-155.

A Sample/Calibration "Pipeline" for the Analysis of Hazardous Cylinder Gases

Jeremiah D. Hogan
Texas Instruments Inc., Dallas, TX

The need to analyze a wide variety of hazardous gas cylinders with an equally large variety of analytical instruments presents a formidable challenge. Analysis of gases such as WF_6, HBr, HCl, HF, NF_3, BCl_3, NH_3, BF_3, and other such hazardous and/or corrosive species causes several immediate problems in the area of sampling. Safety guidelines dictate that these gas cylinders be isolated in high-airflow gas cabinets, which further complicates the sampling process. It is also inadvisable to incorporate lengthy runs of tubing, or a large number of fittings in order to connect each of these cabinets to an analytical instrument.

Development of a novel tubing/valving arrangement has led to the construction of a tubing "pipeline" which enables any of eight analytical workstations to access each of six gas cabinets with a minimal risk of cross-contamination, and with a minimum amount of tubing and fittings. The six gas cabinets are interconnected such that they form three "loops", with two cabinets on each loop. These loops are arranged such that the gases for which these cabinets are designated are interconnected with cabinets containing gases which present a minimized risk, should cross-contamination occur. For example, the HCl cabinet is connected to the HBr cabinet, not to the NH_3 cabinet, and so forth. This network also provides purging of each sample line with inert house-gas when the line is not in use. Each loop is accessible via a manifold located adjacent to the analytical instruments in the lab. Figure 1 is a schematic representation of the one of the loops in the pipeline network, all of which are similar.

There is an additional loop which is designated as a calibration loop. This loop is not tied to any of the cabinets, but provides custom blended calibration gases to each instrument through the same manifolding system as the sample loops. Calibration gas is supplied to this loop from a custom-made gas blending unit which is capable of multiple dilutions of a premixed standard calibration gas used for calibrating the analytical instrumentation.

All four loops were manufactured from electropolished stainless steel tubing, and all joints were orbitally welded to insure integrity and to maintain cleanliness. All valves are ultraclean and contain all-metal seals to prevent valve damaged due to exposure to corrosive gases.

Figure 2 depicts the time required to fill a loop with sample gas, and then to purge the sample from that loop completely, after the analysis is completed. Overall cycle times of less than three minutes are routinely achieved using this system

FIGURE 1

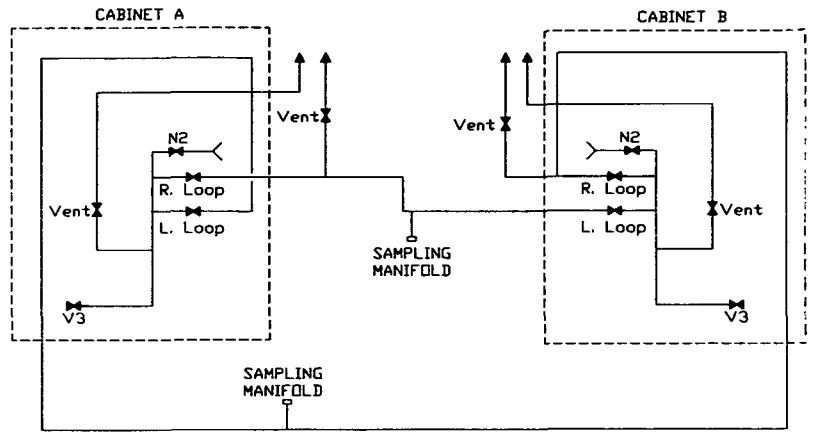

FIGURE 2

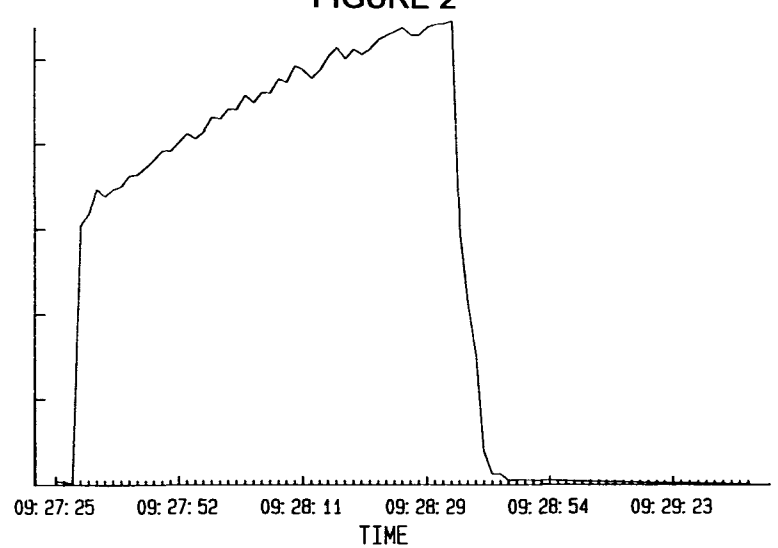

MICROVOLUME GAS ANALYSIS

Julius Perel, Stephen A. Ruatta and John F. Mahoney
Phrasor Scientific, Inc. 1536 Highland Ave, Duarte, CA 91010

The presence of moisture or gases in a sealed atmosphere can be an important factor in the premature failure of semiconductor and other devices[1,2]. Determining the concentration of moisture in the ambient atmosphere of a package volume is complex. Compared to most gases, water has a relatively low vapor pressure which makes extracting it out of a package and into an analyzer challenging. It is well known that measuring the concentration of any compound requires reference materials be available during analyses. Standards covering a range of concentrations have been used for the calibration of samples. Ideally, the standards should be as similar to the sample as possible. In the case of semiconductor package analysis, the internal volume, internal pressure and temperature should be matched and the standard be readily available for both interlab comparisons and blind standards.

A system for the mass spectrometric analysis of the gaseous components contained within a small volume package has been constructed and tested. The key features of the interface between the package and the mass spectrometer is shown schematically in figure 1. This design minimizes the surface area exposed to the analyte water vapor thus reducing adsorption and outgassing effects that could lead to systematic errors. The system exposes a very small surface area to the water containing gas, thus minimizing contamination and loss of analyte water.

As illustrated schematically in figure 1, puncturing of a package releases the gas into about a $0.05cm^3$ volume connected to a fused silica transfer line. This transfer line (40μmID) utilizes viscous (laminar) flow to reduce contact of the analyte vapors with the walls of the tubing as it flows into the Millipore/Extrel Questor III quadrupole mass spectrometer source. The gas is then ionized by electron bombardment and the resulting ions up to 200 Daltons(amu) mass analyzed and detected by a Faraday cup and/or an electron multiplier. Data is collected automatically by a computer which also controls the mass spectrometer operation.

Gas flow in a tube can be characterized as one of two basically different types. At low pressures where few molecules are present, the mean free path between gas molecules is long compared with the dimension of its container. In this molecular flow regime, there are many interactions between a gas species and the container walls as shown in figure 2a. As the pressure increases, the mean free path decreases, eventually becoming less than the distance to the walls of the tubing through which it is flowing. When the mean free path is much less than this distance, the character of the gas flow is determined mainly by gas-gas interactions while gas-wall interactions occur relatively infrequently. This viscous flow regime is shown schematically in figure 2b.

A major problem in the analysis of moisture inside of semiconductor packages is the lack of standards used in calibration. While samples are available for certification purposes, it would be ideal for laboratories to have a standard that could be utilized daily. One possibility which we have begun to investigate is to utilize saturated salt solutions to generate known moisture levels in air or nitrogen inside of small metal and/or Teflon packages. The use of saturated salt solutions to provide constant humidity gases is not new and has been used commercially as secondary standards for calibrating solid state hygrometers in the field. Adapting the idea to the production of a useful calibration tool requires that the design look as much as possible like the package under test. A schematic diagram of a reference device is shown in figure 3. This device is based on a stainless steel Whitey valve, with the addition of a glass salt solution holder and a stainless steel or aluminum reference volume. When the valve is in the open position, the vapor above the solution can easily equilibrate throughout the valve and the gas chamber. This results in all the surfaces being wetted so as to be in equilibrium with the moisture containing gas. Just prior to sampling, the valve is closed, isolating the gas chamber from the salt solution, without moving the solution containing bulb. Using this technique, we have generated concentrations of moisture ranging from 1590 ppmV to 18300 ppmV to compare with results using a two pressure humidity generator and measurements of the humidity in the calibration flow with a solid state sensor.

REFERENCES

1. Cohen, E.C., Ruthberg, S., Eds., *NBS/RADC Workshop Moisture Measurement Technology for Hermetic Semiconductor Devices, II*, Washington, DC, (1980).
2. Schafft, H.A., Ruthberg S., Cohen, E.C., Eds.*ARPA/NBS Workshop V, Moisture Measurement Technology for Hermetic Semiconductor Devices*, Washington, DC, (1978).

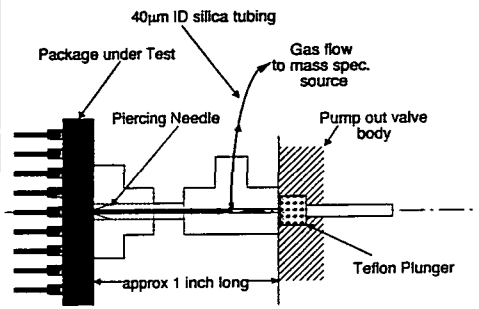

Figure 1. Schematic of the inlet portion of instrument.

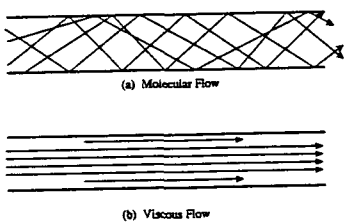

Figure 2. Two basic flow regimes.

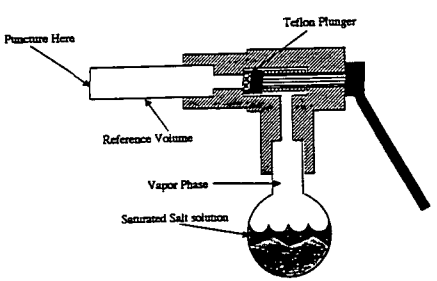

Figure 3. Schematic diagram of a reference device(Valve closed).

FAB MS and HPLC Analysis of Fumonisin B_1 and Fumonisin B_2 in Food Substrate Cultures

Manuel Holcomb, John B. Sutherland, M. Paul Chiarelli, Walter A. Korfmacher*, Harold C. Thompson, Jr., Jack O. Lay, Jr., and Carl E. Cerniglia
National Center for Toxicological Research, Food and Drug Administration, Jefferson, AR 72079, USA
*Schering-Plough Research Institute, Department of Metabolism, 60 Orange St., Bloomfield, NJ 07003, USA

INTRODUCTION:

Fusarium moniliforme Sheldon, which occurs worldwide on grains, is a common contaminant of corn. Fumonisins B_1 and B_2, which are mycotoxins produced by *F. moniliforme*, have been shown to promote cancer in rats. Isolates of *F. moniliforme* from corn have been shown to produce higher concentrations of fumonisins B_1 and B_2 than similar isolates from other substrates.

We grew cultures of a toxigenic strain of *F. moniliforme* on five different substrates (corn, unmilled rice, rodent feed, peanuts, and soybeans) and analyzed them for fumonisins by FAB MS as well as FAB MS/MS and quantitated by gradient HPLC. Corn was used as a positive control for determining if proper conditions were used for fumonisin production. Rodent feed cultures were of particular interest since the National Center for Toxicological Research (NCTR) maintains a rodent colony for research purposes and any toxin in the feed could affect research results.

This study was to determine if FAB MS and FAB MS/MS analysis could be utilized for the determination of both fumonisins B_1 and B_2 in culture extracts. The fumonisins were quantitated by a modified gradient elution HPLC method with fluorescence detection after derivatization with fluorescamine.

EXPERIMENTAL:

FAB MS Analysis. The FAB MS system consisted of a Finnigan MAT TSQ 70 triple quadrupole mass spectrometer, equipped with a Finnigan fast atom bombardment (FAB) source and an Ion Tech fast atom gun. Xenon was utilized in the primary atom beam at energies of 8 to 10 KeV and thioglycerol was used as the matrix. Typically, the matrix was applied to the FAB probe tip followed by 1 μL of the sample. The mass spectrometer was scanned from m/z 200 to m/z 800 at 1 scan/sec.

FAB MS/MS Analysis. The FAB MS/MS analyses were performed under the same conditions as FAB MS, except that the collision gas, argon, was set to about 0.5 mtorr and the collision energy was either 30 or 50 eV. To obtain daughter ion spectra, MS1 (Q1) was set to pass the selected parent ion and MS2 (Q3) was operated under full scanning conditions.

HPLC Analysis. The gradient HPLC system consisted of two Shimadzu model LC-600 pumps (Shimadzu Scientific Instruments, Columbia, MD), a Shimadzu model SIL-9A autoinjector, a Shimadzu model C-R3A integrator, a Waters model 470 fluorescence detector (Waters Chromatography Division), and a Microsorb C_8 column (25 cm x 4.6 mm i.d., 5 μm particle size, Rainin Instrument Co., Woburn, MA).

RESULTS AND DISCUSSION

As expected, the corn cultures produced the highest concentration of fumonisins B_1 and B_2. Significant levels of fumonisins B_1 and B_2 were also observed in the unmilled rice culture extract.

The mass spectra obtained for the FAB MS analyses of the unmilled rice and corn culture extracts showed $[M+H]^+$ ions at m/z 722 and m/z 706 for fumonisins B_1 and B_2, respectively. Additional peaks can be attributed to the K adduct ions; peaks at m/z 760 and m/z 744 correspond to the $[M+K]^+$ ions for fumonisins B_1 and B_2, respectively.

FAB MS/MS analysis was performed on the fumonisins B_1 and B_2 standards as well as the culture extracts. Figure 1 shows the collisionally activated dissociation (CAD) of the $[M+H]^+$ ions for fumonisin B_2 for the standard and the corn culture extract, confirming the presence of fumonisin B_2 in the extract.

FAB MS together with FAB MS/MS was found to be a sensitive technique for the detection of both fumonisin B_1 and B_2 in culture extracts. Also, a modification of an existing HPLC procedure using fluorescence detection after derivatization with fluorescamine has resulted in a sensitive method for quantitating the fumonisins.

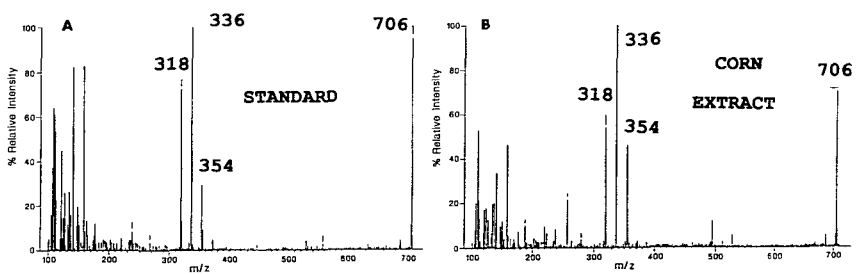

Figure 1 (A) FAB MS/MS of fumonisin B_2; this is the CAD product ion mass spectrum of the m/z 706 ion. (B) FAB MS/MS of the corn culture extract containing fumonisin B_2; this is the CAD product ion mass spectrum of the m/z 706 ion.

The Use of Internal Standards to Improve Linearity and Reproducibility in the Thermospray LC/MS Analysis of Chlorinated Phenoxyacetic Herbicides

*Jeffery S. Hollis, The Hewlett Packard Company, Cincinnati, OH 45242
Alexander B Schilling, The Hewlett Packard Company, Naperville, IL 60566

Introduction.

The EPA Method 8321A recommends the use of thermospray (TS) LC/MS for the identification and quantification of chlorinated phenoxyacid herbicides. Earlier work[1] had examined the use of negative ion TS LC/MS in SIM mode to quantify a series of these herbicides Although good sensitivity and linearity were observed, during the use of thermospray one can observe small source pressure fluctuations under normal operating conditions that can be sources of non-linearity and affect reproducibility This could be a problem using an external standard based assay The use of internal standards might help to compensate for these fluctuations and improve the reproducibility and linearity over the calibration range. Ideally, internal standards should be stable isotope labeled analogs of the compounds being analyzed However since stable isotope labeled standards are not always readily available, structurally similar analogs may be employed One requirement of any internal standard in an LC/MS assay is that it ionize under the conditions employed A variety of alkyl esters of the chlorinated phenoxyacid herbicides are readily available but yielded poor sensitivity under the discharge negative ion conditions employed in this study Dinoseb (2,4-Dinitro-6-sec-butylphenol) is included in the 8321A method and yields the largest response in negative ion mode for the compounds studied previously. This is presumably due to electron capture facilitated by the nitro-functional groups Thus compounds possessing nitro functional groups may be suitable as internal standards for this assay

Experimental

A series of nitro-functionalized phenols, benzenes, toluenes and phenylacetic acids were analyzed using TS/LC/MS using the method protocol. A HP 5989A LC/MS/DS with a thermospray interface and a HP 1090L HPLC with a diode array detector were used to chromatograph the compounds Negative ion mode employing discharge ionization was used in all cases Chromatography was performed on a Zorbax Rx 4 6 x 250 mm column using a solvent system as follows Solvent A 0 1 M NH_4Ac pH 4 5, Solvent B. 0 1 M NH_4Ac in methanol, with gradient elution starting (%A %B) 50.50, hold 2 minutes then to 40.60 at 12 minutes, then to 10 90 at 20 minutes, hold to 25 minutes, then to 50.50 at 30 minutes. The column was at ambient temperature. SIM acquisition was used, monitoring the most intense ion for each compound The internal standards were added at 50 ng each on column. A series of six calibration levels were run with a 3 uL injection volume All samples were made up in acetonitrile

[1]Hollis and Schilling, 40th ASMS Conf on Mass Spec and Allied Topics, 1992, 1699-1700.

Results and Discussion.

Several mono and dinitro-functionalized analogs of Dinoseb and the chlorinated phenoxy acids were examined for suitability as internal standards Amongst these only the dinitro-phenols and toluenes were found to have both a good response and useful retention times with the current chromatographic system These compounds presumably ionize in discharge negative ion mode in a manner analogous to the chlorophenoxy herbicides By using the internal standard based assay an improvement in the reproducibility over the calibration range (3 0 ng-400 ng on column) of the assay was observed There is a possibility that typical hazardous waste samples being examined for herbicide residues may contain one or more of the internal standards as an unexpected but likely trace contaminant Nitrophenols and nitrotoluenes are listed on several EPA RCRA/CERCLA lists as target analytes. Therefore the use of labeled analogs of these compounds, which are commercially available and would yield similar results are recommeded.

LC/MS Chromatogram Of Three Selected Internal Standard Candidates

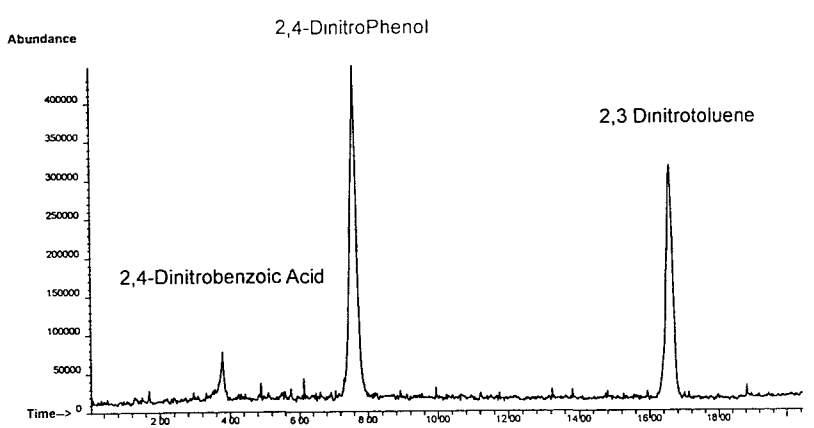

LIQUID CHROMATOGRAPHY/PLASMASPRAY MASS SPECTROMETRY FOR CHARACTERIZATION OF A COMMERCIAL CHLORINATED *n*-PARAFFIN MIXTURE.

G.T.Tomy [a,b], D.C.G.Muir[a], J.B.Westmore[b] and G.A.Stern[a].
[a]Fisheries and Oceans, Winnipeg, MB. R3T-2N6, Canada.
[b]Department of Chemistry, University of Manitoba, Winnipeg, MB. R3T-2N2, Canada.

Introduction. Chlorinated *n*-paraffins (CPs) are used as fire retardants, plasticizers in PVC, adhesives, and as extreme pressure additives in lubricants and cutting oils. They have also found use as replacement chemicals for more toxic and persistent chemicals such as PCB's.

Currently there is limited information on the fate and impact of CPs in the environment, and this is due, in part, to the complexity of CP mixtures and also to the difficulties in measuring low levels.

This report describes preliminary results on the application of liquid chromatography-negative ion plasmaspray ionization (NPI) mass spectrometry to the qualitative determination of a commercial *n*-paraffin mixture.

Mass Spectrometry. A Trio 1000 (VG/Fisons Analytical Ltd.) quadrupole mass spectrometer equipped with a thermospray/plasmaspray interface was used. Ionization was achieved using the plasmaspray interface. Mass spectra were recorded in the negative ion mode with a plasmaspray current of 150μA, a source temperature of 200°C, a nozzle temperature of 170°C, a repeller voltage of 225V and an ion source pressure of 1×10^{-4} mbar. The mass spectrum was scanned from 350 to 650 daltons.

Chromatography. HPLC separations were performed on a Waters Novapak™ 150mm × 3.9mm C_{18} column with 3μm packings at a temperature of 30°C. A gradient elution using tetrahydrofuran (A) and water (B) was used. The initial condition 50%A : 50%B was held for 3 minutes, ramped linearly to 51%A : 49%B over 5 minutes, held there for 15 minutes, and then ramped linearly to 52%A : 48%B over 5 minutes, and held 15 minutes. A constant flow rate of 0.75mL/min was used throughout the gradient.

Results and Discussion. Chloroparaffin huls 70C (CP huls 70C) is a mixture of isomers and congeners with C_{10} to C_{13} chain lengths and chlorine content of 70% by weight. The total ion chromatogram of CP huls 70C separated with the reverse phase column is shown in Figure 1. The broad hill-like shape of the chromatogram is due to the large number of congeners and isomers present in the mixture. Congeners and isomers present in low concentrations cause the rise in the baseline, while congeners and isomers present in higher concentrations give rise to the peaks[1].

The mass spectrum of signal* is shown in Figure 2. The highest mass ion cluster starts at m/z 510, and corresponds to ten chlorine atoms, indicating the molecular formula $C_{12}H_{16}Cl_{10}^{-\cdot}$. The odd-mass peaks in this cluster correspond to loss of a hydrogen atom from the molecular ion. The ion clusters around m/z 496, m/z 476 and m/z 462 correspond to the molecular ions $C_{11}H_{14}Cl_{10}^{-}$, $C_{12}H_{17}Cl_{9}^{-}$ and $C_{11}H_{15}Cl_{9}^{-\cdot}$ respectively. Upon each of these ions is superimposed, at odd-mass, the cluster corresponding to a loss of a hydrogen atom from the molecular ion.

The two isotopic patterns of low abundance are probably fragment ion clusters. The ion cluster starting at m/z 440 corresponds to the formula $C_{12}H_{16}Cl_{8}^{-}$ and could be derived by a loss of Cl_2 from the molecular ion $C_{12}H_{16}Cl_{10}^{-\cdot}$. The ion cluster starting at m/z 441 corresponds to the formula $C_{12}H_{17}Cl_{8}^{-}$ and is derived from dechlorination of the molecular ion $C_{12}H_{17}Cl_{9}^{-\cdot}$.

The isotopic pattern starting at m/z 426 corresponds to eight chlorine atoms and can only be derived from dehydrochlorination of the molecular ion $C_{11}H_{15}Cl_{9}^{-\cdot}$. The ion cluster starting at m/z 425 corresponds to the molecular formula $C_{11}H_{13}Cl_{8}^{-}$ and is derived from dechlorination of the molecular ion $C_{11}H_{13}Cl_{9}^{-}$.

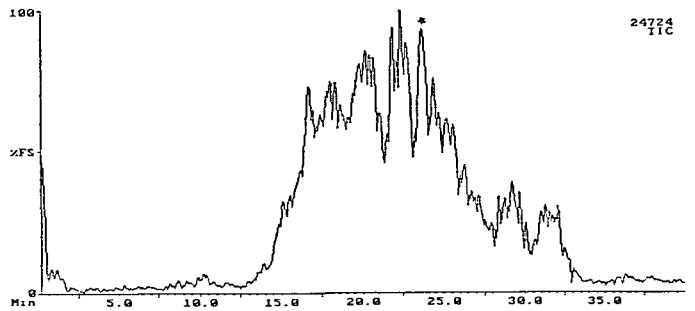

Figure 1. NPI-LC/MS total ion chromatogram of CP huls 70C.

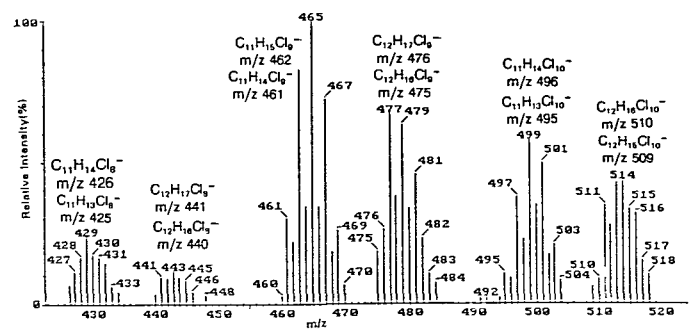

Figure 2. NPI mass spectrum of signal*

Conclusion. These results demonstrate that negative ion plasmaspray ionization (NPI) mass spectrometry is a suitable analytical technique for studying chlorinated *n*-paraffins. Mass spectra are dominated by molecular ions, but also contain ions corresponding to $[M-H]^-$, $[M-Cl]^-$ and $[M-HCl]^{-\cdot}$.

References.

1. Vetter, W. Chemosphere, 1993, **26**, 1079-1084.

CHEMOMETRIC ASSESSMENT OF GC/MS AND GC/MS/MS DATA OF NAPHTHENIC BIOMARKERS

C. S. Hsu(1), A. Lorber(1), S. C. Blum(1),
A. G. Requejo(2), G. Isaksen(2) and G. Hieshima(2)
(1) Exxon Research and Engineering Co., Annandale, NJ 08807
(2) Exxon Production Research Co., Houston, TX

GC/MS has been commonly used to characterize biomarkers to obtain important geochemical information, such as organic matter input (source), geological age, thermal maturity, molecular alteration (such as biodegradation), etc. The use of tandem mass spectrometry further resolves overlapping isomers, particularly for steranes, that are difficult to analyze by GC/MS. We have used chemometric approaches to assess GC/MS and GC/MS/MS data for marine-source rock extracts and oils in Western Canadian sedimentary basin.

The age of the source rocks studied range from Cretaceous (100 million years) to Devonian (400 million years). Principal component regression (PCR) was used to regress age with sterane distribution. Figure 1 represents the regression coefficients obtained by applyting PCR. the magnitude and direction of the regression cofficients are indicative of the importance and direction of the correlation for the particular biomarker. Close look at the figure shows that odd carbon number steranes (except αββ isomers) are positively correlated, while even carbon number steranes are negatively correlated with the geological age of the source rocks. This result is consistent with the results found by Grantham and Wakefield over a wide range of marine-source rocks that the ratio of C_{28} steranes to C_{29} steranes increases with decreasing geological age of the source rocks.[1] In order to improve age modeling, applicability of a neural network model was tested The neural network model succeeded to reduce the prediction error (estimated by cross validation) from 20 million years to 12 million years. Neural network using four principal components and two nodes in the hidden layer (see Figure 2) improves age correlation among the source rocks and between source rocks and oils. Figures 3 and 4 compare the predicted and measured age of the source rocks with and without neural network. The samples coded with a letter O at the beginning are oils. The codes for rocks are K for Cretaceous, J for Jurassic, T for Triassic, etc. With neural network, rock samples are distributed in clusters with smaller ranges. Close scrutiny of Figure 4 reveals that only predicated ages of oils do not agree with the assessed ages based on geological information. OM4, which was thought to be an oil derived from Cretaceous rocks, should be derived from Mississippian rocks. OM3, another outlier, was re-analyzed and found to be indeed a Mississippian oil (as OM3').

For the maturity assessment, PCR shows that 5β and αααR steranes are negatively correlated with T_{max} of Rock-Eval pyrolysis measurement, as shown in Figure 5. This is consistent with the fact that these sterane isomers have configurations similar to their biological origins, and therefore represent low maturity of the sediment. There are redundancies found by PCR between C_{27} and C_{29} steranes and between C_{28} and C_{30} steranes in the maturity assessment. Preganane, a C_{21} βαα sterane, is found to be positively correlated with T_{max} and should be included in the maturity assessment.

Table 1 shows the comparison of age and maturity assessments between using sterane data only and using both sterane and terpane data. For the age assessment, three factors (i.e. principal components) are needed to describe over 90% of variance using only sterane data. At least five factors are needed for over 90% variance if both sterane and terpane data are used. For the maturity assessment, only one factor can describe over 90% of variance if only sterane data is used and at least three factors are needed if both sterane and terpane data are used. Therefore, in the data set studied the addition of terpane data does not help age and maturity prediction by principal component regression based on steranes.

Thus, the utility of principal component regression and neural network for the assessment of GC/MS and GC/MS/MS data of naphthenic biomarkers is demonstrated.

Reference:
(1) P. J. Grantham and L. L. Wakefield, *Org. Geochem.*, **12**, 61-73 (1988)

FIGURE 1

PRINCIPAL COMPONENT REGRESSION YIELDS CORRELATION OF INDIVIDUAL STERANE ISOMERS WITH GEOLOGICAL AGE

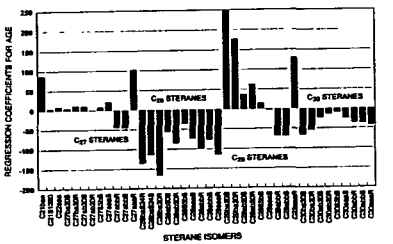

FIGURE 2

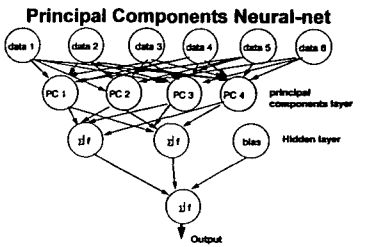

FIGURE 3

PREDICTED AGE TRACKS GEOLOGICAL AGE OF SOURCE ROCKS USING PRINCIPAL COMPONENT REGRESSION

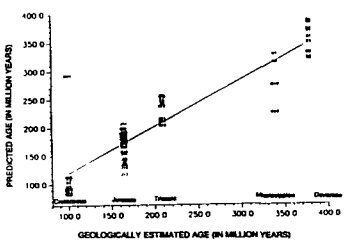

FIGURE 4

NEURAL NETWORK IMPROVES CORRELATION OF PREDICTED AND GEOLOGICAL AGES OF SOURCE ROCKS

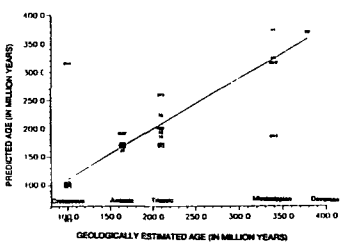

FIGURE 5

PRINCIPAL COMPONENT REGRESSION YIELDS CORRELATION OF INDIVIDUAL STERANE ISOMERS WITH MATURITY (T_{MAX})

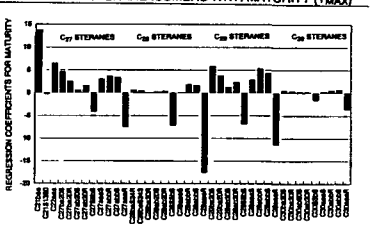

TABLE 1

ADDING TERPANE DATA DOES NOT IMPROVE AGE AND MATURITY ASSESSMENT BASED ON STERANES

STERANES ONLY

Factor	Variance (%)	Accumulated Variance (%)
For Age Prediction		
1	0.38	0.38
2	57.40	57.77
3	24.36	82.13
→ 4	9.56	91.69
5	1.09	92.78
6	4.14	96.93
7	0.18	97.11
For Maturity Prediction		
→ 1	90.38	90.38
2	0.67	91.05
3	0.18	91.23
4	1.60	92.83

BOTH STERANES AND TERPANES

Factor	Variance (%)	Accumulated Variance (%)
For Age Prediction		
1	0.38	0.38
2	0.16	0.54
3	39.84	40.38
4	32.00	80.38
5	9.12	89.50
→ 6	2.15	91.65
7	1.40	93.04
For Maturity Prediction		
1	73.42	73.42
2	12.19	85.61
→ 3	5.07	90.68
4	0.89	91.57

Computer Program for Interpreting Peptide Mass Spectra Utilizing Hydrogen-Deuterium Exchange Information

D.C. Stahl and T.D. Lee, Beckman Research Institute of the City of Hope, Duarte, CA 91010
N.F. Sepetov, O.L. Issakova, and M. Lebl, The Selectide Corp., Tucson, AZ 85737

Recently we reported the use of hydrogen/deuterium exchange to facilitate peptide sequence analysis by mass spectrometry [1]. Information about the number of exchangeable hydrogens can be used to filter the list of candidate sequences obtained from computer interpretation programs, thereby significantly decreasing the number of possible sequences to be considered. We have since developed an efficient peptide sequencing algorithm which utilizes the experimentally determined number of exchangeable protons as a key input parameter. The basic approach is to first calculate possible compositions that are consistent with the molecular weight. A novel method reduces the customary list of 20 amino acids to nine groups and dramatically decreases the time needed to do the calculations. By using information about the number of exchangeable hydrogens, the final list of possible compositions is reduced to a manageable size. Possible compositions are then calculated for each significant ion in the mass spectrum. These subcompositions are then combined to yield a final list of possible sequences. The program was written in the C programming language in conformance with the ANSI programming standard to ensure code portability. The code was generated and tested on a Dell 433DE desktop computer using the Microsoft Quick C compiler version 2.5. Future work will optimize the process of building sequences from composition data and to analyze deuterium exchanged fragment ion spectra.

[1] N.F. Sepetov, O.L. Issakova, M. Lebl, K. Swiderek, D.C. Stahl, T.D. Lee, Rapid Commun. Mass Spectrom., 7 (1993) 58-62.

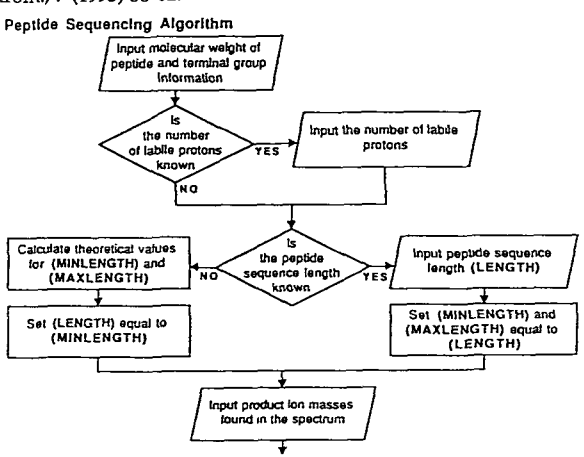

145a

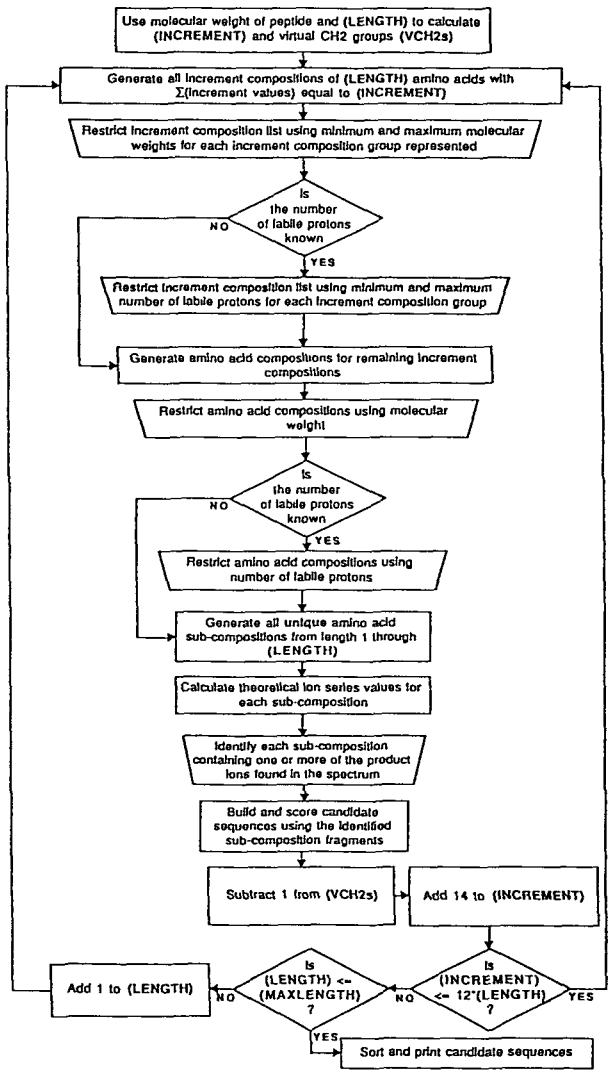

145b

Quantitative Aspects of Maximum Entropy Applied to Multiply Charged Electrospray Data.

J.C Cottrell and B.N. Green, Fisons Instruments, VG BioTech, Tudor Road, Altrincham, Cheshire, UK. and J. Skilling, Cavendish Laboratory, Madingley Road, Cambridge, CB3 0HE, UK.

Introduction. The maximum entropy technique known as MaxEnt has been successfully applied to multiply charged electrospray data giving improved resolution and signal to noise ratio (1). However the quantitative aspects of the technique were not demonstrated. Furthermore, discussion of a different, though entropy based, algorithm (2) implied that this technique would not be quantitative

Here we examine, by way of two examples, the quantitative aspects of the MaxEnt algorithm when applied to mixtures of proteins In the first example, mixtures of two proteins which were resolved in the original m/z data, were examined In the second example, there were three proteins which were unresolved in the original data

Resolved Data. A series of acquisitions was made (m/z 600-1600) on mixtures of horse (16951 5) and whale myoglobins, in which the horse myoglobin concentration was kept constant at 1 pM/µl and the whale myoglobin concentration was varied from 0.1 to 80 pM/µl After baseline subtraction, the m/z data were processed by two methods .-

1 By the transform method. This simply sums all the intensity data from each component in the m/z spectrum and presents it on a true molecular mass scale Thus the transformed spectrum gives a true representation of the intensities of the two myoglobins as they occurred in the m/z spectrum. After smoothing, the heights of the myoglobin peaks above baseline were taken to represent their intensities.

2 By MaxEnt. In this case, the areas under the peaks in the MaxEnt output spectrum (profile spectrum) were taken as measures of their intensities

When the whale to horse myoglobin intensity ratios produced by the two methods were compared, they were within 5% of one another except for the solutions containing 0 1, 0 2 pM/µl of whale myoglobin. The 80 pm/µl data were rejected (the S/N ratio was only 2:1) Fig. 1 is a plot of MaxEnt intensity ratio vs concentration ratio of whale / horse myoglobin from 1 10 to 20 1 Linear regression analysis gave comparable results for the two methods, as shown in Fig 1

Unresolved Data. A series of analyses was made on mixtures of horse and human haemoglobins (Hbs) in which the concentration ratio of horse to human Hb was varied from 1.10 to 10 1 In this case, there are 3 α-globins with molecular masses of 15098 3 (horse α1), 15114 3 (horse α2) and 15126.4 (human α) with mass differences of 16 and 12 Da. They were insufficiently resolved for quantification without the resolution enhancement given by MaxEnt

The m/z data were processed by MaxEnt to obtain intensity data on all three globins and also by the transform method to illustrate the resolution before enhancement by MaxEnt. Two examples are shown in Figs. 2 & 3 for the cases where the horse to human Hb ratios were 1 5 & 1 1 Plots of the intensity ratios of horse α1 and horse α2-globins to human α-globin gave correlation coefficients of 0 9993 & 0.9998 resp. over the concentration ratio range from 1 10 to 5.1 At higher ratios, interferences between horse α1 sodium adduct and human α became significant

References.

1. A G Ferrige et al., Rapid Commun Mass Spectrom , **6**, 707-711 (1992)
2. B.B Reinhold et al , J Am Soc. Mass spectrom., **3**, 207-215 (1992).

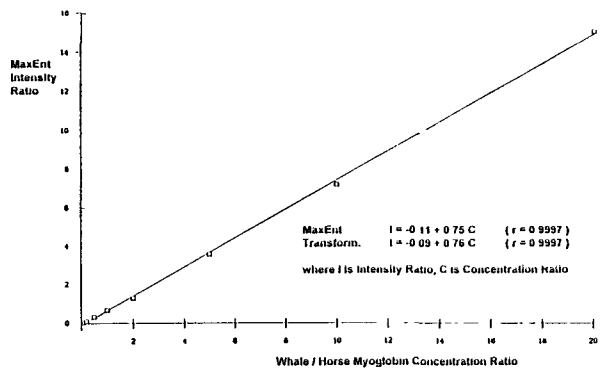

Fig 1 Intensity ratio of whale to horse myoglobin *vs* concentration ratio

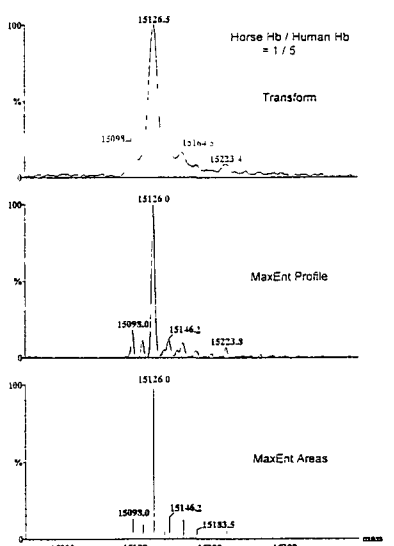

Fig 2 α-globin region from mixture of horse Hb / human Hb in ratio 1 / 5

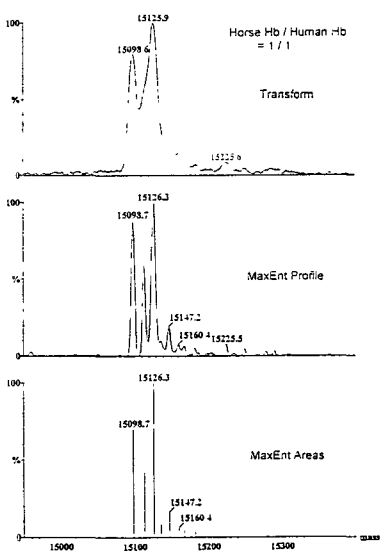

Fig. 3. α-globin region from mixture of horse Hb / human Hb in ratio 1 /1

Curve-Fitting for Resolution of Overlapping Chromatography Peaks in High Precision Gas Chromatography-Combustion Isotope Ratio Mass Spectrometry (GCC-IRMS)

Keith J Goodman and & J. Thomas Brenna
Division of Nutritional Sciences
Cornell University
Ithaca, New York

INTRODUCTION:

In Gas Chromatography Combustion Isotope Ratio Mass Spectrometry (GCC-IRMS) it is general practice to report isotope ratio data only from peaks for which baseline resolution has been achieved because of the stringent requirements for precision and accuracy. GCC-IRMS is increasingly used for biological tracer experiments, chromatography of highly complex mixtures usually results in some overlapping peaks. This is particularly a problem for GCC-IRMS for two reasons First, the system requires plumbing in addition to that required for conventional GC detectors. Second, the carrier gas is restricted to Helium. These factors combine to produce increased peak tailing and somewhat reduced chromatographic resolution, respectively. We have investigated experimentally the effects of overlap using a model system, and the correction of isotope ratios using curve fitting

EXPERIMENTAL:

Isotopically calibrated binary mixtures of methyltridecanoate (Me 13:0) and butylated hydroxytolulene (BHT) were prepared with mass ratios of 1:1, 1:10, and 10:1. Gas Chromatograph conditions were adjusted to produce graded degrees of overlap (10-70% (peak height - % valley)) Chromatograms from each detection channel were fitted using the Marquardt-Levenberg algorithm, implemented in batch processing mode using a commercial computer program Peakfit 3.0 (Jandel Scientific) Isotope ratios were calculated from integrated peak areas. The technique currently employed for peak integration is an automated sequence of peak detection and integration. Peaks are first detected by calculating the slope of a regression line drawn through five consecutive data points and comparing the result to a user defined minimum value. This method is used to define the peak start and stop. Peak areas are calculated as the difference between baseline and signal for the region defined by the peak start and stop.

RESULTS & DISCUSION:

Three functions which model asymmetric chromatography peaks were evaluated for goodness-of-fit Giddings, exponentially modified Gaussian (EMG), and Haarhoff-Van der Linde (HVL) In general, the tail of the peak was poorly modeled for all three functions resulting in an R squared <= 0.996. Modeling the peak with two functions simultaneously resulted in an R squared of 0.9999 Modeling single components with two peaks, however, did not produce accurate peak areas when used for overlapping peaks. The nine possible combinations (three functions, two peaks) were evaluated for fitting of

the 1:1 40% overlap data This screening process revealed that the combinations of EMG/EMG and HVL/EMG gave the best R squared and F statistic.

To further test the resiliency of the fits, both combinations were applied to 1:1 70% overlap. The EMG/EMG fit resulted in a better R squared and F statistic but the shape of the first EMG function distorts and tails into the second peak. This fit resulted in inaccurate (unequal) peak areas. This error would result in inaccurate isotope ratios. The fit achieved using the HVL/EMG combination yielded a poorer R squared but better estimates the peak areas. Based on these data, the HVL/EMG combination was used to model all overlapping peaks

Figure 1 compares R45 obtained for fit and non fit peaks. Each data point represents a mean of at least three replicates chromatographed and fit independently. The non fit data results in 45/44 ratios (R45) that systematically underestimate R45 for Me13 0 and overestimate R45 for BHT The curve fit data preserves accuracy for all peaks >=10% overlap. Similar results were obtained for 1:10 and 10:1 ratio experiments.

CONCLUSIONS:

Overlapping peaks detected by simple algorithms are systematically distorted in isotope ratio even for compounds with closely matched isotope ratios. Curve fitting is effective in restoring isotope ratios for overlaps as high as 70% valley. The quality of ratio restoration depends on relative peak heights.

Figure 1

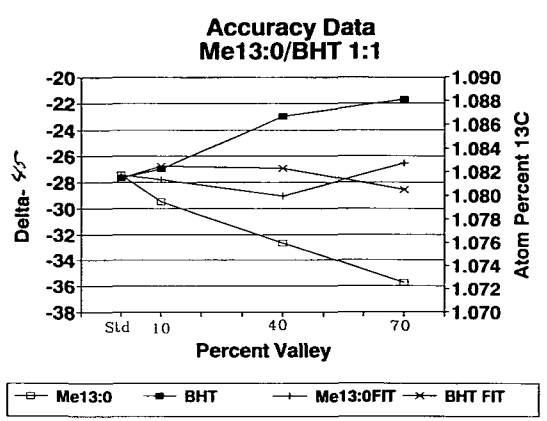

Analysis of Natural and Adulterated Essential Oils by MDGC/FTIR/MS

Kevin A. Krock, N. Ragunathan, and Charles L. Wilkins
Department of Chemistry, University of California, Riverside
Riverside, CA 92521-0403

Introduction:

Gas chromatography has been the analytical tool of choice for the separation and identification of essential oil components for many years. Traditionally, oil analysis has been performed mainly with flame ionization detection (FID) or with a mass spectrometer. However, there are several potential difficulties with both of these methods of analysis. In general, the FID can not provide the specificity required for identifications, and a mass spectrometer is limited in its ability to differentiate isomeric groups. One method to overcome the difficulty of isomeric differentiation is to couple infrared spectroscopy to the analytical system. With the complementary detection scheme, the reliability of the component identity assignments is greatly enhanced. However, the identification process is only as accurate as the separation can provide. In many cases, total component separation is difficult or impossible with a single separation stage, so a solution to this is multidimensional gas chromatography (MDGC). With MDGC, separation efficiencies can be achieved far greater than a single stage separation provides, and when coupled to an infrared/mass spectral detection scheme, accurate identifications are only limited by the library against which the sample spectra are compared.

In the recent past, the use of optical rotation measurements to differentiate between adulterated and natural oils has become obsolete because the adulterated oils now contain a mixture of optical isomers of compounds that occur naturally in the oil to provide an optical rotation similar to that of natural oils. Since the concentration of many components varies somewhat from batch to batch, differentiation between adulterated and natural oils is difficult by either FID or spectroscopic detection. Fortunately, in most cases, the oils that are adulterated to simulate natural oils contain some traces of their true origin, but these traces are usually minimized or masked by high concentrations of compounds that occur naturally. In the research presented here, both natural eucalyptus and adulterated eucalyptus oils, were examined by combined MDGC-IR-MS. Two different known natural eucalyptus oils and a known adulterated oil which derives from camphor oil were analyzed, and compounds present in the adulterated sample but not the natural samples were taken to be "marker" compounds. Using these compounds as a reference point, a suspected adulterated oil and an oil of unknown origin were analyzed to determine the true origin of the oil.

Methods:

The analytical system utilized in this study is a Hewlett-Packard (HP) 5890 Series II Gas Chromatograph-5965B IRD-5970B MSD system modified for multidimensional gas chromatography with multiple cryogenic traps and analytical columns. Each of the five oil samples were separated on each of the three stationary phases by utilizing a *looping* sequence to retrap the column eluents following detection, and then each of the chromatograms were compared with one another. Differences between the natural and known adulterated sample were spectrally identified and considered marker compounds, and in cases where separation was not good, multidimensional separations were employed. The remaining two unknown oils were then analyzed for the presence of the marker compounds using MDGC when required.

Results and Discussion:

The initial separation of the samples on the various stationary phases provided a very rapid and accurate representation of the components in each of the oils (See Figure 1). There were some differences between the two natural oils, but it has been well established in the literature that variations in components and component concentrations vary considerably with several variables such as time of year, geographic location, and tree type. These variations were taken to be a fair representation of components that naturally occur in eucalyptus oils. The known adulterated sample was then compared to each of the natural oil samples, and obvious areas of difference were subjected to an MDGC analysis. The MDGC separations were performed much like the initial examinations. Each of the three chromatographic precolumn areas identified as potential adulterants were trapped and independently reinjected onto one of the analytical columns. The sample

emerging from the infrared lightpipe was then retrapped in an empty cryogenic trap and subsequently separated on the other analytical column after the separation was completed. Thus, with a single sample injection into the GC, three heart cuts were collected, and each heart cut was then separated on both a polar and non-polar analytical column.

After all of the separation steps were completed, the spectroscopic data was examined for differences between all of the components. From these comparisons, the following compounds were identified as adulteration markers for eucalyptus oil: camphor, α-thujene, decane, sabinene, β-phellandrene, and γ-terpinene. Since adulterated eucalyptus oil generally derives from natural camphor oil, camphor is expected to be, and is, the main marker compound. Upon completing the identification of the markers, the unknowns were analyzed for the presence or absence of those compounds. In the analysis of the unknowns, the presence of camphor and/or α-thujene in any concentration was taken to be an immediate indication of adulteration, and absence of camphor or α-thujene but presence of others was considered a strong indication of adulteration of the oil. However, the latter case was not encountered in this study. The results of the examination of the unknowns were that the suspected adulterated oil was indeed an adulterated oil, and the other unknown sample was determined to be a true eucalyptus oil. The suspected oil contained a both camphor and α-thujene as well as small amounts of the other marker compounds. As for the unknown, none of the marker compounds were present at any level.

Conclusions:

- Combined IR-MS systems provide more powerful identification possibilities than mass spectrometry alone, especially for complex isomeric mixtures such as essential oils.
- Multidimensional separations when coupled with spectroscopic detection and the ability to retrap heart cuts provide fast and powerful methods to accurately analyze complex mixtures.

Acknowledgment:

Financial support from the National Science Foundation (CHE-92-01277) is greatly appreciated.
Eucalyptus oil provided by Marc Parilli of the Berjé company.

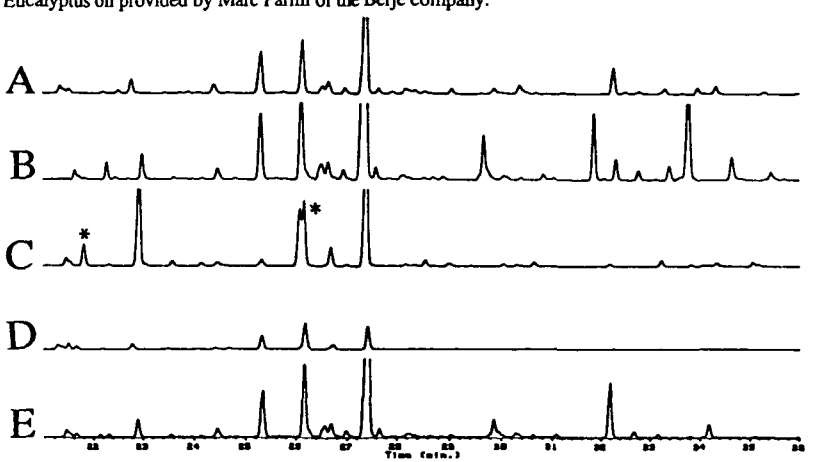

Figure 1. Final half of the precolumn chromatogram for each of the samples. Asterisks mark the largest differences between the natural and adulterated oils. A: Known natural oil, B: Known natural oil, C: Known adulterated oil, D: Suspected adulterated oil, E: Oil of unknown origin.

THE APPLICATION OF SELF-MODELLING MIXTURE ANALYSIS TO AUTOMATED MASS SPECTROMETRY

Alan W Payne, Kodak Limited, Harrow, U.K.
Willem Windig, Eastman Kodak, Rochester, U.S.A.

We are engaged in a programme to automate the process of structure characterisation by mass spectrometry for samples synthesised in a typical industrial research laboratory[1,2] One of the central issues that we are confronting is that many "real world" samples contain mixtures of components. We are using a probe inlet analysis (actually a "DCI" -type probe), and we record mass spectra every second whilst the sample is being temperature programmed; this typically gives us 150 separate mass spectra for one sample. The components of a mixture will generally have different evaporation profiles but the separation with time is invariably incomplete. Traditionally background subtraction techniques are used to attempt to obtain the "pure" spectra. This is of variable success, particularly when applied to any other than binary mixtures, and when applied in an automated procedure.

We have explored the application of self-modelling mixture analysis to this problem[3]. The mathematical technique used for this study is a pure variable method. For this, it is assumed that each component in a mixture has a variable (m/z value) that is unique for that component. With the large number of peaks typically produced in an EI spectrum, this assumption is valid. As has been shown previously[3], a pure variable is basically the variable having the maximum ratio of the standard deviation and the mean (this ratio is termed the "purity") of all the intensities at a given variable (m/z value). The purity values are calculated for each m/z value in the total data set. This shows which masses have varied the most with time as the sample has evaporated. The mass with the maximum value of purity corresponds to the first pure variable. The proportion of the peak intensity that is correlated with the 1st pure variable is then subtracted from every peak in the spectrum, after which the second pure variable can be found. This process is continued until no information is left. In practice, the number of pure variables extracted invariably exceeds the number of components actually present because of noise in the system. However, this is readily obvious both from a noticeable fall-off in the numerical purity values, and also from the appearance of the spectra extracted for these "non-existent" components!

Once the pure variables have been determined, the data set can be resolved into the pure components and the individual spectra extracted. Extraction of the complete spectra , i.e. all peaks relating to the pure variables determined as above, is performed using a least-squares solution, and has been described fully previously[4].

To test the process, data sets were obtained from three separate components, and a mixture of the components. Figs. 1(a), 2(a) and 3(a) show the spectra of the components extracted using the self-modelling approach. Figs 1(b), 2(b) and 3(b) show the reference spectra obtained by analysing the components separately. The comparisons show excellent agreement between the extracted and reference spectra. It was not possible to obtain such "clean" spectra using background subtraction routines, which were of necessity for such a data set, highly interactive and not compatible with our automation scheme.

Fig. 1(a)

Fig. 1(b)

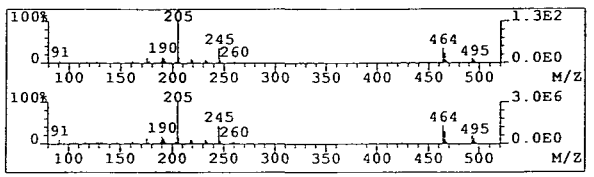

Fig. 2(a)

Fig. 2(b)

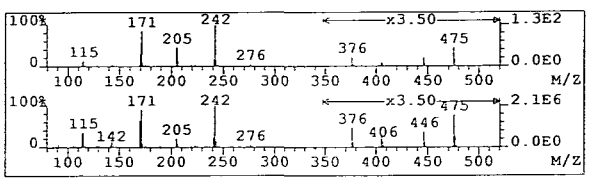

Fig. 3(a)

Fig. 3(b)

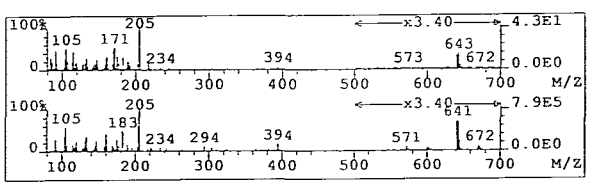

Figs. 1-3 Extracted *vs* Reference Spectra

1. Mannock, K.L., Phalp, J.M., and Payne, A.W., Analytical Applications of Spectroscopy II, eds Davies, A.M.C., and Creaser, C.S., publ Royal Society of Chemistry (1991) pp. 296-302
2. Payne, A.W., McLaughlin, D.R., Phalp, J.M., and Mannock, K.L., 12th International Mass Spectrometry Conference, Amsterdam, August 1991.
3. Windig, W. and Guilment, J., Anal. Chem. 1991, 63(14),1425-1432.
4 Windig, W., Heckler, C., Agblevor F.A., and Evans, R.J., Chemometrics and Intelligent Laboratory Systems, 14(1992)195-207.

EVOLVING FACTOR ANALYSIS AND GC/MS - AN IDEAL COMBINATION.

*Lisa Roach and Michael Guilhaus, School of Chemistry, The University of New South Wales, PO Box 1 Kensington NSW 2033 AUSTRALIA.
Marcel Maeder, Dept. of Chemistry, The University of Newcastle, Newcastle NSW 2308.

Evolving Factor Analysis (EFA) is a recently developed "pattern-matching" deconvolution method which makes use of the intrinsicly ordered nature of chromatographic data. The large amount of uniquely "patterned" information in a mass spectrum makes the combination of EFA and GC/MS data ideal. It offers advantages for the mathematical separation of components in an unknown mixture as it makes no assumptions about the number of components, their identities or their chromatographic behaviour.

EFA is an extension of the classical factor analysis matrix-algebra based methods. Using the EFA method, severely overlapped data from a GC/MS run can be deconvoluted into the concentration profile and pure mass spectrum of each component. This is achieved by performing a forward and backward rank analysis of the data, and plotting the resultant eigenvalues to determine the appearance and disappearance of each component Eigenvalues are intermediate indicators of the significance of the presence of each component or pattern in the data. The larger the eigenvalue, the greater the certainity that the component/pattern is in the data. The number of components in the system can be determined by deciding which of the eigenvalue lines are significant(indicating components) and which derive from noise. The intrinsic fixed elution order of chromatographic components allows the assumption to be made that the order of the onset of elution is the same as the order of the components' finishing elution. i.e. the first component to elute is the first to finish elution, the second to start is the second to finish, and so on. Thus "positive concentration windows" can be formed, which are then used to retrieve the pure mass spectrum of each component. The identity of the resultant spectra can then be ascertained by matching them with the reference spectra in a computerised mass spectral library, such as the Wiley Mass Spectral Database.

EXPERIMENTAL

A system of five organochlorines was studied. A Pye-Unicam Series 204 gas chromatograph with a DB-164, 1.8μm fused silica capillary column(30m x 0.317mmID) was used. A VG-16F single-focussing mass spectrometer was used(70eV spectra, trap current 50μA, accelerating voltage 4kV). The maximum scan speed of the VG-16F was used(0.3 s/scan for a mass range of 40-150 mass units), resulting in 5 -6 scans per GC peak. A series of experiments were run with column oven temperatures ranging between 100°C and 120°C. The data was automatically collected using the Schrader GC/MS data acquisition system on a 286 IBM-PC.

RESULTS

As the following diagram shows, the results produced by the EFA program are accurate and identifiable. The deconvoluted elution profiles retrieved are the correct shape and occur at the correct retention times. The mass spectra are the EFA resultant spectrum and the library-matched spectrum for the most severely overlapped component. The only significant differences between the two are the mass spectral lines in the library spectrum between 20 and 40 mass units, caused by scan's low-mass limit of 40 mass units.

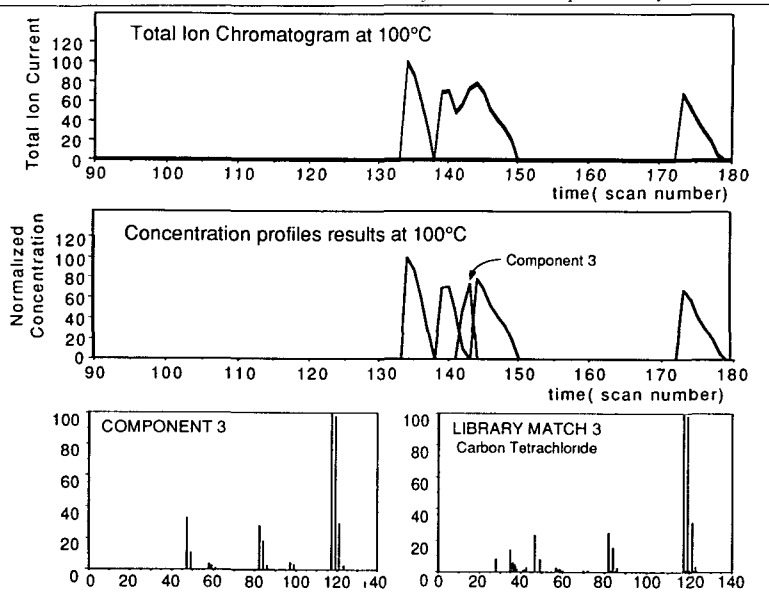

CONCLUSION

The EFA method works successfully with capillary GC/MS data. The elution profiles and mass spectra extracted from severely overlapped GC/MS data are remarkably accurate (in almost all cases, correct matches were given when automated library search procedures were used). The match was incorrect only when the components had precisely co-eluted and a single composite mass spectral pattern of the two components emerged. The limitation of the method at present is the data acquisition speed of the computer software used and the scanning speed of the mass spectrometer. GC/MS/EFA can be used in the analysis of unknown mixtures since no prior knowledge of the system is required. Applications are envisaged such as large-scale pollutant and drug screening where the sample throughput is a problem and accelerated GC/MS followed by automated deconvolution, identification and flagging of target compounds would be efficient as well as cost-effective. Further testing of this method will include data collected from a quadrupole mass spectrometer (faster scan speeds) and fast-spectral acquisition non-scanning instruments.

REFERENCES

1. M F Delaney, Anal. Chem., 56, 261R (1984)
2. L.Roach and M.Guilhaus, Org Mass Spectrom 27,1071-1076(1992)
3. M. Maeder, Anal Chem., 59, 527 (1987)
4. E.R. Malinowski and D.G. Howery in Factor Analysis in Chemistry, Robert E Kreiger Publishing Company, Malabar Florida (1989)

INTRODUCTION

Discrimination and Quantitation of Geometric Isomers by Mass Spectrometry; A Model for Chiral Analysis

Aubrey McIntosh and Jennifer Brodbelt, Department of Chemistry
University of Texas at Austin, Austin, Texas 78712

Introduction

One focus of our research is the development of novel methods of analysis in mass spectrometry that allow the chiral specific analysis of bioactive molecules. Many theraputic agents differ in activity based on their chirality. Thalidomide, for example, gained notariety and fueled the growth in power of the FDA in 1960, due to the tetratogenic properties of an enantiomeric impurity.

Realization of this effort requires significant advances in several distinct areas of Analytical chemistry. Typically, research in Mass Spectrometry has emphasized Apparatus Design. In a few specific instances, such as FT/ICR, the application of existing data analysis methods have been important as well We are exploring the largely underutilized novel reagent development area as it applies to mass spectrometry for this project. The Brodbelt group is developing a suite of novel reagent ions which are typically generated in situ within the instrument and which may have site–selective properties or functional group specificity. Ancillary to the main group effort, this poster reports on post–run data analysis methods that aid in mixture analysis, as applied to a simplified model of the chiral analysis problem.

Data Analysis Concerns

Strong similarities exist between the mass spectra of chiral molecules. However, although there may not be universally a unique mass channel that can be monitored for the presence or absence of an ion, there may be qualitative distinctions that are immediately recognized on inspection. One requirement is to find a mathematical formalism that allows the manipulation of these differences to obtain quantitative results. Two problems present themselves. One is the production of distinct spectra for the enantiomers, and the other is the manipulation of these spectra. The development course that we chose was to use geometric isomers as a model of the ultimate chiral mixture problem, and to develop the data manipulation tools in this known analytical setting. Subsequently, the search for resolving reagents could be accelerated by having the appropriate data analysis tools.

Factor Analysis

Factor analysis, in its most general form, is simply a method to factor a matrix into two more easily interpreted matrices that multiply together to provide the original matrix. This is essentially similar to the elementary algebra operation of factoring a polynomial into more easily interpreted monomial terms. The matrix in question is the covariance matrix formed by multiplying a set of data by itself. In general, this matrix contains all the statistical information about the experiment, and is a rich source of information.

A covariance matrix has certain vectors associated with it that have special properties. The most important property is that the matrix multiplied by this vector gives back a scaled copy of the vector itself. This is simply the familar eigenvector property that plays such a familar and important role in quantum mechanics. In fact, we expect all chemist to recognize the standard eigenvalue equation: $H\psi = E\psi$. In our application, mass spectrum of a pure component are a linear combination of these eigenvectors (and vice versa).

The correspondance between the mass spectrum and the (linear combination of) eigenvectors suggests that it is valuable to "view" the vector as a graphic, rather than a column of numbers. This allows intuitive manipulation of the data during the investigation phase with an economy of programming effort. Decision are often made by the chemist based on interpretations of these graphics. We have reported a tool that does present the factor analysis information graphically, and allows the chemist to manipulate the graphs with a mouse. The graphs may be copied directly into

documents or user as input to additional principle component analysis or other computer processing. The direct visualization of the target factors, as well as the ability to edit them and iterate through the target factor evaluation phase is essential for rapid development of target factors.

Factor analysis is an emerging area of data interpretation, and was not widely known to analytical chemists prior to the Malinowski article in Analy. Chem., April 1977. An entire block of this poster gives an intuitive example of factor analysis targeted toward a mass spectrometrist audience.

Data Manipulation Results

The ultimate goal for the post–run analysis is to accept a data–file which has an evolving series of spectra for a mixture of chiral isomers, modeled in this work as geometric isomers, and produce a list of pure–component mass spectra and corresponding concentration evolution. An additional goal is to have this operation be sufficiently fast that the results are available to evaluate at the conclusion of the experiment. It is convenient language to call this data file a Mass Spectra Chromatogram, although the evolving dimension is not typically a chromatographic separation. Indeed, we envision that many experimental manipulations available to the ion–trapping mass spectrometers may be used as the evolving dimension. In particular, ion–molecule reaction time, pro–chiral reagent concentration, and collisional energy are expected to be key dimensions in the chiral analysis problem. This work, however, reports on initial results verifying the data system.

In this work, we use thermal desorption curves from a temperature programmed solids probe. Responses from various total microgram amounts of 2–Bromobenzoic acid are shown. The 2–Bromobenzoic acid was deposited from solution to a standard glass solids probe vial. After introduction of the probe, a temperature desorption run was effected at 60o/min. Additionally, temperature desorption runs of 4–Bromobenzoic acid and 2–Bromobenzoic acid mixtures are run. Known spectra are compared against the reconstructed spectra. Work continues to address the effects of space charging, charge transfer, and other mechanisms that make the linear model break down.

Improving Performance of Mass Spectral Search Algorithms

***Craig A. Walla, Hitachi Instruments, Inc., San Jose, CA 95134**
Stephen Bradshaw, Teledyne MEC, Mountain View, CA 94039

INTRODUCTION

Comparing an unknown mass spectrum with a database of known mass spectra is commonly referred to as library searching To be of use in industry, library searching must be both fast and accurate There are many library searching algorithms available to determine how well two spectra may match each other. One method, the dot product, has been shown to give the best results[1]. Unfortunately, this method is not practical in all applications because of the amount of time it takes to compare an unknown with each entry in the library. To solve this problem, pre-search methods are used that can select a relatively small number of spectra These spectra are then compared using the dot product method One commonly used pre-search method, INCOS[2], uses the absence / presence of a mass to narrow the number of spectra. Two additional pre-search methods were developed.

METHODS

The NIST Mass Spectral Database was reduced in size from 35.2 Mbytes to 4 2 Mbytes to allow the entire library to reside in RAM for very fast searches The work was done on a 66Mhz, 486 PC with 16 Mbytes of RAM. To reduce the size of the library, each spectrum was limited to include only the most significant 16 masses. These masses were determined by the following steps:

- $I_w(m) = \sqrt{m \times I(m)}$ where $I_w(m)$ is the weighted peak intensity[2]
- normalize the spectrum by setting the maximum peak intensity to 10000
- save only the most significant 16 peaks

To test the results of the 3 pre-search algorithms, the top 10 spectra and top 100 spectra are sent to the main search for further comparison The main search algorithm uses the dot product of the two spectra as a measure of closeness and is described as the Purity[2]

Pre-search Algorithms

INCOS is a widely used algorithm that is based on the number of common masses in both the unknown and the library spectrum. For each unknown mass that is also in the library spectrum a value of 1 is added to the mass total.

We developed two additional methods which expand on the INCOS algorithm by including information about the importance of a peak in the spectrum.

Method #1 - Ranking the Unknown Spectrum

This algorithm is based on the importance of the unknown peak and its existence in the library Each of the 16 or fewer peaks in the unknown is given a ranking based on its weighted intensity. 16 signifies the most important peak while 1 signifies the least important peak If there are fewer than 16 peaks in the spectrum then the remaining positions in the reduced library are set to 0 which signify that there are no more peaks in this spectrum. These rankings are then accumulated as the corresponding peak in the library is found.

Method #2 - Ranking both the Unknown and Library Spectrum

This algorithm is based on the importance of both the unknown and library peak. The library peaks are ranked using the same method as in the previous example. The product of the rankings of common peaks is accumulated. The rank total is doubled if a common peak is found to further distinguish between spectra. The rank total in this example has been scaled to avoid exceeding a 16 bit integer

RESULTS

Ethylbenzene was used as the unknown for comparison of these pre-search methods and was searched against over 62000 compounds in the reduced NIST library. The INCOS method is very fast (0 39 sec) because of the small amount of calculations required to generate a mass total. However, the mass total alone can not discriminate between spectra because this method groups many spectra by assigning an identical mass total While this method selected some very good candidates, a very poor choice was also made. Method #1 is slightly slower (0 49 sec) than INCOS because of the additional calculations required to generate a rank total. However, this rank total is more discriminating than the mass total from INCOS. Method #2 is the slowest (0.55 sec) of all the methods tested because of the multiplications needed to generate a rank total. However, this rank total is much more discriminating than the previous two methods. Unfortunately, this method also selected some very poor choices as possible candidates. The results are shown in the following table. The numbers 1-5 indicate the same 5 best hits

INCOS			Method #1			Method #2		
Mass Total	Purity		Rank Total	Purity		Rank Total	Purity	
16	**.943**	1	136	**.943**	1	1460	**.943**	1
15	840	5	135	896	3	1055	231	
15	865	4	133	840	5	717	897	2
15	896	3	133	865	4	706	896	3
15	897	2	133	897	2	701	865	4
14	750		131	651		679	840	5
14	651		130	.553		660	369	
14	.789		130	712		653	.384	
14	231		129	789		622	189	
13	614		128	.701		547	.553	

CONCLUSION

1) All three methods successfully passed the same 5 spectra to the main search. These 5 spectra appear to be the best matches for the unknown used

2) All three methods are relatively fast. In all cases the pre-search task was completed in less than 1 second This is important for applications where the speed of the library search can affect system throughput.

3) The Ranking methods discriminate between similar spectra

4) Further work needs to be done with specific families of compounds to determine how well a particular method can discriminate between spectra

Acknowledgments

Li-Hsin Zang, Hitachi Instruments, Inc., San Jose, CA 95134
Stephen E Stein, NIST, Gaithersburg, MD 20899

References

1. Stein, S E "Testing and Optimization of Mass Spectral Search Algorithms", Proc. Ann. Conf. Mass Spec. and Allied Topics, 1992.
2. Sokolow, S., Karnofsky, J ; Gustafson, P "The Finnigan Library Search Program", Application Report Number 2, Finnigan Instruments, July 1978

THE CONTROL OF QUALITY IN A COMPREHENSIVE MASS SPECTRAL LIBRARY

A.I. Mikaya*, P.J. Ausloos, S.G. Lias, S.E. Stein, A260/222, NIST Mass Spectrometry Data Center, Gaithersburg, MD 20899

Spectra in comprehensive mass spectral collections come from diverse sources and therefore possess a diverse range of quality. Until recently, spectral quality in the NIST/EPA/NIH Database was monitored solely by a computer-generated "Quality Index," [1,2] which assigned to each spectrum a numerical rating based on selected spectral features and analytical conditions. When multiple spectra of a compound were available, only the one with the highest quality index was included in the distributed library. However, because such algorithms cannot detect a large proportion of serious spectral errors, we found that over a period of time this policy could reduce the overall quality of spectra in the library by replacing good quality older spectra with lower quality, recently-measured spectra that were fortuitously assigned higher Quality Index values. An example of such a replacement is given below.

Here, the spectrum of a pesticide containing major impurity peaks replaced a good quality spectrum of the pure compound. The higher number of peaks in the former spectrum led to a higher Quality Index value.

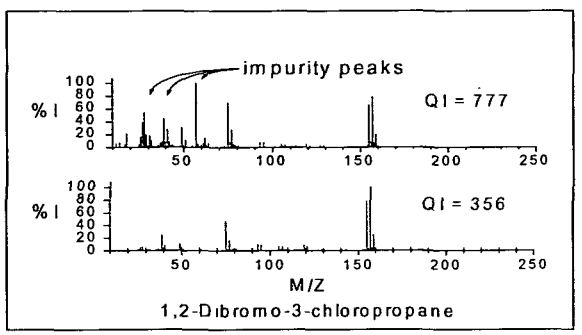

In addition, chemical structure information is not used in the Quality Index. It cannot, therefore, discern many serious errors evident through straightforward application of structure/spectral correlation rules.

For these reasons, we have abandoned the use of the Quality Index for selecting spectra. To deal with quality we have undertaken a program to manually examine all spectra in the database. Suspect spectra are first examined to find the likely origin of the problem. Then, when possible, corrective action is taken. Some correctable errors are name/formula/molecular weight inconsistencies, identifiable impurities and single mass unit displacement of a spectrum. Remeasurements are done for commercially-available compounds and erroneous or seriously deficient spectra are deleted. If a spectrum is not suitable for distribution, but of possible use in later evaluations, it is marked as having low quality and stored in an internal file.

Computer methods, some of which are components of the original Quality Index, are employed only to aid this evaluation process. The accompanying table lists the most commonly encountered varieties of errors.

ERROR CLASS	CAUSE OF ERRORS
Device, Operator	Tuning
	Chemical Ionization
	Saturation
	Column Decomposition
	Inlet Decomposition
	Ion Source "Background"
Data Acquisition	Pressure Change
	Improper Scan Selection
	Improper Subtraction
Data Entry	Chemical Identification Input
	Transcription
Sample	Mislabelled Sample
	Incorrect Structure Determination
	Reaction Prior to Inlet
	Sample Impurity

This chart shows the status of the archive file containing all NIST MS spectra. All replicate spectra have been evaluated, and approximately 60% of the spectra in the main distributable library have been examined so far.

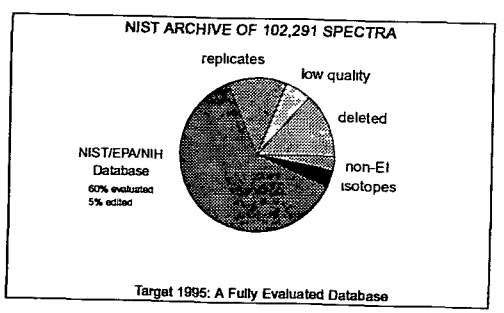

References:
1) D.D. Spect, R. Venkataraghavan, F.W. McLafferty *Organic Mass Spectrometry* **13**, 209 (1978).
2) D.T. Terwilliger, A.L. Behbhani, J.C. Ireland, W.L. Budde *Biomedical and Environmental Mass Spectrometry* **14**, 263 (1987) .

PC-based Modular Data System for Time-of-Flight Mass Spectrometry

*** M. Hubert**
Chips at Work GmbH, Argelanderstr. 36, D-5300 Bonn 1, Germany

A versatile data system for transient recorder based time-of-flight mass analysis is presented.
"ULISSES" originally was developed for matrix-assisted laser desorption mass spectrometry, but is applicable to any ionization method using transient recorders for time-of-flight analysis, such as laser postionization or laser ionization.
The program performes all tasks usually necessary for system control:
laser trigger, transient recorder setup, universal stepper motor control, and allows data handling like: spectra storage, data compression, file managing and offline printing.
The ULISSES-Software supports data manipulation functions like averaging, background subtraction, smoothing, labelling, normalization and line spectra generation Various data analysis features as mass calibration, peak detection, peak integration, peak analysis can be performed

Spectra can be presented by hardcopy-printouts, high-quality postscript or HPGL-plots and exported into PICT-graphics.
The package is written in PASCAL and can be combined with other PASCAL-applications Computer code is optimized for high-speed data acquisition and high-speed display. Data transfer rates to the computer are in the range of 300kByte/s (with digital scopes, such as LeCroy 9450) to 1 MByte/s (using PC-cards, such as Precision Instruments 9825).
Total screen refresh rate can be as high as 10 Hz (depending of the computer and the complexity of display).
Of special importance is the possibility to include user-written routines or units, and to append additional user data to spectra files.

The ULISSES-Software can be run on a MS-DOS-machine, which should be a 386 or higher. The computer should support VGA-graphics-standard. The software works together with various transient recorders. Data transfer can be perfomed via IEEE-interface.
ULISSES runs in an DOS-Box under MS-WINDOWS 3.1. Using this method, the user can drag spectra from the ULISSES-screen and drop into any other WINDOW-application.

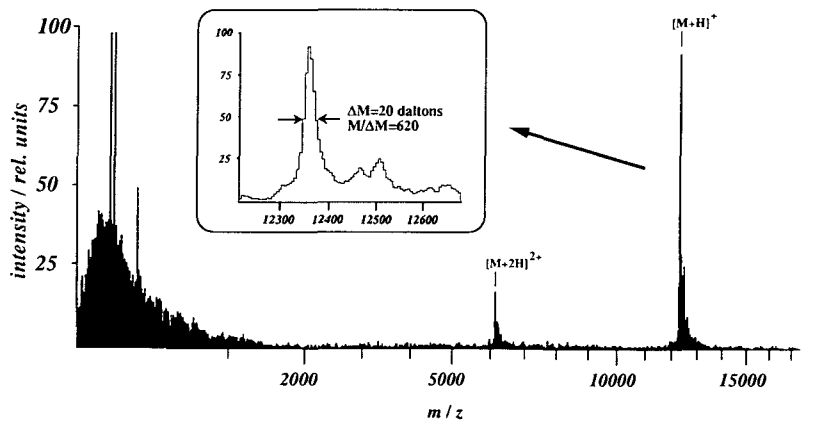

Fig. Matrix-assisted laser desorption mass spectrum of cytochrome c (MW=12360), analysed in a linear instrument with a bare channel plate detector at λ=337nm, at 34keV acceleration energy and a residual gas pressure of $2*10^{-7}$ mbar. Matrix was 2,5-dihydroxybenzoic acid. The from calculated mass resolving power (FWHM) was $M/\Delta M \approx 620$. Data acquisition and peak analysis has been done by ULISSES.

Software for Acquisition and Analysis of TPEPICO - TOF - MS

Bibi Teklehaimanot and Gerry G. Meisels
Department of Chemistry
University of South Florida
Tampa, FL 33620-5250

TPEPICO-TOF-MS, (Threshold photoelectron photoion coincidence time of flight mass spectrometry) is a valuable experimental tool that allows the preparation and study of molecular cations formed in coincidence with zero kinetic energy electrons. It furnishes important information on such diverse areas as thermochemistry, kinetics, unimolecular reaction mechanisms, and on the inter conversion of internal energy among the various degrees of freedom. It is also an invaluable tool for testing theoretical models of ionic decomposition phenomena and for gathering mass spectrometric information on gas phase ion chemistry.

Unfortunately TPEPICO experiments are inherently demanding and tedious. Compounding this inconvenience is the lack of commercially available software for data acquisition and processing specifically suited to TPEPICO.

We have developed TCMS, (Threshold coincidence TOF MS data analysis system) a comprehensive integrated software package, customized for TPEPICO. Major considerations in developing the package were reliability, convenience and ease of data manipulation. TCMS runs optimally on 386/486 series PC compatibles, under the MS - DOS(R) 5.0 operating environment. TCMS is a menu driven, procedure oriented software, consisting of a control module (Fig. 1) and four separate modules each capable of operating in conjunction with the control module or as an independent application. The control module serves as an entry point to the integrated environment. It allows the user to select a particular application.

Module 1 consists of routines for acquiring data, displaying the spectrum on the computer screen, analysis of regions of interest (ROE) such as background subtraction, data smoothing and data deconvolution. Module 2 deals with kinetic energy release analysis based on the shape and width of peaks. Module 3 includes routines for decay rate fitting with one or two component dissociation rates. Module 4 contains routines for the theoretical analysis of data.

Although TCMS was developed to be used with TPEPICO-TOF-MS, the TOF peak analysis routines in modules 1 - 4 can be applied directly with no or minimal modification to analyze TOF MS data from other systems. TCMS has been tested and used extensively in our laboratory for acquiring and analyzing data on the unimolecular dissociation of a number of molecular samples including dimethyl sulfide and furan.

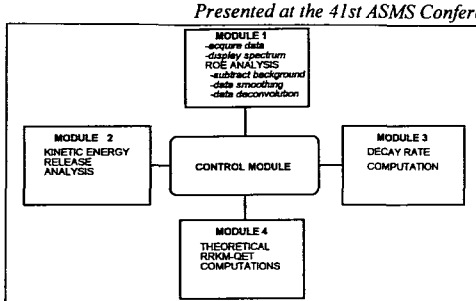

Figure 1 TCMS, Genereal Structure

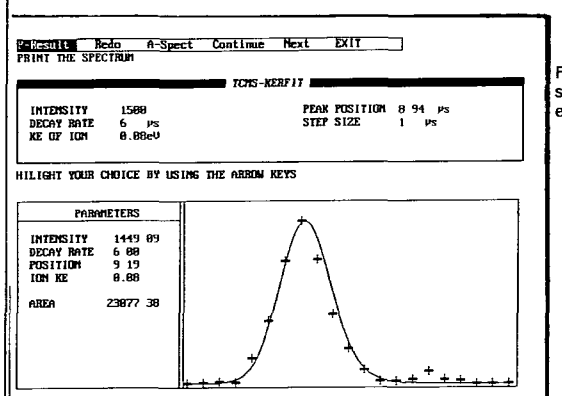

Figure 2. TCMS decay rate analysis screen output, Furan at 14.15 eV photon energy .

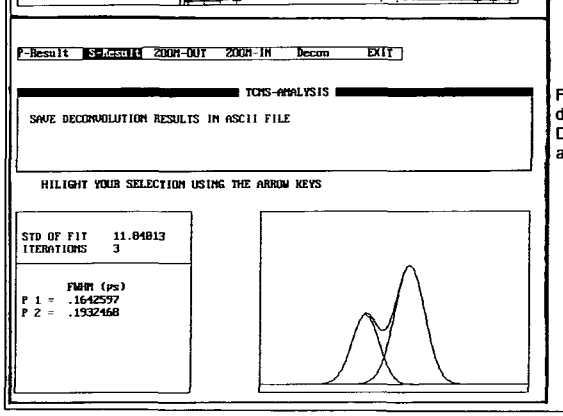

Figure 3. TCMS screen output deconvolution of overlapping peaks Dimethyl sulfide fragment ions m/z 46 and 47 at 11.30 eV photon energy.

Networking a Laboratory Information Management System (LIMS) with Mass Spectrometer Data Systems

*K. Straub and G. Witkop
Syntex Discovery Research, Palo Alto, CA 94304

While the use of autosampling devices on mass spectrometers has become commonplace, procedures for efficient instrument scheduling and sample tracking are still at an early stage of development Most central analytical laboratories make use of a database manager, usually referred to as a Laboratory Information Management System or "LIMS", to facilitate sample tracking and to store final analysis results. The type of information that is stored on a LIMS system includes elements that are normally part of an MS datafile, such as the sample title, notebook reference, project number, and requested analysis. Information stored in a LIMS system prior to actual analysis also includes items that can be useful for instrument scheduling such as expected molecular weight, type of structure, and desired ionization techniques. The practice in most laboratory environments is to use a LIMS for sample tracking and test status, but does not include a physical link between the LIMS and the MS data systems.

Our laboratory operates a number of diverse instruments, including a MAT 8230 high resolution system equipped with an automated solids probe (Audevap™), and several Finnigan TSQ70/700 triple stage quadrupole spectrometers set up for LSIMS and LCMS. The instruments are located in physically distant sites The data systems are based on DEC microPDP-11/73's that use RSX-11M or RSX-11M+ as an operating system (MAT 8230, TSQ70) or Unix-based workstations (TSQ700). All of these spectrometers are connected to the corporate network via ethernet, using either DecNet or TCP/IP.

The large number of samples that are processed by the MS laboratory prompted us to examine methods for achieving a greater degree of integration between the spectrometer data systems and the department LIMS (Beckman Lab Manager, running on a Vax 4000/600). Much of the information that is manually entered into a spectrometer data system prior to data acquisition is already present in the LIMS database We therefore undertook development of a suite of programs to facilitate transfer of this information directly between the LIMS and the various spectrometer systems. We have also explored the complementary process, in which analysis results are automatically entered into the LIMS database following completion of an analysis by the spectrometer data system. The resulting system, when combined with software for analysis and plotting of spectra, permits unattended operation of the instruments for analyzing large numbers of disparate samples.

Lab Manager provides a transaction processing function, LBTRNS, which can be used to transfer information in and out of the LIMS database. The input and output functions are encoded in two 2048 character strings, CRECV and CSEND Specific items of information about a particular sample can be requested by specifying the laboratory reference number for that sample, and then parsing the returned CRECV string. A VAX fortran program was written that, for a given sample reference number, queries the LIMS database and outputs a file containing the requested information In actual practice, each sample submission form is scanned with a barcode reader, and the program retrieves the data and writes a file appropriate for the type of spectrometer that is going to be used Two different file types are constructed, one for the MAT 8230 and another for the TSQ70/700. A flowchart for this process is shown in figure 1.

The MAT 8230 Audevap control program uses a simple text file, in which each line specifies a turret position number, file name, header comment, and instrument parameter file. The latter file contains settings for the instrument such as scan rate, resolution, and other acquisition parameters. The Audevap turret assembly accommodates up to 46 samples, and the normal procedure is to create the control file for a full set of samples. The control text file is actually opened across the network and written directly on the MAT 8230 data system. The samples are then loaded into crucibles and analyzed by EI or CI. After each datafile is acquired, the most intense spectra are automatically selected and plotted. These spectra are then extracted from the original datafile and transferred over the network to magneto-optical disks on the VAX for archival storage.

The TSQ70/700 series instruments make use of a special file, referred to as an "instrument analysis" or ICA file that must be present in a specific subdirectory. This is a 512 byte file specified as *filename.ICA* that contains information about the analysis in a special format. For the TSQ70 this file must reside in UIC [1,102], while on the TSQ700 it resides in the subdirectory */usr/users/finnigan/msi*. In addition to containing the sample description and header comments, these files reference the names of other files that specify the autosampler, instrument control and data analysis methods, and other useful information. The high degree of automation that is implemented on these particular instruments makes it feasible to link the sample with standard data analysis and reduction methods as well as LC or GC programs on the LIMS. For sample scheduling, the VAX fortran program creates the required ICA file after retrieving the appropriate information about each sample from the LIMS. The ICA files are then transferred over the network to the TSQ70 or TSQ700 data system. Following analysis, spectra marked for archival storage are extracted and transferred over the network to magneto-optical disks for permanent storage.

Information flow between the LIMS and MS data systems in this scheme can be bidirectional, since the LIMS system contains an entry for the MS filename, ionization technique, and comments describing the results of the analysis. The MS filename and ionization technique are automatically entered into the LIMS, while the test results are manually entered by the analyst following review of the data.

Retrieval of archived mass spectra data for review is accomplished by transferring a copy of the archived file across the network to the spectrometer data system. Since all of the spectrometers are linked to the corporate network, they can be accessed from any location using PC's with appropriate emulation software.

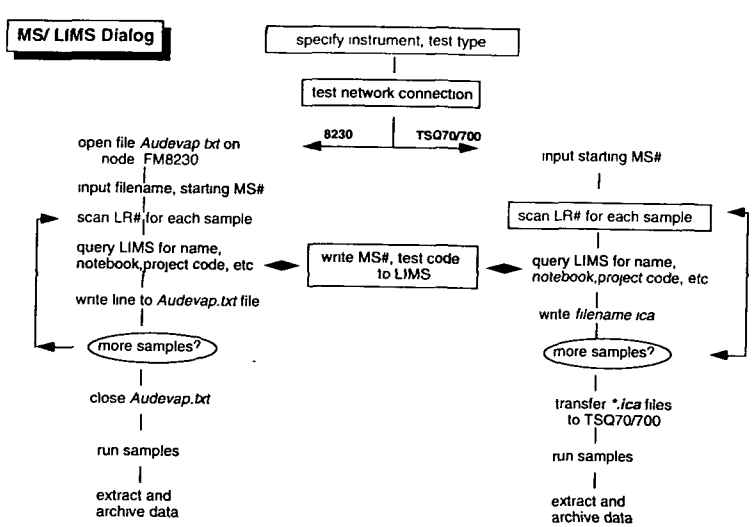

An Instructional HyperCard Stack for Users of the Mass Spectrometry Laboratory at the University of Illinois

Steven L. Mullen, University of Illinois at Urbana-Champaign, School of Chemical Sciences, 505 South Mathews Avenue, Urbana, IL 61801

Why Write a HyperCard Stack?

For many years we have had a lab brochure that explains to our customers how to use the lab and what the lab can do for them. The availability of Macintosh computers and laser printers has made the brochure much more attractive and readable. However, the linear organization of printed text is not always the best way to convey information.

HyperCard 2.1 is a program for the Macintosh computer that allows one to create a stack of cross-referenced index cards. The author of the stack can create cards and link them as he sees fit. Thus, instead of flipping through pages, the reader can jump from card to card in a logical manner and find the required information more readily. The stack also has the advantage of being on a hard disk instead of somewhere in an endless stack of papers.

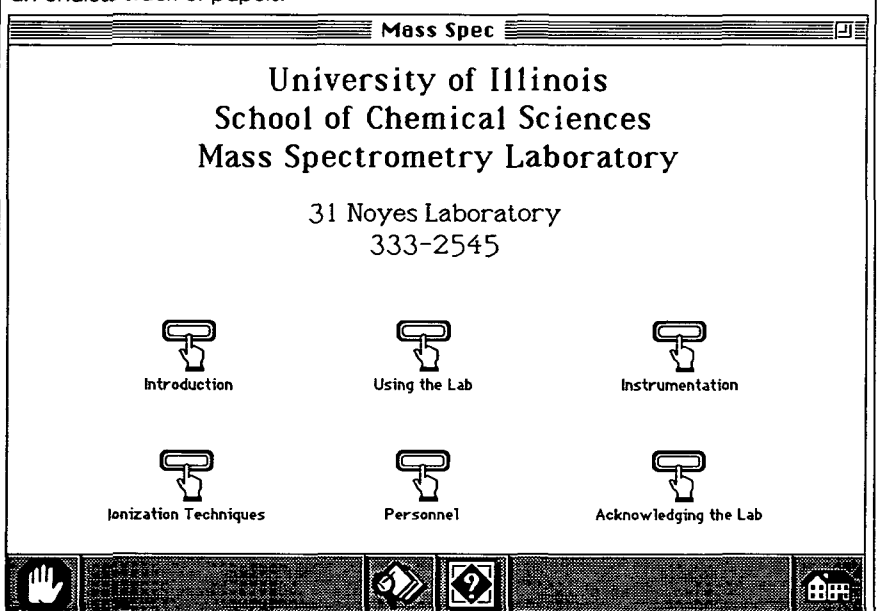

Figure 1. Main card of the Mass Spec stack.

What is in the Stack?

The Mass Spectrometry Laboratory Stack, like the printed brochure upon which it is based, is divided into six main sections. The main card of the stack is shown in Figure 1. By clicking the buttons on the cards, it is easy to move between sections and subsections. The text of the stack is identical to that of the brochure so that users of the printed and HyperCard versions have the same information. Only the means of accessing it is different. However, the stack does have some features that cannot be duplicated in the printed version. For example, clicking on any part of the sample submission form shows instructions on filling out that part. There is also a companion help stack accessible from the main stack and a "Read Me First" stack for novice users. The stack has been distributed to interested research groups in the School of Chemical Sciences.

Construction of the Stack

To be most visually effective, the stack should have a consistent layout. HyperCard allows the creation of a background layer that appears on every card of the stack. Graphics, title and text fields, and the one button that appears on every card were placed on the background. Once the background was in place, buttons and titles were added and text was pasted from the brochure. Buttons that look the same, but perform slightly different functions on each card, were carefully placed at the same position on each card.

Another place where consistency is important is in the visual effect when moving from one card to the next. All cards on the same hierarchal level use the same effect, either a slide right/left or wipe right/left.

Although complex programs can be written in HyperCard, this stack mostly uses simple links between cards. Very little scripting was necessary, and that which was necessary relates to the linking of the cards. For example, information on ionization techniques is accessible from two places in the stack. Pop/push card was used to return the reader to the proper point of origin.

Future Work

There are several additional features that could be incorporated into the stack. More links could be added. A stack can never have too many links. These links could include clicking on key words to go to a card showing more detail. Digitized pictures of the instruments and staff could be added. An index in which the reader could click on the entry of interest to go to that card could also be useful.

Acknowledgements

The printed brochure upon which this stack is based was originally written by Richard Milberg. It has since been modified by this author in collaboration with Dr. Milberg. Beta testing of the stack was done by Furong Sun and Anthony Thompson.

Ion Optical Study of Low Acceleration Ion Source

[1]M. Ishihara and [2]T. Matsuo
[1] Analytical Instrument Division, JEOL Ltd, Akishima, Japan.
[2] Institute of Physics, College of General Education, Osaka University, Japan.

INTRODUCTION

Recent studies have demonstrated the production of large metal clusters (m/z 300,000) by the use of Cs^+ bombardment [1]. In order to extend the mass range of sector mass spectrometers to allow analysis of such massive species, a number of possibilities exist: (i) increase the magnetic sector radius, (ii) increase the magnetic field strength, and (iii) decrease the acceleration voltage. Technical limitations exist for the first two options (we already have a 1.25m radius magnet weighing 9t, and there are limits to the generation of homogeneous, high strength magnetic fields), therefore our only option is to reduce the acceleration voltage. We have previously reported spectra obtained with an acceleration voltage of 70V, but this was severely hampered by the drop-off in ion extraction from the ion source. We have investigated the extraction optics of the ion source region for a unit operating at low accelerating voltage, using computer simulations derived from the computer code 'ELECTRA' [2].

CALCULATION

The block diagram of the prototype ion source used for the calculations is shown in Figure 1. Calculations were performed on an HP-9000-730 and typical computing time was 7 min. It was assumed that ion beam was emitted normal to the target surface, and two parameters (initial energy of the ions, U_0, and target inclination angle, θ_0) were varied.

1. Target angle, θ_0, is fixed (45°) and initial energy, U_0, is varied. (Figure 2a,2b)
2. Initial energy, U_0, is fixed (0 eV) and target angle, θ_0, is varied.
3. Initial energy, U_0, is fixed (5 eV) and target angle, θ_0, is varied.
4. Target angle, θ_0, is fixed (45°) and initial energy, U_0, is fixed (5 eV). Voltage to intermediate plates were varied. (Figure 3a,3b)

DISCUSSION

1. Ion extraction decreases as the initial energy of the ions is increased. Therefore, special attention should be given to very low acceleration voltages (<50V) since the average initial energy of a SIMS-type ion source is of the order of 20-30 eV.

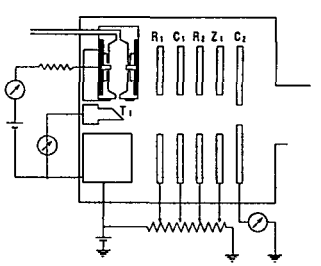

Figure 1: Block diagram of calculated ion source
T1: Target(+50 volt), R_1,R_2.: horizontal lenes (-5v,-80v), C_1,C_2: cylindrical lens (-120v,0v), Z_1: vertical lens (-80v) respectively

2. A smaller inclination angle, θ_0, gives rise to better ion extraction, at low acceleration potentials, but this influence is greatly reduced for sources operating in higher voltage (5-10 kV) régimes.
3. Even in the situation with an inclined target and a larger initial energy, the ion extraction can be improved by changing the potential of intermediate focusing lenses.
4. We are currently verifying the optimized theoretical models by experiment.

REFERENCES

[1] H. Ito, T. Matsuo, I.Katakuse and C.E. Costello. Proc. 40th ASMS Conf. Mass Spectrom., Washington DC 1992, 132.
[2] M.Ishihara and T. Matsuo, Nuclear Instruments and Methods 70B (1992) 445.

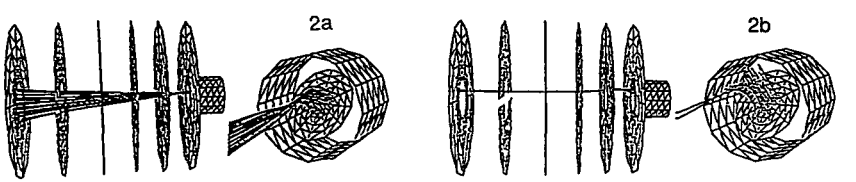

Figure 2. The influence of initial energy a. U_0 =0 eV, θ_0=45°, b. U_0 =5 eV, θ_0=45°)

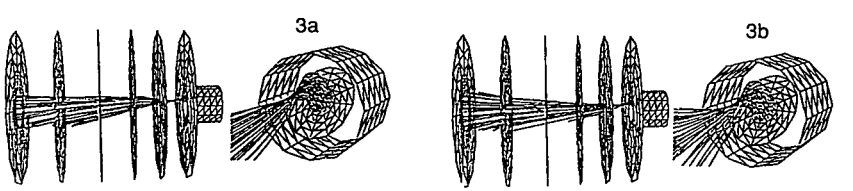

Figure 3: The influence of intermediate potential a: T_1=+50 volt, R_1= -500v ,R_2=-80v, C_1=-120v,C_2=0v, Z_1=-80v, b: T_1=+50 volt, R_1= -500v ,R_2=-800v, C_1=-1200v,C_2=0v, Z_1=-800v.

Identification of Proteins by their Peptide Masses in DNA Databases

Matthias Mann[1], Peter Mortensen[1], Peter Højrup[2] and Peter Roepstorff[2]

[1]Protein & Peptide Group, European Molecular Biology Laboratory, Heidelberg, Germany
[2]Dept. of Molecular Biology, Odense University, DK-5230 Odense M, Denmark

Previously, we have investigated the possibility of correlating partial mass spectral data of proteins with protein databases [1]. It was possible in most circumstances to identify proteins even with very few peptide masses, with moderate mass accuracy (0.1%) and in the presence of masses which were not obviously correlated to the sequence.

In this contribution we wish to extend those investigations to the searching of DNA databases. Such an extension is desirable because virtually all new sequence data that is entered into databases today is DNA data and because projects like the Human Genome Project will yield a wealth of DNA sequence information. For the biological mass spectrometrist these developments represent an opportunity to convert the challenging task of primary structure determination of an unknown protein into the more tractable one of correlating MS measurements to "proposed" sequences in the data banks.

We have adapted the program "PeptideScan" written in C++ and running on the Macintosh family of computers to the task of reading and translating DNA sequences. Figure 1 shows the user interface and a search result from scanning SWISS PROT, a protein database. The user interface was not modified and the main changes to the program were the addition of an "object" (software module) embodying the rules for DNA translation.

Between one and all six reading frame of a DNA sequence can be searched with the program. Digestion (i.e. calculation of peptide masses) is done "on the fly" in all the specified reading frames in contrast to the searches on SWISS PROT which was "pre-digested" to the hard disk according to user specified conditions. In searching DNA sequences open reading frames of a certain length are first determined. A protein match must have all matching peptides in one open reading frame (see below).

The program was furthermore modified to search the 84061 entries of the PIR system of data bases, again using digestion "on the fly". Currently only the search on SWISS PROT is optimized, taking typically 10 seconds or less on a Macintosh Centris 650. The PIR search takes about 10 minutes and DNA database search of the primate division about 12 minutes when specifying all six reading frames (27524 entries and 24 Mbyte sequence).

There are some limitations in the current algorithm that will have to be addressed. They mainly stem from the way the data base is organized. There are some entries where different exons of a gene are separate entries. In such cases a straightforward search might miss a match because some peptides may match in one entry and some in another. Thus it will be necessary to be able to parse (read) the feature table automatically and count up peptide matches across different entries for the same gene. Being able to parse the feature table automatically will in any case be advantageous because it allows the option to use more information about the sequence.

Using the techniques developed for this communication we can now search three categories of databases. (i) Well annotated and established amino acid sequences (i.e. SWISS PROT). (ii) Less certain, mostly auto translated sequences such as PIR III and Patch X. (iii) DNA data bases. The probability for false hits was not found to be very much higher than in amino acid sequence data bases. In particular, there was no need to specify the correct reading frame in advance because wrong reading frames contain enough stop codons to prevent false positives. However, it will in the future be benificial to be able to parse the feature table.

On the basis of our preliminary experience we suggest that MS information be checked against data bases in the order of certainty of entries given above (i.e. (i) to (iii)).

1: M. Mann, P. Højrup and P. Roepstorff, *Proc. 40th Conf. Mass Spectrom. Allied Topics, Washington, DC, 1992, p957*

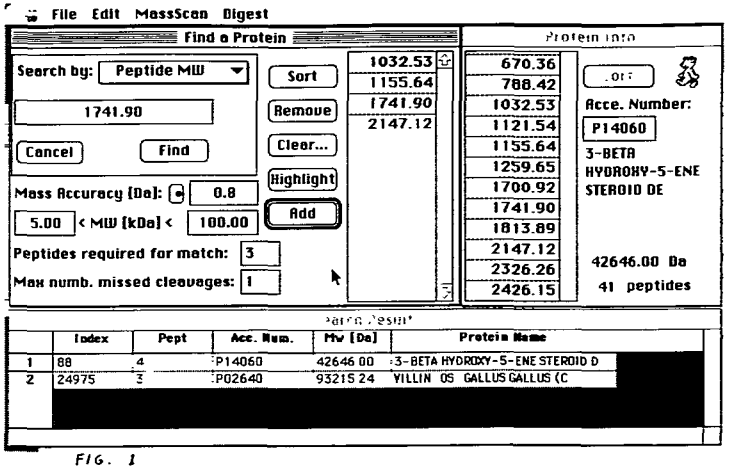

FIG. 1

COMPLEXATION SELECTIVITY OF METAL CATIONS TOWARD ORGANIC MOLECULES BY FAB MASS SPECTROMETRY

D. Giraud, *O. Laprévote and B. C. Das

Laboratoire de spectrométrie de Masse, Institut de Chimie des Substances Naturelles, C.N.R.S., Av. de la Terrasse, 91198 Gif-sur-Yvette, France.

Mass spectrometry using a fast-atom bombardment or a cesium ion beam as ionizing agent (FAB and L-SIMS) has gained increasing success since a dozen of years by virtue of its ability to transfer in the gas phase polar and involatile chemical substances introduced into a liquid matrix. A special feature of the FAB desorption is the generation of ions by attachment of alkali metal cations on various organic compounds (glycosides, oligosaccharides, antibiotics, peptides, etc.). Although the "cationisation" mechanism is not fully understood, some experimental results suggest that the mass spectra may reflect the equilibrium established in the matrix solution (1). This assumption has been developed for studying crown-ethers and other macrocyclic ligands of metallic cations allowing metal cation selectivity measurements and, in some cases, an evaluation of the corresponding stability constants.

Fundamentally, our strategy is based on the study of the variation in concentration of ligand/cation complexes of three different metal ions (M_1^+, M_2^+, M_3^+) competing for a defined amount of ligand (L).

The first step of the work consists in the determination of the theoretical concentration of each complex (LM_1^+, LM_2^+, LM_3^+) starting from fixed stability constants (K_1, K_2, K_3, respectively). The solutions of the three corresponding interdependent equations are obtained by successive iterations. When these calculations are carried out with different values of the ratio R = (total salt concentration)/(ligand concentration), characteristic variations in the relative concentrations ($LM_i^+{}_{calc}$) of the different complexes are observed.

In the presence of an excess of ligand (R<1) almost all the alkali cations are complexed, thus leading to equal complex concentrations and suggesting that, in the initial regions of the curves, the differences in relative intensities of the observed LM_i^+ ion peaks are due to different desorption rates. In order to relate the ion peak heights to each complex concentration in the matrix, the relative intensity values must be corrected by a "desorption coefficient" $D_i = LM_i^+{}_{obs}/LM_i^+{}_{calc.}$ calculated in the initial segments of the curves. Thus, the division of the relative intensities of all the LM_i^+ ion peaks by their corresponding desorption coefficients D_i should draw the observed values nearer to the theoretical curves.

For a ratio R=5, the experimental values LM_i^+ corrected by D_i are very close to the theoretical curves and they can be used directly for calculating new stability constants K_2 and K_3, with only a fixed

value of K_1. The variations in the theoretical curves due to a change of K_2 and K_3 (slightly different from the initial values) lead to new D_i coefficients, then to new LM_i^+ corrected values, and consequently to other K_2 and K_3 values which can be used for the calculation of the theoretical concentrations LM_i^+.

Thus, by fixing one stability constant value, it is possible to determine the stability constants of the two other complexes, and then to measure the selectivity of a particular ligand toward different cations. The reliability of this method is simply demonstrated by the fact that an increase (or decrease) of K_1 by a factor 10 allows only a variation of 0.05-0.1 in terms of $\Delta \log K$ (= selectivity measurement).

The stability constant measurements of a ligand toward different alkali cations are achieved in the same way as for the relative affinities. This is obtained simply by determining the best fit between the experimental data corrected by the desorption coefficients and the theoretical values. Minimisation of the chi-square value is obtained by using the Microsoft® Excel software for searching the best K_1 values. The Figure illustrates the results obtained for various compounds with lithium, sodium and potassium cations, after the complete set of iteration, chi-square minimisation and stability constants determination.

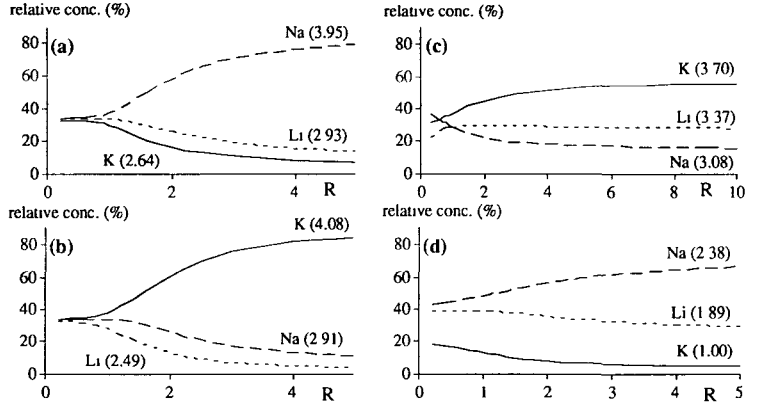

Figure. Relative concentrations (%) calculated for (a) 15-crown-5, (b) 18-crown-6 (c) lasalocid A, and (d) taxotere complexes with Li^+, Na^+, and K^+, along with their log K values. [R = (total salt concentration)/(ligand concentration)].

1) Johnstone, R. A. W., Rose, M. E. *J. Chem. Soc., Chem Commun.* 1983, 1268.

MECHANISTIC INVESTIGATIONS INTO THE ANIONIC OXY-COPE REARRANGEMENT IN THE GAS-PHASE

Jeehiun Lee† and Joseph J. Grabowski‡
Departments of Chemistry
†Harvard University, Cambridge MA 02138
‡University of Pittsburgh, Pittsburgh, PA 15260

[3,3]-sigmatropic rearrangements such as the Cope rearrangement have long been of interest to physical-organic and synthetic chemists alike. The discovery by Evans and Golub[1] that the rate of the oxy-Cope rearrangement (eq 1) could be accelerated by 10^{10}-10^{17} by deprotonation of the hydroxyl substiuent (the aptly named *anionic* oxy-Cope rearrangement, eq 2) led to its widespread use in synthetic chemistry, and to studies to probe the root of the

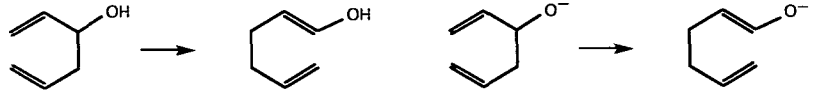

(1) (2)

acceleration. One such theoretical study[2] employed *ab initio* methods to calculate the carbon-hydrogen bond strengths for methanol (H–CH_2OH), sodium methoxide (H–CH_2ONa), potassium methoxide (H–CH_2OK), and the methoxide anion (H–CH_2O^-). It was found that as the substiuent became more "anionic," the C-H bond became weaker (bond dissociation energies of 90.7, 80.6, 79.0, and 74.2 kcal mol^{-1} respectively). This bond weakening effect was suggested as a possible reason for the marked rate enhancements observed. The study of the rearrangement in the gas-phase, where solvent and counterion effects are absent, could potentially provide further insight into the acceleration question.

The greatest challenge in studying any rearrangement in the gas-phase is finding a viable method for discerning whether or not rearrangement has occurred. Since the starting material is an alkoxide and the product is an enolate, methods can be used which capitalize on these structural differences. One such method involves using a reagent, or probe, which can differentiate between the two structures. A well-known example of such a structural probe is the family of deuterated solvents: enolates can exchange protons, alkoxides cannot. A probe of greatest utility would react quickly and efficiently with both alkoxides and enolates, and more importantly, would yield a *unique* product for each.

In our search for the ideal probe, we examined the reactions of alkoxides and enolates with dimethyl disulfide, which is known to undergo fast reactions with both localized and delocalized bases, producing a unique product for each (see scheme). Experiments with

1. Evans, D.A.; Golob, A.M. *J. Am. Chem. Soc.* **1975**, *97*, 4765-4766.
2. Steigerwald, M.L.; Goddard, W.A., III; Evans, D.A. *J. Am. Chem. Soc.* **1979**, *101*, 1994-1997.

model compounds (propoxide and propanal enolate to mimic a secondary alkoxide; isopropoxide and acetone enolate to mimic a tertiary alkoxide) indicated that dimethyl disulfide would be an ideal probe. The alkoxides react efficiently to produce mostly $CH_3SCH_2^-$ (*m/z* 93) while the enolates produce mostly thiomethoxylated product CH_3SA^-.

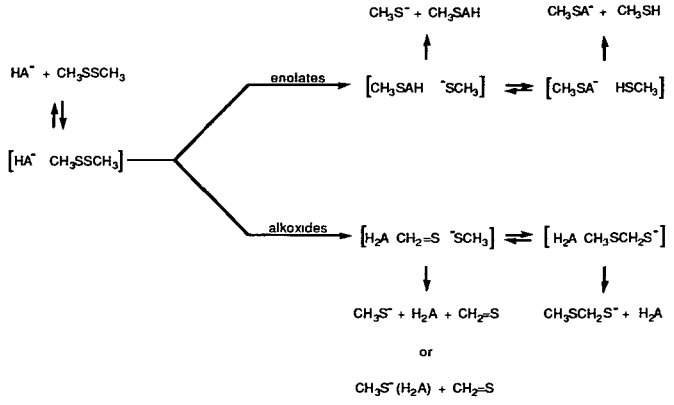

Our experiments were carried out under thermally equilibrated (298 K) conditions attainable in the flowing afterglow. The following procedure was used for both parent alcohols **1a** and **1b**: first, the parent alcohol is deprotonated with a base B^-; then the $(M\text{-}H)^-$ is allowed to react with CH_3SSCH_3. Both alcohols were found to yield thiomethoxylated product upon deprotonation (eq 3), indicating that both the parent secondary and tertiary alkoxides **2a** and **2b** rearrange to the corresponding enolate in our flowing afterglow.

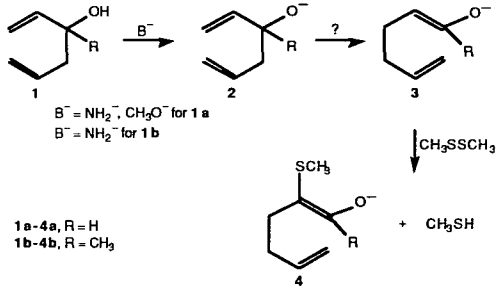

(3)

Complexation Of Alkaline Earth And Transition Metal Ions With Polyethers In A Quadrupole Ion Trap

Hui-Fen Wu, Jeff Liou and Jennifer S. Brodbelt
Department of Chemistry, University of Texas, Austin, TX 78712-1167

The study of molecular recognition has become an increasingly active area of research over the past two decades due to its fundamental importance in many biological and chemical phenomena . The process of complexation, in which a host and guest selectively bind through various types of interactions, is one particularly intriguing aspect of molecular recognition because many different types of binding interactions, including electrostatic, hydrogen-bonding, and covalent, may be involved, and these forces ultimately direct the stability and structures of the resulting complexes.

In the present study, we have undertaken an examination of the types of complexes formed from reactions of metal ions with a variety of crown ethers and their acyclic analogs in a quadrupole ion trap mass spectrometer. The metal ions are generated by laser desorption from a metal foil or metal salts (calcium, magnesium, gold, iron, copper, zinc, cobalt, nickel, silver, tin), and the complexes are formed by subsequent ion-molecule reactions with neutral ethers. Various collision-activated dissociation (CAD) techniques are used to evaluate the structures of both the metal/polyether complexes and sandwich type complexes which contain two polyethers bound to a single metal ion. Ligand-exchange methods were performed to establish the relative order of ligand binding energies for the polyethers. Finally, a comparison of the behavior of transition metal complexes to alkali and alkaline earth metal complexes is made with respect to aspects of host-guest binding.

All experiments were performed in a Finnigan quadrupole ion trap mass spectrometer (ITMS) equipped with a probe-mounted fiber optic laser desorption assembly. Metal ions were generated by pulsed laser desorption of a metal foil or of metal salts applied to a stainless steel sample tip. A Nd: YAG laser operated in the Q-switch mode at 532 nm and 1064 nm provided the desorption pulse. The metal ions are stored in the ion trap and allowed to undergo reactions with neutral polyethers. The metal/polyether complexes are mass-analyzed by operating the ion trap in the mass selective instability mode. A helium buffer gas pressure of 2 mtorr is used to assist in collisional cooling of the complexes The CAD spectra of the metal complexes were obtained by applying a small AC voltage (500 - 1000 mV_{p-p}) across the end-cap electrodes at a q value of 0.3 for 5 - 10 ms.

I: Formation of Metal$^+$/Polyether complexes

In order to compare the reactions of metal ions with polyethers, ion-molecule reactions between metal ions and the polyethers were examined. Typical product spectra are shown in Figures 1-2.

Reactions with Magnesium and Calcium Ions

Many of the reactions between Mg^+ and the crown ethers or glymes result in incorporation of H_2O or a small organic neutral. The C_2H_4O unit is a common skeletal portion of the polyethers Interestingly, reactions of Mg^+ ions with the glycols do not result in hydrated adducts. The lack of H_2O incorporation and general absence of the diverse array of products noted for the crown ethers and glymes may be attributed to the different binding nature of the terminal hydroxy groups.

The results for the reactions of Ca^+ with the polyethers demonstrates that hydration of the complexes does not occur. This absence of hydration may reflect the reduced charge density of Ca^+ ions relative to Mg^+ ions, such that a water molecule is not as strongly electrostatically bound to Ca^+ as to Mg^+.

Reactions with Copper Ions

The major product ions include $(M + Cu)^+$ and $(2M + Cu)^+$, but fragments ions from these complexes are not observed. The dimer ion $(2M + Cu)^+$ is only observed for those crown ethers that have cavity diameters smaller than the diameter of the Cu^+ ion. This result is attributed to a cavity size effect in which the addition of a second polyether ligand can not occur for those $(M + Cu)^+$ complexes in which the copper ion may be completely encircled by the crown ether skeletal, making the coordination of another ether molecule to the copper ion unfavorable.

Reactions with Iron Ions

Many more types of product ions are formed from the reactions with iron ions, and some of these are best rationalized as involving iron insertion into C-C or C-O bonds. Interestingly, the simple dimer ion, $(2M + Fe)^+$, is not observed for several of the polyethers, but instead a dissociation product, $(2M + Fe - C_2H_4)^+$, is formed.

II: CAD spectra of Metal/Polyether Complexes

Each metal/polyether complex was subjected to collisional activation in order to evaluate the types of dissociation reactions that the complexes undergo. The CAD spectrum of the $(12\text{-crown-}4 + Mg^+ + H_2O)$ ions is shown in Figure 3 as one example. Common losses from the complexes of the crown ethers and glymes include losses of several C_2H_4O units.

III: Comparison of Polyether Complexes With Alkali vs. Alkaline Earth Metals

Collisionally activated dissociation of the $(M + Alkali)^+$ complexes results in production of the bare alkali metal ion. These CAD results underscore the fact that the alkali metal/ether complexes are bound by weak electrostatic forces only. CAD of the polyether/alkaline earth complexes shows that the metal ion always remains attached to the polyether fragment. Thus, the alkaline earth metal/ether complexes are bound by very strong electrostatic and/or partially covalent forces. The difference is that the alkali metal ions have inert np6 electronic configurations. For the alkaline earth metal ions, the ionic ns1 configurations promote very strong ion-dipole electrostatic forces and may allow some partial covalent bond development.

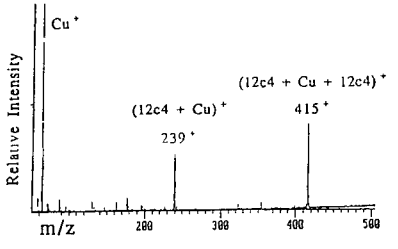

Figure 1 Ion-Molecule Reaction Product Spectrum of Cu^+ with 12-Crown-4

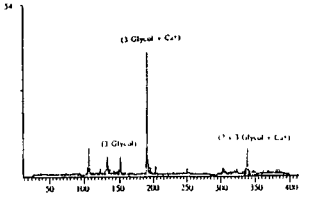

Figure 2 Product spectrum for reactions of Ca^+ ions with triglycol

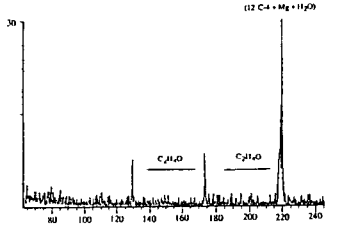

Figure 3 CAD spectrum of $(12\text{-crown-}4 + Mg^+ + H_2O)$

HYDROGEN BONDING INTERACTIONS AND SELECTIVE ION-MOLECULE REACTIONS IN HOST/GUEST CHEMISTRY IN A QUADRUPOLE ION TRAP

Jennifer S. Brodbelt, Hui-Fen Wu, and Chien-Chung Liou, Department of Chemistry, University of Texas, Austin, TX 78712-1167

The ability to examine host-guest chemistry without the influence of solvent effects opens up new avenues for understanding some of the fundamental details of molecular recognition. Intermolecular and intramolecular hydrogen-bonds are arguably the most important interactions in molecular self assembly and molecular recognition. Recently we have undertaken a comprehensive study of hydrogen-bonding interactions in host-guest chemistry in the gas phase with a series of polyethers as model hosts. The model of hosts of interest include the simple crown ethers and their acyclic analogs: the polyethylene glycols and their di-ether counterparts, the glymes, and the more complex "lariat" dibenzo crown ethers with pendant side groups. The latter class of polyethers not only prove to be an interesting set of models for evaluation of multi-site binding interactions but also allow detailed studies of site-selective ion-molecule reactions.

I. Evaluation of Hydrogen-Bonding Interactions

To study the effects of hydrogen-bonding interactions in gas-phase host-guest complexes, proton-bound complexes between a crown ether and amine were formed in a quadrupole ion trap and then probed by CAD. The extent of fragmentation attributed to polyether C-C and C-O bond cleavages is related to the strength and number of hydrogen-bonding interactions of the complexes. Dissociation of many of the ammonium and 2-ethanolammonium ion complexes results in extensive fragmentation of the polyether ligands, especially for the larger crown ethers and glymes. The relative extent of polyether skeletal cleavage increases with the number of oxygen binding sites of the ether. The observation of extensive fragmentation of the acyclic ether ligands supports the idea that the flexible acyclic ligands may participate in the types of multiple bonding interactions already described for the pre-organized crown ethers.

Most interestingly, some of the crown ethers show less extensive fragmentation overall than their acyclic counterparts. For example, the ammonium ion complex involving tetraglyme shows an abundance ratio for $(M + H)^+$: Σ (Fragment ions) equal to 4:5, whereas the ratio is only 5:4 for 15-crown-5 and 7:3 for tetraglycol. The hydrogen-bonds in the tetraglyme complex may be collectively more favorable than those in the 15-crown-5 complex because tetraglyme is a more flexible ligand which can wrap around ammonia whereas ammonia is too large to fit in the cavity of the more rigid 15-crown-5. Also, the kinetics for dissociation may be sufficiently slower for the floppy acyclic ligands, allowing correspondingly more energy accumulation during collisional activation and permitting greater competition from slower dissociation pathways.

In general, the glycols show the lowest extent of skeletal cleavage. This result may be related to the fact that glycols have terminal hydroxyl groups which participate in different types and/or strengths of hydrogen-bonds than do the ether functional groups, thus altering the dissociation dynamics of the complexes. Clearly, the fact that glycols don't exhibit the same extent of skeletal fragmentation as either the crown ethers or glymes indicates that kinetics alone cannot explain the differences in fragmentation patterns because the glycols are also floppy ligands which would be expected to promote slower dissociation kinetics (and thus a corresponding increase in skeletal decomposition).

II. Orders of Gas-Phase Basicities and Ammonium Ion Affinities of Lariat Ethers

There has been great interest recently in the design and evaluation of new and more structurally complex polyethers as ligands for size-selective metal binding. For example, a new class of proton-ionizable macrocycles with pendant groups, termed "lariat ethers" have been synthesized (see Table 1). It is believed that the addition of the pendant groups onto the macrocyclic structures assists in the selectivity and strength of cation complexation due to the ability of the pendant group to stablize the resulting complex in solution via secondary electrostatic interactions. We have measured by ligand exchange methods the gas-phase basicities and ammonium ion affinities of a series of these interesting lariat ethers. The order of increasing is: 7 > 3 > 8 > 6 > 1 > 5 > 2 > 4. The ethers with carboxylic acid pendant groups typically show the lowest gas-phase basicities, whereas the ones with

ester pendant groups show higher basicities. Generally, the ethers with two pendant groups demonstrate higher affinities than those with one or no pendant groups.

III. Site-Selective Ion-Molecule Reactions of Lariat Ethers

The products from reactions of dimethyl ether ions, $(CH_3OCH_3)H^+$ and $CH_3OCH_2^+$, with the lariat ethers are shown in Table 2. Each lariat ether is protonated by protonated dimethyl ether, but only those ethers with a β-hydrogen at the center methylene position may form the diagnostic $(M + 13)^+$ product ion. Those with two pendant substituents, such as compounds **3**, **5**, and **7**, do not form these products. Interestingly, only those macrocycles with phenyl substituents may undergo this reaction. The phenyl groups are inductively electron with-drawing, thus making the methylene carbon atoms more acidic and facilitating the necessary proton migration.

CONCLUSIONS

1) The nature of hydrogen-bonding interactions can be evaluated by examination of CAD spectra for polyether/ammonium complexes. The collective binding interactions of complexes involving acyclic ethers are greater than those involving crown ethers for bulky ammonium ions.

2) The formation of multiple hydrogen-bonds can have striking effects on the dissociation behavior of polyether/ammonium ion-complexes because the multiple hydrogen-bonding interactions allow formation of strongly-bound complexes with relatively large barriers to dissociation.

3) Lariat ethers provide additional information about the structural features which enhance complexation of model hosts in the gas phase. Macrocycles with pendant side groups assist in stabilization of the ionic complexes.

4) Site-selective ion-molecule reactions occur at the methylene position of substituted lariat ethers only if a β-hydrogen is available, thus specifically identifying the nature of this portion of the macrocycle.

ACKNOWLEDGMENTS

This research was supported by grants from NSF, Welch Foundation, NIH, and ACS-PRF.

Table 1. Structures of Lariat Ethers

	Compound Number	R1	R2
Dibenzo-16-crown-5	1	H	H
	2	H	OCH_3
	3	C_3H_7	OCH_3
	4	H	OCH_2COOH
	5	C_3H_7	OCH_2COOH
	6	H	$OCH_2COOC_2H_5$
	7	C_3H_7	$OCH_2COOC_2H_5$
Dibenzo-18-crown-6	8		

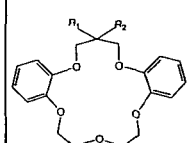

[a] All lariat ethers were provided by Prof. Richard Bartsch of Texas Tech University

Table 2.

Ion-Molecule Reactions of Dimethyl Ether Ions and Lariat Ethers

Ether	Relative Percent Product Ions $(M - H)^+$	$(M - 13)^+$	$(M - 45)^+$
1	50	45	5
2	50	40	10
3	85	< 2	15
4	40	30	30
5	80	< 2	20
6	50	40	10
7	80	< 2	10

RECOGNITION OF CHIRAL AMMONIUM SALTS USING CHIRAL CROWN ETHER HOSTS IN THE GAS PHASE[1]

David V. Dearden, In-Hou Chu, and XueJun Yu
Department of Chemistry and Biochemistry, Box 19065
The University of Texas at Arlington, Arlington, Texas 76019-0065

Introduction. Although mass spectrometry is an excellent technique for determining molecular weights and atom connectivities, it is still a poor means of determining 3-dimensional molecular conformations. Our research group is exploring ion-molecule interactions from the perspective of host-guest chemistry, in hopes of finding ion-molecule reactions which can be used as conformational probes. In this quest, the ability to recognize chiral molecules, and to distinguish enantiomers, is an important and long-sought goal. Although our previous work has successfully shown that host-guest size relationships are important in ion-molecule chemistry, most of those studies have involved atomic ions as guests. Herein we describe some of our efforts to extend our studies into the realm of molecular recognition, using small molecular ion guests. In particular, we note a chiral host-guest system which displays molecular recognition in its ion-molecule chemistry.

Experimental. These experiments employed a Fourier transform ion cyclotron resonance mass spectrometer (Extrel FTMS-1000) equipped with two temperature-controlled direct-exposure solid sample probes. Ligands such as 18-crown-6 or its chiral analog dimethyldiketopyridino-18-crown-6 were introduced into the vacuum chamber on the solid probes. In most experiments, the probes were left at ambient temperature, although the chiral ligands were heated to about 90° C to achieve adequate vapor pressures. Volatile guests and guest precursors (such as water and ammonia) were introduced using precision variable leak valves Guest ions were formed using 70 eV electron impact, followed by a delay to allow proton transfer to generate the hydronium or ammonium ions of interest. The relative initial rates of proton attachment to the two ligands being compared were determined and used to obtain the relative vapor pressures of the two ligands. Equilibrium constants for transfer of guest molecules between two hosts were determined using the host pressure ratios and equilibrium signal intensities for the host-guest complexes. Equilibria were approached from both directions to ensure attainment of true equilibrium conditions.

Results and Discussion. Equilibrium constants for transfer of a number of ammonium ions, as well as H_3O^+, from 18-crown-6 to 21-crown-7 are as follows. ammonium, 11.8 ± 1.9; methylammonium, 2 0 ± 0.2, n-butylammonium, 1.5 ± 0.2; benzylammonium, 0.64 ± 0.03; 2-propylammonium, 0 28 ± 0.04; *t*-butylammonium, 0.07 ± 0.01; hydronium, < 0.01 (transfer was observed in the forward direction only). Among the ammonium ions, a clear trend emerges: as steric bulk increases, *K* for transfer from the smaller host to the larger host decreases. This is a counterintuitive result, especially in light of the fact that *K* is smallest for the sterically smallest guest, hydronium. It is possible that *K* is sensitively dependent on the H-X-H bond angle of the guest (X = N or O). Molecular modeling studies and earlier experimental work suggest that 18-crown-6•H_3O^+ complexes are especially stable due to the C_3 symmetry axes present in both host and guest which allow formation of 3 linear hydrogen bonds

Equilibria for transfer of *R*- and *S*-α-(1-naphthyl)ethylammonium ($NapEt^+$) ions between achiral 18-crown-6 and the chiral analog *S,S*-dimethyldiketopyridino-18-crown-6 were also characterized. Both guests bind more strongly to 18-crown-6 than to the chiral ligand, probably because of greater conformational flexibility and the lack of electron-withdrawing substituents in the case of 18-crown-6. There is a large difference in equilibrium constants for the *R*- and *S* enantiomers (130 ± 15, and 570 ± 70, respectively), indicating a high degree of chiral recognition in this system. If a temperature of 350 K is assumed, this corresponds to a free energy difference of 4.2 ± 0.4 kJ mol^{-1} between the complexes of the two enantiomers with the chiral host, the *R*-$NapEt^+$ complex being more stable. This compares with free energy differences of 2.3 ± 0.5 and 4.6 ± 0.8 kJ mol^{-1}, respectively, in methanol and CD_2Cl_2 solutions,[2] suggesting that strongly solvating achiral solvents such as methanol disfavor the interactions which lead to recognition, while weakly-solvating media give results similar to those observed in the gas phase.

Acknowledgment. We are grateful for the support of the Robert A. Welch Foundation, PRF, and NSF.

(1) Some of this material was very recently published: Chu, I.-H.; Dearden, D. V.; Bradshaw, J. S.; Huszthy, P.; Izatt, R. M. *J. Am. Chem. Soc.* **1993**, *115*, 4318-4320.
(2) Davidson, R. B.; Bradshaw, J. S.; Jones, B. A.; Dalley, N. K.; Christensen, J. J.; Izatt, R. M.; Morin, F. G.; Grant, D. M. *J. Org. Chem.* **1984**, *49*, 353-357.

Presented at the 41st ASMS Conference on Mass Spectrometry

FOURIER TRANSFORM ION CYCLOTRON RESONANCE MASS SPECTROMETRIC INVESTIGATION OF GAS PHASE CRYPTATE COMPLEXES

Qizhu Chen and David V. Dearden, Department of Chemistry and Biochemistry,
The University of Texas at Arlington, Arlington, Texas 76019

Introduction

Cryptands are well known host-guest ionophores. These 3-dimensional ligands are capable of ion encapsulation, because they have cage-like structures. The complexation of cryptands with mono- and divalent cations in solution has been extensively studied. However, there is little or no information about the attachment of alkali metal cations to multidentate cryptand ligands in the gas phase. In the present work, we investigate the underlying factors governing the complexation of alkali metal cations by cryptands. These studies provide evidence that non-covalent attachment can be crucially dependent on the size relationship between the cation and the binding site of an organic host molecule. Fourier transform ion cyclotron resonance mass spectrometry was used to probe the thermochemistry of cation transfer between multidentate macrocyclic crown ethers and cryptand ligands with systematically varying binding cavity size. The relative cation affinities of cryptands and crown ethers of similar size were determined.

Experimental

All measurements in this study were performed using a Fourier transform ion cyclotron resonance mass spectrometer (Extrel FTMS-1000). Alkali metal cations were introduced into the trapping cell via laser desorption using an excimer-pumped dye laser (Lambda Physik LPX 205i/FL 3002). The neutral ligands were introduced into the vacuum chamber through a variable leak valve or by using a mini-tube set in the center of a solid sample probe. Figure 1 shows the structures of cryptands used in this work. Initial rates of proton attachment to the two ligands being compared were measured to determine the relative pressures of the ligands, and this information was used to determine equilibrium constants for cation transfer between the ligands.

Cryptands

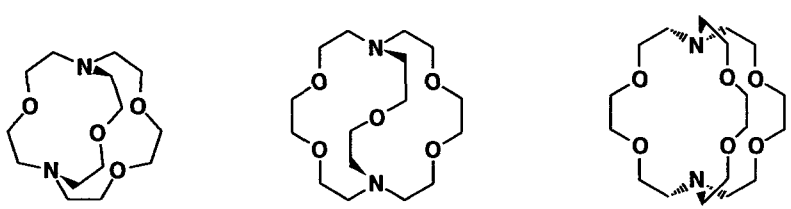

[2.1.1] [2.2.1] [2.2.2]

Results and Discussion

The complexation of cryptands with alkali metal ions in the gas phase has been studied. "Sandwich" 2:1 ligand:metal complexes were observed for cryptand[2.1.1] with K^+, Rb^+ and Cs^+, but only 1:1 complexes were seen for Li^+ and Na^+, suggesting that the latter two small cations enter the binding cavity of cryptand[2.1.1].

As shown in Table 1, among the cryptands, cation affinities were found to be in the following sequences: [2.2.2] > [2.1.1] > [2.2.1] for Li^+, [2.2.1] > [2.2.2.] > [2.1.1] for Na^+, and [2.2.2] > [2.2.1] > [2.1.1] for K^+, Rb^+ and Cs^+ ions. These results can be rationalized on the basis of size-selective complexation by the ligands.

Table 1

Thermodynamic parameters for alkali metal ion transfer reactions between cryptands.

Reaction	Cations	log*K*	ΔG / kJ mol^{-1}
$[M(C_{211})]^+ + C_{221} \rightleftharpoons [M(C_{221})]^+ + C_{211}$	Li^+	-0.18(0.08)	1.17
	Na^+	1.63 (0.09)	-10.9
	K^+	2.51 (0.07)	-16.8
	Rb^+	1.43 (0.10)	-9.58
	Cs^+	1.23 (0.03)	-8.24
$[M(C_{211})]^+ + C_{222} \rightleftharpoons [M(C_{222})]^+ + C_{211}$	Li^+	0.23(0.12)	-1.53
$[M(C_{221})]^+ + C_{222} \rightleftharpoons [M(C_{222})]^+ + C_{221}$	Na^+	-0.02 (0.03)	0.15
	K^+	1.67 (0.20)	-11.2
	Rb^+	1.71 (0.13)	-11.5
	Cs^+	1.94 (0.05)	-13.0

Standard deviations for repeated measurements in parentheses. T = 350 K.

The spatial arrangement of the donor groups was also be observed to be important, in that the 3-dimensional cryptands were observed to have larger cation affinities than crown ethers with the same number of donor atoms. For example, complex stabilities were observed in the following orders: (Na^+[2.1.1]) > (Na^+18C6), and (K^+[2.2.1]) > (K^+21C7).

Acknowledgment

We are grateful for the support of the Robert A. Welch Foundation (Y-1214), the donors of the Petroleum Research Fund, administered by the American Chemical Society (24657-G5), and the National Science Foundation (CHE-9221224).

INFLUENCE OF LIGAND POLARIZABILITY AND LIGAND FLEXIBILITY ON MULTIDENTATE ATTACHMENT OF ALKALI METAL CATIONS: KINETICS AND THERMOCHEMISTRY OF CATION BINDING BY ISOMERS OF DICYCLOHEXANO-18-CROWN-6

In-Hou Chu and David V. Dearden, Department of Chemistry and Biochemistry, The University of Texas at Arlington, Arlington, TX 76019-0065

Introduction:

This work extends our earlier studies of molecular recognition in gas-phase ion-molecule reactions, which have shown that size relationships between neutral hosts and alkali metal ion guests can have profound influences on the kinetics and thermochemistry of the host-guest interactions.[1] For maximum cation binding, the ligand must be flexible enough to allow optimum arrangement of the electronegative heteroatoms around the bound ion. Further, in the gas phase, increasing the number of donor groups in a simple ligand such as a crown ether increases its ability to strongly bind cations. In solution, on the other hand, a much more complicated model is required to predict relative binding affinities due to trade-offs between the intrinsic host-guest interactions and increased solvation energy as the size of the ligand and number of donor groups increases. In addition, kinetic studies imply that ligand polarizability plays a large role in gas phase cation attachment processes.[1] To further explore the relationship between ligand polarizability, ligand flexibility, and cation binding affinity, we have undertaken a study comparing the cation binding properties of 18-crown-6 (18C6) and two isomers of the alkyl substituted ligand dicyclohexano-18-crown-6 (DC18C6). The latter two isomers have the same number of donor groups as the unsubstituted crown, but are less flexible than 18C6 due to addition of the cyclohexyl groups. If ligand flexibility is the determining factor, we would predict that the DC18C6 isomers should bind alkali metal ions less strongly than 18C6. On the other hand, alkyl substitution greatly increases the polarizability of these ligands relative to 18C6 (DC18C6, 39.1 $Å^3$; 18C6, 25.9 $Å^3$, both estimated using the method of atomic hybride components[2]), so if polarizability dominates, we expect the substituted ligands to bind the ions more strongly. Finally, the two DC18C6 isomers, *cis*-syn-*cis* and *cis*-anti-*cis* (referred to hereafter as "syn" and "anti", respectively), differ in the arrangement of the cyclohexyl substituents around the plane of the ligand. It is of interest to determine whether the two isomers can be distinguished mass spectrometrically through their ion-molecule chemistry, and whether guest cation size effects play a role.

Experimental:

Alkali metal cations were generated by laser desorption from salts inside a Fourier transform ion cyclotron resonance mass spectrometer (Extrel FTMS-1000) The two ligands to be compared were introduced into the vacuum chamber on direct-exposure probes, and their relative pressures were determined by measuring the relative rates of proton attachment.[1,3] Crown ether-alkali metal complexes were isolated, and the metal transfer reaction between the two ligands was allowed to come to equilibrium. Equilibria were approached starting from both of the isolated ligand-metal complexes to ensure the attainment of true equilibrium conditions. Equilibrium constants were determined from the product of the ratio of the two ligand pressures times the relative intensities of the two complex ion peaks.

Results and Discussion:

Equilibrium constants for cation exchange reactions between DC18C6 and 18C6 or 21C7 are summarized in Tables 1 and 2. Both DC18C6 isomers have higher alkali metal

cation affinities than 18C6, and in some cases, even the extra donor atom of 21C7 cannot provide it with higher Li^+ or Na^+ affinities than the DC18C6 isomers. These observations clearly indicate that ligand polarizability is more important than flexibility for these ligands. The syn isomer forms more stable alkali metal complexes than the anti isomer, which is consistent with solution results[4] and suggests that the spatial arrangement of the donor groups and ligand flexibility do play a significant role.

Rate constants for cation transfer from 18C6 to DC18C6 were also determined (Table 3). The constants are always larger for the syn isomer than for the anti isomer, suggesting that the arrangement of donor atoms in the syn isomer is better suited for metal binding than in the anti isomer. In general the smaller cations transfer more readily than the larger ones. We are currently performing molecular modeling studies of these systems to gain further insight.

Table 1. Equilibrium constants for $18C6M^+ + DC18C6 \rightleftharpoons DC18C6M^+ + 18C6$

	Li^+	Na^+	K^+	Rb^+	Cs^+
(*cis*-syn-*cis*)DC18C6	*	552 ± 48	7.3 ± 0.6	6.6 ± 0.6	3.4 ± 0.2
(*cis*-anti-*cis*)DC18C6	25 ± 4	11 ± 1	2.4 ± 0.4	1.8 ± 0.4	1.0 ± 0.1
(mixed)DC18C6	*	223 ± 13	4.1 ± 0.3	3.6 ± 0.3	1.1 ± 0.1

'*' indicates that equilibrium was not observed in this system (only the $DC18C6M^+$ complexes were observed at long reaction times).

Table 2. Equilibrium constants for $21C7M^+ + DC18C6 \rightleftharpoons DC18C6M^+ + 21C7$

	Li^+	Na^+	K^+	Rb^+	Cs^+
(*cis*-syn-*cis*)DC18C6	351 ± 27	14 ± 1	1.5 ± 0.1	0.18 ± 0.03	0.11 ± 0.01
(*cis*-anti-*cis*)DC18C6	6.1 ± 0.5	0 40 ± 0.02	0.40 ± 0.02	**	**

'**' indicates that equilibrium was not observed in this system (only the $21C7M^+$ complexes were observed at long reaction times).

Table 3. Rate constants for cation transfer from 18C6 to DC18C6 (* 10^{10} cm^3 mol^{-1} sec^{-1})

	Li^+	Na^+	K^+	Rb^+	Cs^+
(*cis*-syn-*cis*)DC18C6	10 ± 1	10 ± 1	7.0 ± 0.6	6.9 ± 0.7	6.3 ± 0.6
(*cis*-anti-*cis*)DC18C6	8.0 ± 0.5	6.7 ± 0.5	5.1 ± 0.5	4 7 ± 0.6	2.4 ± 0.4

Acknowledgments

We are grateful for the support of the Robert A. Welch Foundation (Y-1214); the donors of the Petroleum Research Fund, administered by American Chemical Society (24657-G5); and the National Science Foundation (CHE-9221224).

References:

1. Chu, I. -H; Zhang, H. and Dearden, D. V. *J. Am. Chem. Soc.* **1993**, in press.
2. Miller, K. J. *J. Am. Chem. Soc.* **1990**, 112, 8533-8542.
3. Chu, I. -H; Dearden, D. V.; Bradshaw, J. S.; Huszthy, P.; Izatt, R. M. *J. Am. Chem. Soc.*, in press.
4. Frensdorff, H. K. *J. Am. Chem. Soc.* **1970**, 4684. Izatt, R. M.; Nelson, D. P.; Rytting, J. H.; Haymore, B. L. and Christensen, J. J. *J. Am. Chem. Soc.* **1971**, 93, 1619. Coxon, A. C.; Laidler, D. A.; Pettman, R. B. and Stoddart, J. F. *J. Am. Chem. Soc.* **1978**, 100, 8260.

FOURIER TRANSFORM ION CYCLOTRON RESONANCE MASS SPECTROMETRIC INVESTIGATION OF CALIXARENES AND THEIR COMPLEXES WITH METAL AND ORGANIC CATIONS IN THE GAS PHASE

Xuejun Yu, Qizhu Chen, Philip Wong and David V. Dearden, Department of Chemistry and Biochemistry, The University of Texas at Arlington, Arlington, Texas 76019-0065.

Introduction

Calixarenes are cyclic ligands consisting of ortho-linked phenol units, which are often studied in solution as biomimetic molecules capable of selective cation binding and as model agents for drug delivery. In a search for gas phase systems exhibiting molecular recognition, we have investigated para-tert-butylcalix[4]arene (PTBC4), shown in Fig.1, and its binding properties using Fourier transform ion cyclotron resonance mass spectrometry. To probe the intrinsic guest-host chemistry between PTBC4 and metal or organic cations, we have undertaken a study of these complexes. For organic cations, the kinetics and thermochemistry of complexation with PTBC4 were investigated. The relative cation affinities of PTBC4 and crown ethers of similar size were also determined.

Calixarene macrocycles serve as receptor models because of their conformational flexibility and the presence of multiple binding sites. These conformations are very important to the study of their host-guest chemistry. PTBC4 has four conformations which are referred to as "cone," "partial cone," "1,2-alternate," and "1,3-alternate" conformations. Due to very favorable electrostatic interactions, only the cone conformation (Fig. 2) is observed for PTBC4 in the solid state. There are at least two cation binding sites (endo and exo).

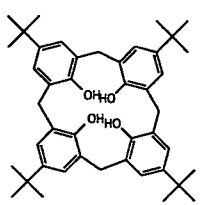

Fig. 1. *p*-tert-butylcalix[4]arene (PTBC4)

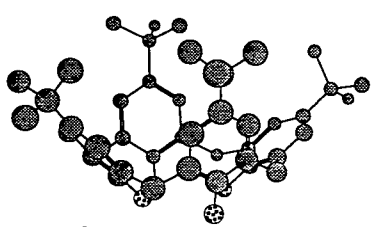

Fig. 2. Cone conformation of PTBC4.

Experimental

All experiments were performed using a Fourier transform ion cyclotron resonance mass spectrometer (Extrel FTMS-1000). Metal cations were desorbed into the gas phase using an excimer pumped dye laser (Lambda Physik LPX 205i/FL 3002). Organic cation precursors and PTBC4 were introduced separately into the chamber via small capillary tubes mounted in the center of a temperature-controlled probe tip. Volatile ligands were introduced into the chamber through a variable leak valve. The relative pressures of the two receptors being compared were determined by measuring the initial rates of proton attachment to them. This information was used with the relative intensities of the two host-guest complex peaks to determine equilibrium constants for guest transfer reactions between the two hosts.

Results

The mass spectra of Fig.3 and Fig.4 show that thermally desorbed PTBC4 can complex with laser-desorbed alkali or divalent metal cations to form mono-metal and bis-metal PTBC4 ion complexes. Complexes of PTBC4 with Na^+, K^+, Rb^+, Cs^+, Ba^{2+}, Sr^{2+}, and Fe^{2+} were observed in 1:1 stoichiometry. In the case of the divalent cations, complexation was accompanied by loss of a proton, such that the overall charge of the complex was +1. Similarly, complexes consisting of two alkali metal ions bound to PTBC4 with loss of one proton were seen, as was a complex involving three Na^+ ions with the loss of two protons.

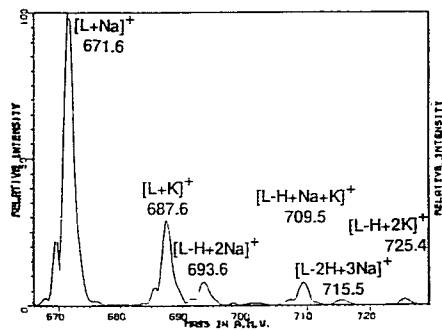

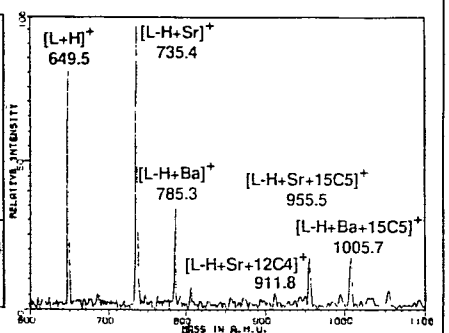

Reactions of PTBC4 with benzylammonium cation were of particular interest, since in this case "ditopic" binding, involving interactions between the ammonium group and the phenolic oxygens of the calixarene, as well as π-π stacking interactions between the calixarene and the guest, is possible. From competition experiments involving cation transfer between PTBC4 and crown ether receptors of similar size, it was observed that the benzylammonium affinity of 15-crown-5 is larger than that of PTBC4, but that the benzylammonium affinity of PTBC4 is similar to that of 12-crown-4.

Acknowledgments

We are grateful for the support of the Robert A. Welch Foundation (Y-1214); the donors of the Petroleum Research Fund, administered by American Chemical Society (24657-G5); and the National Science Foundation (CHE-9221224).

References

1. Gutsche, C. D.; *Acc. Chem. Res.*, **1983,** 16, 161-170.
2. Tabushi, I. *Acc. Chem. Res.*, **1982,** 15, 66-72.
3. Gutsche, C. D.; Dhawan, B.; Levine, J. A.; No, K. H.; Bauer, L.J. *Tetrahedron*, **1983,** 39, 409.
4. Kammerer, H.; Happel, G.; Caesar, F.; *Makromol. Chem.*, **1972,** 162,179.
5. Happel, G.; Mathiasch, B.; Kammerer, H.; *Makromol. Chem.*, **1975**, 176, 3317.
6. Grootenhuis, P. D. J.; Kollman, P.A.; Groenen, L. C.; Reinhoudt, D. N.; Van Hummel, G. J.; Ugozzoli, F.; Andreetti, G. D. *J. Am. Chem. Soc.*, **1990,** 112,4165-4176.

CHIRAL FAB MASS SPECTROMETRY

Masami Sawada, Yasuo Okumura, Yoshio Takai, Hitoshi Yamada, Takahiro Kaneda, and Shigetoshi Takahashi
Material Analysis Center, the Institutue of Scientific and Industrial Research, Osaka University, Ibaraki, Osaka 567, Japan

Enantioselective host-guest complexation has been demonstrated using FAB mass spectrometry. Among several crown ethers, modified chiral crowns **1** and **3** differentiate a chiral alkyl ammonium ion guest such as 1-(1-naphtyl)ethylammonium ion **4** or phenylalanyl ion **5**. On the other hand, chiral crown **2** does not differentiate it.

Relative peak intensity (RPI) method has been principally applied to the evaluation of such host-guest complexations, where the peak intensity of the target host (M)-guest (A^+) complex ion, $[I(M+A^+)]$, is compared to that of the internal standard host (R)-guest (A^+) one, $[I(R+A^+)]$.

$$M + (R+A)^+ \rightleftharpoons (M+A)^+ + R \qquad (1)$$

Here, R is a selected internal standard achiral host, and is added to an equimolar amount of M. Therefore, these two host-guest complex ion peaks appear simultaneously in a FAB mass spectrum. The RPI value is defined as $[I(M+A)^+/I(R+A)^+]$, and might be regarded as a measure of the degree of the ammonium ion transfer equilibrium (eq. 1).

$$M + (R+A_{(R)})^+ \rightleftharpoons (M+A_{(R)})^+ + R \qquad (2)$$
$$M + (R+A_{(S)})^+ \rightleftharpoons (M+A_{(S)})^+ + R \qquad (3)$$

The present enantioselectivity is characterized by the RPI ratio value, $RPI_{(R)}/RPI_{(S)} = [I(M+A_{(R)})^+/I(M+A_{(S)})^+]$, in the range of 1.2 to 1.6, as shown in Table 1 and Fig. 1. The RPI ratio value of 1.0±0.1 is regarded as non-enantioselectivity of the target host. The observed preference of the (*R*)-enantiomer guest ((*R*)-**4** or (*R*)-**5**) is compatible with (i) CPK model examinations toward chiral crown **3** and (ii) related coloration results.

With chiral crown **3**, a close correspondence exists between the enantioselections of FABMS/RPI values and strictly related solution phase energetics

in association equilibria, indicating the potential applicability of the FABMS/RPI approach. The usefulness of this RPI method for searching a new type of enantioselective host compounds has been demonstrated.

Table 1.

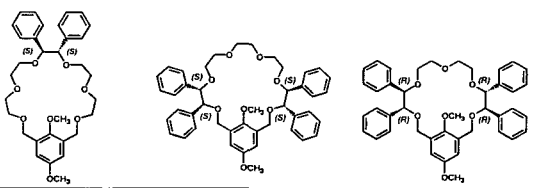

	Chiral A^+	1 RPI_R	1 RPI_S	1 Ratio RPI_R/RPI_S	2 RPI_R	2 RPI_S	2 Ratio RPI_R/RPI_S	3 RPI_R	3 RPI_S	3 Ratio RPI_R/RPI_S
4		0.85	0.69	1.2[a]	1.32	1.32	1.0	3.57	2.89	1.2
5		1.43	1.60	0.9	1.47	1.29	1.1	1.85	1.13	1.6

R=15-crown-5, Matrix=NBA, [M] . [R] . [A] = 1 : 1 : 2.
[a] [M] : [R] : [A] = 1 : 1 : 1.

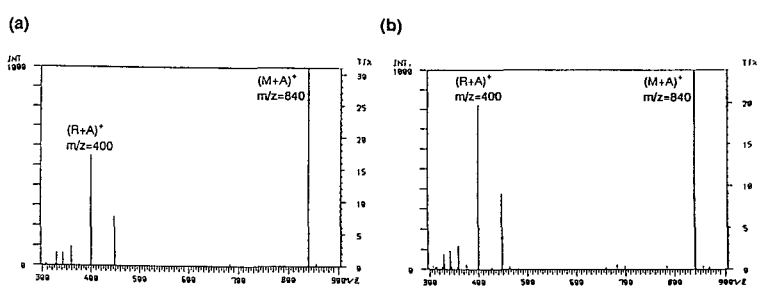

Fig. 1. FAB mass spectra (NBA matrix).
(a) M=3, A^+=(*R*)-5, R=15-C-5. (b) M= 3, A^+=(*S*)-5, R=15-C-5.

GAS PHASE REACTIONS OF THE GROUP 11 IONS WITH SMALL ALKANES

E.E. Ward and W.S. Taylor
Department of Chemistry, University of Central Arkansas, Conway AR 72035
Lucia M. Babcock and Tonya L. McNeal
Department of Chemistry, University of Georgia, Athens, GA 30602

INTRODUCTION

The gas phase reactions of metal ions with small organic species have been the subject of much discussion.[1,2] In the reactions of metal ions with alkanes, an excited association complex is initially formed which can subsequently eliminate small molecules such as H_2 or CH_4. Alternatively, sufficient numbers of collisions between the excited complex and an inert third-body can result in the formation of a stabilized adduct. Access to both the bimolecular and three-body product channels is strongly influenced by the electronic configuration of the metal.[3,4] Significant variation in reactivity can also occur among ions possessing analogous electron configurations.[5] In this work, we have carried out the reactions of Ag^+ and Au^+ with C_2H_6, C_3H_8, and n-C_4H_{10}; and Cu^+ with C_2H_6. The focus of this work is to examine trends in the reactivity of isovalent ions in an environment where both bimolecular and three-body chemistry can occur.

EXPERIMENTAL

The reactions listed above were carried out at room temperature in a flowing afterglow reactor (FA) equipped with a glow discharge ion source.[6] Reactant ions were produced in the discharge as a result of a sputter-bombardment process and injected into the FA along with a carrier gas (He). The reaction environment in the FA is one in which the reactants experience many collisions with the carrier gas. Thus, three-body product channels can be observed as well as bimolecular channels. Further, this environment is one in which only exothermic reactions can occur.

RESULTS AND DISCUSSION

The reactions described here display significant variation, with Au^+ exhibiting facile elimination chemistry not observed with Cu^+ or Ag^+. The systems involving Cu^+ and Ag^+ form the adduct exclusively, while only the reaction with C_2H_6 produces the adduct when Au^+ is the reactant ion. Interaction of Au^+ with all three alkanes yields bimolecular products. In the reaction of Au^+ with C_2H_6, the bimolecular ionic product is $Au^+ \cdot C_2H_4$, which indicates the elimination of H_2. Reaction of this ion with both C_3H_8 and n-C_4H_{10} yields $C_3H_7^+$ and $C_4H_9^+$ respectively - both consistent with the formation of AuH. This product channel has been observed previously for reactions involving Au^+ using ICR techniques.[7] Overall second-order rate constants for the reactions involving Cu^+ and Ag^+ display pressure dependencies (see Figure 1), whereas the Au^+ rate constants are pressure-independent. For reaction with a given alkane, the rate constants

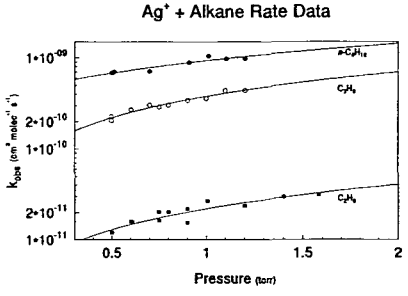

Figure 1

for Ag^+ are approximately an order of magnitude lower than those for Cu^+. In addition, the overall rate constants for Ag^+ increase with the size of the alkane.

Using readily available thermochemical data, it can be shown that formation of the neutral metal hydride is exothermic only for the reactions of Au^+ with C_3H_8 and n-C_4H_{10}, and only when the product ions are i-$C_3H_7^+$ and sec-$C_4H_9^+$ respectively. In the reaction of Au^+ with C_2H_6, AuH formation

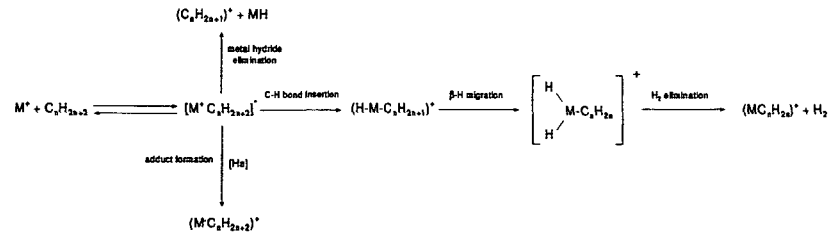

Figure 2

is endothermic, but H_2 elimination is observed in addition to formation of a three-body product. This product channel is also exothermic for the reaction of Cu^+ with C_2H_6 but is not observed in the FA due to the presence of a kinetic barrier most likely arising from C-H bond insertion.[8] Our results suggest a similar situation exists when Ag^+ is the reactant ion. Elimination of H_2 in the Au^+ reaction indicates that this kinetic barrier is lower for this ion; however, some barrier to reaction must exist since H_2 elimination competes with adduct formation. Thus, access to the H_2 elimination channel appears to subject to *kinetic* control, whereas formation of the neutral metal hydride is subject to *thermodynamic* control. The behavior of the systems discussed here can be described by the mechanism shown in Figure 2, which incorporates all observed product channels. It is probable that MH formation occurs directly from the initial association complex, since C-H bond insertion represents a barrier to reaction. Formation of MH after this step would likely result in a competition between this channel and formation of the adduct.

1. Armentrout, P.B.; Beauchamp, J.L. *Acc. Chem. Res.* **1989**, *22*, 315.
2. Russell, D.H. Ed. **Gas Phase Inorganic Chemistry**, Plenum: New York, **1989**.
3. Armentrout, P.B. *Annu. Rev. Phys. Chem.* **1990**, *41*, 313.
4. Tonkyn, R.; Ronan, M.; Weisshaar, J.C. *J. Phys. Chem.* **1988**, *92*, 92.
5. Irikura, K.K.; Beauchamp, J.L. *J. Phys. Chem.* **1991**, *95*, 8344.
6. Taylor, W.S.; Everett, W.R.; Babcock, L.M. McNeal, T.L. *Int. J. Mass Spectrom. Ion Proc.* in press.
7. Chowdhury, A.K.; Wilkins, C.L. *J. Am. Chem. Soc.* **1987**, *109*, 5336.
8. Van Koppen, P.A.M.; Brodbelt-Lustig, J.; Bowers, M.T.; Dearden, D.V.; Beauchamp, J.L.; Fisher, E.R.; Armentrout, P.B. *J. Am. Chem. Soc.* **1991**, *113*, 2359.

Transition Metal Ion Reactions with Laser Desorbed Amino Acid and Peptide Neutrals in a Fourier Transform Mass Spectrometer

Ping P. Wang, Cindy C. Pitsenberger, J. Paul Speir, Gregory S. Gorman*, I Jonathan Amster
Department of Chemistry, University of Georgia
Athens, Georgia, 30602

INTRODUCTION

We have previously reported the reactions of transition metal ions with laser desorbed amino acids neutrals in a Fourier transform mass spectrometer.[1] For these prior experiments, the metal ions were formed by laser ablation of a suitable metal target and were allowed to undergo thermalizing collisions with a single pulse of a bath gas (Ar) resulting in 40-60 collisions/ion. Since many of the metal ions possess long lived excited states, this relatively low number of collisions proved to be insufficient for collisional thermalization of the metal ions to their ground state. Attempts to increase the number of collisions resulted in substantial ion loss due to the expansion of the ions' magnetron radius. Here we report the application of a new technique, quadrupolar excitation,[2] in which the metal ions are subjected to tens of thousands of thermalizing collisions with a bath gas thereby significantly reducing the population of excited state ions with less than a 1% loss in ion intensity

EXPERIMENTAL

All experiments were performed in a Fourier transform mass spectrometer designed and constructed in this laboratory and equipped with an electromagnet operated at a field strength of 1 tesla. Neutral amino acid molecules were produced using the substrate-assisted technique in which 248 nm (KrF) light from an excimer laser is focused onto the sample probe at an irradiance of approximately 1 MW/cm^2.[3] Transition metal ions were produced by laser ablation of a metal target using multiple pulses of 248 nm light at irradiances $\geq$ 10 MW/cm^2 Pulsed valves were used for introduction of the collision gas into the vacuum system. Quadrupolar excitation was performed by applying a r.f quadrupolar electric field to cause interconversion of magnetron and cyclotron motion resulting in tens of thousands of thermalizing collisions between the metal ions and the collision gas. Additionally, this technique axializes the metal ions, moving them to the center of the ICR cell, directly in front of the sample probe, which enhances overlap between the laser desorbed neutrals and the metal ions.

RESULTS

Figure 1 shows the effects of quadrupolar cooling on the reaction of mass selected $^{65}Cu^+$ with laser desorbed phenylalanine molecules. In Figure 1a, in which quadrupolar cooling was not used, the reaction between the metal ions and the amino acid neutrals results exclusively in charge exchange. In Figure 1b, in which quadrupolar cooling was used, we observe metal ion attachment with subsequent loss of the elements of formic acid. The absence of any charge exchange products in Figure 1b suggests that quadrupolar cooling effectively reduces the internal energy of the metal

ions. Figure 2 shows the reaction of quadrupolar cooled, mass selected $^{63}Cu^+$ with phenylalanine neutrals. This spectrum is identical to that in Figure 1b, except that all the peaks appear two mass units lower confirming Cu ion attachment to these ions

REFERENCES

1. Speir, J. P., Gorman, G. S ; Amster, I. J. *J. Am. Soc. Mass Spectrom.* **1993**, *4*, 106
2. Speir, J. P ; Gorman, G. S.; Pitsenberger, C. C.; Turner, C. A.; Wang, P. P.; Amster, I. J. *Anal. Chem.* In press.
3. Speir, J. P.; Amster, I. J. *Anal. Chem.* **1992**, *64*, 1041

Figure 1a

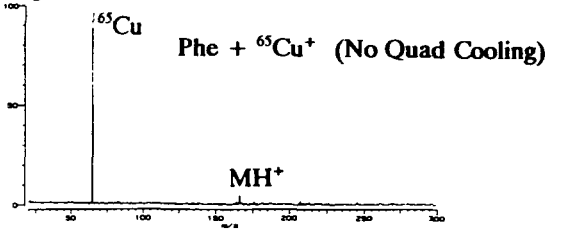

Figure 1b

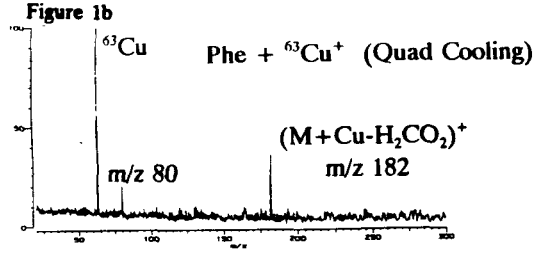

Figure 2

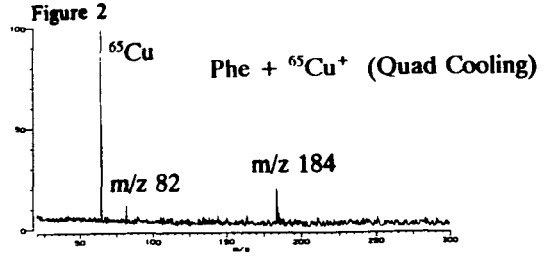

Chemistry of NO and CO Ligands on MCo_n^+ clusters

Yongqing Huang and Ben S. Freiser*
H. C. Brown Laboratory of Chemistry
Purdue University
West Lafayette, IN 47907

The highly reactive nature of small gas-phase transition metal clusters is not only reflected by their abilities to activate a variety of chemical species in the gas-phase, but also by the rich chemistry of their ligated systems where uniquely interesting ligand structures are sometimes observed. One such example is a chemisorbed nitrosyl ligand in Co_nNO^+.[1] This study examines the chemistry of CO and NO coordinated to small heterodinuclear and trinuclear cluster ions with one of the constituent metal atoms being an early transition metal ion, whose strong M-O bond is expected to facilitate dissociated ligand structures.

A. Oxidation of Carbon Monoxide to Carbon Dioxide by Vanadium Oxide Ion

A heterodinuclear complex ion with a CO_2 ligand is formed upon reacting $Co(CO)_3NO$ with VO^+, which is prepared from the reaction of laser desorbed V^+ with O_2, reaction 1. The

(1) $VO^+ + Co(CO)_3NO \longrightarrow VCo(NO)(OCO)^+ + 2CO$ 100% [2]

presence of a CO_2 ligand structure is supported by CID on the isolated product ion from reaction 1, reactions 2-6. The loss of a distinct CO_2 molecule from reaction 3, as opposed to

(2) $VCo(NO)(OCO)^+ \xrightarrow{CID} VCoO(NO)^+ + CO$
(3) $\longrightarrow VCo(NO)^+ + CO_2$
(4) $\longrightarrow VCoO^+ + CO + NO$
(5) $\longrightarrow VO^+ + (Co + NO + CO)$
(6) $\longrightarrow Co^+ + (VO + NO + CO)$

the consecutive loss of CO and an oxygen atom, is verified by the lack of a $VCoNO^+$ fragment upon isolating the product ion from reaction 2 and performing further CID on it. The concurrent loss of CO_2 in reaction 3 and CO elimination in reaction 2 suggest the likelihood of two distinct species for the product ion from reaction 1, with each giving different fragmentation products. Intuitively, an ion with the structure $VCo(NO)(O)(CO)^+$ is expected to give CO elimination readily, reaction 2, while an ion with the structure $VCo(NO)(CO_2)$ is expected to eliminate CO_2 upon CID. Alternatively, the two structures might be very close in energy and interconvert from one structure to the other under CID activation.

Ion-molecule reactions were used to provide further support for the CO_2 structure. Reactions 7-9 were observed upon reacting CH_3CN with the product ion from reaction 1.

(7) $VCo(NO)(OCO) + CH_3CN \longrightarrow VCo(NO)(CH_3CN)^+ + CO_2$ 9%
(8) $\longrightarrow VCo(NO)(O)(CH_3CN) + CO$ 10%
(9) $\longrightarrow VCo(NO)(OCO)(CH_3CN)^+$ 81%

Isolation and subsequent CID of the condensation product ion in reaction 9 gives 19% $VCoNO(CH_3CN)^+$, 13% $VCoNO^+$ and 68% $VCo(NO)(OCO)^+$, suggesting the competitive loss of the acetonitrile ligand.

B. The Structures and Reactivities of NO Ligands

Evidence was presented in an earlier study that the nitrosyl ligand actually exists in both molecularly adsorbed and the dissociated forms in the species Co_2NO^+.[1] This study indicates that this structure may be the favored structure, as opposed to a simple two-electron or three-electron NO ligand for quite a few dinuclear complexes of the ligand. For example, $MCoNO^+$ (M = Sc, Y, La) ions were formed upon reacting $Co(CO)_3NO$ with the respective metal ions. CID on these dinuclear species give MO^+, exclusively, indicating the spliting of the NO ligand under activation. The ion-molecule reactions of several neutral species with $ScCoNO^+$ provided further evidence for the dissociated NO ligand structure. For example, reactions 10 and 11 were observed upon reacting $ScCoNO^+$ with ethylene. Reaction 12 provides another

(10) $ScCoNO^+ + C_2X_4 \longrightarrow ScCoOX^+ + C_2X_3N$ X = H, D
(11) $\longrightarrow ScCoC_2X_3N^+ + OX$

interesting example of a series of unique reactions that give products involving the breaking of the N-O bond.

(12) $ScCoNO^+ + CH_3CN \longrightarrow ScCoOCN^+ + (CH_3N)$

C. Reductive Coupling of Two Nitrosyl Ligands

Simultaneous reduction of two adjacent NO ligands coordinated to small heteronuclear transition metal cluster species occurs. For example, reaction 13 proceeds efficiently upon low energy CID on on $ScCo_2(NO)_2CO^+$, which is prepared from the reaction of $ScCoNO^+$ with

(13) $ScCo_2(NO)_2CO^+ \longrightarrow ScCo_2O_2^+ + CO + N_2$

$Co(CO)_3NO$. Of the two nitrosyl ligands present, only one NO ligand displays reactivity similar to reaction 10-11. For example, the reaction of propene with $ScCo_2(NO)_2CO^+$ gives both ligand displacement of the carbonyl ligand, reaction 14, and products indicating the spliting of the NO ligand, reaction 15.

(14) $ScCo_2(NO)_2CO^+ + C_3H_6 \longrightarrow ScCo_2(NO)_2(C_3H_6)^+ + CO$
(15) $\longrightarrow ScCo_2(NO)(CO)(OH)^+ + C_3H_5N$

The coupled reduction of two NO ligands also occurs for the polynuclear species $ScCo_3(NO)_3(CO)^+$, which is prepared from the reaction of $ScCo_2(NO)_2(CO)^+$ with $Co(CO)_3NO$. $ScCo_3(NO)_3(CO)^+$ readily loses a NO ligand upon CID, with the remaining two NO ligands undergoing reductive coupling and CO elimination to give $ScCo_3O_2^+$. Based on the CID results, it it obvious that multiple patterns of coordination exist for these NO ligands.

In summary, Interesting structures and reactivities are associated with CO and NO ligands coordinated to MCo_n^+ systems with M being an early transition metal atom. The highly reactive nature of the cluster centers definitely plays a key role in promoting these structures and reactivities. Future efforts will focus on using specific ion-molecule reactions to probe unique ligand structures.

References

1. (a).Jacobson, D. B. J. Am. Chem. Soc. **1987**, 109, 6851. (b). Klaassen, J. J.;.Jacobson, D. B. J. Am. Chem. Soc. **1988**, 110, 974.
2. OCO is used to represent both CO_2 and (O)(CO) structures.

FORMATION OF STRONGLY BOUND TRANSITION-METAL MOLECULAR SILANE COMPLEXES. η^2-COORDINATION OF Si-H

R. Bakhtiar and D. B. Jacobson

Department of Chemistry, North Dakota State University
Fargo, North Dakota 58105-5516

The oxidative addition of a Si-H bond to a transition-metal center is an obligatory step in many transition metal-mediated transformations of organosilanes including hydrosilation[1] and silane alcoholysis. Formation of an η^2-Si-H coordination complex (three-center two-electron bond, **1**) is a prerequisite step for formal oxidative addition to yield **2**. Several examples of coordination complexes of **1** have been generated and characterized in solution.[2]

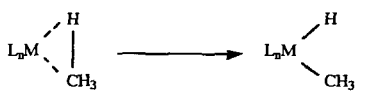

1 **2**

1 is important because it is intermediate toward formal Si-H oxidative addition and is related to the corresponding H-H and C-H three-center two-electron bond complexes.[3] Although Fe^+ reacts with methylsilanes by elimination of simple molecules (H_2 or CH_4),[4] methylsilane adducts can be generated by displacement of CO from $FeCO^+$,

$$FeCO^+ + Me_xSiH_{4-x} \longrightarrow (FeMe_xSiH_{4-x})^+ + CO \qquad (1)$$
$$(x = 0\text{-}4) \qquad \mathbf{3}$$

reaction 1, and it is the exclusive process observed for methylsilanes. **3** may exist either as a molecularly bound iron-silane complex or as an insertion species (e.g., $(HFe\text{-}SiMe_2H)^+$ or $(H_2Fe{=}SiMe_2)^+$ for Me_2SiH_2).

Insight into the structure of **3** can be obtained by studying specific ion/molecule reactions. Ethene and ethene-d_4 react with the silane adducts ($(FeSiH_4)^+$, $(FeMeSiH_3)^+$, and $(FeMe_4Si)^+$) to yield exclusive silane displacement with *no* H/D scrambling observed with ethene-d_4. The silane adduct $(FeMe_2H_2)^+$ yields both adduct formation and silane displacement, reaction 2. Similar results were obtained for reaction with ethene-d_4 with *no* H/D

$$(FeMe_2SiH_2)^+ + C_2H_2 \xrightarrow{0.10} (FeMe_2SiH_2)C_2H_4^+ \qquad (2a)$$
$$(FeMe_2SiH_2)^+ + C_2H_2 \xrightarrow{0.90} FeC_2H_2^+ + Me_2SiH_2 \qquad (2b)$$

exchange. Me_2SiH_2 reacts with $Fe(CH_2CH_2)^+$ to yield both ethene displacement (0.57) and adduct formation (0.43). CAD of the adduct, $(FeMe_2SiH_2)C_2H_4^+$, yields competitive Me_2SiH_2 (0.78) and ethene (0.22) losses at low collision energy. In contrast to the above silane displacement reactions, the $(FeMe_3SiH)^+$ adduct reacts with ethene to yield both silane displacement and formation of $FeSiC_3H_8^+$ (formally a dehydrogenation process), reaction

$$(FeMe_3SiH)^+ + C_2H_4 \xrightarrow{0.74} FeC_2H_4^+ + Me_3SiH \qquad (3a)$$
$$(FeMe_3SiH)^+ + C_2H_4 \xrightarrow{0.23} FeSiC_3H_8^+ + C_2H_6 \qquad (3b)$$
$$(FeMe_3SiH)^+ + C_2H_4 \xrightarrow{0.03} (FeMe_3SiH)C_2H_4^+ \qquad (3c)$$

3. Ethene-d_4 yields similar results with ethane loss exclusively as $C_2D_4H_2$. Reaction of Me_3SiH with $FeC_2H_4^+$ yields competitive adduct formation (0.33) and ethane loss (0.67).

The complete absence of H/D exchange for reaction of the $(Fe\text{-silane})^+$ adducts with ethene-d_4 suggests that insertion into the Si-H bond has *not* occurred. Consequently, the $(Fe\text{-silane})^+$ adducts are believed to consist of molecular silane bound to Fe^+. The displacement of CO from $FeCO^+$ combined with silane displacement from the $(Fe\text{-silane})^+$ adducts by ethene indicate that $D^o(Fe^+\text{-}CO) = 31.3 \pm 1.4$ kcal/mol[5] $< D^o(Fe^+\text{-silane}) \leq D^o(Fe^+\text{-}CH_2CH_2) = 39.9 \pm 1.4$ kcal/mol.[6] The results for Me_2SiH_2 suggest that $D^o(Fe^+\text{-}Me_2SiH_2) \approx D^o(Fe^+\text{-}C_2H_4)$. Hence, Fe^+ forms strongly bound molecular silane complexes with Fe^+! The relative binding energy of the silanes to Fe^+ was determined by silane/silane displacement reactions (e.g., reaction 4).

$$Fe(Me_3SiH)^+ + Me_2SiH_2 \longrightarrow Fe(Me_2SiH_2)^+ + Me_3SiH \qquad (4)$$

These results reveal the following order of relative silane binding energies:

$$\boxed{Me_2SiH_2 > Me_3SiH > MeSiH_3 > Me_4Si > SiH_4}$$

Reaction with mixed deuterated silanes (e.g., $Fe(Me_3SiH)^+$ with Me_2SiD_2) revealed *no* H/D exchange, again consistent with formation of molecular silane-Fe^+ complexes.

We now consider the structure of the $Fe(silane)^+$ adducts. The binding energy of Fe^+ to propane has recently been found to be 19 ± 2 kcal/mol.[7] This binding energy is considerably less than that for the above silanes (> 31 kcal/mol). The strong binding energy suggests that Fe^+ interacts with a Si-H bond instead of a C-H bond of methylsilanes. It has been found that metals that display a weak interaction with C-H bonds may display strong interactions with Si-H bonds. This interaction is presumably in the form of a three-center two-electron bond complex similar to **1**. If the nature of the interaction of the silane with Fe^+ is purely electrostatic, then the binding energy should follow silane polarizability with Me_4Si the strongest bound silane. The above relative order of silane binding energies clearly indicates that the interaction is more complicated than that of a simple ion-dipole model.

References

1. Ojima, I. In *The Chemistry of Organic Silicon Compounds*; Patai, S., Rappoport, S., Eds.; Wiley: New York, 1989, Chapter 25.
2. Schubert, U. *Adv. Organomet. Chem.* **1990**, *30*, 151 and references cited therein.
3. Crabtree, R. H.; Hamilton, D. H. *Adv. Organomet. Chem.* **1988**, *28*, 299.
4. Kang, H., Jacobson, D. B., Shin, S. K., Beauchamp, J. L.; Bowers, M. T. *J. Am. Chem. Soc.* **1986**, *108*, 5668.
5. Schultz, R. H.; Crellin, K. C., Armentrout, P. B. *J. Am. Chem. Soc.* **1991**, *113*, 8590.
6. Armentrout, P. B., Clemmer, D. E. In *Energetics of Organometallic Species*, Simoes, J. A. M., Ed.; Kluwer: Netherlands, **1992**, p. 321.
7. Schultz, R. H.; Armentrout, P. B. *J. Am. Chem. Soc.* **1991**, *113*, 729.

Fe-L$^+$ (L = c-C_5H_6, C_4H_6) MEDIATED EXTRUSION OF CO FROM FURAN. A MODEL STUDY RELEVANT TO CATALYTIC HYDRODESULFURIZATION

R. Bakhtiar and D. B. Jacobson

Department of Chemistry, North Dakota State University
Fargo, North Dakota 58105-5516

Catalytic hydrodesulfurization (HDS), hydrodeoxygenation (HDO), and hydrodenitrogenation (HDN) are important processes for hydrotreatment of liquid fuels.[1] HDS of thiophene and sulfides is particularly significant due to the large sulfur content of many petroleum feedstocks The catalyzed removal of heteroatoms from heterocycles typically involves hydroprocessing petroleum feedstocks over an alumina supported cobalt-molybdenum sulfide catalyst. Model systems have been studied involving thiophene, furan, and pyrrole to better understand the mechanism of heteroatom removal. These species were selected for study because they require the most severe conditions for reaction (i.e , heteroatom removal). The reaction of Fe(L)$^+$ (L = C_4H_6, c-C_5H_5, c-C_5H_6, C_6H_6, and O) with thiophene, furan, and pyrrole was studied by using Fourier transform mass spectrometry (FTMS)

Fe^+, Fe(c-C_5H_5)$^+$, and Fe(C_6H_6)$^+$ yield exclusive adduct formation with thiophene, furan, and pyrrole. The chemistry of the iron-diene complexes, $FeC_4H_6^+$ and Fe(c-C_5H_6)$^+$, is considerably more complicated The most intriguing reaction is the predominant, direct extrusion of CO from furan, reactions 1 and 2. A proposed

$$FeC_4H_6^+ + C_4H_4O \longrightarrow FeC_7H_{10}^+ + CO \quad (1a)$$

$$FeC_4H_6^+ + C_4H_4O \longrightarrow FeC_7H_8^+ + (H_2CO) \quad (1b)$$

$$Fe(c\text{-}C_5H_6)^+ + C_4H_4O \longrightarrow FeC_8H_{10}^+ + CO \quad (2)$$

mechanism for reaction 2 is presented in Scheme I and involves initial C-H bond insertion. Initial C-O bond insertion is also possible.

Scheme I

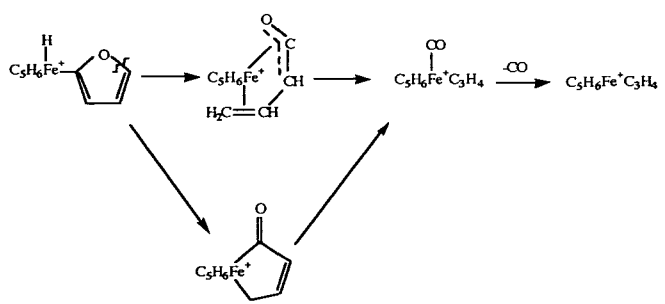

The predominant reaction of both thiophene and pyrrole with Fe(c-C_5H_6)$^+$ is displacement of a hydrogen atom which implies D^o(FeC_5H_5)$^+$-L) (L=thiophene, pyrrole) > D^o(Fe$C_5H_5^+$-H) = 46±5 kcal/mol.[2] Thiophene and pyrrole yield predominant adduct formation and C_4H_6 displacement with $FeC_4H_6^+$. CAD of the adduct, Fe(C_4H_6)$C_4H_4S^+$, yields competitive C_4H_6 (ca. 64%) and C_4H_4S (ca. 36%) loses with an analogous distribution

seen for SORI-CAD.[3] These results suggest that D^o(Fe$^+$-C_4H_4S) ≈ D^o(Fe$^+$-C_4H_6) = 48±5 kcal/mol [4] Finally, CAD of the adducts, Fe(C_6H_6)$C_4H_4O^+$ and Fe(C_6H_6)$C_4H_5N^+$, yield exclusive loss of the heterocycle indicating that D^o(Fe$^+$-C_4H_4O) and D^o(Fe$^+$-C_4H_5N) are less than D^o(Fe$^+$-C_6H_6) = 55±5 kcal/mol.[4]

FeO^+ reacts with C_4H_4X (X = S, O, NH) to yield initial CO elimination followed by loss of CO (furan), C_2H_4 (thiophene), and C_2H_4 (pyrrole), reactions 3-5 A general mechanism for CO extrusion for these heterocycles

$$FeO^+ + C_4H_4O \xrightarrow{-CO} FeC_3H_4O^+ \xrightarrow{-CO} FeC_2H_4^+ \quad (3)$$

$$FeO^+ + C_4H_4S \xrightarrow{-CO} FeC_3H_4S^+ \xrightarrow{-C_2H_4} FeCS^+ \quad (4)$$

$$FeO^+ + C_4H_5N \xrightarrow{-CO} FeC_3H_5N^+ \xrightarrow{-C_2H_4} FeHCN^+ \quad (5)$$

by FeO^+ is presented in Scheme II and involves initial C-X insertion.

Scheme II

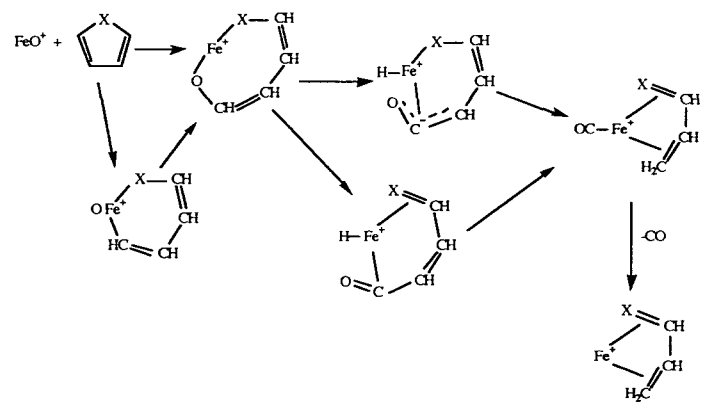

These results indicate that simple iron ion complexes can readily remove the heteroatom from model heterocycles.

References

1. Mitchell, P. C H. *Catal.* **1981**, *4*, 175.
2. Huang, Y.; Freiser, B S. *J. Am. Chem. Soc.* **1990**, *112*, 5085.
3. Gauthier, J. W.; Trautman, T. R.; Jacobson, D. B. *Anal. Chim. Acta* **1991**, *246*, 211
4. Hettich, R. L.; Jackson, T C.; Stanko, W. M., Freiser, B S *J. Am. Chem. Soc.* **1986**, *108*, 5086.

Hydrogenolysis Rates of Group 4 Methyl Metallocenes

*N.G. Alameddin, M.F. Ryan, J.R. Eyler, and D.E. Richardson
Department of Chemistry, University of Florida
Gainesville, FL 32611-2046

The chemistry of organometallic molecules in solution has been extensively studied, while in contrast, the gas-phase reactivity of analogous compounds is just beginning to be explored. Our group at the University of Florida has several projects underway to determine the kinetic and thermodynamic properties of organometallic ions in the gas-phase using Fourier Transform Ion Cyclotron Resonance Mass Spectrometry (FTICR-MS). One array of compounds of particular interest is the Group 4 methyl metallocenes. These complexes have been shown to behave as Ziegler-Natta catalysts in solution, where the presence of the solvent can significantly affect the rate of reaction. The goal of this study is to ascertain the intrinsic reactivity of these important compounds in the absence of the solvent.

In the present work the rates of hydrogenolysis (k_H) for a set of cationic complexes of the general formula, $L_2MCH_3^+$ (M = Ti, Zr, and Hf; L = cyclopentadienyl derivatives) are being measured by FTICR-MS. The least sterically demanding reaction possible, the reaction with dihydrogen to produce the hydride and methane (Fig. 1), was chosen to separate the electronic and steric properties of this system. The compounds were synthesized by A.R. Siedle (3M). A glove box is used for all subsequent sample handling and storage of these air- and water-sensitive complexes

In a typical experiment, a sample is attached to the end of a solids probe and inserted into the main chamber, so that the sample is 3-5 cm from the ICR cell. After setting the sample pressure (~1-5 x 10^{-7} torr), a partial pressure of H_2 (~5-10 x 10^{-7} torr) is established. On electron impact, the neutral, $L_2M(CH_3)_2$, loses a methyl group to form the desired ion, $L_2MCH_3^+$ (Fig. 2). Following a thermalization period, all other ions are

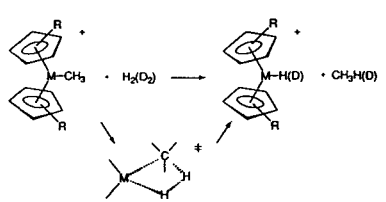

Figure 1

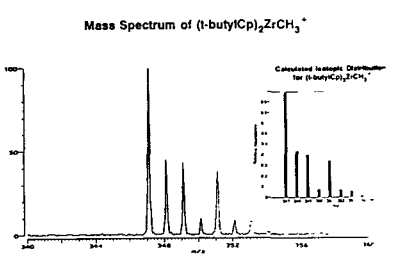

Figure 2

ejected and the substrate is allowed to react with H_2 for a variable time followed by excitation and detection. A pseudo-first order rate constant can be determined by monitoring the disappearance of the reactant and the appearance of the product, L_2MH^+, as a function of time (Fig. 3).

The rate constants are plotted against the sum of the γ parameters [1], a dimensionless parameter quantifying the relative metal-ligand electronic interaction for substituents on cyclopentadienyl (Cp) ligands (Fig. 4). The trend which is becoming apparent (albeit from four points) is that the rate decreases with decreasing γ values. The γ parameters from the ruthenocene study show a decrease in ionization potential with decreasing γ values. Electron-rich substituents (negative γ values) stabilize the oxidation of the substituted ruthenocenes relative to Cp_2Ru. The reactivity of the Zr complexes depends on the electrophilicity of the metal center, and the hydrogenolysis rate is expected to increase with increasingly positive γ values This prediction is illustrated by the three additional points plotted on Fig. 4.

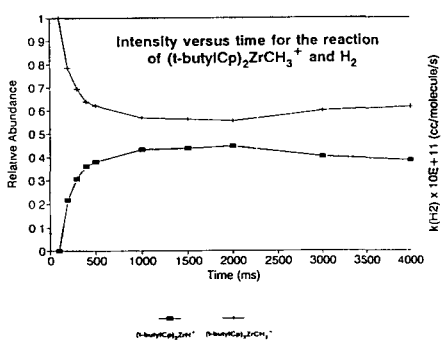

Figure 3

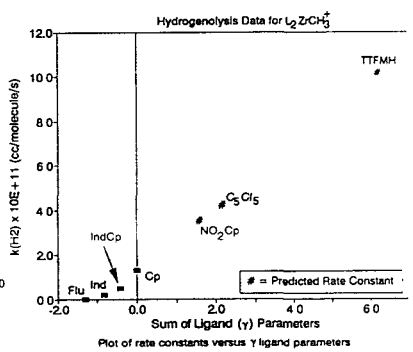

Figure 4

In summary, the hydrogenolysis rate constants for a set of Group 4 methyl metallocenes have been determined. The trend thus far is as expected based on the previously derived ligand parameters In the future, besides continuing the work on the reactivity with H_2, we will explore the reactivity of these complexes with various alkenes and alkynes.

Support for this work by the NSF and the ONR is gratefully acknowledged.

1 Ryan, M.F ; Siedle, A.R., Burk, M J.; and Richardson, D E , *Organometallics*, 1992, 11, 4231.

THE CHANGE IN REACTIVITY OF THE $FeCp^+$ ION AFTER COLLISIONAL THERMALIZATION USING QUADRUPOLAR EXCITATION WITH FOURIER TRANSFORM MASS SPECTROMETRY

Cheryl A. Turner, Charles R. Kutal, I. J. Amster
Department of Chemistry, University of Georgia, Athens Georgia, 30602

INTRODUCTION

We are interested in studying the gas-phase ion chemistry of $FeCp^+$ and its thermal reactions with ethylene oxide and other heterocyclic compounds in order to gain a better understanding of its role in the cationic polymerization of epoxides. We previously reported evidence of two channels for the reaction of $FeCp^+$ and ethylene oxide.[1] Electron transfer yields the radical cation, $C_2H_4O^+$, which rapidly abstracts a hydrogen from a second epoxide molecule to form the observed product, $C_2H_5O^+$; oxygen abstraction forms the metal-containing products, $FeCpO^+$ and $FeCpO_2^+$. There are also two reaction pathways for the reaction of tetrahydrofuran (THF) with $FeCp^+$. Coordination forms $FeCpTHF^+$, while electron transfer, followed by hydrogen transfer with a second molecule of THF, yields $C_4H_7O^+$ and $C_4H_9O^+$. We found that the two reaction pathways could be individually enhanced by changing the internal energy of the $FeCp^+$ ion. However, there was not enough physical data on $FeCp^+$ to determine whether the electron transfer reactions were exothermic or endothermic for $FeCp^+$ in its ground electronic state. Recently, Dunbar et. al. determined the bond dissociation energy of $FeCp_2^+ \rightarrow FeCp^+ + Cp$ to be 3.7 eV,[2] thereby allowing a calculation of the recombination energy of $FeCp^+$ (6.7 eV). As a result, the electron transfer reaction between $FeCp^+$ and ethylene oxide or THF is endothermic by more than 2 eV, which suggests that the $FeCp^+$ ion is formed in an electronically excited state. Recently, we have examined the ratio of the two reaction pathways for both of the heterocyles with $FeCp^+$ as a function of the number of thermalizing collisions using quadrupolar excitation,[3,4] and the results of these studies will be discussed here.

EXPERIMENTAL

A Fourier transform mass spectrometer, equipped with a 1-3/4" cubic cell, a 1 Tesla electromagnet, and an IonSpec Omega data system is used in these studies. The gas/liquid inlet system is equipped with three pulsed valves and a sapphire sealed leak valve which are used for introducing volatile samples into the main vacuum chamber. The gas/liquid inlet system is pumped with a diffusion pump and the main vacuum chamber is pumped with a 330 l/s turbomolecular pump to a base pressure of 2×10^{-10} Torr.

The $FeCp^+$ ion used in these experiments is formed by electron ionization of ferrocene, which is pulsed into the main chamber at a peak pressure of 10^{-7} to 10^{-6} torr. The cation is then collisionally thermalized with a pulse of carbon dioxide for 1200 ms using quadrupolar excitation.[3,4] This technique uses an r.f. quadrupolar electric field to cause the interconversion of magnetron and cyclotron motion. If this interconversion is rapid compared to the collision frequency of an ion with neutrals in the ICR cell, then the ion follows a trajectory that pushes it to the center of the cell. Once at the center of the cell, quadrupolar excitation can be used to allow an ion to undergo thermalizing collisions without the occurrence of radial diffusion. Following thermalization of $FeCp^+$, ethylene oxide or other nucleophiles are pulsed into the system and allowed to react for 2500 ms before ionic reaction products are detected.

RESULTS

Figure 1 shows the ratio of products resulting from the reaction of $FeCp^+$ with ethylene oxide, plotted versus the number of thermalizing collisions $FeCp^+$ experiences with CO_2 prior to reaction. The main reaction pathway for no thermalizing collisions or for a large number of thermalizing collisions is oxygen abstraction, however, electron transfer dominates at every point in between those two extremes. The reaction of $FeCp^+$ with THF is found to have a similar response, except that coordination of the THF molecule, not oxygen abstraction, is the main reaction channel for high and low numbers of thermalizing collisions. Since electron transfer is an endothermic reaction for both of the heterocyclic ethers, and should therefore be a slow reaction for the ground state species, its observation shows that $FeCp^+$ is present in an excited state, even after hundreds of thermalizing collisions with a molecular gas. In conclusion, the results show that thousands of thermalizing collisions are required to relax the $FeCp^+$ ion to its ground state. Therefore, methods for trapping ions while they undergo a large number of collisions, such as quadrupolar excitation or a QUISTOR-type event,[5] are needed to quench the surprisingly long lifetimes of the metal complex's excited states.

REFERENCES

1. Gwathney, W. J.; Lin, L.; Kutal, C.; Amster, I. J. *Organic Mass Spectrom.* **1992** *27* 840
2. Faulk, J. D.; Dunbar, R. C. *J. Am. Chem. Soc.* **1992** *114* 8596
3. Schweikhard, L.; Guan, S.; Marshall, A. G. *Int. J. Mass Spectrom. Ion Processes* **1992** *120* 71.
4. Speir, J. P.; Gorman, G. S.; Pitsenberger, C. C.; Turner, C. A.; Wang, P. P.; Amster, I. J. *Anal. Chem.*, in press
5. Jacoby, C. B.; Holliman, C. L.; Rempel, D. L.; Gross, M. L. *J. Am. Soc. Mass Spectrom.* **1993** *4* 186.

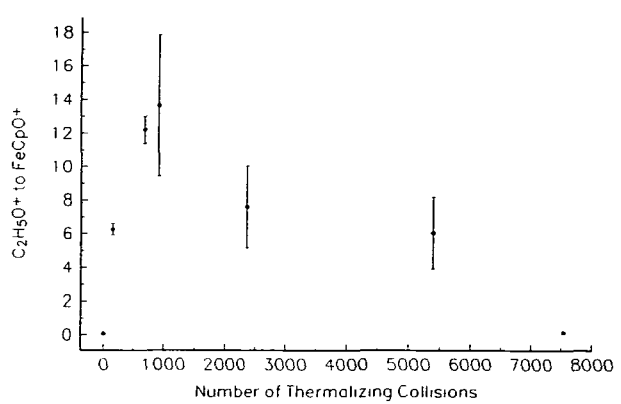

Figure 1: The ratio of products resulting from the reaction of $FeCp^+$ with ethylene oxide, plotted versus the number of thermalizing collisions $FeCp^+$ experiences with CO_2 prior to reaction.

Gas-Phase Ion Molecule Chemistry of η^4-c-$C_8H_8Fe(CO)_3$: Reactivity and Structure

Ziyi Kan and Melvin B. Comisarow, Department of Chemistry, University of British Columbia
Vancouver, B. C., Canada, V6T 1Z1

Introduction. It has been shown that the fully coordinated aromatic hydrocarbon ligands in (η^4-c-C_5H_5)M^+ and (η^6-c-C_6H_6)M^+ from different sources retain their structural integrity in the gas phase [1]. Our ion reactivity study of organometallic complexes bearing non-aromatic olefin ligands, such as (η^6-c-C_7H_8)$Cr(CO)_3$ [2], (η^4-c-C_6H_6O)$Fe(CO)_3$ and (η^4-c-C_6H_8)$Fe(CO)_3$, has revealed an intramolecular β-hydride transfer process from olefin to metal that lowers ion reactivity. An example is the reaction of (c-C_7H_8)Cr^+ shown in Eqn. (1). In this study, the uncoordinated free diene portion of the cyclooctatetraene in (η^4-c-C_8H_8)$Fe(CO)_3$ is demonstrated to be able to lower ion reactivity by fully or partially coordinating to metal center(s). These observations are of importance to a better understanding of the mass spectra of organometallic complexes.

$$(\eta^6\text{-}C_7H_8)Cr^+ \Leftrightarrow (\eta^7\text{-}C_7H_7)Cr\text{-}H^+ \qquad (1)$$

Experimental. A home-built Fourier transform ion cyclotron resonance mass spectrometer equipped with a Nicolet FTMS-1000 console, 2.54 cm cubic trapping cell and 1.9 Tesla electromagnet is used in this study. Sample pressure is maintained at 6.0 x 10^{-7} Torr and monitored by a Varian dual range ionization gauge. 25 eV x 20 millisecond and 2.5 eV x 5 millisecond electron beam pulses are used to generate positive and negative fragment ions, respectively. FT-ICR multiple resonance techniques are used to isolate a single reactant ion to study its reaction pathways. Rate constants for the pseudo-first order reactions between reactive ions and $C_8H_8Fe(CO)_3$ are determined by following the variations of ion intensities with reaction times.

Results and Discussion. The measured rate constants of the major positive fragment ions and ionic products are listed in Table 1. ED in the table is the calculated electron deficiency from an 18-electron closed shell, assuming η^4-C_8H_8 coordination and single metal-metal bonding in polymetallic ions. ED* is the adjusted electron deficiency of rearranged ion structures. The ion reactivity shows increasing trend with increasing electron deficiency of the central metal atoms. Eqn. (2) to (7) summarize the major positive ion molecule reactions determined by ion ejection experiments.

$$C_6H_6Fe^+ + C_8H_8Fe(CO)_3 \rightarrow C_8H_8Fe_2(CO)_2^+ (1) + CO + C_6H_6 \qquad (2)$$
$$\rightarrow C_8H_8Fe_2C_6H_6^+ (2) + 3CO \qquad (3)$$
$$C_8H_8Fe^+ + C_8H_8Fe(CO)_3 \rightarrow C_8H_8Fe_2(CO)_2^+ (1) + CO + C_8H_8 \qquad (4)$$
$$\rightarrow (C_8H_8Fe)_2^+ (3) + 3CO \qquad (5)$$
$$C_8H_8Fe_2(CO)_2^+ (1) + C_8H_8Fe(CO)_3 \rightarrow (C_8H_8)_2Fe_2(CO)_2^+ (4) + Fe(CO)_3 \qquad (6)$$
$$\rightarrow (C_8H_8)_2Fe_3(CO)_2^+ (5) + 3CO \qquad (7)$$

As given in Table 1, the fragment ion $C_8H_8Fe(CO)_2^+$ and the product ions **2-5** in the above reactions are unreactive. As it has been observed repeatedly that 17-electron molecular ions of transition

metal complexes are generally unreactive, we believe that in $C_8H_8Fe(CO)_2^+$, the C_8H_8 ring donates 6 electrons to the metal atom, as shown below.

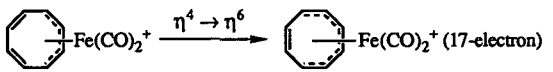

Since this conversion is driven by the electron unsaturation of the central metal atom, the η^6 coordination mode will remain in the fragment ions $C_8H_8Fe(CO)^+$ and $C_8H_8Fe^+$, which explains why $C_8H_8Fe^+$ and $C_6H_6Fe^+$ have the same reactivity. Similarly, the structures of the ionic products **1-5** are proposed to have partial double metal-metal bonds and η^6-C_8H_8 bonding to one Fe or η^4,η^4-C_8H_8 bonding to two Fe atoms, as appropriate to satisfy the measured ion reactivity. All these coordination forms of C_8H_8 to Fe have been observed directly in neutral complexes [3].

The negative mass spectrum of $C_8H_8Fe(CO)_3$ shows two fragment ions, $C_8H_8Fe(CO)_2^-$ and $C_8H_8Fe(CO)^-$. The reactions of $C_8H_8Fe(CO)^-$ with $C_8H_8Fe(CO)_3$ produce two stable ionic products, $(C_8H_8)_2Fe_2(CO)_3^-$ (**6**) and $C_8H_8Fe_2(CO)_3^-$ (**7**). Their structures are proposed in the following reaction sequence in analogy to the structures of neutral complexes $Cp_2Fe_2(CO)_4$ [4] and (η^4,η^4-C_8H_8)$Fe_2(CO)_5$ [3(b)]. Both **6** and **7** have 17-electron stable anion structures [5].

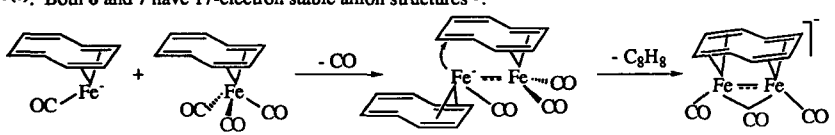

(**6**) (**7**)

Table 1. Rate constants and electron deficiencies

Species	ED	ED*	Rate Constant[a]
Fe^+	11		3.7
$C_6H_6Fe^+$	5	5	1.9
$C_8H_8Fe^+$	7	5	1.9
$C_8H_8Fe(CO)^+$	5	3	1.5
$C_8H_8Fe(CO)_2^+$	3	1	0.0
$C_8H_8Fe(CO)_3^+$	1	1	0.2
$C_8H_8Fe_2(CO)_2^+$	5.5	3	1.3
$C_8H_8Fe_2(CO)_3^+$	4.5	2	0.7
$C_8H_8Fe_2C_6H_6^+$	4.5	1	0.0
$(C_8H_8)_2Fe_2^+$	5.5	1	0.0
$(C_8H_8)_2Fe_2(CO)_2^+$	3.5	1	0.0
$(C_8H_8)_2Fe_3(CO)_2^+$	4.3	1.3	0.0

a. In units of 10^{-10} cm^3 $molecule^{-1}$ s^{-1}.

REFERENCES

1. (a) Parisod, G.; Comisarow, M. B. *Adv. Mass Spectrom.* **1980**, *8A*, 212. (b) Operti, L.; Vaglio, G. A.; R., G. J.; Freiser, B. S. *Organomet.* **1991**, *10*, 104.
2. Kan, Z. and Comisarow, M. B. Proceedings of the 40th ASMS Conference on Mass Spectrometry and Allied Topics, Washington, D. C, **1992**, pp1173-4.
3. (a) Mann, B. E. *J.Chem. Soc. Dalton* **1978**, 1761. (b) Keller, C. E.; Emerson, G. F.; Pettit, R. *J. Am. Chem. Soc.* **1965**, *87*, 1388. (c) Campbell, A. J.; Fyfe, C. A; Maslowsky, Jr. E. *J. Am. Chem. Soc.* **1972**, *94*, 2690. (d) Fleischer, E. B. *et al*, *J. Am. Chem. Soc.* **1966**, *88*, 3158.
4. Harris, D. C. et al, *J.Chem. Soc. Dalton* **1974**, 2389.
5. Squires, R. R. *Chem. Rev.* **1987**, *87*, 623

ACTIVATION OF METAL CARBONYLS BY CHARGE TRANSFER REACTION

Tianlan Zhang and Douglas P. Ridge
Department of Chemistry and Biochemistry, University of Delaware, Newark, DE 19716

Introduction

Metal carbonyls are interesting as prototypical transition metal coordination compounds and are also used as thermometer molecules in mass spectrometry. Their extent of decomposition following activation is used to measure the efficiency of various activation schemes. One method of activation that has not been thoroughly examined is charge transfer. We outline briefly here experiments intended to probe the effect of activating metal carbonyls by charge transfer. Two types of charge transfer processes have been considered. First we consider process where electronic excitation of the neutral product is not possible (eg. $Ar^+ + M(CO)_n$). Second we consider process where electronic excitation (or decomposition) of neutral product is possible ($N_2^+ + M(CO)_n$).

All measurements were made using a double-cell Fourier transform ion cyclotron resonance instrument (FTMS-2000, Extrel, Madison, WI).

Results and discussion

1. Activation of $Cr(CO)_6$ and $Fe(CO)_5$ by charge transfer reaction with NO^+, CS_2^+, OCS^+, Xe^+, CO_2^+, CO^+ and Ar^+. Rate constants and Branching ratios for these reactions have been obtained. Table 1 and Figure 1 show the rate constants and breakdown plot for $Fe(CO)_5$. These curves are consistent with the best data in the literature on appearance potentials. Comparison with the breakdown plot obtained from PEPICO suggests that nearly all of the reaction exothermicity is deposited in the metal carbonyl ions. The total reaction rate constants are fast (10^{-9} cm^3 $molecule^{-1}$ s^{-1}) consistent with an efficient electron transfer.

2. Charge transfer reaction of $Cr(CO)_6$ and $Fe(CO)_5$ with N_2^+, N_2O^+, O_2^+, Br_2^+, ICN^+ and $BrCN^+$. In these cases electronic excitation of the neutral products is possible. The distribution of $M(CO)_n^+$ products suggests a bimodal reaction. Products corresponding to n=0, 1, 2, 4 and 5 may be observed, for example, but the n=3 products is absent. In one mode the reaction exothermicity ΔH is all deposited in $M(CO)_n^{+\bullet}$ which then decomposes to give the distribution of products expected from PEPICO experiments for internal energy $E^* = -\Delta H$. In the second mode a specific product neutral excited state (N_2 $a^3\Sigma_u$) or specific decomposition products ($N_2(X^1\Sigma_g^+) + O(^1D)$) are formed depositing in $M(CO)_n^{+\bullet}$ the difference between $-\Delta H$ and the excitation or decomposition energy, E. The $M(CO)_n^{+\bullet}$ then decomposes to give the distribution of products expected from PEPICO experiments for internal energy $E^* = -\Delta H-E$. this dramatic bimodal behavior is also observed in the reactions of O_2^+, Br_2^+, ICN^+ and $BrCN^+$. The observed products of the N_2^+ and N_2O^+ reactions are consistent with (though not uniquely consistent with) (1) and (2) below.

$$N_2^+(^2\Sigma_g^+) + Fe(CO)_5 \text{ ---> } Fe(CO)_5^{+\bullet}(E^*) + N_2(X^1\Sigma_g^+, v=3) \qquad E^*=-\Delta H-3h\nu=7.0 \text{ eV}$$
$$\text{---> } Fe(CO)_5^{+\bullet}(E^*) + N_2(a^3\Sigma_u, v=3) \qquad E^*=-\Delta H-E-3h\nu=0.8 \text{ eV} \qquad (1)$$

$$N_2O^+(^2\Pi) + Fe(CO)_5 \text{ ---> } Fe(CO)_5^{+\bullet}(E^*) + N_2O(X^1\Sigma_g) \qquad E^*=\Delta H=4.99\text{eV}$$
$$\text{---> } Fe(CO)_5^{+\bullet}(E^*) + N_2(X^1\Sigma g^+, v=2) + O(^1D) \qquad (2)$$
$$E^*=-\Delta H-E-2h\nu=0.8 \text{ eV}$$

Table 1. Rate Constants of Charge Transfer Reaction

Charge Transfer Reaction	$-\Delta H$(eV)	k/k_{no}
$NO^+ + Fe(CO)_5$ -----> $Fe(CO)_5^+ + NO$	1.36	1
$CS_2^+ + Fe(CO)_5$ -----> $Fe(CO)_5^+ + CS_2$	2.20	0.287
$OCS^+ + Fe(CO)_5$ -----> $Fe(CO)_5^+ + OCS$	3.27	0.269
$Xe^+ + Fe(CO)_5$ -----> $Fe(CO)_5^+ + Xe$	4.28	0.157
$N_2O^+ + Fe(CO)_5$ -----> $Fe(CO)_5^+ + N_2O$	4.99	0.364
$CO_2^+ + Fe(CO)_5$ -----> $Fe(CO)_5^+ + CO_2$	5.87	0.303
$CO^+ + Fe(CO)_5$ -----> $Fe(CO)_5^+ + CO$	6.11	0.610
$Ar^+ + Fe(CO)_5$ -----> $Fe(CO)_5^+ + Ar$	7.86	0.373

$k_{no} = 6.74*10^{-10}$ cm^3 $molecule^{-1}$ s^{-1} for reaction of NO^+ with $Fe(CO)^5$

Figure 1. Breakdown Curve of $Fe(CO)_n$

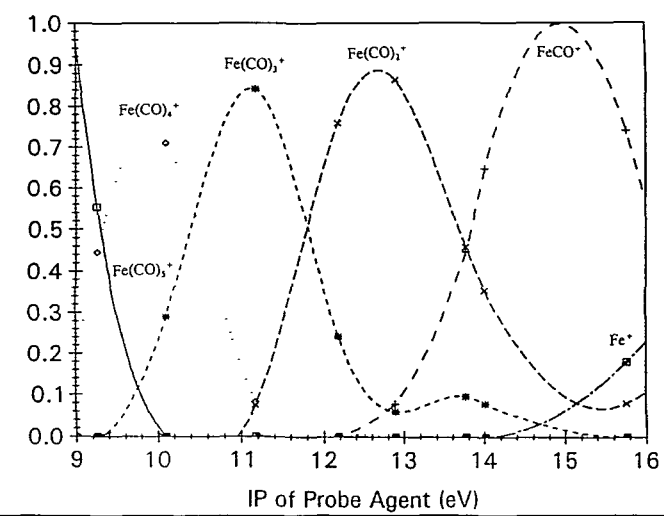

The Chemistry of Methinyltricobalt Enneacarbonyls Radical Anions : Unimolecular and Bimolecular Reactions

David L. Vollmer and M. L. Gross, University of Nebraska-Lincoln, Lincoln, NE 68588
R. Waugh, M. Bruce and J. Bowie, University of Adelaide, Adelaide, South Australia, 5000.

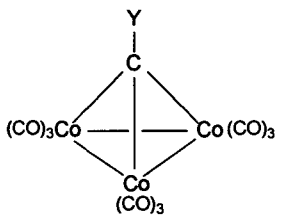

Methinyltricobalt enneacarbonyls are the first examples of heteronuclear cobalt carbonyl clusters[1]. Their stability is indicated by the numerous and facile synthetic routes[2] and can be attributed to the high symmetry of the complexes. The complexes have also been used as catalysts in the reduction of aromatic nitro compounds[3], the hydroformylation of alkenes[4], and the hydrogenation of CO[5].

The synthesis of methinyltricobalt enneacarbonyls was previously shown as the reaction of cobalt tetracarbonyl anion with polyhalogenomethane in the presence of a polar solvent[3]. The mechanism of formation of the cobalt-complexes, however, is not well-understood. Thus, the aim of this study is to investigate the formation of these and higher-order complexes via gas-phase radical anions. The methods for this study are full-scan mass spectrometry, tandem mass spectrometry (MS/MS) and Fourier transform mass spectrometry (FTMS).

The molecular negative ions are absent in the full-scan mass spectra. The principal ions, formed via dissociative electron capture by loss of CO groups, account for nearly 100% of the fragment ions. Each compound shows sequential losses of varying numbers of CO groups; the -Cl derivative loses from one to nine CO groups. The $-CH_3$ derivative, however, has two different fragmentation processes. The first process, similar to the other derivatives, is sequential loss of four CO groups. The second process begins after the loss of three CO groups and involves loss of [nCO + 2H (or H_2)].

CAD spectra of the $[M - 2CO]^-$ for the -H and $-C_6H_5$ derivatives and the $[M - 3CO]^-$ for the -Cl derivative are comparable to those of the negative-ion mass spectra; each shows sequential loss of carbonyl groups with little fragmentation of the YCo_3 moiety (See **Figure 2**). The metastable ion (MI) spectra of $[M - nCO]^-$, where n = 1 - 4, for the $-CH_3$ derivative establish the mechanism of [nCO + 2H] loss to be from $[M - 3CO]^-$ (See **Scheme 1**).

Similar to the negative-ion mass spectrometry experiments, no molecular anions are detected in a normal FTMS experiment, even at low ionizing energy. The principal ions are $[M - 2CO]^-$ for the -H, $-CH_3$, and $-C_6H_5$ derivatives and $[M - 3CO]^-$ and $[M - 4CO]^-$ for the -Cl derivative. Isolation of these radical anions by ion ejection and subsequent reaction delays show that they react with their neutral precursor to form higher-order cobalt

complexes (See **Scheme 2**). The anions also undergo C_2H_2 ligand substitution with one or two CO groups (See **Scheme 3**).

Figure 1. CAD spectra of the -H derivative

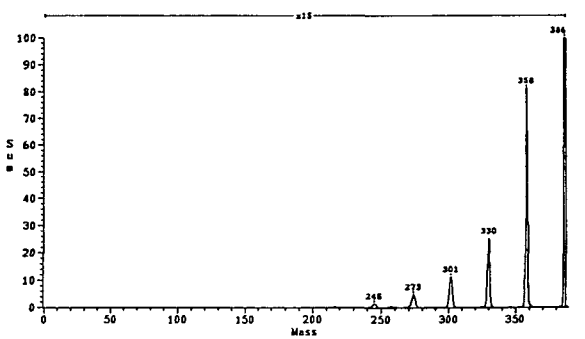

References

1. Markby, R. *et al. J. Am. Chem. Soc.*, **1958**, *80*, 6529.
2. Payli, G. *et al. Inorg. Chim. Acta Rev.*, **1970**, *4*, 109.
3. Miauri, M. *et al. J. Mol. Catal.*, **1988**, *45*(2), 151.
4. Ryan, R. C. *et al. J. Am. Chem. Soc.*, **1977**, *99*, 1986.
5. Myers, G. F. *et al. Inorg. Chim. Acta*, **1987**, *129*, 153,

Scheme 1.

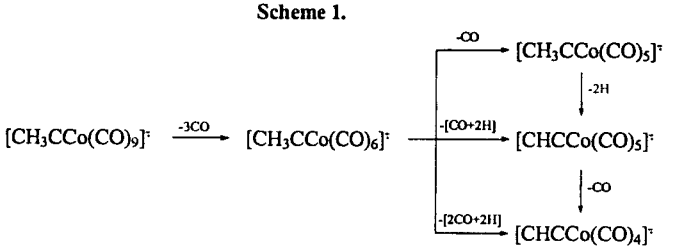

Scheme 2.

Y = H, CH_3, C_6H_5

$$[YCCo_3(CO)_7]^- + YCCo_3(CO)_9 \rightarrow [(YC)_2Co_5(CO)_{11}]^- + Co(CO)_5$$

Y = Cl

$$[YCCo_3(CO)_5]^- + YCCo_3(CO)_9 \rightarrow [CCo_6(CO)_{14}]^- + Y_2C$$

Scheme 3.

Y = H, CH_3, C_6H_5

$$[YCCo_3(CO)_5]^- + C_2H_2 \rightarrow [YCCo_3(CO)_6(C_2H_2)]^- + CO$$
$$[YCCo_3(CO)_5]^- + C_2H_2 \rightarrow [YCCo_3(CO)_6(C_2H_2)]^- + CO$$

Y = Cl

$$[YCCo_3(CO)_5]^- + C_2H_2 \rightarrow [YCCo_3(CO)_4(C_2H_2)]^- + CO$$

Reactions of Metal Carbonyl Anions with Methyl Formate in the Gas Phase

*K. J. van den Berg,[a] I. K. Gregor,[b] S. Ingemann[a] and N. M. M. Nibbering[a]
[a]*Institute of Mass Spectrometry, University of Amsterdam, Nieuwe Achtergracht 129, 1018 WS Amsterdam, The Netherlands,* [b]*School of Chemistry, The University of New South Wales, Kensington, N. S. W. 2033, Australia*

The gas-phase reactions of coordinatively unsaturated metal carbonyl anions ($M(CO)_n^-$; M = Cr, Mn, Fe and Co; n = 0 - 3 and $Co(CO)_nNO^-$; n = 0 - 2) with methyl formate have been studied with Fourier Transform Ion Cyclotron Resonance Mass Spectrometry. The $M(CO)_n^-$ ions were formed either i) in the FT-ICR cell by low-energy electron ionization (EI) on the neutral metal carbonyl compound or ii) by collision-induced loss of one or more CO ligands from the ions generated in an external ion source by EI. The ions formed by collision-induced dissociation were allowed to undergo non-reactive collisions with Ar in order to remove possible excess kinetic/internal energy prior to the reaction with methyl formate.

The products formed in the reactions of the metal carbonyl anions with unlabelled methyl formate are given in **Table I**. No reactions were observed with the $M(CO)_n^-$ (n = 0 , 1) ions and the ions with more than 15 valence electrons. Reactions proceeded in most instances by loss of one or more CO ligands from the collision complex. With the $Mn(CO)_3^-$, $Fe(CO)_2^-$ and $Co(CO)_2^-$ ions, CH_3OH and $[C,H_2,O]$ were also expelled.

Table I. Products formed in the reaction of metal carbonyl anions with unlabelled methyl formate[a)]

Ion	#[b)]	Products[c)]	Losses[b)]	%	Ion	#[b)]	Products[c)]	Losses[c)]	%
$Cr(CO)_2^-$	11	$HCr(OCH_3)^-$	3 CO	<15	$Fe(CO)_2^-$	13	$HFe(CO)(OCH_3)^-$	2 CO	35
		$HCr(CO)(OCH_3)^-$	2 CO	>85			$Fe(CO)_3^-$	CH_3OH	25
$Cr(CO)_3^-$	13	$HCr(CO)_2(OCH_3)^-$	2 CO	95			$Fe(CO)_2(OCH_2)^-$	$[C,H_2,O]$	40
		$Cr(CO)_3(OCH_3)^-$	$HCO^\cdot$	5	$Fe(CO)_3^-$	15	$HFe(CO)_3(OCH_3)^-$	CO	100
$Mn(CO)_2^-$	12	$HMn(OCH_3)^-$	3 CO	<15	$Co(CO)_2^-$	14	$Co(CO)_3^-$	CH_3OH	30
		$HMn(CO)(OCH_3)^-$	2 CO	>85			$Co(CO)_2(OCH_2)^-$	$[C,H_2,O]$	70
$Mn(CO)_3^-$	14	$HMn(CO)_2(OCH_3)^-$	2 CO	50	$Co(CO)(NO)^-$	15	$HCo(NO)(OCH_3)^-$	2 CO	<15
		$Mn(CO)_4^-$	CH_3OH	10			$HCo(CO)(NO)(OCH_3)^-$	CO	>85
		$Mn(CO)_3(OCH_2)^-$	$[C,H_2,O]$	40					

a) No reactions were observed with Cr^-, $Mn(CO)^-$, Fe^-, $Fe(CO)^-$, Co^-, $Co(CO)^-$, $Co(CO)_3^-$, $Co(NO)^-$ and $Co(CO)_2(NO)^-$.
b) Number of valence electrons. c) Assumed structures.

In the reactions of the $M(CO)_n^-$ ions with ^{13}C-labelled methyl formate ($H^{13}CO_2CH_3$), CO as well as ^{13}CO were eliminated. This may be explained as a result of insertion of the metal into both the H-CO and the C(O)-OCH_3 bond of the substrate, forming a five- or six-coordinated intermediate (**Figure I**) which may then expel one or two labelled or unlabelled CO molecules in a statistical ratio as indicated in **Table II**.

Table II. Neutrals formed in reactions with $H^{13}CO_2CH_3$

Ion	Neutrals Lost	Expected	Found	Neutrals Lost	Expected	Found
$Cr(CO)_2^-$	$CO+^{13}CO$ / 2 CO	2/1	1 8/1			
$Cr(CO)_3^-$	$CO+^{13}CO$ / 2 CO	1/1	1.1/1			
$Mn(CO)_2^-$	$CO+^{13}CO$ / 2 CO	2/1	1.8/1			
$Mn(CO)_3^-$	$CO+^{13}CO$ / 2 CO	1/1	1/1	$[^{13}C,H_2,O]$ / $[C,H_2,O]$	1/3	1/2
$Fe(CO)_2^-$	$CO+^{13}CO$ / 2 CO	2/1	1/1	$[^{13}C,H_2,O]$ / $[C,H_2,O]$	1/2	>1/2
$Fe(CO)_3^-$	^{13}CO / CO	1/3	1/3			
$Co(CO)_2^-$				$[^{13}C,H_2,O]$ / $[C,H_2,O]$	1/2	1/1
$Co(CO)(NO)^-$	^{13}CO / CO	1/1	0.25/1			

In the reaction of the ions with $DCOOCH_3$ expulsion of [C,D,H,O] occurred, whereas the reaction with $H^{13}CO_2CH_3$ resulted in a more pronounced loss of $[^{13}C,H_2,O]$ than expected for a statistical process (see **Table II**). This result suggests the occurrence of one reaction leading to the loss of formaldehyde and a competing process in which H_2 and CO are expelled. Moreover, the loss of formaldehyde cannot be explained by a conventional reductive elimination mechanism.

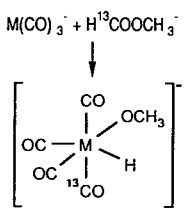

Figure I. Formation of a six-coordinated intermediate

In the reaction of $Fe(CO)_3^-$ with $H^{13}CO_2CH_3$ facile consecutive exchange of all three CO ligands for ^{13}CO was observed in addition to loss of CO/^{13}CO from the collision complex (**Figure II**). This is a unique reaction, which is unlikely to involve formation of a six-coordinated 19-electron intermediate (**Figure I**). The mechanism may be explained for example as oxidative addition to the $^{13}C(O)$-OCH_3 bond and rapid migration of the hydride ligand between the different CO-groups followed by reductive elimination of a methyl formate molecule. The formation of other neutral species is not likely either because of endothermicity, or for kinetic reasons. A possible reason that this novel reaction only takes place with $Fe(CO)_3^-$ may be that initial insertion is very rapid whereas loss of CO, the "exit channel" for the system, is slightly endothermic or has a high kinetic barrier.

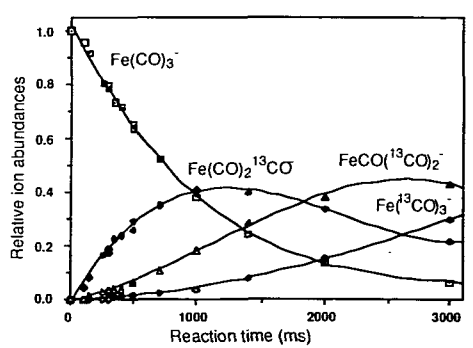

Figure II. Exchange of ligands with ^{13}C-labelled methyl formate

Gas-Phase Ion-Molecule Reactions of $Cr_2(CO)_5^-$ with Ketones and Alkenes

*Larry Sallans, Kelley R. Lane, Robert R. Squires and Ben S. Freiser, Department of Chemistry, Purdue University, West Lafayette, Indiana, 47907

Gas-phase ion-molecule reactions of transition-metal ions and complexes have received significant attention during the last decade. While producing a wealth of important and useful thermodynamic data, these studies have centered predominantly on the reactions of cationic metal species. Nevertheless, anionic species such as atomic metal anions also yield important information (e.g. heterolytic and homolytic metal-hydrogen bond energies).

Previously, we reported the production and proposed structure of $Cr_2(CO)_5^-$ created in the reaction of Cr^- with chromium hexacarbonyl[1]. This study focusses on the reactions of $Cr_2(CO)_5^-$ with ketones, alkenes and other unsaturated compounds. A comparison with $V_2(CO)_3^-$ is also presented.

The reaction between $Cr_2(CO)_5^-$ and 2-pentanone exemplifies the general reaction of the dinuclear species with ketones. Through the use

$$Cr_2(CO)_5^- + CH_3COCH_2CH_2CH_3 \longrightarrow (C_5H_{10}O)Cr_2(CO)_4^- + CO \qquad \text{(eq1)}$$

of deuterated ketone samples and comparisons with alkene reactions, the neutral loss in eq1 originates by CO loss from the ligated chromium. The product ion may represent a simple adduct bound to the bare chromium or, as CID results demonstrate, may involve C-H insertion for additional coordination to the metal. A summary of the reaction and CID results for various ketone reactants are given in Table 1.

TABLE 1. Reaction of $Cr_2(CO)_5^-$ with ketones and CID of the product.

Ketone Reactant (N)	Product $(N)Cr_2(CO)_4^-$	CID of $(N)Cr_2(CO)_4^-$ -CO	-H_2	$OCr_2(CO)_x^-$
Acetone	Yes	1	0	x = 2-4
Butanone	Yes	1-3	1	3,4
2-Pentanone	Yes	1-4	1,2	3
3-Methylbutanone	Yes	1,2	1,2	3
4-Heptanone	Yes	---	---	---

Collision-induced dissociation, CID, of the ketonetetracarbonyldichromium species resulted in losses of CO and H_2, and formation of species presumably involving a strong metal-oxygen bond, $OCr_2(CO)_{2-4}^-$. Secondary reactions of $(N)Cr_2(CO)_4^-$ with ketones yield product ions resembling adduct formation stabilized by CO loss, $(N)_2Cr_2(CO)_3^-$. The reaction of $Cr_2(CO)_5^-$ with 2,4-pentanedione yielded product ions corresponding to two and even three carbonyl ligand losses.

Another group of π-donor ligands, alkenes, are also observed to undergo addition to $Cr_2(CO)_5^-$ followed by CO loss. These results are summarized in Table 2. It is interesting to note that

Table 2. Reaction of $Cr_2(CO)_5^-$ with alkenes and related compounds

Alkene Reactant (N)	Product $(N)Cr_2(CO)_4^-$	CID of $(N)Cr_2(CO)_4^-$ -CO	-H_2
Propene	No	---	---
1-Butene	Yes	1	1,2
Methylpropene	Yes	1	1,2
3-Methyl-1-butene	Yes	1,2	1,2
1-Pentene	Yes	1	1,2
2,3,3-Trimethylbutene	No	---	---
trans-2,4-Pentadiene	Yes	1,2	1,2
Cyclohexene	slow	1,2	1[a]
Cyclooctene	No	---	---
1,3-Cyclooctadiene	Yes	1-3	1-3
1,5-Cyclooctadiene	Yes	1-3	1-3
Benzene	No	---	---
Propyne	Yes	1	1

[a]Loss of C_6H_8 and C_6H_{10} also observed

a number of alkenes are unreactive. There is no explanation that easily rationalizes this observation, however, the π-bonding energy of the ligand in relation to the metal-carbonyl bond strength is currently being investigated.

In comparison, the dinuclear species, $V_2(CO)_3^-$, reacts more vigorously with 2-pentanone (eq2). It appears that these reactions are

$$V_2(CO)_3^- + CH_3COCH_2CH_2CH_3 \longrightarrow \begin{cases} (C_5H_6O)V_2(CO)_2^- + 2H_2 + CO \\ (C_5H_6O)V_2(CO)^- + 2H_2 + 2CO \\ OV_2(CO)_2^- + CO + (C_5H_{10}) \end{cases} \qquad \text{(eq2)}$$

more energetic than the corresponding $Cr_2(CO)_5^-$ reactions since the products in the vanadium system correspond to similar reaction products in the chromium system upon collisional activation. In analogy to ketones, $V_2(CO)_3^-$ reacts with 1-pentene to form products that are characterized by CO loss and extensive dehydrogenation.

[1]Sallans, L.; Lane, K. R.; Squires, R. R.; Freiser, B. S. *J. Am. Chem. Soc.* **1985**, *107*, 4379-4385

Correlation Between Gas Phase Electron Affinities, Reduction Potentials and Catalytic Activities of Halogenated Metalloporphyrins

H. L. Chen, P. E. Ellis, Jr., T. Wijesekera, T. E. Hagan, S. E. Groh, J. E. Lyons and D. P. Ridge
Department of Chemistry and Biochemistry and Center for Catalytic Sciense and Technology, University of Delaware, Newark, DE 19716. Sun Refining and Marketing Co. P. O. Box 1135, PA 19061

Polyhalogenated metalloporphyrins have been the object of a number of recent studies because of their potential as selective oxidation catalysts. The activity of such heme-based biological oxidation catalysts as cytochrome P-450, suggested that metalloporphyrins might be effective homogeneous oxidation catalysts. Readily available iron tetraphenylporphyrin (FeTPP) is essentially ineffective as a catalyst for air oxidation of alkanes to alcohols, but halogenated FeTPPs have been found to be effective and selective catalysts for conversion of isobutane to t-butanol. Both the stability and activity of the catalysts increase with extent of halogenation. In probing the origin of the dependence of catalytic activity on halogenation it was found that catalytic activity increase with the Fe(III) to Fe(II) reduction potential of the catalyst. The importance of the reduction potentials of halogenated FeTPPs led us to measure their gas phase electron affinities. We give a preliminary report of the results of those measurements here.

A FT-ICR was employed to do all the experiments. The measurements were done using the same methods that were used to measure the electron affinities of nickel porphyrins[1]. Syntheses of the halogenated porphyrins have been described elsewhere[2]. Electron affinities of halogenated FeTPPs are listed in table 1. Also listed are the condensed phase reduction potentials for the halogenated FeTPPCl (Fe(III) to Fe(II)) and the halogenated FeTPP (Fe(II) to Fe(I)). It is evident from table 1 that the electron affinities and the reduction potentials vary together. The electron affinities are plotted against the reduction potentials in Figure 1. The Fe(II) to Fe(I) reduction potentials vary approximately linearly with the electron affinities of the neutral halogenated FeTPP. The data for Ni(II) to Ni(I) reduction potentials and the corresponding electron affinities from our earlier study fall approximately on the same line. The Fe(III) to Fe(II) reduction potentials vary approximately linearly with the halogenated FeTPPCl electron affinities, but the line through the III-II data is not collinear with the line through the II-I data. Several of the Fe(III) porphyrins are more easily reduced in solution than would be expected from the gas phase electron affinities. This suggests that reduction of the Fe(III) species is mediated by some solvent effect. One possibility is that on reduction the Fe(III) species reversibly lose the axial chlorine as Cl^- which as an atomic ion has a high energy solvation. The solvent effect also decreases the range of reduction potentials for Fe(III) species (0.50 V) relative to their electron affinities (1.25 eV). The gas phase electron affinities thus uniquely provide an unambiguous measure of the intrinsic electrophilicity of the Fe(III) porphyrin complexes. Finally we note that for those cases for which we have the III-II reduction potential, the electron affinity and the catalytic activity, all three quantities are listed in table 1. The three quantities are clearly covariant.

1. Chen, H. L.; Pan, Y. H.; Groh, S.; Hagan, T. E.; Ridge, D. P., J. Am. Chem. Soc., **1991**, 113, 2766.
2. Ellis, P. E., Jr.; Lyons, J. E., Catal. Lett., **1989**, 3, 389.

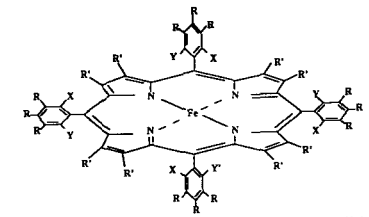

1: X=Y=Y'=R=R'=H
3: X=Y=R=R'=H, Y'= C=O (NH, (CH2)4)
5: X=Y=Y'=R=F, R'=H
7: X=Y=Y'=R'=Cl
2. R=R'=H, X=Y=Y'=Cl
4: X=R=R'=H, Y=Y'= C=O (C(CH3)3, NH)
6: X=Y=Y'=R=R'=Cl, R=H
8: X=Y=Y'=R=F, R'=Cl
9: X=Y=Y'=R=Cl, R'=H

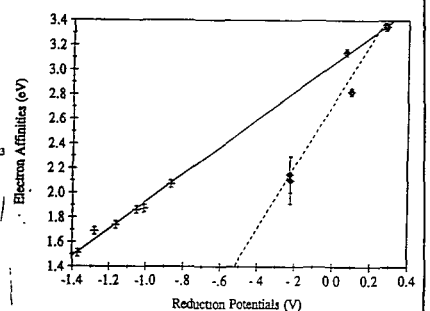

Species[a]	EA(eV)[b]	$E_{1/2}$(V)[c]	TON(60°C)[d]
NiTPP	1.51±0.01[e]	-1.370[f]	
H_2NiTPP	1.69±0.01[e]	-1.280[f]	
NiTPP-CHO	1.74±0.01[e]	-1.165[f], -1.13[g]	
1 FeTPP	1.87±0.03	-1.010[h]	
2 FeTPPoCl$_8$	1.86±0.03	-1.05[g]	
3 FeTPP-val	1.97±0.03		
4 FeTPP-piv	2.07±0.03	-0.866[h]	
5 FeTPPF$_{20}$	2.15±0.15		
6 FeTPPCl$_{28}$	2.59±0.11		
8 FeTPPF$_{20}$6Cl$_8$	3.21±0.03		
1-Cl	2.15±0.15	-0.221[i]	0
2-Cl	2.10±0.19	-0.221[i]	
5-Cl	3.14±0.03	0.07[i]	1160
9-Cl	2.93±0.23		
7-Cl	2.82±0.03	0.10[f]	
8-Cl	3.35±0.03	0.28, 0.27	1800

Photoinduced Gas Phase Ligand Switching

R. M. Pope* and S. W.Buckner, University of Arizona

The gas phase photoinitiated ligand switching reaction of $VC_6H_6^+$ with CH_3CN at 604 nm to generate VCH_3CN^+ has been monitored by FTICR. The $V(C_6H_6)^+$ dehydrogenation product of the reaction between thermalized bare vanadium cation and a pulse of cyclohexene was isolated by swept double resonance excitations. Dissociation of the coordinated benzene occurs by a two photon process in the 585-615 nm region. If, prior to the absorption of a second photon, a $V(C_6H_6)^+$ cation with sufficient internal energy encounters a molecule of CH_3CN (used here as a static buffer gas), competitive elimination from the excited collision complex is possible (scheme I). In spite of the fact that $V(C_6H_6)^+$ is energetically more stable than VCH_3CN^+, a .2 branching ratio for C_6H_6 elimination was recorded. The isolated complex $V(C_6H_6)(CH_3CN)^+$ dissociates exclusively to form $V(C_6H_6)^+$ when irradiated with 585-615 nm light. Photodissociation measurements indicate the reaction proceeds on a single minimum potential surface with an endothermic activation barrier.

The mechanism for the associative ligand switching reaction shown in scheme I can be best understood by reference to a simplified potential surface for the reaction, shown in Figure 1. At thermal energies, CH_3CN does not displace benzene from $V(C_6H_6)^+$ ($k^I I < 10^{-13}$ cm^3/mol-sec) because the reaction is endothermic. The adduct, $V(CH_3CN)(C_6H_6)^+$, does form slowly by collisional and/or radiative stabilization. $V(C_6H_6)(CH_3CN)^+$ undergoes photodissociation

$V(C_6H_6)(CH_3CN)^+ + h\nu$ (488, 514 nm) -> $V(C_6H_6)^+ + CH_3CN$ 80% (1)
-> $V(CH_3CN)^+ + C_6H_6$ 20% (2)

with output from the Ar^+ laser via two channels, reactions (1) and (2). The loss of acetonitrile is the main pathway due to its lower activation energy. Photoexcitation of $V(C_6H_6)(CH_3CN)^+$ with 585 to 615 nm light results in exclusive loss of CH_3CN, as previously stated. This is because the activation energy for benzene loss is greater than the photon energy (46-48 kcal/mol). Initial photoexcitation of trapped $V(C_6H_6)^+$ generates an excited ion (~47 kcal/mol internal excitation) which undergoes interconversion to a vibrationally excited level of the ground electronic state. In the low density environment of the ICR trap, this ion can relax by sequential infrared fluorescence or collisional quenching[1]. Absorption of a second photon induces dissociation to form V^+. However, if the vibrationally excited ion collides with CH_3CN, a highly excited $V(C_6H_6)(CH_3CN)^+$ complex is formed. This ion has internal energy equal to the photoexcitation energy plus the energy of coordination of acetonitrile to $V(C_6H_6)^+$, internal energy A in Figure 1. The highly excited $V(C_6H_6)(CH_3CN)^+$ can then partition between the benzene and acetonitrile loss pathways. The benzene loss pathway effectively results in an associative ligand displacement.

[1] (a) Dunbar, R. C. J Phys. Chem. 1983, 87, 3105. (b) Hanovich, J. P.; Dunbar, R. C.; Lehman, T. J. Phys. Chem. 1985, 89, 2513. (c) Dunbar, R. C.; Chen, J. H.; So, H. Y.; Asomoto, B. J. J. Chem. Phys. 1987, 86, 2081.

Scheme I

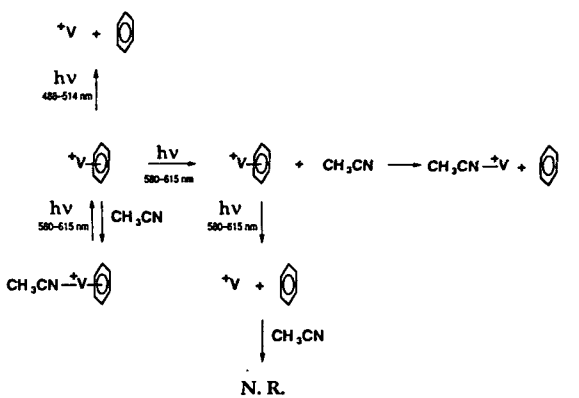

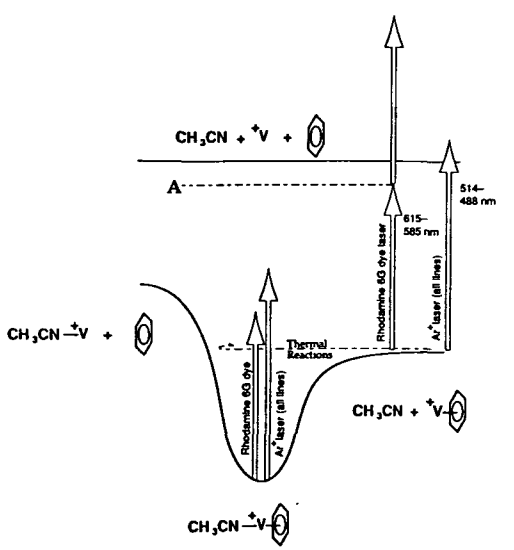

THERMONEUTRAL PROTON AND LIGAND EXCHANGE REACTION RATES FOR PROTONATED AND PROTON BOUND DIMER DIMETHYLTARTRATE IONS

J.P.Honovich*, R.G.Kostanovsky and E.N.Nikolaev
Institute of Energy Problems of Chemical Physics
38 Leninsky Prospect, Bldg.2
Moscow, Russian Federation

INTRODUCTION

As mass spectrometry extends its mass range to larger and more complex species, the question arises whether previously observed ion/molecule behavior and concepts can be extended to larger systems. In this study, three very different ion/molecule reactions involving the neutral Dimethyltartrate (DMT) were studied. This compound approaches a size where geometric factors could be affecting ion/molecule processes. This may be reflected in the fact that the DMT dimer has been found to exhibit an interesting chirality effect.

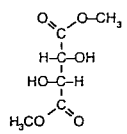

Dimethyl-L-tartrate

EXPERIMENTAL

A Brucker CMX-47 ICR mass spectrometer equipped with a 4.7 T magnet was utilized. The 3cm cell was of cylindrical symmetry and V_t= 3V. The DMT sample was commercially obtained (Fluka AG) while the deuturated (DMTd6) form was synthesized by a reesterfication with CD_3OH. The samples, introduced by separate leak valves, were thoroughly pumped by the high vacuum so as to remove any condensed gases and to fully saturated the vacuum system. A Balzers IMR-132 ionization gauge was utilized for pressure determination. Effort was made to keep ion densities low and comparable for all pressures. Ion ejection was by short (1-10ms) fixed frequency pulses. At the end of the kinetic reaction period the ion of interest was excited by a single frequency pulse and detected in a narrow band heterodyne mode. Repeat experiments with a different excitation pulse were made for each monitored ion. Kinetic delay times were sampled cyclically to give a large number of accumulated transients which allowed an averaging over slow signal variations. Peak heights were taken as proportional to ion intensities.

PROCEDURE

Preliminary Ion: All three reactions of interest are preceded by the electron impact ionization of DMT (or DMTd6) to form ions of presumed formula $C_3H_6O_3$ ($C_3H_3D_3O_3$).

$$\text{DMT (DMTd6)} \quad \text{---}(e^-)\text{--)} \quad 90^+ \ (93^+)$$

Reaction 1: Fragment ions m/e 90 reacts with precursor DMT neutrals to form the protonated DMT species ("self CI").

$$90^+ + \text{DMT} \ \text{---}k_1\text{--)} \ 179^+ \qquad \text{rxn. 1}$$

In the case of the deuterated sample

$$90^+(93^+) + \text{DMTd6} \ \text{--}k_1\text{-)} \ 185^+$$

Reaction 1 is presumed an exothermic process occurring with unit efficiency and is used to determine the collision rate (k_c=k_1/Pt).

Reaction 2: The protonated DMT species undergo proton exchange with the neutral precursor bath gas.

$$185^+ + \text{DMT} \ \text{---}k_2\text{--)} \ 179^+ \qquad \text{rxn.2a}$$
$$179^+ + \text{DMTd6} \ \text{---}k_2\text{--)} \ 185^+ \qquad \text{rxn.2b}$$

To follow the exchange process one of the ion species is ejected from the cell by a double resonace pulse. The original ratio (R_i) will be reestablished as follows

$$R(t) = R_i(1-e^{-kPt}) \qquad \text{eqn.1}$$

Reaction 3: Protonated DMT ions can also react to form proton bound dimers by a combination of collisional and radiative stabilization. The three possible dimer species (m/e 357,363,369) then undergo ligand exchange reactions. The mixed dimer is formed as follows.

$$357^+ + \text{DMTd6} \ \text{---}k_3\text{--)} \ 363^+ \qquad \text{rxn.3a}$$
$$369^+ + \text{DMT} \ \text{---}k_3\text{--)} \ 363^+ \qquad \text{rxn.3a}$$

The mixed dimer reacts as follows.

$$363^+ + \text{DMT} \ \text{---}k_3\text{--)} \ 357^+ \qquad \text{rxn.3b}$$
$$363^+ + \text{DMTd6} \ \text{---}k_3\text{--)} \ 369^+ \qquad \text{rxn.3b}$$

When the fraction of deuterated neutrals (f_d) is around .5 the reestablishment of the ion ratios after ejection of either mixed dimer (m/e 363) or both homodimers (357,369) is given by eqn.2.

$$R(t) = 2f_d(1-f_d)(1-e^{-kPt}) \qquad \text{eqn.2}$$

RESULTS AND DISCUSSION

Column 1 of Table 1 summarizes the determined rate constants.

TABLE 1
Experimental and theoretical rate constants

	$k_i(10^{-10}cm^3s^{-1})$	k_i/k_1	R(calc)
rxn.1	1.14	1	1
rxn.2a	.60	.53	.41
rxn.2b	.69	.61	.41
rxn.3	.71	.62	.48

Absolute values are reported assuming no correction for ionization gauge sensitivity - this is unimportant since only relative values are considered. The normalized values relative to reaction 1 are presented in column 2. Column 3 gives theoretical ratios taking into account the statistical factors (1:1/2:2/3) and the reduced mass effect (1:.81:.7) on the collision rate. Within error limits (+-10%) there is reasonable agreement and correlation between the columns. This suggests that all three reactions are occurring at (or near) the upper limit governed by the collision rate. To presume that three very different reactions would proceed at similar less than unit efficiencies is not reasonable. This would be consistant with reactions 2 and 3 forming a long-lived complex on each collision allowing complete randomization before redissociation. This is the same type of behavior as that observed for smaller organic species such as proton transfer with methanol.

A Redermination of the Proton Affinity Scale from Nitrogen to t-Butylamine by Variable Temperature High Pressure Mass Spectrometry.

*J.E. Szulejko and T.B. McMahon

Guelph-Waterloo Centre for Graduate Work in Chemistry, Department of Chemistry, University of Waterloo, Waterloo, Ontario, CANADA N2L 3G1

In 1991, Meot-Ner and Sieck[1] published a High Pressure Mass Spectrometric based Proton Affinity scale which linked several Proton Affinity "primary standards", viz, C_3H_6, i-C_4H_8 and NH_3. The main finding was that the i-C_4H_8...NH_3 Proton Affinity difference was larger by 4.3 kcal mol^{-1} than previously assigned in the NIST[2] database. This finding was subsequently verified by this work (see TABLE). However, the present work Proton Affinity difference of 13.5 kcal mol^{-1} does not support the Meot-Ner Sieck ΔPA of 16.7 kcal mol^{-1} or the NIST ΔPA of 16.4 kcal mol^{-1} between C_3H_6 and i-C_4H_8. The agreement between the Meot-Ner Sieck and present work ΔG^0_{600} scales is excellent from C_3H_6 to about $(C_2H_5)_2CO$. The agreement is only fair between $(C_2H_5)_2CO$ to $(CH_3)_3CNH_2$. The relative Proton Affinity scales are in excellent agreement from i-C_4H_8 to $(CH_3)_2NH$, but are in rather poor agreement elsewhere.

A completely revised PA scale[3] from N_2 to $(CH_3)_3CNH_2$ is presented in the TABLE. The absolute PA of CO, 141.9 kcal mol^{-1} based on Appearance Energy measurements was used as the *Single* PA reference standard for the entire PA scale. Also presented in the TABLE are, (i) most recent G2 *ab initio* Proton Affinity calculations by Smith and Radom[4] (average deviation 0.6 kcal mol^{-1}), (ii) other recent high quality *ab initio* PA calculations, (iii) the NIST PA values and (iv) Proton Affinities derived from Appearance Energy measurements. One of the main findings of this work is that the PA of i-C_4H_8 has to be revised downward by *ca* 4.0 kcal mol^{-1} compared to the NIST PA table which is in part based on the photoionization AE data of Traeger[5]. The earlier photoionization AE study by Ingraham[6] and an electron monochromator study by Lossing[7] on neo pentane are in excellent agreement with the present finding. The present work leaves the PA for NH_3 (203.5 kcal mol^{-1}) very close to the NIST value of 204.0 kcal mol^{-1}, prior ab initio PA calculations and AE data unlike the Meot-Ner Sieck finding of 208.3 kcal mol^{-1}.

References:

1) Meot-Ner and Sieck; *J.Amer.Chem.Soc.*, **1991** v113 p4448 2) Lias et al; *J.Phys.Chem.Ref.Data Suppl 1*, **1988**, v17 3) Szulejko and McMahon; *J.Amer.Chem.Soc.*, **1993**, in press 4) Smith and Radom; *J.Amer.Chem. Soc.*, **1993** in press 5) McLoughlin and Traeger; *J.Amer.Chem.Soc.*, **1979** v101 p5791 6) Ingraham et al; *J.Phys.Chem.* **1961** v34 p189 7) Lossing and Semeluk; *Can.J.Chem.*, **1970** v48 p955

TABLE Other ***PROTON AFFINITY*** and ΔG^0_{600} Determinations

BASE	PA HPMS This Work	PA *G2 Ab Initio* Radom	PA NIST	PA HPMS Meot-Ner	PA *Ab Initio* Other	PA AE	ΔG^0_{600} HPMS This Work	ΔG^0_{600} HPMS Meot-Ner
$(CH_3)_3CNH_2$	223.5	.	220.8	229.2	.	.	-27.5	-30.5
$(CH_3)_2NH$	222.5	222.7	220.6	227.8	222.8	.	-26.7	-29.1
CH_3NH_2	215.4	215.3	214.1	219.6	216.3	.	-18.7	-19.9
C_4H_5N	209.2	.	207.6	213.4	.	.	-14.9	-15.7
NH_3	203.5	204.0	204.0	208.3	203.7	203.6	-7.8	-9.2
$(C_2H_5)_2CO$	199.3	.	201.4	203.6	.	.	-6.3	-6.8
$CH_3CO_2C_2H_5$	198.1	.	200.7	203.0	.	.	-5.6	-6.2
$CH_3CO_2CH_3$	195.0	.	197.1	199.2	.	.	-2.7	-2.2
$(CH_3)_2CO$	193.7	.	196.7	198.4	193.9	194.0	-1.6	-1.4
i-C_3H_7CN	193.3	.	194.3	194.9	.	.	1.6	1.4
i-C_4H_8	191.7	191.7	195.9	(195.9)	.	193.0	0.0	0.0
$(CH_3)_2O$	189.6	189.3	192.1	192.3	190.7	.	2.8	2.9
HCO_2CH_3	188.1	.	188.9	189.4	.	.	6.6	6.8
$C_6H_5CH_3$	187.7	.	189.8	189.9	.	.	5.5	5.2
CH_3OH	181.7	180.3	181.9	181.9	181.9	.	13.6	13.2
C_6H_6	180.0	.	181.3	181.6	.	.	12.0	12.4
C_3H_6	178.4	177.9	179.5	179.2	177.8	178.7	15.4	15.2
H_2S	168.7	169.1	170.2	.	168.9	168.7	25.0	.
H_2O	165.0	164.5	166.5	.	164.3	167.2	28.6	.
C_2H_4	162.6	163.0	162.6	.	163.8	162.5	29.7	.
CS_2	161.3	163.0	164.4	.	.	.	26.6	.
C_6F_6	153.8	.	177.7	.	.	.	35.1	.
CO	(141.9)	141.7	141.9	.	141.8	142.0	51.0	.
N_2O	137.8	.	138.8	.	138.7	.	52.5	.
CH_4	130.2	129.0	131.6	.	129.6	.	58.8	.
CO_2	129.4	128.9	129.5	.	129.3	129.4	60.3	.
Xe	120.3	.	118.6	.	122.0	.	68.1	.
N_2	118.7	118.0	118.2	.	117.9	119.0	63.1	.

Units: kcal mol^{-1}

Isomers of $CHNO^+$ and the Proton Affinity of NCO at N

Murray J. McEwan, Mark Morrison and Colin G. Freeman
Department of Chemistry, University of Canterbury, Christchurch, New Zealand

Introduction. Four of the most common elements found in the interstellar medium are H, C, O and N. The simplest compound formed from all four is isocyanic acid, HNCO, which has been detected in interstellar clouds and comets, and which is one of several isomeric forms. The radical cations of CHNO, $CHNO^+$ also exist in isomeric forms and at least five structures have been proposed: four acyclic and one cyclic. The order of stability based on ab initio calculations is (ΔH°_f in kJ mol^{-1} in parenthesis)

$HNCO^+$	>	$HOCN^+$	>	c-$HNCO^+$	>	$HCNO^+$	>	$HONC^+$
(1015)		(1165)		(1236)		(1250)		(1407)

This study was undertaken in part to help elucidate the $CHNO^+$ structure of the ion products of the reactions:

$$HNC^+ + O_2 \rightarrow CHNO^+ + O$$
$$HNC^+ + N_2O \rightarrow CHNO^+ + N_2$$

and in part to characterise the reactivity of isomeric $CHNO^+$ ions.

Experimental. A selected ion flow tube (SIFT) was used to investigate the ion-molecule chemistry of $CHNO^+$. Electron impact on one of the species, $H_2NCONHNO_2$, CH_3OCONH_2, $HCONH_2$, HNCO and HNCO polymer generated the $CHNO^+$ ion at m/z = 43. In most cases a mixture of isomeric ions at m/z = 43 were produced as was seen from their decay with appropriate reactants (Figs. 1 and 2).

Results. The $CHNO^+$ ion produced from pure HNCO produced one isomer only which we attribute to $HNCO^+$ (Fig. 1). The curved decay seen in Figure 2 is due to a difference in reactivity between the isomeric forms. The initial fast decay is due to $HNCO^+$ as its proton transfer behaviour with the reactants CH_3Br (PA = 693 kJ mol^{-1}), CS_2 (688 kJ mol^{-1}), CH_3Cl (682 kJ mol^{-1}) and CS_2 (680 kJ mol^{-1}) was identical to that of $HNCO^+$ produced from pure HNCO. The proton affinity of NCO at N established from these reactions was 680 < PA(NCO) < 688 kJ mol^{-1}, which is consistent with tabulated thermochemical data (PA = 669 ± 20 kJ mol^{-1}) and ab initio calculations at the G2 level of theory (PA = 654 kJ mol^{-1}) (Table 1).

The less reactive $CHNO^+$ which was formed by electron impact on all species tried (with the exception of unpolymerised HNCO) exhibited proton transfer with NH_3, $(C_2H_5)_2O$, CH_3COCH_3 but not C_2H_5CN. We conclude from these results that this less reactive isomer will transfer its proton to reactants with PA's in the range 806 – 812 kJ mol^{-1}. None of the known isomers of $CHNO^+$ satisfy these constraints and this isomer has not yet been identified.

The $CHNO^+$ products of the ion-molecule reactions $HNC^+ + O_2$ and $HNC^+ + N_2O$ were each identified as $HNCO^+$.

Table 1. Selected Reactions of $HNCO^+$

			k/(10^{-9} cm^3 s^{-1})
$HNCO^+ + NH_3$	$\xrightarrow{1.0}$	$NH_4^+ + HNCO$	2.2
$HNCO^+ + CH_3Br$	$\xrightarrow{0.85}$	$CH_3Br^+ + HNCO$	1.3
	$\xrightarrow{0.15}$	$CH_3BrH^+ + NCO$	
$HNCO^+ + CS_2$	$\xrightarrow{0.80}$	$CS_2^+ + HNCO$	1.2
	$\xrightarrow{0.20}$	$CS_2H^+ + NCO$	
$HNCO^+ + CH_3Cl$	$\longrightarrow$	$H_2NCO^+ + CH_2Cl$	0.20
$HNCO^+ + C_2H_4$	$\longrightarrow$	$C_2H_4^+ + HNCO$	1.20

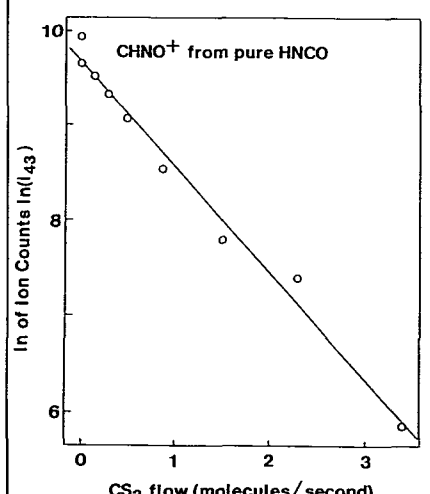

Fig 1

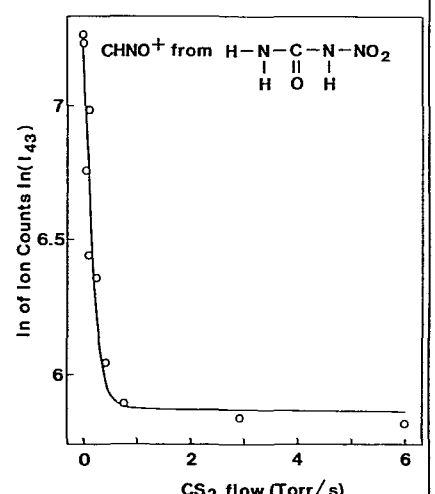

Fig 2

State-Selected Ion-Molecule Reactions in a Quadrupole-Octopole-Quadrupole Mass Spectrometer: Mode-Specific Effects in the Reaction $NH_3^+ + ND_3$

Robert D. Guettler, Glenn C. Jones, Jr., and Richard N. Zare

Department of Chemistry, Stanford University, Stanford, CA 94305-5080

The main goal of our research is to better understand the effect of reactant energy on ion-molecule reactions. In these experiments both the ion vibrational state and kinetic energy are controlled while their effect on product formation is monitored. We have looked in-depth at the ion-molecule reaction system of $NH_3^+ + ND_3$. We have found that product formation in this system has a complex dependence on the ion vibrational state. Distinct differences have been observed between not only ion kinetic and vibrational energy, but also between excitation of differing ion vibrational modes.

This work has been carried out in our quadrupole-octopole-quadrupole mass spectrometer. Ions are generated by intersecting a molecular beam containing the species to be ionized with the frequency-doubled output of a Nd:YAG-pumped dye laser. This ~300-nm laser light prepares the ions in specific vibrational states via (2+1) resonance-enhanced multiphoton ionization (REMPI).[1] The ions are extracted from the molecular beam by a DC quadrupole turning element and focused into a quadrupole mass filter which mass selects the reactant ion. The ions then enter an octopole ion-guide that passes through a collision cell containing the neutral reactant molecule. A second quadrupole mass filter then selects the ion mass to be detected. The octopole ion-guide is essential in insuring that all product ions are collected with nearly uniform efficiency, regardless of their scattered direction and kinetic energy, thus allowing for the direct comparison of product channel intensities. The ratios of the various intensities allow us to calculate product branching ratios and relative cross sections.

The reaction of $NH_3^+ + ND_3$ is seen to have a very interesting dependence on ion reactant energy. By varying both the ion reactant kinetic energy and vibrational state, detailed information regarding the subtle interplay between these two forms of energy is obtained. The three primary product channels of this reaction system are:

$\mathbf{NH_3^+}(v_1,v_2) + ND_3 \rightarrow$	$\mathbf{NH_3D^+} + ND_2$	Deuterium Abstraction
	$NH_3 + \mathbf{ND_3^+}$	Charge Transfer
	$NH_2 + \mathbf{ND_3H^+}$	Proton Transfer

The ammonia reactant ions can be prepared with umbrella bending mode excitation (v_2, symmetric out-of-plane bend) or with combined umbrella and breathing mode excitation (v_1+v_2). We have observed the

[1] W.E Conaway, R.J.S. Morrison, and R N Zare, Chem Phys. Lett 113, 429 (1985).

product channels to show significant sensitivity to the amount of umbrella mode excitation placed into the reactant ion. As the amount of umbrella mode excitation was increased from 0 to 7 quanta, the relative cross sections changed by nearly a factor of two for both deuterium abstraction (enhanced) and proton transfer (attenuated). The same trends were seen with increasing kinetic energy, although the vibrational energy was nearly four times more effective at shifting the reactant intensities.

Of special interest for state-selection of the ammonia ion is a set of nearly isoenergetic vibrational states in which differing amounts of umbrella and breathing motion are excited. The pure umbrella mode ($v_2 = 5$) yields ions with 0.60 eV of vibration energy, while a combination band of umbrella and breathing mode ($v_1 = 1$, $v_2 = 2$) yields ions with 0.66 eV. In addition to depending on the quantity of energy placed into vibration, these experiments show that the intensities of the product channels also depend on the vibrational mode that is excited. At a center-of-mass collision energy of 1.0 eV, the branching ratio for charge transfer decreases from 48 to 37% with stretch excitation, while proton transfer increases from 44 to 57%. The deuterium abstraction branching ratio is slightly attenuated with the stretch excitation.

Although the collection efficiency of the octopole ion-guide is expected to be nearly uniform over the collision energy ranges investigated (1.0-10.0 eV center-of-mass), this cannot be true at all energies. There will be some low collision energy at which the inherent energy spread in the ion beam along with changing collection efficiency will lead to distortions in the measured product intensities. To determine this limit and to rigorously verify our collection efficiencies, we have studied the reaction system of $N^+ + O_2$:

$N^+ + O_2 \rightarrow$	$\mathbf{NO^+} + O$	Oxygen Abstraction
	$N + \mathbf{O_2^+}$	Charge Transfer
	$NO + \mathbf{O^+}$	Anion Abstraction

Electron impact (0.25 mA, 50 eV electrons) was used to generate the N^+ from a beam of N_2. Measuring branching ratios and relative cross sections of the three product channels of this reaction system provides a good test of the instrumental collection efficiency. Comparison of our results to those obtained by techniques that do not utilize RF devices[2] shows that there are no significant biases to collection and detection of the three rather diverse product channels.

The $NH_3^+ + ND_3$ system has demonstrated that vibrational excitation can play an active role in determining product formation in ion-molecule reactions. This influence depends on more than just the amount of vibrational energy, it also depends upon the mode or type of vibration that is excited in the reactant ion. We believe complete interpretation of these results will provide glimpses into the dynamics involved in formation of the different product channels.

[2] F Howorka, I Dotan, F.C. Fehsenfeld, and D.L. Albritton, J Chem Phys 73, 758 (1980)

Electrophilic Bromination of Gaseous Aromatic Compounds: Mechanism and Linear Free Energy Effects on Reaction Rates

Olga Bortolini
Universita Di Ferrara, Dipartimento Di Chimica, Via Borsari 46, Ferrara 44100 Italy.

Sheng Sheng Yang* and R Graham Cooks
Purdue University, Department of Chemistry, West Lafayette, IN 47907, U. S.A.

Electrophilic bromine cation addition to monosubstituted benzenes is studied using $BrCO^+$ and $CH_3NH_2Br^+$ as reagent ions in a pentaquadrupole mass spectrometer[1]. One aim of this study is to seek a correlation between substituent effects and the extent of gas phase ion/molecule reactions under the non-equilibrium, low pressure and solvent free conditions which pertain in quadrupole collision cells. The electrophile $BrCO^+$ was created by electron ionization of acetyl bromide. The protonated electrophile $CH_3NH_2Br^+$ was generated by chemical ionization of CH_3NHBr introduced via a membrane introduction system[2]. The reactions of monosubstituted benzenes with mass selected $BrCO^+$ are dominated by the addition of Br^+. Reaction normally occurs at the ring and the brominated product fragments by Br loss upon collision induced dissociation (Scheme 1). A linear correlation ($r=0.96$, $\rho=-0.23$) between relative reaction rates of bromine cation addition against Brown's substituent constant σ^+ is reported (Table 1 and Figure 1). Nitrobenzene displays unique behavior, NO_2 substitution by Br^+ occurring (Scheme 2). The reactions of $CH_3NH_2Br^+$ with monosubstituted benzenes are characterized by both bromine cation and proton addition (Scheme 3). A good linear correlation ($r=0.98$, $\rho=-0.56$) is observed between the relative reaction rates of bromine cation addition and the σ^+ value (Table 2 and Figure 2). A Hammett type of correlation for protonation is not observed and this suggests that protonation occurs at the ring in some cases and at the substituent in others. Protonation is shown to take place at the substituent for acetophenone, benzonitrile and nitrobenzene. A linear correlation is observed between the relative rate of protonation and proton affinity of the monosubstituted benzenes (Table 3 and Figure 3). Ion/molecule reaction products were characterized by recording sequential product ion mass spectra (MS^3). Electrophilc reaction proceeds via a σ-complex to the ring as suggested by MS^3 spectra. The greater reactivity of $BrCO^+$ is consistent with its weak Br-CO bond and is evidenced by the fact that it reacts even with the strongly deactivated substrates. The much less negative reaction constants in these reactions ($\rho=-0.23$ and -0.56), compared with the reaction constants in solution[3] ($\rho=-12.14$ in acetic acid and -5.78 in hypobromous), is consistent with the much greater reactivity of the electrophiles ($BrCO^+$ and $CH_3NH_2Br^+$) due to the absence of solvation and counterion effects. .

References

1) Schwartz, J. C.; Schey, K. L.; Cooks, R. G. *Int. J. Mass Spectrom. Ion Proc.* **101**, 1 (1990)
2) Kotiaho, T.; Lauritsen, F. R.; Choudhury, T. k.; Cooks, R. G.; Tsao, G. T. *Anal. Chem.* **63**, 1794 (1991)
3) Brown, H. C.; Stock, L. M. *J. Am. Chem. Soc.* **79**, 1421 (1957)

Table 1. Electrophilic Addition of Br^+ ($BrCO^+$) to Aromatic Substrates

Ph-X	σ^+	$Yield_{Br+}$	Rel. $Yield_{Br+}$
Ph-NH_2	-1.3	61	1.6
Ph-OCH_3	-0.78	53	1.3
Ph-CH_3	-0.31	42	1.1
Ph-F	-0.07	32	0.82
Ph-H	0	39	1
Ph-$COCH_3$	0.25	26	0.66
Ph-CN	0.66	22	0.57
Ph-NO_2	0.79	11	0.28

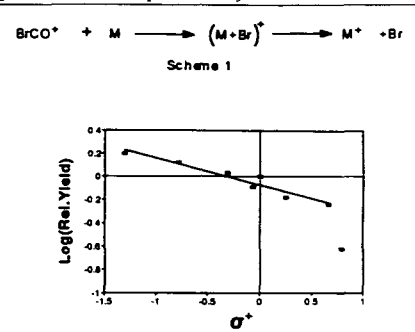

Figure 1

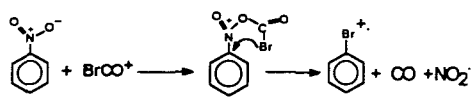

Scheme 2

Table 2. Electrophilic Addition of Br^+ ($CH_3NH_2Br^+$) to Aromatic Substrates

Ph-X	σ^+	$Yield_{Br+}$	Rel. $Yield_{Br+}$
Ph-NH_2	-1.3	38	3.8
Ph-OCH_3	-0.78	21	2.1
Ph-CH_3	-0.31	33	3.3
Ph-F	-0.07	8.5	0.85
Ph-H	0	10.0	1
Ph-Cl	0.11	7.0	0.70
Ph-$COCH_3$	0.25	---	---
Ph-CN	0.66	2.8	0.28
Ph-NO_2	0.79	---	---

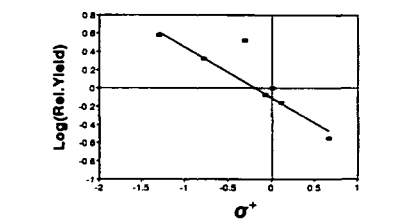

Figure 2

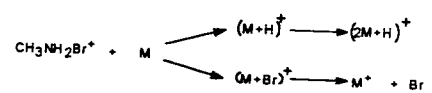

Scheme 3

Table 3. Electrophilic Addition of H^+ ($CH_3NH_2Br^+$) to Aromatic Substrates

Ph-X	PA	σ^+	$Yield_{H+}$	Rel. $Yield_{H+}$
Ph-NH_2	209.5	1.31	32.8	14.9
Ph-$COCH_3$	205.4	0.25	45.0	20.45
Ph-OCH_3	200.3	-0.78	28.0	12.7
Ph-CN	195.9	0.66	9.2	4 18
Ph-CH_3	189.8	-0.31	5.9	2.68
Ph-F	182.6	-0.07	2.0	0.91
Ph-Cl	181.7	0.11	1.0	0.45
Ph-H	181.2	0	2.2	1.0

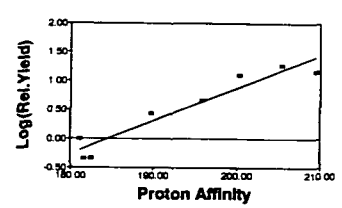

Figure 3

A Study of the Temperature Dependence of the S_N2 Reactions of Cl^- with Methyl Bromide, Ethyl Bromide and n-Butyl Bromide at Atmospheric Pressure using an Ion Mobility - Mass Spectrometer.

*W. B. Knighton, P. M. O'Connor, J. A. Bognar and E. P. Grimsrud, Department of Chemistry, Montana State University, Bozeman, Montana, 59717.

The study of gas phase ion-molecule (IM) reactions at atmospheric pressure is important, because, in conjunction with parallel low pressure measurements insight can be gained into the factors which control the rates of slow IM reactions. In addition, the nature of the potential energy surface for a given reaction system can sometimes be more easily deduced from measurements performed at higher pressures. For instance, in the high pressure limit, if the rate-determining step of a slow gas phase IM reaction is passage over the transition state of interest, theoretical analysis of the rate data requires only knowledge of the reactants and the rate-limiting transition state - no specific knowledge of the reaction intermediates or other minor transition states along the reaction coordinate is then required. Unfortunately, only a modest level of attention has been given to the development of instrumental methods for the measurement of IM reactions under conditions of very high buffer gas pressures, where essentially any IM reaction would be forced into it's high pressure limit of kinetic behavior.

We have recently constructed an instrument called the Kinetic Ion Mobility - Mass Spectrometer (KIMMS) which provides a means for measuring the rate constants of IM reactions at ambient pressure. In this poster, we describe the application of a temperature-variable version of this instrument to the study of a series of nucleophilic displacement S_N2 reactions between Cl^- and three primary alkylbromides (methylbromide, ethylbromide and n-butylbromide), Reaction 1. Measurements of these reactions at 3 torr using a pulsed high pressure mass spectrometer (PHPMS) are also reported.

$$Cl^- + RBr \rightarrow Br^- + RCl \qquad (1)$$

The KIMMS instrument has been previously been described in detail (K. Giles and E.P. Grimsrud, *J. Phys. Chem.* **1992**, *96*, 6680). Ion-molecule reactions occur in the drift tube between the pulses of ions and the reagent molecules that are seeded in the drift gas. If the mobility of the product ions differ from the reagent ions then the ion arrival time spectrum at the Faraday plate will be modified by the reaction. Analysis of these modified spectra as a function of reagent neutral concentration yields a reaction rate coefficient.

The rate constants (k_1) determined here by the KIMMS for the reactions of Cl^- with EtBr, n-BuBr and MeBr are shown in Figures 1-3, respectively. Also, shown in these figures are measurements obtained in the present study in 3 torr methane buffer gas by PHPMS, along with previous measurements by several other groups using a variety of techniques and buffer gas pressures. For EtBr and n-BuBr both the magnitude of and the temperature dependence of the rate constants do not differ over the pressure range of 3 torr to 1.0 Atm. For MeBr it is noted that the measurements of k_1 obtained at 1.0 Atm are significantly greater than all other measurements at lower pressures.

An approximate representation of the reaction coordinates for the reactions of Cl^- with primary alkylbromides is shown in Figure 4. In the reactions of EtBr and n-BuBr with Cl^- (Figures 1 and 2), it is believed that the initially-formed, chemically-activated intermediate, $Cl^-.RBr^*$, is sufficiently long lived that it suffers numerous collisions with the buffer gas at pressures of 3 torr or above, thereby forming a thermalized intermediate, $Cl^-.RBr$. Therefore, the high pressure limit of kinetic behavior is operative at

both 3.0 torr and 1 Atm for these two reaction systems and k_1 is the same at both pressures. For the reaction of MeBr with Cl^-, however, the chemically-activated intermediate, $Cl^-.RBr^*$, is not believed to be efficiently thermalized at pressures of 3 torr or lower. Therefore, at these low pressures, this system appears to be operating within or near its low pressure limit of kinetic behavior. At 1.0 Atm pressure, the distinctly different (higher) k_1 values indicated by the KIMMS measurements in Figure 3 suggest this reaction system has moved towards its high pressure limit of behavior.

The determination of Transition State (TS) energies ($\Delta E^\ddagger$ in Figure 4) from the rate data obtained in the low pressure limit for the reaction of Cl^- with MeBr is difficult using conventional statistical rate theories because simple S_N2 intermediates, including $Cl^-.MeBr^*$, have recently been shown to behave in an non-statistical manner. However, if the buffer gas pressure is made sufficiently high, so that the reaction of interest is moved into it's high pressure limit, where the intermediate is brought into a state of thermal equilibrium with the buffer gas and reactants, then the rate measurements can be interpreted in terms of conventional TS Theory $k_{TST} = \left(\frac{kT}{h}\right)\left(\frac{Q^\ddagger}{Q_{Cl^-}Q_{CH_3Br}}\right)\exp^{\left(\frac{-\Delta E^\ddagger}{RT}\right)}$ (2). By calculation of the partition functions (Q) for the reactants and the envisioned TS, the T-dependence for the combined preexponential factors in Equation 2 can be predicted. If expressed in the form, $\exp(-\alpha/RT)$, this contribution to the T-dependence of k_1 is found to be α = -0.8 kcal/mol. The magnitude of $\Delta E^\ddagger$, where $\Delta E^\ddagger = E_a - \alpha$, can then be deduced from the experimental Arrhenius activation energies, E_a, derived from plot of ln k versus 1/T (Figures 1-3). The $\Delta E^\ddagger$'s thereby determined for each reaction studied here are included in Figures 1-3. Using $\Delta E^\ddagger$ = -2.3 kcal/mol, predictions of k_{TST} for the reaction of Cl^- with MeBr over the temperature range of 35 to 150°C, are shown in Figure 3 to be within a factor of 2 of the KIMMS measurements.

Figure 1. $Cl^- + EtBr \rightarrow Br^- + EtCl$

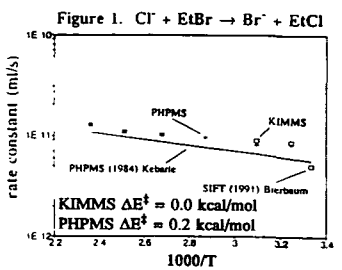

Figure 2. $Cl^- + BuBr \rightarrow Br^- + BuCl$

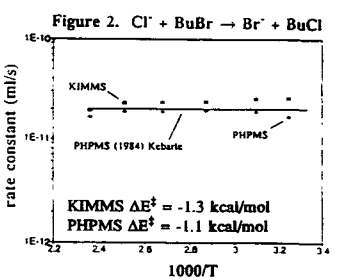

Figure 3. $Cl^- + MeBr \rightarrow Br^- + MeCl$

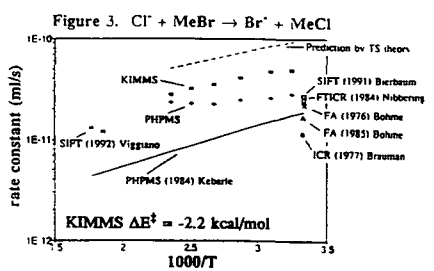

Figure 4. Reaction Coordinate

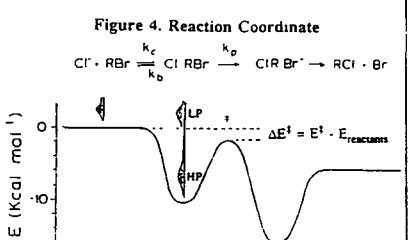

KINETIC ISOTOPE EFFECTS FOR THE S_N2 REACTIONS OF SOLVATED ANIONS WITH METHYL HALIDES.

Thuy Thanh Dang, Charles H. DePuy,
Richard A. J. O'Hair and Veronica M. Bierbaum,

Department of Chemistry and Biochemistry,
University of Colorado,
Boulder, Colorado 80309-0215.

Bimolecular nucleophilic substitution reactions have been the focus of numerous theoretical and experimental studies in recent years due to their central importance in organic chemistry. Nevertheless, there has been relatively little experimental work on the gas phase reactions of solvated nucleophiles and no experimental studies of solvent kinetic isotope effects.

We have studied the S_N2 reactions of F^-, $F^-(H_2O)$, and $F^-(D_2O)$ with CH_3X and CD_3X, where X = I, Br and Cl, using the tandem flowing afterglow-selected ion flow tube technique. The displaced halide ion X^- is the sole product in the reactions of F^-, and the major product in the reactions of $F^-(H_2O)$ and $F^-(D_2O)$, where solvated X^- is also formed. The rate coefficients for these reactions are summarized in Table I.

Table I: Rate Coefficients for S_N2 Reactions

	F^-	$F^-(H_2O)$	$F^-(D_2O)$
CH_3I	2.16 (-9)[a]	1.01 (-9)	1.02 (-9)
CD_3I	2.22 (-9)	9.93 (-10)	1.05 (-9)
CH_3Br	2.02 (-9)	5.31 (-10)	6.06 (-10)
CD_3Br	2.04 (-9)	5.73 (-10)	6.68 (-10)
CH_3Cl	1.44 (-9)	1.45 (-11)	2.04 (-11)
CD_3Cl	1.60 (-9)	1.75 (-11)	2.68 (-11)

[a] 2.16 (-9) represents 2.16×10^{-9} cm^3 $molecule^{-1}$ s^{-1}

These results demonstrate that:

1) S_N2 reactivity decreases as the reaction exothermicity decreases, i.e., for a given nucleophile, the rate coefficients decrease in the sequence $CH_3I > CH_3Br > CH_3Cl$.

2) Reactivity decreases with solvation; this effect is most dramatic for CH_3Cl where solvation lowers the rate coefficient by two orders of magnitude.

3) Kinetic isotope effects are absent for extremely rapid reactions but become evident for slower processes where the height of the central barrier is important.

4) Inverse kinetic isotope effects are observed for deuteration of the methyl halide with k_H/k_D as small as 0.76 ($k[F^-(D_2O) + CH_3Cl]/k[F^-(D_2O) + CD_3Cl]$).

5) Inverse kinetic isotope effects are observed for deuteration of the solvent molecule with k_H/k_D as small as 0.65 ($k[F^-(H_2O) + CD_3Cl]/k[F^-(D_2O) + CD_3Cl]$).

These inverse kinetic isotope effects indicate that the zero point energy difference between hydrogen and deuterium is greater in the transition state than it is in the ground state. Future studies will explore the kinetic isotope effects in reactions of nucleophiles involving higher degrees of hydration as well as other solvent molecules.

COMPETITIVE S_N2/S_Ni REACTIONS OCCURING IN THE COLLISION CELL OF TRIPLE QUADRUPOLE FROM LOW KINETIC ENERGY MH^+ AND $[M+NH_4]^+$ IONS PREPARED FROM THE DIASTEREOMERIC 1,2-INDANEDIOLS.

Bourhis, C., Perlat, M.C., Fournier, F. and Tabet, J.C.*

Laboratoire de Chimie organique Structurale,
Department of Molecular Chemistry, U.P.M.C., Paris, FRANCE.

In the gas phase, ion-molécule réactions were commonly investigated by using either FT-ICR and ITMS (more recently) or Pulsed High Pressure Source Mass Spectrometer and Flowing-Afterglow (and SIFT)[1]. Furthermore, these bimolecular processes can be studied under chemical ionization in high pressure source of tandem mass spectrometer and also in collision cell from selected ions having a low kinetic energy (CAR spectra)[2]. Among the different ion-molecule reactions studied by this approach, proton transfer and nucleophilic substitution are typically generated when the basicity of substrat is lower than of ammonia by less 10 kcal/mol. These réactions can compete from alcohols[3] and esters[4] submitted to CI-NH_3.

$$\text{i.e.}\quad R\text{-}OH + NH_4^+ \rightleftharpoons [R\text{-}OH...NH_4^+] \begin{cases} \rightarrow R\text{-}OH_2^+ + NH_3 & (a) \\ \rightarrow R\text{-}NH_3^+ + H_2O & (b) \end{cases}$$

Different investigations demonstrated that such adduct $[M+NH_4]^+$ ions in ion source lead to the substituted $[M+NH_4\text{-}H_2O]^+$ ions (case of alcohols) *via* nucleophilic substitution which accompanies the unfavored MH^+ formation. The former process occurs from adduct ions either *via* unimolecular S_Ni mechanism (decomposition with retention of stereochemistry) or bimolecular substitution as the "like S_N2" pathway accompanied by Walden inversion of function configuration.

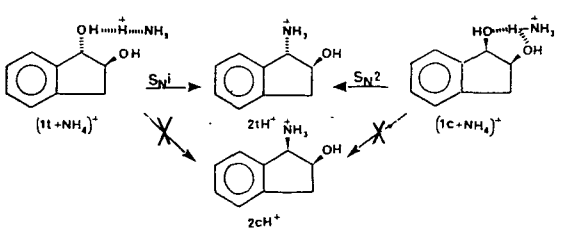

In the present work, the Nucleophilic Substitution is investigated in collision cell of triple quadripole instrument from adduct $[M+NH_4]^+$ ions prepared from *cis* and *trans* epimers of 1,2-indanediol. Methylamine was used as nucleophilic reagent in the cell in order to react with adduct ions under low collision energy. Dissociation (e.g. S_Ni pattern) and ion-molecule reactions take place in competition at E_{lab}=7 eV as well as at lower E_{lab} values. Among the different

bimolecular processes, $NH_3/MeNH_2$ exchange, proton transfer and S_N2 from $[M+NH_4]^+$ are the major bimolecular reactions. Competition occuring between S_Ni and S_N2 processes is influenced by the experimental conditions according to the collision energy used : laboratory energy, methylamine pressure in collision cell etc... The Reaction products of methylamine on the epimeric MH^+ ions is compared to those observed from the adduct ions but mainly proton transfer occurs and the SN appears inefficient. In particular, orientation of competitive reaction such as SN_2 process and proton transfer to nucleophilic reagent, studied according to similar experimental conditions shows that it is strongly influenced by the energy level of the initial state. On the other hand this means that stabilizing collisions are inefficient in collision cell.

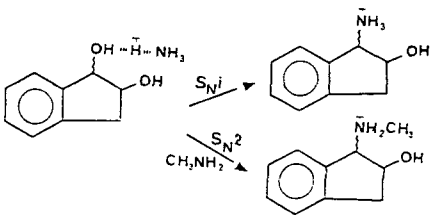

ERMS breakdown from adduct ions $[M+NH_4]^+$ with $MeNH_2$ in collision cell (multiple collision conditions).

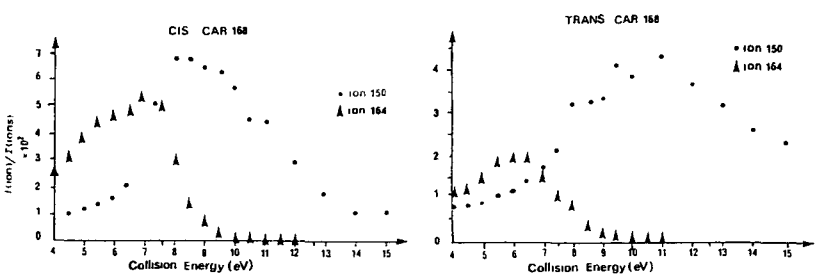

REFERENCES:

1. Bowers, M.T. (1979), in "Gas Phase Ion Chemistry", Bowers, M. T. (Ed), Academic Press.
2. F. Westmore and M. M. Alauddin; Mass Spectrom. Rev. 1986, 5, 381-465. (b). J. C. Tabet; Fundamentals of Gas Phase Ion Chemistry, K. R. Jennings (Ed), 1991, 351-372.
3. (a) J. C. Tabet, H. E. Audier, and J. P. Denhez; Tetrahedron 1987, 43, 873-880. (b) K. R. Madhusudaman, N. Prassad et D. Fraisse, Org. Mass Spectrom. 1985, 220, 630-645.
4. D. Despeyroux, R. B. Cole and J. C. Tabet; Org. Mass Spectrom. 1992, 27, 300-308.
5. W. J. Meyerhoffer and M. M. Bursey; Org. Mass Spectrom. 1989, 24, 169-175.

GUIDED-ION BEAM STUDIES OF REACTIONS OF IONS WITH NO

Susan T. Graul,[a], Skip Williams,[b] Rainer A. Dressler,[c] Richard H. Salter,[c] Edmond Murad[c]
[a] *Department of Chemistry, Carnegie Mellon University, Pittsburgh, PA 15213*
[b] *Department of Chemistry, Stanford University, Stanford, CA 94503*
[c] *Phillips Laboratory, PL/WSSI, Hanscom AFB, MA 01731*

INTRODUCTION

As a consequence of its very low ionization potential (9.26 eV), NO can undergo charge transfer with most atmospheric ions at thermal translational energies. In systems where the charge transfer reaction is very exothermic, the thermal energy reaction rate constant may nonetheless be very small ($k < 10^{-12}$ cm^3-sec^{-1}), which is inconsistent with statistical models for kineticcs of bimolecular reactions. For these charge-transfer reactions where the assumption of energy randomization within a long-lived complex does not apply, alternative models can be considered. The simplest of these invokes two criteria that govern reaction rate constants: *energy resonance* and *Franck-Condon overlap* between reactant and product states. In the present work, we examine the reactions of Ar^+, N_2^+, and Kr^+ with NO at hyperthermal energies, and consider which model best describes the reaction dynamics.

EXPERIMENT

These studies are carried out in a guided-ion beam apparatus.[1] Reactant ions are mass-selected at a Wien filter and injected into an double-octopole beam guide, which runs through a collision cell, where a low pressure of NO gas is maintained. Ionic products are mass-analyzed in a quadrupole mass filter. Time-of-flight distributions are measured by pulsing the reactant ion into the octopole and monitoring flight times of product ions.

RESULTS

Cross sections for the reactions of Ar^+, N_2^+, and Kr^+ with NO are shown below. The total charge-transfer cross sections are significantly less than the Langevin cross section, but below about 1 eV relative translational energy, the energy dependences are similar. In each reaction, N^+ and O^+ fragment ions are also observed at energies above the respective thermodynamic thresholds for dissociative charge transfer.

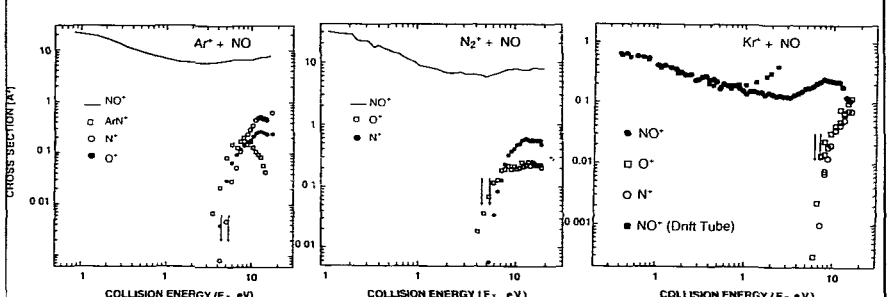

In the Ar^+ + NO reaction, an additional product is observed, corresponding to ArN^+ or ArO^+ (the mass resolution is not adequate to distinguish these products under the high transmission conditions required to detect this channel).

The TOF distributions are transformed to axial velocity distributions using the methodology of Gerlich.[2] Velocity distributions are shown below for the NO^+ product from Ar^+ + NO at a relative translational energy of 1.16 eV. The distributions on the left is obtained with a low octopole guiding field, such that product ions with large components of radial velocity are not trapped. This distribution can be compared with the one obtained for high octopole guiding field (on the right), in which case all product ions are collected. Inspection of these distributions reveals that while most of the NO^+ product ions are formed with very little axial velocity, there is a significant fraction of products that have velocities equal to or greater than the center-of-mass velocity.

The distributions can be analyzed in terms of an "osculating complex" model, in which collisions result in formation of transient complexes. The angular distribution of the products is determined by the lifetime of the complex relative to its rotational period. In addition to momentum transfer, conversion of translational to internal energy. The experimental distributions are compared to distributions calculated for various complex lifetimes and differing amounts of converted energy, until acceptable agreement between the distributions is obtained. The solid and dashed lines in the figures below are the calculated distributions for the internal energy distribution of NO^+ shown.

Most of the NO^+ product ions that are formed with small velocities are likely due to long-range charge transfer reactions, in which little or no momentum transfer occurs. The faster, forward-scattered NO^+ ions are formed in large-impact parameter orbiting collisions, in which varying amounts of energy are converted from translation to internal energy. It is particularly interesting to note that the NO^+ product ions are all highly excited, with internal energies in excess of 6 eV. These ions are probably formed in the excited electronic *a* state.

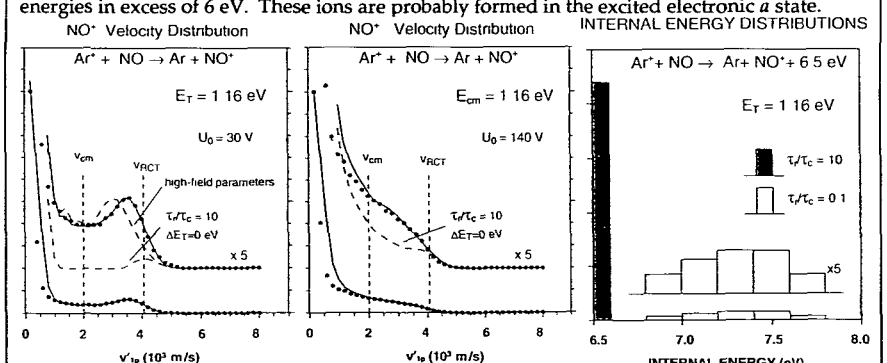

[1] R. A. Dressler, R. H. Salter and E. Murad, *J. Chem. Phys.*, in press. R. A. Dressler, R. H. Salter and E. Murad, *Planet. Space Sci.*, **1992**, *40*, 1695.
[2] D. Gerlich, in "State-selected and state-to-state ion-molecule reaction dynamics", *Adv. Chem. Phys.*, **1992**, *82*, Part 1, edited by M. Baer and C. Y. Ng (Wiley, New York).

Effects Of Reactant Ion Kinetic Energy On Both Endothermic And Exothermic Ion/Molecule Reactions In A Quadrupole Ion Trap Mass Spectrometer

Hui-Fen Wu and Jennifer S. Brodbelt
Department of Chemistry, University of Texas, Austin, TX 78712-1167

Stemming from the first discovery of ion/molecule reactions and the landmark development of chemical ionization, the use of ion/molecule reactions to solve a diverse range of ion structural problems in analytical and organic mass spectrometry has become increasingly widespread. There has been ongoing interest in evaluating the application of endothermic ion/molecule reactions for both fundamental thermochemical and analytical applications. In the gas phase, endothermic ion/molecule reactions require an alternate driving force, and this is typically supplied by accelerating a reactant ion of interest to some particular kinetic energy prior to an ion/molecule collision with a neutral substrate. When sufficient kinetic energy is converted to internal energy during the collision, the barrier to reaction may be surpassed, and product ions may be formed from the intermediate collision complex.

In this study, we have examined a variety of reactions of known endothermicity to determine the feasibility of driving endothermic ion/molecule reactions in a quadrupole ion trap. Both proton-transfer and charge exchange reactions are investigated, and such factors as the activation time, activation voltage, and trapping conditions are described in the context of their effects on the outcomes and efficiencies of endothermic ion/molecule reactions. Additionally, the effects of supplementary activation on the outcomes of exothermic proton-transfer and charge exchange reactions are studied.

All experiments were performed in a Finnigan quadrupole ion trap mass spectrometer. Compounds were admitted into the vacuum chamber to nominally 2 - 5 x 10^{-6} torr. Helium buffer gas was admitted to 1 mtorr. For the reactions, the molecular type ions of one compound were isolated by application of an appropriate combination of dc and rf voltages in order to eject all other ions from the trap. Then during a subsequent reaction interval, the ions were activated by application of a supplementary ac voltage of 0 - 1000 mV_{p-p} across the end-cap electrodes (q_z = 0.2 - 0.6) for 0 - 1000 ms.

Effects of Reactant Ion Kinetic Energy on Endothermic Ion/Molecule Reactions

A survey of various charge-exchange and proton-transfer reactions was performed in order to obtain an initial evaluation of the feasibility of driving endothermic ion/molecule reactions in a quadrupole ion trap. Collisions with either helium or reactant neutrals may lead to two important competing processes, dissociation or neutralization, of the activated reactant ion.

In Figure 1 is shown the endothermic charge-exchange between naphthalene molecular ions (m/z 128) and phenol (net 0.33 eV endothermic). For this experiment, the conditions found to optimize the endothermic reaction consisted of a 20 ms activation period at q_z = 0.35 (600 mV_{p-p} activation at 136,100 Hz). Activation of the naphthalene ions leads to both collisionally-activated dissociation by elimination of C_2H_2 and charge exchange to form phenol molecular ions at m/z 94. The naphthalene fragment ions at m/z 102 do not undergo observable exothermic or endothermic charge transfer reactions with phenol, so evidently the phenol ions must be due to endothermic charge exchange from the naphthalene ions.

Shown in Figure 2 are the spectra illustrating endothermic proton-transfer (18.7 kcal/mole) of protonated propylamine with tetrahydrofuran. Upon activation by a 350 mV_{p-p} voltage (116,700 Hz), protonated propylamine transfers a proton to tetrahydrofuran and does not undergo extensive collisionally-activated dissociation. The conditions found to optimize the formation of endothermic ion/molecule reaction products consisted of a 20 ms activation period at q_z = 0.3.

The effects of activation conditions on competing endothermic ion/molecule reaction and dissociation processes is illustrated in Figure 3 for the case of protonated n-butyl ether. Both n-butyl ether and dimethyl ether were admitted to the vacuum chamber to nominally 4 x 10^{-6} torr. Protonated

n-butyl ether was isolated and activated (q_z = 0.3) by applying a supplementary ac voltage of 0 - 1000 mV_{p-p} for 5 ms. The proton-transfer reaction to dimethyl ether is 11.6 kcal/mole endothermic. The conversion efficiency increases with voltage, reaching a maximum of 6.5 % at 300 mV. At higher voltages, there is a steady decrease in the conversion efficiency, indicating that other competitive dissociation, neutralization and ion ejection processes become more favored.

Effects of Reactant Ion Kinetic Energy on Exothermic Ion/Molecule Reactions

Many exothermic reactions are disfavored as the kinetic energy of the reactant ion increases because the higher velocity of the reactant ion perturbs formation of the collision complex necessary for a successful ion/molecule reaction. Thus, it was of interest to determine whether an increase in the kinetic energy of reactant ions in the ion trap caused observable changes in proton-transfer and charge exchange reactions. For example, shown in Figure 4 is a plot of the relative abundances of the protonated dimethyl ether and protonated n-butyl ether as a function of activation voltage. First protonated dimethyl ether was isolated, then accelerated for 5 ms by application of a supplementary ac voltage (156,000 Hz) from 0 - 800 mV_{p-p}. When protonated dimethyl ether is not activated, it rapidly transfers a proton to n-butyl ether (11.6 kcal/mole exothermic) in the 5 ms interval, and this is represented in Figure 4 by the points of nearly equal intensity at 0 mV activation. With application of a 200 mV supplementary voltage, the abundance of protonated dimethyl ether increases while the abundance of protonated n-butyl ether decreases. At higher voltages, both the abundances of protonated dimethyl ether and n-butyl ether decrease, because the formation of the proton-bound collision complex is disfavored and other ion loss processes occur.

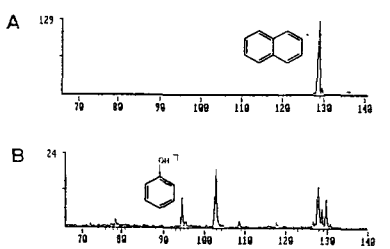

Figure 1

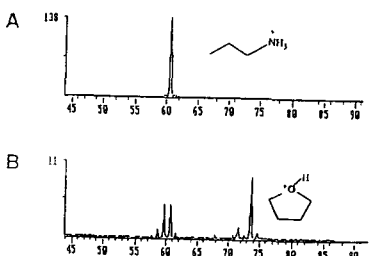

Figure 2.

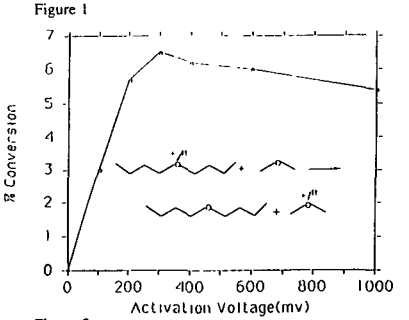

Figure 3.

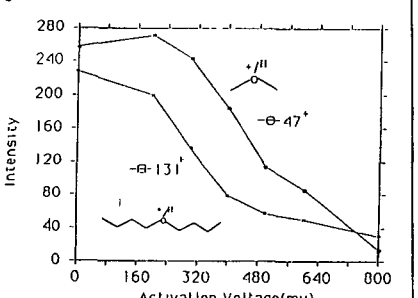

Figure 4.

H/D EXCHANGE IN LOW ENERGY COLLISIONS BETWEEN PROTONATED AROMATICS AND D_2O OR CD_3OD

John A. Stone, Department of Chemistry, Queen's University
Kingston, Ontario, Canada K7L 3N6

H/D exchange can be used to count the number of "active" H atoms in a molecule. The use of both a chemical ionization source[1] and the central quadrupole in a triple quadrupole instrument[2] for this purpose have been demonstrated. We have examined H/D exchange in the hexapole collision cell of a Fisons quadrupole/hexapole/quadrupole triple sector instrument to explore the advantages and limitations of using a triple sector instrument.

A grounded chemical ionization source with grounded ion repeller produced protonated molecular ions MH^+ using CH_4 as reagent gas. The MH^+ ions from the first quadrupole were directed into the hexapole RF only cell which can be set at zero or negative integral voltages with respect to the source. The collision gases employed were D_2O, CD_3OD and C_6D_6. Transmitted ions were analysed by the second quadrupole.

The results demonstrate that the extent of isotope exchange depends on the gas pressure, the difference in proton affinity between M and the collision gas, and the translational energy of the ion.

Table 1 shows the extent of deuteration of various MH^+ by D_2O with 0 V on the collision cell. The extent of deuteration decreases in the order benzene >> toluene > xylene with no deuteration observed for mesitylene. This is the order of increasing proton affinity (PA), i.e. the increasing difference in PA between D_2O (167 kcal mol^{-1}) and M. The pattern of M-d_x ions is not as expected from a statistical point of view since their relative intensities do not fall continuously with increasing extent of deuteration. For benzene there is a minimum intensity at M-d_3^+ and for toluene, p-xylene and 2-F-toluene at M-d_2^+. These patterns does not change drastically over the pressure range 1 to 5 x 10^{-3} mm Hg.

Tables 2 and 3 show the results for similar experiments using CD_3OD and C_6D_6 as collision gases. The same behaviour and conclusions apply as for D_2O. Protonated benzene cannot be studied since it proton transfers to CD_3OD and charge exchanges with C_6D_6.

When a negative potential is applied to the collision cell to accelerate the MH^+ ions, the total ion intensity increases, mainly because the intensity of MH^+ increases. However with D_2O the relative intensities of the M-d_x^+ ions show little change until greater than -4 volts is applied to the collision cell, when their intensities fall to essentially zero (Figure 1). For protonated toluene colliding with C_6D_6, most H/D exchange vanishes at -1 volt; for ethanediol this occurs at -3 volts.

Conclusions

The patterns of M-d_x peaks with changes of pressure and voltage difference between ion source and cell show that some MH^+ ions can survive transmission through the collision cell without exchange while others exchange completely under the same conditions. The dependence on PA(M) can be explained in terms of the change in ion/neutral collision complex lifetime with Δ(PA)[1]. The invariance of the pattern of M-d_3^+ ions with collision energy shows that once an ion is slowed down

by collision inside the cell, its further behaviour is independent of its initial energy. There are, however, cut-off energies above which ions cannot be slowed down sufficiently to take part in any exchange reactions. The intensity of the transmitted MH^+ beam changes little with cell potential from -5 to -200 V.

[1] D.F. Hunt and S.K. Sethi; J. Am. Chem. Soc. **102**, 6953 (1980)

[2] A. Ranasinghe, R.G. Cooks and S.K. Sethi; Org. Mass Spectrom. **27**, 77 (1992).

TABLE 2

EXTENT OF H/D EXCHANGE BETWEEN MH^+ AND CO_3OD (5.3 x 10^{-3} mm Hg AND NOMINALLY OeV COLLISION ENERGY)

M	RELATIVE ION INTENSITIES					PA(M)
	MH^+	M-d_1	M-d_2	M-d_3	M-d_4	
Benzene	100	2	~0.1			
m-Xylene	100	17	50	64	32	
Cumene	100					
Mesitylene	100	5	34	32	14	
α-Me-Styrene	100					

TABLE 3

EXTENT OF H/D EXCHANGE BETWEEN MH^+ AND C_6D_6 (3 x 10^{-4} Mm Hg) AT VARIOUS COLLISION ENERGIES (CE, eV)

M	CE	MH^+	M-d_1	M-d_2	M-d_3	M-d_4	M-d_5	M-d_6
Toluene	0	100	27	8	2.3	0.5	0.04	0.03
	1	100	1.8	0.4	0.5			
Mesitylene	0	100						
	1	100						
Ethanediol	0	100	70	27	7			
	1	100	67	25	6			
	2	100	30	10	2			
	3	100	--	--	-			

Target Capture and Ion/Molecule Reactions in High Energy Collisions between Protonated Peptides and Hydrogen-Containing Targets

Xueheng Cheng* and Catherine Fenselau

Department of Chemistry and Biochemistry, University of Maryland Baltimore County, Baltimore, MD 21228

* Present address: Battelle Pacific Northwest Laboratory, Richland, WA 99352

Recent progress in the methods of ionizing large biomolecules has raised expectations for the application of collision-induced dissociation (CID) in the structural analysis of large biomolecules using mass spectrometry. One limitation of CID is the low efficiency for dissociating large ions. A better understanding of the dynamics and mechanism of CID involving large ions is very important for improving dissociation efficiency and extending applications of CID. Recently, target-capture in high energy CID has been observed for fullerene ions colliding with small target gases and the dynamics of such a process were discussed.[1]

We will present evidence showing that target-capture in high energy CID is likely to be a more general phenomenon and ion/molecule reactions can take place in such a high energy collision. Using a JEOL HX110/HX100 four-sector tandem mass spectrometer (EBEB geometry) modified for the study of variable-collision energy (0 eV-10 keV) ion/molecule reactions, we have studied collisions between protonated peptides MH^+ (generated from FAB ionization) and hydrogen-containing target gases (XH_n) such as ammonia and methane. Peptides (MW, Da) studied include leucine enkephalin (555), leucine enkephalin-arginine (711), valinomycin (1111), renin substrate (1758), ACTH(22-39) (1985) and melittin (2845). Product ions with mass above that of the precursor ion have been observed for all the peptide systems studied and the yield increases with an increase in the MW of the peptides. A major product ion observed had a mass corresponding to elimination of two hydrogens from the ion/target complex $[MH + XH_n - 2H]^+$ (Fig. 1b). The collision energy (E_{cm}) at which maximum yield observed was shown to depend directly on the mass and the thickness of the peptide ions and span from 12 eV to 24 eV (E_{cm}) (Fig. 2). The ion/target complex $[MH + XH_n]^+$ were also observed with a lower yield and lower optimal collision energies (Fig. 3). Isotope labeling experiments established the origin of the two hydrogens eliminated from the ion/target complex with one from the target and the other from the precursor ion (Fig. 1c). Incorporation of 14 Da, $[CH_4 - 2H]$ or 17 Da, $[CD_4 - H - D]$ into some of the fragment ions was observed in CID experiments with renin substrate and CH_4 or CD_4, respectively.

The collision energy dependence showed similarities to the fullerene system. This work renders experimental support to the analysis of collision dynamics of large peptide ions by Derrick and coworkers[2] and suggests that the transition point in target scattering is convergent with the formation of target-capture complexes and maximum kinetic-to-internal energy conversion (Fig. 4).

A model of "loose-woollen-ball" conformation for gas-phase protonated peptides is proposed in which the peptide back-bone wraps around to solvate the proton (Fig. 4). A mechanism based on homolytic bond breaking and reformation in the ion/target complex formed by target-capture is proposed to account for the experimental observations. This work shows that chemical reactions can take place in high energy collisional processes under target-capture conditions.

References

(1) Weiske, T.; Bohme, D. K.; Hrusak, J.; Kratschmer, W.; Schwarz, H. *Angew. Chem., Int. Ed. Engl.* **1991**, *30*, 884-886. Caldwell, K. A.; Giblin, D. E.; Hsu, C. S.; Cox, D.; Gross, M. L. *J. Am. Chem. Soc.* **1991**, *113*, 8519-8521. McElvany, S. W.; Ross, M. M.; Callahan, J. H. *Acc. Chem. Res.* **1992**, *25*, 162-168.

(2) Neumann, G. M.; Sheil, M. M.; Derrick, P. J. *Z. Naturforsch.* **1984**, *39a*, 584-592.

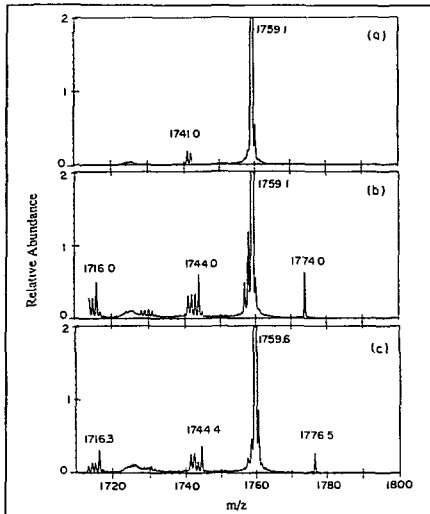

Figure 1. Product ion spectra in the precursor ion region from collision of protonated renin substrate at E_{lab} = 2.2 keV with (a) no collision gas added; (b) NH_3 as collision gas, (c) ND_3 as collision gas

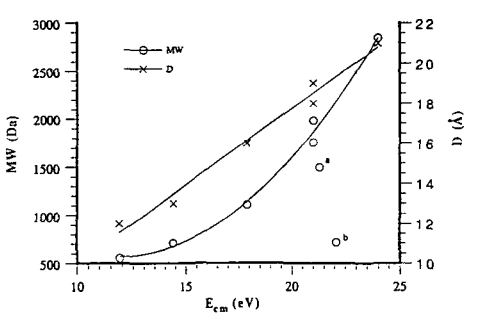

Figure 2. Plot of the molecular weight and the estimated thickness of the 6 peptides studied versus the optimal collision energy (E_{cm}) for the formation of the $[MH + XH_n - 2H]^+$ ion (XH_n = NH_3 and/or CH_4). Point a and b represent data adopted from ref 2 and ref. 1

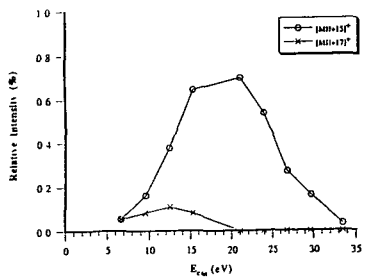

Figure 3. Plot of the yield of the $[MH + 15]^+$ and $[MH + 17]^+$ ions from collision of protonated renin substrate with NH_3 versus the collision energy (E_{cm}).

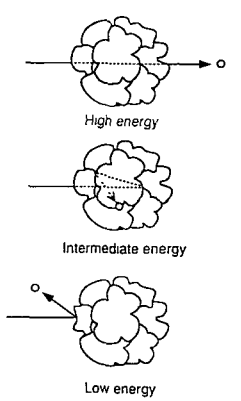

Figure 4. Reaction scheme representing collision of an accelerated protonated peptide with a stationary target at different collision energies. For the convenience of drawing, the protonated peptide was showing to be static and the target moving.

GAS PHASE BASICITIES OF GUANIDINE AND UREA

R. D. Kinser, G. R. Nicol, and D. P. Ridge
Department of Chemistry and Biochemistry
University of Delaware
Newark, DE 19716

Measurements of gas phase basicities (GBs) of the 20 essential amino acids have been the subject of several recent publications.[1,2] Our interest has been focused on the GBs of amino acid amides, since the amide structure incorporates the components of the peptide bond. Studies in our laboratory of proton transfer from the laser desorbed protonated amino acid amide arginamide (ArgA) yielded results indicative of a lower than expected GB for ArgA. Both ArgA and the highly basic amino acid arginine have as R-groups an amino-alkylated guanidine. FTMS studies of proton transfers to the diaminoimine guanidine and its ketone analog, urea, were conducted to increase our understanding of the relationship between structure and GB.

Bracketing techniques were used to establish a proton affinity of urea of 221.0 ± 6.6 kcal/mol. The relevant reactions are:

$$(2,5\text{-diMefuran}+H)^+ + \text{urea} \rightarrow (\text{urea}+H)^+ + 2,5\text{-diMefuran} \quad (1)$$

$$(\text{urea} + H)^+ + \text{pyridine} \rightarrow \text{urea} + (\text{pyridine} + H)^+ \quad (2)$$

$$(\text{urea}+H)^+ + MeNH_2 \rightarrow \text{urea} - MeNH_3^+ \quad (3)$$

Bracketing techniques also were used to establish a proton affinity of 239.6 ± 1.5 kcal/mol for guanidine. Reactions indicative of this are (2,6 - lut = 2,6-lutidine):

$$(2,6\text{-lut}+H)^+ + \text{guan} \rightarrow (\text{guan}+H)^+ + 2,6\text{-lut} \quad (4)$$

$$(\text{guan}+H)^+ + Et_3N \rightleftharpoons \text{guan} + Et_3NH^+ \quad (5)$$

$$(\text{guan}+H)^+ + Pr_3N \rightarrow \text{guan} + Pr_3NH^+ \quad (6)$$

The K_{eq} for Eq. 5 was determined to be 4.22, with $\Delta G° = -0.86$ kcal/mol. From this equilibrium constant, the proton affinity of guanidine was determined to be 240.5 kcal/mol. These values are consistent with the reported GB for arginine and support the need for further refinements in the measurement of the GB for ArgA. Plans for continuing these investigations include measurements of the GBs for N-methyl- and N-ethylguanidine.

[1]Gorman, Greg. S.; Speir, J. Paul; Turner, Cheryl A.; Amster, I. Jonathan. Proton Affinities of the 20 Common α-Amino Acids. J. Am. Chem. Soc., 114, pp. 3986 - 3988 (1992).

[2]Wu, Z.; Fenselau, C. Proton Affinity of Arginine Measured by the Kinetic Approach. Rapid Commun. in Mass Spectrom., 6, pp. 403 - 405 (1992).

BREAKDOWN CURVES FOR THE DISSOCIATION OF PROTONATED PEPTIDE IONS BY LASER DESORPTION/CHEMICAL IONIZATION

J. Paul Speir, I. Jonathan Amster
Department of Chemistry, University of Georgia, Athens, Georgia 30602

INTRODUCTION

The technique of of laser desorption/chemical ionization (LD/CI) has allowed us to obtain fundamental information about the gas-phase properties of peptides and amino acids as well as gain insight into the energetics of fragmentation of peptide ions.[1,2] Here, LD/CI is used to probe the energy dependence of the dissociation pathways of peptides. This technique allows a discrete amount of energy to be placed in the parent ion. By using different reagent species, the exothermicity of the proton transfer reaction can be changed. This allows the product ion distribution to be measured as a function of the reactions's enthalpy, thus producing the breakdown graph. The results of RRKM/QET computations are compared to experimentally obtained breakdown curves in an effort to better understand the dissociation mechanisms of protonated peptide ions.

EXPERIMENTAL

The experiments were performed using a Fourier transform mass spectrometer equipped with a 4.4 cm cubic analyzer cell, a 1 Tesla electromagnet, and an IonSpec data system.[1] For peptide samples desorbed using the substrate-assisted methodology, a 500 monolayer coverage of sinapinic acid, a uv absorbing compound, is first electrosprayed onto the metal substrate. The peptide sample is then electrosprayed on top of the sinapinic acid layer producing an analyte coverage of 500 monolayers.[3] Intact *neutral* peptide molecules are desorbed from a sample stub using either the 248 nm (KrF) or 337 nm (N_2) output of an excimer laser. Proton transfer reagent ions are generated by electron ionization of a high pressure burst of a reagent gas which is admitted through a pulsed valve

The RRKM computer program used for calculating the unimolecular rate constants for the dissociation of peptide ions was written in-house using *Turbo Pascal* ™ The algorithm utilizes the method of steepest-descent for evaluating the reduced energy level densities and sum of states.[4] The vibrational frequencies of the protonated peptide val-pro, used in the RRKM calculations, were obtained by semiemperical (AM1) calculations.

RESULTS AND DISCUSSION

The complete breakdown curve for val-pro (VP), shown in Figure 1, has recently been completed and encompasses the energy range of 16.1 to 136.1 kcal/mol. The dominating fragmentation pathways in this energy range, as a result of proton transfer reactions, is the formation of the y_1 and a_1 fragments. The y_1 is more prominent at the lower energy range (27.7-92.2 kcal/mol) while the a_1 dominates at energies above 99.1 kcal/mol. A plot of the unimolecular rate constant (k(E)) versus internal energy (E), obtained by RRKM calculations, for the formation of the a_1 and y_1 fragments which best model the experimental data is shown in Figure 2. This data is used to produce the theoretically derived breakdown curve which is compared to that obtained

experimentally, as shown in Figure 3 The parameters adjusted to enhance overlap between the theoretical and experimental breakdown curves are the critical energies of the fragments and the degree of 'looseness' or 'tightness' of the transition state. Both the theoretical and experimental data for the formation of the y_1 suggest passage through a tight transition state. This is consistent with a hydrogen rearrangement reaction mechanism for the formation of the y_1 as shown by Orlando etal.[5] The best fit between the theoretical and experimental data for the a_1 was made by assuming that the transition state to form the a_1 gained a rotational degree of freedom, which suggests passage through a loose transition state resulting in direct bond cleavage.

REFERENCES

1. Speir, J. P.; Gorman, G. S.; Cornett, D. S.; Amster, I. J. *Anal. Chem.* **1991,** *63,* 65.
2. Gorman, G. S.; Speir, J. P.; Turner, C. A.; Amster, I. J. *J. Am. Chem. Soc.* **1992,** *114,* 3986.
3. Speir, J. P.; Amster, I. J. *Anal. Chem.* **1992,** *64,* 1041.
4. Forst, W.; Prasil, Z. *J. Chem. Phys.* **1969,** *51,* 3006.
5. Kenny, P. T.; Nomoto, K; Oralndo, R. *Rap. Comm. Mass Spectrom.* **1992,** *6,* 95.

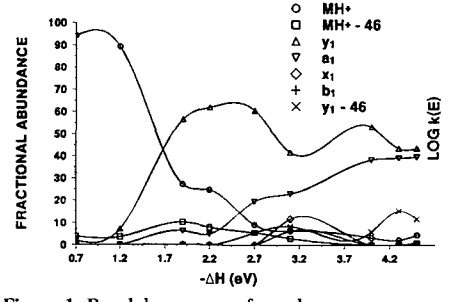

Figure 1. Breakdown curve for val-pro.

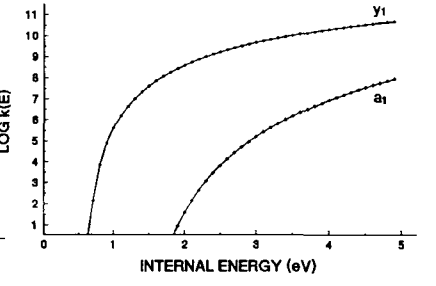

Figure 2. Log k(E) vs. E curve for a_1 and y_1.

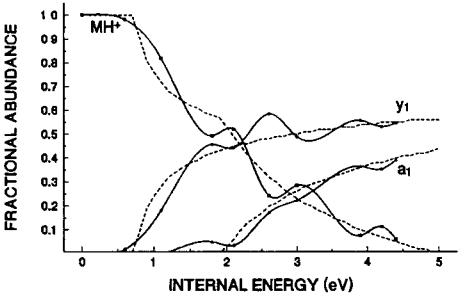

Figure 3. Experimental and theoretical breakdown curves for the MH^+, a_1, and y_1 ions of the peptide val-pro. (broken lines = calculated, solid lines = experimental)

Proton Transfer Rate Constant Measurements of Amino Acids and Dipeptides in a Fourier Transform Mass Spectrometer.

*Gregory S. Gorman, I Jonathan Amster
Department of Chemistry, University of Georgia
Athens, Georgia, 30602

INTRODUCTION

We have previously reported the application of the bracketing method to measurements of the gas-phase basicities (ΔG of protonation) for the 20 common α-amino acids and 22 valine containing dipeptides.[1,2] The basis for assigning gas-phase basicities is the occurrence or nonoccurrence of a proton transfer reaction between a brief pulse of neutral biomolecules with reference base ions previously stored in an ICR cell. When no reaction is observed to occur in the experimental time frame the reaction is considered to be slow and endoergic, while observed reactions are considered to be fast and exoergic. For gas-phase proton transfer reactions, the rate of proton transfer depends on the free energy of the reaction. To determine the thermodynamic value being measured by the bracketing method, a series of kinetic experiments in which the rate of proton transfer is measured under various conditions of free energy and enthalpy were made. Additionally, the transition region between a slow, endoergic reaction and a fast, exothermic reaction, when $\Delta G = 0$, can also be determined.

EXPERIMENTAL

All experiments were preformed in a Fourier transform mass spectrometer designed and constructed in this laboratory and equipped with an electromagnet operated at a field strength of 1 tesla. Protonated amino acid and dipeptide ions were produced by matrix assisted laser desorption/ionization (MALDI) by focusing 337 nm light onto a stainless steel sample probe at an irradiance of 1-10 MW/cm^2. Double resonance eject pulses were used to isolate the protonated molecule ion species from other ions formed in the desorption/ionization procedure. The resulting protonated molecular ions were then collisionally thermalized with Ar, (40-60 collisions), admitted through a pulsed valve, and then allowed to react with reference base, admitted through a leak valve at a static background pressure. The background pressure was measured with an ion gauge, which was corrected for placement and gas sensitivity.[3] Triplicate ion intensity measurements were made at 500 ms intervals from 1 to 5 seconds.

RESULTS

The gas-phase basicity of lysine was determined to lie between that of diethylamine (224.1 kcal/mol) and di-n-propylamine (227.9 kcal/mol) by the bracketing experiments. The proton transfer reaction between di-n-propylamine with protonated lysine (ΔG = -1.9 kcal/mol, ΔH = +5.3 kcal/mol) is both endothermic and exoergic. The measured rate constant was $1.2 \pm .1 \times 10^{-9}$ cm^{3}molec^{-1}s^{-1}, which is essentially the same as the calculated collision frequency of $k_{Langevin} = 1.4 \times 10^{-9}$ cm^{3}molec^{-1}s^{-1}. This entropy-drive reaction is observed to occur essentially at the calculated

collision rate because of the substantial entropy change associated with deprotonation of the cyclic form of protonated lysine. For the reaction with diethylamine (ΔG = +1.9 kcal/mol), the rate constant was measured to be $1.7 \pm .3 \times 10^{-10}$ cm^{3}molec^{-1}s^{-1}, which is approximately an order of magnitude slower than the calculated collision rate of 1.4×10^{-9} cm^{3}molec^{-1}s^{-1}. Since proton transfer was not observed with diethylamine in the bracketing experiments, these results indicate that the free energy (ΔG) of the reaction controls the rate of proton transfer. Table 2 is a comparison between the assigned basicity values of lysine and leucine with those of mono- and diaminoalkane. The upper portion shows the difference between these values assuming the bracketing method is sensitive to free energy, while the lower portion assumes sensitivity to enthalpy. These results indicate that the best agreement between the values is obtained by assuming the bracketing method is sensitive to free energy rather than enthalpy.

REFERENCES

1. Gorman, G. S.; Speir, J. P.; Turner, C. T.; Amster, I. J. *J Am. Chem. Soc.* **1992**, *114*, 3986.
2. Gorman, G. S.; Amster, I. J. *J. Am. Chem. Soc.* in press.
3. Dushman, S. Young, A. H. *Phys. Rev.* **1945**, *68*, 278.
4. Bowers, M. T.; Aue, D. H.; Webb, H. M.; McIver, R. T. *J. Am. Chem. Soc.* **1971**, *93*, 4314.

	GB[a,b]	ΔGB[c]	PA[a,b]	ΔPA[c]
Lysine[d]	**226.0**	**11.2**	**242.6**	**17.6**
Leucine[d]	**214.8**		**225.0**	
1,5-Diaminopentane	**226.6**	**11.9**	**241.3**	**18.1**
n-Hexylamine	**214.7**		**223.2**	
Lysine[e]	**219.0**	**4.2**	**235.0**	**10.0**
Leucine[e]	**214.8**		**225.0**	

All values are in kcal/mol. [a]GB and PA values of the mono-amine/diamine pair are from ref. 4. [b] GB and PA values are from ref. 1. [c]ΔGB and ΔPA values are the differences in basicity and proton affinity between the monoamine-diamine pair or the amino acids. [d]Values for the amino acids if bracketing method is measuring ΔG. [e]Value for the amino acids if bracketing methods is measuring ΔH.

GAS-PHASE BASICITIES OF SMALL CARBOHYDRATES

Carolyn J. Cassady
Department of Chemistry
Miami University
Oxford, OH 45056

The formation of protonated molecular ions is dominant ionization pathway in the analysis of carbohydrates by mass spectrometry. Little is known, however, about the fundamental gas-phase proton transfer properties of carbohydrates. The present study probes the gas-phase basicities (GB) of several disaccharides and glucose by deprotonation reactions with a series of reference compounds in a Fourier transform mass spectrometer.

Gas-phase basicity is the negative of the free energy change for a molecule's protonation reaction:

$$M + H^+ \rightarrow MH^+ \qquad \Delta G_{rxn} = -GB(M).$$

Experimental studies involved bracketing the GBs of glucose, lactose, sucrose, maltose, and cellobiose, using deprotonation reactions in a Bruker CMS 47X Fourier transform mass spectrometer (FTMS). Ions were produced from the carbohydrates by fast atom bombardment (FAB) using a glycerol matrix in an external ion source. The ions were moved into the cell region of the FTMS by electrostatic focusing and then were collisionally cooled. Ion ejection techniques were used to isolate the protonated molecular ions of the carbohydrates. These ions were then allowed to proton transfer to a reference compound of known GB, which was present at a static pressure in the ICR cell:

$$MH^+ + Base \rightarrow M + (Base)H^+.$$

Reaction rate constants were measured, and reaction efficiencies were obtained by comparing these experimental values to the theoretical collision rate constants. For efficiencies of less than 0.10 (less than 10% of all collisions resulting in a reaction), GB(Sugar) was considered to be greater than GB(Base). For faster reactions with efficiencies of greater than 0.10, the reference compound was considered to be the most basic.

Glucose, maltose (two glucose units with an $\alpha(1\rightarrow4)$ linkage) and cellobiose (two glucose units with a $\beta(1\rightarrow4)$ linkage) produced very low abundances of MH^+ by FAB. In particularly, cellobiose was not studied extensively because of difficulties resulting from the low ion yield. (This may be related to its solubility in glycerol.) β-Glucose was found to have a GB between t-butanol and ethyl acetate, bracketing it at 189 ± 5 kcal/mol. This is below the GB of glycerol (196 kcal/mol[1]), which may account for the low formation of MH^+ for glucose by FAB. The GB of mixed anomers of maltose was bracketed between pyrrole and 3-methylaniline, giving a value of 201 ± 6 kcal/mol. All GBs are referenced to the scale of Lias and coworkers[2].

Sucrose and individual anomers of lactose were also studied. The GBs of both sucrose and α-lactose were found to be 203 ± 5 kcal/mol and are bracketed between pyrrole and 3-methylaniline. While in-depth studies have not yet been performed, our preliminary results also suggest that these disaccharides, which have the highest GBs, also form the most intense MH^+ by FAB. β-Lactose was found to be slightly less basic, with a GB of 199 ± 3 kcal/mol, bracketed between i-propyl ether and pyrrole. The higher basicity of α-lactose relative to β-lactose may be the result of enhanced intramolecular H-bonding. α-Lactose contains two sets of OHs that are in proximity in the folded structure, versus one set in the β-form. Intramolecular bonding is known to greatly influence the GBs of crown ethers.[3,4]

Attempts were also made to study galactose and fructose, the monmers which (in addition to glucose) comprise sucrose and lactose. These studies were hindered by low MH^+ formation. Prevous FAB and chemical ionization studies[5,6] have also found that monosaccharides give low MH^+ yields, with H_2O loss dominating. However, the GB of galactose does appear to be near the GB of glucose. As noted above for glucose, this low GB relative to the glycerol matrix may contribute to the poor production of MH^+ by FAB on galactose.

References
(1) Sunner, J.A.; Kulatunga, R.; Kerbarle, P. *Anal. Chem.* 1986, *58*, 1312.
(2)Lias, S.G.; Liebman, J.F. *J. Phys. Chem. Ref. Data* 1984, *13*, 695.
(3) Hedin, P.A.; Phillips, V.A. *J. Agric. Food Chem.* 1991, *39*, 1106.
(4) Clifford, A.J.; De Luca, L.M. *Org. Mass Spectrom.* 1985, *20*, 157.
(5) Meot-Ner, M. *J. Am. Chem. Soc.* 1983, *105*, 4906.
(6) Sharma, R.B.; Blades, A.T.; Kerbarle, P. *J. Am. Chem. Soc.* 1984, *106*, 510.

GAS-PHASE BASICITY STUDIES OF GLYCINE AND DIGLCYINE BY MASS SPECTROMETRY AND AB INITIO CALCULATIONS

Kui Zhang, Alice Chung-Phillips, and Carolyn J. Cassady
Department of Chemistry
Miami University
Oxford, OH 45056

In solution, proton transfer influences the 3-D structure and biological activity of peptides. In the gas-phase, protonation is the dominant ionization pathway during the analysis of peptides by mass spectrometry, with the location of the proton influencing ion intensities and fragmentation patterns. However, very little is known about fundamental thermochemical aspects of the proton transfer process. The present study provides this information for the simples amino acid, glycine, and the simplest peptide, diglycine. The gas-phase basicities (GB) of these species have been determined experimentally and theoretically.

Gas-phase basicity is the negative of the free energy change for a molecule's protonation reaction: $M + H^+ \rightarrow MH^+$ $\Delta G_{rxn} = -GB(M)$.
Experimental studies involved bracketing the GBs of glycine, Gly, and diglycine, Gly_2, using deprotonation reactions in a Bruker CMS 47X Fourier transform mass spectrometer (FTMS). Ions were produced from Gly and Gly_2 by fast atom bombardment (FAB) in an external ion source and moved into the cell region of the FTMS by electrostatic focusing. The ions were collisionally cooled and ion ejection techniques were used to isolate the protonated molecular ions $GlyH^+$ or Gly_2H^+. These ions were then allowed to proton transfer to a reference compound of known GB, which was present at a static pressure in the ICR cell: $Gly_xH^+ + Base \rightarrow Gly_x + (Base)H^+$.
Reaction rate constants were measured, and reaction efficiencies were obtained by comparing these experimental values to the theoretical collision rate constants. For efficiencies of less than 0.10 (less than 10% of all collisions resulting in a reaction), $GB(Gly_x)$ was considered to be greater than GB(Base). For faster reactions with efficiencies of greater than 0.10, the reference compound was considered to be the most basic.

Using this experimental technique, the GB of glycine was found to be 206.2 ± 2.2 kcal/mol and the GB of diglycine was found to be 215.2 ± 2.5 kcal/mol. These values are referenced to the basicity ladder of Meot-Ner and Sieck[1]. The GB value for glycine is in good agreement with previous mass spectral studies that place it between 204 and 209 kcal/mol.[2-5]

Theoretical studies involved high level ab initio calculations using the Gaussian 90 and 92 programs. These studies were primarily performed using the Cray Y-MP8/864 supercomputer at the Ohio Supercomputer Center. In obtaining structures, all geometries were fully optimized. For glycine and protonated glycine, 6-31G* and 6-31 + G(d,p) basis sets were used with MP4 electron correlation. For diglycine and its protonated form, the 6-31G* basis set was used with partial fourth order (MP4SDQ) electron correlation. Gas-phase basicities were calculated from zero-point energies for 298.15 K and 1 atm. Several other levels of ab initio calculations were also performed, but the higher level calculations gave the greatest agreement with experimental results.

For glycine, ab initio research indicates that the preferred protonation site is the terminal amino nitrogen. The calculated GB for this structure is 206.3 kcal/mol, which is in excellent agreement with the experimental results. In addition, a second stable structure, with carboxyl carbonyl oxygen protonation, was found to have a GB of 191.5 kcal/mol.

For diglycine, ab initio research revealed five stable protonated structures. The two most stable structures also involve protonation of the amino nitrogen, differing only in their N13-C12-C9-N6 dihedral angle. Structure I shows the most stable structure. Both structures give strong intramolecular H-bonding from the terminal NH_3^+ to the amide oxygen. This interaction is significantly stronger for diglycine than for glycine and results in a large increase in GB. The calculated GB for the most stable Gly_2H^+ is 215.2 kcal/mol, which is again in excellent agreement with the experimental results.

References
(1) Meot-Ner (Mautner), M.; Sieck, L.W. *J. Am. Chem. Soc.* **1991**, *113*, 4448.
(2) Locke, M.J.; Hunter, R.L.; McIver Jr., R.T. *J. Am. Chem. Soc.* **1979**, *101*, 272.
(3) Meot-Ner (Mautner), M.; Hunter, E.P.; Field, F.H. *J. Am. Chem. Soc.* **1979**, *101*, 686.
(4) Gorman, G.S.; Speir, J.P.; Turner, C.A. Turner; Amster, I.J. *J. Am. Chem. Soc.* **1992**, *114*, 3986.
(5) Wu, J.; Lebrilla, C.B. *J. Am. Chem. Soc.* **1993**, *115*, 3270.

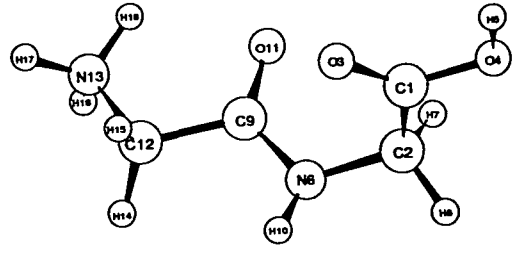

Structure I

Trends in gas-phase basicities of linear oligopeptides Gly_n, Ala_n, and Val_n (n=1-4)

Jiangyue Wu, Carlito B. Lebrilla, Chemistry Department, University of California, Davis. California 95616

The study of the inherent basicities of peptides is important in both chemistry and biochemistry. Basicity is a fundamental property and it affects directly the chemical reactivity and the physical characteristics of peptides. The acid-base properties of various oligomeric peptides in aqueous solution have been studied. It was observed that increasing the peptide length from mono- to di- greatly changes pKa values. Further lengthening the chain from di- to tri- changes the pKa values moderately while tri- to tetra- produces no significant change. In addition, the functional groups on side chains can significantly modify the basicity of peptides.[1] Recently, we reported the gas-phase basicities(GB) of glycine oligomers.[2] Here, we present the continuation of a systemic study of the gas-phase basicities of linear oligopeptides with alkyl side chains.

The gas-phases basicities of peptides are measured in an external source FTMS by using a bracketing method which has been described in earlier pubication.[2] The rate constants and the efficiencies of all the proton exchange reactions are obtained through a kinetic analysis. The efficiencies are large (~ 50%) for the reactions in which the GBs of peptides are lower than that of reference base. The GB values of peptides are assigned according to the efficiencies of the reactions The efficiencies of the reaction are listed for alanine (Table 1) and valine (Table 2). The GB values are listed in Table 3. For comparison, the values for glycine from an earlier study are also shown. The GB values of reference base are assigned from the scale developed by Lias, Liebman and Levin.[3]

In the earlier publication, we reported that the GB values increase from glycine, diglycine to triglycine. However, for the alanine and valine series, the GB values change from amino acid to dipeptide but do not change from dipeptide to tripeptide.

Semi-empirical AM1 calculations show that the increase in GB values between amino acids and dipeptides is due to the hydrogen bonding between the terminal amine and the adjacent amide carbonyl oxygen. The increase in basicity from diglycine to triglycine is due to the second hydrogen bonding between terminal amine with the second amide carbonyl oxygen. This structure is not observed in trialanine due to the Steric interaction of alkyl group and similar behavior is expected for trivaline.

Presented at the 41st ASMS Conference on Mass Spectrometry

Table 1. **Efficiencies of the reactions of ALA_n(n=1-4) with reference bases.**

Reference Base and Gas-Phase basicities *(300K)	ALA	$(ALA)_2$	$(ALA)_3$	$(ALA)_4$
DMF (203.6 kcal/mole)	3	8	9	5
3-F-pyridine (206.2)	100	4	5	5
Allylamine (207.9)	51	2	3	7
n-Propylamine (210.1)	100	7	14	27
i-Butylamine (211.1)	100	84	65	61
s-Butylamine (212.1)	100	100	73	100
Ethylmethylamine (215.1)	100	100	65	63

Table 2. **Efficiencies of the reactions of VAL_n(n=1-4) with reference bases.**

Reference Base and Gas-Phase basicities *(300K)	VAL	$(VAL)_2$	$(VAL)_3$	$(VAL)_4$
DMF (203.6 kcal/mole)	5			
c-Propylamine (206.6)	2			
Allylamine (207.9)	58	10	11	7
n-Propylamine (210.1)	100	9	11	7
s-Butylamine (212.1)	54	18	20	16
Ethylmethylamine (215.1)	93	81	53	44
di-n-Propylamine (219.7)	100	81	87	100

Table 3. **GB values of linear oligopeptides.**

	GB(kcal/mol)		
n	$(GLY)_n$	$(ALA)_n$	$(VAL)_n$
1	202.3	204.9	207.3
2	208.6	210.6	213.6
3	209.7	210.6	213.6
4	209.7	210.6	213.6
5	209.7		

1 Kalman Burger, Biocoordination Chemistry, Ellis Horwood, N.Y., **1990**

2 Jiangyue Wu and Carlito B Lebrilla, J. Am. Chem. Soc. **1993**, 115, 3279

3 Sharon G. Lias, Joel F. Liebman, Rhoda D. Levin, J. Phys. Jef. Data, **1984**, 13, 3

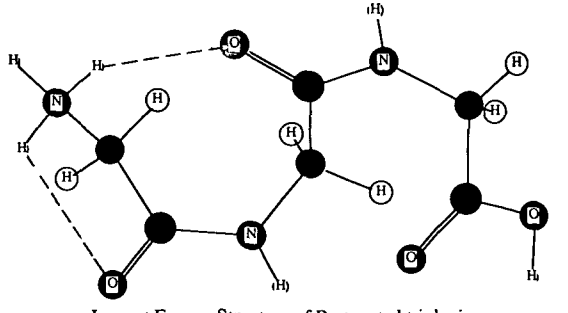

Lowest Energy Structure of Protonated triglycine

Analysis of High Molecular Weight Hydrocarbons by Short Column Gas Chromatography Mass Spectrometry. James G. Moncur, Lockheed Missiles and Space Co. 3251 Hanover St., Palo Alto, CA, 94304.

High molecular weight aliphatic hydrocarbons have been analyzed by high temperature gas chromatographic/MS methods (Ref. 1) in search of "biomarker" up to molecular size C_{60}. In the current study, a commercial oil used as a low volatility lubricant was analyzed by short column gas chromatography mass spectrometry with electron ionization up to molecular size C_{89}. The oil consisted of numerous minor low molecular weight additives and three hydrocarbon components with the following tentative molecular ions and empirical formulas:

644 = $C_{46}H_{92}$ with 1 degree of unsaturation.
910 = $C_{65}H_{130}$ with 1 degree of unsaturation.
1246 = $C_{89}H_{178}$ with 1 degree of unsaturation.

It is possible that the oil was manufactured synthetically, although information on this product was not readily available.

A short length of DB-5 phase capillary column taken from a previously used 30 meter column was used for this work, (3 meter long, 0.25 mm ID, with 0.25μm film thickness). The helium carrier gas pressure was programmed from 10 to 20 psi seconds after sample injection. The current data was obtained using a cool on-column injection technique. The column oven was heated from ambient to 400C at 50C per minute. The injector was set to heat as fast as possible from ambient to 350C soon after injection of the oil. The standard capillary interface of the Fisons VG model 70VSEQ mass spectrometer was operated at 330C and the column was inserted into the ion source for efficient transfer of organics to the 70 eV electron beam.

The mass spectrometer was scanned from 1300 to 50 amu every 5.6 seconds with a 1 second inter-scan delay. A total ion chromatogram is shown in Figure 1. The mass spectrum of $C_{89}H_{178}$ is shown in Figure 2. Low molecular weight additives triphenyl phosphate, tertbutylphenyl diphenyl phosphate, and an unidentified compound were also observed as well separated peaks. A total ion chromatogram of the oil analyzed by direct probe mass spectrometry under the same temperature conditions is shown in Figure 3.

In conclusion, separation of medium to high molecular hydrocarbons by short column GC/MS was found to be much more efficient than direct probe analysis.

1. Lipton, P.A., et al, 40th ASMS Conference on Mass Spectrometry, pp 100-101, 1992.

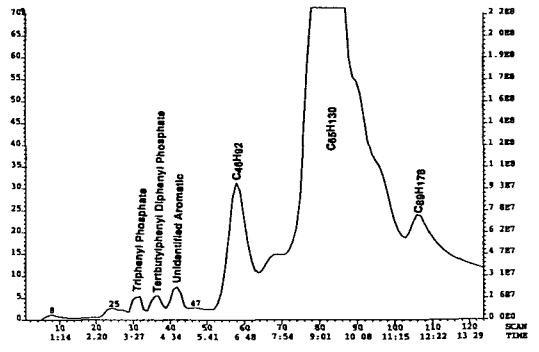

Figure 1, GC/MS TIC of Oil.

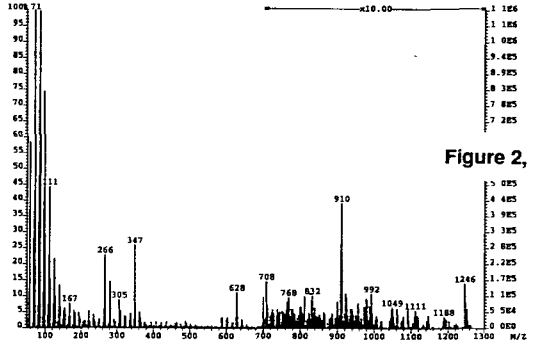

Figure 2, Mass Spectrum of $C_{89}H_{178}$.

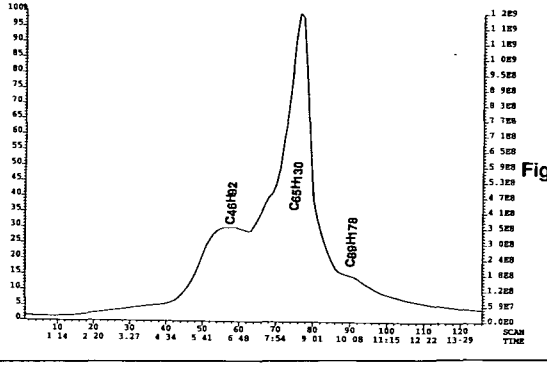

Figure 3, Direct Probe TIC of Oil.

CHARATERIZATION OF WAX FRACTIONS FROM LUBE OIL BASESTOCKS BY THERMAL EXTRACTION-GAS CHROMATOGRAPHY/MASS SPECTROMETRY

J. W. Fedora, S. G. Roussis and T. R. Ashe
Imperial Oil, Sarnia Research Centre, Sarnia, Ontario, Canada , N7T 7M1

The low temperature performance of lube oils is related to the basestock composition, of which wax is a major component. Analytical methods are therefore required for the compositional analysis of wax fractions from lube oil basestocks in order to obtain a better understanding of the relationship between wax composition and low temperature lube oil performance characteristics. GC/MS methods originally developed for conventional lube oil basestock wax characterization proved ineffective when applied to wax fractions from nonconventional lubes (NCL). NCL's are highly complex mixtures of isomeric paraffins and the usual chromatographic procedures cannot provide adequate chromatographic separation which is essential for the correct identification and quantification of the components, due to the similarity of their mass spectra. Consequently, a new characterization approach utilizing thermal extraction prior to gas chromatographic separation (TE-GC/MS) has been examined for use with wax fractions from nonconventional lubes. The study was initially undertaken to examine whether subdivision of the wax fraction into smaller fractions (thermal slices) could improve the chromatographic separation and simplify the mass spectrometric analysis.

The experimental setup used in this work is shown in Figure 1. It consists of a thermal extraction unit (Thermex from Ruska, Houston, TX) coupled, by a heated transfer line, to a conventional HP GC/MS system. The sample is placed into a quartz ampoule with a fritted glass bottom. The ampoule is positioned into a temperature programmable pyrocell which is heated at a controlled rate. The vapourized material is swept through the heated transfer line to the head of the GC column, where it is cold trapped. The thermal extraction step is followed by conventional 70eV EI GC/MS analysis.

The thermal extraction procedure consists of a series of 6 thermal slices, of 30°C widths, taken across a wider boiling range (50° to 200°C). The extraction profiles and optimum chromatographic conditions were determined experimentally, then standardized for all subsequent analyses. Subdivision of the wax fraction into thermal slices allows the large unresolved chromatograms produced by conventional GC/MS to be resolved into simpler chromatograms, shown in Figure 2. The thermal extraction GC/MS system is calibrated using a C5 to C60 blend of n-alkanes. For each thermal slice, a range of n-alkanes of known b.p.'s is vapourized and swept through the GC/MS. The thermex temperature parameters are calibrated by comparison with the actual b.p.'s for the eluted n-alkanes.

The thermal slicing of the wax into smaller fractions has allowed for the identification and quantification of 11 homologous series representing normal, various methyl, dimethylalkanes, naphthenes and alkylbenzenes, across a carbon number range of approximately C10 to C45. Differentiation of waxes based on the isomeric types and their respective carbon number distributions have been obtained (Figures 3 and 4). Correlations of the molecular composition with several physical properties of the lube oil basestock, can now be obtained.

The method developed here, can be applied in a general fashion, in situations where conventional GC/MS experiments are not adequate for the analysis. Complex mixtures of very similar components can be selectively analysed by the on-line thermal slicing procedures reported here. Future work will concentrate on the identification and quantification of other petroleum samples consisting of very similar components (lube oils). Thermal extraction experiments may be coupled with selective separation procedures based on polarity or molecular size.

FIGURE 1 THERMAL EXTRACTION GC/MS SYSTEM

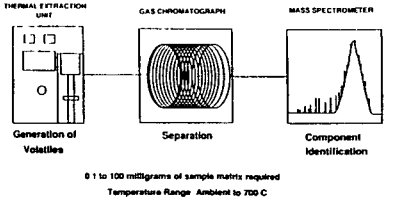

FIGURE 2. (A) TIC OF UNSLICED NCL WAX FRACTION
(B) THERMAL SLICING PROCEDURE IMPROVES CHROMATOGRAPHIC PERFORMANCE

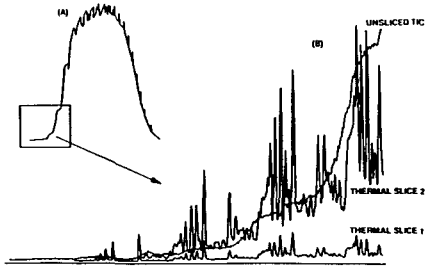

FIGURE 3 ALKANE TYPE DISTRIBUTION IN WAX JWF-1

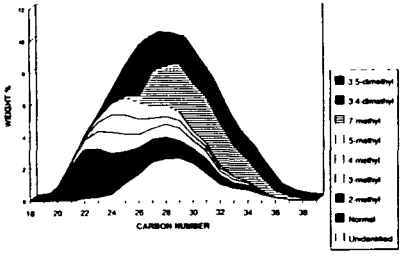

FIGURE 4. ALKANE TYPE DISTRIBUTION IN WAX JWF 2

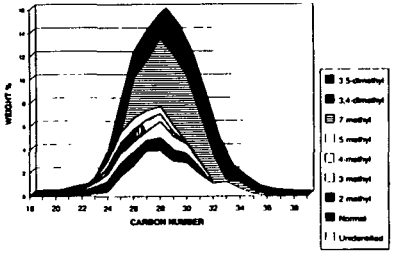

THE ANALYSIS OF A COMPLEX MIXTURE OF ACIDIC MATERIALS DERIVED FROM PETROLEUM BY CAPILLARY ELECTROPHORESIS (CE) AND ELECTROSPRAY IONIZATION-MS(ESI-MS): A PRELIMINARY OFF-LINE INVESTIGATION.*

AI MALLET, INSTITUTE OF DERMATOLOGY, UMDS, UNIVERSITY OF LONDON, , LONDON SE1 7EH. SAUL PARRY*, CF SIMPSON, DEPT. OF CHEMISTRY, BIRKBECK COLLEGE, 29 GORDON SQUARE, LONDON WC1H OPP. .MJC SMITH, BP INTERNATIONAL Ltd, CHERTSEY Rd, SUNBURY ON THAMES, MIDDLESEX, UK.

INTRODUCTION.

A complex Mixture of Mono- and Di-Basic Acids (MMDBA) has been analyzed using ESI-MS . MMDBA is derived from the production of a low molecular weight carboxylic acid, and comprises 25-35% of the production stream. A detailed knowledge of the composition is required to investigate utilization of MMDBA which is currently a waste stream.

EXPERIMENTAL.

ESI-MS: VGTrio-2 quadrupole equipped with a Biotech ESI source (Fisons Ltd,UK). An Isco SFC500 pump delivered buffer at 7.5uL/minute. Standards and MMDBA were dissolved in acetonitrile: methanol (ratios dependant upon sample) . MMDBA was analyzed as solid and liquid fractions , as heating to 100C is required for homogenisation, which might affect sample composition. Results are compared to negative ion CI spectra acquired on an ICR-MS instrument (Nicolet FTMS 2000), using a probe heated to 140C.

*CE: Due to a hardware problem no electropherograms can be shown.

RESULTS.

In contrast to initial experiments with +ve ionization, negative ESI-MS of standards produced strong signals at (M-H)-. Single species were ionized with high efficiency, however equimolar mixtures resulted in reduced ion currents. As the mixture became more complex, individual ion currents were reduced.

In general, acid concentrations were ~0.00001M, resulting in approximately 150,000 counts per 10uL injection of a single standard for the acids studied. When mixtures of different composition were electrosprayed differing response factors were obtained for individual components. Ion counts of standards in mixtures varied from thousands to ten's of thousands dependent upon mixture composition. We ascribed this result to the existence of suppression effects, observing the same effects in the TIC traces.

Succinic acid was retained in the ESI-MS manifold, and may be detected in subsequent injections of other standards. Presumably, this retention results from adsorption on metallic components. The presence of succinic acid in certain mixtures resulted in apparent suppression of some components, whilst other mixtures resulted in increased ion counts. Analysis of an equimolar mixture of di-acids and hydroxy acids resulted in suppression of succinic acid, indicating di-carboxylic and hydroxy acids may act as strong suppressants of succinic acid.

The analysis of MMDBA by ESI-MS resulted in spectra which were comparable to those obtained by distillation from a heated probe by ICR-MS(-ve CI spectra). The major components were present at ratio's consistent with the proposed composition. The ESI-MS results obtained with MMDBA are at present tentative on account of the complexity of response vs composition of standard mixtures. Further work to verify the relationships will be required. The range of mixture compositions studied so far does, however, support the conclusion that the spectra were representative; the components that appear to suppress the major MMDBA components (succinic,adipic,glutaric, and the n-carboxylic acids) were either not present in MMDBA ,or were present at non-interfering concentrations. Suppression effects associated with succinic acid were, however, indicated in the solid fraction sample of MMDBA. Presumably, succinic acid was present at higher levels in the solid fraction. Co-components involved with suppression or enhancement of analyte signals may be present in both fractions, however utilizing ESI-MS alone we are unable to determine this.

CONCLUSIONS.

The present study has demonstrated the potential of ESI-MS for the analysis of complex mixtures; a wide range of carboxylic acids and related compounds having been examined and these produce primarily (M-H)- ions. Despite the suppression effects associated with certain MMDBA components, experimental conditions have been achieved under which ESI-MS spectra reflect the proposed composition of MMDBA. In order to define the molecular composition, including components at the same nominal mass, considerably enhanced resolution will be required. The problem may be simplified if an on-line separation with CE is employed, as this has been shown to be effective in the analysis of complex mixtures. In addition, if employed in the coupled column mode of isotachophoresis(ITP), this could provide a means of selective removal of suppressants from the mixture.

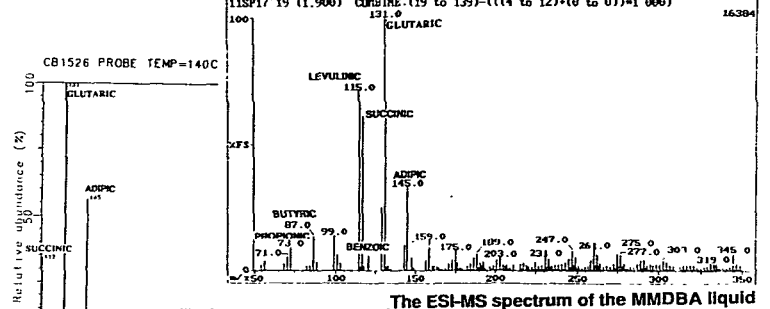

The ESI-MS spectrum of the MMDBA liquid fraction. (~2.8x10-8g/uL)

The negative ion CI spectrum of MMDBA acquired on an ICR-MS instrument.

CHARACTERIZATION OF ASPHALTS AND ESTIMATION OF BOND STRENGTHS BETWEEN ORGANIC COMPONENTS AND AGGREGATES BY PROBE MICRODISTILLATION/MASS SPECTROMETRY

Ronald D.Grigsby

IIT Research Institute
National Institute for Petroleum and Energy Research
P.O. Box 2128, Bartlesville, OK 74005

Arnulf P. Hagen and William D. Lee

Department of Chemistry and Biochemistry
The University of Oklahoma, Norman, OK 73019

The long-term performance of asphaltic concrete as a road-building material is, in part, determined by the bond strengths between components of the organic binder and the surface of the aggregate. To characterize organics and estimate bond strengths, selected whole asphalts and fractions are being analyzed by high resolution mass spectrometry. In addition, pure model compounds and those adsorbed from solution onto aggregates are being studied. Desorption of the mixtures and model compounds from a direct-introduction probe, as a function of linearly increasing temperature, provides apparent activation energies and frequency factors as calculated from first-order kinetics. These parameters are related to bond strengths between organic components themselves and between the components and surface of the aggregate. Binder-aggregate combinations have been selected based on parameters obtained from whole asphalt solubility profile data and zeta potentials of the n-pentane insoluble asphaltenes as well as from the zeta potentials and chemical constitutions of the aggregates.

All data were acquired with a Kratos MS-50 high resolution mass spectrometer. The samples were introduced into the mass spectrometer via a cooled/heated quartz probe with linear temperature programming at 10 ^{o}C/min over a temperature range from ambient to 350 ^{o}C. Ions were generated by low energy (12 eV) and 70 eV electron ionization and by field ionization. A mixture of halogenated compounds was used for calibrating masses in the low eV spectra. Resolving powers up to 20,000 were used.

The mass spectrum of a whole asphalt (without aggregate), obtained at a probe temperature of 346 ^{o}C, is shown in Figure 1. The data were acquired by low energy electron ionization at 14,000 resolving power. Molecular-ion peaks are visible from about m/z 370 to m/z 900 . Intense peaks in the low region of the spectrum are mostly molecular ions from the reference compounds.

Analysis of the data shows that volatiles from the whole asphalt up to a probe temperature of about 350 ^{o}C consist primarily of aromatic hydrocarbons having elemental formulas from C_nH_{2n-26} to C_nH_{2n-38}. Only about 25% of the asphalt is volatile at this temperature. Presumably, the residue consists of higher molecular-weight hydrocarbons and polar compounds.

Figure 2 shows experimental ion intensities vs. absolute temperature for m/z 450, C_nH_{2n-26}, recorded for the whole asphalt (without aggregate). The elimination curve was calculated from least-squares parameters obtained by analyzing intensities as a function of linearly increasing temperature. A four-parameter skewed-gaussian equation was used. From the parameters for the curve shown and for other curves, typical activation energies in the range from 25 to 35 Kcal/mol and frequency factors of about 1 x 10^{10} sec^{-1} are obtained. The relatively low value of the frequency factor is consistent with a model for diffusion of volatile components through a non-volatile matrix, as expected from the theory of asphalt structure.

In contrast, desorption of a model compound such as quinquephenyl from the surface of a solid with a large surface area provides a higher activation energy and a frequency factor in the range of 1 x 10^{14} sec^{-1}. See Figure 3. These values are anticipated from a first-order kinetics model for simple desorption of a volatile substance from a surface.

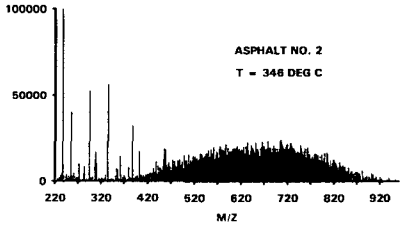

Figure 1. Mass spectrum of asphalt No. 2. Probe temperature = 346 ^{o}C.

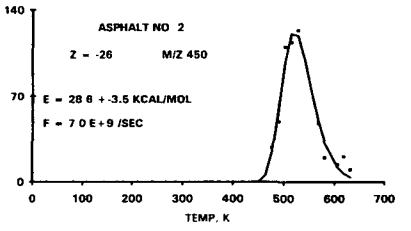

Figure 2. Elimination curve for m/z 450 , C_nH_{2n-26}, asphalt No. 2.

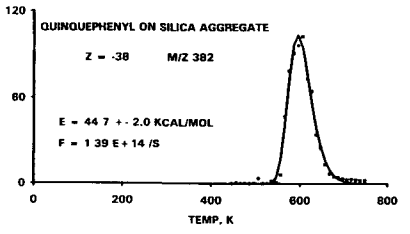

Figure 3. Elimination curve for m/z 382, the molecular ion of quinquephenyl, desorbed from a silica aggregate.

EVALUATION OF MASS SPECTROMETRIC METHODS FOR DETERMINATION OF SULFUR TYPES IN PETROLEUM SAMPLES

S. G. Roussis, J. W. Fedora and W. P. Fitzgerald
Imperial Oil, Sarnia Research Centre, Sarnia, Canada, N7T 7M1

Sulfur compounds of different types such as: mercaptans, sulfides, disulfides, thiophenes and others, are found in petroleum samples in concentrations varying from the percent (%) to the low ppm levels. The presence of sulfur compounds in crude oil and finished products is considered harmful with undesirable metallurgical and environmental consequences. Determination of the individual sulfur types in such samples is therefore important for mechanistic studies and quality assurance. Early mass spectrometric methods utilizing 70 eV Electron Ionization allow for the analysis of aromatic sulfur compounds (1,2). More recently Chemical Ionization GC/MS has also been applied for the identification and quantification of aromatic sulfur compounds (3). However, routine methods for the direct analysis of alkyl sulfur species are not yet available. The present study investigates two different methods for their suitability to analyze both aromatic and saturate alkyl sulfur species in a routine manner. First, 70 eV EI HR by dynamic batch sample introduction, and second, low voltage EI HR GC/MS, are examined using standard sulfur compounds and samples spiked with known sulfur mixtures. The advantages and disadvantages of each method are presented.

High resolution mass spectrometry has the advantage of separating structures with different exact masses. Unfortunately, the resolution required for the separation of ions increases with higher masses. In addition, in sector instruments, where resolution increases by closing the instrument slits, higher resolution usually results in lower sensitivity. Using, however, low mass fragment ions characteristic of the various parent structures, allows detection of different chemical classes with lower resolving power demands. The technique has been used previously (4) to identify sulfur species in complex petroleum samples monitoring the fragment CHS^+ (44.9799 m/z). However, ion CHS^+ can be produced by almost any sulfur compound and cannot be used alone for type analysis. Here, we have used a dynamic batch type introduction system (5) and a set of characteristic sulfur type fragments with known relative abundances and response factors (Figures 1, 2). This set of ions: SH^+ (32.9799), CHS^+ (44.9799), $C_2H_5S^+$ (61.0112), and $H_2S_2^+$ (65.9598) has been found to be produced by the sulfur species under investigation. The concentrations **{Ci}** of the various sulfur types are obtained by HR measurement of the abundances of these ions **{Ai}** and subsequent solution of the equation: (**[M]** is a calibration matrix determined from known sulfur mixtures).

$$\{Ci\} = [M]^{-1}\{Ai\}$$

Low voltage electron ionization is usually employed for selective analysis of aromatic compounds in complex hydrocarbon mixtures. Appropriate selection of the electron kinetic energy (ca. 10 eV) allows ionization of the sulfur types considered in the present study. The advantage of this method is that it forms primarily molecular ions. Low voltage ionization has been studied here, using the same standard mixtures and spiked sample solutions as those used in the study of the 70eV ionization technique. LV ionization produces molecular ions with approximately equal response factors and is an attractive method for the analysis of sulfur species. However, it was found in this study, that analysis using the previous 70 eV EI method is more preferable. This is shown in Figure 3 which displays calibration curves covering typical sulfur concentration ranges found in petroleum samples. Similar results were difficult to obtain using LV GC/MS experiments (Fig. 4). This can be attributed to the fast scanning requirements for GC/MS and the increasing resolution requirements with higher molecular weights.

REFERENCES

(1) Robinson, C J. Anal. Chem 1971, 43, 1425.
(2) Teeter, R.M Mass Spectrom. Rev. 1985, 4, 123.
(3) Dzidic, I.; Balicki, M.D.; Rhodes, A L., Hart, H.V. J. Chromatogr. Sci., 1988, 26, 236
(4) Gallegos, E.J. Anal. Chem 1975, 45, 1150.
(5) Gallegos, E.J., Pazzi, E.C. Proc. 39th ASMS Conf. on Mass Spec and Allied Topics, Nashville, TN, May 19-24, 1991, 1091

FIGURE 1. RELATIVE ION ABUNDANCES OF SELECTED IONS IN THE EI MASS SPECTRA OF RSR, RSH COMPOUNDS

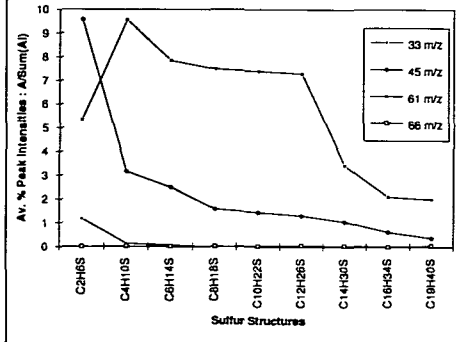

FIGURE 2. RELATIVE ION ABUNDANCES OF SELECTED IONS IN THE EI MASS SPECTRA OF RSSR COMPOUNDS

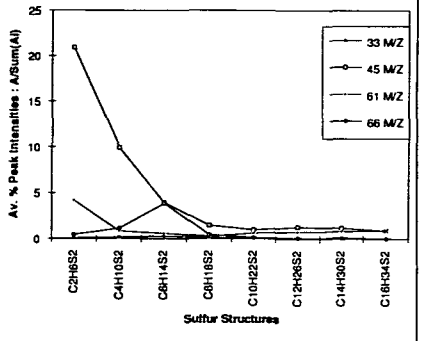

FIGURE 3. 70 eV HR-MS DYNAMIC RANGE-DETECTION LIMIT STUDY (Monitoring C2H5S:61.0112m/z)

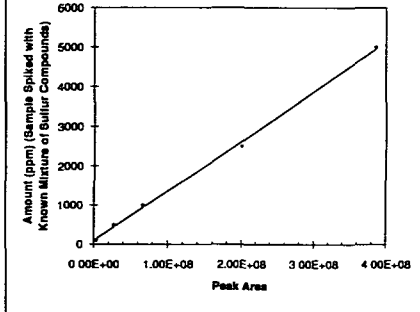

FIGURE 4. LOW VOLTAGE HR-GC/MS DYNAMIC RANGE-DETECTION LIMIT STUDY (Monitoring RSR m/z Series)

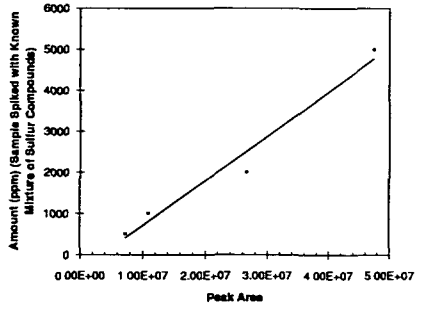

The Determination of 2-Aminonaphthalene in Petroleum Products By High-Performance Liquid Chromatography and Mass Spectrometry

*Nero, V P., D'Antono, J A. and Drinkwater, D. E.

Texaco Research and Development, Beacon, NY 12508

2-Aminonaphthalene has long been recognized as a human carcinogen and as a toxic chemical. It is crucial to establish that it is not present in petroleum products which may come into contact with potable water or food packaging equipment Since these oils are complex matrices containing vast numbers of saturated, unsaturated and aromatic hydrocarbons, their quantitative analyses present a formidable analytical problem. Additionally, these matrices often have many compounds with similar boiling points and molecular weights, making their analyses by GC/MS alone difficult.

The traditional method for quantitative determination of 2-aminonaphthalene is single-ion monitoring of 1-3 major ions in the mass spectrum, preceded by complicated multistep separation procedures to eliminate interferences with similar retention properties and ionic fragments A high-performance liquid chromatography and gas chromatography/mass spectrometry procedure was developed to quickly and unambiguously determine 2-aminonaphthalene in refined oils as well as crude oils at a 1 ppm detection limit. This procedure involves spiking the oil with a deuterated surrogate, removing interferences using an initial HPLC cleanup procedure and then analyzing by selected ion detection

25 uL of a light vacuum gas oil spiked with a deuterated internal standard at the low ppm level is injected onto an Alltech Econosil 5 micron Cyano column 250 mm x 4 6 mm ID. The fraction containing the aminonaphthalene is evaporated to 10-50 uL and 1 uL injected onto a 30 m , 0 25 mm ID, 0.25 um phase thickness fused silica capillary DB-5 capillary column running at a flow rate of 40 cm/sec. The analyte is detected by a Finnigan-MAT SSQ 710 quadrupole mass spectrometer running in electron impact mode with 70 eV electron energy.

The internal standard, 2-Aminonaphthalene, is found to have some interesting H-D exchange properties. One of the labeled aromatic ring positions (but only one, as determined by MS and NMR) can exchange on extended storage in methylene chloride or while passing through an older GC column A 6 week old solution of this compound in methylene chloride is shown to have >80% D6 and <3% D7 in contrast to the expected molecular ion envelope if all aromatic positions exchange with equal ease. It is crucial, therefore, to examine carefully all sample handling, storage and analysis operations to ensure the integrity of this internal standard The undeuterated 1-Aminonaphthalene can also be used as an internal standard since the retention times for this species is well before that of 2-Aminonaphthalene

The Figure shows the response for m/z 143 (aminonaphthalene-d0) and m/z 150 (aminonaphthalene-d7) for **A** GC/MS of the whole oil spiked at 5 ppm D0 and 5 ppm D7, and **B** GC/MS of the HPLC fraction from this oil

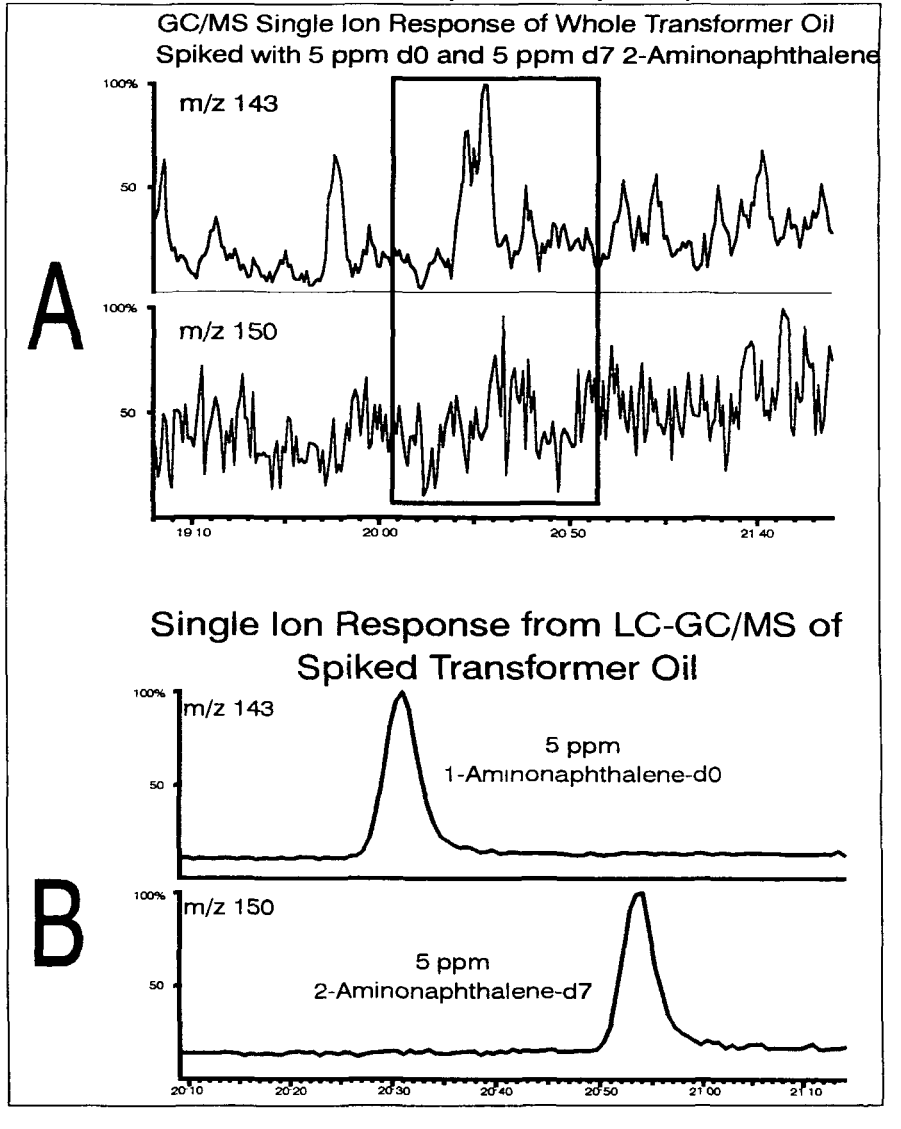

GEOPORPHYRIN ANALYSIS USING ELECTROSPRAY IONIZATION-MASS SPECTROMETRY

G.J. Van Berkel,[1] Miguel A. Quiñones[2] and J. Martin E. Quirke[2]
[1]Analytical Chemistry Division, Oak Ridge National Laboratory, Oak Ridge TN 37831-6365
[2]Department of Chemistry, Florida International University, Miami, FL 33199

Geoporphyrins are found as complex pseudohomologous series of numerous structural types in sediments, fossil fuels, and source rocks. Their potential use as biomarkers in fossil fuel exploration has provided stimulus for determining the relative distributions of the different carbon number species in such geological samples as well as the complete structures of the individual porphyrin species present. In this regard, MS has proven to be one of the more powerful analytical techniques available. EI-MS, which provides the porphyrin molecular weight, has been the most used. CI-MS is also often used because of the ability using this technique to pyrrole sequence a single porphyrin isomer. In a recent paper,[1] we demonstrated the general utility of electrospray ionization-mass spectrometry (ES-MS) for the analysis of a wide variety of porphyrins. In this paper, we examine ES-MS detection limits for geoporphyrins, the use of ES-MS for determination of relative porphyrin abundances within geoporphyrin mixtures, and on-line microbore-HPLC/ES/MS for geoporphyrin analysis. The mass spectrometer employed was a modified version of a Finnigan-MAT ion trap mass spectrometer (ITMS) adapted to sample ambient air. This is not of primary importance except that the ES detection limits that can be obtained with the ion trap might be better than those obtainable with other types of mass analyzers.

Geoporphyrin-like standards, e.g., free-base, nickel, and vanadyl chelates of octaethylporphyrin (OEP) and etioporphyrin-III (etio-III), as well as geoporphyrins isolated from Gilsonite bitumen were analyzed. A single molecular species was produced from these porphyrins and no ES produced fragment ions were observed. Detection limits using continuous infusion at 1-5 μL/min required sampling as little as 1 femtomole of material, while at these same flow-rates, 18 femtomoles of OEP could be detected via flow injection. However, because of sample impurities, spectra with suitable signal-to-background for unambiguous identification of unknowns required injection of about 400 femtomoles. Detection of 500 femtomoles of mesoporphyrin IX dimethyl ester was demonstrated using on-line reverse-phase microbore-HPLC at solvent flow rates of 40 μL/min.

The ability using ES-MS to accurately determine the relative abundances of the porphyrins within geoporphyrin mixtures was demonstrated using standard solutions containing known molar ratios of OEP and etio-III as determined by weighing and UV/visible spectrophotometry (Figure 1). With this methodology established, the porphyrin distribution in Gilsonite Bitumen was determined via three sequential flow injection experiments (Figure 2(a)). Averaged, isotopically corrected and renormalized data from these injections (Figure 2(b)) matched literature values for the porphyrin distribution within this sample (E = etio, D = DPEP or CAP).[2] The major advantages of ES-MS for this determination are the sensitive, rapid and reproducible nature of the measurement.

A reverse-phase separation (300 Å ODS (1 mm X 100 mm), 40 μL/min, 75% MeOH/25% H_2O/0.1% TFA to 95% MeOH/5% H_2O/0.1% TFA in 15 min) was used in the on-line HPLC/ES/MS analysis of the total free-base porphyrin mixture isolated from Gilsonite bitumen (Figure 3). The two porphyrin structural types in the mixture, etio and cycloalkanoporphyrins (CAP) were completely separated from one another. Within each structural type the porphyrins separated by carbon number. All the known porphyrins in the mixture were detected. In addition, minor CAP components of high carbon number (> C_{33}) were also detected in the mixture. Nickel Gilsonite porphyrins separated on-line using different reverse-phase conditions showed similar elution behavior.

1. Van Berkel, G. J.; McLuckey, S. A.; Glish, G. L. *Anal. Chem.* 1991, *63*, 1098-1109.
2. Quirke. J. M. E.; Eglinton, G.; Maxwell, J. R. *J. Am. Chem. Soc.* 1979, *101*, 7693-7697.

Research sponsored by the United States Department of Energy, Office of Basic Energy Sciences under contract DE-AC05-84OR21400 with Martin Marietta Energy Systems, Inc.

Figure 1

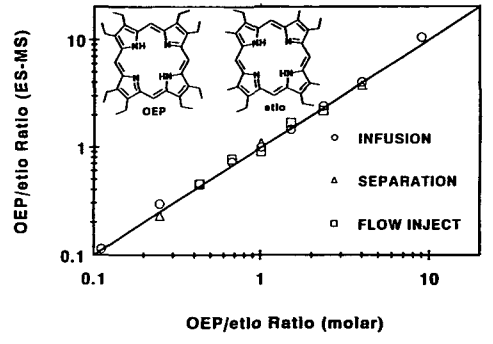

Figure 2

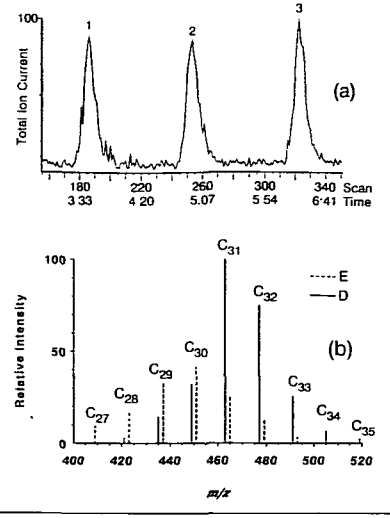

Figure 3

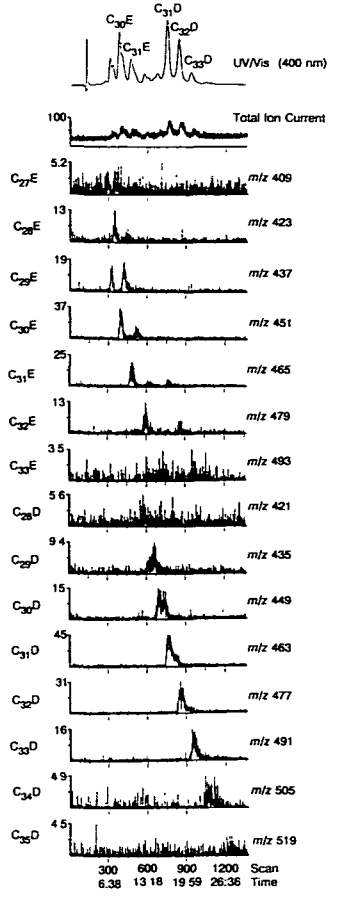

Using in-situ mass spectrometry to study the chemistry of a small scale benchtop minireactor.

J.R. Gilbert, M.A. DesJardin, S.J. Doherty, The Dow Chemical Company
Health and Environmental Sciences Laboratory, Midland, Michigan 48674.

The need for real-time pilot plant data to develop new chemical processes or improve existing production facilities is becoming increasingly important for successful process commercialization. The amount of time spent in the costly pilot plant stage can be greatly reduced through the use of real-time compositional analysis. The application of conventional spectroscopic and chromatographic process instruments often requires some compromise in sensitivity, specificity, or sampling rate. In-situ mass spectrometry offers the advantages of high sampling rate, high sensitivity, wide dynamic range, and good specificity. These characteristics are especially important when evaluating high-speed reactions for product output, catalyst efficiency, catalyst deactivation, and reaction kinetics. We present the application of both in-situ mass spectrometry and off-line GC/MS to study the products of a small scale minireactor.

Several of the trace impurities in thermal chlorination feed streams are oxygen containing compounds. The presence of these impurities in the feed streams may be linked to high corrosion rates in large scale plants. One potential product resulting from the chlorination of these impurities is water, which could be responsible for the observed corrosion. A research study was initiated to determine the fate of these oxygen containing impurities in a thermal chlorination reactor. The products from several different feed streams were studied using the benchtop minireactor system shown in Figure 1.

Figure 1. A schematic diagram of the benchtop minireactor apparatus.

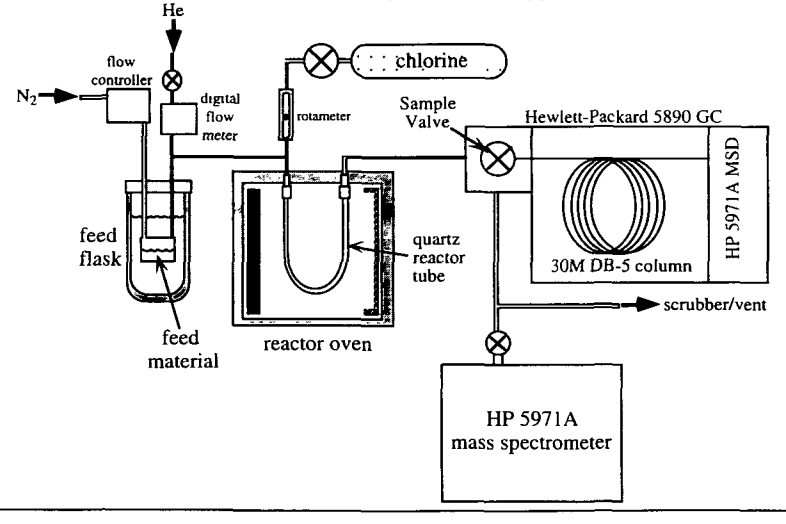

Gaseous oxygenate streams were produced by passing a controlled flow of nitrogen across the liquid oxygenate feed material. The feed material was held at a controlled temperature, producing a constant vapor pressure of the feed material in the nitrogen stream. This stream was combined with fixed flows of ultra-pure helium and chlorine at the reactor inlet tube. The composition of the feed stream entering the reactor was controlled by adjusting the flow rates of these combined streams and the temperature of the oxygenate feed flask. Reaction products were sampled with a heated GC/MS Valco sampling valve and a leak valve coupled to the on-line mass spectrometer. The bulk of the product gases were finally neutralized by bubbling through a caustic bath housed in a fume hood.

Several oxygen containing compounds were studied with the mini-reactor apparatus, the products of these reactions are shown in Table 1. The major oxygen containing products in these systems were CO, CO_2, and phosgene. Carbon tetrachloride, perchloroethylene, and hexachloroethane were also detected as chlorination products. The high concentrations of chlorine in the system produced a large Cl^{2+} signal (m/z 17.5 and 18.5) which interfered with the direct observation of water. Isotopically (^{18}O) labeled methanol was used to determine if water was generated as a product of thermal chlorination. The m/z 20 region of the in-situ mass spectrometer was relatively clear of interfering ions, allowing the direct observation of water ($H_2{}^{18}O^+$) produced from the feed. In all of the systems studied, water was detected at only background levels in the product stream. **These results indicate that the corrosion observed in the large scale plants is <u>not</u> caused by water produced through the chlorination of oxygen-containing impurities in the feed stream.**.

The combination of high-speed acquisition via on-line mass spectrometry with the specificity of GC/MS was ideally matched with the mini-reactor system. The mini-reactor allowed the rapid evaluation of several chemical systems under a variety of reaction conditions. The on-line MS provided rapid response to follow the changing composition of the reactor effluent, and the on-line GC/MS provided sufficient specificity to allow the positive identification of the effluent stream components.

Table 1. A summary of the results from each of the oxygenate systems studied.
The integrated results for GC/MS injections for each compound at a reactor temperature of 600°C. For comparison purposes the peak areas were scaled to account for the percent of oxygenate in the stream. (example: scaled response = (area counts)/(% oxygenate in feed)).

Compound	percent in feed	scaled m/z 44 (CO_2)	scaled m/z 63 (phosgene)	scaled m/z 117 (CCl_4)	scaled m/z 166 (C_2Cl_4)	scaled m/z 201 (C_2Cl_6)
acetone-D_0	3.3	109150	374062	2096798		
acetone-D_6	3.3	157776	422936	2239593		
dichloropropane	2.6	428714	103334	10620322	5491543	168017
epichlorohydrin	**0.1**	2403730	1201770	4935060		
methanol-^{16}O	1.4	404486	837143	2941335		
methanol-^{18}O	1.4	439398*	134065	4018729		
propionaldehyde	5.2	96154	396833	750679	702680	
propylene oxide	6.2	132097	300108	2692927	2916957	125822

* m/z 44 signal shown for methanol-^{18}O is the sum of m/z 44, 46, and 48 signals.

IN SITU MASS SPECTROMETRY FOR PROCESS MONITORING IN CHEMICAL PLANTS

Steve Doherty, Mike DesJardin, Michael Mann
Dow North America, Western R&D Labs, Pittsburg, CA 94565.

In situ mass spectrometry has proven to be an invaluable tool in the characterization of process streams in a chemical plant. Three applications are described, and each highlights a particular strength of mass spectrometry for process analysis.

The first application is a tracer experiment on a large production-scale reactor. In a tracer experiment, an inert compound is injected into a reactor, and its elution profile is obtained (in the form of a selected-ion chromatogram) as it exits the reactor. A mass spectrometer, with argon gas as a tracer compound, is well suited for this type of study on vapor-phase reactors. In the experiments to be described, less than two pounds of argon gas provided a readily discernible signal at the sample point. The real-time data acquisition capabilities of the mass spectrometer allow for continuous monitoring of the tracer compound, making it possible to fully characterize the elution profile. Results from such a study make it possible to describe the macromixing behavior of the reactor or unit operation, which in turn allows for much more accurate reactor modeling calculations. **Figure 1** illustrates how an experimentally obtained trace can be compared to a well characterized macromixing model.

Figure 1

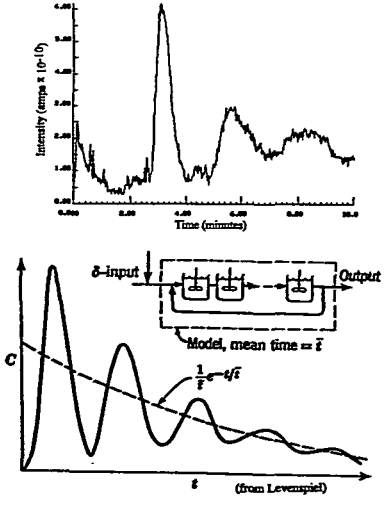

The second application employed the mass spectrometer vacuum system to ensure that a representative sample was obtained. A chemical plant was experiencing operational upsets when it was run at high feedrates. As a result, the plant was facing a substantial loss in capacity. The problem was traced to a vacuum flash separator, but it proved difficult to obtain a sample for off-line analysis, since the process was run at sub-ambient

pressures. Since the mass spectrometer was operated at even lower pressure, there was sufficient pressure drop to draw analyte into the ion source. A calibrated flow of argon gas was introduced into the process as an internal standard, and the mass spectrometer was able to provide real-time composition and flow rate data. Using this method, the source of the capacity problem was deduced.

The last set of experiments describe the apparatus for transfer-line GC/MS of process gases. This combination provides a robust analytical method for unattended operation of catalyst screening reactors and process streams where rapid turnaround and complete sample identification is required. Short lengths of narrow-bore (10-100 micron I.D.) capillary GC column are used to provide pressure drop into the mass spectrometer and to transport the sample from an external sample injector. Separations typically take from thirty seconds to a few minutes (10-100 times faster than conventional GC/MS), with RSD's on replicate injections consistently less than 5%. The apparatus is conducive to automation, making possible unattended operation for runs of up to a week in duration. **Figure 2** demonstrates a typical separation from a catalyst screening reactor for a process that has very high water content and contains corrosive gases. This process has been monitored using this method for several months, without requiring any maintenance on the mass spectrometer system.

Figure 2

$$A + B \xrightarrow[\text{catalyst, } \Delta]{} C + D$$

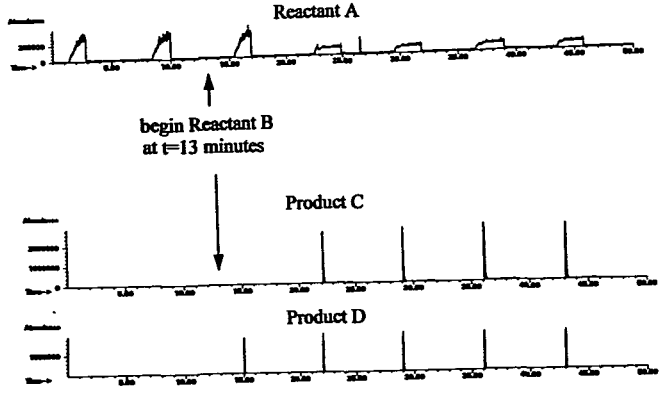

Two Improved Probe Designs and a Modified Source for Desorption Chemical Ionization on the HP5989A Mass Spectrometer

Christopher W. Baker[1] and William J. Jones[2] John A Masucci[2]

[1]Scientific Instrument Services, Inc., [2]R.W. Johnson Pharmaceutical Research Institute

Analysis of samples by direct introduction of the sample into a mass spectrometer via a direct probe is a routinely used analytical tool. Through the years, direct probes have been used on many different mass spectrometers including magnetic sector instruments as well as quadrupoles and ion traps. There have been various designs utilized, many of which have been made available commercially by the mass spectrometer manufacturers.

This article details the design of two new probes for use on the Hewlett-Packard 5989 MS Engine mass spectrometer and demonstrates the usefulness of these two probes for solving analytical problems. The first probe described is a Direct Probe (DP) and the second probe discussed is a Direct Exposure Probe (DEP). The work on the new direct probe design was begun in an attempt to improve on the design of the standard direct probe manufactured by Hewlett-Packard. The standard HP probe has a very slow heating rate which makes it more difficult to use for the analysis of some compounds. The DEP probe is designed and manufactured to provide an additional probe technique which is not currently available from Hewlett-Packard.

Experimental

All experiments were performed on a Hewlett-Packard 5989 MS Engine. The two new probes described below, both designed by Scientific Instrument Services, were utilized to introduce the sample into the mass spectrometer. The standard HP direct probe inlet port was used as the introduction port for insertion of the probes. The probes were ramped at the highest temperature rate that the probe design would allow. All data was acquired using the chemical ionization mode of operation using ammonia as the reagent gas.

Direct Probe

In the new Direct Probe (DP), the heater coil is actually wrapped around the sample vial holder, providing direct heating of the sample. This design eliminates the problem of heat transfer to the sample. Also the probe tip is manufactured from a small, low mass piece of silver which provides good thermal heat transfer to the sample being analyzed. The location of the heater coupled with the relatively small thermal mass of the probe tip allows for ballistic heating of the sample. Control of the temperature in the new designed Direct Probe can be accomplished through the HP data system since the probe is equipped with the same electrical connections and power requirements as the HP original. The thermocouple has also been moved up to the base of the sample cup holder providing the user with an accurate measurement of the sample temperature. The rapid heating rates combined with accurate measurement of the sample temperature provide for more accurate and reproducible results.

The Direct Probe can be used in two different configurations which allows the user to optimize the analysis depending on the type of samples being analyzed. In the standard mode of operation the DP can be used with glass capillary sample vials which are inserted into the end of the probe. They are held in place by a small spring. Quartz sample vials could also be used. Samples are dissolved in a solvent and then the resulting mixture is injected into the sample vial where the solvent can be allowed to evaporate leaving the solid or liquid residue of the sample of interest. Solid samples can also be analyzed directly by placing small amounts of the solid sample directly in the vial. An alternative technique uses a gold plated stainless steel probe tip as a sample cup in place of the glass sample vial. The sample is placed on the very end of the gold plated tip as described earlier. Although the sample is not directly heated in this experiment the relatively short length of the probe tip and the gold plating used on the tip allow for adequate volatilization of the sample when inserted into the mass spectrometer. With both direct probe techniques, control of the temperature can be achieved through the HP data system. Both techniques are used to acquire the data presented in this paper as shown below.

Direct Exposure Probe

A new DEP Probe was also designed for use on the HP 5989A mass spec. This type of probe design is not currently available from Hewlett-Packard. This probe technique has been called direct exposure probe (DEP) mass spectrometry as well as direct chemical ionization (DCI) probe mass spectrometry. In this style of probe, a replaceable probe tip is used which has a small resistance heating wire filament loop which serves to hold the sample. The probe, with the sample in place on the filament heater wire, is inserted into the mass spectrometer placing the sample inside the mass spec source close to the electron beam. After the probe is inserted into the source of the mass spectrometer a small current is passed through the wire loop to directly heat the sample. Since the sample is sitting directly on the filament wire, which is heated to volatilize the sample, this probe design provides for the fastest temperature ramps and a very short analysis time.

Results and Discussion

Analysis of the Drug Topiramate via Direct Probe

The standard Hewlett-Packard Direct Probe (DP) was used to analyze a new drug called topiramate. In the total ion profile the sample comes off in a broad range over a two minute time frame starting at approximately one minute into the analysis. The broad and jagged appearance of the total ion profile is possibly due to thermal decomposition of the sample, created by the slow heating rate of the HP Direct Probe. Topiramate has a molecular weight of 339. The M+NH4 ion at 357 is the base peak, however a significant peak at mass/charge ratio 278 is also present. This is the ammonium adduct ion of the alcohol produced by the cleavage of the sulfamate group from the topiramate. It is theorized that this peak is the result of thermal decomposition of the parent drug due to the slow rate at which the topiramate is heated.

The same analysis for topiramate was done using the SIS designed Direct Probe using the gold plated insert described earlier. The total ion profile is a sharp, symmetrical peak and the sample is completely volatilized in just over 30 seconds. Improvement can be seen over both the standard HP probe as well as the SIS Direct Probe when used with a glass capillary sample vial. The mass spectrum again shows the 357 peak as the base peak, however the peak at 278, is nearly gone. The ratio of the 357 to 278 peaks is much greater due to the rapid heating of the sample which minimizes thermal degradation of the sample.

Analysis of Topiramate via Direct Exposure Probe

Topiramate was also analyzed using the SIS DEP which was used with the sample placed directly on the filament wire loop. The sample was inserted into the mass spec source and then volatilized. The mass spec was again used in the CI mode using ammonia as the reagent gas. The total ion profile shows the sample volatilizing in less than 1.5 minutes, however the peak shape is not as symmetrical as the profiles from the direct probe. The mass spectrum shows that 357 remains the base peak, however the 278 peak is slightly larger than was seen in the SIS Direct Probe data . This suggests that although the DEP probe produced less thermal decomposition than the HP direct probe, the SIS Direct Probe used with a gold plated stainless steel probe tip is the most effective direct probe mass spectrometry technique for the analysis of topiramate.

Conclusion

Analyses via Direct Probe mass spectrometry can be difficult on the Hewlett-Packard 5989 MS Engine with the HP designed direct probe due to the design limitations which do not provide for adequate heating ramp rates. Two new probe designs from Scientific Instrument Services, the Direct Probe and the Direct Exposure Probe, provide increased heating rates, greater flexibility of techniques and therefore allow the analysis of a wider range of compounds. A Direct Probe was designed and manufactured which provides fast heating rates and can be configured for use with either a glass capillary sample vial or a gold plated stainless steel probe tip. A Direct Exposure Probe was also designed and manufactured which allows the user to insert the sample directly into the mass spec source. This probe has replaceable probe tips providing great flexibility. The probe was used with both a filament wire loop and with a glass encapsulated filament loop for this paper.

The Analysis Of Alkylated Diphenylamines By High-Performance Liquid Chromatography / Particle-Beam / Mass Spectrometry

Nero, V. P. and D'Antono, J. A.
Texaco Research and Development, Beacon, NY 12508

Polyalkylated aromatic diphenylamines (DPAs)are commonly used antioxidants in lubricants. DPAs are complex mixtures in which the extent of alkylation, point of attachment of the DPA along the alkane chain, and the positions of the alkyl groups on the phenyl ring will vary. A high-performance liquid chromatograph (HPLC) coupled to a quadrupole mass spectrometer with a particle-beam interface (PBI) was used to resolve and analyze this mixture.

A 0.2% hexane solution of the various alkylated DPAs, ranging up to tetradecyl DPAs, were injected, using a loop injector, onto a Spherisorb 5 um Amino column (15cm X 2mm ID) and eluted with a methylene chloride / hexane gradient. The gradient started as 100% hexane and was increased linearly to 50% methylene chloride. The flow rate was held at 0.2ml /min. The HPLC was directly coupled first to an ultraviolet detector set at 280 nm. Next, a quadrupole mass spectrometer was coupled in series via a Finnigan-Mat particle-beam interface. The interface was held at 40°C and used helium as a nebulizing gas.

Eluting compounds were identified using a Finnigan-MAT SSQ710 mass spectrometer. This instrument was scanned from 100 to 900 amu at 1 scan per 0.8 sec. The source temperature was held at 250°C and was operated under electron impact conditions with an ion current of 200 uA at 70 eV. The mono-, di-, tri- and tetra- DPAs were readily separated and characterized by their mass spectra. (Figure A)

The less polar compounds eluted first, as expected for an amino column when using a non polar solvent. However, the elution sequence was more complex than initially anticipated; Unreacted alkenes, used in the manufacture of DPAs, eluted first. These olefins were transparent to HPLC ultraviolet detector. Next, the more alkylated DPAs eluted. The alkyl groups shield the functionality of the amino group and reduce the overall polarity of these molecules. Finally, the major components followed and were determined to be di- and mono-alkyl DPAs. (Figure B) The point of attachment of the DPA to the alkyl chain also effected its elution time. When the alkylation occurred close to the beta or gamma position on the alkane chain, the corresponding product eluted earlier. If the alkylation occurred towards the middle of the alkane chain, the corresponding product eluted later. Both the ultraviolet and mass spectral detection provide similar, but not identical quantitative results. It appears that the particle-beam interface might discriminate in favor of the heavier components. (Figure C)

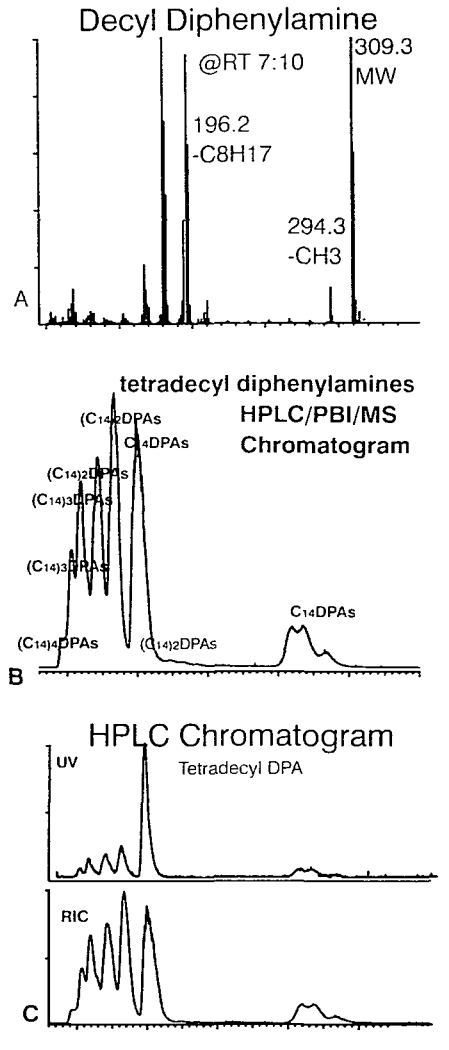

COMPARISON OF FIELD DESORPTION AND THERMOSPRAY MASS SPECTROMETRY FOR THE ANALYSIS OF PETROLEUM RESIDUA

C. S. Hsu, R. V. Kadtke and G. J. Dechert
Exxon Research and Engineering Co., Annandale, NJ 08807

Mass spectrometry has been used in petroleum industry as a powerful analytical technique to characterize hydrocarbon mixtures at molecular levels. Various mass spectrometric techniques have been used to analyze different petroleum fractions, as illustrated in Figure 1. For high boiling petroleum residua, field desorption (FD) has been the method of choice, which does not require vaporization of the sample prior to ionization. In FD, the sample is deposited onto an activated emitter which is made of a fine wire. With a high voltage (10-13 kilovolts) across the emitter and a counter-electrode at a short distance, a high electric field is produced to ionize sample molecules near the surface of the emitter and expelled out of the sample matrix by Coulombic repulsion. If several layers of molecules are present between the surfaces of the emitter and the sample matrix, dimer ions can be formed via ion-molecule reactions. Figure 2 shows a FD spectrum of a 875-1026°F distillate from a vacuum residuum of a Californian crude oil. The average molecular weight of this fraction is near 500. However, the presence of dimers with molecular weights between 700 and 1300 is also apparent. With FD, it is also difficult to perform high/medium resolution mass measurements due to short duration of signals.

We have evaluated thermospray (TSP) as an alternative ionization technique to FD for the characterization of high boiling petroleum residua. In TSP, the sample is carried by a mobile phase which is sprayed out of a heated nebulizer and ionized by a heavy duty filament or a discharge electrode. Solvent molecules which are in excess are ionized preferentially by electron bombardment or discharge ionization. These solvent ions then ionize sample molecules via protonation or hydride abstraction. Since the sample molecules are not directly heated and ionized, intact protonated or hydride-abstracted molecular ions are formed in TSP.

The same distillate as in the FD experiment mentioned above was dissolved in a mobile phase of 75% methylene chloride and 25% hexane. A discharge electrode is used as an external ionization device for TSP, yielding a spectrum shown in Figure 3. The distribution of the ions in TSP is quite similar to that in FD. Most noticeable is the absence of a dimer cluster. However, TSP has a major disadvantage of not being able to ionize saturated hydrocarbons because all of the suitable solvents have similar or higher proton affinity than saturated hydrocarbons.

With TSP a hydrocarbon mixture can be separated by liquid chromatography (LC) and analyzed by MS on-line. Since TSP yields strong and more stable signals than FD, slower scans for high/medium resolution mass measurements are possible. The combination of on-line LC and high/medium resolution MS can provide not only molecular weight determination but also compound class identification. We have successfully applied this combination to a 1120-1305°F fraction of a vacuum residuum from a Middle East crude oil.[1]

Table 1 compares between field desorption and thermospray for the characterization of heavy hydrocarbons.

Reference:

(1) C. S. Hsu and K. Qian, *Energy Fuels*, 7, 268-272 (1993)

FIGURE 1

VARIOUS PETROLEUM FRACTIONS REQUIRE DIFFERENT MASS SPECTROMETRIC TECHNIQUES

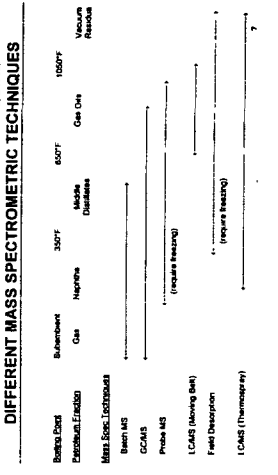

FIGURE 2

FIELD DESORPTION OF A 875-1026 °F DISTILLATE OF A CALIFORNIAN CRUDE OIL SHOWS A CLUSTER OF DIMERS

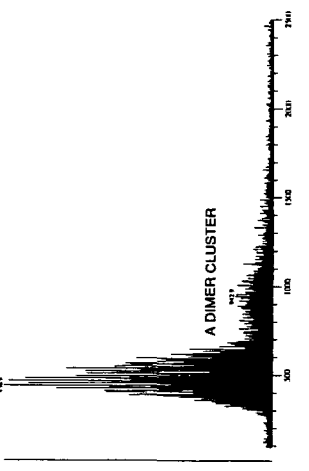

TABLE 1

COMPARISON BETWEEN FIELD DESORPTION AND THERMOSPRAY FOR HYDROCARBON CHARACTERIZATION

	Field Desorption	Thermospray
Solvent Required?	No, But Preferred	Yes
All Hydrocarbon Type?	Yes	Not For Saturates
Signal Duration	< 1 Min	> 1 Min
High/Medium Resolution MS?	No	Yes
On-Line LC Separation?	No	Yes
Possible Dimer Formation?	Yes	No

FIGURE 3

THERMOSPRAY OF THE SAME DISTILLATE SHOWS SIMILAR MOLECULAR WEIGHT DISTRIBUTION WITH NO DIMER CLUSTER

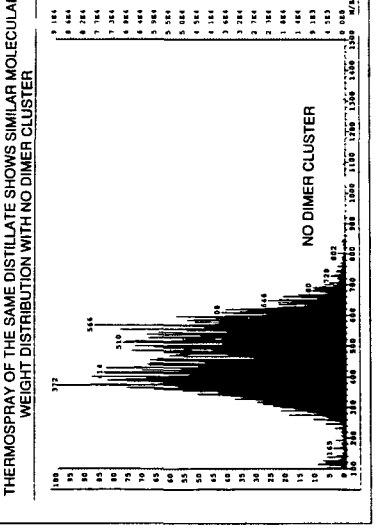

MULTI-SAMPLE PROBE FOR FAST ATOM BOMBARDMENT MASS SPECTROMETRY

Marshall M. Siegel*, Rushung Tsao, William Bouley, Theodore Kornas, Glen Brubaker
American Cyanamid Company, Medical Research Division,
Lederle Laboratories, Pearl River, New York 10965

INTRODUCTION

The traditional method for the analysis of samples by fast atom bombardment (FAB) is to load a single sample onto a probe target and then insert the probe into the mass spectrometer through a vacuum lock. In our laboratory environment, large numbers of FAB samples are analyzed to support pharmaceutical development. An inexpensive and routine method was needed to increase the productivity in generating large numbers of high quality low and high resolution FAB spectra. Flow-FAB and TLC-FAB were evaluated and found not to produce the same quality spectra as by probe analysis. We designed a multi-sample FAB probe for the consecutive analysis of five (or more) samples. With this probe, FAB spectra are produced with equal or better quality than those with the single sample probe but are generated with minimal effort and twice the speed. In addition, the design chosen requires no major modifications to the existing spectrometer system thereby minimizing implementation costs. The new multi-sample probe is an extension of the "reference" probe design introduced by VG for Flow-FAB.

DESIGN DETAILS

A VG ZAB-SE mass spectrometer equipped with an "open" FAB source, originally designed for Flow-FAB, and a vacuum lock perpendicular to the spectrometer beam axis was used. A schematic diagram of the multi-sample probe and source assembly is illustrated in Figure 1. A rectangular probe tip, 72 mm x 5 mm x 1.5 mm, containing five (or more) sample wells was fabricated from stainless steel and polished. A polished surface improves the adhesion of the sample and matrix to the surface and minimizes sample spreading from the confines of the well. The wells are 2.5 mm wide, 1 mm deep and spaced 5 mm apart. About 1 µl of dilute matrix and sample are respectively placed at the top of each well after the probe tip is rotated on its axis and held at about 45 degrees. The samples flow into the wells completely filling them. The multi-sample probe tip is introduced into the FAB source perpendicular to the spectrometer beam axis via the vacuum lock extension. The vacuum lock extension is 3 inches long to accommodate the elongated probe tip for evacuation before introduction to the high vacuum of the spectrometer. "O" rings at both ends of the inlet extension serve to seal the system upon insertion of the probe. After evacuation, the high vacuum valve is opened and the probe is pushed into the high vacuum region until constrained by the probe stop. At this point, the probe guide is locked into place with the thumb screw located on the probe guide extension. The translation of the probe and tip in the source region is controlled by a high performance Mitutoyo vernier dial (Model 297-201). As illustrated in Figures 2A and 3, when the probe tip enters the source block it makes electrical contact with a flexible stainless steel clip. This spring clip attaches securely around the screen plate which floats at the source potential. The clip can be easily disconnected from the screen plate without disassembling the source. (Exploded views of the spring clip and the multiple target tip are also illustrated in Figures 2A and B, respectively.) Each sample well is fully irradiated by the cesium ion beam without cross contamination. Transmission of the secondary ions is very efficient due to the closeness of the irradiated samples to the ion optics.

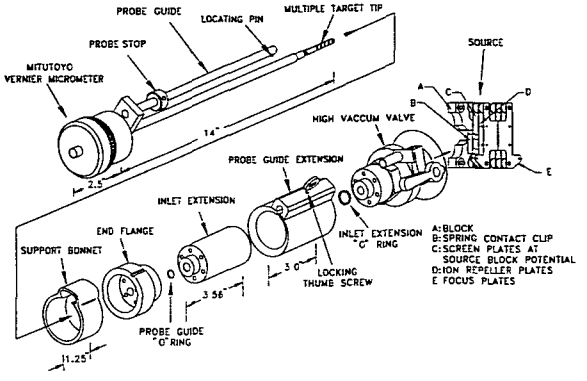

Figure 1. Exploded view of the multiple target FAB probe assembly. The original VG components are the end flange, high vacuum valve and FAB source (excluding the spring contact clip).

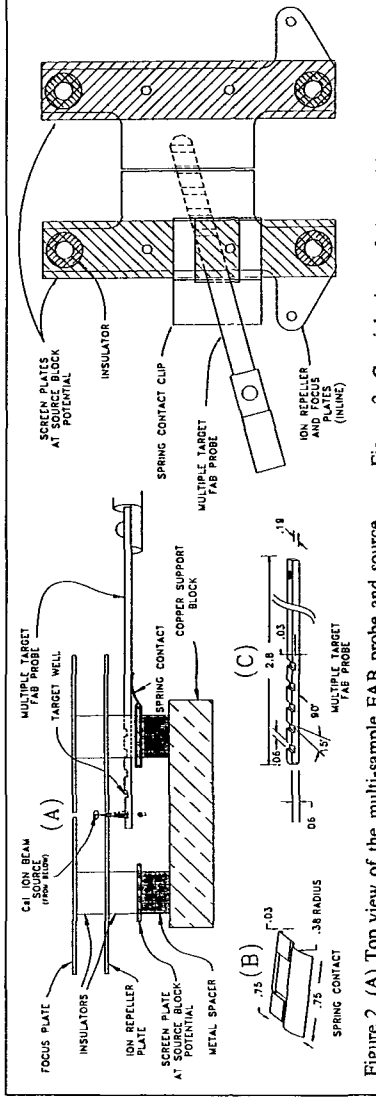

Figure 2. (A) Top view of the multi-sample FAB probe and source assembly. Exploded views of (B) the stainless steel spring clip, and, (C) multiple well target tip.

Figure 3. Coaxial view of the multisample probe tip, spring clip and FAB source assembly.

The multi-sample probe assembly has been in continuous use now in our laboratory for over nine months. The throughput of low resolution FAB samples has increased by about 50%. In the high resolution peak matching mode, pairs of adjacent samples, each with internal standards, can be rapidly analyzed without additional tuning. To maximize the number of samples analyzed, one does not use an excessive amount of FAB matrix so as to keep the source pressure as low as possible during the analysis but not too sparingly so that the matrix does not evaporate before the last analysis. For lengthier analyses, this can be achieved by using slightly more matrix for the later samples versus the earlier samples. The less volatile matrixes *m*-nitrobenzyl alcohol and a 5:1 (w:w) mixture of dithiothreitol:dithioerythritol have been found to work best with the multi-sample probe for a wide variety of pharmaceuticals.

Presently, the multi-sample probe is being automated. The design includes the following modifications. A stepper motor, which is software controlled, is being attached to the manual vernier dial. Rapidly interchangeable probe tips are being designed. With these modifications, up to ten FAB samples can be automatically analyzed without operator intervention. During the automatic operation of the probe, additional samples can be prepared and loaded on to the interchangeable multi-sample FAB probe tips. A net increase in sample throughput of 100% is anticipated upon installation of these improvements.

The Use of a Variable Focus Cesium Ion Source to Facilitate the On-line Generation of FAB Spectra with Particle Beam LC/MS

*Vicki Lanyon and Alexander B Schilling, The Hewlett Packard Company, Naperville, IL 60566

Introduction:

Particle Beam (PB) LC/MS operates by separating solvent from analyte molecules on the basis of differences in their momentum as they pass through a series of skimmers. The net result is an analyte enriched particle beam that enters the source and then is vaporized by source heat and ionized by electron impact or chemical ionization. This has limited the use of PB to compounds that exhibit some volatility The combination of PB with on-line FAB has been previously described using Xe ion sources[1] A focused Cesium ion source provides a higher current density at the sample platform as well as simplifying the alignment procedure needed to successfully interface PB and FAB

Experimental

A Phrasor Scientific cesium ion source was mounted to a HP 5989A MS by means of a clear Lexan(TM) plastic (1" thick) flange that facilitated visual inspection of the source alignment with the primary ion source The flange was tested with the source at 275 C for 2 weeks to ensure that radiant heat from the source would not damage it An inlet for the target probe was constructed to rigidly hold the probe and prevent contact with the repeller The holes on the repeller were enlarged to better accommodate the increase diameter of the target probe shaft The magnetic yoke was removed to give the cesium ion beam a clear path to the target probe tip When used in positive ion mode the target probe tip was allowed to float electrically with respect to the repeller Negative ion mode operation required that the tip carry a potential This was accomplished using either an external power supply or by coupling the tip to the repeller voltage. Two types of probe tips were studied, a bevel ended tip and a flat sectioned tip (referred to here as a spoon tip). Samples were introduced by means of a particle beam interface with a HP 1090L pumping system and methanol as the solvent (0 6 mL/min) using a 2 uL injection The Cesium ion source was operated at an acceleration voltage of 8 kv with a 1 0 uamp current The matrices used were glycerol, thioglycerol and 3-nitrobenzyl alcohol The source temperature was 40C and an HED was used at 9300 V A series of peptides such as the enkephalins, Substance P, Physalaemin and nucleotides such as AMP and GMP were used to evaluate the instruments performance.

Results and Discussion

The work completed demonstrates that a variable focus cesium ion source can be successfully interfaced to a commercially available quadrupole mass spectrometer. The use of a cesium ion source results in lower operating vacuums than are attainable with Xe ion sources because of the increased gas loads produced by using Xe gas When used in conjunction with a particle beam LC/MS interface for sample introduction, the best results were obtained with beveled target probe tips of narrow shaft diameter with a circular depression cut into them These tips allowed continuos operation for an hour , with minimal carryover due to excessive glycerol matrix loading.

[1] Kirk and Browner, Biomed Environ Mass Spec., 18, 355-357 (1989) and references therein.

In order to prevent rapid depletion of the glycerol the source temperature must be maintained at less than or equal to 40 C. This effectively precludes chromatographic separation using buffers as the source fouls very quickly under these conditions The system therefore is currently optimized for flow injection analysis (automated FAB) Ongoing work utilizing a continuos flow probe to ensure the constant supply of glycerol matrix at the target probe tip is underway.

How Particle Beam FAB Is Done

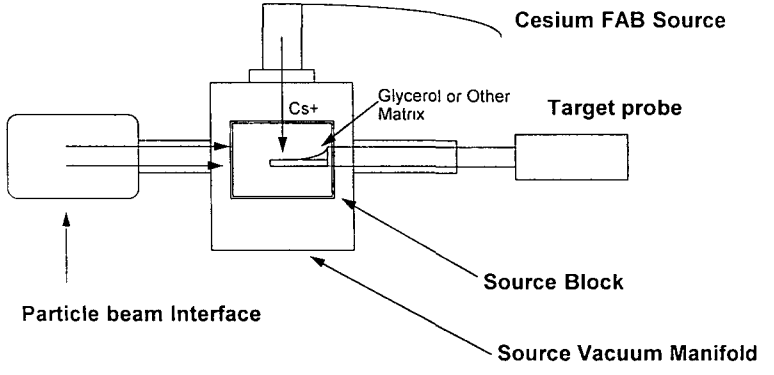

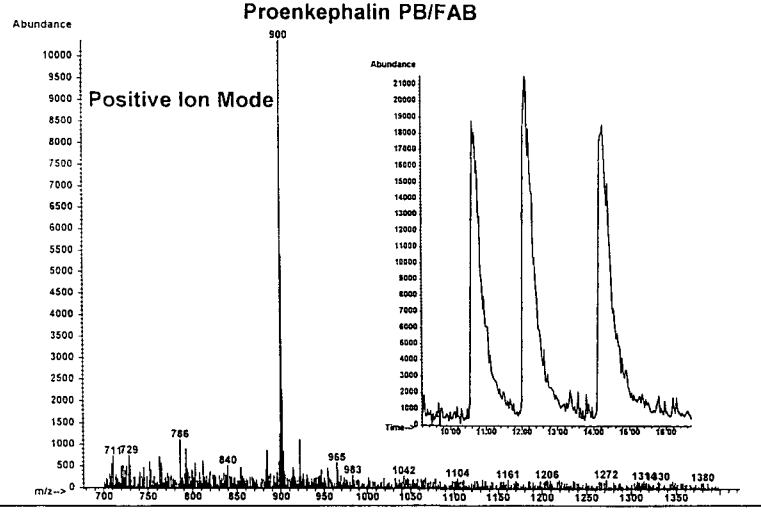

Selective Enhancement of Cationic Surfactant Ion Signal in Fast Atom Bombardment Mass Spectrometry

Yu-Chie Chen and Jentaie Shiea*
Department of Chemistry, National Sun Yat-sen University,
Kaohsiung, Taiwan, 804

The FAB signal of quaternary amines with different surface activity was found to vary with the concentration of sodium dodecylsulfate (SDS) present in the glycerol matrix. By controlling the concentration of SDS in the matrix, the signal of a series of equal concentration of quaternary amines with different alkyl chain can be selectively enhanced. Figure 1 shows the FAB spectra obtained from such samples which contain different concentration of SDS added in the matrix. The spectra show that with increasing SDS concentration, the signal of the less surface active compound increasing gradually. The changes of TIC of C_{16}-trimethylamines with irradiation time is very stable and decreasing with increasing amount of SDS in the matrix. The change of TIC of C_8-trimethylamine with irradiation time shows the reverse trend as that of C_{16}-trimethylamine. The explanation of this observation can be explained as the differences in the rate of formation of ion-pair precipitate from the reaction of SDS with the opposite charged surfactants (quaternary amines) in the matrix.

As we know, the trend to form ion-pair precipitate depends on the chemical properties of the surfactant. For their lower solubility in the aqueous solution and stronger van der waals forces with SDS, longer alkyl chain quaternary amines should form precipitate with SDS faster than that of shorter alkyl chain quaternary amines[2]. The FAB signal of the analyte will decrease when the precipitate was formed by this ion pair reaction. This is the reason why the signal of more surface active amines decrease with adding of SDS. In another word, after adding SDS, the increasing signal intensity of short chain quaternary amines on FAB spectra is not due to increasing of absolute concentration in the matrix. This is actually due to the suppression of the signals intensity of longer alkyl chain quaternary amines by the increasing of precipitate form (with SDS) in the matrix. This explation can be supported by the results from the experiments described below. Equal concentration of SDS was added into the aqueous solution each contained one species of solvated quaternary amines (from C_8 to C_{16} trimethylamines individually). The turbidity of each solution was measured by a turbidimeter. In Figure 2, we can see that the turbidity of the solution which contained C_{16} quaternary amines and SDS shows the highest turbidity. The turbidity of the solution which contained C_8 quaternary amines did not changed even in the solution which contained high concentration of the analyte and SDS. Since the formation of ion-pair precipitate will consume free SDS molecules, we should expect that the signal of SDS decreases for the solution which contain longer alkyl chain quaternary amines. This is clearly showing in Figure 3 where the intensity of SDS signal (obtained by negative FAB analysis) decrease with increasing of the alkyl chain in the quaternary amines.

One of the practice of using the matrix system described in this paper is to properly determining the species of charged surfactants with different surface activity. Figure 4 shows the FAB spectra from a emulsifying agent used in dye industry. The sample is comprised mainly of alkyldimethylbenzene ammonium chloride. It can be seen that, without adding SDS, only one series of peaks (m/z 304-388, m/z 388 as the prominent peak) can be observed in the FAB spectrum (Figure 4a). As the concentration of SDS increasing to 0.3 mM, the peak with m/z 304 turns to be the prominent peak (Figure 4b). When 5mM of SDS was added, a new series of peaks (m/z 248 and 276) were observed on the FAB spectrum (Figure 4c).

References

1. Ligon, W.V. and Steven, B.D., *Int. J. Mass Spectrom. Ion Processes*, 61, (1984) 113
2. Davis, S.S., Bruce, P.E., Baniels, P., Feely, L., *Surfactants in Solution*, (Ed. Lindmany, M.), Vol. 2, (1984), 1391, Plenum Press, New York.

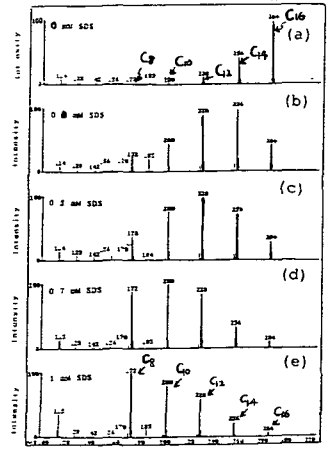

Figure 1. FAB spectra of the solutions which contain 0.2 mM of five quaternary amines (C_8-, C_{10}-, C_{12}-, C_{14}-, C_{16}- alkyltrimethylamine) each in the glycerol matrix by adding (a) 0 mM, SDS; (b) 0.3 mM, SDS; (c) 0.5 mM, SDS; (d) 0.7 mM, SDS; (e) 1 mM, SDS.

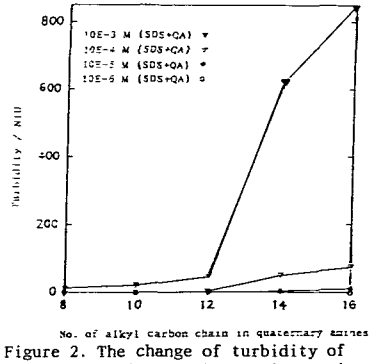

Figure 2. The change of turbidity of aqueous solutions each contain equal concentration of quaternary amine and SDS (from 10E-3 to 10E-6 M) versus the alkyl chain length of the quaternary amine (▼ :10E-3 M; ▽ :10E-4 M; ● :10E-5M; O :10E-6 M; QA:quaternary amine)

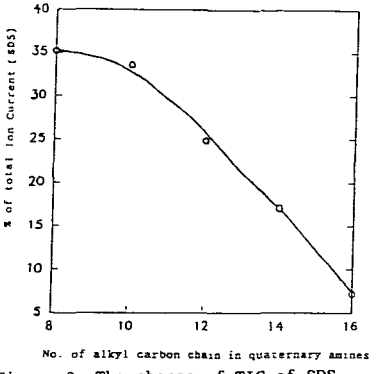

Figure 3. The change of TIC of SDS (dodecylsulfate ion; m/z 265; obtained by negative FAB) versus the alkyl carbon number of the quaternary amines. Each solution contains equal concentration of SDS and quaternary amines (2×10E-3 M).

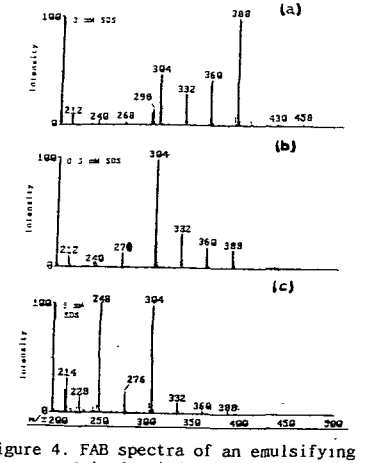

Figure 4. FAB spectra of an emulsifying agent used in dye industry in the presence of (a) 0 mM, SDS; (b) 0.3 mM, SDS; (c) 5 mM, SDS; in the glycerol matrix.

FAB MS OF NON-VOLATILE COMPOUNDS IN THE TRANSITION RANGE BETWEEN LIQUID AND SOLID

K. Anheuser, E. Junker and F.W. Röllgen
Institute of Physical and Theoretical Chemistry, University of Bonn
Wegelerstr. 12, D-53115 Bonn 1, FRG

In Fast Atom Bombardment Mass Spectrometry (FAB MS) molecules are ionized from liquids under conditions of continuous erosion of layers by sputtering. We have investigated the limits of this mode of ionization in the transition range between the liquid and solid state of samples for ammonium nitrate and raffinose.

EXPERIMENTAL

The experiments were performed with a double focusing AEI MS902 mass spectrometer. The Xenon primary particle beam was produced in a saddle field discharge source operated at 6 kV anode potential and 1 mA discharge current. The current density of the Xenon atom beam was 5-10 $\mu A/cm^{-2}$. The probe surface was in a horizontal position allowing the deposition of thick layers.

The change of the physical state of the sample solutions under bombarding conditions was monitored by optical microscopy in a separate experimental setup.

RESULTS

For a concentrated solution of ammonium nitrate in glycerol (molar ratio 1:3) and the onset of Xe atom bombardment immediately after introduction of the solution into the vacuum a steep increase of the intensity of the $[(NH_4NO_3)NH_4]^+$ cluster ion is observed after 10 min (Fig. 1). This intensity increase coincides with an optically observable formation of small crystallites of the salt in solution.

For a concentrated solution of raffinose and ammonium nitrate in glycerol (molar ratio 1:17:54) the same effect of a steep increase of the ammonium nitrate cluster ion signals upon crystallization of the salt in solution is observed. The time dependence of the molecular ion signal of raffinose was similar to that reported before [1] for a raffinose solution of similar concentration without ammonium nitrate.

Abundant and long lasting cluster ion signals are obtained from a "solid" surface layer of ammonium nitrate formed by exposing a concentrated solution of ammonium nitrate in glycerol (molar ratio 1:3) to vacuum for several hours prior to the onset of bombardment.

Long lasting and abundant cluster ion signals with a delayed steep increase during the first minutes of bombardment are also observed for a thick layer (about 1 mm) of ammonium nitrate, with residual water retained in the layer (Fig. 3).

For solvent free solid ammonium nitrate the cluster ion intensities decay within several minutes as shown in Fig. 3. The decay of the cluster ion signal and an increase of the chemical noise level indicate the accumulation of radiation damage during sputtering of the solid layer.

In contrast to ammonium nitrate sputtering of solid ammonium cloride yields an abundant long lasting $[(NH_4Cl)NH_4)]^+$ cluster ion signal with a delayed intensity increase after onset of sputtering [2] (Fig. 4). The delay indicates the effect of loosing the structure of the solid by particle bombardment [3] and the long lasting cluster ion signal shows that no radiation damage accumulates.

CONCLUSIONS

Solutions with precipitated small particles and solid deposits with solvent molecules retained are amenable to FAB MS (dynamic SIMS).

The extent to which FAB MS (dyn. SIMS) can be applied to solutions with precipitated solid particles, or to solids containing solvent residues depends on the decomposition of molecules into volatile products upon sputtering and the accumulation of radiation damage.

The dependence of the sputtering of cluster ions of the ammonium salts from a loose structure of the solid, which is also induced by preirradiation of salts [3], strongly supports a mechanism of pressure pulse sputtering for the formation of the cluster ions. In this mechanism a high pressure (≈10 kbar) generated within about 2 ps in the area of the dense cascade by the incident particle leads to the desorption of neutral and ionized intact molecules and clusters [4].

[1] E. Junker, K.P. Wirth, F.W. Röllgen, Int. J. Mass Spectrom. Ion Phys., 122 (1992) 3.
[2] R.G. Cooks and K.L. Busch, Int. J. Mass Spectrom. Ion Phys., 53 (1983) 111.
[3] B. Schueler, R. Beavis, W. Ens, D.E. Main, K. Standing, Surf. Sci., 160 (1985) 578.
[4] E. Junker and F.W. Röllgen, to be published.

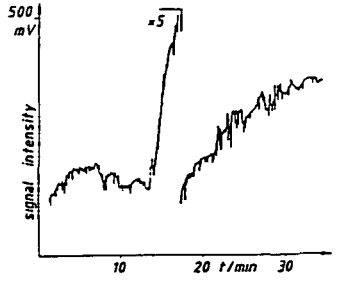

Fig. 1 Intensity of the $[(NH_4NO_3)NH_4]^+$ cluster ion (m/z = 98) as a function of bombarding time for an ammonium nitrate/glycerol (molar ratio 1:3) solution.

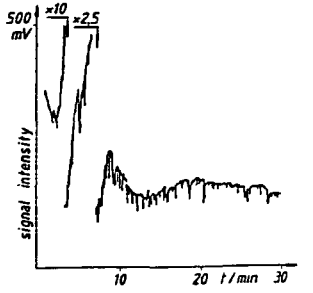

Fig. 2 Intensity of the $[(NH_4NO_3)NH_4]^+$ cluster ion as a function of bombarding time for solid ammonium nitrate containing residual water.

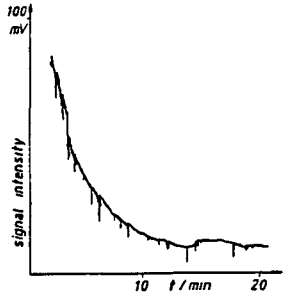

Fig. 3 Intensity of the $[(NH_4NO_3)NH_4]^+$ cluster ion as a function of bombarding time for solid ammonium nitrate free of water.

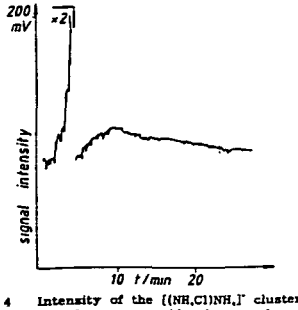

Fig. 4 Intensity of the $[(NH_4Cl)NH_4]^+$ cluster ion of ammonium chloride as a function of bombarding time for solid ammonium chloride free of water.

INVESTIGATION OF [M-H]+ FORMATION IN FAB/LSIMS FOR A COMPOUND WITH HIGH PROTON AFFINITY

G. J. C. Paul, T. Rendon and M. J. Bertrand
Regional Center for Mass Spectrometry, Department of Chemistry, University of Montreal, Montreal, P.Q. H3C 3J7

Recently numerous compounds have been shown to yield $[M-H]^+$ in FAB/LSIMS in addition to the $[M+H]^+$ species normally associated with these techniques A new compound which forms $[M-H]^+$ in FAB/LSIMS is perhydro-3a,6a,9a-triazaphenalene (PHTAP) shown below.

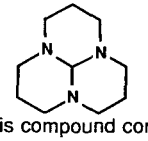

What is especially interesting is that this compound contains three basic amine groups giving it a large proton affinity and exclusive $[M+H]^+$ formation in FAB/LSIMS would be expected. However, the presence of a -CH group α– to three nitrogen atoms is sufficient to provide a site for hydride abstraction in FAB/LSIMS. PHTAP was studied by FAB/LSIMS using several liquid matrices; 1,2,4-butanetriol (BUT), diethanolamine (DEA), glycerol (GLY), 2-hydroxyethyl disulfide (HEDS), 3-nitrobenzyl alcohol (NBA), thiodiglycol (TDG) and thioglycerol (THIO), to gain insight into the ionization processes occurring. CI and electrospray data were taken to complement this study.

A typical FAB mass spectrum for PHTAP is shown in Figure 1. The only significant analyte peaks are in the molecular ion region with $[M-H]^+$ dominant. The relative molecular ion intensities for PHTAP are given in Table 1 for each liquid matrix. For five matrices a dramatic time effect is observed as the relative intensity of $[M-H]^+$ increases relative to $[M+H]^+$. For HEDS and NBA, the duration of fast atom bombardment does not have a significant effect on the $[M-H]^+/[M+H]^+$ ratio. LSIMS experiments have also been performed for PHTAP in TDG and NBA. Similar molecular ion intensity trends to those in FAB are observed (Table 1). The CI (NH_3) mass spectrum for PHTAP is shown in Figure 2. The molecular ions are again dominant but here $[M+H]^+$ is the major species with $[M-H]^+$ weak (Table 1) The CI data makes it difficult to rationalize strong $[M-H]^+$ formation in FAB/LSIMS for PHTAP purely in terms of gas phase ionization processes where the protonated matix is assumed the major reactant species. This is because the hydride ion affinity of NH_4^+ is greater than those estimated for protonated BUT, DEA, GLY and THIO yet the relative intensity of $[M-H]^+$ in FAB in those matrices is greater than in CI (NH_3) (Table 1).

Hence, condensed phase ionization processes appear to be at least partially responsible for $[M-H]^+$ formation in FAB/LSIMS. The time dependence exhibited by the molecular ion intensities in FAB/LSIMS for PHTAP with certain matrices is consistent with this interpretation. In the condensed phase ionization model for FAB/LSIMS a build-up of reactant electrophilic species responsible for hydride abstraction with increasing time of fast atom/ion bombardment would explain the increase of $[M-H]^+$ relative to $[M+H]^+$. The time effect thus suggests the importance of fast atom/ion beam-induced processes in the condensed phase ionization model. It is interesting that a significant time dependence is not observed for PHTAP in HEDS and NBA. These matrices have been seen to inhibit fast atom/ion beam-

induced reduction processes through their proposed electron/radical scavenging properties. These properties may similarly be responsible for the lack of a time dependence for PHTAP in HEDS and NBA as fast atom/ion beam-induced processes are believed responsible for this effect. Indeed, in this work it is seen through negative ion FAB that HEDS and NBA are the only matrices capable of forming radical anions through electron capture.

The ESI mass spectrum for PHTAP is shown in Figure 3. In ESI, ionization occurs predominantly through condensed phase equilibrium processes with no fast atom/ion bombardment taking place. The $[M+H]^+$ is dominant with only a small $[M-H]^+$ peak present, possibly through unimolecular decomposition (Table 1). This again suggests that fast atom/ion beam-induced processes are responsible for the strong $[M-H]^+$ peaks observed in FAB/LSIMS for PHTAP.

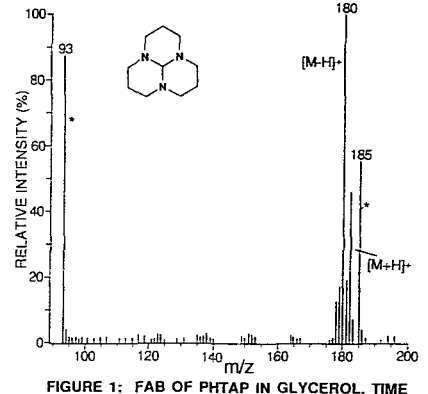

FIGURE 1: FAB OF PHTAP IN GLYCEROL. TIME OF FAB = ~2 MIN. * = MATRIX PEAKS.

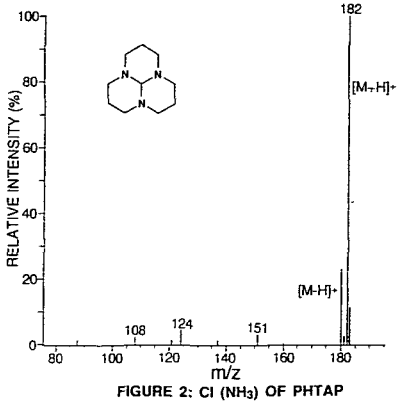

FIGURE 2: CI (NH_3) OF PHTAP

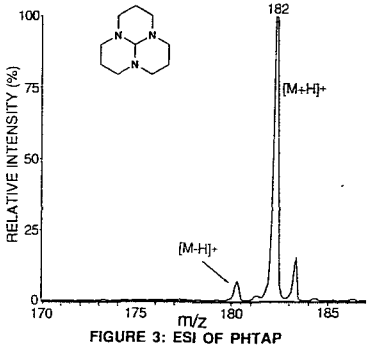

FIGURE 3: ESI OF PHTAP

TABLE 1: RELATIVE INTENSITY (%) OF PEAKS IN MOLECULAR ION REGION OF FAB, LSIMS, CI AND ESI[a]

	Time = ~30sec		Time = ~3min	
	$[M-H]^+$	$[M+H]^+$	$[M-H]^+$	$[M+H]^+$
FAB/BUT/ 08M	67	100	100	28
FAB/DEA/ 15M	50	100	100	66
FAB/GLY/.15M	88	100	100	23
FAB/HEDS/.03M	100	100	100	93
FAB/NBA/.05M	93	100	91	100
LSIMS/NBA/ 05M	70	100	66	100
FAB/TDG/.04M	100	93	100	65
LSIMS/TDG/ 04M	83	100	100	75
FAB/THIO/.08M	25	100	65	100
CI/NH_3	23	100	23	100
ESI	8	100	8	100

[a]Relative intensity of M^+ is between 0-8 % in all experiments

IMPROVED DYNAMIC (CONTINUOUS FLOW) LSIMS (FAB) SENSITIVITY USING A COLD FINGER TO ENHANCE PUMPING

Klaus Eckart, Adrian R. Woolfitt§, Robert S. Bordoli§ and Joachim Spiess
Department of Molecular Neuroendocrinology, Max Planck Institute for Experimental Medicine, Hermann-Rein-Str. 3, D-3400 Goettingen, § VG Analytical, Wythenshawe, Manchester M23 9LE, UK

Dynamic or continuous flow LSIMS (FAB) has a number of advantages compared with static LSIMS, such as improved detection limits, reduced suppression effects, shorter analysis time, and LCMS capability. In favourable cases, such as the peptide substance P (MW 1347), a 200-fold sensitivity improvement has been reported. However, higher mass compounds such as glucagon and the insulin B chain exhibit a weaker response when analyzed with Dynamic rather than Static LSIMS (1). This has been attributed to the adverse effects of source housing pressure on the transmission of such ions. Indeed during experiments with a prototype electrospray interface on a sector instrument (VG AutoSpec) a clear relationship between source housing pressure and ion transmission was established; the effect was most marked for larger proteins such as bovine serum albumin (66 kDA).

We have designed a cold finger in order to overcome the transmission problems associated with the high solvent vapor pressure from the dynamic probe. The factors affecting the performance of the system are investigated and the best operating conditions are presented.

All experiments were carried out on a VG Analytical AutoSpec-T tandem mass spectrometer. LSIMS spectra were obtained using standard LSIMS conditions. The design of the dynamic screen/wick probe has been described in detail (2). The probe was used with a 10μm screen. Samples were continuously delivered in 49.5% water, 49.5% acetonitrile, 1% glycerol, and 0.1% TFA through a 50μm inside diameter capillary. The measurements of the molecular ion intensities were carried out using the peptides Xenopsin in 10ng/μl concentration and the ACTH (18-39) fragment in 100ng/μl concentration. The cold finger was manufactured from stainless steel. It replaces the glass lid above the ion source and incorporates a circular glass window for visual inspection of the ion source under operation. The pumping speed of the cold finger is calculated to be approximately 1000 l/second for water.

Two peptides with molecular weights of 1000 and 2500 dalton were used to establish the dependence of sensitivity and molecular ion intensity (response) from flow rate. A part of these results is displayed in Figure 1. The following aspects should be noted: as expected, the *molecular ion intensity is increased in any case when the cold finger is operated. This increase* amounts to a factor of 1.3 for xenopsin at 1μl/minute and 2.3 at 5μl/minute. For ACTH 19-38 we obtained factors of 2.5 and 8.0, respectively. In addition for glucagon a molecular ion was only detected with cold finger operation. This increase in cross section with increasing mass for collisionally activation observed in these experiments is confirmed by the same behaviour using a collision cell in MSMS experiments.

The sensitivity expressed in coulomb/μg is reduced when the flow rate is increased. This must be attributed to an increasing source housing pressure but it cannot be excluded that the conditions are changing on the probe with the amount of matrix delivered. Independently of the molecular weight the best sensitivity is obtained at the lowest possible flow rate in conjunction with the cold finger operation. We found in addition that reduction of the flow rate from 1.0 to 0.5 μl/min decreases the molecular ion intensity by more than 90%. This indicates that not sufficient glycerol is delivered for LSIMS operation. Earlier experiments showed that

1% glycerol is the best concentration to obtain maximum sensitivity. This finding is in agreement with the results obtained by another group (3).

Increasing pressure reduces the transmission through the ion source housing by scattering and collisionally activated decompositions. This effect is investigated in the linked scan spectra of substance P (data not shown). The operation of the cold finger reduces significantly the amount of collisionally activated fragmentation, but the presence of d-ions even with the cold finger operation indicates a significant amount of high energy collision induced fragmentation. This is completely removed in the linked scan spectrum using the static probe (DTT/DTE matrix). These results support the conclusion that the changes in sensitivity are mainly due to changes in source housing pressure. It should be noted that the molecular ion beam of substance P is more than tripled by the cold finger operation. Nevertheless the linked scan spectrum is less intense compared to the spectrum obtained using 70% reduction with a collision gas in the collision cell. This leads to the conclusion that most of the ions are lost in the acceleration region.

The cold finger enables a sensitivity improvement by a factor of 2 to 10 depending on the sample and operating conditions. Linked scan spectra had shown that even under cold finger operation the ion beam is significantly decreased by collisions with solvent vapor. Highest sensitivity was achieved in all cases by operating the probe with a flow rate of 1μl/min. The cold finger needs five minutes to achieve maximum pumping and is operative for one hour when filled with liquid nitrogen. The advantage compared to a cold trap is that it can be made easily in a machinery workshop and it can be taken out when it is cooled down in order to protect the pumps from acid. The pumping speed of a cold trap which is limited by the diameter of the throat is expected to be in the same range of the cold finger.

Figure 1: Dependence of response and sensitivity from the flow rate
(CF = cold finger)

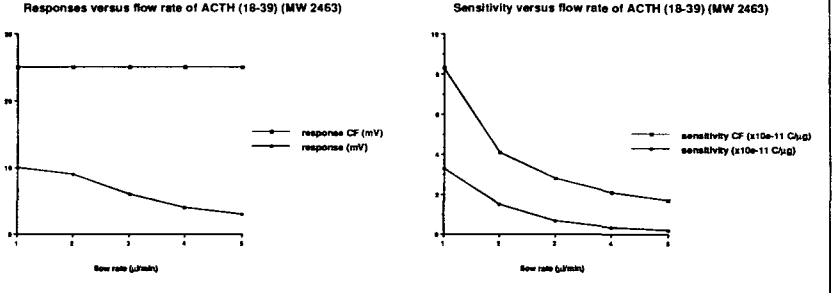

References

1) W. P Johnson, G. Roberts, M E Hemling, M. F. Bean, A. R. Woolfitt and S. Carr, (1990) *38th ASMS Conference on Mass Spectrometry and Allied Topics*, 1315-1316.
2) A. R. Woolfitt and C. A. J. Harbach, (1993) *Rapid Comm. Mass Spectrom.*, 7, 176-178.
3) D B. Kassel, K P. Williams, B D. Musselmann and J. A Smith, (1991) *Anal. Chem.*, 63, 1978-1983

The Effects of Analyte and Matrix Properties on the True Reduction-Oxidation Extents Observed in FAB/LSIMS Analysis of Peptides

J. Visentini*, M.Allard, D. Zidarov and M.J. Bertrand,
Regional Center for Mass Spectrometry, Department of Chemistry,
University of Montreal, Montreal, Canada H3C 3J7

Reduction-oxidation processes which may occur during FAB/LSIMS analysis of peptides are believed to be responsible for the frequent observation of elevated A±n peak intensities [A=(M+H)+, n≥1]. Early work in this area attributed the discrepancy between expected and measured peak intensities entirely to redox products. The reduction extents determined by isotopic peak ratio measurements alone, however, may contain contributions from radiation-induced background signal which may sometimes mask trends in true redox processes. A deconvolution procedure recently developed in our laboratory[1] has proven to be useful for the isolation of actual redox extents and background level from overall measured signals. With the aid of this new tool, the effects of the analyte structure, matrix composition, time of irradiation and sample concentration on the actual redox extents can be studied. All isotopic peak ratio measurements were made using narrow voltage scanning and multi-channel acquisition on a VG Autospec-Q mass spectrometer equipped with a variable energy caesium ion gun. The instrument was operated at an accelerating voltage of 8 kV and maintained at a mass resolution of 2000. Integrated peak areas were averaged over a 5 minute period in order to maximize reproducibility. The computer program SIMBROC[1] (Simulated Background and Reduction-Oxidation Calculations) used to evaluate the individual contributions of redox extents and background signal was written in Fortran 77 and requires only a few seconds for execution. The Red_n and Ox_n values given by SIMBROC represent the extents of those reduction and oxidation processes, respectively, by which *n* hydrogens/electrons are transferred. The redox extents are given as percentages of the sum of all redox processes. The $Back_1$ and $Back_2$ values, however, represent the background level as percentages of the base peak intensity in the molecular ion cluster.

In order to study the effect of analyte structure on redox extents, a series of peptides were analysed under similar conditions and the SIMBROC results are given in Table I. The lack of correlation between redox extents with the hydrophobicity/hydrophilicity indices (ΔF values), indicates that the redox extents are not dependent on the solubility or distribution of analyte in the liquid matrix. The relationship between structural features of the analyte and the redox extents was also examined. Possible reduction sites found in peptides include disulfide bridges which reduce extensively in glycerol or thioglycerol matrices, phenyl rings or other unsaturated sites, and carbonyl groups which are found in the backbone structure of all peptides. The data presented in Table I indicate that as the number of unsaturated sites in the peptide increases, the extent of two-electron reduction also increases. In fact, Figure 1 illustrates that the extent of two-electron reduction varies linearly with the number of unsaturated sites and that each unsaturated site contributes approximately 0.18% of two-electron reduction. The Red_2 values were also found to increase with increasing number of phenyl rings although the relationship was not a linear one. Moreover, SIMBROC results indicated that the redox extents do not vary linearly with the number of carbonyl groups present in the peptide chain. The carbonyl groups and phenyl rings therefore provide sites for reduction without being preferentially reduced. In the cases of substance P and pentaalanine, oxidation processes seemed to be favoured probably due to the presence of more aliphatic groups in the side chains of these peptides. Besides structural features of the analyte, the matrix composition may also play an intimate role in the redox processes. Table II presents data obtained for pressinoic acid and met-enkephalin

in six different matrices. Thioglycerol causes extensive two-electron reduction in pressinoic acid and significant one-electron oxidation in met-enkephalin. Since its behaviour is unpredictable, its routine use is not recommended. When 2-HEDS, 3-NBA and 4-HBSA were used as matrices, the extent of two-electron reduction was significantly decreased while the oxidation extents increase. These results indicate that these matrices are not only inhibiting reduction processes but are also actively involved in promoting oxidation. Results from this study also indicated that actual redox extents do not generally increase with sampling time. Instead, the time dependence often observed in isotopic peak ratio measurements is due moreso to increased radiation-induced background signal with continued bombardment. Measured isotopic ratios typically increase as the concentration is lowered. When the data were treated with SIMBROC however, it was found that the concentration effect remains and cannot thus be explained solely by background interferences at the lower concentrations. By simulating concentration curves, it was found that the extent of reduction observed in peptide samples is proportional to the number of matrix molecules surrounding the analyte species.

[1] J. Visentini, D Zidarov, M Allard and M J Bertrand, *J. Amer. Soc. Mass Spectrom.*, 4, xxx (1993)

*Current address Merck Frosst Canada Inc , P.O Box 1005, Pointe-Claire-Dorval H9R 4P8

TABLE I

The Effect of Analyte Structure on Redox Extents as Determined by SIMBROC Results for Selected Peptides in Glycerol

	$Back_1$ (%)	$Back_2$ (%)	Ox_2 (%)	Ox_1 (%)	Red_0 (%)	Red_1 (%)	Red_2 (%)	ΔF value[a]	# U.S.[b]	# Rings[c]	# CO[d]
Pentaphenylalanine	14 77	17 12	5 13	7.72	76 52	5 96	4 68	-1520	25	5	5
Met-enkephalin	3 88	3 59	3 69	3 24	89 01	2 03	2 03	- 398	13	2	5
Substance P	4 12	5 12	13 32	0 44	86 24	0 00	0 00	- 163	24	2	11
Bradykinin	0 74	0 71	6 51	3 68	86 06	0 05	3 71	- 104	22	2	9
Pentaalanine	9 36	10 96	9 17	8 00	79 83	2 10	0 90	+ 610	5	0	5

Concentration 0 01M, Primary beam energy 14 keV, Primary beam flux 0 032 μA/mm²

a) *Hydrophobicity/Hydrophilicity Index (cal/mole)*
b) Number of unsaturated sites in the peptide
c) *Number of phenyl rings in the peptide*
d) Number of carbonyl groups in the peptide

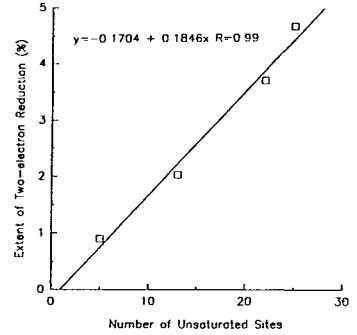

Figure 1
Variation of two-electron reduction extent with number of unsaturated sites present in peptide

TABLE II

The Effect of Matrix Composition on Redox Extents as Determined by SIMBROC for Pressinoic Acid* and Met-enkephalin**

Peptide	Matrix	$Back_1$	$Back_2$	Ox_2	Ox_1	Red_0	Red_1	Red_2
Pressinoic Acid	Thioglycerol	2 76	3 14	0 00	0 00	7 14	4 60	88 26
	Glycerol	2.27	2 33	2 22	2 21	85 58	1 95	8 02
	2-HPEA	0 61	0 64	1.24	2 99	85 87	3 57	6 34
	2-HEDS	1 57	1 12	2 14	7 64	87 75	1 45	1 04
	3-NBA	0 39	0 41	3 79	7 26	87 00	1 17	0 78
	4-HBSA	1 12	0 65	2 97	4 68	85 69	5 35	1 30
Met-enkephalin	Thioglycerol	1 05	0 36	1 28	22 86	75 14	0 16	0 56
	Glycerol	1 03	0 51	1 88	1 94	96 08	0 00	0 10
	2 HPEA	1 21	1 21	1 33	2 04	96 05	0 00	0 58
	2-HEDS	1 18	0.78	3 92	8 45	87 63	0 00	0 00
	3-NBA	0.63	0 70	3 55	3 67	92 78	0 00	0 00
	4-HBSA	0 13	0 16	3 87	2 50	93 63	0 00	0 00

*Concentration 0 06M, Primary beam energy 14 keV, Primary beam flux 0 032 μA/mm²
**Concentration 0 03M, Primary beam energy 14 keV Primary beam flux 0 032 μA/mm²

The Effect of Functional Groups on the Reduction Behaviour of Phenothiazine-related Dyes in LSIMS/FAB Mass Spectrometry.

* M. Allard, J. Visentini, D. Zidarov and M.J. Bertrand, Regional Center for Mass Spectrometry, Department of Chemistry, University of Montreal, Montreal, Canada H3C 3J7

Reduction/oxidation processes in FAB/LSIMS mass spectrometry are frequent for several classes of compound, as for organic dyes. The experimental parameters shown to affect reduction extent include the nature of matrix, the beam density and the analyte concentration. The redox processes manifest themselves by an excess signal in the peaks $(M \pm n)^+$ $(n \geq 1)$ of the isotopic distribution. The real effect of experimental conditions on redox extents can only be seen once the contributions from the background and the other redox species have been isolated. The true rather than the apparent reduction/oxidation extents can be evaluated using the deconvolution program SIMBROC developed in our laboratory. SIMBROC is based on a mathematical model which assumes that each redox process affecting the isotopic distribution occurs by an hydrogen/electron exchange. For a preformed ion in solution, the redox processes are characterized as follow:

Ox_2	M^+	-	$2H^\bullet$	-->	$(M-2H)^+$	[1]
Ox_1	M^+	-	$H^\bullet$	-->	$(M-H)^{+\bullet}$	[2]
Red_0	M^+	-->	M^+			[3]
Red_1	M^+	+	$H^\bullet$	-->	$(M+H)^{+\bullet}$	[4]
Red_2	M^+	+	$2H^\bullet$	-->	$(M+2H)^+$	[5]

Equation 1 and 2 respectively represent the two and one-electron oxidation while equation 4 and 5 define the one and two-electron reduction processes. Results obtained using the SIMBROC deconvolution program are given as Ox_n and Red_n values. These data indicate the extents of oxidation and reduction respectively where n denotes the number of electrons/hydrogens transferred in the process. As for the $Back_1$ and $Back_2$ values, they represent the alternating background levels calculated by the program. Earlier work[1] conducted in our laboratory with Methylene Blue indicated that changes in the experimental parameters affect the true two-electron reduction more significantly than the one-electron reduction process. This would suggest that those two processes are occuring by different mechanisms. Two other dyes, Thionin and Azure A, have been used to monitor the extents of one and two-electron redox processes and to verify the conclusions drawn from the Methylene Blue study Table 1 shows the matrix effect on the redox processes for Methylene Blue, Thionin and Azure A. Glycerol seems to inhibit the oxidation processes for the three dyes while 3-NBA seems to inhibit the extent of reduction. The three compounds gave similar results, thereby suggesting that analyte structure doesn't play an important role in the redox

mechanisms. Figure 1 shows the concentration effect on the redox processes of the Azure A dye. The two reduction processes are increasing with decreasing concentration, while the oxidation processes increase with increasing concentration.

---

1) Allard M., Visentini J., Bertrand M.J., Proceedings of the 40th ASMS conference on Mass Spectrometry and Allied Topics, Washington D.C , 1992, 1409

Table 1

Effect of matrix nature on the redox processes for 0.1M solutions bombarded at 0.018 ($\mu A/mm^2$)

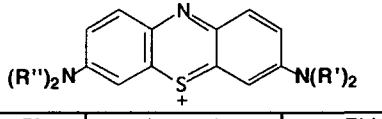

Functionnal Groups	Methylene Blue R' = R" = CH_3		Azure A R'= CH_3 R" = H		Thionin R' = R" = H	
matrix	NBA	GLYCEROL	NBA	GLYCEROL	NBA	GLYCEROL
Red 1	6.87	29.78	7.87	24.39	12.74	31.14
Red 2	0.44	2.95	0.89	7.90	1.48	8.58
Oxy 1	6.89	2.67	8.57	2.38	8.07	1.13
Oxy 2	1.53	1.72	1.59	0.49	0.92	0.06
Back 1	0 20	0.22	0.43	0.87	0.25	0 72
Back 2	0.26	0.38	0.52	2.89	0.29	2.29

Figure 1

Effect of sample concentration in 3-NBA for the a) reduction extents b) oxidation extents of Azure A bombarded at 0.032 ($\mu A/mm^2$)

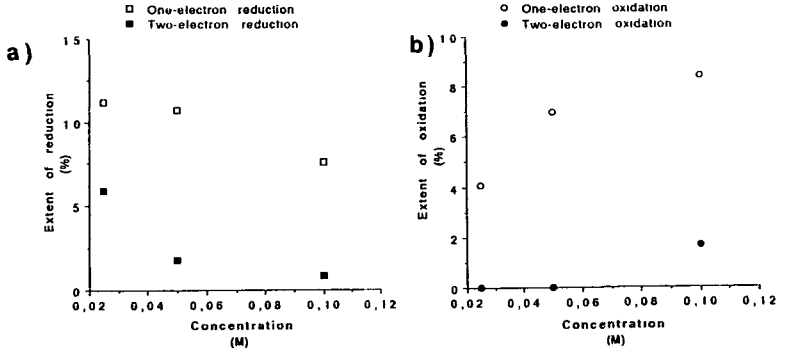

BEAM-INDUCED DEHALOGENATION of ORGANIC COMPOUNDS in LSIMS: EFFECT of ANALYTE STRUCTURE, HALOGEN TYPE, and MATRIX CHEMISTRY.

R. Théberge* and M.J. Bertrand, Regional Center for Mass spectrometry
Department of Chemistry, University of Montreal, Montreal, Canada, H3C 3J7

Dehalogenation reactions of organic compounds during their FAB/LSIMS analysis have been the object of several studies. The importance of these reactions lie in the fact that they can cause the presence of artefacts in the mass spectra. Althought it was suggested that specific experimental parameters influence these reactions, there have been no systematic study of these factors. In a previous study conducted in our laboratory, it was observed that matrix chemistry and analyte structure were the main factors controlling the extent of beam-induced dehalogenation of organic compounds. In our continuing investigation of beam-induced dehalogenation, we have focused on the effect of analyte structure, halogen type, and matrix chemistry. The compounds chosen for this study were the 4-halo-phenylalanine methyl esters (F, Cl, Br, I) 1 and the chlorinated herbicide atrazine 2. The variety of matrices used allowed the elaboration of a rough matrix structure dehalogenation inhibiting efficiency correlation. This correlation can be used to gain insight in the mechanism(s) involved in the beam-induced dehalogenation of organic compounds in FAB/LSIMS. Mass spectra were obtained using an Autospec-Q equipped with a caesium ion gun. The caesium ion beam had an energy of 22 keV and beam density of 2μA. The matrices used were glycerol (GLY), thioglycerol (THIOGLY), thiodiglycol (TDG), , 2-hydroxyethyl disulfide (HEDS), 2-hydroxyphenethyl alcohol (HPEA), 3,4-dimethoxybenzyl alcohol (DMBA), 4-hydroxybenzene sulfonic acid (HBSA), 3-nitrobenzyl alcohol (NBA), 2-mercaptoethyl sulfide (MES), 2-benzyloxy-1,3-propanediol (BOP), 1,4-anhydroerythritol (AET). The last three being new matrix compounds.The extent of dehalogenation was expressed in % as shown in eq (1).

$$\%\text{Dehalogenation} = 100 \times \frac{(M_H+H)^+}{(M_H+H)^+ + (M_X+H)^+} \qquad (1)$$

Where $(M_H+H)^+$ is the relative abundance of dehalogenated molecule (protonated) and $(M_X+H)^+$ is the relative abundance of the intact protonated molecule. As expected, the %dehalogenation observed in glycerol increases in the order I > Br > Cl > F, reflecting the respective leaving group ability of the halogens (Table 1). In fact, the trends presented in table 1 are coherent with the matrix dehalogenation-inhibiting efficiency scale established in our previous study on the LSIMS beam-induced dehalogenation of chlorpromazine. The basis for the rationalization used to explain the dehalogenation-inhibiting efficiency of the respective matrix compounds rests on the premise that keV particle impacts cause the production of electrons (via the ionization of the sample or matrix) and that these electrons can be effective reducing agents. However, the possibility that other beam-generated reactive species might contribute to the dehalogenation process cannot be ruled out. For aromatic matrices, their dehalogenation-inhibiting efficiency can be rationalized in terms of their relative electron affinities. It has been shown that substituted benzenes with electron withdrawing substituents have greater electron affinities than those with electron donating substituents[1]. It is important to note that electron affinitity (a gas phase property) appears to follow the same trend as reduction potentials (a condensed phase property)[2]. However, a dehalogenation mechanism based on beam-generated electrons is of limited use to rationalize the data obtained with the aliphatic matrices since little is known on their electron

affinities or the correlation between their structural features and that physical property. It appears that sulfur plays a role in inhibiting the dehalogenation process since sulfur-containing matrices consistently exhibit a relatively low % dehalogenation with respect to glycerol. The lower extent of dehalogenation observed in sulfur-containing matrices may be explained by the bombardment-induced formation of thiyl radicals which are known to have oxidizing properties. Sulfur compounds are known to be involved in the protection mechanism for biological systems subjected to ionizing radiation or other forms of free radical damage. That sulfur plays a role in inhibiting the dehalogenation process appears undeniable since MES, which has three sulfurs and no other heteroatom, exhibits a low %dehalogenation value.The other new matrices, AET and BOP, exhibit dehalogenation inhibiting trends similar to their structural analogs, glycerol and HPEA respectively.

The effect of the aromatic moiety of the analyte is illustrated by the %dehalogenation obtained for atrazine with respect to the chlorinated phenylalanine compound. Since the capture of an electron is thought to be the cause of dehalogenation, the ability of a molecule to form the radical anion should be commensurate to its propensity to dehalogenate. The one electron reduction potential of s-triazine (-2.0V) is much more positive than that of the chlorobenzene moiety (-2.78V). This is in agreement with the extent of dehalogenation observed in the LSIMS spectra of the compounds.

REFERENCES
1. P. Kebarle and S. Chowdhury, Chem. Rev. **87**, 513 (1987)
2. G. Paul and P. Kebarle, J. Am. Chem. Soc. **111** 464 (1989)

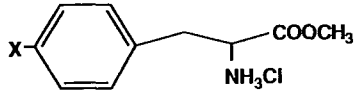

1

2

X= F, Cl, Br, I

TABLE 1 %Dehalogenation values

		4-X-PHENYLALANINE METHYL ESTERS			
MATRIX	ATRAZINE	X=I	Br	Cl	F
GLY	46	50	30	18	9
AET	27	25	20	10	3
THIOGLY	15	17	11	7	0
TDG	16	16	12	6	0
MES	4	NS	NS	NS	NS
HEDS	7	6	0	0	0
HPEA	10	15	6	4	0
DMBA	MI	MI	MI	MI	MI
BOP	11	12	5	3	0
HBSA	0	0	0	0	0
NBA	0	0	0	0	0

NS=not soluble . MI=matrix interference

Sample Charge Compensation on a Large Sample Ion Microprobe

R. T. Short, J. M. McMahon and P. J. Todd
Analytical Chemistry Division
Oak Ridge National Laboratory
Oak Ridge, TN 37831-6365

We have developed a triple quadrupole-based microprobe suitable for secondary ion imaging of biological tissue samples as large as 1 cm diameter. Tissue samples this large, however, are often insulators. Positive charge accumulates on insulating samples, when a positive primary ion beam strikes the surface. Charge compensation is then needed for the analysis of such samples. A charge compensation scheme for large biological samples is necessarily subject to several constraints. The technique must neither damage the sample, nor interfere with secondary ion emission. Spatial resolution cannot be degraded and charge neutralization must be self regulating for variations in sample conductivity across the surface.

One method, which meets these criteria and works well with the large sample microprobe, is described in Figure 1. The secondary ion extraction field is synchronized with a periodic primary Cs^+ beam. A sheet-like beam of 5 eV electrons passes over the sample surface when the extraction field is zeroed. Electrons are attracted to and neutralize any points on the sample which have charged. When the primary ion beam is turned on, the extraction field deflects most electrons away from the sample.

Figure 2 demonstrates the effectiveness of charge compensation on Teflon^R, a well known insulator. Positive secondary ion images were obtained from a 4 mm x 4 mm piece of Teflon^R tape placed on a copper target. The necessity of the periodic extraction field is indicated by the dramatic improvement in secondary ion yield from the Teflon^R in Figure 2c compared to 2b. Figure 3 displays positive secondary ion images obtained from a 50 μm thick slice of dried chicken liver placed on a copper target. The liver sample was spiked with 40 ng of acetylcholine and then analyzed for the acetylcholine secondary ion, *m/z* 146. The location of acetylcholine is easily discernable. This charge compensation technique has worked well with a variety of samples and requires little or no change in operational parameters from sample to sample.

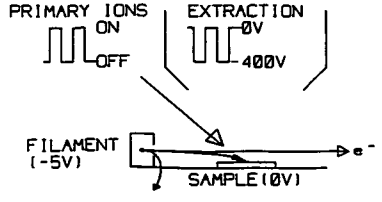

Figure 1. Charge compensation scheme. Electrons strike a charging spot on the sample when the extraction field is zeroed. The primary beam is turned off during charge compensation period (1 ms) to reduce primary ion damage. Data are acquired only during the (3.5 ms) period that the primary beam is turned on. The process is repeated for each spot on the sample to produce an image.

"The submitted manuscript has been authored by a contractor of the U S Government under contract No DE-AC05-84OR21400 Accordingly, the U S Government retains a nonexclusive, royalty-free license to publish or reproduce the published form of this contribution or allow others to do so for U S Government purposes."

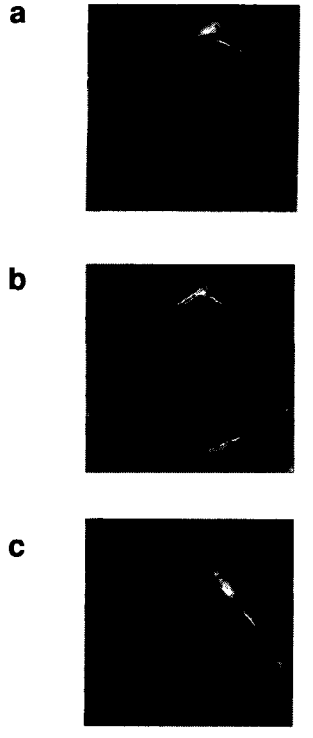

Figure 2. Secondary ion images from Teflon^R a) without charge compensation, b) with electron flood gun only, and c) with electron flood gun and periodic secondary ion extraction field. All images are total ion images and represent an area 5 mm x 5 mm. Gray scale is from least intense (black) to most intense (white).

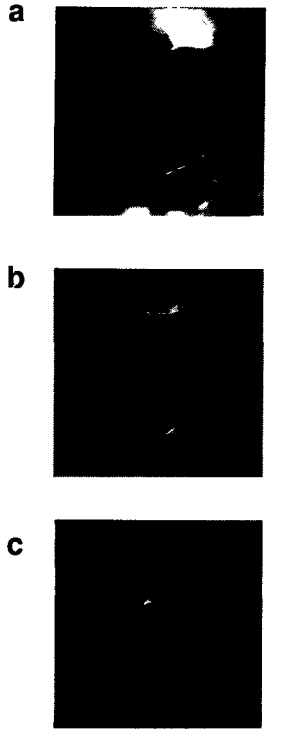

Figure 3. Secondary ion images from dried chicken liver spiked with 40 ng of acetylcholine. a) Total ion image without charge compensation. b) Total ion image with charge compensation. c) Mass resolved image of *m/z* 146, the acetylcholine secondary ion. All images represent a 1 cm x 1 cm area.

This work supported by DOE Office of Basic Energy Sciences under contract DE-AC05-84OR21400 with Martin Marietta Energy Systems, Inc.

Determination of Flux from a Saddle Field Fast Atom Bombardment Gun

Bill Boggess and Kelsey D. Cook, Department of Chemistry, University of Tennessee, Knoxville, TN 37996-1600.

Users of FAB generally list at most the nominal beam energy and "emission current" (load on the FAB gun power supply). Even in LSIMS, it is common to report primary *current* without assessing the beam diameter, thus leaving the *flux* (current/area) undetermined and unreported. The relationship between FAB emission current and particle flux is presumed to be linear, but is not at all well-characterized. Because flux correlates with sensitivity[1] and with the extent of beam-induced damage,[2] it would be useful to have an accurate and simple measure of primary beam flux at the target. Such a measure should improve reproducibility and facilitate interlaboratory comparisons of FAB and LSIMS data. While flux determination using a faraday cup detector with a known entrance aperture is relatively straightforward for primary *ion* beams,[1] a corresponding experiment with the *neutral* primary FAB beam is not possible. This study evaluates the use of the flux-dependent beam-induced reduction of methylene blue[2] as an alternative, indirect measure of flux.

A 15 mM solution of methylene blue (molecular cation, M^+, at m/z 284) in glycerol was exposed to an 8 keV cesium ion beam at various levels of flux (measured using a faraday cup with a 1 mm diameter entrance aperture). The extent of reduction (Fig. 1) was estimated from the excess intensity at $[M+1]^+$ using the enrichment ratio, E, given below:[3]

$$E = \frac{i_m - i_c}{i_c}$$

where i_m is the measured peak intensity for the $[M+1]^+$ ion at m/z 285 and i_c is the corresponding calculated peak intensity based on natural isotopic abundances for M^+. Using the ion at $[M-2]^+$ (m/z 282) as a measure of the peak-at-every-mass background, the estimated signal-to-background ratio exceeds 30; thus, no correction for background[4] was necessary. In a subsequent experiment, E was determined using a FAB gun operating at 8 kV at various emission currents (Fig. 2). During the course of this study, the FAB gun performance deteriorated, requiring higher Xe gas pressure to achieve a given emission current. Electrodes were cleaned, and ultimately replaced. Figure 2 shows data for each set of electrodes. Comparison of Figures 1 and 2 provide an estimate of equivalent flux for each FAB gun operating condition (Table 1). In order to estimate the equivalent particle current emanating from the FAB gun, this flux was multiplied by the area illuminated by the FAB beam, as estimated by viewing the beam-induced luminescence on a flat FAB target coated with CsI. These "currents" are also summarized in Table 1. From Figure 2, it is clear that FAB gun output depended on the condition of the electrodes, even when the emission current and nominal energy indicated on the power supply were constant. The changes are significant in light of the substantial effect of flux on the appearance of FAB spectra.[3] It is obvious that appearance of FAB spectra will depend upon the physical condition of the gun, affecting reproducibility, unless flux is calibrated using a parameter like E.

The decline in FAB gun performance occurs over the matter of months as a result of contamination of the electrodes during use. An investigation into this slow aging process is currently underway.

REFERENCES

1. Todd, P.J. *Org. Mass. Spectrom.* **1988**, 23, 419.
2. *See for example* Pelzer, G.; De Pauw, E.; Dung, D.V.; Marien, J. *J. Phys. Chem.* **1984**, 88, 5065.
3. Reynolds, J.D.; Cook, K.D. *J. Am. Soc. Mass Spectrom.* **1990**, 1, 149.
4. Visentini, J.; Zidarov, D.; Allard, M.; Bertrand, M.J. *J. Am. Soc. Mass Spectrom. in press.*

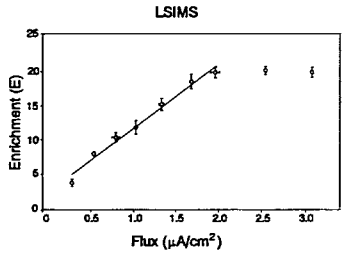

Fig. 1. Enrichment of $[M+1]^+$ of methylene blue *versus* flux from Cs^+ gun. Error bars represent standard deviations of at least 3 samples. Line is least squares fit of first 7 points.

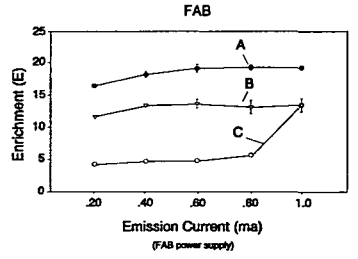

Fig. 2. Enrichment of $[M+1]^+$ of methylene blue *versus* emission current from FAB gun with new (A), cleaned (B), and dirty (C) electrodes. Error bars as in Fig. 1.

Table 1. Important FAB gun parameters with different electrodes

Emission Current (mA)	Dirty, Old Electrodes			Cleaned[d] Electrodes	New Electrodes		
	Flux[a] ($\mu A/cm^2$)	Area[b] (cm^2)	Current[c] (μA)	Flux[a] ($\mu A/cm^2$)	Flux[a] ($\mu A/cm^2$)	Area[b] (cm^2)	Current[c] (μA)
1.00	1.20	0.28	0.34	1.20	≥1.85[e]	0.28	≥0.52[e]
0.80	0.30	0.28	0.084	1.16	≥1.85[e]	0.20	≥0.37[e]
0.60	0.20	0.24	0.048	1.22	≥1.85[e]	0.16	≥0.30[e]
0.40	0.19	0.13	0.025	1.18	1.73	0.11	0.19
0.20	0.14	0.07	0.010	0.98	1.53	0.07	0.11

Notes: [a]Estimated from LSIMS data (Fig. 1) for comparable damage.
[b]Estimated from luminescence area for CsI-coated target exposed to FAB beam.
[c]Current = (Flux) x (Area)
[d]Beam area not available for cleaned, old electrodes.
[e]Lower limit; damage is ~independent of flux above 1.85 $\mu A/cm^2$.

Acknowledgements. This work was supported by NSF (CHE-8822787).

TIME-OF FLIGHT SECONDARY ION MASS SPECTROMETRIC ANALYSIS AND IMAGING OF AVIAN EGG MEMBRANES

C. M. John and R. W. Odom, Charles Evans & Associates
301 Chesapeake Drive, Redwood City, CA 94063

Development of biological applications for surface analysis by time-of-flight secondary ion mass spectrometry (TOF-SIMS) is our goal. The avian egg contains three membranes, inner and outer shell membranes and the yolk membrane These membranes are fibrous, between 20 and 60 μm in diameter and are mainly composed of proteins. A number of minor lipid components of avian egg membranes have been identified.[1] The egg shell membranes are easily prepared in an ordered, intact state for TOF-SIMS.

Positive ion TOF-SIMS analysis and ion imaging of avian egg membranes was performed using a microfocused 25 keV Ga^+ primary ion beam The most abundant ions in the mass spectra were Na^+ and K^+ and various low molecular weight organic fragment ions. Figure 1 presents portions of the positive ion mass spectra of 6 avian egg membranes. Some higher molecular weight ion peaks (> m/z 300), likely fragment and molecular ions from lipids such as cholesterol and cholesterol esters, were also prominent in the spectra Characteristic peaks for cholesterol in positive ion TOF-SIMS spectra have been observed at m/z 369 and 385 The peaks at m/z 413 and 441 are 28 and 56 Da higher than the peak at m/z 385.

Differences were observed in the relative intensities of some of these higher molecular weight ion peaks in spectra from the two sides of an outer shell membrane and the top side of the inner membrane. Spectra of the top side of the outer shell membrane of different birds of the same species and different species were slightly different.

Ion imaging analysis (see Figure 2) revealed topographical features. The Ca^+ and Mg^+ ion images exhibited distinct localization in an outer shell membrane. Organic ion images were obtained from low molecular weight fragment ions. Also, low intensity ion images were obtained of the higher molecular weight peaks such as at m/z 413 and 435, but these images did not reveal localization We are currently working on techniques to increase the secondary ion yield of higher mass molecular ions in TOF-SIMS analysis of biological samples.

1. Burley, R. W and Badehra, D. V The Avian Egg Chemistry and Biology, John Wiley & Sons, New York, NY (1989).

****

NIH support through a Phase I Small Business Innovative Research Grant (#2R44GM47771-02, C. M. John) is gratefully acknowledged

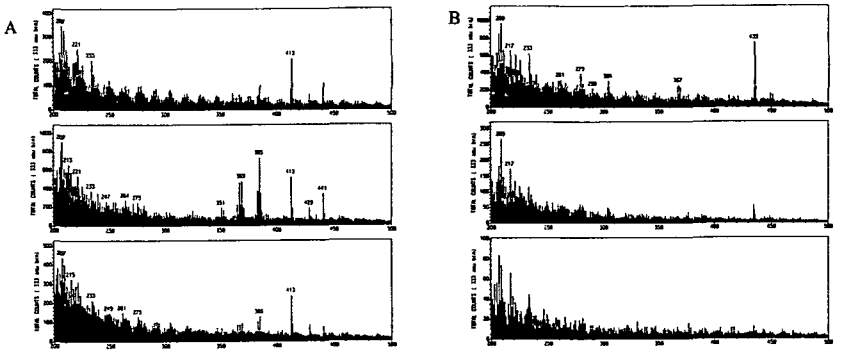

Figure 1 Portions of the positive ion spectra of the egg shell membranes of a chicken are shown in A; the top side of the outer shell membrane (top), the bottom side of the outer membrane (middle), and the top side of the inner membrane (bottom). Spectra from the top side of the outer shell membrane from avian eggs are presented in B, from two different chicken eggs (top and middle), and a quail egg (bottom).

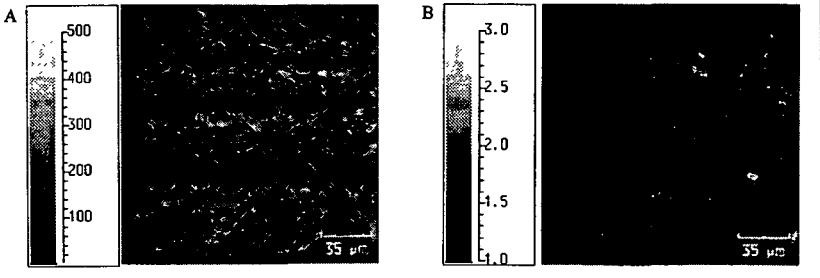

Figure 2 Total ion image (A) and a Ca+ ion image (B) from the top side of the outer shell membrane of a chicken egg are presented.

LIQUID SECONDARY ION MASS SPECTROMETRY OF HYPERVALENT SILICONATES

J. Greaves*, J. H. Small and K. J. Shea. Department of Chemistry, University of California, Irvine, Irvine CA 92717-2025

Introduction

Hypervalent polysiliconates are novel materials that are of interest because of their physical (mechanical and solution), electrical and optical properties. These are due to the dynamic stereochemistry of the silicon, the ion:counterion structure, and the type of organic bridge between the silicon (ionic) components of the compounds. Model building blocks of these ionomeric materials have been synthesized by condensation of catechol with alkoxy silyl derivatives in the presence of triethylamine[1-3]. Penta- and hexacoordinated species with triethyl ammonium counterions have been prepared by this method. Negative ion LSIMS spectra of a related series of compounds - nearly all hexacoordinated compounds with alkali metals as counterions - have been reported[4]. These authors noted rapid interaction between the analytes and glycerol and some interaction with mNBA[5]. The objective of the current study was to use LSIMS to characterise the mass spectrometric behaviour of the model compounds in both positive and negative ion modes and to see if this information would assist in the characterisation of an oligomer whose structure is currently uncertain.

Experimental

The compounds investigated were arylene- (4,4'-biphenylene- [1], 1,4- and 1,3-phenylene- [2,3], and 9,10-anthracylene [4]) and alkylene-bridged (1,2-ethylene- [5], and 1,6-hexylene- [6]) dicatechol siliconates of the form $(C_6H_4O_2)_2SiRSi(C_6H_4O_2)_2^{2-}.\{(C_2H_5)_3NH\}_2^+$ where R = the bridging moiety, and a tricatechol siliconate $(C_6H_4O_2)_3Si^{2-}.\{(C_2H_5)_3NH\}_2^+$ [7]. In all cases the hypervalent silicons are bound with triethylammonium counterions. In addition, an oligomeric compound in which there was assumed to be a spirocatechol:phenyl-silicon triethyl ammonium counterion repeating unit, $\{Si(C_6H_5).(O_2C_6H_2.C_9H_{16}.C_6H_2O_2)\}^-.\{(C_2H_5)_3NH\}^+$ [8], was investigated. The number of repeating units in the structure was uncertain. For compounds 1-6 and 8 the silicon was pentavalent while for compound 7 it was hexavalent. LSIMS was carried out on a Fisons Autospec trisector high resolution mass spectrometer. Cesium ions were used as the bombarding species at either 25 or 35 kV. The cesium ion current was approximately 3 μA. The matrix was mNBA. For accurate mass measurement the matrix was supplemented with 2% polyethylene glycol. For full spectra the instrument was scanned from 2100 - 100 amu (3 second scans) with resolution set at 2000. Accurate mass measurement was performed at 10,000 resolution using voltage scanning over a short mass range.

Results and Discussion

Compounds 1-7. Molecular ions were obtained in both positive and negative ion modes. In the positive spectrum the triethylammonium counterion remained in place and an additional proton was attached to form the charged species. Accurate mass determinations for these ions are given in Table 1. In some cases the positive spectra also showed triethylammonium adduct ions and an ion corresponding to the replacement of a triethylammonium with a proton. In the negative spectrum both triethylammonium groups were lost and replaced with a single proton thus giving a net negative charge. Compounds 5, 6 and 7 also showed a number of interactions with mNBA. Products included a) replacing a catechol with mNBA and b) cleaving the silicon-carbon bond and replacing it with either mNBA or another catechol. NMR studies showed that there were extensive reactions between compounds 5, 6 and 7 and mNBA in solution and, therefore, that the compounds observed in the LSIMS spectra were probably created independently of the ionization process. This does not, however, preclude the possibility that the energy of the cesium ions contributes to these processes in the LSIMS source. The reaction between Compound 7 (with alkali metals as the counterions) and mNBA has been reported previously[5]. These situations do not occur for compounds 1 - 4 which have arylene-bridging.

Compound 8. The positive ion spectrum for Compound 8 showed ions at m/z 1870 and m/z 1768. The major high mass ion in the negative ion spectrum was m/z 1767. The repeating covalently bonded unit has a mass of 441 daltons and triethylammonium is 102 daltons. Assuming that the triethylammonium counterions remain in place in the positive ion mode but are not present in the negative ion mode, as occurred for the other compounds, then the logical structure is a cyclic tetramer with one triethylammonium group and protons as the counterions at the other silicons. Independent confirmation of this structure is currently being sought.

Table 1. Accurate mass values for protonated molecular ions (including two triethylammonium counterions). LSIMS - positive ion mode.

Compound	$[M+H]^+$ calculated	$[M+H]^+$ observed	Δ mmu
1	845.3648	845.3647	0.1
2	769.3337	769.3347	1.0
3	769.3337	769.3320	1.7
4	869.3653	869.3660	0.7
5	721.3340	721.3387	4.7
6	777.3966	777.3930	3.6
7	557.3043	557.3069	2.6

References

1. Shea, K. J., Loy, D. A., Small, J. H. Chemistry of Materials, 4, 255-258 (1992).
2. Shea, K. J., Loy, D. A., Small, J. H. Materials Research Society, Symposium Proceedings, 271, 711 (1992).
3. Loy, D. A., Small, J. H., Shea, K. J. Organometallics, 12, 1484-1488 (1993).
4. Cerveau, G., Chuit, C., Reye, C., Aubagnac, J.-L. Organic Mass Spectrometry, 27, 822-826 (1992).
5. Cerveau, G., Chuit, C., Corriu, R. J. P., Gerbier, L., Reye, C., Aubagnac, J.-L., El Amrani, B. International Journal of Mass Spectrometry and Ion Processes, 82, 259-271 (1988).

Massive Cluster Impact Mass Spectrometry: Source Design and Performance

J.F. Mahoney and E.S. Parilis, Phrasor Scientific, Inc., Duarte CA 91010 USA
T.D. Lee and S. McCullough-Catalano, Beckman Research Institute of the City of Hope, Duarte, CA 91010 USA

Previously we reported on a new method for desorbing large biomolecules that uses a primary beam of massive, multiply charged clusters for sputtering ion from a liquid matrix [1]. A comparison of the MCI spectrum of bovine insulin (Fig. 2) with that of a conventional Xe FAB spectrum (Fig. 1) dramatically illustrates the features of MCI desorption. Abundant ions are observed for the intact insulin molecule (MH^{+1}, MH_2^{+2}, MH_3^{+3}, $M_2H_3^{+3}$) and the B chain fragment (MH^{+1}, MH_2^{+2}). The "chemical noise" background evident in the FAB spectrum is virtually eliminated in the MCI spectrum. Low mass ions in the MCI spectrum are largely the result of debris from the primary cluster beam (obtained by electrohydrodynamic atomization of 1.5M ammonium acetate in glycerol). The proposed mechanism for initiating sputtering events is by shock wave propagation in matrix material subjected to hypervelocity cluster impacts [2]. Cluster which impact liquid matrices with specific energies <5 eV/nucleon (compared to ~75 eV/nucleon for 10 keV Xe atom beams) provide an extremely soft method for sputtering intact biomolecules.

An estimate has been made of the cluster charge-to-mass ratio threshold δ_{tr} for molecular damage. The estimate assumes fragmentation occurs by knocking out target atoms from their positions in the molecule via collions with atoms of the cluster projectile. Spectra for clusters with $\delta > \delta_{tr}$ (Fig. 3) and $\delta < \delta_{tr}$ (Fig. 4) support this model. Different charge to mass ratios were obtained by controlling the flowrate of the glycerol solution. The low flowrate (0.02 µl/min vs. 0.2 µl/min for the high flow rate) favors smaller clusters with higher δ values.

Modifications in the design of the MCI source have resulted in greatly improved performance and more consistent operation. The source is equipped with a focusing lens and an electrostatic deflection system for beam positioning. Depending on the polarity of the applied voltage, primary beams of either positively or negatively charged cluster can be formed. The angle of the sample stage was found to have a significant effect on the strength and character of the spectra. Preliminary studies show that higher desorption yields and more stable operation is achieved using clusters compared to those formed from higher volatility solutions. The primary disadvantage of the MCI mode of operation is that the secondary ion source must be cleaned more frequently (weekly).

Support from the National Institutes of Health (Phase II SBIR grant No. 2R44GM45656-02) is gratefully acknowledged.

[1] J.F. Mahoney, J. Perel, S.A. Ruatta, P.A. Martino, S. Husain, and T.D. Lee, Rapid Comm. Mass Spectrom. 1991, 5, 441-445.
[2] J.F. Mahoney, J. Perel, T.D. Lee, P.A. Martino and P. Williams, J. Am. Soc. Mass Spectrom. 1992, 3, 311.

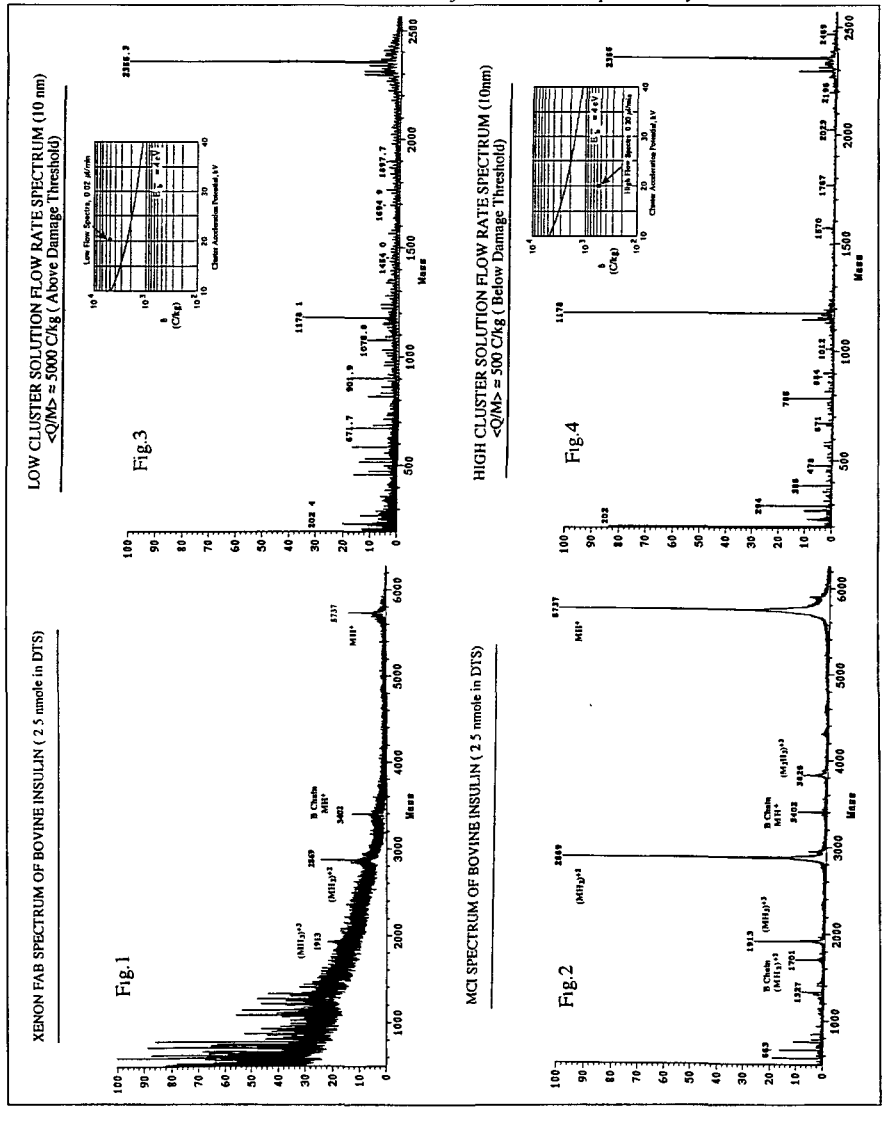

A KINETIC MODEL FOR SENSITIVITY ENHANCEMENT BY SURFACTANT-ANALYTE ION PAIRING IN PARTICLE INDUCED DESORPTION MASS SPECTROMETRY

James G. Pavlovich and Douglas F. Barofsky,
Department of Agricultural Chemistry, Oregon State University,
Corvallis, Oregon 97331

In particle induced desorption-ionization mass spectrometry the strength of an analytes signal under a given set of bombardment conditions is usually considered to be representative of the analyte's relative surface activity. This is the rationale generally used to explain differences in sensitivity between and within various classes of compound under these techniques.

Sensitivity enhancement of ionic analytes in FABMS by ion-pairing with a surface active counterion has been demonstrated by Ligon and Dorn (ref. 1). Previously, we have reported a 10,000 fold increase in sensitivity for adenosine triphosphate using hexadecylpyridinium acetate (HDPAc) in a glycerol matrix. This technique has been utilized in conjunction with a liquid matrix assisted SIMS/time-of-flight instrument to allow detection of femtomole quantities of nucleoside monophosphates (ref. 2). The analyte signal, however, is primarily dependent on the surfactant's bulk concentration (figure 1) and only minimally on that of the analyte. Additionally, the optimum surfactant concentration changes with the analyte concentration indicating that the surface activity of the hexadecylpyridinium ion is not independent of the counterion.

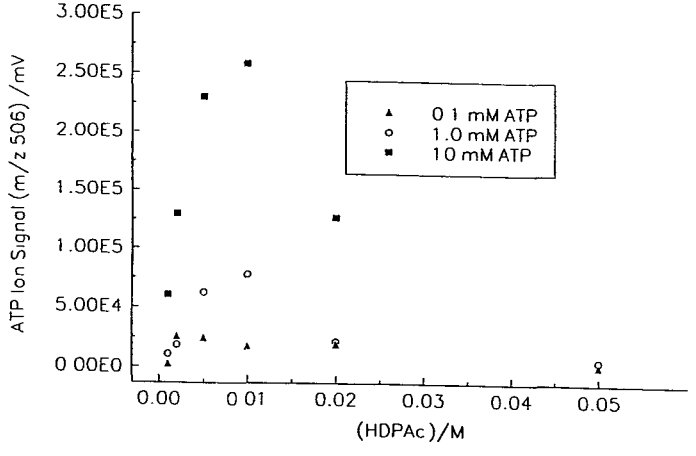

Figure 1. Dependence of ATP ion signal intensity on HDPAc concentration.

We have undertaken to model this phenomenon in terms of conventional solution equilibria and surface chemical principles under the assumption that the initial surface composition and the bulk concentration are the boundary conditions of a steady state established by the competing processes of surface sputtering and surface replenishment from the bulk during analysis.

Fundamentally, the system can be described in terms of two surface active species, the surfactant-

acetate ion pair (HDPAc) and the surfactant-nucleotide ion pair (HDPN), competing for a fixed number of surface sites. The bulk-surface equilibrium for each species is described in terms of a Langmuir type isotherm. In addition, the finite dissociation of each ion pair must be taken into account. The relative stability constants are estimated here from the relative selectivity for each anion on a strong basic anion exchanger. Since the nucleotide is introduced into solution as the free acid, the acid-base equilibrium is also taken into account. Acidity constants in glycerol are estimated based on data reported by Caprioli (ref.3). Equilibrium calculations were carried out using a program called MICROQL (ref. 4).

Figure 2 illustrates the comparison of the MICROQL calculations with the mass spectral data for the dGMP/HDPAc system. Good agreement is seen for the relative abundances of the $(M-H)^-$ ion of dGMP and the calculated surface concentrations of the surfactant-nucleotide ion pair at concentrations below the optimum. At higher concentrations the observed signal decreases faster than expected from the calculations.

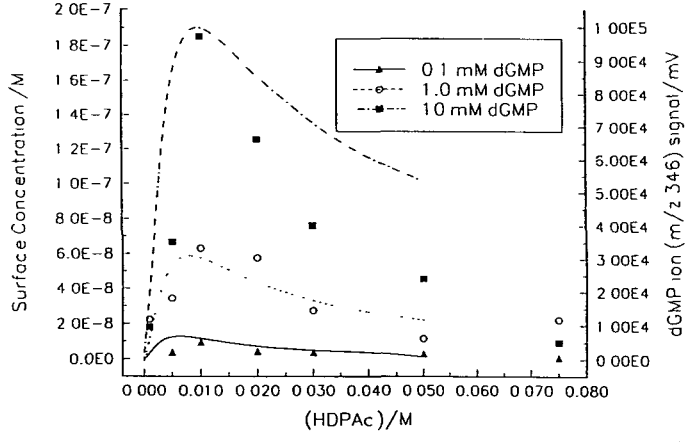

Figure 2. Calculated nucleotide surface activity and relative dGMP ion signal intensity.

References:

1. W. V. Ligon and S. B. Dorn, (1986) *Fresenius Z. Anal. Chem.* **325**, 626-627.
2. J. G. Pavlovich, T. Y. Yen, D. F. Barofsky, J. Kopniczky and B. U. R Sundqvist, In "Proceedings of the 40th ASMS Conference on Mass Spectrometry and Allied Topics," Washington, D.C. June 1-5, 1992.
3. R. M. Caprioli, (1983) *Anal. Chem.* **55**, 2387-2391.
4. J. C. Westall, Department of Chemistry, Oregon State University, Corvallis, Oregon 97331.

Acknowledgement:

This work was supported by US DOE grant DE-FG06-88ER60690

TOF-SIMS STUDIES OF ION FORMATION AND FRAGMENTATION MECHANISMS IN POLYGLYCOLS

Lucinda R. Hittle, Paul A. Zimmerman and David M. Hercules
Department of Chemistry, University of Pittsburgh, Pittsburgh, PA 15260

Ion formation in SIMS typically follows two mechanisms: 1)Simple desorption of cationized oligomers or 2)Desorption of large polymer fragments cationized with a substrate ion (usually Ag). When the second mechanism occurs, it is not clear whether the Ag^+ is attached to the polymer fragment prior to sputtering, or if cation attachment occurs in the gas phase en route to the analyzer. Oligomers may also be cationized with ions from dopant salts such as NaCl, but only oligomers up to ~3000 Da have been detected using this sample preparation. In this study, both mechanisms of ion formation were observed, and the interrelation of polymer molecular weight and cations present to the extent of fragmentation was examined.

The instrument used in these studies was the TOF-SIMS III (Ion-Tof, GmbH, Munster, FRG). The samples were prepared by casting thin films on etched silver, or zinc. A series of poly(ethylene glycol) (PEG) and poly(propylene glycol) (PPG) polymers ranging in molecular weights from 450-100,000 Da were examined.

Fragmentation in Polyglycols

In general, it is possible to detect oligomers from polyglycols with molecular weights up to *ca.* 5000 Da. Main chain fragments in the mass range from 500-3000 Da are observed for samples with molecular weights above 5000 Da. For high molecular weight samples, the primary mode of fragment ion formation involves cleavage of the C-O bond between repeat units to yield fragments corresponding to the formula R_n. Some possible fragmentation modes are shown in Scheme 1. Path A indicates cleavage of the C-O bond within the repeat unit, which would produce 2 fragments, $R_n + \Delta$ and $R_n + 2\Delta$, where Δ corresponds to either an oxygen or CH_2 group. Fragmentation at the C-C bond within the repeat unit (shown in Path B) will also produce $R_n + \Delta$ and $R_n + 2\Delta$ fragments. Similar fragmentation mechanisms may be proposed for the PPGs, including scission of a pendant methyl group to produce $R_n + 3\Delta$ fragments.

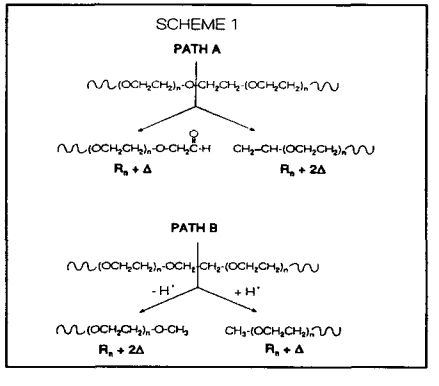

The fragmentation pattern for PPG is shown in Figure 1. Each cluster within the fragmentation patterns contains several peaks, due in part to contribution from the 2 Ag isotopes. The relative intensities of the major fragment clusters were calculated for PEGs and PPGs with a range of molecular weights to determine if the fragmentation pattern will change as a function of polymer size. In general, the relative intensities within the fragmentation patterns of the PEGs were the same regardless of molecular weight.

However, the relative intensities of the fragments resulting from cleavage within the PPG repeat unit (such as $R_n + 3\Delta$) increased with increasing PPG molecular weight. The contribution of pendant groups within the polymer repeat unit must play an important role in fragmentation of high molecular weight polymers.

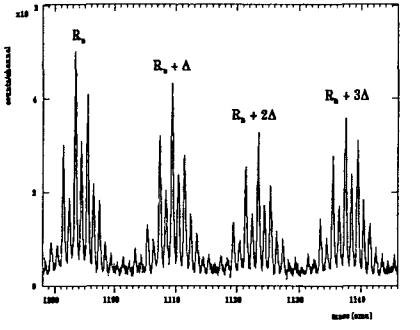

Figure 1. Fragmentation Pattern for PPG

Cationization Effects

Typical TOF-SIMS sample preparation involves casting the polymer film onto a silver substrate which cationizes the polymer samples. Another possible sample preparation method is to add dopant salts to the polymer on an inert metal substrate (e.g. Zn). Both alkali metal salts (Li, Na, K, Cs) and transition metal salts (Fe, Co, Mn, Cu) were examined to determine the optimal method of sample preparation. Directly mixing the polymer with the salt solution provided the best results, using a large excess of the salt in solution. In general, the highest yield of both fragments and oligomers was found for the silver cationized samples. No cationization of polymer species was observed for the other transition metal salts. Since all of the transition metals studied were in the M^{2+} state, the polymer may not be able to stabilize the +2 charge. It may be possible to see cationization with these metals in the M^+ state, similar to what was observed in laser desorption studies.[1-2]

The fragmentation patterns of PEG and PPG samples mixed with alkali metal salts were examined, and in general, the same patterns, containing the clusters R_n, $R_n + \Delta$, etc., were observed. The patterns from the alkali metal (Na^+ or Li^+) are simpler than those from Ag^+ due to the single isotopic contribution of the metal. Comparison of the spectra from several salts may make exact determination of fragments possible. For example, the $R_n + 2\Delta$ cluster may be assigned the formula $H\text{-}R_n\text{-}CH{=}CH_2$ (R_n + 28 Da) rather than $H\text{-}R_n\text{-}OCH_3$ (R_n + 31 Da). Although the choice of appropriate cation will affect the fragmentation pattern observed in the plasma desorption mass spectra[3], no effects on the SIMS fragmentation patterns were observed for different cations. The cations may be attaching to the polymer during the energy transfer from the primary ion impact, rather than in the gas phase, as is observed in PDMS.

Acknowledgement
This work was supported by the National Science Foundation (Grant #CHE-9022135).

References

1. Llenes, C.F.; O'Malley, R.M. *Rapid Comm. Mass Spectrom.* 6(9) 564-570, 1992.
2. Kahr, M.S.; Wilkins, C.L. *Proceedings of the 40th Conference on Mass Spectrometry and Allied Topics*, Washington, D.C., ASMS, East Lansing, 1992.
3. Chait, B.T.; Shpungin, J.; Field, F.H. *Int. J. Mass Spec. Ion Proc.* **58**, 121-137, 1984.

Secondary Ion Mass Spectrometry Depth Profiling of Ti-Implanted AlInAs and InP at Room and at Elevated Temperatures

* P. H. Chi[1], D. S. Simons[1], R. K. Nadella[2], J. Vellanki[2], and M. V. Rao[2]
[1]Surface and Microanalysis Science Division
National Institute of Standards and Technology
Gaithersburg, MD 20899
[2]Department of Electrical and Computer Engineering
George Mason University
Fairfax, VA 22030

There has been considerable interest in the study of ion-implanted InP and AlInAs in recent years due to their potential applications in the fields of microwave, opto-electronic, and high speed microelectronic devices. Ion implantation is preferred over other techniques (MBE, CVD) for introducing a selected dopant at a specific depth with precise control of the implant concentration. Post-implantation treatment is needed to activate the implant and to reduce the radiation damage caused by the implantation[1]. However, the annealing can also lead to the redistribution of the implant in these materials that may hamper the intended applications[2]. In this study, we prepared InP and AlInAs by Ti implantation at room temperature, and at a temperature of 200^0 C. The samples were implanted at energies from 200 keV to 3 MeV with fluences up to 6 x10^{14} atoms/cm^2. These materials were cleaved and then subjected to rapid thermal annealing (RTA) at 825^{0}C, 850^{0}C, 875^{0}C or 900^{0}C. Secondary ion mass spectrometry (SIMS) was used to profile the Ti implant to check whether the Ti in these materials was redistributed after annealing.

Depth profiles of Ti-implanted AlInAs and InP were obtained with a secondary ion microscope using a focused and rastered oxygen primary ion beam. Secondary ions $^{48}Ti^+$ and the matrix signals $^{31}P^+$ (InP) and $^{75}As^+$ (AlInAs) were collected from a circular area 60 µm in diameter that was located at the center of the square raster. For the depth profile of Ti-implanted InP, a 50 V bias was applied to the sample to discriminate the interference at mass 48 from the molecular ion POH^+.

Figure 1 shows the overlay of Ti profiles for the 200 keV/2x10^{13} cm^{-2} room temperature Ti-implanted AlInAs, as-implanted and annealed at 850^{0}C and 900^{0}C. The two high temperature annealed samples show slightly redistributed Ti. There is no major difference between the two annealed samples. The overlaid profiles for the 200 keV/2x10^{13} cm^{-2} Ti implanted at 200^{0}C before and after annealing at 850^{0}C and 900^{0}C are plotted in Figure 2. As shown in this figure, the Ti profiles are similar to the Ti profiles in Figure 1 (room temperature implant) which shows slight in- and out-diffusion after annealing. The elevated temperature implantation at 200^{0}C did not have any significant effect on the redistribution of the Ti.

Figure 3 shows the overlay of plots for the 1 MeV/3 x10^{13} atoms/cm^2 room temperature Ti-implanted InP, as-implanted and then annealed at 825^0 and 875^{0}C. The Ti profiles are similar in all three samples, indicating that the Ti does not redistribute under these annealing conditions.

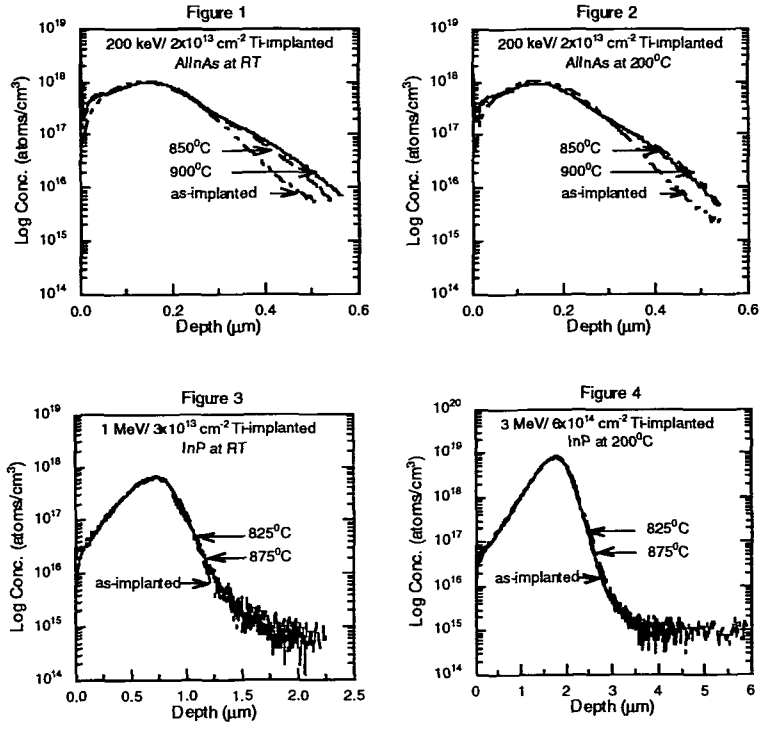

Figure 4 shows the Ti profiles for the 3 MeV/6x10^{14} cm^{-2} Ti-implanted InP at 200^{0}C before and after annealing at 825^{0}C and 875^{0}C. The three Ti profiles are similar, as seen in the room temperature implanted samples, which indicates that the Ti is thermally stable in InP under these annealing conditions.

In summary, SIMS results indicate that Ti-implanted InP is thermally stable but Ti-implanted AlInAs shows a small amount of redistribution under high temperature annealing.

REFERENCES

1- T. O. Sedgwick, J. Electrochem. Soc, **130**, 484 (1983)

2- J. M. Martin, R. Nadella, R. Mulpuri, D. S. Simons, P. H. Chi, and C. Caneau, J. of Electronic Materials, in press.

Measurement of Secondary Emission from Various Materials

*Stephen A. Ruatta, Julius Perel, and John F. Mahoney, Phrasor Scientific, Inc., Duarte, CA 91010

Positive ion detection in mass spectrometry is often achieved by the use of ion/electron multipliers. These devices rely on the ejection of secondary electrons and/or ions upon the impact of the ion of interest on the detector surface. Secondary electron emission results mainly from one of two processes: Kinetic emission or Potential emission. For analysis and detection of very large and thus relatively slow-moving positive ions, the contribution from the kinetic processes to electron and ion emission will be small at energies below about 1eV/amu. Investigation of methods for increasing the potential emission contribution is continuing in our laboratory.

Our interest is in producing surfaces for high mass detection utilizing low work function surfaces to increase the potential electron emission contribution to the total secondary emission. We have also compared the effects of different materials on the kinetic emission and sputtering processes.

In order to compare the total secondary emission contribution from different materials, we have constructed an experiment that allows us to measure the total emission for 3 samples sequentially in situ. Three different samples are held in an insulating holder that can be moved from outside the chamber. The sample is the back surface of a Faraday cup and is isolated from the inner walls of the cup.

A schematic diagram of the potential emission apparatus is shown in Figure 1. Krypton ions (Kr pressure = 5×10^{-5} Torr) are produced by low energy electron impact and accelerated and focussed into the detector

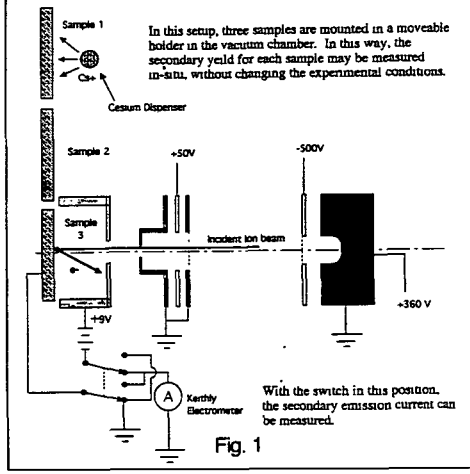

Fig. 1

The Kr^+ ion energy is about 160eV ± 30eV (FWHM) as determined by retarding potential analysis. The walls of the Faraday cup are biased positively to attract the negative secondary electrons and ions.

The kinetic emission experimental setup is shown in Figure 2 below. A cesium ion beam is used at different energies as the incident ion.

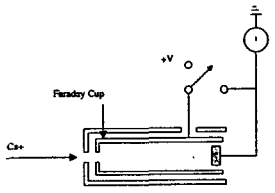

Fig. 2

Secondary electron yeilds can be predicted by Kishinevsky's equation:

$\gamma \approx (0.2/\varepsilon_F)(0.8E_i - 2\varphi)$

and selected results are shown in the Table below:

Material	ε_{Fermi}(eV)	φ[clean surface work function (eV)]	γ (predict)	γ (exp)
Mo	9.28	4.6	.043	.06
Ni	7.39	5.15	.024	.07
Al	11.66	4.28	.045	.06
Mg	7.11	3.66	.109	.06
Li	4.72	2.4	.271	----
W	9.20	4.55	.046	.06
Fe	11.18	4.7	.032	.06 (ss-304)
W/Cs^+	?	?	?	.08

There is no correlation between the expected and observed results. This points to at least 3 possibilities:

1) Experimental Malfunction (unlikely(?)):
   A) MacSimion trajectories indicate that some fraction of secondary electrons can escape the Faraday cup. On the other hand, relative differences between samples should still be observed.
   B) Dosing samples with cesium improves the secondary yield slightly, but only for a short time.
   C) The observed values are in the correct range.
2) Oxide formation at the surface (likely)
   A) Work functions and Fermi energies for oxides needed.
3) Surface dependent adsorbate coverage (likely):
   A) Chamber pressure is 5×10^{-5} Torr

Improvement of kinetic emission by a factor of 3x is easily produced by coating with a material such as NaI or CsI compared to stainless steel, magnesium, PbO glass, AlLi alloys or silicon. The increase should be due to the increased availability of an easily sputterable anion such as I^-.

Work along this line will continue. We need to:
1) Ensure collection of all secondary particles.
2) Operate at lower pressures to minimize adsorption.
3) Continue to try different materials.

Assuming our current setup is operating correctly, it certainly appears that the base material is independent of the actual surface at which the Auger neutralization occurs. In this case, it may be of more use to increase the kinetic contribution.

CHARACTERIZATION OF FINGERPRINT RESIDUES ON SURFACES USING NEUTRAL-BEAM SECONDARY ION MASS SPECTROMETRY (SIMS)

Bryan L. Bentz
David Sarnoff Research Center, CN 5300, Princeton, NJ 08543-5300

To many workers in the fields of spectroscopy and thin film preparation, a human fingerprint inadvertently placed on critical surfaces is a nuisance; it can result in unwanted spectral background, marred optical surfaces, and an inhibition of the condensation of metallic films prepared by vacuum deposition. In our surface analysis laboratory, we have often encountered fingerprint residue on samples submitted for characterization, deposited there accidentally by the submitter through less than careful handling. We became interested in studying fingerprints in their own right, and we have developed a method using static, neutral-beam SIMS for the sensitive detection and identification of trace organic materials that can be found in latent fingerprints. The experiments were conducted using the Sarnoff-developed triple stage quadrupole static SIMS instrument which incorporates a pA level, 3 keV neutral Xe primary beam. Static SIMS spectra in the positive ion and negative ion mode were obtained.

When a human finger touches a surface a sweat deposit - the fingerprint - remains on the surface. The deposited film generally consists of a mixture of natural secretions from eccrine and sebaceous glands in the body. Water, inorganic salts, fatty acids, amino acids, and glycerides are common components of natural fingerprints. In addition, foreign substance contamination picked up on the skin from the environment may be present in the fingerprint. Figure 1 highlights some physical observations concerning fingerprint analysis by our SIMS technique. The quantity of material in a fingerprint is extremely small (low to sub-μg) and it is dispersed over a large area. In view of this form of sample presentation, the response characteristic of our instrument to sub-, mono-, and multimolecular sample layers of a test substance (methylene blue) on silver was investigated. As shown in Fig. 2, quantitative detection of substances at trace levels on solid surfaces appears possible.

We find that the surface-sensitive nature of static SIMS can identify differences in surface composition that are characteristic of a fingerprint. Several metals (Ag, Al, SS) and polymers (PTFE, PP, PE) were studied as collection substrates for fingerprint deposition. Of these, acid-etched silver foil was found to be the most analytically useful for SIMS. Surface energy and wetting were found to play a role in fingerprint adsorption on the substrates.

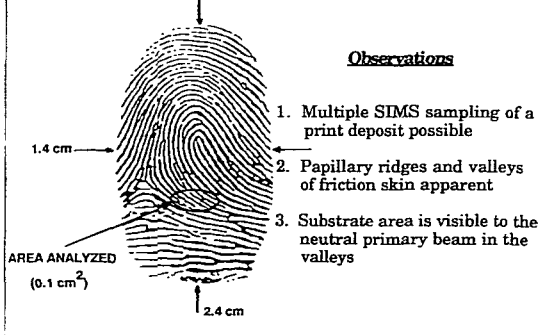

Figure 1

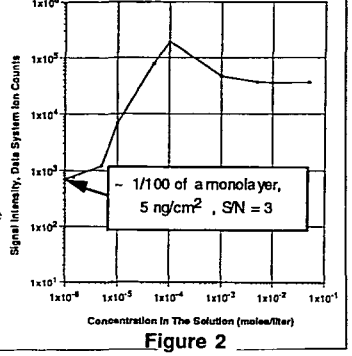

Figure 2

An example of the detection by SIMS of residue from an uncontrolled fingerprint on a silver substrate is presented in Fig. 3. The SIMS method developed can identify the minute amount of chemical constituents present in the deposit. Silicones were found to be a foreign substance contamination in many fingerprints. Additionally, it was observed that deposits from methanol-cleaned fingers and from sweat-rich fingers differed markedly in the amount and type of material (compare spectra of Fig. 4). Solvent cleansing produces dry friction skin and little material is contained in the fingerprint.

A survey analysis of fingerprints from a diverse population of donor individuals was undertaken, including prints from a chef, a machinist, a secretary, a reprographics worker, a plating engineer, and a lab scientist. Interestingly, differences in the amount and identity of foreign substance contamination on the fingers could be observed by SIMS. The contamination detected included species such as aliphatic hydrocarbons, fatty acids, silicones, inorganic salts, and handlotion. Acid-etched silver served as the deposition substrate for these experiments.

In other work, we find that deliberate substance contamination on the finger at the hundreds of nanogram level and greater can be detected in fingerprint residue deposited on a solid surface. Compounds examined for these tests included phenyltoloxamine and 5-methyltryptamine hydrochloride.

The test results of the exploratory studies described here suggest that our static Organic SIMS method has potential for trace substance detection in the fields of forensic science and criminology.

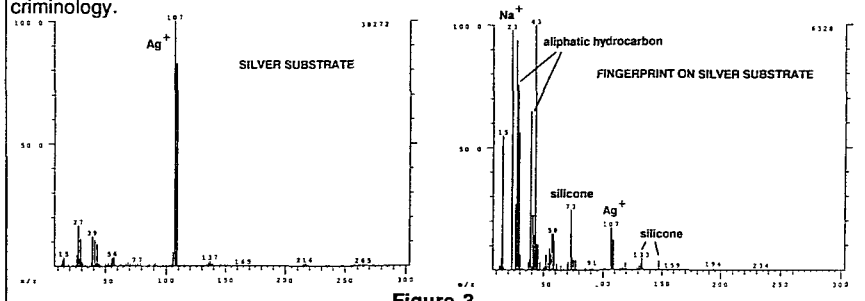

Figure 3

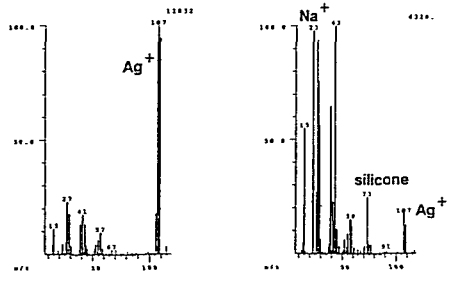

Residue from solvent-cleaned finger

Residue from uncontrolled finger

Figure 4

CORRELATION BETWEEN INITIAL RADIAL KINETIC ENERGIES AND CHEMICAL COMPOSITION OF SECONDARY IONS SPUTTERED ELECTRONICALLY FROM ORGANIC SOLIDS

***P.Demirev, R.Papaléo, H.-F.Kammer, B.Karlsson, G. Brinkmalm, D.Fenyö, J.Eriksson, P.Håkansson, C.Reimann, R. Zoubarev, B.U.R.Sundqvist, Dept. Rad. Sciences, Uppsala University, Box 535, Uppsala, 75121 SWEDEN**

When swift MeV atomic ions interact with organic solids, material is sputtered from the solid. That phenomenon, termed electronic sputtering [1], finds application in mass spectrometry of non-volatile compounds, and is known as plasma desorption. Studies of the properties of ions, ejected as a result of the MeV ion - solid interaction, allow clarification of the mechanisms of the electronic sputtering phenomenon. Systematic investigations of the initial radial energy of low mass positive and negative secondary ions (from 1 to 150 m/z), sputtered electronically from thin industrial polymer films (polyvinylidene difluoride - PVDF, and polystyrene - PS) are reported in this paper. The Uppsala Tandem accelerator provides 72.3 MeV I^{13+} heavy ions for target bombardment at 45° incidence angle. The use of a high resolution time-of-flight mass spectrometer allows separation of peaks, corresponding to ions with same integer m/z (Fig.1). Accurate mass measurements provide unequivocal determination of the chemical composition for different ions.

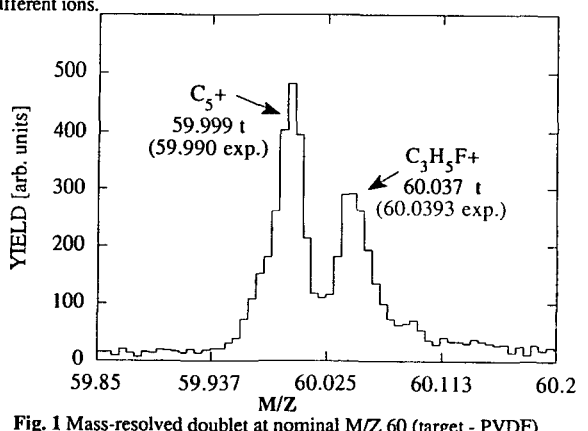

Fig. 1 Mass-resolved doublet at nominal M/Z 60 (target - PVDF).

The low mass ions form homologous series, C_nH_m and $C_nH_mF_p$. The secondary ion yield has been measured as a function of the voltage applied to a set of deflection plates parallel to the ion optical axis. The technique for extraction of the the *initial mean radial velocity* (<v>) *and mean radial kinetic* energy (~<v^2>, connected to the FWHM of the distribution) from the yield versus voltage distribution and the parameters of the experimental set-up has already been described [2]. A plot of <v> and <v^2> as a function of the positive secondary ion m/z results in "oscillating" behaviour due to a systematic repeat pattern (Fig. 2). This pattern is related to the chemical constitution homology of the ions, with 12 as a repeat unit. The degree of hydrogenation for different positive ion series is correlated to their initial mean radial velocity distributions: ions with lower hydrogen content exhibit wider velocity distributions (i.e. higher <v^2>), and they also have <v> directed towards the direction of the primary ion. In its turn ions with higher hydrogen content have lower mean kinetic energies and <v> directed away from the direction of the incident ions. The positive ions from the two targets exhibit somewhat different behaviour: while for

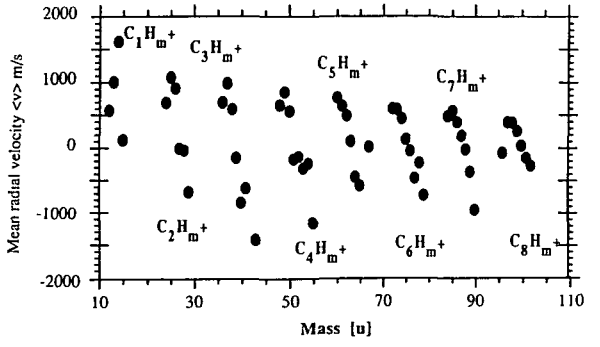

Fig.2 Mean radial velocities for the $C_nH_m^+$ ion series from PVDF.

ions from PVDF there is a dependence of both <v> and <v^2> on the m/z, ions ejected from PS have roughly the same <v^2>, but <v> shows the "oscillating" pattern (with absolute values roughly twice lower than those for the corresponding ions from PVDF). In contrast the negative C_nH_m ions from both PVDF and PS have <v> and <v^2> which does not depend on m/z (Fig. 3).

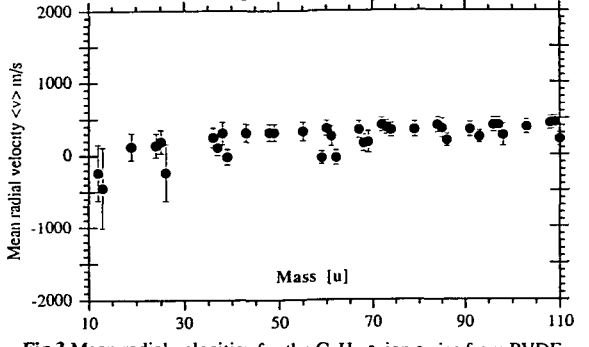

Fig.3 Mean radial velocities for the $C_nH_m^-$ ion series from PVDF.

We argue that these specific properties of the carbonaceous ions ejected in an MeV ion impact provide explicit information for e.g. the spatio-temporal evolution of the deposited energy density after the "big bang" event. The <v> and <v^2> behavior for the ejected positive ions reflects the local temperature (energy density) during the ion formation process thus supplying a specific example of subnanosecond chemistry on an Ångström scale in the MeV ion track. Our results bear also implications on the mechanism of ion ejection, caused by a hydrodynamic type pressure pulse (shock wave), propagating radially from the MeV ion infratrack [1].

[1] R.E. Johnson and B.U.R. Sundqvist, *Phys. Today*, **March** (1992) 28.
[2] G. Brinkmalm, P. Demirev, D. Fenyö, P. Håkansson, J. Kopniczky, B.U.R. Sundqvist *Phys. Rev.* **B47** (1993), 7560.

COMPARISON OF PLASMA DESORPTION- AND THERMOSPRAY-MASS SPECTRA OF MERCAPTURIC ACIDS

*E. Pittenauer, M. Zollinger[1], E. R Schmid and G. Allmaier

Institute for Analytical Chemistry, University of Vienna, Währinger Straße 38, A-1090 Vienna, Austria
[1]Sandoz Pharma Ltd , CH-4002 Basel, Switzerland,
present address Brain Research Institute, University of Zürich, August Forel-Straße 1, CH-8029 Zurich, Switzerland

Detoxification of a wide variety of xenobiotics by conjugation with the tripeptide glutathione (= γ-Glu-Cys-Gly) represents an important metabolic pathway in liver. Hydrolysis of these S-conjugated tripeptides and subsequent N-acetylation of the remaining S-modified cysteines leads to the well known mercapturic acids (= N-acetylcysteine conjugates, S-substituted desaminoglycylcysteine dipeptides) The mass spectrometric characterization of such compounds by different desorption/ionization-techniques like EI, CI, FD, FAB and TS, as well as tandem mass spectrometry, has been subject of several papers. Recently, we could demonstrate the usefulness of positive- and negative-ion PD-MS for the analysis of nine synthetic, structurally simple mercapturic acids (1) In both ionization modes abundant $[M+H]^+$ and $[M-H]^-$ ions, respectively, and significant structurally diagnostic fragmentation of the desamino dipeptide backbone as well as cleavage around the sulfur atom in the side chain are observed. For assignment of these fragment ions we used a slightly modified nomenclature (1) from the one suggested by *Deterding et al.* (2) These spectra obtained by PD coupled to a time-of-flight instrument were compared with those obtained by TS using a triple-quadrupole instrument. In contrast to PD-mass spectra, positive- and negative-ion TS-mass spectra exhibit intense $[M+H]^+$ and $[M-H]^-$ ions, respectively, but little fragmentation in most cases indicating that PD-generated and TS-generated molecular ions contain different internal energies. Interestingly, low-energy CID-spectra (TS-MS/MS) obtained from protonated and deprotonated quasimolecular ions show close resemblance in their product ion patterns to the fragmentation observed in PD-mass spectra Fragmentation of peptides in positive-ion PD-MS was recently compared to fragmentation observed in their corresponding high-energy CID-spectra (3). In the case of the compounds investigated low-energy CID yields comparable product ion patterns as observed in fission fragment-induced decomposition of the molecular ions except that under low energy CID-conditions -C(R)H-C(R)H- bonds where R = -H, -alkyl or a heteroatom do not break apart easily. Finally, for evaluation of suppression effects due to potential competition during the desorption/ionization process of these compounds, an equimolar mixture of eight synthetic mercapturic acids was investigated by positive- and negative-ion PD-MS as well as positive- and negative-ion TS-MS.

References:

(1) E. Pittenauer, A. Pachinger, G. Allmaier and E R. Schmid, Org Mass Spectrom. 26, 1065 (1991)
(2) L. J. Deterding, P. Srinivas, N A. Mahmood, L T. Burka and K. B Tomer, Anal Biochem 183, 94 (1989)
(3) H. Vorst, M W E. M. van Tilborg, P A van Veelen, U R Tjaden and J van der Greef, Rapid Commun. Mass Spectrom. 4, 202 (1990)

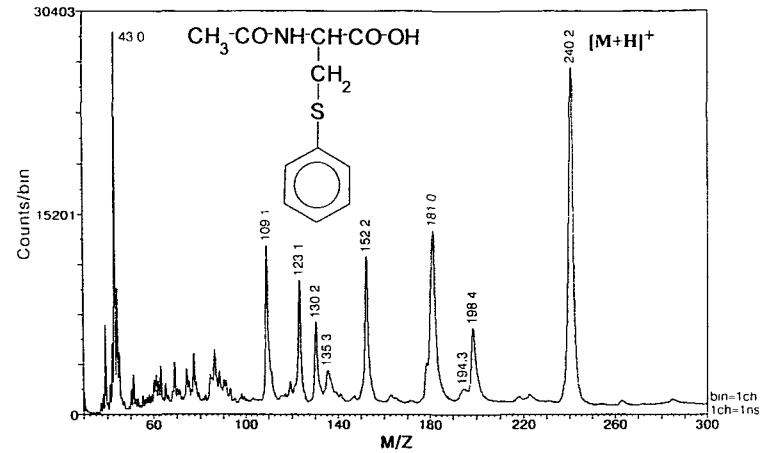

Figure 1: Positive-ion PD-mass spectrum of phenyl mercapturic acid (MWt. 239.06, monoisotopic) electrospray-deposited onto an aluminized polyester backing

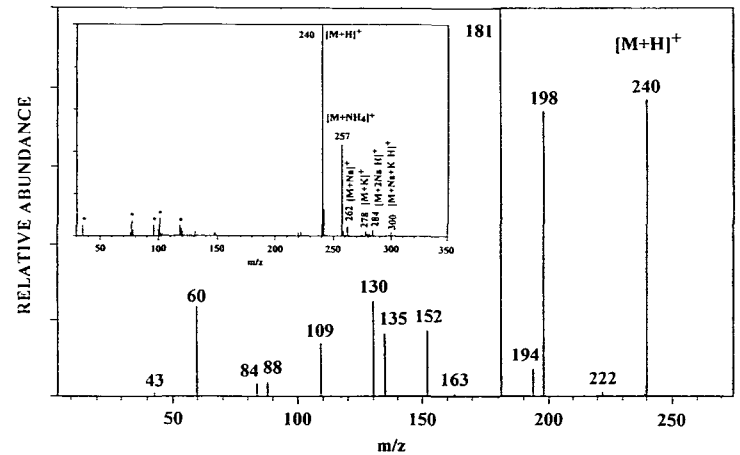

Figure 2: Low-energy CID-spectrum (E_{lab} = 20 eV, 1 06 x 10^{-3} mbar Ar) of the $[M+H]^+$-ion (m/z 240) of phenyl mercapturic acid. The inset shows the corresponding positive-ion TS-mass spectrum (ions labelled with an asterisk are due to contaminants)

Applications of PD-MS in the Analysis of the Genetics of Quaternary Ammonium Compound Accumulation in Plants.

*C.C. Bonham[1], K.V. Wood[2], J.C. Rhodes[1], W.-J. Yang[3], A.J. Wood[3], Y. Samaras[3] and D. Rhodes[3]. Depts. of Biochemistry[1], Chemistry[2], and Horticulture[3], Purdue University, West Lafayette, IN 47907.

A sensitive and selective method for the determination of glycinebetaine and choline is described. The method employs stable isotope dilution plasma desorption mass spectrometry in which a ^{252}Cf ionizing source produces fission fragments which interact with the sample (applied in methanol to a nitrocellulose coated aluminized-Mylar foil) to produce ions which are then mass analyzed by a time-of-flight mass spectrometer. Glycinebetaine is detected as the protonated molecular ion, $(M+H)^+$=118, and the internal standard, $^2H_9$-Glycinebetaine $(M+H)^+$=127 (Fig.1). Choline is detected as the molecular cation, M^+=104 and $^2H_9$-choline (M^+=113) serves as the internal standard (Fig.2). Glycinebetaine is quantified from the ratio of ion intensities at m/z 118 : 127, and choline from the ratio of ion intensities at m/z 104 : 113. The method is applied to the quantification of choline and glycinebetaine pools in two F_6-populations of ***Zea mays* L.** (maize) differing for alleles of a single locus conferring the presence or absence of glycinebetaine. The deficiency gene appears to confer a lesion in choline oxidation (X) to betaine aldehyde in the glycinebetaine biosynthetic pathway (Lerma et al., 1991).

$$(CH_3)_3N^+CH_2CH_2OH \xrightarrow{X,\ CMO} (CH_3)_3N^+CH_2CHO \xrightarrow{BADH} (CH_3)_3N^+CH_2COO^-$$

Choline — **Betaine aldehyde** — **Glycinebetaine**

CMO=Choline monooxygenase ***BADH=Betaine aldehyde dehydrogenase***

Glycinebetaine deficiency in maize is shown to result in a small (<2-fold) but statistically significant expansion of the free choline pool. Choline must down-regulate its own synthesis to prevent a large expansion of the free choline pool in salinized glycinebetaine-deficient plants (Lerma et al. 1991, Weretilnyk and Summers 1992). The results presented here demonstrate the utility of PD-MS in the routine quantification of glycinebetaine and choline in plant extracts.

References

Lerma, C., Rich, P.J., Ju, G.C., Yang, W.-J., Hanson, A.D., and Rhodes, D. (1991). Betaine deficiency in maize: complemen tation tests and metabolic basis. ***Plant Physiology*** **95**, 1113-9.

Weretilnyk, E.A., and Summers, P.S. (1992). Betaine and choline metabolism in higher plants. In 'Biosynthesis and Molecular Regulation of Amino Acids in Plants'. (Eds. B.K. Singh, H.E. Flores, and J.C. Shannon) pp. 89-97.(ASPP Press: Rockville,MD)

FIGURE 1. TYPICAL SPECTRA OF THE BETAINE FRACTIONS FROM THE GLYCINEBETAINE-DEFICIENT F_6-FAMILY (1A) AND THE GLYCINEBETAINE-CONTAINING F_6-FAMILY (1B).

1A) M/Z 127 CORRESPONDS TO THE PROTONATED MOLECULAR CATION OF THE INTERNAL STANDARD $^2H_9$-GLYCINEBETAINE.

1B) M/Z 118 CORRESPONDS TO THE PROTONATED MOLECULAR CATION OF $^2H_0$-GLYCINEBETAINE.

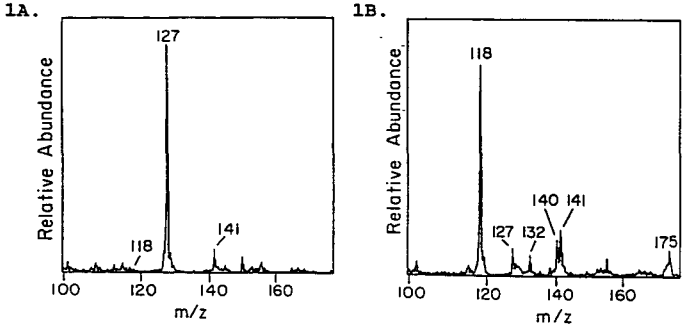

FIGURE 2. CHOLINE FRACTIONS TAKEN FROM THE SAME PLANTS OF EACH FAMILY AS IN FIGURE 1.

2A,B) M/Z 104 CORRESPONDS TO THE MOLECULAR CATION OF $^2H_0$-CHOLINE AND M/Z 113 THE MOLECULAR CATION OF $^2H_9$-CHOLINE (INTERNAL STANDARD).

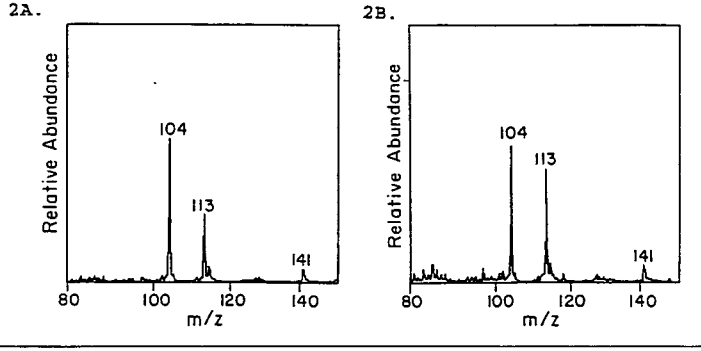

THE CHARACTERIZATION OF TRI-NICKEL CLUSTER COMPOUNDS USING ^{252}Cf PLASMA DESORPTION AND FAB MASS SPECTROMETRY

**A.P. Rothwell, C.C. Bonham, K.V. Wood, D.A. Morgenstern and C.P. Kubiak, Campus-Wide Mass spectrometry Center, Department of Chemistry, Purdue University, West Lafayette, IN 47907.*

The study of metal cluster compounds (molecules containing at least three metal atoms plus coordinating ligands) is among the most active areas of Inorganic Chemistry. Of particular interest is the interaction between small unsaturated molecules and multiple metal centers.

Recently a series of nickel clusters $[Ni_3(\mu_3\text{-}L)(\mu_3\text{-}I)(dppm)_3]^{n+}$ were synthesized (where L = I, CO, $C{\equiv}NiC_3H_7$, etc; dppm = bis(diphenylphosphino)-methane and n = 0,1,2). These clusters were found to be efficient electro-catalysts for the reduction of carbon dioxide. The structural characterization of these new compounds proved difficult on account of their symmetry. Limited information was obtained from IR and NMR data. X-ray crystallography was not possible for several derivatives due to the non-crystalline nature of the materials.

Informative ^{252}Cf Plasma Desorption (PD) and Fast Atom Bombardment (FAB) mass spectral data were obtained. Intense molecular ions were generally observed for the neutral and monocationic tri-nickel clusters using both ionization modes (Figure 1). Fragmentation pathways for the tri-nickel clusters were similar (Scheme 1). The dicationic hexa-nickel clusters gave weak intensity monocations in FAB and ionic aggregates, MI^+, in the PD spectra (Figure 2).

Characterization of the tri-nickel clusters by mass spectrometry was a simple and cost-effective alternative to X-ray crystallography. For the novel, non-crystalline hexa-nickel clusters, molecular weight determinations enabled them to be identified and distinguished from the tri-nickel clusters.

Scheme 1

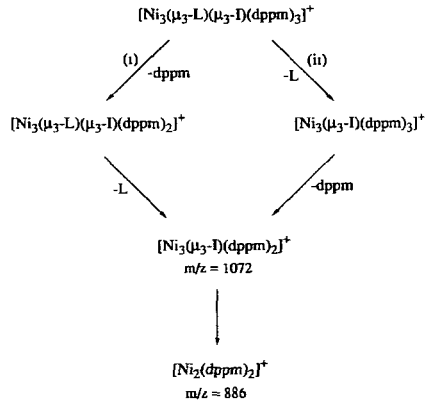

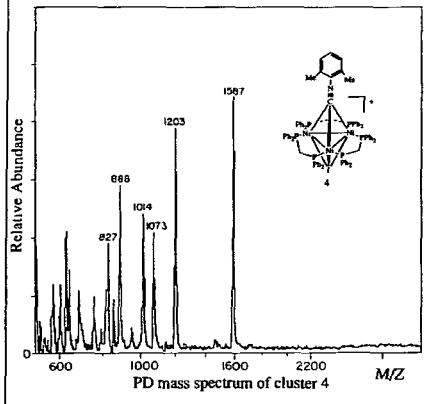

PD mass spectrum of cluster 4

Figure 1

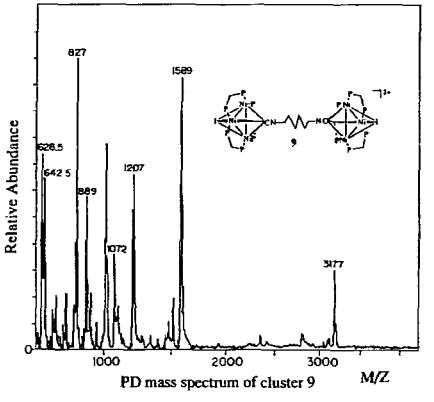

PD mass spectrum of cluster 9

Figure 2

LC-MS ANALYSIS OF SOME PHOTOGRAPHIC COLOUR-COUPLING COMPOUNDS USING A CONTINUOUS-FLOW FAB INTERFACE

Caroline D. Bradley and Alan W. Payne, Kodak Ltd., Harrow, U.K.

Photographic film and paper products employ a mixture of chemicals with one particularly important class being colour-coupling compounds which are the precursors of the colour dyes. Since a complex mixture is present, an analytical technique such as LC-MS is required which combines the ability to both separate and uniquely characterise. Until recently we have been using thermospray as our interface between the liquid chromatograph and mass spectrometer but this can have limitations for higher molecular weight compounds and also limited sensitivity. The nature of colour coupling compounds makes them particularly amenable to ionisation by fast atom bombardment (FAB); they typically have molecular weights of 500-1200 Da and are thermally labile. We have used static FAB for their characterisation with much success but have now combined the advantages of FAB ionisation with the capability of separation of the components immediately prior to analysis. This is achieved using continuous flow FAB as the interface between the HPLC system and a VG-70 mass spectrometer.

The HPLC set up comprises a Hewlett Packard 1050 quaternary pump system to deliver solvent at a flow of 0.3 ml per minute. This is reduced to a flow of 2.5 µl per minute passing through a 320 µm internal diameter (i.d.) LC capillary column by the use of a so-called balance column. The use of a 3 mm internal diameter reversed phase LC column to re-direct the majority of the flow away from the capillary system has been described previously by Balogh and Stacey[1]. Sample is introduced via a Valco C14W injector fitted with a 500 nl slot. Both LC columns and the injector are mounted onto the handle of the mass spectrometry probe. The probe tip is a modified version of the original VG dome design whereby the dome has been reduced in size to enable a wick to be fitted. Solvents used were HPLC grade with 2% glycerol added.

The following example illustrates the use of our LC-MS system in the analysis of a sample from part of a factory process to recover the silver from photographic materials. The final stage of this process results in a dry solid containing silver compounds and silicates but which is contaminated by various organics including colour-coupling compounds

Figure 1 shows the total ion current chromatogram for LC-MS of the sample. Careful analysis of the data revealed at least 10 clearly identifiable organic components. Figure 1 also shows mass chromatograms for two of these components which have MH^+ ions at m/z 909 and 508 (dashed and solid lines respectively).

Fig. 1

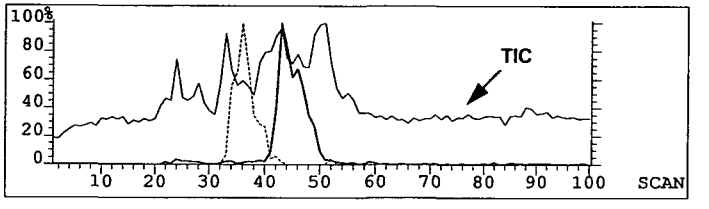

Figures 2 and 3 show the corresponding mass spectra of these two components. Both can be identified as colour coupling compounds with molecular weights 908 Da and 507 Da respectively. All of the major ions present in the spectra can be assigned to characteristic fragmentations of these species.

Fig. 2

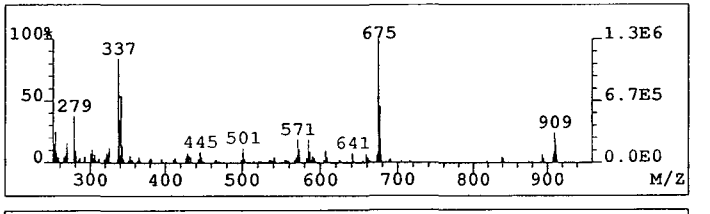

Fig. 3

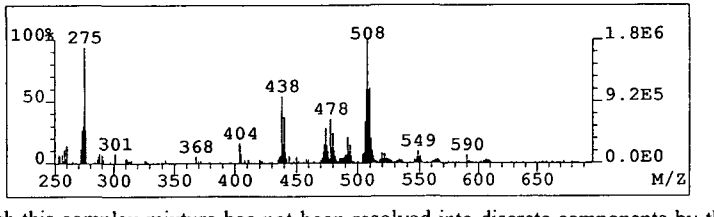

Although this complex mixture has not been resolved into discrete components by the LC, mass spectra of the individual components have either been obtained using background subtraction techniques or alternatively the discriminating ability of linked scanning was employed. We found an order of magnitude improvement in the overall sensitivity with continuous flow FAB as compared to our thermospray system.

1 M P Balogh and C Stacey, J Chromatography 73, 562 (1991)

INFORMATION ON THE IONIZATION PROCESSES INVOLVED IN FAB/LSIMS THROUGH ELECTROSPRAY IONIZATION

G. J. C. Paul, R. Feng[1] and M. J. Bertrand
Regional Center for Mass Spectrometry, Department of Chemistry, University of Montreal, Montreal, P.Q. H3C 3J7
[1]National Research Council of Canada, Biotechnology Research Institute, Montreal, P.Q. H4P 2R2

The formation of dominant $[M-H]^+$ molecular ions in FAB/LSIMS has been observed in our laboratory for two series of ether-type compounds; the cyclic acetals and derivatized monosaccharides.[1-3] This phenomena has been interpreted in terms of condensed phase ionization processes as a consequence of the major $[M+H]^+$ molecular ion formation observed under gas phase CI conditions.[1,3] A remaining question in the condensed phase FAB/LSIMS ionization model for these compounds is whether $[M-H]^+$ formation occurs through condensed phase equilibrium processes prior to fast atom/ion bombardment or through fast atom/ion beam-induced processes. One way to gain information on this subject is through the use of electrospray ionization (ESI). The ions sampled in this technique are formed predominantly through condensed phase equilibrium processes with no fast atom/ion bombardment taking place.

ESI studies have been conducted with two cyclic acetals and two derivatized monosaccharides, shown in Figure 1. The analytes were dissolved in methanol and the ESI experiments were run without and with glacial acetic acid (0.1 M). The ESI mass spectrum for 4-hexyl-2-phenyl-1,3-dioxolane (**1**) without acid is shown in Figure 2. The $[M+H]^+$ is dominant with no significant $[M-H]^+$ formation. Also present is a weak $[M+NH_4]^+$ adduct. The relative molecular ion intensities in ESI and FAB[1,2] for the acetals and monosaccharides are shown in Table 1. In each case, $[M+H]^+$ is the only significant molecular ion in ESI wheras in FAB the $[M-H/D]^+$ is the major ionic species. The absence of $[M-H]^+$ in ESI suggests that hydride abstraction occurs in FAB/LSIMS through fast atom/ion beam-induced ionization processes in the condensed phase. Consistent with this, $[M-H]^+$ was not observed for monosaccharides in either thermospray[4] or electrohydrodynamic ionization mass spectrometry (EHMS)[5] where both techniques rely on the preformation of ions in the condensed phase.

The ESI mass spectrum for α-methyl-2-deoxy-5-0-benzyl-D-ribofuranose (**3**) without acid is shown in Figure 3. In addition to $[M+H]^+$ the $[M+NH_4]^+$ adduct is present in large intensity. The formation of $[M+NH_4]^+$ in ESI (Figures 2 and 3) is through the presence of NH_4^+ in solution as an impurity. The presence of NH_4^+ probably leads to the preformation of $[M+H]^+$ in solution through proton transfer prior to electrospray. This would explain the intense absolute molecular ion signals obtained in ESI for cyclic acetals and derivatized monosaccharides without the presence of acid in solution. Due to the proposed preformed nature of $[M+H]^+$ in solution the addition of acid had little effect on the ESI mass spectra. It is anticipated that $[M+NH_4]^+$ and $[M+H]^+$ are in condensed phase equilibrium where the greater $[M+H]^+$:$[M+NH_4]^+$ ratio for the cyclic acetals (Figure 2) compared to the derivatized monosaccharides (Figure 3) in ESI reflects the greater proton affinity of the former species.

An intense $[M+Na]^+$ adduct was also observed in the ESI mass spectra of the derivatized monosaccharides (Figure 3). It is anticipated that Na^+ is present in solution as an impurity. The $[M+Na]^+$ adduct is also seen in the FAB/LSIMS mass spectra of monosaccharides where

thioglycerol and 2-hydroxyethyl disulfide are the liquid matrices.[2,3] The appearance of $[M+Na]^+$ in ESI indicates when Na^+ is present in the liquid matrix in FAB/LSIMS, preformation of $[M+Na]^+$ occurs through condensed phase equilibrium processes prior to fast atom/ion bombardment. It is believed that no $[M+Na]^+$ is seen for the cyclic acetals in ESI (Figure 2) due to the lower Na^+ affinity of these compounds compared to the monosaccharides.

REFERENCES

1 G.J.C. Paul, S. Bourg and M.J Bertrand, J. Am Soc Mass Spectrom in press.
2. Q Zha, M.D Bailey, and M.J. Bertrand, Can J Appl Spectros **35**, 141 (1990).
3 G J C. Paul, R. Feng, M.D Bailey, R Théberge and M.J. Bertrand, accepted by Org. Mass Spectrom
4 M Liptak, Z. Dinya, F Sztancskai, G Litkei, J Jeko, Org Mass Spectrom. **27**, 1271 (1992)
5 B Stimpson, C Evans Jr., Biomed Mass Spectrom. **5**, 52 (1978).

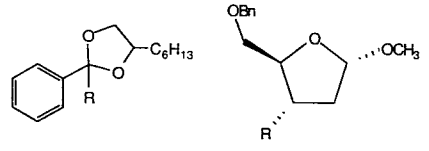

1: R = H
2: R = D
3: R = OH
4: R = OCH_3

FIGURE 1

TABLE 1: RELATIVE INTENSITY (%) OF PEAKS IN THE MOLECULAR ION REGION OF FAB AND ESI[a]

		ELECTROSPRAY	FAB[b]
1	$[M+H]^+$	100	27
	M^+	0	3
	$[M-H]^+$	1	100
2	$[M+H]^+$	100	75
	M^+	0	3
	$[M-H]^+$	0	6
	$[M-D]^+$	0	100
3	$[M+H]^+$	100	11
	M^+	0	0
	$[M-H]^+$	0	100
4	$[M+H]^+$	100	9
	M^+	0	0
	$[M-H]^+$	5	100

[a]Relative intensities corrected for isotope contribution
[b]Relative intensities after ~1 min bombardment

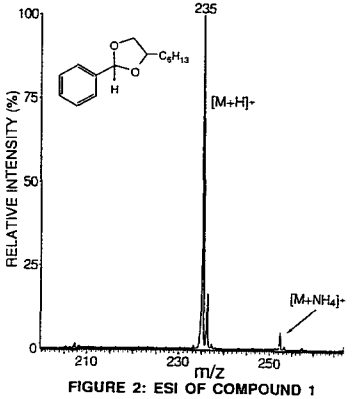

FIGURE 2: ESI OF COMPOUND 1

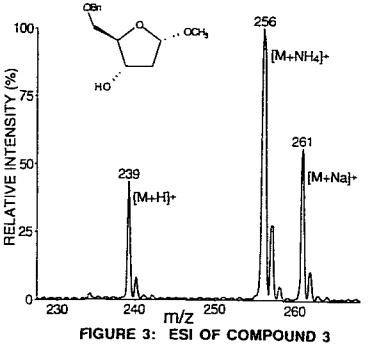

FIGURE 3: ESI OF COMPOUND 3

FORMATION AND SPUTTERING OF FULLERENES BY MeV IONS

I.Bitensky, G.Brinkmalm, *P.Demirev, J.Eriksson, P. Håkansson, R.Papaleo, B.U.R. Sundqvist,
Div. Ion Physics, Dept. Rad. Sciences, Uppsala University, Box 535, 75121 SWEDEN

Swift (with velocities exceeding the Bohr velocity) MeV atomic ions from the Uppsala EN-tandem accelerator are used to bombard different carbon-containing organic solids. A reflectron time-of-flight mass spectrometer is used to analyze the ejected secondary ions in a single ion impact event, and typically several milion MeV ion impact events are collected. Most of the energy of an MeV ion is deposited in a solid target via ionization of the target atoms in times of the order of 10^{-15} s. The energy density in the solid around the MeV ion trajectory is of the order of 1 keV/Å, and thus an infratrack - a short-lived positive ion plasma region with characteristic radius of the order of a few Å - is formed. If the energy relaxation rates from that region are lower compared to the energy deposition rate, as in the case of insulators, material is ejected from the solid in a process termed "electronic sputtering" [1]. As has already been demonstrated [2,3] even-numbered carbon cluster ions (C_n^+, n= 40 to > 400) are ejected from poly(vinylidenedifluoride) - PVDF as a result of this electronic sputtering phenomenon. Both the experimental data [2,3] and a theoretical model [4] suggest that these fullerene ions are formed in the infratrack, resulting from the interaction of a single MeV atomic ion with the solid. So far the PVDF polymer has been unique among the carbon-containing organic solids that produce fullerenes as a result of an MeV ion impact. Here we report the ejection of higher mass positive fullerene ions (C_n^+, n = 40 to > 400) by MeV ions from synthetic $C_{60}F_{2m}$ targets with different degree of fluorination (m = 14 to 24) [5]. The similarity of the spectra from the two targets (Fig. 1) suggests a common formation mechanism. This is also confirmed by studies of the initial radial velocity distributions of the positive ions, ejected from the fluorinated fullerene target. In contrast, the negative ion spectra contain only peaks corresponding to $C_{60}F_{2m}^-$ ions (Fig 2).

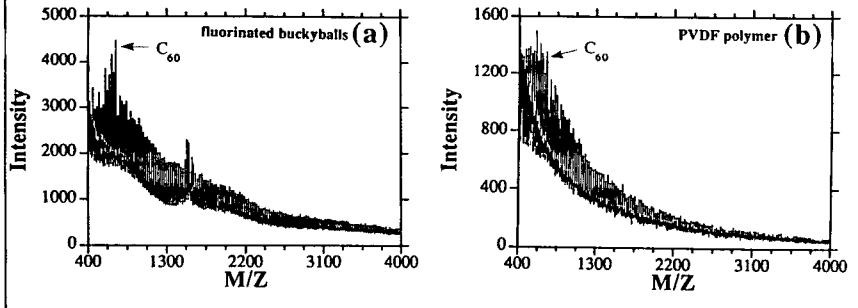

Fig. 1. Positive ion spectra from fluorinated buckyballs (a), and PVDF (b).

Spectra taken from thick films of pure synthetic C_{60} contain higher mass fullerene peaks with increased intensity around multiples of 60. Such peaks are not observed in the negative ion mode, which suggests that these higher mass fullerenes are formed as a result of coalescence reactions between sputtered ions and neutrals of C_{60} and its fragments (we note that the positive and negative ion yields from a film of preformed C_{60} and C_{70} fullerenes are the same [3]). Blends of pure C_{60} with polystyrene (PS) exhibit also higher mass - up to C_{100} - positive fullerene ions that are not present on the target surface (Fig. 2). No "modulation" of the ion intensity around multiples of 60 is observed in this case. The positive and negative ion spectra of a thin layer of pure C_{60} contain only the C_{60} ion peak, and so does the negative ion spectrum of the C_{60}/PS mixture.

Two types of reactions are observed in the electronic sputtering of fullerenes. The first type (as illustrated on the example of $C_{60}F_{2m}$) is the hot carbon atom "gas" condensation in an axially expanding infratrack plasma region, resulting from a single MeV ion impact. Another reaction regime is the coalescence to higher mass fullerenes from preformed C_{60} which occurs most probably in the gas-phase (selvedge). Three points in the electronic sputtering of fullerenes with implications to the fullerene

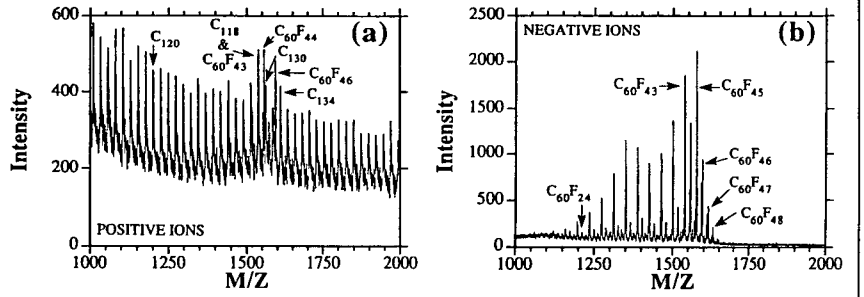

Fig. 2. Positive and negative ion spectra from fluorinated buckyballs in the 1000 to 2000 M/Z.

formation mechanism in general may be stressed: **1.** the typical time (subnanosecond) and spatial (tens of Å) scales for the MeV ion/solid interactions leading to fullerene ejection are orders of magnitude faster and smaller than the corresponding values in laser ablation; **2.** the observation of only positive fullerene ions (not present initially on the target) may be linked to the possible role of a cationic precursor in the fullerene formation pathway; **3.** at least in some instances fullerene growth proceeds through C_{2n} (n=1,2,...) addition to already existing three-dimensional pentagon-hexagon structure.

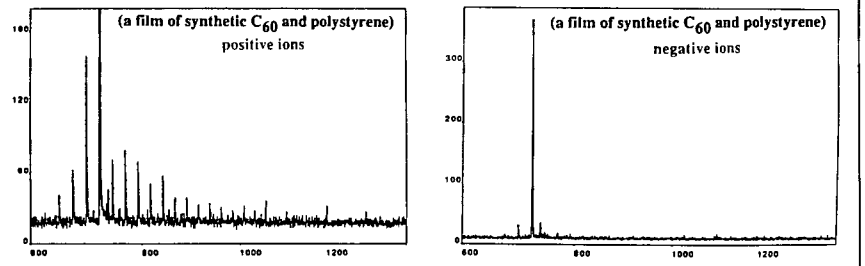

Fig. 3. Positive and negative ion spectra from a mixture of C_{60} and PS.

References

[1] R.E. Johnson, B.U.R. Sundqvist, *Phys. Today*, **March** (1992) 28.
[2] G. Brinkmalm, D. Barofsky, P. Demirev, D. Fenyö, P. Håkansson, R.E. Johnson, C. Reimann, B.U.R. Sundqvist, *Chem. Phys. Lett.* **191** (1992) 345.
[3] G. Brinkmalm, P. Demirev, D. Fenyö, P. Håkansson, J. Kopniczky, B.U.R. Sundqvist, *Phys. Rev.* **B47** (1993) 7560.
[4] I. Bitensky, P. Demirev, B.U.R. Sundqvist, *Nucl. Instr. Meth. Phys. Res.* **B** (1993, July) in press.
[5] A.Tuinman, P.Mukherjee, J.Aldock, R.Hettich, R.Compton, *J. Phys.Chem.* **96** (1992) 7584.

Acknowledgements

The authors gratefully acknowledge A.Tuinman, P.Mukherjee, J.Aldock (University of Tennessee, U.S.A.) for providing the synthetic $C_{60}F_{2m}$ fullerene sample. This work was supported by the Swedish Natural Sciences Research Council (NFR), and the Ångström and Cluster Consortia.

Identification of Degradation Products of the Antibiotic Laidlomycin Propionate by Mass Spectrometry

*David A. Lustig, Syntex Research, Palo Alto, CA 94304.

The ionophoric antibiotic laidlomycin propionate has been found to significantly improve cattle feedlot performance by favorably altering the intraruminal microbe balance and ultimately bovine metabolism. The purpose of this work is to identify the degradation products of this drug to help assess its environmental fate.

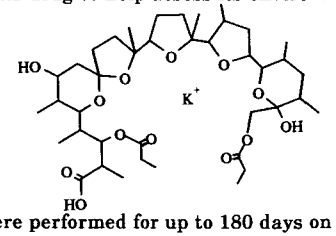

Biodegradation studies were performed for up to 180 days on ^{14}C radio labeled laidlomycin Propionate potassium salt in three regional soils (California, Texas and Mississippi).

An initial separation of the raw soil extracts was performed and fractions were collected. These were further purified by extraction into methylene chloride and subsequently analyzed by HPLC with RAM detection. Phenomenex Ultremex C18 columns (5 µm particles, 4.6 mm x 250 mm) were employed with an acetonitrile / water / THF / acetic acid (70/30/0.5/0.1) mobile phase. Fractions containing the main peaks were collected.

Mass spectral analysis of the HPLC fractions was performed with a Finnigan TSQ70 triple stage quadrupole mass spectrometer. Desorption ionization was accomplished from a glycerol matrix by Liquid Secondary Ion Mass Spectrometry (LSIMS) with 8 keV Cs^+ ions. MS-MS spectra were obtained for parent ions using 25-30 keV collision activated dissociation (CAD) with argon gas.

The ionization and fragmentation of the antibiotic and related models compounds was first studied. The mass spectra and tandem mass spectra were unique in that all molecular ions and fragment ions contained alkali metals, almost exclusively (see Figures 1-3).

It was found that typical fragmentation pathways were dominated by sequential ring cleavages and neutral losses. This information allowed for the identification of the degradation products of laidlomycin propionate. Confirmation was accomplished by comparison of the CAD MS-MS with known standards.

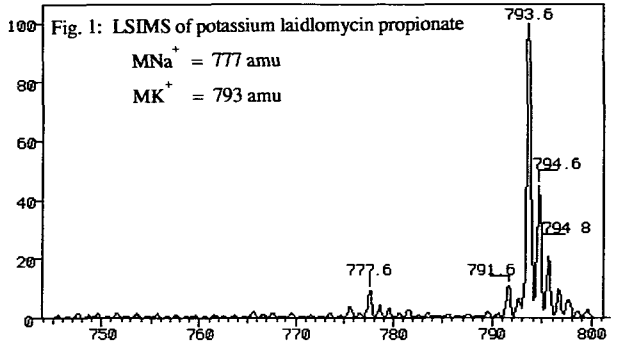

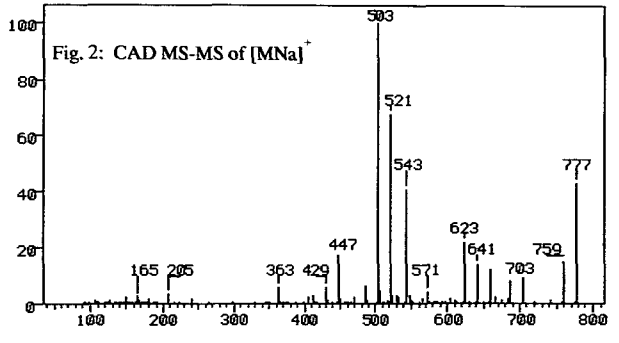

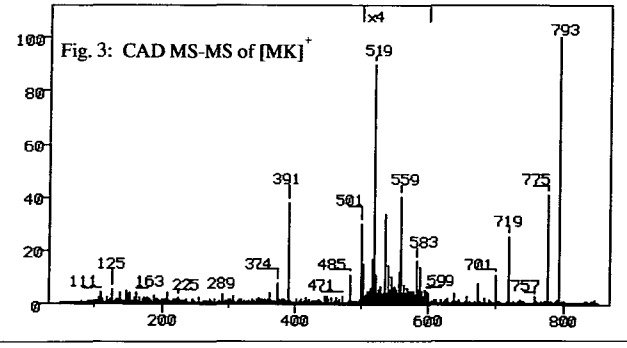

Quantification of malondialdehyde-deoxyguanosine (M_1G-dR) adduct by GC ECNCI MS.

*A. K. Chaudhary[1], H. K. Jajoo[1], L. J. Marnett[1], and I. A. Blair[2].
A. B. Hancock Jr. Laboratory for Cancer Research,
and Departments of Biochemistry[1] and Pharmacology[2]
Vanderbilt University School of Medicine, Nashville TN, 37232.

Exposure to environmental, nutritional and endogenous carcinogens leads to the formation of nucleic acid adducts which have been linked to the induction of mutations and cancer. High dietary fat intake is associated with the development of breast and colon cancer. Malondialdehyde (MDA), an endogenous product of lipid metabolism, causes mutation in bacterial and mammalian cells and cancer in rats. MDA reacts with deoxynucleosides *in vitro* with an order of reactivity guanine > adenine > cytosine > thymine. The monomeric adduct of MDA with guanine (M_1G) is the major adduct formed and induces mutations in bacteria. The possible involvement of MDA in the development of cancer requires a sensitive analytical method to characterize and quantitate the products formed by the exposure to this compound.

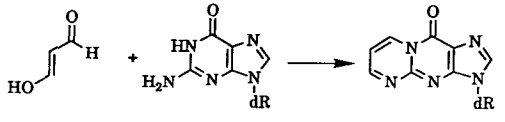

MDA **Deoxyguanosine** **M_1G-dR**

Reduction of M_1G-dR with sodium borohydride produces a dihydro derivative (H_2-M_1G-dR). H_2-M_1G-dR is more stable and exhibits a much improved HPLC profile facilitating the isolation from biological matrices. H_2-M_1G-dR is converted to a monopentafluorobenzyl (PFB) derivative by dissolving in 440 µL of acetone:acetonitrile (1:1), adding K_2C0_3 (2mg) and 35 µL of PFB.Br solution (35 µL PFB.Br in 465 µL acetone acetonitrile mixture) and heating to 60° for 60 min. Reaction proceeds with simultaneous depurination of the nucleoside and yields only one product which was characterized as 3-(2,3,4,5,6-pentafluorobenzyl)-5,6-dihydropyrimido[1,2a]purine-10(3H)-one (H_2M_1G-PFB) using LSI MS/MS and NMR. H_2-M_1G-PFB is converted to H_2-M_1G-PFB-BDMS derivative by heating with N-Methyl-N-t-butyldimethylsilyl trifluoroacetamide (MTBSTFA) containing 1% t-butyldimethylchlorosilane (TBDMCS):Pyridine mixture (1:1) at 120° for 20 min. The PFB-BDMS derivative is purified by SPE extraction and dissolved in n-decane for analysis by EC NCI GC/MS.

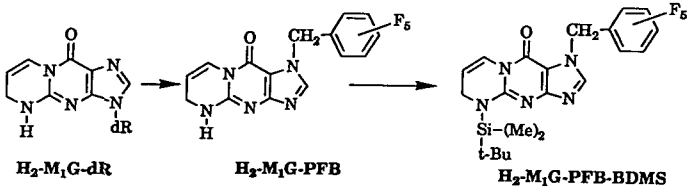

H_2-M_1G-dR **H_2-M_1G-PFB** **H_2-M_1G-PFB-BDMS**

EC NCI GC/MS was carried out on a Nermag R1010C instrument interfaced with a Varian Vista 6000 gas chromatograph using a 10 m SPB-1 fused silica capillary column (0.25 mm ID, 0.25µM film thickness; Supelco). Helium was used as carrier gas at a flow rate of 1 ml/min and methane was used as reagent gas at a pressure of 7 x 10^{-2} torr. Injections were made in splitless mode with the injector

temperature held at 250°C. The instrument was operated with an accelerating voltage of 70 eV, source temperature held at 260°C and emission current at 250 µA. The column temperature was programmed from 150°C (held for 1 min) to 320°C at 20°C/min. The EC NCI mass spectrum showed an intense [M-PFB] negative ion at m/z 302. [$^2H_2$-M_1G] was used as internal standard and exhibited an intense [M-PFB] negative ion at m/z 304. Quantitative analyses were carried out using SIM analysis of ions at m/z 302 and m/z 304. The limit of detection by this method is 10 pg (30 fmol) injected on column. The method was used to estimate M_1G-dR in normal rat liver. DNA was isolated from rat liver followed by enzymatic hydrolysis. The M_1G-dR was isolated by C_{18}SPE extraction, reduced to H_2-M_1G-dR and derivatized to PFB-BDMS derivative. A typical selected ion current profile obtained for analysis of M_1G-dR in rat liver is shown in Figure 1. A full scan mass spectrum of the same sample, to which no internal standard had been added was identical with an authentic standard of H_2-M_1G-PFB-BDMS (Figure 2). This confirms the structure of the isolated compound as M_1 G-dR.

In summary, we have characterized and quantitated M_1G-dR formed *in vivo* in DNA isolated from rat liver. This method is highly specific and sensitive for the analyses of M1G-dR from other biological matrices.

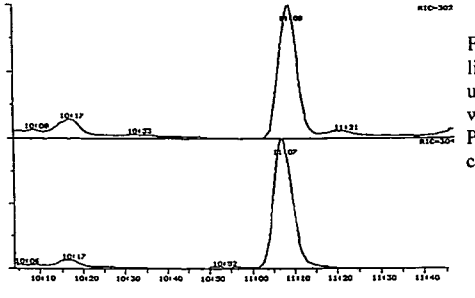

Figure 1. Selected ion current profile for rat liver DNA spiked with 2 ng of [$^2H_2$]-M_1G: upper panel shows H_2-M_1G-PFB-BDMS while lower panel depicts [$^2H_2$]-H_2-M_1G-PFB-BDMS. The concentration of M_1G-dR corresponds to 9 M_1G-dR per 10^7 bases.

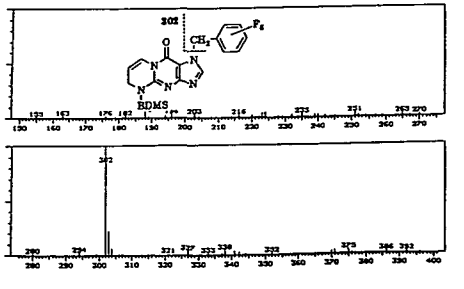

Figure 2. EC NCI MS of H_2-M_1G-PFB-BDMS isolated from rat liver DNA.

This work was supported by NIH grants CA 47479 and ES00267.

Differentiation of Isomeric C8-Substituted Dinitrotoluene Adducts of Guanine by FAB MS/MS

M. P. Chiarelli, R.D. Holland, K. E. Kirtley, and J. O. Lay, Jr., University of Arkansas-Little Rock, Little Rock, AR 72204 and The National Center for Toxicological Research, Jefferson, AR 72709.

Introduction

Mass spectrometric studies of carcinogen-modified DNA are motivated by the hypothesis that these compounds play a major role in the initiation of cancer. In this investigation product ion scans and fragment ion abundance ratios are used to differentiate three different isomeric C8-substituted dinitrotoluene adducts of guanine.

Experimental

All FAB MS/MS spectra were acquired on a Finnigan MAT TSQ70 triple quadrupole mass spectrometer equipped with an Ion Tech fast atom gun. Xenon was employed in the primary atom beam at energies of 8-10 KeV. Argon was employed as the collision gas in the second quadrupole at pressures of ca. 0.8 millitorr. Thioglycerol was used as a matrix for all compounds studied. CAD spectra of the protonated molecules and significant source-produced fragment ions were acquired using 50 eV collision energies. The three guanine adducts used in this study were synthesized using the procedure of Jacobson et al. (1).

Results and Discussion

The major difference between the product ion spectra of these guanine-C8-substituted bifunctional adducts and the product ion spectra of the guanine C8-adducts of simple arylamines (2) is that the primary ion formation processes proceed by fragmentation of the carcinogen, rather than the base, losing the nitro group to produce a distonic radical cation at m/z 256 (Figures 1-3). One aspect of these product ion spectra that distinguishes N-(guan-8-yl)-4-methyl-3-nitroaniline from the ortho-methylnitroaniline adducts is the formation of tropolyium and NH_2-substituted tropolyium ions at m/z 91 and m/z 106 (Figure 1). The two ortho-methylnitroaniline adducts yield an m/z 117 ion in their product ion spectra (Figures 2 and 3) not observed in Figure 1.

The mechanism of formation of the ortho-methyl isomer specific ion at m/z 117 is shown in Scheme 1. After the loss of the NO_2 group, methyl group transfer from the aniline C2 position to the N7 or N9 position of guanine may occur through a six-membered transition state driven by benzyne formation in the aniline ring. Cleavage of the guanine base may then produce the substituted benzyne ion at m/z 117. Alternatively, cleavage of the guanine C8-aniline N^1 bond may produce the methyl-substituted guanine ion observed at m/z 166. Product ion spectra of source-produced m/z 256 ions were acquired from all three isomers to support the proposed mechanisms. The product ion spectra of the source-produced m/z 256 ions from both the ortho-methylaniline adducts show substantial abundances of both m/z 117 and m/z 166, thereby supporting the mechanism of ion formation proposed in Scheme 1.

Although both product ion spectra of the ortho-methylaniline adduct isomers in Figures 2 and 3 show the same major fragment ions they can be differentiated by the comparison of ion abundance ratios of the most prominent fragment ions. Ion abundance ratios, (m/z 117)/(m/z 256), obtained from the product ion spectra of N-(guan-8-yl)-2-methyl-3-

nitroaniline and -5-nitroaniline, were found to be 0.76 ± 0.06 and 0.21 ± 0.02, respectively, when a set of eight consecutive determinations were averaged for each isomer.

References

1. Jacobson, M.D.; Shapiro, R.; Underwood, G.R.; Broyde, S.; Verna, L.; Hingerty, B.E. *Chem. Res. Tox.* **1988**, *1*, 152-159.
2. Chiarelli, M.P.; Lay, J.O., Jr. *Mass Spectrom. Rev.* **1992**, *11*, 447-493.

Acknowledgement

Our work is supported in part by the Center for Indoor Air Research (CIAR #92-002).

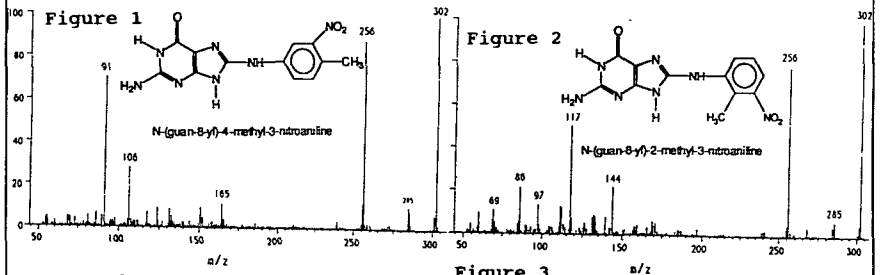

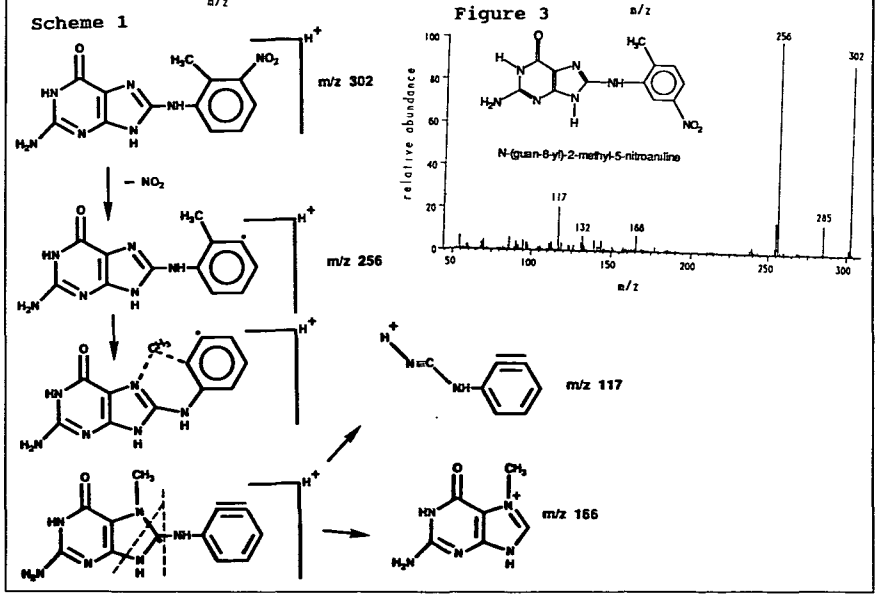

DISTINGUISHING ISOMERIC MONOMETHYL GUANINES BY FAB MASS SPECTROMETRY COMBINED WITH PERMETHYLATION

M. George, *V.M. Sadagopa Ramanujam, R.L. Cerny and M.L. Gross, Midwest Center for Mass Spectrometry, University of Nebraska-Lincoln, NE 68588-0304.

Most of the minor purine constituents of both *transfer*-RNA and DNA consist of mono- and dimethyl derivatives of guanine (2-amino-6-oxypurine). The characterization of these compounds are important because carcinogenic methylating agents are known to cause methylation[1] of guanosine in DNA *in vivo* and can be isolated as methyl guanines. There are seven isomeric *mono*-methyl guanines and it is often difficult to distinguish them especially at submicrogram quantities. Due to high polarity and nonvolatility, the methyl guanines are unsuitable for conventional EI or CI mass spectral analysis. In addition, these compounds have poor sensitivity by fast atom bombardment (FAB) mass spectrometry. The objective of this study is to develop a good method for the characterization of *mono*-methyl guanines at submicrogram levels. In order to achieve this, we have investigated the permethylation of several methyl guanines using **CD_3I** followed by **FAB MS/MS** analysis.

All methyl guanines, except 8-methylguanine, are commercial samples. 8-Methylguanine is a synthetic sample. The permethylation reaction was carried out by reacting each methylguanine with excess CH_3I or CD_3I in DMSO in the presence of *t*-BuOK. The derivatized mixture was directly used for the FAB MS/MS analysis. The collisionally activated dissociation (CAD) experiments were performed by using a VG ZAB-T, a 4-sector tandem mass spectrometer (BEBE configuration), after precursor ion (MS1 resolution 2000) activation in the third field-free region by collision with helium. Sufficient helium was added to the collision cell to decrease the main beam intensity by 50%. Spectral acquisition and data work-up were performed by using a VAX 3100 workstation equipped with OPUS software. Typically 10-15 scans were signal-averaged for each spectrum.

Permethylation of the six isomeric 1-, N^2-, 3-, O-, 7-, and 9-methyl guanines using **CH_3I** yield preformed *tetra*-methyl quarternary ion (*m/z* 222), whereas 8-methylguanine produces a *penta*-methyl derivative (*m/z* 234). The CAD spectra of the *tetra*-methyl derivatives (*m/z* 222) are very similar giving fragments of *m/z* 207, 206, 192, 178, and 85, and hence not suitable for isomer distinction.

If the methylation is carried out with **CD_3I**, however, then the CAD spectra (**Figure 1**) of perdeuteromethyl derivatives (*m/z* 234) are specific for each isomeric *mono*-methylguanine. The changes in mass/charge ratios of the fragments depend upon the position of the original CH_3 group.

Conclusions: (1) The permethyl derivatives of *mono*-methyl guanines give abundant FAB-MS signals corresponding to quarternary ions at submicrogram levels. These quarternary salts are several orders more sensitive to FAB than the respective *mono*-methylguanine. (2) The FAB MS/MS spectra of the perdeuteromethyl derivatives are different from each other thus facilitating the identification of each isomer. (3) Methylation of 8-methylguanine is unique because it is the only isomer yielding a *penta*-methyl derivative.

[1]T.A. Dutta-Choudhury, B.H. Bak and R.C. Guzman, *Carcinogenesis*, **1992**, *13*, 33-39.

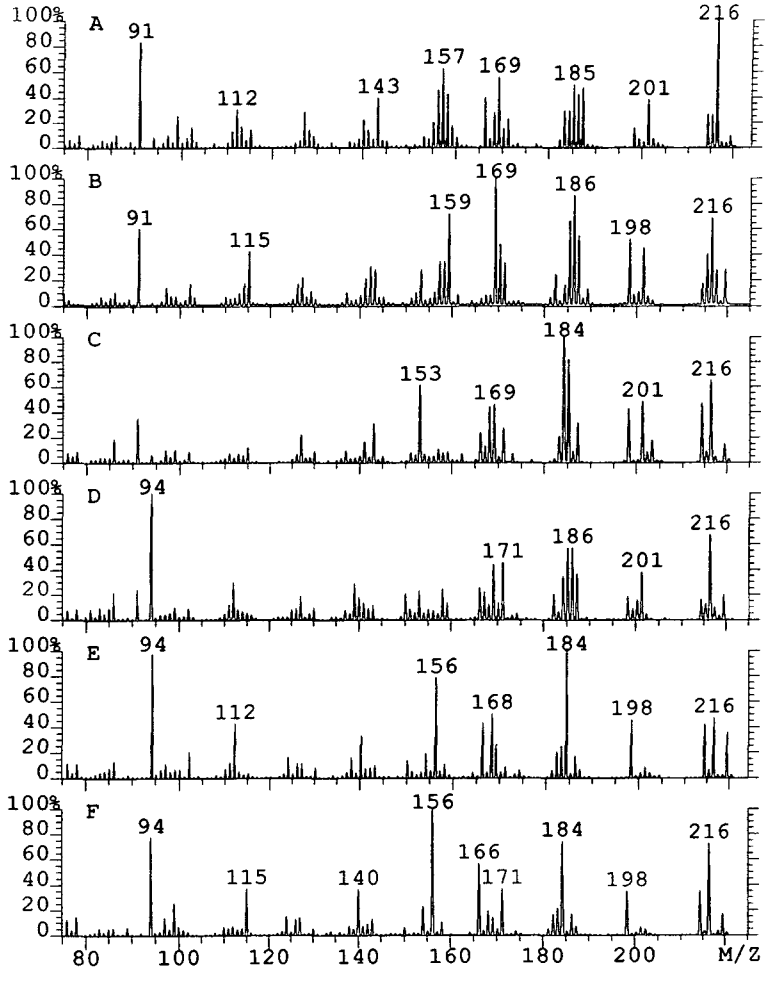

Figure 1. CAD Spectra of Perdeuteromethyl Derivatives (*m/z* 234) of: **(A)** 1-Methylguanine, **(B)** N^2-Methylguanine, **(C)** O-Methylguanine, **(D)** 3-Methylguanine, **(E)** 7-Methylguanine, and **(F)** 9-Methylguanine.

LOW-ENERGY TANDEM MASS SPECTROMETRY OF PAH DIOL EPOXIDE-DEOXYNUCLEOSIDE ADDUCTS

Paula S. Branco, M. Paul Chiarelli, Frederick A. Beland and Jackson O. Lay, Jr.
National Center for Toxicological Research, Jefferson, AR 72079 and
University of Arkansas-Little Rock, Little Rock, AR 72204.

The structural elucidation of carcinogen-deoxynucleotide adducts by mass spectrometry (MS) is motivated in part by the belief that these compounds may serve as biochemical markers of exposure to environmental genotoxins. To date no systematic tandem MS studies of diol epoxide modified deoxynucleoside adducts of polycyclic aromatic hydrocarbons (PAH) have been undertaken. Here we report an analytical strategy using fast atom bombardment (FAB) ionization and tandem mass spectrometry, with collision energies on the order of 30-50 eV, for the characterization of these compounds. Our methodology combines three experimental approaches to charactertize low levels of carcinogen-deoxynucleoside adducts. These include the use of contrast neutral loss (CNL) scans (116 u and 313 u), products ion scans of the protonated molecule or the BH_2^+ ion, and parent ion scans.

Constant neutral loss scans: **The PAH diol epoxide adducts used in this study showed little or no signal for the loss of the deoxyribose by FAB, a fragmentation typically observed with other classes of deoxynucleoside adducts. Nonetheless CNL scans (116 u) were possible and fragments were observed from the mono and di-sodium containing molecule ions as well the protonated molecule. CNL scans of *anti*-benzo(*a*)pyrene diol epoxide (BaPDE) adducts of deoxyguanosine (dG), deoxyadenosine (dA), and deoxycytidine (dC) were acquired using as little as 25 ng applied to the FAB probe. We have also found that another type of CNL spectra (313 u) can be used as a very sensitive probe for dG adducts of PAH diol epoxides (Figure 1).**

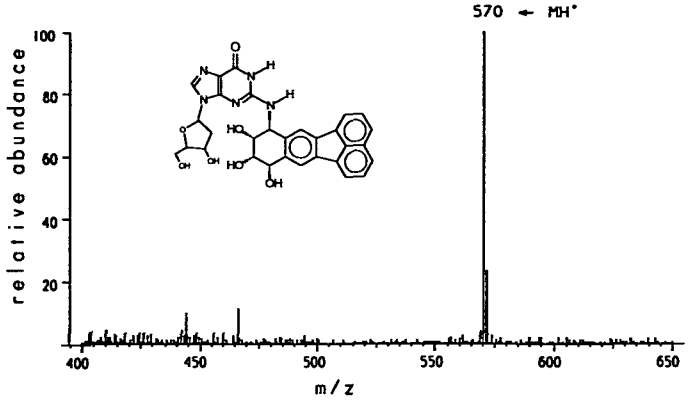

Figure 1. **The FAB constant neutral loss (313 u) spectrum of *anti*-benzo(*k*)fluoranthene diol epoxide-dG adduct.**

Product ion scans: **The $(M+H)^+$ ions of the synthesized PAH adducts showed product ion spectra dominated by fragments derived from the carcinogen group, as shown in the following scheme.**

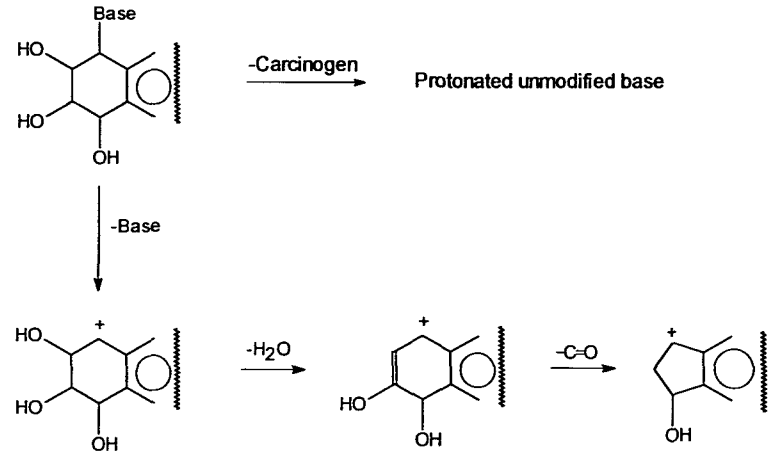

Model compounds for the BH_2^+ ions were synthesized by reaction of BaPDE and the bases guanine, adenine, and cytidine. The major fragments are the same as those observed from the protonated deoxynucleoside adducts.

Parent ion scans: **Another approach can be used to detect PAH diol epoxide deoxynucleoside adducts if the PAH is known. The product ion spectra for the *anti*-benzo(*a*)-pyrene diol epoxide adducts of dG, dA and dC showed a common base peak ion at 257. When a parent ion spectrum (257 u) was recorded for these three compounds, the corresponding protonated molecule ions were observed. (This work was supported in part by the Center for Indoor Air Research, #92-002).**

CHARACTERIZATION OF MODIFIED OLIGODEOXYNUCLEOTIDES BY ELECTROSPRAY MASS SPECTROMETRY

Dasari M. Reddy, Robert A. Rieger, and Charles R. Iden

Department of Pharmacological Sciences, Health Sciences Center
State University of New York at Stony Brook, Stony Brook, NY 11794-8651

DNA may be structurally modified in living cells either by interacting with oxygen free radicals generated as by-products of cellular metabolism and ionizing radiation, or with genotoxic chemicals present in the environment. Recent evidence indicates that these modifications play an important role in degenerative processes such as carcinogenesis, mutagenesis and aging. Consequently, elucidation of the chemical nature of DNA damage is fundamental for understanding the nature of these processes. Mass spectrometry has played an important function in the analysis of modified DNA constituents, and various methodologies have been developed for the characterization of modified DNA constituents. While GC/MS procedures are useful, especially for low level quantitation of known adducts, these methods involve hydrolysis of native DNA to its constituent nucleosides followed by derivatization to increase the volatility and thermostability. New ionization techniques permit analysis of thermally labile and polar molecules and biopolymers at the nanogram level which is required for biological samples. Techniques based on desorption, such as FAB, SIMS and DCI have proven useful for small oligomers, but are often limited by the range of the mass analyzer. Electrospray ionization mass spectrometry (ESI/MS), a sensitive ionization technique useful for the analysis of biopolymers and charged species, provides an alternative method of analysis without need for enzymatic hydrolysis or chemical transformation. Moreover, the propensity of this technique to form multiply charged ions effectively extends the range of mass analyzers and permits accurate molecular weight determination at large molecular weights. We present our preliminary results on electrospray ionization of oligonucleotides containing modified deoxynucleotides.

Analysis was performed on a TRIO-2000 mass spectrometer equipped with an electrospray source. Samples were introduced into the ion source by a continuous flow of solvent (MeOH: H_2O, 90:10) at 6-8 μl/min using a syringe pump connected to a Reodyne injector with a 10 μl sample loop. Prior to analysis samples were dissolved in $MeOH:H_2O:NH_3$ (90:9:1) at a concentration range of 100-200 pmol/μl. An aliquot (10 μl) of each sample was injected into the continuous flow of solvent entering the source. The instrument was scanned in the multichannel analyzer mode (MCB) with a 8 sec dwell time over the mass range m/z 300 to 1200. The mass scale was calibrated in the positive ion mode using polyethylene glycol. Spectra are an average of ten to fifteen scans. Oligodeoxynucleotides were synthesized on a Dupont Coder 300 or Applied Biosystems 394 automated DNA synthesizer using the solid state phosphoramidite chemistry. Oligomers were released from the resin and deprotected by treating with 28% NH_3 at 55^{0}C for 18 h, and purified by HPLC on a reverse phase column (Hamilton PRP-1, 250 x 21.5 mm) using a gradient of 16% to 36% acetonitrile in 0.1M triethylammonium acetate (pH 7.5).

1a.

1b.

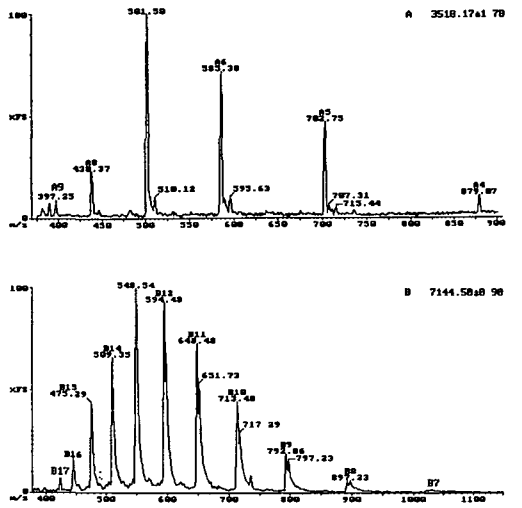

Figure 1. ESI mass spectrum for oligonucleotides a). 5′-GCATGCXTACAG-3′ and b). 5′-CCTTCXCTACTTTCCTCTCCATTT-3′ (see text for definition of X).

Figure 1a shows the negative ion ESI mass spectrum for the dodecaoligonucleotide 5′-GCATGCXTACAG-3′, where X is a tetrahydrofuran moiety, a model for the abasic site in which a nucleobase is replaced by a hydrogen atom. Electrospray ionization produces intact, multiply-charged, molecular ions which result from abstraction of protons from the phosphate bridges to yield even electron ions of the general formula $(M-nH)^{-n}$. This spectrum shows a distribution of multiply charged molecular ions ranging from $(M-9H)^{-9}$ to $(M-4H)^{-4}$. Because of the nature of the purification process, no ions corresponding to sodium or potassium adducts were formed, and well defined peak shapes were observed in the spectrum; however, weak ions corresponding to ammonia adducts are discernable. By increasing the concentration of ammonia in the sample, adduct ions will dominate the spectrum.

Figure 1b illustrates the negative ion ESI spectrum of an oligodeoxynucleotide (24-mer) with the sequence 5′-CCTTCXCTACTTTCCTCTCCATTT-3′, where X is the oxidative lesion 8-oxo-2′-deoxyguanosine. The spectrum exhibits the typical bell shaped molecular ion charge distribution ranging from $(M-8H)^{-8}$ to $(M-17H)^{-17}$. Low intensity ions corresponding to ammonia adducts were also observed. The number of adducts formed with ammonia tends to be greater for the lower charged states of the molecular ion.

Computer-Assisted Interpretation of Electrospray-Tandem Mass Spectra of Oligonucleotides

K.J. Hart, S. Habibi-Goudarzi and S.A. McLuckey
Analytical Chemistry Division, Oak Ridge National Laboratory
Oak Ridge, TN 37831-6120

A computer program is being developed to facilitate the analysis of oligonucleotides by tandem mass spectrometry of multiply charged molecular anions. The nucleotide sequencing program (NSP) currently handles naturally occurring DNA (i.e. deoxyribose & A,C,G,T bases) and RNA (i.e. ribose & A,U,G,T bases). The NSP is being developed in C without, for now, a graphical user interface to allow easy compilations on a variety of computer platforms.

Calculations for a given oligonucleotide sequence include:

- MW and isotopic mass of the neutral free acid
- Expected m/z (s) for ES-MS
- Expected m/z (s) for ES-MS/MS

Calculations for an unknown oligonucleotide sequence:

- Base composition given observed ES-MS m/z, charge state and a user defined mass tolerance (e.g. 1 u)
- Given a selected parent ion, charge state and MS/MS spectrum:
  - ⇒ Identify B- m/z's and -BH m/z's in the ES-MS/MS spectrum
  - ⇒ Identify sets of complementary ions in ES-MS/MS spectrum

The expected ES-MS ions for 5'-d(GTGGCCAC)-3' are:

Ion Desc.	m/z
(M - 7Na+)7-	343.20
(M - 7Na+ + 1H+)6-	400.57
(M - 6Na+)6-	404.23
(M - 7Na+ + 2H+)5-	480.88
(M - 6Na+ + 1H+)5-	485.28
(M - 5Na+)5-	489.67
(M - 7Na+ + 3H+)4-	601.35
(M - 6Na+ + 2H+)4-	606.85
(M - 5Na+ + 1H+)4-	612.34
(M - 4Na+)4-	617.84
(M - 7Na+ + 4H+)3-	802.14
(M - 6Na+ + 3H+)3-	809.47
(M - 5Na+ + 2H+)3-	816.79
(M - 4Na+ + 1H+)3-	824.12

Ion Desc.	m/z
(M - 3Na+)3-	831.45
(M - 7Na+ + 5H+)2-	1203.71
(M - 6Na+ + 4H+)2-	1214.71
(M - 5Na+ + 3H+)2-	1225.70
(M - 4Na+ + 2H+)2-	1236.69
(M - 3Na+ + 1H+)2-	1247.68
(M - 2Na+)2-	1258.67
(M - 7Na+ + 6H+)1-	2408.44
(M - 6Na+ + 5H+)1-	2430.42
(M - 5Na+ + 4H+)1-	2452.40
(M - 4Na+ + 3H+)1-	2474.38
(M - 3Na+ + 2H+)1-	2496.36
(M - 2Na+ + 1H+)1-	2518.35
(M - 1Na+)1-	2540.33

The largest ions observed in the ITMS electrospray mass spectrum are the ions corresponding to (M - 7Na+ + 1H+)6-, (M - 7Na+ + 2H+)5- and (M - 7Na+ + 3H+)4-. The sodiated species in the m/z range below 650 were also observed.

The NSP output for expected ES-MS/MS ions for the triply charged 5'-d(AAAA)-3' parent ion is provided below. The nomenclature used is defined elsewhere [1].

Ion Desc.	m/z
A-	134.05
w[1]2-	164.02
[w[1]-B[4](AH)]1-	195.01
[w[2]-B[3](AH)]2-	253.53
[w[3]-B[2](AH)]3-	273.37
w[3]3-	317.72
w[2]2-	320.55
w[1]1-	329.05
(P-(AH)) 3-	350.73
[a[3] - B[3](AH)]2-	361.07

Ion Desc.	m/z
Parent Ion 3-	395.75
[w[3]-B[2](A-)]2-	410.36
[a[2] - B[2](AH)]1-	410.09
w[3]2-	477.58
[w[2]-B[3](A-)]1-	508.06
(P-(A)-) 2-	526.60
w[2]1-	643.12
[a[3]-B[3](A-)]1-	723.14
[w[3]-B[2](A-)]1-	821.12

The interpretation of ES-MS/MS spectra of oligonucleotides of unknown sequence can also benefit from some simple calculations. There are several spectral features which are useful to recognize when interpreting these spectra. One feature is the presence of ions indicating B^- loss and/or BH loss. Another feature is to correlate complementary ions by using the fact that:

$$(m/z)_{p1} * z_{p1} + (m/z)_{p2} * z_{p2} = (m/z)_p * z_p \quad \text{and}$$

$$z_{p1} + z_{p2} = z_p$$

to derive the ratio of the charges of two complementary product ions:

$$z_{p2} / z_{p1} = ((m/z)_p - (m/z)_{p1}) / ((m/z)_{p2} - (m/z)_p)$$

where p refers to the parent ions and p1 and p2 refer respectively to product ion 1 and product ion 2 of a complementary pair of product ions [1]. The NSP first calculates possible z_{p2} / z_{p1} ratios based on the number of parent ion charges. After MS/MS product ions have been entered, a list of B^-, -BH ions and complementary ions found is displayed to the screen. Future additions to this program are expected to include calculations for neutral sugar loss, loss of PO_3^- and additional rules for interpreting ES-MS/MS spectra. Once sufficient interpretation rules are in place, generation of candidate sequences will be implemented. Also, direct input of spectral data from ITMS data files and a graphical user interface will be added to the program. This program represents a significant step towards achieving automatic candidate sequence generation from ES-MS/MS spectra of oligonucleotides. The authors wish to acknowledge the support of NIH grant number GM45372.

1. McLuckey, S.A.; Van Berkel, G.J.; Glish, G.L.; *J. Am. Soc. Mass Spectrom.* **1992**, *3*, 60.

MALDI MASS SPECTROMETRY OF OLIGONUCLEOTIDES AND NUCLEIC ACIDS

Eckhard Nordhoff, Michael Karas, Franz Hillenkamp
Institute for Medical Physics and Biophysics, University of Münster, Robert-Koch-Str. 31, 48149 Münster, Germany

Finn Kirpekar, Karsten Kristiansen, Peter Roepstorff
Department of Molecular Biology, University of Odense, Campusvej 55 5230 Odense, Denmark

The few results on MALDI mass spectrometry for oligonucleotides and nucleic acids obtained and reported until now show a much lower quality of the mass spectra than typically achieved for peptides and proteins and seem to indicate some fundamental problems in the LDI of this class of compounds.

Formation and desorption of oligonucleotide salt ions with different and differing number of cations has been shown to be one factor responsible for the peak width and degrading signal quality; a simple and highly efficient cleaning of the applied matrix/analyte solution by cation exchange beads replacing metal cations against ammonium ions has been successfully used to overcome this problem (1); ammonium salts of the oligonucleotides enable to reconstitute the free acid in the gas phase and the formation of $[M-H]^-$-ions. DNA pieces of up to 26 mers can now be investigated with a quality and sensitivity comparable to those of peptides enabling e.g. routine analysis of antisense DNA. Susceptibility of larger DNA pieces to fragmentation poses the major problem in the higher mass range. Fragmentation by (multiple) base loss resolved for small pieces of DNA is responsible for the observed limits in performance such as mass range limit, broad molecule ion peaks and systematic errors in mass determination. DNA is much more susceptible to this fragmentation than RNA, enabling intact molecule ion desorption and accurate mass determination for RNAs up to 104 mers (see Figure 1) The advantages documented until now for IR-MALDI (using a succinic acid matrix) vs. UV-MALDI (using

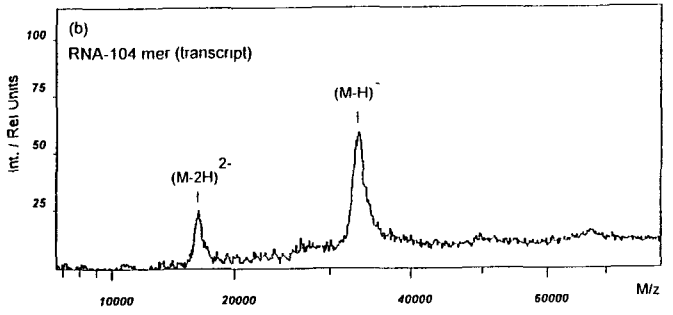

FIGURE 1 : IR-MALDI mass spectrum of a RNA-104 mer (transcript)
Matrix: succinic acid, Er:YAG-laser - 2.94 μm, sum of 10 single shots

typical protein matrices) have been overcome by the use of 3-hydroxypicolinic acid (2) as a UV-matrix.

IR-MALDI of DNA using a succinic acid matrix and working at increased irradiance induces (prompt) fragmentations; this kind of behaviour has never been observed in UV-MALDI. The fragment ions formed are highly specific and significant for the chemical structure; cleavages are observed from both ends of the oligonucleotide chain (X- and Y-series), allowing for a sequencing of the oligonucleotide (see Figure 2). As an explanation for this fragmentation an intramolecular proton-catalyzed elimination of the nucleobase followed by a cleavage of the 3'- or 5'- O-glycosidic bond by a second elimination reaction is proposed. This is substantiated by the fact that cleavages at thymine, the only base which cannot be protonated, are inhibited. Further work will concentrate on optimizing the experimental conditions, until now focused to the desorption of intact molecular ions, for this new aspect of MALDI.

(1) E. Nordhoff, A. Ingendoh, R. Cramer, A. Overberg, B. Stahl, M. Karas, F. Hillenkamp and P.F. Crain, Rapid Commun. Mass Spectrom. 6 (1992) 771.
(2) K.J. Wu, A. Steding, C. Becker, Rapid Commun. Mass Spectrom. 7 (1993) 142.

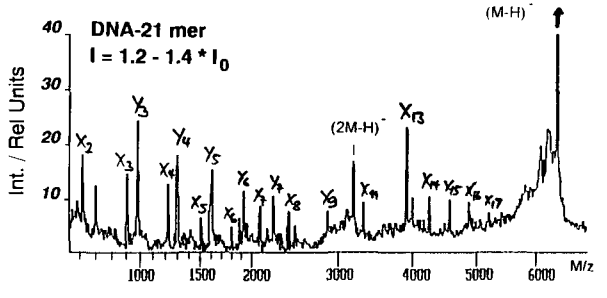

FIGURE 2 . IR-MALDI mass spectrum of a DNA-21 mer at elevated laser irradiance matrix : succinic acid, Er:YAG-laser - 2.94 μm, sum over 10 single laser shots X- and Y-series correspond to cleavages of the 3'- and 5'-O-glycosidic bond.

Acknowledgement

This work was financially supported by the German Fed. Dept. of Research and Technology (BMFT, grant № : 13N5640) and the Commission of the European Communities (grant No.: GENO-CT91-0022(SSMA)) Antisense DNA investigations were done in collaboration with J. Muth and J. Engels (University of Frankfurt, Germany), PEG-DNA-conjugates in collaboration with A Jäschke and D. Cech (Humboldt-University, Berlin) and J.P. Fürste and V.A. Erdmann (Freie Universität, Berlin).

Electrospray LC-MS of Modified Oligonucleotides

LeRoy B. Martin* and Cynthia S. Mamer
Fisons Instruments, 32 Commerce Center, Cherry Hill Drive Danvers, MA 01923

Robert A. Rieger and Charles R. Iden
Department of Pharmacological Sciences, Health Sciences Center, SUNY at Stony Brook, Stony Brook, NY 11794-8641

The purpose of this project was to develop a method for detection of oligonucleotides synthesized by phosphoramidite chemistry. As a chromatographic detector, a mass spectrometer using electrospray ionization can accurately determine the nature of modifications introduced into a sequence during synthesis. The methods developed here are adaptable to HPLC conditions often used in DNA purification.

Detection of DNA from a chromatographic run presents two challenges. The first to overcome is electrospray ionization from highly aqueous, high ionic strength solutions that do not favor the negative ion formation often used in DNA detection. To accurately assign a molecular weight to a species measured by electrospray a strong series of multiply charged peaks is critical. Therefore, a second challenge is the detection of enough peaks in a series to accurately determine their charge state and hence the molecular weight of the measured oligomer. Simple additions after the column can enhance both sensitivity and selectivity by increasing volatility and affecting the ionic form of oligonucleotides. As examples, two modifications were examined by LC/MS. The modifications incorporated into these oligonucleotides have been developed as models for damage leading to carcinogenesis.

Modified phosphoramidites were synthesized in the labs at Stony Brook. Oligonucleotides were purified by HPLC collection of the DMT product. The column used was a Hamilton (Reno, NV) PRP-1 polystyrene divinyl benzene column. Subsequent removal of the DMT protection group afforded product in a state that could be used in the next HPLC separation. Oligonucleotides without DMT were quantitated by UV spectrometry and used directly for HPLC/MS experiments. An HP 1050 LC system was used with a Brownlee (ABI, San Jose, CA) 5µm 220x2.1mm Spheri-5 RP-18 column. The gradient used was 300µl/min 50mM triethylammonium acetate pH 6 in H_2O with 9-15% acetonitrile in 15min. Postcolumn additions were made at the electrospray probe tip and consisted of either 10mM triethylamine in acetonitrile or 50/50 isopropanol/2-methoxy ethanol (IPA/2-MeOEtOH) at 18µl/min using a Phoenix 20 syringe pump (Fisons Instruments SPA, Rodano, Italy). All mass spectra and mass chromatograms were acquired on a VG Platform single quadrupole mass spectrometer. (Fisons Instruments, VG Biotech, Altrincham, UK) operating in negative ion electrospray mode. Infusion experiments used a Harvard Apparatus (South Natick, MA) Model 22 syringe pump at 5µl/min. Dry nitrogen at 300l/hr was used for drying, and 50l/hr was used for nebulization The source was maintained at 30°C.

A series of oligonucleotides with the sequence GCTTXXTTGC was used where the central two nucleosides marked by X are nominally G and A, but have been replaced by one or the other of the derivatives, 8-oxo-2'-deoxyguanosine (8-oxo-dG) and 8-oxo-2'-deoxyadenosine (8-oxo-dA). This replacement increases the mass of the oligonucleotide by 16 corresponding to the addition of a single oxygen. The mass spectra of the 8-oxo-dG and 8-oxo-dA are essentially

identical. The 8-oxo derivatives and the unmodified oligonucleotide are not well resolved chromatographically; the two derivatives coelute. The relative amounts of modified *vs.* unmodified oligonucleotides can be observed by monitoring the triply charged $[M-3H]^{3-}$ ions of the respective sequences (Figure 1). Relative intensities of the two triply charged species at 1010 and 1015 from the coeluting 10-mer and 8-oxo derivatives are indicative of the amount of each species injected on column.

FIGURE 1

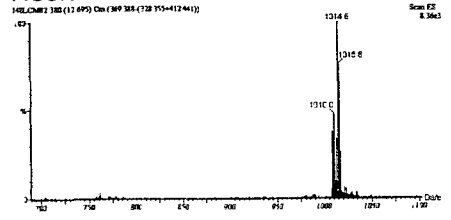

Spectra from coeluting GTTCXXTTGCand GTTCAGTTGC. The base peaks are the triply charged species.

In the second pair of oligonucleotides with the sequence GCTXCT, the adenosine has been eliminated leaving only the furan in the "X" marked site of the 6 base oligonucleotide. The sequence with and without the adenosine base can be easily separated chromatographically as shown in Figure 2. The spectra obtained from these chromatograms are presented in Figure 3. The base peak in each of these spectra are the $[M-2H]^{2-}$ from each of the oligonucleotides. The spectra do not, however, show the triply or quadruply charged species. In such a case, the presence of adduct ions help to confirm the charge state of the ion The spectra in Figure 3 were aquired with a postcolumn addition that enhanced ionization but did not suppress adduct formation. These can be compared with the spectra in Figure 1. If sodium adducts had not been supressed by the postcolumn addition of 10mM TEA in acetonitrile identification of these two coeluting species would be much more difficult.

FIGURE 2

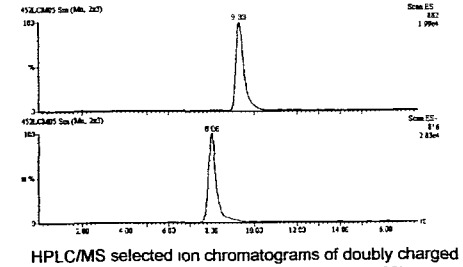

HPLC/MS selected ion chromatograms of doubly charged GCTXCT (m/z 816)and GCTACT (m/z 882)

FIGURE 3

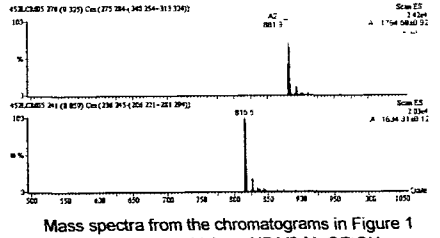

Mass spectra from the chromatograms in Figure 1 Postcolumn addition of IPA/2-MeOEtOH

Conclusions: The methods described here can be adapted for LC/MS analysis for many types of oligonucleotides. Postcolumn addition of volatile solvents facilitates ionization from HPLC systems that are currently in wide use. Volatile salts added after separation can reduce the level of adduct formation.

The Incorporation of Sample Stacking Techniques into the Capillary Electrophoresis-CFFAB-Mass Spectrometric Analysis of DNA Adducts

Susan Wolf and Paul Vouros; Department of Chemistry, Northeastern University, Boston, MA 02115

In previous work, we have examined the utility of CZE-CFFAB-MS for the characterization of DNA adduct mixtures and have observed high concentration detection limits associated with the well-known low injection volume requirement of CZE. Recent attempts to address this limitation have resulted in a number of innovations including a high volume sample stacking technique which is especially suited to the detection of negative ions (1). In this study, we investigated the ease with which this stacking technique could be interfaced with CZE-MS and determined the sensitivity with which a model adduct, AAF-C8-dGMP (the C8 N-acetyl-2-aminofluorene adduct of deoxyguanosine-5'-monophosphate), could be detected in the CZE-CFFAB-MS mode. This methodology was then applied to the analysis of AAF-DNA adducts generated *in vitro* to assess its usefulness for "real" sample analysis.

Experimental. Adaptation of the stacking technique to CZE-MS analysis required the inclusion of a true cathode buffer reservoir in the analytical set-up and the employment of off-line stacking prior to on-line CZE-MS analysis. A modified plexiglass liquid junction interface which relied upon the use of teflon tubing sleeves to allow for the rapid introduction and alignment of the capillaries in the interface was constructed to meet this requirement. A 40 cm x 50 um ID capillary was used to transfer materials eluting from the CE capillary (75 um ID X 75 cm) along with a make-up flow of CFFAB matrix solution present in the interface into the CF probe. A CFFAB solution of 1% glycerol, 39% MeOH, 60% 100mM NH_4OAc at a vacuum induced flow rate of ~ 2.5 uL/min was employed. Electrophoretic separations were conducted at 20kV (15uA) employing buffer of 0.01 M NH_4OAc adjusted with NH_4OH to pH 9.4. A VG Fisons Quattro triple quadrupole mass spectrometer, outfitted with a cesium ion gun, was employed for all mass spectrometric analyses. 1.0 mg of calf thymus DNA was reacted with 1.0 mg N-acetoxy-N-acetyl-2-aminofluorene after which the DNA was enzymatically cleaved to deoxynucleotide-5'-monophosphates (2). A centrifuge filter (MW 3000 cutoff) was employed to remove enzymes and undigested oligonucleotides. Adducts were then isolated using a polystyrene divinylbenzene solid phase extraction cartridge in fractions of low enough conductivity to permit analysis by stacking CZE-CFFAB-MS.

Results and Discussion. *Standard Analysis.* Under typical injection conditions, ~3.5 nL of 5 X 10^{-4}M (1 ng total) AAF-dGMP solution provided a good quality normal scan positive ion FAB spectrum by CZE-MS. With stacking, the concentration detection limit could be lowered by two orders of magnitude as shown in Figure 1. The ~100% recovery at 10^{-5}-10^{-6}M levels indicated that, for the conditions employed, the mobility of the adduct was high enough to prevent losses during the stacking process. When MRM detection was used (m/z 569→373, loss of dRMP from MH+), the signal response obtained was linear over a range from 25 pg (350 nL $1.25X10^{-7}$M injected) to 1.0 ng (35 nL $5X10^{-5}$M injected). Full column (3.3 uL) stacking of 117 pg of AAF-C8-dGMP from a $6.25X10^{-8}$M solution resulted in an 86% recovery of the injected adduct.

Adducts Isolated from DNA In Vitro. Constant neutral loss scanning of the loss of dRMP provided signals corresponding to the MH+ of the two expected dGMP adducts when a 175 nL injection of an adduct extract solution was made (Figure 2). Using the same injection volume, good detectability for the major adduct (AAF-C8-dGMP) was also achieved in full scan and CID (m/z 373) modes. It was not possible to obtain such information on the N^2 species, because mass spectral signals from this compound were obscured by a coeluting unknown related to the C8 adduct.

(1) Chien, R.L., Burgi, D.S. *Anal. Chem.* **1992**, *64*, 1046-1050.
(2) Fu, P.P. et al. *Carcinogen.* **1991**, *12*, 609-616.

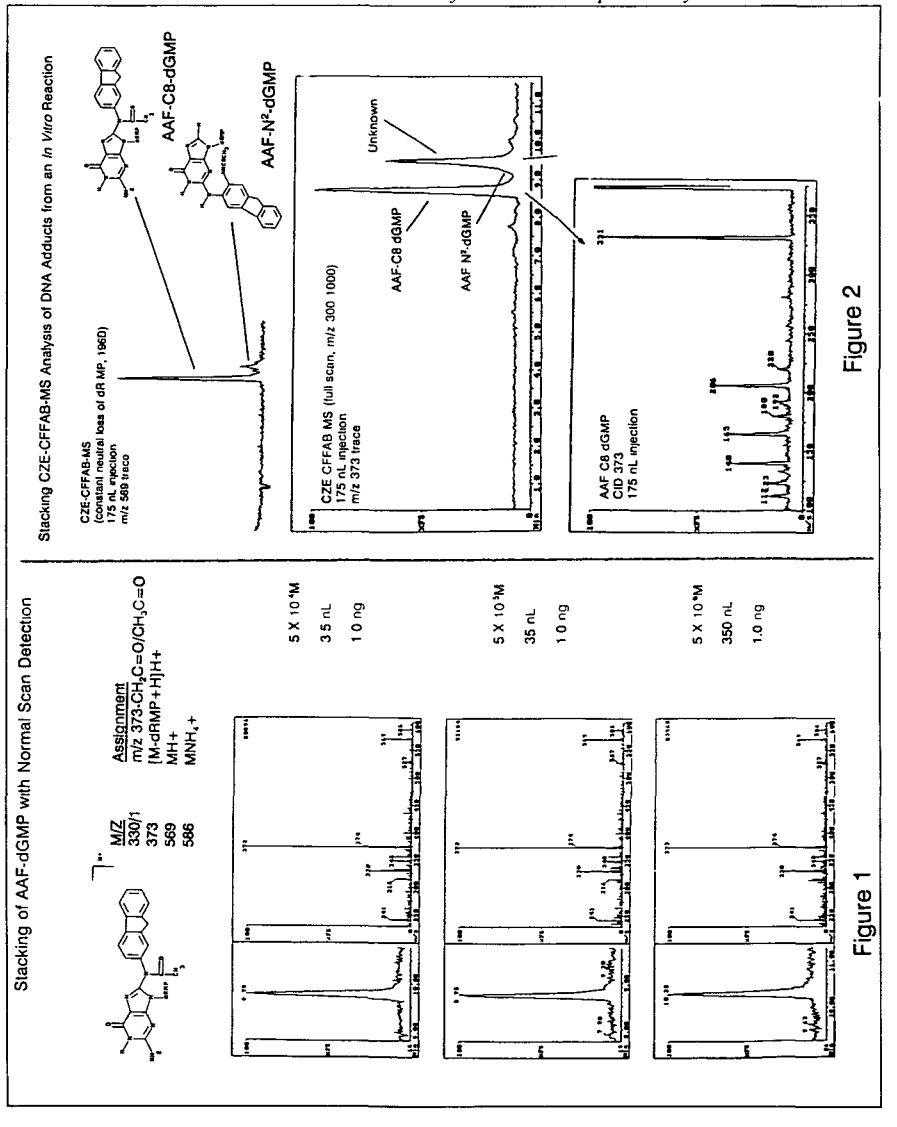

EXPERIMENTAL CONDITIONS FOR THE MATRIX-ASSISTED LASER DESORPTION FTMS ANALYSIS OF MODIFIED OLIGONUCLEOTIDES[a]

E.A. Stemmler*, R.L.Hettich, G.B. Hurst, and M.V. Buchanan**
*Bowdoin College, Brunswick, ME 04011
**Oak Ridge National Laboratory, Oak Ridge, TN 37831-6120.

Matrix-assisted laser desorption/ionization (MALDI)[1,2] Fourier transform ion cyclotron resonance mass spectrometry (FTMS) at 355 nm is being developed for the structural characterization of normal and modified oligonucleotides. Matrix-assisted studies on the FTMS are being duplicated on a newly constructed TOF mass spectrometer to help discriminate between factors influencing ion production (i.e. sample preparation) and ion trapping and detection on the FTMS.

We have found that efficient ion trapping, matrix selection, and laser conditions are critical to the desorption and detection of oligonucleotides by FTMS. The previous upper mass limit for MALDI-produced ions has been addressed by pulsed trapping plate ion deceleration experiments first described by Castoro et al[3]. Previous MALDI-FTMS studies of oligonucleotides were limited to hexamers[4]. By implementing the deceleration technique, the molecular ion for a mixed base 12-mer, 5'-CTGTACCGATTT-3' (MW = 3610.5), was observed in the negative ion mode. In addition, bovine insulin (MW = 5733.5) has been detected in the positive ion mode. The deceleration step used to observing these high mass ions involved setting the source trapping plate at 0 V and the conductance limit at -9.0 V (for negative ions) prior to the laser desorption event. Following the laser pulse a variable time delay (t_D) of 150 to 450 μs is inserted prior to setting both the conductance limit and source trapping plates at -1.5 V for ion detection. The detection of $[M-H]^-$ ions from an oligodeoxythymidylic acid mixture, at two ion deceleration times, is shown in Figure 1.

While ion deceleration methods have extended the FTMS mass range for MALDI-produced ions, the selection of an appropriate MALDI matrix is essential for the generation of intact $[M-H]^-$ oligonucleotide ions. Using dinucleotides as model compounds for preliminary screening experiments we found that basic matrices, such as 1,5-diaminonaphthalene and 9-aminophenanthrene, promoted extensive dinucleotide fragmentation. Fragmentation was reduced using 2,5-dihydroxybenzoic acid; however, the newly introduced matrix, 3-hydroxypicolinic acid[5], significantly improved our ability to detect unfragmented dinucleotides and mixed base oligomers. When FT and TOF mass spectra have been compared, fragmentation on the TOF is significantly reduced relative to that observed by FTMS. This may be a consequence of the longer times (milliseconds) required for FTMS detection.

The characterization of modified nucleic acid constituents in living systems is important for understanding the molecular basis of biological abnormalities, such as cancer. We have applied MALDI-FTMS to the analysis of modified nucleotides, nucleosides and oligonucleotides. For example, we have analyzed the modified hexamer 5'-GCATG^{Me}C-3' (G^{Me} = O^6-methyl substituted guanine), as well as its unmodified counterpart. Using 3-hydroxypicolinic acid, intact $[M-H]^-$ ions were measured for the modified and unmodified hexamers. In contrast, using 2,5-dihydroxybenzoic acid as a matrix, structurally significant negatively-charged fragment ions permit sequence verification. In the positive ion mode, protonated base ions permit further structural characterization of the modified guanine using the trapped ion capabilities of FTMS. While MS/MS of methylated guanine isomers is not sensitive to the site of methyl substitution,

studies by Nourse et al.[6] have shown that H/D exchange reactions can be used to distinguish sites of methyl group substitution. The O^6-methyl guanine isomer is expected to undergo one slow H/D exchange. Only one other isomer, 3-methyl guanine, undergoes one H/D exchange; however, the exchange for this isomer occurs at a faster rate. Experimentally, one slow H/D exchange reaction is observed for the $G^{Me}H_2^+$ ion that appears in the MALDI mass spectrum of the modified hexamer. This supports the assignment of methyl substitution at the O^6-position for the modified guanine in this oligonucleotide.

MALDI-FTMS and TOF have been applied to the structural characterization of deoxyguanosyl and deoxyadenosyl nucleoside and nucleotide PAH triol adducts. These highly polar molecules are difficult to detect by conventional mass spectrometric methods. Using MALDI, abundant $[M+H]^+$ and $[B+2H]^+$ ions were observed by TOFMS. On the FTMS, sodiated molecular and base fragments were more abundant for deoxyguanosyl adducts. Other fragments yield structural information about the nucleoside/nucleotide, nucleic base, and PAH triol.

1. M. Karas and F. Hillenkamp, *Anal. Chem.*, **60**, 2299 (1988).
2. F. Hillenkamp, M. Karas, R.C. Beavis, and B.T. Chait, *Anal. Chem.*, **63**, 1193A (1991).
3. J.A. Castoro, C. Köster, and C. Wilkins, *Rapid Comm. Mass Spectrom.*, **6**, 239 (1992).
4. R. Hettich and M. Buchanan, *J. Am. Soc. Mass Spectrom.*, **2**, 402 (1991).
5. K.J. Wu, A. Steding, and C.H. Becker, *Rapid Comm. Mass Spectrom.*, **7**, 142 (1993).
6. B.D. Nourse, R.L. Hettich, and M.V. Buchanan, *J. Am. Soc. Mass Spectrom.* **4**, 296 (1993).

[a]Research sponsored jointly by the Office of Health and Environmental Research, U.S. Department of Energy under contract DE-AC05-84OR21400 with Martin Marietta Systems, Inc., and the DOE Faculty Research Participation Program under contract DE-AC05-76OR00033 between the U.S. Department of Energy and Oak Ridge Institute for Science and Education.

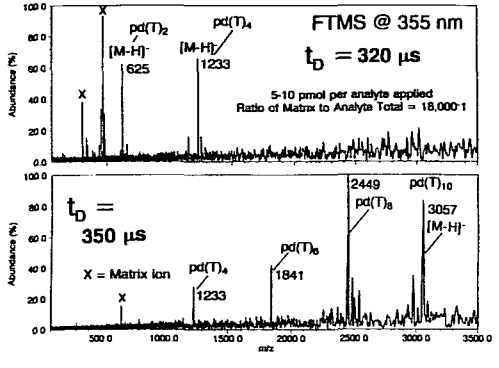

"The submitted manuscript has been authored by a contractor of the U.S. Government under contract No. DE-AC05-84OR21400. Accordingly, the U.S. Government retains a nonexclusive, royalty-free license to publish or reproduce the published form of this contribution, or allow others to do so, for U.S. Government purposes."

Figure 1. MALDI-FT mass spectra of an oligodeoxythymidylic acid mixture using 3-hydroxypicolinic acid as the matrix. The t_D values indicate the ion deceleration times.

MALDI-FTMS FOR THE CHARACTERIZATION OF ULTRAVIOLET AND X-RAY DAMAGE TO NUCLEIC ACID CONSTITUENTS *

Robert Hettich and Hiroko Yoshida
Oak Ridge National Laboratory, Oak Ridge, TN 37831-6120

Both low energy (far-ultraviolet) and high energy (x-ray) radiation can cause DNA damage by inducing strand breaks, base modifications, and sugar alterations. These changes may lead to mutations and ultimately cell death if they cannot be biologically repaired. It is therefore necessary to characterize both the identities (at the isomeric level) and the abundances of the radiation-induced products to probe the nature of DNA damage in these cases. Matrix-assisted laser desorption/ionization Fourier transform mass spectrometry (MALDI-FTMS) is well-suited for the direct detection and characterization of radiation-induced damage to nucleic acid constituents, including oligonucleotides. This technique eliminates the need to hydrolyze and derivatize the samples prior to mass analysis, thereby reducing the possibility of modifying the sample after irradiation. The accurate mass measurement and ion trapping capabilities of FTMS permit the detailed examination of the structures of these products. The experimental approach for these studies focusses on the development of MALDI-FTMS for the sensitive detection (picomole) and structural characterization of radiation-induced products. Reverse phase liquid chromatography (HPLC) is used to purify irradiated samples prior to mass analysis and to quantitate the dose dependent formation of products after they have been identified by mass spectrometry.

Hydroxylated thymines are a common product generated by x-ray irradiation of thymine-containing nucleic acid constituents. In particular, it is important to not only identify a hydroxylated product but also determine the site of hydroxylation on the thymine base. To address this issue, the collision-induced dissociation (CID) spectra of thymine glycol, 5-hydroxydihydrothymine, 6-hydroxydihydrothymine, and 5-hydroxymethyluracil standards were examined. Both thymine glycol and 5-hydroxymethyluracil reveal abundant fragment ions corresponding to loss of water from the $(M-H)^-$ ions. The two isomers of hydroxydihydrohthymine can also be differentiated by CID. Whereas 5-hydroxydihydrothymine fragments to generate NCO^- as the only fragment ion, 6-hydroxydihydrothymine also reveals a fragment ion corresponding to loss of HNCO. Examination of a ^{60}Co gamma ray irradiated sample of d(TpT) revealed the presence of hydroxylated thymines as well as a variety of other products. HPLC was used to purify fractions, and was found to be quite useful for separating the radiation-induced products from the unmodified d(TpT) prior to FTMS examination.

Pyrimidine photodimers are generated by the far-ultraviolet irradiation of DNA. These species consist of the cyclobutane pyrimidine dimers (for example, cis-syn and trans-syn) as well as the 6-4 and Dewar valence isomers. A series of these isomeric dimer standards were examined for d(UpT). MALDI-FTMS was used to generate characteristic negative ions, including $(M-H)^-$, for all of these species. CID of the cis-syn d(UpT) and the trans-syn d(UpT) revealed only one fragment ion, m/z 433 (loss of a sugar ring), and could not be differentiated from each other. In contrast, both the 6-4 d(UpT) and the Dewar valence d(UpT), fragmented to give an ion at m/z 432, loss of H_3PO_4. Figure 1 illustrates the CID of the cis-syn isomer and Figure 2 shows the CID of the Dewar valence isomer. Research is currently directed at development of other ion-molecule reactions which can be used to differentiate these isomers.

* Research sponsored by the Department of Energy, Office of Health and Environmental Research under contract DE-AC05-84OR21400 with Martin Marietta Energy Systems, Inc.

Figure 1

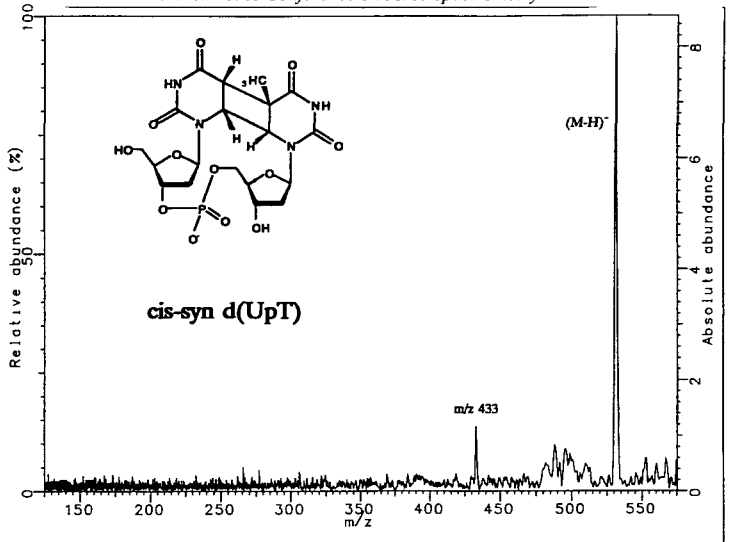

Figure 2

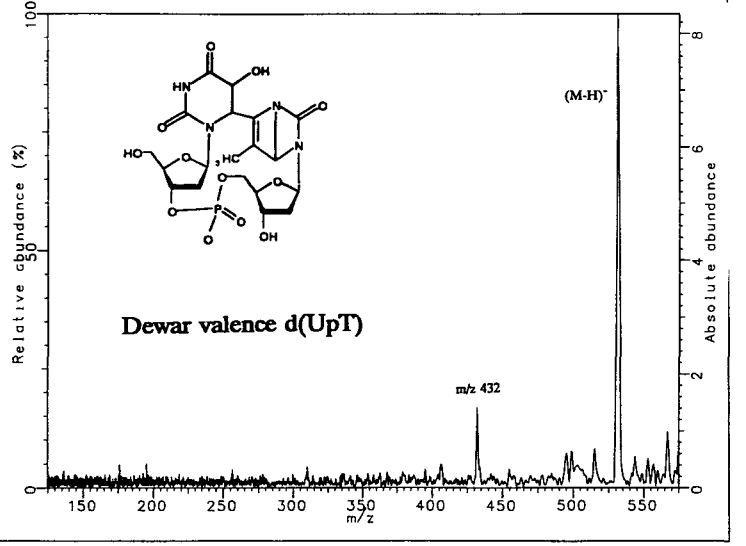

7 Day Low Level Dose Response Study of MeIQx in Rats using Accelerator Mass Spectrometry

CHRIS. FRANTZ[1], ESTER FULTZ[1], JOHN VOGEL[2], AND KEN TURTELTAUB[1]
BIOLOGY AND BIOTECHNOLOGY RESEARCH PROGRAM[1] AND CENTER FOR ACCELERATOR MASS SPECTROMETRY[2], LAWRENCE LIVERMORE NATIONAL LABORATORY, LIVERMORE, CA

2-amino-3,8-dimethylimidazo[4,5-*f*]quinoxaline (MeIQx) is a heterocyclic amine that forms in meats during cooking and has been shown to cause cancer in laboratory animals at high doses. Structurally, MeIQx belongs to a class of heterocyclic amines often referred to as amino-imidazoazaarenes or AIA's. MeIQx, like all AIA-type compounds, is highly mutagenic in the Ames/*Salmonella* microsome-mediated assay, having a potency, depending on the bacterial tester strain, between 56,000 and 99,000 revertants/ ug (Felton and Knize 1990). MeIQx is also mutagenic in mammalian cell systems. Long-term feeding studies in mice (0.06% MeIQx in diet) show an 43% and 99% incidence of liver tumors in male and female CDF_1 mice, respectively (Ohgaki 1987). In F344 rats continuously fed MeIQx (0.04% in diet for 429 days) the incidence of liver tumors was 100% and 53% for males and females, respectively (Kato 1988). A high incidence of zymbal gland tumors in males and females, as well as clitoral gland tumors in female rats, were also found.

Although MeIQx is carcinogenic in rodents at high doses, the significance of these finding for humans is unclear since humans are exposed to much lower amounts of this compound (ngs/g meat) in the diet. We report here on the use of accelerator mass spectrometry (AMS) to trace the absorption, distribution, and elimination of human-relevant levels of [^{14}C]-MeIQx given to animals. We also report on the relationship between DNA binding and administered dose using [^{14}C]-MeIQx (sp. act.=10 mCi/mmol). Using this methodology, we were able to detect sub-pg levels of [^{14}C]-MeIQx in the tissues and DNA of the animals.

The effects of dose on tissue and DNA levels of MeIQx was examined in a sub-chronic feeding regimen by feeding Male Sprague Dawley rats [^{14}C]-MeIQx at concentrations ranging from 1 ng/kg/day up to 34 ug/kg/day in their diet for 7 days. A linear relationship between dose and tissue concentration was found for all tissues at the end of the 7 day exposure. At all dose levels the highest concentrations of [^{14}C]-MeIQx were found in the liver and kidney. The next highest levels were in the intestine, followed by the stomach, then the spleen, thymus, heart, pancreas, blood, and finally the brain.

The relationship between DNA damage and administered dose has also been examined. The dose response is linear ($y= 25.2 + 58302 x$ $R=0.99991$). A comparison of the biologically available [^{14}C]-MeIQx (liver tissue levels) to the biologically active [^{14}C]-MeIQx (bound to liver DNA) suggests that the percentage of MeIQx in the liver tissue that bound to DNA was slightly less at the high doses than the lower doses, though not significantly so. This relationship may be a function of metabolism or DNA repair kinetics.

In summary, AMS has been used to show that the biologically available dose (tissue concentration) decreases proportionally with decreasing administered dose from the high doses used in cancer assays to doses relevant for human exposure. The doses used in this study cover 3 orders of magnitude demonstrating the large dynamic range of the method.

This work performed under the auspices of the U.S. Department of Energy by Lawrence Livermore National Laboratory under contract no. W-7405-ENG-48 and supported by NIH Grant CA55861.

DETECTION OF DNA ADDUCTS BY GC-ECNI-MS. Roger W. Giese, Manasi Saha, Samy Abdel-Baky, Kariman Allam and Amir Abushamaa. Bouve College of Pharmacy and Health Sciences, and Barnett Institute, Northeastern University, Boston, MA 02115.

Covalent damage to DNA by endogenous and exogeneous agents in vivo is termed "DNA adducts". The measurement of DNA adducts in human samples is important to help define the risks to health from exposure of people to carcinogens and mutagens. We are converting DNA adducts at a trace level via chemical transformation and electrophoric derivatization into products which can be detected with high sensitivity by GC-ECNI-MS. A Hewlett-Packard Model 5988A mass spectrometer is being used.

In Fig. 1 is shown a scheme for the detection in general of diolepoxide polyaromatic hydrocarbon DNA adducts, using benzo[a]pyrene as a model. Mild acid hydrolysis of the DNA releases the adduct as a tetrol. The latter is oxidized with potassium superoxide (1) to pyrene-2,3-dicarboxylic acid, which, in turn, is pentafluorobenzylated to DIESTER. The latter can be detected at the low attomole level, as a standard, by GC-ECNI-MS (2). Fig. 2 shows the detection of this particular adduct in human lymphocytes exposed in cell culture to benzo[a]pyrene: 5 adducts in 10^7 nucleotides were found.

Figure 1

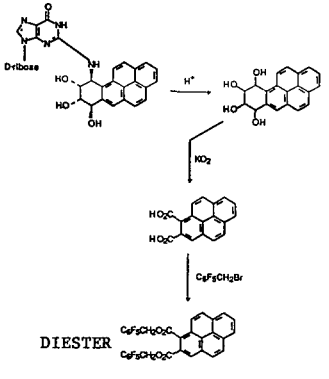

Figure 2

Selected Ion GC-ECNI-MS chromatograms from nonexposed and B(a)P-exposed cells. A. m/z 469 to detect Diester (peak 1) and apparent Diester (peak 1'). B. m/z 477 to detect d8-Diester (peak 2).

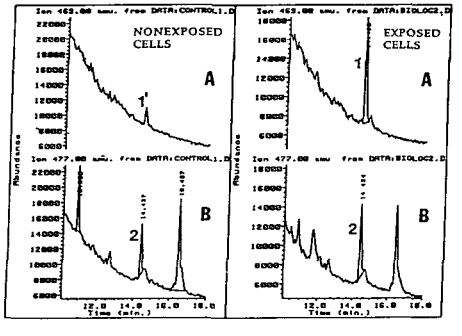

In Fig. 3 is shown a scheme for the detection in general of N7-G alkyl and hydroxyalkyl DNA adducts, using N7-(2-hydroxyethyl)guanine (an ethylene oxide DNA adduct) as a model, along with the detection of 7 fmol of a standard of the latter compound. This type of adduct can be recovered from DNA by neutral thermal hydrolysis. Conversion to a corresponding xanthine by nitrous acid, followed by pentafluorobenzylation, leads to the final derivative. Like the above product, this derivative can be detected as a standard at the low attomole level by GC-ECNI-MS. The detection of 165 pg of this adduct spiked into 100 ug of calf thymus DNA is shown in Fig. 4.

Figure 3

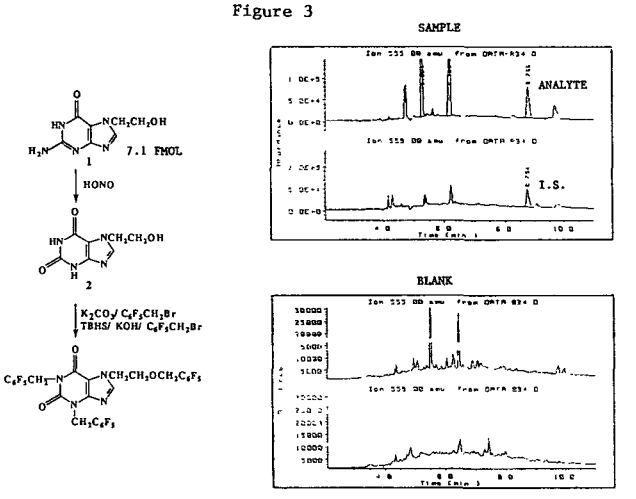

Figure 4

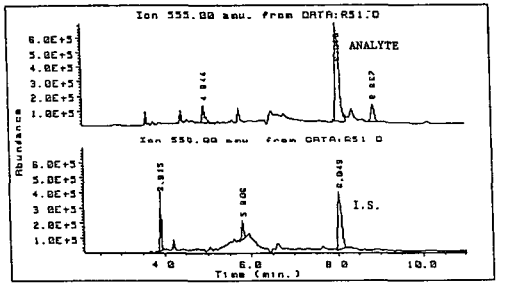

References: (1) Sotiriou, C., Li, W., and Giese, R.W., J. Org. Chem. 55, 2159-2164 (1990). (2) Baky, S.A. and Giese, R.W., Anal. Chem. 63, 2980-2989 (1991).

Spatial Distribution of Nucleic Bases using SIMS

J. M. McMahon, R. T. Short, W. B. Holland, and P. J. Todd
Analytical Chemistry Division
Oak Ridge National Laboratory
Oak Ridge, TN 37831-6365

The Human Genome Project will require rapid analytical throughput to obtain the extensive analytical data required to map the Human Genome. Selectivity, sensitivity, and reproducibility must be linked to rapid throughput for a technique to meet all the analytical demands of the project. Imaging SIMS easily meets these criteria.

Analysis by SIMS is rapid because the primary ion beam can be rastered quickly across the sample. In particular, we have developed a wide-angle secondary ion microprobe that is capable of producing images from samples 1 cm^2. If several thousand spots of nucleic bases were arrayed upon a target, all could be identified, and the DNA strand sequenced by deduction, in ten minutes.

Phase I of this study involves the molecular mapping of an array of one each of the four bases (adenine, cytosine, guanine, and thymine). Figures 1A through 1D illustrate the selective mapping of each base according to its mass-to-charge; Figure 1E is a composite of these four images, and reflects the actual spatial relationship of the spots. These figures demonstrate the ease with which Imaging SIMS can map the molecular distribution of several species and reconstruct the overall distribution.

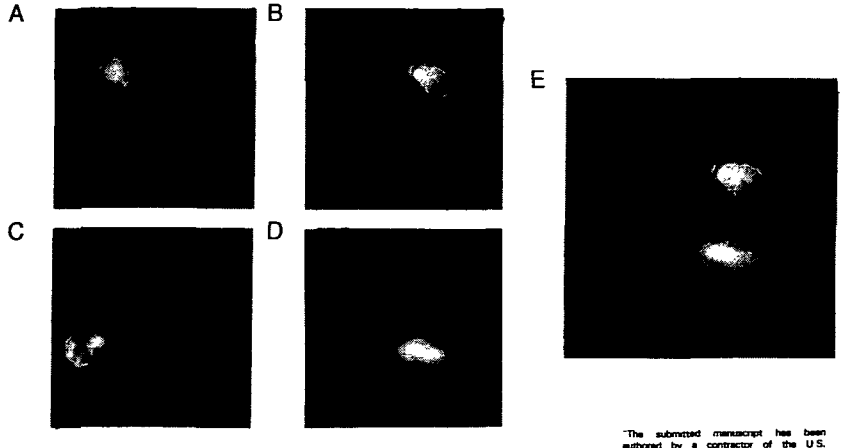

Figure 1. Secondary ion images of array of nucleic bases. A) Image showing position of guanine spot, B) adenine spot, C) thymine spot, D) cytosine spot, and E) composite image of all four spots.

"The submitted manuscript has been authored by a contractor of the U.S. Government under contract No. DE-AC05-84OR21400. Accordingly, the U.S. Government retains a nonexclusive, royalty-free license to publish or reproduce the published form of this contribution, or allow others to do so, for U.S. Government purposes."

As with SIMS in general the nature of the surface proved critical to analytical success, particularly for quantitation and reproducibility. After much experimenting with a variety of surfaces, best results were obtained with electropolished copper targets that were gold coated to inhibit complexation of analyte and metal, and then carbon coated to prevent sample spreading (see Figure 2). When the drop of sample analyte was applied, best results were seen when drying was done rapidly in vacuum. Figure 3 is an example of this surface preparation and sample drying technique.

The concentration profile of cytosine is shown in Figure 4. Using $3x10^{-7}$ liter of 10^{-5} M cytosine on a 1 mm diameter spot (rastered with a 100 µm diameter primary beam) results in a detection limit of $3x10^{-14}$ mol/pixel, or 30 femtomoles.

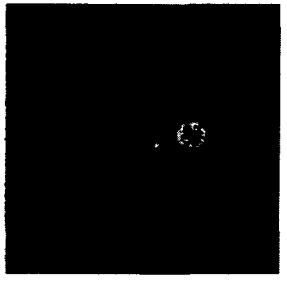

Figure 3. Image of sample prepared as described in Figure 2. Three spots of 10^{-5} M cytosine are easily seen; note even distribution in each circular spot.

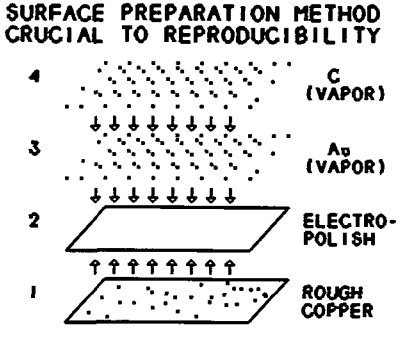

Figure 2. Schematic of surface preparation. An electropolished copper plate is gold coated followed by carbon coating. After applying sample drop to surface, rapid drying in vacuum is employed.

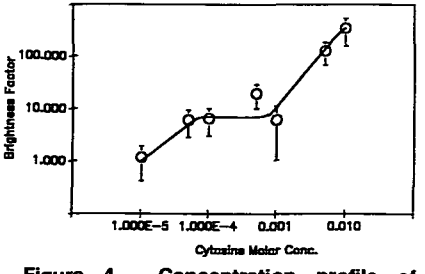

Figure 4. Concentration profile of cytosine. The Brightness Factor (comparable to intensity) vs. Concentration profile of cytosine. The 10^{-5} M concentration represents detection limits of 30 femtomoles.

This work was funded by Grant GM-RO1-41617 from the National Institutes of Health and by DOE Office of Basic Energy Sciences under contract number DE-AC05-84OR21400 with Martin Marietta Energy Systems, Inc.

MASS SPECTROMETRIC IDENTIFICATION OF 2'-DEOXYCYTIDINE ADDUCTS FROM REACTIONS WITH ACROLEIN AND 2-BROMOACROLEIN

Ahmed Chenna and Charles R. Iden

Department of Pharmacological Sciences, Health Sciences Center
State University of New York at Stony Brook, Stony Brook, NY 11794-8651

Acrolein is ubiquitous in the human environment, and a major source is the result of incomplete combustion of organic matter. Studies have shown that acrolein is mutagenic toward *Salmonella typhimurium* and can interact directly with DNA. Several investigators have characterized adducts of acrolein with deoxyguanosine, adenine and cytosine derivatives, deoxycytidine-5'-monophosphate, and thymidine. Halogen substitution at C-2 of acrolein should increase the rate of reaction with nucleobases in DNA; accordingly, 2-bromoacrolein and several chloroacroleins have displayed a higher mutagenic potency than acrolein. 2-Bromoacrolein is a genotoxic metabolite of *tris*(2,3-dibromopropyl)phosphate (Tris-BP) and the nematocide, 1,2-dibromo-3-chloropropane. Tris-BP may be activated by conversion to reactive electrophiles such as 2-bromoacrolein by cytochrome P_{450}. The chemical structure of the products from the reaction of 2-bromoacrolein with 2'-deoxyguanosine and thymidine have been determined, and reaction with DNA produces an unstable thymidine adduct. The goal of the present study was to determine the chemical structures of all major adducts formed in the reaction of 2'-deoxycytidine with 2-bromoacrolein and acrolein under physiological conditions.

2'-Deoxycytidine was permitted to react with either acrolein or 2-bromoacrolein in 0.1 M sodium acetate buffer (pH 4.4 or 7.4) at 37°C. After 38 h the solvent was evaporated under reduced pressure, and silica gel thin layer chromatography (20:80, methanol:methylene chloride) indicated that a single major product was present for each reaction. Flash chromatography on silica gel (15:85, methanol:methylene chloride) permitted separation from 2'-deoxycytidine, but the unknown products failed to crystalize from methanol. HPLC analysis of the reaction mixture separated 2'-deoxycytidine from a mixture of product stereoisomers.

The UV spectrum of the product of the reaction with acrolein was recorded at several pH values, and results are characteristic of 3,N^4-substitution on cytidine. The FAB mass spectrum (Fig. 1a) shows an MH^+ peak at *m/z* 284 (13.5%), a natriated molecular ion at *m/z 306* (17.9%) and a BH_2^+ peak of *m/z* 168 (100%). The 300 MHz ^1H NMR spectrum (Me_2SO-d_6) was compared to that for 2'-deoxycytidine and suggests the formation of a cyclic adduct; however, the position of the hydroxy group, whether at C-7 or C-9, cannot be determined from the spectral data. In order to determine the location of the hydroxy group, the product was hydrolyzed with sodium hydroxide to open the ring and then reduced with sodium borohydride to give the stable alcohol. This product, (N^3-(3"-hydroxypropyl)-2'-deoxyuridine), was identified by UV, FAB/MS and ^{1}NMR. Chemical transformation confirmed the position of the hydroxy at C-7, and the exocyclic adduct is 3-(2'-deoxyribosyl)-7,8,9-trihydro-7-hydroxypyrimido-[3,4-c]pyrimidin-2-one.

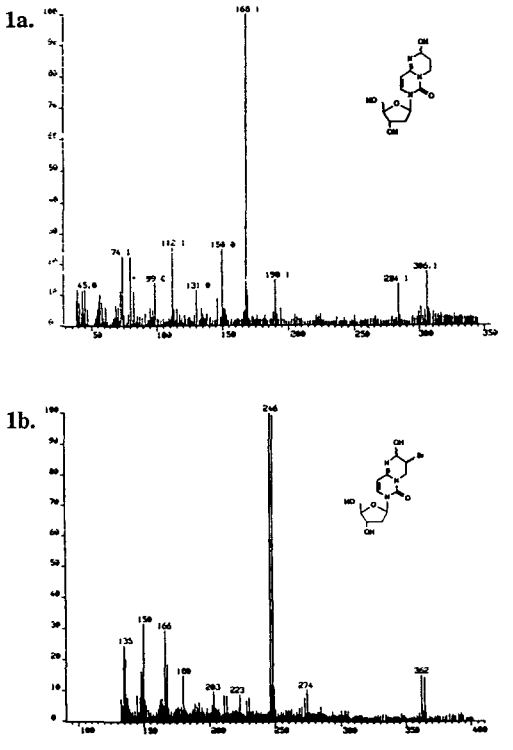

Figure 1. FAB mass spectrum of the exocyclic 2'-deoxycytidine adduct formed by a). acrolein and b). 2-bromoacrolein.

The reaction of 2'-deoxycytidine with 2-bromoacrolein at pH 4.4 gave a single major product which was purified by flash chromatography. The UV spectrum of this substance recorded at pH 2.3 and 4.2 shows λ_{max} at 288 nm, whereas at pH 10.8, λ_{max} of 228 and 274 nm are present. These changes in UV spectral character as a function of pH are characteristic of 3,N^4-substitution on a cytidine residue. The positive ion FAB mass spectrum of this compound (Fig. 1b) has an MH^+ at *m/z* 362 (15.0%) and a corresponding peak at *m/z* 364 (14.4%) containing the ^{81}Br isotope. BH_2^+ peaks at *m/z* 246 (100.0%) and 248 (98.9%) are formed by cleavage of the glycosidic bond. This important fragmentation shows that Br isotopes are present in the modified base moiety. In this reaction two new chiral centers are formed at C-7 and C-8 derived from C-2 and C-1 of 2-bromoacrolein. Because of these chiral centers and those of the sugar ring, the product exists as a mixture of diastereomers which were not separable by HPLC. Consequently, the ^1H NMR is complex and difficult to interpret. However, the spectrum of this mixture does not show any exchangeable protons in the region between 6.2 to 7.5 ppm indicating there is no NH_2 group in the compound. The spectral information did not allow the position of the hydroxy group to be uniquely determined; however, ring opening with sodium bicarbonate gave three N^3-substituted 2'-deoxyuridines which were characterized by UV, FAB/MS, ESI/MS, and ^{1} NMR and confirmed the position of the hydroxy at C-7. The 2-bromoacrolein adduct is 3-(2'-deoxyribosyl)-7,8,9-trihydro-7-hydroxy-8-bromopyrimido-[3,4-c]pyrimidin-2-one.

Enhanced Sensitivity in the Negative Ion FAB-MS Analysis of Polyanionic Organic Compounds Through the Use of Cationic Additives to the FAB Matrix

Zhi-Heng Huang[1], Bao-Jen Shyong[1], Kathleen Noon[2], John Allison[2], and Douglas A. Gage[1]

Departments of Biochemistry[1] and Chemistry[2], Michigan State University, East Lansing, MI 48824

Negative-ion (NI) FAB MS has been the method of choice for characterizing a variety of polyanionic compounds such as nucleotides, oligonucleotides (up to 10 mers), nucleotide sugars, cofactors, sugar phosphates and sulfates, and polar conjugates of xenobiotic substances. However, problems remain. First, the sensitivity is generally poor. Relatively large sample sizes (up to 10 nmoles or higher) are commonly required to obtain a good quality spectrum. Second, the spectra frequently exhibit a variety of pseudomolecular ions, containing various numbers of alkali ions.

It has been proposed that addition of cationic surfactants to such samples can improve sensitivity. For example, it was shown by Ligon *et al.* [W.V. Ligon, Jr. and S.B. Dorn, *Fresenius Z. Anal. Chem.*, 325, 626-627 (1986)] and Barofsky *et al.* (J.P. Pavlovich, T.-Y. Yen, D.F. Barofsky, and B.U.R. Sundqvist, *Proc. 40th ASMS Conference on Mass Spectrom. Allied Topics*, pp. 543-544, 1992) that the $[M-H]^-$ signal for ATP was significantly enhanced when cetyl pyridinium acetate was added to the FAB matrix.

We have evaluated a large number of cationic surfactants for improving the NI-FAB analysis of the title compounds which respond poorly under ordinary conditions, and found that quaternary ammonium-type surfactants having an additional, basic center ("bifunctional" surfactants) increase analyte response more than the simple cationic surfactants that have been investigated previously.

The aims of this work are (1) evaluation of N-alkylnicotinium halides for their ability to enhance the signals of the model compound, coenzyme A; (2) study factors influencing the enhancement effect; and (3) study the scope of application for a potentially useful surfactant, N-octyl nicotinium bromide (ONBr).

RESULTS

Of the various N-alkyl nicotinium halides tested, the analog having a C-8 chain, ONBr, showed the most promising signal enhancement effect for the $[M-H]^-$ of the model compound, coenzyme A (Na salt). When ONBr is added to a polyanionic compound in dilute glycerol, the following phenomena are observed:

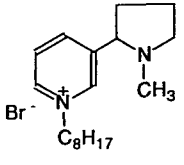

ONBr

- enhanced response of $[M-H]^-$ and the presence of fragment ion peaks in NI-FAB, shown in the spectra below for Coenzyme A, Na salt, FW=767 (for free acid = M);
- reduced tendency of cationization resulting in a much simplified spectral pattern.

Mechanisms have been proposed to explain the phenomena observed:

- Ionic forms of the analyte accumulate at the surface via ion-pair interactions with ON^+, or through establishment of an electrical double layer at the surface.
- ONBr alters the chemical environment from which the analyte desorbs.

CONCLUSION

N-Octyl nicotinium bromide has been shown to be an efficient reagent to assist in the desorption of compounds containing multiple acidic functionalities under NI-FAB conditions. The advantages include: (1) 1 - 2 orders of magnitude gain in intensities; (2) simplified spectra, mostly free of alkali ion clusters; and (3) simple to implement, without requiring other pretreatments like desalting and derivatization.

ACKNOWLEDGEMENTS

This work was supported by the NIH grant (RR-00480) to Professor J.T. Watson. Thanks are also due to Dr. M. Harple, Oak Ridge National Laboratory, for provision of carboxyribose diphosphate.

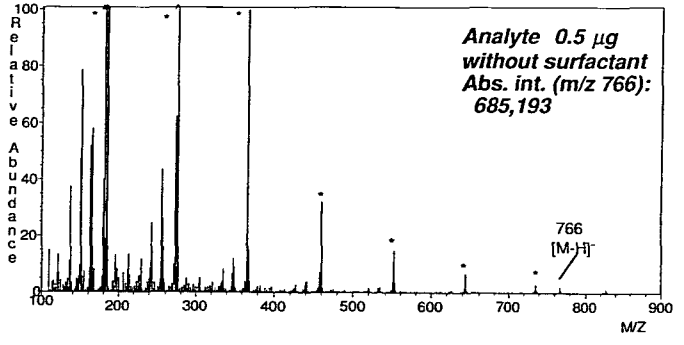

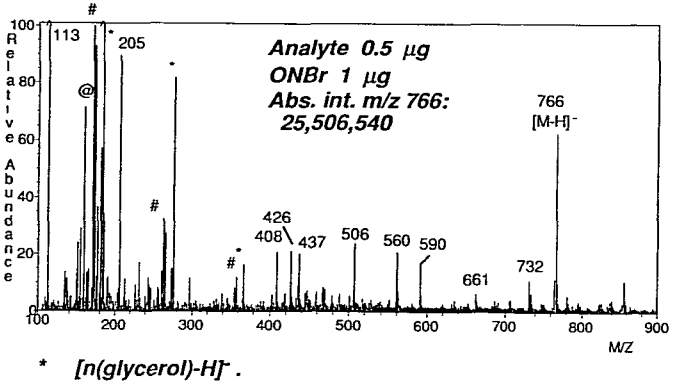

* *[n(glycerol)-H]⁻.*

\# *[Br⁻+ n(glycerol)]⁻.*

@ *[pyrophosphate-H]⁻ and [pyrophosphate-H_2O-H]⁻.*

QUANTITATIVE FAST ATOM BOMBARDMENT MASS SPECTROMETRY: ESTIMATION OF CYCLIC NUCLEOTIDE-DEPENDENT PROTEIN KINASE ACTIVITY

AM Evans [a], FM Harris [b], AG Brenton [b], TJ Walton [a] and RP Newton [a]

[a] *Biochemistry Group, School of Biological Sciences,* [b] *Mass Spectrometry Research Unit, University College of Swansea, Singleton Park, Swansea SA2 8PP, UK.*

INTRODUCTION

Cyclic nucleotides are naturally occurring molecules composed of a heterocyclic base, a ribose ring and a cyclic phosphate group. In mammals one such cyclic nucleotide, adenosine 3',5'- cyclic monophosphate (cyclic AMP), acts as the intracellular mediator of the action of numerous hormones and neurotransmitters, this action leading to its description as a biochemical second messenger, transducing the primary extracellular message from the hormone or neurotransmitter. The response to this message is brought about by the action of a protein which is able to recognise and selectively bind cyclic AMP; this protein is one of two types of cyclic AMP-dependent protein kinase, and when it has bound cyclic AMP it is able to catalyse the phosphorylation of a wide range of substrate proteins:

$$\text{Protein} + \text{ATP} \xrightarrow[\text{Cyclic AMP}]{\text{Cyclic AMP-dependent protein kinase}} \text{Protein-PO}_4 + \text{ADP}$$

The protein so phosphorylated changes shape, resulting in a change in activity, for example in an enzyme or a membrane protein; this change in activity manifests itself as the physiological response to the hormone or neurotransmitter In view of the potency of cyclic AMP and ubiquity of this responsive kinase, this system is a significant potential pharmacological target.

While cyclic nucleotides were not readily amenable to mass spectrometric analysis by more established methods, the advent of fast atom bombardment (FAB) as a method of 'soft' ionization provided a means of generating mass spectra from underivatised cyclic nucleotides which contained a quasi-molecular ion of significant proportion[1,2]. The selection of this quasi-molecular ion and generation of a mass-analysed ion kinetic energy (MIKE) spectrum after its collisionally induced dissociation (CID) has been used successfully to differentiate cyclic nucleotide isomers[2] and to identify putative cyclic nucleotides in tissue extracts[3-5].

The application of FABMS to studies of cyclic nucleotide biochemistry has been extended from qualitative to quantitative analysis by examination of the kinetics of cyclic AMP- and cyclic CMP-phosphodiesterase activities[6,7], and to a protein kinase responsive to cyclic CMP[8]. The latter assay, based upon quantitation of the mass spectrum of enzyme incubate, had the advantage over the alternative radiometric assay in that several incubation components could be monitored in a single incubation. This same approach has now been successfully applied to type II cyclic AMP-dependent protein kinase.

PREPARATION OF CYCLIC AMP-DEPENDENT PROTEIN KINASE

Type II cyclic AMP dependent protein kinase was prepared from bovine heart muscle; a series of incubations were set up containing 1-25 nmol cyclic AMP, 50 μg histone 2A, 0.125 μmol magnesium acetate, 100 μg of protein kinase preparation in a total volume of 400 $\mu\ell$ 50 μM Tris-HCl pH 7.4. The mixture was incubated at 37°C for 10 minutes then the reaction stopped by the addition of TCA; precipitated protein was removed by centrifugation and the supernatant retained for mass

spectrometric analysis. Control incubations containing denatured protein kinase were simultaneously carried out.

EXPERIMENTAL PROCEDURE

Positive-ion FAB mass spectra were obtained on a ZAB-2F mass spectrometer from 5 $\mu\ell$ samples made up in glycerol-water, 1 : 1 v/v. Quantitation of the spectra were carried out by selecting the major ions arising from each component and incorporating their peak heights in the following:-

$$\Delta\ \text{conc} = \frac{\left[\left[\dfrac{\sum I_n\ \text{sample}}{\sum I_n\ \text{matrix}}\right]_{\text{control}} - \left[\dfrac{\sum I_n\ \text{sample}}{\sum I_n\ \text{matrix}}\right]_{\text{experimental}}\right]}{\left[\dfrac{\sum I_n\ \text{sample}}{\sum I_n\ \text{matrix}}\right]_{\text{control}}}$$

where $\sum I_n$ = sum of peak intensities relative to m/z 369 as characteristic ion for sample component or matrix

For cyclic nucleotides and ATP, the peak relative intensities utilized were those corresponding to $[MH]^+$, $[MNa]^+$, $[MNa + Na]^+$, $[M + Gro]^+$, $[MNa + Gro]^+$, $[MNa + GroNa]^+$, plus each of these less 17 mass units and less 18 mass units, corresponding to loss of NH_3 and loss of H_2O, respectively. For the matrix the peak relative intensities used were at $[3Gro + 2Na]^+$, $[4GroH]^+$, $[4GroNa]^+$, $[4GroNa + Na]^+$, $[5GroNa]^+$, $[5GroNa + Na]^+$, $[MH + Gro]^+$ and $[MNa + Gro]^+$, plus each of these minus 18 mass units, corresponding to a loss of H_2O. By this means of monitoring changes in peak heights of diagnostic ions emanating from cyclic nucleotides, it is possible to determine binding of cyclic nucleotides to the protein kinase by FAB analysis, by monitoring changes in the diagnostic ions of ATP and ADP it is also possible to monitor conversion of ATP and ADP and, by means of appropriate controls, to differentiate between ATP hydrolysis due to non-specific phosphorylase activity and that due to protein phosphorylation as a result of protein kinase activity. This approach provides an unique means of determining the specificity of the protein kinase in terms of its cyclic nucleotide-binding capacity and its protein substrate, but also enables the determination of any integral phosphodiesterase activity and the turnover of any low Mr effector molecules. The data obtained has shown that stimulation of cyclic AMP-dependent protein kinase occurred to a lesser extent with other cyclic nucleotides, indicating how the intercellular levels of these other compounds can potentially alter the potency of cyclic AMP in a cyclic AMP-regulated system.

REFERENCES

1. EE Kingston, JH Beynon and RP Newton, Biomed. Mass Spectrom., 11, 367, 1984.
2. EE Kingston, JH Beynon, RP Newton and JG Liehr, Biomed. Mass Spectrom., 12, 525, 1985.
3. RP Newton, SG Salih, BJ Salvage and EE Kingston, Biochem. J., 221, 665, 1984.
4. RP Newton, EE Kingston, NA Hakeem, SG Salih, JH Beynon and CD Moyse, Biochem. J., 236, 431, 1986.
5. RP Newton, D Chiatante, D Ghosh, AG Brenton, TJ Walton, FM Harris and EG Brown, Phytochem., 28, 2243, 1989.
6. RP Newton, TJ Walton, AG Brenton, EE Kingston and FM Harris, Rapid Commun. Mass Spectrom., 3, 178, 1989.
7. RP Newton, JA Khan, D Ghosh, JI Langridge, AG Brenton, FM Harris and TJ Walton, Org Mass Spectrom., 26, 447, 1991.
8. RP Newton, JA Khan, AG Brenton, JI Langridge, FM Harris and TJ Walton, Rapid Commun. Mass Spectrom., 6, 601, 1992.

ULTRA TRACE ANALYSIS OF OXIDIZED NUCLEOSIDES IN BIOLOGICAL MATRICES

A.J.R. Teixeira, G. van de Werken, J.G. Westra [1] and A.P.J.M. de Jong
National Institute of Public Health and Environmental Protection. Bilthoven, The Netherlands
[1]The Netherlands Cancer Institute, Anthonie van Leeuwenhoekhuis, Plesmanlaan 212, Amsterdam.

The study of oxidation of DNA contituents is receiving increasing interest, because they are suspected to be involved in ageing, mutagenesis, carcinogenesis and in a variety of other pathological processes.
Until now approx. 20 oxidized DNA base variants have been identified. Typical examples of oxidized base containing nucleosides are 8-hydroxy-2'-deoxyguanosine (8-OHdG), 5-hydroxymethyl-2'-deoxyuridine (HMdU) and thymidineglycol (dTg).

DNA base oxidation is caused by reactive oxygen species, including hydroxyl radicals and singlet oxygen, and ionizing radiation. Normal aerobic metabolic processes cause a background level of oxidized nucleobases in DNA. Enhanced levels of these compounds have been found in DNA and in urine after *in vivo* exposure to tobacco smoke and to hazardous compounds such as benzo[a]pyrene (PAHs), 2378-TCDD (dioxins), asbestos, phtalates, tobacco smoke and AZT. Reported DNA background levels of 8-OHdG are:

animal	organ	8-OHdG/10^5 dGs	ref.
rat	liver	1.4-1.5	1
	kidney	1.2-1.3	
rat	liver	3-5	2
hamster	liver	3-29*	3
	kidney	6-18*	

* depending on age

Normal urinary excretion rates in healthy adults range between 130–300 pmol/kg/day for 8–OHdG and approx. 100 pmol/kg/day for dTg (4). HPLC with Electrochemical Detection is the most commonly used determination method for base oxidized nucleosides.
Mass spectrometry combined with GC, LC or other separation techniques is becoming increasingly used. GC/MS requires chemical derivatization of nucleosides owing to their polar and thermolabile nature.
Here we report on a GC/MS method based on Electron Capture Negative Ion Chemical Ionization Mass Spectrometry (GC/ECNICI-MS) after acetylation and electrophoric labelling with pentafluorobenzyl groups (PFB).

Results of applications are shown for 8-OHdG in rat liver DNA obtained after in vivo exposure to nitropropane and for HMdU in genomic DNA extracted from Bacillus subtilus bacteriophage H1. Further, first experiences with standard dTg are shown as well as a GC/MS run of a sample containing the three mentioned compounds as a mixture of standards.

We have choosen for Gas Chromatochraphy combined with Electron Capture Negative Ion Chemical Ioniation Mass Spectrometry (GC/ECNICI-MS) as analysis technique as this technique generally provides ultimate sensisitivity when proper derivatives are prepared.
Quantification of 1 modified in excess of 10^6 non-modified nucleotides will require very high sensitivity and selectivity for the low µg DNA sample size range. The method uses nucleosides instead of nucleobases in order to prevent interference from RNA

The results of this show that the method developed is suitable to study the level of 8-OHdG occuring in DNA. This conclusion is supported by:
1. The sensitivity of the method which allowed the detection of background levels of 8-OHdG in DNA;
2. The results obtained with 2-nitropropane, which are in agreement with the findings of Adachi et al. (8) with HPLC-EC;
3. The good inter-assay precision for real samples (13%).

The sensitivity for other oxidized nucleosides is a good support for the development of a multicomponent method allowing analysis of several oxidative products in a single run.

REFERENCES

1. A. Takagi et al. *Jpn. J. Cancer Res.* **81,** 213-215 (1990).
2. H. Kasai, Y. Okada, S. Nishimura, M. Rao and J. K. Reddy *Cancer Res.* **49,** 2603-2605 (1989).
3. D. Roy, R. A. Floyd and J. G. Liehr *Cancer Res.* **51,** 3882-3885 (1991).
4. M. Shigenaga, C. J. Gimeno and B. N. Ames *Proc. Natl. Acad. Sci. USA* **86,** 9697-9701 (1989).
5. M. Crozatier et al. *Mol. Biochem. Parasitol.* **31,** 127-132 (1988).
6. J. C. Klein et al. *Nucl. Acids Res.* **18,** 4131-4137 (1990).
7. J. T. Lutgerink et al. *Anal. Biochem.* **201,** 127-133 (1992).
8. Adachi et al. *Carcinogenesis* **14,** 265-268 (1993).

CHARACTERISTICS OF THE METHOD (STANDARDS)

A. Detection limit

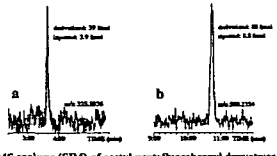

FIG. 4. GC/MS analysis (SIM) of acetyl-pentafluorobenzyl derivatives of HMdU (a) and 8-OHdG (b).

B. Others

	HMdU	8-OHdG
Linearity range	12 fmol – 39 pmol	18 fmol – 0.35 nmol
Correlation coefficient (r)	0.9998	1
Inter-assay precision		
Standards (50pg)	—	10%
Samples (20–100pg)	—	13%

GC/MS OF SOME NUCLEOSIDES

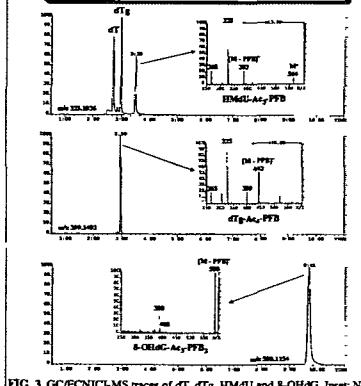

FIG. 3. GC/ECNICI-MS traces of dT, dTg, HMdU and 8-OHdG. Inset: NICI spectra.

ANALYSIS OF 8-OHdG IN RAT LIVER DNA - II

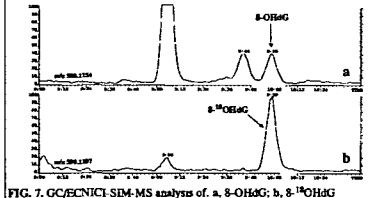

FIG. 7. GC/ECNICI-SIM-MS analysis of. a, 8-OHdG; b, 8-^{18}OHdG (internal standard). The upper trace corresponds to one 8-OHdG in 10^6 nucleosides. Sample size: 20 µg DNA.

ANALYSIS OF 8-OHdG IN RAT LIVER DNA - I

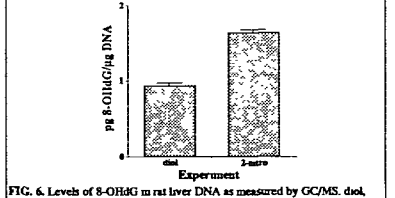

FIG. 6. Levels of 8-OHdG in rat liver DNA as measured by GC/MS. diol, vehicle (propanediol); 2-nitro, rats treated with 2-nitropropane. (Mean ± SD; n ≥ 3).

Estimation of Quadruplex DNA T_M by Electrospray Ionization-Mass Spectrometry

David R. Goodlett[1], Charles C. Hardin[2], Matthew Corregan[2] and Richard D. Smith[3]
[1]Analytical Research, Immunobiology Research Institute, Annandale, NJ 08801
[2]Department of Biochemistry, North Carolina State University, Raleigh, NC 27695
[3]Chemical Methods and Separations, Pacific Northwest Laboratory, Richland, WA 99352

The use of electrospray ionization-mass spectrometry (ESI-MS) to detect non covalent biological complexes has become quite popular.[1-3] It appears to hold some promise in understanding 1) the interaction of subunits within a given structure in solution and 2) the electrospray process itself; in particular the process of ion desolvation. Guanine-rich DNA[4-6] can be found in the telomeric region of certain chromosomes. When removed from the chromosome and analyzed as small oligonucleotides in the presence of cations such as K^+, Ca^{2+}, and Na^+, these guanine-rich sequences form quadruple-stranded structures (quadruplexes); dissociation into single-stranded DNA occurs when all cations are removed from solution. ^{1}H-nmr, circular dichroism and electrophoresis have been used to study the thermal stability of quadruplex DNA. We recently published[1] the detection of quadruplex DNA by ESI-MS. We now present the results of experiments carried out using on-line thermal denaturation to dissociate quadruplex DNA structures in solution followed by observation of the effect of thermal perturbation on the solution structures using ESI-MS. This allowed us to estimate by ESI-MS the melting temperature (T_M); the temperature at which the quadruple-stranded structure dissociates in solution to the single-stranded structure.

For liquid phase thermal denaturation studies, 60 cm of an 80 cm length of 50 µm i.d. x 180 µm o.d. fused-silica capillary was wrapped in heating tape with segments of about 8 cm at the ESI source and 12 cm at the syringe remaining unheated. Temperature was measured with a thermal couple placed inside the heating tape. "On-line" thermal denaturation was conducted by filling a capillary with sample, incubating for ten minutes at a given temperature, then directly infusing (0.5 µl/min.) the sample. The single-stranded DNA oligomer d(CGCG$_4$GCG) was synthesized using phosporamidite chemistry on an Applied Biosystems Model 381A DNA synthesizer. The oligomer was purified from failure sequences using reversed-phase, high-performance liquid chromatography followed by treatment with Amicon Centricon-3 ultra filtration tubes to remove low-molecular weight impurities and residual salt. Quadruplex DNA, d[(CGCG$_4$GCG)]$_4$, was prepared in the presence of 10 mM sodium phosphate, pH 7.6, containing 0.1 mM ethylenediaminetetraacetic acid from single-stranded d(CGCG$_4$GCG) according to a published protocol.[4] All ESI-MS thermal denaturation experiments were done on DNA in this buffer solution.

The single-quadrupole mass spectrometer, operated by a Teknivent data system, was assembled at Pacific Northwest Laboratory from Extrel components and consists of a nozzle-skimmer (+300 V and 0 V) atmospheric pressure inlet, followed by an rf only quadrupole surrounded by a cryopumping surface. Operating pressures in the analysis quadrupole, which was separated from the rf only quadrupole in a second chamber, were typically 10^{-7} torr when a one mm nozzle and a two mm skimmer were used. The front plate was held at ambient temperature and the lens was at +1.0 kV. A counter-current stream of nitrogen gas at ambient room temperature was used to assist desolvation and a coaxial stream of SF_6 within the ESI source was used to prevent discharge when water was used as a sheath solution.

At a solution temperature of 29 °C and a low nozzle-skimmer bias (ΔNS) of -150 volts, unique charge states (e.g. 9- & 11-) for natriated ions of [d(CGCG$_4$GCG)]$_4$ can be observed by ESI-

MS. These ions are absent when ΔNS = -250 volts; presumably dissociated in the desolvation stage of ESI at a high ΔNS, but preserved at a low ΔNS. A solution of [d(CGCG$_4$GCG)]$_4$ incubated at 80 °C and then analyzed by ESI-MS at ΔNS = -150 volts (Figure A) showed the same unique ions of [d(CGCG$_4$GCG)]$_4$ as the solution incubated at 29 °C. However, [d(CGCG$_4$GCG)]$_4$ incubated at 90 °C and analyzed by ESI-MS at ΔNS = -150 volts showed no unique ions (Figure B) for [d(CGCG$_4$GCG)]$_4$. These results agree with circular dichroism experiments which show that [d(CGCG$_4$GCG)]$_4$ dissociates in solution to d(CGCG$_4$GCG) at 90 °C, but not 80 °C. In the mass spectra below "Q" stands for [d(CGCG$_4$GCG)]$_4$ ions and "ss" for d(CGCG$_4$GCG) ions. Also note that as a result of ESI-MS analysis in a sodium phosphate buffer, the 11- ion of [d(CGCG$_4$GCG)]$_4$ has 16 sodium ions attached to it and the 5- ion of d(CGCG$_4$GCG) has 3 sodium ions attached.

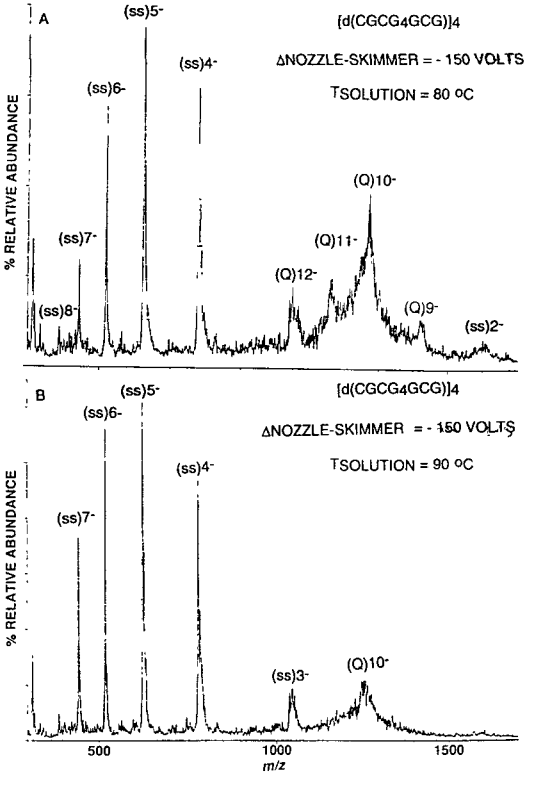

Pacific Northwest Laboratory is operated by Battelle Memorial Institute.

1. D. R. Goodlett, D. G. Camp II, C. C. Hardin, M. Corregan and R. D. Smith, *Biological Mass Spectrometry*, **22**, 181 (1993).
2. K. J. Light-Wahl, D. L. Springer, B. E. Winger, C. G. Edmonds, D. G. Camp II, B. D. Thrall and R. D. Smith, *Journal of the American Chemical Society*, **115**, 803 (1993).
3. B. Ganem, Y. T. Li and J. D. Henion, *Tetrahedron Letters*, **34**, 1445 (1993).
4. C. C Hardin, T. Watson, M. Corregan, C. Bailey, *Biochemistry*, **31**, 833 (1992).
5. W. I. Sundquist and A. Klug, *Nature*, **342**, 825 (1989).
6. E. H. Blackburn and J. W. Szostak, *Annual Review of Biochemistry*, **53**, 163 (1984).

COLLISION-INDUCED DISSOCIATION OF PERMETHYLATED DERIVATIVES OF SITE-SPECIFICALLY ^{15}N- AND ^{18}O-LABELED GUANOSINES

John M. Gregson and James A. McCloskey
Departments of Medicinal Chemistry and Biochemistry
University of Utah, Salt Lake City, UT 84112

In previous reports (1, 2) we showed how permethylation MS/MS could be used to both increase the analytical sensitivity as well as to assign sites of alkylation in nucleosides related to guanosine. Ionic formulas were presented for structurally significant fragment ions that were consistent with — but not proven by — previous workers or by traditional chemical reasoning.

In this report we provide evidence for the veracity of these ionic compositions, based on the results obtained by low energy CID of the permethylated derivatives of guanosines labeled by ^{15}N at N-1, N^2, and N-3; and by ^{18}O labeling at O^6. Microgram level synthesis (10 — 100 nmol) was used for the selective implantation of ^{15}N and ^{18}O into the heteroaromatic ring. Levels of isotope incorporation were high, with [1-^{15}N]guanosine being generally the most difficult to prepare. The synthetic protocols employed (to be published separately) featured exclusive site specificity. Subsequent derivatization and mass analysis were conducted as described (1).

The following figure shows the CID mass spectra of four isotopically labeled perdeuteromethylated guanosines along with guanosine itself (product ion spectra for the base fragments BH_2^+; only the keto forms are shown). The observed patterns unanimously validate the compositions shown previously and help eliminate alternative structures, such as the hypothetical N-3 deammoniated analog of *m/z* 127.

There are several interesting outgrowths of this work. Most important of these is the discovery of widely different fragmentation channels between permethylated and underivatized guanosines. Within these categories is further noted the presence of hitherto unknown decomposition pathways (*e.g.* exclusive retention of N-1 in fragment 152 — not the case for underivatized nucleoside) as well as the absence of certain commonly reported ones (such as the near-absence of H_2O loss in both permethylated and underivatized species).

Acknowledgments: Financial support from NIH (grant GM29812); to J.M.G.: American Foundation for Pharmaceutical Education Fellowship.

References:

1. J. M. Gregson and J. A. McCloskey; "Structure Determination of Modified Guanosines by Permethylation FAB MS/MS"; Proceedings of the 40th ASMS Conference on Mass Spectrometry and Allied Topics, Washington, DC, May 31 - June 5, 1992, pp 539 – 540.

2. J. M. Gregson and J.A. McCloskey; "The Dissociation Chemistry of Permethylated Guanosines as Articulated by MS/MS"; manuscript in preparation.

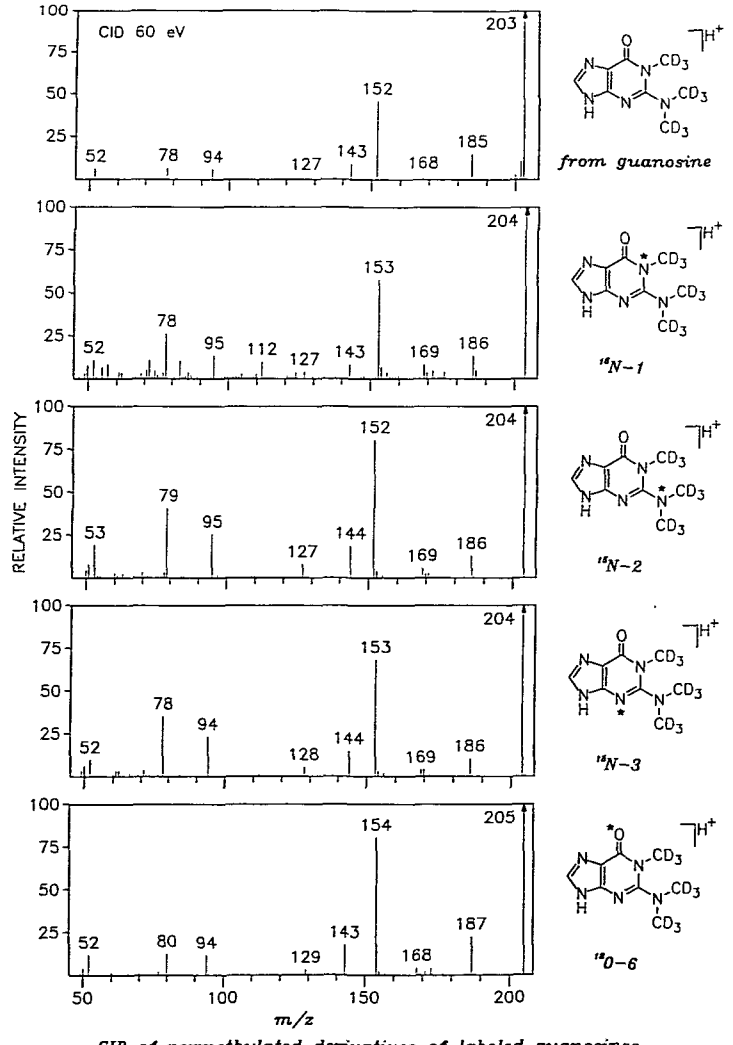

CID of permethylated derivatives of labeled guanosines
(base fragment CID; only the keto tautomers are shown)

EVALUATION OF VARIABLE POST-TRANSLATIONAL MODIFICATION OF HISTONES BY ELECTROSPRAY IONIZATION MASS SPECTROMETRY AND TANDEM MASS SPECTROMETRY. *C.G. Edmonds, M.S. Weir, B.D. Thrall, J.D. Morris and D.L. Springer, Pacific Northwest Laboratory, P.O. Box 999, Richland WA 99352.

The basic subunit of chromatin structure, the nucleosome, consists of 146 base pairs of DNA reversibly wrapped around a central lysine and arginine rich histone protein octamer with an additional histone binding the linker regions. The nature and function of covalent modifications of proteins occurring after translation and simple proteolytic processing is a recurring theme in structural biology. In the case of histone proteins, such post-translational modifications include acetylation, methylation, phosphorylation, mono- and poly(ADP)ribosylation and ubiquitination. These modifications are known to be associated with the alteration in chromatin structure which occurs through the cell cycle and in response to chemical or radiation induced damage and repair to the cell nucleus.

Electrospray ionization mass spectrometry (ESI-MS) permits the direct analysis of the intact modified protein with precise mass measurement allowing the direct and unambiguous evaluation of the nature and extent of post-translational modification. Preliminary experiments on HPLC-purified histones revealed an array of materials, which, when compared to the masses predicted from the gene sequences, had mass values that precisely matched combinations of methylation and acetylation. We have sought to confirm the notion that these measured mass increments are genuine reflections of natural post-translational processes. We have isolated histones from human K562 cells grown in normal cell culture and in the presence of 20 mM sodium butyrate, a deacetylase inhibitor which results in the hyperacetylation of proteins. HPLC isolation and SDS-PAGE separations of these histones show that the proteins are intact but reveal no detectable difference between the proteins from control and butyrate-treated cells. ESI-MS of these materials demonstrate significant increases in heterogeneity of the butyrate treated proteins, consistent with increased levels of acetylation. Differences in predicted masses and the measured values are precisely accounted for by methylation and acetylation. These strongly basic proteins show persistent contamination by noncovalently associated species incrementing the measured mass values by 98 daltons (putatively, sulfate or phosphate). Rigorous exclusion of these contaminants has not so far been possible. Dialysis, ultrafiltration and precipitation according to the method of Chait and co-workers (S.K. Chowadhury, V. Katta, R.C. Beavis and B.T. Chait, *J. Am. Soc. Mass Spectrom. 1*, **1990**, 382-388) have not been completely effective. Reduction of this artifact contribution to the mass spectra may be accomplished by an increase in the collisional activation occurring in the atmosphere/vacuum interface by increasing the voltage bias between the nozzle and skimmer elements. Figure 1 shows an example of the multiple acetylation observable in histone H4 from butyrate-treated cells. Further confirmation of these assignments was possible by employing the triton-acid-urea PAGE method. This method permits the separation of proteins by virtue of the effect of acetylation of a lysyl amino group, reducing the electrophoretic mobility of the protein by decreasing the net charge. The mobility of isolated histone H4 from control and butyrate-treated K562 cells are compared in Figure 2. In both the control and the butyrate-treated sample a series of five proteins are observed. The two principle H4 species present in the control culture are of the highest mobility. Three species migrating at successively slower rates are abundant in the butyrate-treated

sample and present in only trace levels in the control. Correlation with mass measurements identify the two common components (Figure 2, bands 1 and 2) as dimethylacetyl and dimethyldiacetyl H4 proteins and the three additional species (Figure 2: bands 3, 4 and 5) arise from successive acetylations. Further increases in the voltage bias between the nozzle and skimmer elements of the interface causes dissociation of the histone proteins. The success of our interpretive efforts suggest this method has realistic prospects for more direct evaluation of the nature and extent of modification and new information on site of specific modified residues. In future studies we will seek to extend this approach for the evaluation of normal variations in the levels of acetylation and other modification chemistries through the cell cycle in flow cytometry sorted populations. This will be followed by studies which seek to demonstrate the perturbation of these normal variations by physical or chemical insult.

The results of these experiments demonstrate the feasibility of analyzing both natural and altered modifications of histone proteins by ESI-MS. Alterations in chromatin structure which accompany transcription and replication are governed in part by the modulation of DNA-protein interactions through histone post-translational modifications. We hypothesize that the normal temporal profile of these modifications will be measurably and predictably perturbed by physical or chemical insult. These changes are cell cycle dependent and damage induced perturbations in these modifications may be in part responsible for aberrant cell functions. Our technique will permit the full evaluation of the profile of normal modifications by specific detection of perturbations which indicate the response to DNA damage and its repair.

Acknowledgments Work supported in part by Laboratory Directed Research and Development and the National Institutes of Health (GM 47423). The Pacific Northwest Laboratory is operated under Contract DE-AC06-76RLO 1830 with the U.S DOE by Battelle Memorial Institute.

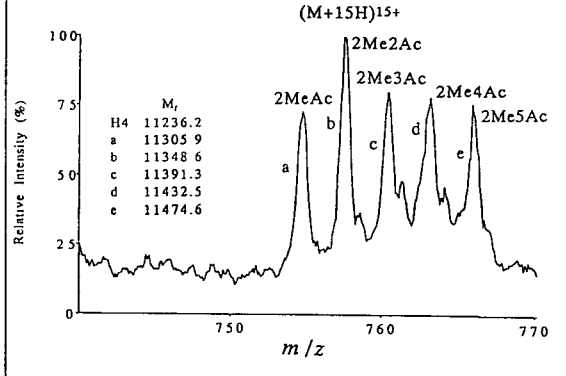

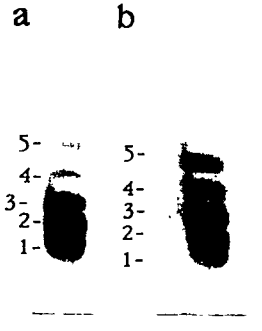

Figure 1 (left). Region of the ESI mass spectrum of histone H4 isolated from human K562 cells grown in the presence of 20 mM sodium butyrate. Calculated and measured masses are tabulated on the left. Figure 2 (right). Triton-acid-urea PAGE of the H4 histones isolated from normal K562 cells (a) and K562 cells grown in presence of 20 mM sodium butyrate (b).

PRODUCT ION SCANS OF THE BH_2^+ ION: A TOOL FOR INVESTIGATING THE STRUCTURE OF DEOXYNUCLEOSIDES MODIFIED BY ARYLAMINE AND DIOL EPOXIDE CARCINOGENS, J.O. Lay, Jr., M.P. Chiarelli, and P.S. Branco, National Center for Toxicological Research, Jefferson, AR, 72079 and University of Arkansas at Little Rock, Little Rock, AR 72204.

ABSTRACT

We have reported nucleoside-base specific neutral losses, from low energy collision induced dissociation (CID) of mass selected BH_2^+ ions of C-8 substituted deoxyadenosine and deoxyguanosine (dG) adducts with arylamine carcinogens. Recently, using arylamine adducts substituted through different positions of the nucleoside base (i.e., N^2), other arylamines, and different classes of carcinogens, we continued our studies using low energy CID of the BH_2^+ ion. Differences were noted in the mass spectral behavior of the BH_2^+ ions of arylamine, arylamide, and polycyclic aromatic hydrocarbon (PAH) diol epoxide adducts. For instance, the formation of the BH_2^+ ion occurs to a lesser extent with PAH diol epoxide adducts than arylamine or arylamide-modified deoxynucleosides. Also, isomeric N^2- and C8-modified adducts are readily distinguished based on both the masses and intensities of product ions. Product ion data obtained in our laboratory was similar to data obtained elsewhere using high energy collisions.

Results and Discussion

Replicate product ion spectra, from the BH_2^+ ions of the model arylamine carcinogens dG-C8-AF and dG-C8-ABP were acquired over 2-3 years. Although variations in the sample loading, matrix, solvent, and collision energy were systematically studied, the variability in signal intensities appeared to increase primarily with the time between experiments. Nevertheless, the specific masses, especially when expressed as neutral losses, were used to provide evidence of structure, based on the large number of common neutral losses. The existence of these common neutral losses reflects cleavage within the base (dG) and the retention of charge on the carcinogen-containing portion of the molecule. Similar losses were also observed with adducts of related compounds, including the heterocyclic amine, dG-C8-PhIP (see table), but not from adducts of arylamide or PAH diol epoxides carcinogens.

Most of the neutral losses observed in our laboratory were also observed by Dietrich et. al. (Carcinogenesis 9, 2113 1988) using high energy CID and a similar arylamine adduct, dG-C8-NFA. Their spectrum showed all these fragments except loss of 42 daltons, although some appeared to be minor peaks. In another study using B/E scans, Annan et. al. (Anal. Biochem. 191, 86 1990), observed several of the same losses, but a few product ions differed in mass by one dalton from the values in our study and others were not observed at all.

Characteristic BH_2^+ Neutral Losses for dG-C8 Adducts

Mass Loss	dG-C8-ABP	dG-C8-AF	dG-C8-An	dG-C8-PhIP
17	302	314	226	357
42	277	289	201	X
44	X	287	(198)	(329)
70	249	261	173	304
72	247	259	171	302
99	X	232	144	275
111	208	220	132	X
124	195	207	119	250
139	180	192	104	235
151	168	180	92	X
166	153	165	77	208

Conclusions

Product ion masses (and neutral losses) taken as a group provided significant structure specificity. As expected, differences were observed when either the class of the carcinogen or the position of substitution were changed. When low energy CID spectra were compared with literature results obtained using high energy, the spectra were surprisingly similar. Previously acquired B/E scans showed more significant differences, whereas high energy product ions from the BH_2^+ of dG-C8-NFA showed 10 of the 11 expected neutral losses. Product ions from the BH_2^+ of arylamine, arylamide, and PAH diol epoxide modified bases showed significant structure specificity. The extent of fragmentation was greatest with arylamine-modified deoxynucleosides. As the structure of the carcinogen was varied, the typical "arylamine-adduct" fragmentation changed, so that only some of the expected fragments were observed using adducts of heterocyclic amines and fragmentation was entirely different using arylamide- and PAH diol epoxide modified deoxynucleosides. Loss of most of the base moiety to give common fragment ions, regardless of the specific base, was observed as a significant fragmentation pathway from the PAH diol epoxide adducts.

(This work was supported in part by the Center for Indoor Air Research (#91-02)).

Studies on the Binding of Actinomycin D to Single-Stranded DNA by Negative Ion Spray Mass Spectrometry . Y.T. Li[1], Y.L. Hsieh[1], H.K. Lim[2], J. Henion[1], and B. Ganem[3]. Drug Testing[1] , Cornell University, 925 Warren Dr., Ithaca, NY 14850. Wyeth-Ayerst Research[2], Princeton, NJ 08543. Department of Chemistry[3], Cornell University, Ithaca, NY 14853.

Recently we reported the detection of the duplex form of an octanucleotide by ion spray mass spectrometry (MS)[a]. By using this promising technique, we have studied the binding of actinomycin D (AMD) to single-stranded DNA for which the binding of complexes has been reported by fluorescence[b]. It has been suggested the biological role of binding AMD to single-stranded DNA might inhibit RNA polymerase via blocking hybridization of RNA-DNA duplex formation, thus terminating DNA transcription. The noncovalent complexes are formed through hydrogen-bonded "outside-binding" model[c]. The intercalation binding of double-stranded DNA by AMD is not reported here.

Several nonself-complementary oligonucleotides and AMD,an inhibitor of RNA polymerase, which has been used as an antitumor drug were studied using negative ion spray MS (1:1 in 50/50 ACN/10 mM NH_4OAc, pH 7) under mild declustering energy (30 V) conditions. Rifampicin (RP), also an inhibitor of RNA polymerase, is used as a control drug for this study. Acetic acid (0.1 %) and ammonium hydroxide (0.1 %) were used to adjust pH.

The noncovalent complex of AMD and single-stranded 5'-CTCGACGG-3' was detectable by negative ion spray MS. When we replaced AMD (hydrophilic) by RP (hydrophobic), no complex was observed (Figure 1), suggesting that the formation of hydrogen bonds is required for the binding of the complex. Moreover, the complex disappeared at pH 3 and reappeared when the pH was adjusted back to pH 7 (Figure 2), indicating that the binding of complexes is pH dependent and reversible. By examining the effect of the DNA sequence on complex binding , G-C or C-G pairs are more favorable to the binding but AMD also could bind to non G-C or C-G sites (Figure 3), reflecting that the presence of deoxyguanine in a DNA is not necessary for complex formation. In fact, no complex formed between AMD and 5'-GGGGGGGG-3' (Figure 3). In summary, the binding of AMD to single-stranded DNA is dependent upon pH, the drug, and the DNA sequence.

Figure 1. Mass Spectra of AMD and RP with 5-CTCGACGG-3'

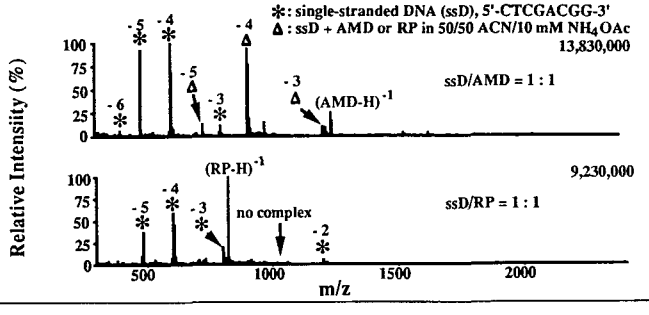

Figure 2. Effect of pH on the Binding of AMD to 5'-CTCGACGG-3'

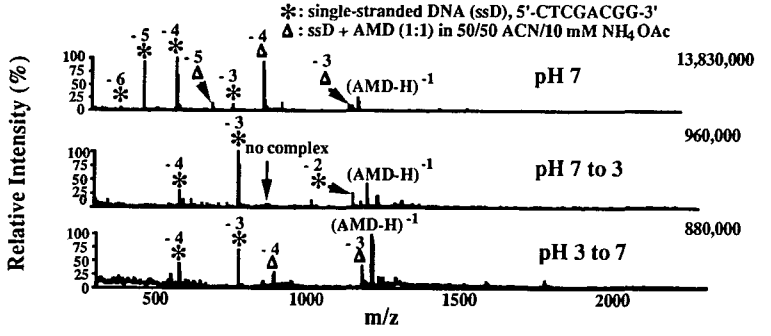

Figure 3. Effect of the DNA Sequence on the Complex Binding

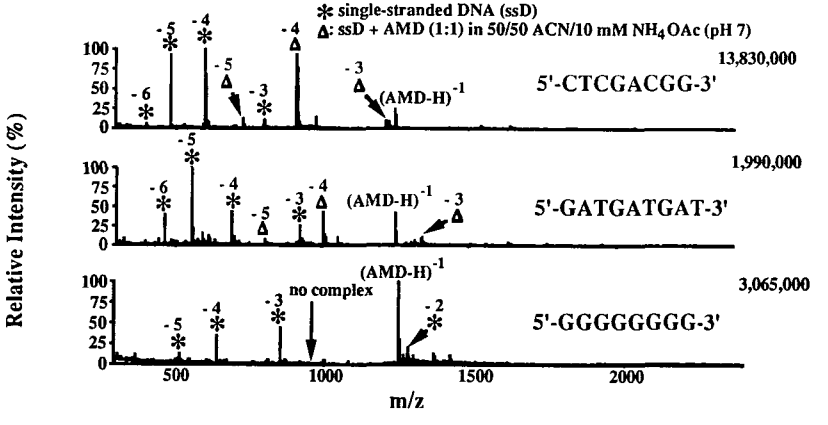

[a]B. Ganem, Y.T. Li, J. Henion. Tetrahedron Lett, 34:1445,1993.
[b]R.M. Wadkins and T.M. Jovin. Biochemistry, 30: 9469, 1991.
[c]L.D. Hamilton, W. Fuller, and E. Reich. Nature, 198: 538, 1963.

Posttranslational Modifications and Mass Spectrometry: What the Well Dressed Protein is Wearing and How to Tell

Steven Carr, Roland Annan, Mark Bean, James Conboy, Mark Hemling, and Michael Huddleston, Physical and Structural Chemistry, SmithKline Beecham Pharmaceuticals, King of Prussia, PA 19406

Protein synthesis can be divided into three discrete stages: i) initiation of the translation process by synthesis and activation of the amino acids into the twenty unique amino(imino)acyl-tRNA adducts, ii) polymerization on the ribosome-mRNA complex of the amino acid moieties of the amino(imino)acyl-tRNA adducts into the sequence specified by the three-nucleotide codons of the mRNA, and iii) processing and release of the resulting polymer. Processing, or posttranslational modification, is almost always required to convert the polymeric end product of translation into a biologically active molecule and for transporting the protein to its proper compartment of action. In this context, posttranslational modifications include all changes to the molecule that are not coded for by the gene whether they have been introduced before, during or after the polymerization step.

Proteins having covalent modifications are the rule rather than the exception in nature. Nearly 200 structurally distinct covalent modifications have been identified thus far, ranging in size and complexity from conversion of amides to carboxylic acids, to the attachment of multiple complex oligosaccharides each with molecular masses up to several thousand daltons. Most posttranslational modifications are introduced by enzymes; the presence of the modification is often required for normal biological function or tissue disposition of the protein, although in many cases the role is as yet unknown. Proteolytic cleavage is perhaps the most common modification in that the amino-terminal Met residue that is the starting point for the synthesis of all proteins is, in most cases, removed through the action of aminopeptidases. Frequently the new amino-terminal residues, or the initiator Met residues if they have not been removed, are acylated through the action of acyltransferases. In addition to acetyl and formyl, longer chain acyl groups such as myristyl have been shown to be attached at the α-amino group. Covalent modifications of the side-chains of amino acids are also common, particularly glycosylation and phosphorylation.

Posttranslational modifications frequently complicate or even prevent the use of classical analysis tools such as automated Edman degradation, the most commonly used method for determining the sequence of peptides and proteins. The presence of lipid or carbohydrate on proteins can also dramatically decrease the accuracy of molecular weight estimates obtained by sedimentation velocity, gel permeation, or SDS-PAGE measurements. Mass spectrometry relies on entirely different principles than these other techniques, and it is uniquely suited for detection and structural characterization of posttranslational modifications in proteins. Many benefits are to be gained when MS-based methods are integrated with more conventional peptide, protein, and carbohydrate structure analysis techniques. For example, in the context of all structural information available for the protein, the molecular mass of the intact, modified protein determined by ESMS or MALDMS can be used to corroborate the overall sequence fidelity and to check for proteolytic processing of the protein, particularly at the C-terminus. Precise location and identification of modifications other than proteolytic processing usually requires a combination of LCMS, tandem MS, and Edman degradation. In our view, the potential for MS in the study of posttranslational modifications is virtually unlimited.

Glycosylation and phosphorylation are two of the most important modifications of proteins, and their characterization is a major emphasis in our laboratory. We have developed several approaches using LC-ESMS with CID for selective detection of glycosylated and phosphorylated peptides in complex mixtures. The most general of these approaches involves scanning or stepping of the collisional excitation potential prior to the mass analyzing quadrupole in order produce characteristic low-m/z marker ions. The orifice voltage, which controls the CID potential in the free-jet expansion region, needs to be adjusted so as to maximize within each spectrum the characteristic fragment-ion signals and to minimize parent-ion fragmentation. These contradictory requirements are met by scanning or stepping the orifice voltage during full-scan acquisition. In the positive-ion mode, collisionally-excited glycopeptides fragment to produce diagnostic sugar oxonium ions, particularly the $HexNAc^+$ and $Hex\text{-}HexNAc^+$ fragments at m/z 204 and 366, respectively. We have used this approach to locate glycopeptides and to characterize the molecular heterogeneity of the carbohydrates at specific attachment sites in numerous glycoproteins including fetuin, gp120 (the surface glycoprotein of the HIV-virus), sCD4 (the soluble receptor to which gp120 binds), sCR-1 (a soluble complement-binding molecule), and various monoclonal antibodies (1,2). A similar approach has now been developed for selective detection of phosphopeptides in complex mixtures (see Huddleston et al., this volume). Phosphopeptides containing the three principal types of phosphate-peptide linkages (i.e., phospho-Ser, -Thr, and -Tyr) yield phosphate-specific fragment ions at m/z 79 and 63 during negative-ion LC-ESMS analysis with stepped collision energy. Figure 1 illustrates the results for a complex mixture of 16 peptides, only three of which are phosphorylated (gray = TIC;

solid = m/z 79 + m/z 63). Once phosphopeptides have been identified, Edman degradation and tandem MS may be used to define the sequence and locate the specific phosphorylation site(s). An example of this is illustrated in Figure 2 for the phosphotyrosine-containing peptide identified by LC-ESMS in Figure 1 (peak 14). Collision energy scanning may find broader application in the identification of other common modifications such as isoprenyl-moieties on Cys and phospholipid membrane anchors on protein C-termini, and for unnatural modifications such as covalently-bound enzyme inhibitors and photoaffinity labels.

1. Carr, S. A.; Huddleston, M. J.; Bean, M.F.; *Protein Science* **1993**, 2, 183-196.
2. Huddleston, M. J.; Bean, M.F.; Carr, S. A.; *Anal. Chem.* **1993**, 65, 877-884.

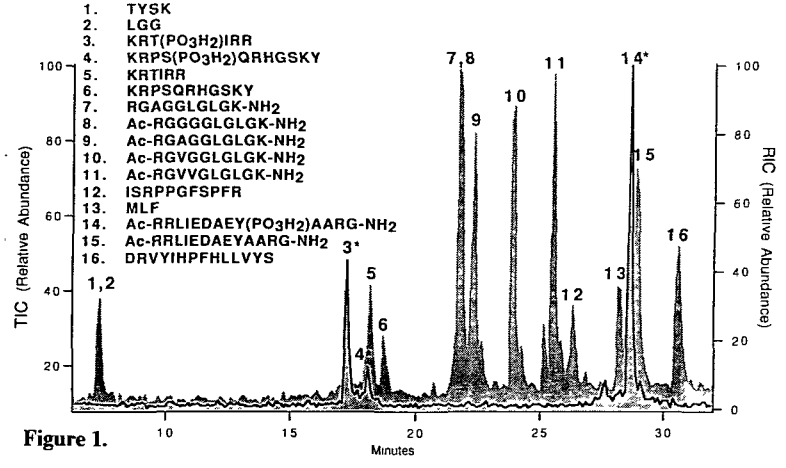

Figure 1.

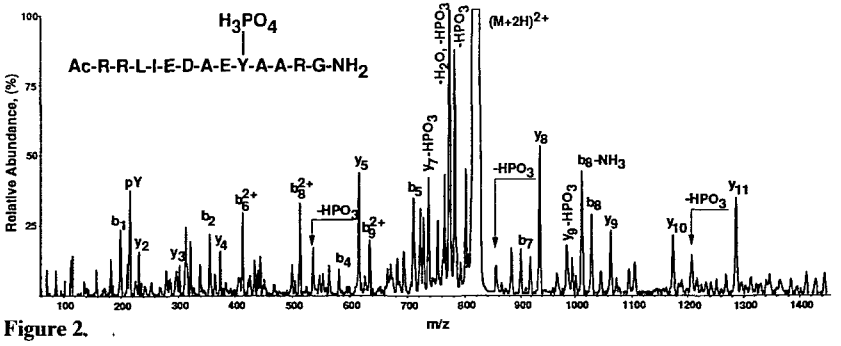

Figure 2.

"Mass Spectrometric Based Strategies for the Structural Characterization of Recombinant Human IL-12"

S.A. Martin, W. Yu, J.E. Vath, B.S. Tangarone, A.S. Harris, E.B. Nickbarg and H.A. Scoble,
Genetics Institute Inc., One Burtt Road, Andover, MA 01810, USA

Interleukin-12 is a pleiotropic cytokine that was originally identified on the basis of its ability to stimulate natural killer cells to kill tumors *in vitro*. Recently, the genes for both the light and heavy subunits of human IL-12 have been cloned and sequenced. When expressed in Chinese hamster ovary cells, heterodimeric rhIL-12 has an apparent molecular mass of 75-80 kD based on SDS-PAGE. Upon reduction, the protein yields light and heavy subunits with apparent molecular masses of 35 and 40 kD, respectively. Recombinant IL-12 has a unique structure among cytokines in that the heavy subunit shows significant sequence homology with the extracellular domain of the IL-6 receptor while the light chain may display a distant relationship with IL-6. Based upon the cDNA sequence of the light and heavy subunits, the heterodimeric protein contains seventeen cysteines, seven consensus sites for N-linked glycosylation and numerous potential sites of O-linked glycosylation.

In this presentation we focused on contributions of mass spectrometric based strategies to the overall solution of the primary structure of this glycoprotein. This strategy utilizes MALD-TOF (a Bruker REFLEX consisting of both linear and reflector modes), FAB MS and MS/MS in addition to protease and glycosidase treatment and various modes of chromatography. The first step in this approach is the determination of the molecular mass by MALD-TOF MS of the intact dimer and the mixture of reduced light and heavy monomers prior to and after treating the molecule with a variety of specific proteases and glycosidases.

MALD-TOF MS is playing an increasing role in the identification and site-specific structural characterization of glycopeptides obtained from proteolytic digestion of recombinant proteins. One feature of this technique, which had not been previously reported, is illustrated with a comparison of the linear and reflected mass spectra of an O-linked glycopeptide from the light chain of rhIL-12 (Figure 1). In the linear mode, abundant ion signals are observed at *m/z* 4299.7 and 4950.1 which correspond in mass to the peptide sequence shown containing a HexNAcHex moiety and one and two neuraminic acid (NeuAc) residues, respectively. In the reflected mass spectrum of the same sample acquired immediately after the linear spectrum, no ion signal is observed corresponding to the bisialylated O-linked species at *m/z* 4590.1 and a weak multiplet of peaks is observed in the mass region corresponding to the monosialylated species (*m/z* 4299.7). The base peak in the reflected mode corresponds to the peptide sequence shown in Figure 1 with one unit each of HexNAc and Hex. The loss of the majority of the neuraminic acid residues in the reflected mode is characteristic of sialylated glycopeptides (both N- and O-linked) and suggest that the species observed in the linear mode are composed of primarily metastable ions. These observations, i.e., the shift down in mass in increments of 291 daltons in the reflected mode as compared to the masses observed in the linear mode, permit the identification of sialylated glycopeptides by a comparison of the linear and reflected mass spectra.

A feature of this reflector instrument is the ability to vary the reflector potential (from its full value to zero in a number of steps) in an effort to identify low energy fragment ions resulting from the metastable decomposition of the desorbed molecule. This is illustrated in Figure 2 which shows a reconstructed metastable reflected mass spectrum of a peptide from the heavy chain of rhIL-12 obtained by stepping the reflector potential from 500 volts to 30 kV. A complete series of b ions are observed as well as a number of a and y ions. In addition to these fragment ion series a number of internal peptide ions and immonium ions are also observed. This technique shows promise for sequencing bioploymers with much less material and under less stringent conditions than are currently possible.

FIGURE 1

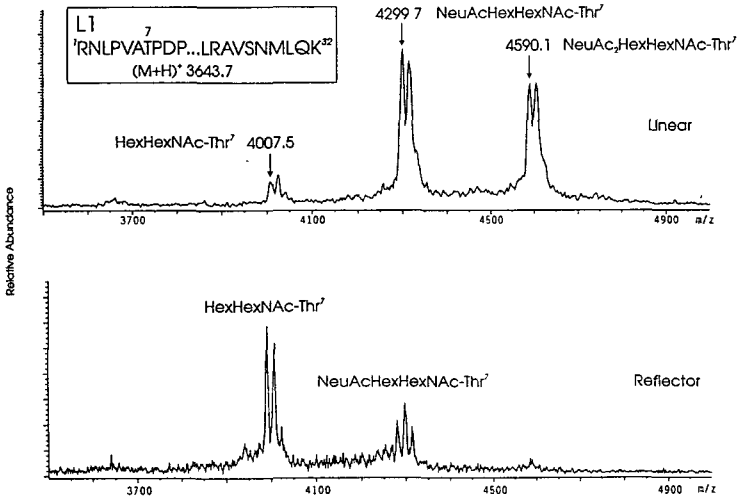

FIGURE 2

Peptide Sequencing by maLD-TOF Mass Spectrometry

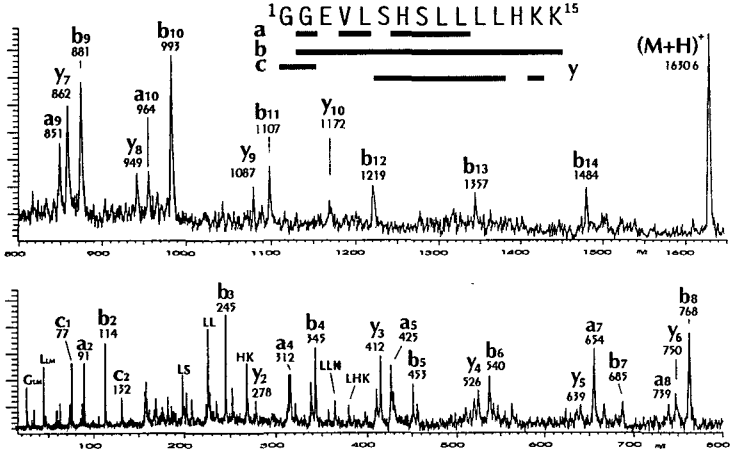

COMBINATION OF MASS SPECTROMETRIC METHODOLOGIES FOR THE DETERMINATION OF PEPTIDE AND PROTEIN STRUCTURE

I.A. Papayannopoulos and K. Biemann, Department of Chemistry, Massachusetts Institute of Technology, Cambridge, MA 02139-4307

The availability of a variety of methods in generating and detecting ions from biological samples suggests a complimentarity of methodologies which can be applied to the determination of peptide and protein structure. Molecular weight data obtained from intact proteins, either by electrospray (ESI) or matrix-assisted laser desorption ionization (MALDI), offer an assessment of the homogeneity and purity of a protein sample. ESI in particular, carried out on a magnetic deflection mass spectrometer, can take advantage of the higher resolution available in sector instruments. The molecular weights of proteolytic peptides often suffice to identify post-translational or other modifications to proteins of known amino acid sequence. For proteins of unknown structure, tandem mass spectrometry of proteolytic peptides provides the sequence.

This is demonstrated first with the structure determination of the thioredoxin from *chloroflexus*. MALDI MS of the protein (Figure 1) attested to the success of its purification, but its ESI mass spectrum (Figure 2) indicated structure inhomogeneities.

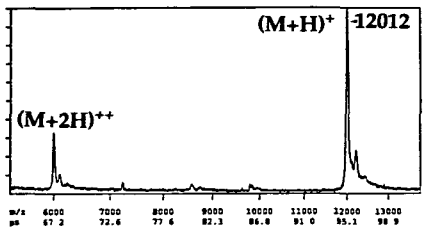

Figure 1. MALDI mass spectrum of *chloroflexus* thioredoxin.

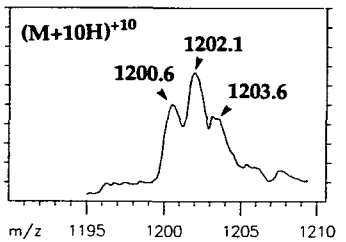

Figure 2. The +10 ion from the ESI spectrum of *chloroflexus* thioredoxin.

Proteolytic peptides, partially fractionated by reversed-phase high performance liquid chromatography, were analyzed by fast atom bombardment (FAB) mass spectrometry (MS). Thus the sequence inhomogeneities, inferred from the ESI mass spectra of the intact molecule, were assigned to positions in the amino acid sequence:

AKPIEVHDSDFNTVLLKSKTPVVVDFWAPWCGPCRVIAPI$^{L}_{N}$DKLTVGYAGRLTIAKV$^{NT}_{DV}$ 60

DDNVQYASQLGIKGLPTLVIFKDGREVGRLVGARPEAMYREIFDA$^{G}_{A}$VLAAM 110

In addition to the inhomogeneities indicated above, which are, presumably, a result of the presence of several gene products, the methionine residues in the protein were found to be partially oxidized; however, this may have been effected unwittingly during isolation and purification of the thioredoxin.

The inhomogeneity at position 41, involving substitution of leucine by asparagine,

was established by collision-induced dissociation (CID) of two protonated peptides (from a tryptic digest) differing by 1 u. One of the two CID mass spectra obtained appears in Figure 3, and the expanded regions of both spectra with sequence-significant ions in Figure 4. The interpretation of the spectra is somewhat complicated by the fact the ion of the ^{12}C isotope of the heavier peptide ($[M+H]^+$ m/z 869.5) also contains the ^{13}C isotope of the lighter one ($[M+H]^+$ m/z 868.5). Nevertheless, the unit mass resolution available on both MS-1 and MS-2 of the four sector tandem mass spectrometer, allows for unambiguous assignment of the fragment ions.

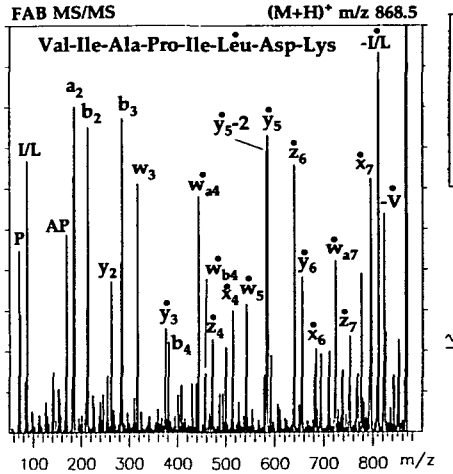

Figure 3. CID mass spectrum of $[M+H]^+$ m/z 868.5; fragment ions marked with a bullet (•) shift by 1 u higher in the CID mass spectrum of m/z 869.5.

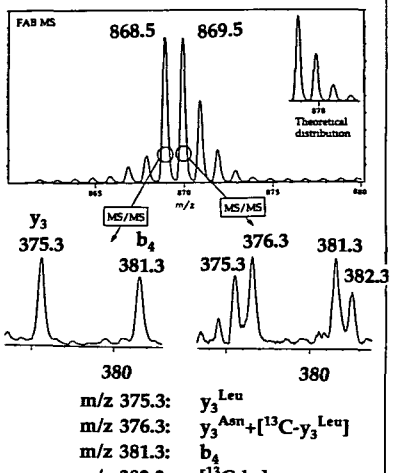

Figure 4. Expanded regions of CID mass spectra of m/z 868.5 and m/z 869.5.

Another modification to protein structure, investigated by MALDI MS, has been the insulin-sensitive phosphorylation of calmodulin in intact cells. Calmodulin was isolated from rat testes cells, half of which had been treated with insulin, and digested with endoproteinase Lys-C. Two peptides were found to have added one and two phosphates in the presence of insulin; calmodulin from insulin-free cells showed no evidence of phosphorylation. These peptides were assigned to the sequence with the aid of the computer program COMPOST, enabling the identification of the amino acids phosphorylated in the presence of insulin as Thr-79 and Ser-81.

Acknowledgements: The support of the MIT Mass Spectrometry Facility by the National Institutes of Health (Grant No. RR00317) is gratefully noted. The thioredoxin sample was provided by Dr. Bob Buchanan and Dr. Hyman Hartman (U.C. Berkeley); samples of calmodulin were provided by Dr. David Sacks (Brigham & Women's Hospital, Boston).

A Strategy for Mass Spectrometric Characterization of Nucleotide-Protein Complexes after UV-induced Crosslinking†

Ole N. Jensen, Department of Biochemistry & Biophysics, Oregon State University, Corvallis, OR 97331; ***Mark C. Young and Peter H. von Hippel***, Institute of Molecular Biology, University of Oregon, Eugene, OR 97403; ***Stephen Swenson and Steven E. Seifried***, Department of Biochemistry & Biophysics, University of Hawaii, Honolulu, HI 96822; ***Douglas F. Barofsky***, Department of Agricultural Chemistry, Oregon State University, Corvallis, OR 97331.

Protein-nucleic acid interactions are involved in important cellular processes such as DNA replication, recombination and repair, RNA transcription and processing, protein synthesis, and regulation of enzyme activities. We present here a novel approach for characterizing the structural details of protein-nucleic acid interactions or, more specifically, for identifying protein domains and amino acid residues in close contact with nucleic acids. The strategy is based on using UV-crosslinking and photoaffinity-labeling techniques to 'trap' a given protein-nucleic acid complex by introduction of a covalent bond between the two molecules and on subsequent mass spectrometric analysis of the newly formed, covalently modified protein.

To demonstrate that this approach is feasible, we have analyzed two systems of UV-crosslinked protein-nucleic acid complexes by MALDI TOF MS.

Experimental: UV-laser crosslinking of gp32 to $(dT)_{20}$ was performed as described previously [Hockensmith *et al.*, *Meth. Enzym.* **208**, 1991] using 10 μL samples containing gp32 (22 μM) and $(dT)_{20}$ (10 μM). Crosslinking yields (4-7% of total protein) were determined by SDS-PAGE and radiodetection of [^{32}P]-labeled $(dT)_{20}$ crosslinked to gp32 Photoaffinity-labeling of rho was accomplished by incubating rho (5 μM) with the ATP-analogue 4sUDP (50 μM) [Favre, in *Bioorganic Photochemistry* (Ed. Morrison), 1989] under 335 nm UV light for 60 min. An ATPase inactivation assay was used to determine the crosslinking yield ($\sim$100%).

MALDI MS experiments (355 nm) were performed using a custom built TOF instrument (60 cm flight tube) equipped with a Nd:YAG laser (Spectra-Physics GCR 11). An ion guide wire potential of -300 V was used to improve ion transmission.

Results: Protein/nucleic acid mixtures exposed to UV-light were analyzed by MALDI TOF MS without prior purification. We have obtained molecular weight information for i) the phage T4 single stranded DNA-binding protein (gp32) crosslinked to the oligonucleotide $(dT)_{20}$ by a single 266 nm laser pulse (figure 1, table 1), and ii) the *E. coli* transcription termination factor rho photoaffinity-labeled with 4-thio-uridine-diphosphate (4sUDP) by exposure to 335 nm light (table 1). The analyses were performed using 1-5 picomoles of protein. The crosslinked gp32:$(dT)_{20}$ complex, consisting of only 5-7% of total protein present in the sample, was detected by MALDI MS after optimizing the matrix-solvent combination used in sample preparation.

Conclusion: Molecular weight determination of intact, covalent protein-nucleic acid complexes by MALDI MS can identify low levels (0.5-2 μM) of crosslinked species present in protein/nucleic acid mixtures as demonstrated with the gp32:$(dT)_{20}$ complex. The choice of solvent system appears to be as important as the choice of matrix compound for MALDI MS analysis of the covalent protein-nucleic acid complexes.

Given our results, it seems feasible to apply strategies used for mass spectrometric characterization of post-translationally modified proteins (MALDI MS peptide mapping, LC-electrospray MS and MS/MS for peptide identification) to the detailed characterization of UV-crosslinked protein-nucleic acid complexes and peptide-nucleic acid complexes in order to identify nucleic acid binding domains of proteins. Structural data obtained this way should be an aid to elucidating the molecular mechanisms involved in protein-nucleic acid interactions.

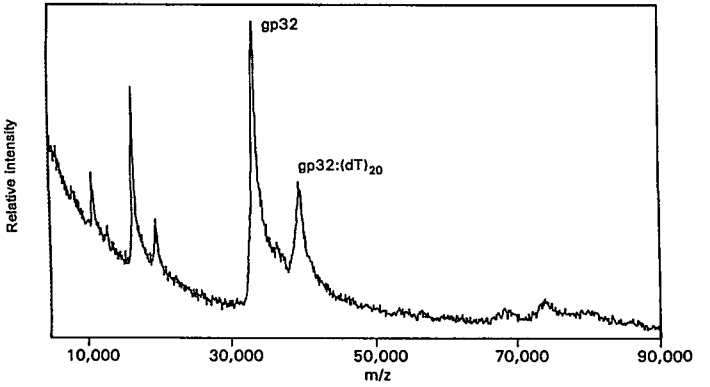

Figure 1. MALDI TOF mass spectrum of a gp32/$(dT)_{20}$ sample exposed to a single 266 nm laser pulse. Matrix: sinapinic acid (10 g/L) in formic acid/acetonitrile/glycerol (66:33:1). The sample was deposited on the probe, allowed to crystallize, and then washed in cold (4°C) water. The crosslinked gp32:$(dT)_{20}$ complex is detected along with non-crosslinked gp32.

Table 1. Molecular weight determinations of nucleic acid binding proteins and UV-crosslinked protein-nucleic acid complexes by MALDI TOF mass spectrometry.

Analyte	MW Measured (Average ± std. error)	MW Calculated
gp32	33,508 ± 3	33,502
gp32:$(dT)_{20}$	39,637 ± 69	39,603[a]
rho	47,004 ± 4	47,003
rho:4sUDP	47,560 ± 37	47,422[b]

[a]Assuming a zero-length photochemical bond. The molecular weight of $(dT)_{20}$ is 6,102.
[b]Assuming a zero-length photochemical bond. The molecular weight of 4sUDP is 420.

† See also: Jensen *et al.* (1993) Rapid Commun. Mass Spectrom. (*in press*)

Application of Electrospray Mass Spectrometry in Probing Protein-Protein and Protein-Ligand Noncovalent Interactions

B.N. Pramanik*, E.C. Huang, A. Tsarbopoulos, P. Reichert, A.K. Ganguly; P.P. Trotta; T.L. Nagabhushan

Schering-Plough Research Institute, 2015 Galloping Hill Rd., Kenilworth, NJ 07033

The newly developed technique of electrospray (ESI) MS represents an important advancement in MS technology which significantly extends the range of MS applications to the field of biomedical research.The unique feature which sets ESI apart from the rest of the available MS techniques is that ESI utilizes highly charged liquid droplets as the ion evaporation medium allowing the sample being analyzed to remain in its solution form prior to MS analysis [1]. We have been studying the noncovalent interaction of human *ras* protein with its guest ligands GDP and GTP, and the successful ESI MS detection of the *ras*-GDP noncovalent complex has recently been reported [2]. An extention of this research is the feasibility study of using ESI MS for probing the noncovalent interaction between protein molecules. We used Interferon (IFN-γ) as the protein-protein interaction model for this purpose. Mature IFN-γ is a protein of 143 amino acids with an excess of basic amino acid residues. The active form of this protein is a homodimer and is also known to be both heat and acid labile [3]. Here, we describe the use of ESI for the detection of the biologically active IFN-γ dimer. The effect of the orifice potential on the detection of this protein dimer and its charge state distribution is also discussed. This effect is further extended to study the *ras*-GDP complex.

Results and Discussion

Our earlier attempts to analyze the IFN-γ dimer under the typical ESI condition (i.e., 50% MeOH, 0.1% TFA, pH ~2.5) resulted in the detection of mass spectrum with a well-defined "bell-shape" multiply-charged ion distribution (+8 charges to +22 charges, data not shown) whose molecular weight corresponded to the monomeric IFN-γ. However, we have recently discovered that the IFN-γ noncovalent dimer can be detected by ESI MS with the use of an alkaline solution.

Since the protein has a pI of higher than 9, the protein was, therefore, prepared in aqueous solution of pH ~9 (adjusted with 30% NH_4OH). Under this condition, the dimeric form of IFN-γ (observed MW 33,819 Da) was preserved and successfully detected (**Figure 1**). The key to determining the presence of a protein homo-dimer is that one should look for the signals corresponding to their multiply protonated *odd* charge states [4]. For easy comparison, the *odd* charged ions are denoted by an asterisk.

It has been shown, with horse heart cytochrome *c*, that random protein aggregation can occur due to high protein concentration [5]. In order to rule out the potential of forming a protein dimer via the *concentration effect*, the MS detection of the protein dimer was further investigated. First, horse heart cytochrome *c* was analyzed at high concentration (40 mM) by ESI MS. The observed signals (**Figure 2A**) at m/z 2061, 1766, 1546, and 1374 correspond to the +6 to +9 charge states, respectively, of the monomeric cytochrome *c*. Signals corresponding to the *odd* charges (+11 and +13) of cytochrome *c* dimer were also observed at m/z 2248 and 1902, respectively. When the protein concentration was diluted to 70 μM, no signals corresponding to the *odd* charges of cytochrome *c* dimer were detected (**Figure 2B**). Next, an equal molar mixture of IFN-γ dimer and cytochrome *c* (each at a final concentration of 35 μM) was prepared, and the mass spectrum was recorded (**Figure 2C**). In addition to IFN-γ dimer, signals corresponding to the +6 to +9 charge states of cytochrome *c* were detected. No signals of the cytochrome *c* dimer were observed. Signals corresponding to the random attachment between IFN-γ and cytochrome *c* were also absent. This result confirmed that the IFN-γ dimer detected by MS under these experimental conditions was the specific noncovalent IFN-γ dimer, and was not the result of the random dimerization due to the *concentration effect*.

Mass spectra of the IFN-γ dimer (pH ~9) were also recorded at **OR** settings from 40 to 200 volts. The percentage of the dimeric form was calculated from the change in intensity of signal corresponding to the *odd* charge states of the dimer. This ratio of ion intensity was then normalized against the value obtained at **OR**=50 volts. The percentage of IFN-γ in the dimer form thus obtained is not an ***absolute*** value; rather, it should be treated as a *relative* measurement of preservation of the protein dimer upon change in the **OR** setting. **Figure 3** shows the percentage of IFN-γ dimer observed against experimental **OR** setting. Dissociation of the IFN–γ noncovalent dimer was triggered by an **OR** setting as low as 60 volts. These results imply that dissociation of the gas phase IFN-γ dimer requires very little energy. A similar experiment was conducted for *ras*-GDP complex at different **OR** setting. The energy required to dissociate *ras*-GDP complex is relatively higher (~ 120 volts) than that applied for IFN–γ dimer.

Conclusion

The noncovalent complexes of IFN–γ dimer and *ras*-GDP have been successfully detected by ESI MS. Dissociation of the gas phase noncovalent complexes can be induced by increasing the **OR** voltage. In the two noncovalent complexes studied, the gas phase *ras*-GDP complex required a substantial amount of energy to initiate the dissociation process while the IFN–γ dimer started to dissociate immediately following the **OR** increase. It has been suggested that covalent and noncovalent complexes observed under electrospray ionization can be easily differentiated by raising the **OR**. Our study of the noncovalent complexes of *ras*-GDP and IFN–γ dimer, however, underscores the importance of careful use of this approach. The ESI MS technique could be extended further to study the complexes between proteins and other compounds of pharmaceutical interest. The extension of this research in probing the various kinetics of enzyme-substrate interactions is the subject of current research in our laboratory.

1. Fenn, J.B.; Mann, M.; Meng, C.K.; Wong, S.F.; Whitehouse, C.M. *Science*, **1989**, *246*, 64.
2. Ganguly, A.K.; Pramanik, B.N.; Tsarbopoulos, A.; Covey, T.R.; Huang, E.C.; Fuhrman, S.A. *J. Am. Chem. Soc.* **1992**, *114*, 6559.
3. Mulkerrin, M.G.; Wetzel, R. *Biochemistry*, **1989**, *28*, 6556.
4. Henion, J.D.; Li, Y.-T.; Ganem, B. *Proceeding of the 40th ASMS on Mass Spectrometry and Allied Topics*, Washington, D.C., **1992**, p.1523.
5. Smith, R.D.; Loo, J.A.; Edmonds, C.G.; Barinaga, C.J.; Udseth, H.R. *J. Chromatogr.* **1990**, *516*, 157.

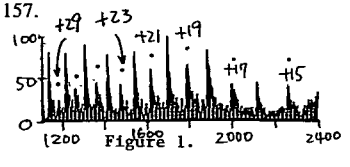

Figure 1.

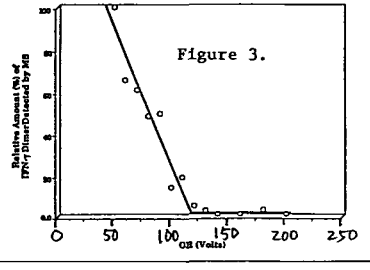

Figure 3.

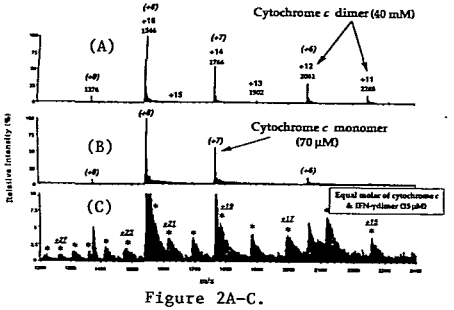

Figure 2A–C.

Identification of Proteins in One- and Two-Dimensional Gels by Mass spectrometric Peptide Mapping

*E. Mørtz, H. H. Rasmussen+, O. Vorm, M. Mann++, P. Højrup and P. Roepstorff.
Department if Molecular Biology, Odense University, 5230 Odense M, Denmark. +Institute of Medical Biochemistry, Ole Worms Allé 170, 8000 Aarhus C, Denmark. ++EMBL, Meyerhofstr.1, 6900 Heidelberg, Germany.

One- and two-dimensional polyacrylamide gel electrophoresis (PAGE) is well established for analytical separation and characterization of complex protein mixtures and is due to its high resolution and reproducibility frequently used for protein identification. Proteins in gels can be identified from their position in the gel, frequently supplemented by partial sequencing. However, in spite of the high resolution a given protein spot may contain several proteins or the proteins are positioned so close in the gel that identification may be ambiguous. To get a fast and reliable identification we have investigated the combination of protein separation by PAGE and identification based on mass spectrometry.

Proteins were separated by 1- or 2-D SDS PAGE. Stained proteins from 2-D gels were cut from several gels and recovered by elution-concentration gel electrophoresis. Proteins were then electroblotted onto polyvinylidene difluoride (PVDF) membranes and visualized by staining. The proteins were either extracted from the membrane with 40% acetonitrile, 10mM octylglucoside and analyzed by MALDI MS, or digested on the membrane with specific endoproteases and the peptides extracted with 5-50% TFA. Mass spectrometric peptide maps were established either by direct analysis of the peptide mixture by MALDI or after peptide separation by reverse phase HPLC followed by PDMS of the fractions. The proteins were identified from their peptide maps using a previously described program[1] that allows identification of proteins by comparing the experimental peptide maps with those generated from protein and DNA sequence databases.

To investigate the applicability of the method we used 6 for us unknown human proteins separated by 2-D SDS PAGE. Proteins No. 1-5 (table 1) were digested with trypsin on PVDF membranes, the peptides separated by HPLC and analyzed by PDMS. The MS peptide maps were used for searches in the transformed database (Protein Identification Resource, PIR) and the proteins identified (table 1 and 2). For protein No. 6, 0.2% of the extracted peptide mixture was analyzed by MALDI, but the peptide map did not resonably match that of any protein in the database and was recorded as unknown. At this point the identification of the first 5 proteins was confirmed by correlation with The Human Keratinocyte 2-D Gel Protein Database and the 6th protein found not to be recorded in the PIR database. A simulated search based on its sequence showed that if the protein had been present in the database it would have been identified. To further investigate direct mapping by MALDI two known proteins (No. 7 and 8) were blotted from gels, digested, mapped (figure 1) and identified.

Table 1. Proteins identified by mass spectrometric peptide mapping.

Sample	Peptide map	Protein identified	MW Da.
1	HPLC + PD	Heterogeneous ribonuclear particle	60176
2	HPLC + PD	Ubiquitin	8450
3	HPLC + PD	Heat shock 27kD protein	22325
4	HPLC + PD	variant	22325
5	HPLC + PD	variant	22325
6	MALDI	Unknown	(27772)
7	MALDI	β-lactoglobulin A	18362
8	MALDI	Carbonic Anhydrase	28980

The specificity of a search by MS peptide maps can be considerably improved if the search is performed within a narrow mass range defined by the approximate molecular weight of the protein. We therefore investigated the possibility to determine the molecular weight of the proteins from gels. 9 proteins were separated by 1-D SDS PAGE, blotted to PVDF membranes, extracted and their molecular weight determined by MALDI MS (figure 2). The mass precision and resolution obtained by MALDI of proteins extracted from gel is not as good as for pure proteins, but by far sufficient for the desired task.

Table 2. Search based on 18 peptides from protein No 1.

Rank	Peptide match	PIR number	MW Da.	Protein
1	11	21725	60176.98	Heterogeneous particle protein L - Human
2	9	13202	89988.17	Topoisomerase 1 - Yeast
3	9	14263	46456.62	Troponin T, skeletal muscle - Fruit fly
4	9	20650	47280.50	Testis determining factor - Human
5	9	21738	90556.47	Testis determining factor ZFY - Human

Figure 1. MALDI spectrum of Carbonic Anhydrase digested with trypsin on PVDF membrane. * indicate peaks used in database search.

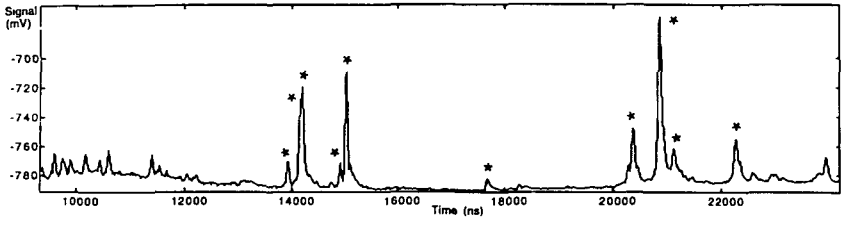

Figure 2. MALDI spectrum of protein blotted from 1-D SDS gel and extracted from membrane. Internal calibration with RNase.

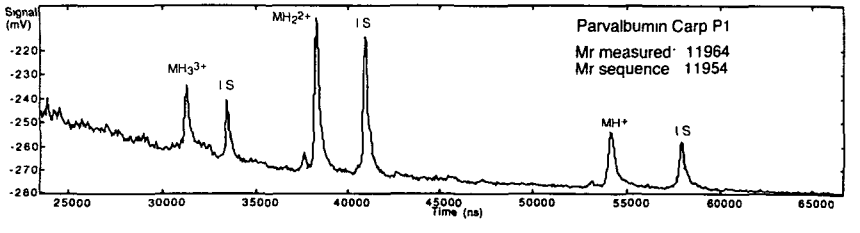

1. M. Mann, P. Højrup and P. Roepstorff, Biol. Mass Spectrometry, in press.

Surface Induced Dissociation of Peptides in a Four Sector Mass Spectrometer

Kevin L. Schey and Kelly R. Thornburg
Department of Pharmacology, 171 Ashley Ave
Medical University of South Carolina, Charleston, SC 29425

A novel in-line surface induced dissociation (SID) device has been constructed for a JEOL HX110/HX110 tandem mass spectrometer in efforts to dissociate larger peptides with greater efficiency than can be accomplished with conventional high energy CAD. The device geometry is shown in Figure 1 and includes an isolated tail electrode to assist in the extraction of product ions from the target surface. The electrodes were made from brass and inserted into a grooved Kel-F plate which mounts on a Kel-F base machined to the dimensions of the commercial collision cell base.

Initial characterization of the in-line SID device involved the measurement of internal energy distributions with the thermometer molecules tetraethylsilane and tungsten hexacarbonyl. Internal energy distributions similar to those measured using previously reported SID geometries were observed. Average internal energies of over 15 eV were deposited in 400 eV collisions. The resolution of MS-2 allowed the observation of both the sputtered $C_2H_5^+$ ion and the product ion SiH^+ in 500 eV collisions of tetraethylsilane. In addition, proton abstraction by $W(CO)_6^{+\cdot}$ molecular ions was observed as evidenced by the protonated product ions WH^+, $WCOH^+$, and $W(CO)_2H^+$.

Peptide molecular ions were generated by LSIMS of typically 1-3 nmoles of material placed in glycerol or glycerol/NBA matrices. The entire sequence of petaalanine and leucine enkephalin were obtained as a_n, b_n, and y_n ions at collision energies of 80 eV. In addition, in 100 eV collisions of pentaalanine, the high energy a_2-16 ion at m/z 99 was generated. The ratio of b_3 to y_2 ions from leucine enkephalin, an indicator of internal energy deposition, increases to 2:1 at 60 eV collisions.

The 130 eV SID spectrum of renin substrate, m/z 1758.9, is shown in Figure 2 where nearly the entire sequence is observed as a_n ions. Furthermore, high energy d_3 and d_{11} ions are also observed. A high energy d_3 ion is observed in 80 eV SID spectrum of substance P. The largest peptide dissociated with this device was melittin, m/z 2846, as shown in Figure 3 for 200 eV collisions. Prominent b_n ions are generated as well as a series of immonium ions in the low mass range for this large peptide.

The dissociation efficiency measured for leucine enkephalin in 80 eV ion/surface collisions was 7.2% with a brass target. Detection limits for peptide dissociation approach 100 pmol. for renin substrate in 200 eV collisions although limited sequence information is available at this high collision energy.

In conclusion, this in-line device has produced promising results on a variety of standard peptides. Peptide sequence information is typically in the form of a_n, b_n, and y_n ions with several high energy d_n ions also being generated. Future studies on the device geometry and, in particular, using modified surfaces should provide higher dissociation efficiencies as well as the ability to dissociate larger peptides.

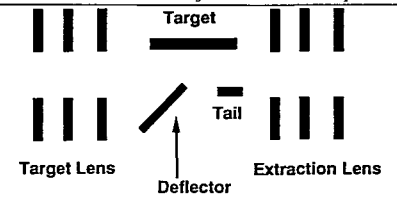

Figure 1. Cross sectional view of in-line SID device

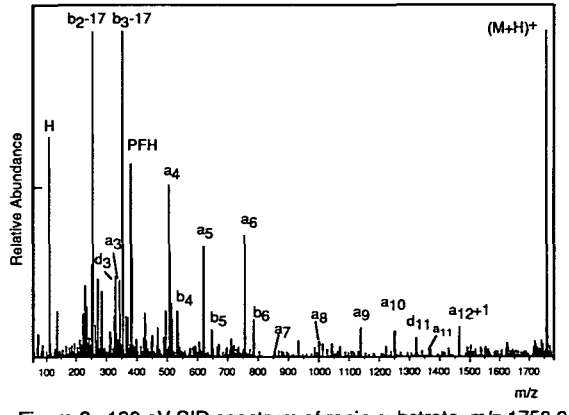

Figure 2. 130 eV SID spectrum of renin substrate, m/z 1758.9

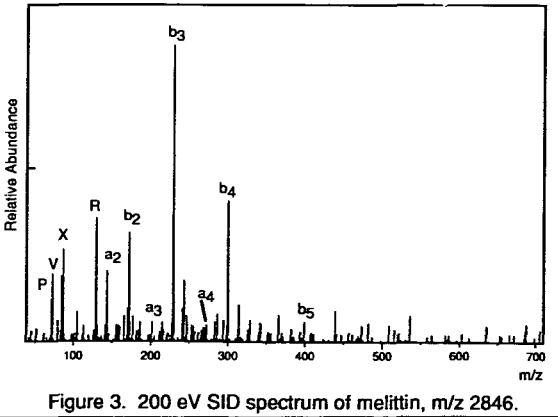

Figure 3. 200 eV SID spectrum of melittin, m/z 2846.

Determination of Posttranscriptional Modification in Ribosomal RNA by Mass Spectrometry

Jeffrey A. Kowalak and James A. McCloskey
Departments of Biochemistry and Medicinal Chemistry
University of Utah, Salt Lake City, Utah 84112

Posttranscriptional modification of nucleosides plays an important, yet incompletely defined role in the structure and function of large ribosomal RNAs. The most compelling evidence for the functional importance of modified nucleosides is the clustering of these residues at the functional center of the ribosome as defined by chemical footprinting and photoreactive cross-linking studies (1).

Experimental approaches have been developed for the structural characterization and the determination of sequence location of modified nucleosides in ribosomal RNAs, based principally on electrospray mass spectrometry (2). Oligonucleotide fragments produced by site specific ribonuclease digestion of RNA are analyzed by ES-MS with sufficient accuracy such that the base composition can be ascertained solely from the measurement of molecular mass (3).

The method has been applied to *E. coli* 16S rRNA (1542 nucleotides, M_r 499,759) in which six different modified nucleosides are located at 10 sequence positions. The chemical identity of these modified residues was confirmed by directly combined HPLC-mass spectrometry (LC-MS) of an enzymatic hydrolysate of the intact rRNA molecule. The rRNA was then digested using RNase T_1, an endoribonuclease which cleaves at Gp↓N sites, and the resultant oligonucleotide mixture fractionated by DEAE anion exchange chromatography. An aliquot of each DEAE pool was then analyzed by LC-MS to determine in which pools the modification-containing oligonucleotides reside Electrospray mass spectrometry (ES-MS) was used to determine the molecular weight of the oligonucleotides in modification-containing DEAE pools. Experimentally determined oligonucleotide mass values, used in conjunction with LC-MS and gene sequence data, were used for characterization and sequence placement of modified residues.

This approach was successfully employed to characterize modification-containing oligonucleotides, of chain length ≥ 4 residues, in *E. coli* 16S rRNA (Table 1).

Table 1. Compositions of Modification-containing Oligonucleotides from RNase T_1 Digestion of *E. coli* 16S rRNA Determined by Electrospray MS.

Modified Nucleoside	M_r Meas.	Oligonucleotide Composition	M_r Calc.	Sequence Position
m^4Cm	1306.35	$C_3Gp+2CH_2$	1306.83	$m^4Cm_{1402}CCG$
m^5C	1646.10	$C_2A_2Gp+CH_2$	1646.04	$m^5C_{967}AACG$
m^6_2A	1994.28	$C_2UA_2Gp+4CH_2$	1994.29	$m^6_2A_{1518}m^6_2A_{1519}CCUG$
m^3U	2305.80	CUA_4Gp+CH_2	2305.44	$m^3U_{1498}AACAAG$
m^5C	3198.30	$C_4U_2A_3Gp+CH_2$	3197.95	$Um^5C_{1407}ACACCAUG$

In the first application of this methodology, the chemical identity and sequence location of the modified nucleoside N^4-acetyl-2′-*O*-methylcytidine (ac^4Cm) were determined in 5S rRNA from a hyperthermophilic archaeon, *Pyrodictium occultum* (4). While ribosomal RNAs have been used for the development and initial applications of the method, the basic principles are generally applicable to characterize covalent structural modifications in any RNA. For example, the chemical identification and sequence position of 2-thiothymine riboside (s^2T) has been determined in unfractionated tRNA from *Pyrococcus furiosus*.

Transfer RNA was isolated from *P. furiosus* cells which were grown at 100°C. LC-MS analysis of an enzymatic hydrolysate of unfractionated tRNA revealed the presence of s^2T, which represents the first occurrence of this modified ribonucleoside in the Archaea. The related nucleoside, thymine riboside, is ubiquitous in bacterial tRNA and is known to occur only at position 54, the first position of the TΨC loop .

Unfractionated tRNA (>50 species) from *P. furiosus* 100°C culture was digested with RNase T_1 and the resultant oligonucleotide mixture was fractionated by DEAE anion exchange chromatography. The molecular weight of one oligonucleotide was determined to be 1324.7 by ES-MS, for which no allowable composition exists. Only after replacement of a sulfur atom for and oxygen atom (Δm 16.02), was a single allowable composition found; $CU_2Gp + 2\ CH_2 - O + S$ (M_r 1324.9 calc.). The oligonucleotide was then completely hydrolyzed and analyzed by LC/MS. The chromatogram presented in Figure 1 indicates that the nucleoside components of the oligonucleotide are Ψ, Cm, G and s^2T. 2′-*O*-methylcytidine is universally conserved at position 56 in Archaeal tRNA, therefore, we conclude that the sequence of the oligonucleotide is 54-s^2TΨCmG-57.

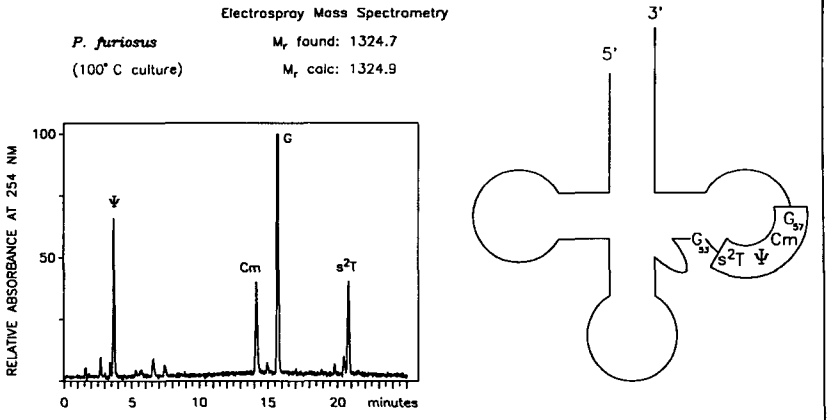

1. Brimacombe, R., Mitchell, P., Osswald, M., and Bochkariov, D., (1993) *FASEB J.*, 7, 161-167.
2. Kowalak, J.A., Pomerantz, S.C., Crain, P.F., and McCloskey, J.A., (1993) manuscript in preparation.
3. Pomerantz, S.C., Kowalak, J.A., and McCloskey, J.A., (1993) *J. Am. Soc. Mass Spectrom.*, 4, 204-209.
4. Bruenger, E., Kowalak, J.A., Kuchino, Y., McCloskey, J.A., Mizushima, H., Stetter, K.O., and Crain, P.F., (1993) *FASEB J.*, 7, 196-200.

The Hows and Whys of Multiply-charged Oligonucleotide Decompositions

Sohrab Habibi-Goudarzi and Scott A. McLuckey
Analytical Chemistry Division, Oak Ridge National Laboratory
Oak Ridge, TN 37831-6365

Multiply-charged gaseous biopolymers, which can be formed by electrospray ionization, constitute new and unusual species. They are unusual in that the unimolecular and bimolecular chemistry of these ions can be highly influenced by the coulombic repulsion arising from the presence of multiple charge sites. This paper emphasizes the unimolecular behavior of multiply-charged single-stranded deoxy oligonucleotides. The objective of this research is to develop an understanding of the influence of charge and sequence on the fragmentation of an oligonucleotide.

Previous work in our laboratory demonstrated that multiply-charged adenosine-containing oligomers tend to lose charged adenine as the lowest energy decomposition followed by cleavage at the 3' C-O bond of the sugar from which the adenine had been lost [1]. Subsequent studies have shown that in general base loss occurs first followed by cleavage at the sugar. Such a sequence can be rationalized by two successive 1,2-elimination reactions to yield a furan attached to the rest of the chain at the 3'-carbon (see Scheme). Two scenarios are depicted in the scheme. In one scenario, proton transfer from a base to a charged phosphodiester linkage precedes base loss. In the other, no proton transfer occurs prior to base loss. Which scenario prevails determines whether or not the base is lost as a neutral or as an ion. Singly-charged mononucleotides tend to lose the base as a neutral under quadrupole ion trap collisional activation conditions. Adenosine monophosphate shows a small signal due to lose of charged adenine. We propose that the coulombic field associated with a multiply charged oligonucleotide can promote intramolecular proton transfer to one or more of the nucleobases depending upon the strength of the electric field. The relief of coulombic repulsion must be sufficient overcome the intrinsic difference in the gas-phase acidities of the nucleobase and the phosphodiester group. Apparently, adenine is the strongest acid of the base substituents followed by thymine. The loss of charged adenine is therefore preferred, followed by loss of charged thymine, because charge is most likely to be transferred to those bases to relieve coulombic strain. The relief in coulombic repulsion provided by loss of a charged base relative to the loss of a neutral base presumably facilitates the loss of charged bases.

As the coulombic field decreases, the likelihood for charge to reside on one of the nucleobases also decreases. For this reason, the appearance of MS/MS spectra can change dramatically with charge state. Figure 1 compares the MS/MS spectra of the triply- and doubly-charged forms of 5'-d(AAAA)-3'. Virtually 100% of the fragmentation of the triply-charged ion proceeds via loss of charged adenine whereas roughly 75% of the fragmentation of the doubly-charged ion fragments through loss of neutral adenine. Similar structural information is present in both spectra despite their remarkably different appearance. This is a common observation in comparing MS/MS spectra of various charge states of the same parent oligonucleotide. This behavior can be understood, at least qualitatively, by the occurrence or non-occurrence of intramolecular proton transfer followed by the reactions depicted in Scheme 1. Further support for these conclusions have been summarized [2].

[1] McLuckey, S.A.; Van Berkel, G.J.; Glish, G.L. J. Am. Soc. Mass Spectrom., 3 (1992) 60.
[2] McLuckey, S.A.; Habibi-Goudarzi, S. J. Am. Chem. Soc., Submitted.

Research sponsored by the National Institutes of Health under Grant GM 45372. Oak Ridge National Laboratory is operated for the Department of Energy under Contract DE-AC05-84OR21400 by Martin Marietta Energy Systems.

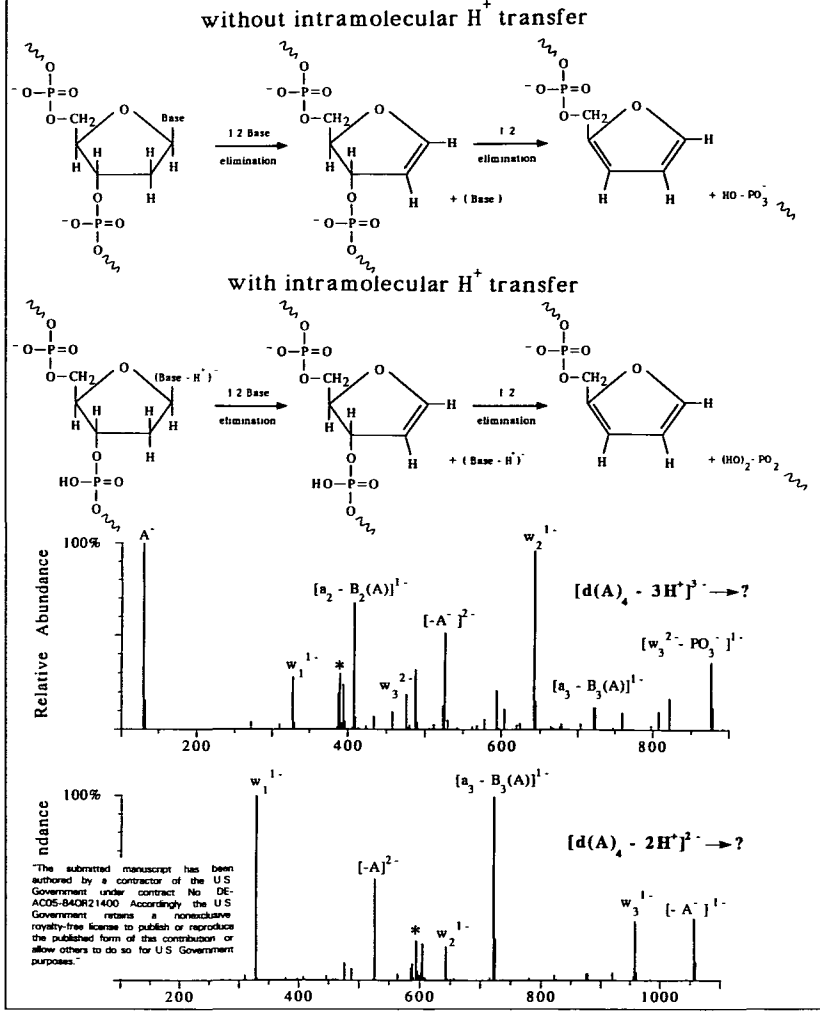

"The submitted manuscript has been authored by a contractor of the U S Government under contract No DE-AC05-84OR21400 Accordingly the U S Government retains a nonexclusive royalty-free license to publish or reproduce the published form of this contribution or allow others to do so for U S Government purposes."

ELECTROSPRAY IONIZATION OF PLASMID DNA AND DETECTION BY MASS SPECTROMETRY. *Charles G. Edmonds[a,b], David L. Springer[b], Brent J. Morris[c], Brian D. Thrall[b] and David G. Camp II[c], (a) Chemical Sciences Departments, (b) Biology and Chemistry, Pacific Northwest Laboratory, Richland WA 99352, and (c) Eastern Oregon State College, Badgley Hall, La Grande OR 97850

We are interested in exploring the limits of electrospray ionization (ESI) for biopolymers. Fenn and co-workers have published examples of the electrospray ionization-mass spectrometry (ESI-MS) of synthetic polymers up to 5 megadaltons in average molecular weight (T. Nohmi and J.B. Fenn, *J. Am. Chem. Soc. 114* **1992** 3242-3246). Ou objective has been to investigate the potential utility of ESI as the basis of a mass spectrometric approach to high speed DNA sequencing. We have successfully employed negative ion ESI-MS to ionize and detect pGem-5S, a 3126 base pair supercoiled closed circular double-stranded plasmid which includes the 5S ribosomal RNA gene from *Xenopus borealis* (Mr 1,945,664 for the free acid). We chose a plasmid for these studies because of the unique topomeric characteristics of these materials which facilitate the purification and provide highly specific characterization of the material on the basis of sedimentation velocity and electrophoretic mobility. DNA samples were purified to eliminate contamination by lower mass DNA, ribonucleic acid and salts. The plasmid was cultured in transformed *E. coli* JM109 and following alkaline lysis the supercoiled DNA was separated by CsCl density gradient centrifugation. Successive 100% ethanol precipitation from ammonium acetate solution was followed by ultrafiltration with Centricon-100 (Amicon, Danvers MA) (100,000 MWCO). Preparations consisted principally of the supercoiled species with small contributions by nicked circular and linearized plasmid. Following final lyophilization plasmid samples were dissolved in deionized water and subjected to ESI-MS using a TAGA 6000E tandem quadruple instrument with a differentially pumped atmosphere/vacuum interface with mild interface conditions. Electrospray ionization of the plasmid DNA sample as illustrated in Figure 1 afforded a single broad envelope of ionized species extending between *m/z* 500 and *m/z* 1400. Maximum relative abundance was found at approximately *m/z* 700. This observation was consistent with the production of gas phase multiply charged molecular anions of more than a megadalton in mass given the low resolving power of the quadrupole mass spectrometer. We further characterized the behavior of the plasmid under ESI conditions by electrospraying the nucleic acid onto targets of stainless steel foil or TRIS-EDTA-Borate buffer droplets stabilized by 1% agarose gel. After electrospray onto these targets, the plasmid was extracted with TEB buffer and examined by 1% agarose gel electrophoresis. The results of this experiment is illustrated in Figure 2. When electrosprayed onto a dry stainless steel target the plasmid was substantially altered with the production of a wide range materials of both higher and lower electrophoretic mobility. However, when the plasmid was prepared onto a liquid buffer surface the plasmid remained substantially intact with the closed circular form of the nucleic acid was opened to the nicked circular. No degradation to material of lower mass was observed. This result substantiates our interpretation of the mass spectrum of pGEM-5S as that of intact nucleic acid of more than 1 megadalton in mass.

Acknowledgment. We thank R.D. Smith for advice and encouragement and G.L. Stiegler for guidance during the early stages of this work. Work was supported by the OHER, Human Genome Program. DGC gratefully acknowledges a Summer Research Grant from Eastern Oregon State College. Pacific Northwest Laboratory is operated for the U.S. Department of Energy by Battelle Memorial Institute under Contract DE-AC06-76RLO 1830.

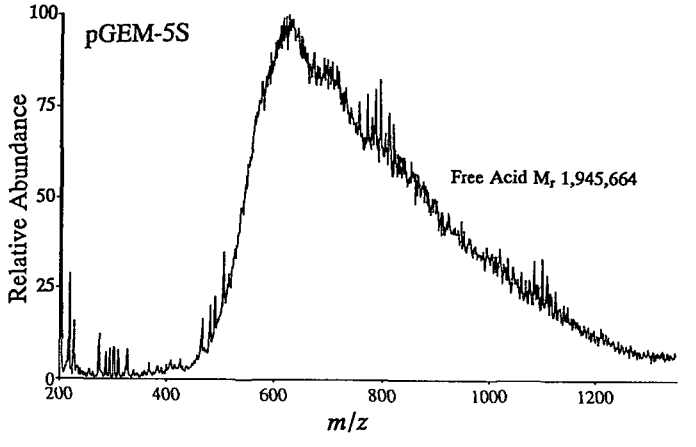

Figure 1. Electrospray ionization mass spectrum of a preparation of the plasmid, pGEM-5S, consisting of 3126 base pairs of closed circular supercoiled DNA, M_r 1,945,664 as the free acid.

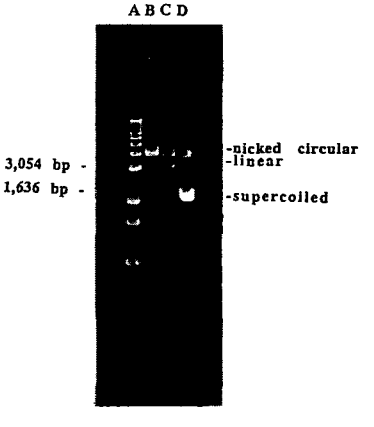

Figure 2. One percent agarose gel electrophoresis of (A) 1Kbase DNA ladder (Bethesda Research Labs.), (B) electrospray ionization preparation of pGEM-5S on to a target consisting of a droplet of TEB buffer stabalized by 1 percent agarose gel, (C) electrospray ionization preparation of pGEM-5S on to a target of chemically clean stainless steel foil, (D) the control pGEM-5S prepartion.

Quantification of Apolipoprotein A-1 by Isotope Dilution FAB MS

John R. Barr, Vincent L. Maggio, Louis, R. Alexander, Donald G. Patterson, Jr.
L. Omar Henderson, Larry L. Needham, Gerald R. Cooper
Centers for Disease Control, Atlanta, GA 30333

Atherosclerosis is the leading cause of morbidity and mortality in the U.S. Major risk factors for atherosclerosis include increased serum cholesterol levels and abnormal distributions of lipoproteins carrying serum lipids. These lipoproteins are composed of both lipid and protein components. As opposed to the variable amounts of lipid material in lipoproteins, the protein structural components remain constant. Recently there has been great interest in measurement of the protein components, called apolipoproteins (apos), as a measure of atherosclerosis risk. One factor which helps to reduce the risk of atherosclerosis is the "good" cholesterol containing lipoprotein HDL. The major protein component of HDL is Apo A-1. Measurement of Apo A-1 has been exclusively done by immunoassay. There is great variation in the clinical measurement of Apo A-1 because of standardization aspects of the assays, primarily the lack of primary reference standard Apo A-I with assigned protein mass values.

We have recently employed isotope dilution high resolution mass spectrometry to assign mass values on an Apo A-1 primary reference standard. The approach utilized enzymatic digestion of Apo A-1 and quantification of three of the resulting peptides with isotopically labeled peptides with the same sequences (Figure 1). The initial portion of this study was to verify the expected molecular weight of Apo A-1 in the reference standard by electrospray ionization MS (Figure 2) and to confirm the sequence via peptide mapping (98% coverage). Enzymatic digestion conditions which yielded reproducible quantitative cleavage at several sites were then determined and three peptides that were found to be reliably formed were chosen for quantification standards. Native and labeled (which range from six to nine mass units higher than native standards) were then synthesized, purified and quantified. The peptide quantification was performed by a combination of amino acid analysis and nitrogen analysis. Peptide purity was determined by a combination of HPLC and CE. The quantification of the standard reference material was then performed by the addition of a known amount of two of the labeled peptides to the Apo A-1 standard, dividing each standard vial into four equal portions, followed by enzymatic digestion of each aliquot. The resulting mixtures were then purified by HPLC and fractions which contain the newly formed native and the labeled peptides were subjected to four replicate FAB MS runs. The third labeled peptide was then utilized as a recovery standard. These results were then quantified against standard curves prepared from synthetic native and labeled peptides. Using this approach, the mean from each standard vial was found to be 1.050 mg Apo A-1. The analytical CV was 3.96% (see Figure 3 for variance component percent of total) and the 99% confidence limits was found to be 1.050 ± 0.010 mg or 1.050 mg ± 1%.

Figure 1: Scheme for the quantification of Apo A-1

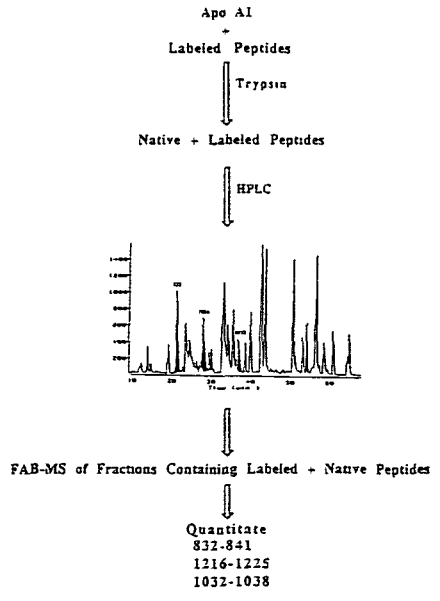

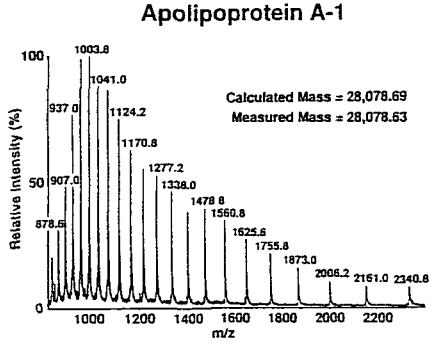

Figure 2: ESI spectrum of Apo A-1

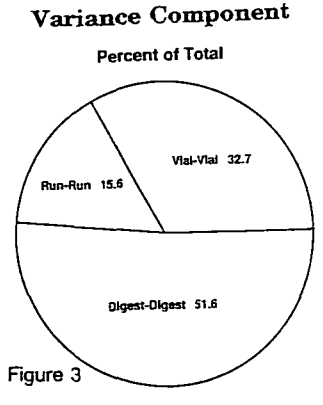

Figure 3

Detailed Structural Characterization of Carbohydrate and Glycoconjugate Oligomers Using Selective Chemical Modification, HPLC-ES-MS-CID-MS.

Vernon N. Reinhold, Bruce B. Reinhold, Stephen Chan
Departments of Nutrition and Biological Chemistry, Harvard University
Schools of Public Health and Medicine. 665 Huntington Avenue, Boston, MA 02115

The functional roles being unraveled in the study of cell-cell interactions point frequently to carbohydrate residues on their surfaces. In part, N-, and O-linked glycans have been shown to influence protein folding during biosynthesis, have a directing control during intra-, intercellular trafficking, stabilize a proteins conformation to the extremes of pH and temperature, protect against proteolysis, provide an effective foil against immune surveillance, and serve as components in signal transduction. As numerous and compelling as these problems are, the analytical effort required to fully understand carbohydrate structural detail can be overwhelming.

The structural characterization of glycoprotein glycans can be considered to fall into three categories: a determination of glycotype, glycoform, and glycomer. A comparative profile of glycoprotein heterogeneity (glycoform distribution) is one of the most critical pieces of analytical information, although appropriate techniques for its measurement have eluded carbohydrate analysts for years. The glycoform distribution mirrors four fundamental characteristics; (i) the complement of glycosyl transferases expressed during glycoprotein biosynthesis; (ii) the *in vivo* physiological milieu of the Golgi; and, (iii) the time frame of elaboration, and (iv) the tissue origin (organelle, intra- or extracellular). Although direct structural differences are noted, the physiological significance is little understood. Production and marketing of recombinant glycoprotein pharmaceuticals have reinforced the need for reliable procedure(s) of product comparison. Chromatographic, chemical and enzymatic techniques all pose the possibility of enriching or excluding particular subforms, thus, given the choice of current analytical techniques, physical methods would be favored over biological measurements for determining a glycoform distribution. Mass measurement of a glycopeptide isolated by reverse phase HPLC may provide the most complete measure of glycan heterogenity since separations are dependent on peptide properties and not influenced by the glycan. Linkage and branching features are hidden as mass isobars and for these features further effort must be invested.

To approach isomeric glycans on N-linked glycoproteins, and glycosphingolipids, and induce molecular specificity we have combined pre-analysis chemistry and chromatography with ES-MS and CID. The altered molecular weights imparted to isobaric structures yield, in some cases, a precise fingerprint of the reacting glycoform without resorting to the classical sample consuming procedures of linkage analyses. As a complement to this improved specificity, the chemically modified glycans are very lipophilic following derivatization, and hence, easily cleaned up by extraction. Electrospray ionization provides multiple charging for lower effective mass measurement, improved signal-to-noise ratios for greater signal amplification and analyte detection, and with the permethylated glycans, a higher efficiency of ionization. The strategies we have found most informative define unique CID fragments from permethylated glycans when infused with alkali metal ions for electrospray ionization by adduction. For determining structural detail, samples prepared in this way are pertinent for several reasons: (i) enhanced ionization efficiency and singularity in adduction type; (ii) mass shifts associated with each glycosidic cleavage to provide a measure of cleavage multiplicity; (iii) adequate detection of cross-ring cleavages that relate to linkage; (iv) the ease of product clean-up by solvent extraction; and (v) consistent with periodate chemistry to enhance molecular specificity.

The location of polylactosamine and N-acetylneuraminic acid residues are positional isomers that are transparent to mass profiling and periodate oxidation, reduction and methylation offers a chemically selective strategy to differentiate linkage and branching patterns, especially when those details are lost among isomeric mixtures. As an example, the linkage isomers of N-acetylneuraminic acid frequently occur as either an a(2—>6) or a(2—>3) to a penultimate galactose, a linkage resolvable by oxidation, reduction and methylation chemistry. Also, the positional isomers of lactosylamine residue (at the 4 or 4' mannose) in triantennary structures yield unique products by oxidation, reduction and methylation chemistry. With these structural entities, each N-

acetylneuraminic acid residue will decrease the glycan mass by 88 amu, and the 4' mannosyl moiety will increment by 2 amu, (4 amu if a 4'-linked triantenna). Furthermore, a terminal fucosyl group will cause a decrease in mass by 42 amu (adjacent glycols), as will all terminal galactosyl residues. Not only does the new pattern of ions unravel difficult isomeric problems, it also provides a reexamination of all structures previously profiled following methylation.

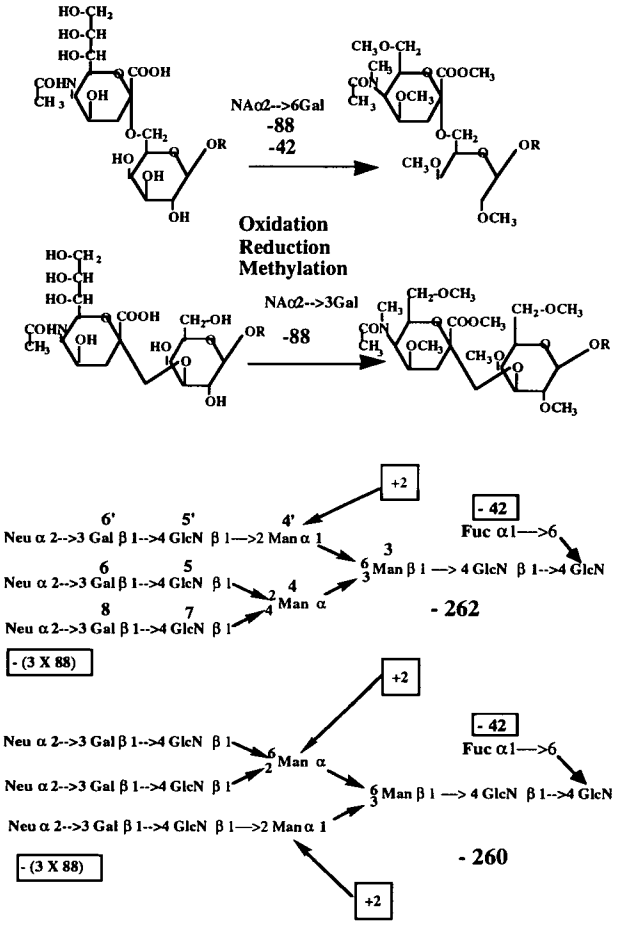

MS/MS of Cobalt-coordinated Branched Pentasaccharide Isomers: Linkage Position Determination using Electrospray Ionization

Julie Leary* and Aberra Fura, University of California, Dept of Chemistry, Berkeley, CA 94720

Our previous research has demonstrated that MS/MS of lithium coordinated oligosaccharides can be used to determine the linkage position in linear glucose polymers (1,2). Extensions of this methodology have also shown that ESI tandem mass spectrometry can be used to distinguish linkages in calcium and magnesium coordinated branched trisaccharides(3). The work described herein is the next step in this characterization process which involves ESI tandem mass spectrometry of cobalt coordinated branched pentasaccharides. In this particular instance, four isomeric pentasaccharides (LNFP I, II, III, and V) were investigated by MS/MS and MS/MS/MS and distinct differences in the linkages were observed. Figures 1 and 2 below are the MS/MS spectra of LNFP-1 and LNFP-V coordinated to cobalt.

In addition to MS/MS, MS/MS/MS of some important intermediate ions was also carried out. By using consecutive mass spectrometric measurements one can sequence the oligosaccharide throughout beginning at the reducing ring. Figures 3 shows the MS/MS/MS spectra for LNFP-V which in addition to MS/MS/MS of m/z 441 (not shown) allows for linkage position determination throughout the molecule.

In all four cases the data suggest that Co^{+2} is partially coordinated to the N-acetyl function of the glucosamine ring. The charge site is clearly located near this ring as evidenced by the dissociation ions detected which also clearly indicate the presence of nitrogen in their composition. Additionally, formation of an aziridine ring always accompanies the facile loss of the substituent vicinal to the N-acetyl group. The nitrogen proton is easily transfered to the adjacent ring which is lost as a neutral.

Experimental: The instrument used for all experiments was a BIO-Q triple quadrupole mass spectrometer equipped with electrospray ion source (Fisons/VG Biotech, Manchester, England). The mobile phase used was a 50:50 mixture of acetonitrile and water. The ratio of metal to oligosaccharide was 1:1 using 1.0 nmole of oligosaccharide. Skimmer voltage was 70 ev except for MS/MS/MS for which it was 150 ev. Optimization studies were not performed on the pentasaccharides but were carried out for the branched trisaccharides which were analyzed at concentrations of 10 pmol/ul (submitted to Anal. Chem.)

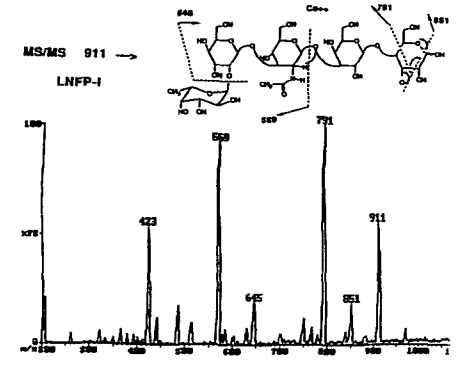

Figure 1

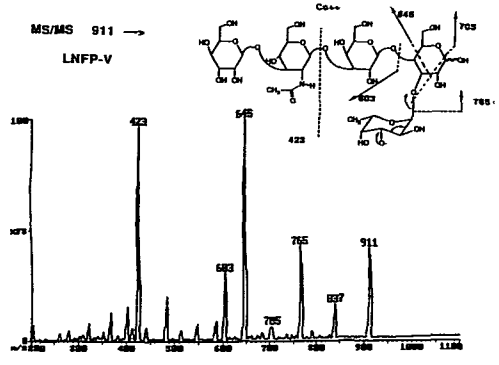

Figure 2

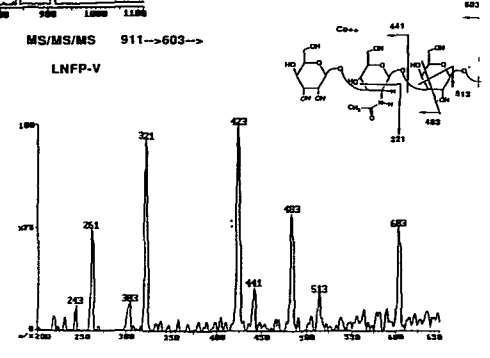

Figure 3

From the Outer Membrane to the Gas Phase: Making Ions of Bacterial Surface Antigens

Bradford W. Gibson*, William Melaugh, Nancy J. Phillips, Jeffrey Engstrom
and Michael Tullius
Department of Pharmaceutical Chemistry
University of California, San Francisco, CA 94143-0446.

Bacterial pathogens interact with their host through a complex set of surface and secreted biomolecules that enable the organism to adhere, invade and multiply in the changing and hostile environment of the host. We are interested in elucidating the roles of bacterial lipooligosaccharides (or LOS), one of the major surface antigens from a group of human mucosal pathogens. These bacterial pathogens include *Neisseria* and *Haemophilus* species that are responsible for an array of serious and often life-threatening illnesses ranging from chancroid and gonorrhea to such respiratory and disseminated infections as pneumonia and meningitis.

LOS are complex biomolecules that contain a largely conserved lipid A moiety and a highly branched and variable carbohydrate domain [1]. The carbohydrate domain can consist of over a dozen different structures from a single bacterial strain. The major analytical challenge facing us is how to best sort out this heterogeneous LOS population and correlate their structures to important biological data. Initially we used liquid secondary ion mass spectrometry (LSIMS) to analyze these LOS as their water soluble O-deacylated derivatives. However, the spectra we obtained were often very weak (particularly at masses above m/z 2000), and usually gave a high level of sodium and potassium adducts (see Fig. 1). If the O-deacylated LOS were also dephosphorylated with aqueous HF, a better spectrum could be obtained, but some glycosidic bonds were hydrolyzed and all information regarding phosphorylation heterogeneity was lost

When electrospray ionization mass spectrometry (ESI-MS) is used, an excellent overall assessment of the LOS components can be obtained with a dynamic range far superior to LSIMS (see Fig. 2) [2]. If these O-deacylated LOS are treated with glycosidases, specific questions concerning structure/function relationships can be readily obtained as well. For example, the identification of LOS containing terminal sialic acid can be readily determined, even in very complex mixtures if these LOS samples are treated with neuraminidase and compared to the original spectra [3]. Unlike most electrospray data, our spectra generally contain a single peak for each LOS component and, therefore, the multiplicity of peaks observed in these spectra arise from heterogeneity of the LOS and not from multiple charge states of specific components.

Literature Cited

1. N. J. Phillips, C. M. John, L. G. Reinders, J. M. Griffiss, M. A. Apicella and B. W. Gibson, *Biomed. Environ. Mass Spectrom.* **1990**, *19*, 731-745.
2. B.W. Gibson, W. Melaugh, N.J. Phillips. M.A. Apicella, A.A. Campagnari and J.M. Griffiss, *J. Bacteriology*, **175**, 2702 (1993)
3. N.J. Phillips, M.A. Apicella, J.M. Griffiss and B.W. Gibson *Biochemistry*, **32**, 2003 (1993)

We would like to acknowledge financial support from the University AIDS Research Program and NIAID (AI 30006, AI 24616, 21620). The UCSF Mass Spectrometry Facility work was supported by grants from the NIH (RR01614) and NIEHS (ES04705).

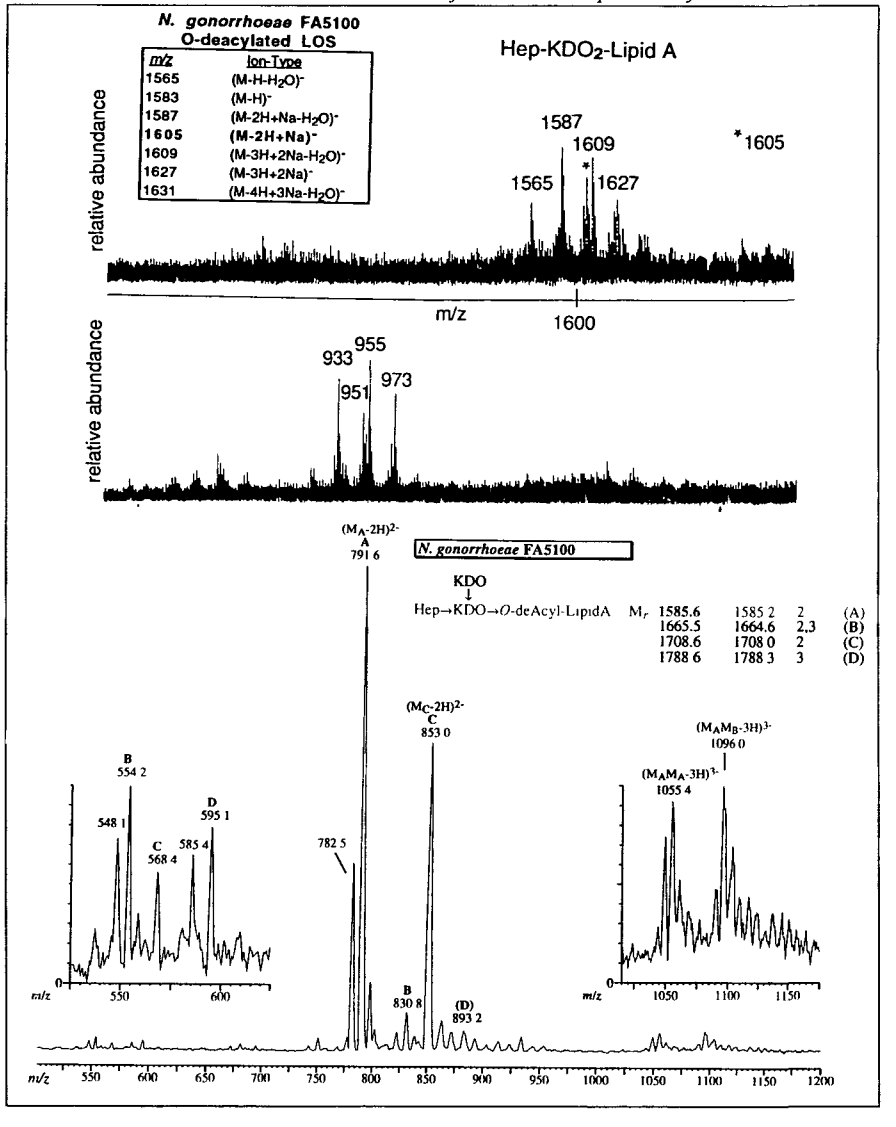

Neutralization-Reionization Mass Spectrometry.

Fred W. McLafferty and Russell A. Chorush. Chemistry Department, Baker Laboratory, Cornell University, Ithaca, NY 14853-1301.

This review is dedicated to my longtime colleague Professor Richard F. Porter[1] who passed away on September 1, 1991. Dick pioneered the neutralization techniques used in our research and unselfishly helped us implement these.

The development of NMRS for molecular species in the last decade has been phenomenal,[2-4] with pioneering research in many other laboratories such as those of Holmes,[5,6] Schwarz,[7] Harrison,[8] Gellene,[1] Wesdemiotis,[9] Turecek,[10] and Terlouw.[5] An original effort was to characterize the neutral species produced in the dissociation of singly charged ions, such as the loss of HCN or HNC from aniline and pyridine. Other research efforts have been aimed at finding ways to characterize ions that isomerize readily, based on the fact that their neutral counterparts can often be dissociated with sufficient rearrangement minimization to provide isomeric charcterization. This was successful in many cases, such as four isomers of $C_4H_4^{+\cdot}$, five of $C_4H_8^{+\cdot}$, and seven of $C_2H_4O^{+\cdot}$.

However, by far the most interesting NRMS application outside of mass spectrometry has been the preparation of a wide variety of unusual neutral species whose reactivity has made them extremely difficult to study by other experimental methods. Detailed energy surfaces for the unimolecular chemistry of carbenes, ylides, diradicals, clusters, organometallics, and hypervalent, sterically strained, and anti-aromatic molecules have attracted broad interest across the chemistry community. A variety of instrumentation developments and refinements, plus computer acquisition and reduction of data, have greatly aided this progress. For example, surface induced neutralization can add more than 20 eV of internal energy to the neutral formed.

1. G.I. Gellene and R.F. Porter, Acc. Chem. Res. **16**, 200 (1983).
2. P.O. Danis, C. Wesdemiotis and F.W. McLafferty, J. Am. Chem. Soc. **105**, 7454 (1983).
3. C. Wesdemiotis and F.W. McLafferty, Chem. Rev. **87**, 485 (1987).
4. F.W. McLafferty, Int. J. Mass Spectrom. Ion Processes **118/119**, 221 (1992).
5. P.C. Burgers, J.L. Holmes, A.A. Mommers and J.K. Terlouw, Chem. Phys. Lett.. **102**, 1 (1983).
6. J.L. Holmes, Mass Spectrom. Rev. **8**, 513 (1989).
7. H. Schwarz, Pure Appl. Chem., **61**, 685 (1989)
8. A.W. McMahon, S.K. Chowdhury, and A.G. Harrison, Org. Mass Spectrom. **24**, 620 (1989).
9. C. Wesdemiotis, B. Leyh, A. Fura and F.W. McLafferty, J. Am. Chem. Soc. **112**, 8655 (1990).
10. F. Turecek, Org. Mass Spectrom. **27**, 1087 (1992).

Presented at the 41st ASMS Conference on Mass Spectrometry

NEUTRALIZED ION BEAM STUDIES OF O_2: A NEW STATE FOR AN OLD MOLECULE

K.S. Griffith and G.I. Gellene, Department of Chemistry and Biochemistry, Texas Tech University, Lubbock, TX 79409-1061

One of the more intriguing applications of neutralized ion beam techniques is its use to produce previously unknown novel molecules or new states of well known molecules. This use of neutralized ion beam techniques is illustrated by a recent study of the O_2 molecule which provides evidence for a new high energy metastable state of O_2. We investigated the charge exchange of O_2^+ with alkali metals using a technique which is sensitive to both dissociative and nondissociative products. Briefly, ions formed by electron ionization in a high pressure source are accelerated to 5 keV and magnetically mass resolved. The ions then enter a neutralization chamber containing a few mTorr of metal atoms (Na or K). Both neutral and ions exit the chamber, and the ions are removed from the beam by a pair of electrostatic plates. The neutral beam, which spreads as species dissociate, travels to a translatable detector, which samples intensity as a function of angle. Metastable products appear as a spike of intensity around $\theta = 0$. In a second experiment, an additional slit is placed after the neutralization chamber, which allows direct investigation of the dissociation of the metastable species by discriminating against signal from promptly dissociative species. A typical set of profiles is shown.

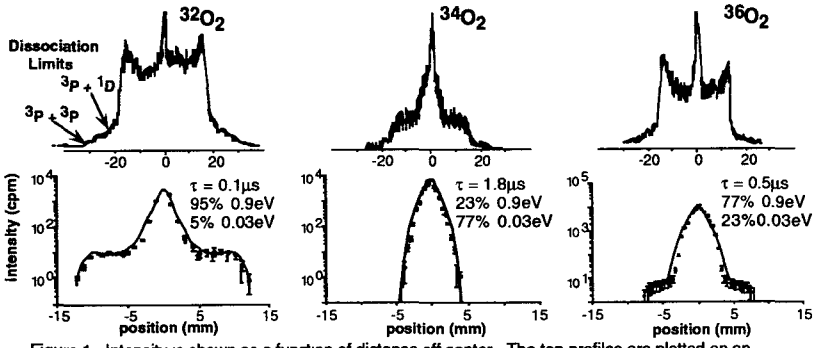

Figure 1. Intensity is shown as a function of distance off center. The top profiles are plotted on an arbitrary linear scale with center heights scaled to be equal. The bottom profiles are from the double slit experiment, and the curves are from the model (see text).

The results for the dissociative products are understandable in terms of previous studies of this charge exchange reaction. Surprisingly, however, undissociated O_2 in a long lived state was also observed. The experimental results of the double slit experiment were simulated using a model that included a geometric apparatus function, a probability of dissociation with time, and a probability of kinetic energy release (KER). The results of the model were not

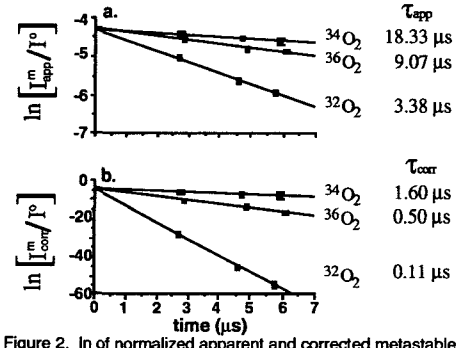

Figure 2. ln of normalized apparent and corrected metastable intensity as a function of time after neutralization. Lifetimes are obtained from the slopes Note the scale change

unique in that a finite range of lifetimes could be modelled. By measuring dependence of the normalized apparent metastable intensity (I^m_{app}/I^o) as a function of time after neutralization, apparent lifetimes were obtained (Figure 2a). These lifetimes were overestimated because of the inability to distinguish between signal from undissociated species and signal from near $\theta = 0$ dissociations. This was corrected for by using the model of the system which allows determination of the amount of dissociative signal, for a given lifetime and KER distribution, that is counted as undissociated. The results are shown in Figure 2b.

Because the metastable relaxes dissociatively, it cannot be identified with any of the known metastable states of O_2, all of which lie below the first dissociation limit. The results of the modelling of the double slit experiment indicate two relaxation pathways, one predissociative (KER = 0.9eV) and one radiative (KER ≈ 0.03eV). Inspection of the predicted bound states of O_2 reveals one candidate that can account for the predissociation, $1^1\Delta_u$. Calculation of the Franck-Condon overlaps of the first five vibrational states of $1^1\Delta_u$ with the state that predissociates it $2^3\Delta_u$, reveals that the v=2 level FCF's vary significantly with mass (Figure 3) and that this variation can account for the difference in the predissociative lifetimes of the isotopic variants. Further, a spin orbit coupling constant of 9(±1) cm^{-1} was determined for the $1^1\Delta_u \sim 2^3\Delta_u$ interaction. *Ab initio* calculations indicate that this small spin orbit coupling constant is reasonable for this interaction. Additional investigation indicates that the only dipole allowed transitions, $1^1\Delta_u \rightarrow 1^1\Pi_g$ and $1^1\Delta_u \rightarrow a^1\Delta_g$, are not efficient relaxation pathways. There are two states to which the $1^1\Delta_u$ state might radiate to which would be expected to give a very small KER, $2;3^3\Pi_g$.

We have identified the metastable species as the previously unobserved $O_2(1^1\Delta_u)$ state. Considering the near 8 eV of electronic energy in this state, the long lifetimes suggest that this metastable state may be capable of unprecedented new oxygen chemistry.

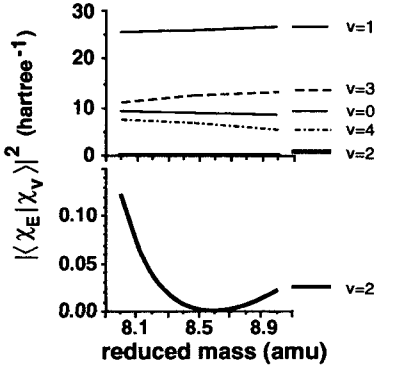

Figure 3. Variation of Franck-Condon factors with reduced mass for $1^1\Delta_u \sim 2^3\Delta_u$.

COLLISIONAL ELECTRON TRANSFER: WHERE DOES THE ELECTRON GO?

Frantisek Turecek, Scott A. Shaffer, Ming Gu, Thuy B. Tran and David W. Kuhns
Department of Chemistry, University of Washington, Seattle, WA 98195

Neutralization-reionization mass spectrometry relies upon fast electron transfer from a thermal neutral target to an ion of keV kinetic energy to produce an intermediate neutral species. The collisional electron transfer may involve the generation of excited electronic states in the neutral formed. The nature and reactivity of these excited states, for example, singlet or triplet biradicals, zwitterion biradicals, and Rydberg states, are discussed for several polyatomic molecules.

Neutralization with Hg of the $^{\bullet}CH_2CH_2CO^+$ distonic ion forms the $^{\bullet}CH_2CH_2CO^{\bullet}$ biradical whose singlet state dissociates exothermically to C_2H_4 and CO (ΔH_r = -358 kJ mol^{-1}). In a parallel reaction the less stable triplet $^{\bullet}CH_2CH_2CO^{\bullet}$ dissociates exothermically to CH_2 and CH_2CO (ΔH_r = -282 kJ mol^{-1}). The latter reaction forming the stable triplet CH_2 is spin allowed whereas the formation of singlet C_2H_4 and CO is not.

Neutralization with CH_3SSCH_3 of the stable $^{\bullet}CH_2NHCH_2^+$ distonic ion forms the $^{\bullet}CH_2NHCH_2^{\bullet}$ biradical which shows remarkable stability. Its reionization produces the survivor ion of a relative abundance exceeding those of the stable $CH_3N{=}CH_2$ and aziridine ions. Ab initio calculations show that the equilibrium C_{2v} structures of $^{\bullet}CH_2NHCH_2^+$ and singlet $^{\bullet}CH_2NHCH_2^{\bullet}$ are very similar, causing negligible Franck-Condon effects upon vertical electron transfer. Dissociation of singlet $^{\bullet}CH_2NHCH_2^{\bullet}$ to the 2-azaallyl radical and H$^{\bullet}$ is 106 kJ mol^{-1} endothermic in keeping with the biradical stability. Triplet $^{\bullet}CH_2NHCH_2^{\bullet}$ geometry shows twisted methylene groups and pyramidization at nitrogen. Vertical neutralization to the triplet state is accompanied with 57 kJ mol^{-1} vibrational excitation causing rapid dissociation by loss of H$^{\bullet}$. The surviving $^{\bullet}CH_2NHCH_2^+$ is therefore due to reionization of the stable singlet biradical.

Neutralization with CH_3SSCH_3, $(CH_3)_3N$, and Xe of aromatic amine cation-radicals induces dissociations which are unparalleled by CAD of the corresponding ions. N,N-dimethylbenzylamine exhibits extensive fragmentations of the aromatic ring to form C_6H_{0-5}, C_5H_{0-5}, C_4H_{0-2}, C_3H_{0-2}, and C_2H_{0-2}, whereas CAD of the cation-radical mostly cleaves the benzylic C-N and phenylic C-C bonds to form $C_7H_7^+$ and $CH_2{=}N^+(CH_3)_2$, respectively. In N-methylbenzylamine a clean transfer of the N-bound H-atom to form benzene is observed for the neutral but not for the ion. A mechanism is proposed considering electron capture by the aromatic ring to form a Rydberg resonance which undergoes dissociative electron detachment accompanied with ring fragmentation.

Hypervalent N-benzyl-N,N-dimethyl-N-hydrogenammonium and N-benzylmethylhydrogen ammonium radicals show extensive cleavages of the bonds in the vicinity of the nitrogen atom, in addition to aromatic-ring fragmentations. The C-N and H-N bond cleavages can result from both electron capture in a Rydberg orbital on nitrogen to form a hypervalent radical, and dissociative electron detachment from the aromatic ring.

Dissociations of *ar*-pentafluorobenzyl- and 3,5-dinitrobenzyl-N,N-dimethylamine following neutralization of their cation-radicals are consistent with this model. The neutral pentafluoro derivative undergoes >6 eV endothermic dissociations forming CF$^{\bullet}$ as the predominant product, while the nitro

derivative yields NO by aromatic fragmentations. The loss of HF and the formation of $CH_2{=}N^+(CH_3)_2$, which are characteristic for ion fragmentations, are absent or negligible in the neutralization-reionization spectra. The neutral fragmentation may be triggered by electron capture in a bound state of the substituted benzene ring (EA ≈ 1.6 eV for 3,5-NO_2, <0.5 eV for F_5). The latter represents a biradical-zwitterion excited state of the neutral which undergoes forbidden electron transition to the ground state accompanied by deposition of >7 eV internal energy.

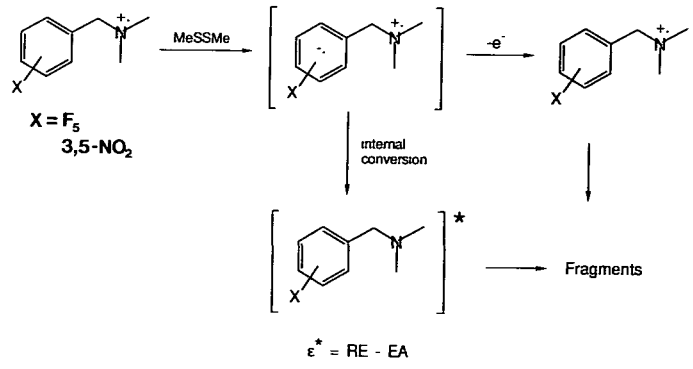

Energy transfer upon neutralization has also been investigated with the newly developed kinetic method that provides phenomenological rate constants for unimolecular neutral and ion dissociations. The kinetic method is based on selective monitoring of ions that have undergone neutralization and reionization at different and variable time scales for neutral and ion dissociations. This is accomplished by applying variable positive and negative potentials on the segments of a long collision cell, so that only ions formed in the segment having the correct potential are detected. In this way the neutral and ion dissociations are distinguished and the rate constants for both the neutral and ion dissociations can be calculated from the time-dependent ion abundances. Neutralization of $CH_3I^{+\bullet}$ with several atomic and molecular targets followed by reionization with oxygen gave different and target-dependent rate constants for the dissociation of neutral CH_3I to $CH_3^{\bullet}$ and I$^{\bullet}$, and ionic $CH_3I^{+\bullet}$ to I^+ and $CH_3^{\bullet}$. In spite of its greater endothermicity the ion dissociation following reionization is faster that the dissociation of the neutral. This points to the dominant role of collisional activation in the reionization process. Neutralization of $CH_3I^{+\bullet}$ with targets of very similar vertical ionization energies (IE_v) results in different excitations of the neutral formed. Resonant neutralization of $CH_3I^{+\bullet}$ with CH_3I (IE_v = 9.54 eV) is less energetic than those with $(C_2H_5)O$ (IE_v = 9.61 eV) and NO (IE_v = 9.54 eV), which cause more rapid fragmentation of the neutral. Endothermic electron transfer from Xe (IE_v = 12.13 eV) results in substantially greater excitation increasing the rate constants of both neutral and ion dissociations.

INVESTIGATION OF ION STRUCTURES BY NEUTRALIZATION-REIONIZATION MASS SPECTROMETRY METHODS

Marcela M. Cordero, Jinnan Cai, Sarka Beranova, Michael J. Nold, Thomas L. Selby, and *Chrys Wesdemiotis

Department of Chemistry, The University of Akron, Akron OH 44325-3601.

Conventional tandem mass spectrometry analyzes ion structures based on the *ionic* products arising upon the unimolecular fragmentation of the studied ion. Neutralization-reionization mass spectrometry (NRMS) offers two alternative means for obtaining complementary structural information: it allows (1) to study the unimolecular reactions of neutralized ions and (2) to also identify *neutral* losses.

Neutralized Ions

The structure of an ion can be determined by examining the stability and reactions of its neutralized form. Since neutrals seldom undergo complex rearrangements, neutralization-reionization (NR) spectra may contain more specific structural information than collisionally activated dissociation (CAD) spectra. This is demonstrated for protonated glycine, $[H_2NCH_2COOH]H^+$. H^+ can attach to the amino or carboxyl functionality. The resulting ions, namely $^+H_3NCH_2COOH$ and $H_2NCH_2C(OH)_2^+$, can best be distinguished from the reactivities of the corresponding neutrals. Neutralization of $H_2NCH_2C(OH)_2^+$ yields a dihydroxy substituted, C-centered radical. Such radicals are stable, as shown by the NR spectrum of protonated acetic acid, $CH_3C(OH)_2^+$, which contains an abundant survival ion (Figure 1b). In sharp contrast, no recovery peak is observed in the NR spectrum of $[Gly]H^+$ (Figure 1a), in agreement with exclusive N-protonation. Based on the fragments observed in Figure 1a, the hypervalent radical generated upon neutralization of $^+H_3NCH_2COOH$ decays mainly to H + Gly, H_2N + CH_3COOH, H_3N + CH_2COOH, and CH_5N + COOH.

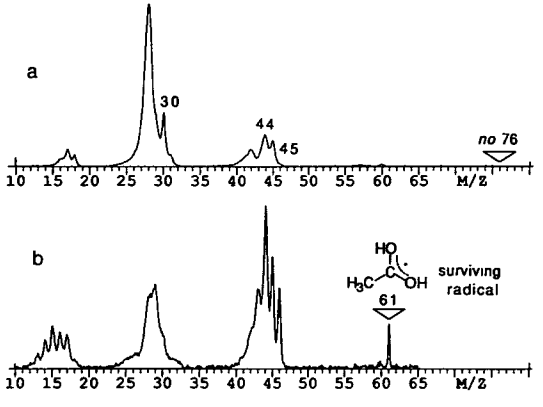

Figure 1. Neutralization-reionization (NR) spectra of (a) $[Gly]H^+$ and (b) $[CH_3COOH]H^+$. Xe is used for neutralization and O_2 for reionization.

Neutral Losses

The neutral products formed upon CAD of a mass-selected ion can be reionized and collected in the corresponding neutral fragment-reionization (N_fR) mass spectrum, which consists of the superimposed collision induced dissociative ionization (CIDI) spectra of the individual neutral fragments. Isomeric ions can be differentiated if they yield different neutral losses.

The interpretation of N_fR spectra and structural assignments are significantly facilitated by the availability of reference CIDI mass spectra of single, important neutral losses. The CIDI spectra of amino acids, which are eliminated as complete units from the *C-termini* of peptides, can readily be obtained by producing them independently from proton-bound dimers. Such CIDI spectra can be used to identify the C-terminal amino acid of isomeric dipeptides. This is illustrated for $[Ala\text{-}Gly]H^+$ and $[Gly\text{-}Ala]H^+$ in Figure 2: their N_fR spectra, combined with the reference CIDI spectra of Gly and Ala, clearly indicate Gly loss from the former but Ala loss from the latter dipeptide. Although protonated Ala-Gly and Gly-Ala can be distinguished from the their normal CAD spectra, the additional N_fR data is essential for confirming the correct sequence. Similar results are obtained for several other isomeric dipeptides, including Asp-Gly / Gly-Asp and Trp-Ala / Ala-Trp.

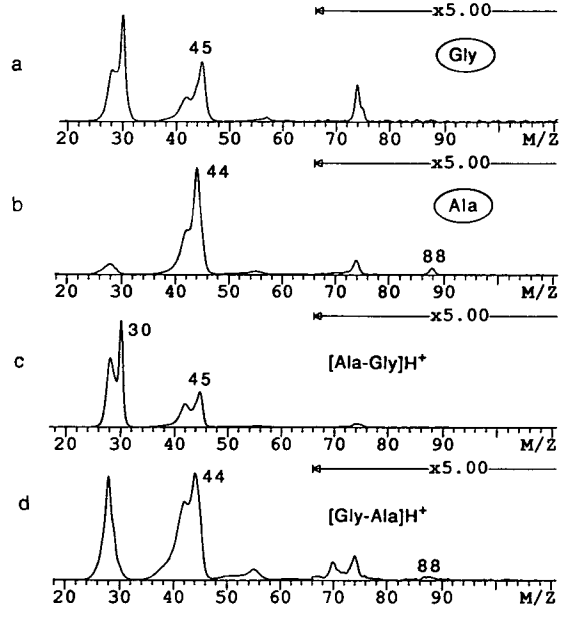

Figure 2. CIDI spectra of (a) Gly and (b) Ala, liberated from the corresponding proton-bound dimers. Neutral fragment-reionization (N_fR) spectra of (c)) $[Ala\text{-}Gly]H^+$ and (d) $[Gly\text{-}Ala]H^+$. He is used for precursor ion dissociation and O_2 for reionization.

NEUTRALIZATION-REIONIZATION MASS SPECTROMETRY; WHAT NEXT?

John L. Holmes, Chemistry Department, University of Ottawa, Ottawa, Ontario, Canada K1N 6N5

Neutralization-Reionization Mass Spectrometry (NRMS) is a technique of great promise, which perhaps has yet to reach its full potential.

The experiment is basically simple, involving the collisional transfer of an electron from a target atom or molecule to a beam of mass selected ions $(M)^{+\bullet}$ and, having deflected remaining ions away, reionizing the (hoped for) neutral (M) by collision with a second target gas. In the resulting mass spectrum, (NRMS), the presence of $M^{+\bullet}$ provides the evidence for the successful production of M. However, the absence of such a "recovery peak" is not conclusive evidence that the neutral is not a bound state.

The NRMS technique has certainly provided some spectacular results, in terms of the generation of novel, stable neutral species, and some recent examples will be discussed in the oral presentation, including a discussion of the elusive stable small molecule OC_2O [1].

Apart from experimental difficulties related to ensuring the structural or even chemical purity of the mass selected ion $M^{+\bullet}$, there are significant difficulties to be encountered in the interpretation of observations.

The first problem relates to the nature of the electron transfer itself. This is a fast event ($<10^{-15}$s) and so is a vertical (Franck-Condon) process. Thus the neutralization step will only produce a significant yield of ground state molecules (or radicals) when the mass selected ion has a ground state geometry similar to that of its neutral counterpart and provided that the majority of the ions are also in their ground state. A good example of this is provided by acetone [2] whose autoneutralization is far from resonant. In general too, mass selected ions from a conventional mass spectrometer's electron impact ion source, will have a range of internal energies from the ground state up to the lowest energy threshold for dissociation. This can be a wide range indeed, as exemplified below. Surprisingly, a lack of resonance in the electron transfer process appears to be far from critical and differences between the ionization energy of the target atom (or molecule) and the vertical neutralization energy of the ion of up to 5eV, can still result in the production of significant neutral yields [3].

Although it appears to be generally assumed that the "recovery peak" in a NRMS is proof of the existence of a stable neutral counterpart of the ion there is very little available alternative physicochemical evidence which provides information as to the state of the "neutral". A good example is the hypervalent $CH_5^\bullet$ radical, believed to exist as a short-lived high Rydberg state [4]. Here, the ion core, of essentially undisturbed geometry,is stable and the acquired electron in its distant orbit gives the system its neutrality.

Good yields of the hypervalent radicals $CH_3O^\bullet(H)CH_3$ and $CH_3CH_2O^\bullet H_2$ have been reported in NRMS experiments [5,6]. There is no evidence from studies of the kinetics of H atom reactions with dimethyl ether and ethanol or methyl radicals with methanol to indicate that the potential hypervalent

intermediate is chemically bound. The energy diagrams below illustrate the internal energy ranges relevant to the NR experiment. Experiments in our laboratory have failed to provide evidence for high Rydberg species and so the nature of these neutrals remains unknown.

It has been found [5], that only $CH_3O^+(H)CH_3$ ions of high internal energy content yield a large "recovery peak". For such species neutralization with Xe to the lower energy radical pair is only about 3 eV endothermic and this energy deficit can readily be provided from the ions' translational energy. With Cd, this neutralization is almost resonant. But are the ground state radical species bound?

These results emphasize the need for an alternative physicochemical method (not another mass spectrum) for characterizing the neutrals.

Measuring their ionization energy is one approach, but the presence of a broad range of excited neutral species could make such experiments difficult to interpret. Spectroscopic measurements certainly hold promise, as exemplified by the experiments of Selgren and Gellene [7] and Helm [8] on the $H_3^\bullet$ radical, but their utility for polyatomic systems remains to be explored.

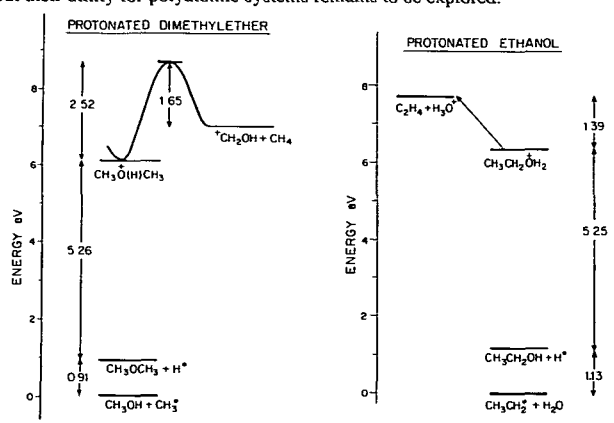

[1] H. Chen and J.L. Holmes, work in preparation for publication.

[2] P.O. Danis, R. Feng, F.W. McLafferty. Anal. Chem. **58**; 348, 355 (1986); R. Feng, C. Wesdemiotis, M.A. Baldwin and F.W. McLafferty. Int. J. Mass Spectrom. Ion Proc. **86**, 95 (1988).

[3] J.L. Holmes, Mass Spec. Rev. **8**, 513 (1989).

[4] S. F. Selgren and G.I. Gellene. J. Chem. Phys. **87**, 5804 (1987).

[5] (a) J.L. Holmes and M. Sirois, Org. Mass Spectrom. **25**, 481 (1990) and (b) unpublished results.

[6] C. Wesdemiotis, A. Fura and F.W. McLafferty. J. Am. Soc. Mass Spectrom. **2**, 459 (1991).

[7] S.F. Selgren and G.I. Gellene. Chem. Phys. Letters **146**, 485 (1988).

[8] H. Helm. Phys. Rev. A **38**, 3425 (1988).

The Quest for the Elusive Iminols with *NRMS* and Multiple Collision Experiments (*MS/MS/MS*)

Graham A. McGibbon, Richard W. Smith, Peter C. Burgers and Johan K. Terlouw*

McMaster University, Department of Chemistry, Hamilton, Ontario L8S 4M1, Canada
Hercules European Research Center BV, Nijverheidsweg 60, 3771 ME Barneveld, The Netherlands

Ionized enols are readily accessible via the McLafferty rearrangement and often their neutral counterparts are easily generated and identified using Neutralization-Reionization Mass Spectrometry [NRMS] [1]. In contrast, iminols or imidic acids, RN=C(OH)R', have so far eluded observation as stable species in the gas phase although their role in the proton exchange of amides, peptides and proteins has been firmly established [2]. In addition, the prototype iminol formamidic acid, H-N=C(OH)H, is predicted by ab initio MO calculations to be separated by high barriers from both its keto isomer H_2N-C(=O)H [3a] and the carbene H_2N-$\ddot{C}$-OH [3b] and the same holds true for their ionized counterparts [3c]. Inspired by these findings, we have explored the use of NRMS for the generation and identification of H-N=C(OH)H and its homologues CH_3N=C(OH)H and HN=C(OH)CH_3.

One of the two methyl analogues, CH_3N=C(OH)H, was readily generated from its ionic counterpart and it has an NR spectrum that is distinctly different from those of its stable isomers, which include the species CH_3N(H)C(=O)H, CH_3N(H)-$\ddot{C}$-OH, H_2NC(=O)CH_3 and H_2NC(OH)=CH_2. We had anticipated that the ionic counterpart of the other methyl analogue, HN=C(OH)CH_3, could be generated by dissociative ionization of an appropriate precursor molecule. However, the m/z 59 ions from acetaldehyde acetylhydrazone produced a CA mass spectrum that was closely similar to that from ionized acetamide and intriguingly the m/z 59 ions from our alternative precursor diacetamide had a CA mass spectrum like that of H_2NC(OH)=CH_2 ions

The identification of formamidic acid was even less straightforward: double collision experiments on ionized formamide, the carbene isomer and the iminol show that formamidic acid **ions** are cleanly generated, but MS/MS/MS type experiments, i.e. CA mass spectra of the survivor ions in the NR spectra, see Fig. 1, do not permit an unambiguous structure assignment of the reionized **neutrals**.

However, from the combined information that (i) the CA spectra of source generated ions of the labelled isotopomers $D_2{}^{15}NC$(=O)D and $D_2{}^{15}N$-C-OD are virtually identical to their corresponding survivor ion CA mass spectra, see Fig. 2, and that (ii) the survivor ion CA mass spectrum of the iminol is characteristically different from those of its isomers it follows that formamidic acid is indeed a stable species in the gas phase.

In addition, Neutralization-Target mass spectra [NTMS] were obtained with the "perpendicular" Quadrupole mass analyser of our ZAB-R instrument of B(⊥Q)EE geometry using formamide, N-methyl formamide, trimethylamine and N,N-dimethylaniline as targets for the neutralization. These spectra confirm distinct structural identities for the three CH_3NO isomers.

[1] For a recent review see : F.W. McLafferty, Int. J. Mass Spectrom. **118/119** (1993) 221.
[2] C.L. Perrin, Acc. Chem. Res. **22** (1989) 268.
[3] a) X-C Wang *et al.*, J. Phys. Chem., **95** (1991) 10419; b) C.A. Kingsmill, P.J.A. Ruttink and J.K. Terlouw, in preparation; c) C.E.C.A. Hop, H. Chen, P.J.A. Ruttink and J.L. Holmes, Org. Mass Spectrom., **26** (1991) 679.

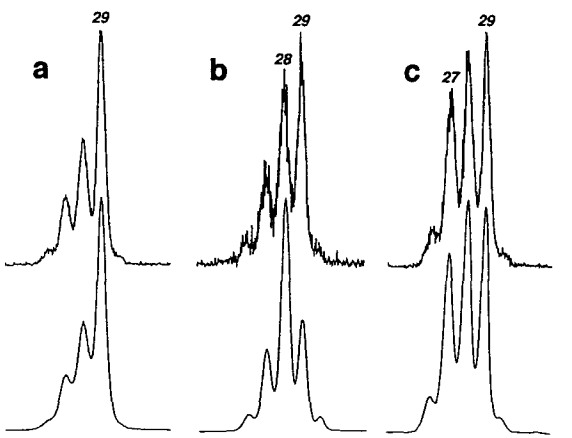

Figure 1 : Partial CA Spectra (He, 3ffr, 8 keV) of NR Survivor Ions (top spectra) and CA Spectra (He, 3ffr, 8 keV) of Source Generated Ions (bottom spectra) of $H_2NC(=O)H^{\bullet+}$ (a), $HN=C(H)OH^{\bullet+}$ (b) and H_2N-C-$OH^{\bullet+}$ (c).

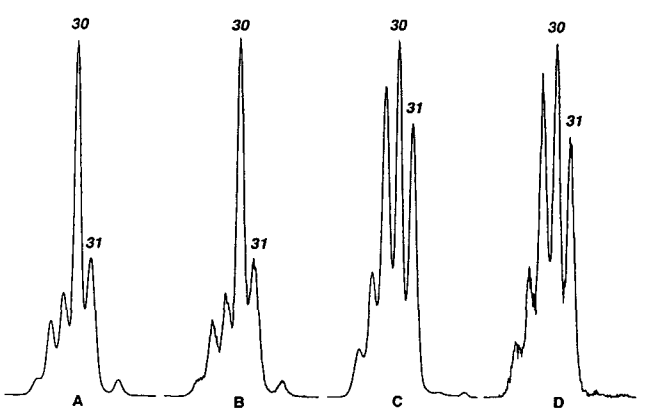

Figure 2 : Comparison of Partial CA Spectra (He, 3ffr, 8 keV) of Source Generated Ions $D_2{}^{15}NC(=O)D^{\bullet+}$ (item A) and $D_2{}^{15}N$-C-$OD^{\bullet+}$ (item C) with those of their NR Survivor Ions (items B and D respectively).

Investigation of Ionized Cyclopropanol. Does it Exist?

*Michael J. Polce, Fred A. Wiedmann, and Chrys Wesdemiotis
Department of Chemistry, The University of Akron, Akron, OH 44325-3601

The molecular cation of cyclopropanol, the simplest cyclic alcohol, has not been characterized unequivocally yet. It is not known whether electron ionization (EI) produces the cyclic ion or a ring-opened $C_3H_6O^+$ isomer or a mixture. Neither has it been determined whether chemical ionization (CI) of cyclopropanol yields an O-protonated ion or a C-C-protonated species

The first question was addressed by investigating ionized cyclopropanol and several of its isomers with the C-C-C-O framework by using metastable ion (MI), collisionally activated dissociation (CAD), and neutralization-reionization mass spectrometry (NRMS) performed on our modified VG Autospec instrument.[1] The studied ions include the molecular cations of cyclopropanol [*cyclo*-C_3H_5-OH]$^{\cdot+}$ (**1**$^{\cdot+}$), allyl alcohol [CH_2=$CHCH_2OH$]$^{\cdot+}$ (**2**$^{\cdot+}$), and propanal [CH_3CH_2CH=O]$^{\cdot+}$ (**3**$^{\cdot+}$), as well as, ionized 1-propenol [CH_3CH=$CHOH$]$^{\cdot+}$ (**4**$^{\cdot+}$) (formed by CH_3CH=CH_2 loss from 2-methylpentanal) and the distonic radical cation CH_2CH_2CH=OH^+ (**5**$^{\cdot+}$) (formed by CH_2=O loss from 3-hydroxytetrahydrofuran).

All of our results show the spectra of **1**$^{\cdot+}$ and **2**$^{\cdot+}$ to be nearly indistinguishable, in agreement with earlier findings of Bombach et al.[2] that they isomerize to a common structure **1**$^{\cdot+}$/**2**$^{\cdot+}$. However, trying to determine what this structure is has proven to be challenging. The major peak in the MI spectra of the studied ions **1-5**$^{\cdot+}$ is at m/z 57 (H$^{\cdot}$ loss), and all exhibit similar peak shape and width. Minor peaks present in the spectra may provide a means to determine differences in ion structure, but more experiments are needed.

The CAD and NRMS spectra of **3**$^{\cdot+}$ are discernibly distinct from those of **1**$^{\cdot+}$/**2**$^{\cdot+}$, **4**$^{\cdot+}$, and **5**$^{\cdot+}$ which eliminates ionized propanal as the structure of **1**$^{\cdot+}$/**2**$^{\cdot+}$. However, the CAD spectra (Figure 1) of **1**$^{\cdot+}$/**2**$^{\cdot+}$, **4**$^{\cdot+}$, and **5**$^{\cdot+}$ are found to be nearly identical within experimental error which contradicts an earlier CAD study in which we found **1**$^{\cdot+}$, **4**$^{\cdot+}$, and **5**$^{\cdot+}$ to be distinguishable isomers.[3] These differences can now be attributed to the earlier use of poor precursors for **4**$^{+}$ and **5**$^{\cdot+}$. [CH_3CH=$CHOH$]$^{\cdot+}$ was formed by C_2H_4 loss from 2-methylbutanal and contained 12% contaminant from isobaric $C_4H_{10}^{\cdot+}$ thus producing a more abundant peak at m/z 42 (from CH_4 loss). **5**$^{\cdot+}$ was provided by CO_2 loss from an 18% aq. soln. of 4-oxobutanoic acid. This generated a very weak ion and therefore background contamination at m/z 43 and 44 The NRMS spectra (Figure 2) for **1**$^{\cdot+}$/**2**$^{\cdot+}$, **4**$^{\cdot+}$, and **5**$^{\cdot+}$ again are very similar, with the major difference being the relative and absolute abundances of the recovery peak (m/z 58). Since no unique fragments are formed it is difficult to deduce the structures of the neutral parents.

All of these results indicate that the incipient $C_3H_6O^{\cdot+}$ cations from EI of cyclopropanol and allyl alcohol initially isomerize to the distonic structure **5**$^{\cdot+}$ via C-C ring opening and 1,2-H shift, respectively. Some further rearrangement to the more stable enolic structure **4**$^{\cdot+}$ seems likely Thus, it appears the structure of **1**$^{\cdot+}$/**2**$^{\cdot+}$ may be a mixture of **4**$^{\cdot+}$ and **5**$^{\cdot+}$.

Our preliminary studies on protonated cyclopropanol indicate that both O- and C-C-protonation occur. The latter is by far the predominant channel and ultimately yields protonated propanal.

References

(1) Polce, M.J.; Cordero, M.M.; Wesdemiotis, C.; Bott, P.A. *Int. J. Mass Spectrom. Ion Processes* **1992**, *113*, 35-58.
(2) Bombach, R.; Dannacher, J.; Honneger, E.; Stadelmann, J.-P.; Neier, R. *J. Chem. Phys* **1983**, *82*, 459-470.
(3) Polce, M.J.; Wiedmann, F.A.; Wesdemiotis, C. *Proceed. of the 39th ASMS Conf. on Mass Spectrom. and Allied Topics* Nashville, TN, **1991**, 1572-1573.

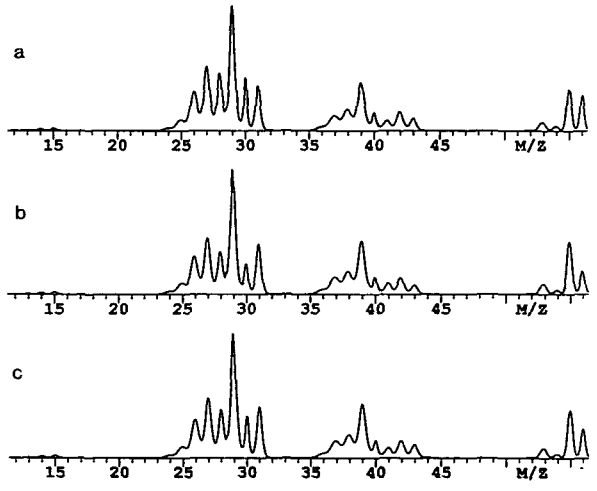

Figure 1. Partial CAD spectra of (a) 1$^{\cdot+}$/2$^{\cdot+}$, (b) 4$^{\cdot+}$, and (c) 5$^{\cdot+}$.

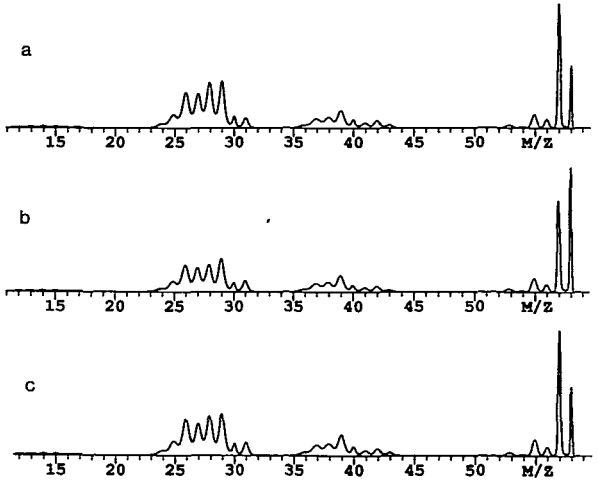

Figure 2. $^{+}$NR^{+} Xe/O_2 spectra of (a) 1$^{\cdot+}$/2$^{\cdot+}$, (b) 4$^{\cdot+}$, and (c) 5$^{\cdot+}$.

Detection and Characterization of Novel $[C_2,H_3,N,O]^{+\cdot}$ Isomers and their Neutral Counterparts

Cornelis E.C.A. Hop* and D.F. Snyder
Department of Chemistry, University of Wisconsin-Madison
1101 University Avenue, Madison, Wisconsin 53706.

Mass spectrometry has distinguished itself as an extremely powerful technique for characterization of the structure of ions. Two complementary approaches are available to determine the structure of ions: (i) ion/molecule reactions and (ii) metastable and collision-induced dissociation. The latter technique will be used here to characterize a variety of $[C_2,H_3,N,O]^+$ ions. Neutralization-reionization (NR) can be to probe the stability of the neutral counterparts of these ions.

Methyl isocyanate, H_3CNCO, is of significant commercial interest because of its role in the large-scale production of insecticides and herbicides. However, its toxicity is of great concern. The isomers H_3COCN, H_3CCNO and H_3CONC have been detected as well, but all three of them are extremely reactive. Glycolonitrile, $HOCH_2CN$, is the second isomer which is commercially available. Via NR mass spectrometry it has been shown that $H_2NC{\equiv}COH$ is a stable species in the gas phase.[1] $H_2C{=}C(H)NO$ has been generated by low pressure pyrolitic deoxygenation of nitro ethene [2] and $H_2C{=}N{-}C(H)O$ has been obtained via flash vacuum pyrolysis of N-formyl-2-azabicyclo[2.2.1]hept-5-ene.[3] Other isomers, e g $CH_2{-}NH{-}CO$ and $O(H)C{-}C(H){=}NH$ have been considered in theoretical studies, but not yet identified.

In Table 1 the metastable ion (MI) mass spectra of nine different $[C_2,H_3,N,O]^+$ isomers are presented as well as their precursors All spectra are distinctly different The isomers can also be distinguished based on their collision-induced dissociation (CID) mass spectra and these CID spectra allow structural characterization. The structures of the $[C_2,H_3,N,O]^+$ ions generated by $\overline{CH_2{-}NH{-}C(O){-}O{-}C(O)}^+$ and $\overline{HN{-}CH{=}CH{-}O{-}C{=}O}^+$ require more attention.

The MI mass spectrum of ionized 2(3H)-oxazolone, $\overline{HN{-}CH{=}CH{-}O{-}C{=}O}^+$, contains an intense signal at m/z 57, $[C_2,H_3,N,O]^+$ *Is CO loss from the molecular ions accompanied by ring closure?* Ring closure leads to $\overline{HN{-}CH{=}CH{-}O}^+$. If no ring closure occurs the m/z 57 ions have the $O(H)C{-}C(H){=}NH^+$ structure Based on the absence of HNO^+ in the CID mass spectrum of the $[C_2,H_3,N,O]^{+\cdot}$ ions we propose that $O(H)C{-}C(H){=}NH^+$ ions are generated The NR mass spectrum of these ions contains an intense signal at m/z 29, which is much more intense than in the CID mass spectrum, and the recovery signal at m/z 57 is extremely small Thus, $HN{=}C(H){-}C(H)O^+$ ions do not survive neutralization-reionization intact The abundant signal at m/z 29 is due to (i) generation of HCO by metastable $HN{=}C(H){-}C(H)O^+$ ions and (ii) fragmentation of neutralized $HN{=}C(H){-}C(H)O^+$ into HCO + HCNH and/or H_2CNH + CO.

The molecular ions of 2,5-oxazolidinedione, $\overline{CH_2{-}NH{-}C(O){-}O{-}C(O)}^{+\cdot}$, undergo only one fragmentation process on the metastable time scale· generation of $[C_2,H_3,N,O]^+$, i.e loss of CO_2 Remarkably, the m/z 57 signal is composite and it is comprised of two broad, dished components of approximately equal abundance ($T_h(A)$ = 128 meV; $T_h(B)$ = 513 meV) Thus there are two ways to lose CO_2 *Is CO_2 loss from the molecular ions accompanied by ring closure?* Ring closure leads to $\overline{CH_2{-}NH{-}CO}^+$ If ring closure does not occur two distonic isomers are generated. $CH_2{-}NH{-}CO^+$ and $NH{-}CH_2{-}CO^+$. The MI mass spectrum of 2,5-

oxazolidinedione-5-^{13}C displays loss of CO_2 and $^{13}CO_2$. The MI and CID mass spectra of the corresponding$[H_3,{}^{12}C,{}^{13}C,N,O]^+$ and $[H_3,{}^{12}C_2,N,O]^+$ ions are not identical! Thus, 2,5 oxazolidinedione yields the distonic ions $\overline{CH_2{-}NH{-}CO}^{+\cdot}$ and $NH{-}CH_2{-}CO^{+\cdot}$. (Note that the isoelectronic compound succinic anhydride, $\overline{CH_2{-}CH_2{-}C(O){-}O{-}C(O)}^{+\cdot}$ yields distonic $CH_2{-}CH_2{-}CO^{+\cdot}$ ions via a similar process.[4]) The NR mass spectrum of these $[C_2,H_3,N,O]^+$ ions is dominated by m/z 28 and the recovery signal is extremely small. Therefore, the distonic ions $CH_2{-}NH{-}CO^{+\cdot}$ and $NH{-}CH_2{-}CO^+$ do not survive neutralization-reionization intact and the m/z 28 signal is due to generation of CO by metastable $CH_2{-}NH{-}CO^+$ and $NH{-}CH_2{-}CO^{+\cdot}$ ions

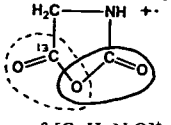

Table 1. Metastable ion mass spectra of $[C_2,H_3,N,O]^+$ ions with the kinetic energy release values ($T_{0.5}$ in meV) in parentheses.

precursor	neutral lost	proposed structure	fragment ions, m/z				
			56	43	29	28	27
CH_3NCO	-	CH_3NCO^+	60 (70)		100 (221)		
$NC{-}C(O){-}OCH_3$	CO	CH_3ONC^+	100 (a)				
$H_3CC(O)N(H)OH$	H_2O	CH_3CNO^+	b (b)	100 (785)			52 (23)
$HOCH_2CN$	-	$HOCH_2CN^+$				100 (29)	
Threonine	C_2H_3OH + H_2O	$H_2N(H)C{=}C{=}O^+$	100 (168)		9 (7 0)		
$H_2C{=}C(H)NO_2$	O	$H_2C{=}C(H)NO^+$					100 (0.8)
$\underline{CH_2{-}NH{-}C(O){-}O{-}C(O)}$	CO_2	$CH_2{-}NH{-}CO^+$ + $NH{-}CH_2{-}CO^+$	76 (265)		100[c] (24/340)		
$\underline{HN{-}CH{=}CH{-}O{-}C{=}O}$	CO	$O(H)C{-}C(H){=}NH^+$				100 (0 5)	

a. Too weak to determine accurately b. The m/z 56 signal is base peak in the spectrum However, it is partially overlapped by an interfering signal of unknown origin. c The signal is composite; it contains a narrow component as well as a broad, dished component

All experiments were performed with VG Analytical ZAB-2F mass spectrometers (University of Wisconsin-Madison and University of Ottawa) The NR mass spectra were acquired with Xe as neutralizing gas and He or O_2 as reionizing gas.

1 J K. Terlouw, P C. Burgers, B.L.M. van Baar, T. Weiske and H. Schwarz, *Chimia* 40, 357 (1986)
2. H. Egsgaard and L. Carlsen, *J. Chem. Res (S)* 18 (1987)
3. M.-C. Lasne, J.-L. Ripoll and A Thuillier, *J. Chem Res. (S)* 214 (1982).
4. J C. Traeger, C E. Hudson and D.J. McAdoo, *Org. Mass Spectrom* 24, 230 (1989)

The Characterization of Labile Metallocenes and Their Neutral Counterparts by Tandem Mass Spectrometry.

Dmitri V.Zagorevskii and John L.Holmes
Department of Chemistry, University of Ottawa, Ottawa, Ontario, Canada K1N 6N5.

Tandem mass spectrometry has been used for the generation and characterization of elusive titanocenium and rhodocenium derivatives and their neutral counterparts. The behaviour of these species has been compared with that of stable analogues of the other transition metals.

Titanocenium has been generated by electron impact dissociation of Cp_2TiI_2. Decomposition of the metastable and collisionally activated Cp_2Ti^+ ions involves metal-ligand bond cleavage, hydrocarbon ligand destruction, and dehydrogenation with H and H_2 loss The mechanism of H_2 loss from Cp_2Ti^+ ion and other metallocenium ions, in particular ferrocenium, are different (Scheme). Cyclopentadienyl ligands coupling precedes H_2 loss in the case of Cp_2Fe^+, whereas decomposition of Cp_2Ti^+ proceeds via formation of the intermediate metalhydrides. The latter is clearly evidenced from the neutralization-reionization (NR) mass spectrum of Cp_2Ti^+ (Fig. 1a). It displays an abundant recovery signal and fragment ions indicative of hydrogen atom(s) migration from the cyclopentadienyl ring(s) to the central metal atom ($C_{10}H_8Ti^+$, $C_5H_4Ti^+$, TiH^+, TiH_2^+).

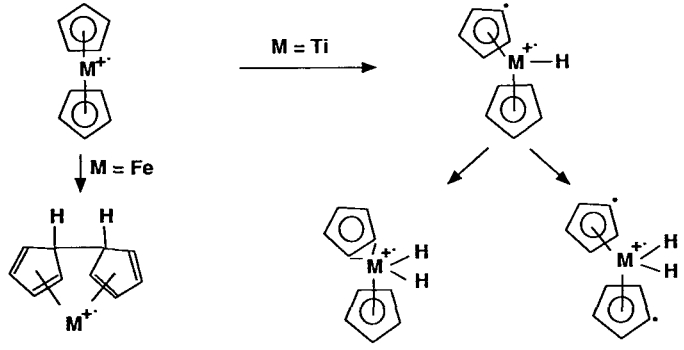

Decomposition characteristics of the rhodocenium cation and its substituted derivatives resemble those of the corresponding ferrocenium derivatives. For example, dissociation of the metastable carboxyl and hydroxymethylrhodocenium ions involves simple metal-ligand bond cleavage with formation of the $CpRh^+$ ion and hydroxy group migration to the metal atom giving rise to the $CpRhOH^+$ ion. The NR mass spectra of unsubstituted rhodocenium (Fig. 1b) and its carboxyl derivative display recovery signals indicating a stability of the corresponding neutral species in the gas phase.

References.
D.V.Zagorevskii and J.L.Holmes, Org. Mass Spectrom., 1993, 28, 49.
D.V.Zagorevskii and J.L.Holmes, Organometallics, 1992, 11, 3224.

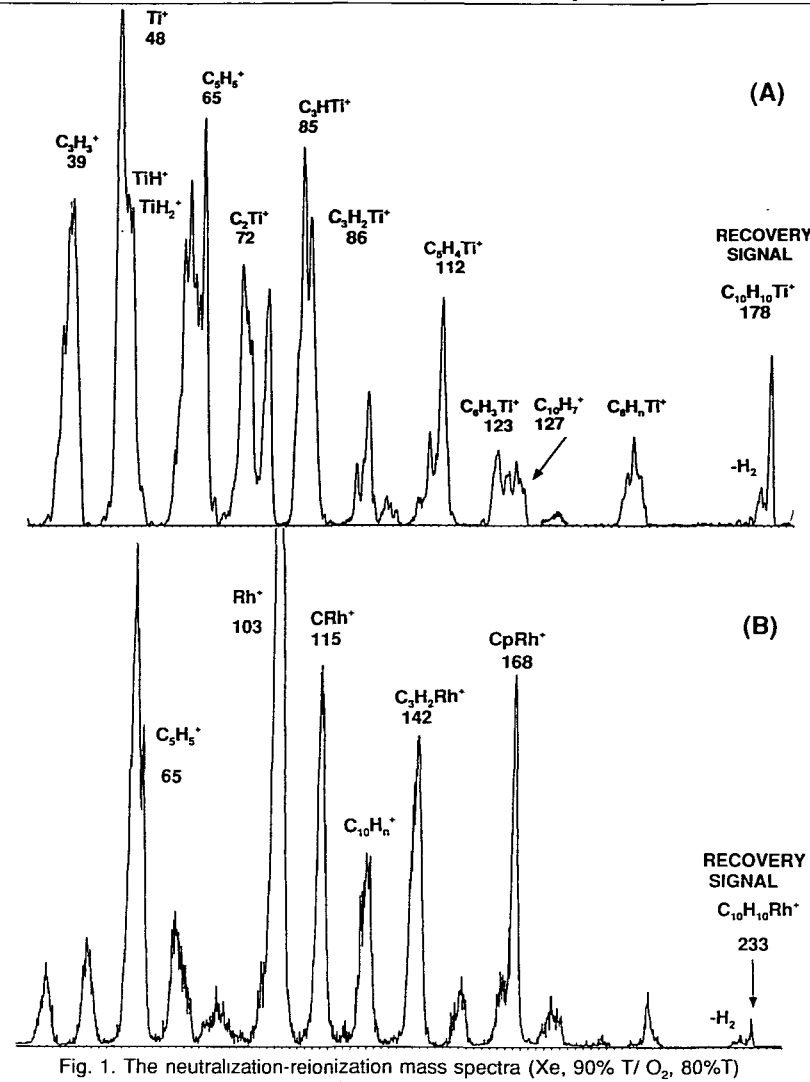

Fig. 1. The neutralization-reionization mass spectra (Xe, 90% T/ O_2, 80%T) of titanocenium (A) and rhodocenium (B) ions.

Current status and new leads in the analysis of small molecules by LC-MS

J. van der Greef, W.M.A. Niessen and U.R. Tjaden, Leiden/Amsterdam Center for Drug Research, Division of Analytical Chemistry, P.O. Box 9502, 2300 RA Leiden, and TNO Centre for Structure Elucidation and Instrumental Analysis, P.O. Box 360, 3700 AJ Zeist, The Netherlands

Introduction

The field of liquid chromatography - mass spectrometry has become mature and impressive results have been obtained for a broad variety of compounds for qualitative as well as quantitative analysis. Various robust interfaces are nowadays commercially available enabling routine laboratories to apply this technology. In fact quantitative analysis of drugs at low levels have been one of the major driving forces in the development of LC-MS or LC-MS/MS. Important in setting up systems aiming at the analysis of large series of samples in an automated way is the optimization of the chromatographic part. Some traditional approaches in bioanalysis will be discussed followed by some possible new trends in the area of small molecules.

Discussion

In general depending on the concentration range to be measured simple chromatographic systems can be used as shown in Figure 1.

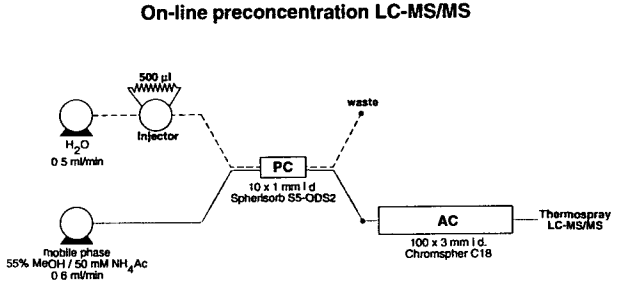

Figure 1. Schematic diagram often used for bioanalytical LC-MS/MS

A precolumn for preconcentration and cleanup purposes is followed by a short analytical column with sufficient separation efficiency to separate the matrix from the analyte and/or metabolites. If for instance direct injection of urine is performed such a system can be used to detect steroids at the ppb level in drug monitoring programmes as shown in Figure 2.

Lower levels down to the fmol/ml level and accurate quantitation can be obtained by TSP for various drugs by more extensive sample pretreatment. However, these levels are more easily obtained using the atmospheric pressure interfaces such as electrospray/ ionspray and the heated nebulizer/APCI. For instance in ESP at the 2-5 ul/min range a chromatographic system consisting of a packed-fused silica column (320 um I.D. x 100 mm) can provide fmol/ml LOQ's for steroids, when peak focusing is used enabling a loadibility of 10 - 20 ul. Such an example is given for two veterinary steroid drugs (20 pg each) in Figure 3.

Developments in this area are the availability of so-called restricted access stationary phases allowing direct plasma injection and on-line protein removal. Depending on the drug-protein binding characteristics such an approach can be attractive.
Another interesting strategy is based on biomimetic chromatography. In such an approach a biological recognition is used in the sample pretreatment of separation process. For instance in screening programs for monitoring illegal use of drugs, it is of interest to use receptor-based technology. We have recently shown this principle for the isolation of analytes such as 17-ß oestradiol and diethylstilbestrol using the oestrogen receptor.
Various approaches have been described to circumvent the incompatibility problem in ion-pair chromatography.
Pseudo-electrochromatography has been inroduced by us as an alternative in such cases. In this methodology a pressure driven system is combined with a electromigration component by applying a high voltage across a packed-fused silica column. This provides an additional selectivity tool for instance by acceleration or deceleration of charged molecules. Even combined effects using voltage programming have been shown to be very useful in the separation of dyes and aromatic glucoronides using ESP LC-MS.

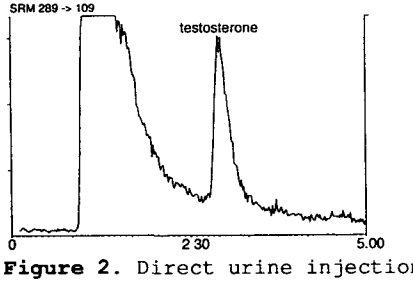

Figure 2. Direct urine injection monitoring testosterone in urine using Thermospray LC-MS/MS at the 1 ppb level.

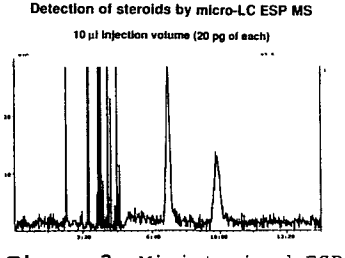

Figure 3. Miniaturized ESP LC-MS/MS detection of veterinary steroid at the low ppt level.

Electrospray Ionization at LC Compatible Flow Rates on a Magnetic Sector Mass Spectrometer

Jeffrey W. Finch[1], Brian D. Musselman[1], J. Fred Banks[2], and Craig M. Whitehouse[2]

[1]JEOL USA Inc., 11 Dearborn Rd., Peabody MA 01960

[2]Analytica of Branford, 29 Business Park Dr., Branford, CT 06405

Introduction: Electrospray Ionization (ESI) for sector mass spectrometers has been limited to low flow rates of typical 2-5 μL/min due to the source design. While these low flow rates are compatible with packed capillary columns, LC/MS applications with larger diameter analytical columns require a split ratio where only a fraction of the effluent is directed into the source, reducing sensitivity. In addition, the use of gradients usually require the use of sheath flow to maintain a stable spray. To overcome these problems, an ultrasonic-assisted electrospray (*Ultraspray*) source has been developed for high-flow LC/MS applications on magnetic sector instrumentation.

Experimental: The ESI source, developed by Analytica of Branford, has been previously described (1) and is shown in Figure 1. The low flow needle has been replaced with an ultrasonic needle operated in "grounded needle" mode, where the needle is held at ground while the capillary entrance is floated at -4.5 kV with the capillary exit and skimmers floated at accelerating potentials. Power for the ultrasonic needle is delivered from a "frequency lock" controller which maintains resonant nebulization regardless of changes in source conditions such as temperature or solvent viscosity. The fine areosol produced at the needle is directed toward the capillary by a stream of N_2 flowing across the needle tip. LC/MS data were recorded on JEOL HX110 (EB), SX102 (BE), and LX2000 (EB) sector mass spectrometers operating at accelerating voltages of 5 kV, 5 kV, and 3 kV respectively. Scan speeds for LC/MS were on the order of 2-5 sec/scan. HPLC separations were carried out using either an Applied Biosystems Aquapore 300 ODS 7 μm 250x1 mm column (tricyclics and peptides) or a Keystone Scientific Hypersil BDS C18 5 μm 150x1 mm column (phenothiazines and triazines). Tricyclic antidepresants were analyzed at a flow rate of 40 μL/min using isocratic elution with an 80% isopropanol/20% H2O solvent with 0.04% NH_4OH. Mixtures of phenothiazines and triazine herbicides were analyzed at flow rates of 50 μL/min using gradient elution where Solvent A =10 or 50 mM NH_4OAc (pH 5.5 or 6.0) and Solvent B = acetonitrile. Peptide mixtures were analyzed using a gradient elution (Solvent A = 0.1% formic acid, Solvent B= acetonitrile with 0.084% formic acid) at a flow rate of 50 μL/min.

Results and Conclusions: Infusion studies of small molecules where ion intensities are measured versus flow rates for full scans indicate optimal flow rates of 100-200 μL/min. Flow injection and LC/MS data indicate good reproducibility for repeated injections. However, if power to the ultrasonic nebulizer is turned off, there is a significant decrease in sensitivity and reproducibility. LC/MS analysis of tricyclic (20 ng/component) and phenothiazine (100-150 ng/component) drug mixtures yield clear ion chromatograms and "clean" mass spectra consisting of the protonated molecular ions. Data for the LC/MS separation of a mixture of four triazine herbicides is shown in Figures 2 and 3.

For LC/MS of peptide mixtures, data can be acquired in real time at sufficient resolution (R=1500, 9 sec/scan, scan range m/z = 200-1400) to resolve the isotopic envelope of doubly and triply charged ions, aiding in the identification and molecular weight determination of the peptides.

[1] Cody, R.B., Tamura, J., and Musselman, B.D, *Anal. Chem.*, 1992, 64, 1561.

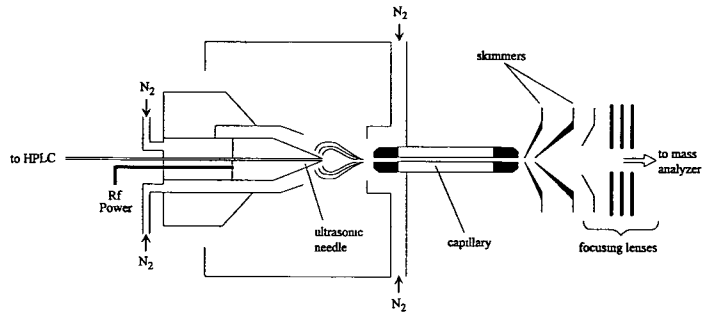

Figure 1

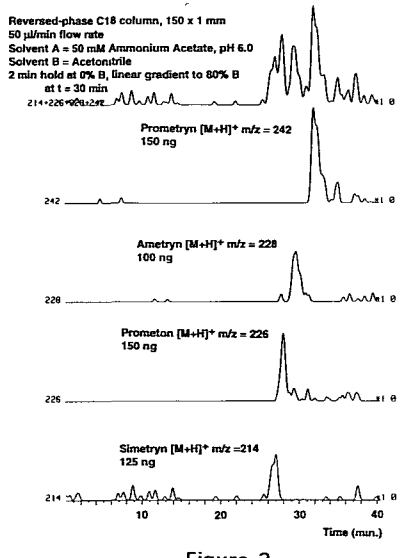

Figure 2

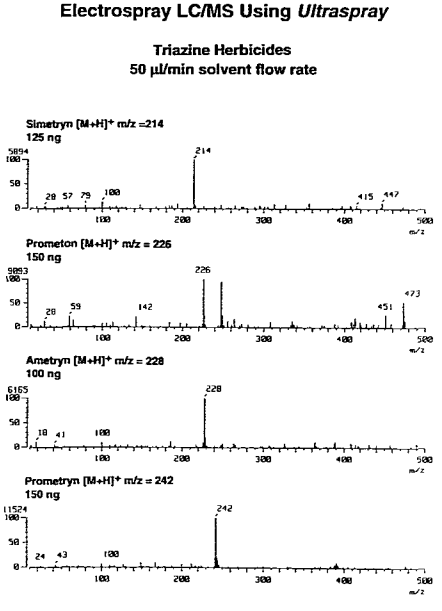

Figure 3

LC/ESMS Characterization of Small Molecule Mixtures in Industry

Kevin L. Duffin, James P. Doom, Fred D. Hileman and David G. Corley, Monsanto Corporate Research, Monsanto Company, St. Louis, MO, 63198.

Liquid chromatography/electrospray mass spectrometry was used to characterize unknown natural product mixtures generated in fermentation broths, These natural products were biologically active in suppressing prostaglandin formation in an inflammation screening assay. LC/MS, LC/MS/MS and LC/CID/MS were used to help identify the structure of the active components. Active fractions were also characterized by ^{1}H and ^{13}C NMR to completely identify the unknown structures.

Two fermentation broths contained compounds that exhibited nanomolar or subnanomolar activity in suppressing prostaglandin formation. When separated by C-18 reversed-phase liquid chromatography, the first broth was shown to contain numerous components, but only one of these components exhibited substantial activity in the prostaglandin assay. The LC chromatogram obtained with in-line UV and electrospray mass spectrometric detection indicated the elution position of the active component, which yielded a $(M+NH_4)^+$ and $(M+H)^+$ at m/z 520 and 503, respectively, in the LC mass spectrum (not shown). A library search of compounds with a molecular weight of 502 amu that exhibited similar UV absorbance tentatively identified the compound as verrucarin A (Figure 1). The MS/MS spectrum of the compound then confirmed this tentative assignment. Verrucarin A is a known potent antagonist of protein synthesis and was active in the prostaglandin assay because it inhibited synthesis of cyclooxygenase, which is an enzyme involved in conversion of arachidonic acid to prostaglandins. A second fermentation broth that also antagonized prostaglandin production was found to contain actinomycin D using the same procedures outlined above. Actinomycin D also inhibits protein synthesis.

Other compounds present in the verrucarin A fermentation broth were found to be structurally related to verrucarin A by a LC/CID/MS experiment. In this experiment the separated compounds are collisionally-dissociated in the mass spectrometry source region. With good chromatographic separation, the CID mass spectrum obtained from this procedure using a single quadrupole mass analyzer closely mimics the MS/MS spectrum of the compound obtained on a triple quadrupole mass analyzer [1]. Figure 2 compares the selected ion LC/CID/MS and parent ion LC/MS/MS chromatograms that are monitoring formation of the m/z 231 product ion. This common product ion results from the conserved ring structure shown in Figure 1. The bioactivity differences between these structurally related compounds suggest that the macrocylic region of verrucarin A is important for its potent activity and that the conserved ring structure is not so important. Figure 3 compares the LC/CID/MS spectrum and MS/MS spectrum of another of the eluents in the verrucarin A fermentation broth. The mass spectra are nearly the same and both contain the product ion at m/z 231.

LC/MS and LC/CID/MS are extremely useful in helping to identify active components in natural product mixtures. Comparison of LC/CID mass spectra of eluents from the same natural product source often leads to identification of structurally similar compounds. Comparison of common structural features of these compounds to their activity profiles leads to structure/activity relationships that can quickly be exploited by medicinal chemists. The efficiency and additional information obtained by LC/MS characterization of unknown natural products makes its use more desirable than mass spectrometric characterization of active components fractionated from an LC column in an off-line fashion.

1. Duffin, K.L.; Wachs, T.; Henion, J.D. *Anal. Chem.* **1992**, 64, 61-68.

Fig 1

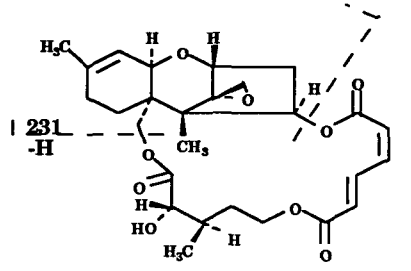

Comparison of LC/CID/MS and LC/MS/MS of Fermentation Broth F21818

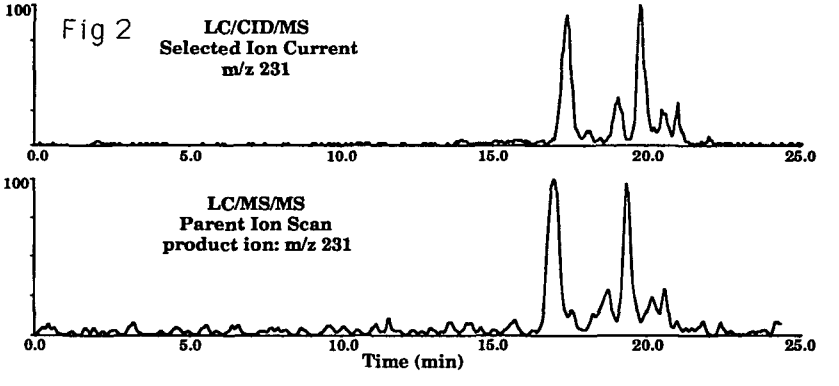

Comparison of Positive Ion LC/CID/MS and LC/MS/MS Spectra of the Compound that Elutes at 19.7 Minutes

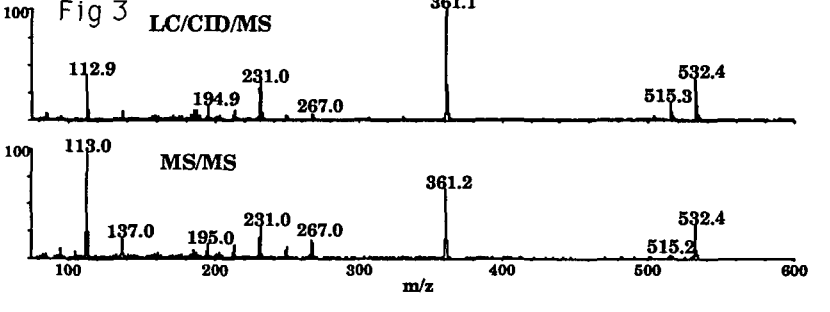

Liquid Chromatography (LC)/Particle Beam (PB) and Thermospray (TSP)/Mass Spectrometry (MS) in Environmental Analyses

*William L. Budde, Thomas D. Behymer, James S. Ho, and Thomas A. Bellar
U. S. Environmental Protection Agency
Office of Research and Development
Environmental Monitoring Systems Laboratory
Cincinnati, Ohio 45268

Most organic environmental analyses are multi-analyte determinations of small molecules (MW < 400) extracted from often complex matrices along with sometimes considerable background material. Users of environmental data are very sensitive to analytical costs but demanding of accurate identifications and accurate and precise concentration measurements at low µg/L or µg/kg concentrations. These "keep it good but cheap" requirements have led to the widespread use of high resolution gas chromatography/mass spectrometry (GC/MS) for the simultaneous qualitative and quantitative determinations of 60 or more analytes in a sample. Because of the typically large number of analytes, the emphasis on qualitative accuracy, and the concern for minimizing costs, selected ion monitoring data acquisition is uncommon and full spectra data acquisition dominates the business.

Although a tremendous amount of research has been devoted to developing LC/MS methods for multi-analyte determinations of non-volatile compounds, no present LC/MS method can match the broad capabilities of present GC/MS methods for amenable compounds. Furthermore, when compared to GC/MS, a significantly smaller number of environmentally significant compounds have been identified as candidates for LC/MS analyses. For example, although over 50 compounds and mixtures are currently regulated in drinking water and have established maximum contaminant levels (MCLs) under Safe Drinking Water Act regulations, only the following 10 are candidates for LC/MS analyses:

Compound	Maximum Contaminant Level (micrograms/L)
carbofuran	40
dalapon	200
dinoseb	7
2,4-dichlorophenoxyacetic acid	70
diquat	20
endothall	100
glyphosate	700
oxamyl	200
picloram	500
2(2,4,5-trichlorophenoxy) propionic acid	50

Currently several different methods must be used to monitor this short list of compounds. The acidic compounds are usually converted into methyl esters and analyzed by GC or GC/MS. The other compounds are determined using high performance liquid chromatography, post column derivatization for some compounds, and detection with conventional detectors such as fluorescence or ultraviolet absorption. In order to minimize monitoring costs and ensure maximum qualitative accuracy, a single LC/MS method for this group of compounds would be ideal. However, no LC/MS method has been developed that can be used to adequately monitor even a few of these compounds simultaneously.

A few additional non-volatile compounds may be regulated in drinking water over the next few years. These include the herbicide, aldicarb, two of its oxygenated metabolites, and a series of chloro-and bromoacetic acids that are formed by chlorine disinfection of drinking water. Although methylation and GC or GC/MS may be used for the acids, no satisfactory LC/MS method is available for the free acids, aldicarb, or its metabolites. A number of other non-volatile compounds appear on various hazardous substances lists, but regulation is unlikely until evidence of significant environmental occurrence is available.

Present LC/MS methods, based on thermospray and particle beam techniques, have been limited to research and a few specialized analyses. Thermospray is useful to distinguish the relatively innocuous diphenylamine from the relatively hazardous N-nitrosodiphenylamine[1]. Particle beam LC/MS has been applied to a quantitative study of the pesticide, rotenone, in river water.

Better and more comprehensive LC/MS technologies are needed for environmental research to aid in the discovery and solution of environmental health and ecological problems. Better and more comprehensive LC/MS technologies are also needed to provide routine monitoring tools and allow expansion of environmental monitoring to more compounds and classes of compounds.

[1]Ho, J. S.; Bellar, T. A.; Eichelberger, J. W.; Budde, W. L. Environ. Sci. Technol. **1990**, 24, 1748-1751

ELECTROSPRAY LC/MS OF LOWER MOLECULAR WEIGHT MOLECULES

Robert D. Voyksner, Markus Linder, Hung-Yu Lin and Rolf Straub
Analytical and Chemical Sciences, Research Triangle Institute,
P.O. Box 12194, Research Triangle Park, NC 27709

INTRODUCTION

The marriage of LC with MS was initially one of compromises. Long analysis times imposed by solvent, buffer or flow rate restrictions and the trade off in MS sensitivity or specificity limited the usefulness of the technique. Developments in the areas of LC, LC/MS interfaces and in MS have overcome some of these problems permitting the monitoring of non volatile and unstable polar organics in complex matrices. This paper will highlight current techniques using (1) high speed LC and (2) electrospray MS (ES-MS) to determine nonvolatile components in biological or environmental matrices.

EXPERIMENTAL

Separations were performed on 2.1 x 150 mm, 0.32 x 150 mm C_{18} columns or 0.32 x 150 mm perfusion LC columns. The 2.1 mm i.d. column was coupled to the ES-MS using a 50:1 split resulting in a flowrate of 4-6 µL/min into the interface. The flow from the 0.32 mm columns (10 µL/min or 60 µL/min for the perfusion column) was directly coupled to the ES interface. The electrospray-MS system was an HP 5989 equipped with a HP electrospray interface and an ultrasound nebulizer (Analytica of Branford) or a Finnigan MAT Ion Trap Mass Spectrometer (ITMS) with an electrospray interface from Analytica of Branford.

RESULTS AND DISCUSSION

The advantages of LC are obvious for resolving nonvolatile components in complex matrices. Incompatibilities between LC and the LC/MS interface due to solvent choice or flow rate and disadvantages of long analysis times have been minimized through the use of high speed perfusion LC columns and ultrasonic nebulization in ES. Perfusion chromatography offers tremendous speed advantages while minimizing problem due to diffusional broadening. Chromatographic separation of six β-lactams in milk, neuropeptides in plasma or aromatic amines in water can be completed in less than 5 minutes. These rapid separations are a result of the high flowrate (60 µL/min) through the 0.32 mm i.d. perfusion column. Normally this flowrate is too high to achieve optimal ES sensitivity, but with ultrasonic nebulization perfusion columns can be directly coupled to the ES interface without a significant loss in signal intensity. Operation of the ultrasonic nebulizer resulted in less than 20% variance in ion current for flow rates from 5 to 60 µL/min flowrate. Furthermore, many solvent and buffer combinations used in the LC separation of the antibiotics, peptides or aromatic amines studied could be employed with minimal compromise of electrospray-MS operation. Ultrasound minimizes the variability in ES response from differences in nebulization of the liquid, due to surface tension or viscosity. Therefore, solvent systems incorporating 80-90% water, 0.1% TFA, or higher molarities of buffer (>10 mM) could be used in ES determinations with minimal losses in sensitivity. On the other hand, operation of the electrospray interface without the

ultrasonic nebulizer resulted in a decrease in ion current by a factor of 5 for 0.1% TFA or a factor of 2-3 for 25 mM heptafluorobutyric acid.

Electrospray ionization has the capability to ionize nonvolatile and thermally unstable compounds without loss of structural information associated with gentle ionization processes. Electrospray can generate molecular ions (e.g., $[M+H]^+$) from pg quantities of β-lactam antibiotics, neuropeptides or aromatic amines. Fragment ions for identification or confirmation can be generated in the electrospray transport region or by the use of ion trap mass spectrometry (ITMS). Collisional activation in the transport region of the electrospray interface resulted in higher product ion yields, a large range of collisional energies and is nearly universal. However, this method is often less specific since all ions present in the transport region undergo collision induced decomposition (CID). The use of the MS/MS capabilities of the ITMS reduces this problem due to the isolation and excitation of a chosen ion. This approach will produce specific CID product ions for the particular compound of interest, but limits the analysis to only a few chosen target compounds. Perfusion LC/electrospray MS using CID provided the specificity to detect target β-lactams (ampicillin, amoxicillin, cephapirin, cloxacillin, cetiofur and penicillin G) in milk, target neuropeptides (α-MSH, ACTH, β-endorphin, α-endorphin and dynorphin A) in plasma or target aromatic amines (chloro, nitro, hydroxy, and methyl anilines; chloro, nitro and amino naphthylamines and benzidine) in wastewater streams. The matrix did not interfere with the LC/MS determination or confirmation of these lower molecular weight molecules.

CONCLUSIONS

LC/Electrospray-MS provides the sensitivity and specificity to determine a variety of lower molecular weight molecules These determinations have been greatly aided using perfusion chromatography to reduce separation times to under five minutes. The ultrasound nebulizer enables near optimal electrospray MS response using flowrates, aqueous levels or buffers used in perfusion chromatography that have historically resulted in up to an order in magnitude decreases in signal intensity.

ACKNOWLEDGEMENTS

This work was supported by EPA Cooperative Agreement No. CR819555 and by NIDA Grant No. 5RO1DA06315.

New APCI Technology Enhances Pharmacokinetics Studies in Biological Samples

M. Wakefield, A. Land, I. Mylchreest, M. Hail, M. Sanders,
K. Mock, M. Uhrich, I. Jardine.
Finnigan MAT, 355 River Oaks Parkway, San Jose, CA 95134

Summary

A LC/MS/MS assay for the quantitation of coeluting corticosteroids in a serum matrix was developed and implemented utilizing a Finnigan MAT APCI source. Pg detection and quantitation levels were easily acheived. The assay was determined to be linear over 3.0 orders of magnitude with precision of <10% RSD over the linear range of the standard curve. Total data system control of critical source, instrument and peripheral parameters provided total automation of the corticosteroid assay.

Introduction

Prednisone metabolizes to prednisolone in a biological system. Accurate quantitation of prednisolone in a serum matrix is a considerable challenge by non-specific HPLC detectors. This is due to the presence of endogenous hydrocortisone in serum which coelutes with prednisolone using a conventional HPLC separation. An LC/MS/MS assay was developed to simultaneously quantitate prednisolone, hydrocortisone and prednisone in a serum matrix.

Experimental

The assay was performed utilizing a Finnigan MAT TSQ® 700 mass spectrometer and APCI source in the positive ion SRM mode. The APCI vaporizer temperature used was 575° C and a capillary temperature of 150°C was utilized for this assay. The SRM conditions specific to each compound are given in Figure 1. HPLC separations were performed on a 50 x 4.6 mm, 3 µm , 20% carbon loaded C_{18} Phenomenex column, utilizing an LDC 4100 MS pump, 4100 UV detector at 240nm, and an Autometric 4100 Autosampler. An isocratic mobile phase of 60/40 MeOH/H_2O at 1.0 ml/min and 20 µl injection volume was employed.

Data

Figure 2. illustrates the MS/MS spectrum of prednisone which is representative of the SRM spectra for the corticosteroids for this assay. Figure 3. shows the chromatography of the methyl-prednisolone internal standard in the serum blank. The UV and SRM chromatograms of 500 pg of the corticosteroids on column are illustrated in Figure 4. Figure 5. is a standard curve for prednisolone which represents a linear range of 3.0 decades. Finally, figure 6. is a table of the statisitcs for the assay which demonstrates precision over the linear range of the standard curve of <10 %RSD.

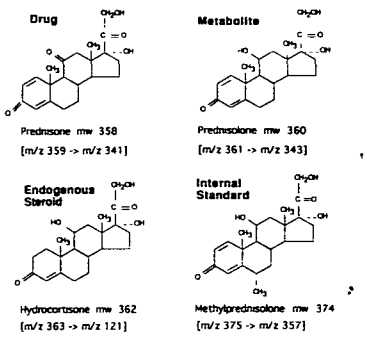

Figure 1. Corticosteroid structures and SRM parameters

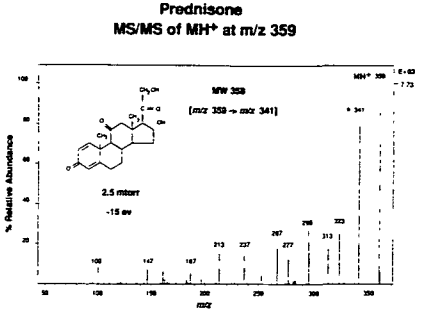

Figure 2. Mass Spectrum of MS/MS of Prednisone

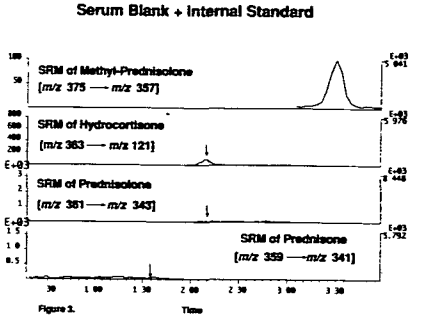

Figure 3.

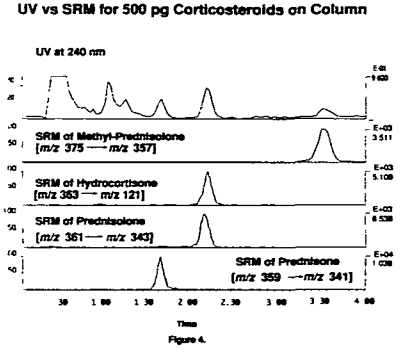

Figure 4.

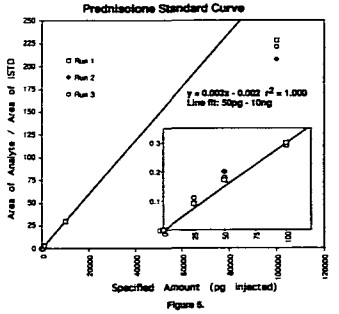

Figure 5.

Corticosteroid Assay Statistics

Std. Amt (ng in-L)	25.0	50.0	100.0	1000.0	10000.0	100000.0
Prednisone						
Mean	21.0	50.7	100.6	1095.3	11148.7	93038.1
Std.Dev	6.8	3.7	3.0	45.7	175.0	2488.5
%RSD	32.2	7.3	3.0	4.2	1.6	2.7
Prednisolone						
Mean	32.2	61.4	99.6	997.8	9829.3	72956.7
Std.Dev	3.6	5.2	3.9	22.0	186.8	3598.5
%RSD	11.2	8.4	3.9	2.2	1.9	4.9
Hydrocortisone						
Mean	74.8	104.5	153.8	1180.3	11615.0	93165.6
Std.Dev	12.3	7.4	7.0	105.1	171.0	3428.0
%RSD	16.5	7.1	4.6	8.9	1.5	3.7

Figure 6.

Comparison of Thermospray and Ionspray for the Analysis of Drug Conjugates. Patrick J. Rudewicz,[1] Robert F. Stack and Charles D. Kennedy, Department of Drug Metabolism and Pharmacokinetics, Sterling Winthrop, Rensselaer, NY 12144; Thomas R. Covey and Takeo Sakuma, Perkin-Elmer Sciex, 55 Glen Cameron Road, Thornhill, Ontario L3T 1P2, Canada.

Since 1985 liquid chromatography-tandem mass spectrometry (LC-MS/MS) has played a significant role in the identification of drug metabolites. The majority of these studies have utilized thermospray ionization (TSP) for LC-MS analysis. Although TSP has proven useful for generating molecular ions for phase I metabolites, it has been unreliable for generating molecular ions for the more polar phase II drug conjugates. The application of heat to the TSP vaporizer often causes thermal degradation of the conjugate. For example, glucuronide conjugates of hydroxylated metabolites are often converted to the corresponding aglycone during the thermospray ionization process, resulting in the formation of an apparent molecular ion for the primary metabolite, not the conjugate. Similar thermal decomposition is observed with sulfate conjugates. Thermal decomposition of the conjugate to the primary metabolite often leads to conflicting results in metabolism profiling studies: the thermospray spectrum indicates a primary metabolite, but the LC retention time is indicative of a more polar compound. Additionally, with thermospray ionization, the weak molecular ion intensities for drug conjugates often preclude the use of MS/MS scans as a screen for these compounds in biological matrices.

The use of ionspray (pneumatically-assisted electrospray) offers an attractive alternative for the analysis of thermally-labile drug conjugates.[1] With ionspray, sample ionization is achieved at ambient temperature; hence thermal decomposition is minimal, facilitating the analysis of polar conjugates. In this study, both TSP and ionspray were used to identify the biotransformation products of zanoterone in man. Zanoterone is an androgen receptor antagonist currently in clinical trials for treatment of benign prostate hyperplasia.

EXPERIMENTAL SECTION

Dosing and Urine Collection. Six healthy male volunteers were administered a single 400 mg oral dose of ^{14}C-zanoterone (0.26 µCi/mg). Urine samples were collected from each subject over various time intervals for 240 hr.

Sample Preparation. 3 mL of combined (0-24 hr) urine containing ^{14}C-labelled metabolites were acidified with 40 µL of glacial acetic acid and applied to a conditioned Bakerbond C8 solid-phase extraction cartridge. The column was washed with 6 mL of water and the metabolites eluted with 3 mL of methanol. The samples were brought to a final volume of approximately 500 µL using a Savant Model AS290 Automatic SpeedVac concentrator. 100 µL of the urine extract was injected onto an LC column for the TSP experiments. 1 µL was used for the ionspray experiments.

The thermospray experiments were done using a Finnigan MAT TSQ 700 triple quadrupole mass spectrometer equipped with a TSP 2 ion source. The operating conditions were: vaporizer, 90 °C, ion source block, 200 °C, repeller, 40 volts. For the CID experiments, argon was used as a collision gas at a pressure of 1 millitorr. The collision energy (quadrupole 2 offset voltage) was 30 eV (E_{lab}).

The ionspray experiments were done on a Perkin-Elmer/Sciex API III triple quadrupole mass spectrometer with an ionspray interface. The ionspray voltage was -3350 V. For the CID experiments, the collision energy (E_{lab}) was 70 eV and the collision gas was argon at a pressure of 8.7 x 10^{14} atoms/cm^2.

DISCUSSION

After oral administration of ^{14}C-zanoterone, 20 % of the dose was excreted as four metabolites (A-D) in urine as determined by LC-flow scintillation experiments. Initially, TSP LC-MS/MS experiments indicated the presence of monohydroxylated metabolites; however, their LC retention times indicated more polar structures. These results and the poor sensitivity of TSP led us to analyze these samples by ionspray LC-MS/MS.

Upon CID, the protonated molecular ion of zanoterone (m/z 417) fragments to give a major ion of m/z 339 which corresponds to loss of the methyl sulfonyl group. This fragmentation corresponds to a neutral loss of 78 amu; hence it was hypothesized that a neutral loss scan of 78 amu could be used to identify any metabolites of zanoterone which contain the methyl sulfonyl moiety. Figure 1 is a contour plot of a negative ion neutral loss (78 amu) ionspray experiment. In this plot, the signal at each m/z is plotted as a function of retention time with increasing ion intensity represented in the Z direction. Although this neutral loss experiment was done using a crude extract of urine, the four metabolites (A-D) are immediately evident. Examination of their ionspray spectra indicated that all four metabolites are conjugates: A is a glucuronide of a hydroxylated metabolite (M-H)$^-$ m/z 607, B is a sulfate of a hydroxylated metabolite (M-H)$^-$ m/z 511, C is a glucuronide of zanoterone (M-H)$^-$ m/z 591and D is a sulfate of zanoterone (M-H)$^-$ m/z 495. One peak in this plot, with a retention time between metabolites A and B had not previously been seen using either TSP LC-MS or LC with scintillation detection. The spectrum of this metabolite, labelled A', is shown in Figure 2 and contains an ion of m/z 527 as the base peak which corresponds to the (M-H)$^-$ ion of a dihydroxylated sulfate conjugate. Examination of the peaks in the contour plot with m/z values less than the molecular weight of zanoterone indicated that they are not drug-related. From this one ionspray neutral loss scan, all of the major biotransformation pathways of zanoterone in man were determined.

1. Bruins, A. P.; Covey, T. R; Henion, J. D. *Anal. Chem.* **1987**, 59, 2642-2646.

FIGURE 1
(-) IONSPRAY NL 78
CONTOUR PLOT

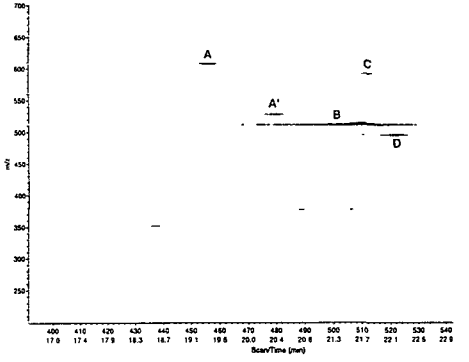

FIGURE 2
(-) IONSPRAY NL 78

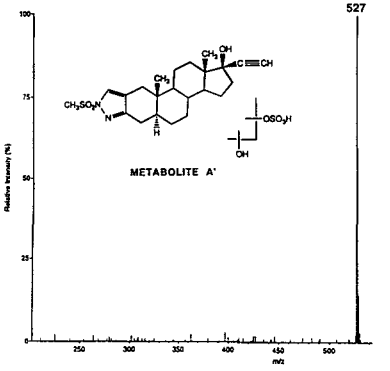

CHARACTERIZATION OF LOW MOLECULAR WEIGHT, THERMALLY LABILE ANALYTES USING CAPILLARY SUPERCRITICAL FLUID CHROMATOGRAPHY/MASS SPECTROMETRY (SFC/MS)

*** J. David Pinkston, Donald J. Bowling, and Claudia A. Smith, The Procter & Gamble Company, Miami Valley Laboratories, P.O. Box 398707, Cincinnati, OH 45239-8707**

With respect to gas chromatography/mass spectrometry (GC/MS), SFC/MS using CO_2 as mobile phase offers a solvating mobile phase, lower analysis temperatures, and reduced volatility requirements. With respect to liquid chromatography/mass spectrometry (LC/MS), packed-column SFC/MS offers greater speed of analysis (thanks to higher diffusion coefficients) and the possibility of using longer columns and achieving higher plate counts (thanks to lower mobile-phase viscosities). Open-tubular-column SFC offers greater column inertness and a simpler interface to the traditional electron/chemical ionization (EI/CI) source, with its flexibility and good sensitivity. This combination of features offers advantages for the characterization of thermally labile or "active" analytes. ("Active" compounds refers here to compounds that interact strongly with active sites in chromatographic systems.) In fact, early workers in the field predicted that SFC/MS might provide a route to the separation and mass spectral characterization of thermally labile compounds [1,2]. The mobile phase most commonly used in open-tubular-column SFC, CO_2, is nonpolar. This limits practical applications of SFC/MS using this mobile phase to relatively nonpolar analytes. But within this realm there exists a multitude of thermally labile or active analytes of significant industrial importance which are not amenable to gas chromatography, but which can be chromatographed and characterized by SFC/MS. SFC/MS thus provides an alternative to LC/MS for the characterization of these types of analytes.

We've used open-tubular-column SFC/MS for the characterization of thermally labile or active compounds such as organic peroxides, derivatized organo-phosphates, amines, and selenium sulfides. The instrumentation consists of a custom-built SFC system, a modified commercial interface, and a TSQ-700 triple quadrupole mass spectrometer [3]. Studies involving peroxides have been especially useful in mapping out the parameters critical for success with thermally labile materials. In fact, SFC with CO_2 mobile phase offers a unique advantage in the characterization of acyl peroxides. Certain degradation pathways of these compounds, such as the unimolecular and the higher order pathways shown below, generate CO_2.

Unimolecular Decomposition:

R-COO-OOC-R ↔ 2 R-COO· (1)

2 R-COO· ↔ **CO_2** + R-COO-R (2)

Chain Reaction:

R-COO· + R-COO-OOC-R ↔ **CO_2** + R-COO-R + R-COO· (3)

We expect that the high pressure of CO_2 in the SFC system will inhibit these degradation pathways. (Evidence that these reactions are reversible exists [pers. comm., D. Bjorquist, P&G].)

In the course of our investigations we have established guidelines for the characterization of peroxides by open-tubular SFC/MS. As would be expected, low column, interface tip, and ion

source temperatures give the best results (maximums of 70 °C, 140 °C, and 140 °C, respectively, for benzoyl peroxide). We use short (2-5 m), thick film (0.5 µm) columns. High linear velocity (10-20 cm/s at 100 atm and 100 °C for a 50-µm i.d. column) *restrictors provide less degradation than* restrictors with linear velocities more typical of open-tubular SFC (1-2 cm/s). The importance of the position of the restrictor aperture with respect to the ion source is illustrated in the figure at left, showing two NH_3 chemical ionization spectra of benzoyl peroxide. In the upper spectrum, the tip of the restrictor is positioned 1 cm from the optimum position in the direction of the oven (away from the ion source). The protonated molecule, 123 Da/unit charge (*m/z*), *and the ammonium adduct ion*, m/z 140, of benzoic acid (the primary decomposition product under these conditions) dwarfs the ammonium adduct ion of the intact benzoyl peroxide, at m/z 260. (The ions at m/z 205 and m/z 279 are in the background.) The lower spectrum shows a dramatic increase in the relative abundance of the ammonium adduct ion of benzoyl peroxide when the restrictor tip is placed at the optimum position. The optimum position for the tip of the restrictor corresponds to the ion-source end of the interface probe, approximately 1 cm from the ion source ion volume. The chromatographic data indicate that the decomposition occurs in the restrictor and ion source region, not on the column. Other influences we have investigated include the co-injection of a free-radical-chain-reaction inhibitor, and the use of an alternate mobile phase, N_2O.

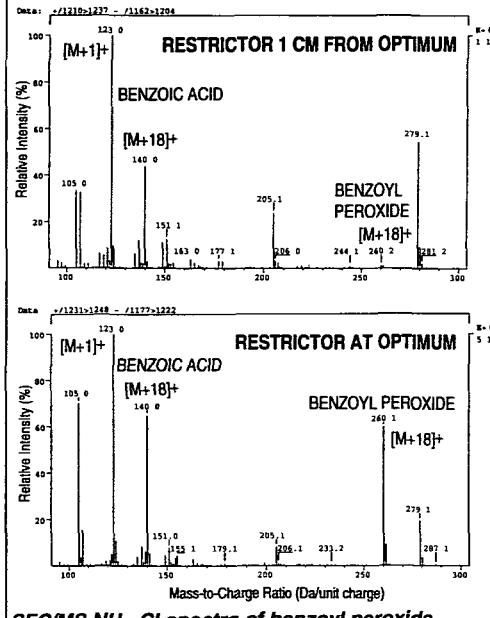

SFC/MS NH_3 CI spectra of benzoyl peroxide showing influence of restrictor position

The straightforward interface of open-tubular SFC to the traditional EI/CI ion source has been useful in experiments involving thermally labile species. For example, negative CI provided the most intense signal in SFC/MS separations of heat- and light-sensitive selenium sulfides [4]. Unfortunately, the negative CI spectra were dominated by low molecular weight fragment ions and provided little structural information. Electron ionization with electron energies of 150 eV, 70 eV, and 20 eV was used to obtain copious structural information [4].

[1] T. A. Milne, *Int. J. Mass Spectrom. Ion Phys.*, 3 (1969) 153.; **[2]** L. G. Randall, A. L. Wahrhaftig, *Anal. Chem.*, 50 (1978) 1703.; **[3]** J. D. Pinkston, D. J. Bowling, *J. Microcol. Sep.*, 4 (1992) 295.; **[4]** J. D. Pinkston, D. J. Bowling, *Journal of Chromatography Library Series*, 53 (1992) K. Jinno (Ed.), Elsevier Science Publishers, Amsterdam, p. 25.

PROFILING OF BACTERIAL METABOLITES BY ON-LINE CAPILLARY LIQUID CHROMATOGRAPHY - ELECTROSPRAY MASS SPECTROMETRY.

G.J. Feistner

Division of Immunology, Beckman Research Institute of the City of Hope, Duarte, CA 91010.

For about fifteen years now, I have been involved in the characterization of bacterial metabolites, with an emphasis on their importance as virulence factors and cell-cell communication. Mass spectrometry has always been an integral part of the structure elucidations, but mostly after extensive isolation and purification protocols. More often than not, I found that the metabolites of interest had been previously described, although at the time, they were not known to be produced by the particular organisms. Thus, the introduction of electrospray was most welcome, because with its assistance it seemed possible to expedite such analyses by on-line LC-ES-MS and LC-ES-MS/MS. I have since used these methods extensively for metabolic profiling of wildtypes, mutants, cosmid bank clones, and the study of environmental influences. These applications are now routine.

For example, I am interested in the evaluation of siderophores as virulence factors in fire blight, a bacterial disease of apples and pears caused by *Erwinia amylovora*. The first step in this investigation was the identification of the siderophores. LC-ES-MS/MS quickly identified them as proferrioxamines based on their characteristic fragmentation at their peptide and/or hydroxamate bonds [1]. A total of 20 proferrioxamines were identified on grounds of, for example, their ability to loose a succinylamino hydroxyaminopentane subunit. Of these, five, namely X_8, X_9, T_{4-6}, remain to be fully characterized. Fifteen have been identified as proferrioxamines D_2, E, G_1, G_{1t}, G_{2a-c}, T_1, T_2, T_3, T_7, T_8, X_1, X_2, X_7, with T_{1-8} being novel tetrameric hydroxamates and T_3 and X_7 being novel diaminopropane containing proferrioxamines. The latter were readily recognized based on their loss of a succinylamino hydroxyaminopropane unit, while the novel tetrameric proferrioxamines were readily identified based on the superimposability of their product ion spectra onto the ones for the trimeric hydroxamates. The fragmentation pattern of the proferrioxamines, which is believed to involve transfer of α-hydrogen atoms from the succinyl subunits, is still under investigation because the latter cannot explain why in the cyclic proferrioxamines every other peptide/hydroxamate bond is especially susceptible to fragmentation. Instead, hydrogen transfer may occur between two nitrogen atoms involving the sterically and energetically favorable formation of succinylimide rings. We plan on corroborating this hypothesis by deuteration studies.

LC-ES-MS was found to be a valuable tool to rapidly confirm the incorporation of deuterium-labeled and other precursors and to study environmental influences on the metabolic profiles. For *Streptomyces* it has been reported that external diamines but not succinic acid analogues are incorporated into proferrioxamines, Thus, it was not a priori clear whether external (deuterated) succinic acid would be incorporated by *E. amylovora*, but this has now been confirmed. On the contrary, malic acid, which is a hydroxylated succinic acid and a prominent constituent of apple and pear, does not get incorporated into proferrioxamines but appears to prevent their cyclization. In the presence of malic acid, proferrioxamine G_1 is the major proferrioxamine, whereas in its absence the cyclic proferrioxamines D_2 and/or E are the most abundant. Siderophore profiles are being used as taxonomic markers. The finding that these profiles are heavily dependent on environmental factors makes it necessary to obtain these profiles under standardized conditions. With regard to our understanding of the virulence mechanisms of fire

blight, it will be necessary to perform corresponding studies in planta. For these, we will be able to take advantage of the excellent sensitivity of our on-line capillary LC system.

Proof that the proferrioxamines are necessary for *E. amylovora* to establish itself in planta has to come from mutants that are unable to produce these siderophores and that can be shown to be avirulent but to regain virulence upon reconstitution of the defective gene. LC-ES-MS has proved to be a good method to verify the phenotype of transposon mutants and recombinants and I have been able to correct several wrong assignments based on less sensitive and less specific assays. It remains a non-trivial problem to distinguish between true biosynthetic and regulatory mutants. Virulence studies with regulatory mutants would not allow us to arrive at a definitive conclusion as to whether proferrioxamines are indeed virulence factors because we would not know how they would behave in planta. The best proof for biosynthetic mutants is the demonstration of accumulated proferrioxamine intermediates. Thus far we have not been able to do so, in part because our present capillary chromatography is not suited for very hydrophilic components such as the expected biosynthetic intermediates. It will be necessary to develop appropriate derivatization schemes or to employ different chromatographic systems. Such modified LC-ES-MS methodology will also be needed for verifying success in generating the desired biosynthetic mutants by homologous recombination. It is important to note that the latter approach has only become feasible with the structural identification. Another lesson learned from the structure determination is that, because of likely multiple biosynthetic routes for the proferrioxamines, several mutations may be necessary to achieve the desired mutants. Previous mutation attempts have all been aimed at generating single site mutants.

Interest in *E. herbicola* arises from the potential use of this epiphyte in the biological control of fire blight. Not all strains of *E. herbicola* are inhibitory. LC-ES-MS showed a clear difference between the metabolic profiles of one inhibitory and two non-inhibitory strains. The non-inhibitory strain produced the same proferrioxamines as *E. amylovora*, whereas the inhibitory strain produced different, as yet uncharacterized siderophores. This lead to the hypothesis that siderophores that cannot be utilized by*E. amylovora* may perhaps prevent it from multiplying due to iron starvation. Because recent taxonomic studies have reclassified the numerous strains in the *E. herbicola/Enterobacter agglomerans* group into *Pantoea dispersa* and *Pantoea agglomerans,* it was of interest to investigate whether there was a correlation between virulence, siderophore production, and *Pantoea* species. It was found that *P. agglomerans* is a proferrioxamine producer whereas *P. dispersa* is not. However, analysis of an additional inhibitory strain revealed that proferrioxamine producing strains of *E. herbicola* may also be inhibitory, consistent with the general consensus in the field that the various *E. herbicola* strains have developed multiple inhibitory mechanisms.

E. persicinus is a newly discovered species and its potential for causing disease is not yet known. LC-ES-MS readily proved that *E. persicinus* produces proferrorosamine A, which has been implicated as a virulence factor in plant diseases caused by *Erwinia rhapontici*. This finding suggests that *E. persicinus* may also be a plant pathogen.

In conclusion, it has been shown that LC-ES-MS can play an important role in the metabolic profiling of bacterial metabolites, in the monitoring of mutageneses and directed fermentations, and, via differential profiling of virulent and avirulent strains, in the elucidation of microbial virulence mechanisms.

[1] Feistner GJ, Stahl, DC, and Gabrik AH, *Org. Mass Spectrom.* **28**, 163-175 (1993)

Electrospray and Plasma Source Ionization Using an Ion Trap Storage/Reflectron Time-of-Flight Mass Spectrometer

*Benjamin M. Chien, Steven M. Michael, and David M. Lubman
Department of Chemistry, University of Michigan, Ann Arbor, MI 48109

The main goal of this work is to interface various API sources including electrospray and plasma source ionizations to time-of-flight devices by using a quadrupole ion trap as a front end source [1]TOF is known for its speed and high mass measurement capability with high transmission. TOF is intrinsically a pulsed ionization technique while ions produced from most API sources are continuous The conventional method in converting a continuous ion beam into a pulse ion beam called beam deflection[2] provides very low duty cycle. Recently, another method called orthogonal extraction[3] was developed to improve the duty cycle. However, the duty cycle is only ~ 0.005% when operated at a pulse repetition frequency of 10 Hz. Higher duty cycle can be achieved by using higher rate such as 5 KHz but this rate is not practical for real time application because the data storage is still limited by the speed of the computer. In contrast, by using a quadrupole ion trap as the front end source for TOF, a nearly 100% duty cycle can be achieved independent of pulse repetition frequency. This is because all the ions that are sampled into the vacuum are stored in the ion trap device and upon applying a dc voltage to the exit endcap all the ions are ejected into the time of flight tube for mass analysis This results in a significant improvement in enhancing the sensitivity over the orthogonal

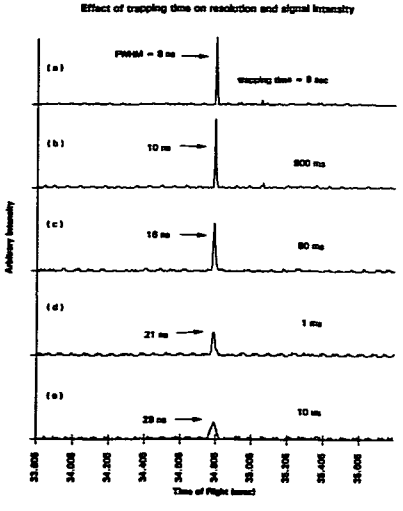

extraction method, especially when operated at a low pulse repetition frequency In addition, high resolution is also achieved in using this method. This can be attributed to a tight ion packet formation owing to the collisional cooling of the ions with background gases inside the trap. It is shown in the Figure 1 that the storage capabilities of the device provide enhanced resolution and sensitivity as the storage time is increased.[4] A resolution of nearly 2100 at m/z 79 is demonstrated using external injection from the atmospheric pressure DC plasma source when a storage time of 9 sec is used before ejection. Further, as shown in Figure 2, a resolution of ~ 3300 at m/z 1060 is demonstrated using external injection from an electrospray ionization source into the trap with a storage time of 931 ms. Figure 3 shows the bovine heart cytochrome C (MW 12,327) spectrum. The multiple charged peaks from +5 to +12 were observed. The charged state of +5 corresponds to a trapped ion of m/z 2,466.[5] The detection limit of this device is also demonstrated with liquid injection techniques for a typical sample and found to be less than a single femtomole.

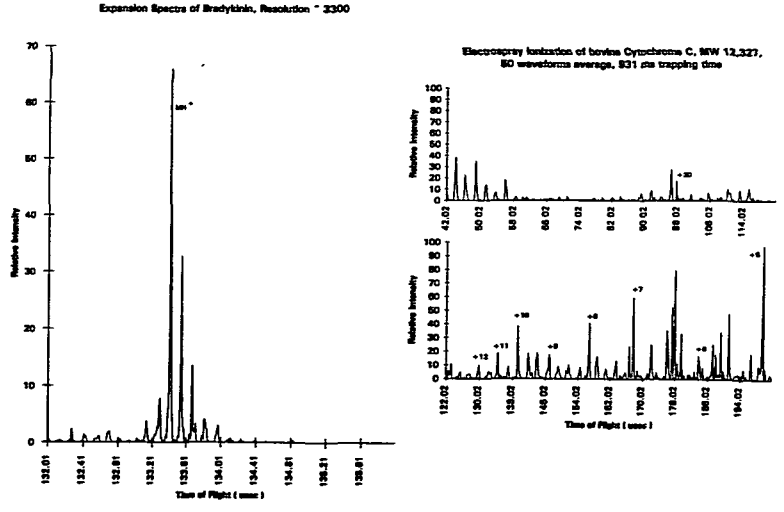

References:

1. S. M. Michael, M. Chien, D. M. Lubman, Rev. Sci. Instum., 63 (1992) 4277.
2. C. Ma, S. M. Michael, M. Chien, J. Zhu, D. M. Lubman, Rev. Sci. Instrum., 63 (1992) 139.
3. J. G. Boyle, C. M. Whitehouse, Anal. Chem., 64 (1992) 2084.
4. B. M. Chien, S. M. Michael, and D. M. Lubman., Anal. Chem., in press July, 1993.
5. B. M. Chien, S. M. Michael, and D. M. Lubman., Int. J. Mass Spectrom. Ion Proc., in press.

STRUCTURE ELUCIDATION STRATEGIES APPLIED TO TAXOL AND TAXANES

Edward H. Kerns, Kevin J. Volk, Susan E. Hill and Mike S. Lee
Bristol-Myers Squibb Pharmaceutical Research Institute, Wallingford, CT 06492

Analytical strategies involving tandem mass spectrometry have been developed for the rapid structure elucidation of trace components of mixtures commonly encountered in pharmaceutical discovery and development research. These strategies provide rapid structural results compared to common lab-scale methods involving scale-up, fractionation and indivividual spectroscopic analysis of each component. However, they are more rapid and require only small samples. The strategies of LC/MS and LC/MS/MS Profiling and MS/MS Screening, developed for screening drug metabolites directly from physiological fluids (1,2) and natural products in crude extracts (3), were applied for the rapid structure elucidation of trace taxol analogs in crude plant extract mixtures, bulk drug substance, and degraded samples. These strategies combine HPLC separation, UV spectroscopy, full scan MS and MS/MS analysis in one instrumental configuration, thus paralleling common lab-scale trace mixture analysis strategies.

LC/MS and LC/MS/MS Profiling was applied to the direct structure elucidation of taxanes in mixtures, such as impurities and degradation products in bulk drug. Photodiode array UV analysis of HPLC separations were obtained for chromatographic comparisons and to obtain class and substructure specific data from UV spectra. Ionspray LC/MS chromatograms are consistent with LC/UV chromatograms Full scan LC/MS, obtained in the same analysis, provided molecular weight and purity analysis. Ammonium acetate in the mobile phase produced abundant $(M+NH_4)^+$ ions for taxanes using ionspray ionization Application of a consistent HPLC separation involving an E.S Scientific pentafluorophenyl HPLC column and gradient elution with acetonitrile and 2mM ammonium acetate buffer provided a consistent database of taxane chromatographic and MS characteristics useful for the rapid identification of taxanes in subsequent samples MS/MS substructural analysis was performed on each unknown component during HPLC elution, eliminating the need to scale-up and isolate individual compounds. Interpretation of the structures of unknown taxanes was based on the CID fragmentation of taxol. Prominent substructural ions of taxol include· m/z 286^+ characteristic of the sidechain, m/z 569^+ characteristic of the taxol core ring structure, and m/z 509^+ characteristic of the deactyl core ring structure Examples of taxanes elucidated include 10-deacetyl taxol and taxol n-pentyl analog (taxol C)

MS/MS Screening was applied to the screening of crude biomass extracts. Using parent MS/MS screens based on CID fragment ions characteristic of taxol substructures the molecular ions of taxanes containing taxol substructures were observed. For example a parent screen of m/z 509^+ indicated compounds containing the taxol core ring substructure Subsequent daughter MS/MS analysis of the molecular ions observed by these screens rapidly provided information used to interpret the structure of the unknonw taxane. An example of a taxane elucidated in this manner is 7-xylosyl deacetyl taxol.

These structure elucidation strategies are applicable to a wide range of pharmaceutical research and development projects, including: natural products, metabolites, impurities, degradation products, biomolecule sequencing, biochemical reaction products, and in-vivo and in-vitro on-line monitoring via direct microdialysis sampling into the mass spectrometer.

References
1 M S. Lee, et al, Proceedings ASMS Conference 1986, p. 929.
2 E H Kerns, et al, Proceedings ASMS Conference 1991, p. 609.
3 M.S. Lee, et al, Proceedings ASMS Conference 1991, p. 1061.

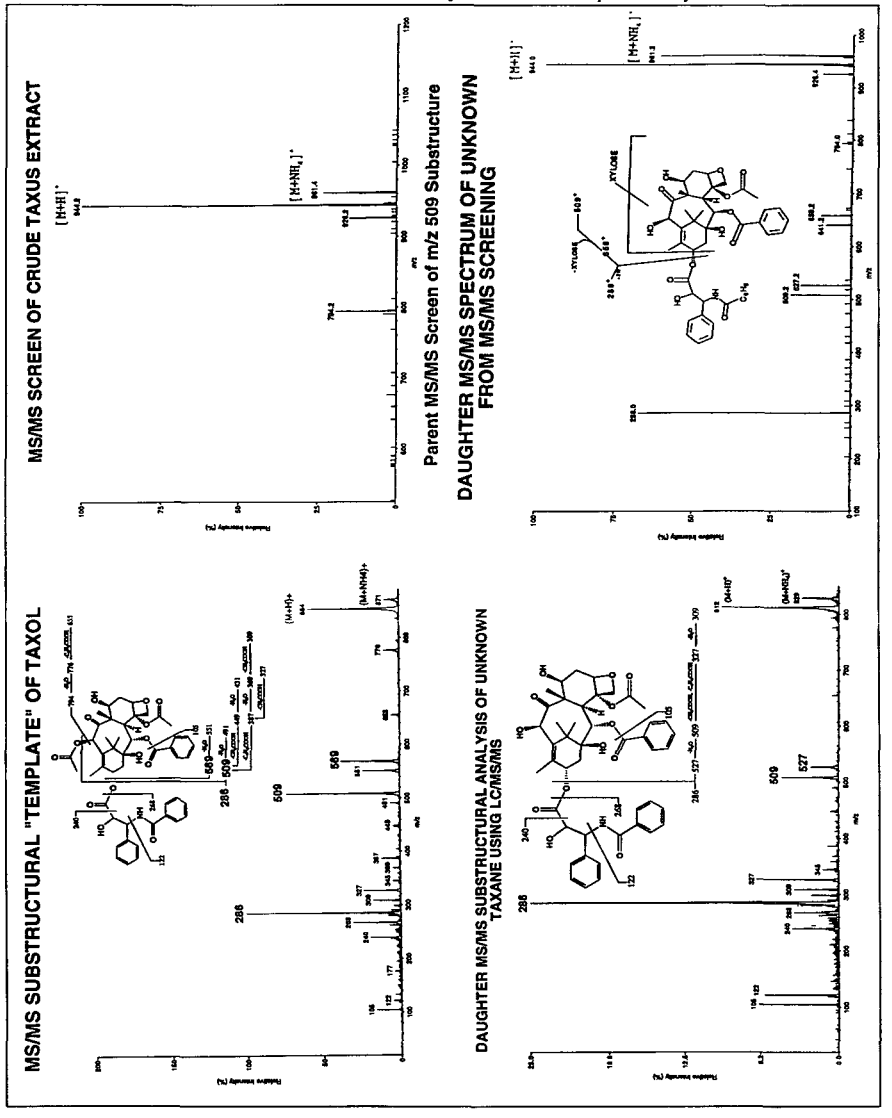

PETROLEUM POLARS CHARACTERIZED BY COMPOUND CLASS SEPARATION AND ON-LINE LC/MS

C. S. Hsu, K. Qian and W. K. Robbins
Exxon Research and Engineering Co.
Route 22 East, Clinton Township, Annandale, NJ 08801

Petroleum polars contain a variety of compounds, particularly hetero-atom containing, which are often difficult to characterize by mass spectrometry because of the complexity, polarity and/or thermal instability of the molecules. The abundance of polars is generally increased with increasing boiling range of the crude oil. Separation into compound classes can eliminate some of the uncertainties of compound identification by MS. Using on-line liquid chromatography-mass spectrometry (LC/MS) the selectivity of separation can also be evaluated. We recently have examined the polars of a 650-1050°F distillate of a Californian crude of high heteroatom content.

A combination of traditional clay and silicic acid chromatographies have been used to isolate three fractions designated "neutral nitrogen", "basic nitrogen" and "complex polars" on the basis of model compounds (see Figure 1).[1] By subjecting the "neutral nitrogen" and "basic nitrogen" fractions to on-line LC/high resolution MS analysis, we have been able to understand some of the overlaps encountered in chromatographic studies. In this instance, we used the normal phase chromatographic system previously described for the resolution of heavy oils into saturates, 1-4 ring aromatics, and polars on a dinitroanilinopropyl (DNAP) silica.[2, 3] Figure 2 shows the compound distribution in these elution regions for the "neutral nitrogen" and "basic nitrogen" fractions. Some diaromatic and triaromatic hydrocarbons are noticeably present in the "neutral nitrogen" fraction due to imperfect Biosil separation. High resolution MS reveals that the nitrogen compounds present are mainly $C_nH_{2n-15}N$ (carbazoles) and $C_nH_{2n-21}N$ (benzocarbazoles) appearing in the tetraaromatic and polars regions, respectively, as shown in Figure 3. Deuterated ammonia chemical ionization (ND_3/CI) demonstrated that all of the carbazoles (pyrrole benzologs) contain one exchangeable hydrogen (see Figure 4) and therefore none has N-R functionality where R is an alkyl substituent attached to the nitrogen atom.

Another interesting result of these combined chromatographies was the finding that the "basic nitrogen" fraction was dominated by NO_x (x = 1 and 2) species rather than pyridine benzologs (Figure 5). Chromatographically, while the open column isolated these components in the "basic nitrogen" fraction the LC technique lumped them in polars. A combination of ancillary techniques, ND_3/CI, x-ray photoelectron spectroscopy (XPS), and infrared (IR), have been used to characterize the NO species as cyclic imides (lactams). In addition, some non-aromatics with NO_2 composition were found; because these compounds show three exchangeable hydrogens in ND_3/CI experiment consistent with molecules containing both amino and acidic functionalities.

At the present time, we are continuing to use the LC/MS approach in evaluating alternative chromatographic techniques in order to obtain better resolution of the petroleum polars. In addition, the existing techniques are being extended to other crudes for comparison with the Californian crude studied here.

References:

1. W. K. Robbins and F. C. McElroy, *Liq. Fuels Technol.*, 2, 113-154 (1984)

2. C. S. Hsu, K. Qian, M. A. McLean, T. Aczel, S. C. Blum, W N. Olmstead, L. H. Kaplan, W K. Robbins and W. W. Schulz, *Energy Fuels*, 5, 395-398 (1991).

3. K. Qian and C. S. Hsu, *Anal. Chem.*, 64, 2327-2333 (1992).

FIGURE 1

SEPARATION OF A CALIFORNIAN CRUDE DISTILLATE BY CLAY AND BIOSIL

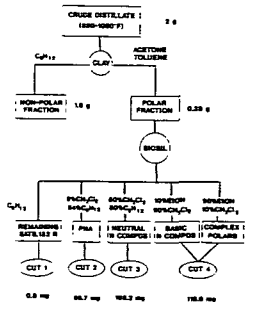

FIGURE 2

LC/MS REVEALS INCOMPLETE N-TYPE ISOLATION WITH BIOSIL SEPARATION

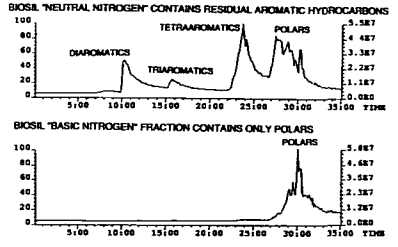

FIGURE 3

DISTRIBUTION OF "NEUTRAL NITROGEN" COMPOUNDS IN TETRAAROMATIC AND POLAR LC REGIONS

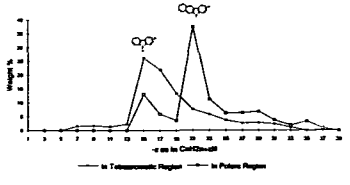

FIGURE 4

ND_3 CI IDENTIFIES "NEUTRAL NITROGEN" COMPOUNDS AS CARBAZOLES (PYRROLIC NITROGEN COMPOUNDS)

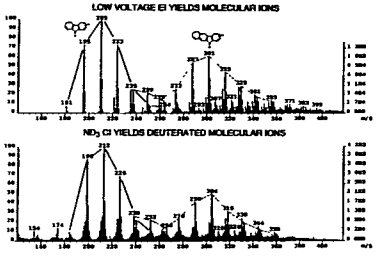

FIGURE 5

MOST OF NITROGEN COMPOUNDS IN "BASIC NITROGEN" CUT ARE NO_X COMPOUNDS BY HIGH RESOLUTION MS

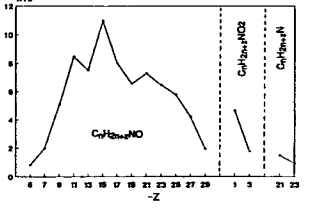

BOND ENERGIES AND ELECTRONIC STATES OF UNSATURATED ORGANOMETALLIC COMPLEXES

F. A. Khan, C. Haynes, N. F. Dalleska, R. H. Schultz, and P. B. Armentrout

Chemistry Department, University of Utah, Salt Lake City, UT 84112

The sequential bond dissociation energies (BDEs) of a series of cationic organometallic complexes in the gas-phase have been measured by collision-induced dissociation (CID) studies in a guided ion beam tandem mass spectrometer [1,2,3,4]. We are interested in two interrelated facets of the resulting information: 1) how do the BDEs vary as the metal approaches saturation (either electronically, in terms of reaching a stable 18-electron valence configuration, or sterically, in terms of reaching a complete solvent shell), and 2) can these BDEs help elucidate how the valence electrons on the metal reorganize to accommodate the ligand shell. The latter consideration may be thought of in terms of ligand field theory and may allow an understanding of how to use ligands to manipulate the electronic configuration at the metal center.

Table 1 lists results for a few representative systems. In addition, complete experimental data has now been obtained for the following systems: $Co(CH_4)_n^+$, n = 1-4; $Ni(N_2)_n^+$, n = 1-4; $Ni(NO)_n^+$, n = 1-3; and $M(H_2O)_n^+$, n = 1-4 where M = Ti, V, Cr, Fe, Co, Ni, and Cu. For the carbonyl results shown in Table 1, the sums of the BDEs agree with literature thermochemistry in all three cases. In general, our results are in good agreement with other CID [5,6] and theoretical [7] work on $M(H_2O)^+$ and $M(H_2O)_2^+$; with equilibrium [8] and CID [9] measurements on $Cu(H_2O)_3^+$ and $Cu(H_2O)_4^+$; and with equilibrium [10] and theoretical [11] work on $Co(CH_4)_n^+$, n = 1-3.

It might be anticipated that if the bonding is largely due to simple electrostatic interactions (as seems likely for all ligands considered here but NO), the BDEs would gradually decrease as the ligand sphere is increased due to ligand-ligand repulsions. Table 1 shows that this is true for the nickel carbonyl cations, but for the chromium and iron carbonyl cations, the sequential BDEs exhibit nonmonotonic changes. $Cr(CO)_6^+$, $Fe(CO)_5^+$ and $Ni(CO)_4^+$ are all expected to have doublet ground states because they are formed by removing a single electron from an 18-electron complex. In contrast, the atomic ions have ground states of $Cr^+(^6S)$, $Fe^+(^6D)$, and $Ni^+(^2D)$, such that only in the nickel system are there no spin changes as CO ligands are added to the atomic metal ion. Therefore, we attribute the nonmonotonic changes observed in the BDEs of $Cr(CO)_6^+$, $Fe(CO)_5^+$, and several other systems to the electronic reorganization that must occur at the metal center as the strength of the ligand field increases with increasing ligation. This explanation is supported by studies that vary the ligand field strength by changing the type of ligand and also by studies of ligand exchange reactions. The comparison of the $Fe(CO)_n^+$ and $Fe(CH_4)_n^+$ systems illustrates the former effect. Note that $D[Fe(CH_4)_2^+\text{-}CH_4]$ *exceeds* $D[Fe(CO)_2^+\text{-}CO]$, a fairly nonintuitive result that can be rationalized in terms of spin changes.

TABLE 1. Sequential Bond Energies of Cationic Transition Metal Ligand Complexes[a]

n	1	2	3	4	5	6
$Cr(CO)_n^+$ [b]	0.93(0.04)	0.98(0.03)	0.56(0.06)	0.53(0.08)	0.64(0.03)	1.35(0.08)
$Fe(CO)_n^+$ [c]	1.36(0.08)	1.57(0.15)	0.69(0.05)	1.07(0.07)	1.16(0.04)	
$Fe(CH_4)_n^+$ [d]	0.59(0.04)	1.01(0.04)	1.02(0.06)	0.76(0.07)		
$Ni(CO)_n^+$ [e]	1.79(0.04)	1.70(0.05)	0.90(0.07)	0.73(0.07)		

[a]Values are at 0 K in eV. Uncertainties are in parentheses. [b]Reference 3. [c]Reference 1. [d]Reference 2. [e]Reference 4.

References

1. Schultz, R. H.; Crellin, K. C.; Armentrout, P. B. *J. Am. Chem. Soc.* **1991**, *113*, 8590.
2. Schultz, R. H.; Armentrout, P. B. *J Phys. Chem.* **1993**, *97*, 596.
3. Khan, F. A.; Clemmer, D. E.; Schultz, R. H.; Armentrout, P. B. *J. Phys. Chem.* in press.
4. Khan, F. A.; Steele, D L.; Armentrout, P. B *J Phys Chem* submitted for publication.
5. Magnera, T. F.; David, D. E.; Michl, J. *J. Am. Chem. Soc.* **1989**, *111*, 4100.
6. Marinelli, P. J.; Squires, R. R. *J. Am. Chem. Soc.* **1989**, *111*, 4101.
7. Rosi, M.; Bauschlicher, C. W. *J Chem Phys.* **1989**, *90*, 7264; **1990**, *92*, 1876.
8. Holland, P. M.; Castleman, A. W. *J. Am. Chem. Soc.* **1980**, *102*, 6174; *J. Chem. Phys.* **1982**, *76*, 4195. Peterson, K. I.; Holland, P. M.; Keesee, R. G.; Lee, N.; Mark, T. D., Castleman, A. W. *Surf Sci.* **1981**, *106*, 136.
9. Magnera, T. F.; David, D. E.; Stulik, D.; Orth, R. G.; Jonkman, H. T.; Michl, J. *J. Am. Chem. Soc.* **1989**, *111*, 5036.
10. Kemper, P. R.; Bushnell, J.; van Koppen, P. A. M.; Bowers, M. T. *J. Phys. Chem.* **1993**, *97*, 1810.
11. Perry, J. K.; Ohanessian, G.; Goddard, W. A. *J. Phys. Chem.* submitted for publication.

Substituent Effects and Solvation Energetics from Electron-Transfer Equilibrium Studies of Gas-Phase Metal Complexes

David E. Richardson, Matthew F. Ryan, Paul Sharpe,
Md. Nazrul I. Khan, and John R. Eyler
Department of Chemistry, University of Florida, Gainesville, Florida 32611-2046

We have focused in this research on the use of gas-phase ion techniques to study the reactivity and thermodynamic properties of gas-phase metal complexes that have direct solution analogs. The opportunity then arises to address several fundamental questions regarding the intrinsic chemistry of such systems as well as to gain insight into the effect of solvation on reactivity and thermochemistry. The principal instrumental technique used in this research is Fourier transform ion cyclotron resonance mass spectrometry (FTICR-MS).

Several electron-transfer equilibrium (*ETE*) studies of organometallic and coordination complexes have been completed.[1-7] This method allows the accurate determination of the free energies of ionization and/or electron attachment of a molecule under thermal conditions in the gas phase (eqs 1 and 2).

$$ML_n \rightleftharpoons ML_n^+ + e^- \qquad \Delta G_i^\circ \text{ (ionization)} \qquad (1)$$

$$ML_n + e^- \rightleftharpoons ML_n^- \qquad \Delta G_a^\circ \text{ (electron attachment)} \qquad (2)$$

The values of $\Delta G_a^\circ$and ΔG_i° can be derived from the equilibrium constant of equilibria of the general type shown in eq 3, where A is a reference compound with known ΔG_a° or ΔG_i° value (for anions or cations, respectively).

$$ML_n + A^\pm \rightleftharpoons ML_n^\pm + A \qquad \Delta G_{et}^\circ = RT \ln K_{eq} \qquad (3)$$

In general, we have used the data to interpret the thermochemistry and bonding of metal complexes, to give quantitative insight into solvation energetics by comparison to solution redox thermochemistry, and to provide a basis for the prediction of electronic substituent effects on the reactivity of transition metal catalysts.

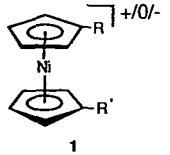

1

Two recent studies[1,6] have addressed the nature of alkyl substituent effects in transition metal complex oxidation-reduction energetics. ETE methods have been used to establish the gas-phase ionization and electron attachment energetics for nickelocene and several alkylated derivatives, (RCp)(R'Cp)Ni (1, R, R'= H, Me, Et, t-Bu).[1] Alkyl substituents larger than methyl decrease the ionization energy and increase the electron affinity relative to the parent (R = H) compound and are thus not uniformly "electron donating" in character. This result was not unexpected, since analogous alkyl effects are well known in the proton affinities and acidities of organic bases and acids in the gas phase. However, the poor solution electrochemical reversibility of the reduction couple for nickelocenes makes direct comparison to solution trends difficult.

Alkyl substituent effects in gas-phase *and* solution redox thermochemistry have *recently been studied for a series of ruthenium coordination complexes.*[6] The gas-phase ΔG_i° and ΔG_a° values (Figure 1) were compared to electrochemical oxidation and reduction half-wave potentials ($E_{1/2}$) for six ruthenium tris(β-diketonate) complexes (2, R = methyl, ethyl, *n*-propyl, *n*-butyl, *i*-propyl, and *t*-butyl). Gas-phase cations and anions are stabilized relative to the neutral by larger alkyl substituents, rendering ΔG_i° less endoergic and ΔG_a° more

exoergic as the alkyl group size increases. Analysis of the gas-phase data by a model of substituent effects based on polarizability and inductive contributions of a group shows that alkyl inductive effects are small in these complexes and that relative stabilities of gas-phase ions are primarily due to differences in polarizability of the alkyl substituents at the β positions.

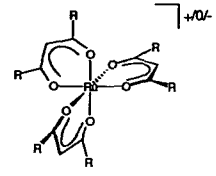

2

Substitution of R = methyl in 2 with larger alkyl groups results in cathodic shifts in both oxidation and reduction $E_{1/2}$ values (in N,N-dimethylformamide), so the trends for solution and gas-phase reduction of the neutral ruthenium(III) complex are therefore reversed. Values of $\Delta\Delta G_{solv}^\circ$(0/-) range from -48 ± 5 kcal mol^{-1} (R = methyl) to -36 ± 5 kcal mol^{-1} (R = *t*-butyl), and these changes in $\Delta\Delta G_{solv}^\circ$(0/-) are identified as the cause of the reversal in the trends for *gas-phase and solution reduction free energies. In contrast,* $\Delta\Delta G_{solv}^\circ$ *(0/+) values all fall in* the range -19 to -16 kcal mol^{-1} and show no correlation with the size of the alkyl substituents.

This work was supported by a grant from the National Science Foundation.

(1) Richardson, D. E.; Ryan, M. F.; Khan, Md. N.I.; Maxwell, K. A. *J. Am. Chem. Soc.* **1992**, *114*, 10482.
(2) Ryan, M. F.; Eyler, J. R.; Richardson, D. E. *J. Am. Chem. Soc.* **1992**, 114, 8611.
(3) Ryan, M. F.; Siedle, A. R.; Burk, M. J.; Richardson, D. E. *Organometallics* **1992**, 11, 4231.
(4) Sharpe, P.; Eyler, J. R.; Richardson, D. E. *Inorg. Chem.* **1990**, *29*, 2779.
(5) Sharpe, P; Richardson, D. E. *J. Am. Chem. Soc.* **1991**, *113*, 8339.
(6) Sharpe, P.; Richardson, D. E., manuscript submitted for publication.
(7) Ryan, M. F.; Richardson, D. E.; Gruhn, N.; Lichtenberger, D. L., manuscript in preparation.

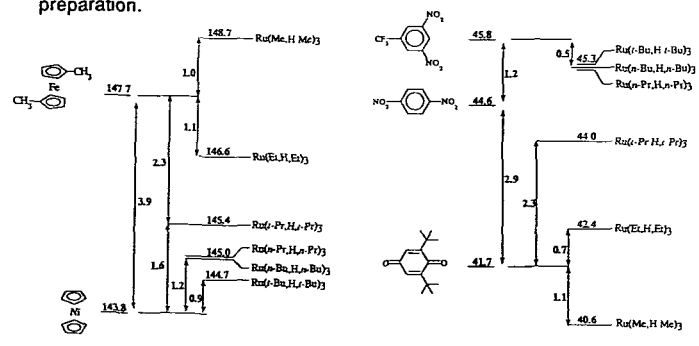

Figure 1. Summary of electron-transfer equilibrium reactions studied with ΔG_{et}°, ΔG_i° and ΔG_a° data (kcal mol^{-1}). (left) Ionization, (right) electron attachment. Numbers next to arrows are experimental ΔG_{et}° values. Numbers *next to compounds are* ΔG_i° *and* $-\Delta G_a^\circ$ *values for reference compounds (left) and ruthenium complexes (right).*

Mechanistic Details of First Row Transition Metal Ions, Sc^+ through Zn^+, Reacting with Propane

*Petra A.M. van Koppen, Paul R. Kemper and Michael T. Bowers
Department of Chemistry, University of California, Santa Barbara, California 93106
Chris Haynes and Peter Armentrout
Department of Chemistry, University of Utah, Salt Lake City, Utah 84112

Introduction

Studies of atomic transition metal ions reacting with simple alkanes in the gas phase have given detailed insight into the mechanism and energetics of these reactions. Metal ions react with propane to form a collision complex, which can be stabilized by collisions with helium or it can dissociate to eliminate molecular hydrogen or methane.

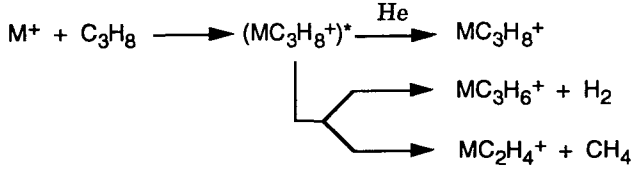

Propane is the smallest alkane to undergo elimination reactions with first row transition metal ions. The electrostatic attraction is sufficient to overcome intrinsic barriers that may be associated with insertion into a C–H or C–C bond. Because these reactions are inefficient, small changes in the potential energy surface greatly effect the reactivity. In a recent study of Co^+ reacting with propane, tremendous progress was made towards the understanding of C–H and C–C bond activation.[1] We have extended this study to include the reactivity of all first row transition metal ions, Sc^+ through Zn^+, with propane.

Observed branching ratios for adduct formation, CH_4 and H_2 elimination were found to vary widely for first row transition metal ions.[2] At 300K and 0.75 Torr of He, adduct formation dominates for V^+ through Zn^+. CH_4 and H_2 elimination are observed for Fe^+, Co^+ and Ni^+ whereas only dehydrogenation and no demethanation is observed for V^+. For Sc^+ and Ti^+, H_2 elimination dominates over CH_4 elimination and over adduct formation. Exclusive adduct formation is observed for Cr^+, Mn^+, Cu^+ and Zn^+.

There are several factors which influence the reactivity of metal ions with propane. The ground state valence electron configuration ($3d^n$ or $4s3d^{n-1}$) of the metal ion, the reaction thermochemistry, crossing to low lying excited state surfaces and sd hybridization are all important factors in determining the reactivity. Several experimental techniques as well as theoretical calculations are necessary to understand the details of these reactions.

Results and Discussion

For Fe^+, Co^+ and Ni^+ reacting with propane, the total cross sections for H_2 and CH_4 elimination are observed to be inefficient, less than 15% of the collision limit, and decrease with the extent of deuteration. The inefficiency of the reaction indicates a rate limiting transition state exists along the reaction coordinate. The decrease in cross section with extent of deuteration indicates this rate limiting transition state is associated with C–H bond activation. Kinetic energy release distributions for H_2 and CH_4 loss from nascent $M(C_3H_8)^+$ complexes for Fe, Co and Ni were measured. For H_2 loss the distribution is bimodal. Studies with propane-2,2-d_2 and propane-1,1,1,3,3,3-d_6 indicate that both initial primary and initial secondary C–H bond activation are involved. The kinetic energy release distribution for demethanation is statistical. Modeling the reaction cross sections, the H, D isotope effect

and the kinetic energy release distribution for demethanation using statistical phase space theory allows for accurate determination of the energy of the C–H bond activation transition state.

The ground state valence electron configurations for Fe^+, Co^+ and Ni^+ are $4s3d^6$, $3d^8$ and $3d^9$ respectively. Adduct formation is the dominant product for all three systems despite the repulsive 4s electron for ground state Fe^+. State selected studies[3] indicate that this is due to a crossing from the $Fe^+(^6D\ 4s3d^6)C_3H_8$ ground-state surface to the $Fe^+(^4F\ 3d^7)C_3H_8$ first excited-state surface where the propane is more strongly bound.

Adduct formation is the most abundant channel for V^+ reacting with propane but only H_2 elimination is observed at thermal energy. A threshold for CH_4 elimination is observed in the ion beam studies. The transition state for C–H reductive coupling was calculated to be 10 kcal/mol higher than the H–H transition state due to the directionality of the sp^3 hybrid orbital on carbon versus the spherically symmetric s orbital on hydrogen.[4] Consequently, it appears the transition state for C–H reductive coupling is very near or above the threshold for reaction.

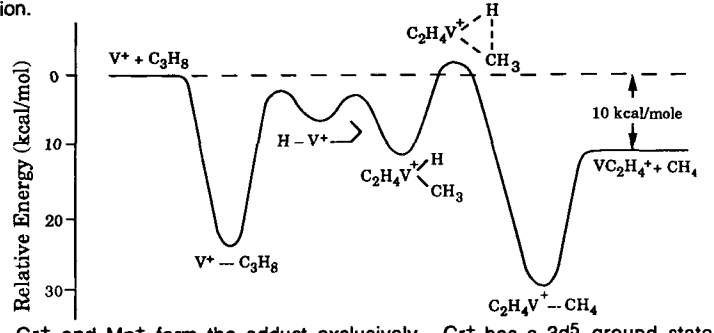

Cr^+ and Mn^+ form the adduct exclusively. Cr^+ has a $3d^5$ ground state electron configuration which is very stable. The elimination reactions are essentially thermoneutral and are therefore not observed. For Mn^+, however, the elimination reactions are more exothermic than for V^+. In this case, the elimination channels are not observed because of the relatively weak electrostatic interaction of the $4s3d^5$ ground electronic state of Mn^+ with propane resulting in the C–H insertion transition state energy being above the energy of the reactants.

$Sc^+(4s3d)$ and $Ti^+(4s3d^2)$ are the only transition metal ions in the first row where the *elimination reactions dominate over adduct formation. The key difference is that for early* transition metal ions, the s and d orbitals are close enough in energy to efficiently hybridize. Ab initio calculations indicate Sc^+ and Ti^+ form two equivalent sd hybrid orbitals with maximum charge density at 90° angles, ideal for forming two covalent bonds.[5] As a result, the C–H bond activation transition state energy is significantly lowered and elimination is favored over adduct formation.

References

1. van Koppen, P. A. M.; Brodbelt, J.; Bowers, M. T.; Dearden, D. V.; Beauchamp, J. L.; Fisher, E. R.; Armentrout, P. B.; *J. Am. Chem. Soc.* 1991, **113**, 2359.
2. Tonkyn, R.; Ronan, M.; Weisshaar, J. C.;*J. Phys Chem.* 1988, **92**, 92.
3. van Koppen, P.A.M.; Kemper, P.R.; Bowers, M.T.; *J. Am. Chem. Soc.*1992, **114**, 10941.
4. Low, J. J.; Goddard, W. A. *J. Am. Chem. Soc.* 1984, **106**, 8321.
5. Bauschlicher, C. W.; Langhoff, S. R.; *Int. Rev.Phys. Chem.*1990,**9**,149.

Accurate Bond Dissociation Energies for $M^+\bullet(H_2)_n$ Clusters

Paul R. Kemper,* J. Bushnell, G. von Helden, and M.T. Bowers
Dept. of Chemistry, University of California, Santa Barbara, CA 93106 U.S.A.

Using temperature dependent equilibrium studies, clustering enthalpies (ΔH°_T) and entropies (ΔS°_T) have been determined for $Na^+\bullet(H_2)_{1,2}$, $K^+\bullet(H_2)_{1,2}$, $Sc^+\bullet(H_2)_{1\text{-}4}$, $V^+\bullet(H_2)_{1\text{-}6}$ and $Co^+\bullet(H_2)_{1\text{-}7}$. In these experiments, the mass selected metal ions (M^+) are injected into a drift reaction cell containing 2-5 torr of pure H_2. The ions are moved through the cell with a small $\vec{E}$ field. At these pressures, sequential clustering readily occurs and

$$M^+\bullet(H_2)_{n-1} + 2H_2 \rightleftharpoons M^+\bullet(H_2)_n + H_2 \qquad (1)$$

equilibrium is quickly established. The ions exiting the cell are quadrupole mass analysed and the resulting equilibrium constants calculated:

$$K_{eq} = M^+\bullet(H_2)_n \cdot 760 \,/\, M^+\bullet(H_2)_{n-1} \cdot P_{H_2} \qquad (2)$$

A plot of ΔG° (= $-RT \ln K_{eq}$) vs temperature has slope = ΔS°_T and intercept = ΔH°_T. The enthalpies are converted to bond dissociation energies (BDE = $-\Delta H^\circ_0$) using a statistical mechanical fit to the ΔG° vs T data.

The Na^+ and K^+ clusters are the most weakly bound (BDE $Na^+\bullet H_2$ = 2.52 kcal/mol, BDE $K^+\bullet H_2$ = 1.88 kcal/mol). The corresponding D_e for $Na^+\bullet H_2$ is in good agreement with theoretical calculations by Siska and coworkers[1] who find the binding to be electrostatic (charge induced dipole and charge-quadrupole) with negligible electron exchange. The H_2 ligands are essentially unperturbed, and are oriented perpendicular to the M^+–H_2 bond axis.

The Co^+ clusters are far more strongly bound[2] (BDEs for $Co^+\bullet(H_2)_{1\text{-}7}$ are 18.2, 17.2, 9.6, 9.6, 4.3, 4.0 and 0.8 kcal/mol, respectively). Theoretical calculations by Partridge and Bauschlicher[3] show that the H_2 ligands are only slightly perturbed. The increase in BDE is largely due to three factors: $H_2\ \sigma \rightarrow Co^+4s$ donation (stabilizes ion); $Co^+\ d\pi \rightarrow H_2\ \sigma^*$ (increases Co^+ d–d exchange); $3d\sigma \rightarrow 4s$ hybridization (reduces repulsion on bond axis). Again, experiment and theory agree well. The pair-wise behavior of the BDEs reflects the symmetry of the clusters. That is, the first and second hydrogens approach the Co^+ 180° apart and experience very similar interactions. The same is true of the third and fourth hydrogens. The reduction in BDEs for this pair is due largely to steric interference. The fifth and sixth hydrogens complete a quasai-

octahedron and are again more weakly bound due to increased ligand–ligand interference.

The $V^+\bullet(H_2)_n$ clusters have BDEs of 10.1, 10.7, 8.8, 8.8, 4.5 and 9.4 kcal/mol for n = 1 to 6, respectively. Preliminary calculations by Maitre and Bauschlicher indicate that the lower BDEs (relative to Co^+) are due to reduced $M^+\ d\pi \rightarrow H_2\ \sigma^*$ back donation. The increase in BDE in $V^+\bullet(H_2)_6$ is accompanied by a large increase in ΔS°, indicating that a large increase in the BDEs in the existing $V^+\bullet(H_2)_5$ occurs when the sixth H_2 is added. This indicated increase in bond strengths is probably due to a transition from a high spin metal center $V^+\ {}^5D$ g.s. ($3d^4$) to a low spin configuration $V^+\ {}^3F$ ($3d^4$). Calculations indicate the low spin cluster should be more strongly bound.

The $Sc^+\bullet(H_2)_n$ BDEs are 5.1, 6.5, 5.7 and 5.3 kcal/mol (for n = 1 - 4, respectively). Theory by Harrison[4] and Upton and Rapeé[5] shows the $Sc^+\bullet H_2$ to be an inserted covalent H–Sc^+–H, however, a large barrier is predicted for the insertion and necessary spin flip.[5] The present experiments indicated that a barrier is present (~10 kcal/mol, based on the forward reaction efficiency). The experimental BDE (5.1 kcal/mol) also agreed fairly well with the 2.0 kcal/mol calculated by Harrison.[4]

Work in progress on other $M^+ + H_2$ systems and on $M^+ + CH_4/C_2H_6$ systems.[6]

---

1. M.F. Falcetta, J.L. Pazun, M.J. Dorko, D. Kitchen and P.E. Siska *J. Phys. Chem.* **97**, 1011 (1993).
2. P.R. Kemper, J. Bushnell, G. von Helden and M.T. Bowers *J. Phys. Chem.* **97**, 52 (1993).
3. C.W. Bauschlicher Jr., H. Partridge and S.R. Langhoff *J. Phys. Chem.* **96**, 2475 (1992).
4. A.E. Alvarado-Swaisgood and J.F. Harrison *J. Phys. Chem.* **89**, 5198 (1985).
5. A.K. Rapeé and T.H. Upton *J. Chem. Phys.* **85**, 4400 (1986).
6. P.R. Kemper, J. Bushnell, P.A.M. van Koppen and M.T. Bowers *J. Phys. Chem.* **97**, 1810 (1993).

Gas-Phase Ion-Molecule Reactions of Atomic Transition Metal Ions with Polar Organic Molecules: Ground Versus Excited Electronic State Reactions

*Vincent J.B. Oriedo, Touradj Solouki and David H. Russell
Department of Chemistry
Texas A&M University
College Station, TX 77843

Studies of gas-phase ion-molecule reaction chemistry of atomic transition metal ions (M^+) with small organic molecules have shown that the ability of M^+ to activate C-C and/or C-H bonds is strongly influenced by the electronic state of the reactant M^+. We recently reported the use of charge-exchange ion-molecule reaction chemistry for measuring the metastable electronic states of M^+.[1] Using this method we estimate that excited states of Fe^+ ions with energies of *ca.* 3.5 eV are formed when Fe^+ is produced by electron impact of $Fe(CO)_5$. We are now using this method to probe the reaction dynamics of Fe^+ with polar organic compounds.

In this paper we report on the reaction chemistry of Cr^+ and Fe^+ with N-methylformamide, N,N-dimethylformamide and N,N-dimethylacetamide. The electronically excited metal ions are denoted $(M^+)^*$ and the ground state metal ions are denoted $(Fe^+)^o$. These studies were performed in a differentially pumped two-section FT-ICR cell. The reactant Cr^+ and Fe^+ were formed in region 1 of the two-section cell by electron impact of $Cr(CO)_6$ and $Fe(CO)_5$, respectively. The reactant M^+ is then isolated using ion-ejection methods and transferred to region 2 of the two-section ion cell where it is allowed to react with the respective neutral amide. The reaction time was varied between 0 and 500 milliseconds.

$(Cr^+)^*$ and $(Fe^+)^*$ ions reacts with N-methylformamide, N,N-methylformamide and N,N-dimethylacetamide to form dissociative and non-dissociative charge-transfer products. The charge-transfer product ion reacts further with a second amide molecule (denoted "A") by proton-transfer to form a protonated amide molecule $[(A+H)^+]$. The enthalpies of the charge-transfer reactions are presented in Table 1.

$(Fe^+)^*$ ions also react with N-methylformamide, N,N-methylformamide and N,N-dimethylacetamide to form C-N bond insertion products. On the basis of molecular orbital arguments[2] we suggest that the $(Fe^+)^*$ ions giving rise to C-N bond insertion products consist of the $3d^7$ electron configuration. That is, $(Fe^+)^*$ ions with the $3d^7$ configuration have an empty 4s-orbital that can accept a pair of electrons from the C-N bond of the amide molecule and spin-paired d-electrons to donate in the C-N antibonding orbital. It should be noted that the $(Fe^+)^o$ ion has a $4s^13d^6$ electron configuration but reacts to form C-N bond insertion products. The reactivity of the $(Fe^+)^o$ ion to form bond insertion products is attributed to the curve-crossing between the ground state $^6D(4s^13d^6)$ and the first excited state $^4F(3d^7)$.[3] The $(Fe^+)^o$ ion also reacts to form the $(Fe\text{-}A)^+$ adduct ion.

In contrast to $(Fe^+)^o$ and $(Fe^+)^*$ ions, the $(Cr^+)^o$ and $(Cr^+)^*$ ions do not react to form C-N bond insertion products. Cr^+ ions reacts to form the $(Cr\text{-}A)^+$ adduct ion. Figure 1 depicts the relative reaction rates of Cr^+ with N-methylformamide, N,N-dimethylformamide, N,N-diethylformamide and N,N-dimethylacetamide. $(Cr^+)^*$ ions also react by collisional relaxation.

In summary, reactions of Fe^+ with amides yield charge-transfer, Protonated, metal adduct, and C-N bond insertion product ions and these ions can provide structural information of the reactant neutral amide. In contrast, Cr^+ does not react with amides to from C-N bond insertion products. Based on the ion-molecule reaction chemistry of Cr^+ with amides, Cr^+ can be used as a chemical ionization reagent for polar organic molecules.

Charge - transfer Reaction Pathway

$Fe^+ + A \longrightarrow A^{+\cdot} + Fe$

$\Delta H = I.E(A) - R.E\{Fe^+[^6D(4s^13d^6)]\}$

(1) N-Methylformamide
$\Delta H = +43.12$ kcal / mol (1.89 eV)

(2) N,N-dimethylformamide
$\Delta H = +27.90$ kcal / mole (1.21 eV)

(3) N,N-dimethylacetamide
$\Delta H = +20.52$ kcal / mole (0.89 eV)

$Cr^+ + A \longrightarrow A^{+\cdot} + Cr$

$\Delta H = I.E(A) - R.E\{Cr^+[^6S(3d^5)]\}$

(1) N-methylformamide
$\Delta H = +69.63$ kcal / mol (3.02 eV)

(2) N,N-dimethylformamide
$\Delta H = +54.42$ kcal / mole (2.36 eV)

(3) N,N-dimethylacetamide
$\Delta H = +47.04$ kcal / mole (2.04 eV)

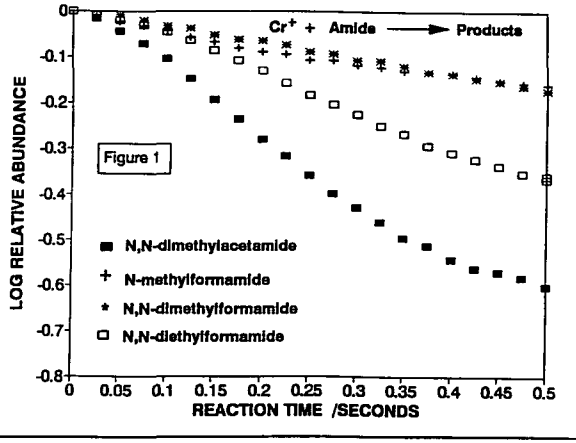

1) Oriedo, J. V. B.; Russell, D. H. *J. Phys. Chem.* **1992**, *96*, 5314-5319.
2) a) Strobel, F. H.; Ridge, D. P. *J. Phys. Chem.* **1989**, *93*, 3635-3639. b) Armentrout, P.B. *Science* **1991**, *251*, 175-179. c) Armentrout, P. B. *Annu. Rev. Phys. Chem.* **1990**, *41*, 313-344.
3) van Koppen, P.A.M.; Kemper, P. R.; Bowers, M. T. *J. Am. Chem. Soc.* **1992**, *114*, 10941-10950.

ISOTOPIC FRACTIONATION IN THE FORMATION OF He_2^+

K.S. Griffith and G.I. Gellene, Department of Chemistry and Biochemistry, Texas Tech University, Lubbock, TX 79409-1061

Recently, it was observed in this laboratory[1] that under some conditions the clustering reaction of O_2^+ and O_2 to produce O_4^+ would equivalently incorporate heavy isotopes of oxygen up to 100 times their natural abundance levels. The explanation of this extraordinarily large non-mass dependent kinetic isotope effect (KIE) required the development of a new symmetry correlation scheme[2] which connected symmetry distinct rovibronic states of the isolated reactants with distinct electronic symmetries of the system in the interaction region independent of the detailed geometry of the collision complex. This correlation scheme provided a framework for identifying systems where non-mass dependent KIE's might be observed. In particular, a potential system is required to have an asymptotic degeneracy arising from either (1) one or both reactants being in a degenerate electronic state or (2) identical reactants in different electronic states. One of the simplest chemical systems which fulfills these requirements is the association reaction:

$$He^+ + He \xrightarrow{M} He_2^+ \qquad (1)$$

which is considered to consist of the two bimolecular reactions:

$$He^+(^2S_{1/2}) + He(^1S) \rightleftarrows (He_2^+)^* \qquad (2a)$$

$$(He_2^+)^* + He \rightarrow He_2^+ + He \qquad (2b)$$

In this case an asymptotic degeneracy arises from the inability to specify which atom is the $He(^1S)$ neutral and which is the $He^+(^2S_{1/2})$ ion when the atoms are the same isotope of He. Decreasing the internuclear separation removes this degeneracy, giving rise to the $^2\Sigma_u^+$ ground and $^2\Sigma_g^+$ first excited Born-Oppenheimer electronic states. This degeneracy is removed at all internuclear distances when the He isotopes are nonidentical because the different ionization energies of ^3He and ^4He energetically distinguish the two possible asymptotes. These energetic considerations are shown in the figure at left.

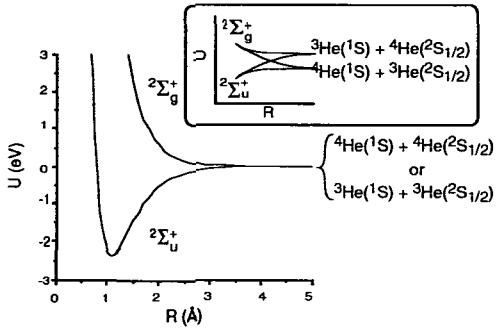

Figure 1. Potential energy curves relevant to collisions of $He^+(^2S_{1/2})$ and $He(^1S)$. The inset is qualitative.

Application of the symmetry correlation scheme to reaction (1) indicates that all of the He/He^+ collisions are capable of accessing the He_2^+ ground electronic state when the He isotopes are nonidentical, whereas only half the collisions of identical isotopes can do so. The direct kinetic consequence of this symmetry restriction is the prediction that the isotopically heteronuclear $^7He_2^+$ ions will be produced at approximately twice the rate of the isotopically homonuclear $^{6,8}He_2^+$ ions. This prediction was tested by a mass spectrometric study. He^+ ions were produced by electron ionization of room temperature $^3He/^4He$ mixtures at ion source inlet pressures of 10-1500 mTorr. Ions exiting the source were accelerated through 5 keV, magnetically mass resolved, and detected by a Channeltron electron multiplier. The results are shown in Figure 2. The near-equivalent enhanced formation of the nonsymmetric $^7He_2^+$ ion relative to that of either symmetric $^{6,8}He_2^+$ ion at low pressure clearly demonstrates the existence of a symmetry dependent (i.e., non-mass dependent) KIE in reaction (1). The apparent loss of the enhancement at increased pressure is best understood not as a loss of the KIE but rather as an increase in the importance of reactions like:

$$^7He_2^+ + {}^4He \rightarrow {}^8He_2^+ + {}^3He \qquad (3)$$

which have no symmetry restrictions and can serve to scramble the nascent isotopic distribution of He_2^+ ions.

Additionally, the results can be used to gain insight into the stabilization step since He is used as the third body. The independence of the zero-pressure KIE on $^3He/^4He$ ratio can be shown to indicate that stabilization occurs primarily without atom exchange, suggesting a role for large impact parameter *l*-changing collisions in the stabilization step. The zero-pressure KIE is approximately 50% larger than can be accounted for by the symmetry restriction alone, implying that an additional KIE is occurring in the stabilization step as well. A likely origin for this additional effect is that *l*-changing collisions for $(^7He_2^+)^*$ for which $\Delta l = \pm 1$ is allowed would be expected to be more efficient than for $(^{6,8}He_2^+)^*$ for which $\Delta l = \pm 2$ is the minimum *l* change.

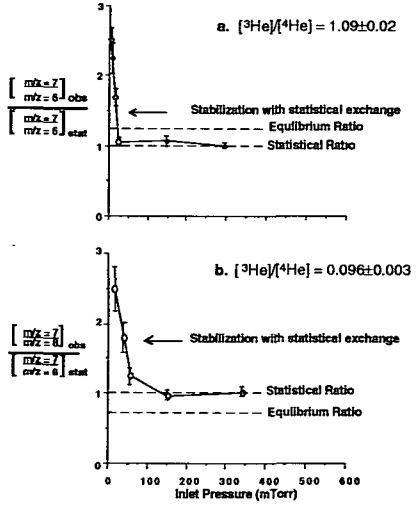

Figure 2. Statistically normalized ratios as a function of ion source inlet pressure.

1 Griffith, K.S ; Gellene, G.I. *J. Chem. Phys.* **1992**, *96*, 4403.
2 Gellene, G.I. *J. Chem. Phys.* **1992**, *96*, 4387.

FUNDAMENTALS OF TANDEM MASS SPECTROMETRY

Anil Shukla and *Jean Futrell
Department of Chemistry and Biochemistry, University of Delaware, Newark, DE 19716

Utilizing an unique crossed beam mass spectrometer apparatus (1), we have completed a suite of experiments providing accurate measurements of energy deposition, angular scattering, fragmentation patterns, and the translational energy dependance of these parameters for several model compounds These experiments have demonstrated dramatic changes in mechanism as a function of collision energy and have identified the "collision time" in which the activation step occurs as the singularly important variable in collisional activation. We have previously drawn attention to the importance of analyzing these experiments in the center-of-mass or collisional coordinates frame in order to separate out mass effects on the interpretation of data which necessarily must be taken in the laboratory frame These studies have shown, for individual molecules, interesting correlations with photoelectron spectroscopy (PIPECO), breakdown graphs, RRKM/QET theories and simple scattering theories. These correlations have been used by us, and others, to discuss such important issues as energy deposition, internal energy randomization, scattering dynamics and activation/dissociation lifetimes

In this paper we review briefly some of the general features of collisional activation mass spectrometry revealed in our experiments and discuss the extent to which simple models can be used to interpret general features of collisional activation of polyatomic ions. In particular, we demonstrate that the Massey Criterion for dependence of energy transfer efficiency on relative velocity provides quantitatively correct results for hydrocarbon ions, such as the propane molecular ion Our conclusion is that CID is accounted for quantitatively, both with regard to energy deposition and fragmentation processes, over a very broad range of collision energies (1 eV to 6 Kev) and a broad selection of scattering gases, by combining a modified Massey distribution with the breakdown graph of propane obtained using PIPECO measurements.

Figure 1 illustrates the remarkable accord between theory and experiment for the three primary dissociation products from collisional activation of propane cations carried out in collaboration with Prof. Gross at the University of Nebraska (2) In this figure the theoretical prediction is botained, as indicated above, by multiplying the breakdown graph for propane by the Massey function

$$P(E) \propto e^{-\frac{\pi \Delta E}{\hbar v}}$$

computer for the collision conditions of Fig 1 The experimental bar graph is in poor agreement as measured; however, when corrected for angular scattering effects measured using our scattering apparatus, the near-perfect agreement between theory and experiment illustrated in Fig 1 is obtained. Accordingly Fig. 1 demonstrates both strong support for the theoretical model and the severe impact of scattering on observed fragmentation patterns in CID.

One detailed test of the theoretical model is a comparison of calculated and experimental energy depositions as a function of collision energy. Essentially quantitative agreement is achieved Closer inspection of the details of the model reveals that the breakdown graph is the controlling factor for propyl ion and ethylene ion formation For ethyl ion the energy deposition function and breakdown graphs are equally important parameters. For more endothermic reactions the energy deposition function is the dominant factor.

The gratifying agreement of experiments with model predictions for the propane cation (and, by inference, other ions following RRKM/QET decay pathways) and the stark disagreement with data for acetone (3), nitromethane (4), SO_2 (5) and benzene (6) molecular ions supports the hypothesis that CID proceeds mainly from isolated electronic states for ions which have intramolecular energy exchange "bottlenecks" which impede energy relaxation. It will be shown that the ensemble of results support the hypothesis that decomposition from the ground state manifold is adequately described by the Massey function/QET model but electronically excited state decay is not.

In these cases coupling of upper and lower electronic state manifolds proceeds on crossing seams of the relevant hypersurfaces We suggest the role of impulsive collisions in inducing remarkably efficient ***T-E*** energy exchange is a very strong dependence of coupling coefficients on nuclear coordinates. According to this hypothesis the Franck-Condon factors for energy transfer in collisionally-perturbed molecular ions is dramatically different from that for isolated ions. Our results for these "pathological" molecules in which this effect is observed is rationalized by combining photoelectron spectroscopy information with molecular orbital descriptions of ground and excited states A predictive feature of this somewhat speculative scheme is that electronic state pathways are commonly found in pi-bonded heteroatomic molecules

These generalizations follow from the microscopic detail on reaction mechanisms deduced from simultaneous measurements of energy deposition and angular scattering in collisional activation mass spectrometry. A completely general feature is that back-scattering and large angle scattering are predominant dynamics features of CID reactions. This clearly implies that most collisional activation processes proceed via small impact parameter collisions, contrary to generally accepted mechanisms used for interpretation of tandem mass spectrometry experiments for the past 20 years. Extrapolation of these results and our conceptual understanding of CID dynamics to large molecule systems provides a partial explanation for the remarkable efficiency of collisional activation mass spectrometry.

References:

1. "A Hybrid Tandem Supersonic Beam Mass Spectrometer for the Study of Collision-Induced Dissociation of Ions in the Energy Range of <1 eV to 3000 eV," A K Shukla, S G Anderson, S L Howard, K W Sohlberg, and J H Futrell, Int J Mass Spec. & Ion Proc , 86, 61 (1988)
2. The Nebraska experiments are described in S. G Anderson's Ph D thesis University of Utah (1992) and interpretation in the Ph.D thesis of R. Zhou, University of Delaware (in preparation, 1994), to be published.
3. "Fundamentals of Tandem Mass Spectrometry A Dynamics Study of Simple C-C Bond Cleavage in Collision Induced Dissociation of Polyatomic Ions at Low Energy," A K Shukla, K. Qian, S. Anderson, and J. H Futrell, J. Amer. Soc. Mass Spec., 1, 6 (1990), "Collision-Induced Dissociation Dynamics of the Acetone Cation: Intraconversion of Translational and Electronic Energy," K Qian, A. Shukla, and J. Futrell, Chem Phys Lett , 175, 51 (1990)
4. "Electronic Excitation in Low Energy Collisions A Study of the Collision-Induced Dissociation of Nitromethane Ion by Crossed-Beam Tandem Mass Spectrometry," K. Qian, A. Shukla, and J. Futrell, J Am Chem Soc., 113, 7121 (1991).
5. # Presented at this Conference
6. # Anil Shukla, Rahul Chawla, and Jean Futrell, to be published.

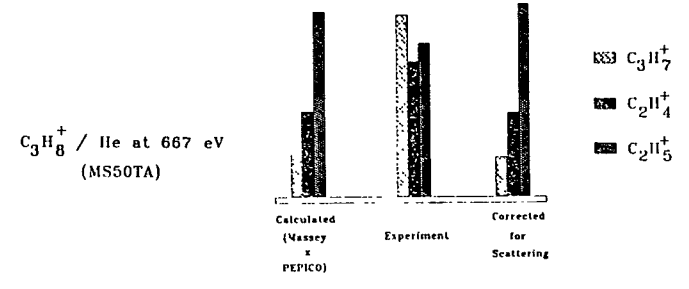

Fig 1 Comparison of theoretical and experimental fragmentation patterns for collision-induced dissociation of propane cations colliding with Ar at 667 eV center-of-mass collision energy (8 KV laboratory energy), with and without scattering correction factors applied to experimental data

Isotopomer Differentiation using Metal Ion Chemical Ionization Reagents

Yongqing Huang and Ben S. Freiser*
H. C. Brown Laboratory of Chemistry
Purdue University
West Lafayette, IN 47907

Catalytic hydrogenation of perdeuterated aromatic species generate selectively deuterated hydrocarbon species.[1] Detailed structural characterizations of these selectively deuterated end products hold the key to understanding the stereochemistry involved in the hydrogenation process. Proton NMR may be employed in limited cases where the sample consists predominantly of one component as a result of high regioselectivity and stereoselectivity during the hydrogenation. Even in these simple cases, however, the interpretation of the NMR spectra is not trivial and high resolution NMR instruments are needed to acquire spectra with enough useful structure information. The task becomes prohibitive for slightly more complicated mixtures of end products. Here we report a versatile technique to address such an analytical problem by using transition metal ions as chemical ionization reagents,[2] in conjunction with Fourier transform mass spectrometry.[3] This technique takes advantage of the intrinsic regioselectivity and stereoselectivity involved in the dehydrogenation of hydrocarbons by transition metal ions. In an elegant paper by Schwartz and coworkers, for example, they reported that in the gas-phase reaction of Fe^+ with octane-1,8-diol, chelation of the metal center by the terminal hydroxyl groups creates conformational configurations inducing regio- and stereo- selectivity during the dehydrogenation process.[4] However, in this work the presence of ring structures on the hydrogenation products creates regio- and stereo-specificity in their dehydrogenation by transition metal ions. Thus, the pattern by which dehydrogenation occurs permits differentiation of isotopomer structures.

All experiments were performed on an Nicolet FTMS-2000 equipped with a 3 Tesla Nicolet superconducting magnet and a dual cell[5] connected through a conductance limit, as well as an array of leak valves and pulsed valves permitting the introduction of various reagents.[6] Metal ions were generated by laser desorption of pure metal targets, mounted outside the magnetic field on the analyzer side, using a Nd:YAG laser operated at its fundamental frequency.[7] A static background pressure of 1-4 x 10^{-6} torr was maintained serving to cool the metal ions and for collision-induced dissociation experiments.[8-9]

The complete characterization of a hydrogenation end product requires the determination of isotopolog distribution and presence of isotopomers for each of isotopolog in the distribution. The former provides information on regioselectivity involved in the hydrogenation process and the latter provides information on stereoselectivity. A tetralin sample obtained from the niobium catalyzed homogenous hydrogenation of perdeuterated naphthalene has been shown by ^1H NMR to be the all cis isotopomer of $C_{10}H_4D_8$. This relatively simple sample was subsequently used to establish and validate the method developed in this study. Its isotopolog distribution was easily determined from its condensation reaction with Ag^+, confirming that tetralin-d_8 is by far the most predominant component, along with only minor amounts of other isotope impurities being present.

The following experiments indicate the presence of the all cis isotopomer of $C_{10}H_4D_8$. The reaction of Co^+ with tetralin gives mostly the double dehydrogenation product ion, Co^+-naphthalene, and a small amount of the condensation product ion, Co^+-tetralin. With the

knowledge that tetralin-d_8 is the main isotopolog, the deuterated tetralin sample gives mostly $2H_2$ and $2D_2$ loss, along with minor amounts of other dehydrogenation products. CID on carefully isolated Co(tetralin-d_8)$^+$ from the condensation reaction gives loss of $2H_2$, $2D_2$, as well as the appearance of Co^+ at higher energies. This indicated that the smaller amounts of dehydrogenation other than $2H_2$ and $2D_2$ are due to the presence of a minor amount of other isotopologs, provided conclusive evidence of regiospecificity and stereospecificity in the dehydrogenation process, and allowed the assignment of the single all cis isotopomer structure.

Subsequently, this methodology was applied to a sample of tetralin obtained by the niobium catalyzed heterogeneous hydrogenation of naphthalene-d_8.[10] While an isotopolog distribution pattern similar to that from the first tetralin sample was observed, the isolation of Co(tetralin-d_8)$^+$ and subsequent CID indicated that two isotopomers were present. Although the isotopomer with four hydrogen atoms on the same side of the ring was still the predominant structure, molecules with two deuterium atoms distributed on each side of the ring were also present, as indicated by a fragment corresponding to $CoC_{10}H_2D_6^+$ (loss of H_2 and D_2, or 2HD). This result is consistent with 1,2-dihydronaphthalene being formed and released during the heterogeneous hydrogenation reaction.[10]

In conclusion, this study indicates the feasibility of using transition metal ions as a class of unique CI reagents, coupled with MS/MS experiments involving isotope selection, to probe isotope distribution and stereo configuration. We are currently applying this method to a variety of other selectively deuterated species.

This work was supported by the Division of Chemical Sciences in the Office of Basic Energy Sciences in the United States Department of Energy (DE-FG02-87ER13766) and National Science Foundation (CHE-8920085).

Reference

1. Yu, J. S.; Ankianiec, B. C.; Nguyen, M. T.; Rothwell, I. P. J. Am. Chem. Soc. **1992**, 114, 1927.
2. Forbes, R. A.; Tews, E. C.; Huang, Y.; Freiser, B. S. Anal. Chem. **1987**. 59,1937.
3. For a review of Fourier transform mass spectrometry, see: (a) Wanczek, K. P. Int. J. Mass Spectrom. Ion. Processes, **1989**, 95, 1. (b) Freiser, B. S. Techniques for the Study of Ion-Molecule Reactions, Farrar, J. M.; Saunders, W. H.; Jr.; Eds.; Wiley-Interscience; New York, **1988**, P. 61. (C) Marshall, A. G.; Verdun, F. R. Fourier Transform in NMR, Optical, and Mass Spectrometry, Elsevier, Amsterdam, **1990**, Chap. 7. (d) Buchanan, M. V., Fourier Transform Mass Spectrometry, ACS Symposium Series 359; Washington, **1987**. (e) Wilkins, C. L.; Chowdhury, A. K.; Nuwaysir, L. M.; Coates, M. L. Mass Spectrom Rev., **1989**, 8, 67. (f) Nibbering, N. M. M. Mass Spectrom. **1986**, 8, 141. (g) Comisarow, M. B. Adv. Mass. Spectrom., **1981**, 8, 1698.
4. Prusse, T. P.; Fiedler, A.; Schwartz, H. Helv. Chim. Acta **1991**, 74, 1127.
5. Gord, J. R.; Freiser, B. S. Anal. Chim. Acta. **1989**, 225, 11.
6. Carlin, T.J.; Freiser, B. S. Anal. Chem. **1983**, 55, 571.
7. Cody, R. B.; Burnier, R. C.; Reents, W. D., Jr.; Carlin, T.J.; McCrery, D. A. Lengel, R. K.; Freiser, B. S. Int. J. Mass Spectrom. Ion Phys. **1980**, 33, 37.
8. Cody, R. B.; Burnier, R. C.; Freiser, B. S. Anal. Chem. **1982**, 54, 96.
9. Burnier, R. C.; Cody, R. B.; Freiser, B. S. J. Am. Chem. Soc. **1982**, 104, 7436.
10. Profilet, R. D. Rothwell, I. P.; Rothwell, I. P. J. Chem. Soc. Chem. Comm. **1993**, 42.

Transition Metal Cluster Anions: Periodic Trends in Oxidation and Chemisorption Reactions

Paul. A. Hintz, Elizabeth G. Kapiloff, Taeck-Hong Lee, Joseph Mwakapumba, and Kent M. Ervin,
Department of Chemistry and Chemical Physics Program,
University of Nevada, Reno, NV 89557

Gas phase transition metal clusters often exhibit strongly size-selective chemical reactivity. Relating the reactivity of clusters to their geometric or electronic structures is important, but problematic because there is limited experimental or theoretical information about the structures. Chemical reactions can probe structural features of the clusters. Chemisorption reactions are particularly useful in this regard, since it may be possible to determine the number and types of adsorption sites on a cluster. Several groups have studied chemisorption on neutral or cationic metal clusters;[1] examining anionic clusters allows us to differentiate reactivity effects due to cluster geometry or size from effects due to electronic configuration. Investigations of selected transition metal elements across and down the periodic table also help elucidate electronic and geometric effects in reactivity/structure relationships.

In this work, we employ Flow Tube Reactor (flowing afterglow) techniques to study the oxidation and chemisorption reactions of transition metal cluster anions. The metal cluster anions are produced by a metal cathode discharge source and are thermalized by 10^5 collisions with the helium buffer gas before interaction with the neutral reagent. The absolute thermal rates of cluster ion reactions are measured, along with product ion spectra.

For most of the metal clusters studied, oxidation by O_2 occurs rapidly via an etching-like process yielding small metal oxide anions containing 1-3 metal atoms. In contrast, the copper-group metals react slowly by addition of O_2. A strong even-odd reaction dependence is found for Ag_n^- clusters—the open-shell even n clusters add O_2 but the closed-shell odd n species are unreactive.

Chemisorption reactions with CO have been studied for titanium-, vanadium-, manganese-, nickel-, and copper-group metal cluster anions. The copper-group clusters are relatively unreactive, yielding only addition of one or two carbonyl groups, but the other metals tend to react rapidly by sequential addition of CO. For the nickel-group clusters, the rate of adsorption of the initial CO molecule on the cluster for all clusters sizes larger than three atoms is efficient, 50% or more of the ion-dipole collision rate.

When the CO concentration is increased, sequential CO additions to the metal cluster anions occur until a limit is reached where no further CO addition is observed. This behavior is shown in Fig. 1, which plots the $Pt_3(CO)_m^-$ product ion intensities as a function of the flow rate of CO in the flow tube reactor. For this case, the saturation limit is reached with the addition of six CO units. The triangular $M_3(CO)_6$ moiety with three terminal and three edge-bridging carbonyls is a common structural unit in condensed phase nickel and platinum complexes.

Fig. 2 plots the observed highest CO coordination numbers for various nickel-group clusters anions. The saturated products can be compared with known organometallic complexes and to the predictions of electron counting theories. In general, Ni_n^- clusters form saturated products that match expectations for a typical for an 18-electron transition metal, while platinum is less highly coordinated both for the gas phase cluster anions and known condensed phase platinum complexes. Palladium appears to be a bridging case, matching platinum for smaller cluster sizes while reaching

higher coordination numbers for clusters with $n > 5$. Cobalt and rhenium cluster anions have higher CO saturation limits, because they have more d-orbital based molecular orbital vacancies into which the CO ligands can donate electrons and form bonds. The skeletal structures consistent with our observed saturation limits for $M_6(CO)_m^-$ (Ni, $m=12$; Pd, $m=12$; Pt, $m=10$; Co, $m=15$) clusters, as predicted by Polyhedral Skeletal Electron Pair Theory, are shown in Fig. 3. For these clusters, compact skeletal structures with near maximum metal-metal bonding are indicated, and more open structures (chains, rings, or planar arrays) can be excluded.

[1] Hintz, P. A.; Ren, X.; Ervin, K. M. *J. Chem. Phys.* **1993** (in press); and references therein.

Fig. 1

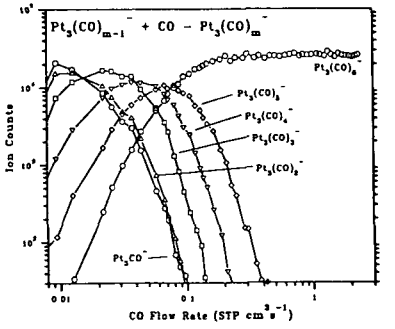

Fig. 2

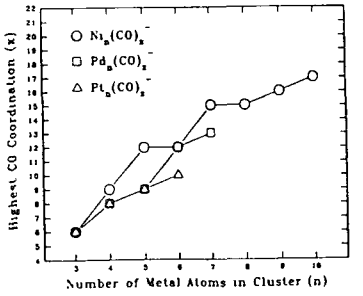

Fig. 3

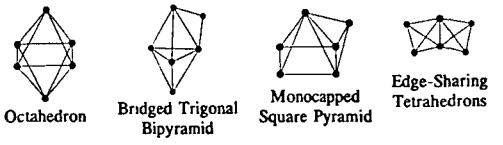

THE NEGATIVE CHEMICAL IONIZATION REACTIONS OF THE ATOMIC OXYGEN RADICAL ANION WITH SELECTED ALKENES.

Joseph J. Grabowski,† Jeehiun Lee§ and Phillip K. Chou†
Departments of Chemistry,
†University of Pittsburgh, Pittsburgh, PA 15260
§Harvard University, Cambridge, MA 02138.

The atomic oxygen radical anion ($O^{\bullet-}$) is an extremely reactive species that is readily produced by electron ionization of nitrous oxide. Because of its importance in ionospheric chemistry and in the chemistry of flames and plasmas of various types, a great number of studies have been carried out on its chemistry with typical constituents of these environments. More recently, $O^{\bullet-}$ has been received attention as a practical reagent in negative ion chemical ionization (CI) mass spectrometry; among its special attributes are the ease of its production from readily available, easily handled, non-toxic precursors and the rapidity with which it reacts with essentially all molecules.[1] A special and unique feature of this *radical anion* is its ability to generate didehydro anions from many organic molecules. A didehydro anion results when a parent neutral, M, which possesses at least two hydrogen atoms, loses the equivalent of $H_2^{\bullet+}$ to generate a ion denoted as $(M\text{-}2H)^{\bullet-}$. For example, $O^{\bullet-}$ CI has been used to generate the radical anions of *o*-benzyne, vinylidene and a variety of carbenes; the radical anions thus generated have been investigated by a variety of techniques including ion-molecule reactivity studies, thermochemical measurements and negative ion photoelectron spectroscopy.

We have been interested in the detailed CI reactions of $O^{\bullet-}$ with organic molecules[2,3] and in the chemistry of the products thus formed.[4,5] As part of this ongoing characterization of the mechanisms and competitions inherent when the atomic oxygen radical anion reacts with organic compounds, we have examined the processes by which it reacts with propene, isobutylene, isoprene and 2,3-dimethyl-1,3-butadiene (DMB) in the flowing afterglow, under thermally equilibrated (298 K) conditions.

Of particular interest is the yield of the $(M\text{-}2H)^{\bullet-}$ from each alkene - these results are summarized in the table on the next page. Hydrogen atom dominates all of the alkenes except DMB, for which the didehydro anion is the major product (see Scheme on next page; similar reactions are observed for the other three alkenes as well). Since all four alkenes are less acidic than $HO^{\bullet}$, no proton transfer is observed *except* as a secondary reaction (the initial HO^- product ion reacting with a second equivalent of the alkene). Deuterium labeling studies have confirmed the structure of the distonic radical anion from DMB shown in the Scheme.

1. J. Lee and J.J. Grabowski, *Chem. Rev.*, 1992, *92*, 1611-1647.
2. J.J. Grabowski and S.J. Melly, *Int. J. Mass Spectrom. Ion Processes*, 1987, *81*, 147-164.
3. Y. Guo and J.J. Grabowski, *Int. J. Mass Spectrom. Ion Processes*, 1992, *117*, 299-326.
4. Y. Guo and J.J. Grabowski, *Int. J. Mass Spectrom. Ion Processes*, 1990, *112*, 253-264.
5. Y. Guo and J.J. Grabowski, *J. Am. Chem. Soc.*, 1991, *113*, 5923-5931.

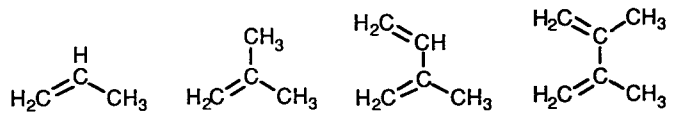

ΔH_{acid}° (kcal mol^{-1})	390.8	390.3	385.8	385.0
% $(M\text{-}2H)^{\bullet-}$	6	7	32	58
k_{obs} (cm^3 molecule^{-1} s^{-1})	1.6×10^{-9}	1.8×10^{-9}	2.2×10^{-9}	2.2×10^{-9}

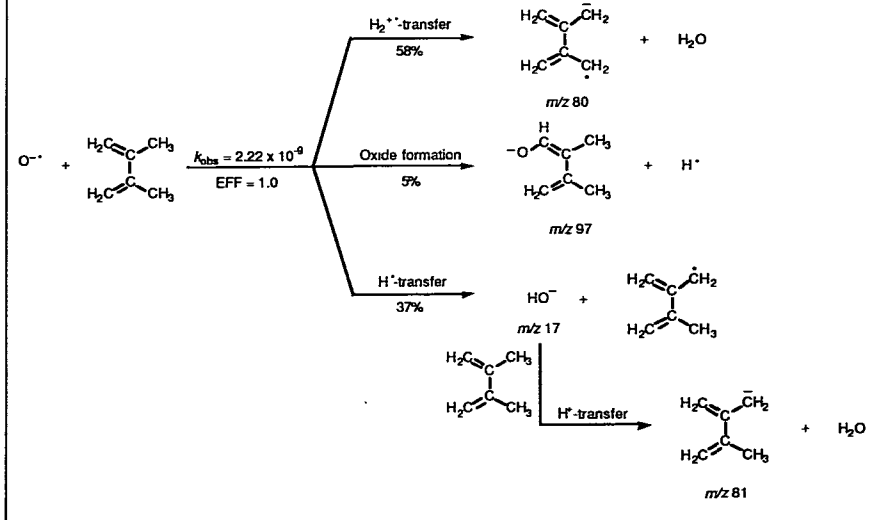

Antiaromatic Ions: The Formation, Reactivity, and Thermodynamic Properties of a Cyclopropenyl Anion

Roseann Kroeker and Steven Kass
Department of Chemistry
University of Minnesota, Minneapolis, MN 55455

The generation of cyclopropenyl anions has been a long standing and elusive goal. The difficulty in forming these species has been attributed to antiaromaticity.[1] Our recent preparation of the diazirinyl anion (c-CHN_2^-) in a flowing afterglow[2] has led us to believe that substituted cyclopropenyl anions should also be accessible.

The reaction of 3-carboxymethylcyclopropene with a base produces the 3-carboxymethyl-1-cyclopropenyl anion (eq. 1). The vinyl position is the most acidic one in this molecule and ΔH_{acid} = 364 ± 3 kcal/mol.

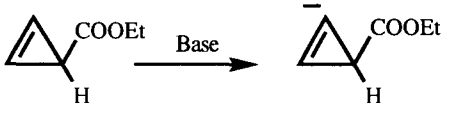

(1)

In order to generate the ion of interest we have made use of a procedure first developed by DePuy and coworkers i.e. fluorodesilylation.[3] In particular, methyl 1-(trimethylsilyl)-2-cyclopropene-1-carboxylate reacts with fluoride to afford 3-carboxymethyl-3-cyclopropenyl anion (eq. 2). This anion has been fully characterized

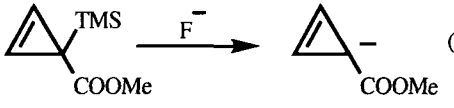

(2)

by reactivity, basicity, collision-induced dissociation, and computational studies. Its proton affinity is 391 ± 4 kcal/mol, it's 13 kcal/mol less stable than its saturated analog (eq. 3) and 14 kcal/mol less stable than it's corresponding acyclic (allylic) isomer (eq. 4). Consequently, this ion is antiaromatic.

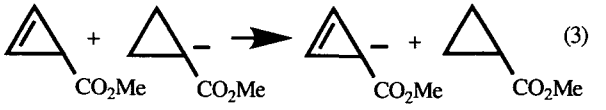

(3)

ΔH = +13 kcal/mol

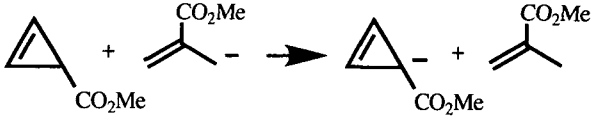

(4)

ΔH = +14 kcal/mol

Not surprisingly, the 3-carboxymethyl-1-cyclopropenyl anion is very reactive. For example, it reacts with carbon dioxide to form >98% of the anion of triafulvenone (eq. 5). The structure of this ion was verified using labeled compounds, examining its

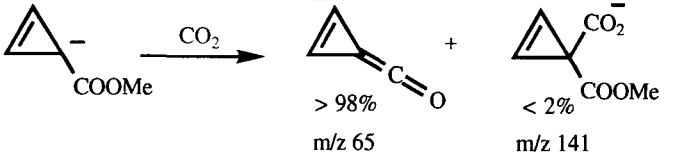

(5)

H/D exchange behavior, and by measuring its proton affinity (345 ± 3 kcal/mol) and comparing the result with theory (346.7 kcal/mol (MP2/6-31+G(d)//6-31+G(d)).

Our results suggest that methylcyclopropene carboxylate has a pK_A of approximately 44, and that cyclopropenyl anions are viable (and attractive) synthetic targets. Efforts along these lines are currently in progress.

1. Breslow, R. *Chemical and Engineering News* **1965**, *43*(26), 90.
2. Kroeker, R. L.; Kass, S. R. *J. Am. Chem. Soc.* **1990**, *112*, 9024.
3. DePuy, C. H.; Bierbaum, V. M.; Flippin, L. A.; Grabowski, J. J.; King, G. K.; Schmitt, R. J.; Sullivan, S. A. *J. Am. Chem. Soc.* **1980**, *102*, 5012.

Ion-Molecule Reactions of Dicoordinated Boron Cations

Hilkka I. Kenttämaa, Thilini D. Ranatunga, James M. Kennady and Varjira Nanayakkara
Department of Chemistry Purdue University, West Lafayette, IN 47907-1393

Boron cations with low coordination numbers are of interest as intermediates in solution reactions of substituted boranes.[1] However, solution studies are limited to ions with bulky substituents and at least one nitrogen-substitient that stabilizes the charge through π-back bonding. This is not true for the gas phase. We have used a dual-cell FT/ICR (Extrel FTMS Model 2001) to study dicoordinated boron cations with no strongly stabilizing substituents. The ions were found to be exceedingly reactive toward oxygen lone pairs in organic substrates, e.g., they rapidly dehydrate organic ethers by elimination of two neutral alkenes.[2] Quite unexpectedly, elimination of an alkene also occurs for carbonyl compounds. The mechanism of this reaction is discussed here.

Electron impact on boron compounds yields abundant dicoordinated boron cations.These ions react to yield two types of primary products with carbonyl compounds (R'C(O)R"; R'= alkyl; R"= H, alkyl): an allyl cation from abstraction of OH from the carbonyl compound by the boron cation, and an adduct of the boron cation and an aldehyde (R"C(O)H) through elimination of an alkene (see Figure 1). The structures of the product ions were verified by CAD through the use of reference ions with known structures.

The reaction of the borocations with carbonyl compounds is facile (efficiencies typically 0.6). The proposed mechanism for the generation of the two product ions are shown in Scheme 1. CH_3-B^+-CH_3 and CH_3O-B^+-OCH_3 yield a similar product distribution; hence, the oxygen atoms in the latter ion do not play an important role in these reactions. Examination of the reactions of CD_3O-B^+-OCD_3 show that the hydrogen atoms in the boron cation do not participate in H/D scrambling with the carbonyl compound.

Both the reactions are estimated to be highly exothermic. Formation of the boron cation as the final product is the faster but less exothermic of the two reactions. The

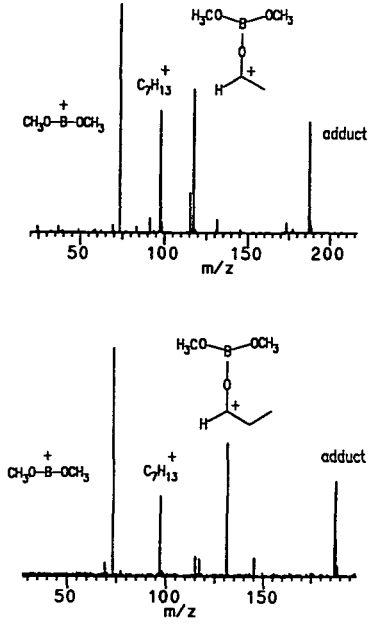

Figure 1. Reaction of (a) 2-heptanone and heptanone and (b) 3-heptanone with CH_3O-B^+-OCH_3.

overall enthalpy change associated with this reaction is fairly unaffected by the size of the carbonyl compound. However, the exothermicity of the reaction leading to abstraction of OH increases dramatically with increasing chain length, being ~19 kcal/mol more exothermic for hexanal than for pentanal. Hence, a strong size dependence is expected and observed: generation of the allyl cation dominates over formation of the boron cation for long-chain aldehydes and ketones (seven carbons or more).

The reactions discussed above are driven by the formation of the very strong B-O bond: generation of the initial addition product (Scheme 1) is estimated to be exothermic by as much as 80 kcal/mol. Much of the chemistry discussed above can be understood on the basis of acid-catalyzed dissociation reactions of carbonyl compounds.

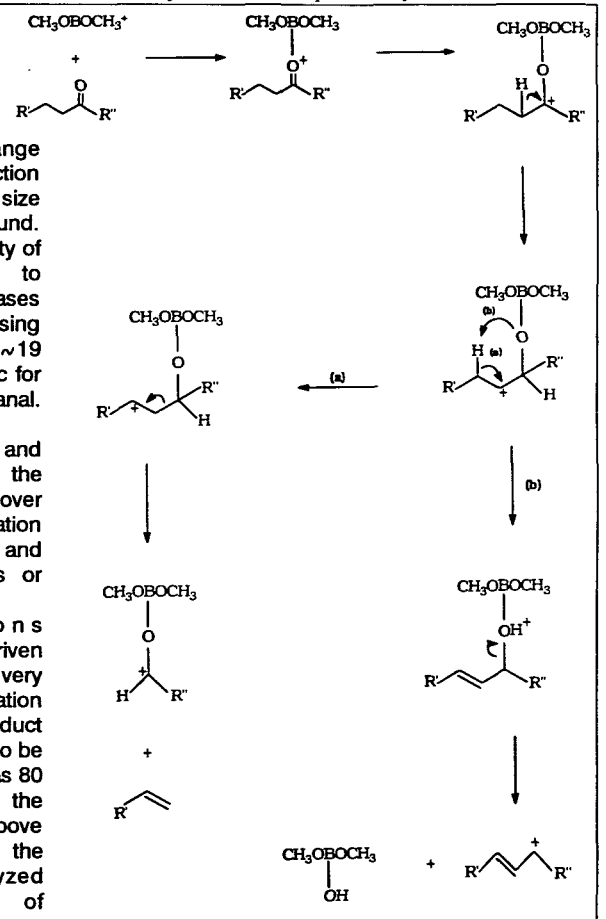

Scheme 1

1) Kölle, P.; Nöth, H. *Chem. Rev.* **1985**, *85*, 399.
2) Ranatunga, T.D.; Kenttämaa, H.I. *J. Am. Chem. Soc.* **1992**, *114*, 8600.

The Structure Elucidation of Taxol Analogs and Impurities Using LC/MS and LC/MS/MS Profiling Protocols

Susan E. Hill, Edward H. Kerns, Kevin J. Volk and Mike S. Lee
Bristol-Myers Squibb Company, 5 Research Parkway, Wallingford, CT 06492

Structure elucidation strategies applied to samples from taxol research studies have resulted in a database of taxol analogs and impurities. This analytical strategy utilizes a systematic approach for the rapid identification of unknown impurities and taxanes which retain the key substructures of taxol. The first step of this methodology utilizes HPLC/UV/MS analysis to obtain chromatographic relative retention times, UV spectra, and full scan mass spectra of each component. Comparison of unknowns to known analogs provides information about polarity and difference in molecular weight relative to taxol. Product ion spectra of each unknown component are obtained on-line (LC/MS/MS) and compared to the product ion spectrum of taxol which is used as a template for subsequent structure elucidation (Figures 1 and 2).

This methodology utilized a Sciex API III triple quadrupole mass spectrometer equipped with an Ionspray interface. Chromatographic conditions included an ES Industries PFP column (25 cm x 4.0 mm) and an ammonium acetate : acetonitrile gradient run at a flow rate of 2.0 mL/min.. The separation was monitored on-line at 230 nm with a Perkin Elmer LC-235 diode array detector. CID was performed on the ammoniated molecular ion of each unknown component.

The database includes knowledge of more than 50 taxanes, including structures, molecular weight from full scan mass spectra, substructural characteristics from MS/MS analyses, HPLC chromatographic behavior, and UV spectra from on-line diode array detection. Taxanes having proposed structures based on LC/MS/MS profiling are often later isolated or synthesized and their proposed structures confirmed by analysis using the same LC/MS/MS protocols. Samples analyzed for the database include taxol degradation studies, taxol bulk drug substance, semi-synthetic taxol, taxol from plant cell culture, taxol from various yew species, and taxol metabolism samples.

The information included in this structural database has been utilized for many aspects of drug discovery and pharmaceutical development on taxol. This methodology allows for the rapid and systematic elucidation of taxol impurities and analogs on-line without the need to scale up or isolate individual components. The added dimension of mass separation allows for the identification of chromatographically co-eluting components which are often found in mixtures containing taxanes.

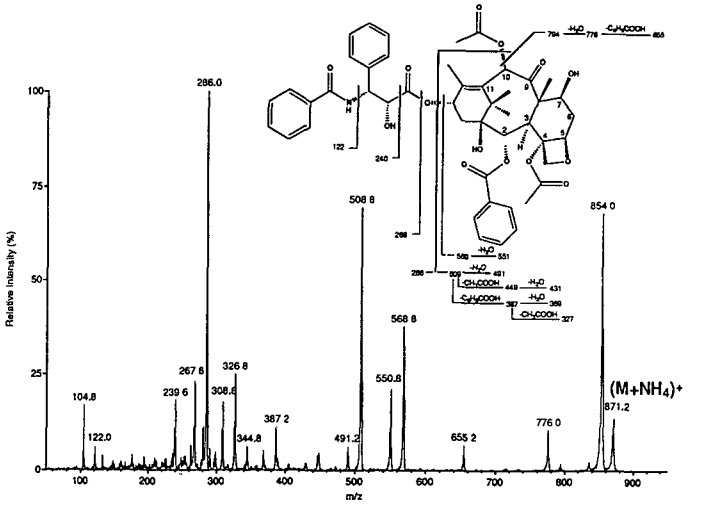

Figure 1. MS/MS substructural template of taxol.

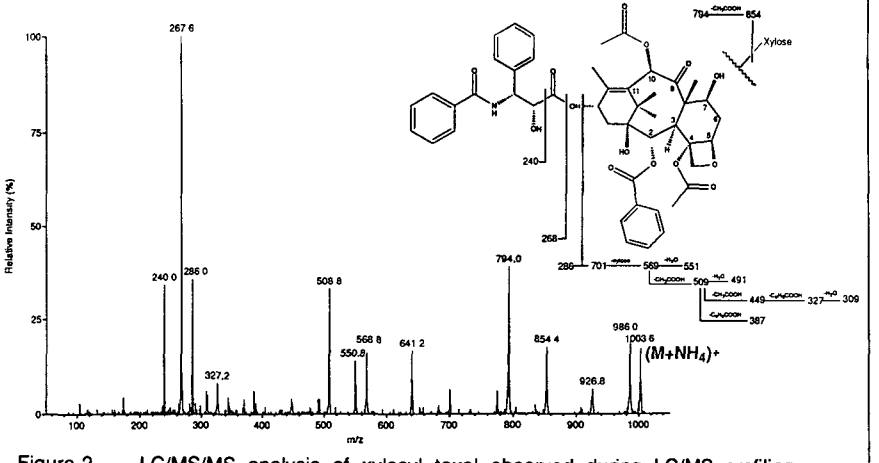

Figure 2. LC/MS/MS analysis of xylosyl taxol observed during LC/MS profiling. Proposed structure is based on comparison to the MS/MS substructural template of taxol.

Detection of Alkaloids by Positive Ion Thermospray LC/MS Using a Nonconventional Ion-Pairing Agent.

Mantai Z. Mesmer, Lorrie A. Lin, Rick A. Flurer and R. Duane Satzger, National Forensic Chemistry Center, United States Food and Drug Administration, 1141 Central Parkway, Cincinnati, OH 45202.

The Forensic Center is frequently called upon to analyze samples of material from incidents of consumer product tampering and counterfeiting. In such cases it is absolutely essential that the identity of adulterants or counterfeit products be unambiguously established when present. In addition adulteration or counterfeiting must be ruled out with certainty when a suspected tampering or counterfeiting has in fact not occurred. Because a false negative or a false positive could have costly consequences, there is no room for error. Therefore, mass spectrometric confirmation of identity is generally required.

Alkaloids are a group of nitrogenous bases that are derived from plants which have application as therapeutics and as rodenticides. Because many alkaloids are Class 6 or Class 5 poisons and are readily accessible to the public, they are potential candidates for misuse. The NFCC is frequently called upon to screen for alkaloids in foods and beverages in cases of suspected product tampering. At the Forensic Center we have been developing RP-HPLC screening methods for classes of compounds using UV-VIS and/or electrochemical detectors. The nature of our work requires that results obtained by these screening methods be confirmed by at least two techniques. The lack of volatility and thermal lability of some analytes preclude the use of GC/MS. Therefore liquid chromatography with mass spectrometry is generally the technique of choice for confirmation. Most of the liquid chromatographic conditions reported in the literature including the ones developed in this laboratory require the use of ion-pairing agents (typically sodium octanylsulfonate) and/or a phosphate buffer. Neither of these substances is suited for thermospray LC/MS. A number of reports in the literature suggest using fluorinated alkanoic acids instead of sodium alkylsulfonates as the ion-pairing agents (1,2) for LC/MS. We have used pentadecafluoro-octanoic acid as an ion-pairing agent for the separation of alkaloids and have obtained good chromatographic separation.

Mass spectra were acquired on a Hewlett-Packard 5989A mass spectrometer using a Hewlett-Packard thermospray probe and ion source. Mass spectrometric conditions: source temperature, 250^0 C; quadrupole temperature, 100^0 C; probe stem temperature, 105^0 C; mass range scanned, 140-360amu; discharge on.

The liquid chromatographic solvent delivery system consisted of a Hewlett-Packard 1090 liquid chromatograph. Separations were carried out on a Supelco Suplex PKB-100, 5 m, 250 mm x 4.6mm ID column. The mobile phase consisted of: (A) Aqueous: 0.1M ammonium acetate with 0.0003M pentadecafluorooctanoic acid and 2% acetic acid. The pH of the resulting solution is 4. (B) Methanolic: 0.1M ammonium acetate with 0.0003M pentadecafluorooctanoic acid and 0.05% formic acid.

The total ion chromatogram for a six alkaloid mixture (codeine, cocaine, yohimbine, strychnine, meperidine and pentazocine) separated using pentadecafluorooctanoic acid as the ion-pairing agent and acetate buffer is shown in Figure 1 (a); (eluent 90:10 A:B to 60:40 A:B at 20 minutes and 50:50 A:B at 30 minutes, flow rate 0.8ml/min). The mass spectrum obtained by averaging across the entire chromatogram is shown in Figure 1 (b).

The predominant ion in all cases is the $[M+H]^+$ ion, except for codeine where the $[M+NH_4]^+$ ion is also significant. Positive ion thermospray LC/MS is an effective technique for the determination of alkaloids and other basic substances. The use of fluorinated ion-pairing agents makes reverse phase HPLC easily adaptable to this class of compounds. Pentadecafluorooctanoic acid ion-pairing agent shows good selectivity for this class of compounds without any apparent adverse effects on the performance of the LC/MS interface.

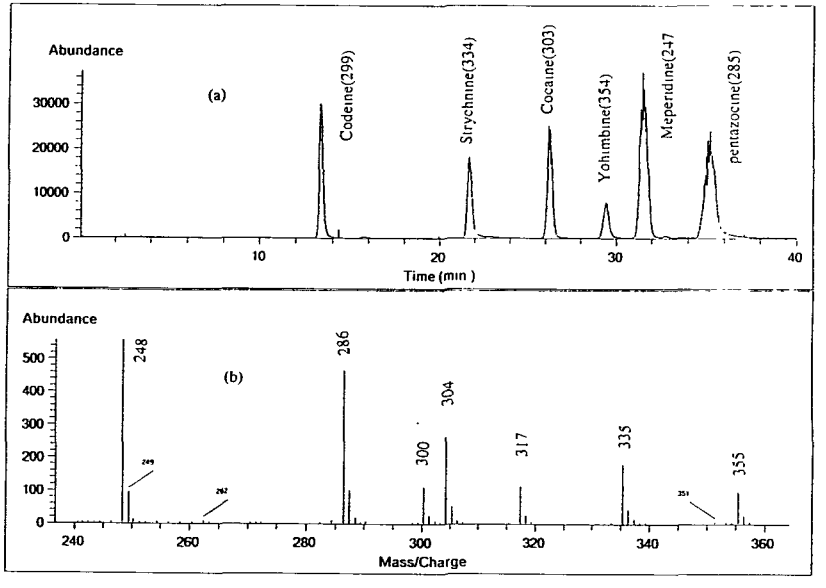

Figure 1. (a) TIC of six alkaloid mixture; (b) Corresponding spectrum.

1. McLuaghlin, L. G. and Henion, J. D.; *Journal of Chromatography*, 591, 195-206, 1992.
2. Alexander, S. B.; The 40th ASMS Conference On Mass Spectrometry and Allied Topics, Washington, D.C., May, 1992.

Coupling of Capillary HPLC with Continuous-Flow LSIMS for the Identification of Flavonoid Conjugates in Plant Extracts

L. W Sumner[1], N L Paiva[2], R A. Dixon[2] and P W Geno[3]

1 Oklahoma State University, Stillwater, OK 74078
2. Plant Biology Division, The Noble Foundation, Ardmore, OK 73402
3. Southwest Research, San Antonio, TX 74078-0047

Flavonoids encompass a wide range of polyphenolic secondary plant metabolites that are found in most plant systems These compounds serve a multitude of functions, and it is now known that the subclasses of flavonoids known as the isoflavonoids, chalcones, and pterocarpins demonstrate phytoalexic or antimicrobial properties These compounds are typically stored in plant cells as O or C-glycoside conjugates Upon infection of the cell, the conjugates are hydrolyzed to yield the free aglycones The newly released aglycones may be biologically active in their hydrolyzed form, or they may be immediately consumed in further syntheses that generate biologically active species Thus, identification of these conjugates will further enhance our understanding of these processes Furthermore, current research is now being conducted to identity these conjugates and to examine there location in the plant tissues, such as surface or subsurface to infected tissue This has resulted in the generation of smaller samples quantities that require new and more sensitive analysis methods

To provide a solution to the mass spectral analysis of flavonoid conjugates, we have developed an on-line capillary HPLC continuous-flow liquid secondary ion mass spectrometry (LC-CF-LSIMS) method The on-line capillary HPLC was interfaced with CF-LSIMS to accommodate the small quantities generated and to avoid the decomposition of flavonoid conjugates associated with HPLC fraction collection followed by mass spectral analysis

Capillary LC-CF-LSIMS was performed on cotyledon acetone extracts from

1 Chickpea (*Cicer arietinum*)
2 Soybean (*Glycine max*)
3 Peanut (*Arachis hypogaea*)
4 Clover (*Trifolium pratense*)
5. Alfalfa (*Medicago sativa*)

and the results from the chickpea experiment are presented A UV chromatogram of the chickpea extract is given below The extract was separated into ten components which were then successfully identified The identification of the components is summarized in the table of Identification of Peaks

Mass spectra of the ten components were obtained Spectrum III, IV, and VII are provided The resulting spectra identify the majority of the components as malonated glucoside conjugates of previously described aglycones found in chickpea The spectra of peaks V and VI have been tentatively identified as IGM and MeBGM respectively and will be further investigated

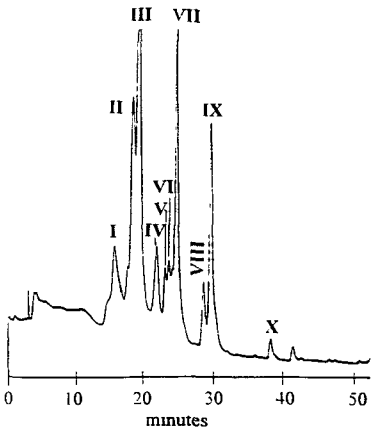

UV Chromatogram of Basic Chickpea Extract

Identification of Peaks

Peak #	Abbrv.	Name
I.	FG	7-O-glucoside formononetin
II.	PGM	7-O-glucoside-6'-malonyl pseudobaptiogenin
III.	FGM	7-O-glucoside-6'-malonyl Formononetin
IV.	MaGM	7-O-glucoside-6'-malonyl Maackiain
V.	IGM	7-O-glucoside-6'-malonyl trihydroxychalcone (isoliquiritigenin)
VI.	MeBGM	7-O-glucoside-6'-malonyl-5-methyl Biochanin A
VII.	BGM	7-O-glucoside-6'-malonyl Biochanin A
VIII.	Pseud	Pseudobaptiogenin
IX.	Form	Formononetin
X.	Bio A	Biochanin A
	MeBio A	5-methyl-Biochanin A

Spectrum III

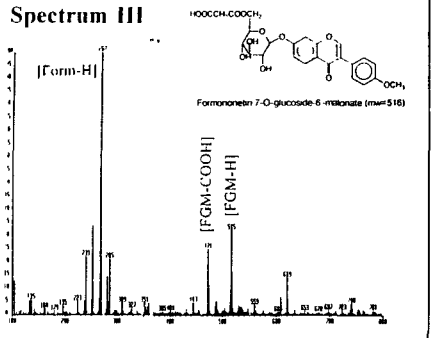

Spectrum IV

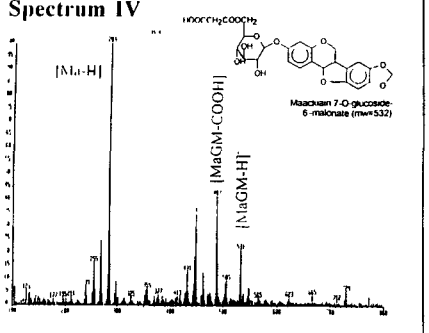

Spectrum VII

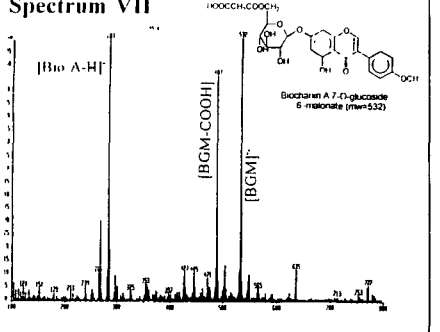

MASS SPECTROMETRY OF THREE NEW TOXINS PRODUCED BY *Alternaria alternata* f.sp. *lycopersici*

***Eloisa D. Caldas[1], A. Daniel Jones[2], Barney Ward[3], Carl K. Winter[1] and David G Gilchrist[3].**
1. Department of Food Science and Technology; 2. Facility for Advanced Instrumentation; 3. Department of Plant Pathology. University of California, Davis-CA, 95616.

The fungus *Alternaria alternata* f.sp. *lycopersici* causes the stem canker disease in tomato, and is a producer of phytotoxins (AAL toxins)[1]. Two toxins, referred to as TA and TB, were isolated in 1981 and shown to be tricarballylic acid esters of amino polyols[2]. The structural similarities of these toxins to the fumonisins, which are mycotoxins associated with animal and human disease[3], have stimulated concerns about their implications to human health.

Liquid culture of *A. alternata* (AS27-3) was grown for 25 days at room temperature. The toxins were extracted using XAD-2 and fractionated on a silica gel column. Final purification was achieved on a SAX (strong anion exchange) column.

Electrospray spectra were obtained in a VG Quattro-BQ (Fisons Instruments), in positive mode. 1% formic acid in 50:50 MeOH/H_2O was used as solvent. Positive FAB mass spectra were obtained using a VG ZAB-HS-2F mass spectrometer (VG Analytical) from a matrix of 3-nitrobenzyl alcohol. Daughter spectra were obtained using helium for collisional activation. For GC/MS method, hydrolyzed toxins were derivatized with BSTFA + 1%TMCS. Electron impact spectra were obtained in a Trio-2 quadrupole mass spectrometer (VG Masslab). The chromatographic conditions were: 15m DB-5, 0.25 mmI.D., 0.25µm film column; splitless injection at 280°C; temperature program - 100 to 220°C at 20°C/min, 220-300°C at 10°C/min.

Mass spectra of isolates obtained from culture filtrates of *A. alternata* revealed the presence of three new AAL toxins (TC, TD and TE). Positive ion Electrospray (Fig. 2) and FAB mass spectra showed $[M+H]^+$ ions at m/z 490, 548 and 532, respectively. Daugther spectra (Fig. 3) obtained for the protonated molecules each yielded abundant daughters at $[M+H-176]^+$, corresponding to a loss of the tricarballylic acid group. The presence of a succession of fragments at $[M+H-176-nH_2O]^+$ is an evidence of the number (n) of hydroxyl groups in the molecule. TD and TE showed in the daughter spectra peaks at m/z 294 and 296 $[M+176-nH_2O-42]^+$, respectively, indicating the presence of N-acetyl group. The final structures were confirmed by 2D ^{1}HNMR and ^{13}CNMR. As is the case of TA and TB, TC, TD an TE are mixtures of two structural isomers of tricarballylic acid esters at either C_{13} or C_{14} of the amino polyol backbone.

Electron ionization spectra of trimethylsilyl derivatives of AAL toxins showed a common peak at m/z 159 and a peak at $[M-159]^+$, which is characteristic of each toxin (Fig. 4 and 5). The use of the 159 peak can be used for trace detection of all of these toxins in foodstuffs using selected ion monitoring (SIM). Electrospray ionization mass spectrometry is a sensitive method that could be used for rapid screening of the presence of AAL toxins in liquid cultures and foodstuffs without the necessity of any derivatization.

REFERENCES

1. Gilchrist, D. G., Grogan, R. G. Production and nature of a host-specific toxin from *Alternaria alternara* f.sp. *lycopersici*, *Phytopathology* **1976**, 66, 880-886.
2. Bottini, A. T, Gilchrist, D. G. Phytotoxins. I. A 1-aminodimethylheptadecapentol from *Alternaria alternata* f.sp. *lycopersici*. *Tetrahedron Letters* **1981**, 22, 2719-2722.
3. Marasas, W. F. O., Jaskiewicz, K., Venter, F. S., van Schalkwyk, D. J. *Fusarium moniliforme* contamination of maize in esophageal cancer areas in Transkei. *S. Afr. Med. J.* **1988**, 74, 110-114.

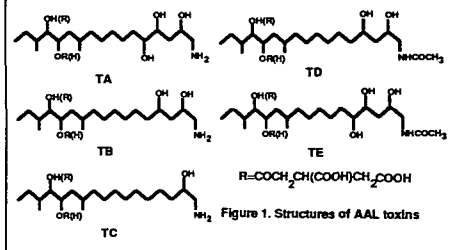

Figure 1. Structures of AAL toxins

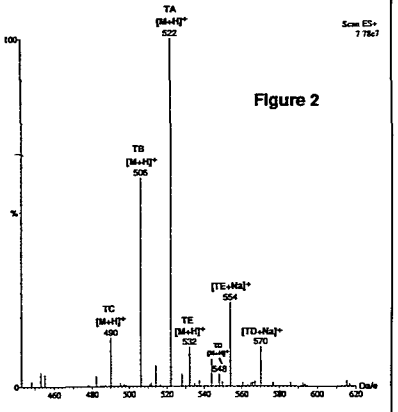

Figure 2

Figure 3. Daughter spectra of TD, TC and TE

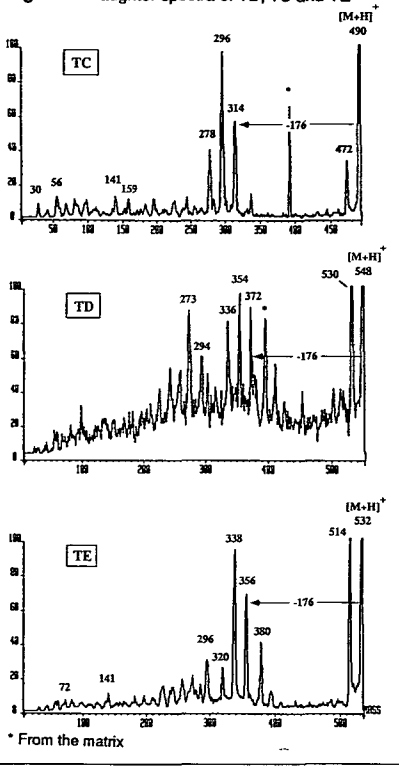

* From the matrix

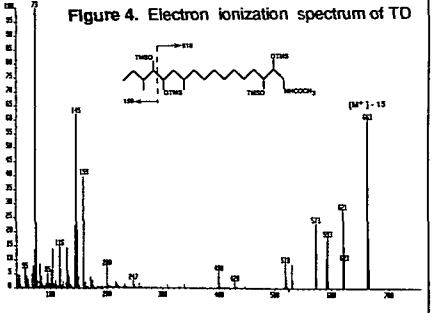

Figure 4. Electron ionization spectrum of TD

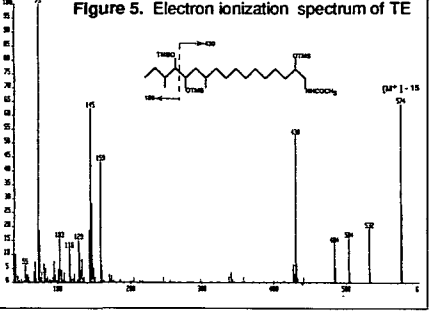

Figure 5. Electron ionization spectrum of TE

Supercritical Fluid Extraction and LC/MS of Thiosulfinates Found in *Allium* Species, *Jean E. Matusik, E.M. Calvey, E. Block & J. Sphon, Food & Drug Admin., Washington, DC 20204.

Characteristic flavors of fresh garlic (*Allium satinum*), onion (*Allium cepa*) and other allium spp. are associated with thiosulfinates, RS(O)SR, and related compounds, formed enzymatically from odorless amino acid precursors when the plants are cut or crushed. Allicin (2-propene-1-sulfinothioic acid-S-propenyl ester), derived from the non-volatile alliim ((+)-S-allyl-L-cysteine-S-oxide), is the major thiosulfinate metabolite found in crushed garlic. Thiosulfinates are further decomposed by heat to form sulfides.

Supercritical fluid extraction(SFE) was used to obtain garlic or onion thiosulfinate containing extracts. A method for the extraction, separation and characterization using SFE, HPLC, TSP\MS and MS\MS techniques is reported here. Various thiosulfinate components in garlic or onion were studied.

The HPLC\TSP\MS of the garlic extract is shown in figure 2. The components at RT 7.2 and 9.3 mins. give essentially the same TSP\MS spectra, i.e., m/z 163. To characterize these compounds HPLC\TSP\MS\MS was performed. The product ion analysis of the ions at m/z 163 from the garlic extract was compared to synthesized standards. Product ion analysis for m/z 137 was also performed. Allicin, ALLSS(O)Propenyl(E) and ALLS(O)SPropenyl(Z,E) were identified and characterized based on the MS\MS mass spectra and chromatographic RT and their comparison to standards.

The HPLC\TSP\MS of the onion SFE is shown in figure 5. The peak at the RT of 7.0 mins. shows a spectra with ions at m/z 163 and m/z 180. The product ion analysis of the m/z 163 reveals that this component is not allicin. Onion is not known to contain allicin. The peaks at RT of 12.5 mins and 13.3 mins are geometric isomers and their spectra exhibit ions at m/z 165. The first compound to elute is the n-Pr-S(O)SCH=CHMe(E) and the second is n-PrSS(O)CH=CHMe(Z,E). The MS/MS spectra of each of these isomers in the onion extract were compared to the spectra from authentic standards for confirmation.

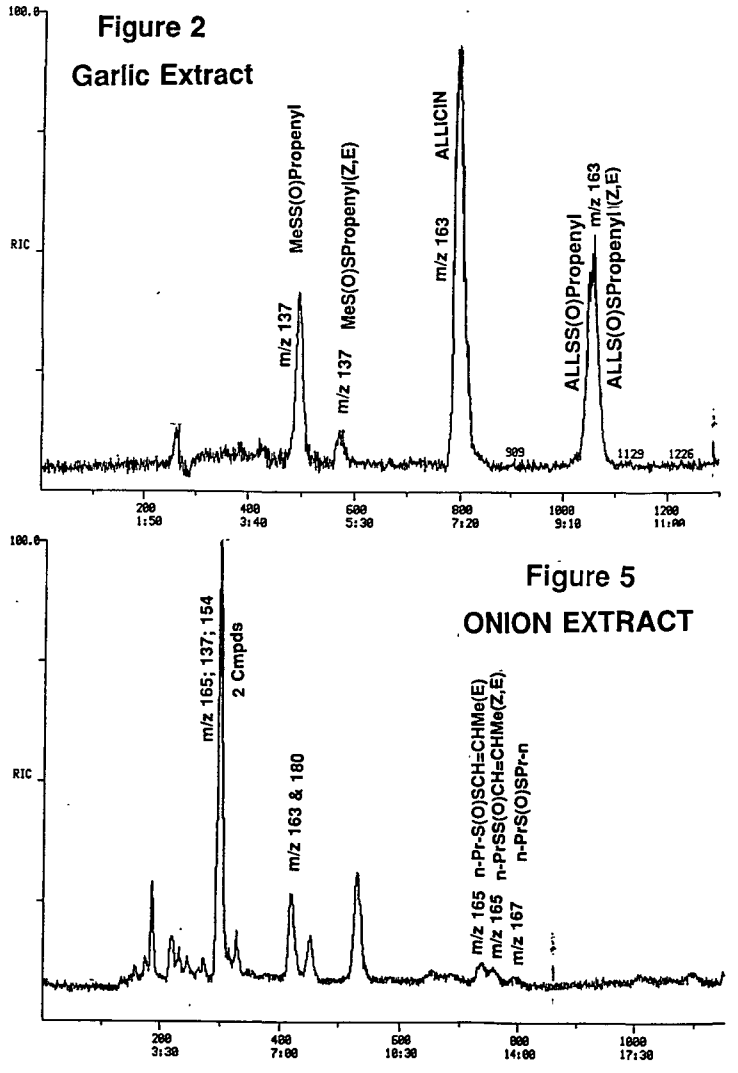

LC/MS Identification and Characterization of Components Isolated from Chaparral, ***Jean E. Matusik, Steven M. Musser, William R. Obermeyer, Jr. and James A. Sphon, FDA, CFSAN, Washington, DC 20204.**

Chaparral is an herbal preparation obtained from the leaves and twigs of the creosote bush (*Larrea tridentata*). This bush is an evergreen desert shrub. The leaves and twigs are ground and used in teas and formed into dietary supplement tablets and/or capsules. This herbal nutritional product has been recommended in non-scientific publications as an antioxidant, a free radical scavenger, as a blood purifier, to retard aging and to treat skin conditions (acne). Also, American Indians use chaparral tea as a medicine.

The U.S.F.D.A. became interested in chaparral products and their respective components because of two patients reported toxic effects. Both patients had taken chaparral tablets and developed hepatotoxic symptoms. After each ceased taking the tablets, their liver enzyme levels returned to normal. The diagnosis of toxin induced hepatitis is supported by the relation between hepatic disease and the patients use of chaparral and by the rapid improvements when they stopped ingesting the formulation.

Our interest has focused on the natural product identification of components in chaparral and toxicity studies to identify the causative agent or agents. A method was developed to separate and identify some of the natural products present. The method and our findings are reported herein.

The HPLC method uses a Ultrasphere C18 column and a gradient run. The gradient was 25% B hold 1 min, then program to 60% B in 50 mins and hold 5 mins. A was 90/10 H_2O/ACN; B was 10/90 H_2O/ACN. For the TSP/MS ammonium acetate was added post UV & prior to MS. MS was done on a Vestec 201 & MS/MS was done on Finnigan TSQ46. Methanolic extracts of chaparral were analyzed by UV & MS after HPLC separation. Our investigations centered on 2 areas, Nordihydroguaiaretic acid (NDGA) and flavonoids. Figure 1 shows the structure of NDGA. NDGA is a potent antioxidant. The retention time for NDGA is app. 28 mins. with its corresponding ion at m/z 303 and an ammonium adduct ion at m/z 320. Figure 2 is a compilation of the UV and MS analysis of a typical chaparral extract. NDGA was confirmed based on its comparison with authentic standard and MS/MS analysis. The TSP/MS of the peak directly after NDGA gives an ion at m/z 331 and was tentatively identified as dihydroguaiaretic acid (DHGA). Additionally the peak at 18 mins. gave an ion at m/z 299, representative of guaiaretic acid diquinone (GADQ). The peak at 21 mins. shows an ion at m/z 301 and is suggestive of guaiaretic monoquinone (GAMQ). The peak at 40 mins. with an ion at m/z 331 is consistent with

desmethyldihydroguaiaretic acid (DMGA) .

Ten authentic flavonoids standards were obtained and analyzed by the HPLC/UV & MS. The extract peak at the RT of 31 mins with an ion at m/z 285 corresponds to RT and MH+ ion for 4',5-dihydroxy-7-methoxyflavone standard.

Toxicity studies of various peak isolates are currently in progress. As this data becomes available we will focus on the respective peak identification and characterization using the various HPLC liquid interface techniques available in our laboratory.

Figure 1

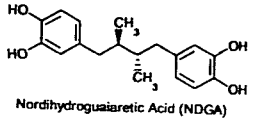

Nordihydroguaiaretic Acid (NDGA)

$C_{18}H_{22}O_4$ = 302.15181

Figure 2

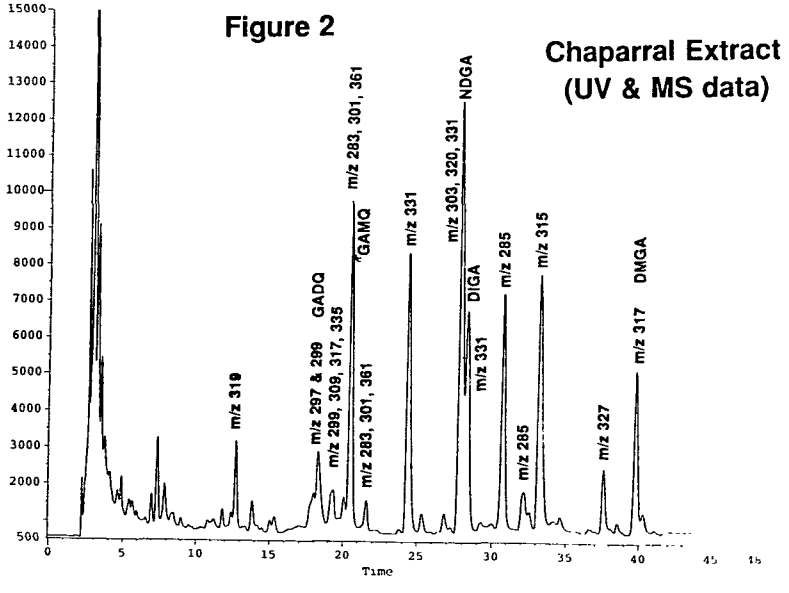

Separation and Identification of Didemnins and Ecteinascidins by On-line Microbore Liquid Chromatography / Continuous Flow Fast Atom Bombardment Mass Spectrometry

K. Janota and K.L. Rinehart,
School of Chemical Sciences, University of Illinois, Urbana, IL 61801.

Didemnins and ecteinascidins are marine natural products which exhibit potent anticancer and antiviral activities. Didemnins are cyclic depsipeptides which were isolated from the extract of the Caribbean tunicate *Trididemnum solidum*. The didemnins have a common ring structure and differ in the amino acid sequence of the side chain. The ring structure consists of commonly encountered amino acids with the exception of two novel subunits: hydroxyisovalerylpropionate (Hip) and isostatine (Sta) (1). Didemnin B, the most potent didemnin, shows strong activity against both L1210 leukemia cells and Herpes simplex virus types 1 and 2 (2). Didemnin B is the first marine natural product introduced as an antitumor agent into Phase II clinical trials.

Ecteinascidins are a group of nitrogen-containing heterocycles which were isolated from an extract of the Caribbean tunicate *Ecteinascidia turbinata*. These alkaloids contain di- and trimeric tetrahydroisoquinoline units and are related to the group of saframycin and safracin antitumor antibiotics. Recently, ecteinascidin 729, which exhibited antitumor activity higher than didemnins and other ecteinascidins against P388 murine leukemia and B16 melanoma (3), has entered pre-clinical evaluation.

Both didemnin B and ecteinascidin 729 are present in mixtures of compounds related to them. Therefore, the development of chromatographic conditions needed for their separation and a method for assessment of their identity and purity on the nanogram scale are necessary. Analysis on such a scale may also be helpful in determining whether or not these compounds are present in the early stages of purification. To achieve these goals, we employed on-line microbore liquid chromatography/coaxial continuous flow fast atom bombardment mass spectrometry.

The analysis of an unknown mixture of didemnins on a 50-ng scale resulted in compounds eluting at 3.2, 4.8 and 8.0 min (Figure 1). The last two components were identified from their molecular ions $(M+H)^+$ at *m/z* 943 and *m/z* 1112 as didemnins A and B, respectively (Figure 2). It is thought that didemnin B was retained longer on the column due to the more hydrophobic character of the additional lactylproline side chain. The third component of the mixture produced a molecular ion at *m/z* 805 (Figure 2).

High resolution measurement of the ion at *m/z* 805 indicated a molecular composition $(M+H)^+$ of $C_{41}H_{69}N_6O_{10}$, which corresponds to hydrolyzed didemnin A lacking a Hip unit. The fragmentation pattern of the ion at *m/z* 805 was obtained by MS/MS. This analysis partially confirmed the amino acid sequence based on the presence of Y" fragments due to the loss of leucine at *m/z* 692, proline at *m/z* 595, and dimethyltyrosine at *m/z* 402. The bioassay against L1210 leukemia cells showed that the linear peptide, acyclo-desHip-didemnin A, is inactive. The bioactivity reported in the short abstract for this meeting was due to contamination with didemnin A, not detected by LC/UV or regular probe FABMS but subsequently identified using LC/CFFABMS. The discovery of the linear peptide, acyclo-desHip-didemin A, related to didemnins yet lacking biological activities characteristic for didemnins, confirms that the Hip unit is necessary for the biological activity.

In the analysis of ecteinascidins, the presence of the ammonium acetate required to obtain partial separation between ecteinascidins 701 and 729 (Figure 3) resulted in formation of a series of adduct ions $(glycerol+NH_4OAc+MeOH+H)^+$ and $(glycerol+NH_4OAc+H_2O+H)^+$. Despite this background interference, most of the components of the ecteinascidin mixtures were identified on a 100-ng scale as ecteinascidins 701, 729, 743, 745 and 736. In comparison to LC/MS using a moving belt interface previously employed by this group (4), LC/CFFABMS yielded mass spectra with a similar fragmentation pattern such as the presence of the base peak at *m/z* 204, and other low molecular weight fragment ions at *m/z* 218 and 234. The fragment ions, including the base peak,

were observed only after the glycerol peaks were subtracted. The bioassay results were consistent with our study that the most active fraction was the one containing ecteinascidin 729.

On-line microbore LC/CFFABMS provided valuable data which were not available by other methods. Separation and identification of closely related components of didemnin and ecteinascidin mixtures, assessment of purity of individual fractions and structural information were obtained using nanogram quantities.

Acknowledgment:

This work was supported by a research grant from the National Institute of General Medical Sciences (GM27029). We are grateful to Dr. R. Milberg for his helpful suggestions and support, Mr. F. Sun for his technical assistance, Dr. R. Sakai for the didemnin and ecteinascidin samples, and Dr. G.R. Wilson for the bioassay data.

References:

1. Rinehart, K.L.; Kishore, V.; Nagarajan, S.; Lake, R.J.; Gloer, J.B.; Bozich, F.A.; Li, K.-M.; Maleczka, R.E.; Todsen, W.L.; Munro, M.H.G.; Sullins, D.W.; Sakai, R., *J. Am. Chem. Soc.* **1987**, 109, 4846-4848.
2. Rinehart, K.L.; Gloer, J.B.; Hughes, Jr., R.G.; Renis, H.E.; McGovern, J.P.; Swynenberg, E. B.; Stringfellow, D.A.; Kuentzel, S.L., Li, H.L., *Science*, **1981**, 212, 933-935.
3. Rinehart, K.L.; Holt, T.G.; Fregeau, N.L.; Stroh, J.G.; Keifer, P.A.; Sun, F.; Li, L.H.; Martin, D.G. *J. Org. Chem.* **1990**, 55, 4512-4515.
4. Holt, T.G., Ph.D. Thesis, University of Illinois, **1986**.

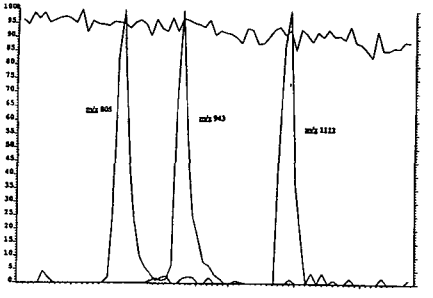

Figure 1. LC/CFFABMS analysis of the didemnin mixture. Selected ion chromatograms correspond to the linear peptide (*m/z* 805), didemnin A (*m/z* 943) and didemnin B (*m/z* 1112) (3:1 MeOH:H2O, 0.1% TFA).

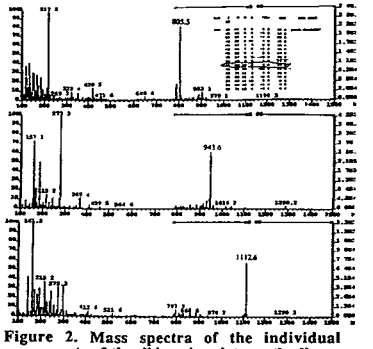

Figure 2. Mass spectra of the individual components of the didemnin mixture: the linear peptide (*m/z* 805) top, didemnin A (*m/z* 943) middle and didemnin B (*m/z* 1112) bottom.

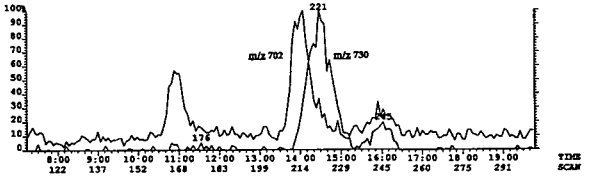

Figure 3. LC/CFFABMS analysis of the ecteinascidin mixture. Selected ion chromatograms of ecteinascidins 701 and 729.

Identification of *S*-linked Conjugates of 2-Chloroethyl Isocyanate as Metabolites of *N,N'-bis*(2-Chloroethyl)-*N*-nitrosourea (BCNU) in the Rat by Ionspray LC-MS/MS.

M.R. Davis, K. Kassahun, C.M. Jochheim, K.M. Brandt and T.A. Baillie.
Department of Medicinal Chemistry, University of Washington, Seattle, WA 98195

The antitumor agent BCNU is known to be unstable in aqueous solution, and to degrade spontaneously to reactive alkylating and carbamoylating intermediates.[1] Whereas the alkylating component is believed to be responsible for the antitumor effects of this drug, it has been speculated that the carbamoylating species 2-chloroethyl isocyanate (CEIC) may mediate some of the serious adverse effects of BCNU therapy.[2] BCNU is known to cause isocyanate-mediated depletion of cellular stores of GSH through mechanism-based inhibition of glutathione reductase.[3] Since GSH plays a key role in the cell's defense against locally-generated reactive oxygen species, it is possible that CEIC-mediated inhibition of glutathione reductase may cause acute lung injury and, ultimately, lead to the development of the pulmonary fibrosis that has been observed in some patients undergoing BCNU therapy.[4]

In a recent study, we found that rats dosed ip with methyl isocyanate excreted the corresponding GSH adduct in bile[5] and the corresponding *N*-acetylcysteine (NAC) conjugate in urine.[6] Interestingly, these *S*-linked conjugates were shown to be formed in a reaction which is chemically reversible at physiological pH. This may explain why the adducts themselves are cytotoxic and act as carbamoylating agents *in vitro*.[7] In light of their reversible formation, it has been speculated that *S*-linked conjugates of isocyanates formed biologically may act as "carriers" of their respective isocyanates.[8]

In order to determine whether CEIC is released from BCNU *in vivo*, rats were administered an i.p. injection of the drug and a targeted search was made by ionspray LC-MS/MS techniques for the GSH conjugate of CEIC in bile and the corresponding *N*-acetylcysteine (NAC) adduct in urine. Following the successful detection of the predicted *S*-linked conjugates in bile and urine, studies were performed to quantify these conjugates in the excreta of BCNU-treated rats. To test the hypothesis that *S*-linked conjugates of CEIC are formed reversibly and may act as "carriers" of CEIC, these conjugates and the parent drug were tested for their ability to inhibit glutathione reductase *in vitro*.

Experimental:

Bile from rats given an i.p. dose of BCNU was collected over ascorbic acid for 4 h after dosing while urine was collected for 24 h after dosing. Samples of bile and urine were analyzed by ionspray tandem mass spectrometry utilizing on-line HPLC (qualitative analysis) or flow-injection (quantitative analysis) for sample introduction. Mass spectrometry and combined liquid chromatography-tandem mass spectrometry (LC-MS/MS) were carried out using a Perkin Elmer-Sciex API III triple quadrupole instrument equipped with an atmospheric pressure ionization source and an Ionspray™ interface. Tandem mass spectrometry was based on collision-induced dissociation of ions entering the rf-only quadrupole region, where argon was used as the target gas.

Product ion spectra of parent ions of synthetic compounds were obtained by directly infusing 10 μg ml^{-1} solutions of the analytes (in methanol / 1% formic acid [1:1, v/v]) into the instrument at a flow rate of 5 μl min^{-1}. Qualitative analysis of biological specimens was performed by LC-MS/MS. 50 μl samples of bile or urine were injected onto a narrow-bore C_{18} HPLC column (150 mm X 2.0 mm i.d.), the effluent from which was split such that 75% of the flow entered a UV detector and 25% was diverted to the mass spectrometer. The mobile phase, delivered at a constant flow rate of 200 μl min^{-1}, consisted of 100% solvent A (0.06% aqueous TFA) for 5 min after injection, followed by a linear increase to 40% solvent B (0.06% TFA in acetonitrile) in 40 min. MS/MS analyses were carried out utilizing constant neutral loss scanning of 129 daltons (derived from the glutamyl moiety of GSH) for the detection of GSH conjugates in bile and parent ion scanning of *m/z* 164 (protonated NAC) for the detection of NAC conjugates in urine. Calibration curves for the quantitative determination of conjugates in bile and urine were generated by selected reaction monitoring analysis of samples of bile or urine from untreated rats to which was added the corresponding synthetic material and the conjugate of benzylisocyanate as internal standard.

Inhibition of glutathione reductase by the *S*-linked conjugates of CEIC *in vitro* was measured in isolated rat hepatocytes. Test compounds (0.1 mM) were incubated with cell extracts and GSSG (50 mM). The reductase reaction was initiated by the addition of NADPH (0.2 mM) and the rate of consumption of this cofactor was measured spectrophotometrically at 340 nm.

Results:

Ionspray LC-MS/MS provided a rapid method for the detection of the GSH and NAC conjugates of BCNU *in vivo*. By the use of ionspray MS/MS, it was found that 3.90 ± 0.64% of the dose of BCNU was excreted as the GSH conjugate of CEIC in bile (4 h post-dose) and 18.1 ± 3.3% was excreted as the NAC conjugate of CEIC in urine (24 h post-dose).

The GSH and NAC conjugates of CEIC were found to be equipotent to BCNU in their ability to inhibit glutathione reductase *in vitro*.

Supported by NIH grants ES05500 and RR05543.

References:

1. Brundrett, R.B. *et al., J. Med. Chem.* **19**, 958-961 (1976).
2. Gibson, N.W. *et al., Biochem. Pharmacol.* **31**, 2795-2800 (1982).
3. Babson, J.R. and Reed, D.J., *Biochem. Biophys. Res. Commun.* **83**, 754-762 (1978).
4. Reed, D.J., In *Oxidative Stress* (Sies, H., Ed.) pp 115-130, Academic Press, New York (1985).
5. Pearson, P.G. *et al., Biochem. Biophys. Res. Commun.* **166**, 245-250 (1990).
6. Lemoine, A. *et al., Xenobiotica* **21**, 775-791 (1991).
7. Pearson, P.G. *et al., Chem. Res. Toxicol.* **4**, 436-444 (1991).
8. Baillie, T.A. and Slatter, J.G., *Acc. Chem. Res.* **24**, 264-270 (1991).

THE UTILISATION OF MODERN LC/MS METHODS TO STUDY THE PHASE I AND PHASE II METABOLISM OF TRIMETAZIDINE IN HUMAN SUBJECTS

R.Brownsill[1], P.Jackson [1], A.Taylor [1] & B.Walther [1] J.Rontree [2], B.Bollen [2] & M.McDowall [2]
1. Servier Research & Development, Fulmer, England
2. Fisons Instruments ,VG Biotech, Manchester, England

INTRODUCTION The use of LC/MS as a method for studying the metabolism of drug compounds has increased rapidly in recent years due to the advent of electrospray ionisation(ESI). Electrosprays' ability to handle gradient solvent systems containing aqueous mobile phases and its wider dynamic range of compound response, is essential when investigating drug biotransformation products, particularly where very polar products are involved eg. conjugated metabolites Trimetazidine(TMZ) is a drug which is extensively used throughout the world for the treatment of ischaemic heart desease. Previous studies have used GC/MS to identify some of the major metabolites, however this technique was not suitable for conjugates unless samples were first hydrolysed and derivatised.
In this study we have investigated the potential of ESI LC/MS and LC/MS/MS to study the metabolism of Trimetazidine in human subjects to:- (i) evaluate the potential of Electrospray ionization with on-line LC/MS and LC/MS/MS for drug metabolism studies, (ii) quantitate TMZ and its metabolites in urine and (iii) study the effects of the biological matrix on metabolite identification and quantitation procedures.

EXPERIMENTAL Urine samples were obtained from subjects participating in a repeat dose pharmacokinetic study of a sustained release formulation of Trimetazidine (80mg). The urine samples were analysed directly, and following BondElut extraction and concentration, using gradient elution LC/MS and LC/MS/MS in the parent-ion scan mode then using the mutiple reaction monitoring (MRM) mode to both identify and quantitate TMZ and its metabolites.All MS analyses were performed using a VG QUATTRO system (Fisons Instruments, VG Biotech, Manchester, England). Quantitation was achieved by reference to a calibration curve produced by the addition of known amounts of Trimetazidine (1ng.ml $^{-1}$ to 20ug.ml $^{-1}$) and an internal standard (S3498) to urine. Quantitation of metabolites was based on their MS response factors relative to TMZ. The levels of TMZ were also quantitated using a validated method based on HPLC with fluorescence detection for comparison with the MRM analyses. Putative metabolites were synthesised and their MS and chromatograhic characteristics were compared with in-vivo metabolites.

RESULTS All the synthesised TMZ reference compounds showed good ESI responses generally within an order of magnitude of the parent drug (see Table 1).LC/MS permitted the detection of five expected metabolites of TMZ from the extracted biological matrix, but LC/MS/MS (parent-ion scan mode) enabled the identification of four new metabolites, including a sulphate and glucuronide conjugate which were detected without initial hydrolysis. The use of LC/MS/MS in the Multiple Reaction Monitoring mode resulted in the confident quantitation of seven of these relatively minor metabolic products (see Table 1,Figure 1),as well as the parent drug which gave results very comparable to those from a validated analytical method (see Table 2). Comparable qualitative and quantitative results were obtained using both extracted and unprocessed biological samples indicating minimal effects of the biological matrix on the ESI LC/MS response.

CONCLUSIONS The Electrospray LC/MS responses for Trimetazidine and its metabolites were generally very comparable. Furthermore, influence of the biological matrix was minimal making it a most usefull ionisation procedure for metabolism studies where compounds of varying polarity and concentration are present in complex biological matrices.

Although quantitative analysis of the metabolites by LC/MS was less conclusive due to the very low levels present within the biological matrix, using gradient elution LC/MS/MS in the MRM mode, definitive data was obtained for most of the metabolites, including two Phase II metabolites not previously identified.

The results clearly show that gradient elution Electrospray LC/MS and LC/MS/MS MRM has a great potential as a robust routine technique for the analysis of drug biotransformation products.

Table 1.

Compound	Retention Time (mins)	ESI Response	Unne Conc^{n} (ng ml^{-1})
TMZ	17.15	1	13054-41292
3 and 4 desmethyl TMZ	15 51	0 56	24 - 44
2 desmethyl TMZ	16.42	0.37	17 - 858
TMZ ketopiperazine	18.06	0.52	36 - 323
N-formyl TMZ	18.76	0.55	83 - 395
N-acetyl TMZ	18.94	1.12	24 - 54
Trimethoxybenzoic acid	4.45	0 07	n/d
Trimethoxyhippuric acid	15.79	0 27	n/d
Tnmethoxybenzaldehyde	20.58	0.22	n/d

Table 2

Sample	MS/MS method ug.ml^{-1}	HPLC method ug.ml^{-1}
02 GB	11.92	6.24
05 BP	19 45	19.77
08 SF	23.07	22.34
10 OS	14.85	14.40

Figure 1.

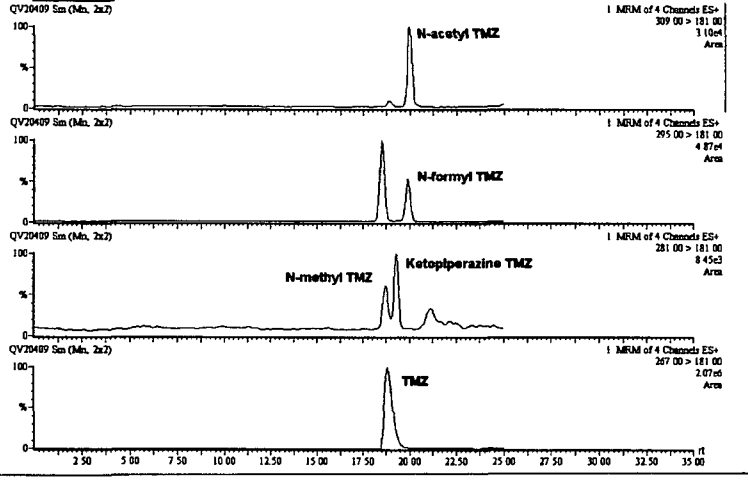

Development of a LC/MS/MS assay for FIAU

*Alan P. Breau[1], Patricia M. Dhahir[2] and Thomas Covey[3], [1]Allergan, 2525 Dupont Drive, Irvine, CA, 92715, [2]Lilly Research Laboratories, Eli Lilly and Company, Indianapolis IN, 46285 and [3]PE/Sciex, Thornhill, Ontario, Canada.

1-(2-Deoxy-fluoro-1-beta-D-arabinofuranosyl)-5-iodouracil (FIAU) (Figure 1), is a potent antiviral agent against herpesviruses and hepadnarviruses that is currently in clinical trials. An assay for plasma levels of FIAU and its metabolite FAU (Figure 2) using the heated nebulizer option and negative ion detection on a Sciex API III mass spectrometer was developed. One hundred microliters of reconstituted extracts were injected onto a 50 mm X 4.6 mm, 5 u particle, 120 A pore size Keystone Hypersil Phenyl-2 reverse phase HPLC column. The column was equipped with a 0.5 micron pre-column filter and a 5 u particle size, 10 mm X 4.0 mm Keystone Deltabond C8 guard column.

The isocratic separation, for the fast-high sensitivity FIAU method utilized a mobile phase of acetonitrile:0.1 % acetic acid (15:85) at a flow rate of 1 mL/min (Figure 3). The slower less sensitive method that separated FAU from serum interferences (Figure 4) was achieved by changing the mobile phase to acetonitrile:0.1 % acetic acid (5:95). The LC eluent was introduced into the Sciex API III APCI source with a quartz transfer line temperature of 500°C and a nebulizer nitrogen gas pressure of 90 psi. The negative charge de-protonated molecular ion at 371 daltons was mass filtered into the collision cell with a collision gas thickness of 671.1 x 200 x 10^{12} atoms/cm^2 of argon gas (Figure 5). Fragment ions at 42 daltons ($N{=}C{=}O^-$) and 127 daltons (I^-) were monitored for quantitation and verification of FIAU (Figure 5). The major metabolite, FAU, produced a negatively charged de-protonated molecular ion at 245 daltons which yielded a robust daughter ion at 42 amu ($N{=}C{=}O^-$) for quantitative purposes (Figure 6). Similarly, the internal standard reference produced a negatively charged de-protonated molecular ion at 277 daltons which yielded a robust daughter ion at 42 amu ($N{=}C{=}O^-$) for quantitative purposes.

A detection limit of 100 pg/mL serum and a quantitation limit of 250 pg/mL serum for FIAU was obtained using the slow non-optimal sensitivity assay option. This assay option was chosen in order to be able to quantitate the metabolite, FAU, simultaneously. The detection limit for FAU was approximately 250 pg/mL serum and the quantitation limit was 500 pg/mL serum using the combined FIAU/FAU procedure. If only FIAU quantitation is desired, a 40 pg/mL detection limit would be feasible.

The calibration of FIAU resulted in a standard curve that was linear from 250 pg to 10 ng/mL serum with a correlation coefficient of 0.999561. The calibration for FAU resulted in a standard curve that was linear from 500 pg to 10 ng/mL serum with a correlation coefficient of 0.999609.

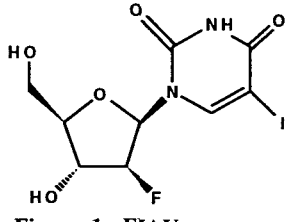

Figure 1- FIAU

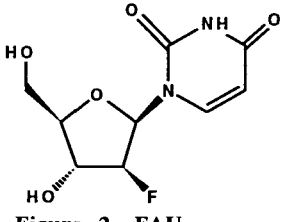

Figure 2- FAU

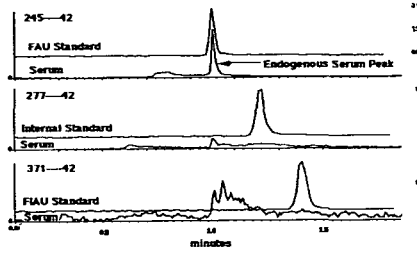

Figure 3

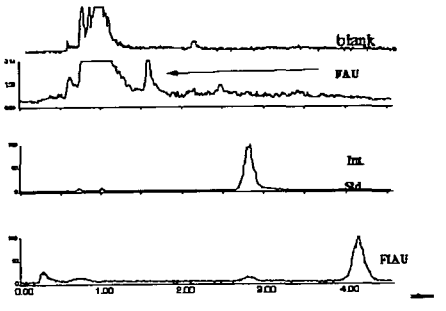

Figure 4

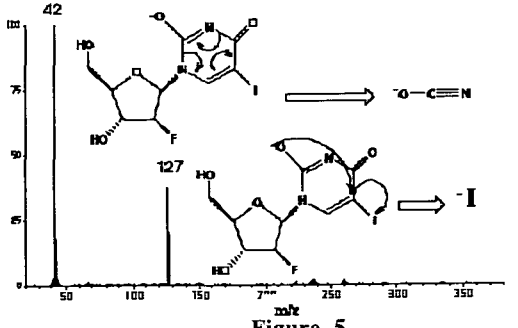

Figure 5

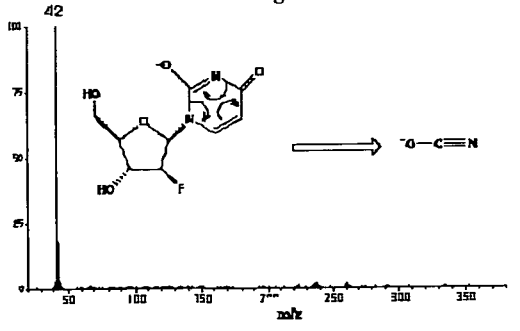

Figure 6

LC/PARTICLE BEAM/NCI MS ASSAY OF KYNURENIC ACID IN THE MEDIA OF CULTURED CELLS

D.B.Naritsin, R.L.Boni, K. Saito, and S.P. Markey,
Section on Analytical Biochemistry, NIMH, Bethesda, MD 20892.

Kynurenic acid (KYNA) is a metabolite of L-tryptophan (L-TRP) that in the central nervous system can act as a non-selective antagonist of excitatory amino acid receptors. In contrast, another L-TRP metabolite, quinolinic acid (QUIN) is an agonist of N-methyl-D-aspartate (NMDA) receptor. Our laboratory is studying the regulation of L-TRP metabolism in order to define the roles of QUIN and KYNA in pathogenesis or neuroprotection in a wide spectrum of immunologically mediated processes which activate the kynurenine pathway. We have previously reported the assay of L-TRP and L-kynurenine (L-KYN) using LC/particle beam/ NCI/MS, and have modified that assay to measure KYNA, which is several orders of magnitude less concentrated than its metabolic precursors. This assay has been applied to the quantification of KYNA isotopomers in the media of cultured cells fed [$^{13}C_6$]-L-TRP, to determine the metabolic activity of various types of human cells in response to cytokines, and the effects of two inhibitors of QUIN synthesis, 6-chloro-DL-tryptophan (6-Cl-TRP) and 4-chloro-3-hydroxyanthranilate (4-Cl-3HAA). In the course of these studies, we compared the relative merits of LC/particle beam/MS with GC/MS for KYNA quantification.

EXPERIMENTAL

Cells were grown with 50μM [$^{13}C_6$]-TRP, either with or without interferon-γ for 48 h [1]. [$^{18}O_2$]-KYNA (exchange labeled) was used as an internal standard, and added to each sample prior to analysis. Culture medium (150μL) was deproteinized, filtered and freeze dried. Pentafluoro-benzylation was effected with phase transfer catalysis as previously reported [2]. A Hewlett-Packard model HP1050 LC coupled to an HP5989 MS system through an HP59980B particle beam interface was used in these studies. GC/MS analyses were performed on the same mass spectrometer using the HP5890 gas chromatograph. The $(M\text{-}PFB)^-$ ions at m/z 368 (KYNA), 372 ([$^{18}O_2$]-KYNA), 374 ([$^{13}C_6$]-KYNA) and 402 (7-Cl-KYNA) were measured by NCI (methane) for quantification. The contribution of different KYNA isotopomers made necessary algebraic deconvolution of overlapped mass spectra, the most significant of which was the contribution at m/z 374 from [$^{18}O_3$]-KYNA. L-KYN was quantified as reported in [2], and QUIN as reported in [3].

RESULTS

The sensitivity of the LC/MS assay was 10pg of KYNA standard (injected) with a signal to noise ratio 10. Reverse phase chromatography using 0.4M ammonium acetate/ methanol/ acetonitrile (28/32/40) produces good separation of L-KYN and KYNA and retains desirable particle beam performance characteristics. The use of ammonium acetate improves significantly transfer through the particle beam interface and eliminates a mass transfer effect (nonlinear dependence between amount injected and absolute response). The absolute response was linear in the range 2pg-10ng KYNA injected (R>0.999).

An important advantage of particle beam LC/MS with respect to GC/MS is for the analysis of polar, thermally labile compounds that are not suitable for gas phase analysis. We had reported that the PFB derivative of L-KYN, which was difficult to analyze by GC, was readily analyzed by LC/MS [2]. The PFB derivative of KYNA is well suited for GC/MS, and we observed excellent chromatographic characteristics and a signal/noise ratio of 55 for the analysis of 4.3pg of diluted standard. Efforts to quantify KYNA in culture media did not give satisfactory results because of interfering unknown chemical background. The large quantity of extractive alkylation reagents limited the portion of the concentrated extract which could be injected into GC. One or more purification steps would be required for GC/MS analysis of KYNA after extractive alkylation. Thus, while GC/MS may exhibit lower limits of detection for pure analytical standards, LC/particle beam/MS analyses are advantageous for the measurement of chemically complex samples because the LC has a high capacity tolerance relative to GC. We have enhanced the capacity advantage of LC by installing a programmed valve that can divert the LC effluent to waste during periods when large quantities of reagents or chemical contaminants are eluting. The LC injection volume can be varied from 0.1 to 100 μL, so that a large proportion of the sample can be injected routinely. In GC/MS analytical procedures, we have generally limited the injection volume to 1-2μL, usually less than 1/5th of a biologically derived sample.

We studied the metabolism of [$^{13}C_6$]-TRP by a variety of human cultured cells lines derived either from central nervous system or peripheral organs. Although interferon-γ increases L-KYN formation in all cell types, only monocytes (THP-1) and liver cells (SKHep1) can convert L-KYN to QUIN [1]. None of the cells derived from central nervous system tissues or lung exhibited metabolic capacity to convert L-KYN to QUIN. In this study, we have quantified the QUIN antagonist, KYNA. All cells studied demonstrated increased synthesis of [$^{13}C_6$]-KYNA from [$^{13}C_6$]-TRP after immune activation.

We also investigated the action of two inhibitors, 6-Cl-TRP (0.5 mM) and 4-Cl-3HAA (1μM), on THP-1 cells. Our data indicate that 4-Cl-3HAA (a known metabolite of 6-Cl-TRP) is a more potent inhibitor of QUIN formation.

Our LC/NICI MS method was suitable for quantification of 6-Cl-TRP and its metabolites, 4-Cl-KYN and 7-Cl-KYNA, without significant modifications. Commercially available 7-Cl-KYNA was used to confirm metabolite identity and prepare standard dilutions. 4-Cl-KYN was identified as one of the major metabolites of 6-Cl-TRP.

REFERENCES

1. Saito, K., Chen, C.Y., Masana, M., Crowley, J.S., Markey, S.P., Heyes, M.P. *Biochem. J.* (1993) 291, 11-14.
2. Boni, R.L., Simpson, J.T., Saito, K., Markey, S.P. *The 40th ASMS Conference on Mass Spectrometry and Allied Topics* (1992), 1460-1461.
3. Heyes, M.P., Markey, S.P. *Anal. Biochem.* (1988) 174, 349-359.

Identification of rat liver microsomal metabolites of Atevirdine Mesylate by Particle Beam LC/MS. ***Phillip E. Sanders, Stephen M. Maio, Richard L. Voorman, Zhiyang Zhao, and J. James Vrbanac. Drug Metabolism Research, The Upjohn Company, Kalamazoo, MI 49001.**
Id

Atevirdine mesylate, (1-[3-ethylamino)-2-pyridinyl]-4-[(5-methoxy-1H-indol-2yl)carbonyl] piperazine, monomethane sulfonate is a bis heteroarylpiperazine inhibitor of HIV-1 reverse transcriptase, and is currently under clinical investigation as an anti-AIDS therapeutic agent. As a part of the pre clinical evaluation of atevirdine, metabolites were generated in incubations of rat liver microsomes and subjected to direct analyses by particle beam liquid chromatography mass spectrometry (PB/LC/MS). Ateverdine (50 uM) was incubated with rat liver microsomes (1 mg protein/ml) in 50 mM tris, pH 7.4, containing 0.1 mM EDTA in a final volume of 1 ml. Following 3 min pre-incubation at 37°C, the reaction was started by addition of an NADPH generating system and was stopped after 30 min by addition of 1mL acetonitrile. The mixture was vortexed, centrifuged, lyophilized, and reconstituted with 0.1 mL of mobile phase. PB/LC/MS was performed on a Finnigan 4500 equipped with a particle beam interface built at the Upjohn Company after the design of Extrel Corporation's (Pittsburgh, PA) Thermabeam© interface (design used by permission). Scan control and data acquisition was accomplished with a Teknivent Vector 2 data system (Teknivent, Maryland Heights, MO). Data was acquired in both electron ionization and chemical ionization (ammonia) modes.

The base peak in the electron ionization mass spectra of atevirdine and its metabolites was the result of cleavage of the piperazine moiety. Atevirdine and its desmethyl metabolite displayed this prominent ion at m/z 150. The desethyl metabolite displayed the analogous fragment at m/z 122. Molecular species were present for the parent drug and both metabolites. The chemical ionization (ammonia) spectra were comprized of the pseudo-molecular ion as the base peak and prominent fragment ions (m/z 207, 235) resulting from cleavage and charge retention from either side of the carbonyl group. The combination of electron ionization and chemical ionization spectra of the metabolites of atevirdine were sufficient to determine their structures.

Electrospray (ESI)/MS, and ESI/MS/MS were also performed on atevirdine to determine its potential usefulness as an analytical tool with this particular class of compounds. Data was acquired on a Finnigan TSQ-70 equipped with an ESI interface developed at the Upjohn Company. Results from the ESI experiments determined that no structural information was present in the simple ESI experiment. However either source induced daughter ions generated by having a DC offset voltage of approximately 150 V (drift tube to sampling orifice offset) or ESI/MS/MS produced the same qualitative spectra obtained from particle beam CI. The difference between PB/CI and ESI/MS is to be found in the relative ease with which informative spectra are generated, and the instrumentation necessary to generate the data. Generally, PB/MS (CI) spectra have been shown to be identical to ESI/MS (source daughters) and ESI/MS/MS (quad daughters). It has been our experience that the necessary offset required to produce ESI source induced daughters is very compound dependent, making screening of unknown samples difficult. Also, in order to obtain ESI/MS/MS data, proper parent ion selection and quad offsets must be determined for each compound in a given LC/MS analysis. PB/MS (CI or EI) will produce the same qualitative results with far less user intervention and without the need for MS/MS instrumentation. However, the relative sensitivity of particle beam is less than ESI and is useful only when nanogram quantities of analyte are anticipated.

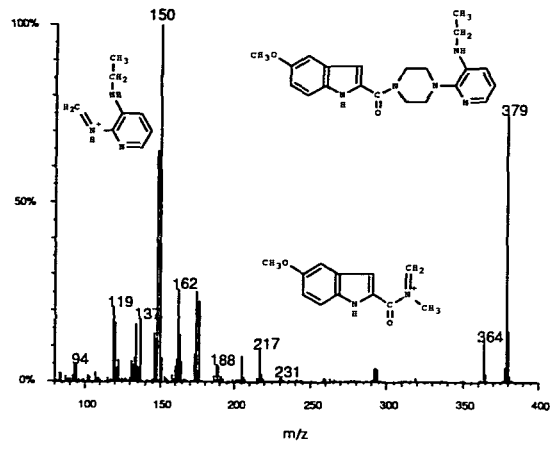

Electron Ionization Spectrum of Atevirdine Mesylate

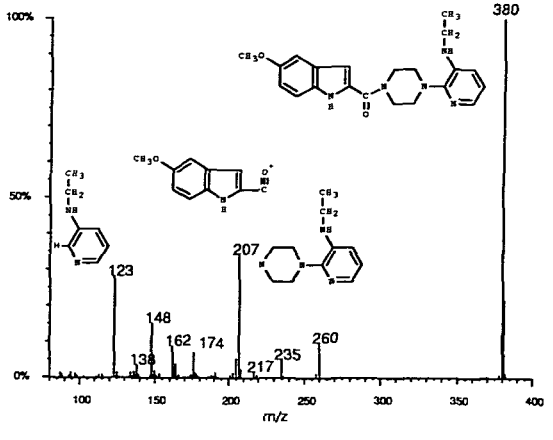

Chemical Ionization Mass Spectrum of Atevirdine Mesylate

Quantitation of Hydroxybenzoates in Biological Fluids as Indices of Hydroxyl Radical Production.

*Jane A. Montgomery, Line Ste-Marie and Julie Brunet, Nutrition Department, Université de Montréal, Notre-Dame Hospital Research Center, Montréal, Canada, H2L 4M1.

Free radical production is increasingly associated with human pathologies, especially those involving reperfusion injury following ischemia as is seen in heart attack, organ transplant or stroke. *In vivo*, hydroxyl radicals are produced from hydrogen peroxide in the presence of metal ions. To estimate hydroxyl radical production, we have developed a method using gas chromatography-ion trap mass spectrometry to quantitate hydroxylation products of benzoic and hydroxybenzoic acids. Analyses were performed on a Varian Saturn II under EI conditions. A DB-5 (30 m x 0.25 mm) column was temperature programmed at 110° for 2 min, 6°/min to 280° which was maintained for 6 min. Helium flow rate was 1 ml/min. The TBDMS derivatives of hydroxybenzoates were quantitated using deuterium labeled internal standards. Retention times and fragment ions are presented in Table 1. Standard curves prepared from extracts of aqueous solutions are linear in the range 0.1-10 μM, R = 0.98-0.999. The detection limit is < 1 pmol injected on-column which is an improvement on HPLC methods with reported limits of 10 pmol (1) and 125 pmol (2). We can simultaneously analyze 13 different hydroxylation products derived from benzoic acid, making the method suitable for screening hydroxyl radical formation. A Fe^{3+}/ascorbate hydroxyl radical generating system was used to evaluate and quantitate hydroxylation of benzoate and 4-hydroxybenzoate *in vitro*. Hydroxybenzoates (Table 2) in urine samples from volunteers were determined to establish normal values prior to assaying these compounds in urine from patients suffering from ischemic disease where hydroxyl radical production is expected to be elevated.

Table 1: Characteristic Ions and Retention Times for the TBDMS Derivatives of Hydroxylate Benzoic Acids.

Compound		MW	RT (min)	Ion (%Intensity)
Benzoate	I	236	9.4	**179**(100),**105**(18)
Catechol	XII	338	15.3	**281**(100),**323**(5.6)
Resorcinol	XIII	338	16.0	**281**(100),**338**(61)
Hydroquinone	XIV	338	16.5	**281**(100),**338**(96)
2-Hydroxybenzoate	II	366	18.23	**309**(100),**351**(6.6)
3-Hydroxybenzoate	III	366	19.31	**309**(100),**351**(3.9)
4-Hydroxybenzoate	IV	366	20.50	**309**(100),**265**(35)
2,6-Dihydroxybenzoate	V	496	25.02	**439**(100),**365**(6.7)
2,3-Dihydroxybenzoate	VIII	496	25.17	**439**(100),**254**(15)
2,5-Dihydroxybenzoate	VI	496	25.37	**439**(100)
2,4-Dihydroxybenzoate	VII	496	26.01	**439**(100),**340**(10)
3,5-Dihydroxybenzoate	IX	496	26.08	**439**(100),**339**(6.2)
3,4-Dihydroxybenzoate	X	496	27.47	**439**(100),**276**(7.3)
[2,3,5,6]-$^2H_4$]Hydroquinone	D4-XIV	342	16.48	**285**(100),**342**(98)
[2,3,5,6-$^2H_4$]-4-Hydroxybenzoate	D4-IV	500	20.47	**313**(100),**269**(22)

Table 2: Excretion Patterns of Hydroxylated Benzoic Acids in Urine Samples (n = 19) from Normal Volunteers.

Compound		Concentration nmol/mmol Cr (SE)	Concentration (BHT) nmol/mmol Cr (SE)
Catechol	XII	174 (38)	224 (54)
Hydroquinone	XIV	12 (1)	7 (1)
3-Hydroxybenzoate	III	69 (26)	100 (48)
4-Hydroxybenzoate	IV	*872 (133)	975 (172)
2,6-Dihydroxybenzoate	V	274 (79)	193 (59)
2,3-Dihydroxybenzoate	VIII	125 (20)	142 (40)
2,5-Dihydroxybenzoate	VI	694 (78)	813 (99)
3,5-Dihydroxybenzoate	IX	#541 (142)	728 (204)
3,4-Dihydroxybenzoate	X	154 (24)	160 (38)

Concentration (BHT), samples were collected into butylated hydroxytoluene
* upper limit of normal range, 16000 nmol/mmol Creatinine
\# upper limit of normal range, 1500 nmol/mmol Creatinine

References

1. G. Takemura *et al*, ***Circulation Res.***, **71**, 96-105 (1992).
2. S. Powell and D. Hall, ***Free Rad. Biol. Med.***, **10**, 439-441 (1990).

Quantitiative Determination of All-*trans* -Retinoic Acid in Rat Serum and Rabbit Plasma by GC/NCI-MS

* C. D'Arienzo, M. Jemal, D. Hawthorne, P. J. Gale and A. I. Cohen, Department of Metabolism and Pharmacokinetics, Bristol-Myers Squibb Pharmaceutical Research Institute, New Brunswick, N. J. 08903

Retinoic acid, a multiply substituted 9-carbon tetra-*ene* carboxylic acid, is known to be chemically unstable with respect to heat, air and full spectrum light. Its quantitative analysis requires conditions suited to the fragile nature of this compound. LC and LC/MS have been employed for such assays to minimize the possibility of isomerization and to provide resolution of the 13-*cis* and all -*trans* isomers of retinoic acid [1].

In this GC/NCI-MS method which utilized the HFIP ester of all-*trans* -retinoic acid (*tr*-RA), no chemical transformation resulting from the use of the GC was evident. The cis and trans isomers are chromatographically resolved, and *tr*-RA can be measured quantifiably at levels corresponding to injection of 1 pg with a S/N of ~ 40:1. With only 2% of the sample injected, this suggests a limit of quanitification (LLQ) of 25 pg/mL with 1 mL extracted.

However, the achievable LLQ in any assay will in part be determined by the volume available for extraction. If only 50 µL of each sample is available, as was the case for the rat study shown here, the LLQ will be raised by a minimum of a factor of 20 - suggesting an LLQ of 500 pg/mL.

For this assay, the LLQ is further limited by the existence of endogenous *tr* -RA. Because the size of the peak representing the endogenous material increases with the volume of matrix extracted, larger sample sizes afford no improvement in the concentration corresponding to LLQ. For the rat and rabbit studies discussed above, 1 ng/mL was the smallest concentration of *tr*-RA that could be distinguished from endogenous *tr*-RA, regardless of extracted volume.

The stable compound β-ionylidene acetic acid (β-IAA) was chosen to enhance accuracy and precision and troubleshoot the extraction and analysis.

All work was done in yellow light because of the light sensitive nature of *tr* -RA

Figure 1.

Structures and spectra for (a) β-IAA, the internal standard and (b) *tr*-RA

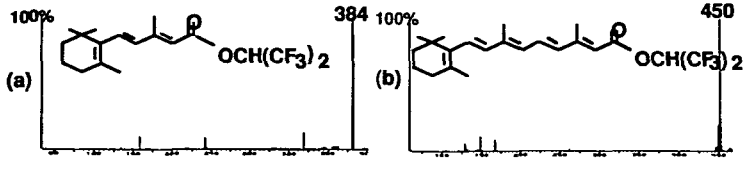

Figure 2.

Chromatograms showing two separate injections of 2 ng of (a) *tr*-RA and (b) 13-*cis* retinoic acid. No isomerization and complete resolution

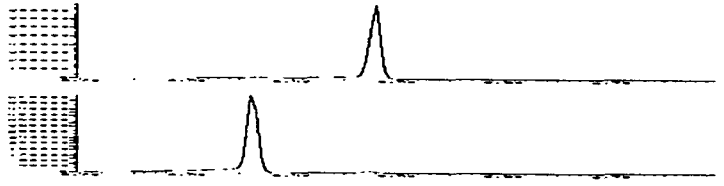

Figure 3.

Chromatogram showing 1 pg injected of the HFIP ester of *tr*-RA

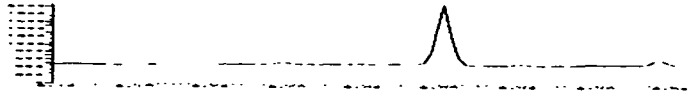

Figure 4.

Chromatograms of two samples extracted from rat serum exposed to full spectrum light. In blank matrix (a) some endogenous level is still seen. When 50 pg are added (b) the difference is still quantifiable

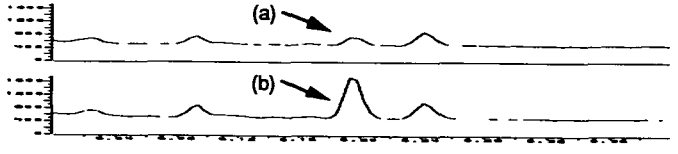

REFERENCES

1. Huselton C. A., Fayer B. E., Garland W. A., and Liberato D. J. *ACS Symposium Series* (1990) vol. 420, no. LC/MS. pp. 166-78

2. Heyes M. P., and Markey S. P. (1988) *Biomed. Environ. Mass Spec.* vol. 15, pp. 291-293

Quantitative Determination of Lanosterol and Dihydrolanosterol in Plasma, Serum and Tissues by GC-MS for Evaluation of Cholesterol Lowering Agents. **S. Murakami, K. Johansen, P. Haroldsen, and I. Massey. Syntex Discovery Research, Palo Alto, CA. 94304**

RS-21607-197 is a specific inhibitor of 14α-lanosterol demethylase, an enzyme in the biosynthetic pathway of cholesterol. Syntex is currently investigating the therapeutic utility of the compound to lower cholesterol. Lanosterol (LAN, structure 1) and dihydrolanosterol (DHL, structure 3) were selected as biological markers to monitor the effect of RS-21607-197 on the 14α-lanosterol demethylase activity. To support these studies, specific GC-MS methods have been developed for the quantitation of LAN and DHL in dog plasma, human serum, and hamster liver.

A brief description of the methods for the determination of LAN and DHL in dog plasma, human serum and hamster liver homogenate is as follows. LAN, DHL, and an added internal standard (D_3-DHL) are extracted from plasma, serum, or liver homogenate into chloroform / methanol. The organic extracts are evaporated to dryness and the residue is reconstituted with chloroform. Following adjustment of the polarity of the organic extract by the addition of hexane, the analytes are further purified using a silica gel mini-cartridge. The analytes are eluted with ethyl ether / hexane, the eluate is evaporated to dryness and the residue is treated with BSTFA-1% TMCS in toluene. A portion of the reaction mixture is injected into a Hewlett Packard 5971 MSD GC-MS operating in the electron ionization mode. Under the ionization conditions employed the trimethylsilyl derivatives of the analytes (structures 2 and 4) produces abundant molecular ions at m/z 498^+ (LAN, Figure 2), m/z 500^+ (DHL), and m/z 503^+ (D_3-DHL). Selected ion monitoring of the molecular ions provides specificity for the quantitation of LAN and DHL with a sensitivity of 0.050 mcg of LAN and DHL per ml of plasma, serum, or amount of tissue. Since there are endogenous levels of lanosterol in the biological media from untreated animals or subjects, calibration curves produced from the biological media would result in a positive offset at the zero level. By producing a calibration curve from buffer the problem of an offset can be eliminated. Since calibration curves produced from buffer have been determined to be parallel with those produced from biological media, calibration curves produced from buffer were used to quantitate LAN and DHL in samples. Linear calibration curves are obtained in the range of 0.050 - 2.00 mcg of LAN and DHL per ml of buffer. The linear range of the method is from 0.050 to 20.0 mcg of LAN and DHL per aliquot of plasma, serum, or liver homogenate using 0.1 to 1 ml of plasma or liver homogenate for analysis.

Quality control (QC) samples (two at each of three concentrations) were analyzed with each set of unknowns to monitor method performance. The inter-assay varibility (%CV) for the plasma and serum QC samples ranged from 4.2 - 7.8 for LAN and 2.3 - 5.9 for DHL. The % recovery of LAN and DHL (found / added) ranged from 93.2 - 104.7 for LAN and 98.6 - 101.9 for DHL. The inter-assay variability (%CV) for the tissue QC samples ranged from 2.0 - 30.6 for LAN and 1.1 - 26.8 for DHL. The % recovery of LAN and DHL (found / added) ranged from 90.8 - 103.7 for LAN and 86.5 -99.6 for DHL.

These methods have been applied to the analysis of samples obtained from dogs, humans, and hamsters following administration of RS-21607-197. Administration of RS-21607-197 to dogs and hamsters increases the concentration of LAN and DHL in plasma and liver up to two orders

of magnitude. The concentrations of LAN and DHL in the plasma of dogs after daily administration of RS-21607-197 for 1 month are proportional to the dose (Figure 3). Liver from hamsters treated with a single dose of ^{14}C-RS-21607-197, shows a postive correlation between the total tissue radioactivity and elevation of LAN and DHL.

In conclusion, specific methods to determine LAN and DHL in dog plasma, human serum and hamster liver homogenate have been developed to monitor the effect of RS-21607-197 on the 14α-lansterol demethylation step in the biosynthesis of cholesterol. These methods fulfill the analytical requirements necessary to support preclinical and clinical studies.

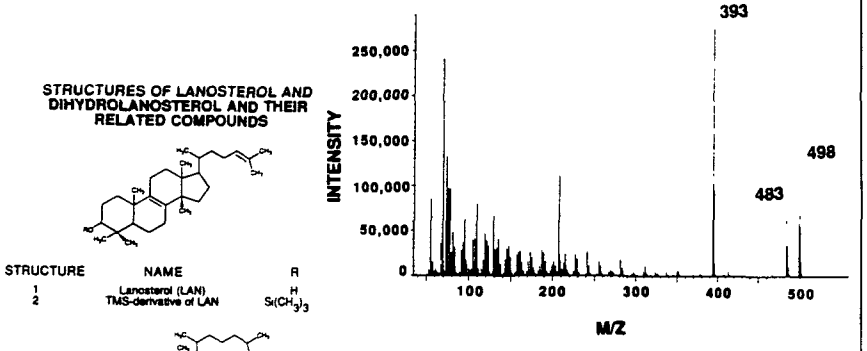

Figure 2. EI Mass Spectrum of the TMS-derivative of LAN (Structure 2).

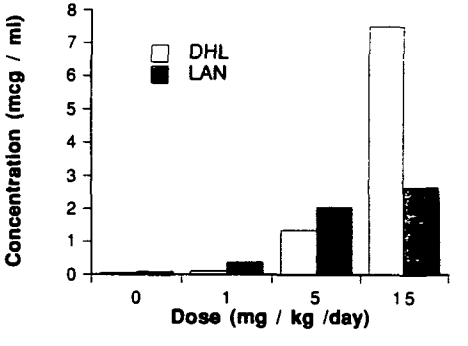

Figure 3. Concentrations of LAN and DHL in Plasma From Dogs Following Daily Administration of RS-21607-197 for 1 Month.

Quantitative Determination of Butorphanol in Human Plasma by GC/ECCI/MS

Daniel E. Mulvana
Bristol Myers Squibb, Pharmaceutical Research Institute
Syracuse, NY 13221

Butorphanol (Figure 1) is a synthetic opioid[1] indicated for the relief of moderate to severe pain. Due to the low transnasal doses administered (1 mg), a very sensitive assay was needed for the determination of complete plasma pharmacokinetic profiles. An assay method was developed which fulfilled this requirement by incorporating solid phase extraction, derivatization, and separation and detection by capillary gas chromatography-electron capture chemical ionization-mass spectrometry (GC/ECCI/MS).

Plasma samples (0.5 ml) containing butorphanol were diluted with 0.5 ml 10 mM ammonium acetate, pH 6.0. The internal standard (Figure 1) was added and the samples were transferred to Bond Elut® CN-N extraction columns. Following two washes with buffer and one wash with 70% acetonitrile in water, the compounds were eluted with 1% triethylamine in acetonitrile with an extraction recovery of 90%. After removal of the elution solvent under nitrogen, the compounds were derivatized by adding 0.1% pentafluorobenzoyl chloride in methylene chloride in the presence of pyridine, capping the tubes and heating the sample in a dry block at 40°C. The solvent was removed under nitrogen and the sample was reconstituted in 30 µl of toluene.

Separation and detection were accomplished using a Hewlett-Packard 5988A mass spectrometer interfaced to an HP 5890 Series II gas chromatograph. The processed samples (3 µl) were injected in the splitless mode onto a 15m DB-1 (0.25 mm ID, 0.25 µm film thickness) GC column at an injection port temperature of 285 °C. The initial oven temperature was 200 °C and was ramped at 25 °C/min to a final temperature of 310 °C for 2.1 min. The molecular ion was the base peak for both compounds (Figure 2). The compounds were detected by selected ion monitoring of ions 521.0 for derivatized butorphanol and 507.0 for the internal standard. The ion source temperature was 200°C and methane was used as the buffer gas at a pressure of 0.75-0.85 Torr.

The assay was linear over the desired concentration range of 20 -2000 pg/ml and all standard curves from the validation (n=7) had r^2 values of ≥ 0.994. The processed samples were stable at ambient temperature for at least 42 hours and butorphanol was stable in plasma when stored at -20 °C for at least 123 days. Analysis of replicates (n=5) of plasma quality control (QC) samples at concentrations of 170, 1100, and 1680 pg/ml over three separate days showed the assay to be precise and accurate. Intra- and inter-assay precisions (%RSD) were within 12% and the grand mean predicted concentrations for all QC samples deviated from the nominal by less then 3%. Intra-assay QC deviations were all within 10%.

The results show that the assay is sensitive, specific, precise, accurate, and reproducible and is expected to be suitable for accurate determination of butorphanol in human plasma.

1. Monkovic', I., Conway, T.T., Wong, H., Perron, Y.G, Pachter, I.J. and Belleau, B. J. Am. Chem. Soc., **95**, 7910 (1973).

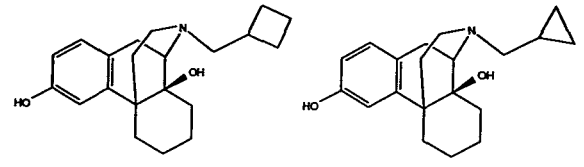

Figure 1

Butorphanol BC-2605

A.

B.

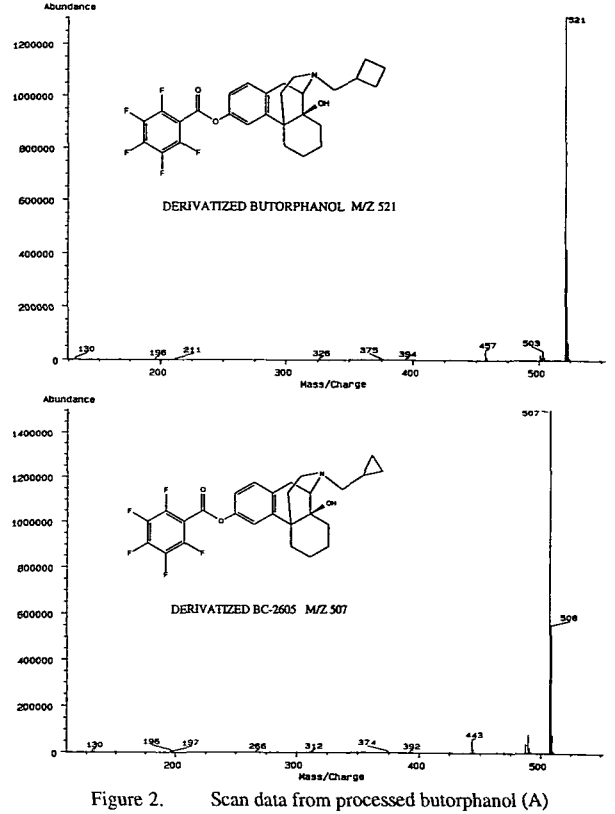

Figure 2. Scan data from processed butorphanol (A) and BC-2605 (B).

Quantitative determination of the antipsychotic agent CP-88,059 in human serum by HPLC/MS/MS.

Hassan G. Fouda, Kimberly Navetta, Elbridge Luther and Richard. P. Schneider
Central Research Division, Pfizer INC, Groton, CT 06340

CP-88,059 is a promising antipsychotic agent currently undergoing clinical evaluation. A specific analytical method for its quantitative determination in human serum was required to support human pharmacokinetic and pharmacodynamic studies. This presentation describes the assay which utilizes on-line HPLC and atmospheric pressure chemical ionization (HPLC-APCI) tandem mass spectrometry (MS / MS). A structural analog served as the internal standard for the assay. The drug and the internal standard are extracted from serum and following a simple clean-up, aliquots are injected onto a standard reverse phase HPLC column. The effluent from the HPLC column at 1ml/min is introduced into the atmospheric pressure source of a SCIEX API III mass spectrometer. The protonated molecular ion undergoes collision induced dissociation to a specific product ion. CP-88,059 concentrations in serum are determined by the selected monitoring of the product ion from the drug and the internal standard.

The assay concentration range extends from 0.5 ng/ml to 50 ng/ml, and its precision and accuracy over that range are 9% or better. It has thus far been utilized for the analysis of several thousand clinical samples.

Analysis of serum samples containing known amounts of CP-88,059: *intra*-assay parameters; 6 samples at each concentration.

fortified drug conc. (ng/ml)	*mean conc found (ng/ml)*	*% RSD*	*% mean accuracy*
0.5	0.51	6.5	102
0.75	0.73	8.8	98
1.0	1.0	5.9	100
2.5	2.4	3.0	95
5.0	5.2	6.4	103
7.5	7.3	4.7	97
10	9.7	2.3	97
15	15	2.7	101
20	20	4.0	102
30	31	2.9	103
40	39	1.9	98
50	49	1.0	99

Positive Ion CID Daughter Spectrum of m/z 413 from CP-88,059

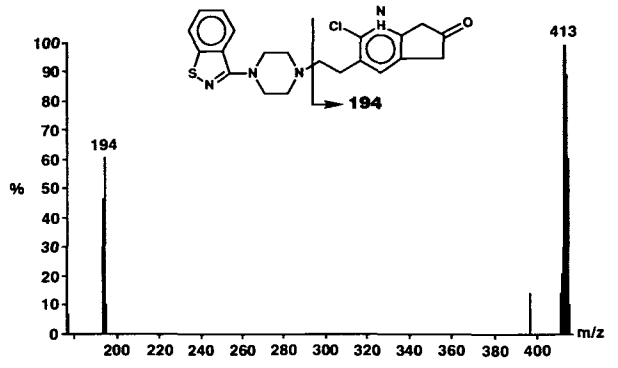

HPLC/API/MS/MS Chromatogram of Serum Extracts

Serum Fortified with the Internal Standard Only

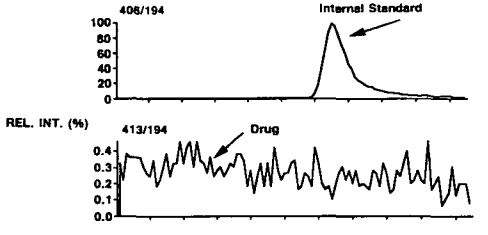

Serum Fortified with 0.5 ng/ml of CP-88,059

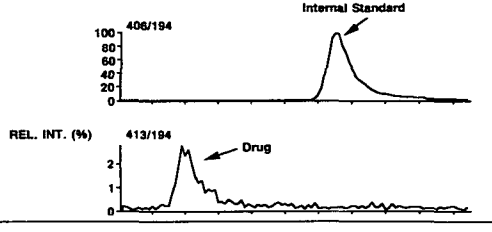

A NCI GC/MS Method for Olanzapine in Human Plasma

R.M. Goodwin, R.D. Barton , T.A. Gillespie
Lilly Laboratory for Clinical Research
Indianapolis, IN 46285

Introduction

Olanzapine is a new drug candidate targeted for the treatment of psychotic illnesses such as schizophrenia and schizophreniform disorder. This antipsychotic compound is an antagonist of dopamine action at D1 and D2 receptors. It also has serotonin antagonist activity at the 5HT2 receptor and thus has anticholinergic properties. This profile suggests that it may provide antipsychotic efficacy without extrapyramidal side effects. Olanzapine is presently being evaluated in Phase II clinical trials in the U.S., Europe, and Asia. A NCI capillary GC/MS method for quantitating Olanzapine in human plasma is described here. The structure of Olanzapine is shown in **Figure 1**.

Extraction & Derivitization

Careful sample preparation is critical for the success of the assay. After addition of 5 ng of an internal standard (I.S.), LY170222, Olanzapine and the I.S. are extracted from 1 ml aliquots of human plasma. To achieve a sufficiently "clean" preparation, the extraction requires several steps. The plasma is first acidified (<= pH 2.0) with 1 N HCL and washed with a 1:1 mixture of ethyl acetate and hexane containing 0.3% butanol. This removes a significant amount of lipids and other chromatographically interferring substances. The wash is discarded and the aqueous phase is alkalinized (>= pH 9.0) with 1 N NaOH. Olanzapine is partitioned into ethyl acetate and removed to a clean tube. The ethyl acetate is acidified with 2 ml of 0.1 N HCl. The ethyl acetate is discarded and the acidified aqueous fraction is alkalinized (pH >= 10) with 1N NaOH. This fraction is then extracted with methylene chloride and reduced to dryness using a Speed Vac. The resulting extracts are treated with heptafluorobutric acid anhydride (HFAA) to form the heptafluorobutyl (HFBA) derivatives of Olanzapine and LY170222 (I.S.). The derivatized materials are dissolved in 200 µl of methanol and separated via GC on a 15 meter DB-5 fused silica capillary column. Injection volume is 1 to 5 µl.

Experimental

Peaks eluting from the GC column are detected mass spectrometrically with a Finnigan 710 or a Finnigan 4500 single quadrupole MS operated in the methane chemical ionization mode (CI) with multiple ion detection of appropriately selected negative ions (MID). The ratio of an ion at m/z=470 (Olanzapine) to an ion at m/z= 484 (LY170222) is is used for quantitation. On the 4500, ions at m/z 370 (Olanzapine) and m/z=384 (I.S.) are used because they are more intense. Plasma concentrations of unknowns are calculated relative to a standard curve constructed from drug-free plasma samples spiked with Olanzapine (0 to 64 ng/ml in 9 steps). Response across the specified range is linear. The limit of detection is 0.1 ng/ml.

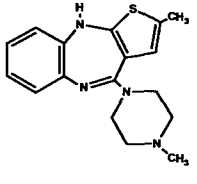

Figure 1

Analysis of Bile Acids and Sterols in Cecum and Colon Contents from the Sprague-Dawley Rat by GC/FID-MS

*M.P. Purdon, R. Takigiku, R.E. Schneider, L.O. Whiteley
Procter & Gamble Co., Miami Valley Laboratory
P.O. 398707, Cincinnati, OH 45239

INTRODUCTION

Bile acids have been implicated as potential indicators of colon cancer risk. They originate from cholesterol metabolism in the liver. There they are conjugated with taurine or glycine before they are secreted into the bile. Once in the intestine the bile acids can be deconjugated into the free acid form and then transformed into secondary bile acid structures by the gut microflora. A significant portion of the bile acids are reabsorbed but some are excreted in the feces. Most studies have been based on bile acid analysis of the excreted feces and not on the actual colon contents. Our study targeted transformation of primary bile acids to their secondary analogs in the cecum and colon of the rat.

Here we present the methodology used to extract, identify and quantify bile acids directly from colon contents.

EXPERIMENTAL

Lyophilized samples were extracted in methanol:chloroform. The extract was hydrolyzed and then saponified to convert all bile acid sulfates and conjugates to the free acid form. The bile acids and sterols were then separated by liquid-liquid extraction and the bile acid fraction cleaned up using reverse-phase, solid phase extraction.

The bile acid methyl esters were formed using diazomethane followed by silylation of the hydoxyl groups with HMDS/TMCS. The sterols were silylated before injection.

Both fractions were gas chromatographed on the same DB-1701 phase. Using a "X" press-tight connector (Restek), the column effluent was split between a flame ionization detector and HP 5971A mass spectrometer. The separation was performed isothermally to insure a consistent spit to both detectors throughout the entire run. Components were quantified on the FID while obtaining structural confirmation with the MSD.

RESULTS AND DISCUSSION

Current methods for bile acid & sterol analyses are complex and time consuming. They cover the range from exhaustive separation of all classes (free, sulfated, conjugated) to total bile acid content only. Our goal was to develop a simplified procedure to quantify total bile acids. Our approach was to chemically convert all species to their free acid analogs before isolation. The finished extracts are extremely clean and chromatography can be performed with minimal interference.

We were not able to obtain all standards that we needed for quantification by SIM. In particular the ω-muricholic is not available and the other muricholic epimers are often of questionable purity. FID can be used to accurately quantify these isomers because all give the same response as other trihydroxy-substituted acids. Nevertheless the complex matrix prompted us to use EI-MS to identify the components we were quantifying by FID.

To meet the above criteria we implemented a post-column splitter to go to both detectors. The splitter is made from a simple press-tight "X" (Restek) and deactivated fused silica tubing. In general the connecting line to the FID needs to be half the length and twice the diameter as the line inserted into the MSD. A flow regulator supplies He make-up gas to the splitter to force sample to the FID. Since the splitter is pressure dependent, the separation must be performed isothermally. Even using constant flow during a temperature programmed run does not provide a consistent split.

Chromatography of the Me/TMS derivatives has been done on non-polar columns simply because the columns are more stable. Typically Carbowax or QF-1 phases give slightly better separation but deteriorate quickly. We needed good separation of our components since we were not using SIM, and in addition, needed a column on which the separation could be done isothermally. A cyanopropyl-phenyl substituted phase (DB-1701) gives baseline resolution of all components of interest even under isothermal conditions. Shown at left is a FID trace of bile acids using the equipment described.

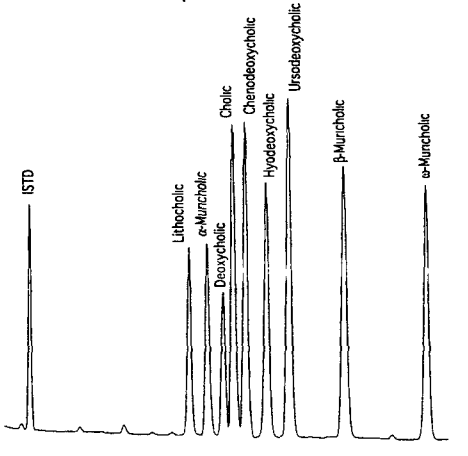

REFERENCES

1. Mitotic aneuploidy as a possible mechanism for tumor promoting activity in bile acids, L.R. Ferguson, J.M. Parry, *Carcinogenesis* 5(4):447 (1984)
2. Bile acid analysis: methods and problems, J.A. Story, E.J. Furumoto, *European Journal of Cancer Prevention* 1(2):29 (1991)
3. General methods for the analysis of metabolic profiles of bile acids and related compounds in feces, K.D.R. Detchell, A.M. Lawson, N. Tanida, J. Sjovall, *Journal of Lipid Research* 24:1085 (1983)
4. Mass Spectrometry of Bile Acids, A.M. Lawson and K.D.R. Setchell, Bile Acids, Volume 4, Chapter 5, K.D.R. Setchell, D. Kritchevsky, P.P. Nair, EDs., Plenum 1988

Quantitative Determination of α-Cyclodextrin in human urine by Electrospray LC/MS.

*K. Michaelis, Z.B. Salama, L.A.B. Inc. Ridgefield, N.J. 07657, U.S.A., J. Rontree, Fisons Instruments, Altrincham, U.K. and H. Bökens, Schwarz Pharma AG, Monheim, Germany

The unique features of cyclodextrins in various pharmaceutical areas have been widely acknowledged in recent years. An improvement in the stability or solubility of drugs using cyclodextrins, reported in the literature, is due to inclusion complexation properties of cyclodextrins. For example, cyclodextrins form inclusion complexes with barbiturates or prostaglandin-E1 is stabilized with α-cyclodextrin (α-CD). Only a few papers have been published on the bioanalysis of cyclodextrins. Therefore, we have developed and validated a highly selective and sensitive Electrospray LC-MS method capable to quantitate α-cyclodextrin (fig. 1) in human urine. MS analysis was performed an a VG Quattro triple stage quadrupole system using the electrospray ion source. An Applied Biosystems HPLC system operated at 200μl/min was coupled to the mass spectrometer via a splitter (20 : 1 split). The urine extracts of the cyclodextrins were separated on a C_{18} 1 x 150 mm column using a acetonitrile/water solvent system containing 1% formic acid. The isolation of α-cyclodextrin and the internal standard ß-cyclodextrin from the biological matrix was carried out by solid phase extraction with C_{18} cartridges. The extracts were derivatized with acetic anhydride. The ES mass spectra (positive ions) of the peracetylated cyclodextrins showed a couple of intense peaks (fig. 2a/b). For the quantitation of α-CD m/z 1748 was used and for the quantitation of ß-CD m/z 1027. Using α-CD standard solutions, separate series of blank urine (1ml) were spiked at concentrations ranging from 0.2 - 20μg/ml (fig. 3). These calibration samples were extracted as described by determining the peak area ratios of α-CD/ß-CD and comparing these ratios with the standard curve obtained from analysis of the calibration samples. The selected chromatograms of a subject sample and a control sample spiked with 1μg α-

CD per ml urine are shown in fig. 4. The analytical method described here provides the appropriate sensitivity and selectivity for the determination of α-cyclodextrin (CD) in human urine, in clinical trials evaluating the fate and pharmacokinetic profile of α-cyclodextrin.

Figure 1

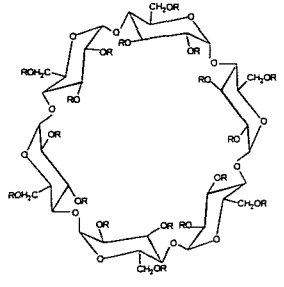

R = H α-Cyclodextrin

R = -CO-CH3 Peracetyl-α-Cyclodextrin

Figure 3

Calibration curve: 1

Intercept: -0.006970654

Slope. 0.184390041

R - square: 0 999539855

Nominal concentration	p.a.r	Backcalc. concentration	Deviation (%)
0 2	0 0322	0 21	6 82
0 5	0 0803	0 47	-5.34
1	0 1757	0 99	-0 93
2	0.3628	2 04	1 92
5	0.8748	4 78	-4.36
10	1 8914	10 30	2 95
20	3 6638	19 91	-0 46

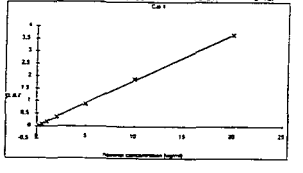

Fig 2a ES+ mass spectrum of α-CD

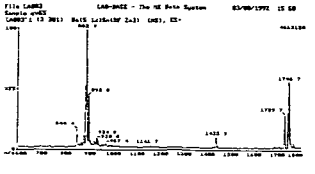

Fig 2b ES+ mass spectrum of β-CD

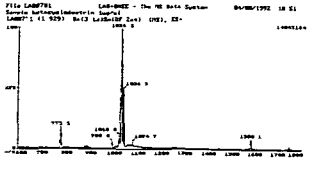

Figure 4
Selected ion chromatogram for a control sample spiked with 1μ/ml α-CD

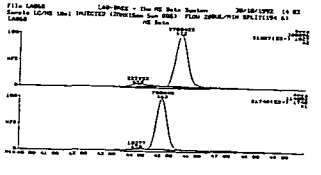

Selected ion chromatogram for a subject sample (subject A)

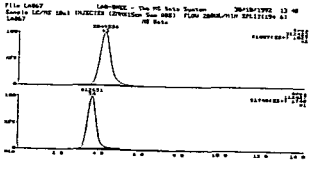

Quantitative Analysis of GR38032 by Isotope Dilution Particle Beam-LC/MS Using Normal Phase and Reverse Phase HPLC

* Brian P. Downey and Daniel L. Norwood, Glaxo Research Institute, Five Moore Drive, Research Triangle Park, NC 27709

Particle Beam-Liquid Chromatography/Mass Spectrometry is a well known technique for obtaining electron ionization (EI) mass spectra from samples separated by high performance liquid chromatography (HPLC). The utility of PB-LC/MS for qualitative analysis is well known, however, quantitative analysis is hampered by the existence of a "carrier effect" in which a coeluting substance enhances the sensitivity of a target compound and may produce non-linear responses. Previous work by this laboratory[1] indicates that reliable quantitation by isotope dilution PB-LC/MS is possible. This report describes the utility of PB-LC/MS for the quantitation of pharmaceuticals by both reverse phase and normal phase HPLC. HPLC assays were developed and characterized for the quantitation of GR38032F (a new $5HT_3$ antagonist) by isotope dilution PB-LC/MS using d_3-GR38032 as the internal standard. This isotope labeled analog coelutes with GR38032 using each of the HPLC systems developed. A linearity comparison with thermospray-LC/MS is also included.

Enhancements in ion abundance for coeluting substances during PB-LC/MS analyses have been observed by several laboratories[2,3,4]. These enhancements are generally recognized as the result of a particle beam "carrier effect" in which increased transport efficiency through the momentum separator is observed for coeluting substances. Formation of molecular clusters in the liquid phase exist as particles in the nebulizer spray and act as particle beam carriers by increasing the effective mass and reducing the vapor pressure of the analytes[2]. The carrier effect potentially results in non-linear response and may limit the applicability of PB-LC/MS for quantitative analysis. This laboratory is currently investigating the quantitative analysis of GR38032F by isotope dilution PB-LC/MS using d_3-GR38032 as the internal standard.

The particle beam carrier effect has negative implications for qualitative analysis as well as quantitative analysis. Selected ion chromatograms (m/z 293, 279, 167, 149) generated from the analysis of GR38032F by PB-LC/MS show a peak that elutes at approximately 9 5 minutes. The molecular ion for GR38032 is m/z 293, while ions 279, 167, and 149 are associated with a phthalate impurity in the mobile phase, and are not part of the GR38032 EI+ spectrum. Therefore, difficulties may exist in obtaining appropriate background subtracted spectra for GR38032, as well as spectra for low level GR38032 impurities.

The utility of PB-LC/MS for the quantitative analysis of pharmaceutical compounds was assessed by examining the linearity and detection limits for both normal and reverse phase chromatography systems. The linearity of response for GR38032F was investigated by injecting five standard solutions of GR38032F containing 13, 52, 258, 512, and 1312 ng of GR38032F (each containing a constant 381 ng of d_3-GR38032) on a normal phase HPLC system. A linear regression was performed on the relative responses obtained for the standard solutions and the response was linear with a correlation coefficient of 0.995. The same experiment was repeated using a reversed phase chromatographic system, however,

the detection limit obtained was higher than that obtained for the normal phase system and thus precluded using standards in the same concentration range. The linearity of response for GR38032F using the reverse phase chromatography system was investigated by injecting five standard solutions containing 0.6, 1.2, 2.4, 4.8, and 9.6 μg of GR38032F (each containing a constant 19 μg of d_3-GR38032). Linearity of response was demonstrated by the correlation coefficient of 0.998 obtained for the reverse phase system. For comparison purposes, the linearity of response for GR38032F was investigated by injecting five standard solutions containing 13 - 1300 ng GR38032F and a constant 381 ng of d_3-GR38032 on the TSP-LC/MS system. Linearity of response was demonstrated and a correlation coefficient of 0.997 was obtained for the TSP-LC/MS analysis.

The effect of different mobile phase buffers on the relative response of GR38032F to d_3-GR38032 was assessed by injecting standard solutions containing 13 ng and 52 ng, respectively, of GR38032F on several chromatographic systems utilizing different buffers. Each standard solution contained a constant 381 ng of d_3-GR38032. The buffers examined included 0.1% trifluoroacetic acid, 0.025 M ammonium acetate, 0.024 M ammonium citrate, and 0.1% ammonium formate. Each HPLC system used a mobile phase of 50% acetonitrile and 50% of the appropriate buffer solution. The relative response for each standard solution was calculated and the results indicate that no significant difference was observed for the relative responses obtained for the 52 ng standard in each of the mobile phases tested. The average relative response was 0.1846 ± 0.0101 (5.5% RSD). However, the average relative response obtained for the 13 ng standard was 0.1199 ± 0.0361 (30% RSD). The higher % RSD obtained for the 13 ng standard is probably due to the irreproducibility of results for consecutive injections in the same mobile phase buffer at this concentration level.

REFERENCES

1. Norwood, D.L., *Downey, B.P., Particle Beam-LC/MS and the Use of Stable Isotope Labeled Internal Standards For Quantitative Analysis; Proceedings of the 40th ASMS Conference on Mass Spectrometry and Allied Topics, Washington, DC, May 31 - June 5, 1992.

2. Bellar, T.A., Behymer, T.D., and Budde, W.L., Investigation of Enhanced Ion Abundances from a Carrier Process in High Performance Liquid Chromatography Particle Beam Mass Spectrometry; *J Am Soc Mass Spectrom* 1990, 1, 92-98.

3. Brown, F.R., Draper, W.M., The Matrix Effect in Particle Beam Liquid Chromatography/Mass Spectrometry and Reliable Quantification by Isotope Dilution, *Biological Mass Spectrometry*, 1991, 20, 515-521.

4. Apfel, A., Perry, M.L., Quantitation and linearity for particle beam liquid chromatography-mass spectrometry; *Journal of Chromatography* 1991, 554, 103-118.

Quantification of Peptide Isotopomer Abundances and Determination of Prottein Turnover Rates by Using Mass Isotopomer Distribution Analysis

K. A. Caldwell[1], C. Papageorgopoulos[1], D. King[2], R. A. Neese[1], E. Roitman[3], C. H. L. Shackleton[3], and M. Hellerstein[1]

[1]Dept. of Nutritional Sciences, U.C. Berkeley, Berkeley, CA 94720
[2]Howard Hughes Medical Institute, U.C.Berkeley, Berkeley, CA 94720
[3]Children's Hospital Oakland Research Institute, Oakland, CA 94606

The notion that body constituents are continually formed and utilized was one of the most far reaching ideas of biology in this century.[1,2] The rate at which a cell, organ, or whole organism synthesizes and degrades biopolymers ultimately controls structure and function, and it is likely that most diseases will reduce to disorders of production or removal of specific molecules such as biological polymers.* Nevertheless, there is currently no comprehensive solution to the measurement of their synthesis rates.

Most previous approaches to the measurement of synthesis rates of biopolymers have used tracers labelled with radioactive isotopes. A major limitation of using radiolabelled monomers, however, is that the ratio of tracer to unlabeled monomer in the pool of monomers used to synthesize the biopolymer is difficult to determine and is usually not known with confidence. Although plasma levels are readily accessible, the tracer is not necessarily distributed uniformly throughout the organism.

MIDA is a new method for measuring the synthesis rates of biopolymers. Monomers labelled with stable isotopes are used, and the perturbed isotope pattern of the biopolymer resulting from incorporation of the labelled monomer is compared to the isotope pattern from the native polymer.[3] The synthesis rate is calculated by determining the fraction of the polymers that are new. By comparing the observed pattern to ones predicted from probability theory, the ratio of labelled to unlabeled monomer that existed *at the site of synthesis* can be determined rigorously, without regard to cell and tissue compartmentalization. MIDA has been applied successfully to the determination of the synthesis rates of cholesterol, lipids, glucose, and fructose in humans and rats.

We have begun to apply MIDA to the determination of protein turnover. Initial studies have focused on the use of an automated peptide synthesizer to model *in vivo* protein synthesis occurring on ribosomes using tRNA amino acids. The peptide SVVLLLR was synthesized from FMOC-leucine containing increasing amounts of the d_3-leucine derivative. SVVLLLR was chosen because it is a proteolytic fragment of human serum albumin, the protein for the human studies.

To apply MIDA to the determinaiton of protein turnover it is necessary to meausue isotope ratios with high precision and, ideally, high accuracy. FAB-MS and electrospray MS were used to measure the isotope ratios of the unlabeled oligopeptide, and electrospray ionization was superior. Accuracy and precision were improved considerably by fitting Gaussian curves to the observed peaks.

*Here, polymer refers to molecules synthesized from repeating units and includes cholesterol from acetate monomers, proteins from amino acid monomers, and glucose from three-carbon monomers.

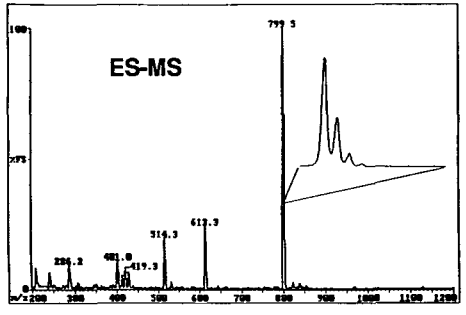

Electrospray mass spectrum of SVVLLLR indicating a negligible abundance of the $[M-2+H]^+$ ion (data for the inset acquired separately).

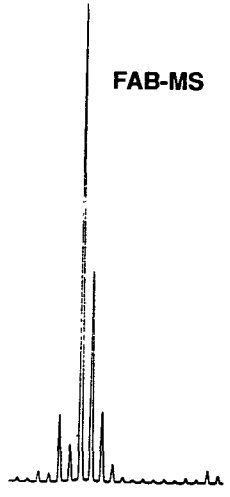

Theoretical vs Observed Ratios of $[M+2+H]^+ / [M+H]^+$

FAB	[(obs - theo)/theo] 100%	ESI	[(obs - theo)/theo] 100%
0.158		0.1136	
0.152		0.1152	
0.155		0.1128	
0.147			
0.153			
0.153 ± 0.004[a]	26.1%	0.114 ± 0.001[a]	-6.0%

1. Hetenyi, G. Jr.; Perez, G.; and Vranic, M. Turnover and Precursor-Product Relationships of Nonlipid Metabolites. *Physiol. Rev.* **1983**, *63*, 606-667.
2. Schoenheimer, R. *The Dynamic State of Body Constituents*. Hafner, New York, 1964. (Reprint of the original of 1942.)
3. Hellerstein, M. K.; Neese, R. A. Mass Isotopomer Distribution Analysis: A Technique for Measuring Biosynthesis and Turnover of Polymers. *Am. J. Physiol.* **1992**, *263*, E988-E1001.

DETERMINATION OF ^{15}N ENRICHMENT OF TAURINE IN CAT URINE BY GC/MS

Andreas A. Stämpfli, Olivier Ballèvre and Laurent B. Fay,
Friskies Research, P.O. Box 44, CH-1000 Lausanne 26, Switzerland

A study of taurine kinetics in the cat was undertaken to understand the physiological basis of taurine requirements. A method was therefore developed for the accurate determination of ^{15}N-taurine enrichment in cat urine by gas chromatography/mass spectrometry.

^{15}N-taurine was given to six animals as an oral bolus dose of 20 mg/kg body weight and the urine was collected over 6 days and pooled on a daily basis. The hydrolysed or non-hydrolysed urine samples (for total and free taurine respectively) were directly derivatised without further purification. The N-pentafluorobenzoyl di-*n*-butyl amide derivative obtained was analysed by GC/MS and the fragment [M-(di-*n*-butyl amide)]+, carrier of the labelled nitrogen atom, selectively recorded at m/z 302 (^{14}N-taurine) and m/z 303 (^{15}N-taurine).

Calibration curves prepared in hydrolysed and non-hydrolysed urine samples spiked with ^{15}N-taurine gave similar slopes to the calibration curve prepared in water. The average coefficient of variation observed for the mole percent excess (MPE) in the non-hydrolysed samples was 1.22 % (n=92) and for the hydrolysed urine 1.00 % (n=98). There was no significant difference between free and total taurine enrichment.

Since the enrichments of free and bound taurine were similar, the half-life and kinetics data were also similar using both non-hydrolysed and hydrolysed samples of urine.

The half-life of taurine in cat body was found to be 29.3 ± 2.9h and 35.0 ± 1.4 h for free and total taurine respectively (non significant). The taurine body pool, calculated by extrapolation of the curve to zero time, had a value of 137 ± 22mg/kg and 157 ± 11 mg/kg for free and total taurine, respectively.

These results illustrate that the bound taurine pool is in equilibrium with the free taurine pool. In these urine samples, 85% of urinary taurine was in the free form. This is related to the fact that taurine intake was in excess of the requirements for cats which is not always

achieved on a diet of unsupplemented commercial petfood. The comparison between free and bound taurine kinetics using both sample enrichment determinations (free and total) should help in the understanding of taurine metabolism in cats and optimise taurine content in different cat foods.

The analysis of urine samples is suitable for taurine kinetics since taurine half-life is longer than a day in the cat. Therefore, any imprecision in the determination of time-related evolution of enrichment in daily pooled urine samples is minimised. Thus the different pathways of taurine metabolism can be determined accurately from taurine pool size and rate constant using a stochastic analysis of the open one-pool model. The presented method allows a fast determination of enrichment in urine samples and can easily be applied to other biological samples, i.e. plasma, whole-blood, since a complete analysis required only 50 nmol of taurine.

Enantioselective Glucuronidation of the Antipsychotic Agent 4-Fluorophenyl-hydroxybutyl-5-fluoro-pyrimidinylpiperazine (5F-FHPP) and Selected Analogs by Rat Liver UDP-glucuronosyltransferases (UDPGTs)

*Frank J. Belas[1], Amin Kamel[1], Lewis J. Klunk[3], Robert Mayol[3], and Ian A. Blair[1,2]. Departments of Pharmacology[1] and Chemistry[2], Vanderbilt University, Nashville, TN, 37232; [3]Bristol-Myers Squibb Co., Pharmaceutical Research Inst., Wallingford, CT, 06492.

The availability of psychoactive drugs has had a profound effect on the treatment of mental illness. However, many of them have significant side-effects when used chronically. The recent development of drugs related to buspirone containing either an azaspirodecanedione or a 1-(2-pyrimidinyl)piperazine (1-PP) moiety has provided a class of drugs with markedly reduced side-effects. The metabolism of the antipsychotic agent 4-Fluorophenyl-hydroxybutyl-5-fluoro-pyrimidinylpiperazine (BMY-14802, 5F-FHPP) has been investigated, and the major urinary metabolites were identified as glucuronide diastereomers. The present study investigated enantioselective glucuronidation in control and phenobarbital induced rat liver microsomes using racemic mixtures and individual enantiomers of 5F-FHPP. Racemic mixtures of 5F-FHPP analogs (5Cl-FHPP, and 5Br-FHPP) were also incubated with phenobarbital induced rat liver microsomes. Structures of the metabolites were confirmed by LSI MS/MS using a Kratos Concept tandem four sector mass spectrometer.

Glucuronidation incubations were carried out in 400 µL of 1M Tris (pH 7), 1.2 mL of 0.1M $MgCl_2$, 0.1M 2-mercaptoethanol, 100 µL Brij 58 solution, 400 µL UDPGA, and 129 µL of rat liver microsomes (1 mg/mL protein) in 0.01M Tris, 0.001M EDTA, 20% glycerin buffer. Enantiomers of BMY-14802 were added to give concentrations of 25 µM to 250 µM. Mixtures were incubated for 20 min. at 37 °C, and the reaction was stopped by the addition of ethyl acetate. Samples were then evaporated to dryness, and the resulting pellet was dissolved in 1.5 mL of methanol/0.01M ammonium acetate (pH 5; 1:1 v/v). After sample clean-up using a C18 SPE column, the eluate was evaporated to dryness, and the residue was re-dissolved in 100 µL of methanol/1N formic acid (2:1, v/v). An additional 100 µL of 1N formic acid was added to this solution. The sample was then spun for 4 min. in an Eppendorf centrifuge. The supernatant was separated and analyzed by reverse-phase HPLC.

Previous studies have demonstrated that BMY-14802 undergoes virtually no oxidative metabolism *in vitro* with human and rat liver microsomes. The major route of BMY-14802 metabolism involves glucuronidation. Glucuronidation was enantioselective *in vivo* with the (-) enantiomer being a better substrate than the (+) enantiomer. Previous studies have also demonstrated that (-) BMY-14802 was a better substrate for UDPGTs from human, bovine, and rabbit microsomes when compared with the (+) enantiomer. Results presented in Figure 1 indicate that in control studies using rat liver microsomes, the (-) enantiomer is preferentially glucuronidated over the (+) enantiomer, but this selectivity was lost upon phenobarbital (PB) induction. Additionally, results suggests that there was

no competitive inhibition between the two enantiomers. Racemic mixtures of 5F-FHPP analogs (5Cl-FHPP, and 5Br-FHPP) were also incubated with PB induced rat liver microsomes. Different substituents at the 5 position of the 1-PP moiety caused differential effects on glucuronidation with Vmax/Km for 5Cl-FHPP>>5Br-FHPP>>5F-FHPP. Structures of the metabolites were confirmed by positive LSI MS/MS using a Kratos Concept tandem four sector mass spectrometer. The positive LSI MS/MS of the BMY-14802-glucuronide is shown as Figure 2.

Supported by NIH grants ES00267, GM31304, RR06254, GM07569, and Bristol-Myers Squibb.

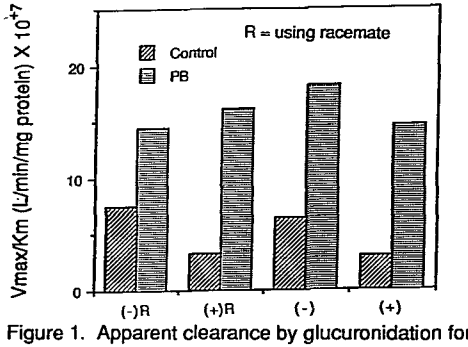

Figure 1. Apparent clearance by glucuronidation for 5F-FHPP.

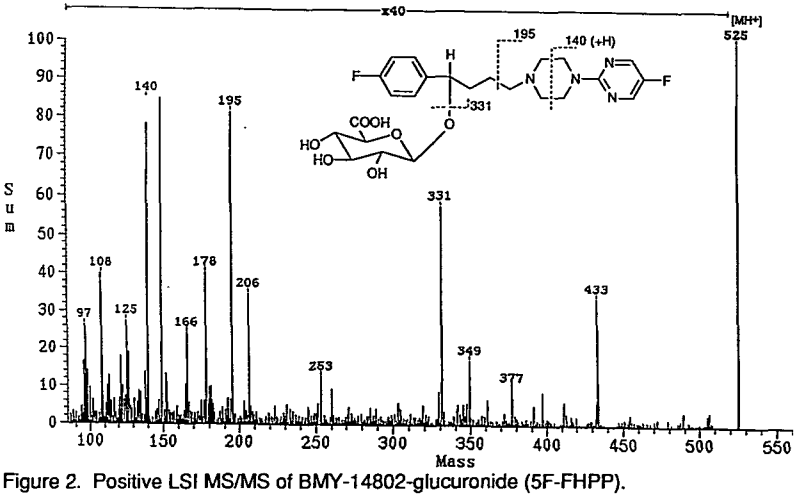

Figure 2. Positive LSI MS/MS of BMY-14802-glucuronide (5F-FHPP).

Derivatizations for Enhanced Detection of N- linked and O- linked Glucuronide Conjugates by LSIMS

P. Haroldsen and I. Massey: Syntex Discovery Research, Palo Alto, CA 94304

Ionization by LSIMS of analytes of biologic origin is often hampered by the presence of interfering substances and by the polarity of the analyte. The greater the polarity, the lower the surface activity of the analyte on the sputtering matrix (1). Modification of analytes by derivatization to improve surface activity for LSIMS has been successsfully employed for both peptides (2) and non-peptide drugs (3). This approach has been extended and applied to the analysis of polar glucuronide drug metabolites and is described herein.

The findings indicate that: a) ester derivatives improve LSIMS sputtering yields of M^+ by greater than 60 fold to allow immediate and unambiguous identification of previously undetectable glucuronide conjugates in extracts of biologic origin; b) the greater the chain length of the alkyl ester derivative of the conjugate, the greater the improvement in sputtering yield (signal to noise ratio) of the M^+ or MH^+ compared to background matrix ions, c) CID and product ion analysis of the M^+ of three quaternary N-linked conjugate esters indicates an unusual type of fragmentation which has been elucidated by stable isotope labeling studies and ester alkyl chain length alteration; d) a key substructural fragment ion elucidates the site of a unique conjugation to be quaternary quinuclidine N-linked.

References:

1. Ligon, W. (1990) Biol. Mass Spectrom: Proceed. 2nd Int. Symp. Mass Spectrom. in Health Life Sci. p. 61.
2. Falick, A. & Maltby, D. (1989) Anal. Biochem. 182: 165.
3. Kidwell, D. et. al. (1985) Biomed. Mass Spectrom. 12: 254.

EXPERIMENTAL: GLUCURONIDES: Quinuclidine N-linked quaternary glucuronides M8, M9 and M12 were isolated from cynomologus monkey urine by C18 Bond Elute cartridges followed by C18 RP-HPLC in tandem with an SCX cation exchange column. HPLC buffer salts were removed with C18 Bond elute cartridges prior to LSIMS. Commercially available glucuronides were obtained from Sigma (Phenothalein, morphine and estradiol).

DERIVATIZATIONS: Dried glucuronide samples, 3 - 20 µg, were treated with 0.1 ml methanol, n-propanol, $^2H_7$-n-propanol (CIL) or n-hexanol acidified with acetylchloride (20 µl / ml alcohol) for 45 minutes at 45°C. The samples were then evaporated to dryness and redissolved in methanol / water (1/1) for analysis by LSIMS.

LSIMS: LSIMS was performed on a Finnigan TSQ-70 mass spectrometer employing an Antek Cesium ion gun operated at 8 keV. Samples were applied to 1µl of glycerol or a glycerol/thioglycerol mixture (1/1).

CID TANDEM MS: Collision induced dissociation was performed in the second quadrupole region employing argon at 0.8 - 1.2 mtorr as collision gas and collision energies of -15 to -25 eV.

RESULTS: Initial attempts to characterize three unknown radiolabeled major components (M8, M9 & M12) of an experimental drug, RS-42358, isolated from monkey urine, by thermospray met with failure. Analysis of the three HPLC purified components by LSIMS did not produce sufficiently intense molecular ions for ready detection of metabolites M8 (Fig 1A) and M9 but did so for M12 . The ion at m/z = 471 for M12 indicated it to be a glucuronide conjugate of the unaltered parent drug RS-42358 (mw = 294). Based on the known structure of RS-42358 the conjugate appeared to be a quaternary N-linked quinuclidine glucuronide.

IMPROVED M^+ and MH^+ INTENSITY BY DERIVATIZATION: Derivatization of M8, M9 and M12 to produce propyl esters and reanalysis by LSIMS resulted in sufficiently intense M^+ for detection of M8 and M9 and a significant improvement in the intensity of the M^+ ion for M12. The M^+ ions for M8 and M9 at m/z = 529 indicated them to be the propyl esters of mono-hydroxylated RS-42358 glucuronides. Calculations of the improvements in signal to noise (S/N) responses for the conjugate free acids vs propylesters indicate a 5 (M8), 22 (M9) and 17 fold (M12) increase. Analysis of M8 (Fig 1B) and M12 as hexylesters indicated an even greater improvement in S/N with ratios of S/N for M^+ of esters vs. M^+ free acids at 54 (M12) and 67 fold(M8). Improvements in S/N responses of MH^+ for commercial glucuronides, phenothalein and morphine, as methyl, propyl and hexylesters vs. free acids have been evaluated. The greatest improvement in all cases is observed with hexylesters, resulting in increased S/N ratios of 29 - 60 fold compared to those for free acids.

ELUCIDATION OF SITE OF CONJUGATION: M8, M9 and M12 were structurally characterized by CID and product ion analysis of the M^+ ions. As propyl and hexylester derivatives, M8, M9 (Fig 2A) and M12 were able to be conclusively characterized as unusual quaternary quinuclidine N-linked glucuronides based on the presence of a weak but diagnostically important fragment ion containing the quinuclidine and glucuronic acid moieties (indicated by *). This ion was observed at m/z = 328 for the propylesters at m/z = 335, for the $^2H_7$-propylesters, and at m/z = 370 for hexylesters of the metabolites. The observed shift in this diagnostic fragment ion with derivative type is consistent with the assignment of these metabolites as quaternary quinuclidine N-linked glucuronides.

CHARACTERIZATION OF A UNIQUE FRAGMENT ION: The CID product ion spectra for the propylesters of M8, M9 (Fig 2A) and M12 indicated a unique fragment ion which was observed at 42 amu above the aglycone

fragment ion (indicated as fragment 'A'). For M8 and M9 this ion was observed at m/z = 353 and at m/z = 337 for M12. The propylester adds 42 amu to the nominal weight of the metabolites and the possibility of this fragment arising from a unique propyl group rearrangement was investigated. Following esterification with $^2H_7$ -propanol, CID and product ion analysis of M9 (Fig 2B) and M12 as $^2H_7$ -propylesters indicated that the aglycone +42 amu fragment ion 'A' did not shift. It is likely that this fragment arises from cleavage through the glucuronic acid ring with retention of the elements C_2H_2O(42 amu) on the aglycone. CID and product ion analysis of the M^+ ions of the hexylesters of M8 and M12 indicated that the aglycone +42amu fragment ion 'A' still formed, demonstrating that this fragment is not unique to propylesters. It is not known if the aglycone +42 amu fragment ion is intrinsic to all quaternary N-linked glucuronides following low energy CID. The presence of the CID aglycone +42 amu fragment ion has been observed in one O-linked glucuronide but has not been observed in the spectra of esters of several other O-linked glucuronides, including those presented here for morphine, phenothalein or estradiol, and warrants further investigation.

Acknowledgement: The technical expertise of Adva Yani in the department of Drug Metabolism is gratefully acknowledged for guidance in the isolation of M8, M9 and M12.

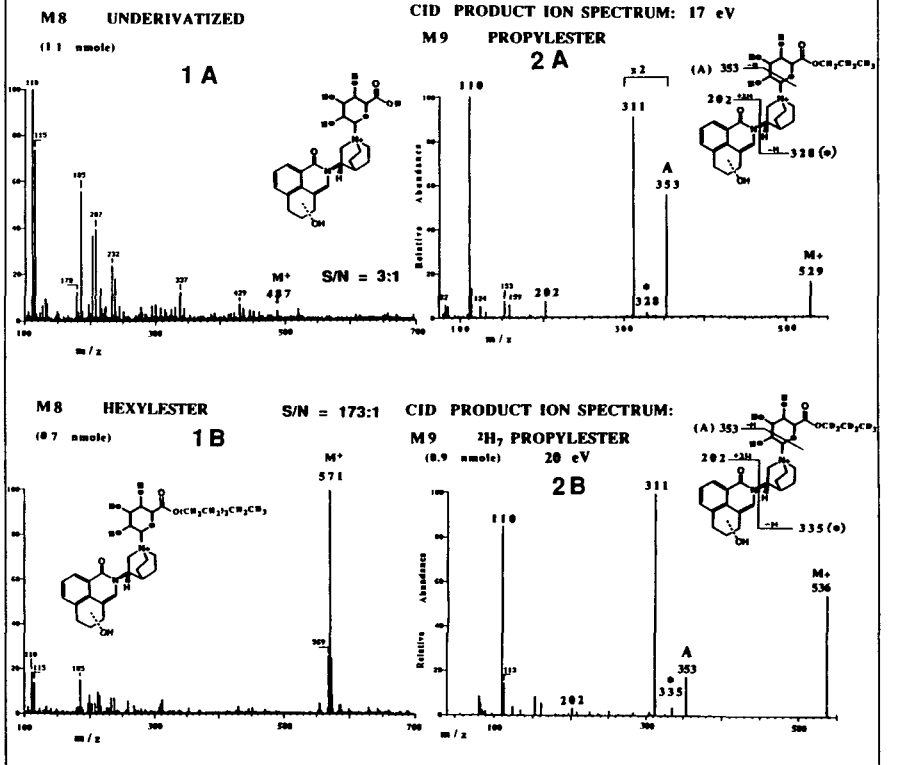

ANALYSIS OF INSULIN - ACYL GLUCURONIDE ADDUCTS BY ELECTROSPRAY IONIZATION / MASS SPECTROMETRY.

*C.D. Márquez[1], J-H. Liu[1], S.T. Weintraub[2], and P.C. Smith[1].
[1]School of Pharmacy, University of North Carolina, Chapel Hill, NC 27599, and
[2]Department of Pathology, University of Texas Health Science Center at San Antonio, San Antonio, TX 78284.

INTRODUCTION

The elimination of acidic drugs, such as the nonsteroidal anti-inflammatory drugs (NSAIDs), from the body often occurs through conjugation with glucuronic acid to form acyl glucuronides. These conjugates are potentially reactive intermediates which may undergo hydrolysis, acyl migration or irreversible binding to plasma proteins[1,2]. Covalent binding of reactive metabolites to cellular constituents is of interest, as it may result in toxicity, hypersensitivity reactions, mutagenesis or carcinogenesis. The objectives of this study are to evaluate model proteins to study reactions of acyl glucuronides, to determine whether ESI/MS can be used to identify the covalent adducts formed between a model protein (insulin) and acyl glucuronides, and finally to determine if a variety of acyl glucuronides react with insulin by nucleophilic displacement or by imine formation.

EXPERIMENTAL

Acyl glucuronide conjugates of suprofen (SG) , zomepirac (ZG), salicylic acid (SAG), etodolac (EG) and tolmetin (TG) were extracted from human or rabbit urine after oral dosing. *Drug acyl glucuronides were purified by HPLC and characterized by FAB/MS. The formation of* acyl glucuronide adducts was examined with a number of model proteins. Insulin, aprotinin, lysozyme, RNAse, bovine lens protein, and human serum albumin were separately incubated with suprofen glucuronide. Insulin was chosen as the model protein since it was successfully resolved from its acyl glucuronide adduct by HPLC. Recombinant human or bovine insulin and drug acyl glucuronide were incubated with and without reducing agent, $NaCNBH_3$, to examine its influence on the extent of adduct formation.

HPLC Fractionation: Insulin and each drug were measured using a Vydac C18 column (4.6mm X 150mm) coupled to two HP-1050 UV detectors connected in series to HP-3396A integrators; fractions were collected via a Gilson FC 204 fraction collector. Separation of insulin and insulin adducts was accomplished using linear gradients consisting of 100% CH_3CN and 0.1% TFA. One UV detector monitored insulin at 214 nm while the other monitored either 295 (SG), 313 (SA), 313 (ZG), 280 (EtG), or 315 nm (TG).

ESI/MS Identification: Insulin and acyl glucuronide adducts were characterized using electrospray ionization/mass spectrometry (ESI/MS). Samples (5 to 10 pmol/µl) were dissolved in methanol containing 0.5% acetic acid and introduced into the ESI interface at a rate of 1 µl/min. Mass spectra were acquired on a Finnigan-MAT model SSQ700 using an electrospray energy of - 3.5 kV. The ESI spectra were obtained after signal averaging for approximately 1 min.

RESULTS

Insulin reacted with a variety of NSAID acyl glucuronides to form adducts. The mechanism of adduct formation between acyl glucuronides and proteins is not well understood. Binding has been proposed to occur through either a nucleophilic displacement mechanism[3-4] or via a process involving intramolecular acyl migration followed by imine formation between the glucuronic acid moiety of the isomeric conjugate and an amino group of the protein[5]. Reducing

agents increased the formation of imine adducts such that when $NaCNBH_3$ was incubated with insulin and drug acyl glucuronide, an increase of approximately 10 to 20 fold was observed for SG, ZG, and EG.

Insulin, insulin-drug acyl glucuronide adduct, and the respective drug were separated and detected using the gradient HPLC system with dual UV monitors. Insulin acyl glucuronide adducts formed multiple peaks which may suggest that acyl glucuronides reacted at more than one site on insulin. The HPLC fraction that contained the multiple peaks was examined by ESI/MS. The results showed that only one molecular species was present. Acyl glucuronides may react with insulin at either the ε-amino group of Lys or the N-terminus of the A and B chains of insulin. If the multiple peaks were due to the attachment of acyl glucuronides to more than one site on insulin, ESI/MS would not be expected to discern such isomeric adducts since all would have the same molecular weight. Representative mass spectra are shown for human insulin (Fig. 1) and ZG-insulin adduct (Fig. 2). The calculated and observed molecular weights of drug acyl glucuronide-human insulin adducts are presented in Table 1.

HPLC and ESI/MS gave no evidence of adducts that might be formed by a nucleophilic displacement mechanism. The reaction appears to be general for reactive acyl glucuronides since five structurally diverse acyl glucuronides react similarly with the model protein, insulin. These results demonstrate that ESI/MS is an excellent means to identify covalent adducts between small proteins such as insulin and reactive metabolites.

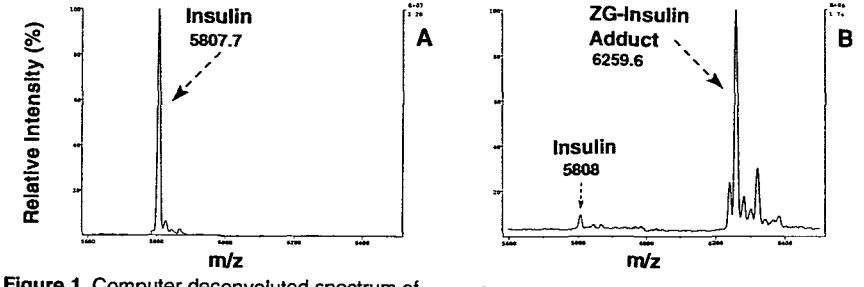

Figure 1. Computer deconvoluted spectrum of (A) human insulin, (B) ZG-insulin adduct by ESI/MS.

Table 1. Calculated and observed mass of drug acyl glucuronide - insulin adducts by ESI/MS.

Acyl Glucuronide Conjugates	Calculated Mass of Insulin Adduct	Observed Mass of Insulin Adduct
Suprofen	6228.1	6227.9
Salicylic Acid	6105.7	6105.4
Zomepirac	6259.5	6259.5
Etodolac	6255.1	6254.8
Tolmetin	6225.1	6225.1

REFERENCES

1. P. C. Smith, A. F. McDonagh and L. Z. Benet, *J. Clin. Invest.*, 77, 939 (1986).
2. H. Spahn-Langguth and L.Z. Benet, *Drug Metab. Rev.*, 24, 5 (1992).
3. R. B. van Breeman and C. Fenselau, *Drug Metab. Dispos.*, 13, 318 (1985).
4. H. W. Ruelius, S. K. Kirkman, E. M. Young, and F. W. Janssen, *Adv. Exp. Med. Biol.*, 197, 431 (1986).
5. P. C. Smith, L. Z. Benet and A. F. McDonagh. *Drug Metab. Dspos.*, 18, 639 (1990).

Supported by NIH Grants GM41828 and AG09594. PCS is a recipient of a PMAF Faculty Development Award.

ASSAY OF THE [^{13}C]ENRICHMENT AND CONCENTRATION OF ACETATE IN BIOLOGICAL FLUIDS

France David, Michel Beylot, Mitchell W. Reider,
Vernon E. Anderson and Henri Brunengraber
Depts of Nutrition and Biochemistry,
Case Western Reserve University, Cleveland OH 44106.

[^{13}C]Acetate is extensively used for investigating intermediary metabolism, particularly for tracing gluconeogenesis. In general, the incorporation of label into products is not correlated to the molar percent enrichment (MPE) of acetate in biological fluids. Its measurement is difficult because of (i) low concentration of acetate in plasma (20 to 60 μM), (ii) poor extractibility of acetate from water into organic solvents, (iii) difficulty to find suitable derivatives for HPLC or GC-MS, and (iv) ubiquitous presence of acetate in the environment and in many reagents.

We tried techniques, involving organic extraction (1,2). These yielded high blanks and low recoveries. We then developed an assay that converts acetate to acetyl-CoA, then to acetyl-glycine (3) which is assayed by GC-MS as methyl or pentafluorobenzyl ester.

METHODS

A clean laboratory is dedicated to the assay. Plasma samples are spiked with 237nmol of [1-^{13}C,^{2}H$_3$]acetate internal standard. Neutralized perchloric acid extracts are incubated for 2 hr with 1.8 mM ATP, 3.0 mM $MgCl_2$, 0.8 mM CoA, 60 mM TRIS/30 mM KCl pH 8.0 and 1.3 U of acetyl-CoA synthetase (final vol: 1.7 ml). Then, 1.7 ml of 1 M glycine pH 9.8 is added to convert acetyl-CoA to acetyl-glycine. After 4h at 60°, the solution is run on a AG-50-X8 Cl^- column. Acetyl-glycine, eluted with water, is dried and reacted with CH_2N_2 or PFBBr + pyridine. The methyl and PFB derivatives are assayed by PCI and NCI-MS, respectively. For acetyl-CoA assay, the latter is reacted with glycine, then with PFBBr.

RESULTS

The PCI spectrum of acetyl-glycine methyl ester has a useful ion at m/z 132 ([M+H$^+$]). The NCI spectrum of acetyl-glycine-PFB has a useful ion at 116 (loss of PFB group). Figs 1-3 show linear standard curves of [2-^{13}C]acetyl-CoA enrichment, acetate concentration in dog plasma (blank 17nmol) and [2-^{13}C]acetate enrichment in dog plasma. Similar sensitivity is achieved with the methyl and PFB esters.

A dog was infused with [2-^{13}C]acetate at 3 sequential rates of 3, 6 and 9 μmol/kg x min. Fig 4 shows the concentration and MPE of plasma acetate. Rates of acetate appearance (corrected for tracer infusion) were 7.5, 5.5 and 4.7 μmol/kg x min, respectively.

1. Rocchichiolli et al (1989) Biomed Environ Mass Spec **18**, 816-819.
2. Kien et al (1990) Biomed. Environ. Mass. Spec. **19**, 554-558.
3. Tamvakopoulos CS & Anderson VE (1992) Anal Biochem **200**, 381-387.

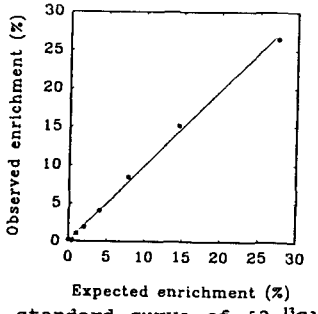

Fig 1: Enrichment standard curve of [2-^{13}C]acetyl-CoA as acetyl-glycine PFB ester.

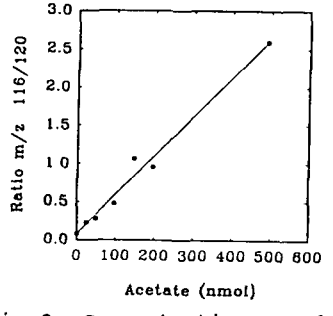

Fig 2: Concentration standard curve of acetate as acetyl-glycine PFB ester.

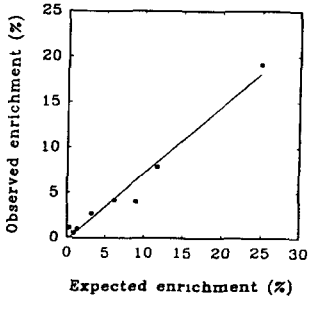

Fig 3: Enrichment standard curve of [2-^{13}C]acetate as acetyl-glycine PFB ester.

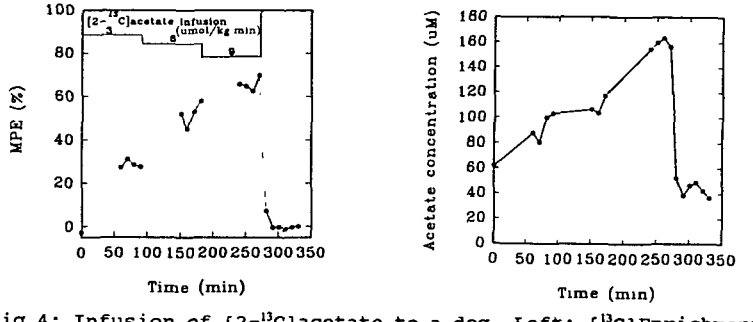

Fig 4: Infusion of [2-^{13}C]acetate to a dog. Left: [^{13}C]Enrichment of plasma acetate. Right: Concentration of plasma acetate.

APPLICATION OF GC-CRIMS IN THE INVESTIGATION OF METABOLIC DISEASE

Donald H. Chace, Diane S. Roe, and David S. Millington, Department of Pediatrics, Division of Genetics and Metabolism, Duke University Medical Center, Durham, N.C. 27710

Capillary Gas Chromatography - Chemical Reaction Interface Mass Spectrometry was utilized in the investigation of biochemical pathways of patients with inherited metabolic disease. A chemical reaction interface (CRI) is primarily a helium plasma generated inside a ceramic tube that is present in a tunable cavity connected to a microwave power supply. The input to the reaction interface consists of a capillary GC and a reactant gas supply and the output is a transfer line connected to the mass spectrometer. Compounds that enter the CRI following gas chromatography are completely decomposed to elemental species. With addition of an oxidizing or reducing reactant gas, low molecular weight polyatomic molecules containing the elements present in the original compound are produced. These small molecules are detected using a mass spectrometer. Isotopic enrichment with the stable isotopes ^{13}C, ^{15}N, and D is detected by monitoring the mass of the low molecular weight molecule produced in the CRI that is representative of the isotope present in the original compound. For example, the isotopes of carbon and nitrogen are monitored at unit mass resolution as $^{12}CO_2$, $^{13}CO_2$, ^{14}NO, ^{15}NO when SO_2 is used as a reactant gas. Isotopic enrichment with deuterium is detected by monitoring HD when hydrogen is used as the reactant gas. A resolution of ca. 1500-2000 is needed to separate HD from H_3^+. Since this resolution was not attainable on the benchtop GC/MS system, a magnetic sector MS was employed. The detection of deuterium-enriched metabolites in the urine of patients with metabolic diseases after the infusion of deuterium-labelled precursors is described.

The metabolic pathways of patients with known metabolic disorders in amino acid catabolism were studied following administration of deuterium labelled (>98%) substrates. Methyl-D_3-leucine was administered to a patient with HMG-CoA lyase deficiency. Methyl-D_3-isoleucine (50:50 isoleucine and alloisoleucine) was administered to patients with β-Ketothiolase deficiency. Control (baseline) urines were collected before the start of these infusion studies. HMG-CoA lyase deficiency is a disorder in the catabolism of L-leucine resulting in the increased excretion of 3-OH-3-methyl glutaric acid (HMG), 3-methylglutaric acid, 3-methylglutaconic acid and 3-OH isovaleric acid. β-Ketothiolase (2-methylacetoacetyl-CoA thiolase) deficiency is a disorder in the catabolism of L-isoleucine. Characteristic urinary organic acid profiles of patients with this disorder usually reveal elevated levels of 3-OH-2-methylbutyric acid and often 2-methylacetoacetic acid with or without tiglylglycine.

1 mL of urine was treated with ethoxyamine-HCl to convert oxoacids to their corresponding oximes, acidified to pH 1, and extracted 3 times with 1 mL of ether and 1 mL of ethyl acetate. The extracts were dried under N_2 and derivatized with 100 μL of BSTFA (bis-trimethylsilyl-trifluoroacetamide) and 5μL of pyridine. One μL of each derivatized sample was analyzed. Various amounts of d_4-glutaric acid, (0.1, 1, 5, 10, and 20 μg) were added to separate vials containing 5 μg of d_3-palmitic acid (external standard) and derivatized with 100μL of BSTFA (85°C for 30 minutes). One μL of sample was analyzed by splitless injection onto a DB-1 column. To test detection limits, 1 μL of serial dilutions of 1 μg/μL of d_{10}- fluorene in CCl_4 was analyzed by splitless injection onto a DB-1 column. A VG 70S mass spectrometer was used at a resolution of 2000 in order to separate HD (3.0219) from H_3^+ (3.0234) and ^3He (3.0160). The amount of H_3^+ produced in the source relative to HD is affected by the amount of hydrogen introduced into the CRI and the repeller voltage. The maximum signal for HD relative to H_3^+ was produced using a high positive repeller voltage. The amount of reactant gas needed in the CRI is determined by the red color of the plasma, ratio of H_3^+ to HD (≈5:1), and the performance of deuterium labelled standards in a test analysis. The raw signal for HD was monitored directly (peak top) using a Shimadzu C-R5a chromatographic data processor.

The metabolic profiles of a patient with HMG-CoA lyase deficiency before and after D_3-leucine administration and metabolic profiles of a patient with β-Ketothiolase deficiency before and after administration of D_3enriched Isoleucine was examined. In each metabolic profile in which D_3-labeled substrate was administered, several deuterium enriched peaks were detected *Figures 1 & 2*. These are catabolites of the D_3-labeled precursors which retain at least 1 deuterium atom. A control chromatograms for each disease profile was determined. These are metabolic profiles of the same patients before administration of the D_3-labeled precursor. The absence of any significant peak in the chromatogram demonstrates selectivity. For a patient with HMG-CoA Lyase Deficiency several deuterium enriched peaks corresponded to the catabolites known to be excreted by a patient with this disease as shown in *Figure 1*. The retention times for each peak were recorded and the peaks at each specified retention time were structurally identified using conventional EI/MS under the same chromatographic conditions. Although a separate instrument was used in this laboratory to obtained EI spectra, it has been previously demonstrated that conventional EI/MS can be obtained using the same instrument

containing the CRI apparatus but with the microwave power turned off. As expected several deuterium peaks were identified as 3-OH-isovaleric acid, 3-methylglutaric acid, and 3-methylglutaconic (2 isomers), and 3-OH-3-methylglutaric acids. Spectra for three peaks (a,b,c) containing enriched deuterium have been obtained but no structure assignment has yet been made. For a patient with β-Ketothiolase Deficiency the peaks detected in the CRIMS chromatogram correspond to 3-OH-2-methylbutyric acid (2 isomers) and 2-ethyl-3-hydroxypropionic acid as shown in *Figure 2*. Identification of each peak was performed by conventional EI/MS in a similar manner as described for HMG-CoA Lyase Deficiency. The linearity of deuterium analysis using GC-CRIMS was examined using $d_3$palmitate (external standard) and serial dilutions of $d_4$glutaric acid. The correlation coefficient of the analysis was 0.93 for a range of 10 ng to 200 ng (on column injection). The detection limit for d_{10}-fluorene was 100 pg was detected with a signal to noise ratio of 5:1.

The ability of GC-CRIMS to selectively detect deuterium enriched substrates has been demonstrated. CRIMS detects deuterium in a structure independent manner which simplifies the search for metabolites of a deuterium labeled precursor. In the metabolic studies described above, several deuterium enriched metabolites were detected. Conventional EI/MS for the major metabolites confirmed the presence of 1 to 3 deuterium atoms. Several additional peaks which contained excess deuterium and gave uninformative EI/MS spectra were also detected.

1 Chace, D.H. and Abramson, F.P., Anal. Chem., 61: 2724 (1989).
2. Chace, D.H. and Abramson, F.P., Biomed. Environ. Mass Spectrom., 19, 117 (1990).
4. Moini, M., Chace, D.H., and Abramson, F.P., JASMS, 2, 250 (1991)
5. Chace, D.H., Roe, D.R., Millington, D.S., ASMS ABSTRACT 1992

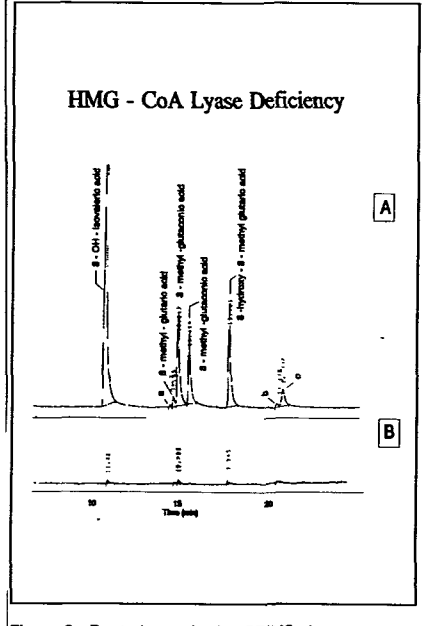

Figure 3: Deuterium selective CRIMS chromatograms for a patient with HMG-CoA Lyase Deficiency. A: post D_3-Leu administration. B: pre D_3-Leu administration

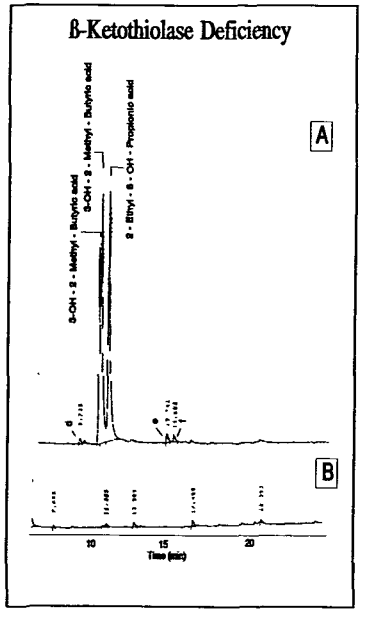

Figure 4: Deuterium selective CRIMS chromatograms of patient with β-Ketothiolase Deficiency. A: post D_3-Ile/alloIle administration. B: pre D_3-Ile/allo-Ile administration

A Comparison of Substituted Phenylboronic Acids as Derivatization Reagents for NCI/MS

J.T. Simpson, S.P. Markey, Yu Ming Pu*, and H. Ziffer*
Section on Analytical Biochemistry, National Institute of Mental Health
and *Laboratory of Chemical Physics, NIDDK, NIH, Bethesda, MD 20892

Introduction

Cyclic boronate derivatives of diols (or other bifunctional compounds), which could capture electrons and stabilize significant structure specific fragment ions are being investigated. The use of these derivatives has been of interest since we observed the potential utility of pentafluorophenylboronic acid (FPBA)[1]. While FPBA exhibited facile boronate formation and excellent chromatographic properties, it did not enhance negative chemical ionization (NCI) detectability for our analytes of interest. Several substituted phenylboronic acids were investigated which could exhibit greater electron affinity and anion stabilization relative to phenylboronic acid (PBA). They were 3-nitrophenylboronic acid (NPBA), 4-bromophenylboronic acid (BrPBA), 2,4-dichlorophenylboronic acid, 3,5-dichlorophenylboronic acid (ClPBA) and FPBA. The four model compounds used for derivatization were methyl 2-methylglycerate, *cis* -1,2-cyclohexanediol, 1,2-dihydroxybenzene (catechol), and 3,4-dihydroxyphenylethylene glycol (DHPG). The derivatives were analyzed by GC/ or particle beam (PB)/ MS in electron impact and negative chemical ionization modes.

Experimental

All the boronic acids used, with the exception of FPBA, are commercially available and were used as supplied without further purification. PBA, NPBA and BrPBA were obtained from Aldrich and the chloroboronic acids were obtained from Lancaster Synthesis. FPBA was synthesized as previously described[2].

A 200 µL aliquot of a boronic acid in dimethoxypropane (DMP) or methylene chloride was added to 200 µL of a dissolved diol in a 7:2 mole ratio. The mixture was vortexed briefly and allowed to stand at room temperature for 15 minutes. An aliquot was then taken for analysis. NPBA was found to have limited solubility in methylene chloride. DMP was preferred in comparison with THF because it scavenges water as the reaction proceeds[3]

Analytical Conditions

Mass spectral analyses were performed on either a Finnigan TSQ-70 (scanning Q1) interfaced with a Varian 3400 GC, or on a Hewlett-Packard 5989 with a particle beam interface. The mass spectrometers were scanned from m/z 50 to 550 for GC/EI and NCI/MS, and m/z 100 to 650 for PB/MS. The ion source temperature was 150°C (250°C for PB/MS). Methane was used as the reagent gas for all chemical ionization experiments.

Typical GC conditions were ramping from 70°C to 280°C at 30°/min, with the injection port and transfer line at 280°C. A DB-5 column (15 m x 0.25 mm x 0.25 µm film thickness) was used for the analyses. The DHPG-boronates did not elute under these conditions and were analyzed by direct flow injection through the particle beam interface on the HP-5989. Hexane was used as the solvent at 0.4mL/min. The desolvation chamber was held at 55°C and helium nebulization pressure was 60 psi.

Results and Discussion

The boronate derivatives formed quantitatively at room temperature and exhibited excellent chromatographic properties. The NPB derivatives gave the best NCI response with methyl 2-methylglycerate/NPB yielding the largest increase in signal enhancement, 26 times that of EI. The remaining NPB derivatives also exhibited NCI signal enhancement of approximately a factor of 10 over EI. NPB derivatives of standards were stable for over one month; the derivatives were also stable to evaporation under N_2 and re-dilution as long as anhydrous conditions were maintained. The NCI mass spectra of the NPB derivatives were dominated by the molecular anion. The EI mass spectra yielded high mass, structure specific ions for all derivatives tested. The chloro- and phenylboronates exhibited the poorest response in NCI. The bromophenylboronate exhibited excellent chromatographic properties, however all of the ion current was the result of facile loss of bromide resulting in an NCI spectrum dominated by the ions m/z 79 and 81. The sensitivity of the boronates follows the order:

NCI: nitrophenyl > bromo-, fluorophenyl > chlorophenyl > phenyl
EI: phenyl > bromo-, chloro-, fluorophenyl > nitrophenyl

The total ion chromatogram (TIC) for the methyl 2-methylglycerate/NPB is shown in Figure 1A, and its NCI mass spectrum is shown in Figure 1B.

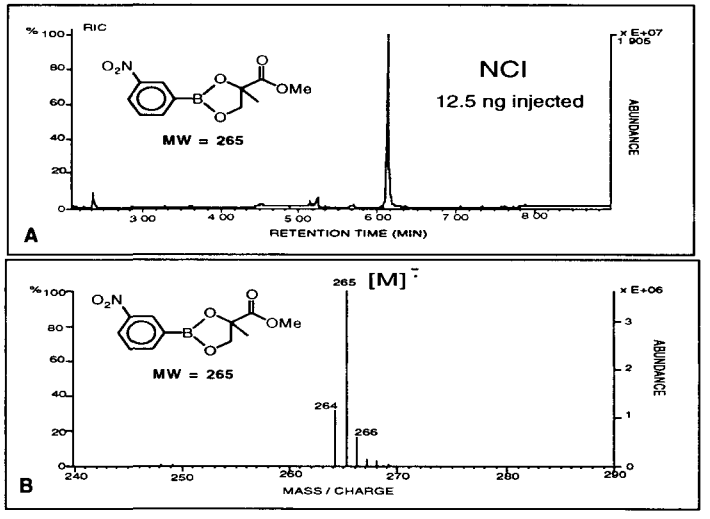

FIG 1: A) TIC of methyl 2-methylglycerate/NPB and B) its NCI mass spectrum.

References
1) J.T. Simpson, S.P Markey, Y.M. Pu and H. Ziffer, *Proc 40th ASMS Conf. Mass Spectrometry & Allied Topics*, 1575, 1992.
2. I.L. Knunyants and G.G. Yakobson, Ed., *Synthesis of Fluoroorganic Compounds*, Springer-Verlag: Heidelberg, 1985, p. 126.
3) C.F. Poole, S. Singhawangcha, A. Zlatkis, *Journal of Chromatography*, 1978, *158*, 33-41.

Quantitative Analysis of Peptido-leukotrienes in Nasal Secretions by Two-Dimensional Gas Chromatography/Mass Spectrometry

Anjula Pamidi, Leonid F. Linberg*, Louis L. Martin
Hem N. Singh, Joseph F. Greer.
Department of Clinical Pharmacokinetics and Disposition, Pharmaceuticals Division, CIBA-GEIGY Corp., 556 Morris Ave., Summit, NJ 07901

Martin Wagenmann, Robert M. Naclerio
Johns Hopkins Asthma & Allergy Center,
301 Bayview Blvd., Baltimore, MD 21224

INTRODUCTION: The peptido-leukotrienes (LTC4, LTD4 and LTE4) have profound effects on bronchial and vascular smooth muscle contractility and also promote extensive plasma extravasation by increasing the permeability of the postcapillary venules. These compounds have been implicated in pulmonary and allergic diseases, inflammation, psoriasis and other disorders. In order to screen the effects of new drugs on peptido-leukotriene synthesis, a simple, selective and sensitive method to measure leukotrienes in various body fluids is required. This report describes a new method for determination of LTC4, LTD4 and LTE4 in human nasal secretions collected on filter paper disks. The method involves separation of the peptido-leukotrienes by HPLC, collection of individual fractions containing each of the compounds, reduction of the compounds to 5-hydroxyeicosanoic acid (5-HEA), derivatization, gas chromatography and detection of the pentafluorobenzyl (PFB), trimethylsilyl (TMS) derivative by negative chemical ionization gas chromatography/mass spectrometry.

EXPERIMENTAL: The method is described briefly as follows. Deuterated analogs (20,20,20-d_3; Cascade Biochem Ltd., Reading, Great Britain) of the leukotrienes were added to 7 mm diameter filter disks containing nasal secretions. Leukotrienes were eluted from the disks with ethanol, separated by HPLC on an Econosphere C-18 column (150 x 4.6 mm x 5 μm) using 65% methanol in 0.1% ammonium acetate buffer (pH 5.4) and collected individually. The leukotrienes were reduced to 5-HEA by bubbling a solution of PtO_2 in methanol (1 mg/ml) with hydrogen. The PFB ester of 5-HEA was prepared and extracted with hexane and water. TMS derivatives were prepared and separated by two-dimensional capillary gas chromatography employing RTx-1701 (30 m x 0.53 mm x 0.25 μm) and Stabilwax (30 m x 0.32 mm x 0.5 μm) fused silica columns. Ions at m/z 399 and m/z 402 were monitored.

RESULT AND DISCUSSION: This method differs from previously published methods in three major ways. First, commercially available deuterated analogs (20,20,20-d_3) were employed instead of unique [^{13}C] or [^{18}O] labeled internal standards. Although concern about the possibility of the exchange of deuterium with hydrogen during the reduction step has been expressed [1], deuterium at the C_{20} position is not exchanged under our conditions and linear calibration curves very clearly demonstrate this (Fig. 1). Second, platinum oxide was used as a catalyst instead of rhodium oxide. Platinum oxide gives a homogeneous solution in methanol and may be pipetted precisely in small amounts,

thereby decreasing irreversible adsorption. Third, two-dimensional gas chromatography combined with mass spectrometry was applied to analyze the final product. Two dimensional gas chromatography eliminated the need for a time-consuming HPLC cleanup step between the two derivatizations. It also significantly increased the sensitivity by reducing background noise. The limit of detection was 100 pg/sample with a coefficient of variation less than 20%. Linearity was indicated by an average correlation coefficient of 0.992 for LTC4 and 0.996 for LTD4 and LTE4.

This method was used to measure leukotrienes in nasal secretions from two seasonal allergic rhinitis patients treated with ragweed antigen. Nasal secretions were collected using filter paper disks, placed in both nostrils 5 minutes before and 2 minutes after vehicle challenge and 2, 4 and 6 minutes after challenge with a disk containing 333 PNU of ragweed antigen in one nostril. Compared to vehicle, antigen administration increased LTC4 release by 17- to 22-fold, LTD4 by 16- to 31-fold and LTE4 by 28- to 38-fold. The time of peak concentration of the peptido-leukotrienes was in the order: LTC4 < LTD4 < LTE4, which is consistent with the synthetic pathway LTC -> LTD4 -> LTE4. Antigen administration also produced higher concentrations of peptido-leukotrienes on the ipsilateral (challenged) side than on the contralateral side, and increases in peptidoleukotriene levels generally occured sooner on the ipsilateral side compared to the contralateral side.

[1] Balazy, M. and Murphy, R.C., Anal. Chem. 58: 1098-1101, 1986

STANDARD CURVES LTD_4 FROM FILTER PAPER DISKS

Theoretical (ng/sample)	Mean (ng/sample)	Standard Deviation	Coefficient of Variation %
0.1	0.111	0.02	18.2
0.5	0.585	0.02	2.8
1.0	0.997	0.03	2.8
2.5	2.270	0.06	2.9
5.0	4.673	0.09	1.8
10.0	10.214	0.04	0.4

STANDARD CURVES LTE_4 FROM FILTER PAPER DISKS

Theoretical (ng/sample)	Mean (ng/sample)	Standard Deviation	Coefficient of Variation %
0.1	0.110	0.02	14.3
0.5	0.598	0.04	7.1
1.0	0.981	0.07	6.7
2.5	2.348	0.10	4.4
5.0	4.674	0.10	2.1
10.0	10.196	0.05	0.5

On the Problem of Sensitivity for Detecting LTC_4, LTD_4 and LTE_4 in CF-LSIMS.

O.A. Mamer, McGill University Biomedical Mass Spectrometry Unit,
1130 Pine Ave West, Montreal Que., Canada H3A 1A3 and
C.S. Li, R. Young and J.A. Yergey, Merck Frosst Centre for Therapeutic Research,
PO Box 1005 Pointe Claire - Dorval Que., Canada H9H 3L1.

Leukotrienes LTC_4, LTD_4 and LTE_4 are present in mammalian tissues and fluids in fmol/g concentrations and because they are unstable and highly polar and they respond poorly in FAB, their detection and determination is difficult especially in situations where sample size is severely limited, as in human studies. Studies with methyl S-benzylcysteine as an LT model have shown that when the free amine function is alkylated with the reagents illustrated below, introduction of a

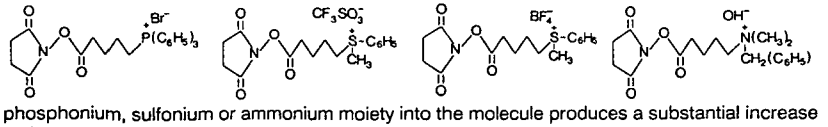

phosphonium, sulfonium or ammonium moiety into the molecule produces a substantial increase in the strength of the signal in FAB (Fig 1). Fig 2 shows the relative signal strengths for an equimolar mixture of the LT model and its triphenylphosphonium valerylamide (TPPV) derivative. We selected for further study the TPPV derivatives of authentic LTs.

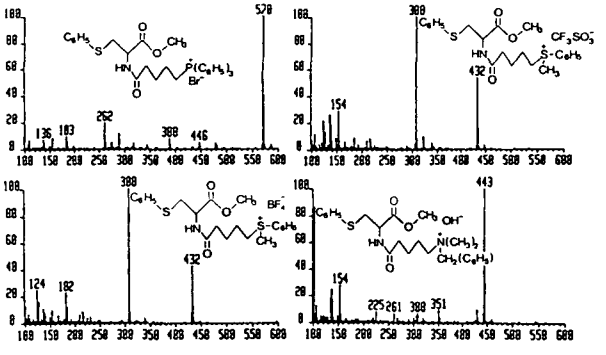

Fig 1

Fig 3 shows the TPPV derivatives of LTE_4, LTD_4 and LTC_4 both as the free acids and the methyl esters. Very prominent ions are noted for the cations produced. When an equimolar mixture is made of the TPPV derivatives of each LT in its acid and ester forms, Fig 4A shows the relative NBA FAB responses obtained immediately after mixing. Fig 4B shows the same mixture run under the same conditions after 21 h at 50° in methanol solution in air. Very little signal degradation has occured for the esters, and only relatively slight loss of intensity is noted for the free acids. The TPPV derivatives therefore are much more stable to oxidation and heat than the underivatized LTs

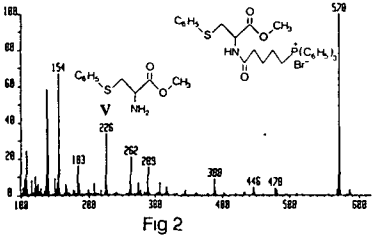

Fig 2

Analysis of a mixture of 5 pmol of free acid LTD_4 and LTD_4-TPPV in CF-LSIMS by HPLC inlet shows (Fig 5a) the TIC for 0-1000 Da, (5b) the RIC for 497 Da and the background subtracted spectrum for the peak, and (5c) the RIC for 841 Da and the subtracted spectrum for the peak. The LTD_4-TPPV peak is obviously much larger than the underivatized LTD_4 peak as seen in the TIC panel. When successive dilutions are made of a solution containing LTD_4-TPPV, 5 pg is easily detected, which corresponds to 3 pg of underivatized LTD_4. Fig 6 illustrates the SIM traces (841.4 Da) for 20 pg, blank, and 5 pg injections of LTD_4-TPPV.

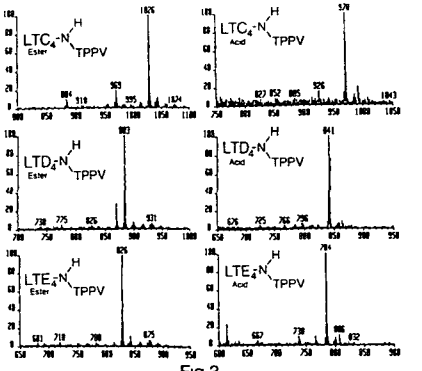

Fig 3

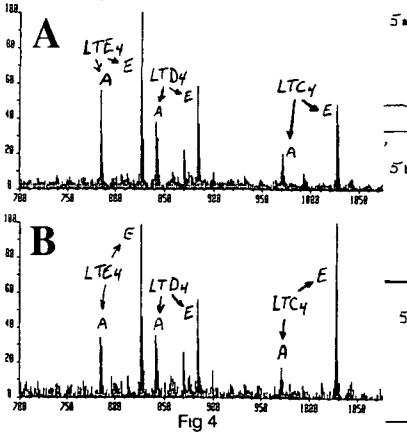

Fig 4

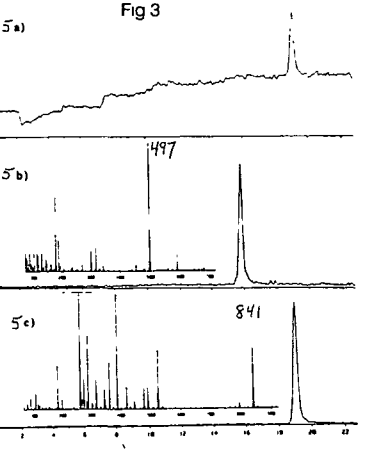

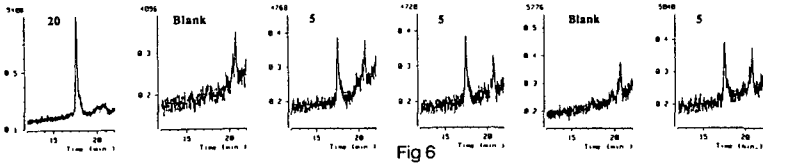

Fig 6

The TPPV derivatives of the LTs provide not only greater molar responses than do the native LTs, but they are also substantially more stable to oxidation and heating. For an example of the use of these derivatives in determining concentrations of the LTs in physiological fluids, please see the poster by Yergey *et al* (TP 43).

Continuous-Flow/Liquid Secondary Ion Mass Spectrometric Characterizationof *in vivo* and *in vitro* Metabolism of the 5-Lipoxygenase Inhibitor L-702,618

C.Li, N.Chauret, Y.Ducharme, L.A.Trimble, J.A.Yergey and D.A.Nicoll-Griffith
Medicinal Chemistry Department, Merck Frosst Centre for Therapeutical Research
P.O.Box 1005, Pointe-Claire-Dorval, Quebec, Canada, H9R 4P8

*Leukotrienes derive from the metabolism of arachidonic acid via the action of 5-*lipoxygenase[1]. The peptido-leukotrienes (LTC4,LTD4,LTE4) are strongly implicated as principal factors in the elicidation of the symptoms of asthma and other pulmonary conditions[2]. LTB4 is a potent chemotatic agent and is believed to be involved in diverse inflammatory conditions[3]. One major class of agents that modulate the effects of the leukotriene portion of the arachidonic acid cascade is the enzyme inhibitors which exercise their action by preventing or reducing the formation of lipoxygenase products. Because of the biological prominence of the 5-lipoxygenase products, great efforts of finding inhibitors of the 5-lipoxygenase enzyme have been undertaken in several pharmaceutical companies. Our search for potent, specific inhibitors of 5-LO led us to *discover a new series of naphthalenic lignan lactones*, exemplified by L-702,539 and its prodrug L-702,618.[4] The open form lactone of L-702,618 was found to close to give L-702,539 both *in vivo* and *in vitro* (the rate of closure is species dependent).

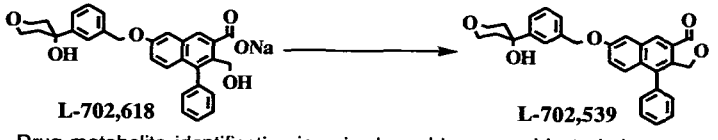

Drug metabolite identification in animals and human subjects is important from both a scientific and product development perspective. Both *in vitro* and *in vivo* metabolism studies[5] of L-702,539 were carried out in order to understand the metabolic stability of the different moieties of this compound. Continuous flow/liquid secondary ion mass spectrometry[6-7] has found its important applications in identification of small amount of polar metabolite. This technique offers great sensitivity compared with thermospray LC/MS. Full scan mass spectra of minor metabolites can usually be obtained rapidly, without sample purification or concentration. In cases where the full scan mass spectra did not give enough information to determine the structures of the metabolites, preparative isolation by HPLC and further characterizations were performed.

JEOL HX110A double focusing mass spectrometer (EB configuration) operated in the continuous flow/liquid secondary ion mass spectrometry mode was used in this study. Waters 600MS HPLC was operated at a flow of 0.9 mL/min, with the flow split just prior to a Rheodyne injector (with a 0.5 µl loop) by the aid of a 60 µm i.d fused silica open tubular column to produce a flow of 3 µl/min through a Spherisorb 0.32x100mm capillary column (Keystone Scientific, Bellefonte, PA) and then to the frit probe of JEOL mass spectrometer. A linear gradient from 55%A : 45%B to 90%A : 10%B in 25 minutes was used for separation (A: 1.5% Glycerol in CH_3OH; B: 1.5% Glycerol in 20 mM NH_4OAc, pH 5). Ions were produced by bombardment with a beam of Cs^+ ions (10 keV), the accelerating voltage was 10 kV and the resolution was set at 1,000.

L-702,539 was found to be metabolized extensively both *in vitro* and *in vivo*, especially on the pyran portion of the molecule. Three major oxidative metabolites were observed and identified to be: hydroxypyran (L-705,212), hydroxylactone (L-705,261) and hydroxyacid (L-745,244).

1. **"Leukotrienes and Lipoxygenase, Chemical, Biological and Clinical Aspects"**, edited by Rokach J. **"Bioactive molecules"** volumn II, (1989).
2. Samuelsson, B. **Adv. Prostaglandin Thromboxane Leukotriene Res.** 11, (1983), 1.
3. Ford-Hutchinson, A.W. **Agents Actions Suppl.** 12, (1983), 154.
4. European patent: EP0501578A, EP0501579A.
5. Chauret, N., Li, C., Ducharme, Y., Trimble, L.A., Yergey, J.A., Nicoll-Griffith, D.A. (manuscript in preparation).
6. Ito, Y., Takeuchi, T., Ishii, D., Goto, M., Mizuno, T. **J.Chromatogr.** 358, (1985), 201.
7. Caprioli, R.M, Fan, T., Cottrell, J.S. **Anal.Chem.** 58, (1986), 2949.

Metabolism Profile of L-702,618 (L-702,539)

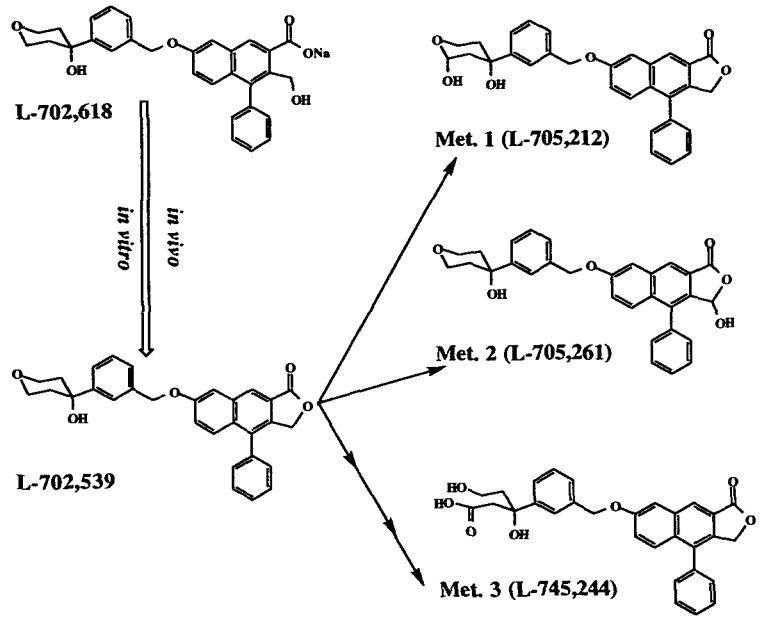

Characterization of Pineal Metabolites by Thermospray LC/MS/MS and GC/MS.

Hee-Yong Kim* and Lisa Edsall, Section of Mass Spectrometry, LMBB, NIAAA, NIH, Building 10, Room 3C-102, 9000 Rockville Pike, Bethesda, MD 20892

Lipoxygenation of polyunsaturated fatty acids leads to the production of many biologically active compounds such as monohydroxy fatty acids and leukotrienes. Since we have previously observed that lipoxygenation in the rat brain occurs only in the pineal, we have investigated the lipoxygenation of major polyunsaturates present in the pineal body.

Pineals obtained after the rat brain was perfused were homogenized in PBS buffer and incubated with 20:4n6, 22:6n3, 18:2n6 or 18:3n3 at 37°C for 30 min. Rat leukocytes were also incubated in parallel. The incubation mixture was extracted with dichloromethane after acidification to pH 3.0. The pineal and leukocyte metabolites were isolated by HPLC and derivatized to pentafluorobenzyl (PFB) derivatives for thermospray LC/MS/MS analysis as reported earlier (1). Subsequently, trimethylsilyl (TMS) derivatives were prepared for GC/MS analysis. In some cases, hydrogenation proceeded trimethylsilylation.

Thermospray LC/MS/MS analysis of PFB derivatives of pineal metabolites in the negative ion mode provided information concerning the position of oxygenation. Likewise, hydrogenated PFB-TMS-derivatives of metabolites analyzed by GC/EIMS in the positive ion mode also provided structural information. Unlike methylester-TMS-derivatives, positional isomers of the metabolites were well separated as hydrogenated PFB-TMS-derivatives. This allowed sensitive quantification of each isomer in the NCI mode based on the $(M\text{-}PFB)^-$. Using these techniques, it was found that rat pineal metabolizes arachidonic (20:4n6) and docosahexaenoic (22:6n3) acid through both 12- and 15-lipoxygenase pathways, primarily through the 12-lipoxygenase pathway.

Linoleic (18:2n6) and linolenic acid (18:3n3) were also well metabolized by rat pineal to primarily 13-hydroxy-derivatives as is shown in the radiochromatogram for 18:2n6 (Figure 1). The thermospray LC/MS/MS spectra obtained from PFB derivatives of 18:2n6 and 18:3n3 metabolites contained peaks resulting from the characteristic a-cleavage of the hydroxylated C-C bond. The cleavage occurred on the conjugated diene side, accompanying the hydrogen transfer toward that side. Characteristic fragments observed in the thermospray LC/MS/MS spectra of various positional isomers of 18 carbon metabolites are shown in Table 1. Production of 9-hydroxy derivatives were also observed in the thermospray spectra, although they occured at a level less than 3 % of 13-hydroxy derivatives, as determined by the NCI analysis. On the contrary to these results, rat leukocytes produced various isomers including 13-, 12-, 16- and 9-hydroxy derivatives from 18:3n3 and 9- and 13-hydroxy derivatives from 18:2n6, using the same incubation condition. Platelets also metabolized 18:2n6 and 18:3n3 to 9- and 13-hydroxy derivatives. These results indicated that the metabolites observed from pineal homogenate were not derived from blood cell components, and the property of 15-lipoxygenase present in the pineal body differs from that in leukocytes or platelets.

1. Kim, H.Y., and Sawazaki, S. (1993) Biol. Mass Spectrom. 22, 302-310.

Table 1. Peaks observed in thermospray LC/MS/MS spectra of pineal 18 carbon metabolites as PFB derivatives.

		Parent ion $(M\text{-}PFB)^-$	$(M\text{-}PFB)^-\text{-}H_2O$	Fragment
18:2n6	9-OH	295	277	171
	13-OH	295	277	195
18:3n3	9-OH	293	275	171
	12-OH	293	275	211
	13-OH	293	275	195
	16-OH	293	275	235

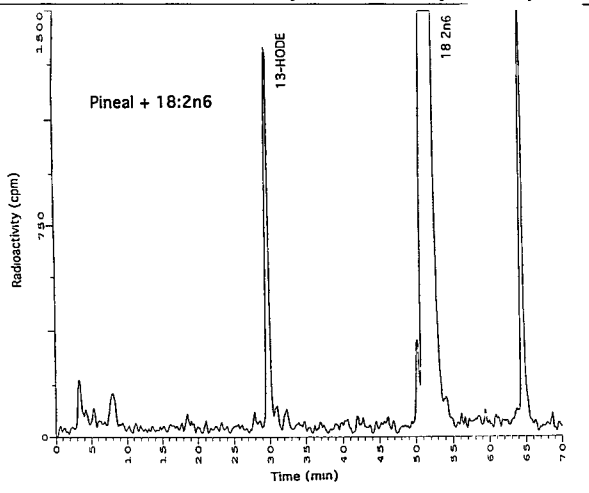

Figure 1. Radiochromatogram obtained after incubation of ^{14}C-18:2n6 with rat pineal homogenate.

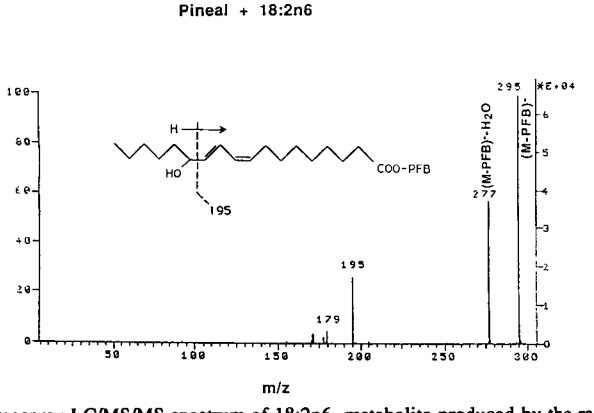

Figure 2. Thermospray LC/MS/MS spectrum of 18:2n6 metabolite produced by the rat pineal. A Finnigan TSQ-70 mass spectrometer was used. The thermospray vaporizer control and source temperatures were 75 and 250°C, respectively. The PFB-derivative was injected into an ODS column with methanol as the mobile phase at the flow rate of 1 mL/min.

CHARACTERIZATION OF SYNTHETIC IMMUNOSTIMULATORY LIPOIDAL PEPTIDES BY FAB-, ESI- AND MALDI-MS

Yoon Seok Chang[1], Patrick Kanda[2] and Douglas A. Gage[3]
[1]Korea Basic Science Center, Seoul, Korea; [2]Southwest Foundation for Biomedical Research, San Antonio, TX; [3]MSU-NIH Mass Spectrometry Facility, Department of Biochemistry, Michigan State University, East Lansing , MI

The introduction of a modified lipoidal residue, N-palmitoyl-S-[2,3-bis(palmitoyloxy)-propyl-cysteine (Pam3-Cys, Figure 1), at the amino terminus of a peptide [1] provides a potent immunoadjuvant which enhances the IgM and IgG antibody response to the rest of the molecule [2]. These synthetic peptides have significant advantages as potential vaccines, since the addition of other adjuvants is not required, and most importantly, because the epitope can be specifically defined. It is critical, however, that these peptides be structurally characterized prior to their use in immunological studies, particularly because the synthesis involves several steps where the peptide is exposed to conditions that promote amino acid side chain modification and/or deacylation. Moreover, the lipoidal nature of these peptides makes them extremely difficult to purify and analyze. On reversed phase HPLC columns, peak broadening caused by their tendency for self-aggregation can obscure contaminating peaks. Thus, amino acid analysis may not be adequate for structural confirmation. Further, because the amino terminal is blocked, traditional Edman degradation cannot be employed. We are currently using several MS techniques to characterize synthetic Pam_3-Cys peptides based on amino acid sequences found in the envelop glycoproteins of HIV-1 and Simian Immunodeficiency Virus (SIV). FAB-MS is useful in some cases for analysis, but the tendency for aggregation, which is somewhat dependent on the particular amino acid residues present, can often preclude detection of ions representative of the Pam_3-Cys peptides present. We have found that the use of nonpolar matrices, such as 3-nitrobenzyl alcohol, together with N-methyl-2-pyrrolidone as the solvent for the peptides, will produce interpretable spectra. Nevertheless, under these conditions some Pam3-Cys peptides yield only weak signals, while others are still refractory. Two alternative techniques, ESI-MS and MALDI-MS, provide much more reliable results with much better sensitivity (picomole level *vs* nanomole level for FAB-MS). The appearance of the ESI and MALDI spectra of Pam_3-Cys peptides can differ significantly, however (see Figures 2 and 3). Salt adducts are more prominent in MALDI spectra, while both techniques seem to have differential sensitivity for various components in a sample. Whether these effects are solvent or matrix dependent is not known. The influence of these factors is currently under investigation.

References

1. Metzger *et al.*, Int. J. Peptide Protein Res. 38: 545-554 (1991).
2. Bessler *et al.*, J. Immunol. 135: 1900-1905 (1985).

Figure 1. N-palmitoyl-S-[2,3-bis(palmitoyloxy)-propyl]-cysteine (Pam_3-Cys).

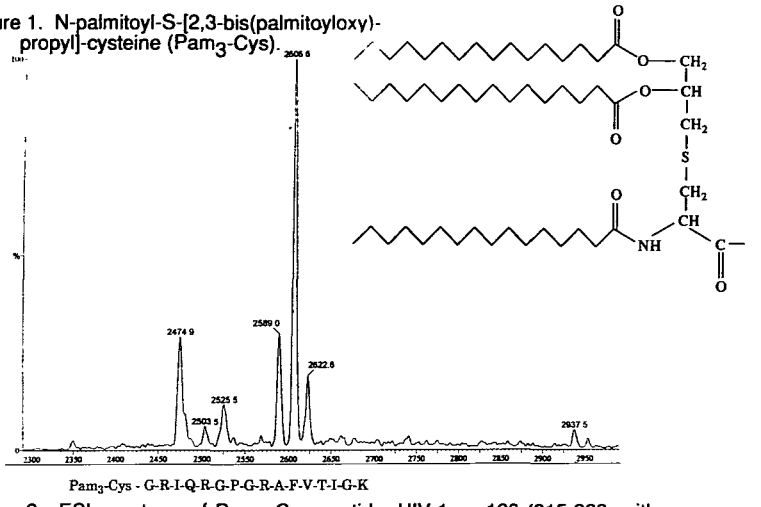

Figure 2. ESI spectrum of Pam_3-Cys peptide, HIV-1 gp 120 (315-329, with an additional G at the N-terminus). The expected MH^+ ion was the largest analyte peak in the spectrum, although other side-products from the synthesis were also detected. FAB-MS analysis of this sample produced no detectable signals.

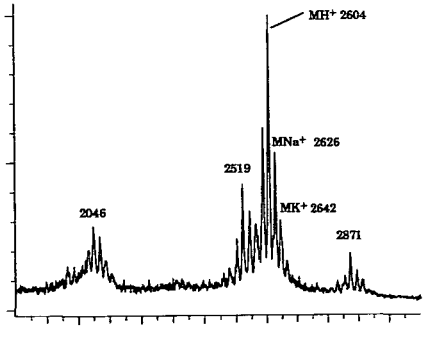

Figure 3. MALDI spectrum of the Pam_3-Cys peptide shown in Figure 2. The expected synthetic product was the largest peak in the spectrum, but the presence of salt adducts was more prominent than in the ESI spectrum. Further, the response of other components in the sample differs significantly from that found in the ESI spectrum.

ENZYMATIC CONVERSION OF NAAG TO NAA *IN VIVO* USING MICRODIALYSIS/MASS SPECTROMETRY

Shen-Nan Lin, [1]John M. Slopis, Li Li, [1]Ian J. Butler and Richard M. Caprioli
The Analytical Chemistry Center and the
Department of Biochemistry and Molecular Biology and
[1]Department of Neurology
University of Texas Medical School, Houston, Texas 77030

In vivo microdialysis with GC/MS analysis is capable of accurately determining stimulated release of extracellular NAA and NAAG from rat hypothalamus. Previous *in vivo* studies have shown stimulated release of NAAG but not NAA from other regions of rat brain, using immunohistochemical methods. Our results demonstrate release of NAA in high concentration but no increase in NAAG concentrations in the hypothalamus. To substantiate these findings, we have addressed the following questions. 1. How reproducible is the methodology? 2. Does rapid catabolism of NAAG occur rendering it difficult to observe in dialysate? 3. Does NAA meet at least one criterion for a neurotransmitter in the hypothalamus?

Male Sprague-Dawley rats were used with pentobarbital anesthesia. A 3 mm microdialysis probe was inserted into the hypothalamus stereotaxically. Artificial CSF dialysis buffer containing 5 mM KCl was delivered at 1.2 μl/min. Microdialysate samples were collected at 30 min intervals. Neuronal depolarization was stimulated in some experiments by infusion of 100 mM KCl for 20 min intervals. Hydrolytic enzyme inhibitor, asp-glu, was administered also by the infusion method. The dialysate samples were derivatized with 3N HCl in N-butanol, separated on an DB-5 fused silica capillary column and analyzed by a Finnigan Incos 50 mass spectrometer with chemical ionization source using ammonia as reactant gas. MH^+ ions of all neuro-compounds were selected for quantitative measurements.

In Fig. 1, microdialysis samples collected in 30 min fraction were divided into two parts, NAA and NAAG concentrations were measured to show the reproducibility of the measurements. The result also shows that NAA is released by the 100 mM KCl perfusion in the hypothalamus but not NAAG. Hydrolytic enzyme activity for degradation of NAAG to NAA *in vivo* was demonstrated by perfusion of NAAG-d3 (977 pmoles) via the dialysis probe and amounts of NAA-d3 break down product in the dialysate was measured. We found substantial amounts (90 ± 15 pmoles) of NAA-d3 in 6 dialysate samples collected from three animals, each rat receiving two NAAG-d3 perfusions. Asp-glu, an inhibitor of NAALADase which is a proposed specific catabolic enzyme system to cleave NAAG to NAA plus GLU, was perfused via the microdialysis probe. Fig. 2 shows that elevated NAAG levels were consistently observed in the fraction collected

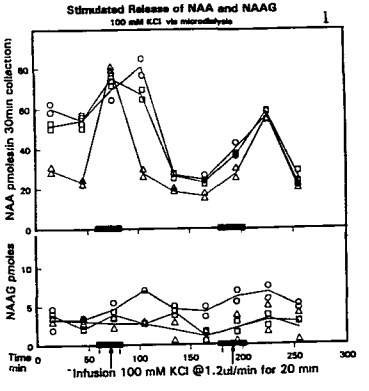

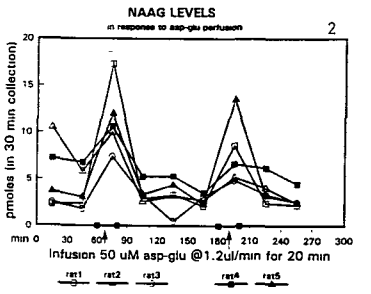

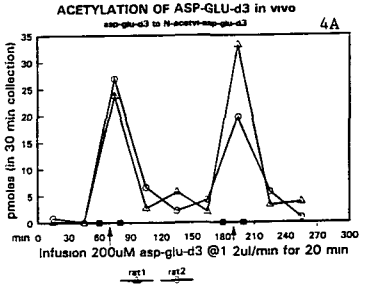

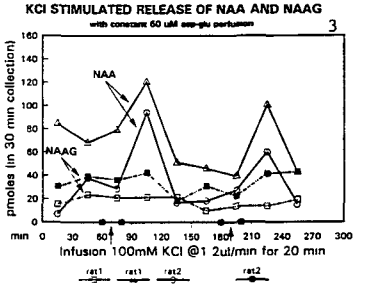

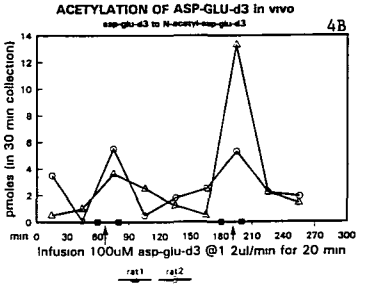

following inhibitor perfusion. When we repeated the catabolic experiments, we did not find differences in the amounts of NAA-d3 produced in the presence (90 ± 15, n=6) or absence (98 ± 20, n=4) of asp-glu. Finally, asp-glu and 100 mM KCl was perfused during the final experiment to stimulate release of NAAG. In Fig. 3, persistently elevated NAAG levels shown appear to be due to constant perfusion of asp-glu. No stimulated release can be observed. The results are in marked contrast to the observation of stimulated release of NAA measured in the same samples. These data suggest the elevated extracellular NAAG levels are not due to KCl stimulated release of NAAG, but instead are directly related to the presence of asp-glu in the perfusate. Our hypothesis is that acetylation of exogenous asp-glu is one of the metabolic events that takes place in the hypothalamus leading to NAAG elevation. Asp-glu-d3 (100 and 200 μM) in artificial CSF was perfused via the microdialysis probe and the acetylated product NAAG-d3 was measured. Figs. 4A and B shows significant amounts of NAAG-d3 proportional to the Asp-glu-d3 concentrations are in the dialysate. In contrast to previous results (Fig. 2), we did not find elevated endogenous NAAG levels resulting from asp-gly-d3 infusion.

In conclusion, we have demonstrated *in vivo* enzymatic conversion of NAAG to NAA. Our observation of KCl stimulated release of NAA support an independent role of NAA as a neurotransmitter in hypothalamus. We have also demonstrated *in vivo* acetylation of infused exogenous asp-glu to NAAG, suggesting the presence of an endogenous N-acetylation enzyme system in hypothalamus.

HYDROLYSIS OF PEPTIDE AND PROTEIN DRUGS BY IMMOBILIZED HEPATIC PROTEASES MEASURED USING CONTINUOUS-FLOW FAB LC-MS AND MS-MS.

Richard B. van Breemen and R. Kevin Blackburn
Department of Chemistry, Box 8204
North Carolina State University, Raleigh, NC 27695

Because biotechnology methods such as recombinant DNA technology facilitate the large scale preparation of pharmacologically active peptides and proteins, the therapeutic importance of peptide and protein drugs is rapidly increasing. Although most protein drugs must be administered parenterally, peptide drugs can often be administered by non-invasive routes, including oral, nasal, or transdermal administration. However, the bioavailability of drugs administered by these methods can be limited by poor absorption or degradation at the site of administration. In order to assess the significance of degradation in the gut prior to absorption of orally administered peptide drugs, we have developed a method using an immobilized digestive enzyme assay and continuous-flow FAB LC-MS to identify proteolytic peptides formed in the gut (1) and the rates of peptide drug degradation (2).

Following absorption from the digestive tract, orally administered peptide drugs must pass through the liver and resist proteolysis before reaching the general circulation. Peptide and protein drugs already in the bloodstream are degraded primarily by proteases in the liver. Therefore, we are developing an *in vitro* immobilized hepatic digestive enzyme assay to study degradation of peptide and protein drugs.

MASS SPECTROMETRY. Positive ion CF-FAB mass spectra were obtained using a JEOL HX110HF double focusing mass spectrometer equipped with a DA5000 data system and frit-FAB version of a continuous-flow FAB interface. Xenon fast atoms at 6 kV were used for FAB ionization. The resolution was 1200 and the ion source temperature was 47°C. B/E Linked Scanning MS/MS was carried out using static FAB and CAD in the first field-free region (helium collision gas). For MS/MS measurements, the range m/z 1-1,500 was scanned in 15 sec. using an equivolume mixture of glycerol/thioglycerol (v/v) as the matrix. Approximately 1 µg of unpurified peptide digest was analyzed per MS/MS measurement.

For CF-FAB measurements, the range m/z 100-1,500 was scanned in 8 sec. An Applied Biosystems Model 140A Microgradient HPLC Pump was used with a Vydac C18 HPLC narrowbore column (25 cm x 2.1 mm) at a flow rate was 100 µL/min. For compatibility with the CF-FAB ion source, the flow was split post-column so that flow rate to the mass spectrometer was 5 µl/min. A 30 min linear gradient from water to acetonitrile was used for reversed phase peptide separations. The mobile phase contained 0.5% glycerol, which functioned as the FAB matrix, and 0.1% trifluoroacetic acid. For each analysis, 10 µL of the incubation mixture was injected.

Enzyme Immobilization and Incubation with Peptide and Protein Substrates. Hepatic microsomes and cytosolic proteases were prepared from homogenized Sprague Dawley rat liver using ultracentrifugation. Microsomal proteases were solubilized in detergent using ultrasound at either pH 7.5 or pH 4.0. Microsomal proteases (pH 4.0 and pH 7.5) and cytosolic proteases (pH 7.5) were immobilized using previously published procedures (1). Each peptide or protein substrate (100 mL; 1 mg/mL) was incubated 8 or 24 hr with 10 mg glass beads containing immobilized proteases prior to analysis using LC-MS. Substrates investigated included recombinant human insulin, substance P, a cyclohexapeptide, and angiotensin II.

The specific activities of each immobilized enzyme preparation were determined by measuring the disappearance of human insulin as a function of time in an HPLC UV absorbance assay (see ref. 2). All fractions showed activity towards insulin. Next, the initial sites of hepatic proteolysis of each peptide substrate were identified using continuous-flow FAB LC-MS and MS/MS. For example, Figure 1 shows the CF-FAB LC-MS analysis of angiotensin II incubated for 24 hr with immobilized rat hepatic proteases, pH 7.5. The peptide eluting at 19.8 min formed a protonated molecule at m/z 775 (see Figure 2), which was shown by MS/MS to correspond to the peptide Val-Tyr-Ile-His-Pro-Phe.

For a given peptide substrate, each of the three enzyme groups displayed similar sites of initial cleavage. This observation suggests that these sites are the most susceptible to proteolysis. Because CF-FAB LC-MS is limited to the analysis of peptides weighing up to approximately m/z 3,000, the proteolytic fragments of human insulin must be identified using another ionization method.

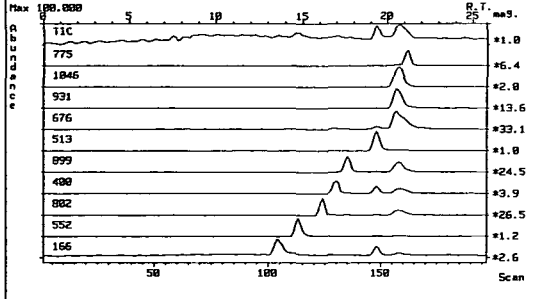

Figure 1.

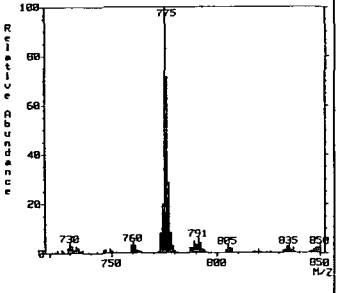

Figure 2.

REFERENCES.
(1) van Breemen, R.B., Bartlett, M.G., Tsou, Y., Culver, C., Swaisgood, H.S., Unger, S.E. *Drug Metab. Dispos.*, **19**, 683-690 (1991).
(2) van Breemen, R.B., Davis, R.G. *Anal. Chem.*, **64**, 2233-2237 (1992).

AN ASSAY FOR URINARY PEPTIDAL LEUKOTRIENES USING IMMUNOAFFINITY EXTRACTION AND CAPILLARY HPLC / CF-LSIMS DETECTION.

***J. A. Yergey, R. Young, C.S. Li, Merck Frosst Centre for Therapeutic Research, P.O. 1005, Pointe Claire-Dorval, Quebec, Canada H9R 4P8, O. Mamer, McGill University Biomedical Mass Spectrometry Unit, 1130 Pine Avenue West, Montreal, Quebec, Canada H3A 1A3**

OVERVIEW: Measurment of urinary excretion of peptidal leukotrienes (LT) is of vital importance in assessing the effectiveness of leukotriene synthesis inhibitors in human clinical studies, and for understanding the role of these potent endougenous inflammatory mediators. Radioimmunoassay of the peptidal leukotrienes requires HPLC separation of the three peptidal leukotrienes (LTC_4, LTD_4, LTE_4) prior to quantification, in order to eliminate cross reactivity[1]. Existing mass spectrometric methods also require HPLC isolation, followed by removal of the peptide part of the molecule, catalytic reduction, derivatization, and GC/MS[2]. The use of continuous-flow FAB for the detection of LT has been demonstrated, but detection limits were not sufficient for the picogram quantities found in many biological fluids[3]. Our goal has been to demonstrate a sensitive and specific capillary HPLC, continuous-flow liquid secondary-ion mass spectrometry (CF-LSIMS) methodology for the detection of urinary LT. We believed that immunoaffinity extraction for initial sample clean-up would provide efficient and clean extracts of the LT in a single step, as has been demonstrated in previous work with extraction of prostaglandins[4]. We also sought to utilize our recently described derivatization of the LT to a precharged triphenylphosphonium amide (Poster TP-36) to provide lower detection limits by CF-LSIMS.

EXPERIMENTAL: Immunoaffinity columns: The gel from Cascade Biochem Limited LTE_4 immunoffinity columns was removed and repacked into 1.5 mL syringe columns fitted with polyethylene frits. The flow rate of PBS through the columns was adjusted with slight pressure to frit / gel to yield about 30-50 µL/min. Columns were stored at 4°C in PBS. **Extraction Procedure:** Urine was adjusted to pH 11 using NaOH and frozen. Thawed urine was adjusted to pH 7.4 using HOAc. Appropriate standards were added (^3H or $^2H_3$ labelled LTD_4 or LTE_4), and some samples were spiked with LTD_4 or LTE_4 for determination of immunoaffinity binding capacity. Urine was centrifuged at 14,000 rpm for 10 min, and the supernatant filtered (0.45 µm). Standards of 1000, 300, 100, 30 and 10 pg LTD_4 plus 200 pg $^2H_3$-LTD_4 were prepared in PBS. Immunoaffinity extraction was automated using a Gilson ASPEC. Previously conditioned columns were allowed to drain and come to R T. Samples were applied in 750 µL aliquots and rinsed with 2 x 750 µL PBS and 2 x 750 µL H_2O. The leukotrienes were eluted with 750 µL H_2O:CH_3CN:NH_4OH (120:40:1) followed by 750 µL $(CH_3)_2CO$:H_2O (90:10). Columns were reconditioned with 2 x 750 µL $(CH_3)_2CO$:H_2O followed by 4 x 750 µL PBS. All flow through columns was by gravity feed. **Microscale Derivatization:** Sample extracts were dried in a Speed-Evap, and redissolved in 15 µL $NaPO_4$ buffer (0.5 M, pH 7.9). Buffer strength and pH were critical; no reaction occurred at pH ≤ 7.4, and the activated ester hydrolyzed too quickly at pH ≥ 8.1. The reaction was initiated by adding 20 µL of the triphenylphosphonium activated ester (TPPAE, 10.0 mg/mL H_2O). After 45 min, the reaction was quenched with 8 µL CH_3OH:NH_4OH (200:1). **Capillary HPLC / CF-LSIMS:** A standard HPLC pump (Waters 600 MS), supplied 1 mL/min of mobile phase consisting of CH_3OH:20 mM NH_4OAc, pH 5 (1.5 % glycerol in each). The gradient was 50:50 linear to 70:30, 5min, linear to 90:10, 15 min, and hold for 10 min. The main flow was split prior to the injection valve using ~ 5 cm of 50 µm fused silica on the open end of a Valco ZDV tee. Flow passed through a 20 µL injection loop on 6-port electrically actuated Valco valve, a 0.25 x 40 mm pre-column, a 0.3 x 100 mm analytical capillary column and into the JEOL HX-110A CF-LSIMS mass spectrometer ion source. Both columns were packed with KAPPA Spherisorb ODS2 (Keystone Scientific). Flow was diverted from the ZDV tee connecting pre-column and analytical column to waste for the first 5 min of each run, with a flow rate of 20 µL/min when passing through the pre-column to waste, and 3 µL/min when flow was reestablished through the analytical capillary column. The leukotrienes were detected by CF-LSIMS using electric-field SIM (m/z 784.38, 787.40, 841.40 and 844.42 for LTE_4-TPPV, $^2H_3$-LTE_4-TPPV, LTD_4-TPPV and $^2H_3$-LTD_4-TPPV, respectively).

[1] P. Tagari, D. Ethier, M. Carry, V. Corley, S. Charleson, Y. Girard, R. Zamboni, Clin. Chem., 35, 1989, 388.
[2] M. Balzy and R. C. Murphy, Anal. Chem., 58, 1986, 1098.
[3] M. J. Raferty, G.C. Thorne, R.S. Orkiszewski, S. Gaskell, Biomed. Environ. Mass Spectrom., 19, 1990, 465.
[4] H. L. Hubbard, T. D. Eller, D. E. Mais, P. V. Halushka, R. H. Baker, I. A. Blair, J. J. Vrbanac, Prostaglandins, 33, 1987, 149.

RESULTS AND DISCUSSION: Immunoaffinity extraction of the peptidal leukotrienes, using 1.5 mL syringe cartridges, gave reproducible recovery of LT; between cartridge SD ≤ 7% in all experiments. It was important to compress the gel slightly during packing, in order to regulate the flow of aqueous solvents to 30-50 µL/min. Extraction efficiency of ^3H-labelled leukotrienes from PBS was greater than 85% using new columns, but degraded to about 60% after 4-5 uses. Extraction efficiency from spiked human urine was greater than 70% using new columns, but degraded to less than 40% after 4-5 uses. After several uses, columns retained their original capacity to bind 50-100 ng of either LTD_4 or LTE_4. The extraction procedure was automated using a Gilson ASPEC, allowing 108 samples to be processed in parallel. Aqueous reaction of the extracted leukotrienes, to produce the triphenylphosphoniumvalerylamide (TPPV) derivatives, required using high buffer strength $NaPO_4$ at pH 7.9 and high concentrations (10 mg/mL) of the triphenyphosphonium activated ester. Under these conditions, the reaction proceeded to greater than 85% completion in under 45 minutes at both nanomole and picomole levels of leukotriene. The reaction was quenched in order to eliminate any unreacted TPPAE. Mass spectra of the derivatized leukotrienes contained strong molecular cations, with sensitivity about three times greater than for the analogous protonated molecule of the underivatized leukotrienes. Utilization of pre-column splitting of the reaction mixture permitted elimination of the large quantities of buffer and reagent present, while concentrating the leukotrienes at the head of the pre-column. Subsequently, the derivatized leukotrienes could be efficiently eluted through the analytical capillary and into the CF-LSIMS ion source. Use of injection volumes of 10-50 µL provided the opportunity to inject a substantial portion of the extracted / derivatized sample. Immunoaffinity extracted standards of LTD_4 could be quantified at the level of 10 pg / sample, and a standard curve was constructed from 10-1000 pg (LLS fit: y = 1.010 x + 10.43 pg, RSD = 17.2 %). Peaks other than the expected derivatives were observed in reagent blanks as well as in standards, but did not interfere with quantification (See Figure 1). Examination of extracted standards without derivatization, monitoring masses corresponding to the underivatized leukotrienes, revealed significantly higher background contamination, obviating the possibilty of detection of the underivatized species. SIM chromatograms of extracted urine samples, both unspiked and spiked with LTD_4, contained significant background peaks, obscuring low-level leukotriene peaks. LTD_4 could be observed in extracted urine only at spiked levels in excess of 300 pg (see Figure 2). The additional contamination observed in urine samples is likely due to non-specific binding in the immunoaffinity extraction, however this possibilty is not yet proven. The polyethylene frits used in the immunoaffinity columns have been reported to be a potential source of non-specific binding. The means to minimize the contamination are being investigated, such that urine samples might be extracted, derivatized and detected with the same efficiency as standard mixtures.

CONCLUSION: This work is the first demonstration of immunoaffinity extraction and mass spectrometric detection of peptidal leukotrienes at sub-picomolar levels. The use of immunoaffinity extraction, aqueous derivatization to cationic amides, and detection using capillary HPLC / CF-LSIMS should provide a useful alternative to GC/MS methods for the quantification of the leukotrienes.

FIGURE 1: Standard C (30 pg LTD_4 + 200 pg $^2H_3$-LTD_4-TPPV)

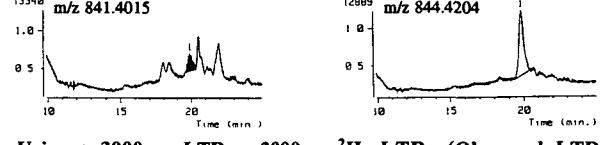

FIGURE 2: Urine + 3000 pg LTD_4 + 2000 pg $^2H_3$-LTD_4 (Observed LTD_4 = 3700 pg)

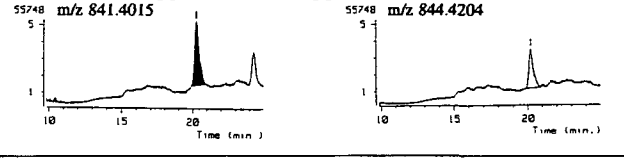

Association of Peptides with Bovine Serum Albumin (BSA) Detected by Electrospray Ionization Mass Spectrometry.

Lubomyr Baczynskyj, George E. Bronson and Teresa M. Kubiak
Upjohn Research Laboratories,
The Upjohn Company, Kalamazoo MI 49001

The recent communication on the detection of noncovalent receptor-ligand complexes by mass spectrometry[1] has generated a great deal of interest. Since then several communications on noncovalent binding of enzyme-substrates have been published and others have been reported at mass spectrometry meetings. All these examples refer to highly specific molecular recognition phenomena which result in the formation of very tight complexes with K_d values in the subnanomolar range. The majority of the studies reported so far has been accomplished using ion-spray (pneumatically assisted electrospray) ion sources where most of the solvent is removed with the help of a curtain gas. Also these investigations were limited to smaller proteins. We were interested in extending these experiments to larger proteins (e.g. albumins) as well as testing other types of electrospray ion sources, where the solvent is removed with the help of heat (thermally assisted electrospray).

Serum albumins are important proteins that circulate in the blood stream and are thought to be responsible for the transport of various substances such as steroids, fatty acids, and hormones. There are some indications that bovine growth hormone releasing factor (bGRF) binds to BSA in vitro[2,3]. BSA has previously been used as a standard for testing mass spectrometers fitted with an electrospray ion source (ESI). It was therefore of interest to use ESI MS for the possible detection of noncovalent complexes formed between BSA and [Leu^{27}]-bGRF(1-29)NH_2 or its more helical, Ala^{15}-substituted counterpart used as model peptides.

All experiments were run on a Vestec 201A instrument outfitted with a Vestec ESI source[4]. The BSA and the peptides, at the 1:10 molar ratio, were dissolved in 10mM ammonium acetate pH 7.4 and incubated at room temperature for 1-3 hours. The solution was then infused at a rate of 2 µL/min. The high mass end of the resulting ESI mass spectrum of the BSA - [Leu^{27}]-bGRF(1-29)NH_2 mixture is shown in Fig. 1. The deconvolution program developed in-house for the determination of mixtures of clusters was applied to this ESI mass spectrum. The association of one, two and three molecules of bGRF with one molecule of BSA was detected as shown in Fig. 1. When the GRF-BSA mixture was treated with acetic acid, the clusters corresponding to the mono-, di- and tri-adducts disappeared and the clusters corresponding to BSA were left which points to the non-covalent nature of these complexes. The Ala^{15}-bGRF analog also formed 1:1, 2:1 and 3:1 molar complexes with BSA.

Under the same conditions as used for the bGRF analogs, insulin and bradykinin (Fig. 2) formed a 1:1 molar complex with BSA. On the other hand, glucagon was more similar to the bGRF analogs in its binding pattern to BSA and formed 1:1, 2:1, and 3:1 complexes with BSA (data not shown). This data shows that BSA does bind various biologically active peptides and such non-specific and non-covalent complexes can be detected by ESI-MS. Our results also indicate that electrospray ion sources of different design are amenable for binding studies.

References.
(1) Ganem, B.; Li, Y.T.; Henion, J.D., *J. Am. Chem. Soc.* **1991**, *113*, 6294.
(2) Zysk, J.R., Cronin, M.J., Anderson, J.M., Thorner, M.O., *J. Biol. Chem.* **1986**, *261*, 1671.
(3) Kubiak, T.M., Martin, R.A., Cleary, D.L., Caputo, J.F. *Proc. 11th Am. Peptide Symposium*, (Rivier, J.E., Marshall, G.R., Eds.), ESCOM Science Publishers, **1990**, 218.
(4) Allen, M.H.; Vestal, M.L., *J. Am. Soc. Mass Spectrom.*, **1992**, *3(1)*, 18.

Fig.1. ESI MS of BSA + [Leu^{27}]-bGRF(1-29)NH_2.

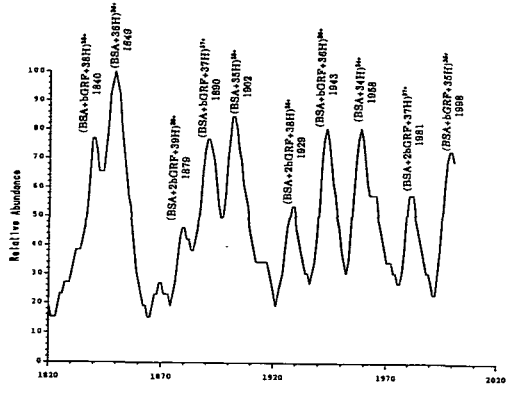

Fig.2. ESI MS of BSA + Bradykinin.

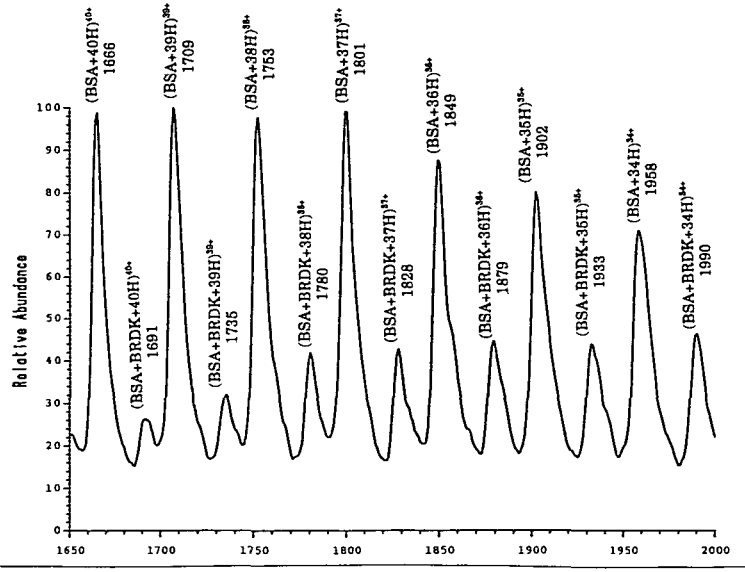

Study of Molecular Association by Electrospray Mass Spectrometry.

Lubomyr Baczynskyj, George E. Bronson, Teresa Kubiak, and Yuanda Zhang.
Upjohn Research Laboratories, The Upjohn Company, Kalamazoo MI 49001.

The recent disclosure of the detection by ion spray mass spectrometry of the formation of molecular complexes between a protein such as FKBP and the macrolide FK506[1)] has attracted a great deal of attention. In the ion spray (pneumatically assisted electrospray) the bulk of the solvent is removed with the assistance of a drying gas. In other source designs, the bulk of the solvent is removed thermally. The Vestec electrospray ion source[2)] belongs to this latter category. In this source the block is heated to 250° C and it was interesting to determine if the complexes formed in the ion source region could survive the thermal treatment. For this reason we repeated the experiments described in the communication referenced above[1)] using calf thymus FKBP (see Fig.1). Here a 1:1 molar ratio of FK506 to FKBP was used. In addition to a cluster at m/z 1799 of 7^+ charges corresponding to the monoadduct, a second cluster corresponding to the association of 2 molecules of FK506 with one molecule of FKBP was apparent at m/z 1914. When the molar ratio of FK506 to FKBP was increased to 3:1, the monoadduct ion cluster became the most abundant cluster in the ESI spectrum and the abundance of the ion cluster at m/z 1914 was 65%. Does this indicate that FKBP has a second binding site for FK506?

Similarly, when a 1:1 molar solution of rapamycin was infused at 2 μL/min at pH 7.4 in 10 mM ammonium acetate, the cluster at m/z 1814 was by far the most intense in the ESI spectrum. This corresponds to the 7^+ charged monoadduct of rapamycin to FKBP. A small cluster corresponding to the bis adduct of rapamycin to FKBP was present at m/z 1945.

The competitive binding experiments of FK506 and rapamycin with FKBP were also repeated (see Fig.2). The abundances of the monoadducts of $(FKBP+FK506)^{7+}$ at m/z 1799 and $(FKBP+rapamycin)^{7+}$ at m/z 1814 were in a ratio of 1·5. In addition to the clusters corresponding to the bis adducts of each macrolide with FKBP, which were present at m/z 1914 and 1945, very strong clusters appeared at m/z 1929 and 1688. The first corresponds to $(FKBP+1FK506+1rapamycin)^{7+}$ and the second to the same adduct but with 8+ charges. The abundance of the first cluster at m/z 1929 was 70% of the most abundant cluster which corresponds to the $(FKBP+rapamycin)^{7+}$ at m/z 1814. We studied the binding of calmodulin with Ca^{++} ions under the same conditions. Competitive binding between the NH_4^+ and the Ca^{++} ions was observed. These unexpected binding of calmodulin with ammonium ions contribute to peak broadening and less accurate MW determinations. However when acetic acid was added to the solution the peak broadening disappeared and a good MW determination of calmodulin was obtained.

α-, β-, and γ-cyclodextrins are known complexation agents of various organic compounds. Here we studied the association of each of them with pyridine, D- and L-Phe, D- and L-Trp and with bradykinin. In all cases strong association between the cyclodextrins and the organic compound could be demonstrated. If the three cyclodextrins were allowed to compete for L-Phe or L-Trp, the β-cylodextrin seem to form the most abundant clusters. The presence of sodium and potassium ions which are present in HPLC water and other solvents yielded sodium and potassium adduct ions with the cyclodextrins and the complexes.

References.

(1) Ganem, B.; Li, Y.T.; Henion, J.D., *J. Am. Chem. Soc.* **1991**, *113*, 6294.
(2) Allen, M.H.; Vestal, M.L., *J. Am. Soc. Mass Spectrom.*, **1992**, *3* (*1*), 18.

Fig. 1. ESI-MS of FKBP + FK506

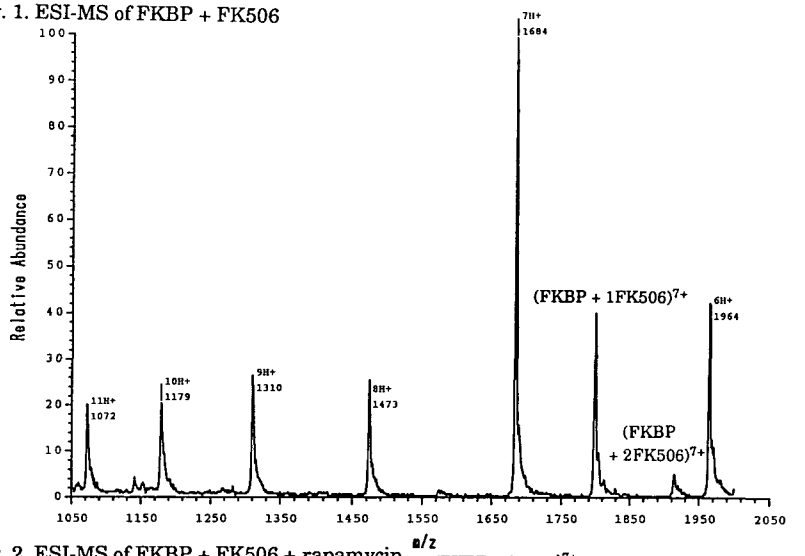

Fig. 2. ESI-MS of FKBP + FK506 + rapamycin

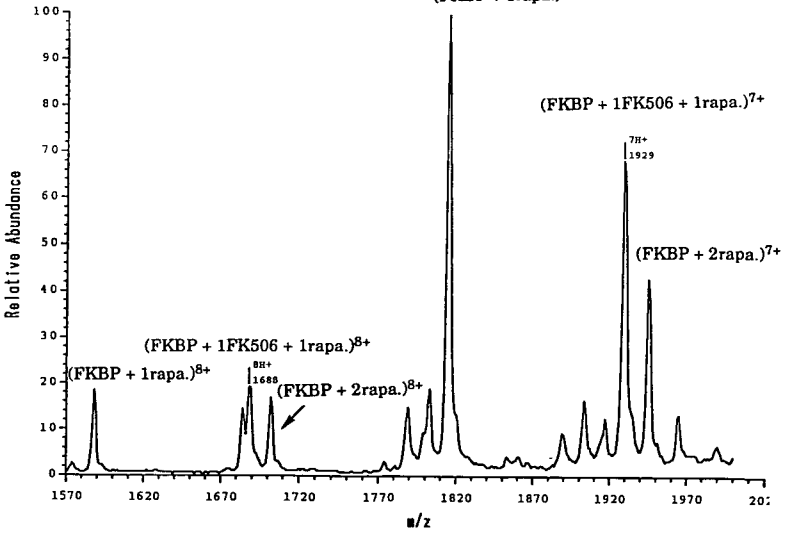

Structural Characterization of the Lung Surfactant Protein SP-B by Mass Spectrometric Methods

K. Baumeister[a], K. Müller[a], C. Maier[a], E Bauer[b], E Hannappel[b], R. Nave[c], U Krüger[c], K.P. Schäfer[c] & M. Przybylski[a]

[a]Faculty of Chemistry, University of Konstanz, P.O. Box 5560, D-7750 Konstanz
[b]Institute for Biochemistry, University of Erlangen, D-8520 Erlangen
[c]Byk Gulden Pharmazeutika, P.O. Box 6500, D-7750 Konstanz

Pulmonary surfactant, composed of ca 95% phospholipids and ca 5% proteins, reduces the alveolar surface tension and is essential for normal lung function and the prevention of alveolar collapse at end expiration. Insufficient surfactant levels or metabolism have been associated with respiratory distress syndrome, a frequent cause of death in premature infants. Among the lung surfactant proteins, the two hydrophobic proteins SP-B (ca 18 kD, unreduced) and SP-C (ca 4 kD) have been identified as essential components for in vivo surfactant activity [1].

Natural SP-B proteins from several mammalian species (tab. 1) have been isolated from lung tissue as well from lung lavage. Extraction from lung lavage was carried out by a modified procedure of Flügge et al. [2]. Initial characterization was obtained by SDS-PAGE for SP-B from several species. Exact molecular weight determinations and structural studies of natural SP-B proteins were perfomed by desorption-ionization mass spectrometric methods (PDMS, ESMS). ESMS enabled the first direct identification of the SP-B monomeric form after reductive cleavage of a covalent disulfide-dimer with dithiothreitol (DTT). The SP-B polypeptide chain consists of 79 amino acid residue (best studied for human-SP-B) and contains a large number of hydrophobic residues over the entire molecule. Furthermore, all SP-B proteins contain an odd number of cystein residues forming one inter- and several intramolecular disulfide bridges (three for human-SP-B).[3] The dimeric and monomeric forms can be distinguished by ESMS by their specific molecular ion series (fig. 1). All natural SP-B proteins investigated so far were identified as disulfide-dimers which can be cleaved by DTT (tab 1).

References:

[1] J. Goerke, Biochim. Biophys. Acta, 344 (1974) 241
[2] D. Wesel, U.I Flügge, Anal. Biochem. 138 (1984) 141
[3] J. Johansson, H. Jörnvall, T. Curstedt, FEBS Lett. 301 (1992) 165
[4] T. Curstedt, J. Johansson, P. Persson, A. Eklund, B. Robertson, B. Löwenadler, H. Jörnvall, Proc. Natl. Acad. Sci. USA, 87 (1990) 2985

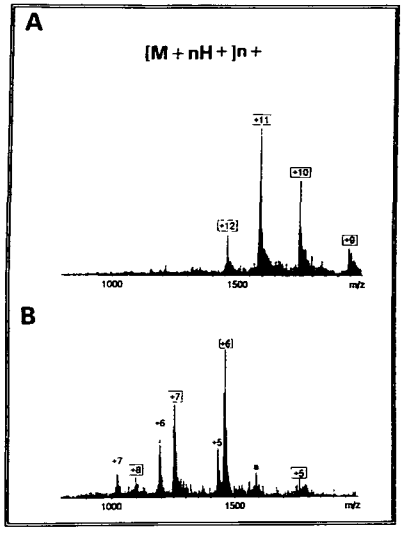

Fig. 1: ES-spectra of (A) unreduced and (B) DTT-reduced bovine-SP-B. The molecular weights identified were 17490 D for the dimer and 8764 D for the monomer.

species	molecular ions PDMS[a] m/z	molecular weight ESMS[b]	dimer	reduced form[c] (monomer)
human	$[M+H]^+$ 8816	$[M+10H]^{10+}$ 1763	17638	+
bovine	$[M+H]^+$ 8716	$[M+10H]^{10+}$ 1748	17490	+
sea lion	$[M+H]^+$ 8666	$[M+10H]^{10+}$ 1740	17388	+
zebra	$[M+H]^+$ 8590	-	17134	+
buffalo	$[M+H]^+$ 8698	-	17396	+
sheep	$[M+H]^+$ 8685	$[M+10H]^{10+}$ 1742	17422	+
rat	$[M+H]^+$ 8467	$[M+10H]^{10+}$ 1703	17045	+
porcine[d]	$[M+H^+$ 8737	-	17474	+

[a]The most abundant protonated molecular ion of the reduced form is shown

[b]Most abundant protonated molecular ion of the dimeric form

[c]The reduced form of different SP-B has been identified by SDS-PAGE after reductive cleavage with dithiothreitol.

[d]*Molecular weight determination has been done by Jörnvall et al. [4]*

Tab.1: Molecular weight comparison of natural SP-B from different species.

Use of Electrospray Mass Spectrometry to Characterize Covalently Modified Proteins

*K. Straub†, L. Antonino†, and M. Levy‡
Syntex Discovery Research† and Syva Corp.‡, Palo Alto, CA 94304

There are numerous examples in protein chemistry where it is desirable to covalently modify amino acid residues to give specifically derivatized macromolecules. For example, immunoconjugates such as haptens linked to carrier proteins are useful for eliciting the production of specific antibodies for use in immunoassays, and hapten-modified enzymes form the basis of many types of enzyme immunoassays. Conjugation of proteins with low molecular weight haptens gives a mixture of macromolecules which differ in the number and site of modified residues. The modification number n describes the average number of covalently modified residues per protein, and is a key parameter that must be carefully optimized when preparing enzyme tracers for use in immunoassays. Methods such as absorption spectroscopy, the use of radiolabeled hapten, and matrix-assisted laser desorption mass spectrometry[1] allow the calculation of an average modification number, but information on the actual distribution of modified proteins is more difficult to obtain

In principle, electrospray MS is an ideal technique for this type of problem, since it can directly give both the average modification number and the relative amounts of each species present. The latter result is useful for optimizing reaction conditions to yield a more precisely defined product for use in immunoassays. We have employed ESI-MS on a quadrupole analyzer to characterize the stoichiometry of covalent binding of small molecules to proteins in the molecular weight range of 50-60 kDa. The results obtained to date show that this methodology can be successfully applied to mixtures of derivatized proteins in this molecular weight range where the modifying hapten has a molecular weight of as little as 150 Da

ESI mass spectra were obtained using a Finnigan TSQ700 equipped with a standard electrospray source. Samples were prepared at concentrations of 1-5 pmol/µl in 10mM NH_4OAc and infused directly into the source at 1 µl/min A sheathing flow of 2-methoxyethanol and a nebulizing flow of nitrogen were used to assist the electrospray process Results obtained with the enzyme glucose-6-phosphate dehydrogenase (G6PDH; mw 54.5kDa) are shown in figure 1A. This protein gives a typical ESI mass spectrum with a distribution of multiply charged species of between +30 and +60, with well-resolved multiply charged ions Modification of the protein by reaction with a carboxylic acid-containing hapten (primarily by reaction with ε-amino groups of lysine residues) yields a mixture of modified proteins, each of which contributes to the overall spectrum The complexity of the resulting spectrum is dependent upon both the modification number and the relative mass of the hapten As the mass of the hapten species decreases, the multiply charged species begin to overlap, eventually reaching a point where individual components can no longer be resolved. An example is shown in figure 1B, obtained on G6PDH modified with a carbamazepine hapten with a residue mass of 290 Da Despite the significant overlap between the series of multiply charged ions, complete deconvolution of the electrospray data to yield a molecular weight distribution is still possible. Figure 1C shows the transformed spectrum obtained from the data in figure 1B. With a quadrupole analyzer, a practical limit to analyzing these types of mixtures appears to occur for a 60kDa protein at a modification number of *ca.* 8 and a hapten mass of approximately 150 Da.

Increasing the resolution of the analyzer does not yield substantial improvements in the deconvoluted data, since the resulting decrease in sensitivity offsets any real gain in signal. It is sometimes possible to improve the quality of the data by employing conditions to shift the entire envelope of multiply charged ions to higher m/z (lower charge number), where the m/z difference between successive charged species is larger This is limited by the decreased sensitivity and resolution of quadrupole systems above m/z 2000, however. In many instances the major factor limiting resolution is not the analyzer, but the presence of non-covalently bound adducts that contribute to broadening and attendant overlap of the multiply charged sample peaks. Removal of these interfering substances using techniques such as ultrafiltration is sometimes successful, but severe loss of sample limits this approach.

Another problem we have encountered is that of proteins that are not soluble under the usual conditions that are employed for ESI An example of this is inosine monophosphate dehydrogenase (IMPDH) This enzyme has a molecular weight of 56 kDa, contains 8 free sulfhydryls, and has very low solubility below pH 7. Treatment with 2-vinylpyridine converted the protein to a derivative with enhanced solubility and which gave a good response with ESI-MS using standard conditions (10 mM NH_4OAC, pH 5, 20% MeOH), as shown in figures 2A and 2B.

(1) I. Wengatz *et al.* , **Anal. Lett. 25**, 1983-1997 (1992).

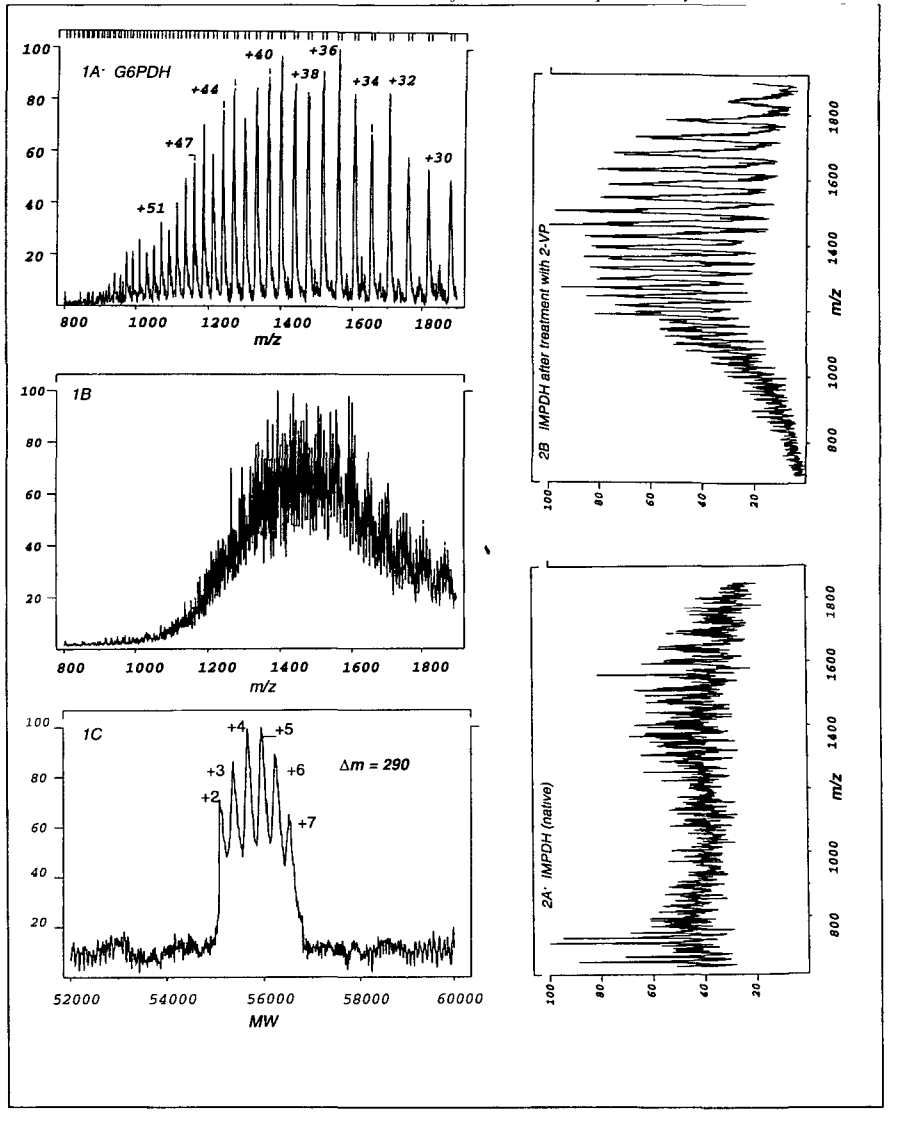

Structural and Functional Characterization of the Lung Surfactant Protein SP-C: Electrospray Mass Spectrometric Identification of "Leucine zipper-Analogue" Dimeric Complexes

C. Maier[a], K. Müller[a], K. Baumeister[a], E. Bauer[b], E. Hannappel[b], R. Nave[c], K. Melchers[c], E. Sturm[c], W. Gernandt[c], U. Krüger[c], K.P. Schäfer[c] & M. Przybylski[a]

[a] Faculty of Chemistry, University of Konstanz, P.O. Box 5560, W-7750 Konstanz;
[b] Institute for Biochemistry, University of Erlangen, W-8520 Erlangen; FRG
[c] Byk Gulden Pharmazeutika, P.O Box 6500, W-7750 Konstanz, FRG

Introduction

Lung surfactant is a complex mixture of phosholipids and proteins (approx. 5 %) that coats the alveoli to effect reduction of surface tension. Lack of surfactant causes respiratory distress syndrom (RDS). Among the LSF proteins, the extremely hydrophobic surfactant-associated protein C (SP-C, approx. 4 kD) plays the crucial role for the development of surfactant preparations, e.g. for the therapy of infant RDS. Therefore, detailed knowledge of the structure and functional characteristics of natural SP-C is necessary to develop corresponding recombinant human SP-C proteins. Based on recent structural data, a molecular comparison of natural SP-C proteins and human identical recombinant SP-C (rh-SP-C, Tab.1) has been carried out by chemical, chromatographic and mass spectrometric methods.

Materials and Methods

Rh-SP-C was obtained by chemical palmitoylation of recombinant SP-C, expressed in E. coli. The molecular homogeneity was established by PDMS and ESMS.
A Vestec A201 single quadrupole mass spectrometer was used for ESMS-analyses. Sample solutions (0.1 µg/µl) were sprayed at a needle voltage of 1 8 kV, a needle temperature of 40 °C and a flow rate of 2-4 µl/min. Mixtures of varying amounts of isopropanol and diluted acetic acid or 0.1 N HCl were used as solvent systems.

Results and Discussion

Natural SP-C was isolated by lung lavage from several species using Sephadex LH60-chromatography [1]. Rh-SP-C and crude natural SP-C proteins were chromatographed by HPLC on a RP-C4 column and yielded comparable retention times. Their primary structures in particular the identification of the thioester-palmitate moiety were established by ^{252}Cf-PDMS-analysis combined with chemical methods, e.g. deacylation by DTT-treatment followed by S-alkylation and N-terminal Edman/PDMS-sequence analysis [2].
New solvent systems for ESMS-analysis were developed and yielded molecular weight data with high accuracy and resolution, enabling the identification of methione oxidation in some of the SP-C proteins. The discovery by ESMS of dimeric supramolecular structures of SP-C ("Leucine zipper-analogue" dimers) via their multiply protonated odd charge states has been an interesting feature for the evaluation of the biological function of SP-C. The formation of the dimeric complexes was shown to be pH- and solvent-dependent. Furthermore, the successful formation of heterodimeric complexes between different recombinant SP-C mutants suggests a structure model of the SP-C dimer, based on the dimerization principle of the "leucine zipper"-proteins [3].

Tab. 1: Primary structures of natural human SP-C (h-SP-C) and recombinant human SP-C (rh-SP-C).

	Primary Structure
h-SP-C	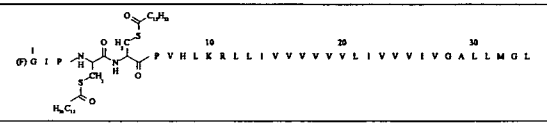
rh-SP-C	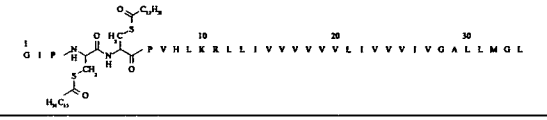

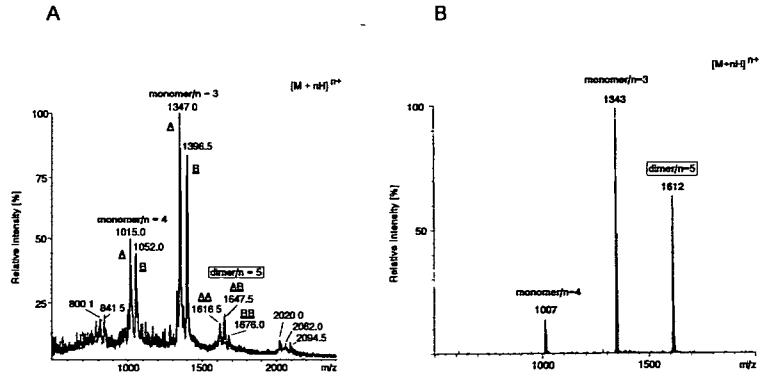

Fig. 1: ES mass spectra of h-SP-C (A) and rh-SP-C (B) showing the 3-fold and 4-fold protonated molecular ions of the SP-C monomer and the 5 fold protonated molecular ions of the SP-C dimer, respectively.

References

1) T. Voss, K.P Schäfer, P.F. Nielsen, A. Schäfer, C. Maier, E. Hannappel, J. Maaßen, B. Landis, K. Klemm, M. Przybylski, *Biochem. Biophys. Acta*, 1138 (1992) 261
2) P.F. Nielsen, B. Landis, M. Svoboda, K. Schneider, M. Przybylski, *Anal. Biochem.* (1990) 191, 302
3) M. Gartenberg, C. Ampe, T. Steitz, D. Crothers, *Proc. Natl. Acad. Sci. USA* (1990), 97, 6034

Reversibility of Heat Induced Conformational Changes of Proteins studied by Electrospray Ionization Mass Spectrometry

*Urooj A. Mirza and Brian T. Chait
The Rockefeller University, 1230 York Ave, New York, NY.10021

Introduction In their native states, globular proteins are tightly folded, compact structures that can be denatured and caused to unfold by subjecting them to extremes of pH, denaturants such as guanidinium hydrochloride, organic solvents, detergents, and high temperatures. A variety of techniques have been applied to the measurement of conformational changes of proteins in solution, including acid-base titrations, calorimetry, spectrophotometry, viscometry, circular dichroism, fluorescence, and nuclear magnetic resonance. Recently, we and others have demonstrated that conformational changes of proteins can also be detected by electrospray ionization mass spectrometry.[1,2] In the present study we demonstrate a new mass spectrometric method for probing the **reversibility** of heat induced conformational changes in globular proteins and the effects of different solutions on the reversibility of these conformational changes.

Experimental The method that we developed for probing the reversibility of heat-induced conformational changes[2] involves comparison of the electrospray ionization mass spectra of a protein acquired under three different conditions. Spectra are obtained from:

1) A solution sprayed at room temperature (25°C), where the protein is expected to be in its native conformation.
2) A solution sprayed at an elevated temperature Td, in excess of that required to bring about the conformational change(s).
3) A solution that has previously been heated in a vial to a temperature Td, maintained at Td for 4-5 minutes, and then cooled to room temperature prior to electrospray MS analysis.

When the spectrum acquired under condition 3 is found to be identical with that acquired under condition 1, we infer that the conformational change is reversible. Conversely, when the spectrum acquired under condition 3 is observed to be closer to that acquired under condition 2, we infer that the change is irreversible.

Results Cytochrome c (MW. 12,229) in an aqueous acetic acid solution at pH 3.6 was found to undergo two separate heat-induced denaturation transitions at temperatures T_1 and T_2 (fig 1). The probe of reversibility outlined above showed that the conformational changes occuring at the lower temperature (T_1) are reversible (fig 2abc), while those occuring at the higher temperature (T_2) are irreversible (fig 3abc) on the time-scale of the experiment (minutes to hours). The presence of (50%) methanol was found to render the high temperature conformational changes reversible on the same time-scale. Analogous reversibility experiments with bovine ubiquitin (MW 8565) indicate that the protein undergoes reversible heat induced conformational changes in all the solutions that were tested. Chicken egg lysozyme (MW 14,306) was found to undergo reversible heat induced conformational changes in an aqueous acidic solution or an aqueous acidic solution to which methanol have been added. By contrast, denaturation of lysozyme in water and 50% methanol was determined to be irreversible on a time scale of hours but reversible over longer time scales (days).

References
1) Chowdhury, S.K; Katta,V.; Chait, B.T. JACS 1990,**112**,9012.
2) Mirza A.U.; Cohen, S.K. and Chait, B.T. Analytical chemistry 1993,**65**,1.

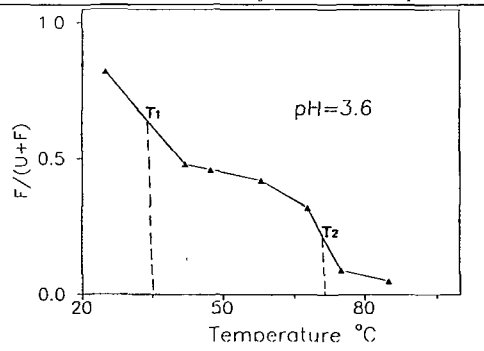

Fig.1 Fraction of folded state of cytochrome c.

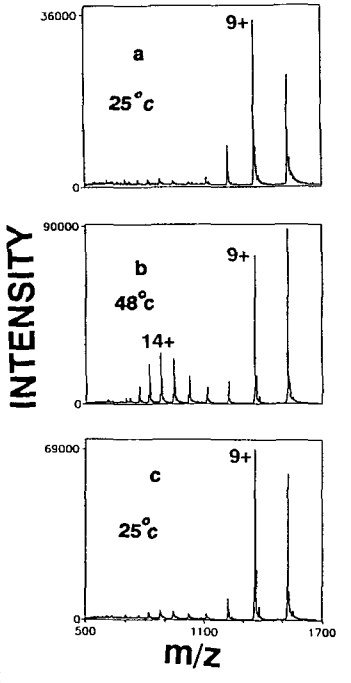

Fig.2 Reversible denaturation of cytochrome c .

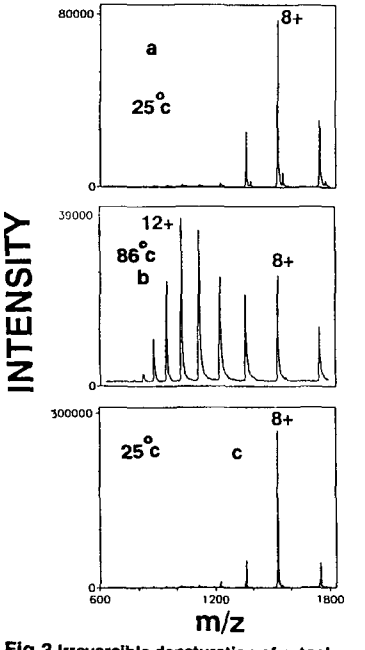

Fig.3 Irreversible denaturation of cytochrome c.

Determination of primary structure and biological activity of different recombinant human epidermal growth factor proteins

*M.Svoboda[a], A.Bauhofer[b], E G.Bade[b] and M.Przybylski[a]
Faculties of Chemistry[a] and Biology[b], University of Konstanz, P.O.Box 5560, D-7750 Konstanz, FRG

Natural epidermal growth factor (EGF) is a 53-aa polypeptide (1) with three intramolecular disulfide bonds. EGF modulates the proliferation and a variety of other functions of almost every cell type studied (2) Recombinant human EGF (rhEGF) is expressed in E. *coli* with an additonal N-terminal Met residue (3). The primary structures and molecular homogeneities of rhEGF's from different manufacturers were characterized using ^{252}Cf plasma desorption (PDMS) and electrospray mass spectrometry (ESMS). Only one protein, rhEGF-A, showed the correct MW of 6346 D, while a second protein, rhEGF-B, had a significantly higher MW of 7020 D both in ESMS and PDMS. Furthermore, the series of multiply protonated ions in ESMS shifted to higher protonation states for rhEGF-B, indicating the presence of additional basic aa in this protein (see figure 1).

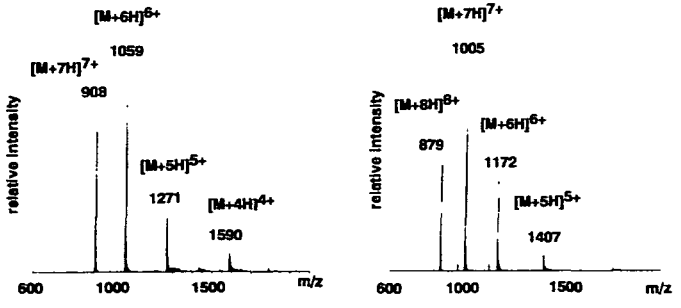

Figure 1: Electrospray mass spectrum of rhEGF-A (left) and rhEGF-B (right) showing the series of multiply protonated molecular ions

Reduction and carboxymethylation of cystines using dithiothreitol and iodacetamide followed by PDMS analysis confirmed the presence of three intramolecular disulfide bridges both in rhEGF-A and in rhEGF-B. Cleavage of C-terminal Arg using Carboxypeptidas B showed a correct C-terminus in both proteins (figure 2). Edman degradation of rhEGF-B combined with PDMS analysis revealed, that this protein had additional Lys residues, because three instead of the expected two phenylisothiocyanates (PITC) coupled to ε-amino groups of Lys residues in the first Edman step. Edman gas phase analysis revealed, that rhEGF-B had 59 aa and an elongated, strongly hydrohilic N-terminus, containing the pentapeptide -**KKYPR**- following the N-terminal Met residue(figure 2)

(1) Carpenter, G., and Cohen, S. (1979) Annu. Rev Biochem. 48,193-216
(2) Carpenter, G. (1989) Handbook of exp. Pharmacology, In Peptide Growth Factors and Their Receptors I (M.B. Sporn and A B. Roberts, Ed.) Berlin, Springer
(3) Kishimoto, F et al.(1986) Gene 45,311-316

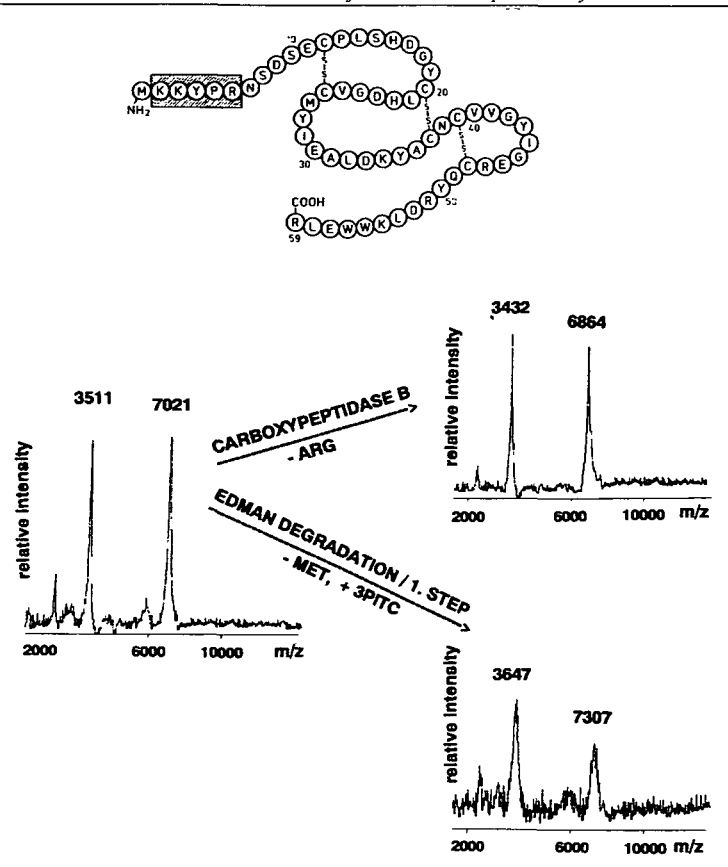

Figure 2 Enzymatic cleavage of C-terminal Arg of rhEGF-B by Carboxypeptidase B and Edman-degradation of intact rhEGF-B showing loss of N-terminal Met but additional coupling of three phenylisothiocyanates (PITC) to intramolecular Lys (K) residues.

This sequence insert leads both to a significant decrease in the proliferation activity as well as to a reduced cell migration activity of this recombinant protein, which can be explained by a change in receptor binding affinity. These results underline the importance of desorption ionization mass spectrometry as fast and accurate molecular analytical method for the structural control of recombinant proteins.

Structural Characterization of Cyclic RGD-Containing Peptides by Ionspray Tandem Mass Spectrometry

Yiping Sun, David J. Eickhoff, Stephen G. Wood, Mark D. Bauer,
Thomas W. Keough and Charles R. Degenhardt
The Procter and Gamble Co., Miami Valley Laboratories,
PO Box 398707, Cincinnati, OH 45239-8707

Introduction

Cyclic RGD-containing peptides and their analogs are important inhibitors of cell adhesion associated with angiogenesis and platelet aggregation. They can be either thioether or disulfide forms. It is very important to establish a method for rapidly identifying these peptides, and for confirming the structure of the final products. The cyclization and blocked N-termini of these RGD-containing peptides make them difficult to analyze by Edman sequencing. Although ionspray ionization mass spectrometry has proven very useful for the structural characterization of peptides and proteins, the mass spectra of the cyclic RGD-containing peptides obtained by ionspray MS/MS analysis showed very little fragmentation. In this study, we report an approach by which cyclic peptides were first converted to their linear counterparts by tryptic digestion or performic acid oxidation (Figure 1), and then sequenced by ionspray MS/MS.

Experimental

Performic Acid Oxidation - Cyclic peptides were dissolved in H_2O and oxidized with performic acid (35% H_2O_2:88% HCOOH, 1:19, v/v) at room temperature for 10 minutes.

Tryptic Digestion - Cyclic peptides were digested with trypsin in 0.1 M NH_4Ac (pH=7.7) at 37 °C for one hour.

Ionspray MS and Ionspray MS/MS - All experiments were carried out on a Sciex API-III LC/MS/MS triple quadrupole instrument. The delivery solvent was CH_3OH:H_2O (1:1) with 0.1% HCOOH using a flow of 5 µl/min. For MS/MS analysis, ultrapure argon was used as the collision gas at a target gas thickness of 3.3×10^{14} atoms/cm^2.

Results and Discussion

Cyclic RGD-containing peptides and their analogs analyzed by ionspray mass spectrometry are listed in Table 1. The molecular masses of these peptides are in the range of 500-1500 Da. Figure 2 is a fragment ion spectrum obtained from an RGD-containing peptide (disulfide form, MH^+=551.0). Unfortunately, this spectrum showed a strong parent ion with little fragmentation. Figure 3 is a fragment ion spectrum of an RGD-containing peptide analog (thioether form, MH^+=649.0), which also showed little fragmentation. Changing MS/MS parameters like the collision gas thickness had little effect on the fragmentation. In order to get sequence information and to confirm the structure of these cyclic peptides, they were first converted to their linear counterparts by tryptic digestion or performic acid oxidation, and then sequenced by ionspray MS/MS. MS/MS data obtained from the disulfide peptide (MH^+=551.0), after performic acid oxidation, is shown in Figure 4. Significantly increased fragmentation is seen in the spectrum compared to that seen in Figure 2. These data confirm the peptide sequence. MS/MS analysis of the RGD-containing peptide analog (thioether form, MH^+=649.0), after tryptic digestion, also showed many fragment ions which provided the sequence of the peptide (Figure 5). This same approach has been used successfully for the characterization of many other cyclic RGD-containing peptides and their analogs.

Conclusions

An approach which combines tryptic digestion or performic acid oxidation with ionspray MS/MS sequencing has been used for analyzing cyclic RGD-containing peptides. The method is simple and rapid. It provides sequence information which is difficult to obtain by classical Edman sequencing.

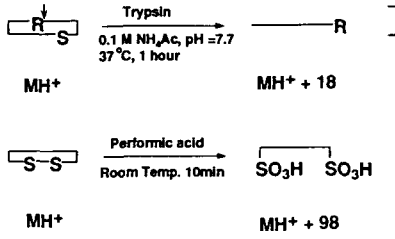

Figure 1. Strategies for the Analysis of Cyclic RGD-containing Peptides by Ionspray MS

Table 1. Cyclic RGD-Containing Peptides and Their Analogs Analyzed by Ionspray MS/MS

Peptide	MH+
CFTPRGDMPGPYC-OH	1441.8
GPen-GRGDSPCA-OH	948.4
CRGDC-OH	551 0
$CH_3C(=O)$-YIGSRC-NH_2	737 3
$CH_3C(=O)$-RGDWP-NH-$(CH_2)_6$	739.2

Pen = Dimethylcysteine

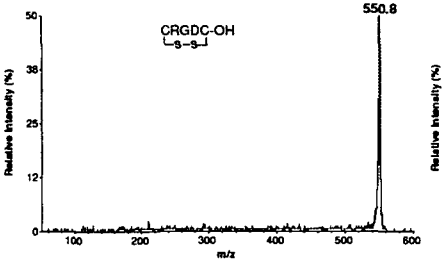

Figure 2. MS/MS Analysis of an RGD-Containing Peptide before Performic Acid Oxidation

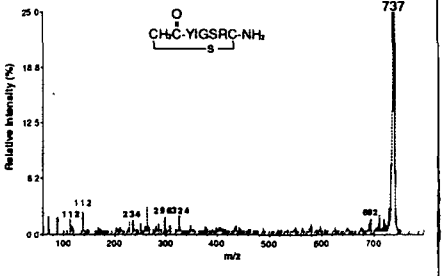

Figure 3. MS/MS Analysis of an RGD-Containing Peptide Analog before Tryptic Digestion

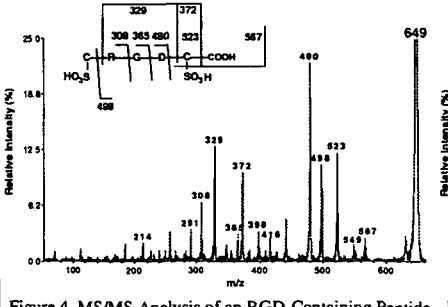

Figure 4. MS/MS Analysis of an RGD-Containing Peptide after Performic Acid Oxidation

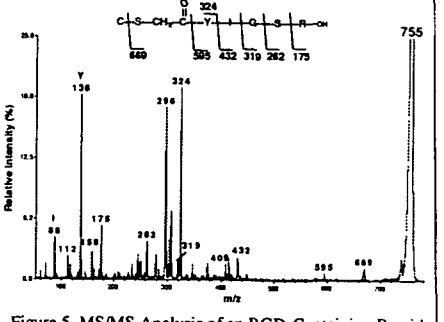

Figure 5. MS/MS Analysis of an RGD-Containing Peptide Analog after Tryptic Digestion

Application of Electrospray Mass Spectrometry to Structure Studies of Bovine Adenosine Deaminase

**Michele A. Kelly, Suming Hua[a] and Catherine C. Fenselau.*
Department of Chemistry and Biochemistry, University of MD, Baltimore County, Baltimore, MD 21228; [a]Department of Biological Chemistry, University of MD at Baltimore, Baltimore, MD 21201

Adenosine deaminase (ADA) is an enzyme required in mammals for the deamination of adenosine to inosine. The genetic deficiency of this enzyme results in severe combined immunodeficiency disease (SCID). Enzyme replacement therapy has been effective in treating victims of SCID as a nontoxic alternative to bone marrow transplantation and red-cell transfusion[1,2]. The primary sequence of bovine ADA is presently unknown although it is used clinically, as an orphan drug. Polyethylene glycol (PEG) is covalently attached to the therapeutic enzyme to increase its lifetime when administered to patients[1,2]. Using the known human ADA gene sequence as a reference[3], the amino acid sequence of bovine ADA is being investigated. Ultimately, the PEG attachment sites on bovine ADA will be determined using experimental methods developed previously in our laboratory[4].

The molecular weight of reduced and carboxymethylated bovine adenosine deaminase was determined to be 40549 ± 16 daltons by electrospray mass spectrometry (ES-MS) (**Figure 1**). This value is close to the calculated molecular weight of human ADA containing 362 amino acids (40933 Da, allowing for 5 carboxymethylated cysteine residues and excluding the initiator, Met). Subsequently, bovine ADA was digested using several proteolytic enzymes and mapped by ES-MS.

Clostripain, which cleaves specifically after arginine residues, was used to digest bovine ADA to produce several proteolytic fragments ranging in molecular weight between 2000-8000 daltons. Few fragments could be mapped perfectly to the human ADA reference; thus, several amino acid substitutions had to be ascertained. Incomplete digestion aided the placement and order of clostripain pieces. For example, two peptides in an ES-MS spectrum of a clostripain fraction have a mass difference corresponding to residues [81-100]. Concluding that the larger peptide (7657 Da) is an incomplete cut from residues [81-141], the smaller peptide (5333 Da) must map onto residues [100-141]. This is 101 Da higher than the value predicted from the human sequence.

Unassigned clostripain fragments were further digested with *S. aureus* V8 protease to produce smaller sized fragments ending in aspartic or glutamic acid residues. This approach provides certainty in mapping resultant peptides within the larger clostripain proteolytic fragment as shown in **Figure 2** and further localizes any mass discrepancies. Tandem mass spectrometry was then used to confirm proposed amino acid changes where mass differences were apparent. Using this approach, residue 351 was assigned as arginine. In the human sequence, the corresponding residue is a glycine so this peptide was not predicted for a clostripain digestion.

CNBr is a useful chemical for obtaining specific cleavage of a protein after methionine residues, resulting in homoserine and/or homoserine lactone termini. Since methionine is not a relatively abundant amino acid in most proteins, fewer fragments are formed. In this case, even if mass variations exist, fragments of distinct sizes can be mapped with confidence against the human gene sequence. Corrected for known mass changes obtained from clostripain experiments, all but five residues from [52-352] can be mapped by CNBr cleavage.

In order to locate the C-terminus of bovine ADA, BNPS-skatole was used to cleave specifically after tryptophan residues. Like CNBr, the infrequent occurrence of tryptophan in protein sequences results a limited number of fragments. The ES-MS spectrum of the C-terminus suggests that this peptide exists as a mixture. Further investigation of this fragment will seek to confirm this result.

Electrospray MS has been used to quickly and conveniently map various proteolytic digests of bovine ADA against a reference sequence. This approach is useful in pinpointing regions with mass discrepancies. Twenty amino acid substitutions have been confirmed by tandem mass spectrometry in the present work. This implies that the sequence of bovine ADA is over 90% homologous to the human sequence. The reproducibility and accuracy of these methods will be crucial when locating the sites of modification on the therapeutic drug, PEG-ADA.

FIGURE 1: ES-MS spectrum of reduced and carboxymethylated bovine ADA.

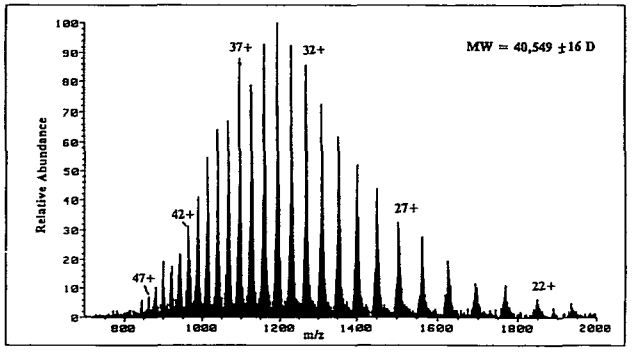

FIGURE 2: *S. aureus* V8 digest of a clostripain fragment

[324-351] MW_{found} = 3282

LNINAAK[330] SSFLPEDEKK[340] ELLDLLYKAY[350] R[351] (G)

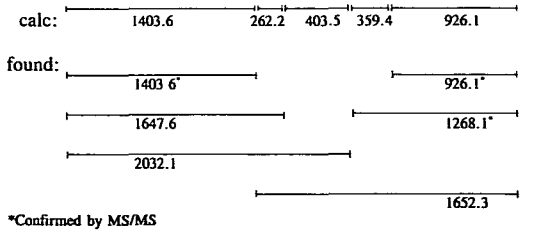

*Confirmed by MS/MS

1. M.S. Hershfield, et al. *New Eng. J. Med.* 316(10), 589-596. (1987)
2. Y. Levy, et al. *J. Pediatr.* 113(2), 312-317. (1988)
3. Peter E. Daddona, et al. *J Biol. Chem.* 259(19), 12101-12106. (1984)
4. Martha M. Vestling, et al. In Press, *Drug Metab. Dispos.* (1993)

ACKNOWLEDGEMENTS: We would like to thank Constance Murphy, Terry Sumpter, and Martha Vestling for their contributions to this work.
This research was supported by the National Science Foundation and the National Institutes of Health.

Electrospray Mass Spectrometry Characterization of Cathepsin B *C*-Terminal Processing

Rong Feng[1], Andrew D. Rowan[2], Yasuo Konishi[1] and John S. Mort[2]
(1) National Research Council of Canada, Biotechnology Research Institute, 6100 Royalmount Avenue, Montreal, Quebec, Canada
(2) Shriners Hospital for Crippled Children, Joint Disease Laboratory, 1529 Cedar Avenue, Montreal, Quebec, Canada

Cathepsin B, an abundant lysosomal cysteine proteinase, has been implicated in the progression of malignant tumor, arthritis, and muscular dystrophy. The DNA coding sequence shows that the enzyme precursor is synthesized as a single-chain polypeptide of 30 kDa. However, as the enzyme matures, the polypeptide chain is shortened and glycosylated. Of particular interest is the finding that, in addition to the usual *N*-terminal extension found in the majority of proteins, the *C*-terminus of the DNA coding sequence of cathepsin B also possesses a 6-residue extension that is not found in the corresponding amino acid sequence of the mature enzyme. It has been *speculated* that the six *C*-terminal residues are removed during the intracellular processing of cathepsin B. In this study we utilized electrospray mass spectrometry (ESMS) in conjunction with site-directed mutagenesis to establish the mechanism of the cathepsin B *C*-terminal processing.

Rat liver cathepsin B was used in the study. It was suspected that the peptidyldipeptidase activity of cathepsin B itself was responsible for the intracellular removal of the *C*-terminal extension. To test this self-processing possibility, a nonactive mutant was expressed in yeast using the recombinant technique. In this nonactive mutant, the active-site amino acid residue, Cys-29, was replaced with a 'dummy' Ser residue to incapacitate the enzyme to determine whether the *C*-terminal extension would survive. However, the mass measurement from ESMS did not produce conclusive evidence, due to the spectral complexity resulted from the heterogeneous glycosylations. To overcome this problem, the glycosylated *N*-terminal pro-region was removed by pepsin cleavage, and a second mutation was introduced to substitute an additional residue, Ser-115, with an Ala residue to alter the *N*-glycosylation consensus sequence (Asn-Gly-Ser) to remove the second oligosaccharide attachment in the middle of the polypeptide chain (see Fig. 1 for a diagrammatic representation). Elimination of the carbohydrate heterogeneity resulted in a greatly simplified electrospray mass spectrum, which in turn clearly showed that the nonactive *double* mutant (with two mutations at residues no. 29 and no. 115) contained the 6-residue *C*-terminal extension (Gln-Tyr-Trp-Gly-Arg-Phe). This evidence suggests that the active cathepsin B is required to remove the *C*-terminal extension.

To further prove that cathepsin B itself is responsible for the removal of the *C*-terminal extension, a trace of the active cathepsin B was added to the nonactive mutant and the mass changes of the mutant were monitored by ESMS (see Fig. 2; only the 21+

charge-state region is shown). The fact that the addition of the active cathepsin B quickly led to the mass reductions of the nonactive mutant established unequivocally that the active cathepsin B served as a processing enzyme for the nonactive mutant. The electrospray mass monitoring data also revealed that the *C*-terminal extension was cleaved two residues at a time and the processing stopped once all six *C*-terminal residues were removed. The reaction kinetics indicated that the dipeptidyl removal became more and more difficult as the *C*-terminal processing progressed, pointing to a possible conformational restriction in fitting the *C*-terminal extension to the cathepsin B active site.

In conclusion, we have demonstrated, using ESMS in conjunction with site-directed mutagenesis, that cathepsin B itself is responsible for removing the 6-residue *C*-terminal extension. It is also shown that the *C*-terminal processing of cathepsin B is stepwise with two residues being cleaved at a time, consistent with the known peptidyldipeptidase activity of cathepsin B.

Fig. 1

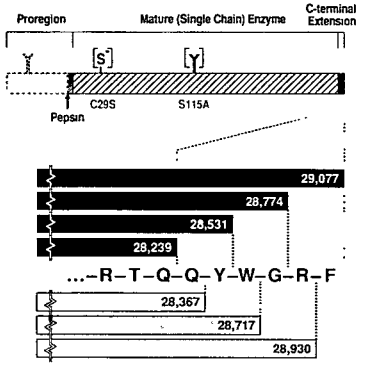

Fig. 2

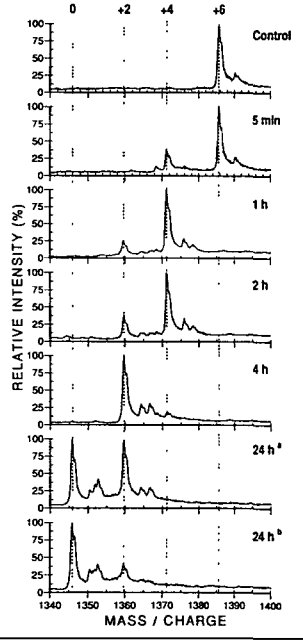

[a] Ten times more active cathepsin B added.
[b] Fifty times more active cathepsin B added.

Studies of the *Ras*-GDP and *Ras*-GTP Noncovalent Complexes by Electrospray Mass Spectrometry

E.C. Huang*, B N. Pramanik, A. Tsarbopoulos, V.M. Girijavallabhan, and S. Liberles[ψ]
Schering-Plough Research Institute, 2015 Galloping Hill Road, Kenilworth, NJ 07033

The *ras* protein can exist in two interconvertible states: GDP-bound and GTP-bound representing the inactive and active forms, respectively. In oncogenic *ras*, the rate of hydrolysis of the GTP to GDP is dramatically reduced, which "locks" the *ras* in the active state resulting in unregulated cell growth. Therefore, the detection and differentiation of the *ras*-GDP and *ras*-GTP complexes is important to the study of abnormal cell growth, as well as to the discovery of organic molecules as anticancer drugs.

To successfully perform direct MS analysis of the pre-formed noncovalent complexes, the MS technique utilized must satisfy the following criteria: (1) the ionization method must be capable of generating intact gas phase protein ions from a solution containing biological buffer; (2) the internal energy transfer to the macromolecule during the ionization process must be minimal to prevent complex dissociation; (3) the MS must have sufficient mass range to observe the ionized complex. Ganem et al.[1] reported the first applications of using electrospray (ESI) MS for the detection of noncovalent interactions. We have been studying the noncovalent complex of *ras*-GDP and *ras*-GTP using ESI, and a preliminary report of the successful ESI MS detection of *ras*-GDP has been published.[2] Here we provide the details of using ESI MS for the detection of *ras*-GDP and *ras*-GTP complexes. The effect of the pH and organic solvent to the stability of complexes is also discussed.

Preparation of ras-GDP Complex

C-terminally truncated normal human *ras* (1-166) was expressed in *E. coli* from a synthetic *ras* gene under the control of both the *lpp* and tac promoters.[3] The noncovalent complex of *ras*-GDP was subsequently purified from fermentor-grown, IPTG-induced cells. The activity of the *ras* in GDP binding assays and GTPase assays was comparable to published data. The final apo-*ras* protein was stored in 750 mM ammonium sulfate, 50 mM Hepes buffer pH 6, and 10 mM 2-mercaptoethanol at a concentration of 6.15 mg/mL. The FPLC isolated *ras*-GDP sample was kept in the solution containing 64 mM Tris HCl pH 7.6, 10 mM $MgCl_2$, 1 mM NaN_3, 0.5 mM DTE, and 250 mM NaCl. All sample solutions were stored at 4°C prior to MS analysis.

Preparation of ras-GTP Complex

An aliquot (100 µL) of apo-*ras* solution was diluted in Hepes buffer (50 mM, pH 7.5, 1 mM DTT) to two mL. To this, 10.2 µL of GTP were added (i.e., 2 - 3 molar excess) from solution of GTP in Hepes buffer. The concentration of the GTP solution was 3.34 mg/mL. This solution was refrigerated overnight and then concentrated to roughly 200 - 250 µL using a centrifuge concentrator. All samples were further treated with 1 mM EDTA and 1 mM $MgCl_2$ prior to MS analysis.

Mass Spectrometry

A SCIEX API III triple quadrupole mass spectrometer equipped with a ESI source (Sciex, Canada) was used. Sample was introduced either through direct infusion of the protein solution or via Rheodyne injector with a preselected solvent. In the latter case, an Applied Biosystems (Foster City, CA) Model 140A micro LC pump was used to deliver a constant liquid flow of 5-100 µL/min.

Results and Discussion

Figure 1 is the ESI spectrum of *ras*-GDP complex obtained at pH 5.8 (no MeOH). The signals at m/z 2396, 2145, and 1931 yielded an average molecular weight (MW) of 19,295 Da which corresponds to the *ras*-GDP complex. Computer deconvolution of this spectrum revealed the presence of a second species with an average MW of 19,344 Da, a component that could have resulted from the addition of two Mg^{2+} to the complex. Nevertheless, this assignment has not yet been confirmed experimentally. When the pH was lowered to ~4.0, the *ras*-GDP complex was still obesrved (**Figure 2**) with the charge distribution apexed at +11 charge state. Further lowering the pH to 3.3 resulted in partial release of GDP, leading to the observation of both the *ras*-GDP and the apo-*ras* signals. When the pH was adjusted to 2.8, the complex was almost completely dissociated.

ψ Undergraduate research participant, Department of Chemistry, Harvard University.

The effect of pH on ESI detection of *ras*-GDP complex is summarized in **Table 1**. It is known that the addition of organic solvent disrupts the well-ordered water molecules, allowing solvent molecules to penetrate into protein's hydrophobic interior and subsequently denature the prtotein. **Table 2** summarizes the effect of the organic solvent (MeOH) content on the ESI detection of the *ras*-GDP complex. This methodology was further extended to monitor the formation of the *ras*-GTP complex. The spectrum obtained from the solution of *ras*-GTP complex at pH 4.0 showed a series of ions at m/z 2154, 1938, 1762, 1616, and 1491, yielding an average MW of 19,374 Da. This indicat es the formation of an 1:1 *ras*-GTP complex. The multiply-charged ion distribution profiles are identical for both *ras*GDP and *ras*-GTP complex. The effect of pH on detection of *ras*-GTP complex was also studied and the results indicated that the *ras*-GDP and the *ras*-GTP complexes possessed the same behavior upon ESI MS analysis. Everything being the same for MS analysis of *ras*-GDP and *ras*-GTP complexes, the data suggest that even though there is a significant difference in biological activity, the change in solution conformation during the transition between the "*on*" and the "*off*" state is not significant enough to allow the differentiation to be made by ESI MS.

Conclusion

The *ras*-GDP and *ras*-GTP noncovalent complexes were successfully detected by ESI MS. This observation indicates that the protein-ligand noncovalent complex (with high association constant) can be desorbed, at its native or very close to its native solution conformation, as multiply-charged ions. From the MW determined by ESI MS, one can readily obtain information regarding the stoichiometry of protein-ligand interactions. The method can be further extended to study the protein unfolding processes associated with the acid-induced, as well as organic solvent-induced, denaturation. Correlation of these changes with specific events in the unfolding is not possible. The ability to observe such noncovalent interactions in solution highlights the potential of using electrospray MS for protein-protein interaction studies, kinetic studies of protein-ligand interactions, and for screening enzymes and receptors for inhibitors and substrates of pharmaceutical interest.

1. Ganem, B.; Li, Y.-T.; Henion, J.D. *J. Am. Chem. Soc.* **1991**, *113*, 6294.
2. Ganguly, A.K.; Pramanik, B.N.; Tsarbopoulos, A.; Covey, T.R., Huang, E.C.; Fuhrman, S.A. *J. Am. Chem. Soc.* **1992**, *114*, 6559.
3. Ghrayeb, J.; Kimura, H.; Takahara, M.; Hsiung, H.; Masui, Y.; Inouye, M. *EMBO J.* **1984**, *3*, 2437.

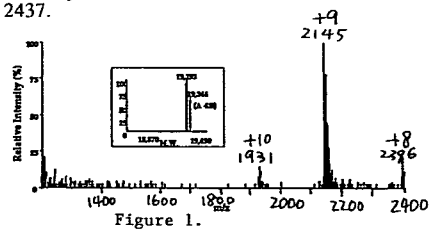

Figure 1.

Solvent	pH	Observation on Ras/GDP Complex System
Aqueous Solution; no organic modifier	~5.8	- Observe Ras-GDP complex - Charge state of complex centered on +9 charge - No unbound Ras protein is observed
Aqueous Solution; no organic modifier	~4.0	- Observe Ras-GDP complex - Charge state centered on +11 charge - No unbound Ras protein is observed
Aqueous Solution; no organic modifier	~3.3	- Observe Ras-GDP complex - Charge state of complex centered on +11 charge - Denaturation occurred
Aqueous Solution; no organic modifier	~2.8	- Near complete denaturation of Ras protein - Charge state of free Ras protein centered on +17 charge - Almost no Ras-GDP complex is left in the solution

Table 1.

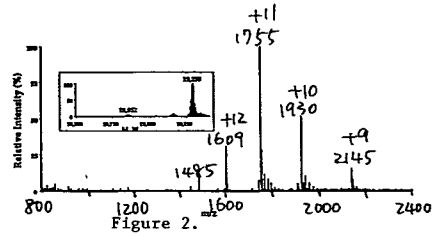

Figure 2.

Aqueous Solution	MeOH	Observation on Ras-GDP Complex System
100%	0%	- Observe Ras-GDP complex - Charge state of complex centered on +9 charge - No unbound Ras protein is observed
90%	10%	- Observe Ras-GDP complex - Charge state of complex centered on +9 charge - Some denatured free Ras protein is observed
50%	50%	- Observe small amount of Ras-GDP complex - Near complete denaturation of Ras-GDP complex
10%	90%	-Neither free Ras protein nor Ras-GDP complex related signals are observed under this condition

Table 2.

Comparison of Charged Peptide Derivatives for High Energy CID MS/MS

*J. Zaia and K. Biemann, Dept. of Chemistry, M.I.T., Cambridge, MA 02139

A comparison of charged derivatives for high energy CID spectra is the purpose of this work. The experiments have been limited to the N-terminal derivatives because it is difficult to prepare C-terminal derivatives without simultaneous alkylation at carboxyl side chains. Specific N-terminal derivatization can be accomplished in the presence of lysine with proper pH control[1].

The structures of the derivatives tested are shown in Figure 1. TPPE[2], TMAA, and DMOAA[1,3,4,5] have been previously described. Trimethylpyridiniumbutyrl (TMPB) is an N-terminal derivative which is a modification of a lysine specific derivative used in earlier work in this laboratory[6,7]. Peptides modified with the derivatives in Figure 1 produce primarily a_n and d_n ions although the abundance of ions produced from the derivative moiety varies widely among them. The abundance of ions containing solely the derivative moiety must be low for a useful charged derivative so that ion current is not diverted from the peptide sequence product ions.

A systematic comparison showed that the TMAA derivative produced the lowest abundance fragment ions containing only the derivative moiety (data not shown). In contrast, these fragment ions were observed to be quite abundant for the TPPE, 4-NMPA, and 3-NMPA derivatives. It was also determined that the effect of TMAA derivatization on ionization efficiency was approximately neutral compared to the underivatized peptide (data not shown). The usefulness of the TMAA derivative is shown in the following example. Consider the CID spectrum of α-endorphin (YGGFMTSEKSQTPLVT), Figure 2a. This spectrum shows lengthy gaps in its product ion pattern which is probably due to the basic lysine in the center of the sequence. The TMAA- derivative (Figure 2b) vastly improves the spectrum. The a_n series is complete for all three with the exception of the glycine residues at positions 2 and 3. Similar results are obtained for ACTH 1-14 (SYSMEHFRWGKPVG) and somatostatin (AGC[*4vp*]KNFFWKTFTSC[*4vp*]), peptides whose underivatized spectra are quite poor (data not shown).

Method. TPPE- derivatives were prepared according to the published method[2]. Trimethylpyridiniumbutyric acid was synthesized according to a literature method[8], and coupled to the peptide N-terminus using 1-Ethyl-3-(dimethylaminopropyl)carbodiimide hydrochloride (EDC) at pH 4.5. 4-NMPA- derivatives were prepared by coupling N-methyl-4-pyridiniumacetic acid to the N-terminus of the peptide using EDC. The same method was used for the 3-NMPA derivatives using N-methyl-3-pyridiniumacetic acid. The TMAA-, DMOAA-, and PyrA- derivatives were prepared by reacting the appropriate amine with an N-terminal iodoacetylated peptide. Peptides were iodoacetylated according to a published method[1].

Acknowledgement. The work was supported by The National Institutes of Health (grant numbers NIEHS ES04675, NIH GM05472 and RR00317).

References

1. Wetzel, R.; Halualani, R.; Stults, J T.; and Quan, C. *Bioconj. Chem.* **1990**, *2*, 114.
2. Wagner, D.S.; Salari, A.; Gage, D.A ; Leykam, J.; Fetter, J., Hollingsworth, R ; and Watson, J.T. *Biol. Mass Spectrom.* **1991**, *20*, 419.
3. Vath, J.E. Ph D. Dissertation, Massachusetts Institute of Technology, **1990**.
4. Vath, J E.; Biemann, K. *Int. J. Mass. Spectrom. Ion Processes* **1990**, *100*, 287-299.
5. Stults, J.T. *Proc. 40th Am. Soc. Mass Spectrom. Allied Topics* **1992**, 1815.
6. Johnson, R.S. Ph.D. dissertation, Massachusetts Institute of Technology, **1988**.
7. Johnson, R.S.; Martin, S.A.; and Biemann, K. *Int. J. Mass Spectrom. Ion Processes* **1988**, *88*, 137.
8. O'Leary, M.H. and Samberg, G.A. *J. Am. Chem. Soc.* **1971**, *93*, 3530.

Figure 1

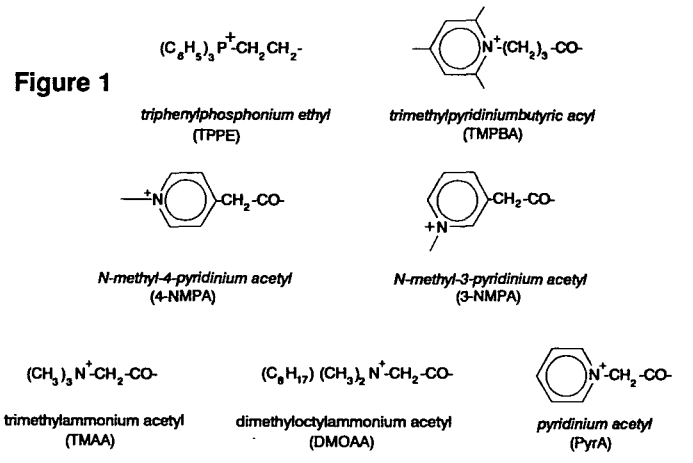

Figure 2

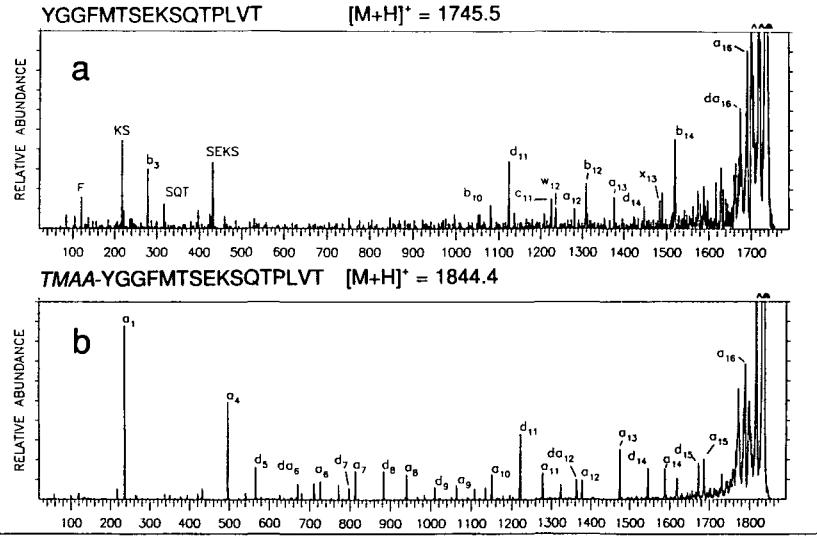

High Resolution and MS/MS Matrix-assisted Laser Desorption on a Fourier Transform Mass Spectrometer

Robert J. Cotter* and Amina S. Woods
Johns Hopkins School of Medicine
Baltimore, MD 21205

J.A. Castoro and C.L. Wilkins
University of California at Riverside
Riverside, CA 92521

Recently, Wilkins and coworkers (1) described a method for trapping *MALDI* ions in a Fourier transform mass spectrometer (*FTMS*) that is used here for the analysis of two synthetic peptides containing amino acid sequences for antigens associated with the Major Histocompatibility Complex (MHC) and displayed on tumor cells genetically engineered to produce specific lymphokines for activating inadequately functioning helper T cells.

Approximately 1-2 nmoles of peptide in a 50 mM 2,5-dihydroxybenzoic acid solution in 0.1% trifluoroacetic acid/methanol was sprayed as an aerosol onto a rotating stainless steel probe tip for homogeneous deposition. Spectra were obtained with 355 nm radiation from a Lambda Physik (Gottingen Germany) FL-2001 dye laser pumped by a Lambda Physik EMG 201-MSC excimer laser (308 nm, 180 mJ/28 nsec pulse) and a Millipore Extrel (Madison WI) FTMS-2000 equipped with a 7 Tesla superconducting magnet. Spectra were obtained using a 9 volt gated trap decelerating potential prior to source side 1-1.5 volt trapping and detection, except for the high resolution spectrum where analyzer side, 0.4 volt trap, heterodyne detection was employed. *SID* spectra were the result of 100 laser shots with a 3 volt trap. No apodization was used. Poly(ethylene glycol) 1000 was used as an external calibrant.

Positive and negative ion mass spectra were obtained for each peptide. For *ASNENMETN* $[M+Na]^+$ and $[M-H]^-$ were detected with a resolution of ~8,000 and a mass error of 8 ppm for the monoisotopic peaks (Figure 1). For *TYQRTRALV* $[M+H]^+$ and $[M-H]^-$ were detected with resolutions of 13,500 and 17,900 and mass errors of 13 ppm and 81 ppm, respectively. A high resolution heterodyne mode mass spectrum of *TYQRTRALV* $[M+H]^+$ was also obtained with an average resolution of 300,000. Surface induced dissociation was carried out on the $[M+H]^+$ ion of *TYQRTRALV* and the $[M+Na]^+$ of *ASNENMETM*. All fragments and impurities below 1000 daltons were ejected prior to an on-resonance excitation of the parent ion. Each ion was excited to a calculated radius of 0.85 cm, resulting in translational energies of 133 eV for $[M+H]^+$ and 141 ev for $[M+Na]^+$, prior to a 25 volt *SID* pulse for around 90 us. For the peptide *ASNENMETM*, ions of m/z 1048 (corresponding to the $M+Na^+$ ion) were selectively excited, producing the product ion mass spectrum shown in Figure 2, containing the sequence ions: A_3+Na (267.1), B_3+Na (295.1), A_4+Na (396.2), B_4+Na (424.1), A_5+Na (510.2), B_5 (516.9), B_5+Na (538.2), A_6+Na (641.2), B_6 (648.2), Z_4+Na (630.2), Z_5 (493.2), X_6 (406.1), Y_6 (380.1), Z_6 (363.1) and X_7 (277.1).

(1) Castoro, J.A.; Koster, C.; Wilkins, C. *Rapid Commun. Mass Spectrom* **1992**, *6*, 239-241.

Figure 1.

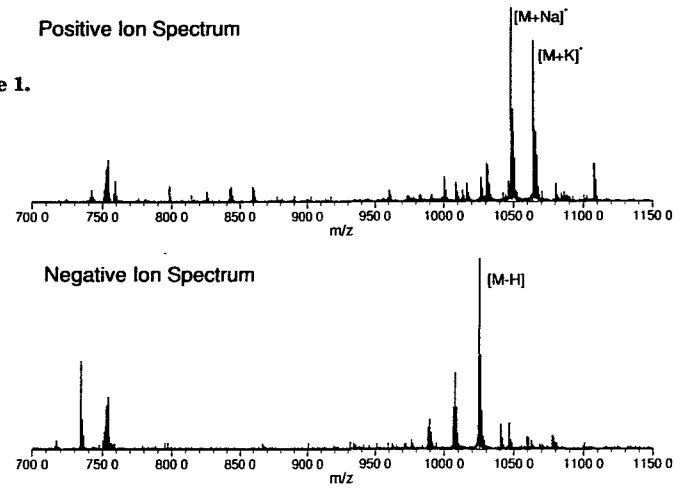

Figure 2.

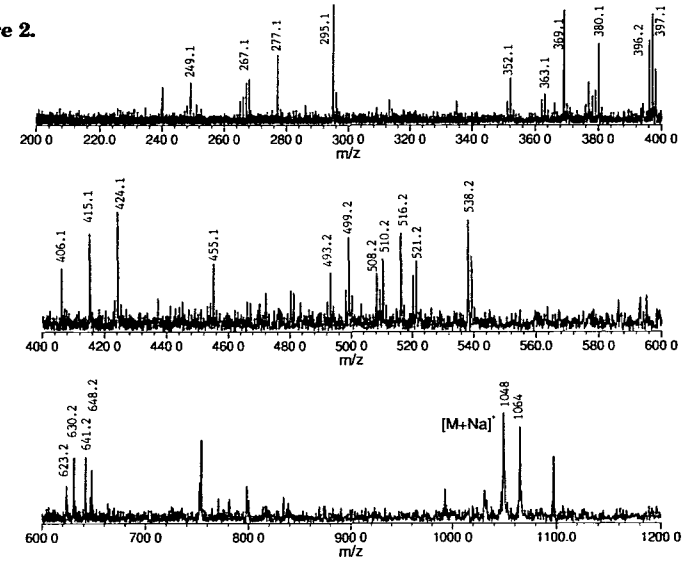

The Analysis of Biomolecules by Electrospray Ionization on a Magnetic Sector Tandem Mass Spectrometer

K.M. Downard, I.A. Papayannopoulos, C.E. Costello and K. Biemann
Dept. of Chemistry, Massachusetts Institute of Technology, Cambridge, MA, 02139

In 1988, Fenn and co-workers showed that the electrospray ionization (ESI) technique developed in their laboratory could be successfully applied to the analysis of large biomolecules to 40 kDa.[1] This mass limit was soon exceeded and to date molecules to 5 million daltons have been ionized by this approach.[2] The success of this technique is due in large part to the phenomenon of multiple charging, where large biomolecules are detected at integral fractions of their mass allowing their detection on spectrometers of limited *m/z* range.

To date most electrospray studies have been performed on quadrupole instruments but recent interest has focused on integrating the technique to other mass analyzers. In this regard sector instruments offer several advantages over quadrupoles; namely higher resolution and the ensuing improvement in mass accuracy, and extended *m/z* range and the potential for high energy CID of multiply charged ions. We have been exploiting the electrospray approach in our studies of proteins, glycoproteins and other glycoconjugates.

The ESI mass spectrum of *Chloroflexus* Thioredoxin is shown in Figure 1. This spectrum indicates that the protein is a heterogeneous mixture containing proteins 14 Da. lower (A to G) and 16 Da. higher (M to M=O) than that of the major protein at M_{av} 12009.

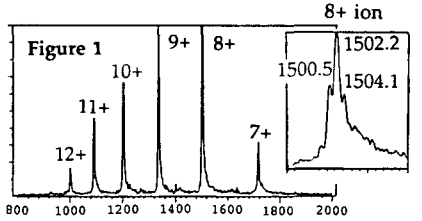

A further site of heterogeneity has been realized upon screening the tryptic digestion products by ESI-MS. The isotopic distribution of a tryptic peptide of M.Wt. 868 is shown in Figure 2. This spectrum indicates that an additional component is present having a molecular weight of one dalton higher. CID spectra of the doubly charged ions $[M+2H]^{2+}$ and $[M+2H+1]^{2+}$ produced by ESI were recorded. The CID spectrum of the $[M+2H]^{2+}$ ion is shown in Figure 3. Examination of this spectrum reveals the smaller tryptic peptide has the structure VIAPILDK. Peaks which shift to higher *m/z* values in the spectrum of $[M+2H+1]^{2+}$ are indicated with a ★.

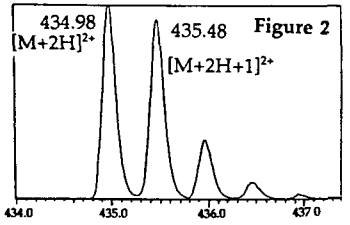

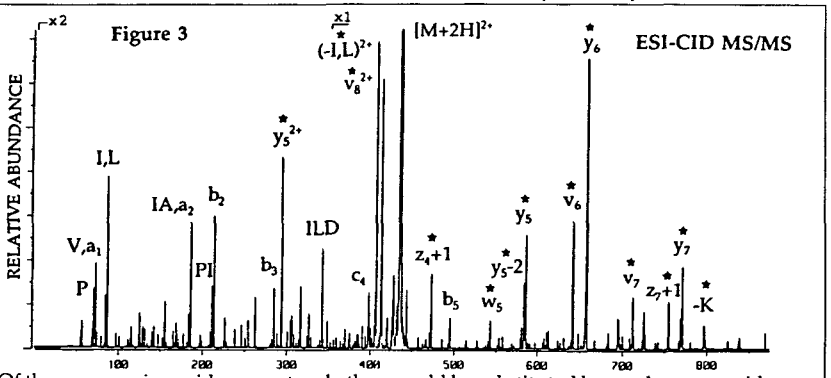

Of the seven amino acids present, only three could be substituted by an alternate residue one mass unit higher. These are I, L and K. Since the peptides were isolated from a tryptic digest, substitution of K for E is unlikely. Note that b_2 and b_5 fragment ions do not shift to higher *m/z* values in the CID spectrum of the $[M+2H+1]^{2+}$ ion, thus heterogeneity exists at position 6 where L is substituted for N.

The ESI mass spectrum of a permethylated ganglioside G_{D1b} is shown in Figure 4. The base peak of the spectrum corresponds to the doubly charged ion $[M+2Na]^{2+}$ of the di-sialylated ganglioside. This peak shows some multiplicity, a consequence of the heterogeneity in the long chain base (-28 Da) and incomplete permethylation (-14 Da)

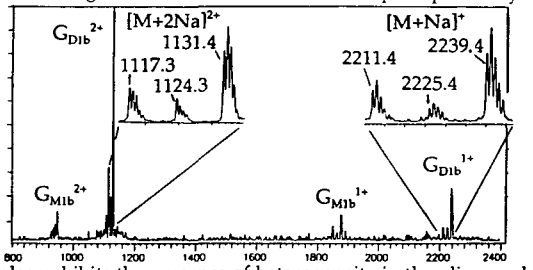

The spectrum also exhibits the presence of heterogeneity in the oligosaccharide portion, where G_{M1b}^{2+} and G_{M1b}^{1+} denote the doubly and singly charged ions of the mono-sialylated gangliosides respectively.

References

1. C.K. Meng, M. Mann, J.B. Fenn, *Proc. 36th ASMS Conf. on Mass Spectrometry and Allied Topics*, San Francisco, 1988, p771.
2. T. Nohmi, J.B. Fenn, *J. Am. Chem. Soc.*, 1992, *114*, 3241-3246.

Acknowledgements

Support from the NIH through grants GM05472 and RR00317 (to K. Biemann) is gratefully acknowledged.

Mass Spectrometry and Tandem Mass Spectrometry Analyses of Pyridinoline and Its Derivatives

Ron Self[1], David A. Pratt[1], Simon P. Robins[1], Su Chen[2] and Peter J. Derrick[2],
[1]The Rowett Research Institute, Bucksburn Aberdeen, AB2 9SB, and [2]Institute of Mass Spectrometry and Department of Chemistry, University of Warwick, Coventry CV4 7AL, UK

Growth and certain disease conditions are related to high turnover rates of collagens. Tissue metabolism results in the release of fragments into blood and urine, some of which contain the collagen-specific, 3-hdroxypyridinium crosslinks. Preliminary studies, using these components to monitor collagen degradation rates, have indicated that a large proportion are present as small peptides. As the crosslinks are found out in a variety of tissues containing different genetic types of collagen, identification and sequencing of these crosslinked peptides would facilitate the development of tissue-specific markers of collagen degradation. By monitoring their natural fluorescence, peptides containing these crosslinks will be isolated from biological materials, such as urine and serum using a variety of chromatographic and electrophoretic techniques. Mass spectrometry analysis of pyridinoline and its derivatives described here.

EXPERIMENTAL

All mass spectra were obtained on a CONCEPT II HH four-sector tandem mass spectrometer (Kratos Analytical Ltd, Manchester, UK) operated at 8 kV ion-acceleration and equipped with a cesium ion gun with 15 keV impact energy, standard LSI mass spectrometry probe and a final scanning-array detector. All experiments were completely controlled by a MACH 3 data system and the data was collected and processed in an identical manner to that obtained from a point detector. Tandem mass spectrometric experiments were carried out by using all four sectors (EBEB) on the instrument. CID of the precursor ions occurred in the flexcicell where a potential of 4 kV related to earth was floated. Argon was used as the collision gas at a pressure sufficent to attenuate the precursor ion beam by 60%.

RESULTS

Structures of the trifunctional crosslink molecules (fig.1), pyridinoline (Pyd), deoxypyridinoline (Dpd) and glycosylated pyridinoline (Glc-Gal-Pyd), have been characterized by positive-ion LSIMS and four-sector tandem mass spectrometry. The naturally-occurring cations are desorbed by LSIMS readily in the positive-ion mode, using G/TG(1:1) or PEG 400 as matrixes, and intense stable M^+ ions dominate the spectra, facilitating an accurate mass measurement of molecular mass (fig.2). Changing matrix to NBA leaves little evidence of the cation since facile decomposition, of Pyd yields $[M-O]^+$, of Glc-Gal-Pyd yields the equivalent $[M-Gal-Glc]^+$, while the $M^+$of the two molecules are drastically reduced in intensity. Electrochemical reaction between analytes and NBA has been evidenced. CID of major ions produced by positive-ion LSIMS (fig.3) gives a wealth of fragmentation for structural elucidation (scheme 1), and the concept of remote-site fragmentation with the charge located on the ring nitrogen (scheme 2) is considered with caution. (M-92) and (M-92-92) peaks in the CID spectra are due to glycerol matrix. It was evidenced by the absence of such ions in the CID MS/MS spectrum of Dpd when NBA was used as the matrix. However, it is unclear how these ions are formed. The study on structures of trifunctional crosslink molecules by MS provide valuable information to identify such markers.

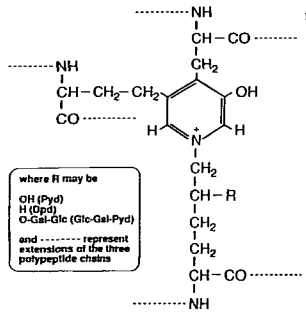

Figure 1 Generalised structure of a collagen pyridinoline-cross linked peptides.

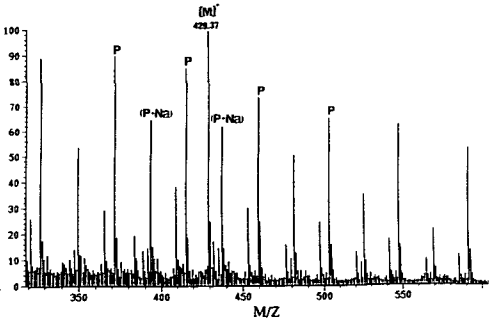

Figure 2. Positive-ion LSI mass spectrum of Pyd. Resolution was approximately 5000 (a) P peaks are due to the PEG 400 (used as the matrix).

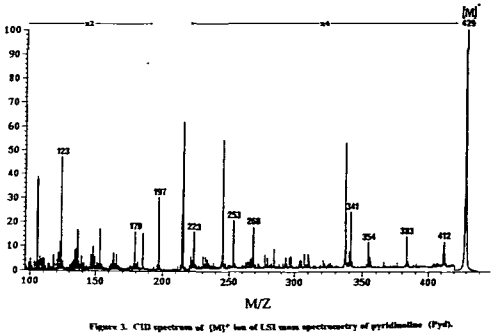

Figure 3. CID spectrum of $[M]^+$ ion of LSI mass spectrometry of pyridinoline (Pyd).

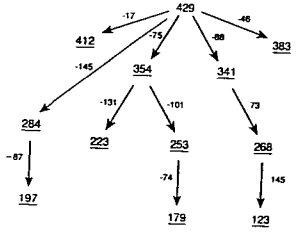

SCHEME 1

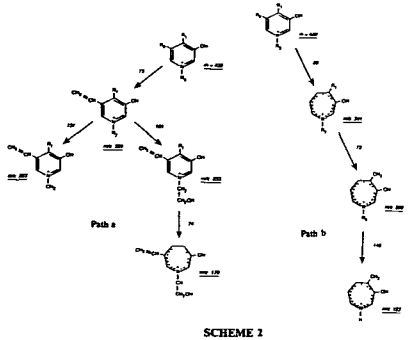

SCHEME 2

HPLC-PB-CI-MS and HPLC-TSP-MS of Linear Peptides (Efrapeptins) and Cyclodepsipeptides (Destruxins) of Fungal Origin

Matt J. Sweeney and Dr. Sandeep Gupta, ISK-MVRC, 1195 W. Fremont Ave Sunnyvale, CA 94087

Introduction-

Efrapeptins and destruxins are fungal peptides which are typically isolated by RP-HPLC and identified by NMR, FD- or FAB-HR-MS and sequence analysis. Particle Beam-MS with an EI/CI source and Thermospray can be used for on-line detection of these metabolites. The fungal genus Tolypocladium includes species which are invertebrate pathogens. Because of this, the genus has attracted interest as a potential biological control agent. The efrapeptins are rich in alpha-aminoisobutyric acid and have an unusual carboxy-terminal blocking group which confers upon them potent mitochondrial ATP-ase inhibitory activity. The molecular weights of these compounds are (efrapeptins C,D,E,F,and G); 1606,1620, 1634, 1634, and 1648. The Destruxins are insecticidal Cyclodepsipeptides originally isolated from an entomogenous fungus.

Methods-

A Waters 600MS pump with a 712 Autosampler was used to inject all samples and for all PBI work. A Waters 6000 pump was used for 0.1 M NH4OAc make up flow with the TSP. Finnigan TSP2 and PBI inlets were used on an SSQ710. Destruxin A was used to optimize He flow, source and desolvation temperature with the PBI interface. Optimizations were done for ends of the gradient run and a suitable value chosen. Efrapeptin F and Destruxin A were used to optimize TSP conditions. Destruxins were dissolved in MeOH and Efrapeptins in ACN:H2O at about 0.5-0.05 ug/ul. Methane was used as the CI reagent gas.

Results

The Efrapeptins were not observable by PB-CI but gave molecular ions with TSP. The Destruxins gave molecular ions with both PB-CI and TSP interfaces. The Destruxins produced greater response in negative PB-CI rather than positive. Attempts with TSP to induce fragmentation of Destruxin A by increasing repeller voltage failed as did variation in the vaporizer temperature. The use of the fragmentation seen in the PB-CI spectra of the Destruxins is useful in confirmation of identities in unknowns and the reduced fragmentation observed in negative CI spectra is helpful in improving detection limits. Shown is an ODS separation of a 4 Destruxin mixture using PB-CI detection in positive and negative modes and a representative Efrapeptin F spectra.

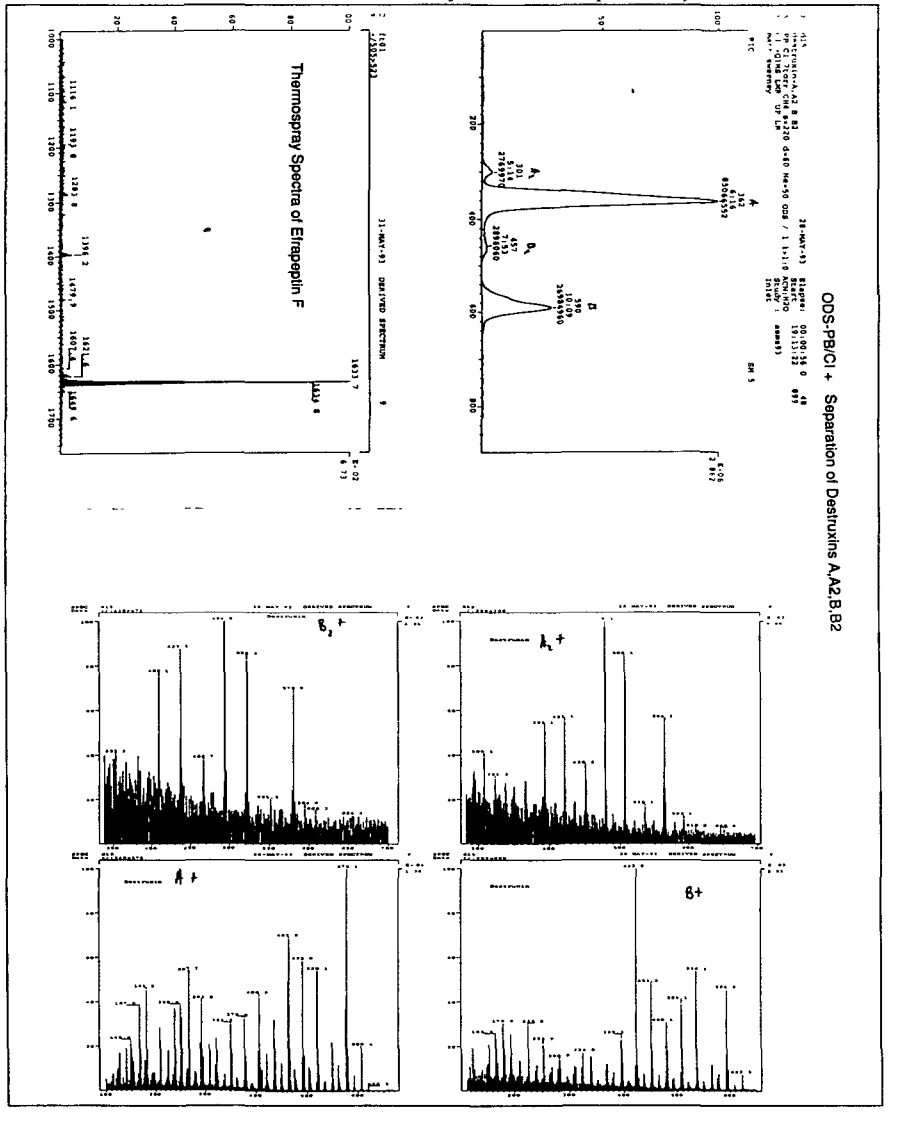

Capillary HPLC/MS Analysis of Hydrophobic Peptides from the α_2-Adrenergic Receptor

*Jane J. Z. Huang[1], Lee E. Limbird[2] and Ian A. Blair[1,2]
Departments of Chemistry[1] and Pharmacology[2], Vanderbilt University
Nashville, TN 37232-6602

α_2-Adrenergic receptor are membrane proteins that bind endogenous epinephrine and norepinephrine and are involved in the regulation of a variety of physiological processes. through molecular cloning, the entire DNA sequence of the α_{2A}-subtype of receptor is known. However, the funtionally important amino acid residues for binding of adrenergic ligands to the α_2-receptor have not yet been identified although there is some evidence that the putative forth transmembrane region is involved. Preliminary experiments have been carried out on the analysis of model peptides that span the putative third and fourth transmembrane domain of the receptor. Six peptides were synthesized that could arise from a combination of tryptic and chymotryptic digestion of the receptor: FGKAW, LALDVLF, WSITQAIEY, TPRRIKAIIVTIW, VISAVISF, PPLISIEKK. The peptides were charaterized by a combination of MALDI TOF MS and LSI MS/MS. The LSI MS/MS spectra of the six synthetic peptides indicated a wealth of sequence ions were present. The peptide spanning reisdues 167-175 (PPLISIEKK) showed the entire series of b and y ions, together with selected a, x, and w ions. Capillary HPLC was then explored for separation of the peptides by using Applied Biosystems 140 B dual syringe pump system. The peptides had excellent chromatographic charateristics when analyzed using a reversed-phase C_{18} column (320 µm i.d. x 50 mm, 300 A, 3 µm; LC Packings). A split of approximately 1:30 was made using an Accurate™ (LC Packings) so that the flow through the capillary column was 3.5 µL/min. It was possible to use a 20 µL loop on the injector because the LC gradient system started with a high aqueous content and the peptides simply adsorbed to the front of the column. High sensitivity UV detection was achieved by the use of a Z flow cell and it was possible to routinely detect 40 pmol of each of the peptides. On line LC/MS analysis of these peptides was successfully achieved by interfacing the capillary LC system with a triple quadrupole mass spectrometer equipped with an electrospray ionization (ESI) source.

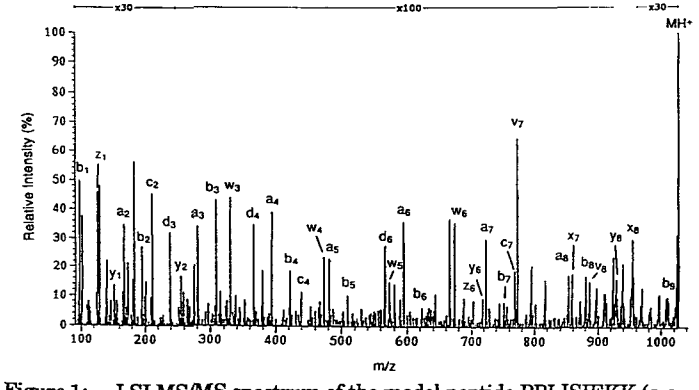

Figure 1: LSI MS/MS spectrum of the model peptide PPLISIEKK (a.a. residue 167-175).

In addition to the model peptides studies, nanomole quantities of α_{2A}-receptor protein were obtained by over-expressing the porcine brain α_2-receptor gene in *LLC.PK1* cells. Purification of the protein was carried out by yohimbine-agarose affinity chromatography. Receptor protein concentration was determined using a binding assay with the α_2-receptor antagonist [^{3}H]-yohimbine. A photoaffinity labelling probe ^{125}I-Rau-AzPEC(17α-hydroxy-20α-yohimbane-16β-[N-(4-azido-3-[^{125}I]-iodo)phenethyl]carboxamide) was bound specifically to the adrenergic binding pocket of the α_2-receptor. The labelled receptor moved as a single band at molecular weight around 66 kDa. on SDS polyacrylamide gel. The radiolabelled tryptic fragments were generated by enzyme proteolysis with immobilized trypsin resin, and separated by 10-21.5% SDS-tricine polyacylamide gel electrophoresis. The fragments were then transferred to nylon membranes and microsequencing was carried out. Unfortunately, the sequence was obscured by autolysis products derived from the trypsin.

Supported by NIH grant ES00267.

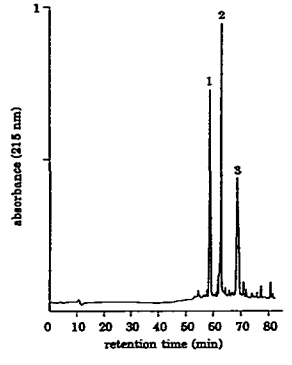

Figure 2: On Line capillary LC/MS analysis of the model peptides span the putative third transmembrane domain of α_2-receptor

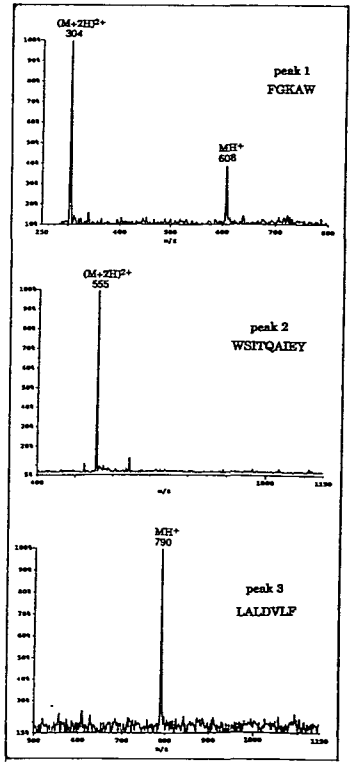

Figure 3: Mass Spectrum from the capillary LC/ESI MS analysis in Figure 2.

Electrospray Mass Spectrometry Analysis of Opioid Peptide Precursors

Lin Yan , Genevieve Fridland, Jih-Lie Tseng and Dominic M. Desiderio
Department of Neurology and Charles B. Stout Neuroscience Mass Spectrometry Laboratory, University of Tennessee, Memphis, 800 Madison Avenue, Memphis, TN 38163

Mass spectrometry (MS) methods are being developed to study the production of several important neuropeptides that derive from the metabolic cascade that occurs in a neuron: DNA → mRNA → various large and intermediate-sized precursors → neuropeptides → inactive metabolites. Those data are needed to clarify the metabolism of neuropeptides that occurs in control and pathophysiological tissues and fluids.

Recently, electrospray ionization (ESI) MS, in combination with gel permeation (GP) chromatography, RIA, HPLC , LSIMS and MS/MS, has been used in this laboratory to characterize intermediate-sized neuropeptide precursor molecules from their respective precursors, preproenkephalin A , which produces methionine enkephalin (ME) and proopiomelanocortin (POMC), which produces β-endorphin (BE)

METHODS

The bovine pituitaries were homogenized at neutral pH with enzyme inhibitors. The homogenate was separated by GP chromatography (G75), and 5% of each aliquot was analyzed for ME-like immunoreactivity (ME-li) following trypsin and CNBr treatments. Those GP peaks that contained immunoreactivity were fractionated further by reverse phase HPLC (RP-HPLC, linear gradient of 15-60% acetonitrile in TEAF buffer pH=3.15 over 90 min.). A portion (5%) of each fraction was used similarly to monitor ME-li after treatment with CNBr and trypsin. Commercial ME RIA kits were used in this study.

Aliquots of all immunoreactive fractions after RP-HPLC were studied by ESIMS on a VG Auto Spec Q (EBE-qQ) mass spectrometer to produce $(M+nH)^{n+}$ ions to determine the molecular weights. The ESI source was operated at 4 kV, and the samples were introduced into the source at a rate of 3 µl/min 1:1 CH_3OH:H_2O containing 1 % CH_3COOH

All remaining immunoreactive fractions were treated with trypsin and were analyzed by ESIMS and LSIMS for detection of $(M+H)^+$ of ME-K, ME-R and LE-K from preproenkephalin A, and BE_{20-24} and BE_{10-19} from POMC.

After separation with HPLC and/or CZE, all tryptic peptides will be sequenced by MS/MS to locate the intermediate-sized precursors within the preproenkephalin $A_{bovine,1-263}$ and the $POMC_{bovine,1-265}$ precursor molecules.

RESULTS AND DISCUSSION

ESIMS analysis of one immunoreactive fraction showed three major components, with M.W. of *ca.* 6550, 8440 and 9855, respectively (Figure 1) Trypsin treatment of this mixture, when analyzed by LSIMS, showed the presence of ions at m/z 558 and 1134 (among others) (Figure 2), which correspond to the tryptic peptides BE $_{20-24}$(=$POMC_{254-258}$) and BE_{10-19}(=$POMC_{244-253}$). The peaks at m/z 558 and 1134 were also present in the FAB spectra from trypsin treatment of endogenous BE (M.W. 3465) in our previous studies.[1] Therefore, that peak may well be an indication that this fraction contains intermediate-sized precursors deriving from POMC. "Intermediate size" means less than the 265 amino acids of POMC but more than the 31 amino acids in BE.

At this stage, we feel that the component with a M.W. of 9,855 is the intemediate-sized precursor of BE. Therefore, this HPLC fraction will be subjected to further HPLC and/or CZE separation, and the putative precursor ion at 9,855 will be studied by trypsin treatment, ESIMS, LSIMS, and MS/MS sequencing of each tryptic fragment. In that manner , we will locate the intemediate-sized precursor of 9,855 mass units within the larger POMC precursor molecule itself. These data will permit the elucidation of the processing of the precursor molecule.

We are also searching for the intemediate-sized precursors of ME by the same method. For example, ESIMS analysis of another active fraction showed the presence of a major peak with a M.W. of *ca.* 15,034 Da, as shown by the series of $(M+nH)^{n+}$ ions 12+-23+ at m/z 1254-655, and a smaller peak (*ca.* 5%) at M.W. *ca.* 14,879 Da. (see Figure 3) Trypsin treatment of this fraction yielded 12 tryptic fragments, which were analyzed by LSIMS and ESIMS and which showed very small peaks at m/z 701 and 729, corresponding to the $(M+H)^+$ ions of ME-K and ME-R.

Finally, this analytical system will be used to analyze human pituitaries (post-mortem controls and post-surgical tumors).

(1) C Dass, J. J. Kusmierz and D. M. Desiderio, Biol. Mass Spectrom. **20**, 130-138 (1991).

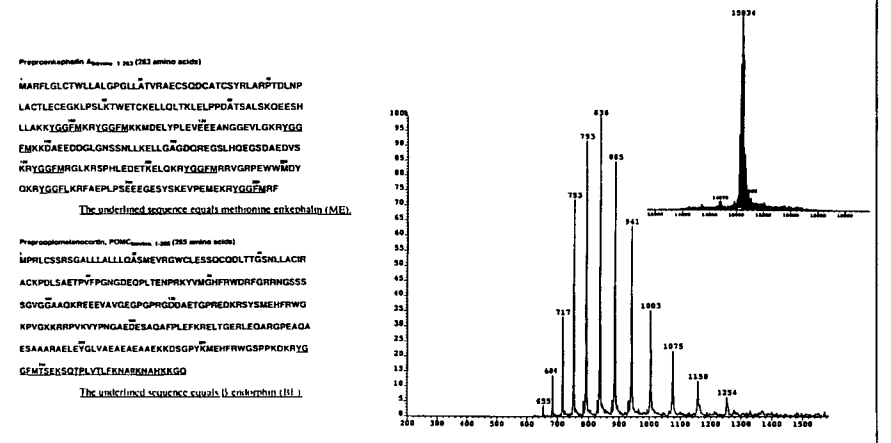

Figure 3

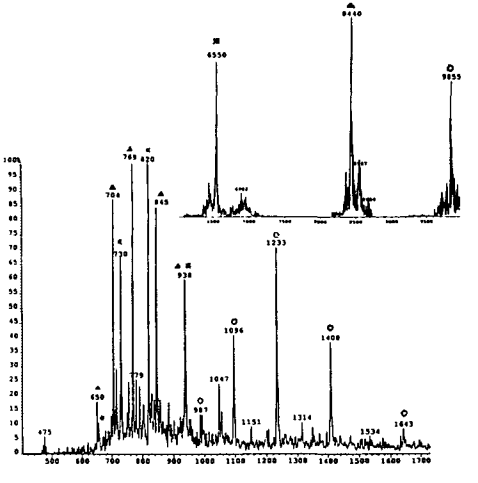

Figure 1

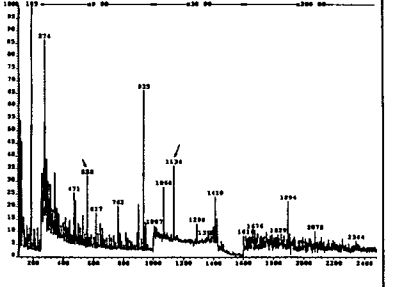

Figure 2

NIH GM 26666

TANDEM MASS SPECTROMETRIC IDENTIFICATION OF A SPECIFIC CYSTEIC ACID RESIDUE IN OXIDIZED LOW DENSITY LIPOPROTEIN.

Odile Burlet, Chao-Yuh Yang and Simon J. Gaskell Department of Medicine, Baylor College of Medicine, Houston, TX 77030.

Low density lipoprotein (LDL), the major carrier of cholesterol in the blood, is composed of a cholesterol ester-rich core which is stabilized by a surface of more polar lipids and protein. The primary sequence of apoprotein B-100, the principal protein constituent of LDL, has been established from the complementary DNA sequence (Chen et al., 1986) and substantially confirmed by classical sequencing methods (Yang et al., 1986). When LDL is subjected to oxidation *in vitro*, significant changes in its biological properties are observed, each of which (if reproduced *in vivo*) may be relevant to the formation of atherosclerotic plaques. Modification of the apoprotein B-100 component, for example, is known to influence receptor uptake. As a first stage in the examination of the undoubtedly complex protein structural changes which accompany oxidation, we have undertaken the detection and location of cysteic acid residues resulting from oxidation of cysteine. LDL was isolated from human plasma, oxidized in the presence of 5 μM copper ions, and delipidated to obtain oxidized apo B-100. The protein was subjected to tryptic hydrolysis and the hydrolysate was fractionated by reverse-phase HPLC; UV-absorbance detection revealed the highly complex profile expected for the digest of a protein of this molecular mass. An aliquot of each of approximately 75 chromatographic fractions was examined by conventional amino acid analysis. Two fractions were identified in which cysteic acid was relatively prominent; these were studied further by FAB MS and tandem MS. Tandem MS with low energy (20-150 eV, laboratory frame of reference) collisional activation was performed using a hybrid instrument of BEqQ configuration. The portions of the hydrolysate used for tandem MS analysis corresponded to approximately 1.5 nmol of the original protein. Each of the tryptic fractions contained multiple components, as judged by FAB MS. Product ion spectra yielded full or partial sequence data; in the latter instances, the partial sequences were sufficient to identify the tryptic fragment of the known apo B-100 sequence. In some instances, data for the native peptide were supplemented by analyses of N-acetylated or esterified derivatives. Table 1 shows the peptides identified in a single HPLC fraction. There are some ambiguities of MS interpretation (such as the inability to distinguish between leucine and isoleucine residues) but for each component the data allow mapping onto the known apo B-100 sequence and the identification of oxidized residues. Figure 1 shows the product ion spectrum for a component yielding an $[M+H]^+$ ion of m/z 1205. The spectrum is readily attributed to the sequence corresponding to residues 4187-4195 in apo B-100 (EELCTMFIR) in which the cysteine and methionine residues are oxidized to cysteic acid and methionine sulfoxide, respectively. (The extraordinary clarity of this product ion spectrum, consisting solely of Y-series ions, is attributed to a gas phase interaction of the cysteic acid and arginine side-chains, promoting a precursor ion population heterogeneous with respect to the site of charge (Burlet et al., 1992)) Coleman et al. (1990) have used a fluorescent probe to identify the cysteine at residue 4190 as one of two cysteines exposed on the LDL surface and therefore potentially available for intermolecular coupling, for example to apolipoprotein (a) via a disulfide bond.

Burlet O, Yang, C-Y, Gaskell SJ (1992) J Amer Soc Mass Spectrom 3: 337-344.
Chen S-W, Yang C-Y, Chen P-F, Setzer D, Tanimura M, Li W-H, Gotto AM, Chan L (1986) J Biol Chem 261: 12918-12921.
Coleman RD, Kim TW, Gotto AM, Yang C-Y (1990) Biochim Biophys Acta 1037: 129-132.
Yang C-Y, Chen S-H, Gianturco SH, Bradley WA, Sparrow JT, Tanimura M, Li W-H, Sparrow DA, DeLoof H, Rosseneu M, Lee F-S, Gu Z-W, Gotto AM, Chan L (1986) Nature 323: 738-742

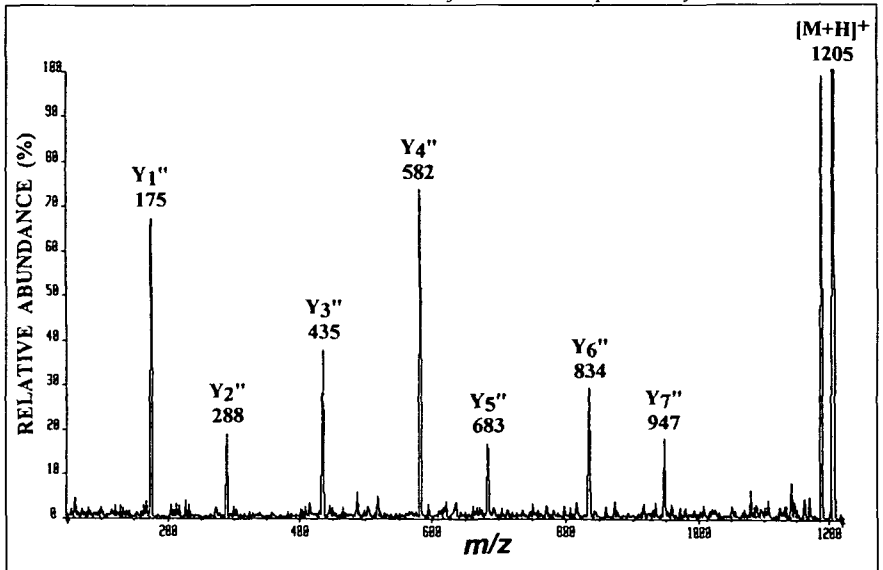

Figure 1. Product ion spectrum obtained by tandem MS of an HPLC fraction (20.8-21.4 min retention time) of the tryptic digest of oxidized, delipidated LDL. Collision activation of ions of m/z 1205 yielded a single series (Y_n") of C-terminal fragment ions consistent with the sequence, Glu-Glu-Leu-(cysteic acid)-Thr-(methionine sulfoxide)-Phe-Ile-Arg.

Table 1. Peptides identified in an HPLC fraction (20.8-21.4 min retention time) of the tryptic digest of apo B-100 from oxidized LDL.

$[M+H]^+$ [a]	Peptide sequence[b]	Residue numbers in apo B-100 sequence
621	*L*T*I*FK	4009-4013
718	*LI*FDPN[c]	632-637
777	SFS*I*PVK[d]	3691-3697
1021	NNA*L*DFVTK	3186-3194
1058	*LSIL*TDPDGK[c]	4425-4434
1205	EE*L*C TM[o]F*I*R	4187-4195
1242	ATGV*L*YDYVNK	4050-4060
1406	*L*QTF*L*DDASPGDK[e]	518-530

[a] *m/z* ratio of the protonated molecule, rounded down to the nearest integral value. [b] C*, cysteic acid; M[o], methionine sulfoxide. Underlined portions of the sequence were deduced from the tandem MS analysis alone; amino acid codes in italics represent ambiguities of interpretation of the MS data. [c] Non-enzymic cleavage following an asparagine residue. [d] Chymotryptic cleavage following an asparagine residue. [e] Chymotryptic cleavage following

Structural Determination of a Modified Membrane Lipopeptide from *Mycobacterium avium* by Using Electrospray, FAB, and Precursor Ion Scanning.

*Denise K. MacMillan, *Robert C. Murphy, #Hee-Joo Park, and #Patrick J. Brennan
*National Jewish Center for Immunology and Respiratory Medicine, Denver, CO 80206.
#College of Veterinary Medicine and Biomedical Sciences, Fort Collins, CO 80523.

Diseases caused by *Mycobacterium avium*, a commonly occurring pathogen, are increasing in recent years, especially among patients already infected with the AIDs virus. Treatment with cycloserine effectively kills *M. avium* by modifying a cell membrane lipopeptide and interrupting peptidoglycan synthesis. However, side effects such as dizziness, headaches and confusion, as well as depression and psychosis, limit the usefulness of cycloserine in the treatment of *M. avium*-caused illnesses (1).

Our goal is to determine the structures of lipopeptides using a combination of chemical and instrumental techniques. Acid hydrolysis of the lipopeptide generated free fatty and amino acids. Trimethylsilyl derivatives of the amino acids were formed and then analyzed by GC\MS. Those experiments indicated that alanine, phenylalanine, N-methylvaline (NMV), leucine, isoleucine and valine are present. Analysis of the methyl ester derivatives of the fatty acids by using GC\MS suggested that four saturated fatty acids occur for both the untreated and modified lipopeptides: octadecanoic, eicosanoic, docosanoic, and tetracosanoic acids. A minor amount of hexacosanoic acid is also observed. As is true with many other biological materials, the lipopeptide is a complex mixture of related compounds.

Both electrospray ionization with single quadrupole mass analysis and FAB ionization with triple quadrupole mass spectrometry were used for molecular weight determination and gave a molecular ion cluster of seven major species, each differing by 14 mass units (M = 1193, 1207, 1221, 1235, 1249, 1263, 1277 amu). The component fatty acids differ by 28 mass units, however, suggesting that the complexity of the mixture extends beyond differences in the acylated acid to the peptide portion of the molecules.

Interestingly, the lipopeptide is not soluble in water but in chloroform. The hydrophobic nature of this molecule posed problems for sample handling, as the material did not behave as a typical peptide. Perhaps for this reason, product ion scans in the molecular ion region gave little characteristic sequence information.

One procedure found to be quite useful for the study of lipopeptide sequence was precursor ion scanning. Precursor ion experiments performed on the most abundant lipopeptide fragment ions provided significant information regarding the complexity of the mixture. Depicted in Fig. 1 is the precursor ion experiment performed on the ion of *m/z* 555.

The precursor mass spectrum suggests that the ion *m/z 555* is produced from three different pathways. One path involves decomposition of m/z 1236 and suggests the sequence 555-NMV-F-A-NMV-A-F. (NMV could also be one of the isobaric amino acids, I or L, as these cannot be differentiated by low energy MS.) Another path starts with *m/z* 1250 to give the sequence 555-NMV-F-A-NMV-A-F-OCH_3. A portion of the ion of *m/z* 1236 may also be a methyl ester. If the C-terminus were methylated, loss of F and methanol would give the ion of *m/z* 1057, a high mass ion along the second path. The sequence which would generate the ion of *m/z* 555 corresponds to 555-NMV-F-A-V-A-F-OCH_3. The contribution to the abundance of the ion of *m/z* 555 has not yet been determined.

Precursor Ion Scan of m/z 555 from the Cycloserine-Treated Lipopeptide

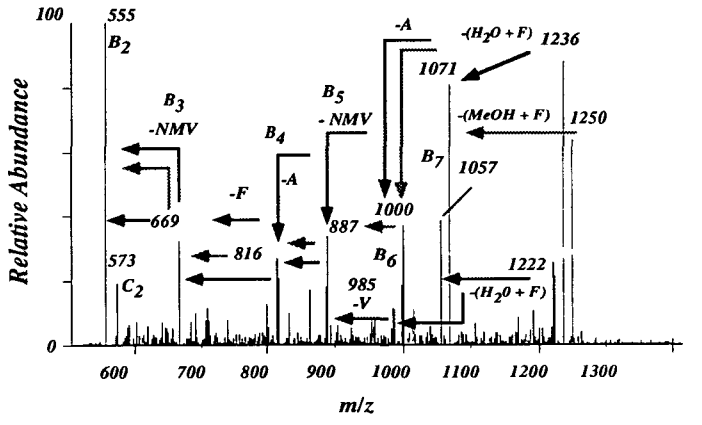

Figure 1: Precursor ion scan of m/z 555 obtained with a tandem quadrupole instrument from the isolated lipopeptide from cycloserine-treated mycobacterium. The ion at m/z 555 corresponds to a dipeptide fragment (F-NMV) acylated with eicosanoic acid.

The ion of *m/z* 1222 can fragment according to the third pathway to give the ion of *m/z* 555. The sequence which fits this route is 555-NMV-F-A-V-A-F. The ion of *m/z* 555 from the treated lipopeptide does not result from decomposition of the ion of *m/z* 1208.

The analysis of this lipopeptide from *Mycobacterium avium* presents unusual analytical challenges not normally faced in elucidating the structure of peptides by mass spectrometry. First of all, the normal methods employed to isolate, purify, and degrade the peptide are not amenable to this chloroform soluble product. Secondly, the mass spectrometry revealed that this product is a complex mixture of peptides differing in amino acid substitutions, methylation sites, as well as fatty acyl molecular species at the amino terminus. While the general motifs in the structure of this lipopeptide are beginning to fall into place, the precise extent of this complex mixture is currently under investigation.

ACKNOWLEDGEMENT
This work was supported, in part, by a grant from the National Institutes of Health (HL25785).

REFERENCE

1. W.B. Pratty and R. Fekety The Antimicrobial Drugs, NY, Oxford University Press, *1986*.

Mass Spectral Analysis of Protein Adducts of the Lipid Peroxidation Product 4-Hydroxy-2-nonenal.

*Bernd A. Bruenner[1], A. Daniel Jones[1], J. Bruce German[2], and T. William Hutchens[3]

[1]Facility for Advanced Instrumentation, [2]Department of Food Science and Technology
University of California, Davis, CA 95616

[3]Department of Pediatrics, Baylor College of Medicine, Houston, TX 77030

Lipid peroxidation in biological systems as a consequence of oxidative stress can result in the formation of toxic and reactive aldehydes, such as 4-hydroxy-2-nonenal (HNE). The double bond of this α,β-unsaturated aldehyde reacts readily with nucleophilic sulphydryl groups by a Michael addition reaction, and the aldehydic moiety can form covalent Schiff base linkages (imines) to amino residues, resulting in loss of protein functionality. The reaction of HNE with macromolecular proteins can form stable, long lived adducts, and their detection may allow for their use as biomarkers of oxidative damage *in vivo*. In order to probe the chemistry of HNE-protein adduct formation, proteins exposed to HNE were characterized by electrospray (ES) mass spectrometry to determine the extent of reaction and to attempt to elucidate the specific sites of modification within the amino acid sequence.

Proteins reacted with HNE *in vitro* included β-Lactoglobulin B (β-LgB), a representative of the lipocalin superfamily of hydrophobic ligand binding proteins, and human hemoglobin A. Several milligrams of each protein were dissolved in 0.01 M HEPES buffer pH 7.4, and HNE was added to the proteins as an 8 mM solution in the same buffer. The final concentration of HNE resulted in a 40-fold molar excess of HNE to hemoglobin and a 60-fold molar excess to β-LgB. Corresponding controls were also prepared using buffer solution only. The mixtures were allowed to react at 37 °C for three hours, and then the samples were extensively dialyzed against 0.01 M ammonium bicarbonate buffer pH 7.4. Heme was removed from the hemoglobin solutions by precipitation in acidic acetone. The proteins were subsequently lyophilized, and taken up in 50/50 MeOH/water + 1% formic acid to give a final concentration of approximately 20 pMol/μl for analysis by ES. Intact proteins were analyzed on a VG/Fisons BioQ mass spectrometer using 50/50 MeOH/water + 1% formic acid as the mobile phase at a flow rate of 5 μl/min using direct flow injection. Capillary voltage was 3.6 keV and source temperature was 60 °C.

The multiple peaks in the mass spectrum of hemoglobin exposed to HNE indicate that a heterogeneous mixture of protein adducts was obtained (Fig.1). Some unmodified α chain was observed, as well as peaks corresponding to addition of from one to four HNE per α chain. Similar results were obtained for the HNE modified β-LgB. A greater number of adducts appear to form in the case of β-LgB, as from three to a maximum of nine HNE appear bound per protein molecule. To confirm that these adducts were not merely the result of hydrophobic binding to the protein, the HNE exposed β-LgB was reacted with dithiothreitol to reduce the two intramolecular disulfide bridges and promote a more "open" structure of the protein and then hexane extracted to remove any HNE which may have been noncovalently bound. No changes in the number of HNE adducts were observed after this treatment.

Sequential peaks in the computer deconvoluted spectra (Fig. 1b) all differ by 156 mass units (within experimental accuracy), the molecular weight of HNE. The

increase of 156 mass units indicates that reaction has occurred via a Michael addition, since the formation of a Schiff base involves loss of water and the corresponding mass shift would be 18 mass units less, or 138, which was not observed. As both proteins have too few free sulphydryl residues to account for the number of Michael adducts, HNE appears to react with amino acids other than cysteine. Lysine and histidine also possess nucleophilic side chains, and Michael addition of HNE to these amino acids may account for the high degree of modification.

These results illustrate the potential of electrospray mass spectrometry for identifying xenobiotic modifications of intact proteins and in relating structural determinants of proteins to their susceptibility towards modification. Future research will involve the analysis of proteolytic digests to determine the specific amino acids of the primary sequence which become modified on exposure to HNE, and to determine if these adducts form *in vivo* under conditions of oxidative stress and can serve as biomarkers of oxidative damage.

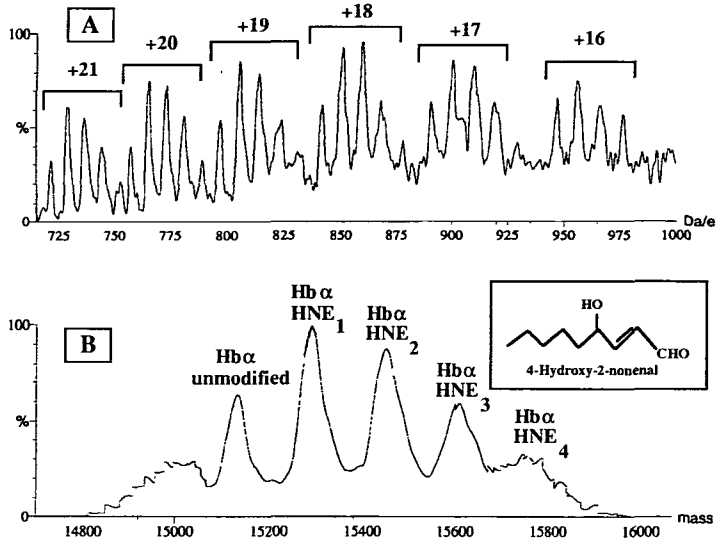

Fig. 1a) Electrospray mass spectrum of globin obtained by incubating hemoglobin with 4-hydroxy-2-nonenal (HNE). b) Computer deconvoluted mass spectrum showing adduct peaks on α chain separated by 156 mass units (molecular weight of HNE). Inset shows structure of HNE.

This work has been supported by NIEHS Superfund grant ES 04699.

STRUCTURE DETERMINATION BY ESI-MS OF PUTATIVE LOCUST DIURETIC PEPTIDES.

A.I. Mallet, G.M. Coast, R.C. Rayne & J.P. Bacon, St John's Institute of Dermatology, UMDS and Birkbeck College, University of London, Lambeth Palace Road, London SE1 7EH and Sussex Centre for Neuroscience, University of Sussex, BN1 9QG, UK.

INTRODUCTION.

Proux *et al* in 1987 **(1)** extracted two arginine-vasopressin-like peptides from over 50,000 suboesophageal and thoracic ganglia of *Locusta migratoria* . These were sequenced and synthesised and reported to be an amidated nona-peptide and its anti-parallel dimer. These were named F1 and F2 **(Figure 1**, A & D). This peptide was reported to have diuretic activity in the insect. Recently a second active diuretic hormone has been identified in the Locust and this is related to corticotropin releasing factor **(Figure 1**, F). Difficulties in obtaining appropriate biological activity from arginine-vasopressin nona-peptide preparations prompted us to examine the activities of a number of defined polymeric peptide structures.

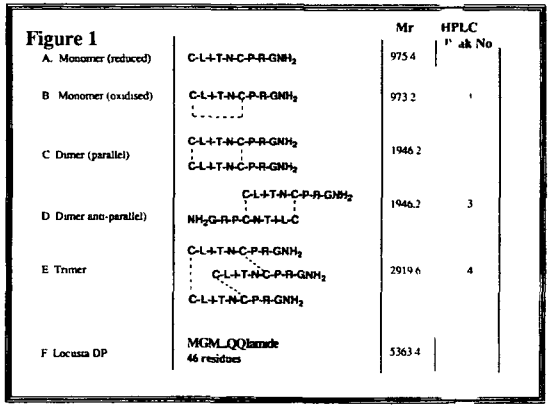

METHODS.

The reduced peptide CLITNCPRG-NH2 was synthesised using fMOC chemistry (Alta Bioscience, Birmingham, UK). The structure was confirmed by sequencing and M_r was determined by electrospray. The oxidised peptides were obtained by glutathione-based oxido-shuffling oxidation system **(2)**. The mixture of products was separated on HPLC (Aquapore C8 RP300 column with a propan-2-ol:0.1% aq. TFA gradient solvent system.

Dimer proteolysis was perfomed with Thermolysin (0.1 mg) in 10 ml of 100 mmol l-1 TES at pH 7.2, 30°C for 2h. Products were purified by HPLC as above.

Electrospray mass spectra were obtained from a VG Biotech source on a VG Masslab Trio-2 mass spectrometer (Fisons Instruments, UK). Peptides were dissolved and run in 50:50:1 water:acetonitrile:acetic acid solvent at 5ml min^{-1}. 1 to 10 pmole were injected.

RESULTS 1.

The electrospray of the reduced monomer peptide confirmed the successful synthesis of this starting product. The oxidation step should lead to the formation of at least three products, an internal bridged monomer, two dimers one parallel and the other anti-parallel **(Figure** 1 B, C and D.). The HPLC trace showed four products and an absence of starting reduced monomer. The electrospray spectra of material from HPLC peaks 1,2,3 and 4 gave Mr values corresponding

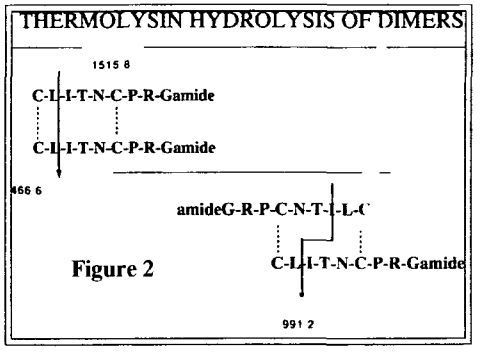

Figure 2

to the oxidised monomer from peak 1 and two identical values for the dimers in peaks 2 and 3. The distinction between the parallel and anti-parallel isomers required further analysis.

Thermolysin proteolysis takes place between the Leu and Ile residues. In the case of the parallel dimer this will lead to two products of M_r 466.6 and 1515.8; in contrast the anti-parallel dimer should only give a single product of M_r 991.2 **(Figure 2)**. The spectra of the products isolated from HPLC confirmed the anti-parallel nature of the material in the original HPLC peak 2.

It was possible to confirm this identification by careful examination of the electrospray spectra of material from peaks 2 and 3 taken at increased 'cone voltage'. The fragment ion patterns were clearly different ions at 701.9 and 758.5 from peak 3 could only have arisen from fragmentation of a parallel dimer. These spectra are shown in **Figure 3**. Peak 4 from the HPLC trace showed a M_r corresponding to the cyclic trimer **(Figure 1** E). All these products were found to be inactive in the relevant biological assay.

CONCLUSIONS.

We have produced unequivocal evidence for the structures of the oxidised products from the nine amino acid peptide. The combination of a number of biological and biochemical techniques together with electrospray mass spectrometry has been essential to the success of this work.

Further studies are now in progress to demonstrate the production of the Locusta -DP peptide from appropriate tissues under the correct biological regimes.

Figure 3

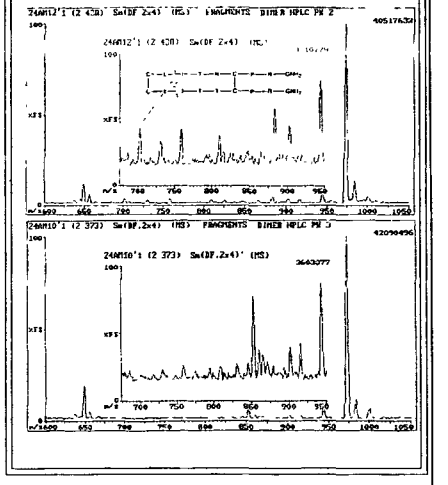

REFERENCES.

1. Proux J.P. et al, (1987) Biochem. biophys. Res. Commun., **149**, 180 - 186.
2. Jaenicke R & Rudolph R., (1989) in Protein Structure, a Practical Approach, pp 191 - 223; Oxford: IRL Press.

CHARACTERIZATION OF THE DRAGLINE PROTEIN COLLECTED FROM THE SPIDER *Nephilia clavipes*

Bernice Yeung* & Paul Vouros
Department of Chemistry & Barnett Institute,
Northeastern University, Boston, MA 02115
Charlene M. Mello & David L. Kaplan
Biotechnology Division, US Army Research Labs, Natick, MA 01760

INTRODUCTION

The spider silk dragline (major ampullate) collected from *Nephilia clavipes* has been a subject of interest in materials research, due to its enormous strength and elasticity. However, little is definitively known about its primary structure and molecular weight. Since dragline is insoluble in almost all solvents, the commonly used enzymatic digest procedures are not applicable for fragmenting the protein. Therefore, we developed a chemical method to digest this protein using N-bromosuccinimide (NBS) in formic acid, which cleaves primarily on the C-terminal side of Tyr[1]. Following the digest, the peptide mixture was characterized by SDS-PAGE, amino acid analysis, HPLC and MS. Also, standard peptides were subjected to the same digest procedure and examined by CFFAB MS in order to identify the modification on Tyr by the NBS digest.

EXPERIMENTAL

Materials: Dragline silk was collected from the abdomens of the live spiders. NBS was purchased from Aldrich (Milwaukee, WI).

Digest procedure: The silk was first solubilized in a minimum volume of formic acid, followed by the addition of ~10x excess of NBS (by weight). The mixture was incubated on ice for 1.5 hours, then another 1.5 hours at room temperature. Next, equal volume of acetone was added to stop the reaction. The solution was then spun at 14000 rpm for 1 hour in a microcentrifuge, after which a white pellet was observed. The supernatant was disgarded and the pellet was washed twice with acetone. At the end, the pellet material was dried in a Speed-Vac and kept frozen until further use. The same procedure was also applied to the standard peptides examined in this work.

HPLC: A Waters 625 LC system equipped with a 991 photodiode array detector and a WISP 722 autoinjector was used in this work. A C_4 column (4mmx25mm) with 5 μm particles and 300Å pore size (YMC, Inc., Wilmington, NC) was used. The gradient was 0-35% B in 88 minutes followed by a 5-minute hold at 35% B (A=H_2O and B=ACN, both containing 0.05% TFA). Flow rate was 1.0mL/min. Sample injections were 200μL, each containing 1 to 2mg of the original protein material in solvent A. Fractions were collected manually.

CFFAB MS: All data were obtained on a VG Quattro triple quadrupole mass spectrometer (VG Biotech, UK) equipped with a CsI gun. Mass range scanned was m/z 100-2300 in 8 seconds.

RESULTS

1. SDS-PAGE on the digest mixture revealed that most of the peptides generated appeared to be in the high mass range (40kDa and above), and that they were generated by reaction with NBS, not hydrolysis by formic acid.
2. Two "silk-like" standard peptides (GLY and GAGAGSGAGAGY) were subjected to the NBS digest procedure and were examined by CFFAB MS and MS/MS. The MS and CID data of the peptide GLY taken before and after the digest are shown in Figures 1 and 2. A mass shift of +158 in the MH^+ ion can be seen in the MS spectra. CID spectra clearly show the modification

to be on the C-terminal side of Tyr, judging from a shift by +158 in only the y ions. The modification is thus similar to that described in the literature[2,3].

3. All HPLC fractions of the digest were screened by CF FAB, using a variety of matrix solutions (glycerol, NBA, thioglycerol, magic bullet, etc.). However, it appeared that none of the fractions contained any peptides in the mass range examined.

CONCLUSIONS

At this stage of our work, we have:

- developed a chemical digest procedure suitable for the dragline silk;
- established the chromatographic conditions for fractionating the digest mixture;
- studied the NBS reaction mechanism and product by MS and MS/MS, and identified the modified y ion series which will aid in future CID data interpretation.

Future work to be carried out includes:

- examination of the present digest fractions by electrospray ionization, and
- increase in incubation time and/or amount of NBS for the digest in order to generate smaller peptides more suitable for examination by FABMS.

REFERENCES

1. R.L. Lundblad, *Chemical Reagents for Protein Modification*, second edition, CRC Press: Florida, 1991, p.52-53, 215-216
2. B. Witkop, *Advan. Protein Chem.*, **16**, p.221-321 (1961)
3. S. Shaltiel and A. Patchornik, *J. Am. Chem. Soc.*, **85**, p.2799-2806 (1963)

FIGURE 1

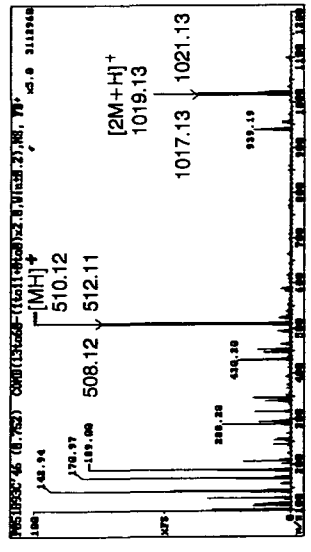

Normal scan spectrum of NBS modified G-L-Y

FIGURE 2

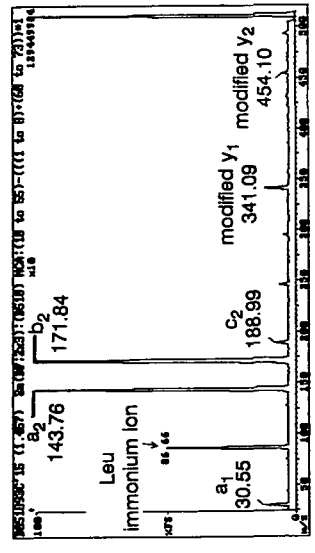

CID spectrum of NBS modified G-L-Y

CHARTING OF PITUITARY GLYCOPROTEINS BY CAPILLARY LIQUID CHROMATOGRAPHY - ELECTROSPRAY MASS SPECTROMETRY.

G. J. Feistner[1], Jens Andersen[2], Ole Vorm[2], Terry D. Lee[1], Peter Roepstorff[2]

[1]Division of Immunology, Beckman Research Institute of the City of Hope, Duarte, CA 91010
[2]Department of Molecular Biology, University of Odense, DK-5230 Odense M, Denmark

Previously, we have successfully charted bovine and rat pituitary hormones as large as the neurophysins (ca. 10 kDa) by plasma desorption and fast atom bombardment mass spectrometry and as large as rat prolactin (22,5 kDa) by electrospray mass spectrometry. We suggested that on-line capillary liquid chromatography - electrospray mass spectrometry may be the method of choice for the qualitative and quantitative determination of entire pituitary hormone profiles [1]. In pursuing this goal, we found that many observed peptides and small proteins could not be readily identified, possibly indicating hitherto unknown neuropeptides. On the other hand, we were not able to identify the physiologically important anterior pituitary glycoproteins, follicle-stimulating hormone (FSH), thyroid-stimulating hormone (TSH), and luteinizing hormone (LH). This did not necessarily mean that the glycoproteins were not amenable to electrospray mass spectrometry because their carbohydrate structures are not yet known and their molecular masses could not be calculated.

In order to address this issue, pituitary glycoprotein standards were obtained from the National Institutes of Health. Initial ES investigations on the α-chain of TSH indicated that the pituitary glycoproteins may be too heterogeneous to be amenable to ES-MS, at least at the low mass resolution typically employed in our charting studies. MALDI spectra revealed average molecular masses of 14.5 kDa (α-FSH), 14.4 kDa (α-LH), and 14.7 kDa (β-TSH), consistent with the reported corresponding DNA sequences plus allowances for glycosylation. As judged by the MALDI spectra as well as inferred from the existence of only one potential N-glycosylation site (versus 2 for the other glycoproteins), β-TSH was the least heterogeneous of the glycoproteins and was thus selected for further off-line ES investigations. These revealed eight major species with molecular masses of 14.5 to 14.8 kDa, which could be separated into two sets of four by RP-HPLC (14542, 14643, 14712, 14815, and 14557, 14660, 14727, 14830 u) (Fig. 1). The same species could be identified by on-line capillary LC-ES-MS. Under RP-HPLC conditions, β-TSH was less protonated than in the H_2O-MeOH-AcOH solvent used for the batch infusions, requiring that the extended mass range of 700-3,000 u had to be scanned for optimum sensitivity (Fig. 2).

Unfortunately, we were not able to confirm the above components as natural products by retroactive screening of our rat pituitary peptide charts. Again, this may be due to insufficient chromatographic resolution and molecular ion crowding that could not be resolved under our low resolution ES-MS conditions. On the other hand, the observed molecular masses of the standard are smaller than the ones expected for the natural product. The two major carbohydrate moieties of *human* β-TSH have reported masses of 1854 (24%) and 2024 u (18%), respectively, with the mass difference of 170 u corresponding to partial terminal sialylation versus sulfation. This diagnostic Δm is observed four times between the rat β-TSH components (14542/14712, 14643/14815, 14557/14727, 14660/14830), suggesting that the carbohydrate moieties in rat and man may be identical. However, addition of these carbohydrate masses to the protein molecular mass of rat β-TSH (13,454 Da) leads to expected molecular masses of 15,308 and 15,478, which are considerably larger than the

observed values. To investigate whether the difference was due to N-terminal truncation, Edman-type sequence analysis on the rat β-TSH standard was performed. Two sequences could be read, one representing the expected N-terminal sequence while the other corresponded to the internal sequence (K)YALSQD.... The latter suggested that some trypsin-like cleavage had occurred but could not explain the observed molecular masses. Reduction-pyridylethylation of the rat β-TSH standard followed by deglycosylation with N-glycosidase F, unexpectedly did not give rise a single protein of mass 14,728 u, but to two small proteins of molecular masses 8131 and 8230. Interestingly, the mass difference between these two products (99 u) is close to the second characteristic mass difference of 101/103 u (give or take a few reduction equivalents) that is observed between the components of the rat β-TSH standard (14542/14643, 14712/14815, 14557/14660, and 14727/14830 u). Further studies, including ES peptide mapping, will be needed to fully characterize the β-TSH standard.

With regard to the feasibility to extend our ES peptide charting to the pituitary glycoproteins, it is probably fair to say that the glycoproteins do not present special desorption/ionization problems but that their successful analysis depends heavily on sufficient chromatographic and mass spectrometric resolution.

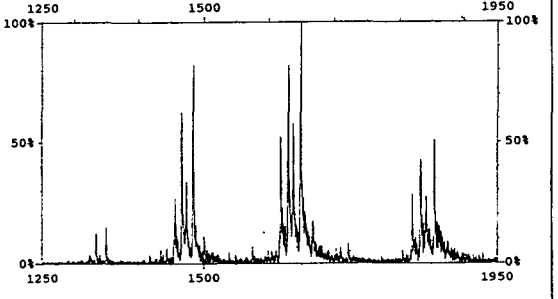

Fig. 1 ES-MS of subset 2 of rat β-TSH acquired on a Vestec instrument; batch infusion of an estimated 10-20 *pmol/μl* at a rate of 0.3 μL/min (1/5 of the corresponding RP-HPLC fraction obtained by chromatography of 600 pmol β-TSH standard, dissolved in 4 μl H_2O: MeOH:AcOH (50:50:1); data averaged over ca. 10 min.

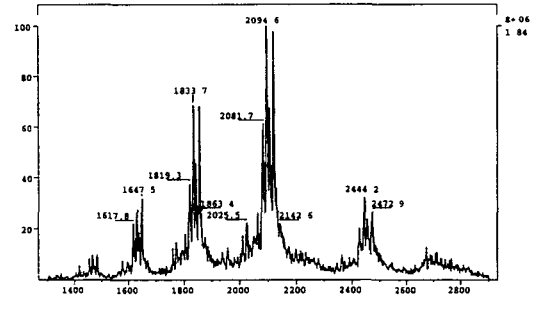

Fig. 2 ES-MS of subset 2 of rat β-TSH (NIH standard) acquired on-line on a capillary-C_{18}-RP-HPLC-Finnigan TSQ700 ES-MS system; 150 pmol rat β-TSH injected, 1-50% CH_3CN in 0.1% TFA/60 *min* at 2 *μl/min*; data averaged over the LC peak (20 scans, total of 1.5 minutes).

[1] G.J. Feistner *et al.* In: *Methods and Mechanisms for Producing Ions from Large Molecules.*, K. Standing and W. Ens (eds.) 1991. Plenum, *pp.* 45-53.

Analysis of Abnormal Glycoproteins of Patients with Carbohydrate Deficient Glycoprotein Syndrome

*Michiko Kanai[1], Katsuko Yamashita[2], Hiroko Ideo[2], Takashi Ohkura[2] and Keiko Fukushima[2]

1 Finnigan MAT Instruments, Inc., 2-5-8 Hatsudai, Shibuya-ku, Tokyo, Japan
2 Dept. of Biochemistry, Sasaki Institute, 2-2 Kanda-Surugadai, Chiyoda- ku, Tokyo, Japan

We applied ESI/MS for the structural characterization of abnormal serum transferrins in patients with carbohydrate deficient glycoprotein (CDG) syndrome.
Transferrin has two potential sites for asparagin-N-liked glycosylation. Transferrin from healthy control mainly has one isoform that has two N-linked disialylated biantennary sugar chains, thus it is tetrasialylated (S4). On the other hand, transferrin from CDG syndrome patients has 3 major isoforms. Yamashita et. al. determined that one of the isoforms has same structure as the major transferrin isoform from healthy control (S4) and abnormal species are missing either or both of two N-linked disialylated biantennary sugar chains using SDS-PAGE, chromatofocusing, lectin affinity chromatography and structural studies of sugar chains linked to these transferrin molecules (1). Thus the abnormal species are disialylated (S2) and desialylated (S0).
Our goals in this study are to determine the molecular weights of transferrin isoforms by ESI/MS providing the direct evidence of the above conclusion, and to determine if the non-glycosylation site in transferrin isoform S2 is <u>not</u> specific by HPLC-ESI/MS analyses of enzymatic digests of transferrin isoforms.

<u>Experimental</u> A TSQ 700 triple quadrupole mass spectrometer (Finnigan MAT, CA) equipped with an ESI source was used. For molecular weight determination, transferrins were dissolved in 0.1% TFA/water at a concentration of ca. 5 pmol/µl, introduced to the ESI source at a flow rate of 1µl/min. Transferrin isoforms S4 and S2 were reduced and pyridylethylated and then digested with trypsin. The tryptic peptides were subjected to the HPLC-ESI/MS analyses. A 4.0 mm x 25 cm, ODS column was used with the 1%/min gradient of 0.1% TFA/water/MeCN at a flow rate of 500 µl/min. Purification of serum transferrin and separation of transferrin isoforms were described in the reference (1).

<u>Results and discussion</u> The ESI mass spectrum of transferrin from a healthy control showed single distribution of multiply charged molecular ions (Fig. 1a). On the other hand, the ESI mass spectrum of transferrin from a CDG syndrome patient showed at least two molecular species (Fig. 1b), one was same as normal and the other was smaller than the normal transferrin. The difference between the molecular weights of two species was just the size of a disialylated biantennary sugar chain, 2206 Da. But the presence of transferrin isoform S0 was not clear in this spectrum. Then we analyzed each isoform separated by chromatofocusing. The molecular weights calculated from the ESI mass spectra of transferrin isoforms S4, S2 and S0 were 79 570 ± 5 Da, 77 364 ± 6 Da and 75 157 ± 6 Da (data not shown). These are very close to the theoretical molecular weights of transferrin polypeptide with 2, 1 and 0 disialylated biantennary sugar chains, respectively. These results consisted with the conclusion of the previous study (1). The proposed structures of transferrin isoforms are shown in Fig. 2.

There are two potential N-linked glycosylation sites in transferrin, so one of them is not glycosylated in transferrin isoform S2. Since desialylated transferrin isoform S0 was detected from the CDG syndrome patients, we supposed that the non-glycosylation occurs randomly at each potential glycosylation site in S2. Analyses of tryptic tansferrin isoforms S4 and S2 were performed by HPLC-ESI/MS. The tryptic fragments containing the potential N-linked glycosylation site are T41 and T67. In the peptide map of S2, we analyzed both T41 and T67 peptides with and without sugar chain (Fig. 3). The result demonstrated that non-glycosylation site in transferrin isoform S2 is not specific.
Accordingly, CDG syndrome can be concluded to be an asparagin-N-linked oligosaccharide transfer deficiency, although the primary deficient enzyme has not yet been determined.

<u>Acknowledgments</u> We would like to acknowledge to Dr. Seta and his colleagues at Tokyo Metropolitan University for valuable technical supports and discussions.

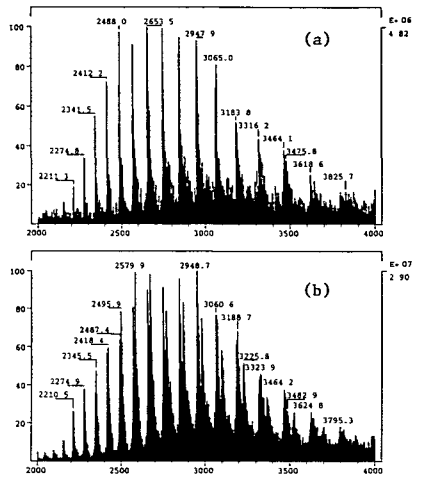

Fig. 1 ESI mass spectra of transferrins.
(a) Healthy control, 79 570±5 Da.
(b) CDG syndrome patient, 79 569±3 Da and 77 363±5 Da.

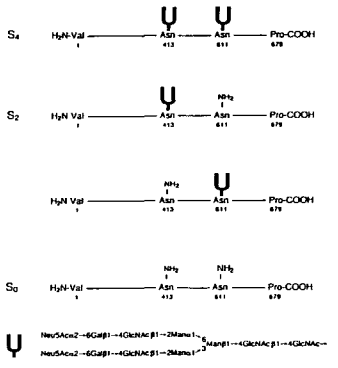

Fig. 2 Proposed structures of transferrin isoforms S4, S2 and S0.

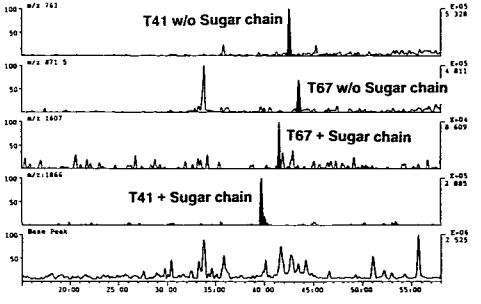

Fig. 3
HPLC-ESI/MS analysis of tryptic peptides derived from reduced and pyridylethylated transferrin isoform S2.

(1) Yamashita, K., Ideo, H., Ohkura, T., Fukushima, K., Yuasa, I., Ohno, K., and Takeshita, K. (1993) *J. Biol. Chem.* **268,** 5783-5789.

Structure of the Disialylated Transferrin Specifically Found in Carbohydrate-deficient Glycoprotein Syndrome

Y. Wada
Research Institute, Osaka Medical Center for Maternal and Child Health.
840 Murodo-cho, Izumi, Osaka 590-02, Japan

INTRODUCTION

Carbohydrate-deficient glycoprotein (CDG) syndrome[1)] is a newly recognized disease with nervous system involvement. The most specific diagnostic marker for this hereditary disease is the increase of an isoform of transferrin (TF) called "disialylated TF"[#] in serum; TF is mostly tetrasialylated in normal subjects. Since similar changes have been demonstrated in many other serum proteins, a structural defect in the N-linked sugar chains of secretory proteins containing sialic acid is suspected in the CDG syndrome.

I characterize here the structure of "disialylated TF" by mass spectrometry and give an important clue to the etiology of the CDG syndrome.

MATERIALS AND METHODS

Profile of Patients: Two unrelated patients were examined. Patient-1 was a severe case. She was 5-year old and have typical manifestations of the CDG syndrome including ataxia and developmental retardation. Patient-2, one of the affected brothers from consanguineous parents was a mild case.

Biochemical Analyses: Following analyses were carried out.

1. Isoelectric focusing followed by western blotting of TF.
2. Purification of TF by affinity chromatography.
3. Hydrazinolysis and reversed phase HPLC of pyridylaminated sugar chains.

Mass Spectrometry of Transferrin:

Electrospray Ionization (ESI) MS: The author reported the ESI mass spectra of human transferrin before[2)]. A magnetic sector mass spectrometer SX102A (JEOL, Japan) equipped with an electrospray ion source (Analytica of Branford, USA) was used. Samples were dissolved in a solution of 49/49/2 methanol/H_2O/acetic acid (v/v/v) at about 50 (20-100) pmol/µl, introduced into ion source at a flow rate of 0.7 µl/min and electrosprayed. Operating conditions were as follows: accelerating voltage was 5 kV, a range from m/z 3,300 to m/z 4,000 was scanned in two minutes and the mass data from ten scans were accumulated. Molecular weight is expressed by chemical mass.

Matrix-assisted Laser Desorption (MALDI) MS: MALDI-MS was carried out by JMS-LDI1700. Sample matrix was sinapinic acid.

RESULTS AND DISCUSSION

Isoelectric focusing of TF identified the increase of "disialylated TF" in both patients (data not shown). The content was larger in patient-1 than in patient-2. "Asialo-TF" was also detected in the patient-1. The HPLC profiles of sugar chains from TFs of patients were not different from those from normal subjects (data not shown).

[#]The term "disialylated" is a classificatory name of an isoform of TF separated by electrophoresis, not indicating true structure.

Molecular weights of the TFs in a complex mixture of normal and defective forms were then measured by ESI-MS. The mass spectrum of a normal healthy control showed multiply charged ions of a single molecular species. On the other hand, the mass spectra of the TFs from the patients revealed both the normal species and a smaller one. In both patients, the relative intensities of the small and the normal ion species correlated with the relative contents of disialo- and tetrasialoTF observed in IEF. The difference between the molecular weights of the normal and abnormal components was calculated to be 2,200 ± 60 Da for patient-1 and 2,200 ± 20 Da for patient-2, and was almost the same as the theoretical molecular weight, 2,206 Da, of disialylated biantennary sugar chain. We therefore conclude that the "disialylated TF" in CDG syndrome is missing a sugar chain at either of two glycosylation sites of the TF molecule[3)]. "Asialo-TF" was identified in patient-1 by MALDI-MS.

Our result signals a new direction for the etiological approach to this disease. The most probable metabolic defect of this disease would be in the early steps of protein glycosylation, from the synthesis of precursor sugar chain in the endoplasmic reticulum to the transfer of the synthesized chain to the nascent polypeptides. Further understanding of these mechanisms will uncover the biochemical cause and pathogenesis of this multisystemic syndrome.

REFERENCES

1. J. Jaeken, et al. (Eds.) *Acta Paediatr. Scand.* Suppl. vol.375 (1992)
2. Y. Wada, et al. *Rapid Commun. Mass Spectrom.* 6, 9-13 (1992)
3. Y. Wada, et al. *Biochem. Biophys. Res. Commun.* 15, 832-836 (1992)

ACKNOWLEDGEMENTS

The author would like to thank Dr. A.Nishikawa and Prof. N.Taniguchi (Biochemistry, Osaka Univ.) for biochemical analyses, N.Okamoto (Osaka Medical Center for Maternal and Child Health), Dr. K.Inui, Dr. H.Tsukamoto and Prof. S.Okada (Pediatrics, Osaka Univ.) for clinical presentation, Mr. K.Nojima (JEOL) for MALDI-TOF measurements, and Dr. H.Ito and Prof. T.Matsuo (Institute of Physics, Osaka Univ.) for mass spectrometry and data processing.

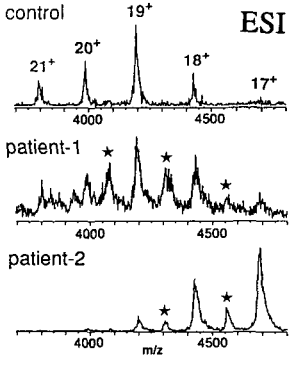

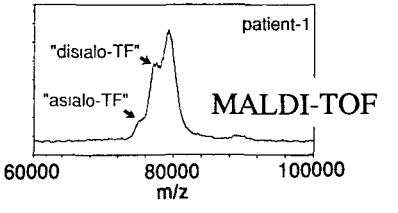

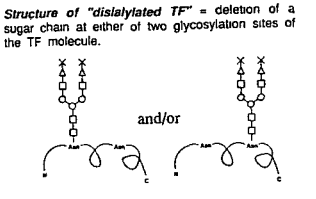

HPLC/ESI/MS of Tryptic Digests on Modified Cytochromes

*Baiwei Lin[a], Joe Sears[b], Jan Sunner[b], Al Jesaitis[c], and Mark Quinn[c],
[a]Lederle Laboratories, American Cyanamid, Pearl River, NY 10965, [b]Department of Chemistry and
[c]Department of Microbiology, Montana State University, Bozeman, MT 59717

INTRODUCTION

A combination of HPLC with electrospray has been used to identify sites of covalent modification in important proteins of the human neutrophil. One such protein is the cytochrome b. This is the electron transferase that delivers energetic electrons to reduce molecular oxygen to superoxide anion. It was recently shown that cytochrome b contains at least 2 hemes. The placement of the hemes is unknown. However, such structural information can be obtained by labeling the protein with fluorescent probes and studying the fluorescent quenching as a function of probe position along the protein chain.

In this work, the experimental protocol for the determination of the labeling site using HPLC/ESI/MS was developed. Horse heart cytochrome c was used as a model protein to develop the experimental procedure for tryptic mapping. Subsequently, the sites of modification in a labeled cytochrome c was determined by the same procedure.

EXPERIMENTAL

The tryptic digestion of unmodified as well as modified cytochrome c was carried out at a pH of 8 and an enzyme-to-substrate ratio of 1:50 (w/w). The digest was performed at 37°C for 16 hours. The HPLC system used consisted of a Gilson liquid chromatograph and a Spectra-Physics UV-detector. Elution was accomplished using a C18 reverse-phase column at a flow rate of 1 ml/min. In a gradient elution, solvent A was 1% HCl in distilled water and the concentration of B (1% HCl in acetonitrile) was increased from 6 to 60% in 30 minutes. ESI/MS was performed in a transport capillary ion source interfaced to VG-TRIO2 quadruple mass spectrometer.

RESULTS AND DISCUSSIONS

(1) Intact Labeled Cytochrome c. The labeled cytochrome c had two series peaks in ESI/MS spectrum. The molecular weight obtained from one series was that of cytochrome c, 12,361 Da. Another series yielded the molecular weight of labeled cytochrome c, 12,860 Da. The mass difference was 499 Da. In this particular sample modification, a Cascade Blue derivative was covalently bonded to the protein. Its molecular weight was calculated to be ca 500 Da. This matches the mass difference between the labeled and the unlabeled cytochrome c.

(2) Tryptic Mappping of Cytochrome c. In the process of enzyme digestion, trypsin breaks the polypeptide chain after the lysine and arginine amino acids. The peptide fragments produced in this digest and their corresponding labels are listed in Table 1, together with their calculated masses. The HPLC of tryptic digests of unlabeled cytochrome c is shown in Figure 1. Fraction numbers are indicated in the same figure. Electrospray mass spectra of each fraction was then obtained and some of them are presented in Figure 2.

Inspection of the ESI spectra in Figure 2 showed that all the expected fragments (except one) were indeed observed, within 1-2 Da of the expected mass. The identification was facilitated by the fact that each peptide has a distinct mass. Results are summarized in Table 1. All those fragments that were observed have "yes" and those that were missing have "no".

(3) Labeling Site Identification. HPLC separation of the tryptic digest of labeled cytochrome c (Figure 3) and mass determination by ESI/MS (Figure 4) was performed using the same experimental

conditions as did in the unlabeled protein. In general, the ions obtained from labeled cytochrome c were very similar to those obtained from unlabeled protein. There was a difference, however, for the peptide fragment T6(His26-Lys27). As shown in Figure 2(E9), the unlabeled protein gave an intense peak at 284 amu due to fragment T6. However, this peak was not detected in any of the fractions from the labeled protein. Instead, a peak at $m/z=392$ amu was observed in fractions L10-L12. This is the expected mass of the doubly protonated ion of His26-Lys27 bounded to the label compound.

CONCLUSIONS

Inspection of the ESI spectra showed that all the expected peptides of unlabeled cytochrome (except one) were observed. The peak observed at 392 is likely due to the His26-Lys27 tryptic fragment, labeled with the Cascade Blue derivative, and doubly protonated. ESI/MS was successfully used to determine the site of covalent modification of a cytochrome by a fluorophore label.

Figure 1. HPLC of Tryptic Digests From Unlabeled Cytochrome C

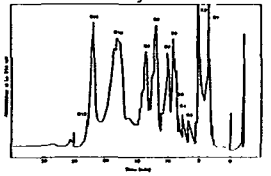

Figure 3. HPLC of Tryptic Digests From Labeled Cytochrome C

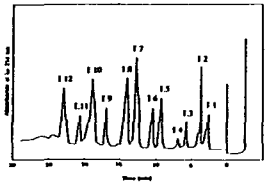

Table 1: Identifications of Tryptic Digests of Cytochromes

Fragment	Peptide	Mass	Ions Observed (Unlabeled)	Ions Observed (Labeled)
T1	GDVEK	588	YES	YES
T2	GK	203	YES	YES
T3	IFVQK	633	YES	YES
T4	GAQCHTVEK	1615	YES	YES
T5	GGK	260	YES	YES
T6	HK	283	YES	NO
T7	TGPNLHGLFGR	1168	YES	YES
T8	TGQAPGFTYTDANK	1470	YES	YES
T9	NK	260	YES	YES
T10	GITWK	603	YES	YES
T11	GGTLMEYLENPK	1495	YES	YES
T12	YIPGTK	678	YES	YES
T13	MIFAGIK	778	YES	YES
T14	TER	404	YES	YES
T15	EDLIAYLK	963	YES	YES
T16	AINE	433	NO	NO

Figure 2.
ESI/MS From HPLC Fractions (Unlabeled)

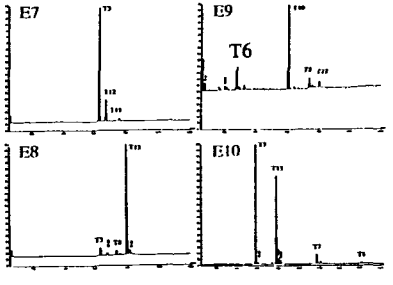

Figure 4.
ESI/MS From HPLC Fractions (Labeled)

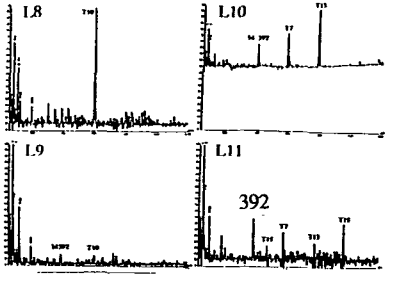

Characterization of Cytochrome $P450_{lin}$ by Mass Spectrometry

Rong Huang, Dipak K. Ghosh, Furong Sun, Anthony G. Thompson, Irwin C. Gunsalus, and Kenneth L. Rinehart, School of Chemical Sciences, University of Illinois, Urbana, IL 61801

Cytochrome P450 enzymes play important roles in the oxidative metabolism of a variety of biologically significant substrates.[1-3] A newly isolated species, $P450_{lin}$(MW=ca. 45kDa), that utilizes the acylic terpene linalool has been sequenced recently by the cDNA technique[4] and mass spectrometry has been used to confirm, or modify if necessary, the primary sequence.

The protein was digested with trypsin or *S. aureus*(Strain V8) and partially separated by HPLC. The HPLC fractions were then analyzed by FABMS. High resolution(HR) and FABMS/CID/MS data were also collected whenever possible to help confirm or assign the sequences of the peptides. The tryptic digest revealed about 83% of amino acids predicted by cDNA study, mostly before position 375. In the meantime, three peptides, with protonated MWs of *m/z* 995, 893, 866 were observed which could not be fitted into the proposed sequence. FABMS/MS spectra and HR data showed the sequences for these peptides as NLNVVLVPK(*m/z* 995), SNFLDGL(I)K(*m/z* 893) and (pyroglutamyl)-RPELLK(*m/z* 866), respectively. The *m/z* 866 peak corresponded to positions 273-279 in the proposed sequence, with glutamine being cyclized to pyroglutamic acid. The corresponding uncyclized peptide ([M+H] = 883 m/z) could also be observed in the same tryptic digest. There were no corresponding positions for *m/z* 995 and 893 peptides. The *S. aureus*(Strain V8) digest revealed about 75% of the proposed amino acids and provided very good overlapping with the tryptic digest, helping the alignment of these peptides. Still no peptides beyond position 375 were observed to confirm the sequence. These results indicated possible mistakes in the sequence proposed by the cDNA study.

The doubt became certain when the MW of intact $P450_{lin}$ was determined by electrospray(ESI) mass spectrometry. As shown in Table 1, the measured MWs were quite consistent from three different sources. The average MW measured was about 1650 Da higher than the calculated average MW. Reexamination of the nucleotide sequencing gel found a guanine that was missed. The omission misidentified an early stop codon. Its insertion corrected the sequence starting at position 378 and extended the protein sequence from 395 residues to 406 residues. The *m/z* 995 peptide was found to be the C-terminus(398-406) in the corrected sequence. The peptide with *m/z* 893 corresponded to positions 390-397 with N^{394} being hydrolyzed to D. The unhydrolyzed peptide ([M+H] = 892 m/z) did not appear under the tryptic digest conditions, but it was observed accidentally in the *S. aureus*(Strain V8) digest because of trypsin contamination in the V8 enzyme. Other peptides in the corrected sequence were also found later and the peptide mapping was completed except for one R at position 387, a mono-peptide in the tryptic digest.

After correction, the calculated average MW was about 160 Da lower than the measured value(Table 1). Also, it was noticed that the ESI spectra generally gave two ion series. The deconvoluted spectra showed two components differing by about 80 Da(Fig.1 & Table 1). The difference coincides with the mass of HPO_3 and SO_3, suggesting possible phosphorylation or sulfation of the protein. Considering the 160 Da difference between the measured and calculated MWs, there are possibly two modifications involved. To the best of our knowledge this is the first evidence of phosphorylation or sulfation to any P450 enzyme. Similar spectra were also obtained on $P450_{cam}$ (Fig.2), indicating a possible common modification among P450 enzymes.

Intact $P450_{lin}$ was also analyzed by MALDI/TOF/MS(Fig. 3). Due to the relatively poor resolution of the TOF analyzer, MALDI failed to identify the two components 80 Da apart. Its mass accuracy with external standards was also not quite as good as ESI, but its sensitivity under normal operating conditions was a little higher(1-10 pmol for MALDI, 100-200 pmol for ESI) and showed capability for mixture analysis(Fig. 4). In Figure 3, an impurity peak was detected along with singly and doubly charged $P450_{lin}$ molecular ions.

Both ESI and MALDI have been used to analyze tryptic digest mixtures. Coupled with HPLC, ESI revealed some peptides that were not observed in normal FABMS, showing the advantage of higher sensitivity, but it did not determine some of the peptides that were detected by FAB due to the difficulties in interpreting some of the peaks. Figure 4 shows the MALDI spectrum of the tryptic digest mixture of $P450_{lin}$. Relatively large peptides were detected without any separation. With internal standards at both the low and high mass ends of the peptides, the accuracy in the spectrum was better

than 1 Da. The resolution in the spectrum was about 700. FABMS is generally less sensitive compared with the other two techniques, but because of its ability to yield HR data and MS/CID/MS spectra on magnetic sector machines, it is still an indispensable tool. For instance, the tryptic peptides with *m/z* 892.49 and *m/z* 893.47 would not have been differentiated by ESI data, which gave *m/z* 892.85±0.4 .

In conclusion, the cDNA-derived amino acid sequence of $P450_{lin}$ was corrected by this MS study. MS data showed evidence of phosphorylation or sulfation of $P450_{lin}$ and $P450_{cam}$, the first indication of this type of modification of any P450 enzyme and implying a possible common modification within the P450 superfamily. Finally, deamidation during hydrolysis may cause a potential problem of misidentification of Q and N. Thus, proper control of the reaction conditions is important.

Acknowledgment: The authors are grateful to Dr.K.T.Yasunobu for sharing unpublished data. We thank Dr.R. Milberg for technical support, P.E.Sciex Co., VG Analytical Ltd., and Finnigan MAT for ESIMS, and VG Biotech for MALDIMS. This work was supported by a grant from the National Institute of General Medical Sciences (GM 27029, to K.L.R.)

1. Coon, M.J.; Ding, X.; Pernecky, S.J.; Vaz, A.D.N. *FASEB J.* **1992**, *6*, 669-673
2. Sariaslani, F.S. *Critical Reviews in Biotechnology* 1989, *9*, 171-257
3. Unger, B.P.; Sligar, S.G.; Gunsalus, I.C. In *The Bacteria*; Sokatch, J.T. and Ornston, L.N., Eds.; Academic: New York, **1986**, *10*, 557-589
4. Ropp, J.D.; Sligar, S.G. International Symposium on Cytochrome P450 of Microorganisms, Berlin, July 24-27, 1991

source	major component (Da)	minor component (Da)	Δm_1[c] (Da)	Δm_2[c] (Da)	Δm_3[c] (Da)
Sciex	45795.0	45720.0	75.0	1650.0	160.9
Finingan	45805.0	45723.0	82.0		
VG	45797.6	45715.5	82.1		
average	45799.2	45719.3	79.7		
Calcd. MW[a]	44149.2 Da				
Calcd. MW[b]	45638.3 Da				

Table 1. ESI data on intact $P450_{lin}$.
[a] Calculated MW before correction.
[b] Calculated MW after correction.
[c] Δm_1 = major - minor component
Δm_2 = MW exptl. - MW calcd.(before)
Δm_3 = MW exptl. - MW calcd.(after)

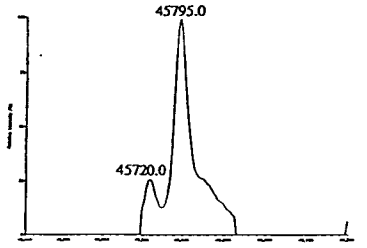

Figure 1. Deconvoluted ESI spectrum of $P450_{lin}$

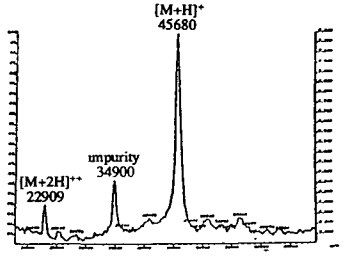

Figure 3. MALDI spectrum of $P450_{lin}$

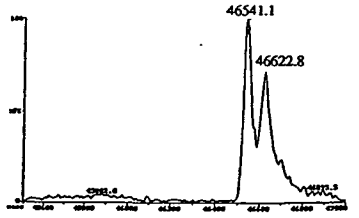

Figure 2. Deconvoluted ESI spectrum of $P450_{cam}$

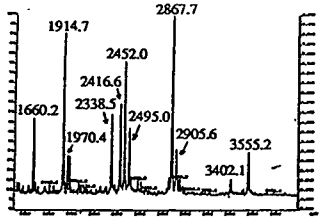

Figure 4. MALDI spectrum of $P450_{lin}$ tryptic digest

Chemical and Mass Spectrometric Characterization of the Heterogeneous N-terminal Lipid Modification of Photoreceptor G-Protein α-Subunit

Toshifumi Takao[1], Koichi Kokame[2], Yoshitaka Fukada[2], Toru Yoshizawa[3], Yoshinori Masatsugu[4], Kaichi Tanida[4], and Yasutsugu Shimonishi[1]

[1]*Institute for Protein Research, Osaka Univ., Yamadaoka 3-2, Suita, Osaka 565,* [2]*Faculty of Science, Kyoto Univ , Kyoto;* [3]*The University of Electro-Communications, Tokyo,* [4]*Shiono Koryo Co. Ltd , Osaka, Japan*

Previously, we and others found a novel posttranslational modification in the α subunit of retinal heterotrimeric G-protein transducin (Tα) [1-3] and recoverin [2,4] with heterogeneous fatty acids. They were modified at the N-termini with four kinds of fatty acids consisting of laurate (C12:0), myristate (C14:0) and unsaturated C14:1 and C14:2. We further suggested that these lipid modifications might mediate formation of the Tα/T$\beta\gamma$ complex. In the present study, we verified the structures of these N-terminal fatty acids of Tα by negative-ion FAB tandem mass spectrometry and chemical synthesis.

Tα was treated with *Achromobacter lyticus* protease I (API) as described previously [1]. In order to get simple fragmentation pattern and to achieve efficient fragmentation on the lipid moieties in MS/MS analysis, the N-terminal API peptides (Gly-Ala-Gly-Ala-Ser-Ala-Glu-Glu-Lys, 0.1~0.5 nmol) isolated by reversed-phase HPLC were completely digested with carboxypeptidase Y to yield the acyl glycine with four kinds of fatty acids. Negative-ion FAB mass spectra of the digests showed the ion signals at m/z=256.2, 284.2, 282.2, and 280.2, which agreed well with the theoretical masses calculated for lauroyl, myristoyl, C14:1-, and C14:2-glycine, respectively. Their negative-ion FAB tandem mass spectra gave highly specific fragmentations [5]. Figure 1 shows the MS/MS spectra of C14:0 (myristoyl), C14:1- and C14:2-Gly. The patterns of the intense peaks marked by asterisks, which correspond to ions arising from cleavage of the carbon-carbon bond allylic to the double bond together with dramatically less intense intervening signals, made it possible to assign the locations of the double bonds, Δ^5 and Δ^5,Δ^8 in C14:1 and C14:2, respectively. Finally, we synthesized the N-terminal nonapeptides modified at the α-amino group with the four kinds of fatty acids (laurate, myristate, *cis*-Δ^5-C14:1, and *cis,cis*-Δ^5,Δ^8-C14:2) and compared them with the N-terminal API fragments of Tα by reversed-phase HPLC. These synthetic peptides were completely identical with the API fragments.

The above results demonstrated the structures of the heterogeneous fatty acids linked to the N-terminus of Tα to be laurate, myristate, *cis*-Δ^5-C14:1 and *cis,cis*-Δ^5,Δ^8-C14:2. It will be interesting to see the role of such heterogeneous lipid modification at the

N-terminus of Tα in a signal transduction process.

References

1. Kokame, K., Fukada, Y., Yoshizawa, T., Takao, T., Shimonishi, Y., *Nature*, 359, 749 (1992).
2. Johnson, R. S., Neubert, T. A., Dizhoor, A. M., Ericsson, L. H., Kumar, S., Olshevskaya, E., Hurley, J. B., Walsh, K. A., *Proceedings of the 40th ASMS Conference on Mass Spectrometry and Allied Topics*, Washington, DC., 1519 (1992).
3. Neubert, T. A., Johnson, R. S., Hurley, J. B., Walsh, K. A., *J. Biol. Chem.*, 267, 18274 (1992).
4. Dizhoor, A. M., Ericsson, L. H., Johnson, R. S., Kumar, S., Olshevskaya, E., Zozulya, S., Neubert, T. A., Stryer, L., Hurley, J. B., Walsh, K. A., *J. Biol. Chem.*, 267, 16033 (1992).
5. Tomer, K. B., Crow, F. W., Gross, M. L., *J. Am. Chem. Soc.*, 105, 5487 (1983).

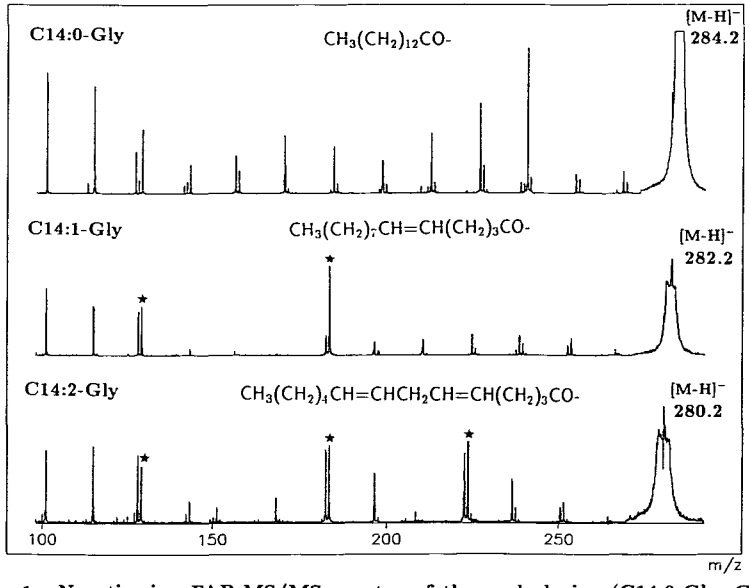

Figure 1. Negative-ion FAB-MS/MS spectra of the acyl glycine (C14:0-Gly, C14:1-Gly and C14:2-Gly) produced by carboxypeptidase Y digestion of the N-terminal API peptides of Tα. The spectra were obtained in a JMS-HX/HX110A four-sector tandem mass spectrometer equipped with a collision cell and an array detector system (JEOL).

Characterization of Peptides Extracted from the Human Class I MHC Molecule, HLA-B7. *Wanda M. Bodnar, Jeffrey Shabanowitz, Donald F. Hunt, Eric L. Huczko, David Benjamin, and Victor H. Engelhard, Departments of Chemistry and Microbiology, Univ. of Virginia, Charlottesville, VA 22901.

Microcapillary HPLC electrospray ionization tandem mass spectrometry has been used to characterize the primary structures of peptides associated with the human class I molecule, HLA-B7 (1). Class I molecules of the major histocompatibility complex (MHC) are a set of glycoproteins which present self and foreign peptides to cytotoxic T lymphocytes (CTLs) of the immune system. It is believed that a small fraction of nascent proteins, both self and viral, are degraded in the cytosol by proteosomes, and that the short peptides which are produced are transported to the endoplasmic reticulum where they bind to newly synthesized class I MHC molecules. The MHC-peptide complex is subsequently transported to the cell surface for examination by CTLs (2). Should a CTL receptor recognize a peptide derived from a foreign protein, the CTL becomes activated, multiplies, and secretes a mixture of enzymes which lyse the infected cell. If only self peptides derived from normal cellular proteins are presented on the cell surface, the CTLs remain inactive and continue to screen other cells nearby.

Although over one hundred structurally distinct class I MHC molecules have been identified in humans, only as many as six different forms will be expressed by the cells of any one individual. Given the limited number of MHC variants per cell, and the fact that a cell synthesizes and degrades thousands of proteins, it follows that each MHC molecule must be capable of binding and presenting a wide variety of structurally distinct peptides. Sequence analysis of the complex mixtures of peptides presented to the immune system by different MHC molecules will lead to a better understanding of how the immune system responds to the presence of foreign proteins. And ultimately, more detailed information about the peptide binding specificities of MHC molecules will be useful in the design of vaccines and therapeutic agents against numerous disease states. This task is challenging however, since each peptide in the complex mixture will only be present at a level of 10 to 1,000 fmol per 10^8 cells.

The development of microcapillary HPLC electrospray ionization tandem mass spectrometry has made possible the sequence analysis of individual peptides present at very low levels within complex mixtures (3). Mass spectrometric analysis of extracts from 10^8 cells bearing the HLA-B7 molecule has revealed that at least 2,000 naturally processed peptides are bound by this MHC molecule. The complete sequences for 18 of these peptides have been determined by collision activated dissociation experiments and the results are presented in table 1. The majority of peptides are nine residues in length and share a consensus motif dominated by Pro in position 2 (P2) and Leu or a small hydrophobic residue at P9. Homology searches in a protein database revealed 7 matches within 6 different human proteins. Synthetic peptides with sequences corresponding to those of the 18 endogenous peptides were tested for association with HLA-B7 in a qualitative binding assay. All were found to increase the expression of a stable conformation of the HLA-B7 molecule on the surface of T2 cells. The sequences obtained by mass spectrometric analysis were used in conjunction with computer modeling to make testable predictions about the binding requirements of HLA-B7. A structure for this molecule with bound peptide was derived from the crystal coordinates of the HLA-B27

Table 1. Partial Listing of Data for Peptides Extracted From HLA-B7

$(M+H)^+$ (m/z)	YIELD (fmol)	SEQUENCE	SOURCE PROTEIN
899	890	A P R T V A L T A	HLA CL.II DP ß-CHAIN PRECURSOR (9-17)
937	580	A P R X P X T G X	---
954	750	A P R A S R P S X	---
979	1078	A P R A X X X X X	---
995	540	A P R T L V L L L	HLA CL.I HEAVY CHAIN PRECURSOR (5-13)
944	310	A P R S N G M V X	---
940	540	A P R Q P G X M A	---
838	130	A P A P T V A V X	---
858	100	A P Y G G P X A X	---
971	360	M P R G V V V T X	---
1039	2310	R P K S N I V L L	CD20 B-CELL SURFACE ANTIGEN (222-230)
909	1850	R P S G P G P E X	---
1127	145	S P R Y I F T M L	DNA TOPOISOMERASE II (801-809)
999	230	L V M A P R T V L	HLA-B7 α-CHAIN PRECURSOR (2-10)
1026	1450	R V M A P R A X X	---
1012	820	A P R T V A L T A L	HLA CL.II DP ß-CHAIN PRECURSOR (9-18)
1080	1110	A P R A F X P X P V	---
1104	327	A A S K E R S G V S L	HUMAN HISTONE H1D (48-58)

molecule by substitution of the appropriate amino acids (4). Modeling of the complex of HLA-B7 with the peptide 899 (APRTVALTA) has allowed us to explain the binding specificity observed for this MHC molecule. Although much of the immune response remains a mystery, mass spectrometry has opened new doors to immunologists by providing a means to a better understanding of the peptide binding interactions of MHC molecules.

References

1. Huczko,E.L., Bodnar,W.M., et al. 1993, accepted *J. Immunol.*
2. Yewdell,J.W. and Bennink,J.R., 1992, *Adv. Immunol.* 52, 1-123.
3. Hunt,D.F., Henderson,R.A., Shabanowitz,J., Sakaguchi,K., Sevilir,N., Cox,A.L., Appella,E., and Engelhard,V.H., 1992, *Science* 255, 1261-1263.
4. Madden,D.R., Gorga,J.C., Strominger,J.L., and Wiley,D.C., 1992, *Cell* 70, 1035-1048.

Structural Analysis of Peptides Associated with the Class I MHC Molecule HLA-A24.1

David Arnott, Jeffrey Shabanowitz, and Donald F. Hunt, Department of Chemistry, University of Virginia, Charlottesville, VA 22901; Ralph Kubo, Allessandro Sette, and Howard M. Grey, Cytel Corporation, San Diego, CA 92121.

Class I molecules of the major histocompatability complex (MHC) bind peptides derived from intracellular proteins and transport them to the cell surface where they are displayed to cytotoxic T-lymphocytes (CTLs or killer T-cells). If a peptide is recognized as foreign the T-cell lyses the infected cell and proliferates in reaction to the discovery of infection. CTLs react against viral infection, cancerous cell transformations, and are implicated in autoimmune diseases Characterization of peptides which bind to class I molecules and the structural features required for efficient binding is therefore of intense interest. Such a characterization is also challenging; over 2,000 peptides may be presented at femtomole levels per 10^8 cells.

A complex mixture of peptides present at the low to subpicomole level was isolated from the class I molecule HLA-A24.1 Microcapillary HPLC/ electrospray ionization and tandem mass spectrometry was used to sequence 10 peptides. In combination with binding assays a binding motif is proposed which requires tyrosine at position 2 and a hydrophobic residue at position nine of nine residue peptides.

Several peptides were sequenced which did not bind to HLA-A24.1 and have a distinct motif of proline or alanine at residue 2 and a small hydrophobic residue at the c-terminus. These peptides, of eight or nine residues may be associated with HLA-B54.

The cell line chosen for study was LKT3, a homozygous cell line derived from the 10th Histocompatability workshop B cell reference panel. Its class I specificities are A24.1, B54, and C1.

Peptides bound to HLA-A24.1 were isolated by immunoaffinity chromatography. A KT3 cell lysate was passed over three columns of monoclonal antibody B1.23.2 to remove HLA -B,-C and then three columns of antibody W6/32 to bind HLA-A. Peptides were eluted under acidic conditions, collected by centrifugation through a 5 kDa filter and concentrated by vacuum centrifugation.

More than 1,000 peptides were recovered from ~600 micrograms of MHC. The complexity of the mixture was reduced by reversed phase HPLC separation:

2.1mm x3 cm Brownlee OD300 cartridge column
200 uL/min flow
0-60% MeCN/0.1% TFA gradient in 40 minutes
Fractions were collected every 60 seconds.

Each HPLC fraction was examined by microcapillary HPLC- Electrospray Ionization- Triple quadrupole mass spectrometry.

10-15cm C18 or POROS II/RH beads were packed in 50 micron i.d. fused silica capillaries behind a glass frit.

Samples were loaded hydrostatically and eluted with a 0-80% gradient of MeCN/0.1M HOAc.

A precolumn splitter resulted in a flow of 0.2 - 0.5 uL/min to the electrospray source where the eluant mixed with a sheath of 90% MeOH/0.1M HOAc flowing at 3 uL/min.

Quadruple 1 of a Finnigan TSQ700 was scanned to acquire spectra; 30 fmol limit of detection. The most dominant peptides in each fraction were subjected to collisionally activated dissociation in the TSQ700 instrument.

Sample was introduced by microcapillary HPLC/ESI as above.

The ion of interest was isolated in the first quadrupole, caused to dissociate in quadruple 2 by collisions with 3 mtorr argon at energies of 15-30v, and the fragments analysed in quadruple 3. Peptide sequences were reconstructed from the product ion spectra. Chemical modifications such as acetylation,esterification and manual Edman degradation facilitated interpretation. MS/MS is typically carried out on 100 - 300 fmol of peptide.

Synthetic peptides were provided by Dr. Ettore Appella or synthesized by F-moc chemistry on a Gilson model AMS 422 multiple peptide synthesizer according to standard procedure.

The binding of peptides to HLA-A24 1 was measured in a competative binding assay. 50% inhibatory concentrations of the test peptides to a 'consensus' sequence peptide which binds well to HLA-A24.1 were measured. The results are reported as a ratio of the 50% inhibatory concentration of the test peptide to that of two standard peptides.

(M+H)+	Sequence	Source Protein
1207	YYEEQHPEL	Unk. protein in natural killer cells
1170	KYPENFFLL	Phosphoprotein Phosphatase I
1103	AYVHMVTHF	
1055	VYXXHPVSX	
1141	DPYEVSYRI	Btg1 Protein
929	VPYEPPEV	Cellular Tumor Antigen P53
886	XPSDXAAEA	
1095	DAHIYLNHI	Thymidylate Synthase
1044	YAFNMKATV	Heat Shock Conjugate Protein
1053	DAEMTTRMV	

The complete sequences of 10 peptides were determined. The source proteins for six were identified by protein or DNA database searches. **Figure 1** lists the sequences The amino acids found at residue nine were in all cases hydrophobic, with Val, Leu, or Ile being most prevalent. Three amino acids were observed at residue 2, the other anchor position Tyr in 4 peptides, Pro in three peptides, and Ala in three. All but one peptide was nine residues long; one had only eight residues.

Seven peptides have been synthesized and assayed for binding to HLA-A24.1. The binding data are illustrated in **Figure 2.** The peptides containing Tyr at position 2 were found to bind well, but those with Pro or Ala at position 2 bound weakly or not at all. Because no monoclonal antibody with high specificity for A24.1 was available it is possible that HLA-B54 or HLA-C1 peptides are found in the preparation.HLA-C1 is expressed at only 10% of the level of HLA-A24.1 so it is unlikely to contaminate the sample, but the non-binding peptides could have been associated with HLA-B54. The sequences of these peptides resemble those of HLA-B7, in which Pro is the dominant amino acid at residue 2, and Ala is also tolerated; these peptides do not, however, bind well to HLA-B7. The differences in binding motifes of the class I molecules are due to polymorphism in the pockets of the binding cleft, but in the absence of crystallographic data it is difficult to draw conclusions about this data. It is, however, possible to assay these peptides for binding to HLA-B54, and these experiments will be carried out.

Microcapillary HPLC coupled with Electrospray Ionization/ triple quadrupole mass spectrometry was used to sequence ten peptides isolated from the class I molecule HLA-A24.1. In conjunction with binding assays this data suggests a binding motif of Tyr and a hydrophobic amino acid at positions 2 and 9 respectively of a nine residue peptide. Those peptides which did not bind to HLA-A24.1 may be associated with HLA-B54, in which case this molecule's binding motif would allow Pro or Ala at position 2 and a small hydrophobic residue at position 9. This hypothesis will be tested with HLA-B54 binding studies.

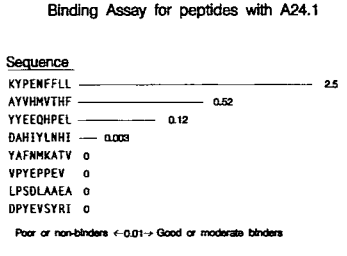

Application of Matrix-Assisted Laser Desorption Time-of-Flight Mass Spectrometry in the Structural Characterization of Proteins

Jimmy R. Calaycay, Tracey A. Dickinson, Richard A. Mumford, and Patrick R. Griffin, Merck Research Laboratories, Rahway, NJ

We present a strategy for structural characterization of proteins that combines the use of SDS-PAGE with matrix-assisted laser desorption time-of-flight mass spectrometry (MALD-TOF-MS). The strategy employed is outlined in Figure 1. Sample was separated by SDS-PAGE and electroblotted onto Cationic Durapore-polyvinylidene difluoride (CD-PVDF, Millipore) membrane. After visualization, bands of interest were excised and analyzed in one of the three pathways illustrated in Figure 1. N-terminal sequence analysis was obtained by placing one excised band directly into a modified ABI 477 gas phase sequencer. Molecular mass information was obtained as follows: Protein was extracted from the CD-PVDF membrane in high salt (2 M citric acid) with sonication followed by a desalting step. In this step, sample was loaded onto a 1 m long fused silica (50 μm) that was derivatized with C18 and the sample was washed with 100 μl water. Protein was eluted directly onto the MALD-TOF sample stage with a solution of MALD matrix in 80% acetonitrile and analyzed by MALD-TOF. Internal fragments of proteins were generated by exposing one excised band to cyanogen bromide in 70% trifluoroacetic acid. Resultant peptides were extracted, desalted and analyzed as described below.

Figure 1.

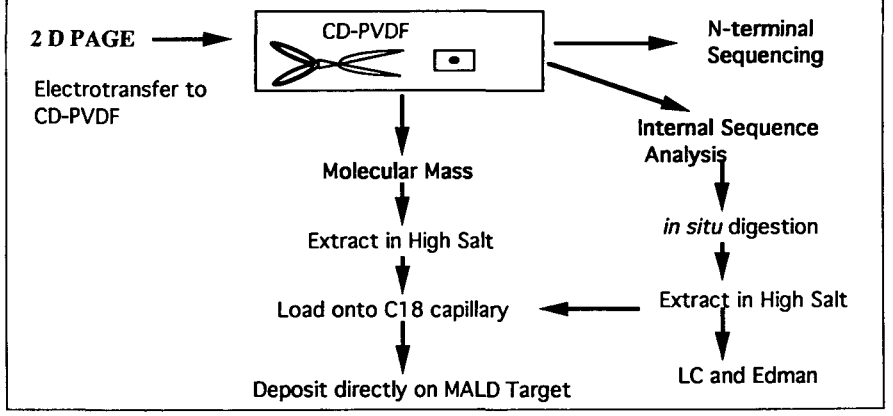

Samples were analyzed on a Finnigan MAT Vision 2000 MALD-TOF mass spectrometer equipped with a movable sample stage (5 kV), Ion reflector, post acceleration detector (20 kV), CCD camera, and a nitrogen laser (337 nm). Data acquistion, instrument control, laser trigger, and beam attenuator are controlled by a Gateway 486 PC. A mixture of 9:1 2,5-dihydroxybenzoic acid (10 g/L) in water : 5-methoxysalicylic acid (10 g/L) in 50% acetonitrile was used as the MALD matrix. Human α1-protease inhibitor (α1-PI) was run on 7.5% SDS gel (60 pmol/lane) and then electroblotted to CD-PVDF. An excised band containing intact α1-PI was placed in an ABI sequencer and N-terminal sequence was obtained out to 18 residues. A second excised band containing intact α1-PI was extracted, desalted and analyzed by MALD-TOF MS (Figure 2). Peptide fragments of α1-PI were also generated by exposing a third excised band of CD-PVDF membrane containing intact α1-PI to cyanogen bromide in 70% trifluoroacetic acid for 2 h. Peptides were extracted in high salt and desalted as described above. Analysis of the fragments by MALD-TOF resulted in the mass spectrum shown in Figure 3. The observed fragments account for over 80% of the amino acid sequence.

Figure 2.

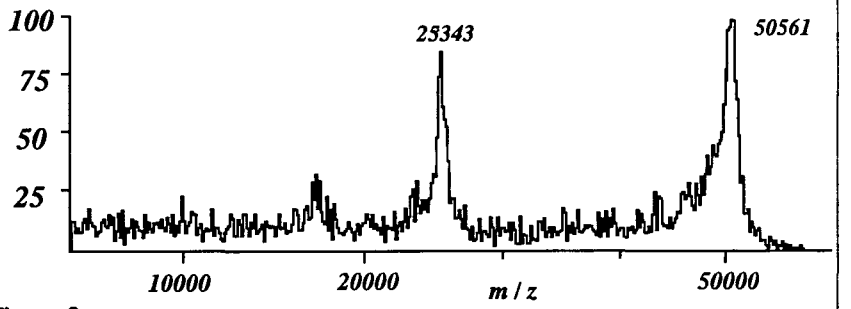

Figure 3.

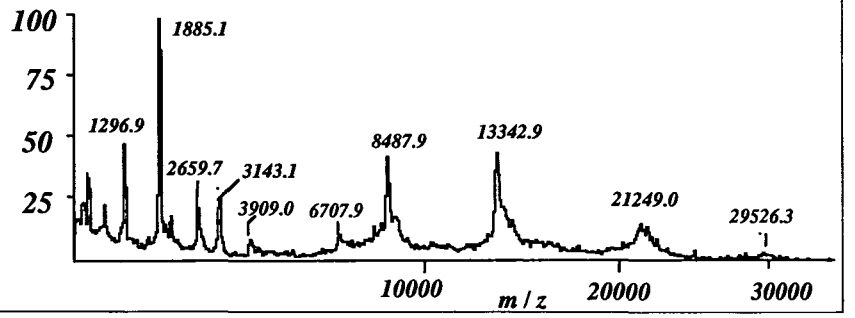

CHARACTERISATION OF RECOMBINANT IL4

D.J.Bell, W.A.Neville, M.Haran and A.West,
SmithKline Beecham Pharmaceuticals, Great Burgh, Epsom, Surrey KT18 5XQ, U.K.

Mass spectrometric analyses formed a considerable part of the effort to define the structure of recombinant Interleukin 4 (IL4) The primary structure of the protein was investigated using on-line HPLC/FABMS to characterise peptides generated in a tryptic digest. Molecular masses could be assigned to the majority of peptides observed by UV aborbance thus much of the sequence could also be verified by correlating the data with the molecular masses of predicted tryptic peptides. In some cases, the background subtracted LC/FAB spectra contained fragment ions of sufficient intensity to confirm the sequence of the peptide. As the protein was digested in the native form, the disulphide bridging could be investigated by calculating the possible combinations of cysteine containing peptides and comparing this with the molecular masses observed in the LC/MS analysis. In addition to molecular mass information relating to the intact bridged peptide, the spectra of peptides with disulphide bridges showed facile cleavage at the -s-s- bond. Comparing this data with the possible masses of disulphide linked peptides, the results were ambiguous as fragment ions corresponding to particular cysteine peptides occurred more than once in the chromatogram suggesting scrambling of the bridges. Using reverse phase chromatography to separate components of the lys-C digest of IL4, followed by re-analysis of reduced LC fractions, the disulphide containing peptides were identified. Analysis of the peptides seen to be affected by reducing agents by FAB allowed the nature of the bridging to be determined. The nature of the bridge peptides was confirmed by on target reduction to generate the two free cysteine containing peptides. Observations in the analysis of the tryptic digest were explained as incomplete digestion of the protein producing partial peptides.

Having determined the primary structure of the protein and the position of disulphide linked residues, ^{15}N and $^{13}C/^{15}N$ labelled IL4 were prepared to allow full structural characterisation of the material by NMR. To investigate the degree of isotopic enrichment, two mass spectrometric methods were used. Initially matrix assisted laser desorption/ionisation time-of-flight was exploited to give an average molecular mass although the resolution limitations of the instrument did not permit observation of incompletely labelled protein or the resolution of adduct ions (fig. 1) The result did suggest a high degree of enrichment (>90%) thus the material was digested using lys-C and the subsequent peptides characterised by FAB. The most intense isotope in the pseudo-molecular ion of the peptides was fully ^{15}N or $^{13}C/^{15}N$ labelled. Ions corresponding to incomplete labelling were also observed and, from the composition of the ion and this isotope pattern, the degree of complete enrichment was calculated as ca. 95%. (fig. 2) The sequence of these peptides was confirmed by linked scanning (B/E=constant), with consideration of the isotope labelling effect in the resulting spectra.

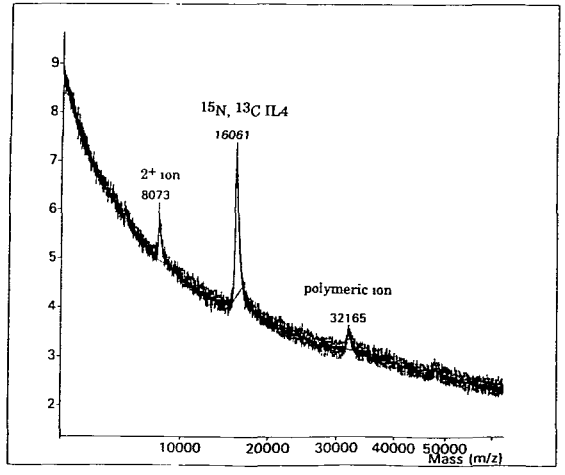

Fig. 1 MALDI ToF spectrum of $^{13}C/^{15}N$ labelled IL4.

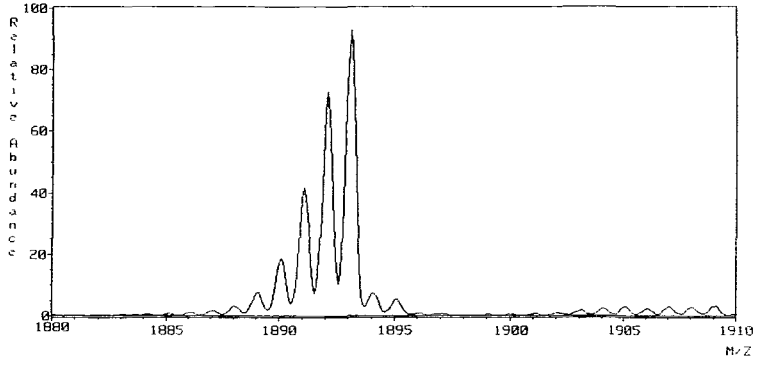

Fig. 2 The pseudo-molecular ion region of a lys-C peptide from $^{13}C/^{15}N$ labelled IL4.

Protein Ladder Sequencing in Solid Phase Peptide Synthesis

Sharon M. Walker*[1], Rong Wang[2], Saskia Milton[1], Brian Chait[2] and Stephen Kent[1]

[1]The Scripps Research Institute, 10666 North Torrey Pines Road, La Jolla, CA. 92037 & [2]The Rockefeller University, 1230 York Avenue, New York, N.Y.10021

Introduction

A technique is descibed through which the primary sequence of synthetic peptides can be routinely and quickly verified. A series of sequence-defining peptide fragments was generated during stepwise solid-phase peptide synthesis (SPPS). The peptide sequence was easily determined in one step using matrix-assisted laser desorption mass spectrometry (LDMS).

Approaches

I. In SPPS, the peptide chain is built up from the C-terminal amino acid (attached to a resin support), by adding successive amino acids one at a time in a stepwise fashion. Peptide resin samples were collected at each step, combined, deprotected and cleaved to form a pool of all possible length peptide intermediates. An aliquot of this mixture was analysed in a single operation by LDMS. Mass differences between successive peaks and their position in the data set gave the amino acid sequence of the peptide synthesized. Peptide resin samples may also be subjected to the quantitative ninhydrin reaction--used to determine the efficiency of the coupling reactions--before combining and subsequent analysis (Figure 1). Terminated by-products are readily detected since they are amplified during the sampling process. Figure 2 shows an example of a terminated peptide by-product. The observed by-product mass of 3339.0 Da corresponds to trifluoroacetylation at His 69 of a fragment from HIV-1 Protease (N$^{\alpha}$-Tfa-(69-99)).

II. An alternative method used to generate a sequence-defining ladder was the incorporation of 5 mole% Fmoc amino acid in a Boc synthesis. In this way, a small fraction of the growing peptide chain was terminated at each step of the synthesis. Removal of the Fmoc group, deprotection and cleavage resulted in a mixture containing a sequence-defining set of peptide fragments of all possible lengths, as well as the full length target peptide (Figure 3).

Conclusions

LDMS readout of ladder sequencing fragment sets from stepwise SPPS was used to confirm the amino acid sequences of synthetic peptides. This method can be used for rapid and routine sequence confirmation and by-product identification. In addition, the method provides easily interpretable data which can be used to identify modified amino acids and terminated by-products. Peptide resin samples may also be combined after quanititative ninhydrin and used for sequence confirmation.

Figure 1

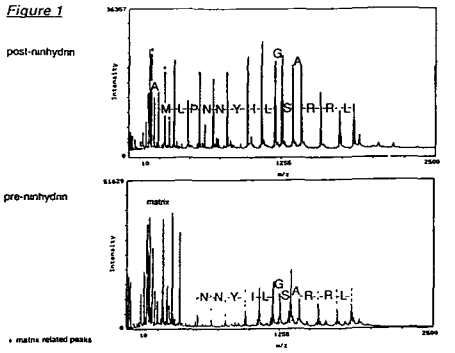

Amino acid mass differences for the peptide *LRRASGLIYNNPLMAR-amide* determined by LDMS

Amino Acid	Pre-ninhydrin Mass Difference (Da)	Pre-ninhydrin Deviation	Post-ninhydrin Mass Difference (Da)	Post-ninhydrin Deviation
Leu[1]	113.2	0.0	113.2	0.0
Arg[2]	156.1	-0.1	156.1	-0.1
Arg[3]	156.3	0.1	156.2	0.0
Ala[4]	71.1	0.0	71.1	0.0
Ser[5]	87.1	0.0	87.0	-0.1
Gly[6]	57.1	0.1	57.1	0.1
Leu[7]	112.9	-0.3	112.9	-0.3
Ile[8]	113.2	0.0	113.2	0.0
Tyr[9]	163.0	-0.2	163.3	0.1
Asn[10]	114.0	-0.1	114.1	0.0
Asn[11]	114.2	0.2	114.0	-0.1
Pro[12]	-	-	97.3	0.2
Leu[13]	-	-	113.2	0.0
Met[14]	-	-	131.1	-0.1
Ala[15]	-	-	70.9	-0.2

Figure 2 LOW MASS REGION OF HIV-1 PROTEASE PEPTIDE LADDER (99-N, WHERE N=66,33)

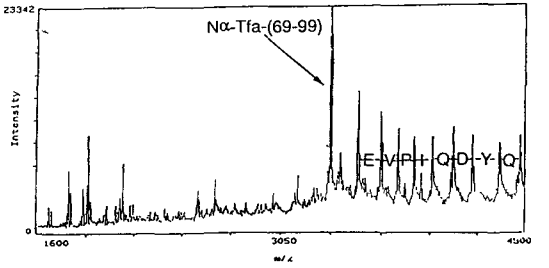

Figure 3

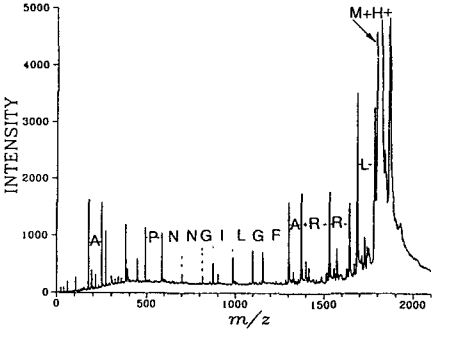

Amino acid mass differences for the peptide *LRRAFGLIGNNPLMAR-amide* determined by LDMS

Amino Acid	Mass Difference (Da)	Deviation
Leu[1]	113.7	0.5
Arg[2]	156.1	-0.1
Arg[3]	155.9	-0.3
Ala[4]	70.9	-0.2
Phe[5]	146.9	-0.3
Gly[6]	56.9	-0.1
Leu[7]	113.1	-0.1
Ile[8]	113.0	-0.2
Gly[9]	57.4	0.4
Asn[10]	113.2	-0.9
Asn[11]	114.5	0.4
Pro[12]	97.2	0.1
Leu[13]	-	-
Met[14]	-	-
Ala[15]	71.1	0.0

Technical Improvements Needed to Fully Integrate MS into the Reference Hemoglobinopathy Laboratory.

*H. Ewa Witkowska[1], Arnold M. Falick[2], Klara M. Kleman[1], Esther Roitman[1], Bing Lau[1], John Kim[1], and Cedric H. L. Shackleton[1]

[1]Children's Hospital Oakland Research Institute, Oakland, CA 94609;

[2] University of California, San Francisco, CA 94143.

Introduction

Implementation of mandatory newborn screening programs in many states is producing a growing volume of uncommon hemoglobinopathies requiring characterization. The cost and efficiency of identification procedures are important factors in the debate whether to pursue all such cases to a final conclusion. The aim of this study is to present advantages of incorporating mass spectrometric techniques at all stages of a hemoglobinopathy analysis: *i.e.* detection, confirmation of the identity of common variants and full structural analysis of uncommon mutants.

Experimental

Mass spectrometry was performed on a VG BioQ quadrupole mass spectrometer (VG BioTech/Fisons, Altrincham, UK). The electrostatic-spray ion source was typically operated at 3.2 kV and the nozzle to skimmer bias was close to 55 V (100 V for the source CID experiments). A Michrom microbore HPLC system (MichromBioresources, Pleasanton, CA) was interfaced with the mass spectrometer through the modified VG BioQ probe and 0.2% TFA in MeOH at the flow rate 2 µl/min was added as a sheath liquid prior to nebulization. Splitting 10:1 of the flow was achieved directly in the UV cell allowing 4 µl/min to be analyzed by mass spectrometer. Globins and peptides were separated on Vydac C4 and C18 narrow bore columns (1x150 mm, 300Å, 5µ), respectively and linear gradients of acetonitrile in 0.1% TFA were employed. Preparative cellulose acetate electrophoresis (CAE) (pH 8) and thin layer isoelectric focusing (TLIF) (agarose plates, Isolab ampholines pH 6-8) were performed using commercially available kits from Helena Laboratories and Isolab, respectively. CAE and TLIF separated hemoglobins were eluted from gels with water and the latter freed from ampholines by ulfrafiltration through Amicon centricon 10 filter units. Either 50% MeOH/1% AcOH or trifluoroethanol were used to deliver separated hemoglobins to the mass spectrometer.

Results

ESI MS has been incorporated into the initial step of hemoglobinopathy evaluation *i.e.* detection of hemoglobin variants in whole hemolysates. MaxEnt® algorithm is being examined as an alternative to deconvolution to provide accurate MW information for variants which are very close in mass and hence poorly resolved from other components of the mixture. An example of a carrier of Hb North Chicago (mass difference between

normal and abnormal β chain 10 Da, measured 10.6 Da) demonstrates the usefulness of the software. Certain mutants cannot be unambiguously analyzed in unfractionated hemolysates. This is the case when variants differ by less than 12 Da from other globin components of the mixture. Also, low abundance mutants which are isobaric with alkali metal adducts of major components pose a serious challenge in routine analysis. Interfacing HPLC of globins with ES MS offers an extension of the screening potential to encompass all hemoglobin mutants regardless of their mass differentials, provided they are separable by reversed phase HPLC.

ESI MS has been interfaced with cellulose acetate electrophoresis (CAE) and thin layer isoelectric focusing (TLIF), the techniques routinely employed in hemoglobinopathy laboratories. Hemoglobins thus isolated are amenable to ESI MS after a very limited work-up although recovery of minor TLIF bands still requires some improvement. Direct mass analysis of abnormal "bands" detected by routine electrophoretic techniques provides a fast way of confirming an identity of a variant hemoglobin or else dismissing certain cases as not being hemoglobinopathies.

Final structural analysis employs micro LC/ESI MS of proteolytic digests derived from the S-carboxyamidomethylated protein, 10% of the material being used for ESI MS and the rest collected for tandem MS sequencing, if required. Selected ion chromatograms aid in locating tentative abnormal tryptic fragments. Whenever possible, CID in the ion source is employed to confirm the sequence of abnormal peptides.

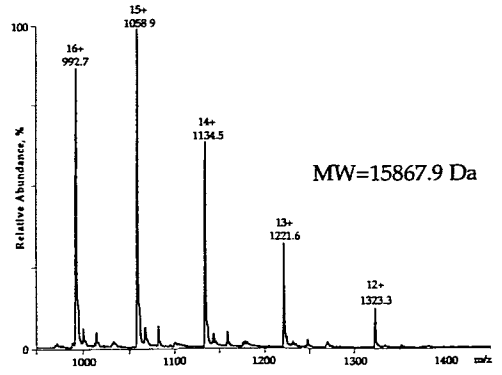

Fig. 1. ESI MS spectrum of Hb H (β_4) isolated by cellulose acetate electrophoresis. The presence of this hemoglobin is indicative of α thallasemia.

The NIH supported these studies through Sickle Cell Center grant HL20985 and a Shared Instrumentation Grant RR06505. CHLS is supported by NIH DK34400.

Amino Acid Sequence Determination of Neuropeptides by using Electrospray Ionization on a Magnetic Deflection Mass Spectrometer

Jih-Lie Tseng*, Chhabil Dass and Dominic M. Desiderio
University of Tennessee, Memphis, 956 Court Ave., Rm 218,
Memphis, TN 38163.

Mass spectrometry techniques have played a very important role in the analysis of biomolecules such as peptides and proteins. In the past, we have used FAB-MS either alone[1] or in conjunction with linked-field scan at constant B/E to determine the amino acid sequence of several biochemically important neuropeptides.[2] In this study, we explore the use of electrospray ionization to characterize a number of C-terminally extended enkephalin neuropeptides, including methionine enkephalin (ME), leucine enkephalin (LE), LE-Arg, ME-Lys, dynorphin (1-7), dynorphin (1-8). All experiments were conducted on a magnetic deflection mass spectrometer of EBE-qQ geometry (VG AutoSpec Q). Electrospray source was operated at 4 kV. The peptides *were introduced into the source as a flowing solution (3μL/min) of 50 pmole/μL in 1:1* $CH_3OH:H_2O$ containing 1% CH_3COOH.

The positive ion magnet scan spectrum contains mainly the singly and multiply charged ions of the peptides as the voltage between the sampling cone and the skimmer (ΔV) was set at 30 V. The ME and LE give MH^+ ions only, whereas, the peptides containing basic amino acid residues such as LE-Arg and ME-Lys yield the MH^+ and $(M+2H)^{2+}$, the latter type of ions are more intense than the singly charged molecular ions. Similarly, dynorphin (1-7) and dynorphin (1-8) give MH^+, $(M+2H)^{2+}$ and $(M+3H)^{3+}$ ions, the $(M+2H)^{2+}$ ions being the most intense As the ΔV is increased, fragmentation of peptides is also increased For example, only a few fragment ions are seen at ΔV = 30 V for ME (see Table 1) and LE (see Fig. 1). When ΔV is raised to 80 V, most of y- and b- type ions can be discerned easily. On raising the voltage further to 100 V, a complete set of y and b series of sequence determining ions is noted for ME and LE (see Fig. 2 for LE). With respect to LE-Arg, a complete set of a- and z- type ions are seen. ME-Lys provides a complete set of b- and y- type ions In addition, multiply charged sequence determining fragment ions are also observed for these two peptides. For example, complete sets of x- type of LE-Arg and c- type of ME-Lys doubly charged sequence ions are observed (see Fig. 3 for ME-Lys). For dynorphin (1-7), no complete set of sequence determining ion series is found. Fortunately, as the ΔV is changed from 30 to 60, 80 and 100 V, most of the a- and y- type series are observed. Besides, all the doubly charged sequence ions of c- series are also found but are less intense (see Fig 4) For the dynorphin (1-8), a complete set of z- type and most of a- type ions are observed as the ΔV is set at 80 and 100 V Multiply charged sequence determining fragment ions are also noticed.

Electrospray ionization can be readily used to determine the molecular weight of peptide from the multiply charged ions. Furthermore, the strategy of changing the inducing voltage between the sampling cone and skimmer provides the MS-MS-like spectra and can be clearly used for amino acid sequence determination for these enkephalin peptides

Acknowledgment:

The finacial support of the NIH (Grant GM 2666 to DMD, and NS 28025 to CD) is highly appreciated

References:

1. C. Dass and D M. Desiderio, Anal. Biochem , 163, 52-63 (1987).
2. C. Dass and D M. Desiderio, Int J Mass Spectrom. Ion. Proc , 92, 267-287 (1989).

Table 1. Fragment Shown at Different Inducing Voltage for ME

	1	2	3	4
ΔV=100				
a	136	193	-	397
b	164	221	278	425
c	-	-	295	-
z	-	-	339	384
y	150	297	352	409
x	177	-	380	-
ΔV=80				
a	136	193	-	397
b	-	221	278	425
c	-	238	295	-
z	133	282	-	394
y	150	297	354	411
x	178	323	380	-
ΔV=60				
a	136	-	-	397
b	-	221	278	425
c	-	-	-	-
z	-	-	-	-
y	150	297	354	411
x	-	-	-	-
ΔV=30				
a	-	-	250	-
b	164	-	278	-
c	179	-	-	-
z	-	-	-	-
y	-	-	-	-
x	-	-	-	-

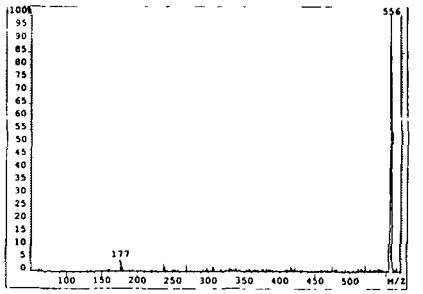

Figure 1 Fragmentation for LE at ΔV = 30V

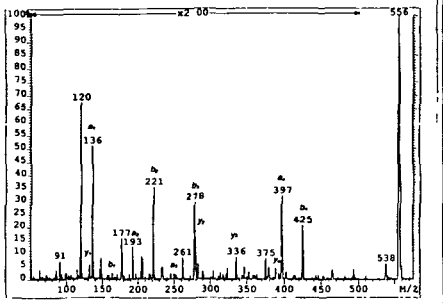

Figure 2 Fragmentation for LE at ΔV = 100V

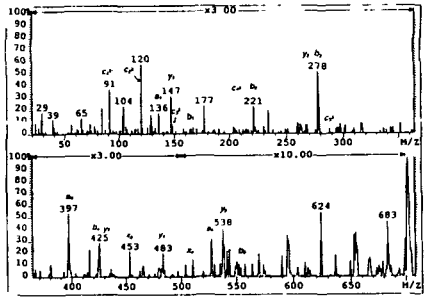

Figure 3 Fragmentation for ME-Lys at ΔV = 100V

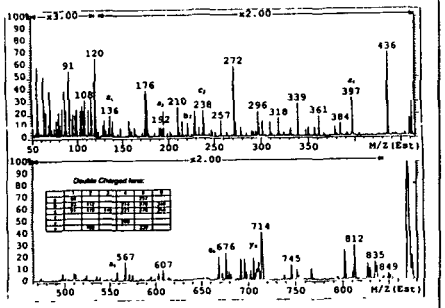

Figure 4. Fragmentation for dynorphin (1-7) at ΔV = 100V

USE OF HIGH RESOLUTION MS^n CAPABILITIES FOR PEPTIDE SEQUENCE DETERMINATION USING A QUADRUPOLE ION TRAP MASS SPECTROMETER

***K.A. Cox and R.G. Cooks, Department of Chemistry, Purdue University, West Lafayette, IN 47907**

Recently developed methods to obtain high resolution and mass measurement accuracy have been combined with the inherent sensitivity and MS^n capabilities of the quadrupole ion trap mass spectrometer for the elucidation of fragmentation mechanisms of some peptides. Generally, the ion trap has less than unit resolution for ions with mass-to-charge ratios greater than 650. However, slowed scan speeds can be employed with the use of an offset/DAC attenuator circuit to dramatically increase the resolution.[1] This method can be used to separate and isolate isotopes of precursor as well as fragment ions in tandem experiments.[2] Calibration methods involving the use of external standards and a peak matching procedure allow masses to be assigned with accuracies generally better than 50 ppm.[3]

These capabilities were utilized in the characterization of bradykinin (MW 1060 dalton) fragmentation. Bradykinin consists of nine amino acids with an arginine residue at each terminus. Since arginine is the most basic amino acid residue, it is assumed to take the positive charge when the peptide is ionized. The MS/MS spectrum of bradykinin reveals a series of structurally characteristic fragment ions including a base peak at m/z 904. This peak corresponds to the loss of an arginine residue from the peptide, but the data is insufficient to determine which terminal arginine is lost.

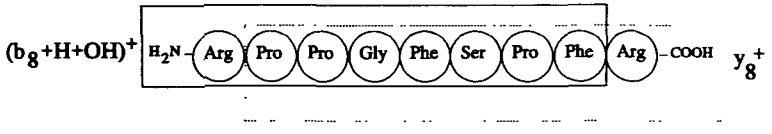

High energy dissociation methods commonly assign this ion as a y_8^+ (or $Y_8^{\cdot}$) ion, corresponding to the simple cleavage loss of the N-terminal arginine.[4] However, recent reports[5] have suggested that the rearrangement product, $(b_8+H+OH)^+$ [or $(B_8^{\cdot}+OH)$], corresponding to the loss of the C-terminal arginine, dominates in low energy dissociations. An MS^3 experiment was performed on bradykinin (1060 --> 904 --> products) to help determine the structure of the m/z 904 ion. Figure 1 shows the comparison of the MS^3 spectrum of bradykinin with MS/MS spectra of commercially obtained fragments, des arg^1 bradykinin (y_8^+) and des arg^9 bradykinin ($(b_8+H+OH)^+$). The similarity of Figure 1 a) and c) provides clear evidence that the N-terminal arginine retains the charge and the low energy rearrangement $(b_8+H+OH)^+$ ion is formed.

High resolution experiments were used to further confirm this assignment. The ITMS scanning speed was slowed with the offset/DAC attenuator circuit[1] to obtain better than unit resolution of the carbon isotopes of bradykinin. The all-^{12}C isotope was then isolated and dissociated greatly simplifying the product spectrum. Figure 2 compares the all-^{12}C MS^3 spectrum of bradykinin with the MS/MS spectra of the commercial standards. The des arg^1 bradykinin standard shows a very small fragment due to ammonia loss, since the only remaining primary amine is on the arginine carrying the charge. On the other hand, the des arg^9 bradykinin standard leaves the primary amine on the N-terminus, and a much larger ammonia loss fragment is observed. Again, this evidence supports loss of the C-terminal arginine residue.

High resolution experiments on the ITMS require a peak matching calibration method to

be used for mass assignments. A calibration line is constructed relating mass and offset voltage using salt cluster ions as standard masses.[3] Typically, CsI is analyzed as an external standard under the same conditions as the peptide in order to obtain the required calibration. Mass measurement accuracies of less than 50 ppm can be obtained. Greater mass accuracies are attainable when an internal standard is utilized.[3] A split probe tip is used to physically separate the peptide analyte and the salt calibrant, but both are injected simultaneously to eliminate small experimental variations.

Utilization of enhanced resolution capabilities and accurate calibration methods are transforming the quadrupole ion trap into a high performance mass spectrometer capable of analyses of complex reaction sequences.

References:

(1) a) J.C. Schwartz, J.E.P. Syka and I. Jardine, *J. Am. Soc. Mass Spectrom.*, **2**, 198 (1991); b) J.D. Williams, K.A. Cox, R.G. Cooks and J.C. Schwartz, *Rapid Commun. Mass Spectrom.*, **5**, 327 (1991).
(2) R.G. Cooks and K.A. Cox in *Biological Mass Spectrometry*, T. Matsuo, R. Caprioli, Seyama and M. Gross, Eds., (1993) in press.
(3) J.D. Williams and R.G. Cooks, *Rapid Commun. Mass Spectrom.*, **6**, 524 (1992).
(4) J.A. McCloskey (Ed.), *Methods in Enzymology: Mass Spectrometry*, Vol. 193, Academic Press, San Diego (1990).
(5) G.C. Thorne, K.D. Ballard and S.J. Gaskell, *J. Am. Soc. Mass Spectrom.*, **1**, 249 (1990).

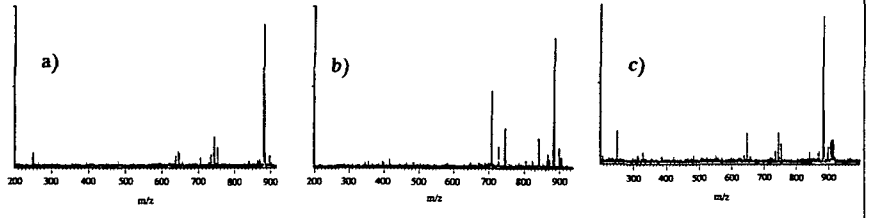

Figure 1 a) MS^3 of bradykinin (1060 --> 904 --> products); b) MS/MS des arg^1 bradykinin (MW 904); c) MS/MS des arg^9 bradykinin (MW 904)

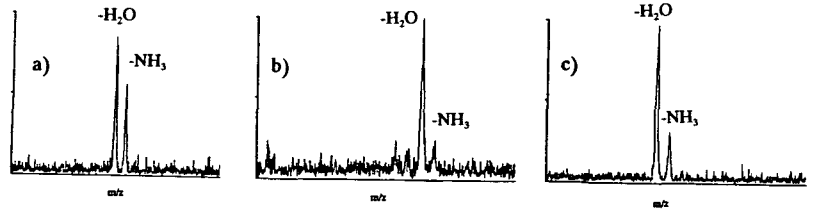

Figure 2 All-^{12}C partial dissociation spectra of a) bradykinin (1060 ---> 904 --> products); b) MS/MS des arg^1 bradykinin (MW 904); c) MS/MS des arg^9 bradykinin (MW 904)

A MASS SPECTROMETRIC ASSAY FOR THE DETECTION OF PYROGLUTAMIC ACID IN PEPTIDES

Klaus Eckart and Joachim Spiess
Department of Molecular Neuroendocrinology, Max Planck Institute for Experimental Medicine, Hermann-Rein-Str. 3, D-3400 Goettingen

N-terminal pyroglutamic acid (Pyr, Figure 1) plays an important role for the function of many neuropeptides. It has been demonstrated that for example the hypothalamic regulatory peptides thyrotropin releasing hormone (TRH) and gonadotropin releasing hormone (GnRH) require for hypophysiotropic activity the presence of an intact N-terminal Pyr residue. It is probable that the N-terminal Pyr residue is formed during posttranslational processing from intermediate glutaminyl peptides by the enzyme glutaminyl cyclase (QC) which has been earlier structurally characterized by our group (1,2). On the basis of Northern blot analysis (2) it was revealed that the highest amounts of QC mRNA were formed in brain regions such as striatum which to date where not known to contain significant amounts of pyroglutamyl peptides. It was therefore speculated that these regions may produce pyroglutamyl peptides unknown to date.

To identify new pyroglutamyl peptides possibly qualifying as regulatory peptides, we are currently developing a chemical assay which is described in detail in this poster. This assay incorporates the release of N-terminal Pyr from peptides using the enzyme pyroglutamyl aminopeptidase. Pyr is than derivatized to the volatile pyroglutamic acid methyl ester (PyrOMe) in order to enable GCMS detection. We found for this derivative detection limits in the low femtomole range. Possible sources for contaminations are investigated and alternative derivatizations for improved sensitivity are discussed.

Figure 1: Main steps in the Pyr assay procedure

HPLC fractions containing peptides

Digestion with pyroglutamyl amino peptidase

Derivatization of Pyr with diazomethane

Extraction of Pyr with ethyl acetate

Detection of PyrOMe using GCMS

The derivatization of Pyr was performed using diazomethane because of its excellent reactivity and the volatility of the reaction byproduct. Experiments with the synthesized standard compound revealed the best ionization efficiency in EI compared to positive as well as negative chemical ionization. The EI mass spectrum consists mainly of the molecular ion with m/z 143 (10% rel. int.) and the immonium ion of the pyrrolidone moiety with m/z 84 (100% rel. int.). We found using the PyrOMe standard significantly more interferences on the m/z 143 trace compared with the m/z 84 trace. Even the m/z 84 trace represents at 1000 mass resolution after application of 1 pg PyrOMe a noisy base line hampering unambiguous identification. A mass resolution of 3000 was sufficient to obtain a base line allowing the identification of 1 pg or less substrate (Fig. 2). Increasing the mass resolution to 5000 did not improve the sensitivity significantly.

Figure 2: 1 pg PyrOMe injection recorded in the SIR mode on m/z 84 with 3000 mass resolution

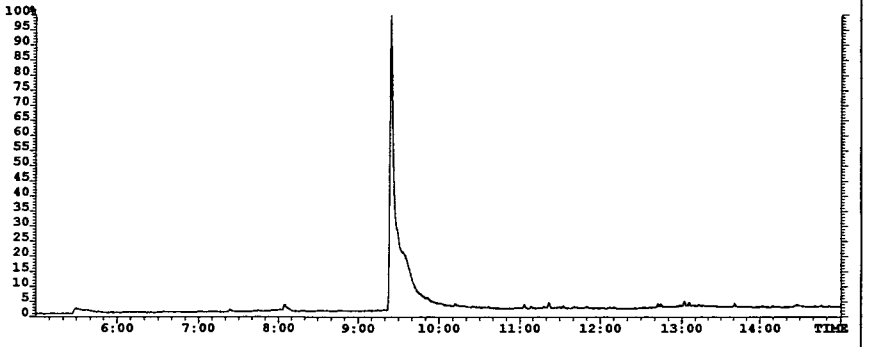

GC SIR recordings showed detection limits in the 100 fg (1 fmol) range for the standard compound. Unfortunately, glutamic acid (Glu) contaminating the pyroglutamyl peptide fraction will probably be derivatized to glutamic acid dimethyl ester (Glu(OMe)OMe) by methylation with diazomethane as descibed above. By splitless injection in a heated injection system Glu treated with diazomethane was found to cyclize to PyrOMe on the basis of gas chromatographic and mass spectrometric data. Thus, this chemical assay for the identification of pyroglutamyl peptides is sensitive to (frequently occurring) contamination of fractions with Glu.

The assay requires highly purified solvents. Especially, minor contaminants present in methanol and diethylether seem to be responsible for the formation of interfering products

As an alternative derivative of pyroglutamic acid the Pyr pentafluoro benzyl ester (PyrPFB) is currently tested with negative chemical ionization. Due to the signal to noise ratio of its mass spectrum we anticipated a detection limit in the 1 to 10 fg (3 to 30 attomole) range. Unfortunately, the resolving power of the column used for gas chromatography was quickly lost, probably by substrate absorption which may be enhanced by hydrogen bridges of the lactame ring of the pyroglutamic acid derivative.

In conclusion, it has been observed that pyroglutamyl derivatives can be detected in the low femtomole range by application of GCMS. Therefore, this detection system proved to be a suitable tool in combination with the enzymatic cleavage of the Pyr residue for screening of pyroglutamyl peptides. Problems such as solvent contaminations and possibly glutamic acid cyclization have been addressed. It is expected that derivatization of the lactame nitrogen or the introduction of a cold injection system will reduce the possible cyclization of glutamic acid significantly. Peptides found by this chemical assay will be subjected to sequence analysis with MSMS which will provide sequence information in the low picomole range without prior removal of the Pyr residue.

References

1) W. Fischer and J. Spiess, (1987) Proc. Natl. Acad. Sci. USA, 84, 3628-3632.
2) T. Pohl, M. Zimmer, K. Mugele and J. Spiess, (1991) Proc. Natl. Acad. Sci. USA, 88, 10059-10063.

Matrix Assisted Laser Desorption/Ionization of RNase Glycation

A.Lapolla,C.Gerhardinger, L.Baldo, D.Fedele
Patologia Medica I,Via Giustiniani 2 35100 Padova (Italy)
*R.Seraglia, S Catinella and P.Traldi
C.N R., Corso Stati Uniti 4, 35100 Padova (Italy)

Interaction between glucose and proteins are relevant processes in both biological and food chemistry fields [1].

The intimate mechanism of such reactions has been proposed to involve a first step in which glucose reacts with free amino groups of proteins to form a labile intermediates (Schiff's base) which undergoes further rearrangements to form a stable adduct usually called "Amadori" product. Its subsequent degradation into a variety of carbonyl compounds, more reactive than the sugar, are responsible for the propagation of the reaction, leading, through a series of rearrangements and dehydration reactions, to yellow-brown, insoluble and fluorescent products, the so called "Advanced Glycation End Products" (AGE)[1]

In the biomedical field these reaction are responsible for the long-term complications of diabetes[1]. In this pathology the high concentration of glucose is responsible for the formation of AGE, indicated as intermediates for cross-linking between proteins [2] and reflecting on severe tissutal modifications.

The relevance of such reactions has induced and induces the development of analytical procedures apt to an evaluation of glycation level of different protein substrates from both qualitative and quantitative points of view

The analytical approaches usually employed pass necessarily through a degradation of the protein (e.g. chemical or enzymatic hydrolysis, pyrolysis): for such reason analytical methods giving information on the intact glycated protein are of high interest.

Matrix assisted laser desorption/ionization (MALDI) mass spectrometry is one of the most powerful methods available for protein structural elucidation [3]. This method is sensitive, rapid and is tolerant of buffers and salts.

In a previous work on glycation of Bovine Serum Albumin (BSA) good results were obtained by MALDI [4]. A clear increase of molecular weight of BSA was found depending on both glucose concentration and incubation time.

In the present paper we report the data obtained by MALDI on the products arising from reaction,under pseudo-physiological conditions, of RNase with two different sugars (glucose and

fructose) at different concentrations (i.e. 0.25 and 0.025 M) for different incubation times (from 0 to 20 days).

The MALDI spectra of samples of RNase incubated with 0.25 M glucose show a progressive increase in molecular weight with respect to incubation time: in fact the maximum of the peak due to RNase passes from 13680 Da at 0 day to 13983 Da at 6 days The latter corresponds to the reaction of 2 molecules of glucose on the protein chain Moreover, after 6 days of incubation, the reaction of 3 and 4 molecules of glucose have been observed, in agreement with what already reported in literature [5] It is to note that just after the addition of glucose (t = 0 day) a small peak, corresponding to the reaction of 1 molecule of the sugar, is well detected With 0.025 M glucose concentration only 2 molecules of sugar react with RNase after 20 days of incubation The glycation reaction is slower, but the presence in the spectra of ions which do not correspond to the simple reaction of glucose suggest that decomposition reactions of the Amadori adducts take place

The MALDI spectra of samples of RNase incubated with 0.25 M fructose are different from those obtained with glucose in the same concentration. A larger peak is always present and, after 6 days of incubation, an indented peak is detected, suggesting that, just after the initial reaction with fructose, decomposition processes take place faster than those observed with glucose With 0 025 M fructose concentration the glycation reaction is slower, but also in this case after 9 days decomposition processes are present. These data are in agreement with literature: fructose reacts faster than glucose in the cross-linking reaction of proteins [6,7].

In conclusion by MALDI technique precious information on extent of glycation can be achieved. Moreover further reactions, different from condensation, can be put in evidence by such technique.

[1] V M.Monnier and A.Cerami, Clin.Endocrinol.Metab **11**, 431 (1982)
[2] M.Brownlee, H.Vlassara and A.Cerami, N.Engl.J.Med. **318**, 1315 (1988)
[3] H.Karas, D.Backmann and F.Hillenkamp, Anal.Chem. **57**, 2935 (1985)
[4] A.Lapolla, C.Gerhardinger, L.Baldo, D Fedele, A.Keane, R.Seraglia, S.Catinella and P.Traldi, submitted to Biochem.Biophys.Acta.
[5] N.G.Watkins, S R.Thorpe and J.W.Baynes, J.Biol.Chem. **260**, 10629 (1985)
[6] H.Kato, F.Hayase, D.B Shin, M.Oinomi ans S.Baba, in "The Maillard Reaction in Aging , Diabetes and Nutrition", Alan R.Liss Inc., (1989) p 69
[7] D J.Walton, J.D.McPherson and B H.Shilton, in "The Maillard Reaction in Aging, Diabetes and Nutrition" , Alan R.Liss Inc , (1989) p.163

AUTOMATED PEPTIDE MAPPING AND SEQUENCING BY LC/ESI/MS

***K. Mock, I. Mylchreest, M. Hail, M. Sanders, M. Uhrich, I. Jardine**
Finnigan MAT, 355 River Oaks Parkway, San Jose, CA 95134

INTRODUCTION

An ideal system for peptide mapping of proteins includes automated on-line LC/ESI/MS of protein digests on HPLC columns used in conventional chromatography (4.6 mm I.D.) to microbore chromatography (1 mm I.D.) to determine peptide and glycopeptide molecular weight. Towards such a system, we have been able to perform full gradients and the solvent flow to the ESI source was direct at 50 μl/min for a 1 mm column, 200 μl/min for a 2.1 mm column and 1000 μl/min for a 4.6 mm column.

In addition, fragmentation of peptides was generated for structural and sequence information in the capillary-skimmer region of the source, in the rf-only octapole region of the source, and in the octapole collision cell of a triple quadrupole system. The product ion spectra were very similar.

The data obtained demonstrated the ability to now couple single or triple quadrupole mass spectrometers to chromatographic systems for routine use in the biochemistry laboratory with high direct flow rates to the mass spectrometer; and in addition, demonstrate new higher sensitivity.

The combination of LC/ESI/MS with CID sequence information was used as an intelligent tool towards obtaining complete structure information on co-eluting peaks. Examples of proteins used were the protein human growth hormone, cytochrome C, and glycoprotein tissue plasminogen activator.

EXPERIMENTAL

Materials: Tryptic digests of native recombinant human growth hormone, reduced carboxymethylated rt-PA, and cytochrome C were analyzed.

Chromatography: The HPLC systems used in this work consisted of a Michrom (Pleasanton, CA) capable of delivering linear reproducible gradients at low flow rates (e.g. 50 μl/min) and an LDC 4100 for gradients at 1 ml/min. Chromatographic separations were accomplished using Reliasil 150 mm x 1 mm; 150 mm x 2.1 mm; and 150 mm x 4.6 mm columns packed with C18 stationary phase. The mobile phase A consisted of 98% water, 2% acetonitrile, and 0.1% TFA Mobile phase B was 10% water, 90% acetonitrile, and 0.09% TFA.

Electrospray Mass Spectrometry: Experiments were conducted on Finnigan MAT SSQ®710C and TSQ®700 single and triple stage quadrupole mass spectrometers fitted with Finnigan electrospray interfaces (ESI). Collisionally-induced dissociation (CID) spectra of peptides were generated between the capillary and the skimmer, and the API octapole on the SSQ 710C. MS/MS of peptides was generated in the octapole collision cell on the TSQ 700.

RESULTS AND DISCUSSION

Figures 1 and 2 are LC/ESI/MS chromatograms of tryptic digest of cytochrome C. The digest was separated on 150 mm x 1 mm and 150 mm x 4.6 mm columns. Flow rates to the ESI source were 50 μl/min and 1000 μl/min respectively.

Figure 3 is an example of source CID spectra obtained from an on-line LC/MS experiment.

CONCLUSIONS

Due to new developments in API technology, LC/ESI/MS analysis of peptides on single and triple stage quadrupole mass spectrometers:

- is routine, accommodating full LC gradients including TFA with excellent sensitivity.
- the system accepts effluent from 1-4.6 mm HPLC columns as well as packed LC or CE with direct flows 1-1000 μl/min.
- the rf only octapole region provides excellent internal sequence information, with good sensitivity.

ESI/LC/MS of Cytochrome C Tryptic Digest
150 mm x 1mm column
50 pmoles injected
Flow Rate 50 ul/min

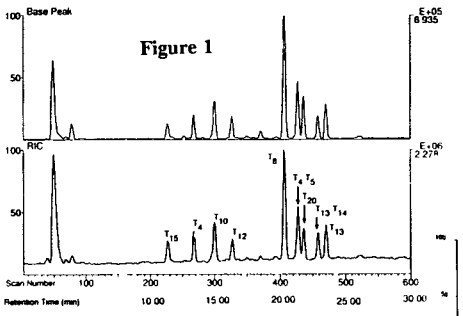

Figure 1

Figure 2

ESI/LC/MS of Cytochrome C tryptic digest

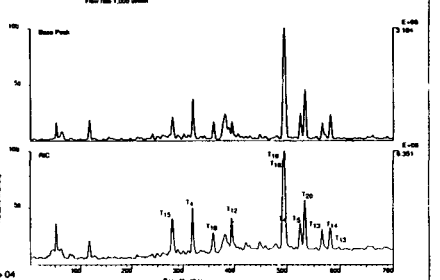

Figure 3

Source-CID Spectrum (API Octapole) of T_{13} Tryptic Fragment Obtained from on-line ESI/LC/MS Experiment (Cytochrome C)
150 mm x 1mm column
50 pmoles injected
Flow Rate 50 ul/min

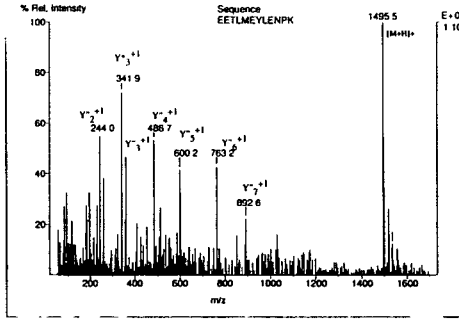

PROBING SECONDARY STRUCTURES OF PEPTIDES BY MASS SPECTROMETRY

D.S. Wagner[1], L. Melton[2], Y. Yan[2], B.W. Erickson[2], and R.J. Anderegg[1]
[1]Glaxo Research Institute, RTP NC 27709 and
[2]Department of Biochemistry, University of North Carolina, Chapel Hill, NC 27599

Recently electrospray ionization mass spectrometry has been used to study conformational changes in proteins and has been shown to be compatible with deuterium exchange experiments. The rates of exchange and the degree of incorporation can be easily observed as mass shifts during an experiment. Since amide proton exchange is becoming a popular method by which to investigate a protein's structure, the study of simpler systems such as helical peptides and β-sheets is useful for understanding more complex proteins. We have been studying model peptides that are well characterized by a more traditional method, circular dichroism. Peptides designed to be random, α-helical, or β-sheets were investigated. The rate of deuterium exchange can be linked to the stability and extent of the secondary structure. The more stable the secondary structure (the stronger intramolecular interactions) the slower the exchange.

The study of α-helicity consisted of a series of isomeric polyanionic peptides (amphiphilic, helical, and random) that have been characterized by CD and determined to have 98%, 34%, and 17% helicity respectively. Deuterium exchange experiments were performed on these peptides. The measured molecular weight of each peptide vs. time during the deuterium exchange experiment is shown in Figure 1. The observed rates of deuterium exchanged is representative of the peptides structure. The peptide with the greatest amount of helicity experienced the slowest rate of exchange while the most random peptide displayed the fastest exchange rate. To obtain information about the rate of exchange, the data can be plotted as ln(number H's remaining) vs. time. If a peptide experiences first order kinetics then the plot would correspond to a straight line, whose slope would be proportional to the exchange rate, but each amide has a different first order exchange rate, producing a curve instead. The curve can be segmented into groups of amides that exchange with similar rates depicted by linear regions on the graph. Curve fitting the first linear region of the graph of ln(number H's remaining) vs. time, one can calculate the percent helicity from MS data where the y-intercepts represent the initial number of slow exchanging amides. The number of H's in the helix is equal to the number of slow exchanging amides plus 4 (to account for first 4 amides in the helix that can not hydrogen bond). The %helicity equals the number of H's in helix divided by number amides in backbone. This gave rise to amphiphilic 100%, helical 45%, and random 27% helicity. These numbers correspond reasonably well with the information obtained from CD.

Two different peptides Betabellin 12M and Betabellin 14M (single chain thiols) were used to study β-sheets. Air oxidation furnished betabellin 12D and 14D, the disulfide-bridged two-chain protein. All four peptides were used in this study. CD data show that the betabellin 12M, betabellin 12D, and betabellin 14D contained no α-helical but substantial β structure while betabellin 14M was a random coil. Although CD can predict the % helicity from α-helical peptides, equations for predicting the % β-sheet are not reliable. A chemical denaturation using guanidine chloride determined that the order of stability is 12D > 12M > 14D. The dimers are more stable than their respective monomers as a result of an increase in the hydrophobic interaction between the two β-sheets. Deuterium exchange experiments were performed on these peptides. In order to compare the stability of these peptides the mass spectral

information was converted to the % unexchanged amides (number of H's remaining / number of amides in peptide) as a function of time Figure 2. The data indicates that the order of stability is 12D > 12M > 14D > 14M. This correlates to the information obtained from the chemical denaturation of these peptides studied by CD.

Determining the % β-sheet from the mass spectral data (similar to that of the helical peptides) by using the y intercept of the first linear region of the graph of ln(%β-sheet) vs. time (graph not shown) corresponds to 12D 118%, 12M 114%, 14D 96% and 14M 90% β-sheet. These numbers are much higher than expected, especially since 14M is a random coil. The first linear region probably corresponds to amides not involved in the H-bonding network but which do not exchange instantaneously because of neighboring effects. Since 14M is a random coil, the section of the %β-sheet vs time (figure 2) where exchange is slow (after 2 min.) should be indicative of the region β-sheet stabilization for the other peptides. Using the regions of the curves from 2-4 minutes indicates 12D 81%, 12M 80%, 14D 36%, and 14M 25% β-sheet. These numbers are more reasonable. Since amides in turns and in exterior regions are not involved in H-bonding, they should not contribute to the % β-sheet, thus the greatest % of β-sheet that these particular peptides can have is 65-70%. The calculated numbers are probably higher because of some shielding effects on the amides not involved in H-bonding.

We have shown that mass spectrometry coupled with deuterium exchange techniques can be used to determine the relative stability of secondary structures. The results obtained using MS are consistent with those obtained by other methods. Although we cannot distinguish between α-helices and β-sheets by mass spectrometry alone, it may be possible to determine the %α-helix or %β-sheet from the deuterium exchange data. This methodology may prove useful for determining the conformation, structural fluctuations, folding intermediates of a protein, the stability of proteins upon structural modifications, and the effects of ligand binding on an enzyme.

FIGURE 1

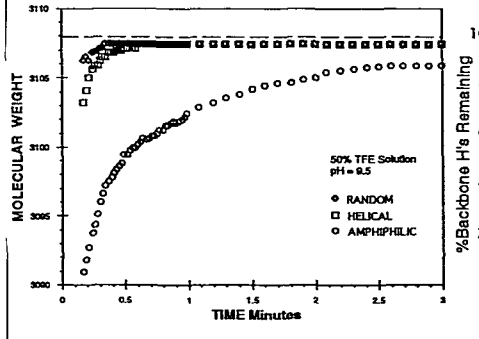

FIGURE 2

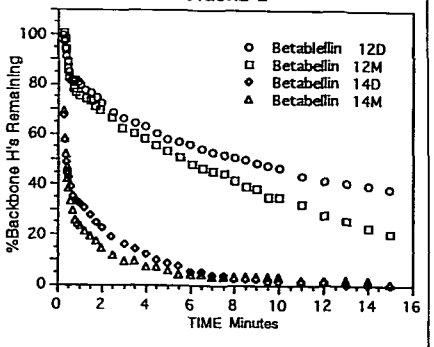

An Atmospheric Pressure Low-Power Microwave Plasma Ionization Source for Liquid Chromatography-Mass Spectrometry (LC-MS)

Nohora P. Vela, Jeffrey J. Giglio and Joseph A. Caruso. Department of Chemistry, University of Cincinnati, Cincinnati, Oh 45221-0172
R. Duane Satzger. U.S. Food and Drug Administration, National Forensic Chemistry Center, 1141 Central Parkway, Cincinnati, OH 45202

Mass spectrometry has developed into a powerful tool for the identification and quantitation of numerous chemical compounds. Because most compounds are thermally labile or non volatile, they are not amenable to GC/MS. There are several LC/MS sample introduction techniques, but most suffer from disadvantages such as high temperatures or introduction of liquid samples into a vacuum system The potential for using microwave induced plasma as a soft ionization source has been previously demonstrated. (1)

The main advantages of this source are that it operates at atmospheric pressure eliminating some of the vacuum pump problems associated with reduced pressure LC/MS sources. It also offers the possibility of obtaining molecular weight information and fragment ions for structural information. This feasibility is demonstrated by varying several operational parameters.

This study demonstrates the effect of microwave power, sample carrier gas flow rate and injector probe configuration in the production of fragment ions using perfluorotributylamine (PFTBA) commonly used for calibration with EI mass spectrometry. A commercial ICP-MS instrument is modified to operate as an MIP-MS system, and there are limitations in the mass range (4 to 246 amu). Response at m/z= 69, 100, 114, 119, 131, 150, 181 and 219 (major fragments in the EI mass spectrum for PFTBA) are selected to monitor the extent of fragmentation obtained with the microwave source.

The use of an injector probe consisting of a stainless steel tube, 1/16" o.d. (Injector Probe "A") produces greater abundance at m/z=69 and minimum of fragments observed at m/z= 219. The use of a ceramic tube inside this stainless steel tube (Injector Probe "B") reduces the interaction between the plasma and the sample with a corresponding reduction in the extent of fragmentation at a given power. A larger diameter stainlees steel tube (1/8") with a ceramic tube inside (Injector Probe "C") used as injector probe produces an increase in the abundance of all fragments. For powers between 22 and 26 w, and considering the limitations in the observable mass range using this quadrupole, there is a shift to greater abundance of higher mass fragments (m/z=219). Ions representing the larger molecular fragments which could not be monitored are expected.

Liquid sample introduction to the MIP is obtained by using a direct injection nebulizer (DIN) that has been designed for ICP-MS. (2) This nebulizer provides a good aerosol, and operates at typical microbore LC flow rates. A 0.025 M tetrabutyl ammonium hydroxide solution is used to demonstrate the possibility of using this nebulizer with the MIP source to obtain structural information in a LC-MS system.

References

(1) Shen W-L. and Satzger D., Anal. Chem, **1991**, *63*, 1960-1964
(2) Wiederin D R., Smith F.G. and Houk R.S., Anal. Chem., **1991**, *63*, 219-225

"A COMPARISON OF ANALYTICAL TECHNIQUES (API/MS, GC/MS AND FTIR), FOR THE MEASUREMENT OF COMBUSTION PRODUCTS FROM A VARIABLE-FUELLED AUTOMOBILE"

O.Vega; Universidade de Sao Paulo, IPEN/USP, Sao Paulo, Brazil.
E.Puckrin, W.F.J.Evans, R.J.Hughes and R.E.March
Trent University, Peterborough, Ontario, Canada K9J-7B8

OBJECTIVE: To examine the relative merits of three analytical techniques applied to analyses of gas exhaust from a Chevrolet Lumina car using methanol and/or gasoline fuels. Analytical techniques; 1) Atmospheric Pressure Ionization Mass Spectrometry (API/MS); 2) Gas Chromatography /Mass Spectrometry (GC/MS); 3) Thermal Emission Spectroscopy (FTIR).

I- THE ATMOSPHERIC PRESSURE IONIZATION/MASS SPECTROMETER (API/MS)

The API/MS analyzer was made by SCIEX Co. model TAGA 3000 and utilizes chemical ionization (CI) to produce ions[1].

Evaluation:

The advantages of the API/MS are;

(i) Performs "Real-time analysis" (see Fig. 1).

(ii) Quantitative analysis of methanol; in the CI mode, the methanol concentration can be measured in the range of 500 ppm to 6 ppb.

(iii) Analysis of formaldehyde.

The disadvantages of the API/MS are:

(i) Limitation of the utilization of the H_3O^+ (and $H_2O.H_3O^+$) as CI agents as the proton affinities of these agents exceed those of many combustion products.

(ii) Low detection limits for unleaded gasoline; gasoline is composed mainly of hydrocarbons of relatively low proton affinities.

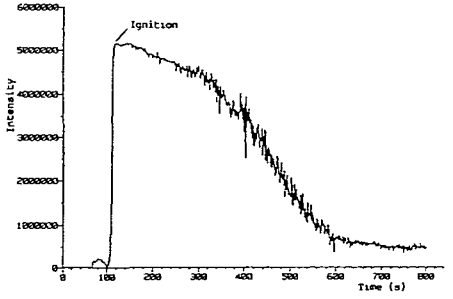

Figure 1: Real-time analysis of protonated methanol (m/z 33) from the M-85 (85% methanol) fuel gas exhaust.

II- GAS CHROMATOGRAPHY/MASS SPECTROMETRY (GC/MS)

The GC/MS analyzer was made by VARIAN Co. model SATURN I which uses an Ion Trap Detector (ITD).

Evaluation: The advantages of GC/MS analysis are:

(i) The range of compounds which could be identified using GC/MS exceeded those of the other techniques discussed here.

(ii) The CI mode presents a greatly simplified mass spectrum, and the degree of fragmentation can be controlled by selection of appropriate protonating agents.

The disadvantages of GC/MS are:

(i) The sorbent/solvent system technique used here blankets the C_2 - C_5 hydrocarbons.

(ii) In this mode, GC/MS does not perform real-time analysis.

III- THE THERMAL EMISSION SPECTROSCOPY ANALYSIS - FTIR

The Michelson-design FTIR analyzer was made by NICOLET Co. (MAGNA-550), having a resolution of 0.1 cm^{-1}.

Evaluation: The advantages of the technique are:

(i) Real-time analysis of the gaseous exhaust products; H_2O, CO_2, C_2H_2, C_2H_4, CH_3OH and CH_4 can be effected (see Fig. 2).

(ii) The light-weight IR emission instrument permits ready portability for analyses outside of the laboratory.

The disadvantages of this technique are:

(i) Emission from compounds other than H_2O, CO_2, C_2H_2, C_2H_4, CH_3OH and CH_4 were not detected.

(ii) Emission data for the observed exhaust gases are sparse.

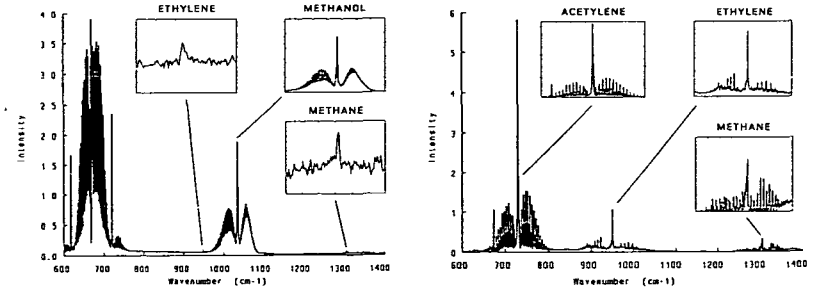

(a) (b)

Figure 2: FTIR emission spectra, obtained from the Lumina car gas exhaust, fuelled with; a) M-100 (100% methanol) in the absence of water, b) gasoline in the absence of water and carbon dioxide.

CONCLUSION: From the results of the present research the following conclusions may be drawn:

(i) A multi-technique approach must be used in order to extend the range of detectable chemical compounds in gas exhaust analyses from a methanol and/or gasoline fuelled vehicle.

(ii) While methanol as a alternative fuel reduces the production of hydrocarbons, new pollutants (methanol and formaldehyde[2]) are liberated into the environment.

(iii) Real-time analyses of the gas exhaust were performed in this work by API/MS and FTIR.

REFERENCES

1- O.Vega, R.J.Hughes and R.E.March, Proceedings of the 40th ASMS Conference on Mass Spectrometry and Allied Topics: Washington, DC, 1992, p.686.

2- R.J.Hughes, R.E.March, J.M.Goodings and D.K.Bohme, Proceedings of the 41th ASMS Conference on Mass Spectrometry and Allied Topics: San Francisco, CA, TP-93.

The Application of HPLC Flow-FAB- and ESI-MS to the Analysis of Pesticide Transformation Products

Robert D. Minard, Guangrui Zou, Jean-Marc Bollag, Penn State University, University Park, PA 16802 and Justin Stroh, Pfizer Central Research, Groton, CT.

INTRODUCTION: The primary goal of this work was to improve the present capabilities for analyzing products from chemical interactions of pesticide-derived anilines and phenols with the organic constituents of soil. The work consisted of two projects:

(1) The assembly of a microbore column gradient HPLC-flow fast atom bombardment (FFAB)-mass spectrometry (MS) system and studies leading to its improved performance.

(2) The utilization of this system for the analysis of the transformation products of the xenobiotic compound 3,4-dichloroaniline and products derived from its coupling with the model humic acid precursor, ferulic acid. Previous research has shown that xenobiotic chloroanilines and chlorophenols can be incorporated into humus substances because of their structural similarity to naturally occurring humic acid constituents (Bollag 1983).

METHODS: A number of parameters are found to be important for achieving the successful operation of combined HPLC-flow FAB-MS. These are shown below along with conditions or interface modifications that were developed in this work. 1.Source temperature, 35-40°C for methanol/water mixtures containing 3% glycerol. 2. Mobile phase flow rate , 30 mL/min (split ratio of 60:1) gave the best compromise between signal intensity and peak width. 3. Sample concentration and injection volume, The best peak shape and sensitivity is obtained at a concentration of ~0.01 M and an injection volume of 3 mL. 4. Peak broadening effects occurring in the LC column and UV detector, Peak widths are approx 10 x's broader than injections directly onto FFAB capillary. 5. Mobile phase degassing , At low flow rates, air is readily absorbed through teflon transfer lines. Use 1/8" O.D. x 1/16" I.D. PEEK tubing. 6. Gradient control for HPLC, The efficiency of solvent blending was improved greatly by using the method of precolumn flow splitting for solvent delivery (Balogh and Stacey 1991).

Enzyme Assay An extracellular enzyme was isolated according to others (Bollag et al. 1979). Enzyme reactions were conducted in 0 1 M phosphate buffer (pH 6 9) with 0 5 unit/mL laccase, 1.0 x 10^{-3} M ferulic acid and 1.0 x 10^{-3} M 3,4-DCA at 30°C for 2 hours. The enzymatic reaction was stopped by adjusting the solution to pH 2.3 with phosphoric acid. The reaction mixture was extracted with an equal volume of ether, the ether extract dried over anhydrous sodium sulfate and evaporated to dryness under a stream of N_2.

High-Performance Liquid Chromatography For the analysis of pesticide transformation products, the dried residue from the enzyme assay was dissolved in 1 mL methanol. Five µL was injected from the injection valve and the reverse-phase separation was achieved on a 30 cm x 1 0 mm Supelcosil LC-18 (bonded octadecylsilane) column of 5 mm particle size. The mobile phase at a flow rate of 30 µL/min was a mixture of aqueous component A (0.5% acetic acid in water, pH 2.75) and organic component B (methanol). Three percent of glycerol was added in both mobile phases as a FFAB matrix. The initial mobile phase composition of 50/50 A/B was held for 5 minutes and then brought to 10/90 A/B in 15 minutes and held at 10/90 A/B for 5 minutes. The column was equilibrated at the initial condition for 30 minutes before each injection.

Flow FAB-MS The 85 cm length of 0.050 mm I.D fused silica capillary (Polymicro Technologies, Inc., Pheonix, AZ) from the flow FFAB probe interface was directly inserted into the 0.030" I.D. x 1/16" O.D stainless steel outlet tubing of the UV detector up to the flow cell exit. The connection between capillary and the stainless steel tubing was not sealed and therefore was at atmospheric pressure. With a pressure differential of one atmosphere across a capillary of these dimensions, the flow in the capillary will be approximately 0.5 µL/min. A split ratio of 1:60 resulted. The FFAB probe used in the system was constructed based on a design by David Smith, Purdue University. A Kratos MS50 RFA mass spectrometer was operated at 4 kV accelerating potential & mass spectra were obtained by magnetic scan at the rate of 3 sec/scan with the range of 130-1500 amu.

HPLC-electrospray-MS The HPLC-electrospray-MS experiment was done by Dr. J. Stroh. A 28 cm x 0.32 mm C-18 column was used for the HPLC separation. (UV detection at 254 nm). The product

mixture of 0 5 mL volume was injected via a micro injector. The mobile phase at a flow rate of 4 mL/min was a mixture of component A (0.1% trifloroacetic acid in water) and component B (80:20:0.075 acetonitrile:water:trifloroacetic acid). The initial mobile phase composition of 50/50 A/B was held for 5 minutes and then brought to 100% B over 30 minutes and held at 100% B for 10 minutes. The column effluent was analyzed on Finnigan TSQ-700 mass spectrometer with an electrospray source. The m/z range 400-2000 was scanned every 2 seconds.

RESULTS: The combined results from HPLC-FFAB-MS and HPLC-electrospray-MS analysis define eight products formed in the reaction of 3,4-dichloroaniline with ferulic acid in the presence of laccase, four of which had been isolated and identified previously(Tatsumi, 1993) Two of these products **1a** and **1b**, are isomeric dimers derived from ferulic acid. A third hybrid dimer, product **4**, involves the loss of the 3-carbon side chain of ferulic acid. Three trimers **2a**, **2b** and **2c** are formed from the cross coupling of two ferulic acids and one 3,4-dichloroaniline. Oligomers derived exclusively from 3,4-dichloroaniline, products **3** and **5**, are also detected in this study but not characterized structurally.

These advantages of HPLC-MS led to the discovery of two oligomerization compounds, **2c** and **4**, not observed by previous off-line analysis.

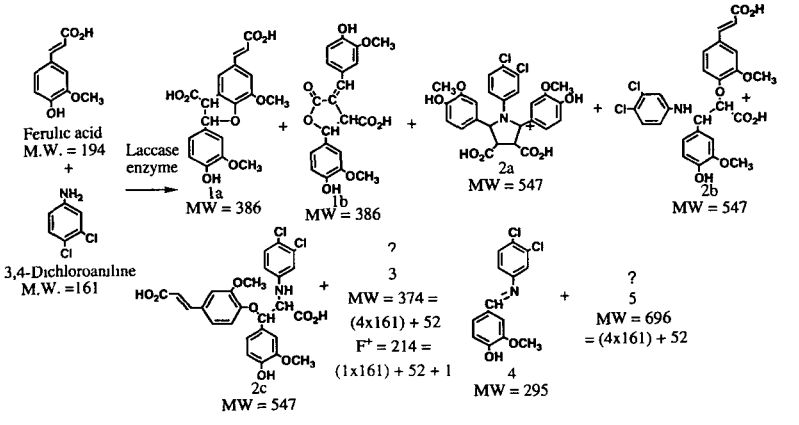

REFERENCES

Balogh, M. P.; Stacey, C. C. 1991, J Chromatogr 562, 73-79

Bollag, J -M.; Sjoblad, R. D , Minard, R D 1977, Experientia 33, 1564-1566

Bollag, J -M, Sioblad, R D ; Liu, S.-Y 1979, Can. J. Microbiol. 25,229-233.

Bollag, J -M , Sjoblad, R D.; Minard, R. D. 1981, J. Agric. Food Chem. 29, 250-253

Bollag, J.-M ; Minard, R D., Liu, S.-Y 1983, Environ. Sci. Technol 17, 72-80

Caprioli, R M , Fan, T , Cottrell, J. S. 1986, Anal. Chem. 58, 2949-2953

Dec, J.; Bollag, J.-M 1990, Arch. Environ. Contam. Toxicol. 19, 534-541.

Fenn, J. B.; Mann, M ; Meng, C K ; Wong, S F.; Whitehouse, C. M. 1989, Science 246, 64-70

Haider, K., Martin, J. P ; Filip, Z 1975, "Humus Biochemistry" in E. A. Paul, A D McLaren(ed) Soil Biochemistry, Vol.4, Marcel Dekker, New York, 195-244

Scott, R. P. W. 1977, J. Chromatography Library Vol. 11, Elsvevier, Amsterdam and New York.

Simmons, K. E.; Minard, R. D.; Bollag, J -M. 1989, Environ. Sci. Technol. 23, 115-121

Tatsumi, K ; Freyer, A., Minard, R. D; Bollag, J -M. 1993 Environ. Sci. Technol. (in press).

A QUANTITATIVE STUDY OF CARBAMATE PESTICIDES USING DIRECT INJECTION/ELECTROSPRAY IONIZATION MASS SPECTROMETRY

J. M. Long, U.S. Environmental Protection Agency, Athens Environmental Research Laboratory, Athens, GA 30613
L. J. Sears, Montana State University, Department of Chemistry and Biochemistry, Bozeman, MT 59717

INTRODUCTION

The electrospray ionization (ESI) source, designed and fabricated at MSU, was installed on a VG TRIO quadrupole mass spectrometer. A combination needle was used instead of the conventional stainless steel variety. A gold-coated 50-μm i.d. fused silica capillary was inserted through and ~ 2 mm past the tip of a 0.129-μm i.d. stainless steel needle. Approximately 3 kilovolts potential is applied to the needle producing a spray of charged droplets which is directed toward a resistively heated 20-cm stainless steel transport capillary (0.5mm i.d.) through which the analyte ions enter the ESI source. This transport capillary is held constant at a potential of 65 volts (v) to minimize analyte fragmentation. The ions after leaving the transport capillary are focused through a set of five electrostatic lenses into the analyzer region of the mass spectrometer. These lenses and their potentials are: skimmer (+11 v), extractor (-16 v), focus 1 (+6 v), focus 2 (+11 v), focus 3 (-80 v), and focus 4 (-18 v). Using this ESI a quantitative study of carbamate pesticides spiked into Yellowstone River water was carried out.

EXPERIMENTAL

Environmentally significant compounds (~ 100 - 500 daltons) such as pesticides/herbicides that are polar, nonvolatile and thermally labile are not readily analyzed by conventional gas chromatography/mass spectrometry (GC/MS). A viable alternative is ESI. This technique was used to quantitatively determine carbamate pesticides spiked into Yellowstone River water. The pesticides studied were carbaryl, carbofuran, methomyl, methiocarb and propoxur. Standard curves were generated for the pesticides in 50/50 mixture of methanol/water both individually and collectively and then various spikes within the analytical range of ~ 0.1 to 20 ng/μL were analyzed similarly. Blank samples were also run and showed no evidence of contamination from these pesticides. The solutions of pesticides in Yellowstone River water were buffered with acetic acid/ammonium acetate to a pH of ~ 5 to minimize matrix effects. Individually spiked samples, after being filtered through 0.45-μm Millipore filters, were diluted to the desired concentration with 50/50 methanol/water and then injected directly into the electrospray ionization interface through a Rheodyne injector valve connected to a 50-μm i.d. gold-coated fused silica transport capillary that measured 10 cm in length. This same procedure was used for the collectively spiked samples without the use of any separation techniques. The solution flow rate was maintained at 2 μL per minute using a Sage syringe pump. The interface was maintained at a temperature of 85 °C and a potential difference of 50 v between the skimmer transport capillary and the skimmer lens was used to maximize the $[M+H]^+$ intensity. Figure 1 shows the ESI spectrum of a collectively spiked sample.

RESULTS AND DISCUSSION

Correlation coefficients for all the calibration curves generated for both the individually and collectively spiked samples were on the order of 0.90 indicating good linearity over the analytical range covering 2 to 3 orders of magnitude. The actual ion counts from individually spiked samples agree within a factor of less than 1.5 with predicted values. Those from collectively spiked samples agree within an order of magnitude with predicted values. This is not unusual and can be explained in terms of matrix effects in the collectively spiked samples. Improvements in these results could probably be made by changing the pH of the buffer system. This work indicates that direct injection/ESI shows promise as a candidate for a rapid method for screening natural waters for pesticide contamination. The minimum concentrations detected in these samples were 0.2 ng/μL and 2 ng/μL in the individually and collectively spiked samples, respectively.

This work on the carbamate pesticides is part of a larger study. Thirty pesticides from 13 different classes were analyzed using ESI/MS. Addition of acid to those pesticides, including these carbamates, produced ion signals that were no more intense than those from the neat samples. This observation and the fact that the majority of these pesticides have extremely low pK_{BH}^+'s, as calculated by SPARC, indicate that many of the protonated analyte ions of these pesticides are formed in the gas phase rather than in the condensed phase. This is the first reporting of this gas phase phenomenon of protonated ion formation.

References:

Karickhoff, S. W., V. K. McDaniel, C. Melton, A. N Vellino, D. E. Nute and L. A. Carreira, *Environmental Toxicology and Chemistry* 10, 1405 (1991).

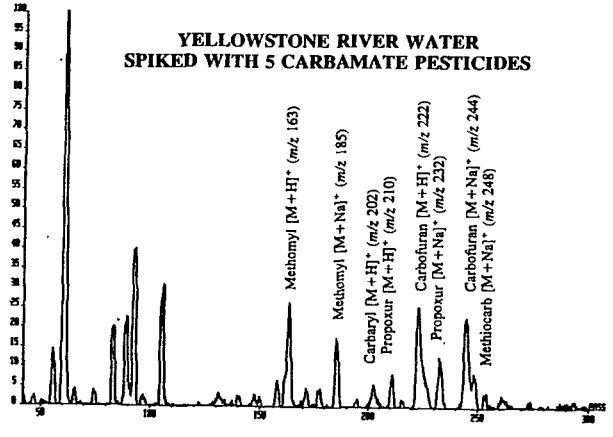

Figure 1. Electrospray Ionization Mass Spectrum of a Mixture of 5 Carbamate Pesticides.

Sensitivity Enhancement in API/MS *via* Gas-Phase Derivatization

R.J.Hughes, R.E.March and P.J. Popp, Department of Chemistry
Trent University, Peterborough, ON, CANADA, K9J 7B8
J.M.Goodings and D.K.Bohme, Department of Chemistry
York University, Downsview, ON, CANADA, M3J 1P3

Our objectives were to collaborate with the Ontario Ministry of the Environment, Air Resources Branch, in order to investigate the possibility of enhancing the sensitivity of their mobile mass spectrometers (Sciex TAGA series) towards certain classes of compounds of environmental interest. The nature of this collaboration was threefold:

1) to investigate the role played by gas-phase chemistry in atmospheric pressure chemical ioniziation (APCI)
2) to suggest modifications to the conventional APCI/MS instrument
3) to suggest alternative methods and protocols for the analysis of problem compounds

A new source arrangement was designed based on the results of our initial experiments. The new source is depicted below and incorporates the following modifications:

1) The sample is injected through a hypodermic needle directly into the corona discharge region which is contained in a glass tube and flooded constantly with high-purity dry air.
2) Samples may be reacted in the gas phase with reagent gases during passage through the heated reactor tube in order to produce derivatives with higher proton affinities and/or more stable hydrates.

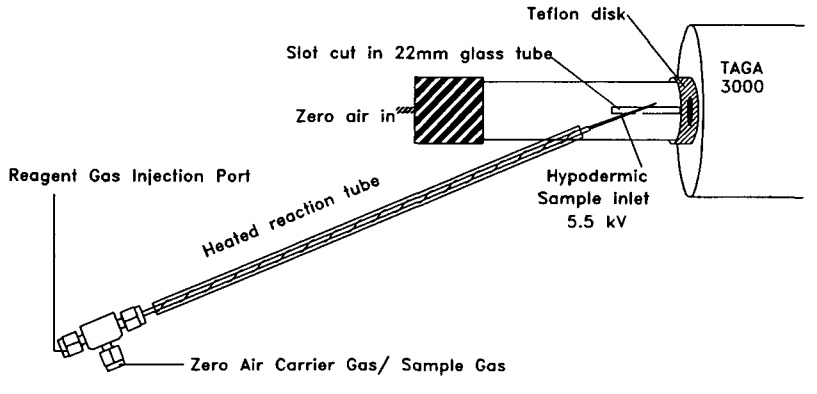

Figure 1 The Low-Volume Heated Reactor Source.

In the dry air environment of the heated reactor source the dominant ionization process appears to be charge exchange ionization with N_{2+} and O_2^+ in the corona discharge region. The resulting mass spectra resemble closely the electron ionization (EI) mass spectra and have been described as *pseudo*-EI mass spectra. These *pseudo*-EI mass spectra are less dependent on the relative proton affinities of the target analytes and may be useful in the detection and quantitation of ion species which produce relatively low signal intensities in conventional proton transfer APCI. For example, a flow of 1 nmole/s of formaldehyde through the heated reactor source produces an ion signal of approximately 10^4 ion counts/second. At this concentration the signal from formaldehyde is not detected in the normal APCI mass spectrum.

By utilizing the gas-phase neutral derivatization reaction of formaldehyde with hydrazine the signal intensity of the hydrazone reaction product is raised to approximately 4×10^6 ion counts/nmole.

Furthermore, the gas-phase neutral derivatization reaction allows one to perform a gas-phase titration. Hydrazine reacts with formaldehyde in the gas phase to produce a product ion signal at *m/z* 45; any excess hydrazine which does not react produces a signal at *m/z* 33. Shown below are the ion signals from both *m/z* 45 and *m/z* 33 in an air sample which contains formaldehyde and hydrazine vapour. The formaldehyde flow rate was 1nmole/s, and it can be seen that the protonated hydrazine signal appears as its flow rate exceeds 1 nmole/s. Such a procedure could be used to determine the approximate concentration of formaldehyde in air in real time.

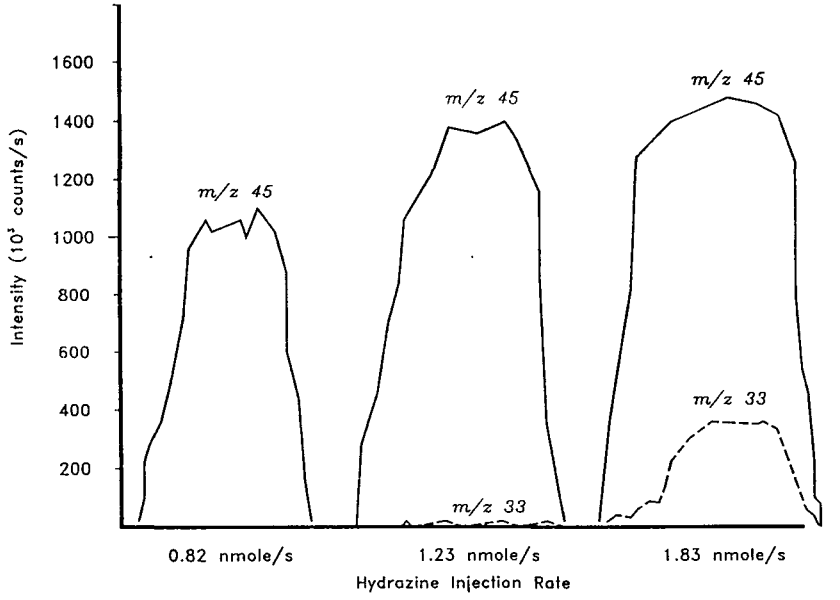

THE APPLICATION OF THERMOSPRAY LC/MS TO THE ANALYSIS OF SMALL ORGANIC ACIDS IN MIXED HAZARDOUS WASTES

J.A. Campbell*, K.E. Grant, R.B. Lucke, and S.A. Clauss
Advanced Organic Analytical Methods Group,
Pacific Northwest Laboratory**
Richland, WA 99352

INTRODUCTION

The Hanford reservation is a 560-square-mile site located approximately 120 miles southwest of Spokane, Washington and 220 miles southeast of Seattle, Washington. The Hanford site was built by the Army Corps of Engineers and the Du Pont Corporation in 1943 to produce plutonium for nuclear weapons in support of World War II. The facility was very successful; within two years after its conception, Hanford had supplied the plutonium used for the bomb dropped on Nagasaki in World War II. Plutonium production continued after the war until January 1987 when the last production reactor ceased operation at the Hanford site. Nine production reactors and five reprocessing facilities operated at the Hanford site to support that mission. These operations created a large quantity of radioactive wastes, much of which was and continues to be stored in underground storage tanks.

There are 177 high-level waste storage tanks at Hanford. Of these, 23 tanks are being watched closely because of the possibility that flammable gas mixtures are being produced from the mixed waste contained in the storage tanks. One tank in particular, Tank 241-SY-101, has exhibited episodic releases of flammable gas mixtures since its initial filling in the late 1970s.

Studies of simulated waste mixtures (SWM) have indicated that the gas generation and retention are influenced by chelator concentration. It was postulated that the chelators form hydrophobic surfaces on solids in the SWM. These hydrophobic surfaces are more conducive to bubble attachment, which leads to flotation of the solids and eventually crust formation. The presence of chelators becomes very important for the understanding of crust formation and gas release. Among the degradation products of the chelators are a number of small organic acids, some of which may be linked to the production of flammable gases such as hydrogen and which also possess chelating properties. As a result, we have analyzed actual waste samples from Tank 101-SY for small organic acids.

EXPERIMENTAL

MS

The thermospray analyses were performed using the HP 5988A LC/MS in the isocratic mode. The ion source was 275° C and the stem initial temperature was 100° C. Typical values for the tip and the vapor were 230° C and 272° C, respectively. Filament operation was in both the on-and-off modes. The multiplier voltage was 2692 V and the scan range was either 79-500 or 92-300 amu, depending on the mixtures being analyzed. The injection volume was either 10µL or 20 µL, depending on the concentration of the sample. The instrument was tuned with polyethylene glycol (PEG) tuning solution to give maximum abundance of ions. It should be noted that the thermospray ion source should be cleaned approximately once a week to remove nonvolatile chloride salts resulting from the use of HCl as the mobile phase. Also, water was

flushed through the entire system at the end of the day. As long as these cleaning and flushing procedures were followed, no detrimental effects of the thermospray or chromatographic equipment were observed.

LC

A Bio-rad HPLC Organic Acids column, Aminex Ion Exclusion, HPX-87H, 300 X 7.8 mm, with compatible guard column was used. The mobile phase for this part of the work was 0.001 N HCl (isocratic). The LC oven temperature was 40°C and the flow rate was 0.6 mL/min. A typical run time was 25 min. Organic acids were analyzed using both direct flow injection and through the analytical column.

RESULTS AND DISCUSSION

The thermospray mass spectra for citric acid and glycolic acid are shown in Figures 1a and 1b, respectively. The total ion chromatogram of an actual waste sample is shown in Figure 2. Figures 2a and 2b show the extracted ion plots of citric acid and glycolic acid, respectively in this sample. In addition, a small contribution from acetic acid is visible at about 16 min.

Research is now focusing on identification of the other peaks in the waste sample, particularly the large peaks at 7 and 8-9 min. Other acid standards obtained through commercial sources or synthesis are being used for this purpose. Diglycolic acid has been tentatively identified as the peak at 7.75 min. Some constituents are clearly co-eluting. Future work will also involve analysis of waste samples taken from different layers in the tank. The composition does not appear to be uniform from top to bottom.

**This work was supported by the Department of Energy under contract DE-AC06-76RLO 1830. Pacific Northwest Laboratory is operated by Battelle Memorial Institute.

Figure 1. Thermospray Mass Spectra of (a) Citric Acid and (b) Glycolic Acid.

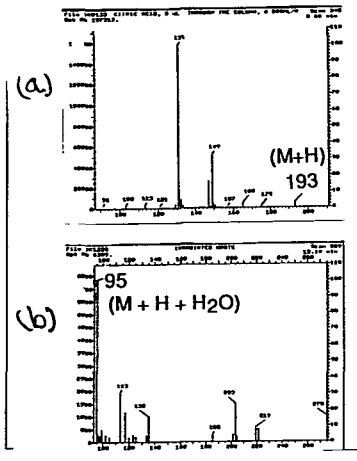

Figure 2. (a) Total Ion Chromatogram of Actual Waste Sample, (b) Extracted Ion Plot of m/z 193 for Citric Acid, and (c) Extracted Ion Plot of m/z 95 for Glycolic Acid

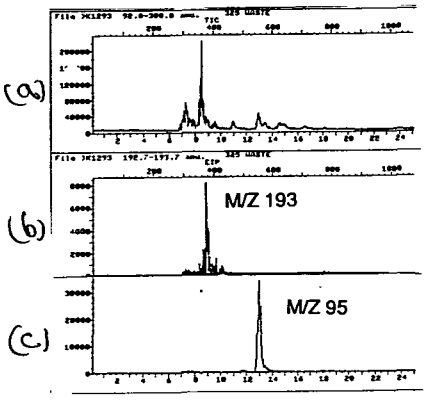

Capillary Liquid Chromatographic Mass Spectrometric Identification of Arsenic Compounds used as Animal Feed Additives

S. A. Pergantis, W. R. Cullen and G. K. Eigendorf
Department of Chemistry, University of British Columbia, Vancouver, B.C., Canada V6T 1Z1

INTRODUCTION

A number of arsenic compounds are approved as additives in feed for poultry and swine. Information concerning the biotransformations of these compounds is very limited. The majority of studies performed to date have been concerned with total uptake and/or excretion of arsenic by animals. The objective of this study is to investigate methods capable of separating and identifying these arsenicals and their metabolites in order to obtain conclusive information concerning the biotransformations of these compounds.

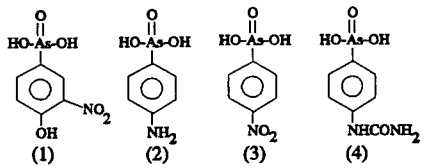

Figure 1 Arsenicals used as animal feed additives for poultry and swine.

METHODS

Capillary columns in a variety of lengths (8, 14.5 cm) and 0.32 mm ID were fabricated and slurry packed with C18 packing material (Spherisorb 3 micron ODS2). Both the microbore (250 mm x 1 mm ID) and the conventional (100 mm x 4.6 mm ID) HPLC columns were C18 Spheri RP-18 (BrownLee Labs). For the Direct Liquid Introduction (DLI) - MS experiments a Nermag R10-10B quadrupole mass analyzer equipped with a desolvation chamber and a cryopump was used. The capillary column was coupled directly to the ion source via a DLI probe equipped with a nickel diaphragm nebulizer. A Kratos Concept II H mass spectrometer was used for off-line Liquid Secondary Ion Mass Spectrometry in both negative and positive detection modes. For the thermospray MS a Kratos MS 80 mass spectrometer was used. A dual syringe pump (Applied Biosystems, Model 140B) was used for the capillary and microbore columns, while a Waters 510 reciprocating pump was used for the conventional columns.

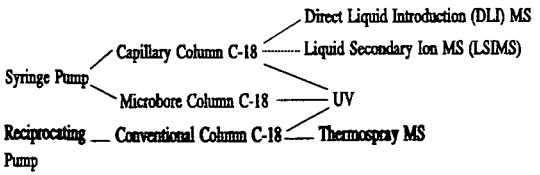

Figure 2 Methods used for the separation and identification of arsenicals used as animal feed additives.

RESULTS

All three column types (capillary, microbore and conventional) showed similar performance characteristics, i.e. resolution, efficiency, although the capillary column allowed for improved detection limits, compared to the others, when used in conjunction with a UV detector.

Figure 3A presents the capillary LC - UV chromatogram of the arsenicals used as animal feed additives, while Fig. 3B contains an additional arsenical (4-Hydroxy), a possible metabolite of 3-Nitro.

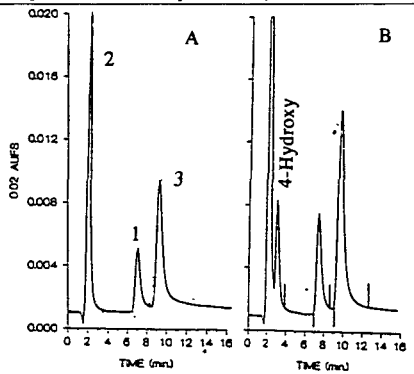

Figure 3(A,B). Capillary LC - UV chromatogram of arsenical mixture

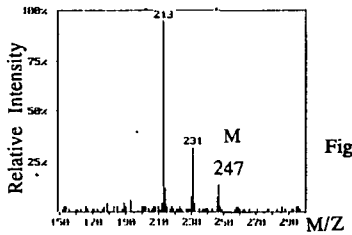

Figure 4. DLI - MS of 4-nitrophenylarsonic acid, mobile phase: water/methanol 90/10, Flow Rate: 20 μL.min^{-1}.

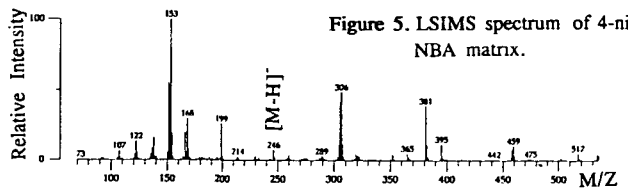

Figure 5. LSIMS spectrum of 4-nitrophenylarsonic acid, NBA matrix.

LSIMS gave spectra that contained the following m/z patterns: $[M+H]^+$, $[M+NBA-H_20+H]^+$, $[M+2NBA-2H_2O+H]^+$ in positive mode, and $[M-H]^-$, $[M+NBA-H_2O-H]^-$, $[M+2NBA-2H_2O-H]^-$ in negative mode (NBA: 3-nitrobenzylalchohol, used as LSIMS matrix).

It was only possible to obtain spectra in negative detection mode for these compounds under DLI-MS experimental conditions.

Thermospray MS spectra resulted in base peak protonated molecular ions, for all the arsenicals analyzed, along with very little fragmentation.

CONCLUSION

The separation and identification of animal feed arsenicals and their metabolites can be achieved with great success using a combination of LC columns and MS techniques. In this study we have shown that these arsenicals exhibit great differences in behaviour when analyzed under different MS techniques (DLI, LSIMS and Thermospray).

Future work will involve the direct coupling of capillary LC to dynamic LSIMS.

Short Path Thermal Desorption GC-MS for the Analysis of Sodium Carbonate and Sodium Bicarbonate

Noreen A. Klitus* and Ronald E. Shomo, II
FMC Corporation, Agricultural Chemical Group, Analytical Department,
Princeton, New Jersey 08543

Short path thermal desorption GC-MS has dramatically changed the process we use for analyzing volatiles and semi-volatiles of solids in our laboratory. Previous to the short path thermal desorber, an extraction was performed on solids before analysis by GC-MS. This was a time consuming task, and some volatiles were lost in the process.

Our current method is less labor intensive and more of the volatiles are observed by this procedure. Typically a preconditioned (heated to 300 C for 4 hours while dry Nitrogen is passed through the tube) 3 mm id GLT desorption tube is loaded with 10-50 mg of sample. A short fused silica lined SS needle is attached and the tube is placed on the desorber. The needle is injected into the GC injection port and the tube is ballistically heated while carrier gas (He in our case) is passed through the tube into the GC. The GC is cooled to -10C to cryogenically focus the volatiles while the desorption is in progress. After the predetermined desorption time, the needle is retracted and the GC temperature ramp is activated. In our case we used the following temperature program: -10 C held for 5 minutes (the desorption period) ramped to 40 C at a rate of 10 C/minute, than heated to 250 C at a rate of 5 C/minute which was held for 15 minutes. The GC column was a DB-5 0.25 mm id by 30 M with a 0.25 µm film thickness.

Figure 1 shows the TIC of a commercially available sodium carbonate and sodium bicarbonate based pet deodorizer.

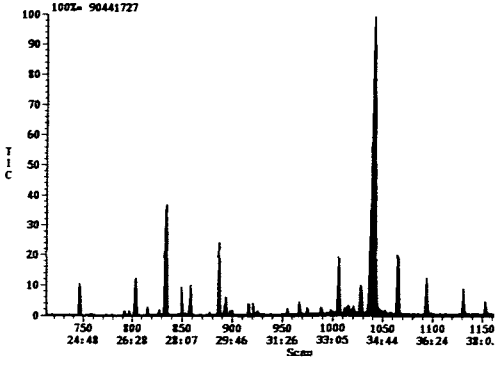

Thermospray LC-MS measurement of brucine in serum and urine

William J. Driskell, Robert H. Hill, Jr., Marianne Gregg, and Sandra L. Bailey
Center for Environmental Health and Injury Control
Centers for Disease Control and Prevention
Public Health Service, U.S. Department of Health and Human Services
Atlanta, Georgia 30333, USA

Denatured alcohol is used in many cosmetic products readily available to the public. One of the most common denaturants is brucine, an alkaloid poison that is a derivative of strychnine. Most commonly used in cosmetic products is the formula "SD alcohol 40", which contains 230 ppm brucine. We developed a thermospray LC-MS method to measure brucine levels in human serum and urine.

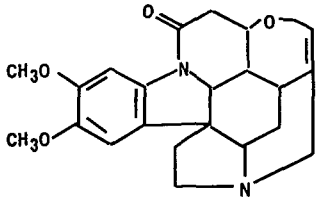

Brucine

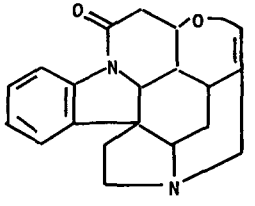

Strychnine

Serum or urine was extracted as follows: Add to 1 ml of urine or serum 10 uL of the internal standard strychnine sulfate (0.2 ug/uL in methanol). Add 0.5 ml of saturated sodium bicarbonate and vortex. To this mixture add 2 ml organic solvent (toluene:n-hexane:isoamyl alcohol; 76:20:4). Repeatedly invert tubes gently for 1 min. Remove the organic layer and evaporate to dryness using a Savant vacuum concentrator. Reconstitute the residue in 100 uL of mobile phase and inject 25 uL.

The chromatography was done with a Hamilton RP-1 reverse phase 15 x 0.4 cm column which was eluted isocratically with a mobile phase of 80% methanol, 19.9% water, and 0.1% acetic acid. The flow rate was 1 ml/min. A UV detector measuring absorbance at 254 nm was online in front of the mass spectrometer. The HPLC equipment consisted of a Waters 600 HPLC pump and controller, a 490 MS UV detector, and a U6K injector. For thermospray the vaporizer was set at 100 C and the block at 240 C. We used filament ionization and alternating single ion monitoring scans of the MH+ ions, 335 amu for strychnine internal standard and 395 amu for brucine. We used a Finnigan TSQ-70 triple quadrupole mass spectrometer with thermospray inlet.

LC-MS Trace of a 1 mL Urine Sample Spiked at 25 ppb with Brucine

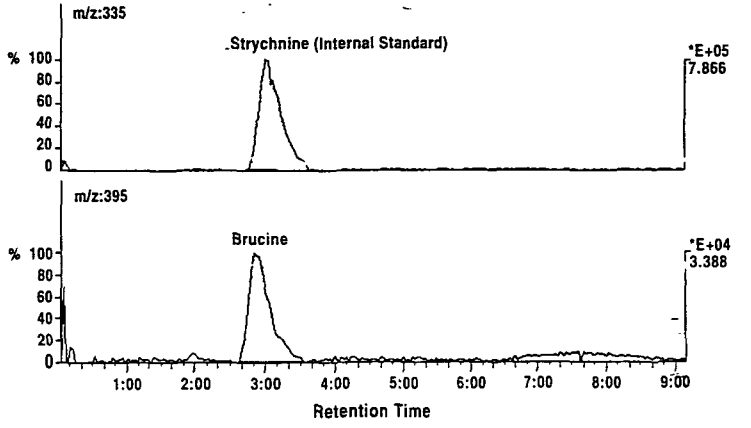

Quantitation is by internal standard quantitation with a strychnine internal standard using response factor averaging with standards equivalent to urine or serum concentrations of 10 ppb to 2500 ppb. The range of linearity is from 10 ppb to 2000 ppb. The extraction efficiency from serum or urine is between 70% and 80%. The detection limit is 10 ppb in 1 ml of urine or serum.

We plan to use this method to evaluate brucine as marker for exposure to denatured alcohol (specifically, SD alcohol 40) in cosmetic products. In addition to a marker role, serum or urine brucine levels may be of intrinsic interest, since brucine is toxic, though less toxic than strychnine. Relating health effects to brucine levels is not possible now since there is little information on brucine poisoning incidences.

Formation of Dialkyl- and Diaryl-tin Buffer Adduct Ions Under Electrospray-LC/MS Positive Ionization Conditions.

*T. L. Jones and L. D. Betowski, U.S. Environmental Protection Agency, Las Vegas, NV, 89193-3478.

INTRODUCTION

The organotins, mainly the triaryltins and triphenyltins, have widespread application as fungicides, anti-fouling coatings for porous and non-porous surfaces, herbicides, and insecticides.[1] It is important to be able to differentiate the organic functional groups, as they can impart varying levels of toxicity to different organisms.[1] Other researchers have used ion-spray (IS) mass spectrometry to characterize the alkyl- and aryl-tin isomers under negative ionization conditions[2] and to isolate tributyltin from a sediment reference material.[3] Under electrospray-LC/MS positive ionization conditions we are able to collect distinctive spectra of the dialkyl- and diphenyl-tins.

METHODS

Electrospray/mass spectrometer. All experiments were performed on a Vestec 201 LC-MS System equipped with a Vestec electrospray probe and source. The optimal ES positive ionization conditions were determined to be: 2.0kV, needle voltage; 220V, nozzle voltage; and 12V, skimmer cone voltage.

Liquid chromatograph/mass spectrometer. A Waters 600MS liquid chromatograph, converted for very low (2 to 4 μL/min) flow rates and a Rheodyne injector, equipped with a 5-μL loop was used to introduce the samples. The probe was interfaced to the ES probe with approximately 25-cm of uncoated 100-μm i.d. fused silica capillary column (FSCC). Eluting conditions were 100% methanol with either 1% acetic or formic acid added as a buffer.

RESULTS AND DISCUSSION

Tin has ten isotopes. In the discussions to follow, only the most abundant ion of the cluster will be mentioned. The results are summarized in Tables 1 and 2.

Acetic acid buffer

The dibutyltin dichloride (DBT, MW = 302 amu) spectrum had as the base peak the acetic acid substitution ion $(M\text{-}2Cl+CH_3CO_2)^+$. Also present, were the dibutyltin ion, $(M\text{-}Cl)^+$, and a small contribution from the $(M\text{-}2Cl+H)^+$ ion.

The spectrum of dimethyltin dichloride (DMT, MW = 218 amu), had as the base peak the acetic acid substitution ion, $(M\text{-}2Cl+CH_3CO_2)^+$. The other ion present is the dimethyltin ion, $(M\text{-}Cl)^+$.

In the spectrum of diphenyltin dichloride (DPT, MW = 342 amu) the base peak was the diphenyltin acetic acid substitution ion, $(M\text{-}2Cl+CH_3CO_2)^+$. There were also contributions from the diphenyltin ion, $(M\text{-}Cl)^+$ and the phenyltin acetic acid ion, $(M\text{-}C_6H_5\text{-}Cl+CH_3CO_2)^+$.

Formic acid buffer

In the formic acid buffer spectrum of dibutyltin dichloride, the base peak was the dibutyltin ion, $(M\text{-}Cl)^+$. Also present in the spectrum was the formic acid substitution ion, $(M\text{-}2Cl+CHO_2)^+$.

In the spectrum of dimethyltin dichloride the base peak was the dimethyltin ion, $(M\text{-}Cl)^+$. Also present was the formic acid substitution ion, $(M\text{-}2Cl+CHO_2)^+$.

The diphenyltin dichloride spectrum was similar to the other two dialkyltin spectra. The base peak was the diphenyl ion, $(M\text{-}Cl)^+$, and present was the formic acid substitution ion, $(M\text{-}2Cl+CHO_2)^+$.

CONCLUSIONS

Detection of the organotins was enhanced by the use of acetic acid buffer. Both acetic acid and formic acid give substitution ions when htey are used to elute these compounds. In the spectra the $(M\text{-}Cl)^+$ ion was the base peak when formic acid was used as the buffer. The substitution ion was the base peak when acetic acid was utilized.

Table 1. Mass-to-charge ratios of Organotins (12V repeller voltage; formic acid buffer)

compounds	Most abundant ion fragment	Other fragment ions*
dibutyltin dichloride	269 $(M\text{-}Cl)^+$	279 [34] $(M\text{-}2Cl+CHO_2)^+$
dimethyltin dichloride	185 $(M\text{-}Cl)^+$	195 [22] $(M\text{-}2Cl+CHO_2)^+$
diphenyltin dichloride	309 $(M\text{-}Cl)^+$	319 [47] $(M\text{-}2Cl+CHO_2)^+$

* Intensities relative to the most abundant ion are given in [ ].

Table 2. Mass-to-charge ratios of Organotins (12V repeller voltage; acetic acid buffer)

compounds	Most abundant ion fragment	Other fragment ions*
dibutyltin dichloride	293 $(M\text{-}2Cl+CH_3CO_2)^+$	269 [33] $(M\text{-}Cl)^+$ 235 [10] $(M\text{-}2Cl+H)^+$
dimethyltin dichloride	209 $(M\text{-}2Cl+CH_3CO_2)^+$	185 [22] $(M\text{-}Cl)^+$
diphenyltin dichloride	333 $(M\text{-}2Cl+CH_3CO_2)^+$	291 [13] $(M\text{-}Cl\text{-}C_6H_5+CH_3CO_2)^+$ 309 [19] $(M\text{-}Cl)^+$

* Intensities relative to the most abundant ion are given in [ ].

REFERENCES

1. John S. Thayer, in *Organometallic Compounds and Living Organisms*, P.M. Maitlis, F.G.A. Stone, Robert West (Eds.), Academic Press Inc., London (1984).

2. Siu, K.W.; Gardner, G.J.; Berman, S.S. *Rapid Commun. Mass Spectrom.* **1988**, *2*, 201-204.

3. Siu, K.W.; Gardner, G.J.; Berman, S.S. *Anal. Chem.* **1989**, *61*, 2320-2322.

NOTICE

Although the research described in this article has been wholly or in part funded by the United States Environmental Protection Agency, it has not been subjected to Agency review and therefore does not necessarily reflect the views of the Agency and no official endorsement should be inferred. Mention of trade names or commercial products does not constitute endorsement or recommendation for use.

Analysis of Ionic Textile Dyes Using Ionspray CE/MS and MS/MS.*

M.D. LeBlanc and L. Ramaley, *Dept. of Chemistry, Dalhousie University, Halifax, Canada B3H 4J3;* R.K. Boyd and P. Thibault, *National Research Council, Halifax, Canada B3H 3Z1;* A. Dietrich, *Virginia Polytechnical Institute and State University, Blacksburg, VA 24061-0246.*

Sulfonated azo dyes are commonly used in the textile industry, and pose environmental problems. Thus, they affect the ecosystem by virtue of their intense light absorption, algal growth and aquatic life are adversely affected, and both the dyes and some of their degradation products (*e.g.* aromatic amines) have been shown to possess mutagenic and carcinogenic properties [1].

Considerable effort has been devoted to developing mass spectrometric procedures for analysis of these dyes and their degradation products in water and wastewater [2-8]. All of these procedures have exploited the facile formation of negative ions from these sulfonated compounds, by LSIMS or Thermospray, or by electrospray and ionspray ionization. Some of these investigators developed LC/MS methodologies. Lee *et al.* [7] exploited the high resolution separatory capability of capillary electrophoresis (CE), for such highly ionized analytes, in a pioneering effort using CE/MS (ionspray ionization).

The present work has extended the approach of Lee *et al.* [7]. All CE development work (Beckman P/ACE instrument) used UV detection at 200 nm in order to ensure detection of impurities with no strong chromophore in the visible -near UV region of the spectrum. It was necessary to find a robust CE buffer system, compatible with negative ion ionspray ionisation (SCIEX API III triple quadrupole). Figure 1a shows a TIC electropherogram obtained by CE/MS for a commercial preparation of Remazol Black B (structure shown, molecular mass of neutral M is 903 Da). Figure 1b shows the mass spectrum acquired at the crest of the major peak in Fig.1a. The spectrum is consistent with formation of doubly-charged anions $[M\text{-}nH+(n\text{-}2)Na]^{2-}$, for n = 4 (m/z 472.5) and n = 3 (m/z 461.5). Also evident is a similar series of ions 120 Da (*i.e.* 60 m/z units), which correspond to expulsion of $NaHSO_4$ in the orifice-skimmer region of the ionspray interface. Support for this assignment was obtained by MS/MS (not shown), in which an intense fragment at m/z 97 corresponded to HSO_4^-, confirming the presence of the sulfate ester groups (see the Remazol Black structure).

When hydrolyzed in base, Remazol Black B yielded a product showing only one set of doubly-charged anions separated by 11 m/z units (replacement of H by Na). No peaks corresponding to expulsion of $NaHSO_4$ were observed. This observation, and the deduced value of 743 Da for the molecular mass of the hydrolyzed product, are consistent with its postulated structure [10], in which the sulfate ester groups are hydrolyzed to the corresponding alcohols. Fragment ion spectra of the $(M\text{-}H)^-$ and $(M\text{-}2H)^{2-}$ ions are shown in Figures 2a and 2b, respectively. Fig.2a is sparse, but Fig.2b shows extensive fragmentation, most of which can be reasonably interpreted as consistent with the proposed structure [10]. The fragment ions at m/z 80 and 81 correspond to $SO_3^{\cdot-}$ and HSO_3^-, characteristic of sulfonates; no HSO_4^- at m/z 97 is observed.

Using these results as a guide similar experiments on an unknown red dye, believed to be structurally related to Remazol Black B, have been interpreted in terms of postulated structures for the dye and its hydrolysis product. Confirmatory experiments are in progress.

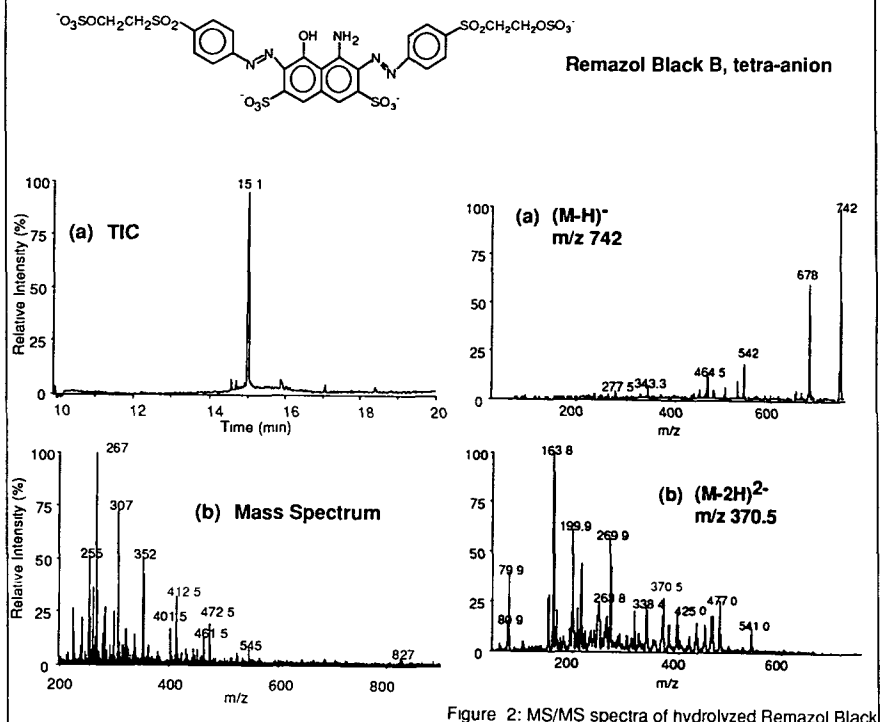

Figure 1: CE-MS analysis of Remazol Black B

Figure 2: MS/MS spectra of hydrolyzed Remazol Black

1. P. Gregory, *Dyes and Pigments* **7**, 45 (1986).
2. J.J. Monaghan *et al., Org. Mass Spectrom.* **17**, 569 (1982).
3. J.M. Ballard *et al., Org. Mass Spectrom.* **21**, 575 (1986).
4. D.A Flory *et al., Rapid Commun. Mass Spectrom.* **1**, 48 (1987).
5. A.P. Bruins *et al., Anal. Chem.* **59**, 2647 (1987).
6. M.A. McLean *et al., Anal. Chem.* **61**, 2054 (1989).
7. E.D. Lee *et al., Biomed.Env. Mass Spectrom.* **18**, 253 (1989).
8. S.D. Richardson *et al., Proc. 39th ASMS Conference*, (1991), p.785.
9. A.J. Borgerding *et al., Proc. 40th ASMS Conference*, (1992), p.1367.
10. C.F. Bell *et al., Proc. 40th ASMS Conference*, (1992), p.1707.

* NRCC No. 34864.

Characterization of Maillard Reaction Products by Capillary Electrophoresis-Mass Spectrometry

L.M.Benson, A.J.Tomlinson, K.L.Johnson, G.F.Scanlan and S.Naylor

Biomedical Mass Spectrometry Facility, Dept. of Biochemistry and Molecular Biology and Dept. of Pharmacology, Mayo Clinic, Rochester, MN 55905, USA

Maillard chemistry is the non-enzymic browning reaction of amino acids/peptides/proteins with reducing sugars. Such reactions are important in the formation of flavor, color, mutagens and antioxidants as foods are cooked. The role of this chemistry in the ageing process of humans has also been postulated.

The matrix of reactions known to occur in Maillard chemistry is complex, and that the products formed (Maillard Reaction Products - MRP's) are hydrophilic and structurally similar. We investigated the model reaction system of 5-hydroxymehylfurfural with glycine by capillary electrophoresis (CE)-ESI-MS.

We characterised a number of such MRP's by this method (Table 1). However, using ^{15}N-labelled glycine we were also able to show that in the ESI process cluster ions are formed during the spraying/evaporation process (see Figure 1). A 1:1 mixture of ^{14}N:^{15}N-labelled glycine with 5-HMF gave isotope distributions that were consistent with cluster formation.

Figure 1. Labeled CE-MS Studies of a Maillard Reaction

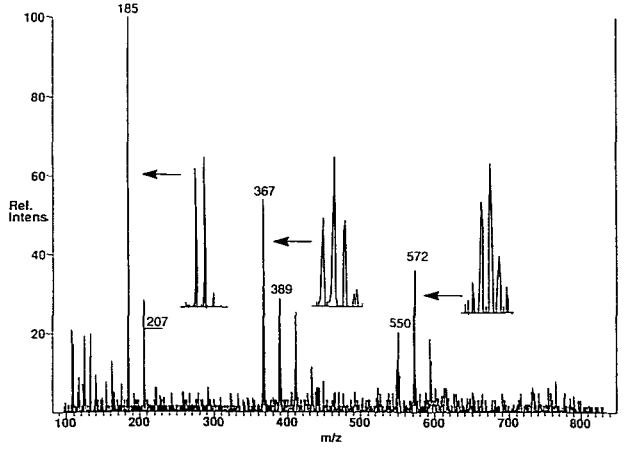

Table 1. ^{15}N-Labelled Studies of MRPs

Detected Ion (m/z)	^{15}N Label Incorporated	Implicated Molecular mass/formula	Proposed Structure
149 (MNa^+)	0	126 $C_6H_6O_3$	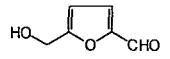
184 (MH^+)	1	183 $C_8H_9NO_4$	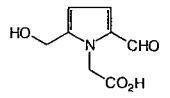
202 (MH^+)	1	201 $C_8H_{11}NO_5$	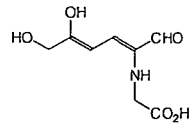
286 (MNa^+)	2	264 $C_{13}H_{16}N_2O_4$	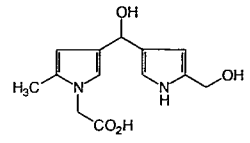

CAPILLARY ELECTROPHORESIS/ELECTROSPRAY MASS SPECTROMETRY OF SOME HAZARDOUS INDUSTRIAL AND AGRICULTURAL CHEMICALS.

Darren Wycherley, Malcolm E. Rose, *Department of Chemistry, The Open University, Milton Keynes, MK7 6AA, UK,*
Duncan Rimmer, *Occupational Medicine and Hygiene Laboratory, Health and Safety Executive, Broad Lane, Sheffield, S3 7HQ, UK,*
Kevin Giles, Stuart A. Jarvis and Mark A. McDowall, *Fisons Instruments, VG BioTech, Altrincham, WA14 5RZ, UK.*

Capillary electrophoresis (CE) coupled to electrospray mass spectrometry (ES) has been applied to environmentally important agrochemicals and industrial diisocyanates which are hazardous to human health. The aims of the investigation are to provide structural specificity, to optimise detection limits and to achieve quantification.

The very low flow rates observed in CE (10 - 40 nl/min) and the higher flow rate (5 - 400 µl/min) required for ES obviate the need for effluent splitting but necessitate a make-up flow. For CE the aqueous phase normally contains an involatile buffer which is detrimental to the ES source. As the solution is diluted considerably for CE/ES, the effect is not serious for involatile buffers such as creatinine and phosphoric acid at low concentration.

Two CE instruments were used for CE/ES work. The ISCO 3850 system coupled to a VG Quattro instrument and the Beckman P/ACE 2100 interfaced to a VG Platform mass spectrometer. Both CE/MS systems, were equipped for electrospray via a triaxial flow probe interface.

Pesticides such as paraquat and diquat when sprayed as a composite, produce an effective contact herbicide used for weed control and pre-harvest desiccation. In this process accidental human exposure may occur. More commonly, exposure is a result of suicide attempts. We have shown them to be separated rapidly by CE at pH values of 3 to 4. As the pesticides are dicationic, only the doubly charged species, M^{2+}, might be expected to be observed by ES, but both doubly and singly charged species can be seen by manipulation of the source parameters. It is postulated that the singly-charged ions result from electron donation by acetate ions in the make-up flow. This observation illustrates the known action of these pesticides as electron acceptors and provides more specific mass spectral information.

At the present time a convenient analytical procedure for analysing non-chromophoric herbicides such as Chlormequat $[HOCH_2CH_2(CH_3)_3N^+]$ and Choline chloride $[ClCH_2CH_2(CH_3)_3N^+]$ in real samples does not exist. The techniques of CE and CE/ES have been used to examine these compounds, their known by-products and appropriate internal standards. For CE, the visualisation of these non-chromophoric herbicides involves indirect UV detection.

The buffer used contains a highly chromophoric agent (creatinine) to provide a large background absorbance. The migration of samples past the UV window causes a decrease in this absorbance, figure 1. When using CE/MS, each quaternary ammonium species is identified unambiguously by its cation in the ES spectrum, (figure 2) despite the low mass ions associated with chemical background.

CE electropherogram of the herbicide mixture illustrating indirect UV detection

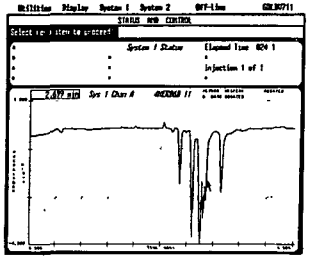

CE/ES of 4 Herbicides and 2 Standard Amines

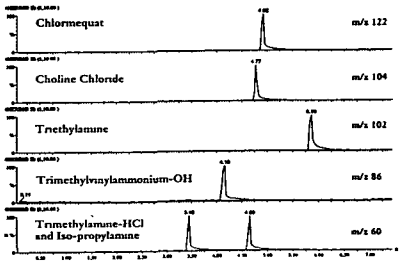

The CE and CE/ES methods applied to these pesticides and herbicides may be exploited in the UK in connection with the enforcement of FEPA (Food and Environmental Protection Act) and COPR (Control of Pesticide Regulations) by the determination of concentrates. Typically, limits of detection were 5 ppm and linear calibration graphs were obtained (all correlation coefficients were over 0.995).

Hazardous industrial diisocyanates are currently trapped from the air and simultaneously derivatised with an aryl-substituted piperazine to produce uv- and electrochemically-active bases which are determined by dual detection HPLC. The accuracy and reliability of the instrumental procedure are under question. We have shown that the same derivatives, which are cations in acidic solution, can be determined rapidly by CE and CE/MS. For example, 4,4'-diphenylmethane diisocyanate (MDI) elutes with high resolution and exhibits $[M + H]^+$ and $[M + 2H]^{2+}$ ions along with one fragment ion. The method can be applied to the monitoring of the workplace exposure to such compounds. Finally we have shown that other isocyanates (e.g. TDI isomers) can be separated and detected as the same derivatives by CE/ES.

Combined on-line CE/ES allows efficient separation and identification of compounds with greater speed and fewer manipulations than fraction collection in an off-line mode. The data shown here demonstrate the utility of the coupled technique for environmentally significant samples.

Both the Beckman CE and the ISCO instrument along with the VG Platform and Quattro spectrometers have produced results illustrating the feasibility of performing these types of analyses at environmentally significant levels.

Determination of Tin Alkylates in Environmental Samples using Thermospray and Electrospray LC/MS

W. Nigge, U. Marggraf and *M.Linscheid,
ISAS Institute for Spectrochemistry, Bunsen-Kirchhoff-Str.11, 44139 Dortmund; Germany

Organo-tin compounds are used in large amounts as fungicides and stabilizers for plastics, polyurethane foams and paints and some of them and their environmental breakdown products are known as highly toxic.

In continuation of preliminary experiments we have used thermospray LC/MS and, recently, a home made electrospray ion source on a sector field mass spectrometer to determine tin species (mono- and dibutyl - cations) after separation on different HPLC columns. For the development of the procedure, we have evaluated different extraction procedures using complex ligands to enhance the extraction and it was necessary to find the most appropriate chromatographic system in order to achieve sufficient separation and specificity. We have used rather polar diol phases, reversed phases, ion exchange columns and straight phases with different eluent systems. We found that a diol phase with methanol/water/acetic acid 75/25/0.5 was superior to all other separations. Using this separation technique and thermospray MS with positive and negative ion detection, detection limits for dibutyl tin and tributyl tin species of ca. 5 ng absolute have been obtained; concentrations of 0.5 to 1 µg of tin species per g sediment have been analyzed, although the recovery can be improved.

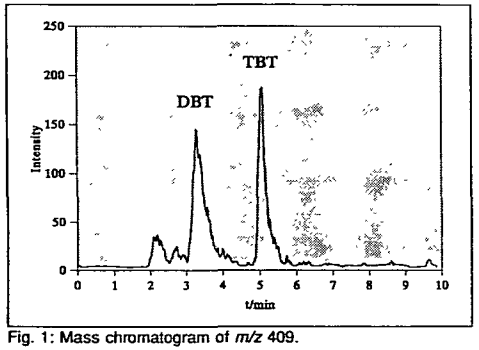

Fig. 1: Mass chromatogram of *m/z* 409.

The determination of the monobutyl tin species still represents a problem in the chromatography and the detection, because that cation has a strong tendency to adsorb to the inner surfaces of the connecting PEEK tubing causing very strong peak tailing.

Our experiments indicate that the detection and quantitation of organo-tin compounds of that type is possible with linear responses down to the low ng level absolute without using an internal standard. To increase the accuracy and the precision of the procedure, internal standards should be used and the synthesis of perdeutero tributyl tin acetate is under way. Furthermore, the use of electrospray MS seems to improve the detection limits by a factor ca. 100 and currently we are developing the required micro HPLC technique to separate the species on a micro column; with that combination, DBT and TBT concentrations in the range of 10 ng/g sediment can be analyzed.

The identification of such compounds by means of their isotopic pattern as a chemometric detector may allow the analysis of complex mixtures from environmental samples.

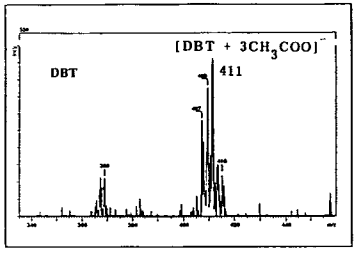

Fig. 2: Thermospray, DBT, neg. ions

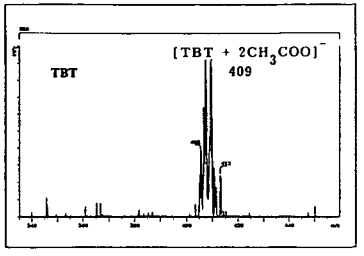

Fig. 3: Thermospray, TBT, neg. ions

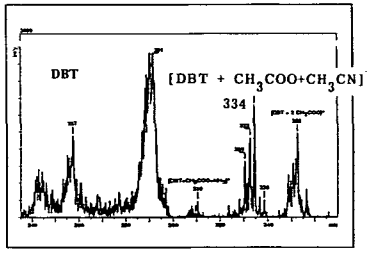

Fig. 4: Thermospray, DBT, pos. ions

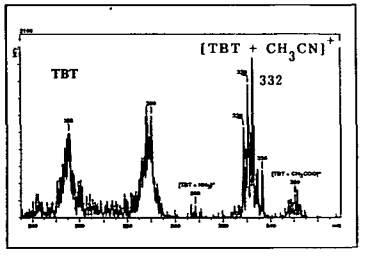

Fig. 5: Thermospray, TBT, pos. ions

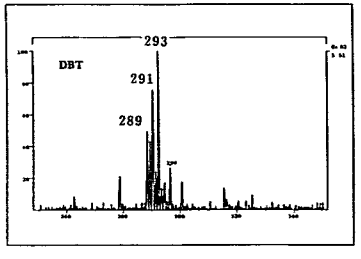

Fig. 6: Electrospray, DBT, pos. ions

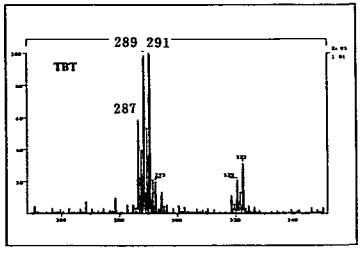

Fig. 7: Electrospray, TBT, pos. ions

Acknowledgements:
Financial support from the "Bundesminister für Forschung und Technologie" and from the "Ministerium für Wissenschaft und Forschung des Landes NRW" is gratefully acknowledged.

A Study of the Relative Particle Beam Transport Efficiency of Typical Commercial Additives in Common Reverse Phase Solvent Systems.

*A. Taaghol, K.T. Ng, R.F. Siegmund, CIBA-GEIGY Corp., Ardsley, NY, 10502-2699

As the use of commercial polymer additives such as anti-oxidants and UV absorbers have become more prevalent, the need for fast and effective identification of these additives, their associated impurities, and degradation products in manufactured goods have increased. LC/Particle-beam/MS, has proven to be an effective method for the analysis of many classes of commercial additives. However, the sensitivity of the technique is a strong function of the transport efficiency across the particle-beam interface[1]. The transport efficiency, in turn depends both on the compound and the mobile phase[1]. Reverse phase liquid chromatography (LC) is the preferred separation technique used in the analysis of commercial additives. In this paper, we have evaluated the relative transport efficiency of a number of commercial additives in the presence of several common reverse phase LC solvent systems. The model additives chosen are :

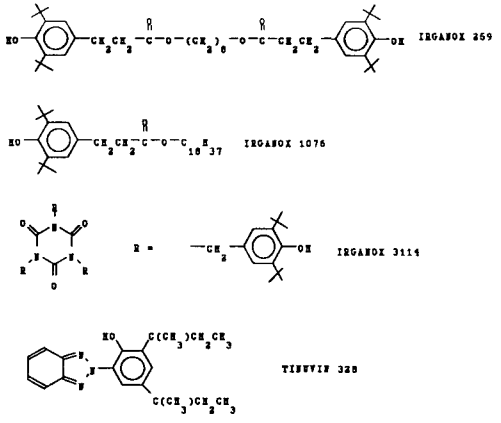

These additives were chosen to represent typical classes of compounds that are used as anti-oxidants and UV absorbers in the polymer industry. We have compared the relative transport efficiency of the above additives in methanol, acetonitrile, ethyl acetate and water/methanol systems. We found that for all of the additives, the best transport efficiency is achieved in the presence of 100% methanol. The following table contains the transport efficiency of each additive studied relative to methanol.

	Methanol	Acetonitrile	Ethylacetate
Irganox 3114	100 %	26%	28%
Tinuvin 328	100 %	49%	48%
Irganox 259	100%	79%	67%
Irganox 1076	100%	66%	48%

The transport efficiency is dramatically reduced when water is introduced into the mobile phase. For example, in a 70/30 methanol/water mobile phase, the transport efficiency of Irganox 1076 is only 10% of it's transport efficiency in pure methanol. We also found that the particle-beam transport efficiency is concentration dependant. In other words the LC/MS response is not a linear function of concentration.

1) T.A. Beller, T.D. Behmyer, W.L. Budde, J.AM.Soc. Mass Spectrometry, 1990, 1, 92-98.

K. Volk, K. NG and J. Karliner, 38th annual Conference. of Mass Spectrometry and Allied Topics, 1990, 1021.

THE IDENTIFICATION OF ORGANOSULFUR COMPOUNDS IN PRODUCED WATER BY MASS SPECTROMETRY

*A. E. Witter[1], A. Daniel Jones[1], and R.M. Higashi[2]
[1]Facility for Advanced Instrumentation, and [2]Bodega Marine Laboratory, University of California at Davis, Davis, CA 95616

Produced water is a chemically complex waste effluent generated by offshore petroleum exploration. Produced water may contain trace amounts of petroleum hydrocarbons, phenols, amino acids, fatty acids, alcohols and humic substances, as well as elevated concentrations of metals[1].

Characterization of produced waters taken from an onshore treatment plant at Gaviota, California, by this laboratory has revealed the presence of sulfur-containing heterocyclic species in concentrations of ~1 ppm, while concentrations of petroleum hydrocarbons were much lower, ca. ppb range. These results led to an interest in 1) identifying and quantifying organic compounds found in produced water generated at a petroleum production site near Gaviota, especially those that may act as potential ligands to modulate metal ion bioavailability; and 2) investigating the reactivities of organosulfur compounds with other biological or chemical species under controlled laboratory conditions.

A suite of mass spectrometric techniques were used to characterize the organosulfur compounds found in the dichloromethane extract of produced water including electron ionization, chemical ionization, accurate mass measurements, and MS/MS experiments. The mass spectra of the constituents indicate the presence of many organosulfur compounds, seen in the [M+2] isotope intensities.

The three most abundant peaks which contained sulfur were chosen for further study. Figure One shows the electron ionization spectra of these three peaks, which have molecular ions at m/z of 128 (Compound A), 132 (Compound B), and 146. (Compound C). Chemical ionization using methane as the reagent gas confirmed these molecular weights. Compound A gave a strong [M+H]+ ion at m/z 129, while compounds B and C gave weak $[M+H]^+$ ions, but measurable amounts of the $[M+C_2H_5]^+$. Derivatization of the produced water using acetyl chloride in methanol revealed that Compound C contained a carboxylic acid moiety. High resolution data for m/z 128, 132, and 146 indicate that Compound A has the molecular formula C_6H_8SO, Compound B has the formula $C_5H_8SO_2$, and Compound C has the molecular formula $C_6H_{10}SO_2$. Linked scanning techniques allowed us to elucidate the fragmentation pathway for the m/z 146 ion (Compound C).

Loss of water from m/z 146 (Compound C), possibly through hydrogen migration, gave the fragment at m/z 128 (Compound A). The peak at scan 399 in the TIC also has the molecular weight 128, which indicates that this may be a dehydration product of Compound C. From the electron ionization and high resolution data, we believe the peak at scan 399 has the structure of 6-methyl-(2H)-thiopyran-2-one. Further loss of CO from the m/z 128 fragment gave an intense base peak at m/z 100, seen in the daughter scan for m/z 128.

The m/z 146 ion can also undergo loss of H_2S through hydrogen migration to form the fragment at m/z 112. Studies are in progress to investigate how these compounds may form in the environment, as well as assessing their environmental relevance.

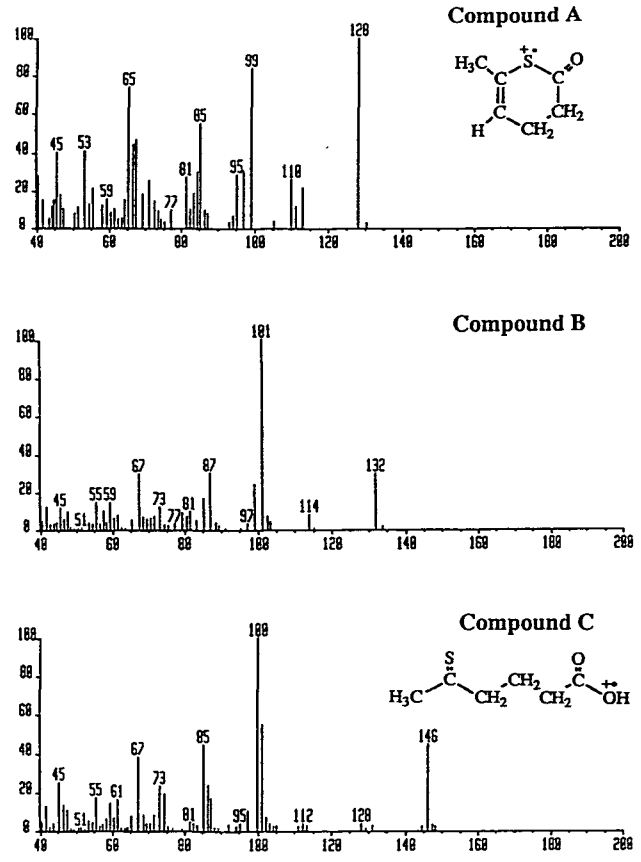

Figure One: The electron ionization spectra of the three most abundant peaks seen in the total ion chromatogram of the dichloromethane extract of produced water are shown above.

1) Menzie, C.A. Environ. Sci. Technol., **1982**, 16(8), p. 458A.

We gratefully acknowledge the support of the U.S. Dept. of the Interior Minerals Management Service.

DETERMINATION OF HYDROXYATRAZINE IN WATER AT LOW-PPT LEVELS BY USING CARBON BLACK CARTRIDGE EXTRACTION AND HIGH RESOLUTION FAB-MS

*Zongwei. Cai[1], V. M. Sadagopa Ramanujam[1], S. J. Monson[1], M. L. Gross[1], and R.F. Spalding[2], (1) Midwest Center for Mass Spectrometry-Department of Chemistry and (2) Water Center, University of Nebraska, Lincoln, NE 68588

Atrazine is one of the most widely used agricultural herbicides in the United States and has been identified along with its metabolites as contaminants in groundwater. Field-applied atrazine is known to undergo abiotic hydrolysis reactions leading to dechlorination and formation of hydroxyatrazine (HA). There are three obstacles to the analysis of HA in water at low parts-per-trillion (ppt) levels: (a) extraction efficiencies by liquid-liquid extraction with CH_2Cl_2 and solid-phase extraction using C-18 cartridges are low (< 10%), (b) the analyte is too polar and hydrophillic for direct analysis by GC or GC/MS, and (c) HPLC lacks the needed sensitivity and specificity for ultra-trace analysis.

This study focuses on three issues of method development for HA: (1) solid-phase extraction with a carbon black cartridge (250 mg, Supelco), (2) high resolution (HR) FAB-MS for quantitative analysis[1], and (3) tandem mass spectrometry (FAB-MS/MS) for further identification.

Water Samples. Groundwater was collected from multilevel water wells in Grand Island, NE. Tap water was obtained from a Lincoln municipal water supply tap at UN-L.

Sample Preparation. Prior to use, the carbon black cartridge was pre-washed sequentially with 2mL each of CH_2Cl_2, CH_2Cl_2/CH_3OH (60/40, v/v), CH_3OH, and organic-free water. The water sample (200 mL) was spiked with a suitable concentration of $^{13}C_3$-atrazine as internal standard. The sample was aspirated through the pre-washed carbon black cartridge at a flow rate of 10 mL/min. The cartridge was first eluted with 1 mL ethyl acetate. HA and the internal standard were then eluted by 5 mL of CH_2Cl_2/CH_3OH (80/20, v/v). Residual water in the ethyl acetate was removed by adding anhydrous Na_2SO_4 and the eluants were combined. The mixture was evaporated to 20-50 uL by using a slow stream of nitrogen. The recoveries of HA on the carbon black cartridge are 88% and 95% for 5 ppt and 500 ppt levels, respectively.

Quantitative High Resolution FAB-MS: A Kratos MS-50TA (EBE configuration) equipped with an Iontech FAB gun and a Kratos FAB source was tuned to a resolution of 10,000 (10% valley definition). One microliter of the sample eluant was placed in 0.5 uL dithiothreitol/dithioerythritol (DTT/DTE) matrix that had been loaded onto FAB probe tip. Narrow scans (300 ppm sweep width) over the following ions were collected by using a Kratos Mach-3 SIM program: $[HA+H]^+$ (*m/z* 198.1355), $[Atrazine+H]^+$ (*m/z* 216.1016), and $[^{13}C_3\text{-Atrazine}+H]^+$ (*m/z* 219.1117). HA was quantified by comparing the peak areas of $[HA+H]^+$ and $[^{13}C_3\text{-Atrazine}+H]^+$ ions (**Figure 1**).

A seven point calibration curve for HA at 25pg/uL to 1000 pg/uL and $^{13}C_3$-atrazine at 250 pg/uL in methanol is linear (r^2 = 0.9926) with relative response factor (RRF) of 0.93 (RSD = 12%). The analytical results are listed in **Table 1**. Due to difference in desorption rates between HA and $^{13}C_3$-atrazine, RRF was found to vary as much as 30%, depending on the state of the instrument (source and FAB gun current). Therefore, RRF was calibrated between each batch of analysis. To eliminate problems of variability, $^{13}C_3$-Hydroxyatrazine has now been synthesized and will be used as internal standard.

FAB-MS/MS: In the HRFAB-MS, the identification of HA was based on measurement of the accurate mass (*m/z* 198.1355) for the protonated molecule, $[HA+H]^+$. This identification may be compromised by interference and background in the sample extract. Therefore, further confirmation is necessary.

The collision activated dissociation (CAD) experiments were performed by selecting the $[HA+H]^+$ ion (*m/z* 198.1355) and activating it in the third field-free region by collision with helium for 50% beam reduction. Typically 10-15 scans were signal-averaged for each CAD spectrum.

Figure 2 (A-C) shows that the CAD spectra of the extracts from groundwater **(A)** and tap water **(B)** are nearly identical to that of an authentic HA sample **(C)**, giving major fragments of *m/z*: 182 [loss of CH_4],169 [loss of C_2H_5], and 156 [loss of C_3H_6]. Thus, the FAB-MS/MS may be suitable for confirming HA at trace levels.

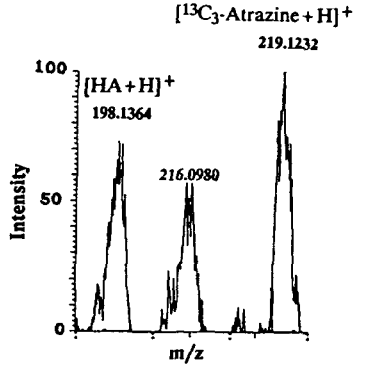

Fig 1. Mass profile spectra from the analysis of a water sample containing 5 ppt each of HA and $^{13}C_3$-atrazine.

Table 1: Levels of HA in Multilevel Well Water and Tap Water Samples.

Sample	HA, ppt
1ML 4-15 FD2	360
1ML 4-18 FD2	320
1ML 4-24 FD2	310
1ML 4-34 FD2	165
1ML 4-46 FD2	130
1ML 4-55 FD2	125
Method Blank 1	ND (3)
1ML 16-17 FD2	300
1ML 16-20 FD2	210
1ML 16-26 FD2	180
1ML 16-34 FD2	200
1ML 16-46 FD2	150
1ML 16-55 FD2	120
Method Blank 2	ND (2)
Tap Water	235

ND (DL) = not detected (detection limit)

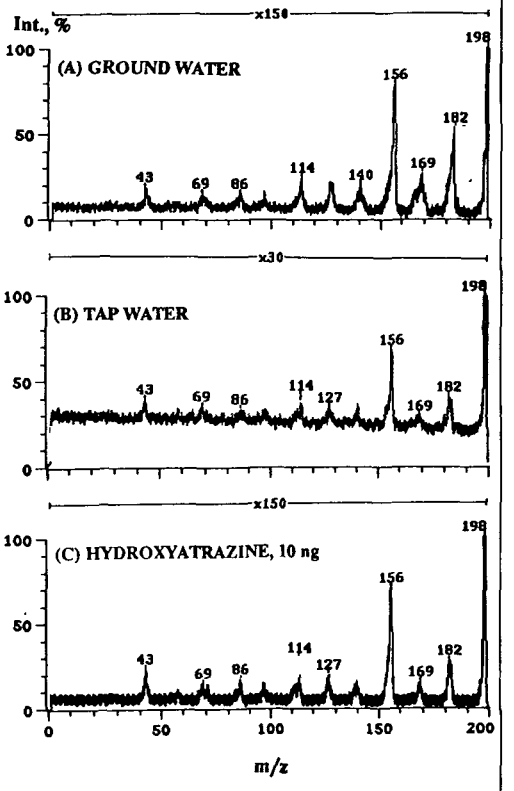

Fig. 2 (A-C). FAB-MS/MS CAD Spectra.

1. K.A. Caldwell, V.M.Sadagopa Ramanujam, Z. Cai, M.L. Gross, and R.F. Spalding, *Herbicide Trace Analysis by High Resolution Fast Atom Bombardment Mass Spectrometry: Quantification of Low Parts-Per-Trillion Levels of Atrazine in Water*, accepted by *Anal. Chem.*, 1993.

Identification of Volatiles and Semi-Volatiles in Honey

Santford V. Overton and John J. Manura
Scientific Instrument Services, Ringoes, NJ 08551-1039

Flavor/fragrance qualities of commercial food products are greatly dependent on the volatile and semi-volatile organic compounds present both in the matrix and the headspace aroma. Today, there is a problem in the food industry as to what constitutes the optimum conditions for harvesting honey so as to provide a consistent quality, flavor and aroma of honey to the consumer. Many factors must be considered such as differences between bee colonies, how they are managed by the beekeepers for a specific honey and time of harvest. The most important factor are the plants used by the bees for the production of honey. The flavor and color of the honey depends on the type of plant that produces a nectarine honey. For example, sourwood produces a honey that is different in color and flavor from that of clover or poplar. Analytical techniques are needed to profile and identify flavors, fragrances, off-flavors, off-odors and potential contaminants that may be present as flavor and fragrance additives. Volatile organic compounds were collected from samples of honey using a purge and trap technique (P&T), followed by trapping on an adsorbent resin and subsequent analysis by thermal desorption-gas chromatography- mass spectrometry (TD-GC-MS).

All experiments were conducted using a Scientific Instrument Services model TD-2 Short Path Thermal Desorption System accessory connected to the injection port of an HP 5890 Series II GC interfaced to an HP 5971 Mass Selective Detector. The mass spectrometer was operated in the electron impact mode (EI) at 70eV and scanned from 35 to 400 daltons during the GC run for the total ion chromatogram. A short 0.5 meter by 0.53 mm diameter fused silica precolumn was attached to the injection port end of a 30 meter x 0.25 mm i.d. DB-5MS capillary column containing a 0.25 um film thickness. The GC injection port was set to 300 degrees C and a 5 1 split was used during the injection step. The GC oven was maintained at -40 degrees C during the desorption and extraction process, after which the oven was temperature programmed from -40 degrees C to 300 degrees C at a rate of 10 degrees per minute for the total ion chromatogram.

Nine honeys (wildflower, blueberry, orange, clover, tupelo, alfalfa, apple spread, mixed, and a mild cream) were analyzed to compare the flavor profiles and to quantify the volatile organics of different manufacturers' brands For quantification, an internal standard was spiked into the adsorbent traps after the sample had been isolated. No correction for extraction efficiency of recovery is achieved using this technique; however, it functions as a useful means of quantifying the levels of components present on the adsorbent traps. Sample sizes of 5-6 g of commercial honey were pipetted into a 10 ml test tube and heated to 80 degrees C. Samples were sparged with high purity helium at 20 ml/min with an additional 20 ml/min dry purge for 45 minutes using a Scientific Instrument Services Liquid Purge System. Volatile analytes were gas extracted and carried to a preconditioned 4.0 mm i.d. glass-lined stainless steel desorption tube packed with 100 mg of Tenax TA. Once the samples were collected they were spiked with 100 ng of d-14 cymene internal standard by injecting 1 ul of a 100 ng/ul of a d-14 cymene stock solution in methanol by

syringe injection into the Tenax matrix. The desorption tubes with sample and internal standard were then attached to the Short Path Thermal Desorption System and a syringe needle attached. The desorption tube was injected into the GC injection port at desorption blocks temperatures of 220 degrees C for 10 minutes at a purge flow of 5 ml/min, and a GC injection split ratio of 5:1.

Nine honeys produced from different plants were analyzed to identify, compare and quantify the volatile organics present The honeys were found to contain numerous mono- and sesquiterpenoid compounds and flavors such as benzaldehyde, furfural, isovaleraldehyde and phenylacetaldehyde. The apple honey spread was found to contain numerous monoterpenoid compounds such as alpha thujene, alpha pinene, delta 3-carene, cymene, limonene, linalool, gamma terpinene, beta phellandrene and alpha terpinolene The Merck Index lists these compounds as constituents of several plant derived essential oils which are used as fragrance materials. The flavor compounds benzaldehyde and furfural have an almond-like odor, isovaleraldehyde has an apple-like odor, and phenylacetaldehyde possesses an odor reminiscent of lilac and hyacinth. Linalool oxide and tetra-furfural alcohol also contributed to the aroma in each of the honeys. Diacetyl, found in bay and other oils, was detected in each of the honeys and is used as a carrier of aroma. Isoamyl alcohol was the most abundant aliphatic compound found. In addition, the aromatic compound toluene was detected in each of the honeys with the exception of the apple spread and mixed honeys. The presence of this compound may be the result of a manufacturing process or occur naturally from essential essences.

Nerolidal, which is present in essential oils of many flowers, was identified in the wildflower honey. The wildflower honey also contained benzonitrile which has an almond-like odor and 1H-Indole which has a pleasant odor in dilute concentrations. 2-methyl propionitrile was detected in wildflower as well as in the blueberry, orange and mild cream honeys. This compound has a pleasant ethereal sweetish odor although is poisoness when heated to decomposition. Trace amounts of dihydro-2-methyl-3 (2H)-furanone, p-mentha-1(7), 8(10)-dien-9-ol and 3,5,5-trimethyl-2-cyclohex-1-one were found in blueberry, orange and clover honeys respectively, and probably contribute to the aromas. High concentrations of the flavors cis-jasmone and beta-damascenone were found in tupelo honey. Cis-jasmone present in the volatile portion of oil from Jasmone flowers has an odor of jasmine while beta-damascenone has a nutmeg-like odor. Trace amounts of 3-phenyl acrolein which has a pungent odor was also detected in tupelo honey as well as in the alfalfa honey. The apple honey spread was found to contain myristicin, an aromatic ether extracted from nutmeg and parsley; safrole, a constituent of several different oils, notably sassafras; and asarones which have a familiar and penetrating ginger odor. 3-phenyl acrolein was also present in high concentrations in the apple honey spread. Trace amounts of benzyl cyanide which exhibits an aromatic odor was detected in the mild cream honey. In addition, other middle-chain aliphatic alcohols, aldehydes, and ketones, which are the degradation products of fatty acids, were found in each of the honeys.

Using GC/MS for the Identification of Volatile and Semi-Volatile Components in Food.

Carol A. Haney[1], Jonathan A. Merkle[2], Duane K. Larick[2], North Carolina State University, [1]GC/MS Laboratory, [2]Department of Food Science, Raleigh, North Carolina 27695.

Introduction: Flavor is a key attribute in the acceptability of foods. The mechanisms responsible for creating the taste sensation are not well understood.[1] In general, many compounds may be involved in the generation of a particular flavor. In addition, it is difficult to establish the quantitative importance each compound of a mixture has on flavor. In meat products fat has a large effect on flavor. When cooked, the fat can be oxidized, generating carbonyl compounds or it can release previously stored compounds.[2]

The popularity of beef products coupled with an increasing concern with dietary fat and cholesterol make identification of beef flavor components an obvious target. Currently, processed low-fat and imitation meat products lack quality meat flavorings. Meat flavor is a complex mixture of compounds which has been difficult to reproduce. This note details an analytical approach for the identification of the volatile and semi-volatile organic components in beef fat.

GC/MS is an ideal choice for the identification of volatile and semi-volatile organic compounds. The complexity of the beef fat extracts is an analytical challenge which requires maximum instrument capabilities. The approach used for volatile organic compounds involves supercritical fluid extraction followed by a purge and trap, GC/MS analysis. The procedure used for semi-volatile compounds involves a Likens-Nickerson extraction followed by concentration and GC/MS analysis.

Experimental: Samples were prepared from subcutaneous fat from the loin of 12 Angus-Hereford steers. Fat was ground, once, through a 3/8 inch plate. Fifty gram (50g) samples were used for the supercritical fluid extractions. A commerically available supercritical fluid extractor was used (Newport Scientific). The sample was immobilized in the 0.850L extraction vessel using glass wool plugs. Carbon dioxide (4000 psi) was held constant using a back pressure regulator. Temperature in the system was maintained at 40°C. The CO_2 pressure was reduced to 1500 psi at the separation vessel to help fractionate the extract. The system was depressurized into a 0.50L flask at room temperature. Upon depressurization, the solute condenses out into the flask. Carbon dioxide flow was maintained at 15 liters per minute. A total of 500L of CO_2 was used to extract the sample.

The purge and trap concentrator (Tekmar LSC-3) was equipped with a 25 mL solids sparger and heating jacket (150°C). One hundred milligrams (100mg) of the supercritical fluid extract was used. The purge time was 14 minutes. Desorb temperature was 200°C. The GC temperature program: -30°C hold 2 minutes ramp at 2°C per minute to 290°C. The scan range was 40-400 daltons.

For the Likens-Nickerson extraction, 100g of fat was weighed into a 0.50L round bottom Pyrex flask containing boiling chips. Distilled deionized water (0.150L) was added. Methylene chloride (75mL) was placed into a 0.10L round bottom on the second extractor arm. The extraction was run for six hours. The methylene chloride phase was separated and condensed using a rotary evaporator to a final volume of 2mL. The extract was further concentrated under nitrogen to 100ul. One microliter of sample was injected.

The GC/MS anlayses were performed on an HP5985B/RTE IV mass spectrometer. The column used was a 30M x 0.32 mm DB5, 1.0um film thickness. For the semi-volatile analysis the temperature program: 45°C hold 1 minute ramp at 4°C per minute to 290°C. The scan range in EI was 40-400 daltons. For positive CI, methane was used as the reagent gas, scan range was 70-500 daltons.

Results and Discussion: Supercritical fluid extraction (SFE) has been shown to be an excellent method for extraction and concentration of volatile components. A wide variety of organic compound classes were efficiently extracted by this method. Identifications were based on library search information and, in some instances, by comparison with standards. As expected, there were strong signals resulting from various aldehydes and alphatic hydrocarbons. Aromatic compounds were also detected, but at fairly low-levels. Several ketones and sulfur containing compounds were also identified. The major component identified (based on peak area) was carbon disulfide. The volatile components detected arise through oxidative and free-radical breakdown of fatty acids or through release of stored chemicals in the fat when heated.

The total ion chromatogram from the GC/MS analysis of the Likens-Nickerson extraction is totally different from the SFE. A comparison of the results shows that the two extraction/analysis schemes provide complementary information. The concentration step of the Likens-Nickerson extraction resulted in significant losses of the volatile components. The major components were identified as aldehydes and terpenes and unsaturated hydrocarbon species. These compounds tend not to give molecular ions, or only very weak molecular ions under electron ionization (EI) conditions. Therefore, it was necessary to analyze this mixture using chemical ionization (CI). Identifications were based on the library search of the EI results and the molecular weights based on the CI results. The major components detected in the semi-volatile analysis are the terpenoid compounds, phytane (2, 6, 10, 14 - tetramethylhexadecane), neophytadiene (7, 11, 15 - trimethyl-3-methylene-1-hexadecene), phyt-1-ene (3, 7, 11, 15 - tetramethyl-1-hexadecene) and phyt-2-ene (3, 7, 11, 15 - tetramethyl-2-hexadecene). These components are derived from a component of chlorphyll and thus, are directly linked to forage feeding. These components appear to be responsible for the "off" flavor reported by the sensory panel.

Conclusions: The analysis of foods is by no means trivial. Fat, in particular, contributes significantly to the flavor of beef. Diet is directly responsible for the organic compounds found in fat. Correlations between diet, organic composition and desirability of flavor are important aspects of food flavor investigations. The approach presented here includes supercritical fluid extraction followed by purge and trap concentration and GC/MS to characterize the volatile components. The approach for the semi-volatile compounds includes the Likens-Nickerson extraction procedure and GC/MS analysis by both EI and methane, postive CI. Thus far, 118 compounds in beef fat have been identified.

References: 1. Compton, S.V., Stout, P. *Application of headspace GC- FTIR; Analysis of flavor oils.* **Am. Lab.** 24 (1992) 38-44.
2. Larick, D.K., Hedrick, H.B., Bailey, M.E., Williams, J.E., Hancock, D.L., Garner, G.B., Morrow, R.E. *Flavor Constituents of Beef as Influenced by Forage and Grain-Feeding.* **J. Food. Sci.** 52 (1987) 245-251.

Photodissociation-Photoionization Mass Spectrometry

Philip L. Ross*, Murray V. Johnston
Department of Chemistry, University of Delaware
Newark, DE, 19716

Introduction

Photodissociation-photoionization mass spectrometry (PDPI/MS) is a technique which probes neutral unimolecular decomposition rather than ionic decomposition. Neutral fragmentation patterns are more directly related to the original molecular structure than ionic fragmentation patterns since rearrangements and isomerizations are less likely to occur. In PDPI/MS, neutral fragmentation is initiated with excimer laser radiation either at 193 nm (ArF) or 248 nm (KrF). The neutral photodissociation products and remaining undissociated parent molecules are photoionized with tunable coherent vacuum ultraviolet radiation (10.5 -9.68 eV) and mass analyzed in a linear time-of-flight mass spectrometer. Recent experiments have focussed on studying the photodissociation pathways of simple alkanethiols in the C_3 - C_8 size range. The primary reactions that have been identified from PDPI/MS experiments involve cleavage of the S-H, C-S and α C-C bond as shown for 1-propanethiol in reactions 1-3 below.

						ΔH_{rxn}
$CH_3CH_2CH_2SH$	→	$CH_3CH_2CH_2S\cdot$	+	$\cdot H$	(1)	368 kJ/mol
	→	$CH_3CH_2CH_2\cdot$	+	$\cdot SH$	(2)	307 kJ/mol
	→	$CH_3CH_2\cdot$	+	$\cdot CH_2SH$	(3)	351 kJ/mol

In this study, the role of structure, molecular size and photodissociation wavelength is elucidated.

Experimental

The photodissociation and photoionization lasers are spatially overlapped between the backing plate and first acceleration grid of the TOF source region. Ions formed by MPI from the UV laser are rejected, and after a suitable time delay, the remaining neutrals are photoionized. The use of tunable VUV radiation (1) makes it possible to reduce the amount of secondary ionic fragmentation so that the photoionized neutral fragments are in most cases observed intact.

Results

A typical PDPI/MS spectrum of 1-propanethiol and 2-propanethiol is shown in **Figure 1**. The primary products from reaction 1-3 are illustrated on the figure. The alkyl radical $C_3H_7\cdot$ (m/z 43) undergoes neutral loss of H_2 to produce $C_3H_5\cdot$ (m/z 41) As seen for 2-

propanethiol, α C-C cleavage to produce a methyl radical as one of the products does not occur. As the molecular size is increased, S-H cleavage appears to be suppressed, and α cleavage gives way to β and γ C-C cleavage.

Figure 2 shows comparative 193 and 248 nm photodissociation of 1-propanethiol. Dissociation of the S-H bond is enhanced with 248 nm radiation, in contrast to the relative energetics of the primary reactions. This increased S-H cleavage is anticipated by SCF and CI calculations (2).

References

1. Van Bramer, S. E.; Johnston, M. V.; *Appl. Spect.* **1992**, 46, 255.
2. Rauk, A.; Collins, S.; *J. Molec. Spect.* **1984**, 105, 438.

This research was supported by the National Science Foundation

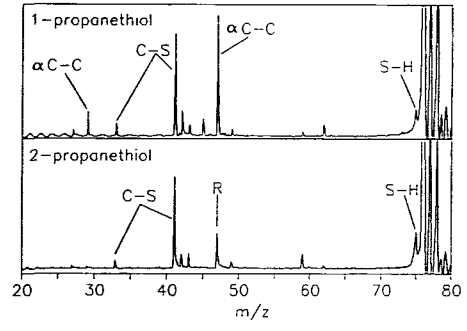

Figure 1 PDPI/MS of propanethiol isomers using 193 nm PD and 121.4 nm PI.

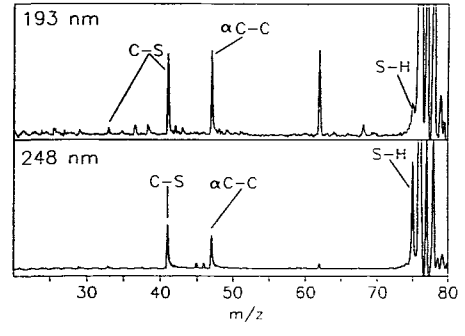

Figure 2 Comparative 248 and 193 nm photodissociation using 128 nm PI.

Protein Phosphorylation Site Study Of OP18

Y. Karen Wang, David Lubman, Samir Hanash, and John Strahler
Department of Pediatrics-Medical School & Department of Chemistry, The University of Michigan, Ann Arbor, MI 48109
Pao-Chi Liao, Douglas Gage
Department of Chemistry, Michigan State University, E. Lansing, MI 48824

Introduction

Protein phosphorylation-dephosphorylation plays a very important role in signal transduction in biological systems. An understanding of the potential role of a protein in signal transduction and of the significance of its phosphorylation requires elucidation of the mechanism of its phosphorylation in response to various stimuli and of the basis for its altered phosphorylation in pathologic states. Of basic importance, is the identification of residues that are phosphorylated in the phosphorylation form(s). While conventional Edman sequencing method can not routinely provide positive identification of the phosphorylated residues, mass spectrometry appears to be the most universally applicable technique to detect protein posttranslational modifications, including protein phosphorylation.

Phosphorylation of the highly conserved cytosolic protein OP18 has been implicated in signal transduction in a wide variety of cell types. While the effect of OP18 phosphorylation on activity of the protein is not known, the findings have emerged that suggest an important role for OP18 phosphorylation. In this investigation we have undertaken an analysis of OP18 phosphorylation in response to treatment of Jurkat T cells with PMA(phorbol-12-myristate-13-acetate), using MALDI/MS combined with enzymatic treatment of the proteolytic fragments.

Methods

Cell culture and metabolic labeling: The human lymphoid leukemic T cell line, Jurkat, was cultured in RPMI 1640 medium supplemented with 10% fetal calf serum. For metabolic labeling, cells($10x10^6$/ml) were suspended in phosphate free RPMI 1640 containing [^{32}P] orthophosphate at 400uCi/ml for 2 h at 37°c. At the end of the labeling period, PMA was added to the cell suspension for 10min and cells were harvested.
Purification of OP18 phosphorylated forms: The major OP18 phosphorylated form , OP18a, was purified by preparative 2-D PAGE using an IPG-based isoelectric separation(pH4-7) in the first dimension and SDS gels with 11.5 to 14% acrylamide gradient for the separation based on the molecular weights in the second dimension. Proteins were then electrophoretically transferred to nitrocellulose.
Proteolytic digestion and peptide isolation: *In situ* tryptic digestion was performed as follows. Nitrocellulose pieces were blocked with polyvinyl pyrrolidone-360 and washed extensively. Digestion was performed with modified trypsin(1:10 enzyme to substrate) in 50mM ammonium bicarbonate pH7.9 at 37°c. At the end of digestion, the solution and a buffer rinse were combined and dried in a Speed Vac. Tryptic peptides were separated using a C18 column. Radioactive fractions were used for phopshorylation site studies.
Secondary enzymatic digestion: Phosphopeptides were dephosphorylated with bacterial alkaline phosphatase at 150 units:0.5-2 pmol enzyme to peptide ratio in 25mM ammonium bicarbonate buffer pH7.9 for 1h at 37°c. Digestion with chymotrypsin and endoproteinase Glu-C was performed in 25mM ammonium bicarbonate buffer pH7.9(1:10 enzyme to substrate ratio) at 37°c for 18h.
Mass spectrometry: Mass spectra were obtained on a VT-2000 linear time-of-flight mass spectrometer with a nitrogen laser. The matrix used for this study was a-cyano-4-hydroxycinnamic acid. 1ul of the peptide solution(0.5-2 pmol/ul in 0.1%aqueous TFA : acetonitrile, 1:1) was added to 1ul of the matrix solution (saturated in 33% aqueous acetonitrile, about 20mM) and applied to a stainless steel probe tip. The mixture was then allowed to air dry before being introduced into the mass spectrometer. Data were acquired with a transient recorder with 5 ns resolution. Potential peptide matches were made to the sequence of OP18 predicted from the cDNA allowing for post-translational modification, using Mac-Pro Mass software.

Results

A highly conserved cytosolic protein OP18 and its phosphorylated forms were first separated by 2-D PAGE, then electrophoretically blotted onto a nitrocellulose membrane. Endopeptidase(trypsin) degradation of the major phosphorylated form OP18a was performed *in situ*, and microbore HPLC was employed to separate the tryptic peptides. An enzyme, BAP, which selectively removes the covalently attached phosphate group aided the identification of this modification. Further proteolytic digests of the tryptic phosphopeptide led to the identification of the phosphorylation site.

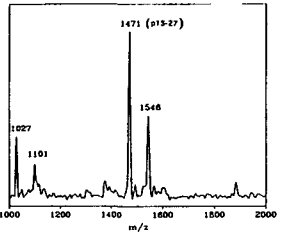

Fig.1 MALDI/MS of TP3.

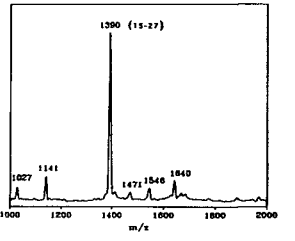

Fig.2 MALDI/MS of BAP treated TP3

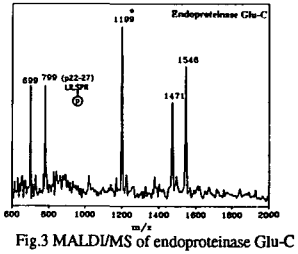

Fig.3 MALDI/MS of endoproteinase Glu-C digested TP3.

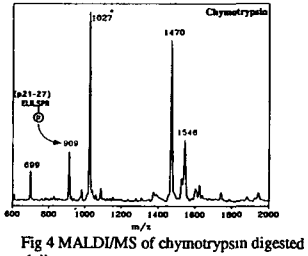

Fig 4 MALDI/MS of chymotrypsin digested TP3

* Present in control digests.

Conclusion

The sequence for TP3 is (R)ASGQAFELILpSPR(S) and the phosphorylation occurred at Ser 25.

In this study we have undertaken the phosphorylation analysis of a highly conserved cytosolic protein OP18, of which the phosphorylation has been implicated in signal transduction in a wide variety of cell types.

We have demonstrated that MALDI/MS in combination with enzymatic digestion can be a useful tool to obtain structural information of phosphopeptides especially in the cases where extremely low sample quantities are available. Each enzymatic treatment and MALDI spectrum in this study consumed 0.5-2 pmol of sample. Other mass spectral techniques may reach this level of sensitivity, but they may not be compatible with the buffer concentrations required for the enzymatic reactions. The relatively poor mass resolution of MALDI/MS makes the multiple enzymatic reactions necessary since many peptides derived from a single protein can yield ions close or identical in mass.

References

1.Zhu, X.X. et al. *J. Biol. Chem.* **264**, 14556(1989)
2. Strahler, J.R. et al. *Methods: A Companion to Methods in Enzymology.* **3**, 109(1991)
3. Aebersold, R. et al. *Proc. Natl. Acad. Sci. USA.* **84**, 6970 (1987)

COMPLEX FORMATION BETWEEN BIOMOLECULES IN MATRIX-ASSISTED LASER DESORPTION IONIZATION

P. Juhasz and K. Biemann
Dept. of Chemistry, MIT, Cambridge, MA 02139

The availability of new soft ionization techniques in mass spectrometry, such as electrospray or matrix-assisted laser desorption ionization (MALDI), now makes possible the study of non-covalently bound complexes of biomolecules. This presentation demonstrates how the existence of ionic complexes ("salts") consisting of strongly acidic and basic biomolecules can be detected and utilized by MALDI.

The experiments were carried out on a modified VT2000 (VESTEC) linear time-of-flight mass spectrometer. sources have been utilized: a N_2 laser (337 nm, 3 nsec pulses) for ultraviolet (UV) MALDI and an Er.YAG laser (2.94 μm, 120 nsec pulses) for infrared (IR) MALDI. The basic components for complex formation experiments, referred to as carrier peptides, were peptides rich in basic residues (arginine first of all): dynorphin (1-9), a tyrosine protein kinase substrate, a synthetic peptide with the sequence RRRRRRPYIL, bovine ubiquitin, *etc.* Acidic components were sulfate and phosphate containing biomolecules: peptides with cysteic acid residues, oligonucleotides, and heparin disaccharides A wide variety of matrix/wavelength combinations have been tested including sinapic acid (UV), caffeic acid (UV), α-cyano-4-hydroxycinnamic acid (αCHCA, UV), succinic acid (IR), and 5-(trifluoromethyl)uracil (TFMU, IR). Samples were generally prepared as a 1:1 molar mixture of the carrier peptide and the acidic component at 1-20 pmol/μL level in the matrix. Typically 10 laser shots were averaged in IR experiments and 30 shots in UV experiments.

Complex formation with the oxidized A-chain of bovine insulin Upon oxidation with a strong oxidizing agent (performic acid) chain A of insulin is turned into a strong acid containing four cysteic acid residues (M=2531.7 Da). Complex formation between the carrier peptides and the oxidized A-chain was observed to be a highly matrix specific process: in UV MALDI sinapic acid, in IR MALDI succinic acid was the most efficient. Figure 1 compares the mass spectra of a 1:1 mixture of ubiquitin and the oxidized A-chain in sinapic acid and αCHCA matrices.

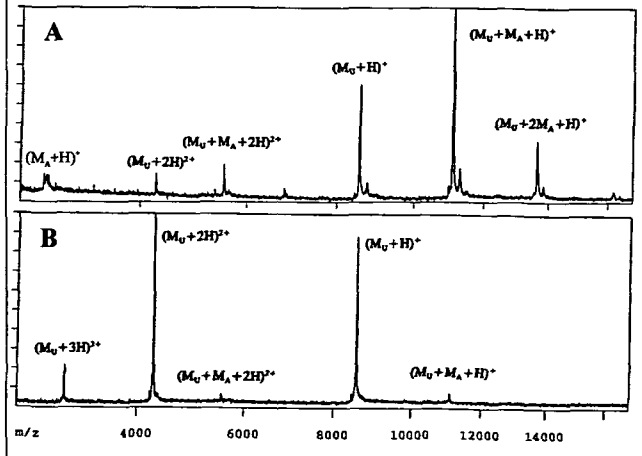

Figure 1 UV MALDI spectra of bovine ubiquitin (M_U) and the oxidized chain A of insulin (M_A) mixed in 1:1 molar ratio. Matrix: **A.** sinapic acid, **B.** αCHCA

Experiments with oligonucleotides. Protein-DNA (RNA) interaction is often driven by the electrostatic interaction of the basic residues on the protein and of the phosphate groups on the nucleotides. Complex formation (mainly 1:1

complexes) could be observed in MALDI for up to about 12mers of DNA and smaller peptides like dynorphin (1-9) (YGGFLRRIR). The relative abundances of the complex ions, however, rapidly declines with the increasing number of nucleotides. For this reason complex formation with the carrier peptides did not improve the sensitivity and efficiency of the analysis of oligonucleotides in the MALDI technique.

Experiments with heparin saccharides. Disaccharide units from glycosaminoglycan heparin have been tested for their complex formation properties. Every disaccharide unit contains 1-3 sulfate groups leading to high density of negative charges in an aqueous solution. These disaccharides attach strongly to basic peptide residues, however the intact complexes could be detected only in IR MALDI using TFMU as matrix (see Figure 2). Loss of the SO_3 group affects the N-sulfated site in the glucosamine residues Unlike oligonucleotides, heparin saccharides can be analyzed with dramatically enhanced sensitivity utilizing a carrier

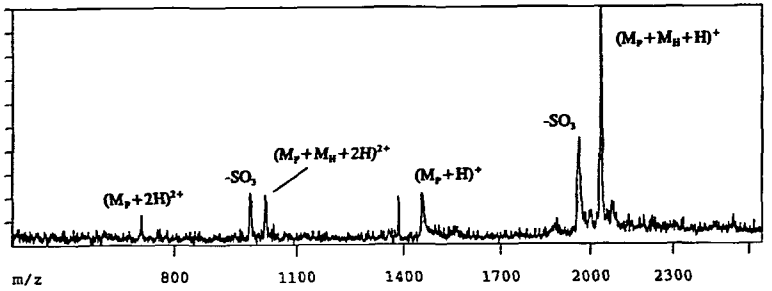

Figure 2 IR MALDI mass spectra of a 1 1 molar mixture of the heparin disaccharide (M_H) ΔUAp2S(1->4)- α- D-GlcNp2S6S [1] with the peptide RRRRRRPYIL (M_P). Matrix. TFMU.

peptide. While for a heparin sample alone at least 100 pmol/μL was necessary to obtain a reasonable molecular ion signal, by admixing a carrier peptide, as low as 150 fmol heparin disaccharide could still be detected. Another advantage of the complex formation that salt contamination does not seem to degrade the quality of mass spectra.

Mechanism of complex formation Several features of the complex formation process (such as matrix specificity, distribution of the abundance of the oligomeric complexes) already suggested that these ionic complexes formed in condensed phase and their structure, in favorable case, was preserved by the matrix. Correctness of this hypothesis was tested by observing the relative abundance of a complex ion as a function of the sample concentration (at 1:1 ratio of the components). Suppression of complex formation with decreasing sample concentration (down to 100 fmol/μL) was observed indeed, however, definite optimum of the relative abundance of complex ions was observed in the range of 1-10 pmol/μL.

References:

1. Mallis, L. M.; Wang, H. M.; Loganathan, D.; Linhardt, R. J. *Anal. Chem.* **1989**, *61*, 1433.

Acknowledgment: This research was supported by a grant from the NIH Center for Research Resources (RR00317).

Structural Characterization of a Cytosolic Glutathione-S-transferase by Fast Atom Bombardment CID and Matrix Assisted Laser Desorption Mass Spectrometry

*Constance M. Murphy and Catherine Fenselau
Department of Chemistry and Biochemistry
University of Maryland, Baltimore County
Baltimore, Maryland 21228

Glutathione-S-transferases are a diverse group of enzymes which catalyze the nucleophilic attack of glutathione in the cells defense against xenobiotic insult. Cytosolic equine glutathione-S-transferase has been reported to be an alpha class homodimer with a subunit molecular weight on the order of 25,500.[1] At the present no sequence information is available for equine glutathione-S-transferase.

The objective of the present study is to compare results obtained in the process of sequencing the cytosolic equine glutathione-S-transferase utilizing matrix assisted laser desorption mass spectrometry (MALD) with those obtained with other mass spectrometric techniques. Total protein molecular weight determinations by MALD and electrospray mass spectrometry (ES) will be compared. Similarly, MALD and fast atom bombardment mass spectrometry (FAB) will be compared for suitability in the mapping of peptides resulting from protein digestion. All MALD spectra were aquired with a Kompact MALD III (Kratos Ltd., Manchester, England). The MALD spectra were then processed using Tofware (Ilys Software, Pittsburg, PA). All FAB and tandem mass spectrometry spectra were acquired with a JEOL HX110/HX110 (Tokyo, Japan). All ES spectra were acquired with an Hewlett Packard 5988A (Palo Alto, CA) retrofitted with a Vestec electrospray source (Houston, TX)

In efforts to deduce the sequence of equine glutathione-S-transferase the mass balance strategy has been applied [2] Initially the total molecular weight of the protein was obtained via MALD and ES mass spectrometry. Subsequently, equine glutathione-S-transferase was subjected to a number of digests including cyanogen bromide, trypsin, and *S.aureus* V8 protease. After minimal separation by reverse phase HPLC the resultant digest peptides have been mapped by FAB and MALD. Due to the fact that no sequence information exists for this equine glutathione-S-transferase the cDNA sequence for human H_{x2} was used as a template.[3] Methylation of the peptides was used to enhance the FAB analysis, and to aid in peptide mapping. The sequences of two large digest fragments were confirmed by Edman degradation. Digest fragments of suitable size were subjected to MS/MS analysis to confirm their sequence.

Matrix assisted laser desorption mass spectrometry was found to be a fast, efficient means of obtaining the molecular weights of both proteins and peptides resulting from protein digestion. The total molecular weight of cytosolic equine glutathione-S-transferase was found to be 25,543 ± 25 daltons by MALD mass spectrometry (0.1% error based on instrument specification). This molecular weight agrees well with the ES mass spectrometry value of 25,554 ± 6 daltons (error based on standand deviation, n=12). The amount of sample consumed in the MALD analysis was approximately 1/15 th of that consumed in the ES analysis, 74 pmoles and 1 nmole respectively.

With regard to large digest fragments, MALD provided a broader effective mass range than FAB. At the higher mass range of 3000 to 10,000 daltons the MALD affords greater sensitivity while maintaining mass accuracy of ± 0.05% (error based on standard deviation, n = 11). With the aid of chemical derivatization, this mass accuracy was sufficient to map the protein. At the lower mass range of 100 to 3000 daltons MALD consistently detected more digest fragments from a given fraction than FAB (Fig. 1). The differences between peptides detected by MALD and those detected by FAB are not in direct correlation to their relative hydrophobicities or their molecular weight. The MALD analysis required 1/10 th to 1/20 th of the sample consumed in FAB. The advantage of the FAB analysis lies in its mass accuracy. FAB generally provided mass accuracy of ≤0.5 daltons throughout the mass range while in these studies MALD gave ± 0.05% mass accuracy (MALD error based on standard deviation, n =37).

Based on protein mapping equine glutathione-S-transferase has been found to be 90% homologous with human glutathione-S-transferase H_{x2}. Of the 221 amino acids present in human glutathione-S-transferase H_{x2} 199 have been confirmed. The remaining 22 amino acids are either substituted, modified, or deleted. From MS/MS data and Edman sequencing 20 of these amino acid substitutions have been identified.

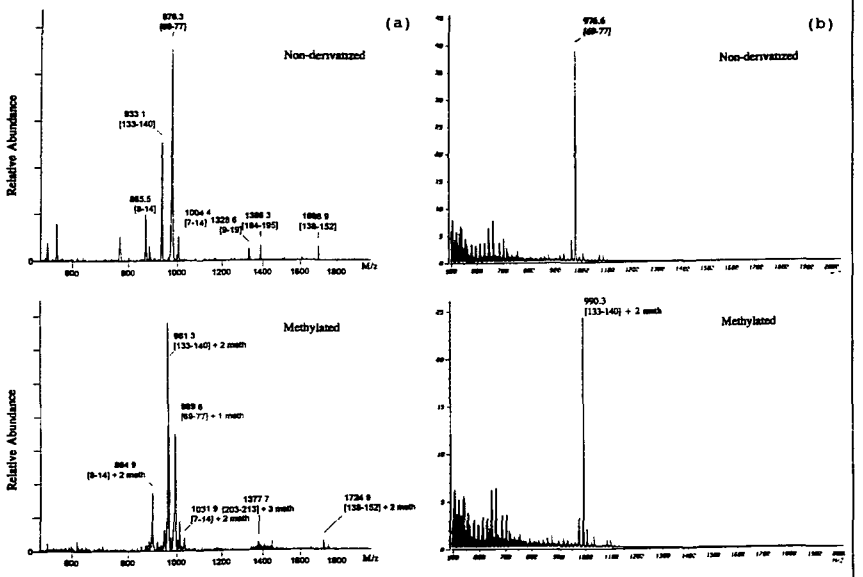

Fig. 1: Mass spectra of Tryptic digest HPLC fraction 4;(a) MALD (b) FAB

1. D'Silva, C., *Biochem. J.*, 1990, *271*, 161-165.
2. Hua, S., M.M. Vestling, C.M. Murphy, D.K. Bryant, J.J. Height, C. Fenselau, J. Thiebert, and J. Collins, *Inter. J. Peptide & Protein Res.*, 1992, **40**, 546-550.
3. Rhoads, D.M., R.P. Zarlengo and C.-P. D. Tu, *Biochem. Biophys. Res. Comm.*, 1987, **145**, 474-481.

Gas-phase Ion-molecule Reactions of Peptide Ions with Small Neutral Molecules

*Touradj Solouki, Vincent J. B. Oriedo, and David H. Russell
Department of Chemistry
Texas A&M University
College Station, Texas 77843.

Results from two methods of biological structural mass spectrometry *via* ion-molecule reactions are described. Previous studies indicate that matrix assisted laser desorbed peptide ions are formed with both excess kinetic and internal energies.[1] A question we wish to address is how do internally excited peptide ions react with small molecules? That is, are there available exothermic ion-molecule reaction channels that yield structurally significant fragment ions or do the ions react *via* collisional relaxation? Another aspect of this work is to explore the specific reaction pathways of laser desorbed metal ions with peptides that are specific to particular amino acids or functional groups:

$[Peptide]^+$ or $([Peptide^+])^*$ + Small Molecule ----------> Products

Small Organic Molecule + $[Metal]^+$ or $([Metal]^+)^*$ ----------> Products

In this paper reactions of laser desorbed peptide ions with NO and other small neutral molecules (*e.g.* CO, CO_2, SF_6) are investigated. We also report on the reaction of laser desorbed Fe^+ with small organic molecules such as formamides as models for peptides. These experiments were performed on 7 tesla FT-ICR system. Small neutral molecules were introduced into the system through a leak valve and peptide ions were formed by MALDI. Fe^+ was generated by direct laser desorption from a stainless steel probe. A cartridge type nitrogen laser (337 nm) was used for both LD and MALDI experiments. The matrix used in this study was α-cyano-4-hydroxy cinnamic acid

Results from reaction of the nitric oxide with matrix assisted laser desorbed angiotensin II are striking. Nitric Oxide has an unpaired electron and is very reactive with functionalized organic molecules. We find it particularly interesting that peptide ions react *via* collisional relaxation with nitric oxide as well as with CO, CO_2, and SF_6. For example, NO suppresses the loss of small neutral molecules (*e.g.*, loss of H_2O and NH_3) and formation of fragment ions from the $[M+H]^+$ peptide ions. Figure 1a and 1b show MALDI/FTICR mass spectra of angiotensin II without and with nitric oxide introduce as a collisional gas. Fragmentation is not observed when NO is introduced into the system under otherwise identical conditions. The primary mode of reaction of NO, CO, CO_2, and SF_6 with matrix assisted laser desorbed angiotensin II ions is *via* collisional relaxation. Reaction pathways that lead to the formation of product ions (*i.e.*, fragment and/or adduct ions) are not observed.

Results from the reaction of laser desorption Fe^+ with formamides suggest that these reactions can provide structural information. For instance, reaction of Fe^+ with N-methylformamide yields both intact ion ($[M+H]^+$ of N-methylformamide) as well as fragment ions. Table I shows the major ions formed by reaction of Fe^+ and N-methylformamide.

In summary, we show that peptide ions formed by MLADI are internally excited and this should be considered when measuring proton affinities. Internally excited peptide ions can

be cooled by collisions with small neutral molecules without leading to formation of fragment ions. However, reactions of Fe^+ with amides (model molecules for peptides) yield structurally significant fragment ions.

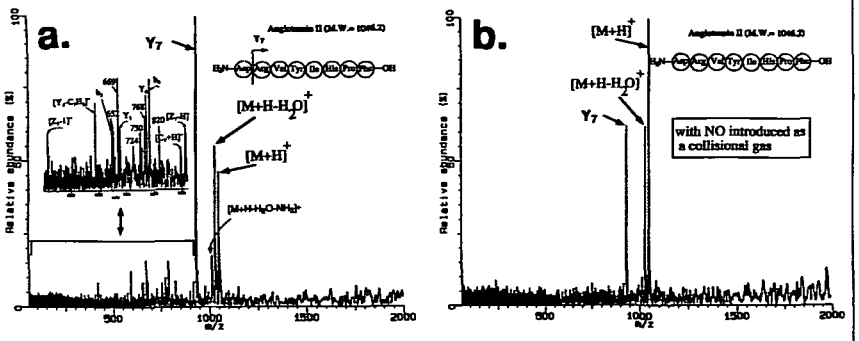

Figure 1. MALDI/FTICR mass spectra of angiotensin II a) without and b) with nitric oxide as a collisional gas. The matrix used was α-cyano-4-hydroxy cinnamic acid. The ions were detected after a two second delay from the desorption event at pressures of $2*10^{-7}$ and $8*10^{-8}$ for a and b, respectively.

Table I. Product ions of the laser desorbed Fe^+ and N-methylformamide.

Ionic Product	m/z	Ionic Product	m/z
$[M+H]^+$	60	$Fe(C_2H_3NO)^+$	114
$Fe(CH_5N)^+$	87	$Fe(C_2H_5NO)^+$	115
$Fe(CH_2NO)^+$	100	$Fe(C_2H_6NO)^+$	116

1. Solouki, T.; Russell, D. H. *Applied Spectroscopy* **1993,** 47, 211-217.

A COMPARATIVE STUDY OF MATRICES FOR MATRIX-ASSISTED LASER DESORPTION-IONIZATION (MALDI) OF TAXOL AND VARIOUS TAXANES

*Mary E. Gimon, Gary R. Kinsel, David H. Russell,
Texas A&M University, Department of Chemistry, College Station, Texas 77843

Matrix-assisted laser desorption-ionization (MALDI) can be applied to classes of compounds other than peptides and proteins. However, conditions necessary for performing MALDI on non-peptides may need to be altered in order to generate analyte ions. Different matrix-to-analyte ratios or even novel matrices may be required. MALDI of the natural product taxol (Figure 1) and its analogs, commonly referred to as taxanes, presents an example where several standard MALDI matrices and matrix-to-analyte ratios do not efficiently produce analyte ions.

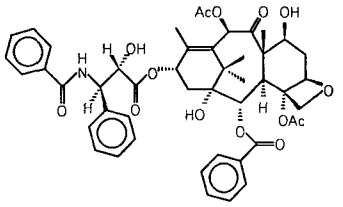

Figure 1: Taxol structure

3,5-Dimethoxy-4-hydroxycinnamic acid (sinapic acid) and α-cyano-4-hydroxycinnamic acid fail to produce useful mass spectra of the taxanes. Sinapic acid generates no intact ions of taxol. Intact ions of taxol are produced when using α-cyano-4-hydroxycinnamic acid. However, α-cyano-4-hydroxycinnamic acid clusters (m/z 200-600) make identification of the low molecular weight taxanes difficult, if not impossible. Successful MALDI is achieved employing either of two less commonly used compounds, 4-nitroaniline and 4-nitrophenol. The optimum matrix-to-analyte ratio is 100:1 and the detection limit is 1 to 2 pmol using either 4-nitroaniline or 4-nitrophenol. Several possible explanations for the different MALDI conditions for the taxanes were investigated.

Sinapic acid and α-cyano-4-hydroxycinnamic acid form monoclinic crystals. 4-Nitroaniline and 4-nitrophenol also form monoclinic crystals having the space group $P2_1/n$-C_{2h}^5 and $P2_1/a$, respectively. Initially, polarized transmission optical microscopy was used to view the crystals of 4-nitroaniline (4-nitrophenol) and 4-nitroaniline(4-nitrophenol) mixed with taxol. The observation of an "hour-glass" included region in the presence of taxol suggests that the matrix-analyte interactions of 4-nitroaniline(4-nitrophenol) and taxol are similar to those observed for sinapic acid and proteins. [1]

4-Nitroaniline produces abundant $[M+Na]^+$ ions of the taxanes. The $[M+H]^+$ ion signal increases by at least a factor of 2 when using 4-nitrophenol. In the case of taxol, enhancement of $[M+H]^+$ by close to a factor of 30 is observed (Figure 2). Enhanced parent protonation suggests that 4-nitrophenol acts as a stronger acid than 4-nitroaniline.

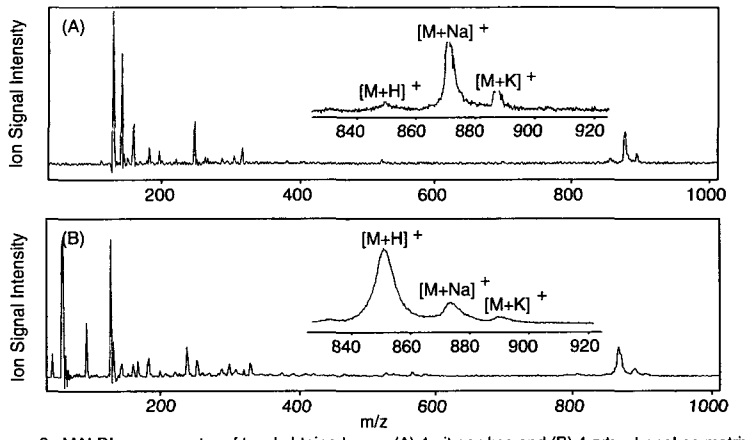

Figure 2: MALDI mass spectra of taxol obtained using (A) 4-nitroaniline and (B) 4-nitrophenol as matrix.

Acidity may be important in determining the effectiveness of a compound as a MALDI matrix. Of equal importance may be the relative basicity of the analyte. A matrix which may be effective for peptides and proteins (*i.e.*, Matrix 1) may not be effective as a matrix for acidic analytes. This may be the case for the taxanes. Taxol and sinapic acid may represent an example of this situation

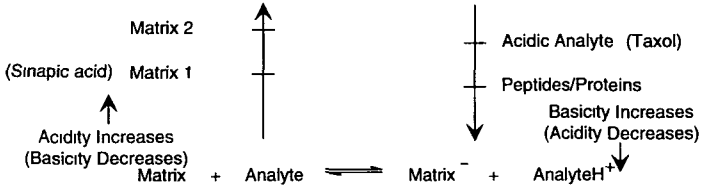

Classical and semiempirical calculations suggest that both the identity of the electron-withdrawing group (EWG) in the position para to the proton donating group, and the proximity of the EWG to the aromatic ring enhances matrix acidity by stabilizing the resultant anion. Studies using semiempirical calculations to quantify the properties that define the effectiveness of a compound as a matrix for MALDI are in progress. The goal of these studies is to understand the role the matrix plays in the mechanism of MALDI ion formation.

Acknowledgments: Taxanes provided by Timothy Prout, NaPro BioTherapeutics, Boulder, CO.

[1] R.C. Beavis and J.N. Bridson, *J.Phys. D: Appl. Phys.* **26** (1993), 442-447.

Matrix-assisted Laser Desorption/Ionization by Fourier Transform Mass Spectrometry.

John A. Castoro and Charles L. Wilkins
Department of Chemistry, University of California, Riverside
Riverside, CA 92521-0403

Matrix-assisted laser desorption/ionization (MALDI) has made possible the generation and observation of molecular ions with masses in excess of several hundred daltons, using time-of-flight mass analyzers. Because of the inherently high mass resolution of Fourier transform mass spectrometry (FTMS) it was logical to adapt MALDI to FTMS. This task was more difficult than anticipated, with the primary difficulty apparently arising from the relatively high kinetic energies of the desorbed analyte ions. However, early last year we reported a procedure (1) involving the use of a carefully timed retarding potential prior to trapping the desorbed ions, which allowed low resolution (50-300 FWHM) FTMS detection of a variety of protein ions including the dimer of myoglobin with a mass of 34,000 daltons. The use of a sugar co-matrix allowed for production of cooler ions which were trapped for longer time periods necessary to obtain high resolution (2).

In this paper, recent studies of the use of a high field FTMS instrument with MALDI techniques designed to yield greater mass range and high mass resolution will be reported. As shown in Figure 1, there is a significant effect of electrostatic deceleration times on signal intensity for single charged MALDI-generated protein ions ranging in mass from 2627 to 29,000 daltons. The optimum deceleration times (intensity maxima) are a linear function of $m^{1/2}$ when a 9.5 V decelerating potential is used. High resolution spectra of small proteins with mass resolution in excess of 150,000 will be presented. As an example, the mass spectrum of α-melanocyte stimulating hormone is shown in Figure 2, with an average resolution of 131,000 for the three most abundant isotopes and a 0.013% mass error for the all ^{12}C isotope-containing ion. Other examples include a synthetic peptide TYQRTRALV, m/z 1107, resolution = 300,000; melittin, m/z 2845 resolution = 99,300; insulin m/z 5734, resolution = 30,000. In addition, positive and negative ion MALDI spectra of a synthetic fulleroid are presented. Slow metastable decay of molecular ions in the absence of a sugar co-matrix is demonstrated for melittin and insulin, with halflives of 11 and 7 msec, respectively. Stability of desorbed insulin molecular ion with respect to energy fluence and the resulting high resolution ca. 30,000 without a co-matrix occurs just above threshold while a broader energy range is possible with the addition of a fructose co-matrix. Detection of a double charged carbonic anhydrase trimer with a mass of 87,000 daltons is also reported.

References

1. Castoro, J.A.; Köster, C.; Wilkins, C., *Rapid Commun. Mass Spectrom.*, 6, 239-241 (1992).
2. Köster, C.; Castoro, J.A.; Wilkins, C.L., *J. Am. Chem. Soc.*, 114, 7572-7574 (1992).

Acknowledgements - We thank Robert Cotter, Johns Hopkins University, for providing the synthetic peptide and Fred Wudl, University of California, Santa Barbara, for providing the synthetic fulleroid. Support from the National Science Foundation (CHE-92-01277) and the National Institutes of Health (GM-44606) is gratefully acknowledged.

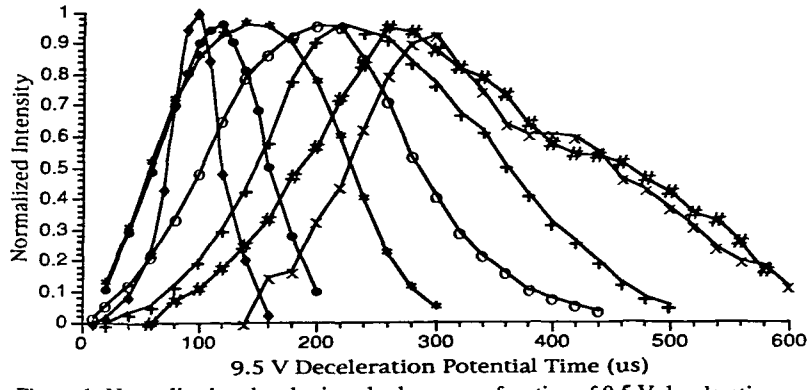

Figure 1: Normalized molecular ion abudance as a function of 9.5 V decelerating potential. A three point smooth was applied to each. ♦ insulin chain a (m/z 2627); • bovine insulin (m/z 5734); * ubiquitin (m/z 8562); o cytochrome c (m/z 12385); + myoglobin (m/z 17,000); # trypsin (m/z 24,000); x carbonic anhydrase (m/z 29,000).

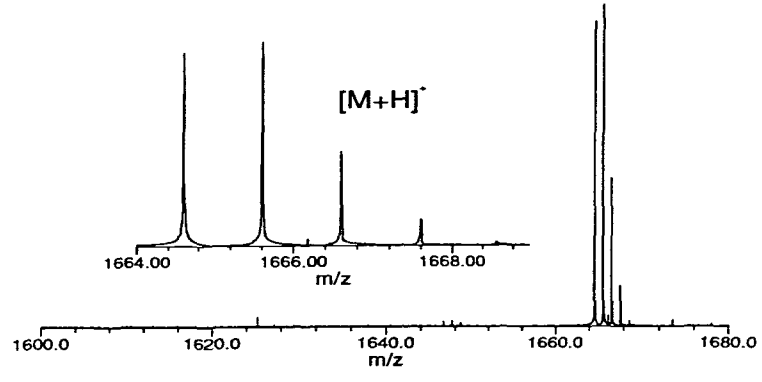

Figure 2: UV-MALDI-FT heterodyne analyzer cell mass spectrum of α-melanocyte stimulating hormone using 1000-fold molar excess of 2,5-dihydoxybenzoic acid matrix. Inset shows the proton-attached molecular ion isotopic multiplet with an average resolution = 131,000.

APPLICATION OF MASS SPECTROMETRY TO THE DETERMINATION OF TERTIARY AND QUATERNARY PROTEIN STRUCTURE

Steven L. Cohen and Brian T. Chait
The Rockefeller University, 1230 York Avenue, NY, NY 10021

We report here the use of 2-iminothiolane, a peptide and protein modification reagent, and its application in determining higher-order protein structure. This study was carried out in two parts. The first was an elucidation of the properties of 2-iminothiolane as a peptide modification reagent. The second part involved probing solvent accessibility of the protein ubiquitin by modification with the 2-iminothiolane reagent and the use of pepsin enzymatic digestions for mapping sites of modification. Matrix-assisted laser desorption mass spectrometry (MALDI) was an important component of the investigation and was used to rapidly monitor and characterize the products of the modification reactions and the enzymatic digestions.

The reagent 2-iminothiolane (2-IT; Traut's Reagents, MM 101 u) is a water soluble chemical modification and cross-linking reagent which specifically amidinates the ε-amino of lysine and the N-terminal amine groups. The reaction introduces a free sulfhydryl group positioned 8 Å from the amine functionality being modified. The amidination reaction can be summarized as follows.

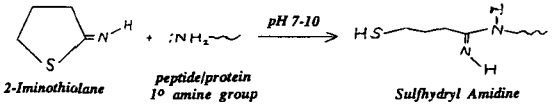

We explored the characteristics of chemical modification with 2-IT by investigating its reactivity with various peptides. **Fig. 1** shows the positive MALDI spectra of the modification of the nonapeptide bradykinin (MM 1060) with 2-IT (1:100 molar ratio peptide:2-IT) in a Tris buffer, pH 10, carried out at 0 °C for various times. Bradykinin has only the N-terminal amine group for amidination, and the peak at m/z 1162, corresponding to the modified peptide appears 101 u above the unmodified bradykinin peak. More interesting, however, is the appearance of a peak at m/z 1145, 17 u below the expected product peak. This degradation product increases with reaction time and appears under acidic as well as alkaline conditions. In fact, the degradation product ultimately dominated for all peptides we studied which underwent 2-IT amidination. The degradation product may be a result of recyclization and hydrolysis of the amidine product back to the thiolane ring. Recyclization would mean the loss of the free sulfhydryl group introduced by the original amidination reaction. This loss has implications for protein cross-linking studies which use 2-iminothiolane as a cross-linking reagent. For the purposes of chemical modification, however, we concluded from the peptide studies that handling 2-IT under ice cold conditions with rapid (1 - 100 minutes) modification reaction times results in minimal complications from degradation.

Having established optimal amidination conditions, we turned to the second part of the study, probing of the solvent accessibility of proteins using the 2-IT amidination modification. **Fig. 2** demonstrates the general approach we considered for proteins. It consists of a modification of the solvent-accessible primary amine groups by 2-IT followed by an enzymatic degradation by pepsin. This part of this study involved an investigation of the solvent accessibility of the protein bovine ubiquitin. Ubiquitin (MM 8565) is composed of 76 resides, 7 of which are lysines and one free N-terminal amine, a total of eight potential sites for amidination modification by 2-IT.

We selected ubiquitin for two principal reasons. Ubiquitin is highly resistant to denaturation so it is likely to retain its native conformation during the chemical modification procedure. Second, extensive analyses of the three-dimensional structure and solvent accessibilities of ubiquitin are available from x-ray crystallographic and 2D NMR experiments. This information is useful in evaluating the mass spectrometry findings.

The amidination of ubiquitin with 2-IT was performed at a high molar ratio of 2-IT to protein (300:1). The modification reaction was carried out over a period of two hours and was monitored by MALDI mass spectrometric analysis. Also during this time, aliquots of the reaction mixture were subject to rapid pepsin digestion. Pepsin digest of ubiquitin yields several prominent peptide fragments. Three of these fragments together cover the full length of the protein consisting of amino acid residues # 1-15, 16-45 and 46-76. Mass spectrometric analysis of the pepsin digests revealed the extent to which the these three fragments underwent 2-IT amidination as the modification reaction proceeded. **Fig. 3** summarizes graphically these findings as the fraction of ubiquitin singly amidinated plotted against the modification reaction time. The graph indicates that ubiquitin residues #1-15 are more solvent exposed whereas residues #16 - 76 are less exposed. These findings are in reasonable agreement with the crystallographic data of solvent accessibilities. There are many considerations in interpreting the mass spectrometric results and relating them to higher-order protein structure and we are currently addressing these issues.

FIGURE 1:
Modification of Bradykinin by 2-Iminothiolane
Positive ion MALDI mass spectra

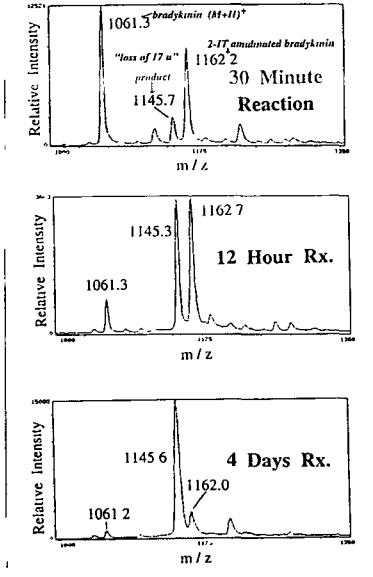

FIGURE 2: General Strategy For Studying Proteins

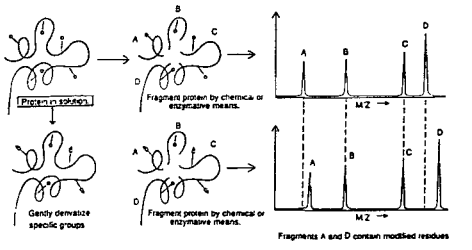

FIGURE 3: Pepsin Cleavage Fragments

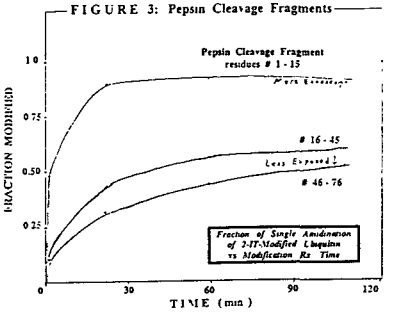

Mass Spectrometric Investigations of Proteins Separated by 2-dimensional Electrophoresis

*Wenzhu Zhang [1], Ruedi Aebersold [2], Tom Yungwirth [2], Daniel Hess [2] and Brian T. Chait [1],

[1]The Rockefeller University, 1230 York Ave., New York, NY 10021,

[2]The Biomedical Research Center, University of British Columbia, Vancouver, BC, V6T 1Z3, Canada

2-D electrophoresis is a technique for high resolution separation of proteins in extremely complex mixtures. The separation is performed in an anti-convective matrix, typically a polyacrylamide gel, after which the separated proteins can be transferred to a membrane to facilitate further structural analysis.

We have continued with our program to investigate how proteins are processed and modified in biological systems by obtaining peptide maps of proteins separated by 2-D analysis.

We have established procedures to map proteins at high sensitivity. The blotting membrane is precleaned with pure methanol to selectively remove SDS and stains. Then, CNBr and/or enzyme digestions are directly performed on the separated protein spots on the membrane. The resulting peptide fragments are extracted from the membrane and subjected to matrix assisted laser desorption mass spectrometry (MALDMS), without further separation. The extraction solution used is 30mM 4HCCA in {2.5% aqueous TFA;30%ACN}.

Bovine synapsins Ia and Ib (fig. 1) are neuronal phosphoproteins (MWs 74,519 Da and 70,441 Da) that coat synaptic vesicles and are believed to function, by means of changes in phosphorylation state, in the regulation of neurotransmitter release. They can be phosphorylated at serine-9 (site 1) by cAMP-dependent protein kinase and Ca^{2+}/calmodulin-dependent protein kinase I, and at serine-568 and serine-605 (sites 2 and 3) by Ca^{2+}/calmodulin-dependent protein kinase II. The capacity of the method for the elucidation of post-translational modifications was investigated for two mixtures of synapsins: (1) synapsin Ia and Ib, both unphosphorylated and phosphorylated (site 1). (2) synapsin Ia and Ib, both unphosphorylated and phosphorylated (sites 2 and 3). In both mixtures, unphosphorylated and phosphorylated forms were present at a ratio of 1:1. 2-D electrophoresis clearly resolved synapsin Ia and Ib, but did not resolve the different phosphorylation states. MALDMS peptide mapping of fragments produced by CNBr and/or enzyme digestions confirmed that the upper and lower bands were Ia and Ib respectively and both unphosphorylated and phosphorylated peptide fragments were detected. The technique also proved capable of resolving the different phosphorylation states that were not resolved by 2-D electrophoresis alone. This resolution was accomplished by dividing each membrane band into 3 segments and obtaining peptide maps for synapsins on each segment. Across each band, changes in the relative population of unphosphorylated and phosphorylated synapsins were reflected by the changes in the relative peak heights of the unphosphorylated and phosphorylated fragments (figs 2). The total amount of synapsins initially loaded onto the 2-D gel was ~45 pmol; ~1-5 pmol of each form of synapsin was estimated to be present on each membrane segment.

The combination of 2-d electrophoresis, digestion and matrix-assisted laser desorption mass spectrometry allowed us to identify the different forms of synapsin I and the sites of phosphorylation. The matrix-assisted laser desorption mass spectrometry also allowed the resolution of different phosphorylation states of synapsins that were not resolved by 2-d electrophoresis. The technique is highly sensitive.

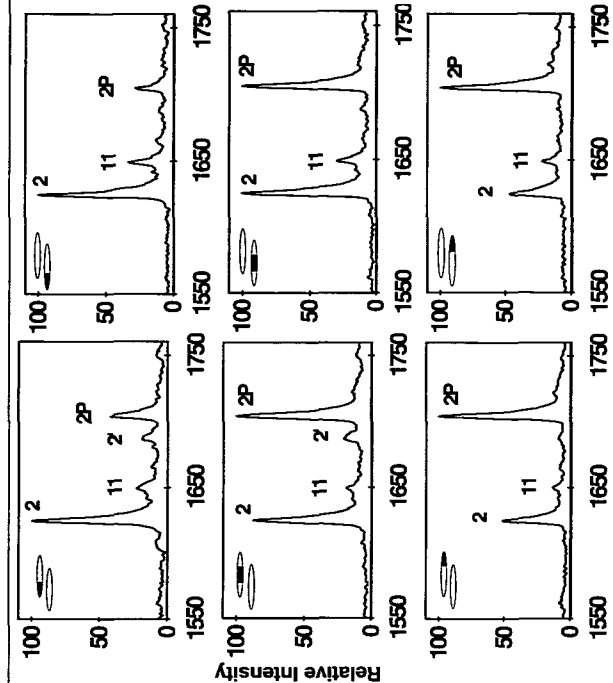

Figure 1. Sequence of bovine synapsin Ib. (Bovine synapsin Ia has 706 amino acids and its 661 n-terminal amino acids are identical to Ib.) Phosphorylation site 1 is contained in CNBr 2 fragment and sites 2 and 3 in CNBr 16 fragment. Endo lys-c digestion can further divide CNBr 16 into two sub fragments 16a and 16b (each containing one phosphorylation site).

Figure 2. MALDMS of CNBr 2 fragment of 2-d electrophoretically separated synapsin mixture (unphosphorylated and phosphorylated at site 1, see fig.1 for sequence). Each spectrum is for a segment as indicated by the darkened region in each cartoon. Relative peak heights of fragments 2 (unphosphorylated) and 2P (phosphorylated) change across each band, indicating changes in relative amount of unphosphorylated and phosphorylated synapsins.

Matrix-Assisted Laser Desorption/Ionization Time-of-Flight Mass Spectrometry as a Probe for Protein Structure.

Matthew A McLean,[1] Randall W. Nelson,[1] Tai-Tung Yip, Jesus Ching and T. William Hutchens
Protein Structure Laboratory, USDA/ARS Children's Nutrition Research Center, Dept of Pediatrics, Baylor College of Medicine, Houston, TX 77030
[1] Vestec Corporation, 9299 Kirby Dr Houston, Tx 77054

Introduction:

Determining change in peptide or protein conformation by mass spectrometry (MS) requires that either mass and/or charge of a given ion is influenced by that conformational change Changes in mass spectral intensity can also indicate conformational change but in the case of matrix-assisted laser desorption/ionization (MALDI) it is difficult to decipher if variations in intensity are related to differences in ionization efficiencies due to conformation or variations in the desorption process. As a result, we have attempted to use changes in the distribution of peptide reaction products to probe protein structure using MALDI MS The first method is to relate the Cu binding stoichiometry of a metal binding protein domain with changes in its conformation Since, biospecific Cu binding stoichiometry is known to change with altered conformation, changes in the ion distribution of the series $(MH+Cu_n-H_n)^+$, as compared to solution-phase metal binding, may indicate changes in conformation The second approach is to selectively react specific, surface exposed amino acid residues within a defined protein domain and determine if the distribution of products are influenced by a change in conformation. Any observed differences in the distribution of the covalently modified products may reflect a change in reactivity of specific residues as a result of conformation

The estrogen receptor dimerization domain (ERDD) was chosen as a model peptide in this work because of its importance in the molecular recognition event leading to estrogen receptor dimerization. It has also been studied extensively for its solution phase metal binding properties and has a known and characterized secondary structure consisting of alpha-helix, beta-turn and beta-sheet structural motifs which can be monitored by vacuum UVcircular dichroism (CD)

Results and Discussion

In the case of ERDD, a dramatic difference in the Cu binding profiles were observed in the MALDI experiment depending on the type of matrix used When sinapinic acid (SA) was used as the MALDI matrix no Cu binding was observed. This was in contrast to results obtained with 2,5-dihydroxy benzoic acid (DHBA) and α-cyano-4-hydroxycinnamic acid (α-CN) matrices where up to eight bound copper ions were observed per ERDD molecule. The Cu binding stoichiometry of ERDD in DHBA and α-CN were, however, different The distribution of ERDD-bound Cu in DHBA closely resembled that observed in solution Based on this result, it appears that the conformation of the ERDD peptide is maintained during the drying, ionization and desorption process when DHBA is used, but may not be retained with the other two matrices investigated Relating the loss of peptide or protein conformation to changes in metal binding stoichiometry is difficult, however, because the matrix influences such variables as pH, localized solvent composition and histidine(His) pKa values which are known to affect metal binding. The retention of metal binding stoichiometry, as with the case of ERDD in DHBA, however, is

evidence that conformation is retained since metal binding is not random but is consistent with solution phase stoichiometry

Covalent modifications of His residues was performed using the selective carbethoxylating reagent diethylpyrocarbonate (DEPC) In this reaction, a $(OCOCH_2CH_3)$ group is covalently bound to the imidizole ring of His resulting in a mass increase of 72 amu per modification The extent of covalent modification appears to be dependent on the conformation of the peptide or protein and can be measured by MALDI MS using SA as a matrix (figures 1 and 2) The reaction products can be driven to a higher degree of substitution by raising the concentration of DEPC in the reaction mixture. The degree of substitution was observed to be limited, however, when the ERDD peptide was reacted in its native conformation and gave a distribution of covalently modified products that is shown in figure 1 When the peptide conformation was altered by sonication prior to and during reaction with DEPC under otherwise identical conditions, a higher degree of modification was observed (figure 2) This may indicate an increased accessibility of the His residues as the peptide unfolds to its denatured state. If this is true, then the conformation of a given peptide or protein can be probed indirectly by monitoring the extent of covalent modifications of specific surface-exposed residues Experiments are currently underway to determine if the increase in the highly modified products is a direct result of conformational change or if the sonication was responsible for increasing the rate of reaction for these products.

In both DHBA and α-CN matrices the selective covalent modification of His residues with DEPC resulted in a loss of ERDD signal The loss of signal cannot be attributed to conformational changes directly, but CD results show that even a slight modification of the His residues results in a loss of conformation. The loss of signal could be due to changes in solubility or crystallization of ERDD in these matrices or could be explained by a change in the net charge of the peptide from an overall positively charged peptide to one that is neutral or negatively charged as the extent of His modification increases Efficient coupling of laser energy into the peptide due to the chemical modifications appears not to be responsible for loss of signal since highly modified species are observed out of SA (figures 1 and 2) Likewise, the overall desorption process was shown to remain intact by including myoglobin into a reaction mixture. In this case, the ERDD signal was lost but there was no apparent loss of sensitivity for myoglobin (results not shown)

Figure 1 MALDI TOF mass spectra of native ERDD after reaction with DEPC at varying DEPC/ERDD molar ratios

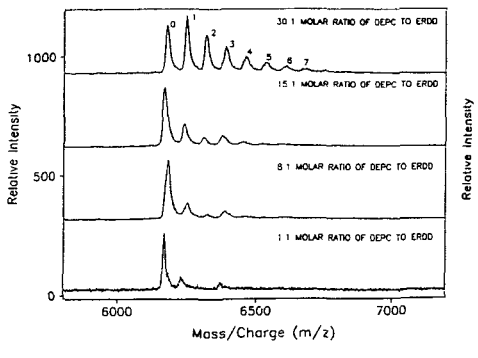

Figure 2 MALDI TOF mass spectra of denatured ERDD after reaction with DEPC during sonication at various DEPC/ERDD molar ratios

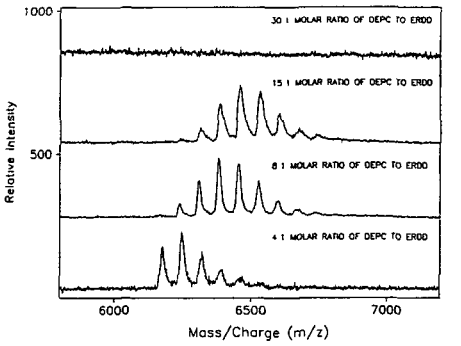

Evaluation of Phosphorylation-dependent Protein Bioactivity by Matrix-assisted Laser Desorption Time-of-flight Mass Spectrometry

Tai-Tung Yip and T.W. Hutchens
Protein Structure Laboratory
USDA/ARS Children's Nutrition Research Center, Department of Pediatrics, Baylor College of Medicine, Houston, TX 77030

INTRODUCTION

An important class of regulatory mechnisms in biology involve the modulation of protein and peptide structure and function by sequence-specific phosphorylation and dephosphorylation reactions. In addition to the widely recognized role of protein phosphorylation as a principal mechanism for signaling, the effect of phosphorylation on metal-binding and the subsequent modulation of molecular recognition and biospecific metal transfer is also of great significance.

We have developed the use of matrix-assisted UV laser desorption/ionization (MALDI) time-of-flight (TOF) mass spectrometry as a fast and sensitive method to map phosphorylation sites in proteins and to monitor protein phosphorylation/dephorylation specificity, stoichiometry and kinetics. In the case of peptides and/or proteins containing multiple possible phosphorylation sites, MALDI-TOF allows the relative ratios of all possible reaction products to be assessed directly

We now report on the further application of this technique to probe the structural and functional changes associated with varying degrees of phosphorylation. Human β casein is a major milk protein with up to five phosphorylation groups. We have mapped the site to be in the N-terminal region of the protein with a concensus sequence SSSEES found not only in human β casein but also in bovine β, αS_1 and αS_2 caseins. It is the major carrier of Fe, Ca and Mg in the milk and plays a key role in regulating mineral and metal ion absorption and cell growth. Again with the MALDI-TOF mass spectrometric technique we have developed to investigate protein/peptide-metal ion interactions we studied the effect of phosphorylation on the specificity and capcity of metal ion binding of human β casein. Parallel studies with electrospray ionization mass spectrometry and UV spectrophotometric titration are used to support the findings.

RESULTS

Fe(II)-binding study of the whole human β casein molecule performed by standard procedure like spectrophotometric tiration revealed that the binding capacity is highly phosphorylation-dependent. In an effort to map this phosphorylation-dependent metal binding site, unfractionated tryptic peptides of human β casein before and after alkaline phosphatase treatment was determined by sequential MALDI-TOF mass spectral analysis. The result showed that the tetraphosphorylated casein peptide (R1-K18 + 4P) was the major Fe(II)-binding entity in the whole digest.

To understand further how the degree and proximity of phosphorylation affect the selectivity and capacity of metal binding, individual peptides were purified from the tryptic digest. The unphosphorylated (R1-K18) peptide could bind only a barely detectable amount of Fe(II). This was confirmed by ESI even when performed in water or dilute buffer. The monophosphorylated (R1-K18 + 1P) peptide could bind Fe(II) much more readily, however, the original peptide with no bound metal was still the predominant species in the mass spectrum. The tetraphosphorylated (R1-K18 + 4P) peptide could bind up to six Fe(II) with the optimum number bound of around 3 and virtually none of the original peptide remained with no metal ion bound. This was again confirmed by ESI even when sprayed in dilute acid. However, Ca(II)-binding apparently was not as dependent on phosphorylation, since both the unphosphorylated and phosphorylated form could bind equally well with not appreciable difference in stoichiometry. This has great implication in the study of bioavailability of both Ca(II) and Fe(II) in the milk since casein is the major binding protein for both these two important metal ions. Therefore we further attempted to study the interaction and competition between these two metal ions for binding to the same phosphopeptide. The result indicated that each could effectively displaced the other from the casein phosphopeptide.

Finally, we adapted this technique to study some clinical samples. Preterm infant gastric aspirate was analyzed by MALDI-TOF directly without any fractionation before and after alkaline phosphatase treatment and then after in situ Fe(II)-binding. The result indicated that the preterm infant could digest an appreciable amount of the casein in the infant formula to generate phosphopeptides that were capable of binding Fe(II)

Evaluation of Matrix-Assisted Laser Desorption/Ionization Time-of-Flight Mass Spectrometry as a Clinical Assay

Randall W. Nelson[1], T.William Hutchens[2], Mathew A. Mclean[1], Tai-Tung Yip[2]

[1]Vestec Corp. 9299 Kirby Dr. Houston TX, 77054, [2]Protein Structure Laboratory, USDA/ARS Children's Nutrition Research Center, Dept. of Pediatrics, Baylor College of Medicine, 1100 Bates St. Houston TX, 77030.

INTRODUCTION

In order for the matrix-assisted laser desorption/ionization technique to be of use in a clinical environment, its practical quantitative abilities and limitations must first be investigated. Presented is a methodology, utilizing simple refinement techniques and matrix-assisted laser desorption/ionization time-of-flight mass spectrometry, for the quantitative analysis of a clinically significant protein, lactoferrin, present in a naturally occurring biological fluid, urine.

RESULTS

Experiments were performed investigating various possible methods to enable the production of lactoferrin ion signal during the matrix-assisted laser desorption/ionization process. Fig. 1 shows a typical MALDI spectrum of lactoferrin containing (3pmol/ul) urine with no prior sample workup. Overall the spectrum is of fairly low quality, with poorly resolved lower mass protein signals and no obvious signal at ~81 kDa (molecular weight of the lactoferrin). The speculated reason for no lactoferrin signal present in the mass spectrum is that lactoferrin ion production was inhibited by the presence of an extreme amount of native protein present in the urine. Fig. 2 shows a mass spectrum of the lactoferrin-containing urine after adjusting the pH to 8.0 and the addition of DEAE-Sephlacel anion exchange resin. At a pH of 8.0 the lactoferrin exhibits minimum binding to the DEAE-Sephlacel anion exchange resin, so it was thought that the rapid mixing of urine and anion exchange resin would perhaps sweep enough of the erroneous proteins out of solution to provide an adequate lactoferrin signal. Fig. 2 shows the resulting mass spectrum. While use of the anion exchange resin did not remove all of the interfering protein, it did refine the urine enough to provide a substantial lactoferrin signal.

After enabling the lactoferrin signal from the urine, quantitative analysis followed in a manner previously described /R.W. Nelson, et al, Proc. of the 40th ASMS Conference on Mass Spectrom. and Allied Topics/. Briefly, the technique involves the addition of an internal reference standard, in this case human serum albumin HSA, followed be successive additions of concentrated analyte solution. Fig. 3 shows a plot of lactoferrin signal (normalized to the HSA signal) versus the resultant lactoferrin concentration. A linear relationship is observed over an order of magnitude with the intercept indicating an initial concentration of, after correction for dilutions occurred throughout the experiment, 0.6 pmol/ul.

CONCLUSION / DISCUSSION

A simple method to enhance the performance of matrix-assisted laser desorption/ionization time-of-flight mass spectrometry of natural biological fluids has been investigated. Because of interferences due to the complexity of the analyzed natural biological fluid, urine, simple off-line fractionation techniques were used to refine the solution with respect to a clinically significant protein

species of interest, lactoferrin. Using the refinement techniques, lactoferrin ion signal was obtained, from urine, at yields sufficient for quantitation, hence accomplishing the original objective of the excersise. Quantitative analysis of the refined urine by matrix-assisted laser desorption/ionization time-of-flight mass spectrometry indicated an approximately 20% recovery of the lactoferrin throughout the procedure. Further investigations need to be undertaken concentrating on ways to improve the lactoferrin recovery throughout the refinement process.

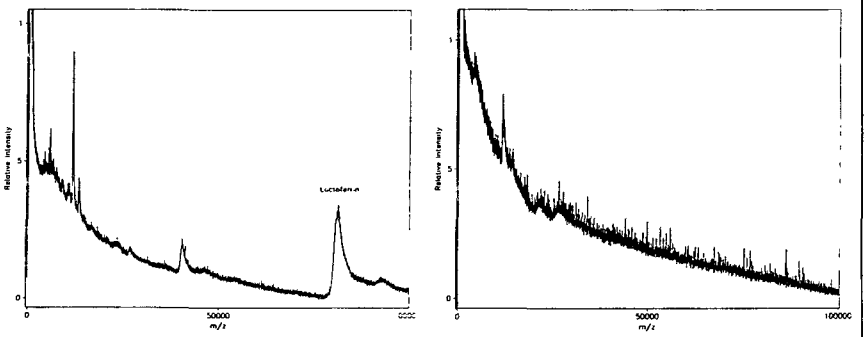

Fig. 1 (left) MALDI spectrum of urine containing human lactoferrin at a concentration of 3 pmol/ul. Fig. 2 (right) MALDI spectrum of the urine used to produce Fig. 1 after refinement by addition of DEAE-Sephlacel anion exchange resin at a pH of 8.0. Reasonable lactoferrin signal is obsered at ~81 kDa.

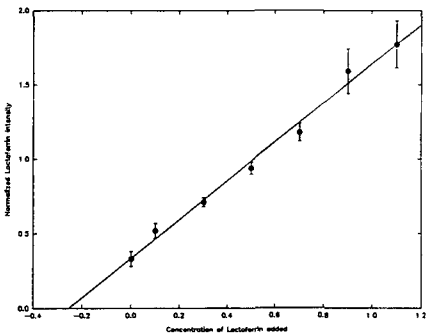

Fig. 3 Plot showing the relationship between the normalized lactoferrin signal intensity and the added concentration of lactoferrin.

REAL TIME ANALYSIS OF SINGLE AEROSOL PARTICLES

D. S. Thomson*, D. M. Murphy, and M. Kalyuzhny*
Aeronomy Laboratory
National Oceanic and Atmospheric Administration Boulder, CO 80303
***also with Cooperative Institute for Research in Environmental Sciences**
University of Colorado, Boulder, CO 80306

We have developed an instrument capable of analyzing individual aerosol particles in real time. Using laser ionization and TOF mass spectrometry, we have obtained mass spectra for a variety of laboratory-produced aerosols. Recent improvements in the instrument as well as in our aerosol production capabilities have allowed us to increase the range of particle types and sizes which we can detect and to increase the resolution of the mass spectra. Further improvements are underway which will allow the instrument to perform field measurements in the near future.

Aerosol particles enter the interaction region of the vacuum chamber through a differentially-pumped multi-stage inlet. The passage of the particles through the focus of a continuous laser beam scatters light into an avalanche photo-diode. This scattered light provides information on the size of the particle and triggers a pulsed excimer laser. The pulsed laser produces several milli-Joules of radiation at 248 nm which vaporizes and ionizes the particle. The ions are accelerated down a time-of-flight mass spectrometer to a pair of ion detectors. Logarithmic amplifiers compress the spectra, which are then digitized and transferred to a personal computer for storage and analysis.

The minimum particle size of the instrument is limited by the scattered light detection. Recently, we have obtained spectra of several types of 0.3 μm diameter particles, including latex spheres, sodium iodide, and ammonium sulfate. Since previous measurements were made on particles from 2 μm to 15 μm diameter, this significantly expands our ability to measure particles of atmospheric interest. Due to the reduction in minimum particle size, we have been able to obtain spectra from ambient aerosols present in the laboratory air. Though we have not yet conducted extensive analysis on ambient particles, we are preparing the instrument for a field measurement campaign which will begin late this summer.

The acceleration fields of the mass spectrometer include a time-dependent field used to increase the mass resolution.[1] As a result, we have obtained spectra with better than unit mass resolution for all masses up to about m = 350 using a flight tube only 67 cm long. In addition, we recently completed the circuitry required for reversing the polarity of the mass spectrometer, allowing us to begin recording negative ion spectra as well as positive.

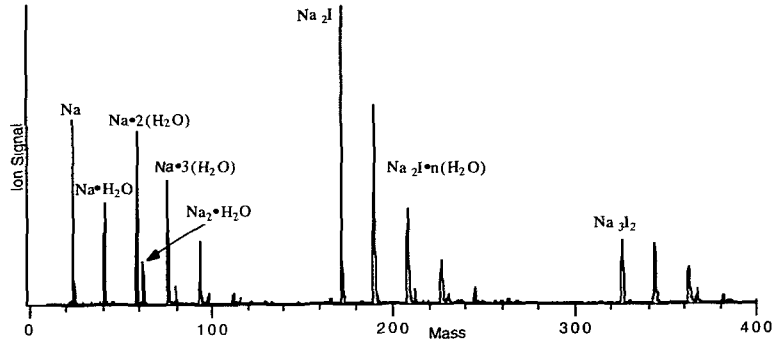

Figure 1) Sample spectrum of 2 μm particle consisting of NaI and water.

As part of the development of the instrument, we have made numerous measurements of the laser energy threshold for ion production as a function of particle type, particle size, and laser wavelength.[2] A limited amount of data were taken with laser wavelengths of 337 nm and 197 nm, and more extensive studies were done using 10.6 μm, 308 nm, and 248 nm. It was found that the shorter wavelengths were more appropriate for this instrument for a number of reasons. Not only were the laser energy thresholds for ion production several orders of magnitude lower at 248 nm than at 10.6 μm, but there was also less variation due to particle size and composition. In addition, at 10.6 μm the threshold for plasma initiation was only a factor of 2 greater than for ion production, while at 248 nm plasma initiation occurs at laser fluences several orders of magnitude higher than ion formation. This allows a broad range of laser energies to be utilized without saturating the interaction region with the space charge effects due to plasma production. The advantages of 248 nm radiation over 308 nm radiation are similar though less pronounced.

We have begun additional measurements on the number of ions produced as a function of laser power. Preliminary data shows that the ion yield is a non-linear function of laser power, but so far the data do not allow for a more precise determination of the functional form.

1) D. M. Murphy, Presented at the 41st ASMS Conference on Mass Spectrometry and Allied Topics (1993).

2) D. S. Thomson and D. M. Murphy, *Applied Optics*, in press.

EXAMINATION OF NATIVE AND DEGRADED IgG ANTIBODIES BY MICELLAR ELECTROKINETIC CAPILLARY CHROMATOGRAPHY AND MATRIX ASSISTED LASER DESORPTION/IONIZATION MASS SPECTROMETRY

Anthony J. Alexander* and David E. Hughes; Bristol-Myers Squibb Co, Pharmaceutical Research Institute, P O. Box 4755, Syracuse, N.Y. 13221.

INTRODUCTION

Monitoring the stability of drug delivery antibodies is a crucial analytical aspect of the IgG production technology. Capillary electrophoresis (CE) has proven valuable for the analysis of proteins (1), and has the potential to separate and detect native antibody components. An ideal complement to CE, which is capable of providing the desired detection specificity, is matrix assisted laser desorption/ionization mass spectrometry (MALDI-MS). Off-line CE-MALDI has been demonstrated (2), but on proteins with molecular weights considerably less than typical for antibodies. Utilizing these techniques we have developed an antibody examination procedure and monitored the degradation of an chimeric (human/mouse) monoclonal antibody.

METHODS

The antibody, at a concentration of 10 mg/mL in buffered saline, was heat-stressed at 60°C for a period of 166 hrs. At discrete time points, sample aliquots were removed and sampled by CE and MALDI-MS. The CE separation was performed using a Beckman P/ACE system with a 50cm x 75µm uncoated capillary. The running buffer was 12 mM borate pH 9 4 containing 25 mM SDS. The separation was performed at 30 kV for 8 minutes at 25°C and monitored at 214 nm. MALDI mass spectra were obtained using a Bruker Reflex Time-of-Flight mass spectrometer equipped with a 337 nm laser. Spectra were obtained using an ion extraction voltage of 30 kV and a time resolution of 10 ns. Samples were diluted 20:1 with an aqueous saturated solution of sinapinic acid (SA) containing 33% acetonitrile. 1 0 µL of this mixture was allowed to air dry on the probe tip Spectra were obtained using the linear detector and represent the summation of 20 laser shots.

RESULTS AND DISCUSSION

Electropherograms of the antibody after 0, 47, 94 and 166 hrs of thermal stress are shown. The unstressed antibody is represented by four major peaks (A,B,C,D assumed to be conformers) and low levels of IgG-related species. As degradation proceeds, peaks 2,4,6 and 7 are formed Peaks 1,3 and 5 also increase in height MALDI mass spectra of the stressed antibody were acquired at the same time points The initial spectrum was obtained from 3.3 pmoles of IgG loaded on the probe tip. At 166 hrs the percentage of ionization carried by the molecular ions M^+, M^{2+}, etc has clearly decreased while that due to additional ion species, particularly below m/z 16,000, has significantly increased. Several ion signals at ca. m/z 125,600; m/z 101,800; m/z 50,900 and m/z 24,070 progressively increase with time. These ions correspond in mass to loss of one and two light chains from the IgG, $(M-LC)^+$ and $(M-2LC)^+$, and formation of separated heavy chain (HC^+) and light chain (LC^+) moieties, respectively.

CONCLUSIONS

CE provides the very selective separation of antibody-related chains and fragments required for the examination of degraded IgG samples MALDI-MS provides a complimentary "fingerprint" or, impurity profile, of an antibody from which it is possible to assess both the degree of degradation, and gain specific MW information on the resulting species formed.

1) Guttman et al; Electrophoresis **88**, 151 (1988) and Grossmann et al; Anal. Chem. **61**, 1186 (1989).
2) Keough et al; Anal. Chem. **64**, 1594 (1992) and Castoro et al; J. Am. Chem. Soc. **114**, 7571 (1992).

Presented at the 41st ASMS Conference on Mass Spectrometry

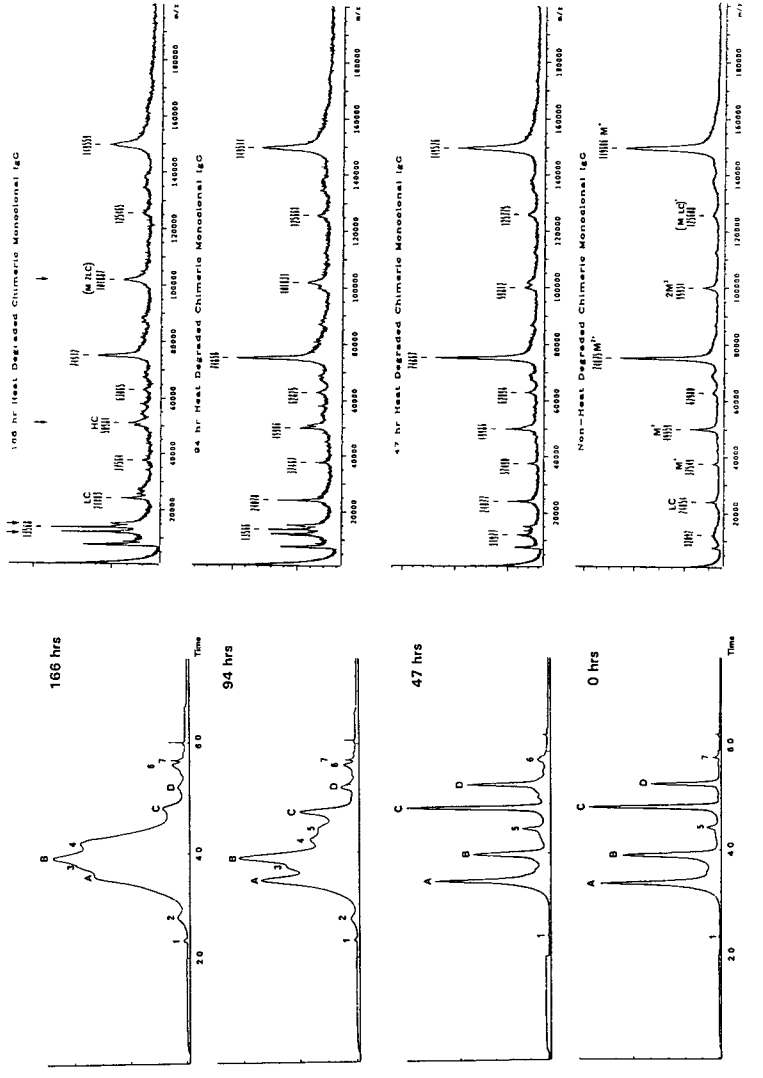

Figure 1: CE electropherograms of a heat degraded chimeric (mouse/human) monoclonal IgG after 0, 47, 94 and 166 hrs of thermal stress at 60°C.

Figure 2: MALDI mass spectra obtained at the same time points shown in Fig. 1. The non-degraded spectrum was obtained from 3.3 pmoles of the IgG. Matrix: SA.

Carbohydrate-Containing Matrices for MALDI: Applications to the Analysis of *in situ* Digests of Proteins from Two-Dimensional Gels

John T. Stults, Todd M. Billeci, William J. Henzel, Susan C. Wong,
Christopher Grimley, and Colin Watanabe,
Protein Chemistry Dept., Genentech, Inc., South San Francisco, CA 94080

Peptide mapping is a valuable tool for the characterization of proteins. Detailed analysis of each of the component peptides in a protein permits examination of the primary structure in considerable detail. Mass spectrometry is now one of the most useful techniques for peptide mapping. In recent years, matrix-assisted laser desorption/ionization mass spectrometry (MALDI) has emerged as an important technique for the analysis of biomolecules. Characterized by sensitivity in the mid-femtomole to low-picomole range, MALDI has a high (>300 kDa) upper mass limit, relative tolerance to many buffer components, and the ability to analyze unfractionated biomolecular mixtures. As a result, the technique is particularly well-suited for analysis of peptide mixtures that result from proteolytic protein digestion. Despite the advantages of MALDI, several limitations have thus far prevented its routine and widespread application. Each of the common matrices discriminates against mixture components in ways which are sample and matrix specific. Some of these matrices yield abundant, interfering matrix ions that extend up to 1000 Da. The lack of a universally applicable matrix lowers analysis efficiency by requiring the comparison of spectra acquired in more than one matrix. One way to surmount the matrix selectivity problem is to improve known matrices by using matrix mixtures.

Based on the favorable results achieved by Köster *et. al.*[1] we evaluated the effect of incorporating glucose, fructose, fucose, b-lactose, maltose and sucrose in various molar ratios with DHB. Fucose/DHB in a molar ratio of ca. 5000:5000 to one part analyte produced the best results achieved to date.[2] The spectrum of recombinant human growth hormone (rhGH) tryptic peptides in sodium acetate/Tris buffer with a DHB/fucose matrix displays a number of striking enhancements over that with DHB alone. The absolute ion signal for many peptides is increased, affording unambiguous detection of more mixture components. The matrix signal, frequently appearing as the base peak for DHB, was dramatically suppressed in the presence of fucose. Further, the rise in baseline at low masses was minimized. The resolution (FWHM) was likewise improved. Signals corresponding to $(M+Na)^+$ were often more abundant than $(M+H)^+$ in preparations with neat DHB. Overall, 96% of the expected tryptic fragments were detected using as little as 280 fmol of unfractionated material. Analysis of <280 fmol showed a decrease in the relative abundance of the higher molecular weight peptides.

The advantages of the carbohydrate co-matrix are applied to the analysis of digests of proteins isolated from two-dimensional gels. Proteins in a gel are electroblotted to PVDF membrane, followed by *in situ* reduction, alkylation and tryptic digestion.[3] The resulting peptides are analyzed by MALDI. The peptide molecular masses are used as input for a computer program (FRAGFIT) that searches a protein sequence database.[4] This approach permits the rapid identification of known proteins at the sub-picomole level.[5]

To demonstrate this approach, proteins extracted from an hGH-producing *E. coli* fermentation were separated by two-dimensional electrophoresis, blotted onto a PVDF membrane, and stained with Coomassie blue. Ten spots were arbitrarily chosen, and two identical gels were run. One gel was used for N-terminal sequence analysis. The second gel was used for tryptic digestion followed by MALDI mass spectrometry. The amounts analyzed ranged from 75 fmol (3% of the total) in spot 1 to 840 fmol (20%) in spot 8. Masses with $900<m/z<2500$ obtained from MALDI analysis were used as inputs for the FRAGFIT program to identify the protein(s) in each gel spot.[5] The FRAGFIT algorithm cleaves >91 000 entries in the protein sequence database using a specified cleavage reagent each time the program is executed. The program then searches the database for a protein with fragment masses that match the user's list of masses within a tolerance of ±4 Da. A molecular mass range based on the second gel dimension is used to limit the size of the proteins searched in the database. The user may specify the number of mismatched fragments allowed for each search. Typically, a protein may be uniquely identified using as few as 3-5 peptide masses as inputs. A complete search is completed in <5 min on a VAX 8650.

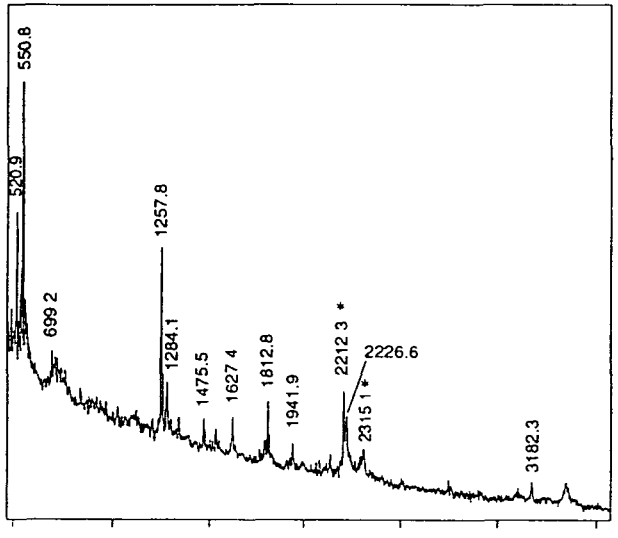

MALDI mass spectrum (above) of spot #1 from a 2-D gel after *in situ* reduction/alkylation/tryptic digestion. Peaks marked with an asterisk are fragments of trypsin that are observed in blanks. The matrix was DHB/fucose. Data were acquired with a Vestec LaserTec ResearcH mass spectrometer using a 337 nm nitrogen laser. The amount loaded on the MALDI probe was estimated to be 75 fmol. The mass range input for the protein was 0.5-45 kDa, based on the SDS-PAGE mass markers. A single protein match was found in the database (Cysteine synthetase *a* from *E. coli*, M_r 34,358). The measured masses input to the program FRAGFIT and the matched sequences are given below.

mass	Δ	sequence from database
1257.8	-0.3	ALGANLVLTEGAK
1284.1	-0.4	NIVVILPSSGER
1475.5	+0.9	VIGITNEEAISTAR
1627.4	-0.5	IQGIGAGFIPANLDLK
1812.8	-0.3	IFEDNSLTGHTPLVR
1941.9		not found

References:
1. Köster, C.; Castoro, J.A.; Wilkins, C.L. *J. Am. Chem. Soc.* **1992**, *114*, 7572-7574.
2. Billeci, T.M.; Stults, J.T. *Anal. Chem*, **1993**, in press.
3. Wong. S.; Grimley, C.; Padua, A.; Bourell, J.H.; Henzel, W.J. in *Techniques in Protein Chemistry IV*, R.H. Angeletti, Ed., Academic Press: San Diego, **1993**, in press.
4. Henzel, W.H.;Stults, J.T.; Watanabe, C. *Presented at the Third Symposium of the Protein Society, Seattle, WA*, **1989**.
5. Henzel, W.H.; Billeci, T.M.; Stults, J.T.; Wong, S.C.; Grimley, C.; Watanabe, C. *Proc. Natl. Acad. Sci. USA*, **1993**, *90*, in press.

An investigation into the advantages offered by an array detector on magnetic sector instrumentation for different ion sources.

R.H. Bateman[1], A.D. Birchenough[1], R.S. Bordoli[1], A.M. Phillips[1], R.G.Vickers[1] and A.R. Woolfitt[1] and D.J. Harvey[2].

[1], VG Analytical, Fisons plc, Floats Road, Wythenshawe, Manchester, M23 9LE, UK; [2]Glycobiology Institute, Department of Biochemistry, University of Oxford, South Parks Road, Oxford, OX1 3QU, UK.

Introduction

Electrospray ionisation (ESI) and matrix assisted laser desorption ionisation (MALDI) are currently preferred ionisation techniques for large molecules. ESI achieves high mass by multiple charging, to give a spectrum that typically appears below 2500 Da. Ion beams are usually weak but, as the noise level is low, the benefits of increased ion collection offered by a multichannel array detector should enable the sample quantity to be substantially reduced.

The MALDI technique is somewhat different in that intermittent bursts of predominantly singly-*charged ions are produced following each laser pulse and, to date, it has not been considered* appropriate to use this ion source with a scanning mass spectrometer. Time of flight (TOF) mass spectrometers are generally preferred but suffer the disadvantage of poor resolution. Even with a reflectron, mass resolution is typically not greater than 2000 (FWHM) An array detector with a mass range of 20% (1.2:1) also appears to offer a solution to the combination of MALDI with a magnetic mass spectrometer for applications up to about 10,000 Dalton. This detector will allow a decade in mass to be covered with 13 separate exposures and multiple laser pulses may be used for each exposure to improve the ion statistics

Experimental

The mass spectrometer used in this work was an AutoSpec-FPDQ (VG Analytical, Fisons plc, Manchester, UK) having E_1BE_2 geometry and a mass range of 5000 Dalton at 8 keV. An inhomogeneous field ESA mounted between B and E_2 allows the beam to be diverted onto a 50 mm microchannel plate (MCP) array detector optically coupled to a 2048 channel photo - diode array. The dispersion of the inhomogeneous ESA and array detector can be adjusted to give 1.2:1 mass ratio at 2000 resolution (FWHM) to 1.07:1 at 5000 resolution.

A 337 nm pulsed (4 nsec, 180 μJ/pulse, repitition rate 20 Hz) nitrogen laser (VSL-337i, Laser Science Inc., Cambridge, MA, USA,) was mounted horizontally above the ion source housing The laser beam was focused by a lens and reflected by an adjustable mirror, downwards through a sapphire window into a standard AutoSpec FAB source with a thin stainless steel strip (6 mm x 1.5 mm) as the sample stage. Two micrometer drives on the adjustable mirror were used to steer the beam around the sample surface to find the optimum production of signal. During acquisition, typically 1 second duration exposures were taken with the laser synchronised with the acquisition cycle so that between exposures the laser was not firing

Oligosaccharide samples (100 pmol) were mixed with 2,5-dihydroxybenzoic acid (2,5-DHB) (1 μl, 50 μM) on the laser target probe. α-Cyano-4-hydroxycinnamic acid was used for peptides. The samples were allowed to evaporate to dryness in air before loading into the mass spectrometer. Samples from 2,5-DHB were further crystallised from ethanol on the target.

Results and Discussion

ESI with continuous sample infusion was used to allow a direct comparison of the detection efficiency of the array and a conventional point detector using serial dilutions of hen egg lysozyme. The scan time was adjusted to be the same for both acquisition modes. For sample consumptions down to about 200 fmol, both the point and array detectors gave useful data although the ion statistics were always better from the array detector. Below 200 fmol, the point data rapidly deteriorated so that at about 50 fmol the signal to noise was about 1:1. Use of the array detector allowed the sample consumption to be further reduced. At about 12 fmol, the array data were superior to that from the point detector at 230 fmol. Even at 1.2 fmol sample consumption the array data were quite usable with a signal to noise of better than 5:1 .

The array detector produced good spectra of peptides and oligosaccharides using MALDI. Both resolution and signal:noise ratio were superior to that from a TOF instrument as shown by the spectrum of released *N*-linked oligosaccharides from ovalbumin (Fig. 1). High resolution was used to confirm the *absence* of the high mannose oligosaccharide $(man)_9(GlcNAc)_2$ ($[M+Na]^+$ 1905.7 Da) from the peak in Fig. 1 at m/z 1909.1 (shown inset in Fig.1). This peak was produced by $(Hex)_4(HexNAc)_6$ ($[M+Na]^+$ 1907.7 Da, average mass 1908.7 Da). This differentiation would not have been possible with a lower resolution TOF mass spectrometer. Detection limits (5:1 S/N ratio) were 5 fmol for the peptide renin substrate ($[M+H]^+$ 1758 9 Da) and 200 fmol for a typical *N*-linked biantennary oligosaccharide $[(Gal)_2(GlcNAc)_4(Man)_3(Fucose)]$ ($[M+Na]^+$ 1809.6 Da).

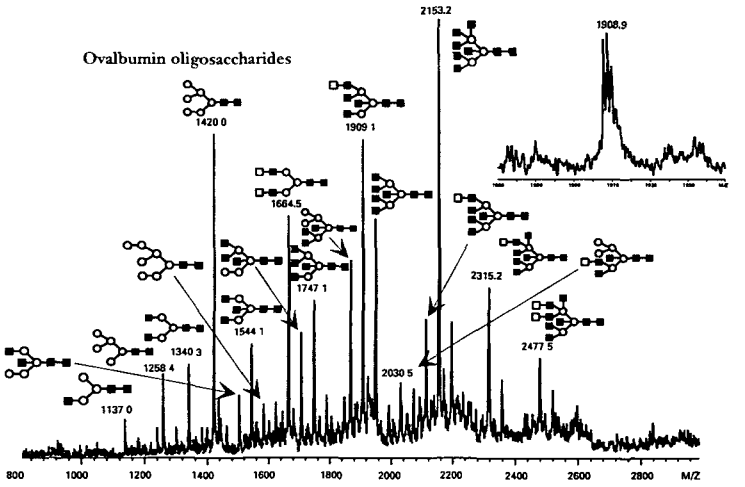

Fig. 1. MALDI spectrum of *N*-linked oligosaccharides released from ovalbumin.

COMPARISON OF FIELD DESORPTION AND MATRIX ASSISTED LASER DESORPTION IONIZATION OF AN INDUSTRIAL OLIGOMERIC ADDITIVE

Kenneth Ng, B. Piatek, C. Shimanskas

Analytical Research Department, Ciba-Geigy Corporation, Saw Mill River Rd., Ardsley, NY 10502

Field desorption is still the technique of choice among many of the available soft ionization techniques to characterize industrial polymers. Since the advent both in its improved performance and cost, matrix assisted laser desorption ionization (MALDI) has been recognized as an alternative to characterize such polymers.

Gel permeation chromatography (GPC) and nuclear magnetic resonance (NMR) are complimentary to one another when used in tandem to characterize these polymers but mass spectrometry is a far more superior analytical technique since it can simultaneously provide molecular weight distribution, both M_w and M_n and structural information during the same analysis. Its only weakness is found in the limitation of handling of many extreme high moleuclar weight polymers.

The objective of this paper is to investigate the usefulness of MALDI in characterizing industrial oligomers of medium molecular weight. Five batches of a commercial light stabilizer (Structure I) whose average MW is usually < 5000 daltons were used in this investigation using both FD and MALDI techniques and their spectra were compared. The FD and MALDI spectra from an identical sample are shown as I and II. Results indicated that both FD and MALDI are useful to provide both molecular weight information as well as specific structural information of this type of compounds. This information can be extracted from the same analysis. Many different oligomeric series were discovered during these analyses. The structures of such series were based on their unique molecular weights as represented by either the M^+ or M^+H ions. The structures of the end capping groups, R and R_1 of series had been tentatively assigned. Some significant differences were observed between the two techniques. While FD can generally provide higher ionization efficiency for the higher molecular weight species, it lacks consistency to reproduce spectra from the same sample thus making batch comparison impossible. On the other hand, since the final spectrum of a MALDI experiment which is the composite of many spectra depending on as many laser shots as being rastered across the sample, the MALDI technique is more likely to reflect the sample characteristics as a whole or at least portion of the sample which ionizes.

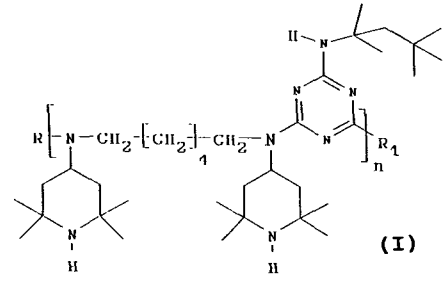

(I)

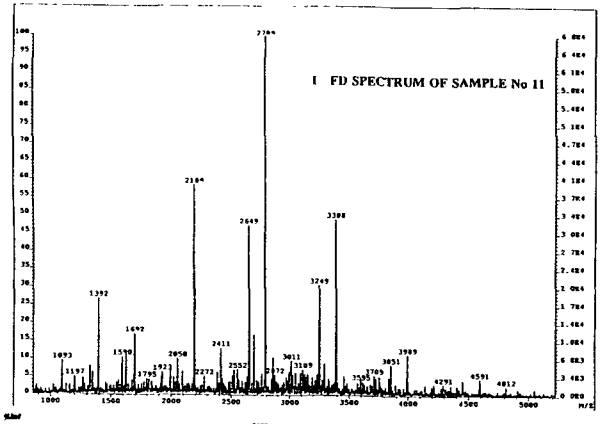

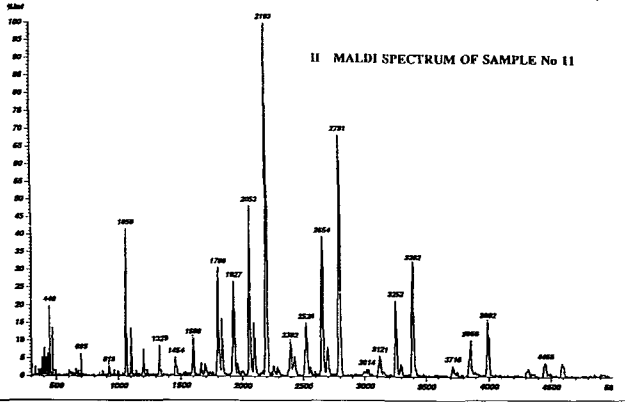

DIRECT MALD MS ANALYSIS OF PROTEASE DIGESTS: COMPARATIVE STUDY OF ANALYSIS PARAMETERS

Paolo Lecchi and Richard M. Caprioli
The Analytical Chemistry Center and the
Department of Biochemistry and Molecular Biology
University of Texas Medical School, Houston, Texas 77030

Introduction

Analysis of biological molecules by MALD MS (1) provides high sensitivity, a wide mass range, relatively facile sample preparation, and short analysis times. For purified peptides and proteins, this technique is quite successful. However, for complex mixtures of samples, application of the technique is more complex.

We have applied MALD MS to the analysis of tryptic digests of proteins up to the 40,000 da. range. Analysis parameters considered were instrument resolution, laser power, m/z scale calibration, choice of matrices, sample concentration, sample preparation, and, overall, mass assignment accuracy. The objective of this work was to assess the value of MALD MS to the protein chemist for the analysis of tryptic digests. Basically, how complete an analysis can be achieved with reasonable care and what instrumental parameters are critical to the analysis? How effective would the technique be in the analysis of a protein of unknown sequence?

Experimental

A Vestec LaserTec benchtop MALD mass spectrometer was used to obtain the spectra shown here. It employs a N_2 laser, 1.2 meter flight tube, and was operated at 26 kv accelerating voltage. The windows version of LABCALC was used for data analysis. Typically, 30 spectra were averaged to obtain spectra.

The matrix compounds (2-6) were prepared in 0.1 M concentrations in a solvent containing 70% acetonitrile, 30% water, and 0.1% trifluoroacetic acid In the case of DHB acid and fucose, a 98:2 water/acetonitrile containing 0.1 trifluoroacetic acid solvent was used (7). Approximately 1.2 μL of matrix solution is mixed on the target with 0.8 μL of sample solution containing 1 pmol/μL of peptide or protein and the sample allowed to dry.

Matrices used in this study were; sinapinic acid (SA), α-cyano-4-hydroxycinnamic acid (α-CCA), ferulic acid (FA), caffeic acid (CA), dihydroxybenzoic acid (DHBA) plus fucose, and 6-aza-2-thiothymine (ATT).

Results

Instrument calibration: Both external standards (separate analysis of standard peptide mixture) and internal standards (peptide standards added to digest) were used. Generally, potassium (m/z 39) and mellitin (m/z 2848.5) were used as mass standards External standard calibration typically provided ± 0.2% mass assignment accuracy, with some cases showing a constant direction of the error (i.e., 0.2% high or low). Optimal calibration was achieved using added internal standards, typically giving ± 0.03% accuracy.

Effect of laser power: For a number of digests, the laser power was varied from 30% to 80% (relative) power. Spectra were compared from the same sample loading, typically 2 pmol total. Altering the power does not appear to significantly change the relative intensities of the fragments observed. It will, however, be advantageous to change laser power depending on the matrix used so as to minimize interfering peaks from this matrix at low mass.

Background interference: All matrices show significant background up to about m/z 600 with laser power sufficient to produce peptide signals. DHBA gave the least interference, although it was typically not the best matrix for the analysis of tryptic digests. At higher laser power, all matrices gave significant background up to (and beyond) m/z 1000.

Effect of sample concentration: The RELATIVE intensities of peaks in the MALD spectrum may change depending on the concentration of the sample. In some cases, peaks not observed at higher sample loading (e.g., > 5 pmol) can be observed at lower loading (e g., 0.5-1 pmol). The opposite can also occur, perhaps due to different amounts of fragments present.

Choice of matrix: Of the several different matrices used in this study, we found αCCA to be most generally useful, and DHBA + fucose to be especially advantageous in the low molecular weight range (< 1000 da). However, no one matrix provided the identification of all of the fragments in the several digests used here. Generally, 60-80% of the fragments could be seen with most matrices, although the specific fragments identified were not the same for each.

Summary and Conclusions

One can consider two kinds of applications for the MALD MS analysis of protease digests:

A) Survey analysis: In this case, the analytical task is not critical in that not all fragments are required to be identified and mass assignment accuracy need only be approximate.
A single matrix can be used (usually, αCCA is a good choice) with 1 pmol of digest. Typically, external calibration is sufficient, giving ± 0.3% mass assignment accuracy and identifying 50-75% of the fragments present. Total time can be expected to be 30 min or less.

B) Optimal performance: In this case, the analytical task is to identify all fragments at high mass accuracy. We recommend; i) use of several matrices (e.g., αCCA, DHBA + fucose, SA, ATT, FA), ii) use several concentrations with the 'best' matrices for the sample (e.g., 8, 1, and 0.5 pmol loaded), iii) acquire data using several laser power levels, and iv) use of internal standards for calibration. Under these conditions, 90-100% of the fragments can be expected to be found, with ± 0.03% mass assignment accuracy. However, an analysis time of many hours would be anticipated for a single digest.

References

1. M. Karas, D. Bachmann and F. Hillenkamp, (1985) Anal. Chem. 57, 2935.
2. R.C. Beavis and B.T. Chait (1989) RCM 3, 432.
3. R.C. Beavis, T. Chaudhary and B T. Chait (1992) OMS Lett. 27, 156
4. K. Strupat, M. Karas, F. Hillenkamp (1991), Int. J. Mass Spec. Ion Phys. 111, 89.
5. P. Juhasz, C.E. Costello and K Biemann (1993), JASMS 4, 399.
6. P. Juhasz, I.A. Papayannopoulos, C. Zeng, V. Papov and K. Biemann (1992) Proc. 40th ASMS Conference on Mass Spectrometry, pg. 1913.
7. T.M. Billea and J.T. Stults (1993) Anal. Chem. 65 (In press).

Acknowledgement

The authors acknowledge the NIH (Grant #GM 43783) for partial support of this work. We also thank P. Bianco (Dept. of Biochemistry, University of Texas, Houston) for providing RecA, and John Stults (Genentech) for recombinant human growth hormone.

Identification of the Facile Gas-Phase Cleavage of the Asp-Pro Peptide Bond in MALD-TOF MS

W. Yu, J.E. Vath, M.C. Huberty, S.A. Martin, H.A. Scoble
Genetics Institute, Inc. One Burtt Road, Andover, MA 01810 USA

Abundant ions corresponding to the gas-phase cleavage of the Asp-Pro bond of peptides in the process of matrix assisted laser desorption were observed using a time-of-flight mass spectrometer (Bruker REFLEX) equipped with both linear and reflector mass analyzers. Peptides containing the N-terminal sequence, Asp-Pro... from an endoproteinase Asp-N digest yielded one peak in the molecular ion region in the linear mode and two equally abundant peaks in the reflected mode TOF mass spectra. The lower molecular masses in the reflected mass spectra could be eliminated by removing the Asp residue or derivatizing its side chain carboxyl group. The observed mass differences did not correspond to any amino acid, however, by lowering the potential of the reflector to correct for the energy loss the mass difference was determined to be 115 daltons, i.e. Asp. These results were compared with those obtained using a JEOL HX110/HX110 tandem mass spectrometer in the MS/MS mode of operation without and with a collision gas. These data suggest the Asp-Pro peptide bond is more labile than other peptide bonds in the gas phase and decays after full acceleration but prior to entering the reflector.

The gas-phase mechanism for this decomposition was derived by obtaining the reflected mass spectrum (Figure 1) of a peptide, whose sequence is listed below, which contains two internal Asp-Pro bonds.

AIPSSDPASVSPHQPLAPSMAPVAGLTW	28	*3B, 7-55, m/z 4935.4*
EDSEGTEGSSLLPGEQPLHTVDPGSAK	55	*3A, 1-50, m/z 5065.5*

The reflected mass spectrum exhibits an abundant peak at *m/z* 5506.4 corresponding to the intact molecular mass of the peptide and two additional abundant peaks at *m/z* 5028.8(3A) and 4917.0(3B). The corrected masses for these two peaks, *m/z* 4935.7(3B) and 5047.7(3A) were obtained by lowering the potential of the reflector. The mass observed for 3B agreed with the expected mass for cleavage of the first Asp-Pro bond with charge retention on the portion containing the proline (see above). The mass corresponding to 3A was 18 daltons less than expected for cleavage of the second Asp-Pro bond with charge retention on the portion containing the new C-terminal aspartic acid (see above). These data support the mechanism shown in the upper left corner of Figure 1.

An application of the specific cleavage of an Asp-Pro bond in a peptide is illustrated with a composite reflector mode spectrum of an asialo O-linked glycopeptide from rhIL-12 (Figure 2). This spectrum is obtained by varying the reflector potential from 30 kV to 5 kV in several steps. The two most abundant peaks in this spectrum correspond to the cleavage of the Asp-Pro bond with a distribution of fragment ions corresponding to the N-terminus (b_9, 1338) and the C-terminus (y_{23}, 2686) of the molecule. The mass of the b_9 peak corresponds to the the peptide backbone and one unit each of HexNAc and Hex. In addition to this ion the are two lower mass fragment ions at *m/z* 1175 and 974 which differ in mass form *m/z* 1338 by 163 and 364 daltons, respectively, which corresponds in mass to the loss of Hex and HexNAcHex. These data as well as the observation of the loss of 364 daltons from the molecular ion suggest that there is an O-linked carbohydrate at Thr^7 of this peptide.

We have also observed the cleavage of 10 of 11 Asp-Xxx bonds in *E.coli* Thioredoxin (*m/z* 11674) with less than 2 pmol of material. These were the only major fragments observed suggesting that the cleavage of the Asp-Pro bond is a subset of a more general pathway of cleavage of Asp-Xxx bonds.

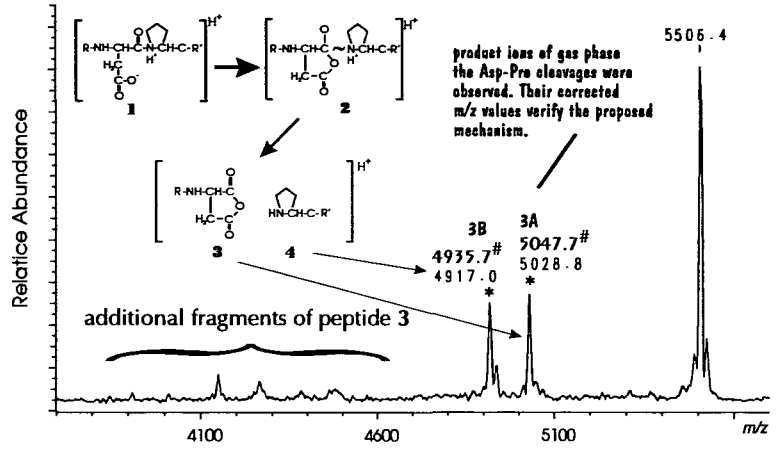

Figure 1. Gas phase cleavages of internal Asp-Pro bond of a peptide are observed in its reflector mode MALD-TOF mass spectrum. The proposed mechanism for such cleavages is shown in the upper left corner. (#: corrected m/z values)

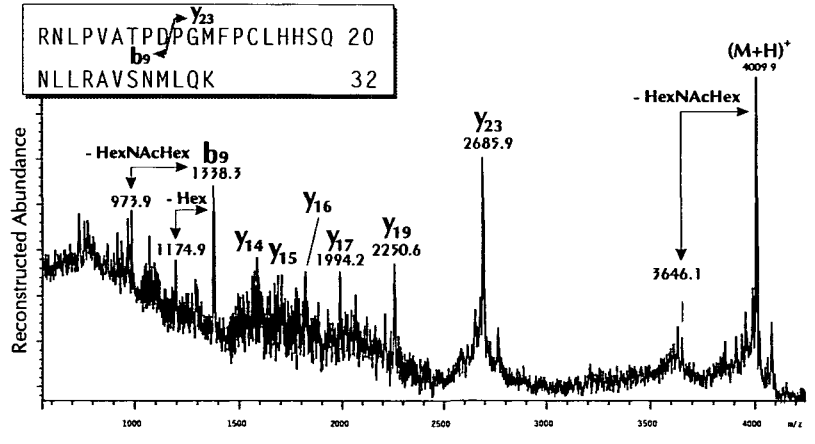

Figure 2. A composite reflector mode MALD-TOF mass spectrum showing the Asp-Pro cleavage (y23 and b9) and other fragment ions for an asialo O-linked glycopeptide isolated from the Achro-K map of the rhIL-12 protein.

MALDI on a Magnetic Sector Mass Spectrometer Equipped with an Integrating Array Detector

R. B. Cody*, J. W. Finch, J. Tamura, and B. D. Musselman
JEOL USA, Inc.
11 Dearborn Rd., Peabody, MA 01960

A commercial matrix-assisted laser desorption ionization (MALDI) source was developed for the JMS-HX110 forward-geometry double focusing mass spectrometer equipped with a "zoom" array detector and quadrupole doublet ion optics. This report describes some of the preliminary results obtained by using the MALDI source.

Experimental A Laser Science Inc. model VSL-337ND laser was used to irradiate the target. This laser operates at 337 nm with a maximum pulse energy of 400 mJ. Beam attenuation and focusing was accomplished by using a dichroic mirror and lens assembly, and visualization of the target surface was made possible by using a CCD camera and video display.

Dihydroxybenzoic acid (DHB) was found to provide the best results as a matrix for laser desorption although mass spectra can also be obtained by using sinapinic acid (SA). The DHB matrix seems to provide a stronger ion signal and the signal persists for a larger number of laser shots than when SA is used as the matrix. Addition of a small amount of ammonium acetate increased the sensitivity for nucleosides detected in the negative-ion mode.

Discussion The results show good mass accuracy (roughly 0.01% without internal calibrant) and resolution (up to 4500 at 5% dispersion). Mass spectral segments can be obtained with a single laser shot, but the best results are obtained by accumulating several laser shots and moving the target during acquisition of successive segments. Although the mass range is substantially less (14,500 at full 10 kV accelerating voltage) than that obtained with time-of-flight systems, the MALDI/sector combination may be useful when good mass accuracy and resolution are needed for small-to-medium sized molecules, or when it is desired to examine a small analyte in the presence of matrix interferences.

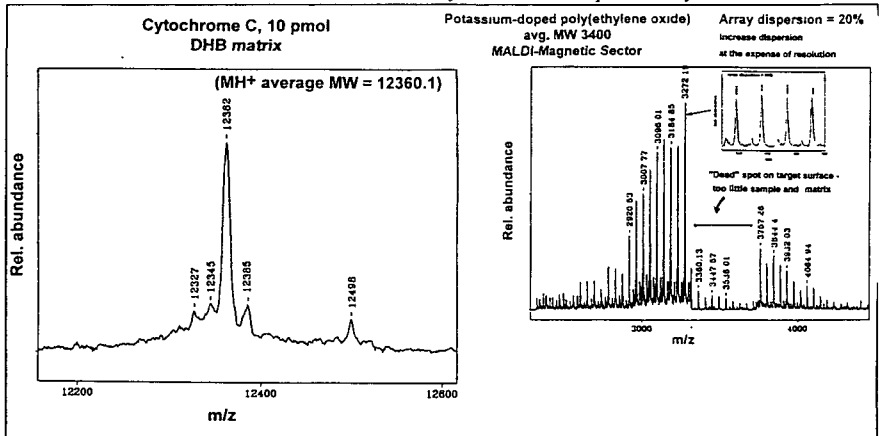

NEGATIVE IONS
Adenosine triphosphate, disodium salt

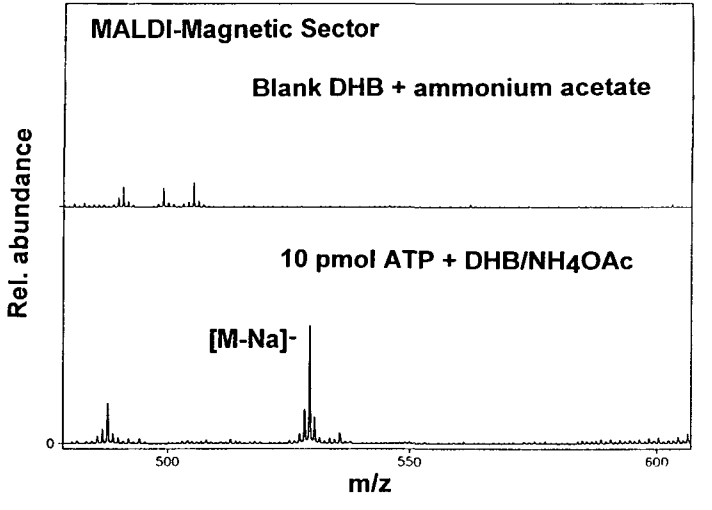

Addition of ammonium acetate improves sensitivity

An Improved Illumination System for Matrix-Assisted Laser Desorption

Ronald Beavis
Department of Physics, Memorial University of Newfoundland
St. John's, Newfoundland
Canada A1B 3X7
beavis@newton.physics.mun.ca

A linear time-of-flight mass spectrometer was described that has a constant field extraction/acceleration ion source and a sensitive detector with no post-acceleration. The ion source had an open geometry, but a rigid orientation alignment system for the sample, to minimize missalignment of the sample with respect to the detector.

This instrument was used to test configurations of laser illumination optics, in an effect to minimize the undesirable effects of using a gas laser (N_2) with a large beam divergence and an inhomogeneous beam fluence profile. The most stable protein ion signals were produced using a Newtonian telescope as a beam collimator/spatial filter, folllowed by a minimum-deflection Fresnel reflection beam attenuator.

The vacuum system, detector and ion source are shown in Figures 1,2 & 3, respectively. The optical system is shown in Figure 4. The "long" focal length and "large" pinhole design of the spatial filter was used because it was very easy to adjust.

The optical system results in a more stable protein ion signal (shot-to-shot), compared with using a single lens. The telescope serves as a spatial filter and allows the use of

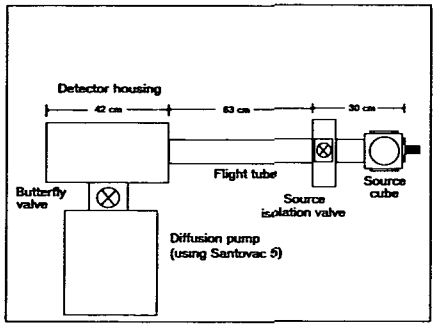

Figure 1 Vacuum system and general layout of the time-of-flight mass spectrometer.

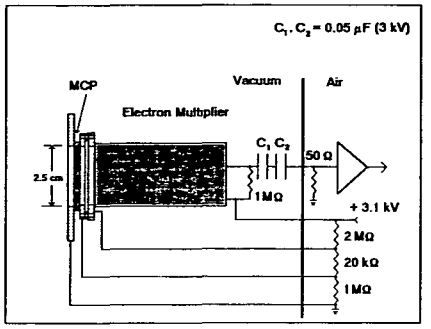

Figure 2 Zero-postacceleration protein ion detector.

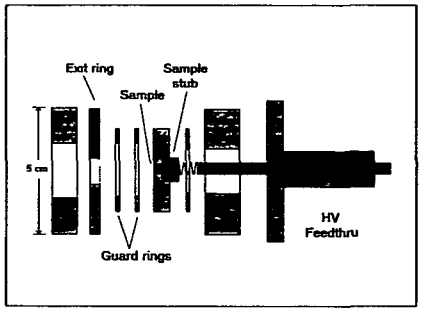

Figure 3 The laser desorption ion source electrode assembly. The ion source was operated at +30 kV on the sample and +20 & +10 kV on the guard rings.

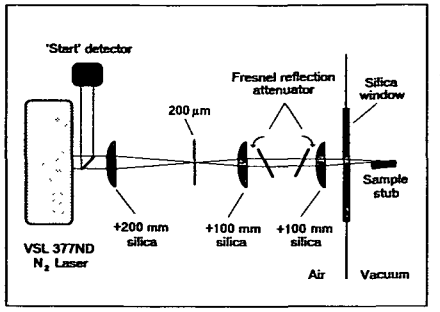

Figure 4 The illumination system of the ion source. Typical incidence angles were >80°.

smaller plates in the Fresnel relection attenuator by reducing the dimensions of the laser beam - this is particularly important at large reflection angles.

Experiments were also performed to determine the effects of raising the sample temperature above room temperature. A copper sample stub was constructed, with a spool section that was wound with 31 Ω/m nichrome wire. The stub could then be loaded with sample, inserted into the instrument and pumped down before heating.

Experiments were performed using sinapic acid. The maximum temperature that could be used was 70° C - higher temperatures produced rapid sublimation of the matrix. Heating the sample did not change the threshold irradiance meaureably. Higher temperatures irreversibly changed the molecular ion peak, by the addition of new adduct species. The peaks obtained were also wider at higher temperatures, but this effect was reversed by cooling.

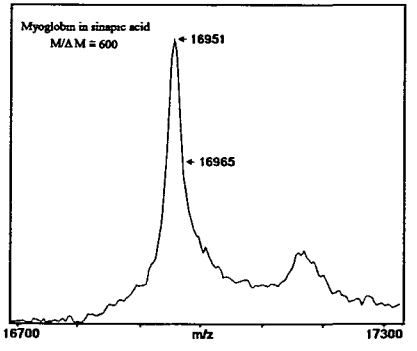

Figure 5 The molecular ion region of a mass spectrum taken using the system described above. The mass resolution is approximately 600 (FWHM).

Spatial Maps of the Polycyclic Aromatic Hydrocarbons (PAHs) in the Allende (CV3) and Bjurböle (L4) Meteorites

C.R. Maechling, S.J. Clemett, and R.N. Zare
Department of Chemistry, Stanford University, Stanford, CA 94305-5080
P.R. Buseck
Departments of Geology and Chemistry, Arizona State University, Tempe, AZ 85287

Chondritic meteorites are extremely heterogeneous. They contain various clasts and inclusions, and the matrix is composed of assemblages of submicron-sized mineral grains. Similary, the organic components of meteorites are distributed in a patchwork manner. To study the spatial distribution of PAHs on meteorite surfaces, we use a microprobe two-step laser mass spectrometer (μL^2MS) [1] with a spatial resolution of 40 µm, mass resolution of routinely 1800 for toluene (92 amu), and zeptomole (10^{-21}) sensitivity.

Meteorite surfaces are prepared for analysis by cutting interior chips of meteorite with a diamond blade saw, using a fresh supply of cold water as a cutting solvent. Checks were performed to ensure that material was not heated or redistributed across the surface. A meteorite wafer was mounted on a sample platter, and introduced into the μL^2MS instrument which is maintained at a base pressure of less than 5×10^{-8} torr. Constituent neutral molecules of the sample were desorbed with a pulsed infrared laser beam (CO_2, 10.6 µm, ca. 10^6 W/cm^2) focused through a Cassegrainian microscope objective to an analysis spot 40 µm in diameter. In a second step, 25 µs after the desorption laser pulse, PAHs in the neutral plume of desorbed material were preferentially ionized by a pulsed ultraviolet laser beam (Nd:YAG, 266 nm, ca. 10^6 W/cm^2) using 1+1 resonance enhanced multiphoton ionization (REMPI). Resultant ions were extracted from the plume and injected into a time-of-flight mass spectrometer. The output of the detector was amplified using a direct-coupled preamplifier and a filter amplifier and digitized every 2.5 ns with a digital oscilloscope. For the PAH mapping studies, five-shot averages were recorded for a spot followed by translation of the sample by 50 µm. After a sample was analyzed, the infrared laser power was increased and position indicators were burned into the surface producing laser-fused beads of the meteorite silicate matrix. These indicators were used to position the sample in the scanning electron microscope (SEM) at Arizona State University.

Previous studies on Allende of the distribution of PAHs were performed *ex situ* [2] and the results were consistent with a study of the spatial distribution of elemental carbon [3]. PAHs occur most abundantly between chondrules and inclusion in the material commonly called matrix. We have performed *in situ* spatial analysis of Allende with our microprobe instrument, and can now to analyze the material surrounding the chondrules and inclusions called dust mantles. This material differs from the matrix (perhaps a remnant of the solar nebula [4]), and we find that the PAH concentrations are larger in this component than the matrix. A mass spectrum is shown for the most PAH-rich region of one of our maps. We have tried to understand our results with respect to the mineralogy of the meteoritic material by performing SEM studies with energy dispersive x-ray detection. The data are not easy to interpret, largely because the 40-µm region analyzed contains many microscopic grains. Although there is a tradeoff between sensitivity and sampling size, we intend to reduce our analysis beam size by using a 1.064 µm Nd:YAG laser beam. This smaller analysis spot size should simplify the comparison between the PAH and mineralogical distribution.

Bjurböle was studied because of its large chondrules, but the meteorite is very friable, and reasonable sample could not be prepared. Not only were we prevented from cutting flat surfaces, but all of the material in the meteorite is grey, which makes it difficult for us to know the type of features we are analyzing. A mass spectrum is shown for what is likely meteorite matrix. The PAH signal is weaker than that of Allende, but shows more high-mass components.

1. L.J Kovalenko, C.R. Maechling, S.J. Clemett, J.-M. Philippoz, R.N. Zare, and C.M O'D. Alexander, *Analytical Chemistry* **64**, 682-690 (1992).
2. R. Zenobi, J.-M. Philippoz, P.R. Buseck, and R.N. Zare, *Science* **246**, 1026 (1989).
3. C.C.A.H. Van der Stap, D. Heymann, R.D. Vis, and H. Verheul, *Proc. Lunar and Planet. Sci.* **XVI**, 3348 (1985).
4. K. Metzler, et al., *Geochim. Cosmochim. Acta* **56**, 2873 (1993).

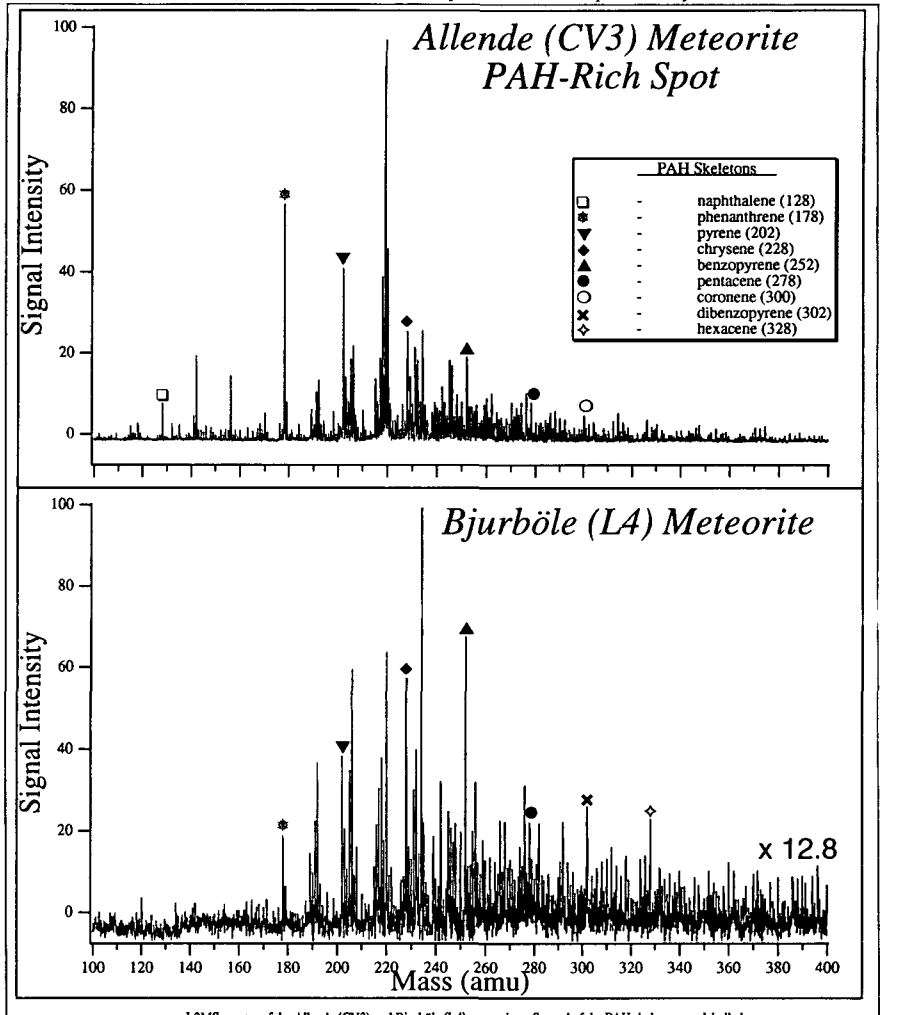

µL2MS spectra of the Allende (CV3) and Bjurböle (L4) meteorites. Several of the PAH skeletons are labelled, and alkylation series [skeleton + n*14, where n=1,2,...] for most of these skeletons are present. Bjurböle contains a smaller concentration of PAHs (scaling factor in lower right of spectrum), but more high-mass components, which is consistentent with its longer exposure to higher temperatures.

Analysis of Polycyclic Aromatic Hydrocarbons (PAHs) in Cosmic Dust

S.J. Clemett, C.R. Maechling, and R.N. Zare
Department of Chemistry, Stanford University, Stanford, CA 94305-5080
P.D. Swan and R.M. Walker
McDonnell Center for the Space Sciences, Physics Department, Washington University, One Brookings Drive, St. Louis, MO 63130-4899

We report the first definitive measurements of specific organic molecules (PAHs) in interplanetary dust particles (IDPs). An improved version of our microbeam-two-step laser mass spectrometer (μL^2MS) [1,2] was used for the analysis. The instrument has a spatial resolution of 40 µm, a mass resolution routinely 1800 for toluene, and zeptomole (10^{-21}) sensitivity.

The upper atmosphere provides an excellent source of cosmic dust, and particles 2-50 µm in diameter are collected from the stratosphere (ca. 20 km) on "flags" mounted on the wings of NASA's high altitude U-2 aircraft [3]. These are later examined in a clean room and particles of interest are removed for further analysis. Extraterrestrial origin is identified by chondritic elemental abundance, that is, similar to class of meteorites referred to as carbonaceous chondrites. In addition isotopic measurements using a modified Cameca IMS-3F ion probe [4] reveals some IDPs to have large isotope anomalies in D/H and $^{15}N/^{10}N$.

The instrument used for the organic analysis is a two-step laser mass spectrometer. In the first step, constituent neutral molecules of the sample are desorbed with a pulsed infrared laser beam (CO_2, λ=10.6 µm) focussed through a Cassegrainian objective to an analysis spot 40 µm in diameter. In the second step, separated both spatially and temporally, PAHs in the desorbed plume of neutrals are preferentially ionized by a pulsed ultraviolet laser beam (frequency quadrupled Nd:YAG, 266 nm) using a (1+1) resonance enhanced multiphoton ionization scheme. Resultant ions are then extracted from the desorbed plume and injected into a reflectron time-of-flight mass spectrometer.

The samples studied were in the form of small, micron sized fragments of original particle that had been pressed into a thin wafer of single crystal KBr. Remaining fragments of the particle were studied by other techniques to gain information on particle morphology, elemental abundances, mineralogy, and isotopes (C, N, and H). The particle fragments were located in the μL^2MS system using sighting markers scribed on to the KBr. Single-shot time-of-flight spectra of each particle were recorded, stored in a computer, and later calibrated and co-added. A minimum of twenty spectra were recorded for each particle, and spectrum acquisition was continued until the signal became indistinguishable from background, this number varied from particle to particle.

A total of seventeen stratospherically collected particles, eight of which are classified as IDPs, seven of which are classified as probable terrestrial contaminants, and two of which have uncertain origins were studied. A rich distribution of PAHs were obtained on two of the eight IDPs, Aurelian (U47-M1-2a) and Florianus (U47-M1-3a), the spectra in each case were similar. Both particles are certainly extraterrestrial; each has a chondritic elemental spectrum and both have large deuterium enrichments (up to $\delta D = 771 \pm 85‰$ for Aurelian and $\delta D = 1120 \pm 100‰$ for Florianus), and in addition Florianus has one of the largest ^{15}N anomalies ever observed ($\delta^{15}N = 441 \pm 20‰$).

The μL^2MS result for Aurelian is shown in figure 1, laser shots made at locations on the KBr mount 100 µm away from the IDP gave integrated signal intensities of less than 3% the value for Aurelian and showed no evidence of PAHs. The spectrum is characterized by three mass envelopes, one near 60 amu, one at moderate mass peaking at 250 amu, and one at high mass peaking at 370 amu. The low mass envelope contains inorganic species such as Na, K, Al and KBr cluster ions which are easily ionized by the UV beam, as well as traces of hydrocarbon fragments (C_4H_x - C_9H_x). It is unlikely that these fragments are decomposition products of PAHs and are attributed to decomposition of other species in the desorbed plume. The moderate and high mass envelopes contain clear signatures of PAHs and there alkylated derivatives, as indicated by sequences of peaks separated by 14 amu as a consequence of the successive addition of methylene (-CH_2-) groups to the PAH skeletons. The virtual absence of low mass PAHs such as alkylbenzenes, alkylnaphthalenes and alkylphenathrenes is consistent with the evaporation of these more volatile, lower mass organic components from an IDP during prolonged exposure in space, as well as loss by heating during atmospheric entry. The distribution of high mass PAHs in the high mass envelope is striking and has not be observed by us before in any other extraterrestrial material we have analyzed which have included, acid residues, meteorites and Antarctic micrometeorites [1,5,2,6].

Due to the zeptomole sensitivity of μL^2MS coupled with the wide scale distribution of PAHs in the terrestrial environment, extensive contamination and blank experiments were performed in order to prove that the observed molecules are not terrestrial contaminants. The silicone oil from the collector panels, materials used in particle selection and curation and samples of lab air were analyzed. All gave no PAH signals. Additional study of terrestrial contamination particles which had

been exposed to the same collection and mounting procedures gave either spectra devoid of PAHs or spectra markedly different to either Aurelian and Florianus.

In conclusion we have demonstrated the application of μL^2MS to the trace organic analysis of micron sized particles with zeptomole detection limits, and have applied this to the organic analysis of cosmic dust. To the extent that IDPs may represent the most primitive materials in the solar system, continued studies of the type described here can be expected to better elucidate the nature of the original organic materials in the solar system. These issues are now amenable to study due to the very high sensitivity and specificity of μL^2MS.

Fig. 1 Analysis of Interplanetary Dust Particle Aurelian

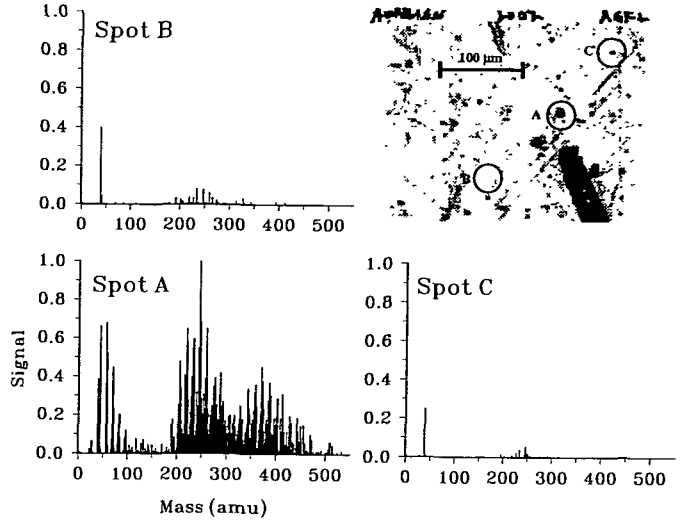

[1] L.J. Kovalenko, C.R. Maechling, S.J. Clemett, J.-M. Philippoz, R.N. Zare, and C.M.O'D. Alexander, *Analytical Chemistry* **64**, 682-690 (1992).
[2] R. Zenobi, J.-M. Philippoz, P.R Buseck, and R.N. Zare, *Science* **246**, 1026 (1989).
[3] D.E. Brownlee in *Cosmic Dust*; J.A.M. Mc Donnell, ED; Wiley and Sons, 1978, pp. 295
[4] K.D. McKeegan, R.M. Walker, and E. Zinner, *Geochimica Cosmochimica Acta* **49** (1985).
[5] S.J. Clemett, C.R. Maechling, R.N. Zare, and C.M.O'D. Alexander, *23rd Annual Lunar and Planetary Sciences Conference*, Houston, TX, March 16-20, 1992.
[6] C.R. Meachling, S.J. Clemett, R.N. Zare, *40th ASMS Conference on Mass Spectrometry and Allied Topics, Washington*, DC, May 31 - June 5, 1992.

LASER DESORPTION STUDIES OF OXIDATIVE DECOMPOSITION IN K_3C_{60}

C.J. Harper, D.C. Sherrod, D.C.Jurbergs, J.T. McDevitt and D. A. Laude, Jr.
Department of Chemistry and Biochemistry, The University of Texas at Austin, Austin, TX, 78712

The development of fullerenes as high temperature superconductors has caused a need for study of their structures, bulk properties and reactions. In particular, K_3C_{60} exhibits excellent superconducting properties; however, when exposed to ambient air or water, K_3C_{60} undergoes rapid decomposition with consequent loss of conductivity. Careful study of this decomposition process is essential to any practical application of fullerene-derived superconductors.

The effect of the K_3C_{60} decomposition reaction on conductivity has been thoroughly investigated. A resistivity of 10^4 ohms is characteristic of K_3C_{60} before exposure to air or water; however, after decomposition, the resistivity is often 10^{10} ohms or more. It also is found that the decomposition occurs faster when exposed to water vapor than when exposed to air or O_2[2].

Some researchers report that the carbon-based product of decomposition is solely C_{60}. Specifically, Haddon, et. al.[1] have noted from Raman studies that after K_3C_{60} is exposed to air and water that the molecular line of C_{60} (1467cm^{-1}) is restored, suggesting that the potassium doping process is reversible with respect to C_{60}.

Eq. 1 $\quad 3K(g) + C_{60}(s) \longrightarrow K_3C_{60}(s)$

Eq. 2 $\quad K_3C_{60} \xrightarrow{\text{Air \& } H_2O} C_{60} + \text{potassium species}$

However, contradictory evidence exists to suggest that this may not be a solely reversible process (Eqs. 1 and 2) and that C_{60} is not the only decomposition product. For example, although C_{60} is highly soluble in toluene, the decomposition products of K_3C_{60} are not. Nor are the products soluble in water. Additionally, the infrared spectrum of the decomposition products differs from that of C_{60} in that it contains a broad absorption band at 1620 cm^{-1}. These differences between IR spectra cannot be attributed to species such as KOH or $C_{60}O$.

In an effort to reconcile these inconsistencies, laser desorption Fourier transform ion cyclotron resonance (LD/FTICR) was used to generate mass spectra of K_3C_{60}, decomposed K_3C_{60}, C_{60} with KOH added and unadulterated C_{60}. These spectra were used to determine whether the decomposition reaction occurs as bulk or surface phenomenon.

In order to fully examine the various compounds to be compared, several experimental parameters were varied. For example, the laser power density was adjusted to three different levels; 2.2×10^7 W/cm^2 (low), 1.1×10^8 W/cm^2 (medium) and 2.3×10^8 W/cm^2 (high). This was done to distinguish between ions desorbed thermally from the sample and species which were formed in the plasma. Additionally, the trapping voltages were varied at positive and negative potentials of 1V, 3V and 5V in order to capture ions of different kinetic energies.

Samples of C_{60} were prepared by J. T. McDevitt's group (University of Texas). Sandblasted, stainless steel probe tips were first cleaned in both methanol and in deionized water. Next, a 60%/40% mixture of gold and palladium was sputtered onto the tips. The C_{60}, purchased as soot from Texas Fullerenes, was extracted with toluene and then sublimated onto the probe tips. To dope samples with potassium, the C_{60} covered probe tips were suspended above a pool of potassium which was heated to evolve potassium vapor.

Comparison of the spectra of the various compounds gave interesting results. For example, studies of the unreacted K_3C_{60} samples showed that it produces small amounts of ions regardless of the experimental conditions used; however, the decomposed sample yields ions in large abundances. Also, a comparison of the decomposed sample and C_{60} yielded two

main differences between the spectra from these samples. First, the C_{60} sample did not generate any ions at the low power density. Lastly, eventhough sample deposition was conducted simultaneously, the decomposed sample generated many ions after 10 firings on the same position; however, C_{60} did not yield ions after 3 or 4 shots on the same position.

It might be expected that as K_3C_{60} decomposes, positive potassium ions would be produced; therefore, the KOH mixed C_{60} sample was used as a control for potassium ions in the sample which might effect the laser desorption spectra. Upon comparison of the decomposed K_3C_{60} and C_{60} - KOH mix, it was determined that the decomposed sample yielded few positive ions.

The depth profiling studies, which were conducted at the three different laser power levels, did not show any difference between the surface and bulk material. Therefore, the decomposition seems to be a bulk phenomenon. It should be noted, however, that sample thicknesses were on the order of 2000 to 5000 agstroms.

The mass spectra of the K_3C_{60} decomposition products yielded ions of C_{60} and C_{70}. The presence of C_{70} is due to incomplete purification of the C_{60}. There were no spectra which indicated a C_{60} species with heteroatoms such as oxygen attached. Nor were there any indications that the fullerene molecules were broken apart. There were also no potassium-attached C_{60} ions detected within this experiment, suggesting that the association of the potassium with the C_{60} is a weak one. However, because the decomposed K_3C_{60} does not yield positive ions as readily as C_{60} or C_{60} mixed with KOH, it is suggested that the decomposition product is a reduced C_{60}. This hypothesis will be tested by comparing decomposed K_3C_{60} with electrolytically reduced C_{60}.

1. Haddon, R.C.; et. al.; "Conducting Films of C_{60} and C_{70} by Alkali-metal Doping"; *Nature*; Vol. 350; Mar 28, 1991; pp. 320 - 322.
2. Riley, D.R; Jurbergs, D.; Zhou, J.; Zhao, J.; Markert, J.T.; McDevitt, J.T.; "Environmental Reactivity of K_3C_{60} and $YBa_2Cu_3O_{7-x}$ High-Temperature Superconductor Thin Films" submitted to *Chemistry of Materials*.

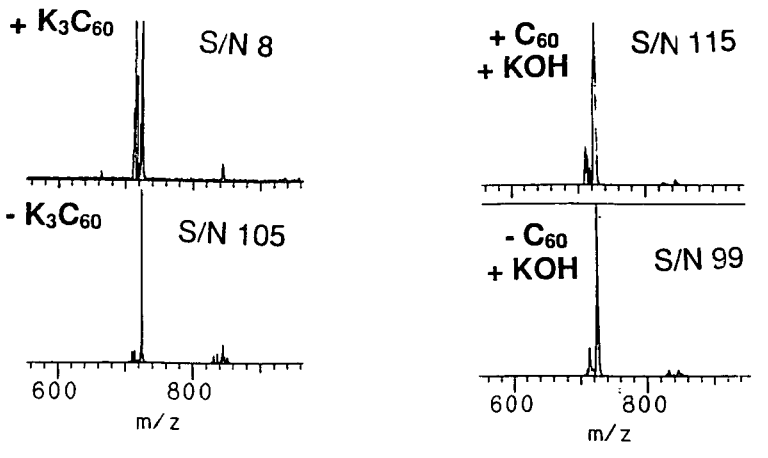

Analysis of Lipopolysaccharides from Gram Negative Bacteria using FAB and MALDI TOF Mass Spectrometry

Xiaoping L. Hronowski and Robert J. Cotter
the Johns Hopkins University, Baltimore MD;
Nilofer Qureshi and Kuni Takayama, VA Hospital, Madison WI.

Liquid Secondary Ion Mass Spectra (LSIMS) and Matrix Assisted Laser Desorption Ionization (MALDI) mass spectrometry have been employed for structural identification of two strains of lipopolysaccharides (LPS) D21f2-ReLPS and D21f1-RdLPS isolated from *Escherichia coli* K-12 mutants.

LSIMS mass spectra were obtained on a Kratos Concept 1H double-focusing electro-magnetic deflection mass spectrometer. MALDI spectra were performed on a Kratos KAMPACT MALDI III TOF instrument with a maximum laser output of 6 mw at a wavelength of 337 nm.

The LSIMS mass spectrum of D21f2-ReLPS is shown in Fig. 1. Molecular ions $(M+H)^+$ and $(M+Na)^+$ were observed at m/z 2238.2 (2238.3) and 2260.1 (2260.3) respectively. The phosphate cleavage reactions from the reducing end, cleavage of acyl-linked fatty acids and loss of KDO were observed. The major fragment ions are oxonium ions with additional losses of one KDO and two KDO units.

Two fractions separated by HPLC from D21f1-RdLPS were methylated. The samples were characterized using LSIMS and MALDI mass spectrometry.

The LSIMS mass spectrum of penta-acylRdLPS is shown in Fig. 2. Protonated molecule ions appear as six peaks at m/z 2425.4, 2439.5, 2453.5, 2467.5, 2481.5 and 2495.5. Fragmentation results in loss of two HEP, two KDO and phosphate. Further fragmentation cleavages hydroxymyristate chain in the 3'-position. Oxonium ions, further loss of two HEP and two KDO, are major fragment ions. The MALDI spectrum of penta-acylRdLPS, as shown in Fig. 3, gives protonated molecule ions and fragment ions by loss of hydroxymyristate group.

The LSIMS spectra of hexa-acylRdLPS have a fragment partern similar to the one of the penta-acylRdLPS with masses greater by 210 units, corresponding to myristate connected to the hydroxy group on hydroxymyristate in the 3'-position. The MALDI spectrum of hexa-acylRdLPS gives protonated molecular ions and fragment ions from loss of fatty acid at the 3-position, the 3'-position, and loss of two KDO and two HEP units.

D21f2-ReLPS has a molecular weigth of 2237.2 and contains two each of glucosamines, KDO and phosphates, four hydroxymyristates, one laurate and one myristate, as shown in the Fig. 4. D21f1 hexa-acylRdLPS has a lipid A protion similar to D21f2 with two additional HEP groups connected to KDO (Fig. 4). D21f1 penta-acylRdLPS has a basic structure similar to hexa-acylRdLPS, but only has five fatty acid chains.

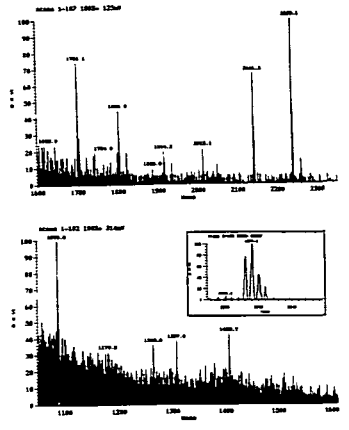

Fig 1. LSIMS spectrum of D21f2-ReLPS

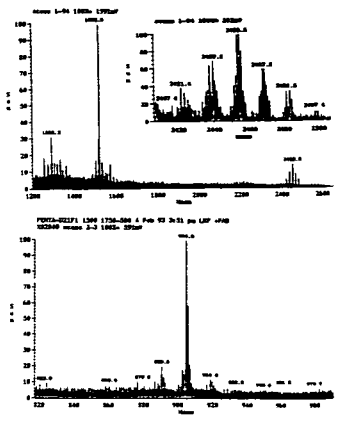

Fig 2. LSIMS spectrum of D21f1 pent-RdLPS

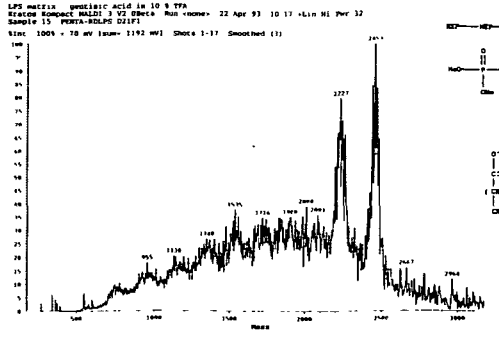

Fig 3. MALDI spectrum of D21f1 penta-acylRdLPS

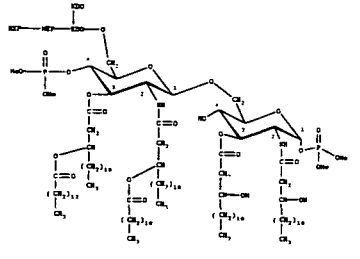

Hex-RdLPS (D21f1)

Fig 4.

Matrix-Assisted CO_2 LD/FTMS of Peptides

Long-Sheng Sheng, Joel P. Covey and Joseph E. Campana
Extrel FTMS, Millipore Corporation, 6416 Schroeder road, Madision, WI 53711-2424

Matrix-assisted laser desorption ionization (MALDI) is an important technique for mass spectrometric analysis of biomolecules. Hillenkamp and coworkers have reported MALDI by using an IR laser with succinic acid, caffeic acid, urea and glycerol as matrices [1,2]. The results were very similar to those obtained with UV lasers.

We have analyzed peptides by using succinic acid (SA) or 2,5-dihydroxybenzoic acid (DHBA) as the matrix in an FT/MS instrument equipped with three types of lasers-CO_2, Nd:YAG and N_2. For example, a synthetic peptide (pGlu-Leu-Trp-Pro-Arg-Pro-Gln-Ile-Pro-Pro, M.W.1214) was analyzed. With SA as the matrix, only the protonated molecule $[M+H]^+$ was observed in the mass spectrum (Fig.1). High signal-to-noise ratio spectra were obtained with a single laser shot, and each spectrum represents the equivalent of 20 attomoles of consumed sample. The collisional dissociation spectra (Fig.2) of the $[M+H]^+$ species were also obtained with argon as collision gas and from which some stuctural information about the peptide can be deduced.

With DHBA as the matrix, similar spectra were obtained by using any one of the three lasers (CO_2 laser at 10.6 microns, Nd:YAG laser at 355 nm and N_2 laser at 337 nm). Figure 3 shows the N_2 MALDI mass spectrum of the peptide.

The MS^n spectra of peptides were obtained by using stored wave inverse Fourier transform (SWIFT) techniques. Figure 4 illustrates the MS/MS analysis of the peptide. It was found that there are a series of a and b type ions in these spectra, and the alkali-adduct ions are the water-loss counterparts of the protonated ions.

References

1. Overberg, A., Karas, M. and Hillenkamp, F., Rapid Commun. Mass Spectrom., 5, 128-131 (1991).
2. Hillenkamp, F., Ehring, H., Overberg, A. and Hassengurger, A., Laser Desorption Mass Spectrometry, in Mass Spectrometry in the Biological Sciences: A Tutorial, 165-197, Gross, M.L. (ed.) Kluwer Academic Publishers, Netherlands (1992).

Figure 1 CO_2 MALDI/FTMS of Peptide 1214
pGlu-Leu-Trp-Pro-Arg-Pro-Gln-Ile-Pro-Pro-OH

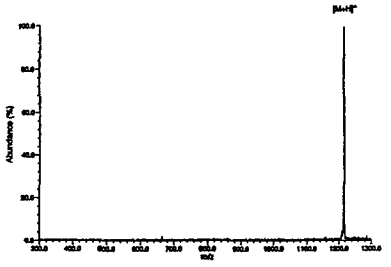

Figure 2 CO_2 MALDI/FTMS of Peptide 1214
with Argon Collision Gas

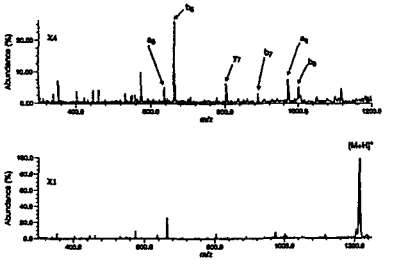

Figure 3 N_2 MALDI/FTMS of Peptide 1214
with Argon Collision Gas

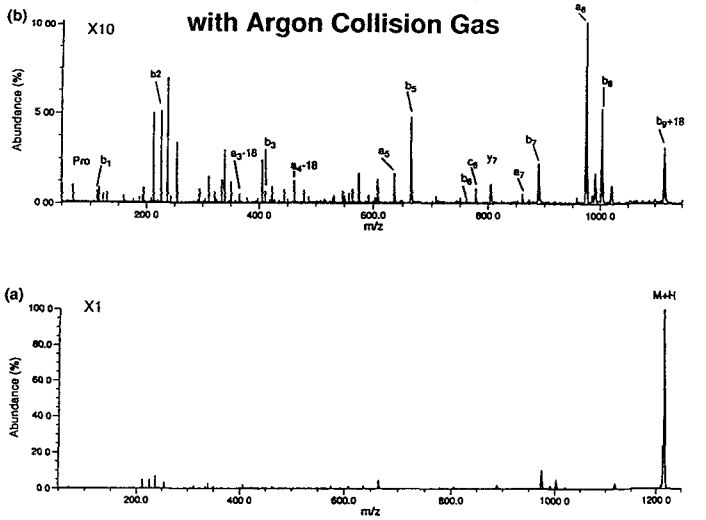

Figure 4 MS/MS of Alkali Adduct Molecular Ions

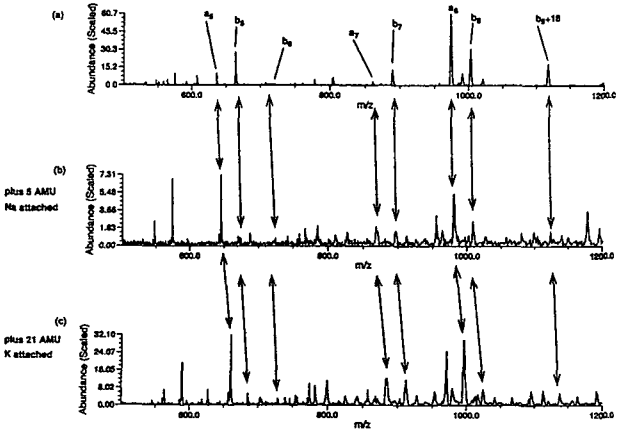

(a) protonated ions; (b) sodium adduct ions; (c) potassium adduct ions

Direct LDI/FTMS of Microbial polyesters

Joel P. Covey, Long-Sheng Sheng and Joseph E. Campana
Extrel FTMS, Millipore Corporation, 6416 Schroeder Road, Madison, WI 53711-2424
and
Jaap J. Boon
FOM Institute for Atomic and Molecular Physics,
Kruislaan 407, 1098 SJ Amsterdam, Netherlands

Introduction

The determination of the sequence of monomeric units in a bacterial polyester, a potentially biodegradable "plastic" with different types of hydroxy fatty acids, is a difficult analytical problem. Boon [1] obtained in-source pyrolysis mass spectra of polyhydroxybutyric acid (PHB) under NH_3 chemical ionization conditions and similarly obtained the in-source spectrum of a polyhydroxyalkanoate (PHA) extracted from octane fed *pseudomonas oleovorans*.

Experimental

These polyester extracts (MW_w = 100,000 to 150,000) were analyzed by Laser Probe FT/MS. A CO_2 laser operated at 10.6 µm was used for these measurements. Direct laser desorption/ionization (LDI) FT/MS spectra and MS/MS spectra confirmed the structures of the samples. The samples were dissolved in chloroform at a concentration of 1 mg/mL. Ten µL of the solution was deposited onto a stainless-steel target and dried at room temperature. A solution of KBr-saturated methanol was deposited onto the sample surface and allowed to air dry.

PHB Analysis

The LDI/FTMS spectrum of PHB was obtained with a single laser shot. The spectrum showed a series of polymer fragments with potassium ion attachment. The peaks observed that are separated by 86 Daltons confirmed the repeating unit is butenoic acid. The m/z 555 peak (hexamer) was isolated by using stored-waveform inverse Fourier transform (SWIFT) techniques. The precursor ion underwent collision-induced dissociation (CID) with argon as the collision gas. The MS/MS spectrum showed sequential loss of butenoic acid moieties

PHA Analysis

Figure 1 shows a LDI/FTMS spectrum of PHA. The spectrum is composed of a series of polymer fragments with potassium ions attached extending up to a mass range of more than 3000 Daltons. The spectrum shows that the peak with highest mass within a repeating unit group is the equivalent to the pure C_8 fatty acid polymer, the lower mass peaks in the group separated by 28 Daltons are the homologures equivalent to 1, 2 and 3 C_6 hydroxy fatty acids mixed into the polymer respectively. The m/z 863 species, which is the copolymer containing five C_8 and one C_6 fatty acid moieties, were isolated by using SWIFT techniques and collided with argon to produce progeny ions. The MS/MS spectrum of the ion shows random loss of the C_8 and C_6 acid as illustrated in Figure 2.

Conclusions

A high-mass molecular fingerprint of these relatively high molecular weight compounds can be obtained easily and rapidly. Multistage mass spectrometry provides another dimension for the structural characterization of the complex copolymer fragment ions observed.

Reference

1. Boon, J., Int. J. Mass Spectrom. Ion Processes, 118/119 755-787 (1992).

Fig. 1 LD/FTMS of Polyhydroxyalkanoates Produced by *Pseudomonas oleovorans*

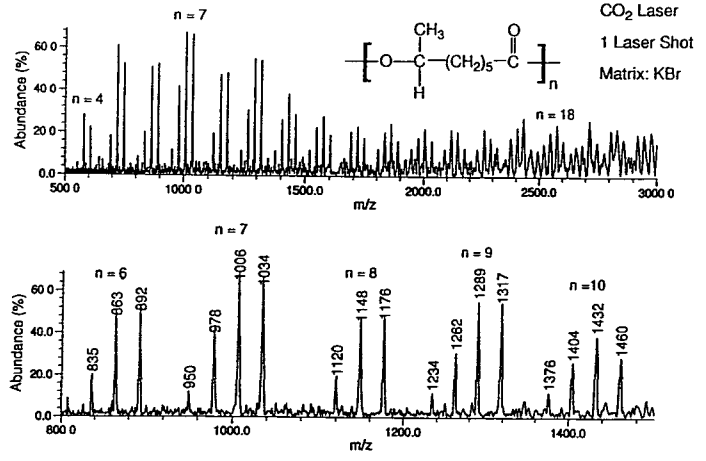

Fig. 2 MS/MS of PHA n = 6 (*m/z* 863) Species

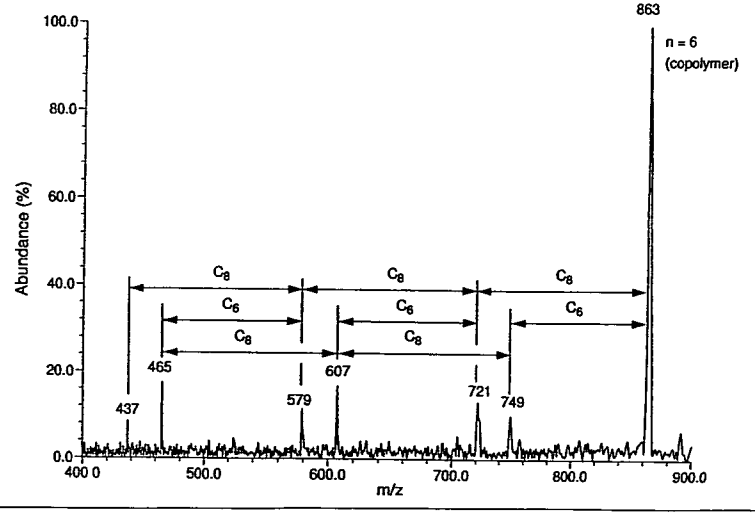

Detection of Large Molecular Ions by Secondary Ion and Electron Emission

G Westmacott, W Ens, K G Standing and A Verentchikov
Physics Dept., University of Manitoba, Winnipeg, Canada R3T 2N2

Detection of molecular ions in time-of-flight mass spectrometry is usually accomplished by secondary electron or ion emission followed by electron multiplication. For a given energy, the ratio of electrons to ions decreases with increasing mass, and for large (singly charged) molecular ions at keV energies, the emission of ions is more likely than the emission of electrons.

We have investigated secondary ion and electron emission using incident molecular ions, produced by matrix-assisted laser desorption, as primary ions in a tandem time-of-flight mass spectrometer (Fig. 1) [1]. Measurements of the ratio of secondary electrons to secondary ions from a stainless steel target were made with a range of projectile masses and energies so that the separate dependence on velocity and mass could be determined. The projectiles ranged in mass from about 300 u to 6000 u (benzoperylene, gramacidin S, LH-RH, and insulin) and in energy from 300 eV to 30 keV. Secondary accelerating voltages down to 20 V were used to reduce spurious contributions to the electron intensity caused by fragmentation of the projectiles or by grid effects.

Fig. 2 shows the electron to ion ratio as a function of velocity for the 4 projectiles. The results indicate that the electron-to-ion ratio is determined almost entirely by the velocity of the projectile; it is largely insensitive to the mass (for a given velocity). The ratio decreases rapidly at first with decreasing velocity but appears to approach as constant value of about 0.10 to 0.20 at a velocitry near 1.4×10^6 cm/s (~ 1 eV/u).

The insensitivity of the ratio to the projectile mass is demonstrated in Fig. 3 which also shows clearly that electrons are observed for projectiles with < 0.5 eV/u. Thus electron emission is a feasible method of detection for large molecular ions.

A strong increase in the absolute electron yield was observed for a fresh CsI target compared to a stainless steel target. We have begun measurements of correlations between the secondary ions and secondary electrons to estimate absolute yields. Preliminary results indicate that the electron yield for 60 keV albumin projectiles (66 000 u) incident on a CsI surface is considerably less than unity, so there appears to be much room for improvement in detection efficiency.

1. A Verentchikov, W Ens, J Martens and K G Standing, Int. J. Mass Spectrom. Ion Processes, in press.

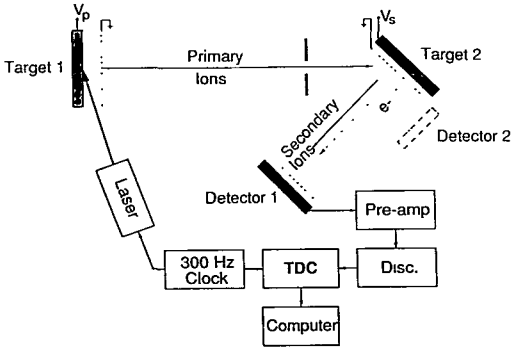

Figure 1 Schematic Diagram of the Experiment

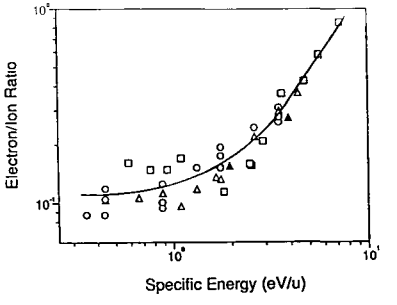

Figure 2 Ratio of secondary electron to secondary ion yield from a stainless steel target with projectiles benzoperylene (squares), gramacidin S (open triangles), LH-RH (filled triangles) and insulin (circles) as a function of the energy per mass unit.

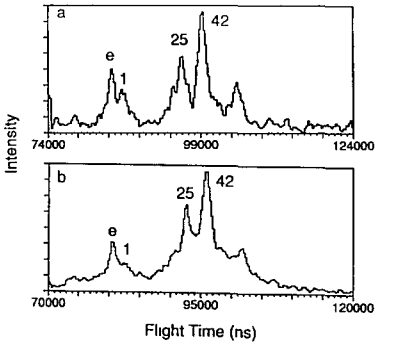

Figure 3 Secondary spectra for (a) gramacidin S and (b) insulin projectiles incident on stainless steel. The velocity of the projectiles corresponds to about 0.44 eV/u for both spectra.

Photodissociation of Precursor Ions Produced by MALDI in a Four-sector Tandem Mass Spectrometer

H.J. Köchling, J.A. Hill, J.E. Biller, and K. Biemann
Department of Chemistry, MIT, Cambridge, MA, 02139 USA

We have previously demonstrated the use of photon-induced dissociation (PID) as an attractive alternative to the more traditional collision-induced dissociation (CID) for the generation of peptide-sequence information in tandem MS/MS experiments on a magnetic sector spectrometer equipped with an integrating focal plane detector. At that time, precursor ions were generated by the fast atom (ion) bombardment (FAB) process. (1)

More recently, we have shown the feasibility of using ions generated by the matrix-assisted laser desorption/ionization (MALDI) process as precursor ions for CID MS/MS experiments on the same instrument. (2) We have continued these investigations to compare the combination of MALDI and PID to MALDI-CID.

EXPERIMENTAL

All experiments were conducted on a JEOL HX110/110 tandem mass spectrometer of $E_1B_1E_2B_2$ configuration, equipped with an integrating focal plane detector. Tandem MS/MS experiments were conducted to record both the MALDI-CID and MALDI-PID spectra of peptides. The desorption/ionization laser generated 600 psec pulses at 337 nm (N_2) at a repetition rate of 10 Hz. Its beam followed the same trajectory as does the Xe^0 beam in the FAB mode, providing an irradiance of approx. $3 \times 10^7 W/cm^2$ at the location of the sample. For CID experiments, a conventional Xe gas collision cell was placed in the region between MS-1 and MS-2. For PID experiments, this cell was irradiated by 12 nsec pulses from an excimer laser at 193 nm (ArF). This beam was attenuated by up to four wire screens (50% transmission each) to produce an irradiance of 10^6-10^8 W/cm^2 at the cell. The excimer laser pulses were synchronously delayed with respect to the N_2 laser desorption/ionization pulses to dissociate the ion packet of precursor ions mass selected by MS-1. The acceleration voltage was 10 kV and the cell was floated at 8 kV.

All samples were dissolved in a saturated aqueous solution of 2,5-dihydroxybenzoic acid (DHB). Several µL of the resulting solution was applied to the gold tip of a FAB probe and allowed to dry in air. The probe was equipped with a micrometer screw for precise translation, allowing different regions of the sample deposit to be irradiated. An integrating detector with variable mass dispersion, placed in the partial focal plane of MS-2, was employed to record the pulsed ion signal generated by MALDI during the experiments, as well as the continuous ion signal generated by the Cs^+ ion gun during calibration. (3)

RESULTS AND DISCUSSION

As expected, the CID product ion spectra of the $(M+H)^+$ ion of a peptide were found to be independent of the mode of ionization that generated the precursor ion. Fig. 1 shows the PID spectrum of the MALDI-generated $(M+H)^+$ ion and it again is in close agreement with the corresponding CID spectrum. This is due to the fact that the PID laser is operated at 193 nm, a wavelength at which the carbonyl group of the peptide bond absorbs. The most remarkable difference is the appearance of a few c_n ions (c_6 and c_7) which are rare in CID spectra. Essentially the same results were obtained when comparing the FAB-CID and MALDI-PID spectra of the $(M+H)^+$ ion (m/z 1296.7) of angiotensin I (D R V Y I H P F H L).

The extent of fragmentation under PID conditions appears to be dependent on the amount of energy contained in the dissociation laser pulse. Fig. 2 shows that the tetra peptide human renin substrate exhibits a MALDI-PID spectrum taken at 8 mJ laser pulse energy that is practically identical with that produced by CID of a FAB-generated $(M+H)^+$ ion. Increasing the PID laser pulse energy to 16 mJ and 32 mJ respectively decreases the abundance of the fragment ions of higher mass in favor of lower mass fragments.

This is most likely due to the higher energy transferred by multi-photon absorption while the ion packet travels through the 25 mm long irradiating region. The proper adjustment of the laser pulse energy is therefore essential, and one should be able to use this feature to optimize fragment ion production by decreasing the laser power while stepping the array detector from low mass to the precursor ion.

CONCLUSIONS

MALDI-PID of several medium molecular weight peptides has been demonstrated. As in earlier PID work @ 193 nm, a correlation between dissociation laser pulse energy and the abundance of product ions was observed (increasing low mass and decreasing high mass ion abundance with increasing laser power and vice versa).

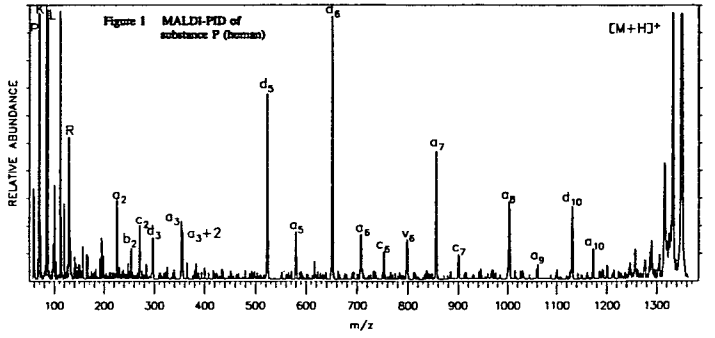

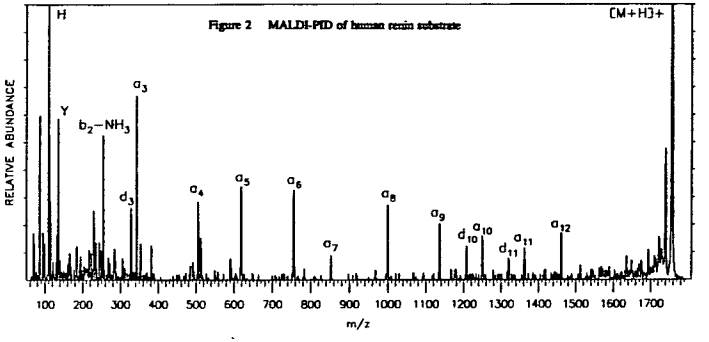

1. S.A. Martin, J.A. Hill, C. Kittrell, and K. Biemann, *J. Am. Soc. Mass Spectrom.* **1**, 107-109 (1990).
2. R.S. Annan, H.J. Köchling, J.E. Biller, J.A. Hill, and K. Biemann, *Proc. 40th ASMS Conf. Mass Spectrom. Allied Topics, Washington, DC* p. 348 (1992)
3. R.S. Annan, H.J. Köchling, J.A. Hill, and K. Biemann, *Rapid Commun. Mass Spectrom.* **6**, 298-302 (1992).

ACKNOWLEDGEMENTS

This work was supported by NIH research grants from the Center for Research Resources (RR00317), and the National Institute of Environmental Health Sciences (ES04675 and ES01640).

MALDI-Mass Spectrometric Analysis of Proteins Immobilized on Nylon-based Membranes

E. J. Zaluzec[1], D. A. Gage[1], J. Allison[2], and J. T. Watson[1,2]
Departments of Biochemistry[1] and Chemistry[2]
Michigan State University, East Lansing, MI 48824

The types of membranes most commonly used for protein immobilization in, for example, automated protein sequencing or the electrotransfer of proteins separated in polyacrylamide gels, are composed of either nitrocellulose, polyvinylidene difluoride, positively charged nylon, or glass fiber filters. Choice of a particular membrane depends upon the requirements that must be met in a specific application because these membranes differ in their binding capacities, sample retention after multiple washing or extractions, and their resistance to chemicals and/or solvents.

In choosing the appropriate membrane for the direct MALDI analysis of proteins initially adsorbed on an immobilization support, desirable characteristics would be retention during sample manipulation and elution under conditions compatible with MALDI sample preparation. We have found both nylon 66 and positive-charge modified membranes (ZETABIND) suitable to fulfill these requirements. The behavior of protein elution from nylon membranes was found to closely parallel that observed in alkyl-silicate chromatography in that proteins are retained in an aqueous environment, and increasing proportions of an organic phase (acetonitrile) favors sample elution. This is in contrast to the harsh conditions that must be employed to elute proteins from other types of immobilization supports.

MALDI spectra were obtained after (*i*) loading protein mixed with matrix on stainless steel probe tips and (*ii*) first adsorbing protein onto nylon membrane fixed to a probe tip, washing by immersing in distilled water, then applying a solution of matrix prepared in 1:1 0.1%TFA/acetonitrile. Detection limits and resolution are apparently not affected by the immobilization/washing procedure. However, there is a lagging time shift of about 200-ns when analysis is performed from membrane fixed to the probe tip.

Applications of MALDI analysis of proteins immobilized onto inert membrane supports include

1) removal of water soluble contaminants by aqueous washings,
2) sample concentration (vacuum or successive application),
3) microscale derivatization reactions,
4) microscale chemical/enzymatic digestions,
5) analysis of proteins electrotransferred to membranes from polyacrylamide gels.

Figure 1a shows a MALDI spectrum of a DNA-binding regulatory protein, SpoIIId, that was isolated by SDS-PAGE. In this instance, elution of SpoIIId from the gel required 6M guanidine for solubilization. Sample dilution provided no useful data. This was likely due to guanidine interference, insufficient sample concentration, or both. Spectra were recorded after both concentration and guanidine removal by 4 sequential applications and water washings on nylon 66 membrane fixed to a probe tip. Figure 1b shows a MALDI spectrum of similarly prepared sample of immobilized SpoIIId that was digested with Asp-N endoproteinase on the probe tip. Peaks for which assignments have been made represent total coverage for cleavage at aspartic acid.

Figure 2a shows a MALDI spectrum of 200 pm of native β-lactoglobulin first immobilized on ZETABIND membrane fixed to a probe tip. Derivatization of a similarly prepared sample with p-hydroxymercuribenzoic acid (figure 2b) showed a minor leading shoulder with a mass corresponding to the unmodified protein, and two signals that parallel results obtained from analysis of the native protein, but with mass shifts indicative of mercurial modification of the single free sulfhydryl group. Mass spectral shifts of 322 u for both the major and tailing shoulder of the native protein suggests a heterogeneous sample lot.

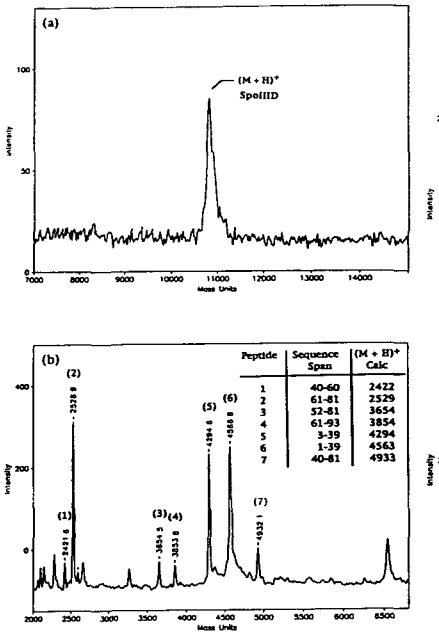

Figure 1
MALDI spectra of a DNA-binding regulatory protein SpoIIID recorded from sample applied to ZETABIND membrane fixed to a probe tip:
(a) after 4 sequential application/washing/drying steps to facilitate guanidine removal and concentration before adding matrix solution, and
(b) same application as in (a) followed by a 6-hr ASP-N endoproteinase digestion on the membrane before adding matrix solution.

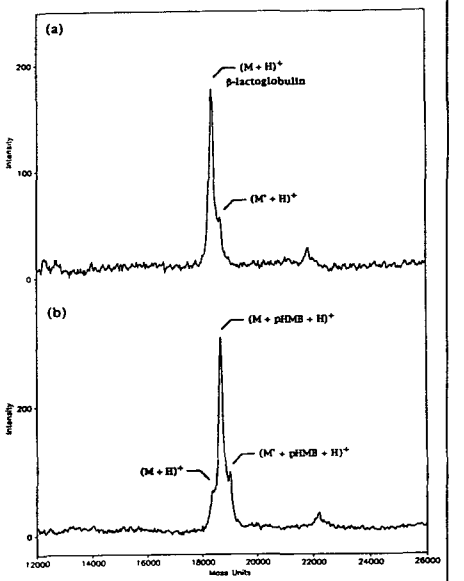

Figure 2
MALDI mass spectra of 200 pm of β-lactoglobulin adsorbed on ZETABIND immobilization membrane fixed to the probe tip:
(a) native protein, $(M + H)^+_{calc} = 18{,}367$,
(b) β-lactoglobulin derivatized with pHMB, $(M + H)^+_{calc} = 18{,}689$. (Mass spectral shifts of 322 u for both the major peak and tailing shoulder of the native protein suggests a heterogeneous sample lot.)

Time-of-flight mass spectrometry studies of laser desorption neutral gramicidin S molecules

*Kuang Jen Wu and Christopher H. Becker
Molecular Physics Laboratory, SRI Internationl, Menlo Park, CA 94025

Experimental

The cyclic peptides Gramicidin S has been studied by time-of-flight mass spectrometry in conjunction with: (1) direct laser desorption by placing the molecules on top of a layer of anthracene, or directly placed on a bare copper sample stage, and (2) matrix assisted laser desorption with several different matrix molecules (e.g., 3-hydroxypicolinic acid, sinapinic acid and DHB). Two wavelengths UV light: 308 nm and 355 nm were used for desorption/ionization of gramicidin S with a typical energy density of 0.1 - 1 mJ/cm^2. Both direct positive and negative ions have been measured with TOF-MS running at linear and reflecting mode. The desorbed neutral material was post-ionized using 118 nm single photon ionization.

Results

We found that the formation of gramicidin S positive ions is much more favorable than negative ions. Direct laser desorption of gramicidin S from on top of an anthracene film has been measured to be very effective in producing/ejecting gramicidin S ions and neutrals with an efficiency generally comparable to matrix-assisted laser desorption under similar laser irradiance. Direct laser desorption of gramicidin S from a bare copper substrate produces weaker signal than desorption from the anthracene layer and requires much higher laser power density. In addition to $[M + H]^+$, the strongest base peak, $[M + Na]^+$, $[M + K]^+$ and $[M + 14]^+$ were always observed, but the intensity of these adduct peaks varied depending upon the sample handling and preparation.

Direct and matrix-assisted laser desorbed neutrals were post-ionized by 118 nm photons. M^+ and series of peaks due to the loss of multiples of m/z 14 as well as an occasional small $[M + 14]^+$ were measured. Since no fragmentation of directly formed ions was observed, these $[M - n(14)]^+$ peaks result from the 118 nm photons. The structure of gramicidin S suggests that such fragmentation is mainly due to the fragmentation of the side groups isobutyl $(CH_3)_2CHCH_2$- from L-leucine and isopropyl $(CH_3)_2CH$- from L-valine.

Discussion

In addition to gramicidin S, we have also investigated a few linear peptides (mass < 2000) such as substance P and gramicidin D in an effort to understand the photoionization of laser desorbed neutrals. We observed no 118 nm photoionized signals above noise for any of the linear molecules. There are two possible explanations for our observation comparing single photon ionization between linear and cyclic peptides.

(1) Both of the cyclic (ring) and linear peptides suffer one random backbone cleavage. This scission results in diminishing signal for linear molecules whereas for gramicidin S ring opening still maintains total mass (except for lose of side chains).

(2) Backbone cleavage occurs in the linear peptides and not in the gramicidin S ring, i.e., ring remains intact.

Linear and cyclic peptides have been successfully photoionized by multiphoton ionization followed by supersonic jet cooling and no significant fragmentation was measured.[1-3] Two major differences exists in experimental conditions employed in this work and those reported previously:[1-3]

(1) the internal temperature and

(2) the photoionization scheme. (single photon event vs. multiphoton ionization)

It is likely that high internal energy of the desorbed neutrals in our non-jet experiment is the main cause for the fragmentation of the cyclic gramicidin S molecules and the null results for linear peptides.

Fig. 1

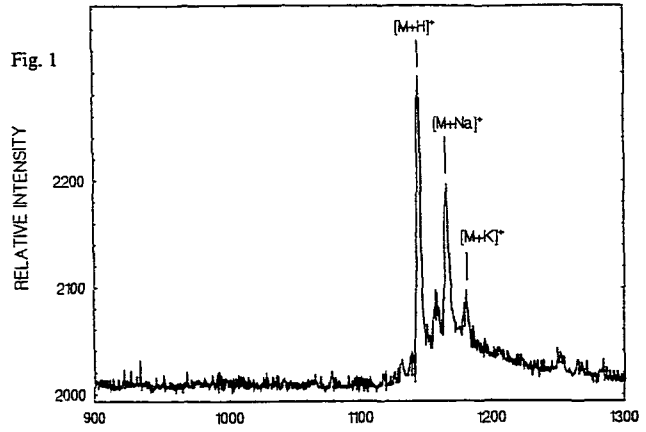

Fig. 2

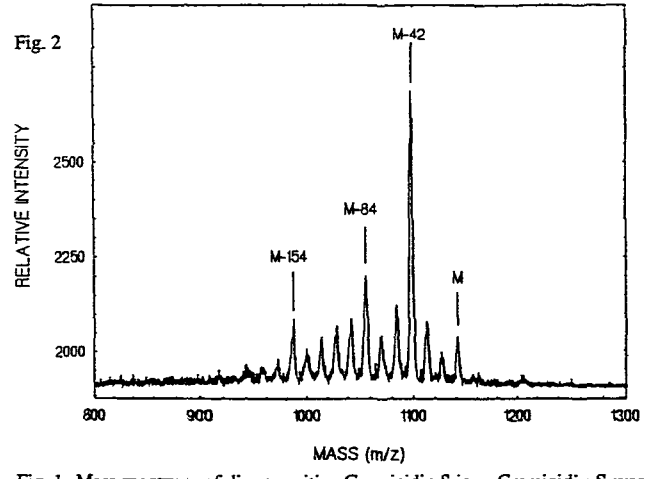

Fig. 1 Mass spectrum of direct positive Gramicidin S ions. Gramicidin S was embedded in a mixture with 3-hydroxypicolinic acid, desorbed/ionized by pulsed 355 nm photons and detected by a linear TOF-MS.

Fig. 2 TOF mass spectrum of post-ionized Gramicidin S deposited on a layer of anthracene film, desorption: 308 nm, post-ionization: 118 nm.

1. G. R. Kinsel, J. Lindner and J. Grotemeyer, Org. Mass Spectrom. 26, 1052 (1991).
2. M. Dey, W. Böhm, S. Prinke and J. Grotemeyer, Proceedings of the 40th ASMS Conference, pp. 332 (1992).
3. R. Frey, A. Holle, F. J. Mayer and R. Schäfer, Proceedings of the 40th ASMS Conference, pp. 334 (1992).

CONSIDERATIONS FOR THE SIZE AND POWER REDUCTION OF A FIELD TRANSPORTABLE ION TRAP MASS SPECTROMETER*

M.B. Wise, M.V. Buchanan, C.V. Thompson, D.E. Goeringer, S.A. McLuckey, R.I. Crutcher
M.S. Hileman, and M.L. Emery, and G.T. Alley
P.O. Box 2008, MS-6120
Oak Ridge, TN, 37831-6120

Introduction

The versatility, sensitivity, and mechanical simplicity of ion trap mass spectrometers makes them an excellent choice for use as field instruments. Applications include on-site environmental monitoring, process monitoring, leak and spill detection, contraband detection, indoor air monitoring, and workplace monitoring, among others. Although modified versions of the Finnigan ITD and ITS-40 have been successfully used as field transportable mass spectrometers, increased analytical capabilities as well as further reductions in size, weight, power consumption, and instrument complexity are needed to expand the range of potential field applications. We have approached this task by modifying the electronics and developing down-sized replacements for many of the associated components. Small, high-efficiency vacuum pumps have also been used to reduce the weight and power consumption. The result has been the development of a field instrument which has all of the capabilities of a full-sized laboratory ITMS in a package occupying approximately 8 ft^3 and weighing approximately 100 pounds.

Instrumentation

Modification of the ion trap electronics has resulted in significant size and power reductions. A major accomplishment has been the development of a considerably smaller rf drive. A fundamental frequency of 550 KHz was chosen in order to reduce the rf power consumption to approximately 1/16 that the 1.1 MHz commercial ion traps (for the same mass range). Peak rf voltage is 1,875 volts which gives a mass range of 10 to 650 amu. The rf coil, tuning capacitor, and drive transistors are enclosed in a shielded box having dimensions of 6" x 4" x 2" and weighing approximately 2 pounds. Modular high voltage power supplies (0 to 5,000 volts) having dimensions of 4" x 6" x 1" are used to bias the multiplier dynodes. A programmable dc power supply for dc mass isolation was developed using high voltage op-amps. The output of this device is +/- 180 volts with 12 BITS of resolution and the components are mounted on a circuit board which is 5" x 5" x 1". The main power supply for the electronics is 24 volts at 8 amps. It is used to power the high voltage modules directly and dc-to-dc converters are used to boost the voltage to 98 volts for the rf driver and reduce the voltage to 5 volts for digital circuits. Mass zoom electronics have also been incorporated into the system which enable the resolution of the mass spectrometer to be enhanced by reducing the mass scan rate.

Weight and power reductions have also been achieved through the use of a light-weight 60 L/s turbopump which is backed by a Drytel Micro molecular drag pump. Power consumption by the pumps after initial pumpdown is approximately 50 watts with a gas flow into the vacuum chamber of 1.5 standard mL/min. The instrument is enclosed in an aluminum cabinet which is 34" high x 20" wide with all pumps and power supplies contained inside. Maximum power consumption is 550 watts which is drawn during the initial pumpdown and manifold heating. The inlet is an open/split capillary restrictor with sampling modules for direct air monitoring, the analysis of water or soil samples, or for the thermal desorption analysis of sorbent tubes. In addition, an atmospheric sampling glow discharge ionization source is being developed for this instrument to enable detection of explosives.

Results:

Initial evaluation of this instrument has indicated that sensitivity is comparable to that of the full-sized laboratory-based ITMS. Even though the fundamental rf frequency is 550 kHz, the MS/MS efficiency is quite good and no significant loss of ion trapping efficiency has been observed. Demonstrated applications have included the detection of volatile organic compounds (VOCs) in water, the detection of PCBs in soil extracts, the detection of drugs of abuse in urine, real-time quantification of chemical warfare agent simulants in air, and real-time detection of VOCs in air.

Conclusion:

A prototype field instrument has been completed which is versatile, rugged, and has all of the features of a full-sized laboratory-based ITMS. Preliminary tests have shown that targeted analytes can be detected in variety of matrices with good sensitivity. Advanced versions of this instrument will include further improvements in the electronics, vacuum pumps, and the development of more efficient manifold heating.

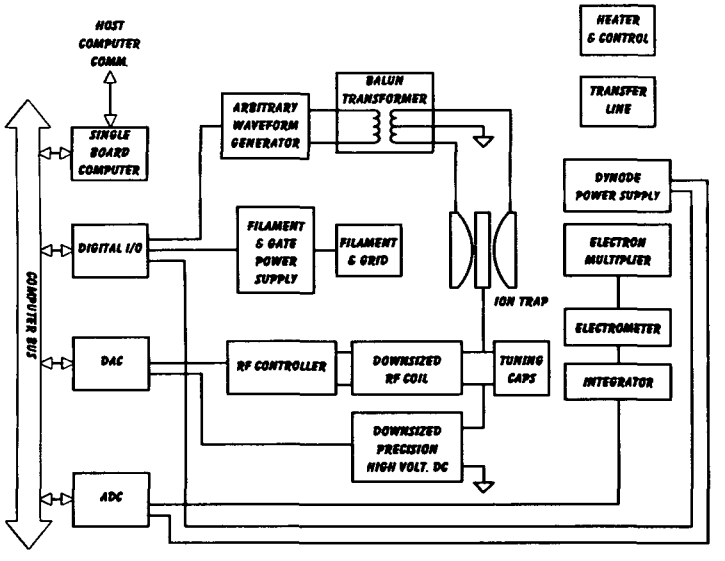

*Research sponsored by the U.S. Department of Energy contract DE-AC05-84OR21400 with Martin Marietta Energy Systems, Inc.

The Next Horizon in Portable GC/MS for Air Monitoring Applications

Wenhu Du, Neil S. Arnold, Paul A. Cole, Bob Watteyne, Dale T. Urban and Henk L.C. Meuzelaar
Center for Micro Analysis and Reaction Chemistry,
University of Utah, Salt Lake City, UT 84112

A fully man-portable TLGC/MS (transfer-line gas chromatography/mass spectrometry) system, based on the combination of an automated vapor sample inlet, a "transfer-line" gas chromatography module and a modified Hewlett Packard Model 5971A quadrupole MS system has been developed in our laboratory [1-3]. The system operates over two hours on a 24 V, 28 A-hr Li battery system with a total system weight of ~45 lbs, utilizing a unique hybrid bulk/ion getter pumping system. Data acquisition is provided remotely via a 200 m coaxial cable using standard HP-Chemstation software. This pumping system will maintain operating pressure for several days.

The GC oven module consists of a heated aluminum oven which houses the capillary GC column; 2 m long, 100 µm i.d. fused silica capillary coated with a 0.17 mm layer of a methylphenyl silicone (DB5) stationary phase. H_2 is approx. 0.3 ml/min. (In the present experiments this column is unheated.) Air samples are introduced using a special automated air sampling inlet [3]. This technique provides very short switching times (i.e., as short as 20 ms, with 100 ms typical) for high speed, high resolution TLGC separations which can be repeated within seconds.

Figure 1 illustrates chromatographic separation of 4 different test mixtures which represent anticipated environmental contaminants. These chromatograms are obtained in full scan mode at ~5 scans/second. While typical concentration in these standards are on the order of 100 ppm, limits of detection typically range between 1 and 10 ppm in full scan acquisitions. Figure 2a shows a similar full scan chromatogram of a gasoline headspace, illustrating identification of various compounds in a complex mixture. The full impact of GC separation is seen in Figures 2b and c where SIM acquisitions at m/z 57 and 55, respectively, are obtained at 15.6 points/second. Initial peak widths are on the order of ~180 ms with a 100 ms sampling pulse (sampling duration in Figure 2a was .5 s).

The SIM offers significantly enhanced detection limits. Figure 3 shows a chromatogram in SIM mode (m/z 91) for the same alkylbenzene mixture shown in Figure 1, but at ~120 ppb concentration. The LOD (S/N = 3) values are between 40 and 100 ppb without any preconcentration technique applied using a .5 s sampling pulse. The result of a field simulation is illustrated in Figure 4. A container with a 5 cm opening, containing 1 l of unleaded gasoline was placed in the center of a semi-enclosed hanger area and allowed to equilibrate for 1 hour. The concentration of several aromatic hydrocarbons were measured based on retention time and SIM (m/z 91). Actual concentrations at a local gasoline station were also measured during a busy spring afternoon (~20 C, calm winds) at various positions about the perimeter of the station. Typical concentrations are listed in Table I. Actual gasoline concentration is estimated from various constituents.

It is clear that this high speed, high sensitivity, low power and light weight TLGC/MS system offers a useful tool for a broad spectrum of field applications ranging from hazardous waste sites and industrial or natural disaster areas to reconnaissance drones, space station, interplanetary probes and autonomous vehicular robots.

Acknowledgements:

This work was sponsored by the U.S. Army ERDEC (DAAA15-90-C-1014) and the Advanced Combustion Engineering Research Center (funded by the NSF, the State of Utah, 23 industrial participants and the U.S. Department of Energy. The authors gratefully acknowledge the help and advice of Jean Luc Truche (Hewlett Packard Corporation) and the technical assistance of Houssine Mihamou.

References:

1. Arnold, N.S.; Urban, D.T.; Watteyne, R.L.; Cole, P.C.; Meuzelaar, H.L.C.; Proc. 39th ASMS Conf. on Mass Spectrom. All. Top., 1991, 671-672.
2. Arnold, N.S.; Cole, P.C.; Watteyne, R.L.; Urban, D.T.; Du, W.; Meuzelaar, H.L.C.; 3rd Intl. Symp. Field Screening Methods for Hazardous Wastes and Toxic Chemicals, Las Vegas, NV, 1993.
3. Meuzelaar, H.L.C.; Urban, D.T.; Arnold, N.S.; Proc. Intl. Symp. Field Screening Methods for Hazardous Wastes and Toxic Chemicals, Las Vegas, NV, 1991, 289-297.

Table I. Concentration of Various Chemicals at a Busy Gas Station

Compounds	Conc. (ppm)
Gasoline	59.0 (est.)
Benzene	6.0
Toluene	4.1
Et-Benzene	0.22
m-Xylene	1.1
o-Xylene	0.25

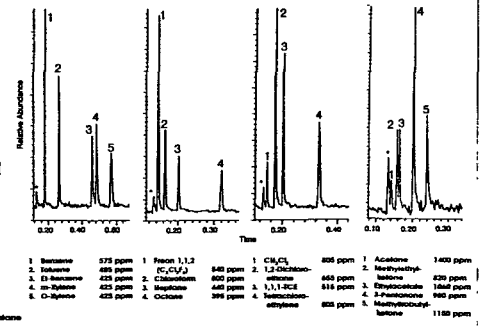

Figure 1. Chromatograms of four chemical test mixtures.

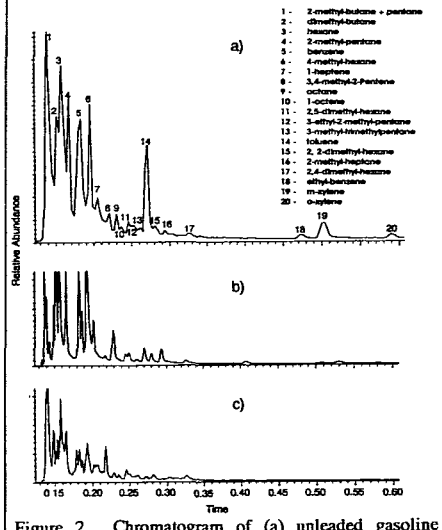

Figure 2. Chromatogram of (a) unleaded gasoline headspace obtained in full scan mode; (b, c) SIM chromatograms of the same headspace for m/z 55 and 57, respectively, at a scan speed of 15.6 scan/sec.

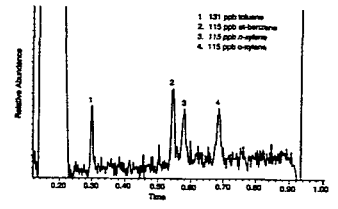

Figure 3. SIM chromatogram of a 120 ppb level alkylbenzene mixture for 91 m/z.

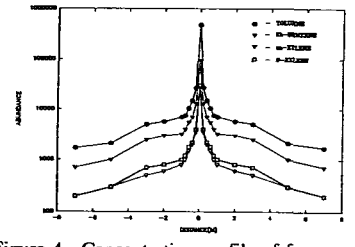

Figure 4. Concentration profile of four alkylbenzenes near a simulated gasoline vapor leak.

LARGER CELLS FOR ICR SPECTROMETERS WITH ELECTROMAGNETS, Joey A. Hatcher and John E. Bartmess, (Department of Chemistry, University of Tennessee, Knoxville TN 37996-1600)

Signal intensity is directly related to the number of ions trapped in an Ion Cyclotron Resonance (ICR) mass spectrometer. Space charge restrictions set an upper limit to the number of ions a reaction cell can hold. Therefore it is postulated that a larger cell would produce signals with greater intensity than a standard cubic cell. There are limitations in construction of such a cell: the z-dimension is limited due to the gap of the electromagnet, and the receiving plates must be relatively close to the ions for appreciable signal linearity at small excitation levels. This leaves only the third dimension for expansion. We have built such a cell, four times the length of the standard cubic cell. In this elongated cell, a uniform excitation rf field gradient is achieved by utilizing segmented trapping plates with appropriate fractions of the excitation rf on them.

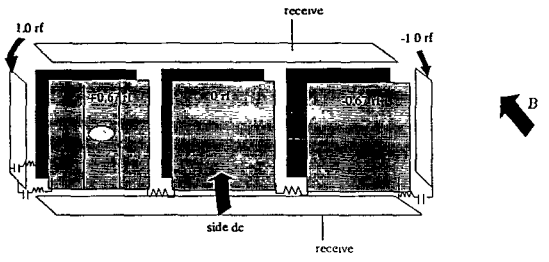

Three dimensional view of three section cell from filament side

Calculations to approximate the cell's treatment of the rf potential were done. It was found that the cell exhibited linearity in the location where the ions would position themselves, the midline of the cell. This proves that three sections will provide the rf levels necessary to cause the ions to accelerate uniformly throughout the cell.

All experiments were done using an ICR mass spectrometer with an electromagnet. Data were collected using an IBM PC interfaced with a Tecmar analog to digital board, under "rapid scan" conditions. Standard experimental conditions were pressure of 1 μtorr, emission current of 1 μA, side plates at 2 V, electron energy of 30 eV, rf amplitude of 178 mV, magnetic field at 10 kG, experiment detect delay of 100 msec, grid pulse length at 20 msec.

Experiments were done to compare the three sectional and standard cubic cells. By observing the benzene molecular ion, information was studied pertaining to the signal intensity, signal to noise ratio, and the signal's full width at half maximum. Experiments were conducted to test the signal dependence on emission current, excitation rf level, side plate voltage, grid pulse length, and transmit plate voltage.

In a study of rf level under standard conditions, the signal intensity of the benzene molecular ion was observed while changing the rf level. It was expected that, under similar conditions for both cells, the sectional cell would have the capacity to hold more ions

and therefore produce signals of greater intensity. By observing the data, the two cells seem to exhibit the ability to contain approximately the same number of ions at different rf amplitude values.

Through further studies it was found that signal intensity in the sectional cell was dependent on the grid pulse length. Another rf study was conducted under standard conditions except the grid pulse length was kept at 100 msec and the detect delay of 200 msec. It was found that the new cell achieved fifty percent greater signal output.

Although we had achieved increased signal intensities with the longer grid pulse length, it was necessary to consider the signal to noise ratio. In studies to compare the two grid pulse lengths it was found that the longer grid pulse achieved the same signal to noise ratio. Therefore the increased signal intensity of the longer grid pulse length had also delivered an increased noise level.

A study of the side dc under standard conditions was conducted. The signal intensity of the benzene molecular ion was observed while varying the side plate voltage. It was again expected that the sectional cell would produce signals of greater intensity. A plot of each cell's behavior shows that there is a linear dependence of signal intensity with side plate voltage up to 3 V. These voltages are within the normal range of experimentation in ICR. The two cells exhibited the capacity to trap the same number of ions.

Further side dc studies were done under standard conditions except the grid pulse length was kept at 100 msec and the detect delay at 200 msec. It was found that the sectional cell at the side dc of 3 V achieved one hundred percent greater signal output.

The signal to noise ratios for the three sectional cell with the two side dc studies were compared. This showed that the signal to noise ratio for the grid pulse length of 20 msec was 15. The signal to noise ratio for the grid pulse length at 100 msec was 45. The increased signal intensity of the longer grid pulse length had not been met with an increased noise level.

The three sectional cell has achieved greater signal output with the extended grid pulse length. With the rf level, it has increased by fifty percent. Through signal to noise ratio studies it has been found that this increased signal output has been met with an increased noise level. The elongated cell reached one hundred percent greater signal output at the tested dc side voltages. It has also been found that the increased signal output has not been coupled with an increased noise level. This is still not the increase expected for the larger cell.

In the future we plan to put a voltage on the upper and lower (receiver) plates, presently at ground. This should result in the ions localized near the electron beam of the cell moving to other areas of the cell to fill the sectional cell with ions more completely, by magnetron motion.

Laser Desorption Ion Trap Mass Spectrometry of the Polymeric Component of Coal

John A. Burroughs, Brian M. Cadre, and Luke Hanley*,
Department of Chemistry, University of Illinois at Chicago,
Chicago, IL 60607-7061.

Coal has long been postulated to be a two component mixture composed of a highly crosslinked polymeric matrix in which are trapped small molecules [1]. However, traditional mass spectrometric methods cannot directly examine the polymeric component because thermal volatilization leads to its chemical decomposition. A laser desorption ion trap mass spectrometer is utilized here to search for this polymeric component.

All experiments have been performed using a modified Finnigan MAT Ion Trap Detector (ITD 700). The ion trap electrodes are mounted inside a new vacuum chamber and equipped with a 6 kV conversion dynode. The end cap electrodes are connected to a function generator (Stanford Research Systems model DS-345) to allow resonant ejection experiments to be performed. The timing and data collection are controlled by custom software through an 80386/AT computer with multifunction data acquisition boards (National Instruments). 266, 355, 532, or 1064 nm pulses from a Nd:YAG laser are focussed onto a stainless steel probe onto which the sample is dried. Samples are prepared by Soxhlet extraction in pyridine of Illinois No. 6 coal from the Argonne Premium Coal Sample Program. These extracts are either used neat or mixed with a UV absorbing matrix or an alkali metal salt.

Figure 1 shows a positive ion spectrum of the coal extract produced by using 355 nm laser pulses, displaying a distribution of ions between roughly 150 and 1500 m/z with the center near 500 m/z. Laser desorption of the extract with 266 and 1064 nm pulses shows similar results, as do negative ion spectra obtained with 355 nm pulses. Polycyclic aromatic hydrocarbons (PAHs) have been used as model compounds for coal in mass spectrometric studies since it is believed that coal is composed largely of aromatic ring systems. Previous experiments have shown laser desorption successful in producing molecular ions from PAH samples [2]. Therefore, we believe the mass distributions found in our experiments to be directly representative of the masses of molecules contained in the extract.

The presence of carbon clusters can be also observed in spectra obtained with both UV and IR pulses. Figure 2 displays a spectrum similar to that shown in Figure 1 except that in addition to the broad distribution near 500 m/z, a number of carbon cluster ions up to 2000 m/z are detected. The carbon cluster ions are shown as sharp peaks in the spectrum spaced by 24 m/z with a particularly intense peak at 720 m/z corresponding to C_{60}^{+}. The appearance of these clusters can be controlled by adjusting the incident laser intensity and the trapping potential during ion injection into the trap.

Matrix assisted laser desorption ionization (MALDI) using sinapinic acid, nicotinic acid, 2,5-dihydroxybenzoic acid, and 3-hydroxypicolinic acid has also been attempted on these coal extracts. No higher mass or other ions are observed in the MALDI experiments beyond those seen in samples of the neat extract. Neither

positive nor negative ions besides carbon clusters have been observed above 2000 m/z in any of these tests. Although species ranging in size from 1000 to 10,000 amu in pyridine extracts of coal have been postulated to exist from results obtained using size exclusion chromatography [3], we have been unable to generate ions higher in mass than those shown here. It is our belief that such high mass compounds are not present in these samples.

References

1) F. Derbyshire, A. Marzec, H.-R. Schulten, M.A. Wilson, A. Davis, P. Tekely, J.-J. Delpuech, A. Jurkiewicz, C.E. Bronnimann, R.A. Wind, G.E. Maciel, R. Narayan, K. Bartle, and C. Snape, Fuel **68** (1989) 1091 and references therein.
2) P.F. Greenwood, M.G. Strachan, G.D. Willett, and M.A. Wilson, Org. Mass Spectrom. **25** (1990) 353.
3) J.W. Larsen and Y.-C. Wei, Energy & Fuels **2** (1988) 344.

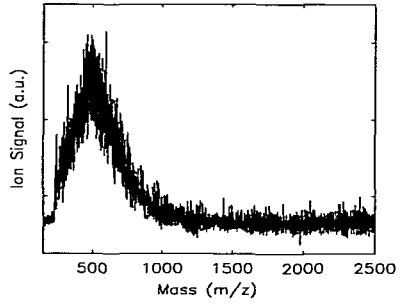

Figure 1: Laser desorption mass spectrum of coal extract at 355 nm showing a distribution of ions centered near 500 m/z.

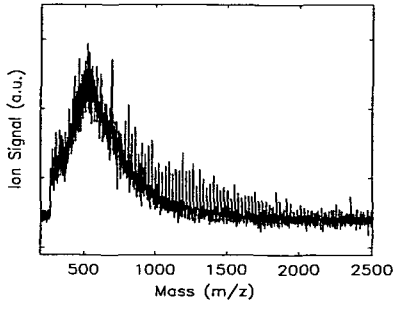

Figure 2: Laser desorption mass spectrum of coal extract exhibiting carbon clusters extending up to 2000 m/z in addition to the distribution of ions near 500 m/z.

Isotopic Masses at ppb Precision (!) from FT/ICR Mass Difference Measurements

Michael V. Gorshkov and Evgeny N. Nikolaev
Institute of Energy Problems of Chemical Physics, Academy of Science, Moscow 117829, Russia
Shenheng Guan, Karl Vermillion, and Alan G. Marshall†
Departments of Chemistry (and Biochemistry†), The Ohio State University, 120 West 18th Avenue, Columbus, OH 43210

FT/ICR mass spectrometry offers the prospect of ultraprecise (10^{-8} or better) determination of the mass difference between two ions of closely-spaced mass-to-charge ratio, because the (otherwise large) systematic error resulting from Coulomb-mediated interactions (namely, ion-ion and ion-image charge forces) may be eliminated from a mass difference determination by appropriate choice of experimental conditions. For more widely spaced mass doublets, even an absolute mass measurement can be highly precise.

The difference between ions of a given mass-to-charge ratio and ions of a second (well-known) mass-to-charge ratio is related to the unperturbed ion cyclotron frequencies, $\nu_{c,1}$ and $\nu_{c,2}$, of the two types of ions according to

$$m_2 - m_1 = \frac{m_2}{\nu_{c,1}}(\nu_{c,1} - \nu_{c,2}) \qquad (1)$$

To use Eq. 1, we must evaluate the shift of the measured FT/ICR cyclotron frequency from the unperturbed cyclotron frequency due to the following effects:

Magnetron shift. In an actual ICR ion trop, non-quadratic terms in the radial component of the trapping electric potential lead to dependence of magnetron frequency shift on the ion radial position. It is therefore necessary to extrapolate the observed cyclotron frequency to zero trapping potential.

Space charge effect. Unexcited ions of other mass-to-charge ratios, if left unexcited on or near the z-axis, ions produce a collective space charge which adds to the electrostatic trapping potential. Following excitation of the mass doublet to larger ion cyclotron orbital radius, the radial component of the space charge potential is directed outward (away from the z-axis) and shifts the doublet ion cyclotron frequencies further downward. This effect may be eliminated by extrapolating the observed cyclotron frequency to zero number of ions.

Relativistic effect. The observed ion cyclotron orbital frequency decreases as the ion cyclotron radius increases due to the relativistic increase in ion mass as the ion speeds up during excitation. This effect may be reduced by extrapolating the cyclotron frequency to zero ion cyclotron radius.

Higher precision in the masses of neon isotopes is important for quantitating energetics of nuclear reactions involving neon isotopes, and as an independent check on nuclear reaction "Q" values (rest mass energy difference between products and reactants in, e.g., an $n \rightarrow p + e + \nu_e$ process). Moreover, systematic error in the masses of neon isotopes can propagate and thereby increase the error in masses determined from other nuclear reactions. Here, we report 24-fold (and 6-fold) improvement in precision of measurement of the mass of ^{20}Ne (and ^{22}Ne), based on FT/ICR/MS. Supported by NSF (CHE-9021058) and Ohio State Univ.

Gorshkov, M.V.; Guan, S.; Marshall, A.G. *Int. J. Mass Spec. Ion Proc.* **1993**, in press.

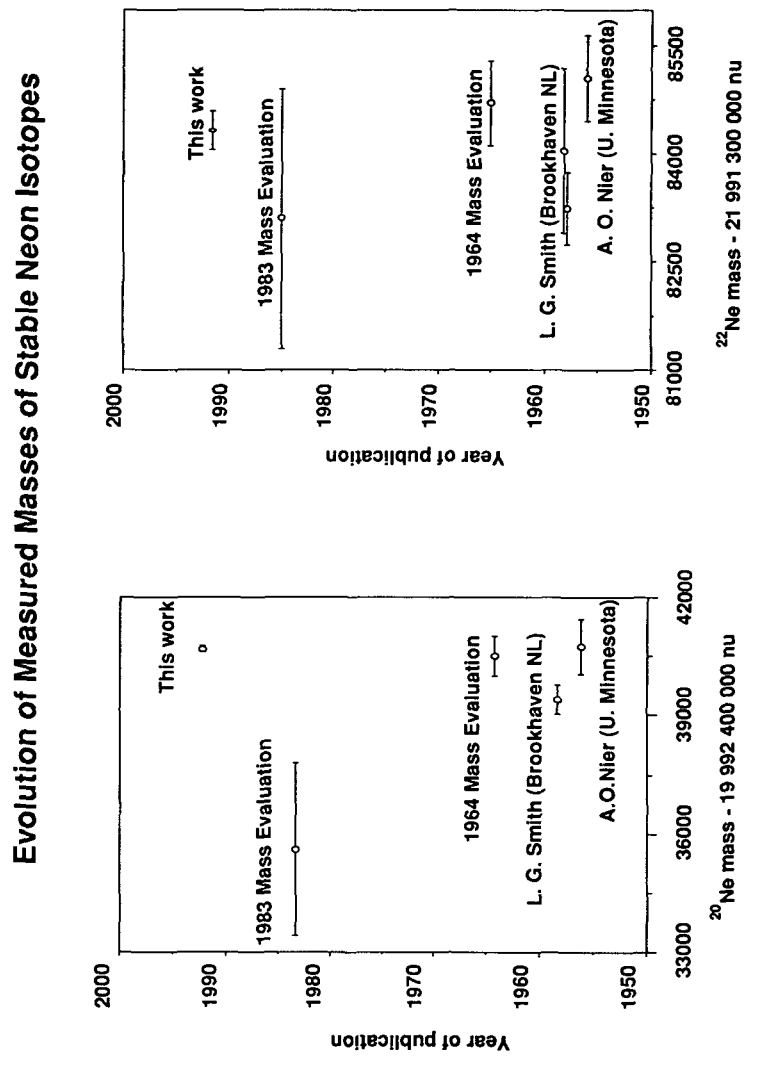

APPLICATION OF A MECHANICAL SHUTTER FOR PRESSURE CONTROL IN EXTERNAL SOURCE ELECTROSPRAY FTICR

*V. L. Campbell, Z. Guan, and D. A. Laude, Jr.; Department of Chemistry and Biochemistry, University of Texas at Austin, Austin, Texas 78712

To achieve the optimum performance of which Fourier transform ion cyclotron resonance (FTICR) mass spectrometry instruments are capable, low pressures are essential. Higher pressures can cause a deterioration of the quality and quantity of ion signal by promoting radial ejection of ions, incoherence of the ion bundle, and ion loss from ion/molecule reactions.

The problem with restricting pressure in the analyzer region is particularly acute for atmospheric sources including electrospray ionization. Low analyzer pressures are typically achieved through the use of numerous stages of differential pumping which extend beyond the magnet bore. As an alternative, it should be possible to insert an inexpensive mechanical shutter along the ion and neutral beam path to reduce the necessary stages of differential pumping. In particular, our use of concentric tubes for differential pumping allows improved ion spray signal to reach the analyzer region by reducing the distance from the source which is positioned in the magnetic field. However the directed flow of neutrals into the source is much higher and the shutter would be expected to provide a substantial benefit in terms of performance.

All spectra were obtained with a 3.0T FTICR mass spectrometer coupled to an electrospray ionization source. The essential components of the vacuum chamber and interface consist of four concentric vacuum chambers of increasing diameter which extend into the high-field region of the magnet. The mechanical shutter was mounted onto the concentric tube positioned adjacent to skimmer. The shutter is a 1.5 cm stainless steel disk with an inset Teflon O-Ring that acted as a self-lubricating seal. The shutter covers a 5 mm conductance limit in the end of the concentric tube, and is manipulated externally via stainless steel bevel gears which control the rotation of the shutter.

The shutter has potential as an alternative to the pulse valve for cooling in the remeasurement experiment. Gating of the ion beam at the skimmer is performed to let a specific ion population into the cell after which the ions are deflected for the balance of the experiment. The shutter is then used in concert with the FTICR pulse sequence to facilitate cooling of the excited ion cloud as an alternative to quenching. In this experiment, rather than employ a separate pulsed valve, the directed neutral beam is shuttered into the cell after FTICR detection to cool the excited ions. The shutter is then closed again for the next detection event.

Typically pressures could be varied over a two order of magnitude from 1 x 10-8 torr to the mid 10-6 torr range with pumpdown times of a few hundred milliseconds. Even when repeated several hundred times for several minutes, the water-methanol spray was pumped away and base pressures with the shutter closed quickly returned.

Variable delay times were inserted between ion injection and detection with the shutter both open and closed. Horse heart myoglobin spectra were compared for 20 and 40 s cooling delays with the shutter opened and closed. It was observed that if the shutter is left open for extended time periods, ion loss occurs, evidently due to radial ion loss at high pressure. However, if the shutter is closed during the cooling, ion signal magnitude remains constant for extended time periods. Once interesting feature of the spectra obtained with the shutter closed is that adduct formation is observed in the low pressure environment.

Using a 30 mm conductance limit between the shutter and cell, the pressure was 4 x 10-6 torr when the shutter was open and 6 x 10-8 torr when closed. The initial S/N ratio was enormous, but at the expense of broader peaks and extremely short ion residence times (Figure 1). Any delay before the excite with the shutter open resulted in complete signal loss due to severe radial ejection (Figure 2). However, if the shutter was closed during the delay, the ions were retained with adequate S/N (Figure 3).

A 4 mm conductance limit delivered 1 x 10-7 torr to the cell when the shutter was open and 1x 10-8 torr when closed. However, the cell pressure was inadequate to trap ions from among the 20 pA of current entering the cell. Instead ions were only trapped when background pressures into the 10-6 torr range were used.

As a compromise between the large and small orifices, a 7 mm conductance limit was evaluated. In this case the cell pressure from the neutral beam was 2 x 10-6 torr when the shutter was open and 2 x 10-8 torr when closed. However, in contrast with the 30 mm case, it was possible to retain ions with the shutter open during a delay. Additionally, improved resolution was obtained with the shutter closed during the delay.

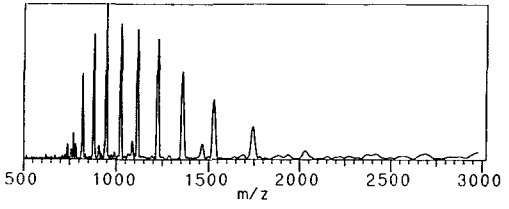

Figure 1 Cytochrome c at high pressure, shutter open, no delay

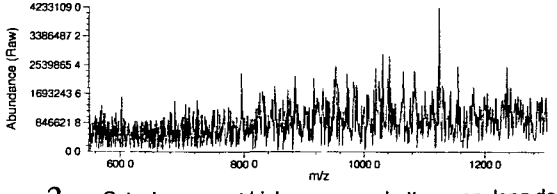

Figure 2 Cytochrome c at high pressure, shutter open, long delay

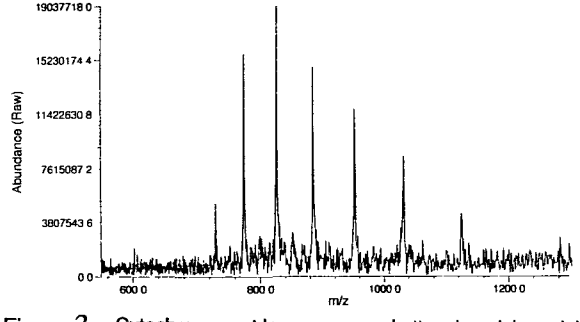

Figure 3 Cytochrome c at low pressure, shutter closed, long delay

A Novel Benchtop Ion Trap Mass Spectrometer for GC/MS/MS

Nathan A. Yates, Timothy P. Griffin, and Richard A. Yost
Department of Chemistry
University of Florida, Gainesville FL 32611-2046

Peggy R. Borum
Department of Food Science and Human Nutrition
University of Florida, Gainesville FL 32611-0370

A new ion trap mass spectrometer has been developed to overcome many of the problems that have restricted the ion trap's use for gas chromatography/tandem mass spectrometry (GC/MS/MS) analyses. In the past, three problems have made ion trap GC/MS/MS impractical: shifts in an ion's secular frequency of motion due to changing ion abundances (1), the need for real-time ionization control to limit space charge for MS/MS experiments, and complicated setup and tuning procedures required for MS/MS scan functions (2).

The instrument used in these studies was a modified Finnigan MAT ITS-40 that has been adapted for MS/MS operation. The key features of this instrument include: Automatic Ionization Control to automatically adjust the ionization time (AGC) and reaction time (ARC) for the amount of sample injected, Two-Step (3) isolation to remove sequentially ions of higher and lower m/z along the $\beta_z = 0$ and $\beta_z = 1$ stability edges, and SWIFT broadband excitation to excite a (10 kHz) range of frequencies, thus minimizing the loss in CID efficiency that can occur over a GC peak due to shifts in the parent ion's secular frequency. Figure 1 shows a diagram of the components that make up the GC/MS/MS ion trap system. Instrument control is handled by a host PC that downloads method files for the autosampler, GC, arbitrary waveform generator, and MS. The new software that we have developed allows the instrument to run unattended, injecting up to 200 samples, while switching between GC/EI/MS, GC/PCI/MS, GC/EI/MS/MS and GC/PCI/MS/MS scan modes.

Figure 2 shows the MS (upper) and MS/MS (lower) calibration curves that were obtained for the parent (m/z 182) and product (m/z 77, 105, 153) ions of benzophenone using electron ionization. The PCI MS (upper) and MS/MS (lower) calibration curves for benzophenone are shown in Figure 3 The 10 fold reduction in signal observed for MS/MS is due to ion losses that occur during the Two-Step isolation process and is not indicative of the efficiency of CID. Figures 4 and 5 show the spectra and selected mass chromatograms for the injection of 83 pg of benzophenone. Note the improvement in signal-to-noise ratio between MS and MS/MS scan modes. The use of SWIFT broadband excitation in place of single frequency resonant excitation results in comparable full scan product ion spectra at 80 pg and 300 ng levels, without manual adjustment of the voltage of frequency. We believe that a benchtop GC/MS/MS instrument that incorporates new features similar to those demonstrated here can reduce GC/MS/MS analysis on the quadrupole ion trap to routine practice. The authors wish to thank Finnigan MAT and NASA Ames Research Center for technical and financial support respectively.

(1) Yates, N.A., Yost, R.A., Bradshaw, S.C., Tucker, D.B., *Abstracts of Papers*, 39th Conference on Mass Spectrometry and Allied Topics, 1991, 132-133.
(3) R.J. Strife and J.R. Simms, Anal. Chem., 1989, 61, 2316-2319.
(3) Yates, N.A., Yost, R.A., Bradshaw, S.C., Tucker, D.B., *Abstracts of Papers*, 39th Conference on Mass Spectrometry and Allied Topics, 1991, 1489-1490.

GC/MS/MS Ion Trap System

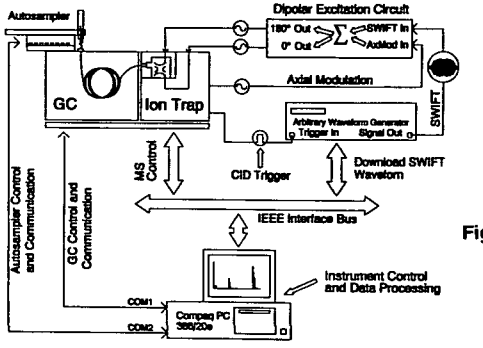

Figure 1

Calibration Curves for Electron Ionization GC/MS and GC/MS/MS of Benzophenone w/ AGC

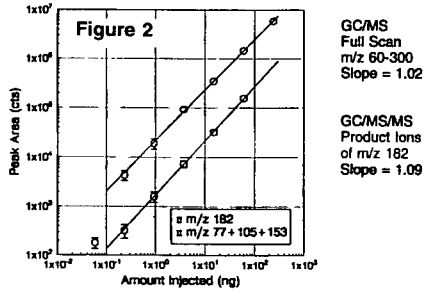

GC/MS
Full Scan
m/z 60-300
Slope = 1.02

GC/MS/MS
Product Ions
of m/z 182
Slope = 1.09

Calibration Curves for Positive Chemical Ionization GC/MS and GC/MS/MS of Benzophenone w/ ARC

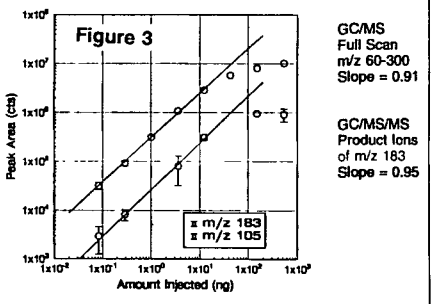

GC/MS
Full Scan
m/z 60-300
Slope = 0.91

GC/MS/MS
Product Ions
of m/z 183
Slope = 0.95

GC/MS EI Mass Spectrum for Benzophenone (83 pg)

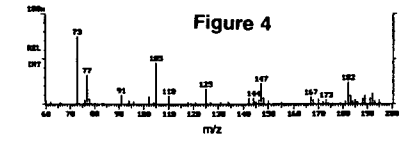

GC/MS Selected Mass Chromatogram for Benzophenone (83 pg

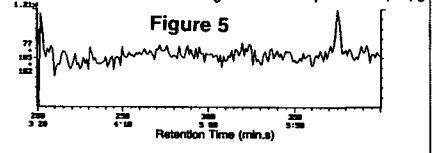

GC/MS/MS Product Ion Spectrum for m/z 182 (83 pg)

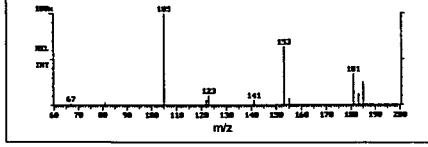

GC/MS/MS Selected Mass Chromatogram (83 pg

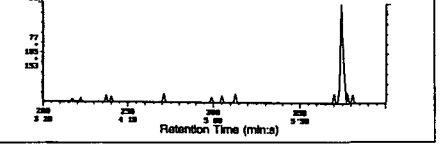

Infrared Multiphoton Dissociation Studies in the Quadrupole Ion Trap using a Multi-pass Optical Arrangement

Stephenson Jr., J.L.; Booth, M.M.; Shalosky, J.A.; Eyler, J.R.; and Yost,R.A.
Department of Chemistry, University of Florida, Gainesville, FL 32611

INTRODUCTION

Infrared multiphoton dissociation (IRMPD) has been used extensively with ion trapping techniques to investigate gas-phase ion chemistry. A continuous wave (cw) CO_2 laser is used in combination with a quadrupole ion trap utilizing resonance ejection The inner surface of the ring electrode is modified with a series of mirrors to facilitate higher photodissociation cross sections than those observed with single pass designs.

EXPERIMENTAL

All experiments are performed on a Finnigan MAT ITMS mass spectrometer. The ITMS manifold is equipped with a modified flange containing a ZnSe window to pass IR radiation. The CO_2 laser employed is an Apollo Model 570, line-tunable over a wavelength range of 9.10-10 82 μm, with a spot size on the order of 1 cm. The ring electrode is modified by incorporation of three spherical concave mirrors mounted on the inner surface of the ring as shown in Figure 1. The modified optical arrangement allows for eight laser passes across the ring electrode of the ion trap, thus increasing the optical path length and the amount of absorption obtained A pulsed valve is mounted on the opposite flange from the ZnSe window and is used to pulse helium into the ion trap to increase trapping efficiency With pulsed valve operation, laser delay times of up to several seconds are needed for the collision-free conditions required by IRMPD.

RESULTS AND DISCUSSION

In a typical IRMPD experiment, a 15 ms ionization period is followed by a reaction time of 400 ms, and the resulting protonated diglyme (m/z 135) is apex isolated. A laser delay time of 0.4 s is included to allow for removal of any excess internal energy by radiative and/or collisional cooling. Depending on the experiment, the laser irradiation time varied from 5 ms to 250 ms, which is then followed by a laser decay table and mass analysis. The characteristic photodissociation spectrum of the $(M+H)^+$ ion is shown in Figure 2 First order kinetics can be applied to the photodissociation process, with typical rate coefficients on the order of 100 s^{-1}. This value is significantly higher than the 2-30 s^{-1} values obtained at higher laser irradiances reported in the literature (see Figure 3). In Figure 4 the wavelength dependence of the IRMPD spectrum of protonated diglyme is shown. The maximum photodissociation efficiency is found at 944 cm^{-1}. Pulsed valve experiments are employed to determine if the increase in trapping efficiency associated with the addition of He buffer gas to the ion trap analyzer would interfere with the collision-free requirements needed for IRMPD. In order for photodissociation to occur, the rate of photon absorption must be faster than that of collisional deactivation. Therefore, long ion storage times are required to sufficiently pump away the He buffer gas used to efficiently trap the protonated diglyme ions. In figure 5 is shown the photodissociation efficiency as a function of the laser delay time. After a 2 s delay between the He gas pulse and laser trigger, the photodissociation efficiency levels off at over 90% The effect of exciting the $(M+H)^+$ ions of diglyme using resonance excitation is seen in Figure 6. With increasing voltage applied to the endcaps, the axial excursions of the ions increase, thus the fraction of time the ions spend in the radial plane of the multi-pass ring electrode and therefore the extent of interaction between the stored ions and photons is decreased. This leads to the decrease in photodissociation efficiency observed for increasing resonant excitation voltage.

Figure 1
Modified Ring Electrode Design

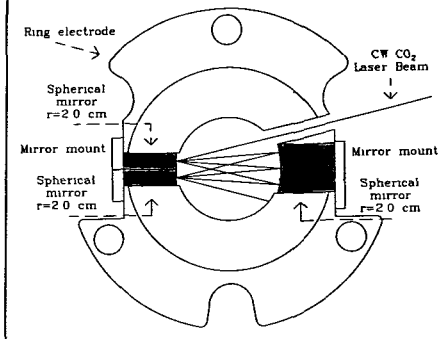

Figure 2
IRMPD of the $(M+H)^+$ Ion of Diglyme

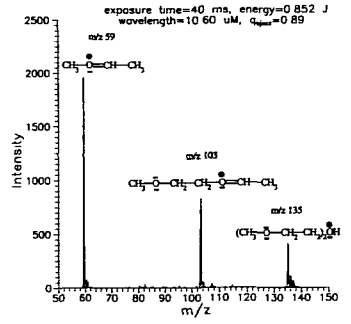

Figure 3
Determination of the Rate Coefficient for IRMPD of Protonated Diglyme

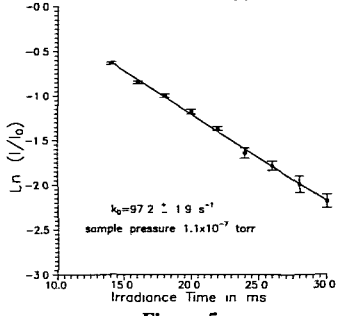

Figure 4
Photodissociation Efficiency as a Function of Laser Wavelength

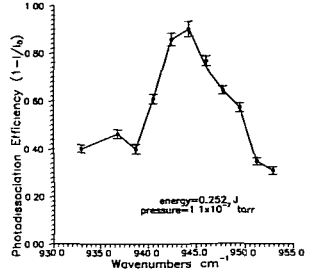

Figure 5
Photodissociation Efficiency for Protonated Diglyme vs He Gas Pulse Delay

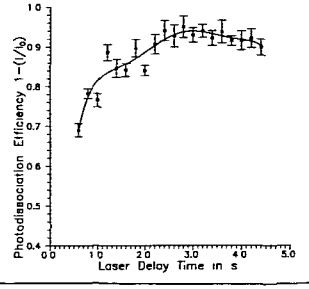

Figure 6
Effect of Resonant Excitation Voltage on the Axial Excursions of Protonated Diglyme

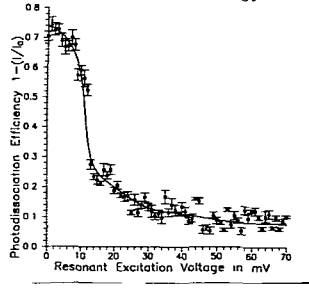

Boundary-Activated Dissociation of Mass-Selected Ions in a Quadrupole Ion Trap

Raymond E. March[1] & Mark R. Weir, Frank A. Londry[2], Silvia Catinella[3] & Pietro Traldi, John A. Stone[4] & B. Jacobs

[1]Department of Chemistry, Trent University, Peterborough, ON, Canada, K9J 7B8, [2]Department of Physics, Trent University, Peterborough, ON, Canada, K9J 7B8, [3]Consiglio Naxionale delle Ricerche, Corso Stati Uniti, 4, Padova, Italy 35020, [4]Department of Chemistry, Queen's University, Kingston, ON, Canada, K7L 3N6.

Introduction. A combined experimental and simulation study is described of the action of a quadrupole field on trapped ions when the working point is moved to the vicinity of a stability boundary, particularly the $\beta_z=0$ boundary. Ions are accelerated under the influence of the field and, as a consequence of collisions with helium buffer, dissociate; this process is known as 'boundary-activated dissociation'[1] or 'border effect'.[2] When ions are subjected to a collisional cooling period prior to the border effect, the duration of the pre-cooling period (or number of collisions) can have a profound effect upon the fragmentation channels accessed subsequently.

Experimental. A simulation study[3] of consecutive ion isolation[4] in the quadrupole ion trap indicated that, when the working point is moved to the proximity of the $\beta_z=0$ boundary of the stability diagram, ion kinetic energy is enhanced. The effect of helium buffer gas during and after the ion-isolation process, for ions with randomly-chosen co-ordinates and velocities, was to moderate ion kinetic energies. Such cooling behaviour in the ion trap is now well-recognised. However, the effect of helium buffer gas during and after the ion-isolation process for collisionally-cooled ions is to enhance rather than moderate ion kinetic energies while the working point is close to a boundary, from an average of 14 *eV* to 34 *eV*. **Thus, contrary to the normal collisional behaviour when the working point is located well-within the stability diagram, the presence of buffer gas leads to kinetic energy enhancement when the ions are cooled previously and the working point is moved subsequently close to a boundary.**

An experimental study of boundary-activated dissociation was carried out by Traldi and Catinella using a Finnigan MAT Ion Trap Mass Spectrometer. The model compound chosen was a benzoquinolizidine derivative (compound **1**, 2,6-dimethyl-9-methoxy-4h-pyrrole [3,2,1-ij] quinolin-4-one) which had been studied previously.[5] The scan function here consisted of a constant ionisation time of 300 μs, a two-step isolation of $M^{+\bullet}$ of **1** (*m/z* 227), a variable cooling time, and a plateau time of 90 μs during which a positive DC potential was applied. This sequence was followed by the usual analytical ramp of the RF potential. The sole scan parameter which was changed during a given set of experiments was the cooling time duration. The cooling time was varied from 0-420 μs for each of the helium pressures, 1×10^{-5}, 4×10^{-5}, 8×10^{-5}, and 1.2×10^{-4} *torr*. The results obtained with the ITMS were compared with those obtained with a triple stage quadrupole in which the selected ion energy could be varied prior to collision.

At 1×10^{-5} and 4×10^{-5} *torr*, only fragments *m/z* 212 and *m/z* 198 originating from CH_3 and CHO losses, respectively, were detected. The situation changed dramatically at 8×10^{-5} *torr*. New fragment ions of *m/z* 183, 184, and 154 appeared and their relative abundances showed almost linear increases with increasing cooling time.

At a helium pressure of 1.2×10^{-4} *torr*, which is the typical helium pressure employed in daughter ion spectroscopy experiments by ITMS, the situation changed further to that which is shown in Fig. 1. The intensities of $[M-CH_3]^+$ and $[M-CHO]^+$ decreased with increasing cooling time but, for this helium

pressure, the dependencies on cooling time of the remaining fragment ions showed a maximum; this behaviour is particularly clear for *m/z* 184 ions and indicates that a specific range of cooling time is most effective for maximizing the yield of a specific collisional product ion.

Figure 1. Boundary-activated dissociation of $M^{+\bullet}$ of 1 as a function of pre-cooling time.

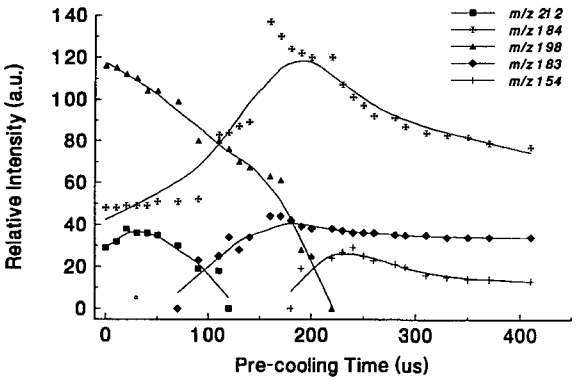

Figure 1 shows a remarkable resemblance to ion break-down curves wherein fractional ion abundances are plotted versus energy in the center-of-mass frame. Clearly, information concerning the appearance energies of fragment ions which can be obtained from such curves should be extractable from the curves shown in Fig. 1, once a suitable calibration procedure can be evolved. In order to estimate the kinetic energies experienced by ions subjected to the boundary effect and to tickling, the above results were compared with those obtained from collision experiments carried out with a triple stage quadrupole (TSQ) instrument. The tickling data were similar to those achieved by ions having 5 *eV* of kinetic energy, while the boundary effect data were similar to those achieved by ions having 100 *eV* of kinetic energy. Further comparison of the ITMS and TSQ data showed an additional and important aspect of instrument performance; daughter ion detection efficiency (60%) for the ITMS experiments exceeded those for the TSQ instrument which were *ca.* 20% and 10% for collisions of 5 *eV* and 100 *eV* ions, respectively.

In a further boundary-activated dissociation study, carried out with M^+ of 4-nitro-o-xylene, similar dissociation behaviour was observed as the cooling time was increased. Again, comparison with a TSQ instrument indicated that boundary-activated dissociation produced a fragmentation pattern which resembled both that obtained with a kinetic energy of 100 eV and upon electron impact.

References

1. C.S. Creaser, private communication, (1992).
2. C. Paradisi, J.F.J. Todd, P. Traldi and U. Vettori, Org. Mass Spectrom., 27 (1992) 251.
3. R.E. March, M. Tkaczyk, F.A. Londry and R.L. Alfred, Int. J. Mass Spectrom. Ion Processes, in press.
4. J. Gronowska, C. Paradisi, P. Traldi and U. Vettori, Rapid Commun. Mass Spectrom., 4 (1990) 306; C. Ardanaz, P. Traldi, U. Vettori, J. Kavka and F. Guidugli, Rapid Commun. Mass Spectrom., 5 (1991) 5.
5. S. Fontana, O. Curcuruto, P. Traldi, A. Castellin, A. Chilin, P. Rodighiero, A. Guiotto, Org. Mass Spectrom., 27 (1992) 1255.

Nature and Effect of Non-Linear Resonances in Ion Traps

J. Franzen, Bruker-Franzen Analytik GmbH, Bremen

The simple physical nature of non-linear resonances in quadrupole fields with superimposed multipole fields is presented in a comprehensable way, and the law for ion ejection by resonances with multipole field of any order is given.

1. The secular oscillations of ions within pure quadrupole fields with an rf driving frequency Ω consist of the basic secular frequency ω and sideband frequencies of the form $\nu\Omega+\omega$ and $\nu\Omega-\omega$, in accordance with the Mathieu theory. The pure quadrupole field behaves as a harmonic oscillator, sometimes called "pseudo-harmonic" because of the additional sideband frequencies superimposed on the basic secular oscillation. The superposition of higher multipole fields makes the storage field non-harmonic and creates higher harmonics $n\omega$ (overtones), as it is known from non-harmonic oscillators in other areas of physics. In addition, sideband frequencies of the general form $\nu\Omega+n\omega$ and $\nu\Omega-n\omega$ (ν and n are arbitrary integers) of the higher harmonics are generated.

The nature of non-linear resonances is extremely simple: ***Non-linear resonances occur if harmonics match with sidebands***. Such matches do not simply consist of two superimposing frequencies, instead, complete series of frequencies come together in a single match.

Fig. 1 below exhibits the frequency spectrum of an hexapole superposition.

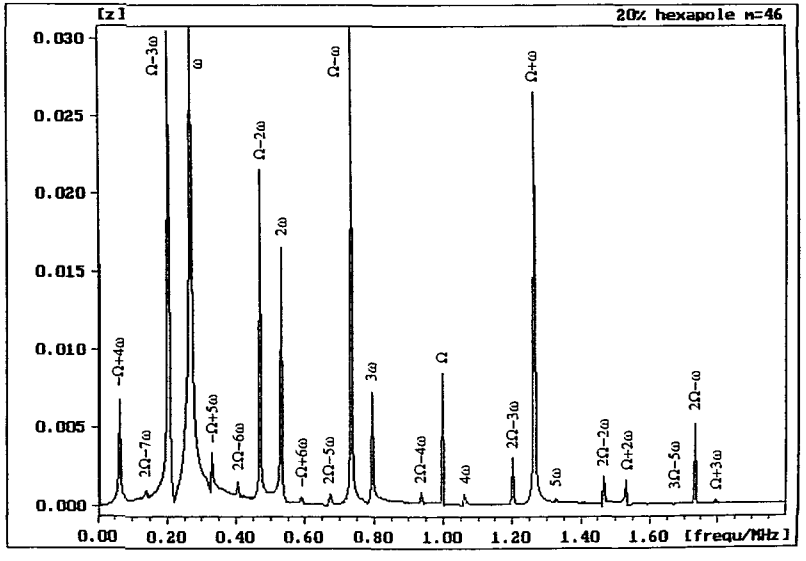

This frequency spectrum was calculated by computer simulation of the ion oscillation in z direction, and a Fourier analysis of the computed oscillations. Superposition of odd multipoles create all higher harmonics, even multipoles create odd harmonics only, as known from non-harmonic oscillators. A rather strong 20 % hexapole field superposition was chosen here to enhance the higher harmonics. The higher harmonics and the sideband frequency series are identified in fig. 1.

2. Simulations of the ejection processes in stationary fields reveal the law for the amplitude growth caused by different types of resonances. The general equation

$$dz/dt = C_{n-1}z^{n-1}$$

is valid for resonances caused by multipole fields of order *n*, as long as the ejection is not disturbed by frequency shifts. This law is valid in all cases of resonances, may it be a resonance with a dipole field generated by an additional AC across the end caps, or may it be a non-linear multipole resonance created by the shape of the electrodes.

The equation can be easily undertstood: The energy pick-up of the ion is proportional to the field strength of the multipole field as seen by the momentary oscillation width of the ion. It clarifies that the energy is taken up from the rf component of the multipole field, not from the basic quadrupole field.

Integration of the basic law of ion ejection gives a linear amplitude growth for the dipolar excitation (with externally applied excitation voltage), an exponential growth for the quadrupole field (in the non-stability area), and a hyperbolic growth (of hyperbole order n-2) in case of non-linear resonances by superimposed multipole fields. Because hyperboles exhibit a mathematical pole, the ejection by higher multipoles is extremely pointed.

Fig. 2 demonstrates the hyperbolic growth of the oscillation in z direction for an ion in resonance with the hexapole non-linear resonance condition $\beta_z = 1/3$.

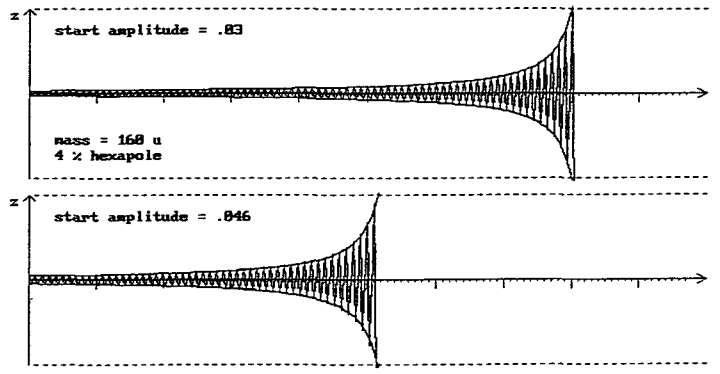

Quadrupolarized ICR Cubic Ion Trap

Hyun Sik Kim, Ruidan Chen and Alan G. Marshall†

Departments of Chemistry (and Biochemistry†), The Ohio State University, 120 West 18th Avenue, Columbus, OH 43210

The electrostatic trapping potential in any ICR ion trap is approximately quadrupolar near the trap center. Away from the center, the deviation of trapping potential from pure quadrupolar form can lead to non-linear response (harmonics, combination modes, peak splitting) [1]. Efforts have been made to improve the electric potentials in various ion traps, as recently reviewed [2]. Here we show that the electrostatic potential field in a conventional ICR cubic ion trap may be shimmed to near-perfect quadrupolar form without change in overall trap shape (cubic in this case) by segmenting the excitation and detection electrodes and coupling them by an appropriate RC network.

The quadrupolar trapping field is established by fitting the electrostatic trapping potentials of every segment to a quadratic function of the distance from the center plane. The electrostatic trapping field is separated from the rf excitation/detection fields by capacitors of carefully chosen values. The trap design has been refined theoretically by use of SIMION [3]. Although the simulated trapping potential well in a conventional trap is deeper than that of a quadrupolarized trap, the overall trapping potential profile in the quadrupolarized trap approaches a perfect quadrupolar field much more closely than does that of a conventional trap.

A striking advantage of the quadrupolarized trap is evident from comparison of benzene molecular ion FT/ICR mass spectral peak shapes for quadrupolarized and cubic ICR ion traps at different ICR orbital radii (Figure 2). (Although FT/ICR peak height increases with increasing ICR orbital radius, each set of plots has been scaled to a common peak height to facilitate comparison of peak shapes.) The elimination of peak splitting in the quadrupolarized trap shows that peak splitting previously observed for conventional ICR ion traps arises from non-quadrupolar electrostatic trapping potential [4], because the splitting is eliminated in the quadrupolarized trap. Moreover, mass resolving power is enhanced by ~10% in the quadrupolarized trap. Finally, even the quadrupolarized trap produces a potential which deviates from pure quadrupolar near the edges of the trap, as shown by the small change in ICR frequency at increasingly large ICR orbital radius (Figure 2, right-hand spectra). This work was supported by NIH (GM-31683), NSF (CHE-9021058) and The Ohio State University.

1. Marshall, A. G, and Grosshans, P. B., *Anal. Chem.* **1991**, *63*, 215A-229A2.
2. Marshall, A. G.; Schweikhard, L. *Int. J. Mass Spectrom. Ion Proc.* **1992**, *118/119*, 37-70.
3. McGilvery, D. C.; Morrison, R. J. S., Dept. of Chemistry, Monash University, Wellington Road, Clayton, Victoria, 3168, AUSTRALIA.
4. Holliman, C. L.; Rempel, D. L.;, Gross, M. L. *J. Am. Soc. Mass Spectrom.* **1992**, *3*, 460-463.

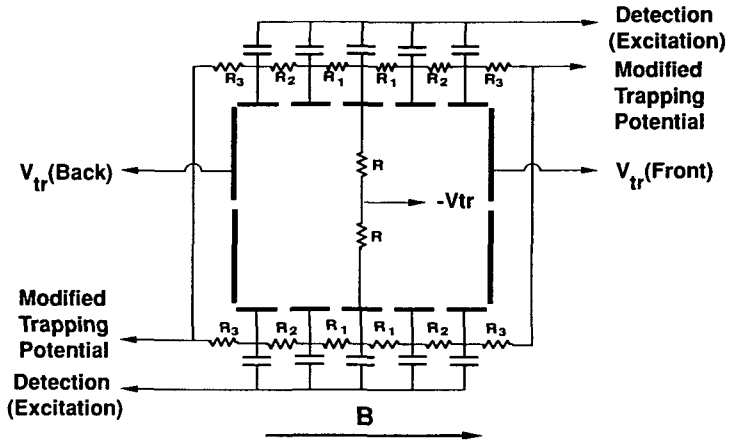

Figure 1. Configuration of the quadrupolarized ICR cubic trap.

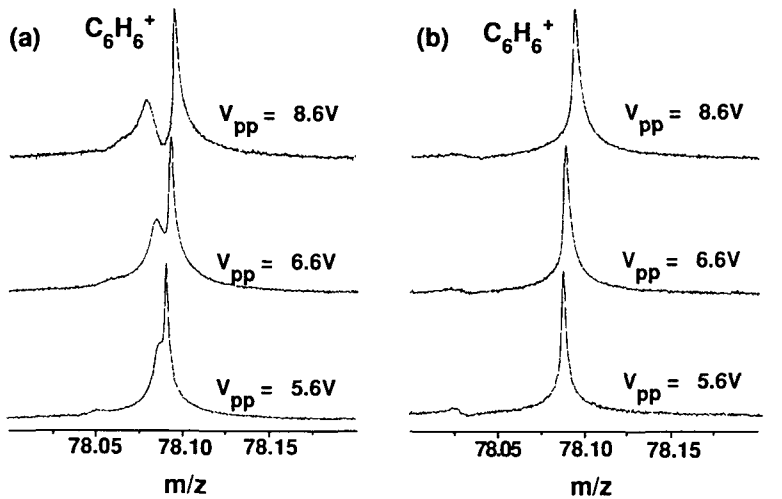

Figure 2. Peak splitting at different radii of cyclotron motion in (a) conventional cubic trap and (b) quadrupolarized cubic trap.

Contaminant Analysis Using Novel Sampling Strategies and Laser Desorption Mass Spectrometry

M.E. Cisper, W.L. Earl, G.C. Eiden, P.H. Hemberger, and N.S. Nogar. Los Alamos National Laboratory, Los Alamos, NM 87545.
J.E.P. Syka. Finnigan MAT, San Jose, CA 95134.

We have combined two sample collection/sample introduction techniques with laser desorption ion trap mass spectrometry for rapid contaminant screening. Direct laser desorption of material affords several advantages over less direct methods: Rapid sample turnaround, little or no sample preparation, reduced waste generation and disposal, and inexpensive and easily prepared sampling materials. Contaminants are sampled in one of two ways: Through zeolite absorption or through solid-phase microextraction on a fiber probe. The two methods are convenient in that they provide both a method to sample for contaminants and a means by which compounds, including volatile organics, are available for laser desorption.

Instrument configuration, described in detail previously,[1] consists of an excimer laser aligned with the ion trap assembly contained in a large vacuum chamber. The ring electrode, drilled through on opposite sides, provides access for a direct insertion probe upon which a pulsed laser beam impinges (308 nm, 15 nsec duration, 3×10^6 W/cm^2). The timing of the laser firing is carefully coordinated with the leading edge of a rising RF step in the scan function to effect a 10 to 100-fold signal increase.[2] Detected signal also tracks the phase of the ring electrode RF.

Zeolites (molecular sieves) are crystalline, alkali-aluminum silicates which form cage-like structures. They are attractive adsorbents because cavity size, determined by the aluminum-silicon ratio, can be controlled for selective sampling of volatile and semi-volatile compounds. The zeolite matrix, after exposure to the suspect airborne contaminant, is tamped into the concave end of a stainless steel probe tip.

Laser sampling of zeolite-entrapped dimethyl methyl phosphonate [$CH_3P(O)(OCH_3)_2$, M.W. 124] produced the mass spectrum shown in Figure 1.

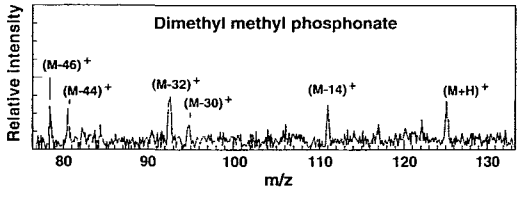

Figure 1. Laser ion trap analysis of dimethyl methyl phosphonate entrapped in zeolite.

Interest in solid-phase microextraction (SPME) on fused silica fibers led to the development of the second sample collection/introduction technique presented here. SPME is a relatively recent method[3] used for the extraction of organic compounds from aqueous samples. A length of optical fiber is exposed to an aqueous solution. Equilibrated partitioning of the organic analytes from the liquid phase to the stationary phase on the fiber can occur within minutes. Conventionally, contaminant analysis by SPME is obtained through thermal desorption in a heated GC injection port.

We used stripped and cleaned fused silica fibers (0.6 to 1 mm in diameter) as sampling probes in organic solutions. The fiber was dipped in solution to a depth of 0.5 to 1 cm, after which it was directly inserted through the drilled-through ring electrode for laser interrogation of the microextracted sample. Pyrene (M.W. 202) served as the benchmark compound for most studies but optical fibers were also used to extract other PAHs, laser dyes, pesticides, trimethyl phenyl ammonium iodide, p-dichlorobenzene, and peptides. Figure 2 shows the typical mass spectrum obtained from laser desorption of a fiber exposed to a soil sample containing 10 ppm anthracene and pyrene. One mL of methanol was added to the spiked soil. The fiber was exposed to the soil/solvent slurry for 3 minutes with no attempt to achieve equilibrium microextraction. We have detected pyrene on fibers exposed to 1 ppb solutions.

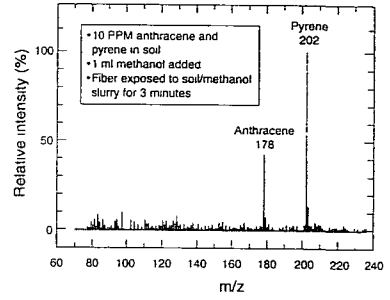

Figure 2. Laser desorption analysis of PAH mixture microextracted on fiber.

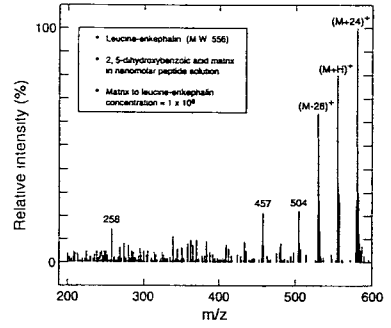

Figure 3. Laser desorption analysis of microextracted peptide on fiber.

Laser desorption of a fiber exposed to a solution containing the peptide leucine-enkephalin and a matrix compound resulted in the mass spectrum shown in Figure 3.

Zeolite absorption and fiber microextraction show great promise as rapid sampling/sample introduction methods. These techniques extend the variety of compounds amenable to laser desorption ion trap mass spectrometry. However, the data are semi-quantitative in nature and zeolite-adsorbed materials may undergo catalysis. We plan to further investigate the fiber surface-laser probe interaction, fiber coatings, improvements in microextraction under equilibrium conditions, and laser ablation/RF step interaction.

[1] P.H. Hemberger, N.S. Nogar, J.D. Williams, R.G. Cooks, J.E.P. Syka. *Chem. Phys. Lett.* **1992**, 191, 405.
[2] G.C. Eiden, M.E. Cisper, M.L. Alexander, P.H. Hemberger, and N.S. Nogar. *J. Am. Soc. Mass Spectrom.* in press. See also Eiden et al, TP 165, 41st ASMS Conference on Mass Spectrometry and Allied Topics.
[3] C.L. Arthur, J. Pawliszyn. *Anal. Chem.*, **1990**, 62, 2145-2148.

AN IMPROVED CALCULATION OF PEAK SHAPE IN FTMS

D. L. Rempel and M. L. Gross

Midwest Center for Mass Spectrometry, Department of Chemistry, University of Nebraska, Lincoln, NE 68588-0304.

In light of recent work for the Fourier transform mass spectrometer (FTMS) that shows that both trap electric field compensation[1] and ion cloud pressure focussing are required to obtain the best improvement in the detection of diffuse ion clouds,[2,3] the connection between experimental parameters and the ions' spectral peak shape needs a more carefull examination.

Here, Lie transforms[4] are used to build a peak shape model with relaxed assumptions and improved rigor over that done in ref 1. The strategy for building peak shapes involves two basic parts.

First, a common factor of 1/m was removed from the single ion Hamiltonian by writing $t=m^*\gamma$. After the Hamiltonian for a single ion was transformed to action-angle variables for the cyclotron, magnetron and z- oscillation modes,[5,6] the Deprit perturbation series[4] was used to calculate a canonical transform for the action-angle variables that removes angle dependence of all terms of the first three orders in the Hamiltonian except those electric field terms which are associated with excitation of the ion motion. The Deprit method was used because old and new variables are not mixed in the generating function for the canonical transform. Because of this, all state variables can be explicitly computed to the desired order.[4] This is in contrast to the perturbation method used by Kretzschmar.[6,7]

The charge displacement caused by the ion's position was "pulled back" to the action-angle variables and then pulled back to the new canonical variables by the inverse of the canonical transform used to transform the Hamiltonian. Only those terms which depend the cyclotron angle and no other angle were retained for computing the peak shape.

The excitation terms in the Hamiltonian were pulled back just as the charge displacement was.

A secular perturbation theory[4] was used in the second basic part to compute the change in state due to an RF-burst excitation. The change in the action-angle variables caused by the excitation was computed by separately transforming the action-angle variables for each mode into "position-momentum" variables, carrying out the secular perturbation calculation to first order, and then converting the result back into action-angle variables. This strategy avoids a result that becomes undefined when the initial actions go to zero.

All results are are written as a function of dimensionless parameters such as MMC = m/m_e, geometry factors, and outer-segment-to-disk voltage ratio.

The effects of compensation, mass and magnetron motion on the cyclotron frequency computed from the tranformed Hamiltonian can be seen by comparing graphs of the cyclotron frequency versus cyclotron and z-mode normalized actions.

The frequency surface of an uncompensated cubic trap shows contours that are tangent to the cyclotron vs z-mode action graph that results from an RF burst excitation only at higher z-mode actions. Only ions with actions in the region where this tangent condition occurs are expected to give high resolution signals. Driving the outer segment of each trap plate of a compensated trap

at 1.7 times the potential of the 50% center disk decreases the frequency variation for low z-mode actions and intermediate cyclotron-mode actions. The region of the tangent condition moves to low z-mode and intermediate actions.

The frequency surface becomes much deeper when the mass is increased by a factor of ten as MMC is increased from 0.01 to 0.1, but otherwise, has nearly the same shape.

Increasing the magnetron mode radius to about 50% of the maximum radius distorts the frequency surface so that the local minima would exist only at lower cyclotron actions and high z-mode actions with lower frequencies. As a result, ion clouds with broader magnetron-mode distributions (high mass ion clouds, for example) are expected to have wider peaks that are shifted to lower frequencies.

The calculated peak shape for which a simple z-mode distribution with a temperature of 1844 K is used shows a dominating high resolution part. This temperature is the expected lowest temperature of the z-mode shortly after electron ionization in a cubic trap with 1 V applied to the trapping plates. The corresponding experimental peak shape (benzene, m/z=78, low ion number, 1x10-7 torr in a 1 V, 0.0254 m cubic trap, 1.2 T) shows the same feature with a resolution of 13.3K for a ionization to excitation/detection delay of 1 ms.

The calculated peak shape for a simple z-mode distribution with a temperature of 300 K shows that the high resolution part of the peak has been lost. The corresponding experimental peak shape also shows the loss of the high resolution part for an ionization to excitation/detection delay of 4 s. The measured half-height resolution has decreasedto 3.2K.

This is a problem for pressure focussed ion clouds that is solved by compensating the trap as shown by calculated peak shapes that show much reduced change with z-mode temperature. Both experimentally measured half-height resolutions are 26.3K for delays 1 ms and 4 s.

The fact that improved performance is achieved while not making the trap more quadrupolar suggests that there is another strategy for improving performance in the trap. This strategy might be described as matching the low z-mode action portion of a level set (contour) of the frequency surface with the low z-mode action portion of the cyclotron action verses z-mode action graph that results from excitation.

1. D. L. Rempel *Proceedings of the 35th ASMS Conference on Mass Spectrometry and Allied Topics*, Denver, CO, 1987, pp 1124-1125.
2. C. L. Holliman, D. L. Rempel and M. L. Gross *WP 163*, this meeting.
3. C. B. Jacoby, C. L. Holliman, D. L. Rempel and M. L. Gross *J. Am. Soc. Mass Spectrom.* **1993**, **4**, 186-189.
4. J. R. Cary *Physics Reports* **1981**, 79, 129-159.
5. D. W. Mitchell *Int. J. Mass Spectrom Ion Proc.* **1991**, 107, 417-434.
6. M. Kretzschmar *Physica Scripta* **1992**, 46, 544-554.
7. M. Kretzschmar *Physica Scripta* **1992**, 46, 555-559.

All symbolic calculations were performed with PC MACSYMA Release 415.25 purchased from Symbolics MACSYMA Division, Symbolics, Inc.

SWIFT Excitation/Ejection of Ion Axial Motion in Quadrupole Ion Trap Mass Spectrometry

Shenheng Guan and Alan G. Marshall†

Departments. of Chemistry (and Biochemistry†),The Ohio State University, 120 West 18th Avenue, Columbus, OH 43210

Stored waveform inverse Fourier transform (SWIFT) excitation is a powerful excitation method for FT/ICR/MS introduced by Marshall and coworkers (1,2). Demonstrated advantages of the SWIFT method over prior excitation methods include: uniform excitation over specified m/z range(s), high excitation/ejection selectivity, extension of FT/ICR detection dynamic range, and convenience in use. The theoretical foundation of the SWIFT method is linear response theory (3,4).

In a quadrupolar Paul ion trap, the high-frequency, high-amplitude rf voltage applied between the ring and end-cap electrodes forms a pseudopotential in the z-direction that may be approximated as a quadrupolar electrostatic potential; ion motion may then be modeled as a harmonic oscillator if $q_z = (4qV_{rf}/mr_0^2\Omega^2)$ is small. The equation of z-motion of ions subjected to dipolar z-excitation in the Paul ion trap is then linear, just as for cyclotron motion in an ICR ion trap.

An important tool for ion trap applications is dipolar (i.e., excitation voltage applied between the two end-cap electrodes) resonant excitation of axial z-motion, applied at the ion "secular" or "natural" z-oscillation frequency corresponding to a given q_z-value. By solving analytically the equation for forced ion z-motion with a collisional damping term

$$\ddot{z} + \gamma\dot{z} + \omega_z^2 z = \eta V_z(t)\ ,\ \eta = \frac{c_1 q}{2 z_0 m}$$

in which γ is a collisional damping factor, ω_z is z-frequency, and c_1 (=0.8) is the trap geometrical factor, we develop a linear response theory for dipolar z-excitation. Post-excitation ion z-oscillation amplitude is proportional to the magnitude spectrum (at the ion secular frequency) of the time-domain excitation voltage signal.

A general algorithm generates an excitation waveform which excites ions to any desired z-amplitude over arbitrary m/z range(s) and provides for selective ion isolation or ejection. The present theory closely follows that previously developed for ICR, except that the ion axial motion in the Paul trap is linear, whereas the ion cyclotron orbital motion is circular. Therefore, SWIFT techniques developed previously for ICR cyclotron excitation (3-7) are easily adapted for high-resolution z-excitation and z-ejection in RF ion traps (8). The effect of collisional damping may be treated theoretically (9). Work supported by Amoco and Ohio State University.

(1) Marshall, A. G.; Wang, T.-C. L.; Ricca, T. L. *J.ACS* **1985**, *107*, 7893-7897.
(2) Marshall, A. G.; Wang, T.-C. L.; Chen, L.; Ricca, T. L. *Amer. Chem. Soc. Symposium Series* **1987**,*359*, 21-33.
(3) Guan, S. *J. Am. Soc. Mass Spectrom.* **1991**, *2*, 483-486.
(4) Grosshans, P. B.; Marshall, A. G. *Anal. Chem.* **1991**, *63*, 2057-2061.
(5) Guan, S. *J. Chem. Phys.* **1989**, *91*, 775-777.
(6) Guan, S.; McIver, R. T., Jr. *J. Chem. Phys.* **1990**, *92*, 5841-5846.
(7) Guan, S. *J. Chem. Phys.* **1990**, *93*, 8442-8445.
(8) Julian, R. K.; Cox, K.; Cooks, R. G. *40th ASMS*, Wash., D.C., **1992**, 943-944.
(9) Guan,S; Marshall, A. G.; *Anal. Chem.* **1993**,65, 1288-1294.

Construction of a SWIFT Time-Domain z-Excitation Waveform for Mass-Selective Axial Excitation and Ejection

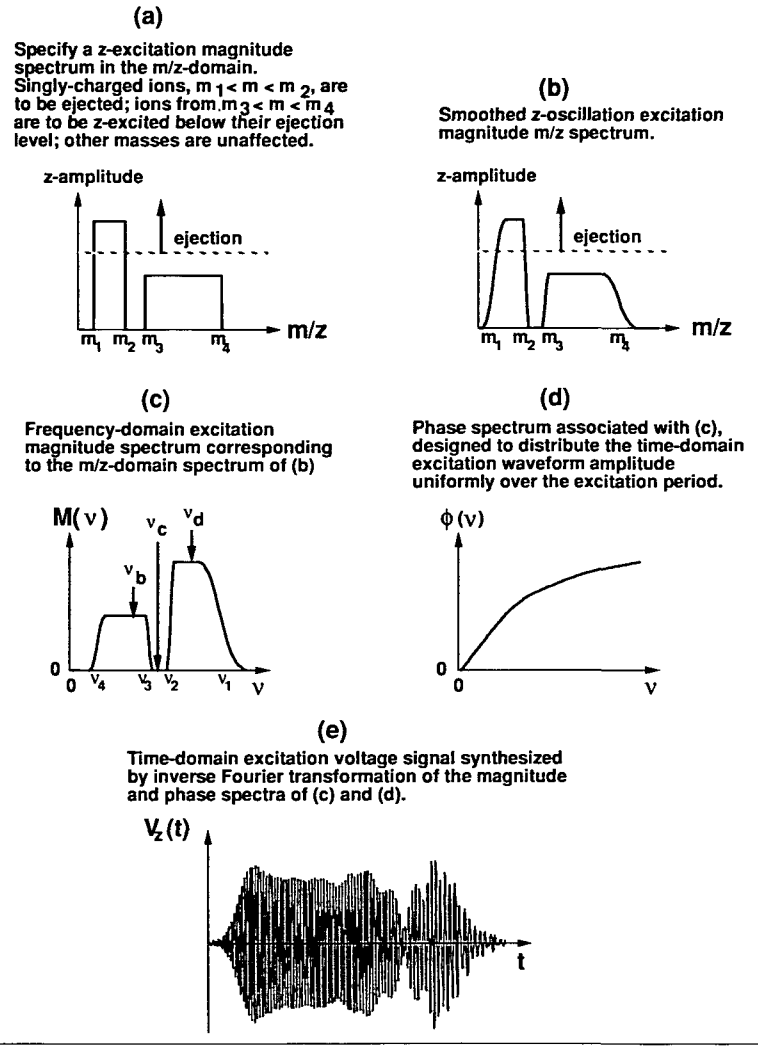

RADIAL ELECTRIC FIELD MINIMIZATION IN OPEN CELL GEOMETRIES FOR EXTERNAL SOURCE FTICR

*Victor H. Vartanian and D. A. Laude, Jr.; Department of Chemistry and Biochemistry, University of Texas at Austin, Austin, TX 78712-1167

The open-ended trap with trap electrodes positioned as a linear extension of the excite and detect electrodes is finding increased use in external source FTICR applications. Advantages include minimal electrode charging, greater gas conductance, and greater charged particle access to the cell interior. One distinction between the conventional closed cell and the open cell is the increased freedom in selecting electrode dimensions used to define the cell geometry. This offers the possibility of finding improved figures of merit for a cell of specified volume constrained by magnetic field homogeneity. Of particular interest is radial electric field minimization.

Five different cell designs were constructed and evaluated to experimentally verify possible reductions in radial electric field including a new type of open cell in which a single trapping electrode positioned in the cell center surrounded by the excitation and detection electrodes with a biased potential of opposite polarity. Thus to trap positive ions a negative potential is applied to the center electrode. This open cell geometry can be classified in a general scheme for open cells as the complement of a cell with positive trap potentials applied to narrow trapping rings positioned at the cell boundaries.

Cylindrical cells were appended to the analyzer side of a dual cell assembly within an Extrel 2000 3.0-T, 150 mm bore superconducting magnet controlled by a Nicolet 1280 data station executing Extrel FTMS software version 6.0r.1. Cells of 0.030" thick OFHC copper were mounted onto aluminum frames utilizing Teflon spacers. For the radial electric field data, benzene was introduced at 7.0×10^{-7} torr. Frequency shifts for the benzene were measured for each spectrum as a function of increasing trap potential.

For an open cell aspect ratio is defined as the distance between potential maxima located at the approximate midpoint of the trap electrodes ***c***, divided by cell width, ***a***. If the gaps between electrodes are considered negligible then ***c*** is approximately c_e (excite/detect dimension) + c_t (trapping dimension). Often the open cell is generalized as having equal electrode segments producing a cell of constant volume for a given aspect. This unnecessary restriction results in a radial electric field for the open cell that is similar to the closed cubic cell but inferior to the elongated cell (Figure 1). However the versatility of the open cell in the selection of electrode dimensions does not require that aspect ratio remain constant for a given cell volume. If ***a*** and ***c*** are kept constant within the homogeneous region of the magnetic field, c_t and c_e can be varied producing cells of varying aspect without changing cell volume. A range of potential well depths and radial electric fields are then possible.

For a cubic configuration where $c_t + c_e = a$, SIMION data indicates that the well depth for a 1.0 V applied trap potential is 0.328 V. Experimental benzene data for a 5 cm cubic open cell exhibits a frequency shift of -74.3 Hz/V at the cell center.

In an elongated configuration where $c_t \to 0$ and $c_e = 1.5a$ the well depth for a 1.0 V trap potential is 0.28 V. Experimental benzene data for a 7.5 cm x 5 cm cell exhibits a frequency shift of -21.8 Hz/V at the cell center. The actual cell was constructed with the actual trap electrode equal to 3/16".

For a compressed configuration where $c_e \to 0$ and $c = c_t$ the well depth is only 0.05 V. A 4 cm x 5 cm cell with aspect ratio of 0.8 exhibits a frequency shift of -380 Hz/V at the cell center. The actual cell was constructed with the excite electrode equal to 3/16".

Shimming is often used to correct for non-ideal fields in the trapped ion cell; specifically an effort is made to reduce the radial electric field. In this case, c_t is sectioned into n slices (here n = 2), electrostatically shimming the cell so that $c = c_{t1} + c_{t2} + c_e$. The well depth is 0.35 to 0.38 V

depending on the voltage on the shim. A 5 cm x 5 cm shimmed open cell with aspect ratio of 1.0 positioned in a 3.0 T magnet exhibits a frequency shift of -27.8 Hz/V at the cell center.

The complementary single trap electrode cell (Figure 2) traps ions in a potential depression of 0.22 V for a 1 volt applied potential. The excite isopotential contour exhibits linearity along the cell centerline despite the presence of the trapping ring in the center of the cell volume (Figure 3). The PFTBA spectrum in Figure 4 was collected at -2 volts applied (about -0.44V effective potential). Additional study is underway to evaluate the performance and potential utility of the trap. One possibility is that because externally generated ions do not have to overcome a potential barrier to enter the cell, a more efficient accumulated trapping process is possible.

SIMION data in Figure 5 reveals that increasing the cell aspect ratio decreases radial electric field and increases the homogeneous excite region. However the potential well depth decreases. A compromise open cell geometry can be utilized in which a cell approaching the geometry of the open elongated cell is used. For this type of cell, the radial electric field approaches the reduced magnitude of the closed elongated cell without the increase in cell length associated with the conventional open cell.

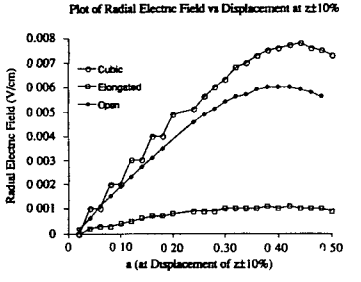

Figure 1

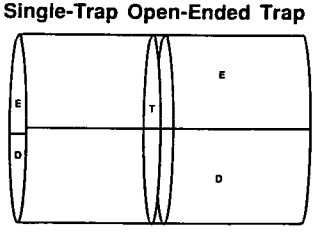

Figure 2

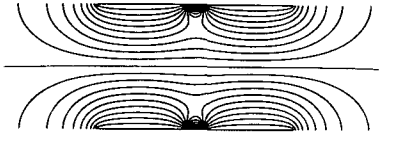

Figure 3

Figure 4

Figure 5

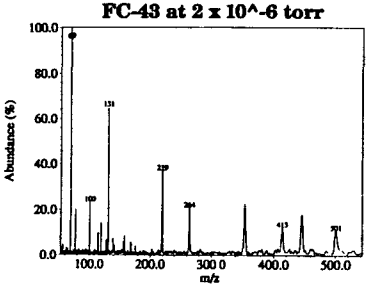

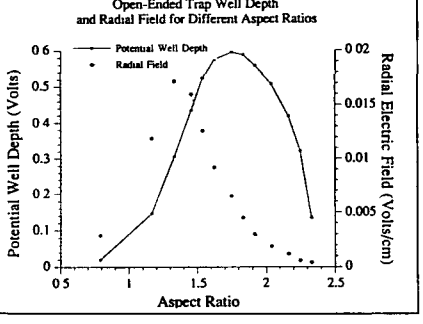

A NEW METHOD OF OPERATION FOR THE QUADRUPOLE ION TRAP

PAUL KELLEY, DON HOEKMAN AND STEPHEN BRADSHAW, Teledyne MEC, 1274 Terra Bella Avenue, Mountain View, CA 94039-7244

We have developed a new method of operation (1) that makes more efficient use of the space charge capacity of ion traps. In this new method, the ion trap is operating using a Filtered Noise Field (FNF). For the quadrupole ion trap, the new field is comprised of a 3-D quadrupole (Q) field and a notch filtered broadband signal (σ) that combines to form the FNF which traps, or operates on, only m/z's or mass ranges of interest (Figure 1). The broadband signal is composed of a sufficient number of frequency components with sufficient amplitude to present, by design, an effective power band that spans the secular motion of the trappable mass range of the ion trap. This broadband signal can be applied with sufficient power to, for example, resonantly eject all m/z's from an ion trap. The broadband signal can be generated by analog or by digital means and can be designed to be a known waveform. If, for example, the broadband signal is constructed by digital means to be a known waveform, it can be notch filtered in real-time to operate on the physical system (Figure 2). The broadband signal needs to be constructed only once and can be used in combination with the 3-D Q field to generate a wide variety of FNFs by using real-time notch filters.

The FNF can be used, for example, during the ion storage portion of an experiment to store only wanted m/z's. The wanted m/z's can be a single m/z, multiple adjacent or non-adjacent m/z's (Figure 3), a mass range, discontinuous mass ranges, or a combination thereof. Since frequency components are present with sufficient power at the unwanted m/z's, they are resonantly expelled while only wanted m/z's are being stored. This allows the dynamic range of an ion trap to be used more efficiently and results in increased sensitivity for the wanted m/z's. We are routinely observing one to three orders of magnitude improvement in sensitivity. The FNF can be used for a host of ion trap experiments such as Selected Ion Monitoring (SIM), Selective Reagent Ion Chemical Ionization (SRI-CI), MS, MS/MS, MS/MS/MS, etc. The development of FNF technology, for use with ion traps, also overcomes the present day limitations of chemical matrix effects such as identifying target compounds that co-elute or are masked by excesses of non-target compounds.

Reference: (1) P. E. Kelley, U. S. Patent 5,134,286;1992

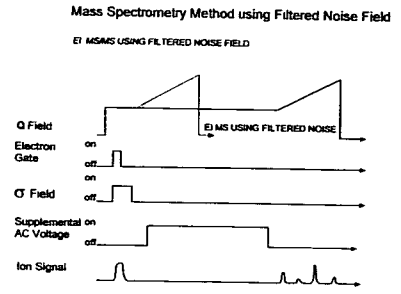

Figure 1 Electron Ionization MS and MS/MS Method of Operation for the Quadrupole Ion Trap using a Filtered Noise Field (FNF) In this example, the σ Field is used in combination with the Q Field to store only m/z's of interest during ionization.

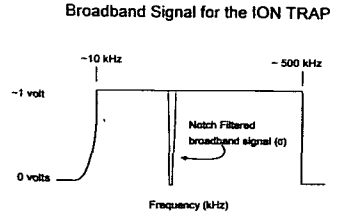

Figure 2. Broadband Signal for the Ion Trap. The broadband signal is composed of a sufficient number of frequency components with sufficient amplitude to present, by design, an effectively flat power band that spans the secular motion of the trappable mass range of the ion trap It can be notch filtered in real-time to create σ Fields The σ Fields can be combined with the Q Field to trap, or operate on, m/z's of interest.

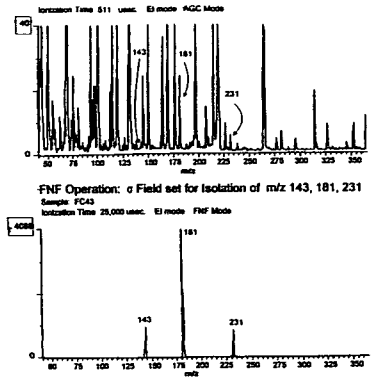

Figure 3. These data demonstrate the ability to isolate m/z's of interest and the resulting sensitivity gain by using an FNF with the quadrupole ion trap. Once isolated, the masses of interest can then be used for SIM or MS/MS.

Time Dependent Behavior of Multiply Charged Electrosprayed Ions Trapped in a Fourier Transform Ion Cyclotron Resonance Mass Spectrometer

James E. Bruce, Steven A. Hofstadler, Gordon A. Anderson, Steven L. Van Orden, and Richard D. Smith Chemical Sciences Department, Pacific Northwest Laboratory, Richland, WA 99352

The technique of electrospray ionization (ESI) has proven to be effective for the production of multiply charged gas phase ions and, as such, has been coupled to many types of mass spectrometers. Recent developments in this laboratory have led to the successful integration of an ESI source with a Fourier transform ion cyclotron resonance (FTICR) mass spectrometer and electrospray mass spectra of many proteins and glycoproteins have been acquired[1]. Time domain signals lasting longer than 80 seconds have been recorded for bovine insulin and ubiquitin. Although the theoretical resolution for these transients is ~3 million, a maximum resolution of only 700,000 was produced by Fourier transformation of the last 40 seconds of the insulin transient. Resolution produced by transformation of the entire data set was much poorer (~100,000, as shown in Figure 1) due to shifts in cyclotron frequencies observed during the evolution of the ion packets after excitation. The broadening as well as splitting of the isotope peaks, as illustrated in the inset of Figure 1, was found to be a result of cyclotron frequencies shifting toward higher frequency. The split appearance of the peaks is an artifact of the Fourier transformation of a time-dependent frequency. Fourier transformation of small segments of data at various times along these transients, shown for the 4+ charge state of bovine insulin in Figure 2, demonstrates very clearly how the detected *m/z*, and thus cyclotron frequency, varies over the course of the detection period.

The present work[2] illustrates successful attempts to correct the frequency shift present in the data and thus realize the ultrahigh resolution potential of long transients. Two different approaches for the correction of observed frequency shifts, both of which involve measuring and fitting the variation in detected *m/z* were employed, as shown in Figure 2. The first technique involved a frequency modulated-discrete Fourier transform (FM-DFT), where each test frequency of the DFT is modulated at the same rate as the measured frequency shift. The second and more highly optimized approach involved time-base correction of the raw data prior to fast Fourier transformation. This technique is effectively a post acquisition modification of the sampling frequency at a rate inversely equal to the fit obtained as described above. Magnitude mode Fourier transformation of the time-base corrected, apodized data produced a significant increase in resolution, 2.5 x 10^6 for the 4+ charge state of bovine insulin, as shown in Figure 3. Results obtained without apodization were of slightly lower resolution and produced slightly worse peak tailing toward lower *m/z*. A poor fit to the frequency shift at early times in the transient has been determined to be the cause of this tailing (apodization reduces the contribution of frequencies at these times) and consequently, a better fit is being developed. The present results demonstrate that correction for frequency shifts can provide higher resolution and, perhaps more importantly, higher mass measurement precision.

References:

1. B. E. Winger, S. A. Hofstadler, J. E. Bruce, H. R. Udseth, and R. D. Smith, *J. Am. Soc. Mass Spectrom.* 4, (1993) in press.
2. J. E. Bruce, G. A. Anderson, S. A. Hofstadler, B. E. Winger, and R. D. Smith, *Rapid Commun. Mass Spectrom.* submitted.

Figure 1

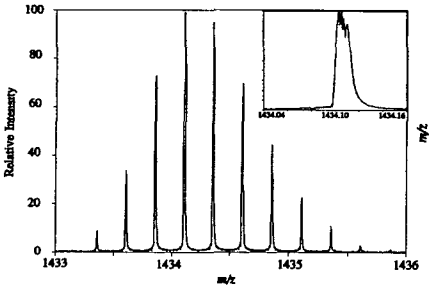

Figure 2

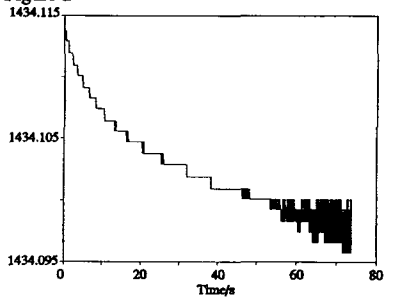

Figure 3

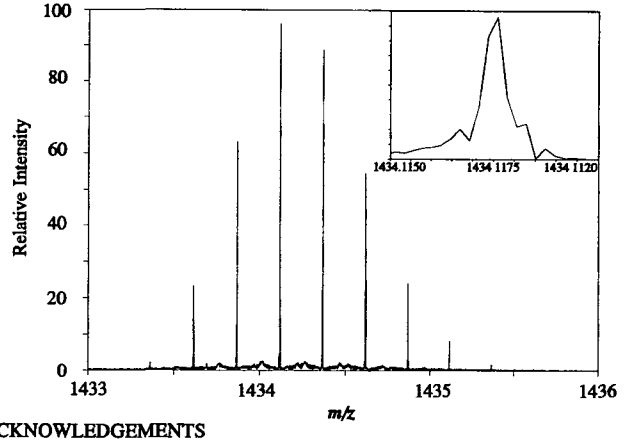

ACKNOWLEDGEMENTS
This research was supported by internal PNL exploratory research and through the U. S. Department of Energy. Pacific Northwest Laboratory is operated by Battelle Memorial Institute for the U. S. Department of Energy, through contract DE-AC06-76RLO 1830.

A Method of Increasing The Sensitivity for Laser Desorption in an Ion Trap Mass Spectrometer

Gregory C. Eiden, Mary E. Cisper, Michael L. Alexander, Philip H. Hemberger, and Nicholas S. Nogar
Chemical and Laser Sciences Division, Los Alamos National Laboratory.

In this work we describe laser desorption, carefully timed with respect to the finite risetime (~175 μsec) of the RF potential in the Finnigan ITMS apparatus.[1] Trimethylphenylammonium (TMA) iodide is ablated by a 308 nm pulse, phase loced to the RF. The probe tip is flush with the inner surface of the ring electrode. Laser desorbed ions, produced when the RF potential is low, can penetrate the trap, but are unable to escape because by the time they have reached the center of the trap, the increase in the RF potential produces a deeper trapping well (Fig. 4). The most intense peaks in the mass spectrum of TMA occur at m/z 58, 121, 136 (parent), 197, 273, 349, 423, 499, and 575; these peaks correspond to methyl loss from TMA (121) and sequential addition of a 76 Da moiety to the 121 mass (197, 273, etc). Compared to the m/z 121 intensity, we observe approximately twice as many ions above m/z 121; that is, most of the observed ions are from ion-molecule reactions occurring in the desorbed plume. Fig. 1 shows the 121^+ signal detected at different values of V_{max}, the steady state RF potential, as a function of laser-to-RF delay. The signal increases by several orders of magnitude at short delays. The maximum signal depends on ion mass, laser-to-RF phase and V_{max}. The maxima shown in Fig. 1 do not coincide when the data are plotted against pseudopotential well depth. However, the pseudopotential well model only applies near the center of the trap and at constant RF potential. Fig. 2 shows the time delay at which the maximum signal occurs (i.e., the maxima of the curves in Fig. 1) as a function of V_{max} and for three different ions. The maximum trapping efficiency occurs at longer delays for heavier ions. This also corresponds to higher RF potentials, since the RF potential is closer to reaching V_{max} at long delay times. We have also measured the signal versus laser-to-RF delay for 20-50 nsec time increments, thereby mapping out the laser-to-RF phase dependence of the signal. Fig. 3 shows the phase dependence for m/z 197 at 40-95 μsec delays, which covers the full range of the 760 V curve in Fig. 1. Zero phase angle corresponds to firing the laser at the positive slope zero crossing of the RF potential. The signal maxima occur at a phase of ~270°, suggesting that deceleration near the ring electrode by the rising RF potential can aid in trapping. The data show that the phase at which the maximum signal occurs shifts to lower values for longer laser-to-RF delays. We have also observed a mass dependence of the phase shift at short delays. For a laser-to-RF delay of 40 μsec and V_{max} = 508 V, the maxima in the 121 and 273 signals occur at 280° and 340° phase respectively. At delays of 75 μsec or longer, the 121^+ and 273^+ signals are in phase. In the future, we will present a quantitative model of these results and new data on the ablation of other atoms and molecules and the effects of different ring DC and RF waveforms and endcap AC voltages on the trapping efficiency.

1. G. C. Eiden, M. E. Cisper, M. L. Alexander, P. H. Hemberger, and N. S. Nogar; J. Amer. Soc. Mass Spectrometry; accepted.

Presented at the 41st ASMS Conference on Mass Spectrometry

Figure 1 121^+ Signal vs Laser-to-RF Delay

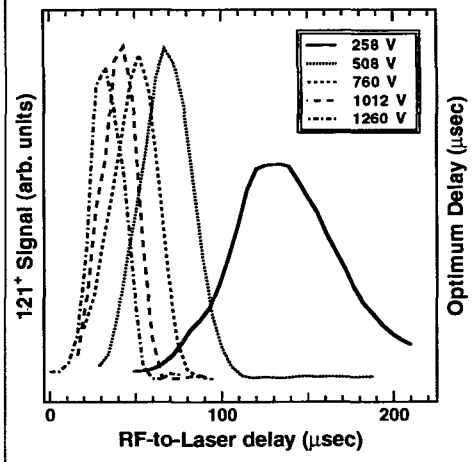

Figure 2 Optimum Laser-RF Delay versus Max RF

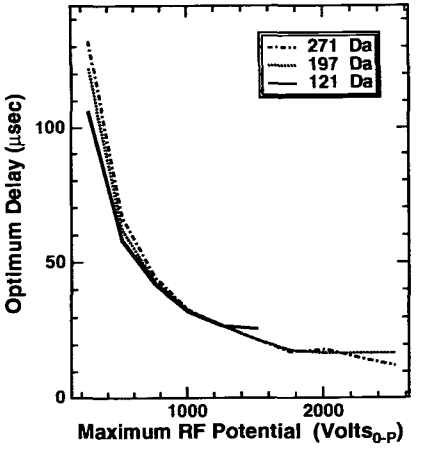

Figure 3 Phase of Max Signal for various Laser-RF Delays

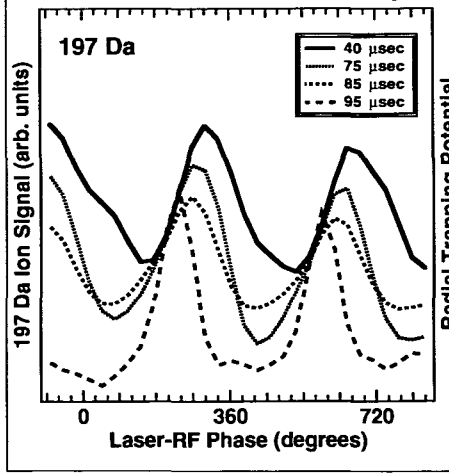

Figure 4 Change in Potential Barrier as Ions cross the Trap

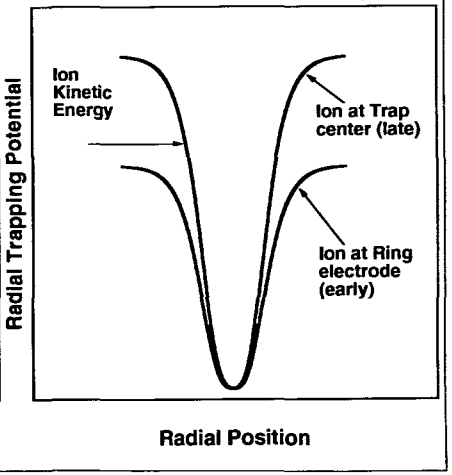

The Reduction of Matrix Effects in Quadrupole Ion Trap Mass Spectrometry

*M.E. Bier, J.N. Louris, D.M. Taylor, J.C. Schwartz, and M.D. Uhrich
Finnigan MAT, San Jose, CA 94025

Matrix effects in ion trap mass spectrometers are the result of a high abundance of non-analyte ions and/or neutral reactive molecules. Matrix ions may be filtered from the ion trap by the application of tailored waveforms, but these waveforms do not directly affect the abundance of neutrals. Neutrals may react with analyte ions and result in "impure" spectra. Ion/molecule reactions occur in the ion trap even at low pressures of neutrals because of the 10 to 1000 ms of ion storage time. Ion/molecule reactions such as self-CI can be reduced by orders of magnitude by placing the ion source external to the trap[1].

Three ion trap configurations were used in this study: a Finnigan ITS40, an external source ion trap system, and an external source ion trap system with a baffle for improved differential pumping. The external ionization systems included: a TSQ-70 ion source, a scan editor, 670 L/sec turbo pumping (split for the differential pumping configuration), and a 10 kv conversion dynode. A GC was interfaced to all instruments.

Figure 1 shows that for 1 μg of hexobarbital (MW 236) no $(M+H)^+$ is observed in an external ionizing ion trap. A 1μg methyl stearate (MW 298) mass spectrum shows m/z 299 $(M+H)^+$ as the base peak using internal ionization. The ratio of $299^+/298^+$ for methyl stearate is dramatically improved using external ionization as shown in Figure 2. An additional reaction time of 500 ms, however, allows time for methyl stearate to form the "self-CI" m/z 299 and adducts as shown in Figure 3. The mass spectrum of 1 μg methyl stearate obtained after replacing the baffle and waiting for the 500 ms shows little evidence of self-CI and very little adduct formation. This adduct formation was further explored by removing low mass EI fragment ions by using a low mass rf cut-off. The data suggest that many fragment ions form adducts with the neutral analyte species. A methyl stearate sample impurity (MW 270) was identified by GCMS and is believed to also contribute to this adduct formation. Ion m/z 227 from methyl stearate was isolated and allowed to react with neutral analytes during a 500 ms reaction period (see Figure 4). The adduct ions formed are from the attachment of MW 270 (impurity) and 298 to the isolated ion m/z 227. Some of the other ions observed are believed to be formed during the isolation period. By increasing the rf low mass cut-off a reduction in the $299^+/298^+$ ratio is observed for methyl stearate (Figure 5). This ratio reduction suggests that m/z 299 may be formed from proton transfer from many EI fragment ions.

Hart and coworkers[2] used 1,4-dichlorobenzene and an ITMS (internal ionization) to study the daughter ion m/z 111 reaction with methane to form m/z 91. In our work, external methane CI followed by MS/MS showed extensive daughter ion/molecule production of m/z 91 in the non-baffled ion trap system. A baffle placed between the source and ion trap reduced the pressure of methane and thus improved the $91^+/111^+$ ratio significantly (see Figure 6).

1. M.E. Bier, R.E. Hartford, J.R. Herron, and G.C. Stafford, *38th ASMS Conf.*, Nashville, TN (1991) 538.
2. K.J. Hart, S.A. McLuckey, and G.L. Glish, *J. Amer. Soc. Mass Spectrom.* 3 (1992) 549.

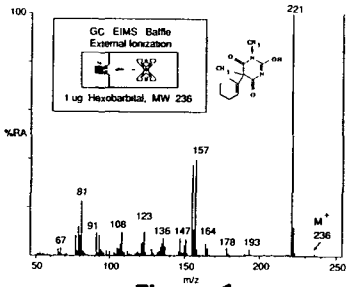

Figure 1

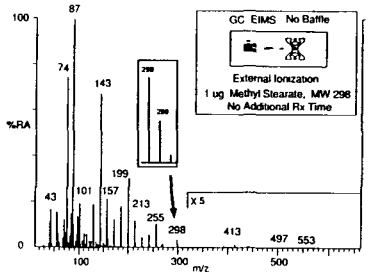

Figure 2

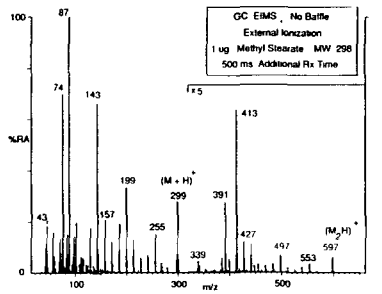

Figure 3

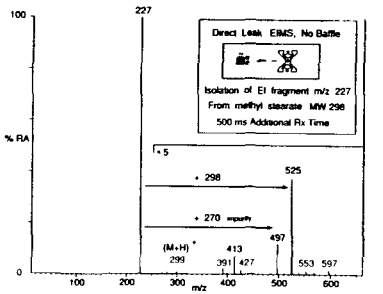

Figure 4

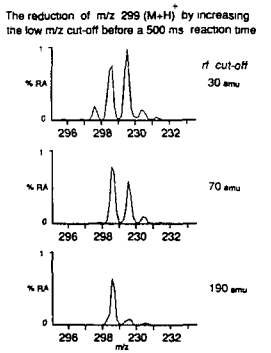

Figure 5

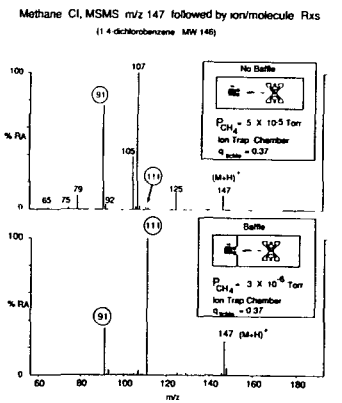

Figure 6

Protein Structural Elucidation by Electrospray Ionization Tandem Fourier-Transform Mass Spectrometry

Deborah S. Gross, Paul D. Mills, Lydia T. Tien, Paul J. Johnson, Evan R. Williams
Department of Chemistry, University of California, Berkeley, CA 94720

Electrospray ionization has become a powerful method for obtaining high accuracy molecular weights of large peptides and proteins. The combination of ESI with Fourier-transform mass spectrometry has many exciting possibilities for extracting even more information from biomolecules through high resolution and MS^n measurements including the ability to identify mutations in proteins, and sequence proteins of unknown structure, even those present in mixtures, using multiple stages of MS. In cases where sample quantity is limited, such as detecting biomolecules separated by capillary electrophoresis, high sensitivity is of key importance.

For this, we are developing einzel lens ion introduction system based on the pioneering work of Smalley (1), for guiding electrospray-generated ions into the FTMS cell (Figure 1). Ions are formed using a two-stage differentially-pumped electrospray source with a heated metal capillary introduction system (2). Ions are trapped in an elongated 5x5x10 cm cell and detected at a cell pressures of ~2 x 10^{-8} and magnetic field strength of 2.7 T.

Spectra of equine myoglobin (MW 16,951 Da) and bovine cytochrome C (MW 12,231 Da) obtained with this system are shown in Figure 2. We find the charge distributions for a variety of peptides and proteins are consistently at a higher *m/z* ratio (lower charge state) than expected. For example, our charge distribution for myoglobin peaks at the +14 charge-state vs +18 measured previously by ESI/FTMS (3). This appears to be a function of our source design rather than our ion introduction/detection system and is currently under investigation.

Ion introduction efficiency is estimated by comparing electrospray current measured on the conductance limit in the first high vacuum stage to the current measured on the back trapping plate. In preliminary experiments with cytochrome C, we measure 7 pA on our rear trapping plate corresponding to a transfer efficiency of ~18%. Acceleration voltages as low as 200 V result in a negligible decrease in ion transfer efficiency, but efficiency rapidly decreases to zero below this voltage.

Ions are trapped using static trapping voltages (4); three volts was found to provide the highest signal for both gramicidin S (MW 1140.7 Da) and myoglobin (MW 16,951 Da), despite the nearly 15-fold difference in mass. This is inconsistent with a supersonic expansion taking place in our electrospray source, as ion energy would be expected to increase nearly linearly with mass resulting in more efficient trapping at higher voltages. For cytochrome C, a S/N of 13 is obtained with 10 s ion introduction corresponding to 9 picomoles of sample introduced. Our trapping efficiency is estimated to be approximately 0.001% for these ions, and remains a key area for future improvement.

With our current cell pressure, a resolution of 14,000 has been obtained for the resolved isotopes of the +3 charge-state of melittin (MW 2845 Da). From the separation between isotopes, the charge-state of an ion can be directly determined, an important advantage for interpreting MS^n spectra of large proteins.

Acknowledgements

We gratefully acknowledge support from the Beckman Foundation, NSF, SACP, Exxon Foundation, and Extrel FTMS, Millipore Corp.

References

1. Alford, J.M.; Williams, P.E.; Trevor, D.J.; Smalley, R.E. *Int. J. Mass Spectrom. Ion Proc* **1986**, *72*, 33-51.
2. Chowdhury, S.K.; Katta, V ; Chait, B.T *Rapid Commun. Mass Spectrom.* **1990**, *4*, 81-87.
3. Henry, K.D.; Williams, E.R.; Wang, B.H.; McLafferty, F.W.; Shabanowitz, J.; Hunt, D.F. *Proc Natl. Acad Sci. USA* **1989**, *86*, 9075-9078.
4. Hofstadler, S.A.; Laude, D.A.Jr *J. Am. Soc. Mass Spectrom.* **1992**, *3*, 615-623.

Figure 1

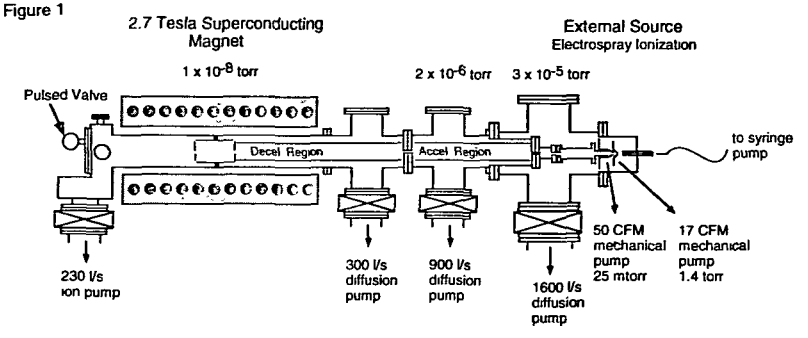

Figure 2

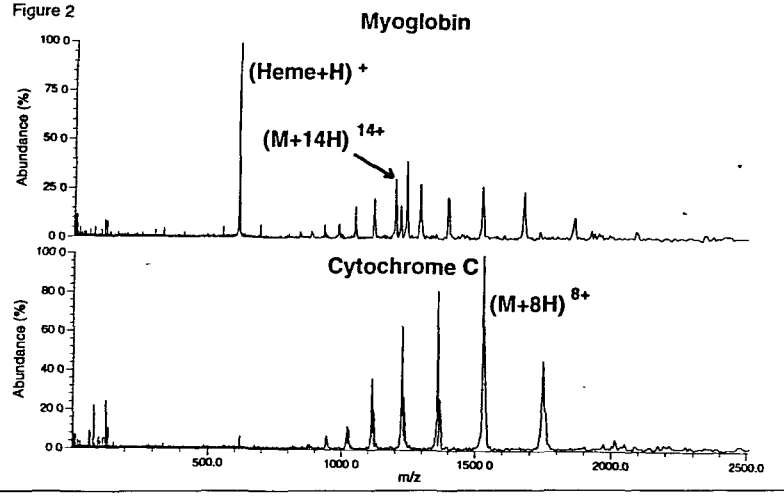

ION TRAP MASS SPECTROMETRY COMBINED WITH INDUCTIVELY COUPLED PLASMA/MASS SPECTROMETRY (IT-ICP/MS)

*Charles J. Barinaga and David W. Koppenaal, Materials and Chemical Sciences Center, Pacific Northwest Laboratory,** PO Box 999, Richland WA 99352

We have been intrigued by the possible gains that might be obtained by combining the robust, intense ion source of an inductively coupled argon plasma (ICP) with the unique features of a three dimensional quadrupole mass spectrometer (ion trap or ITMS), claimed by many to be the most sensitive of mass spectrometers. The effectiveness of an ICP to yield ions at high efficiency using various sample introduction schemes is demonstrated by the exploding use of ICP/MS in elemental analysis (1). The current combination of an ICP with a linear quadrupole mass filter, although very effective, has certain limitations that might be circumvented. The ICP and the vacuum interface yield significant ion currents (possibly hundreds of nanoamps) of argon, argon polyatomics (e.g. Ar_2^+, ArO^+, $ArCl^+$, ArN^+, ArH^+, $ArOH^+$) and other matrix related polyatomics (e.g. ClO^+). The limited mass resolution capability of linear quadrupoles precludes the possibility of separating nominally isobaric ions, both analyte-interferant and analyte-analyte. Sensitivity, although impressive, is limited by instantaneous signal-to-noise levels. The ITMS could help in these areas by providing collisionally induced dissociation (CID) capabilities to reduce the polyatomic ion interferences, by offering greater mass resolution using slow scan techniques, and by improving detection and abundance sensitivity using prolonged trapping times and selected ion ejection techniques.

We were encouraged by the reports of successful external ion injection (2) and atmospheric pressure sampling with ion traps (3). To avoid anticipated complications, including space charge effects and unwanted ion/atom or ion/molecule reactions from the high intensity matrix ions during ion injection, we decided to employ a notch-filtering linear quadrupole (4) preceding the ion trap (5) in order to selectively filter out the unwanted ions (e.g. Ar^+ and others).

A prototype instrument combining an ICP, a notch-filter linear quadrupole, and an ITMS has recently been fabricated, as illustrated in Fig. 1. The IT-ICP/MS utilizes major and modified components from a Fisons/VG PlasmaQuad I and a Finnigan MAT ITMS. Analyte ions from an ICP and prefilter quadrupole can be injected into an ion trap and trapped with a helium pressure of about a millitorr. No estimate has yet been made of transmission and trapping efficiencies, however the current detection limit for lead is better than one part-per-billion. At this time no extensive efforts at sensitivity optimization have been made thus some improvement is expected. Many metals yield good responses as unadducted ions (see Fig. 2), however certain metals (U, Th, La, other strong MO formers) react with background water and oxygen to produce significant levels of metal oxides and hydroxides (Fig. 3). Different pumping arrangements and direct heating of the trap itself will likely decrease this effect. Water from the nebulized aqueous samples appears to not contribute as a dry plasma of laser ablated LaO yielded the same oxides and hydroxides as the aqueous sample. Surprisingly the matrix-related polyatomic interferants do not survive the multiple collision environment in the IT region and are completely eliminated from the spectrum without resorting to MS/MS or high mass resolution techniques. In addition the trapped argon ions undergo relatively fast charge exchange reactions and disappear from the spectrum after approximately 10 ms of unexcited

reaction time thus allowing the observation of ^{40}Ca (6), the most prominently interfered m/z in ICP/MS. The use of rf-only or rf/dc notch-filter modes with the linear quadrupole has also been demonstrated in precluding argon ions from entering the ion trap.

These initial results are encouraging. Additional experiments using improved mass resolution techniques, enhanced abundance sensitivity approaches, and broadband noise filtering methods are planned. Development of an optimized atomic ion trap mass spectrometry system is also underway.

1. Koppenaal, DW *Anal. Chem.* 64 (1992) 320R-342R.
2. JN Louris, JW Amy, TY Ridley and RG Cooks, *Int'l J Mass Spec. and Ion Proc.*, 88 (1989) 97-111.
3. SA McLuckey, GL Glish, and KG Asano, *Anal. Chim. Acta*, 225 (1989)25.
4. RE Reinsfelder and MB Denton, *Int'l J Mass Spec. and Ion Proc.*, 37 (1981) 241-250.
5. KL Morand, SR Horning and RG Cooks, *Int'l J Mass Spec. and Ion Proc.*, 105 (1991) 13-29.
6. SA McLuckey, GJ VanBerkel, DC Duckworth, and RK Marcus, *Anal. Chem.*, 60 (1992) 1606.

**Operated for the U.S. Department of Energy by Battelle Memorial Institute under contract DE-AC06-76RLO 1830

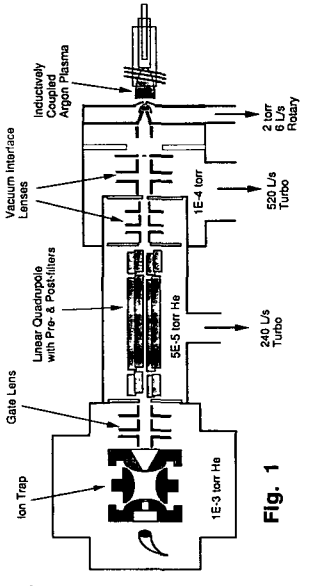

Fig. 1

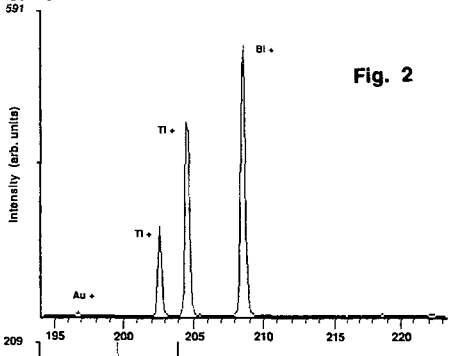

Fig. 2

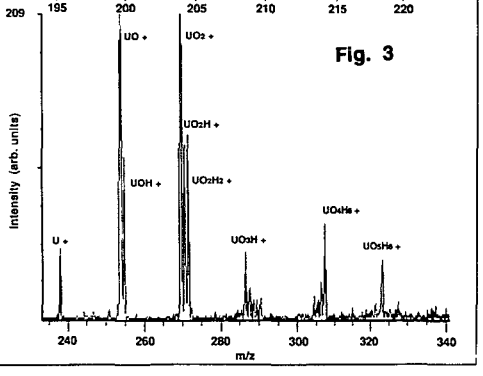

Fig. 3

Effects of Ion Trap Parameters on Mass Axis Stability: Influence of Manifold Temperature, Pressure and Axial Modulation Voltage on Mass Spectra of Hydrocarbons

Robert D. Brittain, David Speltz and Barbara Bolton, Varian Chromatography Systems

Although most molecules analyzed by ion trap GC/MS provide library-searchable mass spectra under a wide range of conditions, some compounds have been reported with low molecular ion abundance and/or non classical mass spectral ion intensities. Lower molecular and fragment ion intensities may be attributed to unimolecular and bimolecular decomposition processes that can occur during the storage process. We have studied several classes of molecules vulnerable to decomposition on the time scale of ion storage. We used a constant analyte flow to rapidly characterize the dependence of ion stability upon instrument tuning parameters. Using this approach, it is possible to recommend ranges of column flow rate, Axial Modulation (A/M) voltage and ion trap manifold temperature which minimize molecular ion decomposition.

A constant flow of analyte was introduced from a heated glass vial connected via the CI port of a Varian Saturn II GC/MS system The mass spectrometer was auto-tuned and spectra in either peak profile or centroid mode were observed in the instrument page as instrument parameters were varied. Helium flow through a DB-5 30M x 0.25 mm ID column was calculated from air sample retention time

Figure 1 shows the menthol ion at 138u with He flow rates from 0.5 to 1.4 ml/min. The peak profile asymmetrically broadens (doubling the FWHM) and appears to shift to lower m/z with increasing helium flow A/M reduction from 4.0V to 3.0V is shown to improve resolution for a given flow rate. Reduction of manifold temperature from 220°C to 100°C also improved resolution of this ion in a similar manner Results for other compounds are shown in the poster presentation The peak broadening phenomenon is consistent with a premature decomposition of unstable ions (subject to collisional dissociation) as they approach resonant ejection from the ion trap into the multiplier. The process would be:

$$(A^+)^* + He \text{ -------> } B^+ + C$$

where $(A^+)^*$ is the unstable molecular or fragment ion and B^+ is a lower-mass fragment that will be ejected from the ion trap and detected by the multiplier as soon as it is formed. High A/M voltage, flow rate, and manifold temperature increase the number and/or energy of bimolecular collisions One possible effect of the asymmetrical peak broadening in Figure 1 is mis-assignment of the molecular ion M to a value of M-1. He flow rate ≤ 1 ml/min, ion trap manifold temperature ≤ 120°C, and A/M ≤ 3V all reduce decomposition of unstable ions. Shown in Figure 2 is the mass spectrum of heptadecane run at optimum trap conditions. Note the excellent levels of molecular ion in the ion trap spectra compared to the NIST library entry. For some hydrocarbons, the molecular ion is an order of magnitude higher in the ion trap spectrum than the NIST library entry.

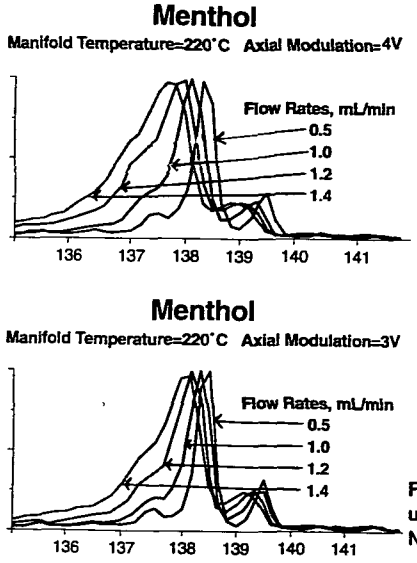

Figure 1. Peak Profile vs. He Flow Rate at Two Different A/M Voltages

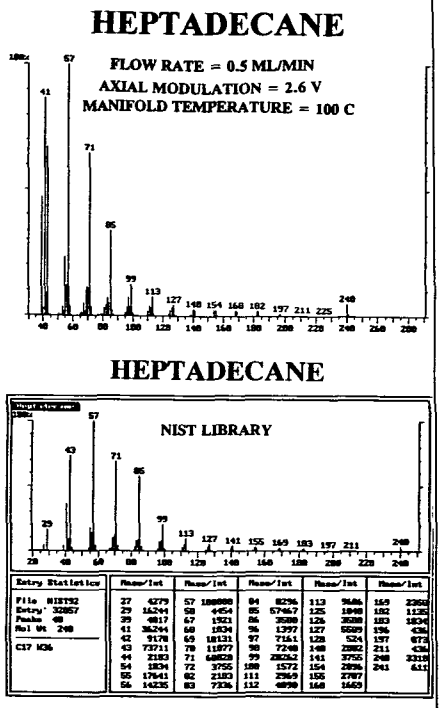

Figure 2. Mass Spectrum of Heptadecane under Optimized Ion Trap Conditions vs. NIST Spectrum

OPTIMIZING ION ACCUMULATION IN EXTERNAL SOURCE FOURIER TRANSFORM MASS SPECTROMETRY

C. F. Ijames and S. P. Markey, Section on Analytical Biochemistry, National Institute of Mental Health, Bethesda, MD 20892.

A differentially pumped external source permits Fourier transform mass spectrometry to incorporate conventional high pressure sources, while maintaining the low cell pressure necessary for optimum performance. Ions are transported through one or more pressure-limiting orifices, through the fringe field of a superconducting solenoid magnet, and delivered to the FTMS cell. Transport can be achieved via radio frequency quadrupoles or electrostatic lenses. The greatest difficulty lies in trapping the injected ions for analysis. Gated trapping (manipulating the trap potentials to admit brief pulses of ions) suffers from a very low duty cycle, 0.5% to 0.01%.

To increase FTMS detection sensitivity, a method of continuously accumulating ions in the cell for an extended period of time, raising the duty cycle to greater than 50 %, is needed. Because the trapped ion cell is a symmetric box, no static arrangement of potentials should result in accumulation of ions injected on the z axis. However, there have been reports of ion accumulation with static trap potentials. To explain this the following mechanism is proposed. Ions whose kinetic energy is slightly less than the trap potential will be able to enter the cell because of the potential depression in the center of the entrance hole in the trap plate. If the entrance is not on the z axis or a potential is applied between the transmitter or receiver plates to move the electrical axis of symmetry off of the z axis, the ions will have a non-zero magnetron radius, and thus will undergo magnetron motion around the electrical axis of symmetry. After reflection at the rear trap plate, the returning ions will no longer approach the potential depression at the entrance hole, but will instead approach a solid region and encounter the full trap potential. The ions will again be reflected and thus trapped. Only if the combined trapping and magnetron oscillations return the ions to the entrance hole will they be able to exit. Any collisions will most likely redirect some energy into the x-y plane and reduce the trapping oscillation amplitude, further closing the trap. Ions whose kinetic energies fall between the trap potential and the minimum potential in the cell opening will be trapped. Deflection plates can be added to the cell opening to move ions off of the z axis (by ExB motion) as they enter the cell, allowing the electrical axis to remain on the z axis for best detection efficiency and maximum ion capacity. Deflection plates also define the potential of the cell opening independently of the trap potential to permit accumulation of ions with a wide range of kinetic energies. The ion cloud will be in the form of an annular cylinder centered on the z axis.

The ratio of the trap oscillation period to the magnetron period in a cubic trap is: $(A\ V_t\ m\ /\ q\ d^2\ B^2)^{0.5}$, where A is a geometry factor (1.3869 for cubic cells), V_t is the trap potential, m is the mass of the ion, q is the charge on the ion, d is the trap plate separation, and B is the magnetic field strength. Under typical trapping conditions an ion with m/z 39 will traverse 1.3 % of a magnetron orbit before returning to the entrance, while an ion with m/z 2000 will traverse 9.2 %. This was experimentally confirmed by determining that the optimum deflection voltage decreases as the mass-to-charge ratio increases. Also, the detected signal intensity was found to increase with increasing pressure, to a maximum at 5×10^{-7} torr where the intensity was 70 times greater than that recorded at 1×10^{-8} torr.

Because the signal increases with accumulation time while the noise remains constant, the maximum signal-to-noise in a given time period will be achieved by accumulating for the entire period, followed by a single excite/detect sequence. For currents of 15 pA and greater, the space charge limit of the cell is reached within approximately 90 seconds. For lower currents, however, longer accumulation periods yield approximately constant signal intensity, so that very weak ion currents can not be completely compensated for by increasing the accumulation time. In this case averaging of 90 to 120 second accumulations is best.

Experiments were performed on a 3 tesla FTMS-2000 (EXTREL FTMS, Madison, WI) with a differentially pumped external source, equipped with electron impact, thermal ionization, and single stage electrospray ionization sources. A computer-controlled gate valve separates the external source chamber and the first trapped ion cell. There are deflection electrodes at the entrance to the cell. To maximize mass resolution without sacrificing sensitivity, the capillary in the ESI interface was chosen to yield a first cell pressure of $2\text{-}2.5 \times 10^{-7}$ torr. Spectra of proteins can be acquired by averaging 2 to 4 accumulations of 90 seconds each, while electrospraying 10 to 100 μM solutions in water/methanol/acetic acid at flow rates of 2 to 8 μL/min.

Results include spectra of Gramicidin S (30 μM, 4 scans, signal-to-noise ratio 50 for the $[M+Na]^+$ ion with m/z 1163) and Cytochrome C (100 μM, 4 scans, signal-to-noise ratio 30 for the $[M+8H]^{+8}$ ion with m/z 1542). The mass resolution can be improved by closing the gate valve after the accumulation period. A 45 second accumulation followed by a 15 second delay to reach the system base pressure, 0.5×10^{-8} torr, allowed the $[M+Na]^+$ ion of Gramicidin S to be detected with a resolution of 90,000. The spectrum of bovine insulin, molecular weight 5733, was recorded at a resolution of 8,500 for the $[M+3H]^{+3}$ ions with m/z 1911, and 14,000 for the $[M+4H]^{+4}$ ions with m/z 1435. Four scans were averaged, with an accumulation time of 45 seconds per scan. The concentration was 100 μM and the flow rate was 3 μL/min.

ELECTROSPRAY ON AN ION TRAP MASS SPECTROMETER: COMPARISON OF AXIAL VS. DIAGONAL INJECTION OF IONS INTO THE TRAP

Robert D. Voyksner and Hung-Yu Lin, Analytical and Chemical Sciences, Research Triangle Institute, P. O. Box 12194, Research Triangle Park, NC 27709

INTRODUCTION

The majority of work using external soft ionization sources involves the axial injection of ions into the ion trap mass spectrometer (ITMS). Axial injection has limited trapping efficiency resulting in a loss of up to an order of magnitude of ion current. An alternative method that may prove more efficient involves injecting the ions diagonally (on the ion trap asymptote) into the trap. This method should minimize the losses from ions with improper energies to cross field lines to enter the trap and provide a longer distance for collisional dampening ions injected into the trap. This paper reports on the optimization of axial and diagonal ion injection for electrospray-ITMS. The parameters that were evaluated for each mode of ion injection include helium gas pressure, q_z value during ion injection, desolvation times and ion energy.

EXPERIMENTAL

Sample: Arginine (mw 174) and gramicidin S (mw 1141) 100 ng/µL introduced at 2 µL/min in 50% ACN in water, 1% acetic acid.

Electrospray: Analytica of Branford Electrospray interface modified with a tubular lens to fit into the end cap and serve as a gate.

ITMS: Finnigan MAT ITMS modified for electrospray interface as described in Anal. Chem., 65, 451-456, 1993, for axial ion injection. The ion trap was modified to rest on a diagonal with the multiplier mounted on the trap assembly for diagonal ion injection.

The following parameters were optimized in the ranges given in the evaluation: end cap aperture 1-6 mm, ionization time 0-200 ms, helium pressure 2-9 x 10^{-4} torr, q_z 0.02 - 0.6, ion energy (skimmer 1), 10-50 V, desolvation time 0-200 ms.

RESULTS AND DISCUSSION

The diameter of the ion entrance aperture in the end cap was varied from 1-6 mm. It was determined that a 3-4 mm end cap opening was optimal for ion injection. Diagonal injection was less dependent on the opening diameter, showing a broad optimum. Larger end cap openings resulted in a decrease in signal levels possibly due to inhomogeneities in the trapping field, which are less important with diagonal injection due to the location of the opening in the edge of the end cap.

Ion injection time into the trap indicated that both axial and diagonal modes had a similar optimal time (50-70 ms) for loading the trap with ions. The diagonal mode appeared to fill the trap faster, possibly indicating better trapping or ion injection efficiency. Longer ionization times appeared to decrease signal levels due to space charging, as well as, decreased mass resolution.

The ion energy (set by skimmer 1, on the electrospray interface) for injecting ions into the trap showed similar patterns between axial and diagonal injection. However, the optimization curve for ion energy was mass dependent. Arginine

showed a broad optimum while gramicidin S exhibited a narrow optimum between 20-30 V. These patterns were most likely due to ion transmission and collisional dampening of the different mass ions.

Helium pressure played a major role in optimizing signal level and the qualitative appearance of the spectra. In general, higher helium pressures were optimal for trapping ions. However, there is a mass dependence in which lower molecular weight ions are trapped at lower pressures while higher molecular weight compounds (gramicidin S) are efficiently trapped at the highest operating pressures. This trend can be explained in terms of the inability of helium to collisionally dampen high mass ions relative to low mass ions. The qualitative appearance of the mass spectra for arginine and gramicidin S could be drastically different, depending on the helium trapping pressure. To enhance trapping of high mass ions, pulsing helium into the trap during ion injection was investigated. In this way, high helium pressure could dampen the ions, then a one second pump out time reduced the pressure before mass analysis was initiated. The pump out time reduced the pressure by a factor of 3-4, minimizing multiplier noise and mass spectral peak broadening.

The q_z for ion injection was nearly identical for axial and diagonal injection. The q_z value was mass dependent for both modes of ion injection with arginine optimizing near a q_z value of 0.15 and gramicidin S near a q_z value of 0.05.

Desolvation time was very important for diagonal ion injection. Diagonal ion injection required a long desolvation time to generate the optimal signal intensity. On the other hand, axial ion injection exhibited about the same signal levels over the desolvation times evaluated. It appears the diagonal ion injection favors trapping lower energy solvated ions (compared to axial mode), therefore requiring some collisional warming to desolvate these ions to generate $[M+H]^+$ ions. It appears that ions trapped in the ITMS that are injected diagonally are less energetic and/or do not undergo collisional activation in the trapping fields. Also, the absolute intensities for parent ions for the test compounds (arginine and gramicidin S) were slightly greater for diagonal ion injection compared to axial injection.

CONCLUSIONS

The optimal ionization time, helium pressure, q_z and ion energy for axial and diagonal injection of ions into the trap were similar. Furthermore, the helium pressure, q_z and ion energy exhibited more dependence on m/z values of the ions that are trapped than the mode of ion injection. The desolvation time was the major difference between the two modes of ion injection. Longer desolvation times were necessary for diagonal injection to minimize cluster formation. Diagonal injection appeared to trap lower energy ions, showing less fragmentation and slightly better sensitivity compared to axial ion injection.

ACKNOWLEDGEMENT

This work was supported by NIDA, Grant No. DA 06315 and EPA Cooperative Agreement No. CR-819555-01.

Off-Center ICR Cubic Ion Trap: Reduction of Space Charge and Manipulations of Coherent Magnetron Motion

Ruidan Chen, Shenheng Guan, and Alan G. Marshall†
Dept. of Chemistry (and Biochemistry†), The Ohio State University,
120 W. 18th Avenue, Columbus, OH 43210.

Here we describe two kinds of experiments based on an ICR cubic ion trap in which benzene molecular $C_6H_6^+$ ions are formed along an axis parallel to the magnetic field, but displaced by a distance (magnetron radius) from the trap symmetry axis (see Fig. 1). First, if the ionization event is long compared to the magnetron period, $(1/\nu_m)$, ions spread out along the surface of a cylinder at the magnetron radius. Space charge (and its resultant shift in the effective cyclotron frequency, ν_+) is greatly reduced (see Fig. 2), and signals at $\nu_+ - \nu_m$, ν_c, and $\nu_+ + \nu_m$ appear due to the strong coupling of ion magnetron motion with ion cyclotron motion (see Fig. 3). Of these, the signal at ν_c yields ion mass-to-charge ratio directly (unaffected by trapping potential): $m = (qB/2\pi\nu_c)$, for simple mass calibration. Moreover, by asymmetric detection, we can in addition detect a signal at twice the trapping frequency.

Alternatively, if the ionization event is short compared to the magnetron period, then magnetron motion is coherent. Conversion of coherent magnetron motion to coherent cyclotron motion [1, 2], may be visualized by either dipolar detection (at ν_+) or quadrupolar detection (at ν_c and $2\nu_+$) as a function of the product of excitation amplitude and duration (see Figs. 4&5). Fig. 4 shows the detected signal after different excitation periods. In Fig. 5, the solid lines are theoretical curves and the circles are experimental data. Coherence of cyclotron motion may be observed directly by measurement of the signals induced by two sequentially produced ion packets. Different peak height oscillation patterns are observed for dipolar detection (Fig. 6a) and quadrupolar detection (Fig. 6b). Work was supported by NSF (CHE-9021058) and Ohio State University.

1. Schweikhard, L., Guan, S. and Marshall, A. G., *IJMSIP* **1992**, *120*, 71-83.
2. Guan, S., Wahl, M., Wood, T. D., and Marshall, A. G., *Anal. Chem.*, **1993**, accepted.

Fig. 1

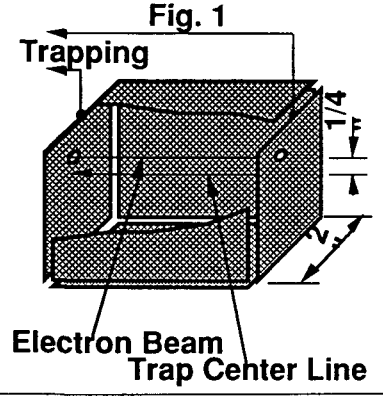

Fig. 2

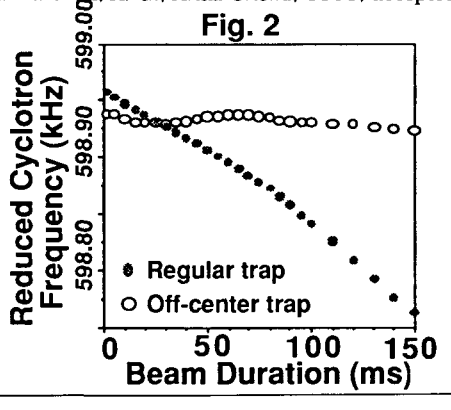

Fig. 3

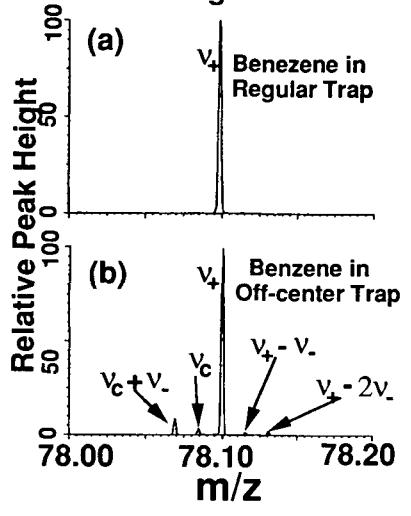

Fig. 4

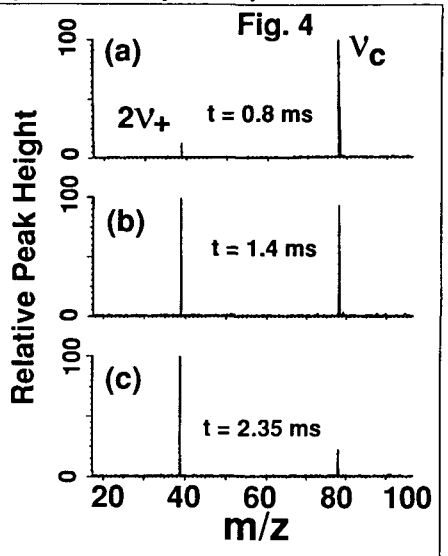

Fig. 5

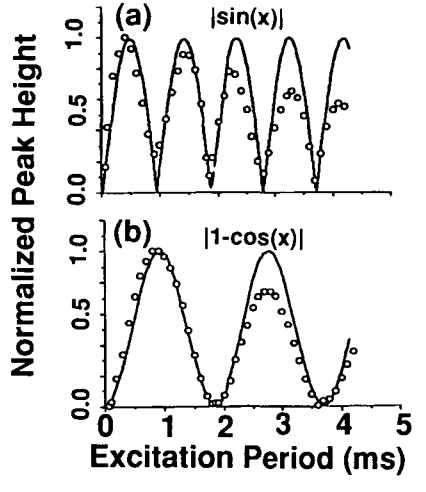

Fig. 6

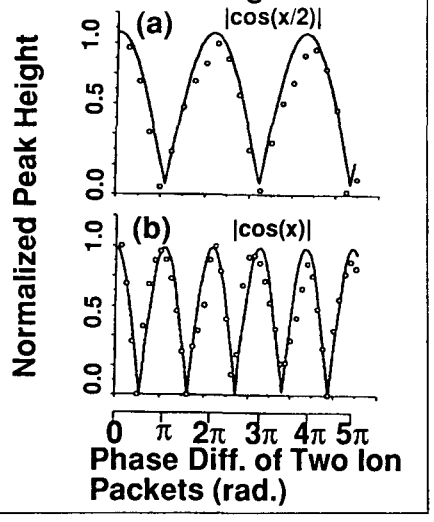

Non-Resonance Excitation and Ejection in Ion Trap

Mingda Wang and Greg Wells

Varian Chromatography System, 2700 Mitchell Dr., Walnut Creek, CA 94598

Tandem mass spectrometry (or MS/MS) has widely been used to identify chemicals and to study ion-neutral reactions in quadrupole ion traps. The single frequency resonance excitation used in current ion trap tandem mass spectrometers requires a manual tune operation for each individual ion studied, because the requirement of the applied excitation frequency matching the secular frequency of the ion motion. Thus, it is difficult to achieve the practical GC/MS/MS operation with a single frequency resonance activation. Based on resonance excitation, several methods[1-6], have been proposed to tackle the problem of secular frequency mis-matching.

We present here a new and novel universal ion excitation and ejection method in an ion trap. The new method is **independent of the ion mass and the number of ions** because it does not require the matching of the supplemental wave frequency (typically, 100-500Hz) with the secular frequency (usually more than 10KHz) of the ions of interest for CID. In the new method, ion energy deposition is achieved by the combination of z direction dipole and rf trapping fields. When the dipole field turns on, the ion oscillation center is moved to a new position[7] instantly with no change of ion space location. Therefore, ions acquire kinetic energy from the perturbation of the trapping field and oscillate around the new center. When ions have lost their energy by collision, they may be re-excited by simply turning off or reversing the dipole field. The process may be repeated for a number of times if needed.

Another disadvantage of resonance excitation process is low energy deposition resulting in ions that preferably decompose through a low energy channel. Our non-resonance excitation provides an effective means of higher energy deposition without compromising yield of product ions. N-butylbenzene has been used as a thermometer to evaluate the amount of internal energy in a variety of activation process. Figure 2 shows that the **91/92 ratio** of product ions can be **more than 100** with our new ion activation method without compromising dissociation efficiency. The highest 91/92 ratio reported by Cooks group[8] is 20 with dissociation efficiency of 5% . Simulations show that ions can easily absorb **a few ev to 40 ev** energy by adjusting the amplitude of the applied dipole field. Figure 1 shows the GC-MS/MS chromatogram of **100pg** N-butylbenzene using the non-resonance excitation method. The signal to noise ratio (**S/N**) in the chromatogram is **3624**.

The method, providing a means to eject ions with mass above a specified mass value, may be applied as a low mass pass filter technique, and be used in the CI mode to eject unwanted sample EI fragments.

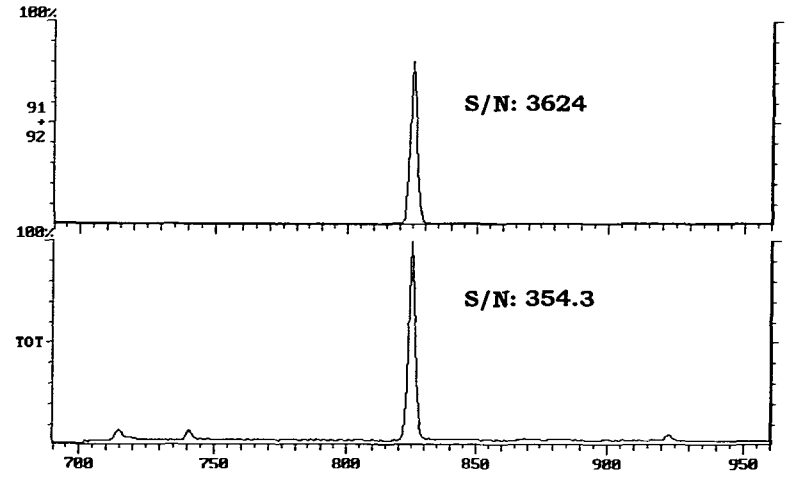

Figure 1: 100pg N-butylbenzene GC-MS/MS chromatogram using non-resonance excitaion

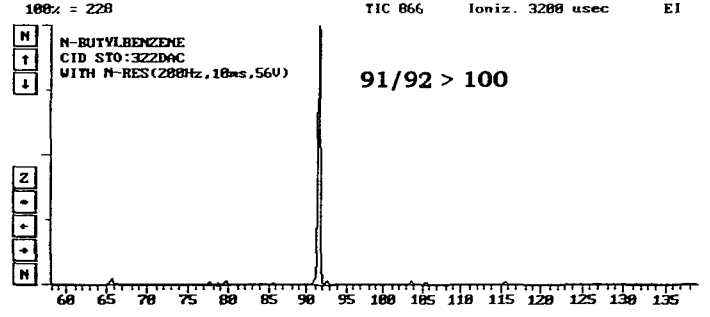

Figure 2: N-butylbenzene MS/MS spectrum by non-resonance excitation

Reference:

1. J. F. Todd et al, Rapid Commun. Mass Spectrom. 4, 108, **1990**.
2. N. A. Yate et al, 39th ASMS Conf. Mass Spectrom. & Allied Topics, pp132, **1991**.
3. A. G. Marshall et al, US Patent 4,761,545, **1988**.
4. S. A. McLuckey et al, Anal. Chem. 64, 1455, **1992**.
5. F. Vedel et al, Int. J. Mass Spectrom. Ion Proc., 108, R11, **1991**.
6. G. Wells et al, 41th ASMS Conf. Mass Spectrom. & Allied Topics, TP185, **1993**.
7. R. F. Wuerker et al, J. Appl. Phys., 30, 342, **1959**.
8. S. A. Lammert et al, Rapid Commun. Mass Spectrom. 6, 528, **1992**.

A SIMPLE MODEL FOR THE ORIGIN OF THE $2\omega_z$ RESONANCE IN FT-ICR

Dale W. Mitchell, Bryan A. Hearn and Stephen E. DeLong
Department of Geological Sciences
University at Albany, Albany, NY 12222

It is well known that for certain ICR cell geometries that there is a major mode of motion at ω_z. ICR excitation on the x-plates at $2\omega_z$ or at $\omega_+ \pm 2\omega_z$ (rather than at ω_z) are the primary frequencies at which this mode is excited. Leading excitation z-force inhomogeneities in a cubic FT-ICR cell[1] is given by[2]

$$f_z \propto xz\cos(\phi_e), \qquad \phi_e = \omega_e t + \beta_e$$

Assuming that x(t) and z(t) remain basically unperturbed from the quadrupolar motion and letting

$$x = r_+\cos(\phi_+) + r_-\cos(\phi_-) \quad \text{and} \quad z = r_z\cos(\phi_z), \quad \text{where } \phi_\pm = \omega_\pm t + \beta_\pm \text{ and } \phi_z = \omega_z t + \beta_z$$

$$\text{Then } f_z(t) \sim r_+r_z[\cos(\phi_+ + \phi_z - \phi_e) + \cos(\phi_+ - \phi_z - \phi_e)] + r_-r_z[\cos(\phi_z - \phi_- - \phi_e) + \cos(\phi_z - \phi_- - \phi_e)]$$

It turns out that the only values of ω_e which give $f_z(t) \propto \cos(\omega_z t)$ are when $\omega_e = 2\omega_z \pm \omega_-$ and when $\omega_e = \omega_+ \pm 2\omega_z$. Therefore, the present model, shown below, carries over to the $\omega_+ \pm 2\omega_z$ resonance as well

The figure shown on the next page illustrates the simple visual model which shows that excitation at $2\omega_z$ on the x-plates gives a force in the z-direction with a strong frequency component at ω_z rather than $2\omega_z$. The force on the ion will drive the ion as a simple harmonic oscillator at ω_z. The behavior at $\omega_+ \pm 2\omega_z$ is more difficult to explain graphically, but the equations given above show that these resonances excite the z-motion in a similar manner.

Also, from the simple visual model, we can see that with a zero magnetron radius, there is no net z-excitation over a cyclotron period. This is due to the z-forces cancelling each other in alternate sectors of the ICR cell: during one half of a cyclotron period, the ions will experience a force in one direction, and the opposite force during the next half-period.

1. M.B. Comisarow, Int. J. Mass Spectrom. Ion Phys., 37 (1981) 251.

2 D.W. Mitchell, B.A. Hearn, and S.E. DeLong, Int. J. Mass Spectrom. and Ion Processes, (in press).

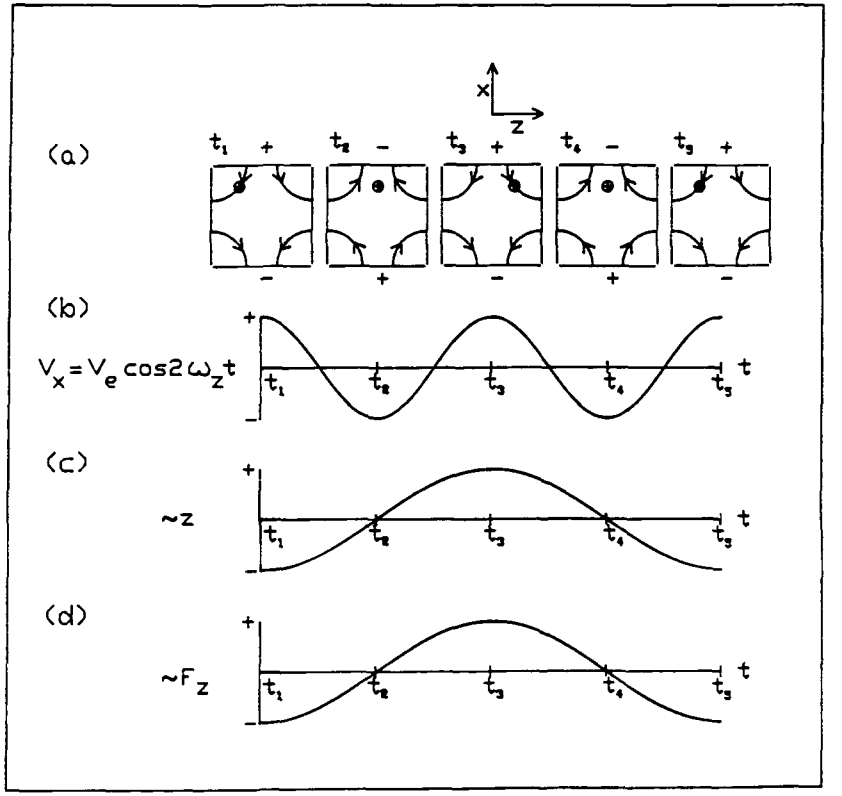

A simple model for z-motion due to excitation at $2\omega_z$: (a) the approximate electric field lines and the ion positions in the x-z plane are shown for five different times in increments of one quarter of the z-oscillation period (b) the excitation voltage as a function of time applied to the +x plate with $\omega_e = 2\omega_z$ (c) the approximate z-position of the ion as a function of time (d) the approximate z-force on the ion due to the excitation.

A Basic Theoretical Approach for the Description of Non-linear Ion Trap

Y. Wang[a),b)] and K.-P. Wanczek[b)],

a) Bruker-Franzen Analytik GmbH, 2800 Bremen 33, Germany

b) Inorganic Chemistry, University, 2800 Bremen 33, Germany

In practice, it is not really possible to generate an ion trap with a pure quadrupole field inside. However, a non-linear ion trap can achiev better performance. Non-linear ion trap can be generated with (1) stretched end-cap distance, (2) modified hyperbolic angle and (3) the superposition of one or two kinds of requried higher multipole fields directely. The potential distrbution in those non-linear ion traps are theoretically expressed with two methods. Method I [1][2]: the variation calculus method described by Ritz. This method transforms the solution of Poisson or Laplace equation with the boundary into the problem of searching an extremum of the variation about the functional. A reasonable approximation of the potential distribution is derived. Method II [1][3]: series expansion with spherical polynoms. With this method, the general potential distribution is expressed in a series of orthogonal functions. Each of them is a solution of Laplace equation. The unknown weight factors of the multipole components are determined by the given boundary. With the least square technique, the weight factors are derived by approximating the series of orthogonal functions to match the special boundary condition of the ion trap until the square deviation is a minimum. The method is applied to the ion trap with stretched end-cap distance and with the superposition of one or two kinds of higher multipoles directely.

A important effect caused by superposition of higher multipole fields is the non-linear resonance of ions. The ion motion can be treated with the Hamilton formalism [1][4]. The original hamiltonian function, at first, is transformed with linear canonical and periodical transformation. This first transformation eliminates the explicit time dependence for the quadrupole component. Its result is a harmonic oscillation with the trap's secular frequencies perturbed by the highter-order multipole components of the trapping potential. The second trasformation is a non-linear canonical and periodical one. Its perpose is to simple the non-linear contributions in the Hamiltion function. The complex variables are intruduced and further expanded with Taylor series. Their coefficients with time are expanded into Fourier series because of the periodicity. The series expanded equations can be solved from lower order to higher order. In final, the non-linear resonance conditions are derived when the expansion breaks down. The non-linear resonance

conditions for the rotationally symmetric ion traps are

$$n_r\beta_r + n_z\beta_z = 2\nu,$$

where n_r, n_z and ν are whole numbers. Due to the symmetry, some resonance lines vanishes. For example, n_r is even integer for all types of multipoles, n_z is even for even higher multipoles and odd for odd multipoles. If in the original Hamilton function (or in the higher multipole potential) terms of order $n \geq 3$ (for example, hexapoles or octapoles) are present, every one of these can in principle excite resonance lines of any order. However, a term of order n will have the strongest effect on the resonance conditions of order $N = n, n-2, n-4$ and smaller effects on the others.

The resonance intensity is defined as the mean rate of energy increase over the time average. The theoretical equation [1][4] expresses that any increase of the mean energy of a trapped ion is due to non-linear components in the trap. With this equation, the intensity of two important non-linear resonance lines for hexapole superposition are calculated and shown in the figures.

References

[1] Y. Wang, PhD Thesis, Bremen University, 1992

[2] Y. Wang and J. Franzen, Int. J. Mass Spectrom. Ion Processes 112 (1992) 167-178

[3] Y. Wang and J. Franzen, Int. J. Mass Spectrom. Ion Processes, (accepted)

[4] Y. Wang, J. Franzen and K.-P. Wanczek, Int. J. Mass Spectrom. Ion Processes 124 (1993) 125-144

An New Type of Structures of Linear Quadrupole Mass Filters and Ion Traps with and without FT Techniques

Y. Wang[a),b)] and K.-P. Wanczek[b)],
a) Bruker-Franzen Analytik GmbH, 2800 Bremen 33, Germany
b) Inorganic Chemistry, University, 2800 Bremen 33, Germany

With conventional method and technique, two- and three-dimensional quadrupole fields were generated by an array of metallic electrodes with isopotential surfaces. The corresponding structures of the quadrupole mass filters consist of four metallic rods with hyperbolic or round cross-secction; and the ion traps consist of a ring electrod and two end-caps.

Indeed, the exact two- and three-dimensional quadrupole fields can be generated by closed boundaries with continuously varied potential [1][2], In principle, if the potential value at each point of a selected curved surface corresponds to the value of the defined quadrupole electric fields at this point, the quadrupole electric fields can be generated within the interior region of the closed boundary.

Especially, the potential value along the boundaries can be linearly varied. For example, Fig. 1 shows the structures of the exact three-dimensional quadrupole field with linearly variable potential. In the ideal case, there exists a simple rhombic closed-plane (curve (D), cone structure in three-dimensional space) with the gradient $\sqrt{8/3}$ V/cm. The quadrupole isopotential curves within the structure (D) are exact quadrupolar. By comparison to the three-dimensional case, there are similar rectangle or square structures for the two-dimensional case [3].

Interestingly, within the same structure (D), a homogeneous ideal field in the direction of the symmetry axis z can be generated and superimposed without interaction with the quadrupole field. The potential lines of electric field are exact homogeneous. In two-dimensional case, there are similar results [3], but the direction of the homogeneous field can be arbitrarily selected.

Fig. 2 shows an example of electrode structure for three-dimensional fields. The upper part of Fig. 3 shows an example of electrode structure for two-dimensional quadrupole fields. The ceramic plates are deposited with a layer of Cr-SiO thin film of the specific resistivity (lower part). The new three-dimensional structure can be employed not only as an ion trap, but also as a FT ion trap. This mass spectrum can be well compared to the spectrum obtained with a FT-ICR mass spectrometer. The FT ion trap is like an ICR spectrometer, but without magnat.

For two-dimensional structure, experiments with electron beam tubes show good agreement with the theory and the practicability of the proposed structures. FT ion trap employed to mass analysis are in progress.

References

[1] Y. Wang, PhD Thesis, Bremen University, 1992
[2] Y. Wang and K.-P. Wanczek, J. Chem. Phys. 98, (1993) 2647
[3] Y. Wang and K.-P. Wanczek, Rev. Sci. Instrum. (1993) (in print)

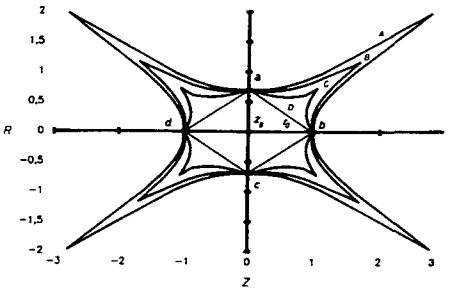

Fig. 1: The plane curves in the symmetric axis coordinate cross-sections as a function of r and z. If the potential value of point b ($r = r_0 = 1$cm, $z = 0$) is 1 (V) and that of point a ($r = 0, z_0 = r_0/\sqrt{2}$cm) -1 (V), the gradient of potential along the curve (A) is constant value of 0.3 V/cm, the curve (B) 0.8 V/cm, curve (C) 1.2 V/cm, and line (D) $\sqrt{8/3}$ V/cm.

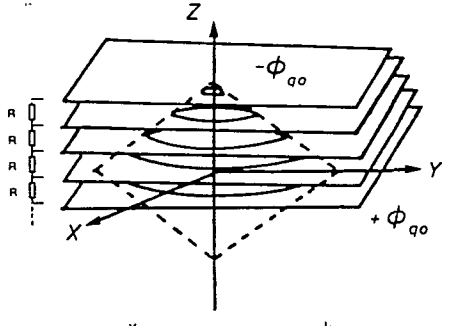

Fig. 4 Realization of the electrode structure by densely placed equidistant metallic sheets with circular holes to form the inner surface of the cone. The electrodes are connected by a network of resistors with resistivity R.

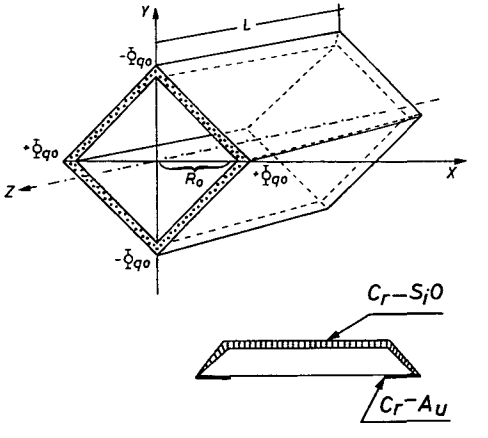

Fig. 5. Upper part: A square structure to generate two-dimensional quadrupole fields. The structure combined with the four plates displayed in the lower part of the figure.
Lower part: The cross-section of a glass or ceramic plate, the upper surface of which has been covered with uniform Cr-SrO resistance thin film. The Cr-Au thin film is use as connector electrod for th applied voltages.

Ion Trajectories Simulations for a Radio FrequencyGlow Discharge Fourier Transform Ion Cyclotron Resonance Mass Spectrometer

Paula R. Cable and R. Kenneth Marcus
Department of Chemistry, Clemson University,
Clemson, SC 29634-1905

J. M. Pochkowski and Robert R. Weller
Environmental Technology Section, Savannah River Technolgy Center,
Westinghouse Savannah River Company,
P. O. Box 616, Bldg 735-A,
Aiken, SC 29808

Introduction

Glow discharge mass spectrometry (GDMS) has expanded in both scope and application throughout the last decade due to the demand for analytical methods for a wide range of sample types. The advent of radio frequency GDMS has expanded sampling capabilities to include not only conductive materials, but also matrices such as glasses and ceramics. A major limitation that still exists for plasma source mass spectrometry is the existence of pseudo-isobaric interferences. One method of effectively eliminating these interferences is to utilize the higher resolving powers afforded by Fourier transform ion cyclotron resonance mass spectrometers (FT-ICR or FTMS). We presented data at the 1992 ASMS meeting from a prototype lensless external ion source instrument which combines the sampling versatility of radio frequency glow discharges with the resolution advantage of Fourier transform mass spectrometry.[1] Ion trajectory simulations have been performed in order to better understand and improve the ion transfer mechanism in the lensless external ion source.

Experimental

Ion trajectory simulations were performed using SIMION Version 4.0. The modeling was broken into two segments due to the limitation on computational array size and the need to maintain scale over a long ion path length. The first modeling phase (Phase I) examines ion trajectories in the GD source, sample cone, and the differential pumping chamber regions. The second modeling phase (Phase II) includes the remainder of the ion flight path from the conductance limit of the differential pumping chamber to the center of ICR cell and is the region where the magnetic field becomes significant. The total distance traveled was ≈ 127.9 cm. Ions starting in Phase I were given a kinetic energy of 15 eV, a mass to charge ratio of 63 (Cu^+), and an angular deviation of 5° in the Y and Z directions. Ion positions in the X, Y, and Z plane, final kinetic energy, and exit angle relative to both the Y and Z axes were used as starting parameters for computing 10 trajectories in Phase II. Trajectory simulations were performed for a variety of conditions including variations in sample cone voltage, conductance limit voltage, ion launch position and angle, and ion kinetic energy.

Results and Discussions

The results of the Phase II modeling indicate that all the ions from Phase I that are transmitted through the conductance limit orifice biased between +5 and -4 volts will follow the magnetic field lines down to and through the analyzer trap plate opening. Hence, for these conditions, the limiting factor for overall ion transmission to the ICR analyzer cell is the throughput characteristics of the differential

pumping chamber conductance limit. A positive DC potential of 25 V or greater on the conductance limit repels ions. An applied potential of -4 V forces the ions to the center of the magnetic field, resulting in stronger magnetic focusing at the ICR cell.

In all cases studied, a maximum of four of the ten ions exiting Phase I were transmitted through the 4.0 mm diameter conductance limit. As a result of poor ion focusing between the sample cone and the conductance limit, it will be necessary to add a lens stack to the differential pumping region to increase transmission efficiency. It does not appear that an additional focusing scheme is required once the ions leave the conductance limit; however, a deceleration grid may be required to optimize ion trapping in the ICR cell.

These simulations demonstrate that ions from an energetically well defined source can be efficiently transferred from an external ion source to an ICR analyzer cell using only the focusing of the converging magnetic field lines. Hence, for an energetically well defined source, high trapping efficiencies can be expected with no external lensing. The results presented here corroborate the experimental data collected in preliminary experiments and presented at the 1992 ASMS meeting.

Acknowledgments

The authors wish to thank Professor Alan Marshall and his research group, with special thanks to Michael May, for providing the magnetic field data and an example of a SIMION magnetic field gradient user program. SIMION Version 4.0 was provided by David Dahl of Idaho National Engineering Laboratory.

This abstract was prepared in connection with work done under Contract No. DE-AC09-89SR18035 with the U.S. Department of Energy. By acceptance of this abstract, the publisher and/or recipient acknowledges the U.S. Government's right to retain a non-exclusive, royalty-free license in and to any copyright covering this abstract, along with the right to reproduce and to authorize others to reproduce all or part of the copyrighted abstract.

References

1. R.R. Weller, J.M. Pochkowski, D.C. Duckworth, R.K. Marcus, and M.V. Buchanan; *"RF-GD/FTMS: An FTMS System with a Lensless External Ion Source for High Resolution Elemental Mass Spectrometry"*; Proceedings of the 40th ASMS Conference on Mass Spectrometry and Allied Topics, Washington, DC, May 31-June 5, 1992

Selected Ion Storage Target Compound Analysis in Complex Matrices Using Ion Trap GC/MS

Barrie A. Shaffer, Joe Karnicky, and S. E. Buttrill, Jr.
E. L. Ginzton Research Center, Varian Associates
3075 Hansen Way, Palo Alto, CA 94304-1025

The high sensitivity of the ion trap results from its ability to accumulate ions for a relatively long time compared to the time required to scan them out into an ion multiplier detector. For fairly clean samples, detection limits can easily be only one or two picograms. However, when the compound of interest co elutes from the gas chromatograph with a large amount of sample matrix, then the fixed storage capacity of the ion trap is occupied by uninteresting matrix ions, and sensitivity for the target compound is reduced. Following a suggestion by J. Franzen [1], this situation can be greatly improved by selectivly storing in the ion trap only the ion masses charactistic of the target compound. The Selected Ion Storage (SIS) capability for the ion trap described last year [2] has been automated,[3] making it a practical technique for target compound analysis in complex matrices.

In setting up a target compound analysis using SIS, there are three factors to be considered: (1) the rf storage level at which ions are accumulated, (2) the mass range(s) to be stored, and (3) the quantitation mass or masses.

The rf storage level determines the lowest mass ion which will be stable in the trap. It also affects the relative efficiency with which ions of higher mass will be stored. Figure 1 shows the signal intensity for some ions in the FC-43 calibration compound spectrum as a function of their q value. $q = 4eV/mr^2\Omega^2$ and thus depends on both mass and rf voltage amplitude V. For most ions, an rf storage level of 300 dacs, corresponding to a low mass cut off of about m/z 48, results in a storage efficiency within a factor of two of optimum

In contrast to the selected ion monitoring experiment used on transmission mass spectrometers, the sensitivity of the ion trap decreases only slowly with the number of masses monitored. Therefore the selection of the mass range or ranges to be stored should be designed to include as many of the target compound's characteristic ions and isotopic clusters as possible while rejecting all of the strong matrix ions A total scan range of 100 to 150 daltons while storing 40 to 60 masses gives excellent results

The lower detection limits of the target compounds will almost always be determined by the chemical noise (from the matrix) at the same mass as the quantitation ion(s). The quantitation ion(s) should therefore be chosen by examining the mass chromatograms of the best candidates in a spiked matrix sample. The best signal to noise will be determined by which ions experience the least contribution from matrix ions at the same integer mass. Figure 2 shows the detection of 20 pg of Aldrin in a bell pepper extract. The signal-to-noise for the less intense ion at m/z 293 is better than that for the more intense ion at m/z 263.

Because of the importance of isotopic chlorine ion clusters in their mass spectra, library searchable spectra were obtained for aldrin, heptachlorepoxide, chlordane, and 4,4'-DDE spiked into bell pepper extract at the 20-40 pg level.

REFERENCES: [1] J Franzen & R -H Gabling, EP 0 362 432, Oct. 7, 1988
[2] . S. E. Buttrill, Jr., Barrie Shaffer, Joe Karnicky and James T. Arnold, Proceedings of the 40th ASMS Conf. on Mass Spec. and Allied Topics. pp 1015-1016.
[3] Barrie A. Shaffer, Joe Karnicky, and S. E. Buttrill, Jr., Presented at the 41th ASMS Conf. on Mass Spectrometry and Allied Topics. (this conference).

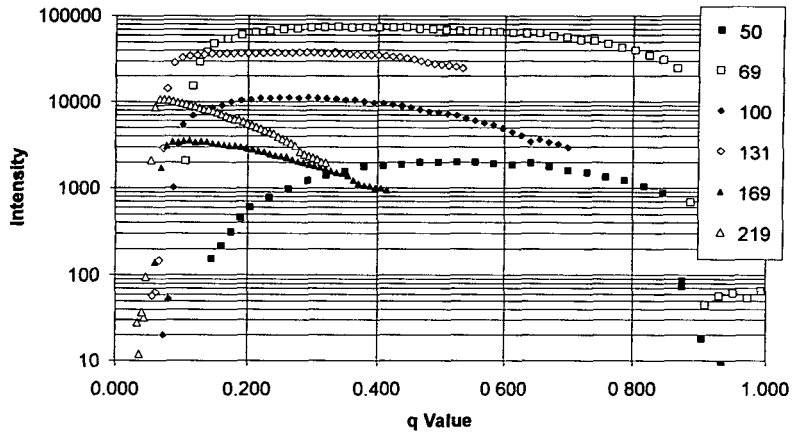

Figure 1. Fixed ionization time· 2 ms; cooldown time· 4 ms. Cal gas ion intensities vs q value (rf storage level from 50 to 500 dacs)

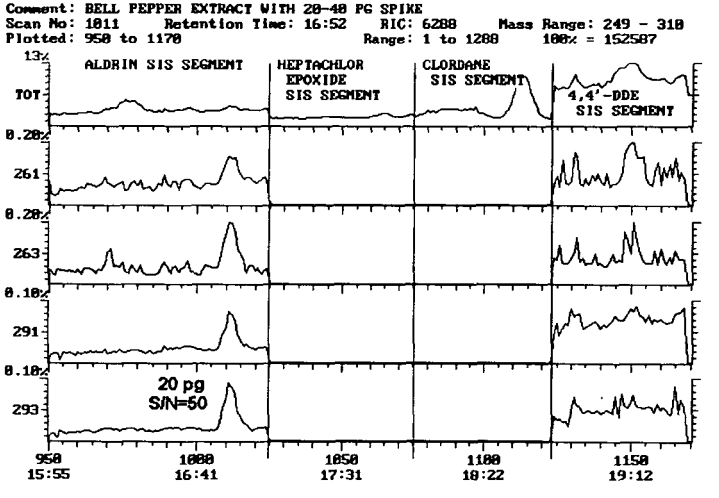

Figure 2. Mass chromatograms of characteristic aldrin ions from SIS analysis.

Optimization of a New API Ion Trap System for On-Line HPLC and CE Applications,

A.V. Mordehai and J.D. Henion, Drug Testing and Toxicology, NYS College of Veterinary Medicine, Cornell University, 925 Warren Dr., Ithaca, NY 14850

Recently we reported a novel design for implementing atmospheric pressure ionization (API) on an ion trap mass spectrometer [1]. Encouraging, low picogram detection limits have been demonstrated for ion spray-micro HPLC and CE applications [2,3]. However, in all applications it was found that chemical noise is the major limiting factor to improving sensitivity. The purpose of this report is to demonstrate system performance with two different API ionization techniques (ion spay [IS] and atmospheric pressure chemical ionization [APCI]) and higher flow rates as well as to address the chemical noise problem by implementation selected window ion monitoring (SWIM).

The previously-designed API ion trap-mass spectrometer was used in all experiments. The spectrometer was equipped with Saturn II data station (Varian, Palo Alto, CA). Thei on trap mass analyzing region was maintained at high helium pressure (5×10^{-3} Torr) to facilitate trapping externally produced ions. For accomplishing selected window ion monitoring (SWIM) a second computer (IBM 486) and arbitrary wave form generator (AWFG) board (Keithley, Taunton, MA) have been used. A fast electronic switch (constructed in house) allows us to connect either an axial modulation circuit from the Saturn electronics or AWFG to the ion trap end-caps. The AWFG board is connected to the end-caps during ionization-accumulation events while the axial modulation circuit is connected to the end-caps during the detection scan. To isolate ions of interest we use the resonance ejection technique with computer designed digital wave-functions (similar to the SWIFT technique in FT/ICR [4]). We have developed a simple mathematical procedure for creating broad-band wave functions with low dynamic range and a given frequency spectrum. Briefly, we use a modified quadratic phase encoding approach (step quadratic phase encoding) where the total frequency range is divided into ~20 equal segments and the quadratic phase encoding is applied separately on each of the segments. The resulting wave function is is produced by direct addition wave functions produced for each frequency segment. In contrast to the SWIFT technique no inverse Fourier transformation has been used; instead we use a direct sum of the harmonic waves separated in 1kHz frequency intervals. Finally, for use in our experiments we synthesize a wave function containing all frequencies in the range from 25 kHz to 500 kHz with a 1 kHz interval and one frequency notch. Frequencies ranging from 40 to 60 kHz have been omitted during the addition process so as to create a 20 kHz frequency notch.

Figure 1 illustrates extending API operation from IS to the APCI ionization. The HPLC analysis of five benzodiopine drugs (10 ng injected on column) performed using standard (Sciex, Thornhill, Ontario) heated pneumatic nebulizer at a low rate of 1 mL/min (40/25/35% CH_3CN/CH_3OH H_2O, using a Zorbax C-18, 4.6 x 150 mm) using no pre or post-column split. The sensitivity in the full-scan mode (no SWIM) is at least twice that previously reported using our Sciex TAGA 6000E updated to API 3 instrument [5].

Figure 2 demonstrates the SWIM technique with ion spray infusion analysis of a model synthetic mixture containing four quaternary ammonium compounds(TBAH, m/z=242; THAH, m/z=354; TOAH, m/z=466; TDAH, m/z=578 [1]) at 500 fmol/μL concentration of each compound dissolved in a common HPLC buffer (50/50% CH_3CN/H_2O; 15 mM ammonium formate). Figure 2a was acquired with full-scan ion trap operation. Figure 2b shows the isolation of two ionic species in the trap by application of a computer-

designed wave function applied to the end caps (SWIM mode). The window for mass selective accumulation is ~ 100 Da width and it can be easily moved across the mass range to accumulate ions of interest by adjusting the main RF storage level.

1. a: A.V. Mordehai, G.H. Hopfgartner, T.G. Huggins, J.D. Henion, *Rapid Commun. Mass Spectrom* , 6, 508(1992);
   b: A.V. Mordehai, J.D. Henion, *Rapid Commun. Mass Spectrom.* 7, 205(1993)
2. J.Henion, A. Mordehai, H. Lim, J. Cai, Fundamentals and Recent Applications on an Atmospheric Pressure Ionization-Differentially Pumped Benchtop Ion Trap, *Proceedings of 41st ASMS on Mass Spectrometry and Allied Topics*, San Fransisco, 93
3. H.K. Lim, W-N. Wu, A.V. Mordehai, J.D. Henion, Analysis of Quaternary Isoquinoline Alkoloids by Ion Spray Ion Trap Mass Spectrometer, *Proceedings of 41st ASMS on Mass Spectrometry and Allied Topics*, San Fransisco, 93
4. T-C. L. Wang, T.L. Ricca, A.G. Marschall, *Anal. Chem.*, 1986, 58, 2935
5. E. C. Huang, T. Wachs, J.J. Conboy, J.D. Henion, *Anal.Chem.*, 62, 713A,(1990)

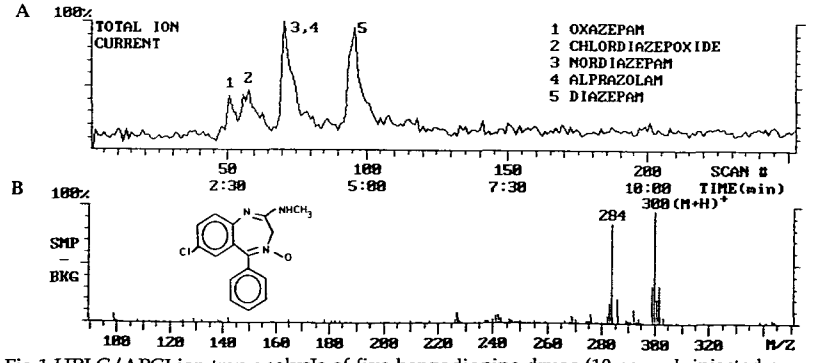

Fig.1 HPLC/APCI ion trap analysis of five benzodiopine drugs (10 ng each injected on-column, flow rate 1 mL/min, no split). Panel A shows the full-scan total ion current profile. Panel B shows the background-subtracted mass spectrum from scan # 58 from panel A (clordiazepoxide). The peak at m/z 300 represents the protonated molecule; peak at m/z 286 may be the result of thermal degradation (loss of oxygen) in the LC/MS interface.

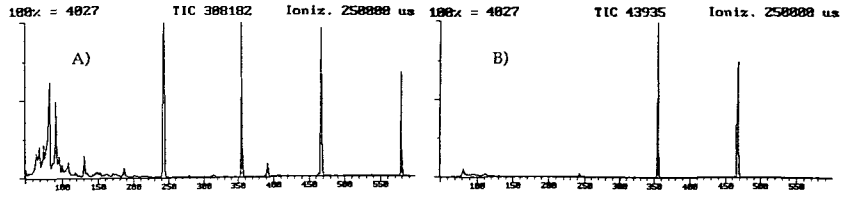

Fig. 2 Ion spray infusion analysis of a synthetic mixture containing four quaternary ammonium compounds (500 fmol/μL each, at a flow 10μL/min). A) shows the full scan mass spectrum of the infused mixture. B) shows isolation of two ionic species in the trap (m/z=354 and 466) by using SWIM.

Particle beam HPLC-MS on ion trap, quadrupole and sector spectrometers for pharmaceutical analysis.

Colin S. Creaser and *James W. Stygall, Dept. of Chemistry and Physics, Nottingham Trent University, Clifton Lane, Nottingham NG11 8NS

A particle beam interface has been used to couple HPLC to quadrupole ion trap (ITMS), sector and triple quadrupole mass spectrometers. These systems have been evaluated by EI, CI and MS/MS analyses of a pharmaceutical sample separated by normal phase chromatography. For HPLC-PB-ITMS operation a novel transfer line design permits particle volatilisation outside of the trap volume by use of an independently heated probe tip. Also, customised ion trap scan routines have been written which minimise space charge and solvent-CI effects in EI acquisition.

A schematic of the interface(1) is shown in figure 1. The nebuliser and heated glass desolvation chamber were constructed in-house. The momentum separator and transfer lines were made by ASH instruments (Manchester, UK) to our design and coupled to two 18 m^3/h 2-stage rotary pumps. The ITMS transfer line consisted of two concentric stainless steel tubes, between which passed the connections for a heater and a thermocouple both located at the probe tip. The assembly was introduced into the manifold via the solids probe lock. The ion trap mass spectrometer was operated at 180°C and 1×10^{-4} torr manifold pressure after addition of helium buffer/collision gas (base pressure with PB in operation was 1.8×10^{-5} torr). The transfer line heated tip was operated at 240°C. The sector (VG 7070E) and quadrupole (VG TRIO 3) transfer line had no internal heater as particle volatilisation occurred in the source, but was fitted instead with a machinable ceramic insulating tip. Connection to both instruments was made *via* the solids probe locks. The 7070E was operated at 4KV source potential, 300°C source temperature. The TRIO 3 triple quadrupole was also operated at a source temperature of 300°C with MS/MS experiments performed using xenon collision gas at 4eV collision energy. Chromatography was performed on a 2.1 x 250mm silica column (HPLC technology, Manchester, UK).

The PB interface was successfully coupled to each spectrometer using the appropriate transfer line, and its performance was evaluated using Fluconazole (I), an antifungal pharmaceutical(2), and its product related impurity(II). Figure 2 shows the normal phase analysis of (I) and (II) on the ITMS system. The spectra obtained are good matches to spectra from probe-EI and HPLC-PB-sector MS analysis, with little interference from solvent observed. To eliminate the adverse effects of excess trapped solvent ions in the ITMS, the scan routine used was composed of repeated ionisation / low mass ejection steps before spectral acquisition, (figure 3). This was found to give good analyte signal without compromising spectral quality.

Ammonia CI was performed on both compounds using the sector machine. Figure 4a shows the spectra obtained, with prominent $[M+H]^+$ ions evident. However the base peak for (I) is m/z 222, which had very low intensity in the probe-EI spectrum, but was similarly intense on another commercial particle beam-MS system. Figure 4b shows the solvent-CI spectra obtained on the HPLC-PB-ITMS system using the RF/DC isolated $[CH_3OH_2]^+$ reagent ion. Surprisingly, as methanol has a smaller proton affinity than ammonia and the methanol-CI reaction is therefore more exothermic, fewer ions are observed in the ITMS spectrum suggesting the presence of processes other than proton transfer in the sector source.

Tandem mass spectrometry was performed on both triple quadrupole and ion trap devices, using collisionally activated dissociation in both cases. Figure 5 compares the HPLC-PB-MS/MS spectra obtained from fluconazole and shows a greater degree of fragmentation occurring in the optimised ion trap routine. Notably, the m/z 169 and 197 products, absent from triple quadrupole MS/MS data, were detected by probe-EI linked scan MS/MS in a previous study, suggesting that the energy imparted during axial excitation in the trap was greater than the 4eV applied in the triple quadrupole experiments.

In conclusion, EI, CI and MS/MS data, on-line with HPLC separations, has been obtained using both conventional and ion trap mass spectrometers coupled to a two-stage particle beam device with an appropriate transfer line. Successful separation and identification of Fluconazole and a related impurity has been demonstrated. Future work will apply the technique to different analytes and explore the use of alternative ionisation and dissociation techniques

References.

1.) C.S.Creaser and J.W.Stygall, *proceedings of the 22nd annual meeting of the British Mass Spectrometry Society*, St. Andrews, 1992.

2.) J.W.Van't Wout, H.Mattie and R.van Furth, *J. Antimicro. Chemother.*, 1988, 21, 665.

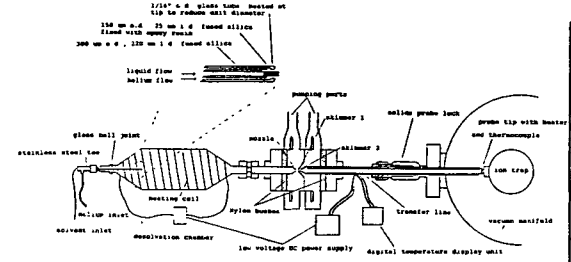

Figure 1 Particle Beam Schematic

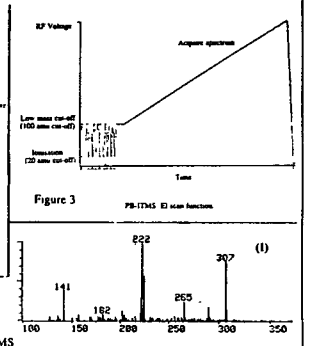

Figure 3

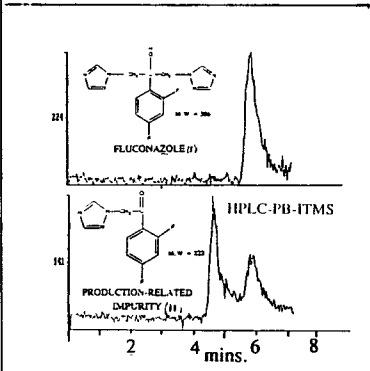

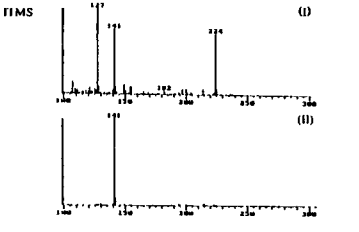

HPLC-PB MS of fluconazole (m/z 224) and related impurity (m/z 141)
Silica column, 2.1 x 250 mm, 0.4ml/min
hexane/methanol/diethylamine (60/39/1)

Figure 2

(a) HPLC-PB-ammonia CI sector MS

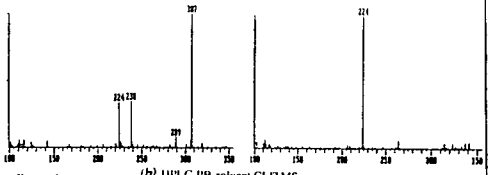

(b) HPLC PB solvent CI ITMS

Figure 4

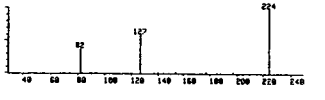

HPLC-PB-MS/MS of fluconazole (triple quadrupole)

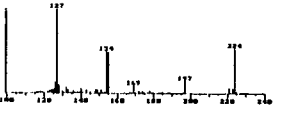

Figure 5 HPLC-PB-MS/MS of fluconazole (ITMS)

An Electrostatic Ion Guide Interface for SIMS with an FT/ICR Mass Spectrometer

Jarrod A. Marto, Shenheng Guan, Patrick A. Limbach, Markus C. Wahl†, and Alan G. Marshall†

Departments of Chemistry (and Biochemistry†), The Ohio State University, 120 West18th Avenue, Columbus, OH 43210

External ion injection for FT/ICR mass spectrometry allows high-pressure ion sources to be coupled, through one or more stages of differential pumping, to the low-pressure mass analyzer region. In this way, the ultra-high resolution capability of FT/ICR/MS is maintained. The magnetic mirror effect, i.e., the repulsive force ions encounter if they are not aligned on the z-axis as they enter the magnetic fringe field, is the chief obstacle encountered in this approach. Quadrupole and Einzel lenses have been used to focus externally generated ions on the z-axis, thereby minimizing their interaction with the radial magnetic field gradient.

Here, we report a Secondary Ion Fourier Transform Ion Cyclotron Resonance Mass Spectrometer (SI/FT/ICR/MS) for the analysis of biological materials. The external ion source consists of a primary Cs^+ beam which allows for pulsed-mode operation at up to 10 keV Cs^+ ion energy. Externally formed ions are transferred to the mass analyzer by use of an electrostatic ion guide, recently demonstrated on an FT/ICR instrument [1]. The ion guide consists of an outer stainless steel tube with a thin wire suspended down the center. The guide extends from the sample probe to approximately 25 cm into the bore of a 3 tesla superconducting magnet. When a small potential difference (~10 V) is maintained between the wire and tube, the electrostatic force on the ions in the fringe field of the magnet is greater than the magnetic force, such that the trajectory of the ions is determined solely by the ion guide, thereby effectively defeating the magnetic mirror effect. In addition, the diameter (3.8 cm) and length (84 cm) of the ion guide allow for an order-of-magnitude pressure differential to be maintained between the ion source and analyzer regions (as determined by ion gauges #1 and #2 in Fig. 1). To maximize the observed ICR signal, an open-ended cylindrical analyzer trap is used.

Figure 2 shows a single-scan broadband FT/ICR mass spectrum of gramicidin S obtained from 1 μl of sample solution (2 μg/μl in methanol) deposited onto a glycerol matrix (2 μl, 0.1N HCl); under these conditions, a pressure of 3.0×10^{-8} torr was realized in the analyzer region. A primary Cs^+ beam pulse 5 s in duration (at 6 keV) was used to desorb the secondary ions. A potential difference of 11 V was maintained between the tube and wire of the guide to transport the ions into the ICR trap; the ions were allowed to accumulate for 20 s prior to excitation (frequency sweep from 5 kHz to 800 kHz at 50 Hz/μs). Besides the abundant protonated molecular ion at m/z=1142, several fragments are readily identified. A standard double resonance excitation sequence, with heterodyne detection over a 20 kHz bandwidth, was used to generate a high-resolution ($m/\Delta m \approx 10{,}000$) spectrum (not shown) of the molecular ion. This work was supported by grants to A.G.M. from NIH (GM-31683), NSF (CHE-9021058) and The Ohio State University.

1. Limbach, P. A.; Marshall, A. G.; Wang, M., *IJMSIP* **1993**, *000*, 000-000.

SI/FT/ICR/MS - Top View

Figure 1

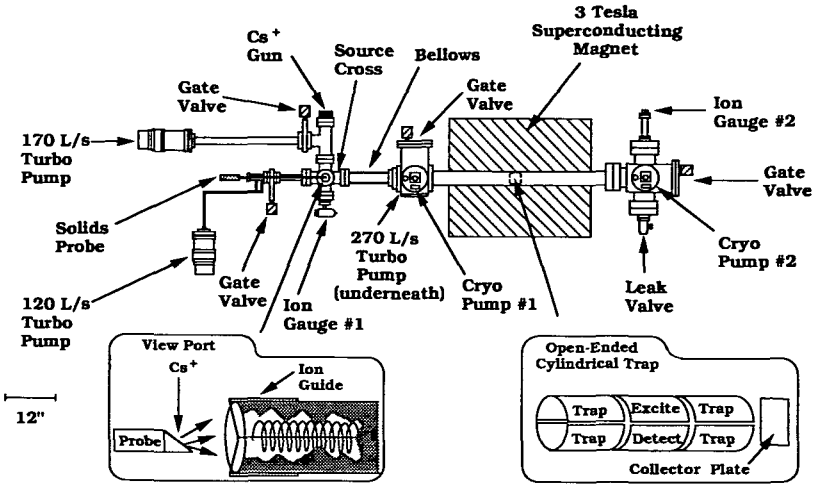

Figure 2

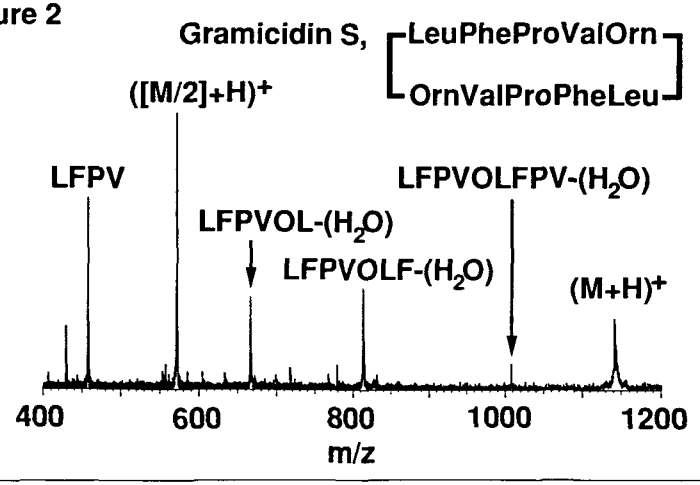

Determination of Ion Frequencies in a Quadrupole Ion Trap Using a Fast DC Pulse as Pump and a Laser Probe

Stephen A. Lammert†, *Curtis D. Cleven, R. Graham Cooks, Purdue University, Department of Chemistry, West Lafayette, IN 47907-1393

†Present Address: Oak Ridge National Laboratory, P.O. Box 2008, MS 6120, Oak Ridge, TN 37831-6120

A new technique has been developed which allows the direct measurement of frequencies of ions trapped in a quadrupole ion trap mass spectrometer. This pump/probe method employs a fast DC pulse (pump) to displace a kinetically cooled ion population from the center of the trap, and a laser (probe) which recognizes when ions reappear at the center of the trap by the formation of photodissociation fragments. The translationally excited ions undergo periodic motion within the confines of the ion trap, and this periodic motion can be followed by recording the intensity of the photodissociation fragment as a function of the delay time between the DC pump and the laser probe. The DC pulse has a rise time of 15 ns; data are taken 1 ms after its application to allow stable ion motion to be sampled. Sampling of the ion cloud is done at 50 ns intervals and Fast Fourier Transform (FFT) of the time-based data yields the ion frequencies and their relative magnitudes. Data are reported for ions derived from acetophenone (m/z 105 -> m/z 77) and 1,4-cyclohexadiene (m/z 80 -> m/z 79) under various trapping conditions corresponding to different Mathieu q_z values.

An example of the data taken is shown in Figure 1 where a DC pulse is applied axially at a q_z-value of 0.6. The measured apparent frequency, f_z, of 502 kHz corresponds to an actual ion frequency of 251 kHz. This agrees surprisingly well, given that the q_z-value is greater than 0.4, with the value of 254 kHz estimated from the Dehmelt pseudopotential well model.[1] Contributions to the ion motion by higher order frequencies increase as the q_z-value is increased as can be seen with $f_{1,z}$ and $f_{-1,z}$ as well as $f_{1,r}$ and $f_{-1,r}$. The fundamental RF frequency, f_{RF}, also contributes to the ion motion.

The measured secular frequencies are found to agree well with those predicted by the Dehmelt pseudopotential model, within the range of its applicability. The ability to experimentally measure ion frequencies under operating conditions provides a new tool for comparing simulated and experimental data. Simulation data from the program ITSIM[2] modified to account for the effects of collisions, are shown to predict all major frequency components observed in the experimental data.

References:

1. Major, F.G., Dehmelt, H.G., *Phys. Rev.*, **1968**, *170(1)*, 91.
2. Reiser, H.-P., Julian, R.K. Jr., Cooks, R.G., *Int. J. Mass Spectrom. Ion Proc.*, **1992**, *121*, 49.

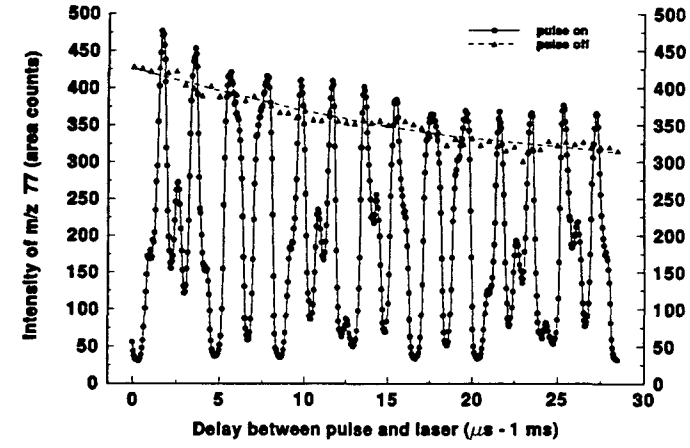

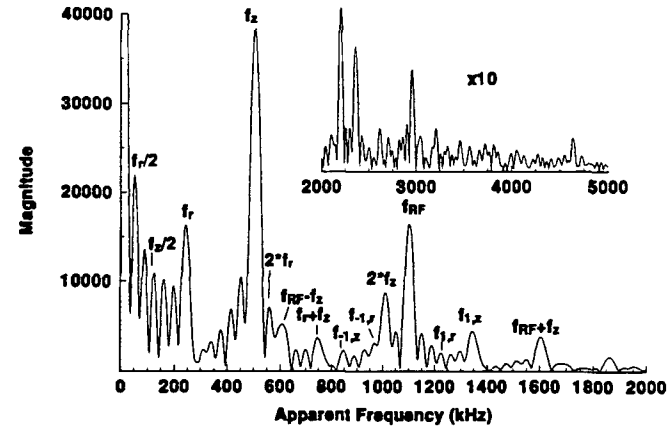

Figure 1: The time-domain (top) and frequency-domain (bottom) data for the DC pulse pump/laser probe experiment using a 25 volt, 2 μs axial DC pulse at a q_z-value of 0.6. The trapped ion is the benzoyl cation, *m/z* 105, and the photofragment is *m/z* 77.

Evidence for "Black Holes" during EI in a Quadruupole Ion Trap Mass Spectrometer

S.A. Lammert*, C D. Cleven and R.G. Cooks
Purdue University, Department of Chemistry, West Lafayette, IN 47907
**current address: Oak Ridge National Laboratory, P.O. Box 2008, Oak Ridge, TN 37831-6120*

Since their observation by Traldi and co-workers in 1991[1], *black holes* in a quadrupole ion trap mass spectrometer have commanded the attention of several research groups[2], including our own[3] In that initial observation, it was reported that during MS/MS in the ion trap, if a parent ion is resonantly excited to produce fragment ions which subsequently appear at specific q_z-values, these fragment ions would be inadvertently ejected from the ion trap In effect, there was a "hole" in the stability diagram through which ions escaped if they were brought near it under certain conditions In a later report[4], these "holes" were reported to be, in fact, "canyons" which occurred not only at the a_z=0 axis, but along non-linear resonance lines[5,6] (at β_z=0.5, β_z=0 67) in the stability diagram. Since the strength of the non-linear fields, which give rise to these resonances, increases as the distance from the center of the trap increases, these ion losses are only observed under the circumstances where the ion's trajectory is moved away from the center of the trap In the above experiments, this was accomplished using a resonant AC to excite the parent ions to a new, larger trajectory It was later reported, however, that the supplemental AC was not needed to promote this ion loss and in fact the *black canyons* could be observed in single stage MS using chemical ionization and no resonance AC.[2]

Experiments discussed in this paper show that electron impact ionization alone can give rise to conditions where ions are lost by way of these *black canyons* through the same non-linear processes discussed above In addition, this effect can be generated and probed using fast DC pulses to rapidly move the ion population away from the ion trap center, either axially or radially, where the non-linear field strength is increased In this way both the ions' β_z-value and its position in the trap can be controlled to examine the ejection process

The scan function for these experiments is represented schematically in Figure 1. The first variation ("RF step" in Figure 1, square data points in Figure 2) employed a low ionization RF level (β_z=0.02 for the m/z 77 fragment from the EI ionization of acetophenone) Under these conditions, no ions are near the βz=0.67 hexapole non-linear resonance line. After the ionization stage, the RF was stepped, in single DAC step increments, across an RF level which corresponds to β_z values of between approximately 0 64 to 0 69 Then, after an approximately 5 ms delay, a small amplitude, 2 μs DC pulse could optionally be applied (either axially or radially) at this new RF value In the second variation ("no RF step" - Figure 1, circle data points in Figure 2), the RF level was held constant throughout the entire ionization period (this time at values which placed the m/z 77 fragment ion near the β_z=0.67 region) The RF level was again stepped in single DAC step increments across the β_z=0.67 region

The results for the axial activation experiment are shown in Figure 2 For both the RF step and no RF step variations, a pronounced dip in ion intensity for the m/z 77 fragment ion is observed at a β_z-value of just over 0.66 The effect of the DC pulse is considerably more pronounced in the RF step experiment where ions formed at larger distance from the center are less likely to be lost during the ionization process Similar results are obtained when the ions are translated radially with the DC pulse.

Ions whose β_z-values are at non-linear resonance points, and which are created at large distances from the center of the ion trap are prone to ejection. Under these conditions, the DC pulse has little additional effect. If the ions are formed under stable conditions, however, and allowed to cool to the center of the trap, subsequent RF level changes which result in an ion acquiring a β_z-value near a non-linear resonance line do not effect appreciable ion loss. These ions can be subsequently ejected if a small DC pulse is used to rapidly move the ion with these β_z-values to positions away from the trap center.

References

1. Guidugli, F , Traldi, P., *Rapid Commun Mass Spectrom* **5** (1991) 343
2. Eades, D M , Yost, R A., *Rapid Commun. Mass Spectrom.* **6** (1992) 573-8
3. Morand, K.L , Lammert, S.A , Cooks, R.G., *Rapid Commun. Mass Spectrom* **5** (1991) 491.
4. Guidugli,F., Traldi, P , Franklin, A.M., Langford, M.L., Murrell, J., Todd, J.F J , *Rapid Commun Mass Spectrom* **6** (1992) 229-31
5. Dawson, P.H , Whetten, N.R , *Int. J Mass Spectrom. Ion Phys.* **2** (1969) 45-59
6. Wang, Y. and Franzen, J., *Int J. Mass Spectrom. Ion Processes* **112** (1992) 167-78

FIGURE 1.

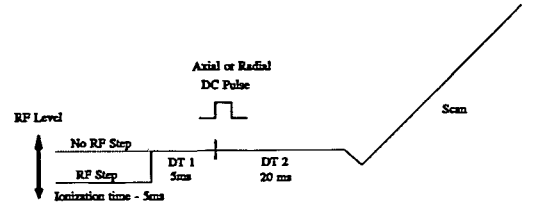

Case 1: Ionization DAC same as DT1, DT2 DAC (No RF Step)

Case 2: Ionization DAC = 150 (fixed), DT1, DT2 DAC varied (RF Step)

DC Pulse applied at beginning of DT2 : V=100 volts for radial, 25 volts for axial

FIGURE 2.

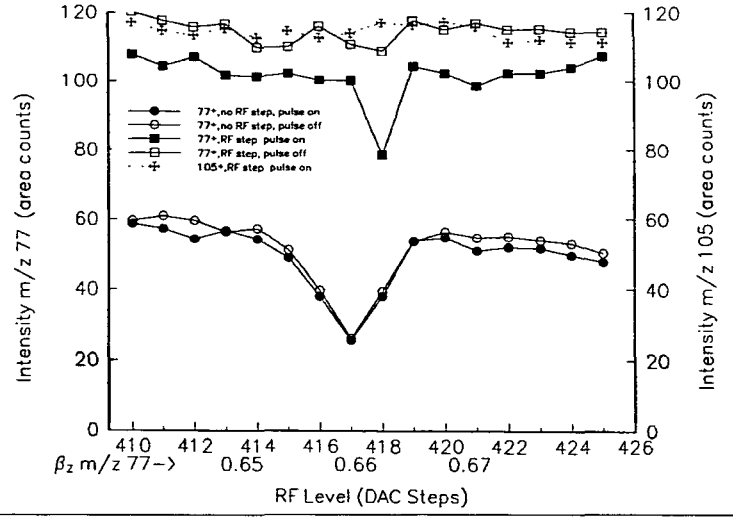

Ion Isolation and Modulated Ion Excitation for GC-MS/MS in an Ion Trap Mass Spectrometer

Barbara Bolton, Gregory Wells and Mingda Wang, Varian Chromatography Systems, 2700 Mitchell Drive Walnut Creek, CA 94598 USA

INTRODUCTION

Several methods(1-2) have been used for parent ion isolation; **Mass-Selective Instability**-where ramping the rf voltage causes ejection of low mass ions. The parent ion as well as ions of higher m/z value will remained trapped; **RF-DC Apex Isolation**-where rf and dc potentials are simultaneously applied which moves the parent ion to the apex of the stability curve, ejecting low and high mass ions; and **Sequential Ejection**-where the parent ion is moved to a high q value and an applied -dc voltage is used to eject low mass ions, return parent ion to low q value and an applied +dc voltage is used to eject high mass ions. These methods have the disadvantage of bringing the parent ion close to one or two stability boundaries which causes their kinetic energy to increase with a concomitant loss of intensity due to CID and ejection of ions outside of the range to be isolated. The limitations of these techniques have been compared(3). This problem can be severe with ions that can dissociate easily (i e. butylbenzene) and when the isolation range of m/z values is a single m/z value For GC-MS/MS applications on the ion trap, the instrumentation requirements must include easy mass calibration for parent isolation, unit mass resolution for isolation of the parent ion, independence of sample concentration and minimal CID losses during the isolation process We describe a novel method of ion isolation and a new method of ion excitation that when coupled with Gas Chromatography meet these instrument requirements for target compound analysis in the ion trap.

METHODS

The scan function is shown in Figure 1. The low mass ions are ejected by resonance scanning using an applied supplemental frequency of 460 kHz to eject up to <m, with a slower scan rate up to the m-1 ion With a small drop in rf level, a multi-frequency wave form was applied to the end caps of the trap to resonantly eject all of the high mass ions simultaneously The rf level is reduced and an off resonance supplemental AC field is applied for CID, simultaneously with the modulation of the fundamental RF trapping field. The next period utilizes normal analytical scanning techniques The multifrequency broadband wave form was generated by a Varian Wave~Board.

RESULTS & DISCUSSION

Figure 2 shows an example of ion isolation for the relatively high mass 502 of PFTBA. The low mass tailing indicates a relatively unstable ion. With broadband ejection the 503 isotope band is eliminated, without peak distortion and minimum attenuation (<10%) of m/z=502.The single frequency dissociation of butylbenzene mass 134 to m/z 92 & 91 is a sensitive probe(4) for excitation since it has two energetically different dissociation channels; the m=92 as the low energy channel and m=91 as the high energy deposition channel. Figure 3 shows a chromatographic peak of n-butylbenzene using rf/resonance ejection with AGC off or on. The mass spectra varied with concentration; both the 91/92 ratio as well as relative intensities of other ions. To control the energy deposition process, a new method of RF field modulation was added during the CID step.RF field modulation causes the secular frequency of the parent ion to successively pass in and out of resonance with the applied supplemental field. The amount of energy coupled into the ion motion is determined by applied field amplitude, the rate of RF field modulation and the number of modulation cycles. Figure 4 shows the peak of n-butyl- benzene using rf/resonance ejection

with rf modulation and AGC is off or on. The mass spectra appeared invariant with concentration; both the 91/92 ratio as well as relative intensities of other ions.

CONCLUSIONS

1. The difficulty of calibration of low volatility samples for isolation and excitation has previously limited the application of MS/MS techniques for GC-MS/MS. A novel method has been developed that provides high resolution ion isolation (unit mass resolution), easy mass calibration (using the PFTBA mass calibration curve) and higher isolation efficiency (minimized ion loss in isolation process).
2. A modulated field for CID has provided controlled energy disposition and uniform fragmentation. Modulating the trapping field compensates for uncertainties and shifts in the secular frequency of the parent ion caused by non-ideal trap geometry and changes in sample concentration, RF trapping voltage and supplemental field frequency.
3. The prescan for AGC has been modified to use the daughter ion TIC in the algorithm so as to maximize sensitivity and minimize space-charge perturbation. This new method of isolation and excitation has provided a GC-MS/MS method that is reliable and easy to implement(5)

REFERENCES

1. N.A. Yates and R.A Yost, Proc of the 39th ASMS Conf on Mass Spectrom. and Allied Topics, Nashville, TN, 1991, pp1489
2. S.A. McLuckey, D.E. Goeringer and G.L. Glish, J Am. Soc. Mass Spectrom. 1991, 2, 11-21
3. K.J Hart, S A. McLuckey and G.L. Glish, J. Am Soc. Mass Spectrom. 1992, 3, 680-682
4. U. Vettori and P. Traldi, Rapid Commun. Mass Spectrom., 1993, 7, 312-314
5. S. Schachterle and R D. Brittain, Poster WP-108, 41st ASMS Conference, San Francisco, 1993

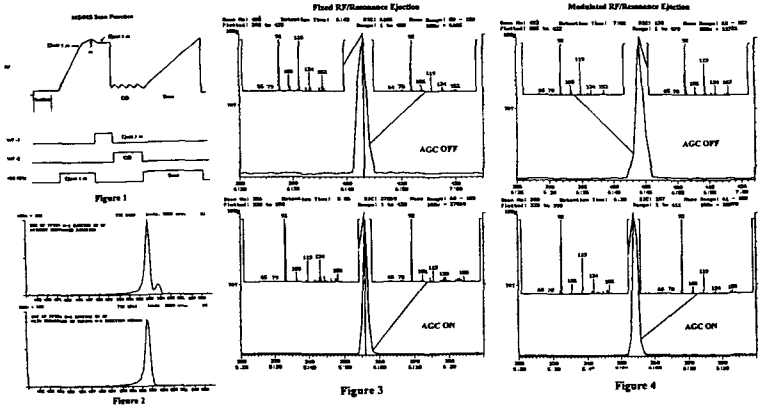

Figure 1

Figure 2

Figure 3

Figure 4

Ion Energy-Modulated Stored Waveform Ion Modulation (SWIM) Two-Dimensional FT/ICR MS/MS

Charles W. Ross III, Shenheng Guan, and Alan G. Marshall†

Dept. of Chemistry (Dept. of Biochemistry†), The Ohio State University, 120 West 18th Avenue, Columbus, OH 43210

Fourier transform ion cyclotron resonance mass spectrometry (FT/ICR/MS) offers high resolution, wide mass range, and the ability to manipulate trapped ions for collision-induced dissociation, MS/MS, and determination of ion-neutral reaction pathways, kinetics, equilibria, and energetics. However, establishing a given ion fragmentation or reaction pathway optimally requires isolation of that ion (e.g., by ejection of ions of all other m/z) followed by a reaction period and then broadband excitation/detection of the various product ions. Thus, the FT multiplex advantage is available for the product ions, but not the various possible parent ions.

With the implementation of Stored Waveform Ion Modulation (SWIM) 2D-FT/ICR/MS[1] it is now possible to identify simultaneously *all* ion-neutral reactions in a single automated experiment. The familiar one-dimensional mass spectrum appears as peaks along the diagonal of a two-dimensional display. Off-diagonal peaks result from forward and reverse ion-neutral reactions. The parent ion cyclotron orbital radii (and thus parent ion speeds, and hence the relative abundances of product ions formed by ion-neutral reactions of those parent ions), may be modulated by applying a series of sinusoidal *single*-pulse excitation magnitude-mode stored inverse Fourier transform waveforms of increasing frequency over a given bandwidth.

However, in some endoergic reactions there is a minimum energy threshold that must be overcome for a reaction to occur. Hence, a simple sinusoidal modulation of parent ion cyclotron radius leads to a clipped sinusoidal signal of the product ion abundance in the second dimension, which upon Fourier transformation produces signals with harmonic and combination ion cyclotron resonance frequencies. Moreover, ion-molecule reaction rates may vary directly with ion kinetic energy rather than with ion cyclotron radius.[2] Since ion kinetic energy varies as the square of ion cyclotron radius and is proportional to the cyclotron frequency, a sinusoidal modulation of ion cyclotron radius will *not* produce a sinusoidal modulation of parent ion kinetic energy (or product ion abundance, Fig. 2) in such a case. However, with SWIM, it is possible to tailor the excitation profile so as to produce a sinusoidal modulation of ion kinetic energy as a function of cyclotron frequency (Fig. 1), so that SWIM 2D-FT/ICR MS/MS could remain linear even in that situation. We denote the energy-modulation SWIM 2D experiment as SMOKE (stored-waveform modulation of kinetic energy).

This work was supported by NIH (GM-31683), NSF (CHE-9021058) and The Ohio State University.

1. Ross III, C. W.; Guan, S.; Grosshans, P. B.; Ricca, T. L.; Marshall,A. G. *J. Am. Chem. Soc.*, **1993**, *000*, 0000-0000.
2. Hop, C. E. C. A.; McMahon, T. B.; Willett, G. D. *Int. J. Mass Spectrom. Ion Proc.* **1990**, *101*, 191-208.

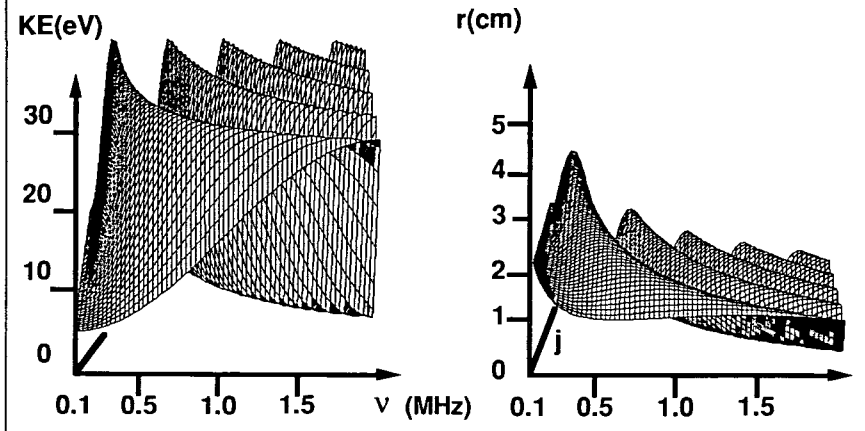

Figure 1. 3D displays of SMOKE waveforms. Each magnitude-mode frequency domain waveform is acquired by taking a slice at integer values of j (axis into the paper). Left is the surface for energy modulation of ions between 5 and 29 eV, and at right the corresponding radius modulation surface. (j=1-10)

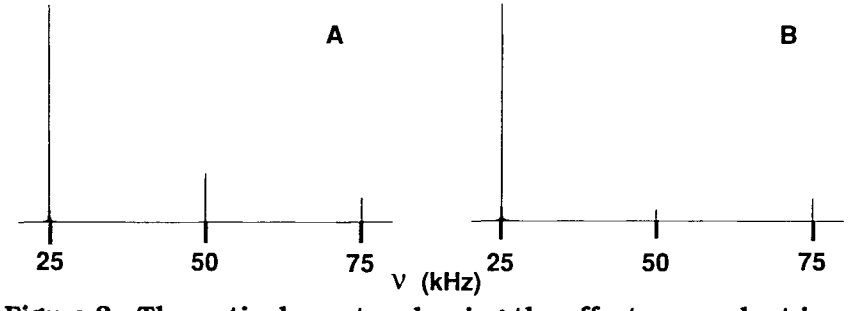

Figure 2. Theoretical spectra showing the effect on product ion signal (cyclotron frequency = 25 kHz) due to sinusoidal modulation of parent ion radius, for the case that the number of product ions varies linearly with energy (spectrum A). Spectrum B shows the additional effect of a non-zero energy threshold for the formation of product ions.

Activation of Aromatic Compounds in Gas Phase Metal Ion Reactions

R. Marshall Pope and Steven W. Buckner, Department of Chemistry, University of Arizona, Tucson, AZ 85721

The activation of aromatic compounds by transition metals has been a topic of recent interest for gas phase chemists. A range of interesting reactivities has been observed including C-H, C-halogen, C-O, and C-C activation, polymerization of halobenzenes[1], and CO extrusion from phenols[4]. Some of these reactions have even found use in the mass spectrometric differentiation of isomeric disubstituted benzenes and isomeric polycyclic aromatic hydrocarbons[3(b)]. We have recently observed the cleavage of stable aromatic rings in the thermal energy reactions of some early transition metal ion complexes in the gas phase[6]. Experimental studies of possible intermediate structures and the effects of methyl substitution on the reactions are discussed here.

Metal ions are generated by pulsed laser vaporization of pure metals and trapped in a FT-ICR mass spectrometer. After a collisional cooling period (> 0.5 sec) or complex formation by appropriate ion-molecule reactions followed by a similar cooling period, the metal ion-arene reactions listed in table 1 are observed. There are two proposed intermediates for this reaction. The first is a metallanorbornadiene complex involving a bent arene and the second is a direct ring inserted structure following the formation of a norcaradiene. The reaction of the quinoline and isoquinoline isomers gives insight into which mechanism prevails. Isoquinoline reacts with Nb^+ and NbO^+ in an analogous fashion to pyridine with HCN loss occurring exclusively. Quinoline, however, is unreactive. If the intermediate is the 7-membered ring structure (structure 1, directly inserted), reaction should be possible with both bicyclic rings. However, for the metallanorbornadiene intermediate reaction is only possible with the isoquinoline. The isoquinoline metallanorbornadiene intermediate is favorable, structure 2, but the quinoline metallanorbornadiene intermediate involves loss of aromaticity in both rings, strucure 3, making this high energy intermediate inaccessible. This suggests the ring cleavage reaction proceeds by the metallanorbornadiene at least for the bicyclic systems.

Reactions with the methylated rings show unusual behavior. Methylation of benzene shuts-off the ring cleavage pathway for Ta^+ with $2H_2$ loss occurring exclusively. This suggests methyl C-H activation is kinetically v\favored over the ring cleavage. Methylation of pyridine also provides for unusual reactivity. In addition to the ring cleavage (by HCN or CH_3CN loss) for picolines and lutidines, a molecule of H_2 is also lost. This occurs when the complex formed by ring cleavage results in formation of a d^2 metal center. This highly reactive metal center can then undergo cyclometallation by C-H attack on the pendant methyl group.

References

1) Dietz, T.G.; Chatellier, D.S.; Ridge, D.P.; J. Am. Chem. Soc., 100, 1978, 4905.
2) Huang, Y.; Freiser, B.S.; J. Am. Chem. Soc.; 1989, 111, 2387.
3) (a) Bjarnason, A.; Taylor, J.W.; Organomet., 1989, 8,; 2020. (b) Bjarnason, A.; Taylor, J.W.; Cody, R.B.; Kinsiger, J.A.; Weil, D.A.; Anal. Chem.; 1989, 61, 189.
4) Schroder, D.; Zummack, W.; Schwarz, H.; Organomet., 1993, 12, 1079.
5) Chen, L.Z.; Miller, J.M.; Org. Mass Spectrom.; 1992, 27, 19.
6) Pope, R.M.; VanOrden, S.L.; Cooper, B.T.; Buckner, S.W.; Organomet., 1992, 11, 2001.

Table 1. Reactions of Early Metal Ion Complexes with Arenes

M^+	d^n	arene	product	implied $D(M^+\text{-}L)$ (kcal/mol)
Ta^+	d^4	benzene	$TaC_4H_4^+$	> 152
			$TaC_6H_4^+$	> 77
Nb^+, Ta^+	d^4	pyridine	$MC_4H_4^+$	> 116
Sc^+, Y^+	d^2	pyridine	$MC_4H_4^+$	> 116
TaO^+, NbL^+ (L=O,N)	d^2	pyridine	$(L)MC_4H_4^+$	> 116
MO^+, NbO_2^+ (M=Sc,Y)	d^0	pyridine	$(L)MC_5H_3N^+$	

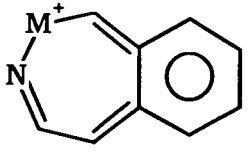

Structure 1.

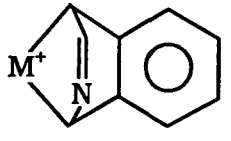

Structure 2.

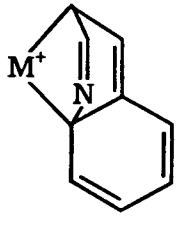

Structure 3.

COMPLEXES IN DISSOCIATIONS OF PROTONATED ALKYL ETHER IONS

Henri E. Audier[1], Dorothée Berthomieu[2], Jeanine Tortajada[2], and T.H. Morton[3]

[1] Laboratoire des Mécanismes Réactionnels, Ecole Polytechnique, 91128 Palaiseau, France
[2] Laboratoire de Chimie Organique Structurale, Université Paris VI, 75230 Paris, France
[3] Department of Chemistry, University of California, Riverside, CA 92521-0403 USA

Unimolecular dissociations of protonated tertiary alkyl ethers are often preceded by hydrogen exchange. For tert-Bu$\overset{H^+}{O}$R, where the R-group is iPr, decomposition to tBu^+ competes with decomposition to $(CH_3)_2C{=}OH^+$ in the metastable ion mass spectrum. The latter ion must be formed concomtantly with isobutane as the expelled neutral, a reaction that is likely to involve an ion-neutral complex. When the parent ion is isotopically labeled, the former ion is found to have undergone partial exchange of the methyl hydrogens of the tert-butyl group and the hydrogen on oxygen. For tert-Bu$\overset{D^+}{O}$R complete exchange between methyl and oxygen would result in an m/z 57: m/z 58 ratio of $\frac{1}{9}$. Experimentally observed ratios are

R	m/z 57:m/z 58
iPr	0.24
Et	0.28
Me	0.8
H	10

Both the exchange and alkane loss can be accounted for by invoking interconversion of [tBu^+ alcohol] and [isobutene protonated alcohol] complexes, but it is not obvious that these are not hydrogen-bonded complexes that need not fulfill the reorientation criterion. Therefore SCF calculations have been performed to explore the stabilities and structures of such complexes. Protonated alcohol···isobutene complexes are found to be quite stable, with dissociation energies that are nearly the same as the heterolytic R—O bond dissociation energies of the corresponding protonated ether. For example, the calculated ΔE_0 values for $(tBu)_2OH^+$ and its isomeric complex (at 6-31G**//6-31G**, including BSSE correction and zero point energies calculated at 3-21G) are summarized at the top of the next page. For this system there is also a stable structure corresponding to tBu^+···HOtBu, with C-O distances of 1.44 and 2.86Å. By contrast, the stable geometry for $(tBu)_2OH^+$ has two C-O bond lengths of 1.56Å, while tert-Bu$\overset{H^+}{O}$Me is calculated to have unequal C-O bond

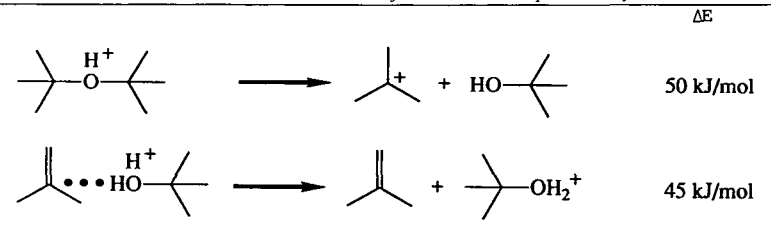

lengths of 1.44 (Me-O) and 1.59Å. The tBu^+···HOtBu complex appears to be hydrogen bonded, and its energy is only 7 kJ/mol higher than that of the protonated ether.

We have been unable to find a similar hydrogen-bonded complex of tBu^+ and methanol. But, because protonated methyl tert-butyl ether nevertheless exhibits hydrogen exchange (although not isobutane expulsion, since the heat of formation of $H_2C{=}OH^+$ is too high), such a complex must intervene. Therefore we infer that the presence of an ab initio potential energy minimum is not essential for a complex to operate.

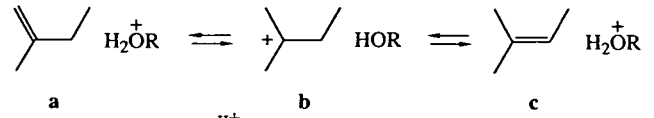

Metastable tert-Amyl-$\overset{H^+}{O}$-R have also been examined. The sites where exchange takes place depend on the identity of R. When the [alkene protonated alcohol] complexes lie close in energy to the protonated ether (as when R=iPr), isotopic labeling shows that both of the reactions a ⇄ b and b ⇄ c take place. But when the complex is higher in energy (as when R=Me) only the exchange corresponding to b ⇄ c is detected. This result is consistent with the fact that 2-methyl-2-butene is more stable than 2-methyl-1-butene.

Calculated carbon-oxygen distances in [alkene protonated alcohol] complexes do not show a great dependence on the identity of the alcohol. In isobutene···H_2^+OMe the distance is 3.18 Å, while in isobutene···H_2^+OtBu it is 3.26 Å. Therefore we discount steric factors in the regiochemistry.

Acknowledgment: This work was supported, in part, by a grant from the UCR Academic Senate Committee on Research.

On the Role of Ion-Neutral Complexes in the Alkene Loss from the Molecular Ions of Alkyl Phenyl Thioethers

Margot W. van Amsterdam, *Steen Ingemann and Nico M. M. Nibbering
Institute of Mass Spectrometry, University of Amsterdam, Nieuwe Achtergracht 129, 1018 WS Amsterdam, The Netherlands

The molecular ions of ethyl and n-propyl phenyl thioether react predominantly by α-cleavage and elimination of an alkene in the ion source and the field free regions (FFR) of a double-focussing hybrid quadrupole mass spectrometer. Deuterium labelling reveals that α-cleavage of ionized ethyl phenyl thioether (eq. 1) occurs without hydrogen atom interchange prior to dissociation and that ethene elimination in the ion source as well as on the μs time-scale proceeds by a specific transfer of a hydrogen atom from the β-position of the ethyl group to the remaining part of the ion (eq. 2).

$$C_6H_5SCH_2CD_3^{+\cdot} \rightarrow C_6H_5SCH_2^+ + CD_3^\cdot \quad (1)$$

$$C_6H_5SCH_2CD_3^{+\cdot} \rightarrow C_6DH_5S^{+\cdot} + C_2D_2H_2 \quad (2)$$

The loss of an ethyl radical from the metastable molecular ions of n-propyl phenyl thioether is to a minor extent accompanied by hydrogen atom interchange between the alkyl and phenyl groups (eq. 3). Moreover, the product ion of propene loss incorporates a hydrogen atom originating from any of the three positions of the alkyl group. A certain preference for transfer of a hydrogen atom from the β-position is observed, however, and this selectivity is particularly pronounced for the metastable ions (see Table).

$$C_6D_5SCH_2CH_2CH_3^{+\cdot} \xrightarrow{94\,\%} C_6D_5SCH_2^+ + C_2H_5^\cdot \quad (3a)$$

$$C_6D_5SCH_2CH_2CH_3^{+\cdot} \xrightarrow{6\,\%} C_6D_4HSCH_2^+ + C_2DH_4^\cdot \quad (3b)$$

The incorporation of a hydrogen atom from the α- or γ-position of the n-propyl group *indicates the occurrence of a reaction sequence involving cleavage of a C-S bond with* formation of an ion-neutral complex of a thiophenoxy radical and a secondary propyl carbenium ion. This complex can react further by proton transfer prior to dissociation into the thiophenol radical cation and propene (eq. 4). Evidence for this mechanism is obtained also by the observation that the metastable ions of $C_6H_5SCH_2CD_2CH_3$ expel $CH_3^\cdot$ and $CDH_2^\cdot$ to a minor extent and in a ratio of approximately 1:1 as expected from the occurrence of an isomerization of the n-propyl group to an isopropyl group (eq. 5).

Table. Normalized abundances of the ions formed by competing transfer of a hydrogen and deuterium atom in the propene loss from the molecular ions of labelled n-propyl aryl thioethers.

compound	H-transfer : D-transfer			
	ion source		2nd FFR	quadrupole section
	70 eV	10 eV		
$C_6H_5SCD_2CH_2CH_3$	82:18		90:10	94:6
$C_6H_5SCH_2CD_2CH_3$	65:35	33:67	30:70	22:78
$C_6H_5SCH_2CH_2CD_3$	70:30		85:15	92:8
$2,6\text{-}(CH_3)_2C_6H_3SCH_2CD_2CH_3$	70:30	70:30	42:58	32:68

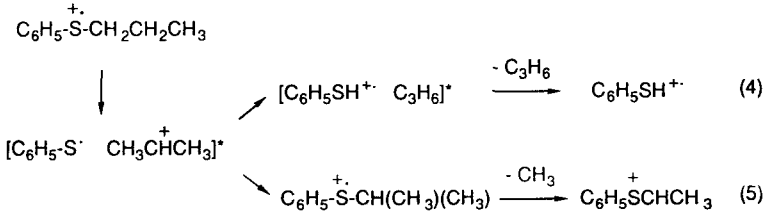

The preference for transfer of a hydrogen atom from the β-position at relatively low internal energies may be a result of a 1,5-H shift to the 2- or 6-position of the phenyl group followed by and/or concomitant with propene loss (eq. 6). This leads initially to the keto-form of the thiophenol radical cation, which subsequently may rearrange to the thiol-form. The preference for transfer of β-hydrogen atom in the propene loss on the μs time-scale is observed also for the molecular ions of 2,6-dimethylphenyl n-propyl thioether (Table) suggesting that a 1,3-H shift directly to the sulfur atom can compete with the *partially reversible 1,5-H shift (see eq. 3b) and the reaction involving ion-neutral* complexes.

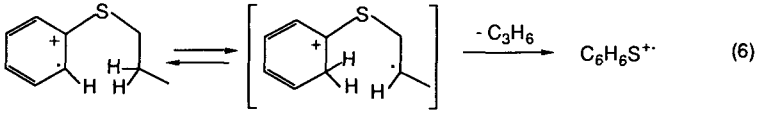

Fluoride Shifts in The Fragmentation of β-fluorophenetole radical cations and in The Rearrangement of 1-fluoropropyl to 2-fluoropropyl cations.

Viet Nguyen and Thomas Hellman Morton
University of California, Riverside, CA92521-0403

The m/z 94 /95 ratios ($PhOH^{+\bullet}$/ $PhOD^{+\bullet}$) resulting from bond cleavage and hydrogen transfer from C_α and C_β of deuterated β-fluorophenetole metastable ions differ markedly from those seen in the mass spectrometer source.[1] Recent studies of neutral vinyl fluorides from $PhOCD_2CH_2F$ and $PhOCH_2CD_2F$ using EBFlow techniques reveal that phenol ion comes from three competing pathways involving ion-neutral complexes: (i) via hydride shift, (ii) fluoride shift to form fluoriranium ion, (iii) vicinal elimination.[2] EBFlow radiolysis has also been done on $PhOCH_2CHDF$. Relative amounts of vinyl fluoride isomers measured from these experiments allow us to determine kinetic isotope effects as well as branching ratios of the three fragmentation pathways. Assuming the same kinetic isotope effects, branching ratios can also be estimated for the corresponding metastable ions.

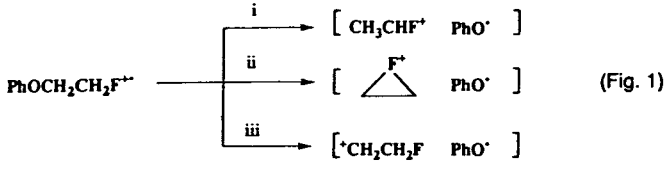

(Fig. 1)

BRANCHING RATIOS	i	ii	iii
Ion source	1.00	0.43	0.18
metastable ions	1.00	0.75	1.30

The difference in peak ratios between the MIKES and the source spectra of β-fluorophenetole can be attributed entirely to an approximately seven-fold increase in the proportion of ions undergoing vicinal elimination in the metastable ion decomposition s as compared to the 70eV ion source. This can account for the reported decrease in the net average kinetic isotope effect with increasing ion lifetime[1] without having to invoke significant changes in isotope effect values for the individual pathways. Threshold energy measured for the simple cleavage to expel $FCH_2^\bullet$ is 11.3 eV , 0.1eV higher than the threshold energy for the complex-mediated pathways.[3] *Ab initio* calculation supports the view that vicinal elimination comes from an ion-neutral complex that contains an unarranged primary carbocation structure.

In the gas phase, 1-fluoropropyl cation converts rapidly to 2-fluoropropyl cation.[4] The reaction of propionaldehyde with CF_3^+, depicted in figure 2 , in EBFlow reactor yields only 2-fluoropropene. CID spectrum of CD_3CH_2CHO with CF_3^+ produces both **1** and **2**. Previous studies have shown that **1** does not transpose deuterium,[4] this means that intramolecular hydrogen exchange takes place prior to or in the course of isomerization of 1-fluoropropyl cation . ^{19}F NMR analysis of collected neutrals from EBFlow radiolysis of

1-^{13}C-propionaldehyde with CF_4 shows all three 2-fluoropropene isomers with the ratio $^{13}CH_2{=}CFCH_3$: $CH_2{=}^{13}CFCH_3$: $CH_2{=}CF^{13}CH_3$ = 1.37:1:1.37. While reaction of 1-^{13}C- acetone only gives $CH_2{=}^{13}CFCH_3$ .To accomodate all available data, equation 1 is invoked as a possible mechanism for the isomerization of 1-fluoropropyl to 2-fluoropropyl cation.

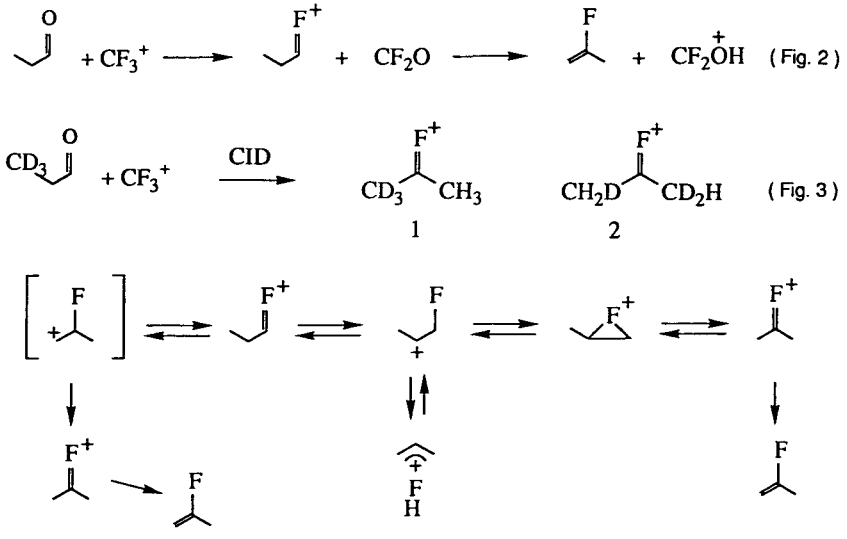

(Eq. 1) Possible mechanism for the isomerization of 1-fluoropropyl to 2-fluoropropyl cation.

REFERENCES:

1) Russell, D.H.; Gross, M.L.; Van der Greef, J.; Nibbering, N.M.M *Org. Mass. Spectrom.* **1979**, *14*, 474-479.
2) Nguyen, V.; Cheng, X.; Morton, T.H. *J. Am. Chem. Soc.* **1992**, *114*, 7127-7132.
3) Holmes, J.L. Private communication.
4) Shaler, T.A.; Morton, T.H. *J. Am. Chem. Soc.* **1991**, *113*, 6771-6779.

Structure and Vibrational Frequencies of Ionized Ethane: A Fluctional Molecule?

Charles E. Hudson*[1], C.S. Giam[1] and D.J. McAdoo[2]
[1]Texas A&M University, Galveston, Texas 77551
[2]Marine Biomedical Institute, Galveston, Texas 77555

In neutral ethane the weakest bond in the molecule is the C-C bond: $2\Delta H_f(CH_3) = 291.6$ kJ/mol while $\Delta H_f(C_2H_5 + H) = 118 + 218.0 = 336$ kJ/mol. However in the ion a C-H bond is weaker: $\Delta H_f(C_2H_5^+ + H) = 902 + 218 = 1120$ kJ/mol while $\Delta H_f(CH_3^+ + CH_3) = 1093.3 + 145.8 = 1239.1$ kJ/mol. This is easy enough to understand if the ionization takes place from an orbital devoted to C-H bonding. However the best calculations have disagreed whether the lowest energy state of $C_2H_6^+$ results from C-C ionization or from the degenerate HOMO devoted to C-H bonding.[2] The ESR spectrum of the ion has been recorded in matrices of low reactivity and is in good accord with the latter prediction and definitely not the result of C-C ionization,[3] but this has been attributed to the effect of the matrix.[4] We have extended the calculations using the general methods of reference 2 with larger basis sets and evaluation of the energies with more extensive treatments of correlations. We have also calculated the vibrational frequencies at the MP2/6-311+G** level to assess zero point effects.

Since the HOMO is a degenerate orbital devoted to C-H bonding, removal of an electron from it gives rise to two states (^2A_g and ^2B_g) after Jahn-Teller distortion. Removal of an electron from the slightly lower C-C bonding orbital gives rise to a symmetrical $^2A_{1g}$ ion. We have characterized all these structures at the MP2/6-311+G(2df, 2p) level of theory. The ^2A_g state with a normal C-C bond length and the $^2A_{1g}$ state with a long (1.9A) C-C bond length are of the same symmetry and can mix. As the bond is lengthened, the structure changes gradually from one state to the other.

Table 1

MP2/6-311+G(2df,2p) parameters of ethane ions

	^2A_g	$^2A_{1g}$	^2B_g
Energy[a]	-79.231005	-79.227955	-79.225833
ZPVE[b]	182.73	183.25	186.20
Rel energy[b]	0	4.70	20.56
RC-C	1.5558	1.9078	1.4272
RCH1	1.1406	1.0809	1.0799
H1CC[c]	82.87	98.38	118.74
RCH_2[d]	1.0804	1.0809	1.1346
H2CC[d]	115.95	98.38	112.26
H2CCH1[e]	70.55	60.0	45.80
QCISD(T) energy[a]	-79.236585	-79.236678	-79.227826
Rel energy[b]	0	0.28	26.47

a. in Hartrees b. in kJ/mol c. bond length (angle) to the two hydrogens on the plane of symmetry. d. bond length (angle) to the other four equivalent hydrogens e. dihedral angle between the plane of symmetry and

the H2CC plane.

The C-C stretching vibrations of the ^2A_g and $^2A_{1g}$ states are easy to identify because their reduced masses are 4 times as large as that of any other. As calculated at the MP2/6-311+G** level the frequencies are 531 and 509 cm^{-1} respectively, with about 3.0 kJ/mol of ZPVE in this mode. Preliminary indications are that this 3.0 kJ/mol exceeds the total variation of electronic energy between C-C bond lengths of 1.56-1.91A, hence the ethane ion may not have a well defined bond length over this range.

ESR theory holds that the hyperfine splittings are proportional to the spin density at the nucleus.

$$a^H(x) = a^H(H)\ \rho^H(x)/\rho^H(H)$$

where $a^H(x)$ is the splitting in question, $a^H(H)$ is the hydrogen atom splitting of 506.86G, $\rho^H(x)$ is the spin density at the hydrogen nucleus in question which is printed in the Fermi contact analyses of the Gaussian[5] output, and $\rho^H(H)$ is the spin density of the hydrogen atom at the nucleus, in electrons per cubic bohr. Our calculated splitting at the MP2/6-311+G(2df,2p) level is 137.2G compared to the experimental value of 152.5G if the analytically correct number ($1/\pi$) is used for $\rho^H(H)$. However if the value of $\rho^H(H)$ as calculated in the same basis set (0.28744) is used, the resulting prediction is 151.9G, in good agreement with experiment.

References

1. Richartz, A.; Buenker, R.J.; Bruna, P.J.; Peyerimhoff, S.D. Mol. Phys. 1977, 33, 1345-1366.
2. a. Lunell, S.; Huang, M-B. J. Chem. Soc. Chem. Commun. 1989, 1031-1033. b. Huang, M-B.; Lunell, S. Chem. Phys. 1990, 147, 85-90.
3. Toriyama, K.; Nunome, K.; Iwasaki, M.J. J. Chem. Phys. 1982, 104, 5700-5702.
4. Bellville, D.J.; Bauld, N.L. J. Am. Chem. Soc. 1982, 104, 5700-5702.
5. Gaussian 92, Revision B.M.J. Frisch, G.W. Trucks, M. Head-Gordon, P.M.W. Gill, M.W. Wong, J.B. Foresman, B.G. Johnson, H.B. Schlegel, M.A. Robb, E.S. Replogle, C. Gonzalez, R.L. Martin, D.J. Fox, D.J. Defrees, J. Baker, J.J.P. Stewart and J.A. Pople, Gaussian, Inc. Pittsburgh, PA, 1992.

Theoretical Study of the Ring Closure of the 1,7-Octadiyne Cation.

Ronny C. Robbins, James Jensen
U.S. Army
Aberdeen Proving Ground
Edgewood Area
APG, MD 21010-5423

The ring closure of the 1,7-octadiyne cation is studied using the GAUSSIAN92 program. The calculations were done at the SCF and CASSCF levels of theory using the 6-31g set. The "Thru-Space" interaction of the pi systems on two alkyne fragments is examined. All calculations were run using Gaussian 92 rev B on a Kubota Pacific ST3000 and a Convex 3820. Possible starting geometries for the open structure were generated using the AVS Chemistry viewer program. These structures were then optimized at the Restricted-Hartree-Fock level using a 6-31g basis set. The structure with lowest energy was then taken for further study. A global search of all geometric configurations was not possible. However, the structure chosen had the largest negatively charge carbon atom as measured by a Mullikan charge in close proximity to the carbon atom with the largest positive charge. The starting geometry for the ring structure was generated by taking the open structure and rotating a single dihedral angle(D5 in the Z-matrix) from 60 degrees to -40 degrees until the carbons on the ends of the two triple bonds were approximately a bond length apart. This rotation of the dihedral angle was monitored using the AVS Chemistry viewer program. In order to make the ring stay closed, the C-C-H angle of each alkyne group had to be manually changed from approximately 180 degrees to 120 degrees. This structure was then optimized at the RHF level using a 6-31g basis set. Using the optimized open and ring structure, a guess structure for the transition state was generated using the Linear Synchronous Transit capability of the Gaussian 92 package. This transition state was then optimized at the RHF 6-31g level. An RHF energy Hessian matrix was generated at each step of the optimization. Single point CASSCF calculations of the ring and open structures showed that the open structure was well described by a single configuration and that the ring structures was somewhat less well described by a single configuration. Therefore, it was decided to optimize all three structures(open, ring, and transition state) at the CASSCF level of theory. An 8 in 8 CAS was used in order to completely correlate the four pi and four pi-star orbitals of the two triple bonds. An RHF energy Hessian was generated for each structure to start the optimization. A frequency calculation (8 in 8 CAS 6-31g) is to be run at the optimized open and ring structures. The ring closure is exothermic by approximately 5 Kcal/mole.

References

1. Nagy-Felsobuki, E., Peel, J.B., Willett, G.D. Chem. "The Photoelectron Spectra of Some Non-Conjugated Acyclic Diynes", Phys. Lett. Vol. 68, No. 2,3, Pages 523-526, 1979

2. M.J. Frisch, G.W. Trucks, M. Head-Gordon, P.M.W. Gill, M.W. Wong, J.B. Foresman, B.G. Johnson, H.B. Schlegel, M.A. Robb, E.S. Replogle, R. Gomperts, J.L. Andres, K. Raghavachari, J.S. Binkley, C. Gonzalez, R.L. Martin, D.J. Fox, D.J. Defress, J. Baker, J.J.P. Stewart, and J.A. Pople, **GAUSSIAN92**, Revision B, Gaussian Inc, Pittsburgh, PA, 1992.

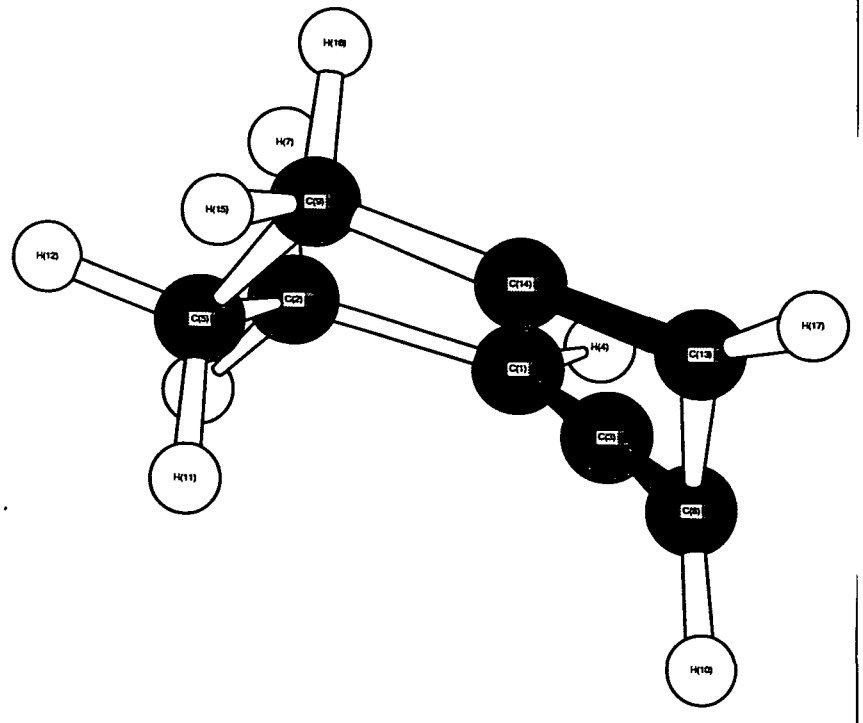

Figure 1: Optimized Ring Structure for the Cyclization of 1,8-Octadiyne

DOUBLY IONIZED STATES OF FLUORINATED METHANES

*W.J.Griffiths, S.Svensson, A.Naves de Brito, N.Correia, C.J.Reid, M.L.Langford, F.M.Harris, C.M.Liegener and H.Ågren Institute of Physics, Uppsala University, Uppsala, S-75121, Sweden.

High resolution Auger-electron, and double-charge-transfer (DCT) spectra have been recorded of the molecules CF_4, CF_3H, CF_2H_2, and CH_3F. Both forms of spectroscopy give information as to the energy levels in dications. Auger-electron spectra are dominated by transitions to states of singlet symmetry and give double ionization energies to such states. In the present work double-charge-transfer spertra have been recorded using the OH+ and the F+ projectile ions. Both of these ions populate triplet states in the dications formed, and double ionization energies to triplet states are measured. DCT spectra have also been recorded using the H+ projectile, where singlet state dications are formed. Auger- electron and DCT spectroscopies provide complimenatry information as to the energy levels in dications. The spectra recorded have been interpreted with the aid new of theoretical calculations obtained by a two-particle Green"s function method. The ageement between theory and experiment is found to be good.

Shown below are the H+, F+, and OH+ DCT spectra of CF_4 and also the C1s Auger-electron spectrum. Double ionization energies are caluclated from Auger spectra by subtracting Auger-electron kinetic energies from core binding energies. In CF_4 the C1s binding energy is 301.96 eV.

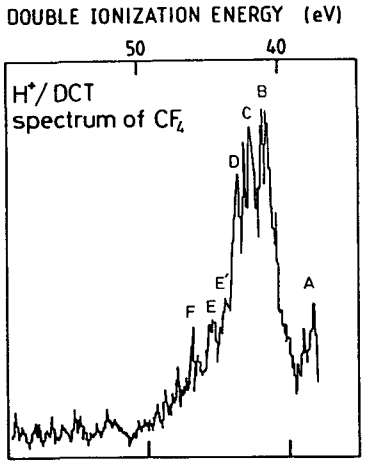

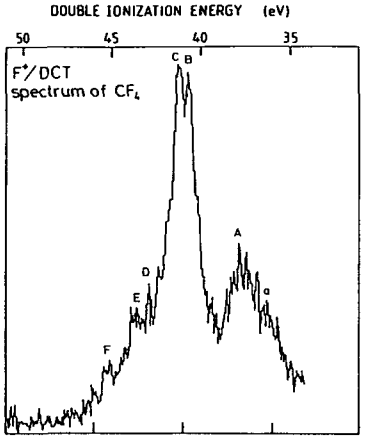

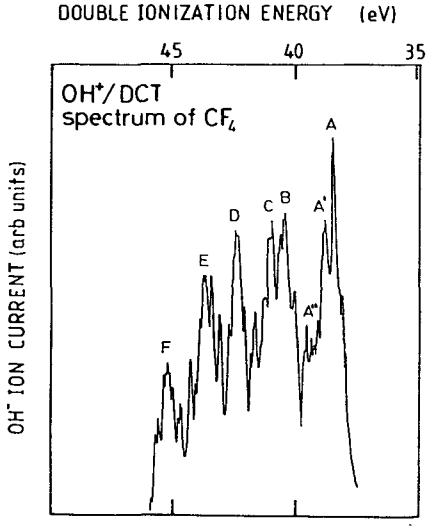

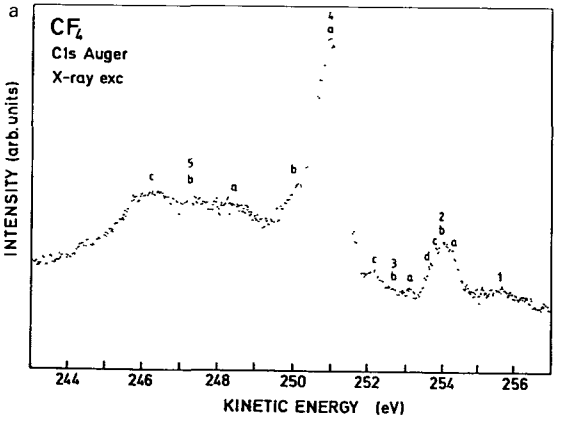

Singlet state energy levels of $C_2H_4^{2+}$

M L Langford[2], P G Fournier[1], J Fournier[1] and F M Harris[3]

[1]Laboratoire de Spectroscopie de Translation, UPS Bat. 478, URA C.N.R.S. 1234, 91405 Orsay, France.
[2]The Chemical Laboratory, University of Kent, Canterbury, Kent CT6 7NH
[3]Mass Spectrometry Research Unit, Chemistry Department, University College of wansea, Swansea.

The Double Charge Transfer (DCT) spectra of singlet states of $C_2H_4^{2+}$ are determined at high resolution and compared with the results of two previous DCT studies [1,2]. Both of these studies were carried out using proton projectile ions but there are substantial differences in the measured energies of the dication states. The present results are also compared with the double ionisation energies and vertical ionisation spectrum predicted using the two particle Green's function method with the second order algebraic diagrammatic construction (ADC(2)) [3].

The present experiments involve the measurement of the translational energy lost by H^+ ions in the reaction

$$H^+ + M \rightarrow H^- + M^{2+} \qquad (1)$$

where two electrons are transferred from a target molecule M to produce a doubly charged ion M^{2+}. The experiments were carried out on a double mass spectrometer. Calibration of the energy scale was carried out with particular care in this experiment in order to resolve the controversy generated by the two previous DCT studies. Due to spin conservation only singlet states of $C_2H_4^{2+}$ are expected to be observed in this study.

The spectral resolution obtained in the present investigation is much higher than in the two previous studies and has enabled an accurate measurement of five singlet states of $C_2H_4^{2+}$ with the energies 30.9, 34.3, 36.2, 38.8 and 42.8 eV. The Figure shows that peak A is a well defined

peak with a sharp onset at approximately 28.8 eV, an energy distribution of 0.8 eV at 90% intensity and a FWHM of 3 eV. (The instrumental broadening in these experiments is 1.3 eV). The energy separations between the three lowest energy singlet states (S1 and S2; S2 and S3) are computed [3] to be 1.73 and 2.62 eV respectively. The energy distribution exhibited by peak A suggests that strong contributions from only one of these states are involved in its generation. Calculations have shown that the ground state of the dication has a radically changed geometry from the planar neutral molecule [3]. Vertical transitions from the neutral ground state would be to an unstable planar configuration leading to poor Franck-Condon transition factors and resulting in a broadened low intensity peak quite unlike peak A. Thus it seems likely that Peak A represents the population of S2 which has a stable planar configuration and not the ground state S1.

References
1. J. Appell, J. Durup, F. C. Fehsenfeld and P. Fournier, J. Phys. B: Atom. Molec. Phys. **7**, 406 (1974).
2. C. Benoit and J. A. Horsley, Mol. Phys. **30**, 557 (1975).
3. E. Ohrendorf, H. Koppel, L. S. Cederbaum, F. Tarentelli and A Sgamellotti, J. Chem. Phys. **91**, 1734 (1989).

The negative-ion spectrum obtained when 5 keV protons are in collision with C_2H_4 molecules.

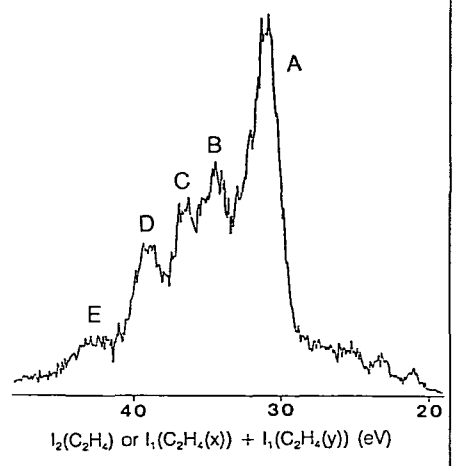

AN EXPERIMENTAL AND COMPUTATIONAL STUDY OF DOUBLE IONIZATION OF CH_2I_2, CHI_3 AND CI_4 MOLECULES

F.M. Harris [a], S.R. Andrews [b], P.J. Jackson [a], M. Vairamani [c], W.J. Griffiths [d] and D.E. Parry [b].

[a]*Mass Spectrometry Research Unit,* [b]*Department of Chemistry, University College of Swansea, Singleton Park, Swansea SA2 8PP, UK.*

[c]*Indian Institute of Chemical Technology, Hyderabad, 500 007 India.*

[d]*Department of Physiological Chemistry, Karolinska Institutet, Box 60400, S-10401 Stockholm, Sweden.*

INTRODUCTION

The results of a combined experimental and theoretical study of the double ionization of CH_3I were reported in 1990[1]. Since that time, similar studies of CH_2I_2, CHI_3 and CI_4 have been completed, the results of which form the basis of this paper. Experimentally, double-charge-transfer (DCT) spectroscopy was used to measure double-ionization energies to various electronic states of the dications. Computationally, these energies have been calculated using a modified form of the Multiple Scattering Xα (MSXα) method[2] of molecular orbital calculations.

EXPERIMENTAL PROCEDURE

In DCT spectroscopy, high-velocity singly charged positive ions undergo double-electron-capture (DEC) reactions in collisions with the molecules under investigation. Since the iodides studied have low volatilities, an MS9 spectrometer was used which has a heated sample reservoir and heated lines to the collision-gas cell. The projectile OH^+ ions had 8keV translational energy so the DEC reaction

$$OH^+ + M \rightarrow OH^- + M^{2+} \qquad ..(1)$$

with a molecule M must, therefore, have taken place very rapidly because of the high velocity of OH^+, resulting in vertical transitions from M to M^{2+}. If E_p and E_n represent the translational energies of OH^+ and OH^-, respectively, then

$$E_p - E_n = IE_2(M) - E(OH^+ \rightarrow OH^-) \qquad ...(2)$$

where $IE_2(M)$ represents the double-ionization energy to the ground electronic state of M^{2+}, and $E(OH^+ \rightarrow OH^-)$ is the energy released in the charge inversion of OH^+. In the experiments, E_n was kept constant and E_p varied; a peak in the OH^- ion current against E_p spectrum was obtained when eqn. (2) is satisfied. Calibration of the energy-loss scale was achieved by obtaining a DCT spectrum with xenon atoms in the cell for which the double-ionization energy is known.

The populating of higher-lying states of M^{2+} will occur at higher values of E_p, giving additional peaks in the DCT spectrum.

COMPUTATIONAL PROCEDURE

Double-ionization energies to triplet states of the dications were calculated since there is now ample evidence[3] to show that the use of OH^+ in the study of closed-shell molecules will populate triplet states of the corresponding dications because of spin conservation in the DEC reaction. Values were obtained by carrying out separate calculations of the total energies of the initial target-molecule ground state and final dication state of interest. It has been found[4] that if the double-ionization process is regarded within a single-configuration approximation as the creation of two holes in molecular orbitals *a* and *b*, which then experience a repulsive interaction energy V_{ab}, then this implies

$$DIE_{ab} = E_{ia} + E_{ib} + V_{ab} \qquad ...(3)$$

where E_{ia} and E_{ib} are the single-ionization energies for each orbital. Experimental single-ionization energies were used in this equation thus rendering the method semi-empirical.

RESULTS

As a result of the computational method, the double-ionization energies to ground and electronically excited states of CH_3I^{2+} were calculated. The data agreed well with the previously published[1] experimental data. Because of space limitations, it is not possible to present all the data for the three molecules studied. One has been chosen (CHI_3), and the calculated and experimental results are presented below.

CHI_3^{2+} state populated	Calculated DIE	Calculated Average	Experimental DIE
$^3A_2$	24.4		
^3E	24.5		
^3E	25.1	24.9	24.8 ± 0.3
$^3A_2$	25.2		
^3E	25.2		
^3E	25.8		
$^3A_1$, $^3A_2$, ^3E	25.9	26.1	26.1 ± 0.4
$^3A_2$	26.6		
^3E	27.8		
^3E	28.2	28.2	28.0 ± 0.5
$^3A_1$, $^3A_2$, ^3E	28.4		
$^3A_2$	29.1		
$^3A_1$, $^3A_2$, ^3E	29.2		
$^3A_1$	29.6	29.6	30.0 ± 0.5
^3E	29.7		
^3E	30.5		

It can be seen that the number of states predicted to exist in the range 24.4 eV to 30.5 eV is large. As shown, logical groupings of the states are possible, and the average state energies of these groups agree well with the energies determined experimentally. For CH_2I_2, the density of calculated states is higher making it more difficult to group the states. For CI_4, however, the density of states is lower than that for CHI_3, so that groups with no more than two components were identified which gave average values in agreement with those measured.

Full details of this investigation will appear in a paper[5] to be published this year.

REFERENCES

1. WJ Griffiths, FM Harris and DE Parry, *J. Chem Soc. Faraday Trans.*, 86, 2801, 1990
2. M Cook and DA Case, XASW, QCPE Program No. 465, Quantum Chemistry Program Exchange, Indiana University, Bloomington, Indiana, USA.
3. FM Harris, *Int. J. Mass Spectrom. Ion Processes*, 120, 1, 1992.
4. SR Andrews and DE Parry, *Chem. Phys. Lett.*, 196, 630, 1992.
5. SR Andrews, PJ Jackson, M Vairamani, WJ Griffiths, DE Parry and FM Harris, *J. Chem. Soc. Faraday Trans.*, - in press.

The Relative Migratory Aptitudes of Fluoride and Methyl in a Gas Phase Carbocation

*Thomas A. Shaler and Thomas Hellman Morton
Dept. of Chemistry, University of California, Riverside, CA 92521-0403

It is well known that carbocations undergo facile rearrangements through the migration of alkyl groups and hydrogens. For carbocations that are substituted by the halogens Cl, Br, or I, there are many examples in the gas phase and in solution of halogen bridging or migration. In contrast, for those that are substituted by fluorine, there are but a few examples of fluorine's participation in bridging or migrating through a bridged transition state.[1]

We would like to report that the recently proposed[2] 1,2-fluoride migration in the decomposition of electron-impact ionized **1** has been confirmed through the use of EBFlow[3] experiements on the ^{13}C-labeled compound **2**. Primary alkyl phenyl ethers such as these are known to decompose through intermediate ion-neutral complexes when ionized.[4] The neutral alkenes that are expelled can be collected and analyzed to allow inferences about the structures and rearrangement pathways of the carbocation within the ion-neutral complex to be made.

Since experiments on **1** could not distinguish between the two possibilities depicted in Scheme 1, one of which involves only methyl shifts and not a fluoride shift, compound **2** was prepared and subjected to EBFlow radiolysis. The formation of C_4H_7F neutral fluoroalkenes having fluorine bonded to ^{13}C has allowed us to unambiguously establish that a 1,2-fluoride migration has occurred. Our results allow us to obtain a direct measurement of the relative migratory aptitude of fluorine and methyl. When corrected for the 2:1 statistical preference for methyl migration, the ratio of the amounts of methyl-shift products to the amounts of fluoride shift products is 2.1:1.

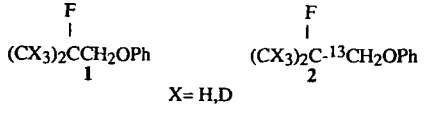

Scheme 1

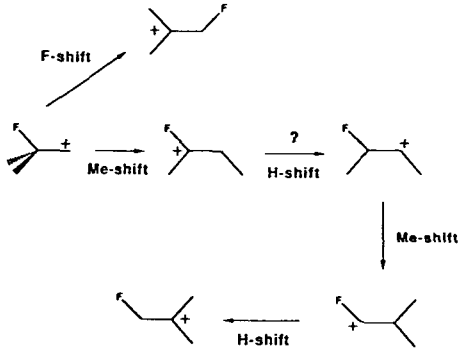

[1] V.Q. Nguyen, X. Cheng, T.H. Morton, *J. Am. Chem. Soc.*, 1992, *114*, 7127
[2] T.A. Shaler, T.H. Morton; *J. Am. Chem. Soc.*, 1990, *114*, 6868
[3] T.H. Morton in "Techniques for the Study of Ion-Molecule Reactions, Farrar, J.M., Saunders, W.H., Eds.; *Techniques of Chemistry*, XX, Wiley, 1988, pp.119-164.
[4] T.H. Morton; *Org. Mass Spectrom.*, 1992, *27*, 353.

Mechanism of Gas Phase Aldose-ketose Isomerization: A Study using Tandem Mass Spectrometry and Theoretical Calculations

*Ya-Jun Zheng and Julie A. Leary
Department of Chemistry, University of California, Berkeley, CA 94720

Fast atom bombardment (FAB) tandem mass spectrometry (MS/MS) of lithium coordinated oligosaccharides has been shown to be an effective method of determining the linkage position of various isomeric oligosaccharides [1-3]. Collision induced dissociation (CID) of either the monolithiated ($[M + Li]^+$) or dilithiated ($[M + 2Li - H]^+$) species produces product ions of the isomers which are different and very specific to the linkage position. In these earlier studies we postulated that in order to observe the different losses for each isomeric disaccharide, the reducing ring hemiacetal must first undergo ring opening to produce the hydroxy aldehyde [2]. Subsequent retro-aldol rearrangement then gives rise to specific two, three, and/or four carbon neutral losses from the reducing ring. In one particular isomer, the 1,3 linked disaccharide, transposition of the carbonyl function from C-1 to C-2 of the hydroxy aldehyde is required prior to the retro-aldol rearrangement [2,3]. Labeling studies employing ^{18}O and ^{2}H indicated that the 1,3 linked disaccharide must rearrange to transpose the carbonyl to the C-2 position prior to the retro-aldol reaction in order to observe the characteristic three carbon chain neutral loss ($C_3H_4{}^2H_2O_3$) as shown in Scheme 1.

Fast atom bombardment (FAB) tandem mass spectrometry (MS/MS) and semiempirical molecular orbital method (MNDO) were used to investigate the mechanism of gas phase aldose-ketose isomerization. Two reaction pathways were investigated. Both involve ring opening, but differ in the aldehyde-ketone isomerization step. In reaction pathway A, the isomerization follows a keto-enol tautomerization via a 1,3 H shift while reaction path B involves a proton transfer from the C-2 hydroxyl to the carbonyl oxygen (C-1) followed by a hydride transfer from C-2 to C-1. The MNDO calculations suggest that Path B is favored over Path A by 29.2 kcal/mol. Metastable and CID studies in all three reaction regions of a hybrid mass spectrometer (BEgQ) indicate this reaction is observed in FFR 2 and 3, but not in 1. Because we do not see this same reaction during CID of the protonated precursor, it is very likely that the hydride transfer mechanism is being catalyzed by the presence of lithium.

References:

1. Z. Zhou, S. Ogden, J. A. Leary; J. Org. Chem. **55**, 5444 (1990)
2. G. E. Hofmeister, Z. Zhou, J. A. Leary; J. Am. Chem. Soc. **113**, 5964 (1991).
3. A. Staempfli, Z. Zhou, J. A. Leary; J. Org. Chem. **57**, 3590 (1992).

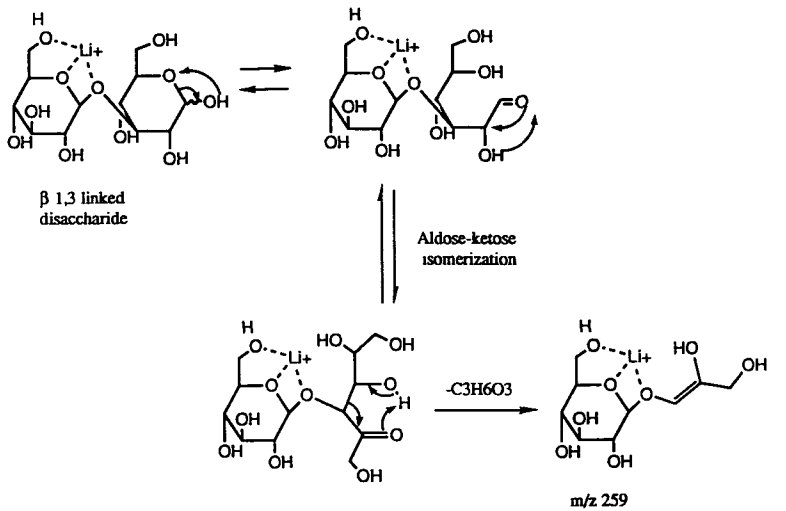

Scheme 1

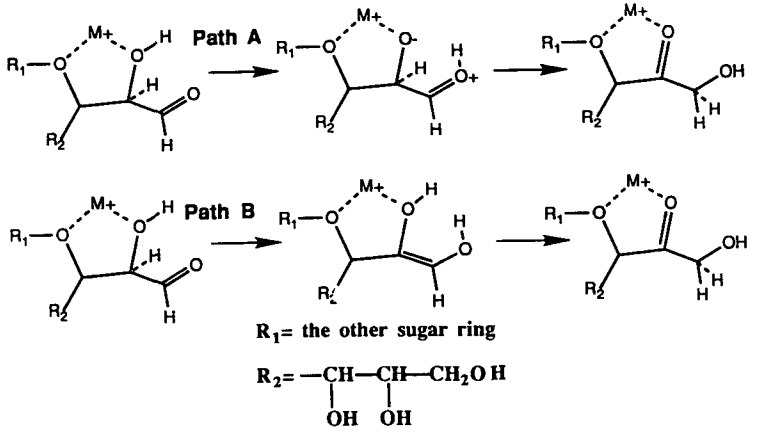

Competing Dissociation of and Bond Formation between CH_3CHOH^+ and $^{\cdot}CH_2CH_3$ formed by Bimolecular Processes.

Mohammed S. Ahmed[a,b], C.S. Giam[b] and David J. McAdoo[a]
[a] Marine Biomedical Institute, University of Texas Medical Branch, Galveston, Texas 77555

[b] Dept. of Marine Sciences, Texas A&M University at Galveston, Galveston, Texas 77553

Introduction

Ion-neutral complexes are often invoked to rationalize unimolecular decompositions of ions in the gas phase. Relationships between those decompositions and corresponding ion-molecule reactions have recently begun to be explored. Whether energetic or angular momentum differences cause significant variations in reactivity between unimolecular and bimolecular processes is of interest. Comparisons between unimolecular and bimolecular processes suggested that they are linked by a common intermediate,, albeit differences in product distribution with mode of reaction exist. These differences have been attributed to reaction on different regions of the potential energy surface.

(1)

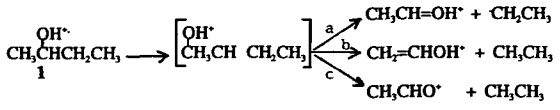

Ionized 2-butanol undergoes complex-mediated decompositions (1a and 1b) which diminish rapidly with increasing energy in the system. We chose to study a variety of ion-molecule reactions to enter the $C_4H_{10}O^+$ potential energy surface in the vicinity of 1 at different energies (Fig. 1). The ion-molecule reactions we characterized include those of $CH_3CH_3^+$ with CH_3CHO, CH_3CHO^+ with CH_3CH_3, $CH_3CH_2OH^{+\cdot}$ with $CH_2{=}CH_2$, and $CH_2{=}CH_2^{+\cdot}$ with CH_3CH_2OH. Our objectives were to determine how closely ion-molecule reactions reproduce the complex-mediated unimolecular decompositions of 1 and how well C-C bond formation and H-transfer compete with dissociation of CH_3CHOH^+ and $^{\cdot}CH_2CH_3$.

Experimental

All experiments were performed on an Extrel FTMS-1000 equipped with a 3 Tesla superconducting magnet. The typical reagent pressures were $5\text{-}7\times10^{-8}$ torr except for ethanol a lower pressure was used ($2\text{-}3 \times 10^{-8}$ torr) to minimize unwanted proton transfer reactions. Spectra were recorded in the broad band mode at a sweep rate of 1 KHz/µs. The reactants were collisionally cooled by pulsing argon to a peak pressure of 2×10^{-5} torr. The ionizing electron energy was 12 eV. All samples were purchased from commercial sources.

Results and Discussion

Reaction of $C_2H_6^{+\cdot}$ with CH_3CHO produced predominantly CH_3CHOH^+, with lesser amounts of CH_3CO^+, $C_2H_4O^+$. (8:5:100:1). These reactants are about 162 kJ mol^{-1} above the threshold for forming $CH_3CHOH^+ + {}^{\cdot}CH_2CH_3$ (Fig. 1).

(2)

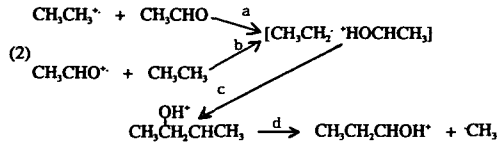

Reaction of $C_2D_6^{+\cdot}$ with CH_3CHO produced m/z 43, 44, 45, 46, 62 and 65 in the relative abundances 11:10:75:100:1:0.3. The formation of m/z 65 demonstrate that reaction 2ac took place. The formation of m/z 65 demonstrate that reaction 3 also occurs at these higher energies.

(3) $CH_3CHO + CD_3CD_3^+ \longrightarrow CH_3CHOCD_3^+ + {}^{\cdot}CD_3$

The oppositely charged ethene/ethanol pairs differ in energy by only 4 kJ mol^{-1} (Fig. 1). $C_2H_4^+$ reacted with ethanol to produce $CH_3CH_2OH_2^+$, $CH_3CHOH^{+\cdot}$ and $C_3H_7O^+$ in about a 2.5:1:10:.05 ratio, but did not produce detectable CH_3CHOH^+.

(4)

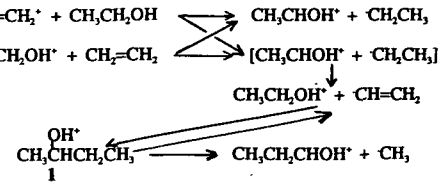

Reaction of $CH_3CH_2OH^+$ with $CH_2{=}CH_2$ also gave $CH_3CH_2OH^+$ and CH_3CHOH^+ but did not yield any detectable $C_3H_7O^+$. The low abundance to absence of C_3 products demonstrate that collapse of CH_3CHOH^+/CH_2CH_3 pair to 1 was slight relative to their dissociation.

Conclusions

1. Bond formation or a second H-transfer infrequently follows initial H-transfer in ion-molecule reactions.
2. C-C bond formation followed by opposite C-C bond cleavage was 12 to more than 50 times less frequent than the prior proton and hydrogen transfers in the reactions studied.
3. Energy and angular momentum in the system generated by ion-molecule reactions could contribute to the differences observed between ion-molecule reactions and metastable decompositions.

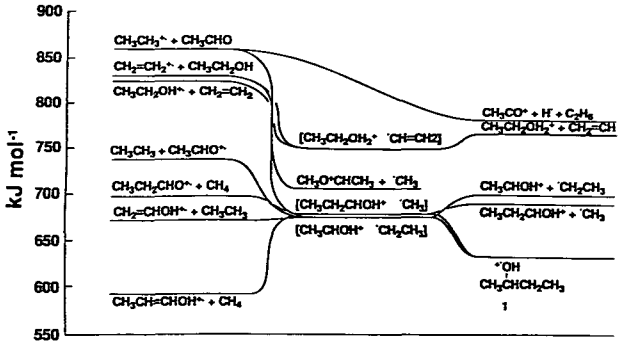

Fig. 1 Potential energy surface for $C_4H_{10}O^{+\cdot}$ system

Gas-Phase Radical Cation Rearrangements of 4-Vinylcyclohexene to Bicyclo[3.2.1]-2-octene

D. L. Vollmer, D. L. Rempel M. L. Gross, Univeristy of Nebraska, Lincoln, NE 68588

The potential energy surface of the C_8H_{12} radical cation has been investigated by several methods including mass spectrometry[1], theoretical calculations[2], and ESR[3]. The reaction of 1,3-butadiene radical cation with 1,3-butadiene neutral was studied by using high-pressure chemical ionization[1] and *ab initio* calculations[3] and was concluded to proceed through an acyclic intermediate to form the 4-vinylcyclohexene radical cation, 1. Investigation by matrix-isolation ESR, however, has shown that 1 undergoes radical cation rearrangement to bicyclo[3.2.1]oct-2-ene, 3 [3].

Here we report the occurrence of this rearrangement in the gas-phase by use of tandem mass spectrometry (MS/MS) on a sector mass spectrometer and a Fourier transform (FT) mass spectrometer. The sector mass spectrometer involves utilization of conventional MS/MS techniques for isomer differentiation. The FT mass spectrometer, however, incorporates a new methodology recently demonstrated in our laboratory[4] which allows for control, in part, of the rearrangement of 1 to 3.

With the sector mass spectrometer, the radical cation of each C_8H_{12} compound was formed, in separate experiments, in a chemical ionization (CI) source by electron-impact ionization. The radical cations were then mass selected by using the first stage of a tandem mass spectrometer, collisionally activated, and a spectrum of its decomposition products taken by scanning the second stage. The collisional-activated decomposition (CAD) spectra are similar; both C_8H_{12} radical cations fragment to form structurally significant ions via losses of ·H (to give *m/z* 107), ·CH_3 (*m/z* 93), C_2H_4 (*m/z* 80), C_2H_5 (*m/z* 79) and C_3H_6 (*m/z* 66).

The addition of a CS_2 bath gas to the CI source in the aforementioned experiment, however, yields distinctive CAD spectra (See **Figure 1**); the abundance ratio of *m/z* 93 to *m/z* 66 is particularly informative. For 1, the abundance ratio changes from 0.5 to 1.8 with CS_2 addition whereas 3 remains constant at 0.4. We attribute this difference to the ability of CS_2 to act as a charge-exchange reagent as well as a collisional stabilization gas to produce low-energy radical cations, which are less likely to rearrange than higher-energy radical cations.

To study the rearrangement further an FT mass spectrometer was utilized. This spectrometer has the ability to form, via the rf-only-mode event, near-thermal ions as well as select and store ions for extended periods of times. In separate experiments, the C_8H_{12} radical cations were produced by low-energy charge exchange with preformed toluene radical cations. During this time, the rf-only-mode event, along with a high-pressure (~10^{-3} Torr) helium pulse, was implemented for collisional stabilization of the radical cations. Following the charge-exchange reaction, the radical cations were isolated by ejecting all other ions. The remaining C_8H_{12} radical cations were collisionally activated by ion excitation in the presence of residual helium.

The CAD spectra of the two C_8H_{12} radical cations display similar fragments to those seen with the tandem mass spectrometer with the exception of loss of ·H (*m/z* 107). The relative abundances of the ions, however, are different for each radical cation. Again, the abundance ratio of *m/z* 93 to *m/z* 66 is the distinguishing feature. For 1, the abundance ratio is 4.9 whereas 3 produces a ratio of 0.1.

Upon addition of internal energy to the aforementioned experiment, by way of ion excitation, during the rf-only-mode event and in the presence of a high-pressure of helium, the CAD spectrum changes for 1; the abundance ratio of *m/z* 93 to *m/z* 66 is 0.5. The abundance ratio remains approximately the same (0.05) for 3, as in the experiment without ion excitation. The higher ratio of 0.5 for 1 in these experiments can be explained by an incomplete rearrangement of 1 to 3.

The ability to excite ions during the rf-only-mode event offers a unique way of controlling, in part, the molecular structure of the vinylcyclohexene radical cation. This is demonstrated by varying the

amplitude of the ion excitation for 1 (See **Figure 2**). At low ion excitation, the relative abundance of *m/z* 66 is greater than that of *m/z* 93 indicating characteristics of 1. Increasing the ion excitation, however, shows an inversion of relative abundances for each mass. At high ion excitation, the relative abundances indicate a structure of 3. A similar experiment was performed on 3 in which no inversion was observed, at low or high ion excitation.

Both MS/MS and FTMS results are in accordance with the matrix-isolation ESR investigation, which suggests that 1 rearranges to 3 at higher internal energy, but is thermodynamically stable at lower internal energy[3]. A mechanism was previously proposed to explain this rearrangement which involves cation attack from the C-2 of the ene radical cation, 1, to form a distonic ion (charge-radical site-separate radical cation), 2, with the carbon skeletal structure of 3 (See **Scheme 1**). A 1,4-H· transfer can then be invoked to reach 3.

Figure 1

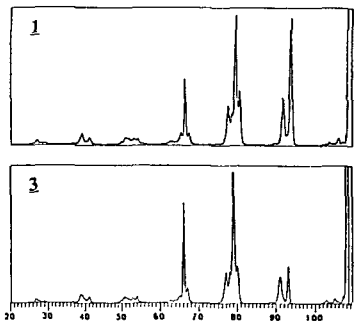

Figure 2

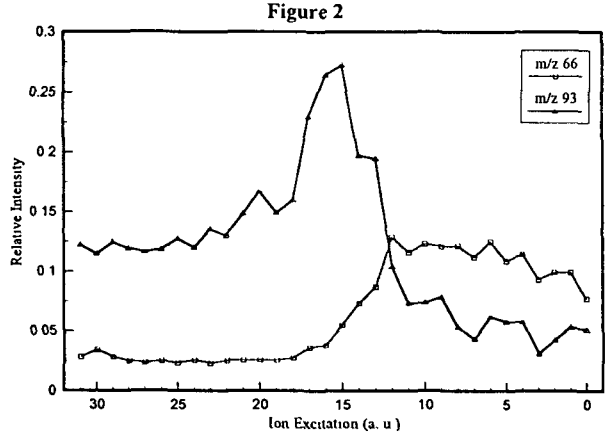

References

(1) Groenwold, G. S.; Gross, M. L. *J. Am. Chem. Soc.* **1984**, *106*, 6569.

(2) (a) Bauld, N. L. *et al.* *J. Am. Chem. Soc.* **1983**, *105*, 2378.

(3) Chen, G.-F.; Williams, F. *J. Am. Chem. Soc.* **1991**, *113*, 7792.

(4) Rempel, D. L.; Gross, M. L. *J. Am. Soc. Mass Spectrom.* **1992**, *3*, 590.

Scheme 1

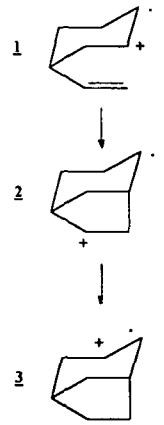

DYNAMICS OF THE UNIMOLECULAR DISSOCIATION OF DIMETHYLFORMAMIDE RADICAL CATION

Susan T. Graul,[a] Jeanette Adams,[b] Joseph Toto,[c] and Michael T. Bowers[c]
[a] Dept. of Chemistry, Carnegie Mellon University, Pittsburgh, PA 15213
[b] Dept. of Chemistry, Emory University, Atlanta, GA 30322
[c] Dept. of Chemistry, Univ. of California, Santa Barbara, CA 93106

INTRODUCTION

In studies of the electron ionization (EI) mass spectra and metastable dissociation spectra of $(CH_3)_2NCHO^+$, Ann and Adams[1] observed products that corresponded to loss of CHO and CH_3 neutral fragments.

$$\left[(CH_3)_2NCHO^+\right]^* \rightarrow C_2H_6N^+ + CHO$$
$$\left[(CH_3)_2NCHO^+\right]^* \rightarrow CH_4NO^+ + CH_3$$

Although the products can be explained readily in terms of simple bond cleavage reactions, deuterium labeling at the formyl position revealed a more complicated mechanism for the CHO loss pathway. For the higher energy EI spectra, d_1-DMF^+ decomposed by loss of 29 amu (CHO), whereas metastable d_1-DMF^+ lost 30 amu (CDO) in this dissociation channel.

Loss of CHO from $(CH_3)_2NCDO^+$ requires rearrangement, whereas loss of CDO requires only N-C bond cleavage. Rate constants for simple bond cleavage typically increase faster with energy than do those for rearrangement reactions. Thus it seems curious that a rearrangement reaction would dominate the kinetics at high energies (EI conditions) but not at lower energies (metastable conditions). Recently, Baer and Riley (UNC Chapel Hill) conducted photoelectron-photoion coincidence (PEPICO) experiments with $(CH_3)_2NCHO$, and observed loss of CHO and CH_3. Based on the time-of-flight spectra, they concluded that the dissociations are nonstatistical.

APPROACH

We decided to study this reaction further, using Mass-Analyzed Ion Kinetic Energy Spectrometry to measure kinetic energy release distributions for the products of metastable unimolecular dissociation. Ab initio molecular orbital calculations were carried out to characterize the potential energy surface and to obtain vibrational frequencies and rotational constants for relevant species. These parameters were then used with statistical phase space theory to model the PEPICO kinetics measured by Baer and Riley, in order to fine-tune the transition state energies. Finally, these modified transition state energies were incorporated into the complete model for the calculations of kinetic energy release distributions.

RESULTS

Metastable dimethylformamide radical cation dissociates to form three sets of products: $C_3H_6NO^+$ + H, $C_2H_4NO^+$ + CH_3, and $C_2H_6N^+$ + CHO. The KERDs measured for these processes are shown below.

Theoretical calculations turned up three low-energy isomers of the DMF^+ ion. These isomers are separated from the molecular ion by energetic barriers of 1.5 eV or more. Investigations of structures for the $C_2H_6N^+$ and $C_2H_4NO^+$ products also revealed multiple

isomeric structures. The singlet products CH_3-N-CH_3^+ and CH_3-N-CHO^+ that would arise from direct cleavage of the carbon-nitrogen bond in DMF^+ were found to be unstable with respect to rearrangement by 1,2-hydrogen shifts. Three transition states for the 1,2-hydrogen shifts in DMF^+ were found. In one, the H-shift is concerted with cleavage of the methyl - nitrogen bond.

Our investigations suggest that simple direct cleavage of the carbon-nitrogen bonds in DMF^+ leads only to high energy species, and that rearrangements of the fragments to lower energy isomers occur spontaneously.

From modeling the kinetics measured in the PEPICO experiments of Baer and Riley, we changed the transition state energies slightly from those calculated by MO theory. All other parameters were used unchanged. Below are shown the calculated KERDs for each of the sets of fragments, plotted over the experimental data. It can be seen that the KERDs are in general nonstatistical, but that each reaction channel has unique dynamics. Hydrogen atom loss results in a broader translational energy distribution than predicted by statistical theory, indicating repulsive interactions in the exit channel. This would be consistent with a reverse activation barrier and the weakness of the attractive interactions expected for an ion with an H atom (due to low polarizability). For the methyl loss channel, the KERD is bimodal, indicative of two or more mechanisms. This is consistent with the results of the ab initio calculations, which show at least two transition states that can lead to methyl loss, one by a concerted pathway, and another by a stepwise H-shift, methyl loss pathway. Finally, the KERD for CHO loss is narrower than predicted by statistical phase space theory, indicating that the products are internally excited. This may result from rotational excitation resulting from the unfavorable ion-dipole interactions that develop as the N–CHO bond is stretched.

Kinetic Energy Release Distribution Calculations

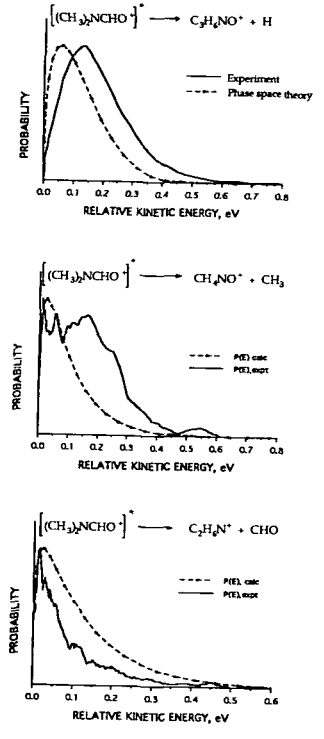

[1] Q. Ann and J. Adams, Int. J. Mass Spectrom. Ion Proc. 1992.

FRAGMENTATION OF DIETHYL DICARBOXYLATES UNDER EI AND CI CONDITIONS

Jan Malát and Alex. G. Harrison
Department of Chemistry
University of Toronto
Toronto, Canada M5S 1A1

The major primary fragmentation route of ionized diethyl dicarboxylates is by elimination of $C_2H_5O^{\cdot}$. The same ion is formed by elimination of C_2H_5OH from the MH^+ ion in Brønsted acid chemical ionization. The present work has concentrated on the further fragmentation of this $[M - OC_2H_5]^+$ ion and on the structures of the fragment ions so-formed. Two sets of isomeric diethyl dicarboxylates were studied, diethyl succinate and diethyl methylmalonate and diethyl glutarate, diethyl ethylmalonate and diethyl dimethylmalonate. Isotopic labelling and metastable ion studies, including kinetic energy releases, have been used as structural probes.

The $[M - OC_2H_5]^+$ ion from diethyl succinate fragments exclusively by elimination of C_2H_4 on the metastable ion time scale. Comparison with the $C_2H_5^+$ adduct of succinic anhydride shows that the $[M - OC_2H_5]^+$ ion has the ethylated succinic anhydride structure and fragments to form protonated succinic anhydride. By contrast, the $[M - OC_2H_5]^+$ ion from diethyl methylmalonate fragments entirely by loss of CO on the metastable ion time scale. The resulting ion is, in part, the destabilized carbenium ion, $CH_3CH^+COOC_2H_5$, although H-rearrangement to form $CH_2{=}CHCOOC_2H_5.H^+$ occurs to a significant extent prior to further fragmentation of the $[M - OC_2H_5 - CO]^+$ ion.

The $[M - OC_2H_5]^+$ ions of diethyl glutarate, diethyl ethylmalonate and diethyl dimethylmalonate, whether formed by EI or CI methods, show different metastable ion characteristics, that from the glutarate fragmenting by loss of C_2H_4 and CO, that from the ethylmalonate fragmenting by loss of CO and $[CH_2CO + CO]$ and that from the diemthylmalonate fragmenting by loss of CO only. The reacting configuration for loss of C_2H_4 from the $[M - OC_2H_5]^+$ ion of the glutarate is ethylated glutaric anhydride and protonated glutaric anhydride is formed. Loss of CO from the $[M - OC_2H_5]^+$ ion of diethyl ethylmalonate forms, in part, the destabilized carbenium ion $CH_3CH_2CH^+COOC_2H_5$, although rearrangement to $CH_3CH^+CH_2COOC_2H_5$ and $CH_3CH{=}CHCOOC_2H_5.H^+$ occurs to some extent prior to further fragmentation of the $[M - OC_2H_5 - CO]^+$ ion. The $CH_3CH^+CH_2COOC_2H_5$ ion fragments on the metastable ion time scale by loss of CH_2CO. Loss of CO from the $[M - OC_2H_5]^+$ ion of diethyl dimethylmalonate forms the destabilized carbenium ion $(CH_3)_2C^+COOC_2H_5$, although some rearrangement to $CH_2{=}C(CH_3)COOC_2H_5.H^+$ occurs prior to further fragmentation of the $[M - OC_2H_5 - CO]^+$ ion.

Presented at the 41st ASMS Conference on Mass Spectrometry

A COMPARATIVE STUDY OF THE DYNAMICS OF LOW AND MEDIUM ENERGY COLLISION-INDUCED DISSOCIATION OF ISOMERIC IONS

Runzi Zhao, Rahul Chawla, Anil Shukla* and Jean Futrell
Department of Chemistry and Biochemistry, University of Delaware, Newark, DE 19716

INTRODUCTION

Isomerization processes are widely known to play an important role in ionic characterizations by mass spectrometry. Isomerization, being slow, usually results in a metastable decay process. Collisional activation and dissociation processes, on the other hand, are fast enough that isomerization is usually not considered important. However, recent studies of the dynamics of CID of nitromethane ions showed that the NO_2^+ fragment, formed by direct bond cleavage, behaves differently than the NO^+ fragment, which is produced following isomerization of nitromethane to methyl nitrite. To explore the role of isomerization processes in CID dynamics, we have studied the CID of methyl nitrite ions to NO^+ and the enolic form of acetone ions to CH_3CO^+. The latter is known to proceed via isomerization to keto form and its metastable dissociation process leads to a bimodal kinetic energy release distribution.

RESULTS AND DISCUSSION

Nitromethane vs. Methyl Nitrite Ion : Figures 1 and 2 show the contour diagrams for the CID of nitromethane and methyl nitrite ions to NO^+ at 3.1 eV collision energy, respectively. Distinct peaks in forward and backward scattering regions in Figure 1 were suggested to be due to two dynamically distinct pathways rather than an orbiting complex formation. Since nitromethane ions have to isomerize to methyl nitrite ions for NO^+ formation (barrier height 0.45 eV), the forward scattered peak, resulting from large impact parameter soft collisions, was suggested to be due to the dissociation of those nitromethane ions that are very near the barrier approaching the transition state configuration. The backward scattered peak is due to dissociation of nitromethane ions that are somewhat lower in the potential well and are activated by small impact parameter hard collisions. CID of methyl nitrite to NO^+ does not require isomerization and dissociation proceeds as soon as sufficient energy is transferred into the ion. The energy transfer into the methyl nitrite ion is close to thermochemical threshold and does not change significantly when collision energy is increased further suggesting no change in the CID mechanism for this process.

Keto v Enolic Acetone Ion : Figure 3 shows a contour diagram for CH_3CO^+ fragment ions formed from CID of the keto- acetone ions at 3.2 collision energy; a similar diagram for the CID of enol- acetone ions at 3.9 eV collision energy is shown in Figure 4. The keto ion has two peaks in forward and backward scattering regions corresponding to transfer of 2.2 eV into internal modes and release of 2.2 eV into translational mode prior to dissociation, respectively. The latter process is due to long-lived excited electronic A state of the acetone which releases excess internal energy into translation. The threshold for this dissociation process is only 0.7 eV, however, energy transfer is 2.2 eV and it increases further with collision energy. Figure 4 for the CID of the enolic ion shows only a single peak corresponding to transfer of 2.8 eV energy into internal modes which is close to the energy barrier to isomerization to keto form. It suggests therefore that after isomerization, dissociation proceeds following complete energy

randomization as against the suggestion that it proceeds from both ground state and first excited state simultaneously. As the collision energy is increased further, dynamical behavior is not changed in any respect in this case. It may be interesting to point out that bimodal kinetic energy release distribution was obtained for metastable dissociation, a slow process with a narrow energy distribution compared to CID process.

These results suggest that CID of both methyl nitrite and enolic acetone ions follow normal dissociation pathway, i.e. dissociation proceeds as soon as internal energy reaches the threshold for dissociation or the isomerization barrier is crossed. Also, the energy randomization process is completed before dissociation takes place.

Fig. 1. CM velocity contour diagram for the CID of nitromethane ion to NO^+ at 3.1 eV collision energy.
Fig. 2. CM velocity contour diagram for the CID of methyl nitrite ion to NO^+ at 3.1 eV collision energy.
Fig. 3. CM velocity contour diagram for the CID of acetone ion to CH_3CO^+ at 3.2 eV collision energy.
Fig. 4. CM velocity contour diagram for the CID of enolic acetone ion to CH_3CO^+ at 3.9 eV collision energy.

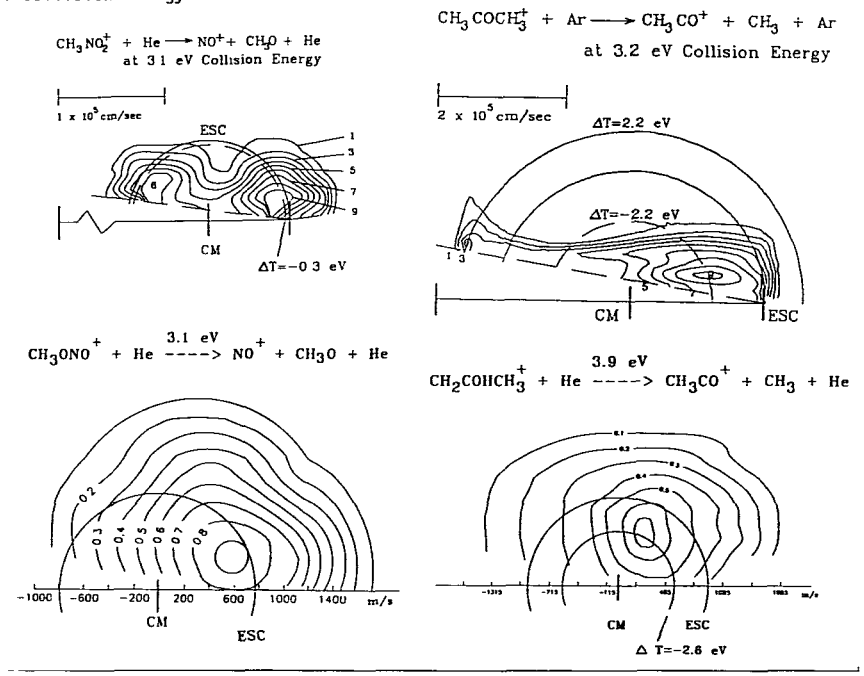

Internal Energy Effects on the Fragmentation of Ions and Neutrals

Ilan Vidavsky,* Russell A Chorush, Fred W. McLafferty
Chemistry Department , Cornell University, Ithaca, NY, 14853-1301

Fatty acid esters were the first "large" molecules whose mass spectra were thoroughly studied [1] Their most abundant peak arises from the McLafferty rearrangement,[2] a rearrangement which should be a low energy process However, Murphy,[3] Harvey[4] and their co-workers found this peak missing in low energy CAD spectra, which we have found true also for metastable ion dissociations of straight and branched chain fatty methyl esters In high energy CAD spectra this peak is present in significant abundance only in the shorter chain fatty acids esters As proposed by Murphy, these results and isotopic labeling suggest a rearranged molecular ion The almost equal abundance of alkyl loss from either end of the hydrocarbon chain suggests a migration of a protonated carbomethoxy group to a radical site within the chain, this is followed by cleavage of one of the two hydrocarbon chains to form an ion of a protonated 2-alkylacrylate structure In contrast to the previous mechanism,[1,3] this is more consistent with that postulated for MI spectra of 2-methylbutyric acid [5] The predicted fragment ion structures indicated by MS/MS/MS of alkyl loss ions in MI and CAD spectra of protonated alkyl acrylates

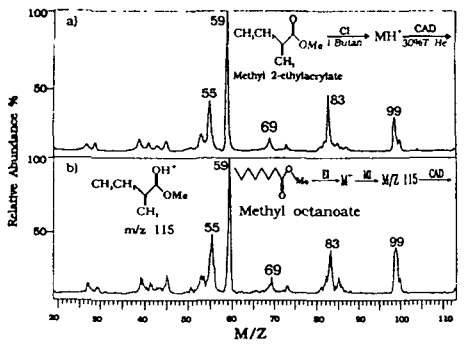

Fig 1 a) CAD of MH^+ in CI of Methyl 2-ethylacrylate. b) MS/MS/MS of m/z 115 from MI of Methyl octanoate $M^{+\cdot}$

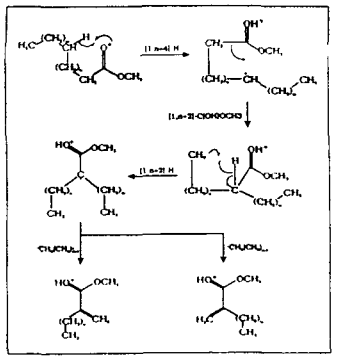

Fig 2 The proposed mechanism for the formation of the alkyl loss ions

Neutralization-reionization mass spectrometry (NRMS) is a uniquely useful technique for the differentiation of isomeric ions that yield similar CAD spectra.[6] Such ionic characterization by NRMS can be improved by increasing the internal energy of the dissociating neutrals,[7,8] enhancing entropically favored direct dissociations over entropically disfavored rearrangements The use of surface-induced

neutralization (SIN) in a NRMS experiment provides a method for increasing the internal energy deposited in the neutrals beyond that currently attainable using gas-phase targets [9] The energy deposited into the neutrals can be approximated by correcting for dissociation following reionization With a Ag surface deposited on an in-line Si substrate, NR efficiencies of 0 01% are achieved using 9.8 keV $CH_4^{+\cdot}$, with ~50% of the neutral CH_4 receiving >14 eV of internal energy; with metallic K vapor neutralization the efficiency is 0 4% with ~50% of the neutrals receiving >8 9 eV The energy deposition can be increased by increasing the potential deflecting ions into the surface (Fig 3), in this way ~15% of CH_4 neutrals can be given >20 eV of internal energy. Thus, despite much lower sensitivity than gas-phase targets (using the present collision cell), SIN is unique in the large amount of energy that can be deposited in the neutral and in the facile control over the average energy deposited In addition, SIN avoids the high gas load and contamination caused by conventional gas-phase targets

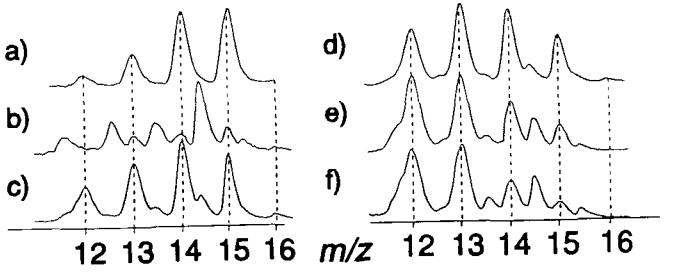

Fig 3 (a) a K(90%T)/O2(50%T) NRMS spectrum of $CH_4^{+\cdot}$, and SINR mass spectra of $CH_4^{+\cdot}$ with the ions deflected into the surface by (b) 70 V (c) 145 V (d) 210 V (e) 350 V and (f) 425 V Peaks at non-integer masses are due to background neutralization

1 Dihn-Nguyen, N , Ryhage, R., Stenhagen, S S,; Stenhagen, E. *Arkiv. Kemi* **1961**, 18, 393-399
2 McLafferty, F W *Anal. Chem* **1959**, 31, 82-87
3 Zirrolli, J A , Murphy, R. C *J Am Soc Mass Spectrom.* **1993**, 4, 223-229
4 Harvey, D J *Org Mass Spectrom* 1993, 28(3), 287-288
5 Weiske, T , Halim, H , Schwarz, H *Chem. Ber.* **1985**, 118, 495-509
6. McLafferty, F W *Science* **1990**, 247, 925
7 Doering, W v E *Proc. Natl. Acad. Sci. USA* **1981**,78, 5279
8. McLafferty, F W.; Turecek, F. *Interpretation of Mass Spectra* Fourth Ed.; University Science Books Mill Valley, CA, 1993.
9 Chorush, R A., Vidavsky, I ; McLafferty, F W submitted.

Decomposition of the Ethyliodonium Ions in the Gas Phase.

Dmitri V.Zagorevski and John L.Holmes
Chemistry Department, University of Ottawa, Ottawa, Ontario, Canada K1N 6N5.

Unimolecular decomposition of EtI⁺R ions produced by ion molecule reactions have been studied by tandem mass spectrometry (MI, CID and NR). Metastable ion decompositions of EtI⁺H and EtI⁺Pr involve alkyl cation formation. EtI⁺Me and Et_2I^+ decompose with ethene loss. PhI⁺Et ion loses I, PhEt and C_2H_4. The latter leads to the 1-iodocyclohexadienyl cation, which is characterized by I elimination.

Collisional activation induces some other dissociations involving simple C-I and C-C bond cleavages and rearrangements with C-C or C-H bond formation. Methyl loss from the ethyl group in EtI⁺D and EtI⁺Me ions leads to the ylid ions, $RICH_2^+$ (R=D, Me). Their dissociation includes CH_2 loss, which is not a characteristic of isomeric RCH_2I^+ ions. Formation of I^+ and RCH_2^+ indicates a partial ylid to alkyliodide isomerization.

The MI and CID mass spectra of D-analogs of EtI⁺R (R=Me, Et, Ph) have been studied in order to elucidate the mechanism of ethene loss. Kinetic energy releases have also been measured. The experimental data obtained can be rationalized by the two barriers in the following energy diagrams (Figs. 1-3; asterisks denote the labelled species). The first barrier (TS_1) corresponds to the irreversible β-hydrogen (deuterium) shift to the iodine atom and the second is responsible for ethene loss (TS_2). The transition states for the species with an I-D bond are higher in energy than those for the species with an I-H bond, i.e. $TS_1^D > TS_1^H$, and $TS_2^D > TS_2^H$. Competition between simple hydrogen migration and hydrogen mixing as well as between H and D migration from the ethyl group is determined by the relative energies of these barriers.

For EtI⁺Me ion TS_1^H, $TS_1^D < TS_2^D$, TS_2^H (Fig. 1), which results in complete hydrogen mixing prior to ethene loss and the preference for loss of the most deuterated ethene.

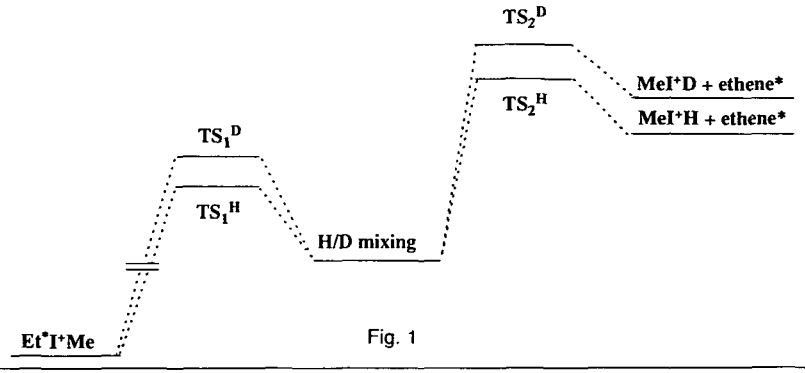

Fig. 1

For Et_2I^+ ion $TS_1^H < TS_2^H$, $TS_2^D \leq TS_1^D$ (Fig. 2), which leads to a large hydrogen isotope effect for ethene loss following H/D-mixing in the CH_3CD_2 group, and makes the direct elimination of $C_2H_2D_2$ from CD_3CH_2 competitive with hydrogen mixing.

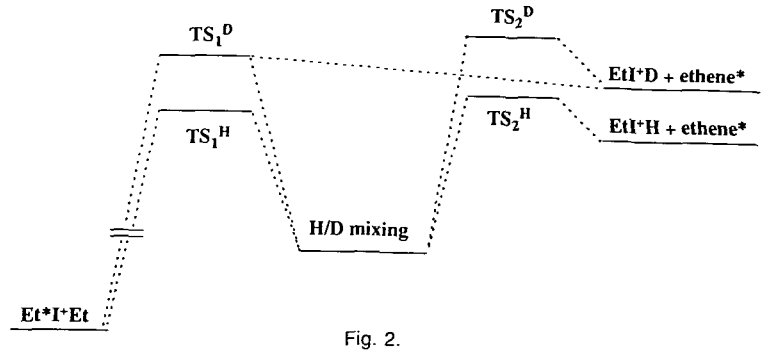

Fig. 2.

For PhI⁺Et ion $TS_1^D > TS_2^D > TS_1^H > TS_2^H$ (Fig. 3), which permits a single step ethene loss from both the CD_3CH_2 and CH_3CD_2 groups to be competitive with hydrogen atom mixing.

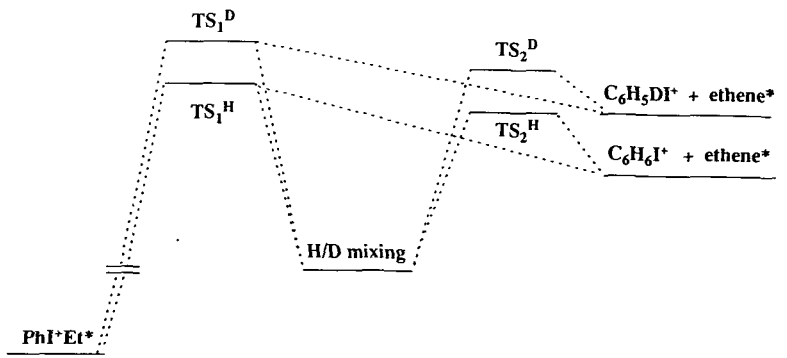

Fig. 3.

The increased $C_2H_3D/C_2H_2D_2$ loss ratio for $CH_3CD_2I^+Et$ ions (originating from $(CH_3CD_2)_2CO$/EtI and $CH_3CD_2NO_2$/EtI mixtures) and $C_2HD_3/C_2H_2D_2$ loss ratio for $CD_3CH_2I^+Et$ and $CD_3CH_2I^+Ph$ ions (originating from $CD_3CH_2NO_2$ mixtures with EtI and PhI) is due to hydrogen pre-mixing in the "classical" form of the ethyl cation reacting with neutral ethyl- and phenyliodide.

Dechlorination of PCB's in Electron Capture Negative Ion Chemical Ionization Mass Spectrometry

***F.Lépine[1], S.Milot[1], M.L.J.Reiner[2] and O.A.Mamer[2]**

1 **Institut Armand-Frappier, Université du Québec, Laval, Qc, Can. H7N 4Z3**

2 **Biomedical Mass Spectrometry Unit, McGill University, Montréal, Qc,Can. H3A 1A3**

The dechlorination mechanism of Polychlorinated Biphenyls (PCBs) was studied using 36 ^{35}Cl mono- and di-labelled penta- and hexachlorobiphenyls. These were synthesized using unselective chlorination with $^{35}Cl_2$ of all the symmetricals tetrachlorobiphenyls, namely congeners **40**, **47**, **52**, **54**, **77** and **80** according to IUPAC nomenclature. Upon chlorination, each of these congeners generates a mixture of penta- and hexachloro congeners containing one and two ^{35}Cl label respectively. The identification of each of these compounds, and consequently the position of the label in these, was performed using their relative retention times as described by Mullin et al. (1,2).

The methane electron capture negative chemical ionization (ECNCI) spectra of the labelled PCBs show ions at $[M-34]^-$ and $[M-68]^-$ which correspond to the loss of one and two chlorine atoms from a PCB molecule which added one and two hydrogen atoms. For pentachloro congeners, only the $[M-34]^-$ ions were sufficiently intense to be analyzed. Within the 27 labelled hexachloro congeners produced, many have the same substitution pattern but for the position of the labels within the pattern. There are three series of such congeners. Being symmetricals, these congeners, upon dechlorination in the mass spectrometer, can only generate three pentachloro intermediates. Assuming that these intermediates are structurally similar to neutral molecules, it is possible to calculate the relative intensities of the $[M2H-2Cl]^-$ ions if the relative proportions of the three pentachloro intermediates contributing to the $[MH-Cl]^-$ ions are known and if the relative intensities of the $[MH-Cl]^-$ ions generated by these pentachloro

intermediates can be obtained. Because the hexachloro congeners are initially produced by chlorination of pentachloro congeners, these corresponding pentachloro congeners can be observed and the intensity of their $[MH-Cl]^-$ ion measured. The relative proportions of the pentachloro intermediates can be obtained from the label loss in the $[MH-Cl]^-$ ions of the hexachloro congener bearing the labels at the corresponding position.

A good correlation can be obtained between the calculated and the observed $[M2H-2Cl]^-$ ion intensities, thus proving that the pentachloro intermediates are similar in structure to the corresponding pentachloro congener. Also, the residual label content of these $[M2H-2Cl]^-$ ions is similar to the calculated value obtained from the $[MH-Cl]^-$ ions of the corresponding pentachloro congeners. These two conclusions strongly suggest that the pentachloro intermediates formed upon dechlorination of an hexachloro congeners are very similar to the corresponding pentachloro congeners studied and that they undergo dechlorination in a similar way. This imply that the incoming hydrogen has to be located at the same position than the departing chlorine atom. This would be compatible with an electrophilic hydrogen radical addition mechanism with rapid loss of the chlorine atom on the carbon undergoing hydrogen attack. The relative intensities of the $[MH-Cl]^-$ ions was found to be dependent of the number of ortho chlorines in the molecules. The relative intensities of the $[MH-Cl]^-$ ions decrease with increasing number of ortho chlorines. However, within a given congener, ortho chlorines, when present, are lost preferentially. These two phenomenon can be explained in terms of the stability of the radical intermediate formed after attachment of the hydrogen radical.

Reference

1. M.D. Mullin, C.M. Pochini, S. McCrindle, M. Romkes, S.H. Safe, L. Safe. Envir. Sci. Technol. 18, 468 (1984)

2. F. Lépine, S.M. Milot, M.L.J. Reimer and O.A. Mamer. Org. Mass Spectrom. 27, 1311 (1992)

EI-LINKED SCAN STUDIES OF DIMETHYLAMINOMETHYLENE-O-TRIALKYLSILYL NUCLEOSIDES

E. Y. Osei-Twum, L. A. Litorja, and N. M. Abbas, Research Institute, King Fahd University of Petroleum & Minerals, Dhahran 31261, Saudi Arabia.

Introduction

The mass spectral fragmentation and rearrangement reactions of the trimethylsilyl derivatives of nucleosides have been extensively discussed. Recent studies indicate that the fragmentation and rearrangement reactions of the dimethylaminomethylene-O-trialkylsilyl nucleosides are much similar to those of the trialkylsilyl derivatives. Present in the mass spectra of these dimethylaminomethylene (DMAM) derivatives are ions that are postulated to arise from the DMAM group.

In this study we have used linked scan techniques to investigate the metastable transitions of the molecular ions (and other ions derived from them) of the DMAM-O-TMS derivatives of dA, dC, dG and N^1-methyl dG.

Methods

The DMAM-O-TMS derivative of each nucleoside (dA, dC, dG) was synthesized by allowing a mixture of 0.1 mmole of the compound and 1 mmole of dimethylformamide dimethylacetal (DMF-DMA) to stand in 500µL of dry DMF at room temperature for approximately 5 hours. Water (100-fold) was added and the sample was evaporated to dryness under a stream of nitrogen. [**Note**: The sample should not be heated during evaporation; doing this may lead to hydrolysis of the DMAM group.] The resulting residue was dissolved in 250 µL of dry acetonitrile and 200 µL of BSTFA was added. The reaction mixture was heated at 80°C for 1 hour (Scheme 1).

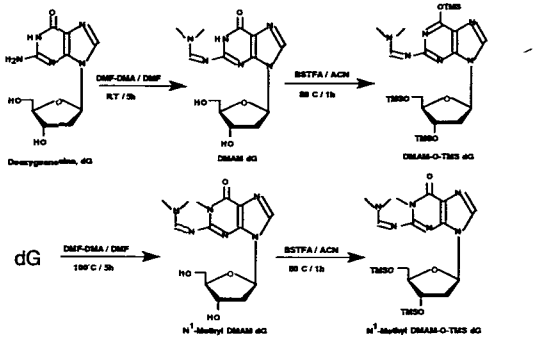

Scheme 1: Derivatization of Deoxyguanosine

The structure of each intermediate DMAM nucleoside was determined by ^1H nmr spectroscopy and by FAB+ MS. The nmr spectra of the samples, dissolved in DMSO-d_6, were obtained on a JEOL (Tokyo, Japan) JNM-GX270 spectrometer.The FAB mass spectra were obtained on a JEOL JMS-HX100 tripple sector (EBE) spectrometer equipped with a

saddle field neutral beam gun. Xenon fast atoms were used to bombard the samples, dissolved in glycerol, on a stainless steel probe.

EI mass spectra were obtained on the HX100 spectrometer. Samples were introduced into the ion source via a direct insertion probe. The probe temperature was programmed from 50°C to 250°C at 30°/min.

Results

The nucleosides react readily with excess DMF-DMA at room temperature to provide the DMAM derivatives. It had previously been observed that at higher temperatures, the guanine nucleosides reacted slowly to yield a product which is methylated at N^1. However, this reaction was never quantitative. In this study, the reaction was repeated at 100°C for 5 hours (Scheme 1). The mass spectrum of the O-TMS derivative indicated that the methylation went to completion.

The region between **M-15** and **BH+29** in the EI mass spectra of these compounds is populated by ions of low intensities. The B/E linked scan spectra of the molecular ions (Fig. 1) show that all four compounds give a prominent **M-28** which may be **M-CO** due to the sugar or **M-CH_2N** due to the base. Another prominent ion common to all the compounds is **M-TMSiOH**. The molecular ions also give the ions **M-C_2H_5N**, **M-C_2H_6N** and **M-C_2H_7N**. The guanine derivatives show ions which are prominent in both the molecular ion and base series. The purine nucleosides give ions of the base series **B**, **B+H**, **B+2H** and **BH+CHO** while the pyrimidine nucleoside, dC, gives the ions **B+C_2H_2O** and **B+C_2H_3O+TMS**.

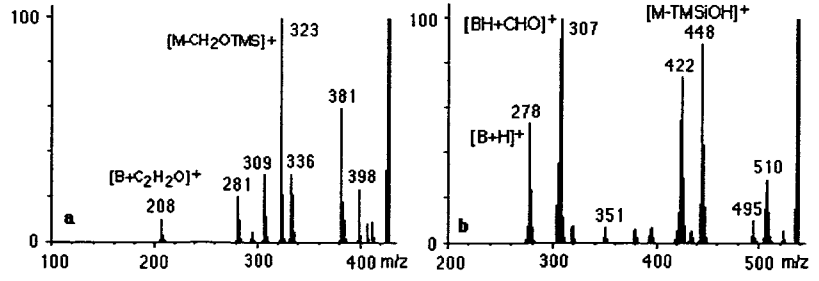

Figure 1: B/E Linked Scan Spectra of M^+ of DMAM-O-TMS (a) dC and (b) dG.

Conclusions

The first-formed ions in the region between **M-CH_3** and **BH+CHO**, a region normally populated by ions of low intensity, appear to be fairly unstable and fragment (rapidly) to other ions.

Fragmentation of dC differs considerably from those of the purine nucleosides, dA and dG; glycosidic bond cleavage is not observed for the molecular ion of the dC derivative. Glycosidic bond cleavage is a prominent feature in the fragmentations of DG and N^1-Me dG.

The nucleobases show fragmentation and rearrangement reactions which are predominantly of the DMAM group.

At higher temperatures the guanine nucleosides react completely with DMF-DMA to give the N^1-Me DMAM derivatives.

The Neutral Products from the Remote Site Fragmentation of Fatty Acid Derivatives.

Marcela M. Cordero and Chrys Wesdemiotis
Department of Chemistry, The University of Akron, Akron OH 44325-3601.

Tandem mass spectrometry (MS/MS) is an established technique for the structural characterization of biomolecules. Since MS/MS reveals only the ionic fragments originating from the biomolecular ion under investigation, a great deal of structural and mechanistic information is forfeited with the undetected neutral losses. Neutralization-reionization mass spectrometry (NRMS) makes possible the study of these neutrals by collisionally ionizing them, so that they can be detected and characterized in the corresponding neutral fragment-reionization (N_fR) mass spectra. In the present study, NRMS is applied to $[M-H]^-$ and $[M-H+2Li]^+$ ions from fatty acids in order to evaluate the information hidden in the neutral products which are simultaneously produced during the CAD process and, thus, obtain insight into the mechanism of charge remote fragmentation.[1-4]

The CAD spectra of the $[M-H]^-$ and $[M-H+2Li]^+$ ions from several saturated (undecanoic, myristic, palmitic, stearic) and monounsaturated (undecylenic, palmitoleic) fatty acids show a series of fragment ions corresponding to formal losses of C_nH_{2n+2}. These eliminations occur at the alkyl (or alkenyl) chain, *i.e.* remote from the charge site residing at the carboxylic group ("charge-remote" site fragmentation). They have been proposed to proceed via 6-membered ring transition states leading to cleavages of H_2 plus C_nH_{2n} (alkenes) instead of intact C_nH_{2n+2}.[3] Alternative mechanisms have been postulated that include loss of alkyl radicals by homolytic cleavages of the fatty acid ion.[4]

The CAD and N_fR spectra of $[M-H]^-$ from palmitic acid are shown in Figures 1a and 1b The CAD spectrum records the ionic fragments produced upon collisional activation with He. The N_fR spectrum shows the coproduced neutrals after reionization with O_2. The N_fR spectrum contains a dominant alkenyl ion series (*m/z* 27, 41, 55, 69) which is characteristic for a mixture of alkenes according to the electron impact spectra of hydrocarbons. The alkyl ion series (*m/z* 15, 29, 43, 57, 71), is much less important

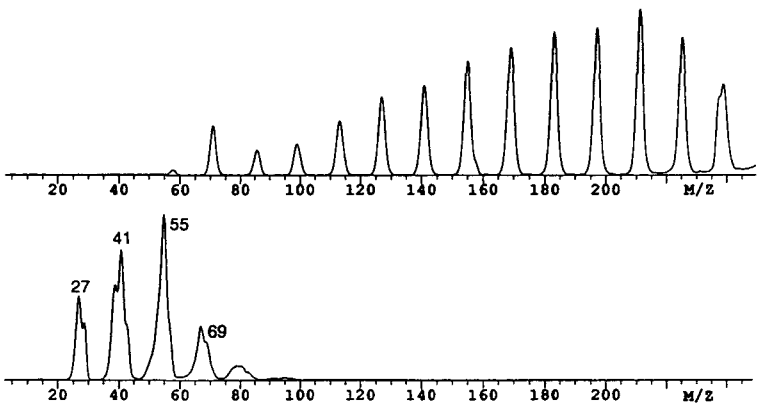

Figure 1. a) CAD, He and b) N_fR He/O_2 spectra of $[M-H]^-$ from palmitic acid.

Undecanoic, myristic and stearic acids also show predominance of the indicative alkenyl ions, consistent with alkene losses. As the chain size increases, so does the abundance of higher mass ions, as expected with the increasing size of the neutral losses.

The N_fR spectra of both $[M-H]^-$ and $[M-H+2Li]^+$ for each fatty acid, shows that the N_fR spectra are very similar, indicating that the neutral fragments from CAD of both precursors are essentially the same. Alkenoic fatty acids (undecylenic and palmitic) present N_fR spectra with more unsaturated ions (*m/z* 39, 54, 67, 79) because *diene* losses are possible with these acids. This is shown in Figure 2 for palmitoleic acid.

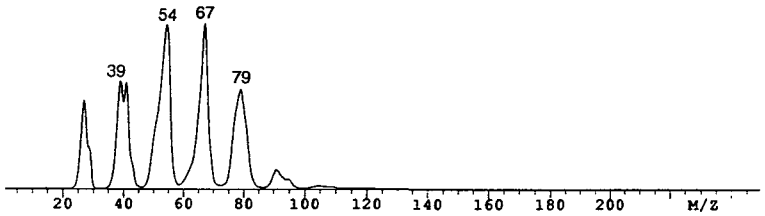

Figure 2. N_fR He/O_2 spectrum of $[M-H]^-$ from palmitoleic acid.

Reference spectra of alkanes and alkenes were obtained for the systems: hexane/1-hexene and heptane/1-heptene, by NR of the molecular ions. The results parallel those of electron impact spectra: alkanes give a predominant alkyl series, meanwhile alkenes preferably produce an alkenyl ions series These findings confirm that if alkanes were present in the neutral mixture, then prominent alkyl ions should be observed in the fatty acid N_fR spectra.

Alkyl radicals reference spectra were obtained from N_fR of ionized cyclohexylamine and cyclooctylamine, which have been found to lose alkyl radical mixtures upon CAD.[5] The spectra show that if alkyl radicals were eliminated during CAD of fatty acids, alkyl ions should also be present.

The relative NR yields (and, hence, R)[6] for isobutane/isobutyl/isobutene ions are similar Therefore, alkanes and alkyls would be expected to produce a detectable alkyl ion series if present in appreciable amounts in the neutral loss mixture.

In summary, the N_fR spectra are complex because many neutrals are eliminated simultaneously. Nevertheless, based on the available reference spectra, it can be concluded that under our experimental conditions the *predominant* neutral losses are *alkenes* (or *dienes*, in the case of monounsaturated fatty acids), not alkanes or alkyl radicals. This is consistent with the originally proposed mechanism for keV CAD of fatty acids ions.[3]

References

1. Adams, J. *Mass Spec. Rev.* **1990**, *9*, 141-186.
2. Gross, M.L. Int. J. Mass Spectrom. Ion Proc. **1992**, *118/119*, 137-165.
3. Jensen, N.J.; Tomer, K.B.; Gross, M.L. *J. Am. Chem. Soc.* **1985**, *107*, 1863-1868
4. Wysocki, V.; Ross, M. *Int. J. Mass Spectrom. Ion Proc.* **1991**, *104*, 141-211.
5. Lefevre, O.; Mollova, N., Longevialle, P. *Org. Mass Spectrom.* **1992**, *27*, 589-596
6. Wesdemiotis, C.; Feng, R. *Org. Mass Spectrom.* **1988**, *23*, 416-418.

Collisional Dissociation Technique for Assignment of Metalloporphyrin Cation Electronic Structure

J. Ha and D. A. Laude, Jr., Department of Chemistry and Biochemistry,
The University of Texas at Austin, Austin, TX, 78712

Our study on porphyrin chemistry has been done using laser desorption/ionization Fourier transform ion cyclotron resonance mass spectrometry(LDI/FTICR). Metalloporphyrin products generated by metallation reactions of free-base porphyrins in plasma ignition LDI are used to study the electronic structure of metalloporphyrin cation. The metalloporphyrin cation has two extreme oxidized forms, a metal-oxidized form and a porphyrin ring-oxidized form (π cation radical), in catalytic and biological system. The metal-oxidized form is important in enzyme systems and has been used as a catalyst. Metalloporphyrin π cation radical play crucial roles in the primary photosynthetic events involving chlorophyll or bacteriochlorophyll which contains magnisium porphyrins and the oxidative metabolism involving heme(iron porphyrin) proteins such as the catalases, peroxidases, and cytochrome P-450s. Furthermore, metalloporphyrin cation radicals are classified into two ground state categories corresponding to removal of an electron from either of two high-lying porphyrin π molecular orbitals, a_{1u} or a_{2u}. The substituents on the porphyrin ring are important factors in determining whether the $^2A_{1u}$ or $^2A_{2u}$ π cation radical will be formed. For example, $[Zn\text{-}OEP]^+$ and $[Mg\text{-}OEP]^+$ belong to $^2A_{1u}$ system, while $[Zn\text{-}TPP]^+$ and $[Mg\text{-}TPP]^+$ belong to $^2A_{2u}$ system. Solution studies indicate that the electronic structure of metalloporphyrin cations depends strongly on many factors including ring substituents, incorporated metal, temperature, counter ion, and solvent. These factors have made the assignment of metal oxidation state in metalloporphyrin cation controversial.

We have developed a gas-phase collision-induced dissociation(CID) technique that readily distinguishes the electronic configuration of a particular metalloporphyrin cation incorporated by a first-row transition metal, Mg or Al. The biological model M-TPP cation in which M is a first-row transition metal, offers the following advantages: (1) It yields simple CID product spectra in which ions are produced by cleavage of the bond between the *meso*-carbon and phenyl substituents. (2) All cation radicals are known to belong to the A_{2u} ground state. (3) It has a planar structure which is not significantly distorted by the incorporated metal. This assumes that collision phenomena are independent of geometrical structures. Thus, CID results predict the effect of incorporated metal on the electronic structure of a metalloporphyrin.

Shown in figure 1 are CID spectra of $[Cu\text{-}TPP]^+$ obtained from controlled translational energy applied to ions. Abundance profiles of fragment ions, $[M\text{-phenyl}]^+$ and $[M\text{-(phenyl)}_2]^+$, *increase with laboratory translational energy. Shown in Figure 2 are the abundance curves for the* ratio of fragment ions to precursor ions obtained from the energy-resolved CID spectra of $[M\text{-}TPP]^+$. $[Zn\text{-}TPP]^+$ favors the cation radical form because Zn(II) has a stable d^{10} electronic structure. $[Cu\text{-}TPP]^+$ favors π cation radical form but exhibits exchange coupling between Cu and porphyrin ring. Determination of metal oxidation state in $[Ni\text{-}TPP]^+$ depends on the temperature in solution (D. Dolphin et. al. J. Am. Chem. Soc. 1975, 97, 5288) with $[Ni(III)\text{-}TPP]^+$ existing at 77K and $[Ni(II)\text{-}TPP]^+$ existing at 300 K. However, in the gas phase $[Ni\text{-}TPP]^+$ appears to be the intermediate between $[Ni(II)\text{-}TPP]^{+\cdot}$ and $[Ni(III)\text{-}TPP]^+$. $[Cr\text{-}TPP]^+$ which has almost same slope as $[Ni\text{-}TPP]^+$ belongs to the intermediate. The closeness of $[Fe\text{-}TPP]^+$ to $[Ni\text{-}TPP]^+$ in fragmentation pattern indicates that $[Fe(II)\text{-}TPP]^{+\cdot}$ is also in equilibrium with $[Fe(III)\text{-}TPP]^+$. This supports the suggestion that in cytochrome *b5* and *c* electron transfer to and from the iron occurs via porphyrin π cation radical transients. $[V\text{-}TPP]^+$ exhibits less fragmentation than $[Fe\text{-}TPP]^+$. $[Co\text{-}TPP]^+$ which has the least fragmentation favors the cation form.

$Fe(II)cyt \rightarrow [Fe(II)(cyt^{+\cdot})]$ (oxidized porphyrin) $\leftrightarrow$ $[Fe(III)cyt]^+$ (oxidized metal)

Two ground state systems (A_{1u} and A_{2u}) which metalloporphyrin π cation radical form has depending on different ring substituents were examined by CID. As shown in Figure 3, bacteriochlorophyll and chlorophyll model porphyrins, Al and Mg porphyrins exhibit quite different CID spectra. Al porphyrin cations, ($[Al\text{-}TPP]^+$ and $[Al\text{-}OEP]^+$), favor $[Al(III)\text{-porphyrin}]^{+\cdot}$, while Mg porphyrin cations, ($[Mg\text{-}TPP]^+$ and $[Mg\text{-}OEP]^+$), favor $[Mg(II)\text{-porphyrin}]^{+\cdot}$. Al(III) and Mg(II) incorporated into the porphyrin ring have the same stable electronic structure as Ne. The $[Mg\text{-}OEP]^+$ fragments more readily than $[Mg\text{-}TPP]^+$. This difference in the extent of fragmentation supports the argument that $[Mg\text{-}TPP]^+$ belongs to the $^2A_{2u}$ ground state, while $[Mg\text{-}OEP]^+$ has the $^2A_{1u}$ ground state. $[Zn\text{-}OEP]^+$ ($^2A_{1u}$ system) favors $[Zn(II)\text{-}OEP]^{+\cdot}$. $[Co\text{-}OEP]^+$ exhibits a similar fragmentation pattern to $[Zn\text{-}OEP]^+$. This suggests that in $[Co\text{-}OEP]^+$ Co has an exchange coupling with the porphyrin ring and $[Co\text{-}OEP]^+$ is inclined to favor the $[Co(II)\text{-}OEP]^{+\cdot}$ form.

It is found that positive charge distribution between metal and porphyrin ring in a metalloporphyrin cation is sensitive to the incorporated metal into porphyrin ring. The above CID results indicate that metalloporphyrin cation has two resonance forms rather than two seperated forms.

Figure 1 [Cu-TPP]+

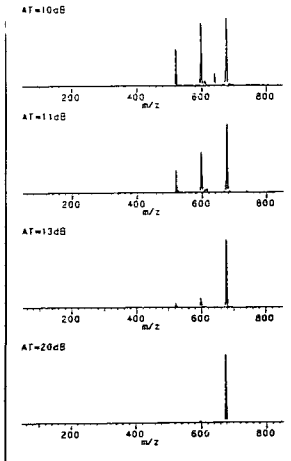

Figure2

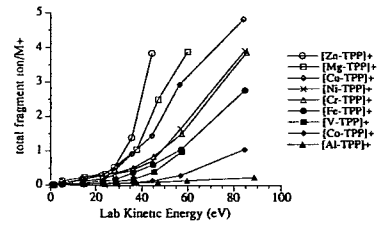

Figure 3 (a) [Mg-TPP]+ (b) [Al-TPP]+

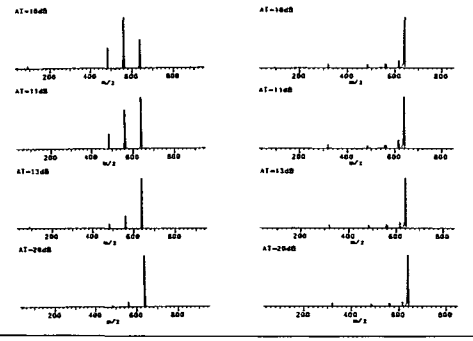

FRAGMENTATION OF TAXANE ANIONS

Steven H. Hoke, II and R. Graham Cooks, Department of Chemistry, Ching-jer Chang, Department of Medicinal Chemistry and Pharmacognosy, Purdue University, West Lafayette, IN 47907, U.S.A.

The ability to promote microtubule assembly exhibited by the natural product, taxol, is associated with promising cytotoxic properties[1]. Taxol has shown significant activity in the clinical trials of many types of cancers[2]. However, the promise of taxol as an anti-cancer drug is offset by its natural shortage. The bark of the Pacific yew tree, *Taxus brevifolia*, is currently a major source of taxol, but it has been estimated that this source of taxol will be depleted within the next 5-10 years[3]. As a result, sensitive and specific analytical methodologies are needed to rapidly screen plant extracts and tissue cultures in the search for alternative sources of taxol. The results presented here describe the development of a rapid method for the quantitation of taxol and the analogs cephalomannine and baccatin III as well as the utilization of other MS/MS scans to screen for known compounds and novel taxol analogs in a methanol extract of *Taxus mairei* needles.

Radical anions of taxanes were produced by desorption chemical ionization with ammonia as the reagent gas A Finnigan Triple Stage Quadrupole (TSQ) 700 mass spectrometer was used for the development of the analytical methodology. Fragmentation patterns of the radical anions of taxol, 10-deacetyltaxol, cephalomannine, and baccatin III are examined with 0.5 mTorr of argon as the collision gas and variable collision energies. Taxol and cephalomannine fragment producing the C13 side chain as an abundant peak in the product ion spectra; however, these compounds also have abundant peaks at m/z 525 and 526 in the collision energy range of 10-40 eV. The product ion spectrum of baccatin III, which has only a hydroxy substituent at the C13 position, shows a neutral loss of 60 mass units, producing an abundant peak at m/z 526. 10-Deacetyltaxol fragments quite differently than taxol as shown in Figure 1 The peaks at m/z 284 and 285 are the only fragment ions with greater than 10 % relative abundance in the mass range from 200 - 900 Da at collision energies ranging from 10-40 eV.

An MS/MS method of quantitation has been developed to simultaneously determine the compounds taxol, cephalomannine and baccatin III in crude plant extracts based on a parent ion scan of m/z 526. Quantitation of taxol, cephalomannine and baccatin III has been achieved by the method of standard addition and the quantitation of taxol has been demonstrated with the use of 10-d_3-acetyltaxol as an internal standard.

For quantitation by the method of standard addition, the sample was analyzed alone followed by analysis at two levels of standard addition, where each level was run in triplicate, for a total of nine runs. The quantitation was performed at the high femtomole to low picomole level with an analysis time of 35 minutes and a relative standard deviation of approximately 30 % for n = 3. 10-d_3-Acetyltaxol was used as an internal standard for the quantitation of taxol. No internal standard was available for cephalomannine or baccatin III; however, the ion current from these compounds was recorded and simultaneous quantitation could be performed with appropriate compounds. Quantitation of taxol with the 10-d_3-acetyl internal standard was demonstrated at the low picomole level with an analysis time of less than 5 minutes per sample and a relative standard deviation of approximately 12 % where n = 3.

Screening for some taxanes, such as 10-deacetyltaxol, cannot be performed with the parent ion scan of m/z 526 because of different fragmentation patterns. As described above, the fragmentation of 10-deacetyltaxol is substantially different from that of taxol. As a result, to

screen for this compound in plant extracts, a parent ion scan of m/z 284 (the C13 side chain of taxol) is performed. This scan was used with a *Taxus mairei* needle extract. The presence of taxol and 10-deacetyltaxol was confirmed in this methanol plant extract. In addition, the presence of several unknown compounds is observed. This parent ion scan reveals analogs of taxol with the same side chain as taxol but with chemical modifications to the diterpene skeleton. In the future, structural characterization of these new analogs of taxol by MS/MS will be studied.

Acknowledgement

This work was supported by the National Cancer Institute, CA 55118. The authors thank Robert Kelly and Samuel Qualls of the UpJohn Company for the preparation of 10-d_3-acetyltaxol.

References

1) Schiff, P.B.; Fant, J.; Horwitz, S.B. *Nature* **1979**, *277*, 665.
2) McGuire, W.P.; Rowinsky, E.K.; Donehower, R.C. In *Accomplishments in Cancer Research-1990*; Fortner, J.G., Rhoads, J.E., Eds.; J.B. Lippincott: Philadelphia, 1991; p. 276.
3) Kingston, D.G.I. *Pharmacol. Ther.* **1991**, *52*, 1.

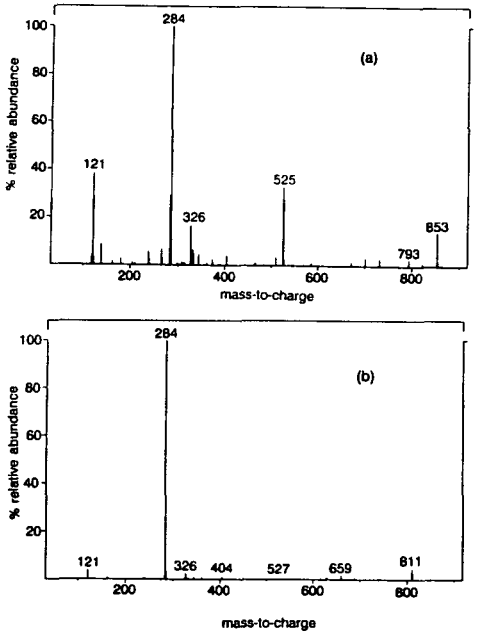

Figure 1: MS/MS product ion spectra of (a) the taxol radical anion and (b) the 10-deacetyltaxol radical anion at collision energies of 30 eV.

Investigation of Fluoroformic Acid, Its Radical Cation, and Its Protonated Form by Tandem Mass Spectrometry Techniques.

Fred Wiedmann, Sarka Beranova, Jinnan Cai,
Marcela M. Cordero, Michael J. Polce, and Chrys Wesdemiotis

Department of Chemistry, The University of Akron, Akron, OH 44325-3601

Fluoroformic acid, FCOOH (M), is a simple molecule that does not exist freely, presumably because of autocatalytic decay into HF + CO_2. Recently, it was predicted to be kinetically stable if a single molecule could be isolated.[1] Neither have the ionized (M^+) nor the protonated (MH^+) forms of FCOOH been detected yet. Here, we report the first experimental characterization of these species.

It was thought that $FCOOH^{+\cdot}$ (*m/z* 64) could be produced from ethyl fluoroformate ($FCO_2CH_2CH_3$), which can be easily synthesized,[2] via the McLafferty rearrangement. However, collisional activated dissociation (CAD) shows that the small *m/z* 64 in the EI spectrum is $CH_3CH_2OF^+$. Thus, $FCOOH^{+\cdot}$ cannot be formed directly from ethyl fluoroformate due to the high ionization energy of fluorinated compounds. FCOOH + $C_2H_4^{+\cdot}$ is produced instead.

Protonated fluoroformic acid ($FC(OH)_2^+$, *m/z* 65) is formed from $FCO_2CH_2CH_3$ via the McLafferty +1 rearrangement. Its metastable ion (MI) spectra contains abundant ^+COOH (*m/z* 45) and FCO^+ (*m/z* 47) fragments, arising by FH and H_2O losses, respectively. Upon CAD, additional products appear, including $FCOOH^{+\cdot}$ (H loss, *m/z* 64). The MS/MS/MS spectra (MI , CAD) of the later radical ion are dominated by the structurally indicative fragments ^+COOH (*m/z* 45) and FCO^+ (*m/z* 47), corresponding to the elimination of $F^\cdot$ and OH, respectively. The neutralization-reionization (NR) mass spectrum of $FCOOH^{+\cdot}$ (see Figure 1) also shows the structurally indicative fragments ^+COOH (*m/z* 45) and FCO^+ (*m/z* 47). Additionally, a peak at *m/z* 44 ($CO_2^{+\cdot}$) suggests that some FCOOH undergoes consecutive decomposition into HF + CO_2 and a recovered parent ion in the NR spectrum shows that FCOOH is stable for at least microseconds. The NR spectrum of $FC(OH)_2^+$ (see Figure 2) contains a recovered parent ion and also all of the peaks found in the NR spectrum of $FCOOH^+$.

The charge reversal spectrum of protonated fluoroformic acid ($FC(OH)_2^+$, *m/z* 65) shows the expected large peaks at *m/z* 16, *m/z* 17, *m/z* 19, and *m/z* 63, that correspond to $O^\cdot$, $OH^\cdot$, $F^\cdot$, and $FCOO^\cdot$, respectively.

1. Havlas, Z.; Kovar, T.; Zahradnik, R. JACS 1985, 107, 7243-7246
2. Tordeux, M.; Wakselman, C. Synthetic Communications, (1982) 12(7), 513-520

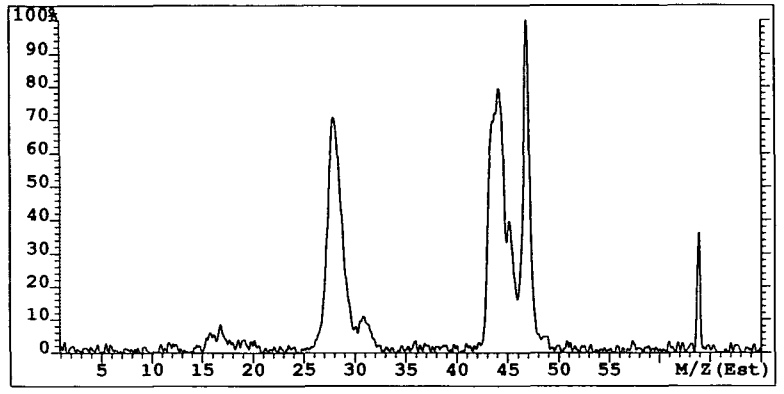

Figure 1. NR Xe/O_2 spectrum of $FCOOH^{+\cdot}$ formed by MS/MS of $FC(OH)_2^+$.

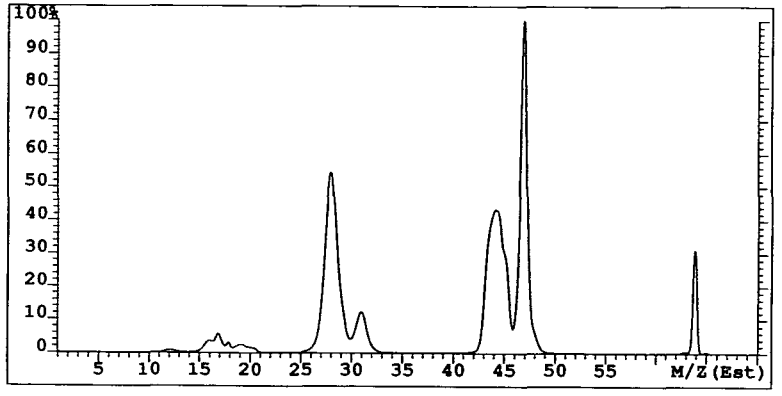

Figure 2. NR Xe/O_2 spectrum of $FC(OH)_2^+$ formed by EI of $FCO_2CH_2CH_3$.

Negative Ion Chemical Ionization/Collisionally Activated Dissociation Studies of Some Aryl Pentafluorobenzoates.

M.-Y. Zhang, N. Molinaro, J. Cantone, T. Cinque and K. Chan
Wyeth-Ayerst Research, Princeton, NJ 08543.

Electron capture negative ion chemical ionization (ECNCI) mass spectrometry can achieve very low detection limits because it is a low energy process as well as a selective process. Pentafluorobenzoyl derivatization is often used to increase the EC cross section of many nonelectrophoric compounds. The ECNCI mass spectrum of phenyl pentafluorobenzoate (PPFB) (1) has been previously reported by Hunt *et. al.*, and only the molecular anion $M^{-\cdot}$ was observed[1]. Apparently the conjugated carbonyl-aromatic system was capable of stabilizing the additional electron, and fragmentation was minimal. However, upon chlorination of the phenyl ring, an increase in the intensity of the fragment ions has been observed by Vouros *et. al.*[2]. In addition to the fragment ions generated by simple bond cleavages, Vouros *et. al* have observed a fragment ion at $[M-64]^{-\cdot}$, and they postulated a rearrangement reaction[2]. However, the site specificity and the mechanism of this elimination process has not been investigated. In this study, ECNCIMS combined with collisionally activated dissociation (CAD) in a triple stage quardrupole instrument has been employed to study the mechanism of the rearrangement-dissociation reaction proposed by Vours[2]. Instead of chlorinated phenyl pentafluorobenzoates, we have studied a similar dissociation mechanism on the following aryl pentafluorobenzoates.

Figure 1

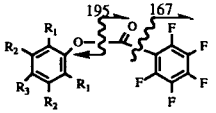

1. $R_1 = R_2 = R_3 = H$
2. $R_1 = R_2 = R_3 = D$
3. $R_1 = R_2 = H, R_3 = D$
4. $R_1 = R_3 = H, R_2 = D$
5. $R_1 = R_3 = D, R_2 = H$
6. $R_1 = H, R_2 = R_3 = CH_3$
7. $R_1 = R_2 = H, R_3 = CH_3$
8. $R_1 = R_3 = H, R_2 = CH_3$
9. $R_1 = CH_3, R_2 = R_3 = H$
10. $R_1 = R_3 = CH_3, R_2 = H$

The molecular anions $M^{-\cdot}$ of PPFB and deuterated PPFB's formed from ECNCI were quite stable, and only yielded a few low intensity fragment ions upon CAD. The daughter ion spectrum of the molecular anion of PPFB (1) showed the $[M-64]^{-\cdot}$ ion, and several fragment ions formed by simple bond cleavages of the ester anion. These ions are similar to those observed in the ECNCI spectrum of chlorinated PPFB reported by Vouros [2]. The exact mass of the $[M-64]^{-\cdot}$ ion obtained by high resolution (HR) measurement is 224.0246, confirming an elemental composition of $C_{12}H_4F_4$ (Δ=0.5 mmu). This observed elemental composition indicated that the $[M-64]^{-\cdot}$ is formed by the loss of CO_2 and HF from the molecular anion. From a parent ion scan experiment, the $[M-64]^{-\cdot}$ ion was observed to be formed from both $M^{-\cdot}$ and $[M-HF]^{-\cdot}$ ions. In the CAD spectrum of PPBF-d_5 (2), the $[M-64]^{-\cdot}$ anion was quantitatively displaced by $[M-65]^{-\cdot}$ indicating the source of the H in the HF loss is from the phenyl ring. However, both $[M-HF,-CO_2]^{-\cdot}$ and $[M-DF,-CO_2]^{-\cdot}$ ions were observed in the CAD spectra of 4-d_1-, 3,5-d_2- and 2,4,6-d_3-PPFB's (3, 4 and 5) with $[M-64]^{-\cdot}/[M-65]^{-\cdot}$ ratios of 95/5, 92/8 and 9/91, respectively. The parent ion spectra of the $[M-HF,-CO_2]^{-\cdot}$ and the $[M-DF,-CO_2]^{-\cdot}$ ions showed that they were produced from $[M-HF]^{-\cdot}$ and $[M-DF]^{-\cdot}$, respectively. The results implied the existence of two possible disso-ciation pathways to form the $[M-64]^{-\cdot}$ ion ($[M-65]^{-\cdot}$ for PPFB-d_n). As indicated in scheme 1, direct loss of HF from the molecular anion formed an intermediate I, and further loss of CO_2 from I produced the tetrafluorobiphenylene anion II. This elimination proceeded by the specific loss of the ortho-H atom and was the major dissociation pathway. On the other hand, the loss of HF could also involve the meta- and para-H atoms and formed an unstable intermediate I' which then rapidly isomerized to I through hydrogen rearrangements.

The proposed mechanism has been further supported by the ECNCI/CAD studies of the methylated PPFB's. In these studies, the $[M-64]^{-\cdot}$ ions were observed in the CAD spectra of 3,4,5-$(CH_3)_3$, 4-CH_3-, and 3,5-$(CH_3)_2$-PPFB's (6, 7 and 8). The parent ion mass spectrum of the $[M-HF,-CO_2]^{-\cdot}$ ion indicated that this ion was formed from the dissociation of the $[M-HF]^{-\cdot}$ and the $[M-CO2]^{-\cdot}$. Apparently, the methyl substitution

on the aromatic ring decreased the bond strength between the carbonyl group and the pentafluorophenyl ring. No $[M-64]^{-\cdot}$ ions were observed in the CAD spectra of 2,6-$(CH_3)_2$- and 2,4,6-$(CH_3)_3$-PPFB's (9 and 10), although the $[M-HF]^{-\cdot}$ ions were formed from both molecular anions upon CAD. The results demonstrated that the elimination of the 64 amu (HF and CO_2) only proceeded by the specific loss of the ortho-H atom (except in 7). Evidently, the hydrogen rearrangement proposed in the minor process was hampered by the ortho-methyl group of the compounds 9 and 10; no $[M-64]^{-\cdot}$ ions could be formed from the further dissociation of the $[M-HF]^{-\cdot}$ ion. These results also suggested that the formation of other ring closed intermediates which would directly produce the $[M-64]^{-\cdot}$ ion by further loss of CO_2 was unlikely.

In conclusion, ECNCI/CAD mass spectral data presented here suggested that there were three possible unimolecular dissociation pathways to form the $[M-HF,-CO_2]^{-\cdot}$ from the molecular anions of the aryl PFB's. The majority of $[M-HF,-CO_2]^{-\cdot}$ was generated from the specific loss of ortho-H atom. Formation of this ion by the loss of meta- or para-H atom through hydrogen rearrangement reactions was a less favorable process. No $[M-HF,-CO_2]^{-\cdot}$ ions were observed in the spectra of ortho-methylated phenyl penta-fluorobenzoates, since the hydrogen rearrangement reactions were hampered by the ortho-methyl group. The intermediates $[M-HF]^{-\cdot}$ (I, I' or I") were detected in the elimination process of all compounds examined; the intermediate $[M-CO_2]^{-\cdot}$ (III) was only observed in the dissociation reactions of the methylated PPFB's. Finally, the presence of the m/z $[M-64]^{-\cdot}$ ion in the ECNCI mass spectra of aryl PFB derivatives might be used as evidence for the occurrence of this system in unknown spectra.

Scheme 1:

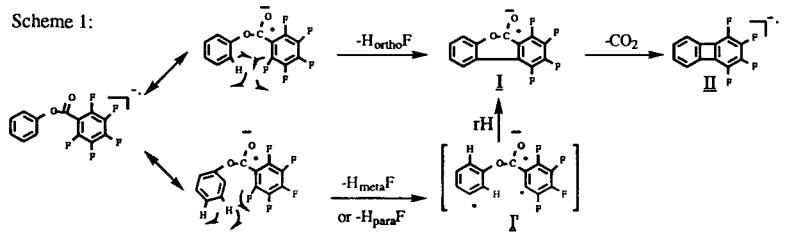

Scheme 2:

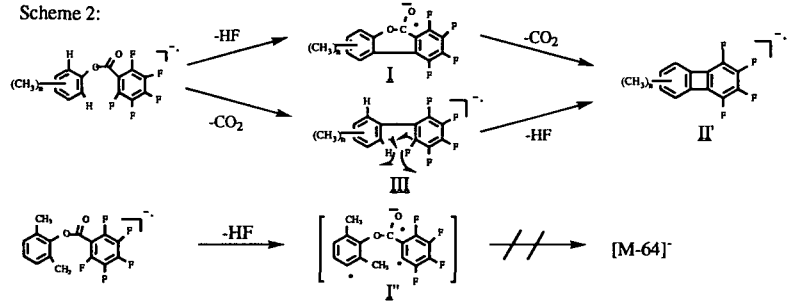

References
1. Hunt, D. F.; Stafford, G. C., Jr.; Crow, F. W. and Russell, J. W. *Anal. Chem.* 1976, **48**, 2098-2105.
2. Trainor, T. M. and Vouros, P. *Anal. Chem.* 1987, **59**, 601-610.

Acknowledgment
The authors gratefully acknowledge Mr. C. Tio and Mr. J. Mattes of Wyeth-Ayerst Research for the useful discussion about the PFB derivative method and the NMR data, respectively.

H-Te-Te-H is stable in the gas phase

Cornelis E C A. Hop
Department of Chemistry, University of Wisconsin-Madison
1101 University Avenue, Madison, Wisconsin 53706.

Hydrogen peroxide, HOOH, has a strongly oxidizing nature and is consequently of significant commercial interest. HSSH has been isolated as well Although HSSH is unstable with respect to the reaction

$$H_2S_2 \rightarrow H_2S + S$$

this reaction, which is believed to be free-radical in nature, is sufficiently slow for HSSH to be stable for considerable periods.[1] Experimental data concerning the properties of the higher homologues, HSeSeH and HTeTeH, is rather sketchy, due to their high tendency towards dissociation into H_2Se + Se / H_2Te + Te. Here the gas phase stability of HTeTeH will be examined It has been suggested that HTeTeH is formed at the tellurium cathode in 0 003-0 02 N HCl solutions, but the evidence is not conclusive.[2] HTeTeH has been the subject of two theoretical studies[3,4] The optimized structure in the most recent study[4] has a TeTeH angle of only 72° and a dihedral angle of 76°. The cis and trans rotational barriers were calculated to be only 13 and 6 kJ mol^{-1}, respectively. These data suggest (i) that the potential energy curve is rather flat around the minimum and (ii) that the structural deformation required for dissociation into H_2Te + Te is remarkably small. No data have been presented regarding the stability of HTeTeH relative to the dissociation products H_2Te + Te

Neutralization-reionization (NR) mass spectrometry has established itself as an effective technique for examining the stability of supposedly marginally stable species in the gas phase. In the NR mass spectrum a signal at the same m/z value as the mass selected ions indicates that the neutral counterparts of the mass selected ions are stable on the time scale of neutralization-reionization experiments.

All metastable ion (MI) and collision-induced dissociation (CID) mass spectra were recorded with a VG Analytical ZAB-2F at the University of Wisconsin-Madison. He (80% transmission) was the target gas for CID The NR mass spectra were obtained with a VG Analytical ZAB-R[5] at McMaster University The NR mass spectra were acquired with N,N-dimethylaniline as neutralizing gas and O_2 as reionization agent

CH_3-CH_2-$CH(CH_3)$-Te-Te-$CH(CH_3)$-CH_2-CH_3 was synthesized as follows Sodium metal was added to liquid ammonia After the sodium had completely dissolved, tellurium was added. Addition of sec-butyl bromide to this solution gave the desired product, CH_3-CH_2-$CH(CH_3)$-Te-Te-$CH(CH_3)$-CH_2-CH_3. Analysis of the material via ^{13}C and ^{125}Te NMR and mass spectrometry confirmed the structure and showed no detectable impurities.

The mass spectrum of CH_3-CH_2-$CH(CH_3)$-Te-Te-$CH(CH_3)$-CH_2-CH_3 displays intense signals due to loss of one and two 2-butene molecules. Loss of Te from the molecular ions is not observed. This behavior contrasts that of other ditellurium compounds such as diphenyl ditellurium, ditolyl ditellurium and dinaphthyl ditellurium[6] The mass spectra of the latter compounds display intense loss of one and two Te atoms.

The molecular ions of CH_3-CH_2-$CH(CH_3)$-Te-Te-$CH(CH_3)$-CH_2-CH_3 lose 2-butene metastably The $[M - 2\text{-butene}]^{+\cdot}$ ions lose 2-butene and sec-butyl metastably in the ratio 10

8 The fragment ions due to the loss of two 2-butene molecules must have the formula $[H_2,Te_2]^{+\cdot}$ and their CID mass spectrum is shown below Since the TeH^+ signal is much more intense than the Te^+ signal, we assume that these ions have the H-Te-Te-H connectivity. (It is noteworthy that the $HTeTeH^+$ ions lose H_2 metastably and not Te.) Next, the HTeTeH ions were mass selected and subjected to neutralization-reionization (see below). An intense recovery signal proves unequivocally that H-Te-Te-H is stable on the time scale of neutralization-reionization experiments. Moreover, the NR mass spectrum resembles the CID spectrum quite closely.

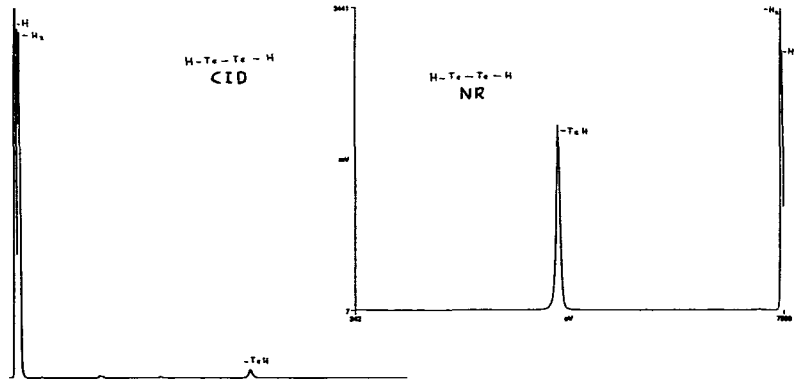

As an extension of this work, the molecular ions were examined as well. The CID spectrum is dominated by signals due to loss of one and two 2-butene molecules Neutralization-reionization gave a spectrum which contains the same fragment ions as the CID mass spectrum (see above). However, obviously more extensive fragmentation occurs in the NR mass spectrum, giving rise to low molecular weight fragment ions. The recovery signal indicates that (a fraction of) the CH_3-CH_2-$CH(CH_3)$-Te-Te-$CH(CH_3)$-CH_2-CH_3^+ ions survives neutralization-reionization intact. The CID mass spectrum of the $[M - 2\text{-butene}]^{+\cdot}$ ions indicates that they have the H-Te-Te-$CH(CH_3)$-CH_2-CH_3^+ structure. The NR mass spectrum closely resembles the CID spectrum and an intense recovery signal indicates that H-Te-Te-$CH(CH_3)$-CH_2-CH_3 is a stable species in the gas phase.

Thus, neutralization-reionization experiments demonstrate that H-Te-Te-H and H-Te-Te-$CH(CH_3)$-CH_2-CH_3 are stable species in the gas phase.

1. F.A. Cotton and G. Wilkinson, *Advanced Inorganic Chemistry*, John Wiley & Sons, New York (1980).
2. S.A. Awad, *J Phys. Chem.* 66 (1962) 890.
3 C.S Ewig, E.H. Mei and J R. van Wazer, *Mol. Phys.* 40 (1980) 241.
4 R. Block and L. Jansen, *J. Chem. Phys.* 82 (1985) 3322.
5. H F. van Garderen, P.J.A. Ruttink, P.C Burgers, G A. McGibbon and J.K. Terlouw, *Int. J Mass Spectrom. Ion Processes* 121 (1992) 159.
6. N.P Buu-Hoï, M. Mangane, P. Jacquignon, J -L. Piette and M. Renson, *Bull. Soc. Chim. France* (1971) 925.

Organic Sulfur Radicals by Neutralization-Reionization Mass Spectrometry

Scott A. Shaffer*, Thuy B. Tran, David Kuhns, and Frantisek Turecek
Department of Chemistry, BG-10, University of Washington,
Seattle, WA. 98195

Photochemical oxidation of atmospheric dimethyl sulfide (DMS) with the hydroxyl radical is presumed to proceed via two competing channels, i.e. hydrogen atom abstraction and attack at the DMS sulfur atom.[1] The former reaction yields the methylthiomethyl radical ($CH_3SCH_2\cdot$). Here we report on the preparation, properties, and dissociations of $CH_3SCH_2\cdot$ and $CD_3SCH_2\cdot$ as studied by neutralization-reionization ($^+NR^+$) mass spectrometry and ab initio calculations.

$CH_3SCH_2\cdot$ radicals are generated by collisional neutralization with a target gas of 8 keV $CH_3SCH_2^+$ formed by α-cleavage of $CH_3SCH_2CH_2SCH_3$, followed by product analysis after reionization with O_2. The measurements were taken on a tandem quadrupole acceleration-deceleration mass spectrometer described previously.[2] The $CH_3SCH_2\cdot$ radical is stable up to 4 microseconds with the highest % surviving ion (38% of CHS^+ base peak after reionization with O_2, Figure 1a.) obtained upon neutralization with trimethylamine or NO while Xe, cyclopropane, and dimethyldisulfide give much smaller yields.

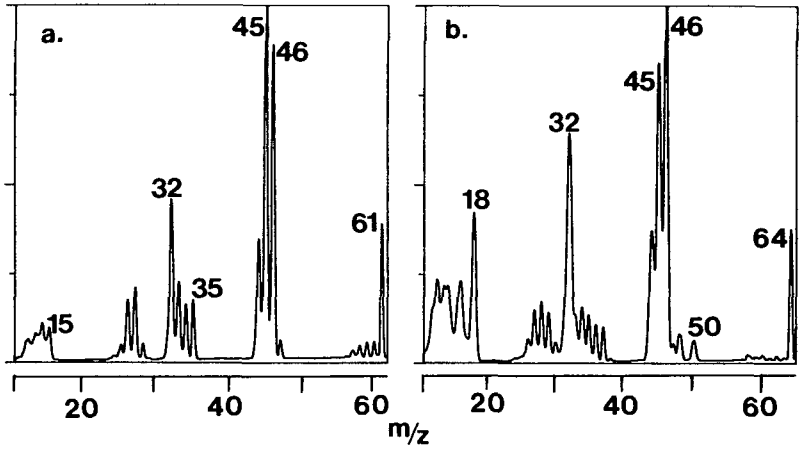

Figure 1 (a.) $^+NR^+$ spectrum of CH_3SCH_2 (TMA/ O_2 70/70 %T) and (b.) $^+NR^+$ spectrum of CD_3SCH_2 (TMA/O_2 70/70 %T).

The radical dissociates by losing CH_2 and CH_3; these are direct bond cleavages unaffected by hydrogen migrations, as evidenced by deuterium labeling (Figure 1b.). The CAD spectra (not shown) of $CH_3SCH_2^+$ and $CD_3SCH_2^+$ show losses of CH_3, CH_4, and C_2H_2 with hydrogen scrambling occuring in a near random manner. The $^+NR^+$ spectra show much less scrambling (-CHD_3 and CH_2D_2, 86.4 % and 13.6%, respectively (60/40% random)). Ion dissociations, such as the formation of H_3S^+, are less abundant in the $^+NR^+$ spectrum. The $^+NR^+$ spectra of other C_2H_5S isomers, generated by α-cleavage of 2-propanethiol and isobutane CI of ethlyene sulfide, differed markedly from CH_3SCH_2 generated above suggesting that isomerization to a common species does not occur.

Ab initio calculations (MP4(SDTQ)/6-311G** + ZPVE + ΔH_{298}) show $CH_3SCH_2\cdot$ as a stable structure with a relatively small Franck-Condon factor (40 kJ/mol, Figure 2.). Its dissociation by loss of methyl requires 103.6 kJ/mol. The calculated vertical and adiabatic ionization energies of the neutral are 6.94 and 6.59 eV, respectively. The calculated vertical recombination energy of the ion is 6.96 eV. These calculations support the overall stability of the radical as do the $^+NR^+$ spectra.

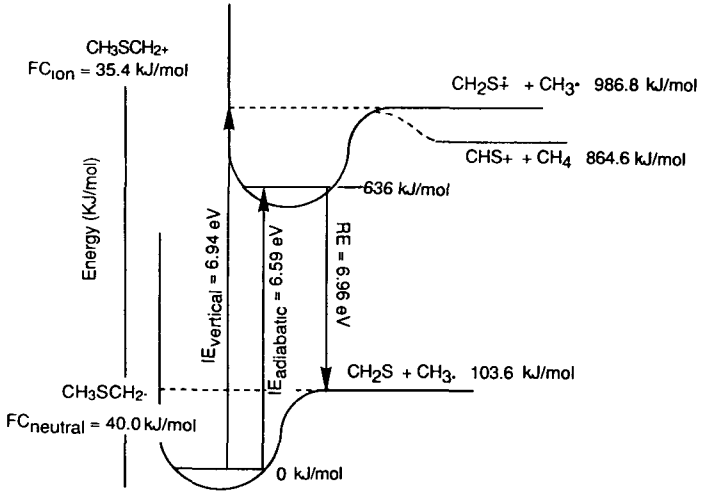

Figure 2 Energy diagram of CH_3SCH_2 radical and ion.

References

1 Lovelock, J.E.; Maggs, R.J.; Rasmussen, R.A. *Nature* (London) **1972**, 37, 452.
2 Turecek, F.; Gu, M.; Shaffer, S.A. *J. Am. Soc. Mass Spectrom.* **1992**, 3, 493.

Neutralization-Reionization Mass Spectrometry (NRMS) Studies of Ethylene Glycol Polymers.

*Thomas L. Selby,[1] Marcela M. Cordero,[1] Robert P. Lattimer,[2] and Chrys Wesdemiotis,[1]
Department of Chemistry, The University of Akron, Akron OH 44325-3601,[1] and BF Goodrich R&D Center, 9921 Brecksville Road, Brecksville OH 44141.[2]

Tandem mass spectrometry (MS/MS) is widely used in the analysis of polymers. Conventional MS/MS, e.g. via collisionally activated dissociation (CAD), reveals only the charged species resulting from the unimolecular dissociation of the precursor ion. Using NRMS, the coproduced neutral species can also be detected. Previous studies of ethylene glycol polymers have been carried out at low energy and revealed a possible fragmentation mechanism by charge-site initiated cleavage. Using NRMS the neutral species resulting from these cleavages were investigated.

For the three linear ethylene glycol polymers polyethylene glycol (PEG), polyethylene glycol methylether (PEGME), and polyethylene glycol dimethyl ether (PEGDME) the ionic fragments from MH^+ were of the form $^+CH_2CH_2$-(-O-CH_2CH_2-)$_n$-O-R (A, R=H; B,R=CH_3). The corresponding neutral fragments resulting from this dissociation were of the form H-(-O-CH_2CH_2-)$_n$-O-R' (C, R'=H;D, R'=CH_3).

For the PEG (R=H) decamer the complete ion series (series A figure 1) was observed in the high energy (8 keV) CAD spectrum (n=0-9). The corresponding neutral-fragment reionization (N_fR) spectrum contains fragments that are characteristic of C (figure 2), which supports the mechanism previously proposed for charge-site initiated cleavage. The CAD spectrum of PEGME shows ions primarily of the form A and B (figure 1). As with PEG, the complete ion series were observed for the decamer. The corresponding neutral losses yielded ions characteristic of C and D (figure 2). PEGDME yielded a complete ion series (figure 1) for the decamer (n=0-9); as expected, the A series was of very low abundance in this case (figure 1). Correspondingly, the neutral losses detected in the N_fR spectrum are consistent with type D. From these results, it is clear that the ionic and neutral fragments for PEGME are a combination of the ionic and neutral fragments from PEG and PEGDME. These results corroborate the proposed mechanism.

A cyclic ether, 18-crown-6, was also investigated under the same conditions. The precursor ion (m/z 265) yielded daughter ions in a complete series separated by 44 Da. The base peak of the spectrum is at m/z 177, indicating a neutral loss of 88 Da. From the N_fR spectrum it is apparent that the fragmentation pathway occurs primarily through the loss of dioxane, all structure indicative fragments of which are found in the N_fR spectrum.

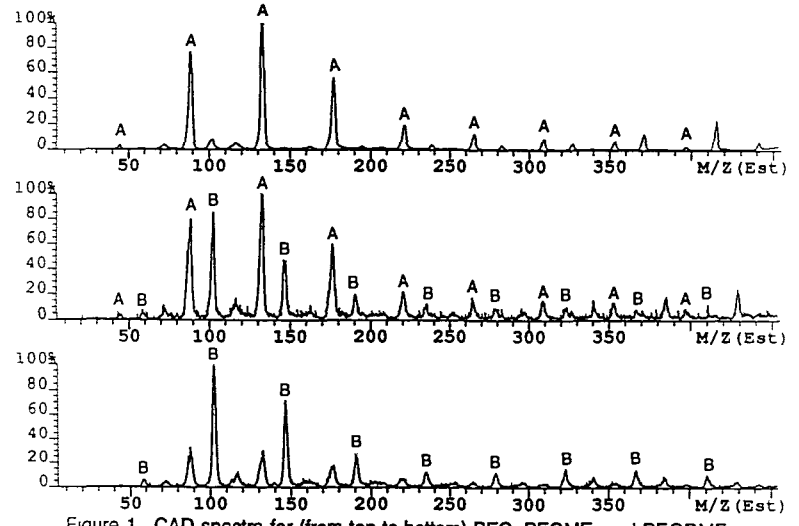

Figure 1. CAD spectra for (from top to bottom) PEG, PEGME, and PEGDME.

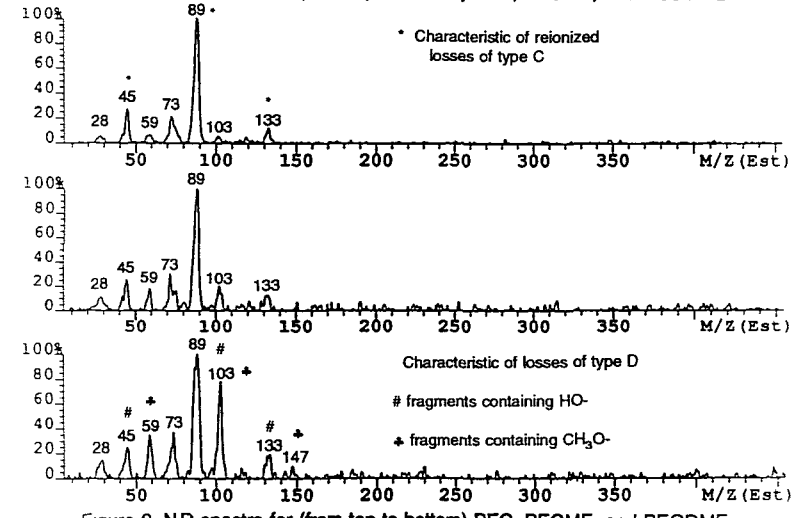

Figure 2. N_fR spectra for (from top to bottom) PEG, PEGME, and PEGDME

A Mass Spectrometric Study of Monoazo dyes

Jia-shen Wang
Clairol Inc., Stamford, CT 06922

INTRODUCTION:

In the dye industry, azo dyes are by far the most important class, accounting for over 50% of all commercial dyes. There is great interest in characterizing the impurities of these dyes in industrial preparation, since these impurities are also color compounds. The monoazo dyes have a common structure of Ar-N=N-Ar'. Disperse Black 9 (shown in Figure 1a) is a typical one. We have successfully applied mass spectrometry to identify the structures of four common impurities of this dye. This report is about the spectral features of these compounds and their common patterns for structural elucidation applications.

RESULTS AND DISCUSSION:

One common impurity of Disperse Black 9 is 4,4'-Diaminoazobenzene. The spectrum (Finnigan 4500 GC/MS) of this impurity is shown in Figure 1b. This compound is a azo dye without a N-substituted amino group. The spectrum shows the typical fragment pattern of this compound type. The main fragment ions of this compound type are formed by cleavage of one Ar-N bond. In conjunction with a molecular ion peak, this spectral feature provides key structural information for one to derive the basic structure of an unknown.

Disperse Red 19 is also an impurity of Disperse Black 9. The mass spectrum of Red 19 is shown in Figure 2a. The base peak is formed by the cleavage of the C-C bond beta to the amine nitogen. We have verified this process by a D-labelled compound (Figure 2b). This fragment ion peak provides the key structural information for the amino functional group ($-NCH_2R$). The fragment ions resulted from this process can be easily found since they appear as M-R peaks for these compounds. In the present case, it is the M-31 peak.

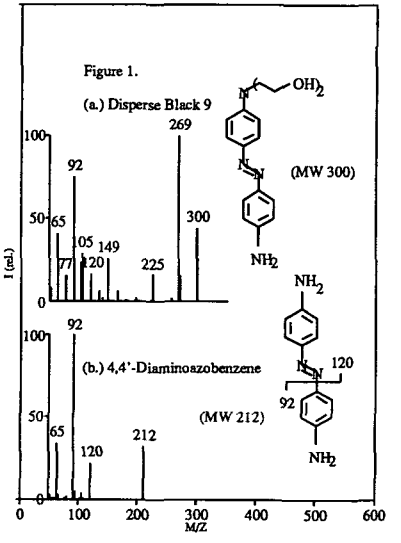

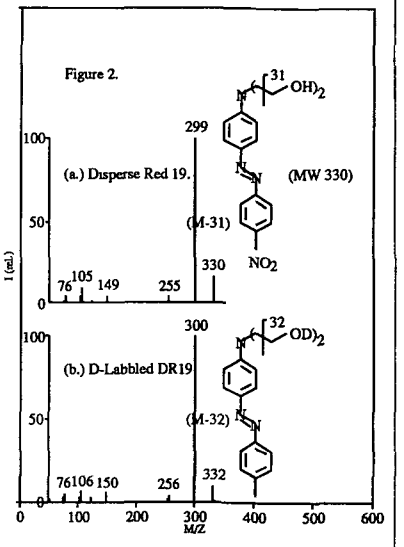

Two other commonly found impurities of Disperse Black 9 are 2-(2-hydroxyethylamino)-4'-amainoazobenzene, 4-(2-hydroxyethylamino)-4'-amainoazobenzene. The basic structures of these two were derived based on the characteristic fragment ion peaks discussed above. The positions of the substituents were assigned by NMR (QE-300, Bruker) analyses.

CONCLUSION:

The results shown here demonstrate that mass spectrometry is a suitable technique for a structural elucidation application of monoazo dyes. The fragment ions initiated from an azo unit and an amino group are two types of peaks most important in this application. Four common impurities of Disperse Black 9 are 4,4'-diaminoazobenzene, 2-(2-hydroxyethylamino)-4'-amainoazobenzene, 4-(2-hydroxyethylamino)-4'-amainoazobenzene, and Disperse Red 19.

Do Reactivity Probes Reveal Ion Structure? The Case Against Dipole-Stabilized Ions

Gregg Dahlke and Steven Kass
Department of Chemistry
University of Minnesota, Minneapolis, MN 55455

The $C_3H_5O^-$ ion can exist in an open (β-formylethyl anion, $^-CH_2CH_2CHO$) or a closed (cyclopropoxide, c-$C_3H_5O^-$) form. We set out to tackle the following questions: What is the preferred structure of this ion? How important is dipole stabilization? and Can chemical probes be used to elucidate the structure? These queries were addressed by carrying out reactivity studies, ab initio molecular orbital calculations, and a negative ion photoelectron spectroscopy investigation.

3-Trimethylsilylpropanal reacts readily with fluoride in our flowing afterglow device to afford a mixture of two ions as shown in equation 1. The reactivity of the $C_3H_5O^-$ ion was explored with a variety of reagents including D_2O, N_2O and O_2 (eqs. 2 - 4). The same results were also obtained when the $C_3H_5O^-$ ion was generated from cyclopropanol and its trimethylsilyl ether (c-$C_3H_5OSiMe_3$).

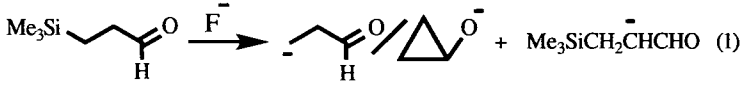

A
~25% 75%

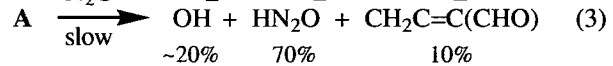

~20% 70% 10%

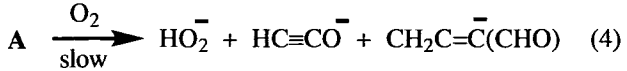

~50% 25% 25%

Molecular orbital calculations reveal that dipole-stabilization is not a dominant factor in stabilizing the open ion, cyclopropoxide is more stable than the open isomer, and that the inter conversion barrier is small (figure below). Consequently, the reactivity studies are misleading i.e. the Curtin-Hammett principle applies.

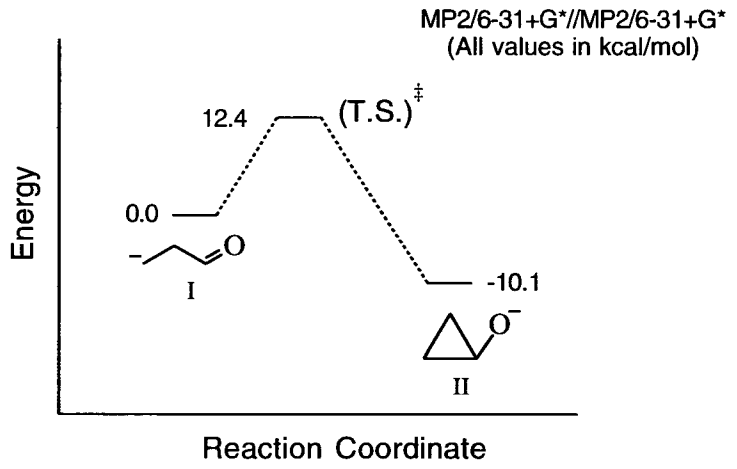

These results are supported by negative ion photoelectron spectroscopy studies which were carried out in collaboration with Professor Doreen Leopold and Mr. Sean Casey. It is also found that conjugation to a cyclopropane ring is nearly as good as to a vinyl group (17.1 vs 22.8 kcal/mol).

THE STRUCTURES OF $C_7F_7^+$ IONS.

Robert W. Holman, Jeffrey P. Kiplinger, Albert A. Tuinman, John E. Bloor, John E. Bartmess*,
Dept. of Chemistry, Western Kentucky Univ., Bowling Green KY 42101
Dept.of Chemistry, Univ.of Tennessee, Knoxville TN 37996-1600

Whether $C_7H_7^+$ has the benzyl or tropyl structure is one of the classic problems in mass spectrometry; variation in the C_7H_8 or C_7H_7X precursor structure results in a considerable change in the benzyl/tropyl ratio produced by electron ionization[1]. The tropyl cation is favored thermochemically by ca. 12 kcal/mol.[2] Perfluorination is known to drastically alter the properties and reactivity of molecules. Access to some rare C_7F_8 species[4] has prompted us to examine the benzyl/tropyl question here.

The benzyl/tropyl ratio of $C_7F_7^+$ ions from EI of the C_7F_8 precursors perfluorotoluene (PFT), perfluoronorbornadiene (PFN), perfluorobicyclo[3.2.0]-2,5-heptadiene (PFH) have been examined, using both chemical reactivity in an ICR spectrometer, and low energy CID.

The ion/molecule work was done on an ICR spectrometer: homebuilt, 1.4 T electromagnet, running in either rapid scan or FT mode. $C_7F_7^+$ ions were produced by 30 V EI; EI at 13 eV did not affect the results. The low energy CID spectra were obtained on a VG ZAB-EQ, BEqQ geometry: EI at 70 eV (no change at 12 V EI or $C_7F_7^+$ from metastable decay); $C_7F_7^+$ ions at 50 eV KE (lab); Ar collision gas pressure: nominally 6 x 10^{-6} torr, actual ca. 10^{-3} torr.

Arene nucleophiles used to detect the protio-benzyl (reactive) and tropyl (non-reactive) populations are not reactive with these stabilized perfluoro cations. $(Me_3Si)_2NH$, more nucleophilic with a structure sensitive to the presence of fluorine atoms, reacts as shown ($k = 1 \times 10^{-10}$ at 305 K. The entire (>96%, based on signal/noise) $C_7F_7^+$ population from PFT reacts in this fashion.

$$\underset{m/z\ 217}{C_6F_5CF_2^+} + (Me_3Si)_2NH \rightarrow \underset{m/z\ 286}{C_6F_5CF{=}\overset{+}{N}HSiMe_3} + FSiMe_3$$

In contrast, $C_7F_7^+$ ions from PFN and PFH are unreactive with $(Me_3Si)_2NH$ ($k < 1 \times 10^{-12}$) no product ion at m/z = 286 is observed above the noise level.

For PFT, the IE in the ICR is 10.2 eV (lit: 9.9 eV[2]), and $AE(C_7F_7^+)$ = 13.6 eV. The relative value of these two measurements is probably more accurate than their absolute values, indicating that fluorine loss requires ca. 3.4 ± 0.4 volts (78 ± 10 kcal/mol) of energy above ionization. This is a reasonable value for a bond strength in a radical cation.

The low energy CID results support the above conclusions: spectra of $C_7F_7^+$ from PFH and PFN are very similar, and somewhat different from that from PFT. Although the CID spectra of all three consist of the same masses (Table), in PFT the m/z 69 (CF_3^+) ion is 60% more intense relative to the base fragment peak at m/z 167 ($C_6F_5^+$) than in the spectra from either PFH or PFN. The latter two CID spectra are identical to within 3%. CF_3^+ is more intense in the spectrum of the (presumed) benzyl form, where there is more than one fluorine atom on some carbon in the precursor structure.

The m/z $69^+/167^+$ intensity ratio for PFT is constant for ionizing electron energies of 70 eV vs. 12 eV: internal energy effects on the

CID results are minimal. $C_7F_7^+$ metastable ions from 1, formed in the first FFR, show essentially the same CID spectrum as those produced by direct EI. The $69^+/167^+$ ratio in this metastable/CID experiment was 10% greater than for the source-produced $C_7F_7^+$ ions, but all other ions' abundances relative to 167^+ were the same to within 3%. There was insufficient sample of PFN and PFH to carry out the metastable/CID experiments with these isomers.

Ab initio MO calculations [enforced symmetry, Gaussian 90] indicate that the $C_6F_5CF_2^+$ is -9.7 kcal/mol more stable 9MP2/6-31G*) than c-$C_7F_7^+$. AM1 semi-empirical calculations [geometry optimized, near symmetric, MOPAC 5.0] put the perfluorobenzyl form 25.5 kcal/mol more stable than the perfluoro tropyl cation. The AM1 minimum energy reaction pathway (MERP) for species on the $C_7F_8^{+\cdot}$ and $C_7F_7^+$ hypersurface is shown below.

Why the reversal of stabilities for protio vs. fluoro benzyl vs. tropyl? Fluorine stabilizes an adjacent cation by a pi-donation interaction, so it should have a larger stabilizing effect when the bulk of the charge is localized at a site where this donation effect can operate. In the perfluorobenzyl cation, by AM1 calculations there are 0.59 charge units on the exo $-CF_2$ group, while in benzyl cation itself there are 0.47 charge units on the exo $-CH_2$ group. The fluorines are thus localizing the charge at the α-carbon, relative to the protio case.

We thank NSF for support of RWH through the Summer Research Program in Chemical Analysis, grant CHE-9023377. We also thank Professors D. M. Lemal and W. P. Dailey for the generous gift of PFN and PFH.

CID Fragments from m/z 217, $C_7F_7^+$.

m/z	Formula	Relative Abundance PFT	PFN	PFH
167	$C_7F_5^+$	100.	100.	100.
148	$C_6F_4^+$	15.	13.	13.
129	$C_6F_3^+$	4.	5.	5.
117	$C_5F_3^+$	45.	37.	40.
93	$C_3F_3^+$	14.	11.	13.
69	CF_3^+	66.	42.	42.

VG ZAB EQ, in the qQ sector, 50 eV parent ion KE (lab), 6 microtorr Ar collision gas.

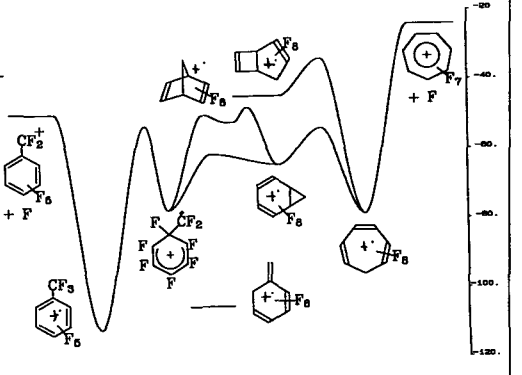

STRUCTURAL INVESTIGATION OF IMPURITIES IN SYNTHESIS OF LY255582.

*A. T. Murphy, A. P. Breau, J. A. Werner, D. K Robbins, Lilly Research Laboratories, Eli Lilly and Company, Indianapolis, IN 46285

Introduction:

Impurities in the synthesis of LY255582 have been shown to originate from the chemical intermediate LY272922. GC/MS analysis of the LY272922 intermediate detected desmethyl and methylated impurities. The site of demethylation of the intermediate presumably occurs at the 4-carbon of the piperidine ring, but was not confirmed in this investigation. The site of methylation was confirmed by solutions of LY272922 in methanol-d_4. The exchangeable protons of LY272922 occur on the phenolic oxygen and the secondary amine. The deuterated and non-deuterated standards were compared by electron impact GC/MS. The LY272922 in deuterated methanol showed the exchange of only one deuterium in the methylated peak imputiry while the peak corresponding to LY272922 incorporated two deuteriums. Analysis of fragment ions confirmed the site of methylation on the secondary amine as evidenced by the relative abundance of the 84, 72, 71, and 70 amu fragments.

Methods:

A Finnigan 4500 GC/MS was used for all analyses. The GC was equipped with a 30m x 0.32mm i.d. fused silica capillary column coated with DB-1 (d_f of 1.0 mm). LY272922 standard solutions were prepared in methanol and methanol-d_4 and injected in the split mode at a ratio of 15:1. The injector temperature was set at 250°C. The column flow was set at 35 cm/sec. The column temperature was set at an initial temperature of 100°C for 1.5 minutes and then ramped at a linear rate of 5°C/minute until the final temperature of 280°C was achieved. The column was held at the final temperature of 280°C for 5 minutes.

The mass spectrometer was operated in the electron impact ionization mode. The source temperature was set at 170°C. The spectrometer was scanned from 30 to 450 amu at a rate of 1 second/scan. The electron multiplier was set at 1150 eV in the positive ion detection mode. The electron energy was set at 70eV while the ionization energy was set at 180 mA. Data were collected using SuperIncos software.

Results and Discussion:

The site of methylation was determined by examination of the fragment ions of the methylated peak in methanol and methanol-d_4 solutions. Comparison of the mass spectra of the methylated 272922 peaks show that only one deuterium was exchanged as evidenced by the increase in molecular weight from 219 amu (Figure 1) to 220 amu (Figure 2). The 84 amu fragment ion of the methylated impurity is the most abundant ion in the spectrum (Figure 1). The proposed mechanism for the formation of the 84 amu ion is shown in Scheme I[1]. The methylated 272922 also shows a 70 amu fragment resulting from the loss of the neutral radical as proposed in Scheme II[1]. The 272922 (unmethylated) shows a major fragment ion of 71 amu which is proposed to originate from the mechanism shown in Scheme III[1].

The deuterium labeled 272922 showed the incorporation of one deuterium on the 3-methyl piperidine as evidenced by the 1:1 ratio of 71/72 amu fragment ion not seen in the 272922 standard in methanol (Figure3 and 4). Failure of the methylated 272922 to incorporate deuterium in the piperdine ring, as evidenced by no mass ratio increase of the 70/71 amu ions, and the relative abundance of the 84 amu ion in the methylated impurity suggest the site of methylation to be the secondary amine.

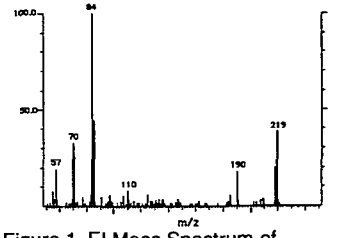

Figure 1. EI Mass Spectrum of Methylated 272922 in methanol.

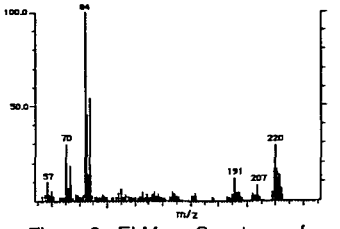

Figure 2. EI Mass Spectrum of Methylated 272922 in methanol-d_4.

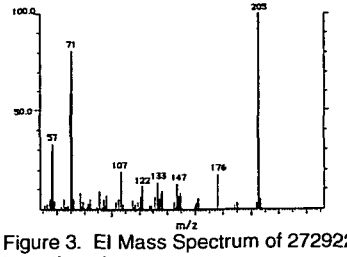

Figure 3. EI Mass Spectrum of 272922 in methanol.

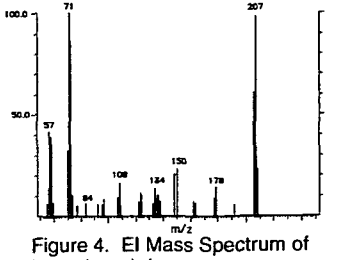

Figure 4. EI Mass Spectrum of in methanol-d_4

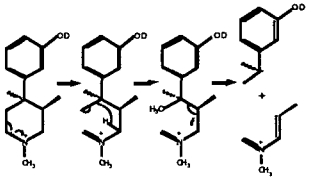

Scheme I.

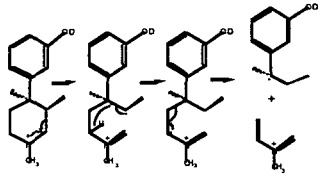

Scheme II.

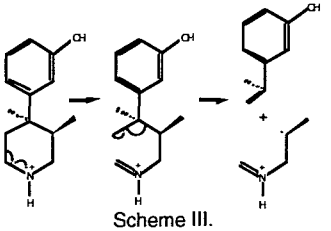

Scheme III.

References:

1. Budzikiewicz, H.; Djerassi, C.; Williams, D. H. *Interpretation of Mass Spectra of Organic Compounds*; Holden-Day: San Francisco, 1964; pp 100-102.

Where do Fullerenes come from, Anyway.

Gert von Helden, Nigel G. Gotts and Michael T. Bowers
Dept. of Chemistry, University of California, Santa Barbara, CA 93106

The structure and stability of carbon clusters and carbon cluster ions have long been a highly debated issue. Small clusters with less than 60 atoms are precursors for fullerene formation and understanding their structure and energetics is therefore crucial for understanding the fullerene formation processes. We recently applied "Ion Chromatography" (IC) to carbon cluster cations[1] and anions.[2] Various structural families have been identified. However, "cup" shaped clusters, that long have been believed to be the precursors for fullerenes, are completely absent for all clusters in our experiment. This results is intriguing since, for large clusters, we do observe high abundances of fullerenes.

We will demonstrate here that IC, in combination with annealing studies and computer modelling, is a powerful tool that allows us not only to characterize cluster structure and isomeric forms but also gives unique insight into the processes involved in fullerene formation.[3] Experimental details can be found in the literature[1,2,3] and only a brief outline will be given here. carbon cluster anions or cations are generated in a laser vaporization/supersonic expansion source. After mass selection using a mass spectrometer, a pulse of ions is injected into a high pressure drift cell. Different isomeric form have different drift times in the cell and therefore exit the cell at different times. Ions exiting the cell are mass analysed and time resolved detected.

A typical "arrival time distribution" (ATD) is shown in Fig.1, trace a. Computer modelling of the drift time allows us the assign the different peaks as resulting from a monocyclic ring (A), a bicyclic ring (B), a tricyclic ring (C), a 3-D ring (D) and a fullerene (E), similar to those in Fig. 2.(see also ref. 1). If the ions are injected into the drift cell at higher energies, annealing and/or collision induced dissociation (CID) can occur. Trace b shows the ATD for C_{35}^+ when injecting C_{35}^+ at 150 eV into the cell (about 5-30 % of this energy will be transfers into internal modes). Clearly, the bicyclic ring (B) and the tricyclic ring (C) are completely absent. Scanning the quadrupole mass filter after the cell, we noticed a substantial amount of fragmentation is occurring. This fragmentation happens right in the beginning of the cell so that, by setting the quadrupole to the right mass, ATDs for the products can be obtained. ATDs for the main CID products C_{34}^+ and C_{32}^+ are shown in Fig. 1, trace c and d.

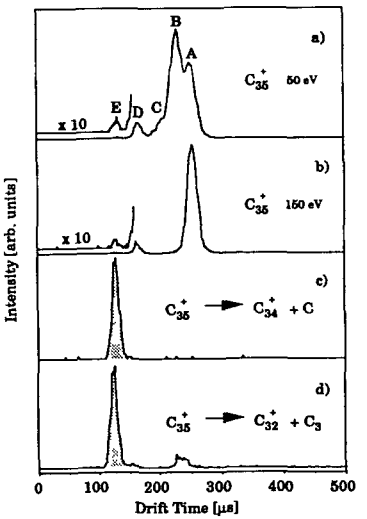

Computer modelling of the drift times allows us to unambiguously assign the shaded peaks in Fig. 1 as fullerenes. From our data it seems that two processes are happening when carbon clusters with more than 33 atoms are injected at high energy into the drift cell:

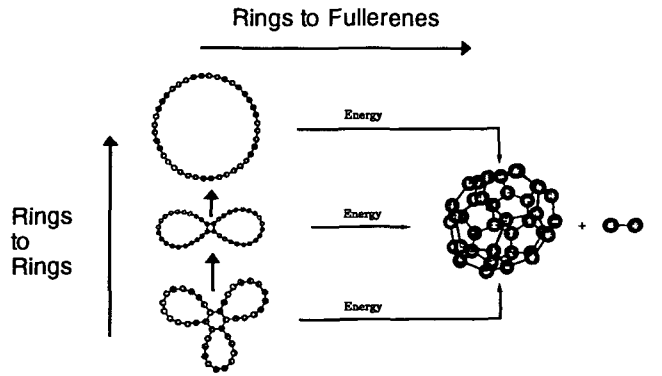

a) annealing of bi- and tricyclic rings to monocyclic rings and b) CID of planar rings with the resulting fragment ions being nearly 100% fullerenes.

We performed annealing experiments with all C_n^+ clusters with $30 \leq n \leq 40$ at 150 eV injection energy. The probability of collision induced dissociation (CID) and fullerene formation increases dramatically as cluster size increases For example C_{31}^+ undergoes only to a small amount of CID (<5%) whereas C_{39}^+ dissociates 77% of the time with almost all dissociation products being fullerenes. The first fullerene observed is C_{30}^+ resulting from C_3 loss in the annealing of C_{33}^+. This process is fairly inefficient for C_{33}^+, with only 13% of all clusters undergoing CID and only 17% of the CID products being fullerenes. For precursors with an even number of atoms, the first fullerene fragment observed is C_{34}^+, resulting from the loss of C_2 from C_{36}^+.

This data implies that the fullerene formation via CID and annealing of large ring systems is not only important in laser vaporization sources but also in C_{60} carbon arc reactors. Fullerene formation via "cup" structures as intermediates is not occurring since none of these structures is observed for either carbon cluster anions or carbon cluster cations.

References:

1) G. von Helden, M.T.Hsu, P.R.Kemper, M.T.Bowers *J.Chem.Phys.* **95** (1991) 3835;
G. von Helden, M.T.Hsu, N.G.Gotts, P.R.Kemper, M.T.Bowers *J.Phys.Chem* (in press)
2) G. von Helden, N.G.Gotts, M.T.Bowers *Science* **259** (1993) 1300.
3) G. von Helden, N.G.Gotts, M.T.Bowers *Nature* **363** (1993) 60;
G. von Helden, N.G.Gotts, M.T.Bowers *J.Am.Chem.Soc.* (in press)

The Resilience of C_{60} Towards Decomposition and Ionization

Y. Gotkis, J. Laskin and C. Lifshitz

Department of Physical Chemistry and The Fritz Haber Research Center for Molecular Dynamics, The Hebrew University of Jerusalem, Jerusalem 91904, Israel

Buckminsterfullerene, C_{60} demonstrates delayed ionization up to the μsec range. C_{60}^+ is very resilient towards SID and CAD. Is C_{60} the most stable large molecule known? The energy required to fragment C_{60} has been calculated to lie in the 11-14 eV range. Experimental values are considerably lower: 4.6 - 7.64 eV.

We have performed two types of calculations: (1) Breakdown graphs were calculated for the decomposition reaction:

$$C_{60}^+ \rightarrow C_{58}^+ + C_2 \qquad (1)$$

(2) Rate energy dependences were calculated for the dissociation and ionization of C_{60}, assuming the latter process is due to thermionic emission. In both sets of calculations, the critical energy for reaction (1) and for the neutral analogue of (1) were varied between two recent extreme experimental values.

Time resolved breakdown curves are shown in Fig. 1. While at $t=1\mu s$ (the typical time under SID) C_{60}^+ is intact even for a transferred energy of 40 eV, it is completely dissociated at t=1S. This result demonstrates that even for a critical energy of only 6.9 eV, the resilience to dissociation under SID is understood - not enough time is available for dissociation - and a higher critical energy of activation need not be invoked. Competition between dissociation and ionization is observed in Fig. 2. Critical energies for the neutral analogue of (1) were calculated through a simple thermochemical cycle to be 0.54 eV higher than those of the ionic reaction. Those for (1) span the range from ~5.2 eV[1] to ~7.1 eV[2]. Neutral products of C_{60} were observed experimentally.[3] Dissociation cannot compete with thermionic emission if E_o is much higher than ~8 eV. The known heat of formation of C_{60} dictates a neutral binding energy[4] of 7.8 + Δ eV, with $\Delta > O$. Theory predicts $\Delta >> O$, but experimental results to date give a rather small Δ value.

[1]P. Sandler, C. Lifshitz and C.E. Klots, Chem. Phys. Lett. **200**, 445 (1992).

[2]M. Follin, M. Lezius, P. Scheier and T.D. Märk, J. Chem. Phys., in press, 1993.

[3]K.R. Lykke and P. Wurz, J. Phys. Chem. **96**, 3191 (1992)

[4]R.L. Whetten and C. Yeretzian, Conf. Proc., World Scientific Publishing Co., Singapore, Clusters and Fullerenes, Trieste, 1992.

Figure 1

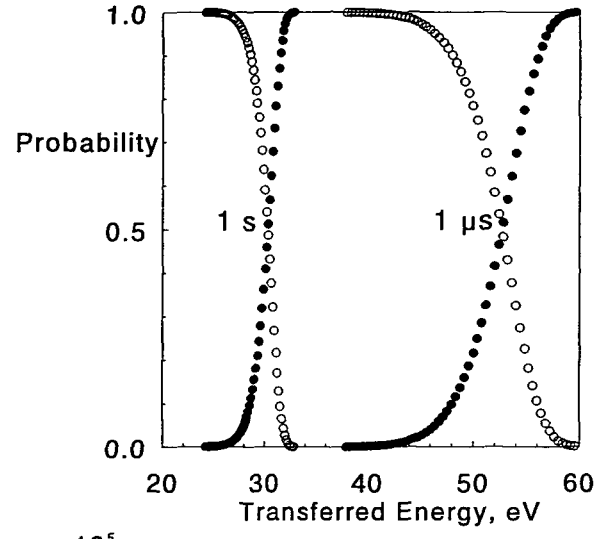

Figure 2

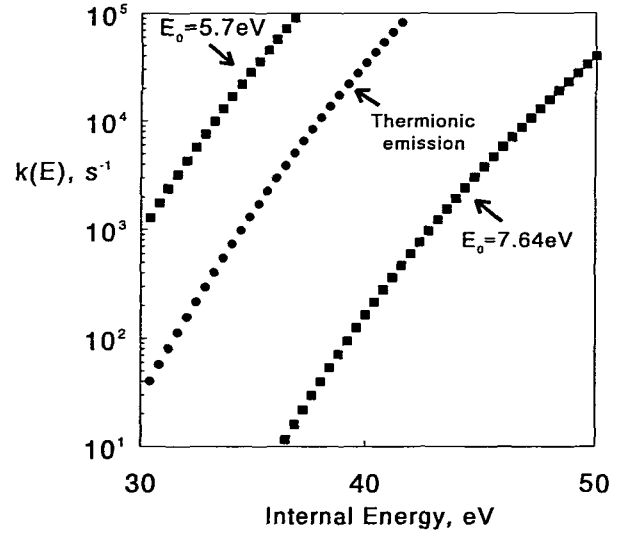

Isotope Effects on the Mass Spectral Fragmentation of the Mixed Glycerol/d_5-Glycerol Clusters

Chhabil Dass
University of Tennessee, Memphis, TN 38163, USA.

Glycerol is the most frequently used liquid matrix in FAB and LSIMS modes of ionization. During desorption/ionization, the energy acquired by the matrix ions in excess of their ground state causes them to dissociate into smaller fragments. Thus, several monomeric and oligomeric ions of matrix and their fragments are observed. All these ions, on one hand, constitute a chemical background noise and often interfere in the FAB analysis. On the other hand, they facilitate mass assignment by acting as reference ions. Therefore, a clear understanding of the fragmentation behavior of matrix ions is very important. Isotope substitution leads to differences in the rates of the gas-phase fragmentation reactions. Therefore, it is important to have knowledge of isotope effects associated with these fragmentations.

To investigate fragmentation characteristics of the proton bound gas-phase ions of glycerol and its oligomers and to determine the associated secondary isotope effect (SIE), the following experiments were conducted: (a) obtain CID-MIKE spectra of the $(M+H)^+$ ions of monomer, dimer, trimer, and tetramer of glycerol (G) and of d_5-glycerol (dG), (b) obtain precursor ion spectra of a few important fragment ions derived from the $(G+H)^+$ and (c) determine the SIE from the CID-MIKE data of the proton bound mixed clusters of G and dG.

This study used a VG AutoSpec Q mass spectrometer of E_1BE_2-qQ geometry and Cs^+ ions of 30-35 keV energy as the source of ionizing beam. The ions were accelerated out of the source to a potential of 8 kV. The precursor ion spectrum was obtained in the first FFR under linked-field scan at constant B^2/E_1. The product ion spectrum was acquired by using MIKES technique; the precursor ion was mass-selected in the third FFR by adjusting E_1 and B and its spectrum was obtained by scanning E_2. Helium was used as the collision gas in both these experiments. All spectra were acquired under computer-control scans.

The gas-phase $(G+H)^+$ ion predominantly fragments *via* the losses of H_2O to yield *m/z* 75 and 57 (Figure 1 and Scheme 1) and *via* the loss of CH_3OH to yield *m/z* 61. The losses of CH_2O, CH_2OH, and CH_3OH from the *m/z* 75 lead to the formation of *m/z* 45, 44, and 43. A loss of H_2O from the *m/z* 61 provides an alternative route to *m/z* 43. The precursor ion spectrum reveals that the *m/z* 31 ($^+CH_2OH$) and 29 (^+CHO) are predominantly derived from *m/z* 45 and 57, respectively. The presence of *m/z* 34 in the CID-MIKE spectrum of the $(dG+H)^+$ ions reveals that a small population of *m/z* 31 also exists as CH_3O^+. The proton bound dimer, trimer and tetramer undergo mainly the loss of glycerol molecules (Figure 2). The *m/z* 93 in these spectra corresponds to the $(G+H)^+$ ion and exhibits all the fragmentations noted in Scheme 1.

Isotope substitution affects the rate of unimolecular gas-phase fragmentations. The effect is very profound when H and D are considered because of a large difference in their mass. The primary isotope effect results when cleavage of the isotopically substituted bond occurs (e.g., C-H, O-H, etc.). The rate of cleavage of the bond remote from the site of isotope substitution is also affected but to a lesser extent and leads to SIE. Isotope effect is caused by the fact that the critical energy of the reaction involving lighter isotope is lower than that involving heavier isotope. These are the direct consequence of the small differences in the zero point energies of the transition states of the two competing reactions.

To determine the SIE associated with fragmentation of the proton bound oligomers of glycerol, the CID-MIKE and metastable ion spectra of $(G+dG+H^+)$, (G_2+dG+H^+), $(G+dG_2+H^+)$, and $(G_2+dG_2+H^+)$ were acquired (Figure 3). The SIE, defined as SIE = k_h/k_d (where, k is the rate of the reaction), was calculated for the competing reactions leading to the loss of labeled and unlabeled glycerol molecules. As shown in Table 1, normal isotope effect was observed. The effect is greater for metastable ions, and is in agreement with the RRKM theory, according to which SIE is expected to increase with decrease in internal energy.

Acknowledgment: Financial support of the NIH (Grant NS 28025) is highly appreciated.

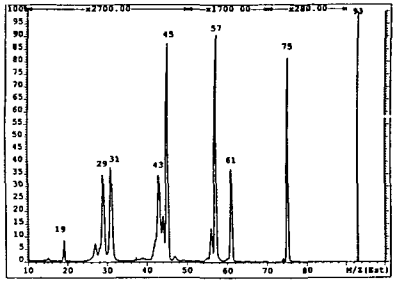

Fig. 1-CID-MIKE spectrum of $(G+H)^+$

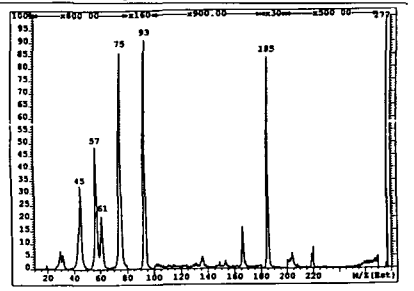

Fig. 2-CID-MIKE spectrum of $(G_3+H)^+$

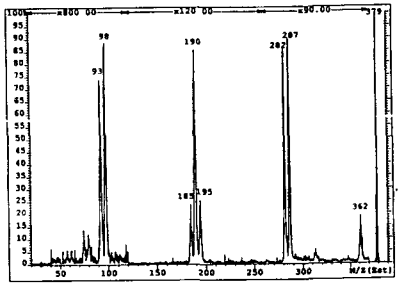

Fig. 3-CID-MIKE spectrum of $(G_2+dG_2+H)^+$

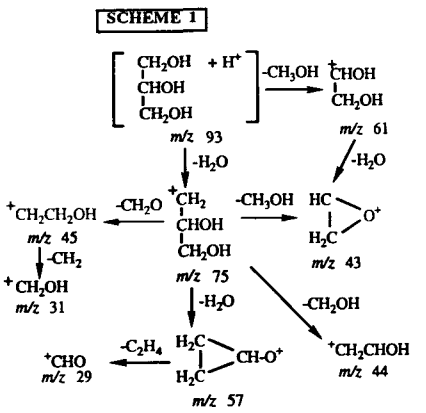

Table 1

Neutral loss	$[G+dG+H^+]$		$[G_2+dG+H^+]$		$[G+dG_2+H^+]$		$[G_2+dG_2+H^+]$	
	A	B	A	B	A	B	A	B
Glycerol	1.167	1.242	1.159	1.161	1.197	1.241	1.115	1.194
$(Glycerol)_2$	-	-	1.152	-	1.136	-	1.136	-
$(Glycerol)_3$	-	-	-	-	-	-	1.183	-

A= CID spectrum, B= metastable ion spectrum

The Effects of Molecular Size, Alkali Metals and Charge Type on the Metastable Unimolecular Decomposition of Oligosaccharides in an External Ion Source Fourier Transform Mass Spectrometer

Lambert C. M. Ngoka and Carlito B. Lebrilla. Department of Chemistry, University of California, Davis, CA 95616.

Studies on the metastable decomposition of oligosaccharides in a liquid SIMS Fourier transform mass spectrometer were reported recently[1]. The present studies examine the effect of molecular size, alkali metal cationizing agents and charge type on the metastable unimolecular decomposition of linear and cyclic oligosaccharides in this instrument.

A 30% solution of thioglycerol in glycerol was used as the matrix. Sample preparation and loading were accomplished by placing about 10 µl of the matrix on a copper probe tip and depositing 5 µl of approximately 0.50 M aqueous solution of the oligosaccharide on top of the matrix drop on the probe tip before introduction into the ion source. A 10-millisecond pulse was used for ion production and injection into the analyzer cell.

Figure 1 shows the metastable decay profiles of Protonated α-cyclodextrin, maltohexaose, maltopentaose and maltotetraose through 10 milliseconds detection delay time. Oligosaccharides studied exhibit an exponential decay of the protonated parent, $[M+H]^+$, which levels off at five milliseconds after ion injection and remains essentially invariant at a background level. These decompositions are accompanied by concomitant increases in the intensities of lower ion fragments. As evident in the diagram, the unimolecular decomposition rate increases with molecular size. This has been attributed to a sequential fragmentation mechanism in which a fragment ion has sufficient internal energy to fragment further. As well, it is conceivable that the energy imparted into the ions by the Cs^+ primary beam is commensurate with molecular size.

Figure 2 shows a plot of the first order rate constants for the metastable decay of cationized and deprotonated α-cyclodextrin. The fact that protonated oligosaccharides decay faster than metallated oligosaccharides could be due to the substantial weakening of the glycosidic bonds by protonation, borne out by the much greater exothermicity of the proton-oxygen attachment reaction. The exothermicity of the ion attachment to the oxygens of the oligosaccharide could be inferred from the aqueous phase hydration energies, which are 1091, 519, 406, 322, 293 and 264 kJ/mol for H^+, Li^+, Na^+, K^+, Rb^+, and Cs^+ respectively[2]. More exothermic ion attachment coordination is seen to bring about greater degree of fragmentation and faster rate of metastable decomposition.

Oligosaccharide anions decay about two times slower than the corresponding cations. This may be due to the weakening of glycosidic bonds by cationization in the latter.

References:

1. Lambert Ngoka and carlito B. Lebrilla J. Am. Soc. Mass Spectrom. 1993, 4, 210-215.
2. Lee, J. D. Concise Inorganic Chemistry, 3rd Edition, English Language Book Society and Van Nostrand Reinhold Company, London, 1977, pp. 122-123, 133.

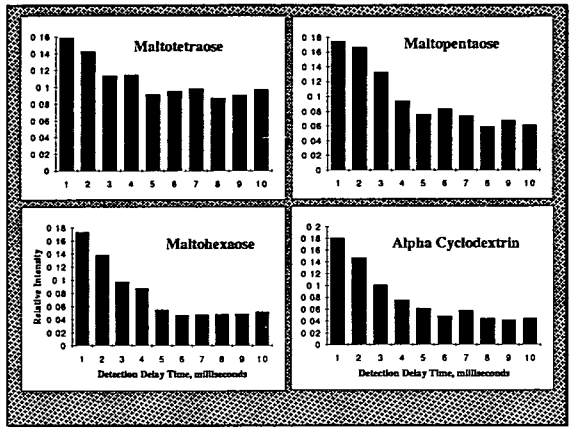

Figure1: Time profile of Some Protonated Oligosaccharides Through the First 10 milliseconds Following Ion Injection into the Analyzer Cell.

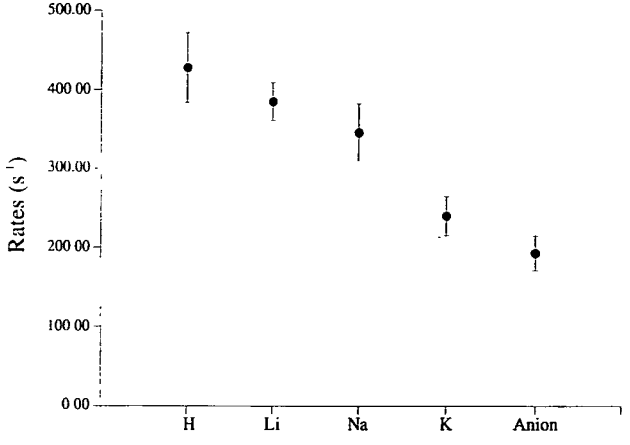

Figure 2: First Order Rate Constants for the Metastable Decomposition of Cationized and Deprotonated α-Cyclodextrin

MECHANISMS OF FRAGMENTATION OF CATIONIC PEPTIDE IONS

Hong Zhao and Jeanette Adams, Department of Chemistry, Emory University, Atlanta, GA 30322.

Sequence-specific product ions are formed by collision-induced decomposition (CID) of either $(M + Cat^{2+} - H)^+$ ions cationized with alkaline earth metal ions (1), $(M + Cat^+)^+$ ions cationized with alkali metal ions (2), or $(M + H)^+$ ions (3). Fragmentation mechanisms that involve hydrogen transfer have been studied and different mechanisms have been proposed. Here, we use deuterium-labelled peptides to address the source(s) of hydrogen transferred in formation of several commonly observed sequence product ions (4). The peptides include GGV, YPFAG, YPFA(CD_3)G, YPFAG(CD_2)-NH_2, G(CD_2)(CD_2)V, and GGV-d_5. Fast atom bombardment is used to form the gas-phase ions. CID spectra of decompositions that occur in the first field-free region of a VG 70-S forward geometry mass spectrometer are acquired by using linked scans at a constant ratio of B/E.

Results from the above peptides indicate that the amide group of the *n-m* amino acid can be a source of hydrogen transferred in the formation of $(a_{n-m} + Ca - 2H)^+$, $(a_{n-m} + Li - H)^+$, and $(a_{n-m})^+$ ions. In addition, the CH(R) group of the *n-m+1* amino acid also can be a source for formation of $(a_{n-m} + Ca - 2H)^+$ ions. Either the amide group or the CH(R) group of either the *n-m+1* or the *n-m+2* amino acids can be the source of hydrogen transferred in the formation of $(y_{n-m} + Ca)^+$ and $(y_{n-m} + Li + H)^+$ ions. Only the former serves as the source in the formation of $(y_{n-m} + 2H)^+$ ions. Either the CH(R) group of the *n-m+1* amino acid or the C-terminus can be the source of hydrogen transferred in the formation of $(c_{n-m} + Ca)^+$ ions.

Our results support some previously proposed mechanisms and provide evidence for others. Our study, however, does not reveal some chemistry that has been observed by others. Thus, it is clear that sources of hydrogen transferred in the formation of particular product ions can vary with both the starting peptide molecule and with the type of positive ion studied (cationized with either Ca^{2+}, Li^+, or H^+). Consequently, our study in conjunction with the previous ones shows that several mechanisms can account for formation of each product ion, and the preference of one mechanism over another will be dictated by peptide structure and the type of cation studied.

References:

(1) Teesch, L. M.; Adams, J. *J. Am. Chem. Soc.* **1991**, *112*, 4110-4120.

(2) (a) Teesch, L. M.; Adams, J. *J. Am. Chem. Soc.* **1991**, *113*, 812-820. (b) Leary, J. A.; Zhou, Z.; Oden, S. A.; Williams, T. D. *J. Am. Soc. Mass Spectrom.* **1990**, *1*, 473-480. (c) Gress, R. P.; Gross, M. L. *J. Am. Chem. Soc.* **1991**, *112*, 5098-5104.

(3) (a) Mueller, D. R.; Eckersley, M.; Richer, W. J. *Org. Mass Spectrom.* **1988**, *23*, 217-221. (b) Kenny, P. T. M.; Nomoto, K.; Orlando, R. *Rapid Commun. Mass Spectrom.* **1992**, *6*, 95-97.

(4) Zhao, H.; Adams, J. *Int J. Mass Spectrom. Ion Processes*, **1993**, in press.

Presented at the 41st ASMS Conference on Mass Spectrometry

FUNDAMENTAL PROCESSES IN DECOMPOSITIONS OF SIMPLE AMINE AND AMIDE IONS

Henri E. Audier[1], Gérard Provot[2], Jean-Pierre Morizur[2], and T. H. Morton[2]

[1]Laboratoire des Mécanismes Réactionnels, Ecole Polytechnique, 91128 Palaiseau, France
[2]Laboratoire de Chimie Structurale, Université Paris VI, 75230 Paris, France
[3]Department of Chemistry, University of California, Riverside, CA 92521-0403, USA

Simple primary alkylamines and simple N-alkyl amides exhibit rearrangements in their mass spectra. Many of these correspond to pathways by which sequence information is lost in the course of CI, FAB-MS, and other techniques used for the mass spectrometric analysis of polypeptide structure. Molecules with primary alkyl groups attached to nitrogen represent a case in point. In studies of metastable protonated n-propyl amines we find that seven alkyl hydrogens scramble, followed by expulsion of propene. Isotopic labeling gives the following proportions:

Parent Ion	Proportion NH_3D^+	Proportion NH_4^+
$CH_3CH_2CD_2NH_3^+$	30%	70%
$CD_3CH_2CH_2NH_3^+$	47%	53%
$CH_3CD_2CH_2NH_3^+$	15.5%	84.5%
$CD_3CH_2CD_2NH_3^+$	81%	19%
$CH_3CHDCH_2CH_3^+$	7%	93%

Given experimental uncertainties on the order of ±1% we infer that all of the α and γ C-H hydrogens scramble with one of the β-hydrogens, and that these 7 are the ones that end up on the ammonium ion, without any exchange between CH and NH hydrogens. This implies that the n-propyl has rearranged to an isopropyl group, presumably via an ion-neutral complex. The question remains whether the [iPr^+ NH_3] complex collapses back to isopropylammonium (which might then eliminate propene via a concerted pathway via a 4-member cyclic transition state[1]). We have examined the dynamics of the reformation of the covalent bond using SCF calculations on the potential energy surface. If the distance between the center of mass of the iPr^+ and the N-atom is held fixed, the most stable geometry looks like the structure 1 for distances > 3 Å (at 6-31G**//6-31G**). A stable energy minimum, in which the N and the three C's are nearly coplanar,

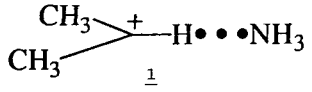

1

is found at a distance of 3.2 Å and is about 60 kJ/mol lower in energy than free iPr^+ and ammonia. To form a covalent C—N bond (which lies about 220 kJ/mol below free iPr^+ and ammonia), the ammonia has to move out of the plane of the carbons. The question posed by rearrangement in n-alkylammonium ions is related to the issue of hydrogen scrambling seen in protonated dialkyl ether ions.[2,3]

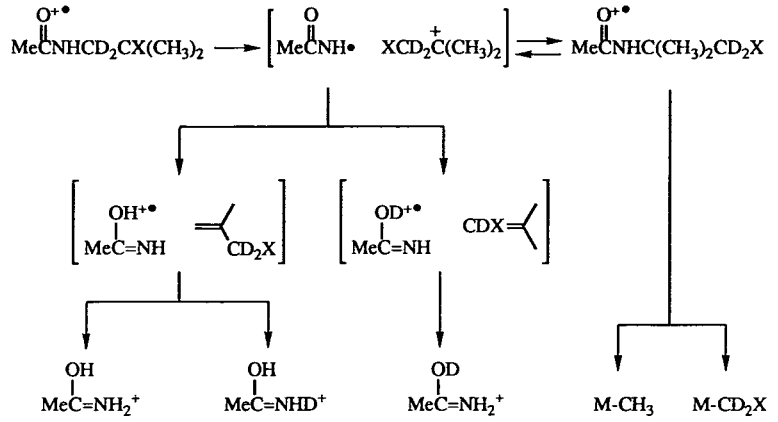

Rearrangements of n-alkyl amides also exhibit hydrogen scrambling. N-Isobutylacetamide yields a "McLafferty + 1" ion (presumably $CH_3C(OH)=NH_2^+$), as a major peak in its electron impact (EI) mass spectrum, as well as in its chemical ionization (CI) mass spectrum. When the parent ion is $MeCONHCD_2CH(CH_3)_2^{+\cdot}$ approximately $\frac{2}{9}$ of these ions contain deuterium. When the parent ion is $MeCONHCD_2CD(CH_3)_2^{+\cdot}$ approximately $\frac{1}{3}$ of these ions contain deuterium. If, as depicted above, tBu^+-containing complexes intervene, the presence of $[M-CHD_2]^+$ in the CAD of the former and $[M-CD_3]^+$ in the CAD of the latter implies that recombination can take place.

1. E.J. Reiner, R.A. Poirier, M.R. Peterson, I.G. Czismadia, and A.G. Harrison (1986) Can. J. Chem. 64, 1652-1660.

2. H.E. Audier, C. Monteiro, D. Berthomieu, and J. Tortajada (1991) Int. J. Mass Spectrometry Ion Processes 104, 145-161.

3. R.W. Kondrat and T.H. Morton (1991) J. Org. Chem. 56, 952-957; R.W. Kondrat and T.H. Morton, Org. Mass Spectrom. (1991) 26, 410-415.

Measurement of Long-Chain Fatty Acyl CoA Species by GC/MS

Keith L. Clay and Christopher A. Johnson

National Jewish Center for Immunology and Respiratory Medicine
1400 Jackson Street
Denver, CO 80206

Long-chain fatty acyl coenzyme A thioesters (FA-CoA) play a central role in many of the important reactions of lipid biochemistry. FA-CoA are important intermediates in catabolic reactions such as beta-oxidation and in synthetic reactions such as triacylglycerol synthesis, phospholipid synthesis, cholesterol ester synthesis and in protein acylation. In addition, these molecules may have such disparate activities as roles in activation of protein kinase C; regulation of cytosolic free Ca^{++}; and modulation of the nucleoside translocase activity. It is clear that this range of postulated activities implies substantial ignorance about the real roles of these molecules in cellular biochemistry.

FA-CoA are established as important intermediates of phospholipid biochemistry. In particular, the activities of Acyl-CoA:phospholipid acytransferase with various substrates has been thoroughly investigated. It is clear that this enzymatic activity is critical to the establishment of the fatty acid composition of membranes and the incorporation of exogeneous fatty acids into cellular phospholipids. Our studies on the composition of membrane phospholipids and the effects of fatty acids on the biosynthesis of platelet activating factor (PAF, 1-O-alkyl-2-acetyl-*sn*-glycero-3-phosphocholine) led to the hypothesis that FA-CoA are critical determinants of the cellular capacity for PAF biosynthesis. To test this hypothesis, direct measurement of FA-CoA is required. The goal of this study has been to identify appropriate GC/MS procedures for the measurement of cellular FA-CoA.

We have characterized a number of derivatization procedures for conversion of FA-CoA into molecules amenable to GC/MS analysis. An extension of an aminolysis procedure and consideration of the unique reactivity of the thioester bond led to the use of heptafluorobutylamine in combination with silver ion catalysis as a useful procedure to prepare volative derivatives of the acyl moiety of FA-CoA. In essence, the procedure involves heating FA-CoA with heptafluorbutylamine and an equimolar amount of silver nitrate in pyridine at 60° for 30 minutes. This procedure has been used to measure the concentration of the two most abundant species of FA-CoA in human neutrophils. Palmitoyl-CoA was present at 6.2 ng/10^7 cells; stearoyl-CoA concentration was 2.3 ng/10^7 cells. Further application of this procedure to measurement of both concentration and turnover of FA-CoA will give valuable insight into the biochemistry of this class of compounds.

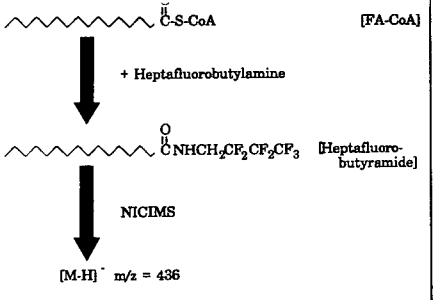

Figure 1. Derivatization procedure for formation of heptafluorobutyramide from acyl-CoA.

The negative ion chemical ionization mass spectrum of the heptafluorobutyramide of nonadecanoyl-CoA is presented in Figure 2. This amide was made by aminolysis with heptafluorobutylamine of nonadecanoyl-CoA on the silicic acid scraped from a TLC plate. 0.25 ml of each solution, 10mM silver nitrate in pyridine and 10 mM HFBA in pyridine were added to a tube containing the TLC scraping and heated at 60° for 30 min. After addition of water, the amide was extracted with ethyl acetate, taken to dryness and re-dissolved for injection into the GC/MS. The reaction will go to completion without silver ion catalysis, but very long times (greater than 24 hours) are required. This reaction does not form the amide from phospholipid oxoesters nor from free fatty acids and is quite specific for the thioester linkage of acyl-CoA species.

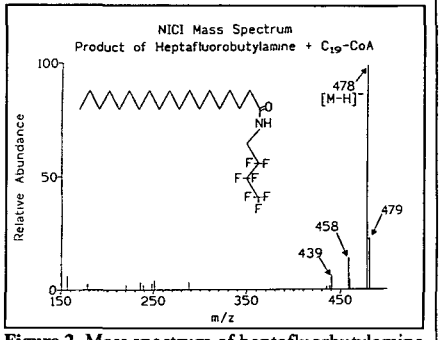

Figure 2. Mass spectrum of heptafluorbutylamine derivative of nonadecanoyl-CoA.

This derivative forms negative ions primarily by proton abstraction rather than resonance electron capture, which increases the minimal detection limit, relative to a species which is formed by electron capture. The minimum amount detected (expressed as acyl-CoA equivalents) was just less than 1 picomole (1 nanogram) of palmitoyl-CoA. This relatively high limit of detection, however, is adequate for experiments with small numbers of cells. Confidence in the procedure is enhanced by the specificity of the reagents for the thioester bond.

The effect of silver ion on the speed of the reaction is quite marked as illustrated in figure 3. Silver ion complexation with the thio group of the thioester of acyl-CoA allows the aminolysis with HFBA to go to near completion in 30 minutes. Without silver ion, the reaction was complete only after more than 24 hours.

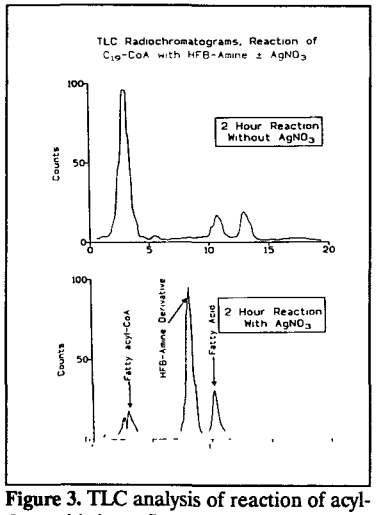

Figure 3. TLC analysis of reaction of acyl-CoA with heptafluorobutylamine. Effect of silver nitrate.

Acknowledgement: This work was supported in part by a grant from the National Institutes of Health, HL34303.

Low-energy Tandem Quadrupole Mass Spectrometry of Unsaturated FAME
A Revealing Study of Unique Ion Chemistry

*Joseph A. Zirrolli and Robert C. Murphy
National Jewish Center for Immunology and Respiratory Medicine
Denver, Colorado, 80206

Introduction: The electron ionization mass spectrometry of fatty acid esters has been studied extensively and, in particular, the EI of saturated fatty acid methyl esters (FAME). The EI spectra of FAME are characterized by the McLafferty rearrangement ion, m/z 74 (the base peak), and a series of carbomethoxy ions, $[(CH_2)_nCO_2CH_3]^+$, observed at m/z 73, 87, 101, 115...., where n=1, 2, 3, 4, ..., etc. The formation of these ions is known to involve complex processes and extensive rearrangements of hydrogen and carbon atoms (1). Collisional activation of the molecular ion and analysis by tandem mass spectrometry yields a different story. Collisional activation of the molecular ion did not yield the McLafferty ion, but extensive rearrangements of the carbon skeleton were observed, using stable isotope-labelled FAMEs (2). A mechanism was proposed to explain these observations which was later refined (3). Independent of this work, a similar mechanism had been reported, based upon the MIKES analysis of deuterium-labelled macrocyclic amines (4,5). These mechanisms propose carbon rearrangement with multiple hydrogen transfers resulting in a symmetrical decomposition pathway. The work presented here extends that previous analysis with new data with FAMEs labelled in the middle of the alkyl chain and with unsaturated FAMES.

Methods: Methyl esters of fatty acids were obtained by treatment with diazomethane. FAMES were introduced into a triple sector quadrupole mass spectrometer (TSQ70, Finnigan Corporation) by solid probe. Collision-induced dissociation of molecular ions of FAMES was performed with varying offset potentials on the second quadrupole (1-50 eV) and argon pressures (0.1-0.5 mTorr). Product ion spectra were obtained by scanning the third quadrupole from m/z 50 to the molecular ion in two seconds.

CID of Saturated FAME: Figure 1 illustrates a typical low-energy CID of a FAME molecular ion generated by electron ionization. No McLafferty ion at m/z 74 appears but rather a regular series of carbomethoxy ions are observed beginning at m/z 101. When deuterium is incorporated into the 2 position, the resulting CID spectra of the molecular ion indicates that the formation of these product ions is not by simple radical cleavage mechanisms but the result of extensive hydrogen and carbon atom rearrangements. For example, the first ion of the series is not observed at m/z 103 but instead at m/z 101 and 102. This is the result of loss of carbons 2,3,4 as well as hydrogen rearrangements.
It is of interest to note that a single radical site can yield complementary ion pairs through symmetrical reactions.

CID of Mono-Unsaturated FAME: A study of six monunsaturated FAMEs also yielded unexpected results. All molecular ions of mono-unsaturated FAME produced similar CID spectra regardless of double bond position and geometry. The fatty acids studied ranged from 14 carbons in length to 24, with the single unsaturation in positions 9, 11 or 15. As shown in Figure 2 for methyl 9(z)-hexadecenoate, these spectra are characterized by the formation of two abundant ions, loss of methanol and formation of m/z 141. The unique ion at m/z 141 was found to contain the carbomethoxy group

from analysis of the ethyl ester derivative and this ion shifted by 14 u to m/z 155. The lack of any influence of double bond position implied a stabilization of the radical site before rearrangement of the $M^{+\cdot}$ and decomposition to this common product ion. This stabilization may occur as an initial allyl radical. After rearrangement it is proposed to yield a cyclohexenylcarbomethoxy ion, as supported by the common abundant ion, m/z 81, observed in the CID spectrum of the ion, m/z 141.

Di- and Tri- Unsaturated FAME: Three series of product ions were formed by CID of molecular ions of di-unsaturated FAME. These ions were all even-mass, odd-electron ions with the most abundant arising from loss of methanol. The other two series of product ions were formed by loss of alkenes and either retained or lost the carbomethoxy group (Figure 3). Decomposition of $M^{+\cdot}$ from tri-unsaturated FAME did not result in the loss of methanol but rather two other ion series; one by loss alkyl radicals from the carbomethoxy group and the other from loss of an alkene from the carbomethoxy group (Figure 4).

1. Dinh-Nguyen, N. *Arkiv Kemi* **1968**, *28*, 289-362.
2. Zirrolli, J.A and Murphy, R.C. *J. Am. Soc. Mass Spectrom.* **1993**, *4*, 223-229.
3. Murphy, R.C. and Zirrolli, J.A. In: Biological Mass Spectrometry: Present and Future. (T. Matuso, Y.Seyma, R. Caprioli and M. Gross, Eds.) John Wiley, **1993**, in press.
4. Mollova, N. and Longevialle, P. *J. Am. Soc. Mass Spectrom.* **1990**, *1*, 238-248.
5. Lefevre, O., Mollova, N. and Longevialle, P. *Org. Mass Spectrom.* **1992**, *27*, 589-596.

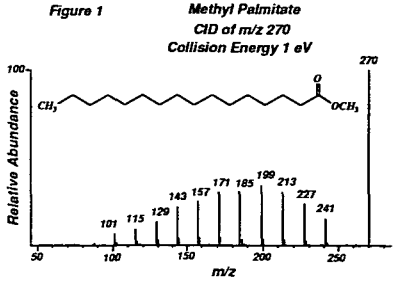

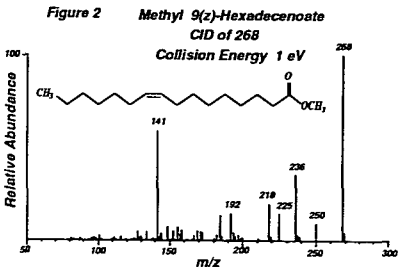

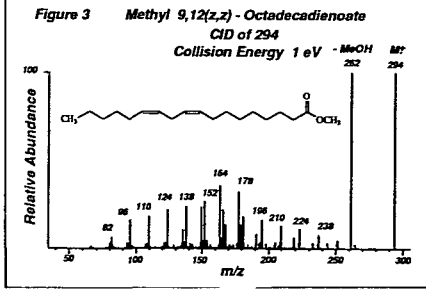

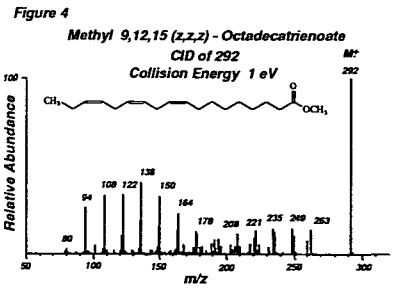

Tandem Mass Spectrometry of Multi-unsaturated Triacylglycerides: Problems and Solutions

L.R. Hogge, S.L. MacKenzie, D.M. Tenaschuk, D. J. Olson and P.J. Brooks*,
National Research Council of Canada, Plant Biotechnology Institute,
Saskatoon, Sask., Canada S7N 0W9
* Scientific Analysis Laboratories, Manchester, England, M3O 0RJ

INTRODUCTION

Angiosperm plants contain complex mixtures of neutral lipids, primarily triacylglycerides, which are used as edible and industrial oils. As part of a seed oil modification project at this Institute, it is necessary to characterize the neutral lipids in the seeds of a variety of these plants.

Currently, the acyl composition of storage lipids is usually extrapolated from fatty acid profiles obtained from trans-methylation experiments, but these experiments reveal little about the structure of the intact neutral lipids. Although gas chromatography/mass spectrometry (GC/MS) has been used for neutral lipid mixtures with some success, preliminary experiments conducted in this laboratory showed that this technique is not useful when the mixture of analytes contain hydroxy-containing fatty acyl components and/or long chains. We have reported a method for the characterization of castor bean neutral lipids (which contain hydroxy-fatty acyl components) using tandem mass spectrometry.

However, when we applied a similar technique to the analysis of triacylglycerides from *Onosmodium hispidissimum*, that are known to contain multi-unsaturated acyl groups without any hydroxy moieties, the CID product spectra of the M^+ ions contained diagnostically important product ions of unexpected *m/z* values.

This report provides a study of the EI and CI (NH_4^+) magnetic scanned spectra as well as the corresponding CID product ion spectra obtained for a set of reference TAGs varying in the degree of unsaturation of the acyl moieties (1 to 4 double bonds) and discusses the usefulness of tandem MS for the analysis of these compounds using these ionisation modes.

EXPERIMENTAL

The triacylglycerides were obtained from Sigma Chemical Company, St. Louis, MO except for the tristearidonin which was synthesized at this Institute. All analyses were done using a VG 70-250 SEQ hybrid mass spectrometer. Samples for EI and CI analysis were introduced (approx. 1 μg) via the solids probe (heated ballistically to 320° C). The source temperature was maintained at 250° C. Magnetic scanned spectra (both EI and CI) were obtained by scanning from *m/z* 1300 to 130 at a rate of 5 sec/decade. Collision induced dissociation product ion spectra were obtained by fragmenting the EI molecular ion or the CI $[M+NH_4]^+$ ion and scanning the quadrupole analyser from *m/z* 100 to 1000 in 7 sec. Xenon was used as the collision gas at a pressure of 9 X 10^{-5} torr. The collision energy was 16 eV (laboratory frame).

RESULTS AND DISCUSSION

Four reference TAGs, *triolein, trilinolein, trilinolenin and tristearidonin*, each varying in unsaturation by one double bond per acyl group, were chosen for this study. The ions $[M-RCOO]^+$ and $[RCO+74]^+$ were considered to be the most important for diagnostic purposes. In the EI magnetic scanned spectra these diagnostic fragment ions occur at the expected *m/z* values in all the spectra except that of tristearidonin. The $[RCO+74]^+$ ion in this spectrum is expected at *m/z* 333 but the only significant ion in this region of the spectrum appears at *m/z* 335.

Furthermore, the collision induced dissociation (CID) product ion spectra obtained from the EI molecular ions only show the correct diagnostic ions for the triolein. In the other spectra, the $[M-RCOO]^+$ ions are not observed and the $[RCO+74]^+$ fragments appear 2 mass units higher than expected (data not shown).

The reference compounds were studied under Fast Atom Bombardment (FAB) and ammonia CI conditions to determine if the same structural rearrangements were observed under the more gentle ionization processes. Although FAB spectra were obtained for these compounds, the protonated molecular ions were of such low intensity that it was impossible to obtain the corresponding CID product ion spectra. The ammonia CI magnetic scanned spectra for the 4 reference compounds showed the diagnostic ions, $[M-RCOO]^+$ and $[RCO+74]^+$ at the expected m/z for each compound. More importantly, the corresponding CID product ion spectra of the $[M+NH_4]^+$ ions (Fig. 1) also showed the expected diagnostic ions.

Therefore, characterization of mixtures of TAGs can be accomplished by subjecting the $[M+NH_4]^+$ ions to CID and studying the product ion spectra. The $[M-RCOO]^+$ and $[RCO+74]^+$ ions in these spectra provide much more reliable structural information than do similar ions in CID product ion spectra derived from EI molecular ions.

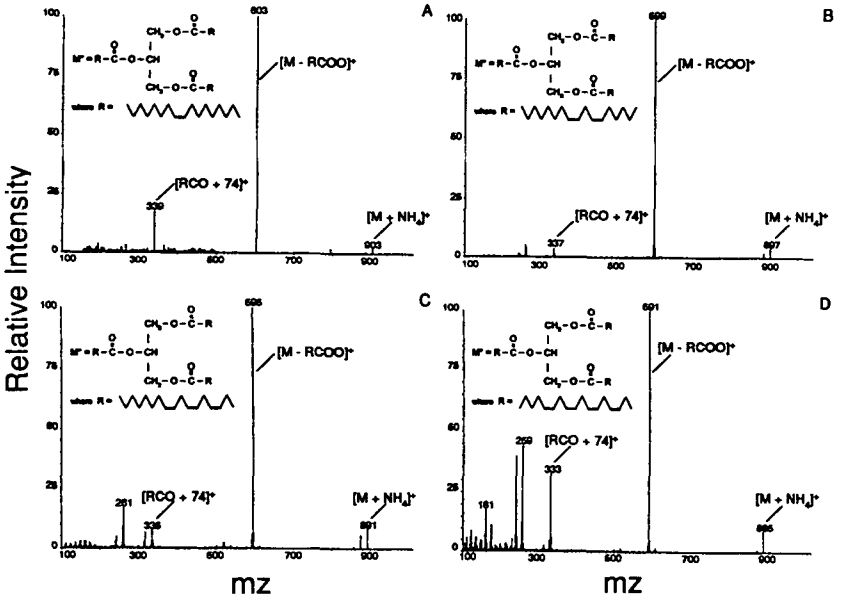

Figure 1

CHARACTERIZATION OF DAIRY TRIGLYCERIDES ISOLATED USING SUPERCRITICAL FLUID FRACTIONATION BY FIELD DESORPTION, DESORPTION CHEMICAL IONIZATION, AND TANDEM MASS SPECTROMETRY

George Spanos, Steven J. Schwartz, and Richard B. van Breemen
Departments of Food Science and Chemistry
North Carolina State University, Raleigh, NC 27695

Although bovine milk fat is a major product of the the dairy industry, its consumption in developed countries has been decreasing due to consumer concern over the high content of saturated fatty acids and cholesterol. In order to expand the desirability and utilization of bovine milk fat, a continuous supercritical carbon dioxide extraction method was developed to isolate milk fat fractions with varied physical properties and triglyceride content. Surprisingly, the triglyceride composition of bovine milk fat has never been determined. Therefore, an HPLC method was also developed to separate as many triglycerides as possible for collection and mass spectrometric identification.

METHODS

Supercritical Fluid Fractionation. Butter oil was donated by Danish Maid Butter Co. (Chicago, IL). Fractionation of butter oil was carried out using a Newport Scientific Inc. (Jessup, MD) continuous supercritical fluid extraction system. Supercritical CO_2 at a flow rate of 12-17 L/min, 900 L/fraction (1 atm, 25°C) was used to sequentially extract a 15g butter oil sample as follows: 1500 psi at 40°C; 2200 psi at 40°C; and 3600 psi at 40°C. Extracts were condensed from depressurized CO_2 in a U-shaped tube.

HPLC. Three Waters Model 510 and 501 HPLC pumps were used with two C18 HPLC columns (Spherisorb and Zorbax), each 25 cm x 4.6 mm, in tandem at a flow rate of 0.7 mL/min. A gradient was used from acetonitrile to propionitrile over 50 min, followed by a second gradient to methylene chloride over 70 min. 900 µg milk fat was injected per analysis. A Varex evaporative light scattering detector was used to monitor elution of triglycerides, which were collected for mass spectrometric analysis.

Mass Spectrometry. Positive ion mass spectra were obtained using a JEOL HX110HF double focusing mass spectrometer equipped with a DA5000 data system. The resolving power was 1,200 for all analyses. Field desorption (FD) mass spectra were acquired using a silicon emitter loaded with approximately 1 µg of supercritical fluid extract. Desorption chemical ionization (DCI) was carried out using isobutane reagent gas and an ion source temperature of 150°C. Approximately 0.5 µg HPLC-purified triglyceride sample was loaded on the DCI filament per analysis. The DCI Filament was heated at 0.25 mA/min. Tandem mass spectrometric measurements were carried out using DCI ionization, and B/E linked scanning with CAD of protonated molecule precursors.

RESULTS

Field desorption mass spectra of each butter oil supercritical fluid extract showed the average molecular weight and mass distribution of the constituent triglycerides. Using reversed phase HPLC with an evaporative light scattering detector, 58 triglyceride peaks were collected, which were then analyzed using DCI mass spectrometry and DCI MS/MS. For example, the positive ion DCI mass spectrum of HPLC Peak 15 is shown in Figure 1. Two different triglycerides were detected in Figure 1 with $[M+H]^+$ ions at m/z 639 and 665. The B/E linked scan of m/z 639 is shown in Figure 2. Fragments ions at m/z 578, 409 and 383 identify this triglyceride as 4,14,18:1.

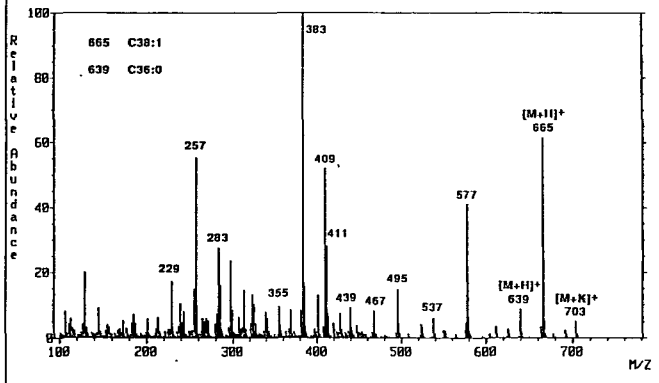

Figure 1.

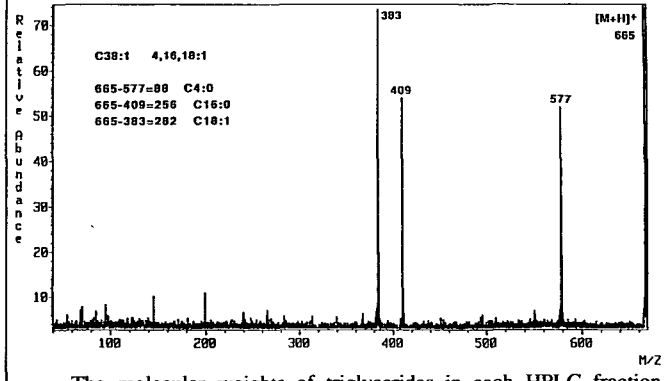

Figure 2.

The molecular weights of triglycerides in each HPLC fraction were determined from $[M+H]^+$ ions in DCI mass spectra. Fragmentation facilitated the identification of fatty acid content of each isolated triglyceride. When HPLC fractions contained triglyceride mixtures or impurities, MS/MS analyses facilitated fatty acid identification. These results are the first identification of the most abundant triglycerides in milk fat.

Analysis of Bull Sperm Plasma Membrane Phosphatidylcholines by Negative Ion FAB-CAD-MS/MS.

T. Tighe, B. Minard, J. Nolan, R.H. Hammerstedt, Departments of Chemistry and Molecular and Cell Biology, Penn State University, University park, PA 16802; D. Fabris, Department of Chemistry and Biochemistry, University of Maryland Baltimore County, Baltimore, Maryland 21228.

The ultimate goal of this research is to better understand the molecular level changes that occur in sperm cells as they mature and become viable after passage through the epididimus. Specifically, changes occur in the biochemical make-up of the cell membrane that allow penetration of the egg cell wall. The phospholipid composition is altered in the process. In order to study these complex compositional changes, an analytical method that is sensitive, universal, and provides structural insight is absolutely essential.

Phosphatidylcholines (PCs) were isolated from the lipid fraction of the plasma membrane removed from the arcosomal region of bull sperm.[1] The phosphatidylcholine fraction was analyzed by FAB-MS, HPLC-Flow FAB-MS, and FAB-MS/MS. Negative-ion FAB-MS/MS with high-energy collisions (CAD) was used to identify the length and position of the fatty acyl side chains. FAB-MS/MS of the $[M-15]^-$, $[M-60]^-$ and $[M-86]^-$ parent ions showed that the major components in the phosphatidylcholine fraction were 1-O-alk-1'-enyl-2-acyl glycerophosphocholines (plasmalogens), specifically $C_{16:0}/C_{22:6}$ plasmalogen and $C_{16:0}/C_{22:5}$ plasmalogen.

METHODS

Isolation of Sperm Cell Membrane Phospholipids was by published methods[2,3]. Normal phase HPLC was used to separate the phospatidylcholine The column used to separate the bull sperm plasma membrane lipids was a 25cm x 10mm id 5 micron silica prep column (Supleco). An isocratic mobile phase, $CH_3CN/MeOH/H_2O$ (50:45:6.5 v/v/v), flowed at 2mL/min. The UV detector was set at 208 nm. The PC fraction was isolated and frozen under N_2.

Probe (-) FAB-MS: Triethanolamine (Sigma Chemical Co., St. Louis, MO) matrix (1-2 uL) was applied to the copper probe tip followed by 2 µL bull sperm plasma membrane phospholipids in chloroform. The matrix and sample were then mixed on the probe target The FAB gun was operated with xenon gas at 4-6 KeV and a beam current of 40-60 µA. A Kratos MS50 RFA double focusing mass spectrometer was operated at a 4 kV accelerating potential and an resolving power of 1000. The mass range m/z 130-1600 was scanned at 10 sec/decade and acquired by a KRATOS DS90 system.

Tandem Mass Spectrometry[4] Negative FAB-MS of plasma membrane phosphatidylecholines (PC) from bull sperm was performed on the first two sectors (EB) of a Jeol HX110/HX110 mass spectrometer (Tokyo, Japan) at an accelerating voltage of 10kV, 100-Hz filtering, a resolution of 1000, a scan rate of 1.5 min./scan and a mass range of m/z 0-1000. The FAB gun was operated at 6kV with xenon. Spectra were recorded with a Jeol DA5000 data system. Negative FAB-MS/MS was performed on the same PC sample by using all four sectors (EBEB) on the Jeol HX110/HX110. Precursor ions were mass selected on the MS1 at a resolution of 1000 and linked B/E scans were made in MS2. Collision-induced dissociation (CID) occurred in the third field free region, with helium used as the collision gas. The CID spectra were recorded at a resolution of 1000. Triethanolamine was used as the matrix.

RESULTS AND DISCUSSION

It has been shown[5,6] that PCs do not give $[M-H]^-$ anions, but reveal a trio of characteristic fragment ions: $[M-H-CH_3]^-$, $[M-H-HN(CH_3)_3]^-$ and $[M-H-CH_2{=}CHN(CH_3)_3]^-$. However, while this information is present in the (-) FAB-MS spectra of PCs, the complexity of the sample and resulting spectra make it impossible to correctly determine the individual PC species. In order to do this, we have tried both HPLC-Flow FAB-MS and FAB-MS/MS. The LC-MS method proved to be quite difficult and non-reproducable, whereas, considerable information was obtained by tandem MS methods in a very short amount of time.

CID tandem MS was carried out on prominant ions derived from two components with molecular weights of **790** and **806**. The corresponding negative pseudomolecular ions $(M-H)^-$ at **789** and **805**

are very low abundance, and rapidly eliminate fragments of the choline moeity to give fragment ions774, 729, 703, 790, 745, 719. The MS-CID-B/E linked scan MS spectra of the six ions above (in bold) were recorded and their interpretation is given in the figures to the right.

The predominant species (MW **790**) gave a very strong spectra that were readily interpretable and very consistent with a plasmalogen PC that had a $C_{16:0}$ alkenyl group at position 1 and a $C_{22:6}$ acyl group at position 2.

MS/MS spectra of the three ions derived from MW 806 species were much more complex and can be interpreted in terms of at least four species being present: two diacyl species ($C_{16:0}/C_{22:6}$ and $C_{16:1}/C_{22:5}$) and two plasmalogens that appeared to have oxidized C_{22} side chains.

On the basis of these results, the single MS-FAB data was rationalized as shown in the table below:

Bull Sperm Plasma Membrane PCs -- Negative Ion FAB-MS Data

$(M-H)^-$	R1	R'1	R2	$[(M-H)^--15]$	$[(M-H)^--60]$	$[(M-H)^--86]$	Comment
835	$C_{18:0}$		$C_{22:5}$	820*	775(56)	749*	
833	$C_{18:0}$		$C_{22:6}$	818*	773(16)	747(12)	
805	$C_{16.0}$		$C_{22.6}$	790(16)	745(19)	719(16)	MS/MS analysis
805	$C_{16:1}$		$C_{22:5}$	790(16)	745(19)	719(16)	→ mixture of normal PCs &
805		$C_{16.0}$	$C_{22:7}O^?$	790(16)	745(19)	719(16)	oxidized
805		$C_{16\,0}$	$C_{22\,6}O$	790(16)	745(19)	719(16)	plasmalogens
803	$C_{16:1}$		$C_{22.6}$	788(16)	743(12)	717(16)	
791		$C_{16:0}$	$C_{22.5}$	776(88)	731(78)	705(66)	Plasmalogen
789		$C_{16:0}$	$C_{22.6}$	774(100)	729(78)	703(75)	MS/MS → Plasmalogen
787	$C_{18:0}$		$C_{18.1}$	772(19)	727(16)	701(16)	
775	$C_{14:1}$		$C_{22:6}$	760(12)	715(9)	689(9)	
761	$C_{16:0}$		$C_{18.0}$	746(12)	701(16)	675*	
759	$C_{16:0}$		$C_{18:1}$	744(12)	699*	673*	
747		$C_{16:0}$	$C_{18.0}$	732(41)	687(12)	661*	Plasmalogen
745		$C_{16\,0}$	$C_{18.1}$	730(44)	685*	659*	Plasmalogen

Numbers in ( ) are % intensities relative to m/z 774 [JEOL data] *Mass not present

REFERENCES

[1]Parks, J.E. and Hammerstedt, R.H., *Biology of Reproduction* 32, 653-668 (1985).

[2]Parks J.E., Hammerstedt R.H. *Bio.Reprod.* 32, 653-668, 1985.

[3]Folch J., Lee M., Sloane-Stanley G.H., *J. Biol. Chem.* 226, 497-509,1957.)

[4]Work done at the Center for Structural Biochemistry, University Maryland, Baltimore. Bryant, D.K.; Orlando, R.C.; Fenselau, C.; Sowder, R.C.; Henderson, L.E. *Anal Chem* 1991, 63, 1114-1118.

[5]Jensen, N.J., Tomer, T.B.;Gross, M.L. *Lipids* 1986, 21, 580-588; Munster, H.;Stein, J.;Budzikiewicz, H. *Biomed. Environ. Mass Spectrom.* 1986, 13, 423-427)

[6]Hayashi, A., Matsubara, T.,Morita, M.,Kioshita, T.,Nakamura, T. J. *Biochem.* 1989, 106, 264-269.; Munster, H.; Stein, J .;Budzikiewicz, H. *Biomed. Environ. Mass Spectrom.* 1986, 13, 423-427

ACKNOWLEDGEMENTS

T.T., R.M., J.N., and R.H. are very grateful to Dr. D. Fabris and Dr. Catherine Fenselau, Department of Chemistry and Biochemistry, University of Maryland, Baltimore for their very gracious assistance with the FAB-MS/MS analysis.

Characterization of Oxidized Phospholipids Using Fast Atom Bombardment Tandem Mass Spectrometry

Kathleen A. Kayganich-Harrison and Robert C. Murphy
National Jewish Center for Immunology and Respiratory Medicine
Denver, CO 80206

Generation of oxygen free radicals in vivo results in peroxidation of polyunsaturated fatty acids esterified in phospholipids. This damages cellular membranes and may also produce biologically active molecules from membrane phospholipids. Peroxidation of endothelial cells has been shown to produce modified glycerophosphocholine (GPC) that activates human neutrophils through the platelet activating factor receptor (Patel, K.D. et al, J. Biol. Chem., 267:15168-15175 (1992). Smiley, P.L. et al, J. Biol. Chem., 266:11104-11110 (1991)). However, the exact identity of the bioactive component(s) has not been determined. The analytical characteristics of oxidized phospholipids are largely unstudied. We are using Cu(I)/H_2O_2 to initiate oxidation of 1-palmitoyl,2-arachidonoyl GPC (PAGPC) in order to determine the FAB and CID characteristics of oxidized phospholipids. Oxygen radicals such as superoxide anion and hydroxyl radical can easily abstract an allylic proton or react directly with the pi bonds in arachidonoyl-GPC. Several types of oxidation products can be obtained, as shown in Scheme I. The FAB and CID characteristics of some of the oxidation products were quite different from those of non-oxidized GPC.

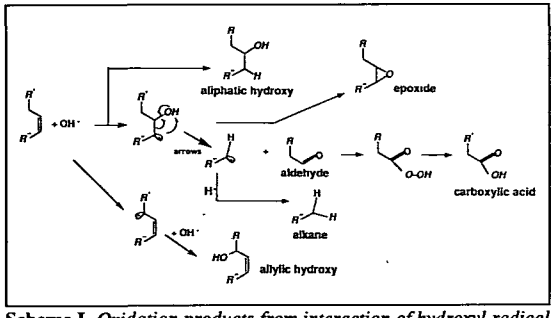

Scheme I *Oxidation products from interaction of hydroxyl radical with unsaturated lipids.*

Methods

Oxidation of PAGPC. PAGPC (2 mg) and 2 μCi of palmitoyl-[1-^{14}C]-arachidonoyl GPC was suspended in 1 ml of distilled water to form liposomes. $CuCl_2$ (100 uM) and hydrogen peroxide (70 mM) were added for 24h. Oxidations of palmitoyl-linoleoyl GPC and $^2H_9$ PLGPC were carried out identically.

Synthesis of $^2H_9$-GPC- 16:0/nonanedioyl-$^2H_9$-GPC was synthesized by treating 16:0/18:2 glycerophosphatidylethanolamine with $^2H_3$-methyl iodide for 50 min, followed by oxidation as described above.

Reverse-phase HPLC- products of PAGPC oxidation were separated using a Beckman 5 micron ODS (4.6mm x 25cm) column eluted at a flow rate of 1.5ml/min for 50 min with methanol:water, 1 mM ammonium acetate, pH 7 (85:15) The gradient was increased to 100% methanol over 40 min. Phospholipids were extracted from HPLC fractions by addition of $CHCl_3$ and water to each fraction (1:1:1,v/v/v).

Mass Spectrometry- FAB/MS (6kV xenon) was carried out on a Finnigan MAT TSQ70B triple quadrupole mass spectrometer. For CID the second quadrupole was pressurized with ca. 0.5 mTorr argon. Collision offset energy was 30eV (E_{lab}). Diethanolamine was used for the FAB liquid matrix.

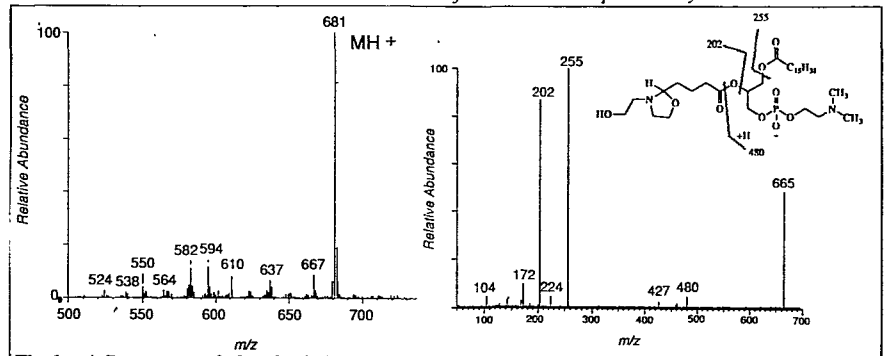

Fig 1. *a) Precursors of phosphocholine ion (m/z 184) in HPLC fraction (13-14 min) from oxidized PAGPC. The odd m/z 681 could arise from reaction with the diethanolamine liquid matrix. b) Negative product ions of m/z 665 [M-CH$_3$]$^-$. M/z 202 corresponds to the carboxylate anion from the sn-2 substituent. Reaction of an ω-aldehyde could result in an oxazole as shown, which would account for the odd m/z and the 87u increase.*

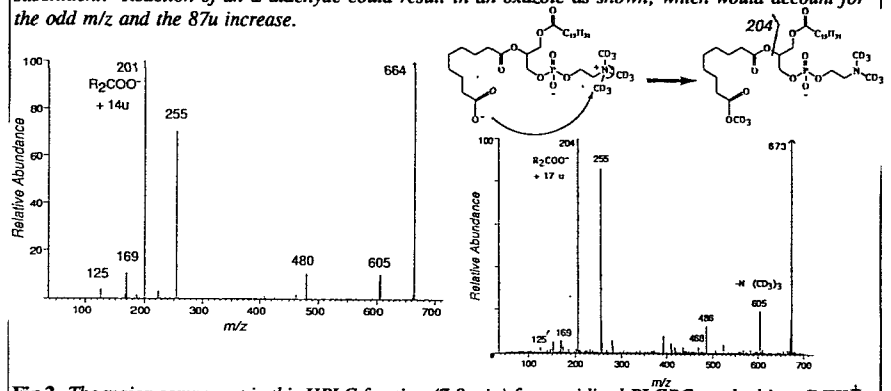

Fig 2. *The major component in this HPLC fraction (7-8 min) from oxidized PLGPC resulted in a [MH]$^+$ ion at m/z 666 and a [M-H]$^-$ at m/z 664. Normally GPC forms [M-CH$_3$]$^-$ ions. This product must possess another ionizable site, such as an ω-carboxyl. a) The CID of m/z 664 results in an sn-2 carboxylate anion that is 14 u higher than expected. b) CID of m/z 673, [M-H]$^-$, from palmitoyl-nonanedioyl-$^2H_9$-GPC shows that this increase is the result of transfer of one of the N-methyl groups to the ω-carboxy of the sn-2 substituent.*

Conclusion - FAB/MS and CID of oxidized phospholipids obtained from Cu(I) /H_2O_2 oxidations of PAGPC and PLGPC suggest that aldehydic compounds form covalent derivatives with the diethanolamine FAB matrix. This can be used to confirm the presence of this functional group. In FAB of oxidized phospholipids having an esterified dicarboxylic acid, [M-H]$^-$ formation is favored over the [M-CH$_3$]$^-$. Also, a methyl group is transferred from choline to the ω-carboxy of the sn-2 substituent resulting in an ω-methylated carboxylate anion.

Thermospray LC/MS Analysis of Phospholipid Molecular Species in Rat Brain Mitochondria

Y. C. Ma and H. Y. Kim, Section of Mass Spectrometry, LMBB, NIAAA, NIH, Bldg. 10, Room 3C-102, 9000 Rockville Pike, Bethesda, MD 20892

Conventional methods of analyzing phospholipid molecular species involve isolation of individual phospholipid classes by either thin layer chromotography (TLC) or HPLC followed by separation of each molecular species using reversed-phase HPLC or argentation TLC. Separated molecular species then have to be identified by GC analysis after transmethylation. The multiple processes are time consuming and results in less accurate analysis. Previous studies (1,2) have shown that with filament on thermospray ionization, phospholipids give simple and characteristic fragment ions which can be used to identify the head group and the constituent fatty acids. In this study, we use thermospray LC/MS to determine the major phospholipid molecular species in rat brain mitochondria. Partial quantification was performed using selected ion monitoring (SIM) in the presence of 18:0d_{35} 20:4-phosphatidylethanolamine (PE) as an internal standard.

Rat brain mitochondria were isolated using sucrose gradient method and the lipids were extracted according to Bligh & Dyer (3). Extracted lipids were dried under nitrogen, redissolved in chloroform, and analyzed using an Extrel ELQ-400 mass spectrometer coupled with a Hewlett-Packard 1050 LC system via a Vestec thermospray interface. Typical analysis conditions were the following: Injection amount: approximately 5 ug of mitochondria phospholipid mixture for SIM. HPLC column: EM Supersphere C18 (4.6 mm i.d. x 12.5 cm, 5 u). Flow rate: 1 mL/min. Mobil phase: 1% NH_4OH in water: hexane:1% NH_4OH in methanol, changing from 10:0:90 to 0:10:90 in 20 min after holding at the initial composition for 3 min. Post-column addition: 2% acetic acid in water at 0.1 ml/min. Vaporizer tip temperature: 200 °C. Source block temperature: 250 °C.

Thermospray LC/MS is a powerful tool for studying phospholipid molecular species. With proper internal standards, both qualitative and quantitative results can be obtained within relatively short time. In this study, the diglyceryl fragment ions were monitored selectively because they were usually the base peak in the spectra and also provided the molecular species information (1,2). Figure 1 shows SIM trace and the relative intensities of the major diglyceryl fragment ions found in rat brain mitochondria, including the diglyceryl fragment ion trace of 1 ug of the internal standard, 18:0d_{35} 20:4-PE. The most abundant phospholipids were 16:0 16:0-PC, 16:0 18:1-PC, 18:0 22:6-PE and 18:0 20:4-PE. Some minor species observed include 16:0 16:1-, 16:0 20:4-, 16:0 22:6-, 18:0 18:1-, 18:0 20:4-, and 18:0 22:6-PC, 16:0 18:1-, 16:0 20:4- and 18:0 18:1-PE, 16:0 18:1- and 18:0 22:6-PS, 16:0 18:1- and 16:0 20:4-PI. Standard calibration of 18:0 18:1-, 18:0 20:4- and 18:0 22:6-PE with 1 ug of 18:0d_{35} 20:4-PE showed a linear response in 20 ng to 1 ug range. Above 1 ug, however, nonlinear calibration curve was observed (Figure 2). With these calibrations, the amount of 18:0 22:6 PE, 18:0 20:4 PE, and 18:0 18:1 PE injected were estimated to be 1.62, 1.48, and 0.15 ug respectively. Using this technique, the effect of ethanol in the composition of phospholipid molecular species as well as decarboxylation of PS to PE in mitochondria is now under investigation.

REFERENCES:

(1) H.-Y. Kim and N. Salem, Jr. *Anal. Chem.* **1986**, 58, 9-14.
(2) H.-Y. Kim and N. Salem, Jr. *Anal. Chem.* **1987**, 59, 722-726.
(3) E. G. Bligh and W. J. Dyer, *Can. J. Biochem. Physiol.* **1959**, 37, 911-917.

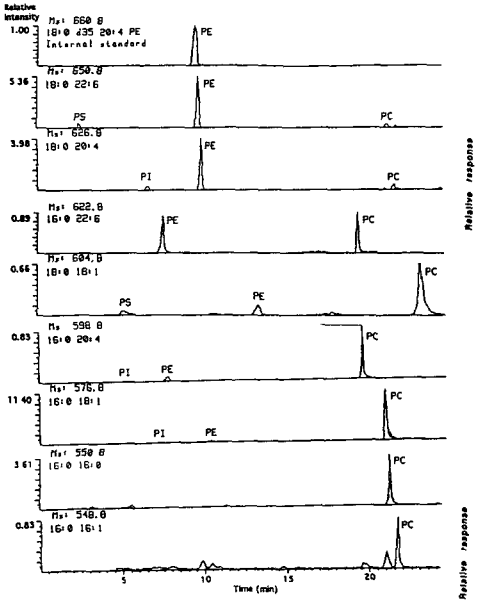

Figure 1. SIM trace of major diglyceryl fragment ions from rat brain mitochondria

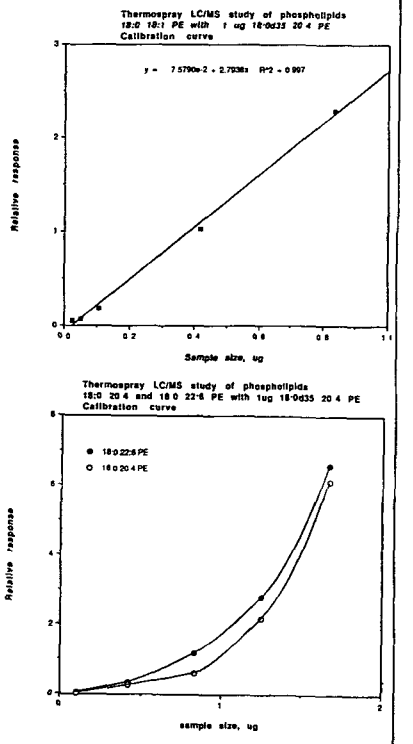

Figure 2. Standard calibration curves using 1 ug 18:0d_{35} 20:4-PE as an internal standard.

Positive Ion LSIMS and Four-Sector Tandem Mass Spectrometry of Aminophospholipids Using Scanning-Array Detection

Su Chen and Peter. J. Derrick, Institute of Mass Spectrometry and Department of Chemistry, University of Warwick, Coventry CV4 7AL, UK

INTRODUCTION

Structures and functions of aminophospholipids in biological system have been widely reviewed. In recent years, studies on the characterisation of the phospholipid molecular species by LSIMS (FAB) coupled to tandem mass spectrometry have been reported. Experiments were performed mostly by negative ion mode since this method can provide structural information including the molecular mass of the species, the characterisation of the polar-head groups, the composition of the fatty acyl chains and the positions of the chains esterified to the glycerol backbone. In this presentation, we report the identification of aminophospholipids (phosphatidyl-serine and -ethanolamine as well as their lyso derivatives) by positive ion LSIMS combined with high-energy collisionally induced dissociation (CID) and four-sector tandem mass spectrometry of $[M+H]^+$ ions of the molecular species of the four classes.

EXPERIMENTAL

Tandem mass spectrometric analyses were performed on a CONCEPT II HH four-sector mass spectrometer (Kratos Analytical Ltd., Manchester, UK) of BEBE configuration. The ion source of MS-I was operated at an accelerating voltage of 8 kV, ionized by a liquid caesium gun with 15 keV translational energy. The experiments were controlled by MACH3 system. The sample was dissolved in chloroform/methanol/water (58/4/0.2), and this solution was transferred to the surface of diethanolamine, used as liquid matrix, without mixing (1). All GPE and GPS molecular species were prepared by the described methods (2). LysoPS and LysoPE were obtained by the treatment of phospholipase A_2.

RESULT and DISCUSS

Fig.1 shows the CID MS/MS spectrum of the $[M+H]^+$ ion of LSIMS of GPE 16:0-18:2. The ion at m/z 575 is formed by the loss of the polar-head group from the species (Scheme 1). The two fatty acids can be detected by the presence of three pairs of fragment ions (ions c,d and e; see Scheme 1), and the location of the chains esterified to the glycerol backbone can be identified by the significant intensity differences of C_1 and C_2 ions, at m/z 307 and 283. Plasmalogen-PE and -LPE are characterised by the absence of the peaks due to the cleavage occurred at the sn-1 position in the spectra (see Scheme 2; spectra not shown). Fig. 2 exhibits the CID MS/MS spectrum of the $[M+H]^+$ ion of LSIMS of GPS 18:0-18:1. The loss of phosphoserine from the molecule gives an ion at m/z 605. Signals due to b, c and d cleavages (Scheme 3) are structurally informative for the analysis of the fatty acid chains. However, abundances of the three pairs of ions show opposite ratio, relative to the GPE 16:0-18:2. This phenomenon was also found for the negative ion CID MS/MS of $[M-H]^-$ ion of LSIMS of GPS. It presumably relates to the diversity of the kinetic energy of the chosen precursors (3). The hypothesis advanced here is that the $[M+H]^+$ "fragment ion" of the GPS species is derived from a solvated protonated molecule, $[M+H+DEA]^+$ ion (4). This is evident by the presence of identical patterns of ions resulting from the MS/MS analyses of glycerophosphatidic acid precursors, the fragmentation of glycerophospholipids (2). Scheme 4 shows the cleavage mode of LysoPS species.

REFERENCES

1) Chen S., Benfenati E., Fanelli R., Kirschner G., and Pregnolato F., *Biomed. Environ. Mass Spectrom.* 1989, 18, 1051.
2) Chen S., Catinella S., Curcuruto O., Traldi P., and Menon G., *Bio. Mass Spectrom.*.1992, 21,65.
3) Ballard K. D. and Gaskell S. J., *J. Am.Soc.Mass Spectrom.* 1992, 3, 644.
4) Chen S., Kirschner G., and Traldi P., *Anal. Biochem.* 1990, 191, 100.

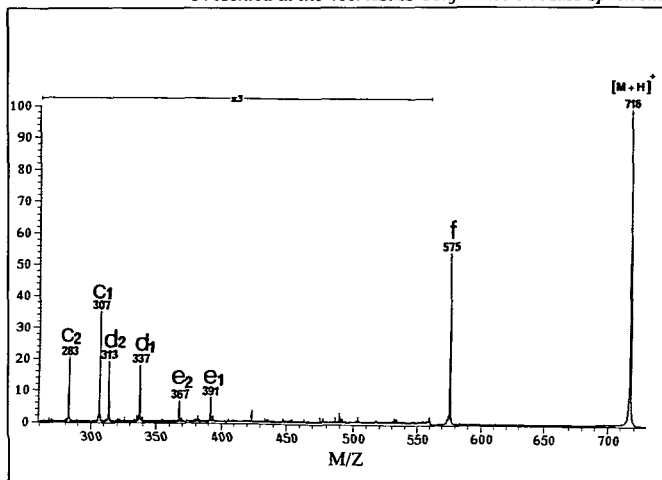

Figure 1 Positive Ion CID MS/MS of $[M+H]^+$ ion of LSIMS of GPE 16:0-18:2.

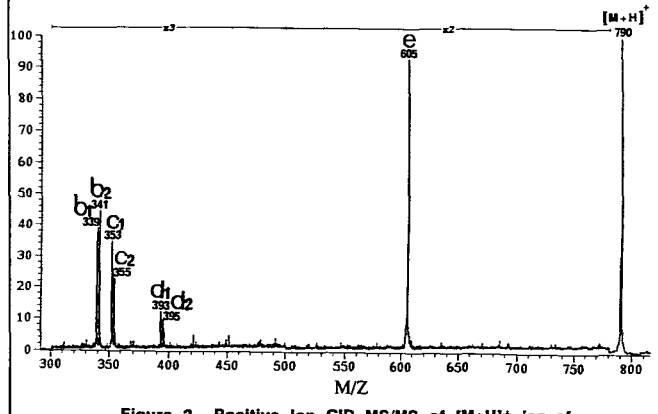

Figure 2 Positive Ion CID MS/MS of $[M+H]^+$ ion of LSIMS of GPS 18:0-18:1.

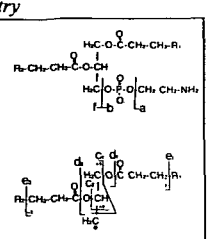

SCHEME 1

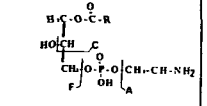

SCHEME 2

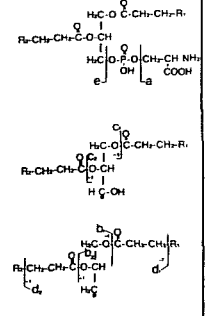

SCHEME 3

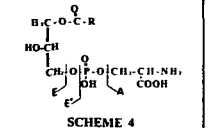

SCHEME 4

Characterisation of glycolipids and sphingolipids by matrix-assisted laser desorption.

D. J. Harvey

Glycobiology Institute, Department of Biochemistry, University of Oxford, South Parks Road, Oxford OX1 3QU, UK.

Introduction.
Lipids have received less attention than other compound types as targets for matrix-assisted laser desorption although a recent report[1] demonstrates the production of good spectra from gangliosides using matrices such as 2,5-dihydroxybenzoic acid (2,5-DHB). This paper examines qualitative and quantitative aspects of several matrices for glyco- and sphingolipids.

Experimental.
Lipids were obtained from commercial sources. Samples were prepared by mixing the lipid (1 - 100 pmol), dissolved in methanol or methanol:chloroform with the matrix solution (1 µl, 50 nmol) on the mass spectrometer target and allowing it to dry at room temperature. Samples with 2,5-DHB as the matrix were further crystallised with ethanol (0.2 µl). Spectra were acquired with a Finnigan Lasermat mass spectrometer (nitrogen laser, 337 nM). Quantitative data were obtained by averaging the signal from 5 laser shots fired at each of 16 target spots.

Results and Discussion.
Good molecular ions were obtained from all compounds at the low pmol level with α-cyano-4-hydroxycinnamic acid, esculetin or 2,5-DHB showing the best matrix properties. Sinapinic acid usually gave weaker spectra. However, the strongest signals from particular compound types showed a considerable degree of matrix and polarity dependence. Sphingosine, cerebrosides, sphingomyelins, ceramides and galactosyldiglycerides produced the strongest signals from α-cyano-4-hydroxycinnamic acid (Fig. 1) with generally good resolution of individual molecular species (Fig. 2). Sphingosine gave a $\{[M + H]^+$ ion with a prominent loss of ammonia whereas compounds containing sugar residues were generally cationised.

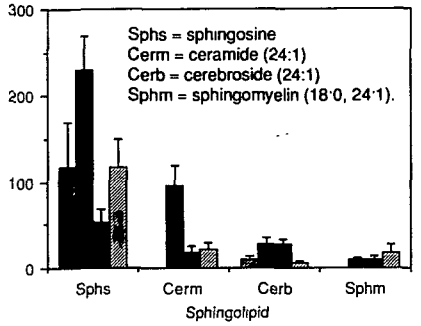

Fig. 1. Responses of sphingolipids (25 pmol) in various matrices.

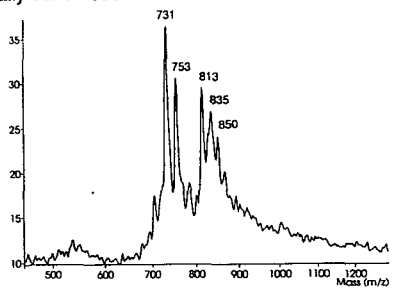

Fig. 2. Molecular ion region of the MALD spectrum (2,5-DHB) of sphingomyelin (10 pmol) from bovine brain. Major peaks are produced by the C-18:0 and 24:1 species.

Monosialylganglioside-M_1 gave a good positive and negative ion signals from 2,5-DHB with the molecular ions corresponding to $[M + Na]^+$ and $[M - H]^-$ respectively. With esculetin and α-cyano-4-hydroxycinnamic acid, fragmentation resulting in loss of sialic acid occurred in the positive ion mode but was absent in the negative ion spectra (Fig. 4).

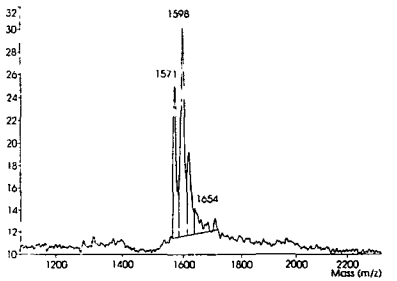

Fig. 3. Positive ion MALD spectrum (2,5-DHB matrix) of monosialylganglioside-G_{M1} (25 pmol) from bovine brain.

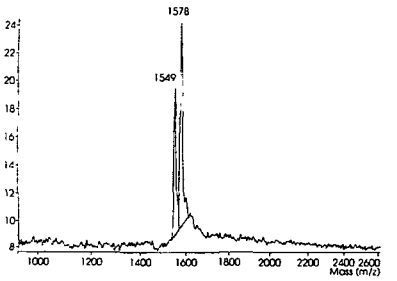

Fig. 4. Negative ion MALD spectrum (esculetin matrix) of monosialylganglioside-G_{M1} (25 pmol) from bovine brain.

Disialylganglioside-G_{D1a} gave similar results. Esculetin and α-cyano-4-hydroxycinnamic acid produced spectra containing, in addition to the molecular ions (mainly $[M + Na]^+$), two broad, unresolved peaks produced by loss of one or both sialic acid groups (Fig. 5). In the negative ion spectra, only one such fragment ion was observed. 2,5-DHB, on the other hand, produced both positive and negative ion spectra that were nearly free of fragment ions (Fig. 6)

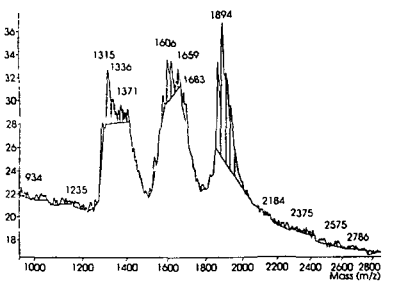

Fig. 5. Positive ion MALD spectrum (α-cyano-4-hydroxycinnamic acid) of disialylganglioside-G_{D1a} (25 pmol).

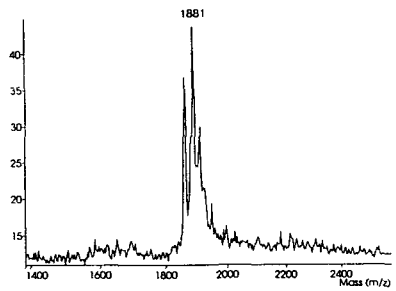

Fig. 6. Positive ion matrix-assisted laser desorption mass spectrum (2,5-DHB matrix) of disialylganglioside-G_{D1a} (25 pmol).

Reference.
P. Juhasz and E. E. Costello, *J. Am. Soc. Mass Spectrom.*, **3**, 785 (1992).

Examination of phospholipids by matrix-assisted laser desorption.

D. J. Harvey

Glycobiology Institute, Department of Biochemistry, University of Oxford, South Parks Road, Oxford OX1 3QU, UK.

Introduction.

Although matrix-assisted laser desorption has been used for examination of many compound types, particularly peptides and oligosaccharides, its utility for lipid analysis has received little attention. This paper presents data on its use for the characterisation of various types of phospholipid using a variety of matrices.

Materials and methods.

Phospholipids were obtained from commercial sources. Samples were prepared by mixing the lipid (0.1 - 100 pmol), dissolved in methanol or methanol:chloroform with the matrix solution (1 µl of a 50 µmol/ml solution) on the mass spectrometer target and allowing it to dry at room temperature. Samples with 2,5-dihydroxybenzoic acid (2,5-DHB) as the matrix were further crystallised on the target with ethanol (0.2 µl). Spectra were obtained with a Finnigan Lasermat mass spectrometer (nitrogen laser, 337 nM) using matrices as described below (obtained from Aldrich Chemical Co. Ltd.,). Quantitative data (100 fmol - 100 pmol) were obtained by averaging the signal from 5 laser shots fired at each of 16 target spots. Methylation was performed by allowing the phospholipid to stand with an excess of an ethereal solution of diazomethane for 15 min. at room temperature.

Results and Discussion.

Phosphatidylcholine, which contained a cationic group, gave very intense signals (M^+) in the positive ion mode (Fig. 1), particularly with α-cyano-4-hydroxycinnamic acid (detection limit 100 fmol) or esculetin as the matrix. These matrices generally proved to be the most satisfactory for the majority of phospholipids tested (Fig. 2). Weaker signals were obtained with 2,5-DHB, 1,4-dihydroxy-2-naphthoic acid and other substituted benzoic acids and coumarins. Phospholipids lacking a cationic site generally gave a mixture of $[M + H]^+$ and $[M + Na]^+$ ions in the positive mode and $[M - H]^-$ ions in the negative spectra. No negative ions were observed with phosphatidylcholines. Where negative ion spectra were produced, these were more satisfactory than the positive ion spectra as molecular weight indicators on account of the absence of sodium adduct ions. However, reduction in the relative abundance of the $[M + Na]^+$ ions in the positive ion spectra could often be achieved by methylation of the phosphate group with an ethereal solution of diazomethane. A good linear response was observed between sample loading and response as shown in Fig. 3 for dilauryl phosphatidylcholine..

Extensive fragmentation occurred with all compounds (see Fig. 1), particularly when α-cyano-4-hydroxy-cinnamic acid was used as the matrix. Fragmentation increased as a function of laser power and was the result of cleavages around the phosphate moiety. This fragmentation produced a prominent diacylglycerol ion which provided information both on the size of the combined acyl chain length and on the nature of the phospholipid (given by the mass loss).

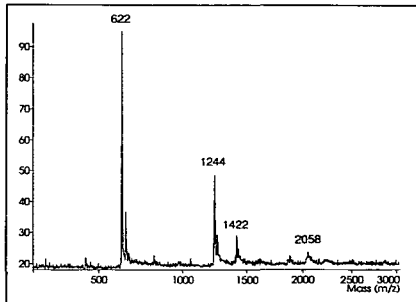

Fig. 1. Matrix-assisted laser desorption mass spectrum (2,5-dihydroxybenzoic acid matrix) of dilauryl phosphatidylcholine (10 pmol).

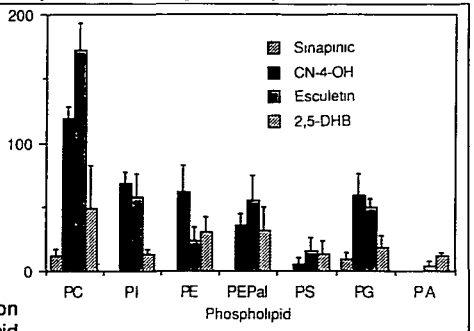

Fig. 2. Relative responses (laser power 25) of phospholipids (25 pmol) in various matrices. Error bars are ± SD of 5 laser shots fired at each of 16 target spots.

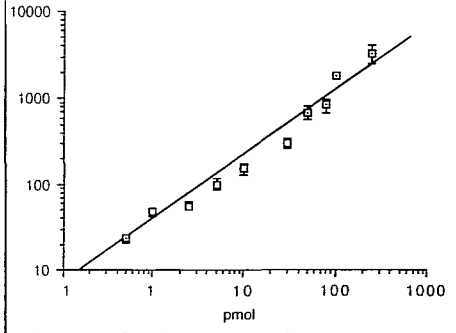

Fig. 3. Graph showing the relationship between sample loading and signal strength for dilauryl phosphatidylcholine in α-cyano-4-hydroxycinnamic acid.

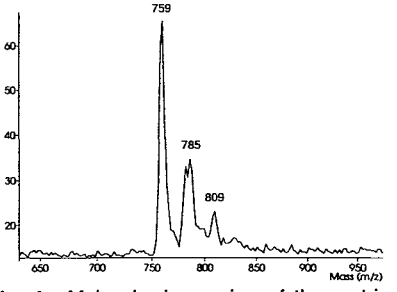

Fig. 4. Molecular ion region of the matrix-assisted laser desorption mass spectrum (2,5-dihydroxybenzoic acid matrix) of di-lauryl-phosphatidylcholine (10 pmol) from egg lecethin.

Phospholipids which had free hydroxy groups, such as phosphatidylinositol and phosphatidylglycerol, tended to form mainly $[M + Na]^+$ ions after methylation of anionic and amino groups with diazomethane. Other phospholipids gave mainly $[M + H]^+$ ions.

In addition to fragmentation, considerable cluster (particularly dimer) formation occurred with many phospholipids. Dimer formation was particularly prominent with phosphatidylcholine, presumably as the result of zwitterion pairing.

Resolution on the TOF instrument was sufficient to resolve many of the molecular species differing in acyl substitution (Fig. 4) but was less satisfactory in assignment of the degree of unsaturation, particularly when adduction with alkali metal ions occurred.

Comparison of Several Contemporary Ionization/Mass Analyzer Techniques for Large Components of Complex Fossil-Derived Materials†

Jerry E. Hunt, Donald E. Drinkwater[a], and Randall E. Winans

Chemistry Division, Argonne National Laboratory, Argonne, IL 60439

[a]Present address Texaco, Inc., Beacon, NY 12508

Introduction

Fossil fuels are a complex mixture of large macromolecular species. Coal- and petroleum-derived samples, therefore, provide a unique mixture for development and comparison of mass spectrometric techniques for high molecular weight analyses. The Argonne Premium Coal samples, a broad array of research grade standards collected, prepared, and stored under controlled conditions, are convenient for assessing classical and novel mass spectrometric techniques. Resiudal compounds from petroleum processing represent complementary high molecular weight materials for such studies. Traditional EI mass spectra of these complex mixtures are dominated by fragment ions and contain little parent molecular ion information.

A number of complementary approaches have been used to investigate fossil fuel-derived materials and model compounds. LD, DCI, and FAB are compared as methods of volatilizing high molecular weight species present in coal and petroleum samples. DCI on a high resolution three-sector tandem mass spectrometer is compared to laser desorption and laser photoionization on a time-of-flight instrument for high mass mixture selectivity.

Experimental

The EI, DCI, and FAB mass spectra were recorded on a Kratos MS 50 triple analyzer. The reagent gas for the DCI studies was isobutane. The solids and extracts were heated in the source on a small platinum wire coil from 200 °C to 700 °C at 100 °C/min. with the source heated at 200 °C. The laser desorption and laser ionization mass spectra were recorded on a linear time of flight mass spectrometer constructed in house. The LDMS spectra were produced by exposing the samples distributed as thin layer on a stainless steel sample holder to laser pulses from either a Nd:YAG or a nitrogen laser. The fluence of the desorption laser is held constant at 10-100 mJ/cm^2 at a repetition rate of 20 Hz. For the prompt ion desorption the laser is operated close to the ionization threshold to minimize fragmentation of the desorbing material. The laser is operated at lower fluences for neutral ion desorption. The neutral molecules are then ionized by vacuum ultraviolet light. The 118 nm laser pulses are produced by third harmonic conversion of 355 nm light from the Nd:YAG laser in a high pressure Kr cell. The flight path is approximately 1.3 m.

Results

Figure 1 shows a broader mass distribution is with FAB than either LD or DCI. where there is a small number of low intensity peaks below m/z=200. The peaks at m/z<200 in the FAB spectra probably result from fragmentation and the matrix (nitrobenzyl alcohol). Several homologous series are observed in the LD and DCI data. Possible structures can be assigned to each of these series based on PyHRMS results from the same coal sample. The prominent series (especially in the LD data) at m/z=230, 244, 258, 272 is assigned to alkyl-pyrenes of fluoranthenes. Another major series contains two different species, alkylphenyl–naphthalenes and alkylhydroxy-pyrenes or fluoranthenes. In contrast, in FAB the major cluster of peaks do not coincide with clusters seen in DCI or LDMS.

At higher masses there is good agreement between all three techniques. Several homologous series appear at these higher masses. A series at m/z=292, 306, 320, 334, 348, 362, 376 is possibly alkylphenylpyrenes. Another series between 306 and 362, form an oxygen containing series with a suggested structure of methylbenzopyrenofuran.

Single photon ionization of neutral molecules desorbed from the sample surface of coal-derived material produce the spectrum shown in figure 2. Coupled with time of flight mass spectrometry, the

spectra exhibit parent ion abundance which conventional 70 eV electron impact lack. The peaks near m/z=800 do not appear in the DCI MS spectra.

Conclusion

The mass spectra show different molecular weight distributions. In general FAB gives the highest molecular weight distribution, while LD, DCI, and EI give progressively lower distributions. Furthermore, the ions present in the LD and DCI spectra are directly comparable, while FAB and EI produce different ion distributions. Information on neutrals is available from PyGC/MS and LD-photoionization/TOF.

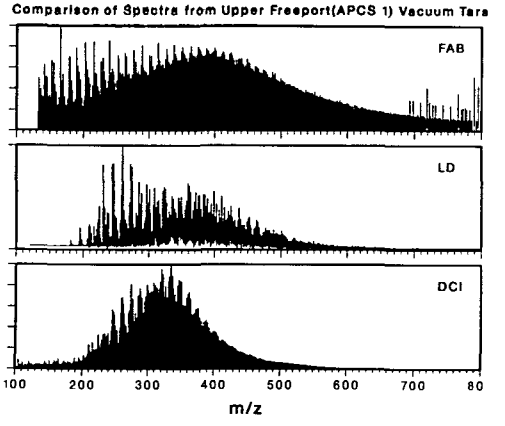

Figure 1. Comparison of FAB, LD, and DCI methods.

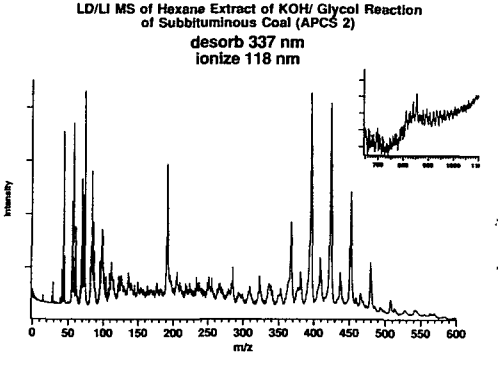

Figure 2. The laser desorption/ laser ionization mass spectrun of coal extract.

†Work supported by the U. S. Department of Energy, Basic Energy Sciences, Division of Chemical Sciences, under Contract W-31-109-ENG-38.

FAB-MS and SIMS Characterization of Polyamic Acid Precursor Formation from BPDA and ODA

J.-P. Wang, Y.-P. Lin, M.-K. Lee, and Y.-C. Ling*

Department of Chemistry, National Tsing Hua University, Hsinchu, Taiwan 30043, R.O.C.

INTRODUCTION Polyimide (PI) synthesized from BPDA (BiPhenyl tetracarboxylic DiAnhydride) and ODA (4,4'- OxyDiAniline) has attracted interest for its process flexibility gained from increasing solubility in organic solvent. The synthesis consists of two reaction steps. First, a soluble, high molecular weight PAA (PolyAmic Acid) is formed. Secondly, the soluble PAA is converted to the PI with the aid of a dehydrating agent. This conversion step affects the property of subsequently prepared PI films in many ways. Hence, a better understanding about PAA formation is crucial to the quality of subsequently produced PI films. This research aims to achieve this goal by using SIMS and FAB-MS to investigate the relationships between the composition of BPDA and ODA reactants, PAA precursor, and PI product.

CHARACTERIZATION All SIMS characterizations were carried out with a CAMECA IMS-4f secondary ion mass spectrometer. FAB-MS characterizations were carried out with a JEOL SX-102A mass spectrometer.

SIMS RESULTS Positive ion SIMS spectra of BPDA and ODA powders are obtained, respectively. In the BPDA spectrum, representative peaks are with m/z ratios of 103, 105, 107, 117, and 152. Peaks with m/z = 113 and 115 are ascribed to the In isotopes. In the ODA spectrum, representative peaks are with m/z ratios of 108 and 199. The peak at m/z = 108 is assigned to $OC_6H_4NH^+_2$, a fragment formed by cleavage of ODA to include the ether oxygen. The peak at m/z = 199 is assigned to $(M-1)^+$ or M^+. Comparing the positive SIMS spectra of PAA and PI,peaks with m/z ratios ranged from 100 to 200 represent characteristic structural fragments. The general appearance of the spectra of PAA and PI are alike. The m/z ranges and intensities of the peaks in PI are narrower and weaker. This is attributed to the increasing hardness in PI after the curing treatments. The sputtering yields are generally lower with harder materials. Peaks with m/z = 115, 117, 119, 153, and 178, which are characteristic of BPDA, appear in both spectra of PAA and PI. We therefore conclude that the surface of PAA and PI are BPDA enriched.

FAB-MS RESULTS In comparison with SSIMS technique, FAB-MS is a bulk analysis technique. In the positive ion FAB-MS spectrum of PAA ,the peaks with m/z = 98, 99, and 100 are from the NMP solvent. Peaks with m/z = 115, 128, 141, 152, 165, 178, and 202 also appear in the SSIMS spectrum of PAA. Other peaks with m/z = 101, 108, 110, 112, 156, 167, 185, 197 do not appear in the SSIMS spectrum of PAA.

Some of them are ascribed to solvents (101, 112, 197) and matrix (185). The remains are equally ascribed to the BPDA (114, 115, 152, 165, 178) and ODA (108, 114, 115, 128, 156). We therefore conclude the bulk of PAA contains equal amounts of BPDA and ODA.

IN-SITU MONITORING OF CURING PROCESS The formation of PI from PAA precursors via curing process was investigated using a home-built FAB probe with heating capability. PAA solutions were placed in the probe which was preheated to 50, 100, 150, 200, 250 and 300 °C. FAB-MS spectra were acquired after the steady-state conditions were observed. Dominant peaks with m/z = 108, 112, 124, 133, 151, 155, 172, 181, and 197 appear in every spectrum. Matrix peaks are not observed because the matrix was not added into the samples. It is noted that the number of fragments decrease with increasing temperature, i.e., peaks with m/z between 400 and 500. It is also noted that the intensity of peak with m/z = 133 decreases with increasing temperature; while that of peak with m/z = 151 shows the reversed relationship. This is expectable because the former fragment comes from the PAA while the later comes from the PI. The degree of imidization increases with higher temperature and therefore fragments from the PI would increase.

ACKNOWLEDGEMENT The financial support by the National Science Council of the Republic of China under grant NSC-82-0208-M-007-101 is gratefully acknowledged.

REFERENCE

1. T. Kaneda, T. Katsura, K. Nakagawa, and H. Makino, J. Appl. Polym. Sci. 32, 3133-3149 (1986).
2. B.N. Eldridge, C. Feger, M.J. Goldberg, W. Reuter, G. J. Scilla, Macromolecules, 24, 3209-3241 (1991).
3. J.-P. Wang, Y.-P. Lin, Y.-C. Ling, Proc. of 1993 Annl. Conf. Chinese Society for Materials Science, 3-43 (1993).

Fig. The FAB-MS spectrum of PAA under 250℃

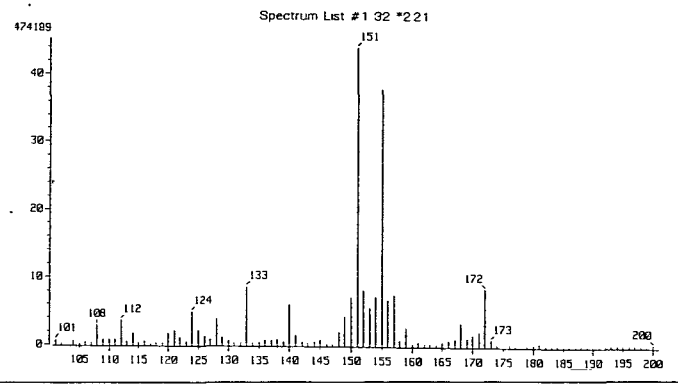

The Detection of Polymer Ions by Matrix-Assisted Laser Desorption/Ionisation Time-of-Flight Mass Spectrometry.

PO. Danis[2] A. Holle[1] D.E. Karr[2], F.J. Mayer-Posner[1] C. Koester[1]
[1]Bruker-Franze.n Analytik GmbH, 2800 Bremen 33, Germany
[2]Rohm and Haas Co., Spring House, Pa 19477, USA

Introduction

The technique of matrix-assisted laser desorption/ionization time -of-flight (MALDI-TOF) has proven to be very powerful for the analysis of biopolymers and synthetic polymers up to a mass range of 10^5 dalton (1-3).
Several investigations of large biopolymers indicate that the dominant detection mechanism is not electron conversion but sputter processes of small surface contaminants of either charge (4,5).
By analyzing a number of synthetic polymers we investigated weather these findings are also applicable to this class of compounds and which kind of the sputtered particles are most suitable for MALDI-TOF analysis. For that purpose we designed a detector which allows the detection of sputtered particles of either charge.
This is achieved by setting the appropriate polarity of the voltage of +/- 5 kV after the conversion dynode. The corresponding particles strike a second conversion dynode and cause another ion-electron- or electron-electron conversion. A successive SEV than provides the analog signal feeding into the data acquisition system.
As opposed to commonly used double channel plate detectors this detector shows no saturation at a high ion current. This prevents a discrimination of high masses which is especially important in the determination of molecular weight distributions of synthetic polymers.

Experimental

Measurements were performed using a Bruker REFLEX™ TOF mass spectrometer. All measurements were performed in the linear mode of the instrument.
A number of polymer standards were analyzed i.e. Polyethylenglycol (PEG 3.4k, 5.0k, 8.0k, 20 k), Polyethylenoxid (PEO 3.0k) and polystyrenesulfonic acid PSSA, 100k. The PEG`s were purchased from Aldrich, Germany , the PEO were provided from MPI für Makromolekulare Chemie, Mainz and the PSSA 100k was purchased from Polymer Laboratories as the neutralized sodium salt of the acids. It than was prepared in the acid form by ion-exchange with a column of Amberlite IRN-77.PEO was dissolved in Chloroform and the PEG`s and the PSSA were dissolved in water with a concentration of about 10 g/l and mixed 1:1 (v/v) with a solution of 1.5 g/l HABA (water : acetonitril ,1:1) as matrix. 2 μl of the mixture was placed on a stainless steel probe tip and air dried.
Ions were produced by a laser desorption at 337 nm (N2-laser, 3 ns, 3 MW/cm2) and accelerated to 15 keV.

Results

The comparison of the mass spectra using the secondary species of opposite charge shows a significant higher detection efficiency for negatively charged particles. Fig. 1-4 shows the mass spectra of PEG recorded by using negatively charged particles (upper spectra) and positively charged ions (lower spectra). Fig. 5 shows the PEO 3k and Fig. 6 the PSSA 100k.

Some of the spectra using negatively charged secondary ions or electrons show a slight shift of the mass centroid of the distribution towards lower masses compared to the mass spectra using positively charged secondary ions. PEO for instance shows a shift of about 10 % (Fig. 5) and PEG (Fig.1-4) a shift of about 1 to 4 %. The PEG measurements do not indicate an increasing shift with increasing mass. The measurement of PSSA (Fig. 6) show a 1 % deviation of the mass centroid.
All the measurement show a significantly higher sensitivity for the detection of negatively charged particles, in favourable cases up to a factor of 20. Fig. 7 shows a comparison of the yield of PSSA 100k . The spectra are sums of 200 single spectra.

Literature

1. F. Hillenkamp, M. Karas, R.C. Beavis, B.T. Chait; Anal.Chem. 63, 1193A (1991).
2. P.O. Danis, D.E. Karr, F. Mayer, A. Holle, C.H. Watson; Org.MassSpectr. 27, 843 (1992).
3. U. Bahr, A. Deppe, M. Karas, F. Hillenkamp; Anal.Chem. 64, 2866 (1992).
4. B. Spengler, D. Kirsch, R. Kaufmann, M. Karas, F. Hillenkamp, U. Giessmann; RapidCommun.MassSpectrom. 4, 90 (1990).
5. J. Martens, W.Ens, K.G. Standings; Proc. ASMS ,348 (1991).

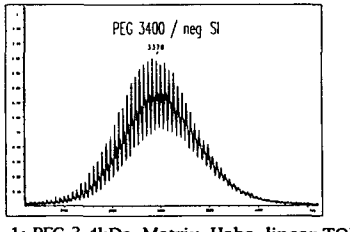

Fig. 1: PEG 3.4kDa, Matrix Haba, linear TOF.

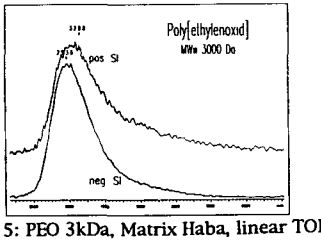

Fig. 5: PEO 3kDa, Matrix Haba, linear TOF.

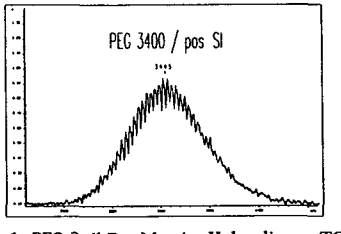

Fig. 1: PEG 3.4kDa, Matrix Haba, linear TOF.

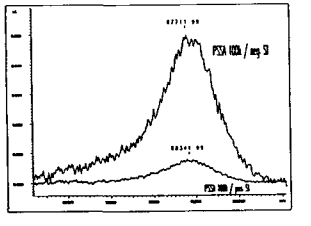

Fig. 6: PSSA 100kDa, Matrix Haba, linear TOF.

RAPID EVALUATION OF POLYMERS USING PARTICLE BEAM/CHEMICAL IONIZATION MASS SPECTROMETRY

Joe M. Wood*, Vistakon Johnson & Johnson Vision Products, Inc.,
P.O. Box 10157, Jacksonville, FL 32247

Ulrich R. Bernier, Jodie V. Johnson and Richard A. Yost,
Department of Chemistry, University of Florida, Gainesville, FL 32611

INTRODUCTION

Mass spectrometry using desorption ionization has become one of the fastest growing techniques for the analysis of low molecular weight polymers. Recent studies using matrix assisted laser desorption ionization (MALDI)[1], fast atom bombardment (FAB)[2], and desorption chemical ionization (DCI)[3] have all demonstrated the power of this methodology. However, these techniques require modest sample preparation and are not suitable for rapid and/or automated sample introduction.

The results presented in this study show that the introduction of polymer samples into a mass spectrometer via a particle beam interface allows rapid evaluation of the samples with results that compare favorably with those obtained using desorption chemical ionization (DCI).

Conventional mass spectra were acquired using both ionization techniques to characterize selected polymers. DCI was employed for MS/MS analysis acquiring both parent and product-ion spectra. Multiple ion monitoring using particle beam/CI was used to demonstrate that both qualitative and quantitative information can be derived in a short period of time with a large sample throughput.

EXPERIMENTAL

Polyethylene glycols (PEG), polypropylene glycols (PPG) and polystyrene (PS) were examined in this study. For particle beam/CI analysis solutions of these samples were injected into an HPLC with no column and introduced into a TSQ-70 triple quadrupole mass spectrometer via a three-stage particle beam interface. $[M+H]^+$ ions of low molecular weight polymers (<2000 Da.) were formed by isobutane chemical ionization following desorption vaporization in the 190°C ion source.

For analysis using DCI, aliquots (μL) of the solutions were deposited upon rhenium wire filaments and the solvent was allowed to evaporate. Temperature profiles of the DCI probe varied between experiments and CI was achieved using ammonia or isobutane.

MS SPECTRA:

Analyses were initially performed using particle beam/CI (iosbutane) and alternating between positive and negative ions (PPINICI). Samples with differing average molecular weights from each of the three polymers were injected into the HPLC and analyzed. Positive CI was shown to be more efficient than negative CI by an order of magnitude. Particle beam/CI of PEG_{600} and PPG_{725} yielded mainly $[M+H]^+$ ions for n>7 and fragment

ions corresponding to $[M+H-H_2O]^+$ for n<7. The positive CI spectrum of PS_{946} (repeating unit = 104 amu) contained two series of ions reflecting a difference in end groups. Extensive fragmentation in the negative CI spectrum of PS makes further characterization difficult.

PPG_{425} was examined using DCI with ammonia as the reagent gas. The positive spectrum was composed of $[M+NH_4]^+$ ions and the negative spectrum was composed of $[M-H]^-$ ions. Both spectra yielded information which can be used to calculate molecular weight distributions.

MS/MS SPECTRA:

Tandem mass spectrometry experiments were utilized to characterize and identify polymers in mixtures. The parent spectrum of the fragment ion m/z 133 (isobutane DCI) in an experiment examining a sample of PEG_{600}/PEG_{1000} was acquired to determine the distribution of protonated molecular ions present in the solution. The product-ion spectrum (ammonia DCI) of the ammonium adduct m/z 442 from a sample of PPG_{425} was acquired to screen samples for the presence of PPG. To further the sensitivity of the MS/MS experiment reaction monitoring of m/z 442 -> m/z 117 was performed. The limit of detection was determined to be 20 picomole.

QUANTITATIVE ANALYSIS:

Particle beam/CI and multiple ion monitoring experiments were employed for detection and quantitation of PEG_{400} in unknown samples. Only the most abundant molecular ions were scanned which led to a lower limit of detection (low picomole) as well as an increase in the selectivity of the experiment. The peak area of the reconstructed ion chromatogram was determined and quantitation was achieved using external standards used to construct a calibration curve. Using this methodology, samples could be evaluated in rapid succession with no detectable carryover. Typical times between injections were two minutes. Further information can be gained by comparing the average %RIC of detected PEG ions in the samples with those from PEG_{400}.

CONCLUSIONS

Particle beam/chemical ionization mass spectrometry is a rapid and sensitive technique for the analysis of low molecular weight polymers (<1000 amu). Very little sample preparation is required and the data obtained using this technique is similar to that acquired using desorption chemical ionization. Both qualitative and quantitative information can be derived in a short period of time. Additionally, the HPLC interface will allow automation of sample evaluation.

References:

1) U. Bahr, A. Deppe, M. Karas, and F. Hillenkamp, Anal. Chem., 1992, 64, 2866-2869.
2) R.P. Lattimer, Tandem MS of Polyethyleneglycol Proton- and Deuteron-attachment Ions, 40th ASMS Conf. on Mass Spectrometry and Allied Topics, Washington, D.C., 1992.
3) M. Vincenti and E. Pelizzetti, Anal. Chem., 1992, 64, 1879-1884.

Structural Characterization of Dimer Fatty Acids by DCI Mass Spectrometry

*Larry Sallans and C. William Blewett
Henkel Corporation, Emery Group
4900 Este Ave., Cincinnati, Ohio 45232

Dimer fatty acids are among the most unusual polybasic acids commercially available. While high in molecular weight, these acids are still liquid and find utility in many diverse applications including surface coatings, synthetic lubricants, polymer modifiers, and polyamides for inks and adhesives. The product is produced by the oligomerization of two unsaturated, mainly C_{18}, fatty acid molecules. The raw product is a complex mixture of oligomers (mainly dimer), structural types (linear, cyclic, aromatic, etc.) with many isomeric forms, homologous chain-length distributions, and a slight amount of other functional groups (interester, lactones, decarboxylation products, etc.). The results presented in this study, are based on hydrogenated Dimer acids purified by distillation. Although low in other oligomers and functional groups, they nevertheless contain a broad distribution of structural types with respect to the dimer linkage. This distribution which correlates with a large variation in performance characteristics, is related to the fatty acid source and manufacturing conditions. The focus of the study is primarily the quantitation of the various structural types in hydrogenated, distilled C_{36} dimerized fatty acid.

These products are difficult to analyze. They represent a very complex mixture of components with low volatility and which may fragment or undergo ion-molecule reactions to yield ions representing other components of the mixture. A technique that is successful, involves electron capture of the pentafluorobenzyl derivatives introduced by means of a Desorption Chemical Ionization (DCI), probe. The pentafluorobenzyl derivatives undergo dissociative electron capture to yield carboxylate anions that are representative of the Dimer's structural types. These pseudomolecular ions, each representing a large isomeric distribution, are deconvoluted for isotopic contribution. Components comprising the various structural types are listed in Table 1 along with the representative carboxylate anion's mass.

Data representing structural types for three hydrogenated Dimer samples from different fatty acid sources are illustrated in Table 1. Immediately evident is the high precision demonstrated by the technique. In addition, a more detailed breakdown of the material's components and quantitation of components (polycyclic aromatics) which have not been previously identified for Dimer, are obtained. The results compare extremely well with other methods and techniques.

McMahon and Crowell[1] combined EI mass spectrometry for nonaromatic components with UV analysis for the aromatic constituents in tall oil and oleic acid based Dimers. They list four structural types, three non-aromatic (linear, monocyclic and polycyclic) and one aromatic. Even though different samples were analyzed, the agreement between the two techniques, is excellent. NMR and UV analysis for the aromatic content of the samples listed in Table 1 also agreed very well with results presented by this study.

Hydrogenated Dimer is not without olefinic unsaturation as Iodine-Value and NMR results attest. In an attempt to further characterize the structural classes, a short-exposure bromination on oleic Dimer was performed. All the Dimer components with the exception of the "polycyclic, nonaromatic" (pseudomolecular ion at 741 amu), remain unchanged. Approximately half of the component at 741 amu underwent reaction. While the results are still preliminary, it is proposed that the olefinic species in oleic Dimer is largely monocyclic with a tetrasubstituted double bond.

In conclusion, electron capture of pentafluorobenzyl derivatives by DCI mass spectrometry, provides an accurate, highly precise technique for the quantitation of the structural components in Dimer acids.

[1]McMahon, D. H., and Crowell, E. P., *JAOCS*, **1974**, *51*, 522-527

Table 1. Hydrogenated Dimer - Comparison with the acid source

Dimer Component[1]	Soya 26-A	Tall 26-B	Oleic 26-C
Linear (acyclic) - 745	23.7±1.1	12.7±0.7	38.2±0.8
Monocyclic, nonarom. - 743	48.2±0.8	57.8±0.9	47.9±1.4
Polycyclic, nonarom. - 741	8.7±0.6	14.7±0.8	7 2±0 9
Polycyclic, nonarom. - 739	1.5±0.6	2.6±0.4	1.0±0.2
Monocyclic aromatic - 737	7.7±0.2	5.2±0.3	3.2±0.4
Polycyclic arom. - 735	8.5±1.0	6.1±0.2	2.1±0.4
Polycyclic arom. - 733	1.8±0.2	1.0±0.1	0.4±0.1
Total acyclic nonaromatics	23.7±1.1	12.7±0.7	38.2±0.8
Total cyclic nonaromatics	58.4±2.0	75.1±2.1	56.1±2.5
Total aromatics	18.0±1.4	12.3±0.6	5.7±0.9

[1]These hydrogenated samples still contain a small amount of olefinic unsaturation (see text). "Polycyclic aromatic" components contain only one aromatic ring with additional saturated ring(s) or olefinic functionality.

Application of MALDI Mass Spectrometry to Different Classes of Synthetic Polymers

Ute Bahr, Andreas Deppe, Michael Karas, Franz Hillenkamp
Institute for Medical Physics and Biophysics, University of Münster,
Robert-Koch-Str. 31, 48149 Münster, FR Germany
Ulrich Gießmann, Andreas Overberg
Finnigan MAT, PO box 140162, 28088 Bremen, FR Germany

The feasibility of using MALDI mass spectrometry for determination of average molecular weight and characterization of the polymer distribution has been shown for various synthetic polymers in the mass range between 1000 and 100,000 Dalton. Different matrix/solvent systems are required to match the specific solubility of e.g. polyanionic compounds or unpolar hydrocarbons. Whereas water- or water/organic solvent soluble polymers are investigated using well-known "protein" matrices, dissolving the polymer sample directly in a liquid nitrophenyl octyl ether matrix yielded best results for e.g polystyrene; Ag-trifluoroacetate addition is used to promote Ag cationization. Reproducible and reliable mass determination of polymers, however, requires a careful control of the experimental parameters. This is documented for same examples :

- a) For polymers of low average molecular mass the determined mass is depending on the ion impact energy at the detector surface with a shift to too low mass at low ion energies. Ion energies of 10 keV and larger are required to avoid these problems. For larger polymers this effect is not observed, higher ion impact energies at the detector, however, are generally preferable because of higher ion intensities.
- b) Cationization of low molecular mass polymers shows a distinct influence on the alkali-metal ion yielding a shift of the polymer distribution to smaller n-values for Li and Na. Sample cleaning by ion exchange and addition of KI yields reproducible results; cationization by K^+ forms the best compromise between obtainable ion intensities (efficiency of cationization) and imaging of the accurate polymer distribution.
- c) Polyanionic polymers, such as poly(methacrylic acids) usually show broad unresolved signals also in the low mass range due to a widely varying number of free acid and salt groups and different cations present. Well-resolved signals displaying the units of repeat are obtained (also) in the positive ion mode by cation exchange (H^+-activated) pretreatment and addition of KI to induce uniform cationization.
- d) Due to locally heterogeneous mixing with the matrix polyanionic polymers, such as poly(acrylic acids) may show different polymer distributions from spot-to-spot. Optical control of preparation and scanning of the sample/matrix layer under microscopic observation is required to avoid misleading results.

Future improvements for MALDI of polymers is possible by searching and choosing new matrices. E.g. 2(4'-hydroxybenzylazo)-benzoic acid yields superior results e.g. for PEOs with respect to signal intensities and mass resolution. In addition, use of IR wavelengths (Er-YAG-laser emitting at 2.94 μm) with a succinic acid matrix showed considerable improvement in the quality of the mass spectra obtained for polyanionic oligomers.

ACKNOWLEDGEMENT : This work was financially supported by the German Fed. Dept. of Research and Technology (BMFT, grant No.: 13N5640)

Direct Analysis of Polypropylene Compounds by Thermal Desorption and Pyrolysis Mass Spectrometry.*

Robert P. Lattimer, The BFGoodrich Research and Development Center, Brecksville, Ohio 44141.

This report describes the mass spectrometric identification of components (particularly residual volatile chemicals, organic additives, and degradation products) in five polypropylene compounds of known composition. Direct probe heating of the compounded polymer was carried out over the range 20-400°C, using a Finnigan MAT 95Q hybrid (BEoQ) mass spectrometer. "Survey" mass spectra were acquired with three different methods of ionization: 70eV electron impact (EI-MS), isobutane chemical ionization (CI-MS) and field ionization (FI-MS). For the polypropylene compounds, residual volatile chemicals and most organic additives were desorbed at lower temperatures (less than ≈300°C), while polymeric components were thermally decomposed (pyrolyzed) at higher temperatures (greater than ≈300°C). It was found that field ionization gives a very convenient overview of the composition of the evolved chemicals, since essentially all of the ions observed are molecular ions for the various components. In some cases, tandem mass spectrometry (MS/MS) was used to obtain fragmentation patterns (product ion scans) for chemical structure elucidation. High resolution mass measurements were also carried out to obtain elemental formulas (or atomic compositions, AC-MS) for particular chemical components.

Of particular interest was the detection of the oligomeric hindered amine light stabilizers (HALS) Tinuvin[R] 622 and Chimassorb[R] 944. It was possible to confirm the presence of Tinuvin 622 in polypropylene by CI- or FI-MS analysis of pyrolyzates evolving in the temperature range 300-350°C. The presence of Chimassorb 944 in polypropylene could be confirmed by detection of one of its low molecular weight components (cyclic monomer) by thermal desorption CI-MS. Pyrolysis products from polypropylene were observed above ≈350°C at every carbon number to masses >1000 Da. Overall, the direct mass spectral analysis of the polypropylene compounds was found to be a very effective means for detection and identification of various organic additives and polymeric components

Our general approach to analysis of the polypropylene compounds was to use field ionization as a "survey" or screening technique to obtain an overview of the chemical composition, *i.e.*, to determine the number of components and their molecular weights. Then the supplemental techniques of MS/MS and AC-MS were used, in EI and/or CI mode, to elucidate or verify chemical structures. To illustrate this approach, a composite FI mass spectrum showing the thermal desorption region for one of the compounds is included. The recipe for the compound is as follows: Himont 6301 polypropylene (100 parts), Irganox[R] 3114 (0.10 parts), Ultranox[R] 626 (0.08 parts), calcium "stearate" (0.10 parts), Tinuvin[R] 770 (0.40 parts). The most intense ion in the FI spectrum is m/z 480, which is $M^{+\cdot}$ for Tinuvin 770, a HALS additive. A small methyl-loss fragment is observed (m/z 465). Other additive molecular ions in the figure are m/z 530 (Irganox 1076), m/z 604 (Ultranox 626), and m/z 783 (Irganox 3114). (The Irganox 1076 is present as an additive in the Himont polypropylene.) Product ion scans for the various components were readily obtained directly from the polymer compound (EI- or CI-MS/MS), despite the fact that the concentrations of the additives were only ≈0.1%. High resolution mass measurements could also be made for ions from the additives directly from the polymer compound. Lower mass ions in the figure include m/z 206, 256 and 284. MS/MS and AC-MS data indicate that these are molecular ions for 2,4-di-*t*-butylphenol, palmitic acid and stearic acid, respectively. The substituted phenol is a degradation (hydrolysis) product from Ultranox 626. The acids arise from degradation of calcium palmitate/stearate.

**J. Anal. Appl. Pyrolysis*, in press (1993).

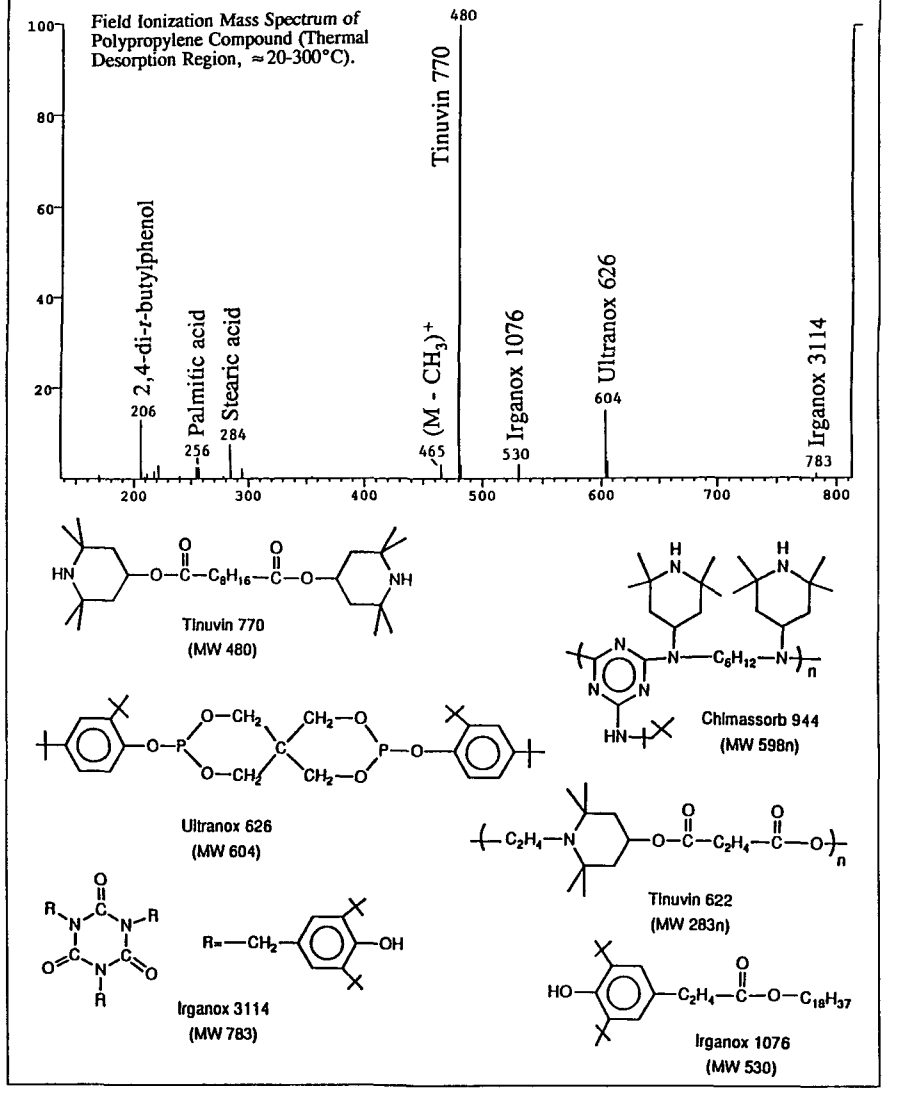

CTD-(GC)-MS SYSTEM [CONTROLLED THERMAL DEGRADATION-(GAS CHROMATOGRAPHY)-MASS SPECTROMETRY]

Ted T. Chang and M. J. Piquette
Cytec Industries, 1937 W. Main St., Stamford, CT 06904

Many industrial products incorporate various additives at small concentrations intended to modify or improve their performance. Typical examples are sizing agents in paper, UV absorbers and plasticizers in polymers and cross-linking agents in coating materials. The thermal behavior of these additives can be as important as the thermal behavior of the major components. Because of their insufficient sensitivity, currently available TGA/MS systems are unable to address these types of problems.

A Controlled Thermal Degradation-(Gas Chromatography)-Mass Spectrometry [CTD-(GC)-MS] system was constructed to overcome the inadequacies relating to poor sensitivity. The sensitivity of this system is approximately 2-3 orders of magnitude higher than that of most commercial TGA/MS systems. Therefore, the proposed system is capable of specifically targeting minor components. A high-resolution mass spectrometer is used to remove interfering ions in the same nominal mass. The system accepts a wide range of sample sizes from low ug to low mg level depending on the target compound concentration. Temperature is controllable within +/- 5°C, which is sufficient to produce thermal degradation patterns comparable to TGA. The system is capable of on-line MS observation of thermal decomposition (similar to TGA/MS), on-line GC/MS analysis of the the degraded mixture, and collection of degraded material for subsequent analysis by other analytical techniques.

The most important advantage of the CTD-(GC)-MS system is its capability to observe the thermal behavior of a selected compound, especially a minor component in a complex sample matrix. The sample size is in the 10 ug range comparing to the 1-10 mg range for pyrolysis GC/MS and TGA/MS. Utilization of a high-resolution mass spectrometer adds a powerful mass ion separation capability.

Thermal degradation products usually are complex mixtures. The unit-mass resolution mass spectrometer used in most TGA/MS systems is highly subjected to interfering ions with the same nominal mass. The collecting device of the proposed system is capable of selecting a desired degradation temperature and obtaining the composition profile of degradation products.

The CTD-(GC)-MS system has many potential applications. It can be used to study the thermal behavior of a sample, the fate of a certain component in a sample, identification of evolved

gases, analysis of complex degradation mixtures, etc. Three typical examples are included in this presentation.
The first example is study on the curing behavior of a commercial monomeric cross-linkng agent. The operation is similar to TGA/MS but with a sensitivity 100 times higher than TGA/MS.

The second example shows the application of the system to study the thermal behavior of a minor component. The sample is a paper containing approximately 0.05% of a common sizing agent. It was found that the sizing agent evolved at the early stage of degradation.

The third example is the CTD-GC-MS operation. It shows the capability of the system to focus on a selected degradation temperature. Many samples exhibit complex thermal degradation processes. Their decomposition products are different at different temperatures and heating rates. Collection of the degradation products and separation by a GC unit prior to MS analysis are essential steps to provide useful analytical information.

Block Diagram of CTD-GC-MS System

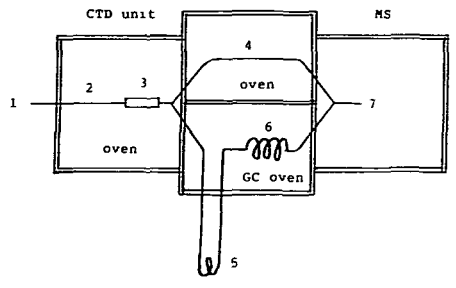

1. Carrier gas
2. Carrier gas preheating tube
3. Thermal degradation chamber (TD chamber)
4. Transfer line
5. Collector
6. GC
7. MS

A Method for Distinguishing Chlorosulfonated Polyethylene from Chlorinated Polyethylene Using Pyrolysis/GC/MS

*Aris A. Gallon and John Glass Green, The DOW Chemical Company, Research and Development, Analytical and Engineering Sciences Laboratory, Plaquemine, Louisiana 70765-0400.

Often it is not possible to distinguish between chlorosulfonated polyethylene (CSM) and chlorinated polyethylene (CPE) by elemental analysis for sulfur content because of sulfur containing additives used in CPE formulations. A method was developed to distinguish between the two based on the formation of sulfur dioxide during the pyrolysis of CSM. Both types of polymers pyrolyze by a side group elimination mechanism. This mechanism of pyrolysis produces SO2 from the pendant -SO2Cl groups on the CSM backbone. The SO2 is detected indicating the presence of -SO2Cl groups in the polymer.

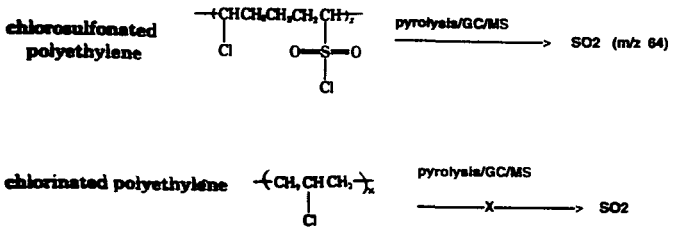

Experimental:

The pyrolysis was done using a CDS 122 coil pyroprobe connected to a Hewlett Packard 5987 GC/MS. The following pyroprobe and GC/MS conditions were used:

Coil Probe:	GC/MS:
Interface= 200 C	column= DB 1701 30 m X 0.32 mm
final temperature= 1400 C	initial temperature= 30 C
rate= 20 C/ms	rate= 15 C/min
interval= 20 sec	final temperature= 250 C
	mass range scanned= 30-500 amu

The pyrolysis/GC/MS chromatograms of a CSM polymer formulation and a CPE polymer formulation that was cured with thiadiazole are shown in Figures 1 and 2. The extracted ion chromatogram for m/z 64 of the CSM polymer pyrolysis products (Figure 1b) shows an intense peak at a retention time of 1.32 min.

The mass spectrum (Figure 1c) indicates that the component is sulfur dioxide. The extracted ion chromatogram for m/z 64 of the CPE polymer that was thiadiazole cured (Figure 2b) also shows a peak at a retention time of 1.35 min. The mass spectrum (Figure 2c) indicates that the component is butadiene.

Comparative results for several other samples will be shown to further illustrate the method. Pyrolysis/GC/MS chromatograms of pure polymers and formulated polymers will be presented.

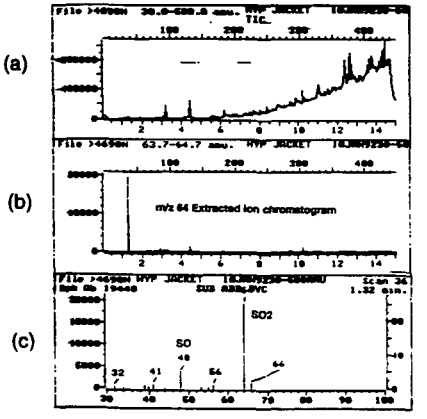

Figure 1:

Chromatogram of chlorosulfonated polyethylene pyrolysis products. (b). Extracted ion chromatogram for m/z 64. (c). Mass spectrum identifying the peak as sulfur dioxide.

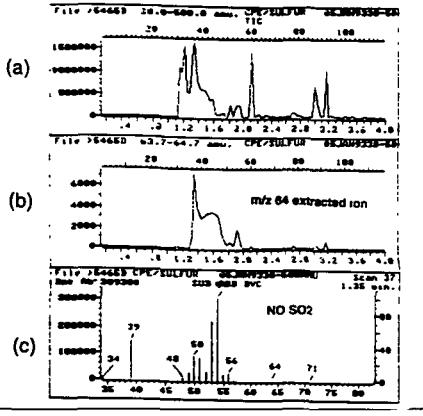

Figure 2:

Chromatogram of chlorinated polyethylene. (b). Extracted ion chromatogram for m/z 64. (c). Mass spectrum identifying the peak as butadiene.

GC/MS Determination of Aromatic Isocyanates and Amines as Degradation Products in Polyurethane Foams Used in Breast Implants.

Frank M. Benoit
Health and Welfare Canada
Ottawa, Ont, Canada K1A 0L2

INTRODUCTION

The Même breast prosthesis consists of a gel filled silicone envelope covered with a thin layer (1-2 mm) of soft polyurethane foam (Microthane TM) which is manufactured from toluene diisocyanates (2,4- and 2,6-TDI ratio 4:1) and polydiethyleneglycol adipate. However, 2,4- and 2,6-TDI react with water to produce 2,4- and 2,6-toluene diamines (TDA) which are commonly found at the ppm (ug/g) level in polyurethane foams. Under harsh conditions of temperature (T = 150 °C) and alkalinity (3N NaOH), polyurethane foams are completely decomposed. We have examined the degradation reaction under the milder conditions of temperature (T = 37 °C) and alkalinity (pH = 7.4) that exist within the human body. In preliminary experiments, we found that the foam contained toluene isocyanate amines (TIA) and TDI in addition to the expected TDA. To test the degradation hypothesis properly, it was imperative that the initial TDA, TIA and TDI contaminants be removed completely from the foam. Despite our best efforts this proved to be an impossible task. Low ppm levels of TDA, TIA and TDI were consistently observed despite extensive washing of the foam. Furthermore, we observed that TDA has a low aqueous solubility; consequently, degradation products from the foam will be preferentially retained on the surface of the foam rather than migrate into the aqueous phase. Hence, in any study of the degradation of the foam in aqueous medium, the foam itself must be examined along with the aqueous phase following exposure.

EXPERIMENTAL

The following protocol was adopted for incubation of the foam. Precleaned (6 days Soxhlet extraction) foam was divided into two fractions A and B. Fraction A was stored in the dark at room temperature while fraction B was incubated in Ringer's solution at 37 °C for periods of 6 to 35 days. Following the incubation both fractions were analyzed and the results compared. A similar experiment wherein fractions C and D were incubated dry at 37 °C was also carried out. The Finnigan MAT-90 GC/MS was operated in EI mode. The on-column injector was operated at 110 °C, hold 0.1 min, ramp to 300 °C at 180 °C/min. The SPB5 30 m x 0.32 mm id column (0.25 micron film) was held at 100 °C for 1 min then ramped to 180 °C at 5°/min, then to 250 °C at 20°/min and held for 3 min. TDA and TDI were identified and quantified as the HFBA amide derivatives by monitoring m/z 514, 495, 345, 317 and 302 for TDA, m/z 344, 325 and 175 for TIA and m/z 174, 145 and 132 for TDI within the appropriate GC retention time windows.

RESULTS AND DISCUSSION

Every foam sample tested in the current study was initially contaminated with 2,4- and 2,6-TDA, TDI and TIA. The TDA levels in the virgin foam samples ranged from 2 to 71 ppm for 2,6-TDA and 18 to 692 ppm for 2,4-TDA. The average sum of TDA, TIA and TDI removed from the foam samples during the cleaning process was 1104 (+/- 644) ppm. The results from the extraction of the Ringer's solution from the foam samples incubated at 37 °C did not show any apparent relationship with the duration (6 to 35 days) of the incubation. On average, 1.88 ppm of total TDA, TIA and TDI were extractable from foam samples into 250 ml of Ringer's solution at 37 °C over periods of 6 to 35 days. In all twelve incubation experiments the levels of TDA, TDI and TIA were all higher in the B fraction than in the A fraction. The average incremental (B - A) amounts of TDA, TIA and TDI produced during incubation and retained on the foam surface were considerably higher (74 ppm) than the average amounts (1.9 ppm) released into the aqueous phase. Not only was there an increase in the levels of TDA but there was also an increase in the levels of TDI and TIA. However, the reaction between TDI and water is slow because of the low solubility of TDI in water. In the present experiments, most of the degradation products are adsorbed on the surface of the foam following the incubation and hence protected from hydrolysis. Nevertheless, TDI and TIA were not expected as products of the hydrolysis of polyurethanes which suggests that the observed degradation process is more complex than simple hydrolysis. The average daily total increments in the amounts of TDA, TDI and TIA was 4.6 ppm. In the dry incubation experiments the foam fraction C was stored at ambient temperature (20 °C) in the dark and fraction D was stored at 37 °C for periods of 7 and 15 days. In both instances (two duplicate samples) the amounts of TDA, TIA and TDI were higher in fraction D than in fraction C. Hence, thermal decomposition of the foam does indeed occur at body temperature. The average daily sum of degradation products was 1.5 ppm, which corresponds to ca 33 % of the daily degradation in aqueous solution.

CONCLUSIONS

The behaviour of polyurethane foams under simulated physiological conditions is complex. The foam surface exhibits strong adsorbent properties and is contaminated initially at the low parts per thousand level with residues of TDA, TDI and TIA, that are difficult to remove completely from the foam. Degradation of the foam occurred under mild hydrolytic (pH 7.4) and thermal conditions (37 °C) and produced an average of 4.6 ppm of TDA, TIA and TDA daily under simulated in vivo conditions and 1.5 ppm under mild thermal conditions (37 °C) alone. Examination of the degradation products showed that TDI and TIA were formed as well as the TDA. Because the ratio of 2,4-TDI and 2,6-TDI used in the production of polyurethane foams is 4:1, 80 % of the TDA, TIA and TDI in the foam have the 2,4-orientation of the nitrogen atoms and, hence, the potential to become 2,4-TDA within the human body. Consequently, the assessment of the risk to health associated with the presence of 2,4-TDA in polyurethane foams must include consideration of the 2,4-TDI and 2,4-TIA precursors as well.

GPC-LC/MS Using a Particle Beam Interface

*R.A. Ludicky, G.B. Kenion, D.E. Doster and P.D. Souchek
Morton International, Woodstock IL 60098

Gel permeation chromatography coupled to mass spectrometry is a technique that is in use in a number of laboratories. This technique requires little development time for analyses of smaller molecules and is a good screening method for such analyses. Many people underestimate the size of molecules which can successfully be transported across a particle beam. A series of polystyrene standards of known molecular weight were passed through a particle beam interface in order to see how transport efficiency varies with molecular weight.

A six component standard made from five polystyrenes of known molecular weight and α-methyl styrene dimer was separated by a two column set of GPC columns. The GPC columns utilized were a Jordi-Gell 300 Angstrom column and a Jordi-Gell mixed bed column. The effluent from the columns was then passed through an Extrel particle beam interface and into an Extrel ELQ 400 mass spectrometer. The six component standard was utilized to perform two different experiments. In the first experiment the standard was analyzed by LC/MS. In the second experiment the components of the six component standard were trapped at the end of the particle beam interface inside the mass spectrometer. The transport efficiencies of the components in the standard were then calculated by comparing the particle beam trappings to the initial standard solution. The particle beam trappings were compared to the initial standard by traditional GPC using a refractive index / viscosity detector operating in the refractive index mode.

The particle beam recoveries are given below in Table One

Table One: Particle Beam Recoveries

Component	% Recovery
Polystyrene MW = 1,600,000	Undetermined, Baseline problems
Polystyrene MW = 400,000	2.7 %
Polystyrene MW = 47,500	6.6 %
Polystyrene MW = 4,000	4.3 %
Polystyrene MW = 826	7.7 %
α-Methyl Styrene Dimer MW = 236	Pumped Away

It appears that most of the components of the six component standard are transported by a particle beam interface. Even the Mw = 1,600,000 can be seen in the particle beam trappings when the sample is analyzed by traditional GPC using a viscometer instead of a refractive index detector.

The GPC-LC/MS total ion chromatogram looks quite different from the GPC refractive index chromatogram of the particle beam trappings. The GPC-LC/MS total ion only features one good sized peak. This peak originates from the MW = 826 polystyrene. The GPC refractive index chromatogram of the particle beam trappings shows good peaks for all the components of the standard except the MW = 1,600,000 polystyrene which appears to get lost in the baseline and for α-methyl styrene dimer, which is pumped away. The difference between the GPC-LC/MS total ion chromatogram and the refractive index trace appears to be due to poor ionization of high molecular weight species by electron impact and chemical ionization. The analysis of high molecular weight compounds by particle beam LC/MS appears more limited by ionization efficiency then lack of transport.

Poly(Amic Acid) Polyimide Characterization Using Both GC/MS and Particle Beam LC/MS

Timothy MacMahon and Mark Chace
IBM, Hopewell Junction, New York, 12533

The analysis of polyimides is becoming increasingly more and more important as this class of polymers become more prevalent in today's electronic packaging technology.[1] Polyimides are noted for their high glass transition temperatures and thermal stability. In some cases, this thermal stability allows heating to temperatures as high as 400°C for many hours without a critical drop in physical or mechanical properties.[1] In addition to the use of polyimides as dielectric layers, there is also interest in developing photosensitive polyimides that could be used as both lithographic and insulating dielectric material; thus, unlike resists currently in use the new polyimide resists would not have to be removed after lithography saving numerous processing steps and shortening cycle times.

The high thermal stability of these polymers make them difficult to analyze by traditional analytical techniques. In particular, mass spectrometry has been able to do little toward understanding these polymeric systems.[2] Plat and Chace developed a mass spectrometric technique for the analysis of these polyimides which uses an Ing-Manske hydrolysis reaction to hydrolyze the polyimide.[3] Once the hydrolysis is complete, information about the amine and acid portion of the molecule can be probed via mass spectrometry. The amine portion can be detected via an ethyl ether extract, but in order to detect the acids their volatility must first be increased through derivatization to the methyl ester or the trimethylsilyl ester making them more amenable to gas chromatography / mass spectrometry (GC/MS).

The advent of liquid chromatography / mass spectrometry (LC/MS) has opened up new capabilities in the analysis of these polyimides. LC/MS can be used on thermally unstable molecules and/or molecules of low volatility i.e. operating temperatures are considerably lower.

In order to evaluate this new technology, a comparison was made between GC/MS and particle beam LC/MS. A number of polymers were hydrolyzed in NH_4OH and studied using gas chromatography / mass spectrometry (GC/MS) and particle beam liquid chromatograph mass spectrometry (LC/MS). The polymers studied in this report were as follows: 3,3',4,4'-biphenlytetracarboxylic dianhydride - phenylene diamine (BPDA-PDA); BPDA-PDA-4'-oxydianiline (ODA); pyromellitic dianhydride - 4,4'-oxydianiline (PMDA-ODA); and finally, 3,3',4,4'-benzophenonetetracarboxylic dianhydride - 1,3-bis(4-aminophenoxy)benzene (BTDA-APB).

Some of the polymer samples were hydrolyzed in both their acid and imide forms to see if any mass spectrometric differences could be detected. In all cases, the acid and imide spectra looked the same. GC/MS was unable to determine either the amine or acid portion of these polymers via a direct injection of the sample, but when the samples were first extracted with diethyl ether and this ether extract was injected into the chromatograph the amine portion of the polymers were readily detected. The acid portion was not detected in either the sample or the ether extract. The LC/MS was able to detect both the amine and acid monomeric units in the non-extracted aqueous sample.

References:

1. a) see "Recent Advances In Polyimide Science and Technology"; Weber, W.D.; Gupta, M.R., Ed.; Mid-Hudson SPE March 1987.
   B) Alston, W.B.; Gratz, R.F. Proceedings of the first pacific Polymer conference NASA technical memorandum 102353 (1989).

2. a) Goldfarb, I.J. Polymer Preprints, 269 (1985).
   b) Van Der Wel, H.; Sondag, A.H.M.; Postma, L.; Roberts, R.C.C. Vacuum, 41, 1651 (1990).
   c) Eldridge, B.N.; Feger, C.; Goldberg, M.J.; Reuter, W.; Scilla, G.J. Macromolecules, 24, 3209 (1991).
   d) Johnson, E.T. J. Appl. Polym. Sci., 44, 1905 (1992).
   e) Dugger, D.C.; Stern, M.B.; Rubico, T.M. Mat. Res. Soc. Symp. Proc., 147, 385 (1989).
   c) Creasy, W.R. Brenna, J.T. Chem. Phys., 126, 453 (1988).

3. a) Chace, M.; Plat, M. Proc. 37th ASMS Conference on Mass Spectrometry and Allied Topics, 264, (1989).

Direct Chemical Analysis of UV Laser Ablation Products of Organic Polymers Using Reflectron Time-of-Flight Mass Spectrometry (Re TOF-MS) and Gas Chromatography/Mass Spectrometry (GC/MS)

Yeong Choi, Heewon Lee, Scott T. Fountain, and David M. Lubman
Department of Chemistry
The University of Michigan
Ann Arbor, Michigan, 48109

The interactions of UV laser radiation with organic polymers have been studied extensively for their potential applications in technology and medicine. Although physical aspects of laser ablation are relatively well understood, direct chemical analysis of the ablation products is still a challenging task that needs to be explored. Some difficulties associated with chemical analysis of the laser ablation products involve the complexity and trace quantities that may result. Even more problematic in some cases is the lack of a technique for direct chemical analysis of laser-induced ablation products in trace quantities.

Recent studies have shown that use of an appropriate masking polymeric fluid in excimer laser surgeries can improve the smoothness of the corneal surface in these surgical procedures and thus there has been an effort to develop new polymer masks for this purpose (1,2). A potential drawback of the use of masking polymeric fluid in excimer laser surgeries is the formation of photochemically induced products which may be toxic. If such species were produced in sizable amounts, then this might preclude the use of these polymers in these surgical procedures, particularly in human subjects. Thus, such problems have motivated us toward developing direct analytical methods for detecting and identifying the UV laser-induced ablation products of polymers.

In the present study, a commercial gas chromatography/mass spectrometry (GC/MS) system has been modified so that trace quantities of ArF excimer UV laser-induced ablation products of a potential masking fluid may be introduced into the capillary column directly for chemical analysis. By obtaining the chromatogram in the SIM (Selective Ion Monitoring) mode which increases the sensitivity of the detector significantly, the presence and/or absence of the potentially toxic fragments that may result from the laser ablation of poloxamer have been monitored.

Poloxamer is an organic polymer which has a potential to be used as a masking fluid. From the photochemistry and structural considerations, the possible laser ablation products of poloxamer include ethylene oxide and acetaldehyde. Upon laser ablation, the chromatogram of the poloxamer shows 4 peaks with different composition as shown in Figure 1. Of particular interest is the peak B in Figure 1 which, when compared with the chromatogram of ethylene oxide/acetaldehyde mixture, shown in Figure 2, has the same retention time as that of acetaldehyde. In addition, the relative ratios of ions, $[C_2H_3O^+(m/z = 43)]/[C_2H_2O^+(m/z = 42)] > 2$ and $[C_2H_2O^+(m/z = 42)]/[C_2HO^+(m/z = 41)] \simeq 3$, identify the peak B as that due to acetaldehyde and exclude the possibility of the presence of ethylene oxide as a laser ablated product of poloxamer.

Complementary information on the laser ablation products of poloxamer was obtained by using the Reflectron Time-of-Flight Mass Spectrometer (Re TOF-MS) and the possible species, which included larger mass fragments, were identified. For comparison, structurally similar polyethylene glycol (PEG) was also studied.

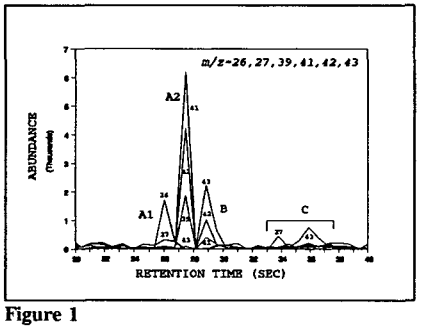

Figure 1

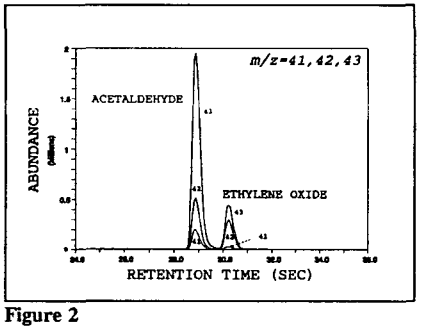

Figure 2

1. Englanoff, J.S.; Kolahdouz-Isfahani, A.H.; Moreira, H.; Cheung, D.T.; Nimni, M.E.; Trokel, S.L.; McDonnell, P.J. *Ophthalmol.* **1992**, *99*, 1201-1208.
2. Kahle, G.; Stödter, H.; Seller, T.; Wollensak, J. *Invest. Ophthalmol. Vis. Sci.* **1992**, *33*, 2180-2184.

Analysis and Quantification of Polymer Additives in Polyolefins by Particle Beam LC/MS

Matthew J. Dilts, Millipore/Extrel Mass Spectrometry,
575 Epsilon Drive, Pittsburgh, PA 15238

INTRODUCTION

The additive packages used for polyolefins can be quite complicated, containing several antioxidants, both primary (such as hindered phenols) and secondary (also called synergistic), as well as antistats, slips, pigments, etc. It is very important to the processing and longevity of the fabricated material that the correct amount of each additive be present. Failure to choose the correct additive package may result in degradation during processing or premature oxidation/aging and early failure in the field.

EXPERIMENTAL

Traditionally, these compounds have been chromatographically separated by reverse phase liquid chromatography and detected by UV. This study will demonstrate the ability to use a mass spectrometer as a secondary detector to confirm peak identification and quantification of additives.

MASS SPECTROMETER

. MILLIPORE/EXTREL benchmark™ mass spectrometer

.Thermabeam™ particle beam LC/MS interface

. Electron Impact (EI) ionization

LIQUID CHROMATOGRAPHY

. WATERS 600-MS solvent delivery system

. WATERS 484 Tunable Absorbance Detector

. WATERS Novapack reverse phase C18 column (2.1 x 150 mm)

Gradient: (A) Water

(B) Acetonitrile

60% - 100% B in 6 minutes hold for 20 minutes

flow rate 0.3 ml/min

CONCLUSION

LC/MS can be used as a secondary detector for quantification of polymer additives. The spectra presented are interpretable electron impact type spectra. The mass spectrometer can also be used for quantification of polymer additives. The next phase of this study is to analyze actual polymer extracts and quantitate the data.

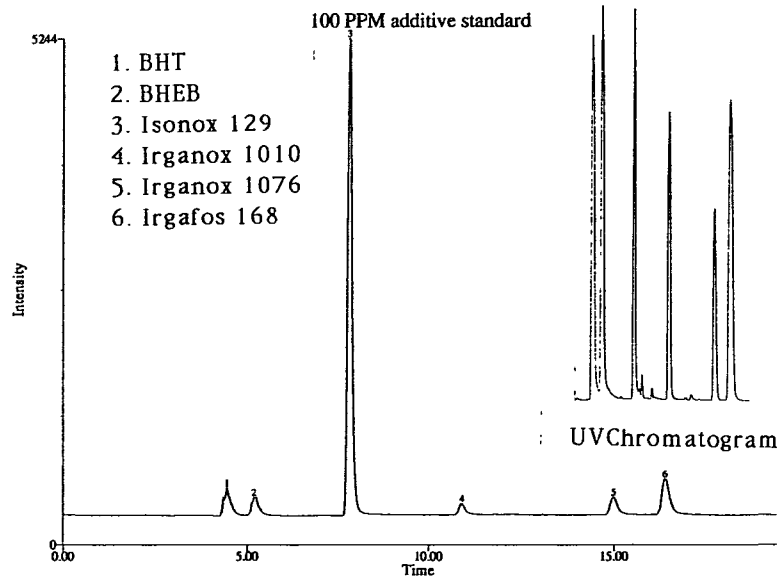

Surface Additives on Bulk PET Studied with High Mass Accuracy ToF-SIMS

S.Reichlmaier*, J.S.Hammond Perkin-Elmer Physical Electronics Division,
Eden Prairie, MN 55344, USA
M.J.Hearn, D.Briggs, ICI Wilton Research Centre, PO Box 90 Wilton,
Middlesbrough, Cleveland TS6 *JE, England

Introduction

The routine analysis of polymer surfaces involves detection of additives that in many cases show molecular ions or unique fragment ions in the mass range up to m/z=1000. The static SIMS technique employing a ToF mass analyzer is most appropriate for the sensitive detection of these materials. The potentials of the technique have been described frequently. For the routine use in a analytical laboratory, however, the reproducibility of the instrument is very important. We studied therefore a very common polymer matrix (poly(ethylene terephthalate), PET) over a 6 month period of time to extract statistical information on the accuracy of the mass assignment as well as on mass resolution and signal intensities. The results obtained from the PET matrix were then used in a study of a very common additive material (glyceryl monostearate, GMS).

Experimental

A Perkin-Elmer PHI 7000 ToF-SIMS instrument was used to analyze the PET polymer films of about 0.1mm thickness. The Cs primary ion gun was used to generate SIMS mass spectra over a range of m/z=10 to 600. The acquisition time per spectrum was less than 2 minutes and the employed primary ion dose was well below10^{12} ions/cm^2. Charge neutralization was established with a low energy electron flood gun. The automated peak finder routine of the instrument software was used to determine the measured masses of selected peaks of known exact mass. The accuracy of the mass assignment was then calculated. The evaluated peaks in positive SIMS and their exact mass are listed in table1.

Species PET	C7H4O	C9H8O2	C10H9O4	M+C2H5O	M+C8H5O3	2M+H	3M+H
Mass	104.0262	148.0524	193.0501	237.0763	341.0661	385.0923	577.1346
Species GMS	C18H35O	C18H37O2	C21H42O3	M+H	M+Na	C39H75O4	
Mass	267.2688	285.2794	341.3055	359.3161	381.2981	607.5665	

Table 1 Evaluated mass peaks of PET and GMS on PET (note that m/z=607 is a low level distearate contamination).

An automated calculation routine was used for the evaluation of the obtained mass resolution and signal intensity. The GMS was studied under similar conditions as the plain PET samples. The analysis was carried out on GMS deposited as thin (non charging) film deposited on an Al disk and as coating on PET substrate. The evaluated peaks are also summarized in table 1. Examples of the routinely achievable mass resolution are shown in figure 1.

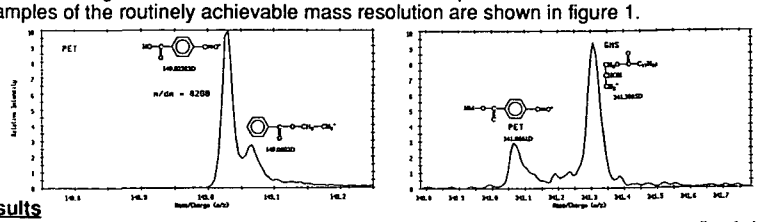

Results

The calibration of ToF-SIMS spectra is performed by calculating a least square fit of data pairs from a set (up to 20) of measured flight times for known mass peaks. In this study we distinguish between a system calibration that was performed before the spectrum was measured and

calibrating the spectrum after the acquisition was finished. The system calibration used only well known low mass fragments (CH_3, C_2H_3, C_3H_5) to calculate the calibration constants. For the calibration of the spectra we investigated different combination of calibration mass peaks. The results from 34 individual spectra acquired between November 1992 and April 1993 evaluating the 238 individual peaks for each calibration are summarized in table 2.

Calibration	System	3Peak	6Peak	8Peak	4Pi
Acc. of Aver [ppm]	11.1	10.4	5.3	6.5	6.2
Standard Deviation	32.2	13.0	13.5	16.2	13.7

Table 2: Accuracy of the mean mass value and standard deviation from 238 evaluated peaks.

Results from five different calibrations are shown. The system calibration was described above, the remaining four were applied to the spectra after the acquisition was finished. The 3Peak calibration involved the same peaks as the sytem calibration. For the 6Peak calibration the C_4H_7 C_6H_5 and C_4H_7O ions were added to the calibration. The 8Peak calibration included also the $C_9H_8O_2$ and $C_{10}H_9O_4$ ions. All these calibrations are regarded as extrapolating, because all evaluated peaks have higher masses than the calibration peaks. In contrast to the above the 4Pi calibration includes the three low mass peaks as the system calibration plus the protonated monomer peak at m/z=193. It therefore includes two peaks with interpolated calibration.
The FWHM mass resolution of the 238 individual peaks was measured and the results are plotted in table 3. The peak areas, calculated within the FWHM around the peak maximum are also included in table 3. The intensities decrease more than 2 orders of magnitude with increasing peak mass.

Peak m/z	29	104	148	193	237	341	385	577	
FWHM m/Δm	6048	7777	7250	7332	6955	6371	7649	8090	
Peak Area	n.a.	20728	5419	2805	631	706	455	115	[cts]

Table 3: Average mass resolution and peak area fom 34 individual measurements.

Results from 16 individual GMS spectra are summarized in table 4. For the typical measured accuracies we calculated the number of possible species assignments for a C,H,O and N containing organic substance at the mass of the GMS protonated molecular ion at m/z=359.3161.

Peak m/z	267	285	341	359	381	607
Accuracy [ppm]	7 6	8 2	5 2	11.2	4 0	37.9
Standard Deviation	10.5	14.6	15 4	11.9	12.1	23.4

Table 4: Average mass accuracy of the evaluated GMS peaks of 16 individual spectra.

The results show that the number of possible choices for assigning a species to a given mass peak is substantially reduced with improved mass accuracy (e.g. 4 @ 10ppm vs. 20 @ 70ppm).
The mean values of mass resolution at m/z=359 of GMS on Al and PET from 16 individual spectra compare as m/dm=10,800 ± 700 on the conductor and m/dm=8400 ± 700 on the PET.

Conclusion

The statistical investigation of the routine performance of the Perkin-Elmer PHI 7000 ToF-SIMS instrument for polymer analysis resulted in achievable mass accuracies better than 20ppm. This kind of perfomance is required for typical additive characterization because it allows species assignments based on accurate determination of the ions mass.
For achieving good mass accuracy it is very important to maintain good routine mass resolution on insulating samples. Only very slight degradation was found in this study on GMS.

Nonpolar Polymer Analysis by Continuous Flow Fast Atom Bombardment Mass Spectrometry (CF-FAB/MS)

Robert L. Dilliplane, Rohm and Haas Company, Spring House, PA 19477

INTRODUCTION

CF-FAB has several advantages compared to static FAB: increased sensitivity, decreased intensity of background and matrix ions, improved background subtraction, and quantitation using flow injection comparisons. Since many compounds are not water soluble and not compatible with the commonly used CF-FAB solvents, I explored alternate solvents to increase the application of CF-FAB to include nonpolar compounds.

The first attempts used organic solvents with 3-nitrobenzyl alcohol, the matrix of choice for many nonpolar compounds analyzed by FAB. Tetrahydrofuran dissolved the compounds of interest and promoted ionization without the addition of a matrix.

EXPERIMENT

Using tetrahydrofuran without additional matrix, CF-FAB was used to determine the molecular weights of both polymer oligomers and polymer additives.

Stable operation can be achieved using 20uL/minute tetrahydrofuran delivered to the FAB tip through a 26um I. D. fused silica line with a source temperature of 30°C. If the flow rate is too low or the source temperature is too high, the rate of evaporation of tetrahydrofuran causes the sample to deposit on the FAB tip. The flow rate of the tetrahydrofuran has to be maintained at a rate high enough to ensure the sample remains in solution for ionization to occur.

The FAB tip is insulated from the ion source so that a potential, independent of the source potential, can be applied.

ADDITIVE RESULTS

Tinuvin 770 was analyzed by CF-FAB using tetrahydrofuran. Applying a potential to the FAB tip was done to enhance ion extraction, a technique reported by M. Linscheid (Ref.). A potential of +9V on the FAB tip had the additional benefit of reducing the solvent adduct ions, enhancing the m/z 481.

CF-FAB of Tinuvin 770
20uL/min THF
26um I.D. fused silica
0.5uL injection volume

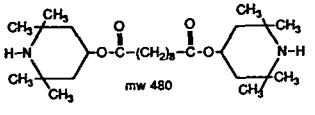

FAB tip at ground

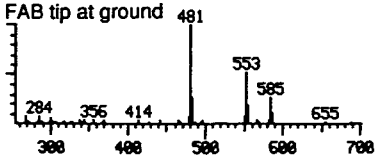

FAB tip at +9V

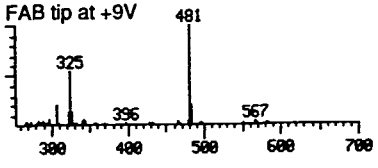

POLYMER RESULTS

Poly(methyl methacrylate) was analyzed by CF-FAB using tetrahydrofuran producing protonated molecular ions at m/z 403, 503, 603, 703, 803, 903, and 1003, corresponding to oligomers 4 thru 10. A second series of ions separated by m/z 100 from 371 to 971 was also detected. When the poly(methyl methacrylate) was analyzed by static FAB, this second series of ions predominated the mass spectrum indicating these ions were not adducts related to tetrahydrofuran since 3-nitrobenzyl alcohol was the matrix. Desorption chemical ionization (DCI) also showed both the m/z 371 series and the m/z 403 series. The m/z 503 ion was collisionally dissociated showing a loss of m/z 32, suggesting a neutral loss of methanol, which corresponds to the m/z 371 series.

The CF-FAB spectrum of poly(methyl methacrylate) enhances the protonated molecular ions while the fragment ions predominate in the static FAB spectrum.

Poly(methyl methacrylate) by CF-FAB using tetrahydrofuran

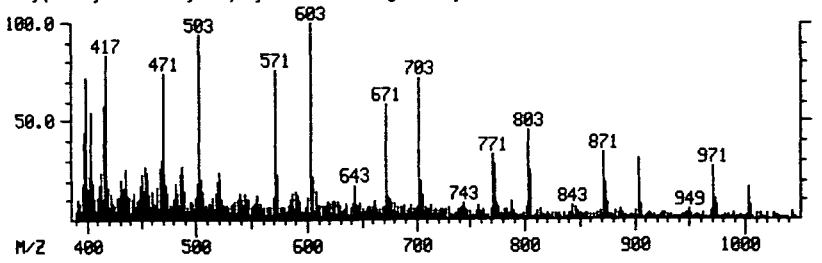

Poly(methyl methacrylate) static FAB using 3-nitrobenzyl alcohol

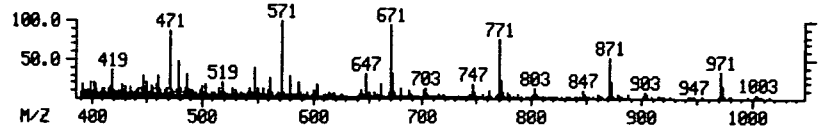

CONCLUSIONS

The use of tetrahydrofuran as a solvent for CF-FAB has made possible the analysis of compounds not soluble in polar mobile phases. Since tetrahydrofuran does not require the addition of a matrix, the mass spectra are not complicated by additional matrix ions. As demonstrated, the background ions produced by tetrahydrofuran are minimal; also stability can be achieved and maintained.

CF-FAB using tetrahydrofuran can be used to analyze both nonpolar polymers and polymer additives providing molecular weight information as demonstrated with poly(methyl methacrylate) and Tinuvin 770.

REFERENCE: J. Hau, W. Schrader, and M. Linscheid, *Continuous Flow FAB/MS: A concept to improve the sensitivity*, presented at the 1992 ASMS by M. Linscheid.

ANALYSIS OF ACYLCARNITINES IN BIOLOGICAL FLUIDS BY ELECTROSPRAY LC/MS: APPLICATION TO HUMAN METABOLISM STUDIES.

Barbara M. Kelly, Malcolm E. Rose, Dept of Chemistry, The Open University, Milton Keynes, MK7 6AA, UK.
Alison E. Ashcroft, Stephen Lowes and Mark A. McDowall, Fisons Instruments/VG BioTech, Altrincham, WA14 5RZ, UK.

Acylcarnitines are important metabolites for the diagnosis of several human genetic diseases, including defects in the ß-oxidation of fatty acids and in the metabolism of branched-chain amino acids.

This poster reports preliminary applications of positive-ion electrospray mass spectrometry to underivatised acylcarnitines. This approach would not require derivatisation and the routine nature of electrospray instruments offers an affordable and attractive method of analysis.

In the carrier solution for electrospray (water/acetonitrile, 50:50), acylcarnitines exist as cations (protonated molecules). The singly charged protonated form of each acylcarnitine gives the only significant peak in its positive-ion electrospray mass spectrum.Octanoylcarnitine is a principal metabolite for the diagnosis of medium-chain acyl-CoA dehydrogenase deficiency (MCADD). Its electrospray mass spectrum consists of $[M+H]^+$ ions at m/z 288. For examining acylcarnitines in humans, the most appropriate medium is blood because the range of acylcarnitine concentrations in blood is much more limited and stable than that in urine. In addition, the profile of acylcarnitines in blood provides a more direct insight into biochemical status. Blood spots are taken from all newborns in the UK and USA, ideally within the first week of life. Typically, four blood spots are taken onto Guthrie paper (a type of filter paper) and in this form are stored and/or transported for analysis. Mass spectrometry was performed using a VG Platform, benchtop, single quadrupole mass spectrometer (Fisons Instruments/VG BioTech).

Prior to the examination of clinical examples, 0.5ml aliquots of fresh blood from a healthy adult were spiked with different octanoylcarnitine concentrations and spotted onto Guthrie paper such that the spots contained down to about 200pmol of the carnitine ester. The acylcarnitine content was then recovered from a spot of 6mm diameter punched from the Guthrie card. Each spot was sonicated twice for 10 mins in chloroform/methanol (2:1). The combined extracts were then dried and the residue dissolved in the solution for LC/electrospray mass spectrometry.

LC/MS was performed using an Applied Biosystems, Aquapore RP-30, 100 x 1.0mm column. Gradient elution at 4µl/min was performed using a linear gradient from 95% 0.01M ammonium acetate, 5% MeOH to 100% MeOH over 20 mins. The LC eluent was introduced directly to the electrospray source.

Figure1 shows the LC/MS analysis results from a) a blood spot spiked with 5nmol of octanoylcarnitine, b) a blood spot taken as a blank from a healthy adult andc) a blood spot from a

neonatal MCADD patient The spiked blood sample gave a peak which eluted at 18.5min. The m/z 288 mass chromatogram clearly shows the acylcarnitine peak and the mass spectrum is consistent with octanoylcarnitine.

The normal blood sample gave a low response on the m/z 288 mass chromatogram at 18.5min. This may be due to the normal levels of octanoylcarnitine present in healthy patients. The peak eluting with a retention time (RT) of 20 mins was attributed to a non-acylcarnitine component.

The sample from the MCADD patient clearly gives an elevated response in the m/z 288 mass chromatogram at the retention time for octanoylcarnitine. From the mass spectrum, it is proposed that an additional component, producing a base peak at m/z 235, co-elutes with the octanoylcarnitine. Other ions recorded in the spectrum are consistent with the acylcarnitine.

Acylcarnitines are readily and directly compatible with electrospray mass spectrometry. To all intents and purposes, the mass spectra obtained comprise only protonated molecules. The limits of detection, reproducibility and linearity of the method have yet to be assessed. These aspects will be studied before the method is applied to quantitative analysis of biological fluids for a broad range of acylcarnitines. However, our initial results suggest that it is worth investigating electrospray mass spectrometry as a new, direct approach to the determination of acylcarnitines in clinical samples.

We thank the Foundation for the Study of Infant Deaths for a research assistantship (to B.M.K.).

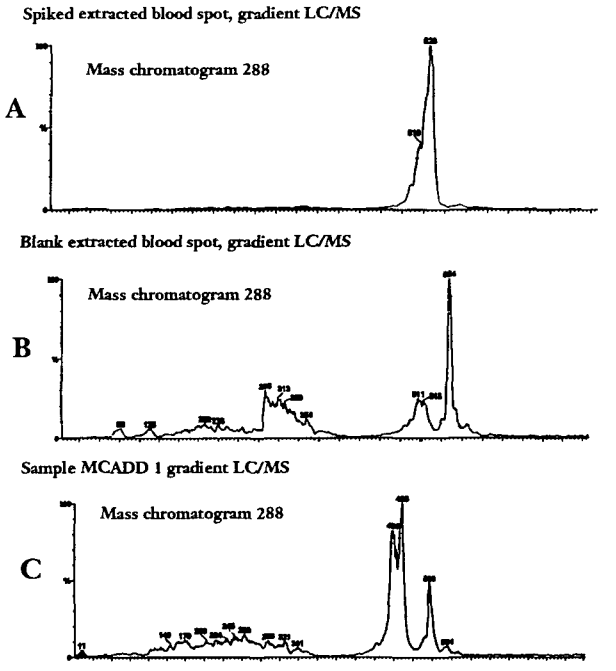

Derivatives for Detection of Anabolic Ketosteroids by Positive Electrospray Mass Spectrometry

Kuruppu A. N. Dharmasiri[1], Z.-H. Huang[2], and J. Throck Watson[1,2], Departments of Chemistry[1] and Biochemistry[2], Michigan State University, East Lansing, MI 48824

In today's society, with the emphasis on physical fitness and "win-at-all-cost" philosophy, it is no surprise that abuse of "miracle drugs" such as anabolic steroids are such a widespread problem. Recent reports show that abuse of performance-enhancing steroids has even reached high school student athletes. This situation creates a practical need for sensitive, selective, and rapid methods for screening and confirmation of steroidal drugs in biological samples.

The atmospheric pressure chemical ionization (APCI) and thermospray approaches are the most widely used in LC/MS techniques to detect steroids and their conjugates. Recently, several research groups have developed negative electrospray mass spectrometry (ESI/MS) for the detection of steroid sulfate conjugates[1,2]. However, positive ESI/MS has not shown advantage in analyses of free steroids because of lack of sensitivity. In this report, we describe modification of anabolic steroids using Girard's T reagent[3] or hydroxyl amine to produce derivatives that greatly enhance their detectability by positive ESI/MS. Girard's T reagent carries a positively charged quaternary ammonium moiety that enhances the ESI response of the derivatives[4]. We have investigated reaction conditions for derivatizing testosterone analogs: testosterone, methyltestosterone, and nandrolone. This procedure is advantageous because it forms water-soluble hydrazone derivatives quickly under mild conditions and it introduces a pre-formed positive charge onto the steroid structure, thereby creating a sensitive means for detecting the steroid using positive ESI/MS. These derivatives are detectable at the low femtogram level using the selected ion monitoring mode. The derivatives are separated by reversed phase HPLC with a C_{18} column and mobile phase gradient of acetonitrile/*i*-propanol/TFA (60/40/0.1 %v/v) and H_2O/0.1%TFA. ESI/MS studies were carried out with a home-built ESI interface coupled to a HP 5985 single quadrupole mass spectrometer. The ESI mass spectrum of testosterone hydrazone is shown in fig. 1. The rate of the reaction with Girard's T reagent is greatly increased (see fig. 2) by adding acetic acid to the reaction mixture. The dependance of reaction rates on temperature and time are as shown in fig. 3.

We also investigated oxime formation of anabolic steroids with hydroxyl amine hydrochloride. Preliminary results indicate that the oxime derivative can be formed

rapidly with ketosteroids, and that it increases the detectability of the steroid to positive ESI/MS. The oxime derivatives can be detected at the femtogram level.

We are presently investigating the applicability of these derivatives to the analysis of other anabolic steroids with the view toward their quantitative determination in urine samples.

References

1. Kletke, C; Roitman, E.; Bitsch, F.; Shakleton, C. *ASMS Proc.* 1992
2. Weidolf, L. O. G; Henion, J. D. *Biomed. Env. Mass. Spectrom.* 15, 283-289 1988
3. Wheeler, O. H *J. Chem. Edu.* 45 (6) 435, 1968
4. Conboy, J. J.; Henion, J. D.; Martin, M. W.; Zweigenbaun, J. A. A., *Anal. Chem.* 62, 800, 1990

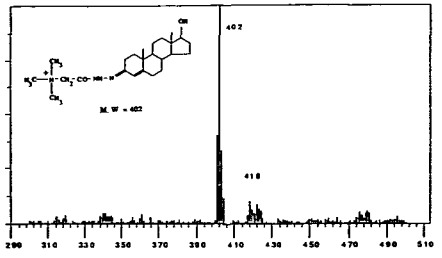

Fig. 1 ESI Mass Spectrum of Testosterone Hydrazone

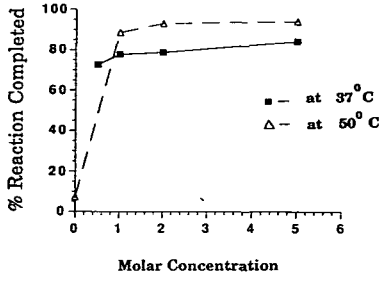

Fig. 2 Dependence of % reaction completed on HOAc conc.

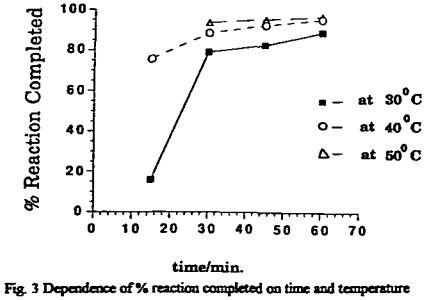

Fig. 3 Dependence of % reaction completed on time and temperature

Determination of 5HT$_3$ Antagonists in Serum Using Heated Nebulizer and Electrospray LC/MS and LC/MS/MS, K.A. Halm, M.A. Moseley and S.E. Unger, Department of Drug Metabolism, Glaxo Inc. Research Institute, Five Moore Drive, Research Triangle Park, NC 27709

5-Hydroxytryptamine (5HT$_3$) antagonists such as ondansetron (GR38032) are effective in the prevention of nausea and emesis in patients receiving chemotherapy and radiotherapy. These selective 5HT$_3$ antagonists are potent drugs, and highly sensitive, selective analytical methods are needed to determine their levels in serum.

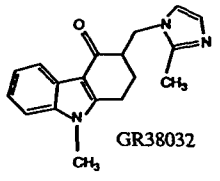

GR38032

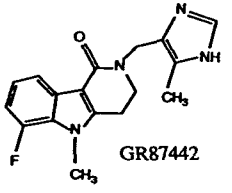

GR87442

Using 1 mL of serum, some 5HT$_3$ antagonists such as GR87442 can be quantified with fluorescence detection to 0.2 ng/mL; others such as GR38032 exhibit weak fluorescence and can only be quantified with UV absorption to higher levels (1 ng/mL). Radioimmunoassay (RIA) has been useful in determining lower serum levels of GR38032 and is capable of detecting as little as 50 pg/mL. The RIA shows cross-reactivity with human metabolites but, by using solid phase extraction to resolve the interfering metabolites, can be made more specific. Mass spectrometry offers both detection sensitivity and specificity in analysis. Provided analysis times are short, it also offers high throughput and therefore can be cost-effective.

While GR87442 is capable of analysis using gas chromatography (GC), it exhibits considerable tailing and poor sensitivity. GR38032 degrades upon injection in either split-splitless or on-column modes, making GC/MS a poor choice for analysis. Both drugs perform well using LC/MS and prior analytical methodology developed for determining higher levels of the 5HT$_3$ antagonists could be adapted to LC/MS.

Thermospray LC/MS was capable of detecting GR87442 in 0.2 mL of serum to 5 ng/mL but showed poor precision and accuracy. The SCIEX heated nebulizer (HN) interface gave significantly better response and allowed drug to be measured accurately to 0.2 ng/mL from 0.2 mL of serum. Similarly, GR38032 showed good promise for detecting low picogram amounts. For GR38032, adsorption on the interface was noted as high nebulizer and orifice temperatures gave best response and peak shape. However, no less than 2 pg (Fig. 1) could be reliably detected using heated nebulizer with LC/MS or LC/MS/MS detection.

Electrospray (ESI) detection exhibited better sensitivity for GR38032 or GR87442 in either MS or MS/MS modes. As little as 0.5 pg could be measured (Fig. 2). Using LC/MS, the electrospray response showed a considerable bias at low levels. It was therefore necessary to use MS/MS detection (10% Ar:90% N$_2$; CGT = 550; 30 eV) to accurately determine low drug levels.

Compound	Parent	Fragment 1	Fragment 2	Fragment 3
GR38032	294	212	184	170
d3-GR38032	297	212	184	170
GR87442	313	219	176	95

Solid phase extraction of drug from serum was used. The strong adherence of drug to the Varian C8 cartridge allowed considerable purification before elution in 80:20 methanol: 2 mM ammonium acetate. Following evaporation, 25 uL of mobile phase, 50:50 2 mM ammonium acetate (pH 4.5):ACN, was used to reconstitute the sample for analysis. Five microliter aliquots were injected from the Alcott 738 autosampler onto a 1 x 100 mm, 5 micron Keystone Hypersil BDS C8 column at 50 uL/min. This allowed a minimum of three injections of analyte.

Several internal standards were evaluated for GR38032. GR38032 in which the 2-methyl had been deuterated was available and chosen as internal standard. Since the internal standard gave identical HPLC retention and MS/MS fragmentation, detection sensitivity was limited by the need to adequately (mass) resolve the m/z 294 analyte from the m/z 297 deuterated internal standard.

Figure 3 shows representative chromatograms at the 20 pg/mL level from serum. A standard curve from 10-200 pg/mL gave acceptable precision with the limit of quantification determined by the need to adequately resolve the stable isotope internal standard. More sensitivity could be gained by degrading mass resolution; however, the resulting bias at the 10 pg/mL level was unacceptable.

For determining low serum levels of 5HT$_3$ antagonists, electrospray LC/MS/MS offers the lowest limits of detection. While the heated nebulizer allows larger injection volumes and LC flow rates, its (on-column) sensitivity is 5x less than electrospray. Both methods have been used effectively with SPE serum extracts. More recently, a heated capillary electrospray interface (Finnigan Corp.) has shown comparable performance for the analysis of GR38032 to the SCIEX API-3.

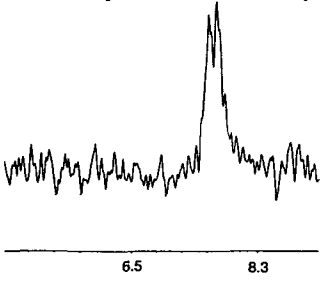

Fig. 1 HN LC/MS/MS of 2 pg GR38032

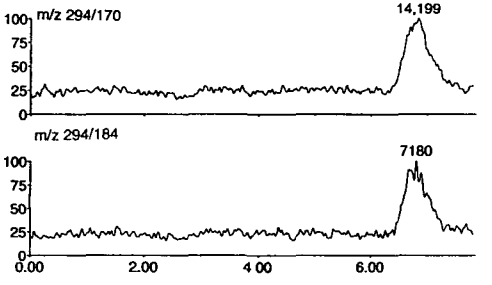

Fig. 2 ESI LC/MS/MS of 1 pg GR38032

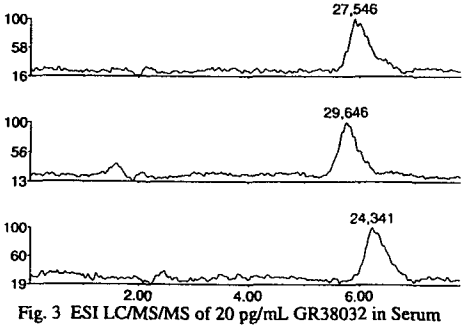

Fig. 3 ESI LC/MS/MS of 20 pg/mL GR38032 in Serum

Identification of Xenobiotic Conjugates by Positive and Negative Ion Electrospray Mass Spectometry

*C. E. Parker[1], L.T. Burka[2], and K. B. Tomer[1]
1. Laboratory of Molecular Biophysics, and
2. Environmental Toxicology Branch,
National Institute of Environmental Health Sciences,
Research Triangle Park, NC 27709

Identification of metabolites is an important component of the characterization of compounds undergoing toxicity and carcinogenicity studies in the National Toxicology Program. Most of these metabolites are polar, non-volatile, and thermally-labile. We have recently been successful in applying electrospray ionization mass spectrometry (ESI/MS) to a variety of xenobiotic conjugates isolated from rat bile and feces, and rat and mouse urine. Compounds studied included oxazepam (an antianxiety agent and a metabolite of Valium), ethoxyquin (used as an antioxidant in pet food and to preserve the vitamin A content in feed), and methacrylonitrile, a monomer used in the plastics industry.

Metabolites identified included glutathione, glucuronide, and sulfate conjugates:

Two sulfate conjugates and a glucuronide of oxazepam were isolated from rat feces, rat urine, and mouse urine, respectively, and identified. The positive ion ESI mass spectrum of one of these is shown in Figure 1. NMR spectra were obtained and were consistent with structures shown.

Five metabolites of ethoxyquin were also identified. These included two glucuronides from rat and mouse urine (one of which is shown in Figure 2), and three glutathione conjugates from rat bile. Positive identification was obtained for the glucuronides and for the EQBM-B glutathione (Figure 3) by a combination of NMR and ESI/MS. The two other glutathione conjugates are positional isomers, whose absolute configurations have not yet been established. Interestingly, in a previous study of ethoxyquin metabolism using GC/MS (1), no sulfur-containing metabolites were found, probably due to thermal degradation.

A glutathione conjugate of methacrylonitrile, and a glutathione conjugate of its cytochrome P450 oxidation product were identified in rat bile. Postulated structures for these two compounds were confirmed by NMR, synthesis, and co-chromatography.

Protonated molecules were obtained by positive ion ESI/MS for the glutathione conjugates. Both positive and negative ion spectra were useful for the identification of the glucuronide conjugates. No useful positive ion ESI mass spectra were obtained for the sulfate conjugates, but these sulfate conjugates did give $(M-H)^-$ ions in the negative ion mode.

ESI/MS has been very useful in providing molecular weight information for these conjugates, but, in general, little structural information was obtained. ESI/MS has assisted in the identification of these conjugates, including some compounds where other mass spectral techniques, including fast atom bombardment (FAB)/MS, had been unsuccessful.

1. Skaare, J.U., *Xenobiotica*, **1979**, 9, 659-668.

Figure 1

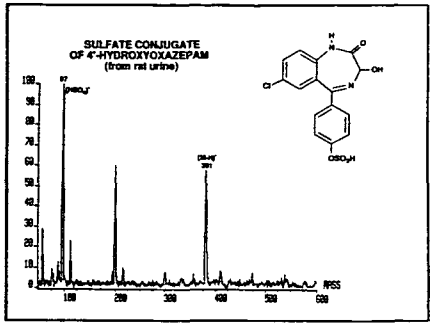

Figure 2

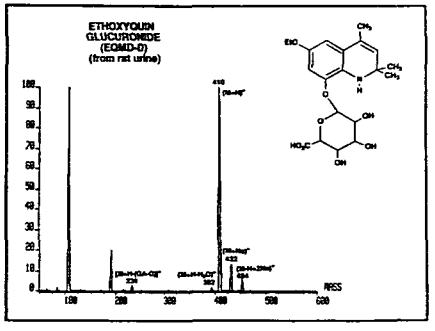

Figure 3

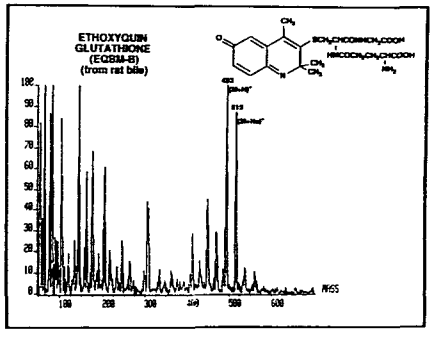

Identification of Metabolites of RG 12915A in Human Urine Using API-LC/MS and LC/MS/MS Techniques

***Tang, S.-Y.; Bordeaux, K.; Berger, P.; Rhone-Poulenc Rorer Central Research, Collegeville, PA, 19426**

RG 12915A, 4-[N-(1-Azabicyclo[2,2,2]octan-3(S)-yl]-2-chloro-5[a(S)-9a(S)-(5a,6,7,8,9,9a-hexahydro)]dibenzofuranocarboxamide hydrochloride, is both an orally and intravenously active anti-emetic agent. Its efficacy has been demonstrated for the prevention of cisplatin-induced emesis in ferrets and dogs, and, it is currently undergoing clinical trials.

Urine samples from human subjects dosed with 200mg of RG 12915A were collected and pooled up to 12 hours after dosing. Samples were lyophilized without any prior treatment or cleaned up by solid phase extraction using CN Bond Elut cartridges. HPLC was performed using a 250 X 4.6 mm column packed with Zorbax CN, 5um bonded phase. The mobile phase was acetonitrile/0.1M ammonium acetate containing 0.2% acetic acid (35:65 v/v). The components were detected by UV absorption at 254nm and then passed into the Heated Nebulizer (SCIEX) interface and ionized by API corona discharge.

The molecular weight of each component was determined by APCI/MS and confirmed by IonSpray using a micro-bore column. LC/MS data have revealed that the protonated molecular ions of two major metabolites were m/z 377 and one other major metabolite was 393, respectively, 16 and 32 amu more than the parent drug. Each contains one chlorine atom.

To elucidate the structure of each metabolite, on-line LC/MS/MS was carried out to obtain the daughter ion mass spectra for each parent ion using argon as a collisional gas at energy of 50 to 100eV. The daughter ion spectrum of RG 12915 has shown characteristic fragments and provided structural information concerning the metabolites. The major metabolite eluted at ~18 min. has been confirmed as the quinuclidine N-oxide of RG 12915 by its molecular weight, retention time, and daughter ion spectra. An N-oxide metabolite is very common with drugs containing a tertiary nitrogen such as a quinuclidine moiety. By comparing of the daughter ion spectra of synthetic standards with unknown metabolites, we have identified two additional major metabolites as a hydroxylated RG 12915 and an N-oxide of hydroxylated RG 12915 . The daughter ions also indicated that the hydroxylation occurred on the tetrahydrobenzofuran ring. The daughter ion spectrum of one minor metabolite has also indicated an isomer of hydroxylated RG 12915.

In summary, the API Heated Nebulizer is a very sensitive LC/MS interface for phase I metabolite identification. Using on-line LC/MS and LC/MS/MS, we have identified the major metabolites of RG 12915 in human urine as 1). N-oxide

of RG 12915, 2). Hydroxylated RG 12915, and 3). N-oxide of the hydroxylated RG 12915. At least two isomers of hydroxylated RG 12915 have been found.

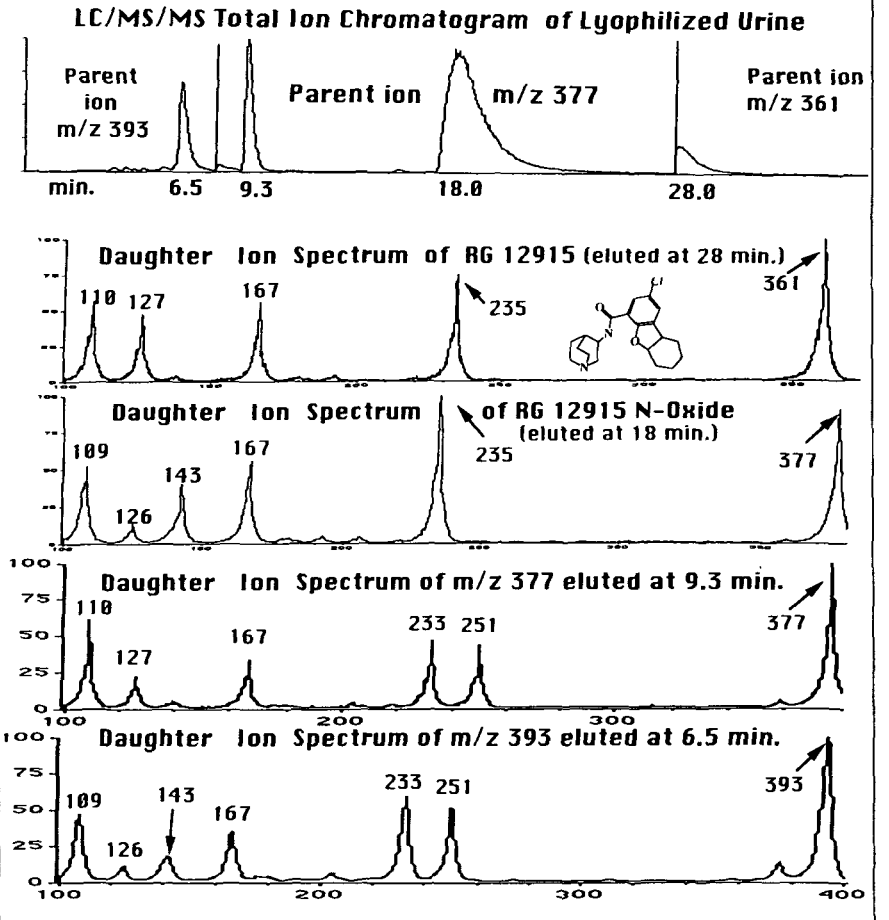

Characterization of Biliary Rapamycin Metabolites by Ionspray Liquid Chromatography / Mass Spectrometry.

K. Chan, P. Wang, †T. Sakuma, J. Scatina, D. Cochran, L. Humber, and S. Sisenwine,
Wyeth-Ayerst Research, Princeton, NJ 08543, and
†Perkin-Elmer Sciex Instruments, Thornhill, Ontario L3T 1P2, Canada.

Rapamycin (AY-22,989) is an antitumor, antifungal, and immunosuppressive agent isolated from the fungus *Streptomyces hygroscopicus*. It is currently under development as an immunosuppressant after transplantation. In metabolic studies related to other immunosuppressants such as FK506 and cyclosporin, some biotransformation products were observed to have activity or toxicity. Therefore, it is important to characterize the metabolites of rapamycin so as to investigate their activity and toxicity. Although two *in vitro* metabolites of rapamycin had been reported by Christians *et. al.* [1], this is the first report of the *in vivo* metabolites of the drug. In the earlier study, Christians *et. al.* isolated the metabolites by HPLC and characterized them by DCI and FAB MS. In addition to DCI and FAB, we have observed that the negative ion ionspray (IS) mass spectrum of rapamycin showed structurally informative fragments [2]. Since IS mass spectrometry can be easily coupled with HPLC, we have employed on-line IS-LC/MS and LC/MS/MS to characterize the *in vivo* (biliary) metabolites of rapamycin in rats.

All LC/MS experiments were carried out on a PE Sciex API III triple stage quadrupole mass spectrometer equipped with the ionspray interface. The bile sample was extracted with ethyl acetate, evaporated to dryness and reconstituted in 65/35 methanol/water. HPLC separations were achieved by a 2 mm x 15 cm Beckman Ultrasphere C_{18} column. The mobile phase consisting of water and methanol, each containing 50 mM ammonium acetate, was delivered by a Perkin Elmer Model 250 Binary LC pump at a flow rate of 200 µl/min. A linear gradient of 58% methanol to 85% methanol in 80 minutes was used. The LC eluant was split 3:1 with 50 µl/min entering the ionizer of the mass spectrometer.

The reconstructed ion chromatogram (RIC) obtained from the LC/MS analysis of the biliary metabolite sample shows more than twenty one peaks (Figure 1). In IS MS, rapamycin generates mostly $[M-H]^-$ and $[M+CH_3COO]^-$. Assuming the metabolites of rapamycin generates the same molecular ion species, the MWs of sixteen of the twenty one components can be deduced from their mass spectra. Simple mathematics then suggests these metabolites are formed by mono- and di- hydroxylation, or a combination of demethylation and hydroxylation of rapamycin as shown in Table 1. The rest of the peaks in the RIC may contain a mixture of unresolved components or some low mass compounds.

In attempts to gain information on the sites of metabolic transformation, LC/MS/MS experiments were carried out. Useful data were obtained on only the five major components, peaks 4, 10, 13, 18, and 19 depicted in Figure 1. For example, Figure 2 shows the MS/MS spectrum obtained from peak 13. The MW of this metabolite has been derived from the LC/MS experiment to be 929.5, suggesting a single hydroxylation. The MS/MS spectrum of this compound shows that the northern fragment is the same as the parent compound at m/z 321. The southern fragment of this metabolite is detected at m/z 606, indicating one additional oxygen relative to rapamycin. The ion at m/z 240 can be assigned as a carboxylate ion containing C12 to C23 of rapamycin. This fragmentation can be promoted by the hydroxylation at any one of the carbon from C8 to C11. Other ions observed in the MS/MS spectrum of this metabolite can be assigned as further decomposition products of the southern fragment.

Our results on the *in vivo* metabolites are in general agreement with the *in vitro* data reported by Christians *et. al.* However, the structures of the metabolites reported here are drawn in the macrolide ring opened form. This proposal is derived from the FAB MS data on isolated samples of these metabolites: macrolide ring closed rapamcycin analogs generate $M^{-\cdot}$ while the ring opened isomers yield $[M-H]^-$.

Furthermore, the addition of 16 amu can also be assigned as epoxidation across a double bond instead of hydroxylation. Data from other spectroscopic techniques such as nuclear magnetic resonance spectroscopy should be obtained to verify these structure proposals.

REFERENCES:

1. Christians, U.; Sattler, M.; Schiebel, H.M.; Kruse, C.; Radeke, H.H.; Linck, A.; and Sewing, K.F. *Drug Metabolism Disposition* 1992, **20**, 186-191.
2. Cantone, J.; and Chan, K. *Proceedings of the 40th ASMS Conference on Mass Spectrometry and Allied Topics*, Washington, DC, May 31-June 5, 1992, 1881-1882.

TABLE 1

SUMMARY OF LC/MS ANALYSIS OF RAT BILIARY METABOLITES OF RAPAMYCIN

Peak number	MW	Possible metabolite[a]
1, 2, 4, 6	945.5	dihydroxylation
3, 8, 10, 12, 19	915.5	demethylation + monohydroxylation
11, 13	929.5	monohydroxylation
5	917.5	2 x demethylation + dihydroxylation
9	931.5	dihydroxylation + demethylation (or hydrolysis product)
17	901.5	2 x demethylation + monohydroxylation
18, 20	913.5	isomer of rapamycin
7, 14, 15, 16, 21	???	unknowns

a. Epoxidation across a double bond can be substituted for hydroxylation.

FIGURE 1

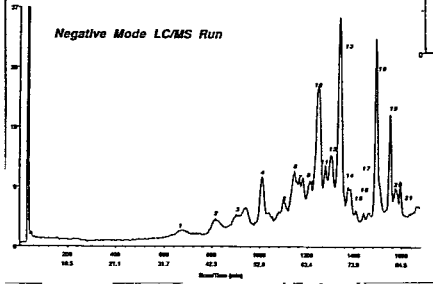

FIGURE 2

MS/MS Spectrum of Peak 13

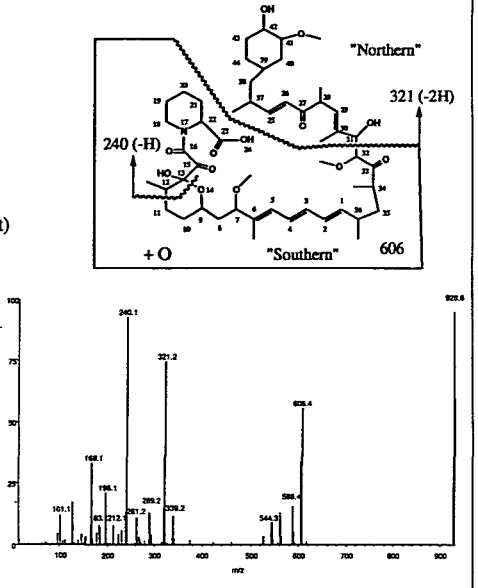

SAXITOXIN DETECTION IN RAT URINE BY HPLC AND CE-ESIMS

H.B. Hines, E.E. Brueggemann, and R.G. Stafford

Toxinology Division, United States Army Medical Research
Institute for Infectious Diseases, Ft. Detrick,
Frederick, MD

Paralytic shellfish poisoning (PSP) is caused by a group of toxins produced by several species of marine dinoflagellates. High toxicity and repeated occurrence have prompted the establishment of shellfish monitoring programs in the United States, Canada, and other countries to prevent PSP. Several instrumental methods were developed to analyze shellfish tissues. In addition to these capabilities, it would also be beneficial to have a diagnostic tool for assessing human exposure. Consequently, we conducted an initial evaluation of HPLC and CE-ESIMS detection capabilities for saxitoxin (STX) spiked in rat urine. STX was chosen because it is typically associated with PSP. Urine was selected because a previous study with tritiated saxitoxinol (reduced STX) demonstrated that excretion may occur principally in urine (Hines et al., Toxicon, in press).

Urine was collected from male Fisher 344 rats housed individually in metabolic cages. One ml aliquots of filtered rat urine were spiked with varying levels of STX and applied to solid-phase extraction columns. A double ion-exchange procedure was used to isolate the toxin. After isolation, HPLC and CE-ESIMS were used to identify STX.

The HPLC method used in this study followed the prechromatographic oxidation method of Lawrence et al. (JAOAC, 74: 404, 1991). Fluorescence detection of oxidized STX was accomplished with wavelengths of 346 and 408 nm for excitation and emission, respectively.

For CE-ESIMS analyses, an untreated fused silica column (50 μm x 100 cm) was fitted to a Finnigan Mat 700 mass spectrometer. An UV detector was placed in-line approximately 45 cm from the anode end of the column. A 1.0% acetic acid buffer and 23 kV were used for CE analysis. Electrokinetic injections were made by applying 8 kV to the sample (dissolved in water) for 15 sec. A sheath liquid consisting of 75% isopropanol and 5% acetic acid was utilized at 2 μl/min as the make-up flow. Either selected ion monitoring of the STX pseudomolecular ion at m/z 300 or scanning from m/z 250 to 350 in 0.5 sec was used to detect STX, depending upon the concentration in urine.

STX recoveries from rat urine averaged 82 ± 1.5 % when STX concentrations were kept below 50 ng/ml. This average recovery from urine was slightly higher than the 75% reported by Mirocha et al. (Rapid Commun. Mass Spec., 6: 128, 1992), who used a weak cation exchange column to isolate STX from urine spikes.

Figure 1 displays results for standard STX, STX from rat urine (2 ng/ml), and a rat urine blank (Fig. 1A, B, and C, respectively). The STX peak is identified with an S.

The most consistent and lowest level of detection with CE-ESIMS was 500 ng/ml (Fig. 2). STX was clearly identifiable in the SIM electropherogram. The peak is marked with an asterisk in Figure 2 in the SIM trace (A), the UV trace (B), and the RIC (C).

These results for HPLC and CE-ESIMS paralleled those obtained previously for shellfish and rat urine. For example, STX detection limits of 10-15 ng/g of tissue (s/n = 3:1) were reported by Lawrence et al. (JAOAC, 74: 404, 1991) with the prechromatographic oxidation, HPLC procedure. A C_{18} SPE procedure was employed for sample preparation for that work. Pleasance et al. (Rapid Commun. Mass Spec., 6: 14, 1992) reported a detection limit of 0.8 - 1.0 μg/ml for STX with nebulization-assisted electrospray ionization, SIM, and reversed-phase chromatography. Mirocha et al. (Rapid Commun. Mass Spec., 6: 128, 1992) established an injection detection of 200 pg/200 nl for standard STX with CF-FAB and SIM. STX was detectable in spiked urine samples at 20 μg/ml with the same conditions. STX identification was verified with HPLC and nebulization-assisted electrospray ionization mass spectrometry.

The prechromatographic, HPLC method was directly applicable to urine analysis. More effort will be required to improve the CE-MS detection limit to achieve the 1 - 5 ng/ml detection limit thought to be required for in vivo assays. It may be necessary to use capillary HPLC combined with ESIMS to achieve the balance between separation efficiency and sensitivity.

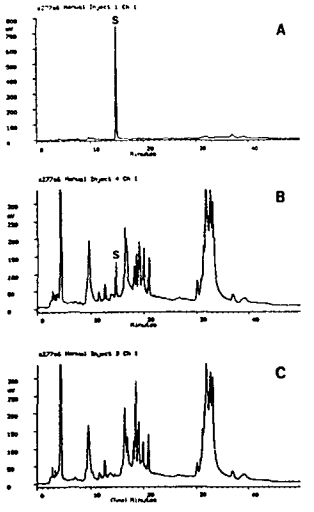

Figure 1. HPLC trace of STX in rat urine.

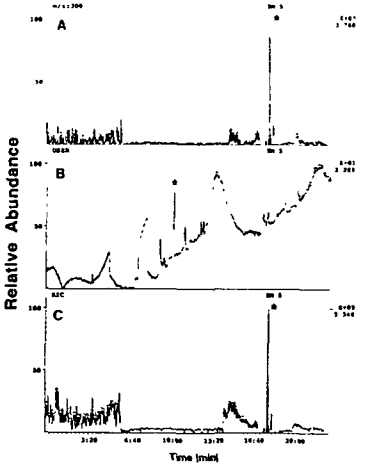

Figure 2. CE-ESIMS SIM and UV electropherograms of STX in rat urine.

Confirmation of Des-Methyl Danofloxacin Residues in Swine Liver by HPLC/ESI-Tandem Mass Spectrometry

Mark J. Cole, John F. Ericson, Hassan G. Fouda, and Marty J. Lynch

Drug Metabolism Department, Central Research Division, Pfizer Inc, Groton, CT 06340.

A specific assay was developed for the confirmation of des-methyl danofloxacin residues in swine liver. The assay utilizes HPLC and tandem mass spectrometry with electrospray ionization. Collisionally-activated dissociation of the des-methyl danofloxacin protonated molecule results in the formation of four product ions, two of which are present in greater abundance (Figure 1). Monitoring the precursor/CAD product reactions for the two most abundant product ions during HPLC provides the specificity and sensitivity required for a confirmatory assay.

Danofloxacin is a novel fluoroquinolone antibacterial agent for the treatment of respiratory diseases in food producing animals. The metabolite des-methyl danofloxacin is considered the marker residue in swine liver. The present assay was developed to satisfy regulatory requirements for the confirmation of des-methyl danofloxacin residues in swine liver. Des-methyl danofloxacin produces a protonated molecule at m/z 344 under positive ion electrospray conditions. Collisionally-activated dissociation of this ion produces the two product ions (m/z 326 and 255) used in this assay. These ions result from intramolecular dehydration (m/z 326) and the subsequent cleavage of pyrrolidine from the bicyclic piperazine moiety (m/z 255).

The present method provides confirmation of des-methyl danofloxacin residues in swine liver at the 50 ppb level. The analysis of blank liver gave no response under the assay conditions. The ratios of the two CAD product ions were similar for des-methyl danofloxacin standard solutions, fortified tissue extracts, and incurred tissue extracts. Representative chromatograms for injections of 6 replicate samples of blank and fortified (50 ppb) extracts are shown in Figures 2 and 3, respectively.

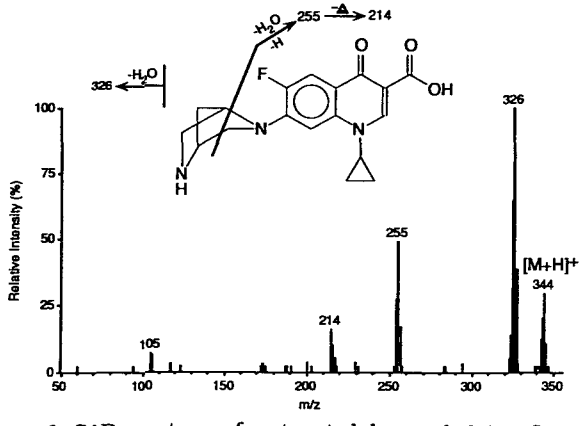

Figure 1. CAD spectrum of protonated des-methyl danofloxacin.

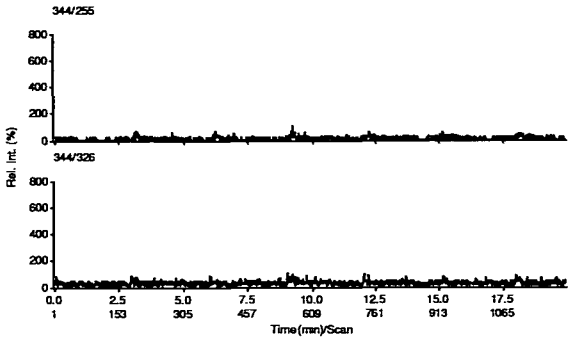

Figure 2. Chromatogram of multiple (n=6) samples of blank swine liver extracts.

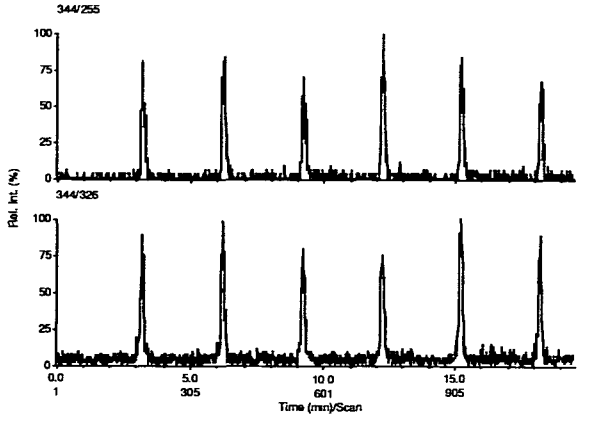

Figure 3. Chromatogram of multiple (n=6) samples of swine liver fortified at 50 ppb.

An HPLC/ESI-Tandem Mass Spectrometry Method for the Confirmation of Doramectin Residues in Cattle Liver and Fat

Mark J. Cole, Joanne Lukaszewicz, Mark A. Nowakowski, and Hassan G. Fouda

Drug Metabolism Department, Central Research Division, Pfizer Inc, Groton, CT 06340.

A specific assay was developed for the confirmation of doramectin residues in cattle liver and fat. The assay utilizes HPLC and tandem mass spectrometry with electrospray ionization. Collisionally activated dissociation of the ammoniated doramectin molecule results in a product ion spectrum rich in structural information (Figure 1). Monitoring the precursor/CAD product reactions for three of these product ions during HPLC provides the specificity and sensitivity required for a confirmatory assay.

Doramectin is a fermentation-derived, broad spectrum ectoparasiticide for cattle and swine. The present assay was developed to satisfy regulatory requirements for the confirmation of doramectin residues in cattle liver and fat. Doramectin produces an ammoniated molecule at m/z 916 under positive ion electrospray conditions. The ammonium is part of the HPLC mobile phase, and its doramectin adduct is formed more efficiently than the protonated doramectin molecule. Collisionally activated dissociation produces the three product ions (m/z 899, 593, and 145) used in this assay. These ions result from loss of ammonium (m/z 899), further dissociation through the loss of the disaccharide (m/z 593), and the formation of the α-L-oleandrosyl product ion (m/z 145).

This method provides confirmation of doramectin residues in cattle liver and fat at the 25 ppb level. The analysis of blank liver and fat gave no response under the assay conditions. The commercial anthelmintic, ivermectin, did not interfere with the assay. The ratios of the three CAD product ions were similar for doramectin standard solutions, fortified tissue extracts, and incurred tissue extracts.

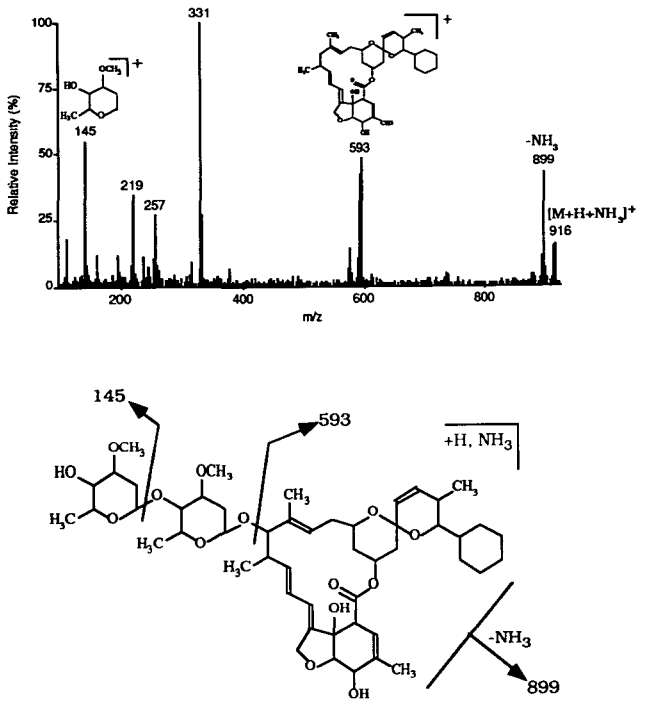

Figure 1. CAD spectrum of the protonated doramectin ammonium adduct. Assignments of the CAD product ions monitored in this assay are shown in the bottom part of the figure.

Identification of the Anticonvulsants Felbamate and Phenytoin and their Metabolites by Thermospray Tandem Mass Spectrometry in Clincial Human Urine Samples.

Robert E. Sparadoski., Leslie A. Romanyshyn, Joseph K. Wichmann, Norbert Kucharczyk, and R. Duane Sofia, Wallace Laboratories, Division of Carter–Wallace, Inc., Cranbury, NJ 08512

INTRODUCTION

Assessment of the metabolite disposition of felbamate, a novel antiepileptic drug currently under clinical development (1,2,3,4), and phenytoin in a drug–drug interaction study required determination of total urinary levels of felbamate, felbamate metabolites, phenytoin and metabolites. An HPLC/UV method was developed and used for analysis of clinical study urine samples following β–glucuronidase hydrolysis. The presence of an unknown and absence of a known phenytoin metabolite prompted the current investigation. The clinical urine sample hydrolysis and extraction procedures and the reverse phase HPLC conditions were presented. The TSP–LC/MS/MS conditions affording positive identification of felbamate, three felbamate metabolites, phenytoin, *p*–HPPH (5–(4–hydroxyphenyl)–5–phenylhydantoin), and partial identification of the unknown are discussed. Only trace levels of *m*–HPPH (5–(3–hydroxyphenyl)–5–phenylhydantoin) were found in the clinical samples.

RESULTS

TSP–LC/MS/MS and DCI tandem mass spectrometry analyses were performed on the clinical human urine hydrolysates, solvent standard mixes and isolated HPLC fractions from the clincial human urine sample. Clinical human urine sample 13608, obtained at steady state felbamate and phenytoin therapy, contained high levels of felbamate, felbamate metabolites and *p*–HPPH as well as detectable levels of the unknown, *m*–HPPH, and phenytoin by HPLC and TSP–LC/MS/MS. Clinical human urine sample 13621, obtained at steady state phenytoin mono–therapy, contained high levels of *p*–HPPH and detectable levels of the unknown and phenytoin by HPLC and TSP–LC/MS/MS. Figure 1 illustrates the simultaneous determination by HPLC/UV and TSP–LC/MS/MS of felbamate, felbamate metabolites, phenytoin, phenytoin metabolites and the unknown. First generation TSP–LC/MS/MS product spectra were obtained for $[M+H]^+$ or $[M+H+CH_3CN]^+$ precursor ions for W–2986, W–2992, W–873, felbamate (W–554), *p*–HPPH, *m*–HPPH, and phenytoin (PHT) confirming the identity of these compounds in the samples. Figure 2 represents the isobutane DCI–MS/MS spectra obtained from the $[M+H]^+$ ions of the isolated HPLC fraction of the unknown metabolite from clincial sample 13621 and from a phenytoin standard.

CONCLUSIONS

The presence of felbamate W–554 (2–phenyl–1,3–propanediol dicarbamate), three felbamate metabolites W–2986 (2–(*p*–hydroxyphenyl)–1,3–propanediol dicarbamate), W–2992 (2–hydroxy–2–phenyl–1,3–propanediol dicarbamate), and W–873 (2–phenyl–1,3–propanediol monocarbamate) and phenytoin (5,5–diphenyl–2,4–imidazolidinedione) and two metabolites *p*–HPPH (5–(4–hydroxyphenyl)–5–phenylhydantoin) and *m*–HPPH (5–(3–hydroxyphenyl)–5–phenylhydantoin) in clinical human urine hydrolysates was confirmed by simultaneous TSP–LC/MS/MS. A new phenytoin metabolite was partially identified by TSP–LC/MS/MS and DCI tandem mass spectrometry techniques. Only trace levels of *m*–HPPH (5–(3–hydroxyphenyl)–5–phenylhydantoin) were found in the clinical urine samples. The TSP–LC/MS/MS, EI and DCI–MS/MS spectra obtained for the unknown support the structure indicated, hydroxylation and methoxylation of a single phenyl ring of the phenytoin molecule. The exact placement of these moieties on the phenyl ring cannot be made from the data.

The use of TSP–LC/MS/MS for analysis of human urine sample extracts confirmed the identity of two drugs and five known metabolites quantitated by an HPLC/UV method. TSP–LC/MS/MS combined with direct probe techniques provided rapid partial elucidation of the structure of an unknown phenytoin metabolite.

FIGURE 1: HPLC/UV CHROMATOGRAMS AND TSP–LC/MS/MS RIC PROFILES

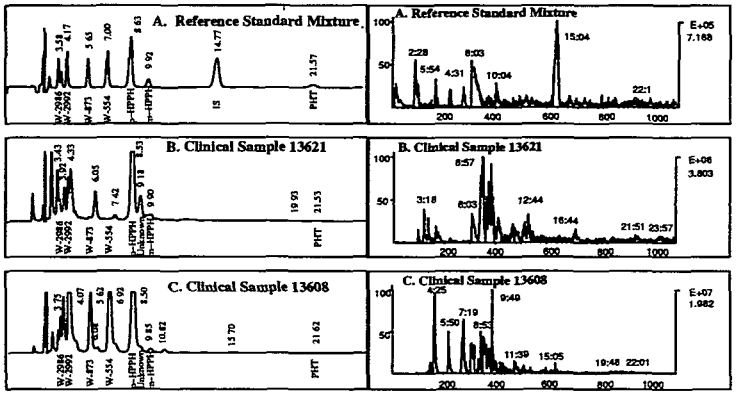

FIGURE 2: Isobutane DCI Spectra of Phenytoin and Unknown

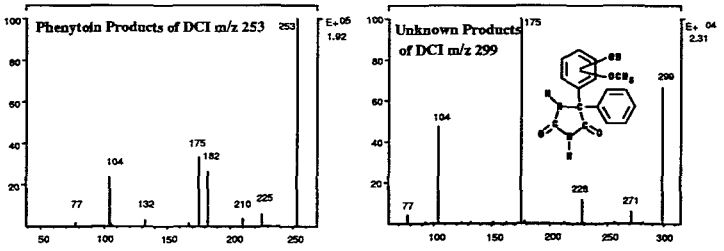

REFERENCES

1. J. T. Yang, V. E. Adusumalli, K. K. Wong, N. Kucharczyk and R. D. Sofia: Felbamate Metabolism in the Rat, Rabbit and Dog, *Drug Metab. and Disp.*, **19**, 1126–1134 (1991).
2. H. S. White, H. M. Wolf, E. A. Swinyard, G. A. Skeen, and R. D. Sofia: Neuropharmacologic Evaluation of Felbamate as a Novel Anticonvulsant, *Epilepsia*, **33**, 564–572 (1992).
3. I. E. Leppik and N. M. Graves, in R. Levy, R. Mattson, B. Meldrum, J. K. Penry and F. E. Dreifuss (Editors) *Antiepileptic Drugs*, Raven Press, New York, 983–994 (1989).
4. I. E. Leppik, F. E. Dreifuss, G. W. Pledger, N. M. Graves, M. Santilli, I. Drury, J. Y. Tsay, M. P. Jacobs, E. Bertram, J. J. Cereghino, G. Cooper, J. T. Sahlrrot, P. Sheridan, M. Ashworth, S. I. Lee and T. L. Sierzant: Felbamate for Partial Seizures: Results of a controlled Clinical Trial. *Neurol.*, **41**, 1785–1789 (1991).

Identification of the Felbamate Metabolite 3–Carbamoyloxy–2–Phenylpropionic Acid (W–3049) in Human and Dog Urine by Negative Ion Thermospray Tandem Mass Spectrometry

**Robert E. Sparadoski., Joseph K. Wichmann, Norbert Kucharczyk, and R. Duane Sofia, Wallace Laboratories, Division of Carter–Wallace, Inc., Cranbury, NJ 08512*

INTRODUCTION

The identification of 3–carbamoyloxy–2–phenylpropionic acid as a biotransformation metabolite of felbamate, a novel antiepileptic drug currently under clinical development (1,2) is discussed. Several metabolites have been previously reported in a quantitative positive ion HPLC/tandem mass spectrometry (TSP–LC/MS/MS) assay for felbamate and metabolites in dog urine (3). Negative ion TSP–LC/MS/MS afforded adequate sensitivity and selectivity to allow positive identification of W–3049 in urine samples without extensive sample preparation or concentration.

RESULTS

Ethyl acetate extraction of acidified urine samples was performed on human urine samples obtained from a bioavailability study in healthy volunteers who received a single oral dose of 1200 mg of felbamate and on dog urine samples collected during a metabolism study from a mature male beagle dog 0–8 hr after a single oral dose of 60 mg/kg of felbamate (unpublished data). The presence of free CPPA (W–3049) in the unhydrolyzed 0–4 hr postdose human urine sample and in the dog urine sample was confirmed by on–line negative ion thermospray tandem mass spectrometry (TSP–LC/MS/MS) of the extracts. Figure 1 illustrates the TSP–LC/MS/MS first generation product spectra of the m/z 208 $[M–H]^-$ ion from the CPPA peak from the standard, the clinical urine sample and the dog study urine sample, respectively. First generation product spectra were also obtained for the TSP fragment ion m/z 165 for the clinical urine sample and the dog study urine. Differences in the product spectrum of m/z 165 were observed in the dog study urine sample. The differences were due to endogenous interferences also found in blank dog urine.

FIGURE 1: TSP LC/MS/MS of m/z 208

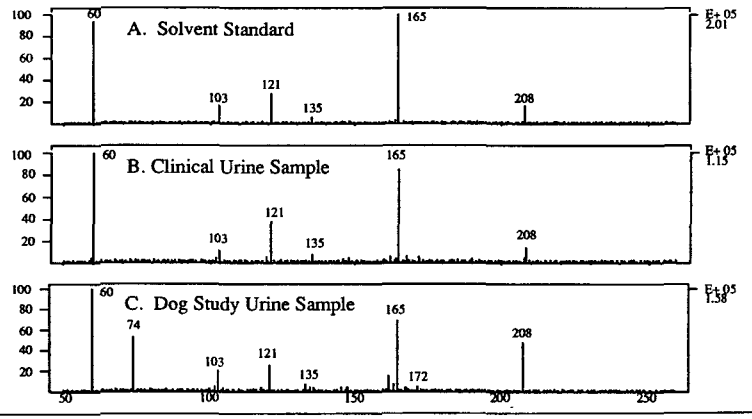

The proposed negative ion CID fragmentation pathway for the m/z 208 $[M–H]^-$ ion of CPPA is shown in Figure 2.

FIGURE 2: Proposed Negative Ion CID Pathway

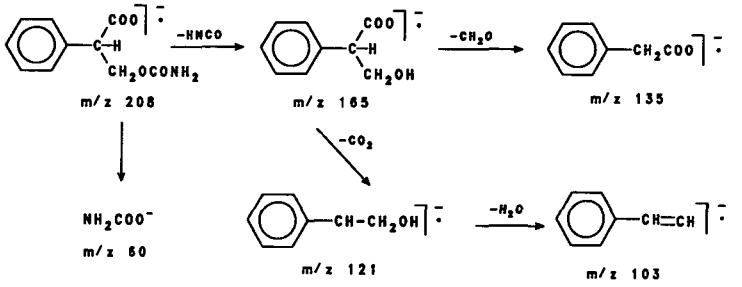

CONCLUSIONS

HPLC separation of CPPA in human and dog urine samples coupled with on–line thermospray tandem mass spectrometric techniques confirmed the identity of the metabolite as CPPA. The negative ion CID fragmentation scheme of the precursor CPPA $[M–H]^-$ ion, m/z 208, is proposed. The base peak in the first generation product spectra of m/z 208 is m/z 60, corresponding to the carbamate anion $[H_2NCOO]^-$.

The metabolite CPPA is the carbamoyl derivative of the natural product tropic acid (3–hydroxy–2–phenylpropionic acid), a constituent of tropane alkaloids, especially atropine. An easy synthetic procedure starting with the monocarbamate felbamate metabolite allowed us to obtain in good yield an authentic synthetic sample of CPPA. The procedure also confirmed the resistance of the carbamate group to chemical oxidation and to strongly acidic media.

We conclude that CPPA is a human urinary metabolite of felbamate contained in free form in the polar, water–soluble metabolite fraction.

REFERENCES

1. J. T. Yang, V. E. Adusumalli, K. K. Wong, N. Kucharczyk and R. D. Sofia: Felbamate Metabolism in the Rat, Rabbit and Dog, *Drug Metab. and Disp.*, **19**, 1126–1134 (1991).
2. I. E. Leppik and N. M. Graves, in R. Levy, R. Mattson, B. Meldrum, J. K. Penry and F. E. Dreifuss (Editors) *Antiepileptic Drugs*, Raven Press, New York, 983–994 (1989).
3. R.E. Sparadoski Jr., J.K. Wichmann, N. Kucharczyk, and R.D. Sofia. (1992) Proceedings of the 39th ASMS Conference on Mass Spectrometry and Allied Topics, Washington, D.C., May 31 – June 5, 1992, p. 1873.

Analysis Of The Squalestatins By On-line Packed Capillary LC-Dynamic LSIMS Mass Spectrometry

*S.J.Lane[1],K.Brinded[1],N.L.Taylor[2]

1. Mass Spectrometry,Structural Chemistry Department.
2. Mass Spectrometry,Department Of Natural Products Discovery .
Glaxo Group Research Limited,Greenford Road,Greenford Middlesex,UB6 OHE.

INTRODUCTION

The squalestatins are novel inhibitors of squalene synthase produced from a species of *Phoma*[1].Their structures were recently determined by a combination of spectroscopic,X-ray crystallographic and chemical methods[2].These structural studies defined the squalestatins as a new class of compounds which incorporate the highly functionalised bicyclic core, [1S-(1α,3α,4β,5α,6α,7β)]-4,6,7-trihydroxy-2,8-dioxabicyclo [3.2.1]-octane-3,4,5-tricarboxylic acid (Fig 1). Mass spectrometric characterisation of this class of compound was achieved using high and low resolution negative ion FAB which typically afforded strong $[M-H]^-$ molecular ions coupled with structurally informative fragment ions.

On-line negative ion thermospray LC/MS methods developed for biotransformation studies and minor metabolite characterisation were found to lack sensitivity and specificity.

The development of a packed capillary LC/UV/DLSIMS negative ion method showed improvements in sensitivity and specificity compared to TSP methods.

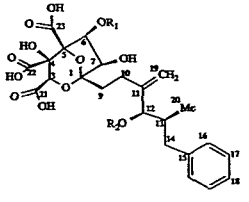

1	R_1 = COCH=CHCH(CH_3)CH_2CH(CH_3)CH_2CH_3	R_2 = Ac
2	R_1 = COCH=CHCH(CH_3)CH_2CH(CH_3)CH_2CH_3	R_2 = H
3	R_1 = H	R_2 = Ac
4	R_1 = H	R_2 = H

Fig 1

EXPERIMENTAL

A gradient of 20%B held for 1min→85% B in 20 mins (A=H_2O + 0.1% TFA and B=CH_3CN + 0.1% TFA,100μLmin^{-1}) from a dual syringe pump was delivered to an Acurate™ micro flow processor (LC Packings,The Netherlands) where it was mixed and split such that 3 μLmin^{-1} was delivered to a 1μL injector (Valco Instruments Co.Inc.TX,USA). The Vydac C18,300A,320μm id X 15 cm packed capillary column with a microguard column (LC Packings) used for the separation was connected to an ABI 759a UV absorbance detector (Applied Biosystems,UK) fitted with a U-Z

view capillary flow cell (LC Packings) The detector was connected to a "Tee" (Valco Instruments Co,Houston,TX,USA). 2μLmin^{-1} of a matrix solution (50:50 CH_3CN/H_2O + 0.1% TFA + 0.5% glycerol + 0.5% thioglycerol) was introduced post column through the "Tee" via a syringe infusion pump (Harvard Apparatus,Mass.,USA). The 5μLmin^{-1}resultant flow was directed to the dynamic LSIMS probe tip of a VG Analytical Autospec. The probe tip featured a screen/wick target The source was heated to 50C.

RESULTS

The in-line LC trace at 210nm and corresponding ion chromatograms resulting from the injection of 40ng of each squalestatin is shown in Fig 2.

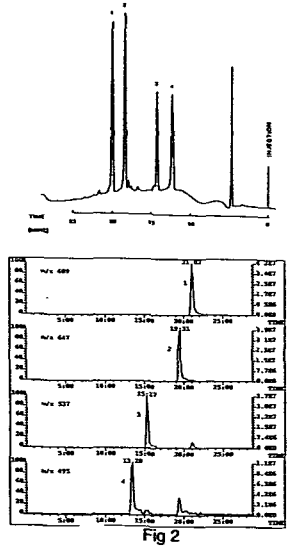

Fig 2

CONCLUSION

Spectra for the individual components were of good quality and the approach provides a routine method for the LC/MS of mixtures where LSIMS ionisation is necessary for the required specificity and sensitivity for a given compound class.

1. M.J.Dawson,J.E.Farthing,P.S.Marshall,R.F.Middleton,M.J.O'Neill, A.Shuttleworth,C.Stylli,R.M.Tait,P.M.Taylor,H.G.Wildman,A.D.Buss, D.Langley M.Hayes *J.Antibiotics.*, 45, 639 (1992).
2. P.J.Sidebottom,R.M.Highcock,S.J.Lane,P.A.Procopiou,N.S.Watson, *J.Antibiotics,* 45,648 (1992).

DCI, ESI and TSP investigations of ß-carbolines

*M.M. Brudny-Klöppel, W. Kuhnz, Schering AG, Berlin, Germany
K.D. Klöppel, GBF, Braunschweig, Germany

Introduction:

Benzodiazepines exhibit sedative, anxiolytic, anticonvulsant and muscle-relaxant effects by binding to the benzodiazepine receptor. ß-Carboline derivatives bind to the same receptor. Some of these drugs act as full agonists, others as partial agonists or antagonists. Abecarnil (isopropyl-6-benzyloxy-4-methoxymethyl-ß-carboline-3-carboxylate, ZK 112119, [1]), a representative of this class of compounds is being developed as an anxiolytic agent and studies in phase III are presently ongoing. During preclinical studies and clinical development it is necessary to determine and identify small amounts of drugs and their mostly unknown metabolites in several biological matrices (plasma, urine, bile, etc.). Because these matrices cause a high background in the mass spectra the knowledge of fragmentation reactions specific for the analyte under different ionization conditions is of great importance. Therefore, abecarnil and other structually related compounds were investigated systematically with several mass spectrometrical techniques. In this paper only a selection of the results obtained in positive DCI, ESI and TSP mode can be discussed.

Materials and Methods:

The experiments were performed on two different TSQ 700 triple stage quadrupole mass spectrometers (Finnigan MAT), one equipped with a DCI or TSP 2 (Finnigan) ion source, respectively and the other with an ESI ion source (Analytica). Standard solutions were prepared from the pure substances diluted in HPLC grade methanol (E.Merck). In all cases except ESI the sample concentration was 1 ng/µl. For the DCI experiments 4 µl of the standard solutions were placed on a rhenium wire dip The DCI probe was heated to a final temperature of 800°C. After each run the wire was cleaned at 1000°C for 30 seconds. The temperature of the ion source was 150°C. Methane was used as reactant gas. For ESI experiments 100 ng of the standards diluted in 10 µl methanol were introduced into the ion source at a flow rate of 2 µl per minute using a Harvard 980 532 syringe pump (Harvard Apparatus). The eluent consisted of a 2:1 (v/v) mixture of 5 % acetic acid and methanol Temperature of the shielding gas (N_2) was 190°C. For TSP analysis the instrument was equipped with a Waters 600 MS HPLC system (Waters Millipore). The ion source temperature was set to 240°C; the vaporizer temperature was found to be optimal at 115°C, the repeller voltage at 160 V, respectively. Routinely 100 µl of the standard solutions were used for each run. TSP-MS/MS experiments were performed using 200 µl of the samples and xenon as collision gas. A collision energy of 15 eV was applied.

Results:

Table 1 shows an overview of the investigated ß-carboline derivatives and figure 1 gives the basic structure of the abecarnil derivatives.The **DCI** results show that nearly in all spectra the molecular ion $[M+H]^+$ is the most abundant ion. The only exception is ZK 113944, because its t-butylester-group can easily be split, resulting in the free acid of abecarnil represented by the ion at m/z 363. Since methane was used as reactant gas, $[M+29]^+$ ions were detected in all cases. $[MH-32]^+$ ions indicate the loss of methanol from the methoxymethyl-group at C4. Very characteristic for the investigated compounds are the ions at m/z 345 and 331 for all those substances carrying an ether group at C5 or C6, and m/z 255 or 241 for the corresponding hydroxy compounds. These "abecarnil-derivative specific" ions at m/z 345 or 255 represent the loss of the alcohol from the ester group at C3. The ions at m/z 331 or 241 were formed by an additional

loss of a methyl group from the chain at C4, according to the neutral loss of the alcohol-methylether. The **ESI** spectra show intense $[M+H]^+$ and $[2M+H]^+$ ions. Application of skimmer fragmentation to these samples produced an additional attachment of sodium to this molecules. In this case also the upper mentioned "abecarnil-derivative specific" ions could be detected with high intensities. **TSP** spectra are dominated by the $[M+H]^+$ ions. Applying **TSP-MS/MS** experiments to the samples yielded the "abecarnil-derivative specific" ions in all cases (fig. 2). An additional ion at m/z 363 represents the free acid of abecarnil or gedocarnil derivatives, that at m/z 273 the corresponding hydroxy compound at C6 or C5, respectively. These results clearly support the structural assignments which were derived from the results obtained with the other ionization methods.

Conclusion:

The mass spectra of the investigated ß-carboline derivatives are characterized by the presence of abundant molecular ions, suitable for molecular weight determination and structure specific fragments. Fragmentation patterns are controlled by the loss of the alcohol from the ester side chain at C3 and an additional loss of a methyl group from the chain at C4, according to the neutral loss of an alcohol-methylether. The appearence of these "abecarnil-derivative specific" ions and the formation of m/z 363 representing the free acid of the benzoylic compounds or m/z 273 for the corresponding hydroxides in all ionization modes can be used for the determination of ß-carbolines and their metabolites in biological matrices.

References:

[1] Stephens, D.N. et al, J. Pharmacology and Exp. Therapeutics 253 (1990) 334

ZK	R3	R5	R6	MW
112119	-COO-CH(CH3)2	H	-O-CH2-Ø	404 17
112138	-COOH	H	-O-CH2-Ø	362 13
138295	- CO-O-CH2	H	-O-CH2-Ø	330 10
110231	-COO-CH3	H	-O-CH2-Ø	376.14
93423	-COO-C2H5	H	-O-CH2-Ø	390 16
113944	-COO-C(CH3)3	H	-O-CH2-Ø	418 19
151185	-COO-C3H6-OH	H	-O-CH2-Ø	420.17
151189	-COO-CHCH3CH2OH	H	-O-CH2-Ø	420 17
153076	-COO-CH(CH2OH)2	H	-O-CH2-Ø	436 16
114536	-COO-CH(CH3)2	H	OH	314 13
116496	-COOH	H	OH	272 08
114539	-COO-CH3	H	OH	286 10
113315	-COO-CH(CH3)2	-O-CH2-Ø-Cl	H	424 12
112135	-COO-CH(CH3)2	-O-CH2-Ø	H	404 17
116827	-COO-CH(CH3)2	-OH	H	314 13

Tab 1: Overview of the investigated ß-carboline derivatives, R_3, R_5 and R_6 indicate the side chains at the corresponding C-atoms, MW the molecular mass of the compounds.

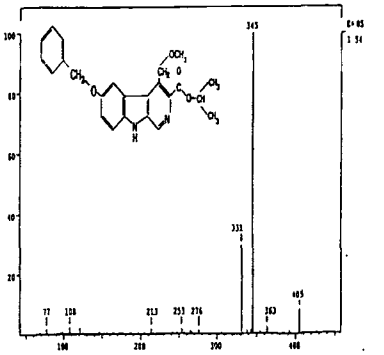

Fig. 2: MS/MS spectrum of abecarnil (ZK 112119) in positive TSP mode

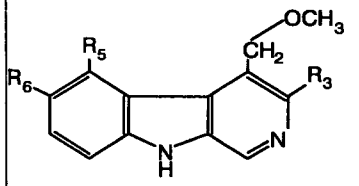

Fig. 1: Basic structure of the investigated ß-carboline derivatives, R_3, R_5 and R_6 indicate the side chains listed in tab. 1

IDENTIFICATION OF FADROZOLE (CGS 16949A) METABOLITES IN HUMAN URINE BY STABLE ISOTOPE PATTERN RECOGNITION GAS CHROMATOGRAPHY/MASS SPECTROMETRY

R.M.Iannucci, M.J.Hayes, B.Walter, D.Lukic and M.L.Powell
Development Department,
Pharmaceutical Division
CIBA-GEIGY Corporation, Ardsley NY 10502

Fadrozole (CGS 16949A), a novel tetrahydroimidazopyridine, is currently under development at CIBA-GEIGY Corporation as an orally active aromatase inhibitor for the treatment of estrogen-dependent mammary tumors. The identification of the human metabolite profile has been studied by pattern recognition stable isotope techniques using both GC/MS and ESI/LC/MS. Six healthy female subjects were given a single 8 mg aqueous solution of a 4:5 mixture of unlabelled Fadrozole:[4-^{2}H]-Fadrozole. Structures are shown in Figure 1.

Figure 1

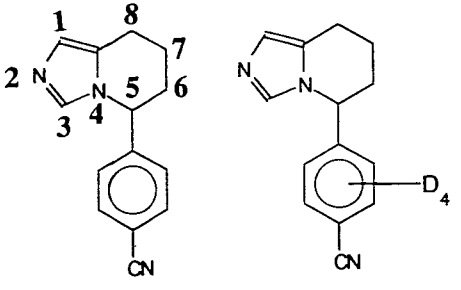

Urine samples were purified by solid-liquid extraction using C-18 reverse phase columns followed by elution with methanol. Extracts were analyzed both by GC/MS and electrospray (ESI) LC/MS. The major compounds found were unchanged parent drug and the 8-O-glucuronide metabolite. The 8-keto metabolite was also identified in significantly smaller amounts when compared with the other major species. The use of both GC/MS and ESI/LC/MS provided complimentary information. ECI/LC/MS was particularly useful for the identification of the 8-O-glucuronide. Figure 2 summarizes the proposed chemical structures of the human metabolites.

Figure 2

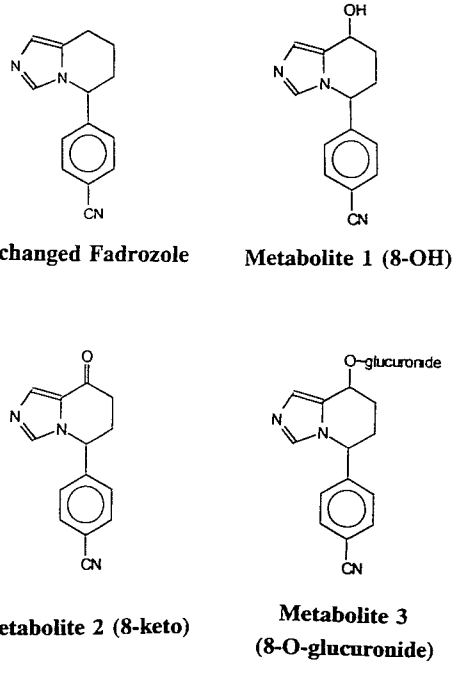

DRUG METABOLISM STUDIES USING "INTRINSIC" AND "EXTRINSIC" LABELS: A DEMONSTRATION USING ^{15}N vs Cl IN MIDAZOLAM

Hengchang Song and Fred Abramson, Department of Pharmacology
George Washington University Medical Center, Washington DC 20037

Introduction: Isotopes play an important role in evaluating metabolic pathways. In this work, we move beyond isotopic tracers to explore the concept that CRIMS (Chemical Reaction Interface Mass Spectrometry) could allow an elemental "label" to trace a drug metabolite pattern. To allow us to simultaneously evaluate the two types of label we used $^{15}N_3$-labeled midazolam, a structure that contains one chlorine, as the intrinsic elemental label, and three atoms of ^{15}N, as the extrinsic isotope label.

The CRI completely decomposes analytes in an effluent flow from a chromatographic column and leads to a reformulation of the atomic species originally contained in each analyte. With SO_2 as the reactant gas, the reactions in the CRI are:

$$C_xH_yO_zN_iCl_j + SO_2 \rightarrow CO_2 + NO + HCl + ..$$

The ^{15}N in the metabolites is determined by the enrichment of NO (m/z 30 *vs* m/z 31) and the Cl is simultaneously detected as HCl (m/z 36 and 38). CO_2 is the nonspecific carbon channel.

Experimental: The GC/CRIMS system consists of a 30m long, 0.25mm id and 0.25 μm film DB-5 column, a microwave powered reaction chamber, and an Extrel C50/400 mass spectrometer. The GC column was initially at 80° for 1.5 min, programmed at 30°/min to 110°, then at 8°/min to 280° and held for 5 min. The ^{15}NO was calculated as:

Enriched ^{15}NO = observed ^{15}NO - (.00403 · observed ^{14}NO).

Urine was collected from two dogs 0-24h before and 0-48h after the oral administration of 5 mg/kg $^{15}N_3$-midazolam. A 10 mL aliquot from each of the urines was spiked with 20 μg unlabeled diazepam, filtered, and incubated at pH 4.5-5.0 and 37° for 24h with glucuronidase/sulfatase. The sample was then extracted with an Amberlite XAD-2 column, eluted with 20 mL of CH_3Cl/iso-C_3H_7OH (3/1, v/v) followed by 20 mL methanol. The dried elute was derivatized with 250 μL MSTFA and 250 μL acetonitrile at 100° for 30 min. 1 μL of sample was injected using the splitless mode.

Results and Discussion: Figure 1 shows the dog urine chromatograms with C, ^{15}N, and Cl detection. The channels for ^{15}N and Cl are highly selective. Although midazolam has three atoms of ^{15}N but only one Cl, the result shows that the intrinsic elemental "label" Cl is equally successful in tracing the metabolites of midazolam as is the extrinsic isotope label ^{15}N.

In contrast to the 4 midazolam metabolites reported in the literature, 14 metabolite peaks were easily detected with CRIMS in both the extrinsic labeling (^{15}N) and the intrinsic labeling (Cl) channels. Since CRIMS detection is quantitative and structure independent, the peak areas of the chlorine channel were used to produce a quantitative metabolite profile of each dog despite not having standards for the unknown metabolites. The result indicates that the metabolite concentrations range from 100 pmol/mL to 10 nmol/mL. Figure 2 is the ratio of ^{15}N/Cl in each metabolite peak with the known α-OH-MDZ as the standard. Peaks 1, 2, 3, 5, 7, and 8 appear to have lost one or two ^{15}N atoms, and this information becomes useful in interpreting mass spectra of these metabolites.

The configuration of GC/CRIMS permits use of the GC/MS in its normal mode by turning

off the microwave power. The sample was reinjected and mass spectra were obtained at the retention times indicated in the selective CRIMS chromatogram. All the four known metabolites (peaks 7, 12, 13, and 14) were easily identified and confirmed by comparing their mass spectra and GC retention times with the reference nonlabeled compounds. Without analytical standards, only tentative identifications are made for other metabolites. However, the mass spectral characteristics of several metabolites strongly suggest that ring opening at bond 5-6 and/or imidazole occurred, and this was supported by the loss of one or two ^{15}N. (Figure 2)

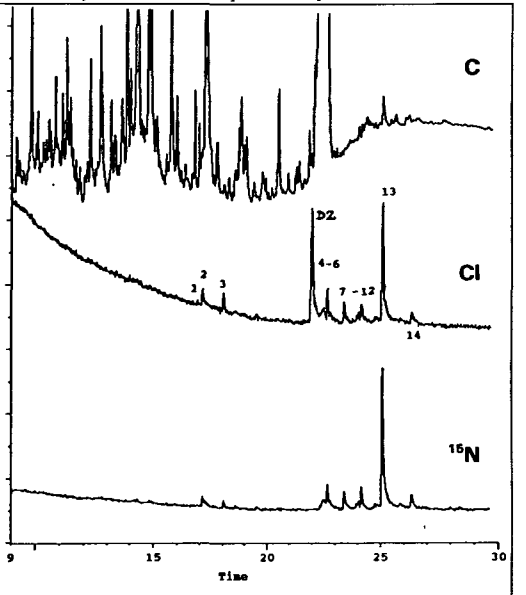

This work clearly shows the equivalence of elemental and isotopic labels in drug disposition. It also provides new information regarding midazolam metabolism. The impact of this demonstration should be greatest for investigations of new chemical entities in the pharmaceutical industry where the totally structure-independent principles of CRIMS permits detection of metabolites without requiring that the analyst make any *a priori* judgements to locate metabolites by traditional means. At the present time, CRIMS can selectively detect Cl, Br, and S, and we are considering analytical strategies to add F and P to the list. Any of these atomic species in an organic compound from a pharmaceutical or biological source makes its detection selective.

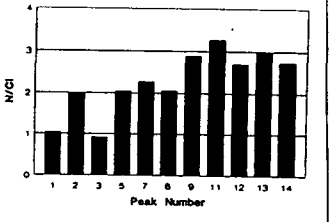

Conclusions: We find equally high selectivity and comparable signal/noise characteristics for chlorine as for isotopic nitrogen. The chlorine in midazolam is itself an effective label; special syntheses to incorporate isotopic labels are not necessary. The power of either mode of CRIMS is shown by detecting 14 metabolites while only 4 had been previously reported. The ratios of ^{15}N/Cl for each metabolite peak along with conventional mass spectra provide clues to the structures of these new metabolites.

Acknowledgements: This work was supported by USPHS Grant R01-GM-36143. We are grateful for assistance from Drs. Dan Liberato, Arnold Liebman, and Arthur Loh of Hoffman LaRoche Inc.

The full manuscript will be published on Drug Metab. Disp. Vol 21(5), 1993

PROFILING OF TRYPTOPHAN METABOLITES IN CELL CULTURE BY HPLC/CRIMS

Y. Teffera, F.P. Abramson, S.P Markey[1], K. Saito[1], and M.P. Heyes[1]
Department of Pharmacology, George Washington University School of Medicine and Health Sciences, Washington DC 20037,
and [1]NIMH/NIH, Bethesda, MD 20892

INTRODUCTION

Quinolinic acid, a kynurenine pathway metabolite of tryptophan, has been found at substantially elevated concentrations both in cerebrospinal fluid and brain tissue of patients with broad spectrum infections, and other inflammatory, neurologic diseases including AIDS. This has led to increased interest in metabolic profiling of kynurenine metabolism in various systems, including interferon gamma (IFN-γ) stimulated cell lines. The various methods developed for analysis lack adequate selectivity, and they assay only single metabolites. In this poster we discuss the development of an HPLC/CRIMS (Chemical Reaction Interface Mass Spectrometry) method that simultaneously detects all known kynurenine pathway metabolites. We have profiled media from six different cell lines with this method.

EXPERIMENTAL

Six cell lines, A-498 (renal carcinoma), H4 (neuroglioma), MRC-9 (lung), U-373MG (glioblastoma), THP-1 (human monocytes), and Macro (human macrophages) were tested. Each cell line grown in D_5-tryptophan-supplemented (100 μM) media was stimulated with IFN-γ (100 U/mL) and incubated for 72h along with unstimulated control cell lines. D_5-methyltryptophan was the internal standard. Tryptophan metabolites were separated by reversed phase HPLC using a C-18, 150 X 4.6 mm Altima column (Alltech). The solvent system was water with 0.1% trifluoroacetic acid (TFA) (A) and 20% acetonitrile and 0.1% TFA in methanol (B). The gradient system for elution was 1-4% B in 6 min, 4-24% in 20 min, 24-54% in 20 min and 54-100% in 10 min. Adequate reversed-phase separation of these compounds required a high carbon load column (15%). The peaks are fully separated and little tailing is observed. In addition, the retention times of the early eluting peaks are markedly increased (Fig. 1). The sample eluting from the HPLC was detected with an HPLC/CRIMS apparatus that used a Vestec Universal Interface and a Dupont 21-492 double-focusing mass spectrometer. Hydrogen was the CRIMS reactant gas and the reaction products C_2H_2 at mass 26 generally monitored carbon and HD at mass 3.022 selectively monitored deuterium.

RESULTS AND DISCUSSION

When stimulated cells are incubated with media containing D_5-tryptophan, the metabolites produced contain deuterium. These metabolites can be detected with deuterium-selective CRIMS methods. We then analyzed various IFN-γ treated cell lines and their respective untreated controls. Area ratios of the various peaks to the internal standard provided quantitation. Most of the stimulated cell lines show peaks due to kynurenine and unmetabolized tryptophan with the occasional appearance of one or two peaks that do not correspond precisely to any known metabolites. In contrast, the chromatogram from media of some stimulated human macrophages contains at least nine peaks only three of which correspond to any of the known tryptophan metabolites (Fig. 2),

however human macrophages do not routinely demonstrate this level of metabolic diversity. The presence of this many unknown metabolites clearly demonstrates the generality of the system including the transmission through the Universal Interface and the efficiency of the CRI. The differences in retention times between Figs. 1 and 2 resulted from having changed columns.

The effect of interferon on tryptophan disappearance at 72 hrs has also been studied. The majority of the cells metabolized more than 90% tryptophan upon stimulation with IFN-γ. A-498 cells have metabolized less than 10% of the tryptophan. Only unstimulated H-4 cells metabolized tryptophan substantially.

CONCLUSIONS

A new HPLC-CRIMS method using deuterium-selective detection has been successful in studying the kynurenine pathway of tryptophan metabolism from media and cell cytosol. Numerous metabolites with markedly different retention times from known metabolites were detected. CRIMS has been used to quantitatively profile the metabolites from various cell lines. In this way CRIMS simultaneously measures the disappearance of tryptophan as well as the appearance of the metabolites. CRIMS could also detect ^{13}C and ^{15}N if they were incorporated in a substrate molecule.

Acknowledgments: This work was supported by a subcontract from Vestec on NIH SBIR Grant GM43669. The internal standard was kindly provided by Dr. Daniel Yohannes, Yale University.

Abbreviations

Quin = quinolinic acid

3-HAA = 3-hydroxy-anthranilic acid

OH-Kyn = 3-hydroxy-kynurenine

Kyn = kynurenine

KA = kynurenic acid

Trp = tryptophan

IS = internal standard

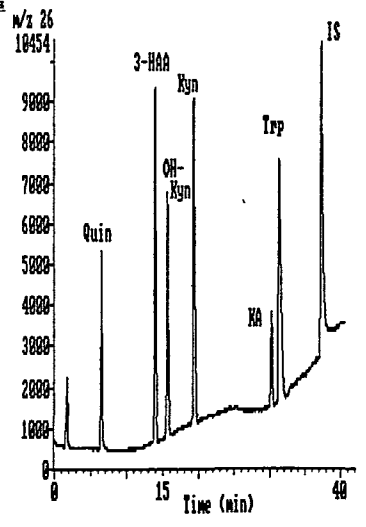

Figure 1. Standards

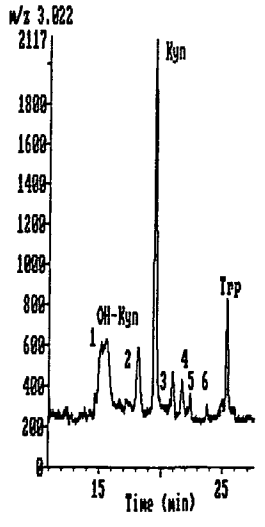

Figure 2. Macrophage medium

The Application of Liquid Chromatography/ Chemical Reaction Interface Mass Spectrometry (LC/ CRI MS) to Quantitative Studies in Drug Metabolism

*Charles A. Goldthwaite, Jr.[1], Brian Nobes[2], Ian A. Blair[1,2], Robert F. Mayol[3] and Lewis J. Klunk[3].
Departments of [1]Chemistry and [2]Pharmacology, Vanderbilt University, Nashville, TN 37203; [3]Bristol-Myers Squibb Co., Pharmaceutical Research Institute, Wallingford, CT 06492.

Chemical reaction interface mass spectrometry (CRI MS) is a new technique for identifying and quantifying stable isotope labeled compounds. The CRI MS unit (Figure 1) consists of a microwave powered device interfaced with an electron impact (EI) mass spectrometer. Compounds are combusted in the microwave chamber and subsequently oxidized by SO_2 to yield stable products such as CO_2, NO and H_2O (Scheme 1). These products are then monitored in a quadrupole mass spectrometer, and the amount of compound is determined by comparing intensity levels with those of a known standard. By using single ion monitoring (SIM), m/z channels corresponding to stable isotope oxidation products (i.e. m/z 31 for ^{15}NO and m/z 45 for $^{13}CO_2$) can be examined.

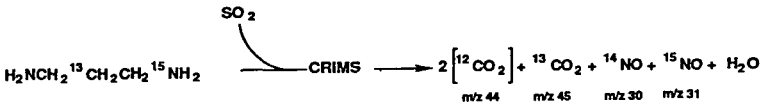

Scheme 1.

A CRI MS unit has been coupled to an HPLC via a Vestec Universal Interface. This interface vaporizes and desolvates the HPLC effluent prior to introduction into the CRI chamber. Analytes are swept through the interface using helium, and a helium particle beam enriched in the sample is formed. This particle beam travels into the momentum separator, where the remaining solvent and the bulk of the helium are removed using a two-stage pumping system. SO_2 is added and the analytes are combusted upon entrance into the microwave-induced plasma (MIP) chamber.

The system was optimized to reduce background in the m/z 30, m/z 31 and m/z 44 channels by employing reduced solvent flow rates (0.2 mL/min to 0.5 mL/min) in addition to optimizing the desolvation gas flow rates and the SO_2 pressure. Several methods of vaporization, including the use of a helium-assisted nebulizer, were examined to determine optimal vaporization conditions. The system has been tested using *in vitro* incubations of $^{14}C/^{15}N$ buspirone (an anti-anxiety agent) with rat liver microsomes as a biological model. Results shown in Figure 2 depict an LC/CRI MS chromatogram of the buspirone incubation mixture. The major sites of hydroxylation of buspirone are the 3', 6' and 5 positions. An intramolecular attack on the carbonyl within the 6' OH metabolite yields oxa-buspirone. Each of these metabolites was identified by comparison with known standards. Independent quantification studies were performed using ultraviolet absorbance data (254 nm) and radioactivity.

The CRI MS technique has been proven to be very precise between injections. Results of quantification studies indicate a large variability in CRI MS response among the buspirone metabolites. This variability is due to solvent composition changes imposed by the gradient used to separate the metabolites. Future studies will focus on methodology aimed at optimizing particle formation during the vaporization process, thus reducing the solvent-dependent variability in the CRI MS response.

Supported by Bristol-Myers Squibb.

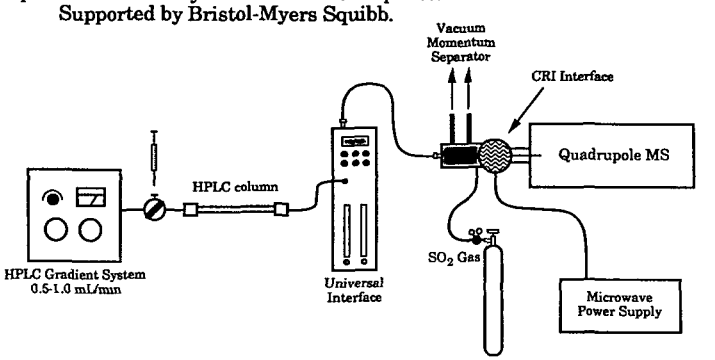

Figure 1. Schematic diagram of the chemical reaction interface mass spectrometer (CRI MS) system.

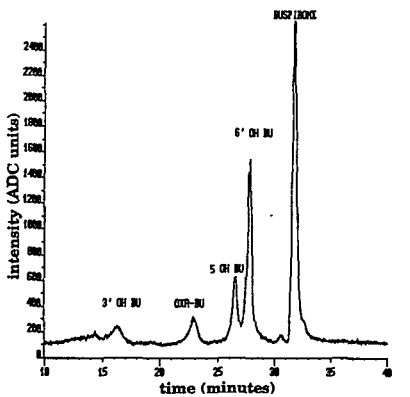

Figure 2. An LC/CRI MS chromatogram of the ^{15}N buspirone incubation mixture measured in the m/z 31 channel.

ANALYSIS OF CATECHOLAMINE METABOLITES BY ELECTRON CAPTURE MASS SPECTROMETRY.

S.T. Weintraub[1], C. Marquez[2], R. Benavides[3] and J.W. Maas[3]
Departments of [1]Pathology and [3]Psychiatry, The Univ. of Tx. Health Science Center, San Antonio TX and [2]Departmentt. of Pharmacy, The Univ. of N. Carolina, Chapel Hill NC.

Long term studies in our laboratories have focused on measurement of endogenous levels of catecholamine metabolites as a means of characterizing various psychiatric conditions, in particular schizophrenia. Quantitative analysis has been accomplished by GC/MS using electron impact ionization of pentafluoropropyl/pentafluoropropionyl (PFP) ester derivatives. The method has proved highly satisfactory for monitoring levels of substances such as 3,4-dihydroxyphenylacetic acid (DOPAC), homovanillic acid (HVA, 4-hydroxy-3-methoxyphenylacetic acid) and 5-hydroxyindoleacetic acid (5-HIAA) in urine and cerebrospinal fluid. However, problems with extraction efficiency and chromatographic interferences have seriously hindered analysis of DOPAC and HVA and have essentially prevented monitoring of 5-HIAA in plasma. Moreover, the derivatives are not very stable; as a consequence, sample analysis must be completed on the same day as derivatization.

Our first attempt to solve this problem involved a switch to electron capture mass spectrometry (ECMS) with negative ion detection as a means of obtaining better sensitivity. Although orders of magnitude increase in response were observed, the anions formed from the PFP derivatives by this ionization technique proved unacceptable for our purposes. One major difficulty is that molecular anions are not observed for these PFP derivatives when methane is used as the chemical ionization reagent gas, and formation of the most intense ion involves loss of deuterium from the internal standard.

A different approach was definitely mandated. In view of the success attained for quantification of extremely low levels of prostaglandins, we next evaluated pentafluorobenzyl (PFB) esters as a way to achieve the necessary sensitivity and sample stability. We found that in a manner analogous to prostaglandins, formation of the trimethylsilyl ethers could be readily accomplished after esterification with PFB bromide, yielding a very stable product with excellent GC/ECMS properties. As expected, $[M\text{-}PFB]^-$ ions predominate, with little additional fragmentation observed. Low pg levels of standard samples were easily detected at modest detector gain settings.

This appeared to be an ideal way to achieve quantitative analysis of these catecholamine metabolites, and when the derivatization was carried out on at least 10 µg of each compound, uniform recoveries were obtained. However, when lower quantities were reacted, the recovery of DOPAC was much less than the other two metabolites (relative recoveries: HVA, 1.0; DOPAC, 0.09; 5-HIAA, 0.5). To see if the decreased yield of DOPAC was occurring at the trimethylsilylation step, 100 ng of each compound was reacted directly with BSTFA/1% TMCS. Analysis by GC/EIMS revealed a similarity in peak heights in the reconstructed total ion current chromatogram as well as in the selected ion retrieval chromatograms for $[M]^+$ and $[M\text{-}15]^+$. These results suggested that formation of the TMS ether/ester derivatives was comparable for all three compounds. We next produced the PFB esters using 10 µg of each metabolite and then removed an aliquot equivalent to 100 ng per component. In most experiments, the yield of DOPAC was significantly less than HVA or 5-HIAA. On occasion, however, better recovery of

DOPAC was obtained. Neither increasing the concentration of PFB bromide, nor using silanized reaction vials yielded any consistent improvement in recovery of DOPAC.

At this point it was decided that even with a reduced yield for DOPAC, there would be sufficient sensitivity afforded by ECMS to permit detection of endogenous levels of DOPAC in 1 ml of plasma. We, therefore, carried out our usual procedure involving ethyl acetate extraction of acidified plasma, followed by formation of the PFB/TMS derivatives. Linear standard curves for analysis of ng levels of metabolite in the presence of 100 ng of deuterated internal standard were obtained, with correlation coefficients routinely ≥ 0.98. Below are typical selected ion retrieval chromatograms for the respective ions and elution times for the PFB/TMS derivatives of HVA (m/z 253), DOPAC (m/z 311) and 5-HIAA (m/z 334) and corresponding deuterated internal standards isolated from human plasma.

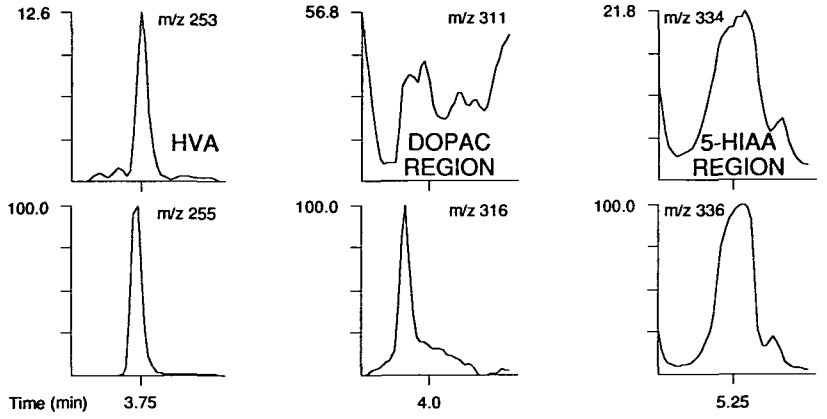

The quantitative results for HVA (10.7 ng/ml) were comparable to those obtained by GC/EIMS analysis after PFP derivatization of another aliquot of the same sample. A distinct advantage of the ECMS method for HVA was that intense signals were observed for significantly smaller aliquots at much lower detector settings than required for the EIMS method. Excellent recovery of HVA was also obtained. However, the traces clearly indicate that our current extraction protocol is not capable of yielding a sufficiently "clean" sample for measurement of DOPAC and 5-HIAA in plasma. It is likely that an additional solid-phase extraction step will provide the necessary purification. In future studies, we also plan to evaluate the phenylboronate/PFB derivative of DOPAC as a means of improving product yield.

Acknowledgements. These studies were supported in part by NIH grant MH40935 to J.W. Maas. We are grateful to Dr. James Yergey for advice on derivatization with PFBBr.

STUDIES OF NITROGEN METABOLISM USING CRIMS 15N-LABELED GLUTAMINE AND ASPARAGINE SUBSTRATES IN CELL CULTURE

Jozef J. Kusmierz and Fred P. Abramson, George Washington University Department of Pharmacology, 2300 Eye Street NW washington D.C. 20037

INTRODUCTION

The unique ability of CRIMS (Chemical Reaction Interface Mass Spectrometry) to selectively detect ^{15}N has been utilized to elucidate metabolic pathways that transfer nitrogen in cultured cell media and cell cytosol. We detect nitrogen selectively as NO using masses 30 and 31 where the natural abundance of M+1 is 0.00403 and atom % excesses as low as 0.004 can be measured. In the present study we demonstrate how CRIMS can trace ^{15}N metabolism, using either α-^{15}N-labeled glutamine or asparagine in the media of cultured hepatoma (HEPG2) cells.

EXPERIMENTAL

Sample preparation. HepG2 cells ($3 \cdot 10^6$) were plated in the 50 ml (25 cm^2) flask (Costar Corp.) and cultured in 10 mL phenol red-free medium (DMEM, Biofluids Inc.) containing 10% calf serum. The cells were incubated in presence of either α-^{15}N-glutamine (12 mM) or α-^{15}N-asparagine (12 mM) respectively. Samples of culture media (100 μL) were taken every 24 hours during incubation and kept at -20° until analysis. The incubation was terminated after 144 hrs. The remaining cells were harvested using 1 ml of methanol. One hundred μL of this was used for analysis of cell cytosol. After protein precipitation, the supernatant was evaporated to dryness and the residue silylated with 50 μL of N-methyl-(N-trimethylsilyl)trifluoroacetamide (MSTFA) and 50 μL of acetonitrile. The mixture was then heated at 80° for 2 hrs.

GC/CRIMS Analysis. The analytes eluting from a capillary GC column are decomposed in the chemical reaction interface in the presence of helium and converted into stable molecules using sulfur dioxide as the reactant gas. The samples were separated on a 30 m long, 0.25 mm i.d., 0.25μ film thickness DB-5 capillary column with 20 psi column head pressure. Four minutes after injection of a 2 μL sample in the split mode (1:10) at 70°, the temperature was programmed 3°/min to 270° and kept constant for 15 min. The microwave power and mass spectrometer were turned on 5 minutes after injection. With CRIMS we monitored carbon as CO_2 using mass channel 44 and nitrogen as NO using mass channels 30 and 31. An enrichment chromatogram of ^{15}N was produced by subtracting the natural contribution of NO at m/z 31. This was generated as follows:

$$\textbf{Enriched } ^{15}N = m/z\ 31 - (0.00403 \cdot m/z\ 30)$$

The percent enrichment of each peak was:

$$100 \cdot \textbf{Enriched } ^{15}N/(\textbf{Enriched } ^{15}N + \textbf{Total } ^{14}N)$$

RESULTS

The CRIMS chromatogram of medium containing ^{15}N-GLN incubated for 144 hrs is shown in Fig.1. The carbon channel chromatogram (top) is complex and difficult to interpret, while the enriched ^{15}N channel (bottom) showed only the relevant peaks. Next, the CRI was turned off and full scan mass spectra of the peaks containing ^{15}N were acquired and

their structure elucidated. The ^{15}N-GLN was completely converted to ^{15}N-glutamic acid during the first 24 hours of incubation. ^{15}N-GLU disappearance (actually measured as pyroglutamic acid), expressed as % of total ^{15}N, and ^{15}N-alanine and ^{15}N-proline production during incubation were measured. GLU was steadily metabolized and declined to 18% of total ^{15}N. ALA peaked at 60% of total ^{15}N after 48 hours of incubation, while PRO maximizes at 20% of total ^{15}N at 144h. The enrichments of ^{15}N of ALA and PRO during GLN incubation reached 46% and 42% at 144h, respectively.

As a substrate, asparagine was degraded more slowly than glutamine. The production of ALA and PRO reached 13% and 5% of total ^{15}N respectively. Glutamic acid contained 2.8% of total ^{15}N. The enrichment of ^{15}N in ALA and PRO increased linearly during course of the incubation and reached 20% and 19% respectively. The enrichment of ^{15}N in asparagine could be measured and was a constant 50.5% during the incubation.

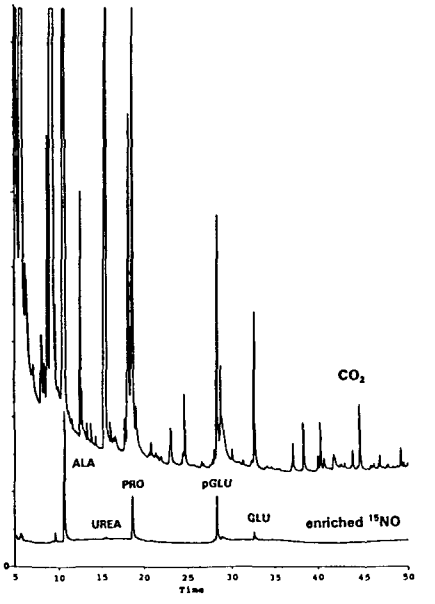

Fig.1 GC/CRIMS chromatogram of culture media incubated with α-^{15}N-glutamine.

The GC/CRIMS analysis of the cell cytosol following asparagine incubation, revealed that the carbon channel is even more complex than from the medium, but the ^{15}N-selective chromatogram is still relatively simple. The cytosol peaks containing ^{15}N were identified by mass spectrometry and were the same metabolites as in the medium in which experiment was performed. The total amount of label in the cell cytosol was estimated at 10% of that in the culture media.

CONCLUSIONS

The special ability of the CRIMS method to trace ^{15}N has been utilized in two studies of amino acid metabolism in cell culture. CRIMS successfully generated ^{15}N-selective chromatograms from both the medium of the cell culture experiment and the cell cytosol. These isotope-selective chromatograms provide both quantitative metabolite patterns from each labeled substrate as well as the fractional enrichment for each metabolite. The selectivity of CRIMS for detecting compounds containing ^{15}N facilitates subsequent experiments to elucidate metabolite structures.

This work was supported by NIH Grant GM36143.

HEPATIC FIRST-PASS METABOLISM OF DIPHENHYDRAMINE IN SHEEP

G. R. Tonn, E. Kwan, C. Hall, F.S. Abbott, J.E. Axelson, and D.W. Rurak
Faculties of Medicine and Pharmaceutical Sciences, University of British Columbia, Vancouver, B.C., Canada.

Diphenhydramine (DPHM) is a H1 receptor antagonist used in the treatment of a variety of allergy mediated conditions. Previous experiments conducted with sheep have shown that DPHM is rapidly removed from the plasma with less than 1% excreted as intact drug in the urine. This data suggests that some form of non-renal clearance is the predominant route of elimination of DPHM in sheep. With the aid of a deuterated stable isotope analog of DPHM (i.e. $^2H_{10}$-DPHM), the *in vivo* hepatic first-pass metabolism of DPHM in sheep was assessed as an indicator of hepatic elimination. Biological studies employed 5 female Dorset-Suffolk cross sheep. Chronic catheters were aseptically implanted in the femoral and mesenteric veins, and the femoral artery. Administration of labelled and unlabelled drug was randomized, such that a dose of either DPHM or $^2H_{10}$-DPHM (50 mg or 52 mg free base, respectively) was administered *via* the femoral vein with the alternate compound simultaneously administered *via* the mesenteric vein. Serial samples were drawn from the femoral artery from -5 to 720 minutes. Following liquid-liquid extraction (0.05M triethylamine in 2% isopropanol: 98% hexane) of plasma samples, both DPHM and $^2H_{10}$-DPHM were simultaneously quantitated by GC-MS (select ion monitoring; m/z 165 DPHM and m/z 173 $^2H_{10}$-DPHM [Fig 1A and 1B]) using a Hewlett-Packard (HP) 5890 series II gas chromatograph equipped with a HP 5971A mass selective detector. The plasma concentration *vs.* time data was fit with PCNONLIN. The area under the plasma concentration *vs.* time curve (AUC) for both DPHM and $^2H_{10}$-DPHM was calculated using the method of trapezoids. The pharmacokinetic data obtained from the five ewes is presented in Table 1, and a representative plot of the concentration vs. time data is presented in Figure 2. The ratio of the AUC obtained from drug administered *via* the mesenteric vein to the AUC following femoral vein administration was calculated as the bioavailability (F) [extraction ratio; E = 1-F]. The bioavailability of DPHM following mesenteric administration was roughly 5% ± 3%, suggesting that roughly 95% of the dose administered to the mesenteric vein was metabolized prior to reaching the plasma. From the data presented, it appears that hepatic clearance (CL_H) is a significant component of the total body clearance (CL_T) of DPHM in sheep. An estimate of hepatic clearance using a literature value for hepatic blood flow (3.3 L/hr/Kg) was 3.1 ± 0.1 L/hr/Kg ($CL_H = Q_H \times E$). The calculated total body clearance of DPHM in these sheep was 3.3 ± 1.1 L/hr/Kg suggesting that, based on our estimate of CL_H, the CL_H accounts for a significant proportion of DPHM total body clearance in sheep. In summary, these results suggest that the ovine liver is very efficient in eliminating DPHM following mesenteric administration, and that hepatic elimination is likely responsible for a large portion of the observed CL_T of DPHM in sheep.

Table 1: Pharmacokinetic parameters of labelled and unlabelled diphenhydramine following IV (femoral vein) bolus administration

EWE #	Weight (Kg)	α-T½ (min)	ß-T½ (min)	CL_{TB} (L/hr/Kg)	Vd_{SS} (L/Kg)	F	E
139	62.6	9.2	39.7	3 3	1.1	0.042	0.96
989	87.6	3.3	28 2	4.5	2.3	0.010	0.99
1158	65.3	5.9	38.9	1.7	1 1	0 093	0.91
1154	63.1	4.4	22.2	3.1	1.2	0 076	0 92
102	72.1	4 5	16.3	4.0	0.9	0.039	0 96
mean	70.1	5.4	29 1	3.3	1.3	0.05	0.95
± sd	± 10 5	± 2 3	± 10.3	± 1 1	± 0.6	± 0.03	± 0.03

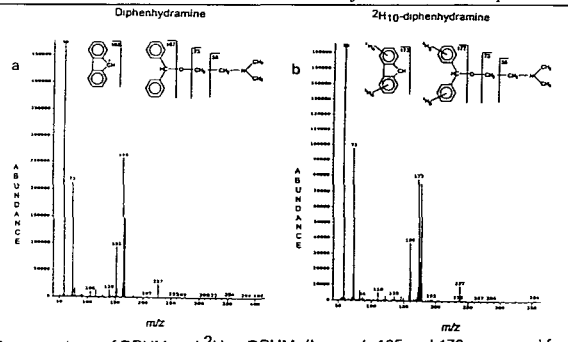

FIG 1A Mass spectrum of DPHM and $^2H_{10}$-DPHM. (Ions *m/z* 165 and 173 were used for GC-MS (SIM) for DPHM and $^2H_{10}$-DPHM, respectively

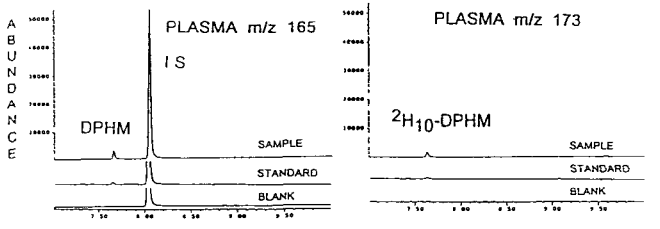

FIG 1B Ion chromatogram of *m/z* 165 (DPHM and internal standard [orphenadrine]) and *m/z* 173 for $^2H_{10}$-DPHM Samples were extracted from plasma The concentration of the spiked standard was 2 0 ng/mL

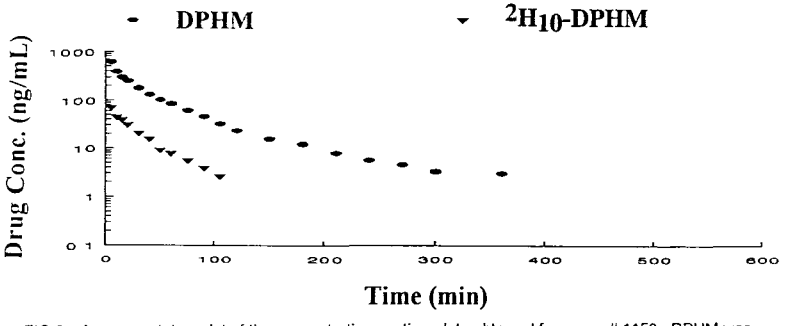

FIG 2 A representative plot of the concentration vs. time data obtained from ewe # 1158 DPHM was administered via the tarsal vein whereas $^2H_{10}$-DPHM was administered via the mesenteric vein

THIS WORK WAS SUPPORTED BY THE MEDICAL RESEARCH COUNCIL OF CANADA PROGRAM GRANT MRC PG-11120

Studies on the Metabolism of Cyoctol: Characterization of the Urinary Metabolites of Cyoctol Present in the Rat by GC-MS. *MJ Hauer, BA Thornburgh, PE Sanders, AJ Wickrema Sinha and JJ Vrbanac*, Drug Metabolism Research, The Upjohn Company, Kalamazoo, Michigan

Cyoctol (Figure 1) is classified as an androgen receptor blocking agent. When administered topically to the rat, rabbit, or human cyoctol was observed to be rapidly absorbed, metabolized and excreted, primarily in the urine. The metabolites of cyoctol present in rat urine following oral administration were characterized by GC-MS. Characterization of metabolites was severely compromised by the complexity of the urinary milieu and by the low concentrations of metabolites. Metabolites were partially purified into eleven fractions by reversed phase HPLC. Attempts at sufficient purification of metabolites for NMR analysis using several approaches were not successful. Attempts to characterize metabolites by on-line LC-MS (particle beam) and by LSIMS analysis of purified fractions were not successful. Suppression of ionization by the biological milieu was a major problem in the failed LSIMS analysis. We describe the characterization of the metabolites found in two of the HPLC fractions which represented approximately 28% of the radioactive metabolites excreted. Structures were assigned based on the interpretation of the EI and PCI mass spectra of the methyl ester-trimethylsilyl (ME-TMS) derivatives. Because of the inability to purify metabolites for NMR analysis we decided interpretation of the EI and PCI mass spectra of the ME-$^2H_9$-TMS derivatives was necessary to facilitate greater confidence in assignment of structures. *Representative metabolite identification:* The EI mass spectrum of the ME-TMS derivative of Metabolite **10A** is shown in Figure 2. The assignment of $M^{+\cdot}$ as 284 was straightforward with the presence of $M^{+\cdot}$ - 15 (m/z 269) and $M^{+\cdot}$ - 90 [$(CH_3)_3SiOH$, m/z 194]. Also, $M^{+\cdot}$ - 31 ($CH_3O\cdot$, m/z 253), $M^{+\cdot}$ - 47 ($CH_3\cdot$ + CH_3OH), $M^{+\cdot}$ - 60 (CH_3COOH, m/z 224) and $M^{+\cdot}$ - 73 (CH_3O-OC-$CH_2\cdot$, m/z 211) were observed indicating this compound was a ME. The acidic structure is consistent with the observed $M^{+\cdot}$ -31, $M^{+\cdot}$ -60 and $M^{+\cdot}$ -73. A neutral losses of 90 daltons from $M^{+\cdot}$ - CH_3-OOC-$CH_2\cdot$ was also observed (m/z 121). The ion at m/z 162 apparently results from loss of methanol by *r*H from m/z 194 and the ion at m/z 135 could result from the loss of $CH_3OCO\cdot$ from m/z 194. The ion at m/z 145 could result from the loss of HO· from m/z 162. Sequential losses of C_2H_4 from m/z 135 produce the ions at m/z 107 and 79. Loss of C_2H_4 from 121 produces the ion at m/z 93. Thus, the ion at m/z 107 represents the intact ring structure, minus $(CH_3)_3SiOH$. The EI mass spectrum of the ME-$^2H_9$-TMS derivative of Metabolite **10A** is displayed in Figure 3. The addition of one TMS group was supported by the observation that $M^{+\cdot}$ has shifted to 293 (CI data supported this assignment). The ion observed at m/z 275 results from an expected neutral loss of 18 ($CD_3\cdot$). The loss of methanol from m/z 275 was also observed (m/z 243) and has shifted by 6 daltons from m/z 237. Loss of 99 daltons, $(CD_3)_3SiOH$, was also observed at m/z 194, the same ion observed in Figure 2. As expected, the ions at m/z 79, 107, 121, 135 and 153 are unchanged from Figure 2 (assignment of structures for these ions was straightforward and their presence was indicative of cyoctol metabolites). Figure 1 displays the structures of metabolites identified in Fractions 9 and 10. In view of the lack of NMR data the use of $^2H_9$-TMS derivatives greatly facilitated confidence in the assignment of structures. These and other metabolites identified indicated that *O*-demethylation, β-oxidation, initial oxidative loss of the terminal 3 carbons, hydroxylation of the cyclopentane ring and reduction of the cyclopentane ring carbonyl to an alcohol were the primary metabolic transformations occurring in the rat.

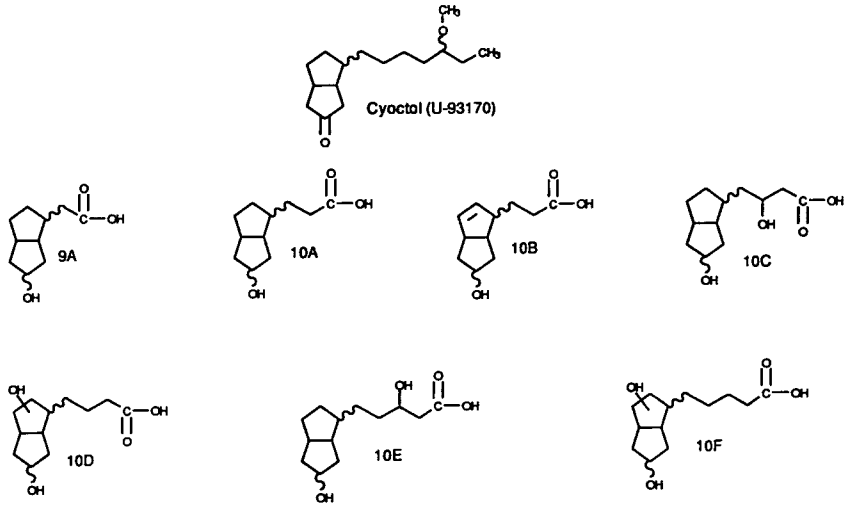

Figure 1. Structures of metabolites of cyoctol observed in rat urine (Fractions 9 and 10) as determined by GC-MS analysis.

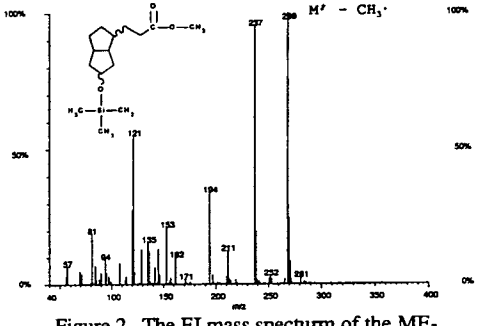

Figure 2. The EI mass spectrum of the ME-TMS derivative of Metabolite 10A

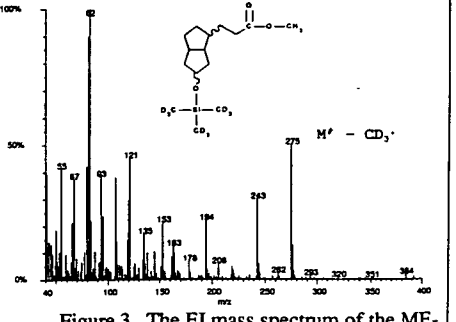

Figure 3. The EI mass spectrum of the ME-$^2H_9$-TMS derivative of Metabolite 10A.

The Metabolism of Essential Fatty Acids in Humans: Studies on the Effects of Dietary Fats on the Conversion of $^2H_5$-18:3w3 & $^2H_5$-18:2w6 to Long Chain Polyunsaturates.

Robert J. Pawlosky, Brent Wegher, and Norman Salem Jr.
Laboratory of Membrane Biochemistry and Biophysics, DICBR, NIAAA, Bethesda, MD. 20892

ABSTRACT

Through a series of elongation and desaturation steps linoleic (18:2w6) and linolenic (18:3w3) acids are metabolized to arachidonic (20:4w6) and docosahexaenoic acids (22:6w3), respectively. Using a negative ion GC-MS technique and the labeled fatty acids, $^2H_5$-18,18,18,17,17-18:2w6 and $^2H_5$-17,17,18,18,18-18:3w3, we investigated the effects of low and high amounts of long chain polyunsaturate fat diets on the *in vivo* biosynthesis of 20:4w6 and 22:6w3 in eight individuals.

Subjects were given a single dose of the isotopes during the first two weeks of the study, at which time they maintained their usual diets and kept food records. Then, for three weeks, subjects were placed on a controlled (low amounts of long chain polyunsaturated fat) diet which included beef and turkey. They were given the isotopes again beginning the fifth week of the study. Subjects were then placed on a second controlled (high amounts of long chain polyunsaturates) diet beginning the sixth week where fish was substituted for the beef. They were given the isotope again during the eighth week. Throughout the controlled diet periods, olive oil and margarine made up much of the remaining dietary fat.

METHODOLOGY

One gram each of the labeled fatty acid ethyl esters were given orally to the subjects and 20 mL of blood was drawn from the forearm at various times throughout a seven day period. The plasma was separated from the red blood cells and the lipids were extracted using the Bligh & Dyer total lipid extraction method. The fats were saponified in a 10% KOH methanolic solution, acidified with HCl, re-extracted into hexane and derivatized to the PFB esters using pentafluorobenzyl bromide. The extracts were analyzed on a Hewlett Packard 5989 gas chromatograph-mass spectrometer in the negative ion mode with methane (99.99%) as the reagent gas. The terminally labeled fatty acids chromatographically resolved from the non-labeled materials using a 25 m X 0.25 mm polar FFAP capillary column (J&W) using splitless injection with an oven temperature program of 80°-185°@20°/min, 185°-240°@10°/min and held for 30 min.. The source temperature was 200° and pressure 4 X 10^{-4} torr. The [M-PFB] ion was used to detect deuterium-labeled metabolites. The fatty acids were quantified using relative response factors and 23:0 as an internal standard (1). The plasma fatty acids were also analyzed as their methyl esters by GC-FID.

RESULTS & DISCUSSION

- The amount of plasma $^2H_5$-18:3w3 was lower than that of $^2H_5$-18:2w6 as measured in the plasma. This suggested that 18:3w3 may be more easily oxidized than 18:2w6 and that based on a per-gram amount more 18:2w6 is available for metabolism than 18:3w3.
- The production of most long chain fatty acids up to and including the 24-carbon compounds were detected using this methodology.
- All deuterium-labelled metabolites could be quantified reliably using a single internal standard.

- The production of 20:4w6 from the time course plots appeared to be diminished while subjects were on fish diet compared to the production when on the beef diet. However,the production of 20:5n3 did not appear to be lowered by the fish diet.

A typical Washington DC diet is more similar to the beef diet where plasma long chain w-3 fatty acids are present in low amount. Our results show that high amounts of long chain polyunsaturates especially those containing w-3 fatty acids (fish diet) contribute to a decreased production of 20:4w6 which may lead to lower amount of 20:4w6 reflected in the plasma. Unexpectdly, the fish diet did not appear to significantly reduce production of the arachidonic acid homologue, 20:5w3.

Table 1. Lipid composition of Controlled diets

	Beef Diet	Fish Diet
18:1	35.23	36.83
18:2w6	4.85	5.43
18:3w3	1.53	1.76
20:4w6	0.06	0.18
20:5w3	-*	0.19
22:5w3	-	0.07
22:6w3	-	0.43

* Data taken from USDA Handbook 8.

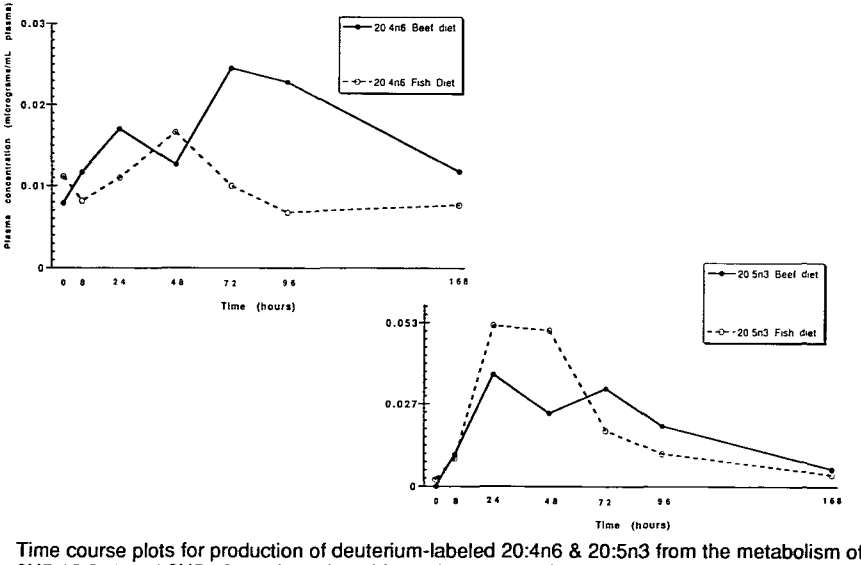

Time course plots for production of deuterium-labeled 20:4n6 & 20:5n3 from the metabolism of 2H5-18:2n6 and 2H5-18:3n3 in eight subjects that were maintained on a Beef diet or Fish diet for a period of three weeks. The data is the result of GC-MS data take at the time points indicated.

The Metabolism of Fluorinated VPA Analogues

Wei Tang*, Guenter Eigendorf+ and Frank Abbott*, Faculty of Pharmaceutical Sciences* and Department of Chemistry+, University of British Columbia, Vancouver, B.C , Canada, V6T 1Z3

Valproic acid (VPA, 2-propylpentanoic acid), an anticonvulsant agent, causes a rare but severe hepatotoxicity which is thought to be induced by one or more metabolites. Two metabolites, 4-ene VPA (2-propyl-4-pentenoic acid) and 2,4-diene VPA (2-propyl-(E)-2,4-pentadienoic acid), were found to induce microvesicular steatosis in rats [1], a feature also evident in patients who died from liver failure while on VPA therapy. As a mechanism for the toxicity, it has been hypothesized that 4-ene VPA-CoA undergoes β-oxidation to 2,4-diene VPA *to either deplete the mitochondrial glutathione pool [2] or to yield an electrophilic intermediate,* 2-propyl-3-oxo-4-pentenoic acid which alkylates and thereby irreversibly inhibits fatty acid β-oxidation enzyme(s) [3] Thus, based on either of these hypotheses, *if the β-oxidation pathway is blocked, the formation of toxic metabolites and the hepatotoxicity of VPA should be prevented.* In order to test this, we reasoned that α-fluorinated VPA analogues would not undergo β-oxidation to form toxic metabolites, because, while fluorine closely mimics hydrogen in size the stronger C-F bond is resistant to many forms of metabolism.

Thus, α-fluoro VPA (2-fluoro-2-propylpentanoic acid) and α-fluoro-4-ene VPA (2-fluoro-2-propyl-4-pentenoic acid) were synthesized through the deaminative fluorination of the *corresponding α-amino acids using Olah's reagent [4]. The in vivo metabolism of α-fluoro* VPA and α-fluoro-4-ene VPA was investigated by GC/MS and compared with their counterparts VPA and 4-ene VPA. Fluorinated or non-fluorinated compounds were administered to rats (Sprague Dawley, 250g) by i.p. injection of 200mg/kg per day for 3 days. Urine was collected over a 24 h period on the second day Blood was collected following decapitation, 2h after the last dose. Urine and serum samples were acidified to pH 2, extracted with ethyl acetate, concentrated under nitrogen, and derivatized with MSTFA or MTBSTFA at 60°C for 1h. GC/EIMS analysis was carried out using a HP 5971A GC/MS: column, DB-1701 (30m x 0.25mm i.d., 0.25μm film thickness), He (15psi), GC program, 80-100°C (10°C/min), 100-130°C (2°C/min), 130-260°C (30°C/min) *Under these conditions, the β-oxidation metabolites 2-ene* VPA (2-propyl-(E)-2-pentenoic acid) and 2,3'-diene VPA (2-((E)-1'-propenyl)-(E)-2-pentenoic acid) were detected in the serum and urine of VPA treated rat (Fig. 1) and 2,4-diene VPA was detected from 4-ene VPA treated rat. The N-acetylcysteine (NAC) conjugate of 2,4-diene VPA was detected in urine using a HP 5989A GC/MS (column: DB-1, 12m x 0 25mm i d., 0.33μm film thickness; He, 3 psi; GC: 50-200°C (30°C/min), 200-300°C (10°C/min)). *The major serum metabolite,* 2-ene VPA could not be detected in serum or urine of the α-fluoro VPA treated rat (Fig. 2). Neither 2,4-diene VPA nor its NAC conjugate was found as a metabolite of α-fluoro-4-ene VPA. Therefore, we have seen a total elimination of β-oxidation products from the metabolism of α-fluorinated VPA analogues

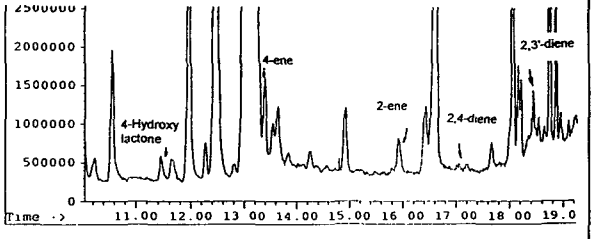

Fig. 1. GC/MS total ion current chromatogram of tBDMS derivatives of an extracted urine sample from a VPA treated rat.

An abundant fragment ion, m/z 77, was found to be characteristic of the TMS or tBDMS derivatives of the α-fluorinated acids (Fig. 3) and proved useful as a diagnostic peak for the detection of metabolites arising from the α-fluorinated compounds. High resolution mass spectra of the derivatives, including the TMS-d_9 derivative, were recorded on a Kratos MS50 or MS 80 mass spectrometer and *confirmed that the m/z 77 ion possessed the chemical structure* $[F\text{-}Si(CH_3)_2]^+$. The mechanism accounting for the formation of fragment ion $[F\text{-}Si(CH_3)_2]^+$ is similar to that proposed by White, et al [5] for the migration of a halogen ion from halo acid TMS derivatives to the silicon charged center (Scheme 1).

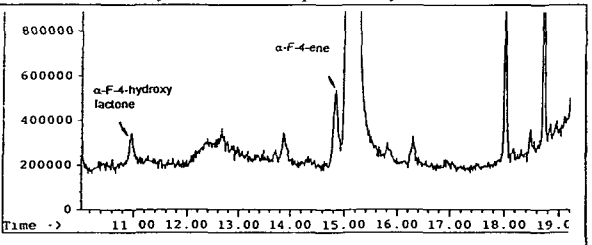

Fig. 2. GC/MS total ion current chromatogram of tBDMS derivatized extract of a urine sample from an α-fluoro VPA treated rat.

This research was funded by a grant from the Medical Research Council of Canada.

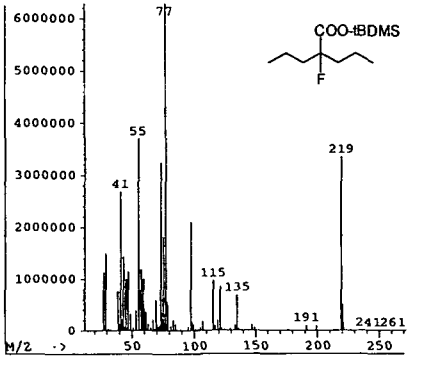

Fig. 3. Mass spectrum of α-fluoro VPA-tBDMS derivative.

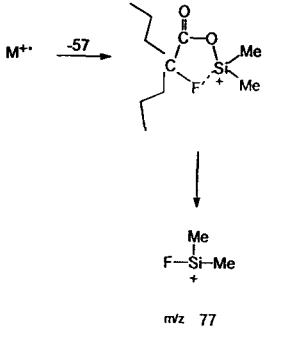

Scheme 1. Formation of the m/z 77 fragment ion from α-fluoro VPA-tBDMS derivative.

References:

1 Kesterson, J. W., Granneman, G. R., and Machinist, J. M., *Hepatology,* 4 (6), 1143, (1984).
2. Kassahun, K., Farrell, K., and Abbott, F., *Drug Metab. Disp.*, 19(2), 525, (1991)
3. Baillie, T., *Chem. Res. Toxicol.*, 1, 195, (1988).
4. Olah, G. et al., *J. Org. Chem.*, 44(22), 3872, (1979).
5 White, E., McCloskey, V. and McCloskey, J., *J. Org. Chem.*, 35, 4241, (1970).

IDENTIFICATION OF GLUTATHIONE CONJUGATES OF *tris*(2,3-DIBROMOPROPYL) PHOSPHATE BY TANDEM MASS SPECTROMETRY: APPLICATIONS OF STABLE ISOTOPES AS MECHANISTIC PROBES

Gregory L. Weber, Sidney D. Nelson[†], and Paul G. Pearson

Drug Metabolism Research, The Upjohn Company, Kalamazoo, MI 49001
[†]Medicinal Chemistry, School of Pharmacy, University of Washington, Seattle, WA 98195

The halogenated alkyl phosphate, *tris*(2,3-dibromopropyl)phosphate (Tris-BP) was used extensively as a flame retardant in children's sleepwear prior to the observation that Tris-BP, or its metabolites, were highly mutagenic. Tris-BP is bioactivated by cytochromes P450 to the potent direct acting mutagen, 2-bromoacrolein (2-BA). In an alternative P450 independent mechanism, it has been proposed that Tris-BP may be bioactivated by conjugation with glutathione (GSH) to form reactive episulfonium ions. The episulfonium ions may interact with critical macromolecules or rearrange to form stable GSH conjugates. The objective of this study was to identify GSH conjugates of Tris-BP to elucidate the respective roles of GSH conjugation and cytochromes P450 oxidation in the bioactivation of Tris-BP. The mechanism of GSH conjugate biogenesis was addressed by the use of a per-deutero-analog of Tris-BP (D_{15}-Tris-BP) as a mechanistic probe and the application of mass spectrometry to assess deuterium retention in GSH conjugates.

Experimental: GSH conjugates excreted in the bile of male Sprague-Dawley rats administered Tris-BP (100 mg/kg) or D_{15}-Tris-BP were converted to their *N*-(benzyloxycarbonyl) dimethyl ester derivatives, separated by HPLC and examined by fast atom bombardment tandem mass spectrometry (FAB/MS-MS) FAB/MS-MS spectra were recorded on a VG AutosecQ hybrid tandem mass spectrometer of EBEqQ geometry. Analytes were desorbed from a dithiothreitol/dithioerythritol (5:3) matrix by bombardment with a primary beam of Cs^+ (10 keV) and conventional FAB spectra were recorded at an accelerating voltage of 8 kV. Collision-induced dissociation (CID) daughter ion spectra of the MH^+ ions of metabolites was performed in the first (rf-only) quadrupole (q) employing argon as a collision gas (2 x 10^{-6} Torr) and collision energies of 20-30 eV. Deuterium retention in the analytes was determined by a precursor ion (MS-MS) scan technique in which precursors of m/z 159 were monitored with Q while a magnet (B) scan was performed across the molecular ion region of the chosen analyte.

Results and Discussion: Three GSH conjugates derived from Tris-BP were identified by mass spectrometry as: *S*-(2,3-dihydroxypropyl)GSH (**III**), *S*-(3-hydroxypropyl)GSH (**IV**) and *S*-(2-carboxyethyl)GSH (**V**). The CID product ion spectra for all the GSH conjugates displayed a series of structurally-informative fragment ions that arose from expulsion of methylglycine (-89u), or the derivatized γ-glutamyl moiety (-277u). Representative product ion spectra of metabolite **III** derived from Tris-BP or D_{15}-Tris-BP are shown in Figure 1a and 1b. In this case ions retaining the alkyl side chain (eg. ion **a** and **e**) were shifted by 5u. Precursor ion scans of m/z 159 demonstrated that metabolite **III** retained 5 atoms of deuterium while metabolites **IV** and **V** retained 3 and 2 atoms of deuterium, respectively. The retention of 5 atoms of deuterium in **III** is consistent with direct GSH conjugation of Tris-BP or Bis-BP and subsequent formation of two reactive episulfonium ion intermediates (Figure 2). The retention of 3 and 2 atoms of deuterium in **IV** and **V** suggest the involvement of cytochromes P450 and possibly the intermediacy of 2-bromoacrolein (Figure 2).

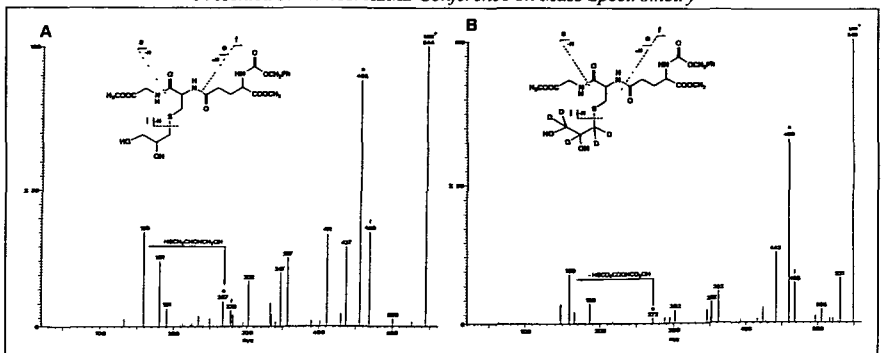

Figure 1. Product ion spectra of *S*-(2,3-dihydroxypropyl)GSH *N*-(benzyloxycarbonyl) dimethyl ester (**III**) isolated from bile of a rat administered (**A**) D_0-Tris-BP; and (**B**) D_{15}-Tris-BP illustrating retention of 5 atoms of deuterium.

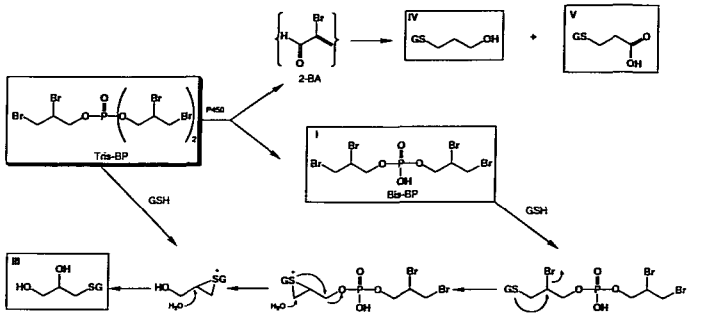

Figure 2. Proposed metabolic scheme for the formation of *S*-(2,3-dihydroxypropyl)GSH (**III**), *S*-(3-hydroxypropyl)GSH (**IV**)and *S*-(2-carboxyethyl)GSH (**V**). Oxidation at C-3 affords 2-bromoacrolein (2-BA) and Bis-BP (**I**). Conjugation of Tris-BP or Bis-BP with GSH, sequential formation of two reactive episulfonium ion intermediates, followed by hydrolysis would afford **III** with retention of five atoms of deuterium from one dibromopropyl side chain of D_{15}-Tris-BP. Conjugation of 2-BA with GSH followed by metabolic reduction affords **IV** with net retention of 3 atoms of deuterium. Additional oxidation of the aldehyde precursor of **IV** affords **V** with net retention of two atoms of deuterium from one dibromopropyl side chain of D_{15}-Tris-BP.

A GC-MS-MS SCREENING STRATEGY FOR THE IDENTIFICATION OF *N*-ACETYLCYSTEINE CONJUGATES DERIVED FROM CHEMICALLY-REACTIVE DRUG METABOLITES OF HALOALKANES

Gregory L. Weber and Paul G. Pearson.

Drug Metabolism Research, The Upjohn Company, Kalamazoo, MI 49001

The endogenous tripeptide glutathione (γ-glutamyl-cysteinyl-glycine; GSH) exists at millimolar concentrations in mammalian systems, and conjugation with GSH serves an important physiological role in the detoxication of reactive electrophilic species. These reactive species, which are generated metabolically from drugs or other xenobiotics, have been implicated in various xenobiotic-induced toxicities. The glutathione conjugates are excreted following a cascade of metabolic events as *N*-acetylcysteine conjugates in urine. As a consequence, therefore, analytical strategies to identify *N*-acetylcysteine conjugates in biological matrices are important, as the structural information thus obtained affords a unique insight into the nature of the chemically-reactive drug metabolite. Analytical approaches based upon fast atom bombardment tandem mass spectrometry (FAB-MS-MS) have been described for the identification of glutathione conjugates in biological matrices (Pearson *et al*, 1990). Here we describe a gas-chromatography tandem mass spectrometry (GC-MS-MS) screening strategy for the facile identification of *S*-(3-chloro-2-hydroxypropyl)-*N*-acetylcysteine (**I**), *S*-(2,3-dihydroxypropyl)-*N*-acetylcysteine (**II**), and *S*-(3-hydroxypropyl)-*N*-acetylcysteine (**III**) derived metabolically from the haloalkane nematocide 1,2-dibromo-3-chloropropane (DBCP).

Experimental: *N*-Acetylcysteine conjugates excreted in the urine of male Sprague-Dawley rats that had received ^{14}C-DBCP (80 mg/kg; 77 mCi/mmol) were converted to methylester derivatives and purified by reverse-phase HPLC. Lyophilized HPLC fractions containing *N*-acetylcysteine conjugates of DBCP were treated with *N*-methyl-*N*-(*tert*-butyldimethylsilyl)-trifluoroacetamide (25µl) in acetonitrile (25µl) at 80°C (60 min.). The samples were evaporated to dryness and reconstituted with acetonitrile (25µl). Aliquots (1-2 µl) were subjected to GC-MS-MS analysis. Separations were performed on a 20 M x 0.18 mm DB-17 column interfaced to a Finnigan TSQ-70 tandem quadrupole mass spectrometer (Finnigan MAT, San Jose, CA) operating in electron ionization mode (70eV). Product ion spectra were recorded by selecting the $M^{+\cdot}$-57 species of choice with Q_1 and scanning Q_3 from 50 - 500 amu. Precursor ion spectra to detect the $M^{+\cdot}$-57 species of **I**, **II** and **III** were recorded by monitoring m/z 144 in Q_3 while scanning Q_1 from 150 - 500 amu.

Results and Discussion: GC-MS analysis of **II** as a *bis*-(*t*-BDMS) methyl ester employing electron ionization afforded a weak M^+ ion (m/z = 479) and an intense M^+ -57 ion (m/z = 422). A product ion (MS-MS) mass spectrum of M^+ -57 ion displayed a series of structurally-informative fragment ions and a base peak at m/z 144 arising by fragmentation adjacent to the sulfur atom (Figure 1A). Analysis of **I-III** by GC-MS-MS indicated that m/z 144 was the base peak in their respective product ion mass spectra. The presence of a common product ion at m/z 144 facilitated a highly specific (GC-EIMS-MS) precursor ion screening strategy for the identification of M^+ -57 of *N*-acetyl-*S*-(hydroxypropyl)cysteine methyl ester derivatives. The reconstructed ion chromatogram (RIC) from a GC-EIMS-MS precursor ion experiment for the identification of NAC conjugates derived from a perdeutero analog of DBCP ($^2H_5$-DBCP) display an intense GC peak at t_r = 10 min. (Figure 1B). Examination of the precursor ion mass spectrum of the GC peak at t_r = 10 min. revealed the presence of a M^+ -57 species at m/z 427, that corresponded to *N*-acetyl-*S*-(2,3-dihydroxy-[$^2H_5$]-propyl)cysteine *t*-BDMS methyl ester (Figure 1C). The general utility of the GC-MS-MS approach was established for a series of *N*-acetyl-*S*-(hydroxypropyl)cysteine conjugates (**I-III**), and *N*-acetyl-*S*-(2-hydroxypropyl)cysteine; GC-EIMS-MS analysis facilitated the separation and identification of $M^{+\cdot}$-57 species for each analyte. Thus by using precursor ion MS-MS scans of m/z 144, $M^{+\cdot}$-57 species of **I**, **II** and **III** were identified in HPLC fractions of urine obtained from rats administered DBCP. These data indicate the selectivity of this GC-MS-MS screening strategy for the identification of *N*-acetylcysteine conjugates as biological markers for metabolic activation of haloalkanes to chemically-reactive drug metabolites.

Pearson, P.G., Howald, W.N., and Nelson, S.D. (1990). Screening strategy for the detection of derivatized glutathione conjugates by tandem mass spectrometry. *Analytical Chemistry*, **62**, 1827-1836.

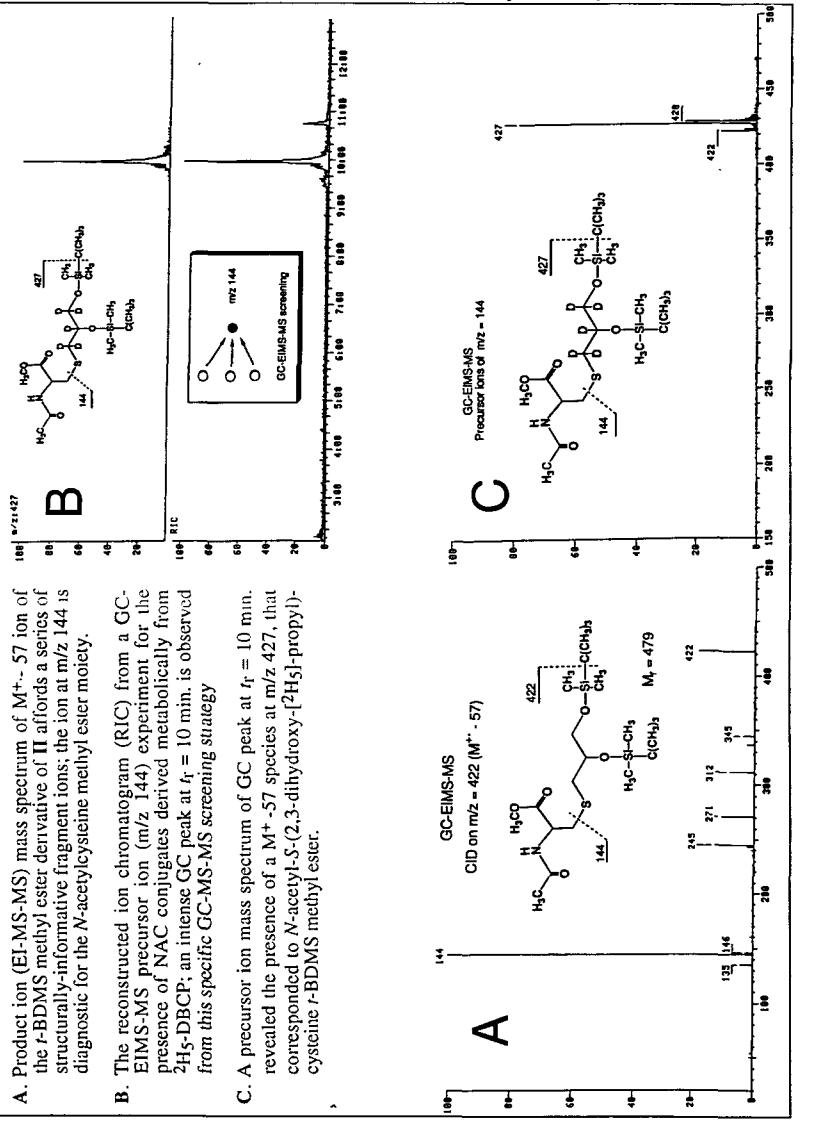

FIGURE 1. *A GC-MS-MS SCREENING STRATEGY FOR THE IDENTIFICATION OF N-ACETYLCYSTEINE CONJUGATES OF DBCP.*

A. Product ion (EI-MS-MS) mass spectrum of $M^{+\cdot}$- 57 ion of the *t*-BDMS methyl ester derivative of **II** affords a series of structurally-informative fragment ions; the ion at m/z 144 is diagnostic for the *N*-acetylcysteine methyl ester moiety.

B. The reconstructed ion chromatogram (RIC) from a GC-EIMS-MS precursor ion (m/z 144) experiment for the presence of NAC conjugates derived metabolically from $^2H_5$-DBCP; an intense GC peak at t_r = 10 min. is observed *from this specific GC-MS-MS screening strategy*

C. A precursor ion mass spectrum of GC peak at t_r = 10 min. revealed the presence of a M^+ -57 species at m/z 427, that corresponded to *N*-acetyl-*S*-(2,3-dihydroxy-[$^2H_5$]-propyl)-cysteine *t*-BDMS methyl ester.

Application of Negative Ion Chemical Ionization Isotope Dilution Gas Chromatography/Mass Spectrometry to Pulse Dose Bioavailability Studies of Mefloquine

W. N. Howald, J. M. Neal, K. L. Kunze, R. F. Lawrence and W. F. Trager

Department of Medicinal Chemistry University of Washington, Seattle, WA 98195

INTRODUCTION

The antimalarial drug mefloquine (I), racemic erythro-α-(2-piperidyl)-2,8-bis(trifluoromethyl)-4-quinoline-methanol, is formulated in both Europe and the United States and has been proven effective against chloroquine- and quinine-resistant strains of *Plasmodium falciparum*. To evaluate the comparative bioavailability of these two tableted dosage forms, each of the unlabeled formulations was orally co-administered with an aqueous solution of isotopically-labelled $^{13}C_3$-mefloquine to adult subjects and blood samples drawn over a 84 day period.

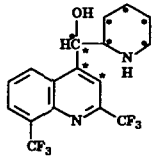

I
(*)mefloquine-$^{13}C_3$
(•)mefloquine-$^{2}H_6$

While an electron ionization (EI) GC/MS method has been reported[1] for the quantification of mefloquine, fragmentation analysis of mefloquine-$^{13}C_3$ using this ionization technique was found to be unsuitable due to significant loss of label in the formation of its diagnostic ion. As a result, a negative ion gas chromatographic mass spectrometric [GC/(NCI)MS] method was developed to quantify the amount of unlabeled mefloquine and co-administered mefloquine-$^{13}C_3$ in plasma in support of this study. This work describes this analytical methodology incorporating a stable isotope labelled internal standard (mefloquine-$^{2}H_6$) and offers an assessment of the sensitivity, precision and accuracy of the technique in the quantification of these compounds.

METHODS

Plasma Extraction and Derivatization

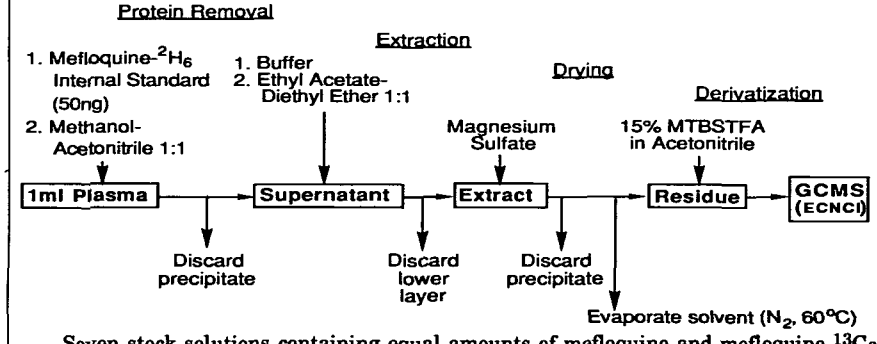

Seven stock solutions containing equal amounts of mefloquine and mefloquine-$^{13}C_3$ at a concentration of 0.02, 0.10, 0.20, 1.00, 2.00 and 4.00 μg mL^{-1} each were used in the preparation of standards by the 50 μL addition of each to 1mL aliquots of blank plasma. Quality assurance plasma samples containing 5, 90 and 150ng mL^{-1} each of mefloquine

and -$^{13}C_3$ were assayed with each sample set to monitor the precision and accuracy of the method.

GC/MS

Analysis of the derivatized extracts was carried out using a VG Trio 2000 quadrupole mass spectrometer (VG BioTech, Cheshire, UK) fitted with an HP 5890 Series II GC and 7673A Autoinjector (Hewlitt Packard, Palo Alto, CA).

GC Parameters:
- Column: J & W 30m DB-1 (0.32mm i.d., 0.25μm film).
- Injector: 250°C with purge on at 1min.
- Oven: 140°C for 1 min, 30°C/min to 290°C, hold 1min.
- Injection volume: 1μL
- Carrier gas: Helium at 10psi head pressure

MS Parameters:
- Ionization mode: ECNCI
- Moderating gas: Methane
- Source temperature: 200°C
- Interface temperature: 300°C
- Data collection mode: SIR with 300ms/ion dwell.
- Ions monitored: [M-TBDMSOH]$^-$; *m/z* 360.1, 363.1 & 366.1

Quantification

Quantification was based upon the ratio of the area measured for each analyte to the the area of the $^{2}H_6$ labelled internal standard. Individual ion intensities were integrated using standard VG Lab-Base™ software. Response ratios for each analyte relative to internal standard were calculated and used for the generation of the standard curves and the determination of analyte concentration in submitted and control samples.

RESULTS

The fragment ions at *m/z* 360, 363 and 366, corresponding to the [M - TBDMSOH]$^-$ ions of the TBDMS derivatives of mefloquine (M_r=492), -$^{13}C_3$ (M_r=495) and -$^{2}H_6$ (M_r=498), respectively, were monitored. These TBDMS derivatives showed a high detection sensitivity in ECNCI for the SIM method with no observed interferences.

Standard curves generated by plotting the peak area ratios of the analyte to the I.S. against known mefloquine concentrations over the concentration range of 1 to 200 ng mL^{-1} were found to be linear with correlation coefficients ≥ 0.990. The intra- and inter-day coefficients of variation were determined by the analysis of duplicate extracts of control samples throughout the study and were found to average ≤ 5% in both cases.

CONCLUSIONS

An ECNCI GC/MS method has been developed which allows the quantification of both mefloquine and its $^{13}C_3$ analog as their TBDMS ethers from plasma.. The high sensisitivity and specificity of the ECNCI GC/MS in combination with the exact control of sample recovery, using mefloquine-$^{2}H_6$ as an internal standard, provides precise and accurate determination of the analytes, with a detection limit of 50fg on-column. The method has proven to be rapid and reliable, and has been utilized to measure over 1000 plasma samples in a three month period.

ACKNOWLEDGEMENTS

We wish to thank Hoffman-La Roche (Nutley, New Jersey) for their gift of mefloquine labeled analogs and support of this work.

1. D. E. Schwartz and U. B. Ranalder, Biomed. Mass Spectrom., 8, 589 (1981).

EXTRACTIVE HYDROGENATION OF BIOLOGICAL SAMPLES PRIOR TO GAS CHROMATOGRAPHY.

Mohammed Itani and Roger W. Giese. Department of Pharmaceutical Sciences in the Bouve College of Pharmacy and Health Sciences, and Barnett Institute, Northeastern University, 360 Huntington Avenue, Boston, MA 02115

INTRODUCTION:

A new technique, "extractive hydrogenation", is combined with gas chromatography (GC) to analyze biological samples. In this method, the sample is subjected to intense hydrogenation under aqueous conditions in the presence of excess (in terms of mass) palladium/carbon catalyst. Products with a saturated hydrocarbon framework result, the larger of which adsorb onto the carbon of the catalyst. These larger products are separately recovered by extracting the washed catalyst with an organic solvent, and then detected by GC. Here, the GC was fitted with a flame ionization or mass spectrometry detector. Unlike pyrolysis (similarly used prior to GC), which tends to convert a biological sample into a char, the hydrogenation reaction turns the sample into a clear, aqueous solution. Most importantly, the technique brings a broad variety of biological samples and organic substances in a simple way into the scope of GC-EI-MS and its computerized library of spectra. The concept is as follows, along with the structures of the compounds that we tested.

CONCEPT FOR
EXTRACTIVE HYDROGENATION / GC-EI-MS

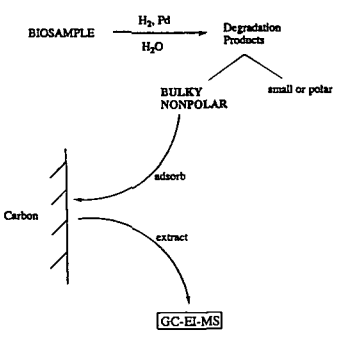

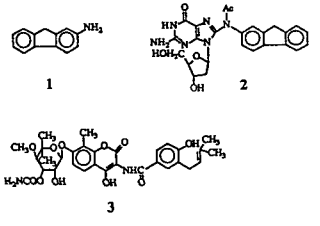

RESULTS AND DISCUSSION:

From 2-aminofluorene (1) a carcinogen, we obtained perhydrofluorene (as a mixture of five isomers), plus a corresponding isomer mixture of 2-hydroxyperhydrofluorene (data not shown). N-(Deoxyguanosin-C8-yl)-2-acetylaminofluorene (100 ug, 2) spiked into 1 mg of DNA was detected (Fig. 2D, cluster of peaks at 14.2 min). The detection by H_2/GC-FID of 1.5 ug of novobiocin (3) spiked into 15 ml of milk is demonstrated in Fig. 2B relative to a blank chromatogram from unspiked milk, shown in Fig. 2A. The former chromatogram is distinguished by the pair of peaks (a, b) which were seen when standard novobiocin was subjected to extractive hydrogenation.

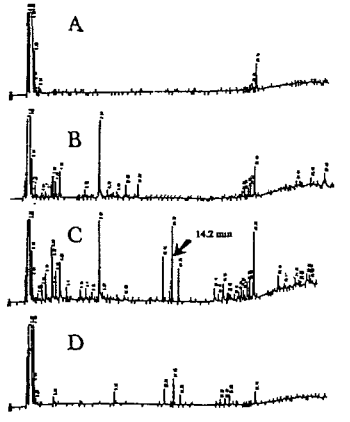

Fig. 1. GC-FID chromatograms from hydrogenation of: A (blank), 50 mg Pd/C in 2.5 ml of water; B,5 mg DNA and 50 mg Pd/C in 2.5 ml H_2O; C, similarly 5 mg DNA spiked with 1 mg of 2; D, similarly 1 mg of DNA spiked with 0.1 mg of 2, but 10 mg Pd/C. Hydrogenation conditions: 150°C, 3 h, 60-80 bar. From a final volume (ethyl acetate solution) of 50 ul, 1 ml was injected.

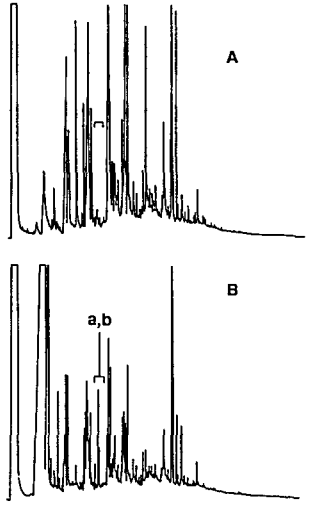

Fig. 2. GC-FID chromatograms from the hydrogenation of: A (blank), sample obtained by extracting 15 mL of skim milk with C18-Si, washing, eluting, evaporating and redissolving in 150 ul of water/2-propanol, 2:1 (prior to hydrogenation); and B, same except the milk was spiked before extraction with 1.5 ug of novobiocin. Hydrogenation conditions: 5 mg Pd/C, 150°C, 60-80 bar, 3 h. Peaks a and b are derived from novobiocin. One ul of a final sample volume of 50 ul was injected.

In Vitro Pancreatic Lipase Hydrolysis of Emulsified Common Fats and Oils by HTGC/FID and HTGC/MS.

Anna J. Sequeira, Experimental Pathology Labs. Inc., c/o Bowman Gray Tech. Ctr., Winston-Salem, NC 27102; Mary S. Uhrig & Bert M. Gordon, R.J. Reynolds Tobacco Co. Winston-Salem, NC 27102; Katherine M. Phillips, TechLab, Blacksburg, VA 24060.

INTRODUCTION

Analytical methods for monitoring lipid enzyme activity are continuously being developed. Many of the present methods are time consuming, cumbersome and involve derivatization. The chromatographic separation of complex Triacylglycerol (TAG) mixtures has been accomplished by TLC, HPLC, GC and SFC. Heretofore, the Free Fatty Acids (FFAs) content has been obtained chromatographically by derivatization to the methyl esters.

In this investigation of lipase metabolism, we describe a simple HTGC method which can simultaneously monitor the disappearance of TAGs and the appearance of Diacylglycerols (DAGs), Monoacylglycerols (MAGs) and long chain FFAs without any chemical derivatization or modification of the extracted emulsions. The characterization of the components was achieved by mass spectroscopy operating in both the EI and CI modes.

EXPERIMENTAL

Cocoa Butter, milk fat, trioleoylglycerol and porcine pancreatic lipase containing 13000 U of lipolytic activity were purchased commercially. Emulsions of these fats were prepared similar to that described by Lindstrom et al, using phosphatidylcholine, sodium taurocholate, sodium taurodeoxycholate, NaCl, $CaCl_2$, NaOH and tris-maleate. Chloroform and methanol were utilized as extraction solvents.

The HTGC system (HP 5890 Series II) was equipped with a temperature/pressure programmable on-column injector and a FID. A 25m x 0.25mm id x 0.1μm film thickness Al-clad methyl 65% phenyl silicone column was used to achieve the separation. For peak identifications the VG 70-VaxSQ system was utilized with NH_3 as the reagent gas for CI. The mass range examined was 50 to 1200u for EI and 300 to 1200 for CI.

RESULTS and DISCUSSION

After emulsion preparation, a single chloroform extraction is performed. A 1μL aliquot of this extract is introduced into the gas chromatograph without any chemical derivatization or modification. The kinetic study was monitored at 0, 2, 5, 10 and 30 minutes (cf Figure 1). Mass spectrometric identifications were made using GC retention times, characteristic fragment ions and the ammonium adduct ion. (T. Murata & S. Takahashi, **Anal Chem**, 45:1816, *1973*).

Quantification of the TAGs, DAGs, MAGs & long chain FFAs was achieved by obtaining the relative response factor ratio (RRF) to Trilauroylglycerol of the saturated TAGs (T6 to T66), C16:0, C18:1, Distearoylglycerol & Trioleoylglycerol. By extrapolation based on Carbon Number (CN), their RRF values and consequently their amounts were calculated at the different time intervals as shown in Table 1 for Cocoa butter.

CONCLUSION

This technique has been successfully utilized to simultaneously monitor (qualitatively and quantitatively) the disappearance of TAGs and the appearance of DAGs, MAGs and long chain FFAs. Sample preparation is a single extraction without subsequent derivatization. Consequently HTGC/MS is a viable technique to characterize complex TAG mixtures and their metabolites. It is believed that this method can be used to monitor any lipase reaction kinetics involving complex TAG mixtures.

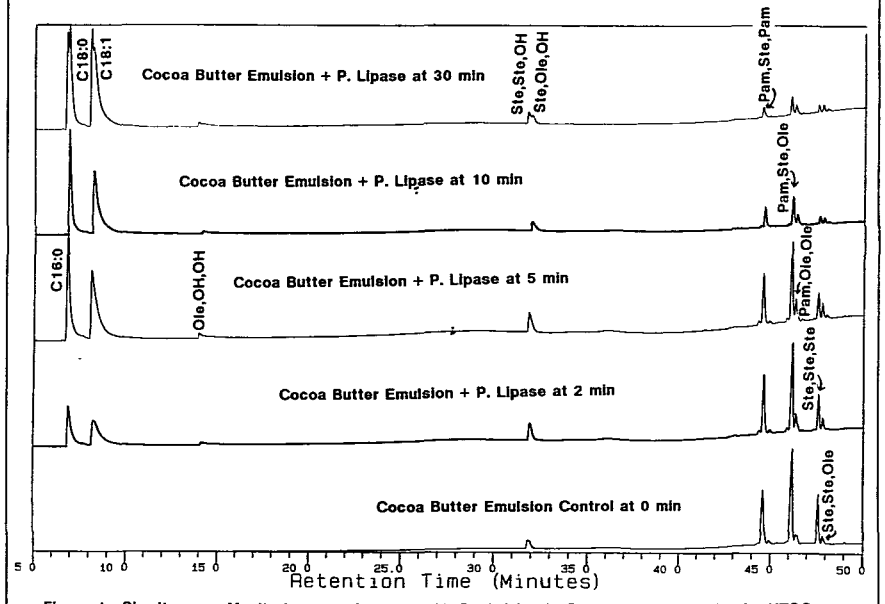

Figure 1. Simultaneous Monitoring of TAGs, DAGs, MAGs & FFAs in Cocoa Butter Emulsion by HTGC

Table 1. Amounts of TAGs & FFAs found in Cocoa Butter at 0 2 5, 10 & 30 mins

Pam,Ste,Pam				
Time min	ug	Amount S.D.	%RSD	nmoles
0	0.42	0.12	28	0.50
2	0.18	0.06	34	0.22
5	0.12	0.06	51	0.15
10	0.12	0.03	22	0.14
30	0.04	0.02	58	0.05

RRF = 0.45 (by extrapolation between T48 & T54)

C16:0				
Time min	ug	Amount S.D.	%RSD	nmoles
0	<0.01			
2	0.13	0.03	20	0.52
5	0.24	0.04	16	0.93
10	0.30	0.04	15	1.19
30	0.39	0.01	2	1.52

RRF = 1.19 (by experimental standard)

Ste,Ste,Ste				
Time min	ug	Amount S.D.	%RSD	nmoles
0	0.37	0.10	27	0.42
2	0.14	0.06	42	0.15
5	0.08	0.03	41	0.09
10	0.12	0.09	70	0.14
30	0.03	0.02	61	0.03

RRF =0.28 (by experimental standard)

C18:0				
Time min	ug	Amount S.D.	%RSD	nmoles
0	<0.02			
2	0.62	0.12	19	2.18
5	1.11	0.17	15	3.91
10	1.44	0.11	8	5.07
30	1.95	1.13	58	6.86

RRF = 0.32 (by experimental standard)

Plasma Testosterone by Negative Chemical Ionization GC/MS

Robert L. Fitzgerald and David A. Herold

VA Medical Center, San Diego, CA 92161 and Dept. of Pathology, UCSD, La Jolla, CA 92134

Introduction Testosterone is the primary androgen responsible for development of sexual characteristics in men and is clinically monitored to diagnose a variety of illnesses which cause hyper and hypogonadism. The majority of methods currently used to quantitate testosterone are competitive protein binding assays based on testosterone binding globulin which can crossreact with a variety of structurally related compounds. We have developed a specific method for the analysis of serum testosterone which uses a trideuterated internal standard and gas chromatography/negative chemical ionization mass spectrometry (GC/NCIMS).

Materials Testosterone was obtained from Sigma (lot #50H0345) and the internal standard testosterone-16,16,17-d_3 was from MSD Isotopes (lot #Md-3793). HPLC grade ethyl acetate was from Burdick and Jackson. HPLC grade pyridine was purchased from Aldrich. The derivatizing reagents BSTFA (N,O,-bis(trimethylsilyl)trifluoroacetamide with 1% trimethylchlorosilane) and Florox (O-(pentafluorobenzyl) hydroxylamine 2.5 mg/mL in pyridine) were from Pierce Chemical Company. Commercially prepared testosterone controls were from BIO-RAD (lyphocheck immunoassay control serum level 1, 2 and 3).

Plasma Extraction The internal standard (50 uL of 0.1 ng/uL testosterone-d_3) is added to 1 mL of plasma and briefly vortexed. Three mL of ethyl acetate are added followed by vortexing for 1 min. Samples are centrifuged (2500 rpm for 10 min), the organic layer is pipetted to a clean 100 x 13 mL screw cap test tube and evaporated to dryness at 40°C under a gentle stream of nitrogen. The pentafluorobenzyl oxime derivative is formed by adding 50 uL of pyridine and 50 uL of Florox reagent to the plasma residues and heating for 1 hour at 70°C. The excess derivatizing reagent is evaporated and trimethylsilyl derivatives are formed by adding 50 uL of ethyl acetate and 50 uL of BSTFA and heating at 70°C for 20 min.

Analysis The GC was equipped with a 15 m DB-1 (dimethylpolysiloxane) capillary column and 1 uL samples are injected in the splitless mode. The initial GC temperature was 160°C (one min. hold) which was temperature programed to 280°C at 20°C per min where it was held for 3 min. Injection port temperature was 265°C and the interface oven was 280°C. The mass spectrometer was operated in the electron capture NCI mode using methane as the reagent gas. The ionizer was maintained at a pressure of 0.35 torr and 100°C. The manifold was 100°C, and the high pressure region was 1.3 x 10^{-5} torr. Tuning was optimized on the m/z 414 and 633 ions of perfluorotributylamine (PFTBA). Testosterone was monitored at m/z 535 and the internal standard at m/z 538. Scans were obtained at 2 Hz with dwell times of 200 ms. The structure of the derivatized testosterone is shown on the bottom of the next page.

Results The chromatogram showed well resolved peaks at 7:33 and 7:43 min which are the geometric isomers of pentafluorobenzyl/TMS testosterone derivative. Since the first peak had a larger signal than the second, it was used for quantitative analysis. The derivatization procedure combined with the selectivity of NCI provided clean extracts which contained no interfering substance at the ions monitored. Typical of NCI, the mass spectrum of pentafluorobenzyl/TMS testosterone was fairly simple, consisting primarily of the base peak at m/z 535 $(M-20)^-$ and an ion cluster at m/z 377 $(M-181)^-$ which are probably due to a loss of HF and $C_6F_5CH_2$, respectively. The m/z 535 ion was chosen for quantitations because it had better signal to noise ratio than m/z 377.

The average extraction efficiency of the the method at 1, 5 and 20 ng/mL was 104±15%. The method is linear from 0.25 ng/mL to 20 ng/mL. The error in the analysis, shown in the table, ranged from 6.0% at 1 ng/mL to 1.4% at 20 ng/mL. A comparison of GC/MS with immunoassay values for a commercially prepared control showed that GC/MS is from 2 to 8 times more precise than the immunoassay values listed in the control package insert.

Discussion Immunoassay values for commercially available testosterone controls have coefficients of variation which range from 33% for a low control (target concentration of 1 ng/mL) to 24 % for a high control (target concentration of 13 ng/mL). This wide variation is probably due to the different crossreactivities of the testosterone antibodies with other endogenous steroids and the lack of uniformity between different manufacturers' testosterone antibodies. Using GC/MS with NCI, only testosterone is measured which increases the accuracy of the method. The one step extraction presented here has significant advantages over previously described procedures which required multiple extractions combined with column chromatography prior to GC analysis.

Conclusion The use of a one step liquid extraction, stable isotope labeled internal standard and NCI GC/MS, provided a method for the efficient, accurate and precise measurement of testosterone in serum.

Table Accuracy of NCI GC/MS for plasma testosterone

Target (ng/mL)	Measured (ng/mL)	±S.D. (ng/mL)	C.V. (%)	Error (%)
1.0	0.94	0.08	9.0	-6.0
5.0	4.83	0.19	3.9	-3.4
20.0	20.28	0.64	3.1	+1.4

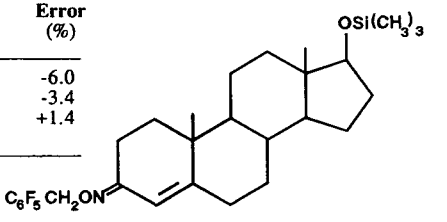

Pentafluorobenzyl/Trimethylsilyl Derivative

Comparision of Electron Impact, Positive and Negative Chemical Ionization Mass Spectrometry of Benzodiazepines

Robert L. Fitzgerald and David A. Herold

VA Medical Center, San Diego, CA 92161 and Dept. of Pathology, UCSD, La Jolla, CA 92037.

Introduction: Benzodiazepines are a group of structurally related drugs prescribed as sedatives, muscle relaxants, anxiolytics and anticonvulsants, which also have the potential for abuse. GC/MS is the standard with which other methods are validated, however the sensitivity of EI GC/MS does not permit the quantitation of low concentrations of the more potent benzodiazepines (and associated metabolites) which have therapeutic concentrations in the low ng/mL range. This lack of sensitivity makes it difficult to detect abuse of these compounds when using EI GC/MS. NCI of benzodiazepines has demonstrated that this technique is very sensitive as compared with EI and PCI, but there are no reports on NCI analysis of some of the newer benzodiazepines or their metabolites. In developing a quantitative GC/MS method for benzodiazepines we compared EI, PCI and NCI to determine which gave optimal sensitivity. These results along with some general rules for interpretation of NCI spectra of benzodiazepines are presented.

Materials: The benzodiazepine standards were all obtained from Sigma Chemical Company except N-1-hydroxy-ethylflurazepam and desalkylflurazepam which were gifts from Hoffman-La Roche (Nutley, NJ) and α-hydroxyalprazolam and α-hydroxytriazolam which were obtained from Radian Corporation. Ethyl acetate was HPLC grade from Burdick and Jackson. N,O-bis(trimethylsilyl) trifluoroacetamide with 1% trimethylchlorosilane (BSTFA with 1% TMCS) was purchased from Pierce.

Methods: Compounds with active hydrogens were silylated by adding 50 uL of ethyl acetate followed by 50 uL of BSTFA containing 1% TMCS and heating at 70°C for 20 minutes. The BSTFA solution was injected into the GC/MS, while compounds which did not require derivatization were injected from a 5 ng/uL methanolic solution. The GC temperature program maintained the initial temperature of 160°C for one minute before increasing at 20°C/minute to 280°C where it was held for 3 minutes. The injection port was maintained at 265°C and the transfer line was 280°C.

Results: The sensitivity of NCI as compared with EI and PCI in the table below shows that the NCI S/N ratio was 4 to several thousand times greater than that of PCI or EI except for medazepam. Medazepam had a EI signal but no NCI signal. Medazepam is also the only compound which did not have a substituent at the 2 position, suggesting that this is important in the electron capture process or stability of the negative ion. Oxazepam, lorazepam, chlordiazepoxide, clonazepam, nitrazepam, oxazolam, lormetazepam, flurazepam, alprazolam and triazolam did not have EI or PCI signals at 5 ng injected; but had NCI S/N greater than 60.

Discussion: Electron capture NCI ionizes compounds with low energy thermal electrons that are formed during the ionization of the reagent gas. The reagent gas also serves a second function by stabilizing the anions formed via a transfer of vibrational energy through collisions. One reason NCI is more sensitive than PCI or EI is that electron capture rate constants can be two orders of magnitude greater than particle ion/molecular reactions. The specificity of NCI is also due to the characteristics of compounds which

capture electrons. Compounds with low electron affinities are not detected by NCI where as compounds with an electronegative functional group such as a halogen are expected to give good signals with NCI. The aromatic rings present in the benzodiazepine structure resonance stabilize the negative charge of these anions, further enhancing the sensitivity for these compounds. The following are a general set of rules which help explain the NCI spectra of benzodiazepines in this study.

Rules for NCI Spectra of Benzodiazepines: Rule 1: Benzodiazepines which form only a molecular ion are characterized by R_7=Cl or NO_2, R_2'=H, 3=CH_2 and N_1 alkyl substituents. This rule applies to alprazolam, flurazepam, diazepam, prazepam, flunitrazepam, estazolam, N-1-hydroxy-ethylflurazepam-TMS, α-hydroxyalprazolam-TMS. **Rule 2:** Benzodiazepines which only form a $(M-162)^-$ ion are di-TMS derivatized with a silyl amine at 1 position and silyl ether at 3 position. This rule applies to oxazepam-diTMS and lorazepam-diTMS. The $(M-162)^-$ ion is probably due to a loss of TMSOTMS. **Rule 3:** Benzodiazepines which only form the $(M-36)^-$ ion have R_7=Cl or NH_2 and R_2'=Cl. This rule applies to triazolam, α-hydroxy-triazolam-TMS, 7-amino-clonazepam-TMS, 7-amino-clonazepam-diTMS, and lormetazepam. The $(M-36)^-$ ion is probably due to a loss of HCl. **Rule 4:** Benzodiazepines which have base peak of $(M-108)^-$ with other major ions at $(M-73)^-$, M^- and $(M-88)^-$ are silylated at the N_1 position with position 3=CH_2 and R_7=Cl. This rule applies to nordiazepam-TMS, desalklyflurazepam-TMS, and delorazepam-TMS. The $(M-108)^-$ ion is probably due to a loss of TMSCl. **Rule 5:** Benzodiazepines which have a base peak at $(M-72)^-$ with major ions at M^- and $(M-88)^-$ are silylated at the N_1 position with position 3=CH_2 and R_7=NO_2.This rule applies to clonazepam and nitrazepam. The $(M-72)^-$ and $(M-88)^-$ ion are probably due to losses of SiC_3H_8 and $SiC_3H_{10}N$ respectively.

Conclusion: NCI provided increased sensitivity when compared to other ionization techniques. Furthermore, the spectra obtained can be readily explained by the structural features of each benzoiazepine.

Compound	NCI S/N	PCI S/N	EI S/N
Nordiazepam	115	25	22
Desalklyflurazepam	270	8	18
Temazepam	2686	25	53
α-OH-alprazolam	2048	10	4
α-OH-triazolam	2314	1	2
α-OH-ethylfluazepam	6868	47	20
Prazepam	408	26	11
Diazepam	440	45	32
Medazepam	-	-	27

General Structure of Benzodiazepines

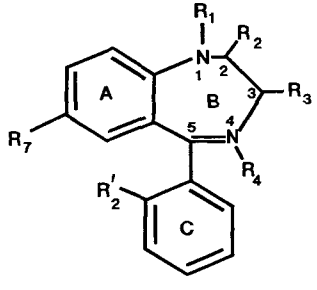

CHARACTERIZATION OF LTD_4 ANTAGONIST METABOLIC PROFILES USING CAPILLARY HPLC / CONTINOUS-FLOW LIQUID SIMS,

***J. A. Yergey, D. Nicoll-Griffith, N. Chauret, M. Belley, M. Labelle, R. Zamboni, Merck Frosst Centre for Therapeutic Research, P.O. 1005, Pointe Claire-Dorval, Quebec, Canada H9R 4P8, S. J. Grossman, E. G. Herold, Merck Research Laboratories, West Point, PA 19486**

EXPERIMENTAL:

Liver Microsome Incubations: Incubations of 200 µM MK-0679 or L-699,392 in 0.5 mL were made with 1 mg microsomal protein. All MK-0679 incubations were with ß-napthaflavone induced rat liver microsomes. L-699,392 oxidation incubations were with Rhesus monkey liver microsomes and L-699,392 glucuronidation incubations were with rat liver microsomes. Co-factors included: Oxidation co-factors (2 mM $MgCl_2$, 2 mM NADP, 20 mM glucose-6-phosphate, in 100 mM PO_4 buffer, pH 7.4 + 2 units glucose-6-phosphate dehydrogenase), Glutathione trapping (Oxidation co-factors + 3mM GSH), Glucuronidation (12.5 mM $MgCl_2$, 12.5 mM UDPGA, 20 mM D-saccharic-1,4-lactone, in 50 mM phosphate buffer, pH 6.6). All reactions were for one hour at 37°C, and were quenched with 0.5 mL of CH_3CN.

Solid-Phase Extraction: SPE was used for MK-0679 studies. 1 mL C_{18} columns were conditioned with 2 mL CH_3OH and 2 mL H_2O. Aqueous samples were applied following dilution of incubations to ≤ 5 % CH_3CN, rinsed with 4 mL H_2O, eluted with 3 x 200 µL CH_3OH and dried in a Speed-Evap.

Capillary HPLC / CF-LSIMS: A Waters 600MS HPLC pump supplied 1 mL/min of mobile phase consisting of CH_3OH:20 mM NH_4OAc, pH 5 (1.5 % glycerol in each). The 1.5% glycerol necessary for CF-LSIMS caused no degradation in chromatographic behavior. The main flow was split prior to the injection valve using ~ 5 cm of 50 µm fused silica on a Valco ZDV tee. The split flow of 3 µL/min passed through a 0.5 µL Valco injection valve or a 20 µL injection loop on 6-port electrically actuated Valco valve, then through the KAPPA Spherisorb ODS2 0.3 x 100 mm capillary column (Keystone Scientific) and into the JEOL HX-110A CF-LSIMS mass spectrometer ion source. Injections were of 0.5 µL of SPE or 10 µL of a 10-fold dilution of incubation mixture. CF-LSIMS spectra were acquired from 0-1000 Da every 4 sec.

RESULTS AND DISCUSSION: Initially, solid-phase extraction was used to concentrate samples, in order to observe smaller metabolites using a 0.5 µL injection volume. This was believed necessary in order to approach the optimal injection volume for a 0.3 x 100 mm capillary column of 100 nL or less. More recently, however, we found that simply concentrating sample components at the beginning of the capillary column using a weaker initial mobile phase strength allowed injections of 10-50 µL with no loss in chromtographic performance (See data for L-699,392). Examination of the total-ion-chromatogram often revealed little regarding a metabolic profile, however, plotting mass chromatograms specific for anticipated oxidative products, or class specific fragments, provided evidence of small metabolites. Spectra of parent drug and oxidative metabolites contained protonated molecules and diagnostic fragmentation which allowed the site of oxidation to be pinpointed to a particular substructure of the molecule. The excellent stability of the system permits background subtraction to work extremely well. For example, following background subtraction, the MK-0679 sulfoxide eluting at 19.9 min could be distinguished from the phenol eluting at 20.1 min, based on their distinctive fragmentation patterns (data shown in poster). The overall sensitivity of the system for full-scan spectra was quite good, excellent spectra being obtained when a total of 50 ng (~100 pmol) of material was injected and the metabolites each comprised 2-8 % of the total material. Phase II metabolites (see data for glutathione adduct of MK-0679 and ß-glucuronide of L-699,392) also produced protonated molecules when examined by CF-LSIMS. In addition, fragmentation leading to the parent drug was observed for both conjugates. Analogous data for the ß-glucuronide of MK-0679 were observed, but were not shown. The MK-0679 glutathione adduct required preparative isolation in order to provide enough material for a good spectrum, while the glucuronides were able to be characterized directly from the incubation mixture; about 20 pmol of the L-699,392 ß-glucuronide was injected in the example shown.

CONCLUSIONS: Oxidative *in vitro* metabolism of the potent LTD_4 antagonists MK-0679 and L-699,392 were predominated by sulfoxidation and oxidation at terminal methyl groups. In addition, evidence for epoxidation of the quinoline substructure of MK-0679 was found in incubations with liver microsomes from animals pre-treated with ß-naphthaflavone. Overall, there was less oxidative metabolism and fewer oxidative metabolites observed for L-699,392. Both antagonists also readily formed acid glucuronides *in vitro*, and the epoxide formed for MK-0679 was shown to be trappable by glutathione. Capillary HPLC / CF-LSIMS was capable of providing full-scan mass spectra for all of the metabolites, thereby allowing characterization of the metabolic profiles for these compounds in relatively few experiments.

CAPILLARY HPLC / CF-LSIMS OF L-699,392 OXIDATIVE METABOLITES

- L-699,392 oxidative incubation diluted 10-fold in mobile phase
- Capillary HPLC gradient: 65 35 linear to 95:5, 35 min

Total-ion-chromatogram

Mass chromatogram for L-699,392 (MH+, 544)

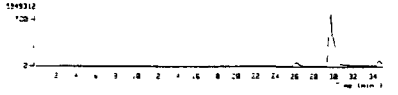

Mass chromatogram for L-699,392 + O (MH+, 560)

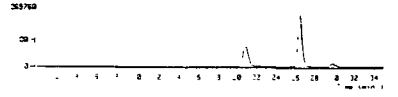

Mass spectrum of L-699,392 (t = 29.7 min)

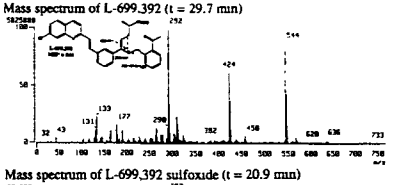

Mass spectrum of L-699,392 sulfoxide (t = 20.9 min)

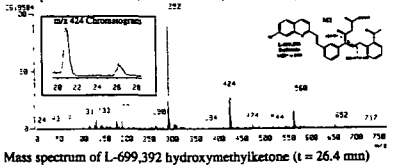

Mass spectrum of L-699,392 hydroxymethylketone (t = 26.4 min)

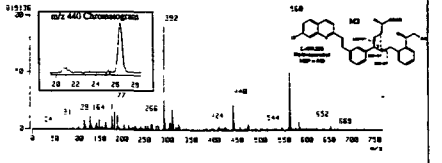

CAPILLARY HPLC / CF-LSIMS OF MK-0679 GLUTATHIONE ADDUCT

- MK-0679 glutathione adduct isolated by SPE and preparative HPLC
- Capillary HPLC Gradient: 40:60 linear to 80:20, 40 min

Mass chromatogram of the MK-0679 glutathione adduct (MH+ = 838),

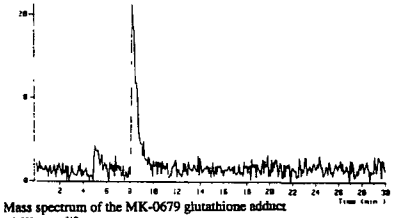

Mass spectrum of the MK-0679 glutathione adduct

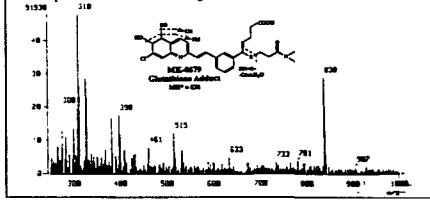

CAPILLARY HPLC / CF-LSIMS OF L-699,392 GLUCURONIDE

- L-699,392 glucuronide incubation diluted 10-fold in mobile phase
- Capillary HPLC gradient: 65:35 linear to 95:5, 35 min

Mass chromatogram for L-699,392 (MH+, 544)

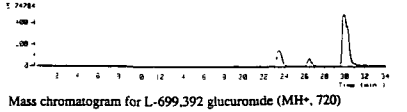

Mass chromatogram for L-699,392 glucuronide (MH+, 720)

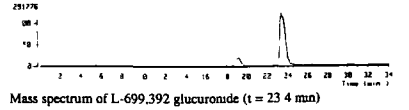

Mass spectrum of L-699,392 glucuronide (t = 23 4 min)

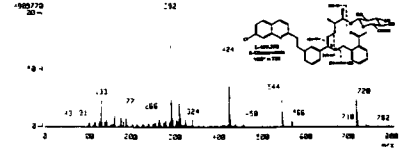

FAB Accurate Mass Measurements Using A Rotating Probe On The VG ZAB-2SE Mass Spectrometer

J.L.Occolowitz* and J.M.Gilliam
Lilly Research Laboratories, Indianapolis, Indiana 46285-1513

INTRODUCTION

FAB is arguably the best ionization technique for determining the accurate mass of molecular species because it is a soft ionization technique which generally gives intense, steady analyte signals and introduces no thermal stress. However FAB is not a colligative ionization technique and the addition of internal mass standards can result in suppression of the analyte or alternately suppression of the calibrant. Additionally cationic impurities in the analyte can cationize the calibrant and give rise to complex spectra where considerable care is required to identify the calibration ions. If it is necessary to measure the accurate mass of fragments of relatively low intensity, which correspond to significant peaks in CID spectra, addition of an internal calibrant can cause trouble because of suppression, cationization, or masking of analyte by calibrant.

At the 1992 ASMS conference[1] we demonstrated that we could make accurate (~2ppm) mass measurements by serial introduction of calibrant and analyte. This involved firstly determining a scan of two bracketing calibrant peaks, a scan of the analyte peak, and a further scan of the two calibrant peaks. A drift correction was applied which was calculated by measurement of the second scan of calibrant peaks using the calibration derived from the first scan of calibrant peaks. Subsequently we decided that introduction of calibrant and analyte on a two-faced rotatable probe would improve the method firstly by reducing the time for measurement and comcomitantly by reducing the mass spectrometer drift between calibrant and analyte scans.

PROBE DESIGN AND ION SOURCE MODIFICATIONS

We had previously described[2] a two-faced rotatable probe for a MAT 731 and were able to adapt this design to the VG ZAB-2SE by changing the probe dimensions, the twin target design, and modifying the mass the mass spectrometer ion source. Drawings describing the probe and ion source modifications are available on request. Essentially the probe consists of a fixed outer probe which is inserted through the EI vacuum lock and an inner probe which is retractable and rotatable and guided by bearing surfaces on the interior of the outer probe. When the outer probe is seated the inner probe is extended so that a gold disc 1/8" diameter having cups machined into its opposing surfaces intercepts the ionizing Cs^+ beam.

MEASUREMENT TECHNIQUE

The calibrant was either PPG 725, 1200, or 1750 dispersed in "magic bullet" containing lithium iodide. This mixture was placed in one of the gold cups, the other cup contained the analyte usually dispersed in "magic bullet". Data were generated by simultaneously scanning the electric sector and accelerating potentials and recording using the VG OPUS data system in the MCA mode. The magnet prescan initiated by the OPUS was suppressed by operating the mode selector in the MS/MS, V,E, and current modes. The lower calibration mass was brought into focus and the magnet moved 2D lower. The data system was programmed to acquire 10 scans at 1.5s./scan with a 0.05s. interscan period. One minute of scanning was allowed before data accumulation. After the 9th recorded scan of calibrant the probe was rotated 180° and 9 scans of analyte accumulated, after the 9th scan the probe was again rotated 180° and a further 10 scans of calibrant accumulated. The analyte mass was measured as described previously[1].

RESULTS

The histogram shown in Fig.1 shows the frequency of errors resulting from a single measurement of 178 separate samples. For 91% of the samples the error was 5ppm or less,

which is acceptable by JACS[3]. 30% of the measurements were within 1ppm and 50% within 2ppm. Increased accuracy was achieved by using one probe introduction and 10 probe rotations of 180° resulting in 5 bracketed analyte scans obtained in 3 minutes of acquisition time. The results of a measurement of this type is tabulated in Table1.

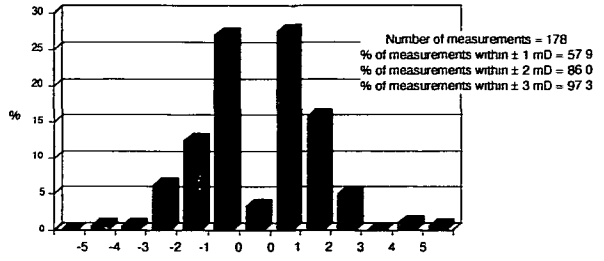

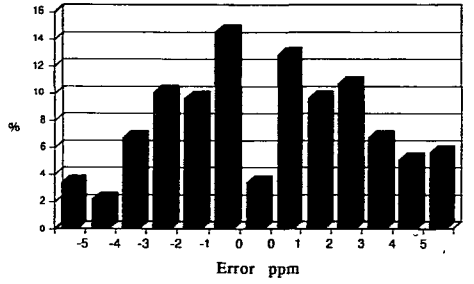

Table 1

Replicate measurements for ion m/z 1662.7651 resulting from a single probe introduction.

Replicate	Uncorrected Mass	Corrected Mass
1	1662.7618	1662.7651
2	1662.7733	1662.7715
3	1662.7646	1662.7663
4	1662.7675	1662.7664
5	1662.7721	1662.7697

Mean mass = 1662.7678, error = 0.0027 D (1.6 ppm)

1) John L. Occolowitz, M.W. Collins, and J.M. Gilliam. Proceedings of 40th. ASMS conference, Washington DC. May 31-June5, 1992. Page 864. 2) J.M. Gilliam, P.W. Landis, and J.L. Occolowitz. Anal. Chem. 1532 (1983). 3) J. Am. Chem. Soc. 114, 10A, 1992.

Structure Determination and Diagnostic Value of Abnormal Bile Acids in Urine from Patients with Generalized Peroxisomal Disease.

*Amit Ghosh, James E. Evans, Jacqueline M. Street, Barbara A. Evans and Marvin R. Natowicz

The E. K. Shriver Center, Mass Spectrometry Facility and Division of Medical Genetics, 200 Trapelo Rd., Waltham, MA 02254.

Detection of taurine conjugates of tri-, tetra- and pentahydroxycholestanoates at m/z 556, 572 and 588 by negative ion FAB-MS analysis of urine extracts is useful for the diagnosis of disorders of bile acid metabolism including generalized peroxisomal disorders (GPD)[1]; other ions have not been reported to be diagnostic. The value of FAB-MS for diagnosis is limited because these ions are not always found in samples from patients with GPD.

We have screened urine samples from normal and diseased controls and from patients diagnosed by other established criteria to have GPD for bile acids by direct injection-continuous flow-negative ion FAB/MS[2]. A number of ions were frequently intense in the spectra from patient samples that were not seen in controls. These included ions m/z 489, and 505, which we postulated correspond to a C29-dihydroxy-monoene-dicarboxylic bile acid and a C29-trihydroxy-monoene-dicarboxylic bile acid respectively. Ions for the glycine and taurine conjugates of the dihydroxy compound were also found at m/z 546 and 596. In addition to these, several patient samples were found that gave high intensity for m/z 625 and 641. These are postulated to be the glucuronides of tri- and tetrahydroxy cholestanoates respectively. Analysis by μHPLC-FAB/MS revealed that several chromatographic peaks are observed for each of these ions presumably corresponding to different positional and/or stereoisomers that are expected to occur for bile acids. B/E product ion CID spectra of these were obtained during μHPLC analyses and are consistent with the proposed structures. Product ion scans were also used to show that an ion at m/z 471 from patient samples lost sodium and is likely to represent the sodium adduct of a trihydroxycholestanoate. The use of m/z 489 and 641 in addition to the previously used m/z 572 significantly increases the sensitivity of FAB-MS for diagnosis of GPD from about 60% to higher than 85%. The table below shows the occurrence of the new ions in spectra from urine samples from normal and diseased controls and from patients diagnosed to have GPD by other criteria.

ACKNOWLEDGEMENT

This work was supported in part by the Department of Mental Retardation of the Commonwealth of Massachusetts (contract # 100220023SC).

REFERENCES

1. Setchell,K.D.R. and A.M.Lawson (1989) Bile Acids. In *Mass Spectrometry*, A.M.Lawson ed., Walter deGruyter & Co., pp.55-125.

2. J.E.Evans, A.Ghosh, B.A.Evans and M.R.Natowicz (1993) Biol. Mass Spectrom., In press.

OCCURRENCE OF DIAGNOSTIC IONS

	PREVIOUSLY USED			IONS REPORTED HERE						
m/z	556	572	588	489	505	546	596	609	625	641
GROUP										
NORMAL CONTROL N=24	0 0%	0 0%	0 0%	3 13%	1 4%	0 0%	0 0%	0 0%	0 0%	1 4%
LIVER DISEASE N=4	0	1	0	1	0	0	0	0	0	0
X-LINKED ALD N=3	0	0	0	0	0	0	0	0	2	2
VARIOUS DISEASES N=33	0 0%	0 0%	1 3%	4 12%	0 0%	0 0%	0 0%	3 9%	5 15%	4 12%
GEN. PEROXISOMAL N=61	24 39%	36 59%	15 25%	38 62%	22 36%	2 3%	2 3%	1 2%	34 56%	38 62%

The Identification of Ketoconazole Metabolites in the Mouse Liver by Liquid SIMS ms/ms.

T.D. Cyr, B. Dawson, A. Menzies and L.W. Whitehouse,
Bureau of Drug Research, Health and Welfare, Ottawa, Canada, K1A OL2.

Ketoconazole is an orally active antimycotic drug often used in immuno-compromised individuals, such as AIDS and transplant patients. Recent research efforts with regard to this drug reflect its potential use for other indications, such as prostate cancer, and problems arising from adverse reactions when used in combination with terfenadine (an antihistamine). Although, this drug is extensively metabolized by the liver, with more than twenty-two metabolites having been detected, only one metabolite, deacetylated ketoconazole, has been identified, to date.

The ketoconazole metabolites were isolated by extracting homogenized mouse livers, then purified by sequential preparative reverse then forward phase HPLC.

The mass spectra were obtained on a VG AutoSpec Q (EBEqQ) tandem mass spectrometer. The samples, in glycerol, were ionized by liquid SIMS using a cesium ion gun (35 kV) and the ms/ms spectra were obtained by programming an increase in the collision energy (Ec = 15 to 25 Ev) as well as admitting argon (7 X 10^{-6} mbar) into the collision cell. The molecular formulae were determined from the high resolution (>5000) accurate mass determinations. Using a combination of techniques (ms/ms, accurate mass ms, and nmr), structures for eight metabolites have been proposed: two of the metabolites result from cleavage and oxidation of the piperazine and the imidazole rings, three metabolites result from transformation of the acetyl group and four metabolites result from oxidation of the piperazine ring and the acetyl group. A proposed metabolic scheme is presented in Figure 1. The CID spectrum for the pseudo-molecular ion as well as the M+2 ion were obtained for each compound. The combination of the two spectra allowed differentiation of the peaks containing the dichlorophenyl group.

The m/z 82 peak was diagnostic for the presence of the imidazole group, and this was generally corroborated by a m/z 255 peak due to scission of the oxygen heterocycle. The m/z 255 fragment also contained the dichlorophenyl group which could be confirmed by the presence of a m/z 257 fragment from the corresponding M+2 CID spectrum.

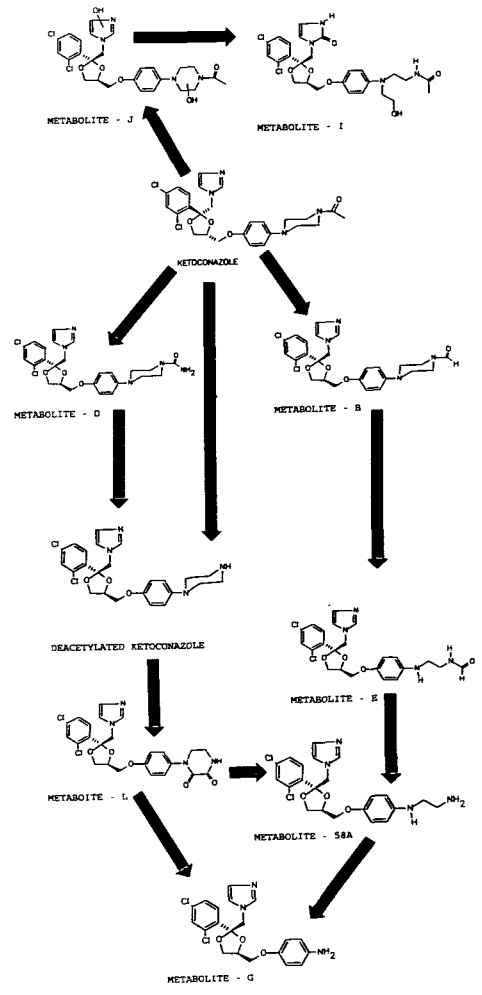

FIGURE 1. Proposed structures and metabolic scheme for ketoconazole.

Complete Mass Spectrometric Structure Elucidation of an Unknown Possible Metabolite

J. P. Kiplinger, L. A. Morehouse, *P.A. Reiche, D.A. Beebe, A. Grodski; Pfizer, Inc., Groton, CT 06340

Mass spectrometry provides useful structural information about unknown compounds, but is usually best combined with other analytical techniques for fast structure elucidation. When the amount of sample is very limited, however, mass spectrometry is often the most convenient tool that can be employed. This poster illustrates the type of structural information that can be obtained using mass spectrometry alone when little other information is available.

A compound being studied as cholesterol lowering agent was tested in African Green monkeys. As part of the study, monkey fecal samples were examined for their bile acid content. Samples were lyophilized and pulverized, then saponified and acidified to deconjugate the bile acids. Bile acids and other lipophilic compounds were extracted with ether and derivatized with p-bromophenacyl bromide.

The derivatized mixture was analysed using HPLC. Many of the bile acids present in the extract may be identified by their retention times, but an unknown peak was observed which comprised more than 50% of the total acidic sterol fraction. The unknown peak was present in the feces of both the control and drug-treated animals, but was more abundant in the drug treated group.

The unknown peak was collected and rechromatographed isocratically to determine it's purity, and was presented purified for mass spectrometric analysis. MS analysis were performed on approximately 2 ug of total sample.

Since the sample was assumed to be related to the other bile acids in the fecal extract, Liquid Secondary Ion Mass Spectrometry (LSIMS) was chosen for the analysis. The spectum shows pairs of peaks at m/z 497/99 and m/z 519/521, the molecular ion species, MH^+ and $(M+Na)^+$, and a pair at m/z 479/81 corresponding to the loss of water. Other Br-containing peaks in the weak spectrum revealed little additonal structural information.

Cholates and deoxycholates have masses in this range, and their bromophenacyl esters exhibit prominent losses of $3H_2O$, and $2H_2O$ respectively. By analogy, the unknown was thought to be a monohydroxy bile acid High resolution analysis of the peak at m/z 497 yielded an exact mass of 497.22878 A formula search of possible elemental compositions (C,H,O, and Br) falling in this range yields only a single formula, $C_{26}H_{42}O_4Br$. This formula contains too many hydrogens to allow the rings of a steroid nucleus; only a saturated monohydroxylated fatty acid ester will fit. Assuming a straight chain, the unknown compound must be a bromphenyl ester of hydroxystearic acid.

To obtain more structural information and identify the position of the hydroxyl group, the remaining sample was analyzed using direct insertion probe EI. No molecular ion is observed; the Br-containing ion pair at m/z 383/85 allowed a tentitive structure to be assigned. This ion, if formed by α-cleavage of the molecular ion and loss of the C_8H_{17} radical, locates the hydroxyl group at the 10 position. High resolution MS confirms the formula assignment.

It is dangerous to base a structural assignment on the appearance of a single peak in a mass spectrum. An available sample of 12-hydroxy oleic acid was analyzed by direct insertion probe EI. The spectrum also shows the α-cleavage fragment at m/z 409/11. This analogy supports the proposed structural assignment of the unknown, and prompted the synthesis of a sample of 10-hydroxy stearic acid for direct comparison.

To confirm the assigned structure, authentic 10-hydroxy stearic acid was synthesised by a known route and derivatized as before. EI and LSIMS spectra of the known material are comperable to the unknown.

Using mass spectrometry alone, a structure has been assigned to an unknown componant from an acidic sterol extract of monkey feces. The early finding that the material was not a bile acid or related compound allowed the study to continue without interruption; the 10-hydroxystearic acid was traced to an oxidized component of the monkeys' diet. The final assignment of the structure was then an academic exercise, and as such illustrates the power of the MS techniques applied to the problem.

STRUCTURE ELUCIDATION OF NOVEL LEUKOTRIENE B_4 METABOLITES FROM CULTURED HUMAN KERATINOCYTES

Pat Wheelan[§], Joseph A. Zirrolli[§], Joseph G. Morelli[‡], and Robert C. Murphy[§]

[§]National Jewish Center for Immunology and Respiratory Medicine
1400 Jackson Street, Denver CO 80206
[‡]University of Colorado School of Medicine
Denver, CO

Metabolism of exogenous LTB_4 by cultured human keratinocytes resulted in the formation of several novel products. The structures of these metabolites were determined by a combination of mass spectrometric techniques including the following:

1) CF-FAB/MS was used to identify the molecular weight of metabolites. Additional information on location and type of substituents was obtained by collision induced dissociation and tandem mass spectrometry analyses. FAB spectra were obtained on a Finnigan TSQ 70 triple quadrupole mass spectrometer. The FAB gun was operated at 1 mA with xenon accelerated to 6 kV. For collision induced dissociation and tandem mass spectrometry analyses, argon was used as the collision gas and the collision offset energy (E_{lab}) was 30 eV.

2) ECI GC/MS was employed to gain molecular weight information as well as information on the number of hydroxy substituents of each metabolite from production of the abundant carboxylate anion and ions derived from losses of trimethylsilyl alcohol. For this analysis, metabolites were derivatized as the pentafluorobenzyl ester/trimethyl silyl ether derivatives. The number of double bonds in metabolites was confirmed by ECI GC/MS analysis of the derivatized reduced metabolite (5% Rh/Al_2O_3 in methanol). Spectra were obtained on a Finnigan SSQ 70 with methane as the moderating gas.

3) EI GC/MS analysis of PFB/TMS derivatized metabolites was employed to provide detailed structural information regarding hydroxy substituent position from abundant fragmentations adjacent to trimethylsilyl ether positions. Confirmation of fragmentation assignments and additional fragment ions were obtained by EI GC/MS analysis of the derivatized, reduced metabolites. Spectra were obtained on a Finnigan SSQ 70 using an electron energy of 70 eV.

Figure 1

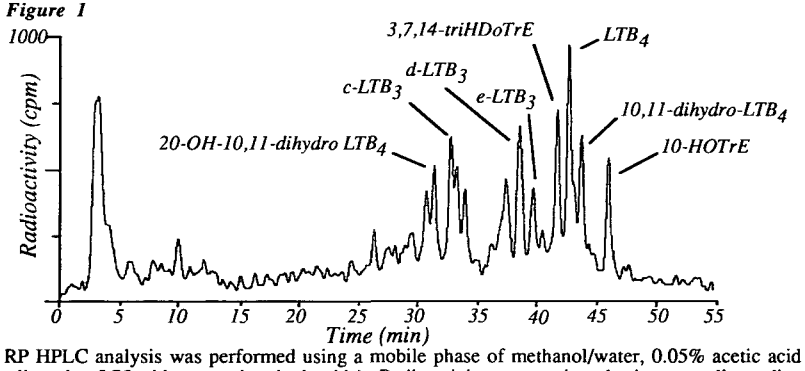

RP HPLC analysis was performed using a mobile phase of methanol/water, 0.05% acetic acid (pH adjusted to 5.75 with ammonium hydroxide). Radioactivity was monitored using an on-line radioactive detector and UV absorbance monitored from 200 nm to 400 nm.

Results: After a 24 h incubation of LTB_4 (3.5μM) and [$^3H_8$] LTB_4 with human keratinocytes, 73 ± 15% (n = 4) of the added radioactivity was recovered in the extracellular supernatant. **Fig. 1** shows a typical radiochromatogram obtained during RP HPLC analysis. The amount of radioactivity corresponding to nonmetabolized LTB_4 ranged from 0% to 8% of the total radioactivity by HPLC analysis. No major radioactive peak other than recovered LTB_4 retained the chromophore indicative of a conjugated triene.

Metabolism of LTB_4 proceeded by two distinct pathways: 1) reduction of the 10,11 double bond resulting in formation of reduced products and 2) glutathione conjugation. Metabolites identified in the first pathway included 10,11-dihydro-LTB_4, 10-HOTrE (10-hydroxy-4,6,12-octadecatrienoic acid), 3,7,14-triHDoTrE (3,7,14-trihydroxy-8-10-16-docosatrienoic acid), and 20-OH-10,11-dihydro LTB_4. Metabolites formed by the second pathway included c-LTB_3 (5,12-dihydroxy-6-glutathionyl-7,9,14-eicosatrienoic acid), d-LTB_3 (5,12-dihydroxy-6-cysteinylglycyl-7,9,14-eicosatrienoic acid), and e-LTB_3 (5,12-dihydroxy-6-cysteinyl-7,9,14-eicosatrienoic acid).

The CF FAB/MS/MS spectrum of e-LTB_3 is shown in **Fig. 2**. The product ion at m/z 235, which was also observed for LTE_4[1], suggested the cysteine moiety was located at C-6 (**Scheme 1**). The product ion at m/z 229 suggested double bonds were located at C-7,C-9 resulting in a favorable charge remote fragmentation. These positions were confirmed by reaction with hypochlorous acid.[2]

Figure 2

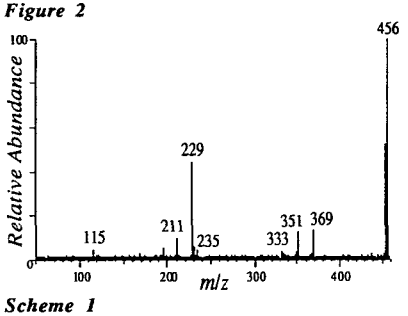

Scheme 1

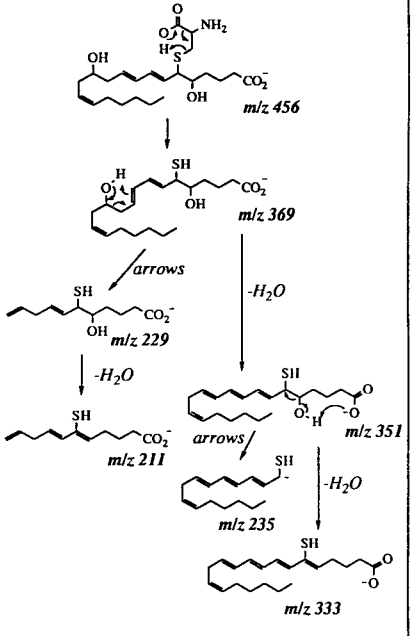

References:

1. Sala, A., Kayganich, K., Zirrolli, J. A., and Murphy, R. C. (1991) *J. Am. Soc. Mass Spectrom.* **2**, 314-321
2. Lee, C. W., Lewis, R. A., Corey, E. J., Barton, A., Oh, H., Tauber, A. I, and Austen, K. F. (1982) *Proc. Natl. Acad. Sci USA* **79**, 4166-4170

Acknowledgement: This work was supported, in part, by a grant from the National Institutes of Health (HL25785).

MULTIRESIDUE ANALYSIS OF SULFONAMIDE ANTIBIOTICS IN MILK USING LC/ATMOSPHERIC PRESSURE CHEMICAL IONISATION/MS

D.R. Doerge, National Center for Toxicological Research, Jefferson, AR 72079 USA.
S. Bajic, S. Preece and S. Lowes, Fisons Instruments/VG BioTech, Altrincham, WA14 5RZ, UK.

Introduction

Sulfonamide antibiotics are widely used to prevent bacterial infections in farm animals. Improper use of unprescribed drugs or improper withdrawal times can lead to the presence of illegal residues in milk and meat. It has been estimated that up to 45% of milk and 5% or pork carcasses contain illegal sulfonamide residues[1]. This is of toxicological and regulatory concern because sulfamethazine (SMZ) produces thyroid tumors in rodent bioassays. Current regulatory methods for detection of sulfonamides in milk utilize preparative HPLC followed by derivatization and GC/MS confirmation[1]. The present study explores the use of APcI as a sensitive and selective on-line LC detector for multiresidue analysis of sulfonamides in milk.

Experimental

Mass spectrometry was performed using a VG Platform single quadrupole mass spectrometer (Fisons Instruments/VG BioTech). Samples were introduced into the atmospheric pressure corona discharge source via a heated nebulizer probe (450°C) using nitrogen as the bath and nebulizing gas. The potential difference between the sampling cone and the skimmer was adjustable from 0-100V. LC was performed using a NovaPak RCM cartridge (5x100mm) with a mobile phase of 25% acetonitrile/ aqueous ammonium acetate (25mM, pH6.8) at a flow rate of 1.0mL/min. Commercial milk samples were prepared for analysis using C18 Sep Pak and Cyclobond I (cyclodextrin) solid phase extraction cartridges. Blank milk extracts were fortified with sulfonamides at the indicated levels immediately prior to APcI/MS analysis.

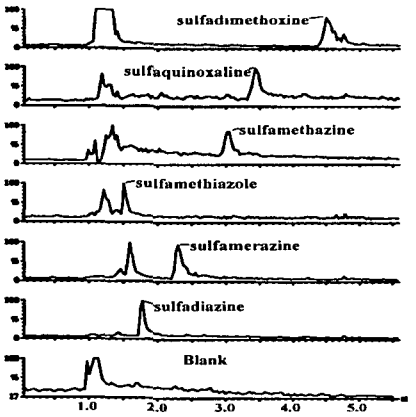

Figure 1. SIR chromatograms for 5ppb of six sulfonamides in a milk extract were obtained by APcI/MS under low cone voltage conditions (30V). The summed ion chromatogram for a milk blank is also shown.

Results

Under conditions of low sampling cone voltage (30V), the mass spectra of all sulfonamides consisted of exclusively $[M+H]^+$ ions. This facilitated high sensitivity by Selected Ion Recording (SIR) of the target sulfonamides. Figure 1 shows the SIR chromatograms produced by 1ng on-column of six sulfonamides along with the corresponding blank summed ion chromatogram. This corresponds to milk containing 5ppb of each component.

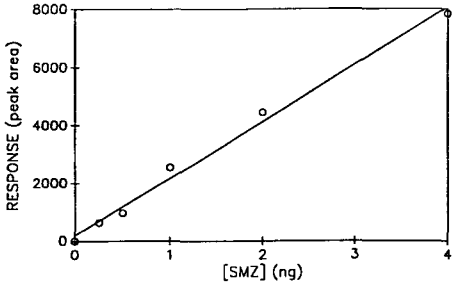

Figure 2. Response curve for sulfamethazine in milk extracts. SMZ was analysed as the [M+H]+ ion formed at low cone voltage (30V) in fortified milk extracts.

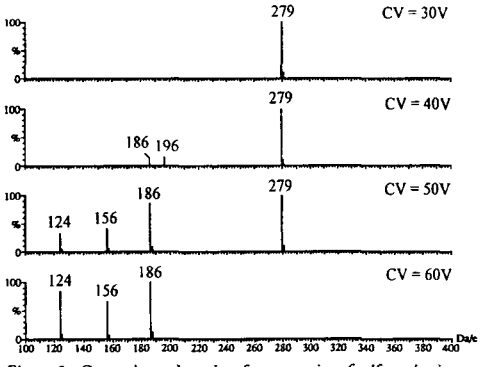

Figure 3. Cone voltage-dependent fragmentation of sulfamethazine. The mass spectrum of SMZ was determined at the indicated cone voltages using flow injection analysis of 100ng injections.

Estimated detection limits for these six sulfonamides in fortified milk extracts ranged from 0.25-2.5ppb. The APcI/MS response curve for a selected analyte, SMZ, was linear (cc = 0.996) over the range corresponding to 1.25-20ppb in milk (see Figure 2). This sensitivity and linearity encompasses the regulatory level of interest for sulfonamides in milk (10ppb).

Another advantage of APcI/MS is the ability to effect collision-induced dissociation by increasing the sampling cone voltage. This can produce information essential for structure elucidation of unknown compounds as well as confirmation of target analytes by using ion intensity ratios from several fragment ions. Figure 3 shows the changes in mass spectrum obtained by increasing the cone voltage. At high cone voltage (80V), only fragment ions were observed from the six sulfonamides tested. Since all sulfonamide antibiotics differ only in the heterocyclic base attached to a constant sulfanilamide portion, the high cone voltage mass spectrum contains a common ion, m/z 156. Selected monitoring of the m/z 156 ion, formed at 80V, permitted class-specific detection of all sulfonamides with minimal loss in sensitivity over that observed for $[M+H]^+$. In addition, the reproducibility of fragment ion intensity ratios from analysis of SMZ in milk at relevant levels (5ppb) suggests that this technique can be used to confirm the presence of sulfonamide residues with a high degree of confidence.

Reference

1. FDA's 1990 Milk Residue Survey. Description of Analytical Methods used for Detecting Sulfonamides and Tetracyclines. Center for Veterinary Medicine, Rockville, MD.

Studies of Secondary Metabolites Newly Identified from *Streptomyces spectabilis* by FABMS, FABMS/MS and LC/FABMS Moving Belt Interface.

*Thompson, A.G.; Sun, F.; Rinehart, K.L.
School of Chemical Sciences, University of Illinois, Urbana, IL 61801

Many metabolites have been previously isolated from *Streptomyces spectabilis*, including the streptovaricins, protostreptovaricins, an acyclic streptovaricin, an atropisostreptovaricin, spectinabilin, tryptophan-dehydrobutyrine diketopiperazine, actinospectacins, deoxymonamycins, and elaiophylin.[1,2] The streptovaricins are the most abundant secondary metabolites and are ansamycin antibiotics. They have strong antibacterial activity, especially against mycobacteria, and inhibit DNA-directed RNA-polymerase (transcriptase) and RNA-dependent DNA-polymerase (reverse transcriptase) of tumor tissues.[1] An extensive mass spectrometric study using positive and negative ion FABMS, FABMS/MS and LC/FABMS with a moving belt interface aided in the identification and structure determination of these known compounds and several newly identified metabolites.[3]

The isolation and characterization began with the detection of molecular ions by LC/FABMS moving-belt experiments which included new signals at *m/z* 1049 and 1065. All subsequent isolation procedures were followed by FABMS. The crude streptovaricin complex was partitioned using 2:3:1 MeOH:H_2O:$CHCl_3$. The methanolic-aqueous layer was purified by amino-silica HPLC and yielded desertomycin A [$(M+H)^+$ *m/z* 1192.7564 ($C_{61}H_{110}NO_{21}$, Δ - 0.6 mDa] and demannosyl desertomycin A , [$(M+H)^+$ *m/z* 1030.7015 ($C_{55}H_{100}NO_{16}$, Δ + 2.7 mDa)].[4] The chloroform layer was purified using a series of C_{18} HPLC solvent systems and yielded oasamycin A [$(M+H)^+$ *m/z* 1027.6585 ($C_{55}H_{95}O_{17}$, Δ - 2.0 mDa)] and oasamycin B [$(M+Na)^+$, *m/z* 1211.6943 ($C_{61}H_{104}O_{22}Na$, Δ -2.6 mDa)] (Figure 1). Other analogs of the oasamycins have been isolated which differ by the number of oxygens, methyl groups, or double bonds.

In positive ion FABMS probe experiments on the oasamycin HPLC fractions, the strong ionophoric capabilities showed almost exclusively $(M+Na)^+$, $(M+K)^+$, $(M+Cs)^+$, and matrix adduct ions. Acidification of the sample yielded more fragment ions, but no $(M+H)^+$. Only the addition of 18-crown-6 to the probe yielded a measurable amount of $(M+H)^+$. Positive and negative ion high resolution FABMS confirmed the molecular formulas of both the oasamycins and desertomycins. Positive ion LRFABMS, HRFABMS and FABMS/MS also showed nine sequential losses of water from the molecular ions, consistent with these polyhydroxy-macrolactone structures. The ^1H and ^{13}C NMR spectra allowed an assignment of oasamycin A,[3] an inhibitor of biosynthesis of cholesterol.[5] A comparison of the FABMS/CID/MS of authentic and isolated desertomycin A also confirmed its identity.

Using FABMS/MS, new fragmentation patterns were also observed for the streptovaricins and deoxymonamycins.[3]

ACKNOWLEDGMENTS
The authors express their appreciation to J. N. McGuire (University of Illinois, Urbana) for performing the ^1H and ^{13}C NMR experiments, and The Upjohn Company for both the *Streptomyces spectablis* and the Streptovaricin Complex Batch No. 11560-3. This work was supported by a grant from the National Institute of General Medical Sciences (GM-27029).

1. Rinehart, K.L., Jr.; Shield, L.S. *Fortschr. Chem. org. Naturstoffe* **1976**, *33*, 232-307.
2. Staley, A.L., Ph.D. Thesis, University of Illinois, Urbana, IL **1991**.
3. Thompson, A.G., PhD. Thesis, University of Illinois, Urbana, IL **1993**.
4. Dinya, Z.; Sztaricskai, F.; Horváth, G. *Rapid Commun. Mass Spectrom.* **1991**, *5*, 534.
5. Zeeck, A.; Phillips, S.; Grably, S. ; Granzer, E.; Eur. Pat. 482543, 29 Apr **1992**.

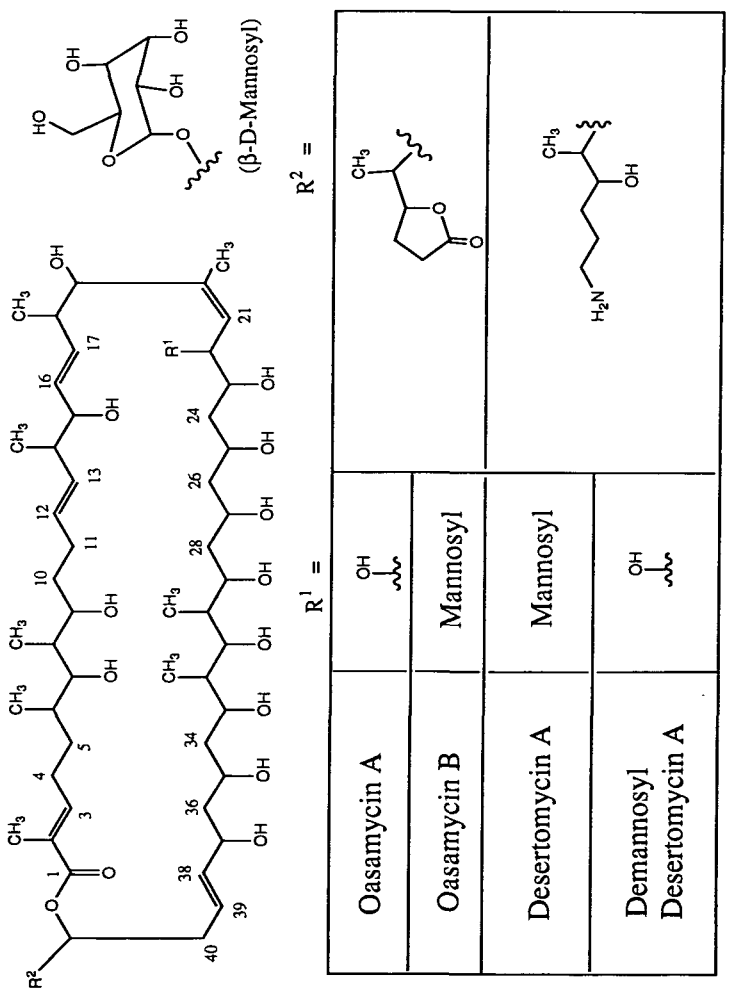

Figure 1. Secondary Metabolites Newly Identified from *Streptomyces spectabilis*[3]

Analysis of very hydrophilic proteins by Electrospray Mass Spectrometry

Jaquinod M.[1], Bitsch F.[1], *Hegy G.[1], Schindler P.[1], Wouters-Tyrou D.[2], Chevaillier P.[2], Sautière P.[2] and Van Dorsselaer A.[1]

[1] Laboratoire de Spectrométrie de Masse Bio-Organique, URA 31 CNRS, Université Louis Pasteur, 67008 Strasbourg, France. [2] URA 1309 CNRS, Université de Lille II, IPL, 59019 Lille, France.

Introduction

Spermatogenesis involves a progressive differenciation of the germ cell toward a terminal stage represented by the mature spermatozoon. During spermatogenesis, histones are replaced by more basics proteins named transition proteins and protamines. These Protamines as well as transition proteins are highly basic proteins, associated with DNA in nuclei (1). They are characterized by a very high arginine or lysine content (more than 50%). Primary structure elucidation of such proteins is therefore particularly difficult when using conventional methods of protein analysis. On purified protamines and/or cleavage peptides, amino acid analysis yields poor information because of the disproportion between the arginines or lysines and the other residues, especially hydrophobic residues. On the other hand serine and threonine, which often appear in the amino acid composition of such polypeptides, are partially destroyed during acid hydrolysis and cannot constitute a reference for the quantitation. Moreover these proteins present an increasing of their heterogeineity by the presence of phosphorylation at different level involved in the modulation of the chromatin decondensation (2). In both case phosphorylation sites can be parttially identified by automatic Edman degradation of the protein after derivatization, but state of these phosphorylation was further demonstrated by electrospray mass spectrometry. Most of the time these proteins are contaminated by phosphate or sulfate buffers and need ionization conditions or non-organic solvent for their mass analysis therefore permitting accurate mass measurement.

Experimental

A VG BioQ triple quadrupole (m/z range of 4000, VG BioTech, Manchester UK) was used to carry out positive ESMS. Extracting cone voltage (Vc) varied from 50 to 100 volts. Samples were dissolved in MeOH or Acetonitrile /water/ 50 / 50 or in pure water at a final concentration of 10 pmol / µl.

Results

Figure 1A shows an ESMS spectrum of the calamar transition protein T1 dissolved in water / MeOH 50/50, containing 1% HCOOH solution recorded at a VC = 50 volts .With the increasing voltage difference between the nozzle and the skimmer of the electrospary interface (figure 1B) an declustering effect of the salt adducts were observed. In those conditions spectrum clearly show the presence of several series identified as multiphosphorylated proteines (+80 Da). Other method such as Edman degradation or method using radioactive elements gave us an average value of phosphorylated sites.

Figure 2 present an human protamine 2 dissolved in water (figure 2A) or in Water / MeOH 50/50 solution (figure 2B). In presence of methanol an important apparition of adduct H3PO4 (+98 Da) was observed and could be due to a local increasing concentration of salt and by stabilization of the protamine charges in presence of organic solvents. Such effect was observed when using other organic solvants such as acetonitrile.

Conclusion

This work has shown that ESMS measurement of molecular masses of hydrophilic proteins such as transition proteins or protamines can be achieved by using water solutions or at higher sampling cone voltage. Nevertheless the biological importance of histones and protamines makes today their analysis by MS an important goal.

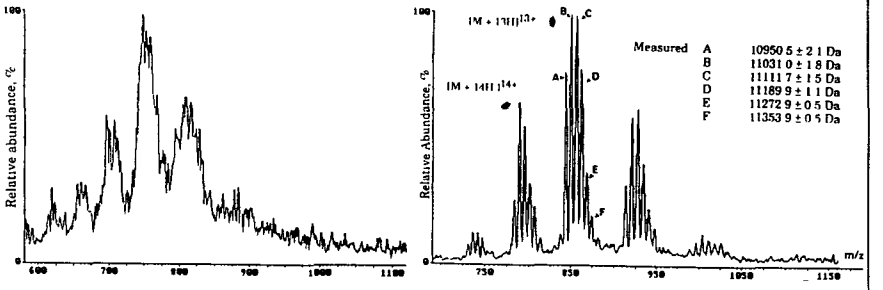

Figure 1A: Electrospray mass spectrum of the calamar transition protein T1 recorded at a low sampling cone voltage (Vc = 55 volts). **B**: ESMS spectrum of calamar transition protein recorded at a Vc = 100 volts

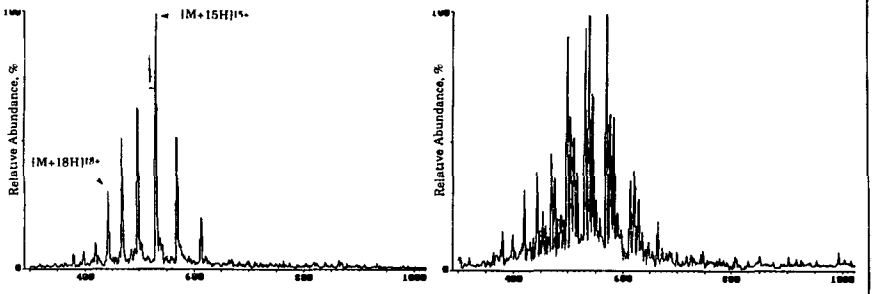

Figure 2 A: ESMS spectrum of human protamine HP2 dissolved in water and in a Water / MeOH 50/50 solution (**B**)

References

1 Wolffe, A. Chromatin structure and function, Academic press, Harbourt Brace Jovanovich, Publischers
2 Chirat, F., Arkhis, A. Martinage, A., Jaquinod, M., Van Dorsselaer, A., Chevaillier, P., and Sautiere, P. Biochim. Biophys. Acta, submitted for publication

Acknowledgments

The financial support of the Region Alsace for the facilities is acknowleged. The authors delight in thanking Dr Martinage for their technical support.

Mass Spectrometric Characterization of a Family of Hydrophobic Peptides with Antibiotic Properties Containing Both L- and D-Amino Acids

C. Moore*, D. Tang, D. Medzihradszky, M. Tullius, R. Mandrell and B. Gibson
Department of Pharmaceutical Chemistry, University of California, San Francisco CA 94143

Previously we have reported the isolation and characterization of a family of amphipathic antimicrobial peptides from the skin of *Bombina orientalis* (Asian Toad) [1,2]. After sequencing the cDNA encoding these precursors, a second family of hydro-phobic peptides were found to be likely encoded on the C-terminus of these precursor poly-peptides. To confiurm this possibility, a set of peptides were isolated with the expected masses.

LSIMS analysis of the skin secretions after HPLC separation revealed several pairs of peptides eluting at different HPLC retention times with the same mass and amino acid sequence as determined by both Edman and MS/MS analyses. In an attempt to determine the basis for their structural differences, we embarked on a more extensive sequencing effort using thermolysin, carboxypeptidase Y and amino peptidase M digestions in combination with HPLC and MS/MS analyses. Figure 1 shows two thermolysin-generated peptide fragments from two different members of this peptide family with the same mass, but different HPLC elution positions. The MS/MS spectra our essentially identical, and rule out the possibility of a isoleucine/leucine difference. Edman degradation confirmed this as well. However, one of these two peptides was not susceptible to aminopeptidase M digestion, suggesting that it may contain a D-amino acid at or near the amino terminus. Our studies eventually concluded that these peptides contained N-terminal isoleucine in both the normal L-configuration as well as the unexpected D-configuration. Given that both D- and L-isoleucine containing peptide forms are present in nearly equal abundances, it is likely that a racemase is involved in their biosynthesis. The biological value of such a modification is suggested from the lack of proteolytic action seen in the aminopeptidase M experiment, thus providing a means to stabilize at least half of these peptides. Circular dichroism studies suggest a type II β-turn structure for these hydrophobic peptides, clearly a departure from the usual α-helices found in other amphibian antimicrobial peptides. Biological assays of these peptides, however, showed very little antibiotic or hemolytic activity, and we are currently expanding our investigations to consider anti-fungal, anti-viral or even mastoparan-like cytotoxic activities for this novel class of peptides.

Literature Cited

1. B.W. Gibson, D. Tang, R.E. Mandrell and E.R. Spindel, "Bombinin-Like Peptides with Antimicrobial Activity from the Skin of *Bombina orientalis*" *J. Biol. Chem.* **266**, 23101-23111 (1991)

2 B.W. Gibson, D. Tang, N. Phillips, D. Medzihradszky, M. Tullius, R. Mandrell, M. Kelly, and E.R. Spindel, "Structural Analysis, Biosynthesis, and Activities of a Novel Class of Antimicrobial Peptides from the Skin of *Bombina orientalis*" Proc. 40th ASMS Conference on Mass Spectrometry and Allied Topics, pp. 1543-1544 (1992)

This work was supported by grants from the UCSF Academic Senate and through the UCSF Mass Spectrometry Facility (National Center for Research Resources RR01614).

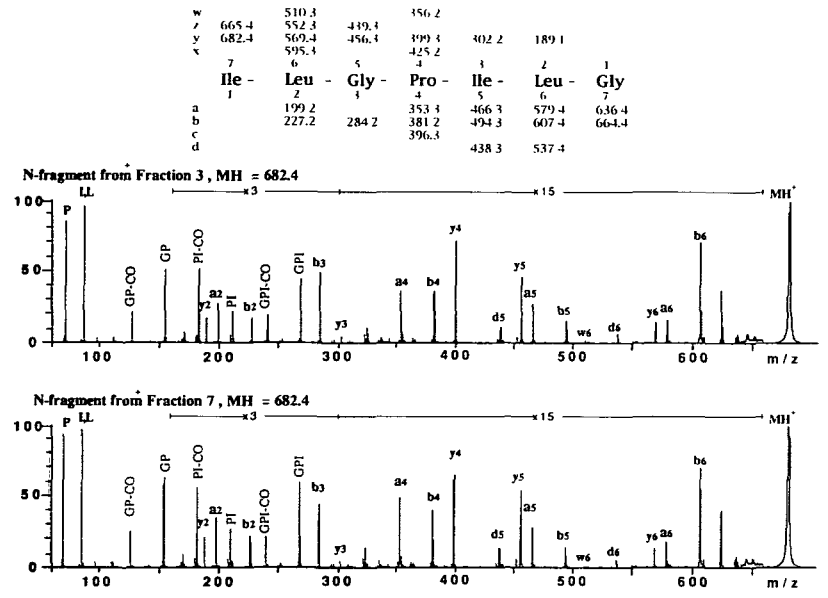

Figure 1. High energy CID spectra of two thermolysin-generated peptide fragments from two members of the hydrophobic peptide family. Although the MS/MS spectra gave identical sequences, these peptides had different retention times by HPLC.

L-Ile-Leu-Gly-Pro-Ile-Leu-Gly-Leu-Val-Ser-Asn-Ala-Leu-Gly-Gly-Leu-Leu-NH_2

L-Ile-Ile-Gly-Pro-Ile-Leu-Gly-Leu-Val-Ser-Asn-Ala-Leu-Gly-Gly-Leu-Leu-NH_2

D-Ile-Ile-Gly-Pro-Ile-Leu-Gly-Leu-Val-Ser-Asn-Ala-Leu-Gly-Gly-Leu-Leu-NH_2

D-Ile-Leu-Gly-Pro-Ile-Leu-Gly-Leu-Val-Ser-Asn-Ala-Leu-Gly-Gly-Leu-Leu-NH_2

Figure 2. The following peptides were synthetised on solid phase using Fmoc chemistry. After the C-terminal 15 amino acids the resin was split in half to facilitate manual Leu and Ile coupling and both resins were then split in half again to prepare D- and L- Ile peptides. Peptides were co-injected with amphibian secretion to confirm identity of native peptides.

Comparative CID Study of MHC Class I and II Peptides using ESI versus CF-LSIMS as the Primary Ionization Method

K.L.Johnson, A.J.Tomlinson, L.M.Benson, G.F.Scanlan and S.Naylor

Biomedical Mass Spectrometry Facility, Dept. of Biochemistry and Molecular Biology and Dept of Pharmacology, Mayo Clinic, Rochester, MN.55905, USA

Major histocompatibility complex (MHC) gene products play an essential role in the immune system through their binding of small peptides and subsequent presentation of these peptides to T-lymphocytes. Although the products of two classes of MHC genes, class I and class II, exhibit peptide binding sites that are similar in structure, they present peptides to two different T-lymphocyte subpopulations:

* class I molecules present peptides to cytolytic T-lymphocytes and
* class II molecules present peptides to cytokine-producing helper T-lymphocytes.

Mass Spectrometry has played an important role in estimating the complexity of such self -peptides as well as providing essential sequence information. In this study we compared the efficiency of ionization (ESI v LSIMS) and low energy CID of a series of Class I and II MEIC peptides. A representative series of results are shown in Figures 1-3 obtained on a Finnigan MAT 95Q.

A) CF-LSIMS with CID in the octapole collision cell
B) ESI with CID in the octapole collision cell
C) ESI with CID in the capillary/skimmer region of the ion source

The striking aspect of this data on the singly charged peptide LSPFPFDL-NH_2 is the similarity of the spectra. However, the overall conclusion was that ESI would be the preferred method of generating a precursor ion for CID experiments in the collision cell.

Figure 1. LSIMS/BEqQ Spectrum of LSPFPFDL-NH_2

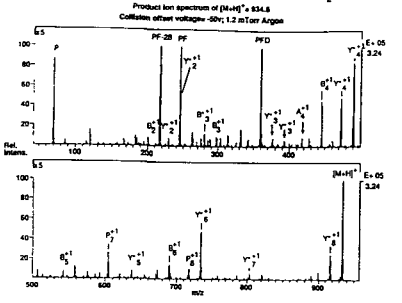

Figure 2. ESI/BEqQ Spectrum of LSPFPFDL-NH_2

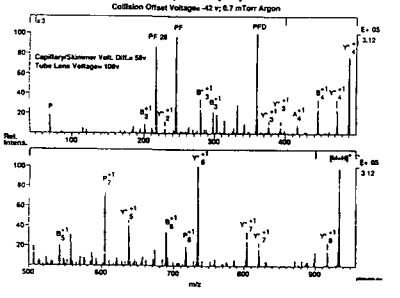

Figure 3. ESI/Source CID Spectrum of LSPFPFDL-NH_2

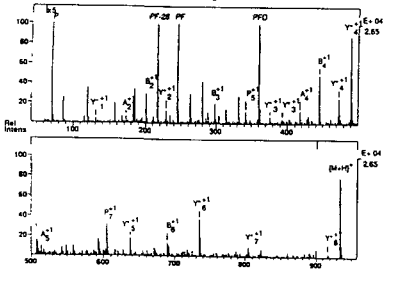

Electrospray Ionization Mass Spectrometry of Peptides and Proteins in the Presence of Detergents

R. R. Ogorzalek Loo, N. Dales, P. C. Andrews

Department of Biological Chemistry, 2552 MSRB II, Ann Arbor, MI 48109

Detergents play a significant role in protein purification with primary applications including solubilization of proteins and disaggregation of complexes. They are employed in applications involving both gel and capillary electrophoresis. Membrane-bound proteins, in particular, require detergent treatment for solubilization prior to chromatography or ultracentrifugation. Unfortunately, some frequently-used detergent solutions perform poorly in bioanalytical mass spectrometry. We undertook a study to evaluate a broad range of commonly used ionic and non-ionic detergents with the goal of finding suitable detergents and conditions for protein applications of electrospray ionization mass spectrometry (ESI-MS). Most of the investigations were performed with detergent concentrations of 0.1% and 1.0% weight:volume (w/v). These are typical concentrations used in biochemical applications.

Except where indicated, mass spectra were acquired on a Vestec 201 mass spectrometer employing the Vestec interface. The solution compositions electrosprayed included 4% acetic acid/50% CH_3CN/46% H_2O and 100% H_2O, selected to reflect conditions frequently used in ESI-MS of proteins. Samples were introduced by injection loop, continuous infusion, and autosampler. Detection was in the positive ion mode.

Horse Heart Myoglobin (M_r 16951) in 4% acetic acid/50% CH_3CN/46% H_2O was continuously infused to evaluate signal suppression at various detergent concentrations. *Severe signal suppression* was observed with the following commonly used detergents at both 0.1% and 1.0% concentrations: *Triton X-100 (Reduced), Nonidet P-40, Taurodeoxycholate, TWEEN-20* and *sodium dodecyl sulfate*. Detergents which yielded better performance in this solvent included: *Octyl Glucoside, Octyl Thioglucoside, n-Dodecyl sucrose, LDAO, CTAB, CHAPS, Thesit, and sodium cholate*. CHAPS, Thesit, and sodium cholate show the least protein signal suppression at the 0.1% detergent concentrations. CHAPS and Thesit are particularly good choices if a 1.0% detergent concentration is used. In continuous infusion studies with other proteins, analyte signal in the presence of 0.1% CHAPS or Thesit was often enhanced by *ca.* 20% over the detergent-free solution. CHAPS is not a particularly good detergent for ESI-MS applications in 100% aqueous solutions, showing significant signal suppression as well as adduct formation. The non-ionic detergent thesit appears to be superior for aqueous applications.

Detergents are well-known for their ability to denature proteins and break up hydrophobic interactions. Figure 1 illustrates mass spectra of myoglobin in 0.01% acetic acid/H_2O without (upper) and with (lower) 0.1% CTAB, a strongly denaturing detergent. The dominant ion in the non-detergent spectrum corresponds to the myoglobin-heme complex, (M_r 17568) while the detergent spectrum shows primarily apo-myoglobin (M_r 16951) in higher charge states; only a small amount of the myoglobin-heme complex is apparent. A similar experiment compared spectra of bovine ubquitin in H_2O with and without 0.1% CTAB; addition of CTAB reduced the intensity of a ubiquitin dimer ion relative to monomer ions. Similarly, the less-denaturing detergent CHAPS has been used to break up protein-protein interactions in noncovalent complexes of concanavalin A.

Significant differences were observed in the ESI-MS charge distributions of cytochrome *c* in water heated off-line with and without 0.1% CHAPS and for lysozyme in 4% acetic acid/50% CH_3CN/46% H_2O boiled off-line with and without 0.1% CHAPS . These differences are attributed to retardation of refolding in the presence of detergent. For unheated solutions of myoglobin in 4% acetic acid/50% CH_3CN/46% H_2O, additions of 1.0% octyl glucoside, octyl thioglucoside, or n-dodecyl sucrose increased charging in comparison to the detergent -free solution. Addition of 1.0% LDAO decreased charging. Higher charging was also observed upon addition of 0.1% cholic acid to myoglobin, ubiquitin, and albumin, but not upon addition of 0.1%

sodium cholate. The mechanism for the apparent increase in charge states observed in the presence of some detergents is not clear. It might arise from better charge separation in more fully-denatured proteins or from effects of the detergents on the dynamics of the electrospray.

Several of the detergents examined in this study should be useful for solubilizing difficult proteins for mass spectrometric analysis, in coupling separations to ESI-MS, and in improving protein recoveries from analytical or purification steps preceeding mass spectometry.

We acknowledge J. A. Loo for the Concanavalin A data acquired on a Finnigan MAT 900.

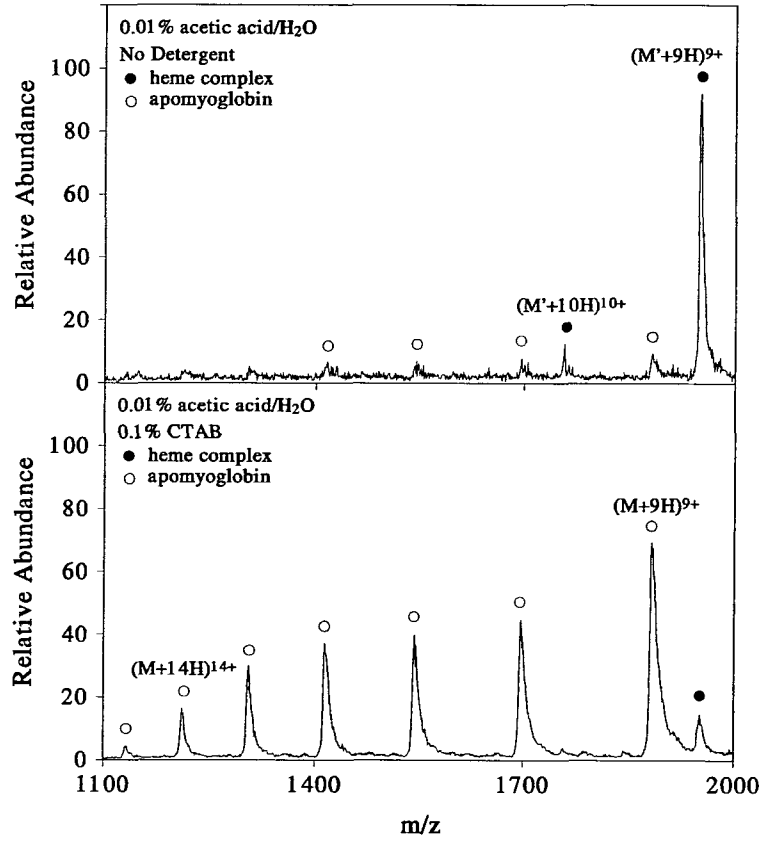

OPTIMIZATION OF LCMS FLOW RATE FOR MAXIMUM MASS SPECTROMETER DETECTION AND MINIMUM RUN TIME

Ken Stoney[1], Kuldip Mock[2] and Mark Sanders[2]
[1]Michrom BioResources, 5673 W Las Positas Blvd, Pleasanton, CA 94588
[2]Finnigan MAT, 355 River Oaks Pkwy, San Jose, CA 95134

Liquid chromatography (LC) flow rates affect the sensitivity and resolution of peak detection and total chromatographic run time Low flow rates maximize sensitivity and resolution but increase run times, while higher flow rates compromise sensitivity and resolution for decreased run time The purpose of this research is to determine if there is an optimum flow range for achieving maximum sensitivity and resolution while maintaining total run times less than 10 minutes. A commercially available microanalytical LC system designed and optimized for low flow rates was used for this study.

Various LC-MS interfaces are currently available which can accommodate a wide range of flows. We restricted our flow rates to 400ul/min, considered to be on the high end of the range for this project In order to maintain total run times less than 10 minutes, only narrowbore (2.1mm inner diameter (ID)), microbore (1 0mm ID), and capillary (0.5 & 0 3mm ID) were used. The small volumes of these columns combined with the minimum dead volume (<100ul) of the microanalytical LC system, allowed for minimum gradient delays, and therefore very short run times.

To determine an optimum flow rate for maximum mass spectrometer detection, UV absorbance and MS ion current (RIC) peak areas were plotted against various flow rates. UV peak areas (sensitivity) increase exponentially with decreased flow rates while it is hypothesized that MS RIC peaks areas (sensitivity) increase in a linear manner. Where these two plots "intersect" should indicate an optimum flow range. Flow rates below this optimum would result in extended run times and overkill for peak sensitivity and resolution. Flow rates above this optimum would result in lower than maximum sensitivity and resolution.

In order to construct the curves, columns of 4 different inner diameters were chosen which allowed for an overlapping range of flows (Table 1). The test sample used to determine sensitivity and resolution for this study is a mixture containing 5 angiotensins with a concentration of 10ng/ul each (50ng/ul total) quantified by amino acid analysis. Peak B was chosen as the peak to integrate for all chromatographs because it was almost always baseline resolved. The same integration parameters were used for each peak area determination. Except for the inner diameter of the 4 columns, all other variables were constant. (Experimental Parameters)

The figure is the plot of the combined UV and MS sesitivity in terms of total peak area. It is clear that the UV trace follows an exponential increase as the flow rate decreases The MS RIC peak area trace appears to be linear over the range of flows so far investigated. The error in integrating the area of peak B was greater at the lower flow rates Each point represents the average area of peak B of 3 duplicate LCMS runs. It appears from this preliminary data that there may be an "optimum" intersect point in the 10 to 20ul/minute flow range. This is based on extrapolation of the MS RIC peak area curve and would be true only if this curve follows a linear path.

Additional LCMS runs are required to determine if there is an optimum flow rate in the 10-20ul/min range Replicate runs would allow an error to be calculated for the integration of each peak, and therefore help in defining the optimum flow range.

The LC chromatographs shown here illustrate that separations of very similar peptides can be quickly accomplished with high sensitivity and resolution in less than 10 minutes The use of small bore columns with their low volumes coupled with a microanalytical LC optimized for these columns contributes to the rapid separations.

UV/MS SENSITIVITY
PLOTTED AGAINST FLOW RATE

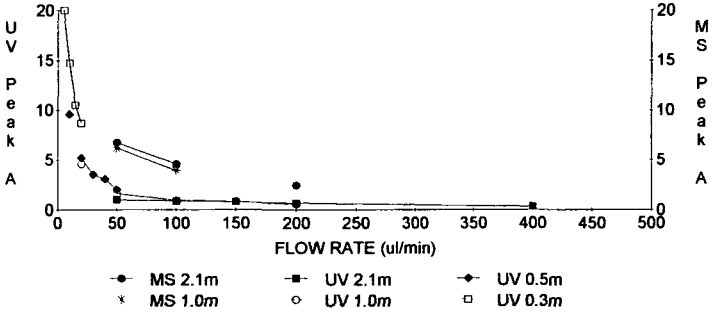

Table 1 FLOW RATE RANGE

Column											
0.3mm ID	2	5	10	15	20						
0 5mm ID			10		20	30	40	50			
1 0mm ID					20			50	100	150	200
2.1mm ID								50	100	150	200	400

EXPERIMENTAL PARAMETERS

Buffers	A) 2% ACN/Water w/ 0 1%TFA B) 90% ACN/Water w/ 0 09%TFA
Gradient	0 minutes 25%B 4 minutes 65%B 10%B per minute 6 minutes 65%B
Column	Michrom BioResources Columns, All were 150mm long packed with Reliasil C18, 300A 5u
Injection	10ul of Angiotensin Standard in fixed loop, 100ng of each Angiotensin
Detection	Fixed Wavelength UV Absorbance , 214nm
Integration	UV Peak Area - EZChrom Software MS RIC Area - Finnigan MAT TSQ 700 Software
LC	Michrom BioResources UMA
MS	Finnigan MAT TSQ 700 w/ new API Interface Tune Tables were very similar for all flow rates.

Analysis of Peptides by the Desorption/Ionization Technique K^+IDS, K^+-Ionization of Desorbed Species

Huaiqin Wu and John Allison
Department of Chemistry, Michigan State University, MI 48824

K^+IDS is a desorption/ionization technique, which is applied here to the analysis of peptides. In the experiment, the analyte molecules are subjected to rapid heating, which leads to desorption of intact analyte molecules (M) and thermal degradation products (D). At the same time, K^+ ions are being generated in the ion source by a thermionic emitter. The K^+ ions attach to the desorbed molecules, yielding mass spectra which contain peaks that represent the $(M+K)^+$ and various $(D+K)^+$ ions. This technique allows us to characterize thermal degradation of peptides, and may be a model for remote-site processes for protonated peptides.

From a typical K^+IDS mass spectrum of *H*-VGVAPG-*OH*, as shown in the attached spectra, K^+IDS spectra show the following features: 1. The dominant ions observed are $(Y_n+H+K)^+$ ions for underivatized peptides. 2. The dominant "fragment" ions observed are $(Y_n+H+K)^+$ ions while their corresponding $(B_n-H+K)^+$ ions are much less abundant even though their corresponding neutral species are formed at the same time and in the same quantities.

In order to understand the dominant cleavages at amide bonds and the dominance of the $(Y_n+H+K)^+$ ions, the thermal degradation mechanism and the K^+ attachment and detachment processes have to be understood. In the study of the thermal degradation mechanism, deuterated peptides, derivatized peptides, and specifically-designed peptides were prepared/synthesized. Our studies on these chemically-modified peptides indicate that thermal degradation of peptides under K^+IDS conditions involves cyclization processes. For example, deuterated peptides show that the shifting hydrogen is not an α hydrogen; For N-terminally acetylated peptides, the characteristic $(Y_n+H+K)^+$ ions are missing in the resulting K^+IDS spectrum and a new $(B_n+OH+K)^+$ ion series dominates the spectrum instead (see the attached spectra). This result clearly indicates that the shifting hydrogen for underivatized peptides is from the N-terminus rather than from internal amide groups. The shift of a hydrogen atom or OH group from a single position in thermal degradation of peptides clearly indicates that the thermal degradation of peptides involves cyclization processes. The differences in the spectra of *H*-AGGFL-*OH* and *H*-(β-A)GGFL-*OH* also confirmed cyclization mechanism. For *H*-AGGFL-*OH*, cyclization generates 3-, 6-, and 9-membered cyclic products and the dominant cleavages occur at the second amide bond from the N-terminus due to the high stability of the 6-membered-ring product formed. For *H*-(β-A)GGFL-*OH*, cyclization generates 4-, 7-,and 10-membered cyclic product. None of these is much more stable than the rest, so the cleavage at the second amide bond is no longer dominant. 2.

The second question is why the $(B_n-H+K)^+$ peaks are so weak in the mass spectra. In our experiments with amino acids, poly-amino acids, cyclic and linear dipeptides, it is found that there exists a response discrimination against small molecules and cyclic molecules. For example, the response of *H*-AA-*OH* is 10 times that of alanine; the response of a linear peptide *H*-GP-*OH* is 6 times that for a cyclic analog, cyclo-(GP). Because the binding energy between K^+ ions and neutral molecules is very small (20 - 40 kcal/mol) and there is no way for nascent K^+ adducts to dissipate the energy released in the binding process other than K^+ detachment or radiative processes, we believe that the relative ion stabilities of the K^+ adducts, thus their lifetimes, are responsible for the dominance of $(Y_n+H+K)^+$ over $(B_n-H+K)^+$ ions.

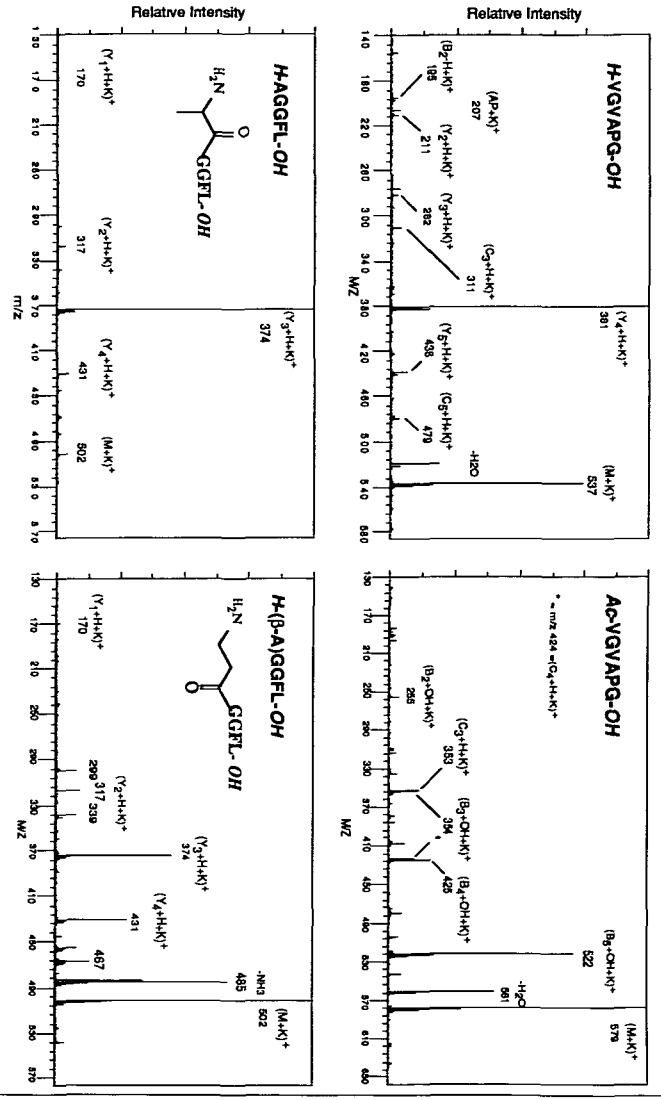

Fast Atom Bombardment Mass Spectra of 2-Iminothiolane Derivatives

M.G. Bartlett and K.L. Busch
Georgia Institute of Technology, Atlanta, GA 30332-0400

Introduction

2-Iminothiolane, or Traut's reagent, is used as a means of introducing sulfhydryl groups into proteins. These groups could be used to determine the number of exposed lysine groups in a protein. Creaing disulfide bonds within a protein with 2-iminothiolane has been used to study the spatial arrangement of ribosomal proteins. The presence of the sulfhydryl group has the added advantage of allowing further derivatization using fluorophores like N-pyrenyl maleimide (NPM).

In addition to introducing the sulfhydryl group into the protein, 2-iminothiolane also introduces a charged amino moiety. This amino group could be used to improve the response of proteins in fast atom bombardment (FAB) mass spectra. It would also allow for the analysis of proteins that have acid labile functional groups like t-BOC.

Experimental

The mass spectra were acquired on a VG-70SEQ hybrid instrument of EBqQ geometry. Samples were ionized using a Cs^+ ion gun operated at 30 keV. Ions were extracted from the source at 8000 eV. Glycerol was used as the matrix for all samples.

Reactions with 2-iminothiolane were carried out in a pH 8.0 triethanolamine buffer. Reactions were agitated for five minutes and then 2 uL of the sample was added to glycerol and analyzed directly from the probe.

Reactions with N-pyrenyl maleimide were carried out as follows. Prepare a solution of NPM in acetonitrile. Prepare a solution with the protein and 2-iminothiolane in pH 8 buffer. Immediately add the NPM solution to the mixture of 2-iminothiolane and the protein. Allow the mixture to sit overnight (12 hours) at 70 C.

Discussion

2-Iminothiolane reacts rapidly with any protein to yield the addition of a sulfhydryl and a precharged amino group. However, the addition of the precharged amino group causes only a two-fold increase in sensitivity for these compounds. The use of trifluoroacetic acid (TFA) as a modifier for FAB yields more intense molecular species than 2-iminothiolane derivatives. However, if the peptide contains an acid labile functional group like t-BOC, 2-iminothiolane may be beneficial.

The mass spectrum of the 2-iminothiolane derivatives show a peak 17 daltons lower than the addition of 2-iminothiolane. This peak becomes more intense with time. This increase corresponds to a decrease in signal intensity observed for the derivatized peptide. This loss of 17 daltons has been attributed to the recyclization reaction shown in scheme 1. This recyclization does not seem to be affected by changes in the buffer pH between 8 and 10. This recyclization may be responsible for the unexpected loss of sensitivity of the derivatized products.

The recyclization side reaction does not affect the ability of 2-iminothiolane to be a linking agent for maleimide fluorophores. The absence of side products, like the recyclization in the reaction of NPM and diphenylalanine and iminothiolane, show that this may be a useful reaction for labeling peptides.

2-Iminothiolane can also be used to derivatize aminoglycosidic antibiotics like kanamycin. Kanamycin A has four amino group. Figure 1 shows kanamycin A 5 minutes after reaction with 2-imnothiolane. After 15 minutes all four amino groups show the addition of iminothiolane.

Conclusions

2-Iminothiolane can be used to introduce both a derivatizable sulfhydryl group and a precharged amino group into peptides. However, because of a recyclization reaction the advantage of the precharged amino group is not recognized. A slight increase in sensitivity over TFA modified sample solutions is observed in the FAB of polyamino oligosacharides. 2-iminothiolane can be used to determine the number of primary amines in a molecule.

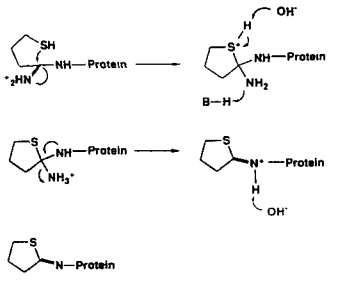

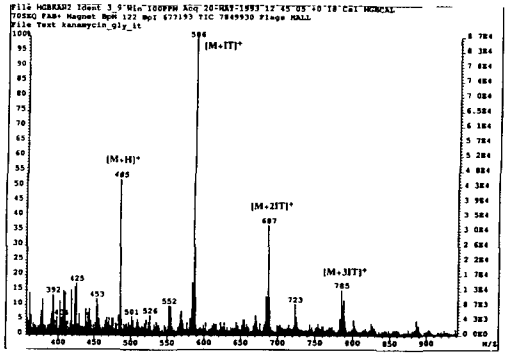

Kanamycin-Iminothiolane in Glycerol

Investigations of a One-step Chloroformate Derivatization Procedure for Small Peptides prior to Analysis by FAB-MS

*Jian Wang[1], Zhi-Heng Huang[2], Douglas A.Gage[2], and J. Throck Watson[1,2]
Department of Chemistry[1] and Biochemistry[2]
Michigan State University, East Lansing, MI 48824

Fast atom bombardment mass spectrometry of peptides is often used for molecular weight determination and sometimes for amino acid sequencing. Several experimental factors can prevent successful analysis, such as the poor ionization efficiency of some hydrophilic peptides. This can be overcome by preparing derivatives of the peptides prior to analysis by FAB-MS. Derivatization methods include a variety of peptide modifications, ranging from esterification to the attachment of a single hydrophobic moiety to a specific site on the peptide. None of the reported methods simultaneously derivatizes both amino and carboxyl groups in a single reaction, and most of the methods are time-consuming.

In earlier work, a rapid procedure was developed and refined in this laboratory using various chloroformate reagents to prepare volatile derivatives of amino acids for analysis by GC-FID or GC-MS [1,2,3]. In an aqueous medium, the chloroformate reagent derivatizes both the amino and carboxyl groups as well as most of the side-chain functional groups (amino, carboxyl, thiol, phenolic OH) of amino acids. Carboxyls are converted to esters, while the other functional groups are converyed to N,O and S-alkoxycarbonyl derivatives.

We have investigated the usefulness of this one-step chloroformate derivatization procedure for increasing the detectability of small peptides by FAB-MS. The FAB response of most of the ethyl chloroformate derivatives (forming N(O,S)-ethoxycarbonyl and ethyl esters) of model compounds (di-peptides to penta-peptides) increased five- to fifity-fold relative to that of the underivatized analytes (see Table 1). (The FAB response of the derivatives formed by chloroformate reagents that introduce a larger alkyl group (e.g., iso-butyl) did not show greater enhancement.) However, we have found that peptides are not quantitatively derivatized under conditions that achieved full derivatization of amino acids in a simple one-step reaction. Our preliminary results indicate that derivatization of amino groups (N-terminal and side-chain) is complete, but conversion of carboxyl groups (C-terminal and side-chain) is not complete, regardless of the size of the peptide (from dipeptides to ninemers in our model compounds). Preliminary investigations on the effect of

reaction medium composition, solvent ratio in the reaction medium, reaction time, and extraction efficiency have been carried out. Variation of reaction conditions had little effect on reaction yield, although the ratio of water/ethanol/pyridine in the reaction medium did influence the degree to which the reaction went to completion. The free carboxyl group was determined by MS/MS to be not specifically localized at either the C-terminal or a side-chain carboxyl (see Figure 1). Investigations of modifified chloroformate reaction conditions are continuing to find those that permit efficient and complete reactions of both amino and carboxyl groups on small peptides.

[1] Zhi-Heng Huang, et.al., *J. Chromatogr.*, 635 (1993) 271-281.
[2] Jian Wang, et.al., *The 40th ASMS Con. on Mass Spec. and Allied Topic*, p1579.
[3] Jian Wang, et al., *J. Chromatogr.*, submitted.

Table 1. Estimation of FAB signal enhancement from small peptides as the ethyl chloroformate derivatives relative to that of the underivatized peptides

Peptide	Enhancement
*RKDVY**	*50 / 80 (one free -COOH)*
*γ-ECG***	*35*
*GHK**	*50*
*YGG**	*20*
*DG**	*30*
VGDE	*10 (one free -COOH)*
KYK	*25 / 40 (one free -COOH)*
*LGG**	*5*
*GGF***	*5*
*SY****	*20*

* Average from 3 samples each with duplicate analysis. ** Average from 4 samples each with duplicate analysis. *** Average from 2 samples.

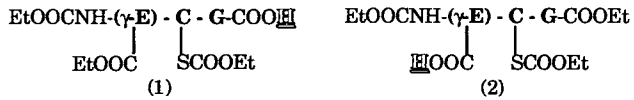

Figure 1. The two products of γ-ECG (glutathione) ethylchloroformate derivative with one free carboxyl either at C-teriminal (1) or on the side-chain of γ-E (2).

Identification of Novel Chemical Modifications in Proteins: Diamino Formation and Guanidino N-Displacement Product in β-Lactamase and Carbonic Anhydrase

R.A. Day, R. Ahluwalia, Y. Du, A.A. Karagözler and M.A. Roberts
Department of Chemistry, University of Cincinnati, Cincinnati, OH 45221-0172:
K. Jayasimhulu, Department of Environmental Health, College of Medicine, University of Cincinnati, Cincinnati, OH 45221-0056
C.J. Metral, NCI-FCROC, Frederick, MD 21701

Cyanogen (C_2N_2) modification of proteins occurs by condensing salt-bridged functionalities into covalent links (1,2). Only intra-molecular condensations occur with no detectable inter-molecular condensation. With identification of the sites modified the C_2N_2 treatment serves as a salt-bridge probe. The resultant covalent links are acylated amino and guanidino groups. Treatment of the acyl guanidino compound with a good nucleophile as a spectroscopic marker gives a product incorporating the nucleophile moiety covalently attached to the guanidino carbon(III). Structures were assigned through exact mass and fragmentation analysis. β-Lactamases, the principle bacterial defense system against β-lactam antibiotics, are irreversibly inhibited by our novel β-lactams. One of these, a monobactam (MB) with chemical bifunctionality, inhibits thorough a covalent cross-link between active site components SER-70 and LYS-234. The cross-linked, enzymatically inactive β-lactamase protein was stabilized to denaturation as measured by circular dichroism. The assignment (I) was made from FABMS analysis of tryptides. A penam with a 3° amino side chain irreversibly inhibited β-lactamase; FABMS showed it to be covalently attached only to SER-70(II) in the LC isolated tryptide.

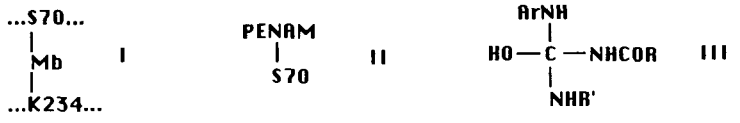

EXPERIMENTAL

β-Lactamase Modification with C_2N_2. *B. cereus* Type I β-lactamase (1.6 mg/ml) was mixed with 3 volumes of 0.14 M C_2N_2. After 30 seconds the excess C_2N_2 was entrained in a stream of N_2. The enzymatically inactive enzyme was treated with a 1% solution of p-anisidine (PAN) for 1 hour at room T. After removing excess PAN by alcohol extraction, it was digested with trypsin after further cold alcohol denaturation. The p-anisidine spectroscopically labeled only one peptide which was isolated by C18-RPLC.

β-Lactamase Modification by Active Site-Directed Labels. The procedures of Ahluwalia and Day (4) and of Du and Day (5) were followed. The tryptides and chymotryptides were produced and isolated essentially as described above. Structural assignments (II and III) were made by analysis of data produced from SIMS.

Acylguanidine Modification

(1) Bovine Carbonic Anhydrase (BCA). Cyanogen modified BCA treated with anisidine as described above yielded a peptide with an ARG-111 modified by anisidine.

(2) Acetylguanidine (AG). PAN treatment of AG yielded a displacement product (III). Exact mass and fragmentation analysis confirmed the structural assignment.

DISCUSSION

Mass spectrometric analyses were crucial in assigning the structures of the modified proteins. The determination of the sites of action of C_2N_2 is facilitated by the development of the guanidino moiety specific reagent, PAN itself a spectroscopic probe. The model compound afforded the information necessary to interpret labeling of C_2N_2 modified protein by PAN.

Representative ions were used to assign the position(s) of attachment of our novel irreversible inhibitors. Not unexpectedly, the β-lactamase protein cross-linked between SER70 and LYS234 by the bifunctional monobactam shows both stabilization to denaturation as demonstrated thru circular dichroic studies and altered retention time by C-18 HPLC (4). The monofunctional inhibitor gave a SER-70 acylated product with no attendant stabilization to denaturation or alter retention time (5).

C_2N_2 modification of proteins takes place through conversion of salt-bridged and H-bonded carboxylate pairs to covalent structures (1,2,3,6). Identification of the site(s) modified by C_2N_2 can be done by a combination of molecular modeling and nucleophile labeling (6). Use of an aromatic amine as the nucleophile affords a means to label the ARG guanidino moiety of a carboxylate-guanidino modification product.

The p-anisidine acylguanidino reaction product involves a novel reaction where one of the nitrogens is displaced from the guanidino groups (Structure IIII). Conventional DI spectral analysis afforded the data to assign this structure III.

C_2N_2 modification of β-lactamase leads to ~50% inhibition in 8 minutes with 0.14 M C_2N_2 at 25°. This is attributed to facile conversion of the GLU-166 carboxylate hydrogen bonded to OH of SER-70 to an ester link.

This work was supported in part by NIH Grant GM-42697.

REFERENCES

1. R.A. Day, J.W. Kirley, R. Tharp, D. Ficker, C. Strange and G. Ghenbot (1989) in "Techniques in Protein Chemistry" (T.E. Hugli, Ed.), p. 517. Academic Press, San Diego.
2. R.A. Day, R.L. Tharp, J.A. Wallace, A. Silanee, P. Hurt and N. Mastruserio (1990) Peptide Res. 3, 169.
3. A.A. Karagözler, G. Ghenbot and R. A. Day (1993) Biopolymers 33, 687.
4. R. Ahluwalia and R.A. Day (1993) Proc. 1993 Miami Bio/Technology Winter Symposium 3, 110.
5. Y. Du and R.A. Day (1993) ibid., 3, 113.
6. G. Ghenbot, T. Emge and R.A. Day (1993) Biochim. Biophys. Acta 1161, 59.

The Characterization of Hydroxyl Radical Oxidized Amino Acids and Peptides by GC/MS

Christa Oberth and A. Daniel Jones
Facility for Advanced Instrumentation
University of California at Davis, Davis CA, 95616

The free radical oxidation of proteins is associated with many degenerative diseases including aging, Alzheimer's', arthritis, immunodeficiencies, and some forms of cancer. Increased oxidative stress can result from exposure to xenobiotic chemicals. The chemistry of protein oxidation, the extent of protein oxidation *in vivo*, and the structural modifications that occur are poorly understood, primarily because previous studies have relied upon indirect methods of analysis.

We have developed a reproducible standardized protocol to investigate the reactions of a model compound, N-acetylphenylalanine, with hydroxyl radical generated by a Fenton system.

Because the products formed by Fenton oxidation have a wide range of physical properties, a single technique is not sufficient to characterize the entire reaction mixture. Several instruments, a quadrupole-GC/MS using electron impact ionization, a magnetic sector instrument using FAB ionization, and a triple-quadrupole instrument using negative electrospray ionization were used to analyze the mixtures. The reaction mixtures were converted to their t-butyldimethylsilyl derivatives prior to analysis by GC/MS. We also analyzed the unfractionated reaction mixture.

The diversity of oxidation products that we have identified by mass spectrometry is the result of the several different modes of hydroxyl radical attack: cleavage of the amide bond, hydroxylation of the side-chain, and products derived from side chain coupling.

An early GC/MS experiment indicated an amide cleavage product, the decarboxylated form of phenylalanine with $M^{+\bullet}$ at m/z 161, as well as products that showed that side chain hydroxylation occurred.

The crude Fenton mixture was placed on a C-18 Bond-Elut cartridge and we analyzed the water fraction directly by GS/MS. Both acetic acid and acetamide, which are two more products of amide bond cleavage were identified.

The mixture was eluted through a strong-anion-exchange cartridge (SAX) to remove the iron in the mixture to improve the yield of TBDMS derivatives. The analyte mixture was eluted with 0.1% aqueous TFA, freeze-dried, and converted to the TBDMS derivatives. The total ion chromatogram (TIC) and the spectra of three major peaks are shown.

The TIC shows three TBDMS-derivatized peaks with scan numbers of 1247, 1277, and 1304, which correspond to the ortho, meta, and para hydroxylated products, respectively. The height of each of these three peaks is important because it gives us an indication of the relative reactivity of each site towards hydroxyl radical in this system. The para isomer was confirmed by comparison with an authentic standard.

Similar reactivity of the *o*- and the *p*- sites, would yield twice as much *o*- isomer to form because there are two ortho positions and only one para. The size of peak 1247 is approximately two times larger than peak 1304 and the meta position is only somewhat less reactive towards hydroxyl radical. This suggests that the hydroxyl radical attacks all aromatic positions in comparable amounts. The spectra of all three isomers have a fragment ion at m/z 221, to yield a benzylic fragment ion. The *o*- and *p*-isomers form this ion to a greater extent because the ortho and para isomers can better stabilize the resultant charge. The relative abundance of this fragment ion in the ortho isomer is lower than that observed for the para isomer presumably due to stabilization of the $[M-57]^+$ ion by neighboring groups.

A unique fragment ion at m/z 147 is present in the spectrum of the *o*-hydroxy isomer. This corresponds to an ion containing two silicon atoms, which forms when silyl derivatives are in close proximity to each other.

For the *m*-hydroxy isomer, one sees fragments that are not seen in the spectra of the other two isomers because the meta isomer generates fragments with few resonance stabilized forms.

Oxidation of N-acetylphenylalanine also yields 1,2-diphenylethane, suggesting formation of benzyl radicals during oxidation.

The FAB spectrum of the SAX-treated-Fenton-oxidized N-acetylphenylalanine verifies the presence of the hydroxyl N-acetyl phenylalanine ($[M+H]^+ = 224$) and the amide cleavage product phenylpyruvic

acid $[M+H]^+ = 165$ was observed. FAB also revealed the dimer product that forms between unreacted N-acetylphenylalanine and hydroxyl N-acetylphenylalanine ($[M+H]^+ = 429$). This product was not seen using GC/MS.

Fenton oxidation products identified by negative ion ES/MS are acetamide, $[M-H]^- = 58$; acetic acid, $[M-H]^- = 59$; phenylalanine, $[M-H]^- = 164$; and hydroxyl N-acetylphenylalanine, $[M-H]^- = 222$.

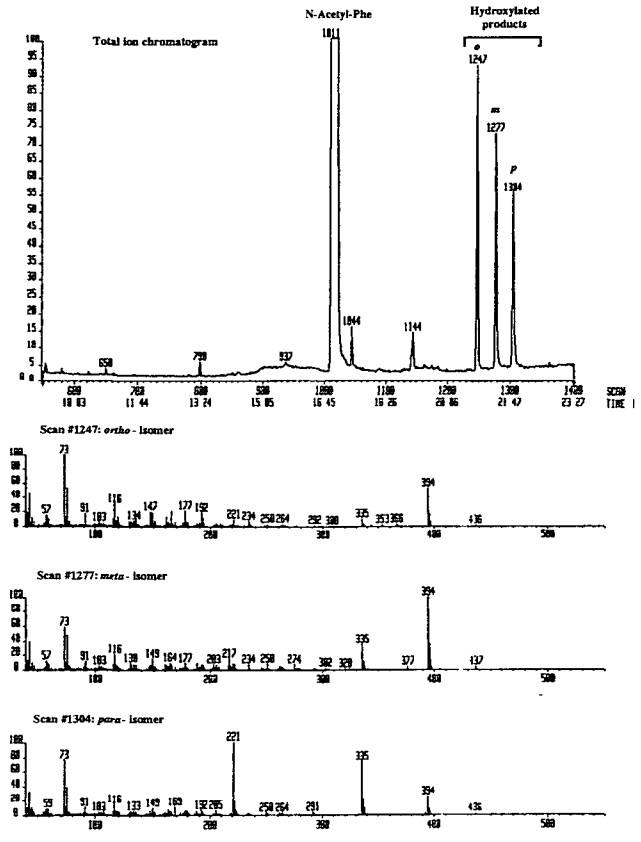

Acknowledgments
This work has been supported by NIEHS-Superfund Grant #ES-04699

ESI/MS Detection and Characterization of Novel Thiohydantoin Amino Acid Derivatives

C. Basic, J.M. Bailey, J.E. Shively, T.D. Lee, Division of Immunology, Beckman Research Institute of the City of Hope, Duarte, CA 91010

Automated N-terminal sequencing of peptides and proteins based on Edman degradation methodology is currently limited to the analysis of samples in the low picomole range (1). This limitation is largely imposed by the use of high-performance liquid chromatography, HPLC, to detect the phenylthiohydantoin, PTH, amino acid derivatives produced as the end products of each degradation cycle. There is increased interest in developing new methods to sequence samples in the mid- to low femtomole range. To this end more sensitive fluorometric (2) and electrospray ionization mass spectrometric, ESI/MS, (3,4) detection methods have been utilized, coupled with requisite modifications of the degradation chemistry.

The ESI/MS and MS/MS spectra of a series of novel thiohydantoin amino acid derivatives in which the phenyl functionality of the standard phenylthiohydantoin ,PTH, derivatives is replaced with a tertiary (dimethylaminopropyl thiohydantoin, DMAP-TH) amine are presented. The development and characterization of these derivatives is part of an on-going effort in our laboratory to couple ESI/MS on-line with protein sequencing.

All ESI mass spectra were obtained on a Finnigan MAT TSQ 700 MS fitted with an Analytica of Branford ESI source. Samples were introduced *via* direct infusion through a stainless steel capillary at a flow rate of 2 $\mu l/min$ and a concentration of 10 $pmol/\mu l$, unless otherwise indicated. The source temperature was ≈ 170° C. Pneumatic nebulization was performed using a co-axial flow of N_2 gas. The ESI/MS/MS spectra were obtained at a collision offset of -20 eV with an indicated Ar collision gas pressure of $\approx 3\times10^{-6}$ torr. The DMAP-TH derivatives were synthesized in our laboratory; the PTH derivatives were obtained from Sigma Chemical Co.

The DMAP-TH derivatives characterized to date include: glycine, valine, leucine, isoleucine, phenylalanine, arginine and histidine. A typical ESI/MS spectra of the DMAP-TH -leucine in 50% $MeOH/H_2O$/1% HAc is presented in Figure 1. Each derivative studied gives rise to a $[M+H]^+$ ion as well as a $[M+H-45]^+$ ion. The $[M+H-45]^+$ ions are attributed to loss of $NH(CH_3)_2$ since none of the -R groups studied give rise to a logical loss of 45 mass units. The relative intensities of the $[M+H-45]^+$ ions can be increased by increasing the capillary/skimmer offset. At higher offsets $[M+H-73]^+$ ions attributed to the loss of $(CH_2)_2NH(CH_3)_2$ are also seen (except arginine which shows no 73 loss). Thus, three characteristic ions for each derivative can be monitored in a single stage mass spectrometer.

The ESI/MS/MS spectra of the $[M+H]^+$ ion of DMAP-TH-arginine is presented in Figure 2. Unlike the other derivatives studied, DMAP-TH-arginine shows fragment ions arising from both the DMAP and -R functional groups. The fragment losses indicate that the $[M+H]^+$ ion may be protonated on both the DMAP and -R groups, *e.g.* the $[M+H-17]^+$ may be attributed to loss of NH_3 from the -R group while the $[M+H-45]^+$ ion is attributed to loss of $NH(CH_3)_2$ from DMAP.

The ESI/MS spectrum corresponding to 21 fmoles of the DMAP-TH derivative of phenylalanine is presented in Figure 3. This spectrum demonstrates that the DMAP-TH derivatives can be detected at the tens of femtomole level. The DMAP-TH derivatives for the remaining amino acids have been synthesized and will be characterized by ESI/MS and MS/MS methods. Future work will also involve the interfacing of a dedicated ESI/MS spectrometer to an N-terminal protein sequencer incorporating the requisite modifications of the degradation chemistry.

1. Calaycay, J.; Rusnak, M.; Shively, J.E., *Anal. Biochem.*, 192 (1991) 23-31; 2. Tsugita, A.; Kamo, M.; Jone, C.S.; Shikama, N., *J. Biochem.*, 106 (1989) 60-65; 3. Aebersold, R.; Bures, E.J.; Namchuk, M.; Goghari, M.H.; Shushan, B.; Covey, T.C., *Protein Science*, 1 (1992) 494; 4. Dharmasiri, K.A.N.; Huang, Z.H.; Watson, J.T, 40th ASMS Conference on Mass Spectrometry and Allied Topics, 1992, Washington, D.C., 1791.

Presented at the 41st ASMS Conference on Mass Spectrometry

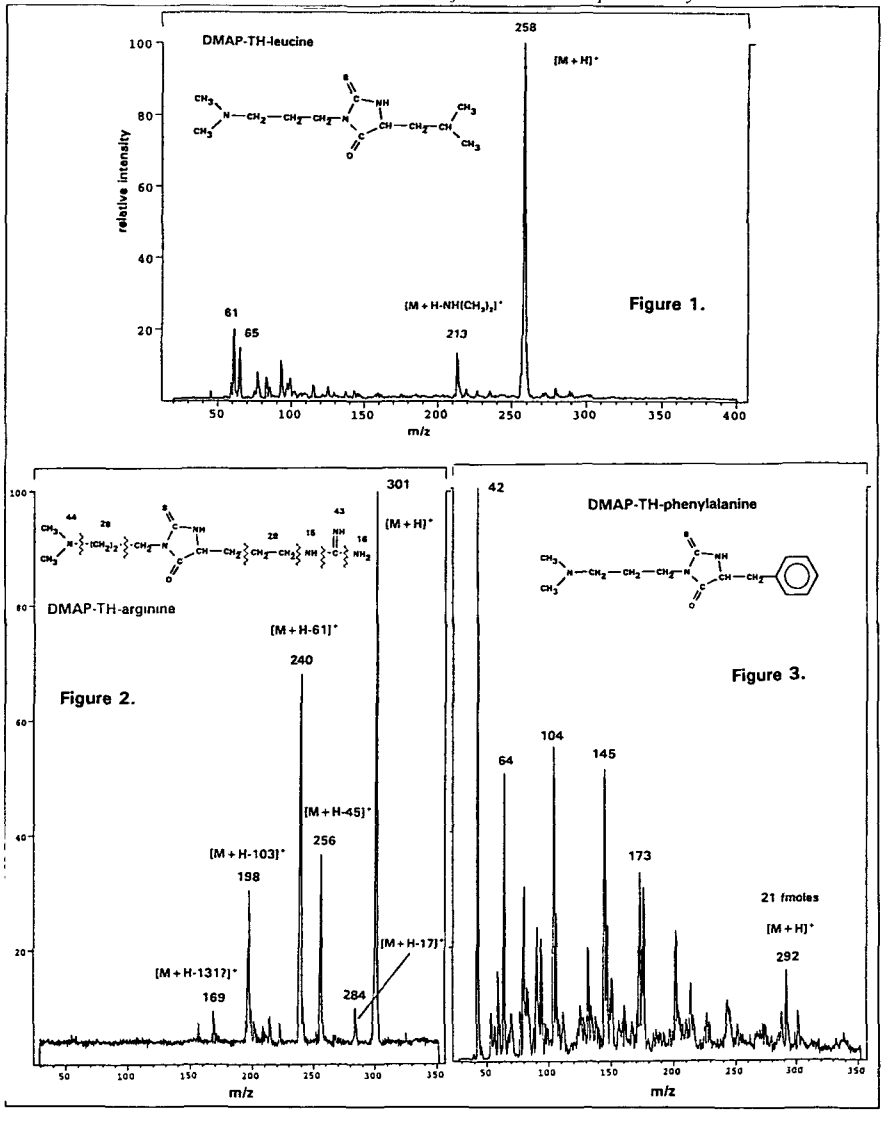

Synthesis and Mass Spectrometric Characterization of Reference Phosphopeptides.

D. I. Papac, J. E. Oatis Jr., & D. R. Knapp
Medical University of South Carolina, Charleston, SC 29425

Introduction: The need for small quantities (few to tens of micromoles) of multiple peptides, including modified (i.e. phosphorylated) peptides for mass spectrometry standards prompted us to devise a simple manual approach for synthesis of multiple peptides using a relatively inexpensive, commercially available solid-phase extraction apparatus. We report here a description of the peptide synthesis apparatus and its use for preparation of a series of monophosphorylated peptides corresponding to fragments obtained from the C-terminal region of bovine rhodopsin. In addition, we report on the tandem mass spectra obtained for these phosphopeptides using high energy CID conditions.

Methods: The synthesis apparatus shown in figure 1 was assembled from a 12-position solid-phase extraction manifold fitted with empty 1.5 ml polypropylene extraction tubes supplied with polyethylene frits and attached to valved teflon needles. A water aspirator vacuum with trap was used to collect the effluents from the extraction tubes into polypropylene tubes held in a rack within the manifold.

Syntheses were performed on "Wang" resin using standard solid-phase Fmoc chemistry as detailed in figure 2. The sidechain groups were all protected as t-butyl derivatives except for lysine which was protected as the ε-amino BOC derivative.

Serine or threonine residues to be phosphorylated were coupled with the hydroxyl group unprotected. The free hydroxyl groups were phosphitylated by treatment for 1-24 hrs with a 10-40 fold molar excess of N,N-diethyl-di-t-butylphosphoramidite in DMF containing a 40-70 fold molar excess of 1H-tetrazole. The resin was washed with DMF prior to oxidation of the phosphite groups with either a 33-fold molar excess of t-butyl hydroperoxide (3M in 2,2,4-trimethylpentane) or a 30-fold molar excess of m-chloroperbenzoic acid in methylene chloride for 0.5-3 hr.

Separation of synthetic phosphopeptides was achieved on a Vydac C-18 column with a mobile phase of (A) 0.1% aqueous TFA and (B) acetonitrile containing 0.084% TFA. The gradient was 98% A held for 10 min then ramped linearly to 89% A over 50 min.

Mass spectra were obtained on a JEOL HX110/HX110. Samples were dissolved in 10 μl of 1N HCl, applied to the probe on a matrix of 1N HCl/thioglycerol, and ionized with 18 kV cesium ions. MS/MS experiments were performed with the accelerating voltage at 10 kV and a resolution of 1500 for MS1 and 1000 for MS2. The collision cell was operated at 3 kV and filled with enough helium to attenuate the ion current of the C-12 monoisotopic peak by 70%.

Results: Using this peptide synthesis apparatus good yields were obtained for unmodified peptides containing up to 19 residues. Low yields (< 10%) were initially obtained for the incorporation of phosphate; however, sufficient quantities of the monophosphorylated derivatives of ASTTVSKTE were prepared for use as mass spectrometric standards using the published phosphitylation and oxidation conditions[1,2,3]. The low yields were most likely attributed to steric hindrance from the bulky t-butyl protecting groups. In subsequent syntheses of monophosphorylated

derivatives, incorporation of the phosphite group was increased substantially by increasing the reaction time and the amount of N,N-diethyl-t-butyl phosphoramidite and 1H-tetrazole. High energy CID MS/MS of the phosphopeptides displayed the characteristic fragment ions and losses[4]. In addition, a novel side chain cleavage loss was observed for phosphothreonine containing peptides (-125 Da) (Fig. 3). This loss was not observed when the phosphate was located on an N-terminal threonine.

Conclusion: A system for small-scale multiple peptide synthesis built from a commercially available solid-phase extraction apparatus was used to successfully prepare several series of monophosphorylated peptides (ASTTVSKTE & TSQVAPA) on the 10-30 μmol scale.

References :

1. Andrews, D. M., et al. (1991) Int. J. Peptide Protein Res. **38**, 469-75.
2. Staerkaer, G., et al. (1991) Tetrahedron Lett. **32**, 5389-92.
3. Perich, J. W. (1992) Int. J. Peptide Protein Res. **40**, 134-40.
4. Biemann, K. & Scoble, H. A. (1987) Science **237**, 992-8.

This work was supported in part by N.I.H. grant EYO8239

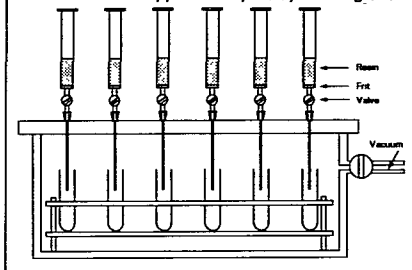

Fig. 1 Diagram of the Small Scale Multiple Peptide Synthesis System.

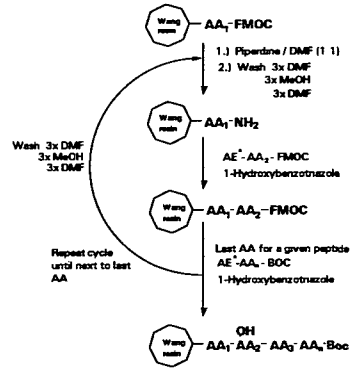

Fig. 2 Synthetic Scheme for Preparation of Peptides. The (AE*) indicates an activated ester; either the pentafluorophenyl ester or the 3-hydroxy-4-oxo-3,4-dihydrobenzotriazine ester.

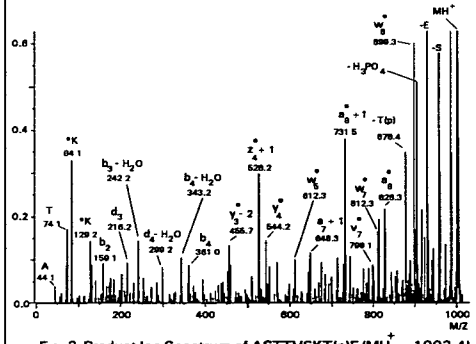

Fig. 3 Product Ion Spectrum of ASTTVSKT(p)E (MH^+ = 1003.4).

Tandem Mass Spectral Decompositions of Protonated N-Acyloligoalanines and N-Acyloligoglycines as Models for Those of the Protonated Free Oligopeptides

Daniel G. Morgan and Maurice M. Bursey
The University of North Carolina at Chapel Hill, Department of Chemistry, Chapel Hill, North Carolina 27599

The decompositions of various n-acylated derivatives of tetraalanine and tetraglycine were studied as models for comparison with their corresponding hexa- and octapeptides using fast atom bombardment (FAB) MS/MS The principle purpose of this study was to compare the dependence of the yields of typical backbone cleavages upon structure in these modified and unmodified peptides This comparison was pursued through increasing the aliphatic chain length of the appropriate acylated tetrapeptide to mimic one or two Ala_2 or Gly_2 units through equal mass or through equal degrees of freedom. Thus, nonanoyltetraglycine approximates octaglycine in the number of degrees of freedom while pentadecanoyltetraglycine approximates octaglycine in molecular weight.

The predominate fragmentation ions noted in the tandem mass spectra for all of the peptides investigated in the study were acylium and ammonium ions, y- and b-type ions as based on the Biemann nomenclature[1] The intensities of these ions in the spectra of the N-acylated oligomers exhibited marked differences when compared with the corresponding free oligomer. Table 1 shows a comparison between Gly_4 and Gly_6 along with the degrees of freedom model for Gly_6, valeroyltetraglycine, and the acylated model of similar mass, heptanoyltetraglycine. Ion, peptides are the fragment ions noted for Gly_4 and Gly_6, while the Ion, models are the labels for the fragments of the acylated peptides For comparison purposes of this study, the b_3 ion of valeroyltetraglycine was considered equivalent to the b_5 ion of Gly_6.

Table 1 Comparison of Gly_4 and Gly_6 with Model Compounds of Similar Mass and Similar Degrees of Freedom (DOF) Based on Total Product Ions

Ion, peptide Ion, models	b_3 b_1	b_4 b_2	b_5 b_3	b_6 b_4	y_2 y_2	y_3 y_3
Tetraglycine	18	21			58	
Hexaglycine		18	40	21		13
Valeroyltetraglycine	1	3	29	10	7	50
Heptanoyltetraglycine	1	4	28	5	6	55

There is a spectacular difference between the spectra of the acylated tetrapeptides and the free tetrapeptides The y_2 ion domination of tetraalanine and tetraglycine is absent and replaced by a domination of the y_3 of the acylated tetraglycine and the b_3 of the acylated tetraalanines Thus the acylation of the terminal amino group prevents the formation of the y_2 ion Yeh et al.[2] argued previously that the intense y_2 ions in the tandem mass spectra of tetraglycine and tetraalanine were due to an especially favorable loss of a diketopiperazine (Scheme 1) This suggests that even though the terminal site of protonation is still favored in the acylated tetrapeptides, as based on proton affinity calculations, the site of protonation has changed from the nitrogen to the oxygen, because of the change of the functional group from an amine to an amide (Scheme 2) Thus the diketopiperazine formation is much less favorable because a transition state ring has increased in size from six to eight Thus, the intensities of the model compounds did not follow statistical or linear free energy relationships as would be expected if they were true homologues.

Diketopiperazine Formation

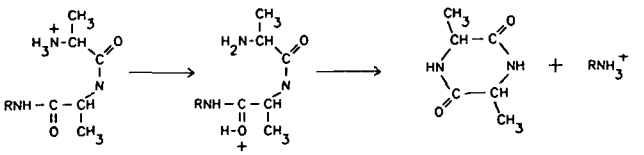

Scheme 1

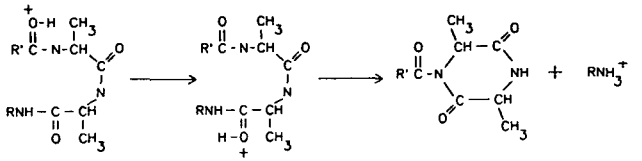

Scheme 2

Labeling studies have been performed to study the formation of the intense y_3 ions in the spectra of the acylated tetrapeptides. The five easily exchangeable hydrogens of nonanoyltetraglycine were replaced with deuterium on the FAB probe tip during analysis of the $[M+D]^+$. These hydrogens were the four attached to the nitrogen amides and the one attached to the carboxylic end. An intense ion observed at 196 amu corresponded to the y_3 fragment, deuterated at the exchangeable sites along with two extra deuteriums, one from the matrix and one from the terminal amide nitrogen This is in agreement with the mechanism as proposed by Kenny, et. al.[3] A labeling study of the aliphatic chain was also performed to confirm this pathway d_{17}-Nonanoyltetraglycine was synthesized where all of the hydrogens of the aliphatic chain were replaced by deuterium The results showed that none of the aliphatic hydrogens were involved in the y ion formation.

This work has provided further evidence for the control of ion intensity by the site of protonation in peptides We have adduced evidence for a difference in structure between the conjugate acids of tetrapeptides, acylated tetrapeptides, and of larger oligomers The difference in the availability of the y2 channel between tetrapeptides and acylated tetrapeptides is consistent with the proposition that amides are protonated on the oxygen atom Finally, we have confirmed the mechanism for y ion formation as proposed by Kenny.

[1] K Biemann, *Biomed Environ Mass Spectrom* **11**, 604 (1984)
[2] R.W Yeh, J.M Grimley, and M.M. Bursey, *Biol. Mass Spectrom.* **20**, 443 (1991)
[3] P.T Kenny, K. Nomoto, and R Orlando, *Rapid Comm. Mass Spectrom* **6**, 95 (1992).

Gas Phase Protein Conformations & Folding

*Francis M. Wampler III, Daniel P. Little, Detlev Suckau, Steven C. Beu , Fred W. McLafferty

Chemistry Department, Baker Laboratory, Cornell University, Ithaca, NY 14853-1301

H/D exchange of electrosprayed protein ions in a Fourier transform mass spectrometer (FTMS) has provided extensive evidence of co-existing conformations of such gaseous ions.[1] Improvements over previous work were made possible by an instrument upgrade including the replacement of the old 2.8 T magnet with one of 6.2 T, in conjunction with the addition of two faster (1500L/s) cryogenic pumps. Utilizing these improvements, all spectra are now isotopically resolved, with the resolution of some approaching 10^5. Single or double SWIFT [2] isolations of a desired charge state were used for the H/D exchange studies. All exchange reactions were carried out at 1.1×10^{-7} torr D_2O for 30 minutes, sufficient time for essentially complete exchange of accessible sites.[1]

20 μM equine cytochrome c was electrosprayed from both denaturing and nondenaturing (pure H_2O) solution conditions. 198 protons of this protein are attached to heteroatoms (N, S, O) and are chemically reactive toward H/D exchange with D_2O. In the gas phase, the number of exchanged sites was shown to depend upon the steric accessibility of those sites, and did not necessarily increase with increasing charge state. Three levels of exchange were observed: ~85 exchanges for 6^+ - 8^+, ~130 exchanges for 8^+ - 15^+, and ~110 exchanges for 8^+, 11^+ - 13^+, 15^+ (trace), and 16^+ -18^+. It is not now clear whether the latter exchange levels represent 1, 2, or 3 different conformations. In solution, two hour reactions with D_2O resulted in deuteration of nearly all 198 exchangeable sites in the resulting ions. At several charge states, there was evidence for co-existing stable conformations, resulting in very dramatic bimodal exchange levels. The 8^+ ion, comprised of high and intermediate exchanging conformers, was primarily in a highly denatured state when electrosprayed from CH_3OH solution, and primarily in the intermediate state when sprayed from aqueous solutions.

In attempting to change the gas phase conformations, a charge state of known conformation was SWIFT isolated. Low pressure pulses of butyl amine (proton affinity = 218 kcal/mol) were used to remove protons (strip charge) from the protein. Sufficient time was left for most of the amine to pump away, and then D_2O was admitted through a separate bleed valve. The interconversion among conformers was achieved. (Figures 1 & 2). The 15^+ ion, shown to be mostly denatured (~130 exchanges) was stripped to 7^+. The low exchange (~85) observed for the 7^+ product was consistent with gas phase folding. In a separate experiment, the intermediate exchanging 16^+ (~110 exchanges)

was stripped to 15^+; mostly high exchanging conformer resulted. The similarity in spectra between the 15^+ from charge stripping and that with no amine added are striking, and provide excellent support in the argument for gas phase unfolding.

1. Suckau, D., et.al., Proc. Natl Acad. Sci. USA, 1993, **90**, 790-793.

2. Marshall, A. G.; Wang, T-C. L.; Ricca, T.C. J. Am. Chem. Soc. 1985, **107**, 7893-7897.

FIGURE 1: DENATURED STATE FOLDING

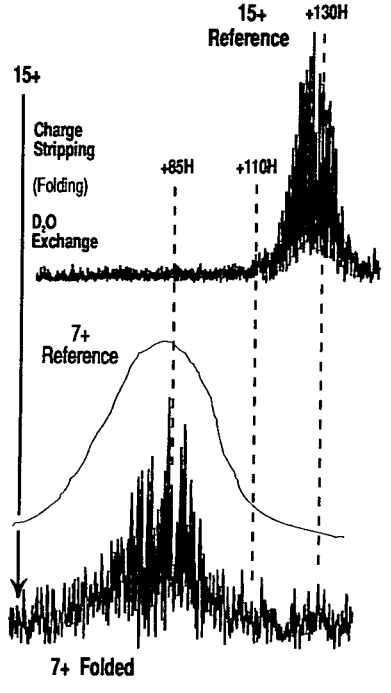

FIGURE 2: "A"-STATE UNFOLDING

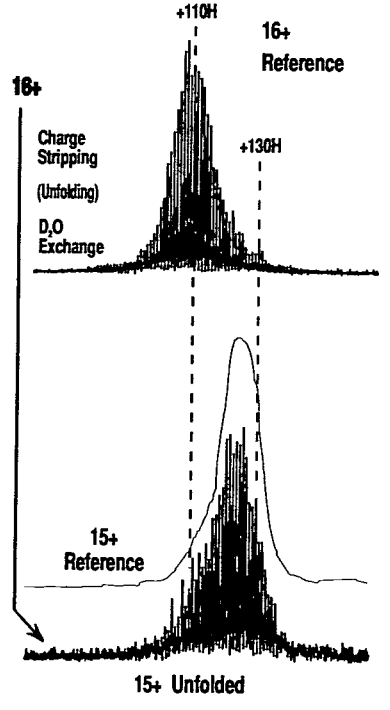

CONFORMATION OF PROTEINS STUDIED BY DEUTERIUM EXCHANGE ESI-MS

D.S. Wagner and R.J. Anderegg, Glaxo Research Institute, RTP NC, 27709

Recently deuterium exchange has been observed with ESI-MS[1,2]; faster exchange being indicative of a more open structure, slower exchange associated with a tightly folded structure or intramolecular hydrogen bonding. Since the experiments performed to date monitor exchange rates for the native and denatured states in different environments (pH, temperature and solvent system), it is not clear whether the variation of the exchange rate is due to the protein's conformational change, to the change in the chemical environment, or to a combination of both. In order to accurately compare the exchange rates for the two different conformations, both the native and denatured states must be analyzed in the same environment. Bovine cytochrome c (MW 12,231) contains 192 labile hydrogens (deuterated molecular weight 12,423). Altering the acid concentration of a solution containing bovine cytochrome c has a dramatic effect on the charge state distribution, CSD, observed in the corresponding ESI mass spectrum: 0% acid (pH=6.0) exhibits 1 CSD ranging between +7 and +11, 2% acetic acid (pH=2.7) displays a "bimodal distribution" one CSD ranging from +7 to +10 charge states and the second CSD ranging between +11 and +18, and 4% acetic acid (pH=2.5) mainly the high CSD. The differences between these spectra have been attributed to changes in the protein conformation, with the tightly folded native states appearing as an CSD at high m/z (low charge) and the denatured state represented by the CSD at lower m/z (high charge). The bimodal charge distribution is interpreted as two conformations in solution, one more tightly folded than the other.

If more than one conformation of a protein exists in the solution, then the more denatured conformation should exhibit a faster rate of deuterium exchange leading to a higher molecular weight at any given time point. Plots of the protein's measured molecular weight versus time for the +8 and +15 charge states in 2% d^4acetic acid (conditions known to produce a bimodal distribution) overlap one another, thus indicating that both charge state distributions have the same rates of H-exchange. Altering the pH and/or organic solvent concentration of the solution changed the observed exchange rate; however, the two charge state distributions always exhibited overlapping curves. This suggests that either the interconversion between the native and denatured states is on a much faster time scale than the exchange reaction, or the protein has only one conformation in solution and the change in the charge state distribution is an artifact of the ESI experiment. Under most conditions the protein's interconversion between conformations is faster than H exchange. Therefore only one overall exchange rate can be observed regardless of the charge state distribution noted in the ESI mass spectrum unless a method for blocking interconversion can be employed.

In order to block the interconversion between the open and closed forms of the protein, samples were partially denatured in an irreversible manner by heating at 95 C for 3 hours[3]. The structural basis for this denaturation probably involves the isomerization of the four proline residues. The mass spectrum of a heat treated sample dissolved in H2O 0% acid (conditions known to produce 1 CSD), displays a bimodal distribution centered around the +9 and +15 charge states. Lyophilized samples of the heat denatured protein were dissolved in D_2O only and the change in m/z as a function of time was monitored. The measured molecular weight versus time for the +8 and +15 charge states clearly shows two unique rates of deuterium exchange for the two charge state distributions (Figure 1). The lower charge state experiences slow exchange representing a tightly folded structure, while the higher charge state undergoes rapid exchange indicating a more denatured structure. This gives unequivocal evidence that two different charge state distributions correspond to two different conformations in solution. A

comparison of the exchange behavior for the native and thermally denatured samples reveals that the high and low CSD of native cytochrome c and the low CSD of the heat denatured protein display similar exchange rates as evidenced by the similarity of their exchange profiles. However, the high CSD of the heat denatured protein displays a markedly faster rate of exchange. Therefore we conclude that there are at least two denatured states of cytochrome c present with approximately the same charge state distribution that have significantly different deuterium exchange rates. The native states that we observe in both experiments are, as far as we can tell, identical.

It is tempting to try to use the ESI-MS exchange data to extract information about the rate of protein unfolding or deuterium exchange. If a uniform first kinetics is assumed, then the observed rate constant $K_{obs}=(k_{unfolding}/k_{folding} * k_{exchange})$ could be obtained for each deuterium exchange experiment. The rate constant for a given experiment can be acquired from a plot of ln[the number remaining of labile hydrogens] versus time. If the protein only contained a single rate constant then the plot would correspond to a straight line, whose slope would be proportional to the exchange rate. However, since each amide has a different first order exchange rate, a curve is obtained instead of a linear plot (Figure 2). The curve can be segmented into groups of amides that exchange with similar rates depicted by linear regions. Although these kinetically isolated sets of protons may have similar exchange rates, this does not indicate they originated from the same structural element.

Deuterium exchange has been shown to be extremely sensitive to protein conformational changes because exchange is irreversible and cumulative. Mass spectrometry can easily monitor the rates of deuterium incorporation by the mass shifts in an experiment. Different conformations do not necessarily have different exchange rates. Data indicates that there are at least two denatured states of cytochrome c which have similar charge state distributions but different rates of deuterium exchange. Therefore the charge state distribution is not a sufficient indicator of the protein's conformation. ESI-deuterium exchange experiments have potential for probing protein folding and obtaining other useful kinetic data. In addition, the stability of proteins upon structural modification, and the effects of ligands, inhibitors or substrates to an enzyme could also be monitored by comparing the appropriate exchange rates obtained by ESI-MS.

FIGURE 1

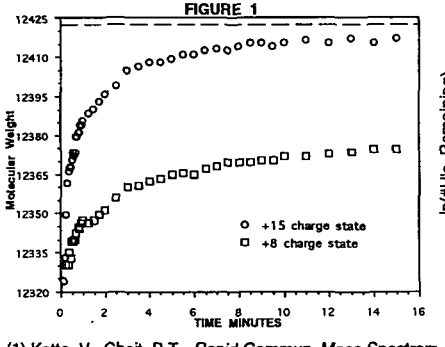

FIGURE 2

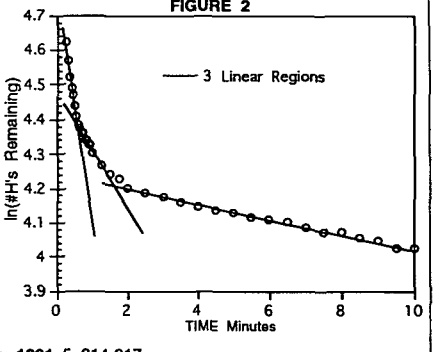

(1) Katta, V., Chait, B.T., *Rapid Commun. Mass Spectrom.*, **1991**, 5, 214-217.
(2) Stevenson, C.L, Borchardt, R.T., R.J. Anderegg, *J. Am. Soc. Mass Spectrometry*, submitted.
(3) Mirza, U.A., Cohen, S.L., Chait, B.T., *Anal. Chem.*, **1993**, 65, 1-6.

Protein Backbone Amide Hydrogen Exchange Determined by HPLC FABMS: Application to Rabbit Muscle Aldolase

Zhongqi Zhang, Carol B. Post and David L. Smith
Department of Medicinal Chemistry and Pharmacognosy, Purdue University
W. Lafayette, IN 47907

Isotopic exchange of protein backbone amide hydrogens has been used extensively as a sensitive probe of protein structure. The principal method for determining rates of hydrogen exchange in small proteins has been one and two-dimensional NMR. However, the use of NMR is restricted to investigations of relatively small and highly soluble proteins.

A new method based on protein fragmentation and HPLC FABMS has been developed in our laboratory to facilitate application of hydrogen exchange to large proteins. We report results obtained when this method was applied to rabbit muscle aldolase and its complex to the N-terminal pentadecapeptide of Band III protein. Aldolase is a protein with four identical subunits and a molecular weight of 157 kDa. Band III protein, a major protein component of erythrocyte membranes, binds to aldolase, thereby inhibiting its enzymatic activity. To better understand the inhibition of aldolase by Band III protein, we are using amide hydrogen exchange to probe conformational changes between bound and free aldolase.

The general procedure used for deuterium exchange-in and analysis is illustrated as follows. The protein was incubated for varying lengths of time in D_2O for deuterium exchange. The exchange was terminated by decreasing the pH of the solution from pH 7.2 to 2.6. The deuterated protein was digested by pepsin for 10 min at 0 °C and analyzed immediately by HPLC FABMS. The extent and location of deuterium exchange-in was determined from the deuterium content of peptides derived from the protein. Conditions used for proteolysis and peptide analysis were selected to minimize hydrogen back exchange (0 °C, pH 2 - 3). The total time required for digestion and analysis was approximately 20-30 minutes, which is substantially less than the half-life for back exchange of amide hydrogens. Since very rapidly exchanging hydrogens (e.g., -OH) undergo back exchange with the HPLC mobile phase, the molecular weights of the peptides are a direct measure of the number of deuteriums located at peptide amide linkages. To correct for exchange occurring during digestion and analysis, nondeuterated and fully deuterated proteins were analyzed by the same procedure. The deuterium levels of the partially deuterated peptides were determined by comparison with the two standards.

Deuterium incorporation into different segments of aldolase was determined as a function of exchange-in time. To investigate the interaction between aldolase and the N-terminal pentadecapeptide of Band III protein, hydrogen exchange into both free aldolase and a mixture of Band III peptide and aldolase were determined. From the rates at which deuterium exchange occurs in different segments of aldolase in free and bound forms, we can see that binding has little effect on the rate of hydrogen exchange in some segments, while increasing the rate of exchange in others (Fig. 1 shows an example for each case). These results suggest that complexation has little effect on intramolecular hydrogen bonding in some regions, while significantly weakens intramolecular hydrogen bonding in others.

Although the present protein fragmentation method is generally limited to determining isotopic exchange rates in segments of proteins, it can be used to obtain more detailed information in some cases. For example, there may be several overlapping peptides from the same region of the protein. Differences in the deuterium contents of such peptides can be used to increase the spatial resolution of the method. For instance, segment 58-64 of aldolase has a significantly increased hydrogen exchange, but segment 58-62 does not change upon binding to Band III peptide. These results show that residues 63 and 64 are responsible for the increased hydrogen exchange of segment 58-64 upon complexation. Fig. 2 shows the difference in the

deuterium levels of segments 58-64 and 58-62, which is a measure of deuterium content in residues 63 and 64. After fitting the curves with an equation of two exponential terms, we found that both exchange rates of the two amide hydrogens increased by approximately a factor of two in the complex (see Fig. 2 insert).

Results described here demonstrate that the amount of deuterium incorporation into a large protein, such as aldolase, can be determined accurately by combining the protein fragmentation method and directly-coupled HPLC-FABMS. Since the rate at which amide hydrogens undergo isotopic exchange is a sensitive probe of the high order structure of proteins, methods described here facilitate use of FABMS in studies of the high order structures of proteins. Although the spatial resolution achieved by this method is not at the single residue level, exchange rates within small segment, sometimes as short as one or two residues, can be determined. Application of this technique to aldolase and its complex to Band III N-terminal peptide have shown that aldolase is locally destablized after binding to the Band III peptide. This may lead to a better understanding of the interaction between aldolase and Band III protein.

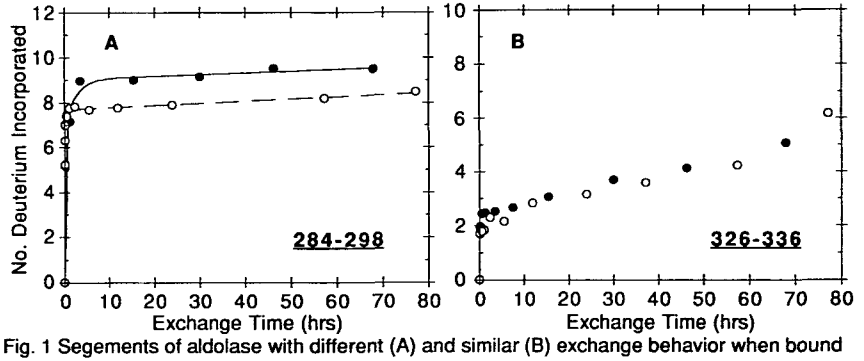

Fig. 1 Segements of aldolase with different (A) and similar (B) exchange behavior when bound (•) and not bound (o) to Band III peptide.

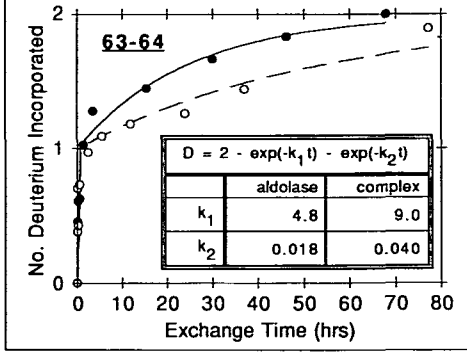

Fig.2 Hydrogen exchange time courses of the 2-residue segment 63-64 derived from segments 58-62 and 58-64. The two curves are fitted by an equation with two exponential terms. (o - aldolase; ● - aldolase plus Band III peptide)

Using AMASS to Localize a Modification on a Peptide. *A. G. Craig, C. Hoeger, S. C. Koerber, J. Porter and J. E. Rivier, The Clayton Foundation Laboratories for Peptide Biology, The Salk Institute, P.O. Box 85800, San Diego, CA 92186-5800.

When fragment ions are assigned manually, the 'simplest' explanations are usually arrived at first. Although, these assignments are generally the correct ones, when assignments cannot be made and a computer is used to generate possible rational assignments, criteria are required for the interpretation. From inspecting possible fragment masses generated by AMASS (ref. 1) for 18 di-, tri-, tetra-, penta- and hexa-peptides we found that almost any fragment mass could be rationalized by carrying out two bond cleavages together with up to 2 proton transfers. However, generally the percentage of the most intense fragment ions which were assigned to double bond cleavage was 17 ± 8 %. We propose that the 'simplicity' of assignments (i.e. single versus multiple bond cleavage) be used as a criterion for distinguishing between these rational explanations.

During the synthesis of Azaline A (Ac-DNal-DCpa-DPal-Ser-Lys(Atz)-DLys(Atz)-Leu-ILys-Pro-DAla-NH_2) (where Nal = 2-napthyl alanine, Cpa = 4-chlorophenylalanine and Pal = 3-pyridylalanine, Lys(Atz) = N^{ε}-(3'-amino-1H-1',2',4',-triazol-5'-yl) lysine, Ilys = N^{ε}isopropyl lysine) and that of an homologous series of novel gonadotropin releasing hormone antagonists an impurity (fraction B) could be isolated together with the parent compound (fraction A) and the LSI mass spectra indicated $[M+1]^+$ and $[M+15]^+$ species respectively. We noted that (a) fraction B when tested in an *in vitro* histamine release assay was significantly more potent than the parent compound, (b) the fraction B impurity had a greater propensity to fragment both in the LSI mass spectra and in the high energy CID spectra than fraction A (Figure 1); (c) different types of fragment ions were formed by the fraction B impurity compared to those of fraction A and (d) almost all of the intense fragment ions derived from the fraction B precursor included the addition of ca.14 Da. Based on these results we concluded that the modification was present on the three N-terminal residues Ac-DNal^1-DCpa^2-DPal^3- which were present in azaline A and common to all of the peptides having this impurity. In order to observe fragment ions attributable only to the three N-terminal residues, we selected the m/z 555 fragment ion (derived from fraction B, which was assigned as the 'a3+14' N-terminal fragment) and measured the CID product ion scan.

We constructed three sets of AMASS input structures with the methyl group located on Nal^1, Cpa^2 or Pal^3 and compared the output of one and two bond cleavages generated by AMASS for these structures with the observed fragment ions. We found that if the modification was located on the Nal^1 or Cpa^2 residues, some of the fragment masses could only be explained by three bonds being cleaved and the assignments generally included significantly more multiple bond cleavages (59 and 53 % respectively) than if the methyl group was located on Pal^3 (35 %). Using nuclear magnetic resonance we were able to further localize the methyl group on the aromatic nitrogen of the Pal^3 residue which would

explain observation (a). We propose that during solid phase peptide synthesis, methylene chloride reacts with the pyridinyl nitrogen to form an immonium ion salt (ref. 2). The formation of an immonium ion salt in corollary with quaternary ammonium ion salts (ref. 3) explained the remaining observations (b)-(d).

Acknowledgments

Work supported by the National Institute of Health (HD-13527, DK-26741, NO1-HD-1-3100, NO1-HD-0-2906, GM-22737) and conducted in part by the Clayton Foundation for Research (California Division) and the Hearst Foundation. We gratefully acknowledge Prof. L. Gierasch and Dr. J. Rizo for NMR measurements. The histamine release assays were carried out under the aegis of the Contraceptive Development Branch, Center for Population Research, NIH.

References

(1) Craig, A. G.; Koerber, S. C.; Porter, J.; Hoeger, C.; Rivier, J. E. *Biol. Mass Spectrom.* **1993**, *22*, 31-44.
(2) Mills, J. E.; Maryanoff, C. A.; McComsey, D. F.; Stanzione, R. C.; Scott, L. *J. Org Chem* **1987**, *52*, 1857-1859.
(3) Vath, J. E.; Biemann, K. *Int. J. Mass Spectrom. Ion Proc.* **1990**, *100*, 287-299.

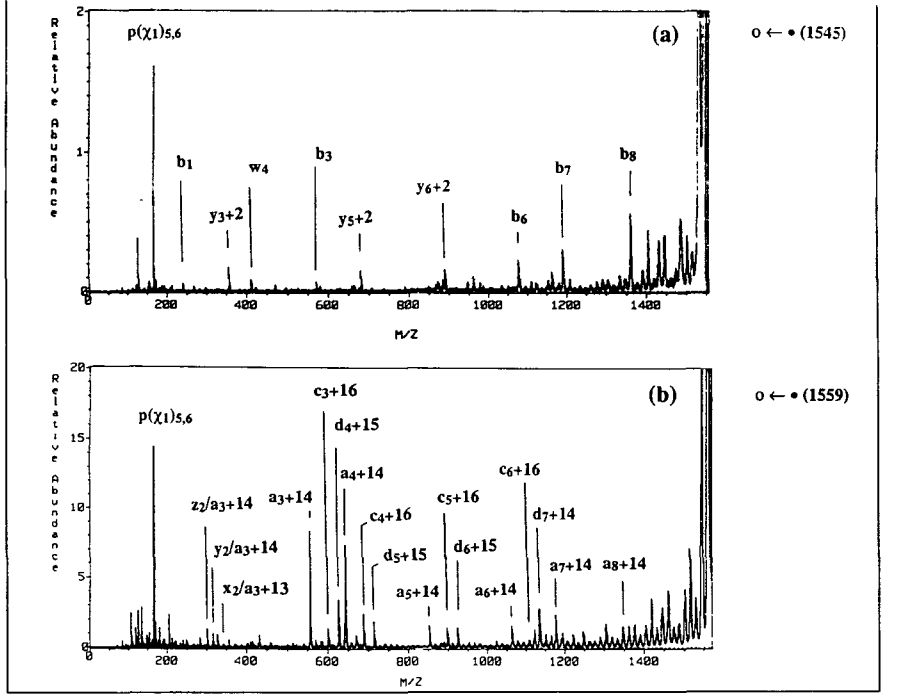

Interpretation of Peptide CID Spectra using Artificial Neural Networks

R. E. Scarberry, Z. Zhang, K. R. Thornburg, and D. R. Knapp
Medical University of South Carolina, Charleston, SC 29425

A recently reported method for computer interpretation of peptide CID spectra is based upon recognition of patterns of related sequence ions.[1] This algorithm classifies peaks by ion type via recognition (using scoring rules) of patterns of related ions. By mathematically converting all classified ions to the corresponding y ions, the spectrum is transformed into an idealized spectrum of only y type ions, which is then interpreted in a conventional manner. We have extended this approach by use of artificial neural networks to identify ion types.

A prototype algorithm has been developed which utilizes two backpropagation networks to, first, classify peaks as being or not being one of the common ion types (a, b, c, d, v, w, x, y, z+1) and, second, to classify the peaks according to ion type. The classified peaks are then used to generate a transformed spectrum of y ions only which is interpreted in a conventional manner. The members of the family of ion types for a given amide bond cleavage site are related mathematically by the following formulas:

$$a_n = MH - y_m - 27 \qquad x_m = y_m + 26$$
$$b_n = MH - y_m + 1 \qquad z_m + 1 = y_m - 16$$
$$c_n = MH - y_m + 18 \qquad v_{m+1} = y_m + 55$$
$$d_n = MH - y_m + 43 + R_a \qquad w_{m+1} = y_m + 53 + R_a .$$

For each peak in a spectrum, the masses of the corresponding other peaks in the family are calculated from the formulas. Nine families are calculated for the peak in question being due to each of the nine ion types. The peak intensities at these masses are used as the input vector for the neural networks. The complete interpretation algorithm is shown in the flow chart on the next page.

In the prototype algorithm, the networks were trained with a set of high energy CID spectra from the following peptides (containing approximately 650 classified peaks): AA, AAA, AAAAA, VLLS, MGMM, SGAGAG, I I I, LLVY, LGG, MAS, IVV, GLLG, MRF, YKT, GGGG, TKY, VLSEG, and FVQWLMNT. The resulting algorithm was tested with spectra from eleven additional peptides. The correct sequence was either the highest (1) or second highest (2) scoring sequence found for the following peptides: ETTTDK(2), TYSK (1), TSQVAPA(1), DDE(1), AKTE(2), and IFVQK(1). The correct sequence was not among the fifty highest scoring sequences found for the spectra of the following peptides: EDLIAYLK, ASTTVSKTE, LRRASLG, YIPGTK, MIFAGIK. The explanation for this dichotomy of results is not apparent, but the high percentage of correct results is encouraging. Work is underway to further explore this approach by training the networks with larger data sets including larger peptides. The method offers the potential for another approach to peptide CID spectra interpretation which could facilitate peptide sequencing by tandem mass spectrometry.

1. W. M. Hines et al. J. Am. Soc. Mass Spectrom. 3:326-336, 1992.

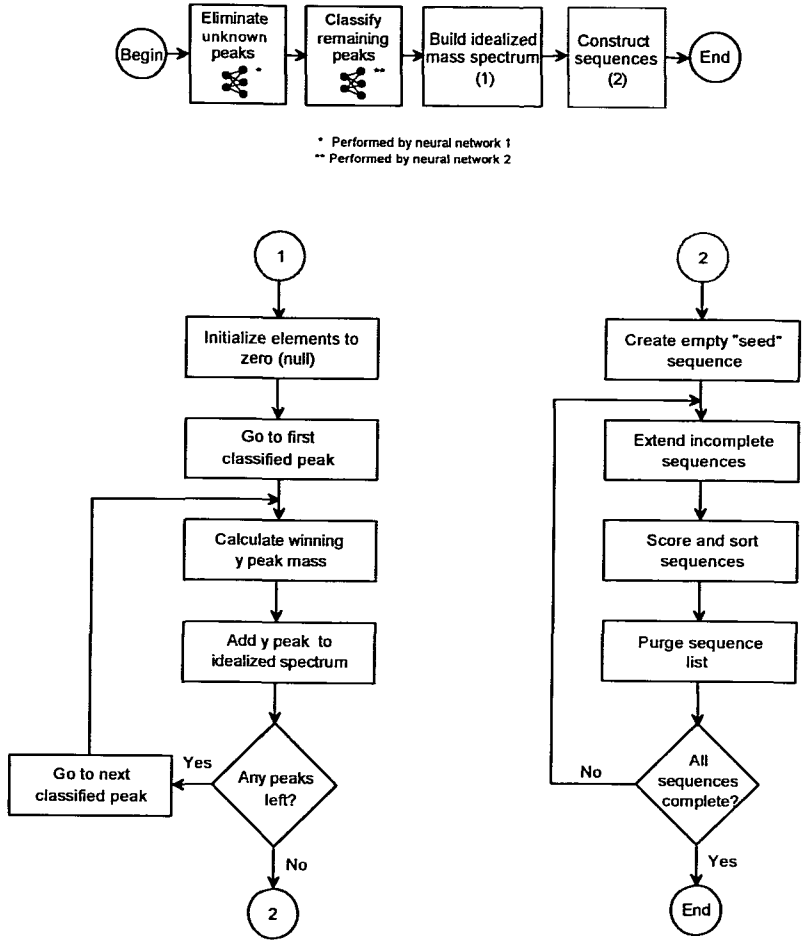

Rapid Identification of Proteins by Database Matching of Proteolytic Peptide Masses.

D. J. C. Pappin[1], A. J. Bleasby[2], C. W. Sutton[3] and J S Cottrell[3], [1]Imperial Cancer Research Fund, London WC2A 3PX, UK., [2]SERC Daresbury Laboratory, Warrington WA4 4AD, UK., [3]Finnigan MAT Ltd , Hemel Hempstead, HP2 4TG, UK.

Previous investigations have demonstrated the possibility of identifying proteins by (i) proteolysis, (ii) mass spectrometric analysis of the digest, and (iii) matching the set of measured molecular weights against a database generated by applying proteolytic cleavage rules to a collection of known protein sequences [e.g. W. Henzel *et. al.* 3rd Protein Soc. Symp. (1989), J. Yates *et. al.* 5th Protein Soc. Symp. (1991), M. Mann *et. al.* Proc. 40th ASMS, 957-8 (1992)].

We report here on the construction of the MOWSE (MOlecular Weight SEarch) database at SERC Daresbury. MOWSE has been extensively tested with data from plasma desorption, electrospray, and matrix assisted laser desorption (MALD). Experience has shown that proteins can be uniquely identified in a database of >48,000 sequences using only 4 or 5 molecular weight values. The greatest selectivity is provided by peptides in the range 700 to 3000 Da. Mass measurement accuracy is not critical, and even errors of several daltons cause little distortion in the results. The incidence of random matches can be reduced to negligible levels by correlating data from two digests using different enzymes. The MOWSE algorithms have also been implemented as a Microsoft Windows program, MassMap, which runs on a standard PC and uses the NCBI composite sequence database distributed on CD-ROM

Table 1 details results obtained from 37 experimental samples supplied by external laboratories. Searches were conducted either "blind" or "double-blind". Of the 37 samples, 33 were correctly assigned. This included the 27 samples listed, and a further 6 samples that were correctly grouped as unknown because they were later found to have no significant sequence homology with any of the database entries. Three samples were grouped as false negatives, and subsequent investigation revealed that, in two cases, the data sets were dominated by partial cleavage products. The one sample recorded as a false positive, (data not shown), was subsequently found to be a mixture.

MALD is an ideal ionisation technique for this application, since it provides low-picomole sensitivity, tolerance to contaminants such as the digest buffer, and requires no chromatographic separation of the digest products. This approach has enormous potential for rapidly identifying the thousands of proteins resulting from whole cell lysis following separation by SDS-PAGE, blotting, and *in situ* digestion. This further raises the prospect of using peptide mass fingerprint analysis to characterise cellular proteins in conjunction with large scale genomic DNA sequencing. Peptide mass databases could accumulate information faster than any linear sequence databases, and become a primary source of information in their own right. Potential DNA reading frames obtained from large scale DNA sequencing could be translated, digested and searched against such databases to discover whether the reading frame corresponds to a mapped protein.

Protein	Source	Size (K)	Method	Enzyme	Peptides used	Hits	Rank (ex 51,093)
Correct designations							
Chlorosome associated protein	Chlorobium spp.	7.5	PD	Trypsin	4	3	1
Diazepam binding inhibitor	Bovine	9.9	PD	Trypsin	5	4	1(Rat)
Fatty-acid binding protein	Bovine heart	14.6	PD	Trypsin	6	6	1
Fatty acid binding protein	Bovine intestine	14.9	PD	V8	7	3	1(Rat)
Cuticle structural protein 8	Locust	15.2	PD	Trypsin	5	4	1
Haemoglobin	Human	15.8	LD	V8	5	3	1
Myoglobin	Sperm whale	17.2	LD	Trypsin	8	5	1
Interleukin 3	Human	17.2	LD	Trypsin	11	6	1
Lactoglobulin beta chain	Bovine	18.3	LD	Trypsin	10	6	1
Metalloproteinase inhibitor	Human	23.1	LD	Trypsin	8	6	1
CAP37 antimicrobial protein	Porcine platelet	24.3	PD	Trypsin	3	3	1
Prolactin	Bovine	25.8	LD	Trypsin	8	6	1
Alternative splicing factor 1	Human	27.7	ES	Trypsin	11	6	1
Annexin V	Murine	35.8	LD	Trypsin	12	7	1(Human)
Actin	Rat cytoplasmic	40.0	ES	Trypsin	7	6	1(Mouse)
cAMP dependent protein kinase	Rat alpha subunit	40.4	ES	Trypsin	7	4	1
Alpha actin	Human skeletal	42.1	LD	Trypsin	15	8	1
P53 cellular tumour antigen	Human	43.6	LD	Trypsin	16	12	1
Beta tubulin	Cod	49.7	LD	Trypsin	20	6	1(Chicken)
Beta-2 tubulin	Cod	49.7	LD	Trypsin	15	5	1(Xenopus)
Alpha tubulin	Cod	50.0	LD	Trypsin	14	5	1(Chicken)
Serum albumin	Bovine	66.5	ES	Trypsin	15	11	1
Heat Shock Cognate Protein 70	Murine	70.8	ES	Trypsin	9	8	1(Hamster)
Annexin VI (P68 protein)	Murine	75.7	LD	Trypsin	13	12	1
Heat Shock Protein 84	Murine	83.2	ES	Trypsin	26	9	1
Initiation factor IF2-alpha	E.Coli	97.3	LD	Trypsin	15	9	1
Acetyl CoA carboxylase	Rat	265.4	ES	Lys C	9	7	1
False negatives							
Acyl CoA binding protein	Rat	9.9	PD	V8	4	2	18
Calcyclin	Murine	10.1	LD	Trypsin	8	2	26
Early light-induced protein	Barley	17.0	PD	Trypsin	4	1	16

Molecular Characterization of Surface Topology in Protein Tertiary Structures by Amino-Acylation and Mass Spectrometric Peptide Mapping.

M.O. Glocker, C. Borchers, W. Fiedler, and M. Przybylski
Faculty of Chemistry, University of Konstanz, W-7750 Konstanz, Germany

Understanding the role of structure-function relationships in proteins today is a topic of intense research. Aside from the intrinsic desire to understand the beauty of nature´s architecture, many exceptionally important applications have been proposed. Industrial, clinical, and agricultural developments may be achieved in the coming years by imitation of the interactions between macromolecules that occur naturally in the living cell. We need to know the threedimensional structure before we can begin to understand protein function at the molecular level. Enzyme catalysis, antibody-antigen interactions and receptor-ligand interactions are prime examples. The most commonly used methods for characterizing protein tertiary structures, X-ray crystallography and multidimensional NMR techniques, both have limitations determining chemical reactivities of specific amino acid residues in proteins.

We have developed a new method (1) for the molecular characterization of intact protein structures by combining specific chemical modifications of amino acid residues with peptide mapping of proteolytic mixtures using desorption-ionization mass spectrometry (PD-MS, ESI-MS). ^{252}Cf-plasma desorption (PDMS) has proved to be a powerful tool for these studies especially when *in situ* reactions were applied. The nondestructive nature of PDMS and the protein-binding capacity of the nitrocellulose matrix makes this method suitable for on-target reactions. Acylation reactions of proteins were carried out at pH 6.5 with up to 100,000-fold

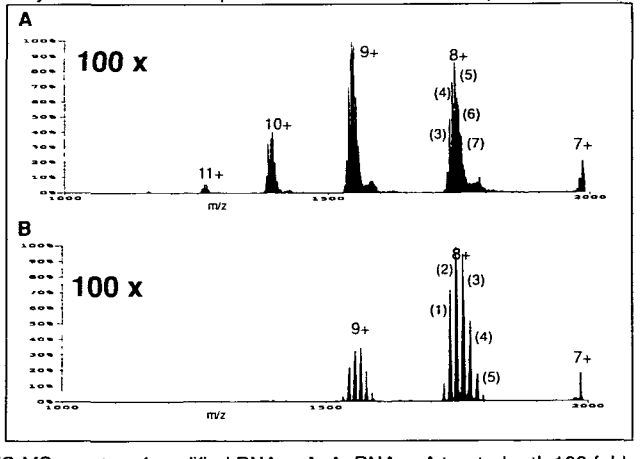

Fig. 1: ES-MS spectra of modified RNAse A. A: RNAse A treated with 100 fold excess acetic anhydride. B: RNAse A treated with 100 fold excess succinic anhydride. The numbers on top of each peak represent the charges. The number of modied residues is given in parantheses.

molar excess anhydride, and the extend of modification was determined by direct PD-MS and ES-MS analyses. A gradual molecular weight increase at increasing reagent concentration was found. Molecular weight determination by ES-MS yielded multiple protonated molecular ion envelopes with varying characteristics. For acetylated protein derivatives the ion envelopes were similar to those of native proteins, indicating a native-like structure for the modified proteins (2). The ES spectra for succinylated RNAse A differ from the acetylated protein spectra. Here, already at a low degree of modification the charge envelope shifts to less charged peaks. Lysines are charged positively at physiological pH (pK≈10.5) and conversion to the amide by acetylation results in charge neutralization, whereas succinylation introduces an additional carboxy function, thereby adding a negative charge to the protein. Peptide mapping analyses of reduced and alkylated protein derivatives were performed by trypsin digestion in solution or on target (3). Molecular ions of most of the relevant tryptic peptides were found. The monitored peptides were assigned and the site of modification in each of the modified derivatives was determined. These results enabled the determination of relative reactivities of the lysine residues in the corresponding protein. The mass spectrometric experiments described here present broad analytical potential in evaluating selectivity of chemical modification agents, the elucidation of reaction pathways, and the analysis of protein surface topology. This new approach may also effectively supplement dynamic methods of surface topology analysis, such as two dimensional NMR techniques and structure simulation approaches.

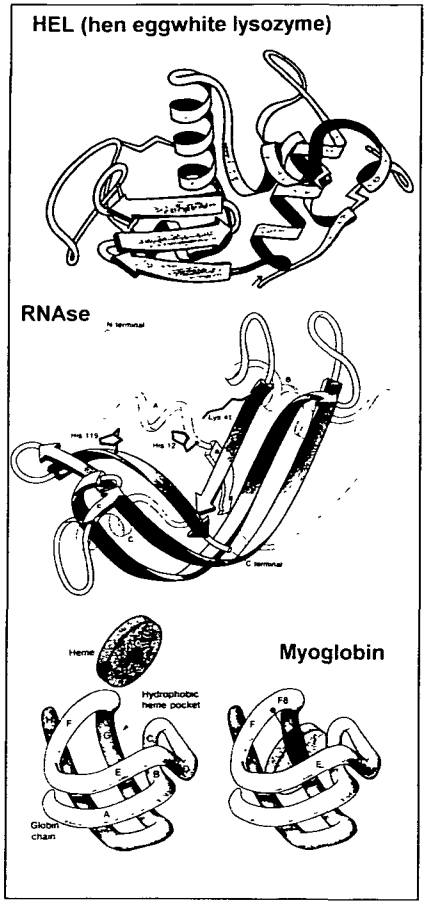

Fig.2: Schematic drawings of protein tertiary structures of the analyzed proteins.

1) D Suckau, M Mak & M Przybylski (1992) *Proc. Natl. Acad. Sci. USA* **89**, 5630-5634.
2) S.K Chowdhury, V Katta & B T. Chait (1990) *J. Am. Chem. Soc.* **112**, 9012-9013
3) B T Chait and F H Field (1986) *Biochem Biophys. Res. Commun.* **134**, 420-426

CHARACTERISATION OF THE WHO INTERNATIONAL REFERENCE STANDARD FOR THYROXINE BINDING GLOBULIN BY ESMS

M.B. Pepys and J.R. Gallimore, RPMS, Hammersmith Hospital, London W12 0NN, UK.
A. Bristow, NIBSC, Potters Bar, Herts, EN6 3QG, UK.
T. Hutton and S. Lowes, Fisons Instruments/VG BioTech, Altrincham, WA14 5RZ, UK.
C. Mamer, Fisons Instruments, Danvers, MA 01923, USA.

Thyroxine binding globulin (TBG, an α globulin) is the major circulating transport protein for thyroid hormones, binding 70% of total thyroxine (T4). A number of different TBG assays have been described with potential clinical usefulness in the characterisation of TBG abnormalities. However the widespread use of such assays has been hampered by the lack of an international standard for TBG.

The National Institute for Biological Standards and Control (NIBSC) was invited be the Expert Committee on Biological Standardisation of the World Health Organisation to establish an international reference material for TBG. We report here the characterisation of several preparations of TBG and the formal establishment by WHO of the International Standard for Thyroxine Binding Globulin 88/638.

TBG was isolated from pooled normal human serum provided by the National Blood Transfusion Service. The purification procedure involved four sequential chromatographic steps. The final product was characterised by sodium dodecyl sulphate 12.5% polyacrylamide gel electrophoresis[1], The extinction coefficient, at 280nm of the isolated pure TBG was determined using refractive index measurements to assess the absolute total protein concentration in the samples prior to mass spectrometry.

Electrospray mass spectrometry was performed on a Fisons Instruments/VG BioTech Platform single quadrupole mass spectrometer.

When 30µg of the purified TBG was run on reduced SDS-PAGE and stained with Coomassie blue, only a single band was seen. N-terminal sequencing revealed a unique sequence which was identical to that reported from the cDNA sequence of human TBG[2]. The concentration of the final bulk preparation of pure TBG determined by refractive index measurement was 3.85µg/µl.

Figure1 shows the raw data obtained from one sample of TBG. Several series of multiply charged ions are observed with between 36 and 49 positive charges. The Maximum Entropy processing algorithm was then applied to this data and produced the MaxEnt spectrum shown in Figure 2. This shows a series of peaks grouped in 3 sets. The major component at 52924.8 is observed together with probably one (+38) and then two (+76) potassium adducts. The second component at 53583.7 also has potassium adducts. The mass difference between the first group of peaks is 658Da and that between the second and third groups also 658Da.

The chromatographic procedure used here yielded TBG which was highly purified by all available

criteria.Characterisation of TBG by electrospray mass spectrometry, which has a precision of better than 0.01% for mass measurement of proteins of this size, showed that the only species present were grouped with masses compatible with those expected from the known protein sequence of TBG (44089.7) together with varying degrees of glycosylation.

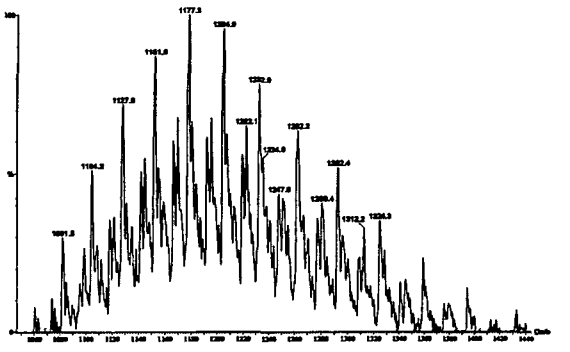

Figure 1. Raw m/z data obtained frim TBG (lot T13). Several ion series observed having between 36 and 49 positive charges.

We cannot exclude the possibility that some of the observed mass heterogeneity may have derived from minor in vitro deglycosylation of TBG, and there is evidence of loss of sialic acid (291Da) from some molecules. However, the mass difference of 658Da between the major sets of peaks corresponds very closely to the calculated mass of a typical chain of GlcNAcGalNeuAc (656Da) such as would form the third arm of a typical complex triantennary N-linked oligosaccharide. It therefore seems likely that there are populations of TBG molecules which are differentially glycosylated with biantennary and triantennary oligosaccharides. Confirmation of this suggestion will require spectrometric and chemical analysis of the structure of the TBG oligosaccharides after cleavage from the protein.

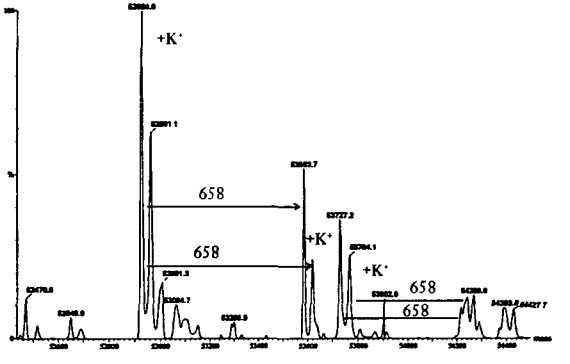

Figure 2. MaxEnt spectrum from human TBG lot 13 probably potassium adducts observed on major component. In addition mass increments of 658 are observed.

1 Laemmli, U.K., 1970. Nature 227, 680-685.
2. Flink et al 1986. Proc. Nat. Acad. Sci., USA 83 7708-7712.
3. Storring, P.L. and Gaines-Das, R.E., 1992. J Endocrinology 134 459-484.

PHOSPHORYLATION OF HUMAN AND BOVINE PROTHYMOSIN α In Vivo.

*L.K. Pannell[1], D.M. Sheeley[2], H.M. Fales[2], S.L. Berger[3], A.R. Sburlati[3], A. De La Rosa[3], D.W. Batey[3], G.L. Kurys[3], R.E. Manrow[3] and B.M. Martin[4]; [1]NIDDK, [2]NHLBI, [3]NCI and [4]NIMH, National Institutes of Health, Bethesda, MD 20892.

Introduction: Prothymosin α is a small (12kD), highly acidic polypeptide found in the nuclei of virtually all mammalian cells. The protein is quite abundant in cells and is required for cell growth. All proteins involved in regulating the cell cycle seem to undergo phosphorylation and dephosphorylation, a step which was thought to regulate the cell cycle. Therefore, it was interesting to see if prothymosin α also under went phosphorylation.

When Prothymosin α was incubated in the presence of [^{32}P]orthophosphoric acid, amongst the labelled material was a single labelled protein of 12kD, and this label was alkaline phosphatase sensitive, but was not destroyed under DNA and RNA hydrolysis conditions. Therefore, the phosphate was amino acid linked. Under partial acid hydrolysis, the label was found to be associated with a single amino acid, a serine. There are 4 serines on human prothymosin α (1,7,8,83) and only three on bovine prothymosin α; the question to be answered - To which serine is the label attached?

Isolation: Calf thymus was homogenized in buffer (50mM Tris-HCl at pH 7.5, 25mM KCl, 3mM $MgCl_2$ and 0.4mM phenylmethylsulfonyl fluoride), filtered through cheese cloth and centrifuged. After the addition of 0.1% sodium dodecylsulfate and 1% NP40, the supernatant was phenol extracted. Nucleic acids were digested with 50μg/ml of RNase A and 130U/ml of DNase, and enzymes were removed by additional phenol extractions. Final purification was performed by C18 reverse phase liquid chromotagraphy.

The [^{32}P]-labelled prothymosin α was digested with Lys C and examined by HPLC. The radioactivity was found to be located on a single peptide. An examination of this peak by FAB showed that the labelled peptide was the N-terminal 14 amino acid sequence and that this corresponded to a large peak for the unlabelled material eluting at a later retention time.

Only a small percentage of the protein was labelled and this was consistent with an electrospray examination of the labelled protein sample which did not reveal any modified protein content. However, a peak representing a loss of water from prothymosin α was present and we have observed this before in phosphorylated samples.

Further digestion of the 14-mer was performed with Asp-N. Cuts could occur at Asp2 and Asp6 but, it is doubtful the first cut would occur.

AcS↑DAAV↑DTSSEITTK

As expected a 5-mer and a 9-mer peptide were produced. By comparing the products of labelled and phosphorylated 14-mer, a first peak was found to be consistent

in both phosphorylated and unphosphorylated 14-mer, and did not contain any [^{32}P]-labelling. A second peptide, which eluted earlier, came out even sooner in the phosphorylated sample. When examined by FAB, the first peak represented the 9-mer and the second peak the 5-mer implying the phosphorylation site was on the terminal acetylserine. However, FAB parent ion of the labelled 5-mer was not detected.

To further clarify the location of the phosphorylation site, the electrospray ions representing the doubly charged 14-mer (m/z 734), and doubly charged phosphorylated 14-mer (m/z 774), were examined separately examined under MS/MS conditions using helium as a collision gas. Considerable sequence information from both ends of the chain were observed from the m/z 734 ion. With the phosphorylated m/z 774 ion, shifts in 80 amu (fragments were all of single charge) were observed in fragments containing the N-terminal acetyl serine, but not in any of those ions not containing Ser 1.

LOCALIZATION OF THE PHOSPHORYLATED SERINE RESIDUE BY MASS SPECTROMETRY

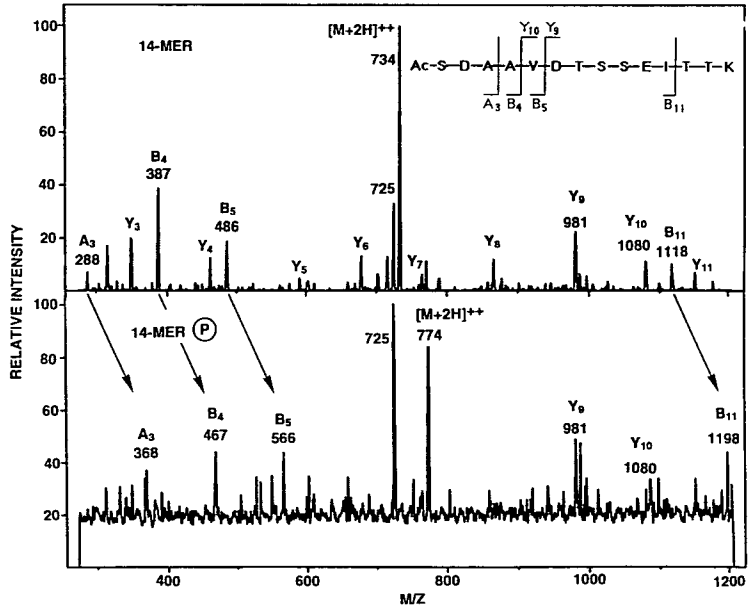

Conclusion: Only the N-terminal acetylserine is post-translationally phosphorylated in Prothymosin α.

Characterization of the phosphorylated ribosomal protein S7 from *Tetrahymena*.

*Lisbeth Palm, Jens Andersen, Henrik Rahbek-Nielsen, Karsten Kristiansen and Peter Hojrup, Department of Molecular Biology, Odense University, DK - 5230 Odense M, Denmark.

The basic ribosomal protein S7 is the only r-protein from *Tetrahymena thermophila* which can be phosphorylated *in vivo*. *Tetrahymena* can be multiply phosphorylated upon starvation by a sodium associated kinase. Previously, it was presumed that *Tetrahymena* S7 was homologous with the most prominent phosphoprotein in the ribosomes of higher eucaryotes, S6, where phosphorylation is presumed to essential for enhanced protein synthesis. Surprisingly, sequence determination of *Tetrahymena* S7 showed that it is homologous to r-protein S4 in higher eukaryotes.

The primary structure of *Tetrahymena* ribosomal protein S7 was determined by a combination of two different approaches. First S7 was separated by two-dimensional polyacrylamide gel electrophoresis (2-D PAGE), digested enzymatically *in situ* in the gel. The generated peptides were eluted by diffusion and separated by narrowbore rp-HPLC. Second S7 was purified by three successive rounds of rp-HPLC using three different column supports and elution-buffers. The purification was monitored by 2-D PAGE after the first step, while the following steps were monitored by electrospray mass spectrometry (ESMS). The electrospray mass spectrum of the purified S7 revealed the mass to be 29,458 ± 6 Da (Fig. 1).

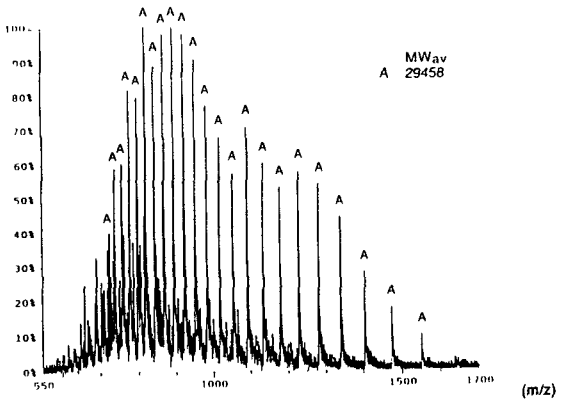

Fig. 1: Electrospray mass spectrum of the column purified *Tetrahymena* ribosomal protein S7.

The *in situ* generated peptides were separated by rp-HPLC and for each peptide the mass was determined by plasma desorption mass spectrometry (PDMS) and the amino acid sequence was determined using automatic pulsed liquid Edman degradation.

The sequence information from the gel purified peptides allowed deduction of 80 % of the *Tetrahymena* S7 sequence. Determination of the remaining sequence was accomplished by sequence determination of the column purified and enzymatically digested protein. A search against the PIR database clearly showed that *Tetrahymena* r-protein S7 is homologous with mammalian r-protein S4 and not to r-protein S6.

In order to determine the phosphorylated sites, starved *Tetrahymena* cell were incorporated with [^{32}P]phosphate and the extracted ribosomal proteins were purified by column chromatography. The molecular mass of the di-phosphorylated S7 was determined by laser desorption mass spectrometry (LDMS) to 29,627 Da, based on the single and double charged molecular ions. This is a derivation of only 0.02% from the calculated mass (29,620 Da) (Fig.2). The laser spectrum is calibrated using a contaminating protein with a known molecular mass of 14467 Da (determined by ESMS).

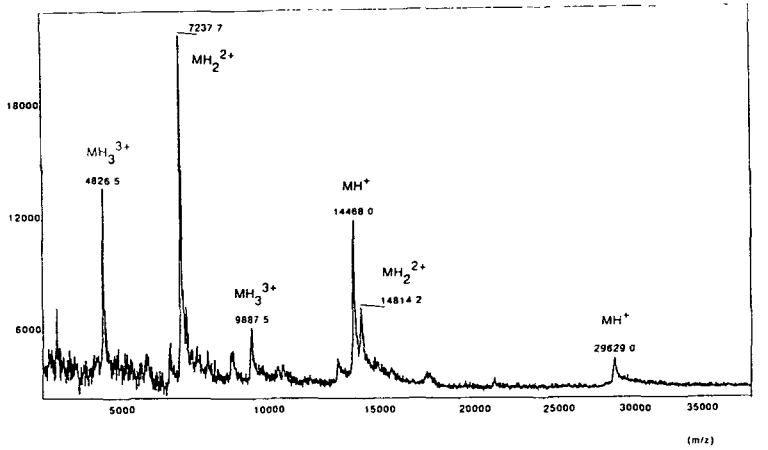

Fig. 2: Laser desorption mass spectrum of the di-phosphorylated *Tetrahymena* ribosomal protein S7.

Phosphorylated peptides were generated by *Staphylococcus aureus* V8 protease digestion and the phosphorylated peptides were monitored using Cerenkov counting. The peptides were analyzed by LDMS and the sequences were determined using Edman degradation. The two phosphorylated residues were located close to the C-terminus.

MASS SPECTROMETRY OF PHOSPHOPEPTIDES ISOLATED BY IMMOBILIZED METAL-ION AFFINITY CHROMATOGRAPHY

Lydia M. Nuwaysir and John T. Stults, Genentech, Inc., South San Francisco, CA

INTRODUCTION

In this study, the feasibility and general applicability of on-line immobilized metal-ion affinity chromatography (IMAC) coupled with electrospray-ionization mass spectrometry (ESI-MS) is investigated for the separation and identification of phosphorylated and non-phosphorylated peptides. The sensitivity and practicality of the technique is demonstrated via the analysis of several synthetic phosphopeptides as well as the phosphoprotein, bovine ß-casein, purified by SDS-PAGE, electroblotted onto a PVDF membrane, and digested in situ with trypsin.

EXPERIMENTAL

SDS-PAGE and electroblotting were performed as described by Wong et. al. [1]. Membranes were digested in 50 μL 0.1 M *N*-ethylmorpholine, 10% acetonitrile, and 0.2 μg of Promega modified trypsin, and incubated for 24 hours at 37°C with the addition of a second aliquot of trypsin after 12 h.

Experiments were performed using a SCIEX (Thornhill, Ontario) API III triple quadrupole mass spectrometer equipped with a pneumatically-assisted electrospray-ionization source (Ionspray). Each scan was acquired over a range of *m/z* 400-2200 using a step of 0.5 u, a dwell time of 1.5 ms, a mass defect of 50 μu , and an 80-V orifice potential.

IMAC was accomplished as follows: A 1.0 mm i.d. x 10 cm long Teflon tube was filled with a 20% ethanol slurry of chelating Sepharose Fast Flow (Pharmacia, Piscataway, NJ). The column was activated by pumping 200 μL of 30 mM $FeCl_3$ solution through the column and excess metal was washed with 2 mL of H_2O. Prior to initial use, two blank runs of all buffers were flowed through the column. Samples were either loaded directly onto the column in acidified (pH 3.5 with acetic acid) digest buffer or in 0.1 M acetic acid. The following buffers were used as eluents to develop the column:

Buffer A: 0.1 M acetic acid
Buffer B: Milli-Q distilled water
Buffer C: 0.1% (w/v) ammonium acetate adjusted to pH 8.0 with 10% NH_4OH
Buffer D: 0.1% (w/v) ammonium acetate adjusted to pH 9.5 with 10% NH_4OH
Buffer E: 2% acetonitrile, 0.1% (w/v) ammonium acetate adjusted to pH 10.5 with 10% NH_4OH.

RESULTS

Figure 1a displays the mass spectrum obtained from a mixture of 10 pmol each of synthetic phosphotyrosine peptides I, II, and III as they eluted together from the IMAC column. The phosphopeptides elute within 15μl of buffer as observed in the TIC (inset).

The application of the IMAC isolation method to a more complex mixture of peptides was studied by analyzing 30 pmol of ß-casein purified by SDS-PAGE, electroblotted onto a PVDF membrane, and digested *in situ* [1]. The peptides that were released from the PVDF membrane upon hydrolysis were loaded onto an IMAC column, washed, and eluted as described earlier. Both the T1-2(4P) and T6(1P) peptides are observed (Figure 1b, and inset: TIC).

CONCLUSION

On-line IMAC separation of the phosphopeptides was found to be crucial in the analysis of low levels of the phosphopeptides. The ability to inject the tryptic digest of an electroblotted protein directly onto the column without buffer exchange and to analyze the eluent directly via on-line IMAC/ESI-MS greatly reduces sample losses incurred through sample handling and provides a convenient method for analyzing phosphopeptides at low levels. With proper optimization of column and solvent conditions, flow rate, and mass spectral scan conditions, better detection limits can be achieved.

REFERENCES

1. Wong, S. C.; Grimley; C.; Padua, A.; Bourell, J. H.; Henzel, W. J. In *Techniques in Protein Chemistry IV*; Angeletti, R. H., Ed.; Academic Press, Inc., San Diego, 1993, pp. 371-378.

Phosphorylated peptides:

I	703.65	GV<u>Y</u>AASG (phosphotyrosine)
II	1126.18	DRV<u>Y</u>IHPF (phosphotyrosine)
III	1586.71	TFLPVPE<u>Y</u>INQSV (phosphotyrosine)
T1-2(4P)	3122.95	RELEELNVPGEIVE<u>S</u>L<u>SSS</u>EESITR (ß-casein 1-25)
T6(1P)	2061.98	FQ<u>S</u>EEQQQTEDELQDK (ß-casein 33-48)

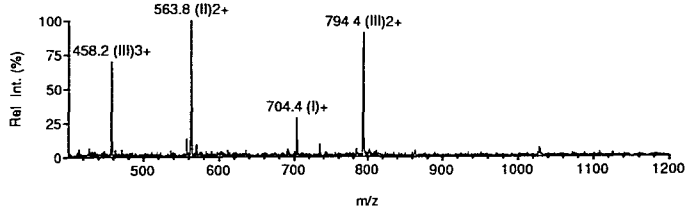

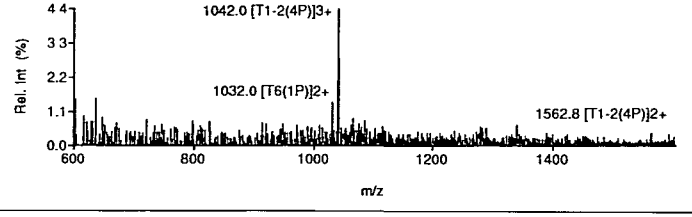

An Approach to Characterize Phosphorylation Sites in Phosphopeptides and Phosphoproteins by Combining Enzymatic and Chemical Reactions with MALDI-TOF Mass Spectrometry

*Pao-Chi Liao[1], Joe Leykam[2], Douglas A. Gage[2] and John Allison[1], Department of Chemistry[1] and Biochemistry[2], Michigan State University, East Lansing, MI 48824;

Karen Wang[3], Philip C. Andrews[4] and John Strahler[3], School of Medicine, Department of Pediatrics[3] and Biochemistry[4], University of Michigan, Ann Arbor, MI 48109

The goal: To develop a fast, picomole-scale methodology to localize the phosphorylation sites in phosphopeptides and phosphoproteins.

Advantages of MALDI-based methods: speed, high sensitivity and mixture analysis capability.

Current methods for locating phosphorylation sites: To locate phosphorylation sites in a phosphoprotein, the most common strategy consists of digesting the phosphoprotein into small peptides, followed by analyzing the products. Unfortunately, phosphoserine, the most abundant, naturally-occurring phosphorylated amino acid residue, breaks down to free phosphate in Edman degradation cycles[1]. To overcome this problem, chemically converting phosphoserine into S-ethylcysteine has been proposed, and is becoming an attractive method to biochemists[2]. Another attractive method under development is combining FAB and MS/MS techniques to induce fragmentation of an ionized phosphopeptide to yield sequence information directly [3].

Identify a phosphopeptide: A reagent is required which removes the phosphate moiety from a phosphopeptide, so a phosphopeptide can be identified from the -80 dalton mass shift ($OPO_3H \rightarrow OH$) in MALDI spectra. Enzymatic dephosphorylation by alkaline phosphatase can serve such a function.

Locate phosphorylation sites in a phosphoprotein: Due to the lack of MS/MS capabilitiy when MALDI is used, phosphoproteins must be cleaved into small peptides and phosphopeptides by enzymatic or chemical reactions prior to MS analysis. The digest mixture of peptides and phosphopeptides from a phosphoprotein can be fractionated by RP-HPLC and then subjected to MALDI analysis. When the protein sequence is known, locating phosphorylation sites is achieved by "mass-mapping".

Results: Three synthetic model phosphopeptides, which are phosphorylated at serine, threonine and tyrosine respectively, were studied. The table below shows their detectabilities in MALDI.

peptides	phosphorylated	dephosphorylated
KRP(p)SQRHGSKY-amide	10 fmol	less than 1 fmol
KR(p-)TLRR	10 fmol	less than 1 fmol
LKRA(p-)YLG-amide	100 fmol	less than 1 fmol

Fig. 1 shows the MALDI spectra of the tryptic digestion of a phosphopeptide to locate the phosphorylation site among possible sites. Time-coursed monitoring of the dephosphorylation reaction of a phosphopeptide and locating phosphorylation sites of ß-casein were also discussed. This work has demonstrated that MALDI-TOF mass spectrometry is a fast, easy and sensitive tool for locating phosphorylation site(s) in a phosphoprotein. The phosphorylation sites of Op18, an phosphoprotein expressed in transformed lymphocytes, had been investigated by this method [4].

Limitations and Future work: A major limitation of MALDI-TOF mass spectrometry is that the signal intensities vary considerably between peptides in a mixture. Some peptides do not give a signal. This hampers the proposed method in certain cases. Suppression effects have been observed in a tryptic digest mixture, which makes interpretation of MALDI spectra difficult. Currently, sample consumption of this method is limited by sample handling in the digestion and separation steps. The incorporation of *in situ* digestion on the MALDI probe and microseparation into the proposed method is under investigation.

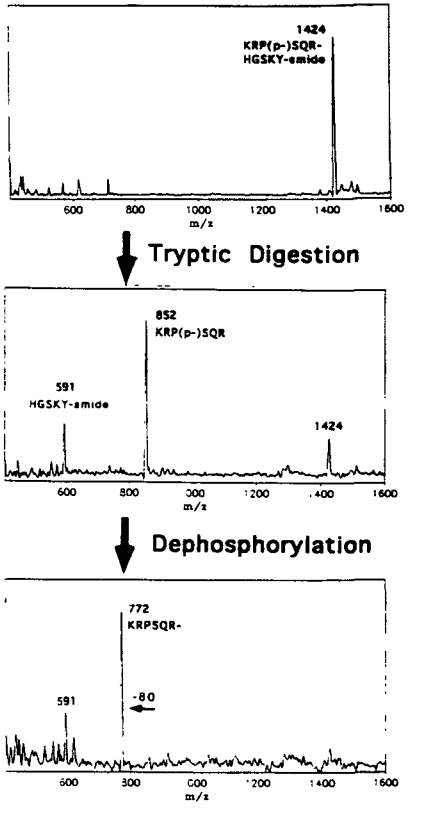

Fig. 1 MALDI spectra of the tryptic digestion of a phosphopeptide to locate the phosphorylation site among possible sites.

References:

1. Campbell, D. G.; Hardie, D. G.;Vulliet, P. R. *J. Biol. Chem.* **261**, 10489 (1986)
2. May, L. T; Sehgal, P. B. *Biochem. Biophys. Res. Commun.* **185**, 524 (1992)
3. Hanspeter, M; Griffin, P. R.; Shabanowitz, J.; Hunt, D. F.; Bennet, J. *J. Biol. Chem.* **266**, 17584 (1991)
4. Wang, K; Liao, P. C.; Allison, J; Gage, D.; Andrews, P. C.; Lubman, D.; Hanash, S. M.; Strahler, J. R. *J. Biol. Chem.* in press.

Analysis of Amylin and Related Peptides from Biological Fluids Using LC/MS and MS/MS

M.A. Moseley, K.A. Halm, S.E. Unger, Glaxo Inc. Research Institute, 5 Moore Drive, Research Triangle Park, NC 27709

Amyloid deposition in the islets of Langerhans is a major pathological feature of non-insulin dependent (type II) diabetes mellitus (NIDDM). The major protein component of the amyloid is a 37 amino acid, carboxyamide peptide designated islet amyloid polypeptide (IAPP), or diabetes-associated peptide, or amylin (1). Amylin shows high sequence homology with human calcitonin gene-related peptide (CGRP) and has been shown to inhibit glycogen synthesis in rat muscle (2). Amylin and related peptides serve to modulate the effects of insulin and, therefore, may be clinically useful. The sequence of rat and human amylin and their average molecular weights are given below:

Rat Amylin	KCNTATCATQRLANFLVRSSNNLGPVLPPTNVGSNTY	3920.4
Human Amylin	KCNTATCATQRLANFLVHSSNNFGAILSSTNVGSNTY	3903.4

Analytical methodologies capable of measuring amylin or related peptides in biological media or determining their metabolic fate are necessary to better understand their effects. Endogenous plasma levels of amylin are low (0.2-5 pM) in most individuals. However, amylin levels are high (150-400 pM) in certain organs such as the pancreas. To measure these low levels, highly sensitive immunoassays have been used (3).

Electrospray (ESI) LC/MS is capable of detecting low nM levels of amylin or related peptides from serum or plasma (Fig. 1). The $(M+3H)^{3+}$ parent of amylin was monitored and referenced to the $(M+2H)^{2+}$ parent of porcine adrenocorticotropic hormone (ACTH) fragment 18-39 as internal standard. Both the 3+ and 4+ charge states were observed with good intensity. The 2+ and 5+ charge states were also observed, but were less than 10% relative intensity. A standard curve for rat amylin extracted from 0.1 mL of rat plasma is shown in Fig. 2.

Due to their facile adsorption and degradation, protein precipitation with 0.2 mL of an ACN/ 0.1% dimethyloctylamine (DMOA) solution was used. The use of DMOA was found to improve the recovery of amylin and related peptides. At sufficiently high (0.1%) concentrations, DMOA associates with the peptide and minimizes its adsorption to glass or polypropylene surfaces. The association was observed by co-elution of DMOA with analyte and inferred by the improved recovery of peptide. This effect may be due to denaturing the peptide as similar results were observed using sodium dodecylsulfate (SDS) for related peptides. The supernatant was dried under nitrogen and reconstituted in 25 uL of mobile phase before injecting 5 uL onto the LC/MS. A gradient of 20% ACN to 50% ACN over 5 minutes with a 10 minute hold at 50% was used. The mobile phase included 0.1% TFA and 5% i-propanol. A 1 x 50 mm Vydac C4 Protein/Peptide column held at 60°C was used.

This procedure minimized sample losses due to handling and provided analyte of sufficient purity for ESI LC/MS analysis. While these concentrations are significantly higher than endogenous levels, they may be useful for toxicology studies. At nM levels, the highly specific LC/MS method could also be used to validate results from a less specific immunoassay.

Little is known regarding the metabolic fate of amylin, and analytical methods which are capable of identifying amylins or their proteolytic fragments *in vitro* or *in vivo* are essential to better understand its mode of action. Abundant fragmentation is observed in the MS/MS spectra of either the 3+ or 4+ charge states of rat amylin. Over seventy fragments were observed with the majority of assignments (b and a series) arising from charge retention on the more basic N-terminus.

Fig. 3 illustrates the reconstructed chromatograms of amylin exposed to immobilized trypsin. Six tryptic peptides were observed; however, the (1-1), (2-18), and (2-37) fragments were not. The fragments are given below with their average molecular weights and observed charge state:

1-1	K	146.2	*
2-37	CNTATCATQRLANFLVRSSNNLGPVLPPTNVGSNTY	3792.2	*
1-11	KCNTATCATQR	1194.4	1+, 2+
12-37	LANFLVRSSNNLGPVLPPTNVGSNTY	2744.1	2+, 3+
2-11	CNTATCATQR	1066.2	1+
1-18	KCNTATCATQRLANFLVR	2008.4	2+, 3+
19-37	SSNNLGPVLPPTNVGSNTY	1930.1	1+, 2+
2-18	CNTATCATQRLANFLVR	1880.2	*
12-18	LANFLVR	832.0	1+

*not observed.

Proteolytic digests of amylin and related peptides have been useful in determining their presence in serum. Similar (nM) detection sensitivites were noted for the tryptic fragments to amylin.

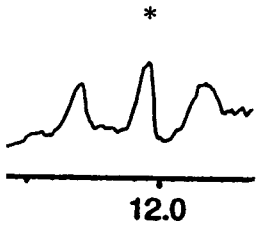

Fig. 1) 8 nM amylin in plasma

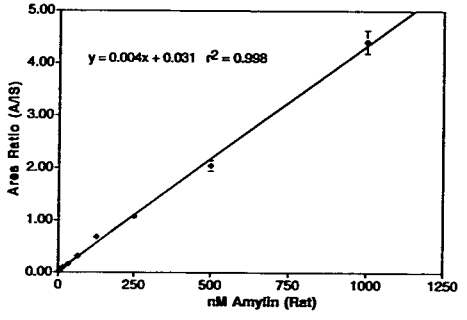

Fig. 2) Standard curve for amylin from plasma

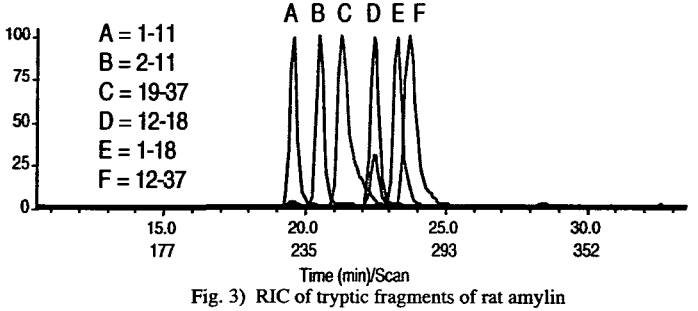

Fig. 3) RIC of tryptic fragments of rat amylin

1. Bretherton-Watt, D., Bloom S.R. (1991) *Trends Endocrinol. Metab. 2*:203-6.
2. Leighton, B., Cooper, G.J.S. (1990) *Trends Biochem. Sci. 15*:295-9.
3. Nakazato, M., Asai, J., Kangawa, K., Matsukura, S., Matsuo, H. (1989) *Biochem. Biophys. Res. Commun. 164*:394-9.

Characterization of β-Amyloid: A Major Component of Cerebrovascular Amyloid Deposits.

Amina S. Woods and Robert J. Cotter
Johns Hopkins School of Medicine
Baltimore , MD 21205

A.E. Roher
Wayne State University School of Medicine
Detroit, MI 48201.

Alzheimer's disease is a neurodegenerative disorder characterized by global cognitive decline. The lesions are formed by insoluble proteinaceous fibers in the brain: extracellular deposits of amyloid in senile plaques and cerebral blood vessels, and in intracellular neurofibrillary tangles in the cytoplasm of neurons.

The β-Amyloid protein (βA) is composed of 39-42 amino acid residues. It is derived from a larger transmembrane protein precursor (695-700 residues. The putative abnormal processing events leading to amyloid accumulation are unknown. However a small proportion of cases occur in families displaying autosomal dominant inheritance of the disorder.

To find post-translational modifications, parenchymal and cerebrovascular βA solubilized in formic acid were digested with trypsin and the generated fragments separated by reverse phase (RP) HPLC using a C_{18} column. The fractions were analyzed by plasma desorption mass spectrometry (PDMS). The carboxy terminal fragment was not detected in the cerebrovascular βA, so βA was purified using superose-12 size exclusion chromatography in formic acid and digested with pepsin or trypsin. The pellet left after the tissue extraction was resuspended in 80% formic acid and cleaved with CNBr. the various digests were separated by RP HPLC and the fractions analyzed by PDMS. Fraction 5 of the trypsin digest shows MH^+=1086.1 amu, MNa^+ =1106.4 amu and MK^+=1125.3 amu ($GAIIGLMVGGVV_{29-40}$). None of the other fractions showed peptide fragments containing residues 41 and 42. The pepsin digest however showed fragments containing residues 35-40 (MVGGVV), MH^+=561.1 amu and MNa^+ =584.0 amu (fr P_1, Fig. 1a), as well as fragments containing residues 36-42 (VGGVVIA), MH^+=613.3 amu and MNa^+ =636.1 amu (fr P_2, Fig. 1b) and residues 35-42 (MVGGVVIA), MH^+=746.1 amu and MNa^+ =768.1 amu (fr P_2, Fig. 1c). The CNBr digest gave fragments 36-40 (VGGVV), MH^+=431.0 amu and MNa^+ =452.9 amu and 36-42 (VGGVVIA), MH^+=614.2 amu and MNa^+ =637.2 amu.

In conclusion cerebrovascular βA carboxy terminal fragment is made of 42 amino acid residues. however the fragments containing the last two residues are less soluble and therefore less likely to be seen. Roher *et al.*, have shown that the modification occurs endogenously (1). Mass spectrometry was a very effective tool in the study of βA because most fractions contained a mixture of peptides which could not always be easily detected by Edman degradation.

(1) A.E. Roher, J.D. Lowenson, S. Clarke, A.S. Woods, R.J. Cotter, E. Gowing G. H. Murdoch and M. J. Ball., *Proc. Nat'l. Acad. Sci. USA* (submitted).

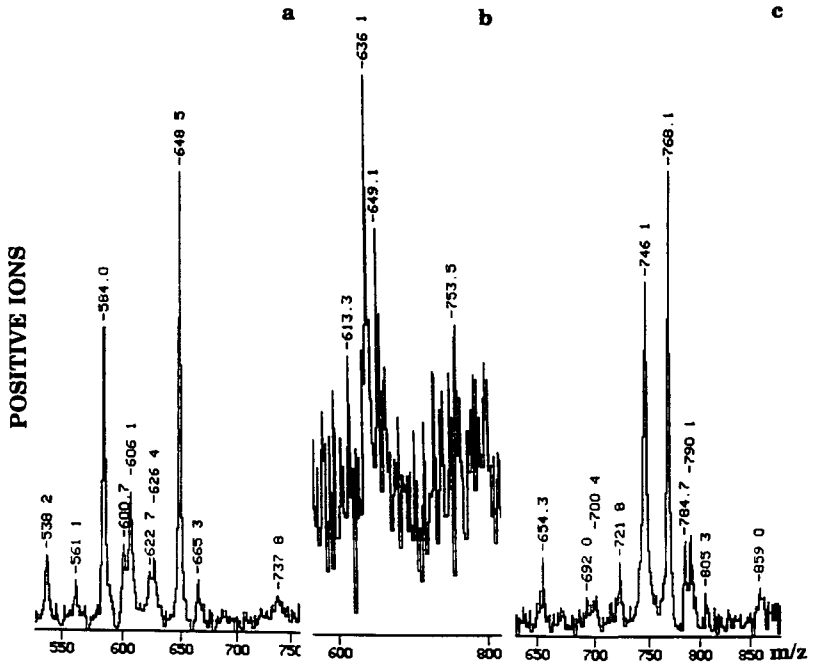

FiG. 1 Peptic Digest Of Cerebrovascular β-Amyloid Protein
a. Fraction P_1: MH^+=561.1 amu, MNa^+=584.0 amu (MVGGVV)
b. Fraction P_2: MH^+=613.3 amu, MNa^+=636.1 amu (VGGVVIA)
c. Fraction P_3: MH^+=746.1 amu, MNa^+=768.1 amu (MVGGVVIA)

ESMS OF HUMAN SERUM AMYLOID P COMPONENT: CONFIRMATION OF THE STRUCTURE AND ANALYSIS OF THE ROLE OF THE GLYCAN.

M.B. Pepys, G. Noble and J.R. Gallimore, RPMS, Hammersmith Hospital, London, W12 0NN, UK.
S. Amatayakul-Chantler, T.W. Rademacher and R.A. Dwek, Glycobiology Institute, Oxford University, Oxford, OX1 3QU, UK.
T. Hutton and S. Lowes, Fisons Instruments/VG BioTech, Altrincham, WA14 5RZ, UK.

The pentraxins are a family of plasma proteins conserved among all vertebrates. In man the two members are C-reactive protein (CRP) and serum amyloid P component (SAP).

SAP is not an acute phase protein but although it is present at rather stable levels its synthesis is highly regulated. Each molecule consists of 10 glycosylated polypeptide subunits arranged in two pentameric discs interacting face to face. Each subunit bears a single typical complex N-linked bi-antennary oligosaccharide chain, which is uniquely homogenous and invariant. SAP is the precursor of amyloid P component (AP) which is deposited together with amyloid fibrils in all forms of amyloidosis.

The structure of the N-linked glycan at Asn 32 has lately been elucidated following hydrazinolysis, and electrospray mass spectrometry has confirmed the mass of the SAP subunit, 25462Da, corresponding exactly to that of the known amino acid sequence plus the oligosaccharide. This investigation was carried out to establish whether any modifications to SAP are associated with the development of amyloidosis and to confirm the desialylation and degalactosylation procedures used in this study.

SAP and AP were isolated and purified by affinity and gel filtration chromatography. SAP was isolated from pooled normal human serum and malignant effusion fluid. AP was extracted from tissues of individual patients with amyloidosis.However, SAP was desialylated and this asialo SAP was the degalactosylated.

Samples were dialysed extensively against distilled water and lyophilised before reconstitution in aqueous acetonitrile with 0.5% formic acid to a concentration of approximately 20pmol/µl. 10µl. The samples were introduced into the electrospray ionisation source of a Fisons Instruments/VG BioTech Platform single quadrupole mass spectrometer.

Studies of the clearance of ^{125}I labelled normal and asialo-SAP were undertaken in 3 normal healthy volunteer controls (all male, ages 32, 33.4 and 36 years) with more frequent early time points for the asialo protein samples. An imaging study after injection of ^{123}I-asialo-SAP was also conducted on the IGE Starcam gamma camera.

The spectrum shown in Figure 1 is that obtained from SAP isolated from pooled normal human serum. The raw data has been subjected to the Maximum Entropy algorithm to produce this spectrum. The major component of SAP has a measured Mr of 25462.5 within 0.1Da of the calculated Mr 25462.4 for the disialated form of the glycoprotein. Serum amyloid P component isolated from a particular

preparation of malignant effusion fluid SAP differed from other preparations in having only 45% of its oligosaccharide moieties disialated, and 40% monosialated and 15% asialated. These differences were precisely confirmed by high voltage electrophoresis of the oligosaccharides released by hydrazinolysis.

The molecular mass of the major component of the AP isolated from amyloid deposits in tissues from two different patients was also consistent with the disialated form of the glycoprotein.

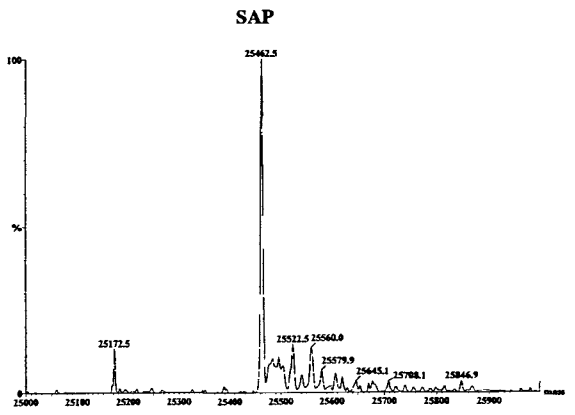

Figure 1

The spectrum obtained in from the neuraminidase preparation confirms that the major component has a Mr of 24882.3Da consistent with the loss of 2 sialic acid (N-acetyl neuraminic acid) groups. Following intravenous injection of ^{125}I labelled asialo SAP there was very rapid clearance from the plasma with 90% of the activity removed by 30 minutes.Whole body scintigraphy after injection of ^{123}I-asialo SAP demonstrated extremely rapid and selective uptake of tracer in the liver which was 'hotter' than the heart blood pool after only 80 seconds. By 40 minutes tracer released from catabolised SAP appeared in the kidneys. Thereafter, radioactivity rapidly appeared in the urine and accounted for 80% of the injected dose by 24 hours and virtually 100% by 3 days. These results contrast sharply with those obtained previously from the same individuals following ^{125}I labelled normal control SAP.

Confirmation of removal of 2 galactose residues from asialic SAP was also demonstrated with the major component molecular mass of 24553.7 consistent with removal of 2 sialic acids and 2 galactose residues from normal control SAP.The clearance rate of this degalactosylated SAP in mice was intermediate between that of asialo and normal SAP.

The results confirm that there is no heterogeneity or polymorphism in either the protein or the glycan moeties of SAP in health and disease, and that AP is unaltered with respect to SAP. Loss of, or deliberate removal of, the terminal sialic acid residues of the SAP oligosaccharide caused SAP to be extremely rapidly cleared from the circulation in vivo, both in experimental animals and in man. Desialated SAP was taken up in the liver by the terminal galactose receptor and catabolised, revealing directly for the first time in man, the carbohydrate-dependent clearance and metabolism of a plasma protein.

Identification of Water Insoluble Human Lens Crystallins by Mass Spectrometry

Laura R. Miesbauer, Jean B. Smith, Zhucheng Yang, Xuanjing Zhou, Yiping Sun†
and David L. Smith
Department of Medicinal Chemistry and Pharmacognosy, Purdue University,
West Lafayette, IN 47907 and
†Procter & Gamble Co., Miami Valley Laboratories, P.O. Box 398707, Cincinnati, OH 45239

In the process of aging or as a factor in disease, the structural proteins in the lens of the eye (the crystallins) become insoluble. Increasing amounts of insoluble crystallins decrease the transparency of the lens by altering the refractive index and scattering light, resulting in cataract. Little is known about the structural changes that occur in the crystallins and the mechanisms that cause them to become insoluble. The goal of our research is to identify the crystallins that are present in the water insoluble portion of the lens and to characterize the post-translational modifications that make these crystallins differ from the water soluble crystallins.

Using ESIMS of intact proteins and FABMS analysis of peptides from tryptic digests, we have identified the major crystallin components in the water insoluble-guanidine soluble portion of human lenses. The amino acid sequences for the primary gene products of α-crystallin, αA and αB, are known, and α-crystallins are thought to be the major constituent in the water insoluble lens. The primary sequences of the human β-crystallins (except βA3, βB2, and part of βB3), are not known, and the γ-crystallin sequences (which include βs, γA, γB, γC, and γD) have not all been confirmed. FABMS analysis of water soluble β- and γ-crystallins allowed a general classification of the water insoluble components that could not be assigned to known crystallin sequences.

Normal human lenses, aged 20-27, were obtained from the National Disease Research Interchange (NDRI) and stored at -70 °C until use. Homogenization of a lens in Tris buffer (pH 7.4, 4 °C) extracted the water soluble portion which could be separated into α- , β- and γ-crystallins by Sephadex G-200 gel filtration The water insoluble pellet was extracted with a Tris buffer containing 6M guanidine hydrochloride, and the guanidine soluble portion was fractionated by gel filtration on Sephacryl S-300 into high molecular weight, dimeric and monomeric species .

The region corresponding to monomers was crudely fractionated into five major fractions (Figure 1) on a C4 HPLC column (0.46 x 15 cm, Vydac, Hesperia, CA) with a gradient of 0.1% TFA in water/acetonitrile. Each fraction was analyzed by ESIMS on a Sciex API III triple quadrupole mass spectrometer. The fractions were also digested with trypsin (1:50 enzyme:protein, 37 °C, 4 hr), separated into peptides on a C18 HPLC column (0.46 x 25 cm, Vydac) and analyzed by FABMS on a Kratos MS-50 mass spectrometer. Peptides were identified by the masses of peptides expected to be generated by trypsin, and by comparison with similar analyses of the water soluble crystallins.

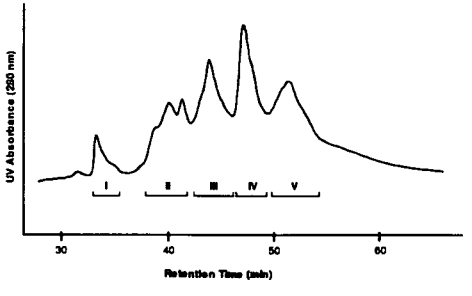

FIGURE 1: C4 HPLC separation of the water insoluble-guanidine soluble portion of human lens.
The five sections collected and analyzed are indicated.

The first water insoluble HPLC section contained βB2 as the major component, as evidenced by ESIMS analysis which gave a molecular weight of 23,290 Da (calculated MW 23,291). The tryptic digest of the second HPLC section identified the complete sequence of βs, portions of γC and γD, and N-terminally degraded αA and αB. The third region contained all of the αB protein with some portions of βs, γC and γD. ESIMS of the third region indicated αB, αB - Lys, αB + PO_4 and αB + $2PO_4$ (Figure 2). The last two HPLC fractions contained αA as a major component, along with some of the βs sequence. The identities of other minor components, possibly β-crystallins whose amino acid sequences are not known, could not be unambiguously assigned. The ESIMS analysis of the fifth section showed the presence of αA at 19,950 (calculated MW 19,952), αA - Ser at 19,865 (calc. 19,865), and αA + PO_4 at 20,030 (calc 20,032).

All major classes of crystallins, α, β and γ were present in the water insoluble-guanidine soluble portion of normal human lenses, with α-crystallin as the most abundant component. Proteins found whose primary sequences are known include αA, αB, βA3, βB2, βB3, βs, γC and γD. Modifications include N-terminal degradation, C-terminal degradation and phosphorylation of αA and αB. Extensive deamidation of Asp and Glu residues, thought to promote insolubilization, was not present, although a small amount of partial deamidation was indicated.

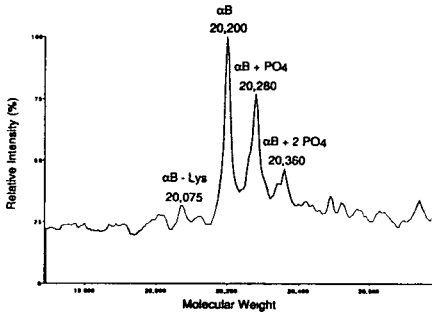

FIGURE 2: ESIMS analysis of Section III from the HPLC separation of water insoluble-guanidine soluble human lens crystallins. The major components of this section are αB (calculated MW 20,201), αB - Lys (20,075), αB + PO_4 (20,081) and αB + 2 PO_4 (20,361)

In spite of denaturing conditions in the chromatographic isolation steps (6M guanidine or 0.1% TFA), it appears that the crystallins still exist, to some extent, as aggregates because some proteins (most notably βs) eluted in nearly all HPLC sections. Since only the monomeric portion of the guanidine soluble extract was analyzed, intermolecular covalent crosslinks were not found but are believed to be the principal components of the higher molecular weight species.

ESIMS was unable to detect the components of sections II and IV, likely because of the large number of components present. Additionally, minor components in the remaining HPLC sections that were indicated by FABMS of the tryptic peptides were not identified by ESIMS. Better separation of the water insoluble proteins will help to identify more of the minor components and modifications that may be present. To this end, we are investigating ion exchange HPLC chromatography in addition to reversed phase HPLC to further purify the guanidine soluble crystallins. The results of this survey of normal human lenses will be used to identify post-translational modifications that may be responsible for insolublization of crystallins in aged and cataractous lenses.

Elucidation of High-order Structure in Lens α-crystallin by Continuous-Flow HPLC FABMS

Yaoqing Liu * and David L. Smith
Department of Medicinal Chemistry
Purdue University, W. Lafayette, IN 47907

α-crystallin consists principally of two gene products, αA and αB. These gene products have molecular weights of approximately 20 kDa, but aggregate to form much larger products with molecular weights of 1,000 kDa. Some of the changes in the eye lens accompanying aging and cataractogenesis have been attributed to changes in the high order structure of α-crystallins. To understand the role of α-crystallin in aging and cataract at the molecular level, it is essential to have analytical methods suitable for detecting and characterizing changes in its high order structure.

We report here a new analytical method based on the rate at which peptide amide hydrogens undergo isotopic exchange as a new probe of the high order structure of α-crystallins. Intramolecular hydrogen bonding, as found in α-helices and β-sheets, dramatically reduces hydrogen exchange rates. Likewise, solvent shielding by hydrophobic residues can decrease the rate of hydrogen exchange. Although the potential of peptide amide hydrogen exchange as a probe of high order structure in proteins has long been recognized, experimental methods for quantifying hydrogen exchange limited applications of the method to relative small proteins. The new method based on protein fragmentation and continuous-flow HPLC FABMS has been applied to α-crystallin. Following a deuterium exchange-in period, isotopic exchange is quenched by decreasing the pH. The partially deuterated protein is fragmented with pepsin into peptides, which are analyzed by HPLC FABMS to determine their deuterium content.

Time course data, as shown in Fig.1, are used to calculate the rate constants for

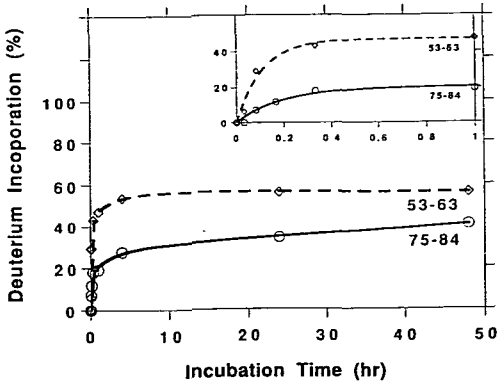

Fig.1

Plot of the deuterium content of 2 segments of αA-crystallin (αA^{53-63} & αA^{75-84}) as a function of the incubation time (2 min. to 48hr). The insertion is a plot of incubation time from 2 min. to 1hr.

hydrogen exchange in specific segments of the protein. Results of this study indicate that many peptide amide hydrogens in α-crystallin exchange rapidly ($k > 10\ hr^{-1}$), while others exchange slowly ($k < 10^{-4}\ hr^{-1}$). As the rates of deuterium exchange into specific segments become available, regions that are either in β-sheet structure, or shielded from the solvent will be identified by their very slow rates of hydrogen exchange. Likewise, regions of random coil and full access to the solvent will be indicated by their high rates of hydrogen exchange.

Since the rate of hydrogen exchange is critically dependent on the hydrogen bonding of the peptide amide hydrogens, it may be used to localize changes in protein structure. The possibility of detecting structural changes has been demonstrated by *determining the rate of hydrogen exchange as a function of the deuterium exchange-in* temperature. The results of some segments (Fig.2) show that hydrogen bonding weakens with increasing temperature, which indicates that this region of the protein is particularly susceptible to thermal destabilization.

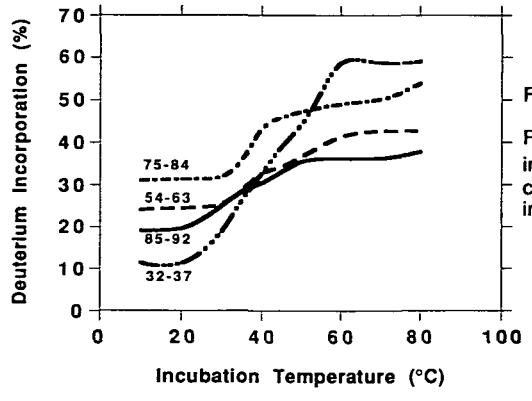

Fig. 2

Plot of deuterium incorporation into specific segments of αA-crystallin as a function of the incubation temperature.

The present results demonstrate that the combination of hydrogen exchange and mass spectrometry may be a useful new tool for investigating the high order structure, and particularly for detecting differences, in various forms of α-crystallin. Hydrogen exchange is a particularly useful probe of high order structure because it may give information about the entire length of the backbone of proteins, rather than a few specific residues.

Disadvantages of the experimental methods described here include: (1) Peptides traceable to all segments of the protein may not be found when pepsin is used to fragment the protein. A possible solution might be to use other acid proteases in addition to pepsin; (2) These measurements are technically very difficult to perform, and require extensive use of a mass spectrometer that is costly to purchase and maintain.

ANALYSIS OF THE BACITRACIN COMPLEX BY LC-IONSPRAY-MS*

M Morris and R K Boyd
Institute for Marine Biosciences, National Research Council, 1411 Oxford Street, Halifax, Nova Scotia B3N 3A8, Canada.

Bacitracin is a mixture of polypeptide antibiotics produced by *Bacillus subtilis* and *Bacillus licheniformis*. The mixture has previously been shown to contain at least ten components, of which only the major component, Bacitracin A, and its oxidized counterpart, Bacitracin F, have been fully structurally evaluated. In a recent study three single substitution sites within Bacitracin A, where Ile has been replaced by Val to form the set of related species known as Bacitracin B, were identified using tandem mass spectrometric methods without any prior separation[1]. Although this type of analysis allowed conclusions to be drawn regarding the sites of substitution, a more definitive method would include separation of the components of the mixture prior to analysis by mass spectrometry. The structure of Bacitracin A with the proposed sites of substitution is shown in Figure 1.

Liquid chromatographic separation of the components of the bacitracin complex has been the subject of study of a number of groups, although the use of buffered solvents was required in these procedures[2,3]. We achieved chromatographic separation using a simple linear gradient elution (acidified acetonitrile water solvent system) that gave reasonable separation of some 18 components of the mixture. Semi-preparative extrapolation of this methodology allowed the eighteen fractions to be collected and concentrated for preliminary MS analysis. Owing to the chromatographic overlap of the components of interest ideal fractionation was probably not achieved, so an on-line coupling of the LC to a mass spectrometer *via* an ESI interface was also attempted.

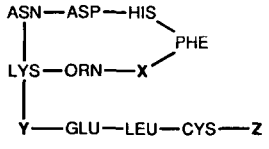

	Bacitracin			
	A	B_1	B_2	B_3
X	Ile	Val	Ile	Ile
Y	Ile	Ile	Val	Ile
Z	Ile	Ile	Ile	Val

Figure 1 Structure of Bacitracins A and B

LC-MS separation and detection was performed on an Hewlett Packard 1090L high-performance liquid chromatograph coupled to a Perkin-Elmer SCIEX API III triple quadrupole mass spectrometer *via* an ionspray interface.

LC Conditions Gradient elution using a solvent ramp of 10-55% MeCN/0.1% TFA in H_2O/0.1% TFA was used at a flow of 0.2ml.min^{-1} into a Vydac 218TP52 column. The eluent from the column was split to allow 10μl.min^{-1} to flow to the mass spectrometer.

MS Conditions Product ion spectra were obtained by selecting the doubly charged precursor ions for the Bacitracins B (m/z 705) and subjecting them to 20V (40eV in the laboratory frame) collisions in the quadrupole collision cell at a collision gas thickness of 3.5 x 10^{14} atoms.cm^{-2}. The resolution of Q1 was set to pass 1.5 Da FWHM, and Q3 was scanned in 0.5 Da steps with 3 ms dwell over the mass range 800 - 1450 (this range was deemed sufficient to provide the information sought), giving a single scan time of 3.9 sec.

* NRCC # 34852

The reconstructed ion chromatogram for the doubly charged molecular ions of the Bacitracin B molecules is shown in Figure 2, extracted from the LC-MS full scan data. This clearly shows the presence of three major components with the molecular weight of 1408 Da, with the possibility of minor components being eluted both before and after the major components (this is probably attributable to the wide resolution used in MS1 to ensure optimum sensitivity.) The MS/MS spectra acquired for these three peaks are shown in Figure 3. The annotation shows the presence of three components where Ile has been replaced by Val, and the points of substitution are clearly confirmed as being at substitution points X, Y and Z in the structure shown in Figure 1.

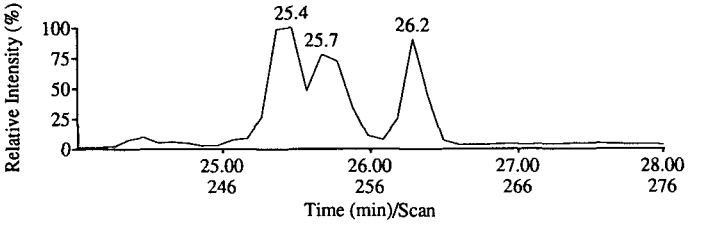

Figure 2 LC-MS Extracted Ion Chromatogram of m/z 705

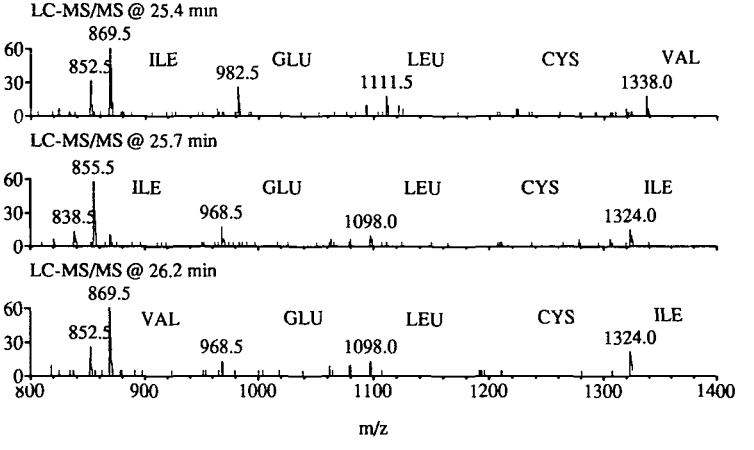

Figure 3 LC-MS/MS spectra of the three components of Bacitracin B shown in Figure 2.

References

1. L W Tetler, S N Davey and M Morris, unpublished results.
2. K Tsuji and J H Robertson, *J. Chromatogr.*, 112 (1975) 663-72.
3. H Oka, Y Ikai, N Kawamura, M Yamada, K-I Harada, Y Yamazaki and M Suzuki, *J. Chromatogr.*, 462 (1989) 315-22.

Post translational modification of recombinant barley α-amylase 1 expressed in yeast, characterized by mass spectrometry.

J.S.Andersen, P. Roepstorff, M. Søgaard* and B. Svensson*.
Department of Molecular Biology, Odense University, Campusvej 55, DK-5230 Odense M, Denmark and *Department of Chemistry, Carlsberg Laboratory, Gamle Carlsberg Vej 10, DK-2500 Copenhagen Valby, Denmark.

The yeast *Saccharomyces cerevisiae* is widely used as a host for recombinant production of heterologuos proteins because desired post translational modification can be obtained in this organism (1). Even though a large number of heterologous proteins are correctly processed in yeast, non-native modifications have also been reported (2). Consequently, structure verification, purity evaluation and determination of post translational modification are important steps in characterizing recombinant proteins. Here we demonstrate the use of electrospray (ES) and matrix assisted laser desorption ionization (MALDI) MS in combination with protein chemical and genetic methods to rapidly assess the nature of post translational modification in the 45 kDa barley α-amylase 1.

Stains, plasmids, plasmid construction and purification of the enzyme followed the described procedures (3 and 4). ES-mass spectra were acquired on a Vestec model 201 single-quadrupole mass spectrometer (Vestec Corporation Houston, TX, USA). The instrument was independently calibrated using β-lactoglobulin. MALDI-mass spectra were recorded on a LDMS prototype instrument (ABI, Sweden AB, Uppsala) with α-cyano-4-hydroxycinnamic acid as matrix and human insulin as internal calibrant. Reduction and alkylation of cysteines followed standard procedures using dithiotreitol and 2-vinylpyridin. Neutral hexose was determined by the phenol-sulfuric acid method and enzymatic activity by Phadebas Blue Starch (Pharmacia, Uppsala). Alkylated rAMY1-1 was cleaved with CNBr (80% TFA at 20°C for 20h) and rAMY1-4 was digested with endoproteinase Lys-C (0.4M urea, 50mM NH_4HCO_3, pH 7.8 at 37°C for 3h, substrate: enzyme ratio 1:100 (w:w)).

Four forms of recombinant barley α-amylase 1 (rAMY1-1 to rAMY1-4) with different pI and enzymatic activities (3,4) are secreted from yeast cells harboring an AMY1 expression vector. M_r determination of the four forms by ESMS indicated that two forms lack C-terminal Arg-Ser and that two forms have been modified by glutathione leading to misfolding and inactivation of the enzyme. The invariant presence of a minor components 324Da below that of the major species suggested the presence of O-glycosylation in the major product. Taking these modification into account, however, a mass discrepancy of 30Da above that inferred from the cDNA sequence could not be explained.

Lack of C-terminal Arg-Ser was in agreement with previous C-terminal sequence data (3). Genetic removal of Arg-Ser resulted in the production of only two forms (rAMY1-1ΔRS and rAMY1-2ΔRS) as verified by M_r determination. Glutathionylation of a Cys residue was verified by reduction and alkylation followed by M_r determination. Furthermore, rAMY1 mutants were expressed with each of the four Cys residues mutated to Ala (C95A, C106A, C125A and C321A). Mutation of Cys 95 to Ala and truncation of C-terminal Arg-Ser (rAMY1ΔRS, C95A) led to the secretion of a single fully active rAMY1 form.

The O-glycosylation was verified by chemical analysis. From MALDI-mass spectra of the peptide mixture obtained after CNBr cleavage and endo Lys-C digest it was possible to locate the O-glycosylation to Thr_{410} and the mass discrepancy to the region Ala_{283}-Met_{298}. Subsequent Edman degradation of isolated peptides identified by MALDI-MS led to the identification of the sequence error Ala_{284}→Val and verification of the O-glycosylation.

References

1 Tekamp-Olsen, P., Valenzuela, P. (1990) Curr. Opin. Biotechnol. **1**, 28-35
2 Hitzeman, R.A., et al.(1990) Meth. Enzymol. **185**, 421-440
3 Søgaard, M., Olsen, F.L., Svensson, B. (1991) Proc. Natl. Acad. Sci. USA **88**:8140-8144
4 Søgaard, M., Svensson, B. (1990) Gene **94**:173-179

Figure 1 ES-mass spectrum of rAMY1ΔRS, C95A. The two series of multiply charged ions show the glycosylated (major) and non-glycosylated (minor) variants.

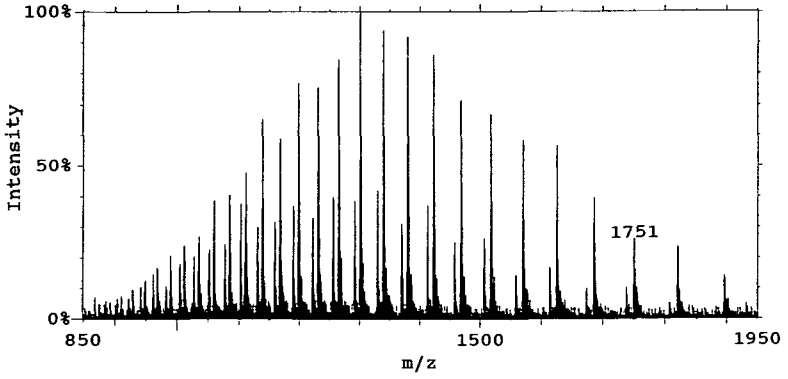

Table 1 M_r of rAMY forms produced from plasmids pBAL7, pBAL7ΔRS and pBAL7ΔRS, C95A measured by ESMS. The M_r difference (ΔM_r) is calculated for selected pairs of rAMY1 forms and compared to the expected ΔM_r (given in parenthesis).

	rAMY1 forms	M_r	Δ	ΔMr	Identification
a	rAMY1-1	45833	a-c	245 (243)	Arg-Ser
b	rAMY1-2	45529	b-a	305 (305)	Glutathione
c	rAMY1-3	46077	c-d	306 (305)	Glutathione
d	rAMY1-4	45774	d-b	244 (243)	Arg-Ser
e	rAMY1-1ΔRS	45839	e-a	6 (0)	
f	rAMY1-2ΔRS	45534	f-e	305 (305)	Glutathione
g	rAMY1ΔRS, C95A	45504	g-f	30 (32)	Cys → Ala
h		45178	h-g	326 (325)	O-glycan

CAPILLARY LIQUID CHROMATOGRAPHY - ELECTROSPRAY TANDEM MASS SPECTROMETRY REVEALS EXPRESSION OF MORE THAN ONE RAT PROOPIOMELANOCORTIN

G.J. Feistner[1], T.D. Lee[1], K.F. Faull[2], P.C. Andrews[3], and P. Roepstorff[4]

[1]Beckman Research Institute of the City of Hope, Duarte, CA 91010, [2]Center for Molecular and Medical Sciences, Mass Spectrometry, University of California, Los Angeles, CA 90024, [3]Department of Biological Chemistry, University of Michigan School of Medicine, Ann Arbor, MI 48109, [4]Department of Molecular Biology, University of Odense, DK-5250 Odense, Denmark.

We have previously suggested the use of peptide charting, i.e. the componential analysis of peptide/protein mixtures in a given tissue (extract), for comparing peptide profiles between different species and/or tissues, as well as to detect responses of the neuroimmunoendocrine system to endogenous regulators, stress, and disease. In the course of exploring the feasibility of peptide charting for experimental models in the rat, we have consistently observed discrepancies between measured and DNA-derived molecular masses for the endorphins (End) and γ-lipotropin (LPH). These discrepancies may be due to pro-opiomelanocortin (pOMC) heterogeneity between different rat strains, to expression of more than one pOMC gene, or to sequencing errors. The DNA data were obtained on Long-Evans rats, whereas we routinely use Sprague-Dawley or Wistar rats for our experiments. Also, the existence of at least two rat pOMC genes was proposed in the original report on the pOMC DNA sequence, but subsequent molecular biological studies suggested that only one gene would be expressed. It is remarkable that no comprehensive analysis of rat pOMC has ever been performed at the protein level. To address this problem, capillary LC-ES-MS and LC-ES-MS/MS studies were performed on Long-Evans rats. No differences to the other two strains were observed.

Summarizing our results, Fig. 1 shows the mass chromatograms for two variants each of joining peptide (JP), γ-LPH, and β-End, in the approximate ratio of 1:7 to 1:10. This ratio was fairly constant between batches and not affected by boiling the extract, thus arguing against artefact generation. Based on molecular mass and LC-ES-MS/MS (Fig. 2) data, the more abundant JP-1 was found to be identical to the one deduced from rat genomic DNA data. The most prominent ion in the LC-ES-MS/MS spectrum of JP-2 was isobaric with Y_5 + of JP-1, whereas the corresponding B_{13} + ion appeared at m/z 1300 in JP-1 but at m/z 1282 in JP-2. Another ion pair, Y_7 + (811)/B_{11} + (1074/1057) confined the sequence difference to the eleven N-terminal amino acids, whereas a series of Y and Z ions (Y_{16} 2+ 842/835; Y_{14} 2+ 713/704, Z_{13} + 1308/1290, Z_{12} + 1236/Y_{12} + 1234, Y_{11} + 1176) further confined the substitution to positions 8-11. A single amino acid substitution of Asp-9 by Pro is likely. The LC-ES-MS/MS spectrum of the pentuply protonated molecular ion of γ-LPH-1 (Fig. 3) shows a series of triply and quadruply charged C-terminal fragments that are consistent with [His12]-γ-LPH. The reported DNA data suggest Gln-12, but we have confirmed His-12 by Edman-type sequencing. The LC-ES-MS/MS spectrum of γ-LP-2 is very similar to that of γ-LP-1 except that many C-terminal Y^{4+}-ions are shifted by about 4 u. Y_{28} 4+ (827/823) and Z_{25} 3+ (979/979) confine the substitution to between residues 25 and 28. No single amino acid substitution can account for the mass difference, but six (fifteen) possibilities for two (three) simultaneous amino acid substitutions exist. With regard to β-End, we find molecular ions that are consistent with the DNA-derived [Val26]-β-End, but more abundant is [Ala26]-β-End as is found in cow and other mammals. Rat Ac-[Ala26]-β-End(1-27) was confirmed by a series of B and Y ions in the LC-ES-MS/MS spectrum of its triply charged molecular ion. Due to low abundance, [Val26]-β-End could not yet be corroborated by a corresponding product ion spectrum.

Fig. 1 Mass chromatograms for rat JP, γ-LPH, and Ac-β-End(1-27).

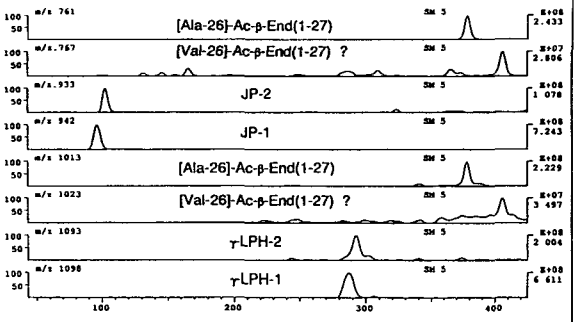

Fig. 2 LC-ES product ion spectrum of the doubly protonated molecular ion of JP1.

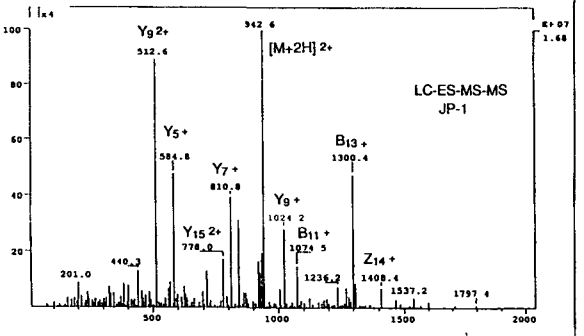

Fig. 3 LC-ES product ion spectrum of the pentuply protonated molecular ion of γ-LPH-1

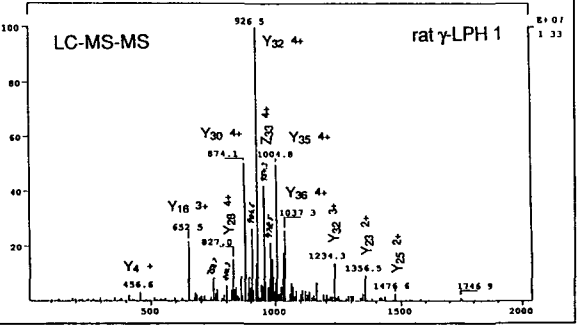

Characterization of Three Isoforms of Soybean Agglutinin by ESI MS.

D.K. Mandal, G.A. Orr, E. Nieves*, Q Yu, J. Roboz and C.F. Brewer
Albert Einstein College of Medicine; Bronx, NY 10461 and
The Mt. Sinai School of Medicine, New York, NY

Lectins are proteins or glycoproteins that bind to specific carbohydrates and are widely distributed in nature. They are found in plants, microorganism, bacteria and animals and may exist as multiple isoforms. Soybean agglutinin (SBA) which is a plant lectin specific for D-galactose and D-N-acetylgalactosamine is a tetrameric glycoprotein with one Man9 oligomannose type chain per monomer. SBA consist of 4-5 isolectins having similar compositions and binding activities. Despite the widespread use of SBA in biological studies, little information is available on the nature of these isolectins.

Our objective was to use electrospray mass spectrometry to characterize three isoforms of SBA and thus provide insight into the structural relationships and hence possible mechanisms of formation of these various isoforms.

Native SBA was purified from the crude extract of soyfluff by affinity chromatography and chromatofocusing. The materials in each peak was pooled separately and the three isoforms of SBA were subjected to (repeated) rechromatofocusing either on a PBE 94 column or a Mono P column. The isolectins SBA-I, SBA-II and SBA-III were denatured in 6 M guanidine hydrochloride and subjected to RP-HPLC using a Aquapore RP-300 (C-8) column. Electrospray mass spectrometry was performed on the separated HPLC fractions and 10-20 μL aliquots injected directly into the electrospray source. The mobile phase was methanol-water (1:1 v/v) with 1% formic acid; flow rate into the source was 5 μL/min.

The HPLC profiles of SBA-I, SBA-II and SBA-III are shown in Figure 1A, 1B and 1C, respectively. The profiles are similar for all three isolectins with two major peaks (peak 1 and peak 3) of approximately equal intensity and one minor peak (peak 2). However, peak 1 of SBA-II (Figure 1B) showed a doublet labeled as 1a and 1b. Electrospray ionization mass spectrometry was performed for each peak from the HPLC runs of SBA-I, SBA-II and SBA-III. A typical reconstructed mass spectrum for the different peaks obtained from the HPLC of SBA-II is presented in Figure 2. The ESI-MS data for the different peaks obtained from the HPLC run of SBA-I, SBA-II and SBA-III are summarized in Table I.

The calculated mass of the intact lectin monomer from the amino acid sequence of the protein deduced from complementary DNA (cDNA) sequencing of the corresponding gene including a Man9 oligomannose type chain is 29,438 daltons. The complete sequence of the protein representing 253 amino acid residues is shown in Figure 3 and is referred to as the intact subunit α. This intact α subunit was found in HPLC peak 3 of all three isoforms of SBA. The lower masses of the subunits are attributed to the fragmentation from the C-terminus of the protein. The formation of a 240 residue subunit is shown in Figure 3 and is labeled as the β subunit. A 243 residue subunit is shown in Figure 3 and is referred to as the γ subunit.

Characterization of SBA-I. HPLC peak 1 would correspond to a 240 residue β subunit. The component in HPLC peak 2 was not detected in ESI-MS. However, the 2 major peaks (peak 1 and peak 2) were of approximately equal intensity, suggesting that SBA-I consist primarily of α and β subunits and it's composition may be considered as $\alpha_2\beta_2$ in terms of major subunits. Also, the β subunit involves loss of 2 acidic residues (D-243 and E-251) which would account for the highest pI (7.0) for SBA-I.

Characterization of SBA-II. HPLC peak 1 is a doublet of which peak 1a represents the 240 residue β subunit, and peak 1b showed 2 strong peaks in ES-MS for 28,022 daltons (β subunit) and 28,352 daltons representing the 243 residue γ subunit. The 243 and 246 residue subunits show a loss of one acidic residue (E-251) and the β subunit a loss of two

acidic residues. As the intensity of HPLC peaks 1 and 3 were about equal, the compositions of SBA-II may be approx-imately considered as $\alpha_2\beta\gamma$ in terms of major subunits present. The presence of both the β and γ subunits would account for the reason the pI (6.85) for SBA-II is lower than that of SBA-I (pI 7.0).

Characterization of SBA-III. HPLC peak 1 yielded a molecular mass for the 243 residue γ subunit along with 2 minor molecular masses of 28,043 daltons (α subunit) and 27,530 daltons (236 residue subunit). The 243 residue γ subunit involves the loss of one acidic residue (E-251) from the intact subunit, suggesting that the approximate composition of SBA-III may be $\alpha_2\gamma_2$ in terms of major subunits accounting for a lower pI value of 6.7 than that of SBA-II.

The results demonstrate that ESI-MS can be used to characterize the isoforms of SBA. The three isoforms of SBA are primarily due to two similar C-terminal fragmented subunits combined with two intact subunits to form a tetrameric isolectin. The major fragmented subunits are shown to be the 240 and 243 residue subunits, which involves cleavage on an aspartic acid residue, namely D-240 and D-243, respectively.

TABLE 1

Molecular masses of 3 Isoforms of SBA

Isolectin	Peak	Observed mass	Correlated nearest mass and number of AA residues: Average mass	# AA residues
SBA-I	1	28,068	28,001	240 (β)
	2	not detected		
	3	29,437	29,438	253 (α)
SBA-II	1a	28,006	28,001	240 (β)
	1b	28,022 (strong)	28,001	240 (β)
		28,352 (strong)	28,326	243 (γ)
		28,667 (moderate)	28,628	246
	2	29,333	29,324	252
	3	29,448	29,438	253 (α)
SBA-III	1	27,530 (moderate)	27,571	236
		28,043 (weak)	28,001	240 (β)
		28,376 (strong)	28,326	243 (γ)
	2	29,372	29,324	252
	3	29,434	29,438	253 (α)

FIGURE 1

HPLC chromatogram of SBA-I, II and III

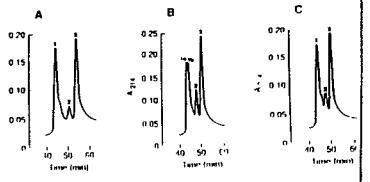

FIGURE 2

Transformed ESI-MS obtained from SBA-II

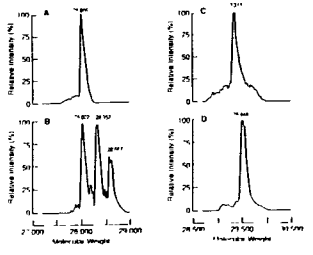

FIGURE 3

Amino Acid Sequence of Soybean Agglutinin

```
AETVSFSWNKFVPKQPNMILQGDAIVTSSG  30
KLQLNKVDENGTPKPSSLGRALYSTPIHIW  60
DKETGSVASFAASFNFTFYAPDTKRLADGL  90
AFFLAPIDTKPQTHAGYLGLFNENESGDQV 120
VAVEFDTFRNSWDPPNPHIGINVNSIRSIK 150
TTSWDLANNKVAKVLITYDASTSLLVASLV 180
YPSQRTSNILSDVVDLKTSLPEWVRIGFSA 210
ATGLDIPGESHDVLSWSFASNLPHASSNID 240
PLDLTSFVLHEAI                  253
```

α subunit - the intact 253 AA residues

β subunit - consisting of 240 AA residues; missing residues 241-253 (PLDLTSFVLHEAI)

γ subunit - consisting of 243 AA residues; missing residues 244-253 (LTSFVLHEAI)

This work was supported in part by USPHS Grant R01 CA16054 from the National Cancer Institute, and Core Grant P30 CA13330 from the same agency.

Profiling Phosphorylation in the High Molecular Weight Rat Neurofilament Protein (NF-H) by ESI-MS

D. M. Sheeley[1], E. Elhanany[2], H. Jaffe[2], W. T. Link[2], H. Gainer[2], H. C. Pant[2], and H. M. Fales[1]

[1]LBC, NHLBI and [2]LNC, NINDS, National Institutes of Health, Bethesda MD 20892

Within the axon, structures essential for maintaining cytoskeletal stability have been identified as neurofilaments, which occur in long straight bundles, and interact with microtubules and other cytoskeletal elements. The neurofilament is composed of three proteins, the light, medium, and heavy neurofilament proteins (NF-L, NF-M, and NF-H), collectively called the "neurofilament triplet". These proteins have head and alpha-helical rod domains which contribute to the neurofilament structure. NF-M and NF-H also have heavily phosphorylated C-terminal tail domains which project outward from the neurofilament body[2]. The phosphorylation of these proteins seems to change during transport and assembly of neurofilaments within the axon. Phosphorylation may regulate the rigidity of the tail domain, and affect its interactions with other structures[1].

In this study, the extent of phosphorylation of the NF-H protein has been partially characterized. The entire NF-H protein has a molecular weight of 200 KDa. The tail domain accounts for approximately 70 KDa, and contains over fifty potential phosphorylation sites. The NF proteins contain a recurring tripeptide motif "Lys-Ser-Pro" (KSP) which appears to be the target for a specific kinase activity. Following digestion with chymotrypsin to remove the head and rod domains, cyanogen bromide digestion breaks the tail domain into three fragments **(Figure 1)**. Peptides obtained by gel filtration following CNBr digestion were analyzed directly by ESI-MS without intervening chromatography in order to evaluate the populations of phosphorylation states present. Phosphorylation at specific sequences has also been evaluated by ESI-MS and Edman degradation.

The C-terminal fragment, CNBr I, contains several serine and threonine residues, but none are in KSP repeats. The molecular weight obtained by ESI -MS for this fragment agrees with the predicted sequence, confiming that it is not phosphorylated. The absence of phosphorylation in this peptide supports the hypothesis that the KSP repeat is a consensus sequence for phosphorylation of the neurofilament proteins and might be the target for specific kinases. The second fragment, CNBr II, contains five KSP repeats. The deconvoluted ESI-MS spectrum for this fragment **(Figure 2a)** shows a mixture of peptides modified with from 3 to 6 phosphates. Because there are only 5 KSP repeats in this fragment, they cannot account for all the phosphorylation observed. There are two sequences in this fragment which are similar to the KSP consensus sequence. One is KTP, and the other is an RSP. One or both of these motifs may be a substrate for phosphorylation. If this fragment is treated with alkaline phosphatase, most of the *phosphate is removed, resulting in a new distribution of peaks in the mass spectrum* **(Figure 2b)**. The molecular weight of the completely dephosphorylated peak corresponds to the anticipated amino acid sequence.

In studies such as this one, MSanalysis provides a particular advantage with repect to mapping and quantification of post-translational modification. By looking at a whole population of peptides, we can get a "snapshot" of phosphorylation. Subsequent characterization of specific peptides can easily assign sites of attachment. Extensive phosphorylation reduces the average charge observed, but not in a one to one relationship, and appears to adversely affect ionization efficiency.

1. R. A. Nixon and R. K. Sihag, TINS 14(11):501-506 (1991).
2. Z.-S. Xu, W.-S. Liu, and M. B. Willard, J. Biol. Chem. 267(7):4467-4471 (1992).

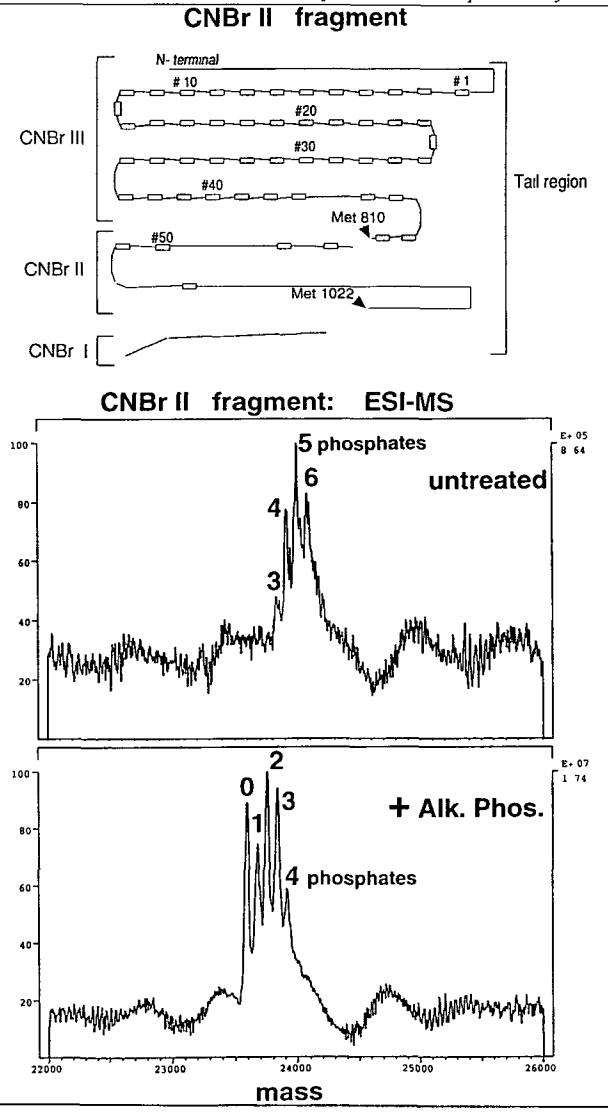

PRIMARY STRUCTURE CHARACTERIZATION OF LEGUME LECTINS; SEQUENCE ASSIGNMENT AND IDENTIFICATION OF POST-TRANSLATIONAL MODIFICATIONS USING LC-MS AND LC-MS-MS+

*P. Thibault[1], D.C. Watson[2], N.M. Young[2]; [1]Institute for Marine Biosciences, National Research Council, 1411 Oxford St., Halifax, Nova Scotia Canada B3H 3Z1; [2]Institute for Biological Sciences, National Research Council, 100 Sussex Dr., Ottawa, Canada, K1A 0R6.

Lectins are a diverse group of proteins of plant and animal origin displaying a high affinity for carbohydrates. These complex proteins were first recognised for their capability to agglutinate a variety of animal cells by binding to cell surface glycoproteins and glycolipids. Considerable interest in these proteins has arisen following the discovery of their important role in cell recognition processes, amongst which are microbial adhesion and adhesion of white blood cells to blood vessels [1].

Most of our current knowledge of the primary structures of lectins has been gathered in the last decade through extensive chemical studies from lectins isolated from leguminous plants. However, such studies are complicated by the diversity in structural features of these complex molecules, and the complete primary sequence is known for only a few. The most well characterized member of the legume lectin family is concanavalin A, a protein isolated from Jackbean. A large number of the legume lectins are single-chain proteins, but sequences deduced from cDNA methods are approximately fourteen residues longer than those obtained from protein sequencing [2], indicating C-terminal trimming. This type of modification was reported recently for the peanut agglutinin (PNA) lectin using ionspray mass spectrometry and indicated that this protein undergoes imprecise C-terminal proteolytic processing resulting in "ragged ends" [3]. In addition to this, many plant lectins are glycosylated which render their complete characterization more difficult.

As an extension to earlier studies on PNA [3], the present investigation evaluated the application of LC-MS and LC-MS-MS with ionspray ionization for the characterization of other leguminous lectins. An example of single-chain lectins examined here is presented in Figures 1 and 2 for a glycoprotein isolated from *Erythrina corallodendron* (ECL). The ionspray mass spectrum (Figure 1) shows an intense series of multiply-protonated ions extending from 15 to 33 charges. The molecular weight of this protein as calculated from the multiply-protonated ion series is 28763 Da, approximately 800 Da more than the mass deduced from the cDNA sequence [4]. Additional components spaced by ≈ 147 Da are also observed in Figure 1 suggesting a pattern of microheterogeneity where different numbers of fucose residues are attached to the ECL glycopeptides. Earlier studies using cDNA cloning and protein analyses [4] have indicated that ECL contains a 26 residue long leader peptide, and the cDNA sequence shows an extra 12 amino acids at the C-terminal end compared to the mature protein. Additional experiments were thus required to answer some of the discrepancies observed between molecular weights determined by ionspray mass spectrometry and those deduced from either protein sequencing or cDNA cloning [4]. The ionspray LC-MS analysis corresponding to the injection of 70 pmols of the tryptic digest of ECL is shown in Figure 2, and permitted identification of most of the predicted peptides. Peptides arising from CNBr cleavage of the ECL lectin were also subjected to LC-MS analyses and provided a complete mapping of the protein sequence. More importantly, these LC-MS analyses permitted identification of glycosylation sites at residues 17 and 113. LC-MS-MS experiments (not shown) confirmed that the carbohydrate attached to residue 113 has the following sequence: GlcNAc-(Fuc)-GlcNAc-$(Hex)_3$ Xyl. The microheterogeneity observed on the ECL lectin is thus likely to arise from the abstraction of fucose on either site of glycosylation.

Similar mass spectrometric analyses were also conducted on a series of more than ten leguminous lectins. In the simplest case, sequence assignments could be made directly by comparing the observed molecular weight with that deduced from published data. This procedure enables a rapid identification of both single chain proteins and other lectins possessing light (α) and heavy (β) chains. However, more complex protein preparations required LC-MS analyses so that overlapping multiply-protonated species could be separated from each other.

+NRCC#: 34857

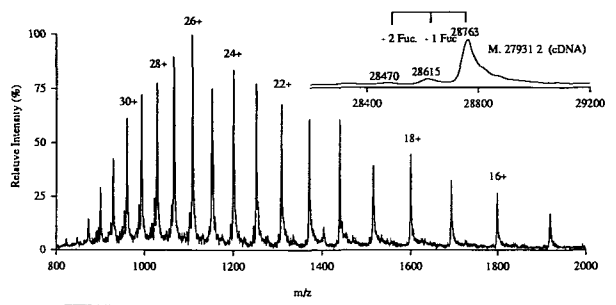

Figure 1: Ionspray mass spectrum of a lectin from *E. corallodendron*. Insert corresponds to the reconstructed molecular weight profile obtained from the mass spectrum.

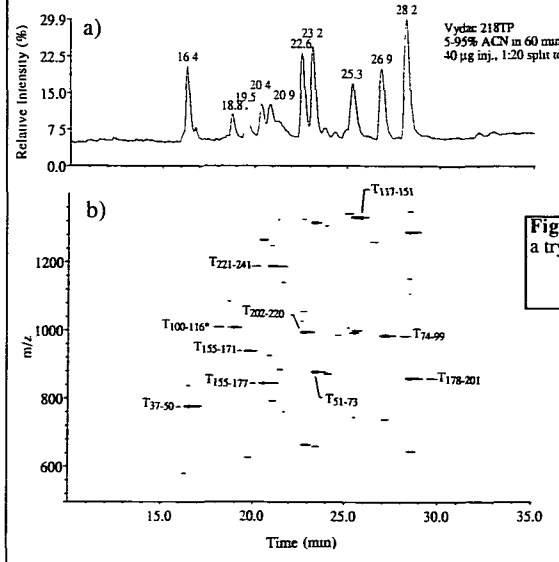

Figure 2: Ionspray LC-MS analysis of a tryptic digest of *E. corallodendron*.
a) Total ion current (m/z 500-1400)
b) Contour profile

[1] Sharon N., Lis H. Science **246**, 227 (1989).
[2] Sharon N., Lis H. FASEB J. **4**, 3198 (1990).
[3] P. Thibault, D.C. Watson, M. Yaguchi, N.M. Young Tech. in Protein Chem. vol. IV, R.H. Angeletti Ed., Acad. Press, NY, p. 91-98 (1993).
[4] Arango R., Rozenblatt S., Sharon N. FEBS letters, **264**, 109 (1990).

Investigations into the Post-translational Modification and Mechanism of Isopenicillin N:acyl-coenzyme A acyltransferase using Electrospray Ionisation Mass Spectrometry.

R T.Aplin, P.L.Roach,C V Robinson and C J Schofield. The Oxford Centre for Molecular Sciences, The Dyson Perrins Laboratory, Oxford University, Oxford, U K. OX1 3QY

The final step in the production of penicillins with hydrophobic side chains in *Penicillium chrysogenum* is carried out by isopenicillin N acyl-CoA acyltransferase (AT) This enzyme removes the α-aminoadipoyl group of isopenicillin N and replaces it with an acyl group from an acyl CoA (Fig 1)

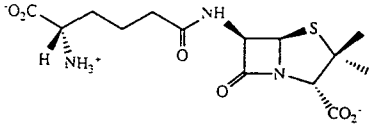

Isopenicillin N (IPN)

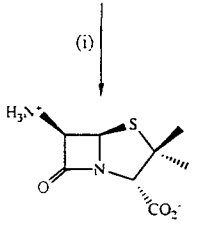

6-aminopenicillanic acid (6-APA)

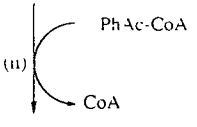

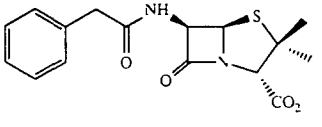

Penicillin G

Figure 1 The biosynthesis of penicillin G from isopenicillin N AT catalyses both steps (i) and (ii)

Post-translational Modifications

The ESI MS of purified AT shows a mixture of four components

A	11497.42 ± 1 01 Da
B	11603 73 ± 1 03 Da.
C	28003 67 ± 1 99 Da
D	28457.35 ± 2 87 Da

The molecular masses of A and D are consistent with the cleavage of a single bond between Gly102 and Cys103 in the preprotein (Calculated masses. A 11498 20, D 28459 67) The mass of component B was consistent with the modification of the α-subunit by the addition of a phenoxyacetate group This was shown to originate from the growth medium by replacement of the phenoxyacetate in the growth medium with phenylacetate or 4-bromophenylacetate.

Acyl Transfer Reactions

A range of acyl CoAs are accepted by AT in the presence of 6-aminopenicillanic acid (6-APA) to yield acylpenicillins ESI MS of AT following incubation with a series of acyl CoAs (hexanoyl, hex-3-enoyl, heptanoyl and phenylacetyl) showed acylation of the β-subunit, both components C and D undergoing acylation That this is a specific process is shown by the addition of the substrate 6-APA to the acylated AT and repeating the electrospray analysis. The species corresponding to the acylated β-subunit are completely absent. Addition of a nonsubstrate amino acid β-alanine has no effect on the abundance of the species corresponding to the acylated β-subunit

In summary, ESI MS has determined the position of the post-translational cleavage of AT and identified the apparent modification by acylation *in vivo* of the α-subunit by exogenously added substituted acetic acids. It has also allowed the direct observation *in vitro* of the specific transfer of an acyl group from a number of acyl CoAs to the β-subunit. Whether this apparent acylation reflects an event in the *in vivo* transformation of isopenicillin N to penicillin G cannot be unequivocally stated at this stage and is the subject of current mechanistic studies

Recombinant Human Neurotrophin-4 (NT-4): Characterization of Protein Folding by Matrix-Assisted Laser Desorption and Electrospray Ionization Mass Spectrometry.

Tanuja Chaudhary, Henryk Cudny, Somesh Nigam, Nancy Tobkes, Candace Seneca and *James E. Labdon,
Regeneron Pharmaceuticals, 777 Old Saw Mill River Road, Tarrytown, NY 10591

Neurotrophic factors are a family of 122-130 residue dimeric proteins which regulate the growth and differentiation of neuronal precursor cells and promote the survival of differentiated neurons in vivo and in vitro. Human NT-4 (also referred to as NT-5) [1-2] is the most recent member of this family, which also includes nerve growth factor (NGF), brain-derived neurotrophic factor (BDNF) and Neurotrophin-3 (NT-3). The neurotrophins exhibit considerable sequence identity and contain six invariant cysteine residues, suggesting similarities in their tertiary structures.

ESI spectra of E. coli derived, human NT-4 (Fig. 1), obtained in unfolded and folded/oxidized forms are in close agreement with their calculated average masses of 13,923 and 13,917 respectively. The deconvoluted spectra differ in mass by 6 amu, reflecting the formation of three disulfide bonds. There are striking differences between the charge envelopes, resulting from a smaller number of sites for protonation in the folded form. Partially-reduced preparations of NT-4 show three peaks by reversed-phase HPLC(Fig.2), resulting from a mixture of the folded, unfolded and partially-folded forms of the protein. ESI-MS analysis of the early-eluting peak 1 (15 min.) was consistent with the native structure while peak 2 had a spectrum with a charge envelope between reduced/unfolded NT-4 (compare to Fig. 1). Fully reduced and unfolded NT-4 (peak 3) had a broad weak ion distribution (not shown) with a charge envelope at low m/z values.

Figure 1. ESI of Unfolded and Folded NT-4

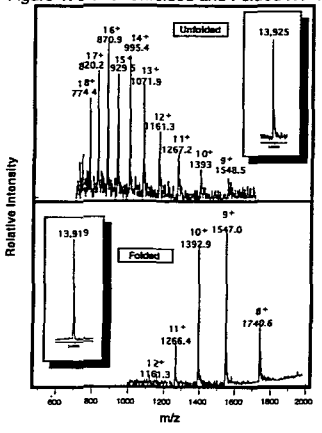

Figure 2. HPLC of Partially Reduced NT4

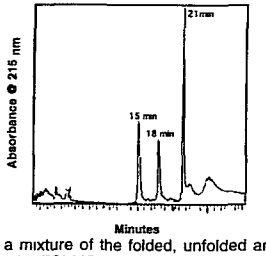

Figure3. ESIMS of HPLC Peaks.

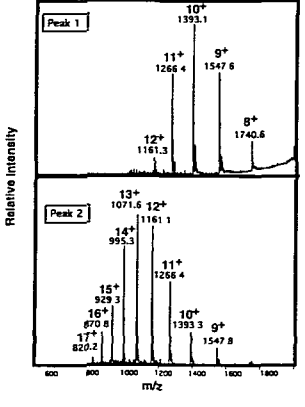

The renaturation of NT-4 requires proper folding, disulfide bond arrangement and non-covalent dimerization. MALDI-MS analysis was performed on a tryptic digest of folded NT-4 to determine disulfide order. The predicted tryptic peptides, in sequence order, are shown in Table 1. Peptide masses confirmed by MS are shown in italics, while the disulfide peptide sequences and masses are shown in bold type. The disulfide arrangement for NGF is 1-4, 2-5 and 3-6, where the numbers refer the order of the cysteine in the sequence.

Samples were prepared using α-cyano 4-hydroxy cinnamic acid as the matrix. With internal calibration, mass accuracy is typically 0.2 %, but order to enhance sensitivity, digest spectra shown here were obtained without using internal calibrant, in order to reduce ion supression effects. Masses of the more intense ions in the digest spectra were confirmed using internal calibration.

MALDI-MS analysis of the unreduced digest revealed ions resulting from cystine (S-S) peptides as a cluster of peaks with m/z values of 2566, 2721, 2782 and 3010 (Fig 3). The first three all result from a Cys 1->Cys 4 disulfide, but include incomplete cleavage products of T-3 with arginine.

Table 1 Tryptic peptides of NT-4.

Tryptic Peptide #	Average Mass	From	To	Sequence		
1	*974 0*	1	10	GVSETAPASR		
2	174 2	11	11	R		
3	*1677.8*	12	27	**GELAVCDAVSGWVTDR**		1
4	174 2	28	28	R		
5	*673 7*	29	34	TAVDLR		
6	231 3	35	36	GR		
7	*1680 0*	37	53	EVEVLGEVPAAGGSPLR		
8	*990.1*	53	60	QYFFETR		*2563*
9	***249.3***	61	62	**CK**	2	
10	***1474.4***	63	79	**ADNAEEGGPGAGGGGCR**	3	
11	445.5	80	83	GVDR		
12	174.2	84	84	R		
13	***888.0***	85	91	**RWVSECK**		4
14	217.2	92	93	AK		
15	*651.7*	94	98	QSYVR		*3014*
16	*901 9*	99	107	ALTADAQGR		
17	*516 6*	108	111	VGWR		
18	*473 6*	112	114	WIR		
19	***1294.5***	115	126	**IDTACVCTLLSR**	5-6	
20	332.4	127	129	TGR		
21	89.1	130	130	A		

Figure 3. MALDI-MS of NT-4 Tryptic Digest

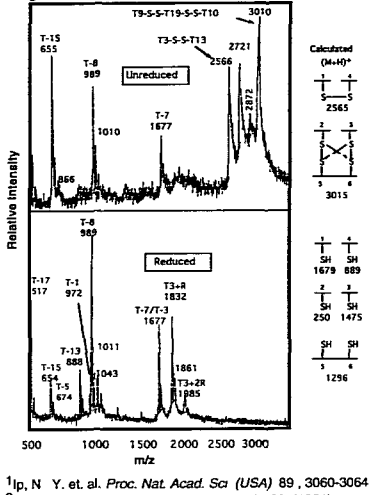

Disulfide arrangements are shown to the right with the cysteine residues numbered 1 through 6 in sequence order from the N-terminus The ion at m/z 3010 results from three peptides, T-9 (Cys 2), T-19 (Cys 5 and 6), and T-10 (Cys 3) joined by 2 disulfide bonds. The disulfide diagram shows the NGF pattern in solid lines, but the dashed lines indicate an alternate arrangement for the triplet which cannot be ruled out in this experiment (Cysteines 5 and 6 occur within the sequence Cys-Val-Cys, which is difficult to cleave enzymatically). The experiment does rule out an intramolecular disulfide between cysteines 5 and 6 in T-19. The disulfide peptides disappeared when the sample was reduced on the target with dithiothreitol (lower spectrum)

The masses of the disulfide-linked peptides were consistent with the disulfide pattern inferred from the crystal structure of NGF[3], suggesting that this pattern is conserved throughout the neurotrophin family.

In summary, human NT-4, expressed in E. coli, has been examined by ESI-MS and has been shown to exist in at least four discrete forms: a fully reduced form, an unfolded form from E. coli inclusion bodies, a folded, biologically active form, and an intermediate, unfolded form from partial reduction The forms displayed unique charge envelope patterns in ESI with an increasing number of ions with lower m/z values as the degree of unfolding increased. MALDI-MS analysis of tryptic digests of NT-4 allowed assignment of most of the predicted peptide fragments, including the disulfide-linked peptides.

[1] Ip, N Y. et. al. *Proc. Nat. Acad. Sci (USA)* 89, 3060-3064 (1992).
[2] Berkemeier, L. R. et al *Neuron* 7, 857-866 (1991)
[3] MacDonald N. Q. et al *Nature (London)* 354, 411-414 (1991)

Effects of Anions on Electrospray Ionization Mass Spectra of Peptides and Proteins

*Urooj A. Mirza and Brian T. Chait
The Rockefeller University, 1230 York Ave, New York, NY. 10021

Introduction Electrospray ionization mass spectra of peptides and proteins are usually obtained from solutions that are acidified and therefore contain relatively high concentrations of anions. The present paper describes a study of the effect of such anions on the electrospray ionization spectra of peptides and proteins and, in particular, on the observed charge distributions.

Experimental Electrospray ionization (ESI) mass spectra were obtained on an instrument constructed at The Rockefeller university and described previously.[1]

Results ESI mass spectra of bovine cytochrome c sprayed from solutions of low pH (2.2 - 1.4) yielded the suprising result that the average charge of the observed ions decreases as the pH of the spray solution is lowered (Fig. 1). Because the spectra taken at the lowest pHs contained trifluoroacetic acid in addition to acetic acid, we hypothesized that the nature of the acid may have effected the charge distribution. In an effort to understand the basis of this phenomenon, electrospray ionization spectra of cytochrome c were obtained from spray solutions containing respectively HCl, acetic, trifluoroacetic, and trichloroacetic acids at a constant pH of 2.2. The distributions of the charge states of ions in the resulting spectra exhibited sharp shifts as a function of the acid used in the spray solution, indicating that the average charge on cytochrome c in the gas phase is effected by the nature of the anion present in the spray solution.

To exclude possible complications from conformational effects, the experiments described above were repeated on small peptides. Thus, for example, the peptide K R Q H P G K R was analyzed from spray solutions maintained at constant pH using respectively acetic, trifluoroacetic, and trichloroacetic acids. The results shown in Fig 2 yielded a similar shift in the charge distribution as a function of the acid used.

These results indicate that the shift in the charge distribution of peptides and proteins is primarily due to the **nature of the anion** present in the spray solution. To further test this hypothesis, ESI spectra of the peptide K R Q H P G K R were obtained in the absence of acid but in the presence of the sodium salts of acetic, trifluoroacetic, and trichloroacetic acid . Again, a similar shift in the charge state is observed suggesting that the anions play a key role in determining the observed charge distribution. We hypothesize that a degree of neutralization was occuring via association of the anion with charge groups on the peptide or protein in solution followed by dissociation of the acid from the peptide or protein in the gas phase. The order of effectiveness of anions to produce such neutralization was **trichloroacetate > trifluoroacetate > acetate chloride.** This series is similar to the electroselectivity series of anions towards anion exchange resins.[2] Association of anions with charge groups were confirmed by comparing the spectra of peptides at relatively low collision-induced desolvation energies with the somewhat higher collision-induced desolvation energies that we normally use to obtain the most intense electrospray ionization mass spectra. At low collision-induced desolvation energies, adducts of the anions with the peptide ions are clearly observed (Fig.3).

References :
1) S.K. Chowdhury, V. Katta and B.T. Chait, Rapid Communi. Mass Spectrom. **4** (1990) 81.
2) Y. Goto, N. Takahashi and A. L. Fink, Biochemistry **29** (1990) 3480

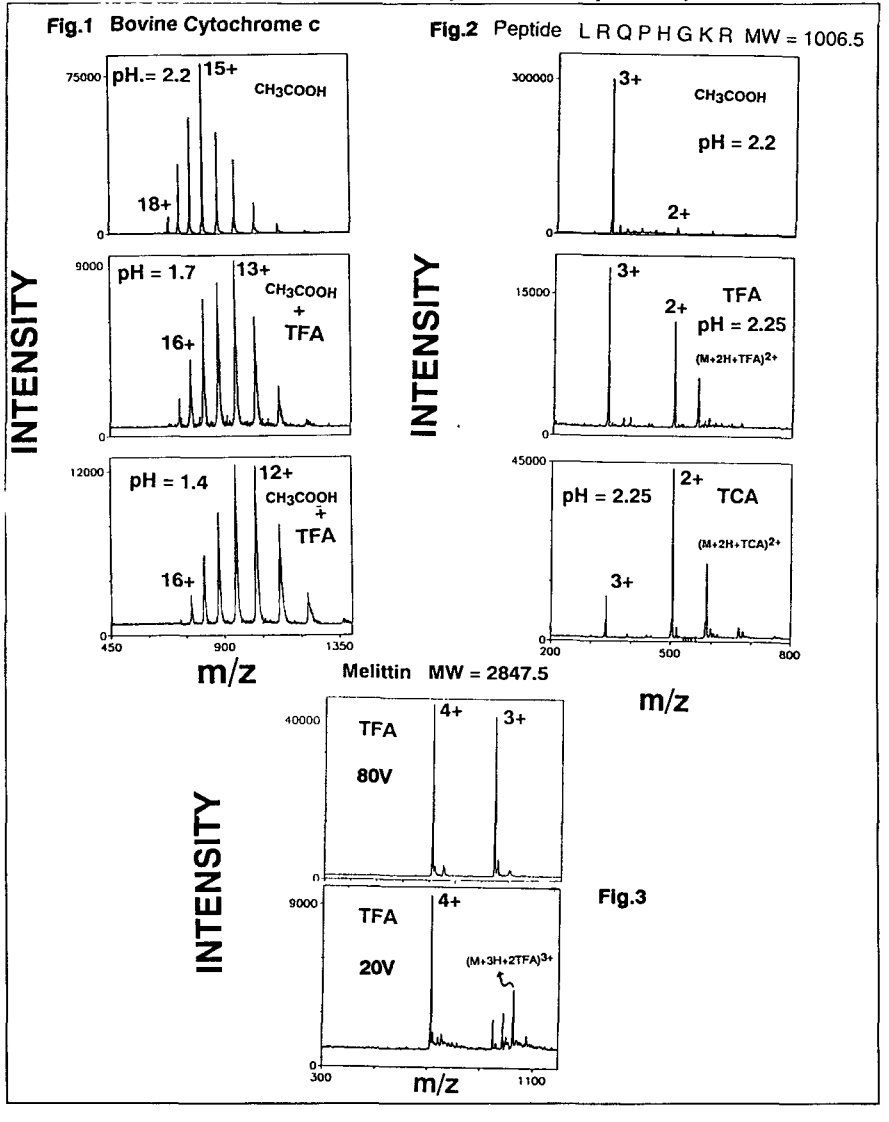

Fig.3

Analysis of Biliproteins by Electrospray Ionization Mass Spectrometry

***Shinya HASHIMOTO and Akira OTSUKI**

Department of Marine Science & Technology
Tokyo University of Fisheries
4-5-7 Konan, Minato-ku, Tokyo 108

Electrospray ionization (ESI) mass spectrometry was used for the analyses of biliproteins. The relative molecular masses of α and β subunits obtained by computer deconvolution were 18,185.9 ± 1.0 Da and 19,236.8 ± 2.9 Da for C-phycocyanin and 18,978.0 ± 0.9 Da and 20,325.8 ± 1.0 Da for B-phycoerythrin, respectively.

Most species of cyanobacteria and red algae contain an antenna assembly called the phycobilisome[1]. This particle consists of proteins-pigment complexes (biliprotein), most of which carry covalently attached, open chain tetrapyrrole pigments. The tetrapyrroles are linked to the polypeptide chains through thioether linkages. These biliproteins are made up of two dissimilar polypeptide chains, α and β.

To date, the molecular weights of biliproteins and their subunits have been roughly determined, for example, by the sedimentation equilibrium method[2]. The molecular weight of these subunits described ranged from 18,100 Da to 22,200 Da. However, determination of a more accurate molecular weight may be necessary. We describe here an application of ESI mass spectrometry[3] for the accurate determination of biliprotein and its subunits masses. ESI mass spectrometry was used for the analyses of C-phycocyanin from *Spirulina sp.* (Sigma P-6161) and B-phycoerythrin (Polysciences 18110). The biliprotein samples analyzed were prepared in 2.5 % acetic acid dissolved in 50:50 (v/v) methanol-water solutions at a concentration of 100 pmol/μL. The solution was continuously infused into the ion source with a Harvard Apparatus syringe pump at 1 μL/min. Full-scan mass spectra were acquired from m/z 200-3000 or 700-2700 in 5 seconds and averaged over 1 min. The ESI mass spectral analysis was performed with a Finnigan MAT model TSQ-700 quadrupole mass spectrometer (Finnigan-MAT Corp., San Jose, CA, 4000 m/z range). The ESI mass spectra and deconvoluted mass spectra of C-phycocyanin and B-phycoerythrin are shown in figure 1-4.

The calculation of molecular mass from the observed m/z values of ions indicates that both samples consist of two different proteins (α and β subunits). The relative molecular masses of α and β subunits obtained by computer deconvolution were 18,185.9 ± 1.0 Da and 19,236.8 ± 2.9 Da for C-phycocyanin and 18,978.0 ± 0.9 Da and 20,325.8 ± 1.0 Da for B-phycoerythrin, respectively. The measurement of mass of biliproteins within ± 0.015% can be performed by electrospray ionization. The electrospray technique provides a sensitive and powerful approach to the determination of accurate mass of biliproteins.

References 1) A. N. Glazer, "Methods in Enzymology", L. Packer et al. ed., Academic Press, (1988), **167**, 291.
2) T. Fujiwara-Arasaki, M. Yamamoto and K. Kakiuchi, Biochim. Biophys. Acta, **828** 261 (1985).
3) B. T. Chait and S. B. H. Kent, Science, **257**, 1885 (1992).

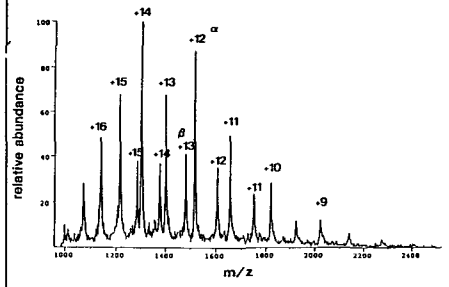

Figure 1
ESI mass spectrum of C-phycocyanin. The calculated charge states of the α and β subunits of this C-phycocyanin are indicated.

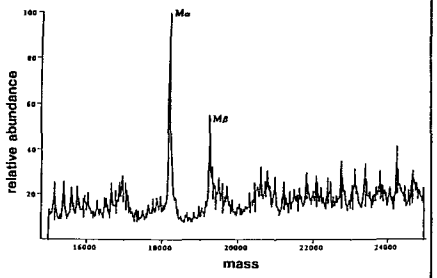

Figure 2
Deconvoluted ESI mass spectrum of the profile data from Figure 1 of the C-phycocyanin. M_α: 18,185.9 ± 1.0 Da, M_β: 19,236.8 ± 2.9 Da.

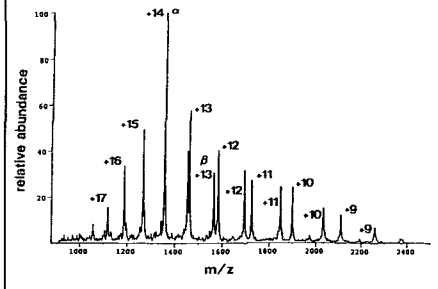

Figure 3
ESI mass spectrum of B-phycoerythrin. The calculated charge states of the α and β subunits of this B-phycoerythrin are indicated.

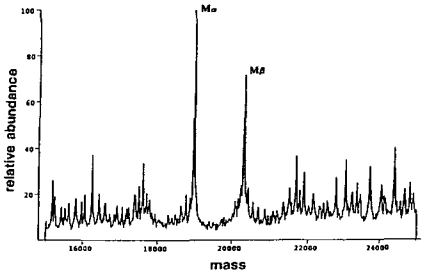

Figure 4
Deconvoluted ESI mass spectrum of the profile data from Figure 3 of the B-phycoerythrin. M_α: 18,978.0 ± 0.9 Da, M_β: 20,325.8 ± 1.0 Da.

Determination Of The Disulfide Bonding Pattern Of Peptide Toxins From The Spider *Agelenopsis Aperta* Using Electrospray Ionization Mass Spectrometry

J.G. Stroh, K.J. Rosnack, N.A. Saccomano, R.A. Volkmann, and D. Phillips
Central Research Division, Pfizer Inc, Groton, CT 06340

Peptide spider toxins are well known Ca^{2+} channel blockers. These peptides contain many disulfide bonds. We reported here on the disulfide bonding pattern of two peptides from the spider *Agelenopsis aperta* Ag-G (Scheme 1) and Ag-H2 (Scheme 2). Both peptides have five disulfide bonds. Trypsinolysis followed by electrospray LC/MS analysis of the partially digested material produced numerous fragments of the proteins (as shown in Figure 1). Based on the molecular weights of the partially fragmented peptides, three of the disulfide bonds could be unambiguously determined in both spider toxins as shown in Table 1.

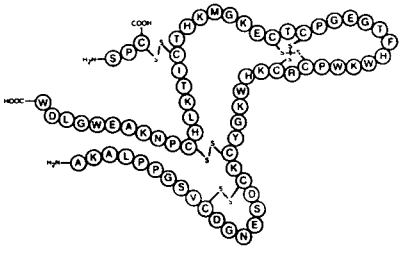

Ag-H2
Scheme 1

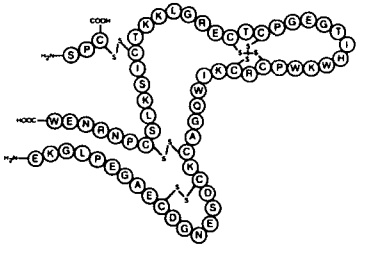

Ag-G
Scheme 2

Figure 1

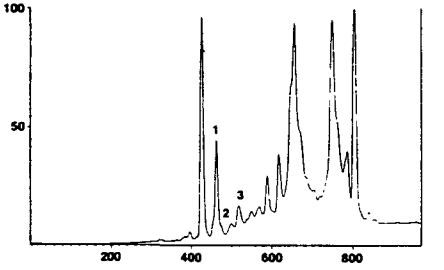

HPLC with UV detection. Data collected after 41 hours of tryptic digestion.

Table 1

HTCIRK | SPC	Peak 1
CYGK | LHCPNK	Peak 2
ALPPGSVCDGNESDCK	Peak 3

Mass Spectrometry Characterization of the Phosphorylated Proenkephalin A-Neuropeptides

*Chhabil Dass and P. Mahalakshmi
University of Tennessee, Memphis, TN 38163.

Post-translational processing of bioactive peptides is an area of significant importance and of growing interest. Protein phosphorylation represents one of the most important and ubiquitous post-translational events. Many metabolic and physiological responses of hormones, neurotransmitters, and extracellular signals are manifested through protein phosphorylation. Phosphorylation of Tyr, Ser, and Thr is mediated by substrate- specific protein kinases. Proenkephalin A (PE-A) is a large 263 amino acids long protein, and is the precursor of enkephalin family of opioid peptides. It contains several Tyr, Ser and Thr, residues embedded within the consensus sequences recognizable by the protein kinases. It is important to have a knowledge whether PE-A peptides undergo phosphorylation and what is the biological significance of this covalent modification.

This study was designed to understand the biological significance of phosphorylation of PE-A peptides. As a first step in this direction, the following specific experiments were undertaken: (a) an experimental protocol was developed to synthesize several phosphorylated PE-A peptides. We used Fmoc chemistry and solid-phase peptide synthesis (SPPS) methodology (on an Advanced ChemTech ACT 90 SPP synthesizer) to synthesize phosphorylated leucine enkephalin (LE-PO_4), methionine enkephalin (ME-PO_4), LE-Lys-PO_4, ME-Lys-PO_4, ME-Arg-PO_4, ME-Arg-Phe-PO_4, ME-Arg-Gly-Leu-PO_4 and (b) the conventional magnet scan and MS/MS spectra (in the MIKES mode) of those peptides were acquired with the objective to obtain sequence-specific information. LSIMS (or FAB) is the method of choice for analysis of thermally labile and polar molecules such as peptides. This study used a VG AutoSpec Q mass spectrometer of E_1BE_2-qQ geometry and 30-35 keV Cs^+ ions as the ionizing beam. Glycerol was used as the liquid matrix.

An abundant $(M+H)^+$ ion is obtained in the conventional magnet scan spectrum of those peptides. The signal due to the loss of HPO_3 to yield the $(M+H)^+$ ions of the unphosphorylated peptides is < 10% of the $(M+H)^+$ intensity. The LSIMS data can be used to obtain AA sequence of those peptides. The typical examples are shown in Figs. 1 and 2. As illustrated in Fig. 1, a complete set of b-type N-terminus sequence ions of LE-PO_4 is observed. The AA sequence determination of LE-PO_4 is also feasible from the C-terminus; all of the y-type ions are seen in the LSIMS spectrum.

The MS/MS provides highly structure-specific data because of the link established between the exclusively mass-selected precursor and its product ions. The MS/MS data, acquired in the MIKES mode, is equally information-rich. As shown in Figs. 3-5 for LE-PO_4, ME-PO_4 and LEK-PO_4, respectively, complete sequencing of these peptides is possible from both ends of the peptides.

Thus, LSIMS either alone or in combination with CID can be used to establish the AA sequence of phosphorylated enkephalin peptides.

Acknowledgment: Financial support of the NIH (Grant NS 28025) is highly appreciated.

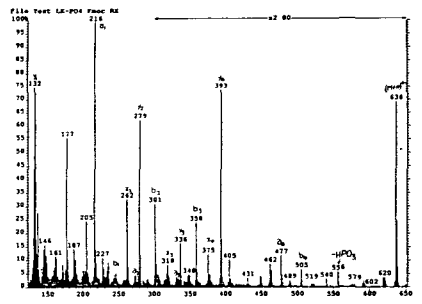

Figure 1-LSIMS spectrum of LE-PO_4

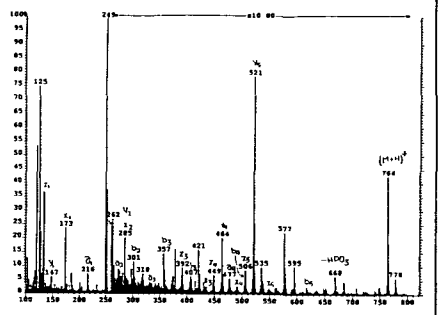

Figure 2-LSIMS spectrum of LE-Lys-PO_4

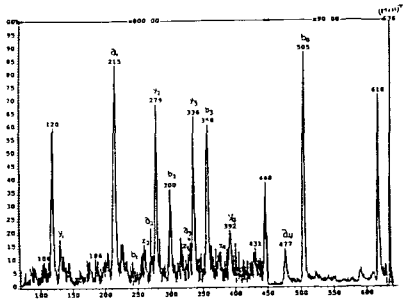

Figure 3-CID-MIKES spectrum of LE-PO_4

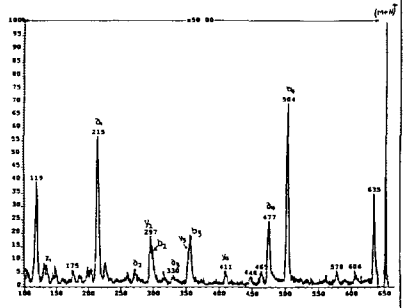

Figure 4-CID-MIKES spectrum of ME-PO_4

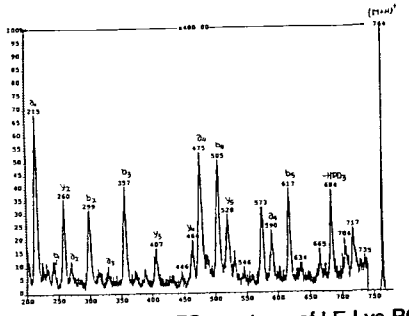

Figure 5-CID-MIKES spectrum of LE-Lys-PO_4

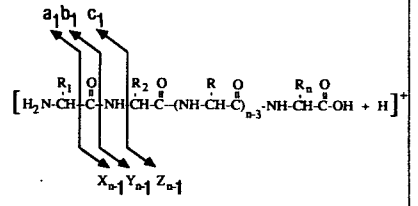

Identification of Two Sites of Phosphorylation in Bleached Bovine Rhodopsin by Tandem Mass Spectrometry.

D. I. Papac, J. E. Oatis Jr., R. K. Crouch and D. R. Knapp
Medical University of South Carolina, Charleston, SC 29425

Introduction: Deactivation of the visual cascade is achieved at multiple sites in the biochemical pathway. One site of deactivation involves the phosphorylation of activated rhodopsin by rhodopsin kinase[1]. Concentrated between residues 333 to 343 in the C-terminus of rhodopsin are seven hydroxyamino acids, the region thought to contain most of the phosphorylation sites[2]. Using mass spectrometry and synthetic reference standards we have identified the two major sites of phosphorylation, serines 338 and 343, within the 19 amino acid C-terminal segment of bleached bovine rhodopsin.

Methods: Rod outer segments (ROS) were isolated from 50 frozen bovine retinae[3]. Following the isolation, half of the ROS were bleached and half were treated as the bleached ROS, except they were not illuminated. Bleaching was performed on the ROS in 0.1 M sodium phosphate (pH 7.4) containing 1 mM $MgCl_2$ and 4 mM ATP under continuous illumination with white light for 30 min at 37°C[4]. After 30 min, 1M NaF was added to a final concentration of 10 mM to inhibit phosphatase activity[5]. The ROS were then washed with 10 mM Tris-HCl (pH 7.8) containing 50 mM NaF and 10 mM NaPPi and cleaved with endoproteinase Asp-N overnight at 37°C employing an enzyme to substrate ratio of 1:6000 (w/w).

Separation of the enzyme digests was performed on a Vydac C-18 column 4.6 x 250 mm. The mobile phase consisted of 0.1% aqueous TFA (A) and acetonitrile containing 0.084 % TFA (B). The gradient was 98% A held for 10 min then ramped linearly over 80 min to 40% B.

Mass spectra were obtained on a JEOL HX110/HX110 four sector tandem mass spectrometer. Samples were dissolved in 10 μl of 1N HCl, applied to the probe in a matrix of 1 N HCl/ thioglycerol, and ionized with 18 kV cesium ions. Single stage mass analysis was performed with an accelerating voltage of 10 kV and a resolution of 1500. The MS/MS experiments were performed with the collision cell operated at 3 kV and filled with enough helium to attenuate the ion current of the C-12 monoisotopic peak by 70%.

Synthetic Phosphopeptides: Monophosphorylated TSQVAPA, ASTTVSKTE, and DDEASTTVSKTETSQVAPA, were prepared as described[6].

Results: Shown in figure 1 is the chromatogram obtained following endoproteinase Asp-N cleavage of bleached ROS. Peaks 2 & 3 when analyzed by LSIMS produced a MH^+ ion of 2016.8 Da corresponding to the incorporation of one phosphate (+80 Da) into the C-terminal peptide DDEASTTVSKTETSQVAPA (MH^+ = 1936.9 Da). The retention time of peaks 2 and 3 were identical to that for synthetic DDEASTTVSKTETS(p)QVAPA and DDEASTTVS(p)KTETSQVAPA, respectively. Treatment of peaks 1 and 2 with alkaline phosphatase shifted the retention time and MH^+ ion to that for the unmodified C-terminal peptide. Due to difficulty in generating sufficient ion signal peaks 2 and 3 were subdigested with endoproteinase Glu-C. The

digests were separated by HPLC and then analyzed by MS/MS to determine the sites of phosphate attachment. Peak 2 was phosphorylated at serine 343 and peak 3 at serine 338. Using this same approach peak 1 was identified as a diphosphorylated derivative with the phosphates attached at serines 338 and 343. Higher phosphorylation states (tri- & tetra-phosphorylated) of the C-terminal peptide were observed but insufficient material was obtained to identify the sites of phosphate attachment. Analysis of the chromatogram obtained from unbleached ROS revealed only a small amount of phosphorylation at serine 338. When phosphatase inhibitors were omitted during enzymatic cleavage, serine 343 was preferentially dephosphorylated.

Conclusions: *We have identified the major sites of phosphorylation in the C-terminal region of bovine rhodopsin (serines 338 and 343), and the data indicate that this region may be constitutively phosphorylated.* Figure 2 shows the two sites of phosphorylation on the cytoplasmic tail of bovine rhodopsin idicated by shaded spheres. Our observations also suggest the possibility of a site specific order in the phosphorylation and dephosphorylation of bovine rhodopsin.

References:

1. Shichi, H. (1989) in *Receptor Phosphorylation* pp 177-98 CRC Press.
2. Hargrave, P. A., *et al.* (1982) Vision Res. 22:1429-38.
3. McDowell, J. H., and Kühn, H. (1977) Biochem. 16:4054-60.
4. Wilden, U., and Kühn, H. (1982) Biochem. 21:3014-22.
5. Cohen, P. *et al.* (1991) Methods in Enzymol. 201:153-68.
6. Knapp, D. R. *et al.* (1993) Int. J. Pep. Prot. Res. (in press).

This work was supported by grants from the N.I.H. (EY08239, EY04939) and N.S.F. (DIR 8804502).

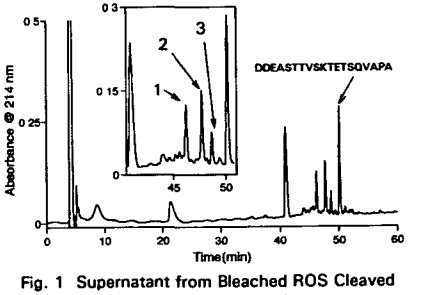

Fig. 1 Supernatant from Bleached ROS Cleaved with Endoproteinase Asp-N.

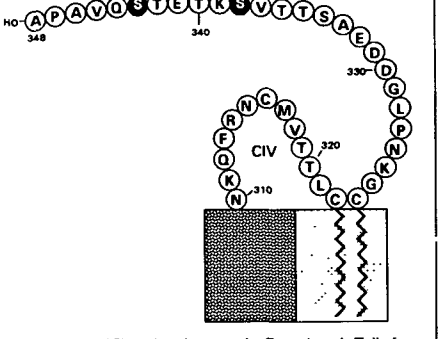

Fig. 2 Sites of Phosphorylation in the Cytoplasmic Tail of Bovine Rhodopsin.

Mass Spectrometry of Protein Samples Containing Detergents

Ole Vorm, Brian T. Chait*, and Peter Roepstorff, Odense University, DK-5230 Odense M, Denmark. *The Rockefeller University, N.Y., New York 10021

Detergents are widely used in protein chemistry because they greatly increase the solubility of peptides and proteins and facilitate purification and/or separation. However, the presence of detergents in peptide and protein samples usually inhibits mass spectrometric analyses of the "purified" compounds.

We have examined a selection of 16 detergents for their influence on the quality of the spectra of peptides and proteins obtained by ^{252}Cf plasma desorption and matrix assisted laser desorption/ionization mass spectrometry. The detergents are broadly characterized (see the table below) into those that: (i) prohibit the acquisition of useful mass spectrometric data [+++]; (ii) reduce the quality of the spectra [++]; (iii) exert little influence on the quality of the spectra [+]; and (iv) often improve the quality of the spectra [+/+]. In general, the most damaging class of detergents to mass spectrometry are those that are ionic (e.g. SDS) and the least damaging or even beneficial are those that are non-ionic (e.g. n-octyl-glucoside).

Detergent	PD	MALDI
n-Octyl-glucoside	+/+	+/+
n-Dodecyl-glucoside	+/+	+/+
n-Dodecyl-ß-D-maltoside	+/+	+
Octanoyl-N-methylglucamide (MEGA-8)	+/+	+/+
Decanoyl-N-methylglucamide (MEGA-10)	+/+	+/+
Octylphenolpoly(ethyleneglycolether)10 (Triton® X-100)	+++	++
Octylphenolpoly(ethyleneglycolether)7 (Triton® X-114)	+++	++
Dodecylpoly(ethyleneglycolether)9 (Thesit®)	+++	+++
Isotridecylpoly(ethyleneglycolether)8	+++	+++
3-[(3-Cholamidopropyl)dimethyl-ammonio]-1-propanesulphonate (CHAPS)	+++	+++
3-[(3-Cholamidopropyl)dimethyl-ammonio]-2-hydroxy-1-propanesulphonate (CHAPSO)	+++	+++
N-Dodecyl-N,N-dimethyl-3-ammonio-1-propanesulfonate	+++	+++
Polyethylene glycol 2000 (PEG)	+++	++
Sodium dodecylsulphate (SDS)	++	++
Tris(hydroxymethyl)amino-methane hydrochloride (TRIS)	+	+
Ethylenedinitrilo tetraacetic acid, disodium salt dihydrate (EDTA)	+	+

Surprisingly, we have found that the addition of some non-ionic detergents, esp. n-octyl-glucoside, to the matrix or peptide sample solutions prior to the sample preparation often *improves the signal-to-noise ratios of peptide and protein peaks. More importantly, this* procedure reduces the peptide specific suppression effects that are frequently observed in MALDI and ^{252}Cf PD mass analyses of peptide mixtures, thereby greatly increasing the likelihood of actually observing all the components that are present in a sample mixture.

A very pertinent example is, characteristic for the cinnamic acid derivative matrices, that relatively small peptides may suppress larger peptides and proteins, as shown below by two MALDI spectra of the same mixture of tryptic peptides from the locust cuticle protein "V4-D1b" (Mr 12684.8). The upper spectrum is taken without and the lower with n-octyl-glucoside present. The detergent is necessary in order to detect the peptide at Mr 5039.8 (aa seq. 1-60) and also the intensity of the peak of the peptide at Mr 2717.2 (aa seq. 92-116) changes remarkably.

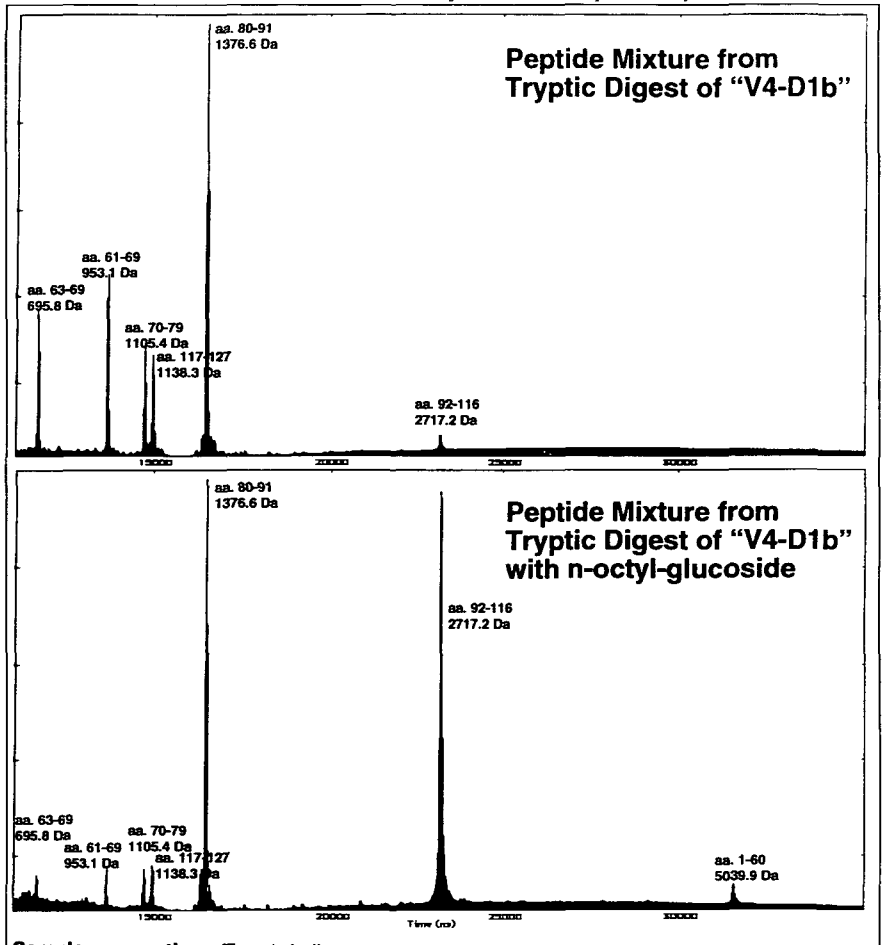

Sample preparation: Two 1µl aliquots of tryptic peptides from V4-D1b (max. 8pmol/µl) in the digest buffer (pH 7.8) were diluted by a factor of five, one of them by water and the other by a 10 mM aqueous solution of n-octyl-glucoside. 0.5 µl of each of these peptide solutions was mixed on a probe tip (of 1.5 mm diam.) with 0.5 µl of matrix solution (saturated solution of α-cyano-4-hydroxy-cinnamic acid in acetonitrile/0.1% TFA 50:50 v/v), i.e. a maximum of 800 fmol of each peptide is applied to the probetip.

Predicting Degratation Products of Environmental Contaminants by On-line Electrochemistry/Mass Spectrometry

Jon A. Jones and Richard A. Yost, Department of Chemistry, University of Florida, Gainesville, FL 32611; Douglas W. Kuehl, U.S.EPA-ERL, Duluth, MN 55804.

Many carcinogenic compounds require metabolic activation to a reactive electrophile before they can alter DNA. The conversion of a procarcinogen into the ultimate carcinogen is generally an enzyme-controlled oxidation-reduction reaction. Many aromatic amines are known to be carcinogenic, and the metabolism of these compounds into reactive electrophiles has been attributed to a variety of enzymes, including cytochrome P-450 [1].

The study of the metabolism of procarcinogens traditionally involves animal studies or lengthy enzymatic digestion followed by solution-phase reactions with DNA. Our interest in this research is to bring the study of procarcinogen metabolism from the solution-phase into the gas-phase. In our laboratory, we have investigated the use of electrochemistry (EC) to activate procarcinogens and mass spectrometry (MS) to analyze the electrochemically generated products. The use of on-line EC/MS to model the enzymatic oxidation of purine compounds has previously been demonstrated, with tandem quadrupole mass spectrometry employed to elucidate the structures of the intermediates involved in the metabolism [2].

In this work, the electrooxidation of some aromatic amines is studied by on-line EC/MS. Of the number of interfaces available for interfacing the solution phase to the mass spectrometer, thermospray (TSP) and particle beam (PB) interfaces were investigated. All EC/TSP/MS experiments were performed using a Vestec Thermospray source on a Finnigan MAT TSQ 45 triple quadrupole mass spectrometer (TQMS) using an Isco LC-2600 syringe pump at a flow rate of 1.0 mL/min. EC/PB/MS experiments were performed with a Finnigan prototype 3-stage PB interface on a modified Finnigan MAT ITS40 quadrupole ion trap mass spectrometer (QITMS) using a Hewlett Packard 1090 liquid chromatograph for sample introduction at a flow rate of 0.15 mL/min. The electrochemistry was conducted using a ESA model 5020 guard cell with a model 173 potentiostat (EG&G Princeton Applied Research). The supporting electrolyte used was ammonium acetate, at a concentration of 0.1 M for TSP and 0.01 M for PB experiments.

EC/MS studies were performed by loop injection of 5-10μL of the sample solution into the electrochemical cell. The electrode potential was held constant for triplicate injections, and the average peak areas for the analyte and any products were calculated at each potential. This procedure was repeated over the potential range of interest by incrementing the electrode potential, thus creating a mass spectrometric hydrodynamic voltammagram (MSHV).

The MSHV obtained for N,N-dimethylaniline (DMA) by TSP/TQMS is shown in Figure 1. The mass spectrum obtained at a potential of +350 mV is shown in Figure 2. The product ion at m/z 241 is thought to be protonated N,N,N',N'-tetramethylbenzidine (TMB). The ion at m/z 227 has previously been attributed to a fragmentation of $(TMB+H)^+$ [3]; however, the mass intensity data for m/z 227 in Figure 1 does not parellel that for m/z 241 as one would expect for a fragment ion. The intensity for the m/z 213 species also does not parallel either of the other two ion intensities, suggesting that this may be a different oxidation product.

The MSHV obtained for benzidine by PB/QITMS is shown in Figure 3. This experiment was performed in a 50/50 methanol/0.01M ammonium acetate solvent system on a new carbon electrode. The ions at m/z 275, 364, and 366, shown in the spectrum in Figure 4, indicate oxidation and further reaction of the benzidine to various products. These products are consistent with those we have observed in on-line EC/MS of p-anisidine. The formation of azo and hydrazo derivatives appears to be the primary reaction pathway for primary aromatic amines at the potentials studied. Repetition of this experiment yielded different results; no products were observed. The absence of EC products for benzidine is thought to be due to adsorption of benzidine or its EC generated products onto the electrode surface. The alteration of the surface appears to have a significant effect on the oxidation of benzidine but does not appear to affect that of DMA or p-anisidine.

Figure 1
MSHV of N,N-Dimethylaniline by EC/TSP/MS

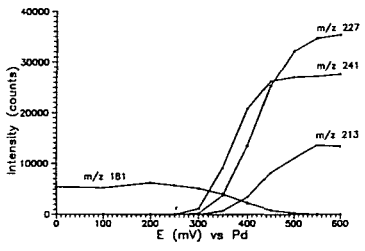

Figure 3
MSHV of Benzidine by EC/PB/MS

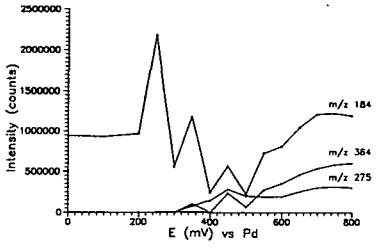

Figure 2
Mass Spectrum of N,N-Dimethylaniline at E=+350 mV

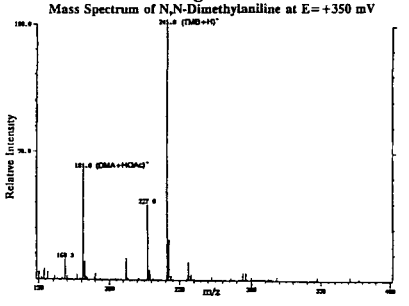

Figure 4
Mass Spectrum of Benzidine at E=+500 mV

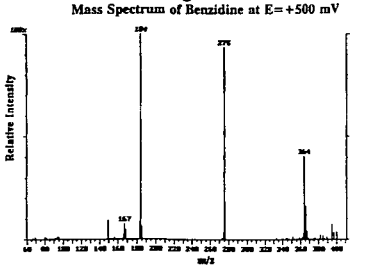

References
[1] Aoyama, T.; Gelboin, H. V.; and Gonzalez, F. J. *Cancer Res.* 1990, 50, 2060-2063
[2] Volk, K. J.; Yost, R. A.; Brajter-Toth, A. *Anal. Chem.* 1989, 61, 1709-1717.
[3] Hambitzer, G.; Heitbaum, J. *Anal. Chem.* 1986, 58, 1067-1070.

A Mass Spectrometer Based Diagnostic to Analyze the Hostile, High Enthalpy Exhaust of a Hypersonic Engine

Albert D. Tomassian and Thomas L. Bunn
Rocketdyne Division, Rockwell International
Canoga Park, CA 91309-7922

A diagnostic application of mass spectrometry has been developed to sample the exhaust of an air breathing supersonic combustion RAMJET engine. This integrated, hydrogen burning engine will power the single-stage-to-orbit, National AeroSpace Plane (X-30). The objective of the gas sampling diagnostic is to analyze the burned and unburned products of combustion emanating from subscale engine components. These engine components (i.e. inlet, combustor and nozzle) are tested in hypersonic, combustion heated wind tunnel facilities. The gas sampling project was undertaken to ascertain the extent of supersonic mixing and combustion as tunnel flow conditions, fuel injection schemes and engine configurations were varied.

Water cooled probes draw gas samples from the test article. Four probes located downstream of the tunnel facility nozzle and eight probes situated in the exit plane of the engine's internal nozzle are mounted on translatable rakes to survey several locations normal to the flow. Each gas sample is transported through the heated, three stage differentially pumped, inlet manifold to a dedicated residual gas analyzer (RGA) for real time analysis. The manifold was designed to prevent water condensation, reduce the pressure and minimize the response time as a gas sample is conveyed from the probe tip to the inlet aperture of the spectrometers. The quadrupole RGA's have independent vacuum systems, utilize open electron impact ionization sources, employ autoranging electrometers and possess a mass range of 1 to 100 amu. The instrumentation is enclosed in an air conditioned and shock isolated cart that is controlled remotely by a data acquisition computer. The computer synchronizes the rake movement with a record of 12 chemical compounds every 1.2 seconds. Spectrometer calibration is achieved for most flow constituents using certified gas mixes and for water vapor by flowing humid nitrogen through the gas sampling diagnostic and a chilled mirror hygrometer simultaneously.

In SCRAMJET tests, fuel is injected through multiple orifices into the engine's parametric (variable geometry) combustor and coerced to mix with the supersonic vitiated air flow by inducing turbulence. The gas sampling

diagnostic is used to analyze the specie concentrations of the vitiated air flow (i.e. O_2 replenished, H_2 combustion heated air flow) at the exit of the facility nozzle and of the combustor exhaust flow at the exit plane of the internal nozzle. Mole fractions, χ_i, are calculated by normalizing the ion signals, which assumes that the diagnostic measured every gaseous component in the flow. An equation for equivalence ratio, ϕ, defined as the ratio of the fuel mass flow rate to the oxidizer mass flow rate, relative to the fuel/oxidizer stoichiometric ratio, is derived in terms of mole fractions. Formulating the "amount of burned hydrogen" term in the ϕ equation as two times the "amount of consumed oxygen" rather than the "amount of water formed" yielded more repeatable and reliable results. Equivalence ratio contours provide data to study fuel penetration as a function of injector location, injection angle and free stream Mach number. Fuel distribution plots also indicate mixing effectiveness as a function of fuel injection schemes and engine configurations. Combustion efficiency, η_c, is also derived in terms of mole fractions and is defined as the percentage of burned fuel in fuel lean locations and as the percentage of consumed oxygen in fuel rich regions.

Using carefully determined calibration sensitivities and background levels, the ion signal versus time data files are reduced to plot contours of specie mole fractions, equivalence ratios and combustion efficiency. N_2 and O_2 mole fraction data for the vitiator (facility) calibration plotted as a function of probe location and H_2, N_2 and O_2 mole fraction contour plots for a SCRAMJET engine test were presented during the poster session. Two equivalence ratio contours were presented in the poster session for different fuel injection schemes. Combustion efficiency contours for these tests were also presented.

The gas sampling diagnostic results are compared with and used to validate computational fluid dynamics codes. Furthermore, combustion efficiency contours are integrated to calculate the overall average (or global) combustion efficiency which is strongly correlated to engine thrust. The global combustion efficiency, $<\eta_c>$, is an important measured property for evaluating performance. Currently, work is under way to understand the vortical mixing process more completely by seeding the fuel with helium through selected injectors and mapping the inert helium to determine the most effective fuel injection scheme.

Identification of Polychlorodibenzothiophenes in Crab Tissues From Raritan/Newark Bay

Zongwei Cai, D. E. Giblin, V. M. S. Ramanujam and M. L. Gross, Midwest Center for Mass Spectrometry, Department of Chemistry, University of Nebraska, Lincoln, NE 68588

Polychlorodibenzo-dioxins and -furans (PCDD/Fs) were found in crab tissues collected from the Raritan/Newark Bay system in New Jersey[1]. Analysis of the samples showed an unknown major component (approximately ten times the level of 2,3,7,8-TCDD) was present in the mass window for TCDD (Figure 1A). The unknown compound has similar chemical and chromatographic properties as PCDD/Fs since it was present in the same sample extract despite many steps of clean-up including three column chromatographic separations. Moreover, the molecular ion clusters of the unknown compound have the same nominal masses and isotopic patterns as those TCDD.

It would be very difficult to determine whether this major peak is an isomer of TCDD or an interference by using the conventional peak top monitoring mode even with GC/high resolution MS at mass resolution of 10,000. The unknown compound has a chromatographic retention time within the window for TCDD isomers. That retention time corresponds to that for at least 16 TCDD isomers.

The mass profile mode provides additional information such as accurate mass about the ions that are being monitored. By using the mass profile mode[2], the unknown compound was not only shown to be an interference but also identified by accurate mass information as a likely isomer of tetrachlorodibenzothiophene (TCDT), a sulphur analogue of TCDF.

Figure 1B shows the profiles of mass peaks of the unknown compound (solid line) and those of 2,3,7,8-TCDD (dashed line). Centroid analysis of the mass profiles for the unknown compound indicates that the accurate masses of the two selected ions are approximately 50 ppm less than those expected for TCDD. The accuracy of masses derived from this analysis have less than 10 ppm deviation. Thus, one can easily determine that the unknown component is not a TCDD isomer. Moreover, the accurate masses (*m/z* 319.8814 and *m/z* 321.8797) match closely those of the molecular ion clusters of TCDT (*m/z* 319.8788 and *m/z* 321.8759) rather than those of TCDD (*m/z* 319.8965 and *m/z* 321.8936). Measurements of the accurate masses along with the isotope distribution pattern suggest that the two ions have atomic compositions of $C_{12}H_4Cl_4S$ and $C_{12}H_4{}^{35}Cl_3{}^{37}ClS$. Similarly, an isomer of P_5CDT was identified in the mass window for P_5CDD.

The mass difference between the molecular ions of polychlorodibenzothiophenes (PCDTs) and PCDDs is 0.0177 mass units, the mass difference between O_2 and S. This small mass difference leads to an interference when resolution of 10,000 in HRMS is used. In fact, a mass resolving power greater than 18,000 is required to separate the PCDTs from the corresponding PCDDs in peak top analysis. Mass Profile, however, can separate an interference from dioxin by the mass difference as low as 0.0032 mass units, for which a resolution greater than 100,000 is needed for the peak top mode.

The identification of the TCDT in the crab samples has been confirmed by using GC/MS (EI) and high resolution peak match combined with GC. The EI mass spectrum of TCDT found in a pancreas sample matched that published in the literature[3]. Exact masses for the three most abundant ions of the molecular ion cluster of TCDT were determined by high resolution peak match performed as the compound came off the gas chromatograph. Mass deviations between experimental and theoretical data in the GC/high resolution peak match analysis were less than 3.0 ppm (Figure 2).

Concentration levels of TCDT and P_5CDT in some pancreas samples are listed in Table 1. The response factors for the PCDTs are unknown owing to a lack of standards. Therefore, we used $^{13}C_{12}$-2,3,7,8-TCDD as internal standard to get preliminary quantitative estimates. The levels of the TCDT are more than 5 times those of 2,3,7,8-TCDD, assuming the relative response factor for TCDT is similar to that for 2,3,7,8-TCDD. In some muscle samples, TCDD/F and P_5CDD/F were not present (detection limits are 1 ppt), whereas TCDT and P_5CDT were easily detected.

PCDTs have been found in other environmental samples[3-5]. The source and potential toxicity of PCDTs remain unknown at this time, but the compounds are expected to be biologically active[3].

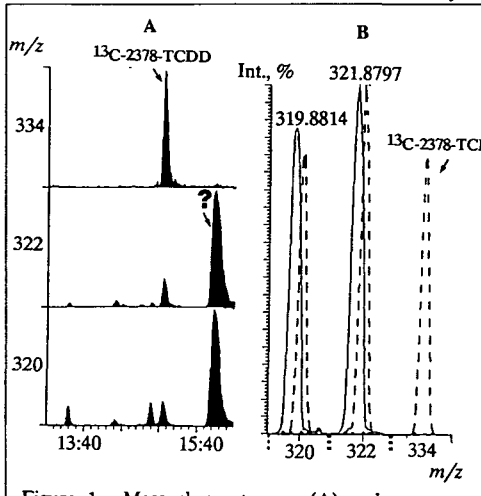

Figure 1. Mass chromatogram (A) and mass profile spectra (B) for TCDT (solid line) and 2378-TCDD (dashed line).

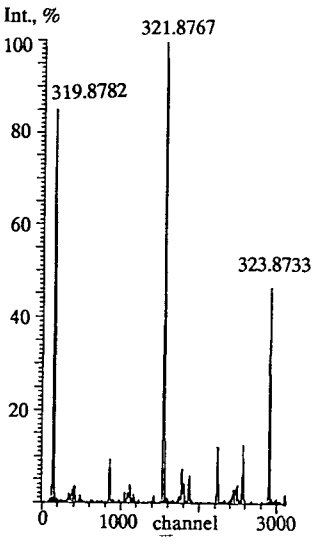

Mass	Int., %	Dev., ppm	Formula
319.8782	85	-2.0	$C_{12}H_4{}^{35}Cl_4S$
321.8767	100	+2.6	$C_{12}H_4{}^{35}Cl_3{}^{37}ClS$
323.8733	43	+1.2	$C_{12}H_4{}^{35}Cl_2{}^{37}Cl_2S$

Figure 2. GC/HR peak match analysis of TCDT found in the pancreas sample.

Table 1. Levels (ppt) of TCDT and P_5CDT in crab pancreas samples.
Date of sample collection: Sept., 1991

Station	2378-TCDD	TCDT	P5CDT
1	50	300	ND
2	90	490	ND
3	940	14,800	350
4	210	1,500	60

Reference:

1. Cai, Z., Ramanujam, V.M.S., Gross, M.L., Cristini, A., presented at the 41st ASMS, 1993.
2. Tong, H.Y., Giblin, D.L., Lapp, R.L., Monson, S.J., Gross, M.L. *Anal. Chem.* 1991, *63*, 1772.
3. Sinkkonen, S., Koistinen, J., *Chemosphere*, 1990, *21*, 1161.
4. Peterman, P.H., Lebo, J.A., Major, H.J., presented at the 36th ASMS, 1988, p240.
5. Buser, H.R., Rappe, C., *Anal. Chem.* 1991, *63*, 1210.

PRECURSOR SCANS IN NEUTRAL DISSOCIATIONS

Ming Gu and Frantisek Turecek, Department of Chemistry, BG-10
University of Washington, Seattle WA 98195

Precursor-ion and neutral-loss scans on tandem sector and quadrupole mass spectrometers have been used for ion dissociation studies, as well as for mixture analysis.[1] We have developed a new technique based on monitoring mass-selected neutral fragments formed by ion and neutral dissociations taking place in the tandem quadrupole acceleration deceleration quadrupole mass spectrometer.[2] To obtain a spectrum of precursors fragmenting to form the given marker neutral, ions formed by electron impact in the ion source are transmitted through the first quadrupole mass analyzer operated in the r.f. only mode. The ions are accelerated to 8 keV kinetic energy and neutralized by collisions with a gas (He, Xe, cyclopropane, or CH_3SSCH_3). The neutral products are separated from the residual ions and reionized by collisions with oxygen. The second quadrupole mass analyzer is tuned at unit mass resolution to pass the ions of mass corresponding to that of the marker neutral (m_M), and the deceleration voltage is scanned from zero to the nominal high voltage (i.e. $U_{dec} \approx U_{acc}$). This allows passage of ions formed by reionization of neutrals of increasing kinetic energy as formed by fragmentation of precursor neutrals and ions according to equation 1, where U_{acc} is the constant acceleration voltage. A linear scan

$$U_{dec} = U_{acc} \frac{m_M}{m_p} \qquad (1)$$

of U_{dec} results in a non-linear mass scale with $U_{dec} \rightarrow 0$ corresponding to $m_p \rightarrow \infty$. This is similar to the B^2/E linked scan on a sector instrument. The precursor mass resolution ($m_p/\Delta m_p$) decreases with increasing m_p according to equation 2, where T is the kinetic energy release in the formation of m_M.

$$\frac{m_p}{\Delta m_p} = -\frac{U_{dec}}{\Delta U_{dec}} = \sqrt{\frac{m_M U_{acc}}{16T(m_p - m_M)}} \qquad (m_p > m_M) \qquad (2)$$

This leads to both peak broadening and a compressed mass scale at higher m_p, resulting in less-than-unit precursor-ion mass resolution.

The precursor spectrum of PO from trimethylphosphate (**1**) (Fig. 1a) shows all important ions at *m/z* 140, 109, 95, 79, 65, and represents a fingerprint of neutral dissociations corresponding to the ions in the EI spectrum of **1**. This characteristic precursor pattern is utilized to distinguish oxidized phosphorus compounds in mixtures. For example, the EI spectrum of a mixture of **1** with equal amounts of 1,6-dichlorohexane, methyl benzoate, 1-nonanone, 3-nonanone, 5-nonanone, 1-aminononane, acetophenone, and benzyl amine shows multiple peak overlaps at *m/z* 65, 79, and 109 obscuring the presence of **1** (Fig.1b). By contrast, there is no isobaric overlap at *m/z* 47, so the neutral precursor scan of the mixture (Fig. 1c) displays only PO^+ corresponding to dissociations of **1**. Isobaric overlaps of PO^+ with $CH_3O_2^+$ and $C_2H_7O^+$ in the EI spectrum of the mixture do not result in interferences in the neutral precursor spectrum due to the instability of the $CH_3O_2^{\bullet}$ and $C_2H_7O^{\bullet}$ radicals during the neutralization and reionization processes. Other possible interferences from stable ^{35}ClC and CH_2SH can be deconvoluted based on their unique peaks in the neutral precursor spectra.

References

1. J.A. Schwartz, A.P. Wade, C.G. Enke , R.G. Cooks, *Anal. Chem.* **62**, 1809 (1990).
2. F. Turecek, M. Gu, S.A. Shaffer, *J. Am. Soc. Mass Spectrom.* **3**, 493 (1992).

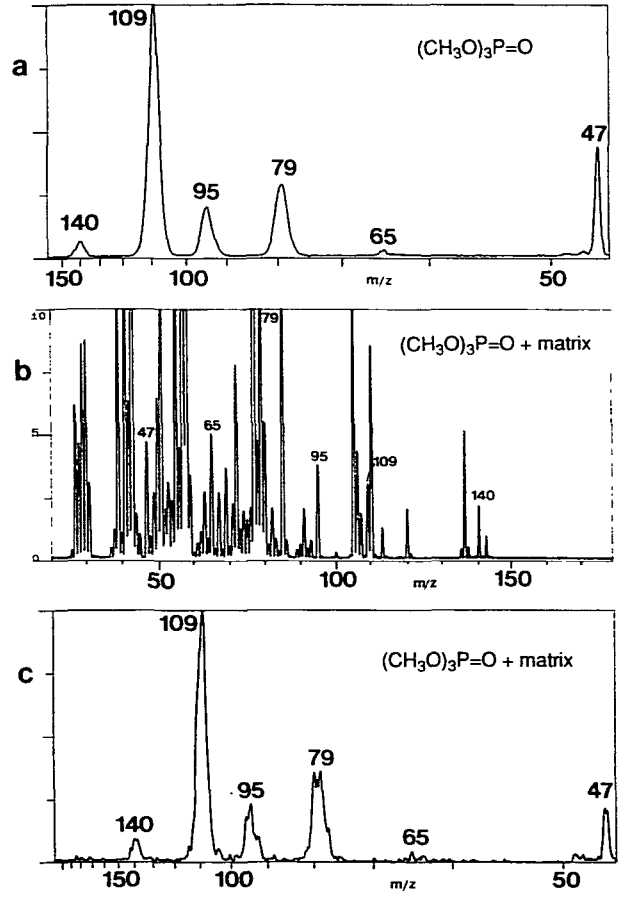

Figure 1. (a) Precursor scan of trimethylphosphate, (b) 70-eV EI spectrum of the mixture, (c) Precursor scan of trimethylphosphate in the mixture

RESIDUAL VOLATILES ANALYSIS OF DEACIDIFICATION TREATMENT OF BOOKS USING ON-LINE SFE/GC/MS

Casey C. Grimm[1], Terry J. Braggins[2] and Conrad Kamienski[3]

A combination of gas chomatography/flame ionization/olfactory analysis and on-line supercritical fluid extraction/gas chromatograph/mass spectrometery were utilized to analyize the residual volatiles present in deacidified paper. Paper treated with magnesium alkoxide solvated in freon (Treatment #1), purified magnesium alkoxide solvated in heptane (Treatment #2), and an untreated book were analyized for residual volatiles.

The initial investigation utilized a purge and trap connected to a GC with the effluent split to a conventional flame ionization detector (FID) and to a sniffer port. Offensive odors were eluted at two different locations. To identify the offending compounds, samples of paper taken from the treated books were extracted at 400 atm and 50°C using supercritical CO_2. The split/splitless injecton port of the GC/MS was adapted to accomodate the SFE restrictor (Figure 1). The volatiles were extracted directly from the sample and deposited at the head of a capillary column which was cryofocused at -150°C. The major limitation of the method was the necessity to use the split injector to vent off gaseous CO_2, resulting in decreased sample loading and loss of low boiling compounds.

Using the FID trace, the two offensive odors were related to compounds observed in the total ion chromatogram. The first was associated with the freon solvent and contaminates, and the second related to residual alkoxide impurities. In addition to residual butoxytriglycol three additional compounds; butoxydiglycol, butoxytetraglycol and a compound similar to butoxytriglycol, but containing an extra oxygen were present (Figure 2). These contaminants were also found in the treatment solution and were traced back to the supplier of the butoxytriglycol.

1. Southern Regional Research Center, Agricultural Research Service, USDA, 1100 Robert E. Lee Blvd. New Orleans, La. 70124

2. Meat Industry Research Institute of New Zealand, East Street - Ruakura Campus, P.O. Box 617 Hamilton, New Zealand.

3 FMC Corporation, Lithium Divison, Highway 161, Box 795 Bessemer City, N.C. 28016

MODIFIED SPLIT/SPLITLESS INJECTOR

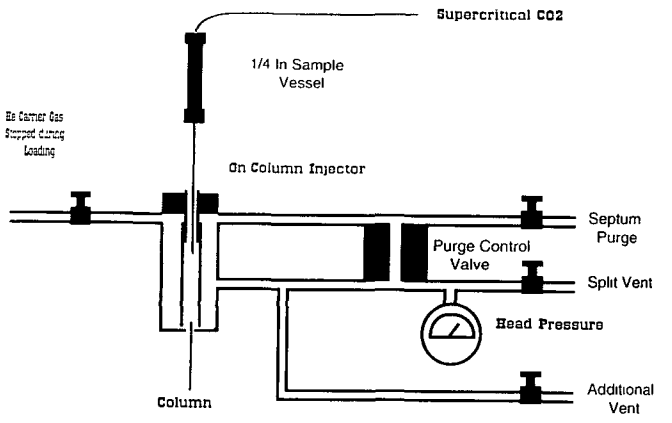

TIC of Semi-Volatiles form De-Acidified Paper

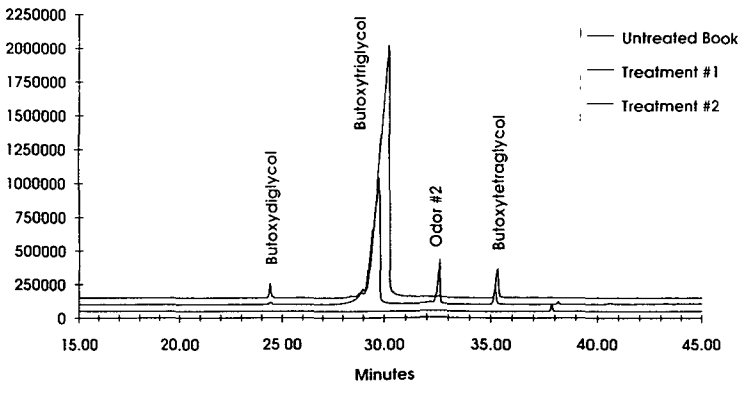

MS/MS CHARACTERIZATION OF PHOSPHATE ESTERS

Paul A. D'Agostino and Lionel R. Provost, Defence Research Establishment Suffield, P.O. Box 4000, Medicine Hat, Alberta, CANADA, T1A 8K6.

The United Nations Chemical Weapons Convention will require sophisticated analytical methods to help ensure compliance by all participating nations. Considerable analytical effort will be directed towards the development and validation of analytical methods for organophosphorus compounds controlled under the Chemical Weapons Convention. For this reason, a homologous series of straight chain C_1 to C_4 phosphate esters, commonly employed as chemical simulants for the organophosphorus chemical warfare agents, was selected for tandem mass spectrometric characterization. These typical organophosphorus compounds, including trimethyl phosphate, triethyl phosphate, tripropyl phosphate and tributyl phosphate, were investigated to ascertain the utility and limitations of tandem mass spectrometry for the detection and identification of phosphate esters.

GC-MS/MS analyses were performed with a VG Autospec-Q mass spectrometer equipped with a H/P 5890 gas chromatograph. A 15 m x 0.32 mm ID DB-1701 J&W capillary column was used with the following program: 40°C (2 min) 10°C/min 280°C (5 min). EI operating conditions were as follows: 3 x 10^{-6} Torr; 200°C; 70 eV; 100 μA and 8 kV. Daughter spectra were obtained for the molecular ion or a higher mass EI fragmentation ion for each phosphate esters with a CAD cell Ar pressure of 8-9 x 10^{-7} Torr and an energy of 25 eV (laboratory scale). This argon pressure reduced the intensity of the PFK ion at m/z 219 to 50% of its original intensity (residual air in CAD cell). The quadrupole was operated at unit resolution and scanned from 250 to 50 u at 1 sec/scan and the sector resolution was set in the 1000 to 3400 range (10% valley definition). RIM data were obtained for tripropyl phosphate by monitoring both the m/z 183 to m/z 141 and m/z 183 to m/z 99 transitions (80 msec with a 40 msec delay). GC-MS/MS specificity was evaluated by spiking the phosphate esters into a complex extract of diesel exhaust emissions (primarily hydrocarbons) collected onto the charcoal bed of a Canadian C2 mask canister.

Daughter spectra were obtained for the principal four to eight EI ions of each phosphate ester with residual air or argon (two different pressures) in the CAD cell by stepping the cell energy from 1 to 100 eV in 1 eV increments (Figure 1 illustrates tripropyl phosphate data). Figure 2 illustrates the GC-MS (EI) chromatogram obtained for the diesel exhaust extract spiked with 2.5 ng of each phosphate ester and the same spiked sample extract during GC-MS/MS analysis. The four phosphate esters were masked by the presence of high levels of chemical interferences and poor quality EI data were obtained for the spiked compounds During the acquisition of daughter spectra for the same spiked extract all the phosphate esters were detected. The increase in specificity afforded by the use of moderate sector resolution was demonstrated during both daughter (Figure 3) and RIM (Figure 4) GC-MS/MS analysis. Reductions in chemical interferences were observed for the daughters of m/z 183.08 ($[M-C_3H_5]^+$ for tripropyl phosphate) by increasing the sector resolution to 2400 (Figure 3). Daughter scanning sensitivity was found to approach typical EI full scanning detection limits (e.g., 100 to 500 pg). Lower levels of phosphate esters were confirmed by multiple RIM (minimum of two transitions). Figure 4 illustrates the RIM chromatograms for the m/z 183 to m/z 141 transition (loss of C_3H_6) with a sector resolution of 1000 and 2400. Chemical interference, due to loss of C_3H_6 from sample components, was reduced with increased resolution and a S/N ratio in excess of 100:1 was observed for 200 pg of tripropyl phosphate at both sector resolutions. GC-MS/MS data obtained for spiked diesel exhaust extracts during parent and constant neutral loss operation were considerably less specific than daughter or RIM operation.

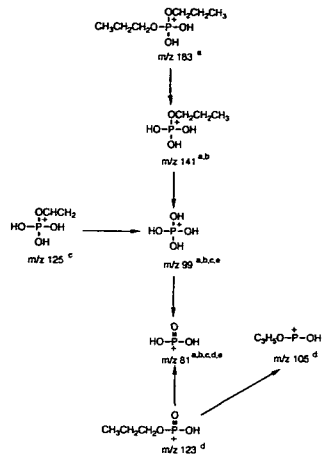

Figure 1. Ions observed in daughter spectra of a) m/z 183, b) m/z 141, c) m/z 125, d) m/z 123 and e) m/z 99 for tripropyl phosphate.

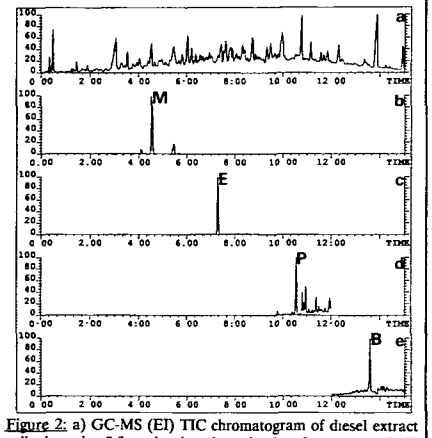

Figure 2: a) GC-MS (EI) TIC chromatogram of diesel extract spiked at the 2.5 ng level with each phosphate ester. CAD chromatograms for daughters of b) m/z 140 (M^+ for trimethyl phosphate (M)), c) m/z 182 (M^+ for triethyl phosphate (E)), d) m/z 183 ($[M-C_3H_5]^+$ for tripropyl phosphate (P)) and e) m/z 211 ($[M-C_4H_7]^+$ for tributyl phosphate (B)) obtained with sector resolution of 1000.

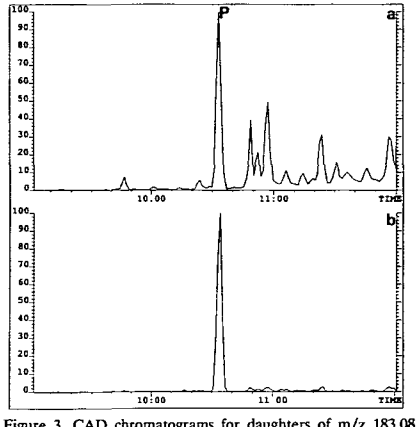

Figure 3. CAD chromatograms for daughters of m/z 183.08 ($[M-C_3H_5]^+$ for tripropyl phosphate (P)) obtained with a sector resolution of a) 1000 and b) 2400.

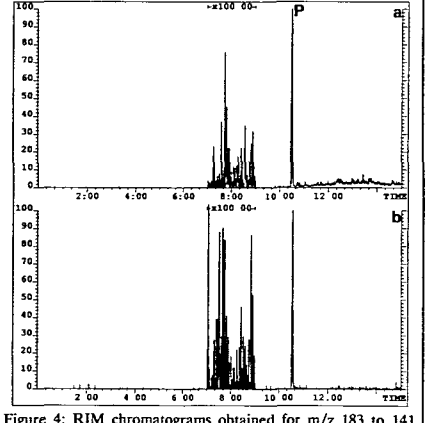

Figure 4: RIM chromatograms obtained for m/z 183 to 141 transition during analysis of diesel exhaust extract spiked with 200 pg of tripropyl phosphate with a sector resolution of a) 1000 and b) 2500.

Extraction of Trace Elements in Coal Fly Ash and Subsequent Speciation by High Performance Liquid Chromatography with Inductively Coupled Plasma Mass Spectrometry (HPLC-ICP-MS)

***Jiansheng Wang, Medha Tomlinson and Joseph A. Caruso, Department of Chemistry, University of Cincinnati, ML 172, Cincinnati, OH 45221-0172, USA.**

There is an increasing demand for the trace element speciation of coal fly ash, due to the toxic nature of many of its components. The toxicological profiles of some of the potentially hazardous compounds depend markedly on the oxidation states of the element and/or their chemical forms For example, chromium (III) is an essential element while chromium (VI) has been known to be toxic; vanadium (V) is much more toxic than vanadium (IV); several arsenic compounds such as arsine, arsenite, arsenate, methanearsonic acid and dimethylarsinic acid are known to have various toxicities.

However, the difficulty lies in the successful extraction of these trace elements from coal fly ash, without changing their oxidation states or chemical forms. Most digestion procedures involve harsh conditions, which would change the original form of the element. In this work, attempts to develop procedures for trace element speciation in coal fly ash will be performed utilizing the following order: (a) extraction of coal fly ash with water (pH=1 to 12), (b) extraction of ground coal fly ash (~ 2 to 3 μm)with water, (c) determination of trace elements in solutions of various pH with inductively coupled plasma mass spectrometry (ICP-MS), (d) speciation of trace elements in coal fly ash by high performance liquid chromatography coupled with inductively coupled plasma mass spectrometry (HPLC-ICP-MS)

Preliminary results have shown that most of the trace elements in coal fly ash are released in small amounts in water under normal environmental conditions (pH= 5 to 7). However, when the pH is below 2 or higher than 10, the solubilities of trace elements in coal fly ash are markedly increased. Speciation of vanadium in

the extracted solution by HPLC-ICP-MS indicates that both vanadium (V) and (VI) exist in aqueous solution. Therefore, this extraction method can be applied to the speciation of As, Cr, Ni and other elements.

Effect of Varying pH on the Solubilities of Trace Elements in Coal Fly Ash

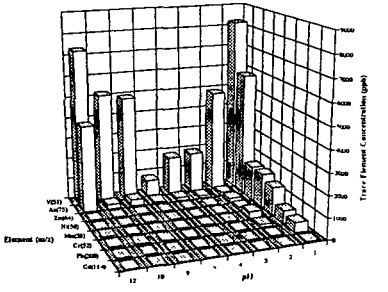

Speciation of Vanadium in Coal Fly Ash

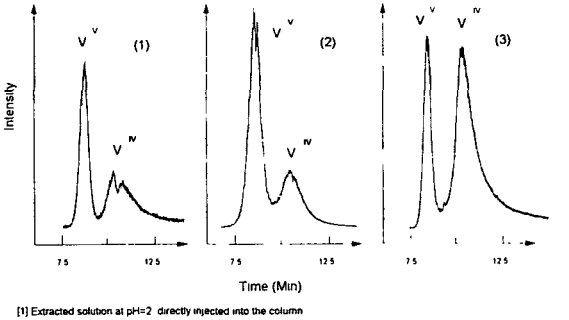

[1] Extracted solution at pH=2 directly injected into the column

[2] Extracted solution at pH=1 adjusted to pH=2 6

[3] Vanadium (V) and (IV) standard solution

Determination of Methanol in Water Samples using a Modified EPA Method 8015, Direct Injection GC/MS, and Purge and Trap GC/MS.

*D.W. Berberich, C.K. Trang, B.M. Hughes, J.L. Briscoe, and R.G. Orth, Monsanto Company, 800 North Lindbergh Blvd., St. Louis, MO., 63167, Mailzone S3C.

Two sets of water samples were analyzed by direct injection GC/MS onto a capillary column, purge and trap GC/MS, and a modified EPA method 8015 with direct injection onto a packed column. The data from this analysis is summarized in Table 1. The analysis methods were compared in terms of sensitivity, reproducibilty, and sample turn around times. The mass spectrometers used for this analysis were the VG ZAB 70E double focusing magnetic sector mass spectrometer and the HP MSD quadrupole mass spectrometer. The modified EPA method 8015 was performed by an outside contract laboratory.

The QA/QC data for triplicate injections of the sample indicated reproducibility of 11% for the direct injection method, 25% for the purge and trap method, and the data for the EPA Method 8015 was not available. The laboratory water blank did not have a detectable level of methanol. The direct injection data indicate an 85% recovery for the field effluent spike, 104% recovery for the field distilled water spike, 109% recovery for the effluent lab high spike, and 100% recovery for the effluent lab low spike. The purge and trap data indicate an 86% recovery for the field effluent spike, 96% recovery for the field distilled water spike, 68% recovery for the effluent lab high spike, and 65% recovery for the effluent lab low spike.

The reported water sample concentrations were corrected for % recovery based on the QA/QC spikes. The methanol level in water prior to treatment was 180 ppm and following treatment was approximately 22 ppm, corresponding to an 88% reduction in methanol. The direct injection GC/MS onto a capillary column method had an 18 minute per sample analysis time while the purge and trap GC/MS method had an 1 hour analysis time.

Table 1. Summary of data obtained for methanol analysis.

Sample Description	Concentration (ppm) Direct Injection	Concentration (ppm) Purge and Trao	Concentration (ppm) Modified Method 8015	Predicted Concentration (ppm)
Effluent - 7/21/92	24 ppm	24 ppm	23 ppm	
Effluent - 7/20/92	21 ppm	24 ppm	21 ppm	
Effluent Field Spike - 7/21/92	63 ppm	64 ppm	NA	74 ppm
Water Field Spike - 7/21/92	52 ppm	48 ppm	39 ppm	50 ppm
Effluent Lab High Spike - 7/21/92	98 ppm	NA	NA	90 ppm
Effluent Lab Low Spike - 7/21/92	37 ppm	NA	NA	37 ppm
Effluent Lab High Spike - 7/20/92	NA	68 ppm	NA	100 ppm
Effluent Lab Low Spike - 7/20/92	NA	41 ppm	NA	63 ppm
DI Water High Spike	NA	52 ppm	NA	79 ppm
DI Water Low Spike	NA	28 ppm	NA	39 ppm
Lab Blank	ND (0.079 ppm)	ND (8 0 ppm)	ND (Unknown)	

NA - This sample was not analyzed using this method.
ND (LOD) - Not detected with Limit of Detection in brackets.
ND (Unknown) - Not detected Limit of Detection is unknown.

Chemical Ionization of Pesticides Using a GC/MS Ion Trap Detector

Y. A. Ranasinghe[1], G. A. Loraine[1], G. L. Glish[2] and M. J. Charles[1]

[1]Department of Environmental Science and Engineering and [2]Department of Chemistry, University of North Carolina, Chapel Hill, NC 27599.

Guidelines to pesticide usage in agriculture and the potential short and long term health risks to biota and humans is a principal topic in environmental science. The major concerns are the detection, control and environmental monitoring of pesticides in ground water, streams and in consumables such as fruits and vegetables.

The use of CI in concert with ion trap mass spectrometry for the analysis of pesticides offers the advantage of providing the needed sensitivity while collecting full-scan spectra to assist in confirming the identity of the compounds. The nature of the ion trap CI experiment results in electron ionization of analyte molecules in the interval that is devised to ionize reagent molecules. Consequently EI ions can occur in the mass spectra that are produced[1]. Difficulties arising due to the "hybrid" spectra can be prevented by using a very low rf trapping level during ionization[2]. Decreasing the rf amplitude during ionization can cause high mass ions to be lost from the trap. In this study experiments were performed to determine the effect of the rf amplitude (cut-off mass) during the electron pulse on the chemical ionization mass spectra of specific pesticides, and comparing these spectra to the electron ionization spectra in the ion trap, and chemical ionization mass spectra obtained on a beam instrument.

A Varian Saturn II GC/MS ion trap detector was used to create a methane CI library for propazine, propanil, prometryne, atrazine, dacthal, dichlobenil, difolotan, dinoseb, vegadex, lindane, DDE and methoxychlor, pesticides recieved from Polyscience Corporation (at > 90% purity). The samples were diluted in either hexane or methylene chloride. Separations were performed on a 30 m, DB-5, .25 um fused silica capillary column, at a He carrier gas pressure of 13 psi. The optimum conditions for the CI spectra were obtained with an electron pulse of 1000-2000 usec for concentrations of ~ 10-50 ng/ul sample, at an emission current of 5 uA, run under automatic reaction control (ARC). The methane was maintained at a constant pressure that yielded equal ion abundances of CH_5^+ and $C_2H_5^+$. Methane pressures giving a similar $CH_5^+/C_2H_5^+$ ratio were used to generate CI spectra for the same pesticides on the Finnigan 4000 quadrupole instrument for comparison.

The effect of varying the cut-off masses from 10, 5, 3 & 2 on the appearance of the chemical ionization mass spectra is exemplified by comparing the electron ionization and the chemical ionization mass spectra for propazine obtained in the ion trap (Table 1). The electron ionization mass spectrum is characterized by the presence of a molecular ion at m/z 229 (Figure 1). The major fragment ions appear at m/z 214 (100%) due to the loss of a CH_3 moiety; at m/z 172 (65%) and at m/z 58 (60%) due to $((CH_3)_2CHNH)^+$. The abundance of m/z 58 decrease in the CI spectrum with a decrease in the rf amplitude and completely disappears at a cut off mass of 2 (Table 1). However this adversely affects the performance of the ion trap by reducing the total ion current (TIC). This could be due to the repulsion of methane ions by He^+ which is trapped at this value.

In general, similar CI mass spectra were obtained on an ion trap and on the quadrupole instrument (Figure 1). Major differences occurred for methoxychlor and difolotan. For methoxychlor the ion trap spectra yielded protonated molecule and fragment ions due to losses of HCl. In contrast the quadrupole spectra contained primarily m/z 227, which is also the the primary ion $(M\text{-}CCl_3)^+$ in

the EI spectrum. For difolotan, the ion trap spectra show $(MH\text{-}HCl)^+$ as the major ion at m/z 314 (100%) and M^+ (8%) at a lower intensity. The quadrupole mass spectrum exhibits ions at m/z 152 (100%) and m/z 79 (60%). The m/z 79 (100%) is also the major fragment in the EI spectrum.

Other investigators are devising changes to scan functions that need both hardware and software modifications to eliminate the EI artifacts[1]. Here data is presented to show that these ions could be eliminated by changing the rf amplitude on the ring electrode. The CI mass spectra obtained under these specific conditions were similar to those using a quadrupole mass spectrometer.

1. Cairns, T. C.; Chiu, K. S.; Siegmund, E. ; Weber, M. Rapid Comm.in Mass Spec. 1992, 6, 449.
2. Hart, K. J.; McLuckey, S. A.; Glish, G. L. J. Am. Soc. Mass Spec. 1992, 3, 549.

Table 1

Cut-off mass	Relatve Abundance (%)				
amu	m/z 58	m/z 172	m/z 214	m/z 229	m/z 230
2	-	-	5	15	100
3	15	-	25	35	100
5	48	2	30	45	100
10	51	30	55	60	100

Figure 1

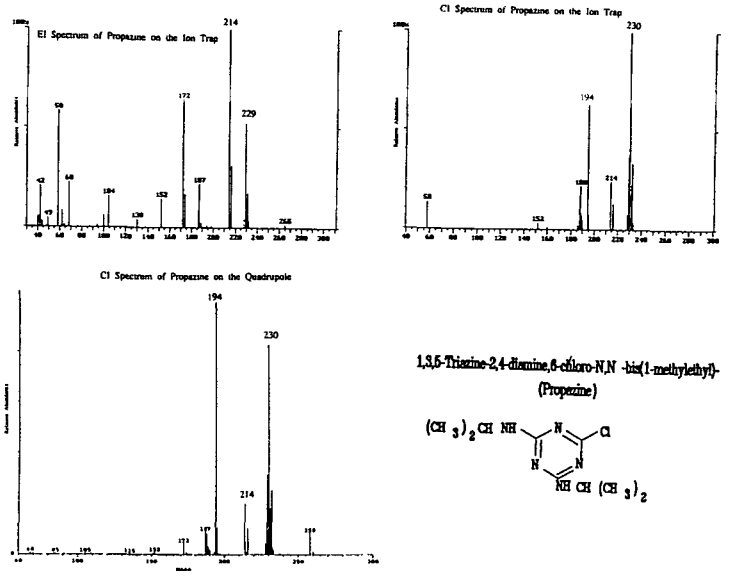

Low PPB Detection Limits for the Analysis of Atmospheric Contaminants in Ultrapure InertGases

Charlene Long, Jeremiah D. Hogan,
Texas Instruments Inc., Dallas, TX 75265

A Hewlett Packard 5988A GC/MS with a Teknivent Vector Two data system is used to detect atmospheric contaminants in several ultra high purity (UHP) and very large scale integration (VLSI) grade inert cylinder gases.

With the aid of a custom-made gas blending system for calibration, five-point calibration curves over several orders of magnitude of concentrations are generated, allowing for ppm to low ppb level detection limits for contaminants such as carbon monoxide, carbon dioxide, methane, argon, neon, and oxygen. A porous layer, open tubular (PLOT) column in series with a mole sieve (MS) column provide baseline separation for all concerned species at ambient temperatures. A single, ten-port injection valve with a 200 mL injection volume provides adequate sample for S/N ratios of approximately ten for concentrations as low as 50 ppb. Figure 1 shows the injection valve scheme in both the inject and load modes. Valve switching permits a reversal of column order to permit the elution of CO_2 prior to the other components. The novel feature of this injection scheme is that the direction of flow is never reversed. Utilizing this sampling scheme allows turnaround times of about half an hour per cylinder, including a purge-down time of approximately five minutes, a standard injection to verify calibration, and a total GC run time of fifteen minutes per sample,

Shown below are: 2A) a reconstructed chromatogram of a calibration standard in helium which contains 2.5 ppm of CO_2, Ne, Ar, N_2, CH_4, and CO 2B) the same run at a concentration of 50 ppb.

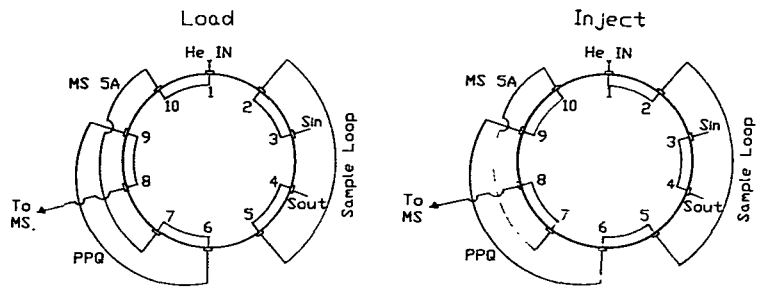

Figure 1

Presented at the 41st ASMS Conference on Mass Spectrometry

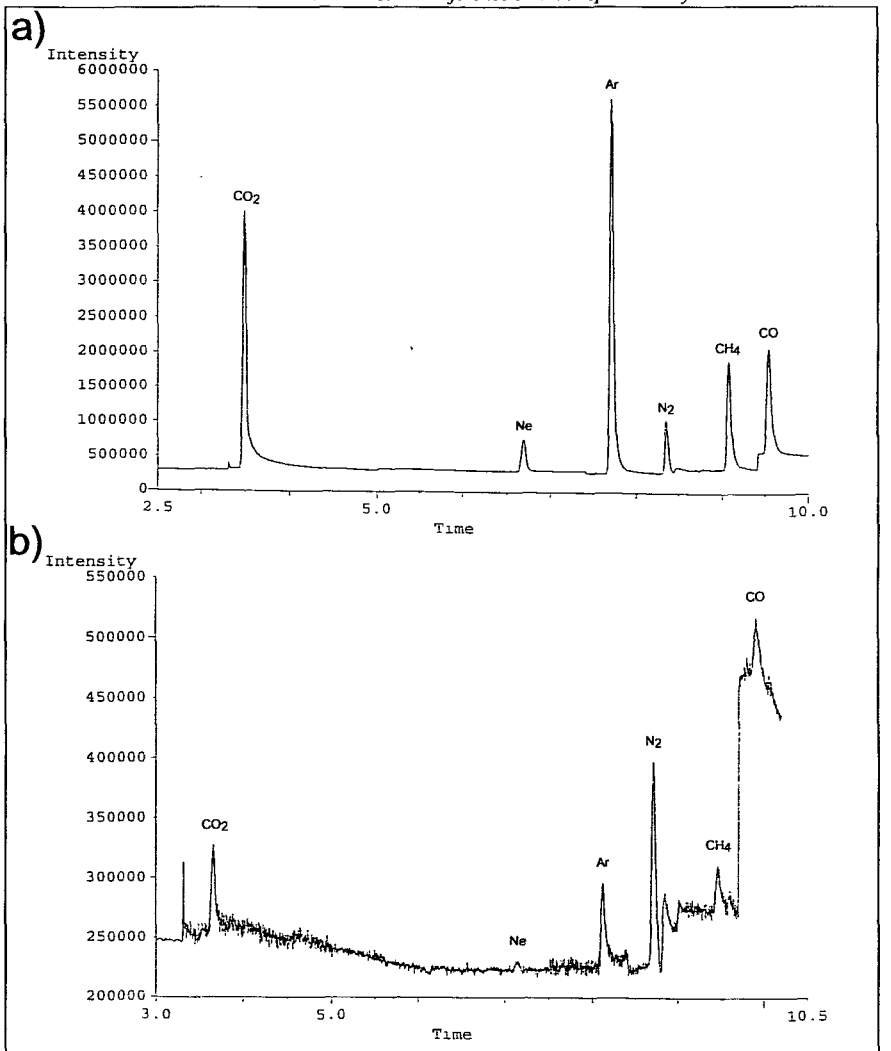

Figure 2

Enhancement of Molecular Ion Detection by Variation of Mass Analyzer Thermal Energy for C_{10}-C_{28} Alkanes by Ion Trap Mass Spectrometry

by **Curtis S. Phinney**, Water Resources Division,
U.S. Geological Survey, 431 National Center, Reston, VA 22092

The qualitative determination of low molecular weight alkanes in natural waters is important in investigations of contaminant geochemistry, fate and transport studies, and aquatic particle-organic chemical interactions. Our efforts to analyze this class of compounds by gas chromatography/ion trap mass spectrometry (GC/ITMS) were hampered by the virtual absence of molecular ions (M+) and excessive fragmentation. This study investigated the effectiveness of varying the thermal energy imparted to the analyte molecules in the Finnigan MAT Ion Trap Device (ITD) mass analyzer manifold as a means of reducing the fragmentation of C_{10}-C_{28} alkanes and enhancing the production of molecular ions.

In this investigation, the thermal energy imparted to ions stored in the ion trap was systematically varied. This was achieved by incremental variation of the mass analyzer manifold temperature. The production of molecular ions (expressed as % of base peak), efficiency of mass transfer, and the degree of similarity to classical electron impact mass spectra were evaluated.

Ionization is achieved in this device by electron impact within the mass analyzer region itself. Ionization times range from .078 to 25.0 milliseconds (mS). Ions in the potential field below the specific threshold mass (20 amu at the initial RF voltage) become unstable and leave the trapping field region. An additional time, on the order of .100 mS, lapses prior to the start of the analytical scan function. It is hypothesized that these residence times in a highly energetic environment can lead to rearrangement decompositions of saturated aliphatic hydrocarbon ions. Hence, experiments were conducted in an effort to reduce the thermal energy imparted to these analyte molecules during storage.

A Finnigan MAT model 800A quadrupole ion trap, directly interfaced to a capillary gas chromatograph by way of the standard flexible transfer line was used for this study. The manifold temperature was initially set to 70°C., and then returned to the standard operating temperature of 200°C. in 6-8°C. increments. The production of molecular ions for a range of n-C_{10} through n-C_{28} alkanes and a branched C_{19} compound (pristane) was measured at each temperature. The effectiveness of the data system at correctly matching the resultant mass spectra with classical electron impact mass spectra was investigated. The reported purity (the resemblance to the library entry for the authentic compound) was measured for each compound as the temperature was varied. The efficiency of mass transfer through the GC/ITD interface region was determined by calculation of total ion current (TIC) relative response factors (RRF), normalized to n-C_{10}, as the mass analyzer manifold temperature was varied. Although independently heated, the interface temperature is influenced by the large thermal mass of the manifold, and was found to be subject to "cold spots" at low manifold temperatures.

The use of brand, firm, or trade names does not constitute endorsement by the U.S.G.S.

Results of this study indicate that the production and subsequent detection of molecular ions is enhanced at reduced manifold temperatures (figure 1). For example, M+ production for n-C_{17} varied from zero at manifold temperatures above 150°C. to above 16% of the base peak at temperatures below 90°C. The production of molecular ions was highest for all of the compounds at a manifold temperature of 101°C. This high production of M+ did not produce adequate additional fragmentation to allow library matching with classical electron impact mass spectra. However, operation in this temperature range may be useful for determination of molecular weights of unknowns, or for analysis of compounds that are not typically analyzed by electron impact ionization due to excessive fragmentation. The ability of the Finnigan MAT ITDS v. 4.10 data system to match the resultant mass spectra with those in the mass spectral library was greatest at low to intermediate manifold temperatures, e.g. 115-140°C, with the highest purity match values being achieved at 123°C. TIC relative response factors for the higher molecular weight compounds generally increased with manifold temperature, with n-C_{24} showing the highest TIC RRF at 184°C. Optimal mass transfer, as defined by a leveling off of response relative to n-C_{10}, was observed for all compounds through n-C_{24} at temperatures of 123°C. and above (figure 2). Mass transfer was low for n-C_{28} at temperatures below 146°C., and some peak tailing was evident at temperatures below 160°C. Hence, the optimal manifold temperature selected is dependant on the type of information desired from a given experiment, i.e. maximization of M+ production or optimal matching of classical electron impact mass spectra. An additional constraint on selection of an optimal manifold temperature is the minimum temperature at which a given analyte demonstrates acceptable mass transfer across the GC/ITD interface.

Figure 1

M+ Production vs. Temperature

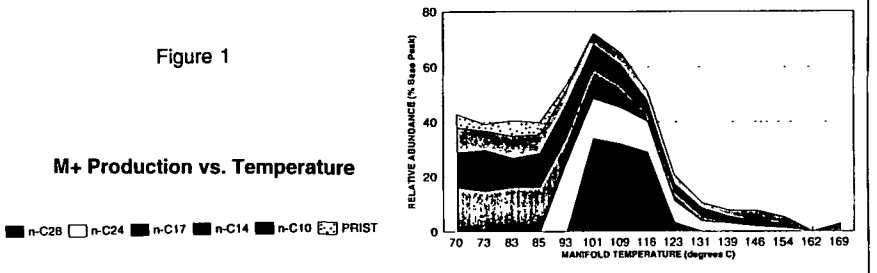

Figure 2

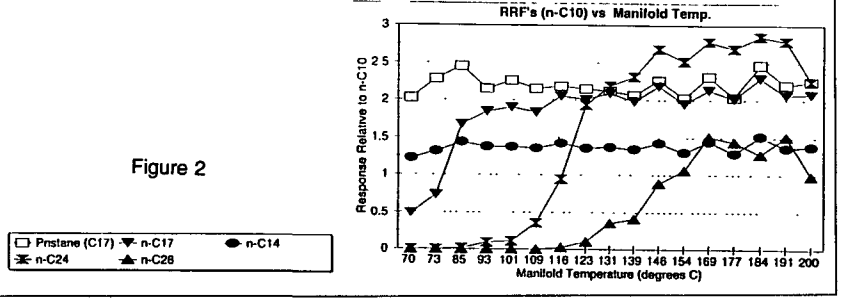

Survey of Volatile Organic Chemical Emissions from Waste Composting Facilities. Brian D. Eitzer, The Connecticut Agricultural Experiment Station, P. O. Box 1106, New Haven, CT 06504.

The proper disposal of solid waste materials is a problem facing many communities and industries. A disposal option for much of the solid waste stream is composting, which is actually a recycling option, taking wastes and generating a usable soil amendment. There are, however, several community concerns which must be addressed before this form of waste recycling can be utilized to its full potential. Some of these concerns relate to potential volatile organic chemical (VOCs) emissions from large composting facilities. In an attempt to answer these concerns we have recently completed a survey on VOCs at eight waste composting facilities.

The facilities span a size range from 5-10 tons/day design capacity to 660 tons/day. Facility types range from in-vessel systems with forced aeration to open windrows with no aeration other than weekly turning. Some facilities only use source separated waste, while others have extensive waste separating on site, and another co-composts sewage sludge. Several of the facilities use biofilters to try to reduce the odorous (and VOCs) emissions. Thus, this set of eight facilities represents a survey of the many possible approaches to MSW composting and provides a first estimate of the types and quantities of VOCs that should concern MSW composting facilities.

At each facility several sampling locations were selected. Where possible these included: the tipping floor, biofilters, different areas of active composting (differing in age of the compost), air near shredders, and curing compost piles. In addition, a field blank was taken at every facility

Samples were taken by using small portable sampling pumps to draw air at a rate of 0.6 liters per minute through sampling tubes containing Tenax-TA or Carbotrap-300. The sampling tubes were placed in the side of a bottomless plastic carboy which was set into the area to be sampled. Thus, the air sampled was isolated so that the sample was correlated to the specific location within the compost pile rather than ambient air in the vicinity of the pile.

In the laboratory these tubes were analyzed by thermal desorption GC/MS utilizing a thermal desorber accessory to a Tekmar LSC-2000 purge and trap, interfaced to a Perkin-Elmer 8500 Series GC/MS (ion trap). After a 2 min dry purge to remove excess water the tubes are thermally desorbed at 250°C for 4 min, and VOCs are transferred to the GC/MS system where they were cryogenically focused in the GC at -10°C. The GC/MS is operated using a J&W 30 meter DB-624, 0.53 mm ID capillary column. The GC oven was temperature programmed as follows; -10°C for 2 min, 5°C/min to 180°C, 10°C/min to 220°C hold for 4 min. The ion trap is operated with automatic gain control on, background 39 amu, scanning from 40-400 daltons at one scan per second.

A set of target compounds was developed which included most of the compounds from EPA method 8240 as well as several other VOCs for which standards were readily available. Standards of all target

compounds were analyzed to determine retention times, and, response factors based on the most intense and/or most distinctive ion for each compound. All target compounds were screened for in every sample with identification based on single ion chromatographic peaks at the proper retention time as indicated by the standards. Compounds were quantified using the external response factors developed with the standards.

The group of compounds producing the largest total ion chromatographic peaks were identified by computer searching of the complete mass spectra. These "largest peak" compounds are classified as terpenes. Due to the large number of structural isomers, similarities in spectra and unavailability of standards these compounds were not specifically identified but quantified as a class using a set of five terpene standards to develop an average response factor.

Two trends were observed in the results. First, though the facilities spanned a range of sizes and composting styles, a consistent pattern of VOCs at similar concentrations were seen at all of the composting facilities. These great similarities also allowed averaging of the data from all of the facilities for comparisons of concentrations within the different areas of a facility. When this was done the second trend was observed, VOCs concentrations were much higher on the tipping floors, by the shredders and at the early composting stages than in older, more mature compost. This indicates that the VOCs are rapidly emitted from the material as the pile comes to its 150 ^{o}C operating temperature. Finally, it should be noted that the observed concentrations remained well below permissible exposure limits for workplace air as defined in the ACGIH handbook (1).

The results from this study indicate that municipal waste feed used for composting has VOCs emissions, but, knowledge of the location of those emissions allows for planning in the design of new facilities

1. 1992-1993 Threshold Limit Values for Chemical Substances and Physical Agents and Biological Exposure Indices. American Conference of Governmental Industrial Hygienists. 1992, Cincinnati, OH.

Acknowledgments: This research was supported by a grant from the Composting Council. The author wishes to thank Terri Misenti for technical assistance.

DIRECT DETECTION OF TRIBUTYL PHOSPHATE ADSORBED ON SURFACES OF ENVIRONMENTAL INTEREST BY STATIC SIMS

G. S. Groenewold, J. C. Ingram, A. D. Appelhans, J. E. Delmore, D. A. Dahl, Idaho National Engineering Laboratory, P. O. Box 1625, Idaho Falls, ID 83415-2208

Tributyl phosphate (TBP) was widely used in the DOE complex to recover U, Pu, Th, Np and Am. The compound is not toxic by itself, but it may be useful as an indicator for the presence of Pu, U and other contaminants at DOE burial sites. TBP can be analyzed by extraction/GC/MS, but this analysis is time consuming. Further, the compound can adsorb strongly onto mineral surfaces, thereby making extraction difficult.

The Idaho National Engineering Laboratory (INEL) and Hanford have sites that are contaminated with TBP. The predominant mineral in both areas is basalt, which is a black aluminosilicate material stutted with Fe and other transition metals. The basalt is very porous, and wet chemical extraction can be difficult.

The objective of the present research is to develop rapid methods and instrumentation for the analysis of TBP on minerals and other refractory materials. Ideally, the technology should be fieldable, and should require minimal sample preparation, thereby avoiding the generation of laboratory waste. Clearly, the ability to directly analyze amorphous, irregular materials like basalt is desirable.

Static secondary ion mass spectrometry (SIMS) instrumentation which employs ***pulsed extraction*** and a ***perrhenate ion gun*** was used for the direct analysis of TBP on basalt. Sample preparation consists of attaching a basalt chip to a target planchette using double-sided tape. Using pulsed extraction, anions and cations are alternately drawn from the sample surface, which prevents charge buildup on the basalt, and also allows for the simultaneous acquisition of anion and cation spectra. The perrhenate ion gun produces a massive, high energy (10 KeV), anionic, molecular particle (ReO_4^-, ca. 250 da), which is very efficient for producing abundant secondary particles at low primary ion currents (typically 100 picoamps).

When basalt is spiked with TBP, or immersed in an aqueous TBP solution, no molecular ion species are observed in the SIM spectrum, but abundant ions are observed at m/z 137^+, 125^+, 119^+, 99^+, 79^-, and 63^- (fig. 1, lower, fig. 2). The analysis can be performed in about 5 minutes with no sample preparation. It is of interest that small quantities of TBP on the surface of basalt do not rapidly pump away, which indicates that the TBP must be strongly bound to the surface of the basalt.

Excellent signal to noise was observed when basalt was exposed to low concentrations of TBP in H_2O (10 ng/ul). In addition, TBP could be easily observed on basalt that had been exposed only to gas-phase TBP.

Figure 1. Cation SIM spectra of unspiked basalt (upper), basalt exposed to TBP solution (lower)

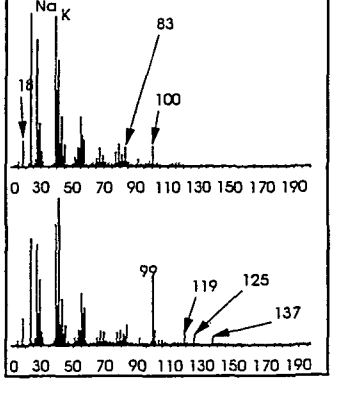

m/z 99^+ is the most abundant ion in the spectrum, and accordingly is the most sensitive ion for low level TBP detections. The abundance of this ion was used to estimate the minimum detectable quantity of TBP on basalt at 1 to 10 ng. Generally, lower quantities of TBP are observable on basalt surfaces which are smoother. The use of m/z 99^+ for low level TBP detections has limitations, because there is a m/z 99^+ ion in the background spectrum of the unspiked basalt, and the uncertainty for any abundance measurement in these experiments was ca. 30% (1 standard deviation).

Abundant cations not derived from TBP are also observed in the SIM spectrum of basalt (fig. 1, upper). Hydrocarbon cations could be observed at odd masses corresponding to C_2, C_3, C_4, C_5, C_6, and C_7. The abundances of the hydrocarbon cations decrease above m/z 100^+. Background ions at m/z 100^+, 83^+, 56^+, 30^+, and 18^+ originate from cyclohexyl amine, which is an atmospheric contaminant in our laboratory that adsorbs to basalt and other minerals. The other abundant cations in observed on the basalt surface correspond to Na^+ and K^+. Significant anions observed in the SIM spectrum originate from the mineral itself, and are are attributed to O^-, OH^-, C_2H^-, SiO_2^-, and SiO_3^-.

Figure 2. TBP fragmentation observed in SIMS analysis.

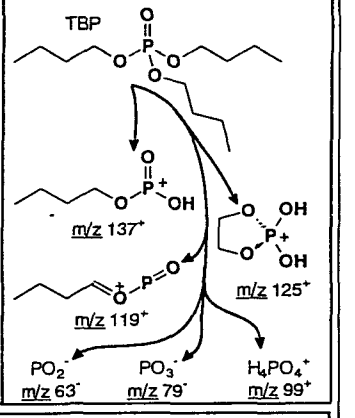

Figure 3. General structure proposed for basalt

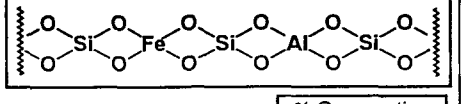

Basalt was analyzed using scanning electron microscopy (SEM) and X-ray powder diffraction to identify surface moieties that might be responsible for interaction with TBP. SEM images revealed a very irregular surface, with significant amounts of Si, Al, Fe, and Ca. An aluminosilicate structure stutted with Fe is proposed (fig. 3), where Ca is the predominant counter ion. We hypothesize that the efficacy of SIMS for analysis of TBP on basalt stems from interaction of the phosphoryl group with Fe in the basalt structure, which immobilizes TBP on the surface, and catalyzes the formation of ions. Alternatively, TBP may be bound on the basalt surface through interaction with silanol groups. We prefer the former hypothesis at this time, because no deuterium uptake could be observed in the TBP ions when the basalt was treated with D_2O. Further, TBP appears to adhere less strongly to quartz (SiO_2) than to basalt.

% Composition of Basalt by SEM	
Na	1
Mg	2
Al	8
Si	22
P	1
K	1
Ca	7
Ti	2
Fe	13
O	43

Funding support of the U. S. Department of Energy, Office of Technology Development, is gratefully acknowledged.

A NEW ANALYSIS TECHNIQUE FOR ENVIRONMENTAL LEVELS OF MERCURY USING ICP-MS

J.E. Halverson and D.M. Beals
Savannah River Technology Center
Westinghouse Savannah River Company
Aiken, SC 29808 USA

Introduction

Mercury is an extremely toxic metal, thus it is important to monitor its concentration in the environment at ppt levels. The speciation of Hg in the environment can affect its toxicity and mobility A procedure has been developed at the Savannah River Technology Center (SRTC) to determine the concentration and speciation of Hg in environmental samples.

Methods

Mercury in its elemental form is quite volatile and will diffuse through membranes. These principles were used by Braman (1971) to develop a membrane probe to detect Hg. At the SRTC, we built a membrane probe based on Braman's 1971 design. The probe is lowered into an aqueous solution so that the membrane is in contact with the sample solution to be analyzed.

A Turner Scientific Sola ICP-MS (now Finnigan MAT Sola) is used for the detection of Hg. We are currently using Au as an internal standard, which is aspirated into a CETAC Technologies U-5000 AT ultrasonic nebulizer. Argon gas incorporates the Au and then flows past the SRTC membrane probe (MP). Elemental Hg diffusing through the membrane is carried to the ICP torch by the argon, along with the Au. The mass/charge (m/z) range of 197 to 202 is scanned for the Au and Hg peaks.

Each sample analysis requires four measurements on the ICP-MS. The elemental Hg in the sample is first determined. After the addition of $SnCl_2$ the inorganic Hg concentration is measured. This is followed by the addition of $NaBH_4$ which gives a measure of the organic Hg. Lastly, a Hg standard is added to the sample. The absolute concentration of Hg in each form may then be calculated by standard addition equations.

To determine the Hg concentration in an aqueous sample 40 mL of sample solution are poured into a 50 mL glass breaker. The sample is typically preserved prior to analysis by the addition of nitric acid (Seastar Chemicals, Seattle WA). Soil or sediment samples are weighed into a 50 mL glass beaker. Distilled water or 2M nitric acid (Seastar) is added to the beaker to a total volume of approximately 40 mL. The SRTC MP is placed in the solution, which is continuously stirred during the analysis.

Results

Analysis of Standards. Standard solutions were prepared by the sequential dilution of a 1000 ug/mL Hg ICP standard (Specpure, Johnson Matthey) with 2% HNO_3. The SRTC MP was lowered into the solution and the Hg concentration measured by standard addition. The results are shown in Table 1

Table 1. Calculated vs. Expected Hg Concentrations in Standard Solutions

Expected (ppb Hg)	Calculated (ppb Hg, 2 sigma)
0.063	0.054 ± 0.018
0.25	0.26 ± 0.15
2.50	2.54 ± 0.78

Soil and sediment samples from NIST and the Canadian Bureau of Standards having certified Hg concentrations were analyzed using the SRTC MP. The results are shown in Table 2.

Table 2. Calculated vs. Expected Hg Concentrations in Standard Soils and Sediments

STD	Expected (ppb Hg)	Calculated (ppb Hg, 2 sigma)
NIST 1806	60	25 ± 7
SO-1	22	11 ± 1.4
SO-2	82	27 ± 3

Comparison with Other Methods. Well samples were collected and then split for analysis. One aliquot was analyzed using the SRTC MP, the other aliquot by cold vapor atomic adsorption (CVAA). A comparison of the results is shown in Table 3.

Table 3. Hg concentration in ppb measured in well water by the SRTC MP and by CVAA

Sample ID	Hg form	SRTC MP	CVAA
TGB-FB	metal	<0.03	
	inorganic	0.03 ± 0.004	
	+ organic	0.055 ± 0.006	<0.5
TGB-4-1	metal	<0.05	
	inorganic	4.6 ± 0.6	
	+ organic	4.1 ± 1.3	5.8
TGB-4-2	metal	<0.04	
	inorganic + organic	1.7 ± 0.6	5.6

Conclusions

The SRTC MP technique for detection of Hg in aqueous samples appears to give accurate results when analyzing standard solutions and compared to the EPA approved method of CVAA. At this time we are uncertain as to the inaccuracy of the technique when analyzing standard soil samples. We are continuing to examine this technique as an alternative to the EPA soil method of sample digestion followed by dilution and CVAA analysis.

Acknowledgments

The authors wish to thank Greg Hall for his help with this project and the ICP-MS. We also thank Laura Tovo for the CVAA results.

The information contained in this document was developed during the course of work done under Contract No. DE-AC09-89SR18035 with the U.S. Department of Energy.

References

Braman, R.S. Analytical Chemistry, 43, p. 1462.

EVALUATION OF ELECTROSPRAY AND FAB FOR MASS SPECTROMETRY OF ORGANOMETALLIC PARASITICIDES

J.V. Headley, M.S. Yong[1], P.W.Brooks[2], K.M Peru and A. Phillips[3]
National Hydrology Research Institute, Saskatoon, Saskatchewan, S7N 3H5 Canada

[1]*Human Safety Division, Bureau of Veterinary Drugs, Health and Welfare Canada, Tuney's Pasture, Ottawa, Ontario K1A 1B7, Canada;* [2]*Scientific Laboratories Ltd., Business & Technology Centre, Green Lane, Patricroft, Eccies, Manchester, M30 0RJ, England, U.K;* [3]*Fisons Instrument, VG Analytical Limited, Floats Road, Wythenshawe, Manchester M23 9LE, England, U.K*

INTRODUCTION

Organometallics containing toxic levels of pentavalent antimony have received extensive use as parasiticides or drugs for treatment of leishmaniasis infected cattle and human beings. The parasiticides, meglumine antimonate and sodium stibogluconate are susceptible to thermal degradation and readily transform to involatile salts. This has precluded their study using electron impact ionization, and hampered the elucidation of mechanistic pathways.

In this work, these parasiticides were studied using electrospray and fast atom bombardment, as part of an on-going program to develop mass spectrometry tools for broad spectrum analysis (BSA) of pesticides. BSA is used in the context of optimizing the information obtainable from analyses of environmental samples.

EXPERIMENTAL

Studies were conducted using a VG AUTOSPEC-Q and a VG 70S-Q mass spectrometers. For the FAB experiments, suspensions of the antimonials in glycerol were deposited on the target of a FAB probe using a pasteur pipette and the target bombarded using argon atoms (6Kv energy). Studies were also conducted using samples acidified with HCl, employing constant neutral loss scan of 121 (atomic weight of Sb 121), parent-ion scans and daughter-ion scans in the mass range 50 - 1500 amu. Similar experiments were performed using electrospray, with loop injection and a mobile phase of 50/50 methanol/water acidified with 1% acetic acid.

RESULTS AND DISCUSSION

Both the electrospray and FAB experiments resulted in diagnostic mass spectral data for meglumine antimonate. No diagnostic ions, however, were observed for sodium stibogluconate. Discussion is thus limited to the results obtained for meglumine antimonate. As shown in Figure 1-2, the positive ion mass spectrum of meglumine antimonate contained ions with characteristic antimony isotope ratios (57:43) at m/z 627, 507, 406, 314. There was also evidence of ion clusters containing antimony atoms (Sb_{1-3}), which revert to Sb_1 under acid pH conditions. The linked scan data was consistent with a molecular weight of 507, for which the Sb_1 pentavalent antimony was oriented predominantly in a coplanar configuration, suspected to be important for efficacy of the parasiticide and transformation products (Scheme 1-2).

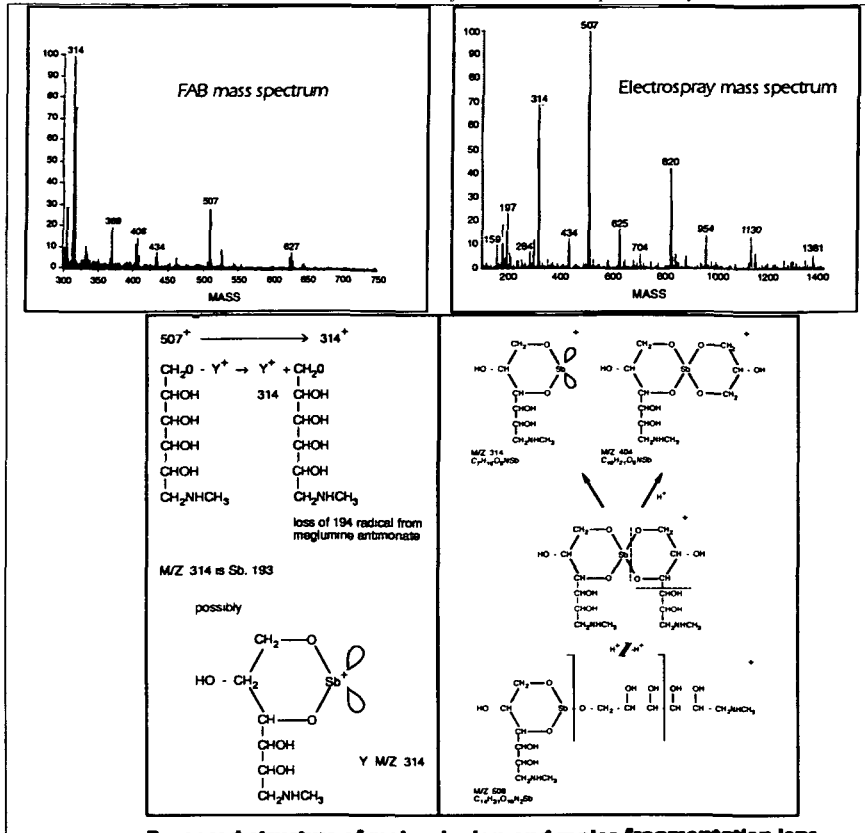

Proposed structure of molecular-ion and major fragmentation-ions

CONCLUSION

The electrospray and FAB techniques provided complementary data for the mass spectral characterization of one of two parasiticides investigated. Further work is required to develop techniques amenable to mass spectrometry studies of sodium stibogluconate and similar compounds for BSA of environmental samples.

ACKNOWLEDGEMENTS

The FAB/MS research was funded in part by the Alberta Environmental Centre, the Geological Survey of Canada and Chemex Labs Alberta Inc.

DETERMINATION OF ACID AND BASE-NEUTRAL PESTICIDES IN WATER BY LC-MS WITH A NEW MICRO PARTICLE BEAM INTERFACE

A. Cappiello, G. Famiglini, P. Palma, A. Berloni and F. Bruner
Istituto di Scienze Chimiche, Università di Urbino
P. Rinascimento 6, 61029 Urbino, Italy

SUMMARY

A new method for the determination of 32 base neutral and 13 acid pesticides in water, which is proved as particularly amenable with High Performance Liquid Chromatography (HPLC), is presented.
A liquid-solid extraction procedure for the isolation of pesticides from acqueous samples is employed.
The LC-MS analysis is carried out with a LC-18 reversed-phase packed capillary column coupled with a Hewlett-Packard 5989A quadrupole mass spectrometer using a new micro Particle Beam interface. Mobile phase flow rates, ranging between 1-5 uL/min, are allowed into the Electron Impact (EI) ion source of the mass spectrometer.

EQUIPMENT

A Kontron HPLC PUMP 420 binary system (Kontron Instruments, Milano Italy) is coupled with a HP 5989A quadrupole mass spectrometer (Hewlett & Packard, Palo Alto, CA, USA) via a modified HP 59980B Particle Beam unit. For UV detection a Jasco UVDEC-100-V, UV-Vis detector (Jasco, Tokyo, Japan) is connected to the column outlet by a 50 μm ID fused silica tubing which is also used as micro-flow cell.

INTRODUCTION

The use of HPLC methods for the analysis of pesticides in various matrices has become imperative after the introduction of a very large series of polar compounds of high efficiency and easily degradable. However, The lack of specificity of the usual HPLC detectors and the large number of compounds to be identified and quantitatively analyzed, push to the use of LC-MS techniques for better analytical results in order to avoid misleading interpretations.
Particle Beam interface provide the variety of structurally significant fragment ions characteristic of conventional electron ionization (EI) mass spectrometry. Furthermore, detection limits were generally in the range of required for enviromental analyses (0.1-30 ppb).
Recently, in our group a modification of the Particle Beam interface has been realized which allows the use of packed capillary columns with a mobile phase flow rates of the order of magnitude of 1 uL/min (1). Improved sensitivity, better response with high water content mobile phases for a greater chromatographic performance during gradient analysis and negligeable instrument contamination are peculiar characteristics of the new device.

EXPERIMENTAL

Figure 1 shows the chromatographic separation of a standard mixture of 32 base-neutral pesticides recorded with the mass spectrometer in the

TIC mode. Figure 2 shows the TIC profile for a mixture of 13 acid pesticides. A 250 um ID C18 packed capillary column (2,3) was employed for both separation. The flow rate was costantly kept at 2 uL/min. It can clearly noticed that no peak broadening is introduced by the the micro interface. The evident peak tailing of most acid pesticides is mainly due to extra chromatographic processes and in particular to thermal decomposition phenomena activated by the electron impact source enviroment. A more extented discussion is reported in reference 4. The performance of micro Particle Beam interface has been improved by adding ammonium acetate in the mobile phase employed for the separation of base-neutral pesticides. As discussed by Bellar et al. (5), the enhancements are attributed to both improved chromatographic efficiency and Particle Beam carrier process.
These beneficial effects can be also found in a enhanced linearity of the calibration concentration plots. Similar effects are obtained by adding a proper amount of TFA in the mobile phase used for acid pesticides separation.
A liquid-solid extraction procedure for the isolation of pesticides from acqueous samples is employed (6). A polyethilene cartridge is filled with a 250 mg of graphitized carbon black (Carbopack B) and is used to sample up 2L of water. By taking advantage of the presence of positively charged active centers on the Carbopack B surface, a stepwise elution system allowed the complete separation of base-neutral pesticides from the acidic ones. After a partial solvent removal the two sample were analyzed by HPLC-PB-MS.

REFERENCES

1) A. Cappiello, F. Bruner *Anal. Chem.* 65, **1993**, 1281
2) A. Cappiello, P. Palma, F. Mangani *Chromatographia* 7/8, **1991**, 389
3) G. Crescentini, F. Bruner, F. Mangani, G. Yafeng *Anal. Chem.* 60, **1988**, 1659
4) L. D. Betowsky, C. M. Pace and M. R. Roby *J. Am. Soc. Mass spectrom.* 3, **1992**, 823
5) J. S. Ho, T. D. Behymer, W. L. Budde and T. A. Bellar *J. Am. Soc. Mass Spectrom.* 3, **1992**, 662
6) Di Corcia, M. Marchetti *Anal. Chem.* 63, **1991**, 580

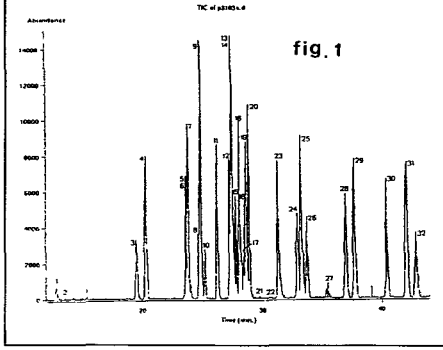

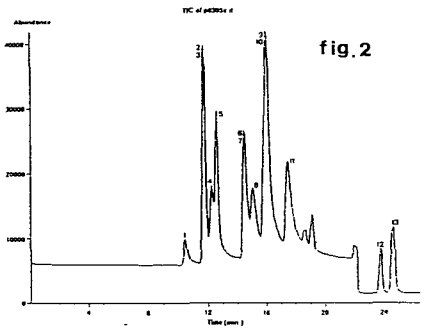

Analysis of Pesticide Residues in Food using GC/MS/MS with an Ion Trap Mass Spectrometer

Steve Schachterle and Robert D. Brittain
Varian Chromatography Systems, 2700 Mitchell Drive, Walnut Creek, CA 94598

Introduction:

Gas chromatography coupled to tandem mass spectrometry (MS/MS) can be used to achieve selective detection of target pesticide components, even in the presence of a complex matrix. Two recent developments in ion trap technology, resonant ejection to remove unwanted ions during the isolation step and modulation of the RF field during CID excitation, make using the ion trap a good choice for MS/MS. These techniques use MS/MS control parameters which are virtually independent of sample or matrix concentration and may be calculated rather than optimized experimentally.

Data are presented showing the linearity and detectivity for malathion by GC/MS/MS. Matrix interferences for malathion-spiked orange extract samples are compared for standard full-scan EI-GC/MS, CI-GC/MS, Selected Ion Storage (SIS), and for this GC/MS/MS approach.

Methods:

A standard Saturn 3 equipped with a Wave-Board was used for all work. Breadboard MS/MS Software was used to insert intermediate segments in between ionization and mass analysis (1). These segments were applied to both the AGC prescan and the analytical scan. A Selected Ion Storage (SIS) waveform was applied during ionization to eject unwanted ions above and below the parent ion and to selectively store a narrow range of ions around the parent ion (2). Off-resonance excitation of 173^+ ion with modulation of the RF trapping voltage was used to provide energy for CID.

Results:

GC/MS/MS was compared to three other GC/MS techniques for the analysis of malathion in orange extract. The techniques differ in the amount of the chemical background that they reject. MS/MS is the most selective technique, virtually eliminating the background. It also gives the best detection limit for malathion.

Using resonant ejection during the isolation step and modulation of the RF during CID excitation, the spectra remain constant across the chromatographic peak.

Calibration curves for malathion standards were also run. Using the major ion of the MS/MS spectrum (127^+) gave a linear response from 2.2 pg/μl to 22 ng/μl.

Conclusions:

Using resonant methods of ion isolation and modulated ion excitation, GC/MS/MS is reliable and easy to automate, offering a convenient way to analyze target compounds in a complex sample matrix.

References:

1. "Ion Isolation and Modulated Ion Excitation for GC-MS/MS in an Ion Trap Mass Spectrometer", B. Bolton, G. Wells, and M. Wang, 41st ASMS Conference.
2. "Development of Automated Selected Ion Storage for Quadrupole Ion Trap Mass Spectrometry", B. Shaffer, J. Karnicky, S. Buttrill Jr., 41st ASMS Conference.

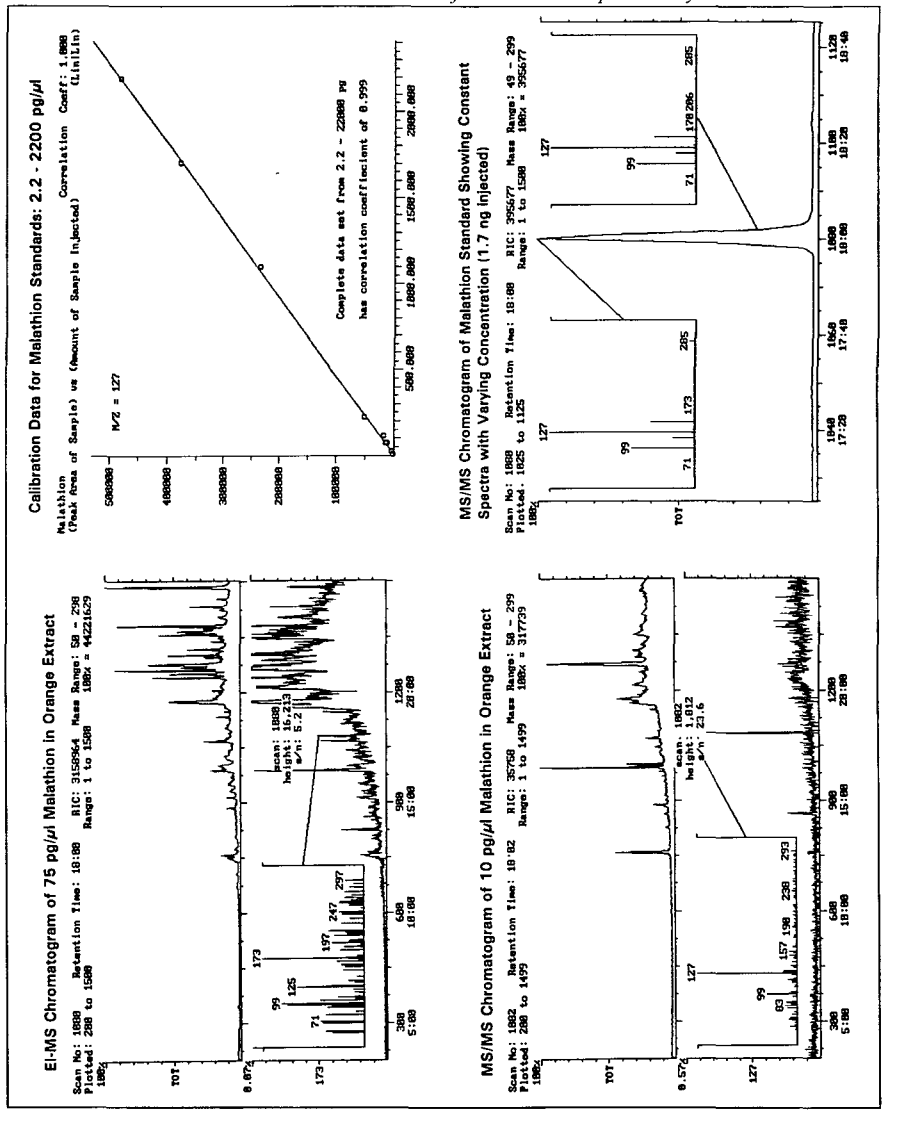

Ion Trap GC/MS Analysis of Pesticides Using Chemical Ionization with Selective Ion Ejection

Robert D. Brittain and Charles K. Huston, Varian Chromatography Systems

Determination by GC/MS of trace level target compounds in complex matrices can be impeded by the interference of matrix components. Chemical ionization (CI) reduces matrix interference without excessive sample cleanup. CI is a "softer" ionization approach, so analyte ions generally fragment to a lesser degree than in EI. CI spectra are often concentrated in a higher mass range than in EI, thus reducing matrix interferences. Also, saturated molecules including hydrocarbons (typical matrix interferences), are poor proton acceptors and respond poorly to CI. We choose the determination of pesticides in food extracts for illustration.

Three steps occur sequentially in ion trap CI: Ionization, Reaction, and Detection First, electrons enter the ion trap to ionize the CI reagent gas (methane for our study). Primary reagent gas ions (CH_3^+ and CH_4^+) react with neutral CH_4 to produce more stable CH_5^+, $C_2H_5^+$, and $C_3H_5^+$. Electron ionization of analyte and interfering matrix can also occur at this time. The EI artifact ions can be ejected during reagent gas ionization by a Selective Ejection wave form applied to the endcap electrodes of the ion trap so that only reagent ions are stored. The maximum m/z for ion storage is set by adjusting the amplitude of the wave form. The elimination of EI artifacts in the CI mass spectrum of Heptachlor is shown in Figure 1. Reagent gas ions then react with GC column effluent for a time determined by an Automatic Reaction Control prescan. High mass product ions are now stored in the ion trap Several classes of reactions can occur between reagent gas ions and analytes during the reaction period. **Proton transfer** produces characteristic M+1 ions which can also undergo fragmentation processes. Although ion traps utilize a low pressure of CI reagent gas, **adduct ions** at M+17, M+29 and M+41 may be observed in good proton acceptors such as Simazine. **Charge transfer** reactions can produce EI-like ions during the reaction period. Figure 2 compares the EI and methane CI chromatograms of a bell pepper extract. The total ion count for the most intense EI peak is over 1,300,000; the mass spectrum at the apex (Scan 1075) is characteristic of hydrocarbon interference from the matrix. The ion count for this peak is reduced to about 40,000 in the CI chromatogram, a reduction of matrix interference at this point in the chromatogram of over 95%.

CI can improve S/N and detectivity in complex matrix samples. Figure 3 shows the extracted ion chromatograms for characteristic ions of methoxychlor in EI and CI The S/N values calculated for each peak demonstrate the advantage gained by shifting ion intensity of the target compound to higher mass. Although the peak heights in CI are reduced from those in EI for this compound, S/N values increase in CI because higher mass ions have less background interference.

Chemical ionization is an option of ion trap mass spectrometer operation which is easy to use; alternating EI/CI segments may be programmed in the same acquisition using programmed acquisition tune events in the Saturn 3 GC/MS. Selective Ejection CI in the Saturn 3 system uses a non-resonant ejection wave form to remove EI artifact ions during the reagent gas ionization process so that a pure CI mass spectrum is acquired Chemical ionization spectra of complex matrices such as food extracts exhibit much less interference than corresponding EI spectra. The reduction of interference can lead to improvements in detectivity, particularly for compounds which are good proton acceptors

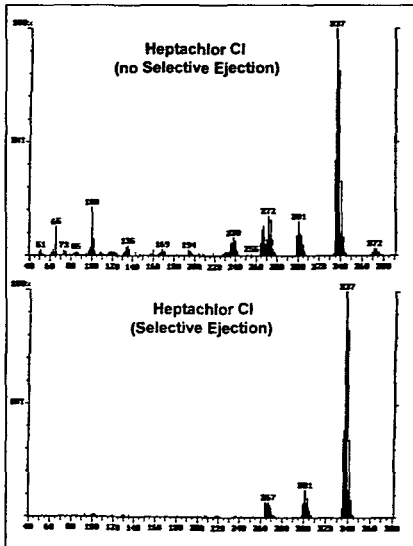

Figure 1. Effect of Selective Ejection on the CI Mass Spectrum of Heptachlor

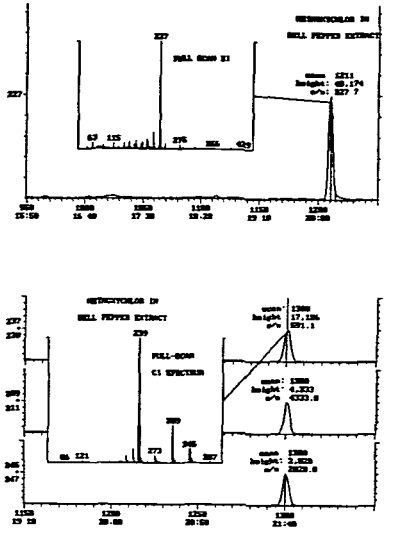

Figure 3. S/N for Characteristic EI and CI Ions of Methoxychlor in Bell Pepper Extract

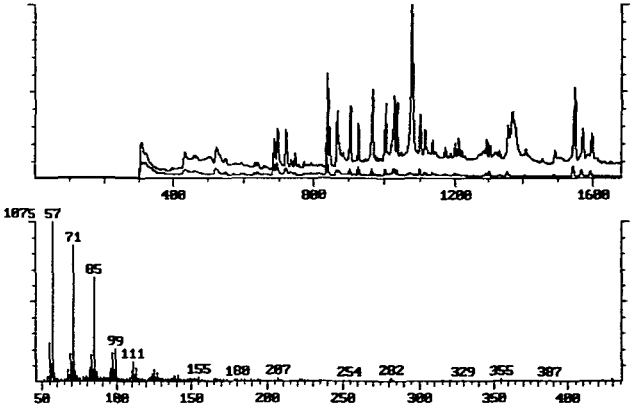

Figure 2. EI vs. CI Chromatograms of a Bell Pepper Extract

COMPOSITIONAL ANALYSIS OF SUBMICRON PARTICLES IN AIR BY TIME-OF-FLIGHT MASS SPECTROMETRY

W. D. Reents, Jr., A. Swanson, S. Downey, A. M. Mujsce, A. J. Muller, B. Emerson, D. J. Siconolfi, and J. D. Sinclair
AT&T Bell Laboratories, Murray Hill, New Jersey 07974

Particles are a major contamination problem in the electronics industry. From plasma processing to clean room conditions, particle formation continues to cause semiconductor device failures. Currently, particle sizes ≥0.05 micron are of concern. As linewidths in devices shrink, particles of even smaller size will create problems. There is no effective way to detect and analyze small particles so as to identify and eliminate their source in clean rooms.

We have built a prototype instrument fo rdetection and chemical analysis of individual airborne particles. A schemiatic of the instrument is shown in Figure 1. Particles are introduced via a 0.53 mm ID x 500 mm long tube and two stages of differential pumping separaaated by 1.0 mm ID orifices. The particles travel 15 cm to the ion source of a time-of-flight mass spectrometer where they are struck by the focused output of a pulsed excimer laser (308 nm, 1-2 x 10^8 W/cm^2). The ions are then accelerated to 4kV and mass analyzed. Teh output of the electron multiplier is digitized with an oscilloscope.

Mass spectra of individual particles have been obtained with the compositions of $(NH_4)_2SO_4$ (Figure 2), SiO_2, $RbNO_3$, and $CsNO_3$. Detection of SiO_2 particles deomonstrates the ability to analyze refractory materials with high ionization potentials. Molecular ion are observed for both $(NH_4)_2SO_4$ and SiO_2 particles. In contrast, $RbNO_3$ and $CsNO_3$ particles produce only the metal cations, Rb^+ and Cs^+, respectively.

We have also obtained mass spectra of particles as small as 0.02 micron. Both $(NH_4)_2SO_4$ and $RbNO_3$ give readily identifiable mass spectra. The ion intensity is proportional to particle diameter for 0.02 to 0.1 micron diameter particles (Figure 3).

In summary, we have demonstrated the ability to detect individual airborne particles as small as 0.02 micron. In addition, we can identify a particle's composition from its characteristic mass spectrum.

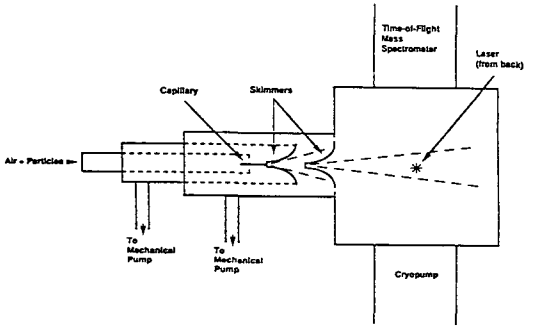

FIGURE 1

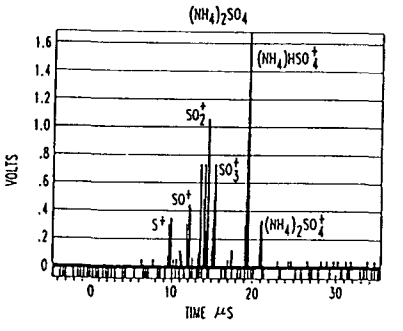

FIGURE 2

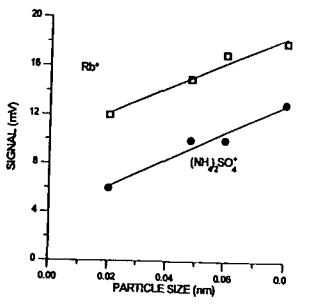

FIGURE 3

MATCHING PROBABILITY OF LIBRARY SEARCH IN SCREENING ENVIRONMENTAL SAMPLES BY GC/MS

Hsia Yung Hur, John R. Oppenheimer and Qingmei Zha
Center for Environmental Science, College of Staten Island
City University of New York, Staten Island, NY 10301

Great concern has been focused on the air pollution. The volatile organic compounds (VOCs) have been detected in ambient atmosphere at certain levels. Some of those compounds have been proven to be toxic, mutagenic and possibly carcinogenic in laboratory studies and have been linked to respiratory cancer in certain occupational settings. In late eighties, Staten Island Air Pollution and Respiratory Disease Study was initiated at our center, which involved a lung cancer case-control study and an air monitoring program. Staten Island, as an urban region of metropolitan New York, is a river apart from New Jersey industrial complex. The world's largest landfill is located in Staten Island. As a consequence, Staten Island has a complex air matrix.

The sampling and analysis of ambient air have been reported previously [1]. Over 24 hours period, air were pumped through the sample traps filled with Tenax at a rate of 8 ml/min (low flow) and 16 ml/min (high flow), respectively. The sample traps were then sealed and send to laboratory for analysis. Sample screening was performed on a thermal desorption-GC/MS system. The volatile compounds trapped in Tenax were released by a thermal desorption unit (Perkin-Elmer ATD-50) and transferred to a GC/MS (Hewlett Packard 5970B) for mass spectral analysis. The capillary column was DB-5, 60m x 0.25mm, 1.0 um thick film. The column was cryo-focused and gradually heated to 225°C over 40 min period for a sample run.

The numbers of chromatographic peaks between summer sample and winter sample were slightly different. The average number of peaks is 264 for summer and 272 for winter. The summer samples showed not only less peaks, but also lower concentrations of VOCs. This behavior probably related to the seasonality of ozone concentration in atmosphere [2]. Among those peaks, 228 compounds were mass spectrally identified and verified. According to their characteristic functional groups, the 228 compounds were placed into 6 classes: alkanes (51), alkenes (37), cycloparaffins (35), aromatics (52), halocarbons (22) and oxygenated compounds (30). In addition, there was one sulfur containing compound.

The first step in screening ambient air samples was computer library search. For every chromatographic peak, library search can narrow down the possible candidates to a reasonable small number in a short period. All the possible candidates suggested by the library search were listed by their percentage matching probabilities. To find the right structure of the unknown, all the candidates need to be carefully considered by their physical properties, and finally verified by the injection of the pure form chemical of the potential candidate. However, a candidate with a high percentage matching probability would most probably be the right structure of the unknown.

The NBS library gave a low overall mean match probability of 56.5%. Among the 6 different classes, aromatics had the highest average matching probability of 70.3%, while the alkenes had the lowest average probability of 41.2%. The average matching probability was 69.6% for halocarbons, 59.1% for alkanes, 50.8% for oxygenated compounds and 44.2% for cycloparaffins. The number of compounds that had high matching probability was very limited. Only 17 compounds (7.5% of the total identified compounds) had the matching probability greater that 90%. Most of them were aromatics (9) and halocarbons (5). Furthermore, there were 24 compounds (10.5% of the total identified compounds) that were indicated by NBS library as "no match".

Oxygenated compounds had the highest percentage 23.3% of "no match" (7 out of 30). Aromatics and cycloparaffins had low "no match" percentage of 0% (0 out of 52) and 2.9% (1 out of 35), respectively.

It was understood that a candidate with a high percentage matching probability may not always be the right structure of the unknown. However, 56.5% of overall mean matching probability turned out too low. In order to assess this valve, the matching probabilities of the compounds in real samples were compared with that from pure chemicals. For the randomly selected 28 compounds, the mean matching probability was 63.9% for real sample while it was 67.4% for the pure chemicals. Although some compounds from pure form chemicals had the higher matching probabilities than that from the real sample, and vice versa, there seemed to be no significant differences in mean matching probability between the real sample and the pure chemicals.

Comparison of NBS library search probablity between samples and pure compounds

		NBS library search prrobablity			
No	Compound Name	Sample	Prob # of >90%	Pure Compoun	Prob # of >90
	Alkanes				
5	Pentane	52		52	
23	Pentane, 2-methyl	27		52	
66	Heptane	41		29	
207	Undecane	96	1	83	
221	Undecane, 2-methyl	58		76	
226	Dodecane	69		86	
	Alkenes				
30	1-Pentene, 2-methyl	30		20	
31	1-Hexene	43		33	
36	2-Hexene(Z)	92	1	94	1
49	1,3-Pentadiene, 3-methyl(E)	30		64	
71	2-Heptene	77		83	
106	2-Octene(Z)	36		86	
	Cycloparaffins				
58	Cyclohexene	51		64	
	Aromatic				
151	Benzene, propyl	84		70	
154	Benzene, 1-ethyl 3-methyl	93	1	83	
155	Benzene, 1-ethyl 4-methyl	86		86	
157	Benzene, 1,3,5-trimethyl	87		41	
159	Benzene, 1-ethyl 2-methyl	93	1	71	
168	Benzene, 1,2,4-trimethyl	57		48	
173	Benzene, iso-butyl	49		71	
180	Toluene, p-isopropyl	43		89	
181	Benzene, 1,2,3-trimethyl	83		69	
186	beta-methyl styrene(E)	30		71	
188	Benzene, 1,3-diethyl	95	1	59	
193	Benzene, 1,4-diethyl	81		75	
196	Benzene, 1,2-diethyl	69		93	1
213	Benzene, 1,2,3,5-tetramethyl	93	1	71	
222	Benzene, 1,2,3,4-tetramethyl	44		67	
	Mean	63 9		67 4	
	S	23 6		19 2	
	#	28	6	28	2

[1] Q. Zha, J. R. Oppenheimer and C. P. Weisel, Proceedings of 38th ASMS Conference on Mass Spectrometry and Allied Topics, (1990) p.618.

[2] J. R. Oppenheimer, D. B. Gerstle, C. P. Weisel and Q. Zha, Measurement of Toxic and Related Air Pollutants, USEPA and Air Waste Management, Pittsburgh (1991) p.267.

Identification of Surfactants in Formulated Detergents By Using FAB and FD on the AutoSpec-Q Mass Spectrometer

J. G. Nowlin, I. Dzidic, L. A. Spino and L. Kravetz

Shell Dev. Company, Westhollow Res. Center, Houston, TX 77082

Introduction

Surfactant characterization in formulated detergents has long been dependent on a combination of both classical chemistry methods and chromatographic techniques. The analytical procedure starts with the extraction of surfactants followed by cleanup steps using a series of ion exchange columns, titrations and analyses by GC and LC.

Instead of using these lengthy procedures, one can rapidly identify surfactants in detergents directly using the combination of positive and negative ion FAB and FD mass spectra. The nonionic surfactants, such as alkyl ethoxylates, R-(OCH2CH2)nOH and polyethylene glycols, H-(OCH2OCH2)nOH can be identified from the positive FAB and FD ions, MH+ and MNa+. These spectra provide the (OCH2CH2)n distribution up to n = 40 as compared to LC, which can determine the distribution up to about n=18.

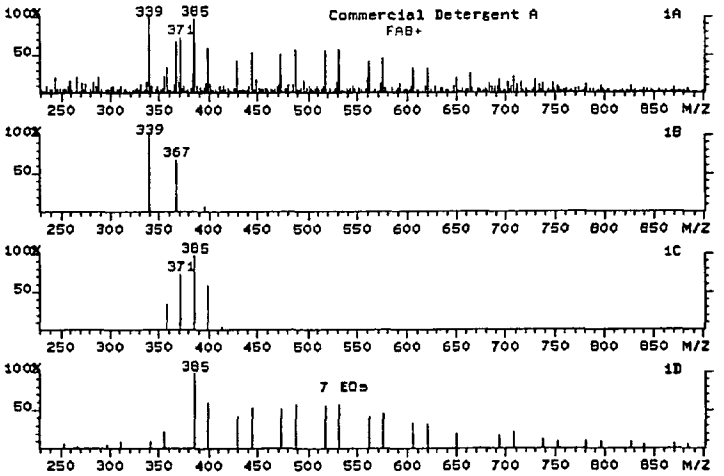

Figure 1

Results and Discussion

Positive ion FAB spectrum of a typical liquid detergent is shown in Figure 1A. This "total" positive ion spectrum indicates that several different surfactants are present in this detergent. By using the data processing "filter", the composite "total" spectrum is sorted out into the spectra B, C, and D, which indicate that at least three distinct surfactant types are present in the sample.

Note that the positive ion spectra shown in Figure 1C and 1D exhibit the same nominal mass ions at m/z 385 and 399. In order to prove that these two ions belong to different molecular formulas, the spectra were acquired again at a higher mass spec resolution, which produced two well resolved peaks at m/z 385.2929 and 385.4988 from which the molecular formulas, C20H42O5Na (spectrum D) and C19H31SO3Na2 (spectrum C) were obtained. From the molecular formulas it was concluded that compounds in the spectrum D belong to the nonionic C12/C13 alcohol ethoxylates and in the spectrum C to the C11, C12, C13, etc., alkyl benzene sulfonates.

Figure 2 compares positive ion FAB and FD mass spectra of a C11 alcohol ethoxylate sample. The FD spectrum (bottom) does not exhibit any fragment ions and is now used routinely for screening high molecular weight surfactants. While the FD spectrum exhibits the higher intensities for the potassium aduct ions, MK+, the FAB spectrum (top) exhibits more intense MH+ ions. The (CH2CH2O) distribution obtained from intensities of MH+ ions is in agreement with the data obtained from the GC/LC analysis.

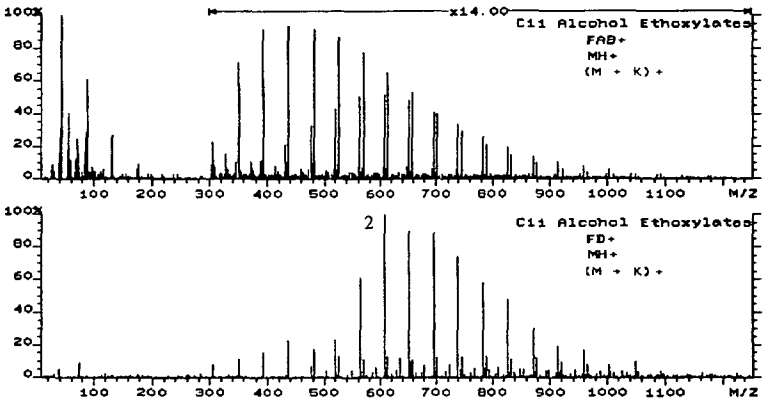

Figure 2

DETECTION OF METAL COMPLEXING AGENTS ON MINERAL SURFACES BY STATIC SIMS

G. S. Groenewold, J. C. Ingram, A. D. Appelhans, J. E. Delmore, D. A. Dahl, Idaho National Engineering Laboratory, P. O. Box 1625, Idaho Falls, ID 83415-2208

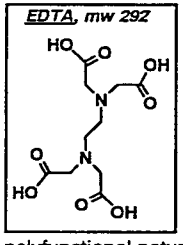

Ethylenediaminetetraacetic acid (EDTA) and related compounds [nitriloacetic acid (NTA) and diethylenetriaminepentaacetic acid (DTPA)] have been widely used at Department of Energy facilities for complexing radionuclides, and have been disposed of together with radionuclides. EDTA is not toxic by itself, but decreases the ability of minerals to adsorb radionuclides, and enhances the mobility of radionuclides in the environment. Additional motivation for studying EDTA is related to its implication in the generation of H_2 in the Hanford nuclear waste storage tanks. EDTA analyses have been effectively performed using derivatization/GC/MS, and electrospray MS. However, due to the polyfunctional nature of the molecule, screening for EDTA on surfaces, and determination of EDTA speciation can be time consuming and difficult.

The objective of the INEL research effort is to develop rapid methods and instrumentation for analysis of EDTA on minerals and other refractory materials, and also having the potential for determining EDTA speciation. Ideally, minimal sample preparationwould be required, and little or no lab waste would be generated.

Static secondary ion mass spectrometry (SIMS) instrumentation which employs ***pulsed extraction*** and a ***perrhenate ion gun*** was used for the direct analysis of EDTA on basalt. Sample preparation consists of attaching a basalt chip to a target planchette using double-sided tape. Using pulsed extraction, anions and cations are alternately drawn from the sample surface, which prevents charge buildup on the basalt, and also allows for the simultaneous acquisition of anion and cation spectra. The perrhenate ion gun produces a massive, high energy (10 KeV), anionic, molecular particle (ReO_4^-, ca. 250 da), which is very efficient for producing abundant secondary particles at low primary ion currents (typically 100 picoamps).

Ionic species of EDTA in solution versus pH	
pH range	predominant species
<0.0	H_6Y^{+2}
0.0 - 1.5	H_5Y^+
1.5 - 2.0	H_4Y
2.0 - 2.7	H_3Y^-
2.7 - 6.6	H_2Y^{-2}
6.6 - 10.2	HY^{-3}
> 10.2	Y^{-4}

EDTA can exist as a variety of species in solution, with the dominant species varying as a function of pH. If the solution-phase ions are preserved on the dry surface of the basalt, then the SIM spectrum will likely be affected. Basalt chips were exposed to EDTA solutions having pH values ranging from 1.4 to 11.5 in order to assess this factor. The pH of the unmodified Na_2EDTA solution (4.7) was adjusted using HCl or NaOH in order to generate solutions of different EDTA species.

When basalt was exposed to EDTA solutions having low pH (2.2 or less), no $[M + H]^+$ or $[M - H]^-$ were observed; instead, m/z 235^+ was observed(fig.1), which corresponds to the loss of one of the CH_2CO_2 moieties. This ion has been interpreted in terms of *a* (fig. 2). Presumably, formation of this ion requires the

presence of excess protons on the surface for the protonation of the carboxyl moieties, because EDTA exists predominantly as a zwitterion with a -1 charge in a pH 2.2 solution.

When basalt was exposed to EDTA solutions having a pH of 4.7, the ion corresponding to the loss of a single methyl carboxyl moiety is observed at m/z 233^+. The formation of an ion having fewer hydrogen atoms is consistent with the idea that there are fewer protons available on the surface for protonation of the carboxyl and amine moieties of EDTA, and with the fact that the predominant species of EDTA in a pH 4.7 solution is H_2Y^{-2}. A cyclic structure *b* is proposed in order to account for the unsaturation dictated by this mass.

When basalt was exposed to EDTA solutions having a pH close to neutral (6.0 - 7.0), the ion corresponding to the loss of a single methyl carboxyl moiety is nearly evenly partitioned between m/z 233^+ and m/z 231^+. The conclusion for this experiment is the same as for the pH 4.7 experiment: fewer protons are available on the surface for protonation of EDTA, and the predominant species in a pH 7 solution is even further deprotonated, HY^{-3}. M/z 231^+ is interpreted in terms of a bicyclic structure *c*, in order to account for the unsaturation dictated by this mass. In both the pH 4.7 and 7.0 experiments, no $[M + H]^+$ or $[M - H]^-$ were observed.

The decrease in mass of the $[M-CH_2CO_2]$ ion from m/z 235^+ ion to m/z 233^+, and then to 231^+ as the pH of the spiking solution increases is interpreted in terms of increasingly deprotonated EDTA species present on the surface. The surface species which give rise to these ions reflect the predominant species originally present in the EDTA spiking solution. We conclude that different EDTA surface species are distinguishable in the SIM spectra of exposed basalt, although we note that intact EDTA is difficult to sputter off a mineral surface because it strongly binds to minerals.

Fig. 1. Partial Cation Spectra of EDTA

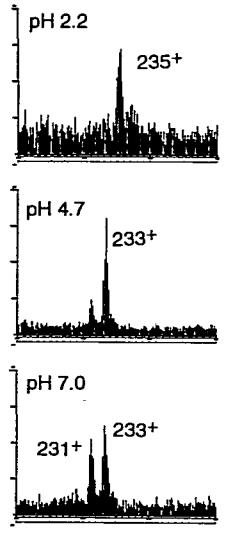

Figure 2. Postulated ion structures for the loss of CH_2CO_2 from EDTA.

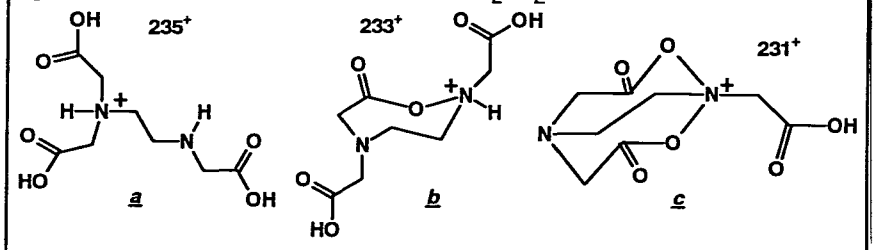

Funding support of the U. S. Department of Energy, Office of Technology Development, is gratefully acknowledged.

INFRARED PYROLYSIS OF POLYMERS FOR GCMS ANALYSIS

B. Wiezorek[1,2], *G. Baykut[1], and K. P. Wanczek[2]
1) Bruker-Franzen Analytik GmbH Fahrenheitstr. 4, 2800 Bremen 33, Germany; 2) Department of Chemistry, University of Bremen, NW2, 2800 Bremen 33, Germany

The analysis of solid samples by mass spectrometry requires special sample introduction techniques. In the on-site environmental mass spectrometry, one prefers to use simple methods, that produce results of high information content. Membrane inlets used in the mobile mass spectrometry, make it necessary use special devices for handling solid or liquid samples. A fast gas chromatographic separation simplifies the mass spectrometric identification of the components in the sample.

The infrared pyrolyzer[1,2], the application of which we present in this paper, is recently developed to use with the environmental mass spectrometry. This device helps to prepare solid samples for the mass spectrometric analysis. It is also used for detemining GCMS contaminants in solid matrices. Soil samples containing environmental pollutants.

In the infrared pyrolyzer (Fig. 1), the sample is heated remotely by an infrared lamp (Osram, Halotherm 500). This rod shaped IR-source and the reaction chamber are mounted along the two focal axes of an elliptic cylinder. The reflecting inner surfaces are covered with aluminum (reflection coeff. 94% for the used IR radiation). The sample is

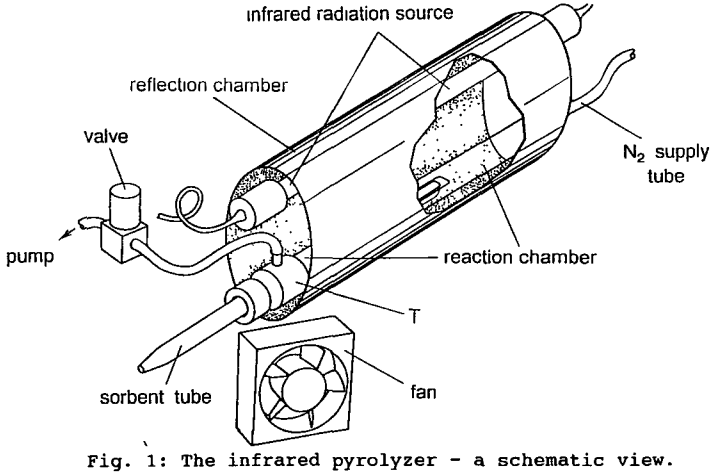

Fig. 1: The infrared pyrolyzer - a schematic view.

1) B. Wiezorek, A. Schiller, G. Baykut, K.-P. Wanczek, 40th ASMS Conference on Mass Spectrometry and Allied Topics, Washington, DC, May 1992
2) B. Wiezorek, A. Schiller, G. Baykut, K.-P. Wanczek, Rev. Sci. Instrum. **1992**, *64*, 5607-5612

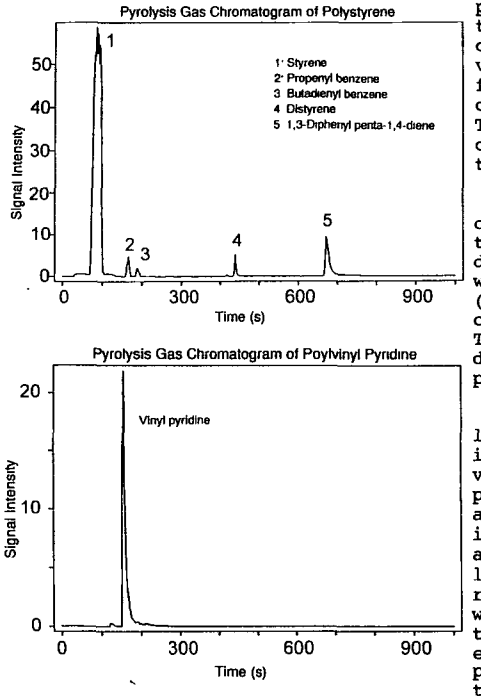

Fig. 2: Two examples of IR pyrolysis chromatograms of polymers

placed in the center of the reaction chamber into a boat-shaped container made of aluminum or Invar. The infrared radiation is focused onto a solid sample placed in a quartz reaction chamber. The programmable heating rate is controlled by pulse modulation of the infrared lamp.

During the experiments a carrier gas flow (9l/h) was maintained in the reaction chamber during pyrolysis. The products were collected in the sorbent (Tenax) tube, which is placed at one end of the reaction chamber. The sorbent tube was kept cool during trapping of the pyrolysis products.

Polyethylene, polypropylene, polystyrene, polyvinyl pyridine, polyvinyl chloride, polyvinyl acetate, polyvinyl alcohol, polyvinyl phenol, polyvinyl carbazole, polyvinyl benzoyl chloride, poly-hydroxyethyl methacrylate and poly ethylene terephtalate have been studied by infrared pyrolysis. Gaseous products were transferred into a sorbent tube filled with Tenax by an inert carrier gas (N_2). Collected products were then desorbed in the desorption oven of the gas chromatograph (4.5m fused silica capillary, stat. phase: RTX 200) and detected after GC separation by quadrupole mass spectrometry.

Most of the studied polymers were relatively easy to identify, since the infrared pyrolysis has led to the corresponding monomers with a high yield. Other polymers like polyethylene terephtalate yield to a multitude of products, which in turn form the characteristic pyrolysis GC pattern for the corresponding compound.

MODULAR INLET SYSTEMS AND SAMPLING DEVICES FOR MOBILE ENVIRONMENTAL MASS SPECTROMETRY

***G. Baykut, G. Weiss, A. Brekenfeld, H.-P. Vetters, G. Heinen, and J. Franzen**
Bruker-Franzen Analytik GmbH, Fahrenheitstr. 4,
2800 Bremen 33, Germany

Environmental mass spectrometry with on-site sampling and analysis capability requires special inlet and sampling systems for various types of natural samples. Most of the analytical investigations in the environmental science are aimed to determine anthropogenic, as well as biogenic contaminants. Studies of contamination dynamics help determine protection and decontamination strategies. In order to avoid losses and possible changes of samples during their transport from sampling site to the laboratory, a large number of analytical determinations can be performed using on-site analysis instruments. In order to obtain a high throughput, these sampling systems must operate very quickly.

A series of inlet and sampling systems (MS peripherals) have been developed in our laboratories to be used in mobile mass spectrometry. These devices are developed in a modular concept. This allows them to be quickly installed and easily operated. A task-oriented combination of different modules is possible. Two examples for the sampling modules are the injector/desorber module and the air sampling module.

A primary peripheral module of the mass spectrometer is the gas chromatographic separator. The GC is mounted on top of the mass spectrometer and has a special quick connection system to the mass spectrometric inlet membrane port. On its other end, a similar quick connector helps to combine it with the secondary peripherals. Injector and desorber units are considered as the secondary periphery. Two versions of the GC is developed. One of them is equipped with a short (3.5m) capillary and is used for semi and low volatile compounds. The other GC has contains a longer capillary (20m) and is developed for volatile compounds. However, volatile compounds can also be run through the short GC, since a special peak separation algorithm in the post-processing software helps resolve overlapping GC signals. The gas chromatographic separator is interfaced to the membrane inlet of the mass spectrometer. This is a heated hollow fiber membrane made of polysiloxane. The GC-separated compounds flow through the hollow fiber and diffuse through its walls into the mass spectrometric vacuum system.

The *injector/desorber module* can be used as a liquids injector for the GC as well as a desorber for sampling tubes filled with sorbents. Sorbent tubes with gaseous contaminants from air or from *spray-and-trap* gas sampling in aqueous samples can be inserted into the desorption port of the module. The automatic gas sampling module *"air sampler"* can be used as an alternative secondary periphery. This module consists of a computer controlled preconcentration system. Here, a sorbent tube filled with Tenax is used to adsorb and desorb compounds in the sample and inject them into the GC. The sorbent tube of the air sampler can be reused several hundred times. In order to sample volatile organic compounds in water, a *spray extractor* is used. The water sample is sprayed in a chamber in form of small droplets, where the VOCs are easily extracted into

the gas phase. The sampled compounds are preconcentrated in the *air sampler*, before the GCMS analysis is performed.

The soil sampler and the *infrared pyrolyzer* are two of the other secondary peripherals. The soil sampler has a heated sampling head with a polysiloxane membrane. The sampler head heats the soil sample on contact and desorbs the volatile organics. They diffuse through the sampler membrane, and will be transferred through a short GC capillary to the mass spectrometric inlet membrane port. The IR pyrolyzer is used for solid samples, contaminated soil and polymer pyrolysis. The soil sample is heated by an infrared lamp and the pyrolysis products are transferred into a sorbent tube by an inert carrier gas.

The following scheme shows the overall view of the sampling and inlet devices in the modular concept of mass spectrometric accessories:

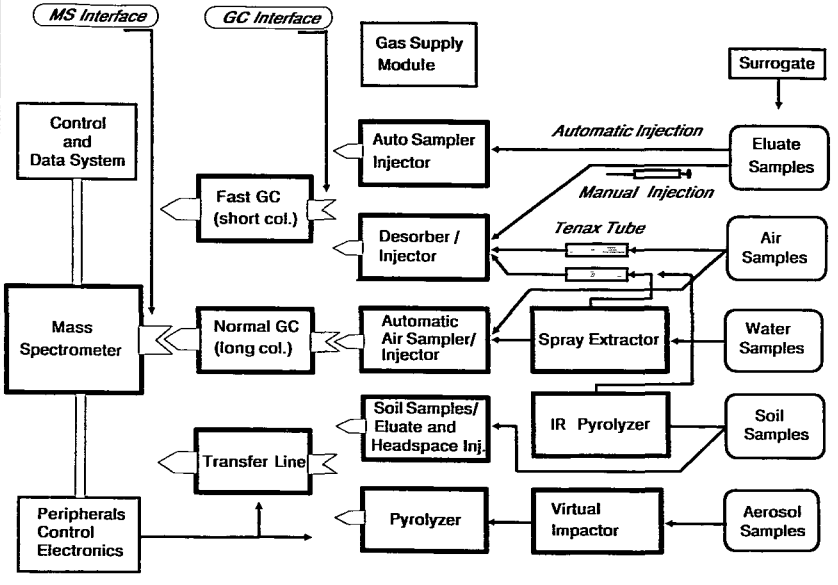

The major difference between these sampling and inlet systems and conventional GC or GC/MS equipment is their modularity. Unlike in the conventional systems, the injector/desorber module can easily be separated from the GC module and replaced with a different injection module, in a very short time just by simple hand operations. Being able to perform fast GC runs of 4-5 minutes with the 3.5 m-capillary GC module, decreases the sample througput time enormously, which is important for on-site measurements.

AUTOMATED ANALYSIS OF SELECTED ORGANIC COMPOUNDS IN URBAN AIR BY AN ISOTOPIC DILUTION GC/MS METHOD

***E. Davoli, L. Cappellini, O. Rossi, S. Ferrari[1], U. Delprato[2] and R. Fanelli, Istituto di Ricerche Farmacologiche Mario Negri, Via Eritrea 62, 20157, Milano, ([1]) RIAL Vacuum S.p.A., Via Novara 6/A, 43100 Parma, Italy and ([2]) ELECOS S.p.A.,Viale degli Eroi di Cefalonia 123, 00128 Roma, ITALY.**

A new technique is presented that allows fast, direct, automated analysis of environmental air enriched with isotopic labelled internal standards. The method is based on a cryofocussing GC/MS technique with a fixed loop 6-way sampling valve and an on-line permeation tube device.

The instrument is based on a modified residual gas analyzer (RGA) (RIAL QM 130) coupled to a DANI 86.10 gas chromatograph equipped with a cryofocussing device (TCT, Chrompack, The Netherlands) and with a 6 way sampling valve with a 100 ml fixed loop(1). A custom made thermostated permeation tube, filled with an isotopic labelled standard, is placed on the sampling line in order to continuously enrich the sample with known amounts of internal standard.

Benzene and toluene were chosen as the target compounds because of regulatory interests and their toxicity. In order to achieve an analytical cycle as short as possible the chromatographic column, a 10 m CP Sil 5, 150 µm ID, 1 µm film thickness has been kept isothermally at 110 °C. The carrier gas was nitrogen.

In fig 1. a chromatogram of air enriched with the internal standard (benzene-d_6) is shown. The instrumental response (5537 ± 1.2 %, mean ± RSD) during the period of the experiments was very good. The amount injected was correspondent, for the permeation tube used during this experiment, to 266 µg/m^3 (with an air sample of 100 cc and a sampling speed of 500 ml/min). We have not observed major interference peaks, even with such a short cycle, in the sample or internal standard time window.

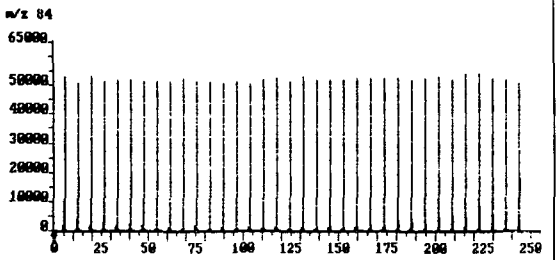

Fig. 1

A calibration curve of benzene/benzene-d_6 and toluene/benzene-d_6 was prepared, with splitless injections of 1 µl of solutions containing 10 ng/µl of internal standard, in the range 50-5000 pg. Quantitation was performed on the

basis of this calibration curve, and of the internal standard peak area. The internal standard added was deuterated benzene at a concentration of 26.6 µg/m^3. Sensitivity was high enough to monitor benzene concentrations in urban air. A 10 pg benzene splitless injection gives a S/N higher than 3, therefore if we assume a 100% adsorption and desorption efficiency of the trap, the lowest detection limit under the same experimental setup, should be 0.1 µg/m^3.

In fig. 2. benzene and toluene concentrations of a 5 days urban air monitoring experiment are reported. The analytical cycle time was 14 minutes.

The monitoring system here described is the first application, at our best knowledge, that takes advantage of an "on line" isotopic dilution technique. The use of an "on line" isotopic dilution technique, in air monitoring, gives not only the accuracy advantages of isotopic dilution, but also a continuous check of the trapping efficiency of the cold trap.

It is interesting to note that a "low end" mass spectrometer, like RGAs are considered from the most of us, might have a role also in solving some analytical chemistry everyday problems, like the one discussed before. We believe that in cases like this, when the technical performances are sufficient, it is even preferable to use RGAs over conventional organic mass spectrometers not only for the lower price, but for a more reliability that comes from a more general mechanical simplicity.

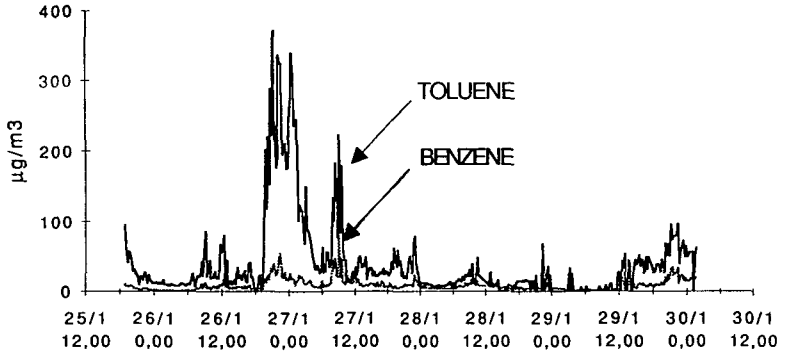

Fig. 2. Urban air benzene and toluene concentrations. Results of five days monitoring.

This study has been supported by the CNR-ENEL project-interactions of energy system with human health and environment. Rome-Italy.

1. E. Davoli, L. Cappellini, S. Ferrari and R. Fanelli.; Proceedings of the 40th ASMS Conference on Mass Spectrometry and Allied Topics; Washington, DC, May 1992; pp 695-696.

A NOVEL HIGH RESOLUTION MASS SPECTROMETER FOR AUTOMATED TARGET COMPOUND ANALYSIS

Schubert R., Pfaff H., Huels W., Pesch R.
Finnigan MAT GmbH, Barkhausenstr. 2, 28197 Bremen, Germany

INTRODUCTION

The analysis of target compounds as halogenated dibenzo-dioxins and -furans is well regulated and standardized. A growing number of samples has to be evaluated for ever lower concentrations of these species. As this trend escalates, analytical instrumentation is required to accommodate greater sample loads with improved efficiency through automation, better sensitivity, and increased stability and reliability.
The QUANTUM is a fully microprocessor controlled high resolution mass spectrometer that incorporates a novel mouse oriented user interface TACO (TArget COmpound Analysis Software) (Fig. 1). This gives the unique advantage to customize complete methods like USEPA 1613 and 8290 including routine MS-setup, automatic data evaluation, reporting and quality assurance. Instrument feedback control from TACO guarantees that only data are acquired which are within user specified tolerances. To validate the QUANTUM a sensitivity and stability test was performed.

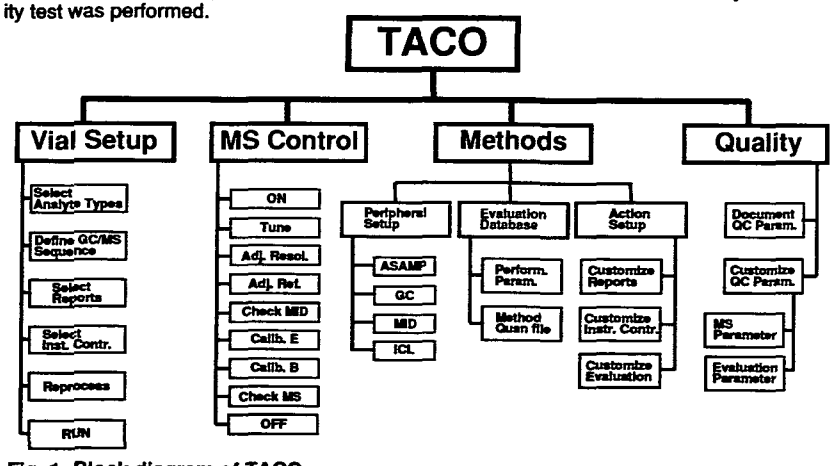

Fig. 1: Block diagram of TACO

SENSITIVITY TEST

The QUANTUM was autotuned via TACO - MS-Control -Tune. In the VIAL SETUP a batch was defined containing solutions from 3 fg/µl to 1000 fg/µl of native 2378-TCDD together with 5 pg/µl $^{13}C_{12}$-2378-TCDD standard as carrier. Triple injections onto a 25m DB 5 capillary column were performed from each vial containing 10 µl. The MID descriptor acquired the M^+

and the $(M+2)^+$ ion for each congener and two reference ions. Cycle time was 500 ms. Each run took about 20 min and the total batch (including blanks 26 injections) was processed unattended over night. The resolution was written into a QC-chart inbetween the different concentrations. Since it was within the specified limits no retuning of the system was necessary. Sensitivity specifications of 30 fg with S/N > 10 : 1 are easily achieved and the response indicates good linearity over the complete concentration range.

STABILITY and REPRODUCIBILITY TEST

An initial calibration was performed as required by USEPA method 1613. This calibration was verified twice a day for one week. The batch for the initial calibration included the window-test GC performance-test and the calibration solutions CS 1 to CS 5. GC and MID setup was performed via TACO as required by USEPA method 1613. MID peak jumping accuracy and resolution at full and reduced accelerating voltage were checked against the limits and documented automatically via TACO inbetween injections. Automatic data evaluation included checks for the isotope ratio, the retention time stability and the reference mass stability. Quantification was performed in respect to USEPA method 1613. TACO also performed reports for individual runs as well as the summary report for the calibration. Batches for verification included the window-test, GC performance-test, and the verification solution CS 3. Instrument parameter and data evaluation limits were specified within TACO in correspondence to USEPA method 1613. There was no need for any retuning of the QUATUM during this week.

	Apr-03 04:37	Apr-03 21:19	Apr-05 20:31	Apr-06 14:23	Apr-06 20:58	Apr-07 14:44	Apr-07 20:32	Apr-08 12:05	Apr-08 19:54	MEAN	%RSD
Native Congeners											
2378-TCDF	9.6	9.5	9.4	9.0	9.0	9.3	9.2	9.5	9.6	9.4	2.2
2378-TCDD	9.2	9.0	9.2	8.8	8.9	9.3	9.2	9.0	9.0	9.1	1.7
12378-PeCDF	48.9	49.4	49.6	48.9	48.3	51.0	49.0	50.0	48.2	49.3	1.7
23478-PeCDF	48.8	48.3	47.7	47.8	46.8	46.9	46.9	47.2	48.0	47.6	1.4
12378-PeCDD	52.5	49.1	49.8	47.2	48.4	48.2	48.3	48.4	48.8	49.0	2.9
123478-HxCDF	50.0	48.9	49.8	48.9	49.6	50.1	49.8	49.2	50.4	49.6	1.0
123678-HxCDF	50.0	49.7	50.3	48.5	49.4	49.9	49.6	49.3	49.9	49.6	1.0
234678-HxCDF	49.1	49.2	49.3	48.8	48.7	48.3	49.1	49.5	49.9	49.1	0.9
123789-HxCDF	50.2	49.6	50.1	49.4	49.4	50.7	50.9	50.8	51.8	50.3	1.5
123478-HxCDD	50.6	50.0	50.4	49.9	49.8	50.4	49.3	50.3	49.8	50.0	0.8
123678-HxCDD	49.5	49.6	50.1	49.3	49.6	48.8	50.3	50.1	49.6	49.7	0.9
123789-HxCDD	48.4	50.3	49.0	47.2	46.7	47.1	47.9	47.7	48.0	48.0	2.2
1234678-HpCDF	48.6	47.1	47.2	47.3	48.0	47.6	48.0	47.3	47.2	47.6	1.0
1234789-HpCDF	48.6	49.5	50.3	49.4	49.2	48.4	50.8	49.1	50.3	49.5	1.5
1234678-HpCDD	49.0	49.7	49.5	48.3	48.3	48.7	49.1	49.3	50.2	49.1	1.2
OCDF	99.3	101.3	104.1	99.8	99.8	100.9	102.4	100.8	101.9	101.2	1.4
OCDD	91.6	95.9	96.8	95.0	95.2	95.7	96.7	94.0	94.7	95.0	1.6
Surrogate Std's											
2378-TCDF 13C12	101.5	98.8	100.3	100.0	98.7	98.6	99.6	99.7	102.0	99.9	1.1
2378-TCDD 13C12	93.4	92.6	94.9	94.8	93.8	89.5	91.4	93.2	93.6	93.0	1.7
12378-PeCDF 13C12	86.7	96.2	95.1	92.8	83.0	79.7	93.6	90.8	91.4	89.9	5.9
23478-PeCDF 13C12	86.3	96.4	95.4	87.4	87.3	85.1	87.2	87.0	98.0	90.0	5.3
12378-PeCDD 13C12	85.2	98.0	90.8	94.3	91.7	87.7	91.0	96.0	91.6	91.8	4.0
123478-HxCDF 13C12	99.5	97.2	101.3	98.7	97.8	95.1	94.4	99.5	100.5	98.2	2.3
123678-HxCDF 13C12	99.7	98.1	100.4	100.2	99.7	101.0	103.4	101.6	108.4	101.4	2.8
234678-HxCDF 13C12	99.0	97.7	101.6	98.4	98.4	100.9	96.8	98.7	101.8	99.3	1.7
123789-HxCDF 13C12	94.4	96.3	96.6	94.4	93.2	91.2	91.8	93.1	94.7	94.0	1.8
123478-HxCDD 13C12	96.5	96.1	97.7	94.7	94.5	93.4	91.5	92.9	95.1	94.7	1.9
123678-HxCDD 13C12	98.7	96.6	99.2	100.5	99.9	101.2	99.9	100.3	103.5	100.0	1.8
1234678-HpCDF 13C12	100.8	99.8	101.5	96.6	99.4	102.5	99.3	104.1	112.5	101.8	4.2
1234789-HpCDF 13C12	96.9	98.4	94.0	92.4	95.3	98.1	95.5	101.1	98.5	96.7	2.6
1234678-HpCDD 13C12	97.9	97.4	98.5	98.0	98.6	98.8	97.6	101.5	97.9	98.5	1.2
OCDD 13C12	186.1	198.7	190.3	185.5	193.9	202.8	193.7	200.8	197.9	194.4	3.0
Cleanup Std											
2378-TCDD 37Cl4	8.7	8.7	8.9	8.6	8.5	8.6	8.6	8.7	8.8	8.7	1.1

Fig. 2: Reproducibility of USEPA method 1613 verification solution over one week

LC/MS Analysis of Mutagenic/Carcinogenic Heterocyclic Aromatic Amines in Food Products

B.P-Y. Lau, D. Lewis, B. Starvic and R. Klassen
Food Research Division, Health & Welfare Canada,
Ross Ave., Tunney's Pasture, Ottawa, Ont. CANADA. K1A 0L2

INTRODUCTION : It is well known that mutagenic and potentially carcinogenic aromatic amines (HAAs) are formed in protein-rich foods during typical cooking procedures. The formation of HAAs depends on the cooking temperature and duration as well as the presence of other food constituents. Precursors are believed to be creatine or creatinine, amino acids (such as phenylalanine, threonine and alanine) and sugars. In order to assess the human risk and to ensure the safety of the consumer, a sensitive and specific analytical method is required to routinely monitor this type of mutagenic/carcinogenic food contaminant. The objective of the present work is to investigate the use of an electrospray (ESI) or a heated nebulizer interface (HNI) coupled to an atmospheric pressure chemical ionization (APCI) mass spectrometer for the analysis of eight HAAs (IQ; MeIQ, MeIQx; 7,8-DiMeIQx; 3,4,7,8-TetraMeIQx; Trp-P-2, PhIP and Trp-P-1) in cooked meat and food flavors. The complete method involves solvent extraction, simple cation-exchange cartridge cleanup followed by on-line HPLC/MS analysis.

EXPERIMENTAL : Acidified food flavor or food homogenate was continuously extracted with CH_2Cl_2 for 48 hrs. The aqueous layer was made basic and extracted again with fresh CH_2Cl_2. The extract was then back extracted into 0.2N HCl and the above extraction scheme was repeated The final extract was evaporated down to dryness and redissolved in 20% CH_3CN and 0.06% HCOOH. It was then transferred onto a HEMA-SB (sulphobutyl) cation-exchange cartridge (Alltech) and subsequently washed with 0.1N HCl; 20% MeOH in 0.1N HCl and H_2O. HAAs were eluted with 40% acetonitrile in 0.5M NH_4Ac/NH_4OH (pH=9.4). Twenty microliters of the final sample dissolved in mobile phase were injected onto a polymer based PLRP-S column (Polymer Lab , 25 cm x 4 6 mm ID, 5µm) which was connected to a UV detector (254 nm) and the electrospray or heated nebulizer interface in series. A TAGA 6000E (SCIEX, Toronto, CANADA) mass spectrometer equipped with an atmospheric pressure chemical ionization ion source was operated in SIM mode to monitor the protonated molecular ions of 8 HAAs in two groups. The electrospray interface was fabricated in-house but fashioned after the commercial version. A splitter with a split ratio of *ca.* 30:1 was used to reduce the LC flow rate of 0.7 mL/min to 20-30 µL/min. A commercial heated nebulizer interface was also used using the following parameters : probe temperature = 480 °C, nebulizer gas (N_2) = 80 psi, aux. gas flow rate = 1 L/min

RESULTS : Both electrospray and heated nebulizer interfaces produce strong protonated molecular ions for all 8 HAAs under investigation. Fig. 1 shows the responses from a 50 ng injection of 8 HAAs using a heated nebulizer interface. The separation of IQ and MeIQ, the two most mutagenic compounds of the isolated HAAs, are highly susceptible to mobile phase composition and column packing. Very fine particles from the cation-exchange cartridge often enter the chromatographic system. Frequent changing of the protective on-line filter and the guard column is required to maintain the peak shape and sensitivity of

these two compounds. Detection limits for the 8 HAAs range from sub-nanograms to low ng per injection which is equivalent to low ppb (ng/g) in samples. Fig. 2 clearly demonstrates that these compounds can be easily detected in a bouillon blank sample spiked with 2.5 ppb each of the eight HAAs. This figure also shows that the simple cation-exchange cleanup method can effectively remove most of the interferences to allow the detection by LC/MS at this low level. The recoveries of the cleanup method range from 105-90% for MeIQ, IQ and MeIQx and 84-67% for Trp-P-1, Trp-P-2, 7,8-DiMeIQx, TetraMeIQx and PhIP.

CONCLUSION : Although both electrospray and heated nebulizer interfaces have been successfully applied to the HAA analyses in cooked meat and food flavors, the latter offers the following advantages :

1) *It accepts the entire flow from a standard 4.6 mm ID analytical HPLC column without* the complexity of using a splitter.
2) It can accommodate a higher concentration of buffer which is present in the sample as a result of the cation-exchange cleanup method.
3) Its rugged design makes the day-to-day operation easier and maintains a more stable and reproducible performance

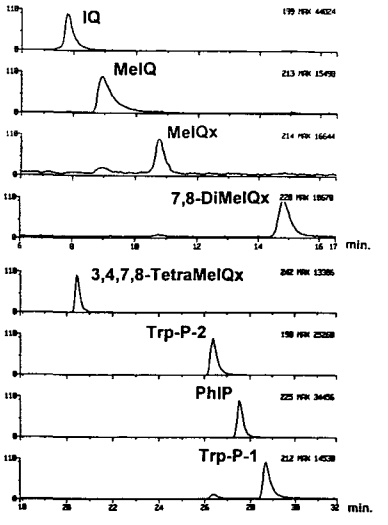

Fig. 1 Responses from an injection of 50 ng of 8 HAAs using a heated nebulizer interface.

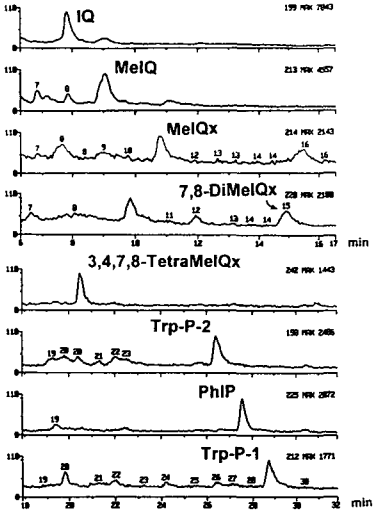

Fig. 2 HPLC/HNI/MS analysis of 8 HAAs in a bouillon sample spiked with 2.5 ppb of HAAs. Conditions were identical to Fig. 1.

Indirect Measurement of Spatial Spread and Initial Velocity Spread of Ions Produced in MALDI.

A.A. Makarov, S.C.Davis and R.J.Greathead
Kratos Analytical, Barton Dock Road, Manchester M31 2LD, UK

Introduction

Recent studies of ion energy distributions[1-3] from matrix assisted laser desorption ionisation (MALDI) have suggested that the process involves ablation of the matrix/analyte mixture with the formation of a fast and collisional gas jet. The objectives of this work were to further explore the origin of time-of-flight spread in the MALDI process using ion-optical measurements, and elaborate a model of the physical processes to account for the findings.

Experimental

The experimental work involved measurement of resolution in linear mode on a Kratos Kompact time-of-flight mass spectrometer as a function of voltage, V, in the ion source (see Figure 1). The ion-optical arrangement consists of two acceleration regions and a drift region. Grids were used to create linear field gradients. Measurements were made on three compounds: gramicidin S, bovine insulin and lysozyme. The matrix used in all cases was sinapinic acid. The measured resolutions as a function of the extraction voltage V are shown in Figure 2. An accelerating voltage of 8kV was used for these particular experiments.

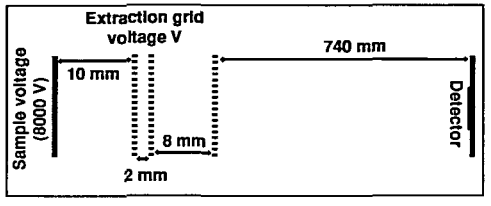

Figure 1: Ion optical arrangement

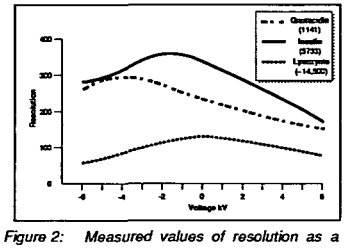

Figure 2: Measured values of resolution as a function of extraction voltage V.

The Model

Models used to try and explain the measured results considered the following possibilities:

(i) Jet-induced initial velocities
(ii) Debye shielding because of space charge
(iii) Spatial spread caused by space charge, length of ion formation and geometrical non-uniformity of the cloud
(iv) Mass-dependent energy losses during expansion because of collisions
(v) Drift of ions in the cloud under the influence of electric field.
(vi) Scattering on grids.

The main factors which need to be involved to obtain a reasonable fit (Figure 3) with the experimental results are (i) and (iv); Jet-induced initial velocities and mass dependent energy losses during expansion because of collisions. The model is illustrated in Figure 4.

Laser irradiation is absorbed by the matrix producing a shock wave in the solid state and a dense ablation jet. Absorbed energy is transformed into jet velocity. Multiple collisions activate proton transfer reactions so that $(M+H)^+$ ions are formed during the initial stage of expansion. At this stage the electric field can't accelerate ions efficiently due to space charge and collisional dissipation of energy. Rapid expansion provides rarification of the cloud (after the first 10 - 15 µm) and more effective extraction of ions by the field. Ions move in the cloud, undergoing multiple collisions and dissipation of energy. This rarified region has an effective length d.

As laser power is increased values of various parameters increase giving reduced resolution. Conversely, laser powers closer to the threshold produce higher resolutions than those shown in Figure 2.

Conclusions

Experimental values are adequately explained by the jet mechanism (velocity ~ 800 ms^{-1}), and a rarified region resulting in a spatial spread and velocity spread (determined primarily from dissipation of the jet velocity). The length d of the rarified region increases with mass since the collisional cross section is larger and energy dissipation will continue to occur in more rarified regions. Lengths used were: d = 15 µm for gramicidin S, d = 20 µm for insulin and d = 30 µm for lysozyme. A higher value for initial velocities (1500 ms^{-1}) is needed to explain the resolution values obtained from gramicidin S. This is feasible since lighter masses have a higher mobility than more massive ions.

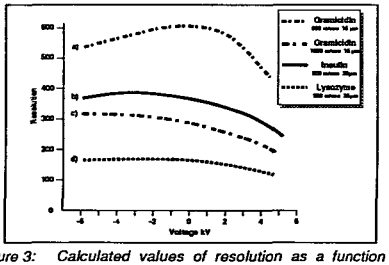

Figure 3: Calculated values of resolution as a function of extraction voltage V
(a) gramicidin: d = 15 µm, v = 800 ms^{-1}
(b) gramicidin: d = 15 µm, v = 1500 ms^{-1}
(c) insulin: d = 20 µmm, v = 800 ms^{-1}
(d) lysozyme: d = 30 µm, v = 800 ms^{-1}

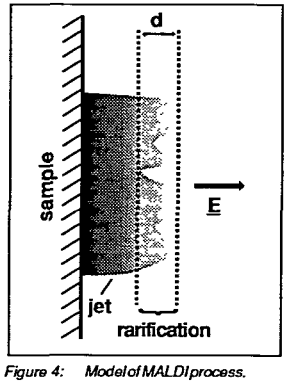

Figure 4: Model of MALDI process.

References

1 R.C.Beavis, B.T. Chait; *Chem. Phys. Lett.*, 181, 479 (1991)
2 A. Verentchikov, W.Ens, J.Martens, K.G.Standing; *Proc 40th ASMS Conf.*, Washington 1992, p360.
3 J.Zhou, W.Ens, K.G.Standing, A. Verentchikov; *Rapid Comm. Mass Spectrom.*, 6, 671 (1992)

High Mass Resolving Power for High-Mass Ions in LD FT/ICR/MS: Quadrupolar Axialization and Ion Cooling

Shenheng Guan, Markus C. Wahl†, Troy D. Wood, Hyun Sik Kim, and Alan G. Marshall†

Departments of Chemistry (and Biochemistry)†, The Ohio State University, 120 West 18th Avenue, Columbus, OH 43210

The high kinetic and internal energies of ions formed by laser desorption may be effectively cooled by collisions of the ions with argon buffer gas atoms at 10^{-6} - 10^{-7} Torr. The collisions expand the magnetron radius. However, magnetron motion may be converted into cyclotron motion by azimuthal quadrupolar excitation; collisions then collapse the cyclotron radius, leaving ions on-axis in the center of the trap where they may be efficiently transferred from the high-pressure source to the low-pressure analyzer of a dual-trap for high-resolution detection [1].

Here we report highly promising initial applications of the quadrupolar excitation/ion cooling technique to Nd:YAG (1.06 μ) laser-desorbed ions [2]. First, ions may be stored for lengthy periods (several minutes or more). Second, high FT/ICR/MS resolution is easily achieved for laser desorbed ions. For example, rhodamine 6G $(M+H)^+$ ions initially detected in the source trap are resolution-enhanced simply by addition of a cooling gas, presumably because the z-distribution of ions is more uniform after cooling so that the pre- and post-excitation cyclotron radius distributions are similar (i.e., all of the ions reside in the same magnetic field environment during detection). On azimuthal quadrupolar excitation in the presence of ion-neutral collisions, ions may be efficiently transferred to the analyzer trap for high resolution detection ($m/\Delta m \approx 144{,}000$ at m/z 443). Third, dramatically improved sensitivity results from the improved trapping efficiency.

Unfortunately, trapping can be so efficient that the resulting high space charge produces a noticeable downward drift in ion cyclotron frequency during the detection period, severely degrading mass resolving power. Although the time-domain signal for laser-desorbed axialized $(M+K)^+$ ions from leucine enkephalin persists for almost 1 min (Fig. 1, top), its corresponding ICR mass spectrum is quite broad (Fig. 1, middle). The observed (and theoretically explainable) ICR frequency drift during detection may be eliminated by a digital quadrature heterodyne technique [3] to yield an ultrahigh-resolution ($m/\Delta m = 1{,}300{,}000$ at m/z 594) mass spectrum (Fig. 1, bottom).

A fourth advantage of this technique is its high ion selectivity. For example, we have isolated ions of a single isotopic mass (e.g. the all-^{12}C isotope of C_{84}^-) [2]. The selectivity advantage may be exploited for MS/MS. For example, single cluster ions, C_{94}^+, may be isolated from a fullerene mixture and transferred to the analyzer trap for high-resolution CID to generate fullerenes which lose either C_2 or C_4, as shown in Fig. 2 [4]. This work was supported by the NSF (CHE-9021058), NIH (NIH GM-31683) and The Ohio State University.

1. Schweikhard, L.; Guan, S.; Marshall, A. G. *IJMSIP* **1992**, *120*, 71-83.
2. Guan, S.; Wahl, M. C.; Wood, T. D.; Marshall, A. G. *Anal. Chem.* **1993**, *65*, 00-00.
3. Guan, S.; Wahl, M. C.; Marshall, A. G., submitted for publication.
4. Wood, T. D. Ph.D. Dissertation, The Ohio State University, 1993.

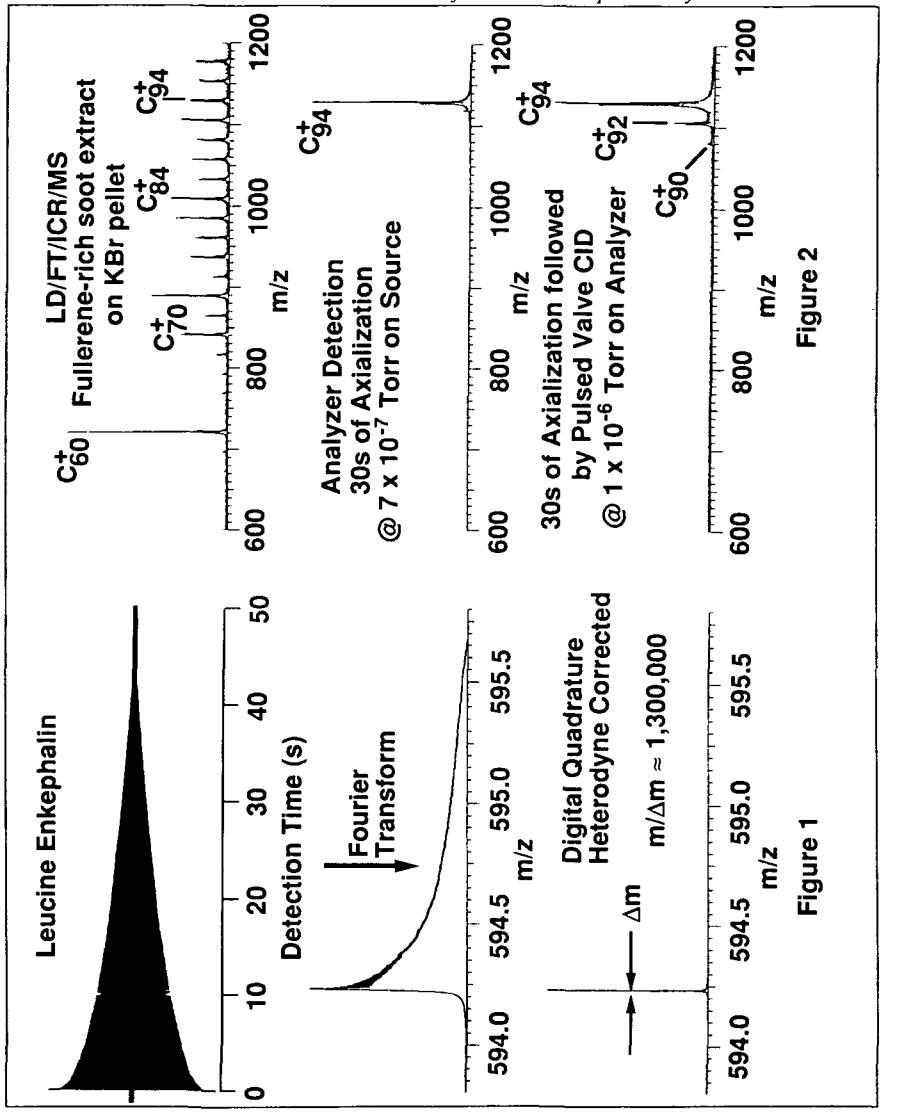

MALDI Fourier Transform Mass Spectrometry

Joel P. Covey, James Haas, Long-Sheng Sheng, Donald Weigt and Joseph E Campana
Extrel FTMS, Millipore Corporation, 6416 Schroeder Road, Madison, Wi 53711-2424

Introduction

Obtaining sequence and molecular weight information on peptides and other biological molecules is a topic of considerable interest to the mass spectrometry community. By performing a combination of MALDI, SWIFT, CID and MS^n experiments on a Extrel Fourier transform mass spectrometer equipped with a 3 tesla magnet and three lasers -- CO_2, Nd:YAG and N_2 -- we have developed techniques that can provide significant and, in many cases, total sequence information on medium to high weight (>2000 Da) peptides.

Small Peptides

The $[M+H]^+$ and the $[M+Na]^+$ species of a synthetic peptide (MW 933 Da) were analyzed in several MS^n experiments and ions that could provide the complete sequence of the peptide were observed. In the spectrum shown in Figure 1(a). the N-terminus (b_1, b_2, b_3) and C-terminus ions (y_4, y_5, y_6, y_7) provide sequence information on the lysine and the triple proline amino acid residues.

In Figure 1(b) the Na-attached y_6 ion of the molecular ion was isolated and underwent CID. Two sets of ions, $[b_6+ Na+ OH]^+$, $[y_4+ Na]^+$ and $[b_5+ Na+ OH]^+$, $[y_5+ Na]^+$ provide sequence information about both the valine residue and its neighboring proline residue. The most abundant species [b7 + Na + OH] +of the first doublet represents a loss of a valine residue (99 Da) from the C-terminus while the satellite peak $[y_5+Na]+$ represents the lost of the proline residue (97 Da) from the other end of the peptide fragment. The second set of ions represent the additional loss of the proline residue next to the C-terminus valine. The b_5 and c_5 ions indicate that the fifth residue is either a leucine or isoleucine.

To obtain further information, the Pro-Pro-Trp-Ile fragment of the Na-attached peptide, i.e. the middle four residues of the peptide, was isolated and underwent CID in a MS^n experiment. The N-terminus ions, $[b_5+Na]^+$ through $[b_4]^+$, shown in Figure 1(c) provide information about the tryptophan residue. In addition, the ion 28 Da below the main peak of the fragment is characteristic for isoleucine (the equivalent ion from leucine would be 42 Da below) and is caused by the loss of part of its side chain. In all these experiments an Nd:YAG laser was used, argon was the collision gas and the collision energy was 25 eV nominally.

By using a N_2 laser, other peptides such as Substance P, (1348 Da), α-Melanocyte Stimulating Hormone (1664 Da) and Ribonuclease S-peptide (2166 Da) were also analyzed with MS/MS techniques. In all cases significant structual information was obtained.

Large Peptides

A modification to allow the trap plates to be raised to 40 volts in less than 2 µs, combined with the use of a cooling gas or a mixed matrix of frucrose and DHBA[1] allowed for efficient trapping of ions to 9000 Da. We have observed the molecular ions of proteins such as bovine insulin (5734 Da) and ubiquitin (8565 Da).

[1] Koster C., Castoro J. A., and Wilkins, C. A. *J. Am Chem Soc.* 1992, *114*, 7572-7574.

Figure 1 MS/MS of a synthetic peptide

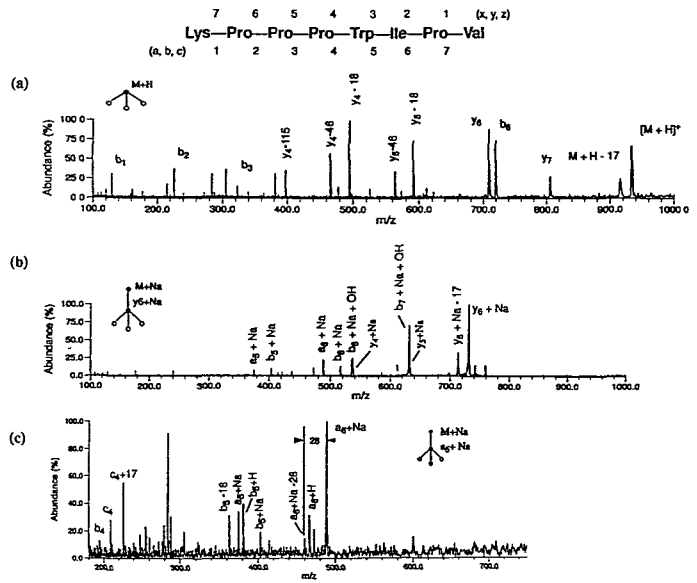

Heavy Atom Effects on Matrices for Matrix Assisted Laser Desorption Ionization Mass Spectrometry

Lisa M. Preston, Kermit K. Murray and David H. Russell
Department of Chemistry
Texas A&M University
College Station, Texas 77843

Ion formation in MALDI can be described as an excited state proton transfer process between an acidic (or basic) matrix molecule and a basic (or acidic) analyte molecule.[1] For ionization to take place in this manner, the proton transfer reaction must occur on timescales similar to other competitive excited state decay processes such as fluorescence. Heavy atom substituents such as bromine and iodine tend to alter the excited state relaxation dynamics of organic molecules either by quenching the state or by promoting triplet transfer.

In this study, we use bromine and iodine substitution to change the excited state relaxation dynamic of MALDI matrices. Absorption spectra (245-600 nm) and fluorescence emission spectra from thin films are acquired, as well as MALDI mass spectra, using absorbing and non-absorbing analytes. The results are analyzed for the correlation observed between fluorescence quantum yields with analyte ion yields of $[M+H]^+$ ions.

Table 1 contains results from spectra of vitamin B_{12} acquired using various heavy atom substituted matrices and their non-substituted counterparts. Note that the relative abudance of the "intact" analyte ion is markedly increased when a heavy atom matrix is used. This increase relative to the fragment ions observed, suggests that the addition of the heavy atom substituent has changed the ionization process, allowing the production of intact ions from compounds with highly labile bonds (the -CN of vitamin B_{12}). The mechanism of ionization may be "colder" due to changes in the relaxation dynamics of the matrices.

Table 2 contains results from fluorescence emission spectra, taken using a SLM Aminco 8000 fluorometer. Comparison of the results shows a consistent decrease observed in the fluorescence quantum yield for iodine and bromine substituted matrices relative to their non-substituted counterparts. It is suggested that the decrease in fluorescence is linked to the observed increase in $[M+H]^+$ observed from the MALDI experiments.

Heavy atom matrices improve the relative $[M+H]^+$ ion yield for peptides as well as UV-absorbing compounds. Figure 1 contains two mass spectra of leu-enkephalin acquired using 4-hydroxy-3-iodo-5-nitrobenzoic acid and 4-hydroxy-3-nitrobenzoic acid. The increase in $[M+H]^+$ ion signal observed when the iodo substituted matrix is used, supports the hypothesis that decrease of fluorescence may enhance the mechanism of proton transfer, perhaps by promoting triplet transfer.

Table 1.

Comparison of Ion Signal Observed for Vitamin B_{12}

Matrix	Total Analyte Ion Signal Ampl.	Rel. Abundance Fragment Ions	Rel. Abundance "Intact" Ion
4-hydroxy-3-nitro-benzoic acid	9 mV	96 %	3 %
4-hydroxy-3-iodo-5-nitrobenzoic acid	13 mV	40 %	60 %
salicylic acid	22 mV	100 %	0 %
5-iodosalicylic acid	22 mV	71 %	29 %
2,4-dinitro-aniline	53 mV	100 %	0 %
2-bromo-4,6-dinitroaniline	21 mV	83 %	17 %
2,4-dihydroxy benzoic acid	3 mV	100 %	0 %
5-bromo-2,4-dihy-droxy benzoic acid	38 mV	95 %	5 %

Table 2.

Comparison of Fluorescence Emission Quantum Yields

(Excitation wavelength = 337 nm)

Matrix	λ_{max}	Fluorescence Em. Quantum Yield	% Q.Y. Decrease with H-atom Subs.
4-hydroxy-3-nitro-benzoic acid	392 nm	2860	
4-hydroxy-3-iodo-5-nitrobenzoic acid	392 nm	2400	16 %
salicylic acid	393 nm	9030	
5-iodosalicylic acid	393 nm	4350	27 %
2,4-dinitro-aniline	389 nm	1900	
2-bromo-4,6-dinitroaniline	389 nm	1480	22 %
2,4-dihydroxy benzoic acid	394 nm	10210	
5-bromo-2,4-dihy-droxy benzoic acid	394 nm	6424	37 %

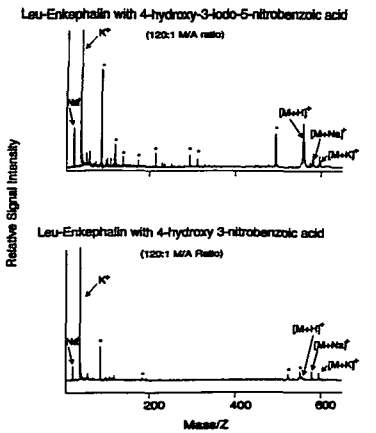

Figure 1. MALDI mass spectra of leu-enkephalin

1. Gimon, M.E., Preston, L.M., Solouki, T., White, M.A., Russell, D.H. *J. Org. Mass Spectrom.*, 27, **1992**, 827-830.

Direct and Matrix Assisted UV Laser Desorption Ionization of Analytes Containing Absorbing Chromophores

Michelle D. Beeson, Gary R. Kinsel, Lisa M. Preston,
Touradj Solouki, Mike A. White and D.H. Russell
Department of Chemistry
Texas A&M University
College Station, Texas 77843

Fragment ions are often observed in direct laser desorption/ ionization (DLDI) mass spectra. Lower molecular weight analytes may also show fragment ion formation during matrix assisted laser desorption/ionization (MALDI) under appropriate conditions. However, the types and abundances of MALDI fragment ions may be significantly different than DLDI fragment ions and prompts the question: "What mechanism(s) of energy transfer leads to fragment ion formation during MALDI?"

A systematic investigation of matrix/analyte ratio and desorbing laser intensity has been performed for several matrices with several smaller DNP substituted peptides and Vitamin B12 as model analytes. Figure 1 contains spectra of vitamin B_{12} by DLDI and MALDI. DLDI yields extensive unresolved fragmentation in the TOFMS. MALDI using α cyano-4-hydroxy cinnamic acid as a matrix, gives the M-CN fragment ion as the most abundant analyte ion, and weaker signal from additional assignable fragments.

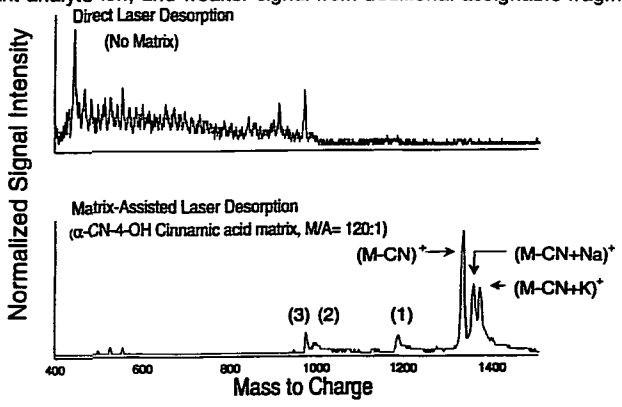

Figure 1. DLDI and MALDI mass spectra of vitamin B_{12}.

Three mechanisms must be considered as potential sources for the fragment ions observed for vitamin B_{12}.

(1) Substrate laser heating with subsequent thermal energy transfer to vitamin B_{12}.

(2) Direct photodissociation of the vitamin B_{12} by the desorbing laser.

(3) Photoactivation of the matrix with subsequent matrix mediated energy transfer to the vitamin B_{12} analyte.

A study of matrix/analyte (M/A) ratio with vitamin B_{12} and α-cyano-4-hydroxy cinnamic acid shows a clear transition from the DLDI type fragmentation to MALDI type fragmentationat M/A of 60:1 or greater. Once this ratio is exceeded little change in either the extent or type of fragmentation is observed at threshold desorbing laser intensities. This behavior suggests that substrate mediated thermal energy transfer is of little significance at M/A of 60:1 or greater.

Comparison of the vitamin B_{12} spectra resulting from use of lasers with different pulse widths (600 ps vs. 3 ns) indicates little change in the extent or type of fragmentation observed. This suggests that the second mechanism of gas phase photodissociation is unlikely. Furthermore, a matrix has been identified (4-hydroxy-3-iodo-5-nitrobenzoic acid) which not only yields an intact parent ion of vitamin B_{12}, but little fragmentation other than the M-CN ion (Figure 2). This result supports the conclusion that fragmentation of vitamin B_{12} is not a result of direct photodissociation. Energy transfer from the photoactivated matrix to the analyte molecule dominates at ratio of 60:1 or greater.

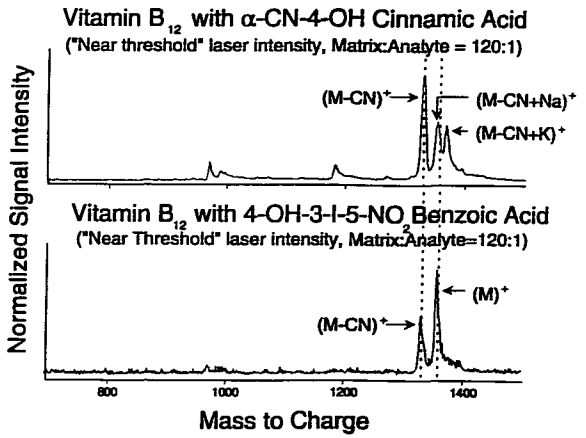

Figure 2. MALDI mass spectra of vitamin B_{12} acquired using two different matrices.

Matrix-assisted Laser Desorption Ionization of Hydrophobic Peptides and Proteins

Kevin L. Schey[1] and Jeff W. Finch[2]
[1]Department of Pharmacology, 171 Ashley Ave
Medical University of South Carolina, Charleston, SC 29425
[2]JEOL USA, Inc., 11 Dearborn Rd, Peabody, MA 01960

Hydrophobic proteins represent an important class of proteins having diverse functions such as ion/molecule transport and signal transduction. The hydrophobic nature of these proteins makes them insoluble in solvents used in standard methods of analysis. The versatility of MALDI makes it an attractive method for molecular weight analysis of hydrophobic peptides and proteins. Two experimental protocols are presented for the analysis of hydrophobic proteins by MALDI. First, formic acid (FA) in combination with hexafluoroisopropanol (HFIP) is used to dissolve hydrophobic proteins present as precipitates, in their native membranes, or even in their native tissues. Second, non-ionic detergents are used to solubilize hydrophobic proteins prior to mixing with the standard MALDI matrix solutions.

Hydrophobic proteins were solubilized by mixing the protein with FA and HFIP in the ratio of 3:7:2. Precipitated proteins can be solubilized using the same ratio of FA to HFIP. Sonication for 5-10 minutes is required for solubilization. The protein solution is then mixed 1:3 with sinapinic acid (50 mM, 70% FA) and spotted on the sample probe tip. Due to deleterious effects of formic acid (discussed below), isopropanol was substituted for FA in the above protocol in several experiments. The second method of sample preparation involved concentrating hydrophobic proteins in non-ionic detergents such as Lubrol-PX and Thesit at concentrations of 0.1%.

Photography of the spotted probe tips indicates drastic differences in crystal formation between the standard MALDI preparation and the preparations described above for hydrophobic proteins. The use of formic acid and HFIP generates a crystalline ring which is lipid coated for solubilized membrane preparations. When isopropanol was substituted for formic acid, a surface of widely dispersed matrix crystals was observed.

Molecular weights were determined for a variety of integral membrane proteins including native and recombinant bacteriorhodopsins; bovine, gecko, and salamander rhodopsins; and the human platelet thromboxane receptor using the FA protocol. A MALDI spectrum of salamander rhodopsin desorbed from solubilized intact retina tissue is shown in Figure 1.

Peptide and protein formylation of serine and threonine residues as well as cleavage of acid labile Asp-Pro bonds are observed in the presence of formic acid. HFIP enhances MALDI signals in this protocol; however, formylation is increased in the presence of HFIP. Substitution of isopropanol for formic acid results in dispersed crystals and oscillatory MALDI signals. Figure 2 shows a MALDI spectrum of bacteriorhodopsin solubilized with isopropanol/HFIP and spotted with sinapinic acid (7:3 isopropanol:HFIP).

A mixture of GTP binding proteins prepared in cholate or CHAPS detergent

micelles produced no MALDI signals. Exchange into non-ionic Lubrol-PX or Thesit provided strong MALDI signals for the gamma subunits of of these proteins.

In conclusion, two protocols have been successfully implemented for the generation of MALDI signals for hydrophobic proteins. Substitution of isopropanol for formic acid was only partially successful. Continued investigation of non-reactive solvents should provide improved MALDI performance for this important class of proteins.

Acknowledgements:The authors thank their collaborators: D. Knapp, D. Papac, R. Crouch, P. Goletz, W. Corson, J. Hildebrandt, M. Wilcox, J. Dingus, P. Halushka, and K. Davis-Bruno.

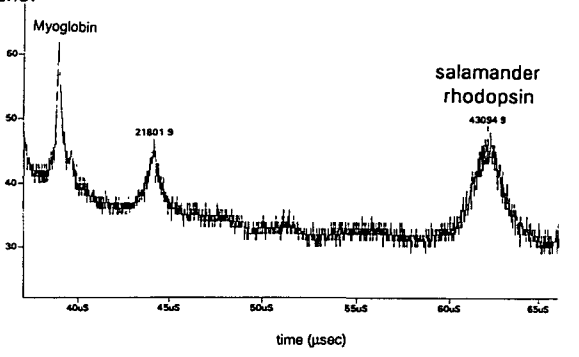

Figure 1. MALDI spectrum of salamander rhodopsin desorbed from solubilized intact retina tissue.

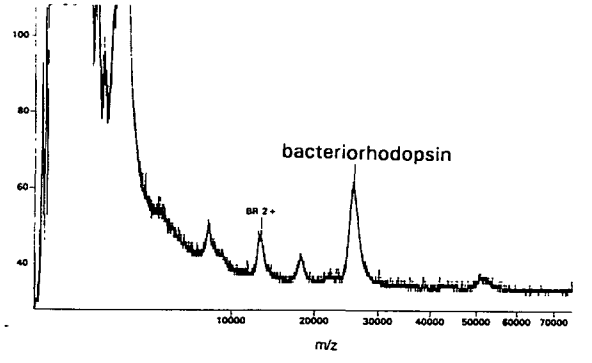

Figure 2. MALDI spectrum of bacteriorhodopsin (BR) solubilized in isopropanol/HFIP and mixed with sinapinic acid in 70% isopropanol/HFIP.

MONITORING BIOMOLECULAR REACTIONS USING MALD MASS SPECTROMETRY

Lee Q. Huang, Robert Tilton, Bart Haigh, and Bill Knowles,
Miles Research Center, Miles Inc., 400 Morgan Lane, West Haven, CT 06516
M. Kimber, A. D. Hoffman, S. C. Davis, C. Moore, D. C. Dingley
Kratos Analytical Inc., 535 East Crescent Ave., Ramsey, NJ 07446

Mass spectrometry has traditionally been reserved for elucidation and confirmation of low molecular weight compounds. However, in recent years mass spectrometry has joined the revolution in the biological sciences, due mainly to the discovery and development of matrix assisted laser desorption (MALD) and electrospray ionization of biological molecules. In this presentation, we report the successful use of MALD mass spectrometry to monitor the biomolecular reactions.

The instrument used in this study is a desktop matrix assisted laser desorption time-of-flight mass spectrometer (Krotos Kompact Maldi III). It comprises both liner and reflectron facilities. The linear facility provides high mass performance as well as highly accurate assignments. Increased resolution is achieved by use of the integral reflection. The system has a 300 Mhz transient recorder for high bandwidth data acquisition. The disposable sample substrate accommodates up to 20 samples and standards. With the MALDI technique only Pico-mol quantities of sample are required. The sample is mounted on a probe that is drawn into the vacuum system under full software control. Interlocked turbo vacuum pump systems provide rapid pump down and a contamination free environment.

The first example is the reaction of a cysteine containing peptide antigen with the protein carrier, BSA. This bioconjugation was monitored by the MALD-MS (Figure 1), and the efficiency of the multiple coupling as determined by mass spectrometry agrees well with independent chemical analysis.

In the second example, MALD-MS was used to monitor the chemical synthesis of peptides containing phosphotyrosine. Analysis of the multiple peaks obtained following HPLC separation allowed us to readily identify the fully deprotected and unmodified phosphopeptide. The kinetics of dephosphorylation by specific phosphotyrosine phosphatases was also examined by MALD-MS. The results demonstrate that MALD-MS has sufficient mass resolution and mass assignment accuracy for monitoring the phosphorylation.

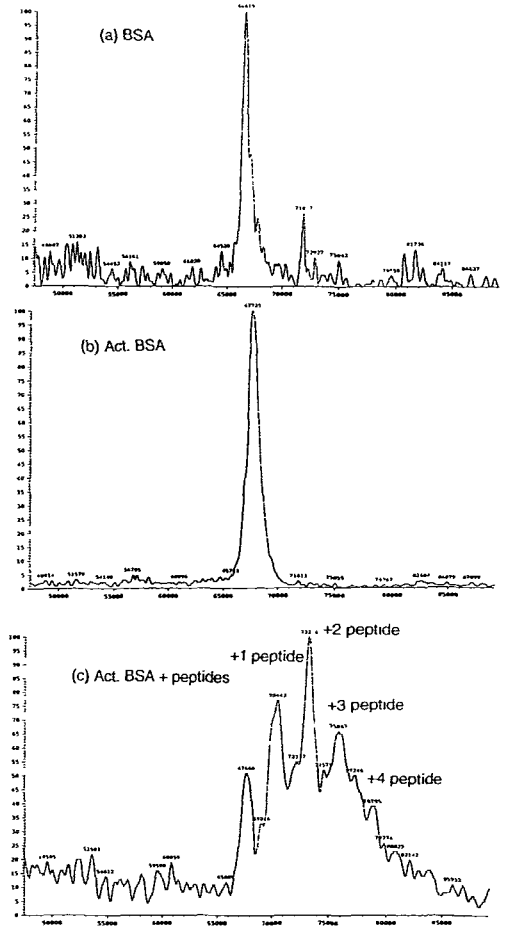

Figure 1. MALD mass spectra of (a) protein carrier, BSA, (b) activated BSA with linking groups, (c) BSA with conjugated antigen peptides.

Geometric Signal Averaging Applied to Matrix-Assisted Laser Desorption/Ionization Time-of-Flight Mass Spectrometry

Randall W. Nelson and Marvin L. Vestal
Vestec Corporation, 9299 Kirby Dr. Houston TX 77054

INTRODUCTION

For some time the matrix-assisted laser desorption/ionization technique has been recognized for its ability to generate time-of-flight mass spectra exhibiting impressive signal to noise ratios (S/N). In numerous examples, spectra resulting from a single laser shot have shown S/N > 10, and in themselves were quite adequate for nominal molecular weight determination. Typically though, spectra are produced by averaging signal from multiple laser shots, either in a computer after single shot acquistition, or during acquisition using a transient recorder capable of fast mathematical operations. The most common signal averaging techniques generally use some form of arithmetic average where the spectra from individual laser shots are added together and the cumulative spectrum divided by the number of spectra used, i.e.

$$[(y)_1 + (y)_2 + (y)_3 + \ldots (y)_n] / n . \qquad \text{Eq. 1}$$

This presentation addresses a new approach to signal averaging, one in which the product of the individual laser shots is used rather than the sum. In this approach, the individual laser shots are multiplied together and the nth root of the product taken (n being the number of spectra used), i.e.

$$[(y)_1 (y)_2 (y)_3 \ldots (y)_n]^{1/n} . \qquad \text{Eq. 2}$$

In principle this approach, termed geometric averaging, offers a variable degree of signal enhancement. Like the arithmetic approach, the signal enhancement for the geometric approach is dependent on the S/N of the individual shots and the number of individual shots taken. Another factor for which the arithmetic approach is independent does however influence the degree of signal enhancement during geometric averaging. This is the absolute offset, above zero, of the individual spectra. At the limits of the absolute offset, zero and infinity, the geometrically averaged spectra approach signal to noise ratios of infinity (for a baseline of zero) and that of the arithmetic average (at a baseline offset of infinity). Practically, the limits of enhancement are reached before either of these extremes, with a significant improvement in S/N, over the arithmetic average, being achieved under proper conditions.

EXPERIMENTAL / RESULTS

Data sets comprised of single laser shot time-of-flight spectra exhibiting similar qualities were generated from samples prepared using sinapinic acid as a matrix, and irradiated at a laser wavelength of 355 nm (frequency-tripled Nd:YAG). Fig. 1 shows five single laser shot time-of-flight spectra of bovine insulin. Each spectrum exhibits a S/N, insulin to baseline noise, of between 5 and 15, with a noticeable amount of single-ion noise. The spectra have been normalized to the insulin signal, giving it a value of 1, and have been given a very small positive baseline offset (~0.01). Adding the five spectra and dividing the summed spectrum by 5 results in Fig. 2, the arithmetic average. As can be seen, an insulin signal to baseline noise enhancement is observed, relative to the individual spectra, and also a significant, but not complete, reduction in the single-ion noise. Because of the nature of the arithmetic average, the characteristics of this spectrum are independent of linear mathmatical operations performed on the individual spectra prior to averaging, i.e., multiplication of, or addition to, the individual spectra before averaging does not affect the cumulative spectra. When geometric averaging (Eq. 2) is applied to the

same data sub-set used in Fig. 2, Fig. 3 results. An almost complete reduction of the single-ion noise is observed.

DISCUSSION

An approach alternate to straight arithmetic signal averaging has been presented. As opposed to using the sum of individual spectral events, the product is used (the approach is termed geometric averaging). In principle, the S/N enhancement of the geometric averaging technique has no limit. The reason for this is that the product of baseline noise crossing through zero, is zero, yielding no noise whatsoever. The product of non-zero coherent signal, on the other hand, yields a signal of something other than zero. Under such conditions a S/N of infinity is expected. In practice, the geometric signal averaging technique mandates an offset of the baseline. A dependence on the absolute value of the baseline, and the single-shot signal to noise ratio, is observed. In general, as the baseline approaches zero, for any data set, increasing signal to noise ratios are observed suring geometric signal averaging. Practical limits at which the geometric S/N equals the arithmetic S/N, and at which a maximum geometric S/N enhancement is obtained, are observed.

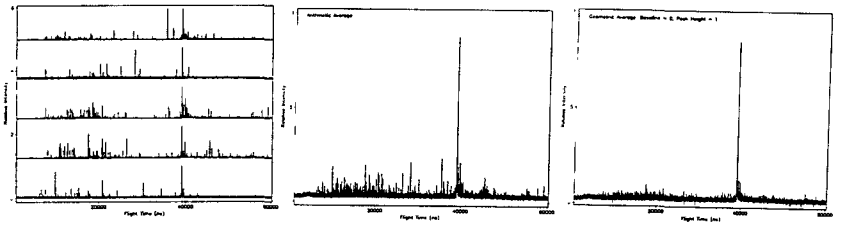

Fig. 1 (left) Five single laser shot time-of-flight spectra of bovine insulin. Sinapinic acid was used as a matrix with 355 nm radiation (frequency-tripled Nd:YAG). **Fig. 2 (center)** Arithmetic average, summed and divided, of the five single shots presented in Fig. 1. The spectra were intensity normalized to the insulin signal (value of 1) and given a slight baseline offset (~0.01). An increase in the insulin signal-to-noise ratio is observed, as well as a reduction in the singl-ion noise contribution. **Fig. 3 (right)** Geometric average of the data set in Fig.1. Again an increase in the insulin signal-to-noise ratio is observed, and an almost complete elimination of the singl-ion noise contribution.

Matrix-Assisted Laser Desorption/Ionization of Oligonucleotides

Kai Tang, Steve L. Allman and Chung H. Chen
Oak Ridge National Lab Oak Ridge, TN 37831-6378

Matrix-assisted laser desorption/ionization (MALDI) has been quite successful in detecting very large protein molecules However, the progress of using MALDI to analyze oligodeoxyribonucleotides is somewhat limited In this work, we report our recent results on this topic for detecting larger homo-oligomeric deoxynucleotides as well as those containing four different bases.

A Nd YAG laser with frequency tripled output of 355nm in wavelength is used for desorption/ionization A linear time-of-flight mass spectrometer was used to analyze the ions produced by MALDI. The typical laser fluence was between 40mJ/cm^2 and 400mJ/cm^2 depending on the absorption coefficient of the matrix used. The typical quantity of the oligonucleotides loaded for analysis was about 2 to 30 picomoles with matrix to analyte ratio of 5000:1 to 10000:1.

Experimental results of poly(dA)$_{12-18}$, poly(dC)$_{12-18}$ and poly(dG)$_{12}$ with ferulic acid (FA), 3-hydroxypicolinic acid (3-HPA) and 2,5-dihydroxybenzoic acid (2,5-DHB) as matrices are shown in Fig 1, Fig.2 and Fig 3 respectively For poly(dA), FA and 3-HPA were better matrices than 2,5-DHB in which one base was cleaved for each nucleotide For poly(dC), base cleavage was observed for both FA and 2,5-DHB matrices, and 3-HPA was obviously a better choice For poly(dG), serious fragmentations due to depurination were observed for both FA and 2,5-DHB as matrices and fragmentations due to the broken of the DNA backbone were also observed in the 2,5-DHB case. Again, 3-HPA was shown to be a better matrix

With 3-HPA as matrix, we have succeeded in detecting oligonucleotides with size up to 60 mer for poly(dA), 30 mer for poly(dC) and poly (dG), and 100 mer for deoxynucleotides containing mixed bases, as shown in Fig 4, Fig 5, Fig 6, and Fig 7 Larger oligomers might be detected if high quality synthetic deoxynucleotides are available. For poly(dT), however, 2,5-DHB continues to be the best matrix when mixed with 10% 5-methoxysalicylic acid as up to 130 mer could be easily detected (shown in Fig.8), although up to 100 mer could also be seen when 3-HPA or FA is used as matrix. These results indicate that deoxynucleotide-matrix interaction is the most critical factor for the success of DNA analysis by MALDI

In conclusion, MALDI has been demonstrated successfully for detection of medium sized deoxynucleotides. We expect it can be used to detect even larger sizes in the near future With further improvement in resolution and sensitivity, DNA sequencing using MALDI-TOF mass spectrometer could become a reality

This work was sponsored by the Office of Health and Environmental Research, US Department of Energy under contract DE-AC05-84OR21400 with Martin Marietta Energy System, Inc. We also wish to acknowledge Kai-Lin Lee, Lan-Yang Chang, Rick Woychik and Mitch Doktycz for valuable discussions

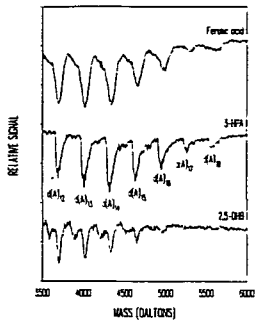

Fig 1

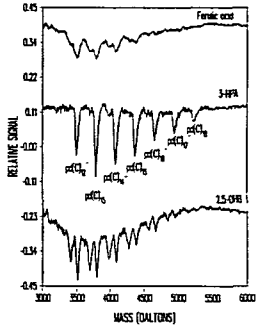

Fig. 2

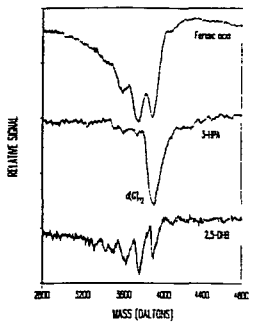

Fig 3

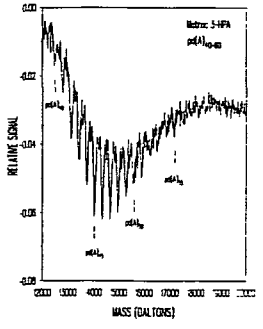

Fig. 4

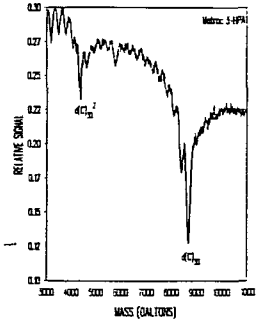

Fig. 5

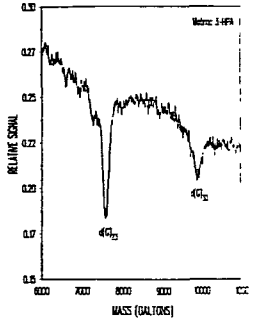

Fig 6

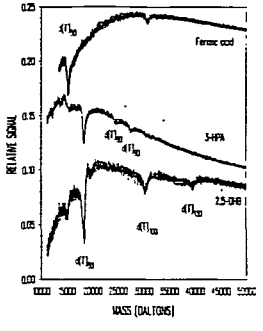

Fig 7

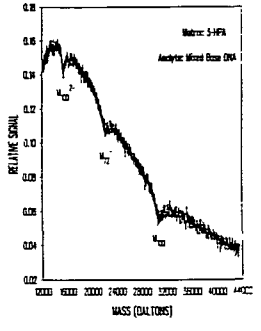

Fig. 8

LADDER SEQUENCING OF POST-TRANSLATIONALLY MODIFIED PROTEINS

Rong Wang[1], Sharon Walker[2], Ronald C. Beavis[3], Stephen B.H. Kent[2], and Brian T. Chait[1]

[1]The Rockefeller University, New York, NY 10021,
[2]The Scripps Research Institute, La Jolla, CA 92037,
[3]Memorial University of Newfoundland, Canada A1B 3X7

INTRODUCTION

The inability to directly identify, locate, and quantify post-translational modifications of proteins is a major shortcoming of the standard Edman sequencing methods,(1,2).

We have recently developed a rapid, highly efficient method for sequencing polypeptides: Protein Ladder Sequencing. In this method, a controlled stepwise chemical degradation is performed on one terminus of a polypeptide. The reactions yield a set of sequence-defining peptides, each differing from the next by a single amino acid. This protein sequencing ladder is read out rapidly in a one-step operation by matrix-assisted laser desorption mass spectrometry. Each amino acid is identified from the mass difference between successive peaks, and the sequence is determined by the position in the data set.

Three peptides with different types of post-translational modifications (serine phosphorylation, tyrosine phosphorylation, and N-glycosylation) were subjected to protein ladder sequencing. The experimental results show that all of these three modifications can be identified and that the sites of modification can be determined. Our experimental results demonstrate that the ladder sequencing method can be used to determine the sites and masses of modified amino acids within peptides and proteins.

In this presentation, we also report the automation of the ladder generating chemistry. In addition, results are presented of using short degradation times to generate the sequencing ladder in the absence of a blocking agent and for parallel degradation of multiple peptide samples

EXPERIMENTAL

I. Generating of protein sequencing ladder. The N-terminal degradation reaction of peptides was performed in the presence of a small amount of terminating agent, phenylisocyanate (PIC). The ratio of PIC to phenylisothiocyanate (PITC) is 1:20.

II. Automation of ladder generating chemistry. The automation of this method was carried out by using the chemical delivery device on an ABI-471A protein sequencer.

III. Ladder sequence read-out. Matrix-assisted laser desorption mass spectrometric analysis was carried out on a device constructed at The Rockefeller University. α-cyano-4-hydroxy-cinnamic acid was used as matrix.

RESULTS AND DISCUSSION

An additional advantage of the ladder sequencing method over conventional Edman sequencing is its ability to determine the sites and masses of modified amino acids within peptides and proteins. To assess the potential of ladder sequencing for the elucidation of post-translational modifications, we have applied the method to an analysis of a 16-residue serine-containing peptide that is a substrate for cAMP-dependent protein kinase. Both the phosphorylated and unphosphorylated forms of the peptide were subjected to protein ladder sequence analysis. The ladder sequencing of the 16 residue synthetic peptide: SWI-57A, L-R-R-A-S^5-G-L-L-Y-N^{10}-N-P-L-M-A^{15}-R-NH_2. are shown in Figure 1, (A) Phosphorylated peptide, (B) Unphosphorylated peptide. Each peptide sample was subjected to ten cycles of ladder-generating chemistry, after which the sequence-defining set of fragments was read out in a single operation by laser desorption mass spectrometry. Data defining the N-terminal 11 amino acid residues is shown. The Ser(P_i) residue was characterized by a mass difference of 166.7 daltons (Ser, calculated residue mass 87.1; Ser(P_i) calculated residue mass 167.1) observed in position five. There is no evidence of loss of phosphate.

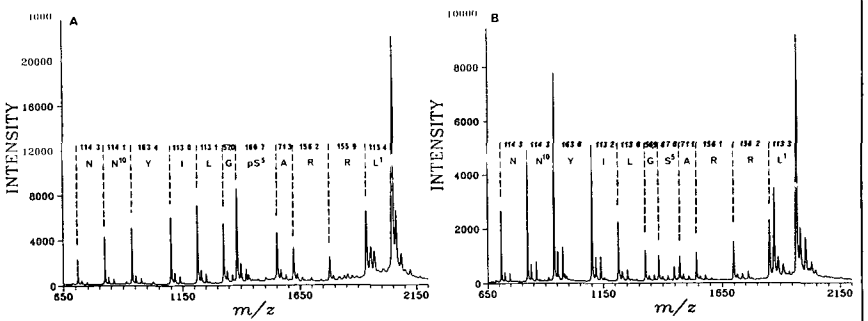

Figure 1. Ladder sequencing of Ser-phosphorylated peptide. (A) phosphorylated peptide; (B) unphosphorylated peptide.

CONCLUSION

The ladder sequencing method has general applicability to the direct identification of post-translational modifications.

REFERENCES

1. R.J. Paxton, G. Mooser, J. Thompson, and J.E. Shively (1987) Methods in protein sequence analysis - 1986, K.A. Walsh Ed., Humana Press, New Jersey, p437-449.
2. B.W. Gibson, A.M. Falick, A.L. Burlingame and et. al. (1987) Methods in protein sequence analysis - 1986, K.A. Walsh Ed., Humana Press, New Jersey, p463-478.

LASER ABLATION OF PROTEINS USING NANOSECOND PULSES OF TUNABLE MID-IR RADIATION

David M. Schieltz, David Dogruel and Peter Williams
Department of Chemistry and Biochemistry
Arizona State University
Tempe, AZ 85287-1604

Previously we demonstrated that massive DNA molecules can be ablated intact from thin frozen films of aqueous solution by nanosecond pulses from a visible laser. The angular distribution of the ablated DNA is strongly forward-peaked, consistent with the idea that the ablated water vapor plume undergoes a supersonic jet expansion which can efficiently cool the entrained biomolecules. Although ionization in this process is highly irreproducible, when a mass spectrum is obtained, the peaks show no evidence of fragmentation, which is consistent with the idea that efficient cooling occurs in the expanding vapor plume. A difficulty with reproducibility in this approach is that, because heating follows energy deposition in the substrate, each laser shot completely ablates the entire sample film in the irradiated area, so that the sample must be moved for each successive shot. In contrast, mass spectra of DNA ablated using UV radiation from a UV chromophore matrix show extensive fragmentation, suggesting that cooling in the vapor plume is far less efficient. Because only a shallow depth is ablated on each shot, multiple shot averages can be obtained from an appropriate region and sample uniformity becomes far less important. However, the small amount of vapor produced on each shot appears not to develop a full supersonic expansion which can cool the ablated biomolecules efficiently.

It would be desirable to combine the best properties of both ablation approaches. If the ice matrix could be heated directly, using ~ 2.9 μm radiation, thick targets could be used and spectra from multiple laser shots could be obtained from a given region of the sample. The relatively large extinction depth of 2.9 μm radiation in ice should result in ablation of a few μm thick water layer, which should evolve into a supersonic jet capable of effectively cooling entrained biomolecules. Recent publications have indicated that ions are formed reproducibly at this wavelength. To date, ablation experiments in the mid-IR have used 150-200 ns long pulses, and we were concerned that the continued irradiation of the vapor plume by the tail of the laser pulse might cause heating which would negate the cooling effects of the expansion. We have now evaluated the effectiveness of ablation of frozen DNA and protein solutions using 2.9 μm radiation from an optical parametric oscillator (OPO). The OPO (STI Optronics Inc., Mirage 3000) is pumped by 1064 and 532 nm pulses from a Q-switched Nd-YAG laser, and produces 1-2 mJ pulses a few nanoseconds wide. In principle the OPO is tunable over a wavelength range from ~ 1.5 - 4 μm, but all our experiments were conducted at 2.9 μm.

We reached the following conclusions about this approach:

a) The OPO is a more complex laser system than is desirable for a robust analytical technique, but with care it delivered 2.9 μm pulses reproducibly over a one-month evaluation period.

b) Ablation depths for aqueous targets at 2.9 μm are certainly far greater than for UV chromophores in the UV; it was estimated from the single pulse ablation of thin frost layers that ablation depths were on

the order of several micrometers.

c) Time-of-flight mass spectra were *not* obtained reproducibly using this approach. For most experiments we used small proteins rather than DNA analytes, and shot-to-shot reproducibility, although significantly better than for our visible laser approach was far worse than in the UV, and was unacceptable for analytical purposes.

d) The most reproducible spectra were obtained using solid matrices such as 2,5-dihydroxybenzoic acid. Even here, reproducibility was worse than in the UV. The mass spectrum of bovine albumin, ablated from succinic acid is shown in Fig. 1. The spectrum contains molecular ions in charge states extending up to at least +7. Disappointingly, the high background signal and the broad peaks suggest that extensive fragmentation is occurring, so that the anticipated greater cooling and reduced post-ablation heating appear not to have the desired effect of producing cool, unfragmented molecular ions. The difference between these spectra and those obtained for DNA from ice using an indirect heating approach may result from coupling a significantly greater amount of energy into the sample volume by direct heating with 2.0 μm radiation.

This work was supported by the US Department of Energy Grant DE-FG02-91ER61127.

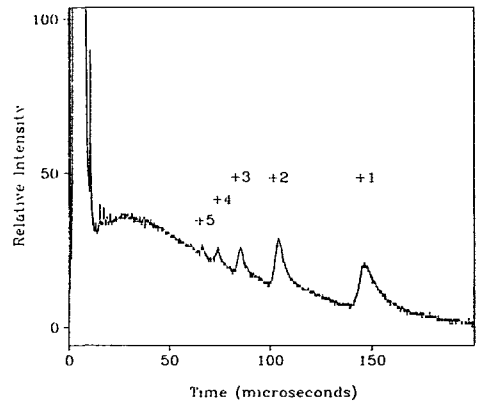

Fig. 1. Bovine albumin, matrix 2,5-DHB, V_{acc}= +30 kV, λ= 2.9 μm, 56 shot average.

Structural Characterization of Oligonucleotides by Matrix-Assisted Laser Desorption/Ionization Time-of-Flight Mass Spectrometry

*Bing H. Wang and Klaus Biemann
Department of Chemistry, MIT, Cambridge, MA 02139

Structural characterization of small oligonucleotides (3-50mer) by mass spectrometry has many applications. For example, the assessment of the homogeneity and correctness of the sequence of a synthetic oligonucleotide is very difficult by conventional methods. We have found that some of these problems can be conveniently solved by measuring the molecular weights of the samples by matrix-assisted laser desorption/ionization time-of-flight mass spectrometry (MALDI-TOFMS). Subjecting the samples to Maxam-Gilbert reactions prior to MALDI-TOFMS analysis yields additional structural information.

Maxam-Gilbert Reactions[1] For "C+T" base-modification reactions in this study, a few microliters of oligonucleotides (50 pmol/μL) was combined with 60 μL of hydrazine. The mixture was incubated in a thermal bath for a selected length of time. For "T" base-modification reactions, 1 μL of pyridine was combined with 1 μL of 5% aqueous solution of OsO_4 and a few microliters of oligonucleotide (50 pmol/μL). The mixture was incubated at 30 °C for 15 minutes. For strand-scission reaction, based-modified oligonucleotide mixture was dissolved in 100 μL of 1 M piperidine and incubated at 90 °C for 30 minutes.

MALDI-TOFMS Analysis Typically, 0.5 μL of oligonucleotide solution ($1\text{-}5\times10^{-5}$ M) was co-deposited with 2 μL of matrix consisting of 1:1 (weight) mixture of anthranilic acid and nicotinic acid in aqueous 30% acetonitrile solution (12 g /L). Ion exchange resin (100-200 mesh) was added to reduce the formation of alkaline-metal adduct. [2] All spectra were obtained with a linear time-of-flight mass spectrometer (VESTEC-2000) equipped with a nitrogen laser (337 nm) in the negative ion mode. Typically 10 laser shots were summed to yield one mass spectrum.

We have been able to observe $(M\text{-}H)^-$ ions up to $d(T)_{40}$, for which a mass resolution (FWHM) up to 500 has been obtained.

The utility of direct molecular weight measurements of oligonucleotides is illustrated by an example involving a 16mer-synthetic oligoribonucleotide, in which one phosphate-diester group has been succesively replaced by a phosphorothioate group. MALDI-TOF analysis revealed that, as the synthesis progressed from 3'-end toward the 5'-end, the sulfur atom was gradually lost, *i.e.* replaced by an oxygen atom (Figure 1).

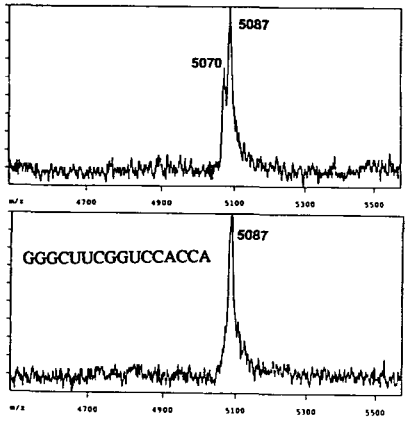

Figure 1. MALDI-TOFMS Spectra of 16mer Oligoribonucleotides. Phosphorothioate Substitution Occurred at the Positions between C11 and C12 (Top); and between G1 and G2 (Bottom).

Combining chemical reactions with molecular-weight data provides additional structural information. An example illustrating this approach concerns a 25mer-synthetic oligodeoxynucleotide, in which one G was replaced by its O^6-n-butyl guanine derivative to study the mutagenic effect of alkylation at the site of modification. The mass spectrum revealed the presence of two products differing by 72 u due to incomplete removal of the protecting butyryl group. This extra component had eluded the detection by gel electrophoresis. "T" cleavage confirmed that the modification site is in the correct region. However, the butyryl group has been lost during the cleavage reactions.

When a synthetic 12mer deoxynucleotide (5'-TCTGGUACCTCT-3') was subjected to "C+T" reactions, U was removed much faster than C or T, leaving TCTGGp (*m/z* 1573) and pACCTCT (*m/z* 1806) as two major products (Figure 2). In contrast, when an oligodeoxynucleotide does not contain a U, "C+T" cleavage occurs much more uniformly at all positions of T and C.

In conclusion, MALDI-TOFMS is a sensitive and convenient technique for the detection of oligonucleotides. Mass resolution up to 500 (FWHM) obtainable by this technique allows the identification of small changes in the structure of an oligonucleotide, which may elude the detection by conventional techniques. Structural information can be obtained by combining Maxam-Gilbert reactions with MALDI-TOFMS.

Acknowledgment

Financial support from the NIH Center for Research Resources (Grant No. RR00317) is acknowledged. Some of the oligodeoxynucleotide samples were supplied by J. Essigmann, MIT. Oligoribonucleotide samples were supplied by P. Schimmel, MIT.

References

1. Maxam, A. M.; Gilbert, W. *Methods Enzymol.* **1980**, *65*, 499-560.
2. Nordhoff, E.; Ingendoh, A.; Cramer, R.; Overberg, A.; Stahl, B.; Karas, M.; Hillenkamp, F.; Crain, P. F. *Rapid Commun. Mass Spectrom.* **1992**, *6*, 771-776.

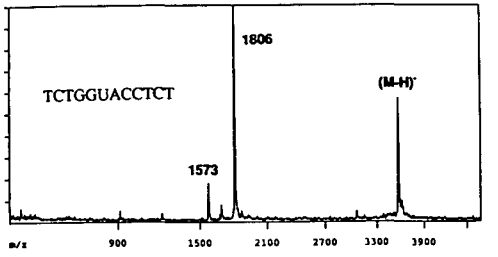

Figure 2. MALDI-TOFMS Spectra of "C+T" Cleavage Products of a Uridine Containing Oligodeoxynucleotide.

COLLECTOR STUDIES OF ANGULAR DISTRIBUTION AND FRAGMENTATION OF PROTEINS ABLATED FROM ICE AND UV-ABSORBING MATRICES

Congwen Luo and Peter Williams
Department of Chemistry and Biochemistry
Arizona State University
Tempe, AZ 85287-1604

Despite the dramatic successes of matrix-assisted laser ablation in generating intact molecular ions of extremely large biomolecules, there still exists no concensus on the mechanism by which the matrix apparently protects analyte molecules from destruction by the intense laser radiation. Suggested mechanisms include a "bottleneck" for energy transfer from matrix to analyte (Vertes), cooling by evaporation of a matrix molecule solvation shell (Hillenkamp) and cooling in a supersonic free jet expansion (Nelson *et al*). There is little experimental evidence concerning the first two models, but evidence does exist that some degree of supersonic expansion occurs. Nelson *et al* showed that angular distributions of radiolabelled DNA ablated from an ice matrix were very strongly forward-peaked. Cooling by a factor of 3-5 could result from such expansions. Velocity measurements have shown that UV-ablated matrix and analyte molecules have similar mean velocities, again suggestive of a jet, although the velocity *spread* is broad, suggesting that cooling may not be strong. Early successes with UV ablation of intact proteins are proving difficult to reproduce with DNA molecules; UV-ablated DNA mass spectra show extensive fragmentation, suggesting that the process produces very hot molecules. We have used a collector approach to determine angular distributions of lysozyme and matrix molecules ablated from 2,4-dihydroxybenzoic acid (DHB) and from ice, and gel electrophoresis to determine the state of fragmentation of the ablated protein. We have also revisited earlier collector measurements of DNA ablated from ice.

UV-ablation samples were prepared as films (~ 1 cm^2) on a stainless steel sample holder, using DHB/lysozyme ratios typical of those used for mass spectrometry. Because a relatively large amount of ablated material is required, the sample was moved mechanically under the laser beam to irradiate an area of approximately 1 cm^2. Frozen solution films were prepared by spreading ~ 20 µL over a 1-2 cm^2 area on a copper block cooled to ~-20 °C and subliming to a few µm thickness in a rough-pumped vacuum system. The samples were then plunged into liquid nitrogen and transferred when cold to the liquid nitrogen-cooled sample stage of a time-of-flight mass spectrometer. The DHB samples were ablated using the tripled output of a Q-switched Nd-YAG laser at 355 nm. Power densities were in the range 10^7 to 10^8 W/cm^2. Ice samples were ablated using 578 nm pulses from a dye laser; power density was ~ 10^9 W/cm^2. Ablated material was collected on a Whatman No. 2 filter paper suspended 2 cm from the sample. The angular distribution of DHB was visualized using UV-induced fluorescence and recorded photographically. The protein was stained with Coumassie Blue and photographed. Photographs were digitized using a slow-scan CCD camera and digital line scans were obtained across the distributions.

A typical angular distribution of lysozyme UV-ablated from DHB is shown in Fig. 1. The data are compared with a power cosine function, $I(\Theta) = I(0)\cos^n\Theta$, for various values of n. The best fit to the UV data was obtained for n = 4-5. The distribution of the lysozyme was slightly narrower than that of the DHB at lower power, but the two distributions became identical at the highest power used. These data may be compared with the angular distribution of lysozyme ablated from a thin ice film (Fig. 2) This

distribution was much more strongly forward-peaked (n = 35 ± 5), consistent with our earlier results for DNA ablated from ice (n ~ 40). Gel electrophoresis of the collected lysozyme showed that fragmentation had occurred, but that the extent of fragmentation decreased as the laser power density increased. This too is consistent with our earlier work.

These data suggest that the cooling effect accompanying the expansion of UV-ablated DHB is quite small. The fact that the supersonic jet expansion is poorly-developed probably is due to the shallow ablation depth resulting from the high extinction coefficient of the UV chromophore. In a true supersonic jet, expansion can only occur in the forward direction. When only a few tens of monolayers of material are ablated, however, expansion can also occur in the reverse direction after the plume detaches from the surface. The asymmetry introduced by the surface imposes a net forward velocity on the system which is typically hyperthermal, but the cooling of translational velocities is much less effective than in a full supersonic expansion. In the frozen samples, typically the entire film in the irradiation area is removed in a single pulse -- a thickness of several µm -- giving a gas pulse that has more of the characteristics of a true supersonic jet.

This work was supported by the US Department of Energy Grant DE-FG02-91ER61127.

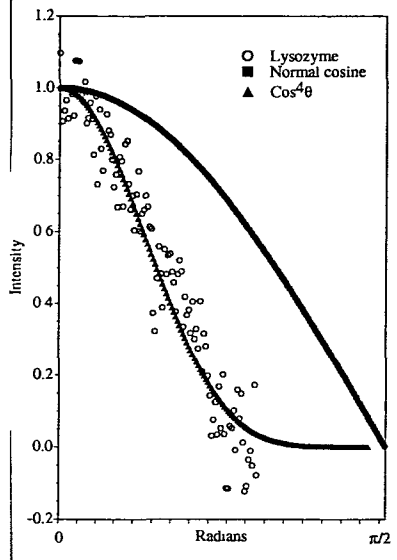

Fig. 1. Angular distribution of lysozyme ablated from DHB matrix. Data are compared to $\cos^4\theta$ angular distribution

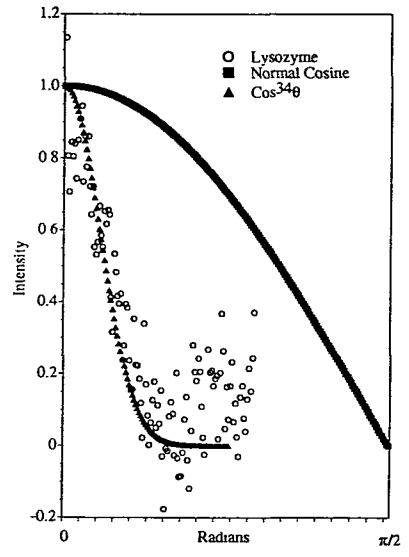

Fig. 2. Angular distribution of lysozyme ablated from ice film. Data are compared to $\cos^{35}\theta$ angular distribution.

Effects of Desorption Technique and Post-Ionizing Laser Pulse Width on Molecular Fragmentation

*C. R. Ayre,[a] L. Moro[b] and C. H. Becker[a]

[a]Molecular Physics Laboratory, SRI International, Menlo Park, CA 94025
[b]Instituo per la Ricerca Scientifica e Tecnologica, Divisione di Scienza dei Materiali, I-38050 Povo-Trento, Italy

The influence of desorption technique and post-ionizing laser wavelength on the fragmentation of *l*-tryptophan and serotonin, two biologically important molecules, has been investigated using time-of-flight mass spectrometry (TOF-MS) and the results compared with positive, static secondary ion mass spectrometry (SIMS) data obtained with the same apparatus. While ion-stimulated desorption using 7 keV Ar^+ was employed exclusively in the SIMS experiments, both ion-stimulated and thermal desorption were used in conjunction with laser post-ionization. Furthermore, laser wavelengths of 118 (10.5 eV) and 266 nm (4.66 eV) were employed to compare the photofragmentation patterns arising from single photon and multiphoton laser post-ionization. Finally, in the 266 nm experiments, the effects of post-ionizing laser energy density were explored by making independent measurements using the fourth harmonic of 5 ns and 35 ps Nd:YAG lasers.

All experiments were conducted in a stainless steel UHV chamber with a typical base pressure of ca. 5×10^{-9} torr which has been described elsewhere [1,2]. Briefly, in laser post-ionization experiments, neutrals desorbed from a sample were photoionized by a focused laser beam passing approximately 1 mm above and parallel to the sample surface. The photoions were analyzed by a reflecting time-of-flight mass spectrometer, which electrostatically rejects secondary ions, and detected by a dual microchannel plate assembly [1]. Alternatively, time-of-flight positive SIMS spectra were recorded after minor adjustments of the mass spectrometer voltages [3]. In ion-stimulated desorption experiments, a pulsed (10μs), 7 keV Ar^+ beam was employed. A typical Ar^+ current of 0.1 μA in a 160μ diameter spot was obtained at the target for a continuous beam. Post-ionizing laser radiation from two different lasers was used. For experiments involving 266 nm post-ionization, the frequency quadrupled output of 5 ns and 35 ps Nd:YAG lasers was used independently. VUV radiation (118 nm; 10.5 eV) was obtained by third harmonic generation of the 355 nm output of the 35 ps Nd:YAG laser in Xe phase-matched with Ar. Samples were prepared by laser post-ionization experiments by pressing *l*-tryptophan or serotonin powder onto indium or tantalum foil. In SIMS experiments, silver foils etched with nitric acid and rinsed in deionized water were dipped in sample solutions of serotonin or *l*-tryptophan (concentration: *ca.* 10 μg/μL), the excess solution was shaken off, and the sample was allowed to dry in air.

The effects of ion-stimulated and thermal desorption on fragmentation pattern were probed by comparing the spectra obtained for *l*-tryptophan and serotonin when each of these techniques was followed by photo-ionization at a particular laser wavelength and

energy density. For *l*-tryptophan *m/z* 130 $(M-74)^+$, which arises from C_α-C_β cleavage of the amino acid side chain, was among the most intense peaks in all spectra. By contrast, for serotonin, the most abundant mass fragments varied as a function of both desorption method and laser wavelength. For positive SIMS, for example, loss of both the hydroxyl (-OH) and amine ($-CH_2CH_2NH_2$) substituents to yield *m/z* 115 $(M-61)^+$ and loss of water and the amine side chain to produce *m/z* 114 $(M-62)^+$ occurred. These peaks were several times more intense than *m/z* 146 $(M-30)^+$ due to α-cleavage of the amine, *m/z* 160 $(M-16)^+$ due to radical loss of $-NH_2$, and the molecular ion M^+ (*m/z* 176). However, the *m/z* 114 and 115 peaks are absent from both the 118 and 266 nm laser post-ionization spectra recorded following ion-stimulated desorption, and the *m/z* 146 $(M-30)^+$ peak is of greater intensity. Yet, in single photon (118 nm) post-ionization following the thermal desorption of serotonin at 200 °C, *m/z* 112 and 113 due to the loss of the amine and hydroxyl substituents plus 2-3 additional hydrogens were stronger than *m/z* 146 $(M-30)^+$. Finally, the *m/z* 112-115 peaks were absent from the 266 nm thermal desorption spectra at all laser energy densities employed.

In general, the use of a pulsed 7 keV Ar^+ beam for desorption was found to cause extensive fragmentation of both *l*-tryptophan and serotonin relative to thermal desorption. The molecular ion (M^+) for *l*-tryptophan (*m/z* 204) was absent from all spectra in which ion-stimulated desorption was employed. A weak M^+ (*m/z* 176) signal was observed in the positive SIMS spectrum of serotonin, but no M^+ peak appeared when either 118 or 266 nm post-ionization of sputtered neutrals was employed following ion-stimulated desorption.

Finally, increased fragmentation of both molecules occurred when the intensity of the 266 nm post-ionizing laser energy density was increased. For example, for both serotonin and *l*-tryptophan, an increase in post-ionizing laser energy from *ca.* 2.5×10^3 mJ cm^{-2} to 8×10^3 mJ cm^{-2} resulted in an increase of an order of magnitude in the ratio of the total yield of fragment ions to the molecular ion yield.

[1] Becker, C. H.; Gillen, K. T.; *Anal. Chem.* **1984**, *56*, 1671.

[2] Schuehle, U.; Pallix, J. B.; Becker, C. H.; *J. Vac. Sci. Technol. A* **1988**, *6*, 936.

[3] Becker, C. H.; Gillen, K. T.; *J. Vac. Sci. Technol. A* **1985**, *3*, 1347.

Laser Desorption and High Temperature Methods for Vaporization and Ionization in Particle Beam LC / MS Interfacing

J. Chris Richardson and Richard F. Browner, School of Chemistry and Biochemistry, Georgia Institute of Technology, Atlanta, Georgia 30332-0400

INTRODUCTION

Particle beam LC/MS is unique in using an aerosol based interface that is solely a "transport" interface. After aerosol generation, the analyte is desolvated and transported to the mass spectrometer as solid crystals or solvent-free drops. Consequently, the technique does not exclusively favor any one ionization technique over another, and a wide variety of vaporization / ionization techniques may be used. Up to this point, the ion formation has been a two step process of vaporization by collision with a resistively heated source block followed by electron impact or chemical ionization. However, many compounds are too involatile or thermally labile to be vaporized and ionized effectively by these techniques. Some have demonstrated decreased thermal degradation with the use of an extremely hot target, consisting of electrically heated nichrome ribbon. Also, softer ionization methods such as FAB and SIMS have been used with varied success in this laboratory. More recently, we have been successful in obtaining laser desorption / ionization (LDI) and matrix assisted laser desorption (MALD) spectra on a quadrupole mass spectrometer using flow injection introduction.

The purpose of this research is threefold: 1) Directly compare laser vaporization / electron ionization to other forms of high temperature vaporization, 2) Test the feasibility of surface ionization (ionization caused by contact with a surface held at temperatures in excess of 1500C), and 3) Explore and improve on current techniques for producing laser desorption ionization spectra with the particle beam interface.

EXPERIMENTAL

Experiments were performed on an HP 5988 quadrupole mass spectrometer. The laser in use is a continuous wave, 3W Argon ion laser, operated in the multi-line mode at 457.9-514.5nm, focused to a power density of ~10^3 W/cm^2. Flow injection experiments were performed using an HP 1090 HPLC pump at 0.4mL/min with a 5 µL injection volume.

RESULTS AND CONCLUSIONS

The loss of water by cholesterol is often used as a measure of the thermal degradation caused by a system. Figure 1 shows the results of a comparison between laser vaporization and other forms of vaporization. Decreased degradation is observed with increasing temperature, with the laser vaporized cholesterol showing at least a three fold decrease in degradation. These results suggest that the coupling of laser vaporization to a softer ionization technique such as chemical ionization, could make the analysis of very thermally labile compounds by particle beam a routine process.

Next, LDI experiments were performed using the argon ion laser. The ion source was completely removed to accommodate the laser. The particles exiting the PB transport tube were directed onto a blackened ceramic probe, where LDI takes place. Thus far, flow injected LDI spectra have been obtained for methyl red, naloxone caffeine, aerosurf, sucrose, and cholesterol. All spectra show little or no fragmentation, with a potassium adduct ion $(M+K)^+$ as the base peak. Several direct insertion spectra have been obtained using the argon laser, including aldicarb, ampicillin, and erythromycin, which is shown in figure 2. These spectra demonstrate the potential of this technique to broaden the scope of compounds amenable to PB-LC/MS.

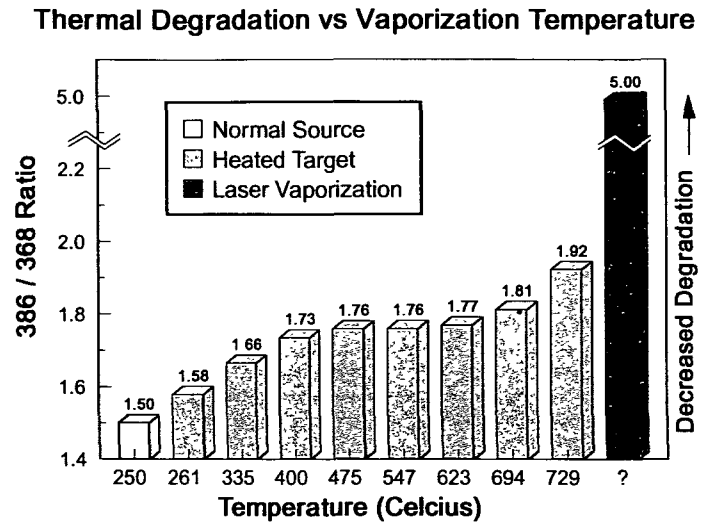

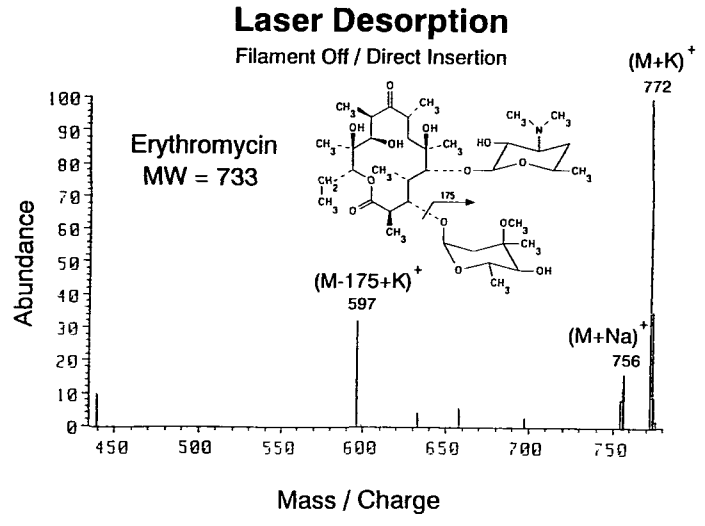

POWER-DEPENDENT CALIBRATION SHIFTS IN LASER ABLATION TIME-OF-FLIGHT MASS SPECTROMETRY

Chau-Wen Chou and Peter Williams
Department of Chemistry and Biochemistry
Arizona State University
Tempe, AZ 85287-1604

Laser ablation time-of-flight mass spectrometry is becoming widely used for molecular weight determination of massive proteins and other biomolecules, and impressive accuracies have been claimed for such mass determinations. Although mass reference standards are often incorporated into the analytical sample, it may often more convenient to attempt to establish an instrument calibration curve using an external standard and to assume, or hope, that this curve is universally applicable. We have recently identified a circumstance where this hope may not always be justified.

A fullerene mixture provides a useful time-of-flight calibration sample at relatively low masses because the mass distribution of unseparated fullerenes is dominated by the C_{60} and C_{70} peaks at masses 720 and 840 Da respectively. In using such a fullerene mixture to calibrate a time-of-flight mass spectrometer, we noticed that the C_{60} and C_{70} peaks could be shifted to significantly longer flight times if the laser power was increased to the point where intense signals from the copper substrate were present at low mass. Figure 1a shows a typical time of flight mass spectrum of an unseparated fullerene mixture. 10-20 µL of a dilute solution of the fullerenes were pipetted onto a copper sample block and allowed to evaporate, forming a thin deposit over an area of 1-2 cm^2. The sample was ablated using 532 nm pulses from the frequency-doubled output of a Nd-YAG laser. Pulse energies were ~ 0.8 mJ/pulse and the beam was focussed to an elliptical spot ~ 100 x 200 µm across, giving an energy density ~ 4 J/cm^2. The C_{60} and C_{70} peaks form a distinctive doublet at 15.2 and 16.3 µs. The position of these peaks is within < 1% of the calculated flight time for these ions through the mass spectrometer. When the laser power was increased to ~ 2 mJ/pulse (10 J/cm^2), a strong signal was generated at low mass from the copper substrate. Accompanying this low mass signal, we saw a significant increase in the C_{60} and C_{70} flight times as seen in Figure 1b. Again, the distinctive signature of the two peaks ensures that we are not seeing the appearance of some new heavier species. These shifts vary with the intensity of the low-mass signal, which depends on the laser power.

Examination of peak shifts at varying laser power revealed the following:

a) Both the C_{60} and C_{70} peaks shift together: the time difference between the peaks is constant to better than 100 ns while the peaks shift by several microseconds.

b) At higher power a mass 1 peak can be seen; the flight time for these H^+ ions is consistent with the flight time calculated from a fullerene calibration *at low power*, i.e. there is no detectable shift in the mass 1 peak at times when the fullerene peaks are shifted by several µs.

c) There is a rough correlation between the duration of the intense low mass signal and the fullerene shift, i.e. the time difference between the upper time limit of the low mass peak and the fullerene peaks is roughly constant.

The mechanism we feel is most consistent with our data is as follows. At high power, the pulse of low-mass ions is sufficiently intense to result in a strong space charge above the sample surface; if we assume that the low-mass ions are distributed over a 100 µm deep region above the sample surface, the ion density in this volume is estimated to be ~ 10^{18} ions/m^3. Because the heavier fullerene ions move away from the surface more slowly, the effect of this charge will be to screen the fullerenes from the acceleration field for a short period until the low mass ions are accelerated away. From the width of the low mass peak it may be estimated that extraction of the ions from the space-charge cloud can take up to ~ 5 µs. Only when this space charge has been dissipated can heavier ions trapped below the cloud be extracted. These ions then see the normal acceleration field, and their *relative* flight times are characteristic of the relative masses accelerated in the full field. However, the arrival times are delayed by the dissipation time of the low-mass pulse. Also consistent with this picture is the fact that the arrival time of the mass 1 peak does not vary significantly in the different spectra.

This space charge effect has serious implications for mass calibration accuracy in any situation where there is an intense low-mass ion flux, which can often be the case in matrix-assisted laser desorption. In such a case, the calibration curve for a set of protein masses will not go through zero time at zero mass but will be offset. If several calibration masses are available, a valid calibration curve may still be obtained. However, if only a single calibration mass is used, with the assumption that the curve passes through the origin, errors will result. Additionally, external calibrations at different laser power settings may be erroneous. In systems where the low-mass ions are suppressed by a deflector pulse after acceleration, the operator may not be aware of the possibility of space charge effects. Finally, if shot-to-shot fluctuations in laser power occur, the effect of varying space charge will be to degrade mass resolution in an averaged spectrum due to the shifting peak positions.

This work was supported by the US Department of Energy Grant DE-FG02-91ER61127.

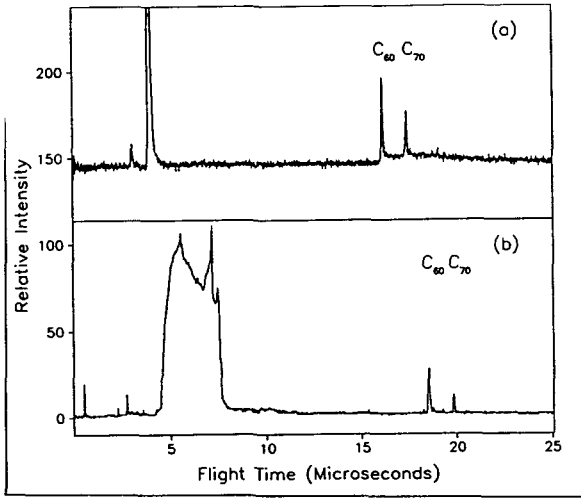

Figure 1. A comparision between low power and high power spectra.

HYPERTHERMAL SURFACE IONIZATION MASS SPECTROMETRY IN SUPERSONIC MOLECULAR BEAMS

Aviv Amirav, Albert Danon and Shai Dagan

School of Chemistry, Tel Aviv University, Tel Aviv 69978, Israel, Fax 972-3-6409293

Organic molecules acquired with hyperthermal (1-20 eV) kinetic energy in a supersonic molecular beam (SMB) undergo efficient surface ionization. The molecular kinetic energy increase the surface ionization yield by several orders of magnitude and thus hyperthermal surface ionization (HSI) can serve as a universal ion source for organic mass spectrometry with tunable selectivity.

Five main types of HSI processes were observed:
(a) Molecule-surface electron transfer, (b) Surface-molecule electron transfer, (c) Hyperthermal surface induced dissociative ionization, (d) Chemically induced hyperthermal surface ionization and (e) local hot spot HSI.
These processes will be described with several examples.

We have found that HSI may lead to extensive ion dissociation and non-statistical negative and positive fragment ion formation. This fragmentation occurs near the surface in small molecules and is affected by it while in large polyatomic molecules such as cholesterol, it is unimolecular far away from the surface. HSI serves as a very efficient mass spectrometry ion source with total ionization efficiency of over 10 percent. This and the lack of vacuum background ionization result in sub-femtogram minimum detected amount. HSI in SMB is also uniquely supplemented by a fast GC-MS inlet and a fly through electron impact ion source. This combination results in a new approach of mass spectrometry in supersonic molecular beams. The electron impact ion source results in EI mass spectra with total fragmentation tunability and enhanced relative abundance of the molecular weight peak. In addition, the in line combination of EI ion source and HSI surface, allow the surface induced dissociation (SID) of EI produced ions on the HSI surface. We have found that rhenium oxide surface is a very good surface for both HSI and SID with 70 times enhanced SID yield in comparison with stainless steel.
Hyperthermal surface ionization is also characterized by a tunable degree of ionization selectivity which is controlled by the surface used (work-function) and molecular kinetic energy. The selective detection of aromatic compounds in gasoline with fast GC-HSI-MS will be demonstrated.

Presented at the 41st ASMS Conference on Mass Spectrometry

pH EFFECTS AND INSULIN CLEAVAGE IN MATRIX-ASSISTED LASER DESORPTION MASS SPECTROMETRY

X. Tang[a], R. Donaldson[b], A.Vertes[a*]
[a] Department of Chemistry, [b] Department of Biological Sciences
The George Washington University, Washington, DC 20052

The effect of pH on matrix assisted laser desorption mass spectrum (MALD-MS) of insulin has been studied to uncover the influence of matrix acidity. UV optical absorption spectra of insulin and four different matrix solutions (sinapinic acid: SA; 2,5-dihydroxy-benzoic acid: DHB, α-cyano-4-hydroxycinnamic acid: CHCA; 2-(4'-hydroxyazobenzene)-benzoic acid: HABA) were investigated while gradually replacing their solvents with NaOH solution. Minor shifts in the absorption maximum were observed. Melting point and pH measurements supplemented the investigations. Characteristic values for melting points, UV absorption maxima, molar absorptivity at nitrogen laser wavelength (337 nm), pH, and pK_a are shown in Table 1 for the matrices and for the corresponding sodium salts.

Table 1. Characteristics of matrices and their sodium salts:

	Matrices					Sodium salts of matrices			
	MP (°C)	λ_{max} (nm)	ϵ_{337nm} ($M^{-1}cm^{-1}$)	pH	pK_a	MP (°C)	λ_{max} (nm)	ϵ_{337nm} ($M^{-1}cm^{-1}$)	pH
SA	203	320	14,000	3.75	6.20	>290	310	7,200	8.60
CHCA	206	335	28,000	2.70	4.08	>300	325	14,800	6.08
DHB	252	330	5,600	2.52	3.76	>290	322	1,940	4.50
HABA	211	359	28,000	3.63	5.96	>300	349	16,800	7.10

MP: melting point; pH was measured at 0.05 M concentration

Matrix sodium salts show significantly increased melting points, elevated pH and somewhat lower molar absorptivity at 337 nm. Insulin absorption maxima were found at λ_{max}=277 nm in 0.1% trifluoroacetic acid solution (ϵ_{337nm} =92,000 $M^{-1}cm^{-1}$) and λ_{max}=295 nm in 0.02 M sodium hydroxide (ϵ_{337nm} =9,000 $M^{-1}cm^{-1}$).

MALD-MS of insulin in the four matrices and in their sodium salts were recorded on a Comstock Model TOF-101 time-of-flight mass spectrometer. The instrument was modified to accommodate laser desorption and 30 kV accelerating voltage. A Laser Science VSL-337ND nitrogen laser was used for ion generation. Spectra were obtained close to threshold irradiance for ion formation. Good protein molecular ion signal was found for neat SA, DHB, and CHCA matrices. Partial or total neutralization of the matrix solutions with NaOH led to declining total ion yields. Diminishing of both insulin related *and* matrix molecular ion signals were observed in the MALD spectra. We could not compensate spectrum deterioration by increasing laser irradiance.

The cool plume model of MALD [1] predicts that minor increase in melting point and/or lowering of the molar absorptivity can be compensated for by elevating the laser irradiance. In fact, model calculations showed that SA and SA sodium salt matrix produced plumes of similar *neutral*

particle densities at 2×10^6 W/cm^2 and 10^7 W/cm^2 irradiances, respectively.

There are several possible explanations of the lack of matrix and protein molecular ions in the salt based MALD-MS. Significantly lower acidity of the matrix salts may explain the lack of protonated insulin ions. Sodiated quasi-molecular ions, however, could be present in these spectra. Another possible explanation is the thermal degradation of the salt matrix. Neat matrices produce plumes by strong sublimation, whereas the salt matrices may decompose before they reach their phase transition temperature. The existence of this process is supported by the presence of low molecular weight non-matrix specific ions in the mass spectrum.

Similar MALD-MS measurements were carried out using neat matrices and insulin dissolved in 0.05 M NaOH. Standard quality spectra were observed showing the kinetics of insulin cleavage. Figure 1 shows a series of MALD spectra of insulin incubated in 0.05 M NaOH for (a) 10 min, (b) 35 min, (c) 60 min, (d) 75 min, (e) 420 min, respectively. The peaks labelled A, B, I correspond to chain A, chain B and to intact molecular ions of insulin, respectively.

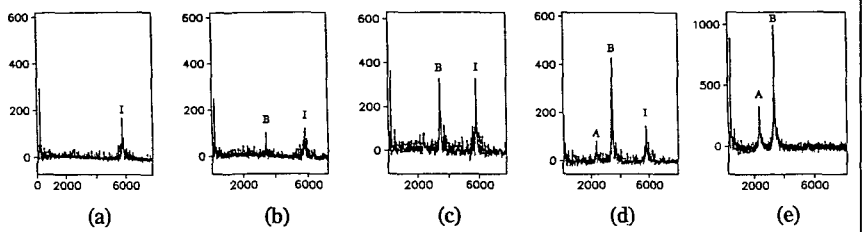

Figure 1.

At 10 min after dissolving the insulin in 0.05 M NaOH only the intact insulin molecular ion peak appeared. After 30 min, both reduced chain B and intact molecular ion peaks were abundant, but no chain A was observed. The domination of chain B in positive-ion spectra was also mentioned by other authors [2]. The intensity of chain B peak increases with increasing reaction time. After 7 hrs, only chain A and chain B species were observed. To study the effect of base concentration 0.004 M NaOH solvent was also used. MALD-MS at 10 min, 30 min, 1 day and 1 month showed no sign of insulin cleavage, only intact molecular ion peak appeared.

To verify that the cleavage is a liquid phase process (i.e. to rule out photochemical effects) gel filtration was used to detect the cleavage products before laser irradiation. Sephadex G-25 gel filtration of insulin (10 mg/ml) dissolved in pH 10.5 phosphate buffer showed no cleavage in the eluent. Complete cleavage was observed in the presence of β-mercaptoethanol (0.02 ml/ml). UV absorption detection after the column indicated three components in insulin incubated in 0.05 M NaOH for 1 hr. Thus, we concluded that the formation of chain A and B in mild base is a liquid phase process. MALD-MS proved to be an appropriate tool to follow the cleavage process.

References:

1. A. Vertes, R. Gijbels, In: Laser Ionization Mass Analysis, A. Vertes, R. Gijbels and F. Adams (eds), Wiley & Sons, New York, **1993**, pp. 127-175.
2. W.H. Fischer, J.E. Rivier, A.G. Craig, Rapid Comm. Mass Spectrom., **7** (1993) 225-228.

Investigating the Ionization Step in MALDI: Matrix-Dependent Formation of [M+H]+ *vs.* [M+Na]+ Ions of Small Peptides

*Pao-Chi Liao and John Allison
Department of Chemistry, Michigan State University, East Lansing, MI 48824;

Matrix-assisted laser desorption/ionization, MALDI, has one feature that links it to other desorption/ionization techniques such as FAB and SIMS - its development and commercial availability preceded our understanding of the chemical and physical processes that are involved. To generate ions in MALDI, analytes must be desorbed and, at some point, ionized. Models to describe the desorption of large, intact molecules from an energized matrix have been pursued, and appear to accurately describe the desorption step[1]. The chemical step, leading to ionization, is still a matter of considerable debate. Data are presented here concerning our pursuits in defining the ionization step in MALDI. We concentrate our efforts here on positive ion formation, using UV laser excitation.

Our initial goal was to attempt to understand why some matrices seem to generate [M+H]+ ions for peptide analytes, M, while other matrices generate predominantly [M+Na]+ ions for the same analytes. An example is given in the three spectra shown. In all three, hexatyrosine is the analyte. In Figure 1a, when sinapinic acid is the matrix, the pseudo-molecular ion is the [M+H]+ ion. In Figure 1b, where α-cyano-4-hydroxy-cinnamic acid is the matrix, both an [M+H]+ and an [M+Na]+ peak is present. In Figure 1c, where 2,5-dihydroxybenzoic acid is the matrix, only an [M+Na]+ peak is present. For a hexatyrosine/α-cyano-4-hydroxycinnamic acid (molar ratio, analyte/matrix = 1:150) system, it is found that [M+Na]+ ion yield increases dramatically when NaCl/α-cyano-4-hydroxycinnamic acid is ~ 1/3 (molar ratio).

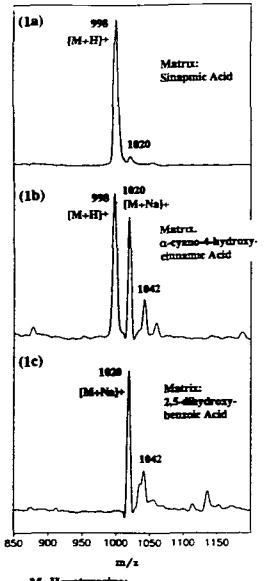

M=Hexatyrosine;
Analyte:Matrix = 1:50 (molar ratio);
NaCl was added to samples to give
NaCl:Matrix = 2.5:1 (molar ratio)

Possible mechanisms for the formation of [M+H]+ *vs.* [M+Na]+ ions in MALDI were considered. Possible mechanisms for protonation are: excited state acid-base chemistry[2], chemistry following matrix photoionization and chemistry following analyte photoionization. Possible mechanisms for the formation of [M+Na]+ ions are: excited state "salt" chemistry, protonation of the sodium salt of the analyte and gas phase capture of Na+ ions by the analyte.

It is known that MALDI spectra cannot be used for quantitation of mixtures. The signal intensity for each peptide of a mixture reflects the efficiencies of both the desorption and the protonation steps. The response seems to correlate with the basicity of the peptides. To investigate this further, MALDI spectra of small molecules with known PA's were obtained. The results indicated that there is a PA requirement for a successful MALDI analysis. The analyte must have a PA that lies above some value, X kcal/mol, where 208 < X < 223.

Triphenylphosphonium(TPP)-derivatives of the peptide *H*-VGVAPG-*OH* were made to investigate the formation of gas phase ion from "preionized" species in MALDI(figure 2). There is no detectable signal for this peptide before derivatization. However, very strong signals were observed for the TPP-derivatives. From this experiment, it was demonstrated that the formation of gas phase ion from "preionized" species in MALDI is possible.

Data are consistent with a model that involves acid/base chemistry for excited matrix molecules in the condensed phase leading to protonation. While some matrices seem to generate predominantly [M+Na]+ forms of the analyte, instead of protonated molecules, these matrices seem to be available with a high salt content. However, it is unclear why the addition of NaCl to MALDI matrices does not <u>always</u> lead to predominant of [M+Na]+ ions over protonated molecules.

References:
1. Vertes, A.; Gijbels, R.; Levine, R. D. *Rapid Commu. Mass Spectrom.* **4**, 228 (1990)
2. Gimon, M. E.; Preston, L. M.; Solouki, T.; White, M. A.; Russell, D. H. *Organic Mass Spectrom.* **27**, 827 (1992)

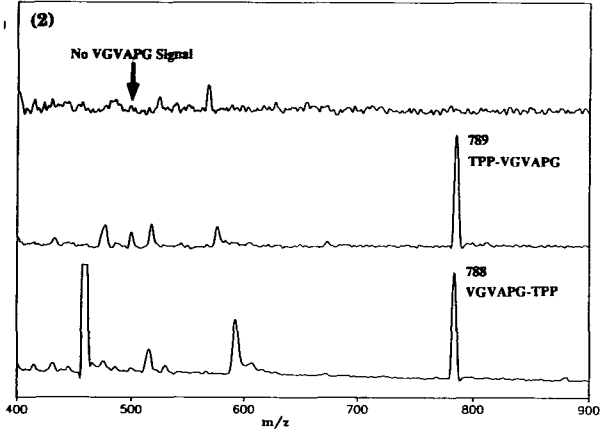

10 pmol VGVAPG, MW= 499; Matrix:α-cyano-4-hydroxycinnamic Acid;
Analyte:Matrix = 1:2000 (molar ratio)

A Postacceleration Detector For Time-of-flight Mass Spectrometry Utilizing Ion To Photon Conversion

*Robert S. Brown, Scott S. Hermsen, John J. Lennon, Department of Chemistry, Colorado State University, Ft. Collins, CO 80523

Three detector designs for time-of-flight mass spectrometry based upon the use of a fast (2.3 ns decay half-life) plastic scintillator (polyvinyltoluene) coupled to a fast response photomultiplier tube (Burle model S83062E) were evaluated in terms of obtainable mass resolution, sensitivity, response vs. mass and the degree of signal perturbation induced by significant (5-20 kV) amounts of postacceleration. All of the designs involved primary ion to secondary electron conversion, followed by secondary electron to photon conversion at the scintillator. The photons were then detected by the photomultiplier tube. Designs 1 and 2 (figure 1) utilized a conventional conversion dynode, either a 3 mm thick CuBe venetian blind dynode or a 1 mm thick CuBe focused mesh (Beckton-Dickinson) dynode. The latter should offer a smaller flight path perturbation due to its thinner size, but in practice gave identical performance to the venetian blind style dynode in terms of mass resolution and sensitivity. In fact, both designs produced limiting mass resolutions of ≈500 (fwhm) for the protonated molecular ion of porcine insulin. Mass resolution is probably being limited by the initial kinetic energy distributions of the ions in the linear TOF-MS utilized (25 kV accelerating potential) rather than the ion detector. Representative spectra for cytochrome C obtained with the venetian blind style conversion dynode in place is shown in figure 2 at various dynode bias up to -15 kV. Unlike what is observed when similar conversion dynodes are coupled to electron multipliers, little signal distortion is observed with the scintillator-PMT design. This signal distortion is thought to be due to the sputtering of secondary ion species off the dynode surface by primary ion impact. These secondary ion species are not uniformly extracted out of the conversion dynode, resulting in significant signal tailing. The improvement in response with the scintillator is believed to be due to the fact that the scintillator requires very fast particles to induce a response, therefor effectively discriminating against secondary ions and preferentially responding to secondary electrons. Some signal distortion is observed at high extraction fields, but it is significantly less than what we have observed with other postacceleration schemes. Increased signal at higher postacceleration is offset by increased noise, believed to be due to random field ionization events caused by high localized electric fields at the thin dynode edges.

The third design evaluated is depicted in figure 3. It utilizes a flat, optically transparent dynode (currently a sapphire window - Al_2O_3) instead of the previous dynodes. It makes use of the fact that the primary ion beam is tightly focused by a wire ion guide (-100 V). An optically reflective 5 mm aperture at the exit of the wire guide is coated with a 0.5 mm thick scintillator film. Secondary electrons sputtered from the dynode surface are accelerated back towards the scintillator and produce photons which the PMT detects. The angular

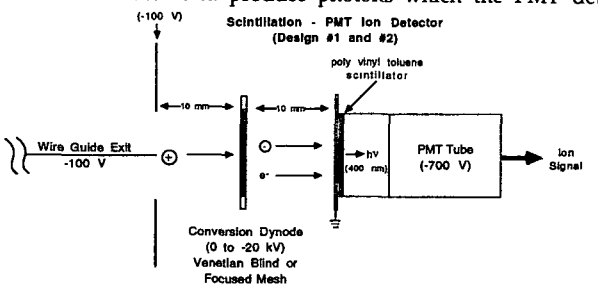

Figure 1

distribution of the emitted secondary electrons is such that the majority miss the small wire guide exit aperture. A typical MALD TOF mass spectrum for porcine insulin with this design is shown as figure 4 (-18 kV dynode bias). Sensitivity and mass resolution are comparable to the previous designs, although some signal tailing and fronting is apparent due to the high postacceleration. Interestingly, the smooth surface of the dynode eliminates field ionization induced noise. This design will be explored more in terms of the effect of coating the dynode with thin films of various materials (such as Cu, Au) to try and enhance secondary electron sputtering. It may also be possible to enhance the response for larger m/z ions by utilizing materials, such as LiF, as the dynode and optimizing the detector for effective sputtering of small secondary ion species.

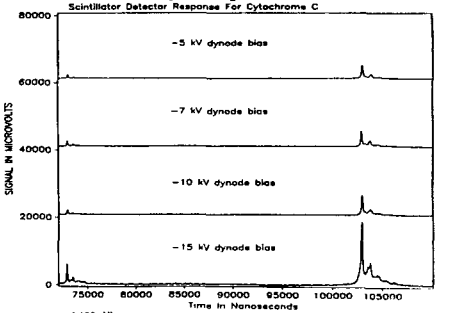

Figure 2

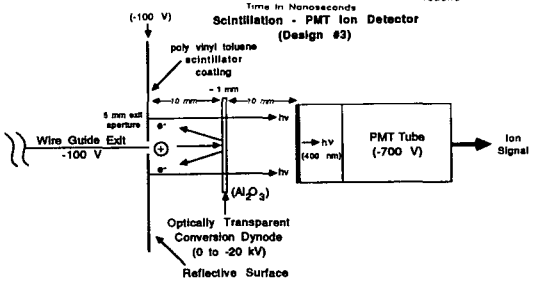

Figure 3

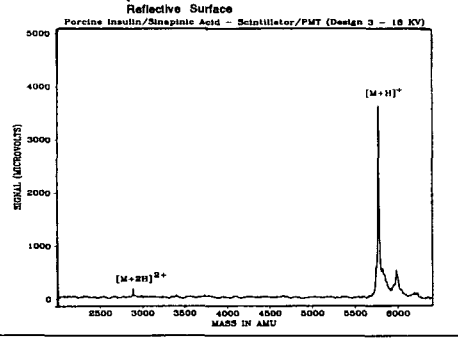

Figure 4

High Mass Resolution and High Mass Accuracy MALD/I Spectra with a Triple Electrostatic Analyzer Time-of-Flight Mass Spectrometer

*J.A. Chakel, E.P Marsh and R.W. Odom, Charles Evans & Associates, 301 Chesapeake Drive, Redwood City, CA 94063

High mass resolution and high mass accuracy analysis of biomolecules using matrix assisted laser desorption/ionization (MALDI) is possible on an innovative time-of-flight mass spectrometer (TOF-MS). A schematic of this TOF-MS is shown in Figure 1. This instrument was originally designed for TOF secondary ion mass spectrometry (TOF-SIMS) applications [1]. It features specialized stigmatic ion optics which transport an image of ions formed at the sample surface through the mass analysis section of the instrument and high precision, fast digital detection circuitry. The three 90° quasi-hemispherical ESAs provide complete first order energy focusing for both ion flight times and ion imaging with very small residual second order aberrations. The ESAs are fitted with field termination plates (Herzog shunts) and Matsuda plates for electrostatic field shaping.

This design is both strongly energy and position focusing having a large spectrometer energy acceptance (~340eV, FWHM) and angular acceptance (±90 mrad) [2]. In addition, an energy slit (between the first and second ESAs) can be used to define the energy spread of transmitted ions. The transmitted ion beam traverses various image points and image planes along the ~2 M flight path. Unlike a reflectron based TOF-MS, the ions are maintained at full acceleration energy throughout their flight path and thus, space charge broadening and ion/neutral collisions are minimal in this instrument. Metastable ions formed before the third ESA are not transmitted to the detector thus minimizing peak broadening or spurious metastable peak detection. The overall transmission efficiency of this instrument is higher than 50%.

A frequency tripled Nd YAG (355 nm) laser was used. The laser beam was attenuated primarily with a variable beam attenuator and by software control of the Q-switch delay The pulsed laser output (4-5 ns FWHM) was focused and transmitted onto the sample Analysis of selected individual matrix crystals was achieved with a tightly focused laser beam (6-7 μm diameter) Ion detection was accomplished with a DMCP detector coupled with a 200 MSample/s (5 ns channels) transient recorder.

A single shot spectrum for gramicidin S obtained with use of the energy slit is presented in Figure 2. The mass resolution (>8000) is difficult to measure with a single channel peak and illustrates the need for faster transient recorders. Accurate mass measurements require accurate determinations of the peak centroids. Fast transient recorders are thus desirable, especially in the peptide mass range. Timing inaccuracies produced primarily by trigger jitter could shift the centroid of higher mass peaks by a few tenths of a mass unit. Mass measurements of the molecular ion of angiotensin produced from a mixture of gramicidin S, angiotensin and substance P in sinapinic acid revealed mass measurement accuracies of 2 to 63 ppm. The absolute mass error in all of these analyses was <0.1 Da which is on the order of a single 5 ns timing channel (0.13 to 0 14 Da at these masses).

High mass resolution and high mass accuracy are desirable in extending the utility of MALD in direct digest mixture analysis. The spectrum from 10 laser shots of a single location of a 3.2 pmole deposit of a hemoglobin α & β chain tryptic digest mixture in dihydroxybenzoic acid is illustrated in Figure 3 The expanded mass range plot in the lower panel shows the β-chain T-5 fragment at mass 2059 The mass resolution for the monoisotopic peak of this fragment is ~12,000 FWHM. Mass accuracies for this digest mixture range from 22 to 108 ppm for the observed fragments and the absolute mass error is less than 0.12 Da. The width of a single 5 ns channel varies from 0 08 to 0.18 Da over the range from 451 to 2226 Da.

1. B. Schueler, P. Sander and D A. Reed, Vacuum, 41, 1661 (1990).
2. B Schueler, Microsc. Microanal. Microstruct., 3, 1 (1992).

This work was funded in part by a Phase I SBIR grant from the National Science Foundation., No. ISI-9160545

Figure 1

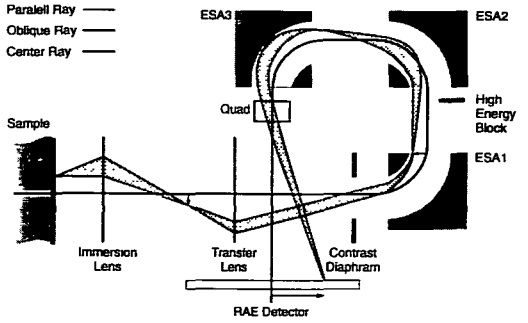

Figure 2

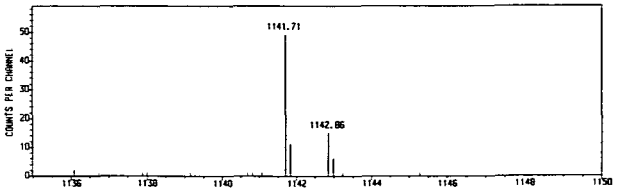

Figure 3

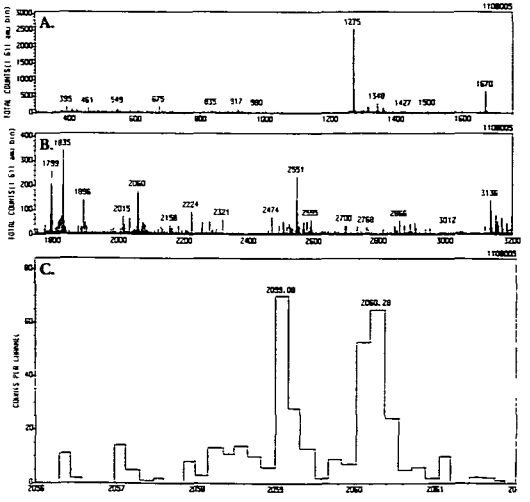

Initial Kinetic Energies of Peptide Ions Formed by MALDI

Dieter Kirsch, Bernhard Spengler, Raimund Kaufmann,
Inst. of Laser Medicine, University of Düsseldorf, Moorenstr. 5, D-4000 Düsseldorf, Germany

Recent results on desorption kinetics of MALDI ions obtained by several groups, suggest the formation of a supersonic jet of matrix ions carrying larger analyte ions with almost mass independent velocities [1-3]. Knowledge of jet velocities, as well as of ion start time profiles will give important information about the mechanism of ion formation and desorption, and will, on the other hand, help to optimize instrumental design with respect to high mass accuracy, mass resolution and sensitivity.

Employing different matrices such as 2,5-dihydroxybenzoic acid (DHB), α-cyano-4-hydroxycinnamic acid (4HCCA) and sinapinic acid, positive and negative ions of matrix, proteins and oligonucleotides have been investigated with respect to initial kinetic energies and mean virtual ion start times. This was done by monitoring the drift time of the ions in a spatially and electrically well defined field free region s_1 of variable length between sample surface and acceleration field (Figure 1). The field terminating grid was specially designed to avoid field penetration from the acceleration region into the field free drift region. By varying the length of the drift region a mean virtual desorption time (relative to the laser pulse event) could be extrapolated precisely.

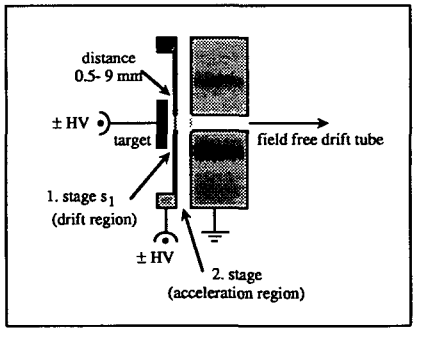

Figure 1: Ion acceleration region of the linear TOF instrument. The electric field of the first acceleration region could precisely be set to zero.

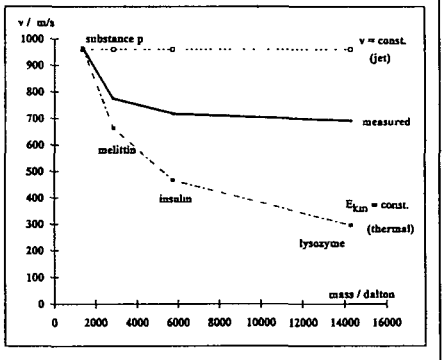

Figure 2: Dependence of analyte ion velocities on their mass, indicating an expansion process with combined thermal and supersonic-jet characteristics.

Initial velocities of analyte ions have been found to significantly depend on analyte mass, irradiance and matrix used. Figure 2 demonstrates the dependence of analyte ion velocities on mass. It shows a behavior characterized by a combination of supersonic jet expansion (v=const.) and thermal desorption (E_{kin}=const.).

Mean virtual desorption times have been found to be non-zero in most cases (Figure 3), imaging probably collision- and acceleration-effects of (slower) analyte ions with (faster) matrix molecules and ions, rather than real ion start time delays (Figure 4). Virtual desorption times are typically 200 to 400 ns at threshold irradiance and approach zero at high irradiance. Evaluating the fastest analyte ions of the velocity distribution leads to zero virtual desorption times at threshold irradiance (Figure 3).

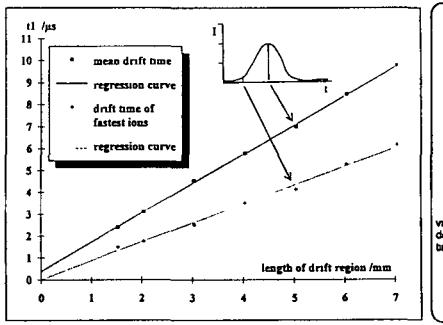

Figure 3: Drift time of the most abundant and of the fastest negative ions of oligonucleotide TTGAC in the field free drift region s_1 at various lengths of s_1.

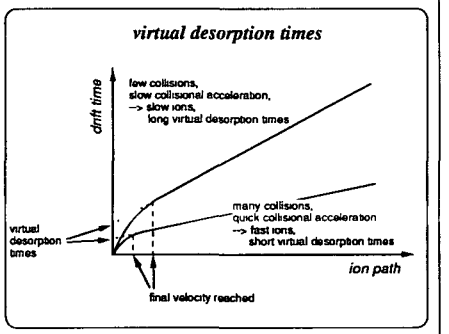

Figure 4 Modell for explaining non-zero virtual desorption times. Collisional ion acceleration extending over different distances leads to different extrapolated flight time values.

REFERENCES

1. A. Verentchikov, W. Ens, J. Martens, K. G. Standing, Proceedings of the 40th ASMS Conference, Washington, DC, 1992.
2. Y. Pan, R. J. Cotter, Org. Mass Spectrom. **27**, 3 (1992)
3. R. C. Beavis, B. T. Chait, Chem. Phys. Lett. **181**, 479 (1991)

DESIGN OF A NEW FLOW PROBE FOR CONTINUOUS-FLOW MATRIX-ASSISTED LASER DESORPTION IONIZATION

Davinder S. Nagra and Liang Li*
Department of Chemistry, University of Alberta
Edmonton, Alberta, Canada T6G 2G2

Matrix-assisted laser desorption (MALD) is a very powerful technique for the generation of ions from large biochemicals. Currently, MALD is usually performed from a solid insertion probe. A desired feature of this technique would be to desorb and ionize molecules directly from a solution. This would permit MALD to be interfaced with various solution-based separation methods for on-line detection and quantitation. Recently, we demonstrated the feasibility of using a continuous flow (CF) probe with a liquid matrix, namely 3-nitrobenzyl alcohol (3-NBA) to introduce solution samples directly into a linear time-of-flight (TOF) mass spectrometer [1]. In this present work we report a much improved design over the previous flow probe for CF-MALD and show that (1) it is now possible to perform flow injection analysis of large peptides with molecular weights above 10,000 with CF-MALD and (2) flow injection ion profiles of these biochemicals in the subpicomole region can readily be obtained.

Figure 1 shows the new design of the continuous flow probe. A capillary tube is inserted into a stainless steel tube and extends from the sample injector to the probe tip. A piece of Kapton (2.8-mm diameter), with a small hole pierced through the center, is mounted at the tip. The capillary tube punctures through the hole in the Kapton and is placed no more than 1 mm above the surface. A piece of filter paper is wrapped around the probe tip to absorb the excess liquid. The flow probe is inserted into the TOF mass spectrometer between the repeller and extraction plates. The sample molecules are carried by a solvent mixture (aqueous trifluoroacetic acid, ethanol, ethylene glycol, and 3-NBA) through the capillary tube and onto the Kapton surface. The resulting MALD ions are recorded on an oscilloscope and the data is transferred in real time to a PC via GPIB. The data transfer and data analysis software are developed in house. After storing all the mass spectra in the PC a selective ion profile can be established.

Figure 2 shows a representative single-shot CF-MALD mass spectrum of cytochrome c (MW ~ 12,360) with a total sample injection of 3 picomoles. Trypsinogen (MW ~ 24,000) aids in the initial optimization of the flow conditions by continuously flowing onto the probe surface. Since more than 500 mass spectra can be obtained and only a portion of the sample flowing onto the probe surface are actually being desorbed, the total amount of sample consumed for generating such a mass spectrum is less than 6 femtomoles. A flow injection ion profile can be obtained by calculating and plotting the peak area of the molecular ion as a function of the elution time. Figure 3 shows the ion profiles of 5 repeat injections of different amounts of cytochrome c. Note that there are some variations in peak heights and areas with repeat injections. We are currently in the process of better optimizing the flow conditions. Figure 4 shows a sensitivity curve for cytochrome c (±1 std deviation). A linear response of one order of magnitude in the low picomole region can be obtained. While the precision still needs to be improved, quantitative CF-MALD shows much promise.

Reference

1. Li, L.; Wang, A.P.L.; Coulson, L.D. Anal. Chem. 1993, 65, 493.

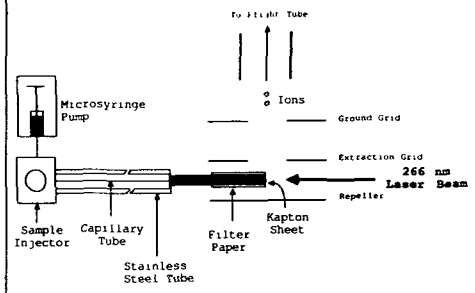

Figure 1
CF-MALD

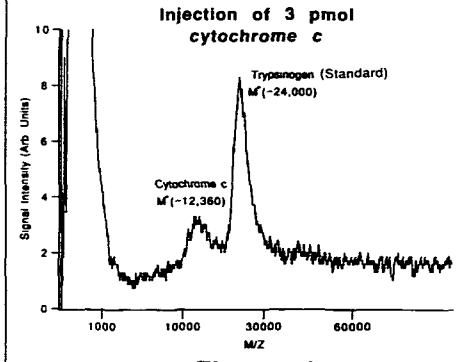

Figure 2

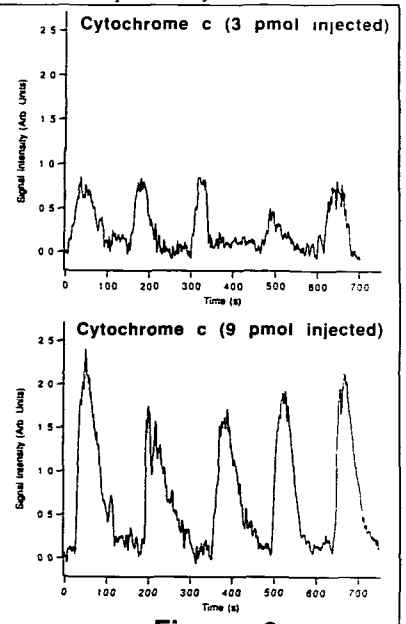

Figure 3

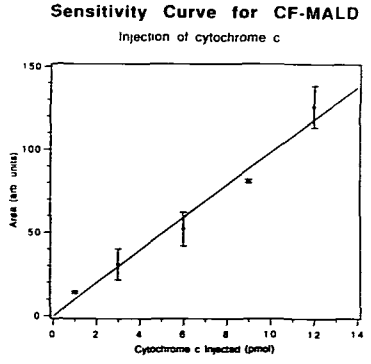

Figure 4

OPTIMIZATION OF ION EXTRACTION AND ION DETECTION FOR CONTINUOUS-FLOW MATRIX-ASSISTED LASER DESORPTION

Randy M. Whittal, Davinder S. Nagra and Liang Li*
Department of Chemistry, University of Alberta
Edmonton, Alberta, Canada, T6G 2G2.

Matrix-assisted laser desorption (MALD) has become an established technique for the analysis of large biomolecules. Recently, we extended this technique by using a continuous flow (CF) probe with the liquid matrix 3-nitrobenzyl alcohol (3-NBA), to introduce solution samples directly into a linear time-of-flight (TOF) mass spectrometer [1]. However, mass resolution was relatively poor due, in part, to the ion extraction geometry. Static MALD spectra are normally generated with the ions extracted in parallel to the direction of ion expansion. This geometry minimizes the initial ion spatial distribution. However, with this geometry, the sample probe is usually floated at a high voltage. In order to avoid possible electric breakdown in the CF probe, we grounded the probe and placed it in between the repeller and extraction grids. Thus, ion extraction is performed orthogonally to the ion expansion direction.

In this report we demonstrate that it is now possible to perform CF-MALD in the parallel ion extraction configuration. The objective of this work is to evaluate the performance of the parallel CF-MALD method in terms of sensitivity, signal stability and mass resolution, with emphasis on comparison to the orthogonal method.

We recently constructed a linear TOF mass spectrometer which can accomodate both the parallel and orthogonal ion extraction geometries. A frequency quadrupled Nd:YAG laser (266 nm) is used to perform MALD. The resulting mass spectra are recorded on a digital oscilloscope and transferred in real time to a PC via a GPIB. The data transfer and data analysis software is developed in house. The design of the flow probe for CF-MALD is described elsewhere [2]. In brief, a solution containing an internal standard in a mixture of 3-NBA, aqueous trifluoroacetic acid, ethanol and ethylene glycol is introduced continuously through the flow probe. A sample injector allows for on-line injection of protein samples.

We first present results with static MALD in order to assess the performance between the different ion extraction geometries. The sample and matrix are mixed together on a probe tip and inserted into the vacuum chamber. Figures 1A and 1B illustrate the static MALD spectra for bovine insulin ß-chain (MW 3496) mixed with 3-NBA for the orthogonal and parallel configurations, respectively. Parallel MALD produces a sharper peak, resulting in a resolution enhancement of approximately 3.5. Sensitivity improves by approximately an order of magnitude in parallel MALD.

Figure 2A shows the orthogonal CF-MALD spectrum produced from an injection of 5 pmol of chicken egg lysozyme (MW~14400). Figure 2B represents the corresponding parallel MALD spectrum. In both cases reproducible ion profiles can be obtained with repeat injections. The ion profile (not shown) shows that 500 spectra can be produced from one injection. Thus, Figure 2 actually represents a spectrum for a few femtomoles of sample. The sensitivity of CF-MALD improves 5 to 10 times in the parallel ion extraction configuration. We are currently in the process of studying the degree of resolution enhancement.

References

1. Li, L.; Wang, A. P. L.; Coulson, L. D. *Anal. Chem.* **1993**, *65*, 493.
2. Nagra, D. S.; Li, L. This volume.

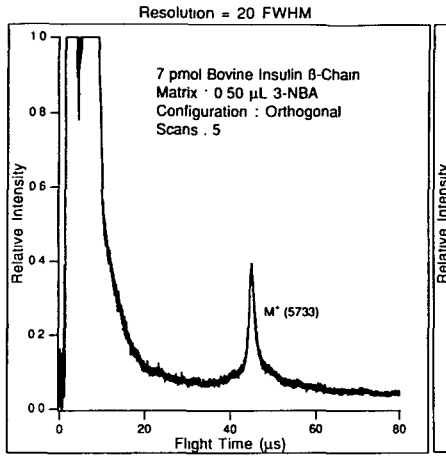

Figure 1A

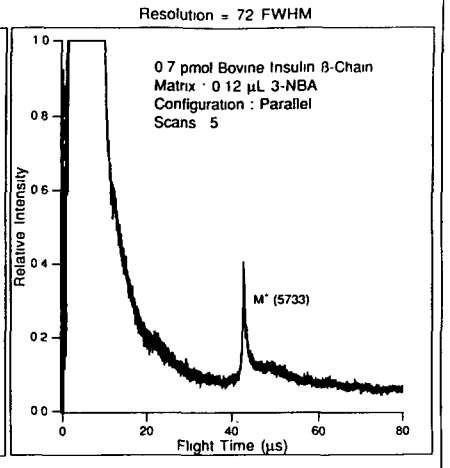

Figure 1B

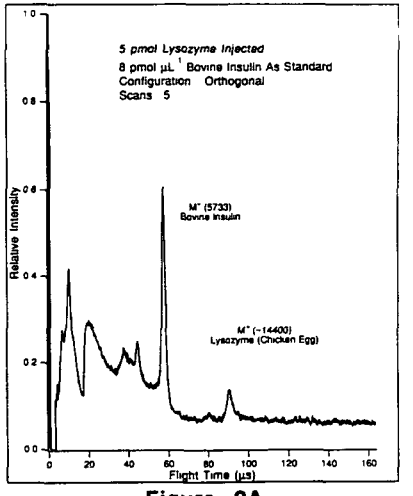

Figure 2A

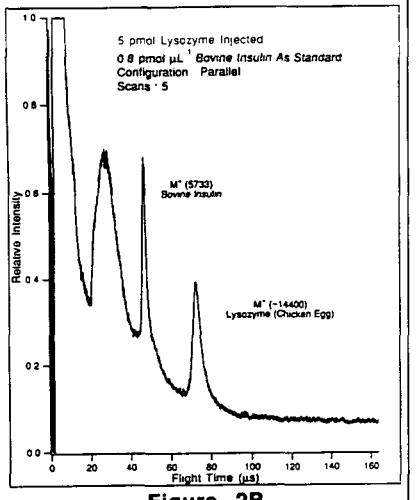

Figure 2B

Basic Matrices for the Matrix-Assisted Laser Desorption/Ionization Mass Spectrometry of Proteins and Nucleic Acids

Michael C. Fitzgerald, Gary R. Parr, and Lloyd Smith
Department of Chemistry, University of Wisconsin, Madison, WI 53706

Matrix-assisted laser desorption/ionization (MALDI) mass spectrometry has emerged as a powerful new analytical technique that permits the mass analysis of high molecular biopolymers (up to 300,000 Dalton). The matrix, a small organic molecule, is a key part of the desorption and ionization process in this mass spectral method. By irradiating the sample with a high intensity, pulsed laser beam it is possible to generate intact, gas phase molecular ions of the analyte. Several matrix materials including nicotinic acid, sinapinic acid, and 2,5-dihydroxybenzoic acid have proven to be effective for the MALDI analysis of a wide variety of proteins. However, these acidic matrices have not been found to be generally applicable to the analysis of nucleic acids. The goal of this study was to determine if pH is an important factor in the MALDI analysis of nucleic acids and proteins.

All mass spectra were recorded using a Vestec Model VT 2000 laser desorption, linear time-of-flight mass spectrometer. The flight tube has been modified with a nickel wire, 0.012 mm in diameter, that spans the length of the 2 m flight path and is biased at 120 volts so ions are efficiently transported along the center axis of tube. Desorption and ionization of samples was accomplished with a Lumonics Model HY 400 Nd:YAG laser. Ions were accelerated in two stages through a total of 30 keV. All spectra were summed over 50 laser shots.

A total of 37 highly substituted pyrimidine, pyridine, and benzene derivatives containing basic amino groups were screened as potential matrices. Several of these compounds were useful for the preparation and analysis of samples under neutral and basic pH conditions. The matrix, 2-amino-4-methyl-5-nitropyridine (matrix solution pH=7.1), gave good results with small proteins (up to about 12,000 Dalton). The best results with nucleic acids were obtained with 2-amino-5-nitropyridine (matrix solution pH=7.3), which was a useful matrix for the analysis of mixed base oligonucleotides smaller than 20 nucleotides in length and homopolymers of thymidine. It is also noteworthy that at neutral and basic pH the prevalence of sodium and potassium salts is high with nucleic acids. However, treatment with an ion exchange resin removes these alkali cations and yields a single molecular ion peak [1]. The resin's effectiveness is illustrated in Figure 1.

Protein analysis using basic matrices is apparently limited to relatively low molecular weight samples (<12,000 Da); oligonucleotide analysis using basic matrices was found to be subject to the same constraints of size and base composition that hold when acidic matrices are used. However, a major advantage of these newly discovered matrices is that they extend the utility of MALDI to the analysis of acid sensitive species. The MALDI analysis of a short oligonucleotide containing an acid labile dimethoxytrityl group at it's 5' terminus is shown in Figure 2 and provides a dramatic illustration of the utility of basic matrices.

References

1. E. Nordhoff, A. Ingedoh, R. Cramer, A. Overberg, B. Stahl, M. Karas, F. Hillenkamp, and P. F. Crain, *Rapid Commun. Mass Spectrom.* **6** 771-776 (1992).

Figure 1. Negative-ion mass spectrum of the octamer, d(AAATATTT) mw =2406.4 Da, using 2-amino-5-nitropyridine as the matrix. The sample was analyzed (A) before and (B) after treatment with a cation exchange resin. Salt formation was significantly reduced after treatment. The resolution (FWHM) of the major peaks in (A) and (B) was 315 and 300, respectively.

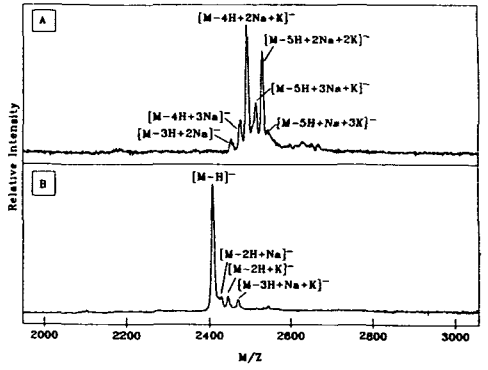

Figure 2. Negative-ion mass spectrum of the octamer, d(CCCGATCA), containing an acid labile dimethoxytrityl (DMT) group on the 5' hydroxyl group (2673.3 Da) using the matrices (A) 2,5-dihydroxybenzoic acid and (B) 2-amino-5-nitropyridine after ion exchange treatment. The resolution (FWHM) of the major peaks in (A) and (B) was 191 and 226, respectively.

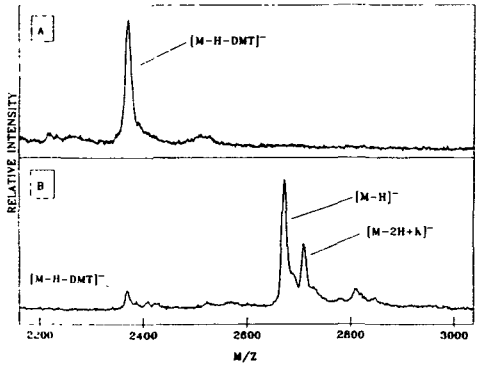

Influence of Amino Acid Gas Phase Proton Affinities on Ion Yield from Matrix Assisted Laser Desorption Ionization (MALDI) by D.R. Phillips, M. Karas, H. Ehring, and F. Hillenkamp, Institute for Medical Physics and Biophysics, University of Muenster, 4400 Muenster, FR Germany.

INTRODUCTION The lack of understanding concerning the mechanism of matrix assisted laser desorption ionization (MALDI) along with the methods increasing popularity for studying mixtures has prompted this study.

If the analyte was closely associated with matrix molecules (ions) and competing for the proton of ionization during the MALDI process, then the gas phase proton affinity of the analyte would partially determine the efficiency of analyte ionization. The idea was tested by measuring the MH^+ ion abundance of 12 amino acids. Each amino acid (a.a.) MH^+ ion abundance was measured and no correlation with gas phase proton affinities was observed. Studies were extended to investigate the presence or absence of ion suppression in a.a. mixtures. When a correlation was observed for a.a. mixtures, several peptides and proteins were selected to test for suppression in protein mixtures.

METHODS All spectra were acquired by a LAMMA 1000 time-of-flight mass spectrometer equipped to visually direct laser shots. The samples were prepared by adding 0.5 µL of each equimolar analyte (a.a., 5.7 mM; peptides, 1.0 mM; proteins 58.0 µM) to 2.5 µL of 10 g/L 2,5-dihydroxybenzoic acid (DHB) matrix. Upon drying, the sample formed a crystallin rim and an amorphous center.

In all cases, 50 spectra were averaged together which were acquired from a minimum of 5 different sights from either the crystalline rim or the amorphous center. The MH^+ ion peak height was measured from the averaged spectrum.

RESULTS Values in TABLES 1-3 correspond to molecular ion peak height in the mixture referenced as a percentage to the peak height of MH^+ when desorbed alone. E.g., the MH^+ ion signal from gln in DHB is 33.9 mV and that of arg in DHB is 80.3 mV. However, in a mixture of gln and arg the MH^+ ion signal from gln is 5.0 mV or (5.0 mV/33.9 mV)*100=15% of the expected value if MH^+ is unsuppressed and arg is (62.7 mv/80.3 mV)*100=78% as intense as when gln is absent (Table 1, bolded). The a.a.s are placed in the order of descending gas phase proton affinity[1] going from left to right and top to bottom. The upper number in each box corresponds to the amino acid listed above it and the bottom number to the amino acid to the left. With few exceptions, the smaller percentage value in the individual boxes results from the amino acid with the lower gas phase proton affinity. In all tables, the upper right portion of the table contains values obtained by sampling the DHB rim and the lower left is by sampling the center of DHB.

TABLE 1 MH^+ Ion Intensities of A.A s Compared to MH^+ Ion Intensities from A.A. Mixtures Obtained by MALDI of DHB

A.A.	Arg	His	Lys	Gln	Pro	Ala
Arg		166 128	0 84	**15** **78**	48 119	0 75
His	134 19		0 184	22 430	55 253	0 177
Lys	126 0	36 0		same mass	110 60	1 29
Gln	56 3	111 13	same mass		76 70	16 129
Pro	20 5	78 3	85 105	93 44		16 134
Ala	35 0	167 0	18 4	95 0	84 0	

Arg, arginine; his, histidine; lys, lysine; gln, glutamine; pro, proline; ala, alanine.

The peptides and proteins TABLES 2-3 were chosen for the ion suppression studies based on their differing arginine content (ß-Lipotropin fragment 1-10 (ß-lip), 0 arg/10 a.a.; neuromedin B (neur), 0 arg/10 a.a.; substance P (sub. P), 1 arg/11 a.a; dynorphin fragment 1-10 (dyn), 3 arg/10 a.a.; insulin 1 arg/51 a.a. = 2% total composition; ubiquitin 4 arg/76 a.a. = 5%; aprotonin 6 arg/58 a.a. = 10%). In each case shown, except one, the relative MH^+ ion current from the protein with the smaller percentage of arg was suppressed more than the other protein in the mixture. These results were as predicted by a simplistic model.

TABLE 2 MH^+ Ion Intensities of Peptides Compared to MH^+ Ion Intensities from Peptide Mixtures Obtained by MALDI of DHB

Peptide	Dyn	Sub. P	Neur	ß-Lip
Dyn		5 52	5 85	0 99
Sub. P	44 7		20 36	0 40
Neur	67 12	100 55		0 78
ß-Lip	55 0	43 0	63 0	

The model makes the assumption that the proton of ionization (H^+) is associated with the most basic a.a. residue (usually arg) in a protein.[2] If a protein contains multiple arg residues, then each arg has an equal chance of obtaining H^+. When two proteins are associated during the MALDI process there is a competition between them for H^+. The protein with the fewer number of arginines has the lowest probability of obtaining H^+ and hence, ion suppression is observed. Note for the mixture neuromedin B and ß-lipotropin, neuromedin contains the more basic a.a., his.

CONCLUSIONS This study shows that there is a suppression effect when using MALDI. Suppression is observed when two a.a.s are present in a sample and it correlates with the a.a.s' gas phase proton affinities. In the case of the protein mixtures, ion suppression relates to the lack of a.a.s with high gas phase proton affinities. Suppression effects are observed in both the crystalline rim and amorphous center of the droplet. Ion suppression correlating to analyte gas phase proton affinity indicates the probability of the analytes being associated at some time during the MALDI process.

TABLE 3 MH^+ Ion Intensities of Proteins Compared to MH^+ Ion Intensities from Protein Mixtures Obtained by MALDI of DHB Droplet

Protein	Aprotonin	Ubiquitin	Insulin
Aprotonin		35 70	48 88
Ubiquitin	58 105		5 69
Insulin	82 45	152 9	

Exceptions to the proposed model in the RESULTS section are expected due to variables not accounted for such as gas phase ion structure of the protein and protein solubility in matrix.

ACKNOWLEDGMENTS The Fulbright Commission.

REFERENCES 1. Z. Wu, C. Fenselau *Rapid Commun. Mass Spectrom.* 1992, *6*, 403.
2. K. Biemann, *Biomed. Environ. Mass Spectrom.* 1988, *16*, 99.

A New Matrix for MALDI Analysis of Water Insoluble Organic Molecules

M.P. Lacey and T. Keough
The Procter and Gamble Co., Miami Valley Laboratories
P.O. Box 398707, Cincinnati, OH 45239-8707

Matrix-assisted laser desorption/ionization has been used by several laboratories to analyze synthetic polymers[1-4]. Most of these polymers (PEG, PPG, PMMA) have been soluble in water, ethanol or acetone, and have been analyzed out of matrices typically used for protein analyses. Unfortunately, a number of important classes of organic molecules are water insoluble and cannot be analyzed from conventional matrices. Here we report the use of a new matrix, 5-chlorosalicylic acid, for high sensitivity MALDI analyses of water insoluble organic molecules.

We have previously been unsuccessful in analyzing water insoluble polymers from aqueous matrix solutions. A typical spectrum of PDMS 3000 analyzed from DHB is shown in Figure 1 (upper trace). The PDMS was diluted in water and mixed with an equal volume of DHB. A total of 10 picomoles was loaded onto the end of the probe, and the sample was run without washing the probe tip. When analyzed from a chloroform solution and 5-CSA, the results improve dramatically (lower trace).

We analyzed a series of PDMS standards from 5-CSA as shown in Figure 2. The measured molecular masses of these standards are about a factor of two lower than those quoted by the supplier (Table 1). Similar results were obtained with vapor phase osmometry, NMR, desorption chemical ionization mass spectrometry, supercritical fluid chromatography and electrospray ionization mass spectrometry.

Mass calibration can be somewhat more difficult than for water soluble analytes. However, small peptides and proteins can be used as internal calibrants for this application by first loading the peptide or protein from an aqueous solution containing a water soluble matrix like sinapinic acid. After that solution is thoroughly dried, an overlayer of analyte plus 5-CSA in chloroform is loaded onto the probe tip. It is possible to find regions of the tip that contain both analyte and standard. Unfortunately, this approach is somewhat irreproducible. An alternative strategy involves the use of high-mass, chloroform soluble compounds that can be mixed directly with the analyte and the matrix. We use various olestras[5], which have molecular masses greater than 1000 Da and have been well-characterized.

The role of the matrix is uncertain in the MALDI characterization of small synthetic polymers. Sensitivity for low-mass PDMS standards is somewhat enhanced relative to laser desorption without a matrix. The spectra obtained in the presence of 5-CSA show mainly MNa^+ molecular ions, while the spectra obtained without matrix show comparable levels of Na^+ and K^+ attachment. Very little fragmentation is evident. In our hands, small water soluble polymers like PEG 3300 also show similar spectra when analyzed with a matrix like DHB or without a matrix (Figure 3).

References

1. U. Bahr, A. Deppe, M. Karas and F. Hillenkamp, **Anal. Chem., 64**, 2866 (1992).
2. P.O. Danis, D.E. Karr, A. Holle, F. Meyer and C.H. Watson, Proceedings of the 40th ASMS Conference on Mass Spectrometry and Allied Topics, Washington, DC, May 31 - June 5, 1992.
3. R. Holm, M. Karas and H. Vogt, **Anal. Chem., 59**, 371 (1987).
4. D.E. Mattern and D.M. Hercules, **Anal. Chem., 57**, 2041 (1985).
5. R.A. Sanders, D.R. Gardner, M.P. Lacey and T. Keough, **JAOCS, 69**, 760 (1992).

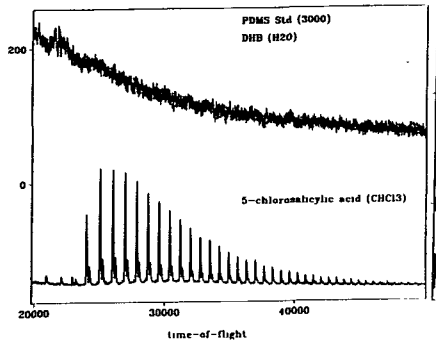

Figure 1.
PDMS 3000 standard analyzed from DHB (upper) and 5-CSA (lower)

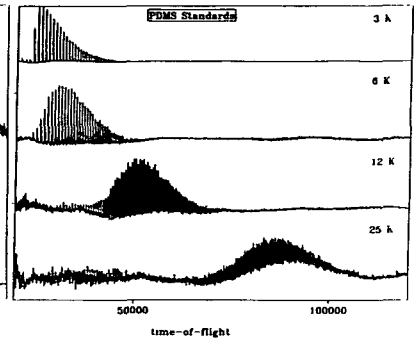

Figure 2.
Series of PDMS standards using 5-CSA matrix

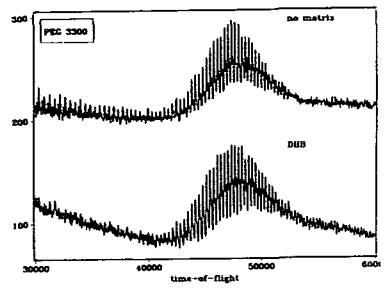

Figure 3.
PEG 3300 standard with no matrix (upper) and with DHB matrix (lower).

Table 1

Number Average Molecular Weight vs. Technique
Low Molecular Weight Polysiloxanes

Technique	DC200	Advertised MW 3K	6K	12K
NMR	1632	985	2222	6491
SFC	1833	1144	2008	5493
MALDI	1549	1303	1604	4235

Studies of oligonucleotides by matrix-assisted laser desorption time-of-flight mass spectrometry

*Kuang Jen Wu, Anna Steding and Christopher H. Becker
Molecular Physics Laboratory, SRI International, Menlo Park, CA 94025

Matrix-assisted laser desorption time-of-flight mass spectrometry has been used to produce quasimolecular ion signals from underivatized mixed-base single-stranded DNA oligomers ranging from 10 to 67 nucleotides in length with the matrix material, 3-hydroxypicolinic acid (HPA). The desorption and simultaneous ionization was by 5-ns pulsed laser at 10 to 50 mJ/cm^2, studied at 266, 308, and 355 nm. HPA is found to be very effective as a matrix material at all three wavelengths examined and demonstrates to be less destructive to the analyte molecules. An examination of the direct positive and negative mass spectra reveals three major mass peaks directly related to HPA: parent, and two features associated with the loss of stable neutrals (H_2O and HCOOH). Unlike some other matrices, HPA is not sensitive to the variation of the base components of oligonucleotides, a property desirable for this application.

Both reflecting and linear TOF-MS operating in positive and negative ion detection modes has been used. A study comparing positive and negative ions signal intensities measured by reflecting and linear TOF-MS under the same desorption condition by 355 nm laser has been performed. The results are summarized as follow.

- Strong and comparable single intensity for positive and negative ions measured by linear TOF-MS.
- Moderate negative ion signal measured by reflectron TOF-MS.
- Weak (or no) positive ion signal measured by reflectron TOF-MS.
- Linear mode demonstrates higher signal intensity and better mass resolution.

We attribute such results to the strong metastable decay of the oligonucleotide ions during the flight path. Such effect causes mass peak broadening and significant loss of signal intensity. Since both positive and negative ion signals in linear mode appear fairly comparable in strength, it thus appears that the formation of positive and negative ions is equally effective, whereas the decay of positive ions is possibly much stronger and become almost unobservable by the detector after reflected. With the advantages of better sensitivity and mass resolution, we therefore conclude that a linear TOF-MS system is better suited for the studying of DNA oligomers.

Measurements of 355 nm laser threshold energy density for desorption as a function of oligomer length has been performed by using reflecting TOF-MS. A trend of increasing threshold energy density as the size of molecules increases is observed.

** Financial support form National Institutes of Health is gratefully acknowledged.

Fig. 1

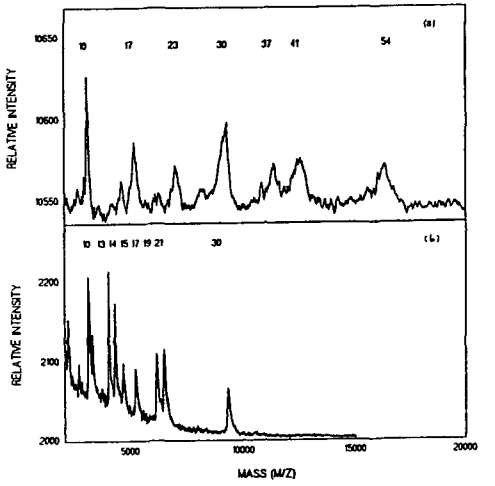

Fig. 2

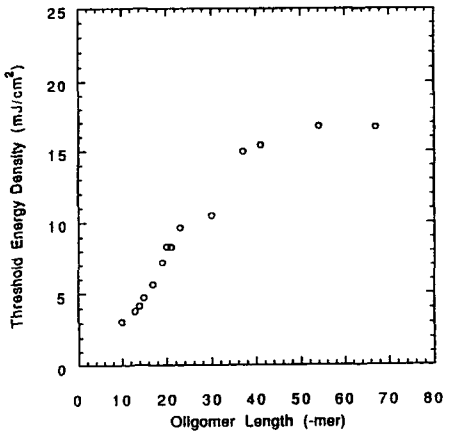

Fig. 1 Negative ion mass spectra of mixed-length oligomers (a) measured by reflecting TOF-MS and (b) measured by linear TOF-MS.

Fig. 2 Threshold energy density of 355 nm photon for desorption as a function of mixed-base oligomer detected by reflecting TOF-MS. Sizes ranging from 10 to 67-mer were measured.

CLEAVAGE OF INTERCHAIN DISULFIDE BONDS FOLLOWING MATRIX-ASSISTED LASER DESORPTION

J. Zhou[1], W. Ens[1], N. Poppe-Schriemer[1,2], K. G. Standing[1] and J. B. Westmore[2]
[1]Physics and [2]Chemistry Departments, University of Manitoba, Winnipeg, Manitoba,Canada R3T 2N2

The assignment of the positions of disulfide bonds in a protein is an important part of the determination of its primary structure. Recently, Bean and Carr examined a number of peptides of masses up to ~2000 u containing single interchain disulfide bridges [1] with tandem mass spectrometry. They observed cleavage at the bridges with retention of zero, one or two sulfurs on the charged fragment. With matrix-assisted laser desorption, we have investigated the cleavage of interchain disulfide bridges of insulin and a digest of tyr-somatostatin, containing two and one disulfide bond(s) respectively.

Targets were prepared from bovine insulin or from a tryptic digest of tyr-somatostatin (Sigma) in matrices of sinapinic acid or α-cyano-4-hydroxycinnamic acid (4HCCA). The digestion of tyr-somatostatin was performed at room temperature for a few minutes. No purification was made of the digestion products. A few μL of sample solution (~0.4 g/L insulin in 0.1% TFA or ~0.5 g/L digested tyr-somatostatin in solution) were mixed with 10-20 μL matrix solution (10g/L in 1:3 water:acetonitrile) and dropped onto a 1 cm diameter etched silver foil, then dried in air.

The measurements were carried out in our reflecting time-of-flight spectrometer (TOF II) [2]. Ions were desorbed from the target by a nitrogen laser (Laser Science ND337) at a wavelength of 337 nm and a power density (~10^6 W/cm^2) slightly above threshold. In the reflecting mode, the mirror V_m is set at higher potential than the target. Undissociated ions as well as charged daughters are reflected by the mirror. A convenient method of measuring the mass of a daughter ion is to reduce the mirror voltage to a value V_m^* such that the flight time of the daughter is the same as that observed for its parent with mirror voltage V_m. The ratio of daughter ion mass m* to parent ion mass m is then given directly by the ratio of the measured voltages, i.e. $m^*/m=V^*/V$ [2].

Figure 1a shows the reflected spectrum of negative ions for insulin. A- and B-chain daughter ions are observed in the spectrum. Some structure is apparent in the peaks and is seen clearly on an expanded scale in figure 1b. The negative daughter ion spectrum, as shown in figure 2, was then measured with a reduced mirror voltage; a considerable improvement in resolution is obtained. Masses of the individual components were determined by varying the mirror voltage as described above. Results are clearly consistent with decay into A- and B- chain daughter ions with retention of zero, one, two or three sulfurs from the interchain bridges, as represented by A_0, A_1, A_2 and A_3 for A- chain daughters, B_0, B_1, B_2 and B_3 for B- chain daughters. There is one intrachain disulfide bridge in tyr-somatostatin (M.W.=1801.1 u) between Cys_4 and Cys_{15}. A tryptic digestion is expected to cleave at Lys_5 and Lys_{10}, but only the latter is observed, yielding a peptide with two chains (1261.6 u and 556.2 u) linked by a single disulfide bond. Figure 3 shows the negative daughter ion spectrum of digested tyr-somatostatin. Calibration results correspond to zero or one sulfur on a B-chain daughter.

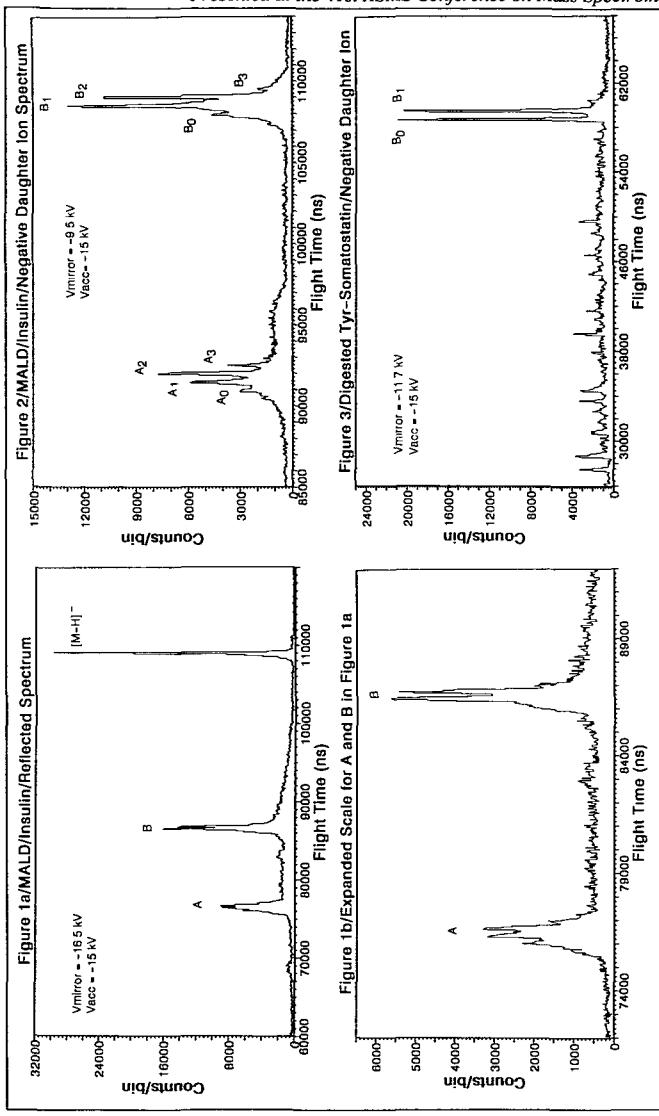

The cleavage of interchain disulfide bridges of insulin and digested tyr-somatostatin has been observed in the negative daughter ion spectra from matrix-assisted laser desorption. The $[M-H]^-$ molecular ion decays into negative A and B chain, or only B chain, daughters with various numbers of sulfurs attached. The observation may provide a simple analytical method for determining interchain disulfide bridges in peptides or proteins.

[1] M. F. Bean and S. A. Carr, Anal. Biochem. 201 (1992) 216.
[2] X. Tang, R. Beavis, W. Ens, F. Lafortune, B. Schueler and K. G. Standing, Int. J. Mass Spectrum. Ion Processes 85 (1988) 43.

ANALYSIS OF MYCOTOXINS FROM *AMANITA PHALLOIDES* BY MATRIX ASSISTED LASER DESORPTION MASS SPECTROMETRY

L. Szente[a], R. Gijbels[b], X. Tang, A. Vertes*
Department of Chemistry, The George Washington University
Washington, DC 20052
[a]Cyclolab, P.O.Box 435, H-1525 Budapest, Hungary
[b]Department of Chemistry, University of Antwerp (UIA)
B-2610 Wilrijk, Belgium

The three most toxic components of *Amanita Phalloides* (green death cap) are usually analyzed by high performance liquid chromatography or radioimmunoassay [1]. Recently, electrokinetic capillary chromatography was used to accurately identify other mycotoxins [2]. Matrix-assisted laser desorption mass spectrometry (MALD-MS) has made the rapid and accurate determination of small peptides feasible [3].

Three cyclic peptides, α-amanitin (inhibitor of RNA polymerase II), β-amanitin and phalloidin (inhibitor of cytoskeletal function) were measured using MALD-MS. 337 nm nitrogen laser excitation of five matrices (sinapinic acid: SA; α-cyano-4-hydroxycinnamic acid: CHCA; 2,5-dihydroxybenzoic acid: DHB; 2-(4'-hydroxyazobenzene)-benzoic acid: HABA; 6-aza-2-thiothymine: ATT) provided molecular ions of all three toxins. MALD spectra were simple and straightforward to interpret. α-amanitin showed peaks at $[M+H]^+$ (m/z 920), $[M - OH]^+$ (m/z 903), and $[M+Na]^+$ (m/z 942). Molecular adduct ions $[M+M' - OH]^+$ (M': matrix molecule) (m/z 1046) also were observed. DHB, CHCA and ATT usually produced good quality spectra.

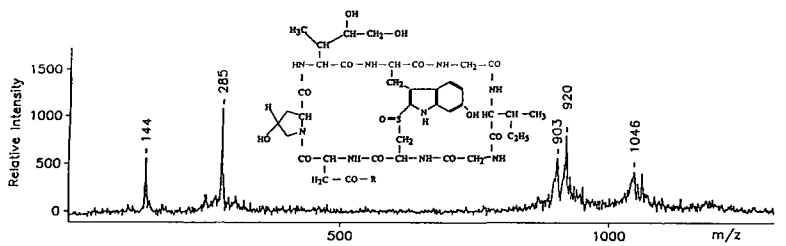

Figure 1. MALD-MS of α-amanitin in ATT matrix and its structural formula. $R=NH_2$ for α-amanitin; R=OH for β-amanitin.

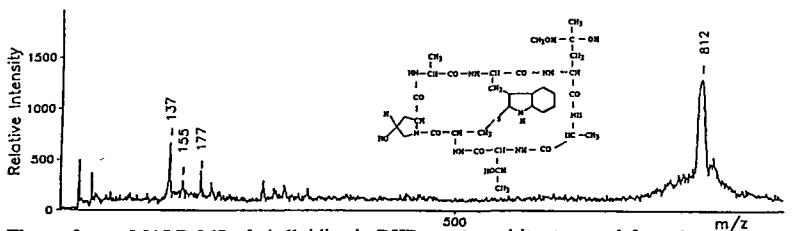

Figure 2. MALD-MS of phalloidine in DHB matrix and its structural formula.

Both protonated and sodiated peptide ions were present in spectra taken in ATT and DHB matrices (Figs. 1 and 2). It is interesting to note that MALD-MS *did* produce fragment ions in some cases. The m/z 903 ion in Figure 1 corresponds to a protonated molecular ion after the loss of an OH group. Similar loss of small functional groups (NO_2, Dns) in MALD was reported earlier [4]. Table 1 summarizes the most abundant ions of the three toxins in ATT and in DHB.

Toxins	Analyte ions m/z	
	ATT matrix	DHB matrix
α-amanitin	903: $MH-OH^+$; 920: MH^+; 942: MNa^+; 1046: $MM'-OH^+$	885: $MH-2OH^+$ (?); 903: $MH-OH^+$; 920: MH^+;
β-amanitin	888: $MH-OH^+$; 905: MH^+; 927: MNa^+	905: MH^+
phalloidin	773: $MH-OH^+$; 790: MH^+; 812: MNa^+	812: MNa^+

Table 1.

Preliminary experiments were carried out to detect α-amanitin in human serum. The major serum protein components like albumin and different globulins were removed from the α-amanitin spiked serum by centrifugal ultrafiltration (Millipore, Ultrafree-MC, 30,000 NMWL). Salts and other low-molecular-weight components (MW < 30,000 Da) accumulated in the filtrate collection tube. The 1μL filtrate, 1μL 1M HCl and 5μL 0.05M DHB matrix solutions were directly applied to the probe tip. The dried deposit was washed by immersing the probe tip into distilled water to remove any water-soluble contaminants, particularly Na^+ ions. α-amanitin ions were detected but the spectrum quality was poor. The sample preparation technique needs further refinement.

Although the specificity of the mass spectrometric determination is better than that of other methods, detection limits are generally higher and quantitation remains difficult.

Support:
This work was supported by the George Washington University Facilitating Fund.

References:

1. F. Jehl, C. Gallion, P. Birckel, A. Jaeger, F. Flesch, R. Minck, Anal. Biochem., **149** (1985) 35-42.
2. R.D. Holland, M.J. Sepaniak, Anal. Chem., **65** (1993) 1140-1146.
3. A. Vertes, R. Gijbels, In: Laser Ionization Mass Analysis, A. Vertes, R. Gijbels and F. Adams (eds), Wiley & Sons, New York, **1993**, pp. 127-175.
4. A. Vertes, L. Balazs, R. Gijbels, Rapid. Commun. Mass Spectrom., **4** (1990) 263-266.

ANTISENSE DNA OLIGONUCLEOTIDES II: THE USE OF MATRIX-ASSISTED LASER DESORPTION IONIZATION MASS SPECTROMETRY FOR THE COMPLETE SEQUENCE VERIFICATION OF METHYLPHOSPHONATE OLIGODEOXYRIBONUCLEOTIDES

Thomas Keough, Timothy R. Baker, Roy L.M. Dobson and Martin P. Lacey, The Procter and Gamble Co., Miami Valley Laboratories, PO Box 398707, Cincinnati, OH 45239-8707.
Timothy A. Riley, Jody A. Hasselfield and P. Eric Hesselberth, JBL Scientific, Inc., 277 Granada Drive, San Luis Obisbo, CA 93401-5809.

Antisense therapy uses modified oligonucleotides, like methylphosphonate oligodeoxyribonucleotides, to bind to messenger RNA, thereby inhibiting the synthesis of specific proteins. The specificity needed to inhibit a particular protein synthesis is thought to require an oligonucleotide 12 to 18 bases in length. Of course, the exact oligonucleotide sequence affects the highly specific binding of these materials, and sequence verification is needed prior to biological testing. A novel matrix-assisted laser desorption ionization (MALDI) approach for complete sequence verification of synthetic methylphosphonate oligodeoxyribonucleotides is reported.

The UV-MALDI mass spectrum obtained from 5 pmols of a representative methylphosphonate oligonucleotide is given in figure 1 (Vestec VT 2000 mass spectrometer, frequency tripled Nd:YAG (355 nm), sinapinic acid matrix, positive ions). Methylphosphonate oligonucleotide MALDI spectra are dominated by the MH+ molecular ions. Mass measurement accuracy of +/- 1 Da is typically achieved, and the mass resolution is >200 (FWHM). The spectra are all quite simple; no fragmentation is observed. Unlike phosphodiester oligonucleotides, the quality of these spectra appears to be independent of base composition. All of the methylphosphonate oligonucleotides examined to date have given spectra of comparable quality to the spectrum given in Fig. 1.

Obviously, the MALDI mass spectra of purified methylphosphonate oligonucleotides exhibit no fragmentation and no structural information. However, detailed structural information can be obtained by direct analysis of the crude synthetic products formed in these solid-phase syntheses. This results because the coupling yield for each added nucleotide is only 96 to 99%. The remaining 1 to 4% that has not undergone coupling in each cycle, the failure sequence, is capped with acetic anhydride to simplify final product purification. Capping also prevents subsequent reaction to produce "mixed" sequences, which would preclude the use of MALDI for this application. After the final cycle, the desired product and the failure sequence mixture are cleaved from the resin. This cleavage procedure also removes the 5'-protecting group from the final product, and the acetate capping groups from each failure sequence that has been formed.

The first step in the MALDI sequence verification involves direct analysis of the crude synthetic mixture. The spectrum obtained from analysis of a crude synthetic 15-mer is given in Fig. 2. An intense molecular ion is observed for the desired final product (1-15)+, where nucleotide 1 is defined as the 3'-end of the molecule. The spectrum also exhibits several abundant series of ions. The most intense corresponds to the failure sequences (1-14)+, (1-13)+, etc. The oligonucleotide sequence is simply established by measuring the mass differences between adjacent members in this series, and comparing these values with the known masses of the four methylphosphonate nucleotides used in the synthesis. If one measures from the (1-15)+ molecular ion toward lower mass, the reading direction is from the 5'-end to the 3'-end as determined by the synthetic procedure. In this particular example, 11 of the 15 nucleotides were easily established. However, the 4 nucleotides near the 3'-end were not observed.

The strategy for obtaining the remaining portion of the sequence can be understood by re-examination of the MALDI spectrum obtained from the crude synthetic mixture. An expanded view of a portion of that spectrum is given in Fig. 3. Each failure sequence molecular ion, the top series of ions, is accompanied by a satellite peak weighing about 78 Da more. These peaks, indicated with asterisks, could be formed by non-specific base-catalyzed hydrolysis during the resin cleavage step. If this interpretation is correct, a

WP 149
Code

complementary set of products containing the 5'-end of the molecule should also be produced. In total, four products should be produced for each hydrolyzed phosphonate group. Re-examination of the MALDI spectrum given in Fig. 3 reveals that indeed, there are many clusters of four ions evident in the spectrum. The failure sequence ions provide information about the 5'-end of the molecule. The complementary set of hydrolysis products, lower series, provide information about the 3'-end of the molecule.

Complete sequence verification is possible by combined use of the failure sequence ions and hydrolysis product ions. However, some crude synthetic mixtures have shown relatively low levels of the complementary hydrolysis product ions. Fortunately, they can be produced rather easily when needed. This is illustrated by the spectrum in Fig. 4, which was obtained by intentionally hydrolyzing a purified methylphosphonate 15-mer in 3% ammonium hydroxide at 50C for 1 hr. The starting 15-mer was highly purified. It did not contain either hydrolysis product ions or failure sequence molecular ions. After hydrolysis, the resulting spectrum reveals all of the complementary information needed to complete the sequence assignment.

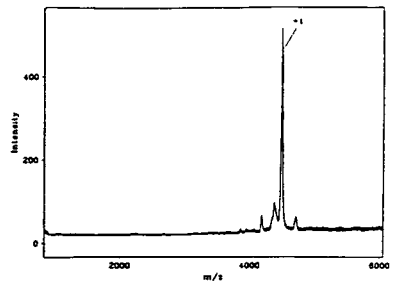

Fig. 1: MALDI mass spectrum of a purified 15-mer.

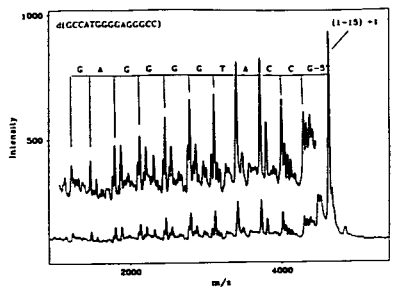

Fig. 2: MALDI mass spectrum of a crude synthetic 15-mer.

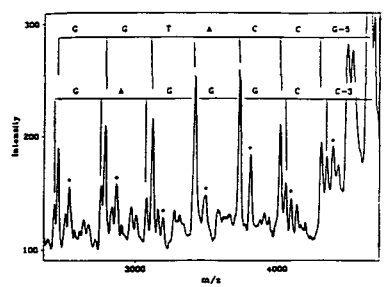

Fig. 3: Expanded view of a portion of the MALDI spectrum of the crude synthetic 15-mer.

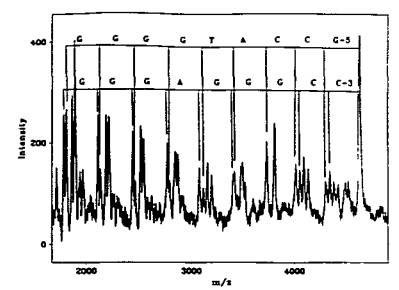

Fig. 4: MALDI mass spectrum of a purified methylphosphonate oligonucleotide after base-catalyzed hydrolysis.

Angular- and Time-resolved Intensity Profiles of Ejected MALDI Ions

V. Bökelmann, R. Kaufmann, *B. Spengler
Inst. of Laser Medicine, University of Düsseldorf, Moorenstr. 5, D-4000 Düsseldorf, Germany

A new time-of-flight instrument was developed for the investigation of spatial and temporal characteristics of the ejected ion jet [1-3] in matrix-assisted laser desorption ionization (MALDI). It consists of a cylindrical vacuum chamber with a fixed laser beam path, focused on to a tiltable sample holder which is located in the center of the apparatus (Figure 1). Two individual Wiley-McLaren-type TOF systems equipped with post-accelerating detectors are placed in the vacuum chamber, one in a fixed reference position and the other rotatable around the sample. TOF system and sample holder are positioned by stepper motors. All surfaces outside the TOF systems are electrically grounded in order to allow field-free ion propagation.

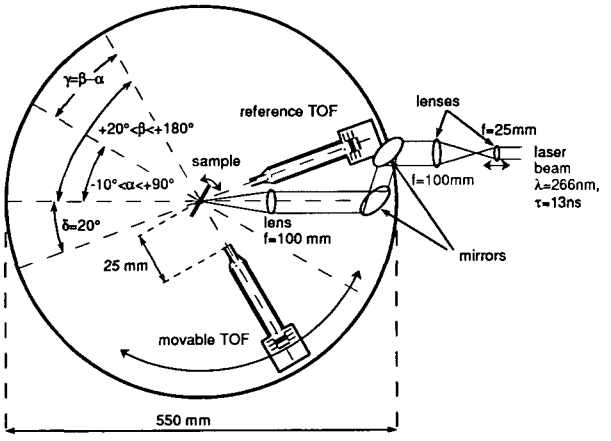

Figure 1: Scheme of the time-of-flight instrument for angular- and time-resolved ion intensity measurements.

In order to investigate the characteristics of the ion jet, the kinetics and spatial distributions of the predominant matrix ions have been analysed. Due to the special construction of the time-of-flight analysers initial velocity distributions of both, the total ion pulse (acceleration voltages turned off) and of mass separated ions (acceleration voltages turned on) could be monitored. Single crystals (size up to 3*5*15 mm) were used as samples in order to provide a topologically well-defined surface.

In the case of 2,5-dihydroxybenzoic acid (DHB) used as a matrix, the most intense ion of the dehydrated parent molecule at M=137 shows an angular dependent intensity distribution $I \sim \cos^{2.39}$ at a focus diameter of 150 µm under threshold conditions (Figure 2). The angle of the laser beam with respect to the surface normal was fixed at 20°. Ion velocities of the dehydrated parent molecule have been measured in the range of 1700 m/s (ion ejection angle 0° to surface normal) to 1300 m/s (ion ejection angle 70° to surface normal). Corresponding kinetic energies were in the range of 2.4 eV to 1.25 eV (Figure 3). Kinetic energies of the dimer ion M=273 were considerably lower in the forward direction, suggesting that the ion jet is mainly energized by the (most abundant) monomer ion (M=137).

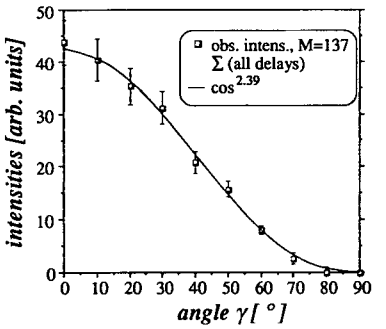

Figure 2: Angular intensity distribution of the dehydrated parent ion of DHB obtained fron a single crystal.

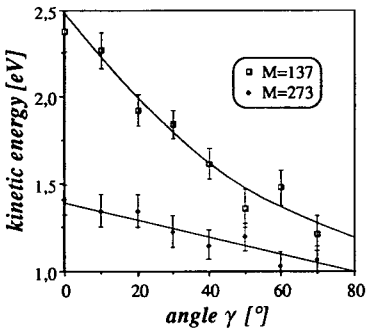

Figure 3: Mean kinetic energies of ions from a DHB single crystal as a function of the angle γ between sample surface normal and TOF axis

It has been observed that both, velocity distributions and angular distributions are strongly dependent on laser irradiance and size of the laser focus. Under focused conditions (focus diameter ≈80 µm) velocities of the dehydrated parent molecular ion range from 2700 m/s (threshold irradiance) to 7400 m/s (5.6 times threshold irradiance). At high irradiances angular distributions are significantly narrower compared to threshold conditions The obtained results support the idea that a nozzle-beam-like supersonic jet is formed by laser irradiation, rather than an effusive one. The spatial and temporal characteristics which are determined by source pressure and size of the nozzle in classical molecular beam systems, seem to be determined by laser irradiance and focus diameter in MALDI systems.

REFERENCES

/1/ R. C. Beavis, B. T. Chait, *Chem. Phys. Lett.*, **5** (1991), 378.
/2/ A. Verentchikov, W. Ens, J. Martens, K. G. Standing, Proceedings of the 40th ASMS Conference, Washington, DC, 1992, pp 1927-1928.
/3/ Y. Pan, R. J. Cotter, *Org. Mass Spectr.*, **27** (1992), 3.

An External Ion Source FTMS for the Analysis of High Molecular Weight Biomolecules

*Brian E. Winger, Bruce L. Becker, Richard E. Hein, James A. Haas and Joseph E. Campana
Extrel FTMS, Millipore Corporation, 6416 Schroeder Rd., Madison, WI 53711-2424.

Ion formation external to the superconducting magnet with subsequent injection through the fringing magnetic field, first demonstrated by McIver et. al., allows for the use of a variety of ionization sources without degrading the high-performance characteristics, i.e., ultra-high resolution and accurate mass measurement, of Fourier transform mass spectrometry (FTMS). Recent demonstrations of coupling FTMS with ionization sources such as electrospray (ESI), continuous-flow fast atom bombardment (FAB), glow discharge and matrix-assisted laser desorption (MALDI) have increased the acceptance of FTMS. Specifically with regards to ESI, the detection of the bovine albumin dimer (M_r 132,532) and resolving powers in excess of 1.0 x 10^6 for bovine ubiquitin have demonstrated the potential of ESI-FTMS for the analysis and subsequent sequencing of biological molecules.

Figure 1 is an illustration of the external source FT/MS system. The design of the ionization source chamber allows for easy interchangeability between EI/CI, FAB and ESI and other ionization sources. The ion injection optics are based upon an acceleration/deceleration electrostatic injection system. An acceleration potential of ~ 2 kV, although voltages in the range of 50 to 2500 have been used succesfully, is used to guide the externally-generated ion beam into the magnetic field. The FT/MS is a commercially available Extrel FTMS Model 2001 based on a 3 Tesla superconducting magnet. All instrument control and data acquisition is accomplished with the Odyssey Data Station.

Polymers are easily ionized by using ESI. Figure 2 is the ESI mass spectrum of a 20 mM solution (MeOH and 0.1% NaBr) of poly(propylene glycol) (PPG) whose weight average molecular weight was listed as 725. The distribution shown here is the sodiated form of PPG. By using a feature of the Odyssey data analysis software, the calculated weight average molecular weight of the sodiated polymer is 709.467 and 686.972 for the nascent polymer.

The data illustrated in Figure 3 of angiotensin II represents our first result of ESI for peptides. The peptide concentration was10 mM and was dissolved in 1:1 MeOH:H_2O with 5% HOAc. The ESI mass spectrum of angiotensin II exhibits an intense monoisotopic $[M+H]^+$ ion at 1046.550, where the calculated value is 1046.542, resulting in an error of 7.6 ppm without using an internal mass reference.

These preliminary results indicate the feasibility of our external source FTMS design, and further developments to optimize sensitivity and speed of acquisition are currently underway.

External Source FT/MS System

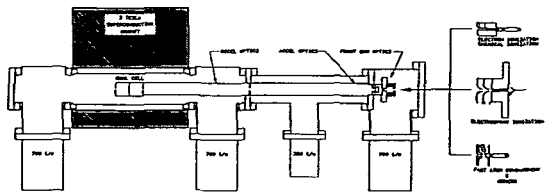

Figure 1

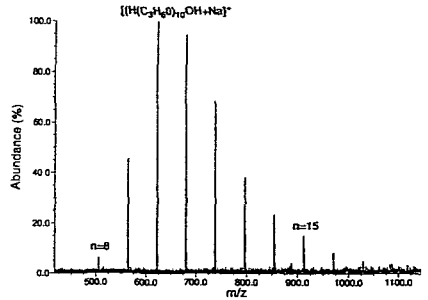

Figure 2

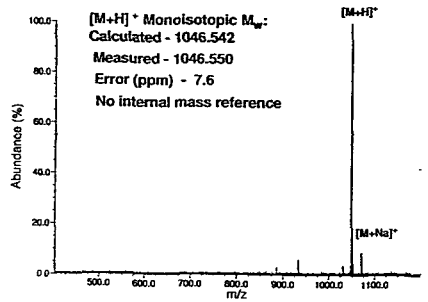

Figure 3

Storage Tandem MS — Nucleophilic Substitutions in the Gas Phase

M. Stöckli, S. König, H. Reinhard, M. Sägesser, P. Kofel and U. P. Schlunegger
Institute of Organic Chemistry, University of Bern, Freiestr. 3, CH-3012 Bern, Switzerland

A purpose built quadrupole, quistor, quadrupole tandem mass spectrometer [1], enhanced by a personal computer equipped with a data acquisition board [2] was used for the experiments. Primary ions were generated in the differentially pumped external ion source under EI, resp. self-CI conditions, mass selected by a first quadrupole mass filter and injected into a quistor. After a variable storage period in the quistor for reaction the product ions were extracted and analysed by a second quadrupole mass filter. For the QRE-experiments (quistor resonant excitation) a supplementary ac voltage of low amplitude (app. 1 V) was applied to one end-cap electrode of the quistor.

The reaction of CH_4^+ with methane was studied for calibration of the gas pressure inside the quistor volume and subsequently for the investigation of the influence of the kinetic ion energy on product ion distribution [3]. A pressure differential of 35 between quistor volume and quistor housing was determined by comparison of the observed rate constant to the literature value of $1.13\ 10^{-9}\ cm^3 mol.^{-1} s^{-1}$. Unselective increase in the kinetic ion energy by increasing the trapping potential as well as selective increase of kinetic energy using the QRE-technique results in the opening of endothermic reaction channels. The kinetic ion energies in the range of 1-2 eV were monitored as a function of the ratio $I_{m/z\ 27} / I_{m/z\ 29}$ [4].

In an H/D exchange study of the ion / molecule reaction between protonated acetaldehyde and methanol the origin of the protons in the reaction products was determined. Besides the adduct ion and formation of methanol cluster ions [5], methylated acetaldehyde ions could be detected, resulting from water cleavage of the protonated acetaldehyde - methanol adduct [6]. The provenience of the hydrogen atoms in the cleaved water molecule could be established in ion / molecule reactions of labelled reagents (d_1-, d_3-, d_4-methanol and d_4-acetaldehyde) with undeuterated counterparts. A reaction rate constant of $1.0\ 10^{-10}\ cm^3 mol.^{-1} s^{-1}$ for the formation of the methylated acetaldehyde ion and a H/D transfer rate constant of $4\ 10^{-10}\ cm^3 mol.^{-1} s^{-1}$ for the hydrogen directly bound to the C1 atom of the carbonyl group could be determined. The hydrogen atoms cleaved with the water molecule were found to be those that are directly bound to oxygen atoms in the intermediate protonated acetaldehyde - methanol adduct (see figure).

References:
[1] P. Kofel, H. Reinhard, U.P. Schlunegger, *Organic Mass Spectrom.*, 1991, 26, 463.
[2] M. Sägesser, Thesis, Bern, 1992.
[3] H. Reinhard, Thesis, Bern, 1992.
[4] G. Lawson, R.F. Bonner, R.E. Mather, J.F.J. Todd, R.E. March, *J. Chem. Soc. Farad. Trans.*, 1976, 72, 545.
[5] J.C. Kleingeld, N.M.M. Nibbering, *Org. Mass Spectrom.*, 1982, 3, 136.
[6] G.G. Dolnikowsky, T.G. Heath, J.T. Watson, J.H. Scrives, C.H. Rolando, *J. Am. Soc. Mass Spectrom.*, 1990, 1, 481.

Support from the Swiss National Science Foundation is gratefully acknowledged.

Reaction scheme for production of methylated acetaldehyde

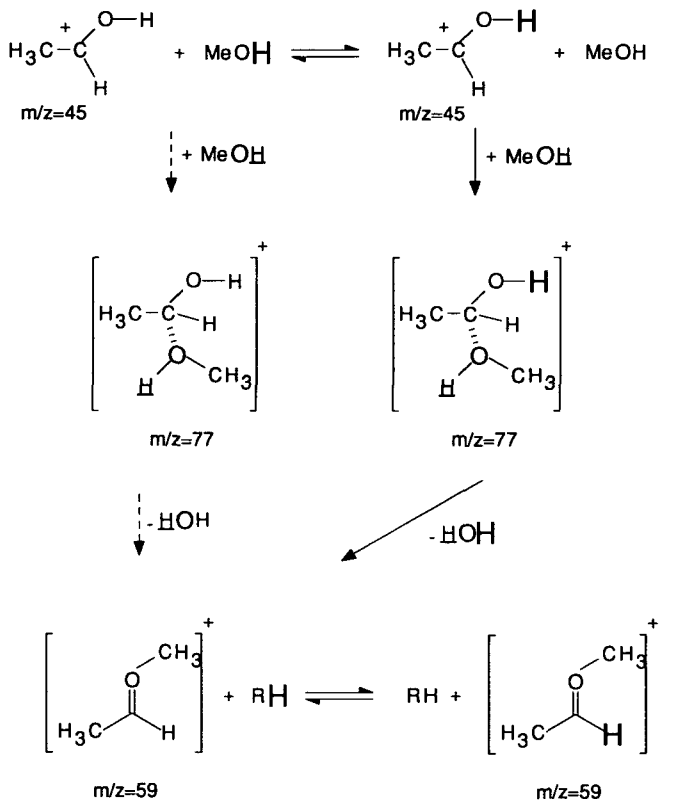

THE EFFECT OF Z-DIRECTION STRETCHED GEOMETRY ON ION INJECTION INTO A QUADRUPOLE ION TRAP MASS SPECTROMETER. Habibi-Goudarzi, S. and McLuckey, S.A., Analytical Chemistry Division, Oak Ridge National Laboratory, Oak Ridge, TN 37831-6365.

Precise electrode spacing is one of the criteria for producing a pure quadrupole potential field in a Paul type ion trap. Symmetrical alterations in the end cap spacing introduces fourth-order distortions (e.g. octapole), and asymmetrical alteration, third-order distortions (e.g hexapole).[1] It has been shown that these higher-order fields may be controlled advantageously.[2] The theoretical and experimental treatments of non-linear fields have not addressed their effects (if any) on the injection of ions into an ion trap. We have performed some preliminary experiments with a "quadrupole" ion-trap mass spectrometer (Finnigan ITMS) in which the trap geometry has been changed via symmetrical stretching in the z-direction This is accomplished by simply changing the length of the spacers which separate the ring electrode from the end caps. Three geometries are reported here and they are: (1) "Pure" quadrupole geometry z_o=0.7071 cm, (2) Finnigan geometry z_o=0.7884 cm, (3) S62 geometry z_o=0 8697. Note that the end cap electrode surfaces were not altered. Therefore, geometries two and three should have strong fourth-order distortions. Ions are formed and injected into the ion trap via the atmospheric sampling glow discharge ionization source (ASGDI) as described previously [3] A series of mass spectra were recorded using DNT and TNT as model compounds. An obvious observation was the mass shift in the spectra which was predicted using Knight's equation[4]: $q_z = -8eV/m(r_o^2 + 2z_o^2)\Omega^2$ In terms of observed mass, m_1, which is proportional to the rf amplitude (V) needed to eject that ion at q_{eject}=0 91 in the mass selective instability mode (a=0), a simple expression $m_2=m_1(d_2/d_1)$ is derived where $d_i=(r_o^2 + 2z_o^2)$ corresponds to the appropriate geometry. For example, TNT with m/z 227 is observed at 201,226, and 257 in geometries 1-3 respectively. Note: Axial modulation is not used and the calculated m/z values could have an error of about 3 u. Injection efficiencies are affected in an m/z dependent fashion The relatively limited set of results reported here indicate that the pure quadrupole trap has a higher injection efficiency for the TNT molecular anion than the Finnigan trap (by a factor of about four; Fig.1). Separate experiments illustrated nearly the same injection efficiency for the DNT molecular anion. The S62 geometry has consistently lower injection efficiency, by at least one order of magnitude, as compared to that in the pure trap. These studies indicate that further stretching of the already stretched Finnigan geometry will provide no benefit in ion injection efficiency and that there appears to be no benefit of the present stretched geometry over the "pure" ion trap in this regard

Since the overall performance of a given geometry is needed to determine whether one should be selected over another, characteristics other than injection efficiency were studied. In the case of MS^n experiments, the larger the fraction of fragment-ions collected leads to higher values of n. MS/MS efficiencies were recorded for the three geometries and the values varied significantly from one geometry to another. In the case of TNT, an efficiency in the range of 50 to 80% was observed in the Finnigan geometry (Fig. 2). This performance was at least a factor of two better than the pure trap and about the same as that in the S62 geometry. All three ion trap configurations had higher MS/MS efficiencies for the DNT molecular ion (m/z 182) than that for TNT. But the "pure" trap geometry again had lower MS/MS efficiency than that of the other two geometries. Another factor considered was mass resolution: $R=m/\Delta m$ where Δm is the full width at half maximum (FWHM). The DNT molecular anion peak was arbitrarily chosen for this purpose which had R values of 250, 320, and 310 for geometries 1-3, respectively. Axial modulation improves the resolution and peak intensity up to a factor of two in the case of the two stretched geometries, however, in the pure quadrupole trap, both

"The submitted manuscript has been authored by a contractor of the U.S. Government under contract No. DE-AC05-84OR21400. Accordingly, the U.S. Government retains a nonexclusive, royalty-free license to publish or reproduce the published form of this contribution, or allow others to do so for U.S. Government purposes."

R and peak intensity are reduced by about 10 to 15 percent. Present experiments indicate that the trade-off between injection and MS/MS efficiencies and resolution need to be examined for geometries in between cases 1 and 2, specially with ions of larger molecules.

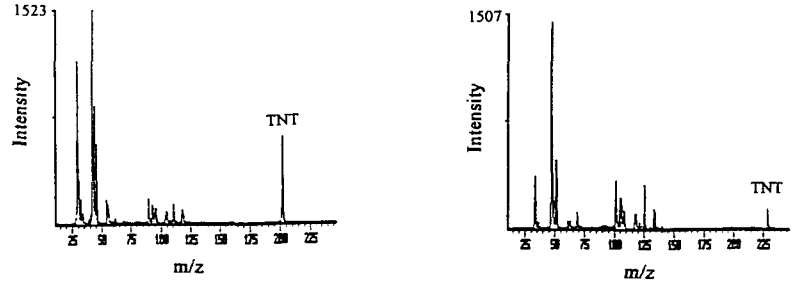

Figure 1. Atmospheric-sampling glow discharge mass spectra of TNT (5 ms injection time) recorded using (from left to right) the "pure" and the Finnigan traps.

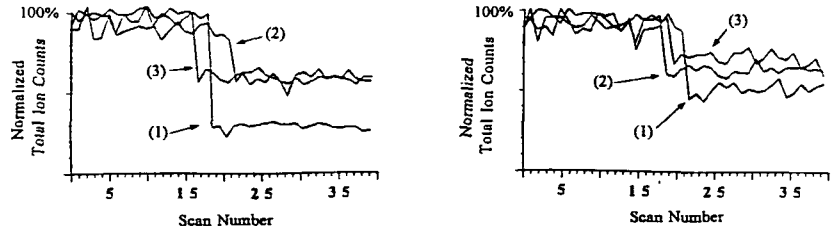

Figure 2. Normalized total ion counts recorded before and after collision-induced dissociation of the TNT anion (left diagram) using (1) the "pure" trap with 30% MS/MS efficiency, (2) the Finnigan trap 67%, and (3) the S62 trap 62% compared with the counts recorded for the DNT anion in (1) 56%, (2) 69%, and (3) 74%.

References:

1 Dawson, P H and Whetten, N.R. Int. J Mass Spectrom. Ion Phys. **2**(1969)45
2. Franzen, J Int. J. Mass Spectrom. Ion Proc. **106**(1991)63.
3. McLuckey, S.A.; Glish, G.L , Asano, K.G. Anal. Chim. Acta **225**(1989)25.
4. Knight, R.D. Int. J. Mass Spectrom. Ion Phys. **51**(1983)127.

Credit:

Research sponsored by the U.S. Department of Energy, Office of Safeguards and Security, under contract DE-AC05-84OR21400 with Martin Marietta Energy Systems, Inc.

Deflection of Laser-Produced Ions in Laser-Desorption/FTMS

Nick A. Thornburg, Ihab M. Abdelrehim, Steven H. Pullins, and *Donald P. Land,
Department of Chemistry, University of California, Davis, CA 95616.

The presence of even small quantities of alkali metals can prevent LD/FTMS studies of monolayer organic adsorbates and surface chemistry. This is because alkalis have low heats of vaporization as well as low heats of ionization. Thus, vast quantities of ions are produced directly by the laser during desorption, thereby filling the cell and making detection of post-ionized organics impossible. However, alkali promotion in catalysis is an important industrial technique which is poorly understood, and one which we would very much like to study using LITD/FTMS. Results are presented here for laser-induced thermal desorption from oxidized Ti foils using a new method for deflection of the laser-produced ions using a static electric potential outside the cell. Desorbed material must pass through this potential on the way (1 cm) to an aperture (1 cm diameter) into the FTMS analyzer cell, as depicted in Fig. 1. Deflected ions do not pass through the aperture into the cell, but neutrals are unaffected and can be postionized (with an electron beam inside the cell) and analyzed, even with significant amounts of K present on the surface.

Fig. 2 compares two laser-desorption spectra from Ti foil surfaces with less than 1% of a monolayer of K plus approximately one monolayer of carbonaceous material. The first spectrum uses no deflection voltage and shows only laser ionized K^+ (m/z 39) and K^{++}. The second spectrum utilizes a 600V deflection potential and does not show K^+, but does exhibit the ions due to adsorbed organics, such as benzene (m/z 78, 77, 52, 51, 50), ethylene (m/z 28, 27, 26), and other, as yet unidentified species. The peak at mass 39 in spectrum (b) is not due to K+ (m/z 38.96) but occurs at m/z 39.02, correct for $C_3H_3^+$ (a common fragment for virtually all hydrocarbons). This uses the high resolution capabilities of the FTMS to obtain information about elemental composition of unknown peaks.

To further characterize the deflection of laser-produced ions, the Ti sample was deliberately ablated to provide a renewable, consistent source of directly formed ions. Three variables are manipulated during these experiments: deflection voltage, laser energy, and sample-to-aperture distance. Deflection plate voltages were varied from 0 to +500 V on one plate and 0 to -500 V on the second. For a sample-to-aperture distance of 1 cm and laser power density 5% above threshhold for Ti ablation, laser produced ions were completely deflected using a minimum of 500V (±250V). When the laser energy was increased an additional 6% above the threshold for ablation, the voltages placed on the ion deflection plates had to be increased from ± 50 V to ± 200 V for complete ion deflection at a distance of 1.5 cm. Thus, as expected, lower ion deflection plate voltages were necessary to deflect ions when the sample was moved away from the cell aperture.

This technique, therefore, allows the detection of postionized species in the presence of easily ionized coadsorbates by deflecting ions formed externally to the cell so that they do not pass through an aperture. This is important for studies of alkali promoted catalysts, as well as environmental samples or samples exposed to biological fluids.

Figure 1

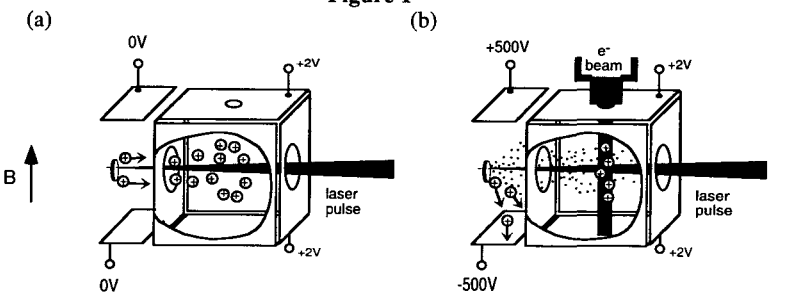

Above is a depiction of the cubic (5 cm) ICR cell with ion deflection plates. (a) Ions formed directly during desorption flood the analyzer cell, preventing detection of postionized neutrals desorbed. (b) Deflection of the laser-formed ions by a DC voltage on external deflection plates allows postionization and detection of desorbed neutrals

Figure 2

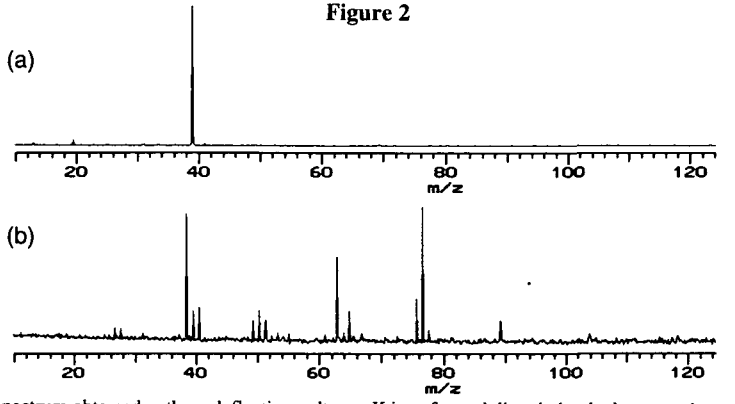

(a) Spectrum obtained with no deflection voltage. K ions formed directly by the laser are the only observable species. (b) With 600V applied to one plate the K ions are completely deflected and the organics are postionized and detected.

Determination of Relative Dissociation Energies in an Ion Trap Mass Spectrometer

K.J. Hart, S. Habibi-Goudarzi and S.A. McLuckey
Analytical Chemistry Division, Oak Ridge National Laboratory
Oak Ridge, TN 37831-6120

The minimum energy required for the fragmentation of a polyatomic ion is of fundamental importance in mass spectrometry. Recently, March and Todd have recognized that collision-induced dissociation as it is typically effected in the quadrupole ion trap can be characterized by the kinetics of parent ion decomposition under various experimental conditions. We were intrigued by this approach for its potential for allowing for quantitative measurements of critical energies of decomposition for the wide variety of ions that can be stored in an ion trap. Such a capability would significantly enhance the value of the ion trap as a tool for fundamental research in gaseous ion chemistry and might also prove useful analytically in isomer differentiation. To investigate the possibility of measuring critical energies, or some parameter that can be related to critical energies, we have studied a number of parent ions with critical energies measured by other means.

The method used to measure relative dissociation energies in the ion trap is: 1) form the molecular ion by EI and isolate, 2) apply an optimized ac signal to the endcap electrodes at several different amplitudes, 3) monitor loss of parent ion versus the duration of the ac pulse, 4) plot $\ln([P]_t / [P]_0)$ versus time and record the slope of a linear regression fit, 5) convert the slope to a dissociation rate constant using the number density of helium, 6) plot dissociation rate constants versus resonant excitation amplitude and 7) extrapolate the resulting curve to $k_v = 0$ to determine the "threshold resonant excitation amplitude" (TREA). The resonant excitation frequency was optimized at each amplitude and a shift of 200-400 Hz over a 200-300 mV range was routinely observed in these experiments. A helium buffer gas pressure of 1.1 mTorr and a trap temperature of 100 °C were maintained for all determinations. The effect of the q stability parameter was studied using n-butylbenzene and only a 4.5% relative standard deviation was observed in the TREA's obtained with a range of q's from 0.2 to 0.4.

A summary of the TREA results obtained for several model systems is provided in Table 1 with the corresponding literature critical energies. Comparison of these thresholds with literature critical energies indicate that the experimentally derived minimum resonance excitation amplitude is indeed related to kinetic stability of the ion as shown in Figure 1. Two hypothetical $P(\varepsilon)$ vs. ε curves, both Boltzmann internal distributions, are shown in Figure 2 reflecting parent ions before resonant excitation and during collisional activation once a steady state condition is reached. Our interpretation of the threshold resonant excitation measurement is that it reflects a parent ion "temperature" at which a negligible number of parent ions have sufficient internal energy to fragment but one in which a slight increase in temperature would dissociate. The k_v values reflect the rate at which parent ions achieve sufficient energy to fragment. If the internal energy distributions can be characterized by temperatures, the TREA is a measure of ΔT. Provided all parent ions start at the same temperature, there is a correlation between ΔT and critical energy because they are proportional. This work constitutes an important first step in developing a means for quantifying ion stability with a quadrupole ion trap. The authors wish to acknowledge the support of the Office of Basic Energy Sciences, U.S. DOE.

TABLE 1

CID of $M^{+\cdot}$

System (dissociation)	E0 lit. (eV)	TREA (mV)
tetraethylsilane (loss of $\cdot C_2H_5$)	0.5 [1]	0*
nitromethane (loss of $\cdot CH_3O$)	0.71 ± 0.03 [2]	52.5 ± 7.9
allyl chloride (loss of ·Cl)	1.01 ± 0.05 [3]	88.40 ± 2.9
n-butylbenzene (loss of C_3H_6)	1.10 ± 0.10 [4]	105.3 ± 9.4
ethylbenzene (loss of $\cdot CH_3$)	1.30 ± 0.02 [5]	137.5 ± 8.7
toluene (loss of ·H)	1.70 ± 0.06 [6]	159.7 ± 6.4
styrene (loss of C_2H_2)	2.43 ± 0.05 [7] (2.7 ± 0.6) [8]	180.6 ± 10.2

REFERENCES

1 de Ridder, J.J.; Dijkstra, G.; *Recl. Trav. Chim.* **1967**, *86*, 737.

2 Nicholson, A.J.C.; Recent Developments in Mass Spectrometry, ed. K. Ogata and T. Hayakawa, University Park Press, Baltimore, **1970**, p. 745.

3 Buff, R.D.; Parr, A.C.; Jason, A.J.; *Int. J. of Mass Spectrom. and Ion Proc.* **1981**, *40*, 31.

4 Chen, J.H.; Hayes, J.D.; Dunbar, R.C.; *J. Phys. Chem.* **1984**, *88*, 4759.

5 McLoughlin, R.G.; Morrison, J.D.; Traeger, J.C.; *Org. Mass Spectrom.* **1979**, *14*, 104.

6 Bombach, R.; Dannacher, J.; Stadelmann, J.P.; *J. Am. Chem. Soc.* **1983**, *105*, 4205.

7 Dunbar, R.C.; *J. Phys. Chem.* **1990**, *94*, 3283.

8 Dunbar, R.C.; Zaniewski, R.C.; *J. Chem. Phys.* **1992**, *96*, 5069.

FIGURE 1

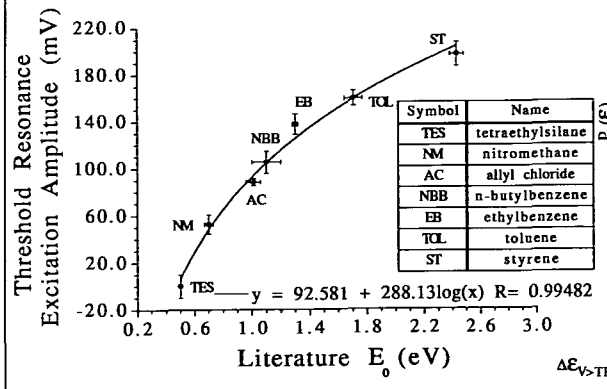

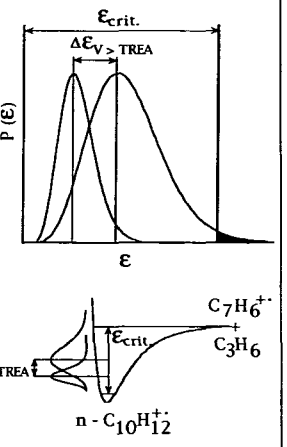

"The submitted manuscript has been authored by a contractor of the U.S. Government under contract No. DE-AC05-84OR21400. Accordingly, the U.S. Government retains a nonexclusive, royalty-free license to publish or reproduce the published form of this contribution, or allow others to do so, for U.S. Government purposes."

FIGURE 2

Trajectory Modeling of Electrosprayed Protein Ions in a FT/ICR

Peter B. O'Connor*, Mike W. Senko, Steven C. Beu, and Fred W. McLafferty; Chemistry Department, Baker Laboratory, Cornell University, Ithaca, NY 14853-1301

Ion trajectory simulations are an attractive method for investigation of space charge effects in a fourier transform mass spectrometer. Several analytical approaches have been used successfully in the past. The models by Marshall [1] and Comisarow [2,3] have been very successful at describing frequency shifts and line broadening, and the model by Beu and Laude [4] describes some peak shape distortions very well. However, it is more satisfying to allow full inclusion of coulombic forces. Recently, Dunbar's group has done so numerically [5], and showed some interesting results, but they had trajectory stability problems. Our Multiple Ion Trajectory Simulator (MITS) uses Runge Kutta fourth order numerical integration with adaptive timestep correction to solve the stability problems and a KSR1 parallel supercomputer to allow the calculation of many ions simultaneously.

MITS has been applied to several problems. Investigations of radial and axial ejection of fragment ions formed in the ICR cell by splitting of multiply charged ions showed that the energies of the repulsion alone should not eject the ions (figure 1). Although the ions are specified to fragment in the axial direction, the two ions here represent a "best case" scenario with respect to the magnitude of the repulsion because the parent ion is assumed linear with evenly distributed charges which minimizes effective charge. The effective charge is calculated by a $1/r^2$ weighted average. Fragmentation of higher charge states or from conformations that are more compact initially will increase the chance of axial coulombic ion ejection, but loss of ions should be easily prevented by raising the trap potentials.

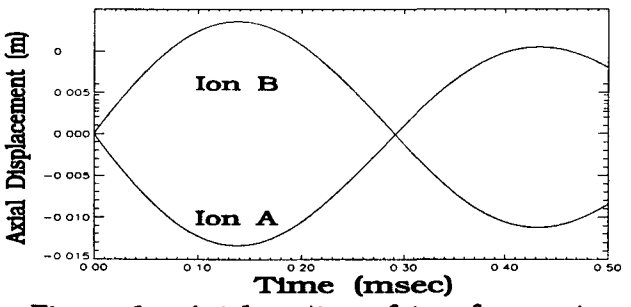

Figure 1: Axial motion of two fragments.

A new trapping mechanism is proposed. If an ion moves axially through a cell that contains trapped ions, the ions will interact coulombically, and the trapped ions can absorb some of the axial energy of the "hot" ion thus trapping it. This mechanism was modeled with MITS, and the "hot" ion was indeed trapped (figure 2).

The effects of increasing mass and cross sectional area at constant m/z was modeled. As mass increases, the effect of collisions with background gas diminishes, and the ions have better resolution. As cross sectional area increases, the number of collisions increases and resolution decreases. However, increasing mass usually implies increasing cross sectional area. Therefore, assuming that volume is proportional to mass, we increasec cross sectional area proportional to mass$^{2/3}$, and resolution still increased at high mass. Therefore, the solution of the problem of achieving high resolution at high mass must concern other line broadening mechanisms such as space charge and field inhomogeneities.

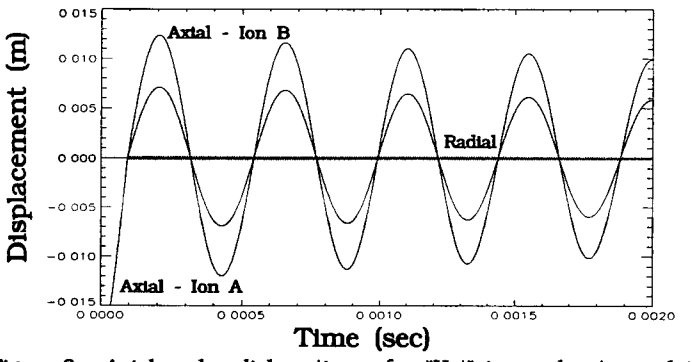

Figure 2: Axial and radial motions of a "Hot" ion and a trapped ion

References:

1. Wang, T. C. L. ; Marshall, A. G. *International Journal of Mass Spectrometry and Ion Processes* **1986**, *68*, 287.
2. Chen, S.P.; Comisarow, M. B. *Rapid Comm. Mass Spectrom.*, **1992**, *5*, 450-455.
3. Chen, S.P.; Comisarow, M. B. *Rapid Comm. Mass Spectrom.*, **1992**, *6*, 1-3.
4. Hendrickson, C. L.; Beu, S. C.; Laude, D. A.; *Proceedings of The 40th ASMS Conference on Mass Spectrometry and Allied Topics*, **1992**, 723-724.
5. Uechi, G. T.; Dunbar, R. C.; *Journal of the American Society for Mass Spectrometry*, **1992**, *3*, 734-741.

Equilibrium Distribution of Space Charge in a Quadrupole Ion Trap

Shenheng Guan and Alan G. Marshall†

Departments. of Chemistry (and Biochemistry†),The Ohio State University, 120 West 18th Avenue, Columbus, OH 43210

Quadrupole (Paul) ion trap mass spectrometry has developed into a powerful technique for mass analysis, with demonstrated high mass range, multi-stage MS, and potentially high mass resolving power. However, poor mass measurement accuracy can result from space charge effects which are difficult to model theoretically and evaluate experimentally. Here, we propose a simple model for ion space charge distribution based on the pseudopotential or Dehmelt approximation.

In a Paul ion trap, the high-frequency, high-amplitude rf voltage applied between the ring and end-cap electrodes forms a three-dimensional pseudopotential that may be approximated as a quadrupolar electrostatic potential, $\Phi_0(r)$ Ion motion in such a potential may be modeled as a harmonic oscillator when $q_z = (4qV_{rf}/mr_0^2\Omega^2) < 0.4$). Unlike the three-dimensional electrostatic potential in free space bounded by closed-surface boundary electrodes, the three-dimensional pseudopotential has a "true" energy minimum at the center of the trap.

At millitorr He buffer gas pressure, ions collide with He atoms several tens of thousands times per second, and those collisions tend to thermalize the ion motions. After a long (several-seconds) ion storage period, one can approximate the ion velocity distribution as a Boltzmann thermal distribution, particularly at small q_z-value for ions located near the center of trap. At thermal equilibrium, the charge distribution depends only on the total number of charges, the pseudopotential, and the temperature), and is independent of the choice of collision gas. As a further simplification, we consider only operating conditions under which the pseudopotential (and thus the ion distribution) is spherically symmetric (see Figure 1a). The potential generated by the space charge must satisfy the one-dimensional Poisson equation

$$\nabla^2\Phi_s(r) = \frac{1}{r^2}\frac{d}{dr}\left(r^2\frac{d\Phi_S(r)}{dr}\right) = -q\,n(r)/\varepsilon_0 \qquad (1)$$

in which r is the position, $\Phi_S(r)$ is the space charge potential, and n(r) is the ion number distribution which should also satisfy the Boltzmann distribution with the respect to the pseudopotential

$$n(r) = N\frac{\exp\left(-q[\Phi_0(r) + \Phi_S(r)]/kT\right)}{4\pi\int \exp\left(-q[\Phi_0(r) + \Phi_S(r)]/kT\right) r^2\,dr} \qquad (2)$$

in which $\Phi_0(r)$ (proportional to r^2) is the pseudopotential. We solve the above problem self-consistently. First, an arbitrary ion distribution is generated and subjected to Eq. 1; the space charge potential is then solved and substituted into Eq. 2. This process is repeated until the solutions agree with each other. A detailed description of the method will be given in an upcoming manuscript. This work was supported by NSF (CHE-9021058), and The Ohio State University.

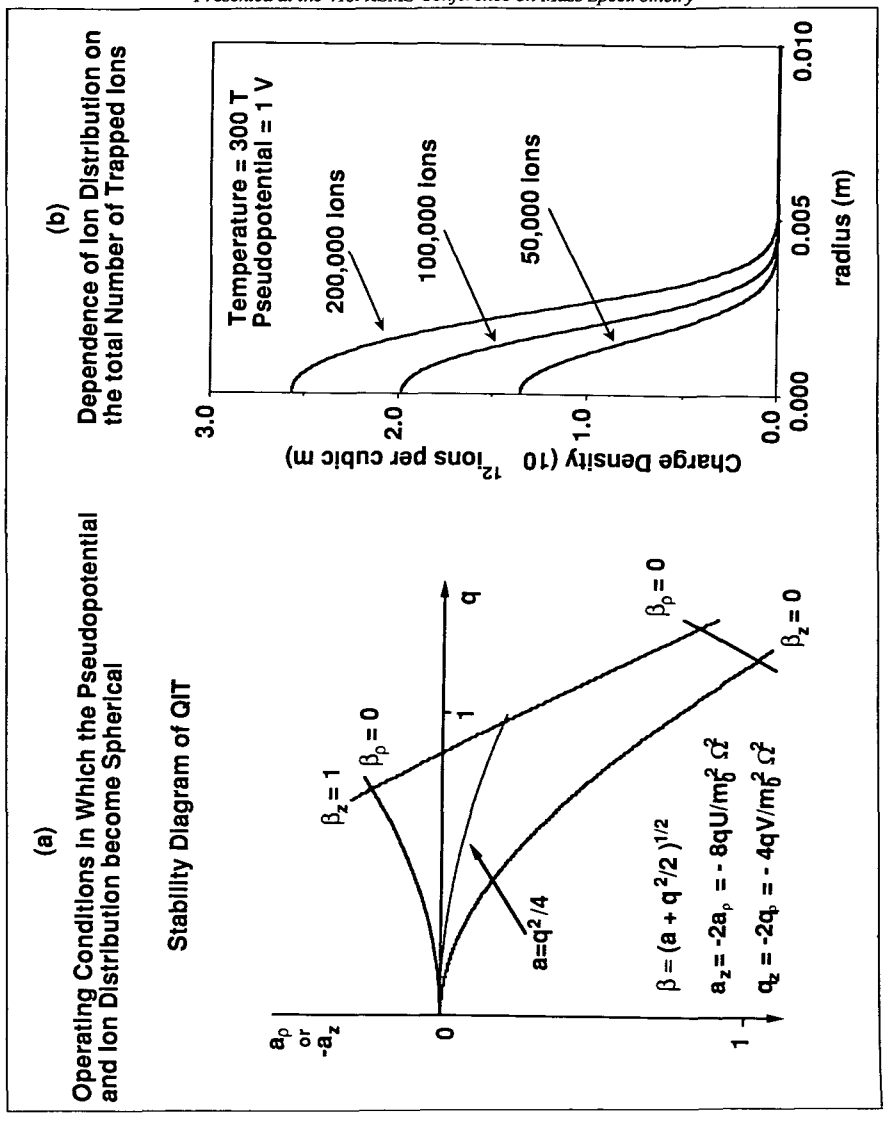

Chemical Ionization in Ion Trap GC-MS Using Selective Ion Ejection Techniques.

Charles Huston, Barbara Bolton, Mingda Wang, and Greg Wells,
Varian Chromatography Systems, WC-14
2700 Mitchell Drive, Walnut Creek, CA 94598 U S A

Introduction

The electron ionization (EI) process used to internally create chemical ionization (CI) reagent gas ions in a quadrupole ion trap mass spectrometer can also produce EI products from the analyte and any contaminants The mass instability CI scan function can use a low ionization rf level to minimize (but not completely eliminate) the storage of EI fragments at higher m/z Complete elimination of unwanted EI products prior to mass analysis can be accomplished by using selective ion ejection techniques

Methods

Wave-Board electronics were added to a Varian Saturn II GC/MS System to provide the flexibility to implement three simultaneous ion ejection techniques Resonant Ejection, Non-Resonant Dipole Ejection, and dc Isolation These techniques caused the reagent ions and their lower mass precursors to be stored, following ionization and prior to CI reaction, while all ions at higher m/z were ejected For **Resonant Ejection**, a complex waveform (containing the resonance frequencies for the ions to be ejected) was applied to the endcap electrodes **Non-Resonant Dipole Ejection** utilized a simple square wave (500Hz) whose amplitude could be characterized in terms of a desired lower m/z cutoff point The **dc Isolation** method applied -2V dc to the ring electrode of the ion trap during the ejection period

Results

The *Ejection Comparison* chart shows that, depending on the compound, the ejection methods gave an apparent 50-65% reduction of selected EI fragments when compared to Mass Instability CI None of the three ejection methods produced significantly different results relative to each other.

Comparison of *EI Spectrum of Methoxychlor* with *Mass Instability CI* illustrates the presence of EI products (i e., the ion at m/z=227) in CI spectra. All of the simultaneous ejection CI methods produced methoxychlor spectra that were similar to that shown for *Non-Resonant Dipole Ejection CI* This CI method reduced the abundance of m/z 227 by more than 50% (relative to mass instability CI), however, its continued presence indicated that it was also produced by a non-EI pathway Confirmation that the remaining fragments at m/z 227 were produced by a CI charge transfer reaction was obtained by observing isobutane CI spectra in *Non-Resonant CI Using Isobutane* The use of a softer CI reagent gas produced a spectrum that was very similar to those produced by simultaneous ejection CI using methane The use of different CI techniques to examine the spectra of other compounds allowed similar qualitative ion chemistry information to be obtained

Finally, CI signals from the three simultaneous ejection CI methods ranged from 8-30% higher than comparable Mass Instability CI results

Ejection Comparison

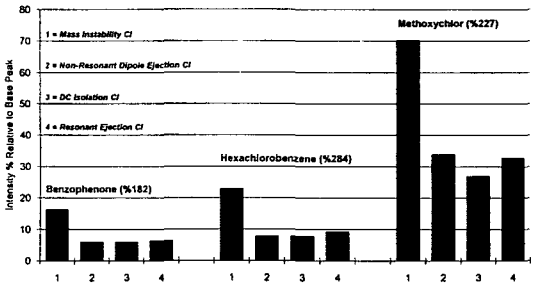

EI Spectrum of Methoxychlor

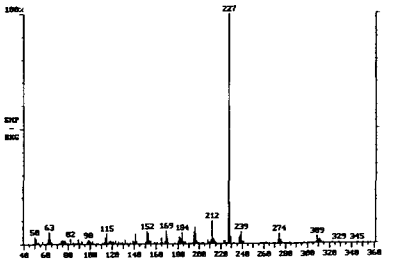

Non-Resonant Dipole Ejection CI

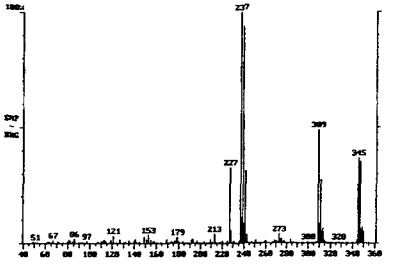

Mass Instability CI

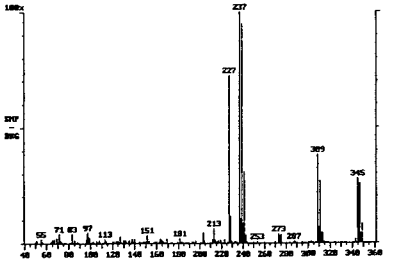

Non-Resonant CI Using Isobutane

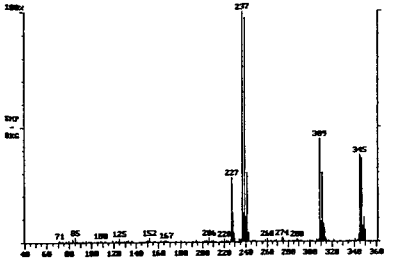

Numerical Computation of Trapping and Excitation Electric Fields and Ion Trajectory Simulations in an ICR Ion Trap

Xinzhen Xiang, Shenheng Guan, Alan G. Marshall†, L. A. Southern, and D. Knight

Departments. of Chemistry (and Biochemistry†),The Ohio State University, 120 West 18th Avenue, Columbus, OH 43210

A numerical method has been developed for computation of trapping and excitation electrical fields in a rectangular/cubic ICR ion trap and for simulation of ion trajectories. Theoretically, the problem of solving for the potential, $\Phi(x,y,z,t)$, inside a rectangular or cubic trap with arbitrary boundary conditions at any given time, t, may be simplified to superposition of "eigen" potentials, $\Phi_0(x,y,z)$

$$\Phi(x,y,z,t) = V_{x+}(t)\,\Phi_0(x,y,z) + V_{x-}(t)\,\Phi_0(-x,y,z) + V_{y+}(t)\,\Phi_0(y,x,z) + V_{y-}(t)\,\Phi_0(-y,x,z) + V_{z+}(t)\,\Phi_0(z,y,x) + V_{z-}(t)\,\Phi_0(-z,y,x)$$

in which the eigenpotential is the solution for the special boundary condition that one trap electrode is set to 1 V and the other electrodes are at groundl; $V_{x+}(t)$ etc. denote potential applied to the electrode (i.e., at $x = +a/2$, a is the trap edge length). Our program also contains routines to generate arbitrary excitation waveforms, including SWIFT algorithms. Ion trajectories for a variety of excitation modes (see Table) and in the presence of collisional frictional force may be simulated. The time-domain ion signal derived from the image current induced on the detection electrodes and its frequency-domain spectrum may also be generated.

The programs are written in Fortran 77 and compiled and executed on a CRAY Y-MP8/864 computer with 8 processors and 512 megabytes of high-speed memory at the Ohio Supercomputer Center. The Supercomputer provides both computational speed and high accuracy. In order to visualize the desired potential, the data are transfered to a SUN SPARC station and converted to a Felix data file format. Both contour and stack plots may be generated within the Felix program. Trajectory data are then transferred to a Macintosh IIsi, where they are displayed and printed from a BASIC program. 3D videos from apE have also been generated.

To produce the "eigen" potential data with high precision, an array of 101X51X51 dimensions is reserved. By symmetry, only one fourth of the eigen potential data need be generated, reducing computation time and storage space. The potential is computed by a simple relaxation method. Over 10,000 iterations (6,300 s of CPU time) were excuted until the maximum deviation of data points between the last two consecutive iterations is less than 10^{-8}. The large computing effort is warranted, since the "eigen" potential need be generated only once, from which the electrical field anywhere in the trap may then be calculated. During the trajectory simulation, the "eigen" potential was extrapolated to double the spatial resolution for the electric field data. The Lorentz equation of ion motion is solved by a 4th-order Runge-Kutta method at 100 ns time increments.

Our simulations have already revealed some interesting nonlinear effects of a real ICR trap and details will be reported in an upcoming manuscript [1]. In future work, we shall investigate the effects of space charge on the temporal evolution of an ion distribution. Supported by NSF (CHE-9021058) and Ohio State University.

1. Xiang, X.; Guan, S.; Marshall, A. G., in preparation.

Table 1. ICR single frequency-excitation experiments supported by the program described in the text.

Experimental Mode	Potentials Applied to Electrodes of an ICR Ion Trap					
	x+	x-	y+	y-	z+	z-
Normal trapping	0	0	0	0	V_T	V_T
Dynamic trapping	0	0	0	0	$V_z\sin\Omega t$	$V_z\sin\Omega t$
Azimuthal linear dipolar cyclotron	$V_x\sin\omega_+t$	$-V_x\sin\omega_+t$	0	0	V_T	V_T
Azimuthal linear dipolar magnetron	$V_x\sin\omega_-t$	$-V_x\sin\omega_-t$	0	0	V_T	V_T
Azimuthal circular quadrupolar cyclotron	$V_x\sin\omega_+t$	$-V_x\sin\omega_+t$	$V_x\cos\omega_+t$	$-V_x\cos\omega_+t$	V_T	V_T
Axial dipolar z-motion	0	0	0	0	$V_T+V_z\sin\omega_zt$	$V_T-V_z\sin\omega_zt$
Azimuthal parametric	$V_x\sin\omega_pt$	$V_x\sin\omega_pt$	$V_x\sin\omega_pt$	$V_x\sin\omega_pt$	V_T	V_T
Axial parametric	0	0	0	0	$V_T+V_z\sin2\omega_zt$	$V_T+V_z\sin2\omega_zt$
Azimuthal quadrupolar ω_+/ω_- conversion	$V_x\sin\omega_ct$	$V_x\sin\omega_ct$	$-V_x\sin\omega_ct$	$-V_x\sin\omega_ct$	V_T	V_T
Azimuthal quadrupolar $2\omega_+$ excitation	$V_x\sin2\omega_+t$	$V_x\sin2\omega_+t$	$-V_x\sin2\omega_+t$	$-V_x\sin2\omega_+t$	V_T	V_T
Azimuthal quadrupolar $2\omega_-$ excitation	$V_x\sin2\omega_-t$	$V_x\sin2\omega_-t$	$-V_x\sin2\omega_-t$	$-V_x\sin2\omega_-t$	V_T	V_T

Non-linear Resonance Conditions and their Relationships to Higher Multipole Fields in Quadrupole Mass Filters and Non-linear Ion Traps

Y. Wang and J. Franzen

Bruker-Franzen Analytik GmbH, 2800 Bremen 33, Germany

It is non-linear resonances, caused by higher multipole fields, which change the stability and instability of ion motion based on the pure quadrupole field. The resonace can be termed as the "internal" resonance.

With theoretical analysis, a general non-linear resonance conditions for three-dimensional non-linear quadrupole systems can be derived:

$$n_x\beta_x + n_y\beta_y + n_z\beta_z = 2\nu \qquad (0 \le \beta_x, \beta_y, \beta_z \le 1) \tag{1}$$

where $\beta_x, \beta_y, \beta_z$ are secular frequency parameters in x, y, z direction and n_x, n_y, n_z, ν are $0, \pm1, \pm2, \pm3, \cdots$ all integers. The resonance conditions (1) can be applied in non-linear ion traps with three-dimensional distortions; and quadrupole mass filters with distortions and/or fringe fields. Distortions mean, for example, any twists, and so on.

Some kind of symmetry of electrode shapes results in the corresponding symmetry of the electric field in the quadrupole system. Therefore, resonance conditions are reduced and some resonances are not produced due to the symmetry. For the ion trap with the rotational symmetry, reduced non-linear resonance conditions are

$$n_r\beta_r + n_z\beta_z = 2\nu \tag{2}$$

with $n_z, \nu = 0, \pm1, \pm2, \cdots$ all integers and $n_r, \nu = 0, \pm2, \pm4, \cdots$ even integers. Specially for the superposition with higher "odd" rotationally symmetric multipoles, there are additional restrictions for resonance conditions (2): n_z are odd integers; and for the superposition with higher "even" rotationally symmetric multipoles, n_z are even integers. In non-linear quadrupole mass filters, reduced non-linear resonance conditions are

$$n_x\beta_x + n_y\beta_y = 2\nu \tag{3}$$

with $n_x, n_y, \nu = 0, \pm1, \pm2, \pm3 \cdots$ all integers. In general, there are no additional restrictions in this case.

There are different types of resonances as following: Type (I): One-dimensional resonances (uncoupling resonances), which fulfil resonance conditions:

$$n_\xi\beta_\xi = 2\nu \qquad (n_\xi, \nu : \text{integers}) \tag{4}$$

where ξ means x or y or z in general three-dimensional cases, r or z in ion traps with rotational symmetry, and x or y in quadrupole mass filters. On this type of resonance, the ion takes up energy in ξ direction only. One-dimensional resonances are strong. Type (II): Sum-resonances (coupling resonances). In Eq. (2) and (3), ν and n are positive integers. On this type of resonance, the ion takes up energy in each direction at the same time. Sum-resonance are strong, too. Type (III): Difference resonances (coupling resonances). In Eq. (1) (2) and (3), there are positive and negative integers for n numbers, respectively. On this type of resonance, energy is exchanged mainly between different directions of ion motion. Difference resonances are weak.

In practice, z direction resonances are dominant in ion traps because ions are damped by buffer gas to the center of the trap, then often excited in z axis. Sum-resonances should be paid more attention in quadrupole mass filters, because they locate within the up-corner of the first stability diagram, which is used to analyse the ion mass. In general, difference resonances will be not easily observed in experiments.

Concentrated on the non-linear resonance conditions, each order of multipoles generates a few resonances which fulfil different group of resonance conditions. However, different orders of multipoles generate resonances which fulfil different and/or same group of resonance conditions. In mass spectrum, a group of mass picks caused by non-linear resonances may be generated by different multipoles or mixtures of them. Therefore, orders N of resonance conditions are defined as

$$|n_r| + |n_z| = N \quad \text{(ion trap)} \quad \text{or} \quad |n_x| + |n_y| = N \quad \text{(quadrupole mass filters)}$$

$N = 2$: $2nd$ order of resonance conditions; $N = 3$: $3rd$ order; $N = 4$: $4th$ order; $\cdots$.

If weight factors of a whole set of higher multipoles decrease with multipole order n asymptotically, resonances with a few lower orders N are stronger. Furthermore, resonances with lower orders, for example, the 3rd and/or the 4th order are always observed even if weight facters of a few more higher multipoles are larger. There exist restraining or encouraging functions for resonances if superimpose two or more than two main higher multipoles.

Each order N of resonance conditions consists of several resonance lines. In non-linear ion traps with rotational symmetry, resonance lines for the hexapole superposition(the 3rd order is main) are $\beta_z = \frac{2}{3}$ and $\frac{1}{2}\beta_z + \beta_r = 1$; and for the octopole superposition(the 4th order is main) are $\beta_r = \frac{1}{2}, \beta_z = \frac{1}{2}, \beta_r + \beta_z = 1$. In non-linear quadrupole mass filters, resonance lines for hexapole superposition are $\beta_x = \frac{2}{3}, \beta_y = \frac{2}{3}, \frac{1}{2}\beta_x + \beta_y = 1$, and $\beta_x + \frac{1}{2}\beta_y = 1$; and for octopole superposition are $\beta_x = \frac{1}{2}, \beta_y = \frac{1}{2}, \beta_x + \beta_y = 1, \frac{1}{2}\beta_x + \frac{3}{2}\beta_y = 1$, and $\frac{3}{2}\beta_x + \frac{1}{2}\beta_y = 1$.

Oscillating frequencies of a ion trapped in the pure quadrupole field are

$$\omega_\xi^m = (m_\xi + \frac{\beta_\xi}{2})\Omega \tag{5}$$

where Ω is frequency of the driving voltage, m_ξ means m_x, or m_y or m_z, which are integers. The main resonance frequency($\omega_\xi^0 = \frac{\beta_\xi}{2}$) conditions are

$$n_x\frac{\beta_x}{2}\Omega + n_y\frac{\beta_y}{2}\Omega + n_z\frac{\beta_z}{2}\Omega = \nu\Omega \tag{6}$$

If main resonance frequencies fulfil resonance conditions (6), all side-bands(ω_ξ^m with $|m_\xi| \ge 1$) also fulfil resonance conditions. Therefore, the non-linear resonance is a kind of resonance of a group of resonance frequencies.

Presented at the 41st ASMS Conference on Mass Spectrometry

Electric Trap Fields and High Mass Ions in FTMS: Peak Ratios

C. L. Holliman, D. L. Rempel, M. L. Gross, Midwest Center for Mass Spectrometry, Department of Chemistry, University of Nebraska, Lincoln, NE 68588-0304, USA.

The effect of the electric trap field increases with mass and can adversely affect resolution and sensitivity at high mass. Peak ratios may also be affected. Pre-detection mechanisms to which inaccurate abundances of low mass can be attributed are: z-excitation [1], chirp amplitude [2], and coulombic interactions [3]. DeLong and coworkers [4] present a damping model for post-excitation isotopic fractionation.

While all of the above may play a role in the analysis of high mass ions, the effect of the electric trapping field must also be considered. The effect of the trapping fields on ions approximately 10% of the cell's critical mass can be investigated with the C60 buckminsterfullerene molecular ion (m/z 720) in a 0.0254 cm cubic cell at 1.2 tesla field (m_c = 8100) and scaling the results. For example, *m/z* 720 at 1.2 T scales to *m/z* 24,500 at 7 T. Because tools like the RF-only-mode event and cell compensation produce quality signals at high mass [5], it becomes worthwhile to turn to more subtle high mass problems.

All experiments are performed with a 2.54 cm. cubic molybdenum cell. The trap plates are divided into disc and ring sections and electrically isolated so that different voltages may be applied. The disc is held at 1 V and compensation is achieved by raising the voltage as indicated on the outer ring. Benzene is introduced to a pressure of $1x10^{-7}$ torr (uncorrected). Default parameters are; ionization at 70eV and 35 nA emission current for 15 msec. The fragment ions of *m/z* 50, 51, and 52 are excited by consecutive rf bursts (high to low mass) for 700 usec at 0.74 V_{p-p}. The outer trap electrode is at 1.7 V. C60 buckminsterfullerene is introduced to the cell by a heated solids probe. Default parameters are; ionization at 70eV and 80 nAmp emission current for 500 msec. The molecular and isotope ions of *m/z* 720, 721, 722 are excited by a single rf burst centered on *m/z* 720 for 300 usec at 1.27 V_{p-p}. The outer trap electrode is at 2.3 V.

Discrimination due to chirp/sweep excitation is avoided by exciting the molecular ion and isotopes with a single rf-burst. The frequencies of *m/z*'s 720 at 25042 Hz to 722 at 24973 Hz differ by only 69 Hz. The bandwidth of the rf-burst is sufficiently wide to excite simultaneously ions 720-722 with retention of their relative abundances. Only by going out 5 mass units *m/z* 727 at 24797 Hz is a modest change observed.

Fractionation due to dampening of the signal is circumvented through the use of complex area measurement [6]. Complex areas, sample the initial envelope of the transient before dampening processes have an effect.

The role of space charge is determined by increasing the beam time and plotting the ratio of areas 720/721. Although there is curvature due to space charge, the coulombic interactions reported by Dunbar do not play a major role under these experimental conditions. Space charge effects during detection are increased by reducing the detection orbit by one third. A lack of significant change in the ratio behavior indicates that space charge during detection is not playing a major role in our measurements.

The role of mass and the electric trapping field can be evaluated by comparing the performance of C60 ions with benzene ions. The excited ion orbit is scanned to observe the the effects of the trapping field. Ions sample different areas of the cell during detection by increasing the excitaion time. The ratios of the benzene fragment peaks 50/51 and 50/52 vary by approximately 40% over a 2-fold increase in excite time. A similar increase in excite time for C60 ions results in a 150% change in the ion ratios indicating that the high mass is more sensitve to changes in the electric field.

The shape of the trapping field is changed with compensation voltage and its effect on detection is observed. The ratios of benzene ions remain relatively constant over a change of 0.8 V on the ring electrode whereas the C60 ratios vary as much as 150%. The dependence of high mass relative abundance measurements on trapping field is further demonstrated by a measure of the deviation from the theoretical C60 isotope ratio Figures A-C. As the compensation voltage is increased, the isotpic abundances can be "tuned" to the proper value.

1. Huang, S. K.; Rempel, D. L.; Gross, M. L., *Int. J. Mass Spectrom. Ion Processes*, **1986**, *72*, 15.
2. Moini, M.; Eyler, J. R., *Int. J. Mass Spectrom. Ion Processes*, **1989**, *87*, 29.
3. Uechi, G. T.; Dunbar, R. C., *J. Am. Soc. Mass Spectrom.*, **1992**, *3*, 734.

Evidence suggests a previously unreported mechanism exists that effects the detected isotope ratios of high mass ions. The mechanism is not dependent on the details during the excitation time and coulombic interactions do not play a significant role. Electric trap inhomogeneity plays a strong role in accurate isotope ratios at high mass and its effects can be moderated by cell compensation.

4. Mitchell, D. W.; DeLong, S. E., *Int. J. Mass Spectrom. Ion Processes*, **1990**, *96*, 1.
5. Jacoby, C. B.; Holliman, C. L. Rempel, D. L.; Gross, M. L., *J. Am. Sos. Mass Spectrom.*, **1993**, *4*, 186.
6. Whalen, A. D., *Detection of Signals in Noise*, Academic Press, New York, 1971, 56-61.

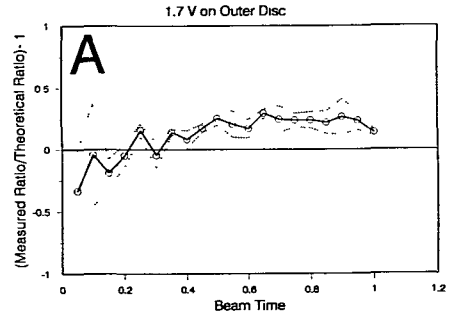

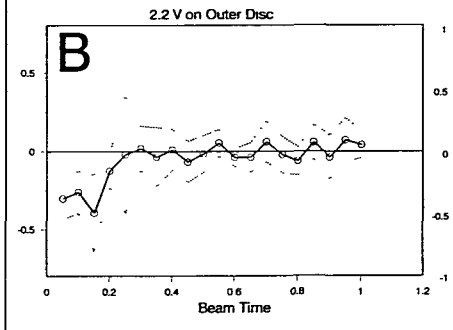

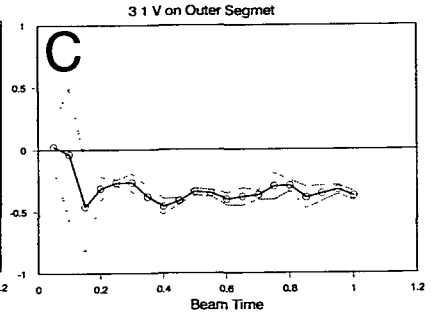

SIMULATION OF EXCITATION PROFILES GENERATED BY EXTERNAL SOURCE FTICR ION DISTRIBUTIONS

F. Hadjarab, D. Riegner, C. J. Harper, T. L. Williams, D. A. Laude, Jr.; Department of Chemistry and Biochemistry, University of Texas at Austin, Austin, TX 78712

The use of Fourier transform ion cyclotron resonance mass spectrometry (FTICR) to examine externally generated ions. Unfortunately, the injection of externally-formed ions increases the likelihood that the trapped ion population is not well-behaved, either in terms of its spatial or kinetic energy distribution. Whereas ideally a low amplitude ensemble of ions will be captured along the z-axis centerline of the cell, it is more realistic to consider for example that laser desorbed ions formed in a region adjacent to the cell might assume a much broader spatial distribution in the cell.

We are interested in understanding the appropriate excitation conditions for an ensemble of ions that enter the cell under non-ideal conditions. Toward that goal a simulation program was written that determines the predicted FTICR signal for an initial ion packet that is subjected to excitation events of increasing magnitude. What distinguishes this simulation from others is the accommodation of statistical ion populations applied to model external ion injection. This increases the reliability of modeled excitation profiles in predicting appropriate excite events for well-characterized but non-ideal ion populations.

In order to simulate the motion of ion clouds under the effect of resonant electric fields inside the ICR trap, we first solve analytically the equation of motion for a single particle, and then write a FORTRAN program that applies this solution to an ensemble of ions. The equation of motion of an ion moving inside the ICR cell under the effect of a single cyclotron excite voltage is known to be :

$$\frac{d^2u}{dt^2} - i\omega_c \frac{du}{dt} - \frac{\omega_z^2}{2}u = F(t)$$

Where $F(t) = F_0 \sin(w_c + q)$ and where $u = x - i\,y$, x and y being the usual Cartesian coordinates describing that component of the ion's motion that is transverse to the magnetic field. The homogeneous solution of this second order differential equation is readily found to be:

$$Z = Z_c + Z_m = r_c e^{(\omega_c t + \delta)} + r_m e^{(\omega_m t + \varphi)}$$

where r_c, r_m, d and j are the cyclotron and the magnetron radii and phases respectively.

In order to find the inhomogeneous solution due to F(t), we use the known mathematical formula:

$$Z_{sol}(t) = Z_c(t)\int_0^t \frac{Z_m(x)F(x)}{W}dx - Z_m(t)\int_0^t \frac{Z_c(x)F(x)}{W}dx$$

This is the inhomogeneous solution for a forced oscillator second order differential equation (like the one above) in which $Z_c(t)$ and $Z_m(t)$ are two independent solutions of the homogeneous problem, F(t) is the electric force, and W is the Wronskian:

$$W(Z_c, Z_m) = Z_c \frac{dZ_m}{dt} - Z_m \frac{dZ_c}{dt}$$

Hence, the time dependent solution under the cyclotron excitation electric field is given by:

$$Z = Z_c + Z_m + A[(\frac{1}{\omega_c - \omega_m} + \frac{e^{-2i\theta}}{\omega_c + \omega_m})e^{i(\omega_m t + \theta)} -$$

$$-(\frac{1}{\omega_c - \omega_m} - it + \frac{e^{-2i\theta}}{2\omega_c})e^{i(\omega_c t + \theta)} - (\frac{1}{\omega_c + \omega_m} - \frac{1}{2\omega_c})e^{-i(\omega_c t + \theta)}] \text{ where : } A = \frac{-iqB\beta}{2m(\omega_c - \omega_m)}$$

q,B,b, m,w_c and w_m are the ion charge, the magnetic field , a coefficient characteristic of ICR cell geometry, and the effective cyclotron and magnetron frequencies respectively.

For the simulation program, the above solution is the basic entity describing the behavior of each ion. The program first starts by setting all the parameters relevant to a typical ICR experiment such as the magnetic field strength, the excite signal voltage, the temperature etc.... It then builds the ion cloud itself taking into account the spatial ion density distribution as well the Maxwell-Boltzmann distribution for the random velocities. It also is capable of handling an initial macroscopic velocity of the ion cloud as a whole. Once this is done, the program calls a subroutine to bring the ion cloud to some desired excited state (through excitation of the cyclotron resonance). Finally a detection subroutine is called to calculate the current induced by the ion cloud on the detection plates, taking into account the gradual disappearance of the ions as they hit the plates. In this initial set of simulation to test the veracity of the simulation, several simplifying assumption were made. First a collision and Coulomb-free environment is assumed. It is also assumed that a uniform distribution of ions is initially formed. Several examples are considered. One is presented here:

Presented in Figure1 is excitation profiles for an ion beam injected on axis but with a spatial distribution extending over the entire cell. This might correspond experimentally to a laser desorption experiment in which the desorbed ions are formed at increasing distance from the trapped ion cell. For this case, the range of r_m increases steadily but the radial kinetic energy remains negligible and r_c ---> 0. Presented in Figure 2 is the predicted optimum excite for each initial ion spatially distributed on-axis. It is observed that a general skewing of the excitation profile to lower optimum excite voltages occurs. This is expected since an increasing fraction of the ions possess a substantial off-axis component The generation of an excitation profile for this uniform distribution verifies that with the application of an excitation event, an asymmetric ion population is generated for detection. of the optimum excite voltage for each of the distributions. The wide range of different optimum excites argues strongly that an understanding of the injected ion population distribution be known to avoid inappropnate application of an rf excitation event that does not generate an FTICR signal. In future work this simulation program will be used to consider the case of ions injected with a substantial kinetic energy distribution. In addition, it will be possible to determine which ions in a particular distribution of injected ions actually participate in generating the detected signal.

Figure 1. Excite profile of an Ion Cloud Uniformly Distributed in the Cell

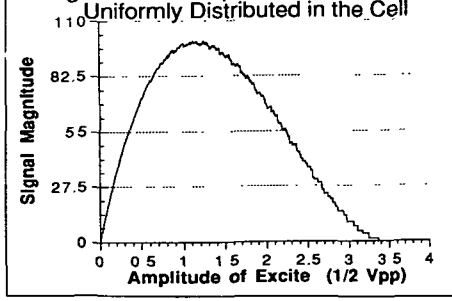

Figure 2 Optimum Excite for Ions Spatially Distributed On-Axis

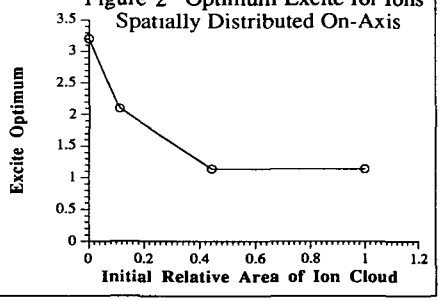

Probing Ion Frequencies in a Quadrupole Ion Trap

Donald M. Eades*, Jodie V. Johnson, and Richard A. Yost
Department of Chemistry, Univeristy of Florida, Gainesville, Fl 32611

Introduction and Experimental

Ion motion in a quadrupole ion trap has been described as a harmonic oscillator in both the axial direction (center-to-endcap electrode) with frequency ω_z and in the radial direction (center-to-ring electrode) with secular frequency ω_r. However, other frequency components, comprised of combinations of ω_z, ω_r, and the drive frequency (Ω), contribute to the total ion motion. The magnitude of each component depends on the location within the Mathieu stability diagram and on the contribution of higher-order fields to both the quadrupolar trapping field and to the dipolar excitation signal. Vedel et al. [1] have reported frequency components of ion motion corresponding to ω_z, $\omega_z/2$, $2\omega_z$, ω_r, $2\omega_r$ and other linear combinations while storing N^+ ions at q_z=0.5, a_z=0 (DC=0V). Franzen has reported [2] calculations of the magnitudes of frequency components in a quadrupole ion trap with superimposed higher-order fields.

The work presented here investigates ion frequency components at points on the Mathieu stability diagram corresponding to regions employed during either mass-isolation (i.e. RF/DC) or resonance excitation (for CID). Specifically, the points chosen for this work were near 1) the apex (q_z=0.78, a_z=0.118), 2) the β_z=1 edge (q_z=0.85, a_z=0.05), 3) the β_z=0 edge (q_z=0.70, a_z=-0.19) and 4) q_z=0.3, a_z=0. At each point, m/z 40 ions of argon were subjected to dipolar resonant excitation of varying frequency. When the excitation frequency corresponded to a component of the ion motion in the axial direction, power was absorbed by the ion resulting in ion ejection. A Finnigan MAT ion trap mass spectrometer, controlled by the ICMS Ion Trap Software v. 2.2 [3], was used for all experiments. The RF drive frequency (Ω) was 1.1 MHz.

Probing Ion Frequencies

The absorption spectrum obtained while storing ions near the apex (q_z=0.78, a_z=0.118) is shown in **Figure 1**. The excitation amplitude and time were purposely increased in order to observe the low magnitude frequency components. The Ω-ω_z component absorbs approximately 84% as much as ω_z. Although the $\Omega+\omega_z$ component does not appear to significantly contribute to the ion motion, it should be noted that the ability to probe frequency components above 1.5 MHz is hindered due to attenuation of the excitation signal by the ITMS frequency synthesizer. Consequently, frequency components in this region contribute more than what is observed. The two small absorption bands between ω_z and Ω-ω_z have not been attributed to any combination of ω_z, ω_r and Ω as of yet, but are currently being investigated. The absorption spectrum obtained near the β_z=1 stability edge (q_z=0.85, a_z=0.051) was similar to the that near the apex. Probing frequency components along the β_z=1 edge in the lower portion of the stability diagram (i.e. a_z < 0) will be the subject of future studies.

The absorption spectrum obtained while storing m/z 40 ions of argon near the β_z=0 edge (q_z=0.7, a_z=-0.186) is shown in **Figure 2**. The frequency components corresponding to the secular frequency (ω_z=126 kHz), $3\omega_z$, Ω-$3\omega_z$, Ω-ω_z, and $\Omega+\omega_z$ are observed to contribute to the total ion motion. Additional spectra obtained in this region verify the identity of the components involving $3\omega_z$. Interestingly, components due to $\omega_z/2$ and $2\omega_z$ are not observed. These components may be hidden in the absorption band due to the strong excitation signal.

The absorption spectrum obtained for q_z=0.3, a_z=0 is shown in **Figure 3**. The observed frequency components can be attributed to $\omega_z/2$, ω_z, and $2\omega_z$, all of which were verified by other absorption spectra acquired in the region. Although not shown, frequency components corresponding to Ω-ω_z and $\Omega+\omega_z$ were also present and of greater magnitude. Absorption due to a $3\omega_z$ component was also present, but required excitation of 10 V_{p-p} from an external waveform generator to be observed. The sharp spikes observed at a slightly higher frequency than the $2\omega_z$ and $3\omega_z$ absorption bands (**Figure 2 & 3**) are believed to be evidence of the collective behavior of the ion cloud [1]. This was further investigated by varying the ion population while storing m/z 40 ions at q_z=0.3, a_z=0. Shown in **Figure 4** is a comparison of absorption bands corresponding to $2\omega_z$. Note that the observed effect increases with increasing ion population (space charge effects) which might be expected to promote the collective behavior of the ion cloud. Inspection of the absorption band shape indicates that the band is not shifting, but is simply splitting as evidenced by the width of the band and by the position of the spike.

The US/EPA (Cincinnati) is acknowledged for funding this research. The authors wish to thank Nathan A. Yates for valuable software development and helpful discussions.

[1] Vedel, F.; Vedel, M.; March, R.E. *Int. J. Mass. Spectrom. Ion Proc.* 1990, 99, 125.
[2] Franzen, Y. *Int. J. Mass. Spectrom. Ion Proc.* in press.
[3] Developed by Nathan A. Yates, University of Florida, 1992.

Figure 1

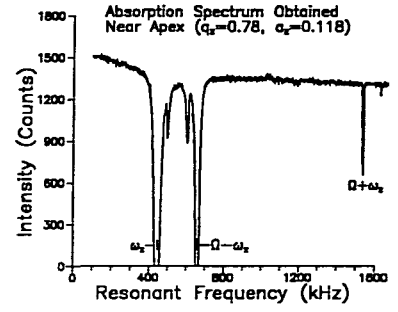

Figure 2

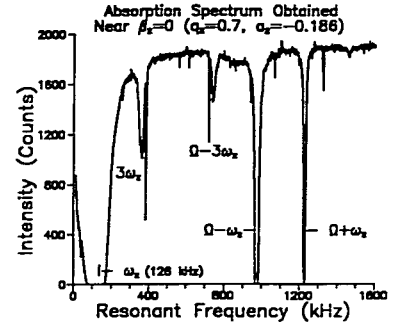

Figure 3

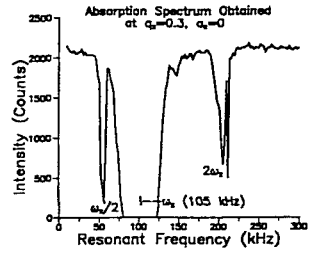

Figure 4

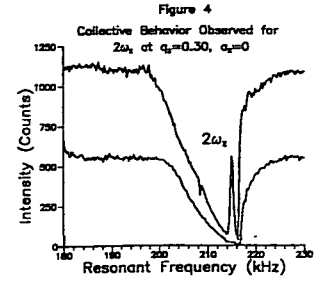

Optimization of simple open cylindrical trapping geometry for FT/ICR

L Schweikhard, M. Lindinger, H. Hartmann, Inst. f. Physik, P.O. Box 3980, 55029 Mainz, Germany

Ion cyclotron resonance (ICR) traps consist of homogeneous magnetic fields allowing mass-to-charge analysis of the trapped charged particles by their cyclotron frequency, and of electric fields providing the trapping in the axial direction (i e. along the direction of the magnetic field, z-direction). The electric field is produced by application of voltages to the trap electrodes A broad range of electrode geometries has been introduced [Mar92]. Whereas the main purpose of the electric field remains the same (axial trapping) these different electrode arrangements differ in the details of the field. The axial electric trapping field implies radial components which lead to a shift in the cyclotron frequency. In most cases (e g. the traditional cubic or cylindrical ion cells for Fourier Transform/ICR, FT/ICR) this shift is position dependent. It is position independent only for a pure axial quadruple potential (i.e. an ideal Penning trap). Such a potential can be approximated by hyperbolical trap electrodes (a ring and two endcaps). However, even for these traps, deviations from the ideal geometry (e.g. truncation of ideally infinite electrodes, entrance and exit holes for the ions, machining imperfections) lead to perturbations of the ideal ion motions and position-dependent frequency shifts. To minimalize the imperfections of the potential, compensation electrodes can be placed between the ring and endcaps (Van76) and additional correction electrodes may adjust the perturbations of the axial holes [Bol90].

Traditionally, emphasis has been on the creation of the best possible quadrupole approximation for the trap center. This is the appropriate approach for experiments with small amplitudes of the ion motion In FT/ICR however, the ions are excited deliberately to relatively large cyclotron radii (on the order of magnitude of the trap radius itself). In order to improve the potential for the purpose of FT/ICR investigations it seems appropriate to fine-tune the trap regions that the ions experience after they are excited

As a first example for a detailed analysis of trapping field optimization at finite cyclotron radius, the "simple open cylindrical geometry" was chosen. By "simple" we mean restriction to the minimum number of electrodes to create a trapping potential, namely three (in general; in special cases two electrodes may do [Sch90]). "Open" traps allow free optical and ion optical access to all trap regions Since the ions are guided by the magnetic field lines this access is accomplished best via the trap axis. There is a long tradition of use of open geometries for the storage of charged particles [Byr65]. Special multi-electrode designs have been developed to allow a shimming of the central trap potential without effecting the trapping frequency [Gab89], and open geometries have recently been introduced to FT-ICR [Beu92] Recent investigations lead to a cylindrical trap design which offers an almost perfect quadrupolar trapping potential not only in the very center of the trap, but also in a rather large region [Har93] The programs developed for the latter studies have been employed for the investigations described below

The simple open cylindrical design investigated by us consists of a center tube (center electrode) and on each side an infinitely long tube (trapping electrodes) of the same diameter The aspect ratio R = L/D (length-over-diameter, Fig. 1) of the center trap was varied for numerical calculations of the trapping potential These calculations give, e g , the potential along the z-axis and as a function of distance r from the trap center in the symmetry plane (z = 0) for several aspect ratios. A byproduct is, e g., the depth of the trapping potential as a function of the aspect ratio (Fig. 2).

The electric trapping field leads to a shift $\Delta\nu = \nu_c - \nu_+$ of the reduced cyclotron frequency ν_+ as compared to the pure cyclotron frequency $\nu_c = qB/2\pi m$ in the absence of the electric trapping field. From the potential (for each given aspect ratio) we can calculate the frequency shift as a function of the ion position in the trap. For a first analysis we chose a pure cyclotron motion (no magnetron motion) in the symmetry plane (z = 0) of the trap (no axial motion). The calculation was performed for a magnetic field

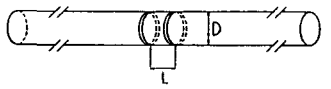

Figure 1: Geometry of 'simple open cylindrical trap'. The aspect ratio is defined as R = L/D.

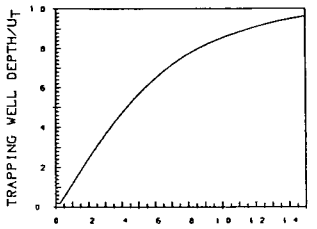

Figure 2: Depth of the trapping potential in units of the voltage difference UT between the trapping electrodes and the centerelectrode as a function of the aspect ratio R.

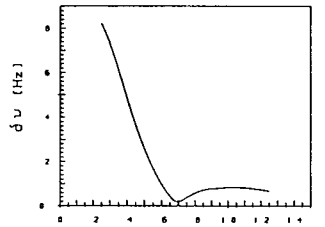

Figure 3: Root-mean-square frequency deviation for a cyclotron radius range of D/6 > r > D/3 as a function of aspect ratio R. For details see text.

of B = 5 T, trap diameter D = 80 mm, and a trapping potential on the trapping electrodes of U_T = 1 V (with the center electrode on ground potential) For a given range of cyclotron radii r of interest (in this example D/6 < r < D/3) we can now calculate the respective range of frequency shifts, or the root-mean-square deviation $\delta\nu$ from the respective average frequency. Figure 3 shows a plot of this measure of the frequency deviations versus the aspect ratio of the trap While the deviations are small in general (a few tenth of a Hertz as compared to cyclotron frequencies from 15 MHz to 15 kHz for ion m/q = 5 to 5000 amu/e) we find a minimum at the aspect ratio R = 0 7 For ultimate mass resolution this is the aspect ratio of choice for this electrode configuration (and the range of radii used), since it minimalizes the frequency deviations of ions that are excited to different cyclotron radii.

This study has dealt with the trapping potential only For FT-ICR the electrodes have to be segmented further to allow for excitation fields and pick-up of image charge signals (again, there are special cases that can do without [Mar92]) 120° seems to be the angle of choice for the pick-up electrodes since it minimalizes the third harmonics components of the signal in the standard (dipole) detection scheme. On the other hand, 60° segments maximize the third harmonics and therefore allow for ion cyclotron radius determinations based on the third-to-first harmonic ion signal [Gro92]. Further segmentation may be needed for special excitation [Sch93] or detection modes [Mar92]. Finally, the electrode segmentation for excitation/detection can be extended to the trapping tubes as well As has been pointed out [Beu92], this avoids z-ejection by the excitation field. It has two further advantages: No dependence of the ICR signal on the amplitude of the trapping motion and an excitation amplitude that is independent of the cyclotron radius.

[Beu92] S.C. Beu, D A. Laude, Jr., Int. J Mass Spectrom. Ion Processes 112 (1992) 215-230
[Bol90] G Bollen, R. B Moore, G. Savard, H Stolzenberg, J. Appl. Phys. 68 (1990) 4355-74
[Byr65] J. Byrne, P.S. Farago, Proc. Phys. Soc. London, 86 (1965) 801-815
[Gab89] Gabrielse, G, Haarsma, L., Rolston, S.L., Int. J. Mass Spectrom Ion Proc 88 (1989) 319 - 332
[Gro92] P.B. Grosshans, A.G. Marshall, Int. J Mass Spectrom. Ion Processes 115 (1992) 1-19
[Har93] H. Hartmann, G Bollen, H.-J Kluge, in preparation for Int. J Mass Spectrom. Ion Processes
[Mar92] A.G Marshall, and L. Schweikhard, Int J. Mass Spectrom. Ion Processes 118/119, 37 (1992)
[Sch90] L Schweikhard, M. Lindinger, H.-J. Kluge, Rev Sci. Instrum 61 (1990) 1055-8
[Sch93] L Schweikhard, A G. Marshall, Excitation Modes for FT-ICR MS, J. Am Soc Mass Spectrom., in print
[Van76] R.S van Dyck, Jr., D.J. Wineland, P.A. Ekstrom, H G. Dehmelt Appl. Phys. Lett. 28 (1976)446

DETERMINATION OF PHOSPHORYLATION SITES ON THE SENDAI VIRUS P PROTEIN BY MALD-ITMS AND MALD-TOF

K.R. Jonscher and J.R. Yates, III, Dept. of Molecular Biotechnology,

University of Washington, Seattle, WA 98195

INTRODUCTION

Protein modifications by phosphorylation are ubiquitous in nature and are often important factors in biomolecular functions such as synaptic vesicle transport, cell cycle progression and signal transduction. Phosphorylation may also play a role in maintaining the structural integrity of the phosphoproteins of *Paramyxoviridae*. Viruses belonging to this family include human parainfluenza viruses, mumps, measles, canine distemper and the Sendai virus. The amino acid sequence of the P protein of the Sendai virus has been deduced from the nucleotide sequence and is rich in serine and threonine residues (~25%), providing ample sites for phosphorylation [1]. The purpose of the present work is to determine the phosphorylation sites on the P protein of the Sendai virus using a combined approach of quadrupole ion trap (ITMS) and time-of-flight (TOF) mass spectrometry. A modified quadrupole ion trap, capable of high resolution and resonant excitation/ejection, provides sequence information for the determination of peptide structure. Mixtures of species with a wide range of *m/z* are analyzed by matrix-assisted laser desorption (MALD) TOF mass spectrometry. The combination of these instruments provides a strong methodology for the investigation of biological problems.

APPARATUS

Quadrupole Ion Trap: Components from an ITMS and TSQ70 (Finnigan MAT) were used in the construction of an instrument employing a quadrupole ion trap as a mass analyzer, a 20 kV collision dynode/electron multiplier detection system and a differentially pumped vacuum housing to provide for the addition of external ionization sources [2]. The trap was filled with a mixture of 10:1 He:Ar at a nominal pressure of 1 mtorr. A supplementary rf voltage placed across the endcaps of the ion trap allows extension of the mass range by resonant ejection of the ions and collision-induced dissociation by resonant excitation and collisions with the He bath gas. A MALD source consisting of a nitrogen laser coupled to an optical fiber was interfaced to the mass spectrometer [2]. Sample was applied to a probe tip then the position of the probe with respect to the fiber was optimized.

Time-of-Flight: A Lasermat (Finnigan MAT) linear time of flight mass spectrometer was employed to supplement information obtained on the quadrupole ion trap. Light from a laser is focused through a rotating stage onto a plate containing the sample. Ions are accelerated by a 20 kV grid then drift through a field-free region and are detected by a 20 kV collision dynode/electron multiplier detection system [3].

SAMPLE PREPARATION

~ 250 pmol of sample was subjected to S-carboxymethylation and proteolytic digestion with trypsin. An aliquot of the digested protein was separated with an ABI 140A reverse phase HPLC equipped with a 2.1 mm x 3 cm C_{18} packed capillary column using a 75 minute gradient of 0 - 55% solvent B (80% acetonitrile/20% 0.1% TFA). Fractions of the eluent were collected and analyzed by MALD - ITMS and MALD - TOF mass spectrometry. The matrix used was a super-saturated solution of α–Cyano-4-hydroxycinnamic acid.

RESULTS AND DISCUSSION

Peptide masses representing 55% of the amino acid sequence of the P protein of Sendai virus have been observed. Approximately 0.1 mtorr Ar was added to the bath gas, allowing some fragmentation to occur during ion injection. Figure 1 illustrates the identification of predicted fragment ions corresponding to *m/z* 2909, confirming the structure of this peptide. Preliminary data indicates the presence of one phosphopeptide, residues 255-282. The mass spectrum is shown in Figure 2 [a) MALD-ITMS and b) MALD-TOF]. The molecular ion was observed at *m/z* 2912 and the phosphorylated moiety (indicated by an asterisk) at *m/z* 2993. The signal of the phosphorylated peptide on the ion trap is reduced by a factor of ~15 compared with that obtained on the TOF. The peak at ~18-19 below the ion at *m/z* 2912 may be loss of water from *m/z* 2912 and/or loss of HPO_4 from *m/z* 2993. Loss of phosphoric acid from the phosphorylated peptide due to energetic injection conditions in the ion trap may explain the reduced signal intensity.

CONCLUSIONS

A modified quadrupole ion trap was employed in conjunction with a TOF mass spectrometer to determine the sites of post-translational modification in the amino acid sequence of the P protein of Sendai virus. Peptide masses representing 55% of the protein sequence have been observed. Preliminary data reported here indicates the presence of one phosphorylation site in residues 255-282. This peptide contains four serines, thus further analysis is required to find the position of the phosphorylated amino acid.

REFERENCES

1. *"The Paramyxoviruses"* (David W. Kingsbury, Ed.), Plenum Press, New York 1991, p. 59.
2. K.R. Jonscher, G.J. Currie, A.L. McCormack and J.R. Yates, III, *Proc. of the 40th ASMS Conf. on Mass Spec. and Appl. Topics* (Washington, DC) 1993, 701.
3. K.K. Mock, C.W. Sutton and J.S. Cottrell, *Rapid Comm. in Mass Spec.*, **6**, 1992, 233-238.
4. J.C. Schwartz, J.E.P. Syka and I. Jardine, *J. Am. Soc. Mass Spectrom.*, **2** (3), 1991, 198.

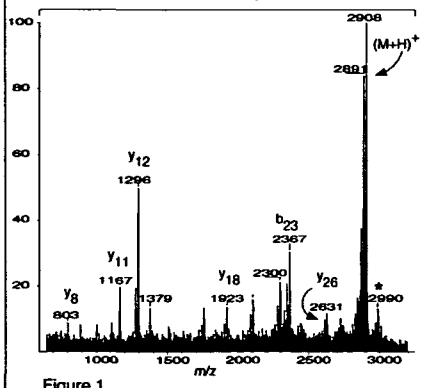

Figure 1

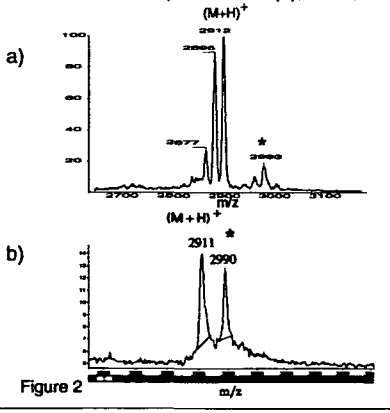

Figure 2

Investigation of Saccharide Anion Fragmentation using Fourier Transform Mass Spectrometry and Semiempirical Calculations (AM1)

James A. Carroll and Carlito B. Lebrilla
Department of Chemistry, University of California
Davis, CA 95616 USA

There is current interest in developing reliable methods for saccharide analysis using mass spectrometry. Several research groups have used fast atom bombardment (FAB) for saccharide ionization, and this has proven to be a powerful technique for their analysis. An area in which significant progress has been made is in the discrimination of the five possible linkage types present between adjacent monosaccharide units in an oligomer, i.e. a 1→4 type linkage versus a 1→6 type linkage. It has been shown that high energy collisionally activated dissociation (CAD) of saccharide anions is useful for distinguishing linkage types using sector mass spectrometers.[1,2] Our results have shown that the external source Fourier transform instrument is useful for saccharide analysis. In the negative ion mode, di- and trisaccharide linkage isomers can be distinguished in a single-step analysis, without the need for CAD.[3] The negative ion spectra of two trisaccharide linkage isomers, isomaltotriose (glcα[1→6]glcα[1→6]glc) and panose (glcα[1→6]glcα[1→4]glc) are shown in figure 1. The two spectra are easily distinguishable due to the different linkages present in the molecules.

We are currently investigating the mechanism of saccharide fragmentation reactions using model oligosaccharides and isotope labeling experiments. It has been proposed that cross-ring fragmentation, which is necessary for linkage discrimination, occurs via a retro-aldol mechanism initiated by ring-opening.[4] Evidence for this is that non reducing saccharides, in which ring-opening cannot occur, show no ring cleavage from the reducing ring. Once the ring has opened, a hydroxyl group beta to the aldehyde can initiate the retro-aldol reaction, leading to the loss of a neutral fragment. The size of the neutral lost depends on the position of the glycosidic linkage between the two saccharide monomers. All of the possible linkage types have different characteristic neutral losses. Analysis of a ^{13}C-lactose compound verifies that it is the anomeric carbon that is lost in the ring fragmentation of lactose, which supports this mechanism.

Using β-glucose as a model, the relative stabilities of the possible intermediate and transition state structures were determined using semi-empirical calculations (AM1).[5] The heat of formation of the fully optimized structure of deprotonated glucose was found to be -309.6 kcal. The barrier to ring opening was determined by increasing the C-O bond distance, as indicated in figure 2, incrementally, and fully optimizing every other parameter at each increment. The gradient was then calculated, and the transition state verified using a force calculation. The barrier can therefore be calculated as 14.8 kcal. The same method was used to calculate the barrier for loss of the neutral as 18.6 kcal. The results are summarized in figure 2.

1 Garozzo, D.; Giuffrida, M.; Impallomeni, G.; Ballistreri, A., Montaudo, G. *Anal. Chem* **1990**, *62*, 279.
2 Dallinga, J. W.; Heerma, W. *Biol. Mass Spectrom.* **1991**, *20*, 215.
3 Carroll, J. A.; Ngoka, L.; Beggs, C. G.; Lebrilla, C. B. *Anal. Chem.*, in press.
4 Spengler, B.; Dolce, J W.; Cotter, R. J *Anal. Chem* **1990**, *62*, 1731.
5 Dewar, M. J. S.; Zoebesch, E. G., Healy, E F.; Stewart, J. J. P. *J. Am. Chem. Soc.* **1985**, *107*, 3902.

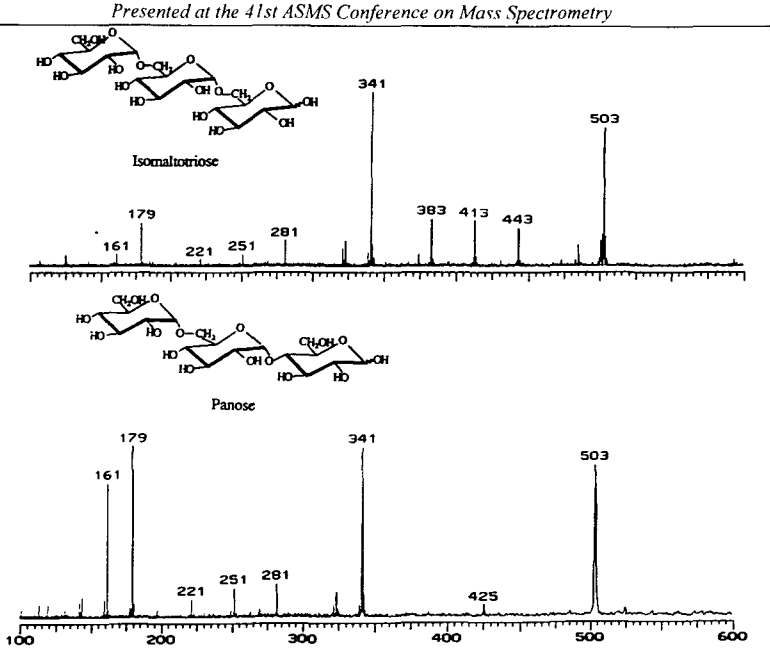

Figure 1. FTMS spectra of isomaltotriose and panose

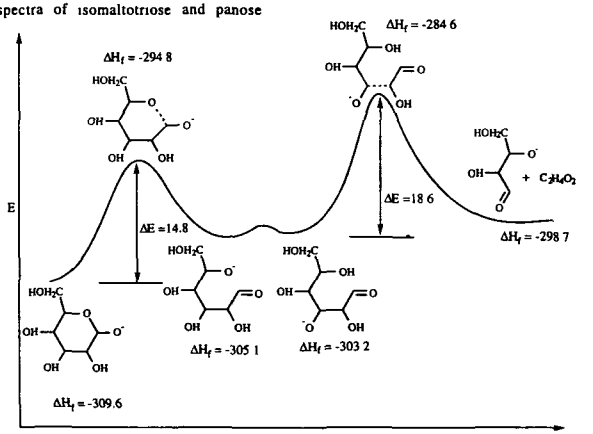

Figure 2. Summary of the AM1 calculations for glucose. All energies are in units of kcal. The barrier to ring opening was determined to be 14.8kcal and the barrier to loss of the $C_2H_4O_2$ neutral was determined to be 18.6kcal

FACTORS WHICH AFFECT THE ACCURACY OF MASS MEASUREMENT OBTAINED WITH THE QUADRUPOLE ION TRAP MASS SPECTROMETER

J D Williams, K A. Cox, C.D. Cleven, R G. Cooks
Department of Chemistry, Purdue University, West Lafayette, IN 47907-1393

Recently, a peak matching technique has been developed to calibrate higher-resolution mass spectra and tandem mass spectra obtained with a quadrupole ion trap mass spectrometer (ITMS).[1] This technique allows both calibrant and analyte ions of differing masses to be brought to the identical point in the stability diagram. Typically, the accuracy of mass measurement is $\leq \pm 0$ 008%, when this method is performed with internal calibration. The goal of these studies was to further determine the underlying factors which affect mass measurement accuracy when higher-resolution mass spectra are acquired with the quadrupole ion trap

All spectra were recorded using a digital storage oscilloscope (Tektronix TDS 540) to monitor the signal produced by the pre-amplifier in the ITMS electronics. The first parameter studied was the change in the ejection time (i e. mass shift) of $Cs_3I_2^+$ (m/z 912.3) and $Cs_3Br_2^+$ (m/z 768 4, 770 4, 772.4, 774.4) ions as a function of ionization time when they were resonantly ejected from the trap. The scan rate was slowed to 1,100 and 628 Da/s, respectively, by using the offset-DAC method [2] Figure 1 shows that the ejection of the isotopes of $Cs_3Br_2^+$ was delayed with increasing ionization time However, this delay varied for each isotopic species. These independent shifts are caused by space-charging of the trap.[2] In the mass-selective instability scan, ions of increasing mass are sequentially ejected from the trap. Thus, space-charging is reduced for ions of higher mass since fewer ions are present when they are ejected from the trap. A reverse RF resonance ejection scan (i e decreasing the amplitude of the RF voltage for ion ejection) was done to invert the order of ion ejection Figure 2 shows the results recorded for this experiment. Mass resolution was much poorer for the reverse scan experiment The cause for this loss in resolution is unclear, but it is suspected that the higher-order field components in the trapping field may be responsible for this effect.[3] Variations in the ejection time of all the isotopes (i.e. mass shifts) in this experiment were small until the ionization time was increased above 300 ms.

In a another set of experiments, it was demonstrated that space-charging affects the ejection time of specific isotopic peaks from one scan to the next Figure 3 shows that the ejection time for m/z 770.4, shifted from scan to scan, while the signal that represented m/z 772 4 remained fixed when the forward scan rate was 103 Da/s and the ionization time was 120 ms When the ionization time (i e the number of trapped ions) was reduced, this shift in peak position was minimized

Figure 4 shows the results obtained when the ionization time was held constant and the pressure of the helium buffer gas was varied These results show that the position of the peaks shifted, most likely due to the increased number of ions that were trapped during the injection period. Mass resolution also decreased as the pressure of the buffer gas was increased.

These studies show that the ionic environment plays an important role in determing how accurately masses are measured with the quadrupole ion trap mass spectrometer The accuracy of mass measurement is improved when internal calibration is performed since the trapping conditions are the same for both analyte and calibrant ions. Reduction of ion-ion interactions along with the use of internal calibrants should allow the accuracy of mass measurement obtained with the quadrupole ion trap to be improved further.

References

1. J.D Williams, R.G Cooks, *Rapid Commun. Mass Spectrom.*, **6**, 524 (1992).
2. J.C. Schwartz, J.E.P. Syka, I.Jardine, *J. Am. Soc. Mass Spectrom*, **2**, 198 (1991).
3. J. Franzen, *Int. J. Mass Spectrom Ion Processes*, **106**, 63 (1991)

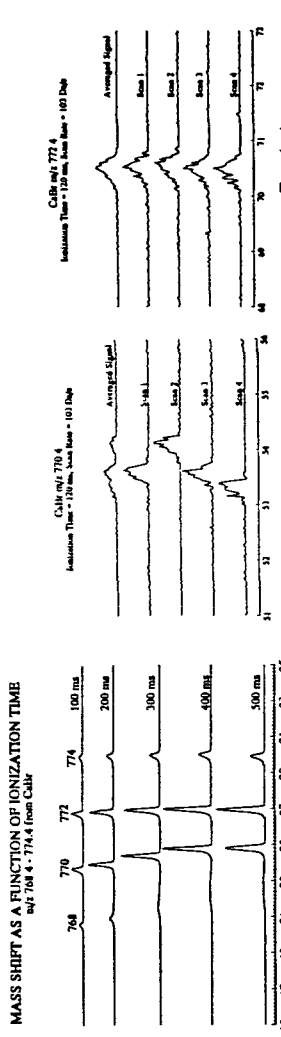

Figure 1 Signals recorded for $Cs_4Br_3^+$ ions (m/z 768.4 - 772.4) when the ionization time was varied. The scan rate was 628 Da/s.

Figure 2 Signals recorded for $Cs_4Br_3^+$ ions (m/z 768.4 - 772 4) at various ionization times The scan rate was -628 Da/s.

Figure 3 Portions of single scan spectra of CsBr clusters when the scan rate was 103 Da/s.

Figure 4 Signals recorded for $Cs_4Br_3^+$ ions when the pressure of He bath gas was varied.

Uni-Directional Ion Ejection in Ion Trap

*Edward Marquette & * Mingda Wang*
Varian Chromatography Systems, 2700 Mitchell Dr., Walnut Creek, CA 94598

In current ion trap mass spectrometry, the symmetry of the electric field causes ions to be ejected towards both end caps so that only half of the ions are collected by the electron multiplier. Since the maximum number of ions stored in an ion trap without degrading mass resolution is limited, the detection limit is reduced by not using the other half of the ions. Franzen [1] showed in his trajectory simulation that ions could exit from one end cap by adding a hexapole term, which was achieved by changing the shape of the trap electrodes.

We have developed a novel and practical unidirectional ion ejection method without any geometric modification of the trap electrodes. In the method, **an RF (not DC) dipole and/or monopole field**, which has the same frequency as that of the trapping field, is applied to the two end caps. The superimposed dipole field shifts the ion packet towards one of the end caps (see Figure 1) and forces ions to exit preferably towards that end cap. This is achieved by minor electronic circuit modifications of the Varian Saturn II GC/MS mass spectrometer. Since it does not rely on the non-linear resonance ejection, this new method places **no constraints on the axial modulation frequency**. For example, in our experiments, the standard 485 KHz was used as the axial modulation frequency. By contrast, the method of reference [1] requires the axial modulation frequency to be 1/3 of the trapping field frequency - the non linear resonance frequency as reported in reference [1]. Figure 2 shows the PFTBA spectra acquired with/without superimposed rf dipole field. The ion signal is doubled when an appropriate dipole field is applied. A computer simulation with the SIMION program also confirms that with a 3% of dipole field, the ratio of ion exiting two end caps is about 4 to 1. With our new approach to ion ejection, **the non-linear field can be switched on and off and the exit direction of the ions is changeable**.

In an ion trap, negative and positive ions are able to be confined simultaneously. With our new method, negative and positive ions are forced to exit in the opposite directions due to their opposite electric polarity. Therefore, **negative and positive ions may be detected simultaneously and separately** by this new method.

[1] J. Franzen, Int. J. Mass Spectrom. Ion Proc., 106, **1991**, 63-78.

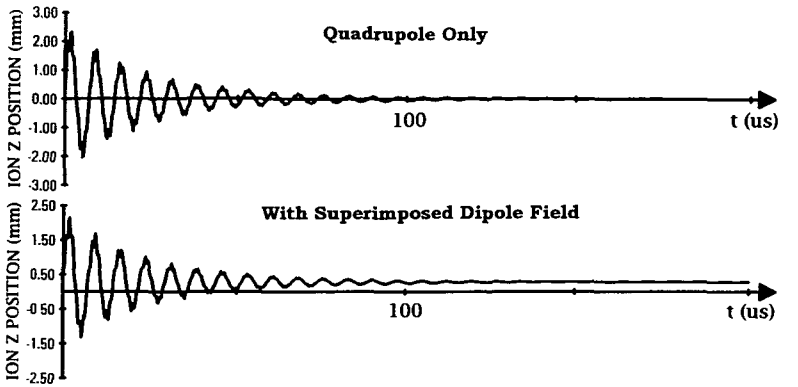

Figure 1: Ion trajectory calculated by the SIMION program. The upper figure shows that ions gradually migrate to the trap center due to collisions. The middle figure shows that if a dipole field is superimposed on the quadrupole field, the ion packet is shifted towards the electron multiplier.

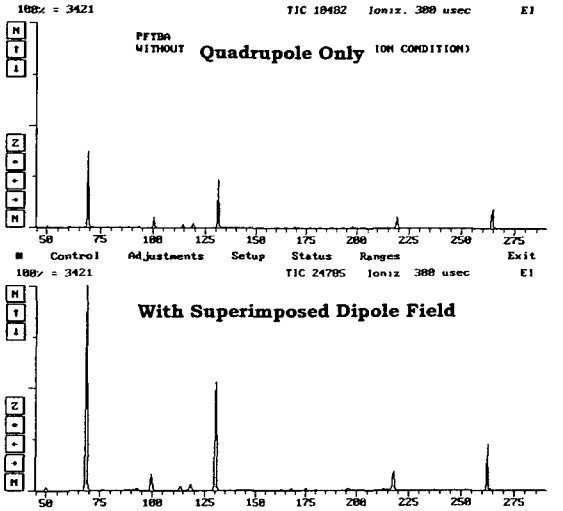

Figure 2: The PFTBA mass spectrum in the lower figure is acquired under the same conditions as the upper one except a dipole field is superimposed on the quadrupole field. Since all ions exit in the direction of the electron multiplier, ion peaks are doubled in the lower figure.

Internal Ion Impact Ionization in FT/ICR/MS

Troy D. Wood and Alan G. Marshall[†]

Departments of Chemistry (and Biochemistry)[†], The Ohio State University, 120 West 18th Avenue, Columbus, OH 43210

Lutz Schweikhard

Institut für Physik, P.O. Box 3980, D-6500, Mainz, Germany

A new method for the generation of ions has been developed for use with FT/ICR mass spectrometry. Low-mass (high ion cyclotron frequency) ions may be excited to high kinetic energy in the form of projectiles to ionize and fragment neutrals species in an ICR ion trap [1,2]. Projectile ions (e.g. H_2O^+, N_2^+, Al^+) are formed inside the trap by standard ionization methods (e.g. electron impact, laser desorption) and are excited to large ion cyclotron orbital radius. High-energy impact of the ion with neutrals in the trap serves to ionize the neutrals, after which standard FT/ICR excitation/detection is employed. Because the projectile ions are themselves trapped within the ICR trap, we denote this MS/MS procedure as *Internal Ion Impact Ionization (IIII, or I^4)*. The primary motivation for these experiments is the availability of high collision energy in the center-of-mass frame, leading to considerable fragmentation of the neutral species.

The first experimental applications of this technique are shown. Figure 1 shows one such demonstration: ions from both N_2 and perfluorotributylamine (PFTBA) are generated by EI in an ICR trap (top); all ions with ion cyclotron frequencies below that of N_2^+ are ejected from the trap (middle); the remaining N_2^+ ions are then excited to larger ICR radius to serve as projectiles for ion impact ionization with neutral PFTBA (bottom). Figure 2 is a plot of FT/ICR magnitude-mode signal peak area as a function of duration of excitation of N_2^+ projectiles; the signal for PFTBA fragment ions clearly increases with the duration of resonant excitation of the projectile ion until the projectiles gain sufficient kinetic energy to be ejected from the trap. Ionization is not achieved merely by menas of thermal gas-phase reactions between N_2^+ and PFTBA, as evidenced by the absence of PFTBA fragment ions even after several tens of milliseconds in the absence of excitation of projectile ion cyclotron motion. Ionization is therefore achieved only by impact of projectile ions on neutrals. Ion impact ionization is effective even with off-resonance cyclotron excitation of the projectile ions. We have also produced ion impact ionization with N_2^+ projectiles onto acetophenone, as well as with other projectiles formed by electron impact (e.g. H_2O^+).

Finally, ions formed by laser desorption may also be employed as projectiles. For example, Al^+ generated by laser desorption from aluminum foil for ion impact ionization of acetophenone produces acetophenone fragment ions as well as $Al(acetophenone)_n^+$ (n = 1,2) ions. Off-resonance excitation of the Al^+ projectile ions seems to be particularly effective in producing acetophenone fragment ions. Work supported by NSF (CHE-9021058) and The Ohio State University.

1. Schweikhard, L.; Alber, G. M.; Marshall, A. G. *Physica Scripta* **1992**, *45*, 598-602.
2. Schweikhard, L.; Alber, G. M.; Marshall, A. G. *JASMS* **1993**, *4*, 177-181.

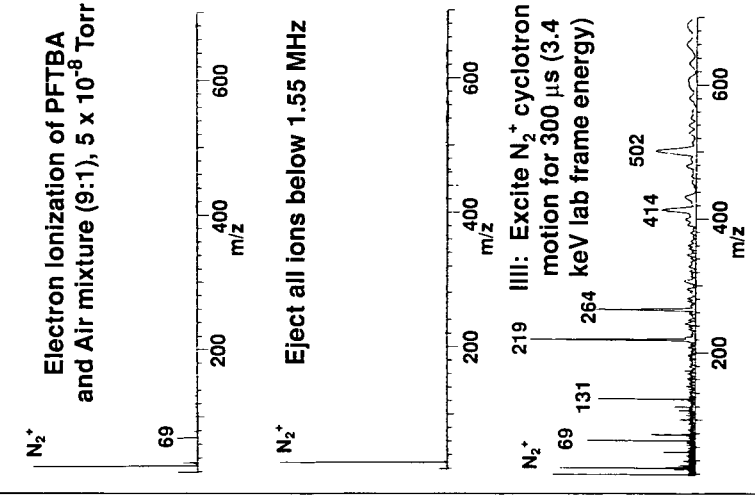

Figure 1

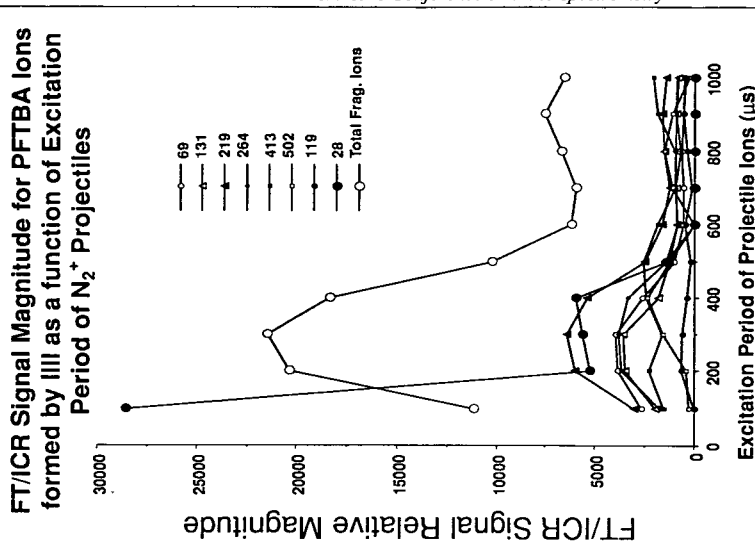

Figure 2

Mass-selective Ion Accumulation in the Ion Trap: Ion Injection using Filtered-Noise Fields

Keiji G. Asano, Douglas E. Goeringer, Scott A. McLuckey
Oak Ridge National Laboratory, Oak Ridge, TN 37831-6365

Don Hoekman, Teledyne MEC, Mountain View, CA 94039
Steven W. Stiller, Hitachi Instruments, Inc., San Jose, CA 95134

The quadrupole ion trap has become a very versatile analytical instrument due in part to its adaptability to various ionization methods as well as its sensitivity and tandem mass spectrometry capabilities. Another characteristic of the ion trap that can be exploited for chemical analysis is the ability to accumulate ions. Specifically, the sample dynamic range can be extended beyond the working range of stored ion number densities by controlling the duration of ion formation or introduction. This method, which allows accumulation times to be maximized for low sample concentrations and limited at high sample concentrations, is most effective in systems such as GC/MS where the analyte ions are the most abundant species in the mass spectrum. However, the degree of dynamic range enhancement is minimal when analyte ions comprise only a small fraction of the total ion signal, the sample dynamic range then being limited by the matrix ion number density. This is the case for our instrument, a Finnigan-MAT ion trap mass spectrometer (ITMS) modified with an atmospheric sampling glow discharge ionization (ASGDI) source, which is used for analysis of trace organics in air. Nevertheless, even in such cases further improvements can be realized if ion accumulation is performed in a selective manner. One such method is a wideband resonance excitation technique using filtered-noise field (FNF) technology recently developed by Teledyne-Hitachi.

In the FNF, a signal having evenly spaced frequency components (250, 500, or 1000 Hz) and spanning the secular frequency spectrum (10-500 kHz) for the entire ion trap mass/charge range is digitally synthesized by the Teledyne-Hitachi HST-1000 module. Subsequent digital processing allows the signal to be notch-filtered to effect mass-selective ion accumulation. In addition to mass-selective accumulation, mass selective ion isolation (single m/z, multiple discrete m/z values, continuous m/z range, and discontinuous m/z ranges), selected reagent CI, and tandem mass spectrometry (ThP 106) are possible with the FNF. This paper reports on our experiments using the FNF during the ion injection process. The mass spectra were taken with a 1 s injection period with trinitrotoluene (TNT) and sulfur as our analyte. The mass spectrum in Figure 1 was taken without applying the FNF and shows very little signal from the molecular anion (m/z 227) of TNT and from sulfur clusters at m/z 64, 96, and 128. Figure 2 shows the same mass spectrum with the FNF signal applied during ion injection. The signal for the molecular anion of TNT is approximately ten times greater. Figure 3 is a magnified view of Figure 1 in the mass/charge range where sulfur cluster ions should appear. The S_4^- ion (m/z 128) can be identified, but ions from S_2^- (m/z 64) and S_3^- (m/z 96) are obscured by the matrix ions. Figure 4 shows the same region when the FNF signal is applied and demonstrates both multiple, discrete ion accumulation as well as improved signal intensity.

Research sponsored by the U.S. Department of Energy, Office of Safeguards and Security, under Contract DE-AC05-84OR21400 with Martin Marietta Energy Systems, Inc.

Presented at the 41st ASMS Conference on Mass Spectrometry

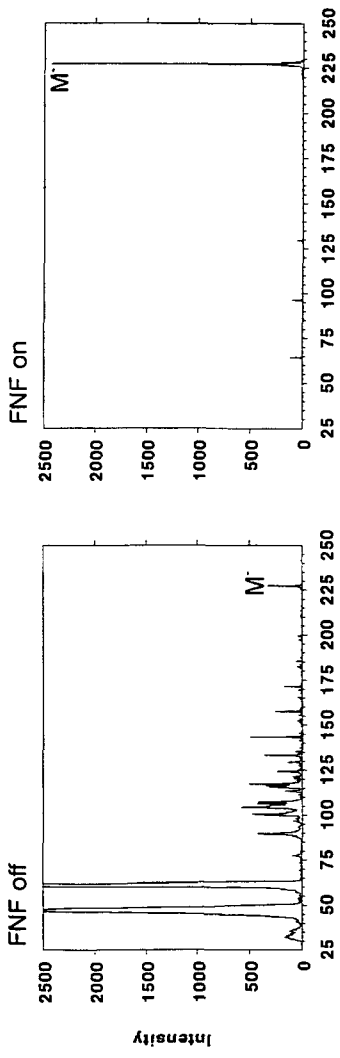

Figure 1

Figure 2

Figure 3

Figure 4

"The submitted manuscript has been authored by a contractor of the U.S. Government under contract No. DE-AC05-84OR21400. Accordingly, the U.S. Government retains a nonexclusive, royalty-free license to publish or reproduce the published form of this contribution, or allow others to do so, for U.S. Government purposes."

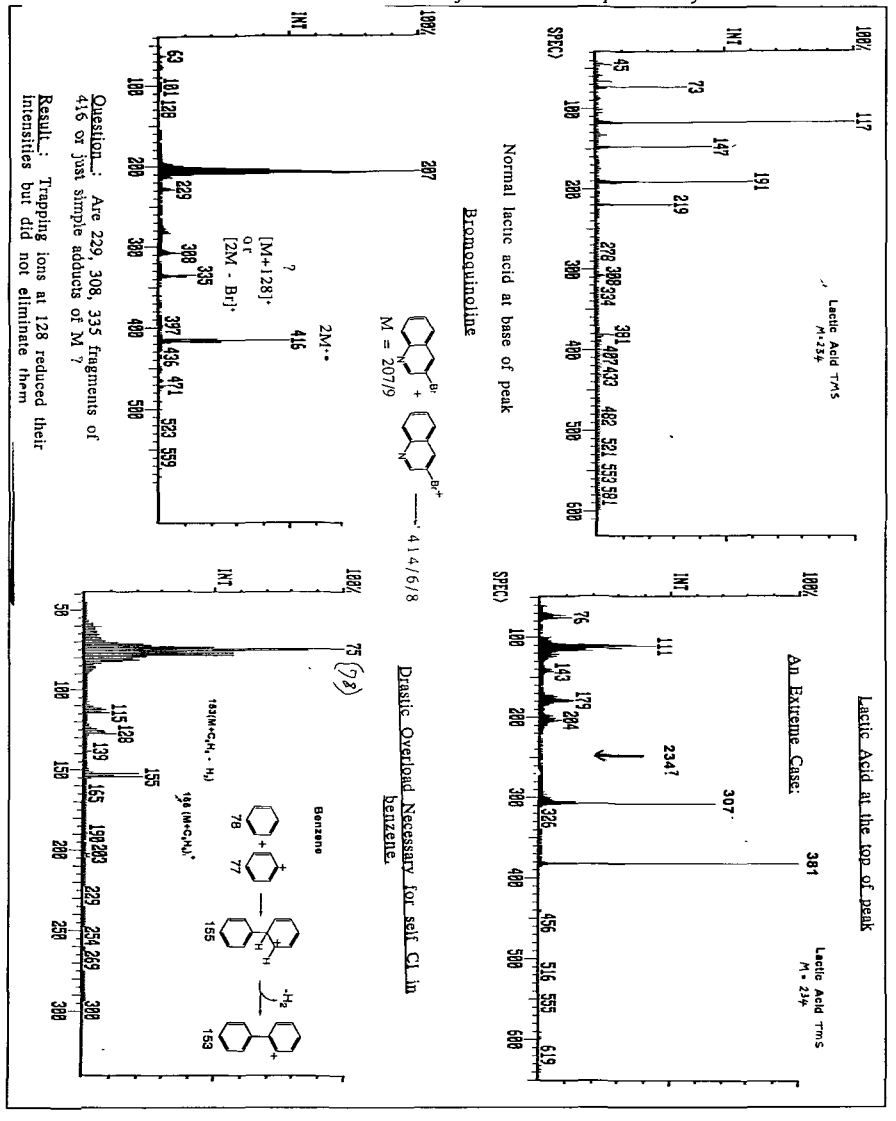

SELF_CI IN THE ION TRAP

Krishnaswany Nagarajan1, Henry M. Fales2, and Lewis K. Pannell3,
1. Armed Forces Institute of Pathology, Washington, DC 20306, 2. NHLBI, NIH, and 3. NIDDK, NIH, Bethesda, MD 20892

The many advanteges of the ion trap mass (high mass range, high resolution, msn capability, sensitivity, etc.) are not bought without certain concurrent disadvantages including susceptibility to space charge effects, ion-molecule reactions ("self-CI"), and difficult mass assignment at high mass. The first problem is overcome with the Finnigan automatic electron gating system ("AGC") while the second requires careful attention to limit the amount of sample admitted to the trap, In practice this is not always convenient, and when a second analyte is present in overwhelming amounts, not always possible.

We have examined self-CI in the trap with a variety of compounds including trimethylsilyl derivatibes of short chain acids of the Krebs cycle, aliphatic and cycloaliphatic amines, esters and various halogenated species to determine the relative concentrations required to cause self-CI. The types of ion-molecule reactions that result are themselves interesting (e.g., M+73 an M+147 in TMS derivatives) and, as in classical CI, occasionally reveal the molecular weight when a molecular ion is not present. In addition, use of the tickling facility provided with the ITMD (Finnigan) version of the ion trap allows selective removal of the adducting ion.

In the accompanying spectra we show the effects of lactic acid trimethylsilyl ether under heavily overloaded conditions compared with the normal spectrum. Space charging has diminished the intensities of the normal ions below 219 and the ions at 73 (TMS) and 147 (TMSIODMS) have adducted to the normal molecule of mass 234. Interestingly, the most intense ion at m/z 117 (COOTMSI) does not adduct under these conditions probably because it is a weaker Lewis acid due to the charge being distributed into the carbonyl. Within the small class of compound types examined here, we were not able to predict the type of reaction that would occur. Thus simple dimerization was seen with bromonaphthalene, M+(M-1) with others, and 2M+H in some cases. The only clear correlation found is that for self-CI to be prominant the molecule needed to be a good Lewis base since, by definition, the cation is a good Lewis acid.

COMBINED RF AND MAGNETIC TRAPPING IN A HIGH PRESSURE FOURIER TRANSFORM MASS SPECTROMETER

C. L. Hendrickson, E. G. Schmidt and D. A. Laude, Jr.; Department of Chemistry and Biochemistry, University of Texas at Austin, Austin, TX 78712

Fourier transform ion cyclotron resonance mass spectrometry (FTICR) traditionally employs collinear static electric and magnetic fields for the purpose of ion trapping. The magnetic field confines ions in the plane perpendicular to the magnetic field axis while the electric field traps the ions along this axis (normally referred to as the z-axis). This type of trapping has proven adequate for successful operation at relatively low pressure. However, the performance of the instrument deteriorates as the cell pressure is increased. This is due to the radial electric field associated with the static z-axis electric field which, in conjunction with collisions, causes rapid ion loss through expansion of their magnetron orbit. Situations in which high pressure is desirable include ion-molecule reactions, ion stabilization and ion cooling. Therefore, methods must be developed for high pressure ion trapping and relaxation.

One high pressure trapping technique which has shown great promise is the "RF-only" event currently employed by Gross and coworkers [1]. This method involves the use of high voltage RF trapping, similar to that of a quadrupole ion trap, during any event which exposes the trapped-ion cell to high pressure. Traps involving both a static magnetic field and an oscillating electric field were developed in the 1950's [2] and are known in the physics community as "combined traps". These traps, which have been investigated for use in laser and microwave spectroscopy, collisional studies and mass determination, have been shown to operate successfully at high pressure [3]. However, relatively little has been done to exploit the analytical utility of such a trap (for one example, see [4]). In this work, efforts to investigate and optimize this method of ion confinement are presented. An FTICR spectrometer which has been designed and constructed specifically for high pressure studies is described. FTICR spectra are presented comparing conventional static electric field trapping, RF electric field trapping and a combination of static and RF electric fields. Evidence for high pressure ion cooling is presented as well as an RF optimization study.

All experiments were performed on an electromagnet system consisting of a 4.1 cm cubic cell mounted within an ultra-high vacuum chamber which is pumped by a 1500 l/s diffusion pump to a base pressure in the mid 10^{-8} torr range. The cell electrodes are made of 80% transmissive hexagonal mesh to maximize conductance. Ionization is accomplished using a laboratory-built electron gun which is mounted on the cell flange. The vacuum chamber is mounted in 90 mm gap between the pole faces of a 1 Tesla electromagnet. The cell flange is equipped with two MHV electrical feedthroughs which allow up to 5 kV to be applied to the trap electrodes. Two leak valves and one set of pulse valves allow for the introduction of analytes and collision gases in both static and pulsed modes. Instrument control and data collection, which are shown in Figure 1, were accomplished using an Odyssey data station which was equipped with an Extended Trap Control Module*. The module allows RF voltage to be gated onto the trap plates from either an internal or an external source. In the internal mode the RF signal is taken from the cell controller and amplified by the module to a maximum of 80 V_{p-p}.

In preliminary experiments with the high pressure trap evidence was obtained which indicates that RF confinement can improve high pressure trapping performance. In these experiments naphthalene was used as the analyte of interest and helium served as the buffer gas. Helium was chosen in order to minimize ion scattering (and potential loss) through collisions with the buffer gas. Because of its high ionization potential it is also easy to exclusively ionize the analyte in the presence of this gas. To collect the data, naphthalene was leaked into the vacuum chamber at a pressure of 2 x 10^{-6} torr and ionized by a 12 eV, 500 nA, 8 ms electron beam

event. Helium was admitted through a second leak valve at a steady pressure of 2 x 10^{-5} torr (readings uncorrected). A 400 ms delay was inserted before excitation as a stringent test of trapping efficiency. Despite the high pressure a clean signal of adequate resolution is obtained.

Successful RF trapping generated spectra similar to the RF-off experiment suggesting similar trapping efficiency and cooling for the two trapping methods. The RF amplitude and frequency values were chosen after an optimization experiment using the previously stated conditions. Since 80 V is the upper limit of the internal RF, it is reasonable to think that higher voltages will improve performance.

The result of a third type of trapping were obtained. Here the combination of a 3 V DC potential and an 80 Vp-p, 600 kHz RF potential is applied during the 400 ms delay. This spectrum shows a significant increase in signal abundance, implying an improvement (~ a factor of three) in trapping efficiency and ion cooling.

As further evidence of ion retention and cooling, excite profiles were acquired in which ions are excited to a moderate cell radius followed by a cooling delay and subsequent excite to detect. The results of RF trapping are shown in Figure 2. As can be seen in the figure, the optimum cooling delay was 600 ms (as opposed to 50 ms for DC trapping) for these experimental conditions. Although the RF cooling is superior at long delays it appears to be less effective for shorter times. No explanation can be given for this anomaly at this time. However, these results are preliminary. In the future the experiment will be repeated while varying the first excite amplitude. This will reveal information about the efficiency of the cooling at different radii in the cell.

References

1. D. L. Rempel and M. L. Gross, J. Am. Soc. Mass Spectrom. 1992, 3, 590.
2. Fischer, E., Z. Phys. 1959, 156, 1.
3. D. J. Bate et. al., J. Mod. Optics 1992, 39, 305.
4. M. V Gorshkov et. al., Rapid Comm. Mass Spectrom 1992, 6, 166.

*We wish to acknowledge the gracious loan of the Extended Trap Control Module by Extrel FTMS.

Figure 1

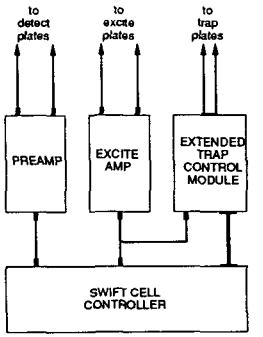

Figure 2

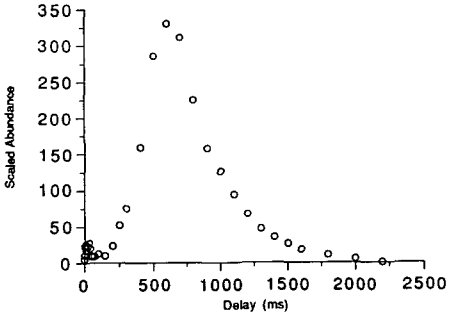

ELECTRON BEAM DEPRESSION AS AN ION TRAP IN FOURIER TRANSFORM ION CYCLOTRON RESONANCE MASS SPECTROMETRY

C.L. Hendrickson, F. Hadjarab and D. A. Laude, Jr., Department of CHemistry and Biochemistry, University of Texas at Austin, Austin ,TX, 78712

Electron beams are commonly used in Fourier transform ion cyclotron resonance (FTICR) experiments as ionization sources. Since the beam is terminated prior to any ion manipulation, excitation or detection, its affect on ion motion is rarely considered. It is known, however, that the space charge of the electron beam creates a potential well and that ions can be trapped for a relatively long period of time in such a well. The electron beam has been used extensively to ionize, trap and excite positive ions in order to measure a variety of properties such as ioization cross-sections and potentials. Recent emphasis has been placed on spectroscopic studies of highly-charged ions in instruments known as electron beam ion traps (EBIT). EBIT experiments are performed using a high magnetic field for radial electron beam compression and a static electric field for axial confinement of any generated ions. Since these conditions are identical to those employed in a typical FTICR experiment, it seems reasonable that ions formed by electron ionization may be trapped in the electron beam until its termination. In this work electron beam ion trapping is demonstrated to occur during the FTICR experiment and a model describing the confinement process is presented. Conditions for ion trapping and escape are demonstrated through the use of resistive-wall destabilization of the magnetron motion of ions in the FTICR cell. Plots of ion retention time versus ion number are consistent with a model in which ions are initially trapped in the electron beam but eventually "fill" the cell and escape into a magnetron orbit. The model predicts a potential well dependent on electron beam current, energy and dimension which is capable of holding a finite number of low energy ions. The model is compared to experimental results in both a qualitative and quantitative manner and good agreement is found. Several analytical applications of the technique are discussed.

An electron beam of energy V_e, current I_e, and diameter a will produce a radial potential depression V_t given by equation 1

$$V_t = \frac{I_e}{4\pi\varepsilon_0 V_e^{1/2}(2\eta)^{1/2}}$$

where η is the electron charge-to-mass ratio and ε_0 is the permittivity of vacuum. If the parameters used in the majority of this work (70 eV, 50μA) are substituted into equation 1, a potential well of about 0.1 V is obtained. This well depth is capable of trapping a substantial number of thermal energy ions. A graphical depiction of the well is shown in Figure 1 for a 70 eV, 50μA, 1 mm diameter beam.

Consider a case in which ions are formed by an electron beam away from the central axis of an FTICR trap. If the ions are not influenced by the electron beam they will start on a magnetron orbit as soon as they are formed and an annulus of ions will result. Therefore, only a small image current will be detected (that which is due to any asymmetry in the annulus). . However, if the ions are trapped in the beam they will be precluded from starting their magnetron orbit until after the beam is terminated. Now the ions are released in a coherent cloud and the image current in the detection circuitry is much greater. This causes resistive damping to occur much more quickly and the ion retention time to decrease. As ionization continues the well will "fill up" and ions will begin to leak into their magnetron orbit. This leakage will degrade the coherence of the cloud, thereby reducing image current and increasing retention time. Eventually, however, there are so many ions in the annulus that the density outside the well is greater than inside the well. Now the ions opposite the well are the source of a monopole which grows with ion number and brings the retention time to a minimum.

The results of experiments in which on- and off-axis electron ionization and subsequent detection of coherent magnetron motion were performed were presented. In Figure 1 ion number was altered by varying the electron beam event time. The on-axis data shows the expected exponential decay in retention time as ion number is increased. The off-axis data reflects the more interesting result expected from the previous discussion. The curve shows an initially rapid decrease in retention time due to efficient ion trapping and subsequent coherence of the magnetron motion. As ion number is increased the well "fills up" and ions leak into their magnetron orbit. This destroys the coherence of the motion and retention time increases. Eventually the retention time reaches a minimum.

Further evidence for electron beam ion trapping came in the form of ion transfer data from two similar dual cell experiments. The results are shown in Figure 2. In the "beam off" experiment ions were formed by electron ionization along the z-axis on the source side of the dual cell with 2 V trapping potentials on the trap plates and conductance limit. After termination of the electron beam the conductance limit was grounded during a variable ion transfer period. After transfer the conductance limit was raised and excitation and detection occurred in the analyzer cell. The data reflects rapid signal loss as the ions are forced to pass between cells more times. A logical explanation for this is that immediately after ionization the ions begin their magnetron orbit which, if not perfectly aligned with the conductance limit, takes many of them on a trajectory that strikes the conductance limit instead of passing through. It is obvious upon inspection of the "beam on" data that this does not occur during this experiment. This experiment differs from the "beam off" experiment in that the conductance limit is grounded throughout the ionization period which continues to occur dunng the transfer period. This data shows that ion abundance grows linearly with time which implies that no ion loss occurs during ion passage through the conductance limit. This observation can be explained by noting that the ions can be trapped in the electron beam. Therefore, if the electrons make it through the conductance limit, the ions will too.

Figure 1

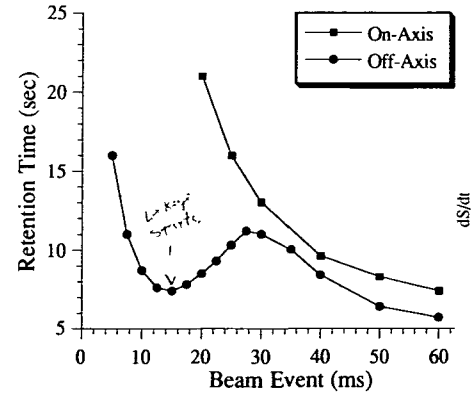

Figure 2. Ion Passage in the dual cell Experiment

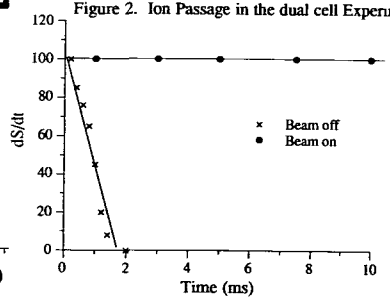

Ion/Molecule Reactions and Electron Detachment of O_2^- in a Quadrupole Ion Trap Mass Spectrometer

J. Murrell†, M.L.Langford†, J.F.J.Todd† and P.Watts‡
†The Chemical Laboratory, University of Kent, Canterbury, Kent, CT2 7NH, U.K.; ‡Chemical and Biological Defence Establishment, Porton Down, Salisbury, Wiltshire, SP4 0JQ, U.K.

Molecular oxygen anions have been the focus of much research as they play an important part in negative ion chemical ionisation, in ion mobility spectrometry and the negative ion processes of the atmosphere. To date there has been relatively little work published on the behaviour of O_2^- ions in the ion trap mass spectrometer, and this presentation reports on preliminary results on the trapped ion chemistry of this species.

The oxygen anions were created in an external DC glow discharge in 'zero grade' air and injected into the quadrupole ion trap (a modified Finnigan ITMS™); following a variable reaction period (utilising the method of 'dynamically programmed scans') the ions were analysed by ramping the amplitude of the RF drive potential. Typically the discharge chamber was maintained at 800 mTorr and the glow discharge current was *ca.* 7.0 mA; the helium buffer gas pressure in the trap was *ca.* 10^{-4} Torr.

There are essentially four major collisional means of increasing the internal energy of an ion in a quadrupole ion trap. These are by altering the q_z value at which the ion is stored, by applying an on-resonant tickle voltage, by boundary excitation and by varying the pressure and the composition of the buffer gas. All these methods can be used to excite ions to either dissociate or to react with a substrate where there is a need to overcome activation energies in order to form products.

The reactions were performed by setting the initial conditions and then incrementing the reaction time. The four types of experiment which were investigated were: (1) holding the O_2^- at constant q_z over a range of values; (2) holding the O_2^- at q_z values of 0.3 or 0.5 with a small on-resonant tickle voltage applied; (3) holding the O_2^- at a q_z value of 0.3 and setting various values of a_z; (4) the effect of removing the helium buffer gas from experiment 1.

For the Type (1) experiment storing O_2^- at a q_z value of 0.4 produces the plot shown in Figure 1. The only observed product of this reaction is NO_2^- which is thought to be formed by the charge-exchange reaction:

$$O_2^- + NO_2 \rightarrow O_2 + NO_2^-$$

involving NO_2 molecules formed in the discharge. The remaining loss of O_2^- is considered to be by electron detachment as the electron affinity of O_2^- is low (0.44eV). The logarithmic plots of O_2^- ion intensity *versus* time show excellent linearity, and Figure 2 shows how the plots depend upon the value of q_z during storage. Similar experiments in which either a low amplitude on-resonant tickle or in which the (a_z,q_z) value for the ion was held near to a stability boundary gave similar graphs. On the assumption that similar rate coefficients for O_2^- ion intensity reflect similar ion kinetic energies it is possible to superimpose the data on the same plot, and thus draw conclusions about the comparable degrees of ion excitation under different conditions (Figure 3). With the removal of helium from the trap and storing the ions at a q_z of 0.3 there is a greater rate of loss of O_2^- and less formation of NO_2. This demonstrates the cooling effect of the helium, indicating a possible competition between electron detachment from the O_2^- and electron transfer to NO_2.

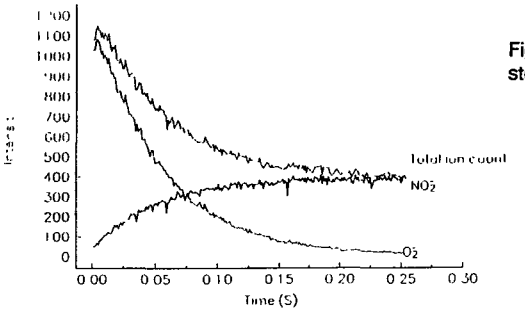

Figure 1: Reactions of O_2^- stored at q_z = 0.4

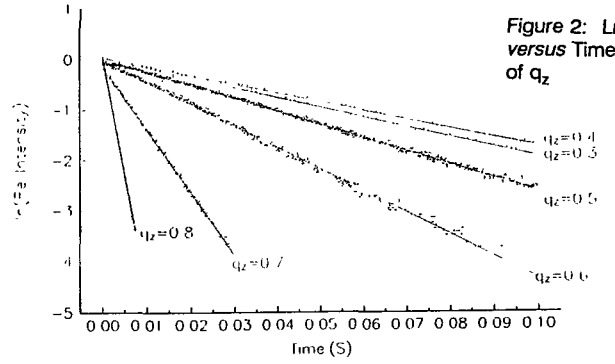

Figure 2: Ln(Rel. O_2^- Intensity) versus Time for different values of q_z

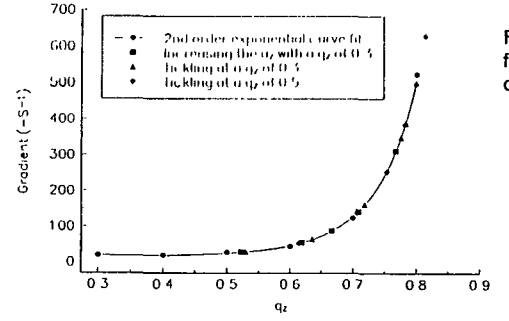

Figure 3: Decay coefficients for the loss of O_2^- under different conditions

Negative-ion fragmentation pathways of four isomers of dinitrotoluene (DNT)

M L Langford and J F J Todd

The Chemical Laboratory, University of Kent, Canterbury, Kent CT6 7NH, UK.

The present study examines the mass spectra and fragmentation routes generated by the dissociation of negatively charged isomers of DNT.

All experiments were carried out on a Finnigan MAT. Ion Trap Mass Spectrometer (ITMS) coupled to an Air Sampling Glow Discharge Ionisation (ASGDI) source. A few grains of either 2,3-, 3,4-, 2,5- or 2,6-DNT were placed inside an unheated sampling chamber and air was drawn over the sample into the glow disharge ionisation source. Collision induced dissociation reactions between energetic electrons and sample molecules gives rise to the production of neutral fragments. These fragments, and sample molecules, may form negative ions by the capture of low energy electrons. Negative ions produced in the glow discharge were directed into a quadrupole ion trap by a series of lenses. The application and manipulation of the RF and DC voltages applied to the ion trap is controlled by the construction of a scan function. This was defined using ITMS software to enable MS/MS/MS experiments to be performed in the ion trap enabling the examination of fragmentation routes down to the 3rd generation.

The negative-ion mass spectra of 2,5- and 2,3-DNT are very similar with base peaks at m/z 182, a strong peak at m/z 46, weak peaks at m/z 152 and 104 and a vanishingly small peak at 122 u. The mass spectrum generated by 3,4-DNT produced a weaker mass spectrum with additional peaks at m/z 135 and 137. The negative-ion mass spectrum of 2,6-DNT shows a base peak at m/z 182 with a

strong peak at m/z 46 and very weak peaks at m/z 122, 152 and 165. The negative-ion fragmentation pathways of 2,3-, 3,4-, 2,5- and 2,6-DNT observed in this investigation are shown the Figure.

It can be seen that the isomers 2,3-, and 2,5-DNT have straightforward fragmentation routes producing four daughter/granddaughter ions. The fragmentation pathways of 3,4-DNT are similar but with an additional fragment with m/z 135. The fragmentation pathways of 2,6-DNT are more complex with an additional fragmentation route initiated by the loss of OH. This additional fragmentation route may be due to the proximity of the two *ortho* NO_2 groups to the methyl group which increases the probability of a rearrangement leading to the loss of OH and the formation of the fragment seen at m/z 165.

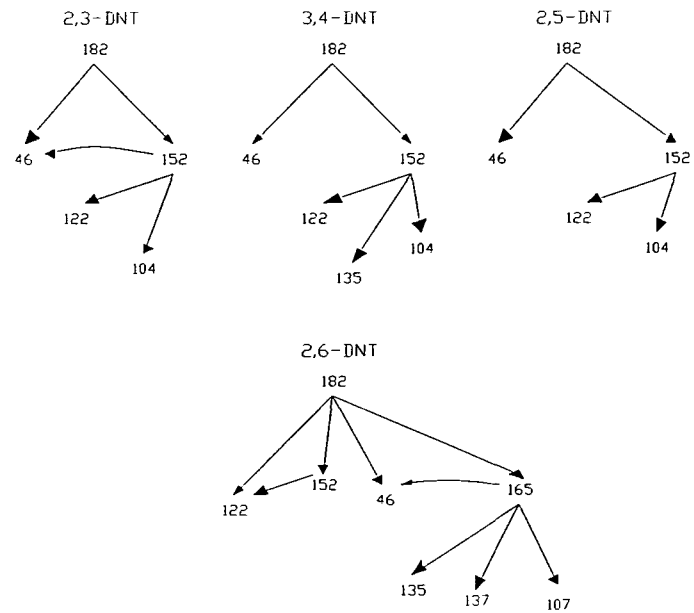

Extended Mass-to-Charge Range Operation of a Non-Linear Quadrupole Ion Trap

Kenneth Morand[1], Michael Schubert[2], Jochen Franzen[2] and Matthias Mann[1]
[1]Protein and Peptide Group, European Molecular Biology Laboratory, Heidelberg, Germany
[2]Bruker-Franzen Analytik GmbH, Fahrenheitstrasse 4, 2800 Bremen 33, Germany

Following the introduction of the Quadrupole Ion Trap Mass Spectrometer in the early 1980's there have been numerous advances. High mass, high resolution and external introduction of ions in particular have enhanced the applicability of the quadrupole ion trap to the analysis of biological compounds, paving the way for the introduction of the ion trap into the molecular biology laboratory.

Unfortunately, while mass spectrometry in general has made great advances in biological analysis and such instruments are now routine in these laboratories, the quadrupole ion trap has seen only limited use in this areas. Therefore, it is a goal of this research group to begin a program for implementing the ion trap and many of the developed methods into mainstream molecular biology analysis, emphasizing practical problem solving.

Figure 1 depicts the cesium ion desorption mass spectrum for the $[M+H]^+$ ion of substance P (Mr 1347.6). The mass spectrum was acquired for 5 pmole of the peptide mixed with 1 μL of the matrix solution on the tip of the direct-insertion probe. Ions were injected into the ion trap for 2 msec in the presence of 1 mTorr of helium bath gas. The scan rate was reduced by a factor of 16X with the results of a measured resolution of > 3000 (M/ΔM, FWHM).

Figure 2 shows the mass spectrum for the $[M+H]^+$ ion of substance P in the presence of 0.5 mTorr of laboratory air. A comparison of this data with the spectrum in Figure 2 reveals some loss of resolution (M/ΔM > 2000, FWHM). However, the loss is offset by an increase in the signal intensity of approximately 25% due to increased trapping efficiency [6]. In addition, the use of laboratory air as a buffer is beneficial for both increased energy deposition during MS/MS experiments[6] and when the ion trap is coupled with electrospray ionization.

Non-linear traps are characterized by a sharp octopole resonance, therefore, analysis utilizing this resonance point is associated with high mass accuracy. For this reason, extension of the m/z range was effected by a reduction of the RF drive frequency[5], instead of the standard method of resonance ejection, and allowed us to maintain mass analysis with the strong octopole resonance. Mass accuracy data is presented in Table 2 for the mass measurements of five peptides covering a period of six consecutive days.

Previous work in which the RF drive frequency was reduced to effect an increase in the mass range, undesirable effects were observed that included poor resolution even when the scan rate was significantly reduced. The results presented in this work suggest that high resolution may be maintained even at a significantly reduced drive frequency.

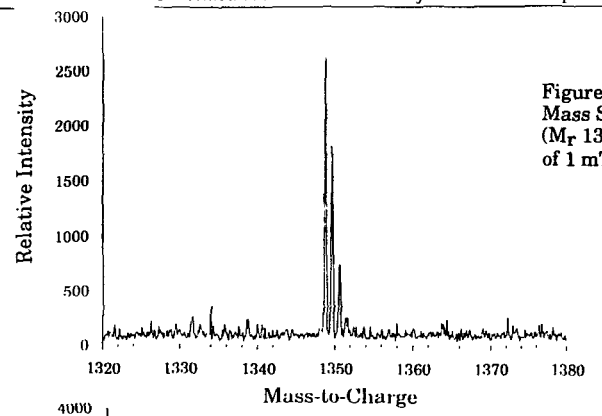

Figure 1: Cs^+ SIMS Ion Trap Mass Spectrum of substance P (M_r 1347.6) in the presence of 1 mTorr of Helium.

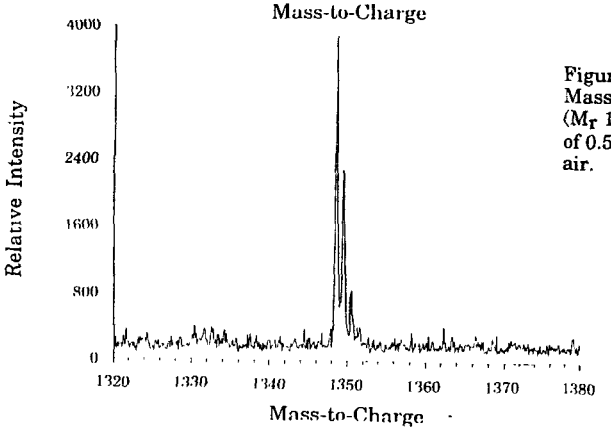

Figure 2: Cs^+ SIMS Ion Trap Mass Spectrum of substance P (M_r 1347.6) in the presence of 0.5 mTorr of Laboratory air.

Table 2: Variation of Experimental Mass Values over 6 Days

Sample	Theoretical Mass Da/e ($^{12}C_n+H$)$^+$	Day 1	Day 2	Day 3	Day 4	Day 5	Day 6	Average Mass	Standard Deviation	Percentage Error
n-acetyl MLF	452 2	452 3	452 2	452 1	452 1	452 1	452 1	452 1_5	0 076	0 011%
Leucine enkephalin	556 3	556 5	556 2	556 2	556 3	556 2	556 3	556 2_8	0 107	0 003%
Eledoisin Related Peptide	707 4	707 6	707 5	707 5	707 6	707 6	707 7	707 5_8	0 069	-0 026%
Bradykinin	1060 6	1060 5	1060 8	1060 3	1060 3	1060 3	1060 7	1060 4_8	0 203	0 011%
substance P	1338 7	1338 6	1338 3	1338 5	1338 5	1338 4	1338 8	1338 5_2	0 157	0 014%

Pulse Sequences for the Study of Simultaneously Trapped Positive and Negative Ions with ICR-Spectrometry

M.Paul, R. Malek, Y. Wang* and K.P. Wanczek,
Inorganic Chemistry, Universtity Bremen, D-28 Bremen 33
*Bruker Franzen Analytik GmbH D-28 Bremen 33

The ICR-Cell constructed by Y. Wang [1] is an effective new device for the study of positive and negative ion interaction. Positive and negative ions are stored simultaneously. Storage is possible for several seconds. Even generation and storage of double positve ions together with negative ions was achieved. Quantitative data on ion abundance can be acquiered. The properties of Xe and SF_6 are studied, with focus on the ions SF_6^- , $SF_5^{+/-}$, Xe^+ and Xe^{++}.

Experiments are carried out using a CMS-47 mass spectrometer with a 7 T superconducting magnet. The system is controlled by an Aspect 3000 microcomputer, and a personal computer.

A new cell parameter control program allows changes of the trapping conditions during the experiment. By this means charge selective axial ejection and thus determination of ion polarity is possible. In Figure 1 is a a broad band spectrum of simultaneously stored positive and negative ions of Xenon and SF_6 shown. ($Xe^{++}$and Xe^+-Isotopes, SF_6^-, $SF_5^{+/-}$, SF_4^+, SF_2^+, SF^+; SF_3^+ is ejected by double resonance). Having quenched positive ions, only SF_6^- and SF_5^- remain.

High resolution spectra can be acquired where positive and negative ions of identical atomic composition are resolved (resolution for SF_5^+/ SF_5^- is >100000). Figure 2 contains a high resolution spectrum of SF_5^+ and SF_5^-.

Combination of a pulsed valve inlet system and storage mode switches (e. g. from a mode storing one charge polarity only to a mode storing both charge polarities) during experiments allows charge selektive ion generation from several neutral species and study of their interaction. Electron ejection using trapping frequency resonance is employed for some experiments. These new features allow even storage of Xe^{++} together with negative ions.

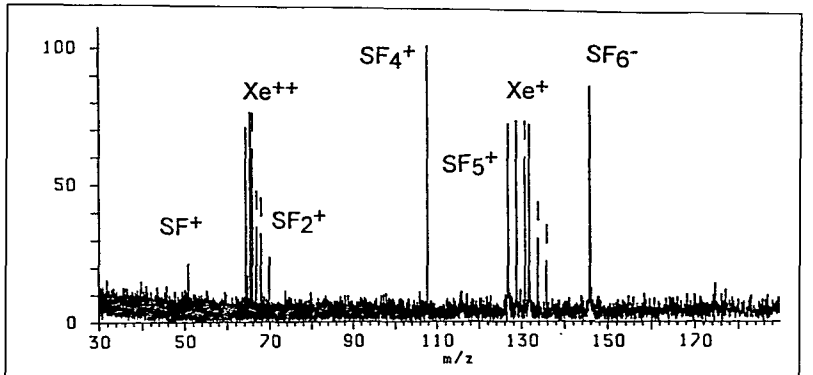

Fig. 1: Spectrum with Positive and Negative Ions Generated from SF_6 and Xe.

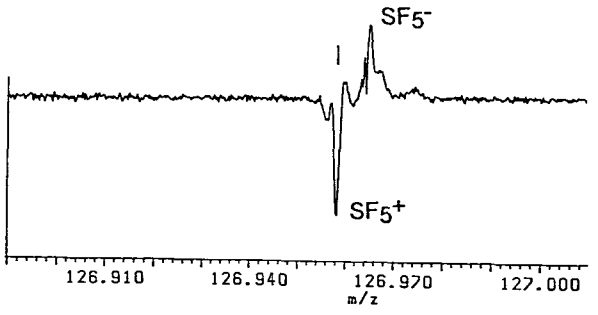

Fig. 2: High Resolution Spectrum of SF_5^+/SF_5^-.

References

[1] Y. Wang and K. P. Wanczek, Rev. Sci. Instrum. 64 (1993) 883-889.
Y. Wang Thesis Bremen 1992

Acknowledgements

Funding by the Deutsche Forschungsgemeinschaft is gratefully acknowledged. For genereous support we thank Mr. K. H. Kaiser from EMG, D-28 Bremen.

Multiparticle Simulations of Operating Modes of the Quadrupole Ion Trap Mass Spectrometer

R.K Julian, Jr., H.-P Reiser, R G Cooks, Department of Chemistry,
Purdue University, West Lafayette, IN, 47907

Small scale multi-particle simulations are used to characterize the ion motion of ensembles of ions under various kinetically excited conditions These conditions include (i) ejection via the $\beta_z = 1$ boundary, the so-called mass selective instability scan [1], (ii) resonant ejection and resonant excitation via an auxiliary (AC) field [2] The spatial and temporal relationships between ions of the same mass-to-charge ratio (m/z) under kinetically excited conditions is important because of the consequences for the mass resolution of the ejected ions. The random nature of the ion secular phase is introduced via an preliminary ionization simulation The key to mapping ion behavior is an accurate description of the motion of the ions within the ion trap under the influence of collisions, and higher order electric fields This study uses Poincaré sections to evaluate the role of buffer collisions during ion storage and resonant excitation. Higher order fields are evaluated via harmonic analysis Simulations of mass spectra collected from octopole field containing traps is also presented

The small scale simulation (ITSIM) is primarily used to visualize ion trajectories, in space as a function of time, and as phase space plots Phase space plots can be plotted directly or simplified by constructing Poincaré sections Figure 1 gives an example of three types of information available from a collection of stable ions of m/z 202 at $q_z = 0\ 4$ The top trace shows the x position, the second trace shows the z position and the third shows the total kinetic energy The fourth plot is a axial (z) phase space plot and the last is a Poincaré section of the phase space taken at the RF drive frequency of 1.1 MHz, sampled at a zero phase angle It has been observed that the mass resolution of the mass selective instability scan can be greatly improved by performing resonant ejection either near the stability limit or much below the stability limit [3] Some explanations for the difference in resolution can be observed by comparing Figures 1 and 2. In Figure 1 a single ion of m/z 202 is just brought to the instability point (q_z=0 908) by applying ~2520 V_{0-p} to the ring electrode. In the presence of a buffer gas, the motion is stabilized within the electrode structure, despite mathematical instability. The trajectory plots for the x and z directions shows that the motion is erratic. The kinetic energy plot (KE) reflects the random nature of the motion The scattered Poincaré section indicates the stable attractor has been replaced with a chaotic attractor, which indicates that ions of the same m/z value with only slightly different initial conditions will have extremely different trajectories leading to a wide range of ejection times and hence to the low mass resolution

The chaotic situation in Figure 1 is to be contrasted by the stable condition shown in Figure 2 for the resonant ejection case Here ions at a $q_z = 0\ 4$ are resonantly excited with a 2 5 V_{0-p} field at a frequency of 160.911 kHz The trajectory plot indicates that in the presence of the buffer gas the motion is being dampened, however in the z direction that dampening is being balanced by the resonant excitation signal As shown in the Poincaré section, a limit cycle is created which all ions are driven

1. G.C. Stafford, P.E. Kelley, J.E P. Syka, W.F. Reynolds, J F.J Todd, Int. J. Mass Spectrom Ion Proc., 60 (1984) 85
2. R E. Kaiser Jr., R.G. Cooks, G.C Stafford, J.E.P. Syka, P H Hemberger, Int. J. Mass Spectrom. Ion Proc., 106 (1990) 79
3. M Weber-Grabau, P.E. Kelley, S C. Bradshaw, and D J Hoekman, Proc. 36th ASMS Conf. on Mass Spectrometry and Allied Topics, San Francisco, CA, 1988, p. 1106.

towards. In phase space, once two trajectories fall on the same limit, they are phase locked. This limit cycle forces the ions to become a coherent ion cloud with a very narrow range of maximum amplitudes and phase shifts. As the ion absorbs energy from the auxiliary field, the limit cycle will increase in diameter until the electrode dimension is reached and the ions are ejected. If the ions are given time to adjust to changes in the RF amplitude, the limit cycle will remain elliptical. When the RF ramp is slow, ions are allowed to equilibrate and to maintain their phase coherence, resulting in the high mass resolution observed when slow RF ramps are used

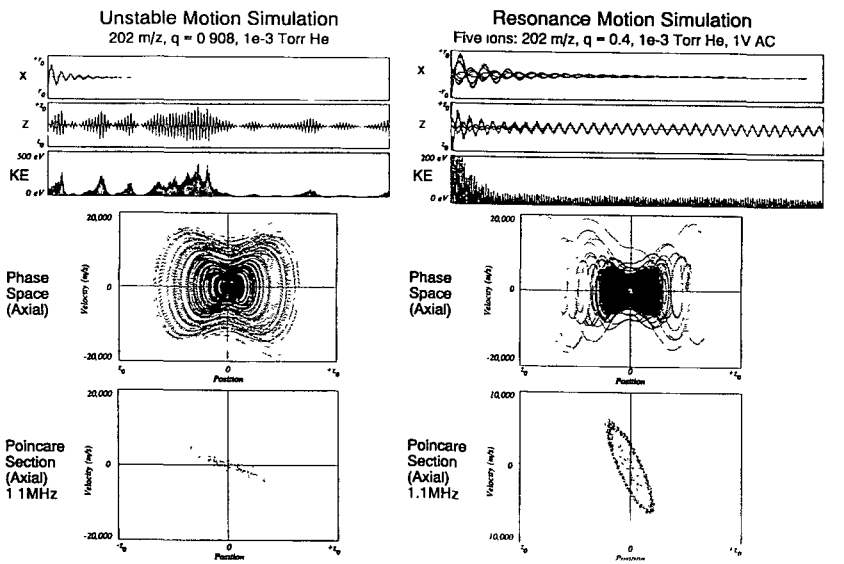

New Applications of Ion Tomography.

P.H. Hemberger,* M.L. Alexander, M.E. Cisper, and N.S. Nogar.
Los Alamos National Laboratory. Los Alamos, NM 87544
J.E.P. Syka. Finnigan MAT. San Jose, CA 95134.
J.D. Williams and R.G Cooks, Purdue University. W. Lafayette, IN 47907.

We have reported the mapping of ion distributions in the axial direction of the ion trap using laser photodissociation of trapped ions.[1] These studies have shown the effects of other molecules and ions on the distribution and the effects of resonant excitation on the distribution. They provide insight into the collisional damping process and provide data from which collision frequencies (300/sec at 10^{-3} Torr) can be obtained. By phase-locking the laser probe with the supplementary AC field, we have also determined experimentally the velocity and kinetic energies of ions subjected to resonant excitation.[2] We present new data that describes ion trajectories in the radial direction. These data are obtained by measurement of photodissociation product ion yield ($C_6H_3Cl_3^{+\bullet} \rightarrow C_6H_3Cl_2^+$) as a function of the radial position of the laser beam, i.e., the laser beam enters the ion trap through the *endcap* electrode. Because the ion trap can operate at relatively high pressures, the spectroscopy of collisionally excited and collisionally relaxed ions can be studied. Fig. 1 shows the photodissociation spectra at 10^{-4} Torr He and 10^{-5} Torr He. Transitions to excited vibrational states observed in the high pressure spectrum are washed out, presumably due to the greater number of excited vibrational and rotational states at lower pressures. The radial distributions of $C_6H_3Cl_3^{+\bullet}$ at $q_r = 0.1$ and 0.3 are shown in Fig. 2. As expected, the distribution at the higher q_r is narrower because the ions reside in a deeper potential well. Fig. 3 shows that ions are collisionally relaxed in the radial direction, just as they are axially. Resonant excitation at ω_z would not be expected to perturb ion motion in the radial direction. Although these motions would be independent in an ideal trap, they could be coupled through collisions with the helium buffer gas or by higher-order fields in the ITMS. Distributions measured at 10^{-4} Torr of helium with resonant excitation are broader than those with no AC voltage applied (Fig. 4). At lower helium pressures (10^{-5} Torr), no (or less) broadening would be observed if the motion in *r* and *z* were coupled solely through collisions. These experiments suggest that higher-order fields do contribute to the coupling of motion. This effect is difficult to quantitatively assess because the product ion abundance decreases at lower pressures.

1. P H. Hemberger, N.S Nogar, J.D. Williams, R.G. Cooks, and J.E.P Syka. *Chem. Phys. Lett.* **1992**, 191, 405-410.
2. J.D. Williams, R.G. Cooks, P.H. Hemberger, N S. Nogar, and J.E.P. Syka. *JASMS.* In press.

Photodissociation Spectra for Trichlorobenzene

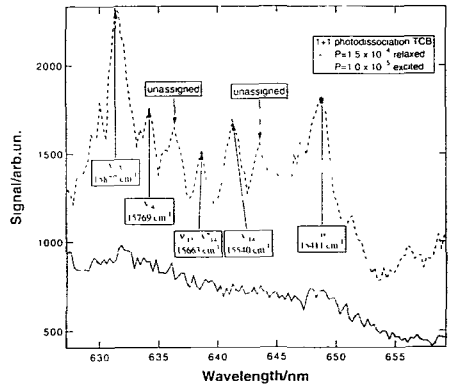

2 Radial Distribution of $C_6H_3Cl^{+\bullet}$ as a Function of q_r

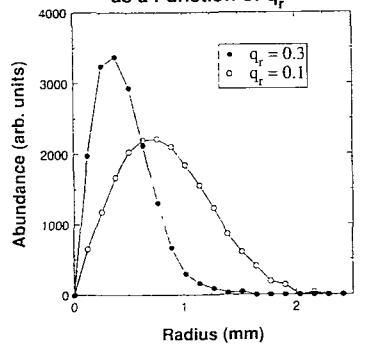

3 Buffer Gas Effects on Radial Distribution

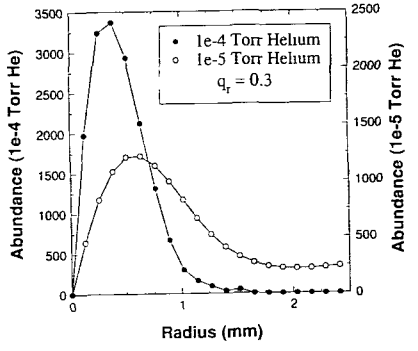

4 Resonant Excitation Broadening of Radial Distribution

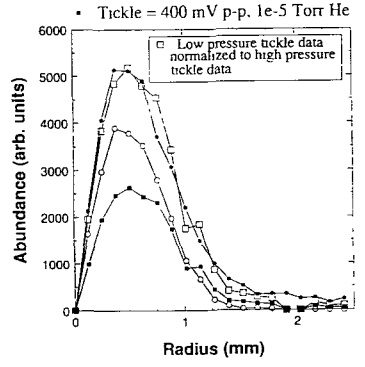

Computer Simulations of Ions in an Electrostatic Ion Guide for FT/ICR Mass Spectrometry

Michael A. May, Patrick A. Limbach, and Alan G. Marshall†

Departments of Chemistry (and Biochemistry†), The Ohio State University, 120 West 18th Avenue, Columbus, Ohio 43210

An electrostatic ion guide (EIG) consists of a conductive outer cylinder and a rigid central wire to which a dc potential difference is applied. Such an EIG can transport ions from an external glow discharge ion source through the strong magnetic field gradient of a 3T superconducting magnet, and ultimately into an ICR trap.[1] Here, we report the use of SIMION[2] to calculate initial conditions (ion mass, ion position, ion entry angle, ion kinetic energy, and EIG cylinder/wire voltage difference) under which low energy ions can enter the ion guide, traverse a strong magnetic field gradient, and exit the guide at the entrance to an ICR ion trap.

Figure 1 shows the geometry of the target, central wire, outer cylinder, and ICR trap electrodes. The nominal dimensions (in mm) of this EIG system correspond to a secondary ion FT/ICR mass spectrometer recently constructed in our laboratory.[3] Figure 3 shows the magnetic field map as a function of axial position (in both the z- and xy-directions) which was input to SIMION. Ion trajectory simulations under various initial conditions demonstate that low kinetic energy ions (1-10 eV) formed near the EIG entrance may be accelerated, transferred through the guide, and decelerated upon exit.

Figure 2 shows an ion trajectory in the xy- and xz-planes under the following initial ion conditions: m/z 1000, KE = 5 eV, entry angle = 10°, z_0 = 1012 mm, and r_0 =3 mm. For this trajectory, the wire was biased at -15 V and the cylinder at -10 V. The xy-plot shows that the ion ends up 7 mm off-axis; ergo an open-ended ICR trap would be experimentally desirable in this case.

At suitable EIG voltage difference, ions of various kinetic energy and entry angle may be efficiently captured in the guide cylinder. Figure 5, for example, shows that a 5 eV ion of m/z 1000 may enter the guide at a maximum angle of 15°–60°, depending upon the EIG voltage difference. The trajectory simulations also suggest that ion transport efficiency through the EIG depends strongly on ion initial position, velocity, mass, and entry angle. Figure 6 shows that 1000 u ions are transported through the EIG at entry angles of 10°–15° under specified conditions. Further simulations indicate that high-mass ions (of sufficient kinetic energy) should be efficiently transported through the EIG. This work was supported by NIH (GM-31683), NSF (CHE-9021058), and The Ohio State University.

1. Limbach, P. A.; Marshall, A. G.; Wang, M.; *Int. J. Mass Spectrom. Ion Proc.* **1993**, *000*, 000-000.
2. Simion PC/PS2, Version 5.0, Idaho National Engineering Laboratory, EG&G Idaho Inc., Idaho Falls, ID 83415.
3. Marto, J. A.; Guan, S.; Limbach, P. A., Wahl, M. C.; Marshall, A. G.; 41st ASMS Conference on Mass Spectrometry and Allied Topics, San Francisco, CA, May 30-June 1, 1993, Abstract #TP 182.

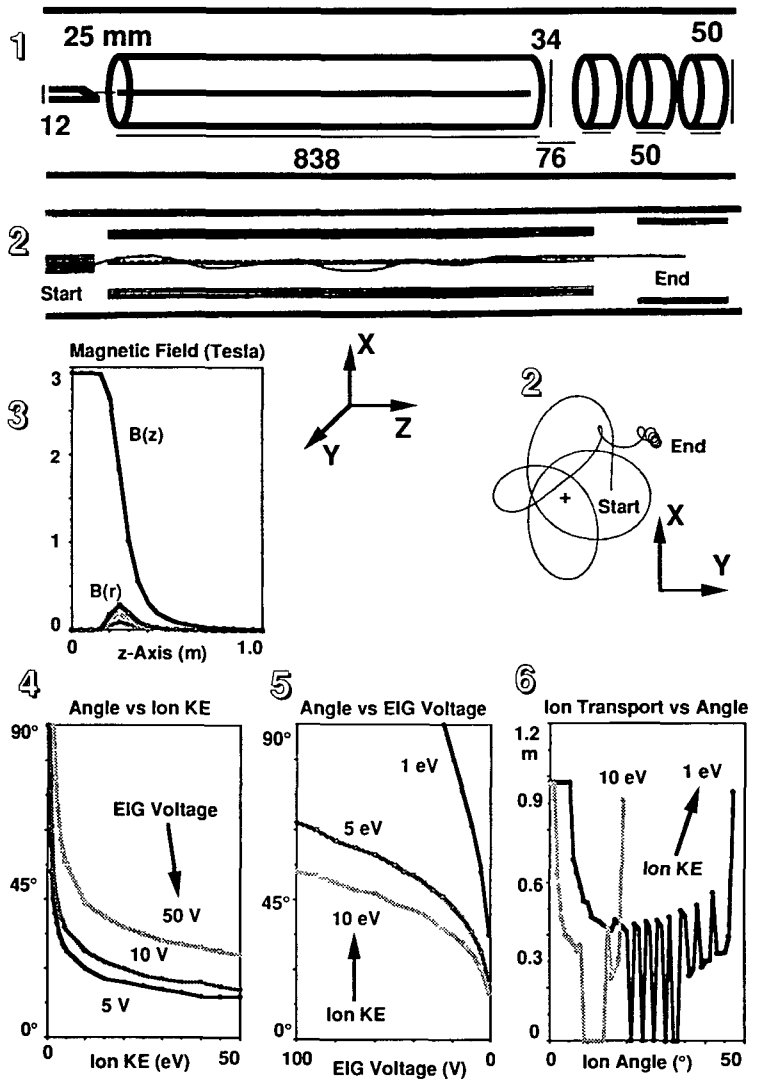

Investigations in Resonance Excitation in the Quadrupole Ion Trap Mass Spectrometer

*Randall E. Pedder[†], Jodie V. Johnson[‡], and Richard A. Yost[‡].
[†]Millipore Corporation, Extrel Mass Spectrometry, Pittsburgh, PA 15238
[‡]Department of Chemistry, University of Florida, Gainesville, FL 32611

Introduction. It has been observed that the effective collision energy in a collision-induced dissociation experiment in a quadrupole ion trap increases with RF trapping potential (the Mathieu parameter q). It has been observed that for small RF trapping potentials (low parent ion q) collision-induced dissociation fragmentation efficiency is poor. March et al.[1] have observed that for a given mass at a given RF trapping potential, the fluence (i.e. the product of resonance excitation voltage and excitation time) is constant to achieve either ion ejection or some degree of collision-induced dissociation. The objective of this work is to identify the dependencies of the resonance excitation experiment on acceptance aperture and pseudopotential well depth (maximum ion kinetic energy), to assist understanding of some of these observations.

Mathematical modeling of ion trap physics was performed using the BASIC computer program Hyperion[2]. Hyperion uses a fourth-order Runge-Kutta algorithm to numerically integrate the Mathieu equation with a dipolar field perturbation term.

Estimation of Maximum Ion Kinetic Energy. The energetics of a resonance excitation experiment are dependent upon the maximum amount of kinetic energy which an ion can have and remain in a stable trajectory within the ion trap cell. The maximum kinetic energy for a given ion increases with increases in the Mathieu parameter q as shown in Figure 1. For low trapping RF voltages (low q's) ions are resonance ejected prior to collision-induced dissociation because the ion collision energy is limited. As RF voltage is increased, the range of ion collision energies increases, resulting in more energetic reaction products.

Acceptance Aperture of a Quadrupole Device. The acceptance aperture of an RF quadrupole device is defined by the superposition of a family of acceptance ellipses calculated from an ion's trajectory. That area in phase space which is common to all phases of RF is identified as the acceptance aperture. For an RF-only quadrupole device, the relative acceptance (acceptance radius divided by inscribed radius) decreases with increasing q, as shown in Figure 2.

Fluence. The fluence required for resonance ejection of m/z 134 at various values of q is shown in Figure 3. The dramatic dropoff at q>0.8 of the fluence curve is attributed to the reduction in the size of the acceptance aperture of the quadrupole ion trap with increasing q. The curve shown in Figure 4 was calculated by scaling the maximum energy curve in Figure 1 by the relative acceptance curve in Figure 2.

For resonance ejection (axial modulation), maximum resolution is predicted to coincide with the maximum of the curve of relative acceptance aperture scaled by maximum kinetic energy a function of q (coinciding with maximum fluence) (q 0.6 to 0.8).

1. March, R.E.; McMahon, A.W.; Londry, F.A.; Alfred, R.L.; Todd, J.F.J.; Penman, A.D.; Vedel, F. *Int. J. Mass Spectrom. Ion Proc.* **1989**, *95*, 119-156.
2. Pedder, R.E.; Yost, R.A. *Proceedings of the 36th Annual Conference on Mass Spectrometry and Allied Topics*, San Francisco, CA, June 5-10, 1988, 632-633.
3. Major, F.G.; Dehmelt, H.G. *Phys. Rev.* **1968**, *170*, 91-107.

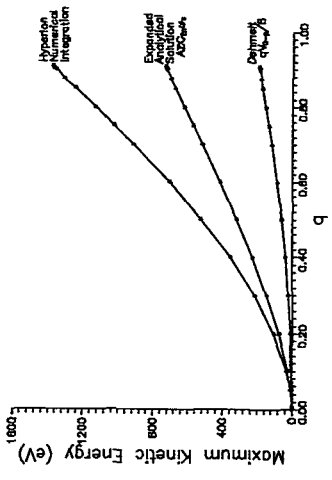

Figure 1: Maximum ion kinetic energies for m/z 134 as calculated via various methods as a function of the Mathieu parameter q.

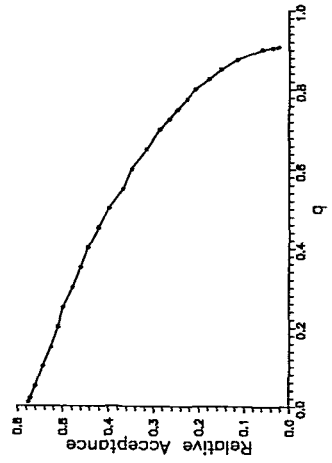

Figure 2: Relative acceptance aperture (ratio of acceptance radius/inscribed radius) for a quadrupole device.

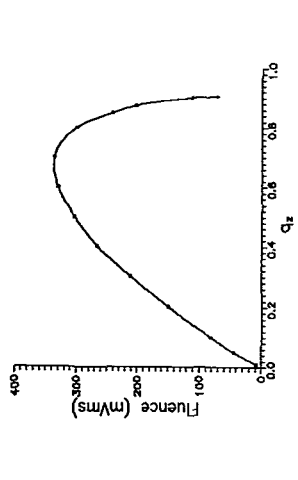

Figure 3: Fluence required for ejection of m/z 134 as a function of q_z as calculated using Hyperion.

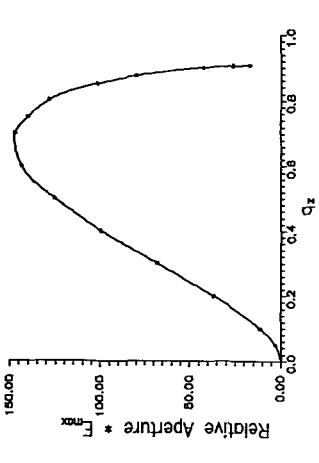

Figure 4: The product of relative acceptance aperture and maximum kinetic energy plotted as a function of q.

HIGH-MASS ANALYSIS ON THE QUADRUPOLE ION TRAP MASS SPECTROMETER

J.V. Johnson, M.M. Booth, J.L. Stephenson, Jr., R.R. Vargas, and R.A. Yost
Chemistry Department, University of Florida, Gainesville, FL 32611

The Finnigan MAT ITMS was introduced with a maximum mass range of m/z 650 using the mass-selective instability scan.[1] Subsequently, in an excellent paper, Kaiser *et al.* demonstrated that **axial modulation** provides the most straightforward and efficient method to increase the mass range of the ITMS[2]. Rearrangement of the definition of the Mathieu q_z parameter shows that the maximum m/z of a quadrupole ion trap can be determined by:

$$(m/z)_{max} = \frac{-8\ e\ V}{(r_0^2 + 2z_0^2)\ \Omega^2\ q_{z,eject}}$$

where, V = RF trapping voltage, m/z = mass-to-charge ratio of ion, Ω = frequency of RF trapping voltage, r_0 = ion trap ring electrode radius, e = charge on an electron, and $q_{z,eject}$ is the q_z value where ejection of ions occurs during the RF scan. **Mass range extension** is achieved by resonantly exciting and ejecting ions during the mass-selective instability RF scan, i.e. axial modulation. By reducing the frequency of the resonance voltage applied across the endcaps, the point on the stability diagram where ions are ejected occurs at a lower $q_{z,eject}$ and the mass range is extended.

The **objectives** for this research are to (1) characterize the mass range extension capabilities of the "standard" ITMS with respect to m/z range, mass resolution and sensitivity, (2) characterize the effect of the resonant excitation voltage on ion ejection, and (3) investigate the implications of resonant excitation for CID of high-m/z ions.

Experimental. The "standard" (unmodified) Finnigan MAT ITMS electronics were utilized for axial modulation. Internal electron ionization (EI) of perfluorotri-N-butylamine (FC43) and a perfluoropolyether (UltraMark 3200F) were utilized for the characterization studies. However, the low intensities of the higher m/z Ultramark EI ions and the contamination of the ITMS by this relatively non-volatile compound precluded its use and results from it are not reported here.

Effect of mass range extension on resolution. As the $q_{z,eject}$ is lowered and the mass range extended, there is a reduction in mass resolution. For example, for the m/z 614 EI ion of FC43, the peak width at 1/2 peak maximum increases from 1 to 5 to 30 mass units with mass range extension factors of 1, 10, and 30, respectively. This is the result of two major factors: increased scan rate and reduced resolution of resonant excitation. The scan rate of the RF voltage and ion signal sampling and integration response rate and times were designed for a m/z 650 mass range and is constant at ≈5550 u/s. With mass range extension, a greater range of m/z is scanned in the same time interval thus reducing the resolution. Below a q_z = 0.2, the effective frequency bandwidth that elicits resonant excitation begins to widen and the difference in secular frequencies of adjacent m/z ions decreases with decreasing q_z, i.e. mass resolution of resonant excitation is reduced with decreasing q_z. The

combination of high resolution techniques (axial modulation at slower scan rates) in conjunction with mass range extension may compensate for the instrumental limitations. However, further characterization of the ion physics is required to overcome (if possible) the limitations of the latter.

Effect of mass range extension on sensitivity. For $q_{z,eject}$ between 0.45 and 0.908, the sensitivity remains fairly constant. However, below a $q_{z,eject}$ of 0.45, the sensitivity decreases dramatically until at $q_{z,eject}$ of 0.1, the ion signal is often less than 1/100 of that at $q_{z,eject}$ > 0.45. It was observed that the sensitivity for higher m/z ions decreased first. This behavior suggests that the lower resonant excitation frequencies may act like a DC voltage resulting in a high m/z cutoff with low $q_{z,eject}$. Although multiple or longer duration ionization events can compensate for this, further characterization is necessary in order to determine the source of this phenomenon.

Effect of resonant excitation voltage on mass range extension. Either resonant ejection does not occur or collision-induced dissociation (CID) does occur at low resonant excitation voltages; both are undesirable. With increasing resonant excitation voltages, the "apparent m/z" of the ions decreases as they are ejected earlier. For example, as the resonant excitation voltage was varied from 1 to 6 volts, the m/z 219 EI ion of FC43 was ejected at an RF voltage level corresponding to low m/z cutoff levels decreasing sequentially from m/z 76 to m/z 71 while it's predicted ejection should have been at m/z 72.5. The resonant excitation voltage for optimum ejection increases with the m/z of the ejected ion. Further characterization is required to delineate the exact relationship between the resonant excitation voltage and the "apparent" m/z such that the m/z of an ion can be accurately assigned.

Resonant excitation CID of high-mass ions. Conventional MS/MS in the ITMS relies upon resonant excitation to increase an ion's axial kinetic energy sufficiently such that upon collisions with the buffer gas, collision-induced dissociation occurs. The efficiency of resonant excitation CID falls off dramatically below q_z (parent ion) of 0.20 for low m/z ions. This is due to the shallow potential well-depth at low q_z values resulting in ejection of parent ions instead of their CID. From the Dehmelt pseudopotential well model, the maximum center-of-mass (COM) collision energies can be estimated for a range of high m/z ions held at the maximum RF voltage (low m/z cutoff ≈650) possible on the ITMS. Even with collision gases more massive than helium, the available COM collision energies are minimal (with Xe, maximum kinetic energies (COM) < 10 eV for m/z < 3000). We have begun to characterize the use of **photo-induced dissociation (PID)** as an alternate means of performing MS/MS in the ITMS (see Stephenson *et al.* TP 155, ASMS, 1993). It offers a number of advantages over CID including being largely independent of an ion's secular frequency and q_z and being most efficient when ions are near the center of the ion trap where the optimum trapping of parent and daughter ions also occurs.

Acknowledgements. Nathan A. Yates (UF) for software modifications to ITMS and Randall E. Pedder (UF; now Millipore-Extrel) for use of his ion energetics program. Funding for this work was provided by EPA-EMSL/Cincinnati, EPA-ERL/Duluth, and the University of Florida Division of Sponsored Research.

[1]Stafford, G.C.; Kelley, P.E.; Syka, J.E.P.; Reynolds, W.E.; Todd, J.F.J. *Int. J. Mass Spectrom. Ion Proc.*, 1984, **60**, 85-98.
[2]Kaiser, R.E.; Cooks, R.G.; Stafford, G.C.; Syka, J.E.P.; Hemberger, P.H. *Int. J. Mass Spectrom. Ion Proc.* 1991,**106**,79-115.

EVALUATION OF A LOW COST, LOW HOMOGENEITY, VERTICAL BORE 7-T MAGNET FOR FTICR

J.S. Anderson, E. G. Schmidt, V. H. Vartanian, and D. A. Laude, Jr., Department of Chemistry and Biochemistry, The University of Texas at Austin, Austin, TX, 78712

INTRODUCTION

The adaptation of superconducting magnets for Fourier transform ion cyclotron resonance (FTICR) mass spectrometry has produced both higher magnetic field strengths and simplified external ion injection compared to conventional electromagnets. In addition, higher field strengths have the analytical advantages of extended mass range, extended mass resolution, and improved mass accuracy. Such utility is theoretically possible due to the increased magnetic flux present in the trapped ion cell at higher field strengths. As a result, coherent ion clouds can be constrained radially to a smaller volume and the detected cyclotron frequency is better defined.

Superconducting high field magnets specifically designed for FTICR have high magnetic field homogeneity and wide, horizontal bores for ready installation of FTICR vacuum chamber and cell. One disadvantage of such magnets is the rather large capital investment. We decided to evaluate a possible solution to such an expense: a vertical bore NMR-type magnet which costs a fraction of the horizontal bore FTICR magnet.

We have constructed an FTICR mass spectrometer based on an inexpensive vertical bore magnet of field strength 7.2 Tesla. Issues of concern in evaluating this magnet for FTICR performance include its narrow 86 mm bore and the poor magnetic field homogeneity of about 1000 ppm.

To be presented here are pilot studies of FTICR performance in our high field magnet. Initial efforts were directed at placement of the trapped ion cell within a homogeneous region of the magnet solenoid to optimize signal detection. A probe-mounted translatable cell was useful for this study.

EXPERIMENTAL

The FTICR instrument constructed around the vertical bore magnet is shown in Figure 1. The magnet was a 7.2 Tesla vertical 86 mm bore superconducting magnet designed and built by American Magnetics, Inc. (Nashville, Tennessee). To maximize bore diameter, a UHV flange was welded directly to the magnet warm bore. The cell flange assembly, electron beam assembly, laser desorption probe, and 1.50 inch cubic trapped ion cell constructed of OFHC copper fit easily inside the restricted bore The vacuum system was pumped by a diffusion pump which due to geometric constraints was located approximately 2 meters from the trapped ion cell. Consequently, overall pumping performance in this system was often inadequate and difficulty existed in reaching the low 10^{-8} Torr region

Of great concern was the placement of the trapped ion cell in the proper region of the superconducting solenoid. Due to large magnetic field inhomogeneities within the solenoid, 1000ppm over 1 cm diameter spherical volume (DSV), misplacement of the cell by a few mm could have deleterious effects with respect to signal detection and mass resolution. Taking this into account we have designed our cell to be translatable over a 12 mm z-axis region of the solenoid.

Using field mapping values obtained from the manufacturer, a plot of axial displacement versus field strength is shown in Figure 2. The optimum cell placement is also shown to illustrate the possible magnetic fields experienced by an ion in the cell at a point away from the suggested solenoid center.

RESULTS A study on the detected frequency of benzene at different axial cell positions shows a distinct change in Δf as the cell is displaced. As illustrated in Figure 3, the frequency change is much more pronounced in the 0-3mm and 8-12mm regions. This would indicate a greater inhomogeneity in these regions and a basis for the more severe frequency change.

Using this information, excite profiles of benzene were performed in two different regions of Figure 4, 4mm and 12mm displacement. Shown in Figures 4a and b are excite profiles which indicate an increase in ion loss at 12mm displacement. Besides the collisional loss mechanism which is also prevalent in the 4mm case, a very promenent reason for the loss of ion signal would seem to be the lack of magnetic field homogeneity as the cell is displaced from the center region of the solenoid.

The ability to better define the magnetic field effects on performance were hampered by the difficulty in achieving a good vacuum. Pressures in the cell typically ranged from high 10^{-8} Torr to mid 10^{-7} Torr. Consequently, the inability to obtain high resolution data at this point cannot necessarily be assigned to problems with the magnet, since every spectrum obtained exhibited a pressure-limited transient. We believe the pressure problem likely rests with an inadequate pumping scheme for our vacuum chamber design. Even if homogeneity is found to limit mass resolution performance for low mass ions, the effects will be less severe for the high mass applications intended with the mass spectrometer, specifically the MALDI experiment.

Short term future concerns will be focused on reducing the system pressure. Probe displacement experiments will then be repeated at sufficiently low pressure to better define performance. Given a magnet cost that is one-tenth the price of a standard 7T, wide bore horizontal magnet, there is a compelling argument for pursuing the performanace capabilities for high mass applications.

Figure 1

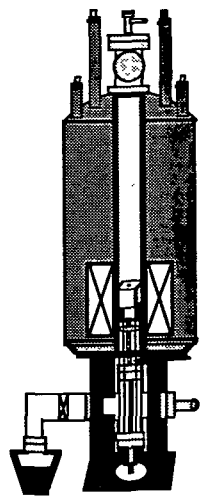

Figure 2

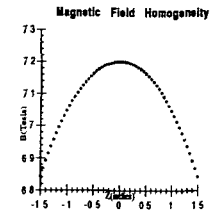

Figure 3

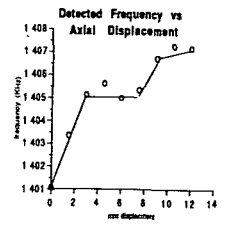

Figure 4a

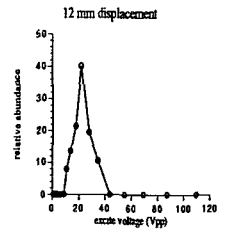

Figure 4b

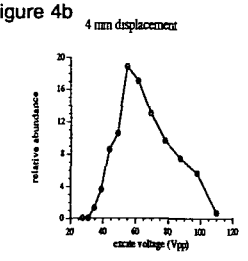

MATRIX-ASSISTED LASER DESORPTION/IONIZATION IN THE QUADRUPOLE ION TRAP: A NEW METHOD FOR TRAPPING ENERGETIC IONS USING CONTROLLED GATING OF THE TRAPPING FIELD

Vladimir M. Doroshenko and Robert J. Cotter
The Johns Hopkins University, Baltimore, MD

The ability of the ion trap to perform $(MS)^n$ experiments suggests broad opportunities for utilizing ion traps in biochemistry, protein chemistry and molecular biology, for elucidating the structures and sequences of biomolecules. MALDI has undoubtably become one of the most promising techniques for the desorption of biomolecule ions. The major problem during an introduction of ions formed external to the ion trap into the trapping field is that the ion kinetic energy needed to overcome the RF field also prevents trapping the ions. So far there has been only one approach to this problem which is to accelerate the ions to kinetic energies sufficient to penetrate inside the active RF field, and subsequently reduce their kinetic energies through collisions with a buffer gas. An additional approach has been discussed in the literature but never realized which involves phase-synchronized gating of the trapping RF voltage during the introduction of ions to the trapping field.

In this work we have developed a novel method for trapping ions formed by MALDI which involves gradual ramping of the RF field amplitude from zero to trapping values during the flight of ions into the center of the cell. The desorbed ions easily penetrate the weak electric field at the initial stage of RF ramping, and are trapped with high efficiency during the last ramping stage, when they reached the center of the trap. It does not require phase synchronization with the trapping field, or use collisions with helium atoms as primary method for reducing ion kinetic energy

A Finnigan MAT series 700 ITD has been modified for MALDI inside the trap using the fourth harmonic (266 nm) laser pulse from a Quantel International Nd:YAG laser. The 0.04" diameter probe tip was inserted inside the ion trap through the existing ~0.05" hole in the upper *end-cap* electrode normally used for introduction of the electron beam. The sample on the probe tip was illuminated by the focussed laser beam through the gap between the *ring* and bottom *end-cap* electrodes. In order to operate beyond the standard 650 u, *resonant ejection* of ions was used. Mass resolution was improved by slowing the RF voltage scan rate. In operation, the firing of the laser and onset of the gated fundamental RF voltage was followed by a 10-20 ms storage period. The rise time of the RF amplitude in response to switching on the control voltage was 20-30 μs. The settling value of the RF voltage at the storage period corresponded to the mass level of 450-520 u. Single-shot laser MALDI spectra were acquired by a digital oscilloscope using TOFWARE, a WINDOWS-based data acquisition system.

Spectra of several peptides obtained at different mass scan rates are shown in Figures 1 and 2. The buffer gas pressure of 10^{-3} torr was typical for normal trap operation and is several times less than that used in previous experiments. Using *Gramicidin S* as a test compound, we were able to observe spectra by our method at buffer gas pressure of $\sim 2\times10^{-4}$ torr. Highest resolution is achieved in a single-shot experiments (Figure 2b) and approached one in 12,000.

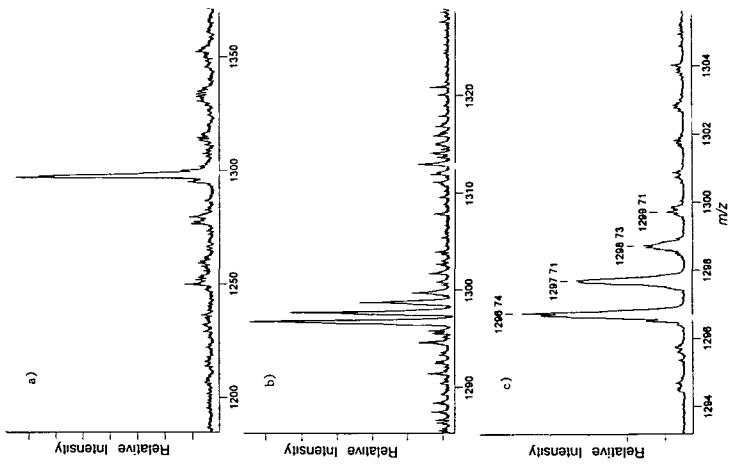

Fig. 1. The MALDI spectra of *Angiotensin I* obtained at the different mass scan rates. (a) 5555 Da/s, 12 laser shots are averaged, mass resolution R=880; (b) 1291 Da/s, 32 shots, R=3,800; (c) 373.3 Da/s, 49 shots, R=7,600.

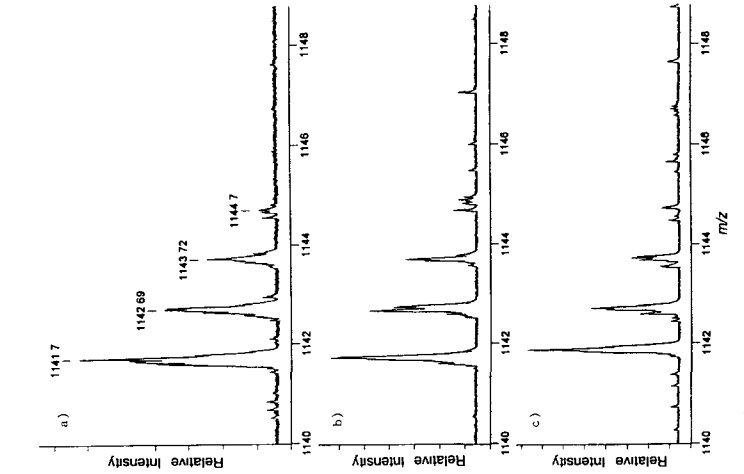

Fig. 2. The MALDI spectra of *Gramicidin S* obtained at the mass scan rate 330.6 Da/s: (a) 16 laser shots are averaged, mass resolution R=7,600; (b) single shot experiment, R=12,000; (c) space charge effect, single shot experiment.

The Development of Mass-selected Automatic Gain Control on a Quadrupole Ion Trap Mass Spectrometer

*Timothy P. Griffin, Nathan A. Yates, Richard A. Yost
Chemistry Department, University of Florida
Gainesville, FL 32611-2046

The quadrupole ion trap is a high performance mass spectrometer that exhibits high sensitivity, low limits of detection, and a large linear dynamic range (LDR). Increasing the ionization time to increase the number of ions can result in space charge effects (poor resolution, incorrect mass assignment) due to the high abundance of ions. To limit the effects of space charge while maintaining high sensitivity, Finnigan MAT developed automatic gain control (AGC)[1]. AGC automatically adjusts the ionization time dependent upon the total number of ions detected. AGC is limited, however, when two or more compounds of widely varying concentrations are present in the trap simultaneously. Since AGC detects the total number of ions in the trap, the ionization time is controlled by the major component, resulting in discrimination against compounds present at lower concentrations.

We are developing mass-selected automatic gain control (MSAGC) specifically for co-eluting compounds and complex mixtures. The scan function for MSAGC (shown in **Figure 1**) can be applied to: 1) co-eluting peaks of widely varying concentrations, 2) complex mixture analysis, and 3) GC/MS/MS. During the AGC pre-scan, two-step isolation was used[2,3]. The factors used to calculate the ionization time were optimized to give the best resolution and response while preventing space charge.

To characterize the MSAGC technique, the signal response for co-eluting compounds was investigated. For example, **Figure 2** shows two spectra for a mixture containing 4 ng of an M+8 analyte (m/z 199) and 525 ng of an M+4 internal standard (m/z 195) using AGC (**Figure 2a**) and MSAGC (**Figure 2b**). The ionization time for MSAGC was 100 times that used for AGC; the increase in ionization time produced more ions and thus, the m/z 199 peak is still easily detected.

To demonstrate the effect of MSAGC on calibration curves, mixtures composed of 525 ng of an M+4 internal standard (m/z 195) and varying amounts of the M+8 analyte (m/z 199) were used to generate the log-log calibration curve for AGC and MSAGC (**Figure 3**); all injections were performed in triplicate. Note that the slope of the MSAGC calibration curve (**Figure 3b**) is 1.0, which is the expected slope for a log-log calibration curve; this is a marked improvement over the slope for the AGC calibration curve (**Figure 3a**). Also, when using MSAGC, data were obtained for all three injections at the 1 ng level, whereas data were obtained for only one out of three injections for AGC.

In summary, mass-selected automatic gain control shows the possibility of automatically adjusting the ionization time dependent upon only the ion of interest. The calibration curves which result are linear (i.e., slope = 1.0 for log-log plot) even when the analyte is not the most abundant ion in the ion trap.

1. Stafford, G.C.; Taylor, D.M.; Bradshaw, S.C.; Syka, J.E.P.; Uhrich, M, *Proceedings of the 35th ASMS Conference on Mass Spectrometry and Allied Topics*, 1987, Denver, CO, pp. 775-776.
2. Gronowska, J.; Paradisi, C.; Traldi, P.; Vettori, U. *Rapid Commun. Mass Spectrom.* **1990**, 4, 306.
3. Yates, N.A.; Yost, R.A.; Bradshaw, S.C.; Tucker, D.B. *Presented at the 39th ASMS Conference, Nashville, TN, 1991, p. 1489.*

Figure 1. MSAGC Scan Function

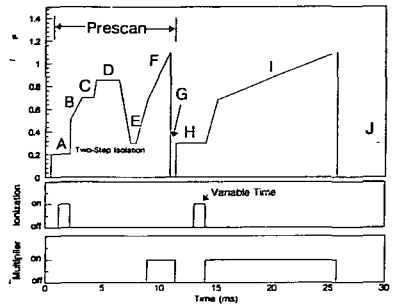

Scan Table List:
A = Ionization Time
B = RF/DC Ramp
C = Eject High m/z
D = Eject Low m/z
E = Cool at q of 0.3
F = AGC Acquistion
G = AGC Reset
H = Variable Ionization Time
I = Acquistion Scan
J = Reset Table

Figure 2. Mass Spectra of point B on the Calibration curves.

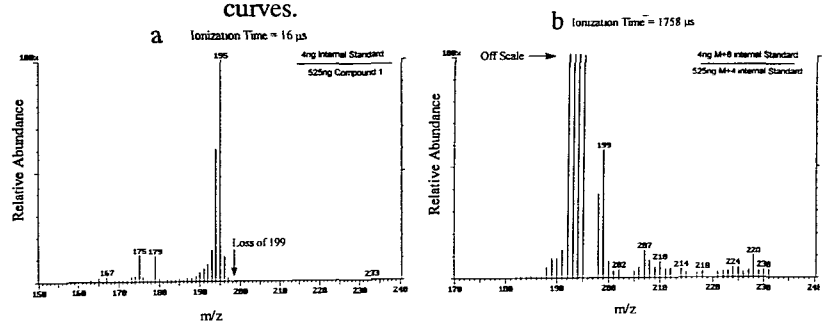

Figure 3. Calibration curves for AGC and MSAGC.

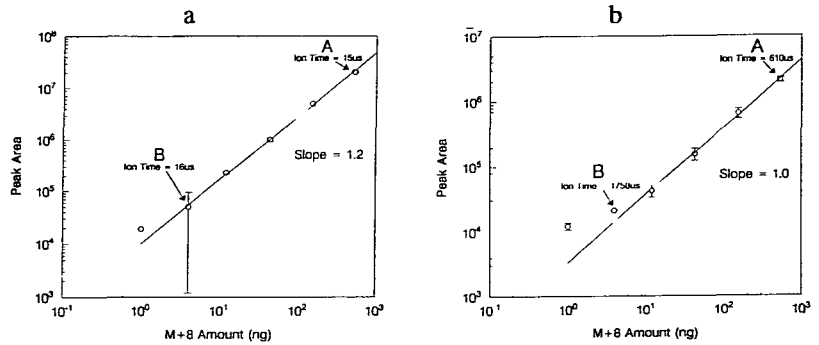

Gas Chromatography/Ion Trap Mass Spectrometry Using an External Ion Source

Matthew M. Booth, James L. Stephenson, Jr., Richard A. Yost
Chemistry Department, University of Florida, Gainesville, FL 32611

INTRODUCTION

When an ion trap is used as a GC detector (**Figure 1**), mass spectral peaks due to ion-molecule reactions are commonly observed for compounds containing oxygen or nitrogen (1) The fragment ions for these types of compounds have relatively high gas-phase acidities, and both proton transfer (creating excessive M+1 abundances) and alkyl group transfer (creating adduct peaks) can occur (see **Figure 5**) In this work, an external ion source is used to limit the number of neutral molecules (either analyte, solvent, or contaminants) present in the ion trap during storage and scanning in an attempt to minimize ion-molecule reactions that may occur during GC/ITMS analyses

EXPERIMENTAL

A schematic of the external ionization system is shown in **Figure 2**. For this work, a Finnigan 4500 ion source was directly coupled to a Finnigan ITMS-style ion trap The only modification to this system was that a tube lens was mounted onto lens L3 of the 4500 source. The Finnigan 4500 ion source, ITMS ion trap, and electron multiplier were mounted inside of a cradle-style vacuum manifold A Varian 3400 GC was interfaced to the vacuum system using a transfer line adapted from a solids probe A Finnigan 4000 quadrupole electronics module (QEM) was used to control the ion source (filament, collector, and lens potentials), and Finnigan ITS40 electronics were used to control the ion trap. Injection of ions was accomplished by grounding the ion source and floating both the endcap and ring electrodes of the ion trap by a variable potential. A standard ITMS electron gate was used as the ion gate for this system. The electron gate TTL signal produced by the ITS40 electronics was inverted and amplified using a custom circuit and a Kepco model 400B variable power supply to produce the ion gate voltage

RESULTS

Since benzophenone forms both protonated molecule (m/z 183) and adduct ions (m/z 216, 231 and 259), it was chosen to evaluate the GC/MS performance of this system. **Figure 3** shows the total ion chromatogram and mass spectrum for 1 ng of benzophenone analyzed on the GC/ITMS external ion source system **Figure 4** compares the M+1/M ratio for the analysis of benzophenone using both internal and external ionization systems The theoretical ratio for this value is 14 6% if only ^{13}C contributes to M+1 As can be seen from this figure, the M+1/M ratio remains constant and very close to the theoretical value for the GC/ITMS system using external ionization The data for the internal ionization system, though, shows that even at 0 5 ng, the proper M+1/M ratio for benzophenone is never obtained

Figure 5 shows the mass spectrum for 100 ng of benzophenone analyzed on the GC/ITMS system using internal ionization At this concentration, both protonated benzophenone molecule and adduct ions can be seen. **Figure 6** shows the mass spectrum for 500 ng of benzophenone analyzed on the GC/ITMS system using external ionization. Even at this high concentration, the proper M+1/M ratio is obtained, and no adduct ions are observed in this spectrum.

FUTURE WORK

Future work will include improving the limit of detection for this system by making ion optic and ion trap changes and by increasing the ion injection time. GC/ITMS using negative ion chemical ionization (NICI) will also be attempted (NICI cannot be performed on an ion trap system using internal ionization due to the lack of thermalized electrons inside the ion trap)

Figure 1 GC/ITMS Internal Ionization

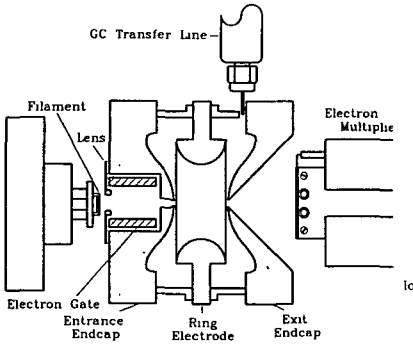

Figure 2. GC/ITMS External Ionization

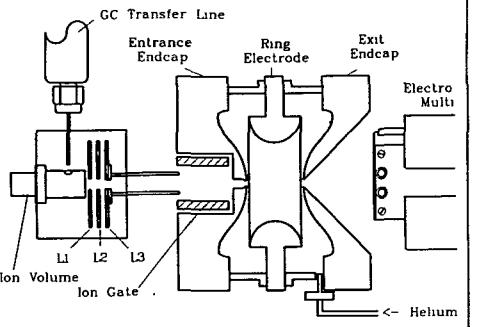

Figure 3. GC/ITMS External Ionization - 1 ng Benzophenone

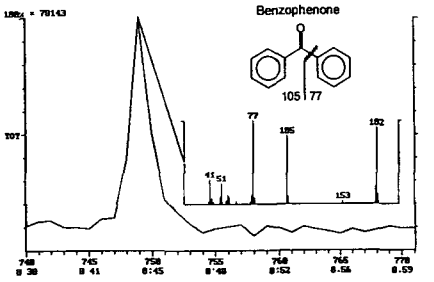

Figure 4. (M + 1)/(M) Ratio vs. Amount Injected

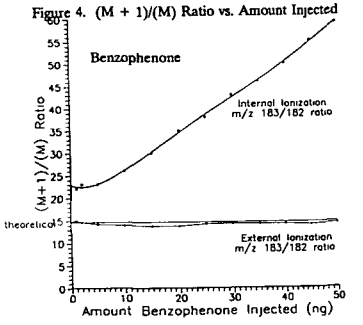

Figure 5. GC/ITMS Internal Ionization

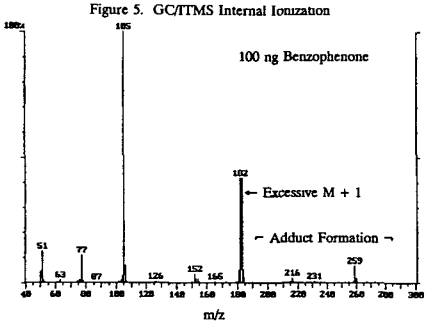

Figure 6. GC/ITMS External Ionization

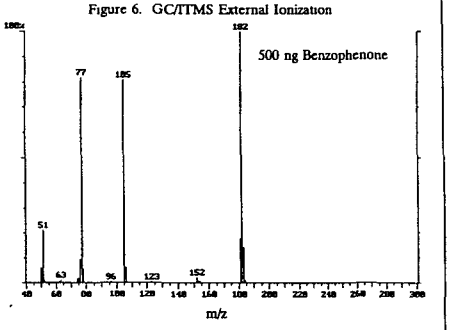

(1) L.K. Pannell, Q -L Pu, H M Fales, R T. Mason, J.L Stephenson,Jr , Anal Chem., 61, 2500 (1989)

A New Model for the Estimation of Ion Kinetic Energy in a Quadrupole Ion Trap

*Randall E. Pedder[†], Richard A. Yost[‡]
[†]Millipore Corporation, Extrel Mass Spectrometry, Pittsburgh, PA 15238
[‡]Department of Chemistry, University of Florida, Gainesville, FL 32611

The Dehmelt pseudopotential well model for the estimation of maximum kinetic energies of ions stored in a quadrupole ion trap is known to be inaccurate for values of the Mathieu parameter q>0.3[1]. The Dehmelt pseudopotential well model is essentially based on a single-term truncation of the analytical solution of the Mathieu equation. A new model, derived from a four-term truncation of the analytical solution of the Mathieu equation, has been proposed for the estimation of maximum ion kinetic energy. This new model, the Expanded Analytical Solution Model, is compared with results calculated using the computer simulation program developed in our lab called Hyperion[2].

Ion motion in a quadrupolar field can be described using the Mathieu equation:

$$\frac{d^2u}{dt^2}=\frac{eu}{mz_0^2}(U+V\cos\Omega_0 t)$$

The analytical solution of this equation can be used to identify position at time t (assuming zero initial velocity):

$$u(t)=A[C_0\cos(\omega_0 t)+C_{-2}\cos(\omega_{-1}t)+C_{+2}\cos(\omega_{+1}t)+C_{-4}\cos(\omega_{-2}t)+...]$$

where the coefficients (C_{2n}) can be calculated as a function of the Mathieu parameters a and q, and the frequencies can be calculated as a function of β and the RF drive frequency Ω_0:

$$\omega_n=(\frac{\beta}{2}\pm n)\Omega_0 \quad \text{where} \quad n=0,\pm1,\pm2...$$

Note that the ripple seen in the classic photomicrograph of Wuerker et al.[3], and in simulated ion trajectories, is not the drive frequency applied to the trapping electrodes, as often identified in the literature. Rather, that ripple is the result of the first and second harmonics (ω_{-1}, and ω_{-2}) beating upon each other.

Ion velocity can be calculated as the first derivative of the Mathieu equation Analytical solution.

$$\frac{du}{dt}=\dot{u}(t)=-A(C_0\omega_0\sin(\omega_0 t)+C_{-2}\omega_{-1}\sin(\omega_{-1}t)+C_{+2}\omega_{+1}\sin(\omega_{+1}t)+C_{-4}\omega_{-2}\sin(\omega_{-2}t)+...)$$

Since the maximum of a sine function is one, maximum ion velocity can be calculated from:

$$\dot{u}(t)_{max}=A(|C_0\omega_0|+|C_{-2}\omega_{-1}|+|C_{+2}\omega_{+1}|+|C_{-4}\omega_{-2}|+...)$$

In the Dehmelt pseudopotential well model, the ion velocity equations are truncated to a single term (C_0=1, $C_{n\neq0}$ =0):

$$\dot{u}(t)=AC_0\omega_0\sin(\omega_0 t)$$
$$\dot{u}(t)_{max}=A|C_0\omega_0|$$

Kinetic energy, calculated as shown below, reduces to Dehmelt's:

$$E_{kinetic,max}=\frac{1}{2}m\dot{u}(t)^2=\frac{mA^2\omega_0^2}{2}=\frac{qV_{RF}}{8}$$

In the Expanded Analytical Solution Model proposed here, the maximum ion velocity equation is truncated to four terms:

$$\dot{u}(t)_{max}=A(|C_0\omega_0|+|C_{-2}\omega_{-1}|+|C_{+2}\omega_{+1}|+|C_{-4}\omega_{-2}|)$$

Kinetic energy can be calculated as: $E_{kinetic,max}=\frac{1}{2}m\dot{u}(t)^2_{max}$

Inclusion of these three additional terms results in a doubling of velocity with a five-fold increase in estimated ion kinetic energy. Although the higher harmonics tend to be small in amplitude, their large frequencies cause them to have significant contributions to velocity and kinetic energy. Indeed, the velocity contribution of the first harmonic frequency, ω_{-1}, is always greater than that of the fundamental frequency.

Conclusions. The harmonic frequencies of ion motion evident in the Wuerker photograph and in simulations contribute significantly to ion velocity and kinetic energy: low amplitudes at high frequencies yield large contributions to ion velocity. The proposed Expanded Analytical Solution Model yields calculated ion kinetic energies five-fold larger than the Dehmelt pseudopotential well model for all values of q. Hyperion numerical integration results yield an additional factor of two increase in estimated kinetic energy, for a total ten-fold increase over the Dehmelt model. While the Hyperion numerical integration results are presumed more accurate, calculations using the Expanded Analytical Solution Model are much simpler to implement.

1. Major, F.G.; Dehmelt, H.G. *Phys. Rev.* **1968**, *170*, 91-107.
2. Pedder, R.E.; Yost, R.A. *Proceedings of the 36th Annual Conference on Mass Spectrometry and Allied Topics*, San Francisco, CA, June 5-10, 1988, 632-633.
3. Wuerker, R.F.; Shelton, H.; Langmuir, R.V. *J. Appl. Phys.* **1959**, *30*, 342-349.

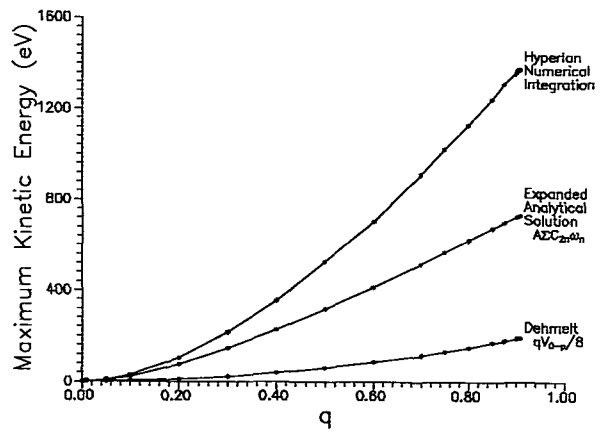

Maximum ion kinetic energies for m/z 134 as a function of q, as calculated via various methods.

FTMS External Ion Source for Ion-Molecule Reactions

C.R. Chris Wang, Anthony M. DeSantolo, Mary L. Mandich and William D. Reents, Jr.
AT&T Bell Laboratories, Murray Hill, New Jersey 07974

Reactivity studies of gas phase semiconductor clusters have provided new insights into the chemistry of nanosize semiconductor surfaces and the chemistry of gas phase semiconductor precursor species which arise during semiconductor processing. The size and stoichiometric dependent reactivities of gas phase semiconductor clusters are under study using powerful trapped ion cell technique of Fourier transform ion cyclotron resonance (FTICR) mass spectrometry in conjunction with an external cluster source and ion guide.

Using an external cluster source and a differential pumping of an ion guide allows for operation of the FTICR at requisite low pressure conditions while extracting clusters generated in a high pressure environment. A fast atom bombardment (FAB) sputtering source was chosen in our early investigations due to its simplicity in construction and capability of producing continuous cluster beams, containing both neutrals and ions, with broad range of cluster sizes. The FAB gun (Phrasor Scientific), capable of delivering a maximum 25 kV and 250 $\mu A/cm^2$ continuous primary Xe/Xe^+ beam, is operated typically at 10 kV and 25 $\mu A/cm^2$. It is aligned with an angle of 70° to the surface normal of the sample target to obtain the maximal secondary ion fluent. Fig. 1 shows the schematic of our external cluster source and ion transfer system. A 6.4 mm diameter target is mounted on a sample holder that can be floated at a source voltage (Vs). The sputtered cluster ions are transferred through the magnet fringing fields into the ICR cell by a newly designed ion guide which permits a high transfer efficiency. The ion guide consists of ion extraction/ acceleration, X&Y deflection (Z defined as the direction of the central magnetic field line), field-free (1 kV) regions, ion focusing elements (Einzel lens), and deceleration region. Most of ion optical lenses are made of 2.3125" (diameter) x 0.125" (thickness) copper discs with a 0.75" diameter central opening on each one. Einzel lens L1 focuses the ions through the differential pumping aperture A2 and Einzel lens L2 refocuses the ion which are then decelerated to their original kinetic energies before entering the ICR cell. A smooth ion deceleration is achieved using an assembly of exponential deceleration lenses connected through a resistive voltage divider.

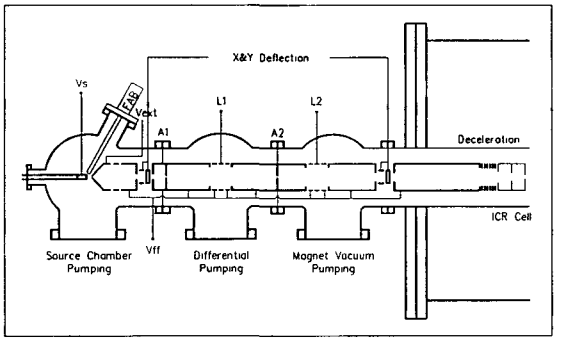

Figure 1. Schematic diagram of the external cluster source and ion transfer system.

Cluster ions from the ion guide are trapped in the ion cell and then specific cluster ions are isolated from the total ion population for reactivity studies. Fig. 2 shows the required pulse sequence for ion loading, trapping, isolation, reaction and detection. Briefly, prior to ion collection in the cell, all ambient ions are quenched from the cell. Since ions are streaming continuously from the source towards the cell, they must be prevented from entering the cell during this quench pulse. This is accomplished by pulsing one of the ion guide deceleration lenses near the ion cell entrance to a large positive voltage (typically +260 V). During ion collection, the ion blocking pulse is removed which allows ions to re-enter the cell. A collection time of 20 ms is found to be sufficient to "fill" the ion cell. Once the cell is loaded, ions are again blocked from reaching the cell until the next experimental cycle. The ion cell is operated with a constant +1.0 V trapping voltage on both the near and far trapping plates except for during the ion collection period. While ions are loading into the cell, the far trapping plate is pulsed to a higher voltage (1-10 V) which is found to assist the trapping process. An isolation pulse is employed in ion-molecule reaction studies to selectively isolate a single size or stoichiometry of cluster ion by strongly irradiating the other cluster ions at their cyclotron frequencies.

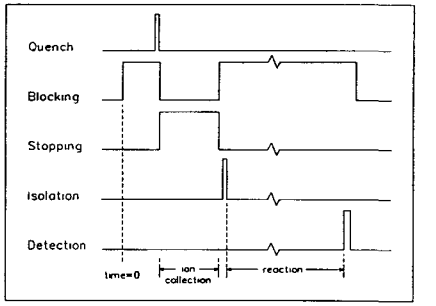

Figure 2. Timing Sequence required for an experimental cycle.

Indium phosphide cluster ions, $In_xP_y^+$ ($x<9$, $y=0,1,2,3$), have been successfully generated, transferred and detected, as shown in Fig. 3. The retarding potential analysis on the total $In_xP_y^+$ ion beam indicates that the kinetic energy distribution is very broad. However, 80% of the cluster ions have kinetic energies less than 20 V. The dis-tribution of the kinetic energies of the remaining 20% of the cluster ions tails out to more than 100 V. Highly selective reactions of these indium phosphide cluster ions are observed with ammonia and trimethylamine. Of all of the $In_xP_y^+$ cluster sizes and stoichiometries studied, only In_2^+ reacts with ammonia. Trimethylamine is much more reactive. However, the reaction probability decreases to zero as the clusters become larger.

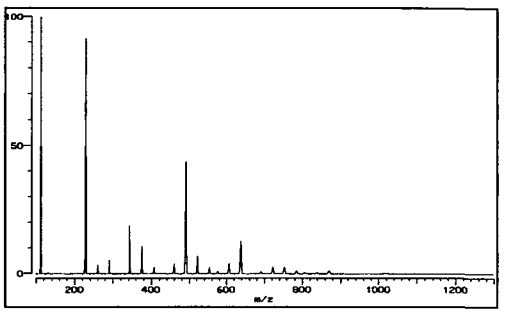

Figure 3. Measured mass spectrum of indium phosphide clsuter cations, denoted as (x,y).

Characterization of an FT/ICR Mass Spectrometer Based on a 0.4 T Permanent Magnet

*Loreen C. Zeller,[1] James M. Kennady,[1] Diane T. Leeck,[1]
Lori M. Castro,[1] Joseph E. Campana,[2] and Hilkka I. Kenttämaa[1]

[1]Department of Chemistry, Purdue University, West Lafayette, Indiana 47907-1393
[2]Extrel FTMS, Millipore Corp., 6416 Schroeder Rd., Madison, Wisconsin 53711-2424

The performance of a Fourier transform ion cyclotron resonance mass spectrometer based on a 0.4 T permanent magnet has been explored. In this mass spectrometer the cell is 3.0 cm along the z-axis and 3.2 cm along each of the x- and y-axes. Several screened cells[1] were constructed and their performance was compared. SIMION calculations were performed to study the effect of the grounded screens on the electrostatic field inside the ICR cell. The mass range, the dynamic range and ion isolation were examined.

SIMION calculations show that the electrostatic field inside the cell is significantly reduced by the introduction of a grounded screen inside the trapping plates (Figure 1). The performance of a screened cell (3 wires/cm placed 2 mm inside the trapping plates) and an unscreened cell was compared by performing electron ionization of perfluorotributylamine (PFTBA) (Figure 2). For similar ionization and trapping conditions, the signal in the screened cell was significantly greater than the signal in the unscreened cell, suggesting that more ions are trapped in the screened cell. The data obtained in the screened cell compares favorably to that obtained in a commercial Extrel Model 2001 FTMS system (4.76 cm cubic dual cells, 2.4 T).

The upper portion of the mass range was examined by using 2,4,6-(perfluorononyl)-1,3,5-triazine (MW 1485) and 2,4,6-(perfluoroheptyl)-1,3,5-triazine (MW 1185). Electron ionization of these compounds produced abundant fragment ions of m/z 1466, 1066 and 866 (Figure 3). A cell in which the wires of the screen were spaced 2 wires/cm proved to have the best performance in this portion of the mass range. Unit mass resolution is achievable at m/z 1466.

The dynamic range of the instrument was studied by measuring the mass spectrum of air in a screened cell in which the wires were spaced 3 wires/cm. Argon was detectable in the presence of nitrogen. In an additional experiment, SWIFT was used to selectively excite the lower abundance components.[2,3] By using this method of detection it was possible to detect CO_2, which is present in air at 0.0033%, thus demonstrating an extended dynamic range in excess of 10^4.

A wide variety of ion chemistries can be studied in this instrument. Of interest to gas-phase ion chemists is the ability to isolate and study highly reactive species, such as organic radical cations. This is demonstrated here for ionized propanal. Propanal was pulsed into the mass spectrometer and the radical cation was isolated by using a SWIFT waveform (Figure 4). The isolated ion was reacted with both dimethyl disulfide and cyclopentanone. Very little interference occurs from ion-molecule reactions with trace levels of the neutral precursor.

References

1. Wang, M., Marshall, A.G., *Anal. Chem.*, **1989**, ***61***, 1288.
2. Poretti, M., Rapin, J., Gäumann, T., *Int. J. Mass Spectrom. Ion Processes*, **1986**, ***72***, 187.
3. Wang, T.-C.L., Ricca, T.L., Marshall, A.G., *Anal. Chem.*, **1986**, ***58***, 2935.

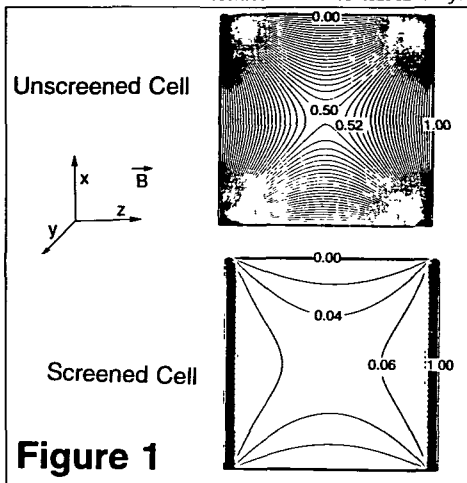

Figure 1

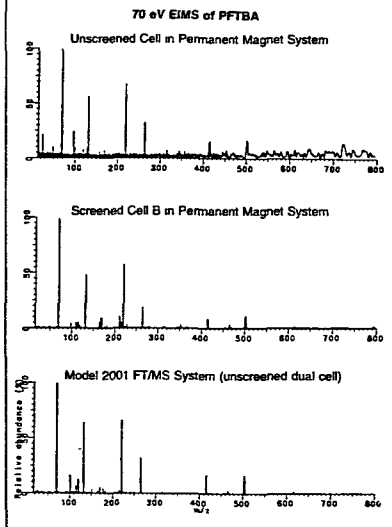

Figure 2

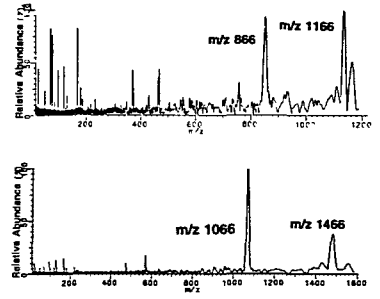

Figure 3

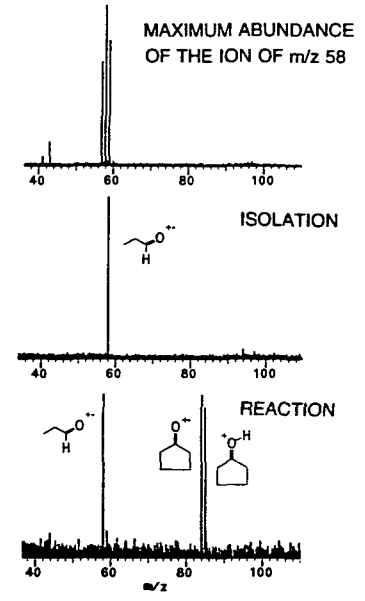

Figure 4

High-Resolution Fourier-Transform Mass Spectrometry of Large Biomolecules

*Michael W. Senko, Peter B. O'Connor, Steven C. Beu, John P. Quinn, and Fred W. McLafferty, Cornell University, Department of Chemistry, Ithaca, NY 14853-1301

Fourier-transform mass spectrometry (FTMS) has features that are appealing for the analysis of large biomolecules: ultrahigh resolution, high mass accuracy, and simultaneous ion detection over a wide m/z range. The benefits of high resolution include mass determination uneffected by unresolved adducts and the unambiguous determination of charge from isotopic peak spacing. The initial coupling of an electrospray ionization (ESI) source to FTMS demonstrated high resolution analysis of multiply charged biomolecules of greater than 15 kDa [1]. Improvements to the instrument have increased resolving power, sensitivity and mass accuracy by an order of magnitude [2]. Resolving powers of $2x10^6$ for ubiquitin (8.6 kDa) and $5x10^6$ for carbonic anhydrase (29.0 kDa) have recently been demonstrated [3].

Performance for molecules larger than 30 kDa has been unexpectedly poor. Potential problems at high mass are the increased charge carried by each molecule, larger collisional cross sections, and increased heterogeneity. Each of these has been investigated in an attempt to extend the range of compounds amenable to high-performance ESI-FTMS analysis.

Optimum resolution is obtained with the FTMS using small ion populations. Larger biomolecules have more isotopic peaks, carry more adducts, and have more charge states, causing a decrease in signal levels for the same number of ions. Ion populations large enough to produce acceptable signal levels degrade resolution. By initially overloading the cell (Figure 1a), then using SWIFT [4] to remove all but a few charge states (Figure 1b), high resolution can be maintained with acceptable signal levels for molecules as large as Protein A (45 kDa).

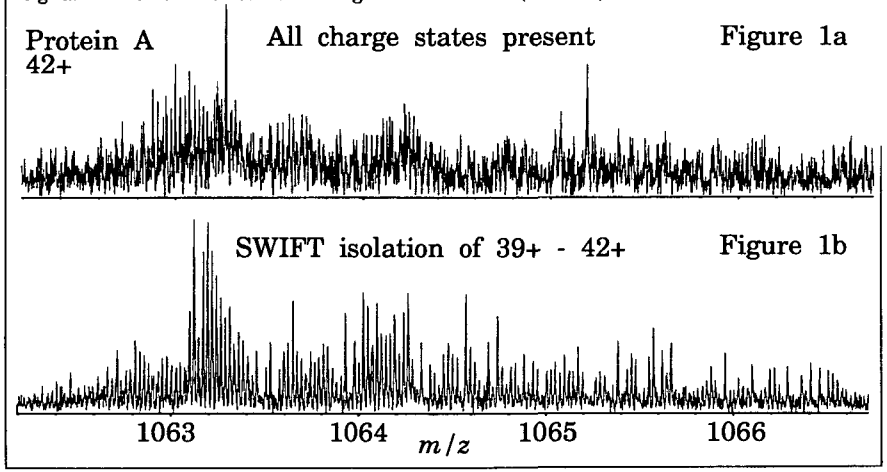

Microheterogeneities for large molecules can arise from various sources including adducts and structural modifications [5]. To minimize the effect of non-covalent adducts, the nozzle-skimmer bias is set high enough to induce some covalent bond fragmentation. Even under these conditions, the molecular weight distribution for porcine albumin (67 kDa) is 1000 Da wide (Figure 2).

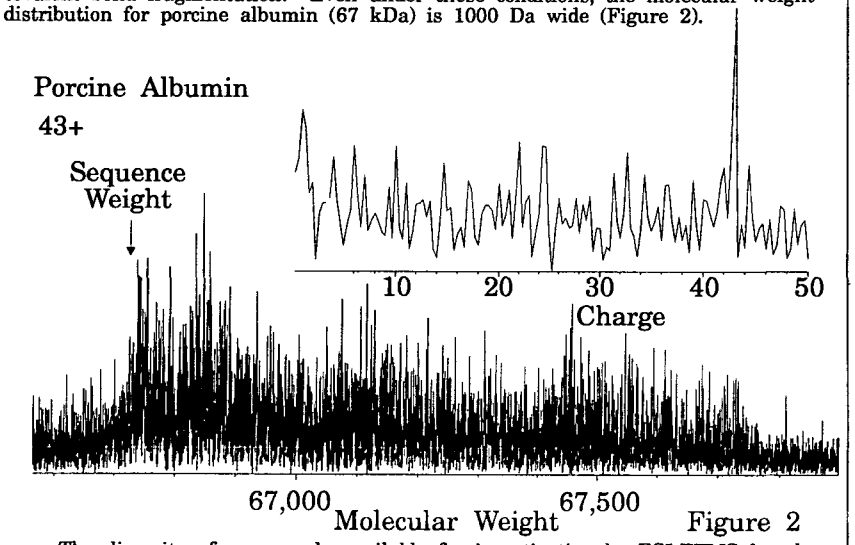

Figure 2

The diversity of compounds available for investigation by ESI-FTMS has been increased by extending the mass limit amenable to high-performance analysis. The main cause of poor performance has been determined to be a combination of space charge effects and microheterogeneities. Larger molecules are more heterogeneous, with wider isotopic distributions and more charge states, and therefore require larger ion populations to produce acceptable signal-to-noise ratios. Larger ion populations have a negative effect on resolution, and it is therefore necessary to remove the majority of charge states before analysis to maintain high resolution. By removing all but one charge state, unit resolution is obtained for molecules as large as porcine albumin (67 kDa).

References:

[1] Henry, K. D.; McLafferty, F. W. *Org. Mass Spectrom.* **1990**, *25*, 490-492.
[2] Beu, S. C.; Senko, M. W.; Quinn, J. P.; McLafferty, F. W. *J. Am. Soc. Mass Spectrom.* **1993**, *4*, 190-192.
[3] Beu, S. C.; Senko, M. W.; Quinn, J. P.; McLafferty, F. W. *J. Am. Soc. Mass Spectrom.* in press.
[4] Marshall, A. G.; Wang, T-C.L.; Ricca, T.L. *J. Am. Chem. Soc.* **1985**, *107*, 7893-7897.
[5] Loo, J. A.; Edmonds, C. G.; Smith, R. D. *Anal. Chem.* **1991**, *63*, 2488-2499.

EXPERIMENTAL AND THEORETICAL RELATIVE ION YIELDS FOR GLOW DISCHARGE MASS SPECTROMETRY

*R. W. Smithwick III, D. W. Lynch, and J. C. Franklin

Oak Ridge Y-12 Plant[1]
Analytical Services Organization
Martin Marietta Energy Systems, Inc.
Oak Ridge, Tennessee 37831-8189

Previous Work

The purpose of this work is to improve quantitative elemental analyses by glow discharge mass spectrometry (GDMS) by predicting the individual sensitivities of the elements. The results reported on this poster reinforce recently published work (JASMS 1993, 4, 278-285). Relative ion yields (RIYs), defined in that work, were experimentally measured for 19 elements in NIST steel reference materials (#661-665) using both pure argon and argon containing 1 vol % H_2. RIYs were also theoretically calculated using the following equation:

$$RIY_s = \frac{(Mass\ factor)_s\ (Ionization\ factor)_s\ (Atomic\ weight)_{Fe}}{(Mass\ factor)_{Fe}\ (Ionization\ factor)_{Fe}\ (Atomic\ weight)_s}$$

The mass factor, taken to be $1 - e^{-0.04\,AW}$, was believed to result mostly from the mass dependence of analog detection. The predicted use of ion counting to eliminate the need for this factor is one of the interesting aspects of the present paper.

The thermodynamic ionization factor, $1/[1 + e^{+(EA+IP-\mu)/kT}]$, involves the electron affinity and the first ionization potential for each element, as well as a chemical potential (μ = 9. ev), the Boltzman constant k, and a temperature (T = 14000 K). The atomic-weight factors are necessary to convert atom % to wt %.

When the theoretical RIYs were plotted versus the experimental RIYs, the correlation was found to be strong when the measurements were made using argon that contained 1 vol % H_2.

Present Results

The following results were obtained using a Concept S32 high-resolution glow discharge mass spectrometer (manufactured by Kratos Analytical, Ltd.):

1. When ion counting was used, theoretical RIYs without a mass-dependent factor correlated well to experimental RIYs when argon was used that contained 1 vol % H_2.

2. When Inconel-steel reference materials (4.5 to 46 wt % Fe) were measured using argon containing 1 vol % H_2, the theoretical RIYs (previously used for low-alloy steels) correlated well. This indicated that the same RIYs apply to a wide variety of steels.

3. When a steel standard was measured using argon containing 5 vol % helium, the results were nearly the same as the results obtained when pure argon was used. This indicated that the physical effect of thermal conductivity (which is similarly high for both H_2 and He compared to argon) does not account for the improved correlation observed for argon containing 1 vol % H_2.

---

[1]Managed by Martin Marietta Energy Systems, Inc., for the U.S. Department of Energy under contract DE-AC05-84OR21400.

Development of a Pulsed-Gas Glow Discharge Ion Source for High Mass Resolution on a Fourier Transform Ion Cyclotron Resonance Mass Spectrometer

Clifford H. Watson,[1] John Wronka,[1] Frank H. Laukien,[1] Christopher M. Barshick,[2] and John R. Eyler[3]; [1]Bruker Instruments, Inc., Manning Park, Billerica, MA 01821; [2]Oak Ridge National Laboratory, Oak Ridge, TN 37831-6375; [3]Department of Chemistry, University of Florida, Gainesville, FL 32611-2046.

ABSTRACT

A new pulsed-gas glow discharge (GD) source has been developed for use with a commercial external ion source Fourier transform ion cyclotron resonance (FTICR) mass spectrometer. Since the gas load in the mass analyzer region was greatly reduced an improvement in mass resolution was observed. Mass resolutions, $m/\Delta m_{\frac{1}{2}} > 1{,}000{,}000$ were achieved for Cu in a brass sample. The pulsed-gas glow discharge source shows promising analytical usefulness for high resolution detection in FTICR mass spectrometry.

INTRODUCTION

The FTICR mass spectrometer requires extremely low pressure in the analyzer region ($< 10^{-8}$ torr) to obtain ultra-high mass resolution. For most FTICR instruments the 1 torr background of argon present in the GD source can severely limit the base pressure in the FTICR analyzer region and degrade the mass resolution. The method most commonly used in FTICR mass spectrometry to eliminate the gas load associated with GD or other high pressure sources is to separate physically the ionization and detection regions[1]. Watson et al.[2], have successfully used a commercial FTICR instrument that utilized 3 kV electrostatic ion focussing to transfer ions from a continuous glow discharge source into the ICR analyzer cell while maintaining a pressure differential of 10^8. Since the FTICR is inherently a pulsed technique a pulsed-gas glow discharge source was developed to further lower the gas load on the system in order to improve the mass resolution and conserve both gas and sample.

EXPERIMENTAL

The glow discharge source was mounted in the normal source housing of a Bruker APEX 47e external ion source FTICR mass spectrometer. The instrument was pumped by cryopumps with separate pumps for the source region (800 l/s,N_2), ion optics and transfer region (400 l/s,N_2), and analyzer region (400 l/s,N_2). The pulsed-gas glow discharge source was mounted on a standard source flange that mates with the external ion source housing. The glow discharge was formed within an enclosed high pressure compartment, much like a chemical ionization (CI) source housing, maintained at a 1 torr pressure of argon that was introduced through a piezoelectric pulsed valve. Ions extracted from a 1 mm ion exit orifice, located 6 mm from the standard external source lens stack, were accelerated toward the analyzer cell by a -3 kilovolt potential.

The samples, usually consisting of metallic rods 1 to 3 mm in diameter and 10 to 15 mm long, were held at a potential of -1000 to -1500 volts at a distance of 5-10 mm from the (grounded) ion exit orifice plate and sputter/ionized in the argon atmosphere. The experimental sequence was as follows. A quench pulse is applied to the ICR cell to remove any ions stored in the trap. The pulsed valve was opened allowing argon to enter

the GD source. Ions were allowed to exit the source once a stable discharge was established. A delay of 0 to 9s allowed time for the background argon to be pumped away before ion excitation/detection.

RESULTS AND DISCUSSION

At higher mass resolutions the ion image current signal is attenuated as collisions with background gas dephase the coherent ion motion resulting in a loss of signal. For the continuous GD source the signal has faded away to noise after ca. 0.75s. By pulsing in the argon gas and waiting 3s prior to detection, the reduction in the gas load allows the signal to last for more than 2s. The mass spectra obtained from a standard continuous-gas and pulsed-gas source are shown below. Since the coherent ion signal for the pulsed-gas source is longer lasting the mass resolution is improved from 380,000 to 1,178,000 (FWHH). The improvement is resolution observed with the pulsed-gas operation is directly proportional to the reduction in the background pressure[3]. The background pressure can be lowered by an order of magnitude with a pump-out time delay of 9s between ion accumulation and detection.

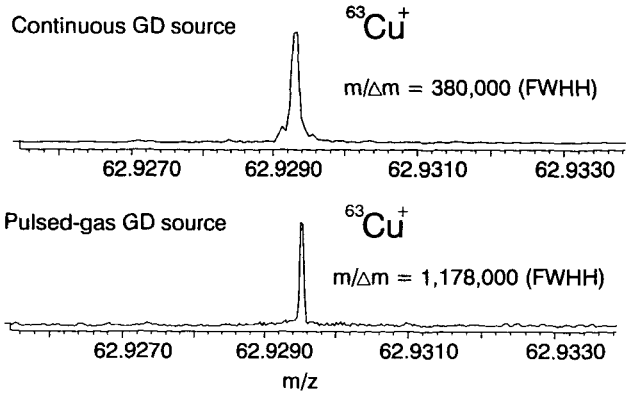

CONCLUSION

Coupling a pulsed-gas glow discharge ion source with an external ion source FTICR mass spectrometer offers a technique that provides ultra high mass resolution to separate closely spaced isotopic peaks. Additional benefits include a reduction in the gas load on the pumping system, and a reduction in the rate of sample consumption.

REFERENCES

(1) Barshick, C.M.; Eyler, J.R. *J. Am. Soc. Mass. Spectrom.* **1992**, *3*, 122.
(2) Watson, C.H.;Barshick, C.M.; Wronka, J.; Laukien, F.H.; Eyler, J.R. *Proc. 40th ASMS Conf. on Mass Spectrom. Allied Top.* **1992**.
(3) Comisarow, M,; Marshall, A.G. *J. Chem. Phys.* 1976, *64*, 110.

THE EFFECT OF CRYOGENIC COOLING ON THE GASEOUS IMPURITY AND ANALYTE ION SIGNALS IN GDMS

*S. K. Ohorodnik and W. W. Harrison
Department of Chemistry
University of Florida
Gainesville, Florida 32611

Glow discharge mass spectrometry (GDMS) is an elemental analysis technique in which atomization, excitation, and ionization of the solid sample occur independently in the discharge. A common problem encountered with a glow discharge ion source is the presence of gaseous impurities, particularly water vapor and air (N_2, O_2, CO_2), that can reduce the amount of sample sputtering as well as quench excitation and ionization reactions. The main source of contamination in the glow discharge is water vapor, which can be introduced into the GD chamber from the following sources: sample cathode, discharge gas, vacuum leaks, and desorption from the ion source surfaces. Elimination of water vapor and other gaseous impurities from the ion source is essential to obtaining reliable quantitative results and has been attempted using one or more of the following methods: (1) high purity discharge gases, (2) gettering reagents in the gas lines, (3) maintenance of high vacuum conditions, (4) frequent baking of the glow discharge system, and (5) cryogenic cooling of the ion source.

This poster described a cryogenic cooling coil that is inserted directly into the glow discharge ion source, resulting in a cooling sink adjacent to the plasma, permitting removal of impurities from the discharge gas by their physical freezing onto the coil surfaces. The coil is a simple and effective design for cryogenic cooling of the glow discharge chamber, which can be adapted to many different types of ion source configurations.

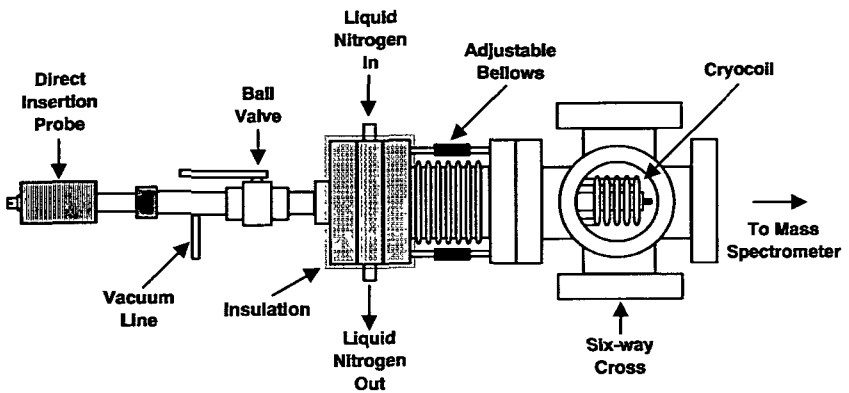

Since the greatest interferences from water and other impurities occur in the m/z range between 10 - 40, an aluminum cathode was chosen for analysis. The mass spectrum of the alloy after sputter cleaning the cathode for 30 minutes included water impurity species at 17, 18, and 19 Da as well as other impurities at 3, 12, 14, and 29 Da corresponding to H_3^+, C^+, N^+, COH^+, and N_2H^+. The major species in the spectrum are H_3^+ and ArH^+, both a result of residual water vapor. A mass spectrum of the sample taken after 30 minutes of cooling with liquid nitrogen is devoid of any of the impurity species except N^+, which is not removed by cryogenic cooling.

The relative sensitivity factor (RSF) values were calculated for a standard low-alloy steel sample (NIST SRM #1264) with and without cryogenic cooling. RSF values calculated for the cryogenic cooled sample had between a 50-95% increase in precision (determined by their %RSD) as compared to the noncooled values (Table I). In addition to the increase in precision, the magnitude of the RSF values also differed between the cooled and noncooled analyses. By controlling the liquid N_2 flow rate through the coil, it was possible to control the temperature of the coil and degree of impurity removal. The effect of the liquid N_2 flow rate on the RSF values of Al, Ti, and Cu was determined. The RSF of Al^+ decreased with increasing flow rate because of the removal of interferences at m/z = 27, while the RSF value of Ti^+ increased probably because of the reduction of TiO^+ production. Copper, a relatively unreactive element toward oxygen, shows a small decrease in RSF value with increasing flow rate, at present unexplained. The effect of liquid N_2 flow rate on the gaseous species was also determined. The ArH^+ and H_3^+ species decreased with increasing flow rate, while the Ar^+ increases.

The cryogenic cooling coil, as expected, is effective at removing water vapor and other gaseous impurities from the glow discharge plasma. The cryogenic coil provides a mean of manipulating the gaseous impurities in the plasma making it possible to investigate the effect the impurities have on the plasma chemistry. Elimination of these impurities results in RSF values of greater precision that should, as a consequence, produce more precise quantitative analyses. The RSF values also varied as the flow rate of liquid nitrogen through the coil and the amount of impurities in the discharge varied. Therefore, accurate and reproducible quantitative analyses also require that the water vapor and other impurities be controlled at a known and reproducible value.

Table I. Relative Sensitivity Factor Values for Low-Alloy Steel NIST SRM #1264 (*n = 3)

	No Cooling		Cryogenic Cooling	
	Mean	%RSD*	Mean	%RSD*
$^{27}Al^+$	4.21	18.6	1.44	8.2
$^{48}Ti^+$	2.10	4.5	4.26	0.41
$^{51}V^+$	1.69	3.2	3.78	0.61
$^{57}Fe^+$	1.00		1.00	
$^{59}Co^+$	0.77	1.6	1.60	0.62
$^{63}Cu^+$	0.38	5.5	0.26	0.94
$^{98}Mo^+$	0.68	2.9	1.54	1.1
$^{181}Ta^+$	0.11	7.4	0.38	1.7
$^{186}W^+$	0.081	5.2	0.23	1.4

CHARACTERISTICS OF RADIO FREQUENCY POWERED GLOW DISCHARGE CELL FOR THE ANALYSIS OF FLAT SAMPLES

Charles R. Shick, Jr. and R. Kenneth Marcus
Department of Chemistry, H.L. Hunter Laboratory, Clemson University,
Clemson, SC 29634

INTRODUCTION: The research interests of this group have focused on the development of radio frequency (rf) powered glow discharge sources which can directly sputter and atomize nonconductive materials such as glasses and ceramics. In addition to the expanded sampling scope, rf sources have proven to be advantageous in the analysis of metals and alloys which tend to form oxide layers, such as Al.

The VG GloQuad (Fisons) quadrupole mass spectrometer is currently equipped with a dc GD source. Recently, we have begun work in the interfacing of an rf GD source to this mass spectrometer system. This report describes the preliminary development and characterization of a direct insertion rf probe (DIP)-flat sample introduction assembly for use with the VG GloQuad. The goals of this research were:

1. To develop an rf-GD DIP flat sample holder for the VG GloQuad.
2. To demonstrate the figures of merit for the rf source through exemplary spectra, pre-sputter time, internal stability, and external reproducibility.
3. To show that rf-GDMS warrants further evaluation for the analysis of both conductive and nonconductive flat sample types.

EXPERIMENTAL: The GloQuad is a quadrupole-based instrument with two detectors installed: a Faraday cup for high ion currents typical of matrix species and an electron multiplier for trace measurements. A novel flat sample holder (Figure 1) was designed to mount onto the end of the DIP allowing for the analysis of flat samples with only slight modifications of the GloQuad ion volume. Preliminary studies were conducted with this rf source to determine pre-sputter times, internal stability, and external reproducibility. Since the sputtering region is defined by a grounded limiting orifice, the use of a 5mm and a 10mm orifice was used for this presentation

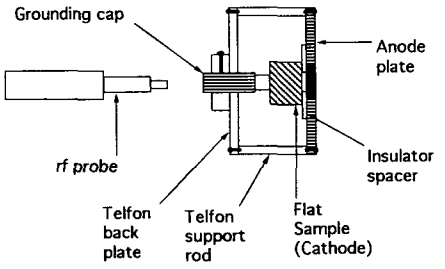

Figure 1. Flat sample holder for rf-GDMS

RESULTS AND DISCUSSION

Conductive sample: An NIST 1243 Waspaloy standard was used with the rf flat sample holder. 5mm and 10mm anode orifice plates were used, with the maximum signal for $^{58}Ni^+$ being 3.5E8 and 4.2E9 counts per second, respectively. For both orifice plates, The temporal profile was collected for 20 minutes while scanning the $^{60}Ni^+$ peak. The internal stability data was obtained by peak jumping the selected elements for 45 minutes. The external reproducibility data was obtained by five different runs whereby the sample was exposed to the atmosphere between each run, and the concentration values calculated with the GloQuad RSF software package. Results show that with both orifice sizes, the analyte signal stabilizes within 4 minutes of the plasma ignition. The 5 mm cell yielded slightly better precision than the 10 mm cell, both internally (4% vs. 7% RSD) and externally (9% vs. 12% RSD).

Nonconductive sample: For this study, an NIST 1412 multicomponent glass standard was used with the rf flat sample holder. Again, the 5mm and 10mm anode orifice plates were used with the maximum signal for $^{28}Si^+$ being 1.4E8 and 3.5E8 counts per second respectively (spectrum from 10 mm plate is shown in Figure 2). These optimized intensities and plasma parameters were used throughout this study. Temporal stability and external precision for nonconductive sample are hindered because the sample surface is prone to contaminated upon exposure to the atmosphere. All oxide-base sample types have a propensity for spectral interferences. For the 5mm orifice plate, the $^{28}Si^+$ isotopic abundance after 20 minutes is 89.5% (accepted value=92.18%), whereas the 10mm orifice plate has an abundance of 91.8% after 20 minutes, indicating that it stabilizes faster after exposure to atmosphere.

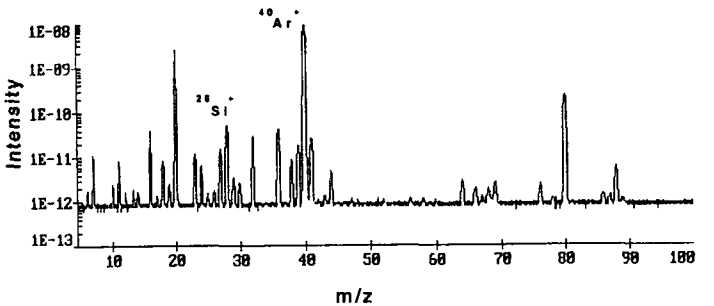

Figure 2 Mass spectrum of an NIST 1412 multicomponent glass using a 10 mm plate.

SUMMARY: An rf source for flat samples has been adapted to a commercial quadrupole mass spectrometer, the VG GloQuad. Preliminary results for both conductive and nonconductive samples indicate that the new source is promising in terms of beam intensity, internal stability, and external reproducibility. These results also support previous observations that the anode orifice plate is a factor in optimizing the plasma conditions.

ACKNOWLEDGEMENTS: Research funding from the National Science Foundation and VG Elemental is gratefully acknowledged.

ANALYSIS OF ELECTRODEPOSITED METAL IONS BY GLOW DISCHRAGE MASS SPECTROMETRY

Charles R. Shick, Jr., Paula R. Cable, Ashley Torrence, and R. Kenneth Marcus,
Department of Chemistry, Clemson University, Clemson, SC 29634

INTRODUCTION: Glow discharge techniques continue to grow in both scope and application; however, the method has thus far been primarily limited to the analysis of bulk solids and thin films. Solution samples may be analyzed as residues which have been dried onto a conductive host matrix. For the latter case, sample preparation is labor intensive, and sample atomization of the resultant oxide material does not necessarily provide a steady state atomic population. Electrodeposition of metal ions onto a cathode forms a more homogeneous thin film of non-oxidized material that produces an abundance of atoms and ions when analyzed by GD methods. We have investigated a technique for electrodepositing thin films of metallic material from solution onto vitreous carbon electrodes. Metal ions are stripped out of solution and are introduced directly into the GD ion source where they are sputter atomized.

EXPERIMENTAL: For this study, five molar concentrations (i.e. 0.01 - 0.5 M) of aqueous $Co(NO_3)_2$, $BaCl_2 \cdot 2H_2O$, and $Pb(NO_3)_2$ solutions were electrodeposited onto vitreous carbon electrodes. The 3 mm x 12 mm electrodes were partially submerged in 5 ml of test solution, which was magnetically agitated during the procedure. Each electrode was electroplated for 5 minutes with an applied voltage of -5 V, oven dryed for 10 minutes, then affixed to a direct insertion probe (DIP) for subsequent analysis by rf-GDMS. A representation of the electrodeposition apparatus is shown in Figure 1. The thin films were analyzed using a VG GloQuad which is a quadrupole-based instrument with a differentially pumped vacuum system. Two turbo pumps produce a final stage vacuum of 10E-7 mbar. A Faraday cup was used for detection.

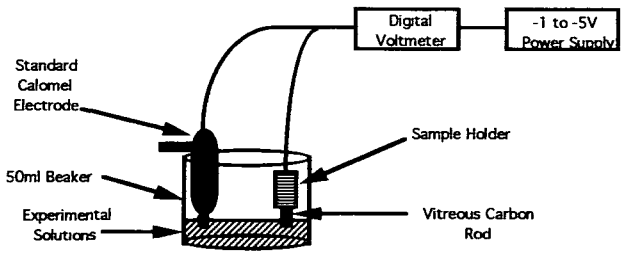

Figure 1. Electrodeposition Apparatus

RESULTS AND DISCUSSION: Deposition of metal ions to form a thin film suitable for GDMS analysis was readily achieved. The films appeared, for the most part, to be homogeneous and metallic in character. Surprisingly, the analyte signals, as measured with a Faraday cup, for the solutions of 0.5 M produced ion beam currents equivalent (>10^{-10} A) to those obtained for sputtering bulk metals. The signals display the anticipated transient nature as shown in Figure 2, though not all of the analyte films are removed at the same rates. At this point, no sort of electrolyte species is employed, and thus nonlinearities in terms of plating efficiencies would be expected. As such, the quality of the generated calibration curves is not as good as hoped.

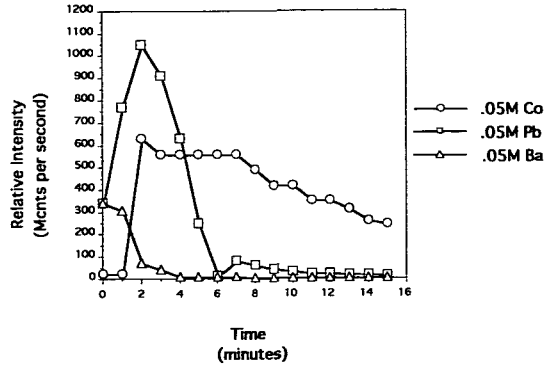

Figure 2. Temporal profiles of analytes sputtered by the rf-GDMS source.

The analyte intensities observed after a 5 minute sputter time are quite encouraging in terms of the beam currents. As these signals are measured on the Faraday cup detector to be on the order of 10^{-11} A, the ability to detect minute beam intensities on the electron multiplier detector (~10^{-17} A) would suggest that this method could be very sensitive. An added benefit of the technique itself is that it is multielement in nature.

SUMMARY: A technique of electrodepositing aqueous metal ions onto a glassy carbon electrode for rf-GDMS analysis seems to be a viable alternative to the current methods of solution residue analysis. Future studies will first focus on improving the deposition methodologies, and then look at the relevant figures of merit. It is hoped the the electrodeposition, rf-GDMS approach may find use in the simultaneous, multielement analysis of volume-limited samples.

ACKNOWLEDGEMENTS: Financial and instrumentation support from the National Science Foundation and VG Elemental is gratefully acknowledged.

AN IMPROVED DOUBLE QUADRUPOLE MASS SPECTROMETER FOR VERSATILE RADIO FREQUENCY GLOW DISCHARGE STUDIES

Yuan Mei and R. Kenneth Marcus
Chemistry Department, Clemson University, Clemson, SC 29634l

INTRODUCTION: The use of rf-GD double quadrupole mass spectrometer in our laboratory has been successful for conducting studies that entail both the application and fundamental aspects of the rf-GD plasma. The original laboratory-constructed mass spectrometer suffered from low ion transmission efficiency. Recently, a new ion optics assembly has been constructed that improves both the ion throughput and the energy defining properties of the instrument, with which collision induced dissociation (CID) studies were carried out using Ar, Xe, and N_2 as target gases to eliminate polyatomic interferences generated in the rf plasma. Studies were also conducted to assess the role of charge exchange in the CID process.

EXPERIMENTAL: The modified double quadrupole mass spectrometer is shown in Figure 1. The old three-element lens stack has been replaced by an ion optics system that combines an accel/decel design and an offset lens insert. The offset lens acts as a photon/neutral stop such that the original ion deflecting unit (ESA) situated in front of the detector has been removed to allow coaxial installation of the detector with respect to the ion beam.

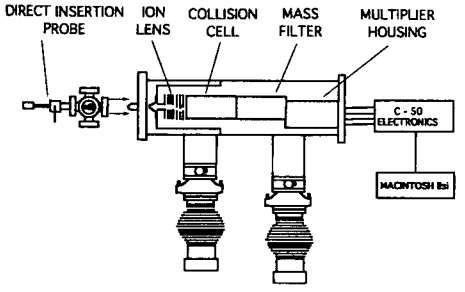

Figure 1. Double quadrupole rf glow discharge mass spectrometer

RESULTS AND DISCUSSION:

I. Ion transmission and energy definition of the new lens: Previous studies have shown that the high negative voltage (-1100 V) applied on the acceleration lens (skimmer cone), combined with the on-axis detector arrangement, improved the ion throughput by a factor of 5. This is especially favorable for the detection of low concentration species such as metal argides and dimers that are of interest in CID experiments. In addition, comparison of the kinetic energy values of several ions measured with both the old and the new lens systems indicate that the new lens system transmits a better defined (5-6 eV narrower) energy range. This property helps optimize a better defined collision energy in the collision quadrupole.

II. Collision energy optimization for target gases: A primary factor affecting the efficiency of CID is the collision energy, related as the center-of-mass energy which is experimentally determined by the dc bias voltage applied on the collision (first) quadrupole (Q1). To select the best Q1 bias for different target gases, the CID efficiency for several ions was studied as a function of the Q1 bias. The best CID results (maximum dissociation of the

molecular species with minimum loss of elemental ions) are obtained when Q1= -8V for Ar, 1V for Xe, and -10V for N_2, corresponding to E_{cm} values in the neighborhood of 4eV.

III. Effect of target gas pressure on CID efficiency: For each of the target gases used, Ion signal intensities were collected across a certain pressure range which is predicted to be on the order of 1 mTorr based on the third stage vacuum gauge reading on the mass spectrometer. Shown in Figure 2 is the CID efficiency of Ar, expressed by the signal attenuation factor $\ln(I_0/I)$, as a function of the indirect collision gas pressure. Ar^+ demonstrated the highest loss which was probably caused by symmetric charge exchange reactions with the target Ar atoms. It is important to note that the analyte ion, Cu^+, is lost to the least degree as compared with the unwanted species, i.e., ArH^+, Ar_2^+, $CuAr^+$, and Cu_2^+. Similar studies with Xe and N_2 as the target gas indicate that the degrees of signal attenuation are comparable between Ar and N_2. The signal attenuation factors obtained with Xe at 1/10 of Ar and N_2's pressure are as high as those of the latter, probably a result of the increased scattering by the heavier Xe atoms.

IV. The role of charge exchange reactions to the ion loss processes: The double quadrupole mass spectrometer used here allowed for further probing of the charge exchange process occurring in Q1 , which can be expressed by the following equations:

$$A_1^+ + A_2 = A_1 + A_2^+ \text{ (symmetric)}, \quad \text{and} \quad A_1^+ + B_1 = A_1 + B_1^+ \text{ (asymmetric)}.$$

The involvement of charge exchange in the total ion loss process of Ar^+, ArH^+, and Cu^+ was studied by monitoring the signal attenuation factors of the three ions while changing the pole bias on the second quadrupole to pass through ions with selective energy ranges. As the Q2 pole bias is decreased (Figure 3), ions resulting from the charge exchange reaction (that posses lower kinetic energies) are more readily passed through the mass analyzer. These ions make up for part of the lost primary ions, resulting in a smaller I_0/I This trend is most obvious with Ar^+, observable with ArH^+, and least apparent with Cu^+, indicating that symmetric charge exchange reactions (Ar^+) occur to a higher degree than the asymmetric ones (ArH^+) in Q1, whereas little charge exchange is involved with the loss of Cu^+ ions.

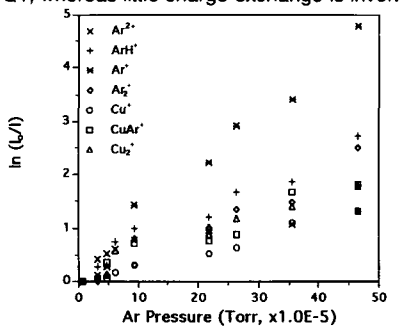

Figure 2. Effect of Ar pressure on CID .

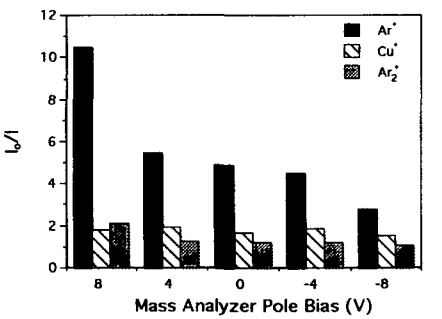

Figure 3. Role of charge exchange in CID

ACKNOWLEDGEMENTS: The financial support received from the National Science Foundation is greatly appreciated.

GLOW DISCHARGE - ISOTOPE DILUTION MASS SPECTROMETRY

***C.M. Barshick and D.H. Smith**
Analytical Chemistry Division, Oak Ridge National Laboratory
Oak Ridge, TN 37831-6375, USA

After developing a glow discharge mass spectrometric (GDMS) method to analyze microliter volumes of solutions as dried residues, we turned our efforts to glow discharge isotope dilution mass spectrometry (IDMS). IDMS is a powerful technique for determining the concentration of a target species in a given unknown, with the crucial step being the establishment of an isotopic equilibrium between the spike and the analyte of interest. With gases and most liquid samples, this step is easy and rapid; all that is needed is to mix the two species prior to analysis. When the analyte is present in solid form, as is typically the case for GDMS, spark source mass spectrometry, or SIMS, equilibration during sample preparation is believed to be impossible. Because glow discharge cathodic sputtering affords a certain degree of mixing during sampling, however, equilibration of the spike and sample, even if both are present as solids, might be possible.

Although our long range goal is to use isotope dilution to determine directly the elemental concentrations of analytes in the solid, in all studies performed to date both the spike and the analyte of interest have been present in an acidic aqueous medium; under these conditions, equilibration is considered to be rapid and complete. Table 1 compares the results obtained using GDMS and inductively coupled plasma optical emission spectroscopy (ICP-OES) in the analysis of lead in three oil leachate samples. Solutions were prepared using EPA Method 3050. Both GDMS calibration curve and GDMS isotope dilution results compare well with those obtained by ICP-OES (EPA Method 6010). IDMS internal precision was found to be better than 5%, even when the concentration was just above the detection limit (LOD ~ 0.3 ppm for GDMS solution residues). External precision was about 2%, better than the precision obtained when using calibration curves or relative sensitivity factors (RSFs).

Table 1. Elemental Lead Concentration in Three Aqueous Leachates Prepared from Contaminated Waste Oils by EPA Method 3050

Contaminated Oil Leachate	ICP-OES Calibration Curve Concentration (ppm)	GDMS Calibration Curve Concentration (ppm)	GDMS Isotope Dilution Concentration (ppm)
†A	2.65	2.68	2.69
†B	3.52	3.97	3.54
†C	81.56	86.68	81.97

†Aqueous Samples

Simultaneous with the isotope dilution investigations of aqueous solutions, we have been evaluating the glow discharge solution residue sampling methodology for analyzing

organic solutions. Early results showed that cathode formation could not be achieved simply by drying and pressing, and an additional step (low temperature ashing) was incorporated. The LFE low temperature ashing system that we are using enables the dry removal of organic materials from a sample, while retaining the inorganic elements. Atomic oxygen produced in an r.f. discharge chemically reacts with the sample material to produce H_2O, CO, CO_2, etc., which is continuously exhausted by a mechanical vacuum pump. The sample temperature never exceeds 120° C, ensuring nearly 100% recovery of trace residual elements. For the initial work reported here, we compared two NIST aqueous reference solutions with two SPEX standard reference oils. After drying and ashing the oil, only small differences in relative ion yields (less than 10% average) were observed between the two types of samples; this is well within experimental error. Table 2 illustrates the results obtained when a second NIST 3172 cathode was used to develop RSFs (1 / RIY) specific for lead (RSF_{Pb} = 1.25, RSF_{Ag} = 1.00). Good accuracy (better than 5% average error) indicates a minimal matrix effect, although it is still too early to speculate about the degree with which the matrix will influence the analysis of other types of solutions (high brines, volatile organic compounds, etc.,). Not shown in Table 2 but also observed, was good agreement between these results and the EPA approved ICP-OES calibration curve methodology.

Table 2. Elemental Lead Concentration in Four Reference Materials Prepared by Drying and Low Temperature Ashing

Sample	Reference Lead Concentration (ppm)	GDMS Measured Lead Concentration (ppm)	Percent Error
*SPEX SPPB8 - 2Y	109.6 ± 2.2	102.0 ± 1.7	7.2
*SPEX MIO - 12B	109.9 ± 2.2	106.2 ± 2.5	3.5
†NIST 3128	100.0 ± 2.0	98.3 ± 8.8	1.7
†NIST 3172	100.0 ± 2.0	104.5 ± 0.7	4.5

*Organic Sample, †Aqueous Sample

Research in this area will continue as we develop a ^{204}Pb isotopically enriched organic spike to improve further the accuracy of GD elemental analysis in organic media. We will also continue to look for ways of delivering small amounts of solid (< 1 mg) spike material directly into the bulk, to extend IDMS's role in GDMS.

Research sponsored by the U S. Department of Energy, Office of Basic Energy Sciences, under Contract DE-AC05-84OR21400 with Martin Marietta Energy Systems, Inc.

"The submitted manuscript has been authored by a contractor of the U S. Government under contract No. DE-AC05-84OR21400 Accordingly, the U S. Government retains a nonexclusive royalty-free license to publish or reproduce the published form of this contribution, or allow others to do so for U S. Government purposes."

Isotopic Analyses by Glow Discharge Mass Spectrometry

Lee R. Riciputi, Douglas C. Duckworth, Christopher M. Barshick, David H. Smith

Analytical Chemistry Division
Oak Ridge National Laboratory
Oak Ridge, TN 37831

Glow discharge mass spectrometry (GDMS) has enjoyed considerable success as an elemental analysis technique, but its potential for the measurement of isotope ratios is relatively unexplored. Analysis of isotope ratios by GDMS offers a number of potential advantages, including limited sample preparation, direct analysis of solids, and relatively high sample throughput. In this paper we evaluate the internal and external precision achievable in the measurement of isotope ratios using a glow discharge, double-focusing mass spectrometer (VG9000). The effects of various instrument operating conditions and sample form on precision will be addressed, as will possible variation in mass biases.

The VG9000 was operated at relatively low mass resolution (~500) to provide flat-topped peaks. Secondary ion signals were measured using either a Faraday cup or Daly detector, peak jumping the magnet to shift masses. Counting times were 1.28 seconds on the Faraday cup, and 2 to 4 seconds on the Daly. One hundred sets of ratios were measured in each analysis, split into 10 blocks of 10 ratios each. Internal precision (discussed below) were calculated on the basis of 10 blocks. Samples were prepared as pins 1.8 cm long, and ranged in diameter between 2 and 5 mm. Isotope ratios, measured using NIST standards when available, include those for B (NIST 951), Cu (variety of samples), Sr (NIST 987), Ag (NIST 978), Re (NIST 989), and Pb (NIST 981). When conductive, analyses were done on solid pins (Cu and Pb as pins, Re wrapped on Pt). Otherwise, samples were prepared as 0.75 to 10 wt% standard mixed with either Cu or Ag powder and pressed into pin shape at high pressure. Most analyses were conducted with the glow discharge in DC mode, although the use of RF power was also investigated.

Cu was used to investigate the influence of pin material and instrument parameters on precision of isotope measurements. The best results on a single sample were obtained in DC mode using a solid Cu pin, with an external precision of 0.035% after correction for linear drift. Results using a single pin of pressed Cu powder were similar (0.046%). Using either constant voltage or constant current in DC mode yielded similar isotope ratios and external precision, although internal precision was slightly better with constant current. Isotope measurements made in RF mode had internal precision (ave 0.19%) that were an order of magnitude worse than those made using DC power (ave 0.026%). The poor internal precision probably results from the poor peak shape associated with RF mode. However, external precision obtained using RF power are only a factor of 2 worse (0.057%, n=5) than those using DC power on the same sample (0.030%, n=7). With improved filtering, both internal and external precision obtained using RF mode should improve. True external reproducibility was evaluated by making four pressed Cu powder pins, and loading and analyzing each one several times. External precision (0.29%) is ten times worse than that achieved using a single pin. These results may be improved by developing a different, more reproducible, sample geometry (flat cell), and by allowing a longer pre-sputter period before starting the analysis. Average daily $^{65}Cu/^{63}Cu$ ratios

ranged between 0.4534 and 0.4466.

Results for a number of NIST standards are summarized in the table below. External precision (single pin) ranged between 0.025% and 0.28%, and generally correspond to the concentration of the element in the matrix. There is no apparent matrix effect on measured Sr isotope ratios using Ag and Cu matrix powder (data not shown). In general, biases are low (<1%), and there is no correspondence between bias and mass or ionization potential. This result is not surprising, since atomization (cathodic sputtering) and ionization take place in two separate steps in GDMS. In fact, the variation in isotopic bias between different elements is similar to the daily changes in the measured isotope ratio for a single element.

GDMS holds promise for the relatively precise measurement (<0.1%) of isotope ratios on solids with a minimum of sample preparation. Current performance may be improved by optimizing sample and cell geometries, improving the stability of the discharge, and by optimizing the detection system. Accurate analyses will require daily calibration of the instrument.

SUMMARY OF SELECTED ISOTOPE ANALYSES USING GDMS

Element (detector)	Material	Ratio	N	Ave.	%External Precision	Accepted Value	Bias
Cu (Fara)	Solid Cu	65/63	22	0.4511	0.035 (corr)	0.4456	0.62%H
Cu (Fara)	Pressed Cu	65/63	10	0.4495	0.046 (corr)	0.4456	0.43%H
	4 pin		10	0.4466	0.295	0.4456	0.11%H
Sr (Daly)	1% NIST 987 (Cu)	84/86	8	0.0573	0.173	0.05655	0.66%L
		87/86		0.7029	0.283	0.71034	1.05%L
Sr (Fara)	5% NIST 987 (Ag)	87/86	4	0.7158	0.205	0.71034	0.77%H
		88/86		8.4274	0.087	8.37861	0.29%H
Re (Fara)	NIST 989 on Pt	185/187	5	0.5980	0.150	0.5974	0 05%L
Ag (Fara)	7.5% NIST 978 (Cu)	107/109	6	1.0689	0.059	1 07638	0.34%H
Pb (Fara)	NIST 981 solid	208/206	9	2.1729	0 034	2.1681	0.11%H
		207/206		0.9159	0.025	0.91464	0.14%H
		204/206		0.0588	0.080	0.5904	0.17%H
B (Fara)	2.8% NIST 951 (Ag)	10/11	2	0.24552	0.055	0.2473	0.73%H

Research sponsored by the United States Department of Energy, Office of Basic Energy Sciences, under contract DE-AC05-84OR21400 with Martin Marietta Energy Systems, Inc.

Design of an Array - Detector Mattauch - Herzog Mass Spectrometer for Atomic Mass Spectrometry

Thomas W. Burgoyne, Gary M. Hieftje, and Ronald A. Hites
Department of Chemistry and School of Public and Environmental Affairs,
Indiana University, Bloomington, IN 47405.

Introduction. The quadrupole is the most common device for mass analysis in plasma source mass spectrometry. However, a major drawback of the quadrupole is that masses are detected one at a time; it is a scanning instrument. For example, 99.6 % of the analyte material is wasted from a continuously operating ion source (e.g. ICP or glow discharge) (not including quadrupole transmission efficiency) if a complete atomic mass spectrum (from mass 7 to 238) is required. This tremendous waste of sample reduces sensitivity and sample throughput. In addition, scanning results in each mass experiencing different conditions due to small fluctuations in the ion source (plasma). This produces a poorer S/N ratio in an isotope - ratioing mode. Scanning also limits precision. Furuta (1) found that with an increase in the mass scanning rate, the precision of lead isotope ratio measurements improved due to the elimination of the effects of drift in the plasma source.

An improvement to the plasma source mass spectrometer would therefore be a mass spectrometer capable of detecting all (or most) of the masses simultaneously; a direct reading mass spectrograph. This improvement could be accomplished by using a mass spectrometer with an array detector that will simultaneously detect ions as they undergo mass analysis by a magnetic field (a sector). Such an instrument should provide better sensitivity, speed, precision, and throughput compared to the commonly used quadrupole mass analyzer.

Methods. A 3 - inch array detector will be used in our instrument, so the mass spectrum will be detected in segments that we call mass windows. We situated our mass windows around argon, an abundant element in the ICP that could blind the detector. Skipping mass 40 (±1) leads to a mass ratio of 5.4 : 1 (analyzing masses 7 to 38) for the first mass window. That window corresponds to a high - mass trajectory radius of 9.5 cm and is the size of our mass spectrometer. We will measure the remainder of the mass spectrum in two additional mass windows containing masses 42 to 224 and 225 to 238 respectively.

The electric sector cancels second - order angular aberrations at the high mass trajectory (9.5 cm). The pertinent calculations, performed by Johnson and Nier (2), specify a ratio of 1.68 between the radii of the electric and magnetic sectors. The electric sector is equipped with shims, sometimes called Rose corrections (3), to correct for a drop in the electric field near the edge of the pole pieces. The electric sector is located between two electrodes called diaphragms or Herzog shunts (4), which produce field-free regions before and after the electric sector.

The mass spectrometer will require a three - stage sampling interface in order to be coupled to an ICP. To accelerate the ions into the spectrometer, the ICP source will float to the appropriate potential by applying a voltage to the sampling cone which sits in the plasma. Electrostatic lenses focus and accelerate the ions to a slit after the sampling process. The source slit should provide adequate resolution yet not reduce throughput excessively. The theoretical resolving power for a Mattauch - Herzog mass spectrometer is (5):

$$R = r_e/2S$$

where R is the theoretical resolving power, r_e is the radius of the electric sector, and S is the slit width. The design criterion for this instrument is a resolution of 500. MacSIMION (Montech, Australia) was used to simulate the ion optics of the ICPMS interface.

Design. All materials are stainless steel except for Macor spacers that separate the electrodes from the instrument body (see Figure 1). The apertures in both the sampler and skimmer cones are 1 mm. An electrically isolated lens tunnel follows the skimmer which acts as a lens and a barrier between the second and third stages. A series of six lenses follows the lens tunnel; three cylindrical lenses and three aperture lenses. The lenses focus the ions onto a slit 0.15 mm by 6.35 mm, producing a theoretical resolution of 533. After the slit, the ions travel through a channel 11.32 cm long to the electric sector. The electric

sector is between shunts 1.14 mm from the electric sector face to reduce fringing fields. The electric sector has a gap width of 1.52 cm and pole face of width 3.81 cm. An electromagnet with a gap width of 8.64 mm and capable of a 8 kilogauss field will be used for the magnetic sector.

Conclusion. A Mattauch - Herzog mass spectrograph has been designed for the inductively coupled plasma. Construction is underway at the Indiana University Mechanical Instruments Services.

Acknowledgements. We gratefully acknowledge the help of Dr. A. O. C. Nier for his help and guidance in this project. We would also like to thank Dr. R. G. Cooks, Dr. J. M. Hayes, Dr. J. P. Reilly for their help. Finally, we thank the Indiana University Mechanical Instrument Services for the construction of the instrument. Supported in part by the National Institutes of Health through grant R01 GM 46853.

Literature Cited.

1) Furuta, N. *J. Anal. At. Spectrom.*, **1991**, 6, 199-203.
2) Johnson, E. G.; Nier, A. O. *Phys. Rev.*, **1951**, 91, 10-17.
3) Rose, M. E. *Phys. Rev.*, **1938**, 53, 715-719.
4) Herzog, R. *Z. Physik.*, **1935**, 97, 596-602.
5) Mattauch, J. *Phys. Rev.*, **1936**, 50, 617-623.

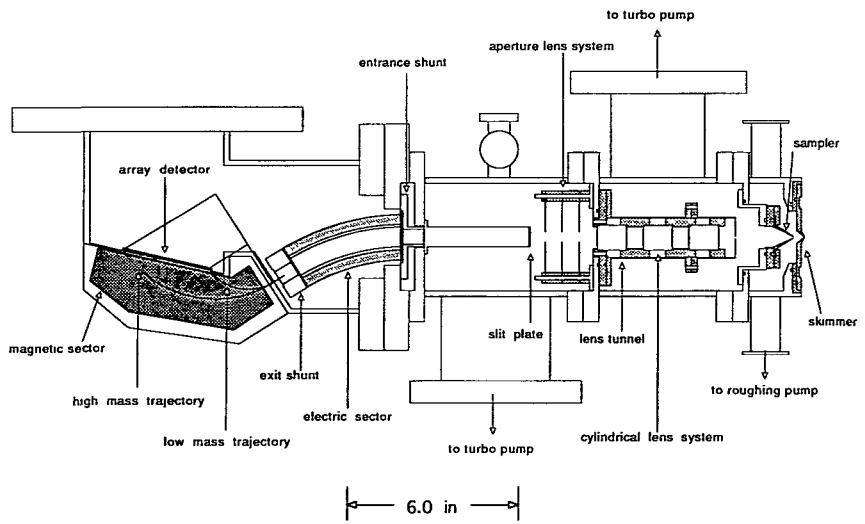

Figure 1. Complete design of the Mattauch - Herzog mass spectrograph for the inductively coupled plasma.

Optimization of an ICP/High Resolution Mass Spectrometer System for Elemental Analysis

Otsuka, K., Kubota, E., JEOL Ltd., Akishima, Tokyo, Japan 196, and Musselman, B.D., JEOL USA, Inc., 11 Dearborn Road, Peabody, MA, USA 01960

The development of a new ICP/High Resolution Mass Spectrometer system has been undertaken. Prior reports have focused on the use of high resolution mass analysis to resolve various atomic ion species in order to obtain more reliable quantitative results through elimination of interferring ion species. This work describes improvements in the instrument control circuitry which have been added to permit more routine analysis of ICP-MS samples while operation in high resolution mode is being utilized.

Experiments describing the use of both magnetic field and acceleration voltage scanning to permit multi-element analysis at low solvent flow rates is also described. Low resolution quadrupole-based ICP-mass spectrometers typically utilize ion counting-based detectors for signal determination. This type of detection system is appropriate with low resolution mass filter systems where peak profile information is not required. The use of scanning methods in quadrupole-based instrument would in effect lead to oversampling of the peak of interest. Magnetic sector instruments with their higher resolution have the capability to resolve the signal from different isobaric ions. The information derived from peak shapes is useful in identification of possible interfering ion species since peak shapes as well as relative ion abundance can be determined from the raw data.

The use of magnetic field scanning desirable for survey scans where a variety of elements are being determined and wide dynamic range for ion detection is desired. The instrument

is operated with the acceleration voltage fixed to 5kV for this experiment. Ions enter the mass analyzer and by applcation of an increasing current through the coil of the electro-magnet the mass of the ions being passed to the detector is changed. By using this scanning method it is possible to detect all of the ions in the desired mass range less than a second. Repetitive scanning over the same mass range is used to effect signal averaging. This method is useful for qualitative analysis but not particularily effective for quantitative analysis.

The reproducibility of the ion current from a specific ion is a function of the ion statistics involved in the formation of that ion, the time period of its detection and the detector response to transitent signals. Using a magnetic field scan severely limits the interval of time that an ions derived from a specific ion specie strike the detector. In the case of a 2 second scan of the mass range 20 to 220 for example, the time period that the maximum ion ion current from an ion with m/z 50 would strike the detector is less than 1 millisecond.

In order to extend the time period for more accurate relative ion abundance determinations, it is necessary to use a different scan function. The control function required for this experiment requires that adjusting the magnetic field to pass the ion of interest, and then completeing an acceleration voltage sweep be effected for each ion abundance being measured. The net result of this action is that all of the ions of a small mass window are passed to the detector. The ion current from the ions is then integrated. In cases where interferring ion species have been observed, the integration of signal from only one of the ion packets in the prescribed mass window can be completed. Changing the time interval of the sweep, and adjusting the mass range passed to the detector yield more quantitative results as shown. The time interval of the sweep, or dwell time, can be set to any time period desired to improve the ion statistics.

ICP/TOFMS SYSTEM FOR USE IN ELEMENTAL ANALYSIS

Mingin Wu, Paul B. Farnsworth, and Milton L. Lee
Department of Chemistry, Brigham Young University, Provo, UT 84602, USA

Chung Hang Sin and Edgar D. Lee
Sensar Corporation, 479 West Universal circle, Sandy, UT 84070, USA

The use of a time-of flight mass spectrometer (TOFMS) with inductively coupled plasma (ICP) ion source offers significant advantages over conventional ICP/MS systems with quadrupole mass analyzers. The attractive features of TOFMS include simplicity, high speed, high transmission efficiency, and instantaneous recording of the full mass spectrum. However, a TOFMS with an on-axis pulsing geometry suffers the shortcomings of low duty cycle and limited resolution.

The problem encountered with on-axis acceleration TOFMS can be overcome utilizing an orthogonal acceleration configuration. The unique right angle pulsing geometry allows the pulsing region to be refilled with extracted ions while a full spectrum is being recorded; this raises the duty cycle significantly. Also the resolution can be improved by accelerating the ions in a direction perpendicular to the ion beam.

In this paper, we describe an ICP/TOFMS system that has been developed based on an orthogonal acceleration configuration. The background spectra obtained with an Ar plasma indicates the current instrument has a mass resolution of 100 at 40 amu. Future work will center on ion focusing schemes and the use of a high speed data acquisition and processing system.

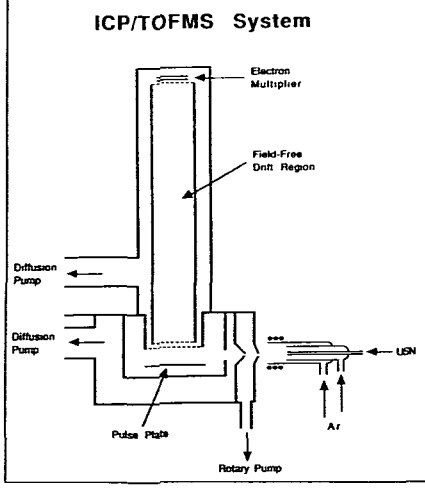

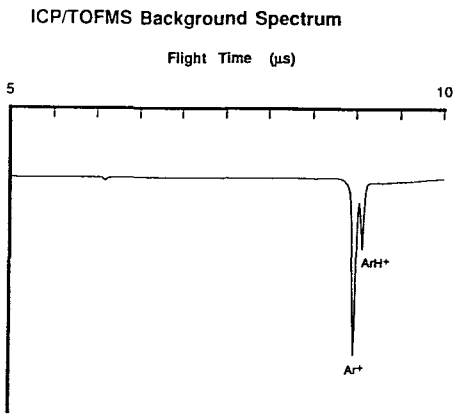

Elemental IonSpray-Mass Spectrometry: Analysis of Solutions of Metal Salts

J.J. Corr and D.J. Douglas, SCIEX, 55 Glen Cameron Rd., Thornhill, Ontario, Canada, L3T 1P2

Recent studies, by Kebarle and co-workers [1] and Agnes and Horlick [2] for example, have indicated that electrospray ionization-mass spectrometry (ESI-MS) has application to the study of the gas-phase chemistry of metal ions. Most recent work has involved spectra typically dominated by ion solvent clusters such as hydrated clusters of the metal ion or methanol/water metal ion clusters. These metal-solvent adducts ions complicate the spectra and increase detection limits by diluting the analyte ions over a number of ionic species. Agnes and Horlick [2] have succeeded in observing a number of spectra where bare metal ions (M^+) were the predominant ions and have demonstrated their ability to control the degree of clustering for a number of different ions.

In the present work some 45 elements ranging in mass from Na at 23 amu to U at 238 amu have been studied by IonSpray-mass spectrometry, the pnuematically assisted version of ESI-MS. Solutions were prepared by dissolving salts in water or from commercially available standards. Dilutions were with water, or methanol, or a water/methanol mixture. A differentially pumped interface was utilized on the front end of a MS-MS system. The N_2 curtain gas and the declustering potential (the voltage difference between the orifice through which the free jet expansion occurs and the skimmer in the differentialy pumped region) were chosen with other operating parameters to allow desired degrees of declustering. Seeking maximum declustering of multiply charged ions promoted charge reduction [1] and hence the observation of bare metal singly-charged ions.

In addition to bare metal ions, metal hydroxides or tightly bound metal oxides and their solvent adducts were easily obtainable and sometimes unavoidable. In many cases spectra such as those in Fig 1 were obtainable by varying the declustering in the interface In most cases the sensitivities obtained for the singly-charged bare metal ions or their oxides were within an order of magnitude of those attainable with inductively coupled plasma-mass spectrometry (ICP-MS). Detection limits of a few ppt to 0.5 ppb were measured for a range of elements. Since this technique does not have the same interferences as ICP-MS, it offers advantages in detection of certain elements, particularly in negative ion mode. Calibration curves (log-log) were linear over a range of four orders of magnitude in solution concentration and did not "roll over" before data accumulation was limited by detector saturation at a few million cps per ppm. The acid content of typical commercial standards increased the conductivity of diluted solutions causing a detrimental effect on analyte sensitivity.

Real world applications of such a technology should be plentiful An example of interest in the nuclear industry is the detection of ^{137}Cs in the presence of Ba, which has isotopes which interfere with Cs detection. To test such a possibilty, solutions containing ^{133}Cs and Ba were sprayed. Taking advantage of the variable declustering available it was possible to "shift" Ba up by 17 amu by detecting $BaOH^+$ while leaving much of the $^{133}Cs^+$ in the bare metal state.

The speciation capabilities of the technique have been demonstrated by selectively detecting selenite and selenate in the negative ion mode.

In this preliminary study the sensitivities and detection limits obtained, the ability to observe bare elemental ions in uncomplicated spectra, and the speciation capabilities indicate that the IonSpray-MS method has great promise as a complementary technique to ICP-MS for elemental analysis.

[1] Blades, A.T., Jayaweera, P., Ikonomou, M.G., and Kebarle,P. *J. Chem. Phys.* **1990**, 92, 5900

[4] Agnes, G.R. and Horlick, G. *Appl. Spectrosc.* **1992**, 46, 401

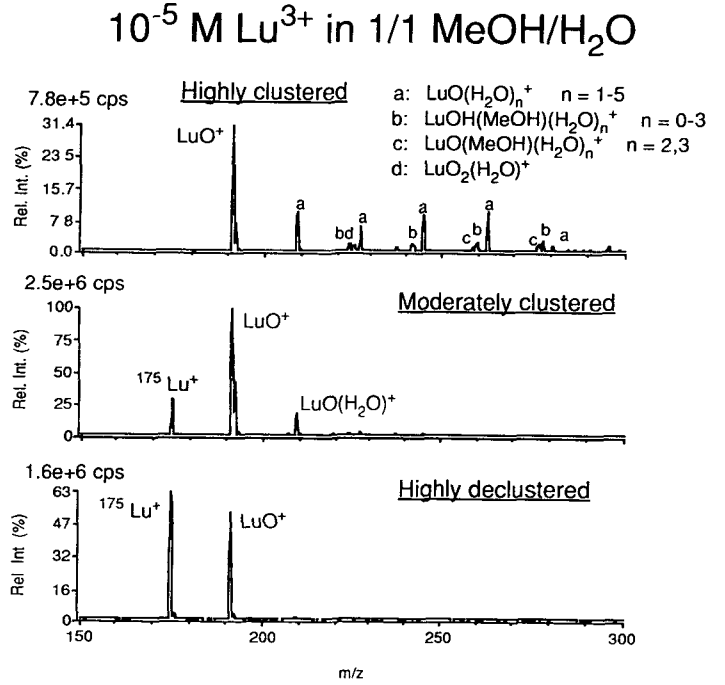

Spectra from 10^{-5} M $LuCl_3$ show that various degrees of declustering are possible. In this case LuO^+ could not be completely dissociated. Other rare earth elements show similar behaviour.

Figure 1

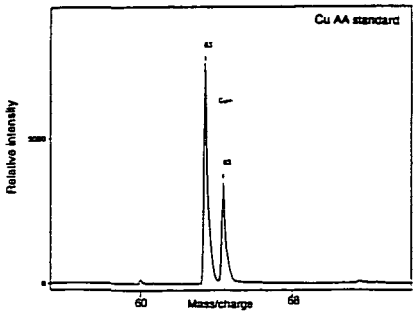

Figure 1. LD/TOF mass spectra of Cu AA standard (1ul of 1mg/ml) on Pt probe tip (250 laser shots averaged).

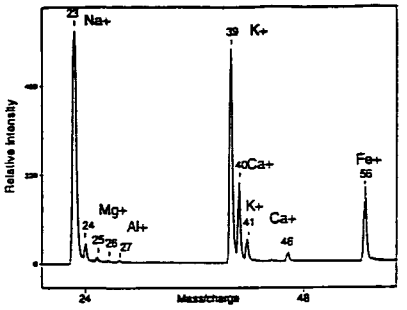

Figure 2. LD/TOF mass spectra of all the metals detected in serum sample enriched in Mg^{25}, on Pt probe tip (1000 laser shots averaged).

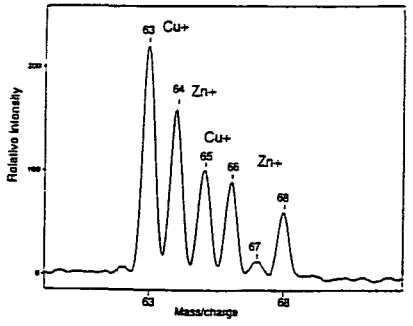

Figure 3. LD/TOF mass spectra of a mixture of Zn and Cu AA standards on Pt probe tip (250 laser shots averaged).

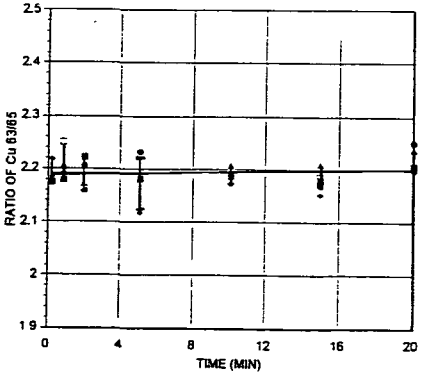

Figure 4. The Cu63/65 ratio in the AA standard remain constant with increasing analysis time (number of averaged laser shots). Twenty minutes of analysis time corresponds to 24000 laser shots. No mass depletion of sample is observed.

METAL ISOTOPE RATIO DETERMINATION WITH LASER DESORPTION TIME-OF-FLIGHT MASS SPECTROMETRY.

Iphigenia L. Koumenis[1], T. William Hutchens[2*] and Marvin L. Vestal[1]

[1]Vestec Corp., 9299 Kirby Dr, Houston, TX 77054 and [2]Protein Structure Laboratory, USDA/ARS Children's Nutrition Research Center, Department of Pediatrics, Baylor College of Medicine, 1100 Bates, Houston, TX 77030, USA.

INTRODUCTION: Laser desorption time-of-flight mass spectrometry (LD/TOF-MS), a technique mainly used for the accurate molecular weight determination of intact macromolecules, is for the first time evaluated for the determination of stable metal isotopic ratios.

The need to eliminate the use of radiotracers for mineral bioavailability studies resulted in the development of several techniques that quantify stable isotope ratios. Current techniques for analysis, such as thermal ionization mass spectrometry (TIMS), inductively coupled plasma mass spectrometry (ICP/MS), fast atom bombardment mass spectrometry (FAB/MS) and resonance ionization mass spectrometry (RIMS), are either inadequate or extremely expensive and time consuming. Because of these limitations and the high cost of tracers, only a limited number of such studies are possible at the present time.

In this work, metal isotope ratios are determined using a LD/TOF mass spectrometer and emphasis is given to the high measurement precision required to permit accurate measurements. The factors that might affect the precision are systematically studied and the results are discussed in this presentation. The five metal ions studied were: Cu, Zn, Mg, Ca and Fe.

RESULTS: With the existing LD/TOF-MS instrument, we show that the technique can overcome the difficulties that the existing methods have: 1) all metals seem to be ionizable, thus overcoming the major drawback of thermal ionization 2) biological matrix components do not seem to cause any interference thus overcoming the major disadvantage of FAB/MS, and 3) accuracy and precision required for tracer work is feasible. Most importantly, the TOF-MS instrument permits all masses to be monitored simultaneously. This permits excellent precision on small quantities of materials, since small changes in isotope ratios can be detected. A substantial reduction in cost can result from using less tracer material.

The two limiting factors for the precision, as determined in these studies, are the digitizer statistics (when not operating in the ion limiting region of the EM gain) and the inadvertent saturation of the signal which distorts the ratio of the peaks.

The RSD is 0.2-0.5% for the higher abundance isotopes and 0.8-2.3% for the lower abundance isotopes. Those values can easily be improved if a 12-bit digitizer is used. The digitizer statistics can be further improved by averaging a higher number of laser shots. We have shown that there is no depletion of sample as a function of analysis time, thus a higher repetition laser can be employed to decrease the analysis time.

A computer-controlled electronic gate can also be incorporated in the digitizer to prevent signal distortion from inadvertent saturation. With this computer-controlled gate a desired window of the signal intensity is preset and any spectra outside the desired window are rejected.

Finally, the technique allows the detection of mixtures of two or more metals to be monitored simultaneously. This is extremely important because two or more metals can be studied at the same time within the same sample. Studies are underway to quantify the ratios of various free and peptide-bound metal ions to establish new approaches for the determination of complex equilibria constants.

DETERMINATION OF SUBPICOGRAM QUANTITIES OF TECHNETIUM-99 IN ENVIRONMENTAL SAMPLES BY POSITIVE THERMAL IONIZATION MASS SPECTROMETRY

J.M. Pochkowski and D.M. Beals
Environmental Technology Section
Savannah River Technology Center
Westinghouse Savannah River Company
Aiken, SC 29808 USA

Introduction

The Savannah River Technology Center's (SRTC) Environmental Technology Section (ETS) has developed a new isotope dilution method to measure ^{99}Tc concentrations in environmental samples. The instrumental detection limit is calculated to be 10 fg (0.17 fCi). The method uses a boric acid/silica gel ion enhancer coupled with positive thermal ionization mass spectrometry (PTI-MS).

Technetium-99 is a by-product of the Savannah River Site (SRS) operations. Technetium, as Tc_2O_7, is extremely volatile. Once in the environment, it readily forms the pertechnetate ion, TcO_4^-, which can be easily transported in hydrologic systems. The long-lived (2.15×10^5 yr) radionuclide is of concern because technetium has been shown to concentrate in the thyroid and GI tract of animals

In the past, most ^{99}Tc measurements have been made by radiochemical separation followed by low-level beta spectrometry. This method is neither specific nor sensitive enough for environmental sample analysis. Other mass spectrometry techniques suffer from hydrocarbon interferences, as well as, isobaric interferences caused by molybdenum and ruthenium not removed during sample preparation. The method developed by the ETS employs a "Delmore" style filament to reduce filament contributions, a rigorous chemical separation and cleanup procedure to reduce chemical blank, and a boric acid/silica gel slurry to allow the sample to be run at a lower temperature with increased ionization efficiency.

Methods

Aqueous samples to be analyzed for ^{99}Tc are spiked with 1.2 ng of ^{97}Tc After equilibration of the tracer, the technetium is separated using a chromatographic resin (TEVA-Spec) method developed by the ETS.[1] Samples are initially screened by isotope dilution/inductively coupled plasma-mass spectrometry (ID/ICP-MS). Five samples per hour can be analyzed with a procedure detection limit of 0.5 pCi/L. Approximately one-half of the concentrated sample is used for the ID/ICP-MS screening

The remaining sample may be further purified and concentrated using a microdistillation technique[2] and analyzed by PTI-MS to confirm a positive result or to decrease the effective detection limit. The microdistillation is performed in a precleaned Teflon vial. After the microdistillation, the technetium is in 4 µL of 0.1 M NH_4OH. The sample is then loaded onto a 0.007" deep "V" dimpled Delmore style zone refined rhenium filament using a camera driven microloader. The technetium is loaded in a 2 µL boric acid/silica gel (1:4) slurry sandwich. The microloader permits consistent point loading of 1 µL solutions onto the filament. The benefit of point loading is that it controls and limits sample contamination and increases sample ionization. This loading procedure gave better reproducibility than previously obtained by other techniques tried by the ETS.

Results

The isolated technetium is analyzed on a National Institute of Standards and Technology (NIST) designed and ETS modified 30.5 cm, 90° deflection, single sector mass spectrometer. We found the maximum stable intensity of the Tc^+ thermal ion signal to occur at a temperature of 1510 ± 50° C using this instrument and

loading procedure. At this temperature, Ru^+ and Mo^+ ions are not formed from the filament This lower temperature also minimizes the time and temperature dependent effects of isotopic fractionation.

Despite rigorous steps to clean the silica gel, organic species were still a minor problem. We found that by heating the sample filament at a temperature of 1100° C for 15 minutes prior to analysis, this interference was significantly reduced.

An average lower limit of detection for ^{99}Tc on this instrument was calculated to be 10 fg (6.1×10^7 atoms, 0 17 fCi) based on the analysis of the ^{97}Tc spike. Several standards containing 10 pg of ^{99}Tc were analyzed using the conditions described above and produced ion count rates of 6000 to 8000 counts per second for over an hour.

The ETS is responsible for performing low level analyses of ^{99}Tc in support of the SRS monitoring programs Air filter samples collected near the administrative area (3/700), the reprocessing areas (200 F, 200 H), and the burial grounds were analyzed for ^{99}Tc using the described technique. As shown in Table 1, the reprocessing areas have as much as 14 times greater ^{99}Tc activity than the site administration area.

Table 1

Location	^{99}Tc Activity (fCi±2σ)
3/700	0.67 ± 0.03
200 F	3.38 ± 0.04
200 H	9.59 ± 0.23
Burial Ground	0.91 ± 0.03

Conclusions

The success of these measurements demonstrates that the use of a highly selective chromatographic resin coupled with a PTI-MS boric acid/silica gel ion enhancer can yield ^{99}Tc measurements as low as 0.67 fCi. This sensitivity approaches that of negative thermal ionization without the need for additional filament preparation and instrument modification. Measurements of SRS environmental samples show that the movement of ^{99}Tc is limited to the SRS plant boundary. Future work includes detailed ^{99}Tc measurements of SRS waters, vegetation, soil, and air filters to study the migration of ^{99}Tc in the Savannah River Site environment.

Acknowledgments

This abstract was prepared in connection with work done under Contract No. DE-AC05-89SR18035 with the U.S. Department of Energy. By acceptance of this abstract, the publisher and/or recipient acknowledges the U.S Government's right to retain a nonexclusive, royalty-free license in and to any copyright covering, this abstract, along with the right to reproduce and to authorize others to reproduce all or part of the copyrighted abstract.

References

[1] Beals, D.M , Determination of Technetium-99 in Aqueous Samples by Isotope Dilution Inductively Coupled Plasma Mass Spectrometry, Proceedings from the 3rd International Conference on Nuclear and Radiochemistry, Vienna Austria, September 1992

[2] Rokop, D J., Schroeder, N.C., and Wolfberg, K., Mass Spectrometry of Technetium at the Subpicogram Level, Anal. Chem., 1990, 62, 1271-1274

Simultaneous Observation of UO^+ and U^+ Ion Ratios via Total Evaporation Thermal Ionization Mass Spectrometry

Douglas D. Jenson
Westinghouse Idaho Nuclear Company, Inc.
Idaho Falls, ID, 83403

Production of UO^+ ions was studied concurrently with isotopic analysis of uranium. A MAT 262V thermal ionization mass spectrometer was used; Faraday cups were positioned to collect data simultaneously at masses 233, 235, 238, 249, and 251. Sample material was NBS U-750 spiked with high purity ^{233}U. The ^{233}U allowed for isobaric corrections to the data. The technique of total sample evaporation and signal integration was used. Filament and sample-handling conditions were varied with an interest toward minimizing the UO^+/U^+ ratio during isotopic analysis.

A "worst-case" situation for UO^+ production is shown in Fig. 1. Oxide ions typically appear at slightly higher filament currents than the metal ions, but they grow rapidly and often dwarf the desired specie. If sample lifetime is sufficient, two U^+ peaks are observed, with corresponding UO^+ peaks.

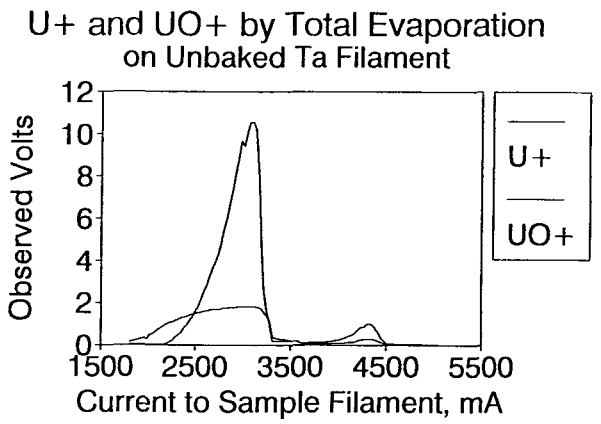

Figure 1. Evolution of U^+ and UO^+ ion beams as a function of current applied to sample filament.

The effects of various experimental conditions on the final integrated UO^+/U^+ ratio are shown in Table 1.

Filament	Condition	Relative Final UO^+/U^+
Ionizing	2250 °C	2
Ionizing	prebake in atmosphere	71
Ionizing	prebake in vacuum	100
Sample	baked Ta	2
Sample	baked Re	16
Sample	unbaked Re	33

Table 1. Relative final integrated UO^+/U^+ ratio compared to reference condition: unbaked ionizing filament at 2100 °C; sample loaded on unbaked Ta sample filament. Reference condition=100.

Small sample size improves the UO^+/U^+ ratio. Fig. 2 demonstrates this effect. Typically, 100 ng total U produces a good U^+ ion current while minimizing the UO^+.

As a "best case" combination, 100 ng U analyzed on a baked Re sample filament produces a final integrated UO^+/U^+ of 0.0002. However, the signal from baked Re tends to tail off gradually.[1]

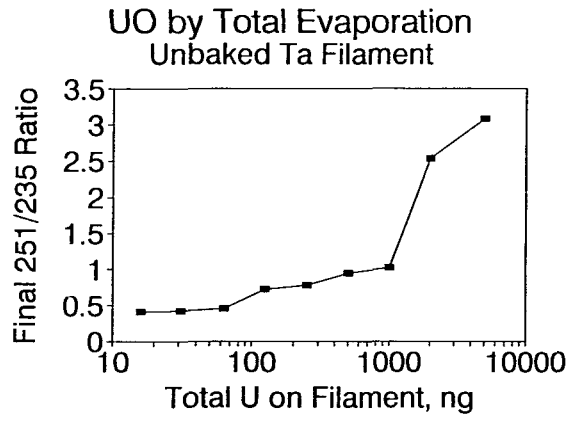

Fig. 2. Effect of sample size loaded on filament.

[1]Callis, E.L. and R.M. Abernathy, Int. J. Mass Spec. Ion Proc. 103, 1991, 93.

Lead Analysis by Electron Capture Negative Chemical Ionization GC/MS

Geoffrey S. Baird, David A. Herold, Suresh K. Aggarwal and Robert L. Fitzgerald
Laboratory Service, VA Medical Center, San Diego, CA 92161
and Dept. of Pathology, University of California-San Diego, La Jolla, CA 92134

Introduction

Studies have shown that Pb may have adverse long term effects on cognitive and motor function at blood concentrations that are significantly below the level that gives rise to clinical symptoms. The potential for long term learning disabilities in several million American children caused by Pb toxicity has prompted the Centers for Disease Control to lower the "threshold of concern" for children from 250 ug/L to 100 ug/L of Pb in whole blood. At this concentration several million children are considered to have poisoning and to be at risk of irreversible mental and physical damage. In order to monitor lead exposure, assays for determining lead concentrations in biological samples are needed. Previously we have used diethyldithiocarbamate for chelating and extracting Pb from biological samples. We found that further reaction with 4-fluorophenyl magnesium bromide (4-FPMB) produced stable derivatives which can be measured with good precision and accuracy as well as very little memory effect when analyzed by GC/MS. Our initial studies were done with a magnetic sector MS instrument using on column GC injections. In the present study, we used a quadrupole GC/MS equipped with an autosampler to study para-substituted aryl lead compounds under EI, PCI and NCI.

Experimental

Reagents: Lead atomic absorption standard solution was from Aldrich. Lead nitrate (70.94 atom% ^{204}Pb, Oak Ridge National Laboratory), the enriched isotope used in memory effect studies was dissolved in deionized water with the addition of a few drops of concentrated HNO_3. Phenylmagnesium bromide (3.0 M), 4-fluorophenyl magnesium bromide (2.0 M), 4-chlorophenyl magnesium bromide (1.0 M), sodium diethyldithiocarbamate, Na(DEDTC), CF_3-phenyl bromide and anhydrous tetrahydrofuran were purchased from Aldrich. Ethyl ether and toluene were purchased from Baxter. Glacial acetic acid was obtained from Fisher, and sodium acetate was obtained from Mallinckrodt.

Grignard Preparation: CF_3-phenyl magnesium bromide was prepared to be a 1.0 M solution in 10 mL of THF. After the glassware was assembled, a stir bar and 0.242 g (0.01 M) Mg turnings were added to the round bottom flask. Under argon, 5 mL of toluene was added and boiled through the system to remove any residual water. After cooling, THF was added through the septum. The CF_3-phenyl bromide (0.01 M) was added dropwise, with stirring and refluxing, until a reaction was visible. After the reaction appeared complete, i.e. the magnesium appeared mostly gone, the solution was removed with a syringe and stored in a dry, argon-filled plastic tube fitted with a rubber septum.

Derivitization: The sample was buffered to pH 4 with acetate buffer and reacted with a 20 mM solution of Na(DEDTC). The $Pb(DEDTC)_2$ chelate was extracted into 1 mL of toluene and evaporated to dryness

under nitrogen at 40°C. The samples were then reconstituted with 100 µL of THF, and 5 to 10 drops of Grignard were added. Excess Grignard was destroyed with 100 µL of 10% isopropyl alcohol in toluene, followed by addition of 1mL of 1N HNO_3. The organic layer was extracted into 1mL of toluene, then dried under nitrogen at 40°C. Samples were reconstituted in 200 µL of toluene.

Instrument Conditions: Samples were analyzed using splitless injection onto a 10m x 0.32mm DB-1 bonded phase fused silica capillary column. The GC was temperature programmed from 160°C (one minute hold), to 280°C degrees at 20°C/min where it was kept for 3 minutes. Total chromatography time was 10 minutes. Approximate retention times for phenyl, 4-Cl-phenyl, 4-F-phenyl and 4-CF_3-phenyl Pb compounds were 5.0, 9.0, 4.8 and 4.3 minutes respectively. For comparison of EI, PCI and NCI, equal amounts of the lead derivatives were injected. EI tuning was optimized at m/z 100 and 502 of perfluorotributylamine (PFTBA) ions. Methane was used as the reagent gas for PCI and NCI. PFTBA was also used to optimize tuning for chemical ionizations; PCI tuning was optimized at m/z 219 and 414 while NCI tuning was optimized at m/z 414 and 633. Studies using NCI for memory, accuracy and precision studies were done by injecting 5 ng of natural Pb or 8 ng of ^{204}Pb as the 4-FP derivative and measuring the $[M-L]^-$ cluster (m/z 489, 491, 492 and 493). Isotope ratios were determined by integrating peak areas.

Results and Discussion

Precision: The precision obtained for $(4\text{-F-phenyl})_4Pb$ in the NCI mode when determining the more abundant isotopes in naturally occurring Pb at the 5 ng level was a C.V. of 0.51% or less.

Memory Effect: The slight memory effect observed from analysis of lead chelates with 330-fold differences in the ratios of m/z 493 to m/z 489, corresponding to ^{208}Pb and ^{204}Pb. Since this limiting case would practically never be encountered, memory effect does not limit this method.

Signal-to-noise Ratio: Using chromatographic peak areas and a base noise level of 10 area units, the signal-to-noise ratios can be calculated. These results for the different Pb compounds are compared according to ionization mode. The $(4\text{-F-phenyl})_4Pb$ compound using NCI conditions gave the most intense S/N ratio. NCI analysis of a sample of natural lead (5 ng Pb on column) in aqueous solution gave a signal to noise ratio of 1089:1 for the weakest signal, ^{204}Pb. This suggests that a sample in the low pg range would give an acceptable signal-to-noise ratio of 10.

Conclusion

Stable isotope dilution NCI GC-MS using 4FMB derivatization of the DEDTC chelate eliminated memory effect. This method enhances the sensitivity by a factor of 75 and increases the precision by a factor of 4. The increased sensitivity and minimal memory effect using an autosampler equipped quadrupole instrument in the NCI mode increases the utility of the GC/MS analysis of Pb in medical and environmental applications.

A STUDY OF MESO-SUBSTITUTED ZINC TETRABENZPORPHYRINS BY FAST ATOM BOMBARDMENT MASS SPECTROMETRY

J.B. Carlson, P. Vouros

Department of Chemistry and Barnett Institute for Chemical Analysis
Northeastern University, Boston, MA 02115

Metallotetrabenzporphyrins are being extensively investigated because of their large and rapid nonlinear optical response[1]. The nonlinear response has applications in the fields of optical communications and optical data processing. The nonlinear optical response is enhanced by the synthesis of metallobenzporphyrins with substituted phenyl rings in the meso position[2].

The structure for zinc tetrabenzporphyrin is shown in Figure 1, where "R" represents the meso position. Nine different meso-substituted zinc tetrabenzporphyrins with a broad range of electron donating or electron withdrawing characteristics were evaluated where R = p-dimethylaminophenyl-, p-hydroxyphenyl-, p-decyloxyphenyl-, p-methoxyphenyl-, phenyl-, p-chlorophenyl-, m-fluorophenyl-, p-trifluoromethylphenyl-, and perfluorophenyl-.

A VG Quattro triple quadrupole mass spectrometer with a cesium ion Fast Atom Bombardment source was used for the analysis. The meso-substituted zinc tetrabenzporphyrins were dissolved in 3-nitrobenzyl alcohol and placed on a static probe for analysis.

FAB/MS provides a rapid technique for structural confirmation of the meso-substituted zinc tetrabenzporphyrins. In addition to molecular weight information, the mass envelope of naturally occurring isotopes is a source of information for the elemental composition of these compounds. The distinctive isotopic abundance pattern unique to each of these compounds compares favorably with theoretically calculated isotopic abundances.

The loss of successive meso-substituents is the primary fragmentation pathway for the zinc tetrabenzporphyrins. The fragmentation is dependent upon the electron withdrawing or electron donating characteristics of the meso-substituent. No fragmentation is observed for zinc meso-tetra-(p-dimethylaminophenyl)tetrabenzporphyrin while the fragment representing the loss of a single meso-substituent is the predominant ion observed in the mass spectrum of zinc meso-tetraperfluorophenyltetrabenzporphyrin. The susceptibility of the zinc tetrabenzporphyrins to fragmentation is related to the nonlinear optical properties of these compounds.

As a representative example, the FAB/MS spectrum of zinc meso-tetraphenyltetrabenzporphyrin is shown in Figure 2. The mass envelope starting at m/z 876 represents the molecular ion and the fragment at m/z 800 represents the loss of a single meso-substituent (R).

Figure 1: The structure of zinc tetrabenzporphyrin where "R" is the meso position.

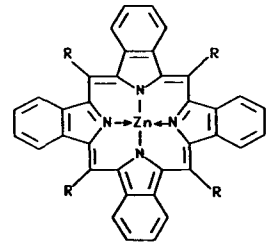

Figure 2: The FAB mass spectrum of zinc meso-tetraphenyltetrabenzporphyrin.

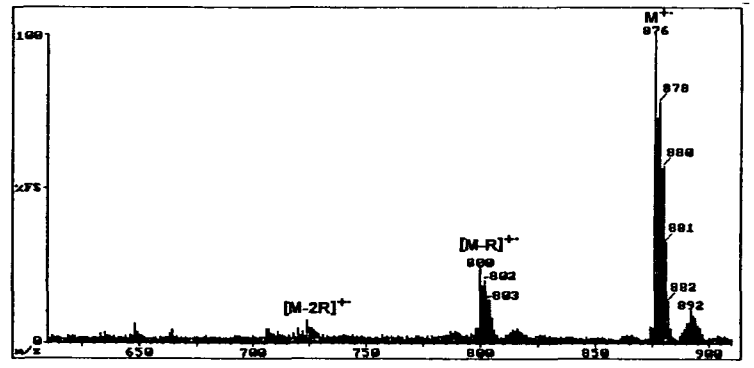

References

[1] Guha, S., Kang, K., Porter, P., Roach, J.F., Remy, D.E., Aranda, F.J., Rao, D.V.G.L.N., *Opt. Lett.*, 1992, 17, 264.

[2] Rao, D.V.G.L.N., Aranda, F.J., Roach, J.F., Remy, D.E., *Appl. Phys. Lett.*, 1991, 58, 1241.

Gas Chromatography-Combustion Isotope Ratio Mass Spectrometry (GCC-IRMS) at Femtomole Carbon Levels and High Enrichments

Keith J. Goodman & J. Thomas Brenna
Division of Nutritional Sciences
Cornell University
Ithaca, New York

Introduction

Since its introduction in 1978, GCC-IRMS (Goodman & Brenna, 1992, Analyt. Chem. 64, 1088) has been employed almost exclusively in studies of $^{13}C/^{12}C$ fractionation due to natural processes. High precision is required in these studies since natural processes usually result in subtle changes in isotope composition. Minimum sample loads of 10ng can be determined to delta (PDB) <0.3°/oo. Terrestrial isotope segregation rarely results in ratios beyond the narrow range of -60°/oo<delta(PDB)<30°/oo.

Recently, we and others have reported application of GCC-IRMS to biomedical tracer experiments using artifically enriched precursors. Such experiments may result in samples with orders of magnitude greater enrichment than natural variation. Therefore, lower precision is often tolerable for investigation of small highly enriched samples. We have characterized the precision and accuracy for enriched samples ≥14°/oo and quantities on column below 250 picomoles carbon

Experimental

The first high sensitivity GCC-IRMS system, a Finnigan 252 interfaced to a Varian 3400 GC, was operated with splitless injection, using the temperature profile 60 °C(1min) to 190 °C(10 min) ramping at 50 °C/min, and a 30 J+W DB Wax 0.25um 0.32mm 30 meter column.

The instrument was operated exclusively in high sensitivity mode with the ion source window closed completely. Methyl stearate (Me18:0) of 36% 13C content was diluted serially with natural abundance Me18:0 to generate a series of eight standards with defined isotope ratio to 14°/oo. Each standard was injected in triplicate at total quantity on-column ranging from about 250 picomoles to 50 femtomoles carbon (minimum sample of less than 1 picogram). Standard deviations and delta-PDB values were generated using vendor-supplied software.

Results and Discussion

"Apparent" delta-PDBs and standard deviations were plotted versus quantity on-column for enrichment levels approximately 14, 50, 100, 500, 1000, 8200, 27000, 37700 °/oo. Typical plots are shown in figures 1 & 2 for the 500°/oo level. Enrichment levels for 1000 °/oo and below plateau above about 1 pmole.

Precision for these levels is usually well within 1°/oo standard deviations, with all data considered and no outliers thrown out. Below this value systematic error is observed. For 100°/oo and below, apparent isotope ratios increase, and for 500°/oo and above apparent isotope ratios decrease. At the highest levels investigated, about 100 pmoles, isotope ratios are offset slightly and in the same direction as is observed at lower levels, which appears to be related to an increasing mismatch between sample and standard CO2 total levels. Below 1 pmole, isotope ratios are a strong function of sample size.

For 8200°/oo and above, isotope ratios do not plateau at any sample size on column. This appears to be due to the limited dynamic range of the detection/electronics, which allow only about 1000. For highly enriched compounds, the mass 45 signal is at very high levels while the mass 44 detector is simultaneously at very low levels.

These data indicate that $^{13}C/^{12}C$ isotope ratios can accurately and precisely be measured for samples sizes above 1 picomole carbon, below 1000°/oo for samples which do not substantially exceed the level of the standard CO_2 Outside these limits measurements can be made with great attention to sample standard matching, dilution of high enrichment samples with natural abundance material to reduce enrichment, and the use of calibrated standards internal to the sample.

Figure 1

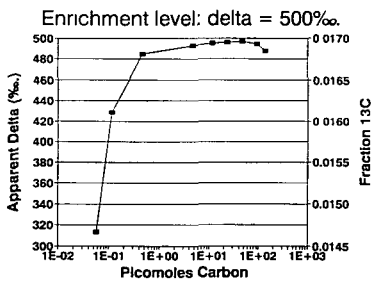

Figure 2

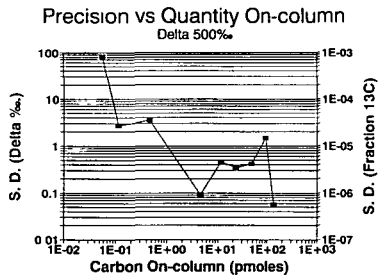

Comparison of Polymer Additives Analysis by High Temperature GC/MS vs. Particle Beam LC/MS

*R.A. Ludicky, G.B. Kenion, D.E. Doster and P.D. Souchek
Morton International, 1275 Lake Avenue, Woodstock, IL 60098

Polymer additives include many compound classes and a variety of molecular weights. Ultraviolet stabilizers and antioxidants include small compounds such as Tinuvin 326 (MW = 315), hindered phenolics such as Ethanox 330 (MW = 774) and phosphite esters such as tris(nonylphenyl) phosphite (MW = 688). The smaller species are on the low end of what can be analyzed using a particle beam LC/MS interface while the largest species are not gas chromatographable. With the advent of high temperature capillary GC columns, the area of common ground between GC/MS and LC/MS has been significantly increased. A comprehensive comparison of quantitative (precision and sensitivity) and qualitative (quality of mass spectra and chromatography) will be presented to facilitate the best choice for analysis of most of the more common antioxidants and UV stabilizers.

All the work described here was performed on an Extrel ELQ 400 GC/LC/MS system. The GC separations were performed on a J&W DB-5 high temperature capillary GC column while LC/MS was performed on a two column set consisting of a Phenomenex 250 cm by 4.6 cm W-Porex 5 phenyl 300 Angstrom column and a 250 cm by 4.6 cm Spherex 5 phenyl 80 Angstrom column. The LC flow rate was 0.5 ml per minute. Fourteen Antioxidants and UV stabilizers were chosen for this study. These additives were Ethanox 330, Irganox 1024, Irganox 1035, Irganox 1076, Irganox 3114, Naugard 445, Naugard 524, Tinuvin 144, Tinuvin 326, Tinuvin 327, Tinuvin 328, Tinuvin 770, Tinuvin 900 and Wytox 312.

Both GC/MS and LC/MS gave nearly identical spectra for the same additives. These two methods, however, gave far different detection limits. The detection limits of the seven compounds which could be analyzed by both techniques are:

Additive	GC/MS Detection Limit	LC/MS Detection Limit
Tinuvin 326	10 nanograms	500 nanograms
Tinuvin 327	5 nanograms	600 nanograms
Tinuvin 328	5 nanograms	600 nanograms
Naugard 445	6 nanograms	300 nanograms
Naugard 524	5 nanograms	600 nanograms
Tinuvin 900	5 nanograms	600 nanograms
Irganox 1076	6 nanograms	1000 nanograms

GC/MS is more sensitive than LC/MS. LC/MS, however, is more universal. Of the fourteen compounds chosen for this study only eight could be analyzed by GC/MS. Twelve of the compounds, on the other hand could be analyzed by LC/MS. The only two compounds which could not be analyzed by LC/MS, Tinuvins 144 and 770, probably could be analyzed if different LC/MS conditions were chosen.

LC/MS was far more precise than GC/MS. Precision data is given below for the seven compounds which could be analyzed by both techniques.

Additive	Relative Standard Deviation GC/MS	Relative Standard Deviation LC/MS
Tinuvin 326	35 %	18 %
Tinuvin 327	36 %	11 %
Tinuvin 328	36 %	11 %
Naugard 445	50 %	11 %
Naugard 524	42 %	22 %
Tinuvin 900	46 %	11 %
Irganox 1076	75 %	14 %

Relative standard deviation for GC/MS was determined by six replicate injections while relative standard deviation for LC/MS was determined by five replicate injections.

Fourteen polymer additives were analyzed by LC and GC/MS. GC/MS is more sensitive but LC/MS is more precise and universal. The data presented here tends to indicate that particle beam LC/MS polymer additive analyses should be done as quickly as possible to give the sharpest peaks. Sharp peaks give better detection limits. The data also indicates that quantitative GC/MS analysis is difficult using standard GC and GC/MS hardware. GC/MS analysis of polymer additives may be improved by use of cold on column injectors which have recently become available. Quick analyses and less thermal stress should improve LC/MS and GC/MS polymer additive analyses.

BASICITY AND SOLVATION EFFECTS IN ELECTROSPRAY MASS SPECTROMETRY

M. Shahgholi and K.D. Cook, Chemistry Department, The University of Tennessee, Knoxville, TN 37996-1600, and M.V. Buchanan, Analytical Chemistry Division, Oak Ridge National Laboratory, Oak Ridge, TN 37831-6120

Several factors have been reported to affect the response of electrospray (ES) MS. For example, hydration energies have been considered in deriving a quantitative model for predicting the response of amino acids[1] and tripeptides[2]. Correlation has also been reported between the pK_b of some thirty amines and their ES response[3]. Furthermore, a role for gas phase chemistry has been suggested in reporting the occurrence of gas phase proton transfer reactions in the drift space between the needle and the mass spectrometer inlet[2]. The present investigation seeks to determine whether thermochemical measures of solvation and basicity are useful in predicting ES response for compounds of varying chemical functionality. Towards this end, two classes of compounds with known thermochemistry, n-alkyl amines and amino acids, were tested for correlation of their ES response with solution phase acidity, pK_a, gas phase basicity, polarizability, and heats of solvation. In this latter case, the heat of solvation, $\Delta H_s^0(BH^+)$, is comprised of a neutral term, $\Delta H_s^0(B)$, and an electrostatic term, $\Delta H_s^0(BH^+)^{el}$[4].

Amines were dissolved in methanol at a concentration of 100 μM. Amino acids were prepared in 50:50 (v/v) methanol:water at a concentration of 100 μM. An ES source similar to Chait's was constructed and interfaced to an Extrel (Model 065-2) quadrupole mass spectrometer. Samples were electrosprayed at 4 μL/min with a needle potential of +3.0 to 3.5 kV. The capillary and skimmer potentials were +90-130 V and 45-65 V, respectively. The inlet capillary was heated to 100-120°C for desolvation of the sampled spray.

The n-alkyl amines used in these correlation studies were propyl- and butylamine (1°); diethyl-, dipropyl-, and dibutylamine (2°); triethyl-, tripropyl-, and tributylamine (3°). The amino acids examined were alanine, isoleucine, phenylalanine, proline, threonine, valine, and glycine. The ES response of the amines and amino acids were tested for correlation with pK_a, gas phase basicity, solvation energies, and polarizability, as estimated from the r^2 "goodness of fit" parameter for a quadratic least squares fit of the data ($r^2=1.0$ for perfect correlation, $r^2=0$ for no correlation). Among the parameters tested, polarizability, pK_a, and the neutral heat of solvation, $\Delta H_s^0(B)$, correlate well ($r^2>0.7$) with the observed ES response of the alkylamines. In considering gas phase basicities and solvation energies of the alkylammonium ions, $\Delta H_s^0(BH^+)$ and $\Delta H_s^0(BH^+)^{el}$, correlation is also observed, and in fact a distinction can be made among 1°, 2° and 3° amines (e.g., Figure 1). The strong correlations observed reflect the general similarity of the various members of this homologous series of compounds.

The amino acids studied, on the other hand, represent a diverse group of compounds. The correlation of the various parameters with the ES response of the amino acids was less well-defined. Only poor correlations ($r^2<0.5$) with pK_a, gas phase basicities, and the electrostatic solvation energies, $\Delta H_s^0(BH^+)^{el}$, were observed (e.g., Figure 2). The only strong correlation observed was with polarizability ($r^2=0.9$).

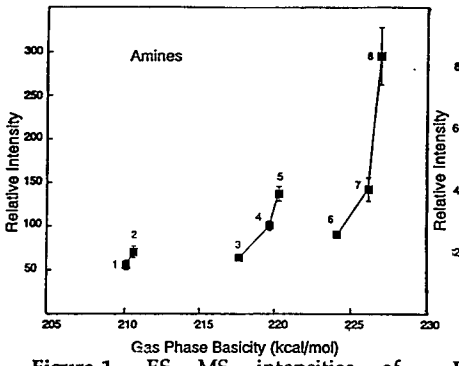

Figure 1. ES MS intensities of alkylamines versus gas phase basicity. (1) propylamine; (2) butylamine; (3) diethylamine; (4) dipropylamine; (5) dibutylamine; (6) triethylamine; (7) tripropylamine; (8) tributylamine

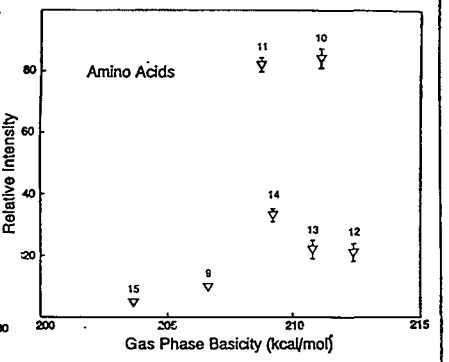

Figure 2. ES MS intensities of amino acids versus gas phase basicity. (9) Ala; (10) Ile; (11) Phe; (12) Pro; (13) Thr; (14) Val; (15) Gly

Thermochemical data utilized for correlations were obtained from J.E. Bartmess[5].

References

1. Sakairi, M; Yergey, A.L.; Siu, K.W.M.; Le Blanc, J.C.Y.; Guevremont, R., Berman, S.S. *Anal. Chem.*, **1991**, *63*, 1488.
2. Voyksner, R.D.; Pack, T. *Proceedings of the 40th ASMS Conference on Mass Spectrometry and Allied Topics, Washington, DC*, 1992, 493.
3. Ikonomou, M G.; Blades, A.T.; Kebarle, P. *Anal. Chem.*, 1990, *62*, 957.
4. Arnett, E.M. *Accounts of Chemical Research*, 1973, *6*, 404.
5. Bartmess, J.E. Unpublished compilation of thermochemical data.

Acknowledgements

Research supported in part by the National Science Foundation under grant CHE-8822787 to UT and by the Office of Health and Environmental Research, U.S. Department of Energy, under contract DE-AC05-84OR21400 with Martin Marietta Energy Systems, Inc., and contract DE-AC05-76OR00033 with ORAU

"The submitted manuscript has been authored by a contractor of the U.S. Government under contract No. DE-AC05-84OR21400. Accordingly, the U.S. Government retains a nonexclusive, royalty-free license to publish or reproduce the published form of this contribution, or allow others to do so, for U.S. Government purposes."

Sensitivity, Dynamic Range and Solvent Effects in Electrospray (Ionspray) Ionization

° R. Kostiainen and * A.P. Bruins, University Centre for Pharmacy, A Deusinglaan 2, 9713 AW Groningen, The Netherlands

In spite of the growing number of publications describing the applications of electrospray, there is a lack of understanding of the details of the ionization process. Fenn and Kebarle and their coworkers have studied aspects of the fundamental limitations of the electrospray process Concerning the dynamic range of electrospray and ionspray, the upper limit of the sample ion signal observed after mass analysis is reached at approximately 10^{-5}M sample concentration[1], both for proteins and for small molecules.

We have used the ionspray version of electrospray in a home built atmospheric pressure ionization source on a NERMAG 3010 mass spectrometer Other equipment: Jasco Familic 100N syringe pump and Brownlee syringe pump operating at 5 or 10 μL/min; Rheodyne injectors with 20μL loops to generate broad and reproducible sample bands, so that peak height is not affected by dead volume or tailing. Sample solutions: tetrabutylammonium bromide in 95% acetonitrile + 5% methanol. The amount of charge on droplets leaving the nebulizer is measured as depicted in Fig. 1.

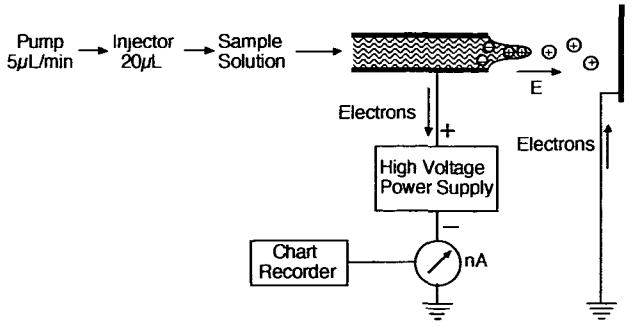

Figure 1 Measurement of spray current

Kebarle et al. have described electrospray as a special case of an electrolysis cell[2]. Positive charge on droplets is the result of removal of negative ions (charge separation). Since the number of available negative ions is proportional to sample concentration, charge separation and spray current are a function of sample concentration. Theory has predicted and experiments have shown that the spray current is proportional to c^n (c: concentration; n= 0.2 – 0.4). Figure 2 shows that the ion signal reaches a plateau at 10^{-5}M, while the spray current (charge on droplets) keeps rising. Insufficient charge on droplets thus does not appear to be the major cause of signal saturation.

The upper limit to the ion signal may also be due to an upper limit on the number of ions

that can be taken from the source into the vacuum of the mass analyzer. By repositioning the sprayer to a longer distance from the ion sampling orifice, the total number of ions transported into the mass analyzer is reduced. Figure 2 also shows that ion signal limitation still exists when the sprayer is placed far away. Thus, limitation in the transport of ions is ruled out as a cause of ion signal limitation.

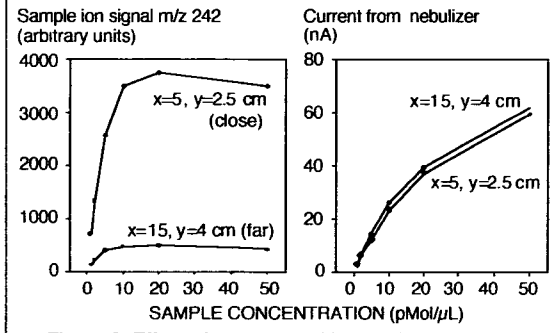

Figure 2. Effect of sprayer position on dynamic range

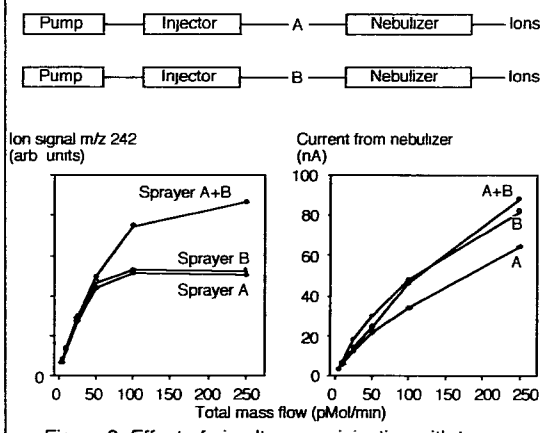

Figure 3 Effect of simultaneous injection with two injectors and two sprayers, after twofold dilution (A+B)

Next, the limitation could be inherent in the nebulization (droplet formation) process By splitting the flow into two sprayers operating in parallel, one could generate more droplets, or spread droplets in order to reduce interaction between droplets. No improvement was obtained in such a simple split into two nebulizers

If on the other hand the sample concentration is halved, and two simultaneous injections are made, a shown in figure 3, so that the total sample mass via two sprayers is equal to the total sample mass injected into one sprayer, at the original concentration, then the dynamic range is extended.

Thus, the dynamic range is not limited by the total amount of sample introduced into the source, but related to concentration *per se*.

For the time being, we conclude that the sample ion signal limitation is due to a concentration dependent limitation in the liberation of ions from charged droplets. The details are still unclear to us.

° On temporary leave from Food and Environmental Laboratory of Helsinki, Finland

1. A. Raffaelli and A.P. Bruins, Rapid Cummun. Mass Spectrom. 5 (1991) 269
2. A.T. Blades, M G. Ikonomou and P. Kebarle, Anal. Chem. 63 (1991)2109

Investigation of Metal-Ligand Aqueous Solution Chemistry using Electrospray Mass Spectrometry

Roger Guevremont, K.W.M. Siu, J.C.Y. Le Blanc[a], and Z.L. Cheng, Institute for Environmental Chemistry, National Research Council of Canada, Ottawa, Ontario, Canada K1A 0R6

The ions observed in electrospray (ES) mass spectrometry appear to originate from preformed ions in aqueous solution. In recent work we have investigated the speciation of metals in aqueous solution, and have considered the role of droplet evaporation in electrospray mass spectrometry. Preliminary results suggest that the ions are formed early in the ES process, and therefore the composition of the aqueous phase from which the ions are evolved more closely resembles that of the bulk solution than previously thought possible. The characteristic profile of multiply charged ions observed in the electrospray spectrum of proteins appears to originate from an array of pre-formed multiply charged protein ions in aqueous solution. An aqueous solution equilibrium model based on the pKa's of acidic and basic sites on proteins can be used to compare the distribution of ions in solution to the shape of the ion abundance profile in the electrospray mass spectrum[1]. We will now consider the extension of this work to the speciation of labile metal-ligand complexes in solution.

Electrospray measurements were performed using a TAGA 6000E (SCIEX Inc., Thornhill, Ont. Canada) triple quadrupole mass spectrometer. To ensure reliable measurement of relative ion abundance data, the mass resolution was decreased from unit mass resolution to the extent that two or more measurements were taken near the apex of every peak. Samples were continuously infused at a rate of 20µL/min through a 100µm ID stainless steel capillary held about 3kV. Stable operation of electrospray was achieved with the needle approximately 1.5 cm from the instrument orifice, and with a measured stable current of between 70 and 120 nA (positive ion mode).

The aqueous solution acid-base chemistry of Deferoxamine (DFA) MW=561 was studied using positive ion electrospray of a series of solutions of various pH (adjusted with piperidine). Simplex calculations were used determine the formation constant which best matched the variation in species concentration as a function of pH. The species concentrations were calculated using COMICS [2]. The pKa for the protonation of DFA (H_3L to H_4L^+) appears in Table I.

Complexation of DFA with La, Yb and Y were investigated since these metals each provided several positively charged electrospray ions. Samples were prepared with 1 or 2 mM of metal ion and 1 mM of DFA and pH adjusted with piperidine (pKa=11.1). Formation constants of species were calculated by Simplex optimization of the constants to achieve the best match between the ES ion abundance and the calculated species concentration as a function of pH. The aqueous solution model included protonation of the DFA (pKa_2=9.7, pKa_3=9.03, pKa_4=8.39 where the fully protonated ligand is taken to be H_4L^+) and several known metal-ligand complexes

and metal-hydroxide complexes (since the samples were between pH 3 and pH 10). Typical species included ML, MHL, MH_2L, MH_3L, and hydroxide species. Table I includes formation constants of several complexes.

Table I. Stability Constants of DFA Complexes.

Complex	DFA	Yb:DFA (1:1)	La:DFA (1:1)	La:DFA (2:1)	Y:DFA (1:1)
H4L/H3L	8.5(8.39)*				
MHL/M.HL		17.1(16.0)	13.6(10.9)	13.3(10.9)	18.5
MH2L/MHL.H		5.4(4.7)	6.0(6.4)	6.3(6.4)	5.8
MH3L/MH2L.H		2.5(4.4)	5.8(6.0)		4.2

*values in parenthesis from [3]

Deferoxamine

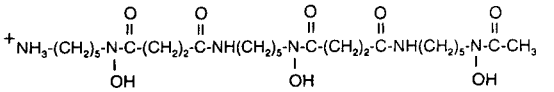

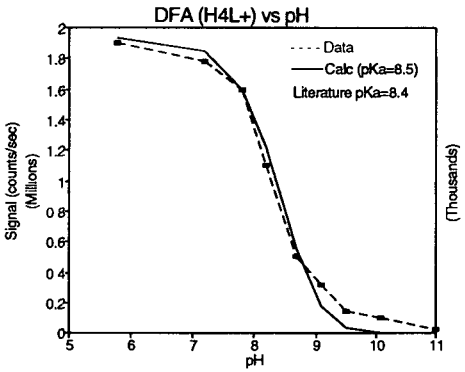

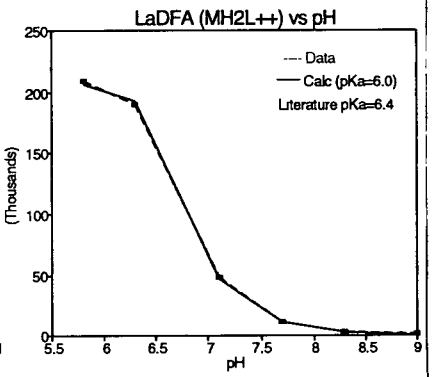

[a] Postgraduate student, Queens University, Kingston, Ontario, Canada K7L 3N6

[1] R.Guevremont, K.W.M.Siu, J.C.Y.LeBlanc, S.S.Berman, J.Am.Soc.Mass Spectrom., **3**, 216 (1992).
[2] D.D. Perrin, I.G. Sayce, Talanta 14, 833(1967).
[3] R.M. Smith, A.E. Martell, Critical Stability Constants, Plenum, New York, 1981.

Peptide Charge State Effects on Electrospray and Capillary Electrophoresis / Electrospray Mass Spectrometry

W. Weinmann[1,2], M. Przybylski[2], C. E. Parker[1], K. B. Tomer[1]

[1]Laboratory of Molecular Biophysics, NIEHS, Research Triangle Park, NC, 27709
[2]University of Konstanz, Postfach 5560, D 7750 Konstanz, FRG

Using a coaxial sheath flow electrospray probe [1] which is stable over several hours of operation, peptides with differing acidities have been investigated by Flow Injection Analysis (FIA) and by capillary electrophoresis (CE) ESMS on aminopropylsilane-treated capillaries [2] The sensitivities of the most abundant mono- or doubly-protonated molecules have been compared. For acidic peptides one order of magnitude less sensitivity than for the basic peptides has been found, both in FIA and CE ESMS. In contrast with peptide mixture analysis by ^{252}Cf-plasma desorption mass spectrometry, where suppression effects of basic, hydrophobic peptides on the ion intensities of acidic, hydrophilic peptides have been observed [3], these effects were not found in the mixture analysis by ESMS.

Coaxial sheath flow ESMS was further applied to proteins (Cytochrome c and Lysozyme), injected in solutions with pH's from 2 to 10 with a constant sheath flow composition (50:50, MeOH 3% acetic acid, pH 2), and with SDS addition in the sample solution. Using basic sample-solutions, a shift in the envelope of mass-to-charge ratios to higher masses is observed. Although the resulting pH at the probe tip is about 3 5 - when measuring the mixture of basic sample-solvent (pH 10) and sheath-flow (pH 2) directly at the needle-tip without spraying - the resulting charge distribution suggests that the conformation is more like that from the pure sample-solution and is not influenced by the sheath flow solvent.

For ES mass spectra aquisition of SDS- or high amounts of salt-containing protein-solutions (10 mM NaOH), higher repeller voltages were used on a Vestec 201A-quadrupole mass spectrometer Repeller voltages of 40 to 80 V can be used for CID-fragmentation of peptides, even higher repeller voltages (100 to 150 V) applied to a mixture of lysozyme and SDS (10:1 / w:w) can lead to dissociation of protein-dodecylsulfate complexes (Fig. 1 a,b) resulting in easily interpretable mass spectra (Fig 1 c,d) and may be advantageous in the analysis of biological samples

[1] C.E. Parker, J. R. Perkins, K.B. Tomer, Y. Shida, K. O'Hara, M. Kono, *J. Am. Soc. Mass Spectrom* 3 (1992) 563
[2] M.A. Moseley, L.J. Deterding, K.B. Tomer, J.W. Jorgenson, *Anal. Chem.*, 63 (1991) 109.
[3] K. Schneider, P.F. Nielsen, D. Suckau, M. Przybylski, in Mass Spectrometry of Large Non-Volatile Molecules for Marine Organic Chemistry (1990), E.R. Hilf and W. Tuszynski, Eds; (World Scientific, Singapore), 176-185.

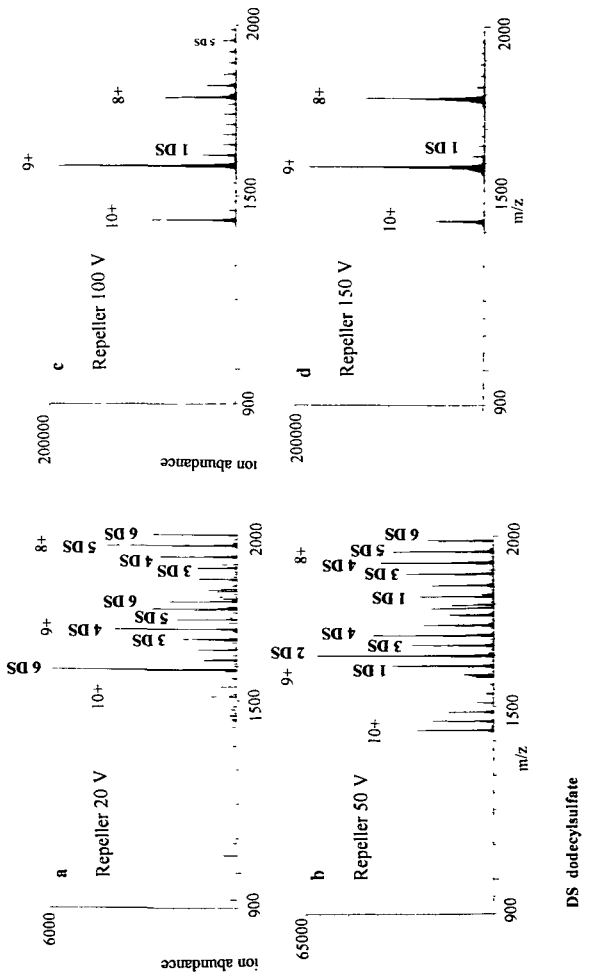

Fig. 1: Coaxial sheath-flow ESMS of lysozyme / SDS (10 1 / w w) in 10 mM ammoniumacetate pH 6.8 Sheath-flow solvent 50 50 MeoH/ 3% acetic acid, pH 2, 5µl/min Sample 0 1 µg/µl SDS / 1 µg/µl hen eggwhite lysozyme (MW 14306 D) Repeller voltage 20 V (a), 50 V (b), 100V (c), 150 V (d)

THE USE OF MULTIPLE SPRAYER SYSTEM IN THE ELECTROSPRAY MASS SPECTROMETRY

R. Kostiainen[1,2] and A.P. Bruins[1]

1. University Centre for Pharmacy, Antonius Deusinglaan 2, 9713 AW Groningen, The Netherlands.

2. Environmental Laboratory of Helsinki, Helsinginkatu 24, 00530 Helsinki, Finland

A limited usable flow rate (2-10 µl/min) in the electrospray mass spectrometry (ESMS) is a well known phenomenon, which is reported to be due to droplet coarsening at high flow rates. In this study we present the use of two and four sprayers instead of one in ESMS and in ionspray (pneumatically assisted electrospray) mass spectrometry (ISMS). In our experiments the flow from a liquid chromatograph (LC) was divided to the sprayers with Valco minimum dead volume T-pieces and fused silica capillaries (Fig. 1). The flow rate in the individual sprayer was decreased with the number of sprayers, while the flow rate from the LC was not decreased Tetrabutylammonium bromide (TBABr, 2 pmol/µl) was used as a reference compound. The measurements were made in MeCN/MeOH 95/5%. The injection volume was 20 µl causing flat topped peaks, which were broad enough to check the stability of the ion current m/z 242 (TBA^+) The instrument was Nermag R 3010 triple quadrupole mass spectrometer equipped with a custom-made atmospheric pressure ionization (API) source.

The dependence of abundance of the ion current m/z 242 (TBA^+) on the flow rate measured with one, two, and four sprayers in ES and IS has been presented in Figs. 2 and 3 Fig. 2 clearly shows that the usable flow rate can be increased in ES by increasing the number of sprayers. This is because the flow rate in the individual sprayer and thus the size of the initial droplet is decreased with the number of sprayers In our experiments it was possible to see the spray against an intense light during the acquisition. We recognized that at the flow rate, where the ion current decreased, also the shape of the spray changed due to sudden coarsening of the droplets The usable flow rates from the LC for one, two, and four sprayers are 4-10, 4-50, and 10-75 µl/min, respectively The flow rate of 4-10 µl/min from the LC (1-2.5 µl/min in the individual sprayer) in the four sprayer system is too low for an efficient dispersion of the liquid

The measurements with one, two, and four sprayers in ISMS (Fig. 3) at fixed position (x=7, y=2.5 cm; x=axial distance, y=off axis distance) resulted in very similar curves in contrast to curves obtained with ES (Fig. 2). The droplet size distribution is less dependent on the flow rate in IS than in ES due to pneumatic nebulization in IS We recognized visually that at high flow rates the size of the droplets in IS are significantly smaller than in ES. The smaller droplet size in IS leads correspondingly to better sensitivity in IS than in ES at high flow rates as shown in Figs. 2 and 3.

Although a reasonably good sensitivity was obtained in ISMS even at a flow rate of 1000 µl/min, the signal becomes very unstable above 200 µl/min leading to noisy background. However, the stability of the signal is highly dependent on the positioning of the sprayer. To keep good stability at high flow rates the sprayer must be removed to more off axis and to a larger distance from the sampling orifice. The positioning of the sprayer is more critical in ES than IS.

The dependence of the ion signal on the flow rate in IS was measured with one, two, and four sprayers and by repositioning the sprayers to achieve the best possible combination of high intensity and good stability for each flow rate (Fig.4). To maintain good stability the sprayer was moved to a longer distance from the sampling orifice, when the flow rate was increased. The operation at a long distance leads to decreased sensitivity. However, we recognized that the four sprayer system can be operated closer the sampling orifice than the one or two sprayer systems This means that the usable flow rate can be enhanced by using several sprayers instead of one.

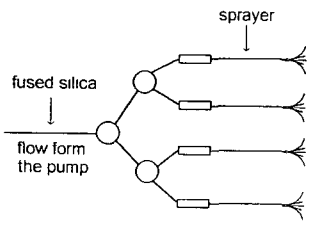

Figure 1 The four sprayer system

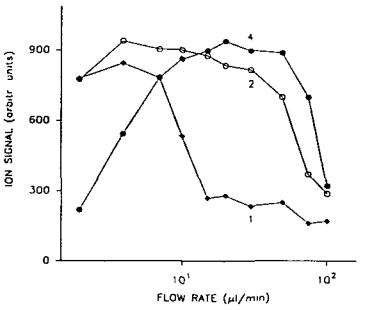

Figure 2 The effect of flow rate on the ion current (TBA^+,m/z 242) for ES using one (1), two (2) and four (4) sprayers.

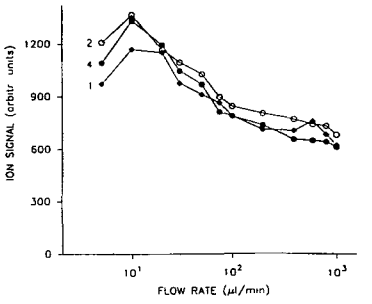

Figure 3 The effect of flow rate on the ion current (TBA^+,m/z 242) for IS using one (1), two (2) and four (4) sprayers. The position of the sprayer was fixed (x=7, y=2.5 cm).

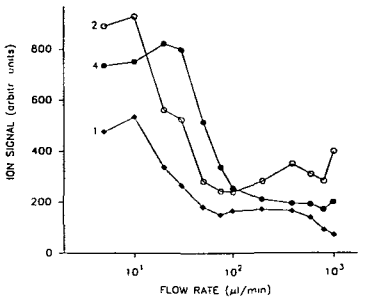

Figure 4 The effect of flow rate on the ion current (TBA^+,m/z 242) for IS using one (1), two (2) and four (4) sprayers. The position of the sprayer was optimized for good stability and sensitivity for each flow rate.

Characterization of a New Atmospheric Pressure Ionization Interface for Liquid Chromatography/Mass Spectrometry

Mark Hail, Iain Mylchreest, Finnigan MAT, San Jose, CA 95134.

In the past few years, the atmospheric pressure ionization (API) interface has emerged as the interface of choice for high-sensitivity LC/MS. Recently, we have designed a new API interface which may be operated in either electrospray (ESI) or atmospheric pressure chemical ionization (APCI) mode with liquid flow rates of up to 2 mL/min. In this interface, ions created via ESI or APCI are desolvated and transported from atmosphere to vacuum through a heated metal capillary tube. The ions exiting the capillary region at 0.7 Torr are focused by a tube lens through a skimmer orifice into the differentially-pumped vacuum manifold of a single quadrupole or triple quadrupole mass spectrometer.

An rf-only octapole, which transports the ions from the skimmer exit to the quadrupole entrance, has replaced the 3 electrostatic lenses used in our previous ESI source. The octapole, which exerts a lateral restoring force on the ions, can efficiently contain ions through this 1 mTorr region with minimal losses due to scattering. This is particularly significant for the detection of low mass ions, which are more susceptible to these collisional scattering losses. For example, the spectra in Figure 1 show that signal response for the tetrapeptide Met-Arg-Phe-Ala increased 70-fold, while that of myoglobin increased 5-fold when the octapole was used in place of the 3-lens system.

The capability to operate in ESI mode over a wide range of liquid flow rates (1μL/min - 1 mL/min) is due to the ability to achieve excellent control of the desolvation process with the heated capillary. By varying the temperature of the heated capillary, one can achieve optimum results at virtually any flow rate, obviating the need for post-column splitting. For example, a capillary temperature of 200 C is typically used for flows of 50 μL/min, while temperatures of 250-275 C are used at 1 mL/min. Higher capillary temperatures dramatically reduce solvent background at high liquid flow rates, as shown in Figure 2. As shown by the chromatograms in Figure 4, the signal intensity actually increases when the entire column flow of 1 mL/min is introduced into the ESI interface as compared to splitting the flow down to 200 μL/min or 50 μL/min. This seems to indicate that the electrospray response may not be purely concentration dependent, particularly in these high flow applications.

Another aspect of the interface that has improved high flow operation is the use of a misaligned capillary-skimmer arrangement which has no line-of-sight from the capillary exit through the skimmer. This dramatically improves the signal-to-noise ratio by preventing aerosol particles which are not desolvated in the capillary from reaching the detector. This is demonstrated in Figure 3 which shows data for the on-axis versus the off-axis capillary-skimmer arrangement for 3 loop injections of 500 pg of reserpine. In the on-axis mode the analyte is completely obscured by the aerosol noise events, while excellent signal-to-noise is obtained in the off-axis configuration.

Presented at the 41st ASMS Conference on Mass Spectrometry

Figure 1. Comparison of MRFA-Myoglobin mixture spectra obtained with (a) new ion optics and (b) ion optics used on previous design

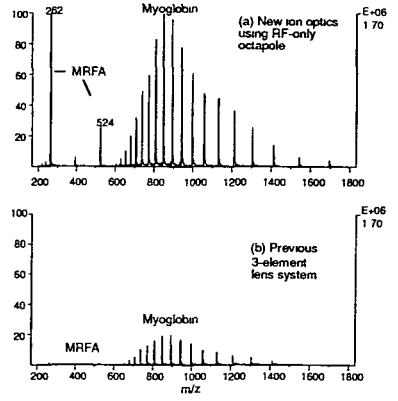

Figure 2 Effect of capillary temperature for loop injections of astemizole in 80/20 MeOH/H_2O 10mM NH_4OAc at a flow rate of 1 mL/min

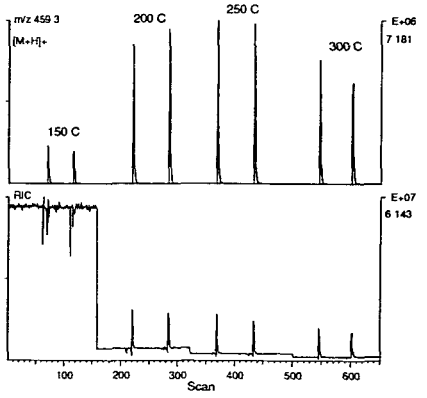

Figure 3 Effect of capillary-skimmer alignment on signal-to-noise for 500 pg injections of reserpine at 50 µL/min

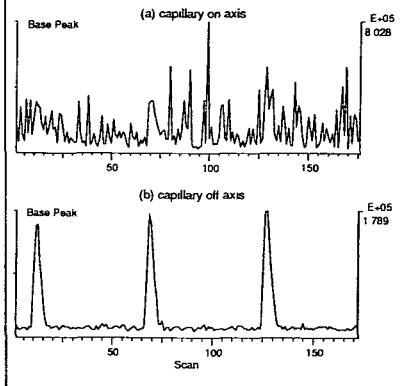

Figure 4 Effects of flow splitting with a 4 6 mm column at 1mL/min Signal increases when the entire flow enters the interface.

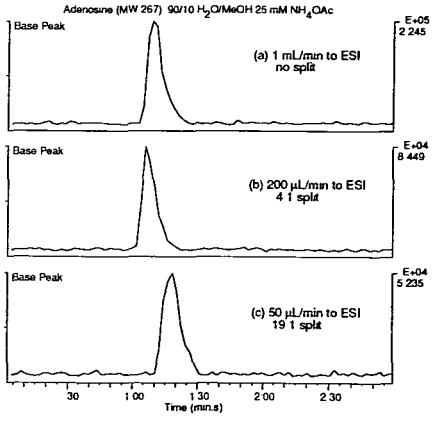

Fundamental Energy Studies of Electrospray Ions Entrained in a Free Jet Expansion

***Erol E. Gulcicek, Craig M. Whitehouse and James G. Boyle**
Analytica of Branford, Inc. Branford, CT 06405

Energy and energy distribution of electrospray ions were studied using a two pumping stage electrospray ion source interfaced to a high vacuum apparatus which may utilize various types of mass analyzers.

Electrospray ions are formed at atmospheric pressure and are entrained in a free jet expansion through several pumping stages before they reach the TOF mass analyzer. In order to increase the transmission of ions, "unconventional" electrostatic fields are utilized in the earlier viscous flow and transition flow pumping regimes. As a result, the final energy and the energy spread of the ions retain components from both the free jet expansion and the electrostatic fields. Although the free jet energy of the ions can be estimated, the electrostatic components are hard to determine since they depend on the voltage gradient around the region where ions attain a collision free path to the mass analyzer. This study determines both of these energy components and their energy spreads experimentally over a wide range of molecular weights. The energies of the ions have been determined as a function of different electrostatic conditions at the transition pressure flow and the free molecular flow interface.

The set-up for the stopping potential experiment is shown in Figure 1. Electrospray ion currents were measured with the conductive plate at the end of the optical lens stack as a function of the plate voltage with respect to the grounded mesh in front of it. The experiments were conducted for gramicidin S (MW 1141 Da), cytochrome C (MW 12,361 Da), and bovine albumin (MW 66,267 Da) at 1 pmole/µl concentrations.

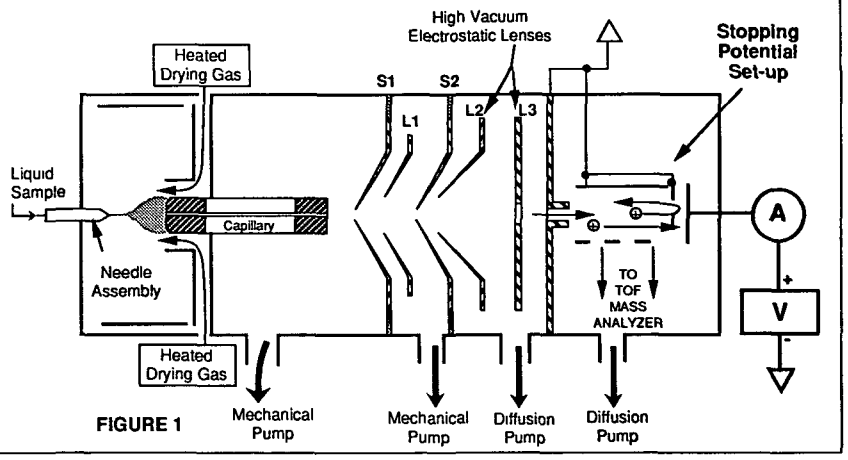

FIGURE 1

A typical plot of the measured current vs stopping potential voltage in the absence of electrostatic fields (all lenses at ground potential) is shown on the top trace of Figure 2; the bottom trace shows the first derivative of this plot for easy observation of the energy spread of the ions.

Figure 3 shows the stopping potential distribution for the gramicidin S ions with all the ion optical lens voltage settings optimized for maximum ion signal. Of the total of 12.7 V required to stop the gramicidin S ions in the mass analyzer, only 0.6 V comes from the free expansion as measured in Figure 2.

By measuring the stopping potential of the ions, one can approximate the location of the ions theoretically where they become collisionally free. The results show that in most cases, the energy of the ions are established approximately within a mm of the orifice of the second skimmer (S2). Furthermore, the correlation between the voltage difference applied to S2 and L1 lenses and the electrostatic field lines created by them near S2 can be used to control the total energy of the ions.

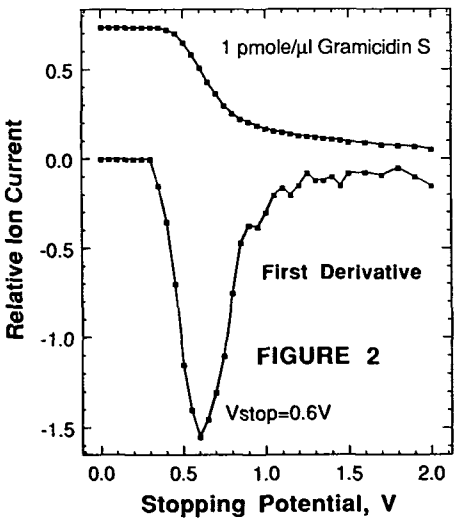

FIGURE 2

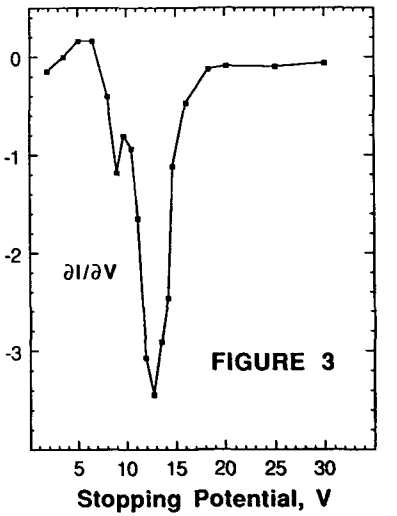

FIGURE 3

This work was supported by an SBIR grant 2 R 44 MH46756-02 from the National Institute of Mental Health

Application of Orifice Potential Stepping for the Sequence Identification of Phosphorylated Proteins

*J.-M. Ding, W. Burkhart, and D.B. Kassel, Glaxo Research Institute, 5 Moore Dr., Research Triangle Park, NC 27709

INTRODUCTION

A number of groups have begun to evaluate non-biochemical methods for identifying sites of phosphorylation (in the absence of radio labeled ^{32}P-ATP). and the majority of these studies have involved mass spectrometric analysis.(1-3) We have investigated an alternative method for identifying the phosphorylation of proteins and sequencing phosphorylated peptides. The method is similar to that described by Carr et al. (4) for the identification of glycoprotein digests. By ramping the orifice potential as a function of m/z ratio, Carr et al showed that it was possible to produce both molecular weight information and fragmentation characteristic of common glycoforms to aid in the rapid identification of glycopeptides. In an analogous manner, we have investigated the utility of orifice potential scanning for the identification of phosphopeptides. Orifice potential "stepping" rather than "ramping" in the negative ion mode was used for the identification of phosphorylation. Results are presented within for a model mixture of non-, mono- and (bis)-phosphorylated peptides, a known phosphorylated protein β-casein and a novel tyrosine kinase.

EXPERIMENTAL

Tyrosine, threonine and serine phosphorylated peptides were synthesized "in-house" (M. Rodriguez, Glaxo Research Institute) following the procedure of Andrews et al.(5). Peptides were dissolved in H_2O containing 0.1% TFA.

β-casein was purchased from Sigma Chemical Company (St. Louis, MO). The tyrosine kinase, SH3-SH2-TK, was expressed in baculovirus and purified "in-house" (M.A. Luther et al., Glaxo Research Institute).

A one nmol protein of SH3-SH2-TK was digested in-situ with subtilisin (Boehringer-Mannheim) following the procedure of Burkhart (6), and a 13 KD fragment was then digested with Staph V8 at pH=8.5. The eluant was speed-vac lyophilized and reconstituted in100 µl of aqueous 0.1% TFA .

A Hewlett-Packard HP1090 microbore HPLC was used for all analyses and operated at a flow rate of 250 µl/min. A 30mm x 320µm packed capillary Vydac reverse phase C18 column (LC Packings, USA, San Francisco, CA) was used for all peptide separations. The column flow rate was adjusted to 5µL/min by aid of a 40:1 pre-column split. A piece of fused silica tubing (75 µm i.d. x 150 µm o.d.) was connected directly to the end of the column and terminated at the ionspray needle assembly. An ABI 785A absorbance detector was used "in-line" between the column oulet and the mass spectrometer, and the peptides were detected at a wavelength 205 nm. A Sciex API-III IonSpray Triple Quadrupole Mass Spectrometer (PE-Sciex, Thornhill, ON, Canada) was used for all analyses.

RESULTS AND DISCUSSION:

A mixture containing 3 mono-, 2 di-, and one non-phosphorylated peptides was readily analyzed in the negative ion mode with orifice potential stepping and the phosphorylation could be identified. The orifice potential (OR) was set to -160 V in the mass range of m/z 74 to 574 and to -120 V in the mass range of m/z 574 to 1074. The low mass fragments generated at high orifice potentials could be used as a diagnostic for phosphorylation. We chose an OR value of -120 V to permit observation of both the $[M-H]^-$ ion and fragments in the molecular ion mass region which are characteristic of phosphorylation (e.g., $[M-H3PO4]^-$). Figure 1 shows a simple extraction of the m/z 79 ion (PO 3) from a TIC trace of a 6-peptide mixture. Five phosphopeptides were selectively identified. In addition, extraction of m/z 159 (HPO3: PO 3)$^-$ from the TIC trace enabled the (bis)-phosphorylated peptides to be identified.

β-casein with known phosphorylated serines was evaluated as a model protein to determine the utility of the orifice potential stepping method for identifying the phosphorylated peptides from a complex enzymatic digest. The phosphorylation was identified readily by negative ion mode LC/ESI/MS with orifice potential stepping method. A reconstructed mass chromatogram of m/z 79 ion produced only the two phosphorylated peptides.

A novel protein which contains non-phosphorylated and phosphorylated proteins was digested in-situ (6) using subtilisin to produce a 13 KD fragment which was determined to be phosphorylated from positive ion mode LC/ESI/MS analysis. This 13 KD protein was isolated and digested using Staph V8 at pH=8.5. Both positive LC/MS and negative LC/MS with orifice potential stepping were performed.

Figure 2 shows the TIC of the Staph V8 digestion acquired in positive LC/MS mode. Two peptides were observed whose masses differed by 80 Da and were suspected to be the phosphorylated and non-phosphorylated peptides. An LC/MS analysis in the negative ion mode with orifice potential stepping enabled the charge state of these peptides to be determined based on the formation of the TFA adduct (ΔMS=57 for a -2 charged ion), Phosphorylation was confirmed by extracting the ion at m/z 79 in Figure 3.

CONCLUSION:

We have demonstrated that negative ion orifice potential stepping provides a rapid way for identifying phosphorylated peptides from protein digests. For small molecular weight peptides, mono- and di-phosphorylated peptides were differentiated by the extraction the characteristic ions at m/z 79 and 159, respectively. For phosphorylated proteins, we demonstrated that the 79 ion could be used to identify the relevant peptides for a model protein, β-casein and a novel protein , SH3-SH2-TK. Additionally, TFA adducts in the negative ion mode were used to establish charge states for peaks in the negative ion LC/MS spectra.

REFERENCES:

1. (a). B.W. Gibson, Biological Mass Spectrometry, 1990, Ed. A.L. Burlingame, Elsevier Science Publishers, B.V., Amsterdam. (b). B.W. Gibson, A.M. Falick, A.L. Burlingame, L. Nadasdi, A.C. Nguyen, G.L. Kenyon, J. Am. Chem. Soc., 1987, 109, 5343. (c). B. W. Gibson, P. Cohen, Peptides and Proteins, Methods in Enzymology, 1990,193, Academic Press, NY.
2. S.A. Carr, M.J. Huddleson, M.F. Bean, Protein Science, 1993, 2, 183.
3. T.-T. Yip, T.W. Hutchens, "Techniques in ProteinChemistry", IV, Ed. R. Angeletti, 1993, Academic Press, NY.
4. J. W. Crabb, C. Johnson, K. West, J. Buczylko, K. Palczewski, J. Hou, K. McKeehan, M. Kan, W.L. McKeehan, M.J. Huddleston, S.A. Carr. "Techniques in Protein Chemistry" IV, Ed. R. Angeletti, 1993, Academic Press, NY.
5. P.C. Andrews et al. Intl. J. Pept. Prot. Res. (1991) 38, 469.
6. W. Burkhart "Techniques in Protein Chemistry" IV, Ed. R. Angeletti, 1993, Academic Press, NY.

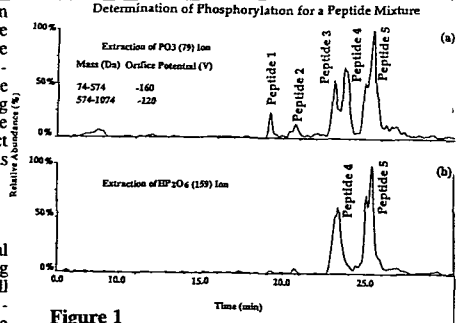

Figure 1

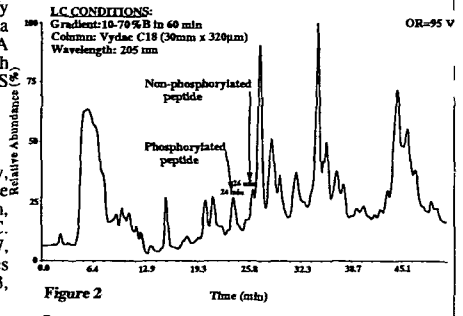

Figure 2

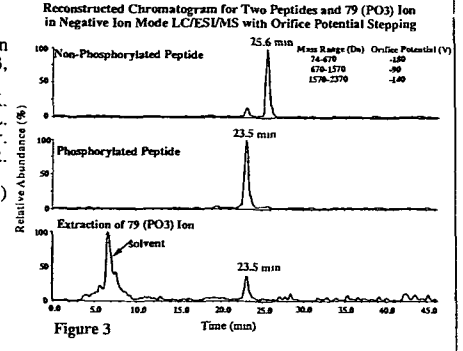

Figure 3

Capillary LC/MS and LC/MS/MS Analysis of Peptides Using a New Capillary LC/MS Interface and a Redesigned Collision Cell

Bruce Thomson, Tom Covey, Bori Shushan, Mark Allen and Takeo Sakuma
Perkin Elmer Sciex Instruments, Thornhill, Ontario, Canada L3T 1P2

There is a strong need for obtaining amino acid sequence information from a small amount of tryptic digest sample (low picomoles or less) by LC/MS and LC/MS/MS. In order to facilitate the sensitive LC/MS/MS data acquisition it is important to generate reproducible chromatographic elution profiles from a small bore column, preferably packed capillary columns for routine analysis.

We developed a low dead volume interface assembly coupling a packed capillary LC column to an API *III* triple quadrupole system using an IonSpray. This interface assembly is mounted on the IonSpray Source Housing. Details of the construction will be shown in the poster.

Capillary columns of 180, 320 and 500 μm ID, 5 to 15 cm in length, were packed with Applied Biosystems Aquapore OD-300 material, 7 μm particle size, 300Å pore size, in our laboratory. Peptide analysis columns of similar sizes but different packing materials were also procured from LC Packings and Keystone Scientific.

An ABI Model 140 B Dual Solvent Delivery System equipped with 2 x 10 mL syringes was used with a 10 μL Lee Visco Mixer for efficient mixing of the two mobile phases. A = H_2O(0.1% TFA), B = 75/25 CH_3CH/H_2O (0.1% TFA). Gradient 20% B (5 min) to 80 %B (60 min). A typical flow rate for a 170 μm ID column was 80 to 100 μL/min with 2 to 3 μL/min going into the capillary column.

Figure 1 is a typical TIC trace obtained from 1 picomole of hGH tryptic digest using a 180 μm ID Vydac C18 column. Figure 2 is an LC/MS/MS spectrum obtained from 1 picomole of T2. A series of Y ions as well as A and B ions were observed.

Figure 1

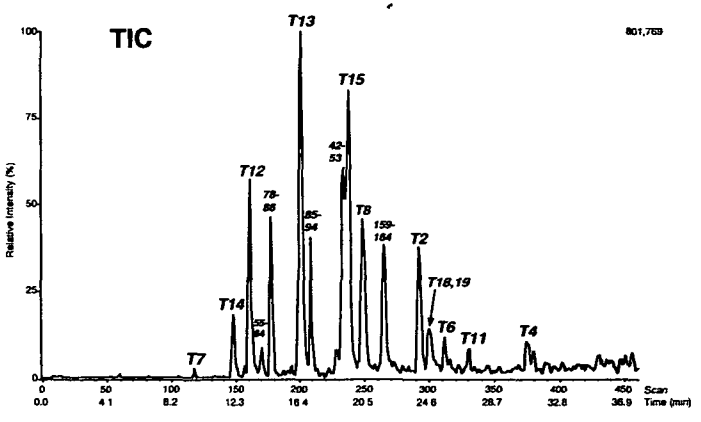

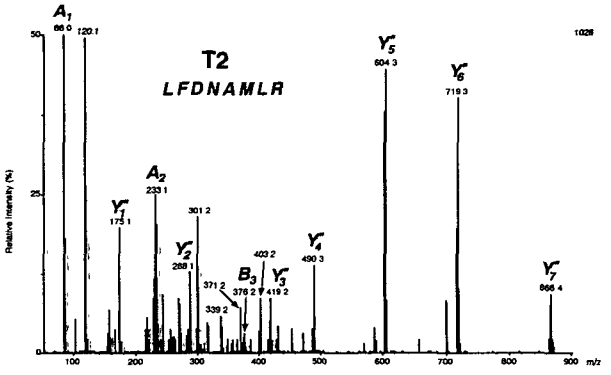

Figure 2

In the past, daughter ion resolution was generally low due to a broad ion energy distribution from the energy release upon fragmentation, thus making unequivocal mass assignment difficult. The collision cell of an API *III* and the surrounding ion optics were redesigned to minimize the ion energy spread, ion scattering loss, and focusing artifacts. A diagram will be shown in the poster. The new ion optics produce unit mass resolution across the entire mass range with up to 20 times greater MS/MS sensitivity over the conventional collision cell.

The daughter ion spectrum of renin substrate shown in Figure 3 was obtained by lowering the Q1 resolution to allow the C13 isotope peak of the quadruply charged parent ion into the new collision cell. The charge state of multiply charged fragmentation with up to 4 charges could be assigned on the basis of the isotope spacing.

Figure 3

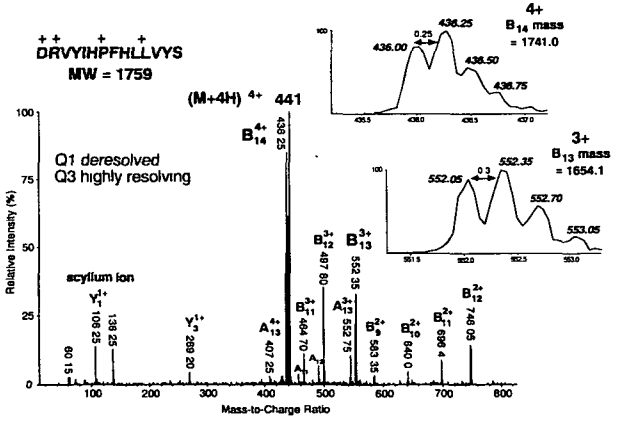

COMBINING CAPILLARY ELECTROPHORESIS WITH ELECTROSPRAY IONIZATION/ION TRAP MASS SPECTROMETRY FOR BIOPOLYMER ANALYSIS

R.S. Ramsey, K.G. Asano, K.J. Hart, D.E. Goeringer
G.J. Van Berkel, and S.A. McLuckey
Analytical Chemistry Division, Oak Ridge National Laboratory
Oak Ridge, TN 37831-6365

Capillary electrophoresis (CE) when combined with mass spectrometry holds considerable potential for the analysis of complex mixtures of biomolecules. CE offers extraordinary resolving power and speed of analysis as compared to more conventional approaches for separations while MS provides the selectivity required for compound identification. Some of the features which make CE attractive for separations, however, impose stringent requirements for MS detection. Small injection volumes require high sensitivity for analysis and the narrow peaks (ca. few seconds at FWHM) given the high column efficiencies demand rapid scan speeds. We have used an electrospray interface with a coaxial sheath to couple CE to an ion trap mass spectrometer (ITMS) for on-line analysis. As compared to other analyzers the ITMS offers enhanced sensitivity and broader capabilities for obtaining structural information (1,2). Full utilization of these capabilities, especially with regard to multiple stages of mass spectrometry, however, are limited in on-line applications when operating the trap under normal modes. Collisional activation (CA) which forms the basis for MS/MS and MS^n experiments is generally effected by applying a single rf frequency, corresponding to the fundamental secular frequency of the ion selected to undergo dissociation, to the end-caps (3). This secular frequency is dependent upon the mass/charge ratio of the ion as well as operating conditions and physical parameters of the trap. To optimize CA several parameters must be "tuned", including selection of the optimum excitation frequency, amplitude, and duration. The implications for on-line analysis are that the mass/charge ratio of the parent must be known for each peak and that tuning has to be performed rapidly during elution. An alternative which we have recently explored is using random noise applied to the end-caps which enables trapped ions to be collisionally activated independent of their mass/charge ratios (4). This approach yields structurally informative MS/MS spectra in on-line CE as demonstrated below.

We have also determined that signal/noise ratios in total ion current (TIC) profiles may be improved by applying low amplitude noise to the end-caps. Chemical noise and background in on-line CE derive primarily from ionic buffer components and clusters, as well as solvent clusters. Buffer ions that consistently appear in the background may be ejected from the trap, reducing overall background, but the application of noise results in further improvements. Figure 1 shows a comparison of the total ion current electropherograms for three peptides, bradykinin, xenopsin, and neurotensin, obtained with and without the application of noise. These results were obtained using a tris-phosphate buffer (pH 7.6) for separation, scanning the mass range from 100 to 1300, and ejecting the predominant background ions at mass/charge 122 and 243, corresponding to protonated tris and its proton-bound dimer. Under the conditions employed, the increase in signal to noise is ca. a factor of three using noise CA. The quantity of material injected was 180, 200, and 220 fmoles for the three peptides, respectively.

To obtain structural information by broad-band CA the noise was applied at higher amplitudes (ca. 2 to 5 fold). Figure 2 shows an example of the structural information obtained for

neurotensin, injecting 0.9 pmoles of material. Some of the product ions that were identified are labeled. The spectrum was found to be similar to that obtained by single frequency CA with continuous electromigration of the peptide. The major differences in the spectra were in the relative abundance of some of the major product ions and the absence of some lower mass/charge ions. Overall, the noise CA spectrum contains a great deal of structural information and is easily obtained in on-line CE. Mass spectral scans where the amplitude of the noise is alternatively turned off and on or varied from low to high during peak elution may also be used to obtain molecular weight and structural data in a single analysis as reported for on-line HPLC (5).

References

1. B.D. Nourse and R. G. Cooks, Anal. Chim. Acta, 282, 1 (1990).
2. R.G. Cooks, G.L. Glish, S.A. McLuckey, and R.E. Kaiser, Chem. Eng. News, 69, 26 (1991).
3. J.N. Louris, R.G. Cooks, J.E.P. Syka, P.E. Kelly, G.C. Stafford, J.F.J. Todd, Anal. Chem., 59, 1677 (1987).
4. S.A. McLuckey, D.E. Goeringer, and G.L. Glish, Anal. Chem., 64, 1455 (1990).
5. G.J. Van Berkel, R.S. Ramsey, S.A. McLuckey, and G.L. Glish, "Proc. 40th ASMS Conf. on Mass Spectrometry and Allied Topics", Washington, D.C., May 31-June 5, 1992.

Research sponsored by the National Institutes of Health under Grant GM 45372. Oak Ridge National Laboratory is operated for the Department of Energy under Contract DE-AC05-84OR21400 by Martin Marietta Energy Systems, Inc.

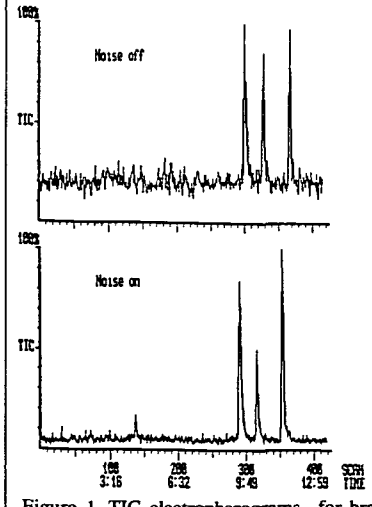

Figure 1. TIC electropherograms for bradykinin, xenopsin, and neurotensin. CE conditions: 24 kV applied field; electro-kinetic inj. 10 sec at 10 kV; 56 cm x 50 μm I.D. column.

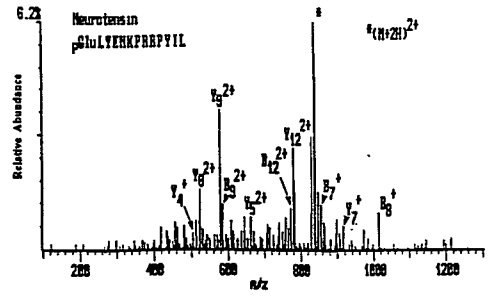

Figure 2. On-line broad-band CA mass spectrum for neurotensin showing structural information.

High Mass Accuracy Electrospray/Fourier Transform Ion Cyclotron Resonance Mass Spectrometer.

CH Watson, GH Kruppa, FH Laukien, J Wronka, M Knobeler[1], K-P Wanczek[1], Bruker Instruments, Inc., Billerica, MA; [1]University of Bremen, Bremen, Germany

Introduction

In addition to being able to ionize a variety of high molecular weight molecules via multiple charging, electrospray ionization (ESI) also provides an efficient means to dissociate high molecular weight ions. Using a commercially available ion source with a Bruker BioAPEX™ 47e external ion source Fourier transform ion cyclotron resonance (FTICR) mass spectrometer both parent ions (with multiple charge states) and fragment ions obtained by increasing the capillary/skimmer voltage difference have been measured for a series of peptide samples. Mass resolved isotopic peaks for multiply charges parent and fragment ions are obtained for ions with up to 20 charges. The charge state of an unknown peak can be determined unambiguously from the mass difference between adjacent isotopic peaks. Mass measurements made on both the parent and fragment ions are extremely accurate. Errors in the mass assignments range from very low ppm (> 5ppm) to ppb using external calibration. An additional advantage of the ESI/FTICR technique is that the calibration procedure is straight-forward and provides reproducible mass assignments with error less than 5 ppm for weeks after calibration.

Experimental

All experiments were carried out using a Bruker Bio-APEX™ 47e mass spectrometer equipped with a 4.7 T superconducting magnet, an external ion source operating at ground potential, and the newly developed RF-shimmed Infinity™ analyzer cell. The external ion source has two stages of differential pumping with one 800 L/sec cryopump for the source, one 400 L/sec cryopump for the electrostatic ion transfer region, and a 400 L/sec cryopump for the mass analyzer region. The pressure between the capillary exit and the first skimmer, where CID ocuurs, was ca. 1 torr. The needle was maintained at ground potential and 4.6-5.0 kV was applied to the capillary entrance. Collision induced dissociation spectra were obtained by increasing the voltage difference between the capillary exit and the first skimmer. A syringe pump supplied a steady 0.8 um/min flow of a 49.5:49.5:1 H_2O, methanol, acetic acid solution to the source. Samples were injected into the flow stream using a standard HPLC injection valve with a 10 ul loop.

Results and Discussion

For all of the peptide and protein samples analyzed to date (up to myoglobin) a capillary/skimmer voltage difference of 200 volts was sufficient to achieve extensive fragmentation. An exact mass analysis was preformed on the parent and fragment ions from samples of Substance P, bombesin, melittin, ubiquitin, and cytochrome C. As an example of the exact mass analysis capability afforded by ESI/FTMS, the most abundant primary sequence fragments from melittin are listed in Table 1. Similar results with average mass error of 2 ppm were obtained for all of the samples.

In addition to the stable and accurate mass calibration the ESI/FTICR technique provides high mass resolution such that the charge state of multiply charged fragment ions

can be readily determined from the spacing of isotopic peaks. Figure 1 shows a typical source CID spectrum of ubiquitin (average molecular weight 8564). The fragments ions generated from the multiple charged parent species have a distribution of charge states ranging from +1 to +8. Without the high resolution capability of FTICR the correct assignment of masses for each fragment ion would be difficult. As an example, Figure 2, shows a portion of the ubiquitin CID spectrum at m/z 1050 showing the presence of several different charge states. The insert shows that at a resolution of 30k, a very moderate resolution by FTICR standards, overlapping charge states of +2 and +8 can be readily resolved and identified.

Table 1. Melittin Exact Mass Analysis

Ion	Formula	Meas. Mass	Charge	Theo. Mass	Error
M^{+2}	$C_{131}H_{230}N_{39}O_{31}$	1423.3873	+2	1423.3873	1.89
y_{19}	$C_{101}H_{176}N_{31}O_{24}$	1104.1811	+2	1104.1789	2.00
y_{17}	$C_{90}H_{157}N_{20}O_{22}$	998.6091	+2	998.6065	2.61
M^{+3}	$C_{131}H_{231}N_{39}O_{31}$	949.2604	+3	949.2590	0.49
y_{15}	$C_{82}H_{142}N_{27}O_{18}$	897.0583	+2	897.0549	3.86
y_{13}	$C_{74}H_{128}N_{25}O_{16}$	812.0050	+2	812.0022	3.08
y_{11}	$C_{66}H_{116}N_{23}O_{14}$	727.9589	+2	727.9572	2.33
y_{10}	$C_{60}H_{105}N_{22}O_{13}$	671.4170	+2	671.4152	2.68
y_9	$C_{54}H_{94}N_{21}O_{12}$	614.8744	+2	614.8732	1.95
y_4	$C_{22}H_{43}N_{11}O_6$	558.3485	+1	558.3471	2.51
b_6	$C_{24}H_{42}N_6O_6$	511.3244	+1	511.3237	1.37
y_3	$C_{16}H_{31}N_9O_5$	430.2426	+1	430.2501	1.28
b_5	$C_{18}H_{31}N_5O_5$	398.2405	+1	298.2398	1.76

Figure 1. Ubiquitin CID fragment ions

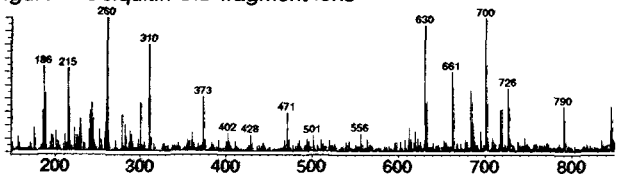

Figure 2. Detection on ubiquitin CID fragment ions

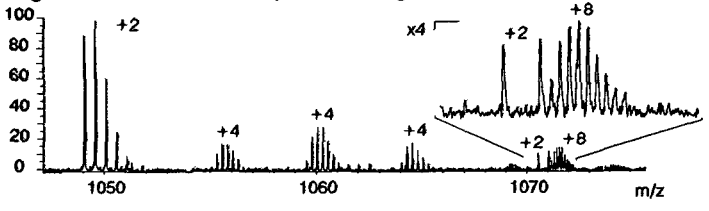

FTICR CHARACTERIZATION OF BEAM DYNAMICS AND ELECTROSTATIC CONTRIBUTIONS TO THE ELCTROSPRAY ION KINETIC ENERGY

V. Campbell, Z. Guan, D. A. Laude, JR.; Department of Chemistry and Biochemistry, University of Texas at Austin, Austin, TX 78712

The kinetic energy distribution of ions exiting the electrospray ion source depends upon the contribution of electric fields experienced by ions in the source and upon the velocity assumed by the ions as a consequence of the flow dynamics in the spray. Understanding and controlling the kinetic energy of electrospray ions is essential for obtaining optimum performance of Fourier transform ion cyclotron resonance (FTICR) mass spectrometry, since the ions have to be captured in a trapped ion cell prior to detection. In the work to be presented, the electrospray ion kinetic energies were evaluated under a variety of experimental conditions by using both variable trapping in the FTICR and retarding grid measurements at a collector behind the trap. Experiments were also performed to determine the effect of ion conformation on kinetic energy achieved in the source.

All experiments were performed with a 3.0T FTICR mass spectrometer coupled to an electrospray ionization source. The spectrometer included a 6" diameter bore into which the vacuum chamber was inserted. The essential components of the vacuum chamber and interface consist of four concentric vacuum chambers of increasing diameter which extend into the high-field region of the magnet.

Two separate pumping arrangements were used to acquire the data in this experiment. Electrospray system 1, a Chait-type electrospray interface, featured a 500μm i.d. resistively heated desolvation capillary and a skimmer with a 400μm orifice. The capillary-skimmer region of this arrangement was pumped to 8 torr. Electrospray system 2 featured a reduced skimmer orifice of 200μm and a increased pressure of 14 torr in the roughing region. These interfaces will be referred as large and small orifice skimmers, respectively.

The primary contributions to the kinetic components to the energy are the velocity component achieved in the supersonic expansion and the electric field component derived from the potential on the skimmer. These are expressed as the first and second terms, respectively, in Equation 1 which predicts the optimum trapping potential for injected ions.

$$V_{trap}=K_{slip}(v^2/2Ae)(m/z)+K_{eff}V_{skim} \qquad \text{eq 1}$$

K_{slip}: correction factor for velocity slip in the expansion

K_{eff} : correction factor for the effective field experienced by the ions

Changing the skimmer orifice size can cause significant differences in ion kinetic energies. This is illustrated by the retarding grid profiles in Figure 1, in which electrospray ions from the larger skimmer exhibit an average kinetic energy that is 1/3 the skimmer potential. In contrast, ions traversing from the smaller skimmer exhibit a kinetic energy that is 60% of the skimmer potential.

Presented in Figure 2 is a plot of optimum m/z trap potential and retarding grid measurement of kinetic energy for the two interfaces shown in Figure 2. The data is fit to eq1 to obtain velocity and effective field data. In general, the larger orifice skimmer promotes an improved expansion and consequently a larger velocity contribution from the flow dynamics. This is reflected in the larger velocity of 900m/s. In contrast, for the smallest skimmer, the reduced slope indicates a weaker expansion and lower electrospray ion velocity 250 m/s achieved from gas dynamics. Instead, the effective electric field is much larger and contributes the preponderance of ion kinetic energy. This is reflected by the large y-intercept.

Kinetic energies for the smaller skimmer is now examined. Retarding grid and FTICR variable trapping profiles indicate that the variable trapping technique yields data that reflect the kinetic energy of trapped ions. Profiles acquired for increasing skimmer potential at a skimmer-capillary distance of 4.5 mm suggest a uniform narrowing of the kinetic energy distribution as the skimmer potential decreases; the contribution to kinetic energy from flow dynamics is apparently small at this close distance and high post skimmer pressure.

One key feature of the instrument is that by placing the electrospray source in the magnetic field, radial motion is confined. Consequently only one focusing potential is employed--the potential applied to the skimmer. Very narrow distributions can then be collected in the cell at small skimmer potentials. For example, using a 3.0V skimmer, a trapping profile for horse heart myoglobin exhibits a trapping bandwidth of only 0.02 V. Signal intensities for ESI spectra are of the same magnitude as for broader kinetic energy profiles.

It is possible that identical molecules that possess different structure would achieve different kinetic energy during the supersonic expansion process. Shown in Figure 3 are variable trapping profiles for the +10 charge state lysozyme of the closed (native) and the open form(denatured, i.e after reduction of the disulfide linkages with dithiothritol). The profiles indicate that the closed form is preferentially trapped at about 0.4 V lower potential than the open form. Velocities were calculated to be 288m/s and 359m/s for the open and closed forms respectively.

Increasing the capillary voltage promotes fragmentation of exiting electrospray ions to yield dissociation products that are detected by FTICR. It was desirable to determine whether a distinction in kinetic energy distributions existed for precursor and dissociation product ions. This difference in kinetic energy would introduce mass discrimination into the resulting spectra and further complicate analysis. The retarding grid and variable trapping profiles were examined for assorted mellitin ions at low and high voltages. Increased fragmentation was observed at 500V as expected. What is important is that the variable trapping profiles for each ion at 500V were identical. This is likely because a 3 mm skimmer-capillary distance was used to sample a subsonic, or higher pressure, region of the spray. The identical profile shapes indicate mass discrimination is avoided.

Figure 1: Old and New Skimmer at 5

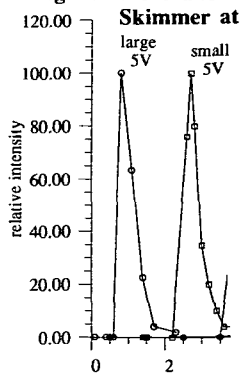

Figure 2:

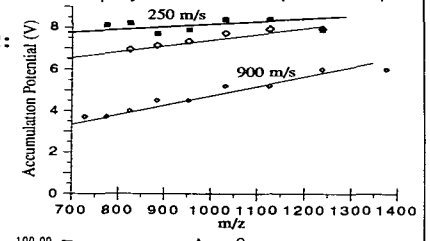

Figure 3:

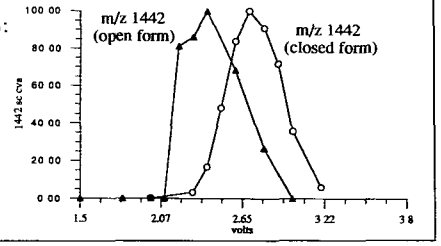

A Direct Injection Electrospray Source for Fourier Transform Ion Cyclotron Resonance Mass Spectrometry

R. Ramanathan, J. A. Shalosky and J. R. Eyler
Department of Chemistry, University of Florida
Gainesville, FL 32611-2046

The multiple charging phenomenon in electrospray ionization allows conventional mass spectrometers with limited mass-to-charge (m/z) range to detect ions having masses in excess of 1,000,000 Da. However, coupling ESI sources with double sector or Fourier transform ion cyclotron resonance (FTICR) mass spectrometers can lead to further benefits from the high mass resolution and mass accuracy of these instruments. Initially, Henry and McLafferty coupled an ESI source externally to a FTICR mass spectrometer and demonstrated its capabilities (1). However, inefficient transfer of ions from the source to the cell limited the use of this instrument for routine experiments. In 1992, Hofstadler and Laude interfaced an ESI source within the strong magnetic field of a FTICR mass spectrometer and showed that this interface can transfer ions from the source to the cell efficiently (2). The ESI source that has been developed in our laboratory is similar to Laude's ESI source.

Figure 1a is a schematic illustration of the ESI source developed in our laboratory. Ionization takes place in the Delrin/MACOR spray cavity. The ESI source is inserted inside a 3/4" stainless steel probe and a vacuum seal is made with a Viton O-ring. When the probe is inserted into the strong magnetic field, the electrospray ionization process occurs 24 cm from the FTICR cell. All experiments were performed using a 2 Tesla FTICR mass spectrometer equipped with a Nicolet FTMS 1000 data station. All the other operating parameters used in these experiments are shown Figure 1b. All the samples were $1x10^{-5}$ M in 50/50 $MeOH/H_2O$ solution (with 1-2 drops of acetic acid for Bradykinin).

It was necessary to measure the ion current along the z-axis to determine where most of the ions are lost during the transfer from the source to the cell. A 50/50 methanol/water solution of Rhodamine 6G perchlorate (1.0×10^{-5} M) was electrosprayed and the total ion current was measured at each component. In addition to ion current information, molecular weight and structural information of Rhodamine 6G ($[M-CH_3]^+$ @ m/z 428) were obtained using the ESI source. The potential difference between the skimmer and the capillary, ΔV, causes the ions exiting from the capillary to undergo energetic collisions with the gases (from the atmosphere) present in the capillary/skimmer region. The primary collisionally induced dissociation product observed was $[M-4CH_3-3CH_2]^+$ (m/z 326).

Recently we have been involved in studies of photodissociation of solvated ions (3). Solvated ions in these studies were produced as products of ion/molecule reactions. ESI could be used as an alternative method to produce solvated ions. As shown in Figure 1c, when the capillary was maintained at 150 °C $[Ru(bpy)_2H_2O]^+$ was observed as the predominant peak following electrospray ionization of a solution of $Ru(bpy)_3(PF_6)_2$. However, when the capillary temperature was dropped to 100 °C peaks due to $[Ru(bpy)_2H_2O]^+$, $[Ru(bpy)_2CH_2O]^+$ (?) and $[Ru(bpy)_2H_2OCH_3OH]^+$ were observed. These preliminary results indicate that ESI can be used to produce solvated ions for further reactivity and dissociation studies. In addition to solvated ions, we were able to produce the doubly protonated molecular ion $[M+2H]^{2+}$ and the porotonated molecular ion $[M+H]^+$ of Bradykinin (Figure 1d). Our future plans include studies of a number of multiply charged organometallic and biological species.

In conclusion, we have demonstrated the potential of electrospray ionization as an ion source for our FTICR mass spectrometer. Our source is still in the early stages of development The following modifications will be implemented before the ESI source can be used for routine experiments : (1) mounting a shutter on z-axis to open only during the ion injection period and (2) reducing the 1st and 2nd conductance limits to ~2mm diameter. This will lead to pressure in the low 10^{-6} Torr range in the cell region and improve mass resolution.

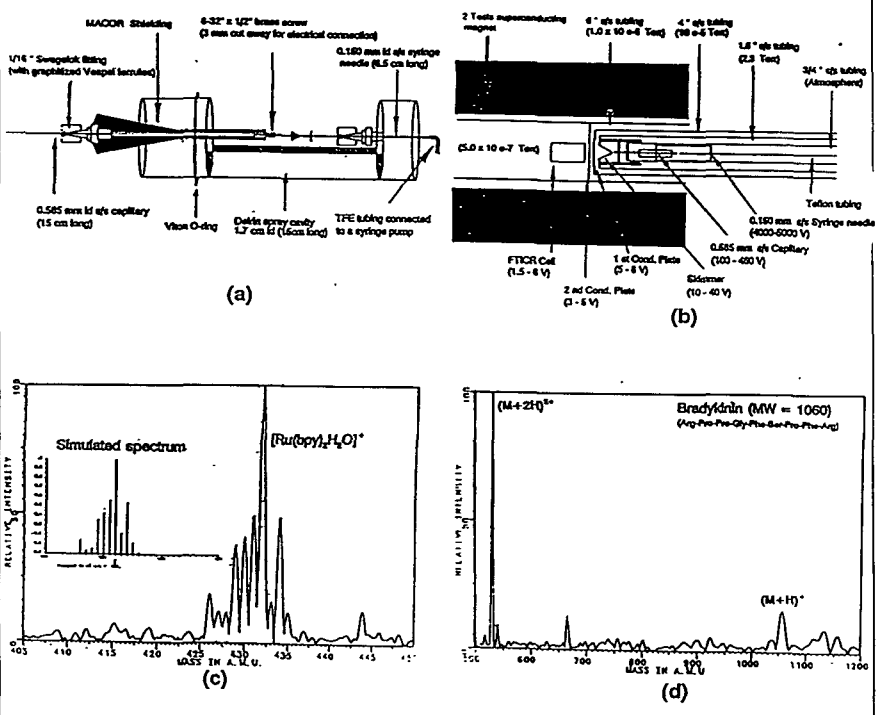

Figure 1. (a) ESI source, (b) ESI/FTICR operating parameters, (c) ESI mass spectrum of $[Ru(bpy)_2H_2O]^+$ and (d) ESI mass spectrum of Bradykinin

REFERENCES

(1) Henry, K. D. and McLafferty, F. W. *Org. Mass Spectrom.* 1990, *25*, 490
(2) Hofstadler, S. A. and Laude, D. A. *Anal. Chem.* 1992, 64, 572
(3) Peiris, D. M. and Eyler, J. R. *41st ASMS Conference on Mass Spectrometry and Allied Topics* San Francisco, CA (ThP 212)

High Energy CID of Multiply Charged Polypeptides and Polynucleotides Produced by Electrospray

D. Fabris*, M. Kelly, C. Murphy, Z. Wu and C. Fenselau
Structural Biochemistry Center
University of Maryland Baltimore County, Baltimore MD 21228

The recent implementation of an electrospray source on a four sector instrument has allowed the present study of high and low energy CID of multiply charged ions[1]. The objectives of the present work are to show a scan scheme allowing the use of kilovolt potentials in both MS-1 and MS-2; to devise an algorithm to accomodate multiple charges in assigning sequence ions; to evaluate structural information obtainable from high molecular weight precursors; to evaluate sites of charge localization in multiply charged ions.

Collisional induced dissociation (CID) mass spectra were obtained on a JEOL (Tokyo, Japan) HX110/HX110 four sector mass spectrometer ($E_1B_1E_2B_2$), under control of DA5000 or DA7000 data systems and equipped with an Analytica of Branford (Branford, CT) electrospray ionization source. Positive multiply charged ions were collided with Xe in the third field-free region within a **grounded** or **floated collision cell**, using 75% primary ion beam attenuation. The resolution was experimentally determined to be 1100 (50% valley). B/E linked scans were performed according to the following **scan scheme**, allowing all the possible fragments produced in a floated collision cell to pass through MS-2 and be detected: $ze(V_a-V_c) = V_2-V_c$ where z is the charge state of the precursor ion, V_a is the acceleration voltage, V_c is the voltage of the collision cell and V_2 is the initial voltage of MS-2. The use of the floating cell on one hand improves both transmission and sensitivity, on the other hand allows to perform different experiments with both high and low collision energy.

The **interpretation** of the spectra is based on the nomenclature presented by Biemann[2], which has been adapted to accommodate multiple charging. In the CID spectrum of a singly charged cation, c, d, v, w and y series ions originate by loss of neutral molecules and the charge is still conferred by the proton added in the original ionization process. For a multiply charged fragment of one of these series, all of the charges are due to additional protons, and the mass of the fragment (m_f) can be calculated as $m_f = m/z * y - y$ where m/z is the position of the peak in the spectrum and y is the charge state of the fragment ion. Singly charged ions in the a, b, x and z series do not retain an extra proton. In a multiply charged fragment of these series all the charges but one are carried by additional protons and the mass is $m_f = m/z * y - (y-1)$ The additional complexity of fragment ions detected with variable charge states strongly recommends computer supported prediction of fragments and interpretation of spectra.

Nine polypeptides were studied in the mass range 2000-5000 daltons, molecular weights that fall across the mass range of most proteolytic peptides. As shown in **Figures 1-2**, both backbone and side chain cleavages occur, immonium ions are formed, and some internal fragments are observed: fragmentation processes are qualitatively similar to those observed in high energy CID spectra of singly charged precursor ions. Fragment ions are detected with all charge states up to that of the precursor.

The general pattern of the spectra (**Figures 1-2**), showing no intense peaks with high mass to charge ratios (large fragments with low charge states) and a only few fragments with low mass and high charge states, suggests that as a precursor loses residues, it also loses charges. In this way, the m/z ratios of the resulting fragments tend to remain close to a constant number and the peaks occur with striking frequency close to that of the precursor ion. If we assume that transmission effects do not overwhelmingly shape the spectra, one feasible explanation is that charges tend to be distributed at rather even spatial intervals across the precursor ions.

Analysis of charge patterns suggests that charges are accommodated as far apart as possible. There is a general correlation with chain length and the number of protonable residues. The position of strongly basic residues influences which fragment ions are detected.

The general features of the low energy spectra are similar to those reported in triple quadrupole instruments[3]: mostly b and y series ions have been assigned in low energy studies. A much richer selection of ions were detected with high energy activation of melittin 4+ and 3+ and of human parathyroid hormone [1-44] 5+ than has

been observed with lower energy activation in either triple quadrupole[3,4] and four sector instruments[1].

Differences noted between low energy experiments in sector and in triple quadrupole[3] instruments are perhaps due not only to the use of different target gas, Xe instead of N_2, but also, most probably, to different numbers of collisions and different time domains.

ACKNOWLEDGMENTS
This research was supported by grants from the National Science Foundation and from Sterling Winthrop Inc

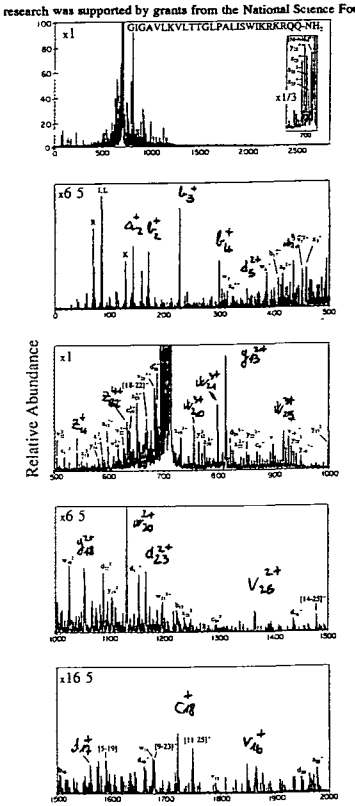

Figure 1. CID spectrum of melittin 4+ (2846.5 da) full range spectrum (0 to 2900 m/z) and enlargements;

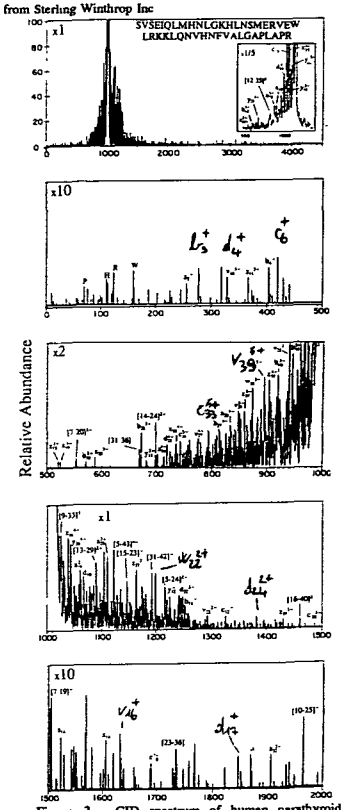

Figure 2. CID spectrum of human parathyroid hormone [1-44] 5+ (5063.0 da): full range scan (0 to 4500 m/z) and enlargements of selected regions.

REFERENCES
(1) Fabris, D , Kelly, M ; Murphy, C., Wu, Z., Fenselau, C *J Am Soc. Mass Spectrom* in press.
(2) Biemann, K. *Annu Rev Biochem.* **1992**, *61*, 977-1010.
(3) Barinaga, C. J., Edmonds, C G ; Udseth, H R ; Smith, R. D *Rapid Commun Mass Spectrom* **1989**, *3*, 160-164.
(4) Smith, R D., Loo, J A.; Barinaga, C. J.; Edmonds, C G , Udseth, H. R *J. Am Soc. Mass Spectrom.* **1990**, *1*, 53-65

High Flow Electrospray LCMS on a High Performance Magnetic Sector Mass Spectrometer

R.H. Bateman, P.A. Bott, A. Phillips, A.R. Woolfitt and D. Peake

Fisons Plc., VG Analytical, Floats Road, Wythenshawe, Manchester, M23 9LE, U.K.

An electrospray/Atmospheric Pressure Chemical Ionisation interface for a VG AutoSpec double focussing mass spectrometer has already been described. The standard electrospray ion source exhibits maximum sensitivity at a flow rate of around 1µl/minute, although is capable of operating at solvent flows of upto 150-200µl/minute. This presentation details the operating characteristics of a modified interface designed to accept solvent flows from 1 to 1000µl/minute.

The key changes that facilitate reproducible, reliable, high-flow or 'Megaflow' electrospray include the following. Firstly, the electrospray is pneumatically assisted using nitrogen at 5-6 bar (earlier studies had typically utilised 2 bar nebulising gas pressure). Secondly, certain of the gas flow passages in the atmospheric pressure region of the interface were enlarged, both to permit a higher gas loading and to expedite the removal of any condensed solvents. Thirdly, the source was heated to 90-100°C, compared to a usual temperature of 50-60°C for low-flow electrospray analysis with the standard version.

Figure 1 shows part of a TIC trace obtained from a magnet scanning experiment in which repeat injections of gramicidin S were made at various flows between 10 and 1000µl/minute. The trace has not been smoothed, so that a true comparison of relative peak heights can be made. Figure 2 clearly demonstrates that the response in terms of injection peak area with increasing flow rate is close to the theoretical value based on the assumption that no loss of performance occurs. Furthermore, no degradation was observed even after several days' continuous operation at 500µl/minute, and the vacuum pressures were unchanged.

Figure 3 shows the UV trace from the repeated gradient separation of a mixture of myoglobin and cytochrome C carried out at a flow rate of 200µl/minute. An Aquapore RP-300 column was used, with a gradient of 30-50% acetonitrile in water + 0.05% TFA. By using the same protein mixture for mass calibration (thus excluding any possible error arising from a discrepancy between the theoretical masses and the actual masses of these protein samples), an RMS error of 32ppm was obtained. This is comparable to the accuracy achieved in low-flow continuous infusion experiments involving similar acquisition parameters. Surprisingly, the required cleaning interval appeared to be independent of solvent flow rate in this study, perhaps because the higher-velocity gas flows tended to keep the sampling cone clean.

Figure 1.

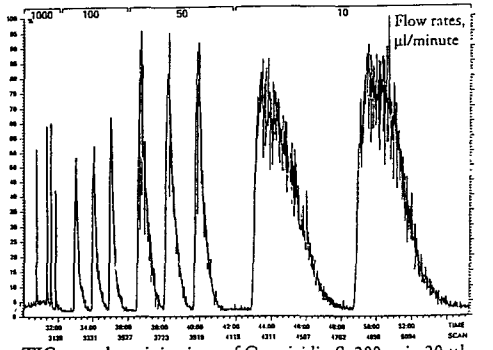

TIC trace: loop injections of Gramicidin S, 200ng in 20 µl

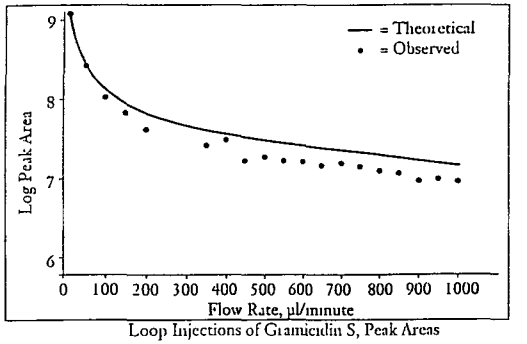

Loop Injections of Gramicidin S, Peak Areas

Figure 2.

Figure 3.

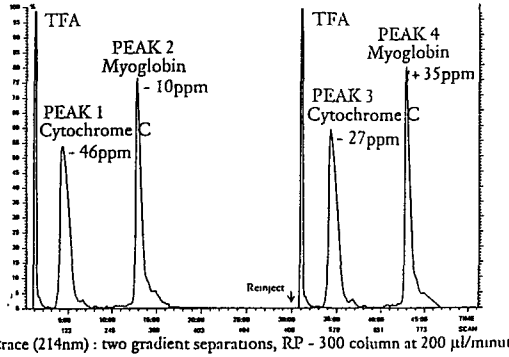

UVtrace (214nm) : two gradient separations, RP - 300 column at 200 µl/minute

Capillary Electrophoresis with Electrospray Ionization Time-of-Flight Mass Spectrometry

L. Fang, R. Zhang and R.N. Zare; Department of Chemistry, Stanford University, Stanford, CA 94305

Capillary electrophoresis (CE) has demonstrated the capability for separating mixtures of large biomolecules (>10,000 Da) with nanoliter samples, but detection and characterization of these components remains a challenge. Mass spectrometry (MS and tandem MS), well known for its high sensitivity, has been used extensively for obtaining molecular weight and structural information from femtomole quantities of biologically important compounds. By combining MS with CE, it may be hoped that analytes could be differentiated not only by their elution time but also by their masses and structures. We are using a time-of-flight MS as the detector because TOF has a fast sweeping speed and a high repetition rate with the ability of measuring a full mass spectrum on every injection pulse. In addition, the TOF device is relatively simple, inexpensive and can achieve a resolution of 1000 or greater by using a reflectron configuration. All these superiorities should make TOF-MS an ideal detector for CE.

To use MS as an on-line detector for CE separations, the exit of the CE column must be removed from the buffer reservoir and have a well defined electric potential.[1] In our preliminary interface arrangement, which is shown in Fig. 1, the fused silica capillary of the CE column was used to replace the original inner stainless steel needle in an electrospray needle assembly. By inserting a gold electrode (25 μm, one end connected to the needle assembly) into the outlet of the CE column (75 or 100 μm ID), the electrical contact for the CE capillary exit was established to that of the needle. Stable electrospray current is generated by maintaining the spray needle at ground while counter-electrodes inside the ES source are maintained at a negative 3 to 4 kV. Effluent from a CZE column is introduced into an electrospray ionization (ESI) source which generates a fine mist of highly charged droplets from the solution. Subsequent solvent evaporation and electrostatic repulsion produces multiply-charged molecular ions. Ion current entering the vacuum through the capillary and two skimmers from atmospheric pressure is essentially continuous. A TOF mass analyzer, conversely, is an inherently pulsed technique requiring spatially and temporally resolved ion packets to conduct mass analyses. To combine ESI with TOF, ions are extracted perpendicular to the axis of the electrospray interface with a pulsed electric voltage applied to the repeller plate, which takes the advantage of the low

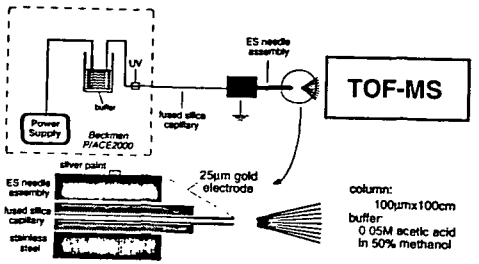

Fig. 1 Schematic diagram for interfacing capillary electrophoresis to electrospray ionization TOF-MS apparatus.

translational energy spread in this dimension. This 0 - 400 V pulsar has a specified rise and fall time of 10 ns, which defines the ion packet.

We have demonstrated that a mixture of peptides can be separated by CE and detected on-line with our TOF-MS. Fig. 2 illustrates a 3-D plot of 15 TOF-MS spectra collected at different elution times during a single CE separation. Lys-bradykinin (B^{3+}, m/z 397; B^{2+}, m/z 595) elutes first from 26.0 to 26.5 minutes. Gramicidin S (G^{2+}, m/z 571; G^{+}, m/z 1142) appears next from 31.0 to 32.5 minutes, and crystal violet (C^{+}, m/z 371) appears from 33.4 to 35.9 minutes. Leu-enkaphalin (E^{+}, m/z 556) elutes finally from 40.5 to 41.0 minutes. Note both gramicidin S (G^{2+}) and crystal violet (C^{+}), which are poorly separated by CE, are resolved simultaneously, a distinct advantage of the CE/MS detection system.

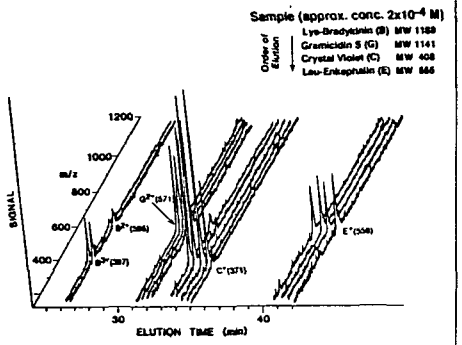

Fig. 2 3-D plot of 15 TOF-MS spectra for peptide mixture by CE-ESI-TOF-MS.

We have found out that by reducing the surface tension interaction between the solution and the outlet of the capillary, the ionization efficiency from the electrospray process can be improved, which is consistent with previous results by others.[2,3] Two ways exist to reduce the surface tension: 1) sharpening the silica capillary tip (decreasing the o.d. of capillary to less than 200 μm), so that the emerging liquid surface area is greatly lessened; and 2) eliminating the coating on outside of the silica capillary tip so that the surface is altered. The ESI-TOF-MS signal for crystal violet has been increased by a factor of 4 to 5. A stable electrospray current has been generated from solvent with a 90% water content, which enables ESI-MS to analyze samples in conditions that are optimal for CE separation. Normally, a 50% water + 50% methanol solvent is needed for operating ESI-MS.

To improve further the sensitivity of our apparatus, our current efforts are focused on modifying the ion optics to increase the ion transmission efficiency. In addition, a reflectron will be incorporated into the system to achieve higher resolution.

1. R. D. Smith, J. A. Olivares, N. T. Nguyen, and H. R. Udseth, Anal. Chem. 1988, *60*, 436.
2. David P. H. Smith, IEEE Transactions on Industry Applications, Vol. IA 22, No.3, 1986, 527.
3. S. K. Chowdhury and B. T. Chait, Anal. Chem. 1991, *63*, 1660.

Electrospray Ionization Collisionally Activated Dissociation on a Bench-Top Mass Spectrometer

*William H. Cusworth, III, and Frantisek Turecek, Department of Chemistry, BG-10, University of Washington, Seattle, WA 98195

A Hewlett-Packard 5971A benchtop mass spectrometer has been modified and furnished with an interface for electrospray ionization as described previously. The overall layout of the instrument, along with the flow-injection sampling system, is shown in (Figure 1). The flow-injection system consists of a linear syringe pump and a 6-port manual switching valve. The electrospray interface consists of a spray chamber containing a 110 μm i.d. syringe needle charged to +4-5.5 kV, an interchangeable stainless-steel capillary (0.4 or 0.5 mm i.d.), which is embedded in an alumina tube resistively heated to 80-120°C and charged to +100-500 V, a skimmer with a 0.5 mm orifice at +20-40 V, and electrostatic lenses. The expansion space between the capillary and the skimmer is pumped to 0.9-1.8 Torr, while the mass spectrometer is pumped differentially to 10^{-4} (skimmer region) and ~10^{-5} Torr (quadrupole analyzer and detector region). Recent modifications have been made to the spray needle and the electrostatic lenses which have resulted in an increase in total signal.

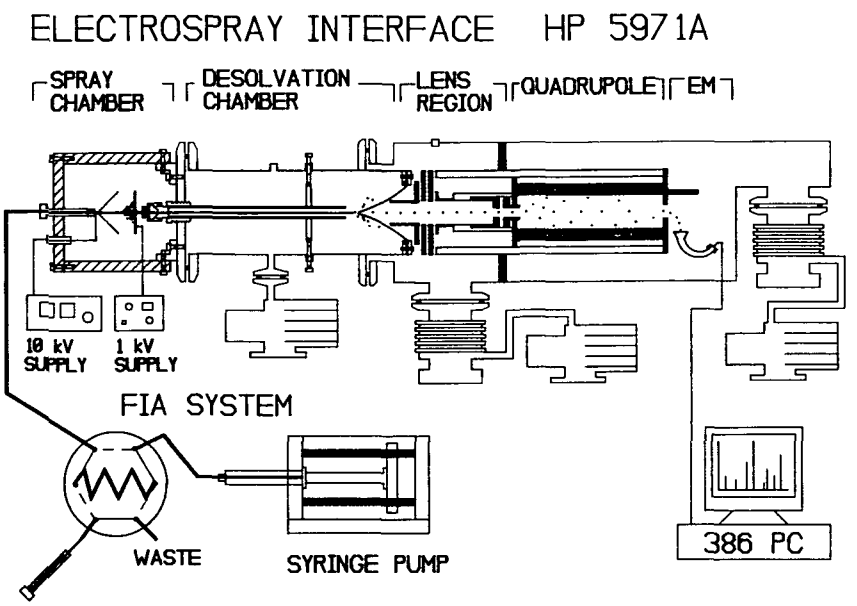

Figure 1. Overall layout of bench-top instrument.

Flow-injection experiments have been carried out and standards of crystal violet have been run. The instrument showed a linear concentration response from 5 μM (present limit of detection) to 100 μM. Above 200 μM, the signal becomes saturated and the response levels off.

We now report an efficient collisionally activated dissociation of the stable cation of crystal violet, $C_{25}H_{30}N_3^+$, *m/z* 372, upon applying bias ($\Delta V = V_{cap} - V_{skimmer}$) between the capillary and the skimmer in the high-pressure region. Spectra taken at increasing bias with a 0.4 mm i.d. capillary are shown in (Figure 2). No dissociation is observed up to ΔV = +85 V, corresponding to E_{CM} = 6.1 eV. Above this voltage elimination of CH_4 is observed (ion **a**, *m/z* 356) which peaks at ΔV = +130 V (E_{CM} = 9.4 eV), where the fragment **a** represents >90% of the total ion current. Elimination of a second CH_4 molecule sets on at ΔV > +130 V and peaks at ΔV = +180 V (E_{CM} = 13 eV) with the ion at *m/z* 340 (**b**) representing >90% of the total ion current. At higher ΔV competitive and consecutive eliminations of CH_4, CH_3N, C_2H_5N, and of an aromatic ring take place to give *m/z* 311, 268, 239, 191, and eventually the fluorenyl ion at *m/z* 165.

The surprisingly step-wise character of the methane eliminations is probably due to their relatively high endothermicities (~1 eV), the absence of competing dissociations, and slow translational heating under multiple-collision conditions. Experiments aimed at utilizing the high pressure CAD for mixture analysis are in progress.

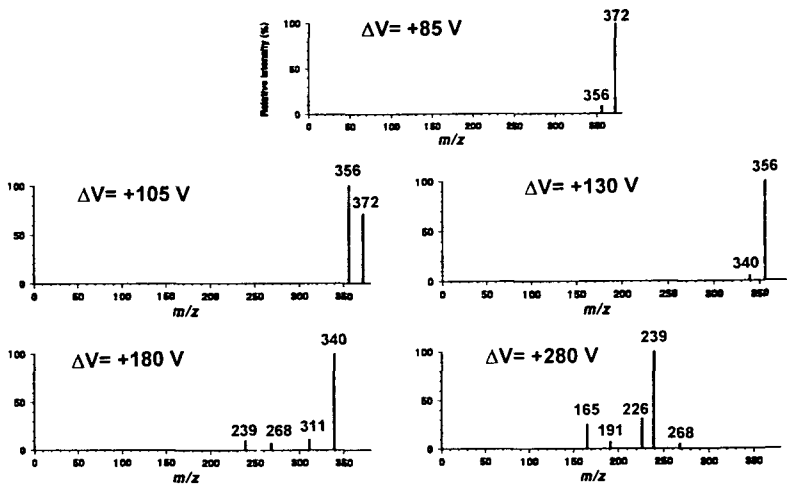

Figure 2. Collisionally-activated dissociation spectra for crystal violet ion taken at increasing capillary-skimmer bias.

Secondary Electron Resolved Mass Spectrometry

Jan Axelsson, Curt T. Reimann, Per Håkansson, Plamen Demirev and B.U.R. Sundqvist
Department of Radiation Sciences, Div. of Ion Physics, Uppsala University, Box 535, S-751 21 Uppsala, SWEDEN

Introduction

In conventional mass spectrometry, all the ions impacting the conversion dynode or the detector are counted irrespective of mass and charge state. Especially with electrospray mass spectrometry of mixed solutions, many ions of different charge states are present. Therefore several masses are likely to fall into the same mass-over-charge (M/Z) channel so that peaks of different masses will overlap in the M/Z spectrum.

In this report we demonstrate a method to resolve such overlapping peaks using the secondary electron yields, i.e. the number of electrons emitted from a single ion impacting the conversion dynode. Using the mass dependence of the secondary electron yield features in the M/Z spectrum can be emphasized for a desired mass region and hidden peaks can be raised from the noise. The method of Secondary Electron Resolved Mass Spectrometry will be referred to as SERMS. Furthermore, a method has been developed where the direct measurement of the secondary electron distribution is employed to give mass information through the mass dependence of the electron yield. This method which has proved useful to probe fragmentation and dimerization will be referred to as 'Direct SERMS'

Method

Secondary electrons emitted from the impact of a positive electrospray ion at the -20 kV conversion dynode are accelerated towards ground potential. The electrons are deflected magnetically into an energy-sensitive silicon surface-barrier detector, where the total energy deposited is proportional to the number of secondary electrons. 'Direct SERMS' is performed collecting electron yields from a large number of impacts with a multi-channel analyzer so that information about the most probable yield and hence the mass of the ion can be deduced.

Feeding the output of the amplified detector signal into a discriminator (or a single-channel analyzer - SCA) and counting the number of pulses per unit time within a certain energy (i.e. electron multiplicity) window allows to measure the number of ions with a mass corresponding to that electron multiplicity. Scanning the M/Z setting of the mass spectrometer and simultaneously registering the pulse rate from the SCA results in a M/Z spectrum in which the masses corresponding to the electron multiplicity window is enhanced. The SCA window can easily be correlated with the secondary electron distribution so that any interesting feature appearing in an electron distribution can be selected for enhancement.

Results

Using the direct SERMS with Cytochrome-C, a distribution of a main peak and a lower intensity peak at higher electron multiplicity is observed. Fitting the distribution to two summed Gaussian distributions gives the position of the two peaks. Applying the empirical dependence found for constant velocity (constant accelerating potential and M/Z) for an Al_2O_3 dynode

$$[\text{electron yield}] \propto [\text{Mass}]^{0.63}$$

on the peak positions yields that the second peak has twice the mass of the main peak, thus the second peak is the dimer peak.

Direct SERMS has also been employed to show that the higher mass poly-ethylene glycols (PEG) do not survive either the process of electrospray, or the transport through the vacuum system (of our experimental set-up). A direct SERMS distribution of PEG 35 000 u shows a main peak at the expected location, whereas a PEG of mass 100 000 u shows low-mass fragments and a main fragment peak at about mass 35 000 u (Fig.1). The same fragment peak has been observed for PEG of mass 300 000 u.

A mixture of myoglobin and insulin (1: 60 molar) in a solution is used to illustrate the possibility to enhance specific masses in an electrospray mass spectrum of a mixture. Setting the discriminator level far above the main peak corresponding to insulin, allows to enhance the myoglobin peaks compared to a conventional electrospray mass-spectrum of the same mixture (Fig. 2).

Similarly, a discriminator level corresponding to the second peak in the Cytochrome-C electron distribution enhances the dimer peaks of odd charges, M/Z=2M/(2N+1), which are residing between the composite peaks of the monomer and the even charged dimer.

Switching to a Myoglobin solution after running Valinomycin (strong peak at M/Z=1131), the Apo-myoglobin peak (M/Z=1134) could not be distinguished from the much stronger traces of Valinomycin. Setting a high discriminator level results in a complete suppression of the Valinomycin peak (Fig.3,4).

An electrospray solution of myoglobin contains three high mass components: native myoglobin (17 567 u), Apo-myoglobin without the 'heme' group (16 951 u) and Apo-myoglobin dimer (33 902 u). In the electrospray spectrum the myoglobin and the Apo-myoglobin dimer peaks are very close in M/Z, so that they will be unresolved. With SERMS a shift in the composite peak towards the M/Z-value of the Apo-myoglobin dimer has been demonstrated when the discriminator level was set to higher masses.

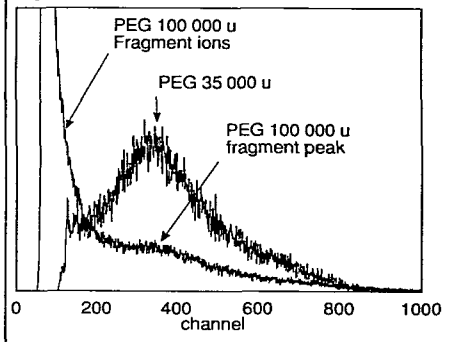

Fig.1. Fragmentation of mass 100 000 u poly-ethylene glycol by 'direct SERMS'.

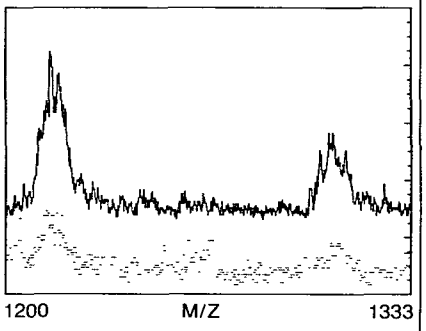

Fig. 2. Low concentration of myoglobin in insulin solution (bottom). Apo-myoglobin peaks are 'lifted' up by SERMS (top).

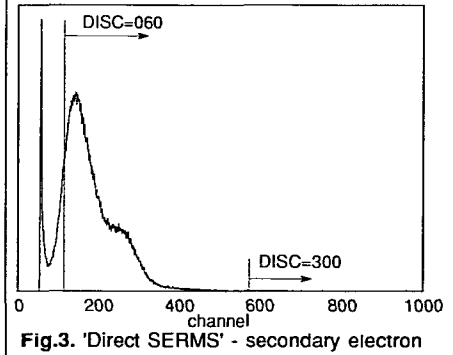

Fig.3. 'Direct SERMS' - secondary electron distribution of apo-myoglobin M/Z=1211, with discriminator levels as referred to in fig.4.

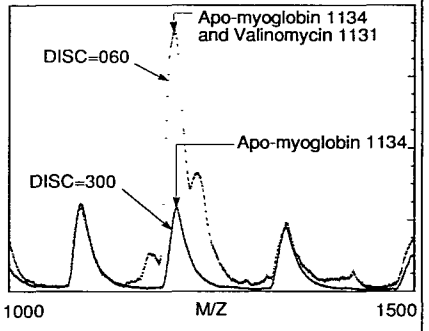

Fig.4. Discriminating against valinomycin makes the apo-myoglobin peak M/Z=1134 appear from the mixed peak of valinomycin and apo-myoglobin.

THE USE OF A FAST SCANNING FOCAL PLANE DETECTOR IN LC-ESI/MS

R. Pesch, E. Schroeder, H. Muenster
Finnigan MAT GmbH, Barkhausenstr. 2, 28197 Bremen, Germany

Focal plane detectors are a suitable means to increase the sensitivity of magnetic sector mass spectrometers. This is particularly true for applications where detection limits are determined by the absolute number of ions transmitted rather than by the ratio of signal to chemical noise.

Electrospray ionization (ESI) produces less chemical noise than many other ionization techniques. Therefore, the use of focal plane detectors is advantageous in many ESI applications.

Since ESI is commonly used in conjunction with on-line separation techniques like liquid chromatography (LC) and capillary zone electrophoresis (CZE), a usable focal plane detector must conform to the time and mass range constraints imposed by the separation technique, i.e. be capable to acquire wide mass range scans with short cycle times.

The focal plane detector used in the experiments is an ion counting device with spatial resolution (PATRIC = Position And Time resolved Ion Counting). The key feature is its capability to be used in rapid wide mass range scans while maintaining mass resolution (> 5,000 FWHM) and the full gain in sensitivity (> 100 over a point detector).

Because the mass scale calibration for the PATRIC detector and the point detector is identical and selection of detectors is electrical with the mass spectrometer used (Finnigan MAT 900), change of detectors takes only about 0.2 sec and can be initiated between scans or within a scan.

Although low chemical noise is produced in ESI, it turned out that for small peptides chemical noise again is the limiting factor in achieving lowest limits of detection. This is especially true with static focal plane detection. The detection limit of 2 fmole bradykinin could not be improved for this reason.

In fast scanning focal plane detection mode, typical detection limits are in the low fmole range for small and medium size peptides (Fig. 1, 3). Because the PATRIC scan cycles of about two seconds compare well to LC and CZE peak widths (Fig. 2), the full sensitivity advantage of focal plane detection can be utilized without restrictions to the liquid separation.

It is expected that ongoing development with the ESI interface, leading to lower noise and higher overall sensitivity, will improve routine detection limits in fast scanning mode into the attomole range.

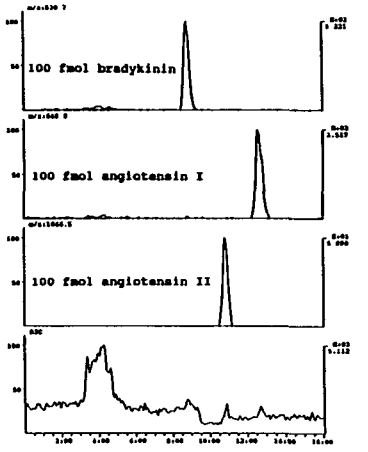

Fig.1 LC/MS with wide range PATRIC scan acquisition m/z 400 -> 1350, 2 sec

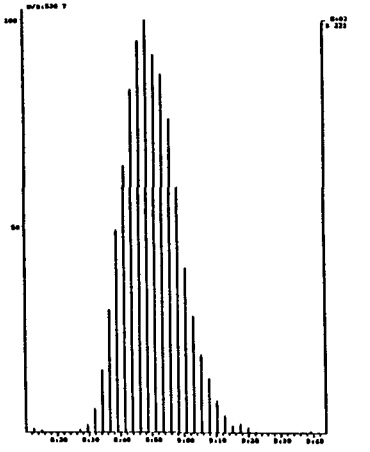

Fig.2 Scan cycles over LC peak

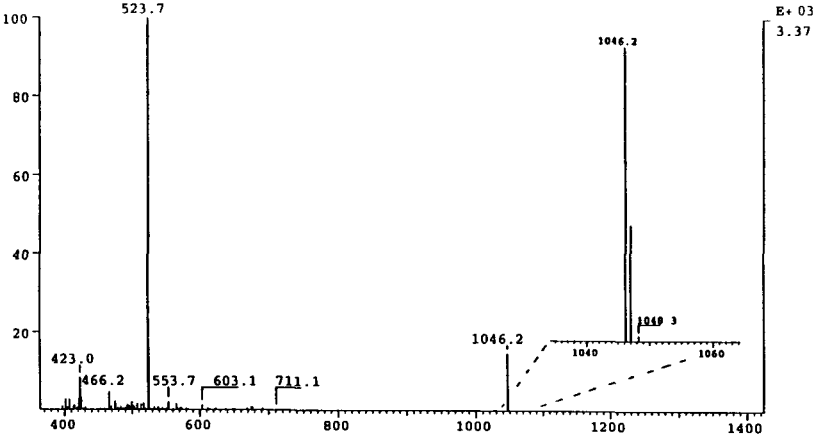

Fig.3 Averaged and background subtracted mass spectrum from 100 fmol angiotensin II

Quantitative Analysis of Pharmaceutical Targets using a CCD Array Detector and Electrospray Mass Spectrometry

S. Kennerley, H. Wight, D. Little, M. Kimber, C. Moore
Kratos Analytical, Barton Dock Road, Manchester M31 2LD, UK

Introduction

Conventional array detectors have had limited use for on-line LC-MS experiments because of their slow acquisition times. In the past it has been necessary to take snap-shots of limited sections of the mass range and then "piece" these together to form a full spectrum. Since the chromatographic peaks may only be a few seconds in duration the time taken to reconstruct a spectra has prohibited the use of these detectors for quantitative analysis.

As most pharmaceutical companies strive to reduce the amount of active compound administered on a per patient basis, the required detection limits fall far below those currently achieved with point detectors .

A new scanning array detector has been developed which achieves the necessary scan speeds and the detection limits required.

How the detector works

Ions strike a microchannel plate multiplier which is one inch long and detects a minimum of ±2% about the m/z value focused at its centre. The microchannel plates are connected by a phosphor and fibre optic link to a charge-coupled device (ccd) array. The ccd has 1152 elements in the dispersive plane. As the analysers are scanned, the ions at each m/z value are electronically tracked across the array so that the resulting signal is integrated 1152 times. The integrated data is continuously transferred to the computer system where it is treated as a normal spectrum and can be processed in an identical manner to data from a conventional detector.

Experimental

The sulphonamide mixtures were analysed by on-line LC-MS using an electrospray interface and a CONCEPT mass spectrometer. Chromatographic separation was achieved using a 15 cm x 2 mm Spherisorb ODS HPLC column operated isocratically with a mobile phase of 70% (1% acetic acid) water and 30% acetonitrile at a flow rate of 100µl per minute.

A post column splitter device was employed to reduce the flow rate to 5 µl per minute before its introduction into the electrospray source. The mass spectrometer was operated with an acceleration voltage of 4 kV. Acquisition was performed over the mass range 100 u to 500 u scanning at 5 seconds per decade with a resolution of 1000 (10% valley definition).

A dilution series was prepared with a mixture of 4 sulphonamides. For the purposes of quantitation, an internal standard (SDM) was added to each of these dilutions. Mass chromatograms were obtained for each of these dilutions using both the point detector and the array detector. Relative response factors were calculated for each compound using peak area measurement.

Results

Examples from the analysis of the sulphonamide dilution series are shown in Figures 1 to 3. The HPLC trace is shown in Figure 1 with the corresponding ion chromatograms from the LC-ESI-MS analysis in Figure 2. An example spectrum of one of the components, sulphamethazine, is illustrated in Figure 3. This is taken from the 2 pmol/µl concentration level.

Conclusions

The CCD array detector enables sufficient scans to be acquired to achieve positive identification and good quantitative analysis on trace level components separated by liquid chromatography. The relative response factors for the experiment illustrate this in Table 1 and Figure 4 shows a calibration curve plotted for one of the components, in this case sulphadiazine (SDZ).

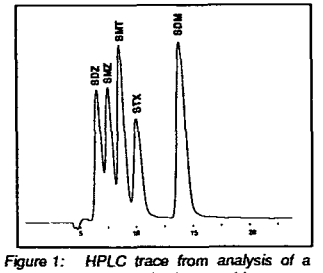

Figure 1: HPLC trace from analysis of a mixture of sulphonamides

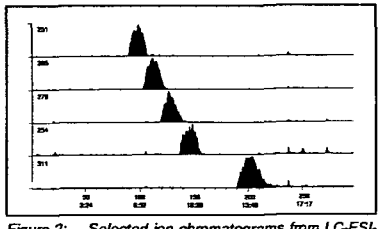

Figure 2: Selected ion chromatograms from LC-ESI-MS analysis of a sulphonamide mixture at the 2 pmole level using CCD array detection.

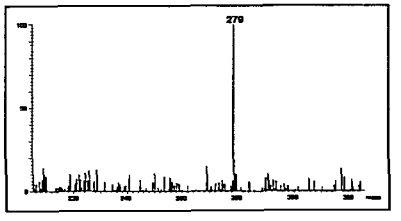

Figure 3: Example spectrum from the 2 pmole level injection. Example shows the response for the sulphonamide, sulphamethazine (SMT).

Compound	name	Concentration (pmol/µl)		
		2	5	10
SDZ	Sulphadiazine	1.66	1.53	2.01
SMZ	Sulphamerazine	3.04	4.02	2.16
STX	Sulphamethoxazole	1.59	1.80	1.74
SMT	Sulphamethazine	4.48	4.13	3.25
SDM	Sulphadimethoxine	(Internal Standard)		

Table 2: Relative response factors obtained for sulphonamide analysis.

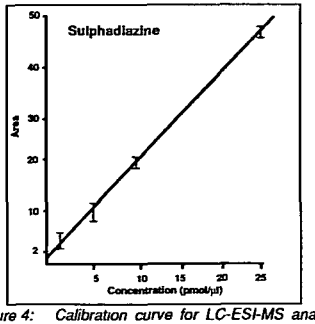

Figure 4: Calibration curve for LC-ESI-MS analysis with CCD array detection of sulphonamides.

NOTES ON THE COUNTER ELECTRODE. The initial design of the electrode had three considerations. Open pumping holes to allow pumping of the nozzle tip and prevent accumulation of material that cause shorts. Make the electrode's exit hole coaxial with the nozzle tip to collimate the ion beam. Make the distance to the nozzle tip adjustable to physically control field strength. Only the latter considerations proved critical.

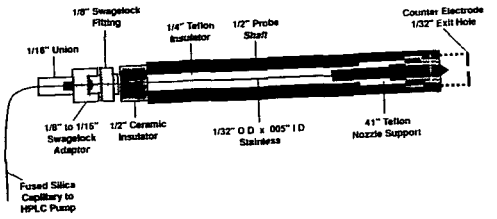

FIGURE 1

Later designs performed well even when pumping holes were omitted This electrode can be made from 1/4"- 3/8" o.d. 1/8" i.d. stainless force fitted into the probe shaft.

DISCUSSION The probe shown was designed as a result of the presentations on ESI, and the related workshop at the 40th ASMS Conference (1992). ESI requires a solvent evaporation system, an electric point source, and a strong electric field. The atmospheric pressure conditions, the long desolvation zones, and the additional lensing present in ESI are brought about by droplet size at the onset of ion formation. The Coulomb explosion seemed governed by physical parameters that could also be correlated to the inital droplet size. Therefore, it was paramount to reduce this initial droplet size and shorten the desolvation zone requirements of ESI. The difficulty in producing multi charged ions may be due to the fast removal of the solvent that seems to favor larger m/z ratios more characteristic of LSIMS. Smaller droplet size brings about two improvements over ESI, namely, a reduced load on the pumping system, and elimination of optics between the probe and the quads As expected, typical operating conditions for FALDI are within those of ESI (<2ul/m flow, 1-3KV). Initial comparisons with ESI have shown FALDI to be 100x more sensitive than our ESI unit for small peptides, CsI, etc. However, for myoglobin and other proteins our ESI unit had no trouble producing spectra while our probe failed A closer look must be taken of intermediate compounds such as medium sized polypeptides to try to find conditions for multi charged ion formation. Compared to LSIMS (i.e., a Cs gun), however, the sensitivity is not as good and the spectrum quality inferior. The peak shape of FALDI spectra is intriguing, it maybe reasoned that without the atmospheric pressure conditions of ESI the only way to thermalize the ions is the removal of excess kinetic energy by evaporation of solvent, and the peak shape is a reflection of the energy spread of the ions entering the quads. However, the observed base line should be extremely high, and peak tops should not be so sharp above the 10% intensity level (high base line and wide peak profiles are observed during small pressure bursts but they disappear completely when the stable conditions return).

CONCLUSIONS. At the present the only conclusion we can make is that the system can be used as an alternative to LSIMS perhaps extending the mass range for polar molecules by a factor of 3 or 4 but not the more striking 20 to 60 of ESI The final word on this technique, maybe its very survival, hinges on finding multi charged ions or an explanationn for their absence. As it stands now, the technique is useful as an interface to an HPLC or CE and as a substitute to CF-FAB but not as a replacement to ESI.

References: 1.Whitehouse et. al., "Electrospray Interface for Liquid Chromatographs and Mass Spectrometers Anal. Chem. Vol 57, pg 675 (1985)
2. J. B. Fenn et.al. 33rd ASMS Conference pg 392 (1985)
3 R.Smith. et.al. Anal.Chem. 60,1948 (1988)

A PROCESS FOR THE DIRECT GENERATION OF IONS FROM POLAR LIQUID SOLUTIONS.

Dr. Climaco J. Metral, PRI-NCI-FCRDC/Dyncorp P.O.Box B. Frederick, MD 21702

INTRODUCTION. Protonated and polymeric molecular ions form directly from polar liquid solutions when the liquid is forced to exit a small nozzle (<100 μm aperture) into high vacuum (<3x10^{-5} torr) in the presence of a field below 5 KV/cm. Larger nozzle apertures are possible by controlling the liquid viscosity with LSIMS matrices such as glycerol, etc.; however, the preferred nozzle apertures are below 50 μm. The ions formed are protonated molecular and polymeric ions characteristic of the compound(s) in solution The higher viscosity solutions allow flow rates of up to 1-2 ul/min. Although field and flow conditions are similar to electrospray ionization (ESI) it takes place in a vacuum without auxiliary pumping, pneumatic gases, desolvation zones or additional lensing [3] The requirements for the process described here are: a) An efficient evaporation of the excess solvent b) A strong electric field in the region immediate to the entrance of the liquid into the high vacuum c) A high viscosity polar liquid solution to control liquid flow. d) A conducting nozzle with apertures below 100μ in diameter. e) A high voltage point electrode A 1/8" i.d. tubing is coupled externally to a 50μm i.d. glass capillary which supplies the pressure from a syringe pump. The spectra observed are almost identical to LSIMS This process is suited for HPLC/MS, CZE/MS, and CF-FAB Although the ion formation process resembles ESI, it is not clear why it could not generate the +17, and higher multiple charged ions for myoglobin observed by ESI[3] The presence of doubly and triply charged ions for angiotensin II suggests that it is possible to generate multicharged ions but we have not found the proper conditions. Several attempts to observe the multicharged ions of myoglobin even under extreme acidic conditions have failed

EXPERIMENTAL Experiments were carried out with the direct probe shown in the inset. Several stock solutions were prepared ranging from 5% to 30% glycerol in acidified methanol. After filling the solvent bottle of a syringe pump with a stock solution, the probe was purged and flow stabilized below at 2 ul/min. The probe assembly was introduced to within 2 cm of the extraction plate of the mass spectrometer adjusting this distance to vary the temperature of the nozzle tip With the probe secured and insulated, power was applied limiting current to <40 μamps and voltage to<2.4KV Once conditions stabilize, analytes are introduced directly into the liquid flow by various methods A practical approach employed for the purpose of this paper was to put the pump in negative flow conditions, load several microliters of the analyte solution into the micropump syringe barrel, and reestablish flow conditions This procedure increases the loading capacity of the system and permits observation of spectrua for a longer time A better approach is to use HPLC injector The spectrum shown in Figure 2 using the first method. The resulting spectrum is similar to the corresponding LSIMS or FAB spectrum, except for a significant difference is the wide base of the peak profile below 10% intensity The effect of this shape on the centroiding algorithms of our 4600 Finnigan quadrupole instrument , at unit resolution, is to produce a noisy base line that obscures and at times deletes the ^{13}C isotope peak.

NOTES ON NOZZLE CONSTRUCTION. It is important to note that there is no need for capillary tubing anywhere in the probe, what is important is a conducting nozzle with apertures below 100 microns. Apertures below 50 microns are difficult to manufacture from conventional tubing, however, 25μ nozzles are commercially available. Nevertheless, it is possible to obtain nozzle apertures <50μ using stainless steel tubing (.004", 003") by grinding the tip of the nozzle with an emery cutting wheel causing it to seal the nozzle and subsequently reopen it with 12000 emery paper under pressure. Alternatively, purposely clogging larger nozzles using a saturated solution of CsI/H_2O also produces smaller nozzles. This approach tends to unclog unpredictably causing severe flash overs

THERMAL SURFACE IONIZATION IN THE PARTICLE-BEAM MASS SPECTROMETRY ANALYSIS OF (ANTI)-CHOLINERGIC DRUGS AND HERBICIDES

A.P. Tinke, R.A.M. van der Hoeven, W M.A. Niessen, U R. Tjaden and J. van der Greef

Division of Analytical Chemistry, Center for Bio-Pharmaceutical Sciences, P.O. Box 9502, 2300 RA Leiden, The Netherlands.

Considering the high ionization efficiencies reported for Surface Ionization (SI), we are investigating whether SI can be achieved by colliding molecules from a (supersonic) molecular beam onto a suitable heated surface [1,2]. This would allow the application of SI in LC-MS interfacing, e.g., via a particle beam interface, as depicted in the schematic representation. In former experiments three types of surface ionization phenoma have been observed [2]:

* hyperthermal surface ionization, resulting in radical cations
* thermal surface ionization, e.g., of quaternary ammonium compounds
* alkali addition

In this presentation, the thermal surface ionization of (anti)-cholinergic drugs and some herbicides (paraquad and diquad) is further investigated. For the experiments a Finnigan MAT TSQ 70 mass spectrometer is equipped with a Hewlett Packard HP 59980 particle-beam interface. An EI ion source is used, operated in filament-off mode. A laboratory-built heatable probe is used with a platinum tip in such a way, that the particle beam collides with the surface at an angle of 45°. A small bias potential (0-5V) is applied to the probe tip. Column-bypass injections (20 µl) into a 0.5 ml.min acetonitrile stream are applied for sample introduction.

Schematic Representation

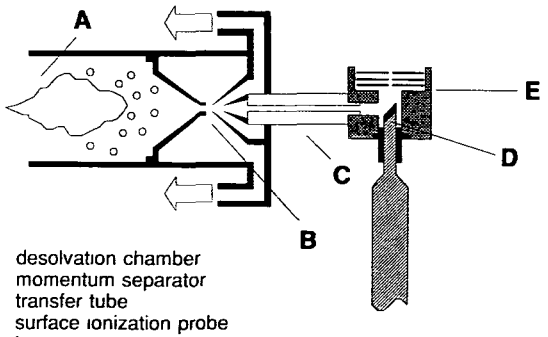

A = desolvation chamber
B = momentum separator
C = transfer tube
D = surface ionization probe
E = ion source

Effects on the response are observed from various surface treatment procedures. Introduction of oxygen into the ion source is believed to clean the probe surface by the rapid oxidation of contaminants. An optimum probe temperature is observed at 600-700 °C after stabilization for 1 hr. Injection of strong acids results in a 2-3x improvement of the signal. The mechanism of thermal surface ionization is assumed to be based on the simple dissociation of ion pairs (salts) by collision with the hot surface. However, in practice the response in negative-ion mode appears to be poor. These observations indicate that the mechanism of thermal surface ionization is more complex. The Surface Ionization spectra of most (anti)-cholinergic drugs do not only contain molecular cations, but give thermally-induced fragmentation. Probe-temperature effects on the mass spectrum of the pipenzolate cation (M_r 354) are shown in the figure

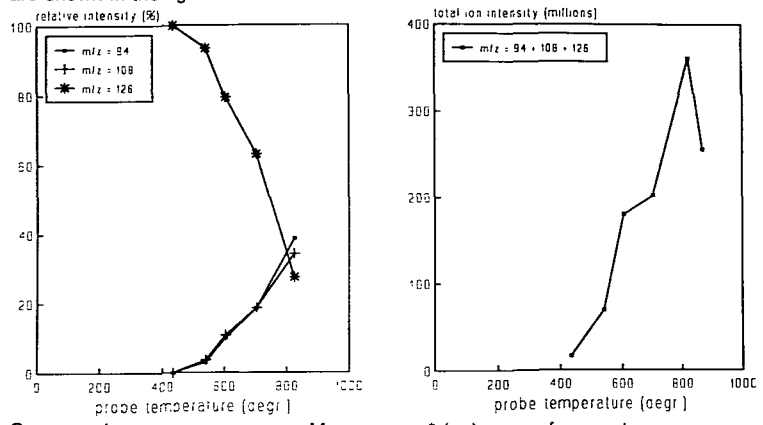

Compound	M_r	* (pg)	fragments
tetrabutylammonium	242	2	242
acetylcholine	146	10	58,72,104,146
isopropamide	353	100	114,264
pipenzolate	354	150	95,108,126
valethamate	306	150	100,114,163,306
diquad	184	10	169,183

* = minimal detectable amount

[1] R.A.M. van der Hoeven, A.P. Tinke, W.M.A. Niessen and J. van der Greef, Rapid. Commun. Mass Spectrom., 7, (1993) 37.
[2] A.P. Tinke, R.A.M. van der Hoeven, W.M.A. Niessen, U.R. Tjaden and J. van der Greef, Presented at the 9th Montreux LC-MS Symposium (november 1992), J. Chromatogr., in press.

The Application of Low Flow Techniques to Particle Beam Liquid Chromatography / Mass Spectrometry

J. Chris Richardson, [†]Matthew A. Tarr, and Richard F. Browner, School of Chemistry and Biochemistry, Georgia Institute of Technology, Atlanta, Georgia 30332-0400

[†] Present Address: USEPA, 960 College Station Road, Athens, GA 30613-7799

INTRODUCTION

Low flow rate chromatography, such as capillary LC, microbore LC, and capillary electrophoresis (CE), has many advantages for the separation of various classes of compounds, including biomolecules. Although very high resolution and low absolute detection limits can be achieved, the major drawback lies in the difficulty of detection. While absorption, fluorescence, and electrochemical detection have been developed extensively for CE, the advantage of more structural information has made mass spectrometry an attractive alternative. Aside from the recent use of FAB, electrospray ionization (ESI) has been the primary method for CE-MS and capillary LC/MS interfacing. ESI provides good detection limits; however, ESI spectra are often difficult to interpret and contain mostly singly and multiply charged molecular ions, with little fragmentation.

In our current study, we have succeeded in directly nebulizing liquid flows as low as 5 µL/min through the use of an ultrasonic nebulizer (USN), and 1 µL/min using a concentric nebulizer. No splitting of streams or addition of makeup solvent is necessary. This method of nebulization results in a neutral aerosol, which can be sampled by the mass spectrometer with the use of a particle beam interface. In this manner, any method of ionization can be utilized, including EI, CI, and others.

EXPERIMENTAL

Experiments were performed on an HP 5988 quadrupole mass spectrometer.The ultrasonic nebulizer used was built in house, and operates at 1.35MHz. Chromatography was carried out on an HP 1090 HPLC, which has the capability of producing liquid flows as low as 1 µL/min. The column used in this study is a 250 x 0.5mm column (purchased from Keystone Scientific) with a 5µm C18 packing. Optimun flow rate for this column is 12 µL/min.

RESULTS

The USN produced very stable aerosols down to 10 µL/min with a slight loss of stability at 5µL/min. The limits of detection for the USN are shown in figure 1. These LOD's are quite good, and are comparable to LOD's at high flow rates.

Similar experiments were carried out using the standard concentric nebulizer. Nebulization at lower flows proved to be very unstable, until the 100 µm capillary was replaced with a 25 µm capillary. After this modification, flows as low as 1 µL/min (the lower limit of the HPLC) could be nebulized. The separation of six phenyl urea herbicides is shown in figure 2.

CONCLUSIONS

The coupling of capillary LC to mass spectrometry using the particle beam interface is a simple process, requiring only the use of a smaller capillary. Sensitivity is comparable, and in some cases better than sensitivity at high flow rates.

The less intrusive nature of the USN may make it more compatible with CE, however, flows lower than 5 µL/min and high buffer concentrations may cause problems in the future.

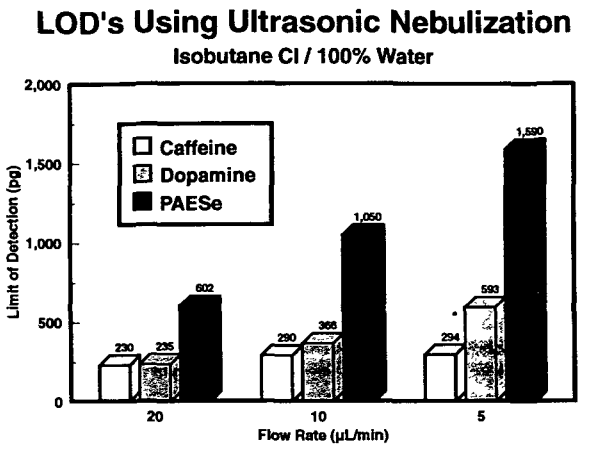

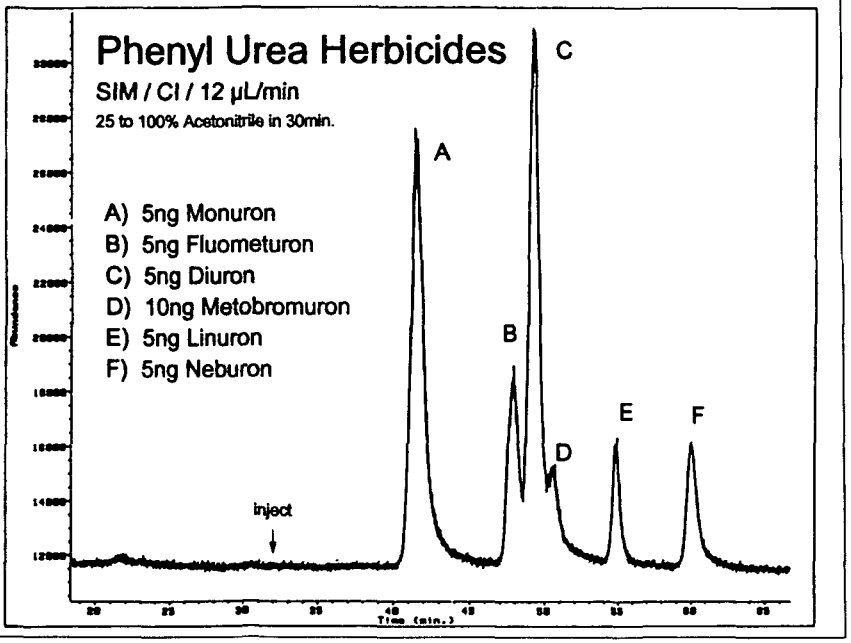

Antisense DNA Oligonucleotides I: The Use of Ionspray Tandem Mass Spectrometry for the Sequence Verification of Methylphosphonate Oligodeoxyribonucleotides

Timothy R. Baker*, Thomas Keough, and Roy L. M. Dobson; The Procter & Gamble Company, Miami Valley Laboratories, Cincinnati, OH, 45239-8707
Timothy A. Riley, Jody A. Hasselfield, and P. Eric Hesselberth; JBL Scientific, Inc., 277 Granada Drive, San Luis Obisbo, CA 93401-5809

Interest in a new pharmaceutical therapy known as Antisense has recently become widespread. This technology utilizes molecules known as oligodeoxyribonucleotides to bind to messenger-ribonucleic acid (m-RNA), thereby inhibiting the synthesis of specific proteins. This highly specific binding to m-RNA is affected by the base content and the exact sequence of the oligomer. Any therapeutic investigations involving these compounds will require verification of the sequences of the synthetically prepared oligonucleotides. Our current interest lies in the use of oligodeoxyribonucleotides having a methylphosphonate backbone, which provides resistance to cleavage by nucleases. Unfortunately, the stability of these molecules precludes sequencing by the Sanger procedure [1].

A variety of mass spectrometric techniques have been utilized to obtain masses of oligonucleotides [2-7]. Recent work using ion trap [8] and fast atom bombardment [9-10] has demonstrated the ability to obtain limited sequence information with small oligonucleotides, but there has been a general paucity of data on larger oligomers. This work demonstates the utility of ionspray mass spectrometry to verify the sequences of these compounds (12-18 mers). Experiments (positive ion) were conducted using a PE-Sciex API III (flow injection).

Initial attempts to generate product ion spectra from multiply charged oligonucleotide precursors focused on maximizing the intensity of product ions. Experiments were conducted using doubly and triply protonated precursors so product spectra would contain ions with fewer possible charge states, facilitating their interpretation. Disadvantages of these constraints were that precursor ions were usually of lower relative abundance and production of fragment ions from doubly and triply charged precursors required collision conditions (high energy and gas thickness) that contributed to the formation of ions of limited diagnostic value. However, these initial experiments did produce a limited series of singly charged ions that were diagnostic of the original oligodeoxyribonucleotide sequence. These ions corresponded to m/z values resulting from simple heterolytic cleavages at the phosphonate-sugar bond with charge retention at the 3'-end of the molecule (defined as y-series fragments). Subsequent experiments proved that these ions could be enhanced relative to nondiagnostic ions by use of milder collision conditions (lower energy and gas thickness). Moreover, these y-series ions could be more readily produced from precursor ions having higher charge states. The product ion spectrum of the $[M+5H]^{5+}$ precursor of d(GGAACTTACCCGACAAGG), not shown, illustrated this point. Although the mild collision conditions resulted in much lower product ion production (<5% of precursor intensity), there was a predominance of diagnostic y-series ions produced. The inefficient yet gentle collision conditions resulted in product ions of all possible charge states.

Visualizing how this MS/MS spectrum relates to sequence becomes more obvious if the diagnostic ions detected in that spectrum are tabulated (see table). There are 17 possible y-ions for this 18-mer. The calculated m/z of the possible multiply charged y-ions are shown in alternating columns, up to the 5^+ state (parent ion charge state). Ions detected in the

spectrum are in bold, in columns for singly, doubly, triply charged, and so on. For this particular oligomer, verification of the sequence was nearly complete. Although there was no sequence information obtained for the y_{11} and y_{12} fragments, there was also no evidence to suggest that these bases were switched (i.e., no peaks at inappropriate m/z values).

Similar results were obtained with other methylphosphonate oligomers and tabulations of results showed the trend of product ion charge state increasing size. The trend is logical since the physically smaller ions prefer to support a single charge (y1-y3), while larger ions that comprise most of the molecule can easily support 3 or 4 charges. Thus far, we have been unable to find convincing evidence of the presence of additional ion series that are indicative of oligomer sequence.

Ion	1^+ calc.	**1^+ meas.**	2^+ calc.	**2^+ meas.**	3^+ calc.	**3^+ meas.**	4^+ calc.	**4^+ meas.**	5^+ calc.	**5^+ meas.**
y_1	345.2	**345.9**	173.1		115.7		87.0		69.8	
y_2	672.5	**672.8**	336.7		224.8		168.9		135.3	
y_3	983.7	**983.7**	492.4		328.6		246.7		197.5	
y_4	1294.9	**1294.7**	647.9	**647.6**	432.3		324.5		259.8	
y_5	1582.1	**1581.7**	791.6	**791.9**	528.0		396.3		317.2	
y_6	1893.3	**1893.8**	947.2	**947.4**	631.8		474.1		379.5	
y_7	2220.6		1110.8	**1110.4**	740.9		555.9		444.9	
y_8	-		1254.4	**1254.5**	836.6	**836.4**	627.8		502.4	
y_9	-		1398.0	**1397.7**	932.3	**932.1**	699.5		559.8	
y_{10}	-		1541.6	**1541.7**	1028.1		771.3		617.2	
y_{11}	-		1697.2		1131.8		849.0		679.5	
y_{12}	-		1848.3		1232.5		924.6		739.9	
y_{13}	-		1999.4		1333.3	**1333.4**	1000.2	**1000.5**	800.3	
y_{14}	-		2143.0		1429.0	**1429.0**	1072.0	**1071.7**	857.8	
y_{15}	-		2298.6		1532.8	**1532.9**	1149.8	**1149.2**	920.1	
y_{16}	-		-		1636.5	**1636.0**	1227.5	**1227.5**	982.3	
y_{17}	-		-		1745.6		1309.4	**1309.2**	1047.7	**1048.0**

The m/z values of proposed y-series ions for the methylphosphonate oligonucleotide d(GGAACTTACCCGACAAGG). A dash (-) indicates an m/z value above the 2400 range of the mass spectrometer. Blank boxes indicates the ion was not detected.

1. F. Sanger, S. Niklen, A. R. Coulson, *Proc. Natl. Acad. Sci.* **74**, 5463 (1977)
2. G. R. Parr, M. C. Fitzgerald, L. M. Smith, *Rapid Commun. Mass Spectrom.* **6**, 369 (1992).
3. K. Tang, S. L. Allman and C. H. Chen, *Rapid Commun. Mass Spectrom.* **6**, 365 (1992).
4. B. Spengler, et. al , *Proceedings of The 38th ASMS* , Tucson Arizona, p. 164 (1990).
5. C. G. Edmonds, et. al, *Proceedings of The 37th ASMS* , Miami Beach, FL, p. 844, (1989).
6. J. T. Stults and L. C. Marsters, *Rapid Commun. Mass Spectrom.* **5**, 359 (1991).
7. T. R. Covey, et. al., *Rapid Commun. Mass Spectrom.* **2**, 249 (1988).
8. S. A. McLuckey, G. J. VanBerkel, G. L. Glish, *J. Am. Soc. Mass Spectrom.* **3**, 60 (1992).
9. R. L. Cerny, K. B Tomer, M. L. Gross, L. Grotjahn, *Anal. Biochem.* **165**, 175 (1987).
10. H. Muenster, et.al., *Proceedings of The 40th ASMS* , Washington D.C. (1992).

EFFECTS OF SURFACE TENSION AND SURFACE ACTIVITY ON ELECTROSPRAY RESPONSE

M.V. Buchanan, Analytical Chemsitry Division, Oak Ridge National Laboratory, Oak Ridge, TN 37831; *M. Shahgholi and K.D. Cook, Chemistry Department, The University of Tennessee, Knoxville, TN 37996

The effect of surface tension on the formation of a stable electrospray (ES) has been studied extensively[1]. However, the impact of this parameter on the sensitivity of ES MS has not been characterized. The present study seeks to assess the effect of surface tension, as well as surface activity, on the mass spectrometric response of electrosprayed ions.

Electrospray experiments were performed with a source designed after that of Chait, interfaced to an Extrel (Model 065-2) quadrupole mass spectrometer. Samples containing 50 μM ($C_6H_{13}N^+(CH_3)_3$) bromide, HTMA, and varying amounts of surfactants were prepared in 50:50 water:methanol or methanol. Each sample was electrosprayed at approximately 4 μL/min through a needle held at +3.2 - 3.5 kV. The drying capillary (heated to 100-120°C) and the skimmer were biased to +90 - 130 V and +45 - 65 V, respectively.

In order to study the effects of surface tension, cationic, anionic, and non-ionic surfactants were added to samples of HTMA. Figure 1 shows the response of HTMA upon addition of varying amounts of the cationic surfactant, ($C_{18}H_{37}N^+(CH_3)_3$) bromide, ODTMA. Up to a concentration of ≈ 30 μM, addition of ODTMA bromide was observed to enhance the signal due to 50 μM HTMA in 50:50 (v/v) water:methanol. The added ODTMA lowers surface tension, presumably resulting in formation of smaller droplets which evaporate more efficiently. At high concentration, the more surface active ODTMA apparently competes with HTMA for surface sites on the droplets, reducing the efficiency of HTMA sampling. Furthermore, the increasing ionic strength may also contribute to the observed decrease in signal for HTMA. When analogous solutions were prepared with 100% methanol, the initial HTMA response enhancement by added ODTMA was not observed, suggesting that ODTMA has a negligible effect on the inherently low surface tension of methanol solutions.

The above experiment was repeated with SHS ($C_{16}H_{33}OSO_2^-Na^+$), an anionic surfactant. This compound should not be transmitted into the positively-charged electrospray and thus compete with the HTMA signal as observed with the cationic surfactant. At concentrations and surface tensions comparable to those in the previously studied cationic solutions, the HTMA signal does not improve. Furthermore, the SHS data reflected instabilities due to clogging of the ES needle, which could have been caused by the oxidation of SHS in the needle or its inherent lower solubility.

To avoid the problem of increasing the ionic strength of the solution, as in the case of the anionic and cationic surfactants, varying amounts of Triton X-100 were added to 50 μM solutions of HTMA in 50:50 (v/v) water:methanol. As shown in Figure 2, the response to 50 μM HTMA is enhanced by the addition of the non-ionic Triton X-100, up to roughly 0.3 mM surfactant. This behavior is attributed to surface tension lowering as also observed with the cationic surfactant, ODTMA. The decline in intensity observed at concentrations of Triton X-100 exceeding 0.3 mM is believed to

result from the onset of micellization (the critical micelle concentration for Triton X-100 is 0.3 mM[2]), which may strip the analyte from the droplet surface. Alternatively, high concentrations of Triton X-100 may interfere with droplet evaporation.

As a test of the role of competition for surface sites (described above), solutions containing equimolar amounts of $C_nH_{2n+1}N^+(CH_3)_3Br^-$ (n=6, 10, 12, 14, 16, 18) were electrosprayed at varying concentrations. When the concentration of each component was less than 2 μM, the responses of the various components were equal. At higher concentrations, the intensity observed for a given member of this series was dependent on its surface activity. This suggests that competition for surface sites induces sampling bias only at high concentrations.

These studies have several important analytical implications. Although it was not generally possible with our instrument to obtain ES mass spectra from aqueous solutions without methanol, this restriction was generally relieved by addition of Triton X-100. Further, these studies suggest that the reported enhancement of ES response resulting from protein denaturation[3] may arise from enhancements in surface activity because denaturation exposes the hydrophobic interior of the protein. Finally, this data shows that caution must be exercised in the quantitative analysis of multi-component mixtures by ES.

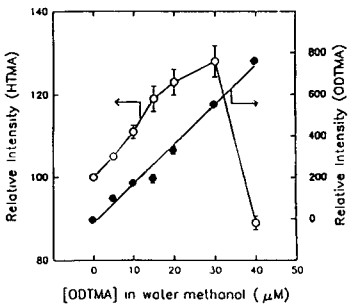

Figure 1. Dependence of the ES response of HTMA and ODTMA on [ODTMA] in 50:50 (v/v) water: methanol.

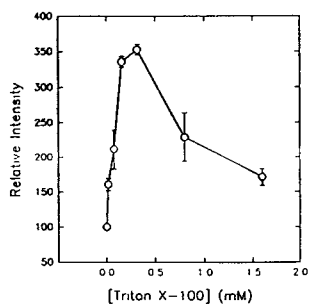

Figure 2. Dependence of the ES response of HTMA on [Triton X-100] in 50:50 (v/v) water:methanol.

ACKNOWLEDGEMENTS

This research was sponsored in part by the National Science Foundation, under grant CHE-8822787 to UT and by the Office of Health and Environmental Research, U.S. Department of Energy, under contract DE-AC05-84OR21400 with Martin Marietta Energy Systems, Inc., and contract DE-AC05-76OR00033 with Oak Ridge Associated Universities (fellowship support).

REFERENCES

1. Tang, L.; Kebarle, P. *Anal. Chem.*, **1991**, *63*, 2709.
2. Rosen, M.J. *Surfactant and Interfacial Phenomena*; Wiley-Interscience: New York, 1978; p.98.
3. Mirza, U.A.; Cohen, S.L.; Chait, B.T. *Anal. Chem.*, **1993**, *65*, 1.

Studies of the Physical Processes of Electrospray

Ross Willoughby, Ed Sheehan, Andy Jarrell,
Randy Peddar, Tom Marecic, and Steve Penn
Millipore/Extrel Mass Spectrometry
575 Epsion Drive, Pittsburgh, PA 15238

Introduction:

An energy balance model is proposed to explain the behavior of the liquid in the electrospray process of aerosol generation and ion formation. Consider that the energy flow on the axis of the electrospray needle and cone is conserved. The system is divided into section a, the needle; section b, the cone; section c, the jet; and section d, the droplets. This condition would be valid for the following assumptions.

Assumptions:

1. The liquid is incompressible, at constant temperature, and in a steady-state geometry.
2. No current flows due to gas discharge, therefore:

   $i_a = i_b = i_c = i_d$ where i = needle current

3. Mass is conserved in the z-axis, flow is constant:

   $dm_a/dt = dm_b/dt = dm_c/dt = dm_d/dt$ where dm/dt = mass flow

4. Energy flux is conserved on the z-axis:

   $dE_a/dt = dE_b/dt = dE_c/dt = dE_d/dt$ where dE/dt = energy flux

5. Energy flux partitions into kinetic, surface, and electrostatic components;

   $dE/dt = dK/dt + dS/dt + d\varepsilon/dt$, where

dK/dt = Kinetic Energy Flux; dS/dt = Surface Energy Flux; and $d\varepsilon/dt$ = Electrostatic Energy Flux

Nebulization Parameters

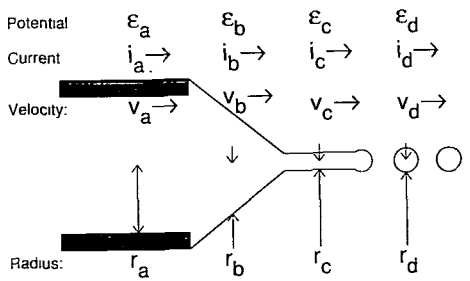

Table I: Partitioning of Energy in Cone

Region	dK/dt	dS/dt	dε/dt
A	$\pi r_a^2 \rho v_a^3/2$	0	$i\varepsilon_a$
B	$\pi r_b^2 \rho v_b^3/2$	$2\pi r_b v_b \gamma$	$i\varepsilon_b$
C	$\pi r_c^2 \rho v_c^3/2$	$2\pi r_c v_c \gamma$	$i\varepsilon_c$
D	$(4\pi r_d^3 \rho v_d^2/6)(dn/dt)$	$0.69(2\pi r_c v_c \gamma)$	$i\varepsilon_d$

Partitioning of Energy with Stable Cone

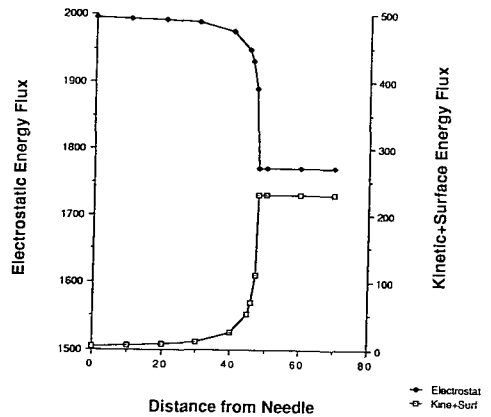

Conclusions:

1 Primary aerosol generation in electrospray can be explained using the Energy Balance Model for a steady state cone .
2. The model predicts that the Rayleigh Limit for surface instability occurs at the point where the liquid jet emerges from the cone. This is an important point in that primary droplets in electrospray are born at (or near) the Rayleigh Limit and consequently little or evaporation is required before subsequent breakup occurs.
3. Secondary droplet formation and geometry is also explained with this model to explain cone formation on the surface of the droplet.
4 The model predicts the observed increase in jet diameter with increased liquid flow rate.

Optimization of the Ionspray Mass Spectrometer as an LC Detector.*

R.K. Boyd, M.A. Quilliam and S. Pleasance[a], *National Research Council, Halifax, Canada B3H 3Z1*; S.J. Vanslyke and P.D. Wentzell, *Chemistry Dept., Dalhousie University, Halifax, Canada B3H 4J3.*
[a] *Present address: Wellcome Research Laboratories, Beckenham, UK BR3 3BS.*

Ionspray (IS, pneumatically assisted electrospray, ES) is an invaluable LC-MS interface for both proteins and small molecules [1]. The pneumatic assistance permits separation of nebulization from droplet charging, and thus greater flexibility. The mechanistic relationships between ES and IS have been clarified [2]. Recently [3] some empirical considerations of the interplay between the sometimes competing demands for chromatographic and mass spectrometric optimization of IS, were presented. The present work expands on this theme by examining the optimization of an ionspray LC/MS interface for both sensitivity and signal/noise ratio, with respect to parameters including needle position and angle, needle voltage, flowrates of nebulizing gas and of nitrogen curtain gas, mobile phase composition and flowrate (including post-column split ratios), *etc.*

Complex interactions of the position parameters were investigated systematically using a central composite design. Figure 1 shows the dependence of both analyte signal (m/z 571.5, $(M+2H)^{2+}$ ion from gramicidin S) and chemical background (cluster ions from aqueous acetonitrile) on the radial distance of the needle tip from the central axis; the signal maximised at about 5mm, but the signal/noise at about 7 mm. This optimum radial position (and also the optimum axial position, not shown) were essentially independent of solvent composition, a finding of significance for gradient elution operation.

Following optimization of the needle position, the dependence of analyte signal on mobile phase flowrate was investigated using the same flow-injection technique (no split). The response maximized at 3-10 µL/min, but dropped off in a quasi-exponential fashion (not shown) to a value about 10% of the maximum at 200 µL/min. Such behaviour of the ionization efficiency has been commonly observed. However, the results shown in Figure 2 were obtained using a full LC/MS method for Diltiazem (m/z 415), with a post-column split controlling the fraction of mobile phase (and thus of the analyte) delivered to the IS interface. At low values of this fraction the signal increases with increasing split ratio, reflecting the increasing fraction of analyte delivered to the mass spectrometer. However this trend is reversed at higher values, where the ionization efficiency effect becomes the dominant factor. There is a fairly broad range where the performance is close to optimal, so this adjustment is not critical. The appropriate choices of column i.d. (and thus of mobile phase flowrate) and of post-column split ratio, are inter-related and complex; the best choice will depend on the analytical problem at hand, *e.g.* how much sample is available, how concentrated is the analyte and its co-extractives, and thus how small an injection volume can be used, *etc.* Simple considerations of ionization efficiency alone do not suffice to optimize LC/MS analyses.

Other parameters investigated included mobile phase acidity (effect on both analyte signal and background), per cent organic content of mobile phase (acetonitrile gives a fairly broad plateau in which response is almost independent of composition), analyte type (*e.g.* small molecules yielding singly-charged ions *vs.* proteins yielding a distribution of charge states). The interactions of all of these parameters with one another have been considered in the context of optimizing LC/MS performance for both chromatographic resolution and overall sensitivity.

1. J.D. Henion *et al.*, *Anal. Chem.* **62**, 713A (1990).
2. M.G. Ikonomou *et al.*, *Anal. Chem.* **63**, 1989 (1991).
3. S. Pleasance *et al.*, *Proc. 38th ASMS Conf.*, 1990, p.381.
* NRCC No. 34863.

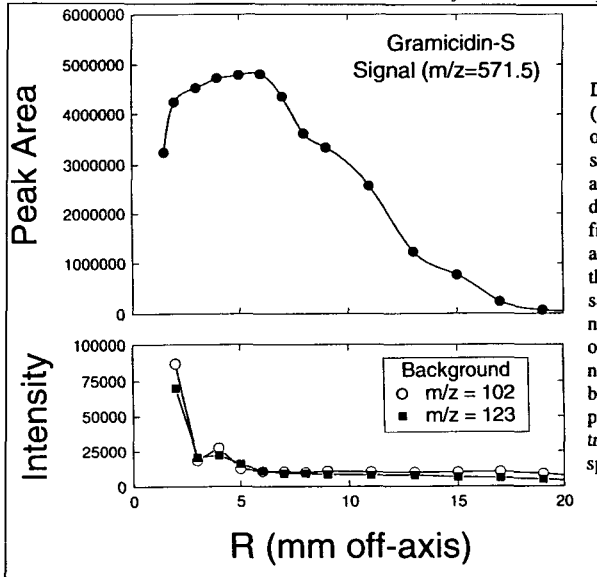

FIGURE 1.

Dependence of the analyte signal (gramicidin S, $(M+2H)^{2+}$ ion), and of the most intense background signals (cluster ions from acidified aqueous acetonitrile) on radial distance of the ionspray needle from the central axis. Both the axial distance of the needle from the interface plate (containing the sampling orifice), and the needle/main-axis angle, were optimized. A sample size of 20 ng in 2 µL was used, introduced by flow injection into a mobile phase flowrate of 50 µL/min transmitted directly to the mass spectrometer with no split.

FIGURE 2.

Dependence of the analyte signal (m/z 415, protonated Diltiezam) on post-column split ratio. A fixed sample size of 100 ng in 2 µL was injected on-column, using a fixed flowrate of 200 µL/min of aqueous acetonitrile (isocratic). The flowrate delivered to the ionspray mass spectrometer was varied *via* a simple post-column split device.

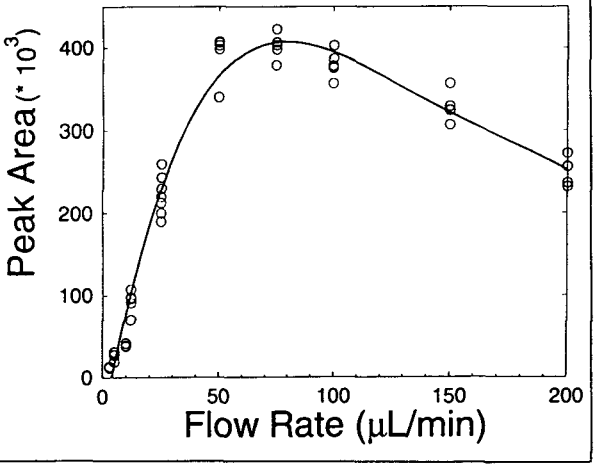

CHEMICAL DERIVATIZATION FOR ELECTROSPRAY IONIZATION-MASS SPECTROMETRY

Gary J. Van Berkel[1] and J. Martin E. Quirke[2]
[1]Analytical Chemistry Division, Oak Ridge National Laboratory, Oak Ridge TN 37831-6365
[2]Department of Chemistry, Florida International University, Miami, FL 33199

The presence of analyte ions in solution appears to be central to the observation of analyte ions in the gas-phase using ES-MS. Therefore, derivatization of neutral analytes to form ionic species should benefit their analysis as has been previously demonstrated for FAB and SIMS.[1] Derivatization along with manipulation of solution chemistry to ionize (or neutralize) a particular analyte has the potential to not only improve the detectability of a particular analyte in ES-MS, but also to add a degree of analyte selectivity to an analysis. In fact, this derivatization approach to the analysis of certain analytes by ES-MS has recently been reported by several groups.[2-6] In this paper, derivatization strategies and specific derivatization reactions for conversion of mono-functional organics to ionic or solution-ionizable derivatives, i.e., "electrospray active" forms of the analyte, are presented. The derivatizations discussed here are not only applicable to the simple, mostly mono-functional molecules used as examples. Rather, these reactions might be used to ionize or transform the selected functionality as part of a larger, more complex molecule. In such a way the ES behavior of these more complex molecules might be enhanced or otherwise altered. The ES-MS instrumentation used in these studies was a modified version of a Finnigan-MAT ion trap mass spectrometer (ITMS) adapted to sample ambient air.[7] Detailed procedures for the derivatizations presented can be found in the papers cited and in most organic chemistry texts.

Three general chemical approaches, collectively referred to as chemical derivatization, are available to effect the solution-phase ionization of analytes. The most straightforward and most often used method takes advantage of the Brønsted or Lewis acid/base properties many molecules possess. Acid/base methods of solution-phase ionization have as their major advantage simplicity, but they are not generally applicable. Another means to ionize analytes in solution is via electron-transfer reactions. For example, chemical oxidants including Brønsted acids, charge-transfer reagents, and Lewis acids can be used to form radical cations of highly conjugated, aromatic, and heteroaromatic compounds. A third approach to generating an ionic form of the analyte is to chemically transform a functional group on the molecule to a solution-ionizable moiety. This transformation might be to a salt (**Figure 1**), to a group that is ionizable via acid/base chemistry (**Figure 2**), or to a group that is ionizable via an electron-transfer reaction (**Figure 3**). Rather than attempt to list possible derivatives, the general synthetic strategies for transformation of a particular functional group to an electrospray active moiety are presented. To aid this discussion, the common functionalities have been placed in groups based on their propensity to undergo similar types of organic reactions.

Hydrocarbons. Alkanes, because of their unreactive nature pose the most ***difficult*** problem for derivatization. In contrast, alkenes and alkynes can be transformed by making use of the propensity of the π-bonded system to undergo ***addition reactions***. In addition, the alkyne carbanion that can be generated from terminal alkynes in strong base is nucleophilic and may take part in ***addition or substitution reactions***. Aromatics are readily amenable to ***electrophilic substitution reactions***, but as a compound class they are relatively easy to oxidize and/or reduce. Therefore, chemical ***electron-transfer reactions*** can be used to form cations/anions of certain aromatics in solution.

R-X Type Compounds. The presence of an electronegative group in RX-type compounds, i.e., a halogen, -OH, -SH, $-NR_2$, and NO_2, provides for a wide range of strategies for generating ionic species for ES-MS. In general, however, the most obvious route to ionic derivatives is to employ

nucleophilic substitution. Some compounds of this type, ***amines and phenols*** in particular, can also be charged by simple ***acid/base chemistry***. Additionally, it is possible to ***transform the "X" group*** of R-X type compounds into an ionic or solution ionizable moiety in a variety of ways.[1]

Aldehydes and Ketones. ***Addition reactions*** across the double bond of these functional groups can be used to form an R-X type compound which can then be transformed to an electrospray active species as outlined above. A second and probably more promising route to a suitable derivative is via ***condensation reactions***. An alternative route for ***aldehydes*** is to take advantage of their facile ***oxidation to carboxylic acids*** which are electrospray active species.

Acyl halides, amides, anhydrides, nitriles, and esters are derived from carboxylic acids and are most easily converted to electrospray active species by ***hydrolysis to the parent acid***. While identification of the carboxylic acid is facile, a second step is required to identify the nature of the "X" group. For example, only one half of an ester can be detected using this approach. An alternative for ***amides*** is ***reduction to the amine*** in which case the product may be further derivatized to an electrospray active species using one of the techniques discussed for R-X type compounds.

Research sponsored by the United States Department of Energy, Office of Basic Energy Sciences under contract DE-AC05-84OR21400 with Martin Marietta Energy Systems, Inc.

1. Busch, K.L., et al. *J. Am. Chem. Soc.* **1982**, *104*, 1507. 2. Lam, Z., et al. *Proceedings 39th ASMS Conf.* **1991**, p. 282. 3. Wilson, S.R., et al. *Proceedings 40th ASMS Conf.* **1992**, p. 1641. 4. Colton, R., et al. *Org. Mass Spectrom.* **1992**, *27*, 1030. 5. Van Berkel, G.J., et al. *Anal. Chem.* **1991**, *63*, 2064. 6. Hiraoka, K., et al. *Rapid Comm. Mass Spectrom.* **1992**, *6*, 254. 7. Van Berkel, G.J., et al. *Anal. Chem.* **1990**, *62*, 1284.

Figure 1

Thiouronium derivative of 1-bromododecane

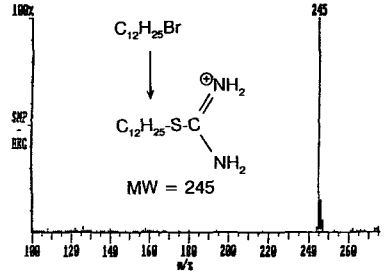

Figure 2

Dodecanoic acid derivative of dodecanol

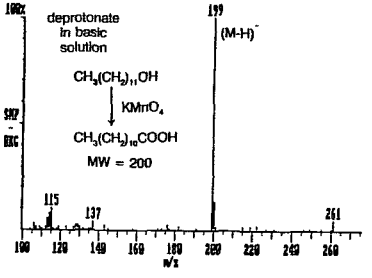

Figure 3

Fluoronone derivative of dinitrophenylhydrazine

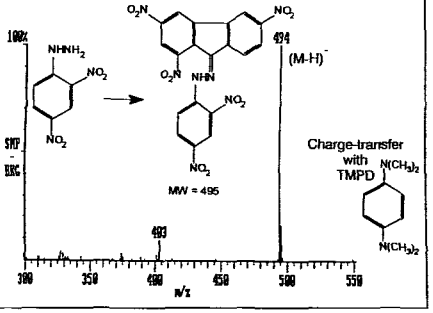

High Resolution Precision Mass Measurements of Noncovalently Bound Protein Aggregates Using Electrospray Ionization Fourier Transform Ion Cyclotron Resonance Mass Spectrometry

Steven A. Hofstadler, James E. Bruce, Brian E. Winger, and Richard D. Smith
Chemical Sciences Laboratory, Pacific Northwest Laboratory Richland, WA 99352

Since its introduction as a viable ionization technique for mass spectrometry of large molecules by Fenn and coworkers, electrospray ionization (ESI) has become a key tool for the analysis of bioanalytically relevant compounds including proteins, peptides, and nucleotides. Aside from the fact that ESI typically generates multiply charged ions, thus lowering the m/z range necessary for detection, the "softness" of the ionization technique allows analysis of large intact biopolymers and potentially provides a direct link between solution chemistry and gas phase conformations. Recently, we have constructed an external source electrospray ionization Fourier transform ion cyclotron resonance (FTICR) mass spectrometer capable of high precision mass measurements and ultra-high resolving power (*i.e.* >> 2 x 10^6 at m/z 1434). The high resolution capabilities of the spectrometer allow simple charge state determination based on the isotopic spacing of molecular ion peaks of a single charge state, thus making it an ideal platform on which to study the abundance and stability of protein aggregates (*i.e.* monomers, dimers, trimers, etc.) based on the observed isotope distribution of aggregate peaks.

Under favorable solution conditions and "gentle" electrospray source conditions, which include minimal capillary heating and low capillary-skimmer potential difference, protein aggregation is often observed. These aggregate peaks correspond to multiply charged noncovalently bound species with molecular weights equal to **n** x $\mathbf{M_r}$, where **n** is the order of the aggregate (eg. **n**=2 corresponds to the dimer species) and $\mathbf{M_r}$ is the molecular weight of the monomeric species. Given that different multimeric species can occupy different charge state distributions, it is often the case that multiple aggregated species are observed at the same nominal m/z. For example, shown in Figure 1 is a mass spectrum of bovine insulin (M_r = 5734) acquired under "gentle" ionization conditions. Even at low resolution it is apparent that additional peaks corresponding to higher order aggregates are evident. A closer look at these peaks reveals that they contain contributions from several multimeric species. It is evident at higher resolution that the peak at m/z 1912 has contributions from the 3+ monomer (***M***), 6+ dimer (***D***), and 12+ tetramer (***T***). Figure 2 demonstrates Bovine cytochrome c (M_r = 12,223) aggregation in the presence of a low concentration of sodium. Under harsher interface conditions less aggregation is observed as is a precipitous decline in the abundance of the monomeric sodiated species. Such aggregates constitute only one example of a broad range of noncovalent associations which should be amenable to study using these methods, including many associations of importance in physiological processes.

This research was supported by internal PNL exploratory research through the U.S. Department of Energy. Pacific Northwest Laboratory is operated by Battelle Memorial Institute for the U.S. Department of Energy through contract DE-AC06-76RLO 1830.

Figure 1

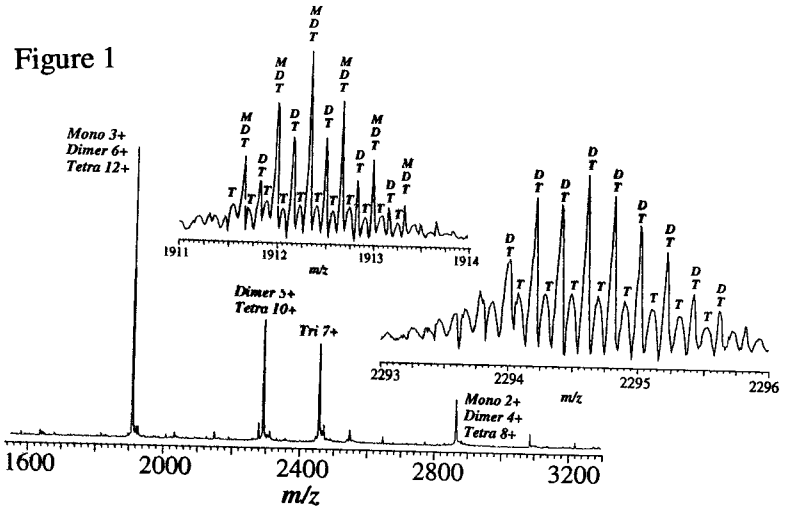

Figure 2

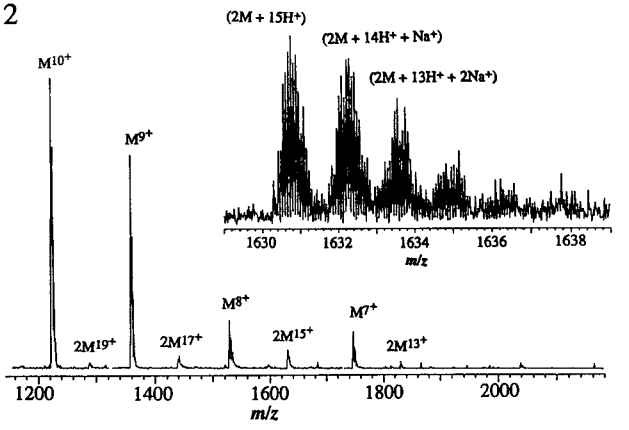

THE DETERMINATION OF A HYPOLIPIDAEMIC AGENT IN PLASMA BY GAS CHROMATOGRAPHY MASS SPECTROMETRY AND LIQUID CHROMATOGRAPHY TANDEM MASS SPECTROMETRY USING ATMOSPHERIC PRESSURE CHEMICAL IONISATION.

I. J. FRASER, R. A. CLARE and S. PLEASANCE,
Department of Bioanalysis and Drug Metabolism, The Wellcome Research Laboratories, Langley Court, Beckenham, Kent, BR3 3BS, U.K.

The compound *N*-Heptyl-*N* '-(2,4 difluoro-6-{2-[-4-(2,2 dimethylpropyl)phenly] ethyl}-phenyl) urea (447C88, Fig. 1) is a member of the new class of potential hypolipidaemic agents, the AcylCoA Cholesterol AcylTransferase (ACAT) inhibitors. Initial attempts to quantitate 447C88 in plasma using both UV and fluorescence detection were unsuccessful and led to the investigation of a sensitive and selective mass spectrometry based method.

A GC-MS method was initially developed to support pre-clinical work requiring the determination of 447C88 in both the rat and dog plasma. Samples were extracted using a phenyl solid-phase extraction cartridge, taken to dryness and derivatised with iodoethane in DMSO. The ethyl derivatives were back extracted into pentane, again taken to dryness and finally reconstituted prior to injection onto a Hewlett Packard 5970 mass selective detector. A deuterated [d4] analogue of 447C88 was used as internal standard and both molecular ions monitored using selected ion recording. While the GC-MS assay was both selective and sensitive, providing a detection limit of 0.4 ng/mL, the extraction and derivatisation procedure was labour intensive and sample turn round was slow due to long chromatographic run times (30 minutes).

The installation of a triple quadrupole instrument with atmospheric pressure ionisation offered the potential of an LC-MS-MS method with increased sensitivity and greater sample throughput. Both 447C88 and its deuterated analogue give an intense deprotonated molecule under negative ion atmospheric pressure chemical ionisation (Fig. 1) and also provided abundant product ions which can be used for multiple reaction monitoring (see Figs. 2-3). The increased selectivity and sensitivity offered by LC-MS-MS has two advantages: firstly, the sample preparation time can be dramatically reduced. Only the solid-phase extraction step is used from the GC-MS method with no concentration steps, no clean-up or derivatisation; Secondly, the run time can be shortened to less than 2 minutes per injection (Figs. 4-6). A short 3 cm C18 column is used with a mobile phase of 20:80 aqueous acetonitrile at 1 mL/min connected directly to the heated nebuliser interface. A 20 µL injection provided the same sensitivity to that obtained by GC-MS, but with a 24 hour turn around of a normal batch of 76 samples (90 with QCs, Stds and blanks) compared with 3-4 days for GC-MS. It has been possible to make 250 injections in a 12 hour period. The LC-MS-MS assay has subsequently been validated in rat, dog and human plasma, showing only limited bias (≤10%) and excellant precision (<10% expressed as pertentage CV) for both inter and intra-assay determinations (Fig. 7). With only minor modifications to the methodology (inclusion of a concentration step, an injection volume of 50 µL and decreasing the mass resolution) the assay can be readily extended to low pg /mL levels should it be required (Fig. 8).

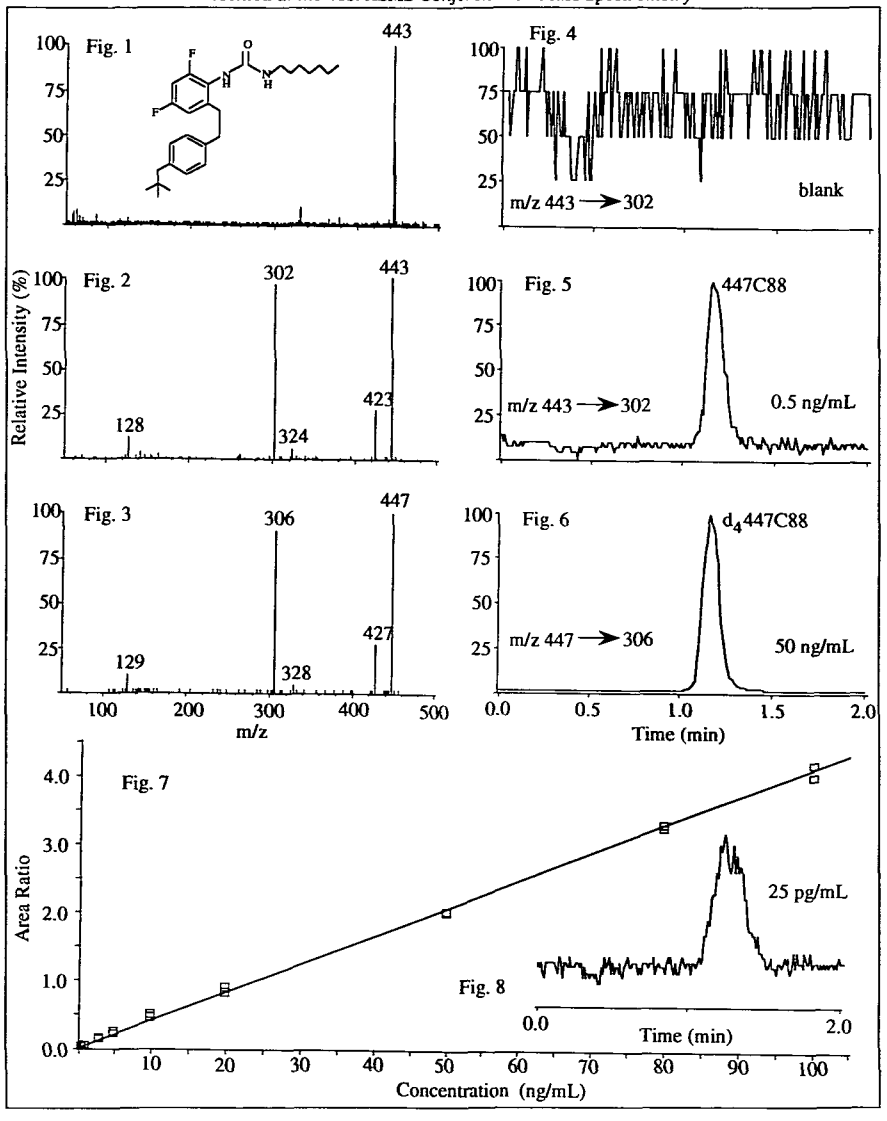

Photographic Studies of Electrospray Aerosols

Edward W. Sheehan* and Ross C. Willoughby
Millipore/Extrel Mass Spectrometry
575 Epsilon Dr., Pittsburgh, PA 15238

Introduction

There have been many models used to explain the electrospray process; including, the "Coulomb Explosion" mechanism by Dole and coworkers[1], and "Ion Evaporation from a Liquid" mechanism proposed by Iribarne and Thomson[2].

The current studies are intended to propose and analyze a more comprehensive model for the physical behavior of electrospray LC/MS. Electrospray has demonstrated unique ability to generate ions of species heretofore thought involatile. We have proposed a three stage process of primary, secondary, and tertiary particle generation. The complete model is addressed in this poster and on poster by Willoughby and coworkers.

The objectives of the present work was to propose a model to explain "Secondary Droplet Production" and "Ion Production" from an aerosol of highly charged droplets based on photographic evidence.

Secondary Aerosol Generation (Figure 1.)

Secondary droplet generation is driven by the (1) evaporation of the primary charged droplet (Maxwell Diffusion), (2) formation of a Taylor Cone, (3) reaching the Rayleigh Limit, (3) forming a jet, and (4) then disruption of the cylindrical jet to form secondary droplets.

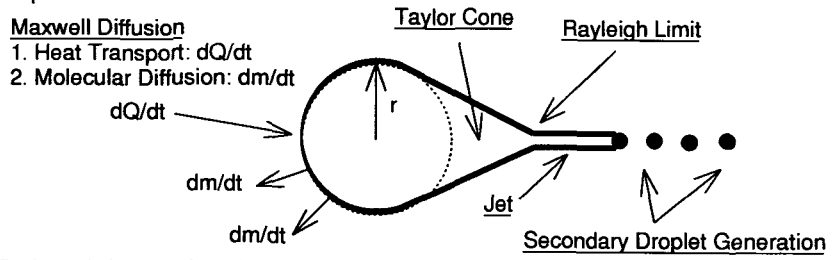

Drying of the droplet with a counter current of dry gas: (controlled by molecular diffusion, dm/dt)
Drying of the droplet with externally added heat: (controlled by heat)

Figure 1. Secondary Aerosol Formation from a Primary Droplet.

1. Dole et al, J. Chem. Phys.(1968),49, p. 2240.
2. Thomson and Iribarne, Reviews of Geophysics and Space Physics (1978), 16, p. 431.

The droplets continue this "cascade" of reaching the Rayleigh instability and generating smaller and smaller droplets till the droplet reaches the Ion Limit. Once the droplet has reached the ion limit, the energy required for evaporation of an ion is considerably larger then the energy needed for ion desorption.

Ion Formation (Figure 2.)

Ion formation is driven by the (1) evaporation of the secondary droplet (Gibbs-Kelvin effect), (2) formation of a Taylor Cone, (3) and reaching the Ion Limit.

Gibbs-Kelvin effect: rate of evaporation (dm/dt) changes from r^2 to r^3 relationship due to curvature.

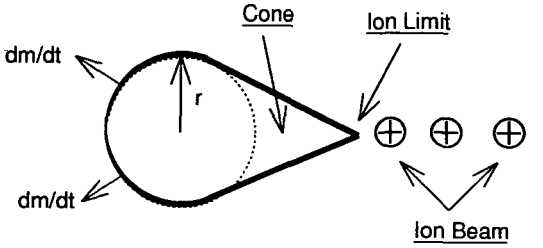

Figure 2. Ion Formation.

Conclusions

1. Secondary Aerosol Generation results from similar processes that occur in the Primary Aerosol Generation from the needle; a cone forms on a sherical droplet which accelerates the liquid to the Rayleigh Limit and a liquid jet emerges breaking into secondary droplets.

2. Secondary Aerosol Generation is initiated by evaporation of Primary droplets. Evaporation is augmented by increasing p_{0S} with heat or decreasing p_{∞} by adding dry gas.

3. Electron micrographic evidence shows significant residue from Primary and Secondary droplet products; thus not all analyte goes into the vapor phase.

4. The size and shape of residue particles supports the "Teardrop" model for ion production.

DOMINANCE OF SOLVENT DIELECTRIC CONSTANT IN DETERMINING ANALYTE CHARGE STATE IN NEGATIVE ION ELECTROSPRAY MASS SPECTROMETRY

Richard B. Cole* and A. Kamel Harrata

Department of Chemistry, University of New Orleans, Lakefront Campus, New Orleans, LA 70148

The choice of solvent has been shown to exert a profound influence on the distribution of charge states in negative ion electrospray mass spectrometry (ESMS) [1]. Conceivably, many solvent characteristics could influence, to varying degrees, the preferred charge states appearing in the ES mass spectrum. Attributing observed electrospray mass spectral characteristics to individual solvent parameters, of course, is complicated by the inability to independently vary a single solvent parameter without simultaneously altering others. Competing forces arising from different solution properties can alter the appearance of the mass spectrum in subtle or conspicuous manners. Certain solvent characteristics, such as specific conductance, surface tension, and viscosity, which are known to influence electrospray performance in a variety of ways, exhibited no obvious correlation to the observed charge state distributions. Rather, experiments point to the dominance of solution polarity in determining the preferred ESMS charge state.

This study has investigated the influence that a series of solvents, having decreasing dielectric constants and increasing solvent basicities, gas-phase basicities and proton affinities, exerts on analyte charge state. Shown in Fig. 1 is the ratio of the abundances of doubly charged/singly charged ions of diphosphoryl lipid A from *Escherichia coli* (✚, 34 °C) and 'cardiolipin' (•, 34 °C) dissolved in various solvents ranked in order of decreasing dielectric constant as given by ε(T °C) [2]. The order of decreasing dielectric constant is also the order of increasing proton affinities and gas-phase basicities, with 2-propanol and 1-butanol (proton affinities and gas-phase basicities virtually equal) exhibiting the only anomaly to this latter ranking. Solution-phase basicities have also been measured [3,4] indicating an order of basicity: methanol < ethanol < 2-propanol which parallels the gas-phase basicity data. A clear trend displaying a decreased tendency toward formation of ions of higher charge state from solvents having low dielectric constants is evident. The fact that the gas-phase basicity and the proton affinity of the solvents are increasing from left to right (except for 1-butanol < 2-propanol) serves to indicate clearly that gas-phase factors are minor, perhaps negligible contributors to the removal of cations from analyte molecules. In other words, even though 2-propanol and 1-butanol have the highest affinity for protons in the gas phase, they exhibited the weakest ability to remove the second proton from diphosphoryl lipid A. Significantly, the importance of solution-phase basicity in determining the predominant charge state is also diminished. In examining methanol, ethanol, and 2-propanol, the higher charge state became less prominent for solutions of increasing basicity, indicating that more highly basic solutions were less effective at removing the second proton from diphosphoryl lipid A.

Evidence suggests that the solution dielectric is the dominant characteristic which dictates the charge state of the two investigated analytes subjected to negative ion electrospray mass spectrometry. For both chlorinated and non-chlorinated organic solvents, the higher the solution dielectric constant, the more the charge state distribution is shifted toward higher charge states. Solvents with high basicities (gas-phase and solution-phase) and high proton affinities, yet low dielectric constants, favor lower charge states in ESMS spectra of lipid A and cardiolipin from *E. coli*. This indicates that gas-phase processes and solvent basicity contribute much less toward ion formation than solution phase solvation via preferred orientation of the solvent dipole. Ionization of these analytes must then be occurring in solution, prior to entering the gas phase. These observations build upon the "electrophoretic" mechanism of droplet charging [5-7]. Solvents with high solution dielectric constants are considered to be most effective at stabilizing multiply charged ions (where charge separation is greatest), and they are likely to increase the level of droplet charging.

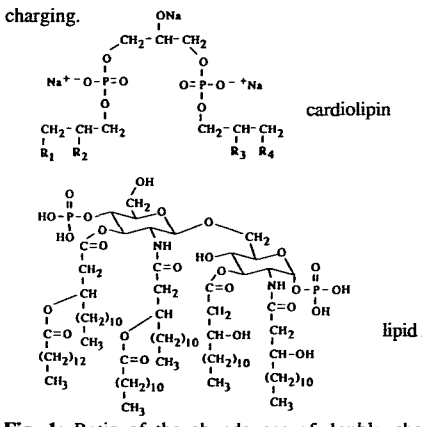

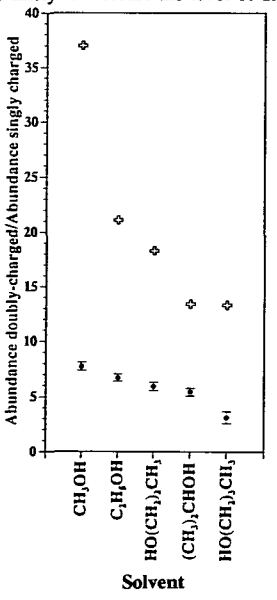

Fig. 1: Ratio of the abundances of doubly charged/singly charged ions of diphosphoryl lipid A from *E. coli* (✚, 34 °C) and 'cardiolipin' (•, 34 °C) dissolved in 10% chloroform and 90% of: methanol ε(34)=30.9; ethanol ε(34)=23.0; 1-propanol ε(34)=18.9; 2-propanol ε(34)=17.2; and 1-butanol ε(34)=16.0. Solvents are listed in order of decreasing dielectric constant [2].

1. Cole, R. B.; Harrata, A.K., *Rapid Commun. Mass Spectrom.*, **1992**, *6*, 536-539.
2. Maryott, A. A.; Smith, E. R., *Table of Dielectric Constants of Pure Liquids*, **1951**, National Bureau of Standards Circular 514, U.S. Dept. of Commerce, U.S. Govt. Printing Office, Washington, D.C.
3. Kolthoff, I. M.; Bruckenstein S., *J. Am. Chem. Soc.*, **1956**, *78*, 1-9.
4. Lowry, T. H.; Richardson, K. S., *Mechanism and Theory In Organic Chemistry*, **1976**, Harper & Row, NY, p. 161.
5. Pfeifer, R. J.; Hendricks, C. D., *AIAA J.*, **1968**, *6*, 496-502.
6. Hayati, I.; Bailey, A. I.; Tadros, Th. F., *J. Colloid Interface Sci.*, **1987**, *117*, 205-230.
7. Ikonomou, M. G.; Blades, A. T.; Kebarle, P., *Anal. Chem.*, **1991**, *63*, 1989-1998.

Elemental Electrospray Mass Spectrometry

George R. Agnes and Gary Horlick
Department of Chemistry, University of Alberta
Edmonton, Alberta, Canada, T6G 2G2

An ideal elemental analysis technique for solution samples would provide both quantitative and qualitative information for all solution components. Solution components include anions and cations in elemental, molecular, and complexed forms. Elemental electrospray mass spectrometry (elemental ES-MS) is being developed with this goal in mind.

Three positive-ion modes have been developed and have been named for the type of information available from the mass spectrum; ion-cluster, metal-ion, and ion-counter-ion mode. The electrospray source operational parameters for positive and negative ion elemental ES-MS are listed in Table 1. The two most critical parameters to control are the sampling plate voltage and the curtain gas flow rate.

	Positive Ion			Negative Ion
	Ion-Cluster	Metal-Ion	Ion-Counter-ion	
ES Tip (kV)	3.5	5.0	5.0	-3.0
Front Plate (V)	700	950	950	-950
Sampling Plate (V)	35	190	190	-80
Skimmer (V)	5	5	5	-5
Curtain Gas Flow Rate (l/min.)	0.3	0.4	0.2	0.4

Table 1. Operational Parameters of the Elemental Electrospray Source.

The process of electrospray generates gas phase metal ion clusters directly from the liquid phase. Operation of the ES source under mild conditions will preserve the ion clusters. Figure 1a is a mass spectrum of a solution of manganese II chloride acquired with ion-cluster conditions. Probing of the solution phase environment for speciation purposes (oxidation state and associated ligands) is possible with the ion-cluster mode.

The metal-ion mode of operating the electrospray source causes the ion-clusters to be subjected to harsh conditions causing decomposition of the gas phase cluster. Figure 1b shows singly charged ions dominating the mass spectrum with few spectral interferences. In this respect, mass spectra obtained with the metal-ion mode of elemental ES-MS are similar in appearance to mass spectra obtained with ICP-MS. Molecular interferences, attributed to incomplete decomposition of the gas phase clusters, have been significantly reduced from that previously reported.[1]

The ion-counter-ion mode is depicted in Figure 1c where $MnCl(MeOH)_n^+$, n=0,1 clusters are detected. Ion-pairing of multiply charged metal ions with counter-ions present in the charged droplet reduces the solvation energy of the ion-counter-ion cluster. A reduction of the curtain gas flow rate decreases the rate of solvent evaporation from the charged droplets allowing more time for formation of the Ion-counter-ion clusters. The rate of ion evaporation from the charged droplets depends on the solvation energy of the desorbing cluster, hence the newly formed ion-counter-ion clusters experience a high rate of ion evaporation.

Negative-ion ES-MS permits direct investigation of solution anions. The halides and sulfur based anions have detection limits in the low ng/ml range. Utilization of both positive and negative ion Elemental ES-MS provides the researcher with a tool with which a complete ionic picture of a solution can be assembled. Positive ion (Figure 2a) and negative ion (Figure 2b) ES-MS was used to differentiate two chromium species. Vanadium and manganese species were similarly differentiated with elemental ES-MS.

Reference 1. George R. Agnes and Gary Horlick, Appl. Spectrosc., **46**(2), 401 (1992).

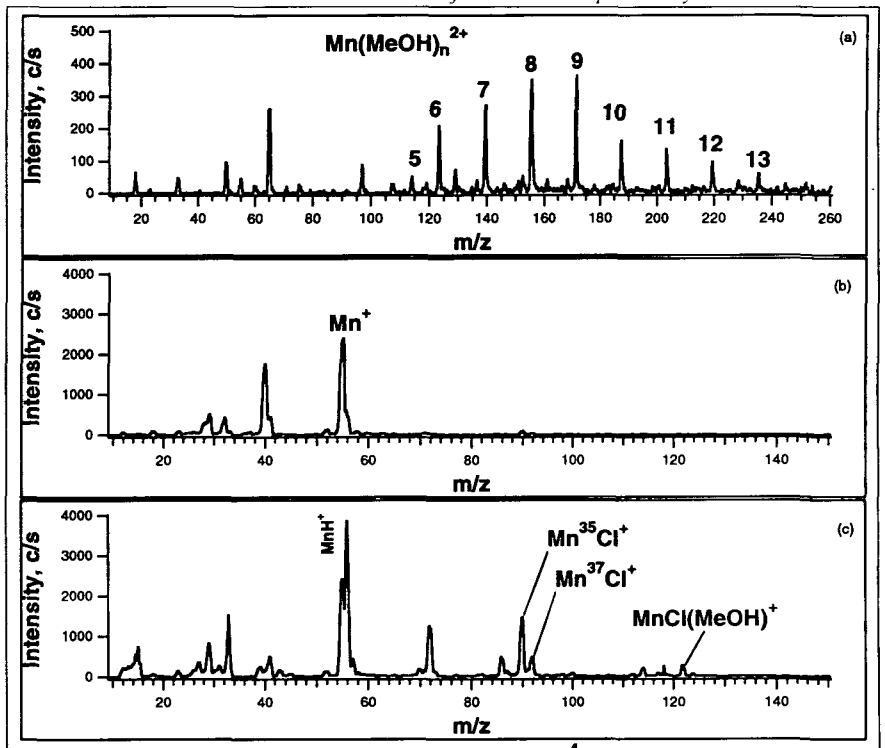

Figure 1. Manganese II Chloride at $1x10^{-4}$ M. a) Ion-Cluster, b) Metal-Ion, and c) Ion-Counter-ion Mode.

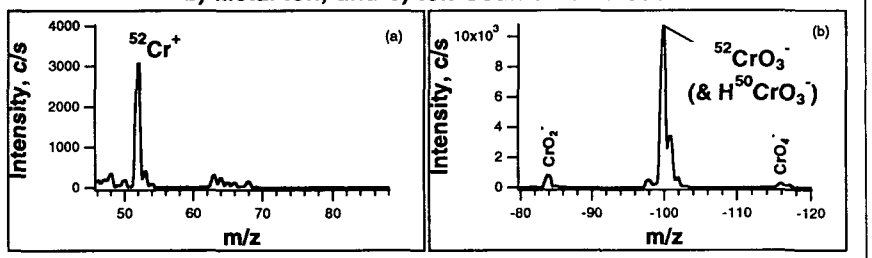

Figure 2. a) Chromium III Nitrate and b) Potassium Dichromate at $1x10^{-4}$ M.

Wavelength-Specific Resonance Enhanced Multiphoton Ionization for Isomer Discrimination via Fragmentation and Metastable Ion Analysis

Scott T. Fountain and David M. Lubman, Department of Chemistry
University of Michigan, Ann Arbor, MI 48109

Resonance-enhanced multiphoton ionization (REMPI) has been shown to be a highly sensitive and selective ionization technique when coupled with mass spectrometry. The spectroscopic dependence of the ionization process and the use of narrow-band tunable laser radiation allows selective ionization with little or no fragmentation. The molecular ion can then absorb additional photons via a ladder-switching mechanism thereby producing molecular fragmentation for structural analysis[1]. Since these fragments are often produced with a relatively narrow energy distribution above the ionization potential of the molecule, unique metastable ions are often observed. By analyzing the energy release associated with these metastable ions using a reflectron time-of-flight mass spectrometer, information on the fragmentation mechanism of the molecule can be obtained[2,3] If metastable ion decay is observed at the isomeric center of two isomers, molecular discrimination is possible[4].

Here it is shown that isomeric dipeptides containing leucine and isoleucine can be discriminated on the basis of their metastable ion decays in a reflectron time-of-flight mass spectrometer when using variable-wavelength REMPI. In particular it is shown that specific metastable ions are observed for the isomeric pairs Tyr-Leu/Tyr-Ile and Leu-Tyr/Ile-Tyr when using REMPI ionization at 266 nm and 193 nm respectively. By using variable reflectron voltages, two complementary spectra can be obtained showing stable ions (produced in the ion source) and lower-energy metastable ions (produced via decay in the drift tube). When a total reflectron voltage in excess of the ion extraction voltage is used, a complete ion spectrum is obtained which includes both stable ions and metastable ions. By decreasing the reflectron voltage to observe lower-energy metastable ions, the energy of these ions can be determined by observing the reflectron turning voltage necessary for ion reflection. Using this information, ion decay mechanisms can be obtained for the metastable transitions.

Figure 1 shows the 266 nm REMPI spectra of Tyr-Leu and Tyr-Ile. Both ions produce two metastable transitions from the molecular ion to give fragments at m/z 277 and m/z 188. However, the 266 nm REMPI spectra of Tyr-Leu contains an additional metastable transition not observed in the isomer which may result from further decay of the m/z 277 product (see Scheme 1). However, the 193 nm REMPI spectra of Tyr-Leu and Tyr-Ile are very similar and neither the stable nor metastable ion spectra show metastable fragmentation allowing isomeric discrimination. The most efficient REMPI wavelength for production of unique metastable ion decays was found to be dependent on the small changes in molecular structure. Figure 2 shows the 193 nm REMPI spectra of Leu-Tyr and Ile-Tyr. Here the 193 nm REMPI spectra provides unique metastable fragmentation allowing discrimination of the two isomers. Both Leu-Tyr and Ile-Tyr show metastable ion transitions from m/z 86 to m/z 30 An additional metastable ion is observed in Ile-Tyr due to rearrangement of the Ile -R functional group (see Scheme 2) thereby allowing isomeric discrimination. The 266 nm REMPI spectra of Leu-Tyr and Ile-Tyr were very similar and neither the stable nor metastable ion spectra allowed discrimination. The correct choice of REMPI wavelength appears to be crucial in optimizing the production of unique metastable ion transitions in such isomeric systems.[5]

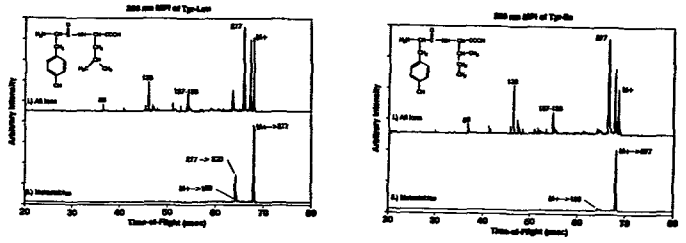

Figure 1: 266 nm REMPI spectra of Tyr-Leu and Tyr-Ile. Metastable ions are shown in bottom spectrum of each figure.

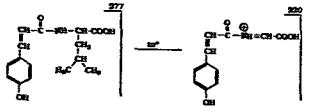

Scheme 1: Proposed metastable fragmentation mechanism for m/z 277 Tyr-Leu fragment using 266 nm REMPI.

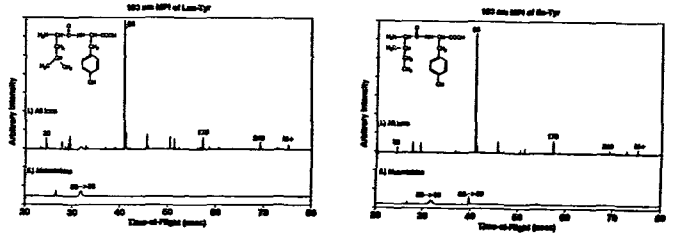

Figure 2: 193 nm REMPI spectra of Leu-Tyr and Ile-Tyr. Metastable ions are shown in bottom spectrum of each figure.

Scheme 2: Proposed metastable fragmentation mechanisms for a) both Leu-Tyr and Ile-Tyr and b) Ile-Tyr using 193 nm REMPI.

[1]Boesl, U.; Neusser, H.J.; Schlag, E.W. *J. Chem. Phys.* **1980**, *72*, 4327.
[2]Boesl, U.; Neusser, H.J.; Weinkauf, R.; Schlag, E.W. *J. Phys. Chem.* **1982**, *86*, 4857.
[3]Brunelle, A.; Della-Negra, S.; Depauw, J.; Joret, H.; LeBeyec, Y. *Rapid Commun. Mass Spectrom.* **1991**, *5*, 40. [4]Segar, K.R.; Johnston, M.V. *Org. Mass Spectrom.* **1989**, *24*, 176.
[5]Fountain, S.T.; Lubman, D.M. *Anal. Chem.*, **1993**, *65*, 1257-1266.

Application of PSD-MALDI to the Localization of Modification Sites in Peptides

Bernhard Spengler, Raimund Kaufmann,
Inst. of Laser Medicine, University of Düsseldorf, Moorenstr. 5, D-4000 Düsseldorf, Germany
Matthias Mann,
European Molecular Biology Laboratory, Meyerhofstr. 1, D-6900 Heidelberg, Germany

A new technique for peptide sequencing and structure analysis, called PSD-MALDI (postsource decay - matrix assisted laser desorption ionization), has recently been developed[1,2,3], taking advantage of the versatility, high sensitivity, short analysis times and low cost typical of time-of-flight instrumentation coupled with the laser/matrix technique. The method is based on mass spectrometrical analysis of daughter ions formed by unimolecular and/or collision induced decay in the first field free drift region of a two-stage grid-reflectron time-of-flight mass spectrometer. The performance of the method has been evaluated for known peptides and has been found to be, in some features, superior to other methods of peptide sequencing. Peptides up to ≈3000u could be sequenced at good spectra quality and with high reliability. Full sequence information of Substance P could be obtained even from single shot spectra (consumed sample amount ≈ 400 attomol).

The method has been applied to localize modification sites of phospho- and lipopeptides of known amino acid sequence Determination of such modifications is an important task in protein and peptide chemistry, and is difficult to achieve with conventional biochemical techniques. Using PSD-MALDI, modifications could be localized unequivocally in all cases.

Figure 1, as an example, shows the PSD-MALDI spectrum of a lipopeptide (15 amino acids) with the most intense peaks labelled. The amino acid sequence was known for this peptide. The position and nature of the fatty acid, however, was unknown. From the parent ion mass the fatty acid has been identified as myristic acid (or an isomer with m=228.4 u) assuming an amide or ester linkage. In the low mass region fragment ions characteristic for the different amino acids appear (immonium ions and smaller fragments). All signals at higher mass correspond to either N-terminal ions containing the fatty acid or C-terminal ions not containing the fatty acid. The smallest ion containing the fatty acid is the b_1 fragment. Since the N-terminal amino acid is glycine, the fatty acid can thus only be located at the terminal amino group forming an amide.

---

[1] B. Spengler, D. Kirsch, R. Kaufmann, E. Jaeger, *Rapid Commun. in Mass Spectrom.* **6** (1992), 105-108.
[2] B. Spengler, D. Kirsch, R. Kaufmann, *Rapid Comm. in Mass Spec.* **5** (1991), 198-202.
[3] B. Spengler, D. Kirsch, R. Kaufmann, *J. Phys. Chem.*, **96** (1992), 9678-9684.

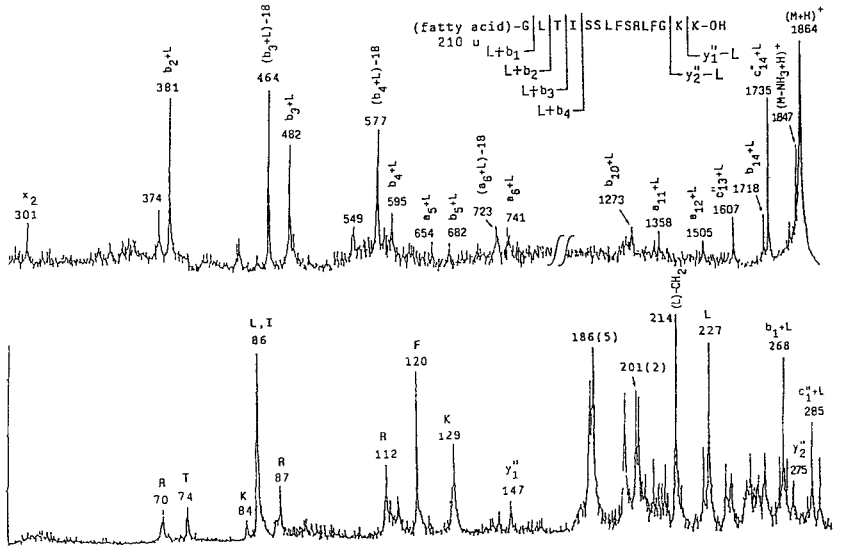

Figure 1 PSD-MALDI spectrum of a lipopeptide Position and nature of the fatty acid have been identified from the fragmentation pattern

Similar to the above example the modification site of a phosphorylated peptide has been identified (Figure 2) N-terminal ions b_2 to b_5 have been observed as unmodified peptide fragments. Larger ions b_6 to b_9 have been found to contain a phosphoryl group (+80 u). Correspondingly C-terminal ions y''_2 to y''_5 appeared as unmodified peptide fragments while larger ions y''_6 to y''_9 were modified by a phosporyl group. From these data the location of the phosphate group could be identified as the tyrosine molecule.

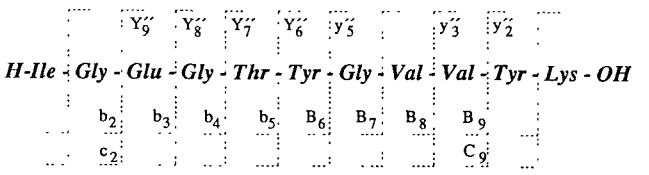

Figure 2 Fragmentation pattern of a phosphorylated peptide Upper case letters indicate fragment ions containing the phosphoryl group. Lower case letters indicate ions of unmodified fractions.

AN EVALUATION OF CRYSTALLIZATION METHODS FOR MATRIX-ASSISTED, LASER DESORPTION / IONIZATION OF PROTEINS

Scot R. Weinberger, Linear Scientific Inc, Reno, NV, USA, 89523

K. O. Boernsen, Ciba-Geigy Ltd., Basel Switzerland

Jeffrey W. Finchy, Vernon Robertson, Brian D. Musselman, JEOL USA Inc., Peabody MA, USA, 01960

The efficiency of MALDI has been shown to be dependent on a number of factors including laser intensity, matrix material, and sample preparation. The dynamics involved in routine formation of homogeneous matrix-analyte co-crystals have been poorly established. This work endeavors to demonstrate the co-crystalization efficiencies of static air dried, heat dried, and vacuum dried sample preparation methods using sinapinic acid and peptide mixtures Sample-matrix co-crystals will be examined for homogeneity using scanning electron microscopy. Additionally, each method will be contrasted in terms of minimal laser desorption fluence, average initial desorption velocity, resultant resolution, and ease of signal production.

Methods and Materials

Sample-matrix co-crystals were formed by mixing equal volumes of 100 mM Sinapinic Acid solutions (*Linear Scientific, MALDI-Grade*) with a 5 uM, peptide mixture of oxytocin, arg-8-vasopressin, angiotensin I, somatostatin, chicken atrial natriuretic peptide, human r-insulin, and r-hirudin (*Linear Scientific Peptide Standard*). One microliter aliquots of this mixture were deposited upon gold-plated probes and allowed to crystalize using static air, 100 watt heat lamp, and vacuum (10^{-2} torr) drying conditions. Resolution and ease of signal production studies were performed using a *Linear Scientific LDI-700 XP* automated MALDI-TOFMS fitted with a nitrogen laser (337 nm). All MALDI-TOFMS analyses were automatically performed by adding successive scans (each scan limited to a 3 - 10 signal to noise window using between one to five microjoules of laser energy) until a 70:1 total signal to noise ratio was achieved for r-insulin. The total number of shots required to produce this signal was taken to be inversely proportional to the ease of signal production. Resolution was calculated as flight time / 2 (half height width time). Minimal laser desorption fluence and initial desorption velocity studies were performed using a Linear Scientific LDI-1700 MALDI-TOFMS fitted with a nitrogen laser (337 nm). Minimum laser desorption fluence was defined as that laser energy of which a five percent decrease resulted in no ion signal. Minimum desorption velocities were extrapolated from a function derived by measuring insulin flight velocities at kinetic energies ranging from 10 to 30 KeV. Scanning electron micrographs were taken using a JEOL JSM 6300 scanning electron microscope.

Results

The average time required for matrix-sample co-crystallization for air, heat, and vacuum drying methods was: 2.66 (+/- 0.04), 1.33 (+/- 0.085), and 0.086 (+/- 0.0025) minutes,

respectively. The average minimal laser fluence required for desorption of air, heat, and vacuum dried sinapinic acid-insulin co-crystals was: 2.99, 2.80, and 2.84 mJ/cm^2, respectively. The average initial desorption velocities of air, heat, and vacuum dried sinapinic acid-insulin co-crystals was 537, 520, and 484 m/sec, respectively. The average resolution of air, heat, and vacuum dried sinapinc acid-insulin co-crystal TOF signals was: 300 (+/- 20.5), 280 (+/- 28.5), and 398 (+/- 19 5), respectively. The average number of laser shots required to create a 70:1 s/n mass-spectrogram of r-insulin for air, heat, and vacuum crystallization schemes was 406 (+/- 85), 485 (+/- 142), and 190 (+/- 50), respectively.

Scanning electron microscopic studies revealed: (1) Heat and air dried co-crystals were hollow hexagonal prisms with average lengths exceeding 100 microns. Vacuum dried co-crystals were irregular shaped, flat sheets with average lengths of 10-40 microns. Heat and air dried co-crystals were circumferentially distributed about the outer probe surface while vacuum dried co-crystals were seen evenly distributed throughout. Heat and air dried co-crystals exhibited a predominance of interco-crystalline voids where vacuum dried co-crystals did not. Heat and air dried co-crystals were observed in various positions upon the probe tip while vaccum induced co-crystals exhibited a smaller variation in their positioning.

Conclusions

It appears that the vacuum crystallization method is 20 - 30 times faster than either air or heat drying methods. Additionally, vacuum crystalized samples required fewer laser shots to create a 70:1 s/n spectra. The latter is postulated to be due to: (1) the overall regular distribution of vacuum-induced co-crystals upon the probe surface; (2) the absence of significant interco-crystalline voids; and (3) the smaller size and geometric pattern of vacuum created co-crystals, making them more easily transluminated by a given incident laser spot. The decreased time period required for sample preparation and signal production results in an overall increase in analytical sample throughput for vacuum induced co-crystalization schemes when compared to those of air and heat.

Vacuum formed sinapinic acid-insulin co-crystals yielded superior resolution for time of flight signals. Because the differences in flight tube pressure, average minimal desorption laser fluence, and average initial desorption velocities between air, heat, and vacuum co-crystalization schemes can not account for these resolution results, we believe the superior resolution of the vacuum co-crystallization scheme to be due to: the lower number of individual scans required to create a given signal; and a postulated narrowed distribution of initial desorption velocities due to the greater regularity of vaccum co-crystal arrangements in space.

Suppression of Metastable Interference in MALDI Spectra Obtained with a Reflecting Time-of-Flight Mass Spectrometer

W Ens, V Spicer, K G Standing and J Zhou
Dept. of Physics, University of Manitoba, Winnipeg, Canada R3T 2N2

The time-of-flight spectra obtained by matrix-assisted laser desorption are often characterized by rather poor mass resolution. In a linear time-of-flight spectrometer, the resolution is usually limited by the initial energy spread caused by the desorption and extraction processes [1 - 3]. Such energy spreads can be largely compensated with an electrostatic ion mirror illustrated in Fig. 1. However, fragmentation of the ions by the loss of small neutral daughters in the field-free region before the mirror causes increased complexity in the spectrum for smaller molecules and peak broadening for larger species (>~ 15 000 u).

We have developed a method to suppress the daughter ion contribution by increasing the acceleration voltage on alternate laser shots so that only daughter ions are reflected. That is, the mirror rejects parent ions on the basis of their higher energy. Two spectra are recorded in this way: the normal spectrum produced by parent and daughter ions, and a daughter-only spectrum. A spectrum of parent ions alone may be obtained by taking the difference. Fig. 2 illustrates the principle of the method. The top panel shows the molecular ion region of the reflected spectrum of bovine insulin. The smaller peak results from a daughter ion formed in the field-free region before the mirror by the loss of a neutral fragment of mass 17 u. The middle spectrum is the sum of transients recorded on alternate laser shots when when the acceleration voltage is increased so that the parent ion is not reflected. The bottom spectrum is the difference spectrum indicating the suppression of the metastable peak.

Fig. 3 shows an example of the method applied to mixture of myoglobin and insulin. The figure shows a linear time-of-flight spectrum, a normal reflected spectrum and the difference spectrum obtained when the daughter ion spectrum is subtracted from the reflected spectrum. The difference spectrum illustrates that much of the background observed in reflected spectra is due to metastable decay, and that much of the metastable broadening observed for larger molecular ions can be suppressed even though the daughter ion peaks are not resolved in time. The resulting mass resolution (FWHM) on the myoglobin molecular ion after subtraction is about 1000.

In order for the energy selection described above to be effective, the parent and daughter ions must have well-defined energy distributions. Since the energy distributions vary considerably from shot to shot, being broader for shots that produce more intense molecular ion signals [3], it is necessary to select shots with approximately the same intensity, preferably rather small. As a result several hundred laser shots are normally required to obtain a good difference spectrum, and each transient must be examined by the computer. To minimize acquisition time, a fast SCSI interface to a CAMAC controller has been configured with a LeCroy TR8828D transient recorder. This arrangement is able to select and accumulate 10 kB transients at a repetition rate of about 10 Hz.

1. R C Beavis and B T Chait, Chem. Phys. Letters 181 (1991) 479.
2. A Verentchikov, W Ens, J Martens and K G Standing, 40th ASMS, Washington DC (1992) p. 360.
3. J Zhou, W Ens, K G Standing and A Verentchikov, Rapid Commun. Mass Spectrom. 6 (1992) 671.

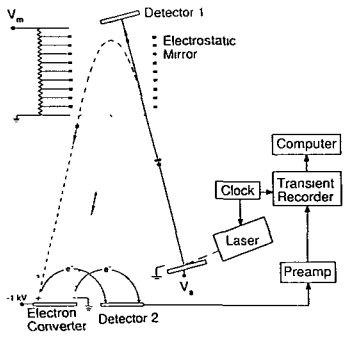

Figure 1 Schematic diagram of the reflecting time-of-flight mass spectrometer

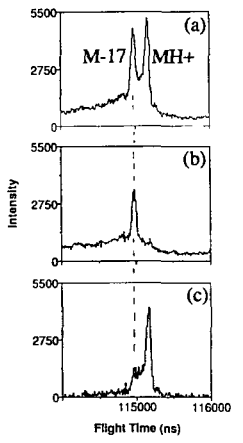

Figure 2 Molecular ion region of the reflected MALDI spectrum of insulin: (a) normal, (b) daughter only with elevated accelerated voltage, and (c) difference.

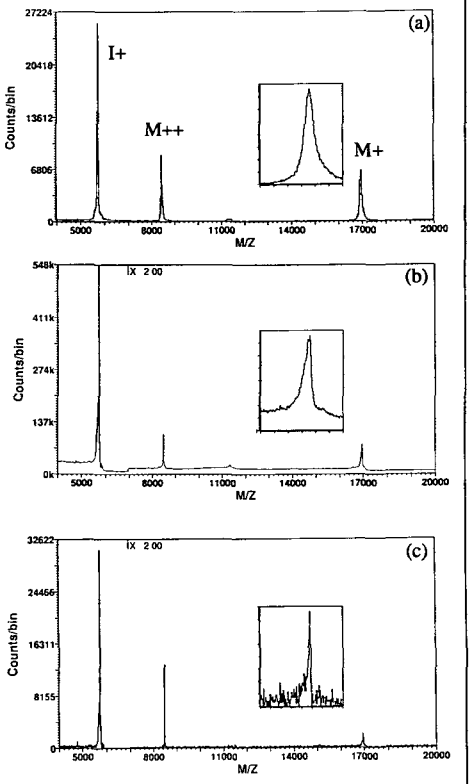

Figure 3 MALDI spectra of a mixture of myoglobin (M+ and M++) and insulin (I+): (a) linear TOF, (b) reflecting TOF, and (c) after subtraction of metastables. The insets are an expansion of the singly charged molecular ion of myoglobin.

HEAT LOAD ON GUEST MOLECULES IN MATRIX-ASSISTED LASER DESORPTION

A. Vertes
Department of Chemistry, The George Washington University
Washington, DC 20052

In a continuing effort to understand the underlying mechanism of matrix-assisted laser desorption (MALD) we investigated the thermal load on "probe" molecules embedded in the matrix. A probe molecule experiences two different environments during the desorption process. The first phase is the period when the molecule is still fixed near to the surface of the matrix. As the laser pulse heats the surface the probe molecule is subjected to energy exchange with matrix molecules. As soon as the phase transition releases the probe molecule its environment changes into an expanding and rapidly cooling plume. Matrix plume temperatures, T_M, can drop to around 100 K in 100 ns [1]. It is the net effect of the first heating and the second cooling phase that determines the internal temperature of probe molecules, T_P.

Heating phase ($T_M > T_P$)

Hydrodynamic calculations of surface heating, plume formation, and expansion were carried out [1] on sinapinic acid, ferulic acid, and nicotinic acid commonly used for MALD in the ultraviolet spectral region. Short transient surface heating was observed followed by expansion cooling of the generated plume.

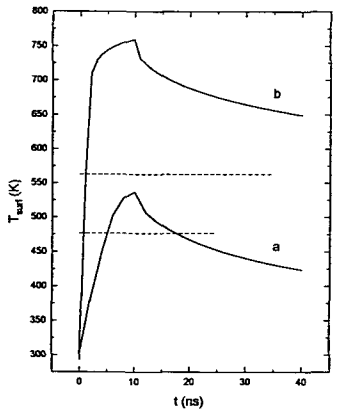

Figure 1 *shows the effect of a 1 MW/cm², 10 ns, 308 nm laser pulse on the surface temperature of sinapinic acid (a). The sublimation temperature of sinapinic acid (477 K) is marked by the dashed vertical line. Superheating of the surface (present for about 12 ns) leads to strong evaporation and plume formation. Irradiation of the sodium salt of sinapinic acid (10 MW/cm², 10 ns, 308 nm) leads to much higher surface temperatures (b) and possibly thermal decomposition.*

Probe molecule temperatures can be lower than the matrix temperature if the probe molecules absorb the laser light less efficiently. The energy exchange between matrix and probe molecules in the solid phase has been discussed earlier [2]. The driving force of the energy exchange is the difference between matrix, and probe molecule temperatures:

$$\frac{c_{p,P}}{V_{M,P}}\frac{dT_P}{dt}=\alpha_s\left(\frac{c_{p,M}}{V_{M,M}}T_M-\frac{c_{p,P}}{V_{M,P}}T_P\right) \qquad (1)$$

where c_p, and V_M denote the specific heat, and the molar volume of the matrix and the probe

molecule indexed by M, and P, respectively. The solid phase energy exchange coefficient, α_s, can be evaluated using the exponential energy gap approximation [2]. The heating phase for a given probe molecule ends when the matrix evaporation entrains it into the gas phase. During the superheated period explosive phase transition also may occur. In this regime the explosive phase transition cuts short the time available for the heating phase.

Cooling phase ($T_M < T_P$)

The cooling phase for a probe molecule starts with entering the gas phase. We assume that the typical probe molecule travels with the maximum density portion of the matrix plume.

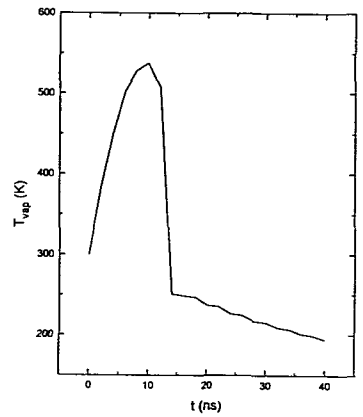

Figure 2 *shows the sinapinic acid plume temperature, T_{vap}, at the maximum of the plume density distribution (laser pulse: 1 MW/cm², 10 ns, 308 nm). During the laser pulse hot matrix material enters the plume. Expansion takes over at the end of the pulse and rapidly cools the plume below room temperature.*

Energy exchange between matrix and probe molecules during the cooling phase also can be described using Eq. (1) by replacing the specific heat, the molar volume, and the energy exchange coefficient with their vapor phase values. The most significant difference stems from the density dependence of the vapor phase energy exchange coefficient, α_v.

The relative duration of the heating and cooling phase, the corresponding matrix temperatures and the energy transfer coefficients determine the net thermal load on the embedded and entrained probe molecules. Calculations on laser desorption with and without matrix indicated higher threshold irradiances for desorption and/or higher heat load on the desorbing molecules in the absence of matrix.

Depending on energy deposition and transfer rates the guest molecules may leave internally "cold," "warm" or even "hot." This coherent description can account for the lack of fragmentation in MALD and for metastable decay of guest molecular ions under certain circumstances.

Support:
This work was supported by the National Science Foundation (Grant CTS-9212389) and by the George Washington University Facilitating Fund.

References:

1. A. Vertes, R. Gijbels, In: Laser Ionization Mass Analysis, A. Vertes, R. Gijbels and F. Adams (eds), Wiley & Sons, New York, **1993**, pp. 127-175.
2. A. Vertes, R. Gijbels, R.D. Levine, Rapid Commun. Mass Spectrom., 4 (1990) 228-233.

Measurement of Neutral Velocities in the Matrix-Assisted Laser Desorption Experiment

Richard C. King & Kevin G. Owens*, Department of Chemistry, Drexel University, Philadelphia, PA 19104

The formation of a molecular beam in the matrix - assisted laser desorption / ionization experiment has been suggested to explain the formation of intact molecular ions with initial velocities of 750 m/sec.[1,2] If a molecular beam is formed, it should have properties similar to molecular beams formed by expansion of a gas from a high pressure region through an orifice into a low pressure region. These systems have been studied extensively and are well characterized.[3] Supersonic molecular beams have several distinquishing properties, the most fundamental of which is that random thermal motion is converted into directed mass motion, causing the mean speed of molecules in the direction of the expansion to increase. The final velocity of the expansion depends on the mole fraction mass of the gas mixture expanding, the size of the orifice and the change in pressure or temperature which occurs during the expansion. Table 1 shows the final velocities of ideal gasses expanding from room temperature calculated for several different masses.

Predicted Flight Time Shifts from Calculated Initial Velocities (Vo) for 1000 volts Acceleration

Expansion Gas Mass (amu)	Vo (m/sec)	Δ TOF (nsec)
15	911	316
17	856	296
18	832	288
28	667	230
44	532	183
180	263	90
224	236	81

Table 1.

Measured Flight Time Shifts and Initial Velocities (Vo) for 1000 volts Acceleration

Delay (usec)	Vo (m/sec)	Δ TOF (nsec)
3.5	1116	309
3.75	1050	284
4	991	274
4.5	890	249
5	809	224
6	683	189
7	581	174
8	521	144
9	467	139
10	422	129
11	385	114
12	354	109
13	327	104
14	305	100
15	285	90
16	268	90
17	325	80
18	239	80
19	226	75
20	215	70
25	173	65
30	144	55
35	124	55

Table 3.

Measured Initial Velocities for Different Mass Analyte Molecules at 1000 volts Acceleration

Compound	Mass (amu)	Analyte Vo (m/sec)	Matrix Vo (m/sec)
Rhodamine B	442.52	566	723
Acridine Orange	265.36	462	741
Cinnamic Acid	148.16	580	759
Indole	117.15	521	723

Table 2.

In the experiments reported here, a post - ionization laser is used to ionize the neutral matrix / analyte released into the gas phase during the matrix assisted laser desorption experiment. Since

the ion time - of - flight depends on the initial velocity of the ion (Vo) as well as the ion mass to charge ratio, ions formed from neutrals having a gas phase thermal velocity distribution (mean Vo = 0) will have a longer flight time than ions formed from neutrals released during the MALD process (mean V0 > 0). Measurement of the flight time shift ($\Delta TOF = TOF_{Vo=0} - TOF_{Vo>0}$) gives a direct measure of the initial velocity of the neutral before post - ionization. Table 2 shows the velocities measured for neutral sinapinic acid molecules at several different delays 4.41 mm above the sample surface.

The large number of collisions that occur during the expansion cause a decrease in the distribution of molecular speeds along the direction of propagation. This velocity narrowing continues until the gas becomes rarified. The narrowness of the velocity distribution is observed in the time - of - flight spectrum as a narrowing in the ion peak width.

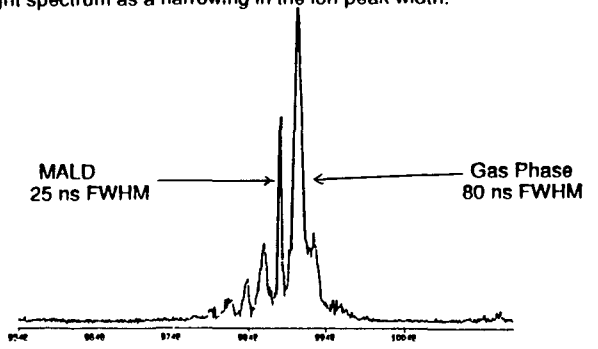

Figure 1 shows the two peaks due to the two different initial velocity distributions, gas phase (mean Vo = 0) and MALD (mean Vo > 0). The peak on the right is produced by ionization of gas phase triphenylene while the peak on the left is produced by post - ionization of neutral triphenylene released during MALD using a sinapinic acid matrix. The narrow velocity distribution of the desorbed neutrals accounts for the difference in width between the two peaks.

When a small amount of analyte is seeded in a large excess of expansion gas, the analyte molecules obtain the same velocity as the expansion gas due to the collision process. This is found to be true for analyte molecules of all masses. Table 3 shows the velocities of the sinapinic acid matrix and the analyte molecules of different masses measured by post - ionization of desorbed neutrals. The results show that the analyte molecules have the same velocity as the matrix neutrals for all masses tested.

Supersonic molecular beams are known to be highly directional. The angular distribution of material is found to approximate a cosine[3] distribution. Results of measuring the width of the released neutrals from MALD at several positions above the sample surface also approximates a higher order cosine distribution.

The measured properties of sinapinic acid matrix neutrals released during the MALD experiment are consistent with known properties of supersonic molecular beams. The values obtained for neutral velocities suggests that small neutral matrix fragments are created during the desorption event and that they are involved in the expansion.

References:

1. R. C. Beavis and B T. Chait, *Chem. Phys. Lett*, 181,1991, p479.
2. A. Vertes, R. Gijbels, R. D. Levine, *RCMS*, 4, 1990, p228.
3. "Atomic and Molecular Beam Methods Vol I", Ed. by G. Scoles, 1988.

LDMS OF PROTEINS AND PEPTIDES ABSORBED ON MEMBRANES

Martha M. Vestling and Catherine Fenselau
Department of Chemistry and Biochemistry
University of Maryland Baltimore County
Baltimore, MD 21228

Colin Moore and Malcolm Kimber
Kratos Analytical
Barton Dock Road, Urmston
Manchester M31 2LD, England

Although gel electrophoresis is probably the most widely used separation technique and the most widely used molecular weight determination technique for proteins, its mass accuracy compares poorly with modern mass spectrometry methods. Currently many labs electroblot proteins from gels to membranes (polyvinylidine difluoride (PVDF), nitrocellulose, and nylon) for further characterization especially by immunological methods. Proteins absorbed on PVDF can be inserted directly into microchemical (Edman) sequencers. Thus membranes are a well established way to handle very small amounts of proteins and a potentially useful way to bring them to mass spectrometry.

Figure 1 shows the "chromatogram" obtained using a Kratos Kompact MALDI III bench top matrix-assisted laser desorption mass spectrometer with a 337 nm nitrogen laser from a strip of PVDF on which cytochrome c had been spotted and then covered with the matrix α-cyano-4-hydroxycinnamic acid. The strip was scanned by firing two thousand laser shots across it. Every fifty shots were averaged. Two spectra from different locations on the PVDF are also shown. After LDMS, the strip was stained with Coomassie Blue confirming that the mass spectrometer could read the membrane to locate the protein (Figure 2).

Figure 3 shows the "chromatogram" (Figure 3a) and one spectrum (Figure 3b) obtained while scanning an electroblotted lane of a gel electrophoresis separation of a BNPS-skatole treated protein under study in our laboratory. This sample was digested with trypsin on the membrane, and the spectrum of a product obtained from the same position is shown in Figure 3c.

Further development is underway to scan electroblotted membranes and to provide molecular weights of proteins before and after digestion directly on membranes.

Figure 2
PVDF Stained with Coomassie Blue after LDMS

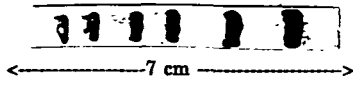

Figure 1

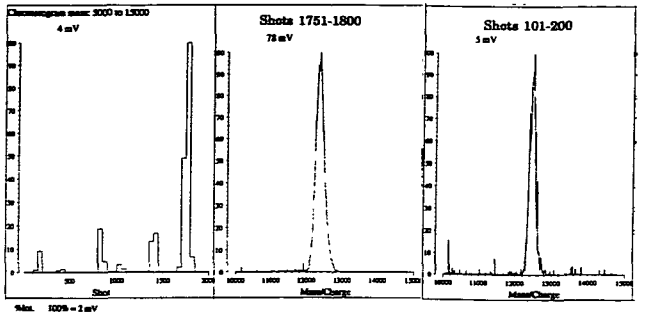

Figure 3a

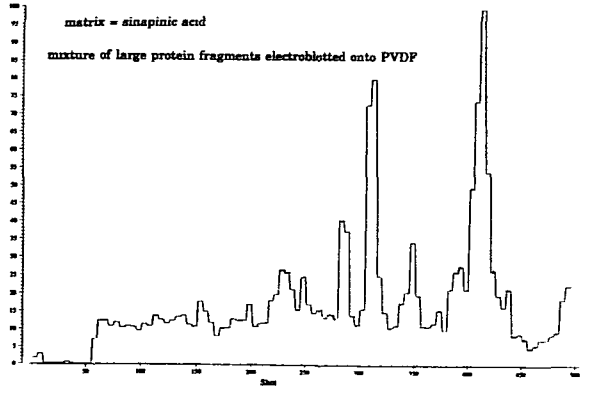

Figure 3b

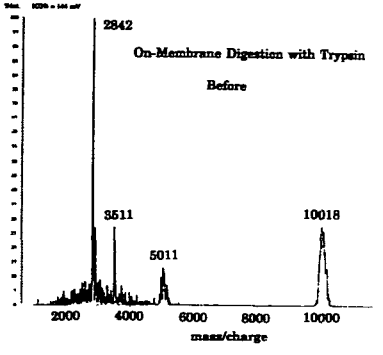

Figure 3c

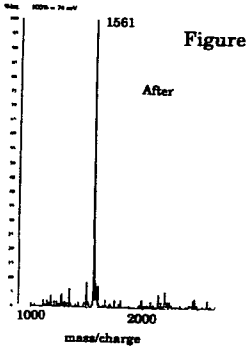

MATRIX ASSISTED LASER DESORPTION IONIZATION OF AEROSOLS

Kermit K. Murray and David H. Russell
Department of Chemistry, Texas A&M University, College Station, TX 77843

We have recently constructed an apparatus that allows continuous liquid aerosol introduction into a matrix assisted laser desorption ionization (MALDI) time of flight mass spectrometer (TOF-MS). The utility of such an apparatus is twofold. First, MALDI TOF-MS has the potential to be an excellent method for liquid chromatography (LC) detection. Second, aerosol MALDI provides a new perspective from which to view MALDI processes. Aerosol introduction provides a continuous and consistent flow of sample for ionization. Ionization occurs without the interference of a metal surface and without the reproducibility problems that often appear in conventional MALDI solid sample preparation.

A detailed description of the aerosol MALDI apparatus is given elsewhere.[1,2] Aerosols are formed by a pneumatic aerosol generator with a liquid flow rate of between 0.5 and 1.0 ml/min. Aerosols are passed through a heated drying tube to remove solvent before ionization. The aerosols are ionized by 355 nm photons from the frequency tripled output of a pulsed Nd·YAG laser focused with a cylindrical lens. Mass separation is achieved in a 1.1 m TOF-MS with extraction voltages of between 5 and 15 kV. Ions are detected with a microchannel plate particle multiplier and the signal is recorded with a digital oscilloscope.

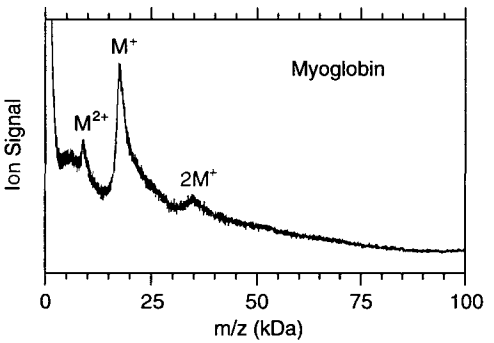

Figure 1. Aerosol MALDI mass spectrum of horse heart myoglobin with α-cyano-4-hydroxy-cinnamic acid matrix.

A number of biomolecules have been ionized by aerosol MALDI including erythromycin, bradykinin, gramicidin S, gramicidin D, vitamin B-12, melittin, bovine insulin, cytochrome C, lysozyme (chicken egg white), myoglobin (horse heart) and bovine albumin. We have had good results using the matrices 4-nitroaniline and α-cyano-4-hydroxy-cinnamic acid. Mass resolution of 125 has been observed for bradykinin (MW = 1060). Figure 1 shows a aerosol MALDI mass spectrum of myoglobin (horse heart, MW = 16,951) with α-cyano-4-hydroxy-cinnamic acid matrix. The aerosol solution contained 100 nmol of analyte and 10 μmol of matrix per mL of methanol solution acidified with 5 % trifluoroacetic acid (TFA). The extraction voltage was 10 kV and the laser irradiance was 160 MW/cm^2. The mass spectrum is the result of averaging over 1000 laser shots. The M^+ peak is the seen at approximately 17 kDa and the peak width corresponds to a mass resolution of 8. There are probably multiple peaks under the M^+ envelope corresponding to $[M+H]^+$, $[M+Na]^+$, $[M+Matrix]^+$ but these are not resolved. Peaks are seen for doubly ionized analyte M^{2+} and for the $2M^+$ cluster. The low mass portion of the spectrum is dominated by peaks corresponding to methanol clustered to H^+ and Fe^+.

The utility of aerosol MALDI with LC/MS was investigated for the separation of bovine insulin and gramicidin S. A 125 μl sample with 40 nmol bovine insulin and 200 nmol gramicidin S in water solution was injected onto a C_{18} column. The column effluent was mixed with a 10 μmol/mL solution of α-cyano-4-hydroxy-cinnamic acid in a TFA acidified methanol solution. Mass spectra were downloaded from the oscilloscope and saved to disk at 10 s intervals. A contour plot of the resulting mass spectra is shown in Figure 2. The x axis is the ion flight time and the y axis is the column retention time. The gray shading indicates the log of the ion signal with darker shades corresponding to larger signals. The individual mass spectra have been smoothed and the number of data points reduced for the purposes of the plot. At a retention time of 6 minutes the total ion signal increases as the first of the effluent comes off the column. Bovine insulin is seen at 10.5 minutes at a flight time of 103 μs. Note that at this time there is decrease in the total ion signal, particularly evident for low mass ions. The peak of the gramicidin S ion signal is seen at 18 minutes and a flight time of 43 μs. Leading and trailing edges of the gramicidin S peak are seen because separation conditions have not been optimized.

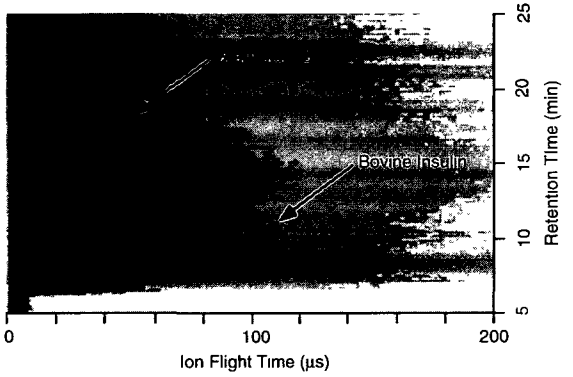

Figure 2. Liquid chromatography separation with MALDI-MS detection for bovine insulin and gramicidin S. Darker shades indicate greater ion signal.

We are currently working to improve the sensitivity, resolution, mass range, and data acquisition rate of the aerosol MALDI apparatus. The basic goal is to maximize the efficiency of aerosol delivery and desolvation while at the same time minimizing the gas load and pressure in the region of ion formation Maximizing data acquisition rate will require a high repetition rate ionization laser and high speed and high capacity data acquisition system. With these and other improvements, aerosol MALDI promises to be a useful method for LC/MS of large biopolymers.

The authors wish to thank T. M. Lewis for help with the LC/MS experiment.

1. K. K. Murray and D. H. Russell, in *Proceedings of the Second International Conference on Laser Ablation*, April 19-22, 1993, Knoxville, TN (in press).
2. K. K. Murray and D. H. Russell, *J. Am. Soc. Mass Spectrom* (submitted).

New desorption strategies for the mass spectrometric analysis of macromolecules

T. William Hutchens and Tai-Tung Yip

Protein Structure Laboratory, USDA/ARS Children's Nutrition Research Center, Department of Pediatrics, Baylor College of Medicine, 1100 Bates, Houston, TX 77030.

Summary

We present two new desorption strategies for the mass spectrometric analysis of macromolecules. These desorption strategies are based on the construction of two general classes of reactive probe surfaces specifically designed to enhance 1) the desorption of intact macromolecules without matrix (neat), and 2) the affinity capture of selected macromolecules directly from unfractionated biological fluids and extracts. Specific examples of Surface-Enhanced Neat Desorption (SEND) and Surface-Enhanced Affinity Capture (SEAC) laser desorption time-of-flight mass spectrometry are presented to illustrate the potential for increased sensitivity (fmol) and mass accuracy. Use of these new probe surfaces as solid phase reaction centers should facilitate protein discovery through molecular recognition *in situ* and also macromolecular structure analysis through the sequential chemical and/or enzymatic modification of the adsorbed analyte *in situ*. The availability of probe surfaces derivatized with or composed of multiple types and defined numbers of energy absorbing molecules should also facilitate investigations of energy transfer and desorption/ionization mechanisms.

Introduction

The ability to measure accurate *differences* in molecular mass enable problems associated with unknown protein structures to be solved more readily. Thus, the future of *biological* mass spectrometry will be defined by simpler and more sensitive means to monitor specific changes in protein and peptide mass.

The introduction of matrix molecules to assist the laser-induced desorption/ionization (MALDI) of intact macromolecules (particularly mixtures) has enabled small quantities (pmol) of large nonvolatile biopolymers to be evaluated by time-of-flight (TOF) mass spectrometry (1). Many new types of investigations have been enabled by this technology. Our laboratory has developed MALDI-TOF to explore various specific ligand-ligate interactions and to analyze protein structure (e.g., 2-9); both approaches have been based largely on biochemical reactions performed directly in situ to expoit the availability of analyte not consumed by previous laser-induced desorption events. However, the required presence of a large molar excess of acidic matrix and the random deposition of embedded macromolecular analytes in and around an undefined array of matrix crystals has limited the use of the probe surface as an effective stationary phase for sequential (i.e., differential) mass spectrometric approaches to the investigation of protein structure and function.

An effective mass spectrometric strategy for protein structure analysis may be realized if each of several diagnostic alterations in mass can be brought about as a result of controlled chemical and/or enzymatic modification events performed directly and sequentially in situ (i.e., directly on the probe surface). In fact, alterations in both covalent and noncovalent structures (including higher order macromolecular assemblies) may be evaluated more readily once 1) conditions are defined to minimize or eliminate the negative influence of matrix molecules, and 2) an active rather than passive means of protein deposition on the probe surface is developed. Our previous experience with the matrix-assisted desorption of peptides and proteins directly from electrophoretic gels and various membrane protein blots provided less than desirable results (e.g., low yield, low resolution). Thus, we have attempted

to advance protein structure and function analyses based on laser desorption TOF MS by redesigning probe surfaces to contain the necessary density of energy absorbing molecules so that the need for matrix can be eliminated.

We introduce here matrix-free methods of introducing large molecular weight biopolymers into the gas phase without fragmentation. We call this approach Surface-Enhanced Neat Desorption (SEND) time-of-flight mass spectrometry. To enhance our investigation of bioregulatory molecular recognition events, we have designed a second class of probe surfaces to be used as affinity capture devices to augment the detection of trace macromolecules present in unfractionated biological matrices, particularly *in vivo*. To distinguish this approach from other indirect strategies we suggest the term Surface-Enhanced Affinity Capture (SEAC) laser desorption time-of-flight mass spectrometry.

Results

We show that macromolecular analytes (proteins/peptides) can be desorbed efficiently from insulating surfaces like nylon, polystyrene, polypropylene, and glass by the normal MALDI process with no apparent fragmentation. Some differences in desorption selectivity were observed among the various surfaces tested

Surface-enhanced neat desorption (SEND) MS experiments performed with myoglobin showed a symmetrical peak with no evidence of matrix adduct, fragmentation, or low molecular weight ions other than those observed from buffer contamination. Other examples of SEND with 6 to 8 kDa synthetic protein surface domains as test analytes showed that cinnamamide was not effective as a matrix when used in the conventional way for MALDI-TOF. When cinnamamide was covalently bonded to the sample presenting surface, however, the resulting structure was transformed to enhance desorption of the peptides in a neat form with no apparent fragmentation and adduct formation.

Surface-enhanced affinity capture (SEAC) laser desorption time-of-flight mass spectrometry was used to detect low quantities (2.5 pmol) of lactoferrin extracted from the urine of a preterm infant. In contrast to the spectrum obtained for the unfractionated infant urine (no lactoferrin signal detected; the use of SEAC resulted in a clean, unambiguous, and significant signal of lactoferrin. The affinity capture and transfer to the probe surface is specific and efficient.

References

1. Karas, M. and Hillenkamp, F. (1988) Analytical Chemistry 60, 2299-2308.
2. Hutchens, T.W., Nelson, R.W. and Yip, T.-T. (1991) J. Mol. Recog. 4, 151-153.
3. Hutchens, T.W., Nelson, R.W., Allen, M.H., Li, C.M. and Yip, T.-T. (1992) Biol. Mass Spectrom. 21, 151-159.
4. Hutchens, T.W., Nelson, R.W. and Yip, T.-T. (1992) FEBS Lett. 296, 99-102.
5. Hutchens, T.W., Nelson, R.W., Li. C.M. and Yip, T.-T. (1992) J. Chromatogr. 604,125-132.
6. Yip, T.-T. and Hutchens, T.W. (1992) FEBS Lett. 308, 149-153.
7. Yip, T.-T. and Hutchens, T.W. (1993) Techniques in Prot. Chem. IV, 201-210.
8. Hutchens, T.W., Nelson, R.W. and Yip, T.-T. (1993) Techniques in Prot. Chem. IV, 210-212.
9. Hutchens, T.W. and Yip, T.-T. (1992) Methods: A Companion to Methods in Enzymology 5, 158-173.

REMPI AND MASS SPECTRA OF COLD PERFLUORINATED POLYETHERS

Deon S. Anex, Mattanjah S. de Vries, H. Russell Wendt, and Heinrich E. Hunziker

IBM Research Division, Almaden Research Center, 650 Harry Road, San Jose, CA 95120-6099.

Laser desorption has become an important tool for the study of complex molecules, making it possible to introduce non-volatile substances into the gas phase. It can be combined with entrainment of the desorbed material in a supersonic expansion to cool the molecular internal degrees of freedom. This enhances the selectivity and sensitivity of resonance-enhanced multiphoton ionization (REMPI), providing a versatile approach to forming ions for time-of-flight mass spectrometry. Unfortunately, many species do not have suitable intermediate states. The polymers that we are interested in, perfluorinated polyethers (PFPE's) of the poly(trimetheleneoxide) type, are such an example. However, if these polymers are substituted with a chromophore-containing end group, they can be ionized using REMPI. We have explored the use of a substituent chromophore as a tag in the substituted PFPE

$$\mathbf{R_a}\text{-}[OCF_2CF_2CF_2]_n\text{-}F \qquad \text{I}$$

where $\mathbf{R_a}$ is the aromatic end group: C_6H_5-O-CH_2CH_2-O-(C=O)-CF_2CF_2-, which absorbs near 274 nm. These polymers are available as Demnum SP® from Daikin Industries. We are interested in whether mass spectrometry through REMPI of a chromophore tag is useful for obtaining polymer length distributions and how the polymer may influence the absorption of the chromophore.

A beam of cold molecules was generated by laser-induced desorption in front of a pulsed jet orifice. The liquid samples were applied to activated charcoal and were desorbed using the 532 nm output from a pulsed YAG laser. A xenon pulse was timed to intercept the plume of desorbed material and entrain, cool and sweep it into the source region of a linear time-of-flight mass spectrometer. There the cold molecules were ionized by either an excimer laser at 193 nm or by a doubled dye laser tunable near 274 nm.

Mass spectra obtained at 193 nm extend to 7000 amu and are dominated by parent ions of the polymer. It is thus possible to determine the parent mass distributions of functionalized PFPE's using this method. Measured distributions resemble those determined with a cationization technique for a similar sample.[1] Minor peaks correspond to van der Waals dimers of **I**, as well as polymers that are substituted at both ends:

$$\mathbf{R_a}\text{-}[OCF2CF2CF2]_n\text{-}O\text{-}\mathbf{R_a} \qquad \text{II}$$

The sensitivity of this technique is sufficient for the measurement of REMPI wavelength spectra for the polymers ranging in size to 1778 amu (n=9), in a short chain length sample, by scanning the ionization wavelength in the vicinity of the electronic origin of the first excited electronic state and monitoring the ion signal at a particular mass to charge ratio. The spectra of **I** consist of a broad feature (about 70 cm^{-1} wide) peaking at 273.4 nm and do not vary with chain length for the measured range of n (5 through 9).

To better understand the polymer REMPI spectra, we studied a series of model compounds that show the evolution of the spectrum from the simplest molecule, phenol, representing the chromophore in the end group of the polymer, through intermediate model compounds representing portions of the polymer of increasing length, to the polymers themselves. The compounds that we used include phenol, anisole, phenoxyethanol, a series of phenoxyethyl esters of straight chain perfluorinated carboxylic acids, PFPE's with n=1 through 3 and having branched repeat units and the straight chain PFPE's themselves (**I**, with n=5 through 9). In this series, the total wavelength shift is about 200 cm^{-1}. The spectra show that this shift is essentially insensitive to structural changes more than six atoms removed from the chromophore. The spectral bandwidth also increases with chain length, due to the presence of multiple conformers and low frequency motions, up to about two repeat units, thereafter becoming independent of length. For the polyethers, no further change is seen in the spectrum for those containing three or more repeat units and no difference was observed between the branched and straight polymer chains. The preferred conformation for each of the three smaller esters (perfluoroacetate, perfluoropropionate and perfluorobutyrate) is strikingly sensitive to the perfluoroalkyl chain length.

The REMPI spectra of the van der Waals dimers of the straight chain PFPE's, **I**, and the spectra of the PFPE's with two phenoxy end groups, **II**, show a striking similarity, suggesting an accompanying similarity in structure. This is evident in the mass spectra collected at two excitation wavelengths. In panel A of the figure the excitation was at 273.5 nm, near the peak of the polymer absorption. The spectrum is dominated by the parent masses of **I**, ranging from n=5 to n=13 and indicated by the closed circles. Moving the excitation wavelength to 274.8 nm, a shift comparable to the well known redshift for van der Waals dimers of aromatic molecules, yields the spectrum shown in panel B. Here the coincidence with the absorption of the van der Waals dimers is demonstrated by the appearance of the peaks indicated by the open circles. These peaks are accompanied by the appearance of a new series indicated by the crosses, corresponding to the masses of **II**. They also exhibit a redshift, characteristic of a dimerized aromatic ring. In fact, scanning the excitation wavelength shows that the spectra of the van der Waals dimer of **I** and the doubly substituted polymer, (**II**) are shifted and broadened relative to the singly substituted polymer (**I**) in essentially the same way.

We argue that in both cases van der Waals complexes are formed between the two chromophores, which are *inter*molecular for the dimer of **I** and *intra*molecular for **II**. The formation of the intramolecular complex is an indication of the flexibility of the polymer chains and the strength of the interaction between chromophores. The barriers to internal rotation in the polymer must be low enough to allow the two ends of the chain to dimerize before the conformations are frozen. This requires a chromophore dimerization energy substantially larger than the critical barrier heights.

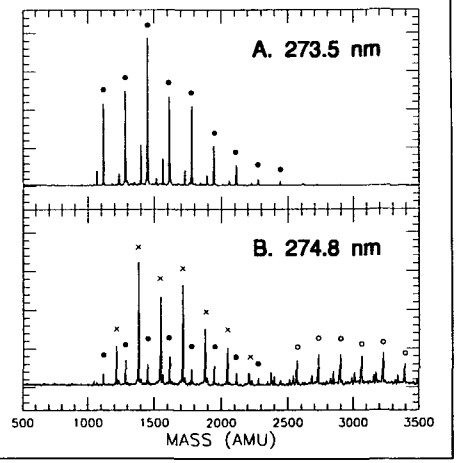

1. E. F. Cromwelli, K. Reihs, M. S. de Vries, S. Ghaderi, H. R. Wendt and H. E. Hunziker, J. Phys. Chem., in press (1993).

Hydrocarbon Polymer Analysis by Laser Desorption/Chemical Ionization Fourier Transform Mass Spectrometry (LDCI/FTMS).

Michael S. Kahr and Charles L. Wilkins, Department of Chemistry, University of California, Riverside, CA 92521

Laser desorption FTMS of nonpolar hydrocarbon polymer samples is generally more difficult than for polar polymers. Polar polymers containing heteroatoms such as oxygen and nitrogen undergo ionization via alkali metal ion attachment. An effective alkali metal ion attachment site often does not exist for hydrocarbon polymers and thus many hydrocarbon polymer samples yield only fragment ions upon laser irradiation. Because the laser desorption event produces intact gas phase neutral analyte molecules, ionization may be accomplished by us of an appropriate chemical ionization reagent.

Silver nitrate is an attractive candidate as a chemical ionization reagent for hydrocarbon polymers and has been investigated in our laboratory. Silver nitrate is a solid that can be codeposited with the sample. Because silver nitrate is a nonvolatile solid, it does not produce a gas load for FTMS analysis. Also, during the laser desorption event, reagent ions are generated in close proximity to desorbed hydrocarbon neutrals, producing spatial overlap between the analyte neutrals and the reagent ions. Finally, the results of this study indicate that silver offers excellent reactivity toward hydrocarbon polymer analytes.

Narrow molecular weight standard samples of polystyrene, polybutadiene, polyisoprene, and polyethylene were obtained for this study. These polymers span the range of hydrocarbon polymer structural categories. Polystyrene represents phenyl functionality and is the least challenging. Polyisoprene and polybutadiene represent branched and linear unsaturated hydrocarbons of moderate difficulty. Polyethylene is linear, saturated, and is the most challenging. Gel permeation data provided by the manufacturer were compared with spectra obtained for silver nitrate LDCI spectra. Figure 1 shows that, even for polyethylene, high quality mass spectra may be readily obtained.
In an effort to extend the mass range capabilities of this technique, a commonly-used matrix-assisted laser desorption/ionization (MALDI) matrix, 2-5 dihydroxybenzoic acid, was added to the sample and silver nitrate. Results for a polystyrene GPC Mn = 8000 sample are presented in Figure 2.

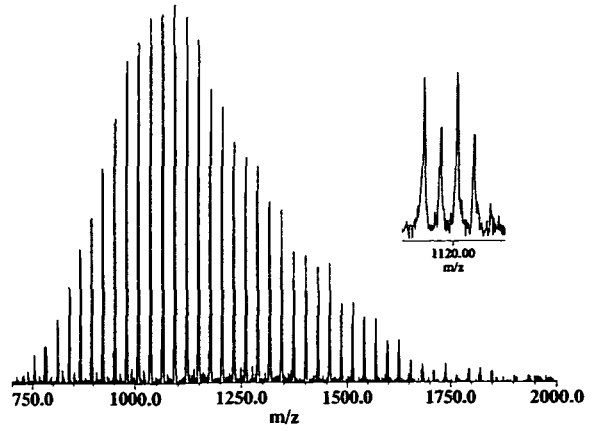

Figure 1: Polyethylene GPC Mw 1214, AgNO3 Mw 1193.
Inset shows the n=36 silver attached oligomer, resolution 7626 at mass 1118.
This spectrum was obtained using SWIFT excitation.

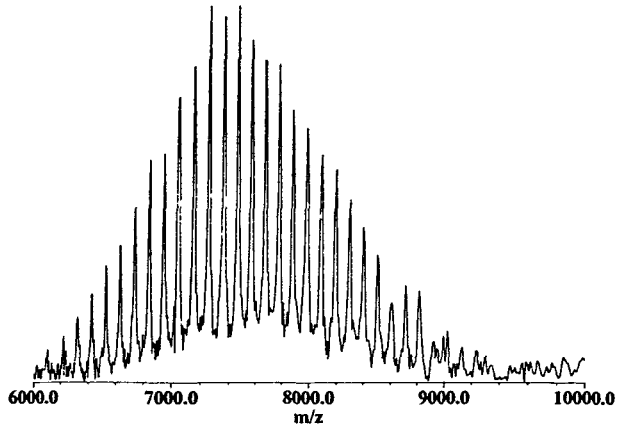

Figure 2: Polystyrene GPC Mn 8000.
This is the MALD/CI spectrum obtained when 2,5-dihydroxybenzoic acid and silver nitrate are present. Excitation was performed using SWIFT.

MALDI MASS SPECTROMETRY OF GEL-ELECTROPHORETICALLY SEPARATED PROTEINS

Kerstin Strupat, Michael Karas, Franz Hillenkamp
Institute for Medical Physics and Biophysics, University of Münster, Robert-Koch-Str. 31, 48149 Münster, FR Germany

Christoph Eckerskorn, Friedrich Lottspeich
Max-Planck-Institute for Biochemistry, 82152 Martinsried, FR Germany

Combining exact determination of the molecular weight by matrix-assisted laser desorption ionization mass spectrometry and the high-separation capacities of gel-electrophoresis forms a challenging analytical approach. Though the use of a laser ablation source to analyze separated immobilized proteins directly in the gel or from blot membranes seems straightforward at a first glance, the elucidation of adequate experimental and preparation conditions in order to fulfil the requirements of MALDI-MS poses a major task to be solved. The ease of MALDI of proteins dot-blotted onto a membrane (1) only proves the general usability of an organic polymer as a substrate for MALDI, but the experimental situation after SDS-PAGE/electroblot is by far more demanding.

In a series of experiments relevant progress for this adaptation was elucidated in a step-by-step procedure. As a general starting point for this work, SDS-PAGE (one-dimensional) and subsequent electroblots onto immobilizing membranes were carried out under standard conditions. Preliminary results have been reported in (2). MALDI mass spectrometry was performed on a laboratory-built reflectron TOF instrument equipped with ports for both UV- (Nd.YAG, 355 nm) and IR-lasers (Er YAG, 2 94 μm)

First promising results were obtained with the IR-laser and from proteins electroblotted onto membranes. Further work therefore followed this line, the mass spectra obtained under standard preparation for IR-MALDI served as a criterion for the quality of the mass spectra to be obtained. In addition, initial experiments were done on unstained proteins in order to avoid foreseeable problems due to peak broadening and mass shifts. In a first optimization cycle, different membranes - differing both in chemical composition and physical structure (pore size and specific surface) -, IR-matrices and preparation conditions (solvents, concentration, moment of matrix incubation) were inspected. The key finding was that soaking of the wet membrane into a saturated aqueous solution of the matrix yielded highly improved results in terms of shot-to-shot reproducibility, signal intensities and width; succinic acid and a number of different aliphatic carboxylic acids were used as matrices. All membranes typically used for electroblots enabled MALDI results, improved signal quality was obtained for polyvinylidene difluoride (PVDF) and polypropylene (PP) of high specific surface (see Figure 1)

The influence of the staining of the proteins usually applied to visualize the protein bands was investigated in an subsequent series of experiments. Whereas organic dyes, such as coomassie blue, resulted in broad peaks shifted in mass and showing a distribution of tagged dye molecules, were colloidal pigments, such as gold and ink, found compatible to MALDI mass analysis (see Figure 2).

The characteristics of IR-MALDI obtained under the above optimized experimental conditions, such as high ion yields, high S/N for single shots and excellent reproducibility

for several shots from the same laser spot and from spot-to-spot, form the necessary prerequisites for a practical SDS-PAGE/MALDI-MS combination; no changes in the standard GE and electroblotting procedures are required. Sensitivity, though not optimized yet, is in agreement with typical protein loads to SDS gels of 0.1 to 1 μg/7 mm. It should be noted that focussing of small protein quantities in high-resolution 2D-gels should enable mass analysis of even fmolar amounts of proteins. The precision of the mass determination given by the correlation of the different molecular ion signals is ± 0.05 % for bovine serum albumin, calibration with proteins on the same blot membrane is suggested to yield the same mass determination accuracy.

(1) Karas, M.; Bahr, U.; Ingendoh, A.; Nordhoff, E.; Stahl, B.; Strupat, K.; Hillenkamp, F. Anal. Chim. Acta **241** (1990) 175.
(2) Eckerskorn, C.; Strupat, K.; Karas, M.; Hillenkamp, F.; Lottspeich, F. Electrophoresis **13** (1992) 664.

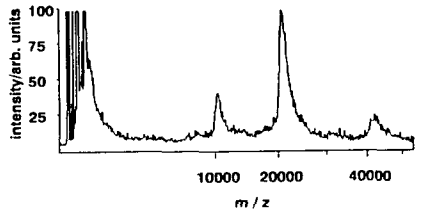

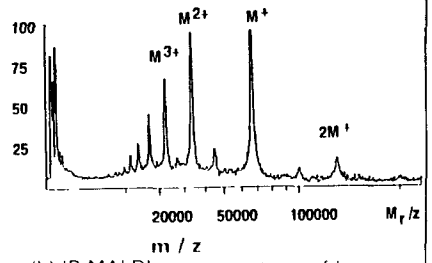

FIGURE 1 : (a) IR-MALDI mass spectrum of trypsin inhibitor blotted onto PP (mean spec. surface), non-stained; succinic acid (2.94 μm) "dry" incubation, sum of 10 single shot spectra

(b) IR-MALDI mass spectrum of bovine serum albumin blotted onto PVDF (high spec. surface) non-stained; succinic acid (2.94 μm) "wet" incubation, sum of 5 single shot spectra

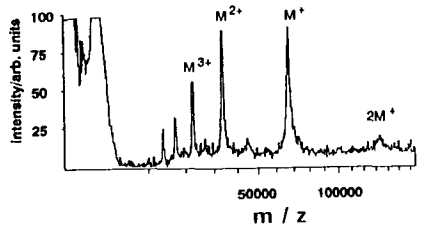

FIGURE 2. IR-MALDI mass spectrum of bovine serum albumin blotted onto PVDF (high-spec. surface); succinic acid, 2.94 μm, sum of 5 single shot spectra stained by colloidal gold (AuroDye)

ACKNOWLEDGEMENT
This work was financially supported by the German Fed Dept. of Research and Technology (BMFT, grant No.. 13N5640) and by Finnigan MAT, Bremen

Laser Desorption/Ionization of Small Biomolecules

P.T.A. Reilly, T. King, and J.P. Reilly
Indiana University, Bloomington, IN 47405

While the development of matrix assisted laser desorption represents a spectacular advance for biomolecule mass analysis, the method has some noteworthy drawbacks. Because the ionization process necessarily involves molecular collisions, it is not precisely localized in space and can significantly affect the velocity distribution of the nascent ions. Selectivity associated with the ion formation process may also not be desirable. In an attempt to improve this situation, we have been exploiting the matrix assisted laser desorption phenomenon simply to introduce neutral macromolecules into the gas phase. Once volatilized, we use resonantly enhanced multiphoton ionization (REMPI) to ionize our samples.

In our initial studies, we have focussed on the ionizing characteristics of small biomolecules. Having previously demonstrated that laser ionization propensities can be strongly influenced by excited state relaxation, we recorded mass spectra of amino acids and small peptides using both nanosecond and picosecond pulses of ultraviolet laser light. Remarkably few differences in the spectra were noted, both exhibiting considerable ion fragmentation. Previously published mass spectra of these same compounds taken with supersonic cooling of the laser desorbed material displayed substantially less ion fragmentation, suggesting that our sample molecules are desorbed hot. In order to probe this issue, we have recorded the wavelength dependence of the two step ionization yield of tryptophan and have measured the velocity distribution of neutral molecules desorbed from the surface. The most noteworthy results are that the velocity distribution is narrowed and the mass spectral fragmentation is reduced upon using higher light intensities. These observations support the theory that some jet cooling of desorbed molecules does indeed take place and that this cooling depends on the incident laser fluence.

LASER VAPORIZATION AND REMPI-TOF DETECTION FOR DNA SEQUENCING

Robert J. Levis, Department of Chemistry, Wayne State University, Detroit, MI 48202.

The mass spectroscopic detection of biological molecules in the gas phase is promoting the development of a number of new biological, biochemical and medical probes. Advances in the vaporization and detection of these fragile molecules are driven in part by emerging laser-based techniques. Our laboratory is investigating two such processes required for mass spectroscopic detection. The first process is laser vaporization and this involves transferring the fragile biomolecule from the solid state into the gas phase with no decomposition. The vaporization is accomplished by directing an intense laser pulse through a thin solid film composed of the biomolecule and a light absorbing chromophore. The second process we are investigating is the subsequent ionization of laser vaporized, neutral biomolecules. This post ionization is accomplished using a series of laser pulses intersecting the plume of cooled biomolecules. Laser ionization is studied in this laboratory because of the potentially high ionization efficiencies (near 100% for atoms) and the considerable increase in ultimate mass spectral resolution (when compared to MALDI, for instance). The ionized molecules are then detected using a linear time-of-flight mass spectrometer.

This laboratory is studying the vaporization and ionization of oligonucleotides to develop a high speed DNA sequencing system based on mass spectrometry. The advantage of a mass spectroscopic sequencing method is that the products of a Sanger dideoxy sequencing reaction for a 500 base DNA strand could be analyzed in less than one second, giving rise to enormous sequencing rates. These rates have been estimated to be 10^4 to 10^7 times faster than conventional gel electrophoresis-based analysis. In addition, with the mass spectroscopic approach, sequence specific irregularities (i.e. missing bands), can easily be identified and corrected. This is because the mass spectroscopic approach precisely and reproducibly determines relative as well as absolute strand lengths. The amount of material required for the sequence may ultimately be less than that required for standard radiographic analysis.

These experiments are performed in a turbopumped linear time-of-flight mass spectrometer. The samples are prepared in aqueous rhodamine 6G (Rh 6G) and are deposited as a ring onto a quartz cover slip. The cover slip is then fixed onto the end of a hollow sample tube and inserted into the four grid ionization and extraction assembly of the spectrometer. The sample is vaporized using a gaussian output coupled, Nd:YAG laser. The 532nm pulse of duration 2.7 ns and intensity 30 mJ/cm^2 to 5 J/cm^2 is directed through the Rh 6G film from the back side (through the glass/film interface first). Ions formed in the vaporization process are removed using axial deflection grids. The neutral sample is then ionized using a two color laser ionization scheme. The pump photon is produced using an excimer-pumped dye laser and is tuned from 350 nm to 400 nm. The probe beam is picked off of the XeCl excimer laser and is fixed at 308 nm. The ionized sample is accelerated in a dual slope extraction field to 1 keV and is then allowed to drift 63 cm to a hybrid high mass detector. The ion current is then amplified and smoothed at 1 MHz and recorded by a LeCroy 7200A digital oscilloscope. The resulting spectra is then transferred to a 486 computer via GPIB . All spectra are recorded in the single shot mode with no averaging.

Our investigations of the laser vaporization process began with an evaluation of Rh 6G as a thin film chromophore for vaporizing fragile biomolecules. This laser dye was chosen so that green light could be employed in the vaporization step, to avoid absorption by the sample molecules. This color (532 nm) is not absorbed by DNA and photochemical complications are eliminated. Initially, gel electrophoretic and direct radiographic analysis of the vaporization products were performed to understand the vaporization process. These studies revealed that the oligonucleotides vaporized molecularly with a $\cos^{120}$ spatial distribution. This tight spatial distribution strongly suggests that the vaporization of macroscopically thick films of material (1000 layers of Rh 6G) mimics the physics of adiabatic expansion in a free jet molecular beam. Vaporization of radio-labeled nucleotides at low powers results in extensive phosphodiester bond scission. Increasing the vaporization laser power to 300 mJ/cm2 leads to molecular vaporization of the nucleotide. Experiments with radio-labeled oligonucleotides reveal the same general trend.

Single strands of DNA as long as 2000 bases have been molecularly vaporized using this technology. These results are favorable for DNA sequencing using a mass spectrometer for several reasons. The highly directed product beam in a small solid angle implies that a large portion of the sample can be interrogated by the ionization beam. Also the large density (10^{12} molecule/mm^3) of material expanding into the vacuum may preclude the need for seeding the sample into a free jet for subsequent cooling.

The strategy for ionizing the laser vaporized, neutral DNA is the same as that for the vaporization step, employ photons which cannot be absorbed by DNA. A photoionization tag molecule is chemically attached to the DNA. This eliminates both multiple charging of a given DNA strand and photochemical fragmentation and reionization of the gas phase DNA. Either process would serve to complicate the mass spectrum and the subsequent determination of the sequence. The tag molecule is chosen to absorb light at wavelengths where DNA does not and also to have a high photoionization cross section. The tag molecule used in this investigation is based on anthracene, a three ring polycyclic aromatic hydrocarbon. The ionization scheme relies on exciting the anthracene into its lowest lying electronic state with one photon and pumping this excited molecule just into the ionization continuum with a second photon. In this way no excess energy is deposited into the ion, limiting fragmentation processes. The study begins with measuring the two color photoionization spectrum of anthracene. Here the pump photon is scanned from 340 to 370 nm and the probe photon, fixed at 308 nm. With this arrangement we measure the 0-0 band of anthracene to be 361.5 nm. Measurements of anthracene molecules with hydrocarbon moieties attached to the 9' position serve to shift the 0-0 band approximately 12 nm to the red (375 nm). A study of the photoionization spectrum of laser vaporized, anthracene-labeled DNA reveals a broad absorption feature centered at 378 nm. Knowledge of the photoionization spectrum of tagged DNA allows us to perform ultrasensitive (<fmol) detection of vaporized species.

Investigations of the velocity distributions of the laser vaporized molecules allow insight into the mechanisms of laser vaporization of biological molecules. Determination of the velocity distribution of the gas phase species is simply obtained by measuring the mass spectrum as a function of delay between the vaporization and ionization lasers. Velocity distributions are extracted from the time distributions using a density weighted Jacobian transformation. These velocity distributions typically peak between 400 and 1200 m/s for DNA and at 2000 m/s for Rh 6G. The full width at half maximum (FWHM) for the velocity distributions is usually 300 m/s. The most probably velocities correspond to Boltzman temperatures of thousands of K while the FWHM of the velocity distributions corresponds to temperatures of hundreds of K. Such nonthermal velocity distributions again suggest adiabatic cooling is present in the vaporization process. Calculations based on the measured velocity distributions suggest that approximately 1/2 of the vaporized material can be interrogated with a 5 x 5mm ionization beam 30 mm down stream from the vaporization region.

Our investigations of velocity distributions result in two significant contributions to understanding the processes of laser vaporization. The first finding results from measurement of the velocity distributions of Rh 6G, labeled nucleotide and various DNA fragment ions. For the thin films the velocity distributions of the fragments were virtually equal to that for the Rh 6G. The peak in the velocity distribution of the tagged-nucleotide was less than half that for the Rh 6G, however. This velocity slip allows us to suggest that the fragmentation observed in the mass spectrum occurs during vaporization, not during ionization. Measurements of the velocity distribution of the labeled nucleotide as a function of film thickness reveal that the peak in the velocity distribution increases monotonically with film thickness until reaching approximately 90% of the Rh 6G peak velocity. This suggests that thicker films have less velocity slip and will more efficiently cool the vaporizing sample. Mass spectra for laser vaporized thick films reveal virtually no DNA fragmentation.

The support of a National Institutes of Health, Human Genome Center grant, RO1 HG00485, of a NIH Research Career Development Award, KO4 HG00006 and of a National Science Foundation Young Investigator Award, CHE-9258193 is gratefully acknowledged.

Matrix-Assisted Laser Desorption Mass Spectrometry of Oligonucleotides

Klaus Schneider and Brian T. Chait
The Rockefeller University, 1230 York Avenue, New York, N.Y. 10021

Several groups have recently reported the use of MALDI to analyze relatively short stretches of single stranded DNA (generally < 60 nucleotides in length). However, a general finding of these experiments is that the mass spectrometric response falls off precipitously for DNA fragments longer than approximately 20 nucleotides in length.

During the past year we have carried out a series of experiments designed to understand this falloff in the mass spectrometric response as a function of oligonucleotide length. We found that dT homopolymers yielded intense mass spectra for species containing as many as 180 bases (i.e. a molecular weight of 54,000 daltons)[1]. By contrast, we found that the mass spectrometric responses to dA, dC, and dG homopolymers were virtually non-existent, except for very short polymers. We discovered 20 different laser desorption matrix compounds that were found to produce mass spectra of dT_{18}. Significantly, none of these matrices produced usable spectra from dG_{18}[1]. These results strongly confirmed the earlier observation of Parr *et al.* that base composition is a critical factor for the analysis of oligonucleotides[2].

We hypothesized three possible causes for the lack of response to polyguanosine: (i) unwanted aggregation of polyguanosine chains and/or "non-ideal" interactions of the polyguanosine molecules with the matrix molecules, (ii) low ionization efficiency, and (iii) high degree of fragmentation. We consider each of these in turn:

(i) Our working hypothesis is that a good matrix-assisted LD mass spectrometric response requires appropriate interaction of DNA with the matrix molecules, leading to the incorporation of analyte into the matrix materials as isolated molecules. To study the incorporation of the oligonucleotides dT_{18} and dG_{18}, we adapted the method developed by Beavis for the study of the incorporation of proteins into crystals of sinapinic acid. In the present experiment, we crystallized sinapinic acid in the presence of acridine orange, which effectively stains single-stranded DNA. Without oligonucleotide present, the sinapinic acid crystals did not become colored indicating that acridine orange was not incorporated. When dT_{18} or dG_{18} were added to the sinapinic acid/dye solution, the crystals obtained were intensely in orange color demonstrating the incorporation of a dT_{18}-acridine orange or a dG_{18}-acridine orange complex. The similar intensity in color of the sinapinic acid crystals indicated a comparable degree of incorporation for both oligonucleotides, which was confirmed by HPLC analysis of the redissolved matrix crystals. Therefore, lack of incorporation of dG_{18} is likely not the primary reason for our failure to obtain a mass spectrometric response for dG_{18}. However, this conclusion assumes that the microscopic environment and the distribution of sample molecules within the crystals do not affect the mass spectrometric response and do not change for dG_{18} versus dT_{18}. Possible causes for microscopic differences in incorporation may arise form the different tendency for association of bases and from differences in the oligonucleotide solution structures.

(ii) Measurements on very short stretches of polyguanosine (e. g. dG_7) gave a reasonably intense response, indicating that low efficiency for ionizing polyguanosine is not the primary reason for our failure to observe longer stretches of polyguanosine.

(iii) The mass spectra of dG_7 showed evidence for a substantial degree of fragmentation of the parent ion in the mass spectrometer Mass spectrometric fragmentation may therefore explain our

inability to observe longer stretches of polyguanosine (e.g. dG_{18}). Experiments on chemically modified polynucleotides provide independent evidence that the detailed chemical nature of the bases have a profound effect on the amount of fragmentation observed. For dU_{18} we obtained a mass spectrum very similar to dT_{18}. The intense peaks for dU_{18} demonstrate that the 5-methyl group in thymidine does not affect the mass spectrometric response. On the other hand, the total lack of response for dC_{18} under identical conditions revealed a major influence of the 4-amino group in cytidine. The spectrum of dI_{18} exhibited distinct broad peaks at masses approximately consistent with the intact molecule (figure), demonstrating that substitution of the 2-amino group of guanosine by hydrogen (or the substitution of the 6-amino-group of adenosine by a keto group, respectively) dramatically improved the response. However, the low-mass tailing of the peaks and the narrower width of the peak corresponding to the doubly charged ion compared with that from the singly charged species strongly indicate a rapid fragmentation of these ions during the time required for ion acceleration (0.8-1.2 µsec). The improved spectrum for dI_{18} compared to dG_{18} (and dA_{18}) may be explained by a lesser tendency for fragmentation for dI_{18} caused by the substitution of the exocyclic amino group.

Of the three hypothesized causes for the lack of mass spectrometric response for polyguanosines in contrast to the strong responses for polythymidines the contribution of fragmentation dominated. The basis for this increased tendency for fragmentation is currently under investigation.

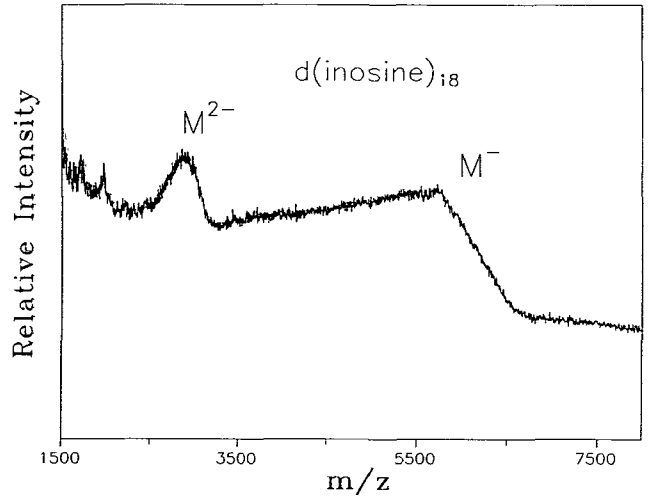

Figure. Negative ion mass spectrum of $d(inosine)_{18}$ (acceleration voltage - 20 kV, matrix: ferulic acid, total amount of sample:1 pmol).

References

1. K. Schneider and B.T. Chait, Proc. 40th ASMS Conference on Mass Spectrom., 1992, pp. 312-313
2. G. R. Parr, M. C. Fitzgerald, L. M. Smith, Rapid Commun. Mass Spectrom. 6, 369-372 (1992)

Fragmentation of Small Oligodeoxynucleotides by MALDI/TOF Mass Spectrometry Using 355 nm Radiation.

*Gary R. Parr, Lin Zhu, Michael C. Fitzgerald and Lloyd M. Smith, Department of Chemistry, University of Wisconsin, Madison, WI 53706, USA

We are investigating matrix-assisted laser desorption mass spectrometry as an alternative to electrophoretic separation of fragments generated by standard DNA sequencing reactions. We have reported that poly $d(T)_n$ samples yield reasonable mass spectra, while poly $d(G)_n$ samples give essentially no response(1). The objective of this study was to determine whether fragmentation might be a factor in the behavior of these molecules.

Poly $d(T)_n$ and poly $d(G)_n$ (n = 2, 4, 6, 8 and 10) were synthesized, purified and subjected to mass spectral analysis. Using 2,5-dihydroxybenzoic acid (2,5DHBA) as the matrix, $d(G)_n$ samples were found to undergo extensive fragmentation yielding a series of peaks represented by the formulae G_n and pG_n and corresponding to cleavage of an O-P bond (fig. 1). A peak corresponding to the loss of a single base moiety is also observed. The intensity of the fragment peaks increases dramatically with the length of the parent molecule, as shown in figs. 2 and 3. For the longer molecule, peaks apparently due to a double fragmentation, represented by the formula pG_np, are also observed. Poly $d(T)_4$ and $d(T)_8$ gave virtually no fragmentation under identical conditions.

The oligodeoxynucleotide, d(TTTTGGGGTTTTTTT), was also sythesized, purified and subjected to mass spectral analysis using 2, 5-dihydroxybenzoic acid and 3-hydroxypicolinic acid (3HPA), (2), as matrix materials. The results are shown in fig. 4. Several peaks corresponding to cleavage of guanine 3' O-P bonds were observed with 2,5DHBA. However, no fragment ions were observed when 3HPA was used as the matrix. These results clearly indicate that the fragmentation process(es) is matrix dependent.

In conclusion, fragmentation appears to account, in large part, for the lack of success in the mass analysis of larger poly $d(G)_n$, and mixed base oligodeoxynucleotides with the MALDI technique using 2,5DHBA as a matrix. Conversely, the absence of fragmentation must be a factor in the successful mass analysis of oligodeoxynucleotides using 3HPA as a matrix.

1. G. R. Parr, M. C. Fitzgerald and L. M. Smith, *Rapid Commun. Mass Spectrom.* **6**, 369 (1992)
2. K. J. Wu, A. Steding and C. H. Becker, *Rapid Commun. Mass Spectrom.* **7**, 142 (1993)

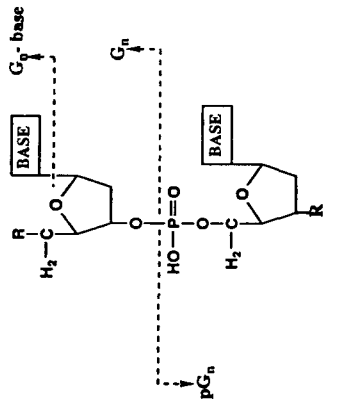

Figure 1

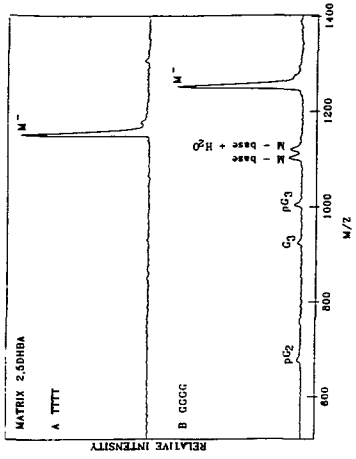

Figure 2

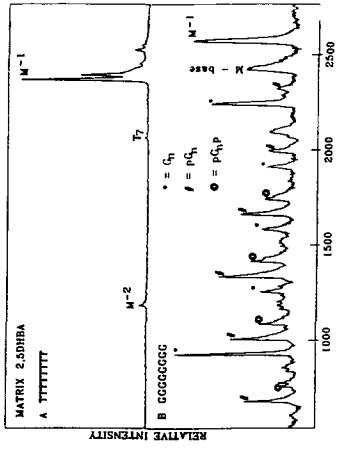

Figure 3

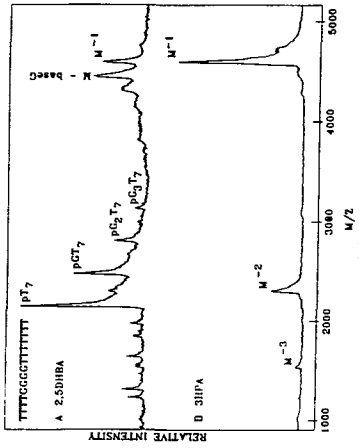

Figure 4

ION TRAP MASS SPECTROMETRY

R.G. Cooks, R.K. Julian, Jr, C.D. Cleven, S.A. Lammert and M. Soni,
Department of Chemistry, Purdue University, West Lafayette, IN 47907

The performance of ion trap mass spectrometers continues to be improved; the current situation is summarized in Table 1. The features listed include best as well as (in parenthesis) usual levels of performance. Areas in which further improvement is clearly needed include (i) internal energy deposition, where DC pulse activation offers prospects for internal energy depositions much greater than the 5 eV values now typical, (ii) mass measurement accuracy, where internal calibration and improved initial conditions are leading to improvements beyond ±50 ppm, and (iii) dynamic range, where selected waveform (SWIFT) and related methods are improving performance.

An important tool in improving performance is simulation of ion motion. In this laboratory two simulation programs have been developed, one, ITSIM, operates on a PC computer and gives animated displays, trajectory and phase space plots for small collections (<100) of ions.[1] The other, NQS, is a program written for supercomputers and designed to simulate mass spectra by following the motion of 10^4-10^5 ions.[2]

The NQS program first showed[2] that ions are ejected only when both the applied RF and AC have the appropriate polarity that an integral frequency relationship between these signals is desirable and that there is a strong phase dependence on ion ejection which has a dramatic effect on mass resolution. A fixed phase experiment has now been implemented[3] (Figure 1) and it shows that ions can be made to eject at each RF cycle.

Hand-in-hand with simulations as a means of characterizing ion motion in the ion trap are tomography experiments. In one such experiment, acetophenone molecular ions are subjected to a rapid DC pulse in the axial direction and their passage through the trap center is detected by photodissociation using a crossed laser beam.[4] Figure 2 shows results from such an experiment in which the photofragment is m/z 77. Fourier transformation of the time resolved data yields the ion frequencies present in the activated ion cloud. An ITSIM simulation of ion motion reveals the secular frequency, f_z, (Figure 3) and additional frequency components occur when the simulation is done using the real as opposed to the ideal fields.

Fast DC pulses can be used to drive ions into the electrodes and cause surface induced dissociation (SID)[5] and simulations are revealing much of interest in this experiment too. Figure 4 contrasts the phase space plots recorded under conditions when n-butylbenzene ions are subjected to a 104 volt and a 187 volt DC pulse. The former experiment shows equal abundances of the low and high energy product m/z 92 and 91, while the latter gives exclusively the high energy product.

The important task of trapping ions of desired m/z ratios (eliminating matrix ions) is facilitated by using the SWIFT technique. Selected multiply-notched waveforms can be applied during ion injection as shown in Figure 5.

While much has been accomplished to develop ion traps into high performance mass spectrometers, much remains to be done. The availability of powerful simulation methods is likely to be an important aid in this future work.

References
1. H.-P. Reiser, R.K. Julian and R.G. Cooks, *Int. J. Mass Spectrom. Ion Proc.*, 121 (1992) 49.
2. R.K. Julian, H.-P. Reiser and R.G. Cooks, *Int. J. Mass Spectrom. Ion Proc.*, 123 (1992) 85.
3. R.K. Julian, Ph.D. Thesis, Purdue University, 1993.
4. S.A. Lammert, C.D. Cleven and R.G. Cooks, *J. Phys. Chem.*, submitted.
5. S.A. Lammert, Ph.D. Thesis, Purdue University, 1992.

Table 1.

Ion Trap Performance

Features

O High Sensitivity	2 attomole peptides (1-10 f mole)
O Desorption and Spray Ionization	SIMS, FAB, LD, TS, ES
O MS^n	n > 10 (n=3,4)
O High Mass/Charge Range	> 70,000 dalton/charge (7,000)
O High Resolution	> 1,000,000 at 3,500 dalton (30,000)
O MS/MS Resolution	10,000 each stage
O High Efficiency Dissociation	approaches 100% (50%)

Issues

O Internal Energy Deposition	~ 5 eV	DC pulse
O Mass Measurement Accuracy	50 ppm	Internal Calibration
O Dynamic Range	10^4	SWIFT

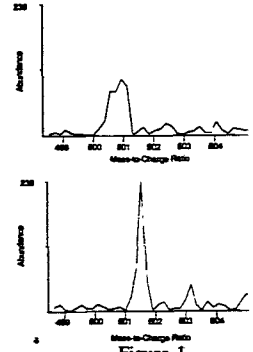

Figure 1.
Ejection of ions occurs at each RF cycle in the fixed phase resonant ejection experiment and results in improved resolution; a) 0° and b) 90°.

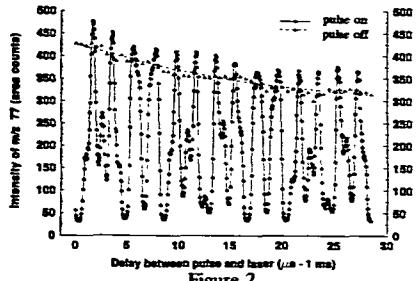

Figure 2.
DC pulse/laser probe experiment showing the time domain spectrum of ion frequencies.

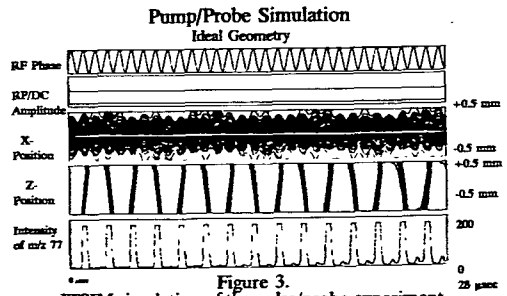

Figure 3.
ITSIM simulation of the pulse/probe experiment. The zero crossings in the z-direction represent times at which photodissociation is detected.

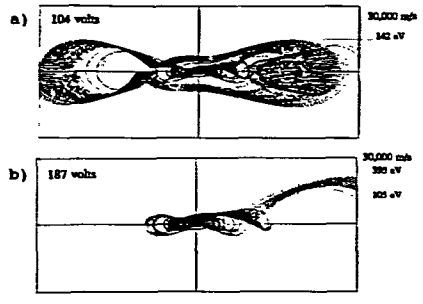

Figure 4.
Phase space ITSIM plots for the DC activation experiment, at a) 104 volts pulse amplitude and b) 187 volts.

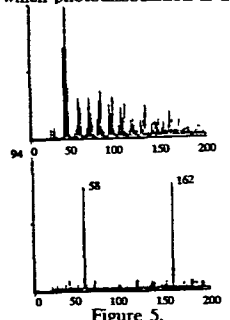

Figure 5.
Cs^+ desorption ionization mass spectrum of l-carnitive hydrochloride a) before and b) after selection of m/z 58 and m/z 162 (C^+) by SWIFT.

Mass Resolution in a Quadrupole Ion Trap

R.E. March[1], F.A. Londry[2] and G.J. Wells[3]

[1]Department of Chemistry, Trent University, Peterborough, ON K9J 7B8 (Canada); [2]Department of Physics, Trent University, Peterborough, ON K9J 7B8 (Canada); [3]Varian Associates, Inc., Walnut Creek, CA 94598-0916 (U.S.A.)

INTRODUCTION

The mass resolution of the commercial quadrupole ion trap, which has a fixed mass scanning rate, is ca. three times the ion mass such that the mass resolution at the mass limit (650 Da) is ca. 2000. The mass resolution may be varied by changing the mass scanning rate in a modified instrument. Mass resolution has been improved by the application of axial modulation,[1] a combination of modest ion trap size and frequency reduction with axial modulation,[2] and reduction of the RF voltage scanning rate.[2,3,4,5,6]

EXPERIMENTAL

The experimental results described here were obtained with a modified version of the standard commercial quadrupole ion trap, model Saturn I gas chromatograph/mass spectrometer, manufactured by Varian Associates Inc. The insrument was modified to permit wide variation of the RF drive voltage amplitude scanning rate. Control of the RF voltage amplitude was transferred from the analogue printed circuit board (PCB) to two external (and externally-controlled) digital-to-analogue converters (DACs), of which one was 16-bit and the other was 12-bit. The summing circuit was configured such that the 16-bit DAC spanned the same mass range as the 12-bit DAC on the analogue PCB which normally controls the RF voltage level; the full range of the 12-bit external DAC was equivalent to one increment of the first.

The integrator on the analogue PCB was controlled by external digital lines and its output was read by an external ADC. Operation of the electron gate, electron multiplier, and axial modulation was controlled also by external digital lines. The axial modulation source on the scan acquisition processor PCB was replaced by an external circuit with a relatively flat response over a range of frequencies from 10 to 500 kHz. By this means, the mass scanning rate for singly-charged ions was varied by a factor of ca. 8.7×10^7, that is, from 1.3×10^6 Da s^{-1}, through the normally fixed rate of 5555 Da s^{-1} to some 0.015 Da s^{-1}. Ion ejection was brought about by resonance excitation applied at a frequency somewhat reduced from that employed in the commercial instrument (q_z=0.86). The pressure of helium buffer gas was not markedly different from the normal pressure of 1 *mTorr*.

RESULTS

While mass resolution, R, is defined as the ratio of ion mass, m, the full width at half maximum (FWHM) of the mass peak, Δm, it is more informative to discuss mass resolution in terms of Δm which is the experimentally-observed quantity rather than the resolution which varies according to the mass chosen. In Fig. 1 is shown the variation of Δm as a function of scan rate (in a log-log format) for four ion species, *m/z* 69, 131, 414, and 614 derived from perfluorotributylamine. Axial modulation was carried out at q_z=0.86 and, for *m/z* 131, at q_z=0.43 also. The arrow marks the normal scan rate of the commercial instrument. As the scan rate is varied over almost 8 decades, the observed variation in Δm spans 6 decades.

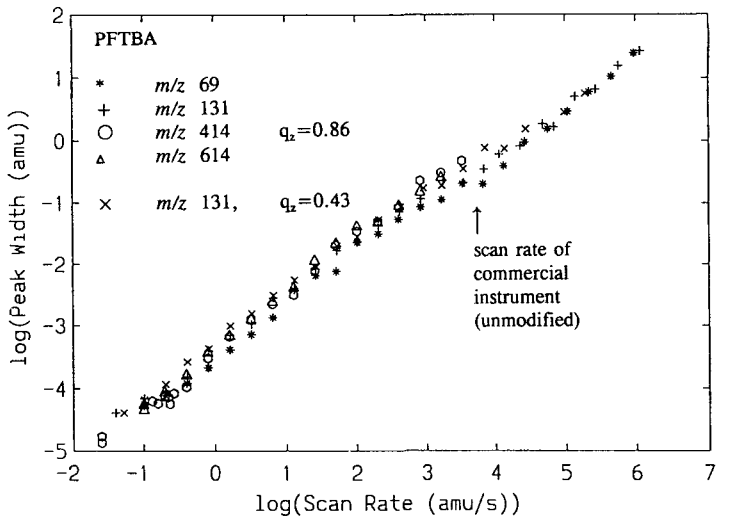

Fig. 1. Variation of peak width as a function of scanning rate, with q_z=0.86: * *m/z* 69; + *m/z* 131; o *m/z* 414; Δ *m/z* 614; and with q_z=0.86, x *m/z* 131.

The maximum RF drive voltage is divided into 2^{27} steps by the ganged 16-bit and 12-bit DACs. Consequently, the smallest increment is 48 μV which corresponds to a minimum peak width of 4.8 μDa. The minimum peak width (FWHM) observed for *m/z* 614 is 52 μDa corresponding to a mass resolution of 1.2×10^7.

A procedure for mass assignment has been explored in which a calibrant ion species and the ion species of unknown mass are isolated in the ion trap using a complex wave-form to eject unwanted ions during ionization. The intensities of the ion species are equalized using two successive ionization periods. Ion ejection is achieved by axial modulation using a composite waveform composed of two frequencies chosen such that the two species are ejected closely in time.

REFERENCES

1. J.E.P. Syka, J.N. Louris, P.E. Kelley, G.C. Stafford and W.E. Reynolds, U.S. Patent 4 736 101, 1988.
2. R.E. Kaiser Jr., R.G. Cooks, G.C. Stafford Jr., J.E.P. Syka and P.H. Hemberger, Int. J. Mass Spectrom. Ion Processes, 106 (1991) 79.
3. J.C. Schwartz, J.E.P. Syka and I. Jardine, J. Amer. Soc. Mass Spectrom., 2 (1991) 198.
4. D.E. Goeringer, S.A. McLuckey and G. A. Glish, Proc. 39th Ann. Conf. Amer. Soc. Mass Spectrom. Allied Topics, Nashville, TN, 1991, p. 532.
5. J.D. Williams, K. Cox, K.L. Morand, R.G. Cooks, R.K. Julian and R.E. Kaiser, Proc. 39th Ann. Conf. Amer. Soc. Mass Spectrom. Allied Topics, Nashville, TN, (1991), p. 1481.
6. F.A. Londry, G.J. Wells and R.E. March, Rapid Commun. Mass Spectrom., 7 (1993) 43-45.

Parallels and Perpendiculars between Magnetic and Non-Magnetic Ion Traps

Alan G. Marshall† and Christopher E. Weaver

Department of Chemistry, The Ohio State University, 120 W. 18th Avenue, Columbus, OH 43210. (†also a member of the Dept. of Biochemistry)

Many of the same sorts of experiments may be conducted in much the same way in ICR and electric quadrupole ion traps (QIT). In their usual configurations, both traps depend on a d.c. quadrupolar potential to trap ions axially (i.e., along a line between the centers of the "end cap" or "trapping" electrodes). Moreover, the natural motion on which mass analysis is based occurs at a frequency which varies inversely with mass in both cases.

Additional insight is provided by analogy to a simple one-dimensional harmonic oscillator (mass-on-a-spring), as shown on the next page. In a conventional harmonic oscillator, the potential is of the form, $U(z) = kz^2/2$, in which the spring force constant, k, is independent of mass. Thus, the "natural" ("secular") frequency varies as $(1/\sqrt{m})$, as for axial oscillation of ions between the two end caps of either a d.c.-only Paul trap or an ICR ion trap. However, both the ion cyclotron frequency in an ICR ion trap and the axial oscillation frequency in an rf-only Paul trap (at low applied rf amplitude) vary as $(1/m)$, a result that may be considered to arise from a harmonic oscillator whose force constant itself varies with mass: $k \propto (1/\sqrt{m})$. Such an analogy explains why thermal ions of higher mass-to-charge ratio, m/z, have higher orbital radius (ICR) or higher axial oscillation amplitude (QIT), because the restoring force weakens as m/z increases (see also bottom right figure). Finally, in an ICR ion trap, the magnetron frequency is approximately independent of mass, corresponding to a harmonic oscillator whose force constant varies as, $k \propto \sqrt{m}$, so that the restoring force actually increases with increasing m/z (bottom right figure).

Based on the above analogies, many techniques originally developed for radial excitation in ICR are now being adapted to the quadrupole ion trap: single frequency, frequency-sweep, and stored-waveform mass-selective excitation and ejection;[1-4] CID; MS_n; and interface with a variety of ion sources. Conversely, dynamic trapping of ions of both charge signs, initially demonstrated for the quadrupole ion trap, has now been implemented in ICR ion traps.[5]

Compared to the QIT, ICR is inherently more linear, and offers higher mass accuracy. Moreover, ions may be trapped (and their chemistry investigated) at much lower temperature (e.g., thermal) in ICR. Also, ions of a much wider m/z ratio (e.g., electrons and negative ions) may be trapped simultaneously in ICR. Work supported by NIH (GM-31683), NSF (CHE-9021058) and The Ohio State University.

1. Marshall, A. G.; Wang, T.-C. L.; Chen, L.; Ricca, T. L. *Amer. Chem. Soc. Symp. Series* **1987**, *359*, 21-33.
2. Grosshans, P. B.; Marshall, A. G. *Anal. Chem.* **1991**, *63*, 2057-2061.
3. Julian, R. K., Jr.; Cox, K.; Cooks, R. G., Proc. 40th ASMS Ann. Conf. on Mass Spectrom. & Allied Topics, Washington, D.C., 1992, pp. 943-944.
4. Guan, S.; Marshall, A. G. *Anal. Chem.* **1993**, *65*, 1288-1294.
5. Gorshkov, M. V.; Guan, S.; Marshall, A. G. *Rapid Commun. Mass Spectrom.* **1992**, *6*, 166-172.

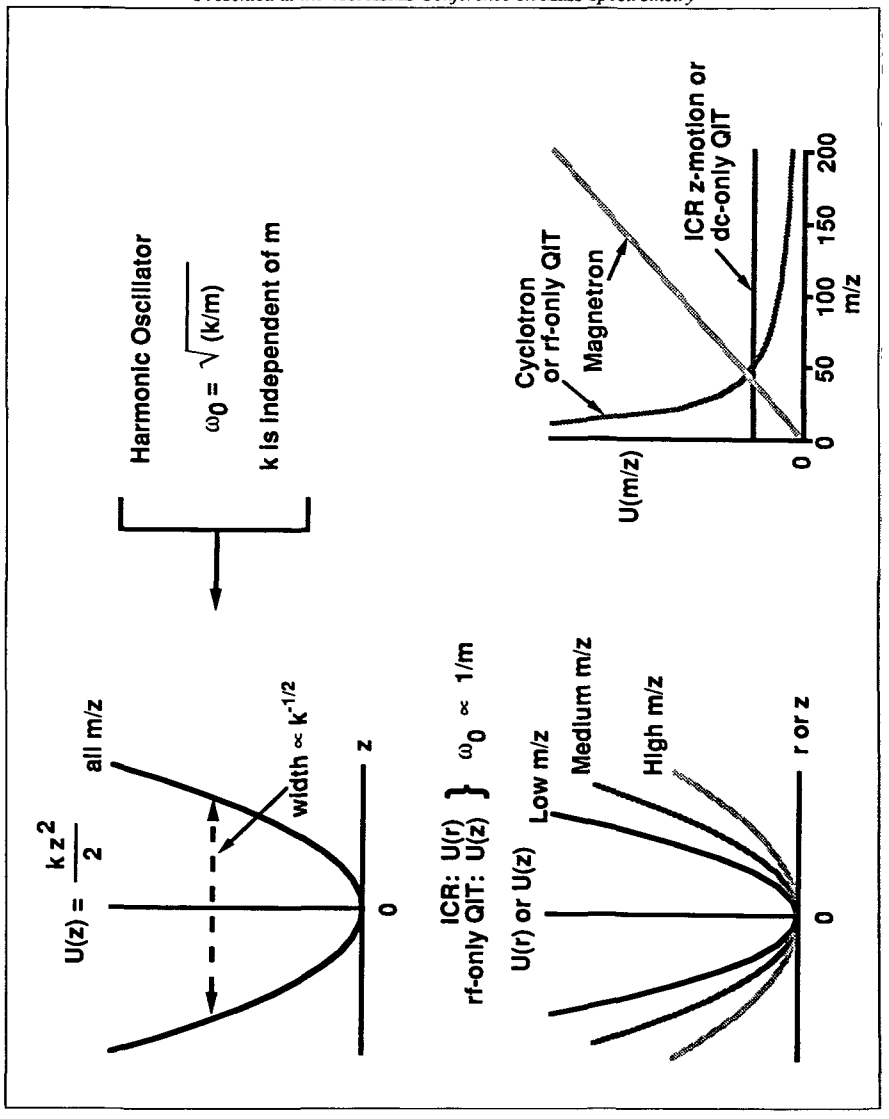

Penning Traps in Physics Research

Lutz Schweikhard, Institut für Physik, Staudinger Weg 7, 55128 Mainz, Germany

Penning traps are ion traps that use the superposition of a static homogeneous magnetic and a quadrupolar electric field which are static - as compared to the radio frequency or Paul traps. (Recently, the 'combined trap', a hybrid form of both Penning and Paul trap has also found some recent interest, e g G -Z Li, Z. Phys. D 14 [1989] 1.) Their name refers to F.M. Penning (Physica 3 [1936] 873) who first described this field configuration. Penning traps have been applied in physics research for a broad range of very different types of experiments, briefly outlined as follows.

They are used as mere storage devices, e g when protons from decaying neutrons are trapped and counted to determine the lifetime of the neutron (J Byrne et al., Phys. Rev. Lett. 65 [1990] 289) The first trapping and monitoring of an individual particle was performed in 1973 (D.J. Wineland et al , Phys Rev. Lett. 31 [19730] 1279) and an electron was continuously trapped for more than ten months (G Gabrielse et al., Phys. Rev Lett 54 [1985] 537). The most impressive of physics experiments on stored charged particles are probably those dealing with the g-value of the electron and the positron which date back to the sixties (H.G. Dehmelt et al , Phys. Rev. Lett 21 [1968] 127, G. Gräff et al., ibid. p 340) and culminated in measurements to 4 parts in 10^{12} (R Van Dyck, Jr , et al., Phys Rev Lett 59 [1987] 26) The stationary traps have furthermore been supplemented by movable systems, trapped electrons have been trucked across the U.S A (C H. Tseng et al., Hyp. Int 76 [1993] 381).

A feature of increasing interest in Penning trap research is the possibility of cooling the ion motions. Several techniques have been developed Light particles are subject to radiative cooling and also to resistive cooling by use of the coupling to an external tuned circuit. Recently, buffer gas cooling, which is very common in Paul traps, has been introduced for Penning traps as well (G. Savard et al., Phys. Lett. A 158 [1991] 247), where different modes of ion motion have to be coupled to prevent ion loss This coupling scheme is similar to the sideband cooling technique (H. Dehmelt, Nature 262 [1976] 777). To achieve extreme low ion temperatures, laser cooling can be employed. By this technique, ion clusters, i e crystal-like structures formed by trapped ions, have been observed (S.L. Gilbert et al., Phys. Rev. Lett. 60 [1988] 2022). Sympathetic cooling (D.J. Larson et al , Phys. Rev Lett. 57 [1986] 70) makes use of the interaction between different ion species where one of them is laser cooled In 'electron cooling' (G. Gabrielse et al , Phys Rev Lett. 63 [1989] 1360) antiprotons loose their energy to simultaneously trapped electrons and these in turn are cooled by synchrotron radiation

A major field of application is mass spectrometry. The cyclotron frequency of charged particles in magnetic fields is an ideal means for mass determination (ICR MS, ion cyclotron resonance mass spectrometry). Here two applications can be distinguished·

The mass (more specifically: the mass-over-charge ratio inferred from the cyclotron frequency) can be used to identify the trapped ion species, e g in investigations of the physical (as well as chemical) properties of atomic and molecular cluster ions. At Mainz, for example, we have developed a system that combines the advantages of ion storage and high-resolution ion selection (by resonant ejection) and/or detection (Fourier Transform ICR) with the sensibility of time-of-flight mass spectrometry (with ion counting techniques) by using the Penning trap as the first acceleration section of a Wiley-McLaren type mass spectrometer It has been used for collision induced dissociation studies and chemical reactions of small gold cluster ions (St. Becker et al , Fragmentation of Gold Clusters Stored in a Penning Trap, in preparation for Z. Phys. D). We will extend these investigations to other elements and other interaction schemes like ion or electron bombardment and photo detachment or fragmentation. Broad band mass spectrometry capabilities are also of interest to the analysis of highly-charged atomic ions (D A Church J Mod Optics 39 [1992] 423; S R. Elliott et al , EBIT Trapping Program, Hyp. Int., in print).

On the other hand, the ions may be already well-known and the investigation may aim at the most accurate mass determination possible. A very impressive example is the recent comparison of proton and antiproton mass which tests fundamental laws of physics. An improvement of a thousand as compared to previous results has been achieved (G. Gabrielse et al., Phys. Rev. Lett. 65 [1990] 1317). At Mainz, a system of two Penning traps has been developed for mass determinations of unstable nuclei for tests of nuclear models (St Becker et al. Int. J. Mass Spectrom. Ion Processes 99 [1990] 53-77; H. Stolzenberg et al Phys. Rev. Lett. 65 [1990] 3104). A similar set-up has been constructed for a metrological application, the accurate mass measurement of ^{28}Si (R. Jertz et al., Highly Accurate Determination of the Mass of ^{28}Si as a Contribution to a New Definition of the Kilogram, in preparation for Physica Scripta). The research groups of Pritchard, VanDyck, and Werth are working on similar problems (see e.g.: E.A. Cornell et al , Phys Rev Lett 63 [1989] 1674; F L Moore, Phys. Rev. A 46 [1992] 2653; Ch. Gerz et al., Z. Phys. D 17 [1990] 119)

The mass-to-charge ratios of the particles investigated range from that of the electron and positron to several (ten) thousands of amu/e for cluster ions, for example; i.e. they extend over almost eight orders of magnitude. Charged particles of matter and antimatter are investigated. And not only the inertial mass is being attacked. Penning traps may also play a significant role in a comparison of the gravitational mass of proton and antiproton (M H Holzscheiter in P. Carlson et al.[eds.] First Biennial Conf. Low Energy Antiproton Phys , World Scientific, Singapore, 1991).

The variety of experiments implies a variety of different trap designs optimized for their specific tasks, e g in respect to the creation and capture of the particles of interest. Ions may be created in the trap or (especially rare species) injected from external sources High energy antiprotons, for example, have to be slowed down from energies of several MeV to energies lower by several orders of magnitude (G. Gabrielse et al., Phys. Rev. Lett 57 [1986] 2504). In another experiment two Penning traps are employed and ion bunches of radioactive isotopes are transferred from one to the other (H. Schnatz, et al., Nucl Instr. Meth. A251 [1986] 17) The trap designs also differ in (optical and ion optical) access to the trap center, perfection of the electric (trapping) potential, magnetic field inhomogeneity and drift, excitation modes for manipulation of the ion motions, and/or detection schemes for the number of ions and/or their resonance frequencies For example, the electric trapping field is often shimmed by compensation electrodes (R S van Dyck, Jr et al., Appl. Phys Lett. 28 [1976] 446; G. Bollen et al , J. Appl. Phys 68 [1990] 4355) For high-accuracy spectrometry single ion detection methods are often used (G Gräff et al , Z Phys A 297 [1980] 35, R M Weisskopf et al., J Appl Phys 63 [1988] 4599). Alternatively, ion interactions are studied in detail (E A Cornell et al , Phys Rev A45 [1992] 3049)

The given space does not allow for a comprehensive review of the subject and the interested reader should refer to the literature given above and below. An overview of ion traps in general has been given by J Allison and R.M Stepnowski (Anal Chem 59 [1987] 1072A), on physics with ion traps by R.C. Thompson (Meas Sci. Technol. 1 (1990) 93-105) The principles of Penning traps have been thoroughly reviewed by Brown and Gabrielse (Rev Mod. Phys 58 [1986] 233) and high precision mass spectrometry with Penning traps by F Vedel and G. Werth (in C R.E. March, J F. Todd [eds.] Modern Mass Spectrometry, CRC Press, in preparation) Some aspects have been discussed in more FT-ICR oriented reviews by A.G. Marshall et al (Int J. Mass Spectrom. Ion Processes 118/119 [1992] 37) and by L Schweikhard et al. (Excitation Modes for FT-ICR MS, J. Am. Soc. Mass Spectrom., in print). Further detailed information can be found in various contributions to several workshops and conferences, as published e.g. in Physica Scripta (vol. T22 [1988] Phys of Low-Energy Stored and Trapped Particles, Stockholm, Sweden, June 1987, vol 46(3,6) Workshop on Physics with Penning Traps, Lertorpet, Sweden, June 1991), Hyperfine Interactions (vol. 76(1-4) Antihydrogen Workshop, Munich, Germany, July 92; Workshop on Traps for Antimatter and Radioactive Nuclei, Vancouver, Canada, Feb. 1993, to be published) and in the topical volume 39(2) [1992] of J. Mod Optics (Physics of trapped ions).

Biological Ion Trap Mass Spectrometry

Scott A. McLuckey
Analytical Chemistry Division, Oak Ridge National Laboratory
Oak Ridge, TN 37831-6365

The capability of the quadrupole ion trap for the analysis of high mass biomolecules has undergone remarkable growth over the past five years. Major advancements have been contributed by research groups at Purdue and Finnigan. A primary goal of our group at Oak Ridge has been to contribute to progress in this area as well. More recently, several other groups have joined in the development of the ion trap for biomolecule analysis reflecting a growing interest in the ion trap for biological research. This paper provides a brief overview of the current status of the ion trap as an analyzer for ions derived from high mass biomolecules and summarizes the efforts at Oak Ridge in this area over the past year.

Ion trap research at Oak Ridge this year directly related to biomolecule analysis can be divided into matrix assisted laser desorption (MALD) studies of mixtures (e.g. protein tryptic digests) [1], capillary electrophoresis combined with electrospray ion trap mass spectrometry [2], and the analysis of multiply-charged anions derived from oligonucleotides via ion trap tandem mass spectrometry [3]. MALD ionization of components of a tryptic digest of glucagon was performed including tandem mass spectrometry experiments. The latter capability makes the ion trap particularly attractive for tryptic mapping relative to time-of-flight mass analysis, for example. MALD ion trap experiments have also been successfully performed to distinguish tryptic digests of cytochrome C derived from horse, tuna, dog, and rabbit. These results, along with those contributed by other groups demonstrate the utility of the ion trap for analysis of ions derived from MALD.

Unlike MALD, electrospray is quite sensitive to matrix effects. For this reason, it is desirable to perform a separation step in the application of electrospray to a complex mixture. We have therefore devoted effort to solving problems associated with the coupling of capillary electrophoresis with electrospray and the ion trap. For example, we have applied random noise collisional activation both to reduce background in the total ion chromatogram and in the mass spectrum and to induce fragmentation in peptides in an on-line separation without mass selection or frequency tuning. In the former application, a relatively low amplitude signal is applied during the ion injection process to induce fragmentation of weakly-bound clusters. These species otherwise tend to fragment on the time frame of the ion trap experiment resulting in chemical noise in the spectrum. In the latter application, a relatively high noise signal is applied to the end-caps after ion injection sufficient to induce dissociation of the analyte ions. The goal of this work is to provide the capability for obtaining extensive structural information from a complex mixture, such as a protein tryptic digest, from a single injection of a sub-picomole/component mixture.

We have expended considerable effort over the past few years in understanding the behavior of multiply-charged oligonucleotides under ion trap collisional activation conditions. We believe that we now have a good overall understanding of these species, at least for oligomers of up to about 20 bases. This size currently constitutes the largest oligomer that we have yet studied. Figure 1, for example, shows the MS/MS spectrum of the $(M-12H)^{12-}$ anion derived from electrospray of 5'-d(AGCTAGCTAGCTAGCTAGCT)-3' acquired using random noise collisional activation. The major fragments are labelled and correspond to those predicted from our previous studies of smaller oligonucleotides. Complete sequencing of this oligomer is not possible from the major

fragment ions. However, all of the lower intensity fragments arise from various sequential decompositions. Perhaps with automated interpretation algorithms based on the rules of decomposition derived from our previous studies, extensive sequence information might be derived from a single MS/MS spectrum such as this one can be determined. We have made some initial steps in this direction [4].

[1] Chambers, D.M.; Ramsey, R.S.; Goeringer, D.E.; McLuckey, S.A.; Glish, G.L. Unpublished Results.
[2] Ramsey, R.S.; McLuckey, S.A.; Van Berkel, G.J.; Asano, K.G. Unpublished Results.
[3] McLuckey, S.A.; Habibi-Goudarzi, S. J. Am. Chem. Soc., Submitted.
[4] Hart, K.J.; Habibi-Goudarzi, S.; McLuckey, S.A., Unpublished Results.

Research involving electrospray was sponsored by the National Institutes of Health under Grant GM 45372. MALDI work was sponsored by the Office of Basic Energy Sciences of the U.S. Department of Energy. Oak Ridge National Laboratory is operated for the Department of Energy under Contract DE-AC05-84OR21400 by Martin Marietta Energy Systems.

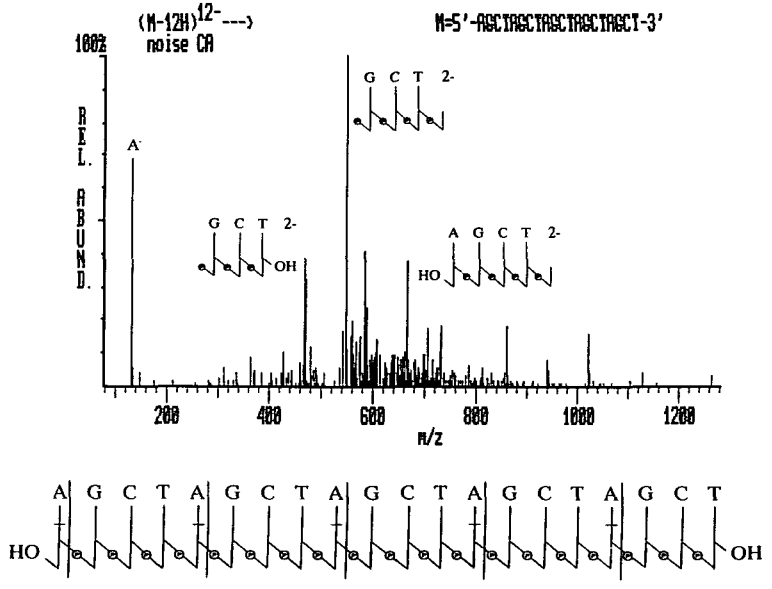

"The submitted manuscript has been authored by a contractor of the U.S. Government under contract No. DE-AC05-84OR21400. Accordingly, the U.S. Government retains a nonexclusive, royalty-free license to publish or reproduce the published form of this contribution, or allow others to do so, for U.S. Government purposes."

Fundamentals and Recent Applications on an Atmospheric Pressure Ionization-Differentially Pumped Benchtop Ion Trap, Jack Henion, Alexander Mordehai, H.K. Lim, and Jianyi Cai, Drug Testing and Toxicology, NYS College of Veterinary Medicine,
Cornell University, 925 Warren Dr., Ithaca, NY 14850

INTRODUCTION

The pioneering efforts which incorporated electrospray ionization capability on the ion trap by the Oak Ridge National Laboratory (ORNL) group[1] has opened entirely new fields of research and applications capability for the ion trap. Recently we implemented atmospheric pressure ionization (API) technology on a benchtop IT mass spectrometer. There are several new features incorporated in our design: a liquid shield API ion sampling interface[2a], differential pumping of ion trap and electron multiplier regions for high helium pressure ion trap operation[2b] and recently two new computer IT operation modes for achieving selected windows ion monitoring(SWIM) mode. The focus of this report includes fundamental and applied aspects of this new system.

The liquid shield API interface provides an efficient means for on-line coupling of modern separation techniques such as capillary electrophoresis(CE) and high performance liquid chromatography (HPLC) with a mass spectrometer. Both micro-(a few uL/min) and megaflows(1mL/min) of HPLC effluents can be accommodated without splitting under ion spray conditions. Recently, we also implemented atmospheric pressure chemical ionization (APCI).

EXPERIMENTAL

One of the fundamental aspects of the new system is operation under high helium pressure (up to 1 x 10^{-2} Torr) to provide optimum trapping efficiency. It was found that the trapping efficiency for externally produced ions increases with increasing helium pressure in the trap with some mass resolution decrease. The optimum conditions were established at a pressure 5 x 10^{-3} Torr to provide unit mass resolution across the mass range (up to 650 Da). This higher helium pressure is unique for ion trap operation in our system so it was of interest to study the possible consequence of this aspect on major principals of ion trap operation such as resonance ion injection-excitation phenomena. To study the resonance phenomena a second computer (IBM 486) with an arbitrary wave form generator was implemented to allow the application of computer-designed wave-functions *(harmonic, chirp or broad-band) to the end-cap IT electrodes. It was found that harmonic* signals of 5-10 Vo-p efficiently eject resonating ions from the trap in the z-direction even at pressures of 5 x 10^{-3} Torr helium. To apply ion ejection technology for chemical noise reduction in analytical applications we synthesized a broad-band time domain signal(10 Vo-p, frequency range 25-500 kHz, step-quadratic phase encoding) with frequency notch at 50 kHz of 20 kHz width. Application of a such time-domain signal to the end-caps during the ionization event allows one to accumulate selectively only ions of interest in ~100 Da mass window while ejecting all other ions from the trap.

RESULTS AND DISCUSSION

The developed system was applied to some simple on-line analytical separations. As an example of micro-flow applications Figure 1 shows the standard curve from the CE/MS analysis of low fmol levels of isoquinoline alkaloids found in the bark of a medicinal tree that grow in Taiwan. This experiment was performed using 10 uL/min sheath-flow (no SWIM). Quantitative CE/MS analysis for berberine was done using

tetrahydroberberine as internal standard (RSD = 0.998). Figure 2 illustrates the use of SWIM for improving sensitivity and reducing chemical noise under on-line ion spray LC/MS conditions with a synthetic mixture containing three Benzodiazepines drugs (1 ng of each injected on-column) at a flow rate of 1mL/min (no split!). These results suggest that conventional-bore HPLC columns and their accompanying 1 mL/min flow rates may be used for high sensitivity LC/MS using the ion trap equipped with this API interface.

1. S.A. McLuckey, G.J. Van Berkel, C.L.Glish, *J. Am. Chem. Soc.*, **112**, 5668(1990)
2. a: A.V. Mordehai, G.H. Hopfgartner, T.G. Huggins, J.D. Henion, *Rapid Commun Mass Spectrom. (RCM)*, 6, 508(1992); b: A.V. Mordehai, J.D. Henion. *RCM*. 7. 205(1993)

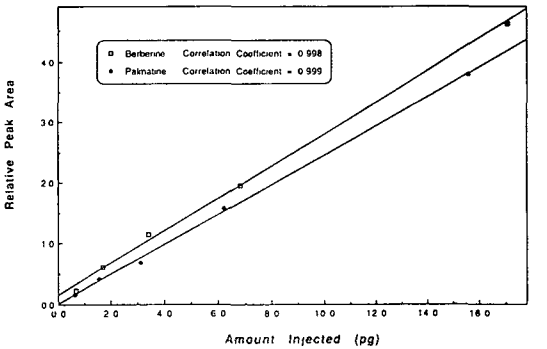

Fig.1 Calibration curve for on-line quantitative CE/MS analyses isoquinoline alkaloids from bark extract. Berberine and palmatine with tetrahydroberberine as internal standard

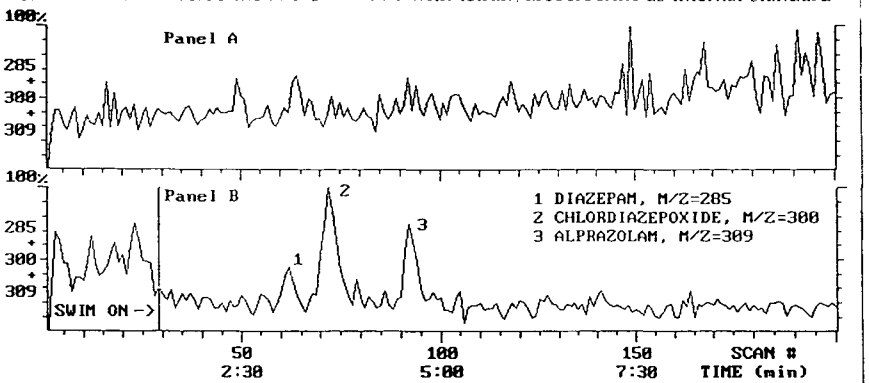

Fig. 2. Ion spray HPLC analysis of a synthetic mixture containing three benzodiopines drugs (1ng of each): flow 1mL/min, column Zorbax C-18, 4.6 x 150 mm, mobile phase 40/25/35 $CH_3CN/CH_3OH/H_2O$ 15 mM ammonium formate. Panel A acquired without SWIM; panel B aquired in SWIM mode.

ESTIMATION OF THE POLARIZABILITY OF GASEOUS IONS BY ION TRAP MASS MEASUREMENTS.

O Bortolini[a], S.Catinella[b], P Traldi[b]

a.Dipartimento di Chimica, Via L Borsari 46, 44100 Ferrara (Italy).
b. CNR, Servizio Spettrometria di Massa, C so Stati Uniti 4, 35100 Padova (Italy).

Significant mass displacements from the expected instrumental value have been observed with several odd and even electron cations[1]. This phenomenon could be, in principle, ascribed to many factors either instrumental or related to the intimate properties or reactivity of the ionic species investigated (space-charge effects, gas-phase ion-molecule interactions, supplementary a.c voltage effects or radiofrequency field effects)

Experiments devoted to the reduction of the ion concentration ruled out the influence of possible space-charge effects[2]. Moreover, the occurrence of chemical interactions among the ions stored within the ion trap was investigated by introducing a reaction time of variable length before the main r f. ramp. Chemical interactions should be time dependent and hence the negligible differences found in the δ_m values for increasing reaction times[2] exclude the involvment of these interactions on the observed mass displacements
The occurrence of an interaction between the ionic species with the auxiliary a.c. voltage was confirmed by two experiments consisting in the reduction of the intensity of selected $[M]^{+\cdot}$ ions with respect to the tickle voltage and in the measure of the mass displacement of the same ion generated either by collision or by the usual mass analysis[2]

Thus the phenomenon of mass displacement must be rationalized in terms of interaction of specific chemico-physical properties of the analytes and the radiofrequency field. The result of this interaction is a small, but well detectable, power comsumption of the r f. field, that reflects on the ejection of the ions at different q_z values (that is at different $V_{r.f.}$ values) This chemico-physical property was recognized to be the polarizability[3] that can lead to interaction with the radiofrequency field on the electron shell about a nucleous (electron polarizability) and/or may result from the forced alignment of the permanent dipoles along the field direction (dipolar polarizability) The polarizability, in fact, is the only property that can account for the different mass displacements observed with isobaric ions of equal elemental composition, but different structure or for the experimental observation that the δ_m increases as the dipole moment of the analyte increases Additional support to this hypothesis was found in the results obtained with isobaric ions of equal elemental composition but different structure analyzed by a quadrupole mass filter. Again, different mass values were found for different isomers, proving that the mass displacement phenomenon is general and occurs when ions experience quadrupole fields[4].

The mass displacements have been measured for a set of substituted benzene molecular cations For ions possessing a small or negligible dipolar component the mass displacements δ_m well correlate with the calculated electron polarizability, as shown in Figure 1 for of alkylbenzene ions[3]

[1] P.Traldi, O.Curcuruto, O.Bortolini Rapid Commun. Mass Spectrom. **1992**, 6, 410
[2] P.Traldi, D.Favretto, S Catinella, O Bortolini Org Mass Spectrom. **1993**, 28, 000.
[3] O Bortolini, S.Catinella, P Traldi Org Mass Spectrom **1993**, 28, 000.
[4] P.Traldi, D.Favretto Rapid Commun. Mass Spectrom **1992**, 6, 543

Figure 1 δ_m as a function of the calculated eletron polarizability α_o.

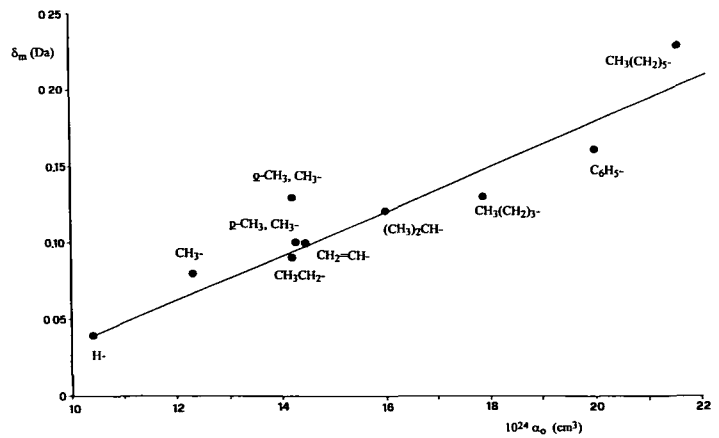

ION REMEASUREMENT IN FOURIER TRANSFORM ION CYCLOTRON RESONANCE MASS SPECTROMETRY

C. L. Hendrickson, V. L. Campbell, Z. Guan and D. A. Laude, Jr. Department of Chemistry and Biochemistry, University of Texas at Austin, Austin, TX, 78712

Mass spectrometric detection is usually characterized as a destructive technique in which ions formed from the neutral analyte are detected by collision at the surface of a current-amplifying device. In contrast, Fourier transform ion cyclotron resonance mass spectrometry (FTICR) is distinguished from other mass analyzers because the basis for signal detection is the mass-dependent periodic fluctuation in image current generated by spatially coherent ion packets that pass in proximity to the detector electrodes of a trapped ion cell. Thus the FTICR detection process is not inherently destructive and the possibility exists that the ion population can be remeasured as a means to enhance the analytical signal or perform more intricate physical measurements. Unfortunately, FTICR remeasurement is complicated by competitive relaxation processes in the cell[8] and in most cases remeasurement efficiency would be small because the spatially focused ion population is not conserved.

Should an efficient approach to relaxation be found, then the remeasurement experiment as depicted in Figure 1 would become feasible. In this pulse sequence an initial population of ions is injected into the mass spectrometer, the axial motion is cooled and then an excite and detect event occur. At this point, rather than quench the ion packet, a remeasurement delay period occurs. This period, whether active or passive, must accomplish the task of returning the ion population to the center of the cell. McLafferty first demonstrated that for large molecules the angular distribution of ion trajectories after collision with small neutrals decreases as ion mass increases. Consequently, an ensemble of large biomolecular ions initially formed in the center of the trapped ion cell would be more likely to return to its orbiting center following excitation of the cyclotron mode for FTICR detection. We have demonstrated that unit remeasurement efficiency can be achieved for electrosprayed protein ions and real gains in signal enhancement can be achieved remeasuring the same ion population. Shown in Figure 2 are comparison FTICR spectra of Bovine albumin dimer remeasured 250 times after a 2 sec. cooling delay to obtain a 15-fold increase in S/N.

We have investigated conditions under which remeasurement efficiency is maximized. In general it is essential to minimize the radial electric field experienced by an ion during the course of the experiment because for this passive experiment there is necessarily a continuous outward movement of the ion as a consequence of each excite event. Shown in Figure 3 is a plot of electric field as a function of radial displacement for several trapped ion cells. What the data suggest is that remeasurement should be most readily accomplished in an elongated closed cell. We find this to be the case. Where unit remeasurement is achieved in a cell of aspect ratio two, both cubic closed and open cells exhibit far poorer remeasurement efficiency.

The remeasurement experiment just described is most effective for large molecules. It would be of great interest if the remeasurement process could be extended to small ions. To accomplish this, however, it is necessary to overcome the growth of the magnetron radius for the ion. Two approaches have been suggested for this type of cooling and therefore offer the potential for use in a remeasurement experiment. For example, following from work by Becker and coworkers, Marshall has recently shown that the magnetron radius can be decreased by inhomogeneous collisional cooling effects upon conversion of motion to the cyclotron mode. Jacoby and coworkers have demonstrated operation of the FTICR trapped ion cell as a Paul trap

to facilitate high pressure cooling of ions to the center of the cell. We have constructed a combined RF-ICR trap based upon an electromagnet system for the purpose of investigating these two types of cooling. The spectrometer was successfully constructed and preliminary data for cooling of naphthalene ions by both quadrupolar excitation and by RF cooling have been attempted. Shown in Figure 4 and 5 are preliminary data for the two techniques that suggest that cooling of the excited ion cloud for a small ion is possible. The effectiveness of the cooling appears to be similar for the data.

Ultimately it is realistic to expect that ion motion in the FTICR trapped ion cell will be sufficiently controlled to arbitrarily create and manipulate any ion population as desired. The present demonstration of nondestructive FTICR mass spectrometry is a specific example of this progress which increases the parallels to FTNMR and should provide new avenues for investigation in FTICR.

Figure 1

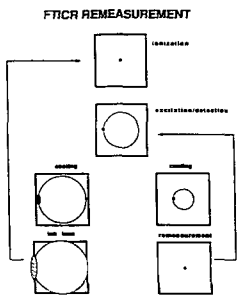

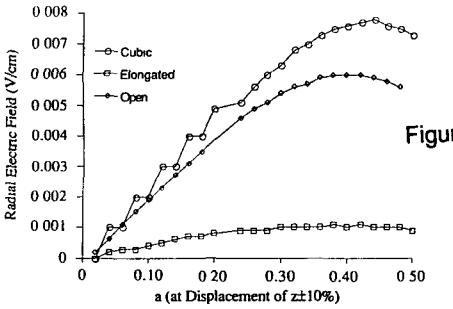

Figure 3

Figure 2

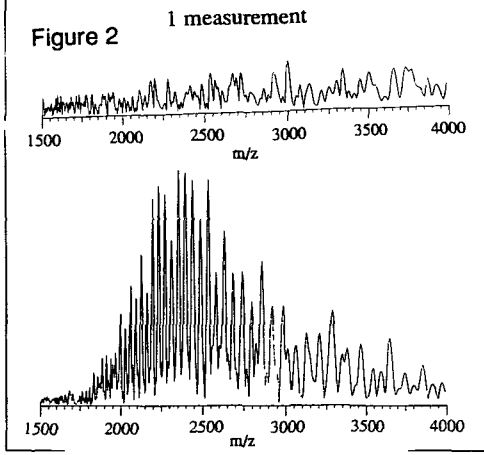

Figure 4 RF-Cooling

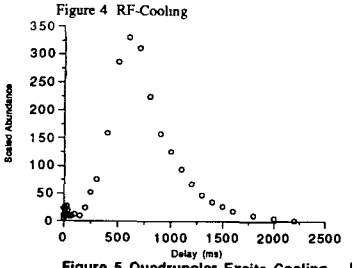

Figure 5 Quadrupolar Excite Cooling

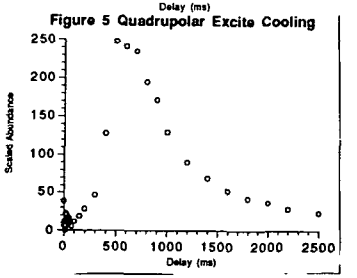

Characterization of Large Linear Molecules by Tandem Mass Spectrometry.

*Fred W. McLafferty, Steven C. Beu, Michael W. Senko, and Peter B. O'Connor. Chemistry Department, Baker Laboratory, Cornell University, Ithaca, NY 14853-1301.

Amino acid sequencing of oligopeptide (<3 kDa) mixtures is now done routinely by tandem mass spectrometry (MS/MS). Soft ionization produces a mixture of molecular ions separated by MS-I; dissociation of each separated ion species and MS-II mass analysis then provides the sequence information for each mixture component. Similar characterization of several kDa carbohydrates, nucleotides, and polymers have also been reported; this describes preliminary results of efforts to extend this technique to molecules at least an order of magnitude larger using electrospray ionization (ESI)/Fourier transform (FT) MS.

ESI has the advantage that even the highest mass ions still have small m/z values of 600-2000; heterodyne FTMS provides simultaneous measurement of all these peaks with resolving powers $>10^5$ and mass measuring accuracy of a few ppm. Such unit mass resolution of isotopic peaks also provides a mass scale to determine both m and z values, which is especially critical for MS-II spectra containing scores of fragment masses. The non-destructive ion detection in FTMS is also unique, so that the trapped ions can be measured repeatedly to improve signal/noise and can also be reacted and mass analyzed sequentially (MS^n); such multiple spectra can be measured simultaneously with Hadamard transform techniques. Characterization of trapped ions can not only be done by a variety of dissociation techniques, but also by ion-molecule reactions indicative of their three-dimensional structure. The potential for sequence information is illustrated using the ionic fragments from nozzle-skimmer dissociation of carbonic anhydrase (29 kDa) measured simultaneously by FTMS, followed by collisionally-activated dissociation of the Y_{67}^{7+} fragment ion.

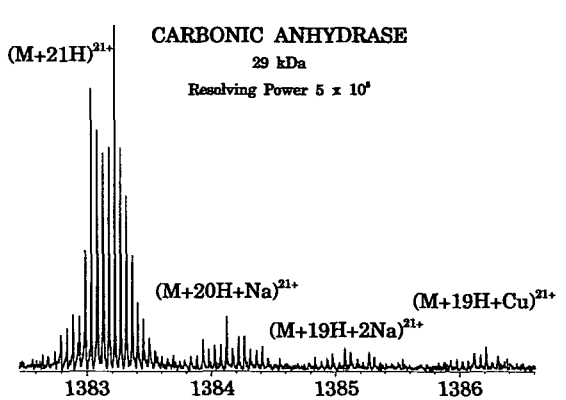

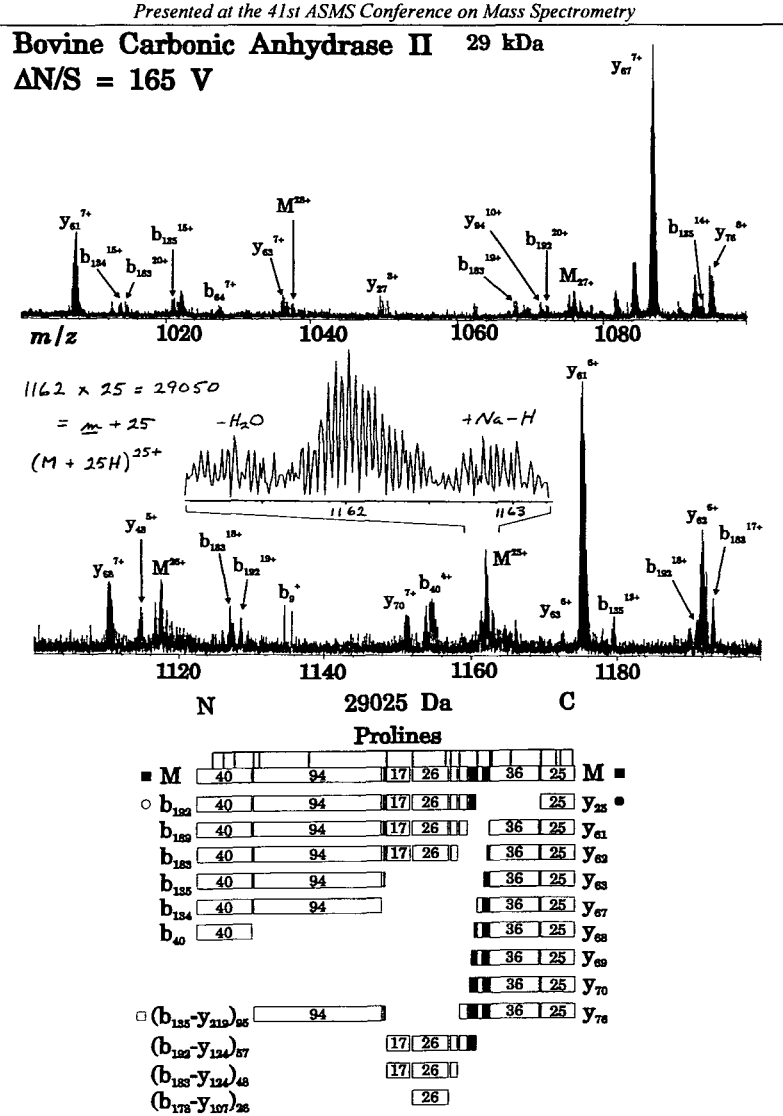

REMEASUREMENT AND COLLISIONAL THERMALIZATION OF IONS BY QUADRUPOLAR EXCITATION IN A FOURIER TRANSFORM MASS SPECTROMETER[1]

Cynthia C. Pitsenberger, Cheryl A. Turner, Ping P. Wang, Greg S. Gorman, J. Paul Speir, *I. Jonathan Amster
Department of Chemistry, University of Georgia, Athens, Georgia, 30602

Quadrupolar excitation of ions with collisional cooling was first proposed by and demonstrated in a Penning trap by Savard et al. More recently, Marshall and coworkers have demonstrated axialization of ions in a dual cell FT-ICR, in which quadrupolar excitation occurred in one cell, and ion detection occurred in a second cell. Here we report quadrupolar excitation in a single cell FT-ICR instrument, and present several examples of the capabilities of this technique, as well as applications to ion chemistry studies.

The axialization of ions is found to occur with high efficiency, by using quadrupolar excitation in combination with collisional cooling. Ions of Rhodamine 6G, formed by laser desorption, can be remeasured over 500 times by axialization of the ions after detection, allowing a substantial increase in the S/N of the detected signal. Figure 1 shows the improvement in S/N that is obtained by remeasuring the m/z 443 ion of Rhodamine 6G 200 times, with signal averaging. The S/N is found to improve by a factor of 12. The remeasurement efficiency for this experiment was found to be greater than 99.5%.

An important feature of this method is that it allows ions to be retained in the ICR analyzer cell while they are exposed to thousands of collisions. Naphthalene ions can be retained after more than 100,000 collisions with methane. Quadrupolar excitation has been used to relax the excited states of transition metal ions, formed by laser ablation of a metal foil, by collisional thermalization. The reactions of thermalized transition metal ions with laser desorbed neutral molecules of peptides and amino acids have been studied. We find that the observed products of such reactions are quite different for metal ions that are thermalized with 5,000-10,000 collisions using quadrupolar excitation than for metal ions that undergo conventional thermalization with 50-100 collisions.

In addition to the capabilities for ion remeasurement and collisional thermalization, we have found that quadrupolar excitation with collisional thermalization increases mass resolution, by increasing the duration of the transients that are produced. Without quadrupolar excitation, laser desorbed m/z 443 ions of Rhodamine 6G produce a transient that lasts approximately 100 ms. When the ions are centered in the cell by quadrupolar excitation before their detection, coherent motion is found to persist for more than 2 minutes. The Fourier limited resolution for a 64 s transient of this mass in our 1 tesla instrument is $1x10^6$, but the observed resolution is $1x10^5$. "Dissection" of the transient reveals frequency drifts of the order of 0.1 Hz/s.

1. Portions of this work have been accepted for publication in *Analytical Chemistry*.

RHODAMINE 6G - EFFECT OF SIGNAL AVERAGING WITH REMEASURED IONS

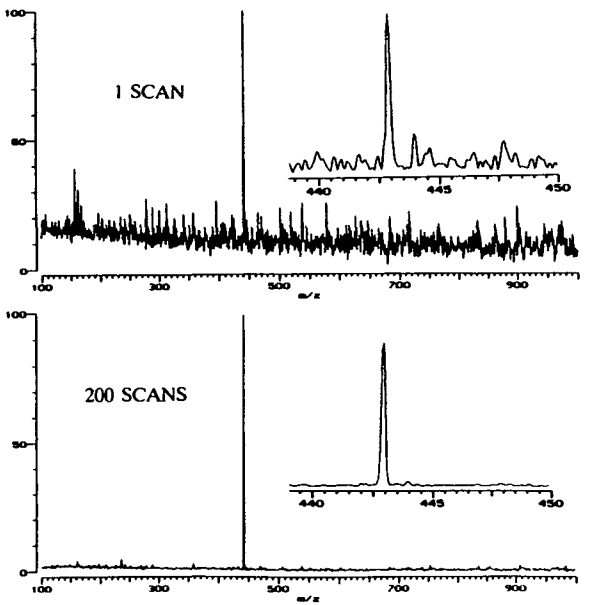

Figure 1. (Top) The mass spectrum obtained from 1 measurement cycle of Rhodamine 6G, formed by laser desorption, after quadrupolar excitation and collisional thermalization. (b) The mass spectrum of the same ions as in a, but remeasured 200 times with signal averaging shows a 12X increase in S/N over the mass spectrum in (a).

AVERAGING THEORY FOR ION MOTION IN A CUBIC FT-ICR CELL

Dale W. Mitchell, Bryan A. Hearn and Stephen E. DeLong

Department of Geological Sciences
University at Albany-S U N.Y.
Albany, New York 12222

The widely employed cubic ICR cell [1] offers an ideal test case for investigating the effects of electric field inhomogenieties and other perturbations on ion motion. This is because the motion of an ion in a cubic cell can be well approximated by simple harmonic oscillations (the quadrupolar approximation) with all other effects treated as perturbations. Also, the electric fields have exact solutions whose lowest order expansions are adequate zero-order approximations. Averaging methods which are based on transforming from a cartesian coordinate system to the amplitude-phase representation whose variables are the mode-radii and phases can greatly simplify the analysis of complicated problems. With the help of these methods, the essential physics can frequently be extracted from an otherwise intractable problem in a consistent manner, thereby allowing for the development of simple yet reasonably accurate models for physical processes. These methods have been applied to the calculation of frequency shifts from trapping field inhomogenieties [2] as well as the effects of excitation field inhomogenieties on ICR ion motion [3]. Here we outline results for the relatively simple case of low mass ions in a linearly polarized electric excitation field with magnitude E, cell length d and magnetic field B as shown in Fig.1 Only the linear terms are retained which allows for comparison with other results. We have only retained the resonance at $\omega_e = \omega_+ \approx qB/m$ which leads to simple solutions For on-resonance excitation, we find that the cyclotron radius $r_+(t)$ is

$$r_+(t) = \{r_{+0}^2 + (Et/2B)^2 + (Etr_{+0}/B)\sin(Q_{+0})\}^{1/2} \qquad (1)$$

where r_{+0} is the initial cyclotron radius and $Q_{+0} = \beta_{+0} - \beta_e$ is the difference between the initial cyclotron phase and the excitation phase, for the geometry shown in Fig.1 ($\beta_{e=0}$ in Fig.1). Figure 2 shows $r_+(t)$ calculated from Eq.(1) for an initial cyclotron radius of 0.25d for different values of initial phase. The phase $Q_+(t) = \beta_+(t) - \beta_e$ is related to $r_+(t)$ by the simple relation

$$\cos(Q_+(t)) = [r_{+0}/r_+(t)]\cos(Q_{+0}) \qquad (2)$$

Figure 3 gives plots of this quantity for different initial cyclotron radii for $Q_{+0} = -\pi/4$. The process of ICR phase synchronization during on-resonance excitation is contained in Eq.(1) and Eq.(2). The phase difference $Q_+(t)$ approaches $\pi/2$ as $r_{+0}/r_+(t) << 1$. From the geometry given in Fig.1 this value for the phase corresponds to the ion velocity being in-phase with the excitation field, as expected

[1] M.B. Comisarow, Adv. Mass Spectrom., 8 (1980) 251.
[2] D.W. Mitchell, Int. J. Mass Spectrom Ion Processes, 107 (1991) 417.
[3] D.W. Mitchell, B.A. Hearn and S.E. DeLong, Int. J. Mass Spectrom. Ion Processes (in Press).

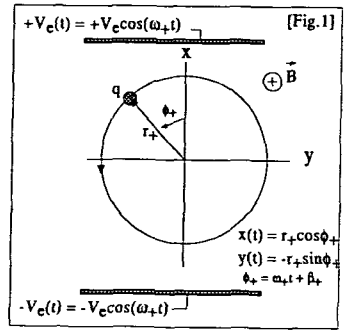

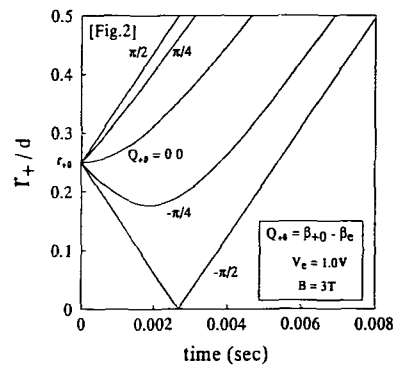

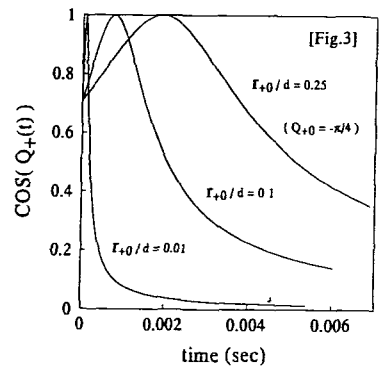

Mass Determination of Trapped Micro-particles and Macro-ions by Optical Techniques (and Subsequent Chemical Analysis by Laser Pyrolysis Mass Spectrometry)

Gyorgy Hars*, Neil S. Arnold and Henk L.C. Meuzelaar
Center for Micro Analysis & Reaction Chemistry
University of Utah, Salt Lake City, UT 84112

* Visiting scientist from TU Budapest, Hungary

Extensive analytical interest in characterization of particulate matter extends in many applications to evalution of individual micro-particles. For complete chemical characterization of individual microparticles adequate measurements of both particle physical characteristics (e.g., size, mass) and chemical constituents are required. Like molecular species, particles may also be readily ionized and manipulated by electrical techniques based on mass to charge ratios. An approach favored by the authors would provide an accurate mass determination which could be followed by laser pyrolysis (ionization) mass spectrometry to determine the chemical composition. Both measurements can be carried out in the same ion trap but they require different electrical operating conditions. For particle mass determination the ion trap operates as an Electrodynamic Balance (EDB) [1] while the compositional analysis is performed in the Ion Trap Mass Spectrometer (ITMS) mode. Figure 1 shows the typical operating parameters for both of the two modes. For macro-ions and submicron particles the distinction between ions and charged particles may become blurred making it profitable to consider the ability to make mass measurements of individual submicropartciles based on optical detection techniques.

The present investigation utilized the apparatus illustrated in Figure 2. A 10 mW HeNe laser illuminates the particle through a 3 mm hole in the ring electrode. A high sensitivity CCD camera with a zoom lens detects 90° scattered light via a second hole in the ring or via a hole in the end cap. Particles are introduced from suspension in water or alcohol by syringe needle inserted through the end cap. Strong electric fields used for trapping provide particle charging in a "quasi electrospray" ionization manner.

In classical EDB operation, gravitational force is offset by a DC potential applied in a dipolar mode to the two end caps making it possible to calculate the mass to charge ratio from the DC voltage applied. To obtain an accurate measurement the particle is damped to a small trajectory at the center of the trap and the end cap voltage measured (see Figure 3). Such measurements have been made to a relative accuracy of 1 in 10^5 [2]. In ITMS mode, secular oscillations of various ions are used to selectively eject ions. These same oscillations could be used to detect macro-ions, but the rapid motion (>100 Hz) and poor light scattering tend to make optical detection impractical. One means to overcome this limitation is to excite "standing" patterns reinforced by repetition of the same trajectory. This is not readily obtained in the r-z plane, but if viewed through an endcap the particle is seen to traverse an elliptical "Lissajous" pattern in the x-y plane. Superimposed on this pattern are drive frequency oscillations forming a "star" pattern as in Figures 4 and 5. This pattern will rotate unless the trapping frequency is an exact integer multiple of the radial secular frequency. By measuring the precession rate the secular frequency is determined allowing the m/z value to be calculated. At present the resolution is limited by a "beating" of 2 radial secular frequencies causing the "star" to collapse to a line every 3-10 seconds. In spite of this limitation current m/z measurements can be made to 1 part in 10^3. Finally, actual mass measurements (rather than m/z measurements) may also be utilizing single electron loss events induced by UV radiation. In principle, therefore it is possible to determine the mass of a single macro-ion in the 10^9-10^{12} a.m.u. range with similar precision. Calculations suggest the possibility of extending this approach to particles in the 10^1-10^2 nanometer range (10^6-10^9 a.m.u.), thus indicating the feasibility of developing a novel optical method for high precision mass determination of a single macro-ion.

Acknowledgements

This work was sponsored by the U.S. Army Research Office (Grant #DAAL03-91-G-0296). The authors would like to acknowledge helpful discussions with Drs. Randy Long (ARO) and Asit Ray (University of Kentucky).

References

1. Davis, E.J. and Ray, A.K., *J. Colloid Interface Sci.* 75, 2 (1980) 566.
2. Philip, M.A., Gelbard, F., Arnold, S. *J. Colloid Interface Sci.* 91,2 (1983) 507.

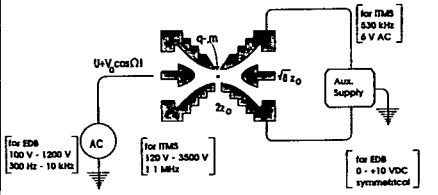

Figure 1. Schematic of the EDB/ITMS arrangement. The operating conditions are displayed in parentheses.

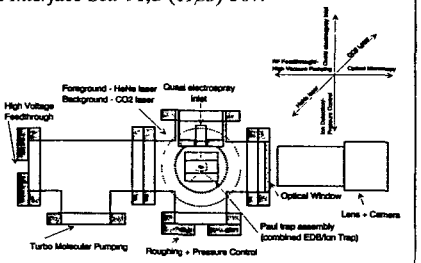

Figure 2. Physical layout of the experimental setup. The direction of optical observation of the particle is normal to the illuminating HeNe beam. The pyrolyzing carbon dioxide laser beam is parallel to the HeNe laser beam. The ions created by the pyrolysis are emitted in vertical z direction.

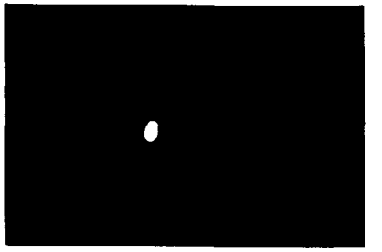

Figure 3. The effect of 10^{-4} torr He buffer gas. The particle is standing still in the center of the trap during the EDB measurement.

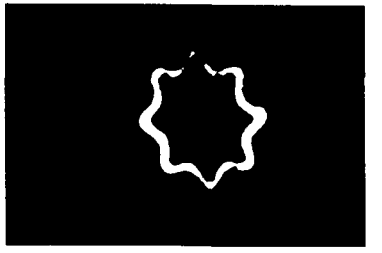

Figure 4. Eight point star pattern of a 1 micron particle in the equatorial plane of the ion trap.

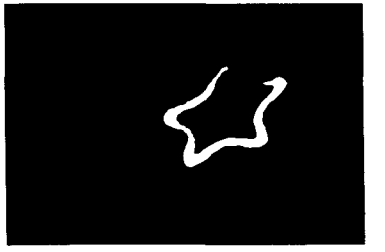

Figure 5. Five point star pattern of a 1 micron particle in the equatorial plane of the ion trap.

Non-Linear Resonance Effects During Ion Storage In a Quadrupole Ion Trap

Donald M. Eades* and Richard A. Yost
Department of Chemistry, University of Florida, Gainesville, FL 32611

Introduction

Realistically, construction of a purely quadrupolar ion trap is both impossible and impractical. Thus, all ion traps possess, to some degree, contributions from higher-order fields due to distortions in the quadrupolar field. Higher-order fields cause the resulting trapping field strength to no longer be linear with distance from the center of the trap. The resulting non-linear resonances (NLR) occur at specific ion frequencies which are unique to the contributing higher-order field. NLR's for hexapolar, octapolar, and dodecapolar fields are shown graphically on the Mathieu stability diagram in **Figure 1**. When stored at values of q_z (RF voltage) and a_z (DC voltage) corresponding to a NLR, an ion can absorb power from the higher-order field resonance causing frequency shifts [1] or ion ejection and/or collision-induced dissociation (CID) [2]. The work presented here shows experimental data used to characterize NLR effects on stored ions. All experiments were performed on a Finnigan MAT ion trap mass spectrometer which was controlled by ICMS v. 2.2 software [1]. The $C_2H_5^+$ ion (m/z 29) of methane was mass-selected and used as a chemical probe.

Results and Discussion

When storing mass-selected $C_2H_5^+$ ions (m/z 29) of methane for 50 ms at various q_z values along the a_z=0 line, m/z 29 ion intensity exhibits minima at q_z=0.65 and 0.80, mirrored by an increase in the ion intensities of m/z 27 and 41. At these points, $C_2H_5^+$ absorbs power from the octapolar (β_z=1/2) and hexapolar (β_z=2/3) NLR's and undergoes CID losing neutral H_2 to yield $C_2H_3^+$ (m/z 27) which then reacts with neutral methane to yield $C_3H_5^+$ (m/z 41). This chemical system was found to be very useful for characterizing NLR effects and was used as a probe to map the *experimental* stability region for $C_2H_5^+$. The results, displayed in **Figure 2**, show that the *experimental* stability region exhibits unstable regions along iso-β lines corresponding to β_z=1/3 (dodecapolar), β_z=1/2 (octapolar), β_z=2/3 (hexapolar), and β_r=1/2 (octapolar).

Factors contributing to the observation of NLR effects include: 1) ion displacement from the center of the trap, 2) ion population, 3) storage time, and 4) storage conditions (q_z,a_z values). Ion displacement influences NLR effects since the field at the center of the trap is nearly purely quadrupolar, with deviations observed only in the outer regions. Thus when displaced, ions interact with higher-order fields more than when in the center of the trap. Ion population directly influences the observation of NLR effects. Ion-ion repulsions cause displacement from the center of the trap and, when stored near a NLR, ions interact with the higher-order fields. This can be seen in **Figure 3** in which the higher ion population of $C_2H_5^+$ shows markedly increased ion losses when stored near q_z=0.65, a_z=0. Ion storage time exhibits a linear relationship to ion loss when storing near a NLR. Longer storage times allow more time for the ions to absorb power and thus undergo CID and ion ejection. This can be seen in **Figure 4** in which compares storage times near q_z=0.65, a_z=0.

Conclusions

Non-linear resonance effects can potentially affect any experiment in which the ions are stored at a q_z,a_z combination corresponding to a higher-order resonance. Factors enhancing NLR effects include ion dispacement from the center of the trap, high ion population, and long storage

times. Due to these factors, experiments such as resonant excitation, kinetic studies, ion injection, and chemical ionization can be particularly affected. It should be pointed out, however, that contributions from higher-order fields are not entirely detrimental. Indeed, Louris et al. [3] have reported improved resolution with the introduction of higher-order by the stretched design. Also, Franzen [1] has reported improved trapping efficiency with superimposed octapolar fields.

The authors acknowlegde the US-EPA/EMSL (Cincinnati) for funding this project. The authors thank Nathan A. Yates for valuable software development and helpful discussions.

[1] Franzen, J. *Int. J. Mass. Spectrom. Ion Proc.* 1991, 106, 63.
[2] Developed by Nathan A. Yates, University of Florida.
[3] Louris, J.N.; Stafford, G.C.,Jr.; Syka, J.E.P.; Taylor,D. *Proceedings of the 40th ASMS Conference on Mass Spectrometry and Allied Topics*; Washington, D.C., May 1992; p 1003.

Figure 1

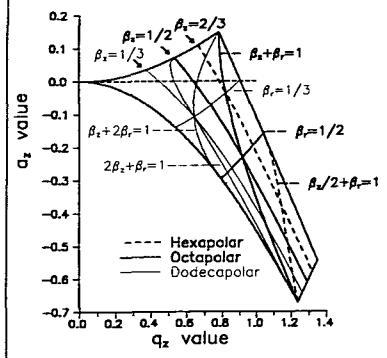

Figure 2

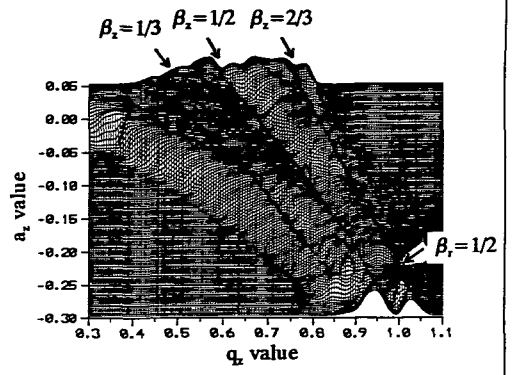

Figure 3

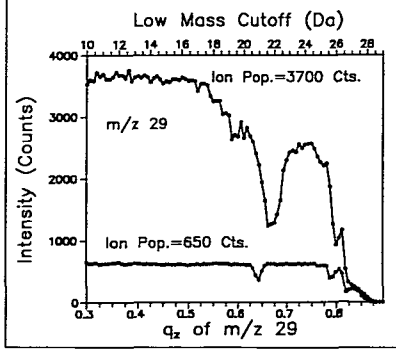

Figure 4

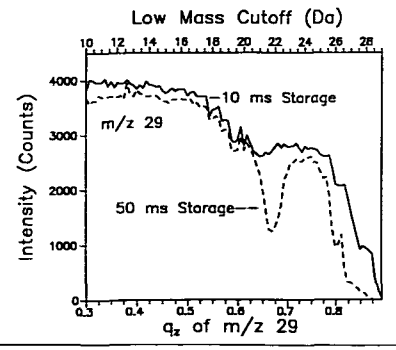

DEVELOPMENT OF AUTOMATED SELECTED ION STORAGE FOR QUADRUPOLE ION TRAP MASS SPECTROMETRY

Barrie A. Shaffer, Joe Karnicky, and S.E. Buttrill, Jr.,
E.L. Ginzton Research Center, Varian Associates,
3075 Hansen Way, Palo Alto, CA 94304-1025

Quadrupole ion trap mass spectrometry has long been known to be an extremely sensitive technique for mass detection. Its sensitivity, however, is limited by the finite capacity of the ion trap for storage of ions. In applications such as gas chromatography/mass spectrometry (GC/MS) the compound of interest is often present at levels small compared to the amount of chemical background resulting from dirty samples or other sources. Selected Ion Storage (SIS) may be used to selectively store a particular ion mass or range of ion masses while ejecting all other species [1]. As a result, the ion trap may be filled to its maximum capacity with only those species of interest

A complex waveform applied across the endcap electrodes of an ion trap causes unwanted species to be resonantly ejected from the trap before mass analysis. The waveform may be calculated by a straightforward procedure, and includes discrete coherent frequency components which correspond to the characteristic oscillation frequencies of the species to be ejected [2]. These frequencies typically lie from 20 to 500 kHz. A well designed SIS waveform will eject all undesired species while leaving the desired ion masses within the trap.

Even a waveform containing only a single frequency can eject multiple ion masses if the amplitude is large enough. Consequently, storage of a single mass by a complex waveform is easily optimized by amplitude adjustment of a waveform having an absence of frequency components in the area corresponding to the secular frequency of that mass. For storage of widely separated masses, performance optimization requires a precisely tailored waveform, so that a single amplitude adjustment will affect the desired result over the entire mass range.

The widths of resonance ejection profiles were measured for several major ion species in calibration gas (perfluorotributylamine, FC-43) Ejection linewidths vary from slightly over 1 kHz at low mass to slightly under 1 kHz at high mass.

Complex SIS waveforms require the following: Each species to be ejected requires a waveform frequency component close to the secular frequency of that mass. This frequency component should have sufficient amplitude for ejection of the mass without broadening the linewidth profile. Each species to be stored requires an absence of frequency components within a frequency range corresponding to the ejection linewidth around the secular frequency. Nearby frequency components should not have amplitudes large enough to affect partial ejection of that mass.

Waveforms have been developed which satisfy these requirements by including discrete coherent frequency components. The calculated secular frequencies are rounded to the nearest 500 Hz (well within the ejection linewidth) and have amplitudes which are weighted as an inverse power of the mass. They may be used to effectively store low and high mass species while simultaneously ejecting all undesired species across the full mass range of the instrument.

Figures 1 and 2 show performance of the same waveform at low and high mass. Mass spectra were recorded (the sample is GC column bleed at 300 C) using Selected Ion Storage (SIS) over a range of applied waveform amplitudes. The percent change in intensity for each mass present is calculated at each applied amplitude. Note that the ejection efficiency is approximately the same for all masses which are to be ejected. The SIS waveform was designed to store m/z 73 and 355. Each of these species maintains nearly constant intensity over the range of applied waveform amplitudes.

[1] S.E. Buttrill, Jr, B. Shaffer, J. Karnicky, and J.T. Arnold, Proceedings of the 40th ASMS Conference on Mass Spectrometry and Allied Topics, May 31-June 5, 1992 pp.1015-1016
[2] Franzen, J. and Gabling, R.-H., European Patent Application EP 0 362 432 A1, filed October 7, 1988

Figure 1.

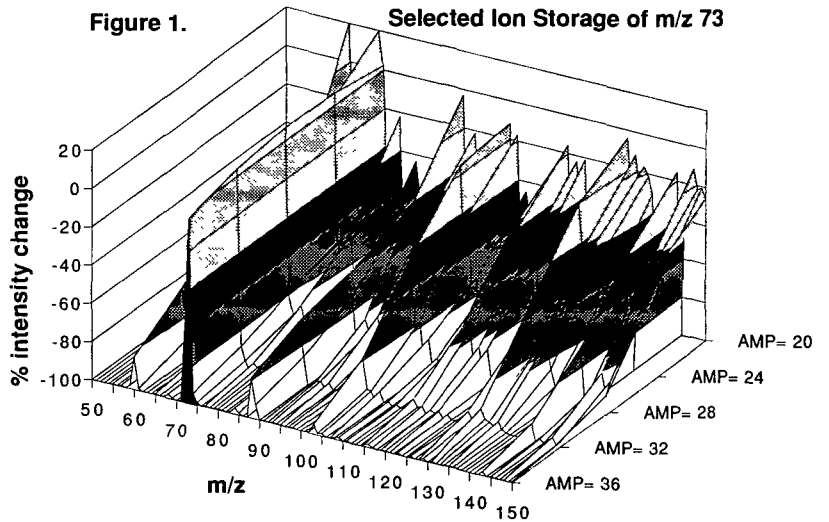

Figure 2.

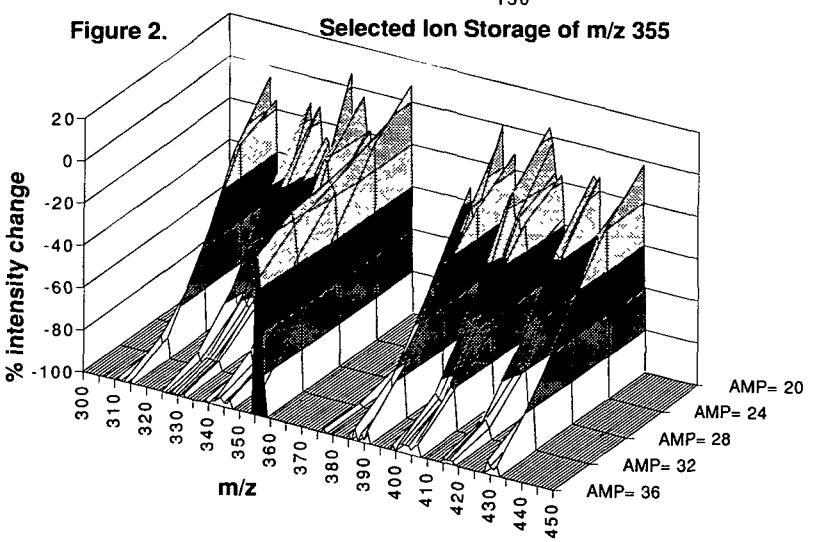

ENVIRONMENTAL ANALYSIS WITH QUADRUPOLE ION TRAPS: PAST, PRESENT, AND FUTURE

Gary L. Glish, Department of Chemistry, University of North Carolina, Chapel Hill, NC 27599-3290.

The quadrupole ion trap was introduced to the main stream of the mass spectrometry community about a decade ago as a GC detector. It immediately made an impact due to its high sensitivity in the electron ionization mode of operation. Since these early days the ion trap has developed into a powerful, multipurpose mass spectrometer. One area in which the future contributions of the ion trap look very promising is in environmental analysis. This is true not because of its high sensitivity as a GC/MS instrument for routine EPA type analysis, but because of its versatility of operation, providing the mass spectrometrist with a number of tools to help solve demanding problems. Three aspects of operation of the ion trap that are important in the application of it to environmental problems are: resonant excitation/ejection, internal/external ionization, and ion/molecule reactions.

Each mass-to-charge ratio that is stored in the ion trap moves with characteristic frequencies in the axial and radial directions. By applying the appropriate frequency in the axial (or radial) dimension of the ion trap, ions moving with that frequency will absorb power and be accelerated. This resonant excitation of ions can lead to one of two possible results. If the rate of resonant excitation is fairly slow, then the ion will likely undergo enough collisions and remain in the ion trap long enough for collision induced dissociation (CID) to occur. This is the basis for CID MS/MS experiments in the ion trap. If the rate of resonant excitation exceeds the rates of activation and dissociation the ion will be ejected from the ion trap. The resonant ejection can be performed in a controlled, sequential manner, which allows a mass spectrum to be obtained. Conversely, the resonant ejection can be used to remove unwanted background ions from the ion trap to allow more analyte ions to be stored.

One of the most dramatic recent advances involving resonant ejection is the ability of obtain high resolution spectra with this mode of operation. By slowing down the scan speed of the ion trap to allow ions longer time to interact with the resonant excitation voltage, very high resolutions have been obtained. It is important to recognize though, that since resonant excitation can also lead to CID, the resolution may be limited by the rate of ion dissociation i.e. when dissociation becomes competitive with ejection. It is also important to note that the detection is done by measuring current from an electron multiplier. When the scan rate is slowed, the same number of ions will be detected over a longer period of time thus giving less current (coul./sec.) at the detector.

Just as the possibility of CID has to be considered when performing resonant ejection, loss of ions by resonant ejection is a possibility during CID MS/MS experiments. This is usually not a problem as evidenced by the high MS/MS efficiencies observed with the ion trap. While the rate of resonant excitation is typically slow for CID experiments, meaning that the collision energy is typically low, the ion trap has a couple of characteristics that lead to its high MS/MS efficiencies. One of these characteristics is that the ions are reaccelerated between collisions. This characteristic along with the long times available for resonant excitation (tens of milliseconds) allows hundreds of collisions to occur. The long activation time also minimizes kinetic shifts by giving ions several orders of magnitude longer time to dissociate versus beam instruments. A potential drawback to the CID process in the ion trap is that often only one or two dissociation channels are accessed, which gives limited structural information. However, because of the efficiency of the MS/MS experiment multiple stages of MS/MS (MS^n) can be performed. This can provide greater selectivity in an analysis since multiple conditions must be met for the final spectrum to be obtained. The MS^n experiment may not be feasible in many environmental analysis schemes, however, because the individual resonant frequencies of the ion depend not only upon

the operating parameters of the ion trap but also upon the number of ions present in the trap. To overcome this problem a broadband resonant excitation source can be used, such as noise. Use of broadband resonant excitation may well be a powerful future tool since this may make on-line chromatography/MS/MS achievable.

The variance in resonant frequency is a result of ion-ion interactions in the ion trap. These ion-ion interactions limit the absolute number of ions which can be stored at one time, which often limits the dynamic range of the ion trap. Resonant ejection can be used to extend the dynamic range by removing unwanted ions during the formation or injection of ions into the ion trap. Two possible scenarios are likely. The first is that the analyte is known and thus all ions except the analyte are resonantly ejected from the ion trap. The other scenario is that the analyte is unknown but there are known background ions from the matrix which are resonantly ejected to allow more analyte ions to be accumulated in the ion trap.

The number and type of background or matrix ions present in the ion trap will depend upon the ionization technique used. Much work has been done demonstrating different ionization techniques with the ion trap. The traditional techniques of forming the ions within the trapping field will work well for some applications. For others external ionization techniques will be desirable. One of the advantages of using external ionization techniques is that higher ionization efficiencies may be achievable because higher pressures can be used. These higher ionization efficiencies have to be considered in the context of the trade-off of the efficiency of injecting the ions into the ion trap. If ion injection can be done with reasonable efficiency, which appears to be the case, then the external ionization can provide increased sensitivity.

Another advantage of external ionization is that the neutral analyte and matrix is separated from the region in which the analysis takes place. This separation helps to minimize unwanted ion/molecule reactions. One example of an unwanted ion/molecule reaction is self chemical ionization. While it is thought by some that self-CI is an inherent problem for ion traps, the usual reason it occurs is from a lack of appreciation of the capabilities of the ion trap. If sample quantities of the same magnitude as used on beam instruments are introduced into the ion trap, self-CI often will readily occur. However, because of the sensitivity of the ion trap sample quantities at least one or two orders of magnitude smaller can readily (and should) be used with the ion trap to eliminate most occurrences of self-CI. Sometimes it is mistakenly assumed that shortening the ionization time will reduce self-CI. However, the majority of the "reaction time" during which the CI process occurs is not during the ionization time but during the scan, until the reacting ion is ejected to the detector. Thus, reducing the ionization time does not reduce self-CI.

While some ion/molecule reactions are unwanted, others can be very beneficial. One limitation of CID is that in activating an ion, it may have a lower barrier to isomerization than dissociation and thus the structure from which the ion dissociates is not the same as the structure of the ion that is being analyzed. Different isomeric structures, however, often have different chemical reactivities to various neutrals. Probing the reactivity of ions toward neutral reagents, which the ion trap is well suited for, could be a major future tool for environmental analysis.

While the ion trap will certainly play a role in future environmental analysis, the degree of success of the ion trap in this arena will depend upon the ability of the analyst to understand and control the processes which occur in the ion trap. The possibility of resonant ejection during CID MS/MS experiments or conversely, CID during resonant ejection must be considered. The competition between excitation and ejection will depend in part upon the nature of the ion and therefore selection of the appropriate ionization technique will be important. Finally, minimizing unwanted ion/molecule reactions and developing structure sensitive ion/molecule reactions will be important to maximizing the information available from ion trap experiments.

ON-LINE ANALYSIS OF SINGLE MICROPARTICLES BY LASER DESORPTION

M.V. Johnston*, K.R. Neubauer, B.A. Mansoori, P.G. Carson
Department of Chemistry and Biochemistry
A.S. Wexler, Department of Mechanical Engineering
University of Delaware, Newark, DE 19716

Aerosol particles affect local and global climate processes as well as human health. Over the past ten years, various microprobe methods have been employed to analyze individual particle that were collected in the field and transported to the laboratory for analysis. These off-line methods offer many advantages over bulk chemical analysis but still suffer from sample transformation between collection and analysis including loss of volatile components, and the relatively long time needed to analyze a significant number of particles We have developed a method to perform on-line analysis of single microparticles by laser desorption. Ambient particles enter the source region of the mass spectrometer and scatter radiation from a helium-neon laser beam The scattered radiation triggers an excimer laser which ablates and ionizes the particle. Instrumental details are given elsewhere in the proceedings. Either positive or negative ions can be detected, both organic and inorganic constituents can be monitored. Figures 1 and 2 show representative spectra of single particles taken with a single excimer laser pulse.

Our current work uses laboratory-generated aerosols to simulate field measurements for characterizing aerosols (chemical speciation, trace metal determination, source apportionment) and to study microchemical reactions of single particles (fractional crystallization, surface vs. bulk partitioning, gas-particle interactions) Methods have been established to distinguish chromium (III) and (VI) based upon the relative signal intensities of ions of the form $Cr_xO_y^-$. The ability of on-line laser desorption to perform semiquantitative analysis of trace metals has been been investigated. Preliminary results with metal salts dissolved in glycerol microdroplets suggest that the precision of on-line laser desorption is similar to that of off-line laser microprobe mass spectrometry (20-50% RSD for absolute signal intensities). Other experiments planned or in progress include fractional crystallization in droplets containing mixtures of salts and the detection of surface active organics Future work will involve chemical reactions between the gas and particle phases in aerosols.

Presented at the 41st ASMS Conference on Mass Spectrometry

Figure 1

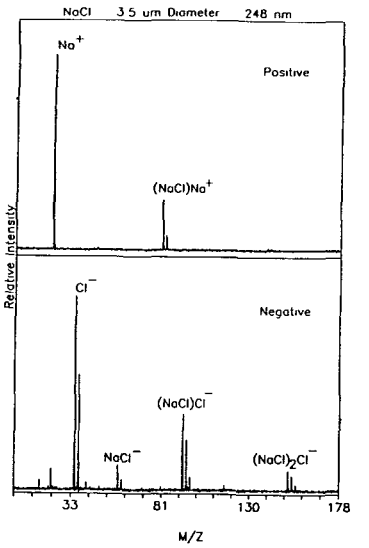

Figure 2

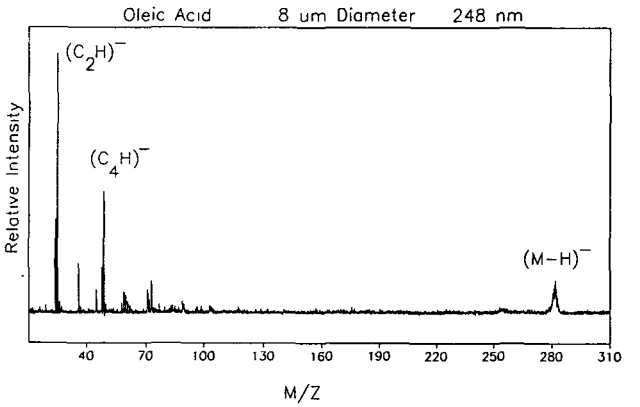

High-Speed Two-Dimensional GC and GC/MS for Complex Environmental Samples

John B. Phillips, Liling Zhang, C. J. Venkatramani, and Christopher Boone, Southern Illinois University, Carbondale, IL 62901.

Environmental samples, especially at trace concentrations, are often extremely complex mixtures. The environmental contaminant to be determined may itself be a complex mixture, a crude oil spill, for example. Or, the matrix containing the contaminant may be complex.

These kinds of environmental samples often require high resolution chromatographic separations which are difficult and time consuming. If many substances are present and must be separated during the analysis, then a long chromatographic column and much time will be required. In special cases, using a sample cleanup before the chromatographic separation or a selective detector such as mass spectrometry after the separation can simplify the problem and save time.

Comprehensive two-dimensional gas chromatography can significantly increase analysis speed for a given resolution. In this technique, a first column separation passes through a second column with fidelity. That is, the presence of the second dimension does not significantly degrade the first dimension separation, all sample substances pass through both dimensions, and the resulting chromatogram consists of peaks on a surface. A comprehensive two-dimensional GC separation can be made orthogonal by tuning the temperature of the second column as a function of progress of the first dimension. Retention in the second dimension then does not depend on the first and the entire plane is accessible. The peak capacity of a comprehensive two-dimensional chromatogram equals the product of the two individual peak capacities and neither column need be especially long to obtain high resolution. The short and fast second column now limits the rate at which peaks pass through the detector. Separation speed in terms of peaks per second does not decrease with increasing sample complexity. In practice, the detector rather than the chromatography limits the overall analysis speed.

Combining this variety of GC with MS will require a fast MS detector such as a time-of-flight. Such an instrument will be capable of generating uncontaminated mass spectra of thousands of individual components separated from a complex mixture in a time comparable to that now required for relatively simple separations. More modest separations involving only hundreds of components may be completed much faster than is now required. Also, this method may eliminate the need for MS detection in many environmental analyses because the two-dimensional GC provides more reliable substance identification. The much greater peak capacity of the plane substantially reduces the probability of interfering substances. The two independent retention times may prove to be nearly as powerful an identification as a mass spectrum for many substances, particularly in hydrocarbon mixtures.

The following is a portion of a high resolution two-dimensional gas chromatogram. The first dimension uses a 50-m long, 250-µm i. d. column with a 2-µm methyl silicone stationary phase. The second dimension uses a 4-m long, 100-µm i. d. column with 0.2-µm OV-1701 stationary phase. The sample mixture is kerosene. Both columns were placed in the same oven and programmed together from 50 °C to 200 °C at 0.8 °C per minute. The shown data is approximately 20% of the entire chromatogram.

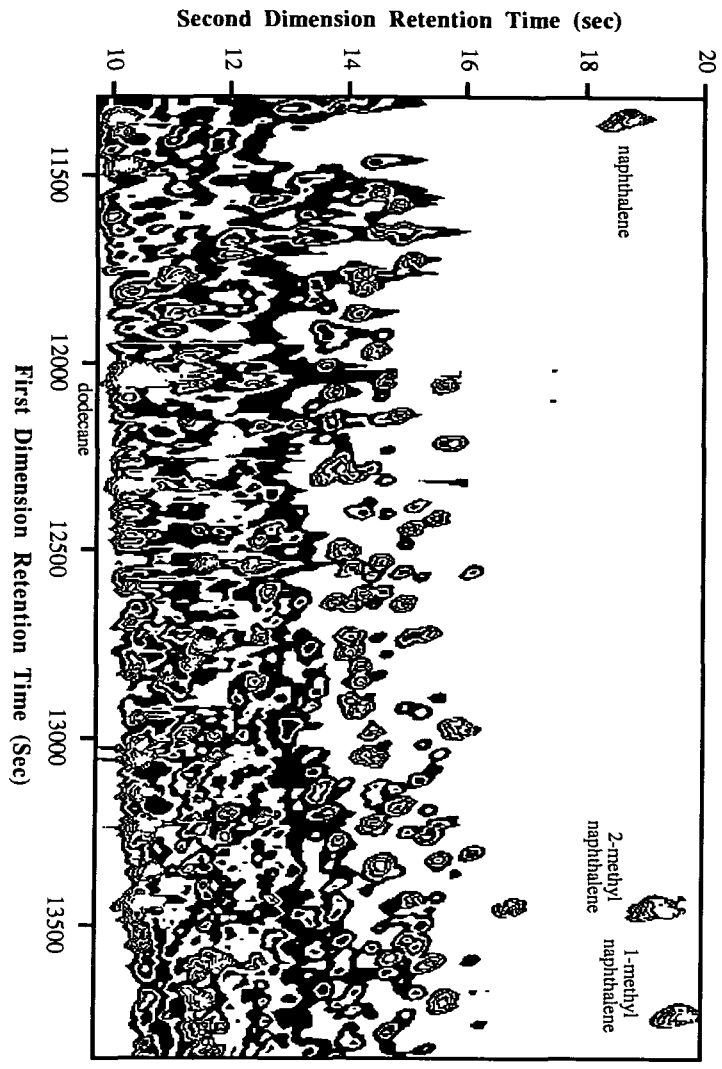

Membrane Introduction Mass Spectrometry and Biomolecular Self-Assembled Monolayers in Environmental Analysis, R. Graham Cooks, T. Choudhury, L. Dejarme, S. Bauer, J. Patrick, Purdue University, Department of Chemistry, West Lafayette, IN 47907

This paper deals in part with advances made in environmental applications of membrane introduction mass spectrometry (MIMS) since a 1992 review (1). Attention is given to the analysis of trace volatile and semi-volatile compounds in water. The advantages of MIMS, as utilized in this work, include: rapid response; selective permeation of analyte; very low detection limits; compound specificity of mass spectrometry; quantitation with external or internal standards; sample handling by flow injection analysis (FIA); simplicity and ruggedness of the method; linear dynamic range of several orders of magnitude.

Two MIMS experiments are described. In one, a direct insertion membrane probe (DIMP) (2) was adapted to an ion trap mass spectrometer (Fig. 1). In the second, a flow-over (3) capillary membrane interface was combined with a jet separator (CM/JS) and used with an ion trap detector (Fig. 2). The jet separator removes water, which permeates the membrane, as well as the helium which is used to pneumatically assist (4) transport of the permeate to the mass spectrometer.

The performance of the membrane probe system is illustrated in Fig. 3 which shows a full scan spectrum taken on a 1 ppb solution of chlorobenzene. The effects of changing experimental variables (such as membrane type and thickness, sample flow rate and probe temperature) were investigated. The effect of changing flow rate on the signal-to-noise ratio is shown in Fig. 4. Table 1 shows the detection limits for a number of volatile organic compounds of environmental under optimized conditions.

Direct comparisons of the DIMP with the CM/JS were made by connecting both systems simultaneously to the ion trap. The jet separator system gave a factor of 3 lower detection limit for selected compounds. For example benzene, chlorobenzene and trans-1,2-dichloroethene were measured directly at concentrations between 200-300 ppt.

In addition, a novel method for the detection of electrophilic alkylating agents is introduced. In these studies nucleic acid constituents are immobilized as self-assembled monolayers (SAM's) (5) then exposed to a dilute solution of an alkylating agent. The reacted samples are then analyzed directly by static secondary ion mass spectrometry. The general concept of the experiment is diagrammed in Fig. 5. The spectra shown in Fig. 6 are of 2'-deoxyguanosine-5'-monophosphate (dGMP) ionically adsorbed to an aminoethanethiol-silver SAM (A) and a similar SAM after exposure to 1 ppth N-methyl-N-nitrosourea (B). The spectra show ions characteristic of the base (GH_2^+, Ag-GH^+) in the control (A) and show reduced intensity for the base peaks as well as ions characteristic of the methylated base (Me-GH^+) in the reacted sample.

This work was supported by the U.S. EPA, BP America and the National Cancer Institute.

References

1. R.G. Cooks and T. Kotiaho, in "Pollution Prevention in Industrial Processes", J.J. Breen and M.J. Dellarco (eds.), ACS Symposium Series, Vol. 508, ACS, Washington, D.C., 1992
2. M.E. Bier, T. Kotiaho and R.G. Cooks (1990), Anal. Chim. Acta, 231, 175.
3. L.B. Westover, J.C. Tou and J.H. Mark (1974), Anal. Chem., 57, 568.
4. L.E. Slivon, M.R. Bauer, J.S. Ho and W.L. Budde (1991), Anal. Chem., 63, 1385.
5. C.D. Bain, E.B. Troughton, Y-T. Tao, J. Evall, G.M. Whitesides and R.G. Nuzzo (1989), J. Amer. Chem. Soc., 111, 321.

Figure 1

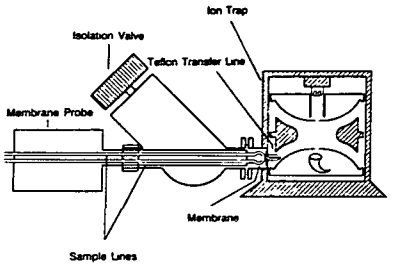

Figure 2

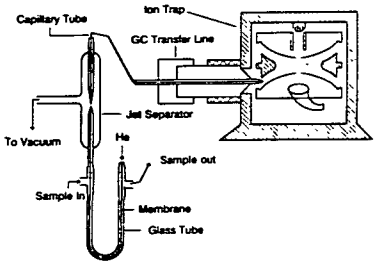

Figure 3

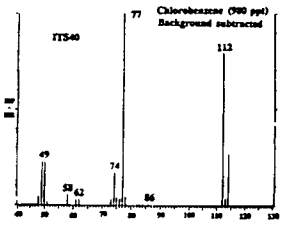

Figure 4

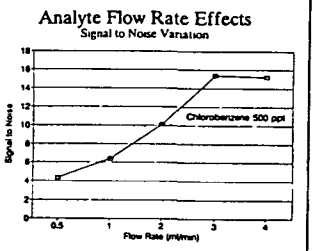

Table 1

Detection Limit using MIMS/ITS40

Organic Analyte	Primary Ion	Detection Limit (ppb)
chloromethane	50	1
vinyl chloride	62	0.5
methylene chloride	84	1
1,1-dichloroethane	63	0.5
chloroform	83	0.5
1,2-dichloroethane	98	1
bromodichloromethane	127	1
1,2-dichloropropane	112	0.5
trans 1,3-trichloropropene	75	0.5
trichloroethene	130	1
1,1,2-trichloroethane	97	2
bromoform	173	1
1,1,2,2 tetrachloroethane	168	2
toluene	92	0.5

Figure 5

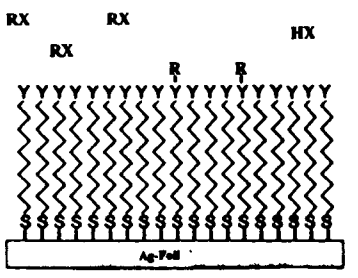

Y = Nucleoside, Nucleotide or Nucleobase

Figure 6

In situ Reaction of Ionically Immobilized Deoxyguanosine Monophosphate (dGMP) (Static SIMS with 15kV Ga^+)

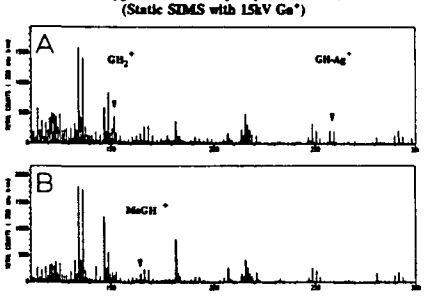

Application of ICP-MS to the Determination of Radioactive and Nonradioactive Trace Constituents in Water from Abandoned Uranium Mines

Vernon Hodge, Megumi Amano and Klaus Stetzenbach
University of Nevada, Las Vegas, Las Vegas NV 89154

Cathleen Webb and Arden Davis
South Dakota School of Mines and Technology, Rapid City, SD 57701

The inductively coupled plasma mass spectrometer (ICP-MS), with ultrasonic sample nebulization, can be used to rapidly determine the concentrations of many metals in environmental waters at part-per-trillion (picogram/milliliter) levels or below, sometimes eclipsing standard radiochemical techniques. As part of an ongoing study of the movement of ground water, samples were collected from standing water in an abandoned uranium mine, an excavation near the mine, a stock dam located down hill about one-half mile from the mine, a drinking water well from a ranch about one and a half-miles from the mine, and the Cottonwood Creek which is about six miles from the mine.

The Diane-A Mine is located on the southern flank of the Black Hills in Fall River County, South Dakota. Uranium was first discovered in the area in 1951 and mined until the late 1960's. Since then, all of the uranium mines have been abandoned, and a uranium mill that operated in nearby Edgemont has been closed and remediated. Annual precipitation is approximately 14 inches and an approximately two-acre pond fills the bottom of the mine. The pond, which holds runoff from the surrounding hills, is perched well above the regional water table and is readily accessible to wildlife. Uranium-bearing ores at the mine include carnotite, tyuyamunite, autunite and uraninite. In an attempt to conduct an initial elemental characterization of the water, samples were collected in the fall of 1992 and the spring of 1993.

The pH values of the samples taken from the mine in the fall of 1992 and spring of 1993 were 4.0 and 3.9, respectively. The low pH of the mine water is indicative of the formation of acid mine water by the interaction of iron bearing minerals with the water. Water from the stock dam also had an acid pH of 4.0, while the ranch well water and water from Cottonwood Creek had pH values of 7.0 and 8.2.

The ICP-MS was used to measure the concentrations of 65 elements and their respective analytical isotopes. In addition, several radiochemical measurements were made to complement the ICP-MS analyses. Preliminary semiquantitative analysis of the mine water indicated that it contained, in addition to uranium, relatively high concentrations of several other trace elements, such as manganese, cobalt, strontium and the rare earth elements. Quantitative measurements demonstrate that the mine water samples that were collected in the fall of 1992 contain 1200 parts-per-billion (ppb) of uranium and those collected in the

spring of 1993, 2600 ppb. As expected, these concentrations are high - about 100 times the maximum concentration proposed for uranium-238 in drinking water in the United States. These values compare to the 2 ppb levels of uranium reported recently for a large number of wells in South Dakota. Concentrations of uranium in waters from the stock dam, ranch well, and Cottonwood Creek are 19 ppb, 34 ppb and 22 ppb, respectively.

The analysis of uranium-238 (the major isotope by mass) and uranium-235 by ICP-MS, along with 32 isotopes of 20 other elements, takes approximately 2 minutes and requires about four milliliters of sample including the wash-in time. All uranium analytical standard deviations are less than five percent. By contrast, if the uranium in four milliliters of mine water is plated onto a stainless steel disk and the uranium determined by a radioactivity technique, alpha spectrometry, overnight counting is needed to get an analytical uncertainty of five percent for uranium-238. Much longer counting times would be required for an accurate analysis of uranium-235. It would be impractical to attempt to measure the uranium concentrations by alpha spectrometry in water from the stock dam, ranch well, and Cottonwood Creek in a four-milliliter sample. Larger volumes, preconcentration, and radiochemistry would be necessary to separate uranium from the bulk salts. Thus, the ICP-MS is the method of choice for quick-accurate determination of uranium-238 and uranium-235 in ground water. However, accurate measurements of the concentration of the shorter-lived uranium-234 would require radiochemical or high resolution mass spectrometry techniques.

The levels of thorium-232 were also measurable by ICP-MS without preconcentration in all samples. The mine water collected in the fall of 1992 contains 2 ppb; that collected in the spring of 1993, 0.7 ppb. Water from the stock dam, ranch well, and Cottonwood Creek contains 0.02 ppb, 0.006 ppb, and 0.09 ppb, respectively. Analysis of the thorium content in these waters by radiochemical techniques would require large volumes of water, tedious separation procedures, and long counting times.

Concentrations of cobalt in the mine water collected in the spring are about 800 ppb, while the concentrations in water from the stock dam, ranch well, and Cottonwood Creek are 25 ppb, 0.03 ppb, and 1.8 ppb, respectively. The concentrations of the rare earth elements (14) in the acid mine water are about 28 times higher than in the stock dam water, 9000 times higher than in the ranch well water, and 1200 times higher than that in the Cottonwood Creek water. The shale normalized pattern for the rare earth elements in water from all of the sample sites is roughly the same - enrichment of the rare earths in the mid atomic mass range relative to the light mass elements and heavy mass elements. A transuranium element, plutonium was found to be present in the mine waters in a concentration of about 10^{-7} relative to uranium-238. The origin of this element may be global fallout.

DETECTION OF TRACE DRUG AND EXPLOSIVE EVIDENCE BY ION MOBILITY SPECTROMETRY

Dean D. Fetterolf, FBI Laboratory, Forensic Science Research Unit, FBI Academy, Quantico, Virginia, 22135 USA

The FBI Laboratory has been involved in the development of new technology and the innovative adaptation of existing technology for use in the war on drugs and terrorism. Due to its small size and versatility, ion mobility spectrometry (IMS) has become the weapon of choice for field support of investigations.

The Barringer IONSCAN Model 250 (Barringer Instruments, South Plainfield, NJ) is capable of detecting as little as 5 ng of particulate cocaine trace evidence. Cocaine, heroin, methamphetamine, THC, LSD, PCP are readily detectable. Samples are collected on a teflon filter using a household vacuum and then thermally desorbed.

The IMS was used to uncover an ingenious new smuggling technique in which cocaine was smuggled in injection molded polystyrene pipe fittings (Figure 1). Three hundred and fifty five pounds of plastic was discovered. A plasmagram for the detection of cocaine in the plastic items is shown in Figure 2. Recently, several fiberglass airline dog kennels were recovered each containing seven pounds of cocaine molded within the fiberglass resin.

Drug detection canines and standard colorimetric tests were unable to detect the cocaine in the plastic and fiberglass matrix. Confirmation of the cocaine and identification of the solvents associated with this investigation was performed in the field using a portable VIKING GC/MS (Viking Instruments, Reston, VA).

The continuing threat of worldwide terrorism as evident by the World Trade Center bombing in New York in February 1993 emphasizes the need for continued efforts at developing improved explosive detectors. Counterterrorism applications of ion mobility spectrometry (IMS) involve detection of pre- and postblast explosive evidence. Laboratory results have determined the limits of detection for most common explosives to be approximately 200 pg. The common commercial and military explosives including NG, TNT, PETN, RDX and ammonium nitrate based explosives are readily detectable.

Detecting residue of explosives on a person or their possessions may be helpful in locating hidden explosives or identifying terrorists. The persistence of explosives on hands and transfer to other surfaces has been examined. An individual handled C-4 (RDX) plastic explosive and then carried out the steps associated with operating a motor vehicle. RDX was detected on all areas that were touched including the keys, car door, steering wheel, gearshift. In addition it required eight hand washings to remove detectable traces of RDX from the hands.

The screening of evidence at a crime scene can greatly reduce the amount of evidence forwarded to the laboratory for confirmation. Post-blast residue of NG was detected on fragments of improvised explosive devices constructed with double-based smokeless powder. Post-blast residue from C-4 (RDX) was detected on clothing from inside a suitcase following detonation. SEMTEX was also identified following the destruction of a portable radio. Figure 3 shows the detection of postblast PETN and RDX residue on the speaker magnet from a portable radio.

Figure 1. Injection molded polystyrene plastic pipe fittings containing cocaine.

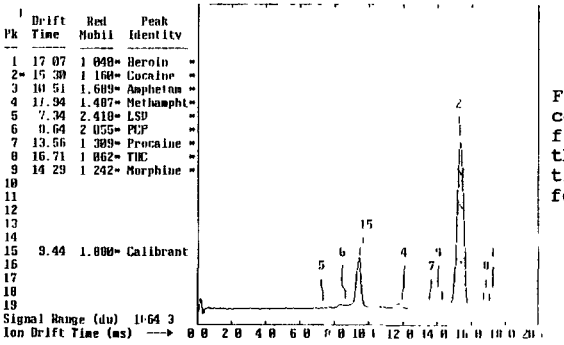

Figure 2. Plasmagram of cocaine in plastic pipe fittings. The table at the left shows the drift time and reduced mobility for the drugs of interest.

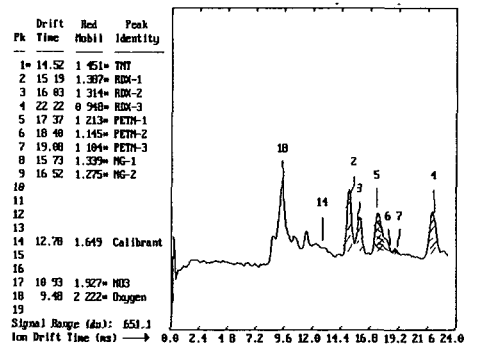

Figure 3. Plasmagram of postblast SEMTEX residue RDX (peaks 2,3,4) and PETN (peaks (4,5,6).

Application of Mass Spectrometry in Monitoring and Identification of Degradation Products of p-Phenylenediamine in Aquatic Environments

Yi Lin, Zamas Lam, and Rosanne M. Kannuck, E.I. du Pont de Nemours
Central Research and Development
Haskell Laboratory of Toxicology and Industrial Medicine
P.O. Box 50, Newark De, 19714

INTRODUCTION Phenylenediamines (PDA) are major industrial intermediates used in manufacturing a variety of polymers and consumer products. The environmental fate and toxicity of these materials are greatly influenced by their subsequent oxidative degradation in aqueous solution. This work focuses on the fate of p-PDA which has the shortest photolytic half-life (0.98 h) relative to the other isomers. The analytical methodology developed in this work utilizes information from HPLC retention time data and mass spectrometry (accurate mass, deuterated labeling, and fragmentation patterns) in confirming the structures present in the complicated environmental mixtures resulting from degradation of the parent compound.

The difficulties encountered in the separation of p-PDA water soluble oxidation products stem from the fact that these compounds are polar, with low volatility and have only slight structural differences. Ion-pair reversed phase HPLC has marked advantages over GC or conventional reverse-phase LC in this type of separation. However, the identification using LC-MS demands the use of volatile ion-pair reagents. To accomplish this, we have employed pentadecafluorooctanoic acid (PFOA) as the ion-pair reagent with LC-MS electrospray[1].

EXPERIMENTAL Separation of the components was achieved with a Zorbax RX-C8 (2.1 mm x 15 cm) column using an Acetonitrile/Ammonium acetate buffer (with PFOA) gradient at a flow of 0.2 mL/min. The optimization of LC and LC-MS conditions with respect to the concentration of PFOA and mobile phase pH shows that pH ≥ 5 and 10 mM PFOA provides satisfactory chromatographic separation. These conditions are adequate for LC-MS, although ionization intensity suppression (approximately 1/4) was observed with 10 mM PFOA vs. 3 mM. Experimental conditions for ESI/MS using a VG Quattro triple quadrapole were capillary, counter electrode and simmers voltages of 3.5 kV, 1.0 kV and 40 V, respectively. For LC-MS experiments, a split ratio to the mass spectrometer of 15:1 was employed. MS-MS experiments were also performed using the VG Quattro, with collision enrgy at 140 eV and attenuation at 60% and Argon as the collision gas. Typical conditions for FTMS experiments using an Extrel FTMS 2000, were CO_2 laser at 10.6 μm, calibrated with an internal standard.

RESULTS AND DISCUSSION LC-ESI/MS and ESI/MS/MS experiments were performed to monitor and identify degradation product formation as a function of time in aqueous solution (Figure 1). Using LC-ESI/MS, the retention time comparison for p-PDA in both water and D_2O provided information as to the number of exchangeable hydrogen. LD/FTMS, was used to distinguish p-PDA (MW 108.0682) from a degradant, quinone (MW 108.0206). The molecular profiles obtained from both LD/FTMS and ESI/MS experimental are comparable (Figure 2). Identification of some oxidation products agree with those previously reported in literature; specifically quinone, 4-4'-azodianiline, and nitroaniline. Additionally, the presence of nitrosodiphenylamine and Disperse Orange 3, were identified from the work.

One of the major oxidation products (referred to as **A**) with molecular formula $C_{18}H_{18}N_6$ (MW 318.1594) was derived from accurate mass measurement using direct probe (M^+= 318.1566) and LD/FTMS in negative ion mode (M-1 =317.1580). Comparison of ESI/MS data for both degraded p-PDA in water and D_2O indicates the structure has eight labile hydrogens. Both data from mass assessment and the labile hydrogen determinations suggest that the structure of **A** is that reported as Bandrowski's Base[2], a linear trimer of p-PDA polymerization. However, the fragmentation pattern obtained from both ESI/MS-MS and direct probe HRMS suggests that the product is benzidineazoaniline rather than the accepted structure of Bandrowski's Base. Comparison of the ion intensities of **A**, and a second product **B** (MW 301), indicates that product **A** is a precursor of **B**. This suggests that the structure of **B** is a highly conjugated azoanaline derivative (Figure 3). The proposed structure of **B** was also evidenced by fragmentation patterns of **B** both in water and D_2O. The formation mechanism of **A** and **B** might be explained by a benzidine rearrangement. Further structure confirmation of products **A** and **B** is in progress.

Figure 1: LC-UV and LC-MS separation and identifiation of p-PDA oxidation products (t = 20 days).

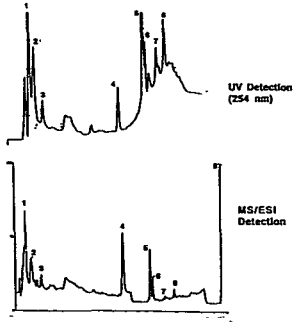

Figure 2. Molecular profiles of degraded p-PDA obtained by ESI/MS (top), and LD/FTMS (bottom).

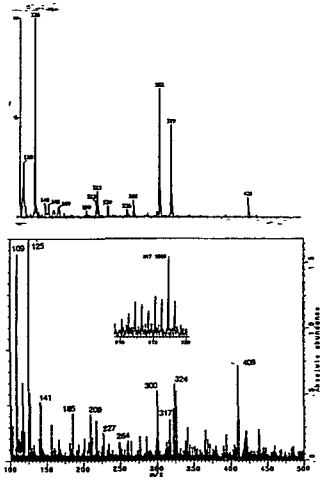

Figure 3. ESI-MS/MS spectra of compound A (top) and B (middle) and (bottom).

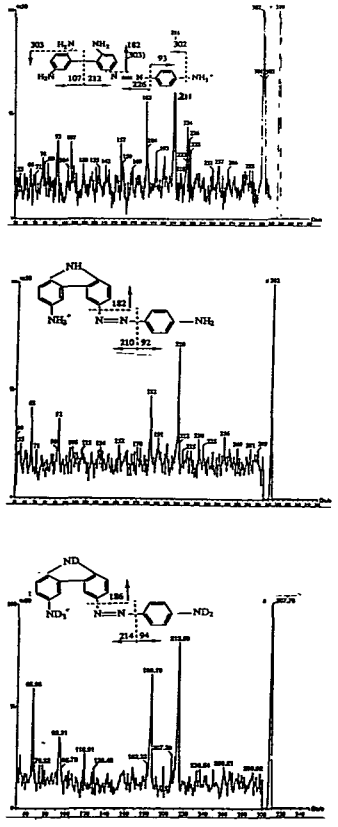

References: [1] Schilling, A.B., The 40th ASMS Conference on Mass Spectrometry and Allied Topics,Washington, DC, 1992.
[2] Corbewtt, J.F., J. Soc. Cosmet. Chem., 23, 683, (1972).

TANDEM MASS SPECTROMETRY STUDY OF CYANO CONTAINING PYRETHROID INSECTICIDES

Ian A. Fleet and *Lee W. Tetler
The Centre for Mass Spectrometry, UMIST, Manchester M60 1QD, UK
and
John J. Monaghan
ICI C&P Ltd, Runcorn Heath, Cheshire, WA7 4QD, UK.

Historically, the synthetic pyrethroids have developed following the discovery of the naturally occurring insecticidally active pyrethrins which are cyclopropane carboxylic acid esters[1]. Work on correlating stereochemical structure and insecticidal activity has led to the discovery of many synthetic pyrethroids having improved photo-stability and potency. Although the low toxicity of these materials to higher mammals makes their use attractive they are extremely harmful to aquatic life[2]. Thus loss of the insecticides and/or their metabolites to the environment requires the unambiguous detection of these materials at sub-microgram levels. To this end we have undertaken a programme of work devoted to the detection of cypermethrin, figure 1, and related materials using tandem mass spectrometry (MS/MS).

A VG Quattro tandem quadrupole mass spectrometer was used for both +EI MS and MS/MS experiments. Ionisation was carried out at 70eV for both sets of experiments with the source set at 180 deg C. All MS/MS experiments were obtained using argon gas in the radio frequency (rf) only hexapole collision cell. The gas pressure within the cell was adjusted so that 50% suppression of the selected ion was obtained. The collision energy was 25eV for each experiment. Ten microgram portions of each pyrethroid (cis/trans mixtures) as dichloromethane solutions were added to a direct insertion probe and the solvent allowed to evaporate prior to analysis.

The fissile nature of the bond between the ester oxygen and alpha carbon of the benzylphenoxy group, results in weak or non-existent molecular ions under EI conditions, (refer to table).

The inherent stability of ions associated with the benzylphenoxy portion of cypermethrin and related insecticides have been investigated by MS/MS using a variety of scan modes. We found that for cypermethrin and cyfluthrin, expulsion of HCN or both HCN and HF (cyfluthrin) occurs. The mechanism by which this neutral loss occurs can be rationalised in terms of proximity effects involving the phenoxy group and either the fluoro or cyano group. Expulsion of the stable species HCN or HF and the formation of a more stable (even electron) tropylium benzofuran type ion occurs by a Wagner-Meerwein type rearrangement involving ring expansion and formation of a more stable carbocation[3].

From MS/MS investigations we have assessed candidate ions for single ion monitoring.

COMMON NAME	MW Da	m/z (% RELATIVE INTENSITY)													
		$M^{+\cdot}$	91	127	129	157	163	165	181	183	199	206	208	209	226
CYPERMETHRIN	415	4.6	80	74	26	--	100	78	87	--	--	--	64	69	--
FLUCYTHRINATE *	451	18	--	--	--	70	--	--	40	--	100	--	--	--	--
CYFLUTHRIN	433	1 4	44	35	12	--	100	76	--	--	53	81	--	--	43

* NON-DIVINYL HALOCYCLOPROPANE TYPE PYRETHROID

For cyfluthrin under +EI conditions using full scan and SIM modes we have found the following limits of detection (spiking experiments using potable water followed by neutral liquid/liquid extraction with dichloromethane):-

FULL SCAN MODE	SIM MODE	(ions m/z)
15ppm	0.05ppm	163; 206; 226

Using ammonia positive CI, cypermethrin shows a quasi-molecular ion $[M+NH_4]^+$.

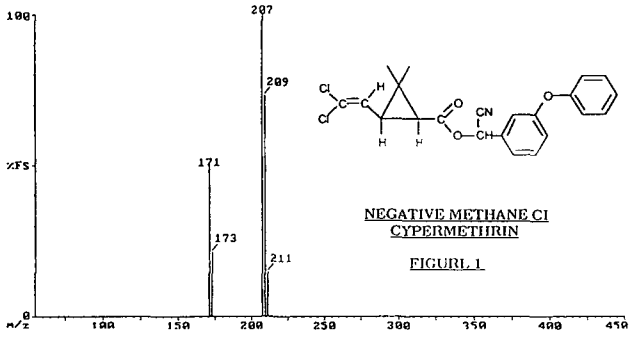

NEGATIVE METHANE CI
CYPERMETHRIN

FIGURE 1

Under negative CI conditions using CH_4 , the spectrum of cypermethrin is dominated by intense ions at m/z 207(base)/209 corresponding to the carboxylate anion and reflecting the correct isotopic abundance (2 x Cl), while the ions at m/z 171/173 correspond to the expulsion of HCl from this ion. A product ion scan of the ion at m/z 207 shows little fragmentation, reflecting a stable species.

REFERENCES

1. N. F. Janes (ed.), *Recent Advances in the Chemistry of Insect Control*, Special Publication No. 53, The Royal Society of Chemistry, London (1985).
2. EEC Directive 78/659/EEC - Fresh Water Directive concerning water quality to support fish.
3. I. A. Fleet, L. W. Tetler and J. J. Monaghan, Org. Mass Spectrom., in press.

CAPILLARY GAS CHROMATOGRAPHIC INTRODUCTION OF ENVIRONMENTAL COMPOUNDS INTO A TROCHOIDAL ELECTRON MONOCHROMATOR/MASS SPECTROMETER

J.A. Laramée, S. Sonnen, and M.L.Deinzer
Department of Agricultural Chemistry and
Environmental Health Sciences Center
Oregon State University
Corvallis, Oregon 97331

A trochoidal electron monochromator attached to a quadrupole analyzer as described by Illenberger and co-workers (1979) recently was tested for the analysis of various environmental chemicals (Laramée et al., 1992). This system produces negative ions by electron attachment. Potentially the instrument provides advantages over the standard practice of moderating high energy electrons from an emitter with a buffer gas in the ion source. High electron capture cross sections are realized with discrete energy electrons that are produced in the ion source and the electron energy spectra are unique for any ion generated which can be useful for identification. Other advantages are anticipated from this device, but most of them can be realized only with additional modifications in the instrument including the interfacing of a gas chromatographic inlet system.

Hexachlorobenzene served as a standard to test the capillary gas chromatographic inlet to the electron monochromator/quadrupole analyzer. This compound captures electrons of optimal energy of 0.6 eV and produces almost exclusively the molecular radical anion cluster. The minimum amount of sample analyzed was 5pg with excellent signal to noise ratio (Figure 1). Narrow range mass scanning between 275-295 amu at a mass resolution sufficient to separate the chlorine isotopic cluster ions was achieved with a 10.8ng sample (Figure 2).

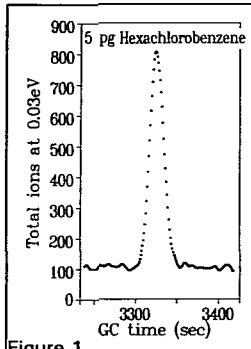

Figure 1

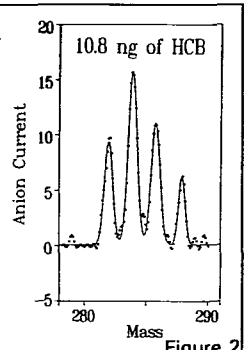

Figure 2

The utility of the system was further demonstrated by injecting Aroclor 1254 into the gas chromatograph and monitoring either the chloride ion or the total ion current. A total ion chromatogram at 0.03 eV electron energy shows a characteristic abundance of peaks due to the PCB isomers and congeners in the mixture. Chloride ion monitoring at 0.03 eV electron energy (Figure 3), shows a similar chromatogram. Excellent signal to noise ratio is observed with 45ng Aroclor sample injected.

The electron energy also was scanned under computer control for compounds introduced through the gas chromatograph. This is demonstrated by the total ion current produced from 2,4,6-trinitrotoluene (TNT) (Figure 4). A 20 eV electron energy range typically was scanned in 0.3 sec. Scanning the intensity of ion peaks at m/z 46 and m/z 47 with respect to electron energy from p-$^{15}NO_2$-labeled TNT showed that the ortho and para nitro groups are ejected at different electron energies (Figure 5). Non-linear deconvolution of the energy spectra revealed a set of negative ion resonances with energy maxima for loss of the para-nitro group at 0.17, 2.77, 4.52 and 7.31 eV, and loss of ortho-nitro groups at 0.13 (minor), 3.31, 4.90, and 7.25 eV.

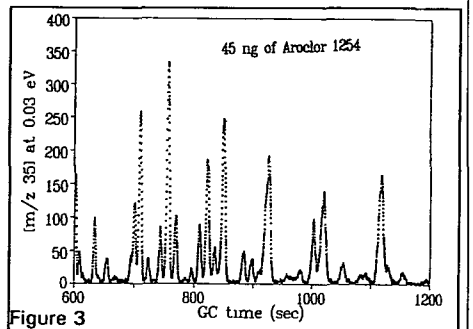

Figure 3

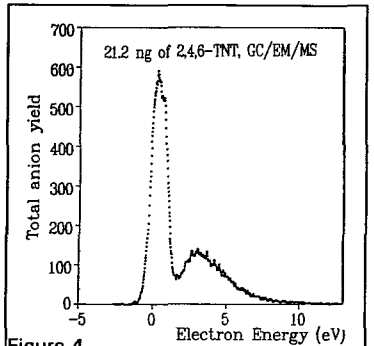

Figure 4

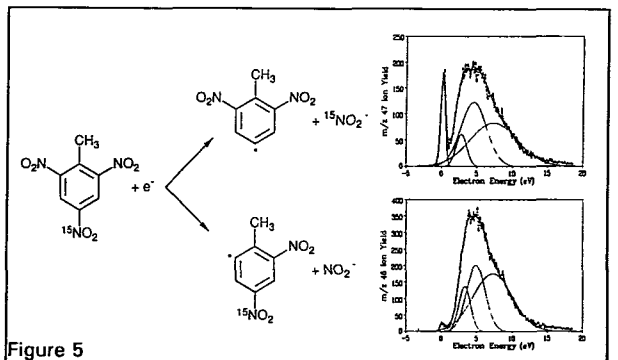

Figure 5

REFERENCES

E. Illenberger, Scheunemann, H.-U., and Baugärtel, H. (1979), *Chem. Phys.* *37*, 21-31.

J.A. Laramée, C.A. Kocher, and M.L. Deinzer (1992) *Anal. Chem.*, *64*, 2316-2322.

CONGENER-SPECIFIC QUANTITATION OF POLYCHLORINATED BIPHENYLS BY GC/MS/MS

J. Lee, J. J. Bradford, T. Victorine, R. A. Lopshire ,and C.G. Enke
Department of Chemistry, Michigan State University, East Lansing, MI 48824

The goal of this study was to develop a rapid, reproducible methodology for the quantitation of the twelve most toxic PCB congeners. The toxicity of PCB congeners varies widely, with non-and mono-*ortho* substituted congeners exhibiting dioxin-like toxicity. The twelve non-and mono-*ortho* PCB congeners are able to achieve a coplanar conformation and hence are loosely referred to as the coplanar congeners. Some of the PCB congeners are stereochemically similar to the planar 2,3,7,8-tetrachloro-*p*-dioxin (TCDD) and, because of this similarity, exert biochemical activity and toxicity comparable to that of TCDD.

For risk assessment, congener-specific analysis is highly desireable. However, in a typical GC/ECD analysis time of 40 minutes several of the most toxic coplanar PCBs coelute with non-planar PCBs of higher chlorination level, precluding congener specific quantitation.[1] Also, electron capture detection is subject to interferences from other halogenated compounds. Due to the tendency for PCBs to undergo fragmention via successive loss of chlorines resulting in a similarity in the fragmentation patterns of the various congeners, only the most highly chlorinated coeluting congener can be quantitated by GC/MS.

The electron capture negative chemical ionization (ECNCI) GC/MS/MS methodology developed employs an oxygen-chlorine exchange reaction in the collision cell of a triple stage quadrapole mass spectrometer to yield a $[M\text{-}Cl+O]^-$ product anion 19 mass units lower than the selected molecular ion $[M]^{-\cdot}$. The reaction scheme is presented in Figure 1. The oxygen-chlorine exchange reaction occurs only with the odd electron molecular anion. By rapidly cycling the spectrometer in the multiple reaction monitoring mode between the unique precursor ion to product ion mass combinations specific to each level of chlorination, simultaneous chlorine number specific mass chromatograms are generated. The reconstructed ion chromatogram (RIC) and the selected reaction monitoring chromatograms for the twelve most toxic congeners are shown in Figure 2. The chlorine-number specific detection allows coeluting congeners of different chlorine numbers to be quantitated with minimal interferences. A surface catalyzed reaction specific for the coplanar congeners produces a $[M\text{-}nCl+nH]^{\cdot-}$ radical anion in the ion source. Being an odd electron anion, the $[M\text{-}nCl+nH]^{-\cdot}$ fragment also undergoes the oxygen-chlorine exchange reaction to produce product ions that appear in the selected reaction monitoring chromatograms of the lower-chlorinated congeners. Since the coplanar congeners are more highly retained on the GC column, and hence do not coelute with any of the lower chlorinated congeners, no loss of selectivity results from this reaction.

The method was evaluated in order to determine the linearity, sensitivity, selectivity, and reproducibility of the assay. Due to the variation of the detector response to the different congeners, multiple ^{13}C-labelled internal standards were employed. The relative response factors for the twelve most toxic congeners with respect to the ^{13}C-

labelled internal standards have been determined. The calibration curves for the twelve congeners are linear in the concentration range 5-100 ppb. Detection limits in the low ppb range have been achieved for each of the twelve most toxic congeners. The method was applied to the quantitation of the "toxic twelve" PCBs in a commercial Aroclor sample, and the results were compared with literature values.[2]

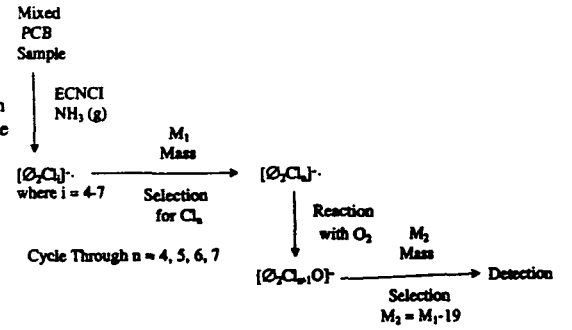

Figure 1. The reaction scheme for the multiple reaction monitoring GC/MS/MS method.

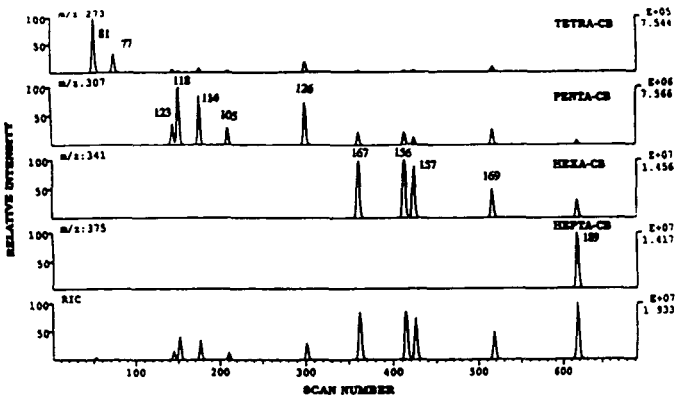

Figure 2. The (RIC) and selected reaction monitoring chromatograms for the coplanar PCB congeners.

1) Duinker, J. C.; Schulz, D. E.; Petrick, G. *Anal. Chem.*, **1988**, 60, 478.
2) Mullin, M. D.; Pochini, C. M.; McCrindle, S.; Romkes, M.; Safe, S. H.; Safe, L. M. *Environ Sci Technol.*, **1984**, 18, 468.

• This work has been supported by grants from General Electric Company and ATSDR.

RELIABLE COMPOUND IDENTIFICATION AT LOW LEVELS IN COMPLEX ENVIRONMENTAL SAMPLES

*Bruce N. Colby, Pacific Analytical, 6349 Paseo Del Lago
Carlsbad, CA 92009 USA

and

Peter H. D'Arcy, Fisons Instruments/VG Masslab, Crewe Road
Manchester M23 9BE England.

The most significant challenge facing the environmental GC/MS analyst today is making reliable compound identifications at low levels and/or in complex sample runs. This problem is the result of spectral contributions from traditional background sources in the mass spectrometer, column and septum bleed from the GC, plus spectral interferences from closely eluted components. These combine to produce major difficulties at very low concentration levels where the TIC trace is primarily the result of instrument background or where important analytes are eluted very close to more concentrated components. The problem lies not with initial location of potential target analytes but with confirming or denying a target analyte's identification. It is also a problem when attempting to identify non-target analytes in a run.

The fundamental problem is removal of spectral contributions from non-analyte species. The challenge is in performing this spectral cleanup process in a reliable and consistent manner. Clearly an expert analyst with many years experience could do the job manually if cost, time and the limited availability of such experts were not prohibitive. Consequently, automated means are essential.

Several background subtraction algorithms are available in commercial GC/MS data systems. These range considerably in complexity and include:

- Subtraction of a scan adjacent to the peak (C-R)
- Subtraction of scans at both sides of the peak (C-LR)
- Evaluation of mass chromatograms for co-maximization[1] (BB+)
- Evaluation of mass chromatogram retention time centroids[2] (Dcn)

In order to evaluate the various background subtraction algorithms experimentally, a series of water samples containing 0.05, 0.5 and 5 µg/L of 57 volatile organic compounds was prepared. To simulate a complex environmental sample, each of these samples was spiked with 2000 µg/L of gasoline. These samples, plus blanks and neat standards, were analyzed according to EPA Method 524.2 on a Fisons MD800 connected to an OI purge & trap via a 20:1 split at the column head. A 75 m x 0.25 mm DB-625 column was used for the separations. The acquired data were inspected manually to identify the location of 45 non-gasoline target analytes. Adjacent scans were identified based on the start and end points for quantitation mass mass chromatogram peaks.

The acquired data were used to generate spectra using each of the above background subtraction techniques. In addition, non-background subtracted data (C) were investigated as a point of reference. The spectrum for each analyte was then compared with the NIST database spectrum of that analyte in order to generate a measure of how successful the background

subtraction had been. The spectrum was also searched against the NIST database to determine whether or not it was sufficiently pure to produce a correct "hit". For the purpose of this study, a hit was correct if the correct compound or a spectral isomer was in the top four hits.

Spectral comparison was accomplished by calculating a statistic consisting of the cosine of the angle between two hypervectors. One hypervector was the reference spectrum and the other was the background subtracted spectrum. Two variations of the statistic were calculated, one which included all mass peaks in the reference and data spectrum, and the other only for mass peaks in the reference spectrum. As a point of reference, these correspond to FOR (or PUR) values in some data systems and REV (or FIT) values in others, respectively.

The statistics for the 45 target analytes in the spiked samples were then combined for each background subtraction technique, sorted and plotted to generate relative cumulative frequency distributions. The same was done for samples which contained no spiked target analytes. The point at which two related sets of distributions crosses is the point at which the probability of generating a false positive equals the probability of generating a false negative. If the statistic value at this point were used as a threshold to accept or deny an analyte's identity, the error rates shown in Figure 1 would be expected. For all background subtraction techniques the REV (FIT) statistic is less effective than the FOR (PUR) statistic. This is important because some manufacturers provide targeting software with their data systems which relies heavily on this less effective statistic. Also, there is a clear trend in the effectiveness of the background subtraction techniques where the more complex ones provide significantly better results.

The library search results were tabulated according to percent of correct hits (Figure 2). The basic trend in background subtraction technique effectiveness follows closely that identified for target analytes. This trend is very noticeable at lower concentrations.

Figure 1 - TARGETING ERRORS

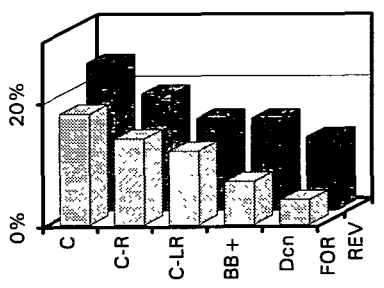

Figure 2 - LIBRARY SEARCH ERRORS

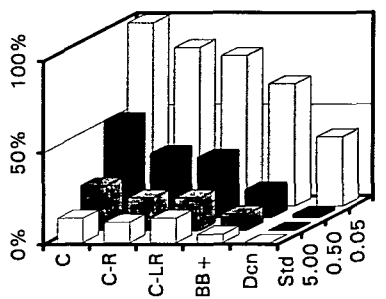

References:

1. Biller, J. E.; Biemann, K. *Anal. Letters* **1974**, 7, 515.

2. Colby, B. N. *J. Am Soc Mass Spectrom* **1992**, 3, 558.

Monitoring Life Support Environments Via Ion Trap Mass Spectrometry

P.T. Palmer and C.M. Wong, NASA - Ames Research Center
MS 239-20, Moffett Field, CA 94035-1000

NASA research in advanced life support has created a significant demand for more powerful techniques to monitor air quality. MS is the method of choice for monitoring air composition and may be employed to evaluate the efficiency of trace contaminant removal subsystems, validate composition data obtained from alternate sensors, and characterize anthropomorphic, biogenic, and material emissions. These applications require the detection, identification, and quantitation of permanent gases, suspected volatile organic compounds (VOC's), and unknown compounds. Ion traps possess a number of characteristics which make them eminently suitable for meeting the analytical and development criteria for these applications [1]. This research describes the use of Thermal Desorption/Gas Chromatography/Mass Spectrometry (TD/GC/MS), GC/MS, and MS/MS methods on a modified version of a Finnigan model ITS40 ion trap instrument for several life support monitoring applications.

TD/GC/MS was employed to characterize the types and concentrations of VOC's in three plant growth chambers used in bioregenerative life support research. A Tekmar 6000 thermal desorption unit and a modified version of EPA method TO-1 were used in these analyses. Figure 1 shows a portion of a reconstructed ion chromatogram (RIC) from the analysis of a 1 L air sample collected from a plant growth chamber. Hundreds of VOC's were evident from this analysis, rendering interpretation a difficult and time-consuming task. Use of library searching on EI data, molecular weight information from CI data, and retention time confirmation enabled reliable identification of many of the VOC's, most of which are ubiquitous in laboratory environments (i.e.;

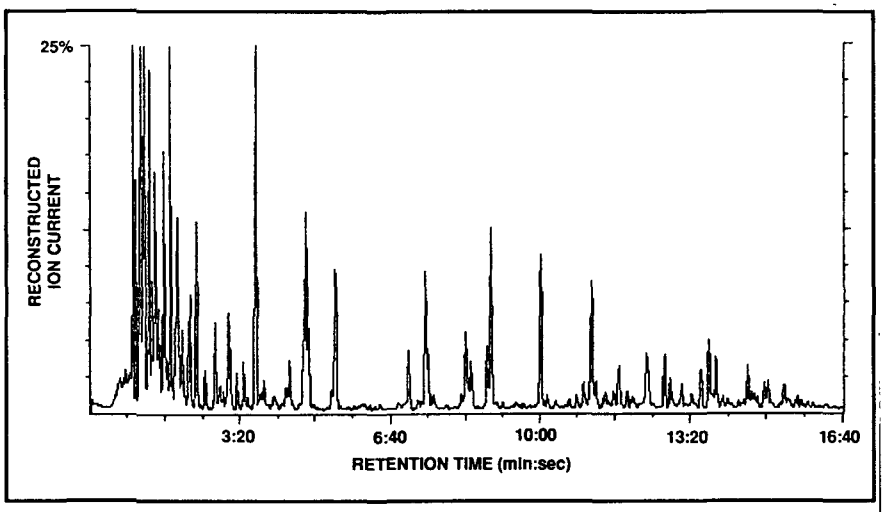

Figure 1. RIC trace from TD/GC/MS analysis of a 1 L air sample from a plant growth chamber.

freons, chlorinated hydrocarbons, aromatic compounds, etc.) and some of which could be attributed to biogenic emission processes (i.e.; terpenes). Nearly all of VOC's were present a concentrations at or below a part-per-billion volume (ppb/v) and individual VOC's could be detected at concentrations as low as a part-per-trillion (ppt/v). Note that these concentrations are well below the Space Maximum Allowable Concentrations (SMAC's) for these species, which are typically on the order of a part-per-million (ppm/v). TD/GC/MS is an excellent method for surveying the types and concentrations of VOC's down to ultratrace levels. However, it is time-intensive, requires stringent quality control procedures, and is unsuitable for in-situ monitoring.

GC/MS analysis of plant growth chamber air samples resulted in the detection of only a few species, as most VOC's in the samples were present at concentrations well below the detection limit of this technique. Note that a GC/MS analysis of a 10 ul injection of a 1 ppm gas standard did provide library matchable spectra for benzene, toluene, and o-xylene. GC/MS was also employed for permanent gas analysis and used to separate and identify oxygen, nitrogen, carbon monoxide, methane, and carbon dioxide. GC/MS will be employed in similar fashion to monitor trace VOC's and permanent gases for Space Station Freedom. Compared to TD/GC/MS, GC/MS is more straightforward in its implementation and its sensitivity is, in most cases, sufficient for monitoring known VOC's to ensure that their ambient concentrations are below their SMAC's.

MS/MS has been heretofore unfeasible for monitoring life support environments, as its size, cost, and complexity have not been competitive with conventional MS for these applications. The ion trap provides a small, relatively inexpensive, and very sensitive means for acquiring MS/MS spectra. Recently, the MS/MS capability was implemented on a Finnigan model ITS40 instrument [2], a benchtop-sized ion trap instrument. This advance is based on the use of a custom MS/MS scan and acquisition editors, the use of a two-step isolation method, and the SWIFT technique for resonant excitation. In recent characterization experiments, this method provided detection limits on the order of 10 pg and a dynamic range of five orders of magnitude. This development has important implications for life support monitoring and is currently being adapted for applications in this area.

The systems used to monitor air quality for manned space missions have, up to this point, been based on MS and GC/MS technology. This research has resulted in the development of the MS/MS capability on a smaller ion trap than is currently available commercially. This development obviates the need for chromatographic separation, provides a means for direct, on-line, real-time monitoring of VOC's, and may revolutionize the manner in which trace contaminant monitoring is performed for life support applications.

[1] P.T. Palmer, C.M. Wong, R.A. Yost, N.A. Yates, J.V. Johnson, and M. Story, SAE Aerospace Transactions, in press.

[2] N.A. Yates, T.A. Griffin, R.A. Yost, and P.R. Borum, *Proceedings of the* 41st ASMS Conference on Mass Spectrometry and Allied Topics, San Francisco, CA, May 30 - June 4, 1993, in press.

The authors thank Peggy Evanich of NASA for support and funding of this research and gratefully acknowledge Dr. Rick Yost, Nate Yates, and Tim Griffin for many fruitful collaborative efforts leading to the development and implementation of the MS/MS capability on the ITS40. The authors also thank Dr. Bill Knott and Barb Peterson from Kennedy Space Center and Dr. Dave Bubenheim, Dave Wilson, and Sonja Cronin from Ames Research Center for providing air samples used in this work.

Trace Element Determination by GC/MS

David A. Herold, Suresh K. Aggarwal and Robert L. Fitzgerald
Laboratory Service, VA Medical Center, San Diego, CA 92161
and Dept. of Pathology, University of California-San Diego, La Jolla, CA 92134

Introduction

Ideally, elemental analysis should be accomplished with precision, accuracy and sensitivity with speciation of the metal on a readily available, easily used instrument. In the last four years we have advanced the analysis of trace elements using chelation followed by analysis by GCMS to explore these areas. The availability of fused silica capillary columns enhances the sensitivity and separation efficiency of different metal chelates. This obviated the need of chemically separating and purifying trace elements as sometimes required by other mass spectrometry techniques. Other advantages of GCMS methods over other MS techniques are as follows. Intensity ratio measurements are made in a mass range where the contributions from the background are very small and, the isobaric interfering elements are usually eliminated since various metal chelates have different GC retention times. Mass discrimination effects are fewer because the isotopic ions used for MS analysis have smaller relative mass differences. When performing isotope dilution experiments using an internal standard, the concentration of trace element can be calculated by employing both the molecular ion and fragment ion peaks, thus enhancing the confidence in the concentration data. Since the tracer calibration is also performed by reverse isotope dilution mass spectrometry, the experimentally determined ratios can be used directly to calculate the concentrations. MS coupled with isotope dilution is a powerful analytical tool for determining the concentration of trace elements in various matrices at levels ranging from major constituent to sub parts per billion. The determination of trace elements in biological materials such as urine, serum, plasma, whole blood, tissues and bone is gaining importance. The IDMS results are free from matrix effects and from the constraints of quantitative recovery of the analyte from the matrix, an essential requirement in other analytical techniques, which is difficult to achieve. This difficulty is due to the complexity of the biological matrices and the volatile or refractory characteristics of some of the trace elements which can lead to poor recoveries.

Experimental

Standards, sample preparation and instrument conditions are given in references 2-9 for the magnetic sector instrument results. Instrument conditions for the Finnigan 4500 quadrupole are given in the extended abstract by G.S. Baird et al in this volume. The preparation of the 4-fluorophenyl Grignard derivative used for the determination of the Pb is given in reference 11. The Pb samples and expected values were supplied by Patrick J. Parsons, Ph.D., State of New York, Department of Health. The extraction of the CH_3Hg^+ from 250 µL of blood was accomplished by adding 200 µL of 0.6 M HCl followed after 5 min with 1 mL of 0.2 M borate buffer (pH 9), then 500 µL of 20 mM fluorodiethyldithiocarbamatewas added to chelate the CH_3Hg^+ followed by extraction into CH_2Cl_2. The CH_2Cl_2 was reduced in volume and analyzed.

Results

The following results show that accuracy and precision of Pb determinations in whole blood and urine has been enhanced by reacting the chelated Pb with a Grignard reagent to form the stable organic Pb.

		Pb (µg/L) Measured	Pb (µg/L) Expected
Urine	(NIST-SRM-2670)	111 ± 7	109 ± 4
Blood	(N.Y. Dept of Health)	160 ± 5	150 ± 40
		431 ± 9	430 ± 40

When ionization is changed from EI to NCI a factor of 4 increased precision and 75x increased sensitivity results (12). The spectra of CH_3Hg(fluorodiethyldithiocarbamate) demonstrates speciation of Hg.

Discussion

In addition to the previously developed applications of GCMS to trace metal analysis, we have demonstrated that negative chemical ionization increased sensitivity by a factor of 75 as compared to electron impact for Pb and that these measurement can be accomplished on a quadrupole mass spectrometer equipped with an autosampler with increased precision as compared to a magnetic sector instrument. These results demonstrate the easy application of stable isotope dilution GC-MS to the measurement of Pb in blood and urine in the clinical laboratory. Additionally we have successfully extracted and analyzed CH_3Hg^+ from whole blood samples in addition to the total Hg in the specimen demonstrating the ability to speciate Hg.

Conclusion

GC/MS analysis of trace elements is maturing into a multielement (10) analytical method with good precision, accuracy and sensitivity and with speciation.

References

1. Aggarwal SK, Kinter M, Wills MR, Savory J and Herold DA. Anal Chim Acta 224:83-95, 1989.
2. Aggarwal SK, Kinter M, Wills MR, Savory J and Herold DA. Anal Chem 62:111-115, 1990.
3. Aggarwal SK, Kinter M and Herold DA. J Am Soc Mass Spec 2:85-90, 1991.
4. Aggarwal SK, Kinter M and Herold DA. Anal Biochem 194:140-145, 1991.
5. Aggarwal SK, Kinter M and Herold DA. J Chrom Biomed Appl 576:297-304, 1992.
6. Herold DA, Aggarwal SK and Kinter M. Clin Chem 38:997, 1992.
7. Aggarwal SK, Kinter M and Herold DA. Anal Biochem 202:367-374, 1992.
8. Herold DA, Aggarwal SK and Kinter M. Clin Chem 38:1647-1649, 1992.
9. Aggarwal SK, Gemma NW, Kinter M, et al. Anal Biochem 210,113-118, 1993.
10. Aggarwal SK, Orth RG, Wendling J, Kinter M and Herold DA. J Anal Tox 17:5-10, 1993.
11. Aggarwal SK, Kinter M and Herold DA. 40th ASMS Conference Proceedings pp 684-5, 1992.
12. Baird GS, Herold DA, Aggarwal SK and Fitzgerald RL. 41th ASMS Conference, 1993.

RADIOFREQUENCY PLASMA IONIZATION TIME-OF-FLIGHT MASS SPECTROMETRY

Mingin Wu, Xiaoli Ren, Milton L. Lee, and Paul B. Farnsworth
Department of Chemistry, Brigham Young University, Provo, UT 84602

Chung Hang Sin and Edgar D. Lee
Sensar Corporation, 479 West Universal Circle, Sandy, UT 84070

An orthogonal time-of-flight mass spectrometer (TOFMS) was developed for sampling ions produced under ambient pressure. Even a mass resolution of only several hundred is sufficient for elemental mass analysis. The simultaneous detection of all ions present also makes the TOFMS more attractive for isotope ratio analysis than other scanning type mass spectrometers. We are currently investigating both inductively coupled plasma and radiofrequency plasma for ionization in this TOFMS. The fast response of the TOFMS also makes it very suitable for detection of transient signals such as those found in chromatographic separation and flow injection analysis.

The radiofrequency plasma possesses several unique characteristics that make it a very promising ionization source. As shown below, the geometry of this plasma discharge cell is very simple. The plasma can be maintained at different power levels (from 1 W to 175 W) in a variety of pure gases or gas mixtures (N_2, He or Ar). By adjusting the power level, both atomic and molecular ions can be produced. Different discharge characteristics, such as direct plasma or afterglow can be obtained by arranging the discharge cell differently. This plasma is therefore flexible enough for different chromatographic systems (gas chromatography, supercritical fluid chromatography, or liquid chromatography).

The following figures show the atomic mass spectrum of chlorine (from methylene chloride), and the molecular mass spectrum of methylene chloride. The molecular and fragment ions were obtained when the sample was introduced from outside the plasma. The radiofrequency plasma can be generated by an inexpensive power supply. Different configurations can be adapted to suit the physical requirements of the mass spectrometer. The same hardware can be used for the determination of molecular species or for elemental analysis.

RPI/TOFMS Mass Spectrum of Chlorine

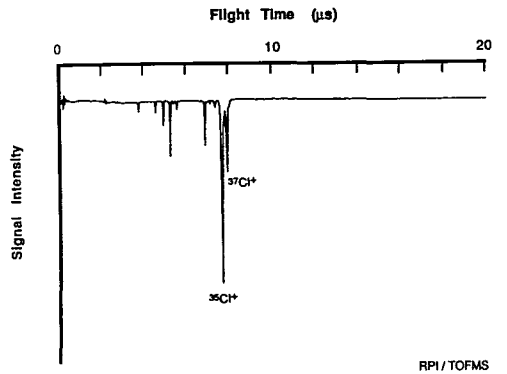

Molecular and Fragment Ions of Methylene Chloride

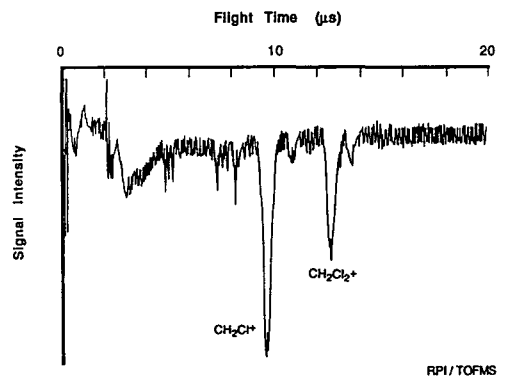

MULTI-CHANNEL He ICP MASS SPECTROMETER FOR ELEMENTAL ANALYSIS WITH TRANSIENT SIGNALS

Evan F. Cromwell and Peter Arrowsmith

IBM AdStaR, San Jose, CA 95193 and
IBM Canada, Toronto, Ontario, Canada

A challenge often encountered in materials applications is the need for elemental analysis of contaminant particles, small areas of deposited material, or inclusions in various materials. One technique that has sufficient sensitivity and is capable of semi-quantitative analysis is inductively coupled plasma (ICP) mass spectrometry with laser ablation sample introduction.[1] Compositional analysis of a small volume of material by the ablation technique requires a single, or small number of laser pulses to avoid sampling the surrounding material. The resulting signal is in the form of a transient and the currently available sequential plasma-source mass spectrometers are too slow to detect more than a small fraction of the ions in the short time available. Hence, these instruments are limited in the number of elements that can be determined.

We report here on the development of a new plasma-source mass spectrometer designed to overcome such problems. The instrument uses either a He or an Ar ICP as an ion source. The plasma is sampled by a differentially pumped vacuum system which maintains the final chamber at a pressure of $<1\times10^{-8}$ torr. The ions sampled are focused with an Einzel lens and a quadrupole lens pair onto the entrance slit of the mass spectrometer. The spectrometer, a Mattauch-Herzog double-focusing instrument comprised of dual electric and magnetic sectors, images ions from the entrance slit to a plane at the exit of the magnetic sector. Ions of different mass-to-charge (m/z) ratios are focused to different areas on that plane. A micro-channel plate (MCP) ion detector, coupled to a photo-diode array (PDA), is placed at the focal plane of the spectrometer in order to simultaneously detect and record all ions. The m/z range of ions detected is determined by the voltages applied to the mass spectrometer. A schematic of the instrument is shown in Figure 1.

The use of a He ICP with mass spectrometry has been demonstrated previously.[2] There are two important reasons for using a He ICP. Spectral interferences are reduced compared to an Ar plasma and, with the mass spectrometer used, the intense He^+ peak is directed off the low mass end of the MCP. Some of the drawbacks of a He plasma are a lower plasma temperature, which results in less efficient atomization and more oxides, and a secondary (pinch) discharge through the sampling cone. The He plasma has been run at a forward power of up to 2.5kW using an end-tapped load coil and a ceramic torch tube. At higher powers the distance from the load coil to the sampler cone must be increased to prevent arcing. The torch box is setup so that it can easily be switched over to a center-tapped load coil for generation of an Ar plasma.

The design of the Mattauch-Herzog mass spectrometer makes it ideally suited for interfacing with a MCP based detector. This combination has been demonstrated previously by different groups,[3,4] although their use has been with low intensity ion sources. This is the first known use with a continuous plasma ion source. In our design the

spectrometer has a 3" long focal plane and the magnet sector has a field of ≈5000Gauss. A 3" x 0.5" dual MCP, which is shielded from the magnetic field, is placed at the focal plane and is coupled, through a phosphor screen and a reducing fiber optic bundle, to a 2" PDA with 2048 elements. The read out time for the PDA is 8msec.

Interfacing the spectrometer to a plasma ion source has presented unique challenges. Background from scattered plasma light was eliminated by coating the electric sector region with graphite and shadowing the mass spectrometer entrance slit. These measures improved the signal-to-noise by >100. Tuning of the mass spectrometer was difficult because of large spreads in the ion kinetic energies. This is believed due to space charge effects in the sampler and skimmer cones. The ion optics had to be tuned to image a "well behaved" portion of the ion beam onto the mass spectrometer entrance slit in order to obtain the desired mass resolution. At an acceleration energy of 500V the m/z range 10 to 130amu was directed onto the MCP with unit mass resolution (FWHM) at m/z=130 (using a 0.004" slit width). At an acceleration of 300V, the range was 20 to 210amu with resolution becoming less than unity for the higher m/z species. The current sensitivity for the instrument is estimated at 10ppb for solution introduced with an ultrasonic nebulizer. The sensitivity is element dependent due to discrimination in the He ICP. It should be emphasized that the purpose of this instrument is to achieve high temporal resolution for a wide mass range, not extremely high sensitivities.

1. P. Arrowsmith, Anal. Chem. **59**, 1437 (1987).
2. A. Montaser, S.-K. Chan, and D.W. Koppenaal, Anal. Chem. **59**, 1240 (1987).
3. D. Murphy and K. Mauersberger, Int. J. Mass Spectrom. Ion Phys. **76**, 85 (1987).
4. M.P. Sinha, Particles in Gases and Liquids 2, ed. K.L. Mittal (Plenum Press, New York, 1990) pg. 197.

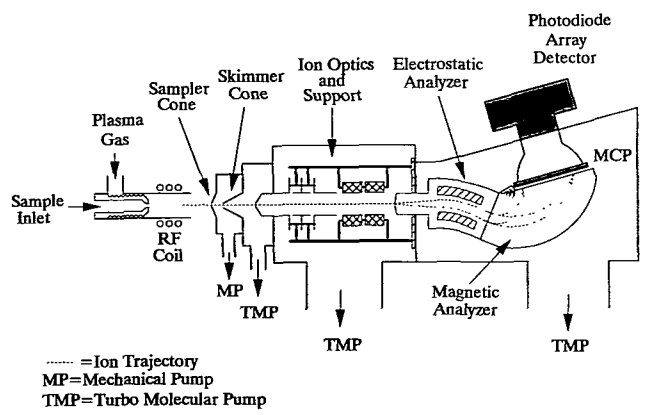

Isotope Ratio Measurement by Inductively Coupled Plasma-Multiple Collector-Mass Spectrometry Incorporating a High Efficiency Nebulisation System.

Andrew J Walder, Dagmar Koller, Nicola M Reed, Robert C Hutton, Philip A Freedman and John E Cantle.

Fisons Instruments Elemental, Ion Path, Road Three, Winsford, Cheshire, CW7 3BX, UK

Isotope ratio analysis by Inductively Coupled Plasma Multiple Collector Mass Spectrometry has been performed utilising a high efficiency desolvating nebulisation system for sample introduction.

Isotope ratio measurements of uranium, lead and hafnium reference materials corrected for mass bias at a concentration of 50 ng/ml are shown in Tables 1, 2 and 3 respectively. Use of the high efficiency device increased sample transmission and hence increased ion signal level by a factor of 10 compared to conventional nebulisation. The analysis of each uranium and lead solution required 29 ng of sample while the analysis of each hafnium solution required 290 ng of sample. The accuracy and precision of the measurements agree with the established values.

Table 1 **Analysis of NIST U010, 50ppb. Values in parenthesis are the SE (%)**
(Isotope ratios corrected for mass bias, acquisition time 50 s/sample)

Sample	234/238	235/238
#1	0.0000542 (2.6)	0.0101519 (0.024)
#2	0.0000560 (3.1)	0.0101507 (0.027)
#3	0.0000637 (2.5)	0.0101507 (0.008)
#4	0.0000506 (5.6)	0.0101511 (0.027)
#5	0.0000576 (2.4)	0.0101453 (0.022)
#6	0.0000618 (2.1)	0.0101481 (0.041)
Mean	**0.0000573**	**0.010149**
2 SD	0.0000097	0.000005
%RSD	8.5	0.024
NIST	**0.0000546**	**0.010140**
2 SD	0.0000005	0.000010

Table 2 **Analysis of NIST Pb981, 50ppb. Values in parenthesis are the SE (%)**
(Isotope ratios thallium corrected for mass bias, acquisition time 50 s/sample)

Sample	208/204	206/204	207/206
#1	36.696 (0.011)	16.942 (0.013)	0.91468 (0.003)
#2	36.696 (0.010)	16.939 (0.010)	0.91462 (0.003)
#3	36.715 (0.017)	16.945 (0.017)	0.91479 (0.002)
#4	36.711 (0.015)	16.946 (0.013)	0.91471 (0.003)
#5	36.683 (0.010)	16.938 (0.009)	0.91459 (0.005)
#6	36.687 (0.011)	16.938 (0.009)	0.91453 (0.002)
Mean	**36.698**	**16.941**	**0.91465**
2 SD	0.025	0.007	0.00018
%RSD	0.035	0.020	0.010
NIST	**36.721**	**16.937**	**0.91464**
2 SD	0.036	0.011	0.00033

Table 3 **Analysis of JMC 475 Hafnium, 50ppb. Values in parenthesis are the SE(%)**
(Isotope ratios internally corrected for mass bias, acquisition time 500 s/sample)

Sample	176/177	178/177	180/177
#1	0.282194 (0.002)	1.46727 (0.001)	1.88637 (0.002)
#2	0.282191 (0.002)	1.46737 (0.001)	1.88656 (0.003)
#3	0.282201 (0.002)	1.46732 (0.001)	1.88620 (0.003)
#4	0.282201 (0.002)	1.46731 (0.001)	1.88635 (0.002)
#5	0.282203 (0.003)	1.46732 (0.001)	1.88627 (0.002)
#6	0.282201 (0.002)	1.46728 (0.001)	1.88629 (0.002)
Mean	**0.282198**	**1.46731**	**1.88634**
2 SD	0.000010	0.00007	0.00025
%RSD	0.0017	0.0024	0.0066
Lit. Value	**0.282195**	**1.46710**	**1.88651**
2 SD	0.000015	0.00010	0.00012

APPLICATION OF ICP-MS TO IMPURITY ANALYSIS OF ROOM TEMPERATURE SEMICONDUCTORS, José A. Olivares, Eugene Mroz, Connie M. Overly, Isotope and Nuclear Chemistry Division, Los Alamos National Laboratory, Los Alamos, NM. and Eilene S. Cross, EG&G Energy Measurements, Inc., Santa Barbara Operations, 130 Robin Hill Road, Goleta, CA., Eugene Mroz, and

INTRODUCTION

Mercuric iodide crystals are semiconductors sensitive to gamma, x-ray, and photon radiation. Detectors manufactured from HgI_2 require no liquid nitrogen to achieve spectral resolutions of up to 1%. Mercuric iodide is synthesized from an aqueous solution of potassium iodide and mercuric chloride. The raw mercuric iodide goes through a series of purification steps which include vacuum sublimations, melts, resolidification, closed system sublimations and zone refining. The purified mercuric iodide is then grown into a single crystal by physical vapor transport. The crystals are cut and are fabricated into room temperature radiation detectors and photocells. Crystals that produce good resolution gamma detectors do not necessarily make good resolution photocells or x-ray detectors. Many factors including elemental impurities may contribute to these differences in performance. A method has been developed to utilize inductively coupled plasma-mass spectrometry (ICP-MS) to determine elemental impurities. Two methods employed to dissolve mercuric iodide. The first is to dissolve the solid HgI_2 crystal in a aqueous solution of 1% KI. This technique dissolves the HgI_2 matrix but is probably not rigorous enough to dissolve particulate contaminants within the crystal structure. This paper discusses these analytical methods as applied to purification methods for HgI_2 and KI.

Sample Dissolution Method

Dissolution of HgI_2 in high purity (Seastar) nitric acid was not successful even with microwave digestion. Aqua regia (3 parts HCl and 1 part HNO_3) is known to readily dissolve HgI_2 . However, for ICP/MS analysis, it is desirable to avoid high concentrations of chloride because the formation of metal chlorides and oxychlorides interferes with the analysis (e.g. $^{35}Cl^{16}O$ interferes with ^{51}V). Therefore, the minimum amount of HCl required to effect complete dissolution of HgI_2 was studied. Experiments showed that 0.5 g HgI_2 treated with 0.1 ml HCl + 5.0 ml HNO_3 + 30 minutes of microwave treatment at 50% power left a solid, black deposit with a metallic luster, presumably $I_2(s)$, on the walls of the Teflon digestion bomb. Addition of 0.5 ml HCl and further heating causes the solid to disappear and a white crystalline precipitate (thought to be I_2O_5) is observed in the concentrated nitric acid. The reaction is nearly stoichiometric. 0.5 grams of HgI_2 containing 2.2 mmoles of iodine requires 0.5 ml HCl to provide a slight excess of NOCl (the oxidizing species in aqua regia) to take the reaction to completion. Samples prepared in this manner show elevated ^{51}V signals possibly due to the formation of $^{35}Cl^{16}O$. Addition of 1.0 ml HNO_3 to the crystalline $HgNO_3$ product and subsequent re-evaporation steps (2) show a marked reduction in the $^{35}Cl^{16}O$ signal.

ICP-MS Instrumentation and Methods

A Finnigan MAT (San Jose, Ca.) SOLA inductively coupled plasma-mass spectrometer (formerly Turner Scientific) is used for elemental analysis. The standard instrument setup is used. The instrument is set to analyze for only one isotope per element of interest. Particular isotopes are avoided due to well known spectral interferences, as shown in Table I. Spectral studies show no interferences above 10 ppt in the Mo mass region due to Hg^{+2}. Furthermore, studies using synthetic solutions of Na, Co, In, Lu, Pb and U in different concentrations of HgI_2, show no significant ionization effects from salt loadings of up to 1% HgI_2 which are not adequately corrected using In as an internal standard. Solutions of mercuric iodide spiked with known concentrations of selected elements were used to determine the analytical accuracy of the method and blank limitations. For most elements recoveries at the 1 ppb level were possible to within a few percent. Notable exceptions were B, Si, and Ca due to blank limitations.

Table I. Known ICP-MS spectral interferences for HgI_2 analyses

Mass	Isotope	Interference
51	^{51}V	$^{35}Cl^{16}O^+$
63.5	^{63}Cu	$^{129}I^{+2}$
67	^{67}Zn	$^{35}ClO_2^+$
69	^{69}Ga	$^{37}ClO_2^+$
142	^{142}Nd	Tail of $^{127}I^{16}O^+$
143	^{143}Nd	$^{127}I^{16}O^+$
144	^{144}Nd	$^{127}I^{16}OH^+$
165	^{165}Ho	Tail of $^{39}K^{127}I^+$
166	^{166}Er	$^{39}K^{127}I^+$
235-238	$^{235}U,^{238}U$	$HgAr^+$

For regular crystal and salt comparisons a semi-quantitative analytical method is used. In this technique 61 elements are selected for analysis. All of the samples and reagent blanks are spiked with 50 ppb In, which serves as an internal standard. The relative sensitivity factors (used for calculation of concentrations) for all of the elements are set to unity. This allows for intercomparison of the relative concentrations of the elements, from sample to sample, without the need for complete standardization for all of the elements. For more rigorous sample intercomparisons and data base archival 15-20 elements are selected for full quantitative analysis. Quantitation is performed using 12 passes/scan, signal averaged, and 8 scans per analysis.

RESULTS AND DISCUSSION

The analysis of the raw synthesized HgI_2 and the six subsequent purification steps show that for most elements the concentrations change by less than 50% over the entire sequence of steps. A handfull of elements are purified up to a factor of ten. In a few cases some of the purification steps seem to show an increase in contamination for some elements. The levels of elemental contamination for the zone refined HgI_2 were higher in the center section than in either the front or rear sections for most elements. However, the rear section of the tube contains the highest levels of impurity contamination for Mg, Ca, Sc, Ti, Mn, Fe, Cu, Zn, and Sb. The front section of KI zone-refined tube contains the highest concentration of impurity contamination for most elements. The only exceptions are Cr, Mn, Ce, and Pb. The total elemental contamination for the front section is approximately 480 ppm, while the center and rear sections each contains 15 ppm total impurities. Presently we have not been able to establish any correlations between elemental impurities and detector performance. A limitation of the technique is that many of the elements are present in solution at blank levels or lower (ppt), making data interpretation very difficult.

SPUTTERED ATOM IONIZATION IN A PULSED RADIO FREQUENCY POWERED GLOW DISCHARGE

Changkang Pan and F. L. King,
Department of Chemistry, West Virginia University,
Morgantown, West Virginia 26506, U.S.A.

Glow discharge mass spectrometry (GDMS) is regarded as a powerful analytical technique for the direct determination of trace elements in solid materials. Although most GDMS systems operate with continuous power to yield a steady-state glow discharge plasma, pulsed power operation of the glow discharge provides some advantages over the steady-state operation. For example, higher instantaneous powers can be applied to increase sputter yields and absolute ion intensities. Interestingly, the ionization processes in the discharge vary in relative contribution during the on-off cycle of the plasma. Such variation permits the temporal discrimination of analyte signals from background signals as well as discrimination against certain spectral interferences.

The present study focuses on the temporal behavior of ionized sputtered atoms produced by a pulsed radio frequency (rf) powered glow discharge. The rf power is pulsed at a frequency of 50 Hz with a duty cycle of 25 %. The resulting temporal ion signal profiles at selected mass-to-charge ratios are monitored with an oscilloscope with sub-millisecond temporal resolution.

The temporal differences in the significance of mechanisms responsible for the ionization of sputtered atoms in a pulsed rf glow discharge are investigated. It is found that modulation of the discharge power generates time-dependent ion signals. Typical ion signal profiles obtained from the pulsed rf glow discharge ion source are shown in Figure 1. Ion signals from both sputtered atoms and support gas atoms exhibit unique, reproducible temporal profiles that do not match the applied rf power step function. As could be seen in Figure 1A, $^{40}Ar^+$ signal undergoes a surge in intensity upon the application of rf power, similar to the observations reported for pulsed dc glow discharges. This prepeak arises from the electric breakdown of support argon gas at the beginning of applied power initiation. Figure 1B is the first derivative of the temporal profile shown in Figure 1A. The negative peak indicates the temporal position of the maximum decay rate for argon ions. In contrast to the behavior of the argon ion signal, the $^{63}Cu^+$ signal shown in Figure 1C does not respond immediately to the initiation of rf power. There is a delay time of about 1 millisecond before the signal gradually begins to increase. This delay time arises because Cu atoms must first be sputtered off the sample surface by argon ion bombardment, and then diffuse to the negative glow region where they are subject to collisional ionization. Comparison of Figures 1A and 1C indicates the temporal correlation between the appearance of argon ion signal and the appearance of copper ion signal. The Cu ion signal only appears after argon ions have been formed by the electrical breakdown of the argon gas. After their initial appearance, it

takes about 2 milliseconds for Cu ion signal to reach a steady-state level. During the steady-state plateau time regime, the plasma is in a quasi-equilibrium condition characterized by constant atomization and ionization. After the termination of applied power, the sputtered ion signal displays a marked increase in intensity, followed by a gradual decay to the baseline value.

It is of particular interest to note that the position of the afterpeak for ionized sputtered atoms, Figure 1C, is temporally coincident with the maximum decay of argon ion, Figure 1B. This indicates that the formation of afterpeak correlates closely with the extinction of argon ions. This extinction arises from the recombination of argon ions with thermalized electrons, a process that generates metastable argon atoms. Upon termination of the applied power, the electric field collapses and the energetic electrons in the glow discharge quickly lose kinetic energy through collisions with other plasma species. The rapid collisional cooling of the electrons and the consequent increase in thermalized electron density favor the ion-electron recombination. As a result, recombination becomes the dominant electron removal process in the afterglow. Metastable argon atom formation is the result of a radiative recombination process. Recombination yields excited argon atoms in the *5p*-level excited state. These excited atoms rapidly decay to the *4s* level through radiative relaxation yielding argon atoms trapped in the metastable $^3P_0$ and $^3P_2$ states, $Ar_{(m)}^*$.

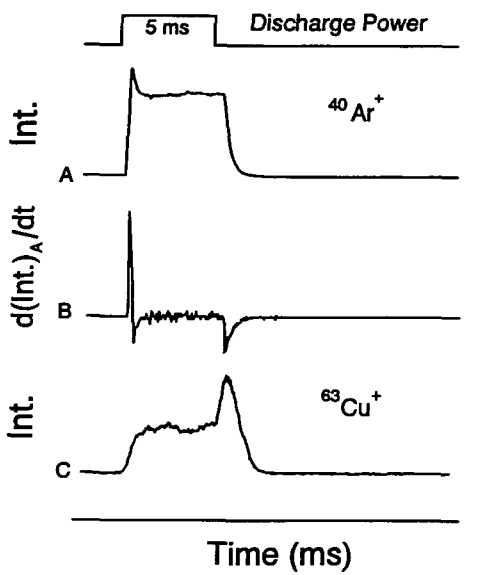

Figure 1. Temporal ion profiles in a pulsed rf glow discharge

The time-dependent production of sputtered ions varies with changes in plasma working parameters, such as rf peak power, sampling distance, duty cycle, and gas composition. The ions produced during the afterpeak appear to have greater average kinetic energies and narrower kinetic energy distributions than those produced during the plateau time regime. The use of time-gated detection with the pulsed rf glow discharge improves the analytical sensitivity and selectivity.

OPTIMIZATION OF A RADIO FREQUENCY POWERED GLOW DISCHARGE MASS SPECTROEMTRY (RF-GDMS) SYSTEM

Charles R. Shick, Jr. and R. Kenneth Marcus
Department of Chemistry
Howard L Hunter Chemical Laboratories
Clemson University
Clemson, SC 29634-1905

Introduction:

Glow discharge mass spectrometry (GDMS) is a technique that has had a long history of application in the area of trace element analysis of metals and semiconductor materials. In recent years, a number of modifications and advances in GD ion source technology have lead to their much wider application; into areas such as atmospheric sampling, GC/MS, and LC/MS.[1] In the area of bulk solids and thin films analysis, the development of radio frequency (rf) powered devices has opened up the realm of materials to glasses, ceramics, and polymeric materials.[2] In this laboratory, we have focussed our recent efforts towards a better characterization of the ion source design and ultimately the analytical figures of merit of different sampling orientations. In this presentation, the operation and analytical characteristics of a pin-type source geometry coupled to a commercial quadruple GDMS system, the VG GloQuad, are detailed.

Experimental:

Figure 1 is a diagrammatic representation of the VG GloQuad system and the developed rf-GD ion source. The GloQuad is a differentially pumped, quadrupole mass spectrometer system which employs a cryo-cooled ion volume as a means of removing residual gases which have deleterious effects in reducing sputtering rates and causing the introduction of molecular species such as N_2^+ and metal oxides into the mass spectrum. No modifications are required to the mass spectrometer or data acquisition electronics. The sample is introduced to the ion volume attached to the end of a 0.5" diameter direct insertion probe (DIP) constructed in this laboratory. In the pin cell geometry, samples of up to 0.25" diameter may be analyzed directly. (The design of a "flat cell" geometry for larger diameter samples is described in a separate presentation.) The plasma is powered by a 13.56 MHz generator (RF 5S, RF Plasma Products, Marlton, NJ) at powers of up to 60 W. A parametric evaluation of the effects of discharge power, argon pressure, ion sampling distance, and cathode size was undertaken as a means of ascertaining the optimum operation conditions.

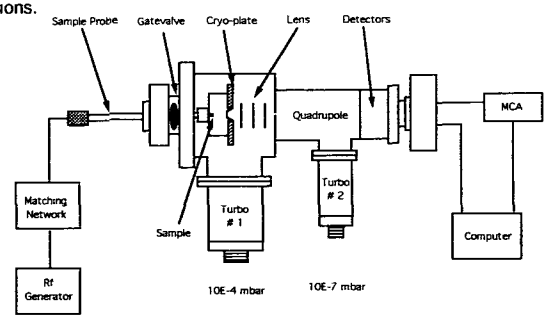

Figure 1. Diagrammatic representation of the rf-GD source coupled to a VG GloQuad.

Results and Discussion:

The results of the detailed parametric evaluation of the rf-GD coupling to the GloQuad are summarized in Figure 2. The pooled data indicate that there is a combination of discharge power density and ion sampling distance (from the tip of the cathode) at which maximum analyte beam intensity is obtained. Additionally, there is a finite range of discharge gas flows (pressures) within which the device operates effectively. The identification of such a set of dependences is useful because not all pin samples will be of the same length or diameter, but either the power density or sampling distance can be predictably set to achieve high (ca. 10^{-9} A) ion beam intensities.

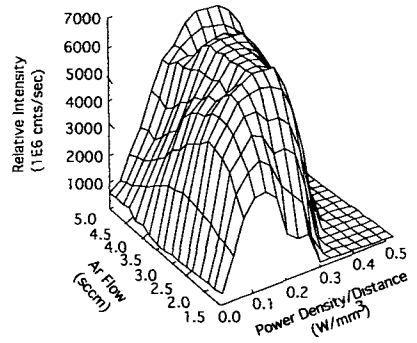

Figure 2. Effect of the discharge power density (per unit electrode separation) on ion beam intensities.

Other characteristics of importance in the implementation of the rf-GD technology include the time required to achieve stable ion beam currents, the relative stability of the beam over the analysis time frame, and the sample-to-sample precision for replicate measurements. Typical values of these characteristics are tabulated below for both conductive and glass samples. As can be seen, the rf glow discharge ion source coupled to a commercial quadruple GDMS system appears to have much promise Future studies will involve extensive methods development and characterization for analysis of wide ranging solid samples.

	stabilization time	beam current	int. precision
NIST 1259 / Al alloy	< 3 mins.	~2 X 10^{-9} A	0.7 % RSD
NIST 1412 / glass	< 2 mins.	~3 X 10^{-10} A	2.2 % RSD

Acknowledgments - Financial and instrumentation support from VG Elemental and the National Science Foundation are gratefully acknowledged.

1. Yuan Mei and R. Kenneth Marcus, "New Developments in Glow Discharge Mass Spectrometry", Tr. Anal. Chem., 12, 86, 1993.

2. R. Kenneth Marcus, "Operation Principles and Design Features for Radio Frequency Powered Glow Discharges", J. Anal. Atom. Spectrom., in press.

RF Glow Discharge Ionization with FT/ICR/MS Detection

Patrick A. Limbach†, Alan G. Marshall†,§, Douglas C. Duckworth‡, and Michelle V. Buchanan‡

† Departments of Chemistry (and Biochemistry[2]), § The Ohio State University, 120 West 18th Avenue, Columbus, OH 43210. ‡Analytical Chemistry Division, Oak Ridge National Laboratory, Oak Ridge, TN 37831

Marcus, Weller, and coworkers recently interfaced an rf glow discharge ionization source with a Fourier transform ion cyclotron resonance (FT/ICR) mass spectrometer for the analysis of conductive and insulating materials [1]. For their experiments, the glow discharge source was attached to the end flange of an FT/ICR mass spectrometer and ions were detected in the ion trap without the use of any external ion injection methods (e.g., quadrupole guide rods or electrostatic lenses).

In order to improve the sensitivity and detection limits for this method, we have added an easy-to-construct and use electrostatic ion guide [2] to focus the ion beam and inject it into the ion trap. The electrostatic ion guide controls the ion trajectories by the use of two low voltage (< 100 V) power supplies. The electrostatic ion guide allows for near-100% injection efficiency and allows for a seven order of magnitude decrease in operating pressure between the source and the detector. The use of this injection device reduces the analysis period relative to that in ref. 1, and improves the sensitivity of the measurement as well.

Figure 1 is a broadband (low-resolution) mass spectrum of a stock brass target. In this low resolution mode, the isotopic distributions of the copper, zinc, and lead present in the sample are easily resolved at a high signal-to-noise ratio. Figure 2 is a broadband (low resolution) mass spectrum of an NIST C1111 Red Brass C sample. Quantitative measurements from this sample are shown in Table 1. These values, calculated without the use of Relative Sensitivity Factors (RSF) normally employed in glow discharge experiments, demonstrate the potential analytical use of this instrument for glow discharge analysis. These results required a beam time half the amount reported in the previous results with a significantly smaller number of transients.

Improvements are underway to improve the sensitivity and resolution which include: replacing the diffusion pumps with cryopumps which should reduce the chemical background noise and reduce the operating pressure in the ion trap, and insulating the conductance orifice to allow for better control of the ion beam energies as they enter the electrostatic ion guide. With a dual cell instrument, we shall perform cooling experiments [3] and we shall also use an open-ended ion trap [4] to improve the ion transmission.

Research sponsored by the Office of Basic Energy Sciences, U.S. Dept. of Energy, under contract DE-AC05-84OR21400 with Martin Marietta Energy Systems, Inc., and The Ohio State University. P.A.L. research supported by the Oak Ridge Associated Universities under contract DE-AC05-76OR00033 with the U.S. Dept. of Energy.

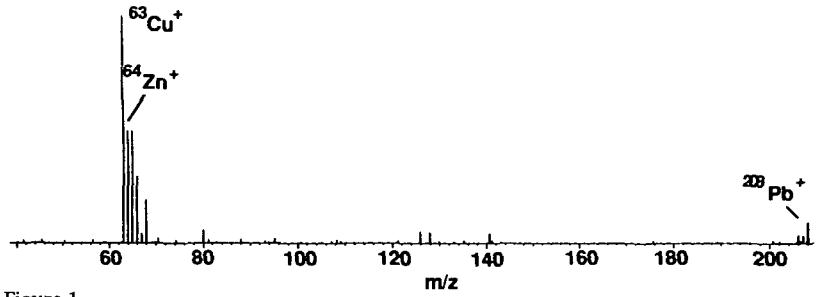

Figure 1.
Broadband mass spectrum of stock brass cathode.

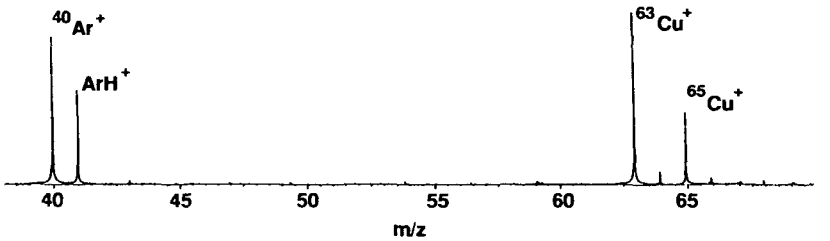

Figure 2.
Broadband mass spectrum of NIST C1111 Red Brass C cathode.

Element	Certified Value	Measured Value
Copper	87.14± 0.01	89.12 ± 2.32
Zinc	12.81± 0.05	10.84 ± 2.24

Table I.
Certified and measured values of copper and zinc in the NIST C1111 Red Brass C sample.

References

1. Marcus, R. K.; Cable, P. R.; Duckworth, D. C.; Buchanan, M. V.; Pochkowski, J. M.; Weller, R. R. *Appl. Spec.* **1992**, *46*, 1327-1330.
2. Limbach, P. A.; Marshall, A. G.; Wang, M. *Int. J. Mass Spectrom. Ion Processes* **1992**, in press.
3. Schweikhard, L.; Guan, S.; Marshall, A. G. *Int. J. Mass Spectrom. Ion Processes* **1992**, *120*, 71-83.
4. Beu, S. C.; Laude, D. A., Jr. *Int. J. Mass Spectrom. Ion Processes* **1992**, *112*, 215-230.

Using Ion-Molecule Reactions to Enhance High Resolution GD/ FTICR Mass Spectrometry

C.H. Watson, Bruker Instruments, Inc., Manning Park, Billerica, MA 01821
C.M. Barshick, Oak Ridge National Laboratory, Oak Ridge, TN 37831-6375,
and J.R. Eyler*, Dept. Chem., Univ. of Florida, Gainesville, FL 32611-2046.

We have been involved in the past two years in a three-way collaboration aimed at exploring many aspects of Glow Discharge (GD) / Fourier Transform Ion Cyclotron Resonance (FTICR) mass spectrometry. In this presentation we describe some experiments carried out at Bruker Instruments, Inc., which demonstrate the utility of coupling high resolution GD/FTICR with the ability of FTICR mass spectrometers to trap ions and allow chemical reactions to take place prior to detection.

Our recent experiments have involved demonstration that GD/FTICR could be used to determine directly (without preseparation) the abundance of ^{238}Pu in the presence of ^{238}U. These two isotopes differ in mass by 1 part in 193,500. We have carried out feasibility experiments on the (non-radioactive) ^{204}Hg / ^{204}Pb isotopic pair, which differ in mass by 1 part in 456,300.

We show in Fig. 1 the separation of the ^{204}Hg / ^{204}Pb isotopic pair which we have achieved. It would be highly desirable in the Pu / U experiments to remove the (expected) excess of U^+ ions from the cell, leaving primarily Pu^+ behind. Direct elimination of ions from one species with retention of those from the other in the FTICR cell will be difficult because the masses (and thus cyclotron frequencies) of the two species are almost identical. It is difficult to eject one ion from the icr cell without also imparting excess energy to another of almost the same frequency. Thus we have explored other means, such as differential chemical reactivity, to help with this problem. An example of this approach is shown in Figs. 2 and 3. By reacting the ions of ^{204}Hg and ^{204}Pb, trapped in the FTICR analyzer cell after glow discharge formation, with benzene for progressively longer periods of time, the ratio of the two peaks is seen to change by almost a factor of 10. This is because the Hg^+ ion underwent charge transfer with benzene, while the Pb^+ ion did not. The Hg^+ ions were thus removed (converted to $C_6H_6^+$ ions), and the latter could be ejected from the cell since they are far removed in mass from the ions (Pb^+ in this case) of interest. Such ejection was not done in the experiments shown in Figs. 2 and 3, but could be implemented with relative ease. Note that the signal-to-noise ratio of the Pb^+ peak remains the same (ca. 3:1) in Figs. 2 and 3, since for these experiments no additional ions were being stored and detected in the FTICR analyzer cell, only the Hg^+were being removed.

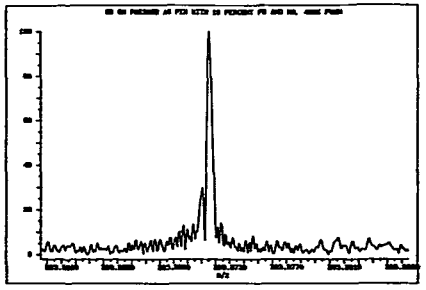

Fig. 1. High Resolution GD / FTICR Mass Spectrum of $^{204}Pb^+$(left) and $^{204}Hg^+$ (right) Ions.

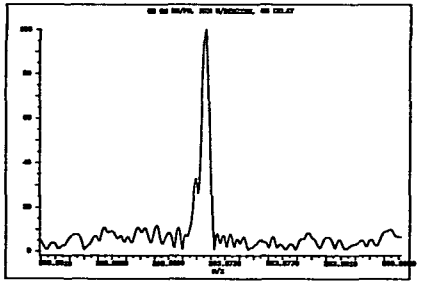

Fig. 2. Pb^+(left) and Hg^+(right) Peaks at m/z 204 before Reaction with Benzene.

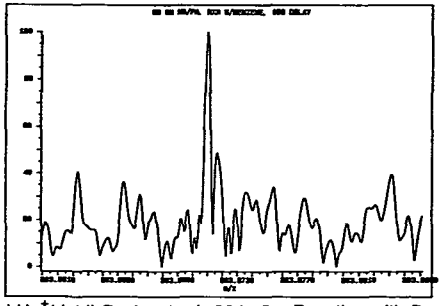

Fig. 3. Pb^+(left) and Hg^+(right) Peaks at m/z 204 after Reaction with Benzene for 15 s.

DIRECT ANALYSIS OF SOILS BY RADIO-FREQUENCY POWERED GLOW DISCHARGE MASS SPECTROMETRY

Douglas C. Duckworth, Lee R. Riciputi, and David H. Smith
Oak Ridge National Laboratory,
Oak Ridge, TN 37831-6375

Introduction

Glow discharge mass spectrometry (GDMS) is a multi-element analysis technique which holds promise for the elemental analysis of soil. Because GDMS is a direct solids technique, arduous dissolution procedures, often required for soils, can be avoided. Such analyses can be performed utilizing direct current (dc) discharges, after mixing the soil with a conducting host matrix, or directly with radio-frequency (rf) powered glow discharges (i.e., no mixing with a conducting host). While the host element serves as an internal reference in dc-GDMS, its addition is undesirable due to dilution of the sample and the additional polyatomic interferences formed. These interferences can be significant due to combinations with the discharge gas and several low mass elements, often present at ≥ 1%. However, the elimination of the host matrix, which serves as an internal reference, requires that an alternative method of quantification be employed. In this study, the feasibility of elemental analysis of soils by rf-GDMS was investigated in terms of spectral characteristics and means of quantification. The use of mass balance quantification, where all minor elements are referenced to the sum of the majors (~100%), was investigated.

Experimental

The rf source was interfaced to a VG9000 double-sector mass spectrometer, which affords a high mass resolving power, beneficial for the analyses of such difficult matrices. Sample preparation for rf-glow discharge analyses consisted of heating the sample at 120 °C for 2 hrs and pelletizing (5mm diam. x 2mm) the soil, without binder. Samples prepared in this manner were nevertheless very rugged.

Results

The number and extent of isobaric, matrix-related polyatomic interferences in the rf glow discharge were determined from the analysis of various oxides, including Al_2O_3, Fe_2O_3, and SiO_2. As expected, a number of polyatomic interferences were observed. Analysis of aluminum oxide (~100%), for example, contributed the following interferences: AlO^+, 1%; Al_2^+, 4%; AlO_2^+, 70 ppm; $AlAr^+$, 0.1%; Al_2O^+, 0.3 ppm; AlO_3^+, 160 ppm; and $Al_2O_2^+$, 30 ppm. For minor and trace oxides present in soils, many such interferences are negligible; however, for the major constituents (SiO_2, Al_2O_3, Fe_2O_3) such interferences are detrimental. With a resolving power of 3 - 4 thousand, many such interferences can be circumvented.

Research sponsored by the U.S. Department of Energy, Office of Basic Energy Sciences, under Contract DE-AC05-84OR21400 with Martin Marietta Energy Systems, Inc.

"The submitted manuscript has been authored by a contractor of the U.S. Government under contract No. DE-AC05-84OR21400. Accordingly the U.S. Government retains a nonexclusive royalty-free license to publish or reproduce the published form of this contribution, or allow others to do so, for U.S. Government purposes."

The results of the mass balance quantification of NIST SRM 2711 Montana Soil are presented in Table 1. Elemental concentrations, based solely on ion beam ratios, are given in column three. Results, including a large error for carbon, differ from the certified values by an average 141%. Given the low relative sensitivity factor (i.e., high relative ion yield), it is likely that the additional carbon arises from residual gases entrained when pressing the pellet. Average error, excluding carbon (52%) is also shown.

Table 1. RF-Glow Discharge Mass Spectrometric Analysis of NIST SRM 2711 Montana Soil

Element	Certified Concen - trations	Elemental Concen - tration	% Error	Measured RSF Value	RSF Adjusted Concen - trations	%Error
C	(2) %	28.0 %	1300	0.067	1.30 %	35
O	-	9.40	-	9.00	57.0	-
Na	1.14	1.70	49	0.792	0.910	20
Mg	1.05	1.90	81	0.695	0.920	12
Al	6.53	7.60	16	0.827	4.20	36
Si	30.44	39.0	28	1.00	26.0	15
K	2.45	4.00	63	0.855	2.30	6
Ca	2.88	4.00	39	1.11	3.00	4
Ti	0.306	0.350	14	2.49	0.59	93
Fe	2.89	3.90	35	1.12	2.90	0.3
P	860 ppm	400 ppm	54	1.85	510 ppm	41
Mn	638	1200	88	0.808	670	5
Cd	41.70	86.0	106	0.563	33.0	21
Ba	726	140	81	3.42	490	33
Pb	1162	1400	21	0.395	370	68
			$\bar{x}$ = 141 (52)			$\bar{x}$ = 28 (27)

Relative sensitivity factors obtained through the analysis of NIST SRM's 2704, 2709, 2710, and 2711 Soils are shown in column five. The RSF adjusted concentrations (column 6) have significantly improved the average error, though some elements fared worse after RSF adjustment, illustrating the need for better characterized RSF values.

Conclusions

Glow discharge mass spectral characteristics arising from the analysis of soils indicate that some means of dealing with isobaric interferences (e.g., high mass resolving power, collision-induced dissociation) is necessary. This is particularly true for rf-GDMS, where most of the low-mass matrix elements have residual gas interferences, and no internal reference is available. (Silicon, the most abundant element, has residual gas interferences at each isotope.) In the absence of an internal reference element, the use of mass balance quantification is promising for semi-quantitative analysis. Carbon and oxygen determinations hinder the technique as errors arising from residual gas species are propagated through the analysis. For solid matrices of less complex composition, this method is even more promising.

THE APPLICATION OF GLOW DISCHARGE-FOURIER TRANSFORM ION CYCLOTRON RESONANCE (GD-FTICR) MASS SPECTROMETRY TO ISOTOPE RATIO MEASUREMENTS

***C.M. Barshick**
Analytical Chemistry Division, Oak Ridge National Laboratory
Oak Ridge, TN 37831-6375, USA

C.H. Watson, J. Wronka, and F.H. Laukien
Bruker Instruments, Inc.
Billerica, MA 01821, USA

J.R. Eyler
Department of Chemistry, University of Florida
Gainesville, FL 32611-2046

Since its introduction at the 1991 ASMS meeting in Nashville, GD-FTICR mass spectrometry has met with a great deal of success. Quantitative capabilities have been shown to be as good as quadrupole and magnetic sector instruments. Detection limits have continually improved to a current level of < 100 parts-per-billion, and resolution, which was always a major advantage of the technique, has recently been shown to exceed 650,000 at m/z = 197.

One area that is absent from this list of accomplishments, however, is reliable isotope ratio measurements. Always suspect in FTMS, isotope ratio measurements are important because they impact a number of areas, including stable isotope enrichment for medical and military applications. Recently, we have begun evaluating how well GD-FTICR mass spectrometry can measure the abundances of several pairs of isotopes. Table 1 compares the results obtained using the VG9000 magnetic sector glow discharge mass spectrometer and the Bruker Apex 47e glow discharge mass spectrometer to measure the lead isotope ratios in a 10% PbO / 10% HgO / 80% silver powder sample. The absolute abundance ratios were not known but were assumed to be natural. Uncertainties given in Table 1 are one standard deviation (1σ). The Infinity Cell® designation in column 5 and column 8 refers to a cell design whose excitation voltages approximate the ideal (i.e., a cell that is infinitely long). In comparing column 7 and column 8, it is clear that the increased control of the ion excitation process afforded by the Infinity Cell® improves the precision of the isotope ratio measurement.

In addition to good precision for any one isotope ratio measurement, it is equally important to demonstrate a small bias between the measured values and the known values. Table 2 illustrates how the VG9000 and the Bruker Apex 47e compare in this regard. Run-to-run precision on the GD-FTICR instrument is poorer than in Table 1, due in part to the lower concentration of the analyte (5% NIST 987 $SrCO_3$ in silver powder). The biases are quite acceptable, although it is still unclear how GDMS biases vary in general.

One question that still remains after this investigation is: "How much precision is lost when measuring isotope ratios at resolution m / Δm > 200,000?" Research is continuing.

Table 1. Isotope Ratio Precision Measurements on VG9000 Magnetic Sector and the Bruker GD-FTICR (10% PbO / 10% HgO / 80% silver powder)

Isotope Ratios	Natural Ratios	Measured Ratios			Percent Relative Standard Deviation		
		VG9000	GD-FTICR Conventional Cell	GD-FTICR Infinity Cell®	VG9000	GD-FTICR Conventional Cell	GD-FTICR Infinity Cell®
$^{206}Pb^+ / ^{208}Pb^+$	0.4612	0.51847 ± 0.00055	0.541 ± 0.017	0.4923 ± 0.0022	± 0.11	± 3.2	± 0.45
$^{207}Pb^+ / ^{208}Pb^+$	0.4218	0.39972 ± 0.00051	0.437 ± 0.014	0.3981 ± 0.0010	± 0.13	± 3.2	± 0.25
$^{207}Pb^+ / ^{206}Pb^+$	0.9146	0.7710 ± 0.0011	0.809 ± 0.013	0.8103 ± 0.0029	± 0.15	± 1.6	± 0.36

Table 2. Isotope Ratio Precisions and Biases for an NIST 987 Isotopic Standard ($SrCO_3$) in Silver VG9000 Magnetic Sector versus Bruker GD-FTICR (Infinity Cell®)

Isotope Ratios	Absolute Abundance Ratios	Measured Ratios			Percent Relative Standard Deviation			Percent Bias	
		VG9000	GD-FTICR Infinity Cell®	VG9000	GD-FTICR Infinity Cell®	VG9000	GD-FTICR Infinity Cell®	VG9000	GD-FTICR Infinity Cell®
$^{87}Sr^+ / ^{86}Sr^+$	0.71034 ± 0.00026	0.71478 ± 0.00010	0.722 ± 0.013	± 0.13	± 1.8	+ 0.61	+ 1.6
$^{88}Sr^+ / ^{86}Sr^+$	8.3786 ± 0.0033	8.4266 ± 0.0080	8.64 ± 0.13	± 0.095	± 1.5	+ 0.57	+ 3.2

Research was sponsored in part by the U.S. Department of Energy, Office of Basic Energy Sciences, under Contract DE-AC05-84OR21400 with Martin Marietta Energy Systems, Inc., in part by the Office of Naval Research, and in part by the Institute for Physical Research and Technology, Ames Laboratory, Department of Energy, Ames, Iowa.

"The submitted manuscript has been authored by a contractor of the U.S. Government under contract No. DE-AC05-84OR21400. Accordingly, the U.S. Government retains a nonexclusive, royalty-free license to publish or reproduce the published form of this contribution, or allow others to do so, for U.S. Government purposes."

IMAGING ISOTOPE RATIO AND TRACE ELEMENTAL ANALYSIS OF GOLD ORE

*Ronald H. Fleming[1] and Barbara M. Bekken[2]

[1]Charles Evans & Associates, 301 Chesapeake Drive, Redwood City, CA 94063.
[2]Barbara M. Bekken, Department of Geological Sciences, Virginia Polytechnic Institute, Blacksburg, VA 24061-0420.

Isotope ratio measurements play a central role in deducing mineral ages and petrogenesis conditions. Different mineral genesis conditions often lead to isotope fractionation in light elements. Multiple petrogenesis episodes can then leave minerals with different isotope ratios in close proximity to each other. Imaging is an ideal way to study the resulting sample heterogeneity. Human observers instinctively comprehend the variability shown in an image.

We have developed secondary ion mass spectrometry techniques for measurement of $^{34}S/^{32}S$ isotope ratio images[1] in pyrite mineral grains. We have also extended relative sensitivity factors to images in order to quantitate gold in the pyrite rims. These measurements employ a CAMECA IMS-4f mass spectrometer operating with Cs^+ sputtering, negative secondary ions, and the ion microprobe (raster) mode of imaging. The imaging has the inherent problem of spreading already limited minor isotope ion signals among many pixels. Image processing methods diminish this problem by treating each image position as the sum of intensities from nearby pixels. In addition, new electron multiplier circuitry[2] accommodates more intense ^{32}S secondary ion signals which allows ^{34}S ion signals to accumulate faster. Dynamic emittance matching provides the high mass resolution imaging required to separate the ^{32}S signal from $^{16}O_2$ interference and the ^{197}Au from $^{133}Cs^{32}S_2$ interference. Although pyrite is a semiconductor, the grains are embedded in insulating minerals. The samples require careful neutralization of ion beam induced charging. For this, we use a combination of a conductive carbon coating on the sample, a normal incidence electron flood gun during sputtering, and low primary ion currents. We also invoke periodic mass recalibration for long data collection periods. Finally, improved software calculates isotope ratio images from multiple images of individual isotopes and element concentration images from trace element and matrix element images. Isotope ratio images of Canyon Diablo Troilite demonstrate that the isotope ratio measurements are invariant as a function of image position. Figure 1 shows the $^{34}S/^{32}S$ isotope ratio image of a pyrite grain from a sample of Carlin gold ore and Figure 2 shows gold concentrations of the same mineral grain.

ACKNOWLEDGEMENTS

The National Science Foundation (Small Business Innovative Research Phase I Grant ISI-9160939) provided financial support for this research.

(1) R. H. Fleming, G. P. Meeker, F. Radicati di Brozolo and D. F. Blake, in Secondary Ion Mass Spectrometry SIMS VII, Wiley, New York (1990) p. 385.

(2) Y. A. Liu and R. H. Fleming, *Rev. Sci. Instrum.*, in press, (1993).

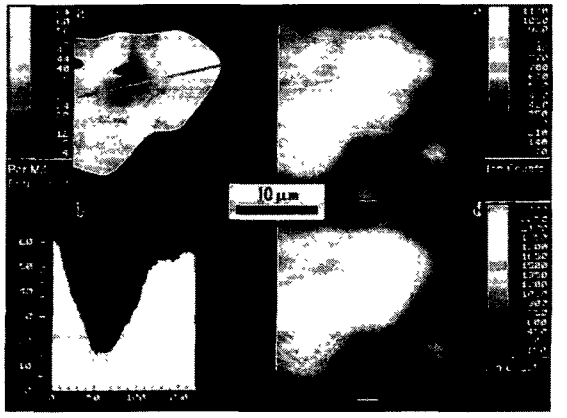

Figure 1. Isotope ratio image of a pyrite grain from a gold ore sample taken from the Carlin mine in Nevada. (a) $^{34}S/^{32}S$ enrichment, parts per thousand (δ) relative to Canyon Diablo Troilite. (b) $^{34}S/^{32}S$ enrichments along the line in Figure 1a. (c) Intensity (ions per pixel) for ^{34}S (m/z 33.968). (d) Intensity (ions per pixel) for ^{32}S (m/z 31.972).

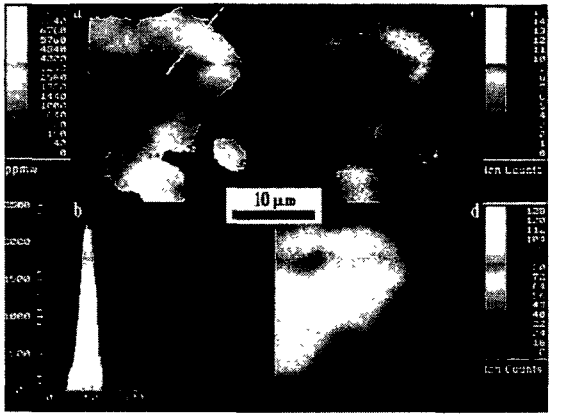

Figure 2. Gold concentration image in a pyrite grain (the same grain as Figure 1) in a gold ore sample from the Carlin mine, Nevada. (a) Gold concentration (parts per million, weight). (b)Gold concentration along the line in Figure 5a. (c) Intensity (ions per pixel) for gold (m/z 196.967). (d) Intensity (ions per pixel) for ^{34}S (m/z 33.968).

High Spatial Resolution Isotope Ratio Imaging Using Secondary Ion Mass Spectrometry

Greg Gillen and David S. Bright, Surface and Microanalysis Science Division, National Institute of Standards and Technology, Gaithersburg, MD 20899

Isotope ratio imaging is a very powerful but as yet underutilized analytical capability of Secondary Ion Mass Spectrometry (SIMS). With recent advances in SIMS imaging systems it is possible to generate isotopic images with high mass resolution and high spatial resolution. The ability to characterize precisely the composition of isotopically heterogeneous materials on a micrometer spatial scale has many potential applications including biological tracer studies, studies of atmospheric particles and identification of isotopic anomalies in geological and cosmological materials.

We are studying the feasibility of high spatial resolution isotope ratio imaging using an ion microscope SIMS instrument (Cameca IMS 4F). In this instrument, the mass-resolved secondary ion image is projected (via ion-electron conversion at a micro channel plate) onto an imaging detector by the secondary ion optics. Precision isotopic ratio imaging has been hampered in the ion microscope by the non-linear behavior of the video cameras used to record the secondary ion images or by the low maximum input count rates that could be processed by the pulse-counting resistive anode encoder detector (RAE). Fortunately, two new imaging detectors that should minimize these problems are now available. The first is a newly designed "fast" Resistive Anode Encoder (RAE) detector (Charles Evans and Associates, Redwood City, CA) that uses a lower resistance anode, "hot" high strip current channel plates and new analog-digital converters to allow input count rates of > 1×10^5 counts/s before pulse pileup effects become significant. The second detector is a scientific-grade slow-scan CCD camera (Photometrics, Tucson, AZ). We have found that this camera is to be highly linear over more than 6 orders of magnitude of input count rate and is sensitive enough to detect single ion events. A significant advantage of this detector is that it can process over 3 orders of magnitude higher input count rates than the fast RAE detectors. This makes it appropriate for imaging of isotope ratios for species in which the low abundance of a minor isotope and the intense secondary ion signal of the major isotope make the use of an RAE detector problematic.

Newer ion microscope instruments can also be used in a microprobe mode of operation. In this mode, the spatial resolution of the image depends on the spot size of the primary beam which, for the 15.0 keV O_2^+ bombardment used in this study, was 0.25 micrometer (with Cs primary bombardment probe sizes of ~0.1 micrometer are possible). Our initial experiments with microprobe imaging have focused on isotope ratio imaging of 5 NIST-prepared research glass standards doped with lithium. Each of these glasses has a different $^6Li/^7Li$ ratio (6/7 ratios 21.6, 1.132, 0.477, 0.193, 0.084). The glasses were ground into fine particles and dispersed onto a carbon planchet with cyclohexane. ^6Li and ^7Li images were obtained from a variety of areas on the sample at various magnifications (180 s image acquisition times for each isotope). Figure 1B shows microbeam images of ^6Li and ^7Li from one of these glass particles. The field of view for this image is 16 micrometers, with the small inclusions being about 2 micrometers in diameter. To display isotope images in a meaningful way, we need to simultaneously present both spatially resolved information and quantitative intensity data to the observer. One way to do this is by using a transformation called Concentration Histogram Imaging (CHI) (1). To generate a CHI, we start with two registered Li isotopic images each represented by an array of pixels(x,y) which contain the intensity information for the given isotope. The CHI is constructed by incrementing an element of the

histogram image array h(i,j) where i and j correspond to the values of intensity for every location (x,y) in the two isotopic images. After the CHI array is calculated, we can display it as an image using a thermal scale constructed so that zero count is black, one count is red, and higher counts range from orange to yellow to white. As an example of the use of CHI for isotopic characterization, Figure 1A shows the CHI for the microbeam image of lithium glass particles. The CHI, which gives the intensity relationship between the ^7Li and ^6Li clearly indicates that the image contains regions with two distinct isotopic compositions. The ratios can be determined from least-squares fits along the displayed line. Having generated the CHI, the observer is likely to be interested in the relationship of features recognized in the CHI to features in the original maps. This relationship can be discovered with a modification of the CHI algorithm called the "traceback" function. The traceback function selects pixels in the CHI images on the basis of intensity correlations; a mask is created which then can be used to mark the original images. We have also found the CHI to be very useful for observing dead-time effects that may affect isotope ratio measurements. In this situation attenuation of the more intense isotopic signal gives a CHI with a curved line that is readily apparent.

In addition to the lithium glasses, we have also been studying the imaging of magnesium isotope ratios from B1 Ca-Al-rich inclusions in the Allende meteorite. These inclusions have been found to have ^{26}Mg excesses of 5-15%. Typically we acquire alternate images of ^{26}Mg and ^{24}Mg (to minimize variations in signal drift) which are summed after the analysis. Total counting times are typically 30 min. for ^{26}Mg and 10 min. for ^{24}Mg. If desired, we can correct for dead-time effects, mass bias and hydride interferences on a pixel-by-pixel basis. For these samples, because of the high secondary ion signal of Mg, it is possible to collect signals for the minor isotope exceeding 20,000 counts/pixel. This allows us to achieve a ratio precision of better than .7% on an individual pixel. Figure 2 shows an isotope ratio image $^{26}Mg/^{24}Mg$ in which a small grain demonstrates on enrichment in the ^{26}Mg of 6%.

1. D.S. Bright and D. E. Newbury, *Anal. Chem.* **63** (4), 1991.

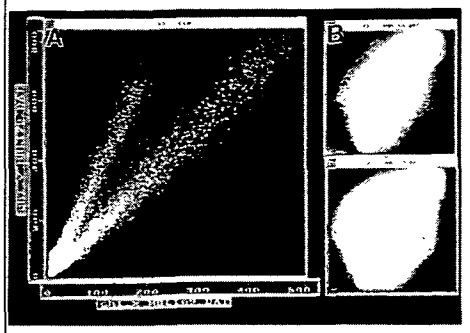

Figure (1B) Image of ^6Li (top) and ^7Li(bottom) from Li containing glass particles. 16 µm field of view. (1A) Concentration Histogram Image generated from isotopic images.

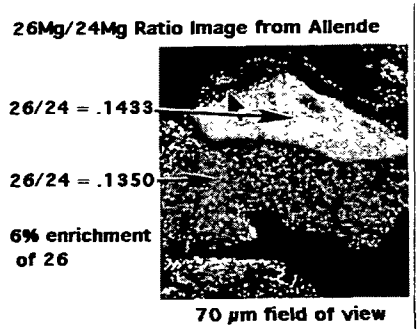

Figure 2. Mg Isotope Ratio Image from Allende meteorite sample.

HIGH PRECISION LIQUID CHROMATOGRAPHY-COMBUSTION ISOTOPE RATIO MASS SPECTROMETRY (LCC-IRMS)

Richard J. Caimi and J. Thomas Brenna
Division of Nutritional Sciences
Cornell University
Ithaca, New York

High precision determinations of carbon isotope ratios in bulk samples (eg–plant parts, petroleum) have been employed for a wide variety of studies of the natural world, and continue to have an important impact on geochemistry, ecology, oceanography and related topics. These measurements are widely employed for tracer experiments in the biomedical sciences, particularly in the context of breath tests and water isotope determinations for total body water and the doubly labeled water technique for energy expenditure. The high precision gas isotope ratio mass spectrometers (GIRMS) used in these applications are designed to analyze a few small molecules (CO_2 , H_2 , N_2) and produce 4-7 significant figures for isotope ratios on sample sizes greater than 100μg.

In recent years the capability to determine carbon isotope ratios at high precision for specific compounds ("compound specific isotope analysis", CSIA) has grown in applications principly because of the commercial introduction of gas chromatography-combustion isotope ratio mass spectrometry (GCC-IRMS) in 1990. Briefly, organic compounds eluting from a GC column are directed to a combustion furnace for quantitative conversion to CO_2 with subsequent drying and admission to the GIRMS instrument. Typical precision for $^{13}C/^{12}C$ determinations is 0.0003‰ (absolute) for sample sizes greater than 10 ng. We recently described a high sensitivity approach to tracer experiments coupling this instrumental method with the use of highly enriched perlabeled tracers (1). Our data suggests this approach is more sensitive than acceptable radiotracer doses for the majority of human applications.

We have recently constructed as system for interface of a liquid source, including liquid chromatography, to IRMS, to extend the technique to non-volatile and thermally labile compounds. The key consideration for such an interface operating at precision and accuracy levels quoted above is reliable removal of carbon-containing compounds, most notably solvents, from the analyte prior to combustion. Although a number of new interfaces have become popular for organic LC/MS in recent years (electrospray, thermospray, direct liquid injection, particle beam), the only interface which can be expected to accomplish this is the moving transport interface. We have modified a commercial moving wire device, originally designed for interface of LC to a flame ionization detector, to remove solvent, combust organic molecules to CO_2 prior to introduction to the IRMS. The combustion furnace is loaded with CuO which exists in equilibrium with Cu metal and O_2 at 800°C and

serves as a source of oxygen. A water trap has been installed in the line prior to the mass spectrometer to dry the stream prior to introduction to the GIRMS instrument.

The instrument is operated in one of two modes: flow injection, in which there is no LC column, or LC mode. Flow injection mode results in sharper peaks that LC mode and therefore is more sensitive and yields more precise numbers for a given sample load. Precision for replicate injections and a calibration curve were determined in flow injection mode. Isotopically calibrated linoleic acid was prepared in graded series from the terrestrial natural abundance range to about 0.1% enrichment above this level $0.010844 < {}^{13}C/{}^{12}C < 0.012285$. Data were calibrated against the known isotope ratio of lowest ^{13}C content. A plot of known isotope ratio versus LCC-IRMS ratio gives a correlation coefficient of 0.9998, with slope=0.996 (theoretical=1) and intercept=0.3 (theoretical=0). Average precision for these determinations was less than δ_{PDB} =0.5‰ .

Liquid chromatography mode was tested with a mixture of isotopically calibrated fructose, sucrose, and lactose. Calibration was made against the known isotope ratio of fructose. Baseline separation was achieved for all sugars. Precision for each was less than 1‰ and accuracy was 0.4‰ and 1.8‰ for sucrose and lactose, respectively. These figures are comparable to errors obtained for similar quantities of material analyzed by GCC-IRMS, estimated to be about 1 ng.

These data represent the first demonstration of on-line coupling of a liquid source with high precision GIRMS, and extend the CSIA to the full range of biomolecules.

(1) K. J. Goodman and J. T. Brenna, *Analytical Chemistry* 64(10), 1088.

Isotope Chemistry in the Jar: Direct Isotopic Analysis from Head Space Gas Mixtures using a GC-IRMS System

A. Hilkert and W. A. Brand,
Finnigan MAT, Barkhausenstr. 2, 2800 Bremen, Germany

Isotope ratio mass spectrometers for gaseous samples offer the highest precision available for isotope abundance studies. For carbon, the limitation of the required large sample size has recently been overcome by combining the isotope MS with a GC and introducing the sample together with the carrier gas (after complete oxidation to CO_2 in a combustion interface) into the ion source[1].
The precision of the method is 0.0003 at% or better. Sample sizes down to 20 pmol carbon in the ion source have been reported[2]. Extension of the method to other isotope ratios like $^{15}N/^{14}N$, $^{18}O/^{16}O$, $^{34}S/^{32}S$ is possible and has been demonstrated.
The technique is also applicable to gas mixtures by replacing the traditional cryogenic gas separation device with a GC.
We have tested this idea by combining a headspace autosampler with a GC-IRMS system. The effluent of the GC is passing through a combustion interface before entering the MS via an open split. The interface has a combustion tube for quantitative oxidation of effluent material, a reduction tube filled with elemental Cu, a water removal system and a means for reference gas injection. The furnaces are hot only when applicable.

Figure 1 shows results from a series of measurements of alcoholic beverages. 200 to 300 µl of liquid were filled in 2ml autosampler vials and septum capped. From the headspace samples were taken using a gas tight 100 µl syringe and injected into a GC (Hewlett Packard model 5890) equipped with a split injector and a capillary column for gas separation (Chrompack Poraplot Q 25m). Following on line combustion the isotope ratio was determined on a gas isotope MS (Finnigan MAT, model Delta S). The Delta values are given versus PDB, the international standard for ^{13}C analysis. The solid points represent the headspace measurements. The two open squares were obtained via total combustion of the respective sample, reflecting the overall ^{13}C value. The agreement between both types of measurement is satisfactory.
Most of the samples have isotope values around -25 permil. Notable exceptions are the synthetic alcohol, the Jamaican brands and two of the Whiskys. Pure Scotch should have a value close to -25 permil as represented by the single malt brands. The value of -16.5 indicates a blending procedure involving approximately 40% Scotch and 60% from another source derived from corn or, less likely, from sugar cain.
It is noteworthy that also beer with an ethanol content of only 5% and thus only 0.4 mb partial pressure can be measured with the technique. The CO_2 is separated by the GC and may be determined simultaneously. The same is true for wines or champaigns.

Figure 2 shows results for a well known classic of isotope ratio techniques, the equilibration of water with CO_2 for ^{18}O determination. The results were obtained on water amounts small as compared to the conventional technique (≈5ml). The Delta values are virtually independent of the sample size.

The technique is suitable for the measurement of methane, CO_2 from breath following oral ingestion of ^{13}C labelled nutrients or drugs, ^{13}C determination of the carboxyl group in aminoacids using the ninhydrin reaction and other analytical problems.

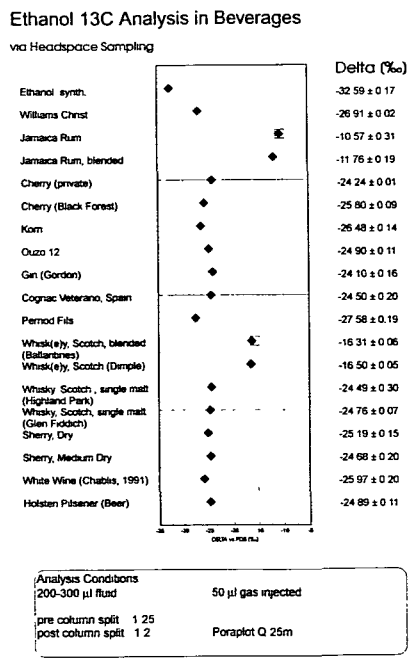

Figure 1

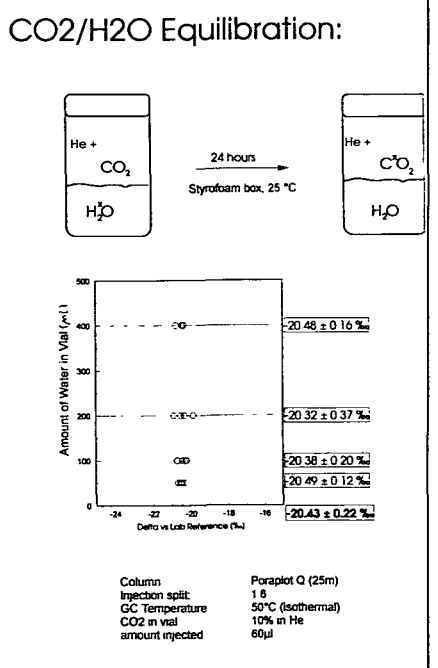

Figure 2

[1] J.M.Hayes, K.M.Freeman, B.N.Popp, C.H.Hoham, Org. Geochem. 16, 1115, 1990
M.Rautenschlein, K.Habfast and W.Brand in: Stable Isotopes in Paediatric, Nutritional and Metabolic Research; eds T.E.Chapman, R.Berger, D.J.Reyngoud, A.Okken, Intercept, Hampshire 1990, 133
W.A.Brand, K.Habfast, M.Ricci, in: Adv.Mass.Spectrom. 11B, ed.P.Longevialle, Heyden&Son, London 1989, 1800
[2] D.Merrit and J.M.Hayes, personal communication

IMPROVEMENTS IN SENSITIVITY AND PRECISION ATTAINED WITH THE APPLICATION OF ION COUNTING TECHNIQUES TO ISOTOPE RATIO ANALYSIS OF ZINC AND IRON USING FAB/SIMS

David R. Flory, Leland V. Miller, Paul V. Fennessey and José A. Olivares.*

Departments of Pharmacology and Pediatrics, University of Colorado Health Sciences Center, Denver, CO 80262 and *Los Alamos National Laboratory, Los Alamos, NM 87545.

Introduction

Stable isotope technology is becoming the method of choice for nutritional studies involving a variety of elements. As study designs increase in complexity (i.e. multiple isotopes delivered, frequent sampling, etc) the sensitivity of isotope ratio measurement can become the limiting factor due to frequent sampling and the small sample volume. We have combined pulse counting hardware with a software control and acquisition system developed at Los Alamos to obtain an increase in both sensitivity and sample throughput. These modifications were made to an organic mass spectrometer (VG 7070EHF) using FAB ionization.[1]

Experimental

A linear-focusing electron multiplier (Thorn EMI C660) pulse counter, was added "on-axis" to the mass spectrometer so as not to interfere with the resident electron multiplier used for organic analysis. The pulses are counted by a counter/timer board (Data Translation DT2827) in an AT-compatible computer. The computer software is a menu-driven program written in HT Basic which acquires data by either ion current or ion counting measurements. This program also has the capacity to do either voltage or magnet switching for operation of the mass spectrometer. Various concentrations of zinc and iron (confirmed by atomic absorption) were used for isotope ratio measurements by magnet switching and the new pulse counting technique.

Results and Discussion

Previous FAB/SIMS techniques[1] using magnetic scanning and EM current measurements were both precise (RSD'S $\leq 2\%$) and accurate ($\geq 99\%$) but required sample loads of from 2 to 8 μg of analyte for analysis. With zinc and iron present in the plasma at ≤ 1 μg/ml, and with frequent sampling used in present studies, 2-3 minutes between samples, this results in a decreased sample volume (2 ml/sample). After loss of analyte which occurs with sample clean-up and isolation, often there was not enough analyte remaining for accurate isotope ratio analysis. The application of pulse counting to isotope ratio measurements of zinc, Figure 1, has increased the sensitivity of measurements while retaining equal precision and accuracy. However, the limits of sensitivity are dependent upon the specific isotope studied. In Figure 1a, the measured ratio $^{70}Zn/^{66}Zn$ remains precise throughout the 20-1000 ng range (RSD's 0.56-3.8%) but is inaccurate below 200 ng of sample. In Figure 1b, for $^{68}Zn/^{66}Zn$, the precision is about equal to $^{70}Zn/^{66}Zn$, but remains accurate to 100 ng with the possibility of getting useful data at only 20 ng sample loads. For ^{68}Zn, this is an actual increase in sensitivity of 1 order of magnitude (at 100 ng) with the potential of 2 orders of magnitude (at 20 ng). The differences between the sensitivities of ratios involving $^{70}Zn/^{66}Zn$ vs $^{68}Zn/^{66}Zn$ are related to natural abundances of each isotope. With a smaller natural abundance (^{70}Zn = 0.62% vs ^{68}Zn = 18.6%) there is a decrease in sensitivity. In Figure 2, the $^{54}Fe/^{56}Fe$ ratio remains very accurate ($\geq 99\%$) and precise (RSD $\leq 1.5\%$) at sample loads down to 50 ng. Beyond this level, the ratio deviates and becomes too

inaccurate for useful measurements. As in the case of zinc, when the least abundant isotope of iron is used, ^{58}Fe, precision is good but accuracy is only retained at sample loads of 200 ng or greater (data not shown).

The application of pulse counting to FAB/SIMS isotope ratio measurement has widened the focus of possible research to infant and initial plasma kinetic studies. These types of studies require increased sensitivity with equal accuracy and precision which is now available with pulse counting techniques.

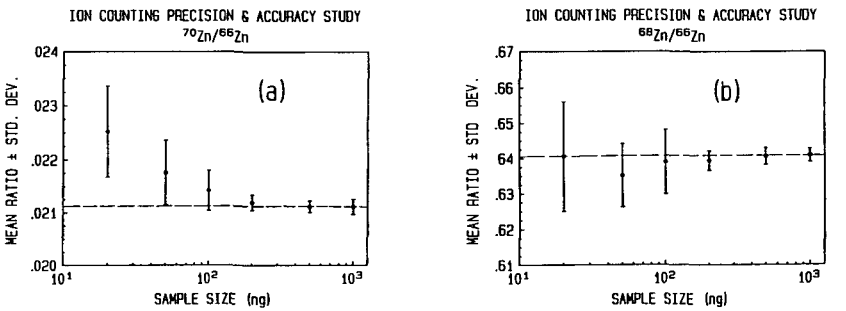

Figure 1. Isotope ratios of (a) $^{70}Zn/^{66}Zn$ and (b) $^{68}Zn/^{66}Zn$ are plotted against sample quantity used for isotope ratio measurement. Each data point is an average of 288 separate measurements at each of the masses. The FAB source was run at 8 kV and 1 mA. The line (-----) denotes the zero enrichment reference ratio.

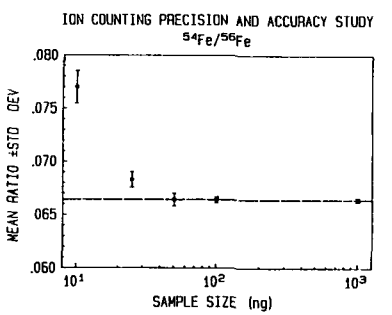

Figure 2. Isotope ratios of $^{54}Fe/^{56}Fe$ are plotted against sample quantity used for isotope ratio measurement. The number of measurements, FAB data, and line (-----) are the same as in Figure 1.

1. Pierce, P.L., Hambidge, K.M., Goss, C.H., Miller. L.V., and Fennessey, P.V. (1987). Fast atom bombardment mass spectrometry for the determination of zinc stable isotopes in biological samples. Anal. Chem., 59, 2034-7.

Metabolism of Δ^4-VPA To Glutathione Conjugates in the Rat: Identification of Novel Adducts Using Ionspray LC-MS/MS.

K. Kassahun, M.P. Grillo, M.R. Davis, L. Jin and T.A. Baillie
Department of Medicinal Chemistry, University of Washington, Seattle, WA, 98195

2-*n*-Propyl-4-pentenoic acid (Δ^4-VPA) is the terminal olefin metabolite of the antiepileptic drug valproic acid (VPA). Δ^4-VPA has been shown to be a teratogen in the mouse and a potent hepatotoxin in the rat (1,2). Several lines of evidence suggest that the hepatotoxicity of Δ^4-VPA may be mediated by reactive intermediate(s) arising from the metabolism of the compound (3,4). Since many electrophilic xenobiotic metabolites react with the cellular nucleophile glutathione (GSH), structural characterization of the resulting conjugates provides a valuable indirect means of identifying short-lived electrophiles. This approach frequently affords a valuable insight into the mechanisms of xenobiotic-mediated toxicity. In this study, we investigated the biliary excretion in rats of GSH adducts from Δ^4-VPA and [3,3-$^2H_2$]Δ^4-VPA.

Bile was analyzed by a Perkin-Elmer/Sciex API III triple quadrupole mass spectrometer equipped with an atmospheric pressure ion source and ionspray interface. Tandem mass spectrometry was based on collision-induced dissociation of ions entering the rf-only quadrupole region, where argon was used as the collision gas. Full scan mass spectra of synthetic compounds and product ion spectra of the corresponding $[M+H]^+$ parent ions were recorded by direct infusion of the sample (10 $\mu g\ ml^{-1}$) into the instrument at a flow rate of 5 $\mu l\ min^{-1}$. LC-MS/MS was performed by injecting 50 μl of crude bile onto a narrow-bore C_{18} HPLC column coupled to the mass spectrometer *via* a splitting tee. Samples were injected at 100% solvent A (0.06% aqueous trifluoroacetic acid) and, after 5 min, solvent B (0.06% trifluoroacetic acid in acetonitrile) was added to the mobile phase at a rate of 1% min^{-1}. The column effluent (flow rate 200 $\mu l\ min^{-1}$) was split such that the flow rate to the ion source was 50 $\mu l\ min^{-1}$, the remainder being diverted to a UV detector. GSH conjugates were detected by operating the instrument in the constant neutral loss scanning mode (loss of 129 Da).

Neutral loss scanning resulted in the detection of four GSH conjugates designated 'A' to 'D' according to their order of elution on HPLC. The major conjugate ('C') was identified as 5-GS-4-OH-VPA-γ-lactone on the basis of its LC-MS/MS properties which were identical to those of the synthetic reference sample, and conjugate 'D' likewise was characterized as the previously reported 5-GS-(E)-Δ^3-VPA (5). Metabolite 'B' was identified as the conjugate of the α,β-unsaturated ketone, 3-oxo-Δ^4-VPA. Metabolite 'A' was the most polar of the conjugates and afforded an $[M+H]^+$ ion 18 Da higher than that obtained for 5-GS-4-OH-VPA-γ-lactone. Hence, on the basis of its HPLC elution order and $[M+H]^+$ ion, metabolite 'A' appears to be 5-OH-4-GS-VPA-γ-lactone.

In a parallel experiment carried out with the deuterium labeled analog, [3,3-$^2H_2$]Δ^4-VPA, metabolites 'A' and 'C', which are considered to derive from a common metabolic pathway (Figure 1), retained both deuterium atoms. Conjugate 'D', which is believed to arise as a result of β-oxidation of Δ^4-VPA, retained only one deuterium and, as expected, conjugate 'B' was formed with loss of both deuterium atoms.

Based on the urinary excretion of the corresponding *N*-acetylcysteine conjugates, the GSH-dependent metabolism of Δ^4-VPA accounted for *ca.* 20% of a single dose of Δ^4-VPA to rats. Because reactive metabolites of Δ^4-VPA appear to be formed both in the mitochondria and endoplasmic reticulum (Figure 1), it may be expected that Δ^4-VPA would deplete both

mitochondrial and cytosolic GSH pools. Oxidative stress as a result of GSH depletion and/or interaction of reactive intermediates with mitochondrial components may contribute to the hepatotoxic effects of Δ^4-VPA.

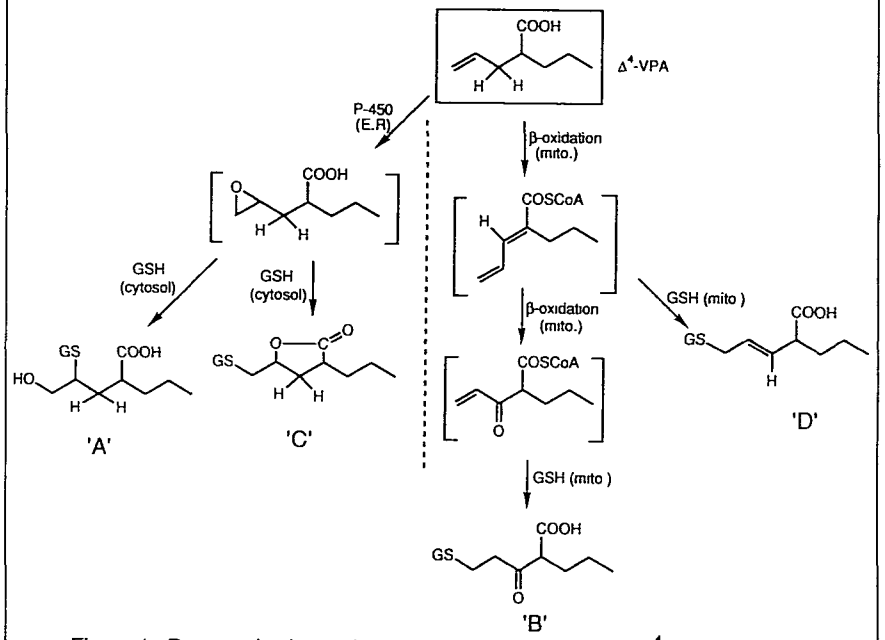

Figure 1: Proposed scheme for the metabolic activation of Δ^4-VPA in rat liver

Supported by NIH grants GM32165 and RR05543

References

1 R.S. Hauck and H. Nau, *Toxicol. Lett.*, **49**, 41 (1989).
2 G.R. Granneman, S.I. Wang, J.W. Kesterson and J.M. Machinist, *Hepatology*, **4**, 1153 (1984).
3 A.W. Rettenmeier, K.S. Prickett, W.P. Gordon, S.M. Bjorge, S.L. Lang, R.H. Levy and T.A. Baillie, *Drug Metab. Dispos.*, **13**, 81 (1985).
4 T.A. Baillie, *Chem. Res. Toxicol.*, **1**, 195 (1988).
5 K. Kassahun, K. Farrell and F. Abbott, *Drug Metab. Dispos.*, **19**, 525 (1991).

Quantification of Topiramate, a Novel Anticonvulsant, in Rat Brain Fluid by In-Vivo Microdialysis and Thermospray Liquid Chromatography/Mass Spectrometry

John A. Masucci, Marta E. Ortegon, William J. Jones, Richard P. Shank and Gary W. Caldwell, The R.W. Johnson Pharmaceutical Research Institute, Spring House, Pennsylvania,19477

Topiramate, 2,3:4,5-bis-*O*-(1-methylethylidene)-ß-D-fructopyranose sulfamate, a potent anticonvulsant, was determined in the extracellular fluid of rat brain by in-vivo microdialysis combined off-line with thermospray mass spectrometry. Since topiramate, and its metabolites are subject to thermal decomposition during GC/MS analyses, and since these compounds have no UV chromophore, LC/MS analysis is the method of choice. Electron ionization and thermospray LC/MS and LC/MS/MS of topiramate has been previously reported.[1,2] The combination of in-vivo microdialysis sampling with thermospray LC/MS has also been previously demonstrated.[3] The purpose of this study was to extend the determination of topiramate to dialysates collected from rat brain extracellular fluid and compare them directly to blood levels. Dialysate samples are typically free from endogenous materials allowing direct analysis without further sample preparation.

Microdialysis was performed using a CMA 12 probe (Carnegie Medicin- diameter-0.5 mm, membrane A, length-3.0 mm) stereotaxically implanted and position later determined histologically. A CMA 100 pump (1 ml syringe) was used to deliver distilled water dialysate at 2 µl/min. Male Wistar rats (~250g) were dosed IV at a 50 mg/kg level of topiramate. Samples were collected at 15 min intervals. Blood samples (100 µl) were collected at 30 min. intervals via cannulized jugular vein. Probe recovery (8.8%) was determined in-vitro following collection.

Thermospray analyses were performed using a Finnigan MAT TSQ-70 mass spectrometer with TSP-2 thermospray source. The detection limit of topiramate by thermospray LC/MS analysis is typically in the 0.1 µM range (20 µl injected) using selected ion monitoring. The ammonium adduct ion $(M+NH_4)^+$, which is the base peak, was used for detection. An internal standard of D_{12} labelled topiramate was added for quantitation.

Dialysate samples were directly injected (20 µl) along with 20 µl (4 ng) of internal standard. Blood samples were diluted 1 to 100 with methanol prior to injection (20 µl) with internal standard (4 ng). This was the only sample preparation required. Results were determined directly from the linear calibration curve.

Extracellular rat brain fluid levels peaked 45 min. after topiramate administration at the 15 µM level, with succeeding levels between 8.5 and 14 µM during the remaining 5 hr collection period. Blood levels peaked 1 hr. after dosage at the 440 µM level dropping to 220 µM after 3 hrs. This limited pharmacological data would indicate that topiramate equilibrates quickly across the blood-brain barrier and brain fluid levels in the micromolar range are maintained over an extended period. These results agree with the previously obtained radioimmunoassay results in which micromolar levels of topiramate were detected over a 24 hr. period.

1. Caldwell, G.W., et al., *Organic Mass Spectrometry*, **1989**, 24, 1051.
2. Masucci, J.A., et al, *Proceedings of the 40th ASMS Conference*, **1992**, 1869.
3. Menacherry, S.D.; Justice, Jr., J.B., *Anal. Chem.*, **1990**, 62, 597

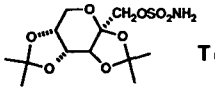

Topiramate

Thermospray LC-MS Calibration Curve

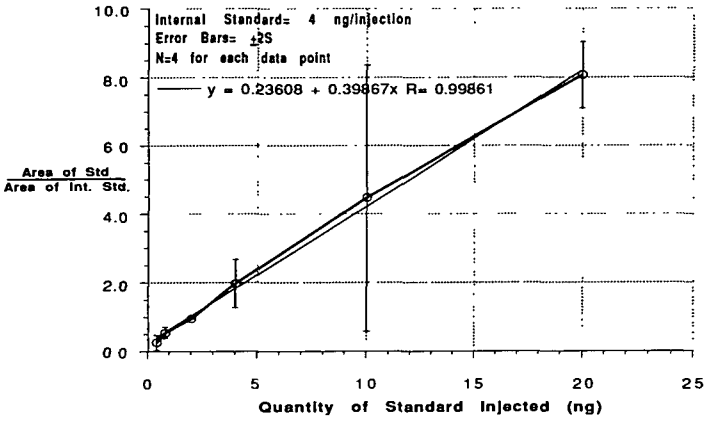

LC/MS Analysis of Topiramate in Rat Brain Fluid Microdialysate and Plasma (50 mg/kg injection)

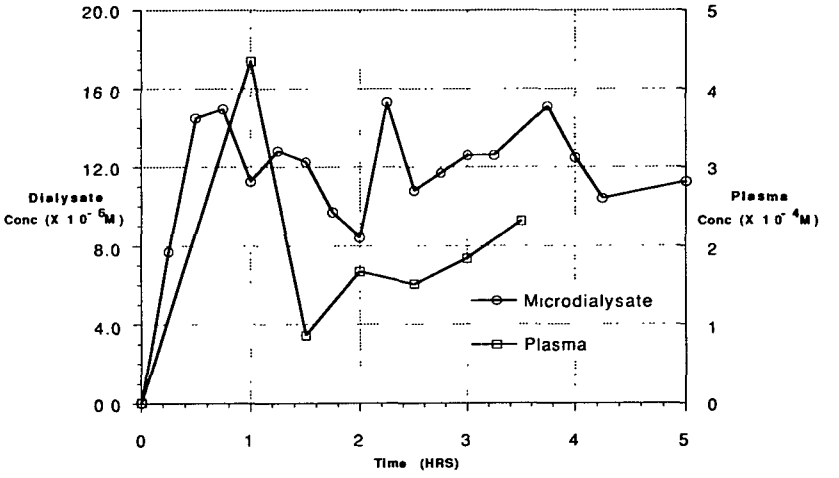

ON-LINE CAPILLARY ELECTROPHORESES-TANDEM MASS SPECTROMETRY OF DRUG METABOLITE MIXTURES

A.J.Tomlinson, L.M.Benson, G.F.Scanlan, K.L.Johnson, K.A.Veverka and S.Naylor

Biomedical Mass Spectrometry Facility, Dept. of Biochemistry and Molecular Biology and Dept. of Pharmacology, Mayo Clinic, Rochester, MN 55905, USA

The structural diversity of modern therapeutic drugs is well documented. However, after entry into the body such compounds are subjected to a series of complex metabolic processes including absorption, distribution, metabolic transformation and excretion. These events modulate the efficacy of the drug in the treatment of disease, as well as determining its pharmacological and toxicological effects, and structural characterisation of resulting metabolites is vitally important to understanding the physical and biological effects of the parent drug.

The use of capillary electrophoresis (CE)-MS in the analysis of small organic molecules (<600-800 daltons) has received scant attention. However, the high efficiency separation of CE (>10^6 theoretical plates) coupled with MS provides a powerful structural analytical tool for drug metabolism studies.

Initial CE-MS studies focused on the metabolism of the neuroleptic agent haloperidol **(1)**. It was possible, using a mixture of **(1)** and six synthetic standards, to baseline resolve all seven components and detect them using CE-MS (Finnigan MAT 900 with PATRIC array detector) at the <100 femtomole level. Further *in vitro* studies demonstrated that differences in the metabolism of different animal hepatic microsomal incubates was possible to detect. A guinea pig incubate revealed the presence of four meabolites plus unmetabolised haloperidol, whereas a mouse incubation revealed CPHP, HP^+, unmetabolised haloperidol, RHAL and HNO. Differences observed were both quantitative and qualitative.

We also investigated the use of non-aqueous CE run buffer in conjunction with MS in the analysis of the H_2 receptor antagonist mifentidine **(2)**. It was demonstrated using 100% MeOH (20mM NH_4OAc) with 1% AcOH that CE-MS analysis of a guinea pig microsomal incubate revealed the presence of five metabolites plus unmetabolised parent drug.

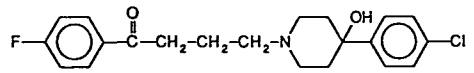

1

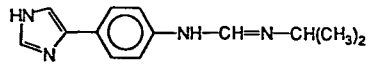

2

Estradiol and Estradiol Metabolites Analysis by Electrospray Mass Spectrometry

Jennifer Duker*, Matthew J. Dilts, Edward W. Sheehan
Millipore Corporation, Extrel Mass Spectrometry, 575 Epsilon Drive, Pittsburgh, PA 15238

As a specific class of structurally complex molecules, steroid hormones have traditionally posed a special challenge to the analytical chemist. Previously, the mass spectral characterization of free steroids was dominated by gas chromatography/mass spectrometry. Less volatile and thermally labile steroids and steroids conjugates required derivatization to more volatile and stable compounds prior to analysis. Successful characterization of underivatized steroids have also been obtained using such techniques as desorption chemical ionization (DCI), fast atom bombardment (FAB), thermospray (TS), and particle beam mass spectrometry.

This prompted an investigation into the possibility of using electrospray ionization along with collisionally induced dissociation (CID) for the analysis of estradiol and estradiol metabolites. Our objectives for this study wereM (1)to demonstrate the utility of LC/MS (2)to alleviate the derivatization step necessary for GC/MS, and (2) to demonstrate quantitation data in the low ppm levels.

EXPERIMENTAL

This study evaluates the feasibility of utilizing a benchtop LC/MS with an Electrospray interface for the analysis of Estradiol Metabolites.

MASS SPECTROMETER
- EXTREL benchmark™ mass spectrometer
- Electrospray LC/MS interface

LIQUID CHROMATOGRAPHY
- WATERS 600MS LC pump and controller
- WATERS 484MS Tunable Absorbance Detector
- WATERS Nova Pak C18 reverse phase column (2.0 x 15.0 cm)

ELECTROSPRAY
- Quenching Gases O_2 and SF_6
- Solvents (A) Methanol/Isopropanol (70/30) (B) H_2O
- Flow Rate 0.2ml min, 100:1 split

Calibration Curve for

β-Estradiol 3-sulfate 17-glucuronide

The response is linear, r=0.998

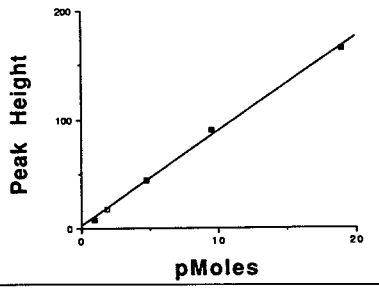

Total Selected Ion Chromatogram of 5 Drug Metabolites by LC/MS

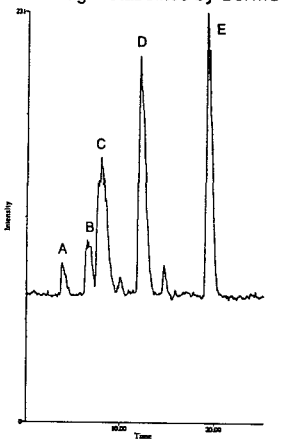

A. β-Estradiol 3-sulfate 17-glucuronide

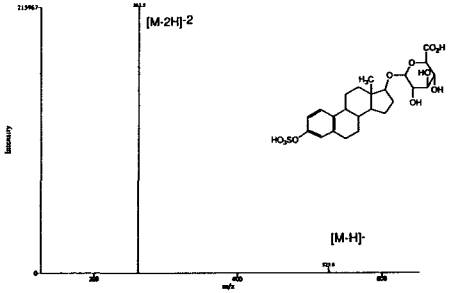

B. Estriol 3-sulfate

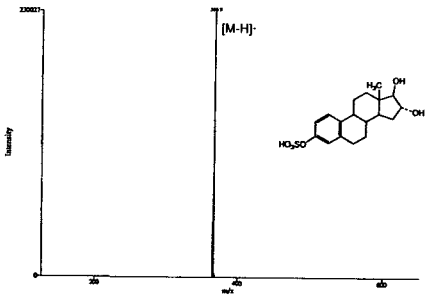

CONCLUSIONS

Negative Electrospray LC/MS Analysis of Estradiol Metabolites

- The compounds were successfully chromatographed and detected by negative electrospray LC/MS
- All five metabolite compounds generated interpretable spectra
- All compounds exhibited sensitivity at pgram levels
- Linear calibration of β-Estradiol 3-sulfate 17-glucuronide was demonstrated

ELECTROSPRAY MASS SPECTROMETRY ANALYSIS OF ISOMERIC C - GLYCOSIDIC FLAVONOIDS

M. Becchi, M. M. Flament SCA, CNRS, BP 22,69390 Vernaison, France
G. Tsoupras HEWLETT PACKARD S.A. Rue de Veyrot 39, 1217 Meyrin, Switzerland

Flavonoid glycosides are an important group of polyphenolic pigments found in plants[1]. They are of interest because of their significance in chemotaxonomy, their biological activity and their use as tracers in medicinal plant preparations.

Mass spectrometry is the method of choice for structure study of C-glycosidic flavonoids because of the resistance of the C-glycosidic bond to hydrolysis. This was achieved in the past by EI mass spectrometry of permethylated derivatives. More recently Fast Atom Bombardment technique in combination with CAD-MIKE or B/E linked scanning[2,3] has been shown to be very useful for the structural characterization of C-glycosidic flavonoids.

The present work is aimed at the differenciation between 6-C and 8-C monoglycosidic flavonoids using Electrospray mass spectrometry. In addition to molecular weight information, HP Electrospray can also provide structural informations through time-programmable collision induced dissociation. In this process the ions are forcefully collided with molecules of the bath gas (Nitrogen) by adjustment of the voltage difference between the capillary exit and the first skimmer. The best informative mass spectra are given by using a capillary exit voltage difference of 200 V. Differentiation between the series of 6-C and 8-C isomers can be directly obtained from the study of the mass spectra, without the need of MS/MS techniques as in FAB ionisation and with a better sensitivity. Leading differences are observed :

* more intense peaks for daughter ions from 6-C isomers than from 8-C isomers
* presence of a $[M+H-60-2H_2O]^+$ fragment ion for 6-C isomers and lack of this ion for 8-C isomers. This characteristic difference was already underligned in positive ion mode FAB mass spectrometry[3].
* the ratio R of $[M+H-150]^+$ / $[M+H-90]^+$ depends of the concerned isomer :

R ~ 1 for 8-C isomers and R ~ 6 to 35 for 6-C isomers

In conclusion Electrospray mass spectrometry is a significant method to analyse C-glycosidic flavonoids. Furthermore this attractive technique can easily be coupled to liquid chromatography for mixtures analysis.

1 - J.B. Harborne, T.J. Mabry and H. Mabry, in *The Flavonoids*, ed. by Chapman & Hall, Londdon (1975)
2 - M. Becchi and D. Fraisse, *Biomed. Environm. Mass Spectrom.*, 18, 122-130 (1989)
3 - Q.M. Li, H. Vanden Heuvel, L. Dillen and M. Claeys, *Biol. Mass Spectrom.*, 21, 213-221 (1992)

Electrospray mass spectra of Vitexin and Isovitexin.
Capillary exit : 200 V.

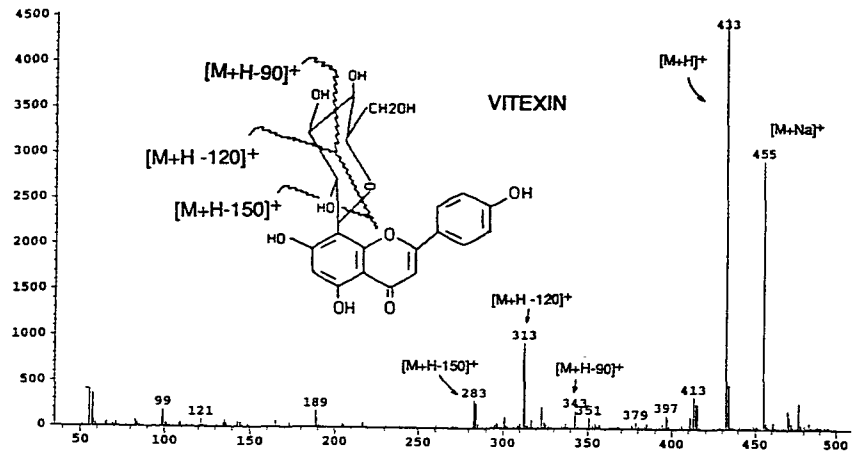

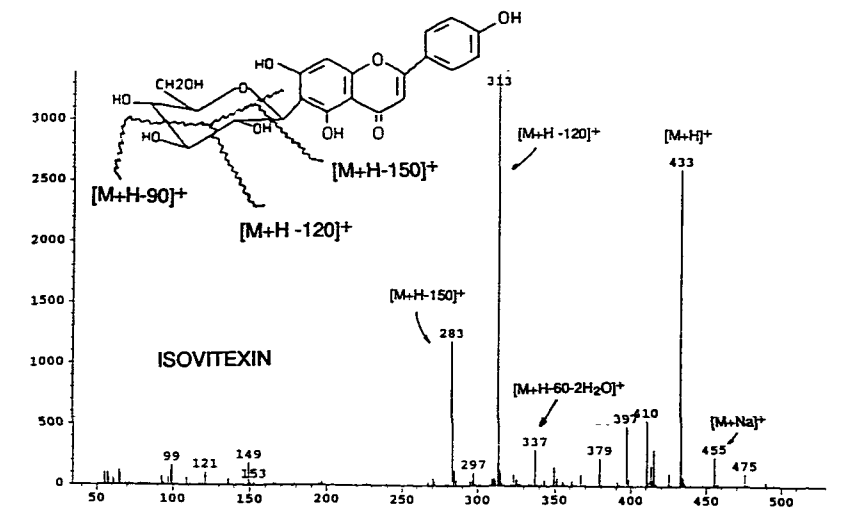

Matrix-Assisted Laser Desorption Mass Spectrometry of Dynorphin A (1-17) Processing in Human Blood (*in vitro*) and Rat Brain (*in vivo*)

James Z. Chou, Isabelle M. Maisonneuve, Mary Jeanne Kreek, and Brian T. Chait
The Rockefeller University, New York, NY 10021.

In preparation for proposed dynorphin peptide pharmacokinetic studies in humans, it is essential to ascertain a) whether the dynorphin maintains its integrity after intravenous administration and b) whether any further processing or breakdown of dynorphin peptides occurs in fresh blood (without or with the addition of enzyme inhibitors) after it is drawn from a patient. To begin addressing both of these questions, we describe a study of *in vitro* processing of Dyn A (1-17) in freshly drawn human blood. We also describe first studies of the processing of exogenously administered Dyn A (1-17) in brain regions of freely moving rats.

The mass spectrometric analysis of the dynorphin peptides was carried out using matrix-assisted laser desorption at a laser wavelength of 355 nm with α-cyano-4-hydroxycinnamic acid as the matrix. The matrix was dissolved to a concentration of 5 g/L in a mixture of 33% acetonitrile and 67% 0.1% trifluroacetic acid (TFA) aqueous solution.

The *in vitro* processing study of Dyn A (1-17) in human blood was carried out by adding 0.5 mM Dyn A (1-17) into freshly drawn human blood to yield a final peptide concentration of 0.01 mM. This spiked blood was allowed to stand for a variable amount of time at room temperature prior to separation and mass spectrometric analysis. A portion of that blood was separated by refrigerated centrifuge (4°C) for 5 min at 2500 g, after different standing time intervals. 300 μl of each resulting plasma sample was then diluted with 1.7 ml of 1% TFA (containing 1.6 μM substance P as an internal standard) and filtered through microconcentrators with a 3000 mw cut off. The filtrate was concentrated in a speed vacuum concentrator before it was combined with matrix solution and analyzed by mass spectrometry.

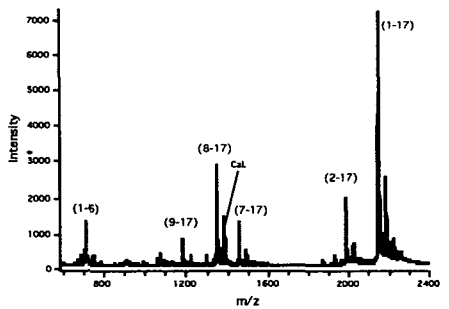

Fig. 1 Mass spectrum of processed products of Dyn A (1-17) in human blood at time=0

The major products resulting from the biotransformation of Dyn A (1-17) in human blood at time 0 is shown in Fig. 1. The most intense peak corresponds to unprocessed Dyn A (1-17). Major processed products identified from their measured nominal masses are Dyn A(7-17), Dyn A(8-17), Dyn A(9-17), Dyn A(1-6) and Dyn A(2-17). More than 10 other processed fragments of Dyn A (1-17) can be readily identified in smaller quantity. Through the use of an internal standard, substance P, the amounts of

processed products were determined as a function of time (Figure 2). The amounts of Dyn A (7-17), Dyn A(8-17), Dyn A(9-17) and Dyn A(1-6) were found to decrease after their maximum values were reached at ~ 20 min. By contrast, the amounts of Dyn A(2-17) and Dyn A (3-17) increased monotonically as a function of time (Fig. 2). This observation suggests that the dynorphin products generated by cleavage between the 6th and 7th amino acid residues are processed (by blood enzymes) differently than the processed products formed by losing the amino acid residues from the amino-terminus of the peptide.

The *in vivo* processing study of Dyn A (1-17) in brain regions of freely moving rats was carried out in striatum and cerebellum. A thin plastic tube (0.67 mm, o.d.) was positioned in close proximity to a microdialysis probe, such that both were located in a brain region of interest. Dynorphin A (10 mM) was delivered (0.1 μl/min) through the plastic tube and the processed products were collected from the microdialysis probe through the constant infusion(1μl/min) of artificial CSF (146 mM Na^+, 2.7 mM K^+, 155 mM Cl^-, 1.2 mM Ca^{2+}, and 1.0 mM Mg^{2+}). The infusion of Dyn A (1-17) was terminated after 60 min of delivery, while the collection of dialysate was continued for another 2 hours. A constant amount of substance P was added to the dialysate as an internal standard.

Mass spectra similar to Figure 1 were obtained, where many processed products (more than 15) were readily identified. The amounts of a processed product, Dyn A (2-17), as a function of time in the living rat striatum and cerebellum are shown in Fig. 3. Similar time profiles were observed for other processed products. The data shows that more time was needed to process the dynorphin peptide in cerebellum than in striatum . This finding is in concert with the expected higher abundance of enzymes, which are believed to be more specific for dynorphin processing, in striatum than there are in cerebellum. [Supported in part by grants from NIDA I-P50-DA05130 and Aaron Diamond Foundation (MJK, IMM and JZC); Aaron Diamond Postdoctoral Fellowship (JZC); NIDA-K05DA00049 (MJK) and NIH RR00862 (BTC)]

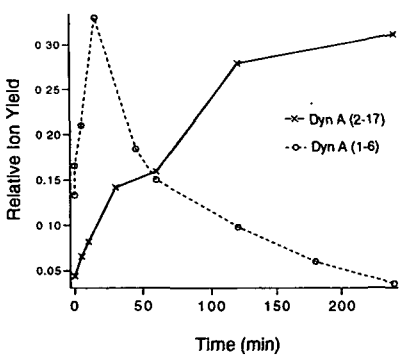

Fig. 2 Time profile of two products from the *in vitro* processing of Dyn A (1-17) in human blood

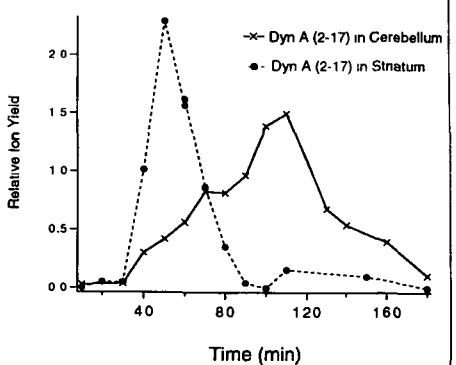

Fig. 3 Time profile of one product from the *in vivo* processing of Dyn A (1-17) in rat brain regions

Rapid Analysis of EA and its Metabolites using LC-MS and MS/MS*

M. Denise LeBlanc[1], Michael A. Quilliam[1], M. Ruth Bailey[2] and David H. North[2]

[1]Institute for Marine Biosciences, National Research Council of Canada, 1411 Oxford St., Halifax, Nova Scotia, Canada B3H 3Z1

[2] Health and Welfare Canada, P.O. Box 1060, 53 Queen St., Dartmouth, Nova Scotia, Canada, B2Y 3Z7

Erythromycin A (EA) is a macrolide antibiotic used in both agriculture and aquaculture to promote optimal health and growth of animals. There are concerns that residues of the antibiotic and/or its metabolites may remain in the edible portion of the tissue if proper withdrawal times are not implemented prior to slaughter.

HPLC analysis of EA is difficult due to the lack of a significant chromophore for detection, its polar, labile nature and its basicity. Earlier work [1] has demonstrated the utility of liquid chromatography coupled to ionspray mass spectrometry for EA analysis and several metabolites in salmon tissue were identified. However, quantitative analysis was limited by the lack of a robust clean-up method and somewhat long analysis times. We have developed a clean-up method for salmon tissue that has permitted the development of rapid LC-MS and FIA-MS/MS methods.

The extraction procedure utilized was similar to that of Takatsuki et al [2]. An additional solid phase extraction step, using a bonded aminopropyl silica cartridge, was developed to decrease the amount of co-extractives present in the final solution for analysis. A 15cm X 2.1mm i.d. RX-C8 column was employed in an isocratic mode with aqueous 30% acetonitrile and 0.2% formic acid. Analysis time was only 8 minutes. Figure 1 displays a typical chromatogram and selected ion chromatograms for EA and some of its metabolites and degradation products.

We have also demonstrated that flow injection analysis coupled with tandem mass spectrometry (FIA-MS/MS) can be used to provide a rapid screening for analytes. Selected reaction monitoring was employed for the following transitions 734 → 576, 734 → 558 and 734 → 158 for EA and 716 → 558, 716 → 540 and 716 → 158 for AEA (anhydroerythromycin A, the principal metabolites of EA). The calibration curves obtained for EA are shown in Figure 2.

Both methods were employed to determine the depletion of EA and metabolites in medicated salmon. Results from the LC-MS and FIA-MS/MS analyses compared favourably (Figure 3).

*NRCC # 34865

References:

[1] S. Pleasance et al., Biol. Mass Spectrom. **21**, 675(1992).
[2] K. Takatsuki et al., J. Assoc. of Off. Anal. Chem. **70**, 708(1987).

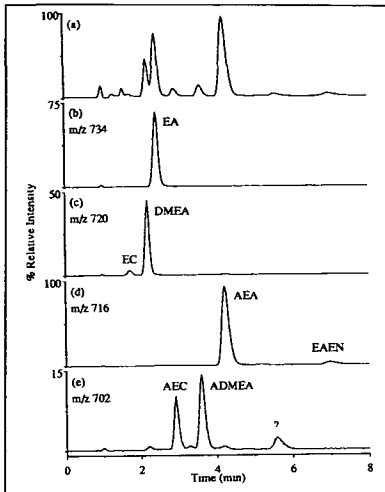

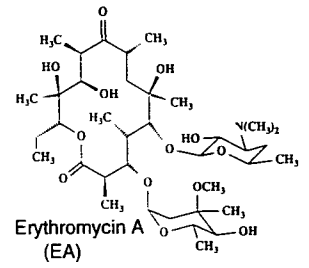

Figure 1: Mass chromatograms from the LC-MS analysis of tissue extracts of salmon medicated with EA.

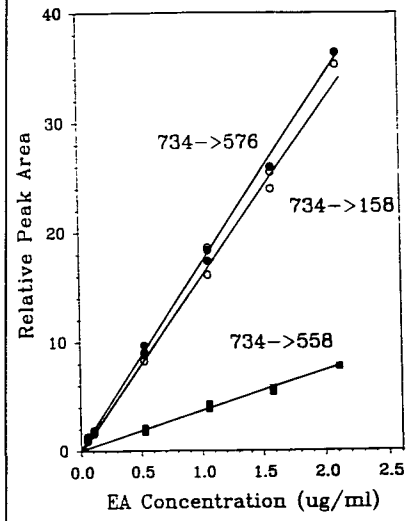

Figure 2: Calibration curves for a series of EA standards obtained by FIA-MS/MS.

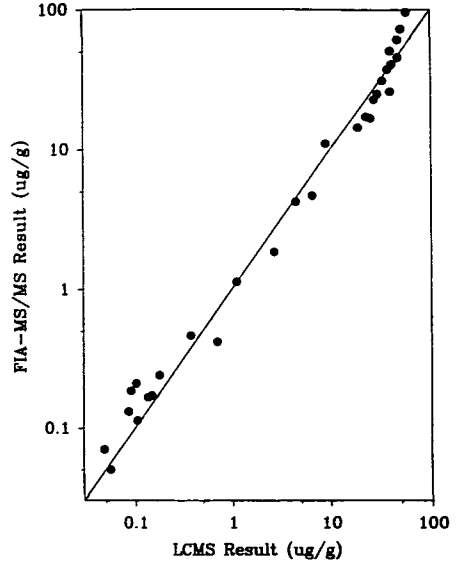

Figure 3: Comparison of results of the analysis salmon tissue extracts by LC-MS versus FIA-MS/MS.

High Performance Liquid Chromatography/Electrospray MS/MS and MS/MS/MS for Metabolite Identification of a Peptide-Based Renin Inhibitor.

R. P. Schneider *, M. J. Cole, J. Wentland, M. R. Nocerini, and H. G. Fouda. Central Research Division, Pfizer Inc, Groton, CT 06340

Renin is an aspartic endopeptidase that is responsible for initiating the angiotensin cascade, resulting in vasoconstriction, sodium and water retention, and ultimately hypertension. Identification of a therapeutically useful renin inhibitor is desirable for the management of hypertension. [1,2]

CP-108,671 is a novel peptide (Figure 1) with promising renin inhibitory activity. We have employed on-line HPLC and triple quadrupole mass spectrometry to gain insight into the metabolic routes of this novel peptide.

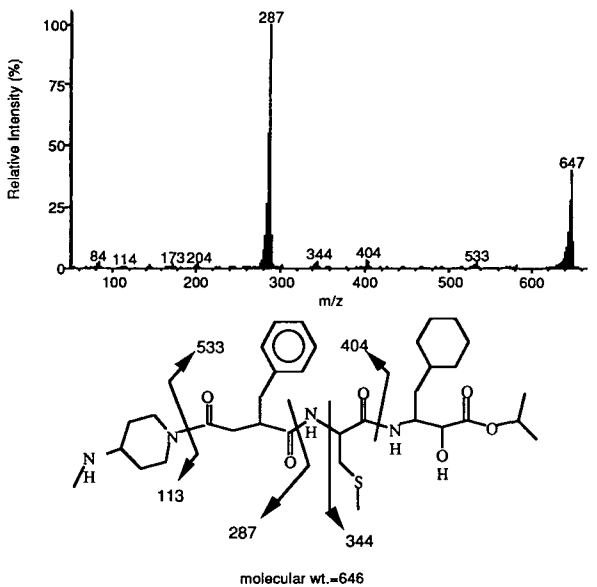

Figure 1. Structure and fragmentation (daughter ion spectra) of CP-108,671

1 D. J Webb, A.M. Cumming, B. J. Leckie, et al. *The Lancet*, December 24-31, 1486, (1983).
2 M. Szelke, B. J. Leckie, A. Hallett, et al. *Nature*, 299, 555, (1982)

Seventeen drug related metabolites were identified in the bile of an orally dosed dog (Summary Table). A variety of mass spectrometric experiments were performed, including precursor, neutral loss, and CAD product ion scans. For several ions of interest, MS/MS/MS conditions were employed by sufficiently raising the orifice voltage to produce the desired CAD product ion prior to the first quadrupole. These experiments were invaluable in assigning numerous sites of metabolism.

Metabolites identified included many Phase I single oxidation products, N and S demethylation, a Phase II O-glucuronide, a sulfoxide, and cleavage of the C-terminus with corresponding formation of a carboxylic acid. Several interesting and unexpected metabolites were found having multiple sites of oxidation on different portions of the molecule. These included N and S oxides, bis-phenyl oxidations, and a significant amount of a tri-oxidized metabolite resulting from a bis-phenyl oxidation and the formation of a ketone on the methylene bridge alpha to the phenyl moiety.

SUMMARY TABLE of CP-108,671 Metabolites found in 0.5 to 1 hr Fraction of Dog Bile Following a 10 mg/kg Dose

Drug or Metabolite	m/z	characterization	% relative to drug related material
I	647	drug	15.5
II	633	N-des methyl	9.6
III	633	S-des methyl	0.3
IV	605	loss of i-Prop to acid	1.6
V	823	O- Glucuronide	0.9
VI a	663	norstatine oxidation	16.1
VI b	663	norstatine oxidation	6.5
VII	663	phenyl oxidation	13.2
VIII	663	sulfoxide	3.3
IX	663	N-oxide on piperidine	0.3
X a	679	phenyl oxid. and	5.0
X b	679	norstatine oxid.	6.7
XI	679	bis-phenyl oxidation	5.0
XII	679	phenyl oxid + sulfoxide	2.5
XIII	679	norstatine ox.+sulfoxide	1.1
XIV	679	bis-norstatine oxidation	1.1
XV	679	N-oxide on piperidine + S-oxide	0.6
XVI	692	bis-phenyl oxidation + hydroxylation of a methylene bridge with dehydrogenation to a ketone	10.7

HPLC/MS Determination Of Components in Black Tea, Robert T. Rosen[1], Douglas A. Balentine[2], Steven Gobbo[2], Richard D. Hiserodt[1], Joseph Lech[1], Elaine K. Fukuda[1], Thomas G. Hartman[1] and Chi-Tang Ho[1], [1]Center For Advanced Food Technology, Cook College, Rutgers University, New Brunswick, N.J 08903 and [2]Thomas J. Lipton Company, 800 Sylvan Avenue, Englewood Cliffs, N.J. 07632

Recent studies have found that polyphenolics in green and black tea have potent anticarcinogenic activity in many laboratory animals. Epigallocatechin gallate (EGCG) has been shown to inhibit nitrosamine induced lung tumors.

Negative Ion Thermospray LC/MS (Negative ion discharge mode) as well as Particle Beam (EI, 70eV) LC/ MS was utilized to identify components in black tea. These components included catechins, theaflavins and flavonoid conjugates. A C-18 column was utilized for the determinations with 0.16% formic acid and 0.20% triethylamine in the aqueous mobile phase. The program started at 100% aqueous, and ended in 75 minutes at 57.5 % methanol. Superior LC resolution was achieved using this modified mobile phase. The triethylamine appeared to complex the polyphenols and appeared to significantly enhance the negative ion mass spectra, especially that of the flavonoids and their conjugates. The particle beam data showed each component eluting as a loosely bound complex with triethylamine. The complex dissociated upon ionization, not giving adduct ions, but rather enhancing the molecular ions of the disaccharides and glycosides.

Superior data was obtained for components such as epicatechin (EG), epicatechin gallate (ECG), epigallocatechin (EGC and epigallocatechin gallate (EGCG) as well as the flavonoid conjugates. Reasonable data was obtained for the compounds theaflavin and theaflavin gallate, but no data was obtained on theaflavin digallates and a class of oligimeric or polymeric compounds called thearubigens. The gallate ester linkage seems too labile and there is no evidence that these compounds even elute from the LC column indicating that the thearubigens may bind to active sites in the metal column. In a separate experiment, no ions were observed by LSIMS above 900 AMU, confirming the difficulty with the oligimeric or polymeric thearubigens. No LSIMS nor LC/MS data was obtained on extracts and other samples known to be enriched in thearubigens. Future work to elucidate the structure of this higher molecular weight class includes derivatization as well as analysis of a degallinated tea.

Acknowledgments: This is New Jersey Agricultural Experiment Station Publication # D-10569-1-93 . The Center For Advanced Food Tecnology is an initiative of the New Jersey Commission on Science and Technology.

CHARACTERIZATION OF FLAVONOIDS BY LC/MS/MS TEA FLAVONOIDS

Yong Y. Lin[1], K.S. Kim[1], Cheng-mo J. Chen[1], and Kwokei Ng[2]

[1]Institute for Basic Research in Developmental Disabilities, Staten Island, New York.
[2]Schering-Plough Research Institute, Bloomfield, New Jersey, USA.

The history of tea in China might started as early as 5000 years ago, when it was discovered as an herbal medicine. Some significant pharmacological and health effects of tea plant, *Camellia sinensis*, have gained supports from scientific research in recent years. Among them, tea appears to have some significant biocidal effects including a strong antiviral effect against human immunodeficiency virus (HIV). Although the mechanism of the antiviral effect of catechins remains unclear, the strong antioxidant activity of the flavonoids as radical scavengers might play some role. In order to study structure-antiviral activity relationship, catechin flavonoids were extracted from *Camellia sinensis*, fractionated by HPLC, and their antiviral activity against herpes simplex 1 and human cytomegalovirus were studied. LC/TSQ-MS was utilized to characterize the catechin flavonoids.

[METHODS]

HPLC Fractionation: Column, reverse phase C-18(10 μm), 7.8 mm x 30 cm; liquid phase: 20 % acetonitrile in water (0.05 % TFA) with a flow rate 1 ml/min; detector, uv 280 nm

LC/MS/MS: Finigan-MAT TSQ 70 mass spectrometer with a thermospray LC/MS interface. CID spectra were obtained at 20-70 ev collision energy.

[REESULTS]

Using the thermospray LC/MS, $[M+H]^+$ ions of four major catechins, (-)epicatechin, (-)epigallocatechin, (-)epicatechin 3-O-gallate, and (-)epigallocatechin 3-O-gallate were quickly identified in a mixture of catechins extracted from the teaplant *Camellia sinensis*. Collision Induced Dissociation (CID) spectra of the $[M+H]^+$ ions gave simple fragmentation patterns, which permitted characterization of the substituents and the ring structure of the molecules.

Thermospray LC/TSQ-MS can be effectively used to identify flavonoids and their glycosides; their CID spectra showed three types of ring cleavages in the pyran ring of the flavonoids, and differentiation among flavanone, flavone, and flavonol was made. (Table 1).

Green tea extract and tea catechins showed strong antiviral activity against Human cytomegalovirus, while other plant flavonoids tested showed little antiviral activity. Polyphenolic antioxidants, such as methyl gallate and tannic acid, have been

reported to have antiviral activity; however, our study shows tea catechins are much potent antiviral agents.

Table 1: Thermospray MS and CID Spectra of Catechins and Flavonoids

Compounds	Thermospray MS		CID Spectra m/z (rel. %)*			
	[M+H]	[others]	[A]	[B]	[C]	[others]
1	291(100)	275(6)	139(100)	165(10)	123(58)	207,147
2	307(100)		139(100)	181(10)	139(100)	223,163
3	443(100)	291(40)	139(24)	165(5)	123(100)	291,273 153,151
4	459(40)	275(100), 273(24) 307(13)	139(100)	181(5)	139(100)	307,289 153,151
5	611(10)	291(100), 285(25) 465(8) 303(100)	153(100) 149(19)	177(68)	-	
6	271(100)		153(89) 119(100)	-	-	
7	287(100)		153(100)	-	121(70)	
8	303(100)		153(100)	-	137(60)	
9	611(8)	465(3)	-	-	-	465,303 165,147 129
	303(100)		153(100)	-	137(70)	

*) CID spectra was obtained with the underlined MS ions.

ANALYSIS OF CAROTENOIDS IN HUMAN SERUM BY USING CAPILLARY COLUMN CONTINUOUS-FLOW FAST ATOM BOMBARDMENT LIQUID CHROMATOGRAPHY-MASS SPECTROMETRY.

Chien-Hua Huang, Steven J. Schwartz*, and Richard B. van Breemen
Departments of Chemistry and Food Science*
North Carolina State University, Raleigh, NC 27695

An essential dietary factor, vitamin A is composed of a number of compounds including vitamin A retinoids and a much larger group of provitamin A compounds called carotenoids. Besides being necessary for human growth, vision, and reproduction, the possible roles of these compounds in cancer prevention, treatment, and tumor prevention are of intense interest. Approximately 600 carotenoids have been characterized, and numerous geometric isomers and degradation products of each are possible. Because carotenoids are unstable in the presence of light heat, HPLC is the method of choice for the separation of carotenoid mixtures. However, HPLC retention times and UV/VIS absorbances are insufficient for positive identification of carotenoids. Therefore we are developing LC/MS and LC/MS/MS methods for identification of carotenoids extracted from food and human serum.

METHODS

High Performance Liquid Chromatography (HPLC). All HPLC analyses were carried out using an Applied Biosystems 140A Microgradient HPLC Pump and an isocratic solvent system consisting of methanol/acetonitrile/ethyl acetate (30:50:20; v/v/v). A Vydac 5 mm C18 narrowbore HPLC column (25 cm x 2.1 mm) was used for narrowbore HPLC separations at a flow rate of 100 μL/min. Sample volumes of 1 mL each were injected using a Rheodyne 8125 injector (see ref. 1). Capillary HPLC was carried out using an LC-Packings 5 mm C18 HPLC column (320 mm x 30 cm; or 320 mm x 50 cm for human serum) at a flow rate of 4 μL/min. The injection volume was 200 nL, and a Rheodyne 7520 injector was used for all capillary column separations (see ref. 2).

Mass Spectrometry. Positive ion continuous-flow fast atom bombardment (CF-FAB) liquid chromatography/mass spectrometry (LC/MS) was carried out using a JEOL HX110HF double focusing mass spectrometer. The resolution was 1,000 and the ion source temperature was 23°C (room temperature) for all measurements. Coaxial-flow addition of matrix solution (ref. 3) was carried out at a flow rate 1 μL/min. The matrix solution consisted of water/acetonitrile/3-nitrobenzyl alcohol (v/v/w). For narrowbore HPLC analyses, the solvent flow was split post-column using a pneumatiac splitter so that 5 μl/min entered the mass spectrometer. The split ratio was 1/20.

Extraction of Carotenoids. Tomatoes (40 g) were pureed in 150 mL methanol, filtered, washed twice with 100 mL portions of methanol, then extracted under N_2 30 min in 100 mL hexane. The extract was evaporated to dryness and redissolved in mobile phase for HPLC. Human serum (5 mL from pooled blood bank serum) was extracted with 5 mL of ethanol/ethyl acetate (1:1). The organic layer was removed, evaporated to dryness, and then redissolved in 1 mL hexane. The hexane extract was loaded onto an alumina solid phase extraction cartridge, eluted with 5 mL acetone to obtain the polar carotenoids, and then eluted with 5 mL hexane/acetone 90:10 to obtain nonpolar carotenoids. Each fraction was evaporated to dryness and redissolved in mobile phase for HPLC.

Compared to post-column addition of the FAB matrix, coaxial-flow matrix addition minimized band broadening. Therefore, coaxial-flow matrix addition was used in all subsequent analyses. As we reported previously for narrowbore CF-FAB LC/MS using post-column addition of the matrix, 3-nitrobenzyl alcohol (1), molecular ions, $M^{+\cdot}$, were detected instead of protonated molecules for all carotenoid species.

Using the capillary HPLC system, separation of lutein, lycopene, α-carotene, β-carotene standards was demonstrated. Next, the CF-FAB LC/MS limit of detection for lutein and α-carotene was determined to be 5 and 15 ng, respectively (see Figure 1).

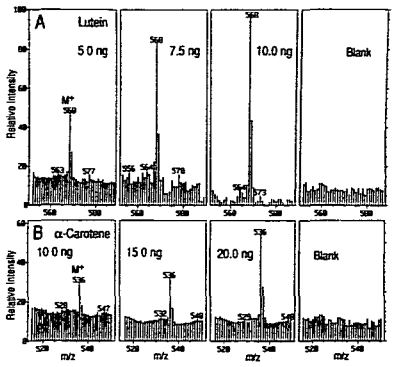

Figure 1.

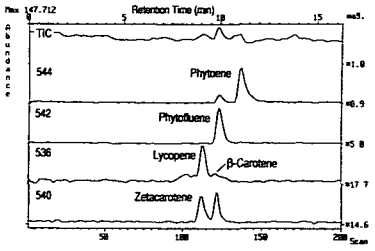

Figure 2.

Because important dietary carotenoids such as lycopene, α-carotene, and β-carotene have identical molecular weights but different HPLC retention times, LC/MS/MS was carried out. Fragment ions were identified that uniquely identified each of these isomeric carotenoids. Next, a tomato extract was analyzed using the narrowbore HPLC system. Abundant carotenoid molecular ions were detected for lycopene, phytoene, phytofluene, and two isomers of zetacarotene (see Figure 2). Finally, extracts of human serum were analyzed using the capillary LC/MS system. Only the most commonly observed carotenoid, lycopene, was detected in these initial analyses.

ACKNOWLEDGEMENTS. This research was supported by grants from the United States Department of Agriculture and the North Carolina Biotechnology Center.

REFERENCES.

(1) Schmitz, H.H.; van Breemen, R.B.; Schwartz, S.J. Methods Enzymol., **213**, 322-336 (1992).
(2) van Breemen, R.B.; Schmitz, H.H.; Schwartz, S.J. Anal. Chem., **65**, 965-969 (1993).
(3) Moseley, M.A.; Deterding, L.J.; de Wit, J.S.M.; Tomer, K.B.; Kennedy, R.T.; Bragg, N.; Jorgenson, J.W. Anal. Chem., **61**, 1577-1584 (1989).

FURTHER DEVELOPMENTS IN NEONATAL SCREENING BY AUTOMATED DYNAMIC LSI TANDEM MASS SPECTROMETRY

Donald H. Chace, Steven L. Hillman, David S. Millington, Department of Pediatrics, Mass Spectrometry Facility, Box 3028, Duke University Medical Center, Durham, NC 27710

Routine analysis of amino acids and acylcarnitines by LSIMS/MS from bloodspotted on filter paper has been demonstrated previously[1,2]. With this method, between 50 and 100 samples can be analyzed manually per day. So that sample throughput can increase, development of automated sample preparation and analysis is required. Blood droplets are spotted onto a special type of filter paper made from cotton fiber. The blood spots (approximately 30 μL) are dried. Two - 3/16" discs (approximately 12.6 μL) are punched from the larger spots into plastic vials. Up to 60 plastic vials are placed in a Gilson code 29 rack which fits into a programmable Gilson model 222 sample changer. The sample changer is used to add 400 μL of isotopically labeled internal standards in methanol. The discs are extracted for 30 min. The blood spot extracts are transferred to a parallel rack of clean vials. Solvent is removed by placing the rack in a custom-built warm air (50°C) evaporator (Grey Line Eng. model 2700). Samples are evaporated to dryness under a gentle stream of N_2. The rack is returned to the sample changer for addition of the derivatizing reagent (100 μL of 3N butanolic-HCl), covered by septum material and a rectangular weight and incubated at 65 °C (15 min) in a forced air oven. The cover is then removed and the reagent evaporated under N_2. The rack is returned to the sample changer and the vials are rinsed with 200μL of hexane. After hexane removal and drying under N_2, 50 μL of a methanol:glycerol (95:5) matrix containing the 0.025% of the surfactant, octyl sodium sulfate, is added to each tube. The sample rack is now placed in the autoinjector (Gilson model 231) for the programmed 2 minute, 15μL load, 500 μL rinse cycle for each sample injected into the dynamic LSIMS/MS system via a Rheodyne injector fitted with a 1μL loop. Matrix (85:10:5 Methanol:Glycerol:H_2O) is delivered at 7 μL/min. by an ISCO model 500D syringe pump The entire injector system is placed on a cart and wheeled into position with the Quattro tandem mass spectrometer The *length of 70 μM i.d., 0.53 mm o.d. deactivated fused silica capillary tubing is 0.75-1 meter. Sample is delivered to* a redesigned dynamic probe tip incorporating a filter paper wick. Our previous work (ASMS '92) was with a mesh screen probe. Problems with flow interruption at the mesh screen surface were overcome with this new design. This tip also uses a septum at closer proximity to an angular tip. A VG QUATTRO triple quadrupole with Lab-base data system was used with a cesium ion gun operated at 10 Kev. Argon was used as the collision gas. Samples were injected every 2 minutes and a neutral loss scan of 102 (scan time=3 sec.) continuously acquired for up to 60 minutes. Six summed baseline scans were subtracted from 6 summed scans over the peak top. The resulting mass spectra were smoothed.

Fifty six normal patient samples and 2 disease controls (PKU (hyperphenylalanemia) and MSUD (hyperleucinemia) and 2 blanks (unspotted filter paper) were analyzed. A Total Ion Elution Profile for a dynamic LSIMS/MS analysis of 60 samples is presented in *Figure 1*. *Figure 2a-f* are NTL 102 mass spectra of patients with normal amino acid profiles and patients with PKU and MSUD.

As is observed in Figure 1, peak shapes were adequately resolved for the first hours. An increase in baseline occurred during the 2nd hour. To insure that one sample spectra does not interfere with the next sample spectra, baseline subtraction to the left the peak top was performed. The adequacy of this procedure is demonstrated in Figures 2a-f, where the high phenylalanine in the PKU patient or high leucine in the MSUD patient did not carry over into the next normal patient sample. Improvements are needed to keep the dynamic LSIMS/MS system optimal for at least an entire rack of 60 (2 hours). We are working to extend this to about 240 samples per day per instrument (240 samples at a rate of 1 sample / 2 minutes = 8 hours). The design of the probe, especially the wick (absorbent material) appears to be important to background contamination. This is probably due to glycerol accumulation which reduces absorbancy. The automated sample preparation procedure described above currently takes approximately 3-4 hours to prepare a rack of 60 samples. The time for each sample analyzed is 2 minutes. The sample preparation procedure will be upgraded to prepare two racks simultaneously (120 samples) in the same time period with the same equipment. The results presented here are the first applications of automated preparation and automated analysis of amino acids in neonatal blood spots using robotic equipment and LSI-MS/MS. The versatility of the method will ultimately enable simultaneous analysis of acylcarnitine and amino acids in the same sample.

Support for this research was provided by a grant from the State of North Carolina, Division of Maternal and Child Health, Department of Environmental Health and Natural Resources (Raleigh, N C No C-05070)

REFERENCES

Chace,D.H., Millington, D S , Terada, N , Kahler, S , Roe, C., and Hofman,L., "Rapid Diagnosis of Phenylketonuria by Quantitative Analysis for Phenylalanine and Tyrosine in Neonatal Blood Spots by Tandem Mass Spectrometry" Clinical Chemistry, 39, 66-71, (1993)

Millington, D S , Kodo, N., Terada, N., Roe, D., Chace, D H. "The Analysis of Diagnostic Markers of Genetic Disorders in Human Blood and Urine Using Tandem Mass Spectrometry with Liquid SIMS" International Journal of Mass Spectrometry and Ion Processes, 111, 211, 1991.

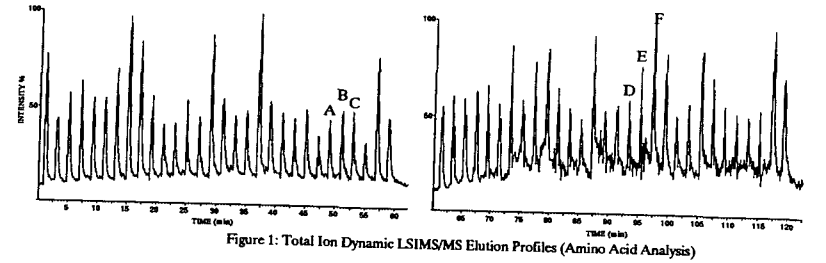

Figure 1: Total Ion Dynamic LSIMS/MS Elution Profiles (Amino Acid Analysis)

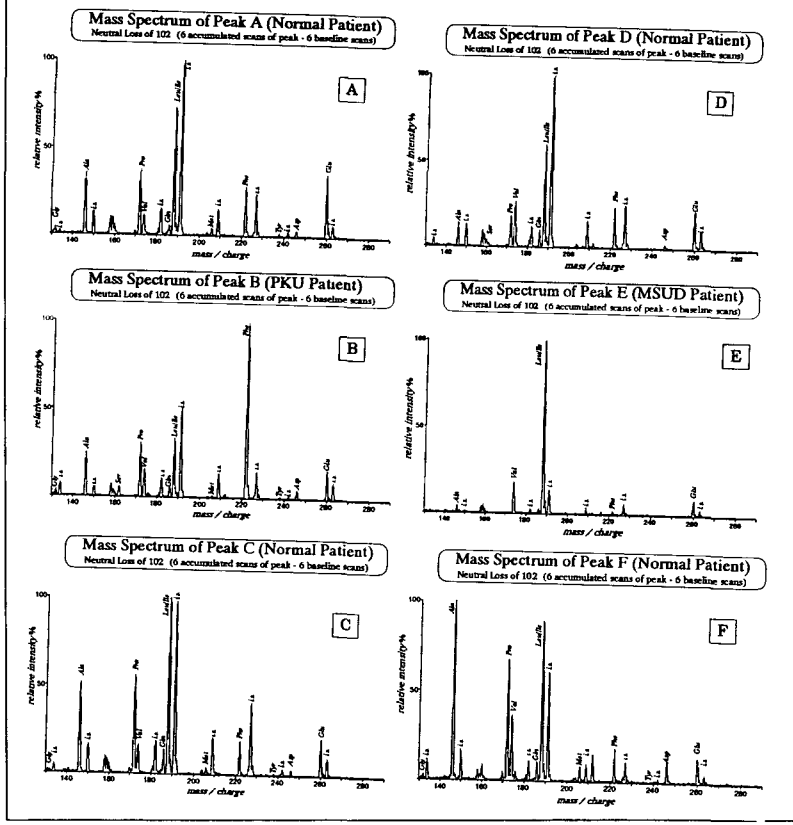

Structure Determination of Metabolites from the Neuroleptic Drug Haloperidol using Ion Trap MS^n

K.A.Veverka, G.F.Scanlan, L.M.Benson, K.L.Johnson, A.J.Tomlinson and S.Naylor

Biomedical Mass Spectrometry Facility, Dept. of Biochemistry and Molecular Biology and Dept. of Pharmacology, Mayo Clinic, Rochester, MN 55905, USA

The structural diversity of modern therapeutic drugs is well documented. However, after entry into the body such compounds are subjected to a series of complex metabolic processes including absorption, distribution, metabolic transformation and excretion. These events modulate the efficacy of the drug in the treatment of disease, as well as determining its pharmacological and toxicological effects, and structural characterisation of resulting metabolites is vitally important to understanding the physical and biological effects of the parent drug.

In this work we used the unique capabilities of the quadrupole ion trap (Finnigan MAT ITMS) to investigate the *in vitro* guinea pig microsomal metabolism of the neuroleptic agent haloperidol. By utilising the ability of the trap to capture and hold ions it is possible to trap all components of a metabolite mixture and then sequentially sweep out component ions, leaving only a specific metabolite in the trap. Such precursor (MH^+) ions remaining in the trap can then be subjected to MS^n experiments in order to acquire structural information.

We demonstrated this for a mixture of haloperidol and five synthetic standards, as well as for a guinea pig microsomal extract. Furthermore, we found five metabolites by using this metabolite mapping technique, namely CPHP (MH^+=212),RHAL (MH^+=378), HP^+(M^+=358), HTPNO ([MH-O]$^+$=358) and an N-oxide ([MH-O]$^+$=376) and this is shown in Figure 1.

Figure 1. Metabolic Mapping of a Guinea Pig Microsomal Incubation of HAL

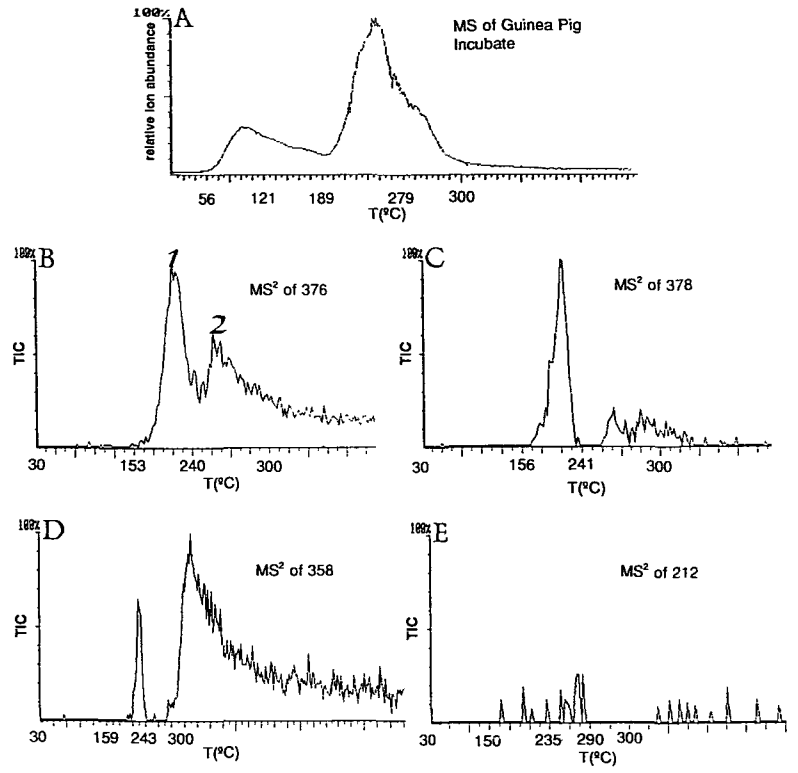

Regioselective analysis of hydroxyeicosatetraenoate in phosphatidylcholines by LSI/MS/MS

*Ji Y. Zhang[1], Brian Nobes[1], Jiemin Wang[1] and Ian. A. Blair[1,2]. Department of Pharmacology[1] and Chemistry[2], Vanderbilt University, Nashville, TN 37232

The hydroxyeicosatetraenoic acids (HETEs) are biologically active eicosanoids derived from arachidonic acid. Three different isomeric compounds, 5(S)-, 12(S)-, and 15(S)-HETE can be formed via different specific lipoxygenase pathways. All three HETEs are incorporated into membrane phospholipids in a wide range of cell types (1). HETE containing phospholipids are lipids peroxidation products (2). Fast atom bombardment mass spectrometry (FAB-MS) and FAB-collision-induced dissociation tandem mass spectrometry (FAB-CID-MS/MS) techniques have been successfully used to characterize the structures of phospholipids. The present study reports a liquid secondary ion tandem mass spectrometric (LSI/MS/MS) method for the qualitative analysis of intact phosphatidylcholines containing HETE moieties.

The esterification of 5-, 12-, and 15-HETE (50 μg) to lysophosphatidylcholine (100 μg) was carried out in 1 ml of 125 mM Tris-HCl buffer (pH, 7.4) containing 2 mM $MgCl_2$ in the presence of coenzyme A (300 μg), ATP (4.4 mg) and rat liver microsome fractions (1.2 mg of protein/ml). The incubation was performed for 1 hr at 37 °C under nitrogen. After the incubation, the lipids were extracted with $CHCl_3/CH_3OH$/acetic acid (2/1/0.05, v/v/v) and then purified using HPLC. Phospholipids containing esterified HETEs were initially separated by normal-phase HPLC and reverse-phase HPLC as described below. Normal-phase HPLC was carried out using an Econosphere silica analytical column (3 μm, 4.6 x 100 mm, Alltech). The mobile phase consisted of a gradient of 70% solvent A (hexane/isopropanol, 3/4, v/v) and 30% solvent B (hexane/isopropanol/water, 4/6/1, v/v/v) held for 20 min then programmed linearly to 100% solvent B over 20 min. The solvent flow rate was 1 ml/min. The esterified HETE-phosphatidylcholines were collected and further purified by reverse-phase HPLC. Reverse-phase HPLC purification was performed using an Ultrasphere ODS analytical column (5 μm, 4.6 x 250 mm, Beckman). The column was eluted by a gradient from methanol/acetonitrile/water (910/40/50; v/v/v) containing 1 mM ammonium trifluoroacetate to methanol/acetonitrile/water (910/80/10; v/v/v) containing 1 mM ammonium trifluoroacetate over 60 min at rate of 2 ml/min. The UV absorbance was monitored at 235 nm.

Collision-induced dissociation (CID) mass spectra of individual HETEs and PCs containing HETEs were obtained from approximately 200 ng of material, which was dissolved in 5 μl DMSO, and placed on a liquid secondary ion (LSI) probe of a Kratos Concept four sector mass spectrometer. Negative ions were produced using triethanolamine as the liquid matrix. Cs^+ ions were accelerated to 2 kV. Argon was used as the collision gas at a pressure of 5 x 10^{-5} Torr. The collision energy was 4 kV. Precursor and product ion spectra were obtained using a Sun data system.

Characterization of phosphatidylcholines (PC) which containing HETEs at the C-2 position was carried out using positive and negative LSI tandem mass spectrometry. In contrast to the positive LSI spectra of these compounds which primarily give a pseudo-molecular ion at m/z 827, more structural information was achieved from their negative LSI spectra. An intense ion at m/z 811 was produced by a loss of CH_3 from the molecular ion. Major ions at m/z 283 and m/z 319 corresponded to carboxylate anions of fatty acids, stearate and a HETE substituent were also observed (Figure 1a). The CID of HETE species yielded fragment ions which indicated the positions of the hydroxyl groups at

HETE molecules. For example, CID of the m/z 319 from 5-HETE-PC produced fragment ions at m/z 115 and m/z 203, which were produced from a four ring rearrangement cleavage and an α-cleavage of a hydroxyl group, respectively. This clearly indicated a hydroxyl group at C-5 position (Figure 1b). For 12-HETE-PC and 15-HETE-PC, their CID spectra of the m/z 319 showed unique ions at m/z 179 and m/z 208, as well as m/z 219 and m/z 248, demonstrating the presence of hydroxyl groups at C-12 and C-15 positions, respectively.

In summary, a direct analysis of the PCs containing HETE molecular species using negative LSI/MS/MS has been developed. This technique allows important structural information of phospholipids containing HETEs to be obtained. This will contribute to the understanding of their mechanism of formation and their physiological significance.

This work was supported by NIH grant DK 38226 & RR06254.

References:

1. A. B. Legrand, J. A. Lawson, B. O. Meyrick, I. A. Blair and J. A. Oates, *J. Biol. Chem.* 266, 7570-7577 (1991).
2. J. M. C. Gutteridge and B. Halliwell, *Trends Biochem. Sci.* 15, 129-135 (1990).

Figure 1. CID spectra of negative LSI of (a) m/z 811 (M-CH_3) and (b) m/z 319 from 5-HETE-PC.

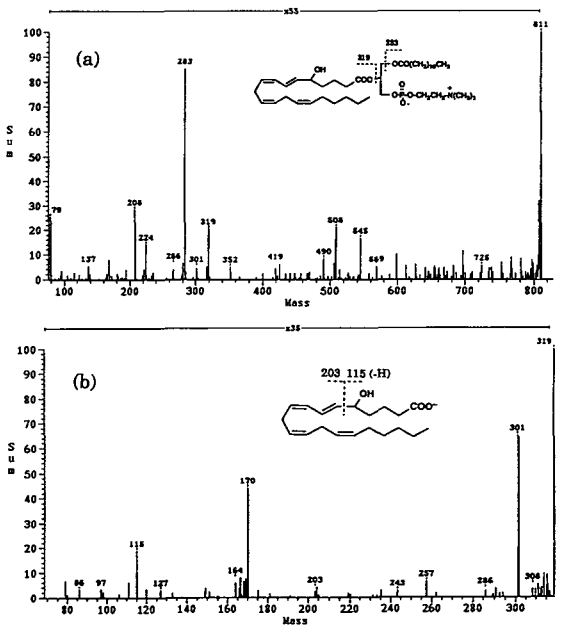

EI, CI and FAB Mass Spectral Characterization and Identification of Noberastine Metabolites

W. N. Wu, J. A. Masucci, A. D. Gauthier, A. J. Streeter, P. L. Stahle, and P. N. Lucas
The R. W. Johnson Pharmaceutcal Research Institute, Spring House, PA 19477

INTRODUCTION: Noberastine (RWJ-27572) is currently being developed as a potential antihistamine agent for seasonal allergic rhinitis. The objectives of the present study were to profile, isolate, and identify noberastine metabolites in dog samples using TLC, HPLC, MS and NMR.

METHODS: Representative samples of plasma (0-24 h), urine (0-48 h) and feces (0-48 h) obtained from the dog (10 mg/kg dose) were pooled and purified for metabolite profiling, isolation and identification. Individual metabolite was isolated using peak collection method. All metabolites were characterized and identified by desorption CI (methane), EI and FAB (thioglycerol) mass spectrometry, and confirmed by NMR. Some of metabolites were further derivatized using diazomethane, and confirmed by MS. Chemical ionization and electron impact were obtained using a VG 7070E. Operating conditions for spectrometer included: Source temperature: 220 degree C; Reagent gas pressure: 2 torr; Ionization potential: 70 eV; Multiplier voltage: 1.8 KeV; Electrometer setting: 10^{-7}A/V; Mass ranges: 18-1000 m/z at 1 sec/decade; Sample inlet: Desorption probe; Sample size: 5 microliter. Fast atom bombardment spectra were recorded using a VG 7070E mass spectrometer. Operation conditions included: Source temperature: 25 degree C; Source type: Ion tech.saddle field design with agron gas at 8 KeV potential and 1 mA current; Multiple voltage: 1.8 KeV; Electrometer setting: 10^{-7}A/V; Mass range: 18-1000 m/z at sec/decade; Sample matrix: 5 microliter; Sample size: 2 microliter.

RESULTS: Approximately 86% of the dose excreted in the urine (48.4%) and feces (37.5%) in the eight days after oral administration of 14C-noberastine. TLC and HPLC metabolic profiles of the plasma, urine and fecal extract samples were obtained. Unchanged noberastine plus ten metabolites were isolated and identified from these samples. Unchanged noberastine accounted for <32% of the dose in excreta samples and >63% of the total 14C in plasma at 0-24 h pool after dosing 14C-noberastine. Identified noberastine and metabolites accounted for >75% of the total 14C in the plasma, urine and fecal samples. MS and NMR spectra of noberastine and representative metabolites are presented.

CONCLUSION: Biotransformation pathways for noberastine in the dog are depicted. Noberastine was substantially metabolized in the dog, and >50% of the dose excreted in urine and feces was represented by metabolites. FAB-MS, CI-MS and EI-MS analysis of the isolated noberastine and metabolites revealed apparent protonated molecular/molecular ions and prominent fragment ions for the structural elucidation of metabolites.

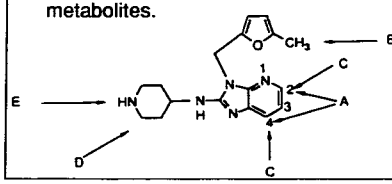

Sites of Metabolic Reactions for Noberastine in Dog

Site of Reaction	Metabolic Reactions/Pathways
(A)	Hydroxylation at the pyridinyl ring
(B)	Hydroxylation at the methyl group
(C)	Conjugation after (A)
(D)	Oxidation/dehydration
(E)	Carboxylation

Structures of Noberastine and Its Metabolites Identified in the Dog

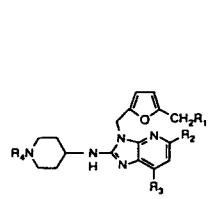

	R_1	R_2	R_3	R_4
Noberastine (RWJ-27572-000)	H	H	H	H
Metabolite 1	H	OH	H	H
2	H	H	OH	H
3	OH	H	H	H
4	H	glucuronide	H	H
5	H	H	glucuronide	H
6	H	H	H	CO_2H
7	H	H	H	CHO
8	H	H	H	CH_3CO

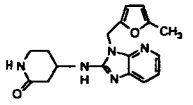

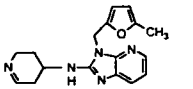

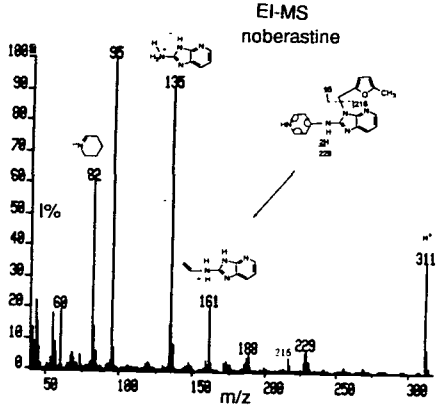

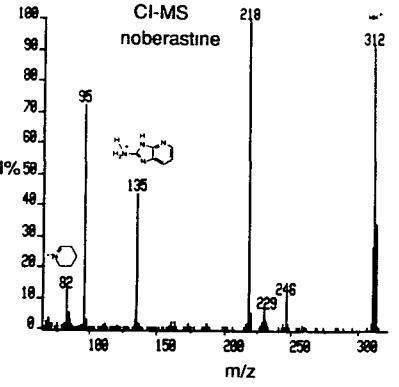

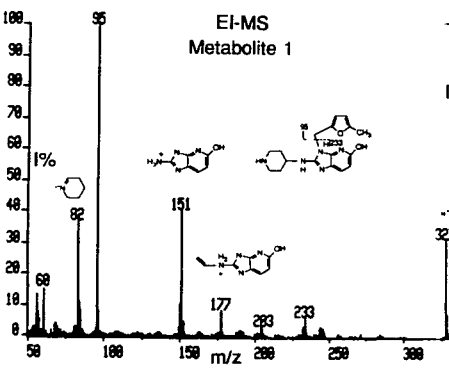

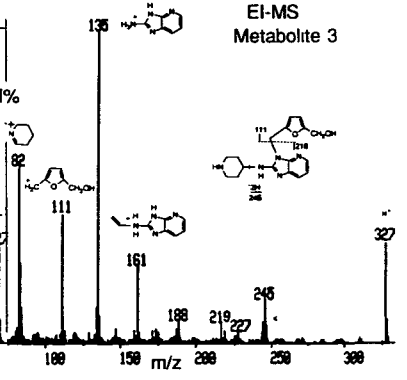

NEGATIVE-ION FAST ATOM BOMBARDMENT / COLLISION-INDUCED DISSOCIATION MASS SPECTROMETRY IN THE STUDY OF URSODEOXYCHOLIC ACID METABOLISM IN MAN

W.J.Griffiths, J.Zhang and J.Sjövall. Department of Physiological Chemistry, Karolinska Institute, S-10401 Stockholm, Sweden.
H-U.Marschall, H.Matern and S.Matern. Department of Internal Medicine III, Aachen University of Technology, D-5100 Aachen, Germany.

Ursodeoxycholic acid (UDCA) is used as a drug in the treatment of cholestatic liver disease. In the present study (24-^{13}C) labeled UDCA has been given to patiets with cholestatis. Their urine has been collected and the lipid content extracted by use of a Sep-Pak C_{18} column. The extract was analysed by negative-ion FABMS. A representative spectrum is shown in fig. 1. It is extremly complex as a result of the presence of steroids, fatty acids and bile acids.

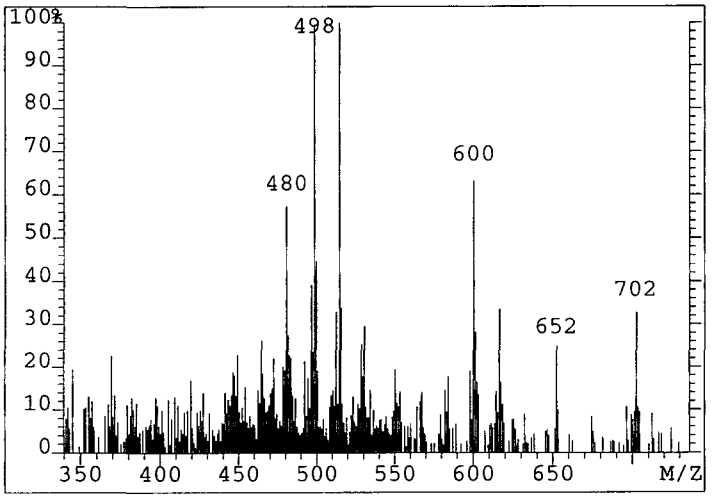

Fig. 1. Negative-ion FABMS of Sep-Pak C_{18} extracts.

To simplify matters the extracts were subjected to ion-exchange chromatography on a Lipidex-DEAP column. The resultant fractions, (1.neutrals and sterols, 2.unconjugated bile acids, 3.glycine conjugates, 4.taurine conjugates, 5.glucuronides, 6.sulphates) were then analysed by FABMS. Intense peaks at m/z 595 Da, 652 Da and 702 Da were observed in the unconjugated, glycine- and taurine- conjugate fractions respectively. These molecular weights are characteristic of the $(M-H)^-$ pseudomolecular ions of the unconjugated, the glycine and the taurine conjugated forms of (24-^{13}C) labeled N-acetylglucosaminyl-ursodeoxycholic acid.

Although FAB spectra give information as to the molecular weight of the bile acids, little information as to their structure is forthcoming. To obtain this, CID spectra are recorded on the $(M-H)^-$ pseudomolecular ions. It has been shown that taurine conjugated bile acid $(M-H)^-$ ions give intense charge-remote fragmentation (CRF) patterns which are of much value in structure elucidations[1]. The CID spectrum of the pseudomolecular ion at m/z 702 Da is shown in fig. 2. From the CRF pattern the ion structure is determined to be (24-^{13}C) labeled (7-N-acetylglucosaminyl)-ursodeoxycholyl-taurine.

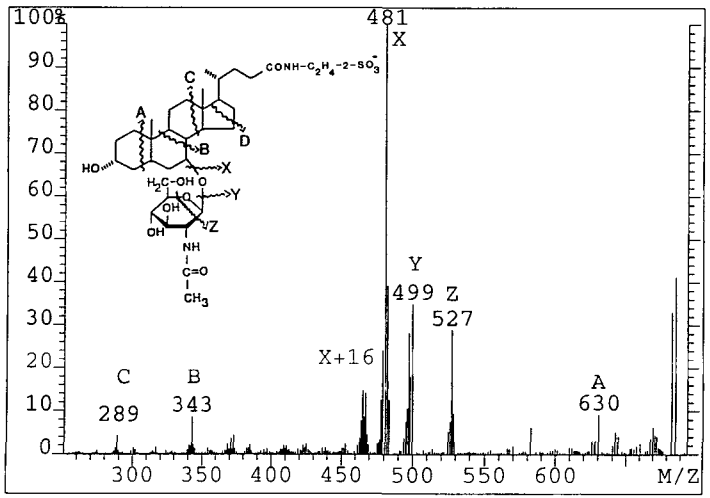

Fig. 2. Negative-ion FAB/CID spectrum of the ion at m/z 702 Da.

Unconjugated and glycine-conjugated bile acids give much less informative CID spectra than the taurine conjugates. To increase the structural information available these chromatographic fractions were derivatized with taurine (2-aminoethanesulphonic acid) using a recently developed rapid and simple method[2]. The derivatives formed were then analysed by negative-ion FAB/CID. In this way it has been established that the position of sugar conjugation in the novel bile acids conjugates N-acetylglucosaminyl-UDCA, and N-acetylglucosaminyl-UDC-glycine is at position 7β.

1.W.J.Griffiths,J.Zhang and J.Sjövall, Rapid Commun. Mass Spectrom., 7, 235 (1993).
2.J.Zhang, W.J.Griffiths,T.Bergman,and J.Sjövall, J. Lipid Res.(1993)

CHARGE-REMOTE FRAGMENTATION OF DOUBLY CONJUGATED BILE ACIDS

William J. Griffiths*, Jie Zhang, and Jan Sjövall. Department of Physiological Chemistry, Karolinska Institute, Box 60400, S-10401 Stockholm, Sweden.

Negative-ion fast atom bombardment mass spectra (FABMS) of bile acids show prominent $(M-H)^-$ pseudomolecular ions, and few fragment ions. Collision-induced dissociation (CID) of such pseudomolecular ions give charge-remote fragmentations (CRF) which are useful in structural identifications. It has been shown that taurine (2-aminoethanesulphonic acid) conjugated bile acids give more intense and informative CID spectra than unconjugated or other aminated bile acids. In this laboratory a procedure for the aminosulphation of biological samples for analysis by mass spectrometry has been developed. In the present study a comparision has been made of the CID spectra of a series of sulphated and glucuronidated bile acids and their 2-aminoethanesulphonate derivatives. Shown in figures 1 and 2 are CID spectra of the taurine derivatized forms of the 3-sulpho and 3-glucuronidyl choloic acid. CRF are prominent, and define the position of hydroxyl and conjugating groups. The structure of 3-sulphocholyltaurine is shown below. When charge is retained at the taurine SO_3^- group fragmentations are defined by capital letters. When charge is retained at the sulphate SO_3^- group small letters define the fragmentations. A similar notation is used for the fragmentation glucuronidated bile acid.

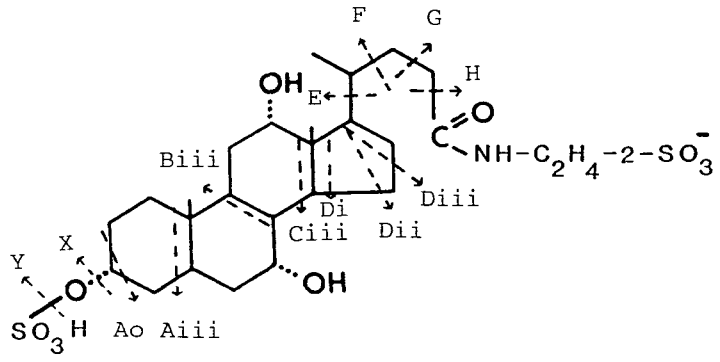

FABMS profiles of human urine reveal that bile acid-glucuronides and -sulphates are often found conjugated to glycine or taurine. Glucuronate and sulphate fractions from human urine have also been analysed CID mass spectrometry and the position of conjugation determined.

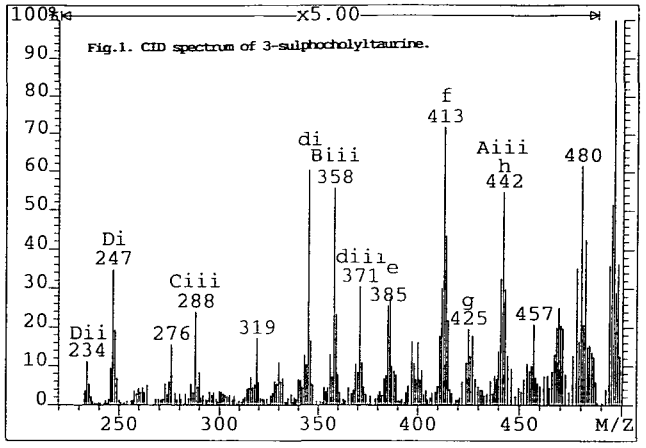

Fig.2. CID spectrum of 3-(glucuronidyltaurine)-cholyltaurine.

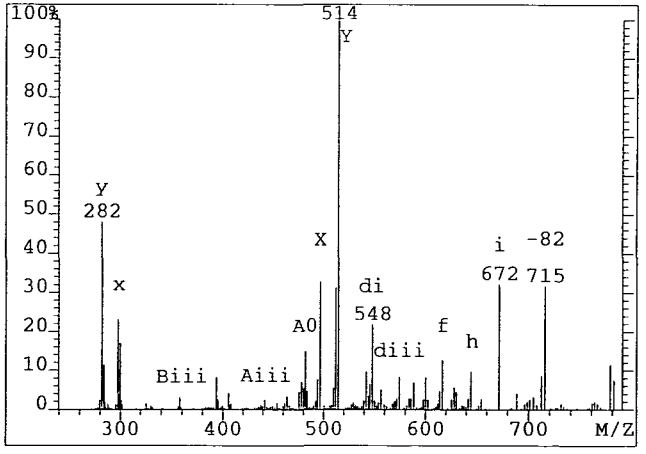

Mass Spectrometry of Sertraline and Related Compounds

Thomas R. Sharp, George J. Horan and Stephen V.O. Day
Analytical R&D, Central Research, Pfizer Inc., Groton, CT 06340 U.S.A.

The antidepressant drug substance sertraline -- 4-(3,4-dichlorophenyl)-N-methyltetrahydronaphthyl-1-amine -- was approved for use in the United Kingdom in 1990 and in the U.S. in late 1991. The hydrochloride salt is marketed under the trade names Lustral® (U.K.) and Zoloft® (U.S.). It is a selective serotonin reuptake inhibitor, departing from the therapeutic line of the tricyclic antidepressants and monoamine oxidase inhibitors.

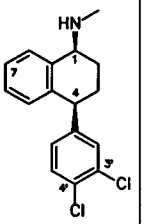

The EI mass spectrum of sertraline is shown in Figure 1. No M^+ is observed, even at low ionization energies. Neutral loss of methylamine produces a base peak equivalent to the dihydronaphthalene. Many of the smaller fragments are those of this related compound, suggesting that the mass spectrum of sertraline is principally the mass spectrum of its primary fragmentation product. The chemical ionization (CI) and fast atom bombardment (FAB) behavior of sertraline are shown in Figures 2 and 3.

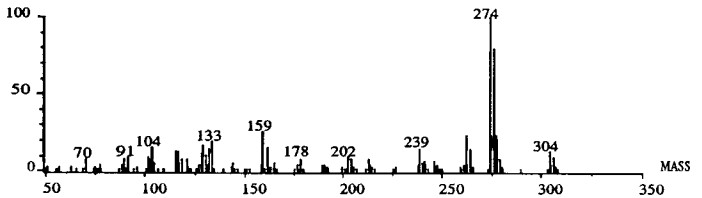

Figure 1: EI mass spectrum of sertraline.

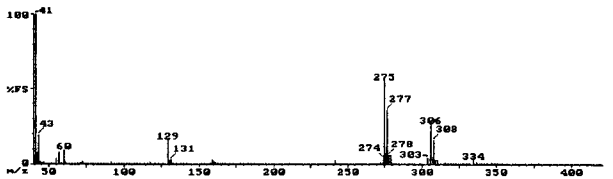

Figure 2: Methane CI mass spectrum of sertraline

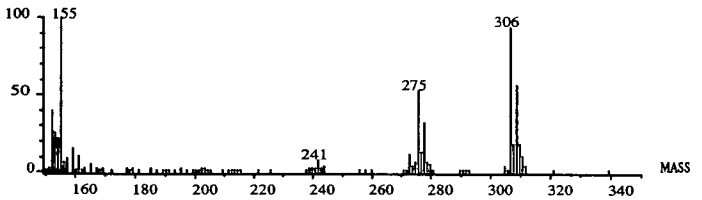

Figure 3: FAB mass spectrum of sertraline

The absence of an M^+ in the EI spectrum is characteristic of all analogs which possess at least one active hydrogen attached to the nitrogen. Replacement of all active hydrogens with alkyl groups stabilizes the M^+ to an observable level. Substitution at position 7 with an OH or OCH_3 also increases the abundance of M^+. Introduction of a double bond, converting the tetrahydronaphthalene ring to a dihydronaphthalene, also stabilizes the $M^{+\cdot}$ so that it is observable. Complete aromatization produces a spectrum typical of a polycyclic aromatic hydrocarbon or a biphenyl, consisting primarily of the intense M^+.

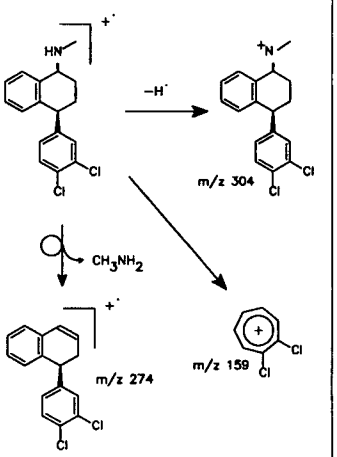

Orientation of the amine group at position 1 with respect to the phenyl group at position 4 does not influence fragmentation, provided that protons are attached to carbons 1 and 4. When a group such as an alkyl or hydroxyl group is attached to carbon 4, the fragmentation changes dramatically. Neutral loss of alkylamine no longer occurs, and is replaced by neutral loss of the appropriately substituted benzene ($M\text{-}Bz^+$ in Table 1). Further, the *cis-trans* orientation of the alkylamine and substituted phenyl ring determines whether $M\text{-}Bz^+$ is the base peak or if it further fragments by loss of 29 daltons (-29 in Table 1).

The methane CI spectrum of sertraline (Figure 2) shows marked sensitivity to reagent gas pressure. EI fragments at m/z 159 and m/z 174 disappear from the spectrum as the reagent gas pressure is increased, the m/z 174 EI-induced methylamine neutral loss being replaced by methylamine neutral loss from $[M+H]^+$ to form the species at m/z 175. The $[M+C_2H_5]^+$ adduct is present at m/z 334 FAB fragmentation echos the true CI fragmentation in that neutral loss of CH_3NH_2 occurs from $[M+H]^+$.

Table 1: EI Fragmentation Relative Abundances

			Substitution Pattern*						EI Fragments (rel. abundance)					
Compound	rmm	stereo	N	N	4	7	3'	4'	M^+	$M\text{-}H^+$	$M\text{-}R_2N^+$	$Trop^+$	$M\text{-}Bz^+$	-29
CP- 25,447	223	cis							0	30	70	38		
CP- 22,185	237	cis		CH_3					0	10	100	42		
sertraline	305	cis		CH_3			Cl	Cl	0	16	100	25		
CP- 53,508	305	trans		CH_3		Cl		Cl	0	10	100	38		
CP- 54,108	301	cis		CH_3		OCH_3			10	10	100	15		
CP- 54,168	287	cis		CH_3		OH			8	10	100	20		
CP- 54,448	319	trans		CH_3	CH_3		Cl	Cl	0	12			100	10
CP- 54,449	319	cis		CH_3	CH_3		Cl	Cl	0	30			50	100
CP-166,400	321	cis		CH_3	OH		Cl	Cl	0	1			25	100
CP-166,400	321	trans		CH_3	OH		Cl	Cl	0	2			100	25
CP- 53,660	285	cis		CH_3	CH_3			Cl	0	10			35	100
CP- 53,661	285	trans		CH_3	CH_3			Cl	0	10			100	10
CP-166,401	303			CH_3	=		Cl	Cl	35	25	100	0		
CP-129,380	319	cis		C_2H_5			Cl	Cl	0	15	100	32		
CP- 57,459	319	cis	CH_3	CH_3			Cl	Cl	15	5	100	58		

* Spaces imply a hydrogen. Numbering scheme shown on sertraline structure.

Fast Atom Bombardment Mass Spectrometry Using a Glycerol Matrix Saturated With a 3:1 Mixture Of Non-Labelled And Trideuterated Tetramethylammonium Hydroxide To Count The Number Of Anionic Sites

* P.L. Jacobs, G.J.H. Schmeits and M.P. de Vries.

AKZO, Organon International B.V., Scientific Development Group, P.O. Box 20, 5340 BH Oss, The Netherlands.

INTRODUCTION

A glycerol matrix saturated with tetramethylammonium hydroxide pentahydrate (TMAOH) was used to obtain FAB spectra of sulphated metabolites of the steroid Org OD 14 [1] in the presence of sodium acetate when glycerol failed. From the mass difference observed in the positive and negative ion spectra of these ion-pair complexes the number of sulphate groups present was calculated[1].

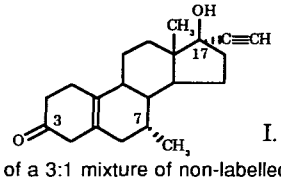

I. Org OD 14

We now report the use of a 3:1 mixture of non-labelled and trideuterated TMAOH in glycerol to produce characteristic artificial isotope patterns for the ion-pair complexes of anionic compounds in the positive ion FAB mode. These observed patterns allow the direct determination of the number of TMA-groups present and subsequently the calculation of both the (minimum) number of anionic sites and the molecular masses from the FAB(+) spectra only.

RESULTS AND DISCUSSIONS

Artificial isotope patterns obtained with this novel matrix of reference steroids with resp. one (Estrone 3-sulfate), two (Estradiol 3,17-disulfate) and three (Estriol trisulfate) anionic groups present are shown in Fig. 1 and the upper part of Fig. 2. The FAB(+) patterns of the ion-pair complexes of these steroids with resp. 2, 3 and 4 d_0/d_3-TMA counter-ions present can easily be distinguished. These patterns were used as reference patterns of mono-, di- and tri-anionic compounds and allowed the determination of the (minimum) number of anionic groups present in unknowns (sulfates, phosphates, glucuronides) as well as the calculation of their molecular masses. As an example the FAB(+) spectrum of 3, 17ß-disulfated Org OD 14 is shown in Fig. 3.

Both FAB(+) profile scans of ß-Estradiol 3-sulfate, 17-glucuronide (Fig. 2 bottom) and ß-Estradiol 3-glucuronide, 17-sulfate were recorded with this novel matrix to demonstrate that isotope patterns characteristic for di-anionic compounds could be obtained despite the low S/N ratio usually obtained for these compounds both with glycerol and TMAOH/glycerol[1]. Without the artificial isotope pattern the unambiguous determination of the molecular masses would not have been possible for these compounds with FAB(+) at the 10 µg level. The enrichment of the TMAOH/glycerol matrix with synthetically prepared d_3-TMAOH, and as a result the 3 Da spacing in the ion-pair clusters, still allowed the recognition of other isotopic contributions e.g. due to the presence of Br and Cl. It was furthermore observed that some compounds were -in part- methylated under these matrix conditions. In those cases a satellite isotope pattern was observed with a mass difference of 14 Da, the degree of methylation was usually <10%.

REFERENCE

1. P.L. Jacobs, G.J.H. Schmeits, M.P. de Vries, L.P.C. Delbressine and H.A.M. Peters, *Biol. Mass Spectrom.* **21**, 491 (1992).

FIGURES

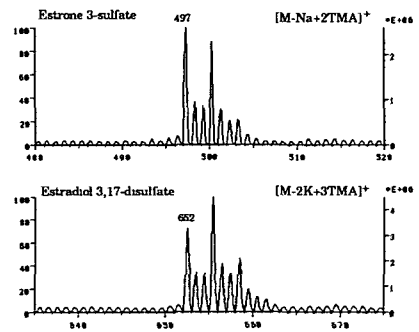

Fig. 1: FAB(+) spectra of Estrone 3-sulfate (upper) and Estradiol 3,17-disulfate (lower), obtained with a glycerol matrix saturated with d_0/d_3-TMAOH in a ratio of 3:1, showing the isotope pattern characteristic for the presence of 2 resp. 3 TMA groups.

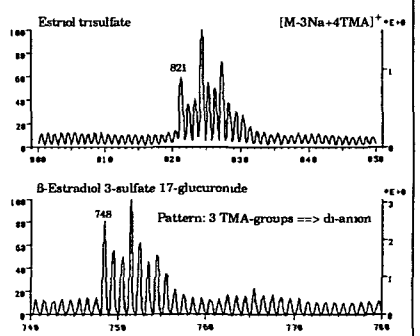

Fig. 2: FAB(+) spectrum of Estriol trisulfate (upper) showing the isotope pattern characteristic for the presence of 4 TMA-groups. The pattern observed for ß-Estradiol 3-sulfate 17-glucuronide (lower) clearly indicates the presence of 3 TMA groups.

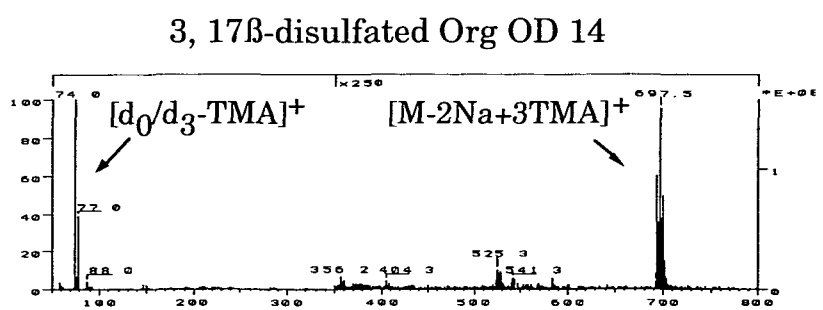

Fig. 3: FAB(+) scan of 3, 17ß-disulfated Org OD 14 showing both the d_0/d_3-TMA cations of the matrix (m/z 74/77) and the artificial TMA ion-pair pattern characteristic for a di-anionic complex.

GC-MS Analysis of Phenylacetic Acid Conjugates in the Rat Brain and Kidney *David A. Durden, Bruce A. Davis and Lillian E. Dyck, University of Saskatchewan, Saskatoon, SK. Canada S7N 0W0.

Phenylacetic acid (PAA), a normal metabolite of phenylalanine and the trace biogenic amine phenylethylamine, has been shown to be a neurotoxic agent damaging neurons and glia when injected into newborn rats and is abnormally excreted by patients with phenylketonuria. Phenylacetic acid is excreted by mammals as a variety of conjugates [1]: primates excrete PAA as phenylacetyl-glutamine (PAGln) whereas carnivores, rodents and other mammals excrete PAA as phenylacetyl-glycine (PAGly) and to a small extent as phenylacetyl-taurine. We have shown that in the rat brain 90% of PAA exists as a conjugate [2]. Neither free nor conjugated PAA levels were decreased by the MAO inhibitor pargyline but probenecid caused a slight increase in total PAA. These studies indicate that conjugates may regulate the amount of free PAA in the brain and thus control its toxic effects.

The conjugate in brain may be one of the excreted conjugates or another such as phenylacetyl-coenzyme A [3]. Since rodents excrete primarily PAGly we have attempted to quantitate it in both rat brain striatum and kidney using the ^{13}C labeled conjugate as internal standard. Several derivatives have been examined for their suitability for GC-MS analysis

Methods

The following derivatives were examined: trimethylsilyl (TMS), t-butyldimethylsilyl (TBDMS), pentafluorobenzyl (PFBz), trifluoroethyl (TFE), pentafluoro-n-propyl (PFnP), hexafluoro-isopropyl (HFIP) esters and these esters combined with the pentafluoropropionyl (PFP) or heptafluorobutyryl (HFB) amides

Tissues from 8 rats were pooled and homogenized in 7 ml of ice cold 2N HCl which contained 50 ng of PAA-d_5. The homogenate was centrifuged at 10,000 x g for 15 min at 4°C and six 1 ml aliquots were taken. Three aliquots were transfered to ampules which were then sealed and heated at 100°C for 4 hrs. After cooling these were transferred to test tubes. To each tube was added 90 ng of PAGly-$^{13}C_2$. The acids were extracted into ethyl acetate and the volume was reduced under a stream of nitrogen. The solutions were then transferred to Reactivials and the volume reduced to 100 µl and 100 µl of 1% triethylamine in benzene added and the solution taken to dryness. Pentafluoropropionic anhydride (50 µl) and trifluoroethanol (50 µl) were added and the sealed Reactivials heated at 80 °C for 1 hr. After cooling hexane (100 µl) and phosphate buffer (100 µl, pH 6.0) were added and mixed for 30 sec.The hexane layer was removed and transferred into a 100ml vial and the volume reduced to 20 ml.

Results

Tests of derivatives were carried out using PAGln and PAGly. PAGln is that it readily cyclizes under heat to form the pyroglutamate. The TMS and TBDMS derivatives decomposed on the GC column. The pentafluorobenzyl derivative gave good spectra for both PAGly and PAGln but the derivative of the latter had poor chromatographic properties. The EI spectra of all the derivatives using TFE, PFnP or HFIP and either PFP or HFB were

similar. The major fragment was m/z 91 and the highest mass ion was the M-91 fragment which had a low intensity. Reaction with PAGln gave many products including the derivatized cyclized product. Again the fragmentation is not very satisfactory.

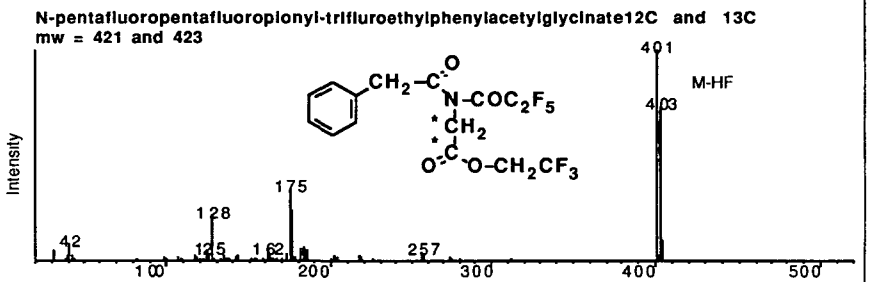

Fig.1 shows the NCI spectra of phenylacetyl-glycine. PAA-TFE exhibits a significant base peak at M-H. These ions were used for quantitation. Table 1. shows the effect of hydrolysis on PAA and PAGly in rat striatum and kidney It appears that in the kidney there is no contribution from another conjugate as the totals are similar. The amount of PAGly in the rat brain is considerable less than the amount of PAA normally measured after hydrolysis. This agrees with other observations [4] that incubation of brain homogenates with ^3H PAA did not synthesize radiolabelled PAGly and with Loo et al [3] that it is probably phenylacetyl-coenzyme A.

Table 1. Levels of phenylacetic acid and phenylacetylglycine in rat striatum and kidney.

	Striatum		Kidney	
	PAA (ng/g)	PAGly (ng/g)	PAA (ng/g)	PAGly (ng/g)
Normal	20	5.7 ±5	80.9 ± 8.1	840 ± 13.3
Hydrolyzed	31.1 ± 2.8	1.0 ± .9	716 ± 34	42.7 ± 6

Conclusions

The TFE-PFP derivative with NCI ionization is the most suitable procedure for analysis of PAA, phenylacetyl-glycine and phenylacetyl-glutamic acid. As expected phenylacetyl-glycine is the major conjugate of PAA in rat kidney and is readily hydrolysed. It appears from this data that the major conjugate of PAA in rat brain is not phenylacetyl-glycine.

References

1. James, M.O., Smith, R.L., Williams, R.T. and Reidenberg, M. Proc. R. Soc. Lond. B. **182**, 25-35, 1972.
2. Dyck, L.E., Durden, D.A., Boulton, A.A. Life Sci. 1993 in press.
3. Loo, Y.H., Miller, K.A., Nowlin, J. and Horning, M.G. Life Sci. **26**, 657-663, 1980.
4. Dyck, L.E., Durden, D.A. and Boulton, A.A. Biosynthesis of conjugates of phenylacetic acid in the rat striatum. Society for Neuroscience, Washington, 1993.

Quantitative analysis of 11-hydroxy,8,9-epoxyeicosatrienoic acid from human umbilical venous endothelial cells (HUVECs) by GC/EC NCI MS

*Ji Y. Zhang[1], Chandra Prakash[1], Richard Hoover[3] and Ian. A. Blair[1,2]. Department of Pharmacology[1], Chemistry[2] and Pathology[3], Vanderbilt University, Nashville, TN 37232

Arachidonic acid is oxidized by the cytochrome P-450 monooxygenase to form four regioisomeric *cis*-epoxyeicosatrienoic acids (EETs). 8(S),9(R)-EET was a potent renal vasoconstrictor, but its activity was abolished by cyclooxygenase (COX) inhibitors (1). It was demonstrated that COX derived from human platelets or ram seminal vesicles metabolized 8,9-EET to 11(R)-hydroxy,8,9-EET (11-HEET) (2). 11(R),8(S),9(R)-HEET is a potent renal vasoconstrictor responsible for the vasoconstrictor activity caused by 8(S),9(R)-EET. In addition, both 11(R),8,9-EET enantiomers are potent mitogens for cultured rat glomerular mesangial cells (3). The present study examines the possibility that endothelial cells generate 11-HEET and convert 8,9-EET to 11-HEET. This study reports a sensitive GC/EC NCI mass spectrometric method to quantify 11-HEET in human umbilical venous endothelial cells (HUVECs).

HUVECs were cultured from human umbilical cord vessels. Confluent HUVEC monolayers were covered with 10 ml of 25 mM HEPES buffer, pH 7.4, containing 150 mM NaCl, 5 mM KCl, 1.8 mM $CaCl_2$, 1 mM $MgCl_2$, 6 mM glucose and substrate 1.5 µM 8,9-EET. The incubation mixture was kept for 4 hrs at 37 °C in an atmosphere of 5% CO_2 in air. In some experiments, cell culture was pretreated with indomethacin or stimulated with calcium ionophore. After incubation, the total lipids were extracted and further purified using HPLC. GC/EC NCI MS was carried out on a Nermag R1010C mass spectrometer using a 5 meter SPB-1 fused silica column (0.32 mm ID, 0.25 µm coating thickness; Supelco). The column was heated at 170 °C for 0.2 min then programmed to 260 °C at 20 °C/min. Methane was used as the reagent gas at a source pressure of $1x10^{-5}$ Torr. Helium was used as a carrier gas, and injection was made in the splitless mode.

A highly sensitive GC/EC NCI MS assay, based on the stable isotope dilution technique, was developed for the quantification of 11-HEET in HUVECs. [$^2H_4$]11-HEET was biosynthesized from [$^2H_4$]arachidonic acid and used as an internal standard. Derivatization of 11-HEET as a pentafluorobenzyl ester (PFB), t-butyldimethylsilyl ether (BDMS) allowed sensitive and specific analyses to be carried out. A 5 meter GC column was employed to avoid thermal degradation of the conjugated double bonds during GC analysis. The EC NCI mass spectrum of derivatized 11-HEET and its tetradeuterated analog showed intense ions at m/z 439 and m/z 443, respectively, which corresponded to a loss of the PFB group from the molecular ions. Quantitative analyses were carried out using SIM analysis of ions at m/z 439 and m/z 443. The limit of detection of the assay was 10 pg/sample with a coefficient of variation less than 10%. A typical selected ion current profile obtained for the analysis of 11-HEET in HUVECs is shown in Figure 1. The results showed that the level of endogenous 11-HEET in four HUVEC dishes were 158 ± 12 pg/$5x10^6$ cells. A dramatic increase of 11-HEET (17.83 ± 0.81 ng) in HUVECs was found when the cells were incubated with 5 µg of 8,9-EET. The formation of 11-HEET was increased in the presence of calcium ionophore and inhibited by indomethacin (Figure 2). These results strongly suggested that HUVEC COX can convert 8,9-EET into 11-HEET.

In summary, a sensitive GC/EC NCI mass spectrometric method to quantify 11-HEET in HUVECs has been established. The results demonstrated that human endothelial cells can convert 8,9-EET to 11-HEET, suggesting they may be involved in the transcellular metabolism of 8,9-EET *in vivo*. Further studies can now be carried out in different patient populations to explore a possible pathophysiological role for 11(R),8(S),9(R)-HEET.

This work was supported by NIH grant DK 38226.

References:

1. T. Katoh, K. Takahashi, J. Capdevila, A. Karara, J. R. Falck, H. R. Jacobson and K. F. Badr, *Am, J. Physiol.* 261, F578-F586 (1991).
2. J. Y. Zhang, C. Prakash, K. Yamashita and I. A. Blair, *Biochem, Biophys. Res. Commun.* 183, 138-143 (1992).
3. T. Homma, J. Y. Zhang, T. Shimizu, C. Prakash, I. A. Blair and R. C. Harris, *Biochem, Biophys. Res. Commun.* 19, 282-288 (1993).

Figure 1. Selected ion current profiles from human umbilical vein endothelial cells: (upper) 11-HEET-PFB-BDMS and (lower) [$^2H_4$-11-HEET-PFB-BDMS internal standard.

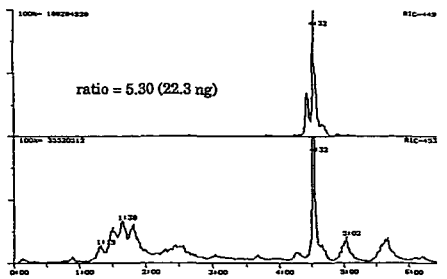

Figure 2. The result of 11-HEET formation in human umbilical vein endothelial cells.

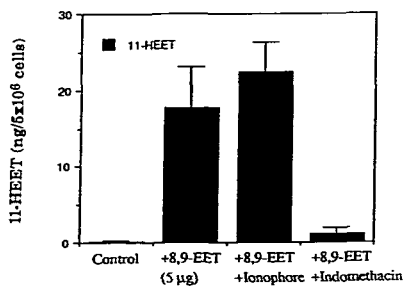

MASS SPECTROMETRY-BASED STRATEGY FOR CHECKING ORIGINALITY OF METABOLITES IN BIOLOGICALLY ACTIVE FERMENTATION BROTHS

C. PONTHUS, JM. PEREILLO, C. PICARD
SANOFI RECHERCHE, 195, route d'Espagne, 31036 TOULOUSE CEDEX

Two main different approaches are used in the pharmaceutical industry to find new, biologically active drugs. The most common one is to test chemically synthetized molecules. Another way is to screen complex mixtures such as fermentation broths from bacteria, moisture..., for activity. With this second approach, the probability is isolating an unknown structure, or family of compounds is quite low and is strongly dependant on (i) the originality of the micro-organism, (ii) the used culture medium, (iii) the relevance of the biochemical screening tests and (iv) the number of screened fractions.

However, the main problem encountered is to rapidly establish whether the active constituant(s) is original or not, even though the quantity of sample available at this early stage is very low (typically 10 to 100 µg).

That is the reason we developped a mass spectrometry-based strategy with the aim to check, as early as possible the originality of the active compound(s) before engaging time-consuming scale-up purifications.

The purified and tested fraction(s) is first analysed with various ionization techniques in order to determine the molecular weight of the compound. In a second step, accurate mass measurements and tandem mass spectrometry are performed on the molecular ion. The data obtained are then used as entry keys for automatic searching in commercial databases (mainly STN International).

Entry keys may be a logical combination of simple data such as possible elemental formula, detected elements in the structure like amico-acids or sugars etc... Assuming that all known structures are referenced in the Chemical Abstract database, an absence of answer form the automatic searching is then a strong presumption for the compound to be original. If answers are retrieved from the database, the spectra and the suggested structures are examined for compatibility of the experimental data with the proposed answers. Any additional information as for example the origin of the proposed molecule (synthetic *versus* natural) is also an item of importance. The following flowchart summarizes our approach :

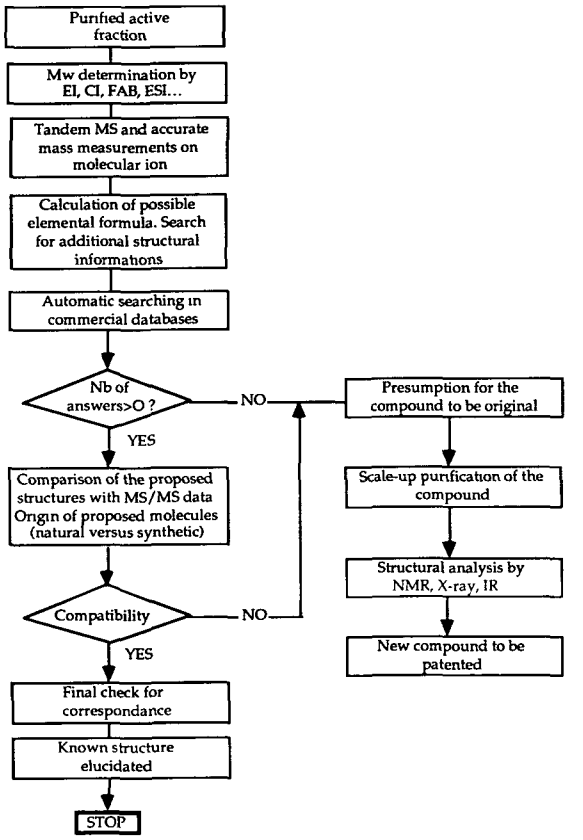

Advantages of using mass spectrometry at the very beginning are its sensitivity and its ability to quickly provide some structural information, as well as possible elemental formula. Starting with an unknown sample, originality checking may, in effect, be completed within 48 hours. Using this strategy, only original compounds have to be prepared in mg-amounts necessary for the complementary but time-consuming structural analysis techniques such as NMR and X-Ray. Examples of compound identification are shown, illustrating the advantages of mass spectrometry as time-saving analytical tool for biologists working in the field of fermentation.

Characterization of 20-hydroxyeicosatetraenoic acid glucuronide by LSI/MS/MS

Yoshiharu Ohyama*[1], Ji Y.Zhang[1] and Ian A. Blair[1,2].
Department of Pharmacology[1] and Chemistry[2], Vanderbilt University, Nashville, TN 37232

Introduction

20-hydroxyeicosatetraenoic acid (20-HETE) is a major metabolite of arachidonic acid from cytochrome P-450 ω-hydroxylase in neutrophils and renal microsomes. 20-HETE is a potent vasoconstrictor and promotes sodium excretion. *In vitro* biosynthesis of 20-HETE from exogenous arachidonic acid by renal microsomes was increased during the development of hypertension in the SHR rat. This suggested a possible role for 20-HETE in blood pressure control. A highly sensitive method has been developed using gas chromatography/electron capture negative ion chemical ionization mass spectrometry for the quantification of 20-HETE in human urine. Using this method, in combination with β-glucuronidase treatment of human urine, 20-HETE was found to be excreted mainly as a glucuronide conjugate. The present study reports the use of LSI/MS/MS for the characterization of the site of glucuronidation of 20-HETE.

Experimental

20-HETE (20 μg), UDPGA (10 mg) and human liver microsomes (200 μl, 17mg protein/ml) in 1 ml of Tris-HCl buffer (pH 7.0) were incubated at 37 °C for 24 hr. The incubation was stopped by addition of 1 ml of ice-cold methanol. Samples were purified using C-18 Sep-pak and HPLC. Reverse-phase HPLC purification was performed using an Ultrasphere ODS analytical column (5 μm, 4.6 x 250 mm, Beckman). The mobile phase was programmed from 100 % solvent A (water/acetonitrile; 80:20, v/v) to 100 % solvent B (water/acetonitrile; 50:50, v/v) over 30 min at a rate of 1 ml/min, then held for another 20 min. Fractions containing radioactivity were collected and evaporated under nitrogen. LSI/MS/MS spectra were obtained using a Kratos Concept II HH (Kratos Analytical Ltd, Manchester, UK) four sector tandem mass spectrometer, which consists of two double-focusing forward geometry instruments (EBEB) that are interfaced to a Sun

computer system. The instrument was equipped with a commercial Kratos ion source. Negative ion data was obtained with Cs^+ gun at 4 kV and the accelerating voltage at 8 kV. The collision cell was floated at 4 kV. The argon gas pressure was 1.5×10^{-6} torr.

Results and Discussion

The negative LSI mass spectrum of 20-HETE glucuronide showed a deprotonated molecular ion at m/z 496. The collision-induced dissociation (CID) spectrum of m/z 496 is shown in Figure 1. Fragment ions at m/z 346, 319, 295, 247, 199, 159 and 87 are produced. The ion at m/z 346 was formed by the loss of {CH(OH)-CH(OH)-CH(OH)-CH(COOH)} from the glucuronic acid moiety of the molecular ion. A loss of glucuronic acid from the molecular ion generated an ion at m/z 319 $[M-175]^-$. The cleavage of the bond between C-16 and C-17 produced a fragment ion at m/z 247, which indicated that the glucuronic acid moiety was conjugated at the hydroxyl group. A loss of H_2O from the glucuronic acid moiety yielded the ion at m/z 159. The fragment ion at m/z 87 was formed from a cleavage between C-4 and C-5 bonds. The results indicated that negative ion LSI/MS/MS was a useful technique for characterizing the glucuronide derivative of 20-HETE.

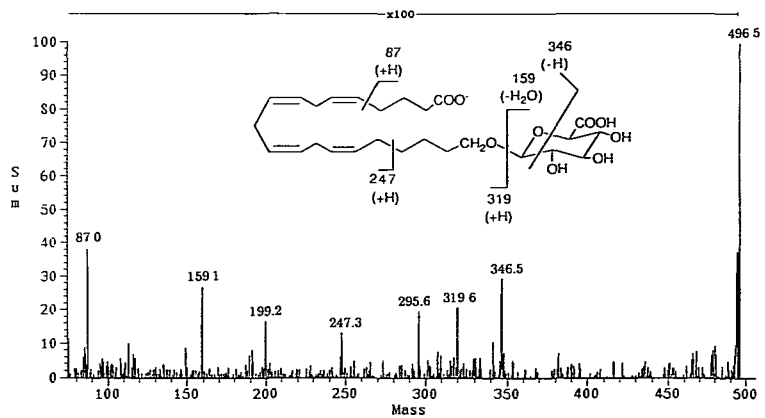

Figure 1. CID spectrum of negative LSI of m/z 496 from 20-HETE glucuronide.

A SINGLE ASSAY FOR THE DETERMINATION OF OXALIC, GLYCOLIC, GLYCERIC, GLYOXYLIC AND HYDROXYPYRUVIC ACIDS IN URINE BY POSITIVE ION CHEMICAL IONIZATION GC/MS

*Mark L.J. Reimer , Orval A. Mamer, E.Y. Osei-Twum, F. Lépine and J.A. Montgomery

Biomedical Mass Spectrometry Unit, McGill University, Montreal, Quebec, Canada H3A 1A3

Introduction. Primary hyperoxaluria encompasses two rare genetic diseases having in common the excretion of large quantities of oxalic acid. The two variants are distinguished by the elevated co-excretion of glycolic and glyoxylic acids (Type I hyperoxaluria) and hydroxypyruvic and glyceric acids (Type II). Ammonia positive ion chemical ionization (NH_3/CI) GC/MS has been used to determine the urinary concentrations of the trimethylsilyl (TMS) derivatives of all five organic acids in a single assay. The method involves the reduction of endogenous glyoxylic and hydroxypyruvic acids by sodium borodeuteride ($NaBD_4$) to ^{2}H-glycolic and ^{2}H-glyceric acids respectively, and these together with endogenous glycolic, oxalic and glyceric acids are quantitated against $^2H_2$-glycolic, $^{13}C_2$-oxalic and $^2H_2$-glyceric acids in a stable isotope dilution assay.

Materials and Sample Preparation. The labeled $^{13}C_2$-oxalate was purchased as the disodium salt from MSD Isotopes, Montreal. $^2H_2$-Glycolate and $^2H_2$-glycerate were prepared by the diazotization of $^2H_5$-glycine and DL-3,3-$^2H_2$-serine, also obtained from MSD Isotopes. Aliquots of urine (1 ml) were made basic (pH>12) with 5N NaOH. To these were added 25 μl of an aqueous standard solution containing 0.25 mg/ml $^2H_2$-glycolic acid, 13.4 mg/ml $^{13}C_2$-oxalic acid and 0.21 mg/ml $^2H_2$-glyceric acid. $NaBD_4$ (2 mg) was added and the resulting solutions were heated at 50°C for 10 min, cooled to room temperature, and extracted with 2 ml of diethyl ether (extract discarded). The aqueous phases were acidified with 2N HCl, saturated with NaCl, and extracted three times with 2-ml volumes of ether. The extracts were combined, dehydrated with anhydrous Na_2SO_4, and concentrated to 1 ml, of which approximately 300 μl was evaporated to dryness in a conical autoinjector vial. Trimethylsilyl derivatives were made by dissolution in 100 μl of a 1:1 mixture of N,O-bis-trimethylsilylacetamide and pyridine.

Instrumental. GC/MS analyses were performed using an HP 5890A gas chromatograph coupled directly to an HP 5988A quadrupole mass spectrometer. Samples were introduced by splitless injection (1.0 μl) onto a fused silica DB-1 capillary column (30 m x .25mm; 0.25 μm) heated from 80 to 160°C at 5°C/min. Ammonia CI spectra were obtained at a source temperature of 200°C and at a source pressure of 0.70 Torr. Selected ion monitoring (SIM) of the $[M+NH_4]^+$ ions for glycolic-$(TMS)_2$ (m/z 238), ^{2}H-glycolic-$(TMS)_2$ (m/z 239), $^2H_2$-glycolic-$(TMS)_2$ (m/z 240), oxalic-$(TMS)_2$ (m/z 252), $^{13}C_2$-oxalic-$(TMS)_2$ (m/z 254), glyceric-$(TMS)_3$ (m/z 340), ^{2}H-glyceric-$(TMS)_3$ (m/z 341), and $^2H_2$-glyceric-$(TMS)_3$ (m/z 342) acids were used for quantitation.

Results. Acid concentrations were calculated using a BASIC program that corrects raw SIM areas for isotopic impurities in the internal standards and for natural heavy isotope substitution in labeled and endogenous acids. Table 1 shows the acid concentrations (expressed relative to creatinine levels) for patients A, T and M, who are thought to have an oxalic aciduria; the values for two controls (O and L) and published normals are also shown.

Table 1. Urinary Oxalic, Glycolic, Glyoxylic, Glyceric and Hydroxypyruvic Acid Concentrations in Three Patients and Two Controls.

	Acid Concentrations (mg/g creatinine)				
Patient	Oxalic	Glycolic	Glyoxylic	Glyceric	Hydroxypyruvic
A	1192.1	72.2	6.8	1004.8	8.3
T	243.4	22.0	0.4	289.4	2.3
M	289.1	80.8	1.2	2039.0	15.8
O	172.0	24.4	1.2	46.6	0.02
L	51.5	22.4	0.4	109.7	0.01
Normals[a]	10-40	22-69	1.4-4.7	ND	U

[a]published normals (mg/day); ND = not detected in normals; U = previously undetermined.

Patient A excretes large amounts of oxalic and glyceric acids, suggesting a Type II oxalic aciduria. Patient T excretes lesser amounts of the acids of interest than A and may represent a Type II in remission or with a less severe deficiency of D-glyceric acid dehydrogenase activity. Patient M, also a Type II, excretes lesser amounts of oxalate than A, but much larger amounts of glycerate and hydroxypyruvate. Control O is remarkable only by its elevated level of oxalate, which is probably attributable to a daily consumption of 1 g. of ascorbic acid The four other acids are in accord with those of control L.

Discussion. The $NaBD_4$ reduction of the α-carbonyl functions in urinary glyoxylate and hydroxypyruvate to 2-^{2}H-glycolate and 2-^{2}H-glycerate respectively allows the analysis of all five acids to proceeed with comparable stabilities and extraction efficiencies. The glyoxylate-to-glycolate reduction may minimize losses of this reactive aldehyde arising from condensation with other urinary constituents; early reduction may also avoid similar losses of hydroxypyruvate, a significant problem because of enolic tautomerism between the keto and hydroxy functions. The method exhibits a high degree of precision as shown in six replicate analyses (%SD): glycolate, 1.1%; glyoxylate, 3.7%; oxalate, 1.0%; glycerate, 0.6%; hydroxypyruvate, 7.5%.

Acknowledgements. This work was supported by the Medical Research Council of Canada.

Thermally-induced Dissociation in the NCI Mass Spectra of Amino Acid n-Propyl Ester, N(O,S)-Heptafluorobutyramide Derivatives (AA-PrHFB).

David L. Hachey, Monica Culea, and Dan Liu
USDA/ARS Children's Nutrition Research Center, Dept. of Pediatrics,
Baylor College of Medicine, Houston, TX 77030

Introduction

Organic molecules with strong electron capture ability give simple negative chemical ionization mass spectra (NCI-MS), but limited structural information. The chief advantage of NCI-MS is the superb analytical sensitivity of some molecular structures. We have used the n-propyl ester, N-heptafluorobutyramide derivatives of amino acids to quantify protein synthesis and turnover in humans (1, 2). This derivative is easy to prepare, it is chemically stable, and it has excellent gas chromatographic separation of nearly all amino acids. In the course of conducting stable isotopic tracer studies of serine and glycine metabolism, we observed a substantial variability in ion production from some amino acids, but not others This variability was due to ion source temperature, as described below.

Methods

The PrHFB derivatives were prepared from a commercial amino acid standard containing 2.5 µmole of each amino acid. The NCI mass spectra were determined using either a Hewlett-Packard HP-5988A or HP-5989A GC/MS. Spectra were recorded near the optimum methane source pressure of 0.65 torr (HP-5988A) or 1.3 torr (HP-5989A), and at 25 °C increments from 100 °C to 300 °C. Ion source pressure strongly influenced sensitivity, but not the fragmentation pattern. The instruments were tuned at the beginning of each day, and only the ion source temperature was changed during the measurements. The samples were chromatographed on a 30 m x 0.32 mm DB-5ms capillary column using a temperature program from 80 - 220 °C at 10 °C/min. About 6.25 pmole of each AA was injected on-column. Spectra were recorded from m/z 100 - 650, at 3 scans/second.

Results

AA derivatives with two HFB groups (Thr, Ser, Lys, Tyr) gave 5-7 times stronger total ion current than AA with a single HFB. At low ion source temperatures (<150 °C), the major ion in most spectra was the $[M - HF]^-$ ion. At higher temperatures, the major fragmentation pathways involved sequential loss of up to 5 HF. Hydroxy AA (Thr, Ser, Tyr) generally produced more complex spectra than other AA, and were more thermally unstable (Figure 1). Hydrophobic and acidic amino acids (Ala, Gly, Leu, Ile, Phe, Asp, Glu) showed the least tendency to dissociate, even at 300 °C (Figure 2) At 300 °C, fragmentation was observed in all amino acids due to sequential loss of HF, loss of propanol, and various C-C fragmentation processes. Although these fragmentation processes may be useful for determining structure, the apparent sensitivity of NCI spectra to temperature may explain sporadic reports in the literature of erratic quantitative behavior. Moreover, selective fragmentation may be useful in quantitative work to distinguish between isotopomers present in different positions in a molecule.

References

1. Patterson BW, Hachey DL, Cook GL, et al. J Lipid Res 1991,32:1063-1072.
2 Lichtenstein AH, Hachey DL, Ordovas JM, et al. J Lipid Res 1992;33:907-914.

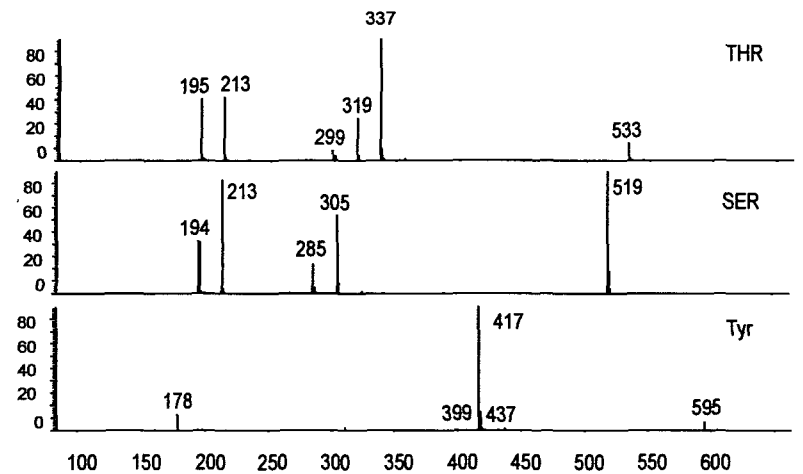

Figure 1 Methane negative CI/GC/MS of selected hydroxy AA-Pr,N-HFB

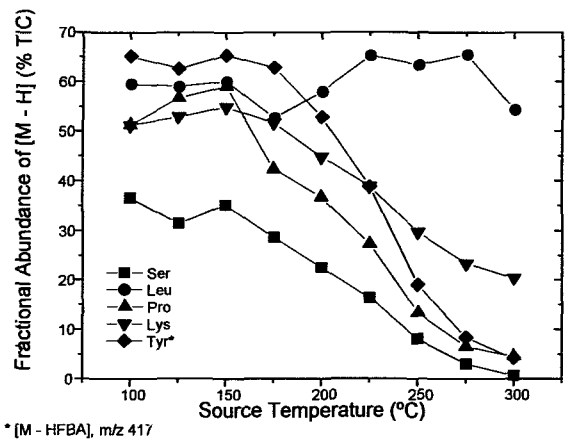

Figure 2. Temperature dependency on dissociation of the AA [M - H] ion.

Interfering Substances in the Gas Chromatographic Analysis of Diamines in Seafood

Edward L.E. Jester, Don E. Mowdy, Anthony M. Guarino, and
F. Aladar Bencsath, Gulf Coast Seafood Laboratory,
Food and Drug Administration, Dauphin Island, AL 36528

The α,ω-diamines cadaverine and putrescine are naturally occurring microbial spoilage products in food of animal origin, and used as indicators of decomposition in seafood.

Traditionally, a gas chromatographic procedure has been used with a packed column and a nitrogen/phosphorus specific detector (NPD) to analyze these diamines in fishery products [1]. The dried and re-dissolved pentafluoropropionylated fish extract is purified by passing it through an AL_2O_3-column and concentrated prior to gas chromatography (GC). The two time-consuming solvent evaporating steps can be omitted and the sample preparation process shortened if the more sensitive electron capture detector (ECD) is used instead of the NPD [2].

93 fish-samples (ground scallop, ground cod, and american plaice) were analyzed using this simplified procedure. Some of the ECD chromatograms showed serious interferences that normally were not seen in the NPD chromatograms. The corresponding samples were re-analyzed using the original procedure with the NPD, and they were also analyzed with capillary GC/MS using electron ionization, and positive and negative chemical ionization. A dozen peaks appeared in the GC/MS chromatograms in the time domain of the relevant diamine-peaks, and most of the eluting components could be identified such as fluoroacylated histamine, hydroxy-methylphenol, di-t.butyl-cresol, di-t.butyl-quinone, and benzthiazol derivatives. All these components were well resolved by the GC capillary. No interference was observed on the mass chromatograms obtained for the molecular ions and several intense fragment ions of the diamines. The results of the quantitative estimations using the protonated molecular ion traces (positive CI) agreed well with those computed from the NPD-chromatograms.

Thus, in order to maintain the high specificity of the analysis, a capillary column should be used with the electron capture detection.

References

[1] W.F. Staruszkiewicz, Jr., and J.F. Bond, J. Assoc. Off. Anal. Chem. 64 (3) 584-591 (1985).
[2] W.F. Staruszkiewicz, Jr., personal communication.

TIC from EI, +CI and -CI spectra
in the scan range of interest (american plaice #0425).

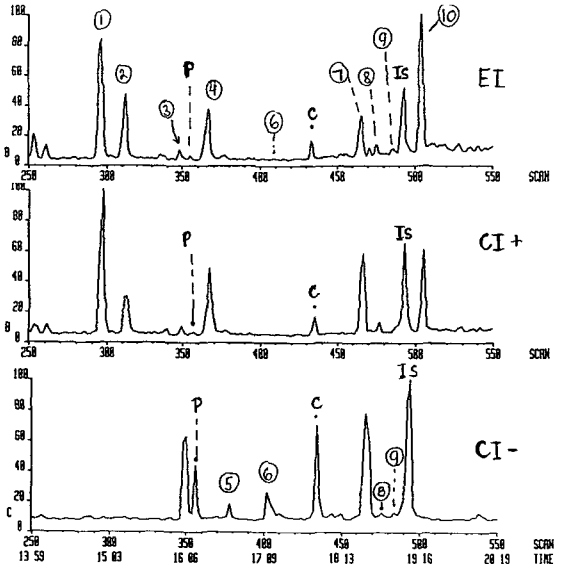

P: putrescine, C: cadaverine,
IS: hexamethylene diamine (Int.Std)

The following tabulation lists the most intense **Interfering Compounds** in one fish sample (american plaice #0425).

Peak #	Name/Description	MW
1	benzothiazol	135
2	2-hydroxy-benzylalcohol	124
3	fluorinated cmpnd	385
4	3-hydroxy-benzylalcohol	124
7	fluorinated cmpnd	258
8	di-(t.butyl)c.hexadienedione	220
10	di-(t.butyl)p.cresol (BHT)	220

VERIFICATION OF LEWISITE EXPOSURE: QUANTIFICATION OF CHLOROVINYLARSONOUS ACID IN BIOLOGICAL SAMPLES

E.M. Jakubowski, J.R. Smith, T.P. Logan, N. Wiltshire, C.L. Woodard, R.A. Evans, and T.W. Dolzine

US Army Medical Research Institute of Chemical Defense, Aberdeen Proving Ground, MD, 21010-5425.

Lewisite (dichloro-2-chlorovinylarsine)is a chemical warfare agent that is capable of causing blisters, immediate pain, and almost immediate systemic arsenic poisoning.[1] Since arsenic can be found in a variety of agricultural chemicals and natural sources,[2] assaying for elemental arsenic is non-specific. At least two metabolites in urine are predicted based on the chemistry of lewisite. The in vitro acid hydrolysis compound, 2-chlorovinylarsonous acid, $ClCH{=}CHAs(OH)_2$, is expected to be the primary metabolite. The polymeric base hydrolysis product of lewisite, 2-chlorovinylarsenious acid (lewisite oxide), $(ClCH{=}CHAsO)_n$, may also be present in trace amounts.[3,4] In general, arsonous acids and their related oxides react with 1,2-ethanedithiol to produce a substituted five-membered 1,3-dithio-2-arseno ring. This reaction can occur even in an aqueous environment. A similar derivatization method was shown to be of value in the analysis of environmental samples.[5] The derivatized lewisite is then analyzed by GC/MS using derivatized phenylarsine oxide (PAO) as the internal standard. The preservation of key structural components in the alkyl sidechain of the analyte make positive identification possible.

Human volunteer and guinea pig urine along with sheep and guinea pig plasma were spiked with CVAA. To 1.0 mL of spiked urine or serum phenyl arsonous oxide (PAO, 1000 ng/mL) was added as the internal standard. Addition of 1,2-ethanedithiol (3 μg/mL) was followed by extraction with toluene (3 x 0.3 mL). The combined extraction volume was reduced to near dryness and redissolved in 0.1 mL toluene. Injections of 1 μL were made onto a DB-5 Gas chromatographic column (20 m x 0.189 mm, 0.4 μm film thickness) using helium as the carrier gas at 33 cm/s. The temperature program was as follows: splitless injector 250°C, initial column temperature of 60°C (0.75 min) increased at 30°C/min, and a final temperature of 250°C (3.00 min). The purge off time was 0.75 min. Electron ionization based data was collected by a Hewlett-Packard model 5970B MSD in the selected ion mode using ions at m/z 107, 165, 167, 228, and 244. Initial assay development and MS/MS studies used a VG Quattro triple quadrapole MS/MS under EI and methane CI conditions.

Derivatization with 1,2-ethanedithiol was optimal when the reagent-to-analyte ratio (EDT/CVAA) was between 2 and 10. Derivatized CVAA had a retention time of 7.25 minutes while derivatized PAO appeared at 8.8 minutes as seen in Figure 1. The very small peaks at 6.97 minutes and 7.28 minutes represented the gem and cis isomers of CVAA, respectively. A huge excess of the dithiol reagent caused the formation of polymers that increased noise in the chromatogram. A dimer of EDT was also visible as a fourth peak in many of the full scan ion chromatograms but does not interfere in the quantitation of analyte or internal standard.

CVAA could be quantitated in urine and serum in the range of 20-

4000 ng/mL. The most remarkable aspect of the assay is the sample preparation and in particular the analyte derivatization. EDT is added directly to the urine or plasma/serum followed by extraction. The stability of CVAA in spiked human urine at room temperature was determined at pH 3.40, pH 6.10, pH 7.97, and pH 9.56. Results are reported for each isomer as a half-life in Table 1. According to this information a pH 6.10 solution would provide optimal stability. Normal human urine is in the range of pH 5 to pH 7 which should ensure adequate stability.

Table 1
CVAA Isomer Half-life versus pH in Spiked Human Urine (in hours)

pH	gem	cis	trans	total
3.40	11.3	32.0	19.1	19.0
6.10	27.9	16.2	41.6	42.5
7.97	5.62	4.09	3.74	3.22
9.56	2.50	1.04	0.767	0.820

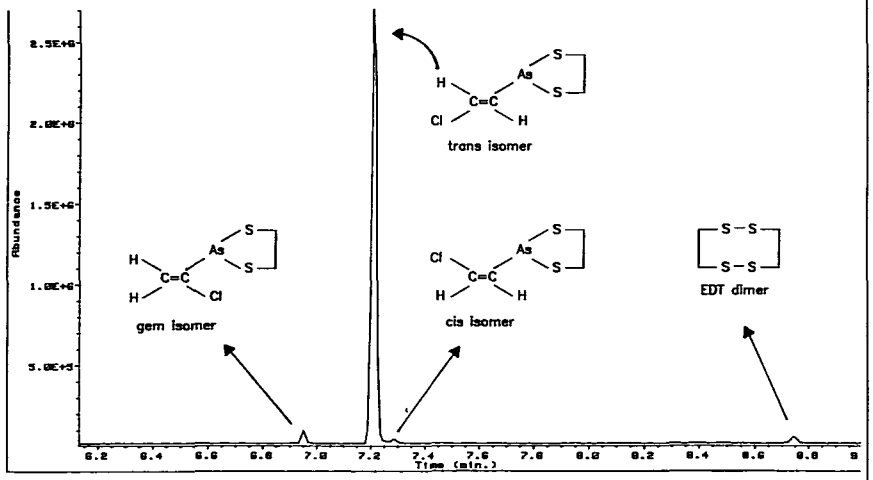

Figure 1.: Full Scan Chromatogram of CVAA-EDT

References
1. Inns, R. H., Bright, J. E., Marrs, T. C., Toxicology, **1988**, 51,pp. 213-222.
2. Cullen, W.R., Eigendorf, G.K., and Pergantis, S.A., Rapid Commun. Mass Spectrom., **1993**, 7, p33-36.
3. Bossle, P. C., Ellzy, M. W., CRDEC-TR-042, **1989**.
4. Lewis, W. L., Stiegler, H. W., J. Amer. Chem.Soc., **1925**, 47, p. 2546-2556.
5. Fowler, W.K., Stewart, D.C., Weinberg, D.S., and Sarver, E.W., J. Chromatogr. 558, **1991**, p.235.

Collision Induced Intramolecular Claisen Condensation In Triglyceride Negative Ions and Assignment of Positional Isomers.

*E. de Hoffmann, R. Rozenberg, E. Deffense# and V. Stroobant.
University of Louvain, Place Pasteur 1, 1348 Louvain-la-Neuve, Belgium.
#Fractionnement Tirtiaux, Chaussée de Charleroi 601, 6220 Fleurus, Belgium.

No mass spectrometric method allows up to now the non ambiguous assignment of the triglyceride positional isomers. Up to now the 2-position analysis via lipolysis remains the only method for determining the fatty acid in the 2-position. It can only be applied to isolated triglyceride or to natural fats, but not to blends, via the Van der Waal-Coleman theory of the 1,3-random distribution ([1]).

We report here a method that allows such a positional assignment through CID fragmentation of triglyceride negative ions at very low collision energy, typically 0.5 eV on Xe (Finnigan-MAT TSQ70). Figure 1 displays the fragment ions obtained by CID of the palmitic-oleic-stearic-triglyceride, abreviated POS, pseudo-molecular negative ion (m/z 859). The ions at m/z 255, 281 and 283 correspond to the three fatty acids, and allow the determination of their masses. The ions at m/z 475, 477 and 503 correspond to anions of ketones containing the hydrocarbon chain of two of the fatty acids and a carbonyl, minus a proton. Scheme 1 displays the proposed mechanism for their formation.

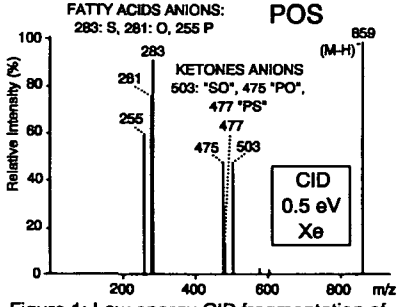

Figure 1: Low energy CID fragmentation of POS triglyceride [M-H]⁻anion. "XY" designate (ketones-H)⁻ containing the hydrocarbon chains of fatty acids X and Y.

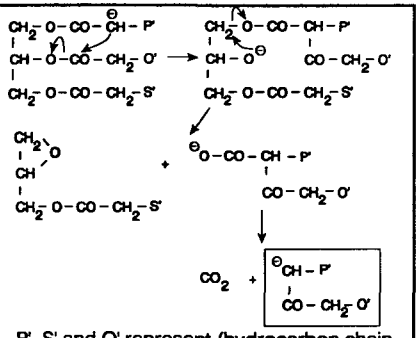

P', S' and O' represent (hydrocarbon chain less CH_2) of the corresponding fatty acids.

SCHEME 1

Figure 1 shows that the "ketone" anions corresponding to fatty acids on vicinal positions on the glycerine moiety, thus for POS, "PO" and "OS", are formed preferentially. Checked on more than 20 triglycerides of known structures, this has been found to be a general rule, thus allowing the assignment of the positions of the fatty acids on the glycerol.

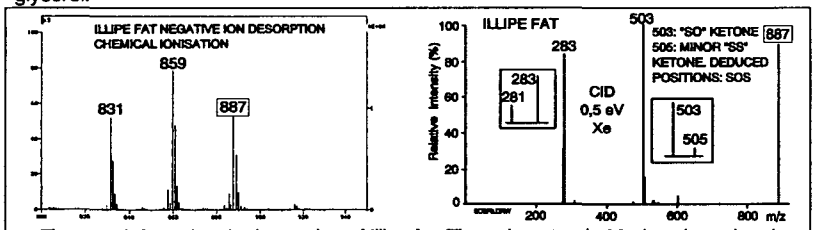

Figure 2: left: molecular ion region of Illipe fat. The anion at m/z 887 is selected and submitted to CID, at the right. From this spectrum, on can deduce the masses of the fatty acids, of the "ketones", and assign the positions on the glycerol moiety.

As shown on figure 2, the method can be applied to mixtures of triglycerides if they contain only one position isomer for each. From their masses at m/z 281 and 283, it can be deduced that the fatty acids are stearic and oleic, and from the molecular mass that there are two stearic and one oleic acids. The "SO" ketone predominates, thus the positions are SOS. This is in agreement with the known structure for this Illipe fat.

This method thus allows to easily assign, for a given triglyceride in a mixture, which are the contained fatty acids and their positions on the glycerol moiety, for so far there is only one position isomer present. No attempt has been made to apply this to position isomers mixtures. No relation has been found between the fatty acids anions intensities and their positions.

The preference for the vicinal condensation has been checked with the diacetates of ethyleneglycol and 1,3 propanediol. The first one yields the acetone anion, while the last doesn't.

References:

1. a. Van Der Waal, R.J. (1963) J. Am. Oil Chem. Soc., 40, 242.
   b. Coleman, M.H. (1981) J. Am. Oil Chem. Soc., 38, 684.

Isolation and Detection of Drugs from Spent Fly Puparia:Drugs in Bugs

**Mark L. Miller, Wayne D. Lord, Brian Donnelly, Laboratory Division, FBI, Washington, D.C. 20535; M. Lee Goff, Dept. of Entomology, University of Hawaii at Manoa, Honolulu, HI 96822*

The forensic use of insects and their remnants has been well established in the determination of time of death, but has only recently been generally recognized as an alternative toxicological specimen. The development of methods for various toxins and controlled substances can make an important contribution to the assessment of cause/manner of death in cases of advanced decomposition. The usual toxicological samples are often absent when mummified/skeletalized remains are found and entomological samples may provide the only clues. A key difference in the extraction of chitinized insect remnants from pathological samples, such as tissue, is the use of strong acids or bases to break down the chitin so the drugs can be released. After the acid or base step and pH adjustment, some of the more routine drug screen extraction methodology can be employed for analyte isolation. GC/MS with chemical ionization was utilized to detect the presence of toxins in extracts.

In October, 1991, the mummified remains of a middle-aged white female were discovered at her residence. Subsequent investigation revealed the decedent had died of multiple drug intoxication in mid-January 1989. Toxicological analysis of desiccated brain and stomach contents revealed lethal concentrations of amitriptyline and its metabolite nortriptyline, as well as diphenhydramine and cocaine. Empty fly puparia(Phoridae), cast beetle skins(Dermestidae), beetle fecal material(frass) were analyzed for amitriptyline and nortriptyline using a modified hair extraction technique. In addition, controlled studies were made for correlating the amount of drugs in tissues with the level in spent fly puparia(Sarcophagidae). Rabbits were injected with zero, 0.5, 1.0, and 2.0 median lethal dosages of drugs. Two sets of experiments were conducted using amitriptyline (tricyclic antidepressant) for the first and phencyclidine (anesthetic) for the second. After the drugs were administered the rabbits were sacrificed and the livers harvested for feeding to the fly larvae.

A comparison was made of acid versus base extraction for the drugs of interest. The base extraction of basic drugs was carried out by using 100 mg of sample and enough 0.1 N NaOH to cover puparial casings. Deuterated internal standards were added and then the sample tubes were heated at 70-80°C for one hour. The NaOH layer was extracted with n-butyl chloride and centrifuged. Back extraction of the organic layer was then accomplished with 1 N HCl. After removal of the organic layer the HCl was adjusted to pH 9.5. Chloroform was added and then the mixture was vortexed and centrifuged. The chloroform was dried with anhydrous sodium sulfate and then evaporated. For GC/MS analysis the residue was reconstituted in methanol. Acid extraction of the basic drugs was performed by weighing out 100 mg of puparial casings and then adding 1 N HCl and deuterated standards. The samples were heated overnight at 65°C and adjusted to pH 4. Using conditioned Tox-Clean RC (Alltech) SPE tubes the extracts were eluted at 1 mL/minute for sample cleanup. The tubes

were washed with water, air dried, and then washed again with hexane and methylene chloride. Elution of the basic drug fraction was accomplished with basic MeOH (2% NH_4OH). The eluent was diluted in water and extracted with 200 microliters of methylene chloride. After centrifugation the methylene chloride layer was collected for GC/MS.

In the case of the amitriptyline controlled studies its metabolite nortrip-tyline was found at a level of about 1/5 to 1/2 that of the parent drug in the puparia. The highest level of amitriptyline was found in the puparia from the one median lethal dosage because the rabbit given the double dosage died rapidly from an overdose. The rapidity of death did not allow enough time for the drug to circulate as fully to the liver as at the lower dosages. This is also supported by the fact only a trace of nortriptyline was found in the 2.0 median lethal dosage puparia.

In conclusion, amitriptyline and its metabolite nortriptyline can be detected in insects and in insect remnants. The ratio of amitriptyline to nortriptyline is consistent with acute ingestion in case findings, otherwise the ratio would be less than one. Acid or base extraction gives very similar results for these basic drugs. No phencyclidine was detected in the PCP controlled studies because its concentration is estimated to be 1000X smaller than the amitriptyline levels (from liver concentrations). A more sensitive method is needed for levels <1 ng/mg.

CASE STUDY FINDINGS

SAMPLE	AMITRIP.ng/mg	NORTRIP.ng/mg	RATIO
DERMESTID SKINS	3.4	NONE DETECTED	
DERMESTID FRASS	3.6	NONE DETECTED	
PHORIDAE PUPARIA	5.4	2.5	2.2
BRAIN TISSUE	25.4	8.1	3.1
STOMACH CONTENTS	112	7.4	15

RESULTS OF CONTROLLED SARCOPHAGIDAE STUDIES

BASE EXTRACTION	AMITRIP.ng/mg	NORTRIP.ng/mg	RATIO
0 MEDIAN LETHAL DOSE	NONE DETECTED	NONE DETECTED	
0.5 MEDIAN LETHAL DOSE	19.7	7.0	2.8
1.0 MEDIAN LETHAL DOSE	154	31.2	4.9
2.0 MEDIAN LETHAL DOSE	7.9	TRACE	
ACID EXTRACTION			
0 MEDIAN LETHAL DOSE	1.0	NONE DETECTED	
0.5 MEDIAN LETHAL DOSE	9.9	5.7	1.7
1.0 MEDIAN LETHAL DOSE	169	51.4	3.3
2.0 MEDIAN LETHAL DOSE	7.0	2.5	2.8

The Characterization of 4- Quinolones by Chemical Ionization Ion Trap Mass Spectrometry.

Armando Colorado and Jennifer S. Brodbelt, Department of Chemistry, University of Texas, Austin, Texas, 78712.

The history of the 4-quinolones began with the synthesis of nalidixic acid, the progenitor of all quinolones. Since then, several new classes of quinolones such as the flouroquinolones have been developed. These compounds are active against 37 different kinds of bacteria and are used in treating various bacterial infections (1). Quinolones are not only used for human related infections. Eel and yellowtail fish farms are treated with these antibiotics for the prevention and treatment of infectious diseases in fish (2).

Up to date, only HPLC/MS, PD/MS, and EI/MS have been used to identify quinolones (3,4). FAB/MS and CI/MS have been attempted with the newer quinolones but no molecular ion information has been obtained(3).

In these series of experiments, nine quinolones, separated into four different groups, were structurally characterized by the utilization of various selective chemical ionization reagents and by performing collisional activated dissociation.

Experiments were performed on a Finnigan Ion Trap Mass Spectrometer equipped with a Hitachi/Teledyne HST-1000 High Sensitivity Trap Accessory. Sample pressures were typically at $2X10^{-6}$ torr. Reagent pressure was nominally at $1X10^{-5}$ torr and raised to nominally 1 mtorr with helium. Trap temperature was set at 120 degrees celcius while the solids probe temperature varied from 120-200 degrees celcius.

Seven chemical ionization reagents were evaluated: dimethyl-ether (DME), vinylmethyl-ether (VME), acetone, allyl alcohol, acetic anhydride, trimethylsilane and propylamine. Of the seven chemical ionization (CI) reagents used, four of them formed characteristic adducts in addition to protonation . Dimethyl-ether formed $[M + 15]^+$ and $[M + 45]^+$ ions while vinyl-methyl ether and trimethyl-silane formed $[M + 15]^+$ and $[M + 73]^{+\cdot}$ ions respectively. The CI reagent that showed the most promising selective behavior was propylamine. Selective adduct formation within each group was observed. Within group I, for example, enoxacin formed only the protonated species, while norfloxacin formed both the $[M + H]^+$ and $[M + 17]^+$ ions. Ciprofloxacin produced the same adducts as norfloxacin plus an $[M + 60]^+$ adduct which corresponded to propylamine attachment. The [M + 17] ions, found only in Group I, were attributed to attachment of ammonia. Cinoxacin (Group 2), piromidic acid (Group 3), nalidixic acid and flumequine (Group 4) were the other compounds producing propylamine adducts. Acetone, allyl alcohol and acetic anhydride did not promote formation of any characteristic product ions.

Unusual and interesting behavior was observed when the protonated quinolones were subjected to collisional activated dissociation (CAD) in the presence of different CI reagents. Depending on the CI reagent used, activation of the protonated quinolones results in the formation of characteristic fragment ions that may rapidly react with the neutral CI reagent, resulting in new adducts. CAD in the presence of DME reagent results only in fragment ions, but acetone, allyl alcohol, acetic anhydride, trimethylsilane and propylamine all undergo attachment to the fragment ions/or to the activated protonated quinolone.

Thus, performing CAD with these latter CI reagents may offer certain advantages. For example, both fragmentation and reactivity patterns are obtained in a single experiment. Secondly, the quinolone ions are selective for reagents possessing certain types of functional groups, such as alcohols and ketones but not ethers. Acetic anhydride was especially useful because both fragmentation and subsequent adduct formation occured with the quinolones. Trimethylsilane and

propylamine, on the other hand, induced complete conversion of quinolone fragment ions to adduct ions.

In fact, after each protonated quinolone has undergone dehydration, it may attach to an intact quinolone neutral. The reason for this self-reaction was elucidated from reactions of models. Further studies with model compounds possessing only carboxylic acid or ketone functional groups show that these do not undergo dehydration and spontaneous attachment of a second ligand. However, if both functional groups are present, then the attchment process does occur. Thus, the quinolones themselves have promise as selective, albeit non-traditional, CI reagents with specific functional group reactivity towards alcohols and acids.

CAD of the product ions formed from selective chemical ionization provides additional structurally diagnostic details. The $[M + 15]^+$ and $[M + 45]^+$ ions from DME chemical ionization fragment in ways similar to the protonated quinolones, and the $[M + 45]^+$ is clearly a direct precursor of the $[M + 15]^+$ ion. The TMS adducts of the group I quinolones are especially intriguing because activation of these adducts may result in formation of even larger product ions.

In conclusion, selective CI reagents afford new opportunities for generating structurally informative mass spectra of quinolones. Although the various reagents often produced similar types of product ions for the different quinolones, in conjuction with CAD each quinolone could be distinguished. Dehydrated quinolone ions are particularly reactive towards molecules containing certain functional groups, such as alcohols and acids, and this may prove to be important for develping a diagnostic scheme which targets the quinolone class, or for developing selective quinolone reactants.

References:

(1) Hooper D. C. and Wolfson J. S., *The New England Journal of Medicine*, (1991), 324, 384.
(2) Horie M., Saito K , Nose N., Tera M., and Kakazawa H , *J. Liq. Chrom* , (1993), 16, 1463.
(3) DiCarlo F. J., Crew M. C. and Greenough R. C., *Arch. Biochem. Biophy.*, (1968), 127, 503.
(4) Cepa S. P., Hill P. and Buko A. M., *Biomed. Mass Spec.*, (1992), 21, 176.

Acknowledgments: NIH, NSF, Welch Foundation, American Cyanamid, ACS-PRF

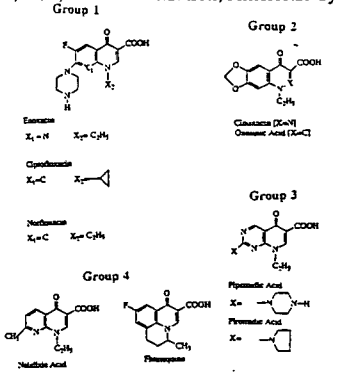

THE ANALYSIS OF 1,4-BENZODIAZEPINES BY SELECTIVE ION-MOLECULE REACTIONS WITH DIMETHYL ETHER IONS IN A QUADRUPOLE ION TRAP

Tracy Donovan McCarley and Jennifer Brodbelt, Department of Chemistry, University of Texas, Austin, TX 78712-1167

The 1,4-benzodiazepines are the most widely prescribed drugs in the world, with diazepam (Valium) being the most well known. They are a class of sedatives and tranquilizers that are used commonly to treat anxiety, insomnia, muscle spasms and seizures. The combination of site selective ion-molecule reactions with collisionally activated dissociation (CAD) offers greater promise for differentiation of related 1,4-benzodiazepines due to the enhanced specificity of ion-molecule reactions. In this study, the chemical ionization of 1,4-benzodiazepines by selective ion-molecule reactions with dimethyl ether and ethylene oxide ions has been examined in a quadrupole ion trap mass spectrometer. The 1,4-benzodiazepines chosen for this study include diazepam, nordiazepam, temazepam, oxazepam, and nitrazepam. As can be seen from Figure 1, they only differ by subtle substituent variations at positions 1, 3, and 7, so they afford a useful set of molecules for systematic evaluation of site-selective bimolecular reactions.

The ion-molecule reaction products of the 1,4-benzodiazepines and dimethyl ether ions are listed in Table 1. Upon reaction with the dimethyl ether ions, all of the 1,4-benzodiazepines were protonated, all compounds formed *either* $(M + 13)^+$ *or* $(M + 15)^+$ adducts, and most formed $(M + 45)^+$ adducts. The selective formation of $(M + 13)^+$ and $(M + 15)^+$ adducts is analytically useful since it allows differentiation of two groups of 1,4-benzodiazepines. Diazepam, nordiazepam, and nitrazepam which do not have hydroxyl substituents at position 3 form $(M + 15)^+$ adducts but <u>not</u> $(M + 13)^+$ products, while both temazepam and oxazepam which have hydroxyl substituents at position 3 form $(M + 13)^+$ adducts, but <u>neither</u> forms $(M + 15)^+$ adducts.

The basis of the selectivity for formation of $(M + 13)^+$ and $(M + 15)^+$ products has been investigated further by studying the ion-molecule reactions of dimethyl ether ions and simpler compounds that serve as models of potential reactive sites in the more complex 1,4-benzodiazepines. The reactions of the model compounds with dimethyl ether ions are summarized in Table 2. Based on the comparison to model compounds, the imine group is the predominant reactive site in the formation of $(M + 15)^+$ adducts.

The determination of gas-phase basicities of compounds is not only fundamentally important for obtaining a correlation of organic structure with thermodynamic properties, but also analytically useful as a further means to predict nucleophilicity and reactive behavior of new classes of compounds. Thus, the bracketing technique was used to estimate the gas basicities of the 1,4-benzodiazepines. Diazepam was selected as a representative of the non-hydroxylated 1,4-benzodiazepine class, and temazepam was selected as a representative of the hydroxylated 1,4-benzodiazepine class. They were each introduced into the vacuum system with compounds of known gas-phase basicities. The standards and 1,4-benzodiazepines were each protonated by dimethyl ether ions. Then each protonated molecule was isolated and held for a reaction period during which the proton could be transfered to the other organic compound. The gas-phase basicities of both diazepam and temazepam are thus determined to be less than 222.2 kcal/mol (from diethylmethylamine) but greater than 220.7 kcal/mol (from 4-amino-1-butanol). This range suggests that the diazepines are most likely protonated at the imine site, not the lactam site.

The ion-molecule reactions of dimethyl ether ions with 1,4-benzodiazepines have been shown to be analytically useful for probing small structural differences in the 1,4-benzodiazepines in a quadrupole ion trap mass spectrometer. Characteristic $(M + 13)^+$ adducts are formed by 3-hydroxy-1,4-benzodiazepines, whereas $(M + 15)^+$ adducts are formed by 1,4-benzodiazepines that do not have hydroxyl substituents. In addition, the 3-hydroxy-1,4-benzodiazepine can be differentiated by the formation or lack of formation of an $(M + 27)^+$ adduct, and the 7-nitro- or 7-chloro-1,4-benzodiazepines without hydroxyl substituents can be distinguished by characteristic high mass fragment ions in the ion-molecule reaction spectra. The CAD spectra of 1,4-benzodiazepines allow further structural identification of the 1,4-benzodiazepines.

Hoffmann-LaRoche is gratefully acknowledged for their donation of 1,4-benzodiazepine samples. This work has been supported by the Welch Foundation (F1155), ACS-PRF (25485-AC5), the NSF (CHE-9122699), the NIH (RO1 GM46723-01), and a grant from American Cyanamid.

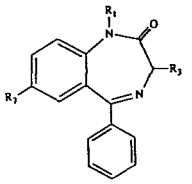

1,4-benzodiazepine	R_1	R_3	R_7
Diazepam	CH_3	H	Cl
Nordiazepam	H	H	Cl
Temazepam	CH_3	OH	Cl
Oxazepam	H	OH	Cl
Nitrazepam	H	H	NO_2

Table 1. Ion-molecule Reaction Products of Benzodiazepines and Dimethyl Ether Ions

Benzodiazepine, MW	$(MH - 74)^+$	$(MH - 63)^+$	$(MH - 46)^+$	$(MH - 30)^+$	$(MH - 28)^+$	$(MH - 18)^+$	$(M + 11)^+$	$(M + 13)^+$	$(M + 15)^+$	$(M + 27)^+$	$(M + 45)^+$
Diazepam, 284	–b	10 (0)	–	–	5 (0)	–	50 (0)	–	0 (5)	–	0 (30)
Nordiazepam, 270	–	<5 (0)	–	–	<5 (0)	–	40 (0)	–	0 (5)	–	0 (50)
Nitrazepam, 281	10 (0)	–	5 (0)	–	5 (0)	10 (0)	35 (0)	–	0 (10)	–	0 (25)
Temazepam, 300	–	–	10 (0)	0 (5)	–	10 (0)	55 (0)	0 (20)	–	–	–
Oxazepam, 286	–	–	5 (0)	5 (0)	–	25 (0)	50 (0)	0 (5)	–	0 (5)	0 (5)

Table 2. Ion-molecule Reactions of Model Compounds and Dimethyl Ether Ions

Model Compound, MW	$(MH - 18)^+$	$(M - H)^+$	$(M + H)^+$	$(M + 13)^+$	$(M + 15)^+$	$(M + 16)^+$	$(M + 29)^+$	$(M + 45)^+$	$(M + 47)^+$
cyclohexanone, 98	5	–	60	–	30	–	–	–	5
N-benzylidenemethylamine, 119	–	5	55	–	15	–	–	25	–
ε-caprolactam[a], 113	–	–	60	5	20	5	–	10	–
N-methyl-ε-caprolactam[a] 127	–	–	20	–	25	–	–	55	–
3-hydroxy-3-methyl-2-butanone, 102	5	–	50	45	–	–	–	–	–
cyclohexanol, 100	35	10	–	–	–	–	35	–	20
chlorobenzene, 112	no reaction								
nitrobenzene, 123	–	–	70	–	10	–	–	–	20

IDENTIFICATION OF METABOLITES OF A NOVEL PLATELET ACTIVATING FACTOR ANTAGONIST BY MASS SPECTROSCOPY

William DeMaio*, D. Cosulich, J. Ashraf, M. Rashed, G. Morton

American Cyanamid Company, Medical Research Division, Pearl River, NY, 10965

A novel platelet activating factor (PAF) antagonist, CL 184,005, is currently under development for treatment of septic shock. Characterization of the metabolism of CL 184,005 was necessary to support this development. Identification of metabolites, determination of metabolic profiles, and *in vitro* species comparison of CL 184,005 were investigated in the rat and in rat, dog and human liver preparations using ^{14}C labeled CL 184,005. Thermospray-MS, GC/MS, high resolution MS and NMR spectroscopy were used to identify four of the metabolites. (See the proposed biotransformation pathway in the Summary Figure.) Prior to structural identification, metabolite samples were prepared by glusulase hydrolysis of rat urine followed by semi-prep HPLC purification. The presence of the ^{14}C label on the thiazole ring and the characteristic fragment $[\underline{m}\text{-HO-}C_6H_4\text{-}CH_2]^+$ (*m/z* 107) assisted structural identification efforts.

^{14}C-CL 184,005 is extensively metabolized by the rat. Several polar radioactive metabolites were observed in rat urine. These metabolites were found to be mainly sulfates and glucuronides of low molecular weight phenolic compounds M1, M2, M4a and M4b. In plasma, up to six hours post-dosing, unchanged drug is estimated to represent 49% of AUC for total radioactivity. The same conjugates observed in urine accounted for the balance of radioactivity found in plasma. From rat feces, 87% of radioactivity was recovered, of which 66% was due to unchanged drug and 32% due to a very polar component. Rat and human liver preparations formed common metabolites, M4. The conjugates of M4 are also the major circulating metabolites as well as being one of the major urinary metabolites. Metabolic cleavage of the phosphate ester linkage resulted in our ability only to trace the labeled portion of the molecule. Further studies are planned with compound labeled on the benzoic acid carbonyl carbon. This would enable us to complete the metabolic profile and the mass balance of CL 184,005.

The proposed metabolic scheme is shown in the Summary Figure. Figure 1 shows a mass spectrum of the M4a metabolite showing the characteristic *m/z* 107 fragment ion and the enhanced M+2 ion at *m/z* 224 from the ^{14}C label. These features were typical of the mass spectra of the CL 184.005 metabolites identified in this work.

Summary Figure

Proposed Biotransformation Pathways of ^{14}C-CL 184,005 In the Rat

Metabolites observed as sulfate and glucuronide conjugates in plasma and urine.

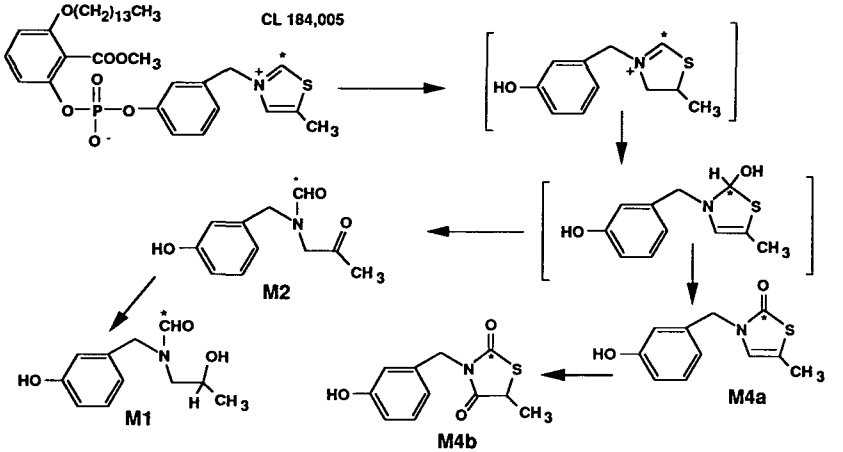

Figure 1

CI Mass Spectrum of the Hydrolyzed M4a Metabolite of CL 184,005

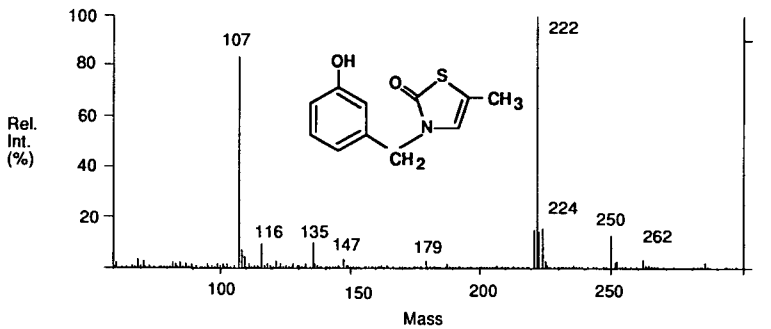

Mechanistic Studies on the Metabolic Oxidation of Terminal Olefins to Carboxylic Acids.

P. R. Sheffels, M. P. Grillo and T. A. Baillie

Dept. of Medicinal Chemistry, University of Washington, Seattle, WA 98195

Terminal alkenes have been reported to form carboxylic acids metabolically,[1,2] yet little is known about the underlying mechanism. It has been postulated that an aldehyde may be an intermediate in the process, although details of the initial oxidation remain obscure. During the course of investigating the metabolism of the hepatotoxic terminal olefin, 2-*n*-propyl-4-pentenoic acid (Δ^4-VPA), in the perfused rat liver, the corresponding dicarboxylic acid, 2-*n*-propylglutaric acid (PGA), was identified as a biotransformation product by GC-EIMS techniques.[1] When an analog of Δ^4-VPA labeled with two atoms of deuterium on the olefinic terminus ([5,5-$^2H_2$]Δ^4-VPA, 97 atom % excess) was employed as substrate with rat hepatocytes, the PGA formed was found to have retained a single deuterium atom (95 atom % excess). This result indicates that metabolic oxidation of the 4,5-double bond of Δ^4-VPA to the corresponding carboxylic acid involved a hydrogen shift, and GC-EIMS methods were employed to localize the deuterium atom in PGA at the sub-terminal (C-4) position. The position of the deuterium was assigned to C-4 based on the shift of the McLafferty rearrangement ion at *m/z* 74 [MeO-C(=$\overset{+}{O}$H)-$\dot{C}H_2$] in the unlabeled spectrum to *m/z* 75 [MeO-C(=$\overset{+}{O}$H)-$\dot{C}$HD] in the labeled spectrum (Fig. 1). These deuterium labeling experiments thus have afforded a valuable insight into the molecular mechanism by which terminal olefins are oxidized to carboxylic acids, and have provided the basis for a revised scheme for the interactions of mono-substituted olefins with mixed-function oxidase enzyme systems. Future work in this area will entail "trapping" the aldehyde intermediate

to confirm that two atoms of deuterium are retained when [5,5-$^2H_2$]Δ^4-VPA serves as substrate.

[1] Rettenmeier, A. W. *et al.*, *Drug Metab. Dispos.* **13**, 81-96 (1985).

[2] Vickers, S. and Duncan, C., *Biochem. Biophys. Res. Commun.* **181**, 1508-1515 (1991).

Figure 1. Proposed mechanism for the biotransformation of [5,5-$^2H_2$]Δ^4-VPA to [4-$^2H_1$]PGA. The intramolecular hydride shift (from C-5 to C-4) is believed to accompany oxidation of the terminal olefin to the putative aldehyde intermediate, which undergoes further oxidation to PGA.

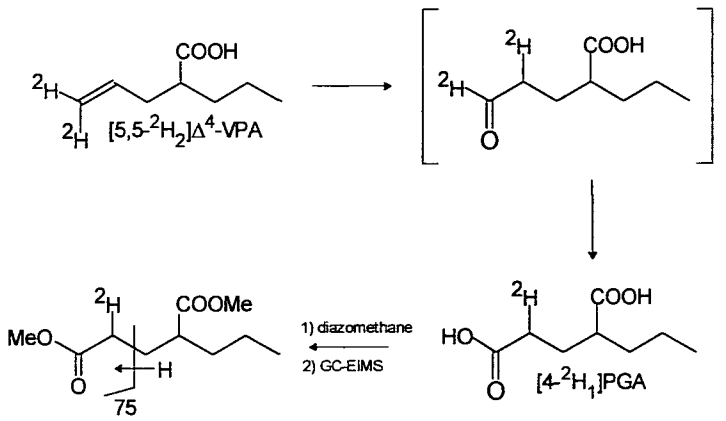

Support by NIH grants GM07750 and GM32165 is gratefully acknowledged.

Automated Static Headspace Sampling With Gas Chromatography - Mass Spectrometry for the Identification and Quantitative Analysis of Volatile Organic Impurities in Drugs and Pharmaceuticals

Kevin J. Mulligan* and Heather McCauley
US Food & Drug Administration
National Forensic Chemisty Center
Cincinnati, Ohio 45202.

Volatile impurities in bulk drugs and pharmaceutical preparations can arise from sources such as: manufacturing byproducts, the degradation of ingredients, and the solvents used in processing. All are of concern from a toxicological perspective and, moreover, may provide a qualitative and/or quantitative chemical profile of a specific manufacturer's product. This can have forensic implications.

Official methods (1) for residual solvents establish limits for select substances at 100 mg/kg in the bulk drug except as shown: benzene, chloroform (50 mg/kg), 1,4-dioxane, methylene chloride and trichloroethylene.

The objective of this work has been to develop some understanding of the performance of a commercial automated static headspace sampler in combination with narrow-bore capillary GC-MS for the identification and determination of residual solvents in bulk drugs.

A liquid sample is confined in a 9-mL glass vial which is sealed with a teflon-lined butyl rubber septum in a crimp cap. After equilibration at a given temperature, helium is added to the vial to raise the pressure to 5 psi whereupon the headspace is vented through a 0.25 mL sampling loop under a backpressure which is roughly equal to the headpressure on the column. Then, the flow to the column is directed through the sampling loop (105°C), transfer line (115°C) and capillary union (180°C) to a cryofocussing trap (-130°C). Sufficient transfer time is allowed for the internal volume of the transfer line to be swept 2.5X. The analytes are revolatilized by rapidly increasing the trap temperature (200°C) and enter the column. Column temperature is maintained at 10°C for 2 min and increased (10°C/min) to 180°C.

The instrument consists of an Equilibrium Headspace Autosampler (7000/7050, Tekmar) which has been plumbed with electroform nickel tubing (Valco). Aliquots of the headspace are cryofocussed on the first 8 cm of the column (Rtx-200, 30m X 0.25mm id X 1000nm film, Restek) by a Cryofocussing Module (Tekmar) attached to the GC-MS (5890 Series II GC/5971A MSD, Hewlett Packard(HP)). Column flow (@ 50°C) is adjusted to 30 cm/s by tracking the elution of CO_2. No special effort is made to optimize the tuning of the MS, rather the standard adjustments returned by the software (1034C, HP) are used.

Although hydrocarbons in water exhibit extremely low coefficients for the distribution of solute between solvent and gas phase (<10), most mixtures have values above 300 so that the volume of solution has a minimal effect on the gas phase concentration (2). For a volume of 0.5 mL, equilibrium is reached within 10 min.

These studies focussed on the solvent, dimethylacetamide (DMAC), since a drug of interest, sulfamethazine, is highly soluble in DMAC (>40% w/v) but only slightly soluble (< 0.1% w/v) in water. The mass

spectrometer was configured for scanning (20 amu to 250 amu at 2.9 Hz). A mixture of standards (0.4 to 2 mg/L) was equilibrated at 105°C for 10 min and after analysis, the S/N ratio at each peak (TIC) was defined as Peak Height/Baseline Width(RMS). For S/N >=3, a PBM(reverse) search of the spectrum against the Wiley Library yielded the compound as the first or second hit. A 20-fold dilution of the test mixture was examined using selected ion monitoring for the major ion in each analyte spectrum (dwell = 50 ms, 12.3 Hz). The sensitivity improved by a factor of 25 to 100. To examine the effect of temperature, solutions were incubated at 25°C, 65°C, 105°C and 145°C. The chromatography degraded substantially at 145°C which may be due to excess DMAC. Plots of ln(Peak Area) vs. T(K) were generally linear (m_r > 0.99) and the relative increase in peak area as a function of temperature was determined to be 2 to 5 %/K. A direct comparison of 10%(v/v) aqueous DMAC (85°C) to DMAC (105°C) showed that while the aqueous system is generally more effective, the difference is not usually drastic particularly for those materials with appreciable solubility in water. Water elutes during the early part of the chromatogram and produces peak broadening of C1 - C3 alcohols.

This system has been applied to the determination of acetone in the sulfonamide antibiotic, sulfamethazine. A 0.2 g portion of the solid sample was dissolved in 0.5 mL of DMAC with 2-pentanone added at 2 mg/L to serve as an internal standard. The sample was incubated at 105°C for 15 min and a 0.25-mL aliquot of the headspace was examined by selected ion monitoring at 43 amu. Calibration curves were prepared from 0 to 6 mg/L by plotting concentration vs. the ratio of the peak area of acetone to that of 2-pentanone (normalized to its concentration). Low level samples were spiked with 300 to 1000 ng of acetone and demonstrated recovery of 89(+/- 4)% (n=8). A system blank limited the LOD (3 X S_{blank}, n=51) to 0.3 mg/kg of acetone in the bulk drug. Within-day precision was 3%(@ 1mg/kg, n = 18) or 2% (@ 13 mg/kg, n = 28) while the between-day precision was about X 3 higher.

Analyte	Concentration for S/N = 3 Scanning (mg/L)	SIM (ug/L)	Temperature Coefficient (%/K)	Relative Signal DMAC vs. H2O
Ethanol	2	60	4.8	3.8
Methylene Chloride	0.5	6	3.3	0.2
Chloroform	1.3	10	2.3	0.07
Acetone	0.4	*	2.9	1
Benzene	0.3	2	3.2	0.1
Trichloroethylene	0.5	6	3.7	0.1
Methyl Ethyl Ketone	0.5	8	3.2	0.4
n-Octane	0.2	6	2.9	0.2
Dioxane	1.2	20	3.6	1.5
Nonane	0.3	10	-3.3	*
Chlorobenzene	1.4	10	3.9	0.02

(1)"<467> Organic Volatile Impurities" in USP XXII NF XVII Supplements 3,4,5 and 6, U.S. Pharmacopeial Convention, Rockville MD.
(2) B.V. Ioffe & A.G. Vitenberg: Head-Space Analysis and Related Methods in Gas Chromatography, John Wiley & Sons (1984).

A COMPARISON OF GAS CHROMATOGRAPHY-MASS SPECTROMETRY ASSAYS FOR *IN VIVO* LIPID PEROXIDATION

W. R. Mathews, R. McKenna, D. M. Guido, T. W. Petry, and R. A. Jolly
Biochemistry and Investigative Toxicology, The Upjohn Company, Kalamazoo, MI 49001
J. D. Morrow and L. J. Roberts, II Clinical Pharmacology, Vanderbilt University School of Medicine, Nashville, TN 37232.

INTRODUCTION

Oxidant stress has been implicated in a wide variety of disease processes. Peroxidation of lipids is a well known sequela of free radical injury. Limitations with methods available to assess oxidant stress and lipid peroxidation *in vivo* are a well recognized problem Peroxidation of cellular arachidonyl lipids results in the formation of hydroperoxy-arachidonic acids (HPETES) and hydroxy-arachidonic acids (HETES). More recently, it was discovered that a series of prostanoids (F_2-isoprostanes) are also produced *in vivo* as products of lipid peroxidation. Both of these classes of lipid peroxidation products are amenable to analysis by GC-MS and sensitive, quantitative assays have been developed. Therefore, we compared these two approaches of measuring HETES and F_2-isoprostanes in rats following induction of lipid peroxidation *in vivo* by administration of CCl_4.

METHODS

GC/MS lipid peroxidation assays. The methods used for the GC-MS analysis of HETES and F_2-isoprostanes have been described previously (1, 2). 12-HETE, 11-HETE, 9-HETE and 8-HETE were assayed as Me ester, TMS ethers by electron impact GC-MS. 16-hydroxy-heneicosatrienoic acid was employed as the internal standard. F_2-isoprostanes were measured as pentafluorobenzyl ester, TMS ethers by negative ion chemical ionization GC-MS. D_7-9α,11β-PGF_2 was used as the internal standard. Tissue samples were subjected to base hydrolysis to release the free acids of the HETES and F_2-isoprostanes prior to GC-MS analysis.
CCl_4 toxicity. Male Sprague-Dawley rats were treated with U74006F, U78517G, or vehicle 24 hrs (200 mg/kg, p.o.) and 5 min (6 mg/kg, i.v) prior to CCl_4 (600 µl/kg, i.p.) administration. Three hours later the animals were sacrificed and blood and liver samples taken. Liver samples were divided in half and frozen immediately in liquid N_2. After addition of the internal standard to the plasma samples they were carried through 2 steps of solid phase extraction. The partially purified plasma samples and half of the liver samples were sent to Vanderbilt for F_2-isoprostane analysis. The remaining liver samples were assayed for HETES.

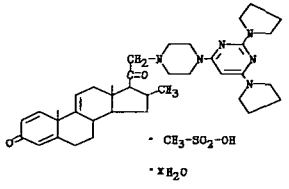

U74006F

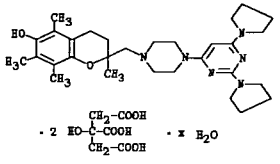

U78517G

RESULTS AND DISCUSSION

Administration of CCl_4 resulted in a significant increase in the amount of HETES (average 7-fold increase) and F_2-isoprostane (75-fold increase) esterified to liver lipids (Table I). Increased levels of the F_2-isoprostanes were also detected in the circulation (25-fold above baseline). Two antioxidant compounds were examined for their ability to inhibit lipid peroxidation in this *in vivo* model. U78517G, when administered prior to CCl_4, inhibited CCl_4 induced lipid peroxidation, while U74006F had no effect. Both assays gave similar results; for example U78517G reduced tissue F_2-isoprostane levels to 37% of the CCl_4 stimulated value while HETE levels were reduced by an average of 38% of the stimulated levels. Plasma levels of F_2-isoprostane were reduced to 35% of the CCl_4 stimulated values.

Table I. Lipid Peroxidation Products in Rats following Carbon Tetrachloride Administration

Sample	F_2-Isoprostane		Tissue HETES (ng/g)			
	Plasma (pg/ml)	Tissue (ng/g)	12-	11-	8-	9-
CONTROL	14±4	7.5±1	120±37	75±19	402±129	644±306
U74006F	16±3	7.8±0.5	139±25	118±35	550±147	411±134
CCl_4	344±90	573±108	1022±142	597±69	2693±497	1955±497
CCl_4 + U74006F	442±106	533±159	1199±172	735±90	3192±458	1923±345
CCl_4 + U78717G	119±42	214±56	352±13	238±17	1009±63	813±91

These results suggest that both methods can detect increases in lipid peroxidation of cellular lipids *in vivo*. Both assays gave qualitatively similar results. The HETE levels detected in the tissue lipids were significantly higher than the F_2-isoprostane levels in all cases. This could be due more facile formation of these compounds or to greater clearance of the F_2-isoprostanes from tissue lipids. Perhaps due to the lower basal levels, the fold increase in lipid peroxidation products was higher for F_2-isoprostane than the HETES. This suggests that the F_2-isoprostane might be more sensitive for detecting low levels of lipid peroxidation. Finally, the ability to measure free F_2-isoprostanes in the circulation to assess lipid peroxidation represents a significant advantage of this assay.

REFERENCES

1. Morrow, J. D., Harris, T., and Roberts, L. J., II: Non-cyclooxygenase oxidative formation of a series of novel prostaglandins: analytical ramifications for measurement of eicosanoids. Anal. Biochem. **184**: 1-10, 1990.
2. Guido, D. M., McKenna, R. and Mathews, W. R.: Quantitation of hydroperoxy-eicosatetraenoic acids and hydroxy-eicosatetraenoic acids as indicators of lipid peroxidation using gas chromatography-mass spectrometry. Anal. Biochem. **209**: 123-129, 1993.

ANALYSIS OF POLYETHYLENE GLYCOLS WITH THERMOSPRAY LC-MS

*S.Auriola, K.-M.Rönkkö, K.Kananen, and A.Urtti, Dept. Pharm. Technology, University of Kuopio, P.O.Box 1627, SF-70211 Kuopio, Finland

After instillation of an eyedrop, typically less than 3 % of the applied drug penetrates the cornea and reaches intraocular tissues. Drug permeability in the membranes is influenced both by the properties of the penetrant and membrane. Permeability is affected by the lipid/water partitioning, charge, hydrogen bonding capacity, and molecular size of the compound.

The dependence of transmembrane permeability on molecular size has been often studied using polyethylene glycols (PEGs) as probes. The structure of this polymer is $H\text{-}(O\text{-}CH_2\text{-}CH_2)_n\text{-}OH$. The physicochemical properties of PEGs do not change drastically with increasing molecular size as happens within a series of alkyl homologues. HPLC is the technique of choice for separation of PEGs, but the detection is difficult as the molecules do not contain a chromophoric structure. PEGs have been widely used in TSP optimization and tuning experiment. TSP LC-MS has also been used for analysis of PEGs in wastewaters [1].

In this study a TSP LC-MS method was developed for simultaneous determination of wide molecular weight range of PEGs (238 - 986). The method proved to be suitable for transmembrane permeability studies performed with an in vitro apparatus. The PEGs were chromatographed with a polymeric PRP-1 column (Hamilton) using isocratic 0.1 M ammonium acetate - acetonitrile (79:21) eluent, and quantitated by SIR of the ammoniated molecules. Polypropylene glycol (PPG) was used as the internal standard.

The TSP mass spectra of PEG oligomers show ammoniated molecules at M+18 as the base peaks and other adduct ions at M+23 (MNa^+), M+39 (MK^+), M+59 (MNH_4^++acetonitrile) and at M+81 (unknown). No significant fragmentation of PEG was observed (Fig. 1). The molecular weight difference between two PEG oligomers is 44 mass units (C_2H_4O). The MNH_4^+ ions (M+18) were diagnostic for each oligomer and there were no overlapping adduct or fragment ions. This means that the various oligomers are well resolved from one another, although chromatographic baseline separation was not achieved for all oligomers. The chromatographic peaks show some tailing, but this might result also from the memory effect, caused by contamination of the ion source with PEG (Fig. 2).

The signal to noise ratio was between 10 and 50 at level of 30ng of PEG 300, 60 ng of PEG 600 and 100 ng of PEG 1000 polydisperse mixture per injection. This means that the TSP LC-MS method is at least hundred times more sensitive than the previously described HPLC methods using refractive index detection or UV-detection.

TSP LC-MS method allows determination of permeability coefficients for a range of PEGs with different molecular sizes. This method may prove useful in the studies of molecular weight dependence in membrane penetration and effects of penetration

enhancers on biomembrane leakiness. Highly purified PEG with narrow molecular weight distribution is not needed, because the method analyses each molecular weight of PEG separately from the sample. This may decrease the need of animals in research, because in each penetration experiment whole series of PEGs can be used and determined simultaneously.

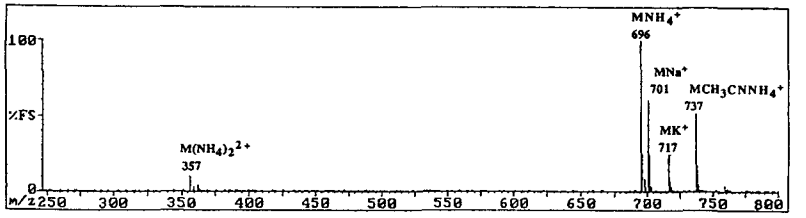

Figure 1. TSP mass spectrum of a PEG oligomer (molecular weight 678).

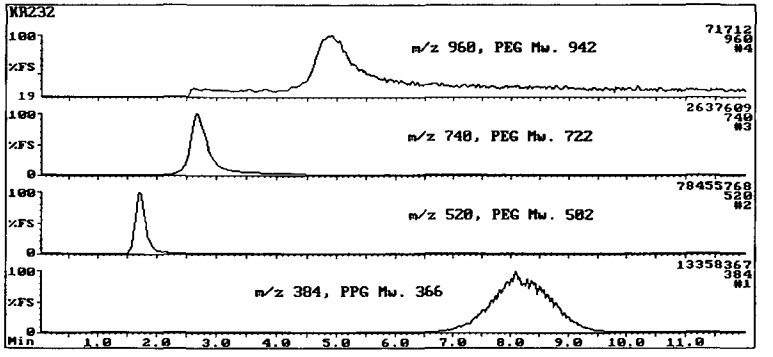

Figure 2. SIR chromatogram of a polydisperse PEG mixture taken from the receptor cell at 60 min. Polypropylene glycol (PPG) is used as an internal standard.

[1] H. F. Schröder, *Gewaesserschutz, Wasser, Abwasser* **112**, 351-384 (1990).

Selective Detection Of Phosphopeptides By Electrospray LC/MS

Michael J. Huddleston, Roland S. Annan, Mark F. Bean, and Steven A. Carr, Physical and Structural Chemistry, SmithKline Beecham Pharmaceuticals, King of Prussia, PA 19406

We have developed an MS-based strategy for selective identification of peptides containing phosphate linked to Ser, Thr or Tyr without the need for radiolabeling. The method involves the generation and detection of phosphate-specific fragment ions while simultaneously acquiring molecular ion information during negative-ion LC-ESMS analysis of protein digests (1). The present work is an outgrowth of our earlier studies on methods for selective glycopeptide detection (2,3).

Positive- and Negative-Ion In-Source CID of Phosphopeptides: Positive-ion and negative-ion electrospray mass spectra of the phosphopeptides were recorded over a wide range of orifice potentials (65V to 250V in positive-ion; -65V to -500V in negative-ion). On the Sciex quadrupole mass spectrometer, the orifice voltage (OR) is the source declustering potential, and this voltage is also used to control the degree of collision-induced dissociation (CID) occurring in the high-pressure region between the orifice and Q1. No characteristic low-m/z fragment ions were observed in the positive-ion data for the three types of phosphopeptides over the range of OR values studied. Fragments formed by loss of H_3PO_4 from the pseudomolecular ions could be observed for the peptides phosphorylated on serine or threonine in both the positive- and negative-ion spectra. The loss of phosphoric acid was more pronounced in the positive-ion data and appeared at lower collisional excitation potentials than in the negative-ion data.

Optimization of Marker-ions and Molecular-Ions of Phosphopeptides by Negative-Ion ESMS: At sufficiently high orifice potentials (collision energies), the negative-ion ES mass spectra for all three varieties of phosphate linkage showed two unique phosphopeptide fragment ions: m/z 79 (PO_3^-) and m/z 63 (PO_2^-) (see Figure 2). Negative-ion ESMS was optimized for detection of the phosphopeptide-specific marker ions using the phosphoserine-containing peptide which gave the weakest response of the three types of phosphorylated peptides. At OR values ranging from -65V to -115V we observed $(M-H)^-$, $(M-H+TFA)^-$ and $[M-2H+(TFA)_n]^{2-}$ ions where n = 1 - 8 depending on the voltage and the peptide composition. TFA adducts to the molecular ion were greatly diminished at -115V in comparison with the standard -65V setting. Minimization of adducts simplifies the spectral data, facilitates molecular weight measurements when dealing with mixtures, and improves the intensity of individual signals.

Selective Detection of Phosphopeptides by Negative-Ion LC-ESMS: The orifice voltage setting, which controls the CID potential, needs to be adjusted so as to maximize within each spectrum the characteristic fragment-ion signals and to minimize parent-ion fragmentation. These contradictory requirements are met by scanning or stepping the orifice voltage during full-scan acquisition in a manner analogous to that previously described for selective detection of glycopeptides in LC-ESMS (2,3). The OR setting of -115V, which is sufficient to effectively reduce TFA-adducts to the parent ions, and the -350V OR setting used for generation of phosphopeptide-marker ions were combined into a single scan by computer-controlled stepping of the OR voltage. This full-scan, stepped collision energy negative-ion LC-ESMS method was applied to the mixture of peptides shown in Figure 1. While both the UV (Figure 1a) and TIC (not shown) traces provide relatively non-specific detection of peptides and phosphopeptides, the reconstructed-ion chromatogram (RIC) for m/z 79 (Figure 1b) is specific for phosphopeptides. The molecular weights of the six peptides were indicated by significant, singly-charged, deprotonated molecular-ions together with their less-intense TFA adduct satellite peaks. Useful data were readily obtained at the low picomole level using packed fused-silica HPLC columns. In cases where even greater sensitivity is required, SIM detection of m/z 63 and 79 may be employed (1).

In summary, negative-ion with CID provides unique phosphopeptide fragment ions for each of the three types of phosphopeptides. SIM of m/z 63 and 79 provides the highest sensitivity for selective detection of phosphopeptides. Stepping the collision energy (orifice voltage) during full-scan acquisition permits detection of phosphopeptide marker ions and molecular-weight related ions for peptides and phosphopeptides. Good sensitivity has been achieved using standard TFA-containing mobile phases for reversed-phase HPLC. Relatively high orifice voltages (> -250V) are required for the best response of the phosphopeptide marker ions. Work is now in progress to use these techniques to identify phosphopeptides in more complex mixtures such as would result from enzymatically digested phosphorylated proteins (4,5).

1. Huddleston, M. J.; Annan, R. S.; Bean, M. F.; Carr, S. A.; *JASMS*. **1993**, in press.
2. Carr, S. A.; Huddleston, M. J.; Bean, M.F.; *Protein Science* **1993**, 2, 183-196.
3. Huddleston, M. J.; Bean, M.F.; Carr, S. A.; *Anal. Chem.* **1993**, 65, 877-884.
4. Annan, R. S.; Miller, T.;Carr, S. A.;**1993**, Proceedings of the 41st ASMS Conference.
5. Carr, S. A. et al.; ibid.

Figure 1. (a) UV @ 215 NM

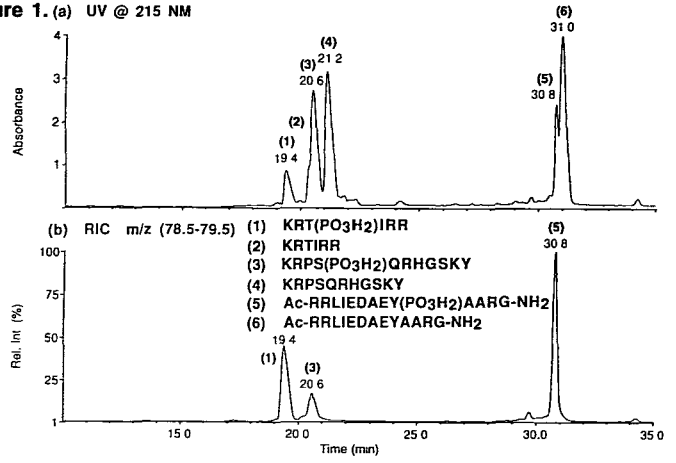

Figure 2.

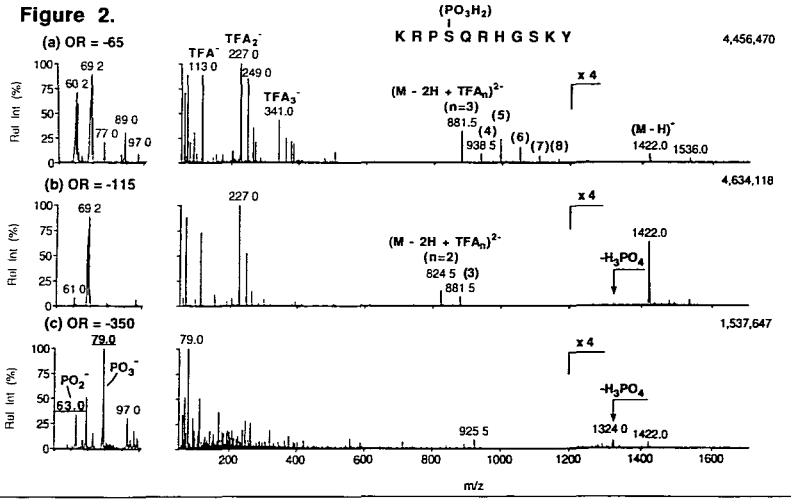

Application of Electrospray Mass Spectromtry to the Identification and Quantitation of a Novel Variant in a Dimeric Recombinant Protein.

* Victor T. Ling, Eleanor Canova-Davis,and Marian L. Eng. Genentech, Inc., 460 Point San Bruno Blvd., South San Francisco, CA 94080 USA

In the biosynthesis of recombinant proteins in mammalian cell systems, unexpected post-translational modifications often result in the occurrence of variants along with the desired product. The development of purification processes is greatly aided by the availability of quick and facile means for the discovery, identification and quantitation of these variants.

NGF normally exists as non-covalent dimers. Post translational C-terminal processing results in the formation of (1-117) and (1-118) variants from the (1-120) polypeptide. These variants then pair up to form homo- and hetero-dimers in all possible combinations. The molecules are readily separated by ion-exchange chromatography in dimeric form. A quick and facile means for definitive identification of the components of each fraction was desirable. C-terminal amino acid analysis is tedious and uncertain because of the -RRA terminal sequence. Reversed phase chromatography proved insufficiently rugged as the variants separate poorly. It was found that when these dimers are examined by electrospray mass spectrometry (ES-MS) in acidified methanol / water, dissociation readily occurs to provide a mass for each monomer, providing unequivocal identifications.

An unexpected post-translational modification was also observed . A peak obtained by cation exchange chromatography showed a component with a loss of 30 mass units. This was consistent with a serine to glycine modification. The transformation was confirmed by MS / MS spectra and Edman sequence analysis of the N-terminal tryptic peptide. It was found to have occurred at the n-terminal serine. Preliminary evidence indicates it may be due to a pyridoxal catalysed serine hydroxymethyl transferase.

ES-MS of the intact protein was also compared to other analytic methods as a technique for the quantitation of variant proteins in a mixture. Intensity measurements on deconvoluted spectra were within 2% of calculated values in samples where normal rhNGF was added back to material containing the glycine N-terminal variant to give defined ratios. MS quantitation also proved to have good reproducibility : the result from 12 observations on a sample at concentrations ranging from 3-30pM was 24.6±1.1 percent. These results proved comparable to quantitation by tryptic mapping or ion-exchange separation.

ELECTROSPRAY MASS SPECTROMETRY OF NON-COVALENT COMPLEXES

Jaquinod M., Leize E., Potier N., Albrecht A.M., Biellmann J.F. and Van Dorsselaer A.
Laboratoire de Spectrométrie de Masse Bio-Organique, URA 31 CNRS-Université Louis Pasteur, Strasbourg, France.

INTRODUCTION:

Electrospray Mass Spectrometry (ESMS) has become a rapid and routine method for the measurement of the molecular mass of proteins up to 100 kDa with an accuracy of 0.01%. At first it seemed that the ESMS ionisation/volatilisation process would not allow the study of non-covalent assemblies. Later, several authors demonstrated that non-covalent complexes could be analysed by ESMS to some extent [1], but it is still difficult to answer the question "How tight must be the complex to resist the electrospray process". In order to help answering that question, we have tried to analyze different types of non-covalent complexes with decreasing stability.

In this study, we would like to show that if several parameters (pH, ionic strength, temperature, source voltage parameters) are carefully controlled, ESMS can be used as a general method for the study of non-covalent interactions. We believe that in fact it is possible to study non-covalent assemblies by ESMS provided that the conditions used before the MS study do not lead to a decomposition of the complexes. Most of the reported ESMS studies make use of MeOH/ H_2O (1/1, 1% AcOH) as solvent. This solvent easily produces a stable electrospray but often destroys weak interactions.

Three types of complexes were tested to determine the ESMS conditions which preserve the integrity of such compounds during the ionisation process:

- a *ferric ion complex with a synthetic analogue* of the bacterial siderophore ferrichrome A (ligand L),
- two *sulphur-ions proteins* (rubredoxin and ferredoxin),
- two *cofactor/protein complexes* (myohemoglobin, aldose reductase/NADPH complex).

EXPERIMENTAL:

Synthesis: Ligand L has been prepared as described elsewhere [2]. Horse heart myohemoglobin and *Porphyra umbilicalis* ferredoxin were purchased from Sigma (St Louis, USA). Rubredoxin was purified from *Clostridium thermosaccharolyticum* [2]. Aldose reductase was purified from pig lens [2].

ESMS: ESMS spectra were obtained by using a Bio-Q quadrupole with a mass to charge (m/z) range of 4000 (VGBioTech Ltd, Altrincham, UK). Values used for the extraction cone voltage (Vc) ranged from 30 to 250 volts. The source temperature was set at 50°C and at 40°C for the aldose reductase. In all cases, electrospray was pneumatically assisted.

RESULTS:

Study of the ligand L/iron (III) complex: Both solutions were prepared in pure methanol and the spectra recorded at Vc = 50 V. For the solution without $FeCl_3$, the major peak corresponds to the doubly-protonated free ligand L (1284.5 Da). For the solution with 2 $FeCl_3$ equivalents, the major peak corresponds to the complex of ligand L with two ferric ions (1389.8 Da). The mass difference measured between the free ligand and the complex with two ferric ions is 105.5 Da and not 111.7 Da (2 x Fe^{3+}). This shows that the complexation of the two ferric ions is accompanied by the loss of six protons from the hydroxamate groups of the ligand L. When Vc was increased to 250 volts, no loss of iron was detected. This fits with the very high affinity of ligand L for iron ions.

Study of the iron-sulphur proteins:

Rubredoxin: The rubredoxin active center consists of one ferric ion surrounded by 4 cysteine thiolates. The spectrum of rubredoxin recorded in MeOH/H_2O (1/1) at Vc = 50 V displayed three series of multiply charged ions corresponding to aporubredoxin (no iron, A series, expected mass: 5936.5 Da), holorubredoxin (one iron, B series) and holorubredoxin with a K^+ adduct (C series).

Ferredoxin: These proteins involved in photosynthesis, are known to carry two possible types of active centers (2Fe/2S or 4Fe/4S). All ferric ions and sulphur ions are complexed by cysteine thiolates. The spectrum of ferredoxin recorded in pure water at Vc = 70 V displayed two major complexes (measured mass: 11232.7 Da and 11177.5 Da) correspond to the proteins with a 4S/4Fe active center and a 4S/4Fe active centre plus one extra unexpected iron atom. Two minor complexes, corresponding to proteins with a 2S/2Fe active centre (11003.9 Da) and a 2S/2Fe active center plus one extra unexpected iron atom (11059.8 Da), were also detected. In MeOH/H_2O (1/1, 1% AcOH), the ESMS analysis detected only the apoprotein.

Study of two cofactor/protein complexes:

Myohemoglobin: Myohemoglobin was dissolved in a pyridinium acetate buffer (50mM, pH = 5.0). Spectrum recorded at Vc = 40 V: at this low voltage, a single peak was detected at 17570.5 Da, corresponding to myohemoglobin (exp. mass: 17568.5Da). A small peak (5%) at 16950.5 Da reveals a minor loss of the heme (616.5 Da) which is normally attached to myoglobine by interaction of one ferric ion with the proximal histidine F8. Spectrum recorded at Vc = 65 V: both species, myoglobin and myohemoglobin were present. The loss of the heme induced by collisions in the interface converts myohemoglobin to myoglobin. At Vc = 100 V, the conversion is complete. Such conversion was also observed , when using organic solvents or pH < 4.5.

Aldose reductase/NADPH complex (Fig. 1): The spectrum of the complex recorded in a 10 mM Tris-HCl buffer at pH = 5.0 and at Vc = 55 V displayed a peak at 36527.4 Da corresponding to holoprotein aldose reductase/NADPH. The spectrum of the holoprotein obtained after RP-HPLC shows that the complex is a non-covalent complex.

CONCLUSION:

In this work, ESMS has been shown to be a useful tool for the study of weak interactions. ESMS also appears to be an easy and general method for ascertaining the number of metal ions present in such supramolecules. A non-covalent complex can resist the ESMS ionization step with only minor dissociation. The experimental conditions allowing such studies depend on the complex analysed. The solvent and the pH used must not decompose the complex and the ESMS interface conditions (Vc, temperature,...) must also be adapted. It is still not possible to evaluate how "tight" must be the complex to stand the ESMS analysis in term of kcal/mol.

ESMS could provide a new and rapid method to evaluate the relative affinity of several inhibitors for a protein.

REFERENCES:

1. M. Baca and S.B.H. Kent, *J.Am.Chem.Soc.*, **1992**, *114*, 3992-3993; B. Ganem, Y.T. Li and J.D. Henion, *J.Am.Chem.Soc.*, **1991**, *113*, 7818-7819.
2. M. Jaquinod, E. Leize, N. Potier, A.M. Albrecht, A. Shanzer and A. Van Dorsselaer, *Tetrahedron Lett.*, **1993**, *34*, 17, 2771-2774.

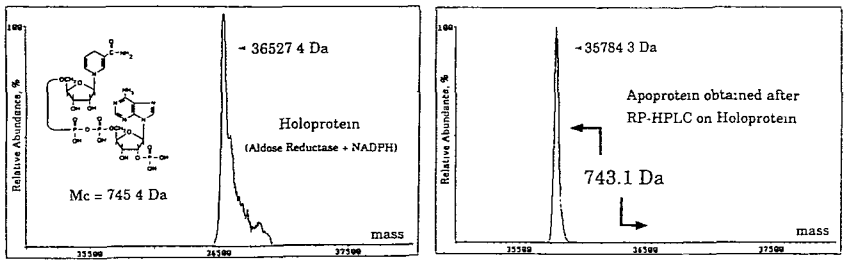

Fig.1: ESMS spectra of the aldose reductase/NADPH complex in Tris-HCl 10mM buffer, Vc = 55 V.

ELECTROSPRAY IONIZATION MASS SPECTROMETRY OF HEMOGLOBIN ADDUCT FORMATION IN RATS

Robert D. Stevens[1], David S. Millington[1], Douglas C. Anthony[2], Doyle G. Graham[2], Joseph Bonaventura[3], and Celia J. Bonaventura[3] Mass Spectrometry Facility, Box 3028[1], Department of Pathology[2], Duke University Medical Center, Durham, N.C. 27710 and Duke University Marine Laboratory[3], Beaufort, N.C. 28516.

Hemoglobin adducts are commonly employed as biomarkers for monitoring exposure to toxic compounds. Typically, characterization and quantitation involves isolation of the globin chains, protein degradation, derivatiza tion and gas chromatography. Electrospray ionization mass spectrometry (ESI-MS) offers the possibility of analyzing hemoglobins for adduct formation without extensive sample preparation. Rats are frequently used as animal models for toxicological studies. The structure of rat hemoglobin is complex and consists of at least six hemoglobins. There are two forms of the globin α chain and three forms of the β chain. We report here ESI-MS studies of hemoglobin adduct formation in rats chronically exposed to the neurotoxin, acrylamide, and the development of complementary in vitro methods to study hemoglobin adduct formation.

In vivo: Sprague-Dawley rats were exposed to different levels of acrylamide (0.1, 0.2, 0.3 mmol/kg/day) by repeated intraperitoneal injection. After 21 days the globin chains were isolated from hemolysates by oxalic acid/acetone precipitation and subjected to Sephadex G25 chromatography prior to analysis. In vitro: Normal Sprague-Dawley rat erythrocytes were washed and lysed. The hemolysate was extensively dialysed prior to the removal of ionic cofactors by Sephadex G25 chromatography. Rat hemoglobins were fractionated by anion exchange chromatography on DEAE Sephadex using a Pharmacia FPLC system. Rat hemoglobins were analyzed directly by ESI-MS. The time course of the reaction of total rat hemoglobin (0.5 mM) and isolated individual hemoglobins (0.05-0.5 mM) with acrylamide (10 mM) was monitored by ESI-MS by direct loop injection of the reaction mixture. ESI-MS: Solutions of rat globins or hemoglobin were electrosprayed in water containing 50% acetonitrile and 1% formic acid. Mass spectra were acquired using a Fisons/VG Trio 2000 quadrupole mass spectrometer. Mass spectra were transformed to molecular mass spectra using the manufacturers' software.

The molecular mass spectra of normal rat globins and those from rats that were chronically exposed to different levels of acrylamide are shown in Figure 1. In the control rat both types of α globin chain are resolved. The β chains, however, are not clearly resolved but appear to be dominated by a major component with a molecular mass of 15848. No acrylamide adduction is found for the α chains of globins from animals exposed to acrylamide. In contrast, the β chains are extensively modified. The molecular mass of the of the adducted globin chain is 15920 This corresponds to an increment of 72 mass units which is close to the expected value of 71 as a result of the formation of the thioether by reaction of acrylamide with the sulfhydryl of cysteine. The extent of adduct formation correlates with the degree of exposure to acrylamide. The results of the in vitro reaction of acrylamide (10 mM acrylamide for 3 hours) with hemoglobin are shown in Figure 2. The results are similar to those from the in vivo experiments and show that in the isolated rat hemoglobin under these conditions only β chains react with acrylamide. The degree of resolution of the β chain region does not permit any conclusions as to which β chains are adducted, as is the case for the in vivo experiments. In an attempt to clarify which hemoglobins react with acrylamide, rat hemoglobin was fractionated by anionic exchange chromatography. Four major fractions were obtained. The globin composition of the hemoglobins in the different fractions are given in Table 1. Only hemoglobins that contain the β_1 globin chain form adducts with acrylamide. The β_1 chains are very reactive and under the experimental conditions the majority of the β_1 chains are converted to the adducted form. Figure 3 illustrates the sequential adduction of fraction 2 ($(\alpha_2)_2(\beta_1)_2$) of rat hemoglobin. Prolonged incubation results in further adduction of the less reactive sites not only of the β_1 globin chain but also of the α_1 globin chain in the hemoglobin tetramer. The molecular mass data from these studies are summarized in Table 2. The general applicability of the approach is illustrated in Figure 4 which shows the molecular mass spectrum of human hemoglobin (HbA_0) before and after prolonged incubation with acrylamide.

The present study demonstrates the potential of ESI-MS to study hemoglobin adduct formation. Previous GC/MS studies of acrylamide adduct formation in rats have shown that the the cysteine residues are the most reactive. The ESI-MS studies show that both in vivo and in vitro exposure of rat hemoglobin to acrylamide leads to the formation of an adduct with a mass that is expected for the for the formation of the thioether and that under under most conditions only hemoglobins that contain β_1 globin chains have any appreciable reactivity towards the neurotoxin. This globin chain has an exposed cysteine at position 125 in the hemoglobin tetramer. The development of a staightforward in vitro -on line- method to study the time dependence of adduct formation allows the comparison of relative reactivities of animal hemoglobin towards acrylamide and other environmental pollutants. Chain separation followed by proteolytic digestion and HPLC/ESI-MS will permit the determination the relative reactivities of specific sites in the hemoglobin tetramer.

In Vivo Exposure To Acrylamide

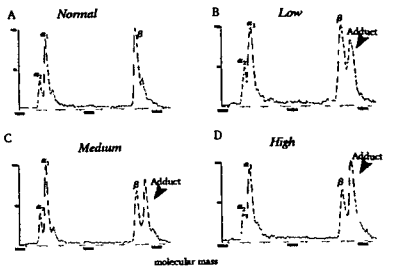

Fig. 1

In Vitro Exposure To Acrylamide

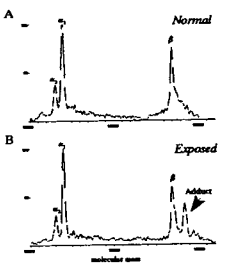

Fig. 2

TABLE 1. RAT HEMOGLOBIN COMPOSITION

FPLC FRACTION	HEMOGLOBIN % TOTAL	GLOBIN CHAINS
1	5	$\alpha_1\beta_2$, $\alpha_2\beta_2$
2	35	$\alpha_2\beta_1$
3	45	$\alpha_1\beta_1$
4	15	$\alpha_1\beta_3$

TABLE 2. MOLECULAR MASS OF GLOBIN CHAIN

GLOBIN	EXPECTED	FOUND
α_1	15197.4	15196.5 ± 1.3
α_2	15153.4	15151.8 ± 0.4
β_1	15848.2	15847.9 ± 1.1
β_2	15861.2	15862.4 ± 1.5
β_3	---	15906.7 ± 0.6
β_1 - Adduct	15919.2	15920.0 ± 0.6

In Vitro Exposure Of Fraction 2

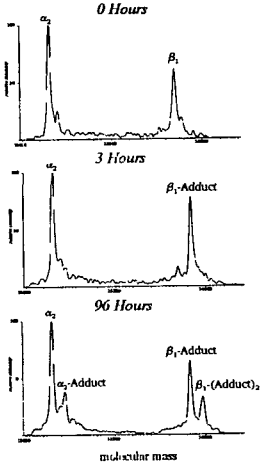

Fig. 3

In Vitro Exposure of Human Hemoglobin to Acrylamide

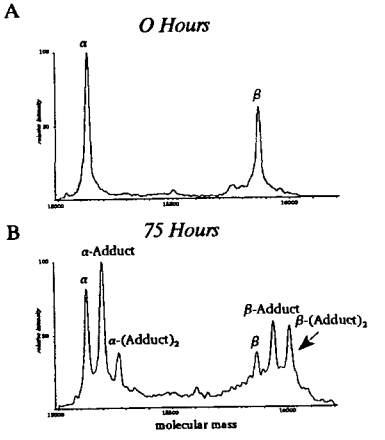

Fig. 4

An Ion Spray Mass Spectrometric Study of Molecular Recognition between the Vancomycin Family of Antibiotics and a Model Bacterial Cell Wall Mucopeptide Precursor.

H. K. Lim[1,2], Y.L. Hsieh[2] and J.D. Henion[2], [1]Wyeth-Ayerst Research, CN 8000, Princeton, NJ 08543 and [2]Drug Testing and Toxicology, Cornell University, Ithaca, NY 14850.

The vancomycin family of antibiotics which include vancomycin and ristocetin are selective towards gram-positive bacteria. Vancomycin is the only member of this family that is still used clinically in the treatment of infections caused by staphylococci, streptococci, enterococci and clostridium. NMR and UV spectroscopies show that antibiotics of the vancomycin family bind specifically and noncovalently to a model precursor of the bacterial cell wall mucopeptide: di-N-acetyl-L-Lys-D-Ala-D-Ala [DALAA] (1,2). Furthermore, a specific C-terminal sequence of the mucopeptide ending in -D-Ala-D-Ala is absolutely required for the host-guest molecular recognition of the bacterial cell wall by the vancomycin antibiotics (2). Such well characterized noncovalent interactions are suited for investigation by the rapidly emerging utilization of ion spray mass spectrometry (IS-MS) to study molecular recognition processes in biology. The aim of this communication is to explore the feasibility of using IS-MS to study this important molecular recognition process in chemotherapy of bacterial infections.

The ion spray mass spectra from infusion of a 1:1 mixture of 25 µM each of either vancomycin or ristocetin and DALAA under relevant aqueous physiological pH and mild declustering conditions (30 V) are illustrated in Figures 1 and 2. The base peak in each mass spectrum is the doubly charged antibiotic+DALAA complex (m/z 911.5 [vancomycin+DALAA] and m/z 1220.7 [ristocetin+DALAA]); other ions present include the protonated DALAA (m/z 373.2), doubly charged antibiotic (m/z 725.4 [vancomycin] and m/z 1034.6 [ristocetin]), and protonated antibiotic (m/z 1449.8 [vancomycin] and m/z 2068.9 [ristocetin]). That the ions at m/z 911.5 and 1220.7 are the noncovalent complexes is supported by collision-induced dissociation of the complex to the protonated DALAA and the respective protonated antibiotic product ions. Furthermore, that this host-guest molecular recognition process is undoubtedly specific is indicated by the dramatic reduction in the noncovalent complex formation upon changing the last C-terminal amino acid residue in the ligand (di-N-acetyl-L-Lys-D-Ala-D-Lys and di-N-acetyl-L-Lys-D-Ala-D-Lactic Acid) used in the binding study with either vancomycin (Figure 3) or ristocetin (Figure 4). Similar reduction in complex formation was obtained upon substituting other polypeptide antibiotics with different mechanisms of action (bacitracin and rifampicin) as host in the study.

Competitive studies between vancomycin and ristocetin for DALAA show the formation of ternary (doubly and triply charged vancomycin+ristocetin+DALAA at m/z 1945.9 and 1297.3, respectively) and quaternary (triply charged vancomycin+ristocetin+2DALAA at m/z 1421.6) noncovalent complexes which apparently result from molecular recognition of the antibiotic-bound DALAA by another antibiotic. Interestingly, no complexes observed involved binding of DALAA with either two vancomycin or ristocetin molecules. The above observation is supported by the absence of these types of noncovalent complexes upon replacing either the ligand DALAA with di-N-acetyl-L-Lys-D-Ala-D-Lys or one of the antibiotic host with bacitracin in the study. Preliminary investigation by MS/MS did not reveal any differences in binding strength between either vancomycin or ristocetin and DALAA.

Acknowledgement: This work is supported in part by Wyeth-Ayerst Research.

References

1. D.H. Williams, M.P. Williamson, D.W. Butcher and S.J. Hammond, *J. Am. Chem. Soc.* **105** 1332 (1983).
2. M. Nieto and H.R. Perkins, *Biochem. J.* **124**, 845 (1971).

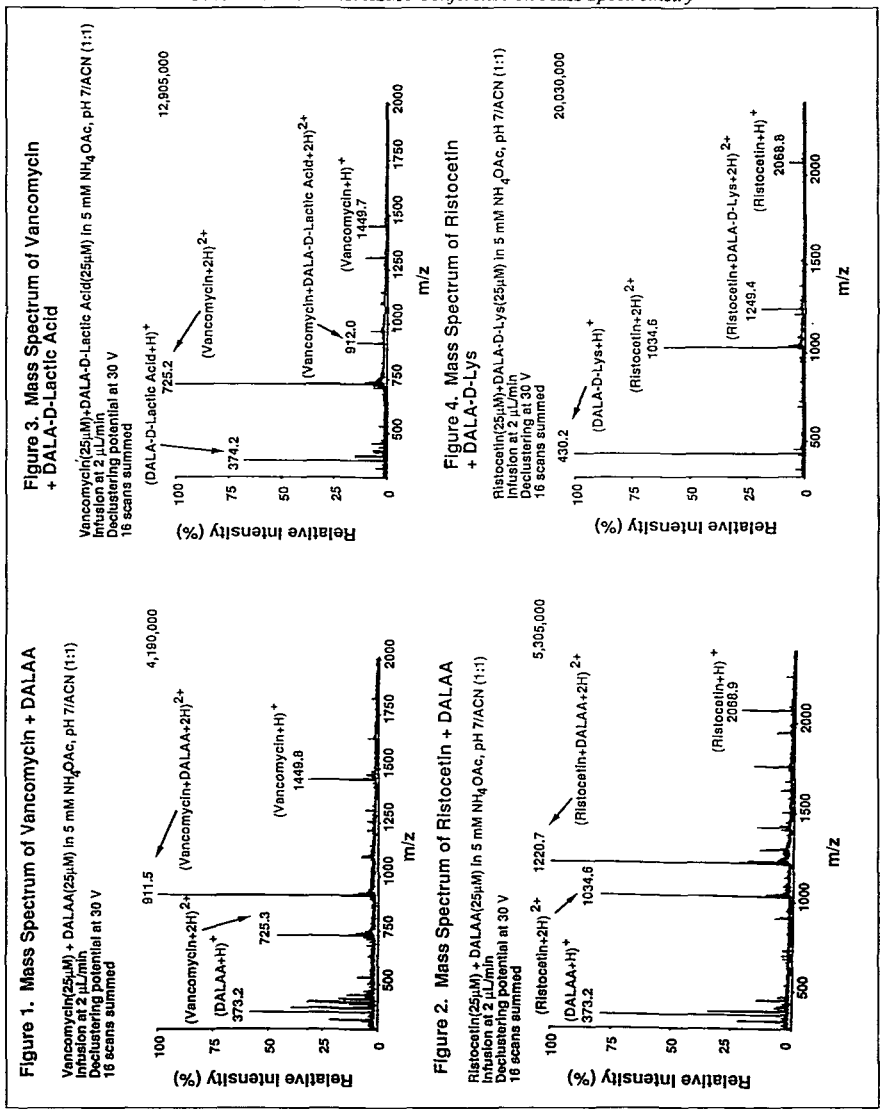

Mass Spectrometry of Bi-Substrate Inhibitors and Their Targeted Protein Kinases

Denes Medzihradszky*, Susan L. Chen, Wade M. Hines,
George L. Kenyon and Bradford W. Gibson
Department of Pharmaceutical Chemistry, University of California,
San Francisco, CA 94143

Several receptor protein tyrosine kinases, including insulin-like growth factor 1 receptor (IGF-1-R), are expressed at high levels in certain tumors, such as breast and ovarian carcinomas [1]. Several receptor kinases including epidermal growth factor receptor (EGF-R), are known oncogenes [2]. Although the kinase domain is presumably responsible for the effects of activation of the receptor, little is known about the biochemistry of the kinase domains. Our studies have concentrated on two areas, the expression of the kinase domain of IGF-1-R and EGF-R, and the development of bi-substrate inhibitors of protein tyrosine kinases. We are in the process of examining several expression systems for production of active, soluble kinase domain of IGF-1-R. Electrospray HPLC-MS is being used for the characterization of expressed IGF-1-R kinase domain, both intact and digested forms. The formation of insoluble inclusion bodies for this kinase domain has presented special problems for our protein characterization efforts. This protein will be used for detailed kinetic studies, inhibitor assays and crystallographic analysis.

We have constructed a new protocol for the synthesis of bi-substrate analogs based on the appropriate peptide substrate with covalently attached AMP, ADP and ATP moieties (**Fig 1**). The peptides were synthetised on solid phase using Fmoc chemistry, phosphorylated, phosphate protecting groups selectively removed, and the activated adenosine-phosphate [3] was coupled to the immobilized phosphopeptide. After TFA cleavage AXP peptides were isolated with good yield. These peptide chimeras are currently being evaluated as inhibitors of cAMP-dependent protein kinase, the only protein kinase for which a crystal structure has been determined [4, 5].

We found that these potential transition state analog inhibitors readily form metal complexes, being detected in abundance in positive liquid secondary ion spectra. Tandem mass spectrometry and CID analysis were used for the characterization of the synthetic peptide analogs for which some unique and characteristic fragment ions have been observed (**Fig 2**).

References:

[1] Rosen, N., et. al. *Breast Cancer Research and Treatment* **18**, S55-S62 (1991)
[2] Farrow, S.N., et. al. *Eur. J. Biochem.* **184**, 361-365 (1989)
[3] Hampton, A., et. al. *J. Med. Chem.* **25**, 801 (1982).
[4] Knighton, D.R., et al. *Science* **253**, 407 (1991).
[5] Bossemeyer, D., et. al. *EMBO J.* **12**, 849 (1993).

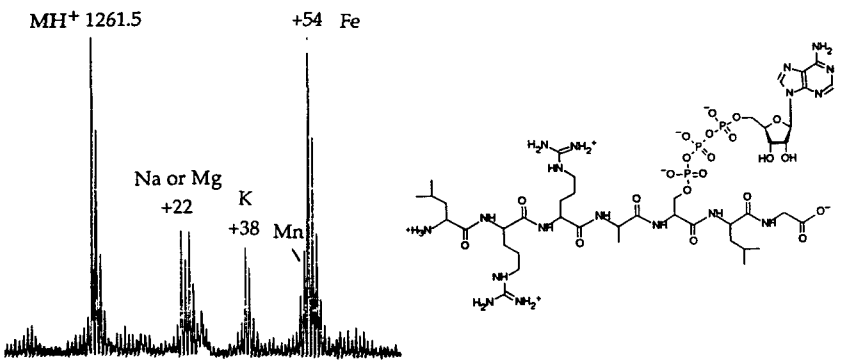

Fig 1. LSIMS spectra and structure of the ATP bi-substrate analog.

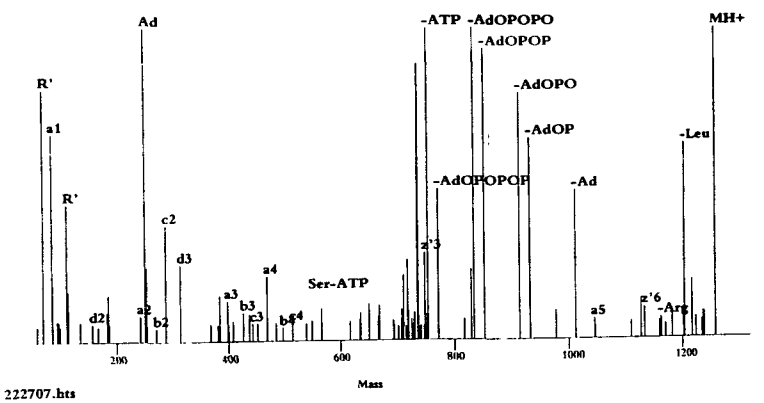

Fig 2. High energy CID spectra of the same ATP-peptide

This work was supported by the Tobacco Related Disease Program (2RT0230) and the Mass Spectrometry Facility (NIH RR01614)

The Use of Packed Capillary LC/MS to Monitor Phosphokinase Activity in Rat Cardiomyocytes

B.L Ackermann, B.T. Regg, J.E. Coutant, K.A. Diekema, and R.J. Dinerstein
Marion Merrell Dow Research Institute, Cincinnati, OH 45215

Protein kinases are an important class of enzymes that regulate cellular responses by changing the conformation of proteins through phosphorylation. Knowledge of which kinases are activated in response to various stimuli is therefore important to understanding the mechanisms of cellular control. Kinases are most often studied in their *isolated* form in conjunction with [γ-^{32}P]-ATP to study the phosphorylation of a particular substrate by a *single* kinase. This presentation describes our initial effort aimed at developing a method to monitor the activity of *multiple* kinases at the *cellular* level. The approach taken involves the addition of five exogenous peptide substrates for target kinases to rat cardiomyocytes immediately upon lysis; the phosphorylated substrates are then isolated and detected through the use of packed capillary LC/MS with electrospray ionization (ESI) using multiple ion detection (MID).

Initial studies were performed to determine the number of cells required for extraction and the working range for analysis. Figure 1 shows the single and doubly protonated ions for phosphokemptide (KT-P) isolated from rat cardiomyocytes stimulated for maximal Protein Kinase A activity in 1 mM cyclic AMP (cAMP). The combined area of these peaks was 67-fold greater than a similar analysis of cells extracted under basal conditions (no stimulus). In an analogous experiment, the ability to detect the phosphorylated forms of all five peptide substrates was demonstrated. For this experiment, the kinase substrates (100 µM ea.) and ATP (100 µM) were added to cells immediately upon lysis and allowed to react at 37C for 20 min. The phosphorylated substrates were isolated by a procedure involving centrifugation, ultrafiltration, and solid phase extraction. The amount injected for LC-ESI-MS corresponded to an extraction of about 5.4 x 10 E4 cells.

In order to demonstrate linearity over the anticipated working range of analysis, standard curves were prepared for all five substrates. Linearity was obtained between 2.5 and 250 pmol for each substrate. Figure 2 shows data from the injection of 250 pmol of the five phosphokinase substrate standards along with 100 pmol of the internal standard leucine enkephalin (LE). Also present is a trace for phosphokemptide (KT-P). This standard was prepared enzymatically using Protein Kinase A. We are in the process of preparing phosphorylated standards for the four remaining substrates. Ultimately, the standard curves used for quantitation will be prepared using phosphorylated standards which are extracted to account for recovery.

Detection of Phosphokemptide in Cells Stimulated for Full Protein Kinase A Activity in the Presence of 1mM cAMP

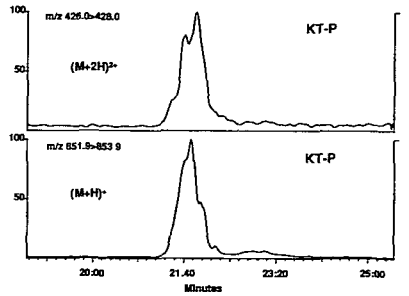

Figure 1

Figure 2

LC-ESI-MS of Kinase Substrates (250 pmol ea.) and Leucine Enkephalin Internal Standard (100 pmol)

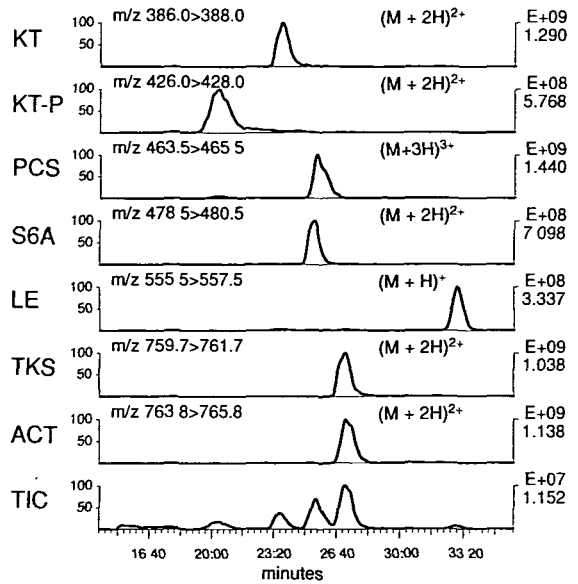

TARGET ENZYME

Protein Kinase A

Protein Kinase C

S6 Kinase

Tyrosine Kinase

CAM Kinase

Probing the Catalytic Domains of Protein Kinases with the Aid of Mass Spectrometry

Roland S. Annan, W. Todd Miller[1], and Steven A. Carr.
Department of Physical and Structural Chemistry,
Smithkline Beecham Pharmaceuticals, King of Prussia, PA.
[1]Department of Physiology and Biophysics, SUNY Stony Brook, Stony Brook NY.

In the mid 1950s, phosphorylation was recognized as a reversible means of modulating protein function. By phosphorylating specific serine, threonine and tyrosine residues, protein kinases alter the functions of their target proteins. The fact that a specific kinase can selectively phosphorylate a wide variety of proteins, has led to the question of how the enzyme recognizes specific residues from among the many hydroxyl groups found in the substrate protein. Additionally important is the identity of the residues and domains in the kinases themselves which are responsible for protein recognition. It is largely the lack of information in this area which has made it difficult to reconcile the frequent exceptions found when attempting to predict protein phosphorylation based on phosphorylation site motifs.

It was nearly 30 years after the discovery of the cAMP dependent protein kinase, that the first tyrosine-protein kinase was identified. Since that time, nearly 20 additional tyrosine phosphorylating kinases have been discovered. Although phosphotyrosine accounts for less than 1% of all phosphorylated amino acids, tyrosine-protein kinases have proved to be intensely interesting since at least eight of them are the protein products of retroviral oncogenes. Because abnormal tyrosine phosphorylation is manifest in cells transformed by many of the viruses, the idea has been put forth, that phosphorylation of tyrosine in critical cellular proteins may be a signal initiating cell transformation. Unfortunately proof of this has not be forthcoming. A large part of the problem in understanding the function of tyrosine-protein kinases has been a lack of success in identifying natural substrates, other than autophosphorylation sites, whose functions have been modified in a way that would explain transformation events. In order to determine optimal peptide substrates for specific protein kinases, amino acids in critical positions of known phosphorylated sequences (e.g. autophosphorylation sites) are randomized. These synthetic peptide "libraries" are then incubated with the enzyme and the phosphorylated peptides determined. We have been attempting to probe the catalytic domains of tyrosine-protein kinases using peptide substrate libraries in conjunction with mass spectrometry.

Cellular and viral Src are members of the non-receptor subfamily of tyrosine-protein kinases. Both proteins are membrane bound via an N-terminal myristoyl. c-Src is phosphorylated by an unknown kinase at Tyr^{527}, allowing a head to tail association of the C-terminal region with the SH2 domain, leaving it inactive. The function of c-Src in normal cells is unknown. The viral form of Src, which is expressed by the Rous Sarcoma virus gene *v-Src*, lacks the Tyr^{527}, and is a potent tyrosine-protein kinase. A peptide covering the autophosphorylation site of vSrc, R^{408}RLIEDAEYAARG^{420} was randomized at position 8, and the resulting "library of peptides" reacted with vSrc. Figure 1 shows the positive ion LC-ESMS analysis of 20µL from the reaction. The expected substrate, the $[Glu]^8$ Src peptide is not phosphorylated. Manual inspection of the data reveals an [M+H]+ ion which corresponded to a $[His]^8$ phosTyr substitution. The RIC of this peptides spectrum is plotted against the TIC. Independent synthesis of the authentic $[His]^8$ peptide and reaction with Src showed it was, in fact, a substrate for the enzyme.

The process of manually inspecting LC-MS data for prospective phosphorylated peptides among substrate libraries is tedious at best. The task becomes daunting when either the number of random positions or the number of templates is increased beyond one. The same can be said for inspecting enzyme digests of large phosphorylated proteins. We have, therefore, been investigating ways to selectively detect phosphopeptides in complex mixtures. In ESMS, at high declustering potentials, the negative ion spectra of phosphopeptides show ions at m/z 63 and 79 corresponding to PO_2^- and PO_3^- respectively (For more information see Huddleston et.al. this volume). Figure 2 shows the negative ion, stepped collision energy LC-ESMS analysis of 20µL of a Kemptide library reaction with the cAMP-dependent protein kinase. In this library, the 2 position in the sequence LRRASLG has been randomized. The MS was scanned discontinuously from m/z 50-100 at OR = -350V and then from m/z 400-1000 at OR= -115. The RIC is sum of m/z 63 and 79 and is plotted against the TIC. The results from this experiment show that

with L*RASLG as a template each peptide in the library is phosphorylated to some extent by cAMK. Furthermore, this suggests that the use of negative ion stepped-collision energy MS is an efficient way to approach the problem of looking for enzyme substrates in peptide library reactions.

ACKNOWLEDGEMENTS The authors are very grateful to Mike Huddleston (SmithKline) for assistance with the negative ion MS and Jeff Till (Stony Brook) for work on the enzyme reactions.

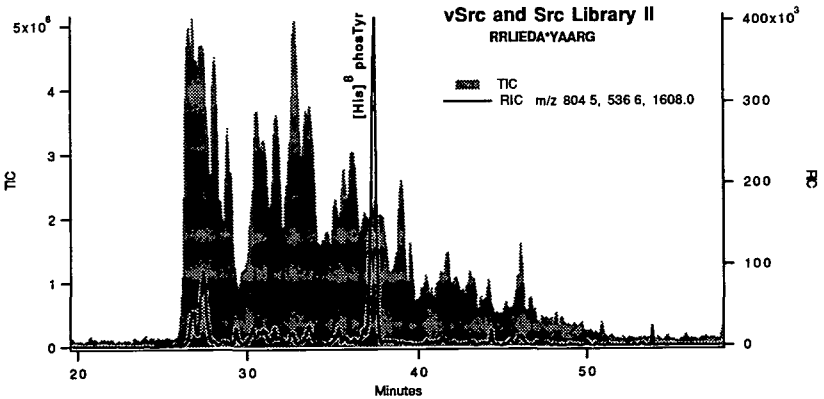

Figure 1.

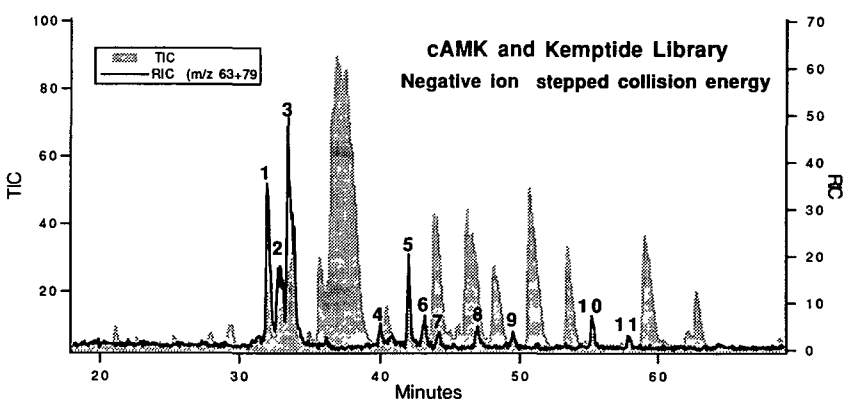

Figure 2.

Analysis of Iron-Sulfur Proteins by Electrospray Mass Spectrometry

***E. Forest[1], Y. Petillot[1], J. M. Moulis[2], J. Meyer[2]**
[1]Institut de Biologie Structurale, [2]Département de Biologie Moléculaire et Structurale, 38 Grenoble, France

In order to characterize iron-sulfur proteins, we have implemented electrospray ionization mass spectrometry (ESI-MS), which has proved to be a valuable technique for precise mass determinations of biopolymers. However, as the interface conditions are selected to provide efficient ionization and sufficient excitation for a good desolvation, labile species are most often dissociated. The iron-sulfur proteins are a typical case of such an occurrence: since the iron-sulfur bonds are weaker than the other bonds involved in proteins, the metal centers are likely to be removed during implementation of the method.

Thus, we have carried out a comparative analysis of several iron-sulfur proteins with various stabilities: a high potential iron protein (HiPIP) from *Chromatium tepidum* (Moulis et al., 1993), a ferredoxin and several forms of rubredoxins from *Clostridium pasteurianum*. Rubredoxins are small proteins, the active site of which consists of an iron atom coordinated to four cysteinyl sulfur atoms. Three forms were analysed in positive and negative modes. With a recombinant rubredoxin expressed in *E. coli*, a partial loss of the iron ion appears in the positive mode spectrum, whereas there is no evidence for apoprotein formation in negative mode. This indicates that the conditions of ionization in the positive mode are somewhat detrimental to the protein. The spectra of the native rubredoxin from *C. pasteurianum* show a major component corresponding to a formylated N-terminal methionine together with an unblocked protein. The ratio of holoprotein to apoprotein is much larger in the case of the formylated rubredoxin than in the case of the non-formylated one. This suggests a greater stability of the formylated rubredoxin, as compared to the non-formylated one. Mass spectra of another protein expressed in *E. coli*, allow to identify it as a rubredoxin with a zinc atom replacing iron. In positive mode, no holoprotein is detected and conversely, in negative mode, no apoprotein is present (Figure 1). With a ferredoxin containing 2 [4Fe-4S] clusters and also extracted from *C. pasteurianum*, the negative mode spectrum also exclusively shows a peak corresponding to the holoprotein, whereas in positive mode, the apoprotein is mainly detected. The influence of the solvent is shown with mass spectra of a high potential ferredoxin contening one [4Fe-4S] cluster and isolated from *C. tepidum* and its expected stability is confirmed through these analyses.

From the data presented in this study, the negative ion mode can be anticipated to be more adapted to the investigation of small iron-sulfur proteins such as rubredoxins and ferredoxins: most of these proteins are acidic, and are therefore negatively charged at neutral pH, where their stability is highest. This opens the way to the detection and analysis, of less stable iron-sulfur proteins. One might then be able, by ESI-MS, to gain access to an often missing and most important piece of structural information, namely the precise composition of the metal centers.

Moulis, J.-M., Scherrer, N., Gagnon, J., Forest, E., Pétillot, Y. & Garcia, D. (1993) *Arch. Biochem. Biophys. in press*

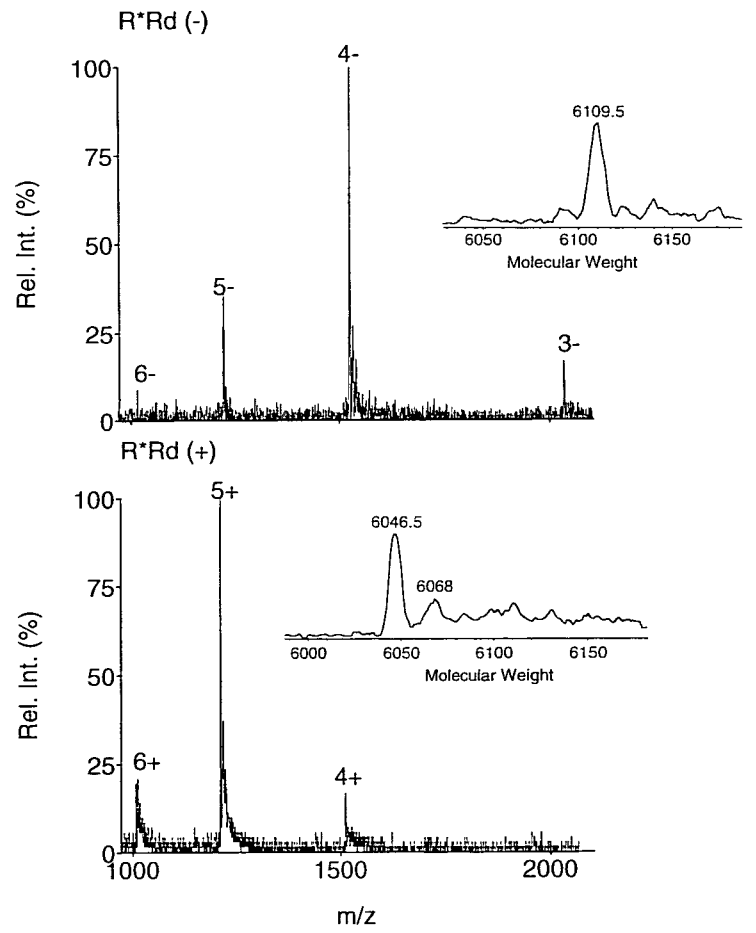

Fig.1 ESI/MS of a recombinant rubredoxin in negative mode (R*Rd(-)),and in positive mode (R*Rd(+)), with reconstructed molecular mass profile of each spectra in the box.

Effect of Proline Residue on Transition Metal Ion Binding in Peptides Studied by ^{252} Cf-PDMS

*Zhaohong Hu and R.D.Macfarlane
Department of Chemistry, Texas A&M University
College Station, TX 77843.

^{252}Cf-PDMS has been used to study the coordinations between transition metal ions and peptides in our group for the past three years. The study of the interactions between Cu(II) and angiotensin (ANG) / bradykinin (BRK) peptides is reported here.

To acquire a spectrum of a peptide, the aqueous solution of 5 x 10^{-4}M of the peptide was prepared and deposited on a sample target. Nitrocellulose (NC) was used as the matrix to adsorb the peptide from solution onto its surface. To obtain a spectrum of a metal-peptide, equal volumes of 1 x 10^{-3}M ANGII and $Cu(NO_3)_2$ solutions were mixed together to gave a Cu-ANGII solution of 1:1 molar ratio and 5 x 10^{-4}M concentration. The solution pH was adjusted from acidic to neutral (*ca.* pH 2 to 7) by trimethylamine. This solution was mixed at room temperature for 10 minutes before it was deposited on a NC sample target.

The ANG peptides studied include ANGII, ANGI, and N$_\alpha$-acetyl-ANGI. Cu(II) is found to bind to ANG peptides primarily at two sites: the N-terminal amino group and its vicinity deprotonated amide nitrogens, and the imidazole ring of His residue and its adjacent deprotonated amide nitrogens. Between the two sites, the N-terminal site has a much stronger affinity towards Cu(II) than the other site. As an example, Figure 1 shows the mass spectrum of Cu-ANGII.

A Pro residue in a peptide functions as the breaking point to metal ion binding due to its lack of NH in the amide bond formed. Both ANG and BRK peptides contain Pro residues. In ANG peptides, the Pro residue is located next to His residue near the C-terminus of the peptides. In BRK, the Pro residue is the second one from the N-terminus. Our study demonstrates that ANG and BRK peptides display completely different properties in Cu(II)-binding due to the location of the Pro residue in the peptides. The Cu-BRK mass spectrum shown in Figure 2 presents this result.

In conclusion, we demonstrate that oligo-peptides in general have multiple Cu(II)-binding sites. The numbers of the sites can be evaluated by the molecular ions observed in the mass spectra. The N-terminal amino group and its adjacent amide nitrogen are important in Cu(II)-binding in oligo-peptides.

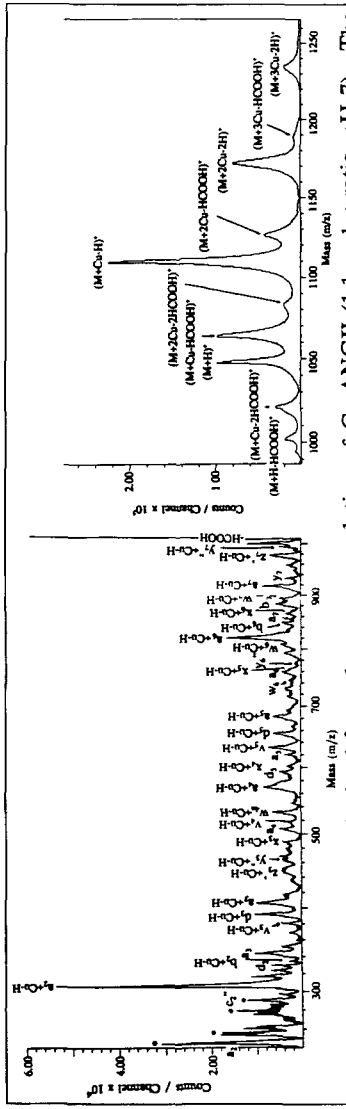

Figure 1. The spectrum obtained from the aqueous solution of Cu-ANGII (1:1 molar ratio, pH 7). The intense a_2+Cu-H peak indicates a strong Cu(II)-binding sites at the N-terminal end. The C-terminal Cu-containing ions provide evidence that His residue is a weaker Cu(II)-binding site. The molecular ions observed reveals three Cu(II)-binding sites.

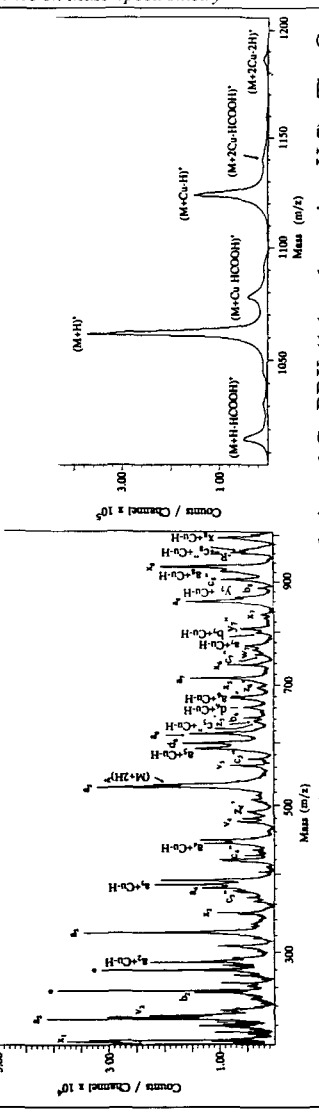

Figure 2. The spectrum obtained from the aqueous solution of Cu-BRK (1:1 molar ratio, pH 7). The Cu-containing ions are of much lower intensities compared to the non-Cu-containing ions. The result indicates that BRK has a much weaker affinity to Cu(II) compared to ANGII.

Studies of Anticancer Drugs Binding with the Metal-Detoxification Protein, Metallothionein II, by Ion Spray Mass Spectrometry

Y.L. Hsieh[1], Y.T. Li Hsieh[1], J. Henion[1], and B. Ganem[2]
[1] Drug Testing, Cornell University, 925 Warren Dr., Ithaca, NY 14850. [2] Department of Chemistry, Cornell University, Ithaca, NY 14853

Metallothionein II (MT II), a cysteine-rich protein with a three-metal cluster (two zinc plus one cadmium) and a four metal cluster (four cadmium)[1,2], coordinates with heavy metal ions and, therefore, confers resistance to metal-containing anticancer drugs, e.g., carboplatin (CP) and cisplatin[3,4]. The three-metal cluster is relatively less stable and exchanges the metal ion with hydrogen ions more rapidly in acid solutions. In this study we investigate the noncovalent coordinate complex formation between platinum from cisplatin and CP with sulfhydryl groups from MT II. The observed molecular weight of apo-MT II is 6119 Da (Figure 1). The molecular weight of the stronger four cadmium binding cluster in MT II, obtained by adding acid (pH~3) to remove the weaker two zinc and one cadmium binding cluster, is 6566 Da (Figure 2).

The mass spectrum obtained from binding of MT II with three CPs is from replacement of the three metal cluster (one cadmium and two zinc) in 10 mM ammonia acetate (pH=7) prior to adding 1% formic acid and 50/50 acetonitrile/H_2O + 1% formic acid shows coordinate complexes with one CP (Mr=6937), two CP (Mr=7308), and three CP (Mr=7679) (Figure 3). Alternatively, two hydrolyzed cisplatin products are shown to coordinate with four cadmium MT II. That this coordination reaction is highly specific for the platinum-based anticancer drugs is indicated by the absence of complex formation with actinomycin D and doxorubicin. The overexpression of MT II is confered to resist the antineoplastic angents, e.g., cisplatin and carboplatin, but only modest resist doxorubicin[5]. Support for a coordination complex between CP and four cadmium MT II was obtained by tandem mass spectrometry (MS/MS) (Figure 4). CID of the 5^+ CP-four cadmium MT II complex (m/z 1388) at 250 eV and 550 eV collision energy produces CP (m/z 372 at 1^+) and four cadmium MT II (m/z 1643 at 4^+). The results of MS/MS are consistent with the concept of a coordinate complex between CP and MT II.

Acknowledgment: This research was supported by the National Institutes of Health (GM47931).

References

1). W.F. Furey, A.H. Robbins, L.L. Clancy, D.R. Winge, B.C. Wang, and C.D. Stout, Science 231, 704-710 (1986).
2). J.F. Riordan, B.L. Vallee, Methods in Enzymology 205, Academic Press, New York (1991).
3). R.R. Bahnson, A. Basu, and J.S. Lazo, Mol. Clin. Adv. Anticancer Drug, 251-260 (1991).
4). A. Pattanaik, G. Bachowski, J. Laib, D. Lemkuil, C.F. Shaw, D.H. Petering, A. Hitchcock, and L. Saryan, J. Biol. Chem. 267(23), 16121-16128 (1992).
5). S.L. Kelley, A. Basu, B.A. Teicher, M.P. Hacker, D.H. Hamer, J.S., Lazo, Science 241, 1813-1815 (1988).

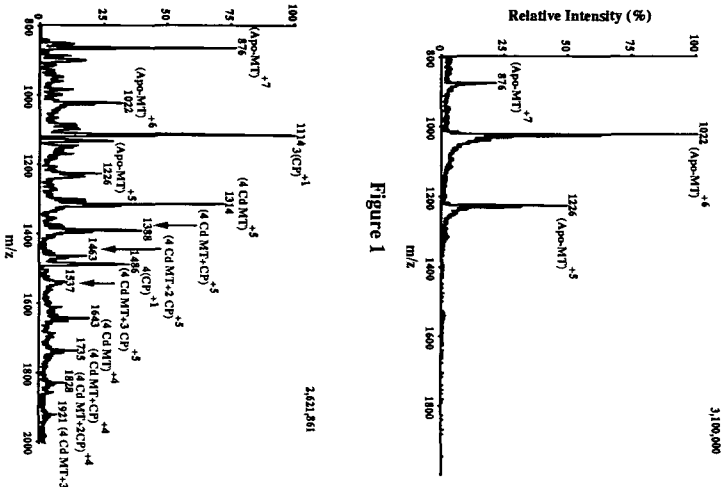

Figure 1

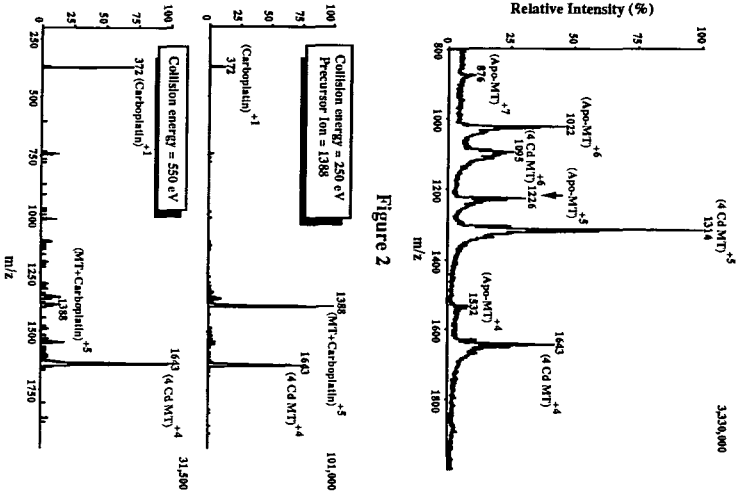

Figure 2

Figure 3

Figure 4

FORMATION STUDY OF METAL COMPLEXES SELF-ASSEMBLY BY ESMS

Leize E.[1], Krämer R.[2], Lehn J.M.[2] and Van Dorsselaer A.[1]
1 Laboratoire de Spectrométrie de Masse Bio-Organique,URA 31 CNRS-Université Louis Pasteur, 2 Laboratoire de Chimie Supramoléculaire, URA 422 CNRS-Université Louis Pasteur, Strasbourg, France.

INTRODUCTION:

Self-assembly is one of the basis of life chemistry. The determination of the different steps and the driving forces involved in the formation of large biological complexes is one of the major goal of modern biochemistry. Weak interactions play a particulary important role in this field. Some important molecule families are: phospholipids (they spontaneously build biological membranes), proteins (they cluster to form active enzymatic complexes and even form extremely complex machinery such as flagella constituted of more than 300 different proteins), DNA (they form the double helix, interact with specific proteins). Electrospray Mass Spectrometry (ESMS) may play an important role in these studies. The study of the polynuclear complexes self-assembly could help understanding the formation of large biological complexes.

Analytical challenge: The task consists in determining the different types of supramolecules formed at different stoichiometries of ligands and metal ions. This is an difficult analytical problem because diluted solutions (10^{-4} to 10^{-6} M) must be used. UV-vis spectrophototmetry is ususally considered as the method of choice for these studies. But in the case of multicomponent systems, spectrophotometric titration data are difficult to interpret. An analytical technique that would allow the identification of the different complexes formed during the titration would permit the interpretation of the UV-vis spectrophotometric data. ESMS seems to be appropriate for this kind of studies. It has been already shown that it is possible to obtain ESMS-spectra of polynuclear complexes in diluted solutions (10^{-5} to 10^{-6} M) without fragmentation and reduction [1].

Description of the model studied (Fig. 1): In this work we will investigate the possibilities of ESMS as a detection method of the different molecular species formed in solution when an increasing amount of Cu(I) is gradually added to a 1/1 mixture of both ligands: L^1 and L^2 [2]. The results from ESMS will be compared to the one obtained from a parallel UV-vis spectrophotometry. Our model is rather simple and UV-vis spectrophotometry can be used to determine the amount of the different species present in solution. This comparison should allow us to answer the key question: *Is it possible to use the intensity of the peudomolecular ions obtained by ESMS for quantization?*

RESULTS:

Spectrophotometric titration: A computer analysis of the titration data revealed that a chemical model including the formation of complexes **1** and **2** (Fig. 2) alone is close to the real situation. The formation constants and the species distribution for **1** and **2** were calculated. The initial formation of the yellow complex **2** and its transformation into the blue complex **1** can also be followed optically.

ESMS (Fig. 3): For the solution with 1.0 equivalent Cu(I), the major peak corresponds to the doubly-charged ion of **2** (m/z = 516.1). For the solution with 2.5 equivalents Cu(I), two intense peaks: the triply-charged ion **1** (m/z = 616.3) and the doubly-charged ion of **2** (m/z = 516.0). For the solution with 6.0 equivalents Cu(I), the spectrum was dominated by the fully assembled complex **1** at m/z = 616.3. The ionization of the complexes consisted in the loss of all the counter-ions PF_6^- and in the protonation of the uncoordinated basic ligands.

Comparison between ESMS and spectrophotometry (Table 1): The ESMS spectra confirm the appearance of complexes **1** and **2** during the titration. Moreover, the relative ESMS peak intensities for **1** and **2** fit well the species distribution obtained by spectrophotometry. A small amount of the complex **3** is revealed by ESMS alone. **3** might not be detectable by spectrophotometric analysis (intensity < 15%).

CONCLUSION:

ESMS appears to be a very valuable technique for the analysis of metal complexes that are in thermodynamic equilibrium in diluted solutions. For the study described here, the results obtained with

ESMS fit very well with those obtained with UV-vis spectrophotometry. The amount of species **1**, **2** and **3** deduced from the UV-vis spectrophotometric data and ESMS spectra are very close. *Then we can conclude that it is possible here to use the ESMS intensity of the peudomolecular ions for a quantization.* Furthermore both techniques show that complex **3** is immediatly transformed in **1** after its formation. This demonstrates *the high cooperativity of this system.*

REFERENCES:

1. V. Katta, S.K. Chowhury and B.T. Chait, *J.Am.Chem.Soc.*, **1990**, *112*, 5348; F. Bitsch et al., *Procedings 40th ASMS*, **1992**, 1643.
2. R. Krämer, J.M. Lehn, in preparation; E. Leize, R. Krämer, A. Van Dorsselaer and J.M. Lehn, *Chem.Comm.*, in press.

Cu (I) equivalent	ESMS relative peak intensities			UV-vis relative abundance		
	1	2	3	1	2	3
1.0	0.02	1.00	<0.05	0.06	1.00	0.00
2.5	1.00	0.50	0.17	1.00	0.53	<0.15
6.0	1.00	0.04	0.02	1.00	0.03	0.00

Table 1: Comparison of relative species distribution obtained by ESMS and by UV-vis spectrophotometry

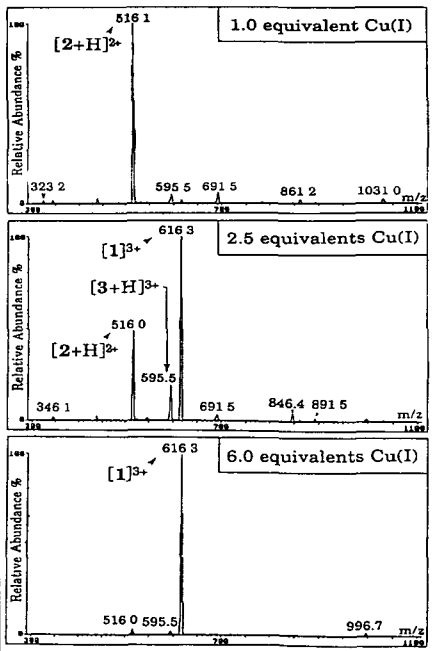

Fig. 3: ESMS spectra of the three titration solutions

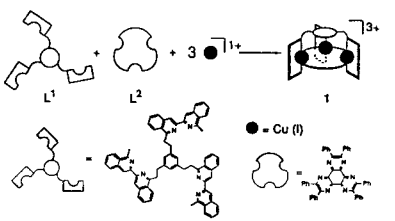

Fig. 1: Formation of the complex **1**

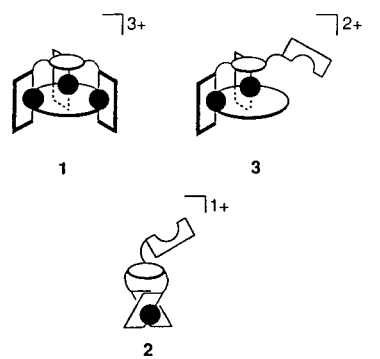

Fig.2: Species detected by ESMS and UV-vis spectrophotometry

STUDIES OF METALLOTHIONEIN AND ANTICANCER ALKYLATING AGENT INTERACTIONS

Xiaolan Yu, Zhuchun Wu, and Catherine Fenselau
Department of Chemistry and Biochemistry,
University of Maryland Baltimore County, Baltimore, MD 21228

INTRODUCTION: Metallothionein (MT) is an important family of metal-thiolate proteins with high metal and cysteine content [1]. It is responsible for much of the intracellular sequestration of Cd and cells tolerate the toxicity of Cd, at least temporarily, by massive amplification of the MT gene. It is our interest, however, to study the hypothesis that MT (also) covalently sequesters alkylating agents. The alkylating agents cis-diamminedichloroplatinum, melphalan, and chlorambucil are commonly used in cancer treatment. Their therapeutic values are attenuated by the development of drug resistance in patients receiving them. Cells with overexpressed MT levels conferred resistance against these alkylating agents [2]. Increased intracellular drug binding is considered to be one of the mechanisms that are responsible for the phenomenon of acquired drug resistance.

EXPERIMENTAL: Rabbit liver metallothionein 2 (MT-2) was purchased from Sigma. Reversed phase high performance liquid chromatography (HPLC) was conducted using a C8 column (Aquapore RP-300, 250 x 4.6 mm). Electrospray ionization mass spectrometry (ESMS) was performed on a Vestec (Houston, Texas) electrospray source fitted to a Hewlett-Packard (Palo Alto, CA) 5988A quadrupole mass spectrometer, with a Phrasor (Duarte,CA) high energy dynode detector and a Technivent (St.Louis, MO) data system. Samples in a mixture of water:methanol:acetic acid (47:50:3) were injected through a Rheodyne (Cotati, CA) 7125 loop injector, with a flow rate of 10 μL/min. The stainless steel needle was held at 2.2 kV and the source temperature was at 240°C. Fast atom bombardment mass spectrometry (FABMS) and tandem mass spectrometry (MS/MS) experiments were performed on a JEOL HX110/HX110 tandem mass spectrometer (Tokyo, Japan), controlled by DA 5000 and DA 7000 (Complement) data systems. The FAB gun was operated at 6 kV and the accelerating voltage was 10 kV. Helium was used as the collision gas and the collision cell was floated to 4 kV in MS/MS experiments. MT was Cys-methylated and HPLC purified before trypsin digest.

RESULTS: Native metallothionein was incubated with the alkylating agent melphalan *in vitro* at near physiological conditions for 30 minutes. The reaction mixture was then desalted and analyzed by HPLC and ESMS. About 10% of the protein was alkylated to form a 1:1 covalent adduct with melphalan. The alkylated MT was also purified by HPLC and weighed by ESMS (Fig. 1). The alkylated MT was then Cys-methylated and digested with trypsin to provide peptide fragments for analysis by ESMS. We were able to map the entire protein sequence and two new fragments from the alkylated MT were characterized to be 1:1 melphalan adducts. MS/MS experiments were then used to locate the exact alkylation site(s). It was determined that one cysteine in each peptide was alkylated by melphalan, as shown in Fig. 2.

CONCLUSIONS: It was determined that MT covalently sequesters alkylating agent melphalan *in vitro*. This is consistent with the hypothesis that induction of MT is involved in the development of drug resistance against melphalan and some other alkylating agents. Computer modeling allows us to rationalize this fairly specific drug-protein interaction.

REFERENCES: [1]. Kagi, J.H.R. et. al., Biochemistry 27,8509-8515. (1988)
[2]. Kelley, S.L. et. al., Science 241, 1813-1815. (1988)

Figure 1. Electrospray ionization mass spectrum of melphalan-alkylated metallothionein

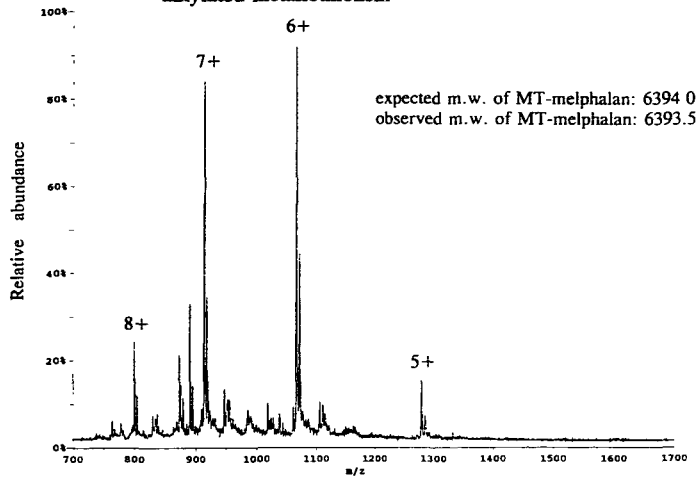

Figure 2. Tandem mass spectrum of a melphalan-alkylated peptide from metallothionein

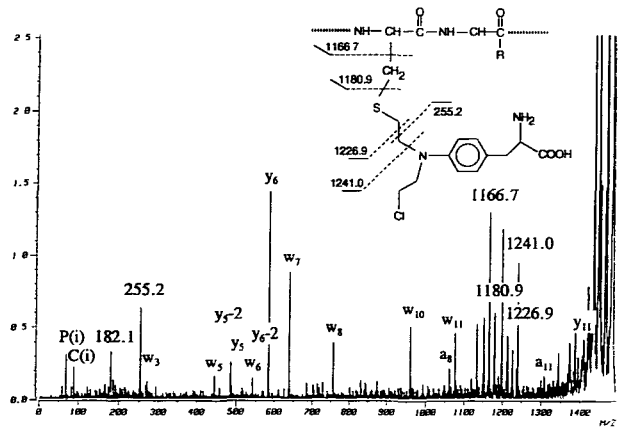

Influences of Peptide Side Chains on the Metal Binding Site in Metal Ion-Cationized Peptides: Participation of Aromatic Ring in Metal Chelation

Peifeng Hu, Curt Sorensen, and Michael L. Gross, Midwest Center for Mass Spectrometry, Department of Chemistry, University of Nebraska-Lincoln, Lincoln, NE 68588-0304

The aromatic residues (Phe, Tyr, His, Trp) influence strongly the fragmentations of the metal-cationized peptides containing these residues when transition metal ions are involved. A metal-bound immonium ion of the aromatic residue and an (a_n - H) ion formed by reactions at the site of aromatic residue are the dominant fragment species. These residues direct the decompositions of alkaline earth metal-cationized peptides in a similar manner only for small peptides (e.g., tripeptides).

We interpret the side chain- and metal-dependent fragmentations to result from specific metal-side chain binding. The metal ion binds to a deprotonated amide nitrogen and chelates to the aromatic ring of the aromatic residue (**1-3**). The participation of the aromatic ring in the metal binding increases the populations of these structures by enhancing their relative stabilities with respect to the structures in which only amide group binding is involved (**4**). The fragmentation of structure 1 gives the (a_n - H) ion (Scheme I) whereas that of **2** produces immonium ions (Scheme II).

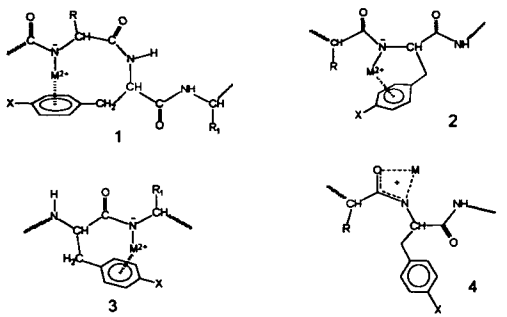

Labelling experiments show that formation of the (a_n - H) ion at the site of aromatic residue from transition metal-complexes involves an amide hydrogen rearrangement which is the opposite to the non-amide hydrogen transfer from alkaline earth metal-complexes. This contrast is explained by the differences of the two metal classes in their ability to bind to an aromatic ring. Transition metal ions (especially Ni^{2+} and Co^{2+} studied here) bind to aromatic ring so strongly that the formation of (a_n - H) ion occurs by the mechanism in Scheme I. Alkaline earth metal ions interact with aromatic ring weakly, and the formation of the appropriate (a_n - H) ion may proceed by a mechanism proposed previously[1] in which a hydrogen on the methylene carbon is transferred.

1. Teesch, L. M.; Adams, J. *J. Am. Chem. Soc.* **1990**, *112,4110.*

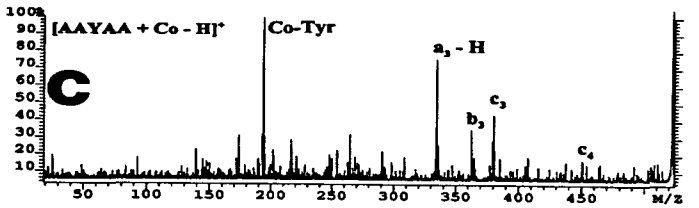

Figure 1 The CAD spectra of Co^{2+}-cationized AAYAA.

SCHEME I

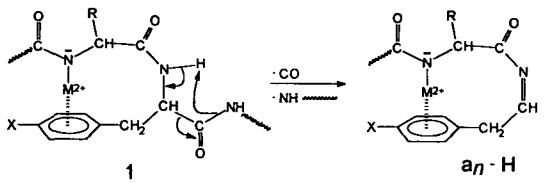

SCHEME II

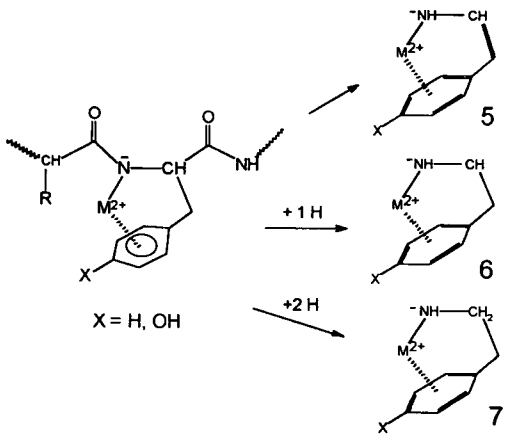

Disulfide Bond Analysis of Recombinant Proteins Using FAB and MALD-TOF Mass Spectrometry, J.E. Vath, E.B. Nickbarg, A.S. Harris, M.C. Huberty, W. Yu, S.A. Martin, H.A. Scoble, Genetics Institute, 1 Burtt Road, Andover, MA 01810

The disulfide bonds between cysteines are covalent modifications which define proximal regions in a protein. An understanding of the disulfide linkages is essential in order to gain insight into features of a protein which extend beyond the primary structure. We have been using mass spectrometry as an integral part of disulfide bond analysis in our laboratory. Two recent examples where it has been applied, in conjunction with N-terminal sequence analysis, are in the analysis of recombinant interleukin-12 human heterodimer (rhIL-12) and murine heavy chain (rmIL-12hc). Both FAB on a sector instrument and MALD-TOF on a reflector instrument were employed for these analyses and served to reveal some of the strengths and weaknesses of the techniques. This presentation focuses on certain aspects of sample preparation and illustrates some of the strengths of FAB and MALD to address disulfide analysis.

Mass spectrometry, as well as other disulfide detection schemes, require cleaving the protein backbone while leaving the disulfide bonds intact. In the case of the IL-12, Achro-K was used to cleave at the C-terminal side of lysine. Coeluting Cys containing peptides on the RP/HPLC map were identified by N-terminal sequence analysis. A strength of mass spectrometry is the ability to detect a mass corresponding to the oxidized state of disulfide-linked peptides, which provides direct evidence that a disulfide bond exists. This conclusion can be substantiated by the observation of the mass of the peptide component(s) under reducing conditions, which should reveal a shift in mass when compared to the oxidized peptide.

Direct analysis of the reduction reaction can be achieved in both FAB and MALD. For FAB, the sample is reacted in 1:1:1 glycerol/thioglycerol/30% ammonia under a heat gun (80-90°C) for 15 sec, followed by an addition of 1 part ammonia and heated again. For MALD, the sample (0.1-2 pmol/μL) is reacted in 20 mM Tris or phosphate buffer (pH 8), 10 mM DTT for 30 min at 50°C and 1 μL of the mixture is mixed with 2 μL of matrix solution, dried in air and analyzed. We have found that FAB is best for the analysis of intramolecular disulfide bonds on a single peptide such as that shown in **Figure 1**. In this case, the mass difference between the oxidized and reduced peptide is 2 u and would not be identified by MALD due to limited resolution and mass accuracy. FAB on a sector instrument is able to resolve the isotopic pattern of the peptide and unambiguously determine such a difference as seen in our example of the ^{12}C isotope shifting from m/z 2716.2 to 2718.3 upon reduction. MALD has a number of advantages including pmol sensitivity, extended mass range and tolerance for additives and buffers. For cases where multiple cysteines are in a single peptide, it is necessary to cleave between them in oreder to assign disulfide pairings and this often involves the use of multiple enzymes. The products of secondary digests can be analyzed by MALD directly from digestion buffers without purification. Furthermore, there is considerable evidence from our laboratory that a significant portion of the signal in MALD is made up of metastable fragment ions. In several examples, we have used a reflector at reduced potential to analyze the fragments for structural information for peptides (TP133) and carbohydrates (TOA910). Fragmentation of disulfides bonds can also be analyzed in this manner yielding information that is equivalent to partial reduction which can be useful for cases of four or more peptides bound together, as in **Figure 2**. This figure shows the reconstructed spectrum from four different potentials applied to the reflector and gives pairing information (i.e. M25 bound to M28 and not M29) that may not be recognized in a conventional experiment.

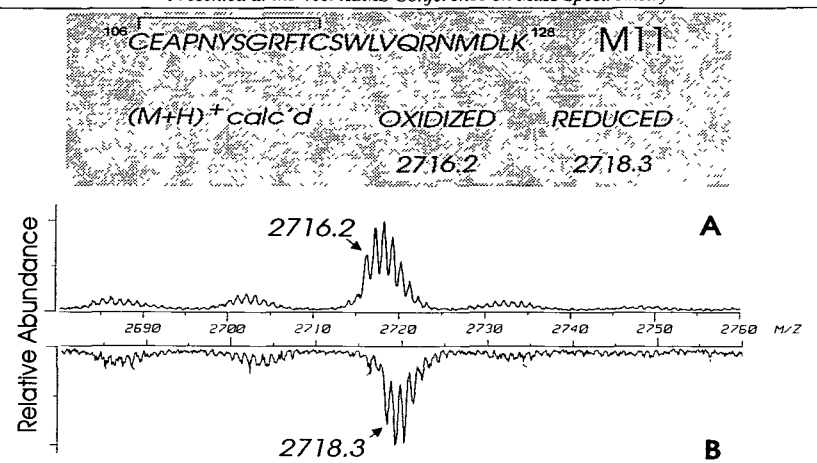

Figure 1 The molecular ion region from the FAB-MS of the Achro-K peptide M11 from rmIL-12hc befor (A) and after (B) reduction with thioglycerol/ammonia.

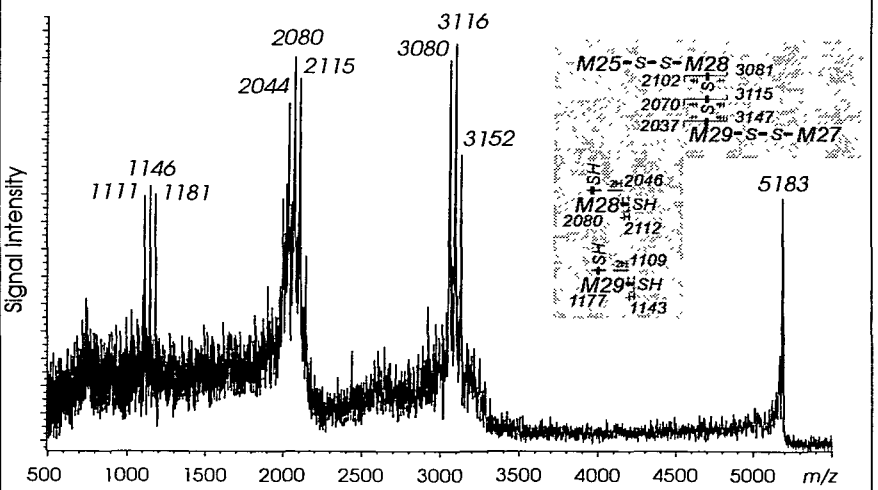

Figure 2. The MALD-TOF reflector spectrum of a rmIL-12hc disulfide cluster of five Achro-K peptides constructed by varying the reflector potential in four steps (30, 18 190, 12 224, and 6.828 kV)

Strategy to Determine Disulfide Bridge Arrangements, Investigation of Selective Reduction of Cystines using TCEP *A. G. Craig, E. Mahe, W. H. Fischer, W. R. Gray† and J. E. Rivier. The Clayton Foundation Laboratories for Peptide Biology, The Salk Institute, P.O. Box 85800, San Diego, CA 92186-5800. †University of Utah, Salt Lake City

One of the advantages of tris(2-carboxyethyl) phosphine (TCEP) [1] is that it reduces organic disulfides to thiols in water at an acidic pH. TCEP was used with matrix assisted laser desorption ionization and liquid secondary ionization mass spectrometry (LSIMS) for the reduction of cystines in peptides. TCEP reduced bovine insulin *in situ* in vacuum when mixed with glycerol and m-nitro benzyl alcohol [2]. Insulin, K-toxin and a large number of other cyclic peptides and toxins contain pairs of adjacent cysteine residues. As a result, these peptides are not amenable to chemical or enzymatic proteolyses that would result in single disulfide bridge containing fragments generally required for determining disulfide arrangements. An alternative approach would be to selectively reduce a particular cystine (e.g. the specifically reduced cystine could be labeled and the connectivity determined if scrambling can be avoided) [3].

In the case of insulin (M = 5729.7 Da) the A-chain and the B-chain (M = 3395.7 Da) are linked by two inter disulfide bridges, while the A-chain (M = 2334.0 Da) contains an intra disulfide bridge. Both inter disulfide bridges must be cleaved to eliminate A-chain and B-chain fragments. As shown in the LSI mass spectra (Figure 1) measured directly after addition of TCEP and introduction into the mass spectrometer the measured mass of the A-chain fragment monoisotopic species (m/z 2338.9) remains constant with time. This measured mass indicated that the intra disulfide bridge of the A-chain was reduced prior to the remaining inter disulfide bridge.

The disulfide bridging arrangement of K-toxin (M = 2428.0 Da, single peptide chain with three bridges) has not been previously characterized. Since all disulfide bridges in a single chain peptide are intra-molecular we investigated proteolysis conditions to produce two fragments (F_1 and F_2) preferably with both inter and intra disulfide bridges. Proteolysis with trypsin in a phosphate buffer at pH 6.5 was found to result in no scrambling The LSI mass spectrum of the crude digest contained a major species at m/z 2175.7. This corresponded with the calculated mass of two fragments (F1 and F2, 1527 6 and 647 2 Da respectively) linked together and containing 3 disulfide bridges (where both F1 and F2 contain three Cys residues). The LSIMS spectrum of the major species after TCEP treatment contained monoisotopic $[F+H]^+$ ions at m/z 1531.6 and 651.2 corresponding with fully reduced fragments (i.e the observed masses were consistent with each fragment containing 3 cysteine residues). We conclude that either 3 inter disulfide bridges link the fragments or the intra disulfide bridges are reduced prior to the single inter disulfide bridge. In the former case the linkage between the two fragments is not useful for investigating the specificity of TCEP.

We have investigated partial reduction with TCEP of the intact K-toxin followed by HPLC purification to isolate three intermediates (R_1, R_2A and R_2B) with retention times intermediate the native (N) and fully reduced (R_3) species. We have alkylated R_1, R_2A and R_2B and observed a number of different species with HPLC. LSIMS analysis of each of the alkylated products of R_1 indicated that each species had 2 alkyl groups added to K-toxin. Similarly all of the R_2A and R_2B alkylated products had masses consistent with addition of 4 carboxy amido methyl (Cam) groups to K-toxin. CZE analysis of R_1 indicated that two species were contained within this broad HPLC peak while only one species was present within both R_2A and R_2B. We are observing four of six possible intermediates suggesting that one disulfide bridge is less readily opened.

We have monitored TCEP reduction of both insulin and a tryptic fragment of K-toxin *in situ* with LSIMS. Using this approach we observed a selective reduction of the intra disulfide bridge of insulin. This and other evidence (e.g. chromatographic and chemical labeling) indicated that TCEP reduction of disulfide bridge containing peptides was at least partially selective. Further studies are planned with peptides of differing disulfide arrangement, in order to generalize these findings and further investigate the level of specificity (e.g. is the intra bridge of insulin opened before or after the first inter bridge). This class of reagent presents unique advantages for elucidating the disulfide arrangement of peptides with adjacent cysteine residues.

Acknowledgment

Work supported by the National Institute of Health (HD-13527, DK-26741, NO1-HD-1-3100, NO1-HD-0-2906, GM-22737) and conducted in part by the Clayton Foundation for Research (California Division) and the Hearst Foundation. We gratefully acknowledge C. Miller for CZE analysis.

References

1 J A. Burns et al. *J Org. Chem.*, 56, 2648 (1991)
2. W H. Fischer et al. *Rapid Commun Mass Spectrom*, 7, 225 (1993).
3 Gray, W. *J Biol Chem* (submitted)

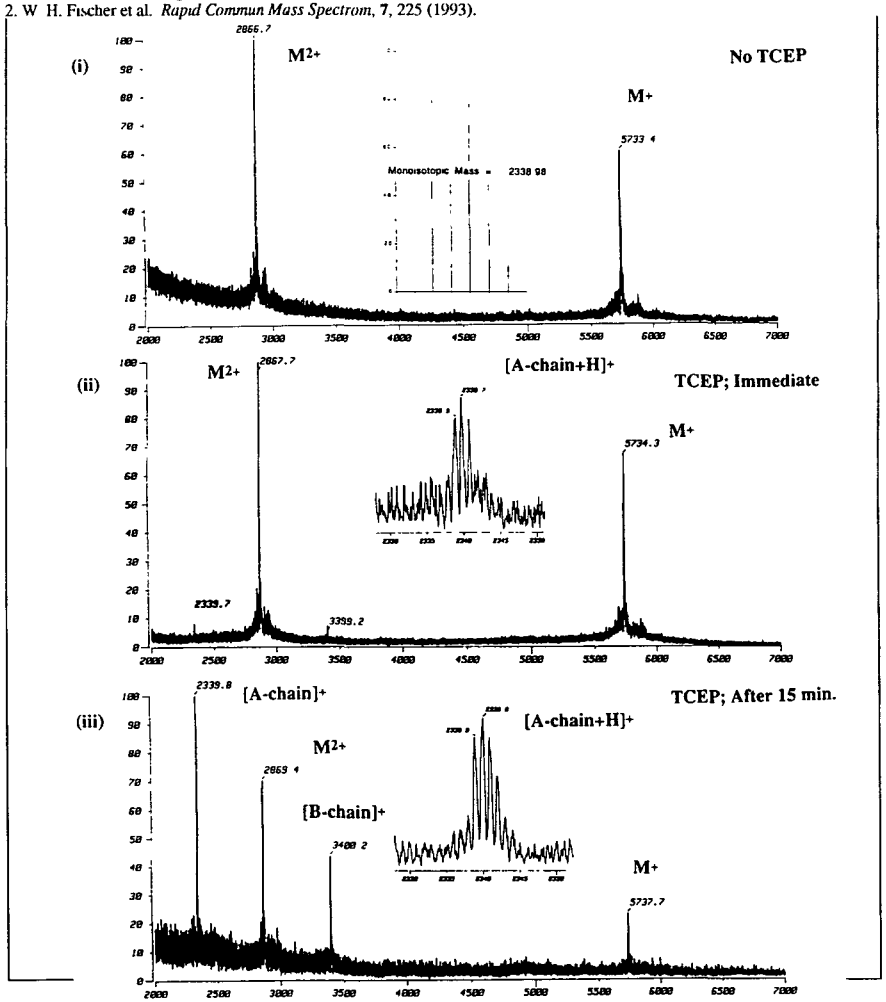

USE OF MASS SPECTROMETRY TO MONITOR CHEMICAL REACTIONS IN PROTEINS

Rong Wang[1], Steven Birken[2] and Brian T. Chait[1]
[1]The Rockefeller University, New York, NY 10021,
[2]College of Physicians and Surgeons of Columbia University, New York, NY 10032

I. INTRODUCTION

Mass spectrometry finds important use in monitoring organic reactions because both final products and reaction intermediates can often be readily detected and identified, and reaction kinetics can be monitored. Such information can be of considerable assistance in the elucidation of reaction mechanisms. The advent of new ionization techniques, like matrix-assisted laser desorption, allows such reactions to be monitored in large complex molecules such as peptides and proteins.

Seleno-methionine (SeMet) is an analog of native methionine (Met) in which sulphur is replaced by selenium. The biosynthetic replacement of methionine residues by selenomethionine has been used in the determination of the three-dimensional structures of proteins by multiwavelength anomalous diffraction. (1)

However, in some cases (e.g. human chorionic gonadotropin), it has been found that crystals of the SeMet-substituted proteins do not produce useful diffraction patterns even though crystals of the Met-containing proteins diffract well. What causes this?

It has been reported (2) that selenomethionine is not as stable as methionine during acid hydrolysis and hydrogen peroxide oxidation. Therefore, one hypothesis to explain the difficulty in the crystallography study described above is that selenomethionine residue undergoes a significantly different oxidation chemistry than methionine. This oxidation of selenomethionine may disorder the structure of the protein or cause the loss of selenium.

II. EXPERIMENTAL

I. Oxidation Peptide samples (5 µg) were dissolved in 10 µL water or desired buffers. 100 µL of 30% hydrogen peroxide was added to the peptide solution and the oxidation reaction was allowed to proceed at room temperature for a desired time. The reaction mixture was then analyzed by mass spectrometry without separation and purification.

II. Matrix-Assisted Laser Desorption Mass Spectrometry Matrix-assisted laser desorption mass spectrometric analysis was carried out on a device constructed at The Rockefeller University. α-cyano-4-hydroxy-cinnapinic acid (4HCCA) was used as matrix. 1 µL of reaction solution was mixed with 10 µL of 4HCCA and 1.0 µL of this mixed solution was applied onto the sample probe.

III. RESULTS AND DISCUSSION

Two model peptides were used in this study. These two peptides share the common sequence Arg-Ala-Ala-Ala-X-Asn-Pro-Thr-Leu-Glu, where the X is methionine for the Met-peptide (M.W. 1073.2 Da) and X is selenomethionine for the SeMet-peptide (M.W. 1121.2 Da) respectively. Figure 1a and 2a are the spectra of these two peptides prior to any chemical treatment.

Figure 1b and 2b are the spectra of these two peptides after 20 minutes oxidation by

30% hydrogen peroxide in water (pH 6.4) at room temperature. The oxidation of the Met-peptide yielded the sulfoxide (M.W. 1089.8 Da) and the sulphone (M.W. 1106.1 Da) as previously reported. (3) However, the SeMet-peptide yields homoserine as the major oxidation product (M.W. 1043.6) rather than the selenoxide and the selenone. Some of the other reaction products were also detected by mass spectrometry (for example, the dehydro-2-aminobutyric acid residue formed by β elimination, peak at m/z 1027.6). These observed products lead us to propose the following reaction mechanism: the oxidation of selenide renders the methyl selenoxide a good leaving group with strong electron-withdrawing tendency. The oxidation can be followed either by a radical reaction forming the homoserine residue or β elimination forming the dehydro-2-aminobutyric acid residue.

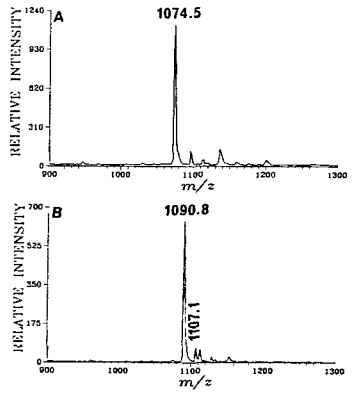

Figure 1 MALDMS spectra of Met-peptide before (a) and after (b) oxidation reaction.

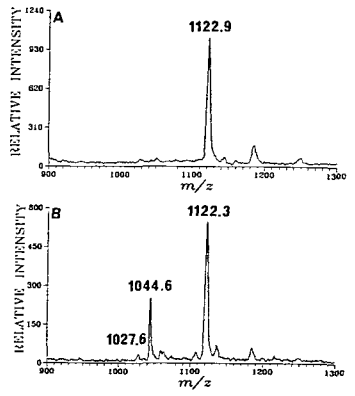

Figure 2 MALDMS spectra of SeMet-peptide before (a) and after (b) oxidation reaction.

We have also tested the sensitivity of the two peptides to oxidation by hydrogen peroxide. Under the same experimental conditions (pH 6.4), the Met-peptide shows a much higher sensitivity to oxidation than the SeMet-peptide. However, when the peptides were exposed to air, the SeMet-peptide is much more sensitive to oxidation than the Met-peptide.

The oxidations of both peptides are affected by the pH of the solution. The oxidation of the Met-peptide is much faster in basic conditions than in acidic conditions. Conversely, the oxidation of SeMet-peptide is much faster in acidic conditions than in basic conditions.

This study shows that mass spectrometry is a rapid, accurate, and sensitive means for monitoring chemical reactions in peptides and proteins

IV. REFERENCES

1. W. Yang, W.A. Hendrickson, R.J. Crouch, and Y. Satow (1990) *Science* **249**, 1398-1405.
2. L. Shepherd, and R.E. Huber (1969) *Can. J. Biochem.* **47**, 877-881.
3. R. Walter, and J. Roy (1971) *J. Org. Chem.* **36**, 2561-2563.

Oxidative Properties of Electrospray Ionization in the Analysis of Peptides

Kenneth Morand, Gert Talbo, *Matthias Mann

Protein and Peptide Group,
European Molecular Biology Laboratory,
Heidelberg, Germany

Electrospray ionization mass spectrometry (ESMS) has seen an increasingly important role in the analysis of large polar and labile compounds such as peptides and proteins. As a result of its wide applicability, many researchers have used ESMS to quantify components present in mixtures. For example, a popular use of ESMS is the determination of the purity of a peptide or protein, such as the determination of protein heterogeneity or the presence of oxidation. In uses such as this it is important that the behavior of the ES source be understood as thoroughly as possible.

Here, we report the observation of an adduct ion of the type [M+H+16]+ present in the electrospray ionization mass spectra of several synthetic and naturally occurring peptides. Initial results have shown that the appearance of the adduct ion is dependent on the field strength at the electrospray needle and the flow rate of the solution passing through the capillary. MS experiments of peptides containing the +16 Da adduct attributed the change to the selective oxidation of either a methionyl, tryptophyl, tyrosl, residue present in the peptide. These results were further confirmed by MS/MS experiments of peptides with a methionyl residue at either the N- or C-terminus, or within the peptide chain. This effect can occur under normal operating conditions and therefore care must be taken in the analysis of samples containing these oxidizable residues. Conversely, the selectivity of the oxidative process may be used to enhance the information obtained from the mass spectrometric analysis. For example, we show results for the analysis of an unknown neuropeptide where the occurrence of the $[M+H+16]^+$ ion is used along with MS/MS data to elucidate the peptide sequence and also that this method may allow one to rapidly screen peptide samples for their occurrence enhancing the information obtained from the analysis of a digestion.

The occurrence of the electrospray-induced oxidation may have further reaching analytical possibilities. While a number of amino acids are subject to oxidative reactions using this method, initial results suggest that methionine and tryptophan appear to give by far the most pronounced effect. More importantly, these amino acids are the only two for which the genetic code is not degenerate (i.e. for which there is only a single neucleotytic base triplet which codes for them). This feature makes them very desired in the construction of oligionucleotide probes used in genetic hybridization studies and, hence, it would be desirable to provide a means of screening unknown peptides for their appearance. Oxidation may also be inducible on the small, polar compounds in the analysis of which ESMS is increasingly used. Similar to the peptide case, our findings may have significance for the avoidance of artifacts created by the ionization method as well as for the selective detection of easily oxidizable compounds. We are currently exploring both of the above possibilities.

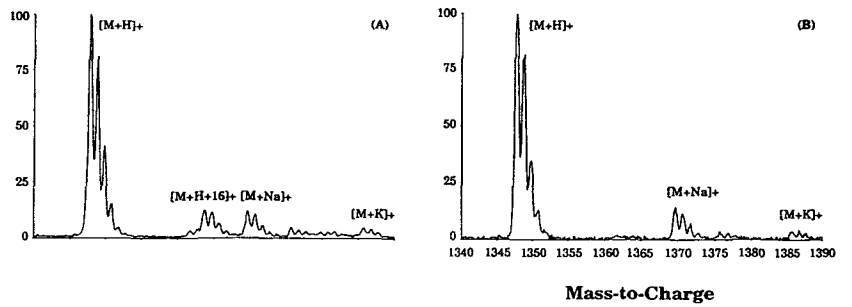

Figure 1: ESMS of substance P (RPKPQQFFGLM, M_r 1347.6) showing the presence of the $[M+H+16]^+$ adduct ion. The flow rate was 5 µL/min and the analyte concentration 25 pmole/µL. The voltage applied to the needle was varied between (a) 5kV and (b) 2.5kV.

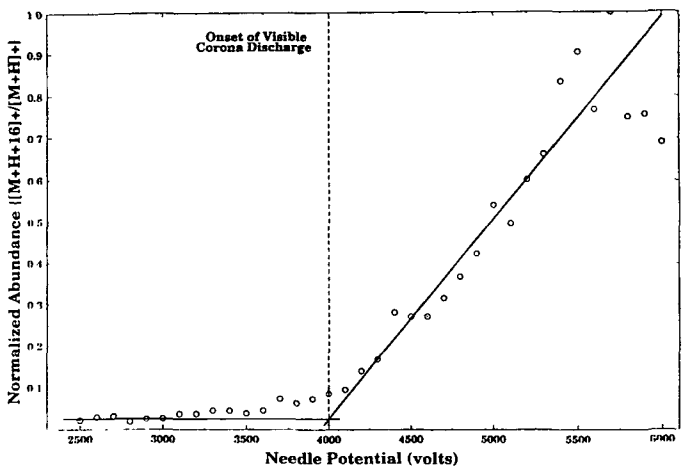

Figure 2: The ratio $[M+H+16]^+/[M+H]^+$ of substance P versus the potential applied to the needle. The vertical hatched line denotes the visual onset of corona discharge.

Gas Phase Reduction-Alkylation For The Identification of Disulfide Bonds At Subnanomole Levels

R.S. Johnson and K.A. Walsh
Dept. of Biochemistry, University of Washington, Seattle, WA 98195

Disulfide bond formation between cysteines is a major post-translational modification of proteins. Identification of disulfide bonds can provide structural constraints within proteins of unknown three-dimensional structure, provide a basis for confirmation (or rejection) of homology between proteins, or provide evidence that a recombinant protein has folded properly. Typically, identification involves proteolytic or chemical cleavage such that peptides connected by single disulfide bonds are obtained; by sequencing these peptides the disulfide bonds can be identified. Usually such cleavage products can only be obtained from non-specific proteases,e.g., pepsin. This has the effect of greatly increasing the complexity of the mixture, making it impractical to purify individual peptides for Edman sequencing. Thus, mass spectrometry has been used to determine pre- and post-reduction molecular weights (1,2). Alternatively, the facile cleavage of disulfide bonds resulting from high energy collisions has been shown to be useful for identifying disulfide bonded peptides (3). Unfortunately, this cleavage has not been observed in low energy collisions, and chemical reduction / alkylation must be carried out when using a triple quadrupole instrument.

A protocol has been developed whereby a proteolytic digest is analyzed by LC/MS to determine the pre-reduction m/z values. A portion of the LC/MS eluent is split and fractions are collected by hand following detection by UV absorption. These fractions are dried and subjected to a single step gas-phase reduction / alkylation (using triethylphosphine and vinylpyridine), and post-reduction m/z values are determined by ionspray mass spectrometry. Correlations are made between pre- and post-reduction m/z values, and MS/MS is used to identify the reduced and alkylated peptides. In many cases, CID gives rise to a very abundant fragment ion of m/z 106 (protonated vinylpyridine); thus parent ion scans for m/z 106 can be employed for rapidly locating peptides containing pyridylethylated cysteine in multicomponent LC fractions. The use of a gas phase reaction reduces the degree of sample contamination and losses such that less than 100 pmol of disulfide-containing peptides can be analyzed. Shown in Fig. 1a is the ESI mass spectrum of a 2 pmol/ul solution of the disulfide-containing peptide oxytocin. Figure 1b depicts the same concentration of oxytocin after reduction / alkylation. The peptide concentration used to obtain Fig. 1b (reduced/ alkylated) was the same as Fig. 1a; indicating that there was little loss of sensitivity upon chemical treatment.

References

1. Morris, H.R. and Pucci, P. (1985) Biochem. Biophys. Res. Comm. 126, 1122-1128
2. Yazdanparast, R., Andrews, B.C., Smith, D.L. and Dixon, J.E. (1987) J. Biol. Chem. 262, 2507-2513
3. Bean, M.F. and Carr, S.A. (1992) Anal. Biochem. 201, 216-226

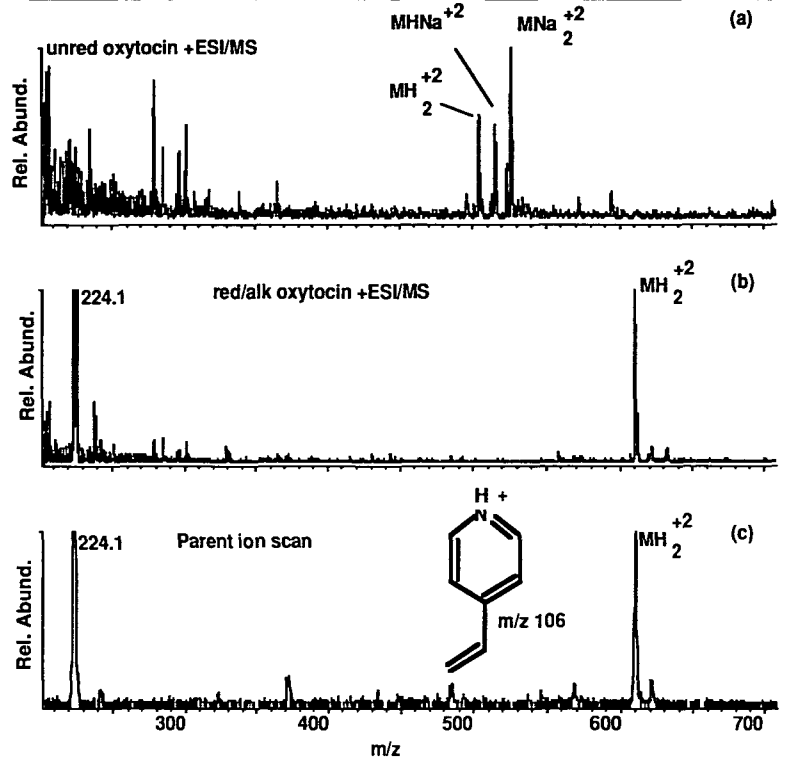

Figure 1: **(a)** +ESI/MS of unreduced oxytocin. **(b)** 80 pmol oxytocin dried in glass tube and subjected to gas phase reduction / alkylation. 500 ul of vinylpyridine (Sigma) and 500 ul of 1 M triethylphosphine in THF (Aldrich) was placed in the bottom of a modified amino acid hydrolysis chamber. A wad of glass wool served to support the sample tubes above the reagent positioned in a bulge of the chamber such that no condensation could run into the sample tubes. The reagents were frozen with liquid nitrogen, evacuated to approx. 130 mTorr, sealed, and warmed to room temperature. The reaction was complete within 1.5 hrs, after which the reagent was frozen, the vacuum released, and the sample tubes briefly placed on a Speed Vac to remove volatile reagent and contaminants. Both reduced and unreduced samples were dissolved in 50% MeOH + 0.1% formic acid at a conc of 2 pmol/ul and analyzed directly by +ESI/MS. **(c)** The same material as in (b), but analyzed by scanning Q1 while statically transmitting only ions of m/z 106 through Q3 (parent ion scan).

The Reactive Site of an Enzyme Inhibitor Complex of the Thiol Protease Cruzain Determined by High Energy Tandem Mass Spectometry

Zhonghua Yu§¶, Ann Eakin§, Patrick R. Jones¶, Charles S. Craik§ and A.L. Burlingame§
§ Department of Pharmaceutical chemistry, University of California, San Francisco, CA 94143, and ¶ Department of Chemistry, University of the Pacific, Stockton, CA 95211

Introduction

A cysteine(thiol) protease, named cruzain, has been found as a key metabolic enzyme in the parasite *Trypanosoma cruzi*, which is the etiologic agent of Chagas' disease, a debilitating disease affecting millions of people in South and Central America. Cruzain's protein sequence has been determined. The native active form of this protease contains 224 amino acid residues. A mutant of this protease, which contains 215 residues having a molecular weight of 22,696 daltons, has the same activity as the wild type [1].

The activity of the protease was effectively inhibited by benzyloxycarbonyl-phenylalanine-alanine-fluoromethyl ketone (Z-Phe-Ala-FMK). The mechanism of inhibition and the reactive site(s) of the protein must be determined to facilitate possible drug designs for the treatment of Chagas' disease. We employed a mass spectrometric strategy to address this issue and determined that one inhibitor is covalently bound to the side chain of cysteine 25.

Procedures

The molecular weight of the inhibited protein was determined by electrospray mass spectrometry. Then the protein was reduced and alkylated. Enzymatic cleavage was carried out by using trypsin, chymotrypsin, V8 and Asp-N protease respectively. The resulting peptides were separated on HPLC and their masses determined by either LSIMS or ESIMS. Subdigestion was performed to cleave the inhibitor containing peptide in order to obtain peptides of appropriate size for MS/MS experiments. High energy CID mass spectra were obtained from a Kratos Concept tandem mass spectrometer of EBEB geometry.

Results

Electrospray mass spectrometry of the inhibited protein showed a molecular weight of 23,062±4 daltons. The mass difference between the inhibited and the uninhibited protein is 365 daltons, which corresponds to one inhibitor residue (M.W.=367daltons). This experiment demonstrated a stoichiometry of one inhibitor per protein molecule.

From peptide mapping of the enzymatic digests, one peptide was found to match the mass of residue 18 to 49 plus one inhibitor. Chymotryptic subdigestion of this peptide generated another peptide, with an MH+ of 1407.5, which corresponds to residue 18-26 plus one inhibitor.

A high energy collisional induced dissociation (CID) tandem mass spectrometric experiment was performed on this peptide. The CID spectrum unambiguously revealed the structure of this peptide, with one inhibitor covalently attached to the side chain of cysteine 25 (Fig.1).

Discussion

Covalent modifications often change the structure and function of a protein, resulting in promotion or inhibition of the protein's biological activity. Characterization of the types and sites of modification is a major step in elucidating the mechanism of a specific process. For characterizing the modification site of cruzain, previous nuclear magnetic

resonance (NMR) experiments suggested that the inhibitor might bind to the side chain of histidine 162. In our work, LSIMS alone has already provided negative evidence for this assignment because the peptide of MH+ 1086.4 only corresponded to the peptide 161-170. However, high energy CID mass spectrometric experiment was required to assign the exact modification site.

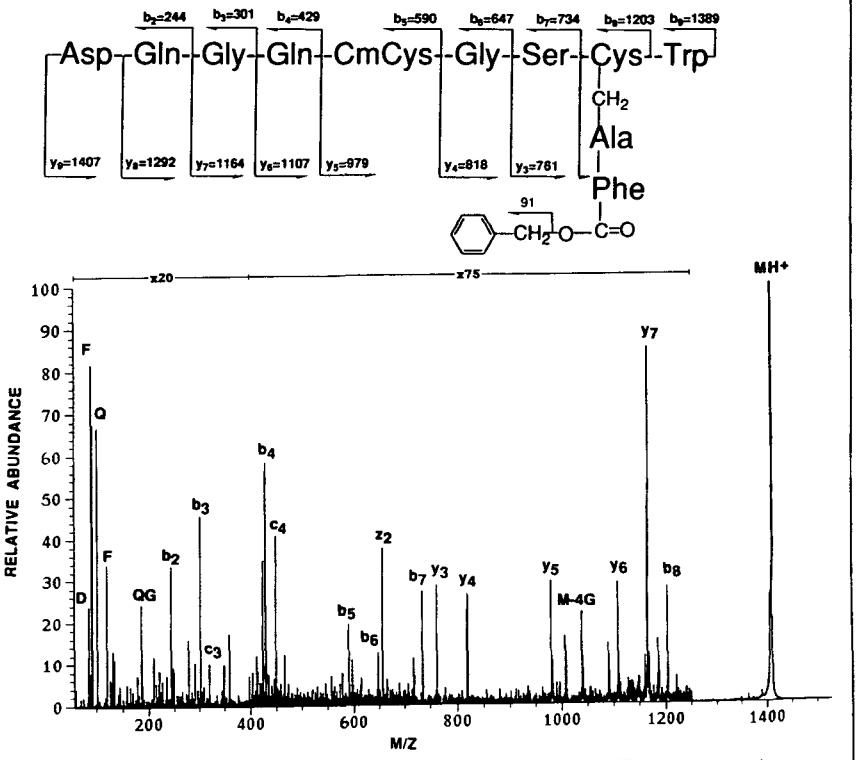

Figure 1. High energy CID mass spectrum of the modified peptide. The b and y series ions were the major products.

Reference

1. Eakin, A.E.; Mills, A.A.; Harth; G.; McKerrow, J.H. and Craik, C.S., (1992), J. Biol. Chem. **267**, 7411.

Acknowledgements

This work was supported by NIH Grant DRR RR01614, NSF Grant DIR 8700766, NIEHS Superfund ES 04705 to A.L. Burlingame and NIH Grant EM 39552 to C.S. Craik.

THE DETERMINATION OF THE PRIMARY STRUCTURE OF THE GLUTAREDOXIN ISOLATED FROM HUMAN ERYTHROCYTES (hErGrx)

Vladimir V. Papov and Klaus Biemann
Dept. of Chemistry, Mass. Inst. of Technology, Cambridge, MA 02139

Glutaredoxins, (also known as thioltransferases), are important in the synthesis of deoxyribonucleotides and are also thought to play a role in cellular sulfhydryl homeostasis. Glutaredoxins exhibit a high degree of homology and are thus of interest in evolutionary studies. A human erythrocyte glutaredoxin has been isolated and characterized by J.J. Mieyal *et al.*, and has been shown to possess catalytic and metabolic properties common to other mammalian glutaredoxins.[1] The human glutaredoxin has been described as a single polypeptide (having an M_r of *ca.* 11,300 by SDS-PAGE) possessing a blocked amino terminus and containing four cysteine residues. The human erythrocyte glutaredoxin is believed to play a role in the maintenance of reduced sulfhydryls in the red blood cells. The primary structure of the human erythrocyte glutaredoxin has now been determined solely by tandem mass spectrometry following a strategy used previously in this laboratory to determine the amino acid sequence of the glutaredoxin from rabbit bone marrow.[2]

Prior to the tandem mass spectrometry experiments, the molecular weight (M_r) of the native human erythrocyte glutaredoxin was determined by matrix-assisted-laser-desorption-ionization time-of-flight (MALDI-TOF) mass spectrometry to be 11,841. The MALDI-TOF mass spectrum of the native glutaredoxin is shown in Figure 1A. The M_r of the S-ethylpyridylated protein, (mass spectrum shown in Figure 1C) increased by 373 u to 12,214. Analysis of the reduced glutaredoxin, (mass spectrum in Figure 1B), revealed that the M_r had decreased to 11,688 and that the mass difference (526 u) from reduced to the S-ethylpyridylated protein now corresponded to the incorporation of five ethylpyridyl groups.

The S-alkylated human glutaredoxin was enzymatically digested and the resultant peptides partially fractionated by reversed-phase HPLC. The molecular weight of the peptides was determined by fast atom bombardment mass spectrometry (FABMS). S-carbamidomethylated glutaredoxin was first digested with trypsin and several of the larger tryptic peptides were further digested with Endo-Asp-N. The amino acid sequences were derived from the collision-induced-dissociation (CID) mass spectra of the peptides. Overlapping sequences from a separate chymotryptic digest of glutaredoxin were used to align the peptides and to assign their position in the glutaredoxin sequence. Lys and Gln (having the same nominal mass) were differentiated on the basis of the specificity of Endo-Lys-C. All of the twenty-one Leu and Ile residues in the human glutaredoxin were differentiated based on the d_n and w_n ions in the CID spectra of tryptic and chymotryptic peptides.

The experimentally determined masses (by MALDI-TOF-MS) for the reduced and S-alkylated glutaredoxin were in close agreement with the calculated masses based on the mass spectrometrically derived glutaredoxin sequence. The human glutaredoxin was found to be highly homologous to the other mammalian glutaredoxins and also contains an acetylated N-terminus. Mass spectrometry has revealed some of the unique features of the human glutaredoxin including five rather than four cysteines, the absence of Met, His at position 52, and a possible heterogeneity (Asp and Asn) at position 51 in the glutaredoxin sequence.

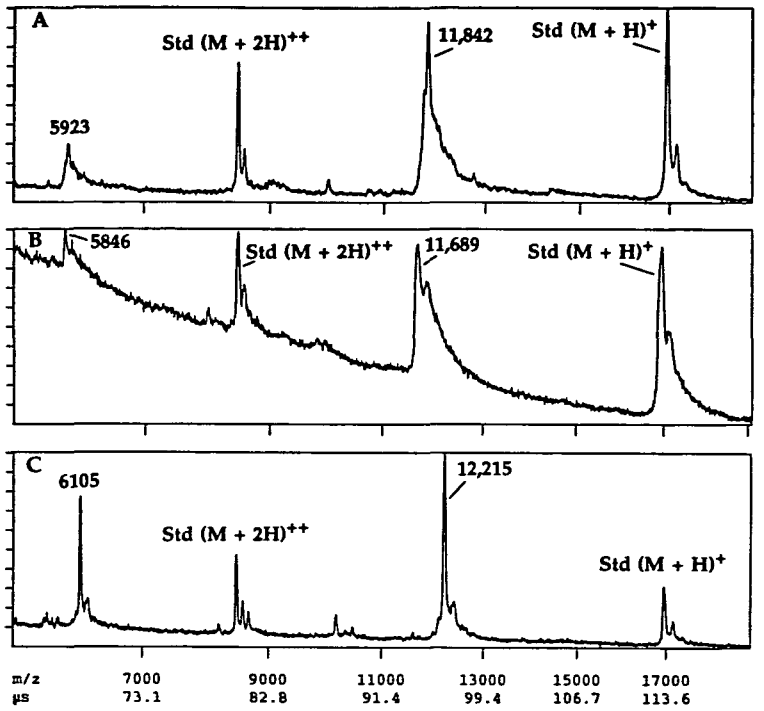

Figure 1. MALDI-TOF mass spectra of glutaredoxin isolated from human erythrocytes. The ions labelled Std $(M + H)^+$ and Std $(M + H)^+$ at *m/z* 16,952.5 and 8476.8, respectively, are due to the internal standard (horse heart myoglobin). **A:** native, **B:** reduced, **C:** S-ethylpyridylated. The matrix was sinapinic acid and the low intensity signals adjacent to the major peaks are adducts of the matrix.

References:

1. J.J. Mieyal *et al.*, *Biochemistry* 30, 6088-97 (1991).
2. Hopper, S., Johnson, R.S., Vath, J.E., and Biemann, K. *J. Biol. Chem.*, 264, 20438-47 (1989).

Acknowledgements:

The authors are indebted to Professor J.J. Mieyal at Case Western Reserve University for providing the human glutaredoxin. This work was supported by NIH grants R37GM05472 and P41RR00317.

THE CHARACTERIZATION OF NATURALLY OCCURING COMPLEX PEPTIDE MIXTURES USING ESI-MS AND MALDI-TOF-MS

J.R. Perkins[1], R.T. Gallagher[1], D.S. Jones[1], S. Davis[1], A.D. Hoffman[1] and K.B. Tomer[2]
1. Kratos Analytical, Manchester, M31 2LD, U.K.
2. NIEHS, Research Triangle Park, NC 27709

Introduction

Mambas (*Dendroaspis*), Cobras (*Naja, Hemachatus*) and Coral Snakes (*Micrurus*) all possess venomous bites, where 90 % of the dried venom consists of small molecular weight protein components. The number of toxins present in snake venoms have been estimated at around thirty by conventional methods[1], but CE-ESI-SIM-MS experiments indicated the presence of around 100 toxins in the venom of *Dendroaspis polylepis* [2]. We are interested in how much preliminary information about complex peptide mixtures (snake venoms) can be gleaned simply from the mass spectra acquired using ESI-MS and MALDI-TOF-MS.

Results and Discussion

Both ESI-MS and MALDI-TOF-MS can provide useful information about the molecular masses of species present within a snake venom. The acquisition of ESI-MS spectra was routine and run to run reproducibility was superior to MALDI-TOF-MS. Ease of acquisition of MALDI-TOF-MS spectra of the snake venoms was dependent on the matrix identity and the polarity of the accelerating voltage.

The low resolution of linear MALDI-TOF-MS means that baseline resolution of peptides with closely related molecular masses can be difficult. The abundant low mass peptides in the venom from *Hemachatus haemachatus* have molecular masses between 6740 and 6940 daltons. In this region of the ESI-MS spectrum we noted 13 peptides including the sequenced toxins 11, 11A, 12A and 12B. In comparison the best MALDI-TOF-MS results noted 6 major peptides Similarly, the major peptides in the venom of *Micrurus fulvius* have molecular masses around 13400, but the low resolution of MALDI-TOF-MS only allows definite mass assignment of the base peaks. In these cases MALDI-TOF-MS provides a useful indication of the approximate molecular weights of groups of ions whereas ESI-MS provides extra resolution for improved characterization of species within the group

The molecular mass assignments provided by ESI-MS and MALDI-TOF-MS have been used to provide confirmation of sequences reported in the literature Spectra of the full venom can definitely confirm the presence of a peptide of a particular molecular mass but cannot prove unequivocally that a toxin is not present because suppression was noted with both methodologies Mass analysis of the individual peptides would be desirable to unequivocally confirm the published sequences. Of the 24 sequenced peptides, for which molecular masses could be assigned from the ESI-MS spectrum the mass accuracy mainly ranges from 0.006% to 0.05%. This compares to a mass accuracy of 0 1% obtained with external calibration for MALDI-TOF-MS

Ion suppression in the MALDI-TOF-MS spectra

The venom of *Dendroaspis polylepis* has been roughly quantified; the major component of the venom, Toxin I (M_r=7132.4), constitutes 20% of the venom[1]. The electrospray spectrum is dominated by the $(M + 7H)^{7+}$ and $(M + 6H)^{6+}$ ions of Toxin I at *m/z* = 1020 and *m/z* = 1190, respectively, but the positive ion MALDI-TOF-MS spectrum using sinapinic acid (+SA) matrix is dominated, instead, by an ion of *m/z* = 6806 resulting from Toxin C (1.5% of venom)[1], while the base peak in the negative ion spectrum, using sinapinic acid (-SA), results from Protein CM-3 (m/z = 7336). The relative abundances of species seen in the electrospray spectrum have been

further clarified by CE-ESI-SIM-MS experiments and other significant peptides in this venom which only show a small response with sinapinic acid, include peptides of molecular weights 7986 (Toxin δ) and 8004 daltons[2]. This suppression of specific peptides can be overcome by use of alternative matrices. The positive ion MALDI-TOF-MS spectrum obtained using α-cyano-4-hydroxycinnamic acid (+CA) as the matrix yielded the $(M + H)^+$ ion of Toxin I as the base peak together with a significant response for both Toxin δ and the peptide of molecular weight 8004. This selectivity is helpful where less abundant peptides yield larger responses than indicated by other methods, such as the enhanced signal, observed using sinapinic acid, for peptides around molecular weight 7300-7400 and 7670 daltons in the venom of *Dendroaspis polylepis* relative to α-cyano-4-hydroxycinnamic acid (CA)

Ion suppression in the ESI-MS spectrum

Reports in the literature state that cobra venoms contain a phospholipase A_2 fraction with molecular masses around 13000 daltons. Two phospholipase A's extracted from the venom of *Hemachatus haemachatus* comprised 10% of the total venom [3]. The ESI-MS spectrum of *Hemachatus haemachatus* provides no indication of larger peptides, but MALDI-TOF-MS spectra, even when acquired at low laser powers to aid the detection and resolution of smaller molecular weight peptides, yielded some response for the phospholipase fraction particularly when sinapinic acid matrix (positive ion) was employed

The ESI-MS spectrum of *Naja melanoleuca* indicated the presence of peptides of molecular masses 13344 and 13432 daltons, but a truer measure of the relative abundances of peptides in the venom of *Naja melanoleuca* was felt to be the total ESI-MS spectrum obtained after CE-MS, where the peptides in the venom were essentially admitted to the source one at a time. The peptides of molecular weights around 13000 daltons had a much higher relative ion abundance than indicated by flow injection analysis

Conclusions

Both ESI-MS and MALDI-TOF-MS provide valuable information for the preliminary characterization of snake venoms. Where many closely related peptides are present ESI-MS is more useful because the resolution of MALDI-TOF-MS is too low to differentiate fully between them, and this can lead to the obscuring of some major components. MALDI-TOF-MS, however, is particularly useful for indicating the full range of peptides present as suppression of higher molecular weight peptides occurs during ESI-MS Suppression during MALDI-TOF-MS is more difficult to predict but can be overcome through the use of alternative matrices. The use of both techniques to provide complementary and confirmatory information is desirable to provide as much preliminary information about complex peptide mixtures such as snake venoms.

1 Schweitz, H , Bidard, J-N.; Lazdunski, M *Toxicon*, **1990**, *28*, 847.
2 Perkins, J.R.; Parker, C.E.; Tomer, K.B. *Electrophoresis*, in press
3. Joubert, F.J *Eur. J. Biochem.*, **1975**, *52*, 539

	ESI	+SA	-SA	+CA	-CA	Total
Dendroaspis jamesoni	22	10	7	20	17	29
Dendroaspis polylepis	31	23	41	40	34	52
Dendroaspis augusticeps	24	29	28	33	29	49
Hemachatus haemachatus	26	20	29	26	25	45
Micrurus fulvius	33	18	18	21	28	45

Table 1. Number of peptides observed using each method with corroboration from other spectra

Analysis of Free Sulfhydryl Content in Proteins by Heavy Atom Derivatization and Matrix Assisted Laser Desorption Ionization Mass Spectrometry

E. J. Zaluzec[1], J. F. Leykam[1], D. A. Gage[1], and J. T. Watson[1,2]
Departments of Biochemistry[1] and Chemistry[2]
Michigan State University, East Lansing, MI 48824

One approach in differentiating cysteine and cystine funcionalities that may exist simultaneously in proteins is to exploit the reactivity of free sulfhydryl groups for metal ions prior to analysis by MALDI-MS. Although many mono- and divalent metal ions can react with sulfhydryl groups, mercurial reagents are known to be especially selective because of the strong affinity of mercury ions for thio groups.

The mass shift determined by comparing the MALDI mass spectrum of the derivatized and underivatized protein can be related to an integral number of free sulfhydryl groups that have reacted with a particular reagent. By using a reducing reagent prior to derivatization, one can further deduce the number of cysteine groups that were originally present in the form of disulfide bonds. Because derivative formation between an organomercurial and cysteine promotes a large mass shift, appropriate use of these reagents to modify the analyte prior to analysis can provide structural information in spite of the limited resolution and mass accuracy in MALDI-TOF-MS, especially in the analysis of proteins over 100 kD.

Free sulfhydryl groups in the protein were derivatized by adding a 5-fold molar excess of mercury reagent and reacting for 10-30 minutes. The total number of cysteines in the protein (those initally free plus those involved in disulfide bonds) were similarly derivatized, but samples were first reduced using either 100mM sodium borohydride, or a 2% solution of tri-n-butylphosphine. Reduction by sodium borohydride permits easy removal of reducing reagent by acidification.

Figure 1a is the MALDI mass spectrum of 100 pm of human hemoglobin A that was dehemed by extraction in acidic acetone, and adsorbed onto ZETABIND immobilization membrane fixed to a stainless steel probe tip. The unmodified protein shows peaks for both the α-chain $(M + H)^+_{calc}$=15,127, and the β–chain $(M + H)^+_{calc}$=15,868. To a similarly prepared sample was added a 5-fold molar excess (over total thio) of p-hydroxymercuribenzoic acid (pHMB). In this case, the MALDI mass spectrum shows mass spectral shifts corresponding to derivatization of the single free cysteine residue of the hemoglobin α-chain, and the two free cysteine residues of the hemoglobin β–chain (figure 1b).

Figure 2a shows the region of the MALDI mass spectrum containing the B- and C- chains of α-chymotrypsin that was first reduced for 30 minutes by 100 mM sodium borohydride prior to analysis $(M + H)^+_{calc}$=13,925 and 10,067, respectively. After sodium borohydride reduction followed by pHMB derivatization, mass spectral shifts corresponding to the derivatization of the 5 cysteine residues of the reduced C-chain and the 4 cysteine residues of the reduced B-chain of α-chymotrypsin were observed..

Derivatization of free sulfhydryl groups can be easily determined at low levels though derivatization with organomercurials prior to analysis by MALDI-MS. In contrast, determination of the total cysteine content has proven to be more difficult experimentally because of the relative poor solubility of reduced proteins, and in that the reducing reagent must be removed before derivatization to prevent reduction of the organomercurial.

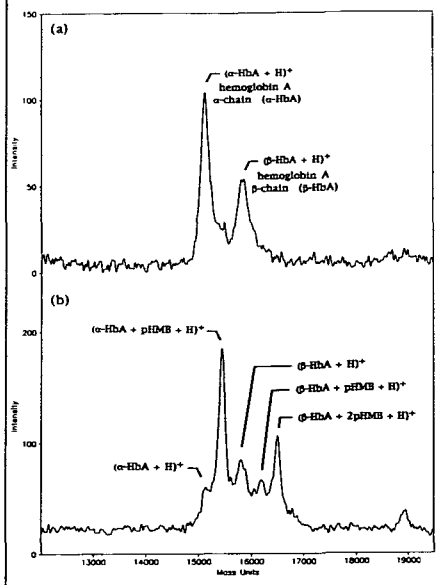

Figure 1
MALDI mass spectra of 100 pm of human hemoglobin A (dehemed) adsorbed on ZETABIND membrane fixed to the probe tip:
(a) unmodified hemoglobin showing peaks for both α-HbA $(M + H)^+_{calc}$ = 15,127 and β-HbA $(M + H)^+_{calc}$ = 15,868,
(b) human hemoglobin A derivatized with pHMB showing mass spectral shifts corresponding to derivatization of the single cysteine residue of α-HbA and the two cysteine residues of β-HbA

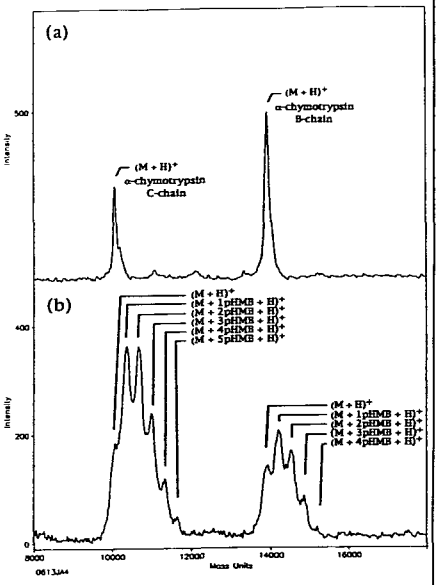

Figure 2
MALDI mass spectra of α-chymotrypsin:
(a) showing the high mass region containing peaks representing the B- and C- subunits recorded after $NaBH_4$ reduction of the native protein, $(M + H)^+_{calc}$ = 13,925 and 10,067, respectively,
(b) after $NaBH_4$ reduction followed by pHMB derivatization at pH=2.0.

TERTIARY STRUCTURE SELECTIVE CHARACTERIZATION OF PROTEIN THIOL GROUPS BY SPECIFIC CHEMICAL MODIFICATION REACTIONS COMBINED WITH MASS SPECTROMETRIC PEPTIDE MAPPING

M.Kussmann[a], T.Knepper[a], D.Wiehr[a], A.L.Burlingame[b] and M.Przybylski[a]

[a]Faculty of Chemistry, University of Konstanz, P.O.Box 5560, D-7750 Konstanz; [b]Dept. Pharm. Chem., University of California, USA-San Francisco, CA 94143

Introduction

Thiol groups in proteins are involved in important biological functions such as protein processing and membrane transport. Chemically and structurally selective thiol reagents acting as thiol markers and protein folding probes are therefore of increasing interest. Phenylarsinoxide (PAO) is a potential candidate to perform these demands. Up to the recent literature, PAO is considered as strongly interacting with thiol groups in proteins[1] and is even applied as a tool for thiol protein purification[2]. In contrast to these various applications, its reactions with sulfhydryl groups have not yet been characterized at a molecular level. In the present study, thiol model peptides and proteins have been modified with PAO and the chemical and structural selectivity of these reactions have been characterized by Fast Atom Bombardment(FAB)- and Electrospray mass spectrometry (ES-MS).

Methods

First, PAO itself was characterized by FAB- and EI-MS. It readily forms adducts with matrices as glycerol and 4-nitro-benzylalcohol and only low intense molecular ions of the monomer were obtained. In contrast EI-MS spectra yielded intense molecular ions of cyclic two- to five-mers.
Oxytocin (sequence: CYIQNCPLG) was reduced with DTT and served as a bifunctional thiol model peptide and its reaction products were compared to those of the monofunctional sequence peptide TCVEWLRRYLKN in order to evaluate the chemical selectivity of PAO Various reaction conditions were tested for applying those found optimum to protein investigations. The structural characterization of the peptide adducts was carried out with FAB-MS using glycerol/0.1% TFA matrices.
Thioredoxin was chosen as a model protein containing two closely spaced sulfhydryl groups in its active site being sterically well accessible due to forming a protruding loop. In addition there is a third thiol group located distant from the active center, so that this protein can work as a mono- as well as bifunctional model system. Thioredoxin is a ubiquituous redox active protein involved in various biological processes, for instance carbondioxide assimilation and protein folding. In this study, recombinant thioredoxin f, a spinach chloroplast's species, obtained by over-expression in E.coli[3], was employed. The molecular weight of the recombinant protein was determined by Electrospray(ES)-MS and its primary structure was characterized by HPLC-ESMS of tryptic and V8-protease digests. The same techniques were applied to determine grade and location of the protein derivatization by phenylarsinoxide comparing the spectra of intact and degraded protein in the native and modified state respectively.

Results

The reduced dithiol peptide oxytocin (m/z 1010) was exposed to 5 - 100-fold molar excesses of PhAsO at pH 2,3...8 and a 5-fold excess PhAsO in the presence of a 10-fold excess of 2-mercaptoethanol at pH 2-4 were the optimum conditions yielding intense molecular ions of the stoichiometric 1/1 peptide-AsPh adduct (m/z 1160) with minor amounts of byproducts. Meanwhile, the monofunctional thiol sequence peptide TCVEWLRRYLKN (m/z 1581) revealed a molecular ion at m/z 1823, due to addition of PhAs+AsO or PhAs+glycerol, a fragment thereof caused by loss of AsO or glycerol (m/z 1733), as well as large amounts of remaining educt, when reacting with PhAsO in a 1:5 molar ratio at pH 2.
Recombinant thioredoxin f was then first characterized in its native state, yielding a molecular mass of 13990 amu (theoretical average mol. mass: 13991) determined by ESMS. After DTT-reduction and carboxymethylation tryptic and V8-protease digests covered over 90% of the protein sequence especially showing intense molecular ions of both cysteinyl peptides of interest (34-53, containing the active site with C^{49} and C^{52}; 74-81, including C^{76}). DTT-reduced thioredoxin was modified with PAO applying standard alkylation conditions (e.g. used for carboxymethylation, enzyme/DTT/PhAsO 1/50/110, pH 8) as well as adjusting pH to 4 (using the same protein/reagent ratios), which turned out to be optimum, when modifying the model peptides. At both pH conditions the active site was selectively derivatized resulting in a stoichiometric 1/1 adduct of PhAsO and the tryptic peptide 34-53, elucidated by LCES data i.e. a selective mass shift from 2282 amu for the carboxymethylated species to 2316 amu for the PhAsO-derivative respectively, meanwhile all other tryptic peptides remained unaffected by the PhAsO-reaction. Furthermore, the HPLC-profile supports this finding showing a delayed HPLC-elution time (about 15 min, water/0.1%TFA//acetonitrile/0.08%TFA gradient, 15-45% B in 60 min, reversed phase C_{18}-column) of the modified relative to the unmodified peptide 34-53 being expected due to the hydrophobic phenyl-arsenic substitution. To confirm the selective addition of PhAsO to the closely spaced cysteinyl residues in the active site, Electrospray mass spectra of PhAsO-modified thioredoxin were monitored and compared with those of the native enzyme mentioned above, revealing a 10 amu mass shift of the $[M+15H]^{15+}$ and $[M+14H]^{14+}$ ions yielding a molecular weight of the PhAsO-modified thioredoxin of 14137 D. This is close to the theoretically expected MW of 14142 D and confirms the selective derivatization of the dithiol containing active site.

Discussion

The present study characterizes **phenylarsinoxide** as a highly **dithiol specific** reagent not affecting other functional groups in amino acid side chains. It can be applied over a wide pH-range (4-8) without loss of selectivity. Its selectivity towards thiol groups differing in the tertiary structure environment is still to be determined. However, phenylarsinoxide is a highly potential candidate for functioning as a protein folding probe due to its preference of inserting into reduced disulfide bridges and, combined with mass spectrometric peptide mapping, it can be efficiently applied in elucidating disulfide bridge patterns. Further investigations with monothiol selective reagents and different model enzymes and mass spectrometric techniques are under way.

References:

[1] R.D.Hofman et al., J.Biol.Chem.1992, 14005.

[2] G.Zhou et al., J.Chrom. 568 (1991), 69.

[3] F.Aguilar et al., Plant Mol.Biol. 20 (1992), 301.

Structures of Recombinant Human Macrophage Colony Stimulating Factor (rhM-CSF) and *in vitro* Refolded Intermediates: Analysis of the Sulfhydryl Alkylation of Free Cysteinyl Residues Using Fast Atom Bombardment - Mass Spectrometry (FAB-MS).

M.O. Glocker[1], B. Arbogast[1], B. Milley[2], C. Cowgill[2] and M.L. Deinzer[1]

[1]Department of Agricultural Chemistry, Oregon State University, Corvallis, OR 97331, USA. [2]Chiron Corporation, 4560 Horton Street, Emeryville, CA 94608, USA.

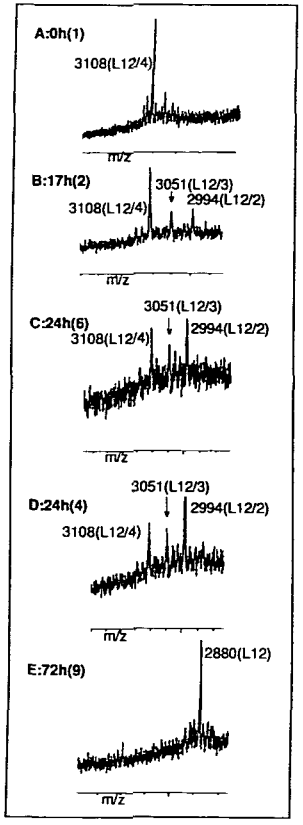

Fig. 1: FAB-MS Spectra of Refolding Intermediates after Lys-C Digestion.

Macrophage Colony Stimulating Factor (M-CSF) is a cytokine of increasing interest within the pharmaceutial and medical communities (1), especially because of its activity as an anti-infective in immune compromised patients (2). It is a hematopoietic growth factor that stimulates the survival, proliferation, differentiation and function of mononuclear phagocytes (3,4). The recombinant human M-CSF (rhM-CSF) we studied here was cloned and expressed from *E. coli* as a truncated form (residues 4 to 221) of the longest cDNA clone (M-CSF β) (5). rhM-CSF contains 9 disulfide bonds, three of them participating in intermolecular bridges resulting in a 49 kD homodimer. We recently reported the locations of the disulfide linkages in rhM-CSF β (6). rhM-CSF is produced in *E. coli* as insoluble and inactive inclusion bodies. Isolated inclusion bodies are reduced, denatured and diluted under appropriate conditions to initiate folding into an active molecule (5). An *in vitro* refolding process is a key step in the production cycle, and therefore, merits special investigation. In order to better understand *in vitro* renaturation and oxidation of rhM-CSF, refolding intermediates were trapped (7) and subjected to proteolysis.

The dimer content of iodoacetamide-alkylated half cystines of trapped refolding intermediates was estimated by SE-HPLC. Intermediates trapped at each of several time points were partially purified using RP-HPLC and were analyzed using FAB-MS in a reducing matrix. The first underalkylation observed occurred at Cys157 and Cys159 and corresponded to the first sample (17 h time point; Fig. 1B) containing disulfide linked dimer. In samples containing only monomer, no disulfide bond formation could be detected (Fig 1A), therefore, disulfide shuffling at the monomer stage can be ruled out under the refolding conditions tested. These results suggest that initial oxidation occurs simultaneously with dimerization. Using the M-NSF-60 analysis (8) no biological activity was found for the monomer M-CSF

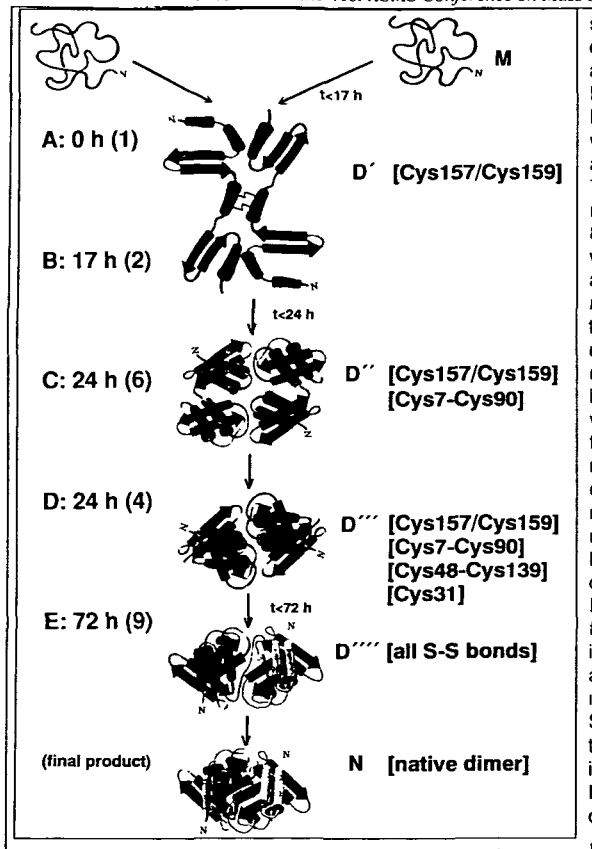

Fig 2: Suggested in vitro refolding pathway for rhM-CSF.

samples. The 24 h time point contained 35% immature dimer and very little biological activity. Four fractions were separated by RP-HPLC and all peptides were partially alkylated (Fig. 1C and 1D) By 72 h of refolding, 79% of the sample was in dimer form and the protein was 86% active. Three isomers were obtained by RP-HPLC and studied by peptide mapping (Fig. 1E). All cysteines were found to be nonalkylated, therefore, all isomers contained nine disulfide bonds. The data from this investigation support the following refolding pathway for rhM-CSF *in vitro* (Fig. 2). In early refolding events, monomers (M) form intermediates that have no disulfide bonds under the redox conditions employed here Initial oxidation leads to the formation of the inactive dimer intermediate (D′) with Cys157 and Cys159 forming the first intermolecular disulfide bonds. Subsequent folding leads to the formation of further intermediates (D″, D‴, and D⁗) that form more and more disulfide bonds until the native homodimer (N) is developed.

1) Aggarwal, B.B & Pocsik, E (1992) *Arch. Biochem. Biophys.* **292**, 335-359
2) Nemunaitis, J , Meyers, J D , Buckner, C D , Shannon-Dorcy, K , Mori, M., Shulman, H., Bianco, J A., Higano, C.S , Groves, E., Storb, R , Hansen, J., Appelbaum, F R & Singer, J.W. (1991) *Blood* **78**, 907-913.
3) Aukerman, S L , Middleton, S., Sampson-Johannes, A. & Ralph, P. (1992) in *Haematopoietic Growth Factors and Interleukins. Biology and Clinical Applications*, eds. Symann, M., Quesenberry, P. & Morstyn, G (Gardiner-Caldwell Communications), pp. 79-93.
4) Clark, S.C & Kamen, R (1987) *Science* **236**, 1229-1237.
5) Halenbeck, R , Kawasaki, E., Wrin, J & Koths, K. (1989) *Bio/Technololgy* **7**, 710-715
6) Glocker, M.O , Arbogast, B., Schreurs, J. & Deinzer, M.L. (1993) *Biochemistry* **32**, 482-488
7) Creighton, T E (1984) *Meth. Enzymol.* **107**, 305-329
8) Nakoinz, I., Lee, M -T., Weaver, J F. & Ralph, P. (1990) *J. Immunol.* **145**, 860-864

MALDI mass spectra of POD derivatives used in an enzyme immuno assay

K.-D. Klöppel, I.Rohm *GBF, D-3300 Braunschweig, Mascheroder Weg 1, Germany*
F.J. Mayer-Posner, U.Rapp *Bruker-Franzen Analytik GmbH, D-2800 Bremen 33, Fahrenheitstraße 4, Germany*

Introduction

Matrix-assisted laser desorption (MALDI) is an established powerful ionisation technique for the mass spectrometrical analysis of biopolymers up to the 10^5 Da mass range. The application of different matrices enables the detection of a large variety of biotechnological relevant compounds. This contribution investigates the application of MALDI for the detection of horseradish peroxidase (POD) derivatives synthesised for a new enzyme immuno assay system for the quantitative determination of mouse immunoglobuline G (IgG) [1]. This enzyme immuno assay is a non competitive homogeneous test system that works on the principle of immuno activation of suitable POD antibody conjugates [2]. Mass spectrometry results of synthesis products were compared with those obtained from photometric techniques usually applied up to now.

Methods

A brief reaction scheme is given in fig.1. Horseradish peroxidase, enzyme immunoassay (EIA) grade, were purchased from Boehringer Mannheim. Further amino groups were introduced into activated POD using 1,4 Diaminobutan. Stabilisation of product was achieved with $NaBH_4$-solution followed by dialysis. Maleimidation of the modified POD was done in a SMCC/dioxan mixture. Purification was achieved by subsequent dialysis against N_2-degased Na-phosphate buffer. $F(ab')_2$-fragment from anti mouse IgG (Dianova) used for the conjugation of maleimid activated POD was reduced with mercaptoethylamine. Conjugates were purified by gel filtration applying TSK G3000 SW (Tosohaas) or Superdex 75 HR columns (Pharmacia). For comparison an activated maleimid-POD was purchased from Merck. Photometry was used to determine the number of free amino and maleimid groups. Amino groups were determined due to the method of Habeeb [3] using lysine solutions as standards. Quantitation of POD maleimid groups was done via calibratrion with solutions of known maleimid (sulfo-SMCC) concentrations [4].

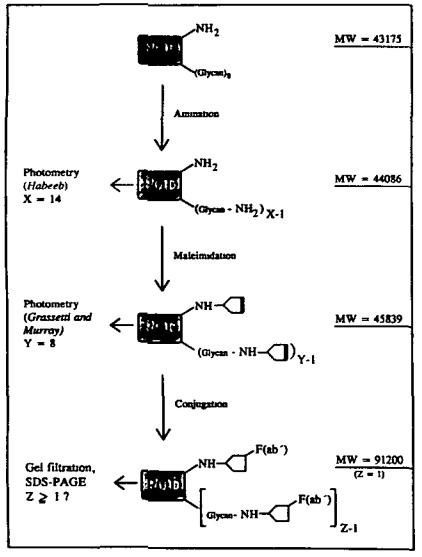

Fig. 1: Reaction Scheme

Mass spectra were obtained using a REFLEX™-TOF mass spectrometer (Bruker-Franzen Analytik GmbH). Ions were produced using a pulsed nitrogen laser at 337 nm using sinapinic acid as matrix. Internal and external mass calibration was achived with bovine serum albumin (BSA).

Results

Basic condition for the successfull synthesis of a POD conjugate for a new enzyme immuno assay test system was the supporting analytic. Hereby, most important is the control with suitable methods of single steps during synthesis of modified POD. Educts, intermediates, products and conjugates have been measured by photometry, gel

filtration, SDS-PAGE electrophoresis and MALDI. Applying photometric methods prove the successful coupling of 12 additional amino groups, and the further incorporation of 8 maleimid groups. For the reference POD 13 maleimid groups were determined, in accordance to specifications of Merck. However, gel filtration and SDS-PAGE electrophoresis of final conjugates only show an average value of 1-3 F(ab') molecules per POD. In contrast to these results mass spectrometric analysis yielded partially lower molecular weights, i.e. lower amino, maleimid and F(ab') amounts in the conjugates (s Table 1). Mass of POD amine was even lower than that of native POD. Peak shapes are broader than expected only by isotopic distribution. Broadening is caused by contributions of adducts of impurities, matrix molecules and especially here the different sample components. Native POD is a mixture of more than 10 isoenzymes. Main component (90%) is the isoenzyme C containing 8 glycans and different amounts of serin. A minor component containing 9 glycans is apparent in the MALDI-MS spectrum (s. Fig. 2). The detected molecular masses of intermediates leads to the assumption that 2 glycans were cleaved off partially at the GlucNAc-GlucNAc bond of the chitobiose unit during amination step, while due to photometric results the remaining glycan residues are multiply aminated (Σ=12). MS-results show further the incorporation of 8 maleimid groups which could be used for conjugate formation. The purchased maleimidated POD contains due to MS-results at least 10 maleimid groups. For final and reference POD a distribution of 1-2 F(ab') molecules per POD were determined by MALDI-measurements, i.e. somewhat lower than average amounts found by gel filtration and SDS-PAGE.

Compound	x	y	z	MW_{theor}	MW_{meas}	MW_{diff}
POD_{nativ}	-	-	-	43.175	43.191	+ 16
POD_{amin}	14	-	-	44.088	42.260	- 1.828
POD_{mal}		8	-	45.839	43.875	- 1.964
POD_{merck}	14	13	-	46.934	46.317	- 617

Table 1: Comparison of MALDI-MS results

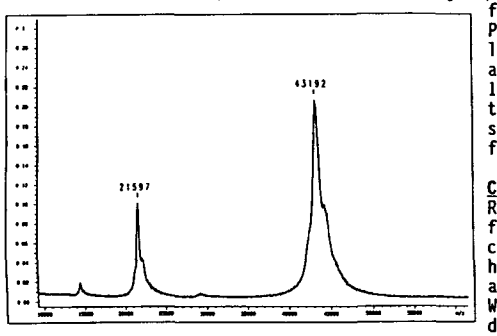

Fig. 2: MALDI mass spectrum POD_{nat}

Conclusions

Results show, that MALDI is a powerful analytic technique applicable for control of steps during synthesis of high molecular weight compounds in addition to conventional methods. While photometric results of intermediates let expect a higher F(ab')-part in the POD-conjugates, the MS-results show that the at least determined amount of 1-3 F(ab') per POD is more realistic. F(ab')-POD-conjugate successfully was established for the set up of a homogeneous enzyme immuno test. Further measurements showing the exact distribution of F(ab')-POD in conjugates of test systems are in preparation.

References

[1] I. Rohm, Diploma, Braunschweig 1992
[2] Ennen, J.; Bäurle R. *MTA* 5 1990, 222
[3] Habeeb, A.F.S.A. *Anal. Biochem.* 14 (1966) 328
[4] Grassetty and Murray *Arch. Biochem.Biophys.*119(1967) 41

MALDI measurements of Intermediate Filament Proteins in Chaotropic Buffers

W.D. Lehmann, J. Schweizer, German Cancer Research Center, D-6900 Heidelberg, Germany

U. Rapp, F.J. Mayer-Posner, Bruker-Franzen Analytik GmbH, D-2800 Bremen, Germany

Introduction

Intermediate filament proteins are the constituent proteins of 10 nm filaments that are part of the cytoskeleton of mammalian cells. They represent highly insoluble proteins. Molecular weights of the keratins are generally determined by SDS-PAGE size estimation or by molecular cloning and calculation on the basis of the derived amino acid sequence. We attempted to use matrix-assisted laser desorption mass spectrometry (MALDI-MS) as additional and independent method for the determination of the molecular weight of keratins. In this approach either total keratin fractions from newborn mouse epidermis or purified individual keratins were investigated.

Methods

Isolation of Total Epidermal Keratins

Total keratins from heat separated newborn mouse epidermis were extracted using a guanidinium thiocyanate buffer as described (1). They were reconstituted by extensive dialysis against water and dissolved in a urea buffer (6M urea, 100 mM Tris pH 7.5, 1% mercaptoethanol) for molecular weight determination.

Isolation of Individual Keratins

Total keratins from adult mouse foot sole epidermis were separated by SDS-PAGE according to Laemmli (2) and visualized by (A) Coomassie blue staining or (B) ammonium acetate staining. Single keratin bands were cut out from the gel and resolubilized by homogenization in guanidinium thiocyanate buffer. After centrifugation, the keratin supernatant was dialyzed against water, freeze-dried and the proteins redissolved in urea buffer for molecular weight determination.

Mass Spectrometric Analysis

Measurements were performed using a REFLEX™MALDI/TOF mass spectrometer (Bruker-Franzen Analytik GmbH, Bremen Germany). Data were acquired in linear mode and positive ionization using 35 kV accelerating voltage. Ions were formed by laser desorption at 337 nm (Nitrogen laser, 3 ns pulse width).

For mass calibration bovine serum albumin (Sigma A-4378) was used as external standard. For calculation the mass value 66,431 Daltons was applied.

The samples were prepared with sinapinic acid as matrix and a total loading of around 5 picomoles of keratins on the target.

Results

1. Total Keratins

Mixture analysis of total keratins of newborn mouse epidermis by gel electrophoresis and MALDI-MS showed a similar pattern of the molecular weight distribution, the range of molecular weights extending from about 50 to 67 kD. The molecular weight of one of the main keratin components in newborn mouse epidermis as determined by MALDI-MS was found to be 58,282 D ± 21 D (S.D.) (n=3). This signal corresponds to keratin 10 with a molecular weight of 57,711 D as determined by molecular sequencing (4). The difference of 571 D is due to a posttranslational modification (e.g. addition of several phosphate groups). Similar comparisons cannot be made for the remaining keratins due to lack of full length sequence data.

2. 70 kD Keratin

Sequence data of the main keratin of adult mouse epidermis predict a molecular weight of 70,980 (5). When this keratin is isolated and analyzed by MALDI-MS a molecular weight around 70,900 D is observed. However, as evident from separations by two-dimensional gel electrophoresis, this fraction is a mixture of up to ten in vivo generated components differing in the degree of phosphorylation and in the proteolytic loss of a few amino acid residues. In the mass spectrum these modifications result in a relatively broad peak exhibiting a fine structure around the peak center.

Conclusions

This study has shown that molecular weight determinations of highly insoluble proteins such as keratins can be successfully performed by MALDI-MS. This is demonstrated by using both total and keratin fractions and isolated individual keratins. The data obtained suggest that by means of the MALDI technique subtle molecular weight changes caused by posttranslational processing or phophorylation can be detected.

References

1. H. Winter et al., Carcinogenesis 1, 391-398 (1980)
2. U. Laemmli, Nature 227, 680-685 (1970)
3. Moll et al., Cell 31, 11-24 (1982)
4. Krieg et al., J.Biol.Chem.260, 5867-5870 (1985)
5. J. Schweizer et al. unpublished results

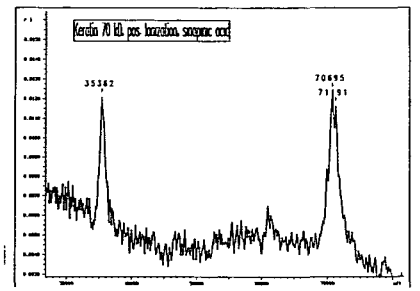

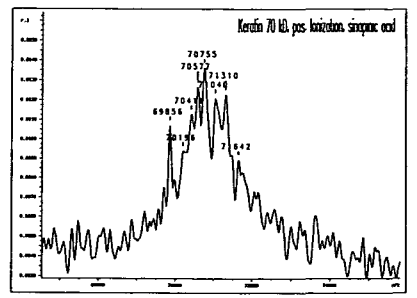

QUANTITATION OF PROTEIN MULTIMERIC SPECIES USING MALD TOF MS

Terry B. Farmer and Richard M. Caprioli
The Analytical Chemistry Center and the
Department of Biochemistry and Molecular Biology
University of Texas Medical School, Houston, Texas 77030

Introduction

Matrix assisted laser desorption mass spectrometry (MALD MS) in conjunction with chemical crosslinking has been used to qualitatively assess the quaternary structure of multimeric proteins[1]. Previous comparison of MALD MS with sodium dodecyl sulfate polyacrylamide gel electrophoresis (SDS-PAGE) with subsequent densitometric scanning of the silver stained gel showed that there were some differences in the quantitation of the multimeric species present in solution after crosslinking[2]. To examine these results more closely multimeric proteins were crosslinked and then separated on a gel filtration column to isolate individual species of the crosslinked proteins. The separated protein multimers were then recombined in a 1:1 molar ratio and examined by MALD mass spectrometry.

Experimental

Protein Crosslinking: Gluteraldehyde (Sigma Chemical Co.) was used as the homobifunctional crosslinking agent for carbonic anhydrase (CA), bovine serum albumin (BSA), and glucose 6-phosphate dehydrogenase (G6PD)(Sigma Chemical Co.). Solutions of 10 pmol/μl protein were prepared and glutaraldehyde was added to 0.8% by volume. The UV absorbance for each uncrosslinked protein was determined before and after the addition of crosslinker using a Gilford 250 UV/Vis Spectrophotometer and no observable change occurred in the absorbance at 280 nm. The crosslinking reaction was terminated after 60 minutes by the addition of an excess of $NaBH_4$ (Aldrich Chemical Co.). The protein solution was dialyzed against Milli Q water for >3 hours using Spectra/Por 6 10000 MCO dialysis tubing (Spectrum) then concentrated against a 20% solution of PEG 20000 (EM Chemical Co.).

Gel Filtration Chromatography: CA was separated on a Sephadex G-100 column (40 cm x 1.5 cm) with a mobile phase of 1% ammonium bicarbonate/0.5 M NaCl and a flow rate of 0.195 ml/min. G6PD and BSA were separated on a Sephadex G-200 column (60 cm x 0.9 cm) with a mobile phase of 0 1 M Tris base/0.5 M NaCl (pH 8.0) and a flow rate of 0.035 ml/min. The fractions were collected and the absorbances were read at 280 nm. The identity of the separated multimers in the fractions was confirmed by SDS-PAGE (Weber-Osborne method[3]) and the gels were silver stained (Bio-Rad). The fractions containing the multimers of interest were dialyzed against Milli Q water until the sodium concentration was below 1 μM and then concentrated against a 20% solution of PEG 20000. Protein concentration was determined using Beer's Law ($A = \epsilon bc$).

Matrix Assisted Laser Desorption Mass Spectrometry: Spectra were obtained on a Vestec ResearcH instrument with a flight tube length of 1.2 m using a N_2 laser and acceleration voltage of 22.5 kV and a multiplier voltage of 4 kV. A saturated solution of sinapinic acid (Aldrich Chemical Co.) in a 70% acetonitrile/30% water/0.1% TFA solution was used as the matrix. The individual protein multimers (2-5 pmol) were added to 1 μl of the sinapinic acid solution, mixed, and dropped onto a stainless steel pin at room temperature. 1.1 molar ratios of the isolated protein multimers were made and added to 1 μl of the saturated sinapinic matrix and then treated as the individual protein multimers. The preparations were mass analyzed (Fig.s 1-2).

Results and Conclusions

In the present experiments we have quantitated protein samples by MALD TOF. These

experiments measure overall mass discrimination from sample preparation to data analysis. Glutaraldehyde crosslinked proteins were separated and recombined in a 1:1 monomer:dimer molar ratio and mass analyzed. Two assumptions were made for this work: crosslinking does not affect any of the MALD MS conditions (drying with the matrix, ionization, etc.) or the extinction coefficient of the UV absorbance of the protein at 280 nm.

The contribution of multimers and multiply charged ions was determined. The peak area of the M^{+2} and $2M^{+}$ ions were calculated from the spectra of the isolated monomers and dimers and used to correct the peak areas obtained from the recombined mixtures.

The effect of laser intensity on peak area was also investigated. Increasing laser intensity decreased the M^{+} peak area slightly, but caused significant deterioration in peak shape and width (resolution).

The spectra of CA 1:1 monomer:dimer indicated mass discrimination is 3:1 monomer:dimer from 30 kD to 60 kD while for BSA the mass discrimination is 2:1 from 66 to 135 kD. These data indicate a 6·2:1 discrimination from 30 to 135 kD. The data were very reproducible (±2 %) as long as the laser intensity remained constant for subsequent mass analysis. Semi-quantitation of crosslinked multimeric species present in solution for the tested mass range can be accomplished. Work is currently in progress to analyze other proteins such as hemoglobin, lactate dehydrogenase and lysozyme to better characterize the process.

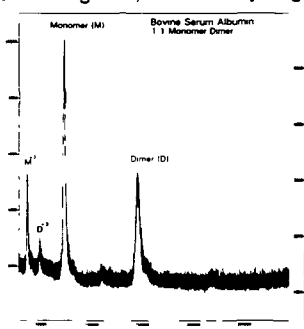

Figure 1

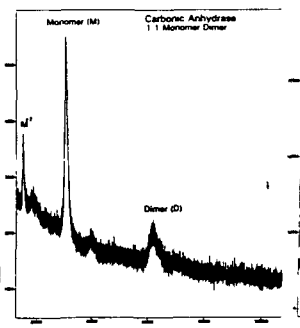

Figure 2

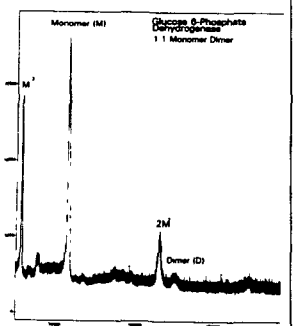

Figure 3

The result of the 1:1 monomer:dimer mix of G6PD showed no overlap of the mass for the monomer $2M^{+}$ peak with the M^{+} dimer peak. This is due to differential addition of glutaraldehyde. Using MALD MS, atypical glutaraldehyde crosslinking can be quickly and easily determined.

References

1. T.B. Farmer and R.M. Caprioli (1991), *Biol. Mass Spectrom.*, **20**, pp. 796-800.
2. Terry B. Farmer and Richard M. Caprioli (1993), Techniques in Protein Chemistry IV, Ruth Angeletti, ed., Academic Press,Inc., pp. 73-81.
3. K. Weber and M. Osborn (1969), *J. Biol. Chem.* **244**, pp. 4406-4412.

Acknowledgements

We would like to thank Dr. C. Vestal and Y.P. Wang of Vestec for their assistance and NIH (Grant #GM43783) for their generous support.

CHARACTERIZATION OF PEPTIDES AND GLYCOPROTEIN DIGESTS USING CAPILLARY ELECTROPHORESIS COMBINED WITH IONSPRAY/TANDEM MASS SPECTROMETRY

Kevin J. Volk, Jinping Liu, Mike S. Lee, Steven E. Klohr, Edward H. Kerns, and Ira E. Rosenberg, Bristol-Myers Squibb Company, 5 Research Parkway, Wallingford, CT 06492

Micro-separation techniques such as capillary electrophoresis (CE) can be used to quickly and efficiently separate complex biological mixtures. These techniques are rapidly gaining acceptance in the bio-pharmaceutical industry for the separation, analysis, and characterization of mixtures such as those produced from protease digestions. The high separation efficiency of CE (1,2) and micro-LC (3) combined with tandem mass spectrometry is an extremely powerful approach for the structural characterization of peptides and proteins in complex mixtures. The profiling strategies we have developed for micro-LC/MS (3) utilizing various enzymatic methods can be applied when CE is coupled with mass spectrometry.

We have coupled a Beckman P/ACE unit to a SCIEX API III triple quadrupole mass spectrometer via a coaxial interface. The conventional Ionspray interface was modified to accommodate standard 360µm o.d. x 50µm i.d. CE columns. All separations were performed at 30kV (25µA) using an uncoated column (100cm) with a running buffer of 25mM ammonium formate, pH 2.5. A make-up buffer (80/20) methanol/0.2% formic acid in water was added at a flow rate of 5µl/min. The mass spectrometer was scanned from m/z 350 to m/z 2200 with a step size of 0.4 Dalton and a dwell time of 0.7 mSec. Deglycosylation was performed using peptide-N-glycosidase F (PNGase F).

The utility of CE coupled with Ionspray tandem mass spectrometry is illustrated with the on-line separation and detection of a peptide mixture (Figure 1). Here we demonstrate the ability to detect peptides at the sub picomole level with a wide scanning range. Various glycoforms of glycoproteins can be separated and characterized using this methodology. The UV electropherogram of a model glycoprotein, Ribonuclease B, is shown in Figure 2. A comparison of the full scan and deconvoluted Ionspray mass spectra of the Ribonuclease A impurity and various Ribonuclease B glycoforms (Figure 3) indicates the molecular weight and heterogeneity of these glycoforms. Products of microscale enzymatic reactions with proteins and glycoproteins were also profiled by CE/MS and CE/MS/MS. Since not all intact glycoproteins yield interpretable mass spectra without deglycosylation, a coordinated approach using a combination of enzymes such as trypsin and PNGase F followed by CE/MS and CE/MS/MS analysis provides complementary information such as carbohydrate composition, sites of N-linked carbohydrates, and sequence information.

In summary, the unique separation mechanism of CE permits the rapid and efficient separation of closely related components such as protein glycoforms as well as structurally similar proteolytic fragments. Coupled on-line with MS, molecular weight information can be rapidly assessed. In addition, MS/MS can provide sequence and substructure information for tryptic peptides and glycopeptide fragments at the sub picomole level. The general profiling methodologies were developed to characterize glycoproteins and are applicable for the characterization other post-translational modifications.

1. P. Thibault et al., 40th ASMS Conference on Mass Spectrometry and Allied Topics, Washington, DC.
2. S. Pleasance et al., J. Chrom., **591**, 325, 1992.
3. J. Liu et al., J. Chrom. **632**, 45, 1993.

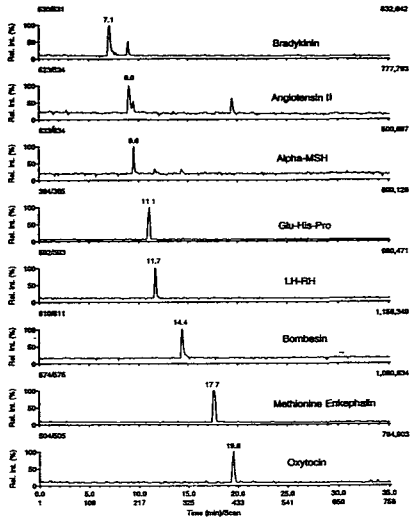

Figure 1. Mass chromatograms (singly/doubly charged ions) of a synthetic peptide mixture (sub picomole levels).

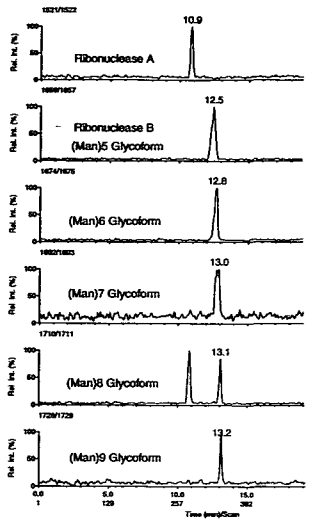

Figure 3. CE/MS mass chromatograms of Ribonuclease B protein glycoforms, $(M+9H)^{9+}$ ions.

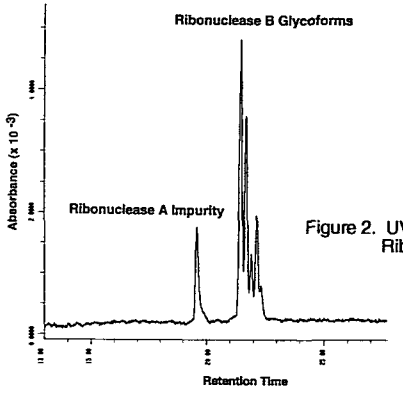

Figure 2. UV electropherogram showing resolution of Ribonuclease B protein glycoforms.

FROM DIPEPTIDES TO OLIGOPEPTIDES : ANALYSIS BY CAPILLARY ELECTROPHORESIS/ELECTROSPRAY MASS SPECTROMETRY.

Darren Wycherley, Malcolm E. Rose, *Department of Chemistry, The Open University, Milton Keynes, MK7 6AA, UK.*
Kevin Giles, Stuart A. Jarvis and Mark A. McDowall, *Fisons Instruments, VG BioTech, Altrincham, WA14 5RZ, UK.*

Capillary electrophoresis (CE) has found application to a broad range of separations including peptides, nucleotides, surfactants and environmental compounds. CE is complementary to standard HPLC but offers rapid high resolution separations with efficiencies between, 10^4 to 10^6 theoretical plates, and can be used for difficult separations. The standard detection method for CE is UV absorption, however, the utility of the technique is greatly enhanced using mass spectrometric detection; more specifically, electrospray ionisation (ES). The system utilised a nebulisation-assisted triaxial flow probe for coupling the CE column to a quadrupole mass spectrometer. Two CE/MS systems were developed for this work: the ISCO 3850 CE instrument coupled to a VG Quattro, and the Beckman P/ACE 2100 CE system fitted with a mass spectrometer interface coupled to a VG Platform benchtop API mass spectrometer. To date, volatile buffers composed of ammonium salts have been most extensively used for CE/ES. However these studies utilized involatile buffers composed of phosphoric acid and β-alanine at low concentrations.

Peptides, in contrast to amino acids, are excreted in urine of healthy individuals only in minute amounts. Strongly increased excretion of some peptides is indicative of dermatological disorders such as chronic skin ulceration. Frequently, susceptibility of dermal collagen to enzymatic degradation appears to be responsible for small peptides and dipeptides in particular, in the urine of such patients. During the course of work on urinary acylcarnitines by GC/MS it was noticed that several neonates excrete high levels of certain dipeptides (e.g. Ala-Leu or Ala-Ile, Pro-Ile or Ile-Pro.) Results have now been obtained by CE/MS for a number of dipeptides leading to the analysis of real neo-natal urine suspected to contain such compounds. In addition, data are presented on the CE/ES analysis of a peptide mixture (Bradykinin, Leucine-enkephalin-Arg, Angiotensin I, Angiotensin II and Angiotensin III) together with a sensitivity study.

A standard mixture of 6 dipeptides was examined by CE/ES. All six dipeptides, despite being very similar in structure, are separated and exhibit peaks for the expected singly protonated molecule in their electrospray spectra.
The urine sample examined was shown to contain various peaks of interest. For instance, the peak corresponding to *m/z* 114 is most likely to be creatinine, which is known to be present in all human urine. The peak at *m/z* 132 is consistent with the protonated molecules of the amino acids, leucine, isoleucine or hydroxyproline. It is hoped that future work will lead to the unambiguous

The reproducibility of the system was examined by introducing three 5-second hydrodynamic injections of Angiotensin II at five different concentrations from 220 pg/nl to 5 pg/nl (630 fmol to 15 fmol injected) as figure 1. A scatter-point calibration graph plotted from the resulting peak heights gave a correlation coefficient of 0.9999.

System reproducibility and sensitivity chromatogram using angiotensin II

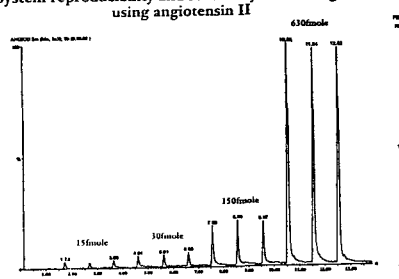

Full scan of the 5 peptide mix, 2.5pmol of each injected

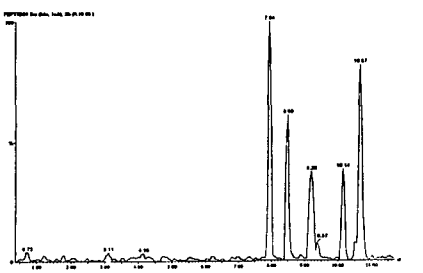

A total ion chromatogram obtained from 2.5 picomoles each of the five peptides by full scanning was recorded, giving baseline separation within a total analysis time of about 15 min, (figure 2). Subsequently, ES spectra were obtained from this chromatogram. The doubly- or triply-charged species of each peptide were most prevalent.

The selected-ion reconstructed chromatogram of the five peptides, 300 femtomoles of each being injected onto the capillary over 5 seconds, was also obtained.

Peptide elution order: Angiotensin III, Bradykinin, Angiotensin I, Leu-enkephalin-Arg and Angiotensin II.

Despite having the largest mass, angiotensin I migrates rapidly through the CE column because it has the largest number of basic residues in its sequence. Consistent with this, its ES spectrum displays a prominent $[M + 3H]^{3+}$ ion.

By combining CE and ES efficient separation and identification of compounds can be achieved. The results shown demonstrate how samples of biochemical significance can be analysed by CE/ES. Coupling of both CE instruments (Beckman and ISCO) to the VG Platform and Quattro mass spectrometers, respectively, produced results illustrating the feasibility of performing these types of analyses at physiologically significant levels.

Mass Spectrometry of Proteins Isolated from Capillary Gel Electrophoresis

R. Takigiku, T. Keough, M. P. Lacey, R. E. Schneider and M. P. Purdon
The Procter & Gamble Co., Miami Valley Labs, PO Box 398707, Cincinnati, OH 45239-8707

We describe our efforts at collecting proteins from capillary gel electrophoresis (SDS-PAGE) and analyzing them by mass spectrometry. Performing SDS-PAGE in capillaries has a number of advantages. Because it is a fully instrumental method, capillary SDS-PAGE offers automation, as well as improved reproducibility and quantitation (relative to traditional slab-gels). Additionally, on-line fraction collection is possible, eliminating the need for staining, destaining, excising and electroeluting proteins. A significant advantage of fraction collection is that it makes protein available for analysis with complementary biochemical methods such as automated Edman sequencing.

Though capillary SDS-PAGE yields molecular mass information, mass spectrometry offers far greater accuracy and precision. In particular, electrospray and matrix-assisted laser desorption ionization mass spectrometry (MALDI) have demonstrated mass measurement accuracies of between ± 0.01 and 0.2%. Hence, we sought to couple the micropreparative capability of capillary SDS-PAGE with the mass measurement capabilities of mass spectrometry.

In order to accomplish this task, we developed a method for removing detergent from protein isolates. This was necessitated because trace amounts of SDS suppress mass spectrometry ionization methods. Purified proteins could then be analyzed by both ionspray (pneumatically assisted electrospray) on a triple quadrupole instrument, and by MALDI on a time-of-flight instrument.

Capillary SDS-PAGE was accomplished with a home-made acrylamide gel-filled capillary, and with a commercially available SDS-PAGE system (Beckman eCAP SDS 200). For comparison, electropherograms of protein standards analyzed on a home-made acrylamide (3%T, 5% C) gel-filled capillary (A) vs. the Beckman eCAP SDS 200 system (B) are shown below.

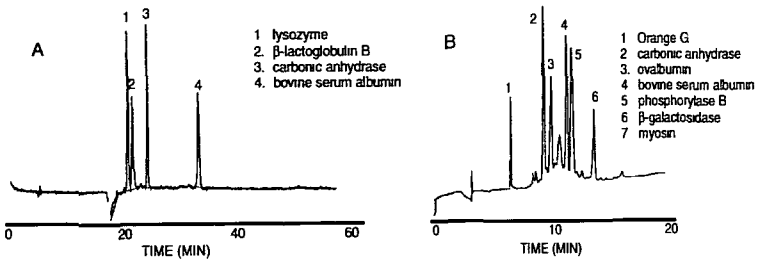

For fraction collection, the migration time of the analytes from the injector to the UV detector were used to calculate the overall migration times to the outlet of the separation capillary. Multiple isolates were pooled by repeated collection of a peak of interest into the same collection vial.

All isolates were collected into an Amicon Microcon 3 (for acrylamide gel-filled capillaries) or Amicon Microcon 10 (for Beckman eCAP SDS 200 gel-filled capillaries). Amicon Microcons are ultrafiltration devices that accept 1.5 ml microfuge tubes (Microcon 3 has a nominal cutoff at 3 kD, whereas the Microcon 10 is at 10 kD).

solates were washed and reduced to approximately 3-5 µL on a speed-vac at room temperature and brought back up to ca. 10 µL with a 1:1 solution of 10% formic acid and methanol.

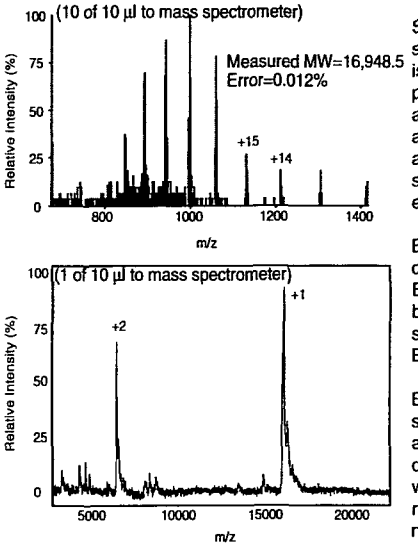

Shown at left are ionspray and MALDI mass spectra of duplicate samples of myoglobin isolates. Although neither quantitation nor percent recoveries of the isolates was thoroughly assessed, a pooled sample of 10 isolates (from an acrylamide gel capillary) corresponds to approximately 4 pmoles (because no internal standard was used for this particular MALDI experiment, a measured mass is not given).

Both carbonic anhydrase and BSA were also collected and analyzed by ionspray and MALDI. Both proteins yielded recognizable spectra from both MS approaches. However, a pooled sample of at least 20 isolates were required for BSA (ca. 8 pmoles).

Both forms of capillary SDS-PAGE used here sieve proteins reproducibly. However, the acrylamide gel-filled capillaries must be discarded after the formation of air bubbles, wherease the eCAP SDS 200 simply requires refilling the capillary with fresh medium (a step normally done prior to each separation).

Additionally, whereas isolates from the acrylamide gel-filled capillary could be prepared using Amicon Microcon 3 ultrafiltration devices, the polymer used in the eCAP SDS 200 system necessitated the use of the Microcon 10 devices. Because the the Microcon 10's have higher nominal cut-offs, smaller proteins may not be recoverable in sufficient quantities for mass spectrometry.

The mass accuracies of the isolated proteins appear to be near those expected for standard preparations (ca. 0.02%), but may be slightly higher. These errors may be due to adduct formation with components not removed with the SDS-cleanup process.

Further work is in progress to determine percent recoveries both from the capillaries and through the isolate preparation. This information will be necessary to determine the overall sensitivity of the method.

Matrix-Assisted Laser Desorption Mass Spectrometric Analysis of a Pegylated Recombinant Protein.

E.Watson, B. Shah, R. DePrince , W. Hendren and *R. Nelson.

Amgen Inc., Amgen Center, Thousand Oaks, CA 91320.

*Vestec Corp., Houston, TX 77054.

Introduction

The administration of proteins for therapeutic treatment is severely hampered by short half-lives in the circulatory system. It has been shown that the covalent attachment of polyethylene glycols to enzymes and proteins has a major effect on their physical and activity properties. Several reports have demonstrated the effect of increased circulating lives from the use of such PEG conjugates without any complications arising from immunogenicity (1-3) and as a result the characterization of these PEG-protein adducts has attracted an ever increasing attention in recent years. While electrophoretic (4) and chromatographic (5) techniques have been reported for separating and characterizing these molecules, there are no satisfactory methods reported for determining the exact number of PEG units covalently bound. We have investigated the use of MALDI as a technique for determing the number of PEG units covalently attached to the recombinant protein.

Mass spectrometry was performed using a Vestec Model VT 2000 laser-desorption time-of-flight mass spectrometer (Vestec Corp. Houston, TX, USA). The PEG-SCF sample was prepared for MALDI using a matrix of sinapinic acid.

Results and Discussion

The reaction of SS-PEG with proteins results in the covalent attachment of PEG (average molecular weight of 6000) at lysine e-amino groups. There are 14 lysines in SCF that can undergo reaction, and since the reaction is not expected to result in complete derivatisation, considerable heterogeneity is introduced into the PEG-SCF complex. Consequently the covalent attachment of PEG to proteins can result in the formation of a species that is both heterogeneous in size and charge. Figure 1 shows the laser desorption mass spectrum obtained from PEG-SCF sample. A series of ion signals are observed with molecular weights of 18770, 24650, 30550 36550 and 42400. daltons, at about 6000 daltons apart. Each PEG attached to SCF will contribute approximately 6000 daltons to the total mass of the modified protein and this information permits the identification of the ions shown in Figure 1 as being consistent with the covalent addition of one, two, three and four PEG units. The ion signal at 18770 Da closely agrees with the calculated molecular weight of SCF (18600). The series of peaks at 18275, 15275 and 12325 daltons are doubly charged species derived from the above parent ions. All of the ion signals can therefore be explained as being derived either from parent compounds or from doubly charged ions. The spectrum permits characterization of all of the PEG-SCF adducts present allowing the number of PEG units covalently bound to be readily determined as well as providing for an estimation of relative amounts present.

The results presented here are of practical importance and demonstrate the utility of matrix-assisted laser desorption as a highly promising technique for determining the number of PEG units covalantly attached to proteins.

REFERENCES

(1) Katre,N.V.; Knauf,M.J.; Laird, W.J. Proc. Natl. Acad. Sci. USA 1987, 84, 1487-1491.

ESI- and MALDI-FTMS of Peptides for the Identification of Proteins

M Mann[a], FH Laukien, GH Kruppa, CH Watson, J Wronka, M Knobeler[b]
[a]EMBL, Heidelberg, Bruker Instruments, Inc., Billerica, MA; [b]University of Bremen, Bremen, Germany

Introduction

We have recently developed a program that allows the rapid identification of proteins in sequence databases by the masses of their tryptic peptides [1]. Briefly, for each protein in the database the masses of all the predicted peptides for a given enzyme specificity are generated. If peptides of a sample of unknown identity are mass analyzed, the program can match the peptide mass pattern against the predicted peptide masses. Such a capability is useful for alleviating the workload in a protein analysis laboratory, because often the task of the laboratory is the confirmation of the identity of a sample. Furthermore, many putatively unknown proteins turn out to be contained in the databases.

The specificity of the pattern matching is determined by several experimental parameters, such as mass accuracy, number of 'correct' peptides (i.e. those obeying the enzyme cleavage rules) and the mass range of the peptides considered for the match. We have previously shown that ESI-FTMS and MALDI-FTMS have the capability for ultra-high mass accuracy measurements (< 3 ppm) of peptides and proteins.[2]

All experiments were carried out using a Bruker Bio-Apex™ 47e external ion source FTMS, which has been previously described.[2] For the myoglobin example, 2 nmol of equine myoglobin was digested by trypsin and fractionated by HPLC. Fractions containing about 1 nmole of peptide material were collected and about 100 picomole was used for ESI-FTMS analysis. The same amount was also applied to the probe tip for the MALDI analysis, but less than 10 picomole of material was actually consumed.

The databases searched were the SWISS PROT release 24 (from the March 1993 EMBL CD ROM; 28154 entries) and the Protein Identification Resource (PIR, release 36), also on CD ROM. The PIR divisions searched were PIR I, PIR II, PIR III, and PATCH X, with a total of 84,000 entries. The program used was a modified version of PeptideScan, running on Macintosh computers with a CD ROM.

For this work, the ESI- and MALDI-FTMS spectra of several of the tryptic peptides from myoglobin were obtained. The calibration was done externally using a mixture of peptides. The mass accuracies for the determination of the myoglobin peptide exact masses are summarized in Table 1, for both the ESI and MALDI-FTMS measurements. In the case of the ESI work all spectra were measured and calibrated in broadband mode. For the MALDI results the calibration was performed and the accurate masses measured in high-resolution mode.

The search by three peptides from the myoglobin digest with a specified error of 0.008 Da resulted in a unique match even though no restrictions were put on the target mass range and two incomplete digestion sites were allowed. The same search at mass accuracies of 0.05 and 0.3 Da resulted in 16 and 108 false matches. These results are in agreement with statistical considerations. Additionally, we repeated the search with 10 arbitrary, non sequence related masses simulate a high "background". Again, myoglobin was the only match. The above results also held when searching the 84000 entries of the PIR database instead of SWISS PROT.

In another experiment we measured the mass of a single peptide from our laboratory practice with high accuracy. Since the protein was known to be small an upper

mass limit of 18 kDa was put on the protein mass range considered. Four matches were found in SWISS PROT two of which were easily discarded on the basis of the species of origin. The two other matches were the correct protein.

In conclusion we have shown that searching with very high mass accuracy had the expected effect of drastically improving the specificity of the search. Accuracies of below 5 ppm could be used to remove all restrictions on the search and still find a unique match with only a few peptides as input. In some cases it may even be possible to identify proteins or contaminants in protein preparation on the basis of the accurate mass of a single peptide. In the near future most of the common peptides will have been sequenced and then the methods described here will be of even more general utility. the successful search of over 80,000 entries in the PIR database suggests that the methods described here will be robust enough to work with expanded future databases. We have further shown that both ESI- and MALDI-FTMS can provide ultra-high mass accuracy data for input to the PeptideScan program. We are currently investigating the use of orifice fragmentation to further increase the specificity of the searches. Laser desorption also results in metastable daughter ions. Since the masses of daughter ions can also be measured to high mass accuracy by FTMS, a single peptide measurement together with some of its fragment masses should be enough to uniquely identify a protein in the database.

Table 1. Myoglobin Peptide Fragment Exact Mass Analysis

Peptide	MASS	ESI	Err(ppm)	MALDI	Err(ppm)
1	1814.896	nm		1814.892	1.7
2	1605.847	1605.848	0.6	1605.839	5.0
3	1270.656	1270.652	3.1	1270.654	1.2
10	1377.834	1377.834	0.0	1377.846	8.7
13	1852.954	1852.961	3.8	nm	
16	1884.015	1844.008	3.8	1884.011	2.1
AVG:			2.3		3.8

note: nm = not measured

1] M. Mann, P. Hojrup, P. Roepstorff, Proc. 40th Conf. on Mas Spectrom. and Allied Topics, Washington D. C., 1992, p. 957
[2] C.H. Watson, G. Kruppa, D. Evard, P. Caravatti, J. Wronka, F. Laukien, Proceedings of the 4th Sanibel Conference on Mass Spectrometry, Jahuary 25-28, 1992. C. Watson, J. Wronka, P. Caravatti, F. Laukien, Proc. 40th Converence on Mass Spectrom. and Allied Topics, Washington, D. C.

Matrix-Assisted Laser Desorption Mass Spectrometry in the Determination of Subunit Stoichiometry of Giant (3,900 kDa) Earthworm Hemoglobin

Klaus Schneider[1], David W. Ownby[2], Hao Zhu[2], Ronald C. Beavis[3], Austen F. Riggs[2] and Brian T. Chait

[1]The Rockefeller University, 1230 York Avenue, New York, N.Y. 10021,
[2]Department of Zoology, University of Texas, Austin TX 78712,
[3]Department of Physics, Memorial University of Newfoundland, St. Johns, Newfoundland, Canada, A1B 3X7.

The giant extracellular hemoglobin of the earthworm, *Lumbricus terrestris*, has ~ 200 chains that form a two-layered hexagonal structure of 3.9 ± .2 MDa. The sequences of the four major heme-binding chains a, b, c, and d, have been determined. Chains *a*, *b*, *c* form a disulfide linked trimer. Additional structural components, "linker chains," deficient in heme, are necessary for the assembly and integrity of the 3900+ kDa molecule. The stoichiometry of the trimer, chain *d* and the linker chains and the heme content of the molecule have been controversial. We report here determination of the stoichiometry of chains and of the heme content by new, unambiguous techniques that utilize high performance liquid chromatography, amino acid analysis and matrix-assisted laser desorption mass spectrometry[1].

Molecular masses of all the individual chains and of the trimer were measured by matrix-assisted laser desorption mass spectrometry. Chain *a* was found to be glycosylated in agreement with earlier results. The molecular mass of chain *d* was found to be 142 u lower than calculated from the sequence indicating that the published sequence may be incorrect. The molecular mass of linker chain L_1 was substantially higher than calculated from the determined sequence[2], indicating glycosylation. To determine the sites of glycosylation chain *a* and linker chain L_1 were subjected to mass spectrometric peptide mapping. Digestion of chain *a* by Lys-C endoproteinase revealed that peptide 68-105 contains the glycosylation site (figure 1). The heterogeneity observed for this peptide agrees well with the heterogeneity observed for the intact protein. The linker chain L_1 was subjected to digestion by several enzymes (i.e. Lys-C endoproteinase, pepsin, trypsin) The results show that the site of glycosylation is within the peptide 88-104, probably at Asn^{103} (N-linked). The mass spectrum of the Lys-C-endproteinase digestion mixture is shown in figure 2.

The proportions of linker chains, trimer and chain *d* were determined by reverse phase HPLC, with simultaneous determination of heme content. A weight proportion of linker chains of 0.163 +/- 0.023 was determined by integration of the absorbance at 220 nm and verified by amino acid analysis. These values, together with sequence- and mass spectrometry derived masses, give a molar ratio of *abcd* chains to linkers of 8:1 corresponding to the minimal unit, $(abcd)_2L$. This ratio suggests that 24 $(abcd)_2$ units and 24 linker chains form the complete structure with a total calculated molecular mass of protein of 3975 kDa composed of 216 chains. The mass spectrometric masses of the chains indicate an additional mass of 133 kDa, attributed to carbohydrate.

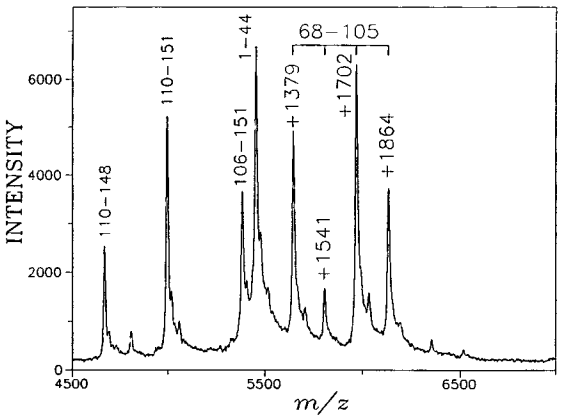

Figure 1
Matrix-assisted laser desorption mass spectrum of earthworm *Lumbricus terrestris* hemoglobin chain *a* after reduction with dithiothreitol and digestion with Lys-C-endoproteinase (matrix: 4-hydroxy-α-cyano-cinnamic acid). Peptide 68-105 was found to be glycosylated.

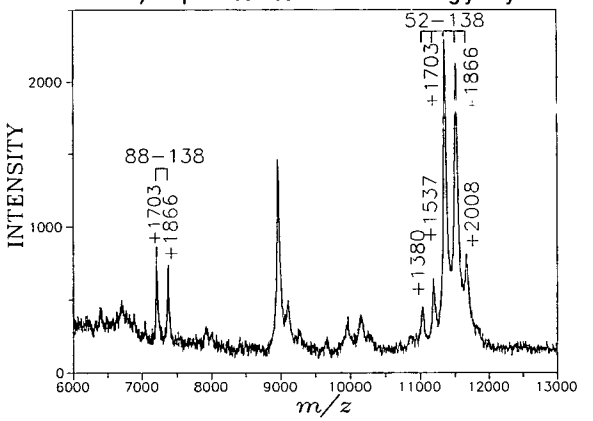

Figure 2
Matrix-assisted laser desorption mass spectrum of earthworm *Lumbricus terrestris* hemoglobin linker chain L_1 after reduction with dithiothreitol and digestion with Lys-C-endoproteinase (matrix: 4-hydroxy-α-cyano-cinnamic acid).

References

1. D. W. Ownby, H. Zhu, K. Schneider, R. C. Beavis, B. T. Chait, A. F. Riggs, J. Biol. Chem. (1993) in press
2. T. Suzuki, A. F. Riggs, J. Biol. Chem. (1993) in press

On-Line Magnetic Sector LC-MS-MS Analysis of a Tryptic Digest of β-Lactoglobulin by CF-LSIMS with Array Detection

P.Ireland, D. Jones, P. Ryan, S. Evans, R.J.Greathead
Kratos Analytical, Barton Dock Road, Manchester M31 2LD, UK

Introduction

Recently, tandem mass spectrometry has been recognised as an analytical technique that enables the primary structure of proteins and peptides to be determined, as well as being suited to the investigation of post-translational modifications. The analytical method usually involves the analysis of the fragmentation products of the protonated molecular ion produced by collision-induced dissociation (CID). The practical limit for sequence analysis of peptides with tandem, high-resolution mass spectrometers is approximately 3,500 daltons, primarily as a result of the inefficiency of the CID process for large molecules.

The strategy for analysis of larger peptides and proteins involves a prior proteolysis stage, usually in the form of an enzyme digestion. This is followed by liquid chromatography (LC) to separate the individual tryptic fragments and then subsequent amino acid sequence analysis by MS-MS.

Often only relatively small amounts of sample are available. In order to achieve the required low levels of detection of fragments ions, an array detector on a tandem, high resolution mass spectrometer is highly desirable.

This study illustrates the use of a magnetic sector, high resolution, tandem mass spectrometer coupled with continuous flow LSIMS interface and utilising array detection. The array detector is of a novel design, incorporating a charge-coupled device (CCD). This enables MS2 to be scanned and the data obtained treated as normal scanning data. This is in contrast to photodiode array detectors which necessitate changing the magnetic field in a stepwise fashion in order to monitor a wide mass range and maintain resolution. The individual windows produced by the photodiode array have to be reconstructed into a continuous spectrum through software processes before interpretation.

The scanning capability of the CCD array also provides a scan time compatible with chromatographic separations whilst retaining the advantages of high sensitivity detection.

A widely available and characterised protein; β-lactoglobulin was used as a model sample to illustrate the general analytical technique outlined.

Experimental Conditions

The 2-sectro analyses were performed at a resoluiton of 1000 (10%valley) with a CF-LSIMS source operating at 70°C. The range 1200 u to 100 u was scanned in 1 second. 4-sector analysis used a cell voltage of 4 kV with helium collision gas at a parent ion attenuation of 70%. The LC column was a 2mm x 150 mm ODS-1 using a flow rate of 0.2 ml/min split to 5 µl/min and a solvent gradient of100% A to 100% B over 30 mins (solvent A: 100% water with 0.06% TFA; solvent B: 80% acetonitrile 20% water with 0.06% TFA)

Results and Discussion

Table 1 shows the BioPolymer Sequence software report for the predicted peptide fragments produced by the enzymic digestion of bovine β-lactoglobulin with trypsin. The fragments are listed in sequence order, but could equally be ordered by molecular weight or HPLC retention index. Figure 1 to 3 show some of the results obtained in this study.

This combination of HPLC and continuous flow LSIMS mass spectrometry is capable of providing speedy analysis with moderate ease, without resorting to off-line separation of components or derivatisation procedures.

The addition of a scanning array detector enhances the detection of amino acid sequence fragment ions in the MS-MS spectra, with a cycle time capability compatible with the chromatographic separation.

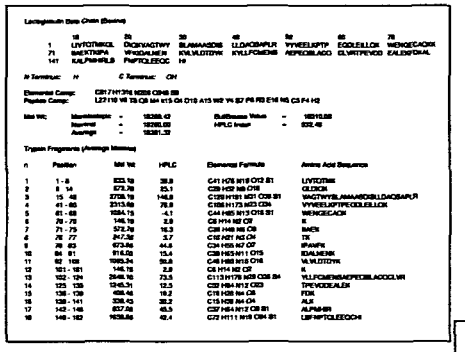

Table 1: BPS software output for lactoglobulin digest.

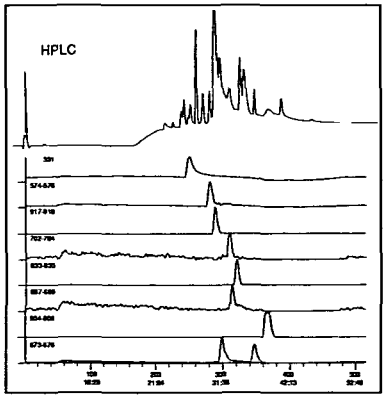

Figure 2: UV and ion chromatograms from the LC-LSIMS analysis of the tryptic digest of β-lactoglobulin

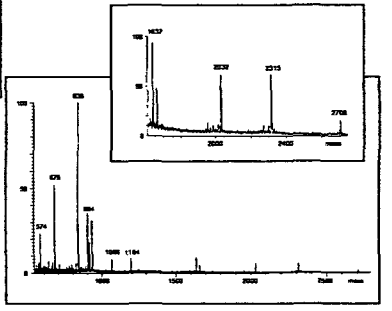

Figure 1: LSIMS spectrum of complete digest.

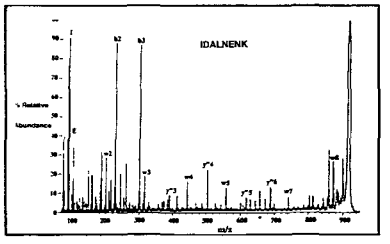

Figure 3: Example of MS-MS spectrum from tryptic digest of β-lactoglobulin

Electrospray Ionization of Trypsin Generated α-Lactoalbumin Peptides

S. Mitrovich, Jr.* & Catherine Stacey
Freedom Area High School, Freedom, PA 15042
Millipore/Extrel Mass Spectrometry
575 Epsilon Dr., Pittsburgh, PA 15238

Introduction

There is a definite need for a quick and relatively simple method to obtain molecular weight information from proteolytically produced mixtures of peptides. For example, a normal protein can be compared with a modified protein containing a substituted amino acid. Protein digest are easily separated by gradient HPLC and detected by UV absorbance, but no structural information is provided. Electrospray (ESI) LC/MS can be used to separate, detect and confirm the molecular weight of the peptides from an enzymatic protein digest.

Protein mapping places high demands on both the chromatographic system and the electrospray interface. The objectives of the present work was to examine the use of two chromatographic approaches to the ESI LC/MS analysis of a tryptic digest of the protein α-lactalbumin.

Experimental

Trypsin Digest: 2 mg/ml α-lactalbumin with 5% trypsin in 0.1 M ammonium acetate buffer (pH 7.8) for 24 hours. The reaction was stopped by the addition of formic acid.

Instrument: Extrel benchmark™ ESI/LC/MS system

Conventional Chromatography: Waters MS600 with a C-18 μBondapak (2 x 300mm) column using a linear gradient of water/2-propanol (95/5 with 1% formic acid) to water/2-propanol/methanol (5/80/15 with 1% formic acid) for 25 minutes, at a flow rate of 0.35ml/min. Flow was split 100/1. Amount of sample injected was 25 μl (3.5 nmoles).

Capillary Chromatography: Protype capillary LC (cLC) system from Waters, designed for gradient chromatography at 1-10 μl/min. A C-18 (0.32 x 150mm, LC Packings) column using a linear gradient of water/acetonitrile (95/5 with 1% formic acid) to water/acetonitrile (40/60 with 1% formic acid) for 40 minutes, at a flow rate of 3μl /min. The entire flow was introduced into the electrospray source. Amount of sample injected was 0.5 μl (3.5 pmoles).

α-lactalbumin Trypsin Peptides

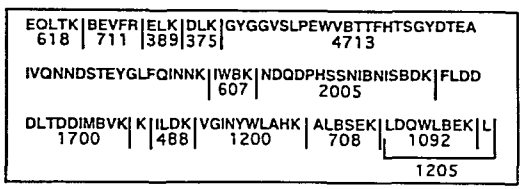

Results:

Shown below are the chromatographic separation of trypsin generated peptides for conventional LC and cLC.

Conventional LC

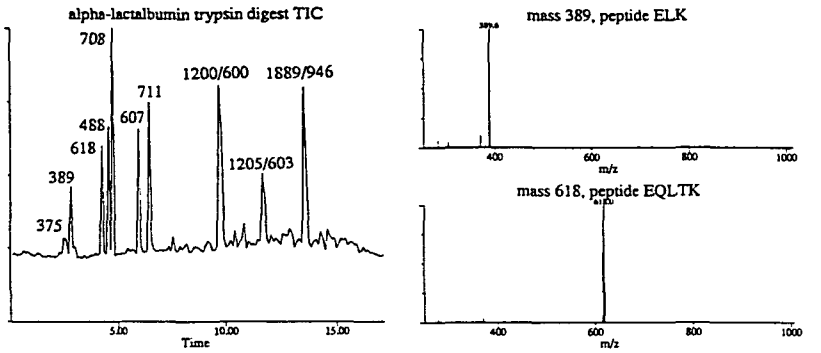

cLC

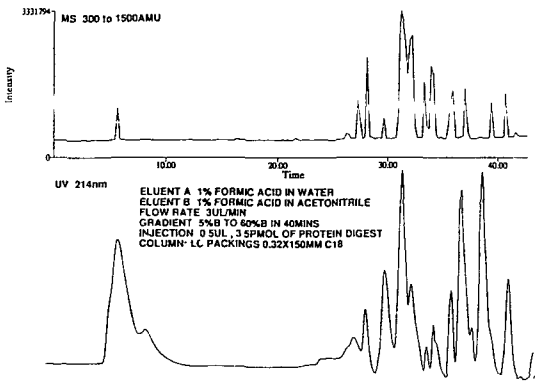

Conclusion:

- Molecular weight analysis of all the tryptic peptides from a protein digest was accomplished at a sensitivity level of low picomole, delivered to the needle.
- With a cLC system, low picomolar amounts were injected.
- Tryptic peptides were detected as the singly or doubly charged ion. One histidine-containing peptide gave a triply charged ion.
- Formic acid containg eluents are a viable alternative to TFA-containing eluents for a peptide mapping and offer sensitivity advantages for ESI/LC/MS

Development of Methods for Structural Confirmation of Peptides

Y. Karen Wang, John R. Strahler, and David M. Lubman
Chemistry Department, The University of Michigan, Ann Arbor, MI 48109

Introduction

Selective removal or addition of certain groups from /to the specific amino acid residues can be characteristic of a mass spectrum for the confirmation of the presence of those residues in the sequences. Both enzymatic digestion and chemical derivatization can be designed to serve the purpose, which is especially needed in the cases where a choice must be made among several possible candidates.

Methods

Carboxypeptidase Y immobilization: CPY(1 mg/ml, 3ml) was stirred with immobilized ConA(1 mg ConA/1g gel) for 30min at 4°c in sodium phosphate buffer(20 mM, 0.15M NaCl, pH7.4). After washing, crosslinking of the ConA-CPY conjugate with glutaraldehyde was accomplished under the following conditions: 0.1M sodium phosphate buffer, pH8, 2ml buffer/1ml settled gel, 0.5% glutaraldehyde, 1h at 4°c. The enzyme activity was determined by the rate of the enzymatic hydrolysis of CBZ-Phe-Ala, which is measured spectrophotometrically by the decrease in absorbance at 224nm.
CPY digestion: A physiologically important protein, OP18, was isolated with 2-D PAGE. *In situ* tryptic digest was then carried out on gels. The resultant peptides were recovered by elution with aqueous TFA-acetonitrile, and separated by reverse phase HPLC. One of the tryptic peptides, TP34, was used in this study. The digest of 10pmol TP34 with about 0.1g immobilized CPY was carried out in 100ul of 50mM ammonium acetate buffer pH6.5 for 2h at 37°c.
***In vitro* phosphorylation of kemptide:** The reaction mixture containing 1mM kemptide, 60mM Mes, 12.5mM $MgCl_2$, 0.25mM EGTA, 5mM ATP, and 10ug/ml of cAMP-dependent protein kinase at pH 6, was incubated at 30°c for 30min. Phosphokemptide was then separated from the non-phosphorylated by reverse phase HPLC.
Methyl esterification of phosphokemptide: 200ul aliquot of a solution containing 1.6ml of acetyl chloride in 10ml of methanol was added to 5 nmol vacuum dried phosphokemptide. The reaction proceeded for 2h at room temperature.
Acetylation of phosphokemptide: About 2 nmol of phosphokemptide was mixed with 45ul aliquot of the reaction solution with 0.102g acetyl anhydride, 0.101g triethyl amine, 0.012g dimethylaminopyridine in 10ml dimethyl foramide. The reaction was carried on for 3h at room temperature under agitation.
Dephosphorylation of phosphokemptide: About 2 nmol phosphokemptide was incubated in 20ul 25mM ammonium bicarbonate pH7.9 with 1ul of bacterial alkaline phosphatase(150units/ul) at 37°c for 1h.
Mass spectrometry: Vacuum dried samples were dissolved in 50%CH_3CN-H_2O for ES/MS and 0.1%TFA-H_2O for MALDI/MS analyses. The laser desorption matrix a-cyano-4-hydroxy cinnamic acid was dissolved in 30% CH_3CN with 0.1% TFA to make a saturated solution at 20°c. The peptide solutions were added to the matrix solution to give a final concentration of 0.5-5uM, and a small aliquot (1.5ul) of this mixture was used for analysis. VT-2000 linear TOF was used for MALDI/MS and VT-201 for ES/MS.

Results

Four possible candidates were given by the search against OP18 sequence for tryptic peptide TP34 (m/z 1549, by MALDI/MS), RASGQAFELILSPR, ENREAQMAAKLER, LREKDKHIEEVR, and NKESKDPADETEAD. The digestion with CPY led to the final identification of the peptide.

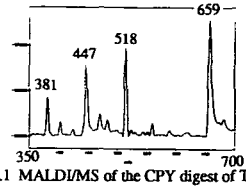

Fig.1 MALDI/MS of the CPY digest of TP34.

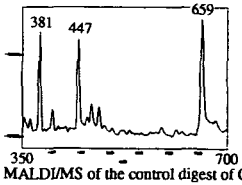

Fig.2 MALDI/MS of the control digest of CPY.

Mass determinations of TP34:

Observed m/z	Sequence position	Theoretical m/z	Sequence
1549	14-27	1545	RASGQAFELILSPR
518	14-18	518	RASGQ

Methods of esterification, acetylation and dephosphorylation of peptides were developed with the model peptide, phosphokemptide. Both ES/MS and MALDI/MS were used in the study.

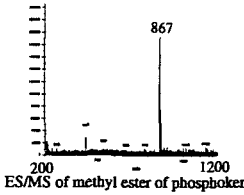

Fig.3 ES/MS of methyl ester of phosphokemptide.

Fig.4 MALDI/MS of methyl ester of phosphokemptide.

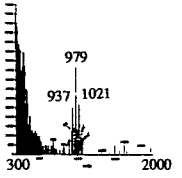

Fig.5 ES/MS of acetylated phosphokemptide.

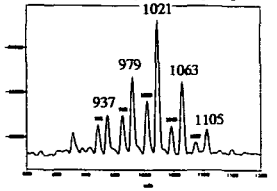

Fig.6 MALDI/MS of acetylated phosphokemptide.

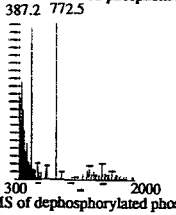

Fig.7 ES/MS of dephosphorylated phosphokemptide.

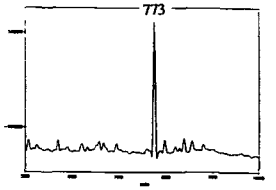

Fig.8 MALDI/MS of dephosphorylated phosphokemptide.

Conclusion

- With the use of carboxypeptidase Y, the number of possible candidate peptides was narrowed down. The identity of a tryptic peptide from a physiologically important protein was given.

- Chemical derivatization and enzymatic digestion proved to be useful for confirming the presence of specific amino acid residues in a sequence, such as acidic, basic, or phosphorylated amino acids.

Reactions may be designed against a specific group on the side chain of a specific residue. Factors, such as volatility of reagents, reaction yield, detectability of the derivatives, all affect the usefulness of a derivatizing reaction on the characterization of an unknown peptide with mass spectrometry.

NON-COVALENT INTERACTIONS OF CROWN ETHERS WITH CYTOCHROME C USING ELECTROSPRAY MASS SPECTROMETRY

Norman Sproch and Terry L. Kruger
Department of Chemistry, Ball State University
Muncie, Indiana, 47306

INTRODUCTION

The soft ionization technique of electrospray mass spectrometry (ESI/MS) has recently allowed the observation of non-covalent complexes between small molecules and proteins. This technique has been used here to study the binding of three different crown ethers to three types of cytochrome c. Previous work has shown the binding of certain crowns to the surface of proteins such as cytochrome c [1]. The suggested binding site on the protein is that of the solvent exposed protonated lysine residue. We report here the binding of 18-Crown-6, Dicyclohexano-18-Crown-6, and Dibenzo-18-Crown-6 to Tuna Heart (Albacore, M_r=12,029 [4]), Horse Heart (M_r=12,360 [4]), and Baker's Yeast (Saccharomyces cerevisiae) Cytochrome c as observed using ESI/MS.

METHODS

The ESI source is of our own design in the configuration of a probe using a standard 1/2 inch vacuum lock (Figure 1), details of its construction will be reported elsewhere. This design uses the heated metal capillary of the type used by Chowdhury, Katta and Chait [2]. An Extrel ELQ 400 (2000 AMU) single quadrupole instrument was used. The experiments showing binding of crowns to cytochrome c were done by adding 1, 2, and 3 mol ratios to a 70 pmol/uL mixture of the three different cytochrome c's. The solutions were prepared with equal parts of methanol/water with 1% acetic acid. Typical sample conditions were, 95 degrees C, 2 uL/min, 4000 VDC on the syringe, 170 VDC on the capillary tube (Figure 1), and 60 VDC on the skimmer (Figure 1).

RESULTS

The binding of crowns increases with increasing concentration (Figure 2) with a large excess producing a spectra showing a pronounced set of peaks corresponding to a protein/protein-crown complex which in addition exhibits a new species with a greater number of charges (Figure 3). This bimodal distribution may be representative of a conformational change in the protein [3]. The molecular weights of the cytochromes were determined from linear plots of each of the proteins set of characteristic m/z peaks vs. 1/z (Figure 4). The slope of the line giving the experimental molecular weight. These values were in close agreement to previously published molecular weights [4]. Similar plots were made to determine the molecular weight of the protein/crown complexes.

CONCLUSION

Signals representing the complex resulting from non-covalent binding of crown ethers to cytochrome c are observed in the ESI mass spectra. Because the crown ethers do not change the proteins charge the characteristic charge envelope remains. The increase in mass of the complex is seen as an intercalated envelope of a slightly higher m/z. The linear plots of m/z vs. 1/z passing through the origin have proven to be a simple method for finding the molecular weight of the proteins, protein complexes and a test for correct charge assignment. The suggested conformational change of the protein with increasing crown concentration is an interesting result and may be due to an increase of the surface hydrophobicity as suggested by recent work using other approaches [5,6]. We are continuing to investigate the suggested conformational changes, the reversibility and stoichiometry of crown binding, and in applying computational/molecular modeling methods using the SYBYL modeling program toward more precise interpretations of the experimental data.

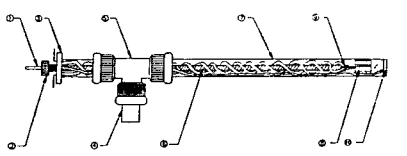

FIGURE 1. Schematic of the Electrospray Ionization Source/Probe: (1) capillary tube; (2) Kurtz-Lok I fitting, (3) endcap with wire feedthroughs; (4) roughing pump connection; (5) Cajon Ultra-Torr Tee, (6) nichrome heater; (7) glass housing, (8) threaded brass spacer for capillary tube; (9) non-contacting thermocouple; (10) brass skimmer cone.

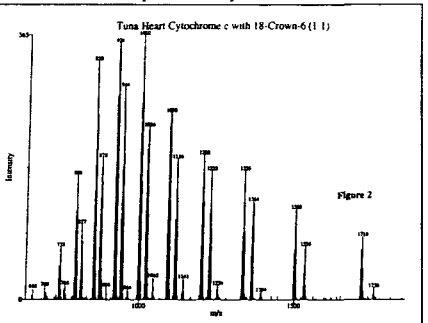

Figure 2

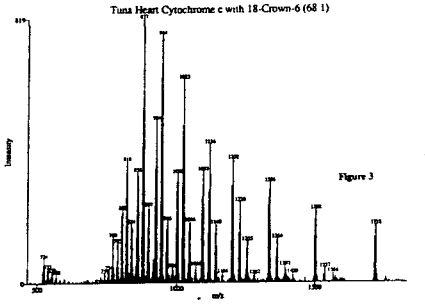

Figure 3

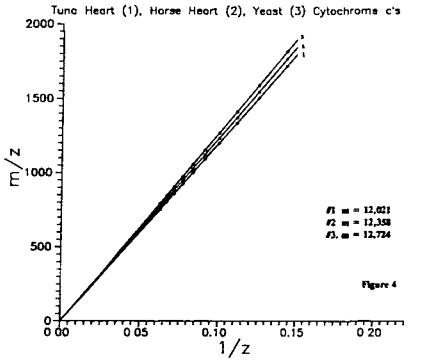

Figure 4

ACKNOWLEDGEMENTS

We thank the Ball State Department of Chemistry, Office of Research Internal Grant Program, Large Equipment Fund and Eli Lilly, our corporate sponsor for the SYBYL modeling program. We also thank Dr. Vicki Wysocki and Jennifer Jones at Virginia Commonwealth University for initial testing of our ESI probe and to the many people at Extrel who have answered questions.

REFERENCES

1. Odell, B., Earlam, G. *J. Chem. Soc., Chem. Commun.* **1985**, 359-361.
2. Chait, B.T., Katta, V., Chowdhury, S.K., *Rapid Comm. Mass Spectrom.*, **1990**, 4, 81-87.
3. Chowdhury, S.K., Katta, V., Chait, B.T. *J. Am. Chem. Soc.* **1990**, 112, 9012-9013.
4. Udseth, H.R., Barinaga, C.J., Edmonds, C.G., Loo, J.A., Smith,R.D., *Anal. Chem.* **1990**, 62, 882-899.
5. Bowler, B.E., May, K., Zaragoza, T., York, P., Dong, A., Caughey, W.S. *Biochemistry* **1993**, 32, 183-190.
6. Shortle, D., Chan, H.S., Dill, K.A. *Protein Science* **1992**, 1, 201-215.

How Big Are Gas Phase Proteins? Collision Cross Sections for Multiply Charged Protein Ions

T.R. Covey and D.J. Douglas, Sciex, 55 Glencameron Rd. Thornhill, Ontario, L3T 1P2 ,Canada

Introduction

Little is known about the physical properties of gas phase protein ions formed by electrospray. Here, we describe a novel method for the measurement of collision cross sections for these ions, based on the energy loss of ions as they pass through a collision cell filled with an inert gas. Results are given for motilin, ubiquitin, myoglobin, cytochrome C, and bovine serum albumin. Cross sections give a measure of the size of proteins. The results here suggest that this new method may be of use for probing the conformations of gas phase protein ions.

Collision Model

Consideration of the kinematics of a collision of an ion of mass m_1 with a neutral of mass m_2 shows that in passing through a collision cell the ion will lose translational energy E as

$$\frac{E}{E_o} = e^{-nl\sigma(ln\alpha')} \tag{1}$$

where E_o is the initial ion energy before collisions, n the number density of gas in the cell, l the length of the cell, σ the collision cross section and α' is given by

$$\alpha' = \frac{(m_1 + m_2)^2}{m_1^2 + m_2^2} \tag{2}$$

Fitting experimental energy losses to equation (1) allows determination of collision cross sections. A Monte Carlo simulation of the energy loss of ions supports this approach (ref.1).

Experimental

Ions formed by ionspray were passed through the collision cell (Q2) of a Sciex API III triple quadrupole mass spectrometer. Stopping curves were obtained with the rod offset of the third quadrupole (Q3) for a range of collision cell pressures. Ratios of stopping potentials with and without collision gas were equated to the ratios E/E_o of equation (1). Cytochrome C ions were formed from aqueous (9:1 water:acetonitrile) and organic (1:1 water:acetonitrile) solutions. Cytochrome C in aqueous solution produced ions in comparatively low charge states (+7–+10) and in organic solution in a broader range of higher charge states (as in ref.2).

Results

Table 1 shows experimental cross sections for all ions studied Collision cross sections generally increase with the charge of an ion. Figure 1 shows cross sections for cytochrome C ions formed from aqueous and organic solutions. Ions formed from aqueous solution show somewhat smaller cross sections than the same ions formed from organic solution and also smaller cross sections than expected from extrapolation from the higher charge states observed from organic solution.

Discussion

It is immediately evident that cross sections for proteins are much larger than those observed for small organic ions (typically 10–100 $Å^2$). Cross sections generally increase with the charge state of the ion. To some extent this might be expected from the larger ion-induced dipole attraction from more highly charged ions. However calculation of ion-induced dipole (Langevin) cross sections gives results 3–8 times lower than those of Table 1. It therefor seems unlikely that the increase in cross section with charge is solely an ion-induced dipole effect; rather, it is plausible that the increase reflects a more open extended structure for the more highly charged ions. The observed charge distributions of cytochrome C imply a more open (denatured) conformation in organic solution and a more closed conformation in aqueous solution. The cross sections of Table 1 and Figure 1 suggest the gas phase ions retain some memory the solution conformation. The energy loss method for determining cross sections may be of use for further studies of the conformations of protein ions.

References

(1) T.R. Covey and D.J. Douglas, *J Am. Soc. Mass Spectrom.*, in press, 1993.
(2) S.K. Chowdury V. Katta, and B.J. Chait, *J.Am. Chem. Soc.* **112**, 9012, 1991

Table 1 Collision Cross Sections in A^2

Motilin

charge	m/z	cross section
3	901	850
4	676	890
5	541	950

Ubiquitin

chatge	m/z	cross section
7	1225	1460
9	952	1900
11	779	2220

Cytochrome C in 9/1 water/acetonitrile

charge	m/z	cross section
7	1748	1450
8	1529	1800
9	1360	1800
10	1224	2020

Bovine serum Albumin

charge	m/z	cross section
30	2222	11400
36	1853	13300
38	1755	13700
41	1626	14000

Cytochrome c in 1/1 water/acetonitrile

charge	m/z	cross section
9	1360	2370
10	1224	2430
11	1113	3230
12	1020	3230
14	875	3830
16	765	3450
18	680	4120
20	612	4310

Myoglobin

Charge	m/z	cross section
8	2118	2520
9	1884	2570
11	1541	3020
13	1305	3550
15	1131	4040
17	998	4290
19	893	4820
21	808	5040

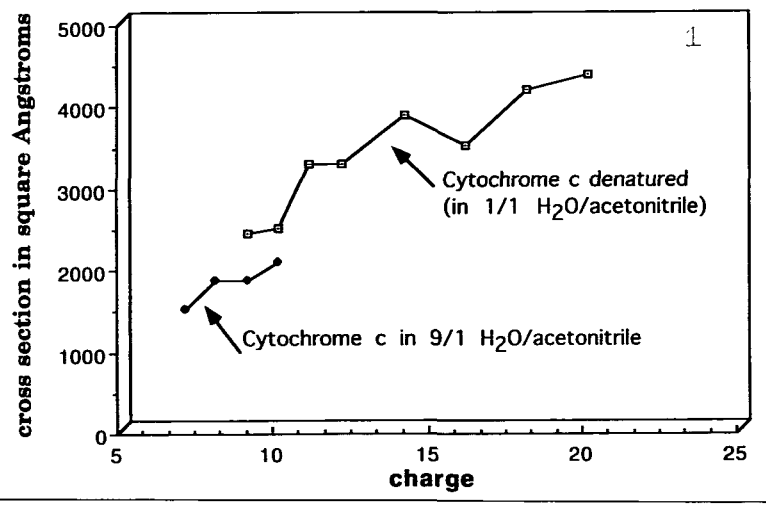

Characterization of histone H1 heterogeneity by electrospray mass spectrometry

J S. Andersen, L. Essalouh*, C. Dechesne*, J. Parello* and P. Roepstorff.

Department of Molecular Biology, Odense University, Campusvej 55, DK 5230 Odense M, Denmark and *Laboratoire de Chimie des Médiateurs et Physiochimie des Interactions Biologiques associée au CNRS, Université de Montpellier 1, 15 avenue Ch. Flahault, F-34060 Montpellier, France.

Histone H1 is involved in the maintenance and regulation of higher order structure in chromatin in relation to its peripheral position along the nucleofilament. Chromatographic and electrophoretic studies have demonstrated that H1 histones contain closely related subtypes. It is believed that the heterogeneity of the H1 histones has important biological consequences (1). Therefore, we have attempted to characterize the molecular heterogeneity of H1 in order to establish to which extent the heterogeneity is caused by variations in sequence or post translational modifications.

H1 extracted from mouse myoblast cells was separated by reverse phase high performance liquid chromatography (RP-HPLC) and capillary zone electrophoresis (CZE). Electrospray (ES) mass spectra were acquired on a Vestec model 201 single-quadrupole mass spectrometer (Vestec Corporation, Houston, TX, USA) with a skimmer voltage of 12 - 20V and a block temperature of 150 - 250°C. H1 histones were digested with endo proteinase Asp-N and Staphylococcus aureus V8 protease (Na_2HPO_4 buffer, pH 7.2 at 37°C for 3h, substrate:enzyme ratio 1:50 (w:w)).

Five sub fractions (F1-F5) were resolved by RP-HPLC. ESMS of F1-F5 resulted in the identification of six major variants. Three of these were in accordance with the nucleotide sequences known for H1.e, H1.c and H1° (Table 1). Fractions F2 - F5 were digested with endoproteinase Asp-N to verify the identity of the components corresponding to H1.c and H1.e and to determine whether the additional components observed were due to sequence variations or post translational modifications. Two peptides (NT and CT) were obtained for each components and analysed by ESMS. Taking into account the formation of fragment ions (see below) the obtained peptides confirmed the identity of H1.e and H1.c and indicated the presence of sequence variations in the additional components.

Extensive fragmentation was observed in the ES-mass spectra of H1 due to dissociation at specific Pro residues in the N-terminal region. Complete dissociation could be induced thermally or by offset of the skimmer voltage in the ES-interface region. Preferential dissociation of the ions with the highest charge states produced characteristic ion abundance profiles observed for the intact proteins (21kDa) as well as for the enzymatically derived N-terminal peptides (6kDa). H1 has an acetylated N-terminal region composed of mainly Ala and Pro residues followed by a sequence with >30% basic residues resulting in highly charged ions. Consequently H1 becomes very susceptible to collision induced dissociation in agreement with previously reported observation of preferential dissociation at Pro residues in charge site-remote regions (2 and references herein). The different fragment ions observed in ESMS confirm the identity of H1.c and H1.e and support the presence of sequence differences in the additional components. Acetylation of the N-terminal Ser residue was also confirmed.

Mass spectrometric peptide mapping showed that H1° was partially acetylated at the N-terminal Thr residue. A mass discrepancy of 15Da between calc. and meas. M_r of H1° suggest an additional modification. Partial phosphorylation of regenerated rat liver histone H1 and the testis specific histone H1.t were localized to the C-terminal region. The relative degree of phosphorylation of H1 histones were determined by ESMS and CZE. This show that ESMS can be used in a quantitative fashion. Changes in the ion abundance profiles were observed only for modifications affecting the number of potential charges.

Our results demonstrate that ESMS in addition to accurate mass determination of intact proteins can provide additional structurale information based on examination of ion abundance profiles and fragmentation patterns.

References

1 Van Holde, K.E. (1989) Chromatin, Springer-Verlag, New York Inc.
2 Loo, J.A., Edmonds C.G. and Smith, R.D. (1993) Anal. Chem. **65**, 425-438

Fig. 1 ES-mass spectrum of histone H1 (fraction F5). Extensive fragmentation is observed due to dissociation adjacent to Pro residue 5 and 8 in the N-terminal region.

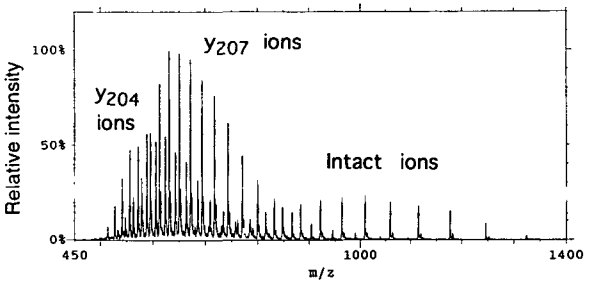

Table 1 M_r of H1 histones and the observed major fragment ions of H1 determined by ESMS. Calculated values inferred from the known cDNA sequences of H1°, H1.e and H1.c (N-terminal acetyated) are given in parenthesis.

HPLC (Type)	M_r intact protein	Fragment ions of intact protein
F1 (H1°)	20733.5 20774.7 (20756.6) 20907.4	
F2	22488.4	22060.2
F3	21700.1	21269.2
F4	22012.9	21580.8 21344.9
F4 (H1.e)	21889.4 (21888.1)	21457.8 (y_{214}) 21219.6 (y_{211})
F5 (H1.c)	21180.2 (21177.4)	20780.5 (y_{207}) 20541.2 (y_{204})

GLYCOPEPTIDE MAPPING AND STRUCTURAL CONFIRMATION BY ELECTROSPRAY LC/MS.

T. Hutton and B.N. Green, Fisons Instruments/VG BioTech, Altrincham, WA14 5RZ, UK.
M.J. Geisow, Biodigm, Bingham, Nottingham, NG13 8SS, UK.

Electrospray mass spectrometry (ESMS) is a fast evolving analytical technique which can be used to determine the molecular weights of intact proteins and glycoproteins. The mass accuracy of the technique is in many instances better than 0.01% and masses differing by as little as 0.1% can be resolved. This resolution can be increased by the application of maximum entropy (MaxEnt) to the data. Electrospray is therefore ideal for detecting and assigning post translational modification of intact proteins. Furthermore, the coupling of liquid chromatography and electrospray mass spectrometry provides a fast and highly sensitive method for the detection of glycopeptides produced from an enzyme digestion of a glycoprotein.

Glycoprotein glycoforms affect the biological activity and pharmacokinetic behaviour of many glycoconjugates. Their detection and analysis has become increasingly important in structure function studies as well as in the manufacture of recombinant glycoproteins. Although full characterisation of glycoprotein glycan requires their release from the protein, it would be of considerable advantage to be able to detect particular glycoforms in the intact protein.

In this study we demonstrate the resolving power of electrospray mass spectrometry using MaxEnt applied to the intact plant glycoprotein horseradish peroxidase showing that the individual glycoforms can be resolved. This can be compared with data obtained from a recombinant horseradish peroxidase and two variant strains. The glycopeptides produced by enzyme digestion of HRP were mapped and analysed by LC/MS and compared to those peptides produced from the recombinant non glycosylated protein produced in E.coli.

The data were obtained on Fisons Instruments/VG BioTech Quattro triple quadrupole and Platform single quadrupole mass spectrometers using electrospray ionisation at atmospheric pressure. The horse radish peroxidase was obtained from Sigma Chemical Co., St Louis, MO. The recombinant HRP and the two variants were supplied as part of a collaboration with Dr Andrew Smith, University of Sussex, Brighton, UK.

HRP and recombinant HRP were digested with trypsin and the resulting peptides and glycopeptides were analysed by on-line LC/MS.

Using the MaxEnt algorithm on the multiply charged ion electrospray mass spectrum of natural horseradish peroxidase, identifiable peaks corresponding to both full length and C terminally truncated HRP molecules with either 8, 7 or 6 Nlinked glycans could be seen in the MaxEnt spectrum. Variants of these differing by one hexose unit (eg. manose) and 13 other peaks were also resolved. These included both hexose, deoxyhexose and Nacetylhexosamine variants. The mean mass error between observed and calculated glycoforms was 1.5Da.

The molecular weight determined for the recombinant protein and variant horseradish peroxidase proteins F142A and R38K were 34041.8, 33965.5 and 33979.3 respectively. The differences between the expected and calculated molecular weights for the recombinant protein and the F142A variant were 0.3 and 0.1Da respectively. The variant R38K is outside this range and may in fact be a double mutant. Other possible mutations accounting for the mass difference could be either His→Cys, Met→Pro, Phe→Ile/Leu or Tyr→Gly.

On line separation of the tryptic peptides and glycopeptides obtained from both recombinant HRP and the natural glycoprotein, analysed in positive ion electrospray, produced the chromatograms shown in Figures 1 and 2. The digested natural HRP was also analysed by on-line LCMS in the negative ion mode). The peaks in the chromatogram are labelled according to the corresponding tryptic peptide or glycopeptide fragment number. Several of the chromatographic peaks contain more than one component. These unseparated components can be easily identified by mass analysis.

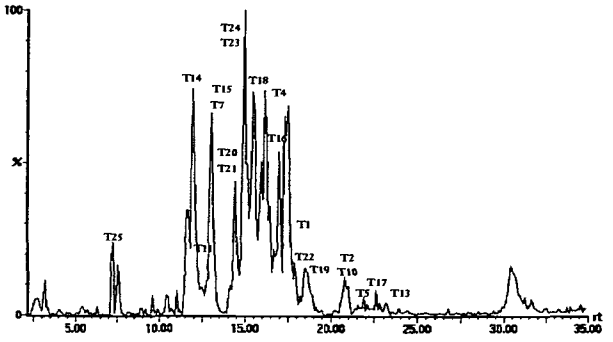

Figure 1. Base peak intensity (BPI) chromatogram of separated peptides from recombinant horseradish peroxidase protein. The peptides are labelled with their tryptic fragment number.

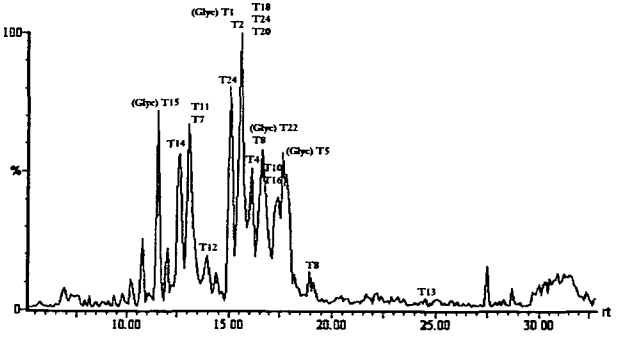

Figure 2 BPI chromatogram of separated peptides and glycopeptides from natural horseradish peroxidase.

A Novel, Rapid and Semi-quantitative Method for the Optimization of Synthetic Peptide Substrates

D.B. Kassel[1], M.D. Green[1], R. Whiebe[2], R. Swanstrom[2] and J. Berman[1]
[1]Glaxo Research Institute, 5 Moore Drive, Research Triangle Park, NC 27709
[2]Lineberger Cancer Research Center, University of North Carolina, Chapel Hill, NC 27599

INTRODUCTION

Knowledge of the subsite specificities (substrate activity relationship) of enzymes is important in the development of both synthetic substrates and inhibitors. Modifications which increase specificity often translate into enhanced inhibitor potency. Identification of high affinity substrates, however, is often the first and one of the more difficult steps in the process of identifying suitable enzyme inhibitors. This problem is particularly evident when attempting to identify favorable substrates for enzyme that exhibit a broad activity range (i.e., proteases which cleave at multiple sites) In an earlier communication (1), members of this laboratory described a novel, systematic approach to optimizing enzyme substrates using defined synthetic peptide substrate mixtures. The method relied principally upon HPLC for the semi-quantitative determination of relative rates of turnover (i.e., enhanced k_{cat}/k_m) for substrates of collagenase. Extensive HPLC optimization and long analysis times (>90 min) was required to achieve baseline chromatographic resolution and quantitate the turnover rates. In order to apply this approach to the rapid optimization of any novel protease substrate k_{cat}/k_m would require tremendous time and effort in establishing optimum HPLC separation conditions. Depending on the complexity of the mixture being screened, baseline separation may not even be achievable by this method This is especially likely if attempting to screen complex mixtures, such as synthetic peptide libraries (2)

We have investigated an alternative approach to screening complex mixtures of peptides This method is based solely on electrospray ionization to screen complex substrate mixtures and quantitate the relative turnover rates. The method requires a simple desalting step and an isocratic elution of all peptide substrates simultaneously into the ion source of the mass spectrometer. This approach has been used to assess the relative k_{cat}/k_m of a defined synthetic HIV protease substrate mixture A mixture of twenty heptapeptides, differing only in a single amino acid substitution (using the 20 common amino acids) at the defined P1' site (Ser-Gln-Asn-Tyr-***Xaa***-Ile-Val) was incubated in the presence of HIV protease and relative rates of turnover were assessed by ESI-MS. The results are presented below HIV protease has been identified previously as a relatively non-specific endoprotease, though the enzyme has shown a preference for cleavage at Tyr-*Xaa* bonds An equimolar mixture of twenty peptide substrates, differing only in their substitution at the P_1' site (C-terminal to the tyrosine residue) (*i.e.,* S-Q-N-Y-X-I-V), was incubated with HIV protease over the course of a 50 min time period. We sought to establish whether mass spectrometry could be used alone to quantitate peptide turnover rates by monitoring the disappearance (turnover) of the peptide substrates as well as by monitoring the appearance of tripeptide products

RESULTS AND DISCUSSION

The averaged mass spectra for incubation time-points A (0 min) and F (30 min) are compared in Figures 1a and 1b. The orifice potential was set to a value sufficient to produce abundant MH+ ions for all twenty peptides (in the m/z range 780-909). The mass spectrum generated for time-point F was characterized by abundant peaks in the low mass region m/z 328, 330, 344, 378 and 394, which corresponded to the cleavage of the peptides by HIV protease at the Tyr-Xaa bond to produce the tripeptide products, P-I-V, V-IV, [L,I]-I-V, F-I-V, and Y-I-V, respectively These peaks were noticeably absent in the zero time-point mass spectrum. The full scan MS spectra acquired at different incubation times (0 min and 30 min) could be used qualitatively to identify the peptides turned over to the greatest extent. In order to determine quantitatively the turnover (rel k_{cat}/k_m) of the individual peptides, we monitored both the disappearance of substrate and appearance of product from their respective selected mass chromatograms. This could be accomplished either by plotting the disappearance of substrate or by plotting the expected masses for product ions *vs.* incubation time for all twenty peptides. Additionally, we could monitor the appearance of product for a number of the peptide substrates. Reconstructed mass chromatograms could be used not only as a tool to rapidly screen the mixture for turnover, but could be used additionally to provide a semi-quantitative assessment of the relative k_{cat}/k_m for this mixture. From these mass chromatograms, integrated areas were then calculated for each peptide at the individual incubation time-points. Figure 2 shows a plot of Integrated Area *vs.* Incubation time for the disappearance of proline substrate (m/z 820) and appearance of its corresponding product (P-I-V, m/z 328). This figure clearly demonstrates that as substrate is consumed by the protease, an equivalent amount of product is produced, thus demonstrating that mass balance is achieved and the method of

electrospray ionization can be used as a semi-quantitative tool. From these data, relative k_{cat}/k_m determinations were made. Most peptides were not turnover at all. Only Pro, Val, Leu, Ile, Phe and Tyr were turned over to any appreciable extent.

The data generated using electrospray ionization alone was consistent with the turnover rates determined from HPLC/MS analyses (data not shown), suggesting that indeed this method could be used effectively as a semi-quantitative tool for assessing turnover for complex substrate mixtures. The major limitation of this method is the inability to distinguish between isobaric or isomeric species Leu and Ile could not be distinguished in the MS analysis nor could Gln or Lys The design and synthesis of defined peptide substrate mixtures should be made in the context of the limitations of the particular screening method. For example, if a goal is to assess the affect of *l- vs. d-* amino acids, then one might consider preparing two distinct mixtures to avoid the problem of the inability to distinguish isomers.

REFERENCES

1. Berman, J , Green, M., Sugg, E., Anderegg, R., Millington, D.S., Norwood, D.L , McGeehan, J. and Wiseman, J., *J. Biol. Chem.* 267, 1434-1437
2 Geysen, H.M , Rodda, S J. and Mason, T.J. (1986) *Molec. Immunol.* 23, 709-715.

Figure 1a

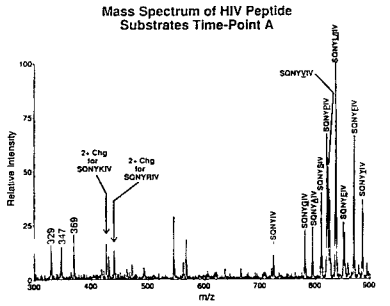

Figure 1b

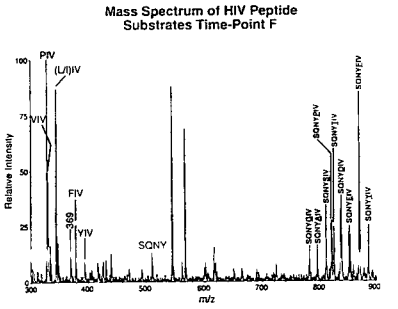

Figure 2

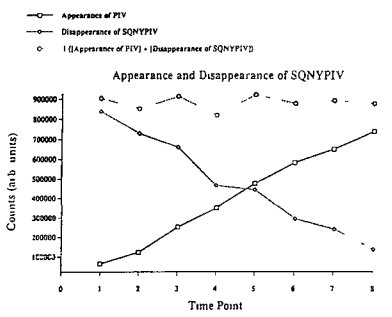

SEQUENCE ANALYSIS of BACITRACIN A and RELATED COMPONENTS by ELECTROSPRAY MASS SPECTROMETRY

Marshall M. Siegel[1]*, Jingfan Huang[1], Russ Tsao[1], Charles G. Edmonds[2]
[1]American Cyanamid Company, Medical Research Division, Lederle Laboratories, Pearl River, New York 10965; [2]Pacific Northwest Laboratory, Chemical Sciences Department, Richland, Washington 99352

INTRODUCTION Bacitracin is a commercially important antibiotic complex consisting principally of bacitracin A and a number of other minor components. Bacitracin A (MW 1421) is a peptide containing a total of 12 amino acid residues, 5 in a side chain and 7 in a ring. The structures of the bacitracin minor components are thought to be related to that of bacitracin A but have not been fully elucidated due to the difficulties in isolating large quantities of high purity materials and the technical difficulties associated with sequencing cyclic peptides with side chains. Preparative HPLC methods were developed for isolating bacitracin A and the minor components which were then characterized by analytical HPLC, amino acid analysis, fast atom bombardment (FAB) mass spectrometry (MS) and electrospray ionization (ESI)/MS. The side chain residues were sequenced by ESI/Nozzle-Skimmer Dissociation (CID)/MS and ESI/MS/MS and the ring sequences were elucidated by ESI/Nozzle-Skimmer Dissociation (CID)/MS/MS.

EXPERIMENTAL The samples isolated and analyzed by the above techniques were bacitracins A, A_2, B_1, B_2 and F. The ESI experiments were performed on a SCIEX TAGA 6000E tandem quadrupole mass spectrometer (Thornhill, Ontario, Canada) equipped with an atmosphere/vacuum interface and ion source previously described [Smith, et al., Anal. Chem. **60**, 1948 (1988), J. Am. Soc. Mass Spectrom. **1**, 53 (1990)]. Nozzle-skimmer dissociation (CID) experiments in the atmosphere/vacuum interface were performed with a difference of 215 volts between the nozzle and skimmer electrodes. MS/MS was performed with a laboraory frame collision energy of 75 volts and an argon collision gas thickness of 1.5 x 10^{14} atoms/cm^2. These two sets of experimental conditions were combined for ESI/nozzle-skimmer CID/MS/MS experiments, Solutions of the bacitracin components were prepared at approximately 1 nmol/µL in 5% aqueous acetic acid and delivered at 0.5 µL/min in combination with a sheath flow of 3 µL/min of methanol.

RESULTS A unique feature of the ESI sequencing experiments of bacitracin components is that the linear side chain can be sequenced with the data from the nozzle-skimmer CID and MS/MS experiments and the cyclic portion of the peptide can be sequenced by selecting that ion and performing a nozzle-skimmer CID/MS./MS experiment. The nozzle-skimmer CID and MS/MS spectra for bacitracin A are illustrated in Figures 1A and 1B, respectively, and for bacitracin B_1 in Figures 2A and 2B, respectively. Two components, bacitracin B_{1a} and B_{1b}, can be detected in the spectra of bacitracin B_1. The sequence ion assignments are illustrated below for the linear portion of the bacitracin B_{1a} sequence. Figures 3 and 4 illustrate the second generation product ion spectrum of the m/z 869 ion of bacitracin A, and the m/z 855 ion for bacitracin B_{1a}, respectively. Each ion corresponds to the cyclic portion of the molecule. The sequence ion assignments for the cyclic portion of the bacitracin B_{1a} molecule are illustrated below. The C-teminus sequence ion assignments for bacitracin A differ by 14 daltons to those of bacitracin B_{1a}. The Table below summarizes the structural assignments for the isolated bacitracin components.

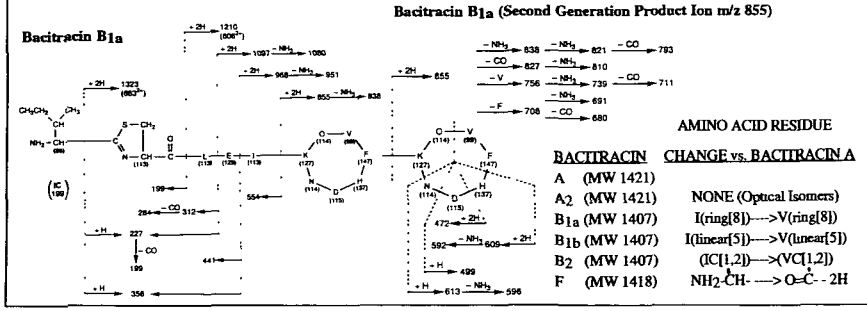

BACITRACIN	AMINO ACID RESIDUE CHANGE vs. BACITRACIN A
A (MW 1421)	
A_2 (MW 1421)	NONE (Optical Isomers)
B_{1a} (MW 1407)	I(ring[8])---->V(ring[8])
B_{1b} (MW 1407)	I(linear[5])---->V(linear[5])
B_2 (MW 1407)	(IC[1,2])---->(VC[1,2])
F (MW 1418)	NH_2-$\overset{+}{C}$H- ---> O=$\overset{+}{C}$- - 2H

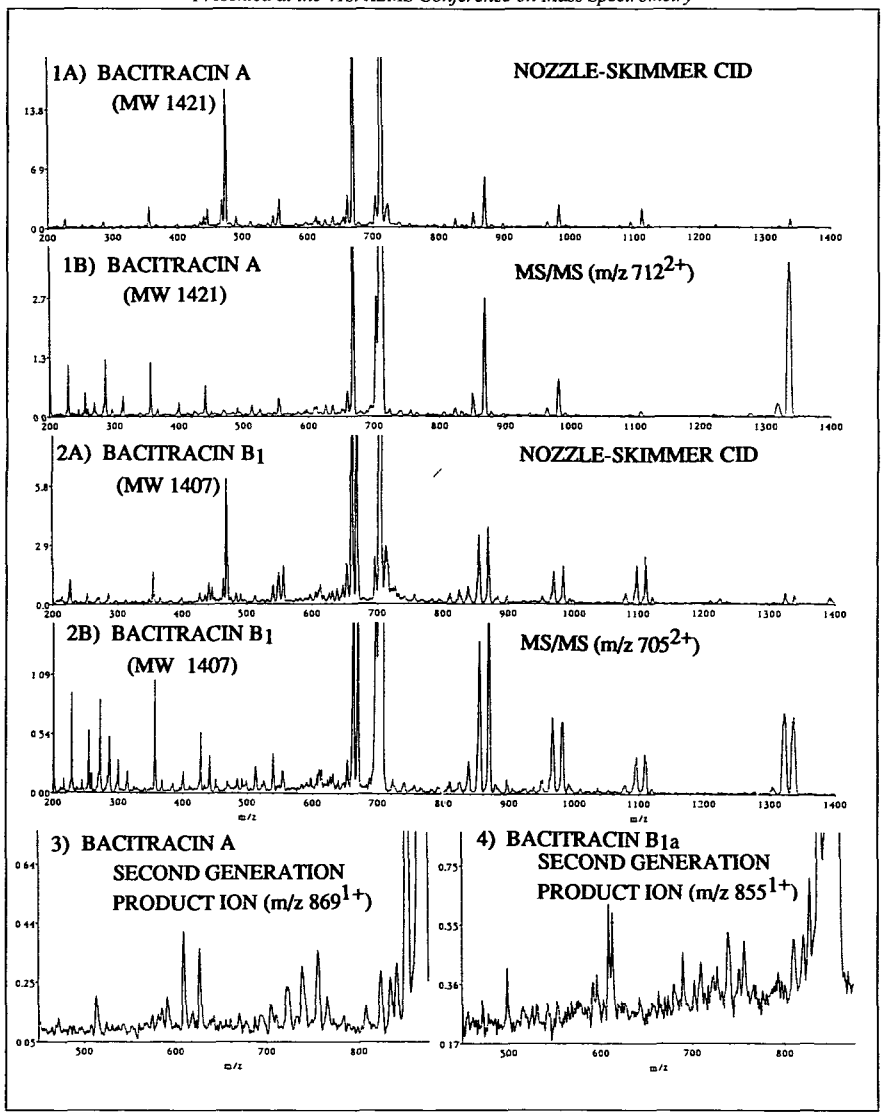

Dilithiated Fragments of a Mono-lithiated Ion? Unraveling B/E Linked Scan Spectra Using Labeled Lithium Ions.

*J P. Kiplinger; Pfizer, Inc., Groton, CT 06340

An investigation of the mass spectral fragmentation of rapamycin (**1**) and related macrocyclic immunosuppressants has been undertaken recently in our laboratory. Negative ion techniques, commonly used with this series, are effective in ionization but offer few structurally useful fragments.[1] In positive ion LSIMS, cationization with alkali metal cations is most effective in determining molecular mass, since these compounds do not readily form MH^+ ions. However, $(M+Na)^+$ and ions formed with larger metal ions do not fragment effectively.[2] Lithium cationization, most often carried out by adding lithium salts to the LSIMS liquid matrix, is becoming an increasingly popular technique in mass spectrometric structure elucidation due to the useful charge-remote fragmentations that $(M+Li)^+$ ions undergo.[3] We have found that cationization of rapamycin with Li^+ ion provides a good yield of $(M+Li)^+$ ions as well as reasonable amounts of structurally significant fragment ions.

The LSIMS spectrum of rapamycin, lithium-cationized using a matrix of 'magic bullet' to which LiCl had been added, is shown in Figure 1. A number of ions in the spectrum were not immediately attributable to the matrix, and were verified as fragments of the m/z 920 ion using linked scanning at constant B/E. Assignment of structures to these ions was undertaken using high resolution and rapamycin analogues.

Intense fragment ions are observed in both the full scan LSIMS spectrum and in the B/E scan at m/z 604 and 586. We attempted to derive structures for these important fragments first, but met with immediate difficulty. No reasonable mechanistic pathway could be derived for monolithiated fragments at these masses. We suspected that these fragments had lost the lithium ion, contrary to the expected charge-remote pathway. Attempted cationization with sodium and other metals produced weak and ambiguous fragment ion spectra. Cationization with $^6Li^+$, however, proved much more helpful

The spectra shown in Figure 2 are partial B/E linked scans of the fragments produced from the $(M+Li)^+$ ion formed from rapamycin. In Figure 2a, the precursor ion is the $(M+Li)^+$ ion at m/z 920. In 2b, the precursor is $(M+Li)^+$ at m/z 919. The strong fragments at 604 and 586 in Figure 2a must contain two lithium ions in order to be shifted by 2 daltons, while the fragment at 591 apparently only contains one It is thus obvious that the B/E scans contain fragment ions produced from two precursors -- the $(M+Li)^+$ ion visible in the LSIMS spectrum, and an $(M+2Li-H)^+$ ion which is not seen in the LSIMS spectrum. The confusion arises from the poor precursor ion resolution obtainable in the linked scanning experiment.

It has often been pointed out in the literature that care must be taken in interpreting B/E linked scanning results due to possible interferences from nearby precursors. However, in this unusual case, no peak for the interfering precursor is seen. This lithium-labeling technique will prove useful in cases where possible artifact peaks exist due to interferences from $(M+H)^+$, $(M+Li)^+$, or $(M+2Li-H)^+$ ions when fragments of only one are desired. Since lithium cationization appears to be a technique which is growing in popularity, as does linked scanning, we can safely assume that these artifacts will be observed more frequently. The use of $^6Li^+$ offers a simple way to deconvolute the fragment ion spectra of lithium-cationized molecules.

1. Cantone, J., Chan, K.; *Proc. of 40th Ann. Conf. on Mass Spectrom. and Allied Topics*, Washington D.C., May 31-June 5 1992, p. 1881.
2. Adams, J., Gross, M. L.; *Anal Chem.* **59**, 1576 (1987).
3. Adams, J.; *Mass Spectrom. Rev.* **9**, 141-186 (1990).

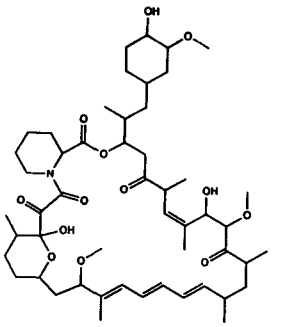

(1)

Figure 1

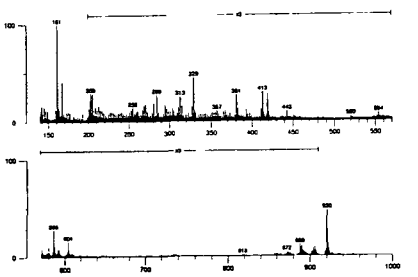

Figure 2

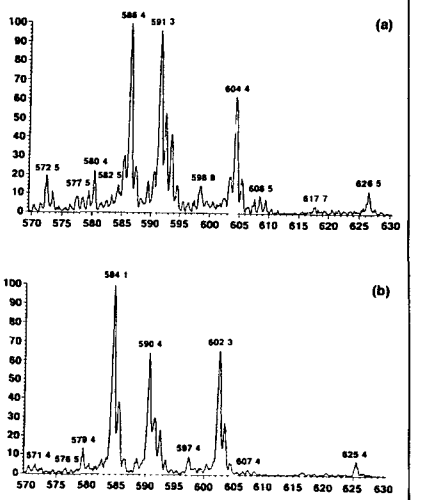

Figure 1. The positive ion LSIMS spectrum of rapamycin from a magic bullet matrix containing ^7LiCl. Note that the ions at 161 and 313 are derived from the matrix, but there are a large number of fragment ions from the $(M+Li)^+$ ion at m/z 920.

Figure 2. Partial B/E linked scan spectra of (a) rapamycin $(M+^7Li)^+$ ion at m/z 920, and (b) the $(M+^6Li)^+$ ion at m/z 919 The dilithiated fragment ions appear 2 daltons lower in spectrum (b).

CHARGE-REMOTE FRAGMENTATION OF POTENTIAL SENSITIVE DYES BY FAB MASS SPECTROMETRY AND MS/MS

Richard E. Carlson, Kenneth L. Busch, and Kenneth D. Hughes
School of Chemistry and Biochemistry
Georgia Institute of Technology, Atlanta GA 30332

A series of fluorescent, potential-sensitive dyes were studied using positive ion fast atom bombardment (FAB MS) mass spectrometry. Such dyes can be used as non-invasive molecular probes to aid in understanding biophysical processes. Typically, absorbance or fluorescent detectors are used to track the progress of these dyes through biological systems, thus sample purity is important. Mass spectrometry has provided valuable results in the characterization of these samples, and produced some interesting fragmentation mechanisms.

All FAB mass spectra were recorded on a VG70-SEQ mass spectrometer of EBqQ geometry using a Cs ion gun operated at 35 keV. m-Nitrobenzyl alcohol was used as a matrix. In the MS/MS experiments, Ar was used as the collision gas and the collision energy was varied from 10 to 300 eV.

FAB MS and CID MS/MS Experiments:

A portion of the MS spectrum of D-275 (3,3'-dioctadecyloxacarbocyanine, perchlorate) is shown in Figure 1. The spectrum shows a singly charged cation at m/z 782, followed by successive losses of CH_4, CH_3, and CH_2 groups, terminating at m/z 529. Consistent with charge-remote fragmentation mechanisms, these losses originate within one alkyl chain on the charged carbocyanine ring.

Figure 2 shows the CID MS/MS spectrum of D-275. The singly charged cation at m/z 782 was selected as the parent ion, and produced major fragment ions at m/z 529, 397, 370, and 277. As previously indicated, m/z 529 arises from cleavage of one alkyl side chain. The peak at m/z 397 originates from cleavage of the alkyl chain between the carbocyanine groups, m/z 370 is produced from the cleavage of a carbocyanine ring with an intact side chain, and m/z 277 results from the loss of both alkyl side chains from the aromatic rings. The MS/MS spectrum of this compound was expected to show charge-remote fragmentation, based on the results obtained in the MS mode. The calculated E_{cm} for the MS/MS experiments is 9.7 eV. In general, charge-remote fragmentation has been observed in several compounds ionized with FAB and then subjected to high-energy collision-induced dissociation. Charge-remote fragmentation is **not** observed in the mass spectrum, but in the MS/MS spectrum. Here we have a **different** case in which the MS shows the charge-remote fragmentation, but we cannot access this process in MS/MS. Some fraction of the **cations** in the source may be highly energized, but those that survive through to the collision cell apparently are not.

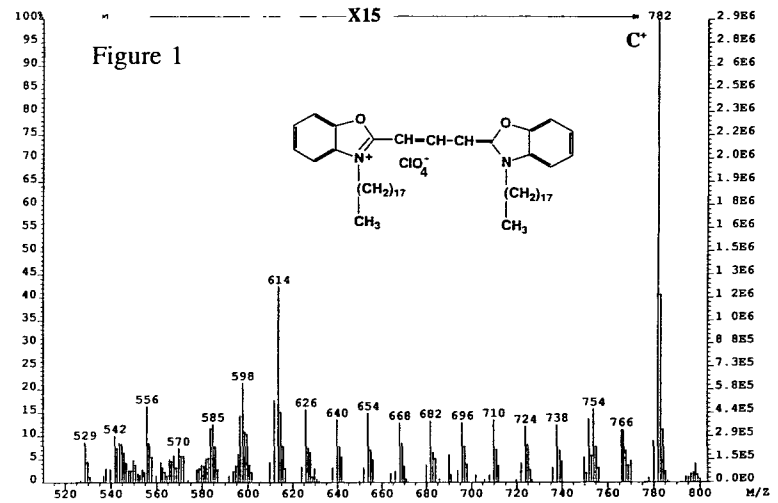

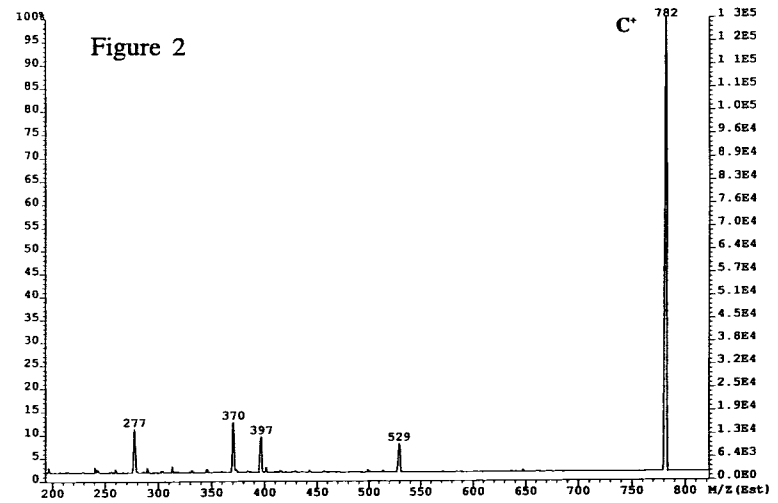

SURFACE-INDUCED DISSOCIATION OF FULLERENES

John H. Callahan and Melvin A. Park, Chemistry Division, Naval Research Laboratory, Washington D.C. 20375. Vicki Wysocki and Arpad Somogyi[a] Department of Chemistry, Virginia Commonwealth University, Richmond, VA.

[a] On leave from Central Research Institute for Chemistry of the Hungarian Academy of Sciences, H-1525 Budapest, P.O. Box 17, Hungary.

From the time of its original discovery by Smalley and coworkers, buckminsterfullerene has been the subject of a variety of studies aimed at studying its physical properties by fragmentation mass spectrometry.[1] With the development of a synthetic technique for the synthesis of bulk quantities of fullerenes,[2] a number of mass spectrometry studies have probed the fragmentation behavior of fullerenes[3]. Most of these studies have shown C_{60} to be relatively difficult to fragment, with successive C_2 loss being the primary fragmentation mechanism. Recently, Whetten and coworkers have used ion-surface collisions to study fullerenes.[4] This work showed that C_{60} is stable toward fragmentation in surface collisions of up to 250 eV. Work by Cooks and coworkers,[5] and by Wysocki and coworkers,[6] has shown that modification of surfaces using perfluorinated self-assembled monolayers (SAM) can significantly increase the amount of internal energy deposited in the parent ion. The explanation for this behavior is not fully known, however, part of the efficiency increase may arise from the increased mass of the atoms (F vs. H) that are struck in the collision. Additionally, differences in the amount of energy taken up by the surface may play a role in the increased energy transfer.

We have used the tandem quadrupole instrument at Virginia Commonwealth University to investigate the behavior of C_{60} in collisions with surfaces treated with self-assembled monolayers formed from derivatized thiols. Collisions with thiol treated surfaces occurr between the first and second quadrupoles in a 90° tandem configuration, at energies between 10 and 160 eV. Fullerene ions were formed by thermal desorption and electron ionization.

Initial studies showed that no fragmentation could be observed between C_{60}^{+} and stainless steel or surfaces covered with octadecanethiol (C_{18}) at collision energies up to 160 eV (consistent with Whetten's results). Some fragmentation could be observed from collisions of C_{60}^{2+} with both surfaces at collision eneries of 250 eV (Figure 1a shows the results for the C_{18} surface). Only singly-charged fragments are observed, due to reduction of doubly charged products. In collisions of C_{60}^{2+} with a perfluorinated surface (PF; $CF_3(CF_2)_7CH_2CH_2SH$), far more extensive fragmentation is observed (Figure 1b). Both singly- and doubly charged fragments are observed, consistent with the higher ionization energy of the perfluroinated surface. The more extensive fragmentation observed from the perfluorinated surface is consistent with greater energy deposition. In fact, the energy deposition is high enough that fragments can be observed from singly charged C_{60} at energies as low as 125 eV. The results indicate that as much as 50% of the translational energy may be converted to internal energy.

We have also obtained results indicating that C_{60}^{2+} undergoes reactions with adsorbates or fragments on SAM surfaces. Collisions of the doubly-charged ion with the perfluorinated surface at 320 eV results in the formation of an ion at m/z 372. This is not likely to be C_{31}^{+}, since it is not readily formed. Thus, it seems likely that this is a reaction product of C_{60}^{2+} with C_2. Evidence that this occurs was also observed on other self-assembled monolayers. Figure 2 shows the result of collisions of C_{60}^{2+} with a surface covered with $NH_2CH_2CH_2SH$. Although the products are reduced to singly-charged ions, the results show evidence for pickup of at least 4 C_2 groups. This indicates that a C_2 growth mechanism is plausible for fullerenes.

1. O'Brien, S.C.; Heath, J.R.; Curl, R.F.; Smalley, R.E. *J. Chem. Phys.* **1988**, *88*, 220.
2. Krätschmer, W.; Lamb, L.D.; Fostiropoulos, K.; Huffman, D.R. *Nature* **1990**, *347*, 354.
3. See reviews in: a. McElvany, S.W.; Ross, M.M. *J. Am. Soc. Mass Spectrometry* **1992**, 3, 268-280; b. McElvany, S.W.; Ross, M.M.; Callahan, J.H. *Acc. Chem. Res.* **1992**, *25*, 162-168.
4. Beck, R.D.; St. John, P.; Alvarez, M.M.; Diederich, F.; Whetten, R.L. *J. Phys. Chem.* **1991**, *95*, 8402.
5. Winger, B.E.; Julian, R.K., Jr., Cooks, R.G.; Chidsey, C.E.D. *J. Am. Chem. Soc.*, **1991**, *113*, 8967.
6. (a) Wysocki, V.H.; Jones, J.L.; Ding, J.-M. *J. Am. Chem. Soc.*, **1991**, *113*, 8969.

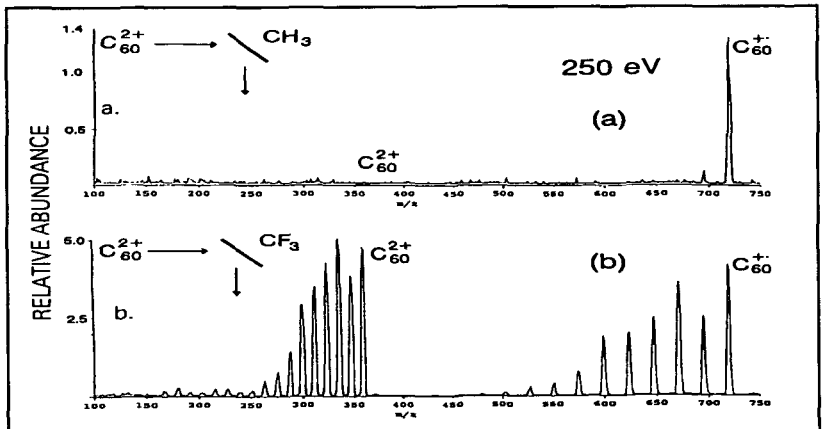

Figure 1. 250 eV collisions of doubly-charged C60 with a surface covered with a) octadecanethiol and b) a perfluorinated thiol.

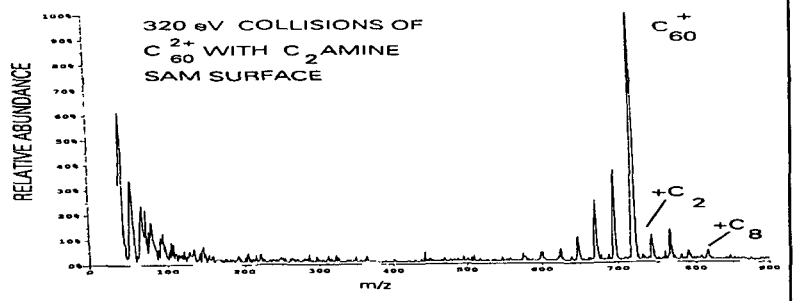

Figure 2. 320 eV collisions of doubly charged C60 with a surface covered with an aminothiol The results indicate addition of multiple C2 units.

TANDEM MASS SPECTROMETRY OF FULLERENE DERVIVATIVES

Simon N.Davey and Lee W.Tetler
Centre for Mass Spectrometry, UMIST, Manchester, M60 1QD
David A.Leigh , Andrew E.Moody and Frances A.Wade
Department of Chemistry, UMIST, Manchester, M60 1QD

The discovery of the fullerenes and their subsequent characterization as the third well defined allotrope of carbon has given rise to a whole new branch of chemistry. Reports have appeared in the literature detailing the reactivity of fullerenes to oxygen, hydrogen, halogens, metals and amines. Mass spectrometry has played a key role in the identification and characterization of these new compounds.

In an attempt to increase the solubility of the fullerenes in polar liquids, we reacted them with a number of water soluble reagents including amines. The reaction with aza crown ethers provides stable monoaddition products. Experimental details of the addition products will be published elsewhere.

Two sources of fullerite were used in the experiment. The first batch was produced at UMIST using a benchtop fullerene generator as described by Koch et al. and the fullerite mixture was soxhlet extracted from the soot using toluene. The second batch was supplied by the Strem Chemical Co. (Newburyport, MA, 01950, USA). The two batches provided identical results.

Mass spectrometry was carried out on a Kratos Concept IIHHM four sector tandem mass spectrometer (Kratos Analytical, Urmston, Manchester, UK) operating under fast atom bombardment ionisation conditions with xenon atoms of 8keV energy. Nitrobenzylalcohol (NBA) was the matrix of choice. MS1 was used to obtain the double focused mass spectrum. Collisional activation (CA) was employed using helium as collision gas such that 70% of the precursor ion beam was attenuated with the collision cell floated at 4kV. Array detection was employed after MS2. All data was obtained in the positive ion mode.

Interestingly the reaction of fullerite (the C_{60} and C_{70} mixture) with dimethylamine has so far only yielded C_{70} products. There appear to be up to eight additions of dimethylamine to the C_{70} ring but the most interesting aspect of these materials is their fragmentation patterns under MS/MS[1]. For up to six dimethylamine groups added onto the fullerene species, the MS/MS spectrum varies according to whether there are an even or odd number of dimethylamine groups attached to the ring. If there are an even number of groups attached to the ring, the fragmentation is stepwise i.e one group is lost at a time. If there are an odd number of groups attached then the loss is two groups at a time. Tandem mass spectrometry of these species reveals the presence of helium incorporation in the substituted precursor ions, whereas the endohedral complexes had previously only been observed for pure carbon compounds.

The complexes formed by the reaction of pure C_{60} with a variety of aza crown ethers yield more readily interpretable tandem mass spectra. The predominant ion in the mass spectra of the $[1A12C4+C_{60}]^+$ complex is m/z 892.3 which is 4Da below the

expected value for the protonated complex. This corresponds to the loss of two hydrogen molecules, a phenomenon also found with the dimethylamine products. We speculate that this may be because of a stabilisation of the ring structure which only becomes apparent when the fullerene molecule has another group attached onto it.

The MS/MS of the m/z 892.3 ion is shown in Figure 1. The predominant fragments correspond to m/z 734 (where the nitrogen atom of the aza crown ether is attached to the C_{60} ring, suggesting this is the site of binding), m/z 720 (C_{60}), and m/z 172, 128 and 100 which are related to fragmentation of the crown ether (crown ether molecule, loss of CH_2CH_2O and further loss of CH_2CH_2 respectively).

The potential of fullerenes for the synthetic organic chemist is exciting but owing to the complexity of the molecular addition products, characterisation by typical methods such as NMR and infrared may prove somewhat difficult. Mass spectrometry has a major future in assisting in the characterisation of this whole new branch of chemistry.

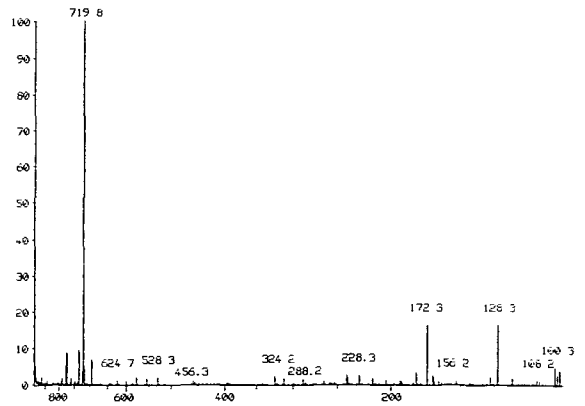

Figure 1. MS/MS of $[C_{60}+1A12C4]$

Acknowledgements
The authors would like to thank SERC, Kratos Analytical Ltd and GEC Marconi for providing financial assistance towards this research.

References

1. S. Davey, D. Leigh, A. Moody, L. Tetler, **Organic Mass Spectrometry**, *in press*.

A Systematic Study of Surface Characteristics Associated With Enhancement of Both Surface-Induced Dissociation (SID), Reaction and Energy Deposition

*Thomas E. Kane, Árpád Somogyi, and Vicki H. Wysocki.
Virginia Commonwealth University, Richmond, VA 23284.

INTRODUCTION Ion-surface collisions deposit high amounts of internal energy into the projectile ion in a process called surface-induced dissociation (SID)[1]. In addition to fragmentation of the selected ion, an ion may (i) neutralize, (ii) exchange its charge with material native to the surface, also known as chemical sputtering, and (iii) react with material from the surface. These other processes are often far less pronounced than SID, particularly when larger polyatomic projectiles are employed. The degree to which these alternate processes occur for a selected ion may better describe the chemical and physical condition of the surface. Organic self-assembled monolayer films provide well characterized surfaces with which to investigate surface-induced dissociation, reaction, and neutralization.

EXPERIMENTAL A tandem quadrupole instrument is arranged in a 90° geometry with the surface positioned 45° to Q1.[2] The collision energy is varied by increasing the source potential relative to the surface potential. Surfaces are highly ordered monolayer films of organic thiols, spontaneously assembled onto gold. Self-assembled monolayers include n-alkanethiolates, and 2-(perfluorooctyl)ethanethiolate. The surface holder allows for the investigation of five surfaces without venting the instrument.

We show that dimethylsulfoxide (DMSO, m/z 78) and its deuterated analog (m/z 84) act as excellent probes of available hydrogen on the surface. Unlike benzene, which was investigated earlier,[3] DMSO is more sensitive towards H-addition, and is capable of detecting trace hydrocarbon on self-assembled monolayer films. Surfaces representing short chain, disordered films (C4 and C8), and long chain, more crystalline films (C12 and C18)[4] were probed with DMSO, and the hydrogen addition measured. The fluorinated surface was probed, and then damaged with a 70eV $Ar^{+\cdot}$ beam for 15 hours. The increase in surface damage was monitored with DMSO-d6.

Atomic ions eliminate the possibility of projectile fragmentation and facilitate the investigation of the processes that compete with SID. All ions appearing in the spectrum, other than the $M^{+\cdot}$, are therefore the result of energy imparted to the surface via the initial collision energy and the ionization energy of the atom. Ions from group I, VII and VIII are collided into monolayer surfaces, and their ionic products are plotted as a function of collision energy.

DISCUSSION Two possible sources of hydrocarbon exist for alkanethiolate monolayers; adventitious material physisorbed to the surface (e.g., from pump oil), and the hydrogen-containing alkanethiolate monolayers. Only trace amounts of hydrocarbon contaminant are expected on the undamaged, low free energy alkanethiolate layers. The amount of H-addition observed for DMSO-d6 decreases with the chain length of n-alkanethiolate monolayer surfaces, suggesting a decrease in the amount of adventitious hydrocarbon on the film (Figure 1). The hydrogens available to DMSO reaction therefore become increasingly limited to the terminal methyl groups of the monolayer. Our data show a decrease in H-addition to DMSO-d6 for all surfaces as a function of the time the surfaces are exposed to the thiol solution. This suggests that a *second* ordering process occurs for monolayer films *in solution,* perhaps as a result of thermodynamically driven repacking of the thiolate chains after the initial self assembly. The magnitude of this second process decreases with increasing chain length. It is therefore likely that this second process depends on the amount of order that occurs during the initial assembly. After extensive bombardment of the fluorinated surface film, hydrocarbon peaks become more

intense than fluorocarbon, suggesting surface damage and increased adsorption of chamber contaminants (Figure 2). SID spectra of large polyatomic ions (peptides) obtained on damaged and unused fluorinated surfaces are virtually identical. For the atomic ions, the amount of chemical sputtering increases with increasing collision energy and recombination energy of the impinging ion.

Figure 1. DMSO-d6, 20 eV; 30 HR. SOLUTION TIME

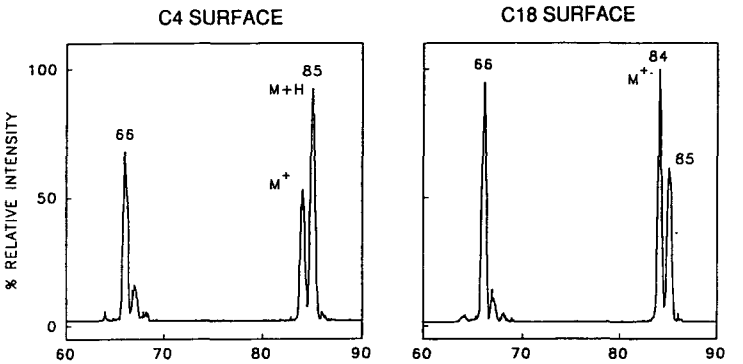

Figure 2. DMSO-d6, 20 eV; FLUORINATED SURFACE

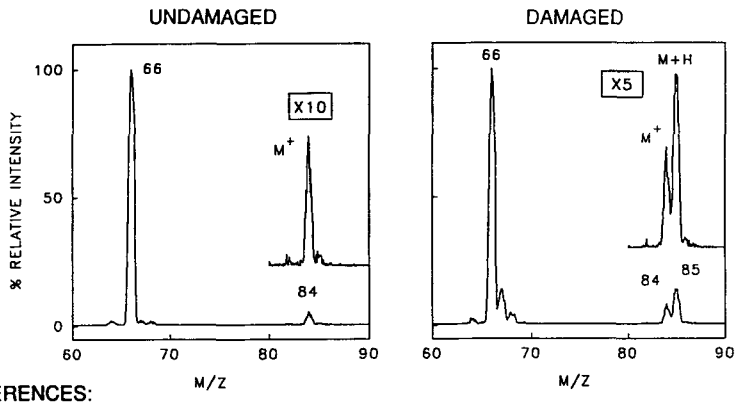

REFERENCES:

1. Cooks, R.G.; Ast, T.; Mabud, Md.A. *Int. J. Mass. Spectrom. Ion Processes,* **1990,** *100,* 209.
2. Wysocki, V.H.; Ding, J.-M.; Jones, J.L.; Callahan, J.H.; King, F.L. *J. Am. Soc. Mass Spectrom.,* **1992,** *3,* 27.
3. Somogyi, Á.; Kane, T.E.; Ding, J.-M.; Wysocki, V.H. *J. Am. Chem. Soc.,* in press.
4. Porter, M.D.; Bright, T.B.; Allara, D.L.; Chidsey, C.E.D. *J. Am. Chem. Soc.,* **1987,** *109,* 3559.

A QUADRUPOLE/TOF MS/MS EXPERIMENTS TO STUDY EFFECTS OF IMPACT OF MACROMOLECULAR IONS ON SURFACES

R.Zubarev, J.Axelsson, J.Eriksson, P.Demirev, P. Håkansson, C.Reimann, B.U.R.Sundqvist,
Dept. Radiation Sciences, Uppsala University, Box 535, Uppsala, 75121 SWEDEN

A "multiply-charged macromolecular accelerator" (MUMMA) is being constructed at Uppsala University for studies of macromolecular ion impacts on surfaces [1,2]. An electrospray ion source and a quadrupole mass spectrometer (MS1) are employed to generate and select positive ions from peptides with mass M from 0.5 to 66.3 kDa and charge Z up to 60, in the M/Z range below 2000. The system is modified by addition of ion optics for transport of the generated ions towards an external target held at a potential U_a of up to - 20 kV. The U_a used in this study was -10 kV, corresponding to primary ion energies Z·10 keV(up to 600 keV for albumin projectiles). A straight time-of-flight (TOF) spectrometer (MS2) has been used for mass analysis of the ejected negative secondary ions as a result of a single macromolecular ion impact on different organic and inorganic targets (Fig.1). The initial experiments, reported here, were performed at a typical pressure in the experimental chamber of $5 \cdot 10^{-7}$ Torr maintained by an oil diffusion pump (an UHV-style experimental chamber is currently under construction).

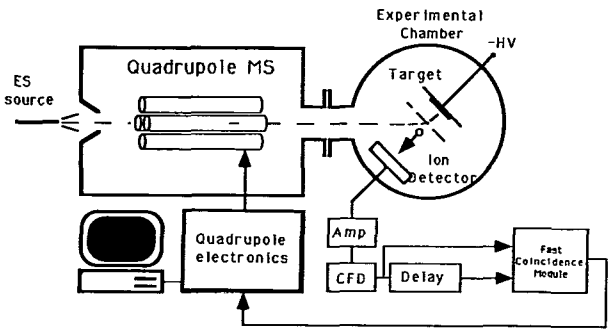

Fig.1 A quadrupole/TOF MS/MS experimental set-up.

Two modes of MS/MS data collection have been developed. Initially MS1 was tuned to a particular M/Z and complete TOF spectra were collected by MS2 (Fig. 2). The negative ion TOF spectra have been obtained using as a start signal either the ejected secondary electrons or H^- ions. Although different target materials have been tested (valine, CsI, bare stainless steel, etc.), 95 to 98 % of the detected secondary ions were not target-specific. Spectra contained mainly peaks of low mass hydrocarbon ions which might have originated from the contamination layer on the target and/or from the projectile. That mode of operation has been employed for estimates of the secondary ion multiplicities (i.e. number of registered secondary ions with different masses per impact event) as a function of different projectile parameters [3]. Our results demonstrate that the average multiplicity of secondary ions ejected in macromolecular impact events scales sublinearly with the projectile velocity [3].

In the second mode fast coincidence electronics is employed to record yields of secondary ions within a predetermined M/Z window (i.e. MS2 collecting ions within a specified arrival time in the TOF spectrum) while the quadrupole (MS1) is scanned through M/Z 500 to 2000, thus resulting in a spectrum of the projectile ions in different charge states (Fig. 3). The secondary electrons emitted during the impact can be magnetically deflected and thus the mass spectrum will contain only secondary ions and/or

fragments from the primary ion projectile. We note the applicability of this approach for resolving the individual components of an electrosprayed mixture (of e.g. peptides), provided that component-specific fragments are detected in the secondary ion TOF spectrum. By choosing a time window for that particular ion the projectile ion spectrum for that component will be accordingly enhanced. So far we have not been able to demonstrate that approach with this particular set-up since we cannot pinpoint a fragment, specific for the primary ion, most probably due to contaminations on the target.

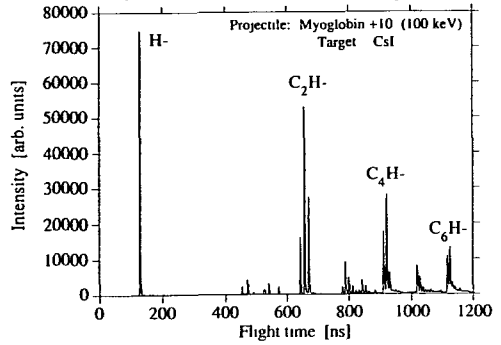

Fig.2 TOF secondary ion spectrum: 100 keV myoglobin ions as projectiles.

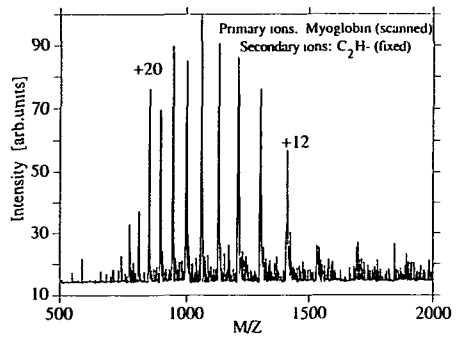

Fig.3 MS/MS mass spectrum of myoglobin, secondary ions: C_2H^-.

1. C.T. Reimann J. Axelsson, P. Demirev, P. Håkansson, J. Kjellberg, B.U.R. Sundqvist, R.E. Johnson, R. Baragiola, B. Donn, in: "*Proceedings of Workshop on Hypervelocity Impacts in Space* ", (ed. J. McDonnell), Kent University Press, Canterbury, (1991) p.58.
2. P. Demirev, C.T. Reimann, J. Axelsson, J. Kjellberg, P. Håkansson, B.U.R. Sundqvist, in: "*Secondary Ion Mass Spectrometry, SIMS VIII* ", (eds. A. Benninghoven, K.T. F.Janssen, J.Tümpner, and H.Werner), John Wiley & Sons, Chichester, (1992) p. 33.
3. R.A. Zubarev, J. Axelsson, J. Eriksson, P.A. Demirev, C.T. Reimann and B.U.R. Sundqvist, paper to be presented at the International Conference on "Polyatomic Ion Impact on Solids and Related Phenomena", St. Malo (France), June 1993.

Separation and Analysis of PAH-DNA Adducts by CE Combined to MS/MS Using an Array Detector.

J. M. Y. Wellemans, R. L. Cerny, M. L. Gross, Midwest Center for Mass Spectrometry, Department of Chemistry, University of Nebraska, Lincoln, NE 68588-0304, USA.

INTRODUCTION. The covalent binding of Polycyclic Aromatic Hydrocarbons (PAH) to purine bases of DNA has been proposed by Cavalieri et al. [1] to be the result of an one-electron oxidation mechanism leading to the formation of a tumor.

Mass spectrometric studies of *in vitro* samples show the attachment of PAH to N7 or C8 of the base to form stable and unstable adducts, respectively [2].

Studies of *in vivo* samples, where less than $1/10^6$ base is modified (femtomole range), involve complex mixtures and low quantities of samples. This necessitates efficacious and sensitive detection techniques. To achieve such detections, we propose to combine capillary zone electrophoresis (CZE) with tandem mass spectrometry via a coaxial continuous flow FAB (cf-FAB) [3]. Because of the high efficiency of CZE and the narrow peaks (half height of 3-10 sec), it is difficult to obtain MS/MS data when scanning MS-2. To overcome the problem, we propose to use a VG ZAB-T tandem mass spectrometer, of reverse Mattauch-Herzog type geometry, equipped with a 15-cm channel electron multiplier array for simultaneous acquisition of major portions of a CAD spectrum.

RESULTS & DISCUSSION. The reference samples, dibenzo[a,l]pyrene-N7-guanine, dibenzo[a,l]pyrene-C8-guanine and 6-methylbenzo[a]pyrene-N7-guanine, were diluted with DMSO/MeOH (1:1). The coaxial cf-FAB was custom-built. The matrix, glycerol/water (25/75) was flowed through a 150-μm i.d. fused-silica capillary at 800 psi by using a μLC Micro Flow pump (ISCO, Lincoln NE). The bomb was pressurized with He at 600 psi to flow the eluent (i.e., water and the samples) through a 10-μm i.d., 140-μm o.d., fused-silica capillary 2 meters in length. For sample injection, the bomb was pressurized at 600 psi for 10 sec., corresponding to a volume injection of 6 nL.

The L-SIMS ion source was at 30 °C and held at 8 kV acceleration voltage. The Cs^+ gun was operated at 30 kV. The collision cell voltage was floated at 4 kV where the collisions with He, as a collision gas, was at a pressure sufficient to reduce the parent beam by 60%. The detection was either a single point or the array detector.

The first goal is to establish the detection limits for the analysis of the PAH-DNA adducts. With the single point detector, MS-2 scans were from 100 u to $[M+H]^+$ at 2 sec/decade. With a 10-sec injection, only 5 scans were recorded. With the array detector, 9 exposures were obtained when covering the same mass range. Each exposure lasted 1 second over a mass ratio of 1.21:1. In addition to a better sensitivity, the array detector allows us to obtain that portion of CAD spectrum that contains most of the structural information with a single exposure, focussing on a specific mass range. For a 10-sec injection, 9 to 10 exposures are recorded for that limited mass range. This way of operating the array detector allows for better detection limits while still obtaining most of the structural information. (See table 1 and spectra 1, 2 and 3).

The next goal is to determine the capability of coupling CZE with the mass spectrometer. The system was tested with model compounds, a tripeptide MLF (methionine-phenylalanine-leucine) and a tetrapeptide FLEEI (phenylalanine-leucine-glutamic acid-glutamic acid-isoleucine). The separation, due to the migration of charged analyte in an electric field, was performed in a 13-μm fused-silica capillary filled with ammonium acetate 5×10^{-3}M at pH 8.5. By using the array detector, 75 fmol of MLF was detected. Most of the major fragments were identifiable.

CONCLUSION. We have shown that, with the array detector, better detection are achieved compared to those with the single point detector. When using the coaxial cf-FAB instead of the static probe, the improvement is approximately three orders of magnitude.

We also have shown, with two peptides, that CZE coupled to our tandem MS can give structural information at low femtomole level. In the future, we will seek better means of desorbing or ionizing the modified nucleobases so that detection limits for MS/MS studies can be reduced to the low femtomole level.

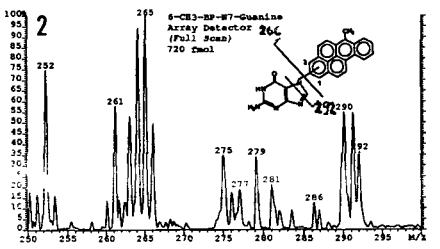

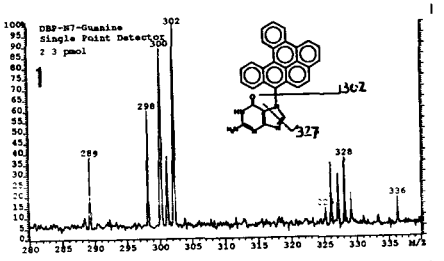

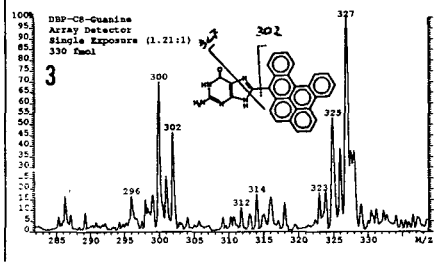

Table 1. Detection limits for coaxial cf-FAB.

Adduct\Mode	Single Point	Array	
	Scan (full scan)	Full Scan	Single Exposure (1.21:1)
DBP-N7 Gua	2.3 pmol	350 fmol	110 fmol
DBP-C8 Gua	1.3 pmol	330 fmol	90 fmol
6-CH_3-BP-1/3-N7Gua	1.4 pmol	350 fmol	86 fmol

REFERENCES

1. Cavalieri E. L. et al. *J. Am. Chem. Soc.*, **1988**, *110*, 4023.
2. RamaKrishna N. V. S. et al. *J. Am. Chem. Soc.*, **1992**, *5*, 293.
3. Moseley M. A. et al. *Anal. Chem.*, **1991**, *63*, 109.

ACKNOWLEDGEMENT

This work was supported by the NIH (Grant No 1P01CA49210-05).

Low-Mass Ions Produced from Peptides by High-Energy Collision-Induced Dissociation in Tandem Mass Spectrometry

A. M. Falick*†, W. M. Hines†, K. F. Medzihradszky†, and B. W. Gibson†
†Mass Spectrometry Facility, Department of Pharmaceutical Chemistry, University of California, San Francisco, CA 94143-0446.

Introduction

High-energy collision-induced dissociation (CID) mass spectrometry provides a rapid, sensitive means for determining the primary sequence of peptides. The low-mass region of the CID spectra of peptides contains several types of fragment ions, including dipeptide ions, immonium ions and other related ions. Immonium ions (general structure $[H_2N{=}CH{-}R]^+$, where R is the amino acid side chain) and related ions characteristic of specific amino acid residues give information as to the presence or absence of these residues in the peptide being analyzed. A data base of 228 high-energy peptide CID spectra has been established, the frequency of occurrence of various ions indicative of specific amino acid residues has been determined, and a model scheme for computer-aided analysis of the amino-acid content of unknown peptides has been developed.

Methods

Mass Spectrometry MS/MS experiments were carried out on a Kratos Concept IIHH 4-sector instrument equipped with an LSIMS source and a multichannel array detector with a 4% mass window. Precursor ions were generated with an 18 keV Cs^+ primary beam. The collision cell (He) was floated at 4 kV.

Data analysis. CID spectra were recorded as peak profiles. A peak detection routine [1] and a threshold were applied to each spectrum. Peaks were classified as strong, medium or weak in the following way. All of the peaks below mass 200 were renormalized such that the largest peak in this range was assigned an arbitrary abundance value of 25. Those peaks with a renormalized abundance of between 5 and 25 were deemed strong, those between 1 and 5 as medium and the remainder were defined as weak. Computer programs for analyzing spectra were written in C and run on a Sun SPARCstation IPX computer. Our database for this study was derived from a larger selection of CID spectra of peptides of known sequence. Programs were designed to suggest residues that were likely absent ("excluded") or present ("required") in the peptide. In cases where no prediction could be made, the residue was "allowed." Predictions were restricted to genetically encoded amino acids. Predictions for Gly and Ala were not attempted as we did not scan low enough to detect their immonium ions. No attempt was made to distinguish the isomeric pair, Leu and Ile, or the isobaric pair, Lys and Gln.

Results

We used the data base to test various possible schemes for computer-aided interpretation of amino acid composition. This "amino acid composition module" was designed to be used in combination with the computer-aided spectral interpretation program developed in our laboratory [1]. The logic for one possible automated scheme for determining amino acid composition is shown in Table 1. This scheme takes account of possible interferences between indicator masses from different residues and also makes use of (crude) ion abundances. In this scheme, peaks are defined as being strong, medium or weak (see Methods).

In developing logic to screen CID spectra for indicator ions, two key points must be borne in mind. First, it is not possible to determine all residues in every case with complete certainty. This conclusion underlines the basic premise of our computer-aided interpretation software, namely that **the computer can be an extremely valuable assistant in the process, but human interaction is essential.** The second key point is that one is required to establish a balance between the desired level of accuracy and the fraction of cases for which a definite prediction can be made. At one extreme, perfect accuracy is required, and all or nearly all tests produce the result "allowed." At the other extreme, definite predictions are required in all cases, but many are incorrect. The scheme shown in Table 1, when tested against the data base, gave 67.5% correct results, 27.7% indeterminate and 4.8% incorrect. In our laboratory we use a variation of this scheme, in which no predictions are attempted for Cys, and Asp, Ser and Glu are never excluded. This reduces the percentage of incorrect results to 2.4%, but at the cost of further increasing the number of cases in which no prediction is made to 39.3%.

AA		Test	Prediction
Simple*		immonium ion mass strong or medium	+
		immonium ion mass absent	-
		all other cases	0
Asn		87 strong or medium and Arg predicted absent	+
		87 absent	-
		all other cases	0
Pro		70 strong or medium and 87, 100 and 112 all absent	+
		70 absent	-
		all other cases	0
Ser		60 strong or medium and Arg predicted absent	+
		60 absent	-
		all other cases	0
His		110 strong	+
	or	110 medium and at least 2 of 82, 121, 123, 136 and 166 present	+
		110 absent	-
		all other cases	0
Arg		100 strong or medium, 87 and at least two of 59, 70, 112 or 129 present	+
		100 strong or medium, 87 and less than two of 59, 70, 112 or 129 present	0
	or	87 or 100 present and at least one of 59, 70, 112 or 129 present	0
		all other cases	-
Lys/Gln		84 and 101 strong and weak (either order) or both medium	+
	or	84, 101, 112, and 129 all present	+
		84 and 101 both absent	-
		all other cases	0
Trp		130 and 159 strong and weak (either order) or both medium and 171 present	+
		130 and 159 strong and weak (either order) or both medium and 171 absent	0
	or	130 and 159 both present	0
	or	171 present and either 130 or 159 present	0
		all other cases	-
Tyr		136 strong or moderate and at least one of 91 or 107 present	+
		136 absent	-
		all other cases	0

Table 1. Scheme for determining the amino acid composition of a peptide. The prediction "+" means that all candidate sequences must contain this residue, "-" means that none may contain it, and "0" means that the sequences may or may not contain it. *"Simple" refers to residues for which only the normal immonium ion peak is used (Cys, Asp, Glu, Phe (91 not used), Ile/Leu (72 not used), Met(61 not used), Thr, and Val).

Conclusions

The low-mass region of high-energy tandem CID spectra of peptides contains information that definitively shows the presence or absence of many amino acid residues, although the complete amino acid composition cannot be deduced in most cases. Both positive and negative conclusions are extremely valuable in generating or narrowing the choice of possible candidate sequences for sequence determination. Logical rules can be developed to provide computer-assisted evaluation of peptide amino acid content. This process can be integrated into an overall computer-aided spectrum interpretation scheme, or used in manual interpretation.

Acknowledgments

We are indebted to Fred C. Walls for acquiring most of the spectra used for this study. This work was supported by grants from NIH (RR01614) and NSF (DIR 8700766) to A. L. Burlingame.

1. Hines, W. M.; Falick, A. M.; Burlingame, A. L.; Gibson, B. W. *J. Am. Soc. Mass Spectrom.* **1992** *3*, 326-336.

Effect of Electrospray Ionization Conditions on Low-energy MS/MS spectra of Peptides.

Greg W. Kilby and Margaret M. Sheil
Dept. of Chemistry, University of Wollongong, Northfields Ave, Wollongong, NSW 2522, Australia

MS/MS spectra of peptides are known to be dependent on collision-induced decomposition (CID) parameters such as ion energy, target gas and target gas pressure[1]. There have been fewer studies, however, of the effect of ionization mode and conditions on MS/MS spectra of peptides[2]. In the case of electrospray ionization (ESI) in particular, the skimmer potential can influence both the the initial internal energy of the ions and the nature of the ions formed and thus may have a significant effect on low-energy MS/MS spectra. In this study we investigated low-energy MS/MS spectra of a range of peptides (500 - 1200 Da) following ESI focussing on: the influence of ESI conditions (solvent pH and skimmer potential) on the type(s) of the ions generated from the peptides for subsequent MS/MS analysis; the effect of varying the electrospray skimmer potential on MS/MS spectra at different collision energies; and the influence of peptide structure on low-energy ES/MS/MS spectra.

In many instances for MS/MS experiments, especially for small peptides and peptides with a number of basic residues (for which multiply-charged species tend to dominate with ESI), it is often desirable to generate $[M+H]^+$ ions. For ESI of most peptides a high solvent pH and high skimmer voltage (B1) has been found to optimize $[M+H]^+$ ion production. Solvent pH also affects the degree of source fragmentation observed in ESI mass spectra. For example, a low pH (2.5) results in more extensive source fragmentation at any given skimmer potential than a high pH (10.5). This effect is much more pronounced with peptides containing a number of basic residues and may in part be due to there being a greater population of doubly-charged species which fragment more readily at low pHs.

That higher skimmer potentials generate ions with increased initial internal energy was reflected in the MS/MS spectra of all the peptides studied. In the MS/MS spectra of Met-Enkephalin shown in figure 1, more extensive fragmentation was observed under the same collision conditions when higher skimmer potentials were employed. This effect was more apparent at lower collision energies, and was found to be a general one for a range of cyclic and linear peptides. For each peptide, however, there was a unique optimum skimmer potential which represented a balance between generating $[M+H]^+$ ions with high internal energy and using too high a potential such that the intensity of $[M+H]^+$ ions was reduced by the onset of other processes *i.e.* source fragmentation etc.

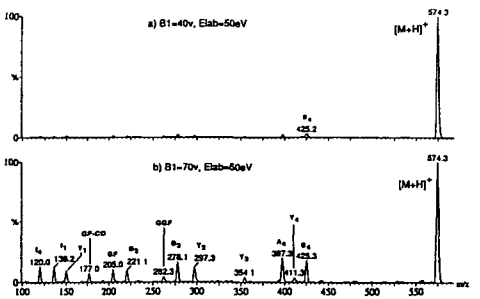

Figure 1 ES/MS/MS spectra of $[M+H]^+$ Met Enkephalin at two different skimmer potentials (B1). E_{lab} = 50 e, argon collision gas.

MS/MS spectra of $[M+cat]^+$ ions of peptides often yield different fragments to $[M+H]^+$ ions. We have found in the case of cyclic peptides which form $[M+NH_4]^+$ ions that these fragment more readily compared with the $[M+H]^+$ ions while still yielding the same structural information. This is illustrated in the ES/MS/MS spectra of valinomycin shown in figure 2. Extensive fragmentation is observed in the MS/MS spectrum of the $[M+NH_4]^+$ ion even with no collision gas. The potential of using NH_4^+ ions to "activate" fragmentation is limited, however, to the small number of peptides that will form $[M+NH_4]^+$ ions.

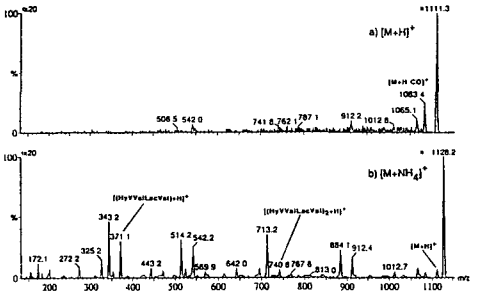

Figure 2 ES/MS/MS spectra of valinomycin $[M+H]^+$ and $[M+NH_4]^+$ ions. No collision gas.

Finally, the influence of peptide structure on low-energy ES/MS/MS spectra was investigated. Gaskell *et al.*[3] have proposed that in order to generate extensive fragmentation in low-energy MS/MS spectra of peptides there must be an even distribution of charged sites within the precursor ion population. This is reflected in the ES/MS/MS spectra of $[M+H]^+$ ions of Arg-Met Enkephalin (RYGGFM) versus Met Enkephalin (YGGFM) and of bradykinin (RPPGFSPFR) compared with des-Arg-bradykinin (PPGFSPFR). The peptides with Arg at the N-terminus (which is probably a preferred protonation site) showed poor fragmentation efficiency compared with the corresponding peptides without an N-terminal Arg. Further, it was not possible to increase the extent of fragmentation in the ES/MS/MS spectra of Arg-Met Enkephalin or bradykinin by increasing either the initial internal energy (increased B1) or the collision energy_ thus supporting the view that it is the charge sites rather than the available energy that is the dominant factor in this case.

Thus low-energy MS/MS spectra of peptides have been found to be very dependent on electrospray ionization conditions. For a given peptide, the source skimmer potential, the solvent pH and the collision conditions all need to be optimized to generate the maximum degree of fragmentation. In some cases, however, especially for basic peptides, the distribution of charged sites within the peptide may have a more significant effect on the fragmentation than either the ionization or collision conditions.

Experimental

All experiments carried out on a VG Quattro triple quadrupole. The solvents were either 50% aq MeCN & 1% Formic Acid or 50% aq MeCN &1% NH_3. Solvent flow rate was 5 µl/min. The collision gas used was argon at a pressure corresponding to ~30% transmission for each MS/MS experiment. The peptides were dissolved in aqueous solutions with concentrations in the range of 300 - 500 pmol/µl.

References

1. S.A. Martin and K. Biemann *Int. J. Mass Spectrom. Ion Proc.* (1987) 78 213
2. J.M. Curtis *et al. Org. Mass Spectrom.* (1992) 27 502
3. S.J. Gaskell *et al.* 40th ASMS, Washington (1992) p1835

CAD/MS/CAD/MS Of Multiply Charged Peptides With Electrospray Ionization

Joseph A. Loo
Parke-Davis Pharmaceutical Research
Division of Warner-Lambert Company
2800 Plymouth Road, Ann Arbor, MI 48105

and

Richard D. Smith
Pacific Northwest Laboratory
P.O. Box 999, Richland, WA 99352

Sequencing of large polypeptides by tandem mass spectrometry has been facilitated by advances in ionization methods such as electrospray ionization (ESI). Multiply charged species from large peptides may be induced to fragment through collisionally activated dissociation (CAD) methods. ESI-product ions may be generated in the collision chamber of a tandem mass spectrometer (low energy collisions with a triple quadrupole instrument or high energy collisions with a magnetic sector instrument) or in the atmospheric pressure/vacuum interface region of the ESI source (low energy collisions) through control of the nozzle-skimmer or capillary-skimmer voltages. Increasing the collision energy in the interface often changes the relative abundance of product ions. For example, at a nozzle-skimmer potential of + 250 V, an abundant series of $b_{2\text{-}10}$ ions are produced for substance P (M_r 1347). At + 350 V, an additional series of $a_{4\text{-}10}$ ions are generated, most likely from further dissociation of b_n ions.

Deciphering the amino acid sequence information is often straightforward, although for more highly charged precursors, multiply charged product ions may be produced. The combination of CAD with higher resolution analyses allows for direct determination of product ion charge state, and therefore product ion mass. For example, low energy CAD in the ESI interface of a magnetic sector instrument (Finnigan MAT 900 with a heated-glass capillary electrospray interface) of melittin (M_r 2846) produces abundant singly- and doubly-charged y_n and b_n type product ions from the first 19 (out of 26) residues. CAD spectra taken at a resolving power of 3000 allows resolution of isotope peaks of the multiply charged molecules and product ions (Figure 1).

Further dissociation of product ions generated in the ESI interface (CAD/MS/CAD/MS) often yields additional sequence information and confirmation of product ion assignments. Figure 2 shows the CAD/MS/CAD/MS spectrum of the y_{13}^{2+} product ion from melittin. The y_{13}^{2+} "parent" ion was generated by low energy collisions and was further subjected to high energy (2.5 keV laboratory energy, B/E linked scan) collisions. In this manner, additional sequence information from the COOH-terminus of melittin was obtained.

In most cases studied, product ions generated in such experiments are the "expected" types (*e.g.*, MS/MS of a b_{10} fragment ion may produce a series of $a_{1\text{-}9}$ and $b_{1\text{-}9}$ product ions.). However, in selected examples such as substance P (RPKPQQFFGLM-NH_2) and substance P analogues, the tandem mass spectra appear to indicate that the peptide has isomerized during or after the initial CAD step. Both low energy and high energy MS/MS of the b_{10}^{2+} product ion of substance P yields fragments from the successive loss of Phe^8, Phe^7, and Gln^6 instead of loss of residues 9 and 10 (Gly and Leu, respectively). Tandem mass spectrometry of the $(M+2H)^{2+}$ ion of substance P (1-9) yields the expected series of a_n/b_n product ions. MS/MS of the b_9^{2+} product ion of full substance P (only 16 Da difference from substance P (1-9) because of the missing terminal amide) produces a more abundant series of ions from loss of Phe, PhePhe, and PhePheGln. For the peptide [His^9]-substance P, MS/MS of the doubly-charged b_{10} and b_9 ions produced no evidence for "isomerization". However, dissociation of the b_8^{2+} product yielded ions

from loss of Gln, GlnGln, and GlnGlnPhe. One possible explanation is that following a dissociation event (occurring in the interface) that energizes the molecule, the gas-phase peptide isomerizes in which the COOH-terminus cyclizes towards residues 4 or 5. Isomerization is hindered by a positively-charged residue near the COOH-terminus (*e.g.*, [His^9]-substance P).

Conclusion. Sequence information for large polypeptides can be obtained by CAD/MS of multiply charged molecules, producing multiply charged product ions. Sequence information from product ion mass spectra can be more easily assigned by assignment of product ion charge states from data taken with higher resolution mass spectrometers. However, for certain peptides, gas-phase isomerization processes may contribute to CAD mass spectra, adding another degree of difficulty to the interpretation process. More work is needed to understand the energetics and structural constraints of dissociation events for large polypeptides.

Fig. 1

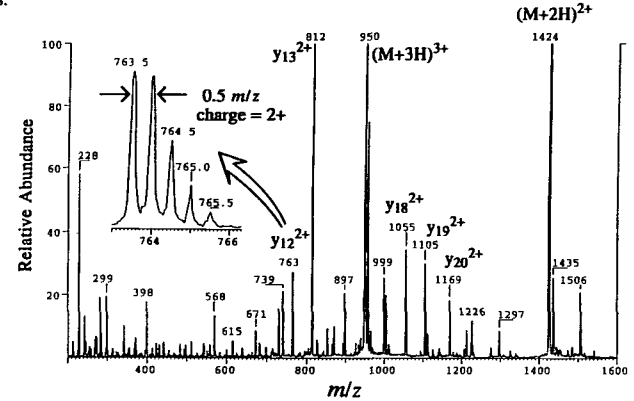

Fig. 2

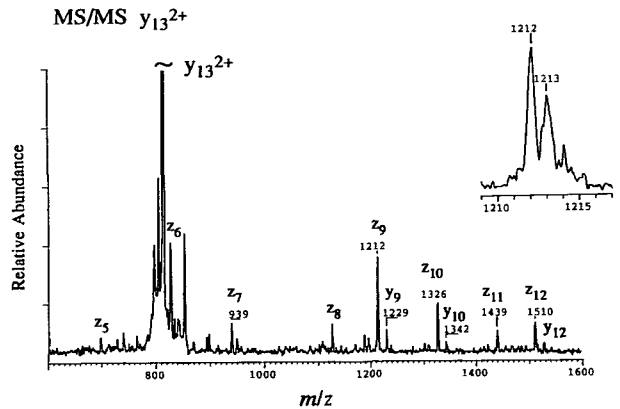

THE MECHANISM OF FORMATION OF PEPTIDE d_n AND w_n IONS EVALUATED BY REACTION INTERMEDIATE SCANNING ON A BEqQ HYBRID

Kevin D. Ballard and Simon J. Gaskell
Center for Experimental Therapeutics, Baylor College of Medicine, Houston, TX 77030

Ions of the d_n and w_n types, *representing side-chain cleavages from peptide [M+H]+ ions* and observed during tandem MS under high energy CAD conditions, are useful for distinguishing isobaric amino acid residues such as leucine and isoleucine. The formation of these ions requires the cleavage of two covalent bonds. When the origins of these ions were first studied[1,2], it was suggested that d_n and w_n ions were formed via the sequential fragmentation of a_n+1 and z_n+1 product ions, respectively. Evidence for this was based upon the observation of d_n and w_n ions *during product ion scanning analyses of source-formed a_n+1 and z_n+1 ions, respectively.* Although those data provided good evidence for the proposed mechanisms, that approach did not directly address the events occurring in the ion beam of the mass spectrometer. Presumed source-formed product ions are not necessarily structurally identical to ions of the same mass formed under high energy CAD conditions in a collision cell. The previous studies also did not consider whether the two sequential fragmentations necessarily require consecutive collision events. These issues have *now been addressed using the sequential MS capabilities of a BEqQ hybrid mass spectrometer.*

Experimental. Tandem MS experiments with synthetic peptides were performed with a VG ZAB-SEQ hybrid instrument of BEqQ configuration. Reaction intermediate spectra were obtained by scanning B and E simultaneously (with B/E constant) over a narrow range encompassing the intermediates of interest formed in FFR1, with Q set to transmit the second generation product ion of interest formed in q.

Results. *Most of the d_n ions studied so far by reaction intermediate scanning are formed via the* intermediacy of the a_n+1 species, with the second decomposition occurring spontaneously. Thus, once the requisite a_n+1 ions are formed by high energy CAD, a proportion can spontaneously decompose to a d_n species. An exception is the d_3 ion from RKDVY, the reaction intermediate scan for which is shown in Figure 1; this signal aligned well with the *m/z*-deconvoluted B/E linked scan of the a_3 ion. Thus, this d_3 ion arises through the initial formation of the a_3 species. Interestingly, when the aspartic acid residue is replaced with glutamic acid, or if the aspartic acid is methylated, the d_3 ion is formed via the a_3+1 species.

All of the w_n ions studied thus far originate through z_n+1 ions, as determined by reaction intermediate scanning. In some cases, however, the signals representing the w_n ions in the reaction intermediate spectra are strong even in the absence of added collision gas. This indicates that, in some instances, w_n ions can be formed from FAB generated $[M+H]^+$ precursor ions without an absolute requirement for collisional activation. This is demonstrated in Figure 2, which depicts the sequential product ion spectrum (obtained without added collision gas) representing the $[M+H]^+ \longrightarrow z_6+1 \longrightarrow$ products reaction sequence for the peptide VHLTPVEK. Here, the w_6 ion and the z_5 ion are clearly detected. Ions of these types are generally not seen in product ion spectra obtained under low energy CAD or unimolecular decomposition conditions. Even with this peptide, the w_6 and z_5 ions are not evident in the low energy CAD conventional product ion spectrum. This is another instance where the higher-order mass spectrometric experiment reveals fragmentation processes not evident in the lower order experiment.

References

1. Johnson, R.S.; Martin, S.A.; Biemann, K.; Stultz, J.T.; Watson, J.T. *Anal. Chem* 1987, *59*, 2621.
2. Johnson, R.S.; Martin, S.A.; Biemann, K. *Int. J. Mass Spectrom. Ion Proc.* 1989, *86*, 137.

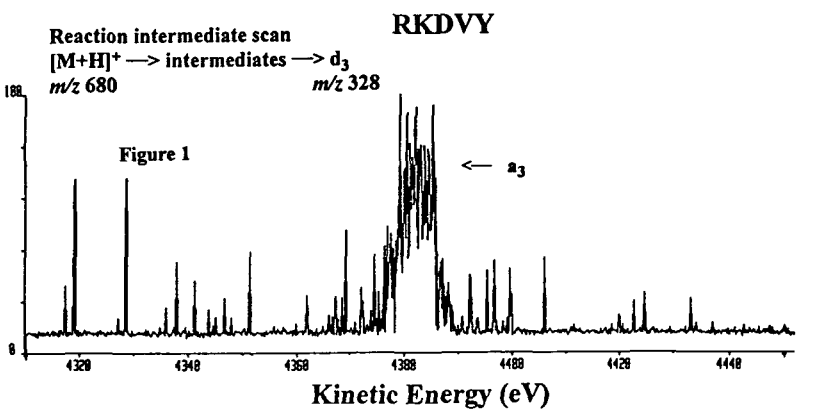

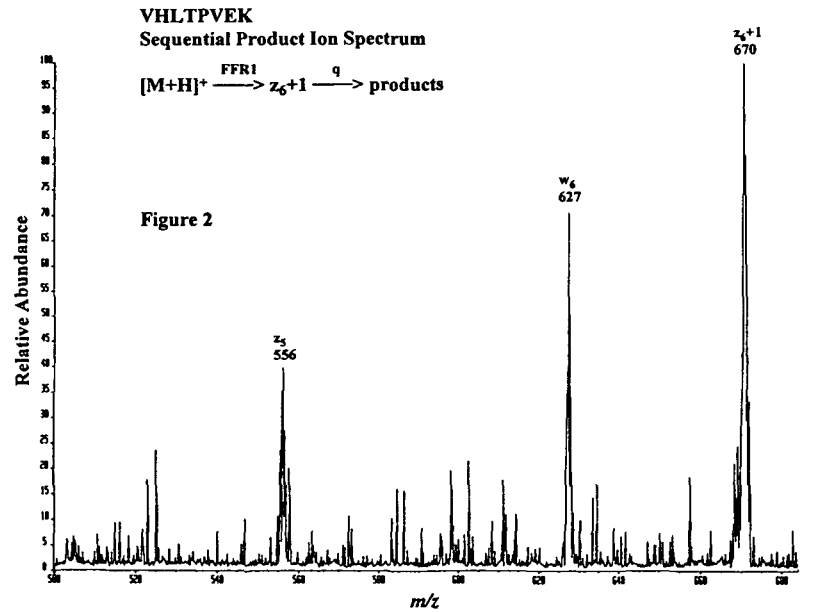

THE TANDEM MASS SPECTROMETRY OF HIGHLY BASIC PEPTIDES*

Jonathan M. Curtis[1], Pierre Thibault[1], Robert K. Boyd[1], Su Chen[2], Peter J. Derrick[2] and Bruce A. Thomson[3]. [1]*Institute for Marine Biosciences, National Research Council, Halifax, Canada B3H 3Z1;* [2]*Institute for Mass Spectrometry and Dept. of Chemistry, University of Warwick, Coventry CV4 7AL, UK;* [3]*SCIEX, 55 Glencameron Road, Thornhill, Ontario, Canada L3T 1P2.*

Determinations of peptide sequence by tandem mass spectrometry (MS/MS) [1] can be routine, but in some cases the method fails. A well known example concerns a round-robin organized by the ASMS [2], in which only one of about 35 participating groups reported any data for an "unknown" peptide stated to have molecular mass of about 1800 Da. An account [3] of the efforts of the (partially) successful group has been published. It turned out that the "unknown" peptide was dynorphin 1-17 (dynorphin A), YGGFLRRIRPKLKWDNQ. The most striking feature of this sequence is the large number of basic residues (3 Arg plus 2 Lys), all located within the central 8 residues. One purpose of the present work was to investigate whether the large number of basic residues was the explanation for the lack of success of a number of expert groups in sequencing this peptide by MS/MS. The original success [3] was achieved using SIMS of a dry sample on a nitrocellulose substrate, with MS/MS achieved by correlation of neutral and ionic fragments from metastable $(M+H)^+$ precursors in a reflecting TOF instrument. Since then two rival techniques have become more widely available. The first exploits high-energy (keV) CID of singly-protonated peptides $(M+H)^+$ produced by LSIMS, in four-sector instruments fitted with array detectors. The second approach exploits the ability of electrospray and ionspray ionization to produce multiply-protonated peptides, in which the Coulombic stress activates fragmentation of the ion, even under low-energy CID (tens of eV) conditions. The present work compared the sequence-specific fragmentations of a series of peptides (endorphins and dynorphins) containing large numbers of basic residues, using both high-energy CID of $(M+H)^+$ ions and low-energy CID of multiply-charged ions.

Figure 1 compares low-energy CID fragment spectra (SCIEX API III triple quadrupole with ionspray interface and a novel collision cell permitting better sensitivity and resolving power for fragment ions) of $(M+2H)^{2+}$ and $(M+3H)^{3+}$ ions from dynorphin 1-13 (YGGFLRRIRPKLK, M=1603.0), while Figure 2 shows the 4 keV fragment spectrum of $(M+H)^+$ (Kratos Concept II-HH EBEB, with scanning array detector). These spectra are representative of most of the peptides studied. The $(M+3H)^{3+}$ provided even less sequence information than the $(M+2H)^{2+}$, demonstrating that coulombic stress alone is not a sufficient condition for useful fragmentation at low energy; in addition it is necessary [4] for one of the ionizing protons to be mobilized along the peptide backbone to permit charge-site initiated reactions. The high-energy spectra (*e.g.* Fig.2) were invariably richer, with abundant sidechain cleavage ions characteristic of a localized ionizing proton promoting charge-site-remote reactions [5]. However, coherent fragment series permitting deduction of the complete sequence were not often observed for these highly basic peptides. In addition, observation of a peak at almost every mass can be a disadvantage, as such a spectrum can be interpreted as consistent with many candidate sequences.

In the case of dynorphin A itself (data not shown) the high-energy CID spectrum was of good signal/noise, with peaks covering the mass range. However, the intense peaks were scattered amongst all of the well-known fragment series [1], providing limited sequence information [2] (no extended coherent fragment series was obtained). When the threshold for peak acceptance was lowered, the "peak-at-every-mass" phenomenon began to be a problem. The low-energy CID spectra of $(M+2H)^{2+}$ and $(M+3H)^{3+}$ of dynorphin A were qualitatively similar to Figure 1, but contained more doubly-charged fragments.

It is emphasised that the problem addressed here is not an artificial one; the dynorphins and other endorphins are important bioactive peptides, which inherently contain large numbers of basic residues.

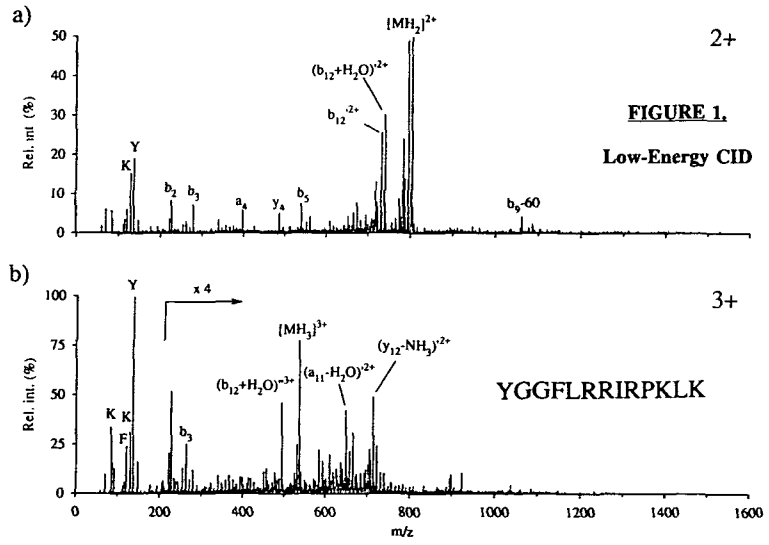

FIGURE 1.

Low-Energy CID

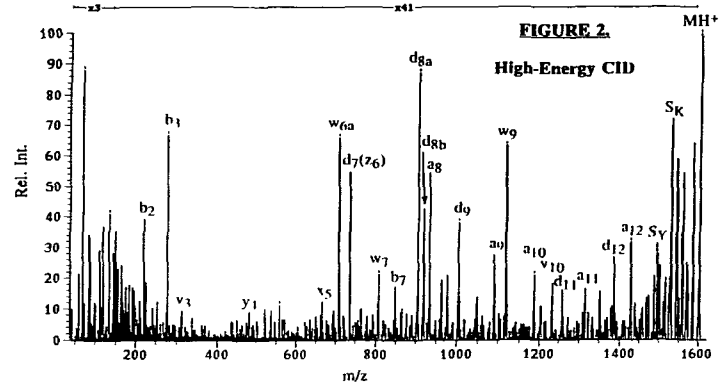

FIGURE 2.

High-Energy CID

1. K. Biemann and S.A. Martin, *Mass Spectrom. Revs.* **6** (1987), 1.
2. S.A. Carr, *Proc. 38th ASMS Conf., Tucson, AZ*, pp.1575-1576 (1990).
3. N. Poppe-Schriemer *et al.*, *Int. J. Mass Spectrom. Ion Proc.* **111**, 301 (1991).
4. X.-J. Tang and R.K. Boyd, *Rapid Commun. Mass Spectrom.* **6**, 651 (1992).
5. R.S. Johnson *et al.*, *Int. J. Mass Spectrom. Ion Proc.* **86**, 137 (1988).

* NRCC No. 34858.

Capillary LC-Tandem Mass Spectrometry of Amadori Compounds

Terry Sumpter and Nancy J. Jensen
Research Center
Philip Morris USA
Richmond, VA 23261-6583

Introduction: Amino-carbonyl condensation reactions (Maillard reaction) and the subsequent slow Amadori rearrangement of the Schiff-base (aldimine) intermediate to give various ketoamine products provide a starting point for pathways leading to a multitude of flavor and aroma agents. There are typically many simultaneous reactions occurring in these processes, generating many components possessing a wide range of molecular weights, volatilities, and thermal stabilities. In addition, the non-enzymatic glycation of proteins has been observed in several cases *in vivo*. This work uses model compounds to demonstrate the application of a variety of MS and tandem MS methods to the characterization of individual components and classes of compounds produced by these reactions.

Experimental: Mass spectra were acquired using a JEOL SX102/SX102 four sector (BEBE) tandem mass spectrometer. Accelerating potential was 10 kV, resolving power was *ca.* 1000, and Xe at 6 kV was used for FAB ionization. Constant neutral loss spectra were acquired by collision of the precursor ions using He (80% precursor ion beam reduction) in the first field free region after the ion source in MS I. Detection of those product ions resulting from the specified neutral loss from the precursor was by the appropriate linked scan function using MS I. For this direct probe work, tetramethylene sulfone was the FAB matrix. For LC-CI experiments, the frit interface was equipped with a CI chamber attachment and an electron energy of 200 eV at an emission current of 300 μA was used. The source temperature was *ca.* 175 °C. For LC-EI experiments, ionization was by EI at 70 eV, 300 μA emission, and the source temperature was *ca.* 175 °C. Capillary HPLC separation of components was accomplished using a Waters 600-MS pump with a precolumn solvent split to reduce the flow into the MS to *ca.* 4-5 μL/min. An LC Packings 0.32 x 150 cm C_{18} column was used, and the mobile phase was 100% A (water, 1% glycerol, 0.1% TFA) to 100% B (MeCN, 1% glycerol, 0.1% TFA) in 20 min for peptide studies. For LC-CI and LC-EI, the mobile phase was 90% MeCN/10% water, with the same column as was used for the peptide studies. MS/MS experiments were accomplished by selecting the precursor ion with MS I, and colliding the mass selected ion in the interface between MS I and MS II. Helium was the collision gas, at a pressure sufficient to reduce the parent ion beam by *ca.* 80%. Detection of the resulting fragment ions was by a B/E scan using MS II. .

Results: The purpose of this study was to combine the separation capability of HPLC, which avoids potential thermal degradation, with the specific structural characterization capability of mass spectrometry to characterize a wide range of compounds. To this end we have applied LC-EI and LC-CI to the analysis of small, volatile model compounds, namely, a series of substituted 1,4-pyrazines. Figure 1 shows a typical LC-EI spectrum obtained, in this case for 10 ng of 2-isopropyl-1,4-pyrazine. This spectrum is dominated by a large $[M + H]^+$ ion, with little fragmentation observed. In most applications of this LC-EI technique, a combination of EI and CI processes is observed. The preponderance

of the CI process for these compounds is due in part to the proton affinity of the pyrazines. In addition, it may be that the large proportion of MeCN used in the mobile phase suppresses radical cation formation by acting as a free radical "scavenger". The LC-CI spectrum of the same compound shows a large $[M + H]^+$ ion as well, though there is a larger chemical background associated with the LC-CI technique under these conditions.

It is also useful to be able to screen for classes of compounds in these reaction mixtures. The amino sugars are characterized by a loss of 17 u upon CID. This permits the use of constant neutral loss (CNL) linked scanning to identify this class of compounds. A CNL spectrum for loss of 17 u by L-rhamnosylamine is shown in Figure 2. This specificity of analysis should provide for functional group identification of components in mixtures.

The non-enzymatic glycation of proteins was investigated using a model system reportedly leading to the dihydroxypropylation of lysine residues and the amino terminus. The use of four-sector MS/MS with rapid linked scans (0-2400 u/5 s) and sequential precursor ion selection has been successfully applied to the model protein, cytochrome c (Figure 3) at the 30 pmol level. However, the expected adducts have not been observed with the treated system. It appears that the adducts are not being formed. Further work in this area is planned.

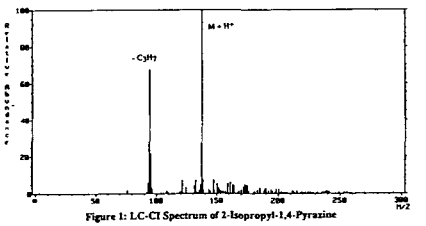

Figure 1: LC-CI Spectrum of 2-Isopropyl-1,4-Pyrazine

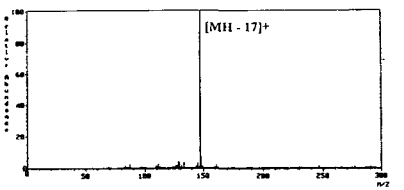

Figure 2: CNL of 17 u by L-Rhamnosylamine

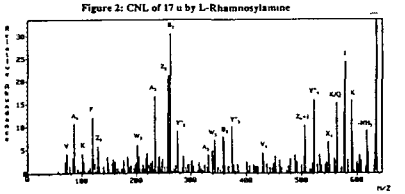

Figure 3: On-Line LC MS/MS of IFVQK

Diastereomeric Selectivity Using Metal Complexes: A MIKES Study

Thuy Thanh Dang and Julie A. Leary
Department of Chemistry, University of California, Berkeley, CA 94720

Chirality is an important determinant of molecular recognition in biochemical systems.[1] While one enantiomer of a molecule shows biological activity, the other enantiomer may show little or no activity. In addition, it is known that in pharmaceutical drugs, the non-desired enantiomer can cause side effects.[2] The increasing need for optically pure compounds has made their synthesis an important focus of current research in both academic and industrial laboratories. New chromatographic techniques, such as enzymatic columns and gas chromatography using a chiral stationary phase, are able to separate enantiomic pairs.[3] However, there have been only a few techniques using mass spectrometry to analyze chiral isomers.[4] We have developed a new technique utilizing fast atom bombardment mass spectrometry (FAB-MS) in combination with MS/MS and kinetic energy release (KER) measurements to distinguish enantiomeric diols.[5]

In this study we have combined various optically pure diols with R,R and/or S,S, threohydrobenzoin (THB) with a racemic mixture of cobalt trisacetylacetonate ($Co(acac)_3$). The complexes formed were analyzed by FABMS and subsequently selected ions were chosen for Mass-Analyzed Ion Kinetic-Enery Spectroscopy (MIKES) study. These experiments were also performed using Mg $(acac)_2$, $Zn(acac)_2$, and $Ca(acac)_2$ to determine whether there were differences in the degree of chiral recognition when the complex studied had either octahedral or tetrahedral geometry.

Table 1 shows the KER values measured for the product ion *m/z* 393 of the $[Co(acac)_2DIPT]^+$ system.[6] The KER values indicate that when the diastereomers $[Co(acac)_2/L\text{-}DIPT]^+$ and $[Co(acac)_2/D\text{-}DIPT]^+$ are formed in the presence of RR- or SS- THB, a chemical kinetic resolution[7,8] effect takes place. This effect occurs when one enantiomer of $Co(acac)_2$ is preferentially coordinated to the DIPT. The KER values of the diastereomic pairs D-DIPT/RR-THB and L-DIPT/SS-THB are the same upon the production of *m/z* 393. In contrast, the KER values for the L- and D- DIPT without of THB are identical, indicating no difference in their structures.

The same chemical kinetic resolution effect is also observed for the $[Mg(acac)_2DET+H]^+$ system.[6] The KER values are reported in Table 2. Both the $[Co(acac)_2DIPT]^+$ and $[Mg(acac)_2DET+H]^+$ complexes have octahedral geometry and clearly show the same trends as discussed above.

The MIKES study was also performed on $[Co(acac)DIPT]^+$. No chemical kinetic resolution effect is observed in the presence of THB. The KER values are reported in Table 3. The geometry of the $[Co(acac)DIPT]^+$ complex is tetrahedral.

Using MIKES in conjunction with KER, we established that chiral recognition of metal coordinated diol complexes requires all of the following conditions: 1) A chiral auxilary agent, threohydrobenzoin (THB) must be present in order to help coordinate the diol to the metal bisacetylacetonate complex. THB acts as a kinetic resolution agent and aids in the enantioselectivity of either D and L forms of the tartrates. 2) The geometry of the metal coordinated complex must be octahedral.

[1] Baldwin, M. A.; Howell, S. A.; Welham, K. J.; Winkler, F. J. *Biomed. Environ. Mass Spectrom.* 16, 357 (1987).
[2] Stinson, S. C. *Chemical & Engineering News*, 70, 46 (1992).
[3] Juaristi, E. Introduction To Stereochemistry & Conformational Analysis. John Wiley & Sons, 1991.
[4] Mandelbaum, A. *Mass Spectrom. Rev.*, 2, 223 (1983).
[5] Hofmeister, A. and Leary, J. A. *Org. Mass Spectrom.* 26, 811 (1991).
[6] Abbreviations : diethyltartrate (DET) and diisopropyltartrate (DIPT).
[7] Sharpless, K. B.; Rossiter, B. E.; Katsuki, T. *J. Am. Chem. Soc.*, 103,464 (1981).
[8] Sharpless, K. B.; Rossiter, B. E.; Katsuki, T. *J. Am. Chem. Soc.*, 110,2978 (1988).

Table 1: MIKES Study of $[Co(acac)_2DIPT]^+$. The KER values* of *m/z* 393 (loss of an acacH neutral and reduction of Co^{+3} to Co^{+2})

A. In the presence of THB

1. RR-THB/D-DIPT = 21.5±1.1 mV
2. RR-THB/L-DIPT = 14.1±1.2 mV
3. SS-THB/L-DIPT = 21.6±0.9 mV
4. SS-THB/D-DIPT = 16.2±0.5 mV

B. Without the presence of THB

5. L-DIPT = 13.3±1.8 mV
6. D-DIPT = 13.7±0.9 mV

*KER values are mean values ($\bar{x}$) for nine experiments.. Error values are standard deviation of the mean ($S_{\bar{x}}$).

Table 2: MIKES Study of $[Mg(acac)_2DET+H]^+$. The KER values* of *m/z* 337 (loss of two neutral ethanols)

A. In the presence of THB

1. RR-THB/D-DET = 13.1±0.3 mV
2. RR-THB/L-DET = 17.2±0.7 mV
3. SS-THB/L-DET = 13.3±0.4 mV
4. SS-THB/D-DET = 18.1±0.6 mV

B. Without the presence of THB

5. L-DET = 12.8±0.4 mV
6. D-DET = 13.4±0.8 mV

*KER values are mean values ($\bar{x}$) for nine experiments. Error values are standard deviation of the mean ($S_{\bar{x}}$).

Table 3: MIKES Study of $[Co(acac)\ DIPT]^+$. The KER values* of *m/z* 349

A. In the presence of THB

1. RR-THB/D-DIPT = 42.1±1.2 mV
2. RR-THB/L-DIPT = 43.1±1.1 mV
3. SS-THB/L-DIPT = 41.9±0.4 mV
4. SS-THB/D-DIPT = 40.9±0.8 mV

B. Without the presence of THB

5. L-DIPT = 40.4±0.6 mV
6. D-DIPT = 41.3±0.6 mV

*KER values are mean values ($\bar{x}$) for nine experiments. Error values are standard deviation of the mean ($S_{\bar{x}}$).

Characterization of Lipids in Marine oils by LSI/MS/MS

*Feng-Yin Hsieh[1], Brian J. Nobes[1], Harry L. Greene[4], and Ian A. Blair[1,2,3].
Departments of Pharmacology[1] and Chemistry[2] and Clinical Nutrition Research Unit[3],
Vanderbilt University, Nashville, TN 37232 and
Mead Johnson Nutrition Group[4], Mead Johnson Research Center, Evansville, IN 47721.

The separation, identification and determination of phospholipids (PLs) in marine oils were based on Solid-Phase Extraction (SPE), HPLC, and Liquid Secondary Ion(LSI) mass spectrometry. SPE using aminopropyl bonded cartridge provided a rapid extraction method and high recovery of PLs. The marine oils contained only trace amounts of PLs and so it was necessary to extract up to 100 mg of the oil. By using a series of columns it was possible to isolate sufficient material for identification of individual PLs. HPLC was carried out using a gradient of hexane/iso-propanol/water in combination with a normal phase silica column. LSI/MS/MS of the purified PLs was carried out on a Kratos Concept IIHH tandem mass spectrometer operating in the positive and negative ion modes. Confirmation of PL class and the molecular weights of individual PLs was carried out by positive and negative LSI MS. The total fatty acid composition of the PLs and the fatty acids attached to individual PLs were identified by negative LSI MS and LSI/MS/MS, respectively. Three major docosahexaenoic acid (DHA) containing phosphatidylcholines (PCs) ($[MH]^+$ *m/z* 879, 833, 807) were identified. In addition, a mixture of structurally similar new glycerolipids was isolated from the PC region during HPLC purification. The mass spectra of the PC mixture and the mixture of new glycerolipids each contained intense ions at *m/z* 58, 86, and 104 indicating the presence of choline. Structures of the PCs, together with assignment of the fragment ions are shown in Figure 1.

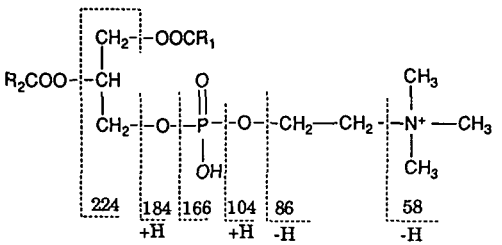

phosphatidylcholine

	MW	R_1/R_2
M_1	878	22:6ω3/22:6ω3(DHA)
M_2	832	18:1/22:6ω3(DHA)
M_3	806	16:0/22:6ω3(DHA)

Figure 1: Fragment ions observed in the positive LSI mass spectrum of PCs from marine oil.

The positive LSI mass spectrum of the mixture of new glycerolipids (Figure 2) lacked ions at *m/z* 166, 184 and 224 observed with PC, but contained ions at *m/z* 132, 178 and 218. The ions at *m/z* 178 and 218 were six daltons lower than expected for a PC. The $[M+H]^+$ ions were also six daltons lower than expected for PCs. The negative LSI spectra lacked ions at *m/z* 79 (PO_3^-) and 97 ($H_2PO_4^-$), but an ion appeared at *m/z* 73. These data indicated that the compounds lacked a phosphate group but contained a choline moiety. LSI/MS/MS analysis suggested that the three new choline-containing glycerolipids ($[MH]^+$ 873, 801, 773) all contained DHA. After methylation of the glycerolipids with diazomethane, the positive LSI spectrum contained $[M+CH_3]^+$ ions and an ion at *m/z* 232 instead of at *m/z* 218. Ions

at *m/z* 58, 86, and 104 were unaffected by methylation. This suggested that there was carboxylic acid group between the choline group and glycerol backbone. The presence of a carboxylic acid group was further established by a deuterium exchange experiment using D_8-glycerol/D_6-dimethylsulfoxide as the LSI matrix. $[M+D]^+$ ions and an ion at *m/z* 219 replaced the $[M+H]^+$ and *m/z* 218 ions in the positive LSI spectrum. These data suggested that the choline-containing glycerolipids contained a [OCHO-COOH] group instead of the phosphate residue found in PCs.

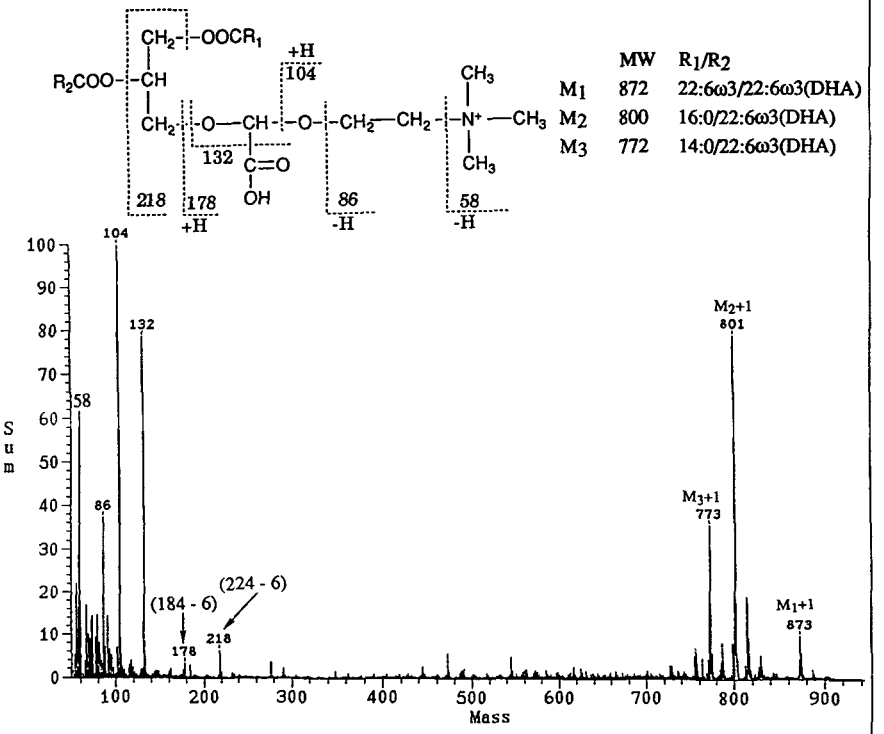

Figure 2: Positive LSI mass spectrum of choline-containing glycerolipids from marine oil.

In summary, LSI/MS and LSI MS/MS were useful for characterizing individual lipid classes in marine oils and for providing fatty acid composition of the lipids. During the course of these studies a new group of glycerolipids was identified that contained glyoxylic acid acetal in place of the phosphate normally found in PCs.

Supported by NIH grants DK26657 and RR06254 and Mead Johnson.

A Kinetic Treatment of Resonant Excitation in the Ion Trap Mass Spectrometer

A M Franklin†, J F J Todd† and R E March‡.
†Chemical Laboratory, University of Kent, Canterbury, UK, CT2 7NH. ‡Department of Chemistry, Trent University, Peterborough, Ont., Canada. KJ9 7B8.

Collisional excitation of mass-selected ions in the ion trap may be brought about by applying a supplementary RF 'tickle' field to the endcap electrodes. Computer simulations of the ion motion during tickling revealed that, in the absence of buffer gas collisions and for constant operating conditions, the product of [tickle time]x[tickle amplitude] needed for ions to acquire trajectories which exceed the boundaries of the trap was a constant for ions of different starting conditions. This product has been termed the 'fluence', and the reciprocal the 'absorbance'[1]. An ion with a large absorbance readily absorbs energy and rapidly leaves the trap; comparison of the three tickle modes showed that the absorbance for dipolar:monopolar:quadrupolar excitation are approximately 4:2:1.

Experimentally it is found that during tickling the rate of decrease in parent ion intensity with tickle time for constant tickle voltage is exponential, and from measuring the rate of decay at different tickle voltages, a value for the absorbance may be obtained; this has led us to develop a 'kinetic' model in order quantify the tickling process. In practice, of course, an optimised pressure of a buffer gas such as helium is present in the trap to enhance performance, and tickling of the ions may then induce them to undergo collisional dissociation so that the decrease in precursor ion signal may reflect both the loss of ions from the trap and the formation of product ions. Initial accounts of the model [2,3] were restricted to treatment of the rate of loss of the precursor ion; this presentation examines the intensities of both precursor and product ions during tickling.

The process of resonant excitation may be represented in the following manner. Ions are created internally, or externally, some are lost but those captured by the RF drive potential undergo collisions with the helium buffer gas atoms which will remove some of the ions' energy and the cooled ions migrate towards the centre of the trap. Upon tickling these ions, those in resonance with the tickle frequency are drawn from the centre of the trap. The amplitude of the tickle voltage is generally <1eV yet the collision activation requires ~3-4eV therefore this process must derive kinetic energy from the drive potential. While the ion is tickled it may either collide with a helium atom, lose energy and migrate to the centre or be energised by the RF drive potential, become internally excited and possibly fragment through a high energy collision with an atom.

This scenario gives rise to the idea of 'mean free time' which is the time within which the ion can move to a position in phase space where it gains energy from the drive field before it experiences a low energy collision returning the ion to the centre. The fact that as the helium pressure is increased the tickle amplitude at which CID occurs must also be increased supports this idea. At high tickle voltages the ion may be accelerated out of the trap before CID can occur. This suggests that for high energy CID collisions to occur it may be necessary for there to be a collision in order to arrest the ion before it is ejected from the trap. In practice tickle times of several milliseconds are required to achieve a reasonable degree of fragmentation and so it is probable the ions are 'simmered' involving many cycles of collisions. Ion loss may occur at low tickle voltages after a collision as the ion may not be at a favourable coordinate lying within the phase space ellipse corresponding to that relevent phase angle of the drive potential.

The experiments were carried out with an ITMS™ at *ca* 10^{-4} Torr of helium buffer gas. The scan function comprised an ionisation step (5ms); DC isolation of the parent ion; a tickle step during which the parent ion is held at q_z=0.45, a_z=0 or q_z=0.25, a_z=0 and tickled by dipolar excitation; finally a data acquisition step. Sample was introduced via a calibration gas valve and bled into the trap at a constant pressure of *ca* 10^{-6} Torr. Samples used were **o-dichlorobenzene** and *n*-butylbenzene with parent ions *m/z* 146 and *m/z* 134 respectively. Dynamically programmed scanning was utilised to tickle the parent ions from 0 to 10 ms in 0.05ms steps at a range of tickle voltages. The resulting data were converted to text files by a DWRITE© program and these files converted by a simple BASIC program into a format which could be read by a graph plotting program AXUM© V2.0.

Plots of $-\ln(X_t/X_o)$ *versus* t were obtained for a range of tickle voltages (V_t) and for each sample. At low tickle times there is a flat portion, the length of which becomes shorter as the value of the tickle voltage is increased. This induction period is followed by two approximately linear portions after which the curve begins to flaten out at long tickle times. From these plots the first linear portions are utilised and the gradients k_1 are recorded. The slopes of the plots of k_1 *versus* V_t have the units of absorbance, and are equal to 2.101 and 10.647 $(V\ ms)^{-1}$ for *o*-dichlorobenzene and *n*-butylbenzene respectively at q_z = 0.45. A parallel first order reaction method was used so the rate of product ion formation could be characterised. This leads to values of the absorbance (and fluence) for both the disappearance of the precursor ion and the formation of product ions.

From this study we conclude that the curves representing the loss of parent and the formation of daughter ions seem to obey the first order kinetic theory enabling the calculation of absorbances and fluences for the respective ions of *o*-dichlorobenzene and *n*-butylbenzene. Comparison of the absorbances of *m/z* 134 and *m/z* 146 from *n*-butylbenzene and *o*-dichlorobenzene respectively for both q_z values shows that *m/z* 134 has a higher absorbance which is possibly due to weaker bond strengths compared with that of the *m/z* 146 ion. The absorbance of *m/z* 134 from *n*-butylbenzene at q_z = 0.45 is lower than that at q_z = 0.25, this could be due to more ions being lost at the lower q_z value as the Dehmelt's pseudo-potential well depth is shallower at low q_z values. From the calculation of the absorbances of the parent and daughter ions of *o*-dichlorobenzene at q_z = 0.45, 46% of the absorbtion of *m/z* 146 is responsible for the formation *m/z* 111, 8% for the formation of *m/z* 75 and 4% for the formation of *m/z* 74, 43% is responsible for ion loss.

ACKNOWLEDGEMENT

A M Franklin wishes to thank the British Mass Spectrometry Society for the John Beynon Studentship Award.

REFERENCE

1. R.E.March, F.A.Londry, R.L.Alfred, A.D.Penman, J.F.J.Todd, F.Vedel and M.Vedel, *Int. J. Mass Spectrom. Ion Processes*, 110, 159-178 (1991).
2. J.F.J.Todd, R.E.March, A.M.Franklin and A.D.Penman, 9th Informal Meeting on Mass Spectrometry. Padova, April 1991, p.M4.
3. A.M.Franklin, J.F.J.Todd, A.D.Penman and R.E.March, 19th Annual Meeting, British Mass Spectrometry Society, St Andrews, September 1993, p.261.

Mass Spectral Fragmentation of 1,9-Decadiyne, and 1,2,9,10-^{13}C-1,9-Decadiyne

* Ronny C. Robbins, James Jensen
U.S. Army
Aberdeen Proving Ground
Edgewood Area
APG, MD 21010-5423

The peculiarities of 70 eV mass spectra with Dempster mass spectrometers of alpha-omega diynes were previously noted in a program to obtain reference mass spectra for exhaust gas component identifications by the United states Bureau of Mines, Bartlesville, Oklahoma.[1] The 70 eV mass spectra of 1,6-heptadiyne (Mol. Wt. 92), 1,7-octadiyne (Mol. Wt. 106), and 1,8-nonadiyne (Mol. Wt. 120) contain an intense peak at m/Z 91 and a weak peak at m/Z 45.5 which suggests the presence of tropylium ions. A tropylium ion has a single ring and a composition of $[C_7H_7]^+$. The mass spectrum of 1,9-decadiyne (Mol. Wt. 134) contains an intense peak at m/Z 91, but no peak at m/Z 45.5 suggesting that the m/Z 91 ions in its spectrum may not be tropylium ions.

From classical fragmentation pathways of hydrocarbons that contain a terminal triple bond, one might expect that the main fragmentation process is cleavage beta to the triple bonds.

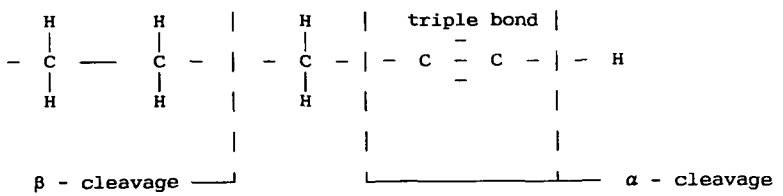

Previous work with carbon-13 labeling strongly indicate that the 1,8-nonadiyne molecule curls into a "U-shaped" configuration and that two carbon atoms are lost from the center of the ring structure.[2] This linear chain curling takes time. Tropylium ions may appear in the spectrum of 1,9-decadiyne if more time is allowed between ionization and detection. Much longer residence times for ions can be obtained in "ion trap" type mass spectrometers.

1,9-Decadiyne was labeled with carbon-13 in the 1,2,9,10-positions and analyzed in a Finnigan ITMS system at 70 eV. The comparison of the labeled versus unlabeled spectra shown in figures 1 and 2, indicate that the tropylium ion was formed from the terminal carbon atoms.

References

1 . R.F. Kendall, B.H. Eccleston, USBM Report of Investigation, No. 6854 (1966).
2. R.C. Robbins, N.G. Foster, Org. Mass Spectrom., **20**, 189-93, 1985

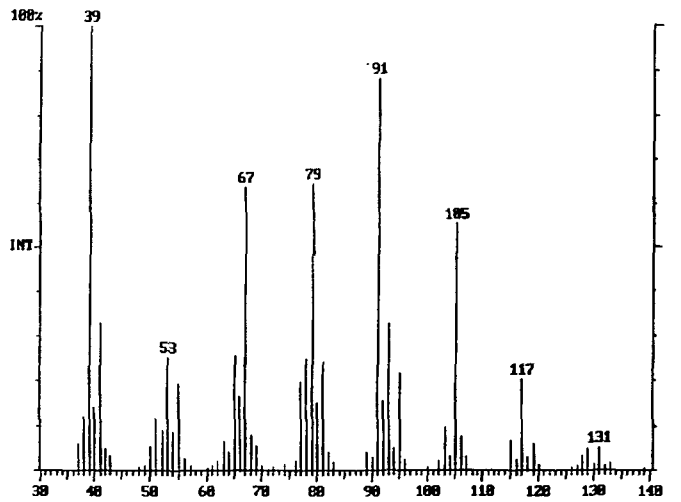

Figure 1: Finnigan ITMS Mass spectrum of 1,9-Decadiyne

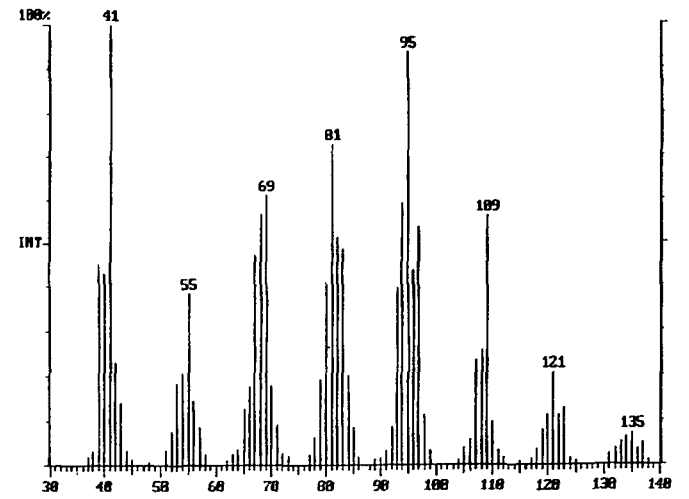

Figure 2: Finnigan ITMS Mass spectrum of 1,2,9,10-^{13}C-1,9-Decadiyne

Unimolecular Kinetics of Neutrals and Ions

*David W. Kuhns and Frantisek Turecek, Department of Chemistry,
BG-10, University of Washington, Seattle, WA 98195

A new technique is described to measure the rate constants of ion and neutral dissociations in the 10^4 - 10^7 s^{-1} range. The neutral species is prepared by charge exchange from a precursor ion transmitted through MS-I of the tandem quadrupole acceleration-deceleration (QADQ) mass spectrometer and accelerated to 8 kV. The neutrals are allowed to drift through an ion conduit maintained at a variable potential. Oxygen is leaked into the conduit region as a reionization gas and cuts the beam to 70%. Reionization of the neutral within the conduit electric field produces the corresponding ion whose total energy depends on the neutral kinetic energy and the conduit electrostatic potential. The conduit is segmented to allow a combination of four potential settings (Figure 1). This allows one to change simultaneously the drift time for the neutral species while extending that for the ions (and vice versa) by applying positive and negative potentials on different segments of the conduit.

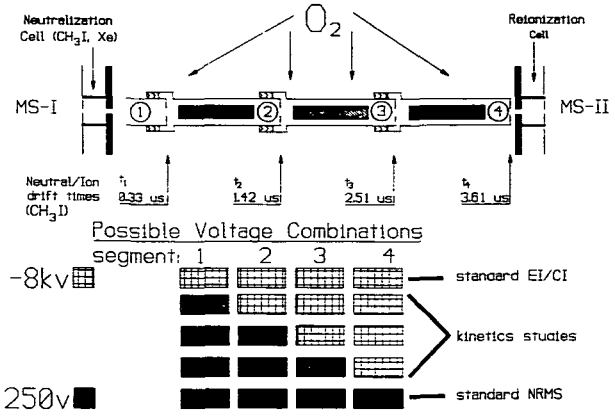

Figure 1

Only ions of a preselected total kinetic energy and mass are transmitted through MS-2 and detected. Therefore neutrals ionized in a 250 volt region will retain their high (keV) kinetic energy and be energy filtered by a chicane lens. Only stable neutrals and their fragments that pass the 250 volt region will be seen because they will be reionized in the -8kV region with the proper energy and not be energy filtered. Increasing the length of the 250V region (setting 1-4) increases the neutral lifetime and decreases the ion lifetime. By monitoring the ratio of the precursor to the daughter fragment we can observe the amount of dissociation as conduit settings are changed. A stable neutral will show little change in $[AB^+]/[A^+]$ even as the neutral lifetime is extended, as long as after reionization the ion fragmentation is not extensive. If the neutral has a rate of dissociation within experimental parameters then as the drift time is increased the

$[AB^+]/[A^+]$ ratio should decrease corresponding to the rate. However this ratio will also depend on the ion rate of dissociation upon reionization. The neutral rate (k_n) and the ion rate (k_i) constants are therefore convoluted. However, the ratios are measured at four conduit settings, thus the system is overdetermined, and the constants can be deconvoluted. The products AB^+, A^+ and B^+ can be formed by the pathways shown in (Figure 2). Equations 1 and 2 describe the dependence of AB^+ and A^+ on time and the rate constants. The velocity (v_{AB}) and the number density of the reionization gas (N) will cancel upon taking the ratio of $[AB^+]/[A^+]$.

$$\overline{AB^+} = \frac{1}{(t_2-t_1)\,k_n} AB_o S_{AB} N v_{AB} \int_{t_1}^{t_2} \left[e^{(-k_n t_1)} - e^{(k_n t)}\right] e^{(-k_i(t_2-t))}\,dt \qquad (1)$$

$$\overline{A^+} = \frac{1}{(t_2-t_1)\,k_n} AB_o S_{AB} N v_{AB} \int_{t_1}^{t_2} \left[e^{(-k_n t_1)} - e^{(k_n t)}\right] e^{(-k_i(t_2-t))} \left[1-e^{-k_i(t_2-t)}\right] + S_A(t_2-t)\,(1-e^{-k_n t})\,dt \qquad (2)$$

Comparing the experimental ratios with the theoretical ratios calculated at each conduit drift time while inputing a matrix of k_n vs k_i produces a plot of the residuals of the model (Figure 3).The minimum gives the best fit for the experimental data.

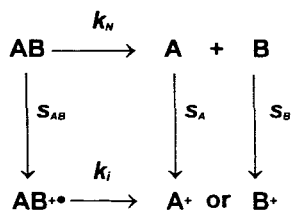

Figure 2

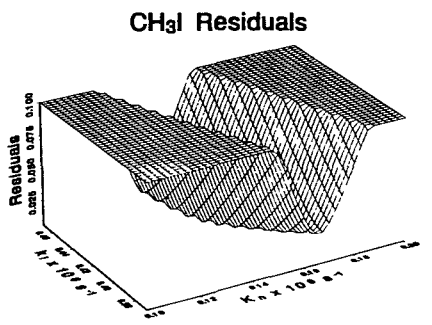

Figure 3

Initially the simple system of $CH_3I^{+\bullet}$ to I^+ and CH_3 was tested with different neutralization gases. Neutralization of $CH_3I^{+\bullet}$ with CH_3I leads to k_n = 1.33 x 10^5 s^{-1} and k_i = 3.70 x 10^5 s^{-1} corresponding to neutral and ion effective temperatures of 2111 K and 3130 K, respectively. Neutralization with Xe gave higher rates of k_n = 3.69 x 10^5 s^{-1} and k_i = 6.09 x 10^5 s^{-1} corresponding to higher temperatures of 2283 K and 3260 K, respectively.

A Comparative study of MS-MS data produced by tandem magnetic and hybrid MS-MS instruments and the implications of the conclusions on the design of a hybrid magnetic sector-orthogonal acceleration time-of-flight MS-MS instrument.

R H Bateman, R S Bordoli and C Braybrook, VG Analytical, Manchester, UK.,
E Clayton, Zeneca Pharmaceuticals, Alderley Park, Macclesfield, Cheshire, UK.

Molecular structure determinations by MS-MS require full product ion spectrum with highest achievable sensitivity over the whole spectrum, unit mass product ion resolution, reliable nominal mass assignments and acquisitions within chromatography time scales.

Gas phase ion-molecule collisions with high "centre of mass" collision energy have been the most commonly used and generally most successful method for generating structurally informative decomposition products. To generate "d" fragment ions in peptides a minimum value of E_{com} of 15 ~ 20 eV is required (Ref 1,2). Figure 1 shows the normalised average d_n/a_n ratios for n = 5,10,11 and 12 as a function of E_{com} for the product ion spectra of Renin Substrate acquired on a VG Analytical AutoSpec-T tandem system. This relationship holds irrespective of target gas mass or laboratory collision energy. It also holds for so called "low energy" quadrupole type collisions cells. Figure 2 shows the presence of the "d" fragment ions in the product ion spectrum of Renin Substrate acquired on a VG Analytical AutoSpec-Q hybrid system at 500 eV collision energy using Xenon as the target gas, for which E_{com} = 35 eV. At a laboratory collision energy of 800 eV when using Xenon collision gas, E_{com} is greater than 25 eV for precursor ions up to mass 4000 Da.

In time-of-flight (TOF) mass spectrometers, unlike scanning instruments, all ions are transmitted to the detector. This offers the potential for fast, high sensitivity full spectra acquisitions thereby meeting several of the requirements for MS-II in MS-MS instrumentation. Conventionally the ion source needs to be pulsed, and resulting ions should not have excessive spatial, energy and temporal spread, a combination which TOF instruments cannot accommodate without severe limitations in resolution. However, the product ions have a relatively large energy spread in the direction of travel, and large spatial and temporal spread owing to the uncertainty as to where and when within the gas cell each decomposition takes place. An alternative approach is to use an orthogonal acceleration(OA) TOF mass analyser (Ref 3). Ions selected by a magnetic sector mass analyser may be decelerated to 800 eV (or less) energy before passing through a gas collision cell. The precursor and product ions would then pass into the orthogonal acceleration chamber of the TOF analyser. The ion source is in the form of an ion beam with spatial and energy spread orthogonal to the direction of travel, and which may be accomodated by the OA-TOF arrangement. The equal velocities of precursor and product ions leaving the gas cell results in equal sampling efficiences for all masses. The OA-TOF mass analyser allows operation with continuous (and pulsed) ion beams and in combination with a sector instrument appears to meet the requirements for MS-MS instrumentation listed above.

(1) S A Martin, *Proc. 37th Conf. on Mass Spectrom. & Allied Topics*, p.858, (1989)
(2) R S Bordoli and R H Bateman, *Int. J. Mass Spectrom. Ion Proc.*, 122, 243, (1992)
(3) T H J Dawson and M Guilhaus, *Rapid Commun. Mass Spectrom.*, 3, 155 (1989).

Average normalised d/a ratios for d5, d10, d11 and d12 from Renin Substrate

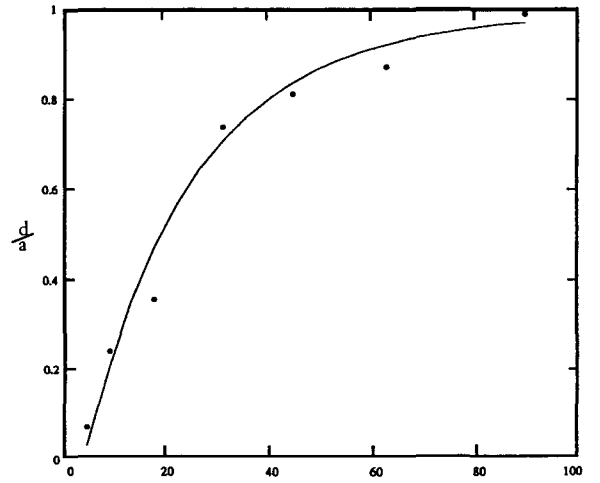

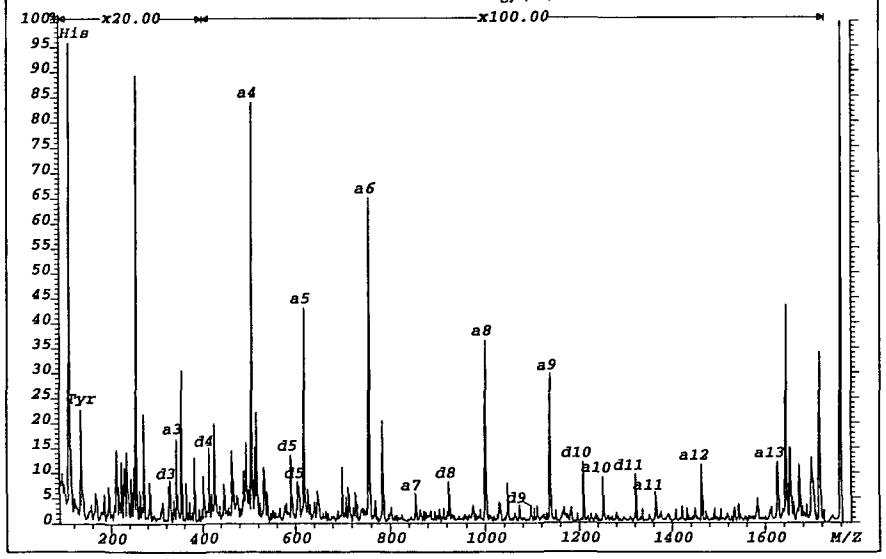

A HYBRID TANDEM MASS SPECTROMETER.

A Duhr, R. Guckert and H. Wollnik
2. Physikalisches Institut der Justus–Liebig–Universität, 6300 Gießen, Germany.

A new hybrid tandem mass spectrometer (Tandem–MS) has been build for the study of molecular fragmentation reactions. The first stage of the Tandem–MS is a reversed–geometry sector field type. The second stage is a Time–of–flight(TOF) Instrument that allows simultaneous detection of the fragment ions. Special emphasis was laid on optimizing the interface between the two different mass spectrometers. The collision cell was build by using a microchannel plate as collision target in order to obtain high fragmentation efficiency and high ion transmission [1, 2, 3, 4].

The purpose of the interface is to cut the continuous ion beam that leaves the first stage MS into discrete bundles or bunches. These bundles can then be mass analyzed in the time of flight MS. TOF start pulse was generated by the ions impinging on the collision microchannel plate. The spectrum is aquired by measuring the time difference between the start pulse and a stop signal generated by a second detector at the end of a drift tube (see Fig. 1).

For the detection of the secondary electrons that are emitted from the surface while primary ions transfer some energy two different setups are tested. In one setup crossed electric and magnetic fields of variable strength in front of the channel plate guide the electrons to a detector. The flight time is numerically optimized to be 10± 2 ns for electrons emerging from the channels with angels of ± 20°normal to the microchannel plate and with an energy range of 1 to 100 eV relativ to the surface of the microchannel plate.

Only electric fields are used to direct the electrons to the detector in another setup tested for the purpose as interface. This setup uses no magnets or coils together with the advantage of better vacuum characteristics. The electron flight time variation however was calculated to be slightly larger.

First results were obtained by using the pyrene mother ion ($C_{16}H_{10}$, 202 u) as precursor. Extensive fragmentation is shown with fragmentation efficiencies in the order of 75 %. Charge transfer is also obvious in the presence of a double charged mother ion at mass 101. At masses smaller than about 60 the spectrum is overlapped with SIMS products that are desorbed from surfaces and grids in the collision cell.

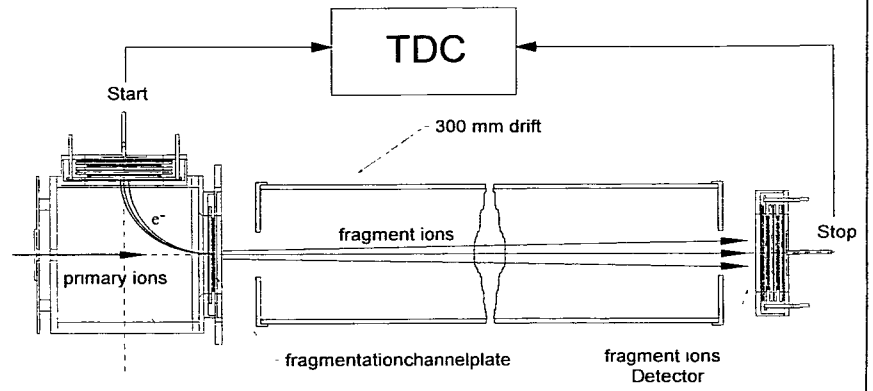

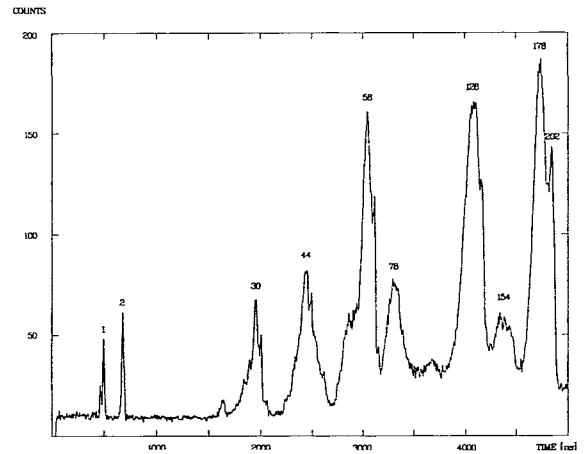

[1] G. Li, A. Duhr, and H. Wollnik. J. Am. Soc. Mass Spectrom., 3, 487–492, 1992.

[2] G. Li, A. Duhr, and H. Wollnik. In Proc. of the 40th ASMS Conf. on Mass Spec. and Allied Topics, page 1438, 1992.

[3] W. Aberth. In Proc. of the 36th ASMS Conf. on Mass Spec. and Allied Topics, pages 73–74, 1988.

[4] William Aberth. Analytical Chemistry, 62, 609–611, 1990.

MS^n IN THE QUADRUPOLE ION TRAP USING FILTERED NOISE FIELDS

Douglas E. Goeringer, Keji, G Asano, and Scott A. McLuckey
Oak Ridge National Laboratory, P.O Box 2008, Oak Ridge, TN 37831-6365.

*Steven W Stiller
Hitachi Instruments, Inc., 3100 N. 1st St. San Jose, CA 95134

Don Hoekman
Teledyne MEC, 1274 Terra Bella Av Mountain View, CA 94039

Although the protocol for tandem mass spectrometry in the quadrupole ion trap is well established, the versatility of the technique is still limited in some instances The parent ion isolation portion of an MS/MS experiment has typically been post ionization or ion injection. As the ion number density in the trap changes, the optimum frequency for fragmentation also changes. Tuning of excitation frequencies is, therefore, always required. Furthermore, for MS^n the tuning difficulties are even greater. Using the filtered noise fields method of Kelley [1] allows analyte ions to be selectively stored during formation or injection The stored ions can then be fragmented by the application of an FNF which is constructed with a finite bandwidth to account for the changes in secular frequency due to the formation of product ions. For MS^n FNFs can be used to simultaneously fragment the parent ion, trap and fragment the product ion(s). This paper describes the use of FNF during the ion injection period to isolate ions of interest formed in an atmospheric sampling glow discharge ionization source. The mass selective ion accumulation step is followed by the application of subsequent FNF to induce fragmentation in targeted ions The MS/MS experiment can also be simplified by combining ion accumulation, isolation and fragmentation using a single FNF.

A Finnigan ITMS modified to include an Atmospheric Sampling Glow Discharge Ionization Source (ASGDI) was used for all experiments and is described elsewhere [2]. FNF capability was added to the system using a TELEDYNE/HITACHI HST-1000 Enhancement Kit. A diagram of the system is shown in Figure 1 The ion trap was operated in negative ion mode for all experiments The scan function used for these experiments is shown in Figure 2 In all experiments, an isolation FNF is applied during the ion injection gate to accumulate only ions of interest Unwanted ions are expelled by the FNF Tickle frequencies can be applied by the ITMS or Tickle frequencies or frequency bands can be applied using FNF. In the case of MS/MS the Fragmentation FNF need have only one band. For MS/MS/MS two bands are used, one for the fragmentation of the precursor ion, another to fragment a product ion. The resulting product ion(s) are then scanned out and detected.

Figure 3 shows the MS/MS of DNT using FNF for both selective ion accumulation and fragmentation. An advantage of using FNF to provide fragmentation frequencies is that the FNF can provide multiple frequencies or frequency bands to allow simplified MS/MS without the need for careful tuning for each experiment. In MS/MS/MS and higher orders of MS^n the problems of tuning and frequency selection are further magnified. FNF can easily be used for any number of steps of isolation and fragmentation. There are several methods of using FNF for MS^n, one is to use subsequent FNF to sequentially isolate, fragment, isolate, fragment, etc. Another method is to combine fragmentation steps into a single FNF. This is demonstrated in Figures 4 and 5. In Figure 4, the m/z 123 (loss of C_2H_5) anion of diethyl methylphosphonate (DEMP) is selectively accumulated using an FNF then fragmented to m/z 95 which is then fragmented to m/z 79 using the same FNF.

The use of FNF for both selective ion storage and fragmentation yields multiple benefits over earlier techniques. The combination of ion storage/accumulation and ion isolation yields much higher sensitivities for ions of interest Unwanted ions are expelled from the trap and the space charge capacity of the ion trap can be used for ions of interest FNF can be used to provide frequency bands to allow fragmentation of selected ions without the need for careful tuning. FNF offer great flexibility in designing experiments as they can easily be used, as in these experiments, to combine steps, but also can be used to sequentially isolate and fragment ions Since all of these experiments were competed without using DC operation, MS^n can now be a reality on rf only instruments. FNF provide a new flexible tool to greatly extend the use of the ion trap for enhanced and simplified MS^n.

[1] P E. Kelley, U.S. Patent 5,134,286; 1992
[2] S.A. McLuckey, G L. Glish, K G. Asano, B C Grant, *Analytical Chemistry*, 60, 2220 (1988).

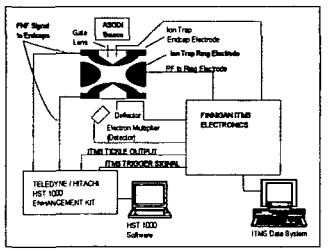

Figure 1

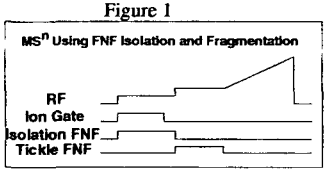

Figure 2

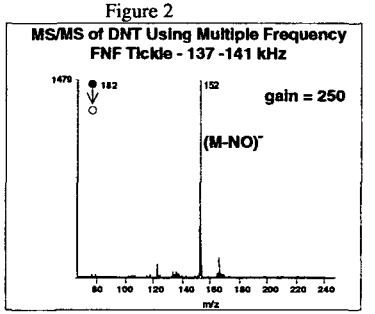

Figure 3

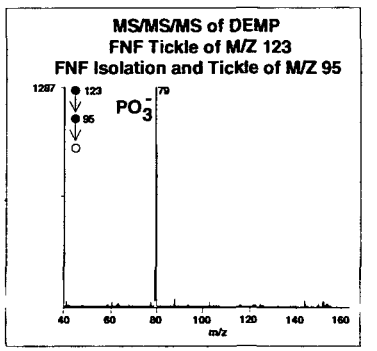

Figure 4

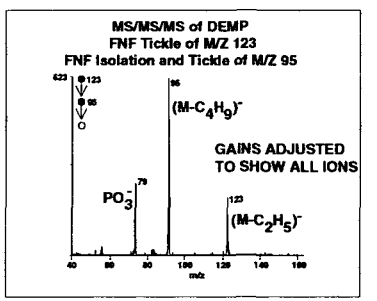

Figure 5

Research Sponsored by the U.S. Department of Energy, Office of Safeguards and Security, under Contract DE-AC05-84OR21400 with Martin Marietta Energy Systems.

GAS CHROMATOGRAPHY-TANDEM MASS SPECTROMETRY IMPLEMENTED ON A BENCH-TOP QUADRUPOLE ION TRAP-BASED INSTRUMENT USING RANDOM NOISE TO EFFECT COLLISION-INDUCED DISSOCIATION

Gary J. Van Berkel and Douglas E. Goeringer
Analytical Chemistry Division, Oak Ridge National Laboratory
Oak Ridge, TN 37831-6365

A next logical step in the advancement of quadrupole ion traps as detectors for gas chromatography (GC) is implementation of routine methods for inducing fragmentation so as to perform MS/MS analyses. The protocol for MS/MS in the ion trap mass spectrometer (ITMS™) is well-established with collision-induced dissociation (CID) being the general method of choice for effecting fragmentation. CID is typically accomplished by resonance excitation of ion secular motion; as the amplitude of oscillations grows, ion-bath gas collisions become more energetic causing a gradual increase in ion internal energy which ultimately results in fragmentation. Resonance excitation is commonly performed via application of an auxiliary, single-frequency signal to the endcap electrodes. Although the same method for CID could be incorporated into commercial bench-top quadrupole ion trap instruments, several factors limit its practical utility. Recently, our group[1] demonstrated that random noise, tailored via amplitude and bandwidth adjustment and applied to the endcaps of an ITMS, is an effective means for inducing CID of trapped ions. We have now adapted the technique on a commercially available, bench-top quadrupole ion trap to implement GC-MS/MS. This new CID methodology provides an instrumentally simple means to overcome the need for frequency tuning, space-charge related frequency shifts, limited fragmentation, and the inability to fragment ions of unknown mass/charge that are inherent in the single-frequency CID method.

The Finnigan-MAT ITS40 quadrupole ion trap mass spectrometer equipped with a Varian Model 3400 GC was used in these experiments. A broadband noise generator (NoiseCom Model NC6103) with a flat power spectrum from 10 Hz - 500 kHz served as the random noise signal source. The scan function used for CI-MS/MS was the nominal CI-MS function provided with the instrument, but used without the ARC feature. The random noise signal, triggered from the electron gate pulse, was applied to one endcap during the final 10-20 ms of the CI portion of the scan function. The standard axial modulation signal was applied to the other endcap.

The particular scenario used here to demonstrate the application of random noise CID in bench-top GC-MS/MS involves the analysis of amphetamines. Amphetamines as a compound class, when ionized by EI, tend to fragment extensively such that no molecular species is readily discernable. In such cases, CI is often used to form a molecular species so as to determine molecular weight. However, little structural information is available from CI due to limited fragmentation, or from EI fragment ions since only low mass/charge species are generally observed. A more direct method for obtaining useful structural information is to acquire a random noise MS/MS spectrum of the protonated molecule.

1. McLuckey, S.A., Goeringer, D E.; Glish, G.L. *Anal. Chem.*, **1992**, *64*, 1455-1460.

A major advantage of random noise CID over single-frequency CID is the capability for acquisition of MS/MS spectra of each component in a separated mixture without the need for parameter tuning for each individual component. This is demonstrated in Fig. 1 which shows the extracted ion current profiles (a-c) and random noise CI-MS/MS spectra acquired during an on-line separation of methamphetamine (d, 100 pg) and amphetamine (e, 200 pg). Although no frequency tuning was necessary in this experiment, the noise power spectrum was adjusted with a low-pass filter (20 dB/decade roll-off above 30 kHz) to avoid excessive fragmentation and potential ejection for low *m/z* ions. Note that the two compounds yielded the same major CID product ions at *m/z* 119 and *m/z* 91. The MS/MS spectra are much more informative than the CI mass spectra (not shown), which contain only very low abundance signals for fragment ions at the previously noted *m/z* values, and than the EI mass spectra (not shown), which have intense signals only at low (< 60) *m/z* values. The data in Fig. 2 also point out the greater demand on separation efficiency imposed by the use of random noise CID for MS/MS. Because the excitation is non-mass selective, coeluting species will undergo simultaneous fragmentation. As such, the MS/MS spectra represent a combination of each molecular species and their respective product ions. A method that at least allows the possible determination of coeluting species is to switch the noise signal on and off, thereby acquiring mass and MS/MS spectra in an alternate fashion during peak elution.

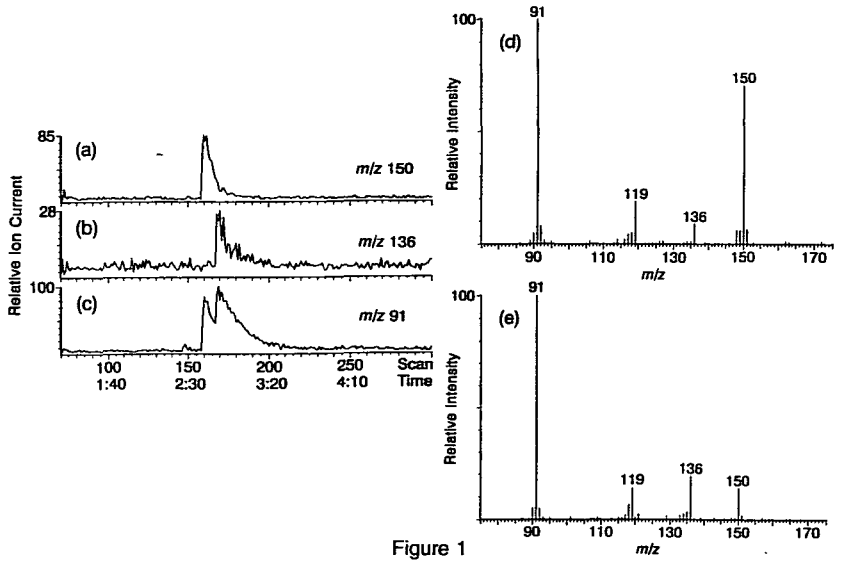

Figure 1

Research sponsored by Grant No. R01GM45372 from the National Institutes of Health.
Oak Ridge National Laboratory is operated by Martin Marietta Energy Systems, Inc.
under Contract DE-AC05-84OR21400 with the United States Department of Energy

Comparison of an Octopole with a Quadrupole as a Collision Cell in a Hybrid Instrument Todd D.Williams[1], Geoffrey Bott[2], Julie A. Leary[3], Carl Braybrook[4]; [1]University of Kansas, Lawrence, KS 66049; [2]GB Scientific, Novato, CA 94945; [3]College of Chemistry, UC Berkeley, Berkeley, CA 94720, [4]VG Analytical, Manchester, UK M23 9LE.

Introduction: The substitution of a quadrupole with an octopole rf only collision cell in a hybrid mass spectrometer has been shown to improve CID performance in a VG ZAB2E-Q (1). In this study, the performance of the same octopole design has been compared to the standard quadrupole collision cell in a VG AUTOSPEC-Q.

Experimental: Mass Spectra were obtained on an AUTOSPEC-Q tandem hybrid mass spectrometer (VG Analytical Ltd, Manchester, UK). This instrument is of EBEqQ configuration. Fast atom bombardment ionization was performed using a cesium gun. Collision induced decomposition (CID) experiments were conducted with precursor ions attenuated 50% with xenon in the collision cell. The analyzer quadrupole was tuned to 1.5 amu full width at half height and the precursor ion was transmitted with MS1 tuned to 1500 resolution. The scan rate was 1sec/100 amu and 3-6 scans were integrated. The standard quadrupole was replaced by an octopole (GB Scientific, Novato, CA) fitted directly in the quadrupole housing. The detector after MS2 was maintained at the same gain for all experiments. MS^3 experiments were carried out by performing CID in the FFR2 collision cell using He collision gas (50% attenuation) and selecting the ESA2 energy to transmit a fragment ion into the rf only cell. CID in the rf cell was with Xe (50% attenuation). The peptides used were Renin Substrate (MW 1758), Substance P (MW 1347), Gramicidin S (MW 1141), FLEEI (MW 649) & Leucine Enkephalin (MW 554).

Results: Fragmentation Efficiency: MS/MS

A series of peptides with molecular weights of mass 500 to 1700 amu was used to compare the fragmentation efficiencies (FEs) of the two cells as a function of collision energy. FE is defined here as: FE = [sum of all product ion current / (sum of product ion+precursor ion current)] *100). The difference in performance is demonstrated in figures 1 and 2. The octopole provided significantly enhanced low mass product ion abundance and greater over product ion yield (see table 1). **The octopole generally provide significantly better product ion yield and much better low mass ion abundance.**

Transmission: To test the relative transmission behavior of the two rf only cells, CsI ions of masses 133 to 2472 were passed from MS1 through to MS2 with no gas in the cell while maintaining the same detector gains for each configuration. The ratio of signals MS2/MS1 was the same for the octopole compared to the quadrupole for all ions. **The transmission characteristics for unattenuated precursor ions are identical.**

MS^3: A MS^3 experiment in which a MIKES generated fragment is transmitted into the collision cell requires focusing of a diverging beam from ESA2 into the rf only cell. Two MIKES product ions were transmitted to explore two energy regimes entering the rf only cells. The FEs for the product ions from the transitions of 650 -->519 (or 390) --> are found in table 1 at two collision energies in the rf only cells. The sample load on the FAB probe for each of these experiment was approximately the same (a "saturated" sample was used) to keep the precursor ion current approximately the same throughout the MS/MS/MS experiments. Precursor ion current at the MS2 detector was constant within a factor of 2 for all

Figure 1. Octopole: 500 eV CID of Renin Substrate (MH^+ 1759; DRVYIHPFHLLVYS)

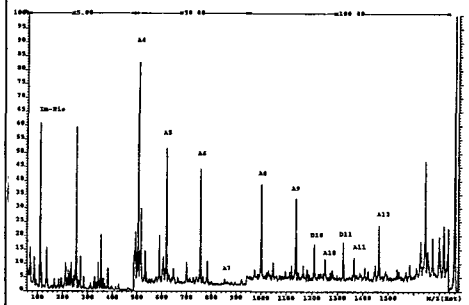

Figure 2. Quadrupole. 500 eV CID of Renin Substrate

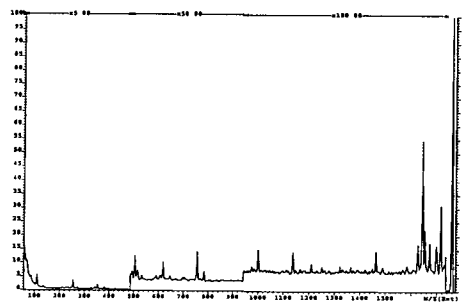

Table 1: FEs (%) of Octopole & Quadrupole

Peptide	CID Energy eV	Oct.	Quad.
Leucine Enkeph.	50	63	22
	175	12	30
	300	15	9
	500	10	60
Gram. S	50	67	23
	175	40	27
	250	38	25
	500	20	11
Subst. P	50	7	4
	150	27	10
Renin Subst.	35	12	11
	175	17	13
	355	35	5
	500	38	9
MS^3 of FLEEI 650(MH^+) --> 519(B_4) -->			
	60	75	63
	200	70	42
650 --> 390 (B_3) -->			
	60	66	40
	200	47	23

experiments. **The octopole provided more efficient fragmentation than the quadrupole.** These experiments further suggest that the optics of the instrument provide a well focused beam sufficient for the octopole.

Nodes: The variation of intensity of precursor and fragment ions of CsI m/z 1952 with collision energy demonstrated that the quadrupole had significantly sharper nodes in transmission of the precursor ion. In the quadrupole the fragment ion nodes tended to coincide at the same energy. The appearance of nodes became much less pronounced with lower mass fragments and higher collision energies in the octopole. **Tuning was easier with the octopole** because it is harder to fall into a nodal "well" using the octopole while searching for an optimum collision energy.

Conclusions: At higher collision energies the low mass region of the CID spectra from the higher mass peptides was significantly enhanced in the octopole relative to the quadrupole. Overall the octopole provided better quality collision data except from the low mass peptide.

References (1) J.A. Leary & G. Bott, Data presented at the Manufacturers Poster session 39th ASMS conference, Nashville, (1991)

Acknowledgements: The instrument was purchased with the aid of a NIH grant (TDW) S10 RR0 6294-01. The authors thank VG Analytical.

Performance Characteristics of a New Hybrid Mass Spectrometer System

M. Ishihara, and F.. Kunihiro, JEOL Ltd., Akishima, Japan and B. Musselman*, JEOL USA, Inc., 11 Dearborn Road, Peabody, MA 01960

A novel MS/MS interface has been fabricated for use in hybrid mass spectrometer systems. The novel feature of the lens system used in this interface is that it facilitates both directional focusing, and ion deceleration as required in such instruments. A quadrupole doublet lens assembly is located immediately after the exit slit of the high resolution mass spectrometer to provide for directional focusing of the ions exiting the double focusing instrument. This directional focusing was attempted in order to reduce the height of the ion beam exiting the sector-based mass analyzer without using a restriction slit. Reducing the beam height was desired in order that we could inject the ions into the quadrupole-based RF-only collision cell with maximum efficiency. A series of cylindrical lenses are then employed to provide for uniform deceleration of the ions to the ion energy suitable for CID in the RF-only quadrupole. The combination of these elements improves the transmission efficiency for ions between the two mass analyzers, thus improving the performance of the hybrid instrument.

Ion optical calculations were completed by using the MSPLEX and ELECTRA programs developed at Osaka University. The values of the potentials of the nodes on the lenselectrodes are given by MSPLEX, followed by using ELECTRA-based calculations for the electric field and ion trajectories.

Characteristics of the ion optics of the quadrupole-doublet had been know from initial calculations on the use of this type of ion focusing element on our tandem mass spectrometer instrumentation. The problem of effecting both the deceleration and focusing of ions was approached iteratively solving for individual ions with ion energies varying from 10 to 250 eV. Based on the results of those calculations the lens system was fabricated and tested.

Collision induced dissociation was completed on a variety of different molecular ions. The results were comparable with those expected for this instrumentation. Unit resolution was observed for all product ions as expected, even at scan speeds in excess of one per second. Product ion m/z mass assignments were within +/- 0.3u.

Studies on Reducing the Scale of a Double Focusing Mass Spectrometer*

David M. Chambers, Hugh R. Gregg, Brian D. Andresen
Lawrence Livermore National Laboratory
P.O. Box 808, Livermore CA 94551

Introduction

The need for portable mass spectrometers has increased in recent years primarily for use in environmental monitoring applications. The widespread application of quadrupole and ion trap mass spectrometers has encouraged several groups to adapt commercial systems into portable units. Similarly, with the advent of high-energy-product magnet materials, fabricating a miniature sector mass spectrometer becomes more feasible. A reduced-scale-sector instrument has the potential to be robust, requiring only simple electronics and less power than those requiring an rf field. Sector mass spectrometers have already been developed with the goal of remote sensing in confined spaces or portability [1–3]. Although theory for high resolution and mass accuracy is well understood, such specifications have not yet been achieved on a reduced-scale instrument. These shortcomings are the result of compromises made to achieve the objective for a low-cost, simple and robust instrument.

In our laboratory, experiments were conducted to develop and optimize a miniaturized sector mass spectrometer. The instrument studied in this work is similar to the ones developed for the Viking project [2], but was further modified to be low cost, simple and robust. Design features that highlight the simplicity of our instrument include the use of a modified Varian leak detector ion source, source ion optics that use a single extraction voltage and an unshunted fixed nonhomogeneous magnetic sector. The effects of these design simplifications on ion trajectory were studied by manipulating the ion beam through the electrostatic energy analyzer (ESA) and translatable magnetic sector.

Experimental

The mass spectrometer design included a Nier-Johnson configuration with a 90° angular deflection through each the electric and magnetic sector. The magnetic sector could be translated perpendicular to the incoming ion beam. The instrument studied is similar to the one described by Andresen *et al.* [4]. The present instrument has a mass range of 230 m/z and a resolution m/Δm of over 300 (full width half maximum). A significant drop in resolution was seen at m/z values above 100 and is attributed to electronic ripple as well as nonhomogeneous and fringing field effects. The accelerating potential was scanned linearly down from 1500 V and the ratio of the accelerating potential to ESA potential was varied from 4.446 to 4.611.

Results and Discussion

One obstacle encountered with incorporating nonhomogeneous fixed magnets into a sector mass spectrometer is estimating the effective flux density, B_o. For the initial design, we estimated the flux density to be approximately 7000 G. The effective flux density determined from this study was 7178 G. Having the ability to adjust the magnet assembly position made it possible to correct for differences between estimated and effective values. Because B_o was

[1] M.P. Sinha and A.D. Tomassian, Rev. Sci. Instrum **62**, 2618 (1991).
[2] D.R Rushneck *et al.*, Rev. Sci. Instrum. **49**, 817 (1987).
[3] A. Bacs, B. Eckenrode, and R. Drew 38th ASMS Conference on Mass Spectrometry and Allied Topics; Nashville, TN; May 19–24, 1991; p. 164
[4] B.D. Andresen, J.D. Eckels, J.F. Kimmons, W.H. Martin, D.W. Myers and R F. Keville, U.S Patent 5,153,433 (1992).

assumed to be 7000 G in the initial design, signal and resolution had to be optimized by shortening the radius through magnetic sector, r_m. This adjustment could be made either by moving the magnet assembly or by deflecting the ion beam out of the ESA to bisect the magnetic sector at a smaller entrance radius. Although this action complicates ion movement by increasing the velocity and angle of trajectory for ions leaving the ESA, the configuration could be optimized by fine-tuning the magnet assembly position.

At a fixed l_{e1}, r_e, r_m and l_{m2}, the experimental system exhibits an $l_{e2}+l_{m1}$ of 9.407 cm, which is 5.75 mm shorter than what theory predicts (i.e., 9.982 cm). This discrepancy is within an acceptable range with respect to potential errors from extrapolating experimental results and a broad optimum range. Breadth of optimum range can be seen in Fig. 1 for the Xenon doubly charged ions where resolution and signal remain relatively unchanged when moving the magnetic sector position nearly 5 mm perpendicular to the incoming ion beam. For the above calculations, the effective field boundary for the magnet was approximated to the lowest order at the magnet boundary itself. From the accelerating potentials and experimentally determined r_m values, the effective magnetic flux density was determined to be 7178 G.

Conclusion

The mass spectrometer instrument presented here is highlighted by its inexpensive and simple analyzer and electronics design, especially the use of fixed nonhomogeneous magnets for the magnetic sector. Because the magnetic flux density cannot be accurately predicted, a key to successful ion beam focusing is flexibility in instrument geometry. In the system presented, focusing was achieved by manipulating the ESA potential and magnet position. From these studies it was determined that the estimated flux density was lower than the effective value derived from our experiments. To correct the instrument geometry, r_m should be reduced. Future modifications could include decreasing l_{m2} as well as the horizontal position of the detector assembly.

Figure 1 **Ion Beam Focusing by Translating the Magnetic Sector Xe^{+2} Isotopes**

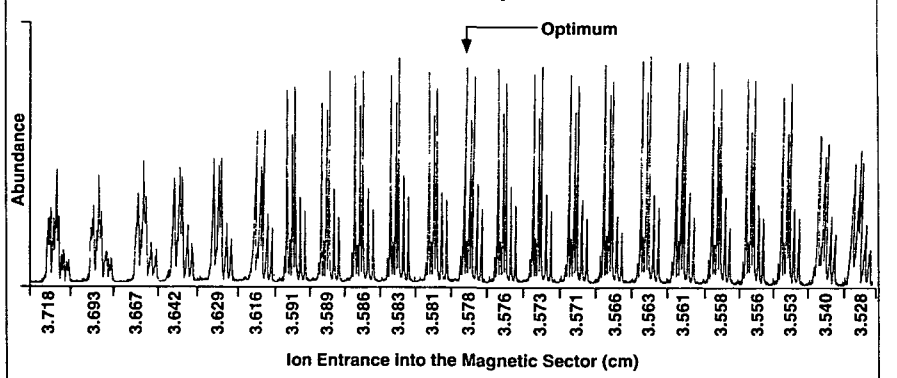

*Work performed under the auspices of the U.S. Department of Energy by the Lawrence Livermore National Laboratory under contract W-7405-ENG-48.

PHOTODISSOCIATION OF MALDI GENERATED PROTEINS VIA 193 NM AND 118 NM PHOTONS IN A TOFMS

Gary R. Kinsel, Mary E. Gimon, Ricky D. Edmondson, and David H. Russell
Texas A & M University, Department of Chemistry, College Station, TX 77843.

Extremely large proteins have recently become amenable for mass spectrometry through the development of the Matrix Assisted Laser Desorption Ionization (MALDI) technique. In general, MALDI is found to be an efficient method for introducing large biomolecules into the gas phase under soft ionization conditions. Little or no structural fragmentation of the protein is typically observed in the molecule mass spectrum. An appropriate evolutionary goal is the development of efficient methods of dissociating large proteins to produce structurally significant product ions. Pulsed laser photodissociation offers an attractive approach to addressing this need due to its inherent compatibility with the pulsed ion formation nature of MALDI in a time-of-flight mass spectrometer (TOFMS).

We have recently developed a two-stage linear TOFMS instrument which allows photodissociation of MALDI generated ions to be performed. In this instrument MALDI generated ions are accelerated from 15 kV to 5 kV across the source region and then drift down a 0.4 m flight tube liner floated at 5 kV. Analyte ions and matrix ions separate in this first drift region. Simultaneously, intact parent ions may metastably dissociate to form metastable product ions and neutrals which drift together with the intact analyte ions. A 193 nm photodissociation light pulse is timed to intersect the analyte ions in a field free photodissociation region at the end of the first drift region. The photodissociation product ions and remaining intact parent ions are then accelerated from 5 kV to ground. All ions then drift through a second 0.6 m drift region where the product ions and parent ions separate in time. All ions are then detected at the end of the flight tube by a microchannel plate detector. The resultant mass spectrum combines ion signals from all of the described processes.

Initial investigations focused on identifying and quantifying the background metastable processes which must be subtracted before identification of photodissociation product ions can be attempted. Retarding grid investigations, where analyte ions are deflected at the end of the flight tube, showed that a large fraction of MALDI generated analyte ions may metastably dissociate during their passage through the combined ca. 1.0 m flight path from the ion source region to the ion deflector. Up to 40 % of the parent ions for a given analyte have been observed to metastably dissociate in these experiments. The results of these studies for several analyte ions are given in the table below.

Analyte	Molecular Weight (Da)	Neutrals/Total Signal X 100 (%)
Arg-Lys-Glu-Val-Tyr	693.7	39 +/- 19
Bradykinin	1040.7	17 +/- 6
Mellitin	2844.8	16 +/- 3
Bovine Insulin	5733	23 +/- 6

Once the metastable processes were identified, 193 nm photodissociation of intact analyte ions was attempted. When the timing for the photodissociation laser pulse was properly adjusted a significant depletion of the analyte ion signal was observed. An example is shown below for the pentapeptide R-K-E-V-Y. In addition, a depletion of the neutral signal was also observed and was attributed to photoionization / dissociation of the neutral metastable product molecules.

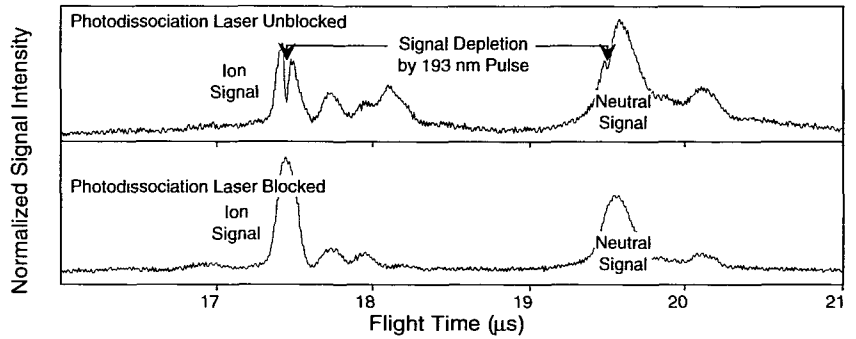

Successful photodepletion studies have also been performed on several larger analyte ions. Photodepletion of analytes as large as bovine insulin has been observed experimentally and an example of the signal obtained is shown below. This result suggests that even relatively large proteins may be photodissociated in the instrument described.

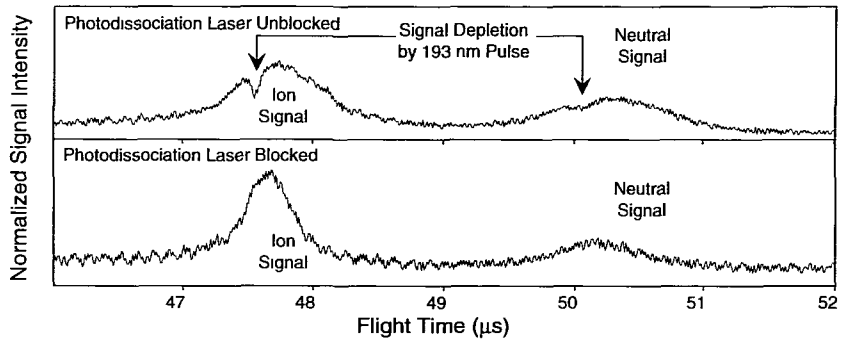

Initial studies have demonstrated the feasibility of photodissociation of large peptides and proteins in a linear TOFMS. Future studies will focus on improving both ion and laser optics to enhance the photodissociation product ion yield. Methods for separating and identifying the product ions are also under development. The results presented here demonstrate that photodissociation is a promising approach to initiating fragmentation of MALDI generated peptides and proteins.

MS/MS OF MULTIPLY CHARGED IONS: DETERMINATION OF CHARGE STATES BY MEDIUM RESOLUTION LINKED SCANS

R. Pesch, E. Schroeder, H. Muenster,
Finnigan MAT GmbH, Barkhausenstr. 2, 28197 Bremen, Germany

ESI-MS and ESI-MS/MS are widely used techniques for the analysis of biopolymers, technical polymers and a variety of other polar and labile compounds.

Using high resolution magnetic analyzers with ESI offers high mass resolution and accurate mass assignment. These capabilities have already been described elsewhere for main beam ions.

Sector analyzers exhibit higher mass resolution not only in main beam experiments, but also under MS/MS conditions. This opens the possibility of reading the charge states of daughter ions from multiply charged precursors directly by evaluating the isotopic clusters. This is true, because isotope peaks are spaced by 1/z dalton, with z being the charge state of the ion. For a peptide with a molecular weight of 3000 dalton, the required mass resolution would be at least 3000 (FWHM).

The experiments have been performed with a Finnigan MAT 900 forward geometry mass spectrometer, using the standard fast scanning focal plane detector (PATRIC).

Because of the large distance between collision chamber and entrance slit (about 600 mm) virtually all daughter ions are formed before the entrance slit and very few decompositions occur between entrance slit and ESA. For this reason, the MAT 900 maintains its double focussing condition also for linked scan daughter ions. As a result, daughter ion resolution in excess of 10,000 (FWHM) is possible.

The capability of determining charge states in the above described way has been tested by fragmenting the quadruply charged molecular ion from melittin. Ionization mode was ESI, collision gas was He, MS main beam resolution was set to 4000 (10% valley)

The daughter ion spectrum, acquired under these conditions exhibits a resolution of 6000 (FWHM). It is shown below (Fig. 1), along with two zoomed-in parts of the mass scale (Figs. 2 and 3).

From the data it is obvious, that charge states of daughter ions can be directly read from B/E linked scan spectra; a possibility significantly easing interpretation.

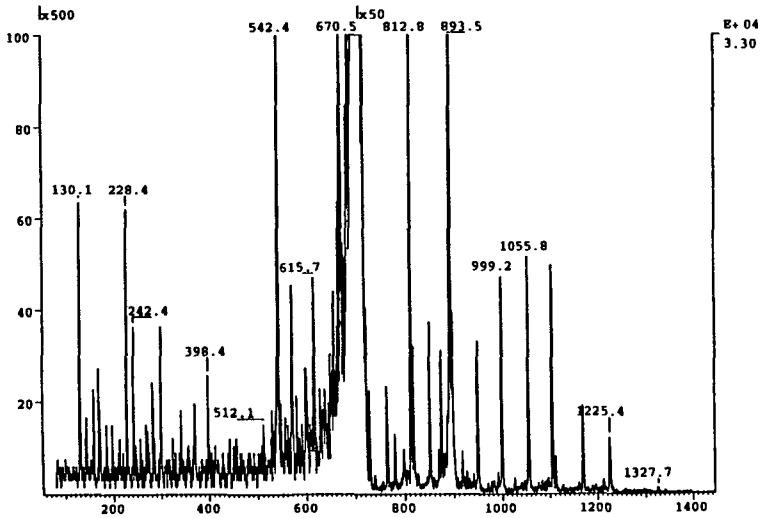

Fig.1 B/E = const. linked scan spectrum of MH_4^{4+} from melittin

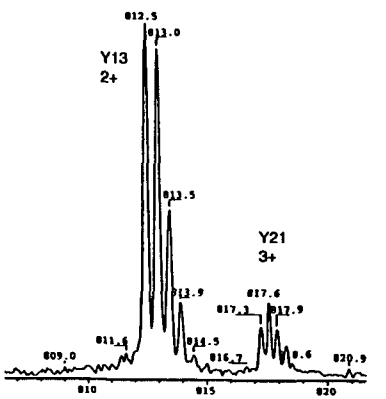

Fig.2 Partial spectrum showing doubly and triply charged daughter ions

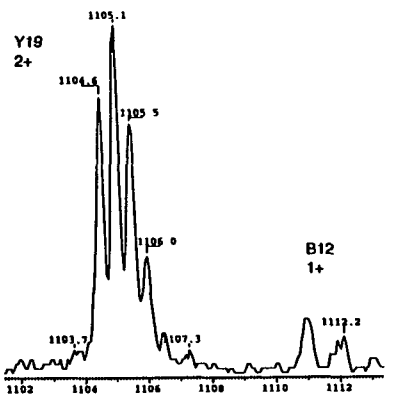

Fig.3 Partial spectrum showing singly and doubly charged daughter ions

Rapid, Continuous Recording of High Energy Collision-Induced Dissociation Spectra Using Charged Coupled Device (CCD) Detection Under Mach 3 Control On A Kratos 4-Sector Concept IIHH: Application to Peptide and Protein Sequence Analysis

F.C. Walls, S.C. Hall, K.F. Medzihradszky, Z. Yu, and A.L. Burlingame
Dept. of Pharmaceutical Chemistry, University of California, San Francisco 94143

S. Evans, A.D. Hoffman, R. Buchanan, S. Glover,
Kratos Analytical, Manchester, England

Primary structural characterization of proteins isolated from natural sources continues to push the detection limits of 4-sector mass spectrometers to lower levels because many times isolation procedures yield only a few picomoles of purified protein. Having to work at such low sample levels necessitates improving ion detection capabilities such that good quality CID mass spectra can be obtained routinely on femtomole quantities of peptides. We have accomplished this goal by making two major modifications to our 4-sector instrument. The first modification involved sample introduction using a continuous flow probe. Since liquid secondary ion mass spectrometry (LSIMS) is a surface sputtering technique, the signal size and lifetime depend on the surface activity of the analyte. Using a conventional batch LSIMS probe for less surface active molecules produces poor signal-to-noise ratios at low sample levels, while hydrophobic samples frequently give intense precursor ion intensities whose lifetimes are shorter than the duration of the MS-2 scan time when our stepped photodiode array is used for detection. Recently, CID sequencing of peptides in the femtomole range has been reported by Kenny and Orlando [1] using a continuous flow probe and 20% array detection. The improved signal-to-noise ratio was attributed to the reduction in chemical background noise which was accomplished by the ability to use a lower concentration of matrix with dynamic sample introduction compared to conventional batch methods. In our laboratory, using a continuous flow probe for sample introduction on our 4-sector instrument has resulted in a dramatic improvement of data quality and overall sensitivity.

The second modification of our 4-sector instrument involved replacing the conventional stepped photodiode array detector with a scanning CCD [2, 3]. The photodiode array consisted of a microchannel plate of one inch in length in the dispersive plane consisting of 1048 channels and detecting signals simultaneously from ±2% of the mass-to-charge ratio focused at the center of the detector. The CCD consists of 1152 channels, spanning 4% of the mass range, which are clocked sequentially through the device and are read out at the last channel. The array clocking speed is synchronized with the ion beam movement across the array face such that the ion current associated with each ion accumulates as the beam travels, which eliminates stepping dead time. Thus, significant time savings is realized since recording of a single CID spectrum can be taken in less than five seconds compared to approximately three minutes using the stepping mode. Also, the capability of scanning rapidly plus the addition of the continous flow probe as our standard method of sample introduction permits on-line HPLC/MS/MS experiments to be performed on a 4-sector mass spectrometer. Incorporating a continuous flow probe and CCD detector on our 4-sector instrument has resulted in a 10-fold increase in detection sensitivity. As an illustration, Figure 1 shows the high energy CID spectra of tryptic peptide (MH^+ = 1033.6 Da) from Galβ1,3(4)GlcNAc α2,3-sialyltransferase isolated from rat liver. Approximately 100 picomoles of this peptide was loaded using the conventional batch mode probe and photodiode array detector. It took approximately three minutes to record this single scan.

In comparison, Figure 2 represents the high energy CID spectra of a synthetic peptide of the same sequence recorded in twenty seconds with the continuous flow probe and the scanning array detector. Approximately 8 picomoles of peptide were consumed during this scan. This spectrum is of equal quality to the 100 picomole spectrum of the same peptide obtained using the batch mode probe and stepped photodiode detector.

References

1 Kenny, P. T. M., Orlando, R. *Anal. Chem.* **64**, 957-960 (1992).
2 Hoffman, A. D., Ryan, P A., Moore, C. *Proceedings of the 40th Conference on Mass Spectrometry and Allied Topics*, May 31-June 5, 1992, Washington DC, pp. 519-520
3 Evans, S., Buchanan, R., Hoffman, A., Mellon, F A, Price, K. R, Hall, S., Walls, F. C., Burlingame, A. L., Chen, S., Derrick, P *J. Org. Mass Spectrom.* **28**, 289-290 (1993)

Acknowledgments

We thank S. Glover (Kratos Analytical) for technical assistance. Financial support for this work was provided by the NIH NCRR (Grant RR01614), the NSF Biological Instrumentation Program (Grant 8700766), the NIEHS Superfund Program (Martyn Smith, UCB, PI) Grant E504705 and the UC TRDRP (Grant 2RT0089).

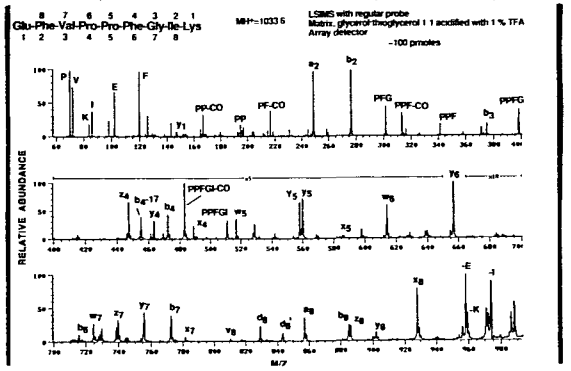

Figure 1.

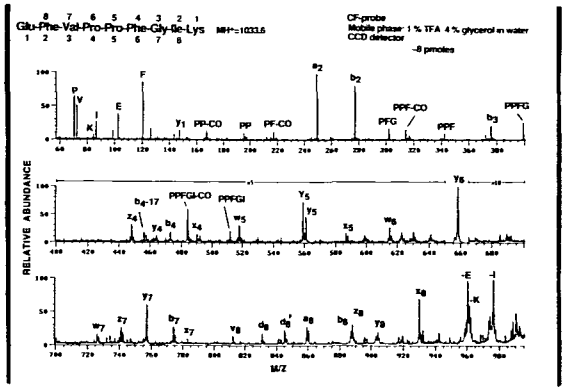

Figure 2.

A Tandem Time-of-Flight Mass Spectrometer Using Photodissociation

M. A. SEETERLIN, R. D. MCLANE†, P. R. VLASAK, D. J. BEUSSMAN, and C. G. ENKE,
Department of Chemistry, Michigan State University, East Lansing, MI 48824

The tandem time-of-flight (TOF) instrument constructed in our laboratory has been designed to obtain complete MS/MS spectra from compounds eluting from a capillary gas chromatographic column, while maintaining unit mass resolution for both precursor ion selection and product ion analysis. To meet this goal, the instrument needs to acquire at least 10 product spectra per second. Such spectral generation rates require maximum utilization of sample molecules and ions, efficient fragmentation of precursor ions, and array detection of the product ions produced. The use of continuous electron impact ionization with ion storage between pulsed extractions, TOF separation and reflectron focusing of precursor ions at an interaction region, pulsed laser induced fragmentation, TOF separation and reflectron focusing of product ions, and array detection of all products formed, meets each of these criteria. Details of instrument design have been presented [1]. Here we present a preliminary report of the achievement of high resolution laser selection of precursor ions and high-efficiency photo-induced dissociation (PID) consistent with the overall instrumentation goals.

For precursor ion selection we rely on the laser pulse interacting with exactly one precursor *m/z* value. The laser pulse is focused to a width of approximately 1 *mm*. The isomass ion packets are also focused to 1 *mm* in length (resolution = 1200 FWHM). At *m/z* 1000, the trailing edge (FWHM) of the *m/z* 1000 ion is separated from the leading edge of the *m/z* 1001 ion by 0.2 *mm*. During the 17 *ns* temporal length of the laser pulse, the *m/z* 1000 ion packet travels 0.2 *mm*. At higher *m/z* values, the distance between ion packets becomes smaller than the distance traveled in 17 *ns*, and unit resolution for precursor selection is not achieved. Figure 1A is a spectrum of the molecular ion region of bromobenzene. With the laser on and the delay time between source extraction and laser firing set such that the laser pulse arrives at the interaction region at the same time as the precursor ions, interaction between the ions and photons occurs. Selection of a new precursor ion simply involves changing the laser delay time to the calculated value for the desired precursor *m/z* value. Figures 1B-1D are the spectra obtained when the laser delay times are set to coincide with the ion packet arrival times for *m/z* 156, 157 and 158 successively. The ion depletions associated with each of these times, being limited to the selected ion, demonstrate the effectiveness of precursor selection by laser timing adjustment.

The high degree of spatial and temporal overlap obtained by this instrument also provides optimal PID efficiency. The laser used in this system is a Questek 2580vβ excimer, in this case operating with ArF (193 *nm*) at 30 *Hz*. The efficiency of the PID process is determined by the efficiency of fragmentation and the efficiency of collection of the ions. We can let P and P_O represent the precursor ion current with and without laser excitation, respectively, and $\sum F_i$ the total current of all fragment ions. The fragmentation efficiency is $E_F = \sum F_i / (P + \sum F_i)$, the collection efficiency is $E_C = (P + \sum F_i) / P_o$, and the overall PID efficiency is $E_{PID} = E_F \times E_C = \sum F_i / P_o$. Product spectra from precursor ions for several compounds were collected. Efficiencies are given in Table 1. In most of these studies, the ions were focused at a temporary detector placed approximately 20 *cm* beyond the interaction region, rather than at the interaction region. This configuration improved product ion resolution, but resulted in lower PID efficiencies. When reflectron 2 is used in the final instrument configuration to focus the product ions, space focus will be achieved at both the interaction region and at the final detector. To determine the effect of improved focusing on PID efficiency, two precursor ions (indicated by asterisks in Table 1) were studied with the focus at the interaction region. As hypothesized, PID efficiencies were increased.

Collection efficiencies of greater than 100% were sometimes observed. This is believed to be the result of greater detector gain for ions with higher velocity (lower *m/z*) [2]. The overall PID efficiency of 104% achieved for bromobenzene is comparable to the high efficiencies achievable in the CID process in a triple quadrupole instrument. These results give evidence that PID can be an analytically useful fragmentation technique when implemented in a system with high ion/photon overlap.

Figure 1

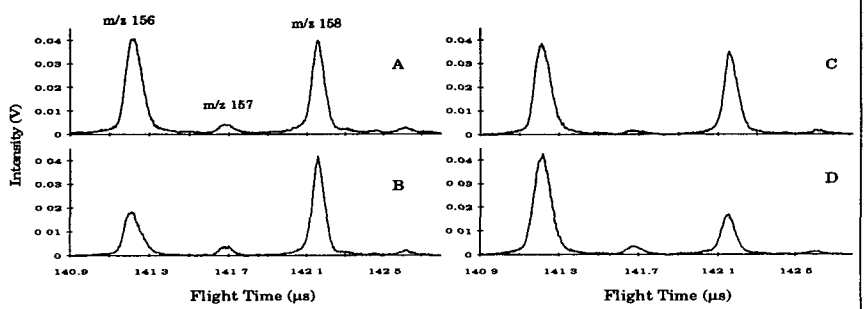

Table 1

Compound	Precursor Ion *m/z*	Laser Pulse Energy (*mJ*)	Fragmentation Efficiency (%)	Collection Efficiency (%)	PID Efficiency (%)
bromobenzene	156	150	56	116	65
	77	160	30	93	28
	156*	130	79	132	104
	77*	130	44	113	50
toluene	91	110	39	103	40
nitrobenzene	123	140	66	137	91
acetophenone	105	140	54	107	58
triethylamine	86	110	27	119	32
N,N-diethyl-formamide	86	100	24	99	24
N-methyl-acetamide	73	120	29	94	27
cyclohexene	67	140	12	91	11

*Precursor ions were focused at the interaction region instead of at the temporary detector.

This research was supported by NIH grant GM 44077.

† *Present Address: The Procter and Gamble Company, 11450 Grooms Road, Cincinnati, OH 45241*

1 Puzycki, M.A., McLane, R.D., Vlasak, P.R., Enke, C.G. *Proceedings of the 40th ASMS Conference on Mass Spectrometry and Allied Topics*; Washington, DC, June 1992; p 1338.

2 Meier, R.; Eberhardt, P. *Int. J. Mass Spectrom. Ion Processes* **1993**, *123*, 19-27.

The use of tandem mass spectrometry in the study of complex mixtures

J H Scrivens, H Yates, K Rollins, R J K Jennings, J Lewis
ICI Materials PO Box 90 Wilton Cleveland England TS6 8JE

1. Introduction

Many industrial formulations are in fact complex mixtures. This reflects the use of inexpensive, multicomponent feedstocks and the need to address a variety of properties in one product. Tandem mass spectrometry techniques have been used to characterise a series of complex ester formulations. These are made up from a variety of cyclic polyhydroxy compounds reacted with various mixed acid feedstocks. A combination of product and precursor ion scanning has been used to simplify the data obtained with both derivatised and non derivatised systems. LSIMS has been the ionisation method of choice combining stability, longevity of spectra and sensitivity.
Many of these formulations have a variety of isomers present and experiments have been carried out to evaluate the ability of tandem mass spectrometry to differentiate similar structures.

2. Experimental

This work was carried out on a Fisons VG ZAB-T four sector instrument of BEBE geometry[1]. The instrument incorporates an inhomogeneous ESA in MS2 enabling the mass range simultaneously detected using the array detector to be varied up to 1.4:1. All product ion scans were obtained with a ratio of 1.2.1 and a resolution of >1000 (FWHH). The collision energy was 4kev. Precursor ion scans were carried out by selecting an ion with MS2 and scanning MS1[2]. A collision energy of 2kev was used and the wide energy transmission of MS2 (1.34:1) enabled all precursors to be detected. Sequential product ion spectra were obtained using the first and third collision cells. First generation products formed in FFR1 were selected using B1 and E1 and the product collisionally activated in FFR3[3]. LSIMS using 35kev caesium ions was the ionisation method employed.

3. Results

Precursor ion scans have been shown to be very useful in simplifying the complex formulations. Both alcohol type and acid component can be picked out by selecting appropriate ions from the LSIMS spectra. Residual unreacted OH groups can result in water loss which can mask the presence of other alcohol components. This has been demonstrated by sequential product ion spectra. Forming derivatives can help but has to be used with caution in unknown systems. Acetylation can often give dominant (M-60) ions which can complicate interpretation. The potential of tandem mass spectrometry in distinguishing closely related structures has been demonstrated for a number of systems. Figure 1 shows a series of $C_6H_{12}O_5$ isomers typical of alcohols used in these formulations. Figure 2 shows the product ion spectra obtained from the m/z 165 ions. All eight isomers can be differentiated using this method The differences are outside those that can be attributed to the normal reproducibility variations (which have been studied). The major source of variation was found to be the tuning of MS2.

References

1. K Rollins, J H Scrivens, R C K Jennings, W E Morden, J K Welby,R H Bateman RCMS 4 454 (1990)
2. J H Scrivens, K Rollins, R C K Jennings, R S Bordoli, R H Bateman RCMS 6 272 (1992)
3. K D Ballard, S J Gaskell, R C K Jennings, J H Scrivens, R G Vickers RCMS 6 553 (1992)

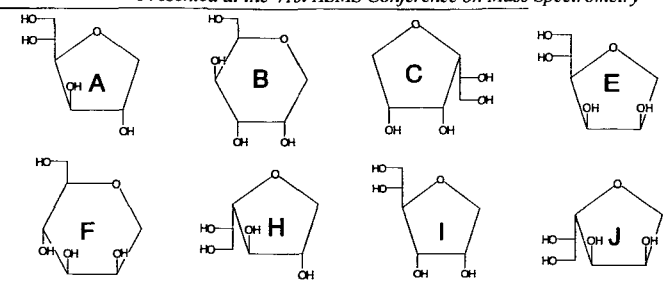

Figure 1 Structures of isomers studied

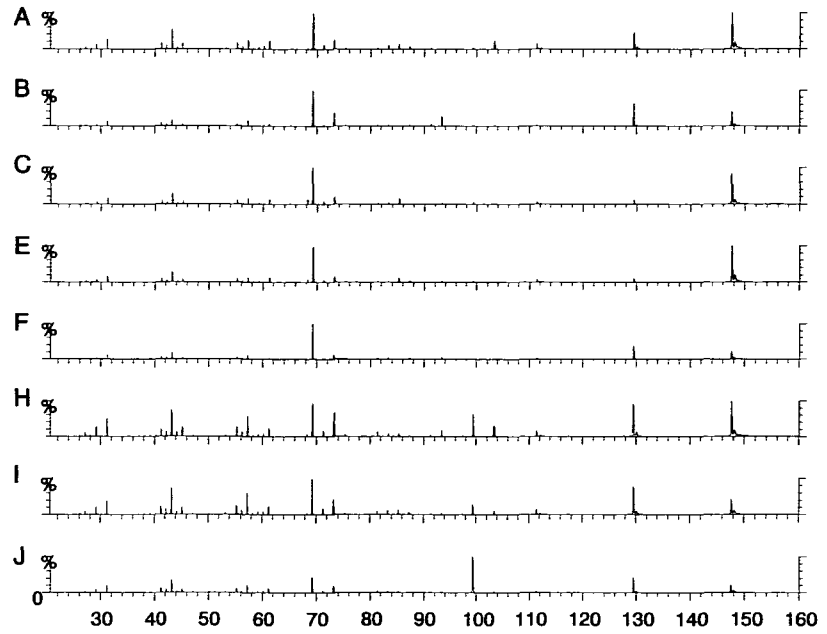

Figure 2
Product ion spectra of m/z 165

USING CLUSTERS AS A TOOL TO PROBE MALDI MASS CALIBRATION

R.D. Edmondson, G.R. Kinsel, L.M. Preston, K.K. Murray,
T. Solouki, and D.H. Russell
Department of Chemistry
Texas A&M University
College Station, Texas 77843

Mass Calibration of TOF spectra of large molecules is hampered by the lack of high mass standards with accurately determined molecular weights. Recently, MALDI spectra of bovine insulin which contain clusters as large as twenty monomeric units were obtained on a linear TOF instrument in our laboratory. These cluster peaks offer an approach to producing high mass species with accurately determined molecular weights. A calibration curve that extends past 100,000 mass units can be created by using these cluster peaks as standards. We are now using this method to accurately determine molecular weights of high mass analytes. In this paper, the method of calibration is presented, discussed, and applied to an "unknown" analyte, Subtilisin (M.W. 27288). Sample preparation methods that enhance cluster ion formation are also discussed.

Figure 1 shows a mass spectrum of bovine insulin clusters, and was obtained as follows: a methanol solution that contains 3% Trifluoroacetic acid was used to dissolve 1 mg of bovine insulin. 2 μl of this solution was added to the probe tip. Then 2 μl of a 15 mg/ml solution of α-cyano-4-hydroxycinnamic acid was added. The laser beam power was varied by a neutral density wheel to optimize the relative abundance of the cluster ions.

The bovine insulin cluster peaks were curve fitted to determine their centroids. Figure 2 shows that a two component fit results in a smaller residual trace (a better fit) than does a single component fit. Figures 3 and 4 show plots of time (t) versus $(M/Z)^{1/2}$ for bovine insulin clusters. In Figure 3 the centroid was determined by the curve fitting method mentioned above, whereas in Figure 4 the centroid was determined by the center of mass method. The mass calibration equation ($t = k\,(M/Z)^{1/2} + b$), shows that a plot of (t) versus $(M/Z)^{1/2}$ should result in a straight line with a slope of k and a y-intercept of b. The b arises from the delay between laser firing and data acquisition. It is evident that a better correlation coefficient (R^2) was obtained from the plot in Figure 3 as opposed to Figure 4. Comparing the b values from these plots suggests that Figure 3 provides a more accurate calibration curve. Typical values for b on this instrument should fall between -0.03 to 0.03. The value of b in Figure 3 (-0.0248) falls in this range, while the value for b in Figure 4 (0.4108) is unrealistic.

A mass spectrum of an "unknown" analyte, Subtilisin, is shown in Figure 5. Subtilisin was chosen because its accurate molecular weight has previously been reported by Beavis and Chait.[1] This spectrum was mass calibrated in the conventional manner of using a low mass ion (Na^+) and an internal standard (bovine insulin) to generate a calibration curve, which resulted in an M/Z value of 27301. The same spectrum was mass calibrated using three bovine insulin cluster peaks, which resulted in an M/Z value of 27289. The value reported by the curve fitting method gives a value closer to the 27288 reported by Beavis and Chait. This shows that using cluster peaks as calibration standards provides a more accurate calibration curve than the conventional extrapolation based on low mass ions.

It should be noted that cluster ions of other proteins can also be produced. For instance, we have been able to acquire mass spectra of lysozyme (M.W. 14306) containing cluster ions as large as 14 monomeric units. Future plans include finding other, larger proteins that will form cluster ions. In addition, a study is planned to measure the neutral content from metastable decay under the cluster peaks.

(1) Beavis, R.C.; Chait, B.T., Anal.Chem. 1990, 62, 1836-1840.

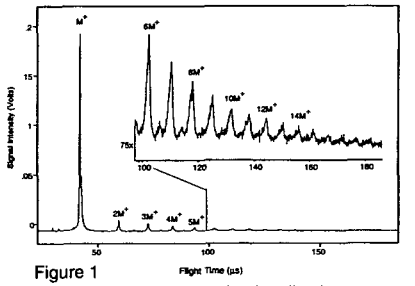

Figure 1
A mass spectrum of Bovine Insulin clusters. M=5734 Da

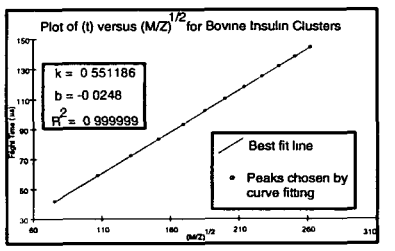

Figure 3
A plot of flight time versus $(M/Z)^{1/2}$ for Bovine Insulin clusters, where the centroids of the cluster peaks were chosen by curve fitting.

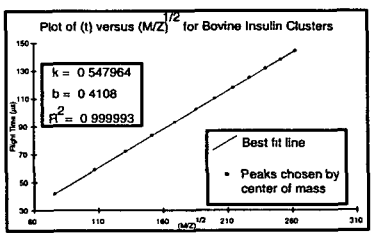

Figure 4
A plot of flight time versus $(M/Z)^{1/2}$ for Bovine Insulin clusters, where the centroids of the cluster peaks were chosen by their center of mass

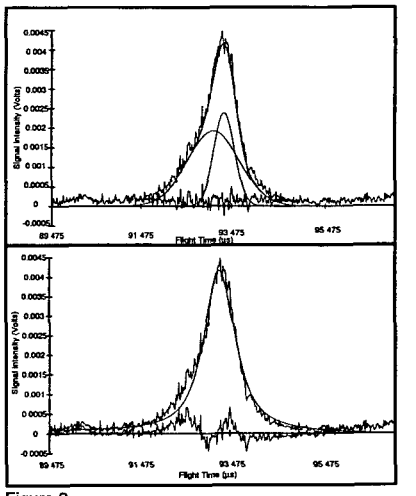

Figure 2
The upper trace shows a two component fit to the 5th Bovine Insulin cluster peak. The lower trace shows a single component fit Note the smaller residual (a better fit) on the upper trace.

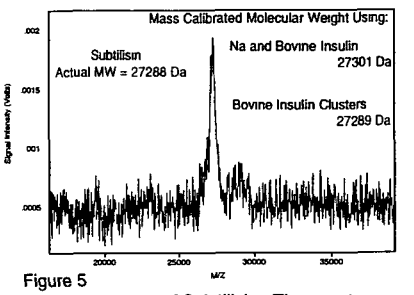

Figure 5
A mass spectrum of Subtilisin. The spectrum was calibrated by two methods: the conventional extrapolation from low mass, and the new method of using Bovine Insulin clusters. Note the calibration by clusters gives a more accurate value for the molecular weight of Subitilisin.

Post Source Pulse Focusing with Linear Time Of Flight Mass Spectrometry and Laser Desorption Ionization

J.M. Grundwürmer, M. Bönisch, G.R. Kinsel* and J. Grotemeyer

Institut für Physikalische Chemie, Universität Würzburg, Marcusstr. 9/11,
D-8700 Würzburg, Germany
*present adress : Texas A&M University, Dep.of Chemistry, College Station, Tx, 77843

Non-volatile molecules are successful introduced into the gas phase by Laser Desorption / Ionization.This method is easily combined with a linear TOFMS for mass spectral analysis.

However a major drawback of the linear TOFMS, particularly severe for LD experiments, is the poor resolution of the detected ion signals. There is need for higher resolutions to be obtained, particularly when investigating high mass ion signals. Higher resolutions are required for improvements for distinguishing between various protonated, sodiated and/or adduct ions which may be formed during LDI and accurate mass determination.

Post Source Pulse Focusing (PSPF) is a method which is expected to improve the resolution of the ion signals in a linear TOFMS by applying a compressing voltage pulse to the ion packet of interest after accelerating the ions from the TOFMS source region using conventional electric fields [1, 2]. Investigations under direct LD/I and matrix assisted LD/I conditions all demonstrate the dramtic improvements in ion signal resolution which could be achieved using this simple technique in a linear TOFMS. A mass resolution of 4800 (FWHM) has been achieved for Zn-mesoporphyrin (MW 656) and 800 (FWHM) for Cytochrome c (MW 12360).

Identifying the mass of the detected requires a well defined mass calibration. The kinetic energy of molecules affected by PSPF depends from the delay time between the desorption laser pulse and the time, when the post source pulse field is turned on. This relation requires a non linear

equation. Therefore, following equation is extrapolated, which allows to calibrate the postsource pulsed TOFMS well with three or more calibrating masses:

$$t = c_0 + c_1 * m^{\frac{1}{4}} + c_2 * m^{\frac{1}{2}} + c_3 * m^{\frac{3}{4}}$$

The constant factors c_i can be found by gaussian minimation of the square of the errors. This equation allows a mass determination of less than 0.02 % [3].

Acknowledgement

This work is supported by the Deutsche Forschungsgemeinschaft (Grant Gr 917/6-2). The authors thank for the support of Fonds der Chemischen Industrie.

References

[1] G.R. Kinsel and M.V. Johnston, Int. J. Mass Spectrom. Ion Proc., 91 (1989) 157.

[2] G.R. Kinsel, C.D. Mowry, P.J. McKeown and M.V. Johnston, Int. J. Mass Spectrom. Ion Proc. 104 (1991) 35.

[3] J.M. Grundwürmer, M. Bönisch, G.R. Kinsel, J. Grotemeyer and E.W. Schlag, Int. J. Mass Spectrom. Ion Processes, in press

Ion Trap Storage/Reflectron Time-Of-Flight Mass Spectrometer Performance with Various Ionization Sources

Steven M. Michael, Benjamin M. Chien, and David Lubman
The University of Michigan
Department of Chemistry
Ann Arbor, MI 48109

An ion trap storage/reflectron time-of-flight mass spectrometer's performance with electrospray, atmospheric pressure plasma discharge, reduced pressure plasma discharge and resonance enhanced multiphoton ionization sources is displayed. This instrument combines the high mass capability, speed, and resolution of the time-of-flight device with the sensitivity and selectivity of the quadrupole ion trap. The innovative feature of this device is that the trap enables coupling of time-of-flight, an inherently pulsed technique, with continuous ionization sources, electrospray and plasma discharge, with 100% duty cycle. This duty cycle is independent of the experimental repetition frequency thus allowing this instrument to serve as a real time on line detector for GC, LC, and CZE without the need for special high speed data collection electronics as the experiment can be run at a low enough frequency to allow for manageable data collection without sacrificing duty cycle.

Figure 1 shows the instrumental configuration with the electrospray ionization source in place Resolution >3000 and detection limits (S/N = 3) less than a single femtomole of analyte are typical for the electrospray experiment.

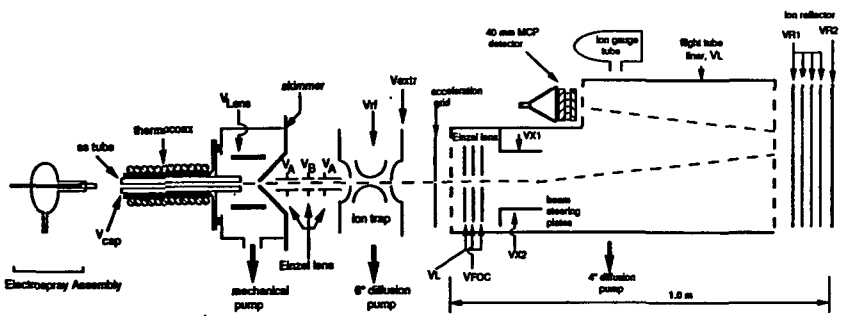

The selectivity advantage of the quadrupole ion trap as a front end source for TOF is demonstrated in figure 2 where, above, the spectrum is dominated by background peaks with only a trace of the peak of interest, however, by increasing the RF amplitude, the stable trapping region is shifted towards higher m/z thereby eliminating the unwanted background and enhancing the now dominant peak of interest.

Reduced Pressure Glow Discharge Ionization of Dibenzothiophene, MW 184. 5 ms trapping time.

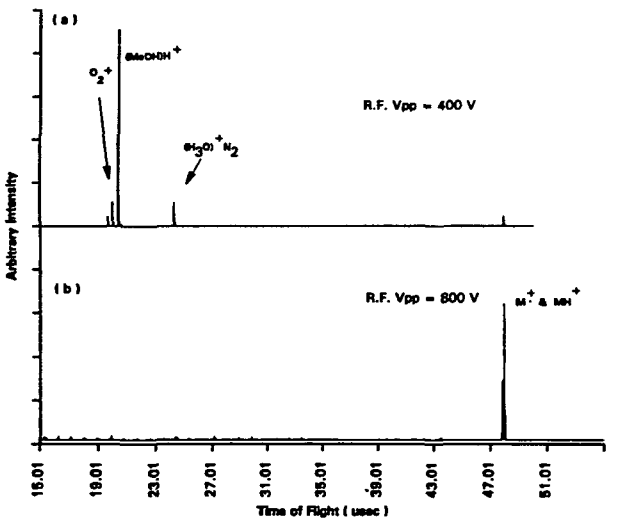

A Compact, High Performance Time of Flight Mass Spectrometer

D. M. Murphy
Aeronomy Laboratory, National Oceanic and Atmospheric Administration, Boulder, CO 80303.

A new design is presented for a compact (67 cm) time of flight mass spectrometer, to be used in field measurements of the composition of aerosol particles. This application poses three challenges: The spectrometer must be portable, the initial ion temperature is very high (>6000 K), and different particles produce widely varying ion yields. An extended post source pulse focus region is used to obtain better than unit resolution for m/e from 1 to 300, covering most species of atmospheric interest. The mass spectrometer uses a two stage detector with nonlinear electronics to attain a dynamic range of over 10^5 from a single laser shot with a precision of approximately 5%. The design presented here is optimized for very hot ions produced in a highly confined region. However, the design is flexible and can compensate for other causes of low resolution.

A wide variety of techniques have been used to improve the resolution of time of flight mass spectrometers, with the most common being the reflectron and time lag focusing. The design presented here uses post source pulse focusing (PSPF), described by *Kinsel and Johnston* [1989]. This technique was chosen over a reflectron because of its simplicity, the ability to compensate for a spread in ionization time, and because a reflectron cannot fully compensate for differences in the initial *directions* of energetic ions. Kinsel and Johnston applied PSPF to obtain the highest possible resolution for one or two mass peaks. The design presented here is, to my knowledge, the first application of PSPF to a wide mass range.

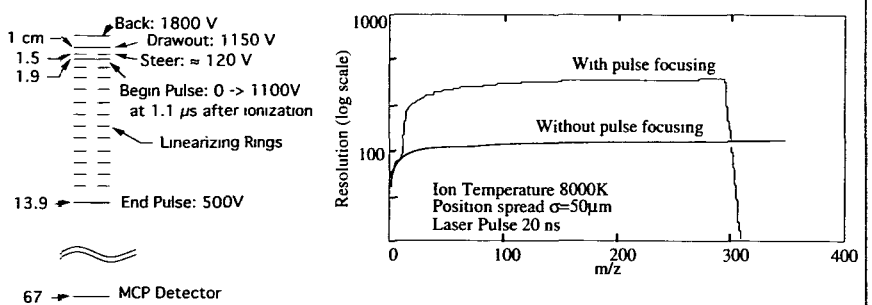

Figure 1: Design and theoretical resolution of the spectrometer for conditions typical of ionization from aerosol particles. Positions of the plates are in cm relative to the backing plate. As shown on the right, PSPF has different effects on three classes of ions. Ions below about m/e 10 u are in the drift region when the pulse is applied and are not affected. Ions with m/e 10 to 300 u are in the pulsed region at the time of the pulse and are observed at enhanced resolution. Finally, heavy ions have not yet reached the beginning of the pulsed region and are either defocussed or are unaffected.

The spectrometer is fully operational and is being used for the analysis of single aerosol particles with laser ionization. The design has also been optimized for near unity ion transmission and convenient operation of steering voltages. The predicted enhancement in resolution has been

observed, as indicated in the next figure:

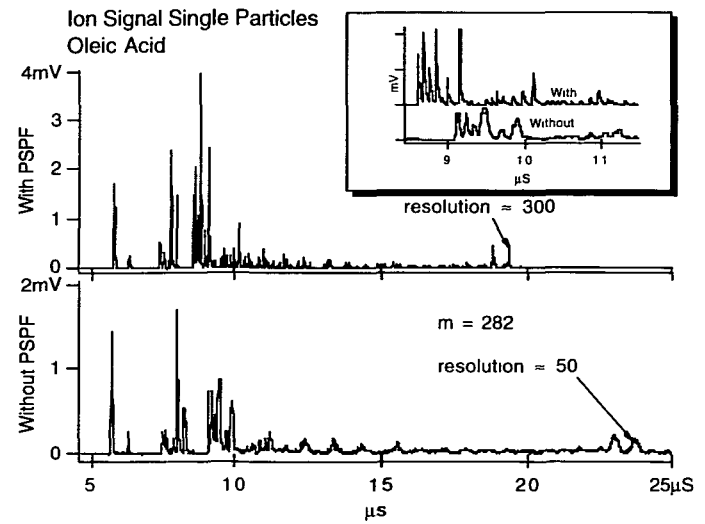

Figure 2: Observed spectra of oleic acid particles with and without PSPF. The PSPF both improves the resolution and changes the mass scale due to the extra acceleration from the pulsed voltage. The inset shows a small area of the two spectra near 10 μs delay.

It is also possible to optimize a design for ions with less kinetic energy but more initial spatial spread. This is accomplished merely by changing the drawout voltage from 1150 to 1650 V and delaying the pulsed voltage to a later time. The range of masses with enhanced resolution can be adjusted with the time delay, as shown below.

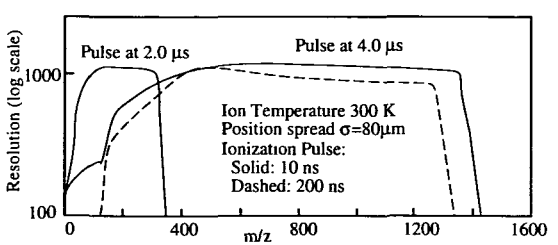

Figure 3: Performance of a compact PSPF spectrometer optimized for cooler ions. It is also possible to obtain good resolution with quite long ionization pulses.

References: Kinsel, G. R., and M. V. Johnston, *Int. J. Mass Spec. Ion Proc.*, *91*, 157-176, 1989.

TIME-OF-FLIGHT MASS SPECTROMETER FOR ON-LINE SINGLE PARTICLE ANALYSIS

M.V. Johnston*, P.G. Carson, K.R. Neubauer, Department of Chemistry and Biochemistry
A.S. Wexler, Department of Mechanical Engineering
University of Delaware, Newark, DE 19716

A new mass spectrometer has been constructed to detect single micron-size particles on-the-fly by laser desorption. Particles enter the source region through a differentially pumped inlet and scatter radiation from a continuous helium-neon laser beam. The scattered radiation triggers an excimer laser (193 or 248 nm) which ablates each particle in-flight and the time-of-flight mass spectrum is recorded. Hundreds of particles can be analyzed per minute with each particle giving its own unique mass spectrum Figure 1 shows the basic experimental setup Figure 2 shows the scatter collection and mass analyzer components in more detail Applications of this instrument to aerosol chemistry and example spectra are presented elsewhere in the proceedings

Aerosols are generated with a vibrating orifice aerosol generator (liquids) or a powder dispenser (solids, particulate matter on filter media). The aerosol is sampled by selectively transmitting particles through a two-stage momentum separator The transit time between the inlet and source region is approximately 0 5 ms, so loss of volatile components is minimized Indeed, cluster ions corresponding to $H(H_2O)_n^+$ can be observed from particles containing a substantial water content The helium-neon and excimer lasers are aligned to give the largest frequency of particles that are detected by light scattering and subsequently ionized by laser desorption. The laser beam waists are estimated to be between 100 and 200 μm diameter Since the particle velocity is approximately 200-300 m/s and the time-delay between detecting a scatter pulse and firing the excimer laser is 0 5 μs, minimal displacement of the excimer laser beam relative to the helium-neon laser beam is required. Ions can be generated and mass analyzed in a number of ways. Normally, ions formed directly from the desorption event are detected It is also possible to postionize neutrals with a pulsed electron beam. Mass analysis can be performed with linear, reflectron, or post-source pulse focusing time-of-flight modes. Each mode has specific advantages and disadvantages relative to mass resolution and sensitivity. Both positive and negative ions can be detected To aid in quantitative analysis, mass spectra can be pre-selected on the basis of the helium-neon laser scatter signal, or the excimer laser pulse energy

This instrument was designed for studies of laboratory-generated aerosols Development of a more compact version for field measurements is feasible Space and electrical power constraints are primarily determined by the vacuum pumps

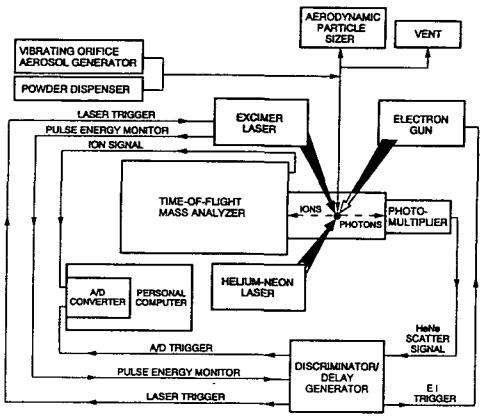

Figure 1

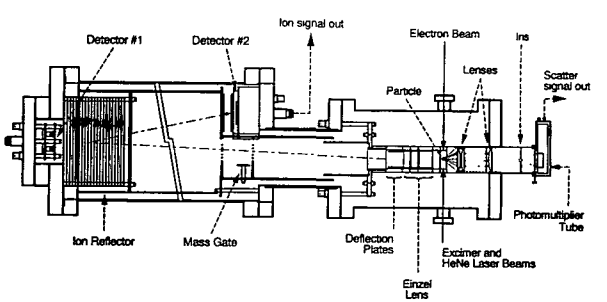

Figure 2

Tandem Time-of-Flight Mass Spectrometry of Organic Molecules by Surface Induced Dissociation

David Fenyö and Brian T. Chait,
The Rockefeller University, 1230 York Avenue, N.Y., N.Y. 10021

Surface induced dissociation, i.e. dissociation of molecules due to high internal energy acquired in a collision with a surface, provides a means for the study of the fragmentation of organic molecules [1]. Most commonly a plane surface is used for the collisions but also the walls of the channels of a microchannel plate (MCP) has been utilized [2]. The use of an MCP allows an in-line geometry which is suitable for time-of-flight mass analysis. Such a time-of-flight analysis provides a highly efficient means for detecting the products of surface induced fragmentation.

The aim of this study was to construct a simple tandem time-of-flight mass spectrometer for the investigation of the fragmentation of molecular ions produced by matrix assisted laser desorption. For this purpose, a thin (250 μm) MCP, with grounded grids on each side, was placed as a collision cell in the field-free region of an existing time-of-flight mass spectrometer (Figure 1). The potential on each face of the MCP could be independently varied to set the collision energy ($q[V_a-V_c]$) as well as the extraction field (ΔV_c) in the channels. The MCP used had an angle of 0° between the channel long axis and the surface normal (the ion beam axis). The potential on the channel plate was pulsed to allow only ions of interest to reach the channel plate and undergo fragmentation. The fragmentation was studied for the cationic dyes brilliant green (MW 386 u), methyl red (MW 270 u) and Janus green (MW 476 u) as well as for the peptides Substance P (MW 1349 u) and [Arg^8]-Vasotocin (MW 1050 u) in a matrix of α-cyano-4-hydroxycinnamic acid. The fragmentation pattern was studied as a function of the collision energy and the extraction field in the channels.

For low energy collisions (0-200 eV) intense fragmentation spectra characteristic of the structure of the organic dyes were obtained (Figure 2). The fragmentation efficiency was approximately 10%. The fragmentation pattern could be varied by changing the collision energy. Smaller fragments were obtained when using higher collision energy. The size of the extraction field (ΔV_c) is critical for efficient extraction of the fragment ions.

In contrast to the results obtained for the dyes, the fragmentation spectra of the peptides were dominated by low mass ions that do not provide useful sequence information. Possible reasons for the difference in the information content of the fragmentation spectra of dyes versus peptides include: (i) differences in internal energy (the dye molecules absorb the laser light) and (ii) differences in charge neutralization upon impact with the surface.

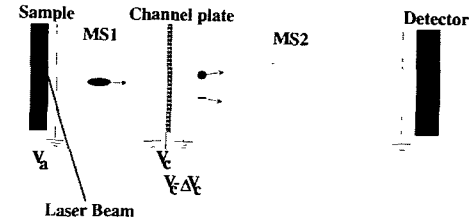

Figure 1. The experimental setup.

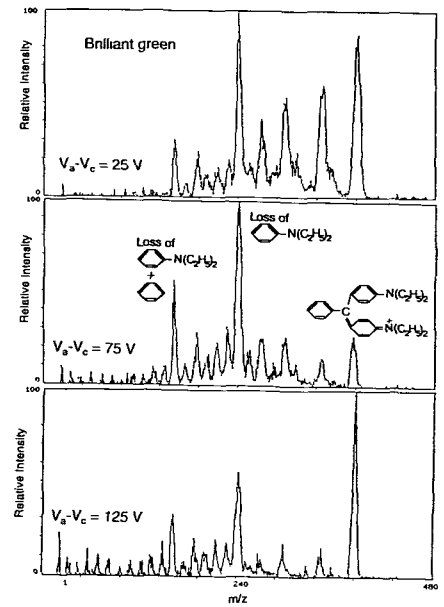

Figure 2. The fragmentation spectrum of the cationic dye brilliant green (MW 386 u) for different collision energies.

1. R.G. Cooks, T. Asf, MD. A. Mabud, Int. J. Mass Spectr. Ion Proc. 100 (1990) 209.
2. W. Aberth, Anal. Chem. 62 (1990) 609.

On-line Laser Mass Spectrometrical Analysis of Atmospheric Particles

K.-P. Hinz, R. Kaufmann, *B. Spengler

Inst. of Laser Medicine, University of Düsseldorf, Moorenstr. 5, D-4000 Düsseldorf, Germany

Investigation of atmospheric aerosol particles is an important task for e.g. air pollution research or the understanding of chemical processes taking place in the atmosphere. Until recently, analysis of individual single particles was possible only by sampling them in the atmosphere with impactors followed by transport to and preparation in the laboratory. Volatile components were not detectable with this method. This limitation can be overcome by interfacing the aerosol phase directly to a laser time-of-flight mass spectrometer [1]. We developed a new instrument for automatic detection, ionization and mass analysis of single particles (Figure 1). The instrumental setup consists of a differentially pumped nozzle system [2] for particle introduction into the mass spectrometer's ion source and a linear time-of-flight analyser with two-stage acceleration. Particles traversing a certain ionization volume are detected by scattered light from a He-Ne laser beam. The discriminated signal from the photomultiplier is used to trigger a UV laser for ionization. The total residence time of particles in the apparatus is less than 1 ms. A liquid phase covering the particles will thus be partially conserved by freezing.

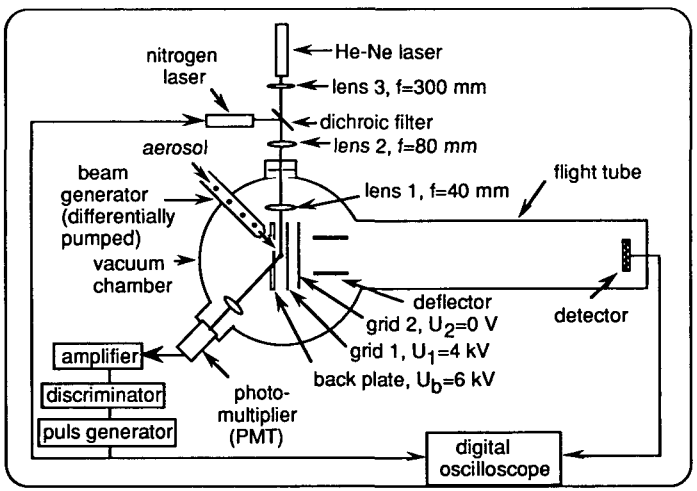

Figure 1: Instrumental setup of the laser time-of-flight mass spectrometer for on-line analysis of airborne particles.

Preliminary investigations of particles from alkali halides, smoke and other available sources gave good sensitivity and a mass resolving power of several hundred.

Particle-size selectivity can be achieved by choosing a proper delay between the photomultiplier signal and the ionization laser trigger, due to the mass dependence of the particle velocity.

Figure 2, as an example, shows a typical mass spectrum of small aerosol particles (<1µm) from room air, characterized by carbon cluster ion distributions. Larger particles from room air, on the other hand, predominantely contain silicate structures. A mass spectrum of a tobacco smoke particle (diameter ≈0.2 µm [3]) is displayed in Figure 3. Besides signals of alkali salts and hydrocarbon compounds it contains a characteristic peak of the nicotine radical ion.

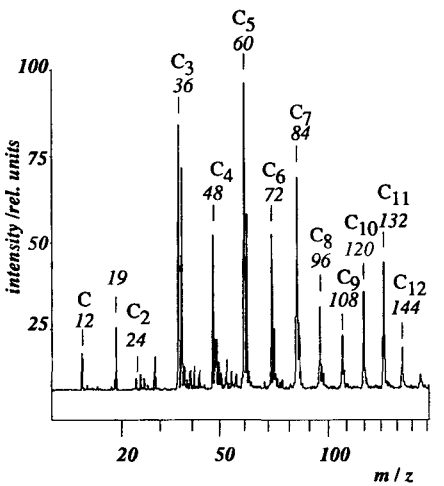

Figure 2: Positive ion mass spectrum of a typical aerosol particle from room air (particle diameter <1µm).

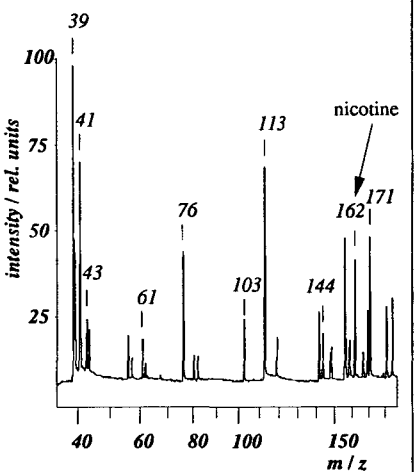

Figure 3: Positive ion mass spectrum of a tobacco smoke particle (particle diameter ≈ 0.2 µm).

ACKNOWLEDGEMENT:
This work has been supported by the Ministry of Science and Research, Nordrhein-Westfalen.

REFERENCES

/1/ P. J. McKeown, M. V. Johnston, D. M. Murphy, *Anal. Chem.* **63** (1991), 2069-2073
/2/ O. Kievit, J. C. M. Marijnissen, P. J. T. Verheijen, B. Scarlett, *J. Aerosol Sci.* **21**, Suppl.1 (1990), 685-688
/3/ Y. Ishizu, K. Kaneki, T. Okada, *J. Aerosol Sci.*, **18** (1987), 123-129

Accurate Mass Measurements in a MALDI Reflector Instrument Using External Calibration

Gert Talbo, Kenneth Morand, Laura Margis and *Matthias Mann

Protein and Peptide Group,
European Molecular Biology Laboratory,
Heidelberg, Germany

MALDI TOF is a fast and simple method for peptide and protein analysis in the life science laboratory. It is in principle capable of high mass accuracy when used with internal calibrants. However, in practice several factors often prevent the use of such calibrants: (i) it is difficult to determine the correct nature and amount of calibrant that leads to a spectrum of comparable peak height and peak shape as the unknown. (ii) the measurement is complicated and prolonged by the necessity of mixing other proteins into the solution containing the unknown. (iii) when dealing with very small amounts the calibrants may suppress the sample peptides. Here we investigate the possibility of obtaining high mass accuracy with MALDI TOF using external calibration.

An ion reflector was used in these studies because some of the mass measurement errors are due to the energy uncertainty of the ions which the reflector compensates. Further experimental parameters to control include the acceleration voltage and the laser irradiance as well as the type of matrix but not the sample concentration.

MALDI TOF experiments were performed on a Bruker REFLEX instrument equipped with a reflectron and two double channel plate detectors. A 400 MHz digital storage oscilloscope (LeCroy 9450) was used to digitize the detector output and the "LaserOne" data system running on a Macintosh Quadra 950 controlled the instrument. A 16 bit high precision controller (FUG Probus III) was used to set the analog input voltage with an accuracy of 20 ppm of a long term high stability power supply (FUG). With this combination the voltage stability and reproducibility should at least be in the low 10^{-5} range and hence not be a limiting factor in mass determination.

To study the influence of laser irradiance we measured peptide mixtures at different attenuation settings of our filter for two matrices.. Figure 1 shows the result for a peptide of mass 1854. Da. Curves for all other measured masses were similar. The observed increase in flight time with increased laser irradiance is much smaller than it is in linear mode (data not shown) but it needs to be taken into account for reflector measurements as well. There is furthermore a difference in flight time between matrices which uncorrected would lead a difference in assigned mass of about 0.5 Da in this case.

We conclude from out investigations that the following factors have to be carefully controlled

- Accuracy and reproducibility of the acceleration and reflector **voltages**.
- Level of the **laser irradiance**. For routine, high accuracy measurements with a reflector it is best to measure in a range somewhat above threshold, where there is little dependence of flight time on laser irradiance.
- Change between **different matrices**. Correction factors between matrices or different sets of calibration constants for different matrices have to be used.

Results from repeated measurements over several days (see figure 2) suggest that it is then possible to obtain unit mass accuracy from reflector MALDI TOF using external calibration. For best results it may be advantageous to perform several independent analysis on the same sample.

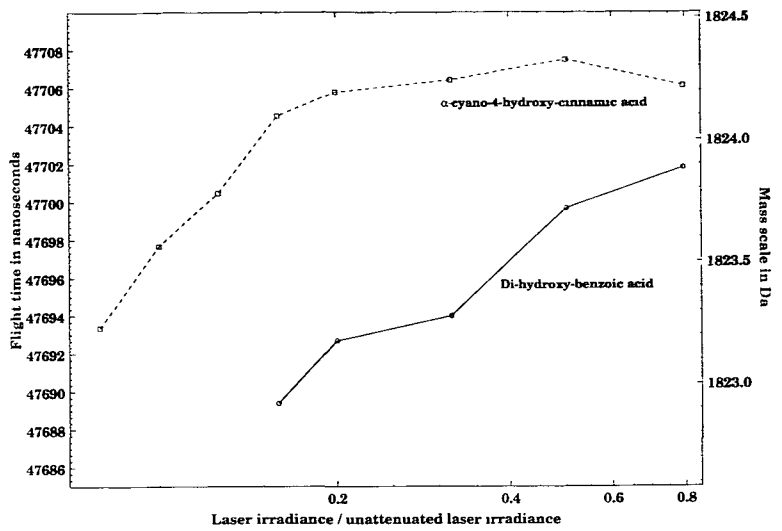

Figure 1 Influence of the irradiance and matrix type on measured flight time and assigned mass of a peptide. Measurements are in the reflector mode and the right hand y axis is based on constant calibration values

Calculated	1 day	2 day	3 day	4. day	5 day	Average	Stdev	Calculated - Measure
777 38	777 29	776 89	777 30	777 30	777 23	777 20	0 18	**0.18**
961 34	961 56	961 20	961 18	960 78	961 30	961 20	0 28	**0.14**
1008 51	1008 74	1008 56	1008 29	1008 29	1008 42	1008 46	0 19	**0.05**
1117 25	1117 20	1117 12	1117 24	1116 85	1116 92	1117 07	0 17	**0.18**
1141 13	1141 59	1140 70	1141 60	1141 41	1140 96	1141 25	0 40	**-0.12**
1516 52	1516 31	1516 70	1516 71	1516 22	1516 50	1516 49	0 22	**0.03**
1674 91	1674 54	1674 90	1674 90	1674 90	1674 67	1674 78	0 17	**0.13**
1702 87	1702 35	1702 48	1702 48	1702 39	1702 57	1702 45	0 09	**0.42**
1876 08	1876 00	1875 65	1876 11	1876 14	1875 67	1875 91	0 24	**0.17**
2062 42	2062 40	2061 81	2061 82	2062 70	2061 96	2062 14	0 40	**0.28**
2346 74	2345 54	2345 58	2346 20	2345 61	2345 24	2345 63	0 35	**1.11** *
2444 90	2444 80	2444 51	2444 85	2444 97	2444 75	2444 78	0 17	**0.12**

* The measured molecular weight was confirmed by electrospray mass spectrometry.

Table I. Masses assigned to twelve synthetic peptides on five consecutive days.

A DUAL REFLECTRON TANDEM TIME-OF-FLIGHT MASS SPECTROMETER

Timothy J. Cornish and Robert J. Cotter
Johns Hopkins Medical School, Baltimore, MD 21205

While CID analysis of biomolecules is becoming routine on magnetic sector instruments, the expense and expertise required to generate high resolution CID data is prohibitive for many biochemistry laboratories. The application of simpler time-of-flight technology to this type of analysis would significantly reduce the complexity of the instrumentation needed to generate CID data. We have been developing a dual reflectron tandem TOF mass spectrometer incorporating a pulsed molecular beam of neutral gas to promote fragmentation of gate selected ions.[1] In the CID mode of operation, the first reflectron is used to energy focus the precursor ions, while the second is used to both energy focus and mass disperse the fragment ions.

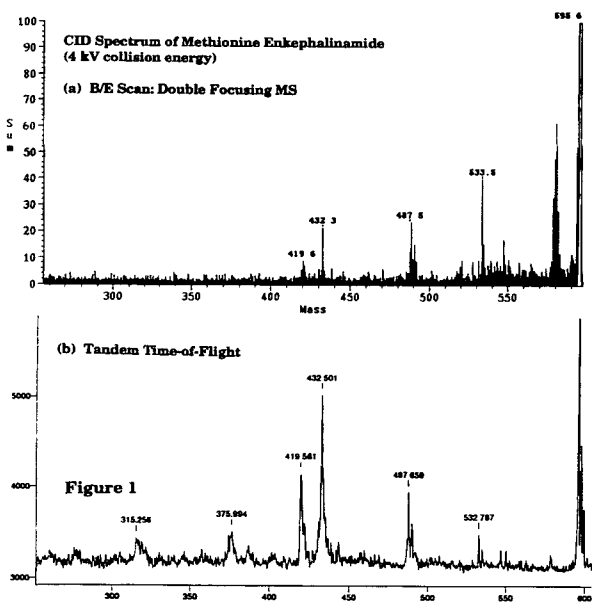

Figure 1

The first successful CID spectrum of a peptide is shown in Figure 1. The ($M+Na^+$) ion of methionine enkephalinamide (594 Da) is mass selected and reacted with helium (4kV collision energy) to generate the product ion spectrum. While the relative peak intensities in the two spectra are somewhat different, the pattern and mass of product ions formed are nearly identical. Likewise, the spectrum of the peptide dermorphin, shown in Figure 2, is also quite similar to the B/E scan. Modifications of the instrument to produce high resolution product ion spectra, as well as isotopically resolved mass selection in MS 1, are currently under development.

1. T.J. Cornish and R.J. Cotter, *Anal. Chem.*, 65, 1043 (1993).

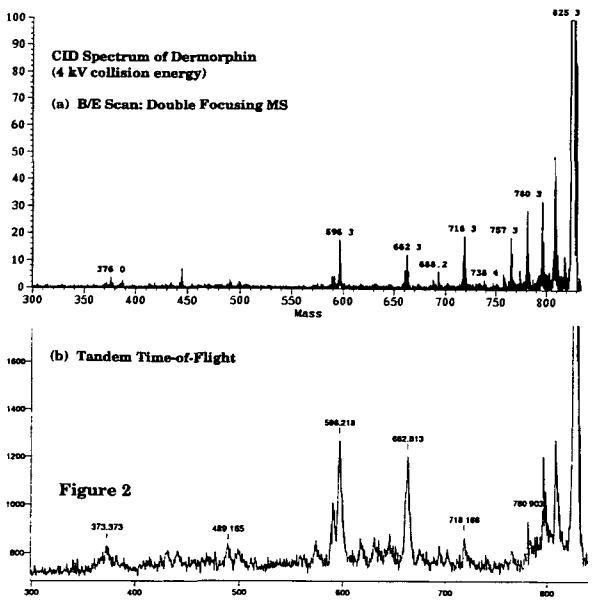

Figure 2

Kinetic Energy Measurements Of Matrix Assisted Laser Desorption Generated Ions With An Electrostatic Analyzer Based Time-Of-Flight Mass Spectrometer

*Robert S. Brown, Katherine H.A. Bogart and Donald L. Dick, Department of Chemistry, Colorado State University, Ft. Collins, CO 80523

The measurement of both the average ion kinetic energy and ion kinetic energy distributions for matrix assisted laser desorbed (MALD) ions can offer significant insights into the ionization mechanism and processes involved in this increasingly important new ionization technique. Recently, the Manitoba group has reported on the ion energies of MALD generated ions in the presence of a strong extraction field. This work indicates MALD generated ions have an actual ion energy deficit relative to the applied extraction field. This ion energy deficit was observed to be dependent on the mass of the ion and also depended upon the relative signal strength. These studies utilized a reflecting time-of-flight mass spectrometer to deduce ion energies. This poster presents preliminary results with an electrostatic analyzer based time-of-flight (ESA-TOF) mass spectrometer for the measurement of ion kinetic energies of MALD generated ions.

The ESA-TOF mass spectrometer was constructed by modifying a VG 7070F mass spectrometer. This entailed removal of the magnetic sector and placing a suitable ion detector (discrete dynode type) at the exit of the ESA. The ion source was removed and replaced with a conventional two stage TOF ion source which could be operated at a maximum accelerating voltage of 18 kV (limited by the electrical feedthroughs). The laser beam was brought in through a quartz window attached to an existing port and the field ionization port was utilized to bring the sample via a direct insertion probe on axis to the ESA's ion flight path. Variable ESA power supplies were added to accommodate the higher ion energies of the new ion source. A suitable transient digitizer and computer were also added. Relatively large exit apertures (1 mm minimum) are employed at present to insure adequate ion signal transmission. This produces an ion energy resolution with the ESA of ≈ ±38 eV at 15 kV accelerating potentials. While this limits the accuracy of determining the width of the ion kinetic energy distribution, average ion kinetic energies (and therefor the measurement of ion kinetic energy deficits of MALD generated ions) are not affected. While both sensitivity and mass resolution are not yet optimized, they are sufficient to measure the kinetic energies of MALD generated horseheart cytochrome C (mw=12360.1 Da) ions and to resolve the matrix adduct ions from protonated molecular ions.

A problem with the systematic examination of a parameter, such as applied ESA voltage or ion accelerating voltage, during MALD ion generation is the sample to sample variations in ionization intensity and the effect of sample history (i.e., extent of laser irradiation) on the observed ion signal intensity. This makes a systematic study of ion energies very difficult. To minimize this problem, a complicated sampling scheme is utilized. The sample is divided typically into 12 regions (like the face of a clock) and at each sample point, the average of several laser shots (typically 5) are taken and the intensity of the ions of interest are recorded. The variable is then changed and the process repeated on the same sample surface over the entire range of the variable to be examined (in this case ESA voltage). A new spot is rotated into the laser beam and the process repeated except the parameter is offset so that the first value is moved to the end of the order. This is repeated for each successive spot examined. The signal is then summed for each variable examined.

Our initial results with this instrument indicate significantly higher ion energy deficits (as much as 200-400 eV) for MALD generated ions than have previously been reported. These differences may arise from differences in the laser power utilized, ion extraction field strength and geometries and even the numbers of laser pulses employed. This latter effect can be observed in the ion energy distribution for porcine insulin shown in Figure 1. This data shows that the ion energy deficit get smaller and the ion energy distribution gets narrower when the ions produced by the first 50 lasers pulses are compared to the ions produced by the second 50 laser pulses on the same surface. This decrease in the ion energy deficit tracks the corresponding narrowing of the ion peaks observed in the TOF mass

spectra themselves. The narrowing always occurs at the high time side of the peak which would correspond to ions with lower velocity (i.e., larger ion energy deficit). Figures 3 and 4 show the most precise and accurate measurements we have made to date in terms of ion energy resolution and kinetic energy deficits. These results, as well as results with porcine insulin indicate that at laser irradiances slightly above threshold (8×10^6 watts/cm^2), the ion energy deficit appears to be independent of mass.

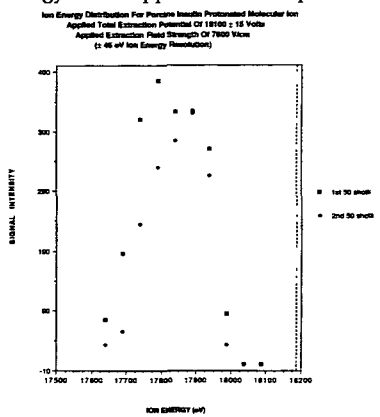

Figure 1

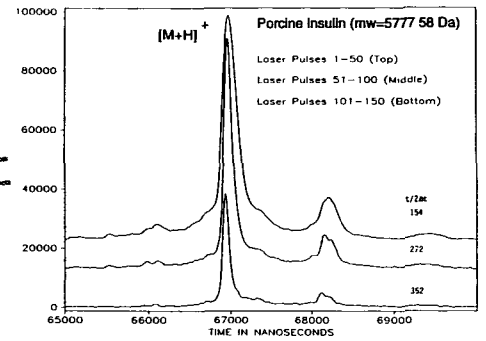

Figure 2

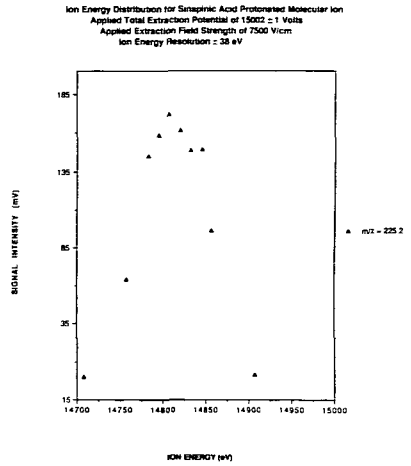

Figure 3

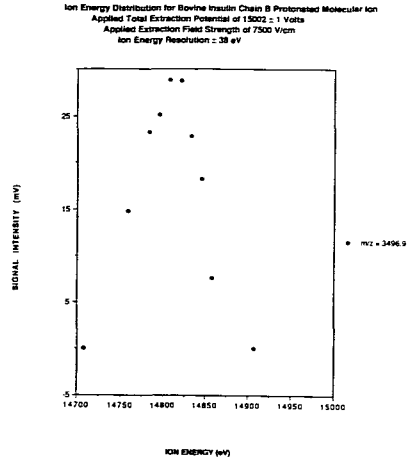

Figure 4

Variable Distance Time-Of-Flight Mass Spectrometer

W.C. Blanchard, Blanchard & Co., Inc., 27 Glen Alpine Rd., Phoenix, MD 21131

A new mass spectrometer configuration is being developed that provides a variable time-of-flight distance. The configuration can provide an increased flight length as the mass is increased. The problem addressed is how to focus ions that are created at different times, different locations, and with different energy levels, thus increasing resolution as mass increases.

Ions created in an electric field are normalized to zero initial velocity. This simplifies the problem to two variables. Two independent methods are then used to focus the ions: A. Focusing the ions created at the same time but at different locations, and; B. Focusing the ions created at the same location but at different times.

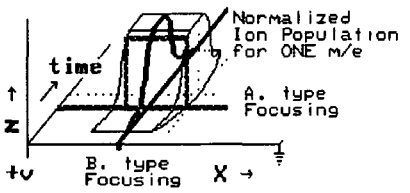

One MS configuration compatible with the above focusing requirements is:

The reflector grids use symetrically positioned wires for maximum repeated ion reflections. A vacuum of 10^{6} torr is used for long ion life.

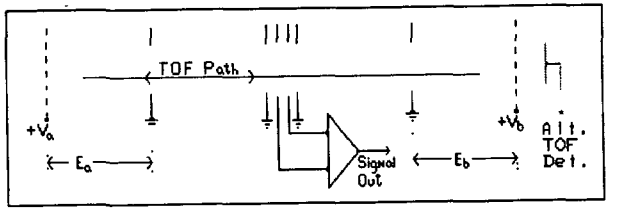

Additional features of this configuration are: low resolution one pass TOF (w/ $E_b=0$), or high resolution cumulative TOF (w/ $E_a=E_b$); repeated detection for enhanced signal/noise, like ICR, with signal processing using a Fourier series; various ionization; trapping of mass ranges (using $E_b=0$); small size/vacuum chamber, 10-50 in^3.

A. For ions created at the same time but at different equipotentials, at X_A and X_B, the ions at the lower equipotential will exit the electric field first but at a lower velocity than the ions exiting later. These later exiting, faster ions will catch up to the slower ions in the TOF region and become focused. They will focus at a TOF distance of:

$$X_{focus} = 2\sqrt{X_A * X_B}$$

X_{focus} is independent of m/e and the electric field.

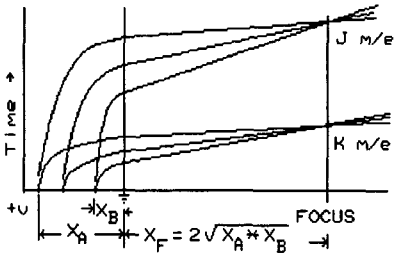

When they focus, the ions are detected not by impact but by induced charge, like ICR. The structure is mirrored for multiple reflections and detections to obtain the desired TOF. The ion population is a geometric distribution, and this arithmetic focus technique introduces errors that will limit resolution after 10,000 m/e.

B. For ions created at the same location (equipotential) but at different times, the ions are made to experience a small increasing electric field early in their flight, such as their first time through the reflecting field. The ions exiting later will catch up to the slower ions, becoming focused after many detector passes.

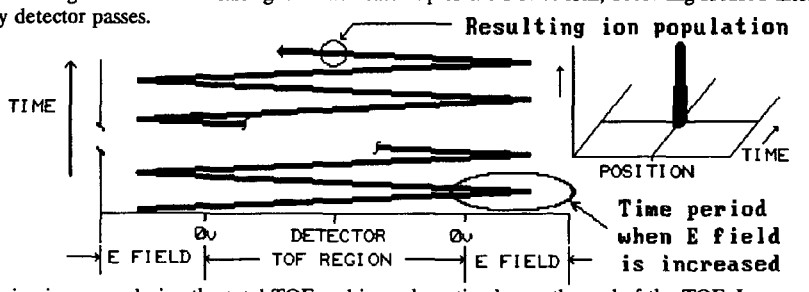

Focusing improves during the total TOF and is made optimal near the end of the TOF. Larger m/e's have broader normalized time spreads. Larger m/e's are slower and therefore experience this increasing electric field over a longer time. The longer time required to focus larger m/e's is compatible with the longer TOF distance required to provide separation. The focusing m/e range is limited by a smaller and faster m/e approaching this focusing electric field a second time as a larger m/e is just exiting the field.

A small detector size maximizes the induced charge caused by the passage of the focused ions. Two parallel detector rings with guard rings, and differential detection, are used to detect and obtain the ions' direction. A detector assembly has been tested by placing it between the filter and the Faraday cup of a UTI 100C Quad. MS. Room air was sampled and N_2 was detected at approx. $1*10^{-11}$a. This detector has been incorporated into a Variable Distance TOF MS structure described and is undergoing tests. The structure under test is 7 cm. long (excluding an external electron impact ionizer).

One signal processing approach is for constructive/destructive interference of the signal I(t), contributing to the intensity for all masses. A weighting phase factor depends on the true periodicity of each mass t_m. A Fourier series, not at discrete frequencies but at discrete "effective mass" intervals that are inversely proportional to the mass, is used. The higher the mass, the more terms (detections) must be included to resolve the m/e. The intensity of mass m:

$$S(m) = \sum_{j=1}^{n} I(t)\exp(2\pi i j t/t_m)$$

Many related works on the reflection and focusing of ions are available, including: F. Melzner, US Patent 3,226,543; B.A. Mamyrin, US Patent 4,072,862; and M.L. Muga, US Patent 4,458,149.

Ion Peak Shape Calculations and Time-of-Flight Mass Spectrometer Instrument Design

Richard C. King and *Kevin G. Owens, Department of Chemistry, Drexel University, Philadelphia, PA 19104

In previous work[1], a simplex optimization routine was used to design a reflectron time - of - flight mass spectrometer (TOFMS). The program uses minimum and maximum power supply voltages and the overall instrument length as the only limits for design. All voltages and distances inside the instrument are allowed to vary within these limits. The simplex response is calculated using a Monte Carlo method to simulate an ion peak from input initial temporal, potential energy and kinetic energy distributions. In addition to these initial distributions, the program takes into account the effect of electric field inhomogeneities near wire mesh grids on the detected ion peak width.

This work indicated that the use of grids to separate regions of different electric field does affect the performance and optimum design of a reflectron TOFMS. The work suggested that a grid material with more wires per inch would improve the instrument performance. The results also indicated that very long reflecting fields would improve resolving power. Unfortunately, both of these conditions will also work to reduce the ion transmission of the instrument. Since the previous version of the program did not consider the ion transmission as part of the simplex response, the optimum designs could show excellent resolving power but unrealistically low ion transmission. The work presented here uses the initial off axis velocity distribution along with the off axis velocity gained by passing through a grid to predict the loss of ions due to the off axis velocitiy. This, along with the optical transmission of the grid material, is used to estimate the ion transmission of the instrument.

Table 1.

	Ideal	70 LPI	110 LPI	300 LPI
TOF (ns)	115353.6	115279.2	115301.4	115337
Peak Width (Std Dev.)	2.88	23.7	7.53	3.21
Resolving Power	11.12	1.350	4.25	9.97
Optical Transmission (%T)	100	43.52	9.54	1.88
Initial Off Axis Velocity (%T)	54.30	25.26	6.06	1.08
Grid Effect (%T)	N.A.	3.70	2.14	0.12

Table 1 shows the results of placing different mesh size grids in an instrument designed on the assumption that the grids create no electric field inhomogeneities (ideal grids). The results shown are for gas phase laser ionization of a room temperature gas with a mass of 300 amu. When the grid effects are included, the resolving power decreases from that predicted by the ideal case. The resolving power increases by more than a factor of seven as the mesh size is increased from 70 LPI (90% optical T) to 330 LPI (61% optical T) while the ion transmission is reduced by 97%. Replacing the 70 LPI grids with 110 LPI grids will improve the resolving power

by a factor of three and reduce the in transmission by 42 %. To improve our understanding of the trade - off between ion transmission and resolving power in a TOFMS the effect of each source of ion loss was calculated at each grid in the instrument. This is shown in figure 2.

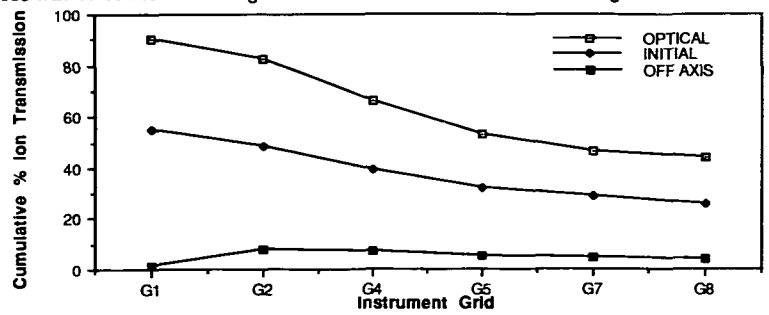

Figure 2.

The figure shows that for gas phase intial distributions with this instrument design, the off axis velocity gained by going through a grid is the largest contribution to the loss of ions; exceeding the losses due to the initial off axis velocity distribution and the optical transmission of the grids.

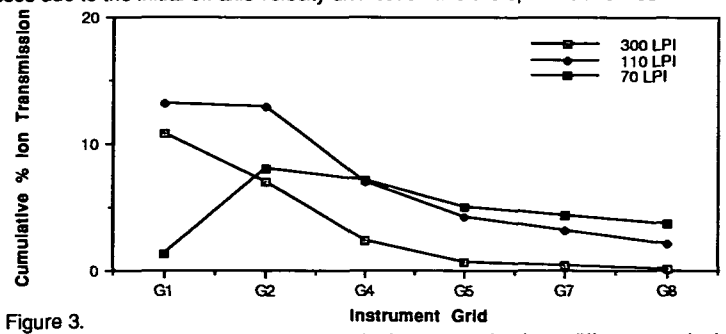

Figure 3.

Figure 3 shows the loss at each grid in the instrument for three different mesh size grids when all three contributions to ion loss are considered. The results indicate that replacement of the 70 LPI grid material in the source region (G1 and G2) will improve the ion transmission and possibly the resolving power of this instrument design.

Replacement of 70 LPI mesh grids with other grid materials may be a way of improving the performance of an existing design but a more efficient approach is to design the instrument taking grid effects into account. When the effects of electric field inhomogeneities are accounted for, a different instrument design is suggested by the simplex optimization routine. This design with 70 LPI grids has ten times better ion transmission and resolving power that is five times better than that found when 70 LPI grids were placed in the instrument designed assuming ideal grids.

References:

1. R.C. King and K. G. Owens, "Ion Flight Time Calculations and Instrument Design", LeCroy Instrumentation for Time - of - flight Symposium, Chestnut Ridge, NY, Nov. 11 - 12, 1992.

Automation of Sample Analysis by Matrix Assisted Laser Desorption Mass Spectrometry.

J. P. Ricketts, C. W. Sutton, and *J. S. Cottrell, Finnigan MAT Ltd., Hemel Hempstead, Herts. HP2 4TG, UK.

Matrix assisted laser desorption mass spectrometry has become a widely accepted technique for the analysis of peptides, proteins, carbohydrates, and related materials. Time per analysis can be as short as three or four minutes, but much of this time is spent waiting to achieve a working vacuum after the sample has been introduced into the instrument. One approach to increasing throughput is to load multiple samples onto a single substrate so that they can be introduced into the vacuum system simultaneously.

We have developed an automatic sample handling system in which up to 48 samples may be deposited along a flexible strip which is then wound onto a rotatable drum inside the ion source. Sample loading spots are defined by concentric rings of surface roughness, (Figure 1). A droplet of half a microlitre will sit comfortably within the central spot, while larger drops, up to 1.5 microlitres, will overflow to fill the surrounding rings. Between each loading position is a cutout, which acts as a gutter to prevent adjacent samples mixing, should spots be grossly overloaded. The autosampler mechanism just hooks onto the side of the Lasermat in place of the standard sample loading hatch One feature of the design is that the autosampler mechanism permits one of the standard single sample targets to be placed in front of the drum even though a strip is already wound onto the drum. This means that it is possible to interrupt the analysis of a long sample strip to slip in a single "emergency" sample.

For unattended operation, the Lasermat software uses a spreadsheet approach. This enables all instrument control and data processing parameters to be manipulated for individual samples while still providing an overview of the entire analysis at a glance. Figure 2 shows a portion of this spreadsheet, termed a "Sequence Table" Each row of the Sequence Table represents a single analysis and the columns delimit the parameter sets which control each aspect of instrument operation and data processing At the top of the Sequence Window is general header containing information such as the filename root which will be used to generate filenames when saving data to disk. The Sequence Table allows for up to 999 rows, equivalent to 20 sets of independent analysis conditions for each of 48 samples Each cell of the Sequence Table contains the name of a parameter set. For example, AUTOSAMP REP is the name of a disk file containing a unique set of parameters to control the display of data on the screen, the saving of data to disk, and the generation and printing of reports. By clicking the mouse on any cell of the Sequence Table, a dialog box is invoked containing the full parameter set for inspection or editing.

The throughput of the autosampler has been benchmarked at 1 minute per sample using a 486 PC. This is for averaging 10 laser shots, performing peak detection and calibration, saving the data to disk, and printing out a single page summary containing the spectrum.

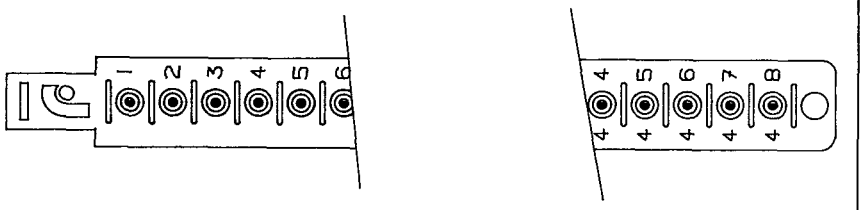

Figure 1

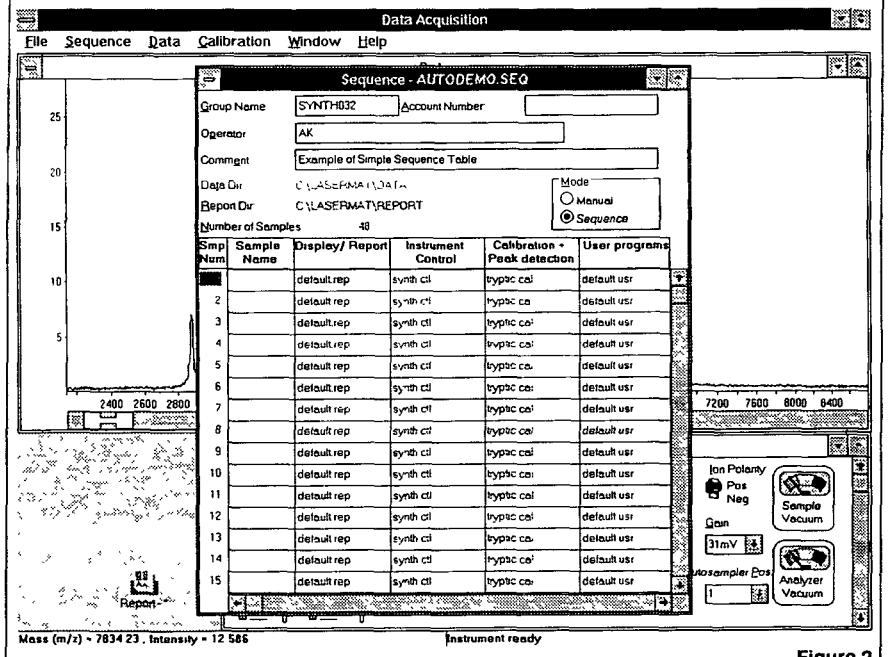

Figure 2

PRIMARY ION PRODUCTION FROM VARIOUS GASES FOR SPONTANEOUS DESORPTION MASS SPECTROMETRY

M.A. Park and E.A. Schweikert, Chemistry Department, Texas A&M University, College Station, TX 77843

It is now apparent from the literature that the spontaneous desorption (SD) of spontaneous desorption mass spectrometry (SDMS) is due to a backsputtering process [1]. According to the backsputtering mechanism, primary ions are generated by field desorption from the wires of a grid immediately in front of the sample. These primary ions are accelerated to keV kinetic energies by the electric field between the sample and grid. When the ions strike the sample, they cause the emission of secondary ions and electrons. In the large majority of studies, the secondary electrons are used to identify the time of impact of a primary ion.

One of the difficulties associated with SDMS is that the nature of the primary ions striking the sample is largely unknown. In the present study, we examine the nature and origin of the primary ions by measuring the count rate and yield of secondary particles as a function of the pressure of residual gases in the chamber. The instrument used for these SD studies has been described in detail elsewhere [2]. Briefly, it consists of a sample deposited on a flat, stainless steel sample holder, a high transmission grid at ground (90% transmission, Buckbee-Mears, St. Paul, Minn.) parallel to and a few millimeters from the sample surface, a field free drift region, and a microchannel plate (MCP) detector. The sample and MCP detector are located on opposite sides of the drift region. Ion flight times were measured using a time-to-digital converter produced at IPN in Orsay, France [3]. A single CsI sample was used throughout these experiments.

For the purpose of these experiments, it was assumed that the number of primary ions corresponds to the number of start signals. Both the primary ion and I^- secondary ion count rate were measured as a function of the pressure of methanol and trichloroethylene (TCE) in the chamber. The primary ion and I^- count rates show a roughly linear increase in primary ion count rate with pressure. This is what one would expect if field ionization were responsible for primary ion production. The rate of ion production by field ionization is proportional to the concentration (pressure) of molecules in the ionization region.

For methanol, the increase in primary ion count rate is observed above the contaminant type primary ion count rate only at pressures of methanol above about 2 X 10^{-5} torr. In contrast, TCE shows no such "appearance" pressure. This may be explained within the field ionization model as due to a difference in ionization potentials (IP_{MeOH} = 10.85 eV, IP_{TCE} = 9.47 eV). That is, a molecule of higher ionization potential would have a lower probability of being ionized in a given time period thus a higher pressure would be required to produce a given ionization rate.

The count rate of I^- does not increase as rapidly with pressure when methanol is used as the introduced gas as when TCE is used as the introduced gas. This may be an indication that primary ions produced from TCE are more efficient at sputtering I^- than those produced from methanol. This difference in efficiency can readily be explained as

an effect of the difference in the mass and complexity of TCE and methanol molecules (132 amu vs. 32 amu) and therefore presumably the primary ions produced.

The percent yield of I^-, $\%Y(I^-)$, as a function of pressure was calculated using:

$$\%Y(I^-) = \{ N(I^-_e) / S \} \times 100\%$$

where $N(I^-_e)$ is the number of counts in the I^-_e peak, and S is the number of starts signals. The change in percent yield with pressure was roughly linear. However, yields calculated this way are not the I^- yields due to methanol or TCE type primary ions but the average of yields from all primary ions produced at a given pressure. By subtracting the I^- and primary ion counts due to contaminant type primary ions, the "true" yield from introduced gas type primary ions can be calculated. The "true" I^- yield from methanol and TCE type primary ions was found to be 0.16 ± 0.01% and 0.42 ± 0.02% respectively compared to 0.6 ± 0.1% from contaminant type primary ions. This seems to indicate not only that the TCE type primary ions are more massive/complex than methanol type primary ions but that the contaminant type primary ions have a higher mass/greater complexity than methanol or TCE type primary ions. The results of PDMS analyses of frozen residual gas show that this may be the case. This analysis produced ions indicative of pump oil (m/z = 149, m/z = 393).

The order-of-magnitude larger error bar seen above on the I^- percent yield from the contaminant vs. TCE type primary ions is due to the fact that over the course of about one day, the I^- yield from the contaminant type primary ions changed from 0.75 ± 0.02% to 0.52 ± 0.02% while that from TCE changed from 0.44 ± 0.01 to 0.40 ± 0.03%. This indicates the nature of contaminant type primary ions changed over the course of the experiments. Most likely, this is a result of a change in the composition of the contaminant near or on the grid wires.

The $\%Y(I^-)$ from TCE type primary ions is observed to become constant vs. pressure at 0.43 ± 0.02% (the "true" yield from TCE type primary ions) at pressures above about 1.5 X 10^{-5} torr. This indicates that the contaminant type primary ions do not influence the measurement above this pressure. This opens the possibility of performing reproducible quantitative SDMS measurments in a manner similar to that of secondary ion mass spectrometry.

The reversibility and reproducibility of both the primary ion count rate and secondary ion yield were shown by measuring the primary ion count rate and secondary ion yield as a function of time while changing the pressure of the introduced gas from about 10^{-7} to about 4 X 10^{-5} torr or vise versa at irregular intervals. The results for both methanol and TCE show little change in the primary ion count rate or yield from one cycling of the pressure to the next.

1. S. Della-Negra, C. Deprun, Y. Le Beyec, F. Rollgen, K. Standing, B. Monart, G. Bolbach, *Int. J. Mass Spectrom. Ion Proc.* **75**, 319(1987).
2. M.A. Park, A.Y. Yau, E.A. Schweikert, *Int. J. Mass Spectrom. Ion Processes*, in press.
3. E. Festa, R. Sellem, and L. Tassan-Got, *Nucl. Inst. Meth. Phys. Res.* **A234**, 305(1985).

Analytical Characteristics of an Inductively Coupled Plasma-Time-of-Flight Mass Spectrometer (ICP-TOFMS)

***D. P. Myers, G. Li, G. M. Hieftje, Department of Chemistry, Indiana University, Bloomington, IN 47405**

Introduction

Research in our laboratory has recently focused on coupling an atmospheric-pressure plasma with a time-of-flight mass spectrometer (TOFMS). Specifically, we have employed an inductively coupled plasma (ICP) as the ion source. In general, the inductively coupled plasma-mass spectrometer (ICP-MS) has emerged as a powerful instrument for performing trace multielement analysis. Historically, ICP-MS instruments have employed quadrupole or double-focusing sector mass analyzers. Yet, a TOFMS potentially offers more speed, simultaneous extraction/analysis of all masses, and equal or better sensitivity than quadrupole mass spectrometers now used in ICP-MS. The TOFMS constructed in our laboratory employs right-angle extraction of the continuous supersonic ion beam generated by the ICP. This orthogonal sampling of the beam is similar to that in instruments described previously (1-5), and offers improved resolution, sensitivity, and duty factor over in-line beam-modulation techniques (2,5).

Instrument Description/Methods

The mass spectrometer includes a three-stage differentially-pumped vacuum chamber interfaced to a time-of-flight mass spectrometer constructed by R.M. Jordan Co. (Grass Valley, CA). The ICP is sampled through a 0.75-mm orifice to create a supersonic expansion, which is skimmed 10 mm downstream of the sampling orifice. These ions are extracted through a 1.3-mm orifice into the low-pressure stage (1 X 10^{-5} Torr) of the interface. In this stage the ions are focused into the right-angle extraction zone with a simple einzel lens arrangement. A 2.5-mm slit placed in the last element of the einzel lens reduces divergence of the ions entering the orthogonal sampling zone. Three extraction configurations were tested for the mass spectrometer. Each configuration was compared for ion noise, sensitivity, and resolution. The best configuration is shown in figure 1. In this setup the acceleration field (G2) was dropped linearly across 4 rings (2.54-cm) to the entrance grid (G1) which was maintained at ground while the repeller (R) is pulsed positive.

Results

Ion noise from the continuous ion beam has been an ongoing problem in our ICP-TOFMS, and all three extraction geometries produced different levels of ion noise in single-shot spectra. Unfortunately, the highest level of ion noise was seen in the configuration shown in figure 1. This ion noise is largely due to the highly divergent ion beam exiting the last element of the einzel lens. Still, the best resolution and sensitivity were seen with this configuration. A resolution (FWHM) of 500 has been obtained with proper optimization of the center element of the einzel lens. However, this optimization causes a resulting loss in signal intensity. Figure 2 shows the resolution of Pb and Bi, the two heaviest non-radioactive elements which are separated by one mass unit. Figure 3 shows resolution (R) and signal-to-noise ratio (S/N) versus the potential of the center element of the einzel lens.

Another interesting characteristic of this mass spectrometer is the effect of mass-independent velocities in the supersonic beam. The steering plates shown in Figure 1 compensate for the velocity component of the ion beam orthogonal to the TOF direction. Because the supersonic beam has all ions of the same velocity, ions of higher mass have greater energy. Therefore, the steering of these ions with electric fields is biased. In figure 4, ion signals for light to heavy ions as a function of steering voltage show this effect. The current sensitivity of the instrument is about 500 ppb for lighter elements and increases to about 1 ppm for heavier ions.

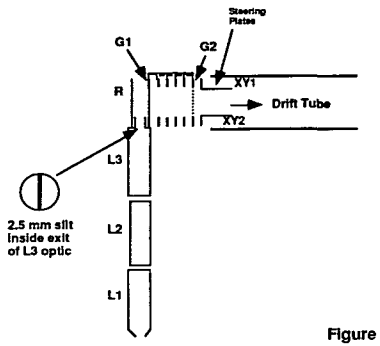

Figure 1

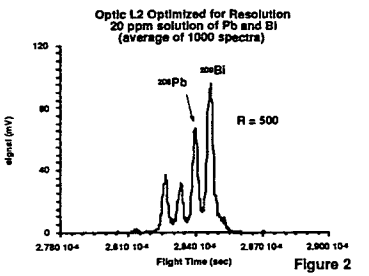

Figure 2

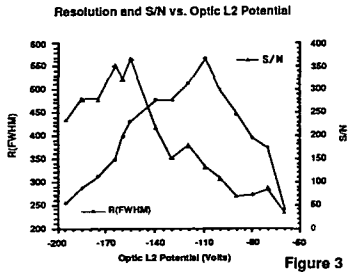

Figure 3

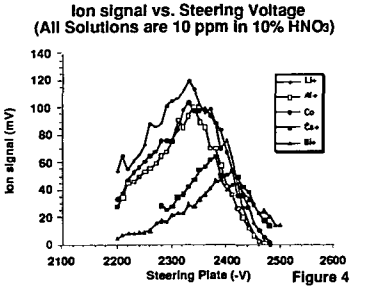

Figure 4

Conclusions

The orthogonal TOFMS we have constructed exhibits unit-mass resolution for the elements; however, the sensitivity is still much worse than quadrupole-based ICP-MS instruments. Presumably, the sensitivity will improve by incorporating better ion optics which focus ions in the supersonic beam into the plane of orthogonal extraction. In addition, the current resolving power of 500 may not insure the abundance sensitivity expected in conventional ICP-MS instruments. Work is underway to use an ion mirror to improve resolution.

(1) O'Halloran, G.J.; Walker, L.W. Technical Document Report No. ASD TDR 62-644, Part I and II, **Nov. 1964**; prepared under Contract No. AF 33(657)-11018 by the Bendix Corporation, Research Laboratories Div., Southfield, MI.
(2) Sin, C.H.; Lee, E.D.; Lee, M.L. *Anal. Chem.* **1991**, 63, 2897.
(3) Coles, J.; Stutsel, M.; Guilhaus, M. *Proceedings of the 40th ASMS Conference on Mass Spectrometry and Allied Topics*, Washington, D.C., **1992**, p.10.
(4) Dodonov, A.F.; Chernushveich, I.V.; Laiko, V.V. *Book of Abstracts from the 12th International Mass Spectrometry Conference*, Amsterdam, Holland, Aug. **1991**, p. 153.
(5) Boyle, J.G.; Whitehouse, C.M. *Anal. Chem.*, **1992**, 64, 2084.

CORRELATION MEASUREMENTS FOR THE DETERMINATION OF THE STRUCTURE OF SOME ALAMETHICIN PEPTIDES

N. Poppe-Schriemer[1,2], W. Ens[1], J.O'Neil[2], K.G.Standing[1], J.B.Westmore[2], A.Yee[2],
Departments of Physics[1] and Chemistry[2], University of Manitoba, Winnipeg, Canada.

Introduction

The alamethicins are a series of antibiotic peptides produced enzymatically (*ie* not from RNA) by the fungus *Trichoderma viride*. The amount of each peptide produced, and perhaps also its sequence, is sensitive to the environment in which the fungus is grown. The sequences of the two main components of the alamethicins grown under standard conditions are known. An alternative preparation method gives a different mixture of components[1]. We report our work on some of these components.

Experimental

Secondary ion mass spectrometry was used with both the linear and the reflecting modes of our time-of-flight spectrometer, TOF II[2], to give sequence information for alamethicin III. In the reflecting mode, correlation techniques[3,4] were used to examine the daughter ion spectra of the molecular ion and the prompt fragments.

Much of the peptide sequence could be inferred from the direct spectrum with the mirror off. Since the alamethicins are unusually metastable, most of the sequence was confirmed using the correlation technique.

Results

An extensive series of B ions, as well as some A and C+2 ions, was observed in the direct spectrum, with corresponding neutral peaks in the neutral spectrum. The only C terminal ions observed clearly were Y_7+2 and Y_{19}+2, both corresponding to cleavage before Pro residues.

Many correlation spectra were taken to study the unimolecular decay of parent ions for several of the alamethicins. A few examples of alamethicin III are shown in figure 1. All other alamethicins examined show similar decay patterns and a comparable wealth of sequence information.

The $(M+H)^+$ ion decays into a partial series of B ions, the Y_7+2 ion and a few internal fragments beginning at Pro_2. The daughters of the B ions were predominantly B ions and a series of ions with Pro_2 at the N terminal end. The daughters of the Y_7+2 ions are predominantly (Y_7B_n) fragments.

The molecular ion region of the 23.33 minute HPLC fraction has *two* peaks. Examination of the correlation spectra shows that an amino acid substitution occurred at position 6 as shown in figure 2. The mass differences are consistent with a partial interchange between Ala and Aib. Other correlation spectra and the molecular ion peaks suggest that a partial interchange between Glu and Gln at residue 18 has occurred, in conjunction with the first interchange. Subsequent chromatography confirmed that two peptides were present and that one had an ionizable group.

The first fourteen amino acids of the 24.53 minute fraction are like those in the 23.33 A and B fractions. The Y_7+2 coincidence spectra suggest a partial interchange between Aib and Val at position 17 which would be consistent with the molecular masses if an interchange between Gln and Glu is also present.

Conclusions

All of the alamethicins examined so far are rich in α-aminoisobutyric acid(Aib), and have an acetyl group at the N terminus and a phenylalaninol at the C terminus.

The 21.34 minute fraction (alamethicin III) has the following sequence:

$$Ac\text{-}Aib_1\text{-}Pro_2\text{-}Aib_3\text{-}Ala_4\text{-}Aib_5\text{-}Ala_6\text{-}Gln_7\text{-}Aib_8\text{-}Val_9\text{-}Aib_{10}\text{-}Gly_{11}\text{-}Leu_{12}\text{-}Aib_{13}\text{-}Pro_{14}\text{-}Val_{15}\text{-}Aib_{16}\text{-}Aib_{17}\text{-}Gln_{18}\text{-}Gln_{19}\text{-}Phe_{20}\text{-}ol$$

The 23.33 minute fraction, A (alamethicin I) is as above, except for a Gln/Glu interchange at at position 18. The 23.33 minute fraction, B(not yet named) has an Aib at position 6 and a Gln at position 18. Investigations are continuing to finalize the sequence determination of the three peptides in the 24.53 minute chromatography peak.

The overlapping peptide maps obtained by the correlation method are a useful means of determining the sequence and also provide information regarding the decay of closely related ions. The peptides were very susceptible to cleavage before the Pro residues, as was also observed for neutralized bradykinin[5]. This cleavage occurred more often for unimolecular decay than for fast fragmentation. However, fast fragmentation allowed the charge to be on either side of the broken bond. We plan to investigate all these effects in greater detail.

References

1. A. Yee and J.O'Neil, Biochemistry, 31(1992) 3135.
2. X. Tang, R.Beavis, W.Ens, F.Lafortune, B.Schueler and K.G.Standing, Int. J. Mass *Spectrom. Ion Processes*, 85 (1988) 43.
3. S.Della-Negra and Y.LeBeyec, Int. J. Mass Spectrom. Ion Processes, 61 (1984) 21;Anal. Chem., 57 (1985) 2035; Springer Proc. Phys., 9 (1986) 42.
4. K.G.Standing, W.Ens, R. Beavis, G.Bolbach, D.Main, B.Schueler and J.B.Westmore, Springer Proc. Phys., 9 (1986) 37; X. Tang, W.Ens, K.G.Standing, and J.B. Westmore, Anal. Chem., 60 (1988) 1791..
5. D.Bunk and R. Macfarlane, Int. J. Mass Spectrom. Ion Processes, 111 (1991) 55.

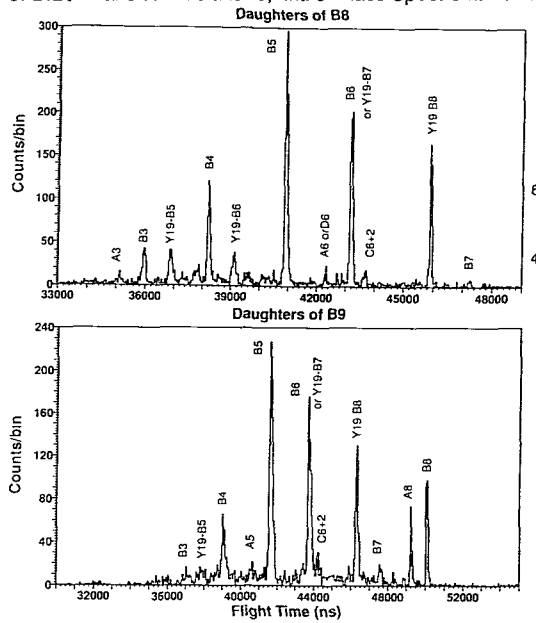

Figure 1, daughter ion spectra for alamethicin III

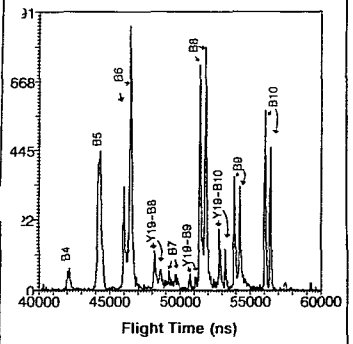

Figure 2, B13 correlation spectrum showing the presence of two peptides

HIGH-SPEED DATA ACQUISITION AND PROCESSING SYSTEM FOR TIME-OF-FLIGHT MASS SPECTROMETRY

Edgar D. Lee and Harold G. Lee, Sensar Corporation, Sandy, Utah 84070

One of the limitations of time-of-flight (TOF) mass spectrometry in the past has been that the majority of the data generated was lost because the acquisition system could not acquire and save the data at the same rate as it was produced from the mass spectrometer. In the recent past processor based timed array detection schemes and digital storage oscilloscopes have been developed and continue to improve to accommodate larger and larger amounts of data.

The ideal data acquisition system for TOF-MS would want to be as flexible as possible allowing for a wide rang of experiments to be performed. These would include both static such as laser desorbtion mass spectrometry and dynamic such as chromatography mass spectrometry applications. Also the ability to profile the peak shapes in the mass spectrum, collect and save mass spectra simultaneously, process data as it is acquired, assist with user interpretation, and be expandable for future improvements in technology would be desired characteristics of such a system.

This data acquisition system (Figure 1.) acquires an analog signal, converts it to digital data, and compresses the large volume of accumulated data into a format that can be handled in a microcomputer environment. The system can operate in two modes:

1. Burst mode, optimized for speed (500 Msamples/sec), in which data is continuously collected with 2 nanoseconds of resolution without loss of data.

2. Pass through, optimized for signal averaging and data storage (up to 2 gigabytes), in which data is continuously collected and averaged with 2 nanoseconds of resolution for long periods of time and no data loss.

The uniqueness of this system lies in its ability to rapidly and continuously acquire and process large volumes of data and to compress and store that data uninterruptedly. Because of its signal averaging and data compression algorithms, the system can be used for applications that require uninterrupted high-speed sampling over long periods of time.

This high speed data acquisition system is designed to take advantage of the major benefits of both non-averaging and averaging. That is, when single shot data (no averaging) is desired, the system acquires and passes data uninterrupted. When averaging is required, the system acquires, averages, and passes averaged data, again, uninterrupted.

There are several paths that can be taken, depending upon the type of data requested in the long term storage area. Because averaging occurs in real time, the averaging decision has little impact on the balance of operations. The decision to average is made prior to each test and cannot be changed during a test. If averaging is to occur, the lone variable associated with it is the number of averages to be taken. Again, if averaging is active, it occurs essentially as a background task to the remaining operations and has little or no influence over their timing.

A second variable in the main system flow is the decision of whether or not to use the burst storage area. The burst storage area is a high speed memory storage area designed to accommodate single shot data through the ADC in real time. As it is very high speed, it is also depth limited. Additionally, its use precludes the downloading of data into the long term storage area without terminating the acquisition cycle. Therefore, the accepted tradeoffs for using burst storage are twofold: the test length is limited, and the test must stop during the period when data is being offloaded from the burst storage to the long term storage.

The decision of whether or not to use the burst area is based on the data throughput requirements. If the burst mode is not used, data flows *via* a high speed bus to the long term storage area. Therefore, if the transfer speed is sufficient, the burst area need not be used. Note also that the data is transferred after averaging has occurred, providing extreme advantage if averaging is in place.

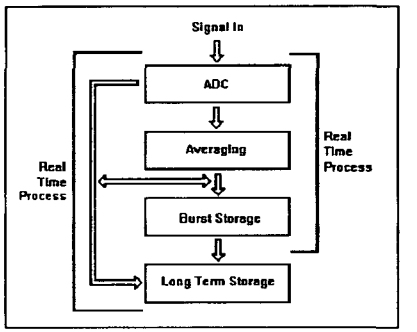

Figure 1

SUB-PPB DETECTION OF IMPURITIES IN HIGH PURITY GASES BY ATMOSPHERIC PRESSURE CHEMICAL IONIZATION TIME-OF-FLIGHT MASS SPECTROMETRY

Karin E. Markides, Fred J. Haydock, Chung Hang Sin, and Edgar D. Lee,
Sensar Corporation, 479 West Universal Circle, Sandy, UT 84070, USA

Sensitive and fast detection of impurities in gases are becoming more and more important in semi-conductor manufacturing industries. A new type of time-of-flight mass spectrometer (TOFMS) has been developed to meet these challenges. This TOFMS utilizes an efficient corona discharge source for ion production. Also, the flight tube is configured perpendicularly to the ion beam so that the duty cycle is dramatically improved.

In the ion source, the corona discharge initiates a series of ion-molecule reactions at atmospheric pressure. Nitrogen and water are the major reactant ions. Through charge transfer, ions are produced from the analytes. The ionization efficiency can be as high as 100% for trace analytes. The ions are then introduced into the mass spectrometer chamber by supersonic expansion through an orifice. As the ion beam fills up the ion pulsing region, an electric pulse will push all of the ions in that region into the flight tube. Because the ion beam is perpendicular to the flight tube, no neutrals will be sent to the detector. The perpendicular orientation also makes it easier to prevent the ion beam from interference. The mass resolution in a TOFMS depends very much on the velocity distribution of the ions. The supersonic expansion also helps in narrowing down this distribution and thus improves the mass resolution.

Another advantage of the perpendicular orientation is that the duty cycle of ion sampling can be improved dramatically. If the ion beam is parallel to the flight tube, very narrow pulses (*e.g.*, 100 ns) must be used for maintaining a reasonable mass resolution. This is because the flight time is in the μs regime. However, in a perpendicular orientation, an electric pulse can be applied long enough for all of the ions inside the pulsing region to enter the flight tube without worsening the mass resolution. Unlike the on-axis case, all ions in the region will move at the same time once the pulse is switched on. As a result, the number of ions sampled per pulse are orders of magnitude greater than in the case of on-axis beam introduction. The ion sampling duty cycle can actually approach 100%. The use of an atmospheric pressure ion source makes it very convenient for direct gas and vapor monitoring. The current emphasis is to develop this TOFMS for gas impurities analysis. As shown in the following figure, sub-ppb detection limits are achievable for trace impurities in high purity nitrogen.

In addition to sensitivity, this TOFMS is also extremely fast. It is useful for capturing transient signals such as those found in chromatography and flow injection. A fast data acquisition system is being developed for storage and averaging the fast incoming data from this instrument. Due to its sensitivity and speed, this TOFMS is also suitable for on-line monitoring in processing stream and detection of illegal chemicals.

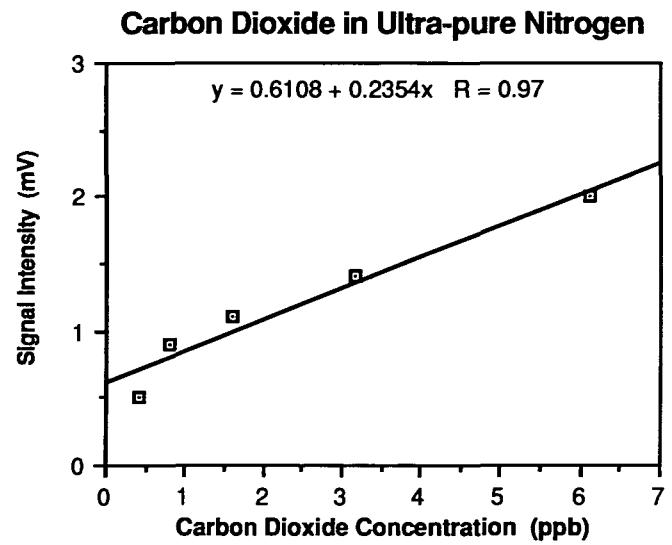

THE E_2/E_1cb MECHANISM IN THE GAS PHASE: COMPETITIVE LEAVING GROUP EFFECTS. John E. Bartmess*, Terry Sumpter, John Farrar, Kurt Wiegel, and Robert Holman, Dept. of Chemistry, Univ. of Tennessee, Knoxville TN 37996-1600, and Dept. of Chemistry, Western Kentucky Univ., Bowling Green KY 42101.

A persistent problem in ion/molecule chemistry is the narrow time/pressure window that is available for reactivity measurement. Reactions with small transition state barriers are insensitive to structural effects, proceeding at collision rate. A method is needed to probe the TS effect on the observed kinetics, separate from the dominating effect of the collision rate.

For example, CH_3CH_2Cl and CH_3CH_2Br both yield halide at collision rate on reaction with hydroxide. Even for Et_2O as substrate, the rate constant for the poor leaving group ethoxide is only a factor of four slower, giving a Brønsted coefficient of 0.02! Only if ΔH_{rxn} is less than ca. 10 kcal/mol (much weaker base) are large leaving group effects on the rate constant seen. No general differentiation of kinetic leaving group ability can thus be made.

The solution to this is to use <u>competitive reactive groups</u> within a single molecule. The collision rate cancels out, and the ratio of two possible products reflects the internal barriers leading to each. We choose the elimination reaction as a demonstration of this effect.

All ion/molecule work was done with the Tennessee ICR spectrometer, using rapid scan detection. This is a more accurate mode than FT-ICR for intensity measurements. Care must be taken to avoid contamination of the neutral compound RY with HY impurities. This could be detected as a rapid rise of one leaving group anion (proton transfer), and a more gradual increase in the other (elimination). For pure compounds, both leaving groups appeared at the same rate, but in the varying ratios.

We must also define the thermochemistry of the systems involved. Leaving group abilities are evaluated as ΔH_{elim}, the enthalpy of:

$$CH_3CH_2Y \rightarrow H^+ + CH_2{=}CH_2 + Y^-$$

This, minus ΔH_{acid} for the conjugate base of some acid XH, yields ΔH_{rxn} here:

$$X^- + CH_3CH_2Y \rightarrow XH + CH_2{=}CH_2 + Y^-$$

Thermochemistry of EtY Elimination:

Y-	ΔH_{elim}	Y-	ΔH_{elim}	Y-	ΔH_{elim}
MeO-	396.3	$MeCO_2$-	364.3	Cl-	350.3
$tBuCH_2O$-	387.3	$EtCO_2$-	363.2	Br-	342.7
CF_3CH_2O-	377.7	$iPrCO_2$-	361.8	CF_3CO_2-	339.6
PhO-	364.8	$ClCH_2CO_2$-	352.2		

Due to the entropy factor (2 species -> 3 species), a base with ΔH_{acid} up to 9 kcal/mol weaker than ΔH_{elim} should still be able to react.

$ClCH_2CH_2CH_2Br$ was first chosen, as a molecule with a common proton leading to elimination of either halide; the <u>molecule</u> chooses the better leaving group.

Base	$\Delta H_{rxn}(Br^-/Cl^-)$	Br^-/Cl^-
$MeCO_2^-$	-5.9/+1.7	>100
$iPrCH_2CH_2O^-$	-32/-23	ca. 95
HO^-	-48/-40	4

At equilibrium, Br^- would be favored by 10^6. It requires ca. 40 kcal/mol of exothermicity to even start to approach parity in reactivity/ selectivity.

Carboxylate esters were then chosen as the leaving groups. These can be closely balanced as leaving groups so should be more sensitive probes. Also, (1) the thermochemistry is precisely known, (2) the atoms forming the breaking bond are constant, and (3) the change in reactivity is due solely to a "distant" substituent.

Results:

	$MeCO_2$-$CH_2CH_2CH_2$-O_2CR				$MeCO_2$-CH_2CH_2-O_2CR		
R	ΔH_{rxn}	Base	$RCO_2^-/MeCO_2^-$	R	ΔH_{rxn}	Base	$RCO_2^-/MeCO_2^-$
Et	-16.3/-17.5	MeO^-	1.6	Et	-18.0/-19.1	MeO^-	1.26
	-6.6/-7.7	F^-	2.45		-8.1/-9.2	F^-	2.37
iPr	-16.3/-18.8	MeO^-	10.0	iPr	-18.0/-20.5	MeO^-	4.0
	-6.6/-9.1	F^-	50.0		-8.1/-10.6	F^-	12.0
CF_3	-16.3/-41.0	MeO^-	>100.0				

Note that the better leaving group is always favored, and the moreso, the less exothermic the reaction is.

For the glycol substrate, where the protons being lost are not the same, the selectivity is less. We attribute this to polarizability effects:

$MeCO_2$-$\bar{C}HCH_2$-O_2CR is less stable than $MeCO_2$-$CH_2\bar{C}H$-O_2CR based on the size/ polarizability of the proximal alkyl groups. To the extent that negative charge is present in the transition state, the poorer leaving group is favored. This parallels our earlier studies of E_1cb reactions.

For Cl-$CH_2CH_2CH_2$-O_2CCH_2Cl, the leaving groups are comparable thermochemically (Cl^- 2.1 kcal/mol better in ΔH_{elim} than $ClCH_2CO_2^-$). Cl^- is the only product observed for reaction with MeO^- or F^-. This is a more subtle transition state probe, using electronegativity.

For Cl-$CH_2CH_2CH_2$-O_2CCF_3, now the $CF_3CO_2^-$ group is the major product (36:1 with MeO^-): thermochemistry overcomes the electronegativity effect at 10.7 kcal/mol better leaving group ability.

We thank the National Science Foundation for support of RWH through the Summer Research Program in Chemical Analysis, grant CHE-9023377.

BY WHAT MECHANISMS DO ANIONIC NUCLEOPHILES REACT WITH DI-*tert*-BUTYL PEROXIDE?

Joseph J. Grabowski,† Jeehiun Lee§ and V. Murugesan†
Departments of Chemistry,
†University of Pittsburgh, Pittsburgh, PA 15260
§Harvard University, Cambridge, MA 02138.

The organic chemistry of peroxides has a long history; such species are key players in many areas, ranging from the immune response to polymerization initiators to bleaches and disinfectants to key ingredients in stereospecific synthetic procedures to oxidation chemistry in atmospheres. Inorganic peroxides are also widely involved as intermediates in a variety of processes; for example, Cl_2O_2 is a intermediate in the catalytic destruction of ozone. While the synthesis, characterization and transformations of peroxides are well-documented in the literature, surprisingly little consensus is available about the detailed mechanisms by which organic peroxides react. Many condensed phase mechanistic studies have been hampered by the high reactivity of these compounds (low O-O bond dissociation energy) and the difficulty in distinguishing between electron transfer and nucleophilic pathways. In an effort to improve our understanding of the mechanisms of these molecules, we have been investigating their reactions in the gas-phase.

We have examined the thermally-equilibrated (298 K), gas-phase, ion-molecule reactions of di-*tert*-butyl peroxide with a large number of anionic nucleophiles by means of the flowing afterglow technique. Special care was taken to ensure proper identification of any chemical reaction occurring via free electrons. Inspection of the data set (not shown) reveals that a E2 mechanism by which dialkyl *ethers* react is essentially absent for the peroxide (only minor amounts of $t\text{-BuOO}^-$ is ever found). Further examination of the data reveals that there are two classes of reactions: the first of which yields primarily *m/z* 73 ($t\text{-BuO}^-$) from ions such as H_2N^-, RO^-, $C_6H_5^-$, $CH_3SCH_2^-$ and $PhCH_2^-$; and the second of which yields primarily *m/z* 131 and 146 from ions such as $H_2C{=}CH\text{-}CH_2^-$, NO^- and O_2^-. Reaction rates vary, representative data are: H_2N^- displaying a reaction efficiency of 95%; HO^-, 99%; $H_2C{=}CH{-}CH_2^-$, 1.1%; MeO, 88% and NO^-, 37%.

The predominance of the *m/z* 131 product for anionic nucleophiles that are relatively weakly bound (EA < 0.5 eV) is diagnostic of a dissociative electron transfer process since *t*-butoxy radicals are well known to undergo unimolecular fragmentation to acetone and a methyl radical. We therefore postulate that $H_2C{=}CH\text{-}CH_2^-$, NO^- and O_2^- react primarily, if not exclusively, by the DET process shown in the bottom half of the scheme. This assignment is further supported by the correlation of the rates of these reactions with the anion binding energy.

The other pathway that produces *m/z* 73 as the predominant ion could either be a nucleophilic substitution at oxygen, a concerted proton transfer-internal displacement at oxygen to produce *m/z* 73 and an epoxide, or an E2 followed by fast and extremely, efficient epoxidation by the formed peroxide anion of the alkene product *within* the product ion-molecule complex. There are difficult aspects with each of these three mechanisms; the attached scheme shows the simplest of these three mechanisms for convenience. It seems likely that additional work now in progress will allow us to rule out the concerted proton transfer-internal displacement while initial examination of the second step of the third mechanism suggests that it too is an unlikely process.

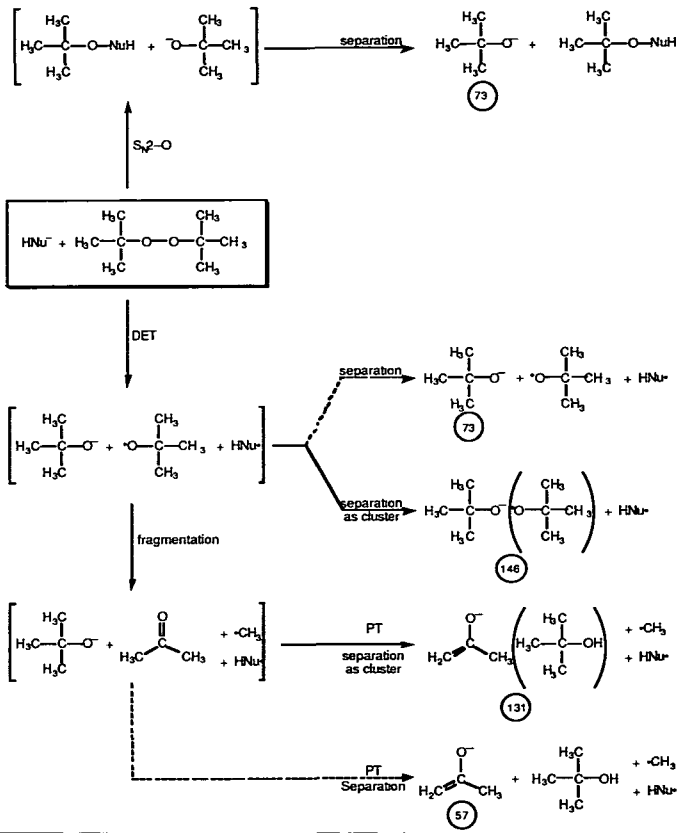

New Insights into the Gas Phase Anion Chemistry of Nitrous Oxide.

*Richard A.J. O'Hair, Scott Gronert and Charles H. DePuy
Department of Chemistry & Biochemistry, University of Colorado, Boulder CO 80309-0215

Nitrous oxide has proven to be a useful reagent gas for the determination of carbanion structure via gas phase ion-molecule reactions. Previous studies have demonstrated its utility at distinguishing isomeric anions and have revealed its diversity of reactions.[1, 2] The mechanistic pathways for such processes are not immediately obvious since all three atoms of N_2O are potential sites of attack.

We have studied the kinetics and products of a wide range of reactions between various anions and N_2O (Table 1) in a flowing afterglow-selected ion flow tube (FA-SIFT).[3] Many of these reactions are best explained by mechanisms involving initial attack of the anion at the terminal nitrogen of N_2O to form an energized diazenyl oxide anion intermediate [R-N=N-O$^-$] which then undergoes either proton transfer or rearrangement followed by decomposition (eqn. 1). Recently we have discovered a way of synthesizing the proposed intermediate (eqn. 2).[4] By carrying out this reaction in the source flow tube of the FA-SIFT, we are able to subject the diazenyl oxide anions to CID reactions (eqn. 3). The products of these CID reactions (eqn. 3) are the same as those observed in the direct reaction of R$^-$ with N_2O (eqn. 1).

Further evidence to support the intermediacy of the diazenyl oxide anion comes from a study of the reaction of the phenyl anion with N_2O. Two products are observed: the phenoxide ion and an adduct. The structure of this adduct was probed by CID (Figure 1a). It exhibits a virtually identical CID spectrum (Figure 1b) to that of the diazenyl oxide anion Ph-N=N-O$^-$, synthesized in the source (eqn. 2). We therefore propose the mechanism shown in Scheme 1 to account for this reaction.

$$R^{\cdot} + N_2O \longrightarrow [R\text{-}N{=}N\text{-}O^{\cdot}] \longrightarrow \text{PRODUCTS} \qquad (1)$$

$$RNH^{\cdot} + R'ONO \longrightarrow R\text{-}N{=}N\text{-}O^{\cdot} + R'OH \qquad (2)$$

$$R\text{-}N{=}N\text{-}O^{\cdot} \longrightarrow \text{PRODUCTS} \qquad (3)$$

References.
(1) Kass, S.R.; Filley, J.; Van Doren, J.M.; DePuy, C.H. *J. Am. Chem. Soc.* **1986**, *108*, 2849.
(2) Andrist, A.H.; DePuy, C.H.; Squires, R.R. *J. Am. Chem. Soc.* **1984**, *106*, 845.
(3) Van Doren, J.M.; Barlow S.E.; DePuy, C.H.; Bierbaum, V.M. *Int. J. Mass. Spectrom. Ion. Proc.* **1987**, *81*, 85.
(4) King, G.K.; Maricq, M.M.; Bierbaum, V.M.; DePuy, C.H. *J. Am. Chem. Soc.* **1981**, *103*, 7133.

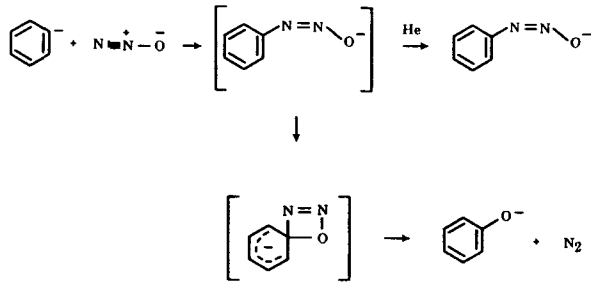

Scheme 1: Mechanism for the reaction of $C_6H_5^-$ with N_2O.

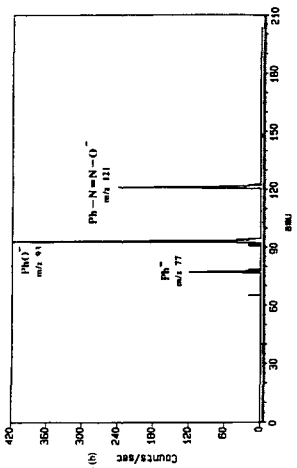

Figure 1 (a): CID of Ph−N=N−O$^-$ formed in source flow tube via the reaction: Ph$^-$ + N_2O ⟶ Ph−N=N−O$^-$

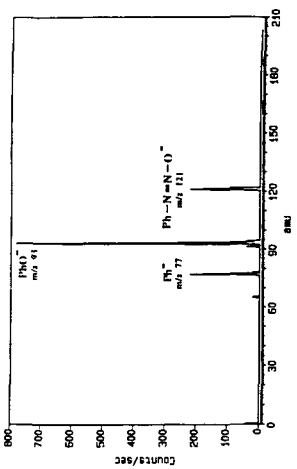

Figure 1 (b). CID of Ph−N=N−O$^-$ formed in source flow tube via the reaction: PhNH$^-$ + ($tBuCH_2ONO$) ⟶ Ph−N=N−O$^-$ + $tBuCH_2OH$

Table 1: Reactions of anions with nitrous oxide. Products, branching ratios, rate constants and efficiencies

ANION (A$^-$)	ΔH^o_{acid} (AH) kcal mol^{-1}	PRODUCTS	BR	k_{exp} (a)	Efficiency (b)
Ph$^-$	400.7	PhN_2O^-		4.4	0.057
		PhO^- + N_2			
Me_2N^-	396.2	$Me_2N_2O^-$	1.00	0.21	0.002
$ClCH_2^-$	396.1	Cl^- + CH_2N_2O	1.00	4.92	0.058
$MeSCH_2^-$	393.2	$MeSCN_2^-$ + H_2O	1.00	0.66	0.008
$BrCH_2^-$	392.8	Br^- + CH_2N_2O	1.00	0.83	0.011
$CH_2CHCH_2^-$	390.8	HO^- + CH_2CHCHN_2	0.20	1.1	0.012
		$CH_2CHCN_2^-$ + H_2O	0.70		
		CH_2CCH^- + N_2 + H_2O	0.10		
$CH_2CCHCH_2^-$	391	$CH_2CHCN_2^-$ + CH_2O	1.00	0.6	0.007
$CH_2C(CH_3)CH_2^-$	390.3	$CH_2C(CH_3)CN_2^-$ + H_2O	1.00	1.4	0.017
$CH_3CHCHCH_2^-$	390.0	$CH_3CHCHCN_2^-$ + H_2O	0.55	0.98	0.012
		$CH_2CCHCH_2^-$ + N_2 + H_2O	0.45		
$Me_3SiCH_2^-$	388.3	Me_3SiO^- + CH_2N_2	1.00	0.84	0.011
ICH_2^-	386.4	I^- + CH_2N_2O	1.00	<0.1	<0.001
$CH_2C(CN_2^-)CHCH_2$	385.7	$CH_2C(CN_2^-)CHCH_2$ + H_2O	1.00	0.24	0.003
$PhCH_2^-$	380.8	$PhCN_2^-$ + H_2O	1.00	<0.1	<0.001
$HCCCH_2^-$	381.1	$HCCCN_2^-$ + H_2O	1.00	<0.1	<0.001
$NCCH_2^-$	372.9	$NCCN_2^-$ + H_2O	1.00	<0.1	<0.001

(a) x 10^{-11} cm^3 molecule^{-1} s^{-1}
(b) calculated using the ADO theory of Su and Bowers

Structures of CHS_2^- Anions and Reactivities with CS_2 Molecules.

#Gimbert, Y., ¤Dive G, #Moradpour A., °Tabet J.C. and *de Hoffmann E.
#Laboratoire de Physique des Solides, University Paris-Sud, F-91405 Orsay, France
¤Centre d'Ingénérie des Protéines, Univ. Liège, B-4000 Sart Tilman, Belgium
Lab. de Chimie Organique Structurale, Univ. Pierre et Marie Curie, F-75230 Paris, France
*Mass Spectrometry, Univ. de Louvain, Pl. Pasteur 1, B-1348 Louvain-la-Neuve, Belgium

CS_2 is often used to probe the reactivities of gas phase ions, and especially as an electrophile with anions. Regioselectivity has been often observed. For example, Sheldon et al. have studied the reaction of H_3Si^- with CS_2, which by a regioselective attack at a sulfur atom leads to H_3SiS^- and CS.

In the course of a study on gas phase anion-molecule reactions induced by CS_2 as an electrophile, we have observed that in a CH_4/N_2O chemical ionisation source CS_2 yields two anions, $CS_2^{\cdot-}$ and CHS_2^- in about a 3/1 ratio. The latter ion is generally referred to in the litterature as being the dithioformate anion. We have got evidence that it is actually a mixture of HS-CS$^-$ and H-CS_2^- having both a regiospecific reactivity toward CS_2. These findings have been confirmed by 6.31G^{++} ab initio calculation.

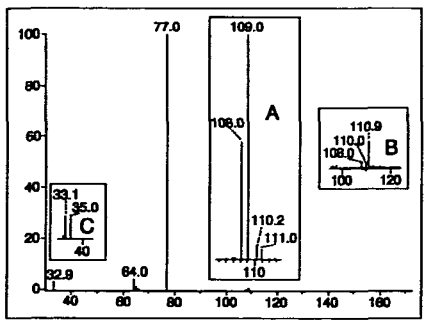

Figure 1: Collision activated reaction spectra of $HC^{32}S_2^-$ (main spectrum and A) and $HC^{32}S^{34}S^-$ (B and C) with CS_2.

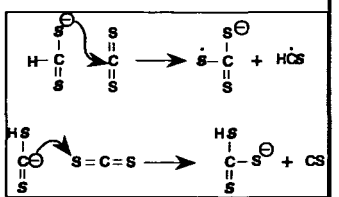
H
C
S
S
S
S
S
C
S
S
S
S
S
C
S
S
S
S
C
S
S
S
S
C

Gas-Phase Chemistry of Halocarbene Radical Anions: Acidities of Radicals and the Related Molecules

Monique Born, *Steen Ingemann and Nico M. M. Nibbering

Institute of Mass Spectrometry, University of Amsterdam, Nieuwe Achtergracht 129, 1018 WS Amsterdam, The Netherlands

The gas-phase ion/molecule reaction of the atomic oxygen radical anion with halogen substituted methanes, CH_3X (X = F, Cl, Br and I), in a Fourier Transform Ion Cyclotron Resonance (FT-ICR) instrument results in the formation of $^{-}{}^{\cdot}CHX$ carbene radical anions by a formal $H_2^{+\cdot}$ abstraction (eq. 1).

$$O^{-\cdot} + CH_3X \longrightarrow {}^{-}{}^{\cdot}CHX + H_2O \qquad (1)$$

Based upon the occurrence/non-occurrence of proton transfer in the reactions of the halocarbene radical anions with selected reference acids, the gas-phase acidities (ΔH^{o}_{acid}) of the $^{\cdot}CH_2X$ radicals have been determined (see Table).

Table. Gas-phase acidities of the CH_3X and $^{\cdot}CH_2X$ species together with C-H bond dissociation energies (BDE) and electron affinities (EA) (all values in kJ mol^{-1})

X	ΔH^{o}_{acid} $^{\cdot}CH_2X$	BDE $^{\cdot}CH_2X$	EA CHX	ΔH^{o}_{acid} CH_3X	BDE CH_3X	EA $^{\cdot}CH_2X$
F	1662 ± 9	402	52 [a]	≈ 1716 [b]	423 [c]	19
Cl	1607 ± 10	412	117 [a]	≈ 1657 [b]	422 [c]	77
Br	1589 ± 8	417	140 [a]	≈ 1643 [b]	427 [c]	96
I	1559 ± 11	409	162 [a]	≈ 1617 [b]	433 [d]	128

[a] Taken from ref 1. [b] From ref 2. [c] From ref 3 [d] Taken from ref. 4

The acidities of the $^{\cdot}CH_2X$ radicals in combination with the known electron affinities (EA) of the CHX carbenes[1] (Table) lead to the following heats of formation of the CHX carbenes: ≈ 150 kJ mol^{-1} (CHF), ≈ 320 kJ mol^{-1} (CHCl), ≈ 370 kJ mol^{-1} (CHBr) and ≈ 420 kJ mol^{-1} (CHI). The acidities lead also to the homolytic C-H bond dissociation energies (BDE) of the $^{\cdot}CH_2X$ radicals with use of eq. 2. An approximately constant value

for the C-H BDE is obtained indicating that the increase of the acidity in the series $^{\cdot}CH_2F$, $^{\cdot}CH_2Cl$, $^{\cdot}CH_2Br$ and $^{\cdot}CH_2I$ is determined by the electron affinities of the carbenes.

$$\Delta H^{o}_{acid} = BDE(^{\cdot}CH_2X) - EA(CHX) + IE(H^{\cdot}) \qquad (2)$$

A similar situation applies to the CH_3X molecules, i.e. the increase of the acidity in the series CH_3F, CH_3Cl, CH_3Br and CH_3I is a result of the trend in the electron affinities of the $^{\cdot}CH_2X$ radicals (Table).[2] For a given halogen, the acidity increases with roughly 55 kJ mol^{-1} when going from the molecule to the radical mainly as a result of a larger electron affinity of a given CHX carbene than of the corresponding $^{\cdot}CH_2X$ radical.

The $^{-}{}^{\cdot}CHX$ ions react with the parent compounds to form X^{-} ions predominantly by direct nucleophilic attack (eq. 3a) and only to a minor extent by initial proton transfer yielding a $[^{\cdot}CH_2X + {}^{-}CH_2X]^{*}$ complex, which reacts further by nucleophilic substitution (eq. 3b).

$$^{-}CH^{35}Cl + CH_3Cl \longrightarrow Cl^{-} + CH_3\dot{C}H^{35}Cl \qquad (3a)$$

$$\downarrow$$

$$[CH^{35}Cl \;\; {}^{-}CH_2Cl]^{*} \longrightarrow {}^{35}Cl^{-} + CH_3\dot{C}HCl \qquad (3b)$$

In addition to overall proton transfer (eq. 4a), the reaction with aliphatic alcohols results in X^{-} ions by a process, which involves initial proton transfer and a subsequent nucleophilic attack on the generated radical as indicated in eq. 4b.

$$^{-}CHX + ROH \rightarrow [RO^{-} \;\; {}^{\cdot}CH_2X]^{*} \nearrow R\text{-}O^{-} + {}^{\cdot}CH_2X \qquad (4a)$$

$$[RO^{-} \;\; {}^{\cdot}CH_2X]^{*} \searrow [R\dot{O}CH_2 \;\; X^{-}]^{*} \rightarrow R\dot{O}CH_2 + X^{-} \qquad (4b)$$

1. M. K. Gilles, K. M. Ervin, J. Ho and W. C. Lineberger, *J. Phys. Chem.* **96**, 1130 (1992).
2. S. Ingemann and N. M. M. Nibbering, *J. Chem. Soc. Perkin Trans. 2*, 837 (1985).
3. S. G. Lias, J. E. Bartmess, J. F. Liebman, J. L. Holmes, R. D. Levin and W. G. Mallard, *J. Chem. Phys. Ref.Data* **17** (suppl. 1) (1988).
4. J. L. Holmes and F. P. Lossing, *J. Am. Chem. Soc.* **110**, 7343 (1988).

MECHANISM OF REACTION OF Fe^+ WITH ORGANOSILANES. GENERATION AND CHARACTERIZATION OF TRANSITION METAL-SILYLENE AND -SILENE CATIONIC COMPLEXES IN THE GAS PHASE

R. Bakhtiar and D. B. Jacobson

Department of Chemistry, North Dakota State University
Fargo, North Dakota 58105-5516

Transition metal-silylene complexes ($L_nM{=}SiR_2$) are postulated intermediates in a number of transition metal-mediated transformations, including Rochow's direct process, catalytic redistribution of silanes, various silylene-transfer reactions, and in dehydrogenative coupling reactions of silanes with transition metals [1] Although transition metal-carbene, germylene, -stannylene, and -plumbylene complexes are well known, the corresponding -silylene species have been synthetically elusive in solution with silylene-metal complexes only recently generated and characterized. The related transition metal-silene complexes ($L_nM(R_2Si{=}CR_2)$) have been proposed as intermediates in metal-mediated rearrangement of organosilicon ligands, including β-hydrogen transfer of a bound silyl group.[2] *Stable transition metal-silene complexes have recently been synthesized and characterized.*[3] The difficulty in synthesizing stable metal-silylene and -silene complexes has prevented detailed studies concerning their involvement in organosilicon chemistry. The mechanism of reaction of Fe^+ with organosilanes was studied in the gas phase by using Fourier transform mass spectrometry (FTMS). The structures of the resulting products were probed by specific ion/molecule reactions (isotopically labeled ethene) with isomeric iron-silylene and -silene cationic complexes ($FeSiCH_4^+$ and $FeSiC_2H_6^+$) characterized.[4]

The predominant reaction channel for reaction of Fe^+ with ethenylmethylsilane and silacyclobutane is loss of ethene, reactions 1 and 2. Reaction of 1 and 2 with isotopically labeled ethene indicates that 1 is an iron-silylene

$$Fe^+ + CH_2{=}CH\text{-}Si(CH_3)H_2 \longrightarrow \underset{1}{FeSiCH_4^+} + C_2H_4 \qquad (1)$$

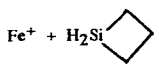

$$Fe^+ + H_2Si \longrightarrow \underset{2}{FeSiCH_4^+} + C_2H_4 \qquad (2)$$

complex ($Fe^+{=}(CH_3)H$) and that 2 is an iron-silene species ($Fe^+(CH_2{=}SiH_2)$). A mechanism for reaction 1 is proposed in Scheme I and involves initial vinyl C-Si insertion. A mechanism for reaction 2 is postulated in Scheme II and involves initial insertion into the strain weakened Si-C bond.

Scheme I

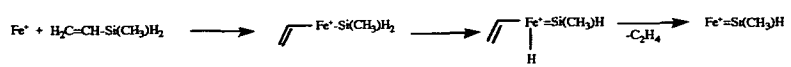

Scheme II

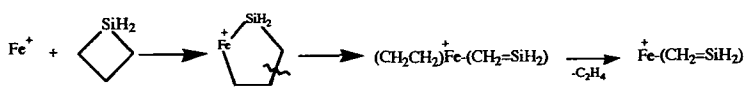

Fe^+ reacts with dimethylsilane to yield exclusive dehydrogenation whereas 1-methylsilacyclobutane gives exclusive loss of ethene, reactions 3 and 4. Structural studies indicate that 3 consists of the silylene complex,

$$Fe^+ + (CH_3)_2SiH_2 \longrightarrow \underset{3}{FeSiC_2H_6^+} + H_2 \qquad (3)$$

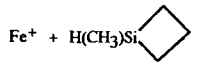

$$Fe^+ + H(CH_3)Si \longrightarrow \underset{4}{FeSiC_2H_6^+} + C_2H_4 \qquad (4)$$

$Fe^+{=}Si(CH_3)_2$, while 4 is the silene complex, $Fe^+\text{-}(CH_2{=}Si(CH_3)H)$. A mechanism for reaction 3 is proposed in Scheme III and involves 1,1-dehydrogenation from silicon. Reaction 4 presumably proceeds by a mechanism

Scheme III

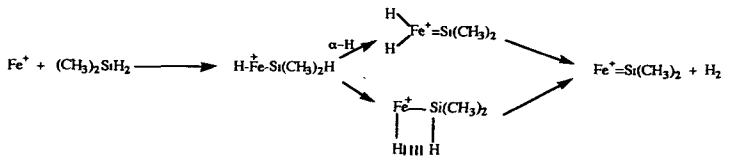

analogous to that in Scheme II.

Fe^+ reacts with $(CH_3)_3SiH$ to yield both demethanation and dehydrogenation, reaction 5.

$$Fe^+ + (CH_3)_3SiH \longrightarrow FeSiC_2H_6^+ + CH_4 \qquad (5a)$$

$$Fe^+ + (CH_3)_3SiH \longrightarrow FeSiC_3H_8^+ + H_2 \qquad (5b)$$

Structural studies indicate that the product of reaction 5a is an iron-silylene complex ($Fe^+{=}Si(CH_3)_2$) and the structure of the product of reaction 5b is an iron-silene complex ($Fe^+\text{-}(CH_2{=}Si(CH_3)_2)$. A mechanism for reaction 5 is presented in Scheme IV and involves initial Si-H bond insertion.

Scheme IV

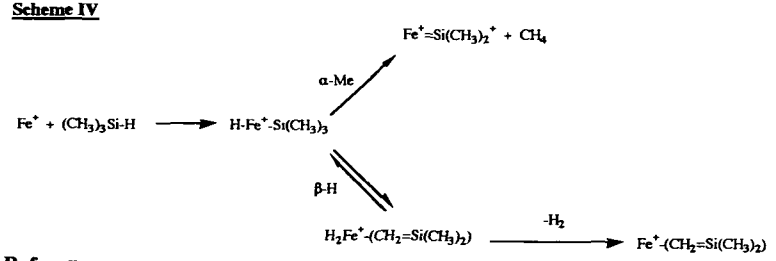

References

1. Tilley, T. D. In *The Silicon Heteroatom Bond;* Patai, S.; Rappoport, Z., Eds.; John Wiley and Sons: New York, 1991, 309 and references cited therein.
2. Randolph, C. L.; Wrighton, M. S. *Organometallics* **1987**, *6*, 365.
3. Koloski, T. S.; Carroll, P J., Barry, D. H. *J. Am. Chem. Soc.* **1990**, *112*, 6405.
4. Bakhtiar, R.; Holznagel, C. M , Jacobson, D B. *J. Am. Chem. Soc.* **1993**, *115*, 345.

SELECTIVE ION-MOLECULE REACTIONS OF LACTAMS WITH DIMETHYL ETHER IONS

Tracy Donovan McCarley and Jennifer Brodbelt, Department of Chemistry, University of Texas, Austin, TX 78712-1167

A variety of molecules containing a lactam ring system are essential in the polymer and pharmaceutical industries. In this study, the selectivity of ion-molecule reactions of four- to seven-membered ring lactams, both unsubstituted and with methyl substituents in various positions, with dimethyl ether ions was characterized to correlate reactivity with ring size and substitution pattern. The ion-molecule reaction products of the lactams with dimethyl ether reagent ions in the ion trap are summarized in Table 1. All of the lactams were protonated by dimethyl ether reagent ions and formed $(M + 15)^+$ product ions by methyl cation transfer, and most of the lactams formed $(M + 45)^+$ adduct ions. Other products formed include $(M + 3)^+$, $(M + 13)^+$, and $(M + 16)^+$ ions.

Although simple protonation or formation of $(M + 15)^+$ products shows no dependence on ring size or substituent position, formation of the $(M + 13)^+$ and $(M + 16)^+$ products appears to be highly selective. For instance, of the five, six, and seven membered ring systems, the $(M + 13)^+$ and $(M + 16)^+$ products were formed *only* by lactams which do not have a methyl substituent on the nitrogen atom. For the lactams with an *N*-methyl substituent, neither $(M + 13)^+$ nor $(M + 16)^+$ adducts were formed.

Unlike the $(M + 13)^+$ and $(M + 15)^+$ products, the formation of the $(M + 16)^+$ ion by dissociation of an $(M + 45)^+$ adduct has not been reported prior to this study. To assist in the elucidation of the structure of this intriguing $(M + 16)^+$ adduct, the $(M + 16)^+$ adduct of each lactam was collisionally activated and compared to the spectra of lactone analogs. For example, the CAD spectrum of the $(M + 16)^+$ adduct of 2-pyrrolidinone shows a base peak at m/z 59 and less abundant ions at m/z 55 and 83 (Figure 1a). This spectrum is strikingly similar to the CAD spectrum of the $(M + 15)^+$ adduct of γ-butyrolactone (see Figure 1b). Based on this observation, the structures of the lactam $(M + 16)^+$ products and the lactone $(M + 15)^+$ products are presumed to be identical.

A mechanism showing the formation of the 5-methyl-2-pyrrolidinone $(M + 16)^+$ adduct is proposed in Scheme I. Such a mechanism also accounts for the absence of an $(M + 16)^+$ product in the ion-molecule reaction spectra of the lactams which have a methyl substituted nitrogen atom. If the $(M + 45)^+$ adducts of these *N*-methyl compounds dissociate according to the mechanism shown in Scheme I, the neutral eliminated would be $CH_2{=}N{-}CH_3$, a

loss of 43 amu, rather than $CH_2{=}NH$, and the resulting final product would be observed at $(M + 45 - 43)^+$, or $(M + 2)^+$. In fact, collisional activation of the $(M + 45)^+$ adduct of each of the nitrogen-substituted lactams produces an ion at $(M + 2)^+$, which offers additional support for this unusual process.

The ion-molecule reactions of lactams with dimethyl ether ions show a high degree of selectivity that was not observed in the ion-molecule reactions of lactones or amides with dimethyl ether ions. All of the lactams were protonated by dimethyl ether ions, but the formation of additional adduct ions shows selectivity based upon ring size and the presence or absence of a methyl substituent on the lactam nitrogen atom. Each protonated lactam exhibits a unique set of dissociation pathways and product ions, making the discrimination of structural isomers possible.

Acknowledgements

This work was supported by grants from the Welch Foundation (F-1155), ACS-PRF (25485AC5), and NSF (CHE-9122699).

Table 1.

Lactam (MW)	Reaction Products (Relative Abundance) $(M + H)^+$	$(M + 3)^+$	$(M + 13)^+$	$(M + 15)^+$	$(M + 16)^+$	$(M + 45)^+$
2-azetidinone (71)	50%	15%	30%	5%		
2-pyrrolidinone (85)	70%		<5%	20%	5%	<5%
1-methyl-2-pyrrolidinone (99)	55%			40%		5%
3-methyl-2 pyrrolidinone (99)	45%		10%	30%	10%	5%
5-methyl-2-pyrrolidinone (99)	50%		5%	30%	10%	5%
1,5-dimethyl-2-pyrrolidinone (113)	60%			35%		5%
2 piperidone (99)	55%		<5%	35%	<5%	5%
1-methyl-2-piperidone (113)	20%			55%		25%
ε-caprolactam (113)	60%		5%	20%	5%	10%
N-methyl-ε-caprolactam (127)	20%			25%		55%

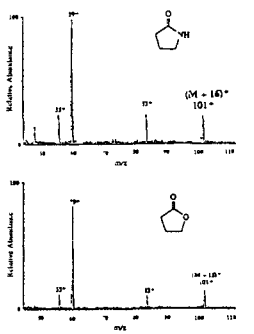

Figure 2. CAD spectra of a) the $(M + 16)^+$ of 2-pyrrolidinone and b) the $(M + 15)^+$ γ-butyrolactone in the ion trap mass spectrometer

Scheme I. Mechanism for formation of lactam $(M + 16)^+$

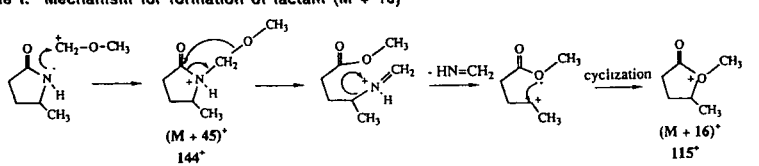

APPLICATION OF SITE-SELECTIVE ION-MOLECULE REACTIONS TO THE IDENTIFICATION OF ALKALOIDS

Erika Eichmann and Jennifer S. Brodbelt, Department of Chemistry, University of Texas, Austin, TX 78712-1167

The alkaloids quinine and quinidine, along with cinchonine, cinchonidine, have been widely used in medicine longer than many modern drugs. Cinchonidine (**1**), cinchonine (**2**), quinine (**3**), and quinidine (**4**), all exhibit similar antimicrobial activity (See Figure 1). These compounds can be viewed as α,β-amino alcohols with aromatic substituents and tertiary amino groups. The major difference within each pair of stereoisomers (**1/2** and **3/4**) is the distance separating the hydroxyl group from the vinyl group. The interaction between the hydroxyl and vinyl groups in quinidine (**4**) and cinchonine (**2**) has long been recognized, and thus reagent ions which selectively target either the vinyl group or the hydroxyl group may be affected by the degree of interaction between them. In this study, we have examined structurally-selective ion-molecule reactions between (DME) dimethyl ether ions **5** and **6** and the cinchona alkaloids in a quadrupole ion trap mass spectrometer.

The product spectra for reactions of **1**, **2**, **3**, and **4** with DME ions are qualitatively similar to each other (Table 1). Each molecule yields an abundant $(M + 1)^+$ ion, as well as $(M + 13)^+$, $(M + 15)^+$ and $(M + 45)^+$ products. Also present in each spectrum is an ion at m/z = 136, which is due to cleavage of the vinylquinuclidine group from the molecular ion. The two pairs of stereochemically similar pairs (**1/3** and **2/4**) show moderate differences in the $136^+/(M + 45)^+$ and $(M + 1)^+/(M + 45)^+$ ratios and especially in the relative formation of $(M + 13)^+$ and $(M + 15)^+$ ions. The $(M + 13)^+$ product is known from previous studies to form only at sites with available protons that can be donated in the necessary elimination of methanol. This rules out any of the potential reaction sites except the aromatic carbon atoms, the vinyl group, and the hydroxyl group. The fact that some selectivity is observed in reactions of these compounds with DME ions indicates that the interaction between these two functional groups is involved in determining the outcome of the DME/alkaloid ion-molecule reactions, as discussed later.

The DME ions $CH_3OCH_2^+$ and $(CH_3OCH_3)H^+$ were each selectively reacted with the neutral alkaloids. Reaction of the alkaloids with $(CH_3OCH_3)H^+$ yields only the protonated species. Reaction with $CH_3OCH_2^+$ results in formation of $(M + 45)^+$ adducts as well as the $(M + 13)^+$ and $(M + 15)^+$ product ions. The products result via elimination of CH_2O or CH_3OH from the $(M + 45)^+$ precursor.

$$M + (CH_3OCH_3)H^+ \longrightarrow (M + H)^+$$

$$M + CH_3OCH_2^+ \longrightarrow (M + 13)^+,\ (M + 15)^+,\ (M + 45)^+$$

The $(M + 45)^+$ adduct is the precursor for both the $(M + 13^+)$ and $(M + 15^+)$ product ions; however, in all cases, activation of the $(M + 45)^+$ adduct yields predominantly the $(M + 13)^+$ ion via loss of methanol. A representative CID spectrum is shown for the cinchonidine $(M + CH_3OCH_2^+)$ ion in Figure 2. Interestingly, the fact that activation of the $(M + 45)^+$ adducts does not result in formation of $(M + 15)^+$ ions suggests either that the stable $(M + 45)^+$ adduct is not the appropriate structural precursor for the $(M + 15)^+$ ions or that the elimination of CH_3OH to form $(M + 13)^+$ ions is substantially kinetically favored over the elimination of CH_2O to form $(M + 15)^+$ ions.

The reactivities of the individual functional groups within the complex alkaloids are modelled by examination of smaller sub-units of the molecules (Figure 3) in order to understand the reactivity and intramolecular interactions of the complete molecule, and to predicting site-

selectivity. Reaction of the alkenol compounds **7**, **8** and **9** with DME ions yields proton-bound $(M + 47)^+$ adducts and $(M + 13)^+$ products. Additionally, it was determined that both the vinyl groups and the hydroxyl groups are necessary for the reactions of alkenols with DME to proceed in the ion trap. None of the tertiary amine compounds give $(M + 13)^+$ product ions, except *N,N*-dimethylethanolamine (**14**). For all of the tertiary amines, there is no way of forming the $(M + 13)^+$ ions because there is no accessible proton attached to the nitrogen atom. *N,N*-dimethylethanolamine (**14**) produces $(M + 13)^+$ ions, rather than $(M + 15)^+$ ions because of the presence of a reactive hydroxyl group. Naphthalene **16** and 2-methoxynaphthalene **17**, unlike their nitrogen-containing counterparts **10** and **11**, forms $(M + 13)^+$ ions instead of $(M + 15)^+$ ions. The reactions of these models show that methylation is only favored when a tertiary nitrogen atom is present and no other reactive heteroatom site is available. Additionally, the formation of $(M + 13)^+$ ions is kinetically favored.

With respect to the alkaloids, these model studies suggest that methylation occurs at the quinoline nitrogen position, whereas formation of $(M + 13)^+$ ions occurs at the hydroxyl group, with assistance by a second functional group, such as the vinyl group. The fact that the formation of $(M + 15)^+$ ions is preferred for cinchonidine and quinine but the formation of $(M + 13)^+$ ions is favored for cinchonine and quinidine suggests that the functional group interaction between the hydroxyl group and vinyl group plays a significant role in determining the selectivity of the ion-molecule reactions of the cinchona alkaloids.

ACKNOWLEDGEMENTS

This research was supported by grants from NSF (CHE-9122699), Welch Foundation (F1155), NIH (R01-GM46723-01), and ACS-PRF (25485-AC5).

Figure 1. Structures of cinchona alkaloids.

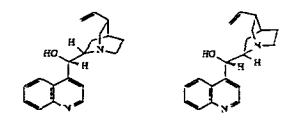

Cinchonidine 1 — Cinchonine 2

Table 1.

		% Total Ion Current				
	Compound	$(M+45)^+$	$(M+13)^+$	$(M+15)^+$	$(M+47)^+$	$(M+1)^+$
1	cinchonine	30	5	10	---	35
2	cinchonidine	35	10	5	---	30
3	quinine	40	5	10	---	20
4	quinidine	40	10	5	—	25

CAD spectra of $(M + 45)^+$ ion of cinchonine.

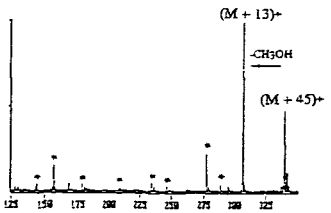

* analogous to $(M + 13)^+$ CID fragments

Figure 2

Figure 3

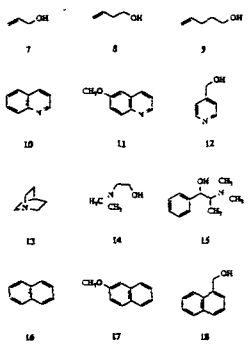

ION-MOLECULE REACTIONS AND DISSOCIATION OF GLYCOLS IN A QUADRUPOLE ION TRAP: EVIDENCE OF INTRAMOLECULAR INTERACTIONS

Erika Eichmann and Jennifer S. Brodbelt, Department of Chemistry, University of Texas, Austin, TX 78712-1167.

Polyethylene glycols serve as important precursors in the polymer industry and as models in the field of host-guest chemistry. In general, glycols of different chain lengths are not easily distinguished by mass spectrometric methods because they yield similar fragmentation patterns. Glycols have the special ability to participate in multi-site binding of ions. In our quest for obtaining a more detailed understanding of the significance of functional group interactions in mediating gas-phase ion-molecule reactions, we have examined the selective reactions of the methoxymethylene cation, $CH_3OCH_2^+$, with a homologous series of glycols. It was of additional interest to determine the analytical value of derivatizing the glycols through ion-molecule reactions in the gas phase in order to promote greater differentiation of the glycol chain length.

Ion/molecule reactions were examined by using a Finnigan quadrupole ion trap mass spectrometer (ITMS). Collisional activation involved the application of an ac voltage of 0.3 - 1.0 V_{p-p} at the axial frequency of motion of the ion of interest (i.e. 120 kHz at q = 0.3). The dimethyl ether (DME) pressure was nominally 1 x 10^{-5} torr, and the helium buffer gas pressure was 0.8 mtorr. Reaction of the $CH_3OCH_2^+$ cations with each of the glycols resulted in formation of $(M + 13)^+$ product ions. The $(M + 13)^+$ ions likely result from formation of short-lived $(M + CH_3OCH_2)^+$ intermediates which spontaneously dissociate by loss of CH_3OH (Scheme I). Although the terminal hydroxyl groups of the glycols are separated by from five to fifteen atoms, several nucleophilic ether oxygen atoms are present within the chain of the molecule, and this structural feature may offer alternative routes towards stabilization of the necessary $(M + CH_3OCH_2)^+$ complex (Scheme 1).

Multi-stage CAD techniques were used to characterize the structures of the $(M + 13)^+$ ions and their protonated counterparts $(M + H)^+$ (see Figure 1). In contrast to the CAD spectra of the $(M + H)^+$ ions, the CAD spectra of the $(M + 13)^+$ ions show a much richer and more structurally diagnostic variety of fragments (see Table 2). Four major fragmentation routes are observed, each involving elimination of a small neutral molecules in conjunction with losses of C_2H_4O units. The most straight forward pathway involves elimination of $(CH_2O + nC_2H_4O)$.

One type of dissociation process that is observed only for the triethylene glycol and tetraethylene glycol $(M + 13)^+$ ions involves the elimination of $(HCOCH_2OH + nC_2H_4O)$ (n = 0 or 1). Initial hydride transfer from a methylene carbon of the glycol adduct to the positively polarized methylene end group results in an oxonium ion. The elimination of $HCOCH_2OH$ occurs after C-O bond cleavage and may then be followed by loss of a C_2H_4O unit.

Each of the final dissociation routes involves cyclization of the $(M + 13)^+$ ions, followed by intramolecular hydride transfer. The ion may undergo direct cleavage of CH_3OH, followed by elimination of zero, one or two C_2H_4O units. The losses of C_2H_4O units are increasingly favored as the length of the polyether chain increases. Alternatively, the cyclization of the $(M + 13)^+$ ion is followed by a hydride transfer reaction and rearrangement in which an ether oxygen abstracts a proton from a β-carbon atom. Then C-O bond cleavage occurs, resulting in the net loss of $C_3H_6O_2$ (86 u). Because this process does not occur in conjunction with losses of ethylene oxide units, it uniquely identifies the size of the glycol polyether chain.

The perdeuterated reagent CD_3OCD_3 was used to assist in elucidation of reaction and dissociation mechanisms and to determine the extent of rearrangment in the glycol ions. The reaction of tetraglycol, triglycol, and diethylene glycol with $CD_3OCD_2^+$ ions led exclusively to

formation of $(M + 15)^+$ ions, assigned as $(M + CD_3OCD_2^+ - CD_3OH)$. The absence of $(M + 13)^+$, $(M + 14)^+$ and $(M + 16)^+$ ions demonstrates that interchange between deuterium and hydrogen atoms does not occur, and thus the reaction of interest proceeds by attachment of $CD_3OCD_2^+$ to the glycol, followed specifically by loss of CD_3OH (see Scheme 1).

CONCLUSIONS

Polyethylene glycols afford a useful set of model structures for the further examination of functional group participation in ion-molecule reactions. On the basis of the specific fragmentation pathways described in this report, it is apparent that the glycols may undergo intramolecular cyclization upon formation and dissociation of the $(M + 13)^+$ ions. Furthermore, the deuterium labelling experiments demonstrate that the intramolecular cyclization and rearrangements do not result in scrambling of atoms. This study has also provided an example of how derivatization of an organic substrate by selective ion-molecule reactions may offer supplementary structural information to that provided by the spectra of protonated analogs. In the present case, the substitution of a methylene cation for a proton results in modified glycols that undergo many more rearrangements upon collisional activation. For the glycols with longer carbon chain lengths, the loss of 86 amu ($C_3H_6O_2$) from the $(M + 13)^+$ ion is a structurally specific elimination that does not occur in conjunction with C_2H_4O losses, and thus unambiguously identifies the glycol chain size.

Acknowledgment
This work was supported by the Welch Foundation, the Petroleum Research Foundation, NIH and NSF.

Figure 1 CAD spectra of (A) $(M - H)^+$ and (B) $(M + 13)^+$ ions of triethylene glycol

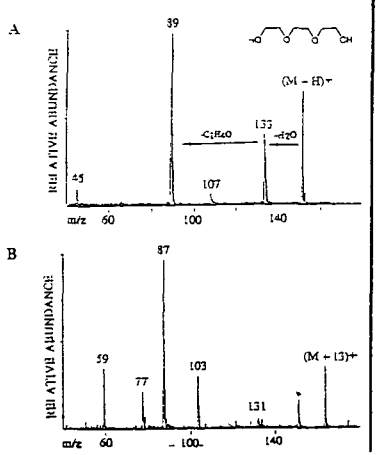

Scheme 1. Mechanism for formation of $(M + 13)^+$ ions.

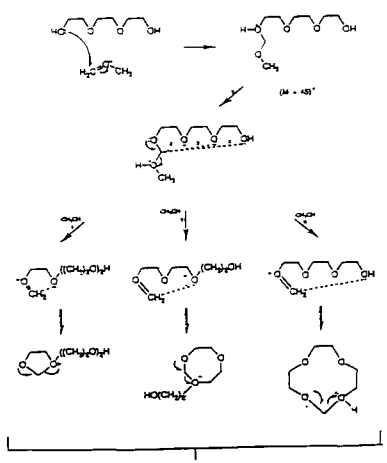

ISOMER DISTINCTION IN A QUADRUPOLE ION TRAP: FUNCTIONAL GROUP INTERACTIONS OF DICARBOXYLIC ACIDS AND ESTERS.

***John J. Isbell, Jeff Liou, and Jennifer S. Brodbelt, Department of Chemistry, University of Texas, Austin, Texas 78712.**

Functional group interactions are among the most important classes of substituent effects in both solution and gas phase chemistry[1-6] The term "intramolecular catalysis" has been used to describe those types of functional group interactions which facilitate specific reaction or dissociation channels [7]. Such effects have been observed for a variety of difunctional molecules, including diols and amino alcohols [2,3].

Some of the most striking functional group interactions have been observed for dicarboxylic acids. The ability of the functional groups to interact can be correlated with distinctive fragmentation patterns upon electron ionization [1] or with the extent of dehydration of the diacids upon chemical ionization [6,9]. Similar results have been reported for related esters [8,9] and fatty acids [10]. Low-energy CAD of the protonated diethyl esters of fumaric and maleic acids resulted in stereospecific dissociation pathways: the protonated cis isomer eliminated ethanol, while the trans diester lost one or two molecules of ethylene [11].

The primary goal of our systematic study of functional group interactions is to gain a better understanding of structure/reactivity relationships in gas-phase ion molecule reactions. As with our earlier work, we are particularly interested in the chemistry of complex biomolecules. By studying diacids and their corresponding dimethyl esters, the effect of methyl substitution on isomer distinction can be determined and the extent of functional group interactions can be evaluated. Dimethyl ether was used as a chemical ionization reagent because of its proven selectivity towards certain functional groups and its capability for probing functional group interactions [12,13].

A Finnigan Ion Trap Mass Spectrometer was operated in the positive ion mode at a typical temperature of 100-120°C. Samples were introduced using a solids probe heated to 80-100°C or through a leak valve at a pressure of 1×10^{-6} torr. Dimethyl ether served as a chemical ionization reagent gas and was introduced at a pressure of $1\text{-}2 \times 10^{-5}$ torr. Helium was added as a buffer gas and was added to increase the pressure to the millitorr regime.

For comparison, results were also obtained using a Finnigan Triple Stage Quadrupole (TSQ). Adducts were formed with dimethyl ether by introducing it at 1.2 torr. Argon served as a collision gas and was introduced into the quadrupole at 1.5 millitorr. Electron ionization was performed using nominally 70 eV electrons and the collision energy was typically 10 V.

Reactions of Acids with Dimethyl Ether Ions in an Ion Trap

Using dimethyl ether as a reagent gas, one can easily distinguish between fumaric acid and maleic acid in an ion trap. Fumaric acid produces $(M+13)^+$ ions while maleic acid forms $(M+15)^+$ ions. The postulated mechanism for the $(M+13)^+$ product formation is given in FIGURE I, while that for $(M+15)^+$ is given in FIGURE II.

Not surprisingly, succinic acid adopts a conformation that is somewhat similar to that of maleic acid, presumably to take advantage of the additional electrostatic interaction of the second carboxylic acid to lower the energy of the product ion. It is interesting to note that succinic acid also forms an $(M+45)^+$ adduct while the other two diacids do not. This suggests that flexibility plays an important role in adduct formation and that models of functional group interactions should be chosen carefully.

CAD of Product Ions in an Ion Trap

It is also interesting to examine the nature of fragment ions formed upon collisional activation of the various product ions and the effect of structural rigidity of the acids. After activation of the rigid protonated diacids, dehydration, followed by a subsequent loss of carbon monoxide is observed. The low CAD yield of protonated fumaric acid supports the high-energy, symmetry-forbidden proton transfer.

Protonated succinic acid loses only water. This difference is attributed to the inability of functional group interaction in fumaric acid, and the increase in strain of maleic acid for functional group interaction. It is the increased flexibility of the protonated succinic acid which enables it to lose water and then cyclize to stabilize the resulting fragment ion.

The methylated product ions $(M+15)^+$ predominantly dissociate by elimination of water. The analogous loss of methanol does not occur. This result is especially intriguing with respect to the trans isomer for which a functional group interaction to allow the necessary proton migration would not be expected to be favored.

Reactions of Acids with Dimethyl Ether Ions in a Conventional CI Source and CAD

Reactions between the acids and dimethyl ether ions in a conventional chemical ionization source afford qualitatively similar product spectra. Products are observed for $(2M+H)^+$, $(M+H+DME)^+$, $(M+45)^+$, $(M+15)^+$ and $(M+H)^+$ for both fumaric and maleic acids. CAD of many of the products ions are qualitatively identical; however, the CAD spectra of the $(M+45)^+$ adducts are strikingly different. The $(M+45)^+$ adduct for maleic acid dissociates to the $(M+15)^+$ ion by elimination of formaldehyde, whereas the $(M+45)^+$ adduct for fumaric acid dissociates to the $(M+13)^+$ ions by loss of methanol. This dissociation behavior mimics the initial product formation observed in the ion trap environment.

The formation and dissociation of dimethyl ether adducts of diacids and diesters is dependent on functional group interactions within the adducts. These effects are most apparent for the competitive formation of the $(M+13)^+$ and $(M+15)^+$ ions of fumaric and maleic acid. Only those substrates with two functional groups that may interact preferentially undergo the methylation reaction.

SELECTED REFERENCES

1. Benoit, F., Holmes, J. L., Isaacs, N. S., Org. Mass Spectrom. **1969** *2* 591. 2. Fenselau, C. C., Robinson, C. H., J. Am. Chem. Soc. **1971** *93* 3070.
2. Harrison, A. G., Krishna Mohan Rao Kallury, R., Org. Mass Spectrom. **1980** *15* 277.
3. Wysocki, V. H., Burinsky, D. J., Cooks, R. G., J. Org. Chem. **1985** *50* 1287.
4. Bowie, J. H., Williams, P., Madsen, G., Schroll, G., Lawesson, S. O., Tetrahedron **1967** *23* 205.
5. Benoit, F., Holmes, J. L., Org. Mass Spectrom. **1972** *6* 541.
6. Krishna Mohan Rao Kallury, R., Org. Mass Spectrom. **1980** *15* 277.
7. Vainiotalo, P., Harrison, P. J., Org. Mass Spectrom. 1987 *22* 687.
8. Harrison, A. G., Nacson, S., Mandelbaum, A., Org. Mass Spectrom. **1987** *22* 283.
9. Weisz, A., Mandelbaumm A., Shabanowitz, J., Hunt, D. F., Org. Mass Spectrom. **1984** *19* 238.
10. Weinkam, R. J., J. Am. Chem. Soc. **1974** *96* 1032.
11. Tu, Y.-P., Lin, Y.-Q., Yang, G.-Y., Org. Mass Spectrom. **1992** *27* 44.
12. Brodbelt, J., Donovan, T., Liou, J., Anal. Chem. **1991** *63* 1205.
13. Donovan, T., Brodbelt, J., J. Am. Soc. Mass Spectrom. **1992** *3* 47.

Acknowledgement

This work was funded by NIH, NSF, ACS-PRF, and American Cyanamid.

FIGURE I: MECHANISM FOR THE FORMATION OF THE $(M+13)^+$ PRODUCT

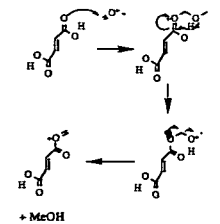

FIGURE II: MECHANISM FOR THE FORMATION OF THE $(M+15)^+$ PRODUCT

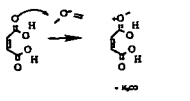

FIGURE III

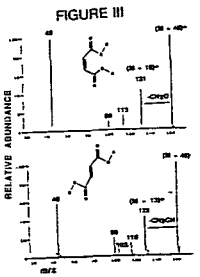

Isomer Distinction of Disubstituted Benzenes in a Quadrupole Ion Trap.

***Niloo Asgharian and Jennifer Brodbelt, Department of Chemistry, University of Texas, Austin, Texas 78712.**

Theoretical calculations[1] have been used extensively to predict the possible stable isomers of $C_2H_3O^+$ composition. It was determined that the lowest energy $C_2H_3O^+$ isomer is the acetyl cation $CH_3C{\equiv}\overset{+}{O}$. The next stable structure was predicted to be protonated ketene, $CH_2{=}C{=}\overset{+}{O}H$ which lies 181 kJ/mol above the acetyl ion. More recently, Cooks et al.[2] determined the structures and reactions of isomeric $C_2H_3O^+$ ions through ion-molecule reactions in a pentaquadrupole mass spectrometer where MS^3 could be achieved. Their results showed that the major $C_2H_3O^+$ isomer formed from acetic anhydride as well as methyl acetate, acetone, and acetaldehyde is the more stable acetyl ion, which formed $(M + 43)^+$ products upon reaction with isoprene and various aromatic substrates.

What led us to continue the investigation of $C_2H_3O^+$ ions was the intriguing observation that of all the precursors of type CH_3COR, only acetic anhydride led to the formation of $(M + 43)^+$ product ions upon reaction with neutral aromatic substrates in a quadrupole ion trap. All the others such as acetaldehyde, 2,3-butadione, acetone, and methylacetate only promoted formation of $(M + H)^+$ protonated substrates. In order to understand the contrasting results obtained in a quadrupole ion trap environment, we undertook a detailed study of reactions of $C_2H_3O^+$ isomers with monosubstituted aromatics and isoprene. A Finnigan Ion Trap Mass Spectrometer (ITMS)[3,4] was used for all experiments. Samples were introduced through a heated leak valve system, and typical pressures used were 2×10^{-6} torr Helium buffer gas was admitted at 1 mtorr. All spectra were recorded at the same manifold temperatures of 45°C and 150°C. The $C_2H_3O^+$ (43^+) ions were generated by 70 eV electron ionization and allowed to react with the neutral sample vapor.

In all cases where isoprene was used as the analyte substrate, both $(M + 43)^+$ and $(M + H)^+$ product ions are formed for all $C_2H_3O^+$ ions. This result replicates the results obtained in a previous study.[2] However, for the reactions of the aromatic substrates with various $C_2H_3O^+$ ions, the $(M + 43)^+$ products are only formed when the $C_2H_3O^+$ ions are generated from acetic anhydride. Figure 3 shows a typical product spectrum for the reaction of $C_2H_3O^+$ ions produced from acetic anyhdride with a neutral substrate, in this case isoprene. According to Cooks and coworkers,[2] there was no difference between $C_2H_3O^+$ ions originating from acetic anydride or other precursors of CH_3COR type. They reported that all of these produced the more stable acetyl isomer as the major structure. The replication of the test substrate used in the previous report[2] (isoprene) duplicated the expected behavior for the CH_3COR precursors in the quadrupole ion trap at ambient temperature. However, the $C_2H_3O^+$ ion generated from acetic anhydride remained unique in its ability to produce $(M + 43)^+$ ions for isoprene at higher temperatures and for aromatic substrates at all temperatures.

There are several possibilities for explaining these discrepancies. Firstly, the translational energy of the $C_2H_3O^+$ ions may be different when generated from different precursors in the ion trap, even if the structures are the same. However, translational energization of each $C_2H_3O^+$ ion by application of a supplementary ac voltage to the ion trap failed to promote changes in the reactive behavior of the ions. The internal energies of the $C_2H_3O^+$ ions could also vary upon formation from

different precursors. Thus the internal energies were varied systematically by increasing and decreasing the helium pressure and by increasing the "cooling" time for $C_2H_3O^+$ relaxation. These efforts caused no change in the reactions of the $C_2H_3O^+$ ions in the ion trap. Structural differences in the $C_2H_3O^+$ isomers are the most obvious reason for differences in reactivity. Yet, CID experiments did not yield structurally distinctive information about the $C_2H_3O^+$ isomers. Translational excitation also failed to induce isomerization of the various $C_2H_3O^+$ ions to more or less reactive forms.

The puzzle that remains is why the precursors respond differently in the ion trap compared to a conventional ion source. In a multiquadrupole instrument, all ionizaton processes occur in an ionization source separate from the mass analyzers. On the other hand in an ion trap, formation of ions and their analysis both occur in one place, the trapping volume. The typical pressure in an electron ionization source is around 10^{-5} to 10^{-7} torr, corresponding to a nearly collision-free environment. In an ion trap, the pressure is around 10^{-3} torr, consistent with a collision frequency of 30 collisions/ms. Thus in the conventional source, the $C_2H_3O^+$ ions undergo no further collisions after formation, whereas the ions may undergo many collisions and thus rearrange in the ion trap. In the pentaquadrupole the collision energy is nearly 0 eV for ion-molecule reactions. In a quadrupole ion trap, ion temperatures have been estimated as 1000 K - 3000K.[5] Thus the average kinetic energy of an ion stored in an ion trap may range from 0.1 - 0.3 eV. All of these factors suggest that the environment of the ion trap is more conducive for promoting isomerization or rearrangement of reactant ions. Moreover, the fact that the formation of $(M + 43)^+$ product ions is temperature dependent in the ion trap supports the idea that the relative extent of isomerization of the $C_2H_3O^+$ ions plays an important role in the outcomes of the reactions.

In light of the consistent discrepancies in the reactive behavior, it seems most plausible that at least two different $C_2H_3O^+$ structures are generated from the different precursors, and these do not intraconvert under any conditions in the ion trap. From our results, it appears that ionization of acetic anhydride results in protonated ketene, whereas all the other precursors generate the more stable acetyl ion.

References

1) R.H. Nobes, W.J. Bouma, and L. Radom, J. Am. Chem. Soc., 1983, 105, 309.
2) M.N. Eberlin, T.K. Majumdar, and R.G. Cooks, J. Am. Chem. Soc., 1992, 114, 2884.
3) J.N. Louris, R.G. Cooks, J.E.P. Syka, P.E. Kelley, G.C. Srafford Jr., J.F.J. Todd, Anal Chem., 1987, 59, 1677.
4) R.E. March and R.J. Hughes, "Quadrupole Storage Mass Spectrometry", John Wiley & Sons, New York, 1989.
5) C. Basic, J.R. Eyler, and R.A. Yost, J. Am. Soc. Mass Spec., 1992, 3, 716.

Acknowledgements

Welch Foundation, NIH, NSF, Petroleum Research Fund

CHARACTERIZATION OF DISSOCIATION BEHAVIOR OF GAS PHASE PROTONATED AND ALKYLATED ORGANOPHOSPHORUS COMPOUNDS BY TANDEM MASS SPECTROMETRY

ANTTI HESSO [1,2], JARKKO TORNAEUS [1] AND HEIKKI BJÖRK [2]

1) INSTITUTE OF OCCUPATIONAL HEALTH, TOPELIUKSENKATU 41 aA, SF-HELSINKI, FINLAND
2) CW-PROJECT, DEPT. OF CHEMISTRY, UNIVERSITY OF HELSINKI, VUORIKATU 20, SF-00100 HELSINKI, FINLAND

INTRODUCTION

The solution chemistry of simple organophosphorus compounds is a well studied topic, but relatively few studies of gas phase ion chemistry of protonated and alkylated organophosphorus compounds have been reported.

The condensed phase studies of organophosphorus compounds in strongly ionizing media have shown that phosphates and thiophosphates are protonated on the phosphoryl oxygen and thiophosphoryl sulphur. Trivalent phosphorus compounds, phosphites are protonated on the phosphorus atom.

In this study methane chemical ionization (CH_4/CD_4) was used for generation of substrate ions. In addition to the protonation products, $[MH]^+$ or $[MD]^+$, adduct ions, $[M\ C_2H_5]^+$ or $[M\ C_2D_5]^+$, were included for low energy collision activated (CAD) MS/MS analysis.

The site of protonation vs alkylation and dissociation behaviour of products of triethylphosphate, triethylthiophosphate, triethyltetrathiophosphate, diethylethylphosphonate, triethylphosphite, diethylphosphonate, diethylethylphosphonate, dimethylethylthiophosphonate and O-methyl, S-methylethylphosphonothiolate were studied by collision activated dissociation tandem mass spectrometry.

RESULTS

The $[MH]^+$ ions of triethylphosphate and triethylthiophosphate dissociates by loosing C_2H_4 consecutively producing m/z 155^+, m/z 127^+, m/z 99^+ and m/z 171^+, 143^+, m/z 115^+ respectively. The product ion spectrum of $[M\ C_2D_5]^+$ of triethylphosphate shows loss of 3 x C_2H_4 and C_2D_4. These results indicates that C_2D_5 group has become equivalent with the C_2H_5 groups originally present in the substrate molecule. The adduct ion $[M\ C_2D_5]^+$ of triethylthiophosphate shows fragmentation where C_2H_4 is lost three times, but C_2D_5 group bonded to thiophosphoryl sulphur do not show any significant fragmentation under 10 eV collision energy. The dissociation behaviour of triethyltetratiophosphate shows different fragmentation behaviour than triethylphosphate and triethylthiophosphate. The main fragmentation channel is loss of C_2H_5SH which supports ester sulphur protonation. ERMS of MH^+ shows loss of C_2H_4 in the second step when CIE >10 eV. The protonated diethylethylphosphonate dissociates by fragmenting C_2H_4 and C_2H_4. The adduct ions $[M\ C_2H_5]^+$ and $[M\ C_2D_5]^+$ show in the CAD fragmentation that all three ethoxy groups have become equivalent. Dissociation of $[MH]^+$ of triethylphosphite shows loss of C_2H_4 three times as main fragmentation channel which indicates phosphorus protonation. Also the ion corresponding loss of C_2H_5OH is present, which supports the oxygen protonation.

For confirmation of ion structures some reference ions were synthetized. The site of alkylation by $[C_2H_5]^+$ at diethylethylphosphonate is propably phosphoryl oxygen (SCHEME 1).

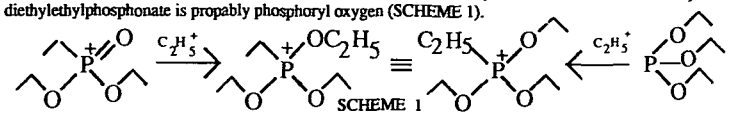

SCHEME 1

The product phosphonium ion contains three equal ethoxy groups . The corresponding deuterated reference ion was synthetized by alkylation of triethylphosphite (SCHEME 2).

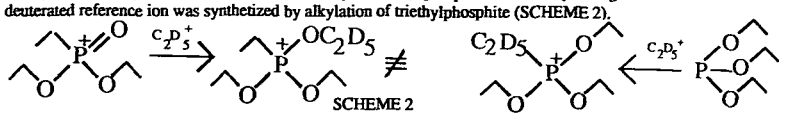

SCHEME 2

The main site for reaction is trivalent phosphorus. The reaction products using $[C_2D_5]^+$ -ion as alkylating agent have not any more the same ion structures as the CAD spectra confirm. Dimethylethylthiophosphonate is bifunctional for protonation reaction. The $[MD]^+$ gives as fragment ion m/z 123, which corresponds to loss of CH_3OD. The ion $[MC_2D_5]^+$ fragments by giving losses C_2D_4 and $CH_3OC_2D_5$. This supports two alkylation sites for thiophosphoryl sulphur and methoxy oxygen.

O-methyl, S-metylethylphosphonotiolate is a three-functional compound for alkylation reaction. The adduct ion $[MC_2D_5]^+$ gives two primary fragment ions; m/z 156 and m/z 107, corresponding to losses of C_2D_4 and $CH_3SC_2D_5$. The fragmentation indicates phosphoryl oxygen and thiomethoxy sulphur alkylation.

CONCLUSION

The protonation and alkylation products of several organophosphorus compounds were synthetized in conventional CI-source. The structures of reaction products and sites of protonation and alkylation were studied by low energy tandem mass spectrometry. The results show that phosphates and thiophosphates alkylates mainly at phosphoryl oxygen and thiophosphoryl sulphur, respectively. Tetrathiophosphates alkylates mainly at ether sulphur. The main reaction site of phosphites is the trivalent phosphorus atom and as minor site ether oxygen. Multifunctional thiophosphonates give mixture of ions, where reaction sites have been phosphoryl and thiophosphoryl groups and also ether oxygen and thioether sulphur.

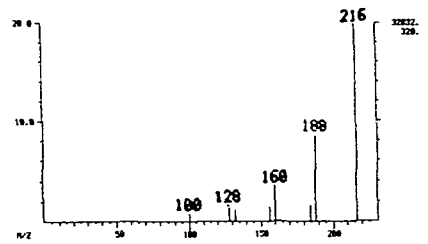

10 eV CAD spectrum of $[M\ C_2D_5]^+$ ion of triethylphosphate

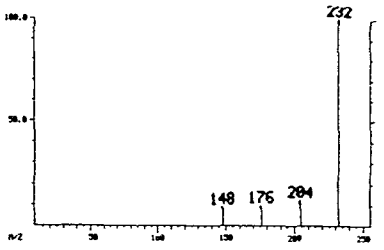

10 eV CAD spectrum of $[M\ C_2D_5]^+$ ion of triethylthiophosphate

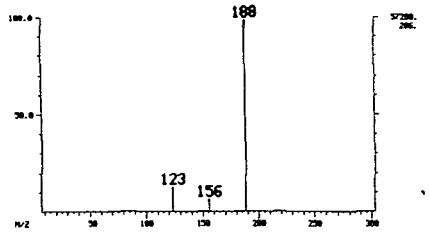

10 eV CAD spectrum of $[M\ C_2D_5]^+$ ion of dimethylethylthiophosphonate

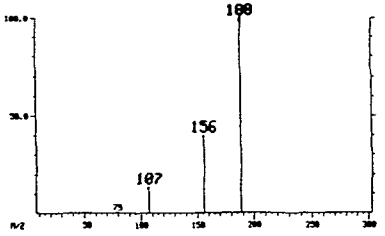

10 eV CAD spectrum of $[M\ C_2D_5]^+$ ion of O-methyl, S-methylethylphosphonothiolate

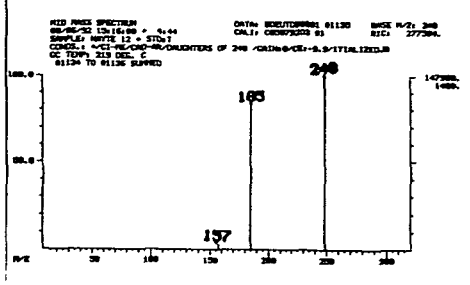

10 eV CAD spectrum of $[MD]^+$ ion of triethyltetrathiophosphate

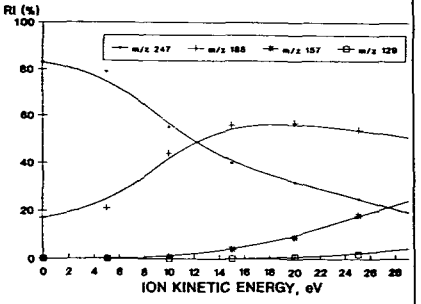

ERMS of $[MH]^+$ ion of triethyltetrathiophosphate

Ion-Molecule Reactions of Dicoordinated Boron Cations With Alcohols

Thilini D. Ranatunga and Hilkka I. Kenttämaa
Department of Chemistry, Purdue University, West Lafayette, IN 47907

Dicoordinated boron cations are proposed to exist as transient intermediates in solution reactions. Condensed phase studies of these highly electrophilic species are limited to ions with bulky substituents which are strongly π- back bonded to boron. On the other hand, dicoordinated boron cations are easily generated in the gas phase upon electron ionization of boron compounds. Therefore, mass spectrometric methods are useful in the study of the properties and reactivity of highly reactive boron cations, such as $CH_3BCH_3^+$ and $CH_3OBOCH_3^+$. Our earlier studies on the reaction of these boron cations with organic ethers revealed that $CH_3BCH_3^+$ and $CH_3OBOCH_3^+$ dehydrate ethers by stepwise elimination of two alkene molecules from a proton bound intermediate.[1] An adduct of a neutral alcohol and the boron cation is expected to occur as an intermediate in the reaction. Therefore, reactions of alcohols with the boron cations have been studied.

The boron cations $CH_3BCH_3^+$ and $CH_3OBOCH_3^+$ undergo very fast reactions with alcohols, most of which occur by abstraction of a water molecule from the alcohol, leading to elimination of an alkene from a proton bound intermediate **b** (Scheme 1). The proton affinity (PA) of $(CH_3O)_2BOH$, determined by proton affinity bracketing experiments to be 198 kcal/mol at OCH_3 and 178 kcal/mol at OH, is greater than that of $CH_2{=}CH_2$. Thus the proton is more strongly bound to $(CH_3O)_2BOH$. This results in elimination of ethylene from the proton bound adduct, resulting in $(CH_3O)_2B(OH_2)^+$ (m/z 91) as the major product. The product ion of m/z 91 is proposed to rearrange to a more stable form $(CH_3O)(OH)B(HOCH_3)^+$ via intramolecular 1,3-hydrogen transfer. Support for the proposed mechanism was obtained from several experimental approaches, such as CAD, deuterium labeling and reactions with several other alcohols. Alcohols such as methanol that cannot lose an alkene molecule are not dehydrated by boron cations. Reaction of $CH_3OBOCH_3^+$ with d_4-methanol yields product ions $CH_3OBOCD_3^+$ (m/z 76) and $CD_3OBOCD_3^+$ (m/z 79), showing that an intramolecular 1,3-hydrogen transfer occurs in boron cations of type **c** in Scheme 1. The ion $CH_3OBOCH_3^+$ reacts with neopentyl alcohol by abstraction of water which rules out the possibility of the reaction proceeding via a four membered transition state. The secondary products from the reaction of $CH_3OBOCH_3^+$ with ethanol are proposed to arise from replacement of methanol with ethanol as shown in Scheme 1.

In addition to elimination of a water molecule from the alcohols, a facile abstraction of OH was observed upon reaction of the ions $CH_3BCH_3^+$ and $CH_3OBOCH_3^+$ with certain alcohols. For example, $CH_3BCH_3^+$ abstracts OH from n-propanol while $CH_3OBOCH_3^+$ abstracts OH from cyclohexanol and n-pentanol. Abstraction of OH is proposed to occur via the same proton bound intermediate which occurs during water elimination reaction. The relative extent of the water and

OH abstraction reactions depends on the relative exothermicities of the reactions, which is determined by the relative stability of the alkyl ion formed. The formation of the very strong B-O bond is likely to be the driving force for all these reactions.

1. Ranatunga, T. D.; Kenttamaa, H. I. *J. Am. Chem. Soc.* **1992**, 114, 8600.

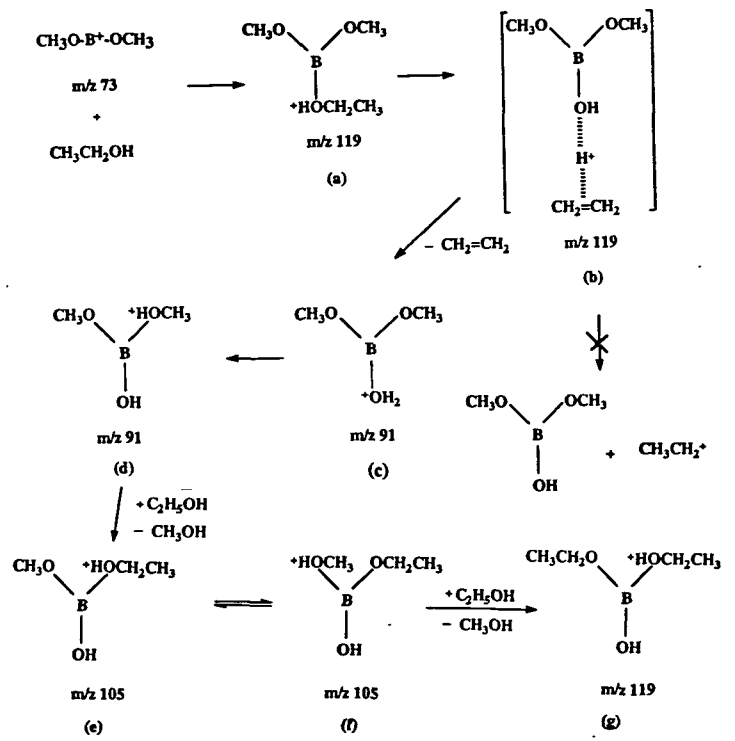

Scheme 1

Two-Center Three-Electron Sulfur-Sulfur Bond Energies in Gas-Phase $[(Me)_2S\therefore S(Me)_2]^+$ and $[(Et)_2S\therefore S(Et)_2]^+$.

Andreas Illies, Mary A. James, Michael Peschke, and Ying Deng
Department of Chemistry,
Auburn University,
Auburn, Al 36849.

The sulfur-sulfur bonds in $[Me_2S\therefore SMe_2]^+$ and $[Et_2S\therefore SEt_2]^+$ are examples of two-center three-electron (2c-3e or a $2\sigma/1\sigma^*$) bonds; these 2c-3e bonds were first described in 1931 by Linus Pauling.[1] A simple molecular-orbital representation of this form of bonding is shown by the potential-energy diagram.

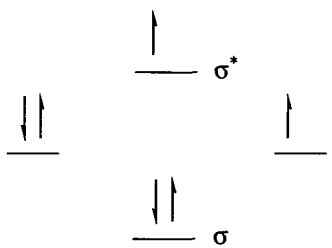

Here we present a thorough study of the experimental sulfur-sulfur bond energies for $[Me_2S\therefore SMe]^+$ and $[Et_2S\therefore SEt]^+$. The goals of our studies are to determine ΔG°_{rxn} from equilibrium studies and, hence, the bond enthalpy (ΔH°_{bond}) from the temperature dependence. For an association reaction, the bond enthalpy (ΔH°_{bond}) is the negative of the reaction enthalpy (ΔH°_{rxn}), and the values of the bond enthalpy and bond energy are nearly the same. The gas-phase ion-molecule reactions:

$$[Me_2S]^+ + SMe_2 + M \Leftrightarrow [Me_2S\therefore SMe_2]^+ + M$$

$$[Et_2S]^+ + SEt_2 + M \Leftrightarrow [Et_2S\therefore SEt_2]^+ + M$$

were studied in SF_4 and CF_4 bath gases as a function of temperature. The reaction enthalpies and entropies, were determined from the van't Hoff equation;

(1) Pauling, L. *J. Am. Chem. Soc.* **1931**, *53*, 3225.

$$\ln Kp = -\Delta H^\circ_{rxn}/RT + \Delta S^\circ_{rxn}/R$$

The van't Hoff plots for the two reactions are shown.

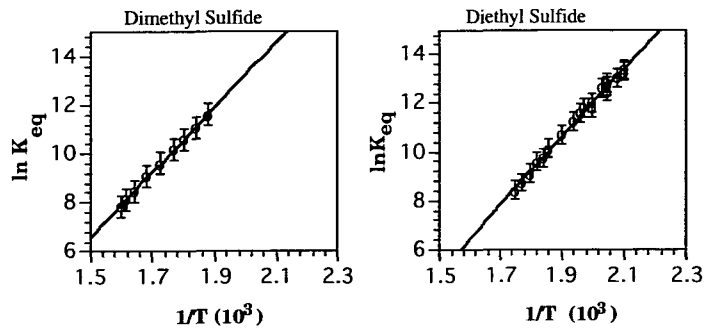

The reaction enthalpies and entropies determined from our data are ΔH°_{rxn} = -26.5 kcal/mol and ΔS°_{rxn} = - 26 cal/mol K for $[Me_2S\therefore SMe_2]^+$ and ΔH°_{rxn} = -27.6 kcal/mol and ΔS°_{rxn} = - 31.4 cal/mol K for $[Et_2S\therefore SEt_2]^+$. The bond enthalpy is the negative of the bond reaction enthalpy and is ≈ 40% of an ordinary two-center two-electron (2c-2e) S-S bond.

Ab initio calculations predict a bond energy of 27.4 kcal/mol and the geometry shown for the $[Me_2S\therefore SMe_2]^+$ molecule. *Ab initio* calculations on $[Et_2S\therefore SEt_2]^+$ are in progress.

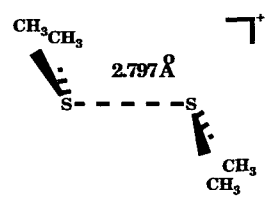

The S-S$^+$ bond enthalpies reported here are about 40% of that for an average S-S 2c-2e covalent interaction. These data represent the first reliable gas-phase measurement for a sulfur-sulfur 2c-3e bond in an organic molecule. Research on other S∴S$^+$ interactions are in progress.

PRODUCT FORMATION AND FRAGMENTATION PATHWAY FOR THE REACTION OF BENZENE AND *N*-METHYLIMIDAZOLE

A.B. Whitehill, M. George, D. Giblin, and M.L. Gross, Midwest Center for Mass Spectrometry, Department of Chemistry, University of Nebraska-Lincoln, Lincoln, NE 68588-0304.

Mass spectrometry has been used extensively to study gas-phase ion-molecule reactions. This is due in part to the ability of mass spectrometers to generate ionic species and to carry out controlled reactions with neutral species. This study deals with gas-phase ion-molecule reactions between polyaromatic hydrocarbon (PAH) radical cations and *N*-methylimidazole.

Radical cations are known to take part in biological chemistry, often occurring as intermediates in metabolic pathways. These radical cations are thus necessary to living species. However, it has been proposed by Cavalieri and coworkers that enzymatically created radical cations of PAH's such as benzo[*a*]pyrene and 7,12-dimethylbenz[*a*]anthracene may be the ultimate carcinogens derived from these species. If radical cations of PAH's are of biological significance, then mass spectrometry could play an important role in understanding the reactivity of these species. It is also for these reasons that the current investigation involving the reactions of benzene, as the simplest member of the PAH's, was initiated.

This study was initiated as a starting point for evaluating the gas-phase reactivity of radical cations derived from PAH's toward model biological nucleophiles. Now that this simple system is understood we can extend this study to a series of PAH's ranging from non-carcinogenic to carcinogenic. Once a series of PAH's have been analyzed it can be determined of the gas-phase reactivity of radical cations correlates with their biological activity.

Chemical ionization (CI), fast atom bombardment (FAB) and MS/MS experiments were performed on a Kratos MS-50 triple analyzer equipped with a MACH3 data system. CI experiments were performed at a source pressure of approximately 0.1 torr. Activation was achieved in the third field-free region (between magnet and second ESA) with helium as the collision gas at 50% beam reduction.

To enhance the metastable decomposition of some ions preheating of the FAB ions was accomplished by collisional excitation in the first field-free region (between source and first ESA). Helium was employed as the collision gas at pressures sufficient for 50-80% beam reduction. To select the collisionally activated ions, the outer member of the beta slits (after the first ESA) was used to eliminate the uncollided ions, which occur at higher energy, The 'hot' precursor ions were then transmitted to the third field-free region for metastable and CA experiments.

FTMS (Fourier transform mass spectrometry) experiments were performed on a custom-built instrument equipped with a cell capable of RF-only mode experiments. During the RF-only experiments, helium was used as the bath gas.

Early CI experiments showed that an adduct of *m/z* 160 formed in an ionized mixture of benzene and *N*-methylimidazole. FTMS experiments proved that the *N*-methylimidazole radical cation and neutral benzene were the reactants.

Once the reactants were established, the structure of the adduct ion was pursued. CAD spectra of the adduct provided little information as the fragment ions were mainly reactants; however, hydrogen atom loss was shown to occur to produce an even-electron ion of *m/z* 159. Experiments with d_6-benzene proved that the hydrogen atom loss was from the benzene moiety.

Because the CAD spectrum of the *m/z* 160 adduct provides little information, the structure of the even-electron ion at *m/z* 159 was pursued. The hydrogen atom loss allows us to postulate the *m/z* 159 ion as the C_6H_5 moiety attached to the imidazole ring. With this in mind, three reference compounds were synthesized for comparison. Their structures are shown below.

Standard *1*

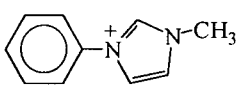

Standard *2*

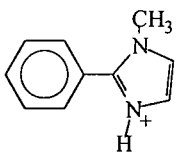

Standard *3*

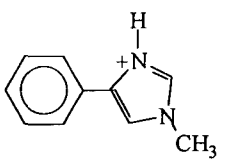

Comparison of metastable and CAD spectra of the adduct and the three standards allowed us to rule out standard *3* as a possibility. Standards *1* and *2* have similar spectra to each other and the CI adduct which does not allow differentiation.

To differentiate between standards *1* and *2* , the methyl groups in both were substituted with a CD_3 group. For comparison, benzene was reacted with *N*-CD_3-imidazole to produce a radical cation at *m/z* 163. In a MS3 experiment, this ion produced one at *m/z* 162 via CAD. The daughter ion at *m/z* 162 was then CAD analyzed for comparison. After analysis it was determined that the *m/z* 159 CI ion closely resembled standard *3*. This information is summarized in the scheme shown below.

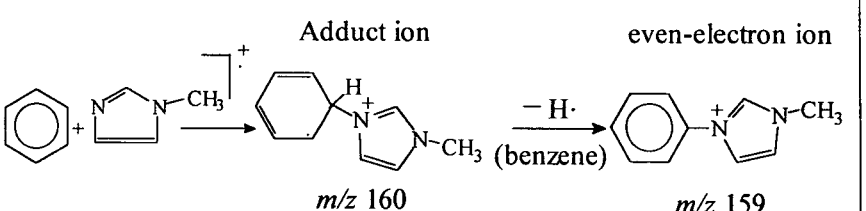

Investigation of Electrophile/Nucleophile Reactions of Polyheteroatomic Organic Cations with Allylic Molecules in Q2 of a Triple Quadrupole Mass Spectrometer

B V Rozynov[1], R J. Liukkonen[2], R.M. Carlson[2], and D W Kuehl[3]

1. Shemyakin Institute of Bioorganic Chemistry, Moscow, 117871, Russia
2. University of Minnesota-Duluth, Duluth, MN, 55812
3. U.S. EPA ERLD, Duluth, MN, 55804

Introduction

An ever increasing need exists to characterize chemical contaminants in complex environmental samples for those chemicals that are potential mutagens and/or carcinogens. Analyte specific detection must be rapid, sensitive, and cost effective. Our approach to this problem was to evaluate the use of mass selective ion-molecule reactions in the center quadrupole of a triple quadrupole mass spectrometer (1,2). Chemicals containing a nucleophilic heteroatomic center (N,S,O) which represents biomolecules such as DNA or protein are introduced into the ion source. Unknown environmental contaminants, electrophiles which may covalently react with biochemicals, are introduced into Q2 via a direct line or GC column. Analytes reacting with model nucleophilic cations are characterized by scanning Q3.

Experimental

All experiments were conducted on a Finnigan-MAT TSQ-70 triple quadrupole mass spectrometer. Neutral compounds were introduced into Q2 via the CIO transfer line. A sample introduction probe was constructed to provide introduction of liquid samples from the right side of the ion source. Analyses were conducted by Q3MS or Daughter ion experiments where Q1 was used to focus on an ion, Q2 passed all ions, and Q3 scanned for reaction products.

Results and Discussion

Compounds selected as model nucleophiles for this study were low molecular weight N and S containing cyclic compounds. Model electrophiles included a series of allylic compounds with greatly different chemical reactivity and mutagenic potential (3), as well as twelve different epoxides. Two reaction processes were observed, charge transfer and electrophilic addition/elimination. Associative reaction product spectra of three typical model nucleophiles, 5-menthyl-2-thiouracil, quinoline and 2-methylpyrazine are shown in figure 1. In each case, the radical cation molecular ion of the heterocycle was generated in the ion source and allowed to react with allyl bromide in Q2. The spectra show the reaction product 41 daltons greater than the m/z value of the nucleophilic reagent This increase was from the addition of the allyl moiety of allylbromide and loss of bromine.

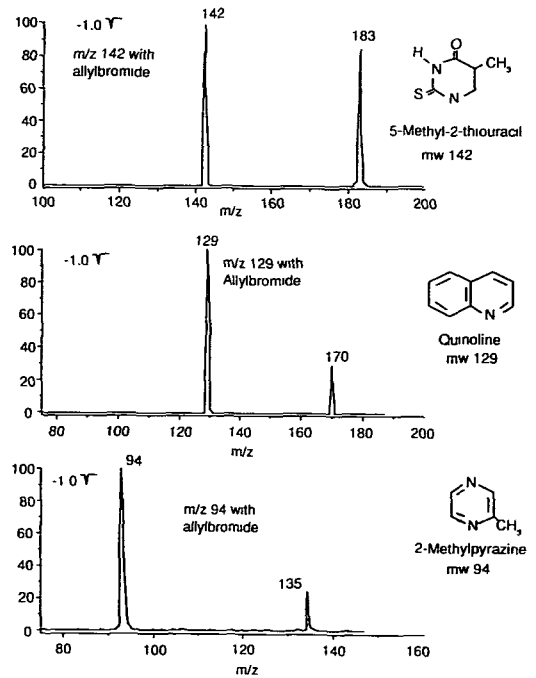

Conclusion

It has been shown that gas-phase ion-molecule reactions in Q2 of a tandem quadruple mass spectrometer may be used to produce reaction products similar to solution phase chemistry. The interaction of ions of N and S containing compounds, which are model compounds for biomolecules such as DNA and protein, with neutral electrophilic reagents can predict in vivo endpoints such as mutagenesis.

References

Freeman, J.A., et. al. J. ASMS 1(1).110 (1990)
Coppersmith, B.I., et. al. 40th ASMS Conference, Washington, D.C., (1992)
Eder, E., et. al. Xenobiotica 12:831 (1982)

An Experimental and Theoretical Study on the Existence of the $H_3C—S\equiv O^+$ Ion as a Stable Gas Phase Species.

*Fábio Cesar Gozzo and *Marcos N. Eberlin*
Universidade Estadual de Campinas, Instituto de Química, CP 6154 Campinas, SP 13081-970 Brazil

Acylium ions are important and stable ionic species both in solution and gas phase. The acetyl cation, $H_3C—C\equiv O^+$, is one of the most important and simplest acylium ions and the most stable among the $C_2H_3O^+$ isomers. One of its sulfur analogs, the thioacetyl cation, $H_3C—C\equiv S^+$, is also a stable and well characterized gas phase species. There is, however, no clear evidence for the existence of $H_3C—S\equiv O^+$ (**1**), another possible sulfur analog of the acetyl cation. Gas phase generation of ion **1** could in principle be easily achieved by loss of methyl from ionized dimethyl sulfoxide but a further loss of water from ion m/z 63 has been interpreted as evidence for generation of the $H_2C=S=OH^+$ isomer (**2**). Recently,[1] the $CH_3—S\equiv O^-$ anion was characterized as a stable gas phase species. This finding opens the possibility that the corresponding cation **1**, as well as many other members of this potentially important class of sulfur analogs of acylium ions, can be also observed as stable gas phase species. Toward this end, this present experimental and theoretical study was undertaken.

Routes to m/z 63 formation from ionized dimethyl sulphoxide. Methyl loss from ionized DMSO could occur by three alternative routes, as shown in Scheme 1. Ion **1** should be formed in case no rearrangement takes place (**I**). A [1,3-H] shift would lead to **II** which upon methyl loss should yield ion **2**. A [1,2-CH_3] shift would lead to **III**, an ion that bears two non equivalent methyl groups and therefore could fragment to ions **4** and/or **1**. Ab initio calculations (Table 1) show that both rearrangements lead to more stable ions, the [1,2-CH_3] shift being the most thermodinamically favored process. The calculations show also that the O-CH_3 group would be lost preferentially from **III**. Therefore, formation of ion **1** is predicted either from **I** or from the more stable isomer, **III**. To evaluate the occurence of a further isomerization of ion **1**, the relative stabilities of ten CH_3SO^+ ions were estimated (Table 1). Among them, only ions **2-4** have the same C-S-O connectivity as that of ion **1**. Isomerization to ions **6-10** would change this connectivity and likely require the participation of the cyclic ion **5** as the intermediate. However, the calculations show that ion **5** does not lie in a potential well, ring opening without barrier to **2**. This makes the isomerizations to **5-10** unlikely, although some of these ions are more stable than **1**. Ion **1** is considerably less stable than **2**, and so the isomerization **1→2** has to be considered. However, transition state calculations show a relative high energy barrier (54.2 Kcal/mol) for this interconversion. Thus, the ab initio calculations indicate ion **1** as the most likely constituent of the m/z 63 population from ionized DMSO.

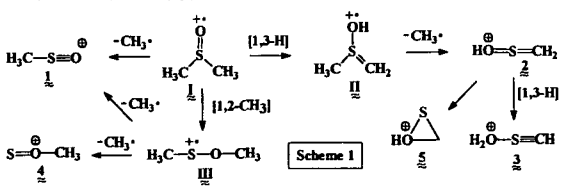

CID decomposition of ion m/z 63. Both high and low energy CID spectra of ion m/z 63 show fragmentation to occur mainly by loss of H_2O, S and SO. The latter fragmentation is no doubt a strong evidence for the presence of ion **1**, since the isomerization **2→1** should not occur (Table 1). The fragmentation by loss of water could be interpreted as presence of ion **2**, but its formation from isomerization of ion **1** induced by collision in the CID cell can not be dismissed.

Ion/Molecule reaction of m/z 63. Recently,[2] ion/molecule reactions with 1,3-dioxolanes were demonstrated to be a general approach for gas phase identification of acylium and thioacylium ions. The acetyl cation reacts to form a very abundant "oxirane addition" product at m/z 87, while its isomers, the oxarinyl cation and the $H_2C=C=OH^+$ cation, react mainly by proton tranfer. Ion m/z 63 from ionized dimethyl sulfoxide reacts with 1,3-dioxolane (Scheme 2) forming an abundant oxirane addition product ion at m/z 107. This , in analogy with the results for the $C_2H_3O^+$ isomers, indicates that the ionic beam consists mainly of ions **1**. The MS^3 spectrum of m/z 107 (Figure 1) shows fragmentation mainly to CH_3SO^+, as expected from the CID behavior of analog ions.

Table 1- Relative Energies (in Kcal/mol) for the ionic species at the MP2/6-31G**//6-31G** + ZPE level

I	25 0	1	42.0	6	42.8
II	18.0	2	22.2	7	45.0
III	zero	3	13.8[1]	8	zero
		4	65.4	9	15.7[3]
		5	22.8[2]	10	21.8

1- HCS^+ + H_2O 2- ion 2 3-HCO^+ + H_2S

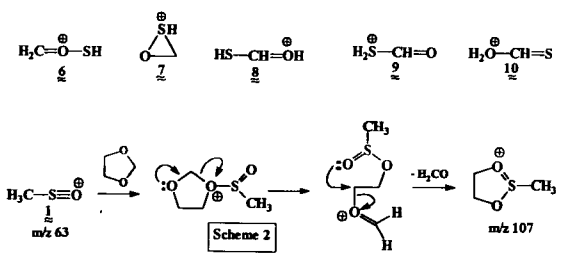

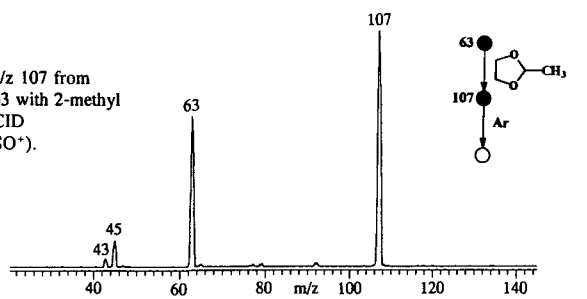

Figure 1 - MS^3 spectrum of m/z 107 from ion/molecule reaction of m/z 63 with 2-methyl 1,3-dioxolane, showing main CID fragmentation to m/z 63 (CH_3SO^+).

1-Downard,K.M.; Bowie,J.H.; O'Hair,R.A.J.; Krempp,M.; DePuy,C.H. *Int. J. Mass Spectrom. Ion Processes.* **1992**, 120, 217.
2- Eberlin, M.N; Cooks, R.G., *Org. Mass Spectrom.*, in press.

FAPESP

The Rich Gas Phase Ion/Molecule Chemistry of The Distonic Radical Cation $^{\cdot}CH_2$—O—CH_2^+ Revealed By Multiple Stage (MS^2 and MS^3) Mass Spectrometry Experiments.

Marcos N. Eberlin Universidade Estadual de Campinas, Instituto de Química, CP 6154 Campinas, SP 13081-970 Brazil

Distonic radical cations are chemically fascinating species since they possess, in a formal sense, spatially separated positively charged and radical sites and therefore could display a diverse and rich reactivity induced by both of these sites. The $^{\cdot}$CH2—O—CH2$^+$ ion (**1**) is one of the simplest distonic radical cations, displaying a peculiar ion/molecule reactivity characterized mainly by net $CH_2^{+\cdot}$ (sometimes net CH^+) transfer. No ion/molecule reaction where both the potentially reactive sites of ion **1** participate has yet been observed. In this study, reactions of the mass selected, pure ion **1** with several neutral compounds are investigated by multiple stage mass spectrometry (MS^2 and MS^3) experiments performed in the versatile pentaquadrupole instrument.[1] Two unprecedent reactions are observed and several structures of ion/molecule reaction products are determined.

The bydented character of ion 1. Reactions with Benzene and Anisole: The MS^2 product spectra for reaction with these two compounds reveal an interesting ion/molecule reaction in which both of the reactive sites of ion **1** participate. The ions observed at m/z 121 and m/z 151, respectively, are the products of a reaction occuring by net $C_2H_3O^+$ transfer, or in other words, proceeding by loss of a hydrogen atom from the intact adducts. Formation of ions **3** are determined by MS^3 experiments (Figure 1) and supported by high level ab initio calculations. The proposed mechanism (Scheme 1) involves an initial electrophilic attack of the positively charged site of ion **1**, followed by a [1,4-H] shift promoted by the radical site which is now incorporated into the adduct structure. This hydrogen shift regenerates the ring aromaticity and leads to formation of the ionized benzyl methyl ether **2**. Further loss from **2** of an hydrogen atom forms **3**. No rearrangement of **3** to the tropylium ion **4** or, alternatively, of ions **2** to the ionized cycloheptatriene **5**, are noted.

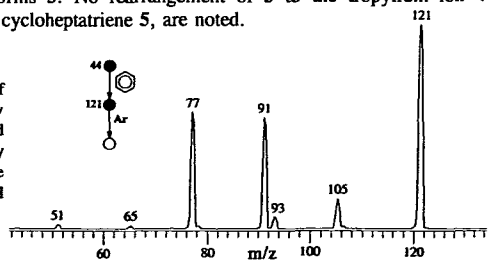

Figure 1- MS^3 sequential product spectrum of ion m/z 121 (assigned as **3**) formed by ion/molecule reaction between mass-selected ion **1** and benzene. This spectrum is very similar to the MS^2 CID spectrum of the authentic ion produced from ionized benzyl methyl ether.

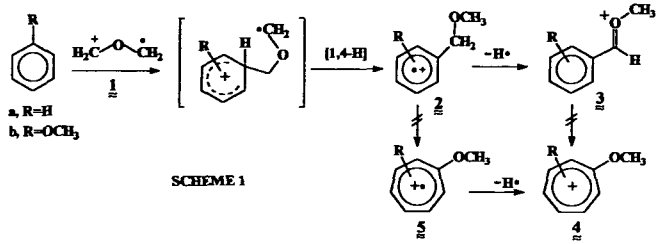

SCHEME 1

A "hole-catalysed"[2] 1,3-dipolar cycloaddition to Ketones: Ion m/z 99 is by far the main product of the ion/molecule reaction between ion **1** and cyclopentanone (Figure 2). This reaction corresponds to net addition of 15u, best assigned to loss of 29u from the intact adduct. Abundant products from similar reactions are also observed for other ketones, i.e. acetone, 2-butanone and 3-pentanone. This reactivity can be accounted for by addition of ion **1** to the carbonyl group (Scheme 2) yielding the ionized 4,4-disubstituted dioxolane intermediates **6**. **1** is the ionized form of the simplest carbonyl ylid $^{\cdot}CH_2$-O-CH_2^+ and by using the terminology introduced by Bauld,[2] this reaction can be classified as a "hole-catalysed" 1,3-dipolar cycloaddition, an unprecedent gas phase reaction. The cycloadducts **6** fragment completely to the cyclic oxonium ions **7** by loss of one of the 4-substituents. Only loss of methyl for acetone and ethyl for 3-pentanone are observed, while 2-butanone shows losses of both methyl and ethyl, the latter being largely predominant. The intermediate for cyclopentanone would be the ionized spiro compound **6d**. This radical cation, in analogy to the fragmentation behavior of 1,4-dioxospiro[4,5]-decane and several analog ions is expected to fragment mainly by loss of ethyl to form m/z 99 and also by loss of a neutral molecule of C_3H_6 to form m/z 86 (Scheme 3), as indeed observed. Formation of ions **7** are also supported by MS^3 experiments and high level ab initio calculations. A stepwise mechanism similar to that presented in Scheme 2 has been proposed for the ionized methylene transfer reaction of the distonic ion $^{\cdot}CH_2CH_2$—O-CH_2^+ to acetonitrile.[3]

Figure 2- MS^2 product spectrum of ion/molecule reactions between mass-selected ion **1** and cyclopentanone, showing product ions corresponding to net CH^+ (m/z 97) and $CH_2^{+\cdot}$ (m/z 98) transfers and the ones assigned to the products of a "hole-catalysed" 1,3-dipolar cycloaddition (m/z 99 and m/z 86).

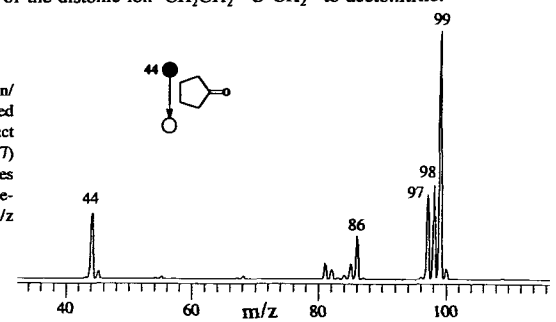

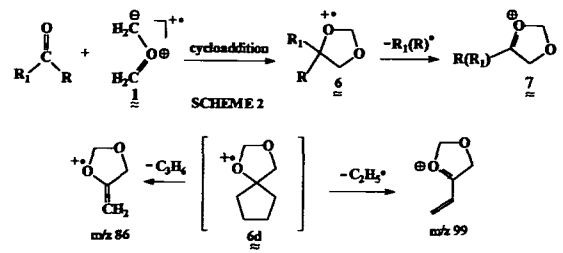

SCHEME 2

SCHEME 3

1- Schwartz, J.C.; Schey, K.L.; Cooks, R.G *Int. J. Mass Spectrom. Ion Proc.* **1990**, 101, 1
2- Kim, T.; Pye, J.; Bauld, N.L. *J. Am. Chem. Soc.* **1990**, 112, 6285.
3- Wittneben, D.; Grützmacher, H.-F. *Int. J. Mass Spectrom. Ion Proc.* **1990**, 100, 545

FAPESP

Gas Phase Addition / Elimination Reactions of Carbanions with Carbonyl Groups measured on the Quadrupole, Quistor, Quadrupole Tandem Mass Spectrometer

M. Stöckli, P. Kofel and U. P. Schlunegger
Institute of Organic Chemistry, University of Bern, Freiestr. 3, CH-3012 Bern, Switzerland

Nucleophilic addition of carbanions **1** to carbonyl groups is of considerable importance in organic chemistry. In the general form, the reaction proceeds by a tetrahedral intermediate. The tetrahedral intermediate **2** has been found in a few cases in solution. However, since such addition ions are formed with excess energy, they either revert to reactants or fragment to different products in the absence of stabilising collisions, which is typical for the low pressure conditions used in gas phase ion chemistry. In the presence of a good leaving group L this group is eliminated from the intermediate **2**. Depending on the proton affinity of the leaving group a proton is transfered to the leaving group, and correspondingly either the leaving group anion **3** or the deprotonated addition / elimination product anion **4** is observed [1,2]:

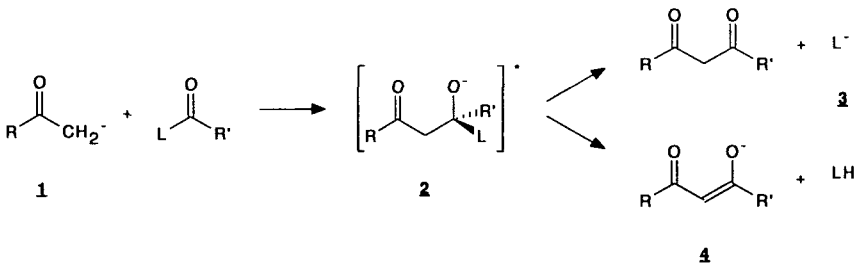

For the study of such reactions a purpose built quadrupole, quistor, quadrupole tandem mass spectrometer [3] was modified for operation in negative ion mode.
Primary ions were generated in a differentially pumped external ion source under negative CI conditions with ammonia, mass selected by a first quadrupole mass filter and injected into a quistor. After a variable storage period in the quistor for reaction the product ions were extracted and analysed by a second quadrupole mass filter. Experimental parameters were: pressure differential 30'000 (between source and quistor chambers); ionization / injection time 10 ms; nominal injection energy 1 ... 2 eV; helium pressure 10^{-3} mbar; reagent pressure $1\ 10^{-6}$ ... $2\ 10^{-5}$ mbar; reaction time 10 ms ... 1 s; quistor radius 1 cm; radiofrequency 1.3 MHz; rf amplitude 370 V (exclusion limit *m/z* 24).
For the detection of negative ions with a secondary electron multiplier the electron current collector has to be floated at a high voltage potential (typically + 5 kV). For operation of the amplifier and recording electronics close to ground potential the electron current was decoupled by a high voltage capacitor. This simple solution could be chosen because the ion currents arrive as a pulse during the extraction event of the pulse sequence:

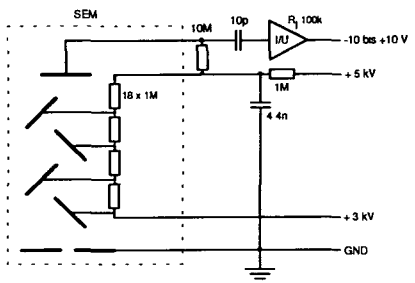

The following reactions were studied and their rate constants determined:

Reagent	Anion **1** ****	Anion **3**	PA Anion **3** / [kJ/mole]	Anion **4**	Rate constant / [cm^3/s/mol.]
2,2,2-Trifluor-ethyl acetate	$CHOCH_2^-$	$\{CF_3CH_2O^-\}$	1551	$CHOCH{=}COCH_3^-$	$5\ 10^{-11}$ *
Vinyl acetate	$CHOCH_2^-$	$\{CH_2{=}CHO^-\}$	1531	$CHOCH{=}COCH_3^-$	$1.4\ 10^{-11}$
Chloral	$CHOCH_2^-$	CCl_3^- **	1494	$\{CHOCH{=}CHO^-\}$	$7\ 10^{-10}$
Ethanoyl chloride	$CHOCH_2^-$	Cl^-	1393	$\{CHOCH{=}COCH_3^-\}$	$2\ 10^{-9}$
Vinyl acetate	$CHOC(CH_3)_2^-$	$CH_2{=}CHO^-$	1531	***	$3\ 10^{-10}$

{ } Corresponding m/z not observed.
* Compares to $1.25\ 10^{-10}$ cm^3/s/mol. obtained in an ICR study [1].
** A second major product ion $CHOCCl_2^-$ (Cl^+ transfer) has been observed, too.
*** Possibly O^--attack, β-dicarbonyl product contains no α-hydrogens.
**** $CHOCH_2^-$ was produced from acetaldehyde and $CHOC(CH_3)_2^-$ from isobutyraldehyde.

These results are consistent with the mechanism given above. The addition / elimination product is only observed as an ion if the leaving group has a high proton affinity. The measurement of the pressure in the quistor has to be improved in the future to remove the large uncertainty in the measured rate constants.

References:

[1] J.E. Bartmess, R.L. Hays, G. Caldwell, *J. Am. Chem. Soc.*, 1981, 103, 1338.
[2] H. van der Wel, Thesis, Amsterdam, 1988, Chapter 8, p. 113.
[3] P. Kofel, H. Reinhard, U.P. Schlunegger, *Organic Mass Spectrom.*, 1991, 26, 463.
[4] H. Reinhard, Thesis, Bern, 1992.
[5] R.L. Summers, Technical Note TN D-5285, NASA, Washington, D.C., 1969.

Support from the Swiss National Science Foundation is gratefully acknowledged.

METHANE LOSS IN DIMETHYL AND TRIMETHYL OXONIUM IONS

H. E. Audier,(1) D. Berthomieu (2) and T. B. Mc Mahon (3)

(1) DCMR, Ecole Polytechnique, Route de Saclay, 91128 PALAISEAU Cedex - FRANCE
(2) LPCR, Centre Universitaire d'Orsay, 91405 ORSAY Cedex - FRANCE
(3) University of Waterloo, Waterloo, Ontario, CANADA N2L 3G1

Dimethyl and trimethyl oxonium ions, **1** and **2**, eliminate CH_4 to yield CH_2OH^+ and $CH_3OCH_2^+$ respectively. On the basis of threshold collision induced decomposition studies, Wang, Squires and Farcasiu[1] have previously proposed that the fragmentation of $(CH_3)_3O^+$ "occurs by a heterolytic cleavage mechanism, with the critical transition state strongly resembling a $CH_3^+/(CH_3)_2O$ complex." Farcasin and Pancirov[2] have also studied the unimolecular dissociation of labelled $(CH_3)_3O$ but have cautioned than in their studies they" are not sure that the mixture of ions have reached equilibrium." In the present study several different complementary approaches have been used to probe the mechanism of CH_3^+/CH_3OH and $CH_3^+/(CH_3)_2O$ reactions.

Unimolecular Dissociation in a Reverse-Geometry Mass Spectrometer

Ions **1** and **2** were generated in the ion source of a VG ZAB-2F mass spectrometer by reaction of CH_3X(X=OH or I) with either methanol or dimethyl ether using H_2O as the chemical ionization reagent gas and their subsequent fragmentation examined in the 2nd field free region.

(1) The similar behaviour of $C_2H_4D_3O^+$ ions generated from either CD_3OH/CH_3I, CD_3OH/CH_3OH or CH_3OH/CD_3I mixtures shows that these reagents all yield the protonated dimethyl ether, $CH_3OHCD_3^+$.

(2) This $CH_3OHCD_3^+$ ion subsequently eliminates either CHD_3 or CH_3D in a ratio of 45:55. Similarly generated $(CH_2D)_2OH^+$ loses CH_3D or CH_2D_2 in a ratio of 63:37, revealing the existence of an important secondary isotope effect and a minimal primary isotope effect. These data can be rationalized either by the intermediacy of a $[CH_3^+{\cdot}CH_3OH]$ complex or by a concerted asynchronous process in which the transition state closely resembles such an ion-neutral complex.

(3) In the case of labelled trimethyloxonium ions, similar experiments lead to the conclusion that the primary isotope effect is more important that in the preceding, dimethyloxonium, case and the secondary isotope effect remains significant, indicating that the elongation of the C-O bond plays a determinant role in the mechanism.

Bimolecular Ion-Molecule reactions in a FT-ICR Cell

The ion-molecule reactions between various isotopically labelled methyl cations, generated in an external ion source, and labelled neutral methanols and dimethyl ethers have been studied in the FT-ICR

cell of a Bruker CMS-47X spectrometer Such experiments clearly demonstrate that two competitive processes occur under ICR conditions: (i) the formation of an oxonium ion intermediate which dissociates *via* loss of methane, and (ii) a direct reaction in which the initial methyl cation abstracts a hydride from a methyl group of the neutral molecule.

(1) The reaction of CD_3^+ with CH_3OH leads to CHD_3 and CH_3D losses in a ratio of 59:41, while in the reaction of CH_3+ with CD_3OH these same neutrals are lost in a ratio of 46:54.

(2) $^{13}CH_3^+$ reacts with $(CH_3)_2O$ to yield CH_4 and $^{13}CH_4$ in a ratio of 56:44 whereas a mechanism involving statistical losses from a trimethyloxonium ion intermediate would yield a ratio of 2:1.

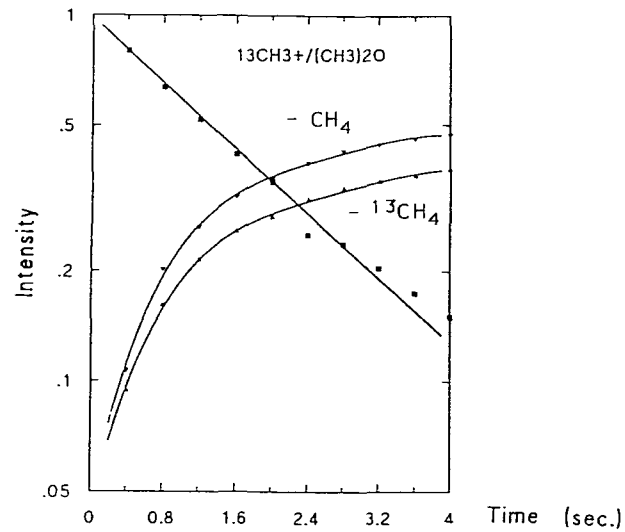

Ab Initio Calculations

Ab initio calculations have been carried out on $(CH_3)_2OH^+$ wich indicate that CH_4 loss may occur *via* a concerted process involving a transition state which has the structure of a $[CH_3^+,CH_3OH]$ complex. For the moment, although no minimum corresponding to a stable ion-neutral complex has been located on the potential energy surface, it cannot be definitively stated that such complexes are not present. On the opposite a $[CH_4,CH_2OH^+]$ complex has been shown to be a stable structure.

(1) D. Wang, R. Squire and D. Farcasiu
Int. J. Mass Spectrom. Ion Proc., **107**, R7 (1191)
(2) D. Farcasiu and R.G. Pancirov
Ion Proc. , **74**, 207 (1986)

DEPROTONATION OF $^{\bullet}CH_2(CH_2)_nXH_2^+$ DISTONIC IONS ($n = 0, 1$; $X = OH, OCH_3, NH_2$)

H.E. Audier[1], D. Leblanc[1], P. Mourgues[1] and S. Hammerum[2]
1 D.C.M.R. Ecole Polytechnique, 91128 Palaiseau Cedex, France
2 University of Copenhagen, DK 2100 Denmark

Is there a significant difference between the Proton Affinities (PA) of the radicals $^{\bullet}CH_2(CH_2)nXH$ (X = O ; NH) and those of the corresponding alcohols or amines ? In order to answer this question we have determined the acidity of the α and β-distonic radical cations $^{\bullet}CH_2XH^+$ and $^{\bullet}CH_2CH_2XH^+$ (X = OH, OCH_3, NH_2) by studying the proton transfer from these ions to a serie of neutral molecules of known proton affinities; this allows us to bracket the proton affinities of the corresponding radicals.

α-Distonic radical cations

$^{\bullet}CH_2OH_2^+$

This ion does not protonate CS_2, CH_3Br and water. On the opposite, protonation of CF_3COOH, CF_3CD_2OD and CH_3I is observed.

These results show that the proton affinity of hydroxymethyl radical, $^{\bullet}CH_2OH$ is between that of H_2O and that of CF_3COOH. Based on the proton affinities recently published, we suggest that PA($^{\bullet}CH_2OH$) is 166 ± 2 kcal.mol^{-1}. By comparison, the PA of methanol is 182 kcal.mol^{-1}.

$^{\bullet}CH_2NH_3^+$

This ion does not protonate acetone-d_6 nor tetrahydrofuran-d_8, while C_6H_5CDO, and NH_3 are protonated.

These results for $^{\bullet}CH_2NH_3^+$ allow us to derive a proton affinity of 199 ± 2 kcal.mol^{-1} for $^{\bullet}CH_2NH_2$. By comparison, the PA of methylamine is 214 kcal.mol^{-1}.

Our results show that the hydroxymethyl and the aminomethyl radicals are considerably less basic in the gas phase than methanol and methylamine, which agrees well with measurements reported for these and related species in condensed phase.

β-Distonic radical cations

$^{\bullet}CH_2CH_2OHCH_3^+$

The PA of $^{\bullet}CH_2CH_2OHCH_3$ lies between that of acetonitrile and that of dimethyl ether; slow proton transfer is observed to toluene-d_8 and to acetic acid. This leads us to suggest that PA ($^{\bullet}CH_2CH_2OCH_3$) is 191 + 1 kcal.mol^{-1}. By comparison, the PA of methyl ethyl ether is 196 kcal.mol^{-1}.

$^{\bullet}CH_2CH_2NH_3^+$

This ion protonates methylamine (rapidly) and dimethyl sulfoxide (more slowly), which leads us to propose that PA ($^{\bullet}CH_2CH_2NH_2$) is 212 + 2 kcal mol^{-1}. PA(ethylamine) is 217 kcal mol^{-1}.

Our results indicate that the proton affinities of β-aminoalkyl and β-hydroxyalkyl radicals are lower than those of the corresponding even-electron molecules. The difference is, however, not nearly as pronounced as for the α-substituted radicals.

Studies of the proton transfer reactions of β-distonic ions are frequently complicated by rapid, competing reactions, such as charge exchange and transfer of ethylene$^{+\cdot}$. Furthermore, a number of very recent observations suggest that the reactions of α- and β-distonic ions with neutral species of similar acidity may be accompanied by isomerization. If substantiated by further studies, this phenomenon may require reinterpretation of some of the present results.

REACTION OF TERT-$C_4H_9^+$ CATION WITH ARENES : INTERMEDIACY OF Π-COMPLEXES

D Berthomieu[1], V Brenner[2], G. Ohanessian[1], J P. Denhez[1], P. Millié[2] and H E Audier[1]

(1) D C M R. Ecole Polytechnique, 91128 Palaiseau Cedex, France

(2) C E A.-C E Saclay, 91191 Gif-sur-Yvette, France

Introduction

The intermediacy of π-complexes in the fragmentation of metastable protonated alkylbenzenes has been suggested for three reactions :

1. The production of a tert-alkyl fragment from protonated n (or sec)-alkylbenzene (1)

   C_6H_6-n-$C_nH_{2n+1}^+ \rightarrow [C_6H_6, \text{n-}C_nH_{2n+1}^+] \rightarrow [C_6H_6, \text{tert-}C_nH_{2n+1}^+]$

2. The H-exchange preceding the dissociation of C_6H_6-iso-$C_3H_7^+$ (2)

   $C_6H_6\text{-iso-}C_3H_7^+ \leftrightarrow [C_6H_6, \text{iso-}C_3H_7^+] \leftrightarrow [C_6H_7^+, C_3H_6]$

3. The isobutane elimination from protonated tert-butyl alkylbenzenes (3)

   $[\text{tert-}C_4H_9\text{-}C_6H_5\text{-}C_2H_5^+ \rightarrow [\text{tert-}C_4H_9^+, C_6H_5C_2H_5] \rightarrow C_6H_5CH^+CH_3 + C_4H_{10}$

Reactions of tert-$C_4H_9^+$ with arenes

These reactions were performed in the ion-source of a VG-ZAB-2F mass spectrometer (B/E) and the decompositions of the adduct were studied in the 2nd FFR.

1. When the encumbrance is small (Ar = benzene or toluene), there is no difference between the MIKE spectrum of the adduct (tert-$C_4H_9^+$+ arene) and that of the isomeric protonated alkyl arene.

2. On the opposite, it has been shown by radiolytic technique that tert-$C_4H_9^+$ does not react with paraxylene by C-C bond formation.

The adduct (paraxylene + tert-$C_4H_9^+$) leads predominantly (90 %) to a benzylic ion through isobutane loss while the protonated tert-butyl paraxylene leads to tert-$C_4H_9^+$ and to the protonated xylene by the way of isobutene loss. We therefore conclude that the adduct essentially corresponds to a π-complex which is the precursor of the isobutane elimination.

3. The adduct (4-tert-butyl toluene + tert-$^{13}CC_3H_9^+$) yields to i) tert-$C_4H_9^+$ and tert-$^{13}CC_3H_9^+$ (50/50) ii) C_4H_8 and $^{13}CC_3H_8$ losses (50/50) iii) only to tert-$^{13}CC_3H_{10}$ elimination (no C_4H_{10} elimination).

This result proves that the adduct corresponds in this case to two structures

i) The covalently bonded structure which is the precursor of tert-$C_4H_9^+$ and of the isobutene loss

ii) The π-structure which leads to a benzylic ion with elimination of a labeled isobutane molecule.

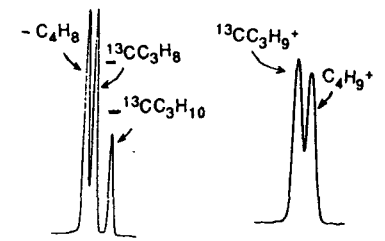

MIKE spectrum of the adduct

Calculations

The results clearly show that the π-complexes are stable enough to survive from the ion source to the 2nd FFR.

Ab-initio and simulated annealing calculations confirm that π-complexes correspond to local minima on the potentiel energy surface. Electrostatic and dispersion energies represent the more important contribution to their stabilization energies. This stabilization energy is calculated to be 11.6 kcal.mol^{-1} for the [benzene, tert-$C_4H_9^+$] complex.

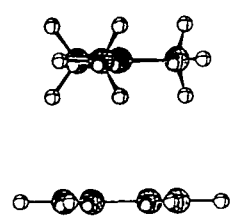

[C_6H_6, tert $C_4H_9^+$] complex

(1) J A. Herman, A. G Harrison, *O M S. 16, 423 (1981)*

(2) D Berthomieu, V Brenner, G Ohanessian, J. P Denhez, P Millié, H. E Audier, *J A. C. S 115, 2505 (1993)*

(3) H E Audier, C. Monteiro, P Mourgues, *O. M. S. 25, 245 (1990)*

Selective Identification of Benzyl and p-Tolyl Ions in the Mixture of C_7H_7+ Ions By Ion/Molecule Reactions

Tomas Vaisar
Inst. Org.Chem.Biochem., Prague Czech Republic
Present address: Molecumetics Ltd., Bellevue, WA

Ion/molecule reactions represent one possible route to identification of isomeric ions. Herein, gas-phase reaction of C_7H_7+ isomeric ions with anisole is presented.Reactivity of each isomer differs, while tropylium ion is nonreactive and benzyl and p-tolyl ions for adduct ions at the same m/z, however with different structure as is visualised by CID spectra.

Anisole as a reagent combines two possible reactive sites, etheric oxygen, where tolyl ions are supposed to react[1], analogy to dimethylehter, and phenyl ring where reactivity of benzyl ions should be directed[2], analogy to toluene.

For the reaction individual isomers were generated from source compounds as mixtures of isomers where one isomer prevails. Tolyl ions were generated from p-nitrotoluene, benzyl from bibenzyl or from benzylbromide by EI (70 eV). Thermal degradation of tropyliumtetrafluoroborate at approx. 220 oC gave tropylium ion.

For the observation of the reaction anisole vapours (giving ion source pressure 3 x 10^{-6} bar) were mixed in the ions source with vapours of source compounds to give the overall pressure 3-4 x 10^{-5} bar. EI spectra of these reaction mixtures showed for both benzyl and tolyl ions peak at m/z 199 corresponding to addition of the ion to anisole molecule, while for tropylium no such ion was observed. CID spectra of this ion from the field free region between magnetic and electrostatic analyzers obtained by scanning ESA show strikingly different features for both reacting isomers. For tolyl the most abundant ion at m/z 184 corresponds to methyl loss with weak peaks at m/z 91 and 121 probably from benzyl ion impurities (fig 1b). the structure of oxonium ion is suggested for this adduct ion. For the reaction of benzyl there are only these peaks at m/z 121 and 91 from losses of benzene from benzyl moiety (as proved by use of d8-toluene as C7D7+ source) and from reversed association reaction,respectively. Structure of the adduct in this case can be described as an intermediate of Friedel-Crafts alkylation of anisole, where benzyl is attached either to o- or p- position. Surprisingly, the ion corresponding to methyl loss was also observed in the CID spectrum of the adduct when toluene was used as C7H7+ ions source. Thus from the adduct of anisole with C7D7+ ions identity of lost benzene molecule was determined (vide supra) as well as it was shown that the methyl radical lost comes from anisole.

This reaction seems to be easy prove for isomeric identity of the ions studied and can be possibly transffered in to the collison cell of triple stage quadrupole mass spectrometer for more easy use.

References:

1. Heath T.G., Allison J., Watson J.T., J.Am.Soc.Mass Spectrom. 2, 270 (1991).
2. Giacomello P., Angelini G., Sparapani C., Speranza M. J.Phys.Org.Chem. 2, 467 (1989).

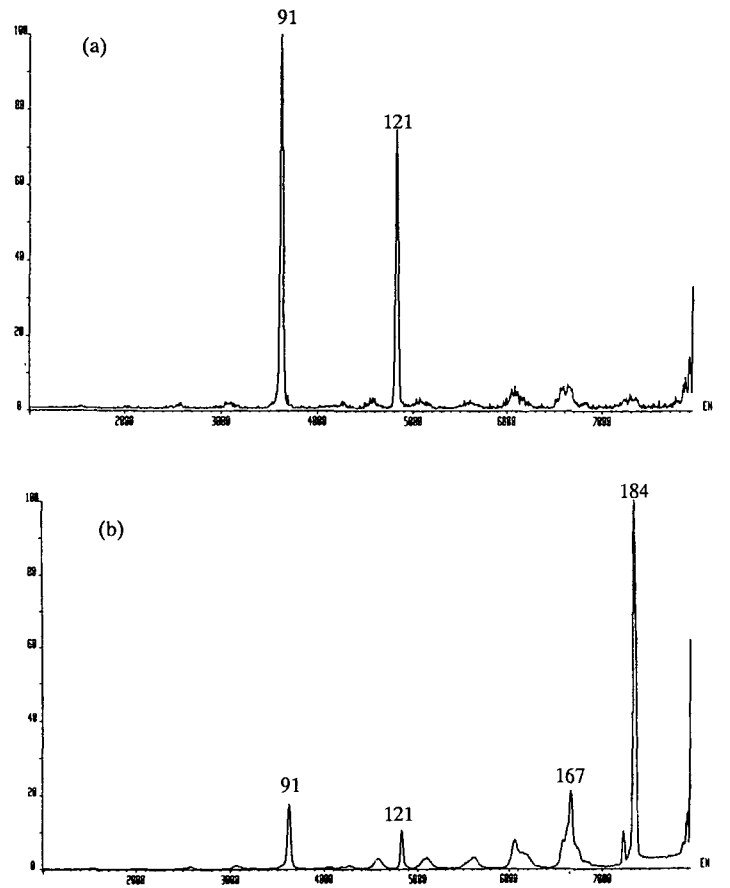

Fig. 1. CID daughter ion spectra of the adduct ions of benzylium and anisole (a) and p-tolylium and anisole (b) obtained with collision gas helium at 30% attenuation of the main ion beam(acc. voltage 8 kV, EI 70 eV, 200 μA)

Electron Impact Induced Self-Protonation and Self-Condensation of Allenic Ketones

*Chung-Ping Yu, Elisa Rambo, and Jack K. Crandall, Chemistry Department, Indiana University, Bloomington, IN 47405

INTRODUCTION Gas phase ion-molecule reactions of allene (C_3H_4)[1] and various carbonyl compounds (n-propyl acetate[2] and benzyl acetate[3]) have been studied using CIMS, MIKE, and CAD techniques. In the earlier reports formation of allene dimer $[2M-H]^+$ ions and protonated acetate dimer $[2M+H]^+$ ions are observed via [2+2] cycloaddition and nucleophilic addition, respectively. To further study these dimerization processes, we investigated several allenic ketones using the conventional electron impact method. The results of these experiments provide evidence for the competition between nucleophilic addition and [2+2] cycloaddition in the allenic ketone system.

EXPERIMENT The EI experiments were performed with a Kratos MS80 mass spectrometer at 30 eV in a high pressure EI/CI source ($5X10^{-5}$ ~ $1X10^{-4}$ Torr) with the source temperature at 40-50 °C. Samples were introduced into the instrument via direct insertion probe. All mass spectral data presented herein are single scans and are representative of several scans recorded during each experiment.

RESULTS AND DISCUSSION The EI mass spectra of allenic ketones **1-6** (Table1) show a prominent $[M+H]^+$ peak as compared to $[M]^+$ peak, indicating the occurrence of self-protonation in the ion source. The predominant fragmentation of $[M+H]^+$ is loss of 16 and 44 u, except for compound **2**, possibly due to elimination of CH_4 and CO as shown in the Scheme 1 (Scheme 1 is not a representative mechanism of **2**). The mass spectra of compounds **1-4** also display an intense signal for the ion $[2M+H]^+$ peak corresponding to possible structure **a** formed from nucleophilic addition of one M molecule to the $[M+H]^+$ ion and/or proton-bond dimer **b**. The proposed structure **a** is supported by the sequentially analogous loss of 16 and 44 u. Investigation of mass spectra of compounds **5** and **6** leads to an interesting phenomena observed for increasing formation of $[M]^+$ and $[2M]^+$ ions. It is believed that [2+2] cycloaddition corresponds to the appearance of the $[2M]^+$ ion. This is rationalized by consideration of decreasing intramolecular interaction between carbonyl group and allenic double bond with increasing distance between these two groups to produce both "independent" functions.

CONCLUSION In this preliminary work, we report that with decreasing carbon chain length increases abundance of $[M+1]^+$ and $[2M+1]^+$ ions in the EI mass spectrometry under high pressure conditions. A possible dimerization mechanism is proposed on the basis of fragmentation patterns of protonated dimers. Self-protonation of allenic ketones is believed to be responsible for the formation of $[M+1]^+$ ions following nucleophilic addition, rather than [2+2] cycloaddition.

ACKNOWLEDGMENT The assistance of Paula Wood is gratefully acknowledged.

REFERENCES

1. Brian J. Shay, Marcos N. Eberlin, R. Graham Cooks and Chrysostomos Wesdemiotis *J. Am. Soc. Mass Spectrom.* **1992**, *3*, 518.
2. Minoru Kumakura, Kazuo Arakawa and Toshio Sugiura Int. *J. Mass spectrom.* **1978**, *27*, 149.
3. D. Cameron and R. G. Cooks *J. Am. Chem. Soc.* **1979**, *101*, 3162.

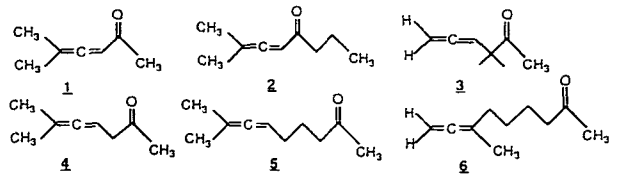

Table 1 Mass spectra of allenic ketones 1-6. m/z (intensity %)

Cmpd	$[2M+H]^+$	$[2M]^+$	$[2M+H-16]^+$	$[2M+H-44]^+$	$[M+H]^+$	$[M]^+$	$[M+H-16]^+$	$[M+H-44]^+$
1	221(98)	220(4)	205(26)	177(13)	111(100)	110(23)	95(38)	67(12)
2	277(12)	276(1)	------	233(16)	139(100)	138(10)	——	95(92)
3	249(6)	----	233(41)	205(3)	125(92)	124(13)	109(83)	81(100)
4	249(4.6)	——	233(1)	205(2.4)	125(78)	124(11)	109(100)	81(28)
5	305(1.5)	304(2)	289(1)	261(4)	153(71)	152(62)	137(13)	109(42)
6	305(1)	304(1)	289(1.4)	261(3)	153(56)	152(24)	137(19)	109(67)

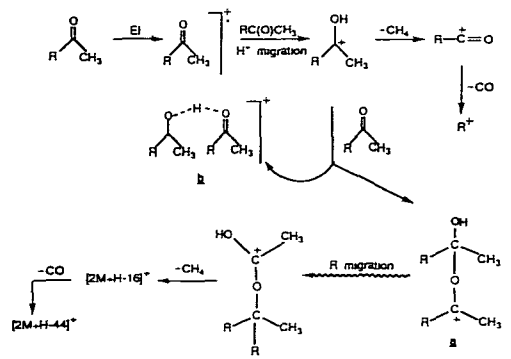

Scheme 1

Differentiation of Isomers through Energy-Resolved CID and Ion/Molecule Reactions in an Ion Trap Mass Spectrometer

*Brad I. Coopersmith and Richard A. Yost, University of Florida
Gainesville, FL. 32611

The quadrupole ion trap mass spectrometer (QITMS) has several features which make it an ideal instrument for allowing comparisons between gas-phase and solution-phase reaction mechanisms. Being tandem-in-time, the QITMS can act as a reaction vessel to form reaction products and is able to perform MS^n (n>2) on these products. This latter ability has been used to determine product ion structures based upon the fragment ions (and their abundances) formed following resonant excitation collision-induced dissociation (CID)[1]. However, the use of fragment ion formation for isomer structure differentiation is limited, because in many instances the isomers will yield identical fragment ions. An alternative method for isomer differentiation is the use of selective ion/molecule reactions, as has been employed in the identification of $C_7H_7^+$ isomers [2]. We have investigated the use of a combination of energy-resolved CID (ER-CID) with selective ion/molecule reactions to differentiate between several even-electron secondary and tertiary carbocation isomers.

In the QITMS, CID is thought to occur in a stepwise manner, meaning that energy deposition into the ion occurs through successive low-energy collisions rather than through a single high-energy collision. As a result, the time between collisions allows the deposited energy to be distributed throughout the ion. Therefore, isomer ions which yield the same fragment ions are believed to pass through a common transition state before fragmenting. This mechanism limits the ability of CID to distinguish between isomers based solely upon the fragment ions formed.

ER-CID is shown conceptually in the reaction coordinate in Figure 1. If the isomer ions have different ground state energies, the activation energies (E_{a1} and E_{a2}) required for each isomer to reach the common transition state should also be different. The difference is based on the assumption that the energy barrier to isomerization, E_I, is not exceeded during ion formation. If E_I is exceeded, the ions will be able to isomerize to assume the lower energy conformation. Once the common transition state is achieved, each isomer will fragment at the same rate with respect to the amount of energy deposited. Figure 2 shows the two cases. When E_I is not exceeded during ion formation the activation energies are different and each isomer has a crossover point at a different energy. When E_I is exceeded, there is only one isomeric structure, therefore both isomers have the same crossover energy.

The effects of the mass isolation and the CI reagent ion used were examined. Of the two mass isolation methods studied, apex isolation was found to impart less energy into the ion as compared to two-step isolation. Using a gentle protonating reagent ion, the m/z 57 ion from isobutane, the two-step mass isolated ions had lower crossover energies than the apex isolated ions. Since the same CI reagent ion was used, the only other factor which could impart energy into the ion was the isolation method. The lower crossover energy indicates that the two-step mass isolated ion must have a higher initial energy, which could only occur if two-step mass isolation is more energetic than apex isolation. Two-step isolation was not found to be energetic enough to cause isomerization. On the other hand, it was found that the use of a stronger protonating reagent ion, for example the $C_2H_5^+$ ion from methane, can cause isomerization.

Another method of isomer differentiation examined was the use of selective ion/molecule

reactions. The concept of selective ion/molecule reactions is to use a reactant (ion or neutral) which will only react with the desired component (neutral or ion) of the system under analysis. Based upon previous studies [3], *tert*-butanol was chosen as the neutral reactant to distinguish between secondary and tertiary carbocations using the proposed scheme shown in Figure 3. When *tert*-butanol reacts with a secondary carbocation, the basic oxygen can remove the hydrogen from the carbocation center resulting in the formation of an $[A+56]^+$ product ion. Tertiary carbocations have no hydrogens at the carbocation center, thus the driving force for this reaction is removed and there should be no reaction. This method was found to be effective for both sets of isomers investigated.

[1] Coopersmith, B.I.; Yost, R.A.; Kuehl, D.W. *40th ASMS Conference on Mass Spectrometry and Allied Topics*, Washington D.C., May 31-June 5, 1992; p.180.
[2] Heath, T.G., Allison, J., Watson, J.T. *J. Am. Soc. Mass Spectrom.* **1991**, *2*, 270.
[3] Beauchamp et al. *J. Am. Chem. Soc.*, **1974**, *96*, 6243.

Figure 1
Energy Diagram Depicting ER-CID

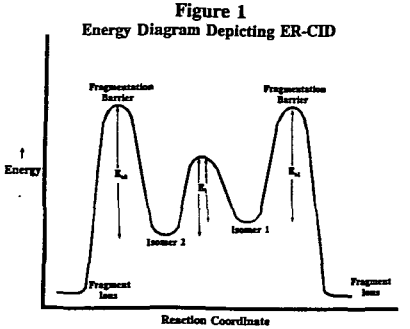

Figure 2
ER-CID Breakdown Curves

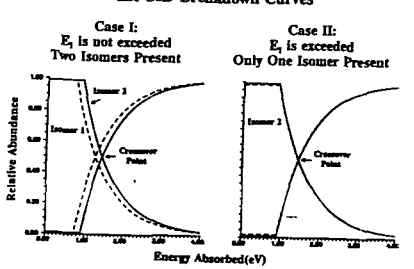

Figure 3

Reactions with *tert*-Butanol

Secondary Carbocation

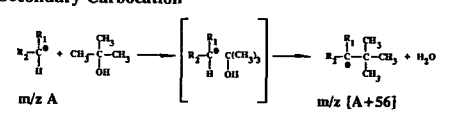

Tertiary Carbocation

Further Investigations of Nucleophile/ElectrophileIon/Molecule Reactions in an Ion Trap Mass Spectrometer

*Brad I. Coopersmith and Richard A. Yost, University of Florida
Gainesville, FL 32611
Douglas W. Kuehl, U.S. Environmental Protection Agency,
Duluth, MN 55804

Gas-phase ion/molecule reactions between potential carcinogens and mutagens (electrophiles) and model DNA bases (nucleophiles) in a tandem mass spectrometer can be analytically useful as an environmental screening technique. Previous work in our laboratory [1] investigating such reactions of carcinogenic allyl halides with piperidine and pyridine on a triple quadrupole mass spectrometer (TQMS) showed good correlation with the Ames Test, a bioassay used to determine mutagenicity. The inability to obtain MS/MS structural information on the product ions formed in the TQMS collision cell led to the use of a tandem-in-time instrument, the quadrupole ion trap mass spectrometer (QITMS) [2]. However, the lack of spatial separation allowed side reactions, especially the self-protonation of the nucleophile, to dominate the product spectra for all nucleophiles investigated.

The desired reaction with the allyl halides (EX), is the addition of the allyl group (E) to the nucleophile ion ($N^{+\cdot}$, m/z N) through an S_N2' mechanism to form a product ion (NE^+) at m/z [N+41]. It became evident that the only method to prevent unwanted side reactions would be to prevent any neutral nucleophile from being present during the reaction period. This goal could be accomplished through two methods, either spatial separation or temporal separation of the nucleophile from the reaction region. The QITMS chamber was modified as shown in Figure 1 for temporal separation using pulsed valve introduction of the nucleophile. The timing required for temporal separation is shown in Figure 2. After pulsing the valve open and closed, the nucleophile is ionized to produce the largest number of nucleophile ions possible. After ionization, the nucleophile ions are isolated as the neutral nucleophile pressure drops back to its base pressure. At that point, the partial pressure of the electrophile will be higher than that of the nucleophile and the reactions due to the neutral nucleophile should be minimized. Using a timing sequence similar to that in Figure 2, the spectrum shown in Figure 3 was obtained for the reaction of pyridine ions (m/z 79) with allyl iodide neutrals. The unwanted side reactions leading to the formation of product ions at m/z 80 and m/z 285 have been minimized while the desired reactions with the allyl iodide leading to the production of ions at m/z 120 (NE^+) and m/z 206 dominate the spectrum. This spectrum indicates that almost all of the pyridine neutrals have been removed prior to the reaction period, thus allowing the pyridine ions to react primarily with the allyl iodide.

To model the DNA/carcinogen reactions in the gas-phase more effectively, nucleophiles with more than one possible site of reaction need to be examined. Three multi-functional nucleophiles were investigated. Their names and structures are shown in Table 1. The information from MS^4 experiments for the reactions of these nucleophile ions with allyl bromide was used to determine the site of reaction. The fragmentations suggest that the allyl group bonds to the sulfur atom as opposed to the nitrogen atom for both the 2-thiohydantoin and the ω-thiocaprolactam $N^{+\cdot}$ ions. For the case of 2-imidazolidinethione, it was not possible to determine to which atom the allyl group is bonded. The hard-soft acid-base (HSAB) theory was used to explain all of the

electrophile/nucleophile ion/molecule results obtained thus far.

[1] Freeman, J.A.; Johnson, J.V; Hail, M.E.; Yost, R.A.; Kuehl, D.W. *J. Am. Soc. Mass Spectrom.*, **1990**, *1*, 110-115.

[2] Coopersmith, B.I.; Yost, R.A.; Kuehl, D.W. *40th ASMS Conference on Mass Spectrometry and Allied Topics*, Washington D.C., May 31-June 5, 1992; p. 180-181.

Figure 1
Hardware Configuration for Pulsed Valve Introduction

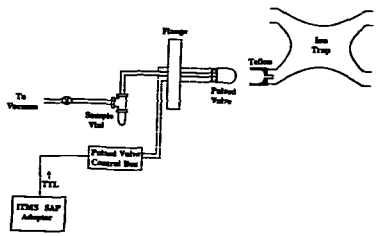

Figure 2
Timing Required for Temporal Separation

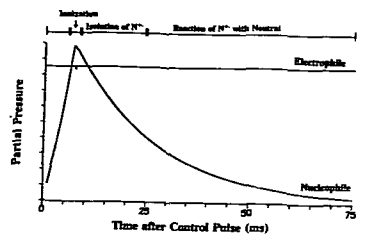

Figure 3
Reaction of Pyridine Ions with Allyl Iodide Neutrals (Pulsed Valve Introduction)

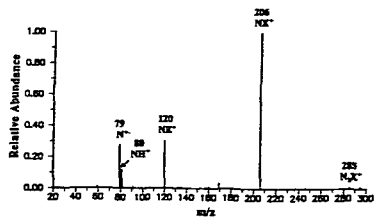

Table 1

Structures of Multi-Functional Nucleophiles

Nucleophile	M.W.	Structure
2-Imidazolidinethione	102 g/mol	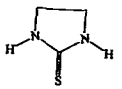
2-Thiohydantoin	116 g/mol	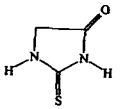
ω-Thiocaprolactam	129 g/mol	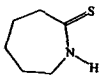

Sample Ion/Sample Molecule Reactions in Chemical Ionization Mass Spectrometry

Burnaby Munson, Adebayo Onigbinde, and Gordon Nicol
Department of Chemistry and Biochemistry
University of Delaware
Newark, DE 19716

The electron ionization (EI) mass spectra of oligomeric polyethylene glycols (PEG's) are very similar. The base peak is at m/z 45 and there are virtually no detectable $M^{+\cdot}$ ions in the spectra. The majority of the fragment ions are at low molecular weight and are not helpful for structure identification or confirmation.

The CH_4 CI (chemical ionization) mass spectra are somewhat more useful than the EI spectra for identification of the PEG's. The base peak is at m/z 45 and there are structurally useful fragment ions. There are two series of ions corresponding to $(C_2H_4O)_nH^+$ and $(M-(C_2H_4O)_o)^+$. With the larger PEG's an additional series corresponding to $HO(C_2H_4O)_nH_2^+$ becomes significant. There are low relative abundances of MH^+ ions and the relative abundances of the MH^+ ions do not obviously increase with increasing molecular weights of these oligomers. Interpretation of any molecular weight dependence in the relative abundance of MH^+ ions is hampered by the dependence of the abundance of MH^+ on sample size.

The relative abundances of the MH^+ ions increase dramatically with increasing sample size because of sample ion/sample molecule reactions. These sample ion/sample molecule reactions can be easily detected and studied in GC/CIMS studies. For somewhat larger than usual samples, one can record many (20 - 30) spectra for each chromatographic peak and note the relative abundances of the major ions in the spectra as the sample size varies throughout the chromatographic peak. The extent of conversion, $\Sigma I_i(\text{Sample})/\Sigma I_i(\text{Total})$, is proportional to the concentration of the sample in each spectrum.

Plots of relative abundance vs extent of conversion clearly show the products of sample ion/sample molecule reactions. Sample ions whose relative abundances decrease with increasing extent of reaction (sample concentration) are clearly reacting to form those ions whose relative abundances increase with increasing extent of reaction. For the polyethylene glycols the major reactions are the proton transfer reactions,

$$C_2H_5O^+ + PEG \rightarrow PEGH^+ + C_2H_4O$$

Small amounts of the proton-bound dimers, PEG_2H^+, are also observed. Little evidence is observed for adduct ions.

Similar observations were made for the dimethyl ethers of the polyethylene glycols. The EI spectra of these compounds are quite similar and contain virtually no detectable M^+ ions, and have a base peak at m/z 59. Most of the fragment ions occur at low mass and are not useful for structure determination.

Presented at the 41st ASMS Conference on Mass Spectrometry

The CH_4 CI mass spectra of the dimethyl ethers of the polyethylene glycols also contain m/z 59 as the base peak. There are low abundances of MH^+ ions and structurally useful higher mass fragment ions in two major series, $(C_2H_4O)_nCH_3^+$ and $(C_2H_4O)_nH^+$. The relative abundances of the MH^+ ions do not obviously increase with increasing molecular weights of these oligomers. The relative abundances of the MH^+ ions increase dramatically with increasing sample concentration.

GC/CIMS studies on the di-methyl ethers of polyethylene glycols, like those mentioned above for the PEG's, clearly show reacting sample ions and ions which are products of sample ion/sample molecule reactions. For these compounds, the major new product ion is MH^+. The reaction sequence is somewhat more complex for these compounds. GC/CIMS studies with ethylene glycol di-methyl ether suggest that $C_2H_5O^+$ reacts to form $C_3H_7O^+$ at m/z 59 and perhaps MH^+. $C_3H_7O^+$ also appears to react to form MH^+. FT/ICRMS studies establish this sequence.

Sample ion/sample molecule reactions may occur relatively frequently under commonly used CI conditions, particularly with polar compounds. These reactions are quite useful in forming MH^+ ions for molecular weight determination. These sample ion/sample molecule reactions will not be noticed unless studies are made about the variation of CI mass spectra with sample size. These analytically useful ion/molecule reactions can be recognized and studied in GC/CIMS experiments for complex molecules with only slightly larger samples than are commonly used for analysis.

ThP nr.1674.

Evaluation of ion formation of carbamate pesticides in TSP- and ESP MS using different eluent additives and proton affinity calculations

M.Honing[1], D.Barceló[2] and J.Abian[3]; Dept. Environmental[1]- and Neuro[2] Chemistry, CID/CSIC, Jordi Girona 18-26, 08034 Barcelona, Spain.
B.L.M. van Baar[3], R.T.Ghijsen[4], U.A.Th. Brinkman[4]; Dept. Organic[3] and Analytical[4] Chemistry, Free University, de Boelelaan 1083, 1081 HV Amsterdam, The Netherlands.

The carbamate pesticides show in various ionisation techniques a specific fragment ion, $[M+H-CH_3NCO]^+$, which is formed after the loss of methylisocyanaat from the protonated molecular ion. As will be reported [1], addition of ammonium to the eluent in TSP-MS causes the loss of this fragment ion. In this presentation the effect of addition of nicotinic acid and the use of aceton, instead of methanol or acetonitrile, is discussed. For comparison studies, ESP experiments were performed. With both interfaces a list of 19 carbamate pesticides and 12 of their degradation products were investigated.

Results and discussion

Use of Aceton as organic modifier in a 50:50 mixture with water, lead to the formation of the $[M+H]^+$ and the $[M+CH_3COCH_3+H]^+$ ions. Contrary to methanol and acetonitrile, the typical fragment ion, $[M+H-CH_3NCO]^+$, for the N-methyl carbamate pesticides except for dioxacarb and the carbamoyl carbamates, was not observed, as is illustrated in figure1. This difference can be explained by the softening of the ionisation process. Hence the PA of aceton is 825 kJ/mole, whereas the PA of methanol is 761 kJ/mole.
Other studies, using nicotinic acid as additive to 50:50 mixtures of methanol or acetonitrile with water, show the same effect. The abundance of the typical fragment ion is decreased completely. Also the formation of a cluster ion, $[M+\text{nicotinic acid}+H]^+$, was observed. In contrast to ammonium acetate addition, no $[M+H]^+$ ion was present, when nicotinic acid was added to the eluent (see figure 2).
For the metabolites V, VI and VII, of the N-dimethyl carbamate pirimicarb, cluster ions with methanol, acetonitrile and aceton were observed. Decrease of the methyl substitution, on the amine group, lead to a increase of the relative abundance of these cluster ions. This increase of cluster ions can be explained by the decrease of the PA values of these compounds. This is supported by the fact that the effect is also observed for N,N-dimethyl aniline (PA = 935 kJ/mole [2]), N-methyl-aniline (PA = 913 kJ/mole [2]) and aniline (PA = 876 kJ/mole [2]). In Contrast to these clusters ions, no cluster ions with ammonia or nicotinic acid were observed for the metabolites and the aniline compounds.
Additionally electrospray experiments with the carbamate pesticides were performed. With this ionisation technique all carbamate pesticides form $[M+H]^+$ or $[M+Na]^+$ ions, whereas no fragment ions, except for methomyl, are observed.

Conclusion

Use of aceton as organic modifier and nicotinic acid as additive suppresses the formation of fragment ions for N-methyl carbamate pesticides. The abundance of cluster ion of the metabolites V-VII is dependent on their PA values.

Acknowledgement
Miss M. Carrascal is thanked for performing the ESP results.

References

1. M.Honing, D. Barceló, B.L.M. van Baar, R.T. Ghijsen and U.A.Th. Brinkman, Ion formation of carbamate pesticides in thermospray mass spectrometry: The effect of additives to the eluent and the vaporizer temperature, submitted
2. S.G.Lias, J.F.Liebman and R.D.Levin, *J.Phys. Chem. Ref. Data*, **17**, suppl. 1, 1988

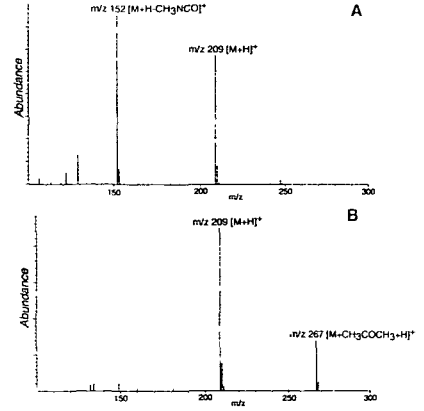

Figure 1. The filament-on TSP mass spectra of the N-methyl carbamate aminocarb, using a 50:50 mixture of water with methanol (A) or aceton (B) as organic modifier.

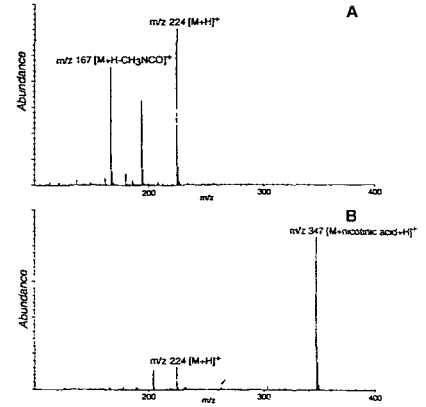

Figure 2. The filament-on TSP mass spectra of the N-methyl carbamate dioxacarb, using a 50:50 mixture of methanol:water without (A)and with (B) addition of 12.5 mM nicotinic acid

Fate of Selected Negative Ions Following Electron Capture at Atmospheric Pressure.

J.A. Culbertson and E.P. Grimsrud, Department of Chemistry and Biochemistry, Montana State University, Bozeman, MT 59717

Many previous studies have focused on the determination of rate coefficients and the ionic products of electron capture (EC) reactions. However, one point which has received very little attention but can be important to the response of an EC transducer is the fate of the negative ion following EC. At atmospheric pressure the dominant mechanism by which ions are destroyed is ion-ion recombination (IIR). Therefore, if a molecular anion formed by resonance EC is regenerated upon IIR (reaction 1a), the EC transducer response will be enhanced relative to the case in which IIR produces neutral fragments of the parent compound that do not attach electrons (reaction 1b).

$$M + e \rightarrow M^- \xrightarrow{p^+} M + \text{neutrals} \quad (1a)$$

$$M + e \rightarrow M^- \xrightarrow{p^+} Z + \text{neutrals} \quad (1b)$$

In this work an experiment has been devised to determine the amount of parent neutral remaining after an electron capturing species has been passed through an ionizing cell at atmospheric pressure. From these measurements, the extent to which the molecular anions are converted back to the original molecule upon IIR has been determined.

The apparatus used in this experiment is shown in Figure 1. It consists of a Hewlett Packard 5890A gas chromatograph (GC) equipped with an ECD. Housed within the GC oven is a stainless steel block which contains two cylindrical cells with a volume of 1.5 cm^3 each. The first cell, or ionizing cell, contains a 13 mCi ^{63}Ni-on-Ni foil which forms its cylindrical wall, while the second, or dummy cell has a non-radioactive Ni foil. The cell temperature was maintained at 120°C by the use of a temperature controller equipped with a heater cartridge and a thermocouple feedback control. A gas flow of 32 cm^3/min of argon-10% methane measured at the ECD exhaust was typically used.

All nitrobenzene (NB) samples were prepared in toluene, while gaseous samples of perfluoromethylcyclohexane (C_7F_{14}), SF_6, and $CHCl_3$ were prepared in pressurized glass carboys. An 18m x 0.53mm SE-54 capillary column (liquid samples) or stainless steel packed column (gaseous samples) were used to introduce the compounds into the cell, and a 12m capillary was used to transport the cell effluent to the ECD.

The results of a typical experiment are shown in Figure 2a and 2b. Figure 2a and 2b are the chromatograms for meta-dinitrobenzene (m-NO_2NB) when it is passed through the dummy cell and ionizing cell respectively. The decrease in response to m-NO_2NB when it is passed through the ionizing cell can be related to the amount of m-NO_2NB being regenerated by IIR in the ionizing cell by Equation 2

$$\alpha = (1-\chi)\beta = \frac{F}{N_e}(H_1/H_2 - 1) \quad (2)$$

where χ is the fraction of recombination events occurring by reaction 1a, β is the EC rate coefficient of M, F is the gas flow through the cell, N_e is the average number of electrons in the ionizing cell and H_1 and H_2 are the peak heights of M when it is passed through the dummy and ionizing cell, respectively. The term $(1 - \chi)\beta = \alpha$ is the experimentally determined quantity. By comparing α to known values of β, the magnitude of χ can be determined from $\chi = 1 - \alpha/\beta$. Listed in Table 1 are values of α, β, H_1/H_2, and χ for the compounds studied in this research.

Compound	α (cm^3/sec)	β (cm^3/sec)	H_1/H_2	χ
NB	1.2×10^{-9}	2.6×10^{-8}	1.4	0.95
o-NO_2NB	5.3×10^{-8}	1.3×10^{-7}	16.1	0.59
m-NO_2NB	2.4×10^{-9}	2.2×10^{-8}	1.7	0.89
p-NO_2NB	8.9×10^{-8}	1.4×10^{-7}	25.0	0.37
p-FNB	5.7×10^{-9}	3.5×10^{-8}	1.4	0.84
C_7F_{14}	1.5×10^{-8}	1.1×10^{-7}	5.2	0.86
SF_6	0.0	3.8×10^{-7}	0.0	0.0

Table 1. Values for α, β, H_1/H_2, and χ for compounds studied.

Values of β for the nitrobenzenes at 4 Torr are from reference 2 while that of C_7F_{14} and SF_6 at 1 Torr are from references 3 and 4. Table 1 demonstrates the varying degree to which the parent molecule is regenerated by IIR following EC. For example, SF_6^- is completely destroyed by IIR and proceeds solely by reaction 1b. On the other hand, NB^- proceeds almost completely by reaction 1a to regenerate NB.

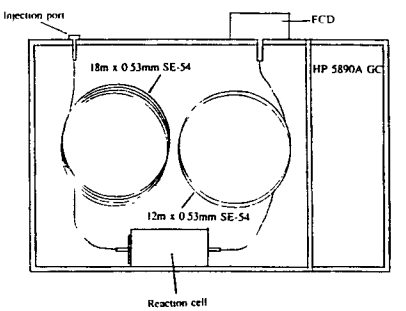

Figure 1. Experimental apparatus to determine fate of negative ions.

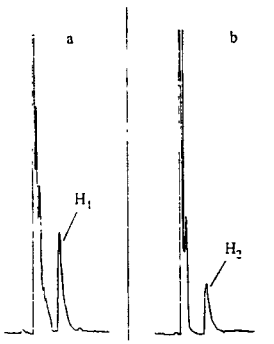

Figure 2. Chromatograms of m-NO_2NB after passing through the dummy cell (a), and ionizing cell(b)

REFERENCES

1. C.A. Valkenburg, L.A. Krieger and E.P. Grimsrud, J. Chem. Phys. 86 (1987) 6782.
2. W.B. Knighton and E.P. Grimsrud, 40TH ASMS Proceedings p.1240.
3. E. Alge, N.G. Adams and D. Smith, J. Phys. B: At. Mol. Phys. 17 (1984) 3827.
4. D. Smith, N.G. Adams and E. Alge, J. Phys. B: At. Mol. Phys. 17 (1984) 461.

ATMOSPHERIC PRESSURE CHEMICAL IONIZATION (APCI) USING PHOTOIONIZATION

Glenn E. Spangler

Environmental Technologies Group, Inc.
1400 Taylor Avenue
Baltimore, MD 21284-9840

INTRODUCTION - Alternate approaches to ionizing sample using atmospheric pressure chemical ionization (APCI) mass spectrometry were investigated. The approach being reported here is photoionization in combination with acetone reagent chemistry.

EXPERIMENTAL - The design of the ionization source is shown in Figure 1. An EG&G XFX-480 flashlamp (2 atmospheres krypton sealed with a magnesium fluoride window) was side-mounted to a ceramic reaction chamber. Fired onto the walls of the chamber was a thick film resistor across which was applied an extraction electric field. Sample was introduced into the chamber through a membrane (1 mil microporous Teflon impregnated with OV101) inlet using purified laboratory air ($\leq$ 2 ppm H_2O) for sample and carrier gases. The sample was further diluted by a purified laboratory air diluent gas ($\leq$ 2 ppm H_2O), which also served as a curtain gas flowing across the 25 micron ion sampling pinhole leading into an EXTREL CM-50 quadrupole mass spectrometer. Diffusion tube generators were used to supply known concentrations of DMMP and methyl salicylate to the membrane inlet. The reactor temperature was nominally 50° C.

A second configuration for the source is shown in Figure 2 where the addition of a ^{63}Ni radioactive source "up-field" from the photoionization flashlamp was used.

RESULTS - DMMP was inefficiently ionized without acetone. After 36-58 ppm of acetone was added to the reactor, Figures 3 and 4 show that the reactant ions are $(Ac)_nH^+(N_2)_m$ and the product ions are $(Ac)H^+(DMMP)$ and $(DMMP)_2H^+$. The results were similar with and without the radioactive source. After addition of acetone, the photoionization technique appeared to be as sensitive as the radioactive source without photoionization. For photoionization unassisted by ionization from the radioactive source, the reactant ions are formed by the following reactions:

$$Ac + h\nu\ (>9.69\ eV) \rightarrow Ac^+ + e^-$$
$$Ac^+ + Ac \rightleftharpoons AcH^+$$
$$AcH^+ + Ac \rightleftharpoons Ac_2H^+$$

The product ions are formed from the ion/molecule reactions:

$$Ac_2H^+ + DMMP \rightleftharpoons (Ac)H^+(DMMP)$$
$$(Ac)H^+(DMMP) + DMMP \rightleftharpoons (DMMP)_2H^+$$

Methyl salicylate could not be ionized using photoionization alone (even with acetone). Figure 5 shows the negative ionization of methyl salicylate in the presence of the radioactive source with the flashlamp off. The product ions are $(MS)_nO_2^-(N_2)_m$. When the flashlamp irradiated these product ions, the results of Figure 6 were obtained. The reactant ions are $(AC)_nCO_3^-(N_2)_m$ which did not ionize methyl salicylate. The CO_3^- ions are formed from:

$$O_2^-(H_2O) + CO_2 \xrightarrow{h\nu} CO_3^- + H_2O_2$$

This reaction is endothermic by 23.4 kcal/mole ($\approx$ 1 eV).

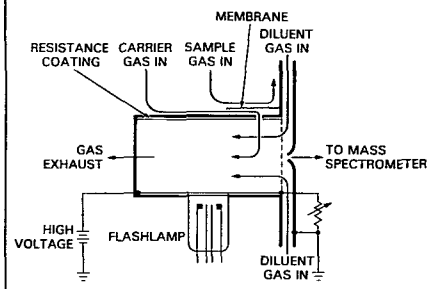

FIGURE 1.

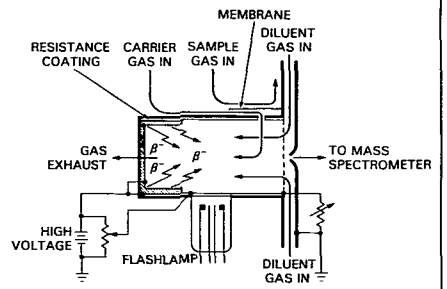

FIGURE 2.

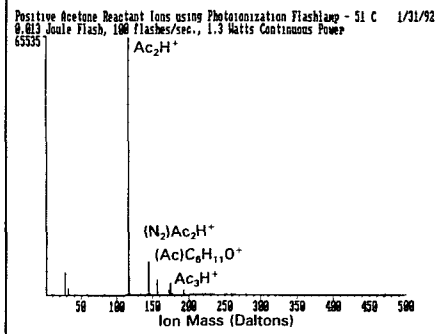

FIGURE 3.

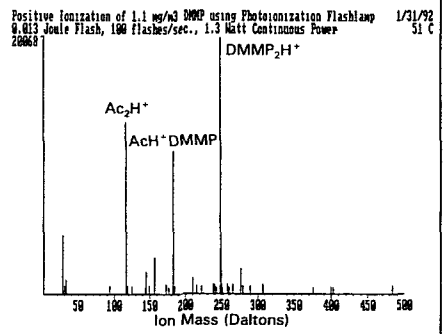

FIGURE 4.

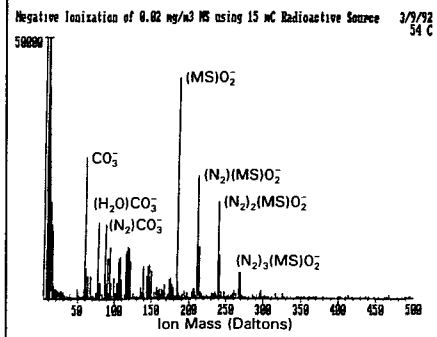

FIGURE 5.

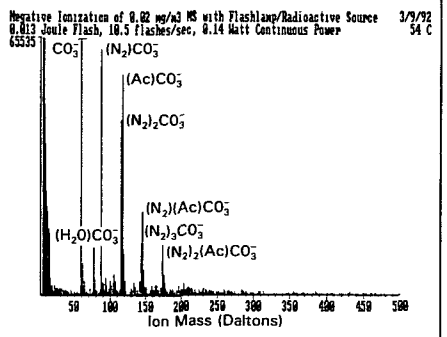

FIGURE 6.

ANALYSIS OF PHENOL AND CHLOROPHENOL ISOMERS BY ATMOSPHERIC PRESSURE IONIZATION AND MASS SPECTROMETRY TECHNIQUES

A. Peter Snyder, Charles S. Harden and Donald B. Shoff, U.S. Army Edgewood Research, Development and Engineering Center, Aberdeen Proving Ground, MD 21010-5423,
Philip B.W. Smith, GEO-CENTERS, INC., Gunpowder Br., P.O. Box 68, Aberdeen Proving Ground, MD 21010-0068 and
Gary A. Eiceman, New Mexico State University, Las Cruces, NM 88003-0003

Phenol and polychlorinated phenols are environmentally significant compounds that are used in vast quantities in the manufacture of resins, polymers, bacteriocides and wood preservatives. Phenol is one of the top 50 chemicals produced, and as water pollutants, phenol and chlorophenols are among the most widespread. Rapid field screening and laboratory analysis techniques are required for this important class of materials. The compounds are amenable to negative ion atmospheric pressure ionization (API) and were subjected to exhaustive studies using API-tandem mass spectrometry (MS/MS) and ion mobility spectrometry/mass spectrometry (IMS/MS). In addition to the $(M\text{-}H)^-$, Sciex API III MS/MS and PCP IMS/MS systems delineated various ions for the title compounds, including MO_2^-, $M_2O_2^-$, $(MO_2\text{-}H_2O)^-$, $(MO_2\text{-}OH)^-$ and $(M\text{-}H+H_2O)^-$ (Figures 1, 2; Table 1). Collision-induced dissociation analyses suggested other peaks in the API mass spectra to be benzoperoxide and orthobenzoquinone. Tuned ion IMS/MS provided evidence that neutral phenol adducts with the phenoxide, chloride and oxygen ions (Figure 3). Information on the mechanisms of ionization, ion-molecule reactions, and collision induced dissociation processes has provided significant insights into the behavior of phenolic type ions, including identification of isomers by MS/MS.

MONO-CHLORO-PHENOLS

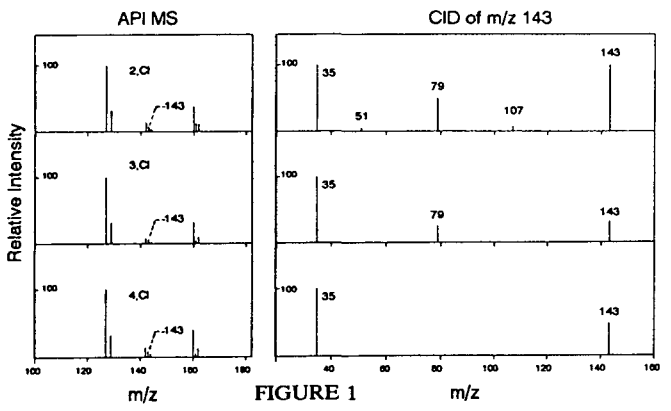

FIGURE 1

TRI-CHLORO-PHENOLS

FIGURE 2

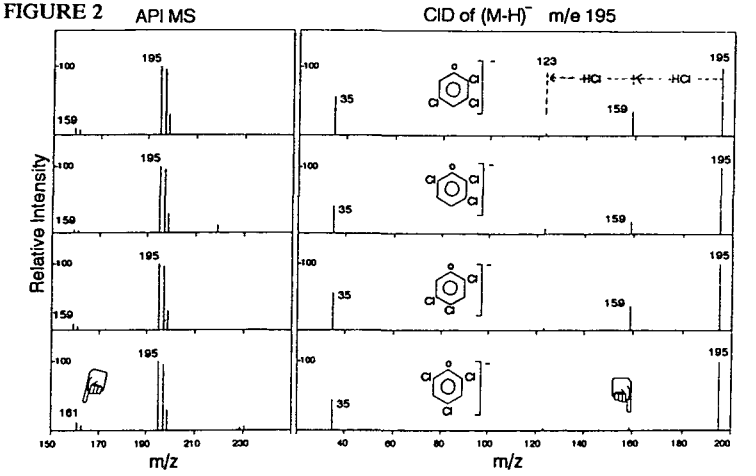

TABLE 1

API (vertical listing) and API-CID (horizontal listing) Mass Spectra of di-chlorophenols given as m/z(Relative Intensity) with base peaks in bold type. Parent ions are listed first in CID spectra

Isomer	API	CID
2,3-Cl	125(3) 127(8) 129(3) 161(100) 176(3) 177(3)	... 127(100), 35(96) ... 161(98), 125(3), 89(2), 35(100) .. ...
2,4-Cl	125(10) 161(100) 176(7) 177(9)	125(98), 89(38), 61(26), 35(100) 161(100), 125(6), 35(<2) ... ...
2,5-Cl	125(14) 161(100) 176(11) 177(9)	125(100), 89(16) 161(100), 125(6), 35(<2) .. 177(100), 141(23), 113(29)
2,6-Cl	161(100) 176(2) 177(3)	161(100), 125(<2) ... ...
3,4-Cl	125(13) 161(100) 176(6) 177(5)	125(100), 89(12), 35(3) 161(100), 125(11), 89(<2), 35(<2) 176(100), 104(8) ...
3,5-Cl	125(7) 161(100) 176(7) 177(4) 239(13) 241(22) 243(12)	125(100), 89(17), 61(<2) 161(100), 125((8), 89(<2), 35(<2) 176(100), 104(<2) 177(100) 239(100), 203(9), 167(3), 159(12) 241(100), 205(8), 203(3), 169(2), 167(<2), 161(5), 159(7) 243(100), 207(4), 205(5), 169(<2), 167(<2), 161(12)

FIGURE 3

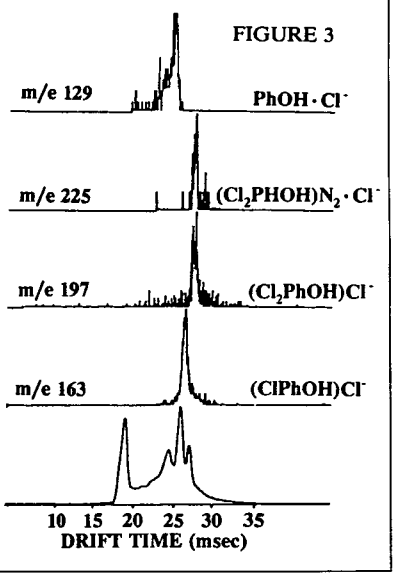

Positive Ion Chemical Ionization of Polycyclic Aromatic Hydrocarbons and Related Compounds.

J. Bazdikian[a,b], R. E. March[a] and A. Mendez.[b]
a. Department of Chemistry, Trent University, Peterborough, ON, Canada K9J 7B8.
b. Department of Analysis and Evaluation, Intevep S.A., Apdo. 76343, Caracas 1070A, Venezuela.

INTRODUCTION. The gas phase ion chemistry of polynuclear aromatic hydrocarbons (PAHs) has been investigated extensively, owing to their biological and environmental importance.[1] However, the differentiation of isomeric structures by mass spectrometry (MS) has met with limited success.[2] Basic research into fundamental gas phase ion-chemistry has stimulated interest in the use of unusual reagent gases for greater selectivity and sensitivity analysis. Chemical ionization (CI) can be used for the differentiation of isomeric compounds on the basis of their reactive behaviour. The use of dimethyl ether (DME) as a reagent gas, has been examined for some PAHs,[3] mono- and bi-substituted oxiaromatic compounds[4] and a group of isomeric polysubstituted nitrobenzenes[5], were found to exhibit isomer-specific DME CI spectra.

EXPERIMENTAL. All experiments were performed on a VG Analytical ZAB-2FQ mass spectrometer of BEqQ configuration. Using the following conditions: ionizing electron energy 50 eV, ion source temperature 250°C, and accelerating voltage 6 kV. The ion of interest was mass-selected by the magnetic sector at 6 keV kinetic energy, with He as collision gas in collision cell 2 (CC_2). The ionic fragmentation products were mass-analyzed according to their kinetic energy-to-charge ratio by scanning the electric sector, with detection of the ions following the electric sector; in the absence of collision gas, this process is referred to as the Mass-analyzed Ion Kinetic Energy Spectrometry (MIKES) technique.

RESULTS AND DISCUSSION.

1. DME-CI SPECTRA. In the CI spectra of PAHs obtained with reagent DME, there are a number of ion species that can be attributed to ion/molecule reactions; these species are: $[M]^+$, $[M+1]^+$, $[M+13]^+$, $[M+15]^+$, and $[M+45]^+$. Production of these ions can be associated with charge transfer, proton transfer, and adduct formation. The ion/molecule reactions appear to involve an electrophilic addition reaction. DME-CI mass spectra show only small differences of the $[M+1]^+/M^+$ ratio. On the other hand, these spectra indicate different spectral patterns of the relative abundances of $[M+13]^+$, $[M+15]^+$ and $[M+45]^+$. The relative abundances of ion species

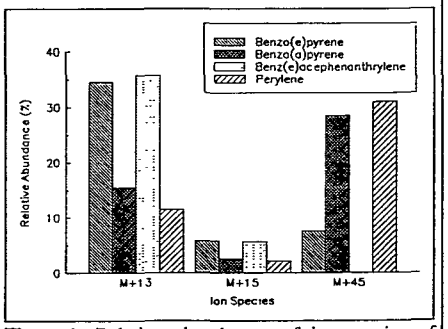

Figure 1. Relative abundances of ion species of PAH isomers of $C_{20}H_{12}$ in DME-CI mass spectra.

from PAH isomers of $C_{20}H_{12}$ are shown in Fig. 1. In the case of $[M+13]^+$ and $[M+45]^+$ are produced more abundantly in perylene and benzo(a)pyrene than the other isomers, benzo(e)pyrene and benz(e)acephenanthrylene.

2. MIKE AND CID-MIKE SPECTRA. The unimolecular metastable decomposition of $[M+45]^{+\bullet}$ to form $[M+13]^+$ is common to such adducts. In some cases, metastable decay led to observation of $[M+15]^+$ and M^+. Similarly, collision-induced dissociation of $[M+45]^+$ results in fragments at $[M+13]^+$, $[M+15]^+$ and M^+, suggesting that the adduct exists as a bound complex involving formation of covalent bonds. A potentially interesting comparison is provided by the MIKE spectra of $[M+45]^+$ ions from heterocyclic PAH isomers containing nitrogen. The $[M+45]^+$ ion of 5,6-benzoquinoline preferentially loses CH_2O, while that of acridine loses CH_2O, CH_3OH and CH_3OCH_2 with comparable intensities. The MIKE spectrum of $[M+45]^+$ from 7,8-benzoquinoline is dominated by the loss of CH_3OH with only a trace due to loss CH_2O. The observed kinetic energy releases, $T_{0.5}$, for loss of CH_3OH and CH_2O from $[M+45]^{+\bullet}$ ions were small, and indicate clearly that these fragmentation reactions involve but a small kinetic shift and reverse activation energy.

CONCLUSION. This study of the reactivity of various types of PAHs with DME has revealed that all of them exhibit $[M]^+$, $[M+1]^+$, and $[M+13]^+$ while some of them exhibit $[M+45]^+$ and $[M+15]^+$ product ions. The relative abundances of these product ions indicate that the PAHs differ in their reactivity with DME. Variation in reactivity is likely due to the topology of PAHs toward electrophilic aromatic addition. The loss of CH_3OH has been shown to be the dominant neutral expulsion reaction of most of the $[M+45]^{+\bullet}$ ions studied. Furthermore, metastable decomposition $[M+45]^{+\bullet}$ of nitrogen-containing compounds were highly individualistic which readily facilitated the isomer differentiation. The KER measurements have provided circumstantial evidence supporting the molecular elimination mechanism.

BIBLIOGRAPHY

1. A. Bjørseth, Ed., Handbook of Polycyclic Aromatic Hydrocarbons, Marcel Dekker Inc.(1983) New York.
2. W. J. Simonsick, Jr., R. A. Hites, Anal. Chem., 56 (1984) 2749.
3. T. Keough, Anal. Chem.,54 (1982) 2540.
4. J Brodbelt, C. C. Liou, T. Donovan, Anal. Chem., 63 (1991) 1205.
5. E. P. Burrows, Org. Mass Spectrom. 27 (1992) 763.

NICI of Selected PCB Congeners : Moderating Gas, Temperature, and Contamination Effects.

Rob O'Brien, Roger Guevremont, & K.W.M. Siu.
Institute for Environmental Chemistry
National Research Council of Canada
Ottawa, Ontario, Canada. K1A 0R6

Introduction :

The utilisation of NICI has been limited because of an inherent reproducibility problem. Electron Capture based processes would appear to represent the simplest case, however, even under these conditions, complex and poorly understood reaction mechanisms are required to explain common structural features.

Subsets of PCB congeners have been examined using different gases and conditions to provide insight into both the EC-NICI mechanisms and PCB structure-reactivity relationships. It is expected that well constructed PCB structure-reactivity relationships will lead to the development of congener selective analysis.

Experimental Methodology :

All PCB's congeners were obtained from Ultra Scientific (Kingstown, RI), with the exception of BZ203 and BZ116 which were obtained from AccuStandard Inc. (New Haven, CT). Samples were introduced into the VG ZAB 2F ion source using the solids probe. Sample flux was restricted by sealing home made vials (containing sample and glass wool) around a fused silica capillary (5-30μm id). All ports to the source with the exception of the probe and septum inlet were blocked. Nitrogen (UHP) and Carbon Dioxide (Bone Dry) were purchased from Liquid Carbonic, Methane (UHP) from Matheson, and Acetylene (Industrial Grade) from Air Products. All gases were used without further purification. Gas pressure was measured at the source ion gauge typically 1×10^{-5} torr. Temperature by a thermal couple connected to the ion block. The instrument was operated in the CI -ve mode, emission current .2 ma, electron energy 150V, and resolution ~1000. Tetracyanoquinodimethane (TCNQ) was obtained from Aldrich. TCNQ, used to indicate the relative radical concentration and reactions[1,2], was introduced using an open vial packed with glass wool.

Observations and Discussion :

As reported previously[3], PCB's of higher chlorination tended to produce sets of [M-nCl+nH] clusters which decreased in relative abundance at higher source temperatures (fig. 1a,b). Some radical addition reactions in the TCNQ spectra also decreased with higher source temperatures (fig. 2a,b). These observations indicate these reactions could be occurring on the source walls, supporting the mechanism presented by Grimsrud et al[4].

PCB's of lower chlorination tended to yield [Cl]- as the base ion. Changing moderator gas influenced the ratio of parent ion [M]- to [Cl]-. This effect could be directly related to the complexity and thus the internal degrees of freedom in the moderator gas.

References :

1. McEwen, C.N., & Rudat, M.A., JACS, **1981**, *103*, 4343.
2. Sears, L.J., & Grimsrud, E.P., Anal. Chem. **1989**, *61*, 2523-2528.
3. Stemmler, E.A., & Hites, R.A., Biomed. & Envir. Mass Spec., **1988**, *17*, 311-328
4. Grimsrud et al., Organic Mass Spec., **1992**, *27*, 277-283.

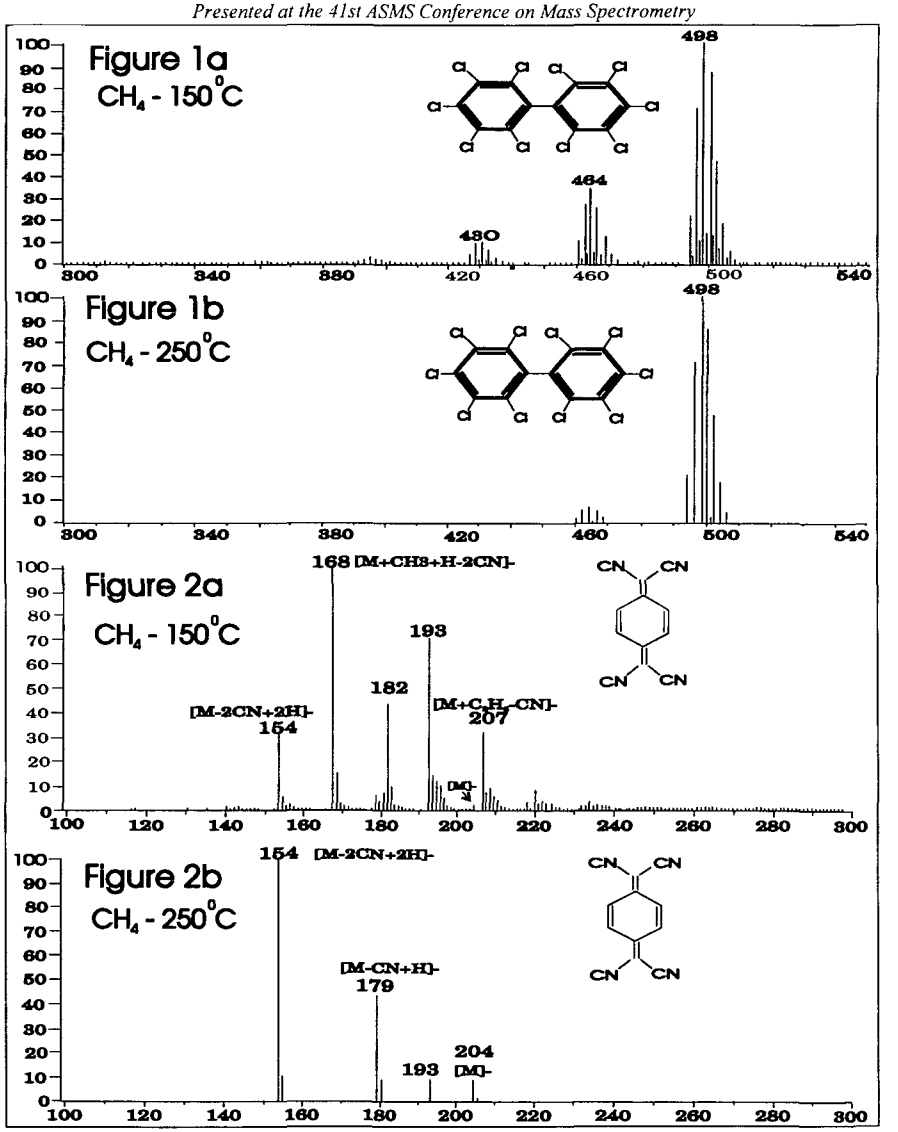

CHARACTERIZATION OF NOVEL CHEMICAL IONIZATION REAGENTS BY QUADRUPOLE ION TRAP MASS SPECTROMETRY

*Erwin J. Alvarez, Jin Duan, Aubrey McIntosh and Jennifer S. Brodbelt; Department of Chemistry and Biochemistry; The University of Texas at Austin; Austin, Texas 78712.

INTRODUCTION

The search for alternative means to differentiate classes of compounds and the increase in the fundamental knowledge and understanding of selective ion/molecule reactions have provoked interest in the evaluation of new chemical ionization reagents. Structurally diagnostic information can be obtained from certain types of chemical ionization processes that may derivatize analytes into characteristic adducts. We have begun an extensive systematic evaluation of many promising new chemical ionization reagents as selective probes of several classes of compounds. A Finnigan MAT Quadrupole Ion Trap Mass Spectrometer (ITMS) has been used to investigate the chemical ionization capabilities of reagents such as 1,1-difluoroethylene, 2,3-butanedione, dimethyl sulfoxide, and ethylene oxide with analytes such as lactones, diols, amines, and aminoalcohols. Our long term goal is to develop ways to distinguish isomeric biomolecules and to elucidate the structures of newly synthesized or isolated compounds, including pharmaceutically active quinine alkaloids and glucuronolactones, through the use of selective ion molecule reactions.

EXPERIMENTAL TECHNIQUES

A Finnigan MAT Quadrupole Ion Trap Mass Spectrometer (ITMS) equipped with a Hitachi/Teledyne HST-1000 filtered noise field accesory device for optimization of ion isolation was used to study the ion/molecule reaction processes. The typical reagent gas pressure used was nominally ~1-1.5 x 10^{-5} torr as measured by an ionization gauge positioned in the vacuum chamber; the reagent gas was introduced through a leak valve. The organic analytes were introduced via leak valve or by a heated solids' probe to about 1-2 x 10^{-6} torr.

After its introduction into the trap, the reagent gas was ionized with a short electron ionization pulse. The ions formed were then allowed to undergo ion/molecule reactions with the organic neutrals for a period of about 50-500 ms. Alternatively, a reagent gas ion was isolated by using the appropriate application of DC and RF voltages and allowed to undergo ion/molecule reactions with the organic neutrals for a period of 10-500 ms. This latter method was used to identify reaction pathways.

Collision activated dissociation (CAD) experiments were performed on each isolated adduct ion after completion of the ion/molecule reactions. Collisional activation was performed by the application of an ac voltage of 0.3-0.4 V_{p-p} at the axial frequency of motion of the ion of interest; activation times were typically 10-20 ms. The mass-selective instability mode was used to eject the fragment ions from the trap onto an electron multiplier for detection.

SELECTIVE PRODUCT FORMATION

For this study, eleven organic molecules with simple functional groups were chosen as representative substrates: 1-butanol, 1,3-propanediol, 3-amino-1-propanol, 1-propylamine, 1-pentene, benzene, butyraldehyde, cyclohexanone, γ-butyrolactone, ethylacetate and diethylether. Ten different chemical ionization reagent gases were used: dimethyl ether, dimethyl sulfide, dimethyl sulfoxide, ethylene, propene, 1,1-difluoroethylene, ethylene oxide, ethylene sulfide, 2,3-butanedione and acetone. Dimethyl sulfoxide, ethylene sulfide and acetone reagent ions proved to be unreactive with most of the organic analytes, and generally only resulted in formation of $(M+H)^+$ products. 1,1-difluoroethylene showed initial promise as a selective reagent for the identification of aromatic compounds; it reacts with benzene to form $(M+45)^+$ and $(M+25)^+$ adducts. However, it failed to be useful for substituted aromatic compounds. Substrates with either electron donating or electron withdrawing groups show less reactivity than benzene for the electrophilic adduct formation. For compounds with electron donating groups, only $(M+25)^+$ adducts were seen with less than 1% of the total ion current. For compounds with electron withdrawing groups

no adducts were observed. Results for chemical reagent gases that showed selectivity towards particular functional groups are presented below.

$(M+41)^+$ FROM ETHYLENE

Ethylene can form selective $(M+41)^+$ adducts for carbonyl containing compounds which do not contain an α-hydrogen like ketones, lactones and esters. Among them, the relative abundances of the $(M+41)^+$ adducts are highest for ketones (~40% of the total ion counts) whereas for lactones and esters the $(M+41)^+$ ions are less than 15% of the total ion counts. This difference may be due to the oxygen atom adjacent to the carbonyl group which enhances the basicity of the analyte and thus promotes proton transfer from the intermediate $(M+41)^+$ ion. The allyl cation is also selective for alcohols, whose $(M+41)^+$ adducts constitute less than 15% of the total ion counts. No stable formation of $(M+41)^+$ ions was observed for ethers and aldehydes, which instead form mainly $(M-1)^+$ ions due to hydride abstraction.

$(M+45)^+$ FROM ETHYLENE OXIDE

Ethylene oxide shows special ring-size selectivity for lactones. It can induce $(M+27)^+$ adducts for four-membered ring lactones, $(M+45)^+$ adducts for five-membered ring lactones and mainly $(M+1)^+$ adducts for six-membered ring lactones. The reactions may involve a loose hydrogen-bond intermediate which can subsequently undergo different reactions for four, five or six-membered (proton transfer only) ring lactones, partially based on the basicity of the lactone relative to ethylene oxide. For the smallest rings, the spontaneous dehydration of the intermediate $(M+45)^+$ adduct is favored, resulting in stable $(M+27)^+$ ions. For the five-membered rings the dehydration process is not spontaneous, resulting in intact $(M+45)^+$ adducts.

$(M+25)^+$, $(M+43)^+$ AND $(M+87-18)^+$ FROM 2,3-BUTANEDIONE

Both reagent ions from 2,3-butanedione, $(C_2H_3O)^+$ m/z=43 and $(M+1)^+$ m/z=87, react with hydroxyl containing compounds to form characteristic adducts. $(M+43)^+$ acetylation adducts are observed for alcohols whereas $(M+25)^+$ products are observed for diols. The intact $(M+43)^+$ adduct formed by acetylation was not observed for diols because spontaneous dehydration following acetylation ocurred, resulting in $(M+25)^+$ ions. The m/z=87 ion from 2,3-butanedione is selective for both alcohols and diols by forming $(M+87-18)^+$ adducts. The reaction leading to the $(M+87-18)^+$ ion was found to be favored for small molecular weight compounds with decreasing conversion efficiency as the size (molecular weight) increases.

CONCLUSIONS

This systematic survey of ten novel chemical ionization reagents has shown that there is great promise for the development of alternative chemical ionization reagents for specific applications. Those reagents which show characteristic reactivities with certain classes of compounds, such as ethylene oxide with lactones, are preferable to those which show non-specific reactivities, like acetone and ethylene sulfide. Finally, selective chemical ionization in conjunction with collision activated dissociation for detailed structural elucidation provides a powerful means of characterizing analytes and should prove to be particularly advantageous for distinguishing complex molecules that contain several types of functional groups.

ACKNOWLEDGMENTS

Financial support from the Welch Foundation, the American Chemical Society Petroleum Research Foundation, the National Institutes of Health, and the National Science Foundation are gratefully acknowledged. E.J.A. acknowledges a Fellowship from the National Institutes of Health.

Fragmentation and Ion-Molecule Reactions of Ethanolamine Using FTMS

Sung-Seen Choi and Hun-Young So
Division of Chemistry and Radiation
Korea Research Institute of Standards and Science
P.O.Box 3, Taedok Science Town, Taejon 305-606, Korea

A FT/ICR spectrometer was used to study fragmentation path and ion-molecule reactions of ethanolamine. The reaction between product ions and neutral molecule were studied by varying experimental conditions such as electron impact energy, pressure, and ion trapping time. The major fragment ions observed under 70 eV energy were $C_2H_6N^+$, $C_2H_4N^+$, CH_4N^+, CH_2N^+, $C_2H_3O^+$, CH_3O^+, and CHO^+. The nitrogen containing fragment ions were found more abundant than oxygen containing ones. By comparing the heats of fragmentation reactions calculated by AM1 semiempirical calculations, it was found that formations of nitrogen containing fragment ions are more favorable than those of oxygen containing fragment ions.

The experimental results of SWIFT ejection technique showed that $C_2H_6N^+$ and $C_2H_5O^+$ ions are formed from protonated molecules while CH_4N^+ and CH_3O^+ ions are formed from all three precursors, $M^{+\cdot}$, $[M+H]^+$, and $[M-H]^+$.

The decrease of fragment ions under longer ion trapping time is considered due to dissipation of internal energies by collisions and to the proton transfer reactions. All fragment ions are decreased at a longer ion trapping time while the intensity of the protonated molecules increase. The rate constants for proton transfer reactions between neutral molecules and fragment ions are listed in Table 1.

Table 1. Rate constants for proton transfer reactions

Fragment Ion	k (X $10^{-9}cm^3molec^{-1}s^{-1}$)
$C_2H_6N^+$	1.56
$C_2H_4N^+$	3.43
CH_4N^+	2.70
CH_2N^+	3.84
$C_2H_5O^+$	1.66
$C_2H_3O^+$	2.91
CH_3O^+	3.53
CHO^+	4.26

The mass peaks of $C_2H_7N^{+\cdot}$ (m/z 45) and $C_2H_9NO^{+\cdot}$ (m/z 63) are appeared by changing ion trapping time from 10 ms to 200 ms as shown in Figure 1(a). From thermodynamic parameters, the structure of these two ions could be postulated as $\dot{C}H_2CH_2\overset{+}{N}H_3$ and

$H_2\dot{O}CH_2CH_2\overset{+}{N}H_3$, respectively. The $\dot{C}H_2CH_2\overset{+}{N}H_3$ is found to be formed from $H_2\dot{O}CH_2CH_2\overset{+}{N}H_3$ by oxygen-carbon bond breaking and loss of H_2O. According to calculational results, the distonic ion $\dot{C}H_2CH_2\overset{+}{N}H_3$ is more stable than its isomer $CH_3CH_2NH_2^{+\cdot}$ by 38 kJ/mol.

Product ions larger than molecular ion are also observed. They are considered as ion-molecule reaction products. We could observe $H_2C{=}\overset{+}{N}H_2$ and protonated molecules as the most abundant ion with short and long ion trapping time. This made us to consider the ion-molecule reactions between $H_2C{=}\overset{+}{N}H_2$ (or protonated molecule) and neutral molecule important. The product ion $H_2NCH_2CH_2\overset{+}{N}H{=}CH_2$ (m/z 74) was observed in mass spectrum, as shwon in Figure 1(a). This ion is generated by ion-molecule reaction between $H_2C{=}\overset{+}{N}H_2$ and neutral ethanolamine and subsequent loss of NH_3.

There are three ion-molecule reactions between protonated ethanolamine and its neutrals. They are the formations of $(H_2NCH_2CH_2OH)_2{\cdot}H^+$ (m/z 123), $HOCH_2CH_2\overset{+}{N}H{=}CHCH_3$ (m/z 88), and $HOCH_2CH_2\overset{+}{N}H_2CH_3$ (m/z 76) as shown in Figure 1(b). Among the three product ions, the $(H_2NCH_2CH_2OH)_2{\cdot}H^+$ is the most abundant ion and the next is HOCH2CH2$\overset{+}{N}$H=CHCH3. The $HOCH_2CH_2\overset{+}{N}H{=}CHCH_3$ ion can be formed by loss of H_2O and NH_3, while the $HOCH_2CH_2\overset{+}{N}H_2CH_3$ ion can be formed by loss of NH_3 and $H_2C{=}OH$.

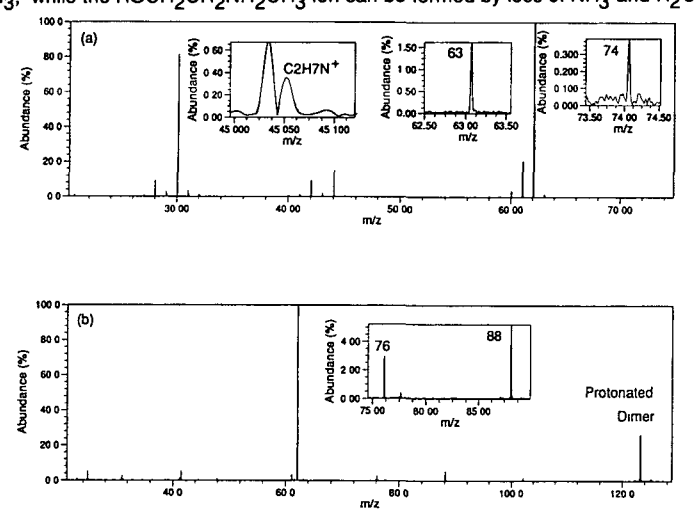

Figure 1. Electron impact ionization mass spectra of ethanolamine with 70 eV of electron impact energy. The pressure and ion trapping time are (a) 2.4 x 10^{-7} Torr and 50 ms and (b) 3.5 x 10^{-7} Torr and 10 s.

The ion chemistry of nitrosamide

Helge Egsgaard[a] and Lars Carlsen[b]

[a]Department of Combustion Research, Risø National Laboratory
DK-4000 Roskilde, Denmark
[b]National Environmental Research Institute,
Department of Environmental Chemistry, DK-4000 Roskilde, Denmark

The nitrosamide, NH_2NO, apparently is the key intermediate in the reaction between amidogen, NH_2, and NO, which is crucial in the highly effective processes developed to remove NO from flue gases [1]. However, the reaction between NH_2 and NO leaves NH_2NO in a highly excited state, causing a rapid decomposition of the latter. The NH_2 + NO has until recently been assumed as the only route to the elusive NH_2NO molecule. Thus, despite its importance, the chemistry of NH_2NO is virtually unknown. However, very recently the nitrosamide has by neutralization-reionization mass spectrometry been demonstrated to be a viable molecule in the dilute gas phase [2]. The isoelectronic CH_3NO_n (n=1,2) system is, on the other hand, one of the most widely studied and a comparison with the general fragmentation of $NH_2NO_n^{+\bullet}$ (n=1,2) appears appropriate.

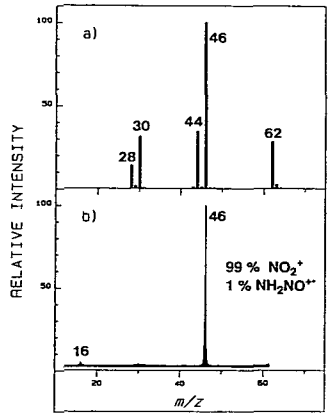

Figure 1. EI mass spectrum of nitramide a) and the collision induced spectrum of the $NH_2NO_2^{+\bullet}$ ($M^{+\bullet}$) b).

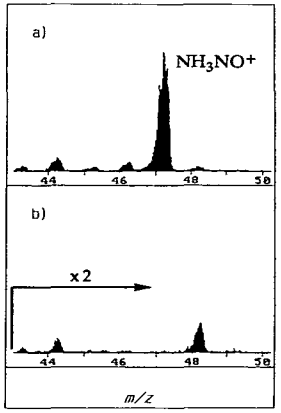

Figure 2. Partiel mass spectrum of a NO^+ plasma following addition of NH_3 a) and the background spectrum b).

The electron impact mass spectrum of nitramide and the collision induced spectrum of the molecular ion, $NH_2NO_2^{+\bullet}$, are given in Figure 1. The nitromethane radical cation shows in

addition to the the simple cleavage concurrent fragmentation via the *aci*- and methylnitrite isomers [3]. In contrast to this, the collision induced fragmentation of nitramide gives rise only to the simple cleavage without any indication of isomerization, possibly resulting in elimination of, e.g. H_2O. The observed m/z 44 ($N_2O^{+\bullet}$) in the electron impact spectrum (cf. Figure 1a) is, owing to the apparent absence of the analogous ion in the collision induced spectrum, assigned to a surface promoted decomposition within the ion source of the relatively labile molecule prior to ionization. The virtual absence of isomerization of $NH_2NO_2^{+\bullet}$ was unexpected since the substitution of CH_3 to NH_2 should make the isomerization processes energetically more favourable. However, the introduction of the relatively weak N-N bond may account for the observed differences. This assumption is, however, somewhat contradicted by the fragmentation of $MeNO^{+\bullet}$ and $NH_2NO^{+\bullet}$; both ions fragmenting by simple cleavages exclusively. On this background it is worthwhile to consider the excited $CH_3NO_2^{+\bullet}$ ion as being described as a methyl cation complexed to a NO_2 radical, thus, giving the nitromethane system unique properties [4].

We have searched for alternative routes to the "NH_2NO" system. Thus, it appears that the NH_3NO^+ is generated through a reaction between NO^+ and ammonia under CI conditions. This ionic reaction constitutes an interesting counterpart to the well-established radical route in the thermal DeNOx process. The reaction may in addition have some implications in heterogeneous processes since NO form complexes with the NO-ligand formally ionized with a number transition metals.

MO calculations strongly support the formation of N-protonated nitrosamide; the reaction being exothermic by 31 kcal/mol [5]. A high energy barrier (86 kcal/mol) prevents the isomerization of NH_3NO^+ to NH_2NOH^+ [5]. The partial CI mass spectra given in Figure 2 demonstrate that the protonated nitrosamide is the primary product of the reaction between ammonia and NO^+. The elemental composition was verified by using ND_3 and $^{15}NH_3$, the protonated nitrosamide being shifted accordingly.

The intensity was found to be very depended on the ammonia pressure, i.e. ammonia acts as a highly effecient sink in the proton transfer from NH_3NO^+ which leaves the elusive nitrosamide. This may be regarded as a novel route to NH_2NO opening up for spectroscopic studies of the parent nitrosamide - the apparent key to the DeNOx chemistry.

References

1. J.A. Miller and C.T. Bowman; *Prog. Energy Combust. Sci.*, **15** (1989) 287.
2. H. Egsgaard, L. Carlsen, T. Weiske, D. Sülzle and H. Schwarz; *Chem. Phys. Letters*, **199** (1992) 643.
3. H. Egsgaard, L. Carlsen, H. Florencio, T. Drewello and H. Schwarz; *Ber.Bunsenges. Physik. Chem.*, **93** (1989) 76.
4. C. Lifshitz, M. Rejwan, I. Levin and T. Peres; *Int. J. Mass Spectrom. Ion Processes*, **84** (1988) 271.
5. H. Egsgaard, J.Ø. Madsen and L. Carlsen; submitted for publication.

Accurate Mass Measurements in Desorption Chemical Ionization (DCI) Mode

S.A. Pergantis, L.L. Madilao, C.A. Emond and G.K. Eigendorf
Department of Chemistry, University of British Columbia, Vancouver, B.C., Canada V6T 1Z1

INTRODUCTION

Desorption Chemical Ionization (DCI) is a mass spectrometric technique capable of providing molecular weight as well as structural information on a variety of compounds not amenable to EI-MS. Depending on the structural features of the analyte a variety of reagent gases can be used. We have found ammonia to be a very effective reagent gas in DCI, particularly for the analysis of oxygen containing compounds such as esters, ethers, and hydroxylated compounds. Under these conditions abundant $(M+H)^+$ and/or $(M+NH_4)^+$ pseudo-molecular ions, along with structurally informative fragment ions, are observed.[1] Under ammonia DCI conditions none of the normally used mass deficient reference standards, such as, heptacosafluorotri-N-butylamine, perfluorokerosene (PFK), or tris(perfluoroheptyl)-S-triazine, gave adequate mass spectra. However, PFK has been successfully used with methane in the CI[2] and DCI mode. Others[3,4] have reported the use of mass sufficient compounds (esters, carbowax) as reference materials in high resolution CI/DCI MS.

In this work we have demonstrated the successful use of PFK as a reference standard with a gas mixture of methane and ammonia. This procedure allows for accurate mass measurements in the full scan and peak matching modes for a variety of compounds. Polyperfluoropropylene oxide (Fomblin) was also used as a reference standard either with iso-butane, methane or ammonia. This allowed for the routine accurate mass measurement of higher molecular weight compounds, up to 1730 amu, in DCI mode.

INSTRUMENTATION

Low resolution DCI measurements were carried out on a quadrupole mass spectrometer (Delsi-Nermag R10-10C / Technivent PC Data system). Both low and high resolution (10,000) DCI measurements were carried out on double focusing mass spectrometers (Kratos Concept II H (Q) / Dart Data system, and Kratos MS 80 RFA / DS 55 Data system). Three reagent gases were used: i-butane, methane and ammonia. Figure 1 shows the Negretti SS-Needle Valve system used to introduce gas mixtures into the ion source. During the high resolution measurements the reference compound (PFK, Fomblin) and sample are introduced simultaneously.

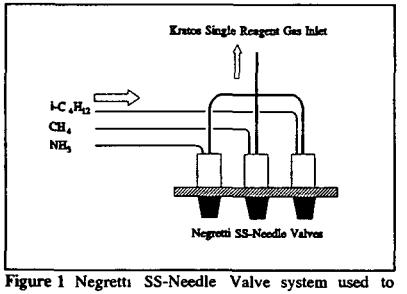

Figure 1 Negretti SS-Needle Valve system used to introduce gas mixtures.

RESULTS

The spectrum obtained for PFK using a mixture of NH_3 and CH_4 gases is presented in Figure 2, the reagent gas ion ratios used are presented in Table 1. The gas ratios could be adjusted using the Negretti SS-Needle Valve system (Fig. 1).

A number of compounds have been analyzed using NH_3 and CH_4 gas mixtures with PFK and

Fomblin as references, the results obtained are presented in Table 2.

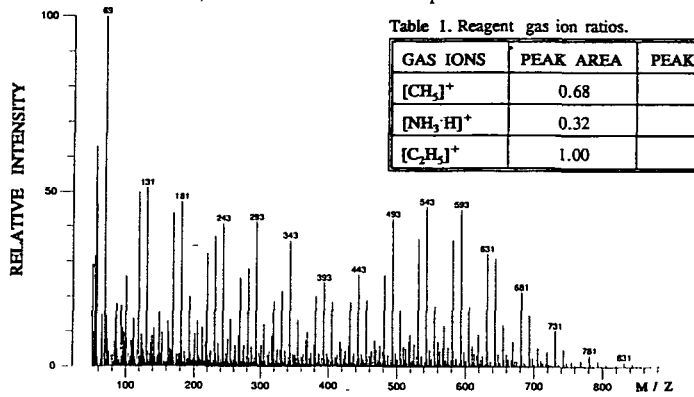

Figure 2. CI spectrum of PFK with ammonia and methane gas mixture.

Table 1. Reagent gas ion ratios.

GAS IONS	PEAK AREA	PEAK HEIGHT
$[CH_5]^+$	0.68	0.86
$[NH_3 \cdot H]^+$	0.32	0.43
$[C_2H_5]^+$	1.00	1.00

Table 2. Accurate mass measurements of compounds from several compound classes

Compound / Formula	Reference / Reagent gas	$[M+Gas]^+$ / $[M+H]+$	Theoretical m/z	Measured m/z	Error, ppm
Disaccharide / $C_{24}H_{33}FO_{15}$	PFK / NH_3 & CH_4	$[M+NH_4]^+$	598.21472	598.21173	5.00
Terpene Precursor / $C_{25}H_{44}O_5SSi_4$	PFK / NH_3 & CH_4	$[M+NH_4]^+$	588.24869	588.24851	0.31
Monosaccharide / $C_{18}H_{26}O_{12}$	Fomblin / NH_3	$[M+NH_4]^+$	452.1768	452.17699	0.43
Organoarsenical / $C_5H_{11}O_2As$	PFK / NH_3 & CH_4	$[M+H]^+$	179.00533	179.0046	3.91
Hemicarcerand / $C_{97}H_{95}O_8N_3$	Fomblin / i-C_4H_{12}	$[M+H]^+$	1430.71974	1430.72006	0.29

CONCLUSIONS

Data presented in this study indicate that mass deficient calibration reference compounds such as PFK and Fomblin can be used in conjunction with a number of reagent gases for high resolution accurate mass measurements in positive DCI (CI) mode. These compounds are generally preferred as reference materials because of their good volatility compared to other compounds reported in the literature.[4,5] We have demonstrated that a gas mixture of NH_3 and CH_4 can be successfully used with PFK, while Fomblin can be used with either i-C_4H_{12}, NH_3 or CH_4. Experiments are under way to evaluate perfluorinated mass deficient reference compounds under negative DCI (CI) conditions.

REFERENCES

1. W. R. Cullen, G. K. Eigendorf and S. A. Pergantis, Rapid Commun. Mass Spectrom., 7, 1, (1993).
2. I. Dzidic, D. M. Desiderio, M. S. Wilson, P. F. Crain and J. A. McCloskey, Anal. Chem. 43,1877, (1971).
3. J. A. Ballantine, J. D. Barton, J. F. Carter and B. Fussell, Org. Mass Spectrom. 22, 316, (1987).
4. G. J. Langley, Org. Mass Spectrom. 25, 429, (1990).
5. H. Maeder and K. H. Gunzelmann, Rapid Commun. Mass Spectrom., 2 (10), 199-200, (1988).

ALKALI METAL CATIONIZATION OF SOME AROMATIC AMIDES

Yu Cao, Kenneth L. Busch, and John Haseltine
School of Chemistry and Biochemistry
Georgia Institute of Technology, Atlanta GA 30332

A series of organic aromatic pyrrolidine compounds has been used as model compounds to study the cationization of group I alkali metal ions in liquid SIMS. Since the pyrrolidine molecules are relatively small, only a few possible sites are available for interaction with metal ions. We hope that the study of mechanism for cationization of these compounds will facilitate the application of cationization for determination of molecular weights for other organic or biological compounds.

All liquid SIMS mass spectra were recorded in m-NBA matrix doped with four alkali metal (Na, K, Rb, Cs) salts in equimolar ratio. Immediately before the mass spectra were measured, the sample and solvent matrix were mixed together on the probe tip in solutions with a constant molar ratio.

Cationization in SIMS and in EI:

Cationization is strongly affected by the number of pyrrolidine amide groups on the benzene ring. The trend of affinities for alkali metals to the target molecules is *mono* < *bis* < *tris*. The increased cation affinity is due to the increased number of carbonyl functionality groups. Larger cations are more favorably attached than smaller cations for those precursor molecules that have multi-functional (carbonyl) groups. It is possible that larger cations can bind to these compounds more effectively than the smaller ones due to the spatial organization of the carbonyls in these molecules.

Cationization of these same model compounds has also been studied by EI with a direct exposure probe. Alkali cations and precursor molecule both appear in the mass spectra, but no cationization has been observed for any precursor molecules, which indicates that cation adduction occurs in the condensed phase rather than through gas phase ion/molecule reactions.

Double Cationizations:

In many instances, multiply cationized ions can occur through multiple proton-alkali metal exchange, leading to ions of the type $[M+nCat-(n-1)H]^+$. In the current study, doubly cationized ions $[M+2Cat]^+$ have been observed for 3-nitro-isophthalic pyrrolidine amide without intervention of the proton exchange or creation of a doubly-charged species (Figure 1). The doubly cationized ions with all four cation combinations have been observed. However, the ions containing cesium are relatively more abundant than those ions with other alkali cation combinations. A CID MS/MS study has been performed for the doubly cationized molecules. One striking feature of product ion spectra for the doubly cationized ions is that the major fragments of dissociation are the doubly cationized NO_2 ions, viz m/z 312 ($[NO_2Cs_2]^+$, Figure 2) and m/z 264 ($[NO_2CsRb]^+$) respectively. However, under similar experimental conditions, (same collision cell pressure and similar collision energy) the dissociation for the singly cationized ion is predominantly through alkali cation loss. Double cationization reactions has also been observed for m-NBA doped with alkali cations. Again, those double-cationized ions containing cesium are of higher intensities. Our study shows the nitro group is the initial site of attachment for at least one of the alkali cations.

Figure 1: Liquid SIMS mass spectrum for 3-nitro-isophthalic pyrrolidine amide in NBA matrix doped with alkali metal salts.

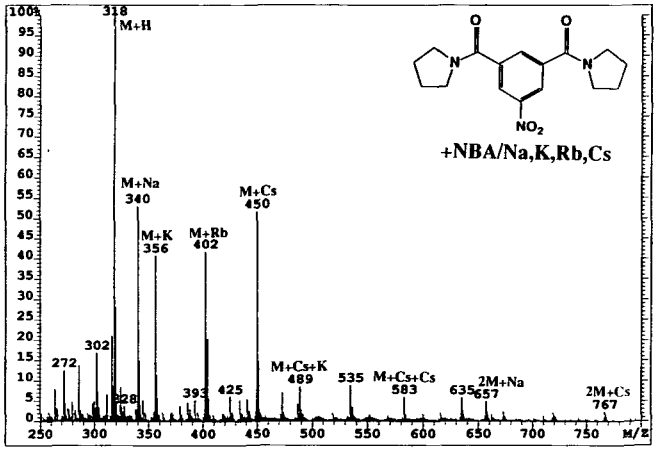

Figure 2: CID MS/MS spectrum for parent ion [M+Cs+Cs]+ of 3-nitro-isophthalic pyrrolidine amide.

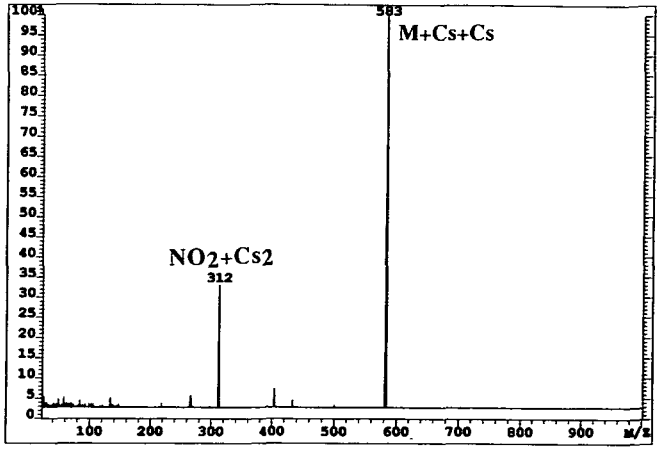

Cluster Ion Formation in Liquid Secondary Ion Mass Spectra of Diquaternary Pyridinium Oxime Salts

Gary J. Kunkel and Kenneth L. Busch
School of Chemistry and Biochemistry, Georgia Institute of Technology,
Atlanta, Georgia 30332-0400, USA

Alkyl phosphates, used as insecticides, cause inhibition of acetylcholinesterase, an enzyme needed for the propagation of nerve impulses. Diquaternary pyridinium oxime salts are effective reactivators of the enzyme and thus effective antidotes for organophosphate intoxication. In our studies of these compounds using Liquid SIMS, extensive cluster ion formation has been noted. These cluster ions are ascribed to interactions between positive ions from the sample and the liquid matrix. We have used Liquid SIMS to acquire mass spectra for several diquaternary pyridinium oxime salts in the high mass range to study adduct formation reactions.

When glycerol was used as the matrix, no sample related high mass clusters were seen. However, when CSA (camphorsulfonic acid) was added to the glycerol solvent, a multitude of high mass cluster ions are observed. An explanation of these ions is given in Figure 1 for the mass spectrum of AB-8.

Figure 2 is the mass spectrum of AB-13 when NBA (m-nitrobenzyl alcohol) is used. The counter anion is observed for several cluster ions in the mass spectrum. If CSA is added, chlorine-containing adducts are no longer observed. Apparently, the chloride preferentially reacts with CSA and is no longer able to participate in cluster formation. However, a large number of CSA-containing clusters are observed.

When thioglycerol is used, the number of different high mass ions decreases dramatically because fragment ions apparently do not participate extensively in cluster ion formation. The anion is present in many of the cluster ions observed.

Sample were the gift of A. Vincze from the Israel Institute of Biological Research.

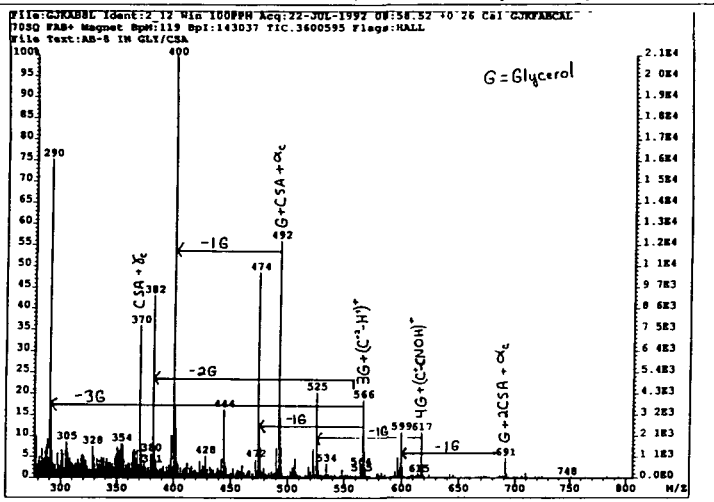

Figure 1

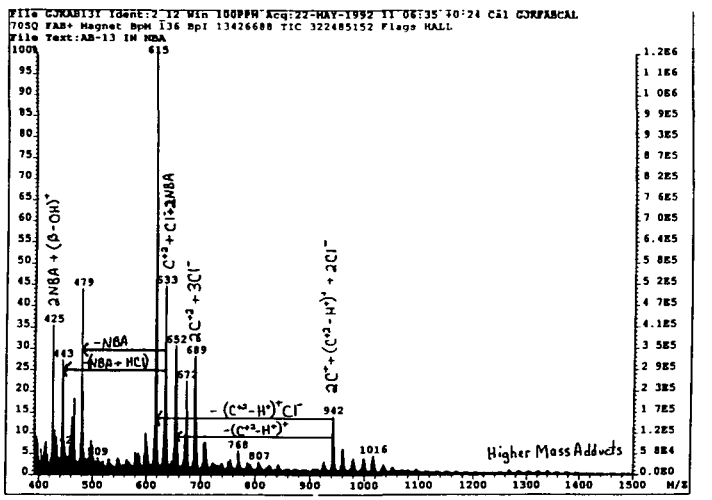

Figure 2

INVESTIGATION OF THE PENNING IONIZATION PROCESS USING THE RARE-GAS METASTABLE BEAM SOURCE

D. Faubert, G.J.C. Paul and M.J. Bertrand
Regional Center for Mass Spectrometry, Department of Chemistry,
University of Montreal, Montreal, Canada, H3C 3J7

Penning ionization (PI) involves the electrophilic reaction of a metastable atom (A*) with an analyte (BC) resulting in an ionic state of the analyte (BC^+), the ground state of the atom (A) and the ejected electron in a continuum state (e^-).

$$A^* + BC \rightarrow A + BC^+ + e^- \quad (PI) \quad (1)$$
$$A + B + C^+ + e^- \quad (PI) \quad (2)$$

Reaction (2) occurs if the excitation energy transferred to the analyte is high enough to effect bond breakage within it. Experimental evidence suggests that Penning ionization is the major ionization process which takes place in the ion source where the metastables are formed through a corona discharge.[1] The apparatus employed consists of a metastable beam source and single quadrupole mass spectrometer. Equipment and working conditions are similar to that reported previously[1] except for the initiator. A high voltage pulse (-6 kV), superposed on the DC voltage of the cathode, between the cathode and the auxiliary electrode was used to initiate the discharge. This new modification makes ignition of the discharge easier and prevents arcing in the source housing. The metastable beam source was obtained from Dephy Technology (Que., Canada). The same analyte partial pressure was used in each experiment.

In this study the utility of the metastable beam source has been extended to the investigation of over fifty organic compounds including substituted aromatics, ketones, aldehydes, alkanes, alkenes, esters, ethers, alcohols, nitriles, amines and fullerene. All compounds were analyzed by the five rare-gas metastables with varying excitation energies (Table 1). Upon collision with Xe*, it has been observed that all molecules which yield a signal generate only the molecular ion. For Kr*, aromatics do not give fragment but all aliphatics give at least one fragment with low intensity. As you go up to Ar*, Ne*, He*, fragmentation increase greatly reflecting the higher energy transfer. Higher fragmentation is observed for aliphatics relative to aromatics which is a consequence of lower APs for aliphatics and, possibly, a faster rate of decomposition of excited aliphatic molecular ions to their characteristic fragments. Exception is fullerene where the only ions present in the mass spectrum of C_{60} with He* are the molecular ion ($M^{+\cdot}$) and the doubly charged ion ($M^{2+\cdot}$). These results show that the second ionization potential of C_{60} is lower than 20.61eV. Lifshitz et al. have previously given a second ionization value of 19.85eV for C_{60} which is consistent with our observations.[2] By varying rare-gases, both hard and soft EI-like fragmentation was achieved yielding molecular weight and structural information.

The metastable beam source pressure greatly influences the metastable beam density and consequetly the TICs (Total Ion Currents) obtained. An exemple of pressure study is shown in Figure 1, for each gas an optimum pressure exists for maximum sensitivity. As each gas gives a similar TIC curve, the shape of those curves is probably explained by the same phenomena. At low pressure, either the metastable production is weaker due to the low density of rare-gas atoms or the metastable transport is less effective at the lower differential pressure. At high pressure, the mean free path is much smaller for the metastable atoms as well as ions formed in the ion source and the sensitivity decreases.

A comparison was made of the TICs for various organic analytes to gain information on the proportion of the two metastable states for xenon ($^3P_0$, $^3P_2$) present in the ion source (Table 1). Two classes of compounds are shown in the Table 2, one with ionization potentials lower than

both metastable states and the other with IPs between the excitation energies of the metastables. As only the highest energy xenon metastable can ionize the compounds with IPs between both metastables, the small TICs for this class of compounds reflects (Table 2) the small proportion of the highest metastable in the source. The same phenomenon is observed for the krypton metastables. These observations mean either the production of the highest energy metastable ($^3P_2$) is weak or their lifetime are short relative to the lower energy states.

The TICs detected for aromatic and saturated molecules upon collision with the krypton metastable are shown in Table 3. These results are of interest as they provide insight into the Penning ionization process for molecules of different structures. It is important to mention that all IPs for molecules in Table 3 are lower than both krypton metastables. The TICs for aromatic molecules are at least a factor of five greater than that for saturated molecules. These observations can be explained in terms of electron distributions for the relevant molecular orbitals of the analyte. For the unsatured aromatic molecules, the spacially extended π-orbitals are expected to have higher electron densities on the molecular surface than the spatially limited σ-orbitals for saturated molecules.[3] Hence, the possibility of electron transfer from the analyte to the metastable atom is greater for aromatic molecules than saturated molecules, as shows by the TIC values in Table 3. The number of unsaturated bond in a molecule also affects the sensitivity of the analyte upon interaction with Kr*. The TIC increases from cyclooctane (saturated bonds) to cyclooctatetraene (4 double bonds), as shown in Table 4.

1. D. Faubert, G.J.C. Paul, J. Giroux and M.J. Bertrand, Int. J. Mass Spectrom. Ion Phys., 124 (1993) 69.
2. C. Lifshitz, M. Iraqi and T. Peres, Rapid Comm. Mass Spect., 5 (1991) 238.
3. K. Ohno, H. Mutoh and Y. Harada, J. Am. Chem. Soc., 105 (1983) 4555.

Table 1 - Metastable states of rare gases

gas	Helium		Neon		Argon		Krypton		Xenon	
Metastable	$^1S_0$	$^3S_1$	$^3P_0$	$^3P_2$	$^3P_0$	$^3P_2$	$^3P_0$	$^3P_2$	$^3P_0$	$^3P_2$
energy (eV)	20.61	19.82	16.72	16.62	11.72	11.55	10.56	9.92	9.45	8.32

Table 2 - Total ion current detected for various organic compounds with Xe*(8.32, 9.45eV)

Molecule	Ionization Potential	Total Ion Current
benzene	9.24	9
fluorobenzene	9.20	7
bromobenzene	8.98	0
1-octene	9.43	6
1-decene	9.42	0
aniline	7.72	737
2-chloroaniline	(8.50)	429
3-chloroaniline	8.09	433
p-Me-anisole	7.90	843
piperidine	8.05	195

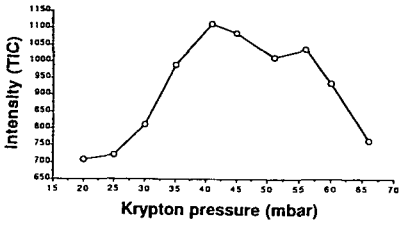

Figure 1- Intensity (TIC) variation with krypton pressure

Table 3 - Total ion current detected for aromatic and saturated molecules upon collision with Kr*

saturated molecules	TIC	aromatic molecules	TIC
1,1-dimethylcyclohexane	106	benzene	500
1,2-dimethylcyclohexane	109	chlorobenzene	480
ethylcyclohexane	102	toluene	452
cyclooctane	60	anisole	666

Table 4 - Total ion current detected for a family of compounds upon collision with Kr*

molecule	Total Ion Current
cyclooctane	61
cis-cyclooctene	143
1,3-cyclooctadiene	217
cyclooctatetraene	325

CHARACTERIZATION OF Ar/CH_4 GLOW DISCHARGE PLASMAS

L. R. Meadows and F. L. King
Department of Chemistry, West Virginia University
Morgantown, West Virginia 26506, U.S.A.

INTRODUCTION

Plasmas sustained in mixtures of methane with a rare gas diluent are employed in the deposition of thin diamond films. Such plasma enhanced chemical vapor deposition affords the ability to deposit films on temperature sensitive substrates because the energy required to promote film growth is imparted to gas phase precursor species through collisions within the plasma. A key limitation to the widespread application of plasma based deposition methods is the poor reproducibility of films obtained from this procedure. This problem is a direct consequence of an inadequate understanding of plasma chemistry and the dependence of this chemistry on plasma operating parameters. Investigations were undertaken to characterize these reactive plasmas. The production of various hydrocarbon species within the plasma was correlated with two observables, plasma energy content and precursor internal energy, derived from mass spectrometric measurements. The long term goal of this work is the correlation of such observables with film quality to permit intelligent control of plasma processing systems.

RESULTS AND DISCUSSION

Two methods were employed in the assessment of plasma energy content. Atomic emission measurements of argon lines in the wavelength range from 425 nm to 435 nm provided data from which argon excitation temperatures were determined. As the plasma composition was varied from 95% argon and 5 % methane to 75% argon and 25% methane, the argon excitation temperature dropped from 7500° to 4700°, Figure 1. Relative argon

Figure 1

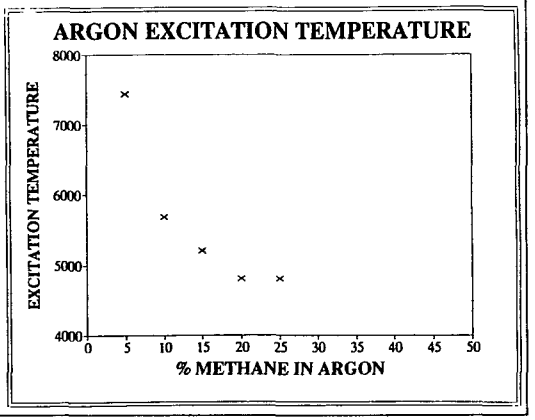

ionization temperatures were obtained from the ratio of mass spectrometry signal intensities, (singly-charged argon species)/(doubly-charged argon species). These values exhibited the same trend as observed for the excitation temperatures. It is important to note that although these are not absolutely quantitative values they do provide qualitative measures of the change in plasma energy content. The production of ions corresponding to methyl fragments and the products of condensation of those fragments decreased with decreasing argon excitation and ionization temperatures.

Figure 2

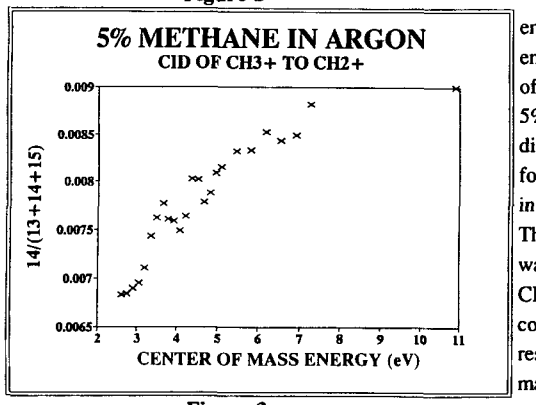

Figure 3

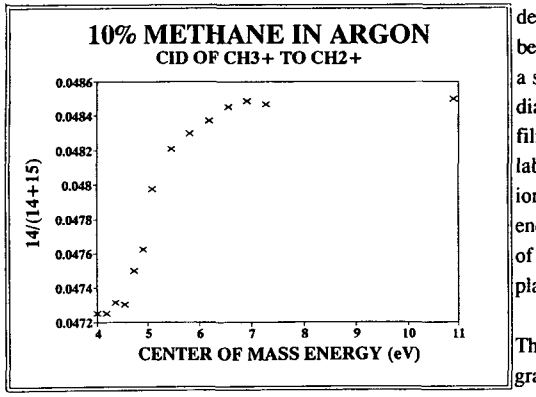

Tandem MS experiments were employed to probe the internal energy of CH_3^+ species as a function of discharge gas composition. With 5% methane the threshold for the dissociation of CH_3^+ to CH_2^+ was found to correspond to a maximum internal energy of 2.2 eV, Figure 2. The same maximum internal energy was found for the dissociation of CH_3^+ to CH^+. Increasing the concentration of methane to 10% resulted in a decrease in the maximum internal energy to 0.5 eV, Figure 3. The ability to track the internal energy of species in these deposition plasmas is important because precursor molecules require a specific internal energy to produce diamond films rather than graphite films. Future investigations in our laboratory seek to correlate argon ion temperatures and internal energies with the diamond character of thin films deposited from these plasmas.

The Office of Naval Research is gratefully acknowledged for support.

REARRANGEMENT OF α-SILYL-SUBSTITUTED CARBENIUM IONS IN THE GAS PHASE. AN INVESTIGATION OF RELATIVE MIGRATORY APTITUDES

R. Bakhtiar and D. B. Jacobson

Department of Chemistry, North Dakota State University
Fargo, North Dakota 58105-5516

The rearrangement of carbenium ions by 1,2-migration is ubiquitous in organic chemistry with a rich body of information concerning the relative migratory aptitude of various groups [1] α-Silyl-substituted carbenium ions ($R_3Si\text{-}CH_2^+$) have been implicated in rearrangements involving 1,2-group migration in α-functionalized silanes in solution (e.g., reaction 1), however, there is virtually no information regarding the relative migratory aptitude of

$$(CH_3)_3SiCH_2Cl \xrightarrow{AlCl_3} (CH_3)_2ClSi\text{-}CH_2CH_3 \qquad (1)$$

various groups [2,3] This is a consequence of the instability of organosilylenium ions (R_3Si^+) in solution under conditions where analogous carbenium ions are long lived [4] We have initiated studies involving 1,2-group migration of α-silyl-substituted carbenium ions in the gas phase by using Fourier transform mass spectrometry (FTMS) [5]

Nascent α-silyl-substituted carbenium ions are generated from the corresponding (chloromethyl)silane by either protonolysis with CH_5^+ or by chloride abstraction with $Si(CH_3)_3^+$. For example, protonolysis of $(CH_3)_2HSiCH_2Cl$ by CH_5^+ yields primarily HCl loss, reaction 2 The incipient carbenium ion (1) subsequently

$$(CH_3)HSiCH_2Cl + CH_5^+ \longrightarrow (CH_3)HSi\text{-}CH_2^+ + HCl + CH_4 \qquad (2)$$

1

rearranges to thermodynamically more stable silylenium ions by either 1,2-hydrogen or 1,2-methyl group migration, reaction 3. Theory has revealed that there is essentially no barrier for the highly exothermic (ca. 40 kcal/mol) 1,2-

$$(CH_3)_2HSi\text{-}CH_2^+ \xrightarrow{H} Si(CH_3)_3^+ \qquad (3a)$$

$$(CH_3)_2HSi\text{-}CH_2^+ \xrightarrow{CH_3} SiH(CH_3)(C_2H_5)^+ \qquad (3b)$$

hydrogen migration for $H_3Si\text{-}CH_2^+$ to yield $H_2Si(CH_3)^+$ [6] In addition, 1,2-methyl migration for $(CH_3)_3Si\text{-}CH^+\text{-}CH_3$ to yield $(CH_3)_2Si^+\text{-}CH(CH_3)_2$ is highly exothermic (ca. 32 kcal/mol) and has little or no barrier [7] These results suggest that both 1,2-hydrogen and 1,2-methyl migration are accessible processes for carbenium ion **1**

Probing the rearrangement channels for carbenium ion 1 (reaction 3) requires that the two distinct silylenium ions be distinguished. Although CAD does not discern silylenium ion structural isomers, specific ion/molecule reactions with methanol and isotopically labeled ethene readily differentiates these isomers. For example, methanol reacts with *authentic* $Si(CH_3)_3^+$ to yield exclusive loss of CH_4 whereas $SiH(CH_3)(C_2H_5)^+$ yields competitive elimination of H_2 (0.49), CH_4(0.23), and C_2H_6(0.28). In addition, ethene-$^{13}C_2$ reacts with silylenium ions containing a two carbon or longer alkyl chain by elimination of the corresponding olefin, reaction 4.

$$(CH_3)_2Si(C_nH_{2n+1})^+ + {}^{13}C_2H_4 \longrightarrow (CH_3)_2Si(^{13}C_2H_5)^+ + C_nH_{2n} \qquad (4)$$

For the two $SiC_3H_9^+$ isomers, $Si(CH_3)_3^+$ is inert with ethene-$^{13}C_2$, whereas, $SiH(CH_3)(C_2H_5)^+$ yields clean elimination of unlabeled ethene (i.e., m/z 73 goes to m/z 75 cleanly). By combining these two specific ion/molecule reaction probes, nearly any silylenium ion structural isomers can be distinguished.

We have generated a host of nascent α-silyl-substituted carbenium ions and studied the relative migratory aptitude of various groups. These include $(CH_3)_2HSi\text{-}CH_2^+$ (1), $(CH_3)_3Si\text{-}CH_2^+$ (2), $(CH_3)_2(C_2H_5)Si\text{-}CH_2^+$ (3), $(CH_3)_2(CH{\equiv}C)SiCH_2^+$ (4), $(CH_3)_2(CH_2{=}CH)Si\text{-}CH_2^+$ (5), and $(C_6H_5)(CH_3)HSi\text{-}CH_2^+$ (6). **1** yields *exclusive* 1,2-hydrogen migration to give $Si(CH_3)_3^+$, **2** undergoes 1,2-methyl migration to yield $Si(CH_3)_2(C_2H_5)^+$, **3** gives roughly 65% 1,2-methyl migration to form $Si(CH_3)(C_2H_5)_2^+$ and 35% 1,2-ethyl migration to give $Si(CH_3)_2(C_3H_7)^+$, **4** yields *exclusive* 1,2-ethynyl migration to give $Si(CH_3)_2(CH_2C{\equiv}CH)^+$, **5** gives *exclusive* 1,2-ethenyl migration to generate $Si(CH_3)_2(CH_2CH{=}CH_2)^+$, and **6** yields both 1,2-phenyl migration to yield $SiH(CH_3)(CH_2C_6H_5)^+$ (94%) and 1,2-hydrogen migration to form $Si(CH_3)_2(C_6H_5)^+$ (6%). The results for **2** and **3** suggest that methyl and ethyl groups have similar relative migratory aptitudes. **1** clearly indicates that hydrogen has a much higher migratory aptitude than a methyl group. **4** and **5** indicate that the migratory aptitude of ethynyl and ethenyl groups is much greater than that for a methyl group Finally, **6** indicates that the migratory aptitude of a phenyl group exceeds that of hydrogen. These results suggest the following relative group migratory aptitudes:

Aryl > hydrogen >> methyl ~ ethyl

ethynyl >> methyl

ethenyl >> methyl

The preferred orientation for 1,2-group migration is presumably coplanarity of the empty p orbital of the carbenium ion center with the sigma orbital of the migrating group (Z) with the transition state involving a three-center, two-electron bond. 1,2-Group migration may be concerted with formation of the carbocation center or may

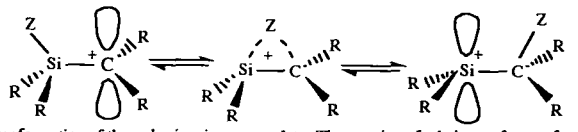

proceed after formation of the carbenium ion is complete. The question of relative preference for migration of different groups, "migratory aptitude", is a complex one, and there is no absolute order. The preference for migration of groups containing pi systems may be due to initial interaction of the pi electrons with the developing empty 2p orbital on the carbon atom This would yield a structure in which the unsaturated group is coplanar with the empty 2p orbital of the carbenium ion and, consequently, is predisposed to migration.

The relative migratory aptitude of hydrogen to that of ethynyl and ethenyl is under investigation as well as the relative migratory aptitude of ethynyl, ethenyl, and phenyl groups.

References

1. Fry, J. L.; Karabatsos, G J. In *Carbonium Ions*, Olah, G. A.; Schleyer, P. v. R., Eds.; Wiley: New York, 1970, Vol. II, p. 521.
2. Tamao, K.; Kumada, M. *J. Organomet. Chem.* **1971**, *30*, 339.
3. Robinson, L. R.; Burns, G. T.; Barton, T J *J. Am. Chem. Soc.* **1987**, *107*, 3935.
4. Cowley, A. H.; Cushner, M. C.; Riley, P. E. *J. Am. Chem. Soc.* **1980**, *102*, 624
5. Bakhtiar, R., Holznagel, C. M, Jacobson, D. B. *J. Am. Chem. Soc.* **1992**, *114*, 3227.
6. Hopkinson, A. C.; Lien, M. H. *J. Org. Chem.* **1981**, *46*, 998.
7. Apeloig, Y.; Karni, M, Stanger, A, Schwarz, H, Drewello, T., Czekay, G. *J. Chem. Soc., Chem. Commun.* **1987**, 989.

AN EXPERIMENTAL AND THEORETICAL STUDY OF THE HYDROGEN-BRIDGED RADICAL CATION $[CH_3C{=}O{\cdots}H{\cdots}O{=}CH_2]^{+\bullet}$

Jaana M.H. Pakarinen,[1] Krista M. Stirk,[2] Pirjo Vainiotalo,[1] Tapani A. Pakkanen[1] and Hilkka I. Kenttämaa[2]

[1]Department of Chemistry, University of Joensuu, SF-80101 Joensuu, Finland
[2]Department of Chemistry, Purdue University, West Lafayette, Indiana 47907, USA

During the past ten years, hydrogen-bridged radical cations have been frequently proposed as intermediates in the dissociation/isomerization pathways of a wide range of radical cations. Although high-level *ab initio* molecular orbital calculations indicate that many hydrogen-bridged -O···H···O-, -C···H···O- and -N···H···O- radical cations correspond to an energy minimum, not much experimental evidence exists to support the existence of such long-lived species.

From the combination of mass spectrometry experiments and *ab initio* calculations, we suggest that the hydrogen-bridged radical cation $[CH_3C{=}O{\cdots}H{\cdots}O{=}CH_2]^{+\bullet}$ is formed from the long-lived and low-energy molecular ion of ionized hydroxyacetone, $[CH_3C(O)CH_2OH]^{+\bullet}$. The isomerization occurs via a [1,4]-hydrogen shift, accompanied by a C-C bond cleavage. The experiments were performed in a differentially pumped dual-cell Fourier-transform ion cyclotron resonance mass spectrometer (FT/ICR) in a magnetic field produced by a 2.3 T superconducting magnet. Aldehydes, ketones and alcohols react with ionized hydroxyacetone by replacement of $CH_3CO\bullet$. For example, propanal replaces $CH_3CO\bullet$ in the ion $[CH_3C{=}O\ \ H\ \ O{=}CH_2]^{+\bullet}$ to form the ion $[CH_3CH_2C(H)O{\cdots}H{\cdots}O{=}CH_2]^{+}$. This product ion reacts by a further replacement of CH_2O with propanal, giving rise to $[CH_3CH_2C(H)O{\cdots}H{\cdots}OC(H)CH_2CH_3]^{+}$ (Figure 1). These results strongly suggest that the long-lived molecular ion of hydroxyacetone partially isomerizes to the hydrogen-bridged radical cation $[CH_3C{=}O{\cdots}H\ {\cdot}{\cdot}O{=}CH_2]^{+\bullet}$

The formation of another hydrogen-bridged ion, $[CH_3C(H){=}O{\cdots}H{\cdots}O{=}CH]^{+\bullet}$, by a [1,5]-hydrogen shift in the ion $[CH_3C{=}O{\cdot}{\cdot}\ H\ {\cdot}{\cdot}O{=}CH_2]^{+\bullet}$, can occur for some of the molecular ions under certain conditions. Ethyl iodide, D5-ethyl iodide, allyl iodide and dimethyl disulfide react by replacement of formyl radical •CHO, in addition to charge exchange. These findings suggest that some of the ions of $[CH_3C{=}O{\cdots}H{\cdots}O{=}CH_2]^{+\bullet}$ rearrange to the structure $[CH_3C(H){=}O{\cdots}H{\cdots}O{=}CH]^{+\bullet}$ prior to or during the reaction.

High-level *ab initio* molecular orbital calculations were performed up to the MP2/6-31G**// 6-31G**+ZPVE level of theory. The hydrogen-bridged species $[CH_3C{=}O{\cdots}H{\cdots}O{=}CH_2]^{+\bullet}$ and $[CH_3C(H){=}O{\cdots}H{\cdots}O{=}CH]^{+\bullet}$ were found to be more stable by 10.2 kcal/mol and 13.5 kcal/mol, respectively, than the covalently bonded, ionized hydroxyacetone. The two enol isomers of ionized hydroxyacetone, $[CH_3C(OH){=}CHOH]^{+\bullet}$ and $[CH_2{=}C(OH)CH_2OH]^{+\bullet}$, which were not observed experimentally, were calculated to be the most stable structures (by 41.2 kcal/mol and 22.3 kcal/mol relative to the covalently bonded, ionized hydroxyacetone).

Figure 1.

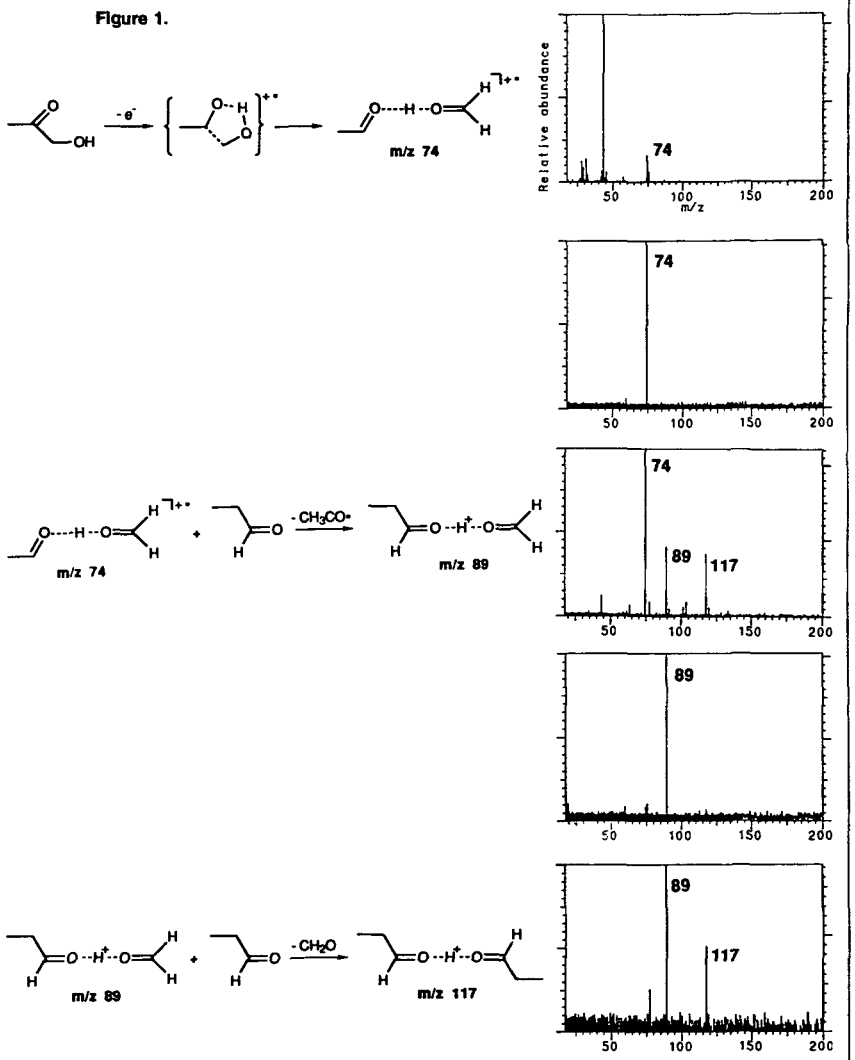

The Gas Phase H/D Exchange Kinetics of Protonated Amino Acids: Trends Within the Alkyl Side Chain Series

Eric Gard *, Jennifer Bregar, Dale Willard, Carlito B. Lebrilla,
Chemistry Department,
University of California, Davis California 95616

The gas phase H/D exchange kinetics of protonated amino acids with organic deuterium sources (e.g. CH_3OD) are studied using an external source Fourier transform mass spectrometer. The amino acids studied are those containing simple alkyl side chains and trends within this group are examined. Rate constants for the H/D exchange of hydrogen atoms associated with specific functional groups are determined within a given compound and compared to analogous rates associated with hydrogen atoms in other amino acids within this series. The trends in rate constants are compared with known gas phase proton affinities differences between the deuterium source and the amino acid.

Both the forward and reverse exchange experiments were carried out using glycine and no kinetic isotope shift is discernible. Comparison of glycine, alanine, and their methyl esters shows the acid hydrogen is exchanged most rapidly. This holds true for the entire series.

Table 2 shows the approximate rates for the hydrogens on both the acid and amino positions within each amino acid. The acid exchange rate has a small dependence on basicity. In contrast, the amino position shows a clear trend with Proton Affinity (PA) difference. The exchange rate at the amino position becomes slower with increasing P.A. difference. This trend is consistent with previous literature information.

The most basic site in these molecules is the amino group which is also the site of protonation in the molecule. It is interesting that the acid hydrogen exchanges when the protonation site is rather far removed from its location. More work in this area will help determine the mechanism for the exchange process.

Table 1: Experiment Rate Constants for Selected Amino Acids

Amino Acid	P.A. Kcal/mole Relative to CH3OH(181 9)	k1	k2	k3	k4
Glycine	29.7	10.3	3.2	2.0	1.1
Glycine (D_4)	29.7	9.6	3.1	2.0	1.1
Glycine methyl ester	N/A	1.9	1.2	b	b
Alanine	32.9	13.3	0.9	b	b
Alanine methyl ester	N/A	1.3	b	b	b
Valine	35.1	12.8	0.2	b	b
Leucine	36.2	9.0	0.2	b	b
iso-Leucine	37.0	9.0	0.2	b	b
Proline	38.3	9.2	b	b	b
Proline methyl ester	N/A	b	b	b	b

*all k's x 10^{-11} cm^3 s^{-1}.
b) Exchange is not observed, k < 0.1 x 10^{-11}

Table 2: Approximate Exchange Rates for the Acid and Amino Hydrogens for each Amino Acid

Amino Acid	P.A. Kcal/mole Relative to CH3OH(181 9)	k Acid	k Amino
Glycine	29.7	7.0	1.0
Alanine	32.9	12.5	0.3
Valine	35.1	12.5	0.07
Leucine	36.2	8.8	0.07
iso-Leucine	37.0	8.8	0.07
Proline	38.3	9.2	N/A

*all k's x 10^{-11} cm^3 s^{-1}.

SPONTANEOUS UNIMOLECULAR DISSOCIATION OF WEAKLY BOUND IONIC CLUSTERS UNDER LOW-PRESSURE CONDITIONS

Detlef Thölmann and Terrance B. McMahon

Department of Chemistry, University of Waterloo, Waterloo, Ontario N2L 3G1

Gaseous ions trapped under low-pressure conditions, e.g. in an ICR cell, usually are regarded as stable species which exchange energy mainly by collisions. The time between collisions in an ICR cell at typical background pressures of 10^{-9} mbar lies in the range of 10 s to 40 s. Metastable ions, on the other hand, usually have lifetimes of 10^{-4} to 10^{-5} s. This is much shorter than the trapping time of an ICR mass spectrometer. Even for large oligosaccharide molecular ions metastable ion lifetimes do not exceed 2 ms[1].

We generated various ionic cluster ions of the type L_nH^+ and L_nCl^- (n = 1–5) in the home-built high-pressure external ion source of our Bruker Spectrospin CMS 47 FT-ICR mass spectrometer and trapped them in the ICR cell for up to 500 s During the trapping time a spontaneous unimolecular dissociation with loss of one or two ligands was observed. The unimolecular dissociation rate constants varied from 2.4×10^{-3} to 0.83 s^{-1} (see Table 1). This is much slower than any metastable dissociation. For a similar cluster ion, the proton-bound dimer of diethyl ether formed in an association reaction, Fisher and McMahon[2] found a metastable dissociation rate of 550 s^{-1}.

The energy required for the dissociation process, the bond dissociation energy, is 20 to 37 times R·T (T = 298 K), i.e. it is considerable larger than thermal energy. In an exchange of energy with the walls of the ICR cell via black-body radiation, however, the high-energy part of the Boltzmann distribution may continuously be re-populated, yielding some ions with energies above threshold. From preliminary RRKM calculations we estimate the minimum dissociation rate constant for a cluster ion at threshold energy to be on the order of 10^2 to 10^3 s^{-1}. This is at the same order of magnitude as metastable dissociation rate constants and very fast compared to the observed unimolecular rates. Therefore the rate of energization of the cluster ions must be rate determining.

Presented at the 41st ASMS Conference on Mass Spectrometry

Table 1. Unimolecular rate constants k_{uni} and thermodynamical data for the loss of a ligand from cluster ions (**W**: H_2O; **E**: $(CH_3)_2O$)

reaction	k_{uni} [s^{-1}]	ΔH°_{298} [kcal·mol^{-1}]	ΔG°_{298} [kcal·mol^{-1}]	ΔS°_{298} [cal·mol^{-1}K^{-1}]
$W_5H^+ \rightarrow W_4H^+$	0.49±0.01	13.9	5.8	27.2
$W_4H^+ \rightarrow W_3H^+$	$4.6(\pm0.1)\times10^{-3}$	17.4	9.6	26.1
$EW_3H^+ \rightarrow EW_2H^+$	0.23±0.03	12.9	6.1	22.7
$EW_2H^+ \rightarrow EWH^+$	$3.3(\pm0.3)\times10^{-2}$	16.7	7.4	31.1
$E_2W_2H^+ \rightarrow E_2WH^+$	0.44±0.07	14.3	6.2	27.2
$E_2WH^+ \rightarrow E_2H^+$	0.83±0.2	12.4	4.3	27.2
$E_3WH^+ \rightarrow E_2WH^+$	$9.5(\pm1)\times10^{-2}$	21.7	9.3	41.6
$W_3Cl^- \rightarrow W_2Cl^-$	$8.6(\pm1)\times10^{-2}$	11.8	5.1	22.3
$W_2Cl^- \rightarrow WCl^-$	$2.4(\pm0.4)\times10^{-3}$	13.0	6.6	21.4

In order to examine and confirm the supposed mechanism, the pressure and temperature dependence of the observed dissociation rates were investigated. A static pressure of 3×10^{-9} to 1×10^{-6} mbar of CH_4 was used in the ICR cell. A small pressure dependence was observed, originating from some collisional activation. This is **not** due to initial excess kinetic energy of the ions, however, because the bimolecular rate for this process is constant over a time period of 400s at 10^{-6} mbar CH_4. Both unimolecular and bimolecular rates were obtained from rate *vs.* pressure plots. The bimolecular rate of the reaction $W_4H^+ \rightarrow W_3H^+$ with CH_4 as the bath gas is as low as $(6.3\pm0.6)\times10^{-14}$ $cm^3molecule^{-1}s^{-1}$.

The unimolecular dissociation rate constants expectedly show a strong increase with temperature. Heating the ICR cell from 298 K to 320 K increases the unimolecular dissociation rate by about a factor of 2. This shows indeed that the energy required for the dissociation is of thermal origin.

References

1. L. Ngoka, C.B. Lebrilla *J. Am. Soc. Mass Spectrom.* **4**, 210 (1993).
2. J.J. Fisher, T.B. McMahon *Int. J. Mass Spectrom. Ion Processes* **100**, 701 (1990).

Photodissociation and Relaxation of Gas-Phase Aluminum Cluster Ions

*Brian T. Cooper and Steven W. Buckner
Department of Chemistry, University of Arizona, Tucson, AZ 85721
Denise C. Parent
Chemistry Division/Code 6113, Naval Research Laboratory, Washington, D.C. 20375-5000

Presented here are studies of the oxidation, near-infrared photodissociation and electron photodetachment of the aluminum cluster anions Al_n^-, where $3 \leq n \leq 23$, as well as studies of the relaxation and oxidation of the photoexcited ions. Highly vibrationally excited aluminum cluster anions may be prepared for those clusters that require the absorption of more than one photon to dissociate, and the excited fraction can be estimated from the extent of dissociation using a Poisson distribution. The effects of vibrational excitation on bimolecular reactivity can be used to gain mechanistic insight; conversely, measurements of this kinetic perturbation can be used to determine the internal energy and relaxation rate of the ions.

All experiments were performed with a Fourier transform ion cyclotron resonance mass spectrometer (FT-ICR). The instrument uses a single trapping cell in a 3.0 T magnetic field, and experiments are controlled by an Extrel Odyssey data station. Aluminum cluster anions were formed by direct laser desorption/ionization from an aluminum nitride pellet held on a solids probe, using the unfocussed, Q-switched second harmonic from a Nd:YAG laser. The unfocussed, non-Q-switched, fundamental output pulse of the YAG was used for photoexcitation. Care was taken to ensure the colinearity of the desorption and ion photoexcitation beams. A static Ar background provided collisional cooling for the ions, while for the oxidation reactions O_2 was admitted through a pulsed valve, since oxygen gettering by desorbed aluminum neutrals made it difficult to maintain a static O_2 pressure.

All of the cluster ions studied, with the exception of the "magic number" cluster Al_{13}^-, absorb at 1064 nm. All but n = 3, 6 and 7 (which predominantly photodetach) photodissociate, losing a single aluminum atom. In general, smaller clusters (n < 13) require the absorption of 1 photon to dissociate, and larger clusters require 2. The effects of photoexcitation on the oxidation reactions of Al_{16}^- and Al_{18}^- were investigated; results are given below:

TABLE 1: Kinetic Behavior of Vibrationally Excited Al_n^-

	$Al_n^- + O_2$			Relax		
	k_{therm}/k_{hot}	therm X(n-5)	hot X(n-5)	k_{rad} (s^{-1})	$k_{coll,\ Ar}$ ($cm^3\ s^{-1}$)	eff*
Al_{16}^-	2.5 ± 1.0	0.32 ± 0.04	0.90 ± 0.08	0.47 ± 0.10	(9 ± 2) x 10^{-12}	1.7 ± 0.4
Al_{18}^-	5.0 ± 2.0	1.0	1.0	-	-	-

*k_L for Al_{16}^-/Ar = 4.96×10^{-10} $cm^3\ s^{-1}$.

These clusters react by the following scheme:

$$Al_n^- + O_2 \xrightarrow{-2Al_2O} Al_{n-4}^{-*} \longrightarrow Al_{n-5}^- \text{ or } Al_{n-4}^-$$

These reactions are found to slow down with cluster internal excitation, while preliminary anion experiments and published cation experiments find that the reaction rate increases upon translational excitation. This non-equivalence of different types of energy must mean that vibrational excitation, dispersed throughout the cluster's 3n-6 internal degrees of freedom, does not efficiently couple into the reaction coordinate, while translational excitation can on the other hand be used to overcome an activation barrier (corresponding to dissociative chemisorption) on the entrance channel. The nonstatistical nature of these reactions will be the subject of a future investigation.

The "branching ratio" measurements of Table 1 are not truly branching processes, but rather are sequential. As it is expected that any excess vibrational excitation in the Al_n^- cluster would be largely and proportionally partitioned into the Al_{n-4}^- product, we are justified in using this ratio as a measure of the cluster internal energy. Therefore, it is possible to measure the relaxation rate constants (radiative and collisional), using the experiment of Figure 1, below.

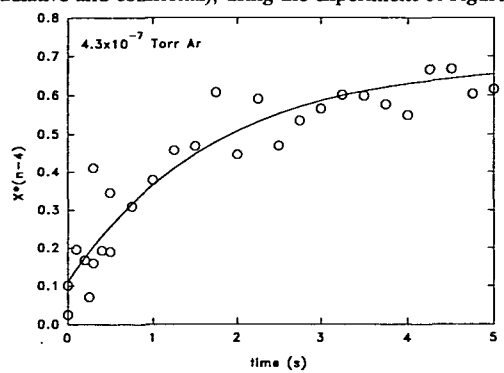

Figure 1. Initial Branching Ratio for the Reaction of Photoexcited Al_{16}^- with O_2 as a Function of Cooling Delay. Open circles: experimental data. Solid line: exponential fit; k_{relax} = 0.60 s^{-1}.

The radiative component of the rate constant measured above, 0.47 s^{-1}, is in the range that would be expected for a typical molecular ion with ~1 eV of excess internal energy, although it is also predicted that this rate constant is *independent* of internal energy, since all vibrational modes are readily populated even at thermal energies. Finally, collisional quenching by Ar is rather inefficient (although this is not unprecedented); more remarkable is that the collisional quenching efficiency for SF_6 is, preliminarily, about the same.

Mass Spectra of Mercury/Alkali and Cadmium/Alkali Clusters and Their Structure

*H. Ito[1], T. Sakurai[1], T. Matsuo[1] and I. Katakuse[2]
[1]Institute of Physics, College of General Education, Osaka Univ. Toyonaka, Osaka, 560 Japan
[2]Department of Earth and Space Science, Faculty of Science, Osaka Univ Toyonaka, Osaka 560 Japan

INTRODUCTION:

Mass spectrometric studies are useful to reveal the size specific properties of micro clusters, such as an electronic shell structure or an atomic shell structure. The structure of cluster ions of group IA, IIA and IIB metal can be explained by the electronic shell structure depending on delocalized electron orbits. That of group 0 rare gas can be explained by the atomic shell structure depending on close-packed atoms (outer form is an icosahedron or a double icosahedron). The cluster size indicating of the specific properties of cluster is called "magic number". In the case of IIB metal cluster ions (Zn, Cd), the total number of valence electrons at their experimental magic numbers differed ±1 from the theoretical shell closing number (2, 8, 20, 34, 40, 58,...)[1]. On the contrary, we expect that in case of IIB/cesium clusters, their total number of valence electrons at experimental magic number could agree with theoretical shell closing number. We report here the investigation of the mass spectra of mercury/cesium, cadmium/cesium and zinc/cesium clusters and discuss the structure of the clusters.

EXPERIMENTAL:

Cluster ions were produced by the bombardment of an appropriate metal sheet with 15keV Cs^+ ions. The primary cesium ions were produced using a thermal ion source. The cluster ions were mass-analyzed using a grand-scale sector mass spectrometer[2]. The identification of clusters was performed using a comparison between high resolution mass spectra at low mass region and calculated isotope patterns. The component of cluster ions at high mass region were determined to be similar pattern as low mass region.

RESULT and DISCUSSION:

We observed the mass spectra of mercury/cesium, cadmium/cesium and zinc/cesium clusters. Figure 1 shows a mass spectrum of zinc/cesium cluster ions. This spectrum is not completely resolved between Zn_nCs^+ and $Zn_{n-2}Cs_2^+$. However, the peak abundance pattern of *zinc/cesium cluster ions can be explained by the electronic shell structure. The abundant cluster* ions, $Zn_{10}Cs^+$ and $Zn_9Cs_2^+$ are attributed by the electronic shell (shell closing number = 20). The abundant cluster ions, $Zn_{20}Cs^+$ and $Zn_{19}Cs_2^+$ is attributed by the electronic shell (shell closing number = 40). Figure 2 shows a mass spectrum of cadmium/cesium cluster ions. The total numbers of valence electrons of Cd_4Cs^+(8), $Cd_{10}Cs^+$(20), $Cd_{17}Cs^+$(34), $Cd_{20}Cs^+$(40) and $Cd_{29}Cs^+$(58) agree with the theoretical shell closing numbers depending on delocalized electron orbits. The electronic shell structure clearly appears in the peak abundance pattern of cadmium/cesium cluster ions. Figure 3 shows a size distribution of Hg_nCs^+. For small clusters, a step-like feature is observed in the abundance distribution. The magic numbers (12, 18, 22, 25, 28 and 31) indicate a symmetrical geometric structure arising from close-packed atoms. For large clusters, a smooth periodic variation is observed. The size distribution of Hg_nCs^+ ions provided information of shell closing effect of neutral mercury clusters, Hg_n^0. The magic numbers (47, 70, 100, 132, 137, 170, 223, 280, 348, 430, 528, 648 and 764), which indicate the stability of neutral clusters, Hg_n^0 depending on the electronic structure, are reflected in the undulated abundance pattern of cluster ions, Hg_nCs^+.

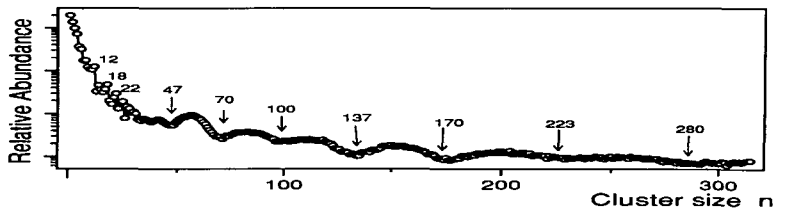

Figure 1. Size distribution of $(Hg)_nCs^+$

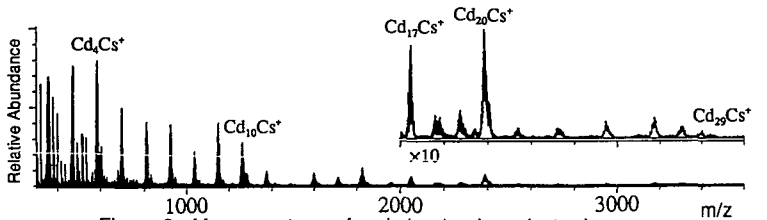

Figure 2. Mass spectrum of cadmium/cesium cluster ions

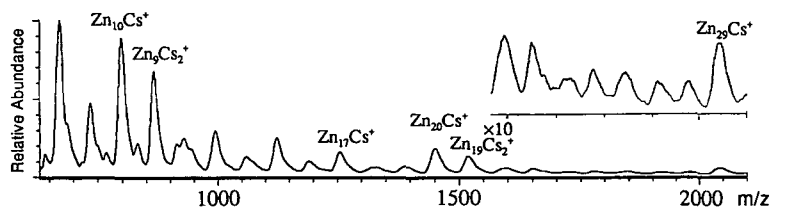

Figure 3. Mass spectrum of zinc/cesium cluster ions

CONCLUSION:

[1] The total number of valence electrons at the magic number of cadmium/cesium and zinc/cesium clusters corresponds to the theoretical electronic shell closing numbers at the low mass region. These clusters are bounded the metallic bonding forces.

[2] The total number of atoms at the magic number of Hg_nCs^+ (n<30) corresponds to the total number of atoms in double icosahedral structure(DIC). Mercury/cesium cluster ions in this region is bounded the van der Waals bonding forces.

[3] The size distribution of Hg_nCs^+ (n>30) ions provides information of the neutral mercury clusters, Hg_n^0. The abundant neutral mercury clusters are originated by the electronic shell structure.

REFERENCES:

1. I. Katakuse et. al., Int. J Mass Spectrom. Ion Processes, 69, 109 (1986)
2. H. Matsuda et. al , Int J. Mass Spectrom. Ion Processes, 91, 1 (1989)

Positive and Negative LC/MS Analysis of C_{60}, C_{70} and C_{84} Fullerenes

[1]T. Matsuo,[1]H.Ito,[2]H.Shinohara,[3]Y.Saito,[4]K.Matsuura and [4]K.Nojima

[1]Institute of Physics, College of General Education, Osaka Univ, Toyonaka 560 Japan
[2]Department of Chemistry, Faculty of Science, Nagoya Univ. Nagya ***, Japan
[3]Department of Chemistry for Material, Mie Univ. Tsu 514, Japan

INTRODUCTION

Mass spectrometric techniques have been successfully used to detect and characterize fullerenes since they yield specific molecular information. It should be noted, however, that mass spectrometry can only determine the mass-to-charge ratio of ions which are mass separated, and that mass spectra can not always give accurate information regarding the composition of the material. It is important to confirm whether detected ions are produced directly from the material itself, or produced as secondary products during the ionization process, especially in the case where ion or laser bombardment is used. In order remove such ambiguities, the following procedures are possible:

1. Use different types of ionization methods.
2. Combine mass spectronetry with chromatographic techniques.
3. Measure both positive and negative ion spectra.
4. Measure a purified sample of a single component.

We have taken LC/MS and FD (field desorption) mass spectra of carbon fullerenes and compared and contrasted the results.

EXPERIMENTAL

The fullerene rich carbon soot was prepared by a contact arc method. The separation (purification) was achieved liquid chromatography.

A JEOL SX102A mass spectrometer with a DA7000 data system was used for mass separation and detection. The frit-FAB ion source was coupled on-line to an HPLC system (Yokokawa LC-100). The eluent was ionized on the frit surface using 6keV Xe^0 bombardment. The flow rate was 5µl/min. A syringe pump (Harverd Apparatus Model 22) was also used to infuse the seprated single component into the frit-FAB system. Mass spectra were acquired at every 5 seconds over the mass range m/z 400 to 2200 at 8kV accelerating potential. A carbon emitter (10µm diameter) was used for the field desorption measurements, and the emitter current was increased by at a program rate of 2 mA/min up to 50 mA.

RESULTS AND DISCUSSION

[A] FAB mass spectra of C_{60}, C_{70}, C_{84}

Mass spectra were obtained through LC or direct inlet system. Positive and negative ion mass spectra of C_{84} by direct inlet mode are shown in Figures 1a, 1b respectively.

1. Fragmentation and aggregation phenomena occurred during ionization for purified C_{60}, C_{70} and C_{84} fullerenes. Fullerene-like carbon clusters (C_{2n}^+ n= 30, 31, 32, 33, 34, 35, 36, 37, 38, 39, 40,41, 42, 43, 44, 45, 46 for C_{84} were produced as gas-phase ions. The intensity of such ions change monotonously according to generation from C_{60}, C_{70} or C_{84}. The intensity at m/z 720 and 840 increase rapidly, which suggests that these peaks are composed of both clusters and fullerenes.
2. Adduct ions (C_{70}+O, C_{70}+CH) were produced.
3. Fragmentation and aggregation were observed less in negative ion mode than in positive ion mode.
4. LC/MS method can distinguish between (1)ions which were produced directly from the material itself and (2)ions which were produced as secondary products during the ionization process,

[B] FD spectra of C_{60}, C_{70} and C_{84}

FD (positive) mass spectra of C_{70} and C_{84} are shown in Figures 2 and 3.

1. Almost no fragmentation or aggregation peaks were observed for C_{60} or C_{70}.
2. Doubly and triple charged ions were observed for C_{60} and C_{70}.
3. For C_{84}, there are some minor components are detected even by FD. This may suggest the purification process for C_{84} was not completed.

Though we can not say definitely whether these peaks are fragment ions or molecular ions of fullerene of these size, we can only say the possibility of latter case is large from the FD mass spectra of C_{60} and C_{70}. In conclusion, (1) LC/MS methds can distingush secondary product ions. (2) FD ionization is more suitable for quantitative analysis of fullerene.

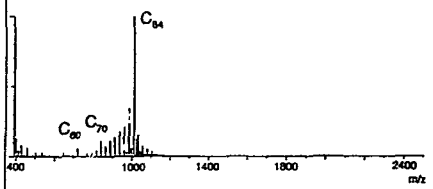

Fig.1a FAB mass spectrum of C_{70} in positive mode.

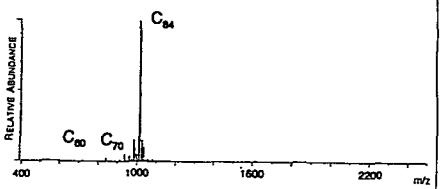

Fig.1b FAB mass spectrum of C_{70} in negative mode.

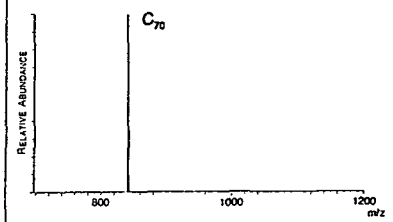

Fig.2 FD mass spectrum of C_{70}.

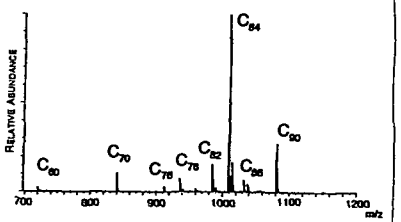

Fig.3 FD mass spectrum of C_{84}.

Presented at the 41st ASMS Conference on Mass Spectrometry

MASS SPECTROMETRIC CHARACTERIZATION OF SYNTHETIC DERIVATIVES OF BUCKMINSTERFULLERENE

J.H. Callahan, M.A. Park, A. Purdy, J.A. Milliken, M.M. Ross, S.W. McElvany, Naval Research Laboratory, Washington, D.C. 20375.

The development of widespread interest in fullerenes since 1990 has led to a wide variety of studies involving C_{60}, including the synthetic derivatization of fullerenes, which may serve as precursors for new materials and polymers. Analysis of these derivatives poses a significant analytical challenge, to which the application of new and established mass spectrometric techniques has proven and should continue to prove useful. We have used mass spectrometric techniques to characterize the products of two types of reactions. In the first, the products of the reaction of catecholborane (CB) with C_{60} are observed by negative desorption chemical ionization (Figure 1). Hydrogenated fullerenes, $C_{60}H_x$, are observed as products of this reaction, with the number of hydrogens (x) exceeding 16 in some cases. Additionally, we have been able to observe intact C_{60}/catecholborane products, $C_{60}CB_n$, where n=1-3. Collision-induced dissociation (CID) of the $C_{60}CB$ product confirms the addition of 120 mass units (corresponding to the addition of CB). The results suggest that the CB reaction may serve as a useful initial step in the synthesis of additional derivatives.

A second reaction of interest is the alkylation of fullerenes with $NaZn(R)_3$ and $Zn(Et)_2$ where R is an alkyl group such as CH_3CH_2 or neo-pentyl (Figure 2). When the reaction mixture in benzene is hydrolyzed with water, DCI analysis shows the resultant products to consist of $C_{60}R_nH_m$, where n=1-15 and m<n. These reactions are similar to those reported by Kahr and coworkers.[1] In general, the lowest molecular weight derivative is $C_{60}RH$, but the addition of a second R group results tends to result in the predominant formation of $C_{60}R_2$, a pattern (even/odd) that continues to higher values of n. CID of the hydrogenated products shows that the alkyl groups are lost preferentially, leaving $C_{60}H_m$- as the products. NMR studies show that thermal dealkylation can similarly occur in solution.

We have also used mass spectrometry to study unusual fullerene derivatives that are formed by reactions of fullerenes with other fullerenes. The products of these reactions are odd-numbered fullerenes with molecular weights corresponding to C_{119} and C_{129}. These are observed in some soots formed by arc-discharge or resistive heating synthesis. They have also been observed in toluene extracts of these soots. We have been able to synthesize these products in solution by ozonolysis, in collaboration with the Huffman group at the University of Arizona.[2] Ozonolysis of C_{60} solutions results in the formation of C_{119}, while ozonolysis of C_{70} solutions results in the formation of C_{139}. Ozonolysis of mixtures of C_{60} and C_{70} result in the formation of a mixed fullerene derivative, C_{129}. Although the mechanism of this reaction is unknown, it is thought to result from the oxidation of C_{60} to C_{59} + CO_2, followed by the reaction of C_{59} with C_{60}.

1. S.H. Hoke, et al. *Rapid Commun. Mass Spectrom.* 1991, 5, 472-474.
2. S.W. McElvany, J.H. Callahan, M.M. Ross, L.D. Lamb, and D.R. Huffman, *Science*, in press, 1993.

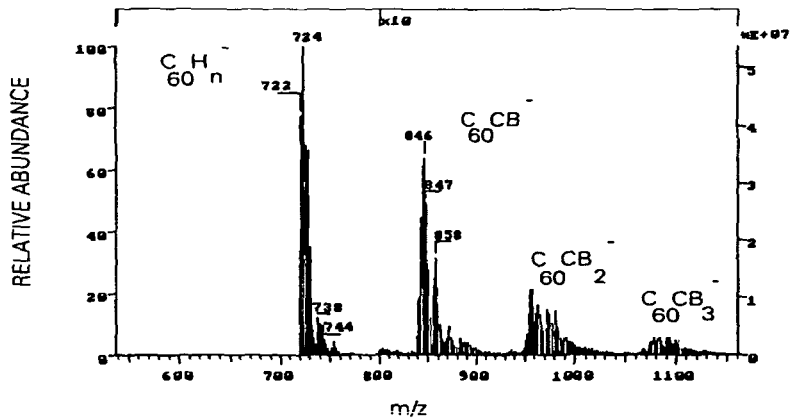

Figure 1. Thermal desorption negative chemical ionization mass spectrum of the reaction products of buckminsterfullerene and catecholborane.

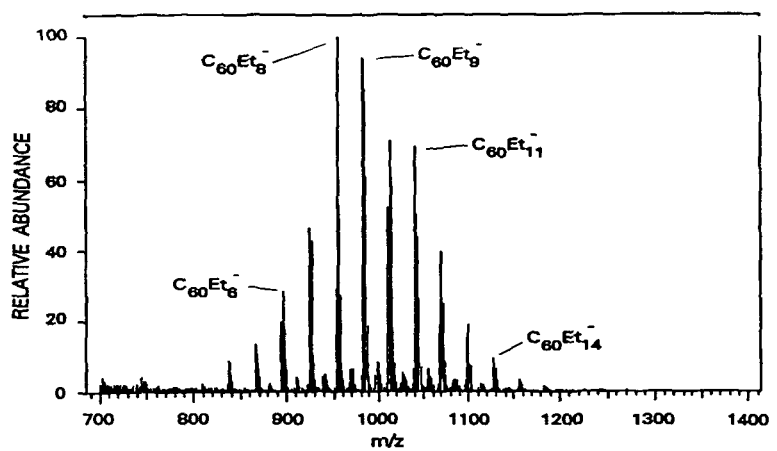

Figure 2. Thermal desorption negative chemical ionization mass spectrum of the reaction products of buckminsterfullerene and $NaZn(Et)_3$.

GENERATION OF FULLERENE-BASED COMPOUNDS AND CHARACTERIZATION BY FTMS*

Changming Jin, Robert Hettich, and Robert Compton
Oak Ridge National Laboratory, Oak Ridge, TN 37831-6120

The synthesis and characterization of fullerene-based materials are areas of active research due to the potential applications in areas such as nanotechnology, new organic materials, as well as other novel uses. A variety of fullerene-based compounds have been prepared and subsequently characterized by Fourier transform mass spectrometry (FTMS). These studies have focussed on the synthesis, stabilities, and properties of fullerenes which have been modified by fluorination and coalescence. Charge exchange reactions can be examined in the FTMS to probe the electron affinities (EA) and ionization potentials (IP) of the modified fullerenes to determine how chemical modification affects the properties of the fullerenes.

Fluorinated fullerenes, $C_{60}F_x$ and $C_{70}F_y$ where x=44-48 and y=52-54, have been synthesized by reaction of fullerenes with fluorine gas. Although several theoretical investigations have been directed at predicting the properties of highly fluorinated fullerenes, to date there has been only very limited experimental information about these species. We have used FTMS to investigate charge exchange reactions of these fluorinated fullerenes in order to determine their electron affinities. As listed in Table 1, a variety of charge exchange reagents ranging from phenoxy to rhenium oxide (corresponding EA=2.36 -- 4.46 eV) have been used in these experiments. It was found that fluorination of fullerenes substantially alters the electronic properties of the species. The electron affinities were bracketed to be EA ($C_{60}F_{46}$) = 4.0 +/- 0.25 eV and EA ($C_{70}F_{54}$) = 4.0 +/- 0.25 eV, which is more than 1 eV higher than the corresponding pure fullerenes. Charge exchange reaction results between $C_{60}F_x$ and $C_{70}F_x$ indicated that EA ($C_{60}F_{46}$) is slightly lower than EA ($C_{70}F_{54}$), reminiscent of the fact that EA(C_{60}) < EA (C_{70}).

In an effort to explore alternate methods of generating hydrogenated fullerenes, we have also pioneered a method to generate C_{60} coalescence products in the solid phase (compared with gas phase synthesis). Pure C_{60} films prepared by drying C_{60} toluene solutions were placed on the electrode of a hydrogen plasma discharge chamber. Examination of these samples by FTMS after the hydrogen discharge did not reveal hydrogenated fullerenes, but rather displayed mass peaks corresponding to C_{120}, C_{180}, C_{240}, etc (see Figure 1). These mass peaks were attributed to the coalescence of C_{60} into higher fullerenes under the environment of hydrogen plasma discharge (C_{60} --> C_{120} --> C_{180} --> C_{240}). In the hydrogen rf discharge chamber, C_{60} molecules were bombarded by ions and electrons. This process most likely fragmented some of the C_{60} bonds and allowed bond formation between neighboring C_{60} molecules. Such coalescence reactions between two or more C_{60} molecules are expected to produce fullerenes in the sizes of C_{120}, C_{180}, C_{240} etc. Preliminary experimental results suggested these coalescence products may have the spherical or tubule structures. The coalescence of C_{60} is energetically favorable because larger fullerenes have higher cohesive energy per atom than C_{60}. This discovery may lead to the mass production and isolation of higher fullerenes like C_{120}, C_{180} etc which do not exist as special species in the conventional carbon arc products.

* Research sponsored by the Oak Ridge National Laboratory Director's R&D Fund and the Office of Health and Environment Research, U.S. Department of Energy under contract DE-AC05-84OR21400 with Martin Marietta Energy System, Inc.

Table 1. Charge exchange (CE) reactions of fluorinated fullerenes

$$C_{60}F_x^{\circ} + A^- \longrightarrow C_{60}F_x^- + A^{\circ}$$

Compound A	E.A. (eV)[1]	C.E. observed?	Back reaction observed?
Phenoxide	1.89	yes	-
NO_2	2.30	yes	no
C_{60}	2.65	yes	no
Fluoranil	2.7	yes	no
TCNQ	> 3.0	yes	no
Iodine	3.06	yes	-
Bromine	3.36	yes	-
Chlorine	3.60	yes	-
NO_3	3.92	yes	-
CF_3COO	4.15	no	
ReO_4	4.46	no	

E.A. ($C_{60}F_{46}$) = 4.0 +/- 0.25 eV
E.A. ($C_{70}F_{54}$) = 4.0 +/- 0.25 eV
E.A. ($C_{60}F_{46}$) < E.A. ($C_{70}F_{54}$)

[1] S.G. Lias, J.E. Bartmess, J.F. Liebman, J.L. Holmes, R.D. Levin, and G. Mallard, **J. Phys. and Chem. Ref Data** 17, Suppl. 1, (1988).

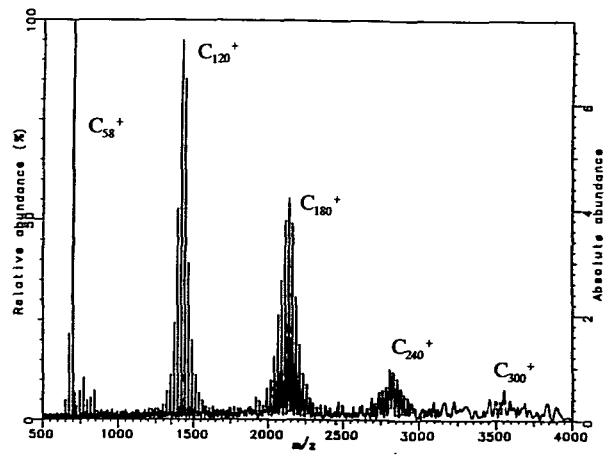

Figure 1. FTMS mass spectrum of C_{60} coalescence products generated by exposing a C_{60} film to a hydrogen rf discharge for 20 min (sample placed on the electrode). The C_{60}^+ peaks were ejected away prior to ion detection.

Radial Velocity Distribution Measurement of Ions Ejected by Laser Desorption

**Wenzhu Zhang and Brian T. Chait*
The Rockefeller University, 1230 York Ave. , New York, NY 10021

Matrix-assisted laser desorption mass spectrometry involves the production of gas phase ions by the absorption of laser energy in small organic molecules. Determination of the velocity distribution of ions is of interest to gain an understanding of the fundament physical process. It is also of practical importance in the design of mass spectrometers because the axial velocity distnbution set limits to the achievable resolution and the radial velocity component governs the divergence of ions of interest as they transverse the mass spectrometer.

Previously Beavis and Chait measured the ion axial velocity distribution, demonstrating that the axial ejection velocity of polypeptide ion was essentially independent of the mass. Supersonic expansion was suggested as a model for the matrix assisted laser desorption process.

To measure the radial velocity distribution, we have designed an experimental setup where the position of ions striking a detector could be measured accurately. In the present experiment, it is necessary to use an acceleration field devoid of any radial component that could obscure the intrinsic radial velocity distribution. Such field can be obtained by a series of ring electrodes with appropriate potentials on them. In the setup shown in fig. 1, the ions produced by laser desorption accelerate in acceleration field, transverse the flight tube and impact on a dual microchannel plate detector that allows both the time-of-flight spectrum to be measured and individual impacting ions to be visualized as bright dots on a phosphor screen. A video camera synchronized with the laser pulses records the images of ion impacts from each laser pulse, whereupon the image is transferred to a computer for subsequent analysis. The radial velocity distribution can then derived from the measured position of dots, the physical axial distance that ions travel and the accelerating potential.

Shown in fig. 2, the radial velocity distribution has been measured for the cationic dye brilliant green (MW 386 Da) at various extraction fields (3, 5 and 10 kV across 4.3 cm). The distribution is independent of the applied extraction field and is an intrinsic property of the laser desorption process. The full width at half maximum of the distribution is about 200 m/s. The angular distribution (fig. 3) is also derived using a previously measured value for the mean axial velocity (~750 m/s). The ejected ions are extremely forward peaked, with a half width at half maximum of ~ 13°.

We have designed an experimental setup and measured the radial velocity distribution for brilliant green. The distribution is independent of the extraction field. The extremely forward peaking distribution of the ejected ions supports the supersonic expansion model in the laser desorption process. In future experiments, the radial velocity distribution for peptide ions produced in matrix-assisted laser desorption will be measured.

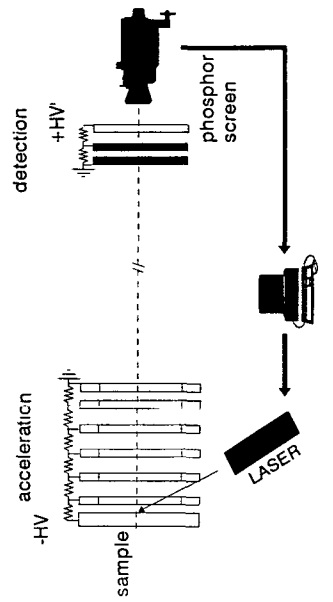

Fig. 1. Experimental setup for radial velocity distribution measurement.

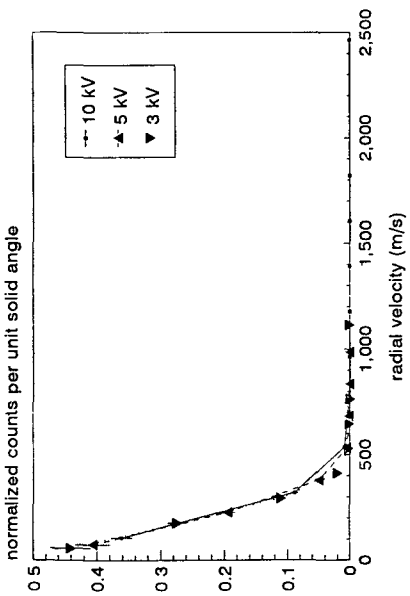

Fig. 2. Radial velocity distribution measured at 10kV, 5kV and 3kV acceleration potentials

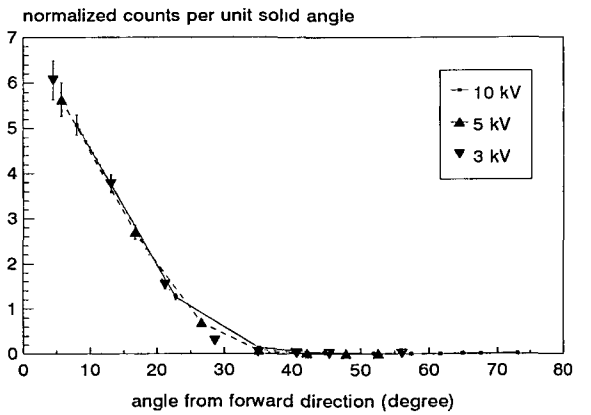

Fig. 3. Angular distribution derived from measurements at 10kV, 5kV and 3kV acceleration potentials.

Gas-Phase Proton Affinity Modifies Molar Response Factors in Fast Atom Bombardment

*Tanya M. Lewis and David H. Russell
Department of Chemistry, Texas A&M, College Station, TX

There have been several studies suggesting that quantitative analysis using fast atom bombardment (FAB) mass spectrometry is subject to discrimination effects that result in signal suppression for some components. Variations in ion yield have been attributed to differences in analyte concentration at the vacuum/surface interface. A direct correlation has been shown between hydrophilicity and signal suppression using glycerol as the matrix. Ionization discrimination has been observed in preliminary studies of mixtures of carboxylic acids using FAB ionization.

In this paper, several mono- and dicarboxylic acids were used as model compounds to determine yields of protonated molecules. We report that ionization discrimination has been observed in both the positive and negative ion mode for equal molar mixtures. Using the surface concentration concept to predict FAB sensitivity the monocarboxylic acid should be preferentially ionized. However, FAB ionization experiments with mono-/dicarboxylic acid mixtures yield exclusively the $[M+H]^+$ of the dicarboxylic acid. These findings are inconsistent with the hypothesis that matrix-acid solubility interactions preferentially ionize hydrophobic compounds. The goal of this study is to determine the nature of ionization discrimination effects of mono- and di-carboxylic acids in FAB.

The experiments discussed here are performed on a modified sector instrument consisting of a Kratos MS-50, as MS-I and a one meter reflectron time-of-flight as MS-II. The Kratos MS-I is operated at an accelerating voltage of 8 KeV with a mass range of 1-2,000 amu. The instrument is equipped with a conventional direct insertion probe source. A variable energy (0-25 KeV) cesium ion gun (Phrasor Scientific) is attached to the ion source housing. The Cs^+ beam is operated continuously at 15 KeV.

We have used metastable ion spectra to bracket the proton affinities of mono- and dicarboxylic acid-glycerol clusters. [Adipic-H^+ (147)] is detected in the metastable spectrum shown in Figure 1. This indicates that the proton affinity of adipic acid is higher than that of glycerol. [Hexanoic-H^+ (117)] is not detected in the spectrum shown in Figure 2. The conclusion is that the proton affinity of glycerol is higher than that of hexanoic acid. Interpretation of these results suggests that gas-phase proton affinity is responsible for the discrimination effects for mixtures of mono- and dicarboxylic acids. Future studies will focus on pulsed-jet/tandem time-of-flight experiments. The application of the principles utilized is being considered for other analyte systems.

Presented at the 41st ASMS Conference on Mass Spectrometry

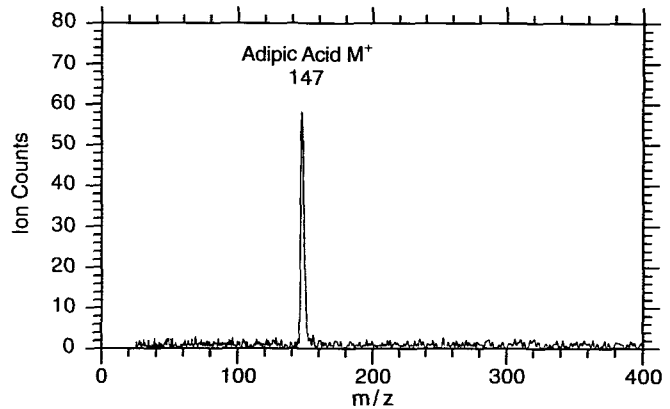

Figure 1 Metastable decomposition of [Adipic-H^+-Glycerol (239)] is detected as the protonated species [Adipic-H^+ (147)]

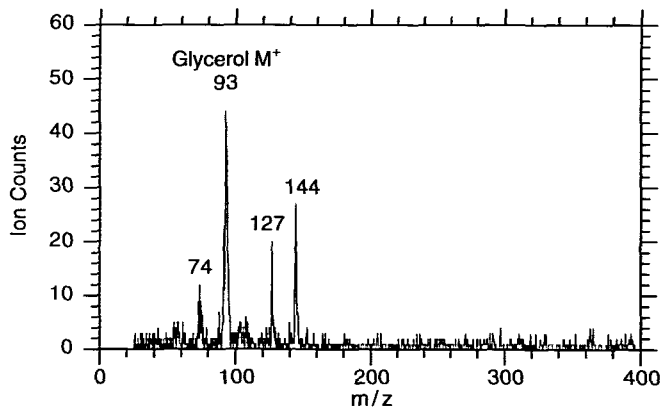

Figure 2 Protonated hexanoic acid (117) is not observed in the metastable decomposition of [Hexanoic-H^+-Glycerol(209)].

THE FORMATION OF NITRIC ACID AND NITRIC ACID COMPLEXES FROM GAS-PHASE AMMONIUM NITRATE CLUSTERS

Robert J. Doyle, Jr., Chemistry Division, Code 6110-D,
Naval Research Laboratory,Washington, DC, 20375-5000.

The sputtering of condensed-phase ammonium nitrate by fast-atom bombardment results in the desorption of ionic ammonium nitrate clusters of the form $(NH_4NO_3)_nNH_4^+$, where n=1,2,3,...,>25, and $(NH_4NO_3)_nNO_3^-$, where n=3,4,5,...,>25. In addition, the well-known nitric acid complexes $(HNO_3)NO_3^-$, $(HNO_3)_2NO_3^-$, and $(HNO_3)_3NO_3^-$ are observed. The absence of anionic ammonium nitrate clusters with n<3 suggests that they are unstable and rapidly decompose to form the observed nitric acid complexes via the reaction:

$$(NH_4NO_3)_nNO_3^- \rightarrow (HNO_3)_nNO_3^- + nNH_3,$$

where n=1 or 2. Indeed, these reactions are confirmed by collision-induced dissociation (CID) of much larger clusters where, under multiple collision conditions, the loss of n NH_3 molecules is observed only from product clusters with n<4. The reactions require an unusual rearrangement of central NH_4^+ (which is hydrogen bonded to nitrate anions) that results in the formation of proton bound nitrate anions and enables the loss of NH_3. A proposed reaction schematic, for n=1, is shown in Figure 1.

In contrast, cationic ammonium nitrate clusters with n<7 show the direct loss of a nitric acid molecule via the reaction:

$$(NH_4NO_3)_nNH_4^+ \rightarrow NH_3(NH_4NO_3)_{n-1}NH_4^+ + HNO_3,$$

where n=1,2,3,...,6. CID experiments under multiple collision conditions show that only one nitric acid molecule is lost from a parent ion and further dissociation occurs by losses of NH_4NO_3 molecules only [1,2]. Collisional activation of large clusters, n=25 for example, shows sequential losses of NH_4NO_3 until an n<7 cluster is formed, at which point one nitric acid molecule is lost. A comparison of metastable and CID spectra of $(NH_4NO_3)_nNH_4^+$ ions shows that the loss of nitric acid is predominantly a metastable process. This implies that nitric acid is formed by a rearrangement of the parent ion.

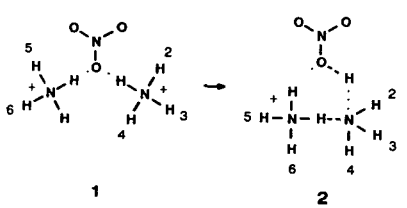

1 2

Figure 1. The rearrangement of $(NH_4NO_3)NO_3^-$ to form $H(NO_3)_2^-$.

The mass spectrum of sputtered ammonium nitrate (cations) establishes that a major stair-step decrease in the ion-abundance distribution occurs at the $(NH_4NO_3)_7NH_4^+$ ion[1]. If the first solvent shell is filled at n = 7, then a cluster-ion core must exist to which NH_4NO_3 molecules are hydrogen bonded to all available hydrogen atoms. The simplest ion configuration that fits this criterion is the first member of the series, $(NH_4NO_3)NH_4^+$, shown in Figure 2. The core ion is fully solvated by the hydrogen bonding of six NH_4NO_3 molecules to the six available hydrogen atoms of the two ammonium ions (indicated by the sites numbered 2-7 in Figure 2). This arrangement results in a structure consisting of seven ammonium nitrate units and an additional ammonium ion which provides the overall positive charge. Ligands are seen to be lost as NH_4NO_3 ion pairs. The ionic mechanism for the formation of nitric acid by proton transfer is through a rearrangement of the core ion through the transition-state structure proposed as Structure **2** in Figure 2 below.

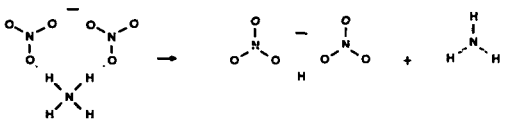

Figure 2. The structure of the core ion (**1**) showing hydrogen-bonding sites and the proposed transition-state (**2**) for rearrangement.

In summary, the experimental evidence established that: (1) the first important structural transition occurs at the $(NH_4NO_3)_7NH_4^+$ ion, (2) only ions with n < 7 dissociate by the direct loss of nitric acid, (3) the loss of nitric acid is predominantly a metastable process, and (4) that a nitric acid molecule is lost only once in the chain of dissociation steps. In conclusion, an ammonium nitrate cationic complex forms and loses nitric acid by an internal rearrangement that is ultimately quenched by the continued addition of ammonium nitrate solvent molecules.

Acknowledgement

This work was supported by the Propulsion and Energetic Materials Program of the Mechanics Division of the Office of Naval Research and the Naval Research Laboratory Energetic Materials Accelerated Research Initiative.

References

(1) Doyle, R. J., Jr. *J. Am. Chem. Soc.* **1993**, *115*, in press.

(2) Doyle, R. J., Jr. *J. Am. Chem. Soc.*, in press.

TETRAALKYLAMMONIUM CATIONS AND THEIR NEUTRAL COUNTERPARTS

Šárka Beranová and Chrys Wesdemiotis
Department of Chemistry, The University of Akron, Akron OH 44325-3601.

Tetraalkylammonium cations are simple polyatomic ions, readily accessible by desorption ionization of the corresponding quaternary ammonium salts. Neutralization of these ions provides a route to hypervalent peralkylated ammonium radicals. The present study investigates the unimolecular chemistry of gaseous tetraalkylammonium ions R_4N^+ ($R=CH_3$, CD_3) by metastable (MI) characteristics, collisionally activated dissociation (CAD), and neutralization-reionization mass spectrometry (NRMS).

The tetramethylammonium ion dissociates into two primary fragments, namely $(CH_3)_3N^+$ (m/z 59) and $(CH_3)_2N{=}CH_2^+$ (m/z 58). The MI spectrum of $(CH_3)_4N^+$ (Fig. 1a) indicates that in the metastable time-frame the production of m/z 59 (i.e. loss of a methyl group) dominates. In the CAD spectrum (Fig. 1b), $(CH_3)_2N{=}CH_2^+$ emerges as the most prominent product. This ion can be formed by two mechanisms, a rearrangement elimination of methane and a consecutive loss of $^{\cdot}CH_3$ + $^{\cdot}H$ (Scheme I).

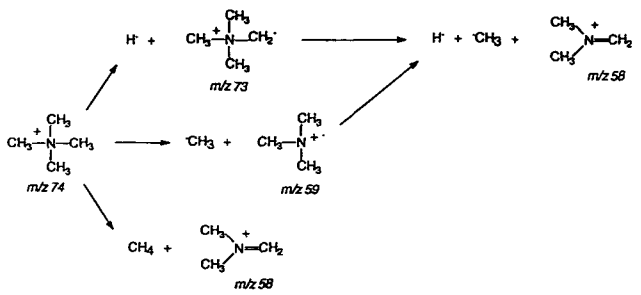

Scheme I.

The B^2/E scans reveal that under MI conditions (Fig. 2a) both $(CH_3)_3N^+$ and $(CH_3)_4N^+$, and to a lesser extent $(CH_3)_3N\text{-}CH_2^{+\cdot}$, are the source of m/z 58. In contrast, upon CAD (Fig. 2b) the predominant portion of $(CH_3)_2N{=}CH_2^+$ arises directly from the molecular ion.

The increase in the abundance of m/z 58 in the spectra of $(CH_3)_4N^+$ is accompanied by substantial peak broadening (Fig. 1b), suggesting that upon CAD, formation of $(CH_3)_2{=}CH_2^+$ proceeds via a process with high reverse activation energy, resulting in a large kinetic energy release. A large reverse activation energy is possible if m/z 58 is reached by CH_4 loss directly out of the molecular ion either in a one step process, or possibly through an ion-molecule complex between $(CH_3)_2N{=}CH_2^+$ and CH_4. Since m/z 59 and 58 compete in the MI frame, the transition state for the concerted CH_4 loss cannot be more than ~50 kJ/mol below the thermochemical limit of the consecutive losses (1025 kJ/mol).

Parallel experimental results obtained for the $(CD_3)_4N^+$ analog support the above findings

Based on the combined MI, CAD, and linked scanning results the conclusions reached here differ from those reported previously (Glish et al., ASMS Conference, San Diego 1985). We find that at internal energies near the dissociation threshold the major decay channels of $(CH_3)_4N^+$ include formation of both $(CH_3)_3N^{+\cdot}$ and $(CH_3)_2N{=}CH_2^+$, the latter ion arising most likely by stepwise direct bond ruptures, as a relatively narrow peak is observed (Fig 1a vs. 1b) The predominant fragmentation pathway of the collisionally activated $(CH_3)_4N^+$ is production of $(CH_3)_2N{=}CH_2^+$ by rearrangement loss of CH_4.

Our first NRMS results on $(CH_3)_4N^+$, showing that its neutralization with trimethylamine yielded a stable $(CH_3)_4N^{\cdot}$ radical, could not be reproduced under various experimental conditions The present study finds that $R_4N^{\cdot}$ ($R=CH_3$, CD_3, CH_2CH_3) decompose fully prior to reionization, primarily via loss of $R^{\cdot}$.

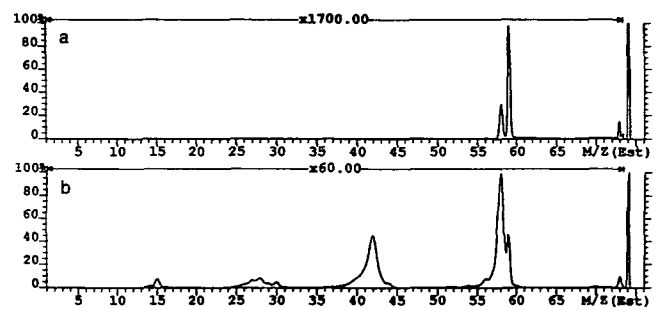

Figure 1. a) MI spectrum of $(CH_3)_4N^+$; b) CAD spectrum of $(CH_3)_4N^+$

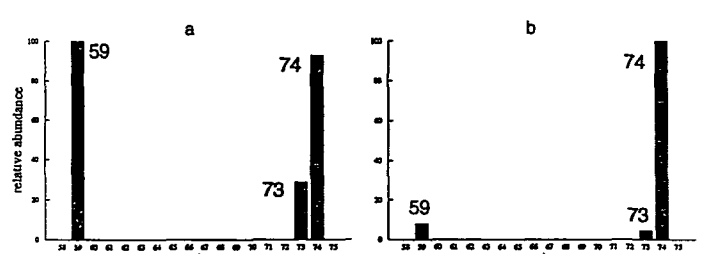

Figure 2. B^2/E parent ion scans of m/z 58 formed by (a) metastable or (b) collisionally activated dissociation of $(CH_3)_4N^+$.

POSITIVE FAB MASS SPECTRA OF SEVERAL COBALT AND CHROMIUM β-DIKETONATES

L. Plaggenborg[a], B. Wenclawiak[a], W. D. Buchannon[b] and J. B. Westmore[b]

[a]*Chemie-Biologie, Universitat-GH-Siegen, W-5900 Siegen, Germany*
[b]*Department of Chemistry, University of Manitoba, Winnipeg, Manitoba R3T 2N2, Canada*

With β-ketoenolate ligands the transition metals chromium and cobalt form kinetically inert, neutral complexes. Metal chelates have been extensively studied under electron ionization (EI) conditions [1]. Since these chelates are soluble in organic solvents, and separable by HPLC, it is apparent that these compounds can be ionized under fast atom bombardment (FAB), i.e. liquid secondary ionization (LSI), conditions.

Chelate complexes of chromium(III) and cobalt(III) with the following ligands were studied: acetylacetone, 1-(2-thienyl)-4,4,4-trifluoro-1,3-butanedione, 1-phenyl-4,4,4-trifluoro-1,3-butanedione, 1-(2-thienyl)-1,3-butanedione, 1-(2-thienyl)-4,4-dimethyl-1,3-pentanedione (Hthdmpd), 1-phenyl-4,4-dimethyl-1,3-pentanedione (Hphdmpd) and 2,2-dimethyl-3,5-hexanedione (Hdmhd).

The FAB mass spectra of samples in a 3-nitrobenzyl alcohol (3-nba) matrix, bombarded by 8 keV xenon atoms, were recorded with a VG 7070E-HF double sector (EB geometry) mass spectrometer, equipped with an 11-250J data system based on a PDP 11/73 microcomputer. Product ion mass spectra of selected collisionally-activated precursor ions were obtained by linked-field scanning (B/E constant). Helium was admitted to the collision cell preceding the electric sector so that the precursor ion current was reduced to about 50% of its original value.

Representative spectra of some of the cobalt complexes are shown in Figs. 1-3. Their characteristic features, together with those of the chromium complexes, can be summarized as follows:

- excellent matrix-free FAB mass spectra of Cr^{III} and Co^{III} chelates are obtained.
- the chromium complexes show protonated molecules and only small yields of polymeric ion species
- the FAB mass spectra of the cobalt complexes, in contrast to the EI mass spectra, show abundant monomeric molecular ions (not protonated molecules), and high yields of the dimeric ion species, $Co_2L_4^+$ and $Co_2L_3^+$
- on CAD the dimeric Co-containing ions decompose to other dimeric ions rather than to mono-Co-containing ions
- a mixture of two different cobalt complexes yields dimeric ions containing mixed ligands

Financial support from the Natural Sciences and Engineering Research Council of Canada (NSERC) and the Graduiertenkolleg "Chemische Reaktivität und molekulare Ordnung" of the University of Siegen is gratefully acknowledged. We also thank NSERC and the Faculty of Graduate Studies, University of Manitoba, for grants to purchase the mass spectrometer.

[1] J. B. Westmore, Chem. Rev. **76** (1976) 695-715

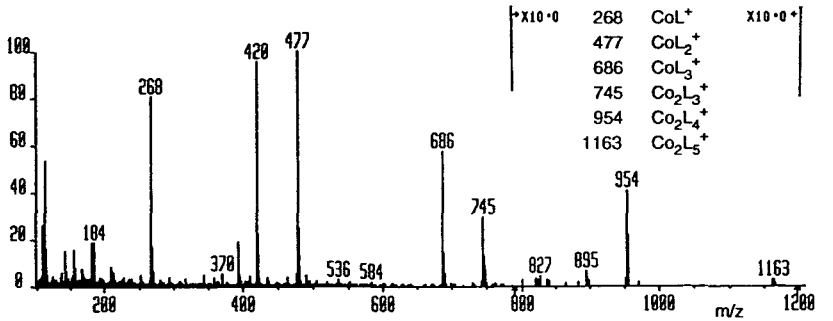

Fig. 1. FAB mass spectrum of $Co(thdmpd)_3$

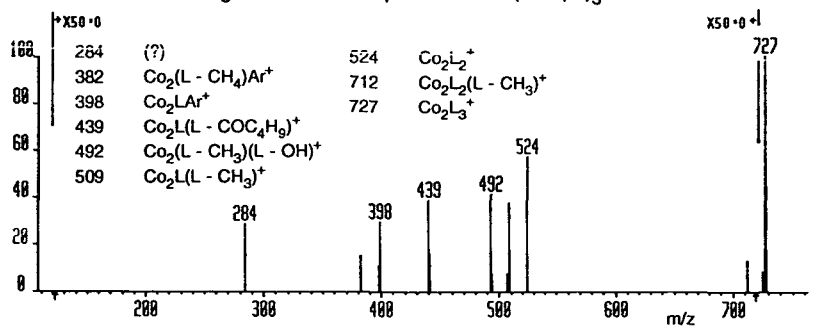

Fig. 2. CAD mass spectrum of $Co_2(phdmpd)_3^+$

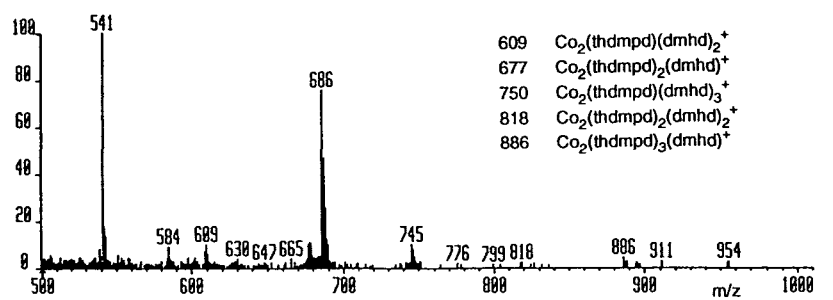

Fig. 3. FAB mass spectrum of a mixture of $Co(thdmpd)_3$ and $Co(dmhd)_3$

Study of Co(III) Clusters Using FAB Mass Spectrometry

*Chung-Ping Yu, Katerina Dimitrou, and George Christou
Chemistry Department, Indiana University, Bloomington, IN 47405

INTRODUCTION

In conjunction with elemental analysis and NMR spectrometry, we have employed Fast Atom Bombardment mass spectrometry as a routine analysis tool to assist in the identification and structural determination of a series of Co(III) clusters : $[Co_2(OH)_2(OAc)_3(bpy)_2]ClO_4$ (1), $[Co_3O(OH)_3(OAc)_2(bpy)_3](ClO_4)_2$ (2), $[Co_4O_4(OAc)_2(bpy)_4](ClO_4)_2$ (3), $[Co_4O_4(O_2CC_6H_4CH_3)_2(bpy)_4](ClO_4)_2$ (4), and $[Co_4O_4(O_2CC_6H_4CH_3)_2(bpy)_4](ClO_4)_3$ (5); bpy=2,2'-bipyridine and $OAc=O_2CCH_3$. In most cases, X-ray crystallography has confirmed the predicted structure of these compounds

EXPERIMENTAL

FAB mass spectra of complexes 1-5 were obtained with a Kratos MS-80 mass spectrometer that was interfaced with a Kratos DS90 data system. Xenon at 8 KeV was used to produce the primary beam with Ion-Tech saddle field atomic gun. Data for each compound were acquired for 10-20 scans at 10 s/decade. Either 3-Nitrobenzyl alcohol (NBA) or a NBA/DMSO mixture was used as matrix. The syntheses of the Co complexes have been described elsewhere[1]

RESULTS AND DISCUSSION

The FAB mass spectrum of the dinuclear complex 1 shows the formation of $[M-ClO_4^-]^+$, $[M-ClO_4^-\text{-}HOAc]^+$, $[M-ClO_4^-\text{-}2HOAc]^+$, and $[M-ClO_4^-\text{-}2HOAc\text{-}OAc^-]^+$ ions at m/z 641, 581, 521, and 462, respectively The cobalt metal centers appear to retain their formal oxidation state of +3. However, the observation of m/z 462 peak indicates that it is formed by a one-electron reduction which possibly originated from the radiation-damaged matrix[2]. The FAB mass spectrum of the trinuclear complex 2, reveals a number of informative fragments at m/z 929, 869, and 674 which correspond to the ions $[M-ClO_4^-]^+$, $[M-ClO_4^-\text{-}HOAc]^+$, and $[M-2ClO_4^-\text{-}bpy]^+$, respectively. The appearance of m/z 674 peak also indicates the existence of a one-electron reduction; this also agrees with the previous observation.

FABMS studies provided the most powerful evidence that compound 3 is tetranuclear possessing a novel $\{Co_4O_4\}^{4+}$ core, when X-ray quality crystals could not be obtained. That led to the synthesis of compound 4 from 3 via a ligand exchange reaction. The X-ray crystal structure of 4 proved the cubane architecture of this complex. In FABMS the analogous fragmentation paths of complexes 3 and 4 are found to produce ions such as $[M-ClO_4^-]^+$, $[M-ClO_4^-\text{-}bpy]^+$, $[M-2ClO_4^-\text{-}bpy]^+$, $[M-2ClO_4^-\text{-}2bpy]^+$, $[M-2ClO_4^-\text{-}3bpy]^+$, etc.., indicating that complex 3 has the same cubane structure. It is also interesting to note that the ions $[M-2ClO_4^-\text{-}bpy]^+$, $[M-2ClO_4^-\text{-}2bpy]^+$ and $[M-2ClO_4^-\text{-}3bpy]^+$ contain the cobalts in a reduced oxidation state. However no peak was observed for the reduced ion $[M-2ClO_4^-]^+$, where the whole cation would remain intact. This suggests that reduction can be associated with the loss of bpy ligands from the clusters and consequently structural changes in the geometry around the metals. This observation is compatible with the irreversible reduction in cyclic

voltammetry (CV) for both complexes 3 and 4. It is worth noting that these two complexes have a reversible one-electron oxidation in CV studies, and theoretical calculations show this oxidation to be metal based. Compound 5 produced from the electrochemical oxidation of 4 was isolated and analyzed by FABMS. Careful comparison of mass spectra for 4 and 5 reveals that both spectra are superimposable. Thus we believe the reduction of complex 5 back to complex 4 occurs in FABMS.

CONCLUSION

As we expected, the highest mass observable ions of Co(III) complexes in FABMS are $[M-ClO_4^-]^+$ ions. A series of diagnostic fragment ions resulting from sequential loss of intact ligands are observed and these fragmentation patterns can provide a better understanding of the identity of these complexes. It is also recognized that some of these fragment ions are reduced by one electron in the fragmentation processes.

ACKNOWLEDGMENT

The assistance of Paula Wood is gratefully acknowledged.

REFERENCES

1. Katerina Dimitrou, Kirsten Folting, William E Streib and George Christou, *J Am. Chem. Soc.*, in press.
2. Jack M. Miller, Kesagapillai Balasanmugam, Jeffrey Nye, Glen B. Deacon, and Nicholas C Thomas *Inorg Chem.* **1987**, *26*, 560.

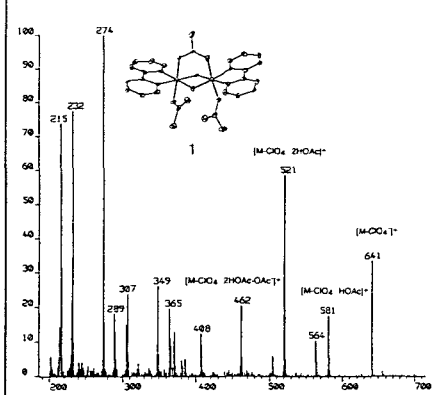

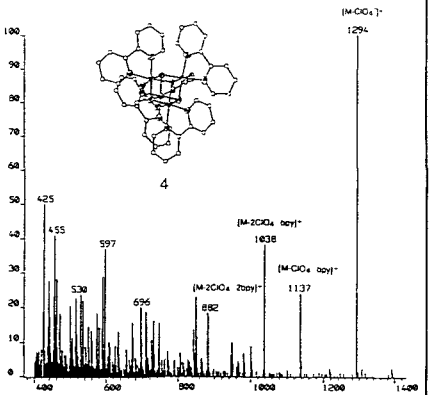

FRAGMENTATION REACTIONS OF MULTIPLY-PROTONATED PEPTIDES+

*Xue-Jun Tang[1,2], Pierre Thibault[2], Robert K. Boyd[2] ; [1]Albert Einstein College of Medicine, Department of Biochemistry, 1300 Morris Park Av., Bronx, NY 10461, [2]Institute for Marine Biosciences, National Research Council, 1411 Oxford St., Halifax, Nova Scotia Canada B3H 3Z1

Ion evaporation techniques such as ionspray have found application in protein chemistry, not only for precise molecular weight determination (within 0.01% for MW of up to 200 kDa) but also for primary structure characterization. A striking example of this latter application has been demonstrated by Loo *et al* [1] who conducted MS-MS experiments on multiply protonated (up to $(M+49H)^{49+}$) albumins. However, sequence information obtainable from these complex MS-MS spectra is limited by uncertainties in determining the fragment mass (within < 0.5 Da) and corresponding charge states. Practical exploitation of MS-MS for such structural investigations will depend upon further understanding of the dissociation mechanisms and development of sensitive methods for determining charge-states of fragment ions.

Under low-energy CID conditions, the fragmentation of protonated peptides is found to be highly dependent on the number and location of basic residues and more particularly of Arg. In the case of tryptic peptides the initial formation of the doubly-protonated species appears to involve obligatory protonation at the N-terminus while the second proton is conveniently positioned on the side chain of the C-terminus residue [2]. This favorable case yields (b + y") complementary pairs via charge-site initiated fragmentation where the ionizing proton of the y fragment ion is anchored on the side-chain of the basic C-terminus residue. The formation of $(y''')^{2+}$ ions is explained by a charge-site-remote mechanism where an extra proton is located on the C-terminus side of the cleaved bond. Product ion spectra corresponding to dissociation of higher protonated forms of precursors are dominated by cleavages occurring near the middle of the peptide chain. Protonation at mid-chain sites presumably minimize Coulombic repulsions and lead to charge-site initiated fragmentations. For peptides possessing basic residues near the N-terminus, such as angiotensin I and substance P, the product ion spectra of $[M+2H]^{2+}$ and $[M+3H]^{3+}$ are dominated by a and b ions with almost no accompanying y ions. It is proposed that these b_n ions could have a different structure from those observed for tryptic peptides and that a charge-site induced mechanism could account for their formation. An example of this is shown in Figure 1 A, the product ion spectrum of $[M+2H]^{2+}$ from substance P. The unusual stabilities of the doubly-charged fragments $b_{10}'^{2+}$ and $b_9'^{2+}$ were investigated using intermediate ions formed in the orifice-skimmer region of the mass spectrometer (Figure 1 B). The product ion spectra of $b_9'^{2+}$ and $b_{10}'^{2+}$ gave abundant fragment ions corresponding to b_n+57 and b_n+170, respectively. These unusual rearrangement reactions were found to arise from wholesale transfer of one or two residues from the C-terminus end of the doubly-charged b fragment to the side chain of a Lys residue.

The fragment ion spectrum of $[M+2H]^{2+}$ from γ-endorphin, another non-tryptic peptide, is shown in Figure 2. Some of the salient features of this spectrum can be rationalized assuming that one external proton is localized on the Lys sidechain while the second proton can be transferred to amide nitrogens on the N-terminus side of this basic residue. Charge-site initiated fragmentation reactions would favor the formation of (b_j plus y''_{17-j}) complementary pairs for j=3-8. However, if the second ionizing proton is located on the C-terminus side of Lys, the same mechanism will lead to formation of $(b_j')^{2+}$ fragments for j=12-16. The difficulty of obtaining sequence ions from each amide bond was even more evident for peptides possessing a large number of basic residues such as dynorphin1-13 (YGGFLRRIRPKLK). In this latter case the fragment ion spectra of $[M+3H]^{3+}$ and $[M+4H]^{4+}$ yield abundant a_1, y''_1, $(y_{12}''')^{2+}$ and $(y_{12}''')^{3+}$ ions with almost no other structurally informative fragment ions, although intramolecular Coulombic repulsion is likely to be significant. It appears that mobilization of ionizing protons along the peptide backbone must also be possible, in order to promote charge-site initiated dissociation mechanisms, and that low-energy CID is not effective in achieving this if the protons are anchored on highly basic sites.

[1] Loo J.A., Edmonds C.G., Smith R.D. Anal. Chem. **63**, 2488 (1991)
[2] Tang X.-J., Boyd R.K. Rapid Commun. Mass Spectrom. **6**, 651 (1992)

+NRCC#: 34856

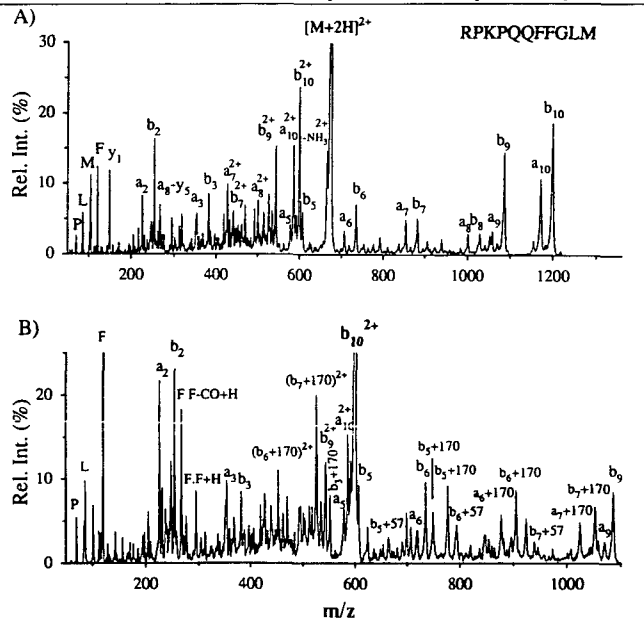

Figure 1: ISP-MS-MS spectra of substance P: Product ion spectrum of $[M+2H]^{2+}$ (A) and $b_{10}'^{2+}$ ion formed in the nozzle-skimmer region of the API/III mass spectrometer. Conditions: Ar target gas, 4×10^{14} atoms cm^{-2}, Elab: 150 eV

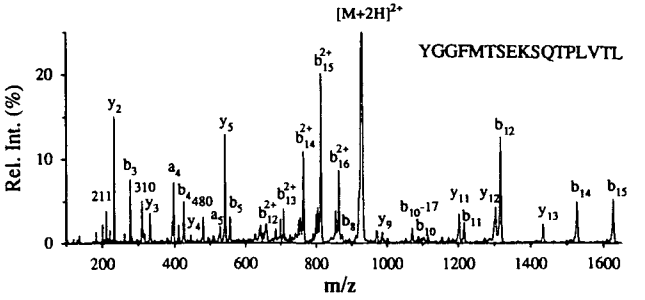

Figure 2: Product ion spectrum of the $[M+2H]^{2+}$ ion from γ-endorphin. Conditions same as above.

FRAGMENTATIONS OF DOUBLY-CHARGED ALKALI METAL-PEPTIDE COMPLEXES

Xue-Jun Tang[1,2], Pierre Thibault[2] and Robert K. Boyd[2]; [1]Dept. of Biochemistry, Albert Einstein College of Medicine, 1300 Morris Park Ave., Bronx, NY 10461; [2]Institute for Marine Biosciences, National Research Council, 1411 Oxford St., Halifax, Canada B3H 3Z1.

Electrospray ionization of peptide solutions doped with alkali metal salts X^+Y^- produces abundant doubly-charged ions $(M+H+X)^{2+}$ and $(M+2X)^{2+}$. For X = K, Rb, Cs, CID of these ions yields mainly X^+ plus the charge-separation complement, with increasingly sparse fragmentation as X increases in size. For tryptic peptides M in which the C-terminal residue is Arg, and for X = Li or Na, a major CID fragmentation pathway leads to $(M+X-60)^+$ and/or $(y'+X-60)^+$ ions. This behaviour is specific to peptides containing a C-terminal Arg residue, such as des-Arg[1]-bradykinin (Fig.1), while *e.g.* des-Arg[9]-bradykinin (RPPGFSPF, Arg at N-terminus, not shown) yields no such fragments nor do peptides containing Arg within the sequence. Many peptides which do not contain any Arg residues yield singly-charged $(M+X)^+$ ions which fragment to give abundant $(b+X+OH)^+$ ions (for X = Li, Na) whose origins are now well understood [1]. The present work has concentrated on elucidating the nature of the 60 Da neutral fragment associated with lithiated or sodiated peptides containing an Arg as the C-terminal residue. Typical fragment spectra (low-energy CID, SCIEX API III triple-quadrupole instrument) are shown in Fig.1.

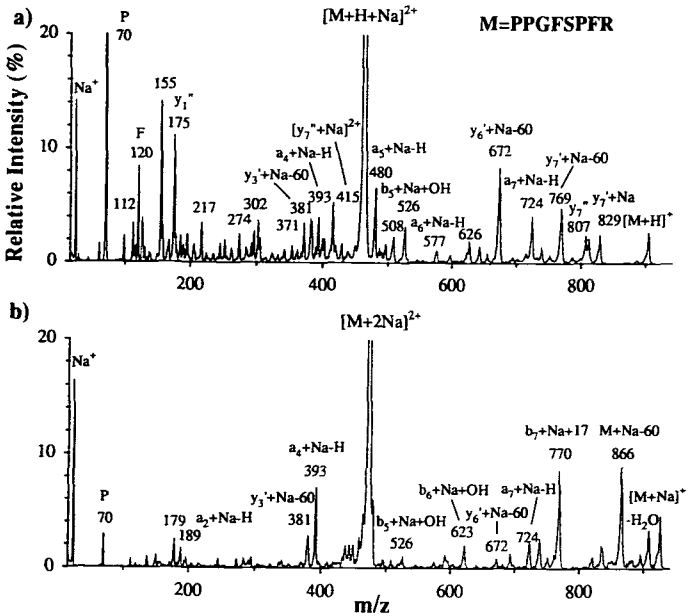

Figure 1. Fragment-ion spectra of (a) $[M+H+Na]^{2+}$ and (b) $[M+2Na]^{2+}$ precursor ions from ionspray ionization of des-Arg[1]-bradykinin.

The singly-charged lithiated peptide $(HGLGAR+Li)^+$, produced by LSIMS, was shown previously [2] to yield an intense fragment corresponding to loss of 60 Da, but no attempt was made to characterize this process. Similar CID experiments [3] on the intense $(b_4+Li+OH)^+$ fragment (which has a C-terminal Arg residue) of $(LWMRF+Li)^+$ showed that it readily lost 18 Da followed by a further loss of 42 Da; a mechanism was proposed [3] for the first of these steps (H_2O expulsion).

The present work has extended these earlier findings [2,3] to include both X = Li and Na, to both singly- and doubly-charged precursors, and has elucidated characteristics of the reaction in which a 60 Da neutral fragment is expelled. The main findings may be summarized as follows:

(a) the reaction is restricted to peptide-X^+ complex ions, where X = Li or Na;
(b) the reaction is characteristic of Arg residues, which must be located at the C-terminus;
(c) experiments using D_2O, in which exchangeable hydrogens were replaced by deuterium, showed that the 60 Da neutral fragment contains 4 exchangeable hydrogen atoms;
(d) it was possible to produce the $(M+X-60)^+$ fragments by CID in the post-orifice expansion region; precursor-ion scans showed peaks corresponding to $(M+X)^+$, $(M+2X)^{2+}$, and more interestingly to $(M+X-18)^+$, though this last intermediate ion was of only moderate intensity.

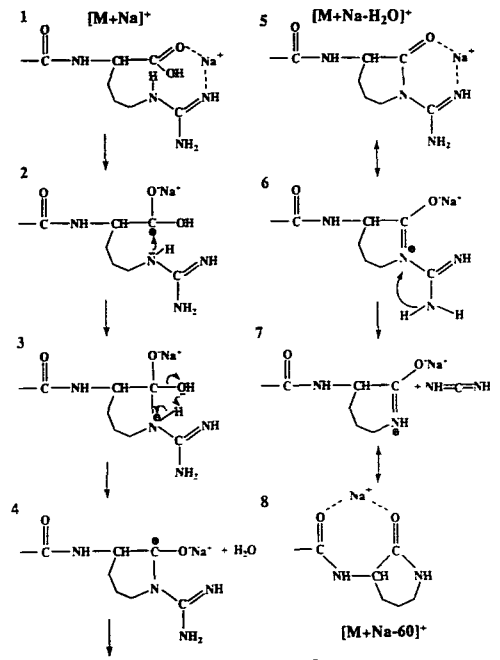

Scheme I

Scheme 1 shows a mechanism proposed to account for findings (a)-(d), drawn for sake of simplicity for a singly-charged precursor; steps 1-5 are slightly modified from those proposed by Grese *et al.*[3] to account for loss of H_2O. The overall loss of 60 Da is thus accounted for by successive losses of H_2O and of a 42 Da fragment from the Arg sidechain, suggested here to be HN=C=NH (isoelectronic with CO_2). The alternative neutral structures are those of diazomethane, *cyc*-(-CH_2-N=N-) (diazirine) and NH_2-CN (carbamonitrile), which are less feasible on both energetic and mechanistic grounds.

1. X. Tang, W. Ens, K.G. Standing and J.B. Westmore, *Anal. Chem.* **60**, 1791 (1988).
2. L.M. Teesch and J. Adams, *J. Am. Chem. Soc.* **113**, 812 (1991).
3. R.P. Grese, R.L. Cerny and M.L. Gross, *J. Am. Chem. Soc.* **111**, 2835 (1989).

NRCC No. 34859.

GAS-PHASE FRAGMENTATIONS OF ANIONIC COMPLEXES BETWEEN PEPTIDES AND TRANSITION METAL IONS: COMPARISONS WITH ALKALINE EARTH METAL IONS

Hong Zhao, Alex Reiter, and Jeanette Adams, Department of Chemistry, Emory University, Atlanta, GA 30322

We showed previously[1] for gas-phase anionic $(M + Ca^{2+} - 3H)^-$ complexes that Ca^{2+} can bind at two sites in peptide molecules. One site is the deprotonated C-terminal carboxylate and the other is the deprotonated side chain of either the protic amino acid Asp, Glu, His, Tyr, or Trp. Here, our goals are to determine the preferential binding site(s) for the transition metal ions Co^{2+} and Ni^{2+}. CID spectra were acquired of peptide-metal ion complexes desorbed by LSIMS using a VG 70-S, forward geometry mass spectrometer. Spectra of decompositions that occurred in the first field-free region were acquired by using linked scans at a constant ratio of B/E. Twenty-two peptides were studied, which include YGGFL, VAAF, YPFAG, VHLGP, and *N*-acetyl-YGGFL.

CID spectra of complexes between the three metal ions and the simple peptide VAAF, which contains only aprotic (hydrocarbon) side chains, is shown in Figure 1. The spectra show that Ca^{2+} can only bind to the deprotonated C-terminus (C-terminal *y* ions), whereas both Co^{2+} and Ni^{2+} can bind to both the C- and N-termini (*y* ions plus N-terminal *a* and *c* ions). For *N*-acetyl-YGGFL (Figure 2), Ca^{2+} can still bind to the deprotonated Tyr side chain to give an abundant *c* ion[1]. The Co^{2+} can likewise bind to the side chain, but Ni^{2+} now only binds to the C-terminus. More information about the binding can be obtained from the chemistry of peptides that contain Pro. When the N-terminal binding site is disrupted (Figure 3), Ca^{2+} still can bind to the N-terminal deprotonated Tyr side chain, but Co^{2+} and Ni^{2+} can only bind to the C-terminus. When the C-terminal binding site is disrupted (Figure 4), Ca^{2+} can still bind to the C-terminus, whereas Co^{2+} and Ni^{2+} can only bind to the N-terminus.

From these data, important conclusions can be drawn about the metal ion-peptide complexes Formation of the complexes requires the metal ion to first "anchor" or bind to a specific site in the peptide. Following anchoring, catalytic deprotonation of the amides occurs to form the final $(M + Cat^{2+} - 3H)^-$ complex. For Ca^{2+}, the primary anchoring sites for YGGFL are either the deprotonated C-terminus or the deprotonated Tyr side chain. The N-terminal amine is not an anchoring site. The anchoring of Ca^{2+} to a deprotonated C-terminus as observed here in the gas phase is also known to occur in aqueous solution.[2] For Co^{2+}, there are no preferential anchoring sites: Anchoring can occur at either the N-terminal amine, at the deprotonated C-terminus, or at the deprotonated Tyr side chain. Anchoring either to the amine or to the C-terminus has also been observed in aqueous solution.[2] For Ni^{2+}, the most important anchoring site is the N-terminal amine. To a much lesser extent, the deprotonated C-terminus can also serve as anchor. The deprotonated Tyr side chain is not an anchoring site. The strong preference of Ni^{2+} for an anchoring N-terminal amine also occurs in aqueous solution.[2]

Another important conclusion can be drawn about geometric constraints on metal ion complexation. For Ca^{2+}, there are little or no constraints on complex formation. The gas-phase results are analogous to those in aqueous solution.[3] For Co^{2+} and Ni^{2+}, however, two adjacent deprotonated amides are required for complex formation. The gas-phase results are similar to those in aqueous solution.[2]

The gas-phase and aqueous-phase chemistry of Ca^{2+}, Co^{2+}, and Ni^{2+} is thus fundamentally the same. The differences that are observed in aqueous solution result from acid-base equilibria that are imposed on the system by the solvent. Weakly acidic sites, such as amides or side chain hydroxyl groups, cannot be deprotonated in water without precipitation of the metal ion as its hydroxide. One could envision that without such equilibria, the intrinsic, gas-phase chemistry would be precisely mimicked in aqueous solution.

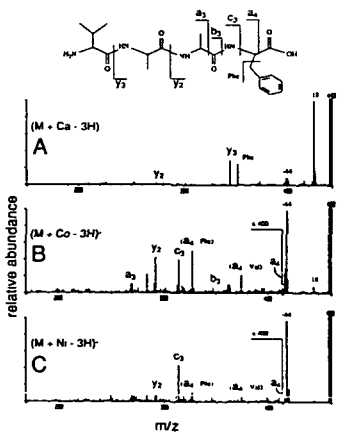

Figure 1. CID Spectra of VAAF.

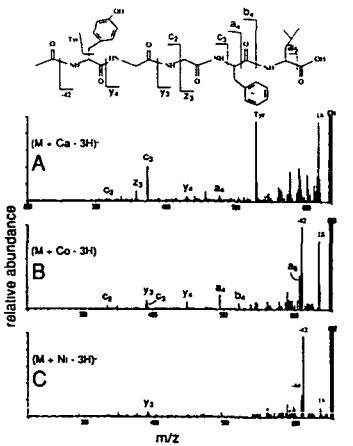

Figure 2. CID Spectra of Ac-N-YGGFL.

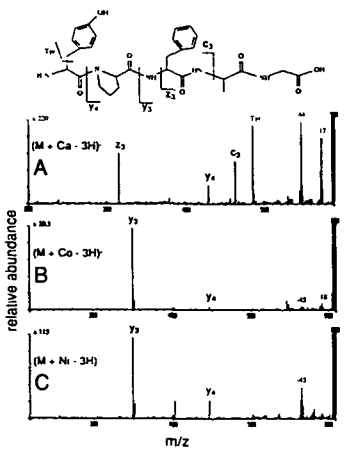

Figure 3. CID Spectra of YPFAG.

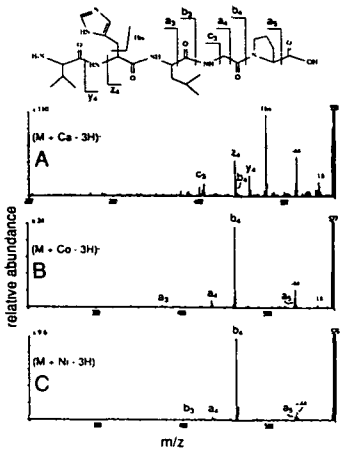

Figure 4. CID Spectra of VHLGP.

References

1. Zhao, H.; Reiter, A.; Teesch, L. M.; Adams, J. *J. Am. Chem. Soc.* **1993**, *115*, 2854-2863.
2. Kiss, T.; Sovago, I. In *Biocoordination Chemistry: Coordination equilibria in biologically active systems*; Burger, K. (Ed.); Ellis Horwood: New York, 1990, pp 56-184.
3. Martin, R. B.; Einsphar, H.; Bugg, C. E. In *Metal Ions in Biological Systems*, Vol. 17; Sigel, H. (Ed.); Marcel Dekker: New York, 1984, pp 1-127.

STRUCTURAL DETERMINATION OF PRECURSOR IONS IN THE COLLISION-INDUCED DECOMPOSITION OF Ca^{2+}-SPECIFIC PEPTIDES BY MOLECULAR MODELING

Alex Reiter, Hong Zhao, and Jeanette Adams, Department of Chemistry, Emory University, Atlanta, GA 30322.

We have previously studied the gas-phase chemistry of anionic complexes between alkaline earth metal ions (Mg^{2+}, Ca^{2+}, and Ba^{2+}) and peptides.[1,2] It was found that fragmentations of the complexes are the same, but product ion abundances change. The relative abundances of fragment ions increase with increasing size of metal ion.

To determine whether there is a relationship between the gas-phase fragmentation chemistry and known solution chemistry, this work was extend to Ca^{2+}-specific peptides. The Ca^{2+}-specific peptide sequences of -Asp-Val-Pro- (-DVP-) and -Tyr-Thr-Pro- (-YTP-) were investigated by CID and molecular mechanical calculations. These two sequences are found in the calcium proteins staphlococcal nuclease and thermolysin, respectively.[3] CID of -YTP- containing peptides, however, fragment to give primarily $(M + Cat^{2+} - 3H - C_2H_4O)^-$ ions,[2] which is a new peptide with the sequence -Tyr-Gly-Pro- (-YGP-).[2] Therefore, this sequence was also studied. The peptides investigated include **ADVPAA**, **AADVPA**, **AYTPAA**, **AAYTPA**, **AYGPAA**, **AAYGPA**, and **YPFAG**.

For **ADVPAA**, the formation of the c_4 product ions, which contain the intact -DVP- sequence, is more abundant when Ca^{2+} is the metal ion. This is in sharp contrast to our previous results.[1] Conversely, the peptide **AADVPA** cannot be cleaved to give a c_4 ion because it would require cleavage of the -DVP-Pro ring. Instead, a c_3 ion is observed even though it involves cleavage of the -DVP- binding site. In this latter case, formation of the c_3 product ion is least abundant when Ca^{2+} is the metal ion. For **AYGPAA** and **AAYGPA**, the trend seen is similiar to that observed for **ADVPAA** and **AADVPA**.

Molecular mechanical calculations were performed to address possible precursor ion structure. The calculations show that for **ADVPAA** (Figure 1), the most favored structures for Mg^{2+} and Ba^{2+} contain the metal ion bound to the Asp deprotonated side chain and to two adjacent deprotonated amides that would be distant from the site of cleavage. Thus, the most abundant precursors do not contain the metal bound in immediate proximity to the bond being cleaved. Therefore, these most abundant precursors decompose to give other product ions. For Ca^{2+}, however, the most favored precursor contains the metal ion in the -DVP- binding site immediately adjacent to the site of cleavage, and thus it decomposes to give highly abundant c_4 ions. The calculations show that for **AADVPA** (Figure 2), the most favored binding site for Ca^{2+} is again the -DVP- sequence. For Mg^{2+} and Ba^{2+}, the most favored binding site is the deprotonated Asp side chain and the two N-terminal amides. (The energy for the Ca^{2+} complexed similarly to Mg^{2+} and Ba^{2+} is shown in brackets, in Figure 2). The most abundant precursor structure for Ca^{2+}-**AADVPA** cannot undergo fragmentation to produce c_3 ions. In contrast for Mg^{2+} and Ba^{2+}, the c_3 ions arise from a high abundance of low energy precursor ions that are shown in Figure 2. Molecular mechanical calculations failed to reveal any useful information for the Tyr-containing peptides because of complications arising from calculated structures that have the Tyr-phenyl ring puckered upon complexation to the metal ions.

References

1. Zhao, H.; Reiter, A.; Teesch, L. M.; Adams, J. *J. Am. Chem. Soc.* **1993**, 115, 2854-2863.
2. Reiter, A.; Teesch, L. M.; Zhao, H.; Adams, J. *Int. J. Mass Spectrom. Ion Proc.*, **1993**, in press.
3. Einsphar, H.; Bugg, C. E. In Metal Ions in Biological Systems, Vol. 17; Sigel, H. (Ed.); Marcel Dekker: New York, 1984; pp 51-97.

ADVPAA

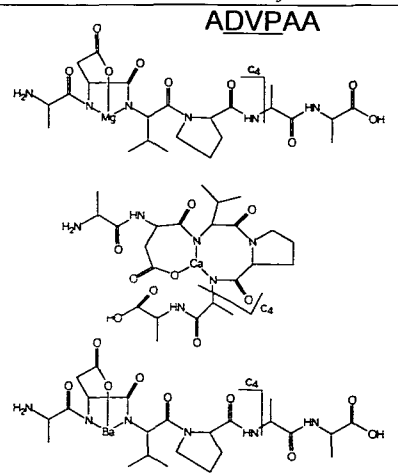

Energy	% ab.
31.4	0.63
18.1	0.91
28.3	0.76

Figure 1. Calculated structures of (ADVPAA + Cat2+ - 3H)- ions

AADVPA

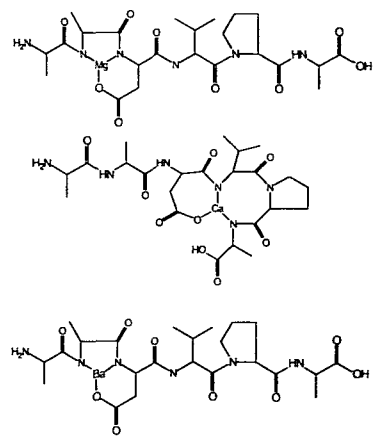

Energy	% ab.
23.7	0.091
25.2 [31.3]	0.083
19.3	0.12

Figure 2. Calculated structures of (AADVPA + Cat2+ - 3H)- ions

COLLISION INDUCED DISSOCIATIONS OF DEPROTONATED PEPTIDES. DIPEPTIDES AND TRIPEPTIDES CONTAINING PROLINE

*Russell J. Waugh[a], John H. Bowie[a] and Michael L. Gross[b]
[a]Department of Organic Chemistry, The University of Adelaide, Adelaide, SA 5001, Australia
[b]Department of Chemistry, University of Nebraska, Lincoln, NE 68588-0304, U.S.A.

The presence and position of proline in underivatized di- and tripeptides may be determined from a consideration of the collisional activation mass spectra of the $(M-H)^-$ ions , formed by fast atom bombardment. Product ion and deuterium labelling studies utilizing a Kratos MS 50 TA and a VG ZAB 2HF instrument have been used in an attempt to elucidate fragmentation mechanisms. The fragmentation mechanisms presented have been rationalized by 'anionic processes' based on the basic fragmentations of even-electron anions of simple organic compounds,(1) however in certain cases other reaction types (*e.g.* 'charge remote' processes) may possibly occur.

Deprotonated dipeptides, upon collisional activation, fragment by the characteristic process :- $NH_2CH(R^1)CONHCH(R^2)CO_2^- \rightarrow NH_2C(R^1)CONHCH(R^2)CO_2H \rightarrow {}^-NHCH(R^2)CO_2H + NH_2C(R^1)=C=O$ when R^1 and R^2 = H or alkyl, to identify the C-terminal amino acid.(2) When one α-substituent (R^1 or R^2) is H or alkyl and the other is an alcohol (Ser, Thr),(3) an acid (Asp, Glu),(4) an amide (Asn),(5) aryl (Phe, Tyr),(6) heterocyclic (His, Trp),(6) an amine (Arg, Lys),(5) or is a sulphur group (Cys, Met),(7) three main fragmentation types have been found to occur. Two questions are addressed, viz i) do Pro peptides undergo the usual cleavage shown above, and ii) are there any cleavages characteristic of Pro?

The spectra of five isomeric pairs of Pro dipeptides and the isotopically labelled derivatives where all the acidic hydrogens are exchanged with deuterium have been recorded. The spectra illustrated in Figures 1 and 2 are typical of all deprotonated Pro dipeptides studied where the α-substituent of one amino acid residue is H or alkyl. When Pro is N-terminal, the fragmentation pattern is consistent with that reported previously for simple dipeptides.(2) For example, Figure 1 is dominated by ion peaks formed by the competitive loss of CO_2 and formation of $(Leu - H)^-$ at *m/z* 130 [see above]. In contrast, the spectra of those isomers containing a C-terminal Pro are quite complex [illustrated by $(Leu\text{-}Pro - H)^-$ in Figure 2]. The base peak is always *m/z* 114 $(Pro - H)^-$ formed by the basic peptide cleavage shown in equation (1). An interesting fragmentation worth noting here is the formation of *m/z* 130 $(Leu - H)^-$. This ion formation involves transfer of the carboxyl oxygen to the carbonyl group of the N-terminal amino acid residue. The process is rationalized for the general case in equation (4), involving the attack of HO^- at the carbonyl group of the N-terminal amino acid residue followed by deprotonation within complex (d).

Proline di- and tripeptides are shown to undergo the basic peptide fragmentation given above. Care must be taken when there is a C-terminal Pro, because in addition to the expected Pro^- peak [*i.e.* ${}^-NHCH(R^2)CO_2H$], there is also a peak corresponding to $NH_2CH(R^1)CO_2^-$ formed by nucleophilic attack of HO^-. Also there are no fragmentations of Pro di- and tripeptides, apart from the basic backbone fragmentation shown in equation (1), which specifically identify a Pro residue irrespective of its position in the peptide.

REFERENCES

(1) J.H. Bowie, *Mass Spectrom. Revs.*, 1990, 9, 349.
(2) M.Eckersley, J.H.Bowie, R.N.Hayes, *Org. Mass Spectrom.*, 1989, 24, 597.
(3) R.J. Waugh, M. Eckersley, J.H. Bowie, R.N. Hayes, *Int. J. Mass Spectrom. Ion Proc.*, 1990, 98, 135.
(4) R.J. Waugh, R.N. Hayes, J.H. Bowie, *Org. Mass Spectrom.*, 1991, 26, 250.
(5) R.J. Waugh, J.H. Bowie, M.L. Gross, *Austral. J. Chem.*, submitted for publication.
(6) R.J. Waugh, J.H. Bowie, R.N. Hayes, *Int. J. Mass Spectrom. Ion Proc.*, 1991, 107, 333.
(7) R.J. Waugh, J.H. Bowie, M.L. Gross, submitted for publication.

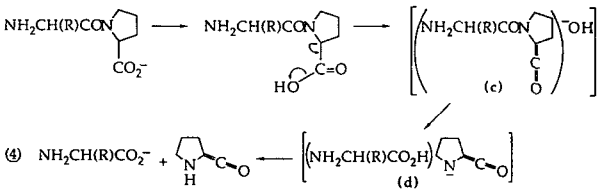

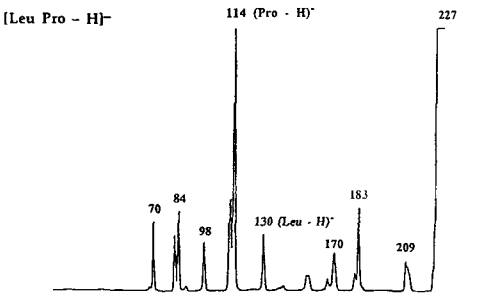

Figure 1: CA/FAB Mass Spectrum of (Pro-Leu – H)⁻

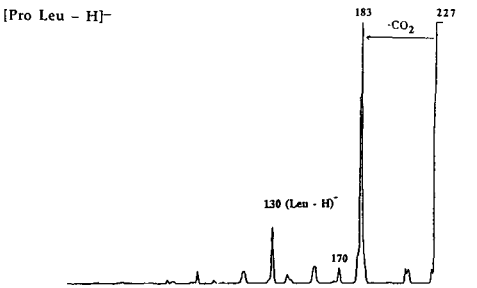

Figure 2: CA/FAB Mass Spectrum of (Leu-Pro – H)⁻

Kratos MS 50 TA instrument, University of Nebraska-Lincoln

FRAGMENTATION OF PROTONATED PEPTIDES: AGREEMENT BETWEEN SURFACE-INDUCED DISSOCIATION SPECTRA AND QUANTUM CHEMICAL PREDICTIONS

Jennifer L. Jones, Ashok R. Dongré, Árpád Somogyi, and Vicki H. Wysocki
Virginia Commonwealth University
Department of Chemistry
Richmond, Virginia 23284-2006

Protonated peptides can be effectively dissociated by collisions with a surface.[1,2] The goal of the work described here is to combine electrospray ionization (ESI) and liquid SIMS (LSIMS) ionization with surface-induced dissociation (SID)[1] to investigate the energy dependence of peptide fragmentation as a function of SID collision energy. The total internal energy acquired by the peptide during both the ionization and activation steps is reflected by the number and relative abundances of fragment ions in the product ion scan. For a given collision energy, the MH^+ ions formed by electrospray ionization do not fragment as extensively upon collision with a surface as do ions formed by LSIMS. A plausible explanation for this observation is that ESI produces protonated peptides that are "colder" than those produced by LSIMS. For similar fragmentation patterns, arginine-containing peptides formed by ESI require a SID collision energy ≈ 40 eV higher than those formed by LSIMS. If additional energy is imparted to the ions by collisional activation in the ESI capillary-skimmer region before mass selection for SID, more extensive fragmentation is apparent in the SID spectrum.

The great sensitivity of the SID spectra to the ionization method suggests that the low internal energy content of the ions produced by ESI, coupled with the narrow movable internal energy distribution associated with SID, can be used to predict the population of different protonated forms (of the same peptide) that fragment under given conditions. Results presented in Figure 1 show the influence of the number, type and location of basic groups on fragmentation threshold. SID thresholds vary with peptide structure; higher thresholds are observed for peptides with basic residues at the amino terminus. This suggests that the majority of the ion population have a stable H-bridged structure (side-chain...H^+...amino terminus).

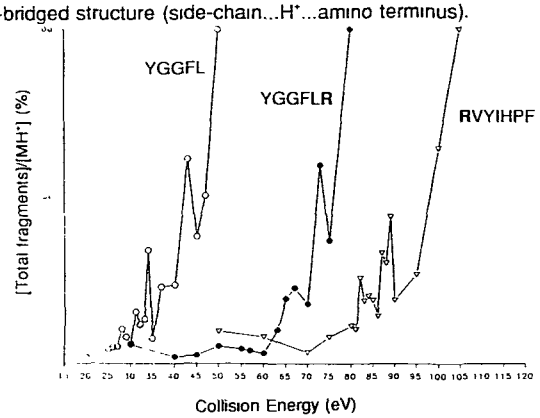

Figure 1

MNDO bond orders have been proved recently to be useful for the description of ion structures and primary fragmentation processes.[2,3] Although bond orders cannot be regarded as direct reactivity indexes, it is generally agreed that smaller bond orders represent weaker bonds. This is illustrated by the bond order values for a $\mathbf{b_2}$ ion (Structure I). Easy loss of CO from **b** ions to produce **a** ions is predicted by experimental results and by the small bond order value (**0.789**) for the C-C≡O bond of Structure I.

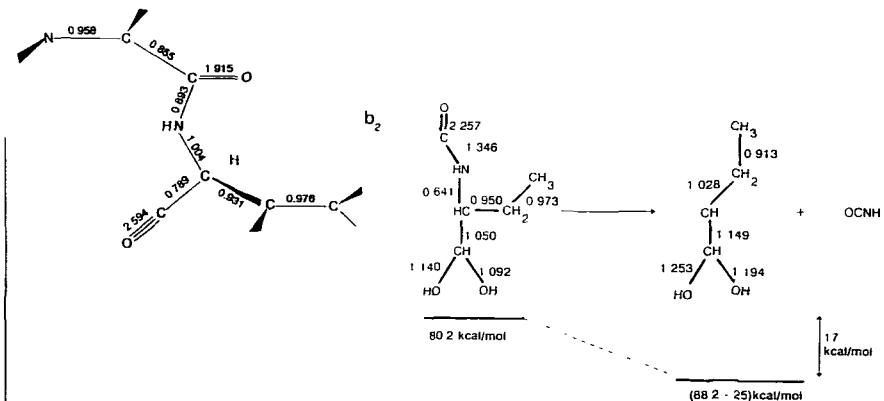

Structure I Structure II

Calculations for a number of different protonated forms of model peptides led to the following conclusions: The protonation has a local effect; only the bond orders of the α, β and γ bonds change significantly due to protonation The protonation on the amide nitrogen leads to a significantly weakening (by about 30%) of the amide bond. Accordingly, the cleavage of this bond, which can lead to the formation of ions **b**, **y**, and **a**, is preferred energetically. Protonation on the amide oxygen makes the amide bond stronger, so the formation of the above fragment ions is less likely from this form. Charge-remote backbone cleavages can be modeled by neutral peptides; the weakest bonds in the neutral peptides are the carbon-carbon bonds of the backbone. Charge remote backbone cleavage, followed by side-chain cleavage, is less favorable that the cleavage of the amide bond of a nitrogen-protonated form, in agreement with experimental observations. If the remote charge is located on the carboxy terminus, we propose that cleavage of the same C-C backbone bond, with subsequent loss of HNCO, would lead to a **z+1** ion (the suggested precursor of the **w** side-chain cleavage ions)(Structure II).

1 Cooks, R G., T. Ast, Md.A. Mabud *Int. J. Mass Spectrom. Ion Proc.* 1990, 100, 209-265.
2. McCormack, A.L., Somogyi, Á.; Dongré, A.; Wysocki, V.H. *Anal. Chem.*, submitted.
3. Császár, A.G.; Somogyi, Á.; Pócsfalvi, G.; Traldi, P. *Org. Mass Spectrom.* 1992, 27, 1349-1356, and references therein.

Gas-Phase Conformational Studies of Multiply Charged Cytochrome c Ions Using Collisional Activation and Ion-Molecule Reaction

*Rong Feng and Yasuo Konishi, National Research Council of Canada, Biotechnology Research Institute, 6100 Royalmount Avenue, Montreal, Quebec H4P 2R2, Canada

Electrospray-produced multiply charged protein ions usually form one (or more) charge-state distribution in the mass-to-charge ratio (*m/z*) range of 500-2500. The charge-state distributions are sensitive to protein conformational changes in solution. Typically, the ions from a protein having the native conformation form a charge-state distribution in the high *m/z* region because the molecule can carry only a limited number of charges while still maintaining its conformational integrity. On the contrary, an unfolded protein, which is capable of holding more charges, always places its charge-state distribution in the low *m/z* (high charge-state) region. The unfolded protein exposes more of the molecular interior and occupies more space than its native counterpart. It is of fundamental interest whether these two classes of multiply charged protein ions can maintain their conformational differences in the gas phase, where solvent stabilization is absent and increased Coulombic repulsion among the charges may force the coiled polypeptide chain to stretch. In this study we used collisional activation and ion-molecule reactions to probe the gas-phase conformational differences of the multiply charged cytochrome c ions.

A triple quadrupole mass spectrometer (Sciex API III) was used for the protein conformational studies. Horse heart cytochrome c (MW 12,360 Da) that was denatured under acidic condition (10% acetic acid v/v, pH 2.2) produced a low *m/z* charge-state distribution centered around the 16+ charge state (Fig. 1a). In contrast, the native protein that was preserved in a neutral stabilizing buffer (10 mM ammonium acetate, pH 6.7) gave a high *m/z* charge-state distribution centered around 7+ (Fig. 1b).

The collisional fragmentation patterns of the cytochrome c ions originated from the denatured and native solution conformations showed sharp differences, which could not be entirely attributed to the charge disparity between them. At the same collision energy (corrected for the charge difference), the former preferentially shed the covalently-bound heme group, producing two intense singly charged fragments at *m/z* 617 and 649 (Fig. 2a), whereas the latter did not dissociate appreciably (Fig. 2b). Thus, it appeared that in the former the heme group was exposed to the impinging argon atoms because the polypeptide chain remained unfolded, while in the latter the heme group was still wrapped in the polypeptide chain and protected from the collisions.

The size difference between the denatured and native cytochrome c molecules in solution appeared to be carried over to the gas phase, as indicated by the collisional scattering cross-section measurements. Under non-dissociative collision conditions and using the same collision gas density, the ions from the denatured solution conformation were more prone to scattering loss than the ions from the native solution conformation. This indicated that in the solvent-free vacuum, the gaseous ions originated from the native cytochrome c in solution still maintained a more compact size, despite the

Coulombic repulsion among the charges.

The multiply charged cytochrome c ions from the denatured and native solution conformations were also subjected to ion-molecule reactions in the gas phase. The former lost protons to ammonia at a rate much higher than the latter (see Figs. 1a and 3a, and Figs. 1b and 3b). In addition to the variations in the charge-transfer energy barrier due to the charge disparities, this large difference in reaction rate also reflected a substantial gas-phase structural difference between these two classes of ions. In the latter, its more compact structure might have restricted the charge-transfer reaction, as the positive charges on the folded protein could be protected by hydrogen-bonding and internal "solvation" from the electron-donating groups.

The above results suggest that, despite multi-charging and lack of solvent stabilization, protein conformational differences still exist in the gas phase; the multiply charged ions from the native conformation in solution appear to retain more folding features in the gas phase than the ones from the denatured conformation in solution.

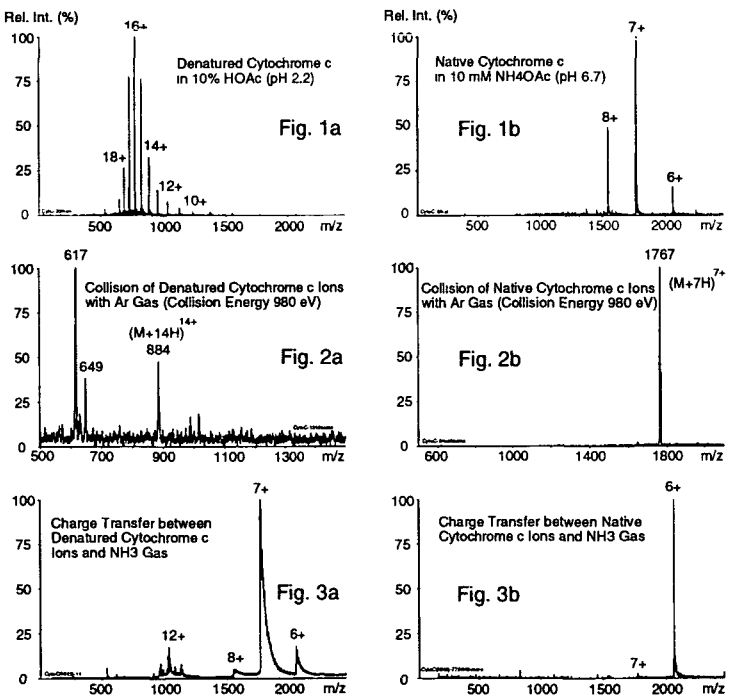

ROLE OF KINETIC ENERGY IN COLLISION-INDUCED DISSOCIATION OF CS_2^+

YiBai Chen, Kevin Norbash, Ronald Tosh, Anil Shukla* and Jean Futrell
Department of Chemistry and Biochemistry, University of Delaware,
Newark, DE 19716

INTRODUCTION

CID of CS_2^+ ions has been a subject of ongoing controversy since first studied by angle-resolved mass spectrometry [1]. The relative abundances of fragment ions CS^+ and S^+ showed two crossovers when monitored as a function of scattering angle. It was suggested that this behavior results from the excitation of CS_2^+ ions into higher electronic states which dissociate independently. Later studies at low energies using crossed-beam [2] and at high energy using z-deflection [3] showed only one crossover which was also reproduced by theoretical calculations of relative abundances based upon kinetic energy release [4]. The low energy experiments showed that relative intensity of CS^+ increased with collision energy but decreased with scattering angle. Since ions with higher internal excitation on collision are scattered at larger angles, it was suggested that collisional excitation results in specific electronic states of CS_2^+ which are associated with unique dissociation behavior. All these studies, however, did not measure the kinetic energy of fragment ions and based their conclusions on the variation of relative abundances only. We have therefore studied the low energy CID of CS_2^+ ions using our tandem crossed-beam mass spectrometer where we can measure kinetic energy of fragment ions also.

RESULTS AND DISCUSSION

S^+: CM velocity contour diagrams for S^+ measured at 7.7, 17.2 and 34.5 eV collision energies show a single peak centered at non-zero scattering angles. Figure 1 shows such a contour diagram at 17.2 eV energy. The energy transfer for this dissociation process, determined by integrating these contour diagrams over all scattering angles, is close to thermochemical threshold of 4.8 eV. Since, energy transfer is nearly constant at all energies, there is no change in the collisional activation and dissociation process.

CS^+: CM velocity contour diagrams for CS^+ show quite a different behavior. Although, the threshold for this process is 5.7 eV, we could not get enough fragmentation at and slightly above this energy. At the lowest energy of 8.6 eV, we found a very broad peak with most probable energy transfer of 8 eV. As the collision energy was increased, energy transfer for this process also increased. At 12.4 and 17.2 eV, the energy transfer into internal modes corresponded to nearly 11.5 eV. At 17.2 eV we also notice a shoulder which corresponds to 5.7 eV energy transfer as shown in Figure 2. At further higher energies, this low energy process again disappears.

Since CS^+ is the high energy process, there may be a competitive shift associated with this process resulting in transfer of higher energy for dissociation. The energy depositions of 8 and 11.5 eV suggest that dissociation proceeds from higher excited state(s) and probably results in excited fragment ions. We suggest from known and speculated potential energy diagrams that CS^+ is formed in excited A and C states respectively at 8.6 and 17.2 eV collision energy.

CONCLUSIONS

These results suggest that CID of CS_2^+ to CS^+ follows a complex pathway that is strongly dependent upon ion's kinetic energy and results in excited fragment ions. Dissociation to S^+, however, proceeds via lowest energy pathway at all energies.

REFERENCES:

1. Laramee et al., Int. J. Mass Spectrom. Ion Phys., 33, 231, 1980.
2. Hirst et al., Int. J. Mass Spectrom. Ion Proc., 63, 119, 1985.
3. Mason et al., Int. J. Mass Spectrom. Ion Phys., 43, 327, 1982.
4. Todd et al., Int. J. Mass Spectrom. Ion Phys., 50, 299, 1983.

Fig.1. CM velocity contour map for the CID of CS_2^+ to S^+ at 17.2 eV collision energy.

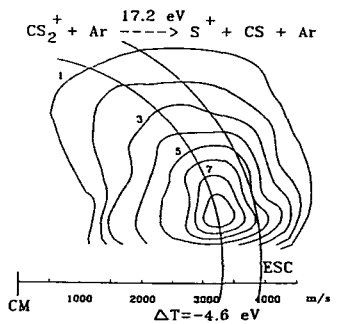

Fig.2. CM velocity contour map for the CID of CS_2^+ to CS^+ ion at 17.2 eV collision energy.

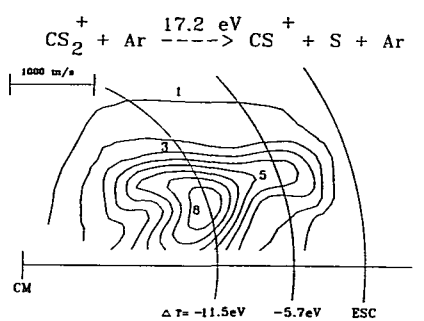

Fundamental Studies Of Molecular Ion-Surface Collisions: Pyridine Ions on Self-Assembled Monolayers

Sam Wainhaus, John A. Burroughs, Qinyuan Wu, and *Luke Hanley,
Department of Chemistry, m/c 111, University of Illinois at Chicago,
Chicago, IL 60607-7061.

Self-assembled monolayer covered gold surfaces have been used as collision targets for surface induced dissociation (SID) of molecular ions since they can be reproducibly prepared outside of vacuum using wet chemical methods [1,2]. Furthermore, the low sticking coefficients of self-assembled monolayers to most vapors allow these collision targets to remain clean on the molecular level, regardless of the atmospheric or vacuum environment in which they are placed. However, the constant bombardment of such monolayers by energetic molecular ions during SID experiments is likely to lead to their chemical modification.

We compare here the SID spectra of pyridine ion scattering off the simplest self-assembled monolayer film, methyl thiolate (MeS) adsorbed on a clean single crystal of silver, Ag(111), with the ion beam damage of same. These experiments are performed in a tandem mass spectrometer which is coupled to an ultrahigh vacuum surface analysis chamber [3]. This apparatus is also equipped with thermal desorption MS and infrared reflection absorption spectroscopy (IRAS) for monitoring the MeS coverage on the Ag(111) surface. The MeS monolayer is prepared by gaseous dosing of dimethyl disulfide.

Figure 1 displays the vibrational spectrum of MeS/Ag(111) recorded by IRAS. By measuring the 2912 cm^{-1} (symmetric C-H stretch of the methyl group) IRAS peak area following ion bombardment of the surface, we have determined the MeS coverage remaining on the surface after a 5 ± 2 nA/cm^2 pyridine ion exposure at 55° off the surface normal:

Beam Energy	Exposure Time	MeS Remaining
32 eV	30 min	76 %
32	60	65
64	30	62
64	60	49

Figure 2 shows SID spectra of $C_5H_5N^+$ scattered off a monolayer of MeS/Ag(111) at 32 and 64 eV. Both spectra display strong MH^+ (80 m/z) and $[M-CN]^+$ (53 m/z) peaks. In addition, the 32 eV spectra displays a $[MCH_3]^+$ peak (94 m/z) which results from reactive scattering off the MeS monolayer. At 64 eV, reactive scattering does not occur but more extensive fragmentation of the incident ion is observed.

We have also monitored individual scattered ion peaks as a function of incident ion exposure time. Although all scattered ion signals slowly increase over 60 min as the methyl groups on the surface are sputtered away by the incident beam, these peaks each increase at the same rate. Therefore, even though the self-assembled monolayer has been significantly damaged by the ion beam, the SID spectra are not affected. These results further indicate that self-assembled monolayers are excellent targets for SID experiments since they give reproducible spectra even after continual ion beam exposure.

References

1) A. Somogyi, T.E. Kane, and V.H. Wysocki, Org. Mass Spectrom. **28** (1993) 283 and references therein.
2) M.R. Morris, D.E. Riederer, Jr., B.E. Winger, R.G. Cooks, T. Ast, and C.E.D. Chidsey, Inter. J. Mass Spectrom. Ion Proces. **122** (1992) 181 and references therein.
3) Q. Wu and L. Hanley, J. Phys. Chem. **97** (1993) 2677.

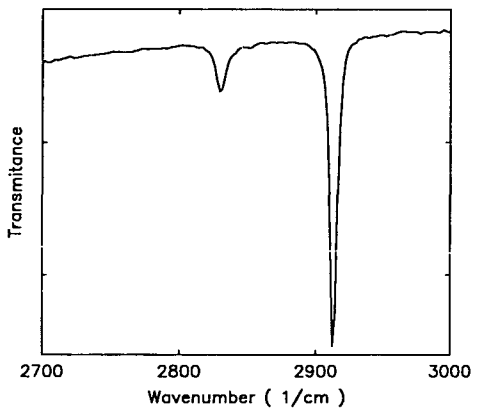

Figure 1: Vibrational spectra by IRAS of a monolayer of MeS/Ag(111).

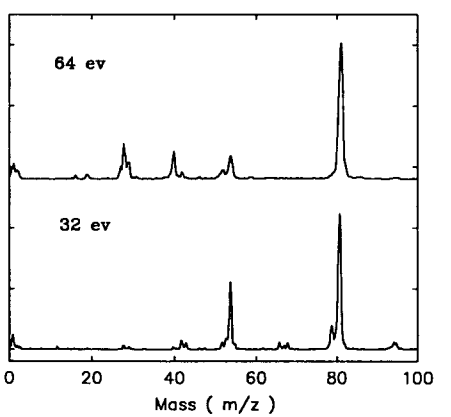

Figure 2: SID spectra of $C_5H_5N^+$ scattered off MeS/Ag(111).

Surface-Induced Dissociation of Ferrocene at Self-Assembled Monolayer and Single Crystal Surfaces

S.A. Miller, D.E. Riederer, Jr., and R.G. Cooks
Department of Chemistry, Purdue University, West Lafayette, IN 47907, USA
W.R. Cho, H.W. Lee, and H. Kang
Department of Chemistry, Pohang Institute of Science and Technology, Pohang, Korea 790-600

Comparative studies are reported for surface-induced dissociation (SID) of ferrocene molecular ions performed on a hybrid BEEQ tandem mass spectrometer and a Wien filter/quadrupole (WQ) combination. Ferrocene molecular ions (m/z 186) undergo dissociation upon collisions at Si(100) and alkylthiol self-assembled monolayer surfaces (SAMs) and the resulting SID mass spectra compare well between the two different instruments. Energy resolved mass spectrometric (ERMS) studies were completed on a perfluorinated alkylthiol (F surface) and a perdeuterated alkylthiol (D surface) SAM surface, while a similar study was done on a clean Si(100) single crystal surface. The Si(100) and the D surface had remarkably similar ERMS curves while the F surface indicated a larger internal energy deposition (Figure 1). Ferrocene was used as a thermometer ion[1] to probe the translational to vibrational (T-V) energy conversion efficiency on the F and D surfaces. T-V energy conversion efficiencies of 15% and 24% for the D and F-surface, respectively, were estimated by a method previously described[1]. These efficiencies are reasonable with previous results for other systems in which the T-V energy conversion is greater for the F surface (19%) than the D surface (13%).[2] The larger T-V energy conversion for the F surface is attributed to the larger effective mass and rigidity of the surface compared to the D surface. The similarity between the Si(100) and the D surface suggest that the effective mass of these collision partners is nearly the same.

Ferrocene has also proven to be a model ion for SID in three respects; i) simple fragmentation patterns (ii) relatively large secondary ion survival probability and iii) lack of ion/surface reactions. This study as well as others[3,4] have shown the main fragmentation pathway of ferrocene to be the loss of one cyclopentadienyl radical followed by a second loss of a cyclopentadienyl radical. Structural assignments were checked by recording SID mass spectra of two ferrocene isotopes (m/z 184 and 186) under identical conditions (Figure 2).

Ferrocene has a relatively low ionization potential and high proton affinity. The low ionization potential accounts for the large secondary ion yield and ion/surface reactions, such as hydrogen (or deuterium) atom pick-up, are also allowed by the high proton affinity. The absence of this reaction suggests that charge exchange is a prerequisite for hydrogen atom transfer in agreement with the mechanism suggested elsewhere.[5] Further insight into this mechanism was obtained by colliding 1,8-bis(dimethylamino)naphthalene (a "proton sponge") on the D surface. The "proton sponge" has a slightly lower ionization potential and a much higher proton affinity than ferrocene. Again, ion/surface reactions did not occur despite the very large proton affinity of the compound.

References:

1. V.H. Wysocki, H.I. Kenttämaa, R.G. Cooks, *Int. J. Mass Spectrom. Ion Processes*, 75, 1987, 181.

2. M.R. Morris, D.E. Riederer, Jr., B.E. Winger, R.G. Cooks, T. Ast and C.E.D. Chidsey, *Int. J. Mass Spectrom. Ion Proc.*, 122, 181 (1992).
3. H. Budzikiewicz, C. Djerassi, and D.H. Williams, *Mass Spectrometry of Organic Compounds*, 1st ed.; San Francisco: California, 1967; Chapter 27.
4. G.D. Flesch, G.A. Junk, and H.J. Svec, *J. Chem. Soc. Dalton Trans.*, 11, 1102, (1972).
5. B.E. Winger, R.K. Julian, Jr., R.G. Cooks, and C.E.D Chidsey, *J. Am. Chem. Soc.*, 113, 8967, (1991).

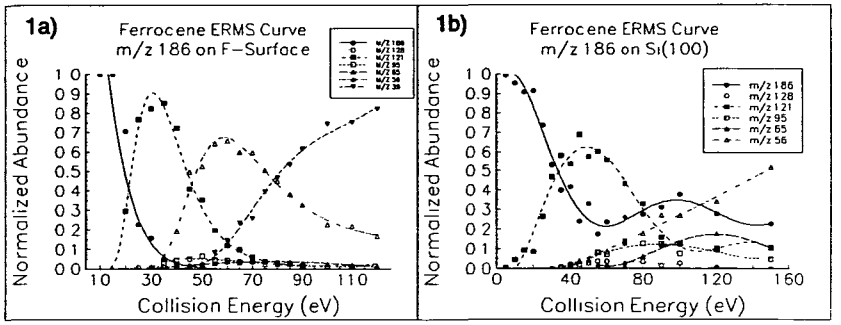

Figure 1. ERMS curve showing scattered ion abundance as a function of collision energy for $Fe(C_5H_5)_2^{+\cdot}$ (m/z 186) on (a) a perfluorinated SAM surface and (b) on a clean Si(100) surface. Figure (a) was recorded using the BEEQ instrument and (b) using the WQ instrument.

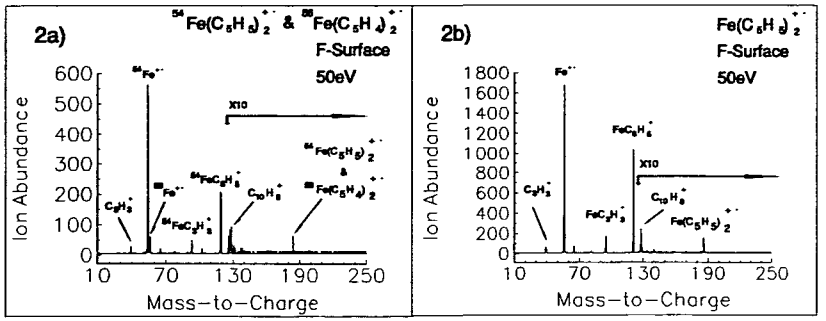

Figure 2. SID mass spectrum of (a) 50eV $^{54}Fe(C_5H_5)_2^{+\cdot}$ (m/z 184) and $[^{56}Fe(C_5H_5)_2 - H_2]^+$ (m/z 184) ions produced by scattering from a perfluorinated SAM surface and (b) 50eV $^{56}Fe(C_5H_5)_2^{+\cdot}$ (m/z 186) ions scattered from the same surface under identical conditions.

COLLISIONS OF PERFLUOROPROPYLENE IONS WITH SOLID SURFACES

T. Ast, D.E. Riederer, Jr, S.A. Miller, M. Morris and R.G. Cooks, Department of Chemistry, Purdue University, West Lafayette, IN 47907

The perfluoropropylene molecular ion $C_3F_6^{+\cdot}$ (m/z 150) yields two fragment ions of similar appearance energies: $C_3F_5^+$ (m/z 131, AE 14.8 eV) and CF_3^+ (m/z 69, AE 15.0 eV). However, depending on the activation method employed, these two ions can be formed in vastly different proportions. In particular, $C_3F_5^+$ is observed only in methods involving a significant degree of electronic excitation (e.g. electron impact, high energy CID, charge exchange), while it is absent, or formed in very low abundance, in methods proceeding predominantly through vibrational excitation (e.g. low energy CID). These observations were rationalized invoking an isolated electronic state of $C_3F_6^{+\cdot}$ which fragments preferentially and directly to $C_3F_5^+$, and which can be populated only by an electronic excitation mechanism.[1,2]

Early attempts to study the surface induced dissociation (SID) of $C_3F_6^{+\cdot}$ were not successful; collisions at an adsorbate covered stainless steel surface gave no projectile fragments and only beam neutralization and chemical sputtering were observed.[3] These experiments have now been repeated on a newly constructed hybrid BEEQ tandem mass spectrometer[4], which, among other features, provides a 100-fold better vacuum in the target region (4×10^{-9} torr). The performance of a stainless steel, as well as of three self-assembled monolayer surfaces, has been examined: $CH_3(CH_2)_{15}SH$ (the H surface), $CD_3(CD_2)_{15}SH$ (the D surface) and $CF_3(CF_2)_{11}(CH_2)_2SH$ (the F surface). The yields of m/z 69 and m/z 131 from the molecular ion have been studied over the collision energy range 20-70 eV for all four surfaces and the results are shown in Figure 1. At low collision energies, H and D surfaces (Figure 1a) yield predominantly the m/z 131 ion, pointing to the prevalence of electronic excitation. As the collision energy is increased, the m/z 131/69 ratio is reversed, suggesting a change over to fragmentation from a vibrationally excited state. These results support the conclusions of Futrell et al. reached in a similar CID study.[5] This effect is much less pronounced for the SS and F surfaces (Figure 1b); the m/z 69 ion now dominates at all collision energies, implying that the main mode of activation leads to vibrational excitation.

The behavior of other major ions generated from C_3F_6 has also been examined. As an example, Figure 2 shows the product ion spectra obtained upon 50 eV collisions of $C_2F_4^+$ at all four surfaces. The F surface provides largest energy deposition; only slightly smaller is observed for the SS surface, in which surface adsorbate sputtering is also evident. The H and the D surfaces are least efficient in energy transfer, as manifested by the presence of the reflected projectile ion at m/z 100. On the other hand, a significant amount of chemical sputtering is observed for both the latter surfaces, reminiscent of the earlier study.[3] The extent of chemical sputtering shows a large dependence on the nature of the projectile; this should be born in mind when assessing the surface cleanliness on the basis of the sputtering experiment. Thus, most organic ions exhibit no or little sputtering upon collisions at the H and D self-assembled monolayer surfaces[6]; as opposed to this, organofluorine ions, CH_3I^+, I^+, I_2^+, and Xe^+ are some examples of ions that induce intense sputtering off these surfaces under identical experimental conditions.

References

1. S.A. McLuckey and R.G. Cooks, *Int. J. Mass Spectrom Ion Proc.*, 56, 223 (1986).
2. S. Habibi-Goudarzi, T. Kotiaho, R.G. Cooks and T. Ast, *Org. Mass Spectrom.*, 26, 1008 (1991).
3. M. Vincenti, and R.G. Cooks, *Org. Mass Spectrom.*, 23, 317 (1988).
4. B.E. Winger, H.-J. Laue, S.R. Horning, R.K. Julian, Jr, S.A. Lammert, D.E. Riederer, Jr, and R.G. Cooks, *Rev. Sci. Instrum.*, 63, 5613 (1992).
5. A.K. Shukla, K. Quiau, S. Anderson and J.H. Futrell, *J. Am. Soc. Mass Spectrom.*, 1, 6 (1990).
6. M.R. Morris, D.E. Riederer, Jr, B.E. Winger, R.G. Cooks, T. Ast and C.E.D. Chidsey, *Int. J. Mass Spectrom. Ion Proc.*, 122, 181 (1992).

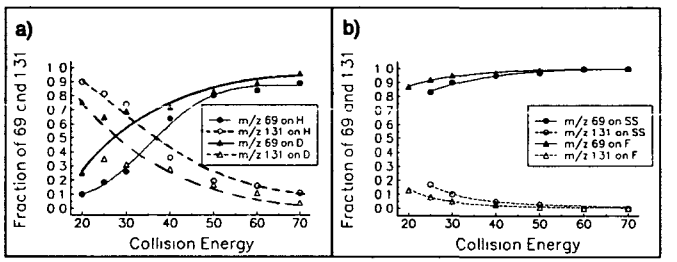

Figure 1. Fraction of CF_3^+ (m/z 69) and $C_3F_5^+$ (m/z 131) obtained upon collisions of $C_3F_6^{+\cdot}$ at (a) H and D surfaces; (b) stainless steel and F surfaces, as a function of projectile collision energy.

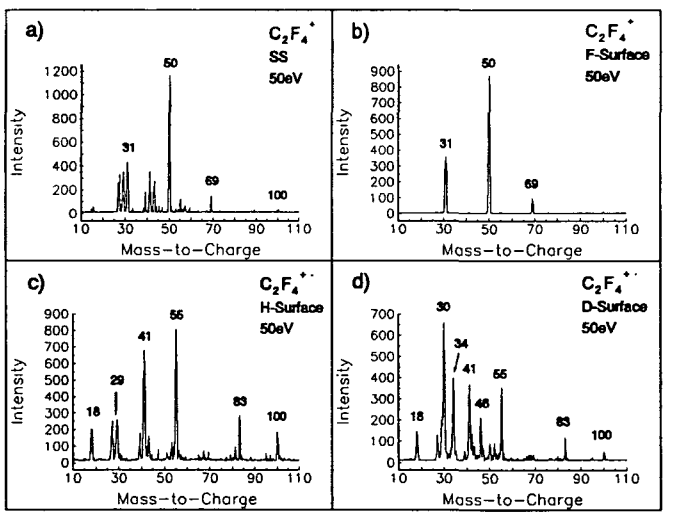

Figure 2. Product ion spectra obtained upon 50 eV collisions of $C_2F_4^+$ ions (m/z 100) upon (a) stainless steel, (b) F, (c) H and (d) D surfaces.

Reactions of Organosilanes with Self-Assembled Monolayers

Ashok R Dongré, Árpád Somogyi, and Vicki H. Wysocki
Department of Chemistry, Virginia Commonwealth University,Richmond, VA 23284-2006

Introduction

Collision of mass-selected projectile ions with chemically-modified surfaces leads to extensive fragmentation. In addition to fragmentation, other processes, like ion- surface reactions, chemical sputtering and neutralization, are observed.[1] Several ion-surface reactions have recently been observed between small organic ions (benzene,[2] pyrazine[3]) and self-assembled monolayer surfaces.

The aim of this investigation to study the reactions of silicon containing ions with various self-assembled monolayer surfaces. Given the preferred formation of Si-F and Si-O bonds over Si-C bonds, the reaction peaks observed for CF_3 and OH terminated surfaces could, expectedly, be more intense than those detected for CH_3 terminated surfaces.

Experimental

The instrument used in this investigation is a tandem quadrupole instrument in a 90° arrangement with the surface intersecting the ion optical path at 45°.[4] The self-assembled monolayers are prepared by immersing plasma-cleaned vapor deposited gold in 1mM ethanol solution of the given thiol. The monolayer surfaces used in this investigation were prepared from 2-(perfluorooctyl)-ethanethiol, octadecanethiol, perdeuteroeicosanethiol, and 1-hydroxyundecanethiol. The silicon containing ions selected to collide with the organic monolayer surfaces were $(CH_3)_3Si^{37}Cl^+$ m/z 110, $(CH_3)_2Si^{37}Cl^+$ m/z 95, and $(CH_3)_3Si^+$m/z 73.

Results and Discussion

The silicon-containing ions react with the fluorinated alkanethiol monolayer. Several reaction peaks are observed for all the three selected ions. Reaction products at m/z 47(SiF^+) and m/z 49 (H_2SiF^+) are fairly intense peaks in the spectra (eg. see Figure 1). The reaction peak at m/z 47 is the base peak at collision energy of 80 eV for m/z 95. The breakdown curve for m/z 95 shows that the peak at m/z 47 is 17-18% of the total ion abundance. No appreciable reaction products are observed when the ion is collided with the n-alkanethiol monolayer surfaces. Silicon also reacts with the hydroxy-terminated surface but reactions are not as enhanced as those observed on the fluorinated surface. A peak at m/z 75 is observed which could be due to the formation of a $(CH_3)_2SiOH^+$ adduct. The absence of the m/z 75 peak in spectra obtained with n-alkanethiolate and fluorinated alkanethiolate monolayers indicates that m/z 75 is formed via reaction with the hydroxy group and not by fragmentation of the selected ion. Peaks at m/z 45 ($SiOH^+$) and m/z 47(H_2SiOH^+) are more intense than those observed on alkanethiolate monolayer surfaces, which indicates that a fraction of the ion intensity results from the reaction and the rest from the fragmentation of the precursor ion.

Comparison of the selected silicon-containing ions with carbon analogues ($(CH_3)_3C^+$ and $(CH_3)_2CCl^+$; generated from *terc*-C_4H_9-Cl) suggests that the d orbitals of silicon play a role in the reactivity of silicon compounds with fluorinated alkanethiolate monolayers.

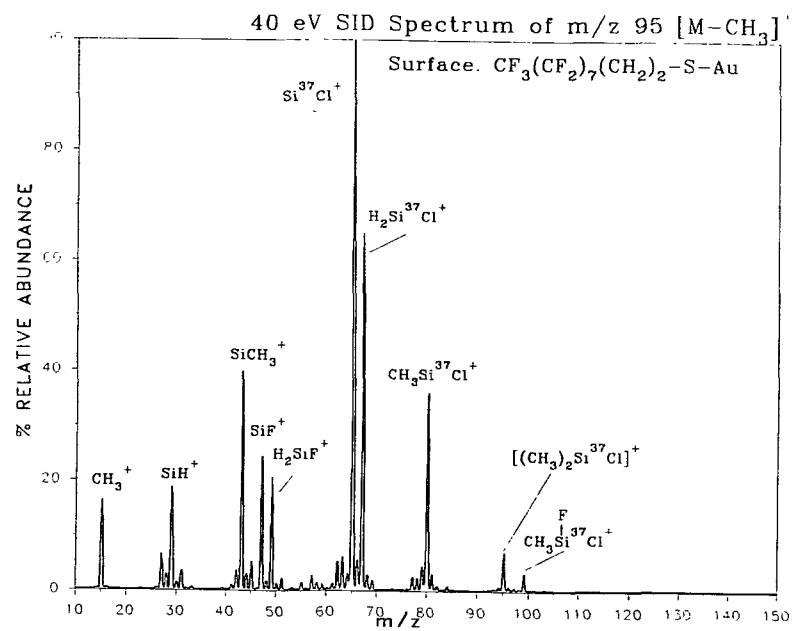

Figure 1 Ion-surface collision spectrum obtained by a 40 eV collision of $(CH_3)_2Si^{37}Cl^+$ with the 2-(perfluorooctyl)-ethanethiolate surface

REFERENCES:

1. Cooks, R. G.; Ast, T.; Mabud, Md. A. *Int. J. Mass Spectrom. Ion Processes* **1990**, *100*, 209.
2a. Somogyi, Á., Kane, T E., Ding, J.-M.; Wysocki V H. *J. Am. Chem. Soc.*, in press.
2b. Morris, M.; Riederer, D. E., Jr.; Winger, B. E.; Cooks, R. G.; Ast, T.; Chidsey, C. E. D *Int. J. Mass Spectrom. Ion Processes* **1992**, *122*, 181.
3. Winger B E ; Julian R.K.Jr ; Cooks R.G.; Chidsey C.E.D. *J. Am. Chem. Soc.* **1991**, *113*, 8967.
4. Wysocki, V H., Ding, J.-M.; Jones, J. L.; Callahan, J. H., King, F. L. *J. Am. Soc. Mass Spectrom.* **1992**, *3*, 27

Reactions of Immonium Ions with Self-assembled Monolayer Films

*Rebecca L. Franklin, Árpád Somogyi and Vicki H. Wysocki, Virginia Commonwealth University, 1001 West Main Street, Richmond, VA 23284

Several processes can occur when a polyatomic ion collides with a surface. These processes include (i) surface-induced dissociation (SID), (ii) ion/surface reactions, (iii) charge exchange (i.e. chemical sputtering) and (iv) neutralization. Recently, self-assembled monolayer (SAM) films of alkanethiolates on gold were shown[1,2] to be effective surfaces for the study of ion/surface interactions.[3] Monolayers used in this investigation include 2-(perfluorooctyl)-ethanethiol, 1-octadecanethiol, and 1-eicosane-d_{41}-thiol covalently bonded to vapor-deposited gold. Here we compare the ion/surface collision products formed by collision of various even-electron immonium ions (e.g. $CH_2{=}NH_2^+$) and their methyl, deuterium, and oxygen analogues with fluorinated alkanethiolate and alkanethiolate films.

Spectra of immonium ions studied exhibit SID, ion/surface reactions, and chemical sputtering, as a function of laboratory collision energy and surface film type. SID of $CH_2{=}NH_2^+$ leads to CH_2^+ and NH_2^+ with some NH_4^+ produced Similarly, SID of $C_2H_4^+$ produces CH_2^+ and CH_3^+. All ions studied exhibited peaks at m/z 69 on the fluorinated surface; this ion corresponds to the chemical sputtering of CF_3^+ from the surface. Typical sputtering peaks from the 1-octadecanethiol surface include m/z 39, 41, and 43.

Chemical reactions of the ions studied include addition of F or CH_3 followed by H and H_2 losses to produce mainly even-electron ions. The reaction product of F addition to $CH_2{=}NH_2^+$ is observed at m/z 46. When $CH_2{=}ND_2^+$ is the projectile ion, the reaction product is detected at m/z 47 (see scheme 1 and figure 1). When the m/z 58$^+$ immonium ion formed from tertiary butylamine is collided with the fluorinated surface, m/z 46 is one of the products formed. This ion (m/z 46) corresponds to the product peak for fluorine addition to $CH_2{=}NH_2^+$. The ion CH_2OD^+ also reacts with the fluorinated surface to add fluorine with loss of HD and H to form FCO^+.

1. B.E Winger, R.K. Julian, R.G. Cooks *J. Am. Chem. Soc.* **1991**, 113, 8967-8969.
2. V.H. Wysocki, J.L. Jones, J.M. Ding *J. Am. Chem. Soc.* **1991** 113, 8969-8970.
3. For a review of SID, see: R G. Cooks, T. Ast, MD.A. Mabud *Int. J. Mass Spectrom. Ion Proc.* **1990**, 100, 209-265.

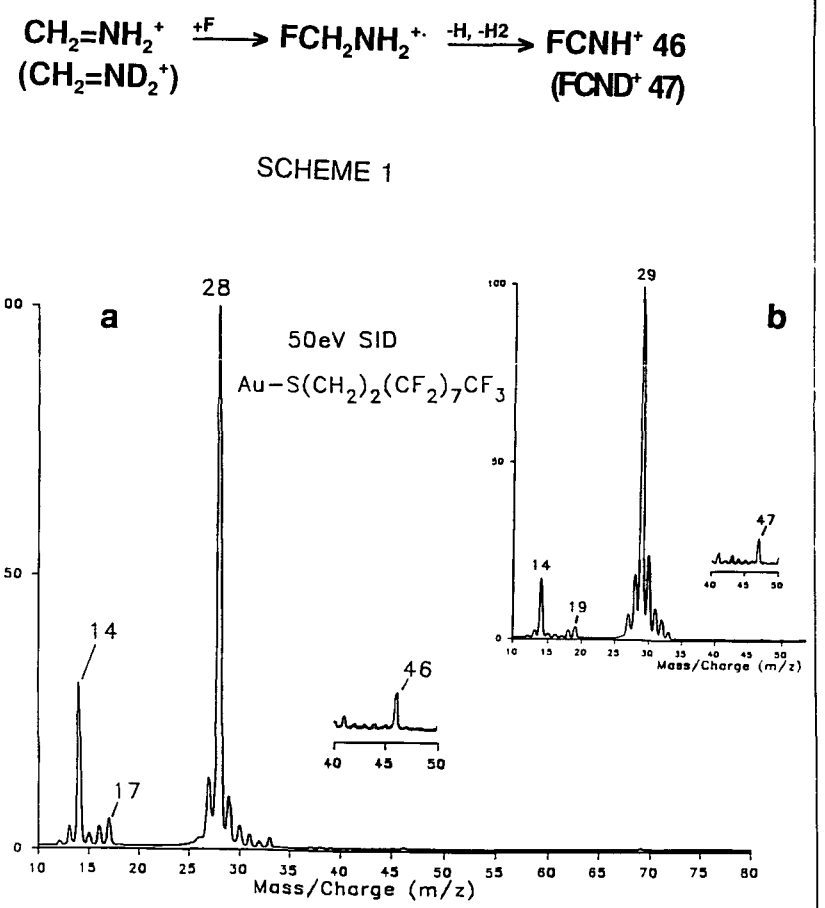

Figure 1. Ion/surface reactions obtained by 50eV collisions of (a) $CH_2{=}NH_2^+$ and (b) $CH_2{=}ND_2^+$ with a surface prepared from 2-(perfluorooctyl)-ethanethiol on vapor-deposited gold.

Surface-Induced Dissociation Spectra of Ketones

Árpád Somogyi, Thomas E. Kane, Vicki H. Wysocki
Department of Chemistry, Virginia Commonwealth University, Richmond, VA 23284-2006

Introduction Surface-induced dissociation (SID)[1] is a promising ion-activation technique. Recent studies[2-4] proved the advantages of self-assembled monolayer films for ion-surface collisions. These monolayers can be easily prepared by the spontaneous assembly of 1-alkanethiols and their derivatives on gold. The monolayers can reduce the neutralization of the projectile ions which leads to higher scattered ion abundance. They also can improve the energy transfer to the projectile, to date, fluorinated alkanethiolates proved to be the most effective monolayers for high kinetic energy - internal energy conversion.[1, 1-4] Chemical reactions between the projectile ions and the monolayers have also been described.[1-4] These reactions, together with the measurement of the total ion current at the detector and the current at the surface, make the SID method unique for the characterization of the self-assembled monolayers in vacuum.

As a continuation of our recent work,[4] we present here the SID spectra of simple ketones (acetone, acetophenone, and benzophenone). The main fragmentation processes of these molecular ions are well known, and acetophenone was also a subject of a recent SID study of Cooks et al [3] Therefore, the main aim of this study is not the description of the fragmentation of these simple ketones but rather the investigation of the effect of different monolayers and collision energies on the fragmentation and ion-surface reactions.

Experimental The instrument used in this investigation consists of two quadrupoles (Extrel, Pittsburgh, PA) arranged in a 90° geometry, with a surface placed to intersect the ion optical path of each quadrupole.[5] The covalently bound monolayers were prepared by the spontaneous assembly of octadecanethiol (C_{18} surface), perdeuteroeicosanethiol (CD_3 surface), and 2-(perfluorooctyl)-ethanethiol (fluorinated surface) on plasma-cleaned vapor-deposited gold. 70 eV electron impact ionization was used to form the molecular ions of acetone, acetone-d_6, acetophenone, acetophenone-methyl-d_3, acetophenone-ring-d_5, and benzophenone.

Results and Discussion

Breakdown curves and energy deposition

The breakdown curves obtained for the acetophenone molecular ion on the fluorinated surface are shown in Figure 1. Similar sharp curves were obtained for the acetone molecular ion, and for the selected acetyl cation (m/z 43). The breakdown curves obtained on the C_{18} and CD_3 surfaces are not as sharp as those on the fluorinated surface and they are shifted to higher collision energies. For example, in the case of the acetyl cation (m/z 43), to get a similar [m/z 15]/[m/z 43] ratio, higher collision energy was required for the alkanethiolate (C_{18} and CD_3) surfaces (by about 10 eV) than for the fluorinated surface. These results support the narrow and relatively high internal energy distribution associated with fluorinated alkanethiolate surfaces, as has been reported e.g., for $W(CO)_6$.[3]

Ion-surface reactions

i) H(D) addition In contrast with benzene molecular ion,[3,4c] the H(D) addition to the ketone molecular ions is estimated to be slightly exothermic. Accordingly, in the low-energy SID spectra (10-30 eV) of these ions with alkanethiolate surfaces $[M+H(D)]^+$ peaks are observed, and molecular ions are of very low intensity. In addition, acetone molecular ion proved to be a sensitive probe to detect *trace* H-containing contaminants on the fluorinated surface. The appearance and pressure dependence of the $[M+D]^+$ peak in the SID spectrum of acetone-d_6 with the fluorinated surface

indicate that the acetone is also physisorbed to the monolayer surface.

ii) $CH_3(CD_3)$ addition The 25 eV SID spectra of acetophenone molecular ion with the C_{18} and CD_3 surfaces are shown in Figure 2. In contrast with benzene,[3,4c] intact adduct ions are observed, together with the $[M+CH_3-H_2]^+$ and $[M+CD_3-HD]^+$ peaks. For acetone molecular ion, the adduct ion peak is dominant in the reaction region of the SID spectra. Results for the molecular ions of acetophenone, acetophenone-methyl-d_3 and acetophenone-ring-d_5, suggest that two different methyl adducts may be formed: an O-adduct and a ring-adduct Preliminary MNDO and *ab initio* quantum chemical calculations predict the O-adduct more stable than the ring(ipso)-adduct.

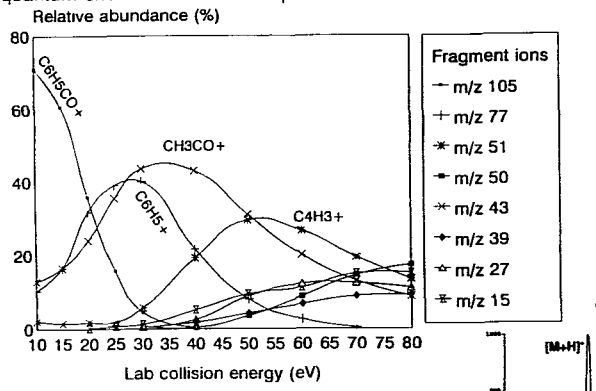

Figure 1

Figure 2

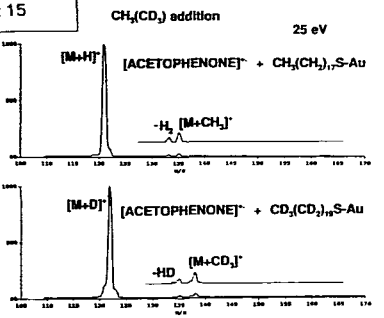

References

1 Cooks, R.G.; Ast, T.; Mabud,Md. A. *Int. J. Mass Spectrom. Ion Processes* **1990**, *100*, 209.
2 Winger, B.E.; Julian, R.K., Jr.; Cooks, R.G.; Chidsey, C.E.D. *J. Am. Chem. Soc.* **1991**, *113*, 8967.
3 Morris, M.; Riederer, D.E., Jr ; Winger, B.E.; Cooks, R.G., Ast, T.; Chidsey, C.E.D. *Int. J. Mass Spectrom. Ion Processes*, **1992**, *122*, 181.
4 (a) Wysocki, V.H., Jones, L.J.; Ding, J.-M. *J. Am. Chem. Soc.* **1992**, *113*, 8969. (b) Somogyi, Á.; Kane, T E.; Wysocki, V.H. *Org. Mass Spectrom.* **1993**, *28*, 283. (c) Somogyi, Á ; Kane, T.E., Ding, J.-M., Wysocki, V.H. *J. Am. Chem. Soc.*, in press. (d) McCormack, A.L.; Somogyi, Á.; Dongré, A.R.; Wysocki, V.H., submitted for publication. (e) Callahan, J.H.; Somogyi, Á.; Wysocki, V.H., submitted for publication
5 Wysocki, V.H., Ding, J.-M.; Jones, J.L.; Callahan, J.H.; King, F.L. *J. Am. Soc. Mass Spectrom.* **1992**, *3*, 27.

Determination of Bond Energies by Collisional Dissociation of Electrospray Ions in Free Jet Expansions

S.D. Fuerstenau* and **J.B. Fenn** *Dept. of Chemical Engineering*
Yale University, New Haven, CT 06520

We present a method for measuring bond dissociation energies of ions which fragment due to collisions in the nozzle-skimmer region of an electrospray ion source. The approach is applicable to any differentially pumped, atmospheric pressure ion source. We consider the multi-collisional excitation of the ion in the jet to be essentially a heating process in which the extent of excitation, or temperature, is directly proportional to the applied voltage. When properly normalized , plots of ion current vs. voltage are interpreted as the result of a unimolecular decomposition. We relate the extent of decompositon to the voltage with an Arrhenius rate expression to arrive at an activation energy for the fragmentation process.

J. French and co-workers observed twenty years ago that the focusing potential applied between the nozzle and skimmer of a high pressure ion source could lead to desolvation of analyte ions. More recently, researchers in R.D. Smith's laboratory found that thermal excitation in the jet region aided in subsequent CID of large peptides in tandem MS experiments. R.Voyksner has demonstrated that at higher voltages covalent bonds may be broken with this CID technique that is both efficient (> 90% yield) and reproducible.

In contrast to single collision CID, ions accelerated in low pressure jets are subjected to hundreds or thousands of energetic collisions over a short time period (10 µs.) During this time the temperature and density of the surrounding gas drop drastically along the ion's path of travel through the jet. At first glance the energetics of this process appear to be hopelessly complex and undefined. Jarrold has pointed out, however, that the product of many collsions, each with a broadly distributed excitation probability, can result in a very narrow distribution of internal energies in the excited ions. We proceed with the problem by making the following simplifying assumptions:

- The amount of energy deposited into an ion, due to the sum of all collisions may be represented by a temperature, Tp, and is proportional to the applied voltage, ie,

$$Tp = \Omega(Vn-Vs)$$

  where Ω is a source dependent constant of calibration.

- The amount of decomposition occurring during and after excitation may be treated as the result of a unimolecular reaction occuring at a single temperature, **Teff**, which we assume scales with voltage.

$$dC/dt = -kC \;\text{--->}\; C(t)/Co = \exp\{-k(Teff)t\} \qquad (1)$$

- The flight time, t*, between excitation and sampling at the quadrupole entrance is fixed but unspecified, and is the same for all ions of similar mass at a given skimmer potential. It follows that:

$$-\mathrm{Ln}\,(C(t^*)/Co) = kt^*$$

Assuming that the rate constant k follows an Arrhenius form, we may express the extent of decomposition as :

$$\mathrm{Ln}\,(C(t^*)/Co) = At^* \exp(-Ea/RTeff) \qquad (2)$$

Taking the log and substituting ΩV fot Teff we get

$$\mathrm{Ln}\,(-\mathrm{Ln}(C/Co)) = \mathrm{Ln}\,At^* - Ea/R\Omega V \qquad (3)$$

A plot of Ln(- Ln(C/Co)) vs. 1/V will have a slope of - Ea/RΩ . The constant Ω can be found by using a calibration compound with a known Ea of dissociation.

Normalization of Ion Currents

It follows from (3) that a plot of C/Co vs. V should have the form

$$C/Co = \exp(-At^* \exp(-Ea/R\Omega V)) \qquad (4)$$

This is an S shaped function which starts at one and decays to zero.

Unfortunately the response of the parent ion vs voltage rarely has this shape. Typical response curves show a rise due to focusing and then a decay attributed to fragmentation. We postulate that the response of a parent ion , Ip , may be represented as the product of two functions of nozzle-skimmer voltage. These are a focusing transfer function, T(V), and a loss function, L(V), which follows the extent of decompositon. Because focusing and decay can occur simultaneously, the function of interest , L , cannot be separated without some additional information. This is provided by the response of the daughter ions which, it may be reasonably argued, follow the same focusing function of the parents. Assuming the disappearance of one parent ion results in the appearance of one daughter ion, we may write a mass balance:

$$Ip = TL$$
$$Id = T(1-L) \;\text{-->}\; L = Ip/(Ip+Id) \qquad (5)$$

Note that T is never specified explicitly. Eqs. (5) represent the algebraic basis for extracting L(V) functions from more complicated systems.

Experimental

The system used in this study employed three stages of pumping with a VG 1200 micromass quadrupole. The pressure in front of the first skimmer was about 1 torr and that in the second pumping stage 1 millitorr. The nozzle to skimmer distance was 3mm with fields in the jet region as high as 50,000 V/M. The ions explored here were SF6-, WCO6+ and MCO6+, all generated by corona discharge in the atmospheric pressure region of the source. ES ions studied were clusters of the amino acid Arginine and metal cations solvated with Acetonitrile. Literature values are available for the gas phase dissociation of all ions except Arginine. Responses were typically recorded with the mass resolution set to its minimum value to minimize discrimination effects.

DISSOCIATION PROCESS	SLOPE	REPORTED Ea	Ω (^{0}K/V
$SF_6^- \text{--->} SF_5^-$	-173	1.05 eV (ref. 1)	70
$WCO_6^+ \text{--->} WCO_5^+$	-207	1.39 eV (ref. 2)	77
$MoCO_6^+ \text{--->} MoCO_5^+$	-152	0.97 eV (ref. 2)	73
$Na^+(ACN)_2 \text{--->} Na^+(ACN)$	-157	1.06 eV (ref. 3)	78

1. F.C. Fehsenfeld, J. Chem. Phys. 1970, 53, No.5 p.2000
2. D.R. Bidnosti and N.S. McIntyre, Can. J. Chem. 1967, 45 p.641
3. R.G. Keese and A.W. Castleman 1986 , J. Phys. Chem Ref Data 15

THE EFFECT OF CHARGE ON ION STABILITY A QUANTITATIVE COMPARISON. Sohrab Habibi-Goudarzi, Kevin J. Hart and Scott A. McLuckey, Analytical Chemistry Division, Oak Ridge National Laboratory, Oak Ridge, TN 37831-6365.

Multiply-charged biopolymers derived from electrospray have yielded useful structural information upon collision-induced dissociation [1] It has been noted that more highly charged species tend to fragment more readily due, presumably, to the additional strain associated with a high coulombic field. A quantitative comparison of the threshold for dissociation of gaseous multiply-charged ions as a function of charge in an MS/MS experiment, however, has not yet been reported. We have been evaluating collisional activation in the quadrupole ion trap for studying the threshold behavior of singly-charged parent ions[2] and have extended this work to multiply-charged biopolymers.

Specifically, we have studied in detail the behavior of the oligonucleotide anions $d(A_pA_pA_pA)^{3-}$ and $d(A_pA_pA_pA)^{2-}$. The former anion fragments exclusively through loss of A^- upon resonant excitation whereas the latter fragments mostly via loss of neutral adenine (Figure 1). We have employed a kinetic method[3] to determine the difference in the threshold resonance excitation amplitudes which can be correlated to literature E_o values based on the calibration curve developed in reference 2. The kinetic method for each of the two parent anions involves the following steps. First, the parent ion is isolated and subjected to collision-induced dissociation at constant resonant excitation amplitude (tickle voltage) and varying excitation duration (tickle time). The rate of decay of the parent anion (k_v) is the slope of the linear region of $-\ln(P_t/P_0)$ vs. tickle time curve. Second, the time dependent decay experiment is then repeated at all other pertinent excitation amplitudes. Finally, the k_v data obtained from each of the above experiments are plotted against the excitation amplitudes.

Ideally, the threshold resonance excitation amplitude is obtained by extrapolating to zero k_v the initial, non-linear region of the k_v vs. tickle voltage curve. Since we are interested in the difference between the two cases (i.e. the triply and the doubly charged anions), and since more data points are need to make accurate estimations, we extrapolated the linear region of the latter curve (Figure 2). The values obtained for each case are then converted to their equivalent literature E_0 values according to the equation TREA= 92.58 + 288.13*[log(E_0)], where TREA is the threshold resonance excitation amplitude in mV (see reference 2). The $d(A_pA_pA_pA)^{3-}$ anion had a threshold resonance excitation amplitude of 187 mV or E_0 of 2.14 eV and the $d(A_pA_pA_pA)^{2-}$ anion 207 mV or 2 50 eV. This suggests that the difference in the threshold energies of these parent anions is about 0.4 eV. The procedure we used to obtain these values should provide an upper limit to the difference in critical energies The results of this work, which should correlate with CID cross-section on beam-type instruments, illustrate the important role that coulombic repulsion plays in the ability to fragment multiply charged ions. For this reason, this case study may have relevance in a variety of electrospray ionization mass spectrometry applications.

"The submitted manuscript has been authored by a contractor of the U.S. Government under contract No. DE-AC05-84OR21400. Accordingly, the U.S. Government retains a nonexclusive, royalty-free license to publish or reproduce the published form of this contribution, or allow others to do so for U.S. Government purposes."

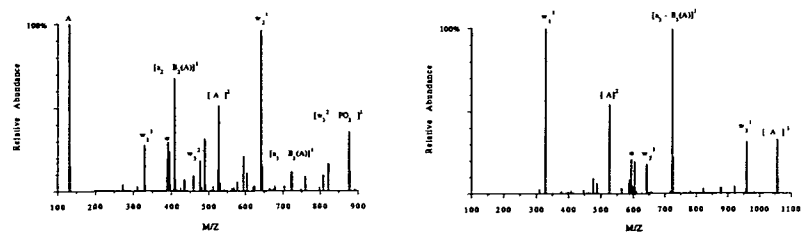

Figure 1. MS/MS spectra of (from left to right) $[d(A_pA_pA_pA) - 3H^+]^{3-}$ and $[d(A_pA_pA_pA) - 2H^+]^{2-}$.

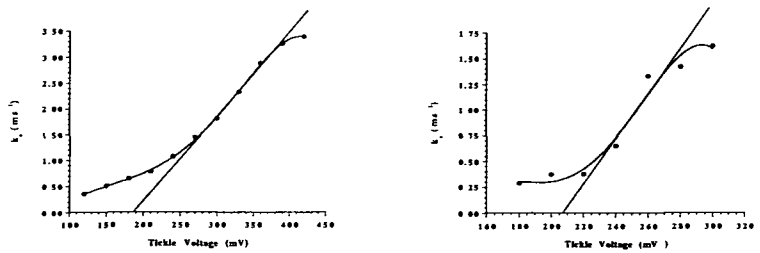

Figure 2. The decay rate constant k_v of (from left to right) $[d(A_pA_pA_pA) - 3H^+]^{3-}$ and $[d(A_pA_pA_pA) - 2H^+]^{2-}$ as function of resonance excitation amplitudes.

References:

1. McLuckey, S.A.; Van Berkel, G.J.; Glish, G.L. J. Am. Soc. Mass Spectrom 3(1992)60
2. Hart, K.J.; McLuckey, S.A. in preparation.
3. Franklin, A.M.; Todd, J.F.J., March, R.E.; to be presented at this meeting.

Credit:

Research sponsored by the U.S. Department of Energy, Office of Basic Energy Sciences, under contract DE-AC05-84OR21400 with Martin Marietta Energy Systems, Inc.

Photodissociation of Solvated Ions

*Y.J. Yang, D.M. Peiris and J.R. Eyler
Department of Chemistry, University of Florida, Gainesville, FL 32611-2046.

Several methods have been used to measure the binding energies of solvated ions, including equilibrium measurements in both high pressure[1,2] and ICR[3] mass spectrometers and photodissociation measurements in a TOF mass spectrometer[4]. An alternate way to study ion/neutral binding energies is photodetachment measurement in ICR mass spectrometry. By measuring the depletion of the parent ion as a function of photon energy, the threshold of photodetachment, related directly to the binding strength of solvated ions, can be determined. Since the electron affinities of the halides are well known, bonding in halide solvates can be studied by using UV-visible photodetachment. The initial stages of work in which the 266 nm 4th harmonic output of a Nd:YAG laser was used to induce photodetachment of alcohol solvated halides are presented here.

The experiment was performed in a FT ICR mass spectrometer with a data system which includes an external trigger option. Thus the Nd:YAG laser was synchronized with the mass spectrometer through the use of a photodiode. Laser energy at 266 nm was *ca.* 17-25 mJ/pulse. The solvated halides were formed by the ion-molecule reactions:

$$ClCO_2C_2H_5 + e^- \rightarrow CO_2Cl^- + C_2H_5$$
$$CO_2Cl^- + CH_3OH \rightarrow \mathbf{CH_3OHCl^-} + CO_2$$
$$CO_2Cl^- + C_2H_5OH \rightarrow \mathbf{C_2H_5OHCl^-} + CO_2$$

where the pressure of $ClCO_2C_2H_5$ was about 4×10^{-7} torr and the total pressure maintained at 1×10^{-6} torr. The chloride donors were formed using an electron beam pulse, followed by a period for ion-molecule reaction formation of the solvated chlorides and relaxation of internal energy before firing of the laser.

Figures 1 and 2 show mass spectra of CH_3OHCl^- and $C_2H_5OHCl^-$ under identical conditions with and without laser irradiation of the ions. By measuring the disappearance of the parent ions, the extent of photodetachment was found to be 49% and 59% for CH_3OHCl^- and $C_2H_5OHCl^-$, respectively (Figs.3 and 4). No increase in the intensity of chloride ion was seen upon laser irradiation for either solvate, which means no photodissociation channel is involved.

Generally one would expect the relative binding strength of the solvent-halide ion to be substantially greater than that in the solvent-halogen. Also, the structure of the neutral solvates may change so that the equilibrium internuclear distance increases compared to that of the solvated ions. Given that the EA of chlorine is 3.62 eV and that we observed photodetachment at 266 nm (4.6 eV),

an upper limit of 1.0 eV can be placed on the difference between ion and neutral solvation energies. To obtain more information on the binding energies and structures of halides solvated by different solvents, we plan to use a doubled dye laser to find the photodetachment threshold and also carry out *ab* initio calculations to understand the structure of both neutral and ion solvates. The binding energies obtained from gas phase equilibrium and photodetachment studies will be compared. The shifts of the binding energies for solvated anions will be also determined, giving a clue as to the structures and bonding interactions in these species.

Fig. 1 MASS SPECTRUM OF CH_3OHCl^-

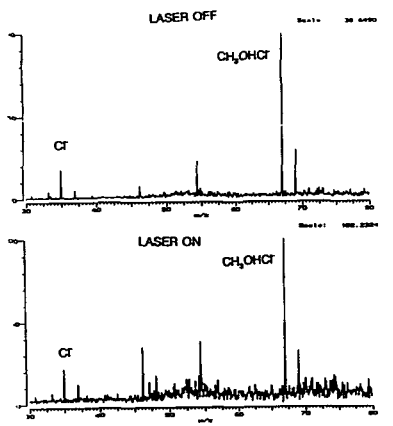

Fig. 2 MASS SPECTRUM OF $C_2H_5OHCl^-$

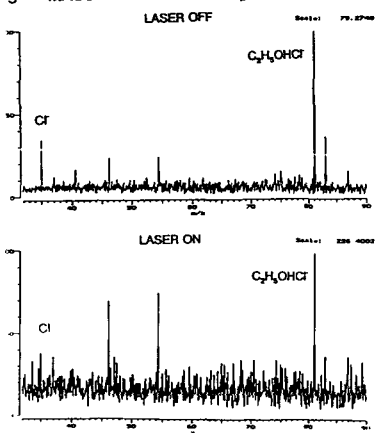

Fig. 3 Photodetachment of CH3OHCl-

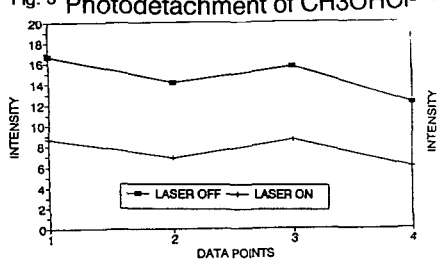

Fig. 4 Photodetachment of C2H5OHCl-

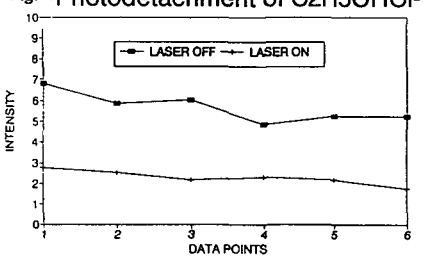

[1]R. Yamdagni, J.D. Payzant and P. Kebarle, *Can. J. Chem.*, 1973, **51**, 2507.
[2]M. Mautner, *J. Am. Chem. Soc.*, 1988, **110**, 3854 and 7604.
[3]J.W. Larson and T.B. McMahon, *J. Am. Chem. Soc.*, 1988, **110**, 1087.
[4]F. Misaizu, M.Sanekata, K.Tsukamoto, K Fuke and S.Iwata, *J. Phys. Chem.*, 1992, **96**, 8259.

Infrared Multiple Photon Dissociation Spectra of Solvated Ions

D. M. Peiris, J. M. Riveros[1] and J. R. Eyler
Department of Chemistry, University of Florida
Gainesville, FL 32611-2046
[1]Inst. of Chemistry, University of Sao Paulo, Sao Paulo, Brazil

There have been a number of studies of gas-phase ions solvated with single neutral molecules to begin following the transition from gas to solution phase ionic behavior. In particular, solvated halide ions have been studied (1) due to their structural simplicity and their existence in solution. In past work we have used CO_2 lasers to excite gaseous ions and photodissociate them. Fortunately, the C-O stretching band of methanol at ν = 1034 cm^{-1} overlaps the CO_2 laser spectrum. Thus, methanol serves as a good solvent candidate for infrared photodissociation studies of solvated ions.

In the past, we have utilized the technique of infrared multiple photon dissociation (IRMPD) in a Fourier transform ion cyclotron resonance mass spectrometer (FTICR) to obtain spectra of gaseous ions (2). A similar approach was used in this study to obtain spectra of halide ions solvated by methanol and deuterated methanol (CH_3OHX^- and CH_3ODX^-, where the halide X is F or Cl).

Experimental apparatus associated with FTICR and its modifications for the IRMPD technique have been previously discussed in detail (2). The background pressure was maintained at 5 x 10^{-9} Torr. CF_4 *or* $ClCO_2C_2H_5$ was admitted in up to 5.5 x 10^{-7} Torr and CH_3OH *or* CH_3OD was then admitted in up to a total pressure of 1.1 x 10^{-6} Torr. The anion of interest was isolated by a series of ejection pulses and then irradiated with the unfocused output of a line-tunable pulsed CO_2 laser. The photoproduct X^- was ejected during the laser pulse in order to prevent it from reacting with excess solvent molecules present in the cell. *The IRMPD spectra of the halide solvated anions were obtained by monitoring the depletion* of the parent ion as a function of a laser wavelength with constant laser energy. CH_3OHX^- and CH_3ODX^- were generated by the reaction sequences shown in reactions 1 through 8.

Methanol solvates of the **fluoride** ion:

$CF_4 + e^- \longrightarrow CF_3 + F^-$ (1)
$F^- + HCO_2CH_3 \longrightarrow CH_3OHF^- + CO$ (2)

Deuterated methanol solvates of the **fluoride** ion:

$CF_4 + e^- \longrightarrow CF_3 + F^-$ (3)
$F^- + DCO_2CH_3 \longrightarrow CH_3ODF^- + CO$ (4)

Methanol solvates of the **chloride** ion:

$ClCO_2C_2H_5 + e^- \longrightarrow ClCO_2^- + C_2H_5$ (5)
$ClCO_2^- + CH_3OH \longrightarrow CH_3OHCl^- + CO_2$ (6)

Deuterated methanol solvates of the **chloride** ion:

$ClCO_2C_2H_5 + e^- \longrightarrow ClCO_2^- + C_2H_5$ (7)
$ClCO_2^- + CH_3OD \longrightarrow CH_3ODCl^- + CO_2$ (8)

Irradiation of CH_3OHX^- and CH_3ODX^- ions results in photodissociation via reaction 9

$CH_3O(H,D)X^- + nh\nu_{ir} \longrightarrow F^- + CH_3O(H,D)$ (9)

IRMPD spectra of CH_3OHX^- and CH_3ODX^- in the 920 - 1060 cm^{-1} region (10.6μm - 9.6 μm P and R branches of the CO_2 laser) are presented in Figures 1a, 1b, 1c, and 1d. Comparison of IRMPD and neutral IR spectra must be done with care due to limitations in resolution and spectral coverage in the IRMPD experiments. Furthermore, peaks seen in the IRMPD spectra will be the result of coincidences between sharp absorption bands and the sharp laser lines.

All IRMPD peaks are red shifted when compared with the neutral. Peaks in the neutral spectra range from 975 - 1075 cm^{-1} whereas IRMPD spectral peaks range from 945 - 1050 cm^{-1} Unfortunately, there is no structural information available for the CH_3OHX^- species (except one isolated study of CH_3OHF^- (3); the spectrum from that study differs somewhat from ours) for comparison with our results At this point, it is difficult to compare the shifts in either CH_3ODX^- or CH_3OHX^- peaks with the respective neutral peaks.

In this study, we have successfully utilized the technique of IRMPD in a FTICR mass spectrometer to obtain spectral information for solvated halide ions. Theoretical calculations and further studies are ongoing to assist in unambiguous assignment of these peaks.

Future experiments include probing the OH stretching modes of these solvated halide ions. In this study we will employ the probe-pump technique which has been proved in our *early experiments* (2). A Nd: YAG *laser with a newly-installed ir extension package in* conjunction with a cw CO_2 laser will be used for these experiments.

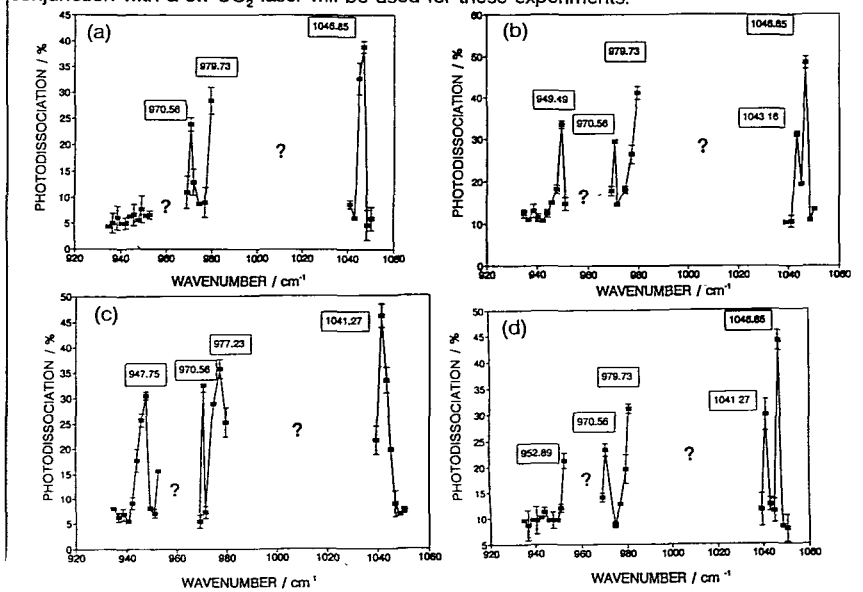

Figure 1. IRMPD spectra of (a) CH_3OHF^-, (b) CH_3ODF^-, (c) CH_3OHCl^-, and (d) CH_3ODCl^-

(1) Isolani, P. C. and Riveros, J. M. *Chem. Phys. Lett.* **1975**, *33*, 362.
(2) Peiris, D. M ; Cheeseman, M A., Ramanathan, R. and Eyler, J. R. *J. Phys. Chem.* in press.
(3) Rosenfeld R. N.; Jasinski, J. M.; and Brauman, J. *J.Am Chem.Soc.* **1982**, *104*, 658.

Obtaining Structural Information on the Aglycones of Macrolide and Azalide Antibiotics by ESI-Tandem Mass Spectrometry of Lithium-Attachment Ions

Mark J. Cole

Drug Metabolism Department, Central Research Division, Pfizer Inc, Groton, CT 06340.

Macrolides are a class of antibiotics containing an amino sugar, a nitrogen-free sugar, and a 14- or 16-membered lactone. Azalides are similarly glycosylated and contain a 15-membered azalide ring. The tandem mass spectra of protonated macrolide and azalide antibiotics provides almost no information on the structures of the aglycone moiety (Figure 1). Only the localization of a substituent to the aglycone can be inferred from a CAD spectrum. This is true for both high and low-energy CAD conditions (1). Intense $[M+Li]^+$ ions of the macrolides and azalides are produced by adding lithium to the samples and increasing the sampling orifice voltage. The $[M+Li]^+$ ions dissociate during low-energy (≈ 50 eV) CAD to produce a wealth of structural information about their aglycones. An example of macrolide dissociation is shown in Figure 2. Most of the dissociation occurs through two major pathways, which are distinct for the azalide and macrolide classes. Product ion structural assignments for the azalides were facilitated by comparison of CAD spectra from analogs containing aglycone substitutions. Collisionally-activated dissociation can be induced in the skimmer region by increasing the voltage applied to the skimmer cone. The spectra obtained are composed of CAD product ions from both protonated molecules and lithium-adduct ions, as well as some ions from the chemical background. Skimmer-induced CAD provides much of the same information as CAD in the second quadrupole region, but the process is not as efficient. A comparison of azithromycin $[M+Li]^+$ CAD spectra obtained from both CAD regions is shown in Figure 3.

1. Y. Shida, *et al.*, 40th ASMS Conference on Mass Spectrometry and Allied Topics, pp. 1351-1352.

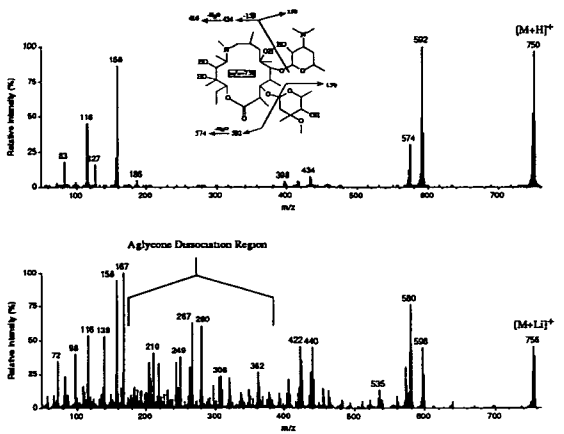

Figure 1. Comparison of CAD spectra from the $[M+H]^+$ and $[M+Li]^+$ ions of azithromycin.

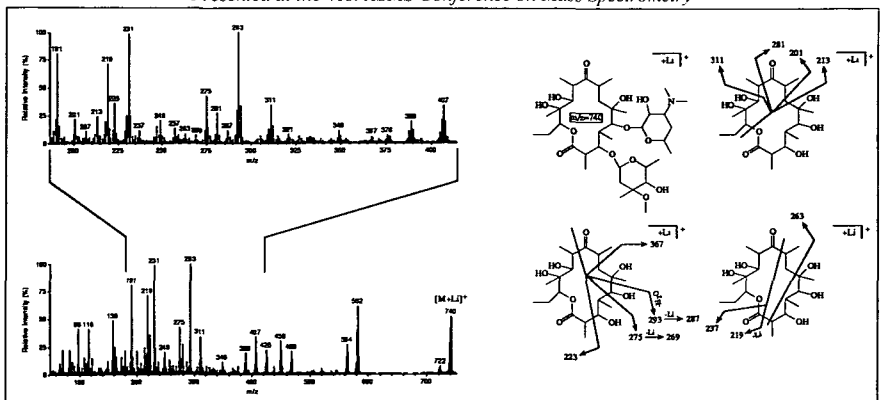

Figure 2. CAD spectrum of erythromycin and proposed dissociation.

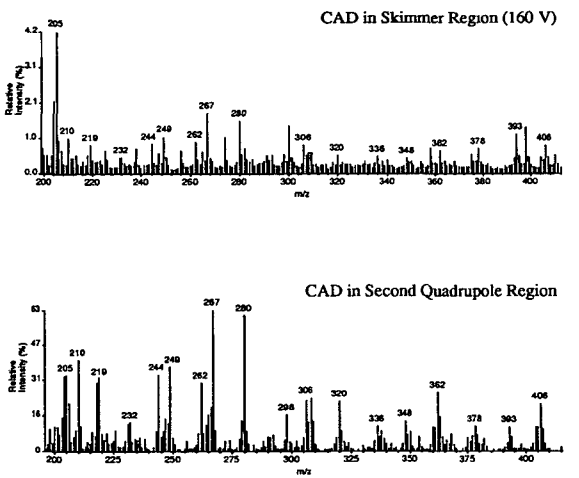

Figure 3. Comparison of the aglycone dissociation region form CAD spectra of azithromycin obtained from the skimmer region (top) and the second quadrupole region (bottom).

A Study of Air Sensitive Compounds Containing Low Coordinate Cationic Phosphenium and Arsenium Centres by Electrospray Mass Spectrometry.

*Jonathan M.Curtis[1], Pearl Blay[1], Neil Burford[2], Trenton M. Parks[2] and Simon Mason[2].
[1]*Institute for Marine Biosciences, National Research Council, Halifax, Canada B3H 3Z1.*
[2]*Department of Chemistry, Dalhousie University, Halifax, Canada. B3H 4J3*

Several salts of the arsolidinium cation (**1**) have recently been isolated. These are novel examples of arsenium centers, a Group 15 analogue of a carbene [1]. The X-ray crystal structures of these compounds have revealed that they exist as the weakly bound dimers $(\mathbf{1})_{2a}$ and $(\mathbf{1})_{2b}$ in the solid state. In solution, the conclusions drawn from NMR studies are that the dimeric species $(\mathbf{1})_2$ either exist as monomers or that the dimer is fluxional. Since these compounds are ionic, analysis by electrospray mass spectrometry was attempted to shed some light on the nature of the species existing in solution. However, the compounds are also extremely sensitive towards moisture and oxygen, so there are a number of challenges involved in their handling and introduction into the mass spectrometer.

Electrospray mass spectrometry used a SCIEX API-III mass spectrometer in the ionspray mode of operation. The nebuliser gas used was ultra-pure nitrogen, and the exhaust gases from the sealed spray chamber were pumped away to ensure a dry atmosphere. Dry, distilled dichloromethane only was used both as the solvent to dissolve the samples and for electrospray. Sample concentrations were in the millimolar range. The API-III was operated with potentials which minimise source fragmentation. The sample solution in an evacuated flask was introduced into a nitrogen filled glove bag. A portion of the solution was tipped into a second flask via a bridge, and withdrawn through a septum into a syringe. Sample introduction into the API-III was by means of a syringe-driver housed within the glove bag. A background spectrum of the solvent could be obtained using the flow from the LC pump before starting the flow of sample solution.

The electrospray spectrum of $[(\mathbf{1})_{2b}(GaCl_4)_2]$ in 100% dichloromethane is given in the figure which illustrates the complexity of the situation. The dication $(\mathbf{1})_{2b}$ is not seen but in addition to the monocation **1b** (the base peak, *m/z* 167), a monocation at twice the molecular mass of **1b** is observed (*m/z* 334) which may be the dimer $(\mathbf{1})_{2b}^{+\cdot}$. Some of the other peaks can be interpreted as fragments of the solid-state structure (eg *m/z* 259 is loss of As), but many are not easily identified. The glove-bag atmosphere is seen to be sufficiently pure, since 90 minutes after first exposing the sample to it, both monomeric and dimeric forms were still observed, although some hydrolysis products became evident. The electrospray spectrum of the aza-dimer $(\mathbf{1})_{2a}$ gives a prominent ion at *m/z* 161, corresponding to the monomer (not shown). Again, no evidence for the dimeric dication was seen. Similar results have also been obtained for the phosphorus analogue of **1a** (a phospholidinium gallate salt) which does not have a dimeric structure in the solid state.

In the present experimental arrangement, poor reproducibility is the major obstacle despite the apparently adequate sample handling procedures. This is mainly due to erratic liquid flow through the capillary. Blockages may be a result of undissolved material in suspension, but filtering the solutions is not trivial given their reactivity. Also, the use of dichloromethane creates additional problems since, for example, it is reactive towards a number of polymeric components used in coupling tubing etc. Nonetheless, it has been demonstrated that the dimeric arsolidinium cations $(\mathbf{1})_2$ are dissociated in solution.

[1] N.Burford et al., J. Am. Chem. Soc. **114**, 8147-8153 (1992)

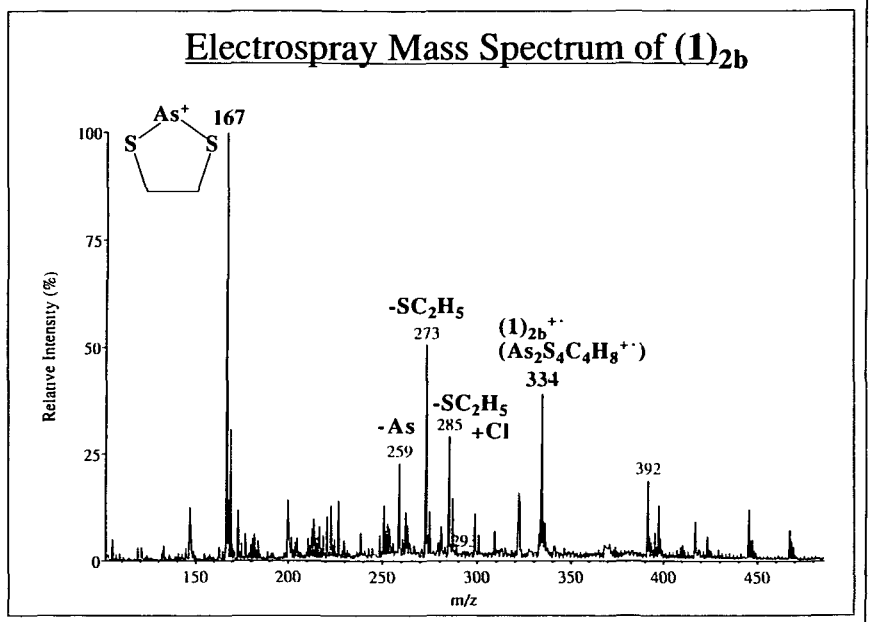

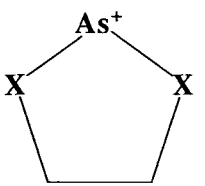

1
a: X = NMe
b: X = S

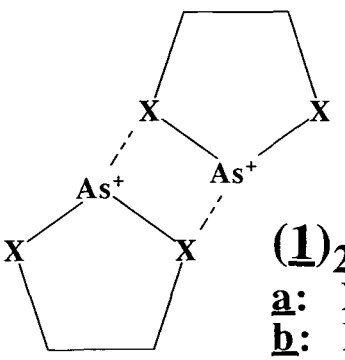

$(\mathbf{1})_2$
a: X = NMe
b: X = S

SELECTIVE MULTIPHOTON IONIZATION STUDIES OF DEUTERIUM-SUBSTITUTED β-FLUOROPHENETOLES

Timothy K. Shin, Thomas A. Shaler, Bryan E. Kohler & Thomas H. Morton
Department of Chemistry, University of California, Riverside, CA 92521

β–Fluorophenetole exists predominantly as a mixture of two conformational isomers, *anti* (which should have Cs symmetry) and *gauche* .[1]

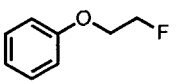

β-Fluorophenetole
MW = 140

Because it is crystalline, it can be prepared in high purity, and supersonic jet expansion followed by laser induced, resonance excitation multiphoton ionization (REMPI) allows selective ionization of individual conformers. From the S_1 vibrational progression as a function of laser wavelength in a one-color experiment, analysis of the excitation spectra of the unlabeled compound and its deuterated analogues $PhOCD_2CH_2F$, $PhOCH_2CH_2F$, $PhOCH_2CD_2F$ and $PhOCH_2CHDF$ allows the assignment of the longest wavelength band (which happens also to be the most intense absorption) at 274 nm to the *gauche* and a band 82 cm^{-1} to the blue to the *anti*.

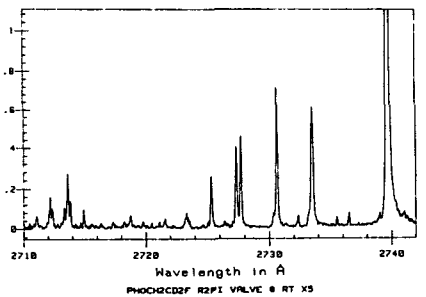

In part this assignment is based on two small peaks between these, 41 cm^{-1} and 56 cm^{-1} to the blue of the *gauche* (0,0) band in $PhOCD_2CH_2F$, which can be correlated with the calculated lowest-frequency torsions (3-21G) of the ground-state, unlabeled molecule (58 and 78 cm^{-1}), as contrasted to the calculated lowest torsional frequencies for the anti, 26 and 52 cm^{-1}. Other vibrational progressions can also be assigned on the basis of the *ab initio* calculation for the ground state.

Two-photon absorption in the 260-274 nm range leads only to formation of molecular ions, while three photon absorption leads to fragmentation (in addition to the molecular ions). The predominant fragmentation pathway in one color experiments is expulsion of vinyl fluoride to produce phenol$^{+\bullet}$ ions, and the ratios of $PhOD^{+\bullet}$ to $PhOH^{+\bullet}$ from the deuterated compounds are very nearly the same as those seen in the 70 eV source mass spectra. Measurements of the ratios of those two fragment ions as a function of laser wavelength permit assessment as to whether the mass spectrum is significantly affected by changes in photon energy or by the conformation of the neutral parent molecule. No significant effect is obserbed.

Mean $PhOH^{+\bullet}$ / $PhOD^{+\bullet}$ (94/95) RATIO

	MPI	70 eV EI
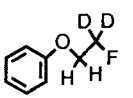	1.3	1.3
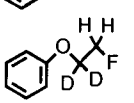	1.0	1.0

The total energy of two 274 nm photons is 9.06 eV which is 0.56 eV higher than the ionization potential of β–Fluorophenetole (8.5 eV). Any *anti-gauche* interconversion has to happen after the molecule has absorbed a second photon. In order to confirm this process two color experiments are in progress.

References

1. Nguyen, V.; Cheng, X; Morton, H.M. *J. Am. Chem. Soc.* **1992**, 114, 7127

Excited State Dynamics of 2,2'-Bithienyl Studied by Resonance-Enhanced 2-Photon Ionization

Wybren Jan Buma, Bryan E. Kohler, and Thomas A. Shaler
Department of Chemiistry, University of California, Riverside California, 92521

Conjugated organic polymers like the polyacetylenes and polythiophenes are currently the subject of intensive investigation as a result of their ability to conduct electricity under certain conditions as well as for their nonlinear optical properties.[1] In the course of our continuing spectroscopic investigations of the electronic states in simple polyenes, the molecule 2,2'-bithienyl (bithiophene) has been studied. Previous high resolution spectroscopic studies of bithiophene in our laboratory have shown that in hydrocarbon matrices at liquid helium temperatures the lowest excited singlet state of bithiophene is the 1B state[2]. Here we report a study of the excited states of bithiophene under isolated conditions in a supersonic expansion by the technique of resonance-enhanced multiphoton ionization.

Our apparatus and techniques for obtaining one- and two-color high resolution electronic excitation spectra of jet-cooled molecules have been described in detail previously.[3] The bithiophene used in these experiments was commercially available material that was purchased from Aldrich and used without further purification. In one-color experiments, the frequency-doubled output of DCM dye provided frequencies appropriate for excitation of bithiophene to S_1 with subsequent ionization by a second photon of the same color. Two-color experiments used in addition, 193 nm pulses of light from an ArF excimer laser.

The origin of the electronic transition from the ground state to S_1 in jet-cooled, isolated bithiophene was found to be at 321.42 nm (31,112 cm^{-1}). The excitation spectrum has been measured up to 1700 cm^{-1} above the S_1 origin. An almost identical spectrum has also been obtained in our laboratory by fluorescence excitation in a free jet. During the early part of these studies it was noticed that the relative intensities of certain peaks in the spectrum were sensitive to the expansion conditions that were used. A thorough study by fluorescence techniques subsequently confirmed that two conformers of bithiophene, s-cis and s-trans were frozen out in the expansion, and careful temperature dependence studies allowed the relative excited state stabilities and interconversion barrier to be estimated.[4] An expanded view of the one color [1+1] MPI spectrum is presented in Figure 1, showing the relative locations of the origins of the s-trans and s-cis spectra.

Another interesting observation made in one color [1+1] MPI scans was a laser intensity-induced splitting of the more intense lines in the spectrum as shown in Figures 2a and 2b. Similar intensity-induced line splittings in MPI spectroscopy have been reported by Syage and co-workers for methyl iodide.[5] Those results were explained as being due to excited methyl iodide's undergoing predissociation. Although the same process is unlikely in bithiophene, the key to observing the splitting is a transformation of the initially formed excited state to a non-ionizable species. This is possible in bithiophene by either internal conversion back to S_0, or by intersystem crossing into the triplet manifold. It was found that the dip in the line was absent when using 193 nm light to perform the ionization, as shown in Figure 2c.

The lifetime of the S_1 state in bithiophene is much shorter than the 10 nsec pulses that were used in attempting to measure it by fluorescence, as expected for such a strongly allowed transition. When the decay of the excitation was measured by 2-color MPI at the s-trans origin, the profile shown in Figure 3 was obtained. From simply considering the shape of the the decay, qualitative conclusions about the excited state dynamics of bithiophene can be deduced. The early part of the decay curve is characterized by an unexpectedly slow rise time. The maximum ion intensity is not reached until about 200 nsec after the signal begins to increase. Since the S_1 state had decayed away by very early time delays, this slow rise time must be coming from some state other than S_1. Additionally, since the intensity continues to increase for delay times up to 200 nsec, yet a third state must be giving rise to the ion signal, and it must further be the case that this third state has a much larger ionization cross section than either of the other states. Further work is underway to attempt to identify the species involved and to determine the rates and cross sections of the various proceesses in the excited state dynamics of bithiophene.

These results therefore support the conclusion that bithiophene excited to the zero point vibrational level of its first excited singlet state undergoes intersystem crossing or internal conversion rapidly to form an intermediate excited state. The intermediate state undergoes a slower conversion or crossing to form a state that has an ionization cross section much larger than the other states involved, and which has a relatively long lifetime.

1 Kohler, B.E. in "Conjugated Polymers", Bredas, J.L. and Silbey, R. (eds.), Kluwer, 1991, pp 405-434..."
2 Birnbaum,D. and Kohler, B.E. *J. Chem Phys.* 1989, *90*, 3506.....
3 Buma, W.J.; Kohler, B.E.; Shaler, T.A. *J. Chem Phys.* 1992, *96*,301 and references contained therein.
4 Chadwick, J.E., Ph.D. Thesis, University of California, Riverside, 1992.
5 Syage, J. and Steadman, J.; *J. Phys. Chem.*, 1990, *94*, 7343.

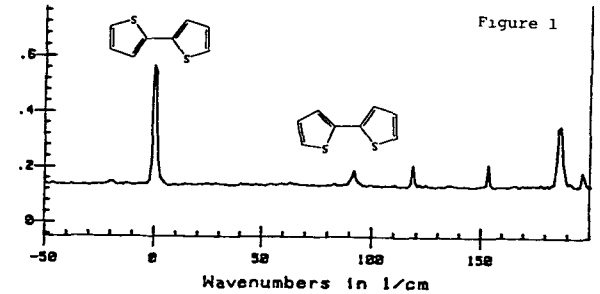

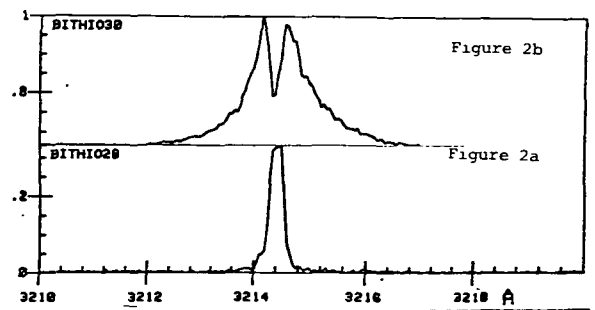

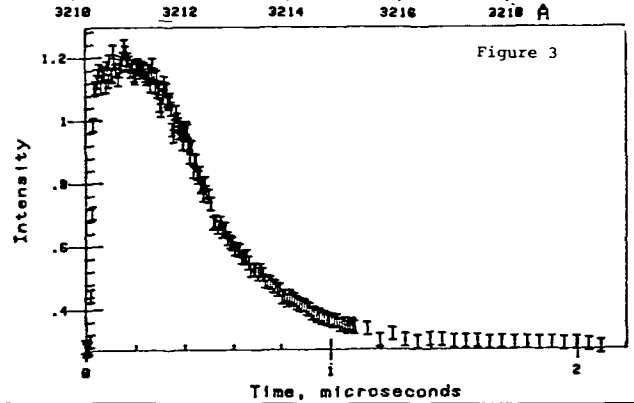

Base Pair Formation of Free Nucleobases and Mononucleosides in the Gas Phase

M. Dey, J. Grotemeyer*, E.W. Schlag**

* Institut für Physikalische Chemie, Universität Würzburg, Marcusstr. 9/11, 8700 Würzburg, Germany
** Institut für Physikalische Chemie, TU München, Lichtenbergstr. 4, 8046 Garching, Germany

The famous Watson-Crick structure of the double-stranded helix of nucleic acids now celebrates its 40th annivesary. The forces causing the double-stranded structure of the DNA are hydrogen bonds between bases of the strand, hydrophobic forces between each strand and interactions between the phosphate ions and solvent molecules. The famous specific interactions A-T and C-G may be a result of of these forces or of specific affinities of the nucleic acid bases.
To examine the partial contribution of the nature bases to form definite base pairs we investigated the pure base interactions in the gas phase. We used the pure bases without derivatization or solvation in order to exclude solvent and side group interactions.

In order to examine the dimer formation behaviour we desorbed mixtures of two bases at the same time. The mass spectra of all 10 possible base combinations have been observed.The base pairs are formed during the desorption of the nucleobases into the jet. In the jet the translational velocities of all molecules are very similar due to the multiple collisions between jet gas atoms and sample molecules. Therefore also weak bonded dimers can be formed by collision of two base molecules. Due to the multiple collisions the equilibrium of the dimer formation is reached faster than the desorption time of about 100 µs As the excess energy deposited in the molecular ion is rather small for MUPI (less than 1.7 eV), these dimers can be observed in the RETOF mass spectrometer.
As seen from the mass spectra below, specific clusters of adenine and thymine as well as cytosine and guanine are formed in the supersonic jet prior ionization.
Association constants are calculated with the assumption that we have the following equilibrium

$$B_1 + B_2 \rightleftharpoons (B_1\text{-}B_2)$$

$$K = [B_1\text{-}B_2]/([B_1]x[B_2])$$

with $[B_1]$, $[B_2]$ and $[B_1\text{-}B_2]$ being the corresponding peak intensities (see table 1).
As can be seen clearly from these results, the base pairing in the gas phase is base specific. A-C, C-T and G-T hetero dimers are not formed . Thus stacking or π-complexes of the bases has little contribution in stabilizing the dimers in the gas phase.

The double hydrogen bonded A-T as well as the triple bonded G-C base pair in the DNA are not only formed because of sterical reasons due to the phophate-sugar chain but show themselves a natural affinity already in the gas phase. Similar results have been obtained for the nucleosides.

References: M. Dey, J. Grotemeyer, E.W. Schlag, J. Am. Chem. Soc. in press

Acknowledgement
This work has been supported by a grant from the Deutsche Forschungsgemeinschaft (GR 917/6-2).

	free bases in the gas phase	hydrogen attached bases in the gas phase
A-A	0.6	0.5
T-T	0.6	0.5
A-T	1.1	19
C-C	1.9	18
G-G	8.1	5
C-G	17	20
A-G	0.6	0.5
A-C	not observed	not observed
C-T	not observed	not observed
G-T	not observed	not observed

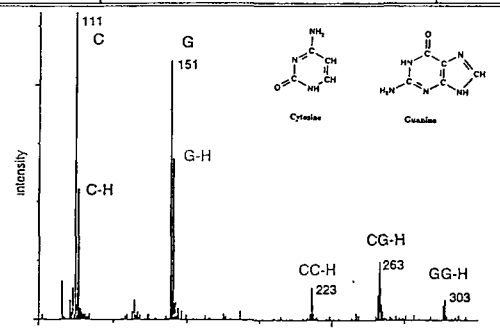

Cytosine, Guanine

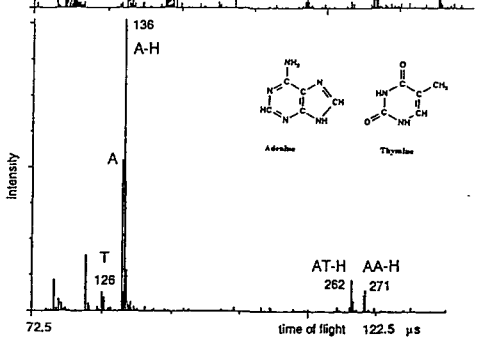

Adenine, Thymine

Nanosecond and Femtosecond Multiphoton Ionisation - Comparison of Fragmentation Behaviour

K.P. Aicher, R. Weinkauf, E.W. Schlag*, J. Grotemeyer**
* Institut für Physikalische Chemie, TU München, Lichtenbergstr. 4, 8046 Garching, Germany
** Institut für Physikalische Chemie, Universität Würzburg, Marcusstr. 9/11, 8700 Würzburg, Germany

Using commercially available ns-laser systems MUPI has become a very useful and generally accepted ionisation technique in mass spectrometry in the last few years. However, recent experiments have shown that the ionisation efficiency of MUPI and other techniques decresases rapidly with the mass of the investegated samples [1]. Therefore this ionisation techniques are rather unsatisfactory for high masses like large proteins or enzymes. A recent theory [1] proposes an increase in the mass range accesible to cation radical formation by using fs- instead of ns-laser pulses.

Femtosecond laser systems provide a convenient way of increasing the laser intensity by at least three orders of magnitude. Conventional ns-Laser systems like excimer or YAG pumped dye lasers have intensities of about 10^4-10^5 W/cm^2, whereas our fs-dye laser provides intensities of about 10^8 W/cm^2.

In order to investigate the effects of laser intensity on the ionisation process as well as on the fragmentation behaviour we compared the results of nanosecond (YAG pumped dye laser with a pulsewidth of 6-7 ns; output energy about 40 µJ) and femtosecond (tuneable fs-laser with a pulsewidth of 500 fs; output energy 8 µJ) laser pulse ionisation for samples up to 1900 Dalton. The experimental setup has been described in detail elsewhere [3]. The samples are desorbed by a CO_2-laser and transfered into the ionisation chamber by a pulsed argon jet. Liquid samples are mixed with the argon and the mixture is expanded through the jet valve into the desorption chamber. A Reflectron-Time-of-Flight mass spectrometer (Bruker TOF-1) is used for recording the mass spectra.

In order to compare ns- and fs-laser ionisation it is essential to produce the ions under similar conditions. Thus the ns- and the fs-pulses are adjusted such a way that both pulses hit the stream of neutrals nearly at the same point in the ionisation chamber.

First we investigated the resonant (λ=259 nm) and non resonant (λ=260.5 nm) ionisation of "cold" (jet-cooled) and "hot" (effusive inlet) benzene.

In the resonant case no difference is observed between ns- and fs-laser pulse ionisation for "cold" benzene. Applying a non resonant wavelength the same result is observed for "hot" benzene. Using a non resonant wavelength and "cold" benzene, however, ionisation is only observed for the fs laser pulse.

These results can be explained as follows. Using a resonant wavelength the same long-lived intermediate state is populated both for "hot" and "cold" benzene. Thus the time between absorption of the first (population of the excited state) and the second photon (ionisation) is not critical. In the non resonant case for "cold" benzene ionisation takes place through a virtual state. Thus the ionisation efficiency depends strongly on the laser intensity, and ions are observed only for fs-pulses delivering much higher intensities. In "hot" benzene due to the higher temperature higher rovibrational states of the electronic ground state are populated allowing for ionisation through hot bands. Therefore, a long-lived intermediate state is reachable and ionisation is again possible by both ns- and fs-pulses.

Comparing ns- and fs-ionisation for tryptophan one can see that due to the other ionisation mechanism (autoionisation ladder instead of ladder switching) fragmentation is more intense for fs-pulses.

Furthermore the determination of the threshold energies for ns- and fs-ionisation (λ=260.5 nm) of β-carotene, gramicidin s and gramicidin d shows that fs-pulses are about 40 times more "efficient" in ionisation than ns-pulses.

Eventually it is shown that the unique features of MUPI (easy change between "hard" and "soft" ionisation; molecular ion being the base peak in the mass spectrum) are also valid for femtosecond pulse ionisation. Figure 1 shows the "hard" and "soft" mass spectra of gramicidine d.

[1] E.W. Schlag, J. Grotemeyer, R.D. Levine, Chem. Phys. Letters 190 (1992) 521.
[2] J. Lindner, J. Grotemeyer, E.W. Schlag, Int. J. Mass Spectrom. Ion Proc. 100 (1990) 267.

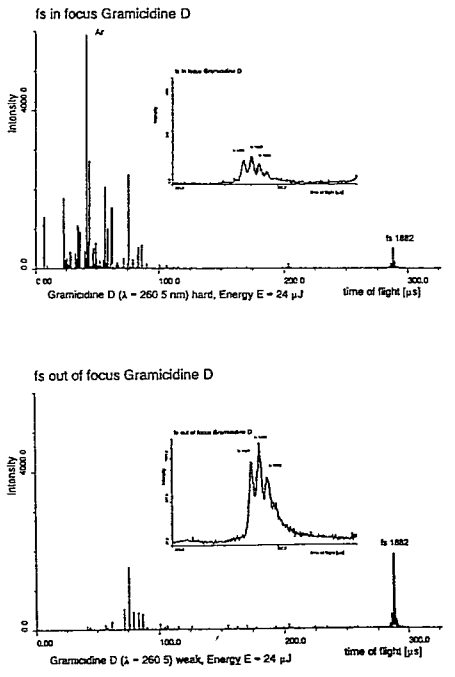

figure 1: fs-ionisation hard and soft mass spectra of gramicidine d

$[M-2H]^{+\cdot}$ Formation in the FD-MS Analysis of Hydrocarbons

C. E. Heine and M. M. Geddes
Exxon Research and Development Laboratories
P.O. Box 2226, Baton Rouge, LA 70821

Intense $[M-2H]^{+\cdot}$ signals have been noted in FD-MS analyses of various compounds. High-boiling hydrocarbon molecules, such as long-chain n-alkanes and squalane, may give rise to particularly abundant $[M-2H]^{+\cdot}$ ions (1). This phenomenon complicates the interpretation of FD-MS data obtained from waxes (2) and other hydrocarbon mixtures, especially when the exclusive formation of molecular ions (M^+) is assumed. The present study compares the magnitude of $[M-2H]^+$ formation in the FD-MS analysis of several pure hydrocarbon standards, including saturated and aromatic compounds. Key experimental parameters are then investigated with respect to their influence on this phenomenon. These parameters include the emitter current program, electric field strength, and quantity of sample loaded onto the emitter.

All experiments were performed on a Kratos MS50 (EB) mass spectrometer equipped with a DS55 data system. Data comparison took place after the individual mass spectra obtained in each FD-MS analysis were summed. The 10 micron tungsten emitters used were activated in our laboratory The activation procedure (using indene) was controlled by a Linden Emitter Activator Samples were applied to the emitter from hexane or methylene chloride solutions by the "syringe technique". The FD anode voltage (+8 kV) also served as the ion acceleration voltage. The cathode voltage (applied to the source block) was -2 kV in normal operation, but varied between -2 and +4 kV for experiments involving alteration of the electric field strength. The standard emitter current program incorporated a current ramp of 1 2 mA/min

The compounds analyzed in this study are shown in Table 1 The intensity of the $[M-2H]^+$ signal relative to the M^+ signal (from the summed mass spectrum) is listed next to each structure, along with the sample quantity loaded onto the emitter. Table 1 shows that equal quantities of C30, C33, and C36 n-alkanes (analyzed separately) gave rise to $[M-2H]^+$ formation which increased with the length of the alkyl chain. Comparison of results obtained from a branched C30 alkane (squalane) and a linear C30 alkane reveal increased $[M-2H]^+$ formation for the branched compound An aromatic ring, however, strongly suppressed $[M-2H]^+$ formation in n-heptadecylbenzene relative to that observed from its saturated analogue (n-heptadecylcyclohexane) in another interesting comparison None of the aromatic compounds tested in this study provided evidence of significant $[M-2H]^+$ formation. Analyses of compounds which did give rise to abundant $[M-2H]^+$ ions indicate that the $[M-2H]^+$ desorption profiles track those of the M^+ ions as a function of emitter heating current

Figure 1 displays the dependence of $[M-2H]^+$ formation for squalane on the potential difference between the FD anode and cathode. 20 nmols of squalane were used in each analysis represented in Figure 1. The data reveal a pronounced diminution in $[M-2H]^+$ signal intensity (relative to the M^+ signal) as the applied potential difference is reduced. Since the electric field strength is linearly related to the applied potential difference (3), $[M-2H]^+$ formation exhibits a strong field dependence. In contrast, no thermal dependence (investigated by widely varying the emitter current program) was documented for this phenomenon

Another experimental parameter shown to influence the magnitude of $[M-2H]^+$ formation is the amount of sample initially loaded onto the FD emitter. Figure 2 shows that $[M-2H]^{+\cdot}$ formation (relative to M^+ formation) decreases as the sample quantity of squalane decreases. Both the field dependence (illustrated in Figure 1) and the sample quantity dependence (illustrated in Figure 2) were confirmed by

similar experiments conducted with the C36 n-alkane.

In summary, this study suggests that $[M-2H]^+$ formation in hydrocarbon molecules may be minimized by appropriate choice of the applied potential difference (hence, field strength) and the amount of sample loaded onto the emitter in the FD-MS analysis Of course, practical limits exist for each of these approaches. In our experiments, when the potential difference between anode and cathode was reduced to 4-5 kV, a significant decrease in ionization efficiency resulted in a serious loss in sensitivity. Likewise, a loss in signal accompanies the practice of loading less sample onto the emitter Yet, FD-MS results of high quality (with misleading $[M-2H]^+$ signals essentially eliminated) were obtained for all compounds analyzed in this work by manipulating these two experimental parameters. The nature of the $[M-2H]^+$ ions is unclear at the present time. They may be formed by converting the alkyl chain into a cyclic or olefinic structure in a field-dependent process. The trends of increased $[M-2H]^+$ formation documented for saturated molecules of increasing chain length and branchiness may implicate a cyclic structure. This issue may be clarified by MS/MS experiments conducted with suitable standard compounds

(1) Schulten, H.-R., Murray, K. E.; Simmleit, N. *Z. Naturforsch, C: Biosci.*, 1987, *42* (3), 178-90.
(2) Thomson, J S.; Grigsby, R. D.; Doughty, D A ; Woodward, P. W.; Giles, H. N. Presented at American Chemical Society Meeting, Dallas, Texas, April 9-14, 1989
(3) Prokai, L *Field Desorption Mass Spectrometry*, Marcel Dekker, Inc., New York, New York, 1990

Table 1

Compound	$I[M-2H]^{+\cdot}/I[M^+]$ (%)	nmols
C 30 n-Alkane	12	2
C 33 n-Alkane	16	2
C 36 n-Alkane	24	2
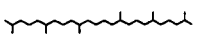	19	2
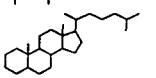	3	4
	5	15
	1	15
	-	24
	1	220
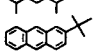	-	75
	-	5
	-	44

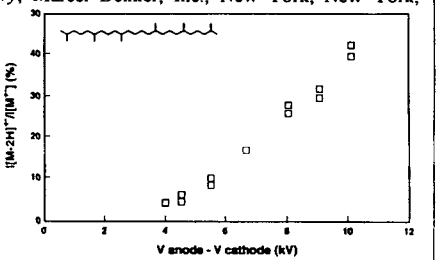

Figure 1. Relative intensity of the $[M-2H]^+$ signal for squalane as a function of applied potential. 20 nmols of squalane were used in each analysis

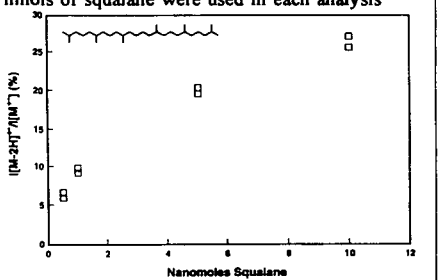

Figure 2. Relative intensity of the $[M-2H]^+$ signal for squalane as a function of sample quantity.

Infrared Spectroscopy of Matrix-isolated Products Following Charge Exchange Ionization of Dihalomethanes with Ar

X.K.Zhang* J.M.Parnis and R.E.March
Chemistry Department Trent University Peterborough ON Canada K9J 7B8
* *Registered at Queen's University Kingston ON Canada K7L 3N6*

INTRODUCTION The ionization, fragmentation and isomerization processes of dihalomethanes CH_2X_2 (X=Cl,Br) following charge-exchange (CE) ionization with Ar has been investigated. The various ionic and neutral products of CH_2X_2 generated were characterized through a combination of matrix-isolation infrared spectroscopy and mass spectrometry.

EXPERIMENT The experimental arrangement consists of a modified EI ionization device inside a vacuum chamber containing a closed-cycle helium cryostat system (Fig.1). A stream of CH_2X_2 and Ar was subjected to ionization directly above the surface of a cold CsI matrix window, where the product species condensed subsequently with the excess neutral precursors at 12 K. Vibrational spectra of matrix-isolated species were obtained with a FTIR Spectrometer.

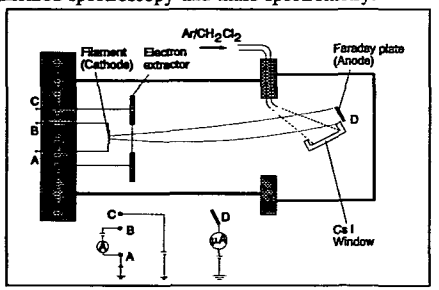

Figure 1 Diagram of EI device and cryostat assembly

RESULTS Various products, such as $HCCl_2^+$, $HCCl_2$, CCl_2^+, and Ar_nH^+, were identified in the spectrum of Matrix-isolated species following CE ionization of CH_2Cl_2 with Ar. Of most interest, a group of strong absorption features was observed, which corresponded to the fundamental absorptions of isodichloromethane H_2CCl-Cl,[1] and showed great photosensitivity to irradiation in the 590-1000 nm range (Fig.2); The ionization of an equimolar mixture of CH_2Cl_2/CH_2Br_2 revealed no scrambled product, *i.e.* H_2CCl-Br, was observed, though the isomers of each were clearly identified (Fig.3).

The MIKE and CID experiments of $CH_2X_2^{+\cdot}$ showed that the expulsion of CH_2 to form X_2^+ is mainly, though not exclusively, a collision-activated decomposition process since the intensity is proportional to the pressure of collision gas in the cell. NRMS experiments showed that no significant amounts of neutral or ionic species having structures other than tetrahedral existed in the gas phase.

Three experiments were carried out by exposing the neutral Ar/CH_2Cl_2 matrix to resonant emissions of excited Ar, Kr and Xe formed by EI. The contribution to isomerization from the resonant emission of excited Ar atoms was found to be less than ca. 10% of that contributed by CE ionization.

DISCUSSION The generation of isodihalomethanes through CE ionization with Ar could be explained by three mechanisms:

1) Molecular ions having structures other than tetrahedral and of diminished stability are created during the ionization process in the gas phase, and are neutralized during the condensation process.

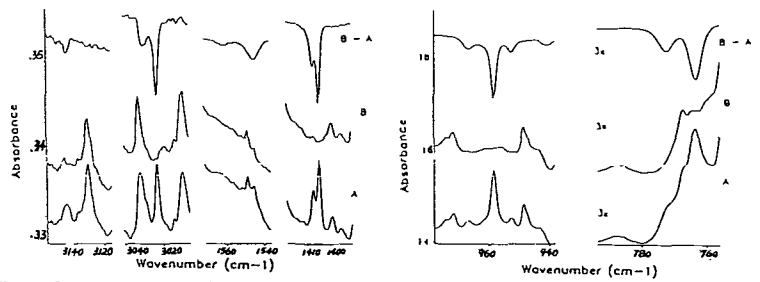

Figure 2. A: spectrum after deposition; B: spectrum after exposing the matrix to irradiation of red light; B-A: difference spectrum of B and A.

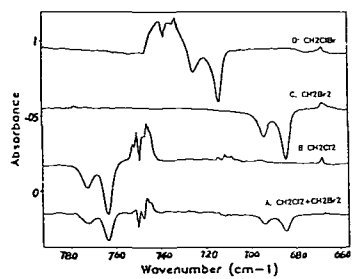

Figure 3. Comparison of CH_2 wagging mode of isodihalomethanes. Spectra shown are the net difference spectra after irradiation with red light.

2) Molecular ions having a tetrahedral structure are neutralized, and these energetic neutral species undergo isomerization during the matrix trapping process. The mass spectrum obtained by reionization of neutralized molecular ions showed a slight increase in intensity of Cl_2^+, which may indicate that some of the isomer are generated in the neutralization process.

3) The isomers are products of fragment recombination. This mechanism is not plausible due to lack of the observation of scrambled H_2CCl-Br product when a mixture of CH_2Cl_2 and CH_2Br_2 was subjected to CE ionization.

CONCLUSION The isodihalomethanes H_2CX-Y (X,Y=Cl, Br) have been generated through CE reaction of CH_2X_2 with Ar, and their back-isomerization upon irradiation with red light has been observed also. The formation of the isomers may be evidence for the existence of molecular ions which have structures other than tetrahedral, and have a diminished stability.

REFERENCE 1. Maier,G., Reisenauer,H.P., Hu,J., Schaad,L.J. and Hess,B.A.Jr., *J. Am. Chem. Soc.*, 1990, *112*, 5117.

Ultra Small Volume and Flow Rate Electrospray Ionization / Mass Spectrometry with a Sheathless Source

David C. Gale, Charles G. Edmonds, and Richard D. Smith
Chemical Sciences Department
Pacific Northwest Laboratory
Richland, WA 99352

The co-axial liquid sheath electrospray ionization (ESI) source is widely used and has advantages for CE and LC interfacing. However, the use of a co-axial sheath liquid has several disadvantages. The sheath liquid contributes additional ionic and neutral species that compete in the ESI process for available charge, and depending on the mixing of the analyte and sheath streams, lowers the maximum sensitivity obtainable. Past experience from our laboratory has also shown that stable signals from sheath type sources can in certain applications be difficult to obtain for extended periods of time.

A new low volume sheathless ESI source (Figure 1), utilizing an etched tip small diameter fused silica capillary (5 to 20 μm), has been developed. This sheathless source for pressure infusion applications is constructed from a 25 μL gas-tight syringe and a modified 1/16 in. bored-through stainless steel reducer. ESI-MS data from both sheathless and sheath sources were acquired on a modified triple-quadrupole mass spectrometer (Sciex TAGA 6000E). Samples were pressure infused at set flow rates with a Harvard Syringe pump. For the sheath source, methanol, at a flow rate of 2.5 μL/min, was used as the sheath liquid. Horse heart myoglobin (M_r = 16951) in 5% acetic acid, 5'-dCCTCTCCTCCCT-3' oligonucleotide (M_r = 3470) in distilled H_2O and oxidized bovine A-chain insulin (M_r = 2532) in 10 mM ammonium acetate were used in this study.

Shown in Table 1 are data acquired with the methanol sheath and sheathless sources respectively. *Identical samples were used to compare the sheathless and sheath* source designs. In obtaining the data shown in Table 1, a 50 μm capillary was used in the sheath source. An HF etched 20 μm capillary was used in the sheathless source. Sample flow rates of 0.50 μL/min and 0.20 μL/min were used for the sheath and sheathless sources respectively. A total of 500 scans (time = 17.2 minutes, scan range = 10 *m/z*) were acquired over the most intense peak in the electrospray mass spectra to obtain the average intensity and % RSD.

Several tentative conclusions can be drawn from the data given in Table 1. First, the sheathless source requires a significantly lower potential to generate a stable electrospray. Second, the signal intensity for the sheathless source ranges from 3.0 to 7.4 times greater than that observed for the methanol sheath source from a flow rate 2.5 times smaller. Third, the percent relative standard deviation of the measured ion currents is substantially lower for the sheathless source, indicating that it is more stable.

The total amount of sample consumed during the mass spectrometric analysis with the sheathless source can be quite low. Shown in Figure 2 is an electrospray mass spectrum of 5'-dCCTCTCCTCCCT-3' acquired with a 5 μm etched tip capillary. The flow rate used for this analysis was 50 nL/min. The mass spectrum represents the consumption of 20 nL of sample, corresponding to 50 femtomoles of the oligonucleotide. Thus, the new

sheathless ESI source is more sensitive and stable compared to the sheath source design and has the ability to operate at lower flow rates and with lower overall sample consumption.

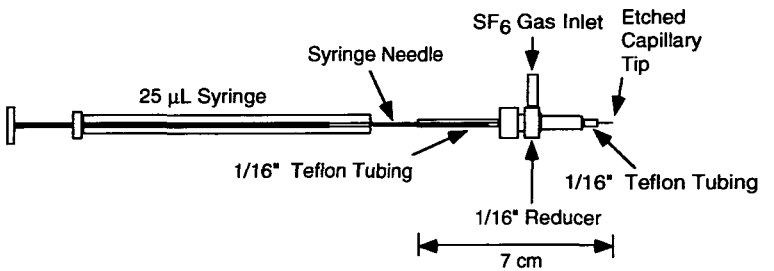

Figure 1

TABLE 1	ESI Potential	Relative Intensity	% RSD
POSITIVE ESI - horse heart myoglobin (0.5 mg/mL)			
Myoglobin - Sheath Source	+ 4.0 kV	1.167×10^6	9.5%
Myoglobin - Sheathless Source	+ 2.15 kV	8.650×10^6	4.4%
NEGATIVE ESI - 5'-CCTCTCCTCCCT-3' (8.6 μg/mL)			
5'-CCTCTCCTCCCT-3' - Sheath Source	- 4.0 kV	75,814	33.1%
5'-CCTCTCCTCCCT-3' - Sheathless Source	- 3.0 kV	393,039	3.8%
NEGATIVE ESI - Oxidized A-Chain Insulin (0.5 mg/mL)			
Oxidized A-Chain Insulin - Sheath Source	- 3.5 kV	4.004×10^6	11.9%
Oxidized A-Chain Insulin - Sheathless Source	- 2.5 kV	1.299×10^7	2.0%

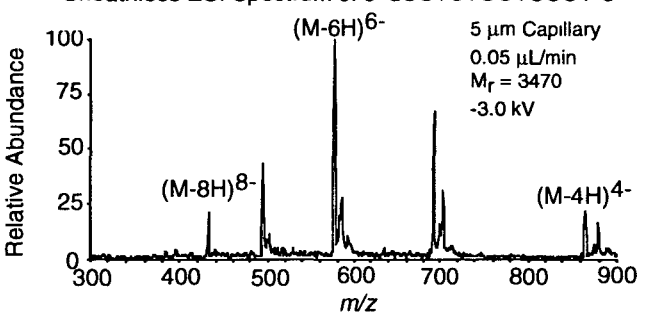

Figure 2

Pacific Northwest Laboratory is operated for the U.S. Department of Energy by Battelle Memorial Institute under Contract DE-AC06-76RLO 1830.

OPTIMIZATION AND EVALUATION OF A CAPILLARY ELECTROPHORESIS - ELECTROSPRAY MASS SPECTROMETRY INTERFACE EMPLOYING OPPOSITE POLARITIES AT THE INJECTOR AND ION SOURCE

Johnson Varghese and Richard B. Cole*

Department of Chemistry, University of New Orleans, Lakefront Campus, New Orleans, LA 70148

A capillary electrophoresis - electrospray mass spectrometry (CE-ESMS) interface coupling a Dionex CE System I unit to a Vestec 201 electrospray mass spectrometer has been constructed. The interface design utilizes the sheath liquid electrode approach [1]. Components of the constructed interface were taken through systematic optimization procedures defining the placement of the fused silica CE capillary exit relative to stainless steel electrospray needles. Maximum sensitivity conditions were found to be rather different from maximum stability conditions. Optimum sensitivities were obtained with the CE capillary tip protruding 0.1 to 0.2 mm outside the electrospray needle. Despite some loss in sensitivity, placement of the capillary tip about 1 mm inside the needle afforded increased ruggedness to the interface and stability to generated signals. Under these conditions, fluctuations in the applied voltages or variations in buffer properties did not degrade electrical contact at the interface.

The combined instrumentation has been used to evaluate the purity of cationic and anionic laser dyes. Solutions of organic dyes are used in laser sources to enable laser operation over a continuum of wavelengths (from the near-UV to the near-IR). The purity of the laser dye can profoundly affect the laser efficiency and the usable lifetime of the dye. Secondary products contained in laser dyes are quite likely to be of inferior efficiency. Impurities may quench laser activity at variable rates, leading to a deterioration of laser power. Assessment of laser dye purity can thus be of high importance to dye laser users.

For on-line analysis of anions, positive CE voltages were used in combination with negative ESMS potentials. On-line cation analysis was performed using a surfactant buffer additive, cetyltrimethylammonium chloride, and negative CE voltages in conjunction with positive ion ESMS Using opposite polarities at the CE source vial and the electrospray needle enabled electroosmotic flow towards the detector in each case. Successful separations of impurities contained in the cationic laser dye Rhodamine 6G were demonstrated. These included isomeric impurities as well as structural analogs which were deficient in an ethyl substituent. Negative ion ES in conjunction with normal polarity CE (positive potential at source vial) proved to be the most difficult due to intrinsic difficulties associated with negative ion ESMS. The anionic laser dye Eosin Y (containing four bromine atoms) was first analyzed by direct infusion (Fig. 1). A major impurity corresponding to a three bromine analog was detected in the sample. This impurity was separated from Eosin Y using positive voltage CE-selected negative ion monitoring ESMS (Fig. 2). Peptide mixtures were also successfully analyzed by negative voltage CE-positive ion ESMS.

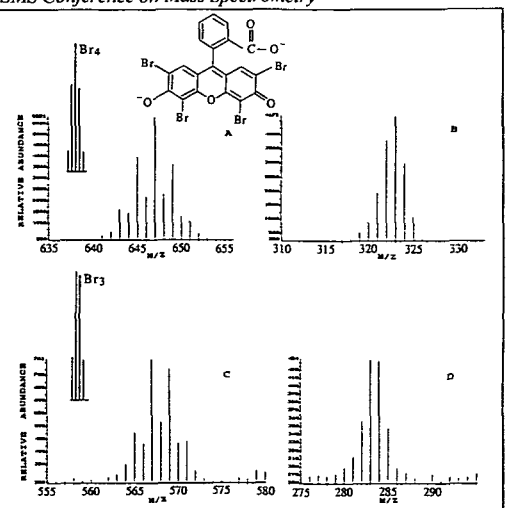

Figure 1. Negative-ion ES mass spectrum of 100 ng/µL Eosin Y (dianion mol wt. = 646 Da) sample generated by direct infusion. A) Singly charged Eosin Y wherein one anionic site has been protonated. B) Doubly charged Eosin Y. C) Singly charged impurity of Eosin Y. D) Doubly charged impurity of Eosin Y.

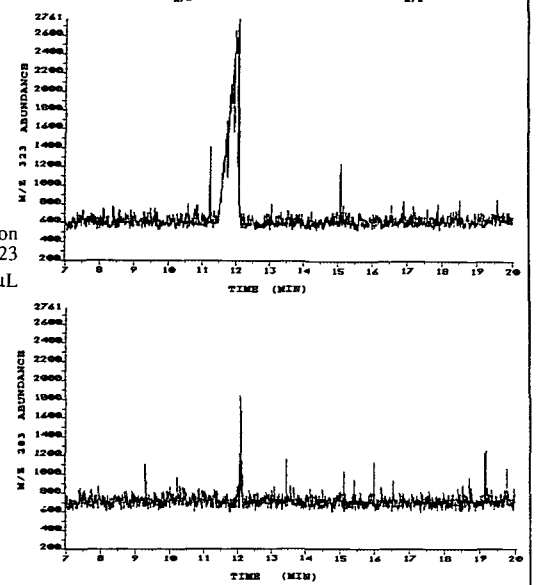

Figure 2. CE-ESMS single negative ion monitoring electropherograms of m/z 323 (top) and m/z 283 (bottom) from 600 ng/µL Eosin Y

Reference:

1. R. D. Smith, C J. Barinaga, H. R. Udseth, *Anal. Chem.* (1988) 60: 1948.

Improved Microbore HPLC Electrospray Mass Spectrometry Interface.

**Igor A. Kaltashov and Catherine Fenselau*
Department of Chemistry and Biochemistry,
University of Maryland Baltimore County, Baltimore, MD 21228.

On-line high performance liquid chromatography (HPLC)/electrospray ionization mass spectrometry (ESIMS) offers a great number of advantages. Since electrospray is a very "soft" ionization technique, it forms molecular ions predominantly, making the corresponding mass spectra easy to interpret. The combined technique also allows identification of analytes that are not completely separated by chromatography. Electrospray ionization permits analysis of heavy molecules by multiply charging them, in which case a deconvolution procedure can be used to calculate the molecular weight of the analyte.

Microbore reversed phase HPLC columns can be operated at very low flow rates (below 50 μL/min.), which are easily adopted by ESIMS without post-column splitting. This increases the overall sensitivity of the system as all injected material is directed to the ion source. In the present work, an on-line microbore reversed-phase HPLC/ESIMS system has been developed to interface a thermally assisted electrospray source and a quadrupole mass analyzer.

In our experiments an ISCO (Lincoln, NE) μLC-10 system equipped with two 100DM syringe pumps and a Synchrom (Lafayette, IN) C18 1.0x15.0 mm column was used. To achieve stable low flow rates through the column, both pumps were operated at relatively high flow rates and, after mixing, the flow of eluent was split (see Fig.1). Use of a second C18 column of larger diameter as a ballast column allowed a constant splitting ratio to be maintained across the gradient. The typical flow rate through the working column was 20 μL/min. The mobile phase consisted of (A) 0.25 % acetic acid in water and (B) 0.25 % acetic acid in acetonitrile. All eluent coming out of the UV flowcell was directed into the electrospray ion source through a piece of fused silica (0.1 mm ID). A Hewlett Packard (Palo Alto, CA) quadrupole 5988A mass spectrometer equipped with a Vestec (Houston, TX) electrospray ion source and a Phasor (Duarte,CA) ion multiplier was used. All mass spectral data was collected and processed by a Vector II data system from Technivent Corp. (Maryland Heights, MO).

To evaluate the performance of the system and to estimate its limit of detection, a mixture of synthetic peptides and proteins was used. The UV-chromatogram and the mass spectrum of positive ions in a 200-1400 amu mass range were recorded simultaneously. Comparison of a UV-chromatogram with total ion current (TIC) chromatogram and reconstructed ion chromatograms for particular ions shows that chromatographic fidelity was maintained when the eluent flow was directed to the ES ion source. We were able to detect all the compounds of the mixture by ESIMS (using reconstructed ion chromatograms) when the mixture was diluted so that only 10 pmol of each component was injected into the column. At that point only half of the mixture compounds had been seen by the UV detector at 215 nm.

The developed system was also employed for peptide mapping. A tryptic digest of melphalan-treated metallothionein (total concentration of material ca. 50 μM, injection volume 2μL) and *S. aureus V8* protease-digested microsomal glutathione S transferase were analyzed by the HPLC/ESIMS system. Mass spectrometry provided information on the molecular weights of digest fragments and allowed identification of species that were not clearly separated by chromatography.

The system has been also evaluated for on-line identification of drug-related components of a rat bile extract. Fig. 2 shows a UV-chromatogram and mass spectra of each UV-peak. The presence of fragment ions in each spectrum helps to identify the analytes. In addition to these two species detected by their absorption, mass spectrometry allowed us to detect 6 more compounds, which lack chromophores.

ACKNOWLEDGEMENTS. Samples were generously provided by Dr. Leonard J. Shore (Univ. of MD Baltimore County), Xiaolan Yu (Univ. of MD Baltimore County) and Dr. Ronald Dickinson (Univ. of Queensland, Brisbane, Australia). Special thanks to Dr. Martha Vestling for very helpful discussions. The work was supported in part by grants from National Science Foundation and National Institutes of Health.

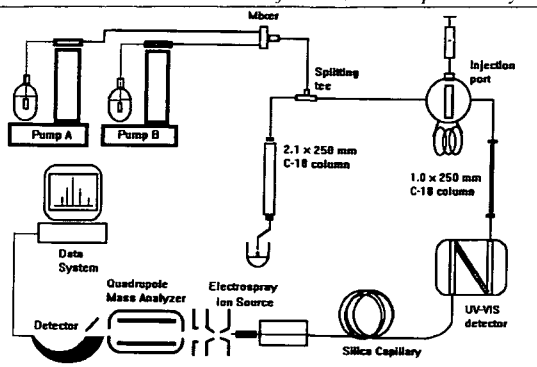

Fig. 1. Schematic diagram of the interface.

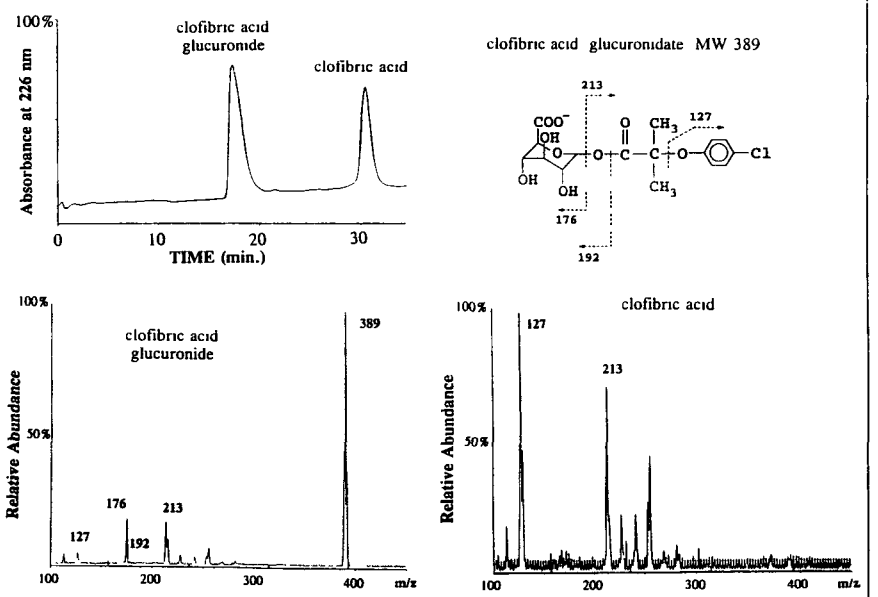

Fig. 2. HPLC/ESIMS identification of clofibric acid and clofibric acid glucuronide in a rat bile extract.

A Performance Evaluation of Several Ion Introduction Techniques Used For Electrospray Ionization.

*Steven M. Musser and James A. Sphon.

Division of General Scientific Support, CFSAN, U.S. Food and Drug Administration, Washington, DC 20204.

Electrospray is now used routinely in HPLC/MS analysis for ionization of a variety of compounds, primarily large biomolecules. Since the introduction of electrospray and its complementary process, ionspray, a variety of methods have been presented for desolvating and transporting ions from atmospheric pressure to high vacuum. The three most common methods are direct introduction of the electrosprayed droplets into the mass spectrometer via a small orifice ; desolvation at atmospheric pressure followed by transport into the analyzer via a quartz tube; and transport/desolvation of the ions through a stainless steel capillary. Although all three ion introduction techniques have been used successfully to obtain mass spectra of both high and low mass compounds, a direct comparison of the techniques has not been reported. Because of the variety of electrospray interfaces now available commercially, and the increasing importance of electrospray to the analytical laboratory, this investigation was undertaken to determine the effect of each ion introduction technique on the mass spectra obtained for both small and large molecules.

A Vestec Model 201A quadrupole mass spectrometer with a Teknivent Vector2 data system was used for all experiments. A standard Vestec electrospray ion source was modified for direct ion introduction (figure 1). Additional modifications of the inlet tube permitted various capillary tubes to be used for heated capillary ion introduction (figure 2). For all experiments the ion source was held at 125 °C and a 2.9 kV needle voltage used. Sample solutions were pumped to the needle tip at a rate of 5 µl/min using a Sage Instruments syringe pump. A 500 ml/min coaxial flow of air over the needle was used for nebulizer assisted electrospray. An Aalborg Instruments flow meter was used to measure all gas flow rates. For direct ion introduction experiments a 0.40 mm orifice was used which resulted in a flow of air through the orifice of ≈ 23.5 ml/sec. To simulate a quartz tube type of interface, a glass lined stainless steel capillary (GLT) having an i.d. of 0.70 mm and a length of 20 cm was used. This configuration resulted in an air flow through the GLT tube of ≈ 26.3 ml/min. When an uncoated stainless steel (SS) capillary having an i.d. of 0.76 mm and a length of 20 cm was used the resulting air flow through the tube was ≈ 30 ml/sec. Capillary tube temperatures for both GLT and SS were operated in the range of 105 - 120 °C.

While the charge distribution for myoglobin and an amine test mixture remained constant regardless of which introduction technique was used, the sensitivity was higher with the direct introduction method, despite similar air sampling rates. Comparison of the absolute sensitivities of the transfer tubes with the direct introduction method showed that use of the GLT transfer tube resulted in a 4-5 fold loss in sensitivity for both myoglobin and low mass compounds (< m.w. 500). Conversely, use of the stainless steel transfer tube resulted in a 5-6 fold decrease in sensitivity for myoglobin and approximately an order of magnitude decrease in sensitivity for low mass compounds. These results show that no significant advantage other than sensitivity is gained by using any of the three ion introduction methods. Additionally, low mass sensitivity using stainless steel tube interfaces can be improved by replacing them with similar inner diameter glass lined stainless steel tubing.

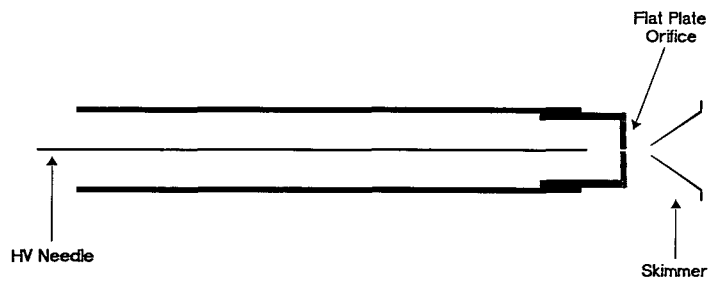

Figure 1. Schematic drawing of the direct ion inlet.

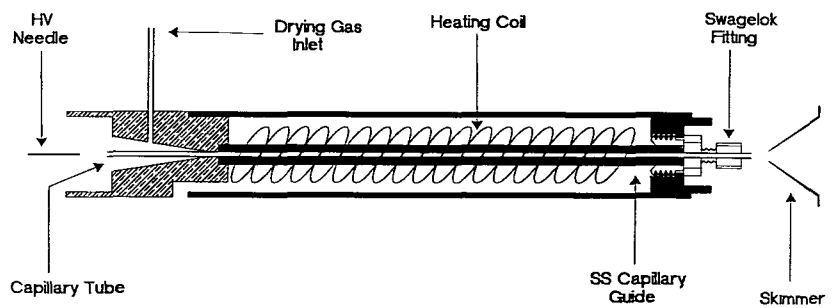

Figure 2. Schematic drawing of the heated capillary ion inlet.

NEGATIVE ION FORMATION IN ELECTROSPRAY MASS SPECTROMETRY

Rolf F. Straub and Robert D. Voyksner, Analytical and Chemical Sciences, Research Triangle Institute, P. O. Box 12194, Research Triangle Park, NC 27709

INTRODUCTION

Electrospray (ES) ionization is rapidly developing as a method to produce gas-phase ions from analyte species in solution for subsequent analysis by mass spectrometry (MS). It is a soft ionization method capable of providing positive ions of many synthetic drugs, dyes, natural products, high molecular weight biopolymers and a variety of other compounds. In contrast to this, only a few examples have been reported so far using negative ions for the characterization of compounds with acidic functionalities such as carboxylic, phosphoric, and sulfonic acid groups.

One crucial reason for this is the fact that, for otherwise equivalent conditions, an electric (corona) discharge occurs, presumably caused by electrons emanating from the sharp edges of the electrospray needle held at a few thousand volts negative relative to a counter electrode. For aqueous or highly conductive solutions, it becomes even more difficult to maintain stable electrospray in the case of negative polarities because, generally, higher voltage is necessary to electrospray the liquid. This situation makes negative-ion mode ES-MS more difficult than ES-MS in the positive-ion mode. This paper describes negative-ion ES-MS operation on a single quadrupole mass spectrometer and compares the results to some positive-ion operations. Also, the ability of common chromatographic solvents to stabilize ES current and to promote intense analyte signals was determined.

EXPERIMENTAL

Sample Introduction:	Flow injection at 4 µL/min for indicated solvent systems and samples.
Electrospray:	Analytica of Branford designed for an HP 5989 operated for the formation and transmission of negative ions.
Mass Spectrometer:	Hewlett Packard 5989 operated in negative ion detection mode.

RESULTS AND DISCUSSION

Optimizing the Generation of Negative Ion in ES

The three layered electrospray needle used consisted of a 50 µm i.d. stainless steel inner tube to deliver solvent, and a 125 µm i.d. second layer tube to deliver an additional solvent as a sheath flow to enhance ES negative ion operation, especially when using high percentages of water. The third and outer tube was used to coaxially add gas to aid in nebulization. In negative-ion operation, oxygen was generally used as an electron scavenger gas.

An evaluation of eight representative chromatographic solvents (methanol, ethanol, 2-propanol, methoxyethanol, acetone, tetrahydrofuran, chloroform and acetonitrile) indicated that 2-propanol (IPA) added with oxygen in the electrospray bath gas is best-suited to suppress electrical (corona) discharge phenomena in negative-ion operation while aiding in solution nebulization, desolvation and transfer of ions in solution to the gas phase. For positive-ion mode no such precaution was necessary. The use of 2-propanol leads to the most abundant $[M - H]^-$ ion with few background ions in the electrospray spectrum of 37 ng/µL adenosine-5-

monophosphate (AMP). Therefore, IPA is an ideal choice as a mobile phase additive in negative-ion ES-MS operation. Also, AMP dissolved in methanol or 2-methoxyethanol exhibits an abundant $[M - H]^-$ ion, few fragment ions, and a low background. Less suitable solvents such as chloroform, acetone and acetonitrile produce higher background throughout the mass range, but in particular at lower m/z ratios. The nucleotide dissolved in ethanol or tetrahydorfuran yielded a low abundance $[M - H]^-$ ion and comparatively abundant background ions.

Application of Negative Ion ES-MS for the Detection of Various Compounds

Negative ions with varying degrees of solvation and structurally relevant fragments can be obtained from a variety of solute species including β-lactam antibiotics, aminoglycosides, aminocyclitols, tetracyclines, sulfonamides, nucleotides, peptides and explosives. No fragmentation of parent species, except those from some labile explosives, was observed as low potential differences were applied between the capillary and the first skimmer, and electrical discharge was avoided in the gas phase. An increase of the capillary voltage resulted in collision induced decomposition to produce structurally relevant fragment ions in both operation modes. Negative-ion electrospray offers the advantage of providing complementary structural information to help in characterization of an unknown compound or to confirm a certain tentatively proposed structure. Nucleotides and explosives were best characterized in negative-ion mode owing to the ease with which they form anions in solution; they could be detected down to the 1 pg/µL level. Other compounds (antibiotics and peptides) were more sensitive by positive ion detection, particularly when no acid sites were present on the molecule to form an anion. Compounds that had both basic and acidic sites (β-lactams) resulted in ion currents within a factor of 2-3 between positive ion (low pH solution) and negative ion (high pH solution) detection. Conditions that promote the formation of anions in solution usually improved the electrospray ion current for negative ion detection. Therefore, the best ion currents for all the conditions evaluated were obtained at solvent pH values of 9-10 (pH adjusted with ammonium hydroxide).

CONCLUSIONS

Negative-ion electrospray mass spectrometry provides a means to characterize a wide variety of compounds such as antibiotics, synthetic drugs, nucleotides, peptides, and explosives. Conditions which promote the formation of anions in solution (high pH with NH_4OH) usually improve ES response. Also, an appropriate choice of the solvent (isopropanol) or the sheath fluid has a substantial effect on the stability of the current produced by the electrospray and the intensities of the recorded signals. This can be attributed to enhancements in the nebulization and desolvation processes resulting in higher ion evaporation yields.

ACKNOWLEDGMENTS

This research was supported in part by the U.S. Food and Drug Administration Cooperative Agreement No. FD-U-00581 and by the NIDA Grant No. 5 R01 DA06315.

Comparison of Buffer Systems in Capillary Electrophoresis - Electrospray Ionization / Mass Spectrometry

Jon H. Wahl, David C. Gale, Steven A. Hofstadler, Harold R. Udseth, and Richard D. Smith
Chemical Sciences Department
Pacific Northwest Laboratory
Richland, WA 99352

The combination of capillary electrophoresis (CE) with electrospray ionization mass spectrometry (ESI/MS) is becoming a powerful technique for the study of biomolecules. In general, a wide selection of buffer systems are used for CE separations. In CE-ESI/MS, however, volatile buffer systems, which are at the lowest practical concentration and ionic strength, generally produce the best detector response. Consequently, a balance must be achieved between a high buffer concentration that degrades solute detectability in ESI/MS and a low buffer concentration that causes solute zone broadening due to conductivity differences.

A variety of ESI approaches are used for interfacing CE with MS. For example in the coaxial sheath flow design, a small flow of liquid serves to establish the electrical contact. Several disadvantages, however, exist with this interface design; for example, the coaxial liquid invariably provides additional electrolyte to the ESI source that may decrease the analyte response and will contribute to the chemical background. Presently, our laboratory is re-examining a sheathless CE-ESI interface approach using a conductive capillary terminus. These two different ESI interface designs are compared and their dependence on solute detectability for three different buffer systems at three different concentrations are examined for capillary i.d.'s of 100 and 10 µm.

The experimental system for these initial studies consists of a modified Sciex TAGA 6000E mass spectrometer and an in-house built capillary electrophoresis system. The coaxial electrospray design used a 75% MeOH / 24% H_2O / 1% HOAc as the sheath fluid, and the sheathless design used a conductive coating at the analytical capillary terminus to establish electrical contact with the CE effluent. In all studies, aminopropylsilane treated fused-silica capillaries of various inner diameters (i.d.) are used. The buffer systems examined are HOAc, NH_4OAc/HOAc, and Na_2HPO_4 at concentrations of 1, 10, and 100 mM and ranged in pH from 3.0 to 6.0. The solute chosen for these experiments is Methionine(M)-Lysine(K)-Bradykinin (1320 Da) at a concentration of 1 µM in all buffer systems used. The solute was electroosmotically infused at ~ -275V cm^{-1} in all studies to approximate the actual conditions in a CE-ESI/MS experiment.

The results for the 3^+ charge state of M-K-Bradykinin obtained using the NH_4OAc/HOAc buffer systems (pH = 4.7) are summarized in Figure 1 where the signal-to-background (S/B) is shown as a function of buffer concentration for both a sheath and sheathless ESI interface. The lighter and darker shaded bars represent the results obtained using 100 µm and 10 µm i.d. capillaries, respectively. From Figure 1 several important observations are made: 1) analyte signal intensity decreases with increasing buffer concentration and ionic strength, as commonly known, 2) the use of smaller i.d. capillaries does not degrade analyte detectability and in some cases enhances detectability (cf. the 10 mM case), and 3) the sheathless interface appears to offer better analyte detectability for this buffer system (cf. the 1 mM case).

Shown in Figure 2 are the total ion electropherograms obtained from a tryptic digest of *Candida krusei* cytochrome *c* when 10 mM HOAc (pH 3.4), 10 mM NH_4OAc/HOAc (pH 4.7), and 1 mM Na_2HPO_4 (pH 6.0) are used.; in addition, the mass spectra acquired for the solute zones 2 and 8 while using 10 mM NH_4OAc/HOAc are also shown. The separations are performed in a 20 µm i.d. capillary at -270 Vcm^{-1} with a sheathless ESI interface. The mass spectrometer in each case was scanned from *m/z* 400–1100 in 2 *m/z* steps at 1 s/scan. As noted previously, and as

can be seen in Figure 2 from the relative intensities, the analyte response decreases as the concentration and ionic strength increases for a buffer system. Still, the S/B is sufficient to allow detection of the tryptic fragments with the three buffer systems.

We have examined and demonstrated that a variety of buffer systems may be utilized for CE-ESI/MS. Moreover, in many cases where a buffer system has a high ionic strength the combination of small i.d. capillaries, which provides a simple method to reduce the effluent mass flow entering the electrospray interface and enhances the overall ionization efficiency, and a sheathless ESI interface server to provide significantly better analyte detectability.

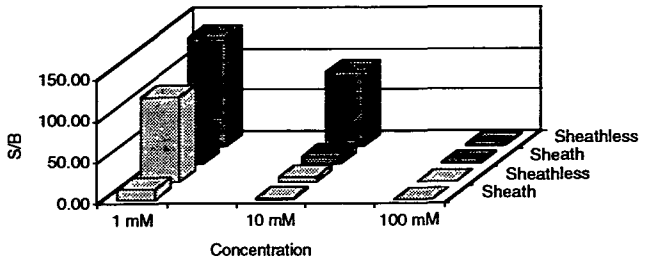

Figure 1 The signal-to-background (S/B) results for the 3^+ charge state of M-K-Bradykinin using the NH_4OAc/HOAc buffer systems. Legend: 100 µm i.d. ▒ 10 µm i.d. ■

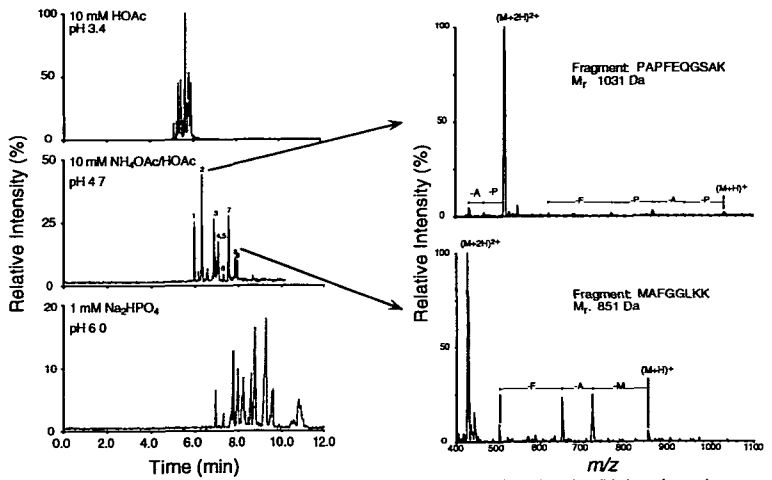

Figure 2 Total ion electropherograms and acquired mass spectra of a tryptic digest from *Candida krusei* cytochrome c. Conditions: 20 µm i.d., -270 Vcm^{-1}, Sheathless, *m/z*: 400-1100, 2 *m/z* step, 1 s/scan.

This research was supported by internal exploratory research and the Director, Office of Health and Environmental Research, and the U. S. Department of Energy. Pacific Northwest Laboratory is operated for the U.S. Department of Energy by Battelle Memorial Institute under Contract DE-AC06-76RLO 1830.

On-Capillary Isotachophoresis for Sample Clean-Up and Loadability Enhancement in Capillary Zone Electrophoresis/ Electrospray Mass Spectrometry

M.H. Lamoree[1], N.J. Reinhoud[1], U.R. Tjaden[1], W.M.A. Niessen[1] and J. van der Greef[1,2]

1. Division of Analytical Chemistry, Leiden Amsterdam Center for Drug Research, P.O. Box 9502, 2300 RA Leiden, The Netherlands
2. TNO-CSIA, P.O. Box 360, 3700 AJ Zeist, The Netherlands

Introduction

The coupling of capillary zone electrophoresis (CZE) to mass spectrometry (MS) provides an analytical technique that combines the high separation efficiency characteristic of CZE with the high selectivity of mass spectrometric detection. A major drawback of CZE is the limited loadability, resulting in poor concentration detection limits. An increase in sample loadability can be achieved by electrophoretic analyte focusing procedures such as isotachophoresis (ITP) and stacking. On-line ITP-CZE-MS in a dual capillary system for improvement of detection limits in CZE-electrospray-MS has been presented at this conference last year. In this presentation, an ITP-CZE procedure in a single capillary prior to electrospray MS analysis is described. The applicability of ITP-CZE-MS as a trace analysis technique is illustrated for some β-agonists. The ITP-CZE-MS approach is applied to the analysis of β-agonists in calf urine.

Experimental

A Finnigan MAT SSQ 710 mass spectrometer, equipped with an electrospray interface and operated in the positive ion mode, was used.
ITP analyte focusing and CZE were carried out in a 740 mm x 100 µm I.D. fused-silica capillary. The capillary inlet served as the anodic end, while the electrospray needle was at ground potential. Buffer systems: CZE buffer: 80% methanol in 50 mmol/l ammonium acetate (also ITP leading buffer), ITP terminating buffer: 80% methanol in 50 mM β-alanine (pH 4.8).

ITP-CZE

The procedure of single-capillary ITP-CZE consists of 4 steps (see Figure):

1. injection of the sample between leading and terminating buffer, starting isotachophoresis with hydrodynamic pressure from detector side (via height difference, Δh) to counteract both the electroosmotic flow and the electrophoretic migration.
2. hydrodynamic mobilization of sample zone towards the inlet side, removal of terminating buffer, sample cleanup by removal of slowly migrating ionic constituents.
3. *replacement of terminating by leading buffer.*
4. separation of analytes by zone electrophoresis and detection by electrospray mass spectrometry.

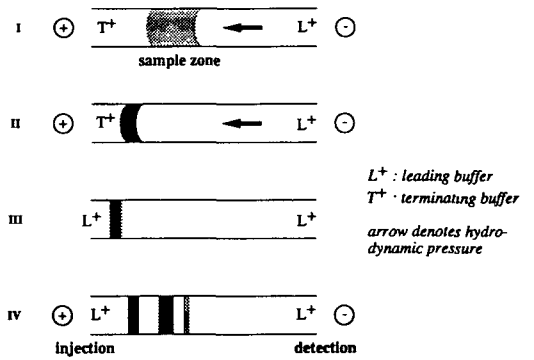

ITP-CZE-MS

In ITP-CZE-MS it is important to have identical composition of leading buffer and sheath flow to allow application of hydrodynamic pressure in the ITP step without disturbing the continuity of the buffer system.

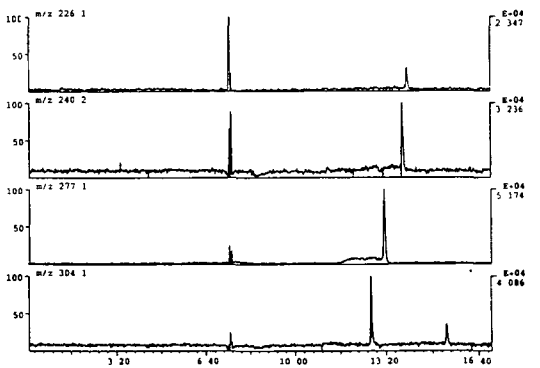

Injection of 870 nl of a 80 ppb test mixture containing all β-agonist (injected amount 70 pg of each analyte); ITP conditions: 5 kV, 600 s, Δh=100 mm

Conclusions

Enhancement of sample loadability by ITP leads to a 100-fold improvement in concentration detection limits for the β-agonists. On-capillary ITP shows to be a promising approach for loadability enhancement in CZE-MS. Further optimization of the system is currently under investigation.

Design and Construction of a Thermospray-type Interface for On-line Capillary LC/MS.

Alain carrier and Michel J. Bertrand, Regional Center for Mass Spectrometry, Department of Chemistry, University of Montréal, Montréal, Canada, H3C 3J7.

The development of techniques allowing the introduction of liquid samples into the ion source of a mass spectrometer has considerably increased the range of compounds that can be analysed by mass spectrometry. Previous work (1) in our laboratory has lead to the development of a simple and inexpensive DLI system that uses a conventional GC/MS interface. Experiments conducted with this system have demonstrated that it is extremely stable, reproducible and allows picogram range sensitivity for low molecular weight compounds. However, this interface has limitations for the analysis of polar compounds. In order to allow the analysis of thermally labile or involatile compounds the design and the construction of a capillary thermospray-type interface such as that developed by Vestal and coworkers (2) was undertaken. The capillary thermospray-type interface developped is schematicaly shown in Figure 1. The interface consists of a fused-silica capillary tubing (10µm) which is introduced directly into a CI source throught the solid probe inlet and is oriented in the beam axis. The heating of the interface is provided by the ion source and ionization is achieved using external mode ionization (filament-on mode). In order to evaluate the system and to determine its optimum operating conditions, the influence of several parameters that are known to have an effect on the overall performance was studied.

The effect of the temperature of the interface, which is provided by the heating of the ion source, was studied. As it can be seen from Figure 2, which shows the intensities of the solvent ions versus the source temperature, all ions reached a maximum intensity in the same region (140-160 ºC). This region was found to provide extremely stable operating conditions. Partial to severe instability was encountered on both sides of this temperature range. Another factor that was found to have an effect on the stability is the flow rate. The flow rate in the system has an effect on the ion source pressure which can affect the composition of the plasma and therefore the ionization characteristics of the system. Result indicates that the range of flows corresponding to stable conditions is found to be between 2 and 6 µL/min. Experiments were also conducted at

different distance between the orifice of the interface and the ion exit slit to determine its effect on the overall performance. It has been found that the ion intensities increase with the sampling distance up to a certain point (12,5 mm) at wich a drop in intensities occurs. In order to evaluate the potential of the interface for the characterization of organic compounds several experiments have been conducted. Mass spectra obtained for a series of test compounds were found to be in all points comparable to those obtained under typical thermospray conditions as shown in Figure 3. Good sensitivity was obtained with the interface developped. Detections limit of 5 to 30 pg were obtained for caffeine, adenosine and chloramphenicol in single ion monitoring. The performance of the capillary thermospray-type interface developped is satisfactory. It is easy to operate and provides reliable results.

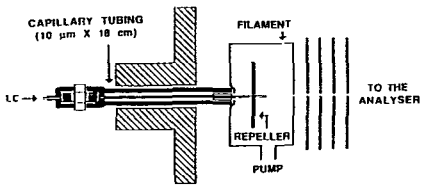

Figure 1. Schematic of the thermospray interface.

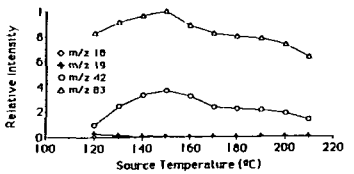

Figure 2. Relative intensity of solvent ions as a function of the source temperature.

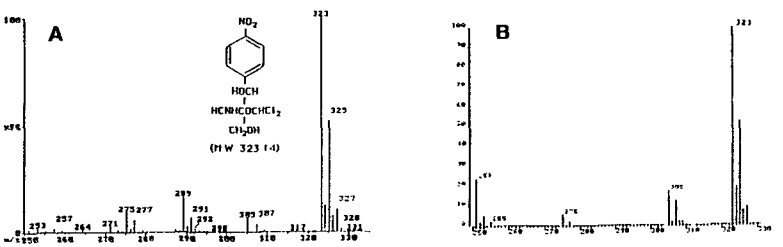

Figure 3. Mass spectrum of chloramphenicol.
A) Capillary thermospray.
B) Conventional thermospray (3).

References
1- J.P. Gagné, S. G. Roussis and M. J. Bertrand, J.Chromatogr.,554 (1991) 293-294.
2- C.R. Blakley and M.L. Vestal, Anal. Chem.,55 (1983) 45.
3- J.R. Chapman, J.Chromatogr.,323 (1985) 153-161.

Design of Electrospray Interfaces for Finnigan-MAT TSQ-70 and VG-ZAB MS

Sharon Jackett, Longfei Jiang, Mehdi Moini
Department of Chemistry and Biochemistry, University of Texas at Austin, TX 78712

The design of an electrospray interface for the Finnigan-MAT TSQ-70 and VG-ZAB mass spectrometers is described.

A. The thermospray (TS) ionization feature of a Finnigan-MAT TSQ-70 mass spectrometer was converted to electrospray ionization (ESI) utilizing the existing source, pumping capacity (using only one mechanical pump), flanges and temperature controller of the TSQ-70 TS feature with a few minor modifications.

The solid-probe design of the ESI interface (Figure 1) produced the pressure required in the first stage of pumping to obtain adequate signal intensity, resolution, and peak shapes. The adequacy of this design in terms of pressure is demonstrated using gramicidin S as the analyte. The doubly charged gramicidin S produced a very strong signal at 572 m/z at picomole level. The optimum signal intensity, resolution, and peak shape were obtained by adjusting the distance between the end of the heated capillary tube and the skimmer. At a distance of ca 4 mm, the pressure in the first stage of the vacuum system was ca 3-5 torr. This pressure along with the existence of a 0.5 mm orifice between the first and second stage, produced vacuum conditions identical to the normal operating conditions of the MS in the chemical ionization mode.

Overall quality of the ESI-generated spectrum is shown in the spectrum of cytochrome C from horse heart (Mw 12,361 Da) in methanol+water+acetic acid (Figure 2). This spectrum is similar to spectra of cytochrome C reported in previously published literature, but shorter scan rates are used in the present experiment The high signal-to-noise ratio of this spectrum allows much faster scan rates. At a scan rate of 1 scan/sec, a signal to noise ratio of approximately 3:1 was observed. Fast scan times (< 1 s) are especially useful when ESI is combined with separation techniques such as capillary zone electrophoresis in which chromatographic peak widths are only a few seconds

In summary, we attribute this enhanced sensitivity and greater ease of operation to the alignment of the ion optics, use of a single mechanical pump, and the mounting of the system on a solid probe. Conversion of the commercial TS option to a simple and economically viable ES option, has made the analysis of large biomolecules possible without expensive upgrades. Mass spectrometric results of low and high molecular weight biomolecules, the mass accuracy, sensitivity, and charge states of the observed ions are comparable to existing published results by other laboratories.

B. The electrospray interface for the VG-ZAB double focusing mass spectrometer is as follows: The electrospray needle is held at a potential of +5 kV relative to the potential of the heated stainless steel capilary tubing. The charged droplets enter the stainless-steel heated capillary tube which is held at a potentail of ca. 4200 V, through which they are transported into the ESI source. The electrospray source consists of two pumping stages. The region between the heated capillary and the first skimmer defines the first stage and is pumped by a mechanical pump to a pressure of ca. 20 torr. This pressure is advantageous because it is too high to sustain an electric discharge. The second stage of pumping, the region between the

first and second skimmers, is pumped by a small diffusion pump to pressures at which molecular flow predominates (<10^{-3} torr). The use of the two pumping stages held at these pressures allows overstepping of the discharge zone, and thus there is no need to float pumps. The other focusing elements of the source are those of the commercial FAB source of the ZAB mass spectrometer. The entire source including heated capillary, skimmers and lens elements are mounted on the source flange, and all voltages are provided by the existing VG power supplies. This feature makes it possible to quickly change from ES to other ionization modes. The system is also capable of operating in counter flow of heated gas modes of desolvation. Figure 3 shows our preliminary results of ES ionization of gramicidin S.

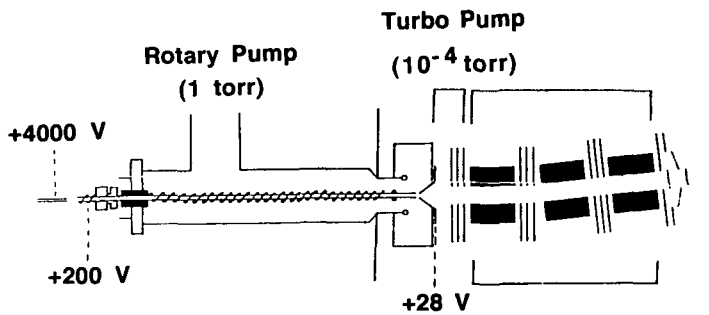

Figure 1: Schematic of electrospray design for TSQ-70 mass spectrometer

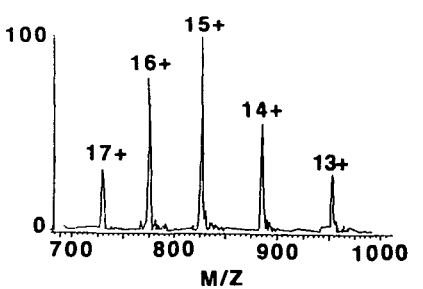

Figure 2: TSQ-70 electrospray mass spectrum of cytochrome C from horse heart.

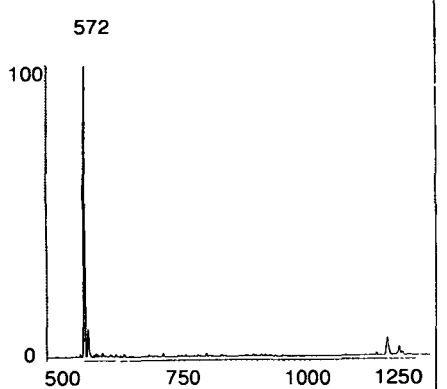

Figure 3: VG-ZAB electrospray mass spectrum of gramicidin S.

Linear Calibration curves using Particle Beam LC/MS.

***Thomas C. Marecic, Ross C. Willoughby, Stephen M. Penn , Millipore/Extrel Mass Spectrometry, 575 Epsilon Drive , Pittsburgh, PA 15065**

Introduction: It has been reported that, as a quantitative tool particle beam is hindered by non-linear calibration curves. Linearity has been achieved through the coelution of a compound with an excess of its isotopically labeled analog[2]. In our laboratory we have demonstrated linear calibration curves for benzidine and caffeine using a particle beam LC/MS system without the use of coeluting compounds. These data support a Band Pass model which relates analytical response with transmission efficiency of the interface.

Band Pass Model: The Band Pass model correlates analytical response to mass transport efficiency of a particle beam LC/MS interface. Figure 1 shows analytical response curves from the model. The ideal curve shows the upper limit of response assuming 100% transport of the analyte through the interface. The band pass limit curve shows three distinct regions of response. There are two non-linear regions at the ends of the curve with a linear one in the middle. A transmission curve can be constructed from the analytical curve (figure 2) using the following equation for transmission efficiency of particles through the interface.(ε_{trans}),

$$\varepsilon_{trans} \propto \text{Intensity/concentration}$$

From this band pass curve it is evident that as long as the interface is operating in the linear region, transmission of analyte is independent of particle size, hence a linear analytical curve. On the other hand, if the analytical region of interest is in the lower region of the curve, response of the analyte is particle size dependent, and the resulting curve will be non-linear. It has also been demonstrated[2] that an interface can be operated in the lower concentration region of the Band Pass curve and give linear response. This is provided there is a carrier compound to increase the particle size into the region of constant transmission efficiency. It is worth nothing that the shape of the Band Pass curve is interface dependent.

Experimental: The linearity data was run on an Extrel **benchmark** LC/MS using a prototype particle beam interface. The HPLC system was a WATERS 600ms. The mobile phase was a 50:50 mixture of water and acetonitrile flowing at 0.5ml/min.

Results: Plotted in figure 3 are the analytical curves for benzidine on two different interfaces. Over the concentration range shown the data from the Extrel interface is linear to ≈ 5ng. This concentration range is near the limit of detection for benzidine on this instrument, while the data from reference 2 is curved with lowest data point at 18 ng.
The linearity of the Extrel data can be attributed to the interface operating in the flat region near the volatility/dispersion loss end of the Band Pass curve, while the other interface is apparently operating in volatility/dispersion loss region of the Band Pass curve. Plotted in Figure 4 are the transmission efficiency curves for both interfaces. The curve for the Extrel interface shows a flat region where ε_{trans} is independent of particle size and hence concentration. For the interface used in reference 2 it appears that there is a dependence of ε_{trans} on particle size over the specified concentration range.

Conclusion: The Band Pass model can be use to explain both linear and non-linear particle beam data based on the dependence of the transmission efficiency on particle size . On the Band Pass curve there are regions where transmission is independent of particle and hence the analytical curves tend to be linear. With the new Extrel particle beam interface it is possible to quantitate linearly close to the detection limits of the mass spectrometer.

1)Willoughby, R. C,; Browner, R. F. Anal. Chem. **1984**, 59, 2626-2631.
2) Ho, J. S.; Behymer, T. D.; Budde, W. L., Bellar, T. A. *J. Am Soc Mass Spectrom.* **1992**, 3, 662-671.

Analytical Curves from Mass Transport Model for Particle Beam LC/MS

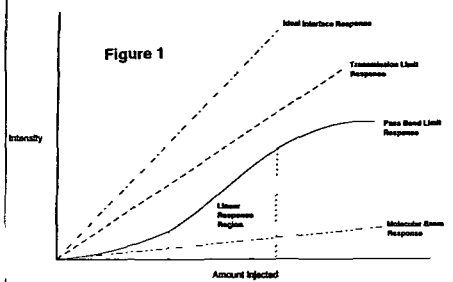

Particle Beam Calibration Curves for Benzidine

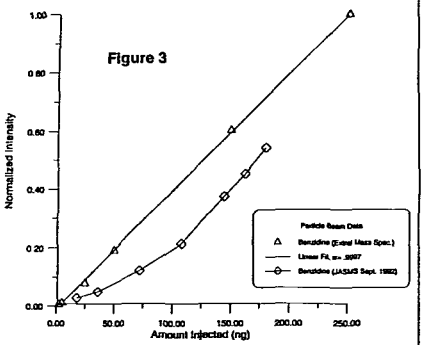

Mass Transport Model for Particle Beam LC/MS

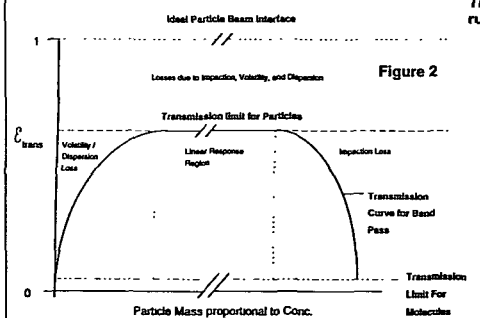

***Transmission Efficiency vs Amount for Benzidine* run on Two Different Particle Beam Interfaces**

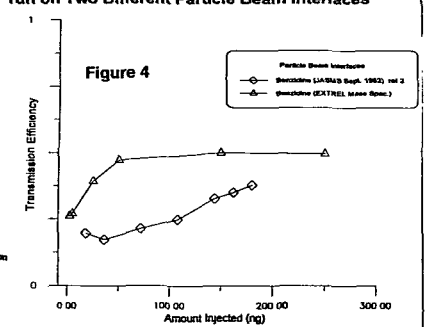

Hydrogen /Deuterium Exchange in Electrospray Ionization Mass Spectrometry as a Practical Tool for Structure Elucidation

James J. Conboy, Mark F. Bean, Mark E. Hemling, and Steven A. Carr,
Department of Physical and Structural Chemistry,
SmithKline Beecham Pharmaceuticals, King of Prussia, PA 19406

Measurement of the number of active hydrogens in a molecule by various types of hydrogen/deuterium exchange experiments has for a number of years proven useful in the elucidation of compounds of unknown structure, in the determination of the mechanism of chemical or biological reactions, and in the interpretation of fragmentation pathways in mass spectra [J. A. McCloskey, *Methods in Enzymology*, **193**, 329 (1990)]. Various means for making such measurements have been developed for nearly every ionization/sample introduction method that has been widely used including EI, CI, FAB, thermospray, particle beam, GC/MS, and LC/MS. Recent work in the analysis of protein conformation by ESIMS has made use of both solution phase and gas phase (atmospheric pressure or *in vacuo*) hydrogen/deuterium exchange methods. The gas phase exchange experiments were performed either on FTMS instrumentation to achieve the long residence times required for exchange or with a heated dual-capillary inlet reactor interface for desolvation and then exchange of the sample molecules. We have implemented methods for hydrogen/deuterium exchange which require only simple changes to the plumbing of our Sciex API-III Ionspray source. Effective exchange of active hydrogens may be achieved by replacing either all of the nebulizer gas or part of the curtain gas or both with a deuterated exchange agent such as ND_3. These methods provide for essentially complete exchange of all active hydrogens on the types of small molecules (e.g., alkaloids, glycosides, etc.) for which H/D exchange has been of proven utility in structure elucidation work; larger molecules, or at least those with a large number of potentially exchangeable hydrogens, proved to be more challenging particularly in regard to completeness of exchange. These methods also appear to work without the need for dissolving the sample in deuterated or aprotic solvents. A simple ESIMS H/D exchange experiment is a useful addition to the mass spectrometrist's armamentarium for the elucidation of unknown structures. With it, H/D exchange is now extended to classes of compounds not amenable to FAB or DCI, especially in cases where sample is limited.

EXPERIMENTAL Nebulizer Exchange: Samples were dissolved in elution solvent (50/50 CH_3OH/H_2O with 0.2% HCOOH; or 50/50 CH_3CN/H_2O, 95/5 CH_3CN/H_2O, or 90/10 $CHCl_3/CH_3OH$ with 5 mM NH_4OAc) and introduced by loop injection (2-3 µL/min) into the ion spray interface. Nebulizer gas (30-35 psi) was toggled from zero air to ND_3 (29-30 psi) after the signal maximized and then back to zero air after ~10 scans. Residual gas was removed from the interface region by the exhaust fan.

Curtain Exchange: Samples were introduced as described above. ND_3 exchange gas was added to the N_2 curtain by a flow controller (1--10 %curtain flow) with simultaneous increase of the declustering potential (OR - R0 = 120--220 V) to reduce clustering and adduction and to increase the extent of exchange. Residual gas was removed completely only after a recycle of the cryopumping system.

General: All components used in the modifications to the interface plumbing were selected to be compatible with ND_3, e.g., stainless steel, indium, Teflon, and glass. ND_3 was obtained from Isotec (99+%; Miamisburg, OH) or Cambridge Isotopes (99%, Woburn, MA).

RESULTS/DISCUSSION Nebulizer Exchange: During flow injection of a sample, H/D exchange is readily effected by switching the nebulizer flow from air to ND_3 for several scans, then switching back to air, thereby providing both normal and exchanged data in a single experiment. For some compounds this leads to noticeable suppression or enhancement of ionization which can be useful for selecting scans for analysis. The exchange is effected very quickly which can be important for reducing gas consumption -- the nebulizer method uses ~0.7 L/min of ND_3. Effective exchange can be observed for most of the molecules tested (Table I) including exchange of amides on the smaller peptides.

Curtain Exchange: H/D exchange can also be effected by introducing ND_3 as a portion (1-10%) of the curtain gas. It was thought that H/D exchange at the atmosphere/vacuum interface would be a way to reduce possible back exchange and to decouple the exchange reaction from any effect the ND_3 gas might have on the desorption/ionization process. Introduction of ND_3 in this region can cause significant clustering $[n(ND_3) + ND_4^+]$ and adduction $[(M + D)^+ + n(ND_3)]$ to be observed. Increasing the declustering potential helps to eliminate the clustering and reduces the adduction. If increased too much, fragmentation may also be induced as evidenced by the water loss ($-D_2O$) peak observed. Increased

declustering potential can also be used in combination with increased curtain ND_3 concentration to drive the exchange process toward completion for the more refractory molecules. Curtain H/D exchange is effective for small molecules with "active" hydrogens. The larger molecules are more difficult to exchange effectively as were the peptides which contain less active amide hydrogens. Notable exceptions to this are the nucleotides which were both exchanged nearly completely in the negative ion mode.

Curtain H/D exchange suffers from residual gas effects, particularly when the plenum is configured with a Teflon/Viton O-ring seal rather than the Macor/indium configuration used in most of the experiments. Residual ND_3 can be observed to exert its effects for several hours after the gas has been turned off. Nevertheless, the reduced gas consumption (1-10% vs. nebulizer exchange experiments) makes this method suitable for cases where prolonged lifetimes of exchanged species are required, e.g., MS/MS experiments; if done at the end of the day, the instrument is completely recovered by the next morning. Other ways of introducing the ND_3 to the orifice more directly may reduce the recovery time.

General: ESI gas phase H/D exchange compares favorably with our experiences with DCI and FAB H/D exchange results. Both of these other methods work well for small molecules or molecules with few exchangeable hydrogens. ND_3-DCI seems to be limited mainly by the type and size of molecules that are amenable to DCI; however, it can be a more vigorous process, exchanging hydrogens on carbons which are activated by other substituents. FAB exchange experiments seem to be limited by more basic problems including possibly slow exchange, back exchange, reduction processes, radiation damage related processes, etc. Our initial experiments with ESI solution phase H/D exchange showed relatively poor exchange. This may have been due to back exchange problems or poor initial exchange conditions; we have not yet attempted to pinpoint the source of the incomplete exchange results

CONCLUSION ESIMS gas phase H/D exchange is an effective way to determine the number of exchangeable hydrogens on small molecules and to exchange many of the active hydrogens on larger molecules. For compounds containing more than a few active hydrogens, ESI gas phase exchange via the nebulizer is, in practice, simpler and more efficient than FAB H/D exchange. Improvements to the curtain exchange experiment to improve the effectiveness of the exchange process and combination of one or both of the gas phase experiments with an optimized solution exchange technique may provide a universal method for complete and effective exchange of molecules of all types and sizes.

ACKNOWLEDGEMENT The authors wish to thank M. Mentzer for providing the DCI measurements and for assaying the ND_3 gas prior to use

Table I. Hydrogen/Deuterium Exchange Results

Compound	mw	theo. xc H	#xc H, neb.	#xc H, curt.	#xc H, soln.	#xc H, DCI/FAB
norphenylephrine	153	4	4	4	3-4 (heat)	4 (DCI)
ascorbic acid (pos)	176	4	4	4		
ascorbic acid (neg)	176	4	4	4		
riboflavin	376	5	5	5	1	
piperidine alkaloid	317 / 331	2 / 1	2 / 1			
MLF	409	5	5	5 max	2-3	4-5 max (FAB)
TYSK	497	11	11	10 max	6? (w)	10-11 max (FAB)
renin substrate	1757.9	25	24	13 max		
ox. insulin B (pos)	3493.6_m 3495.9_a	51	47_m 46_a	16 avg 18 max		
sucrose	342	8	8	8		8 (DCI)
raffinose	504	11	11	11		
stachyose	666	14	14	14		
maltopentaose	828	17	17	17 max		
digitonin	1228	17	17	17 max		ca.16 max (FAB)
holothurin B (neg)	860	7	7	4 or 7		
$(dTp)_7dT$ (neg)	2370.4_m	17	17	17		
$(dTp)_{19}dT$ (neg)	6021.9_a	41	40	40		
ox. insulin B (neg)	3493.6_m 3495.9_a	51	45 avg 48 max	14 avg 18 max		

Ion Source Effects on β-Lactam and Macrolide ESI Mass Spectra

*Y. Shida[1] and K. O'Hara[2], Depts. of Chemical Analysis[1] and Microbiology[2], Tokyo College of Pharmacy, Tokyo, Japan, and
C.E. Parker and K.B. Tomer, Laboratory of Molecular Biophysics, N.I.E.H.S., P.O. Box 12233, Research Triangle Park, NC 27709

Penicillins, cephems, and macrolides are important antibiotics for both human and animal use. As part of a study on the utility of electrospray mass spectrometry for the structure determination of the β-lactams and macrolides, ESI/MS spectra of a series of these compounds were obtained on a VG 12-250 mass spectrometer equipped with a Vestec electrospray source and controller, using skimmer voltages of +10V to 40V. ESI/MS and ESI/MS/MS spectra of the same compounds were obtained on a Finnigan/MAT TSQ700 triple quadrupole mass spectrometer using argon as the collision gas, and a series of collision energies from 0 eV to -40 eV.

Vestec skimmer-induced CID ESI/MS spectra of penicillins and macrolides were in good agreement with ESI/MS/MS spectra obtained on a triple-quadrupole mass spectrometer. There was no selection of the parent ion in the single quadrupole, however, so a composite spectrum resulting from CID on all of the ions present in the source was observed.

Because the Vestec skimmer also functions as a repeller, it is not possible to obtain spectra with zero skimmer voltage or zero collision energy. While this effect may not be as apparent on larger molecules, such as proteins, it leads to some CID contribution to the ESI/MS mass spectra of easily-fragmented molecules.

Thus, while we were able to closely match the TSQ MS/MS spectra with the Vestec CID spectra, we found that we were unable to duplicate the TSQ ESI/MS spectra on the VG 12-250 with the Vestec source. In general, the Vestec ESI spectra most closely matched the TSQ spectra obtained at ~5-10 V higher collision energies (Figure 1).

An additional effect noted was that the sodiated species were often of higher relative abundance in the TSQ700 mass spectra. In some cases, this effect was so pronounced that CID and MS/MS spectra could not be obtained from the same parent ion in both instruments.

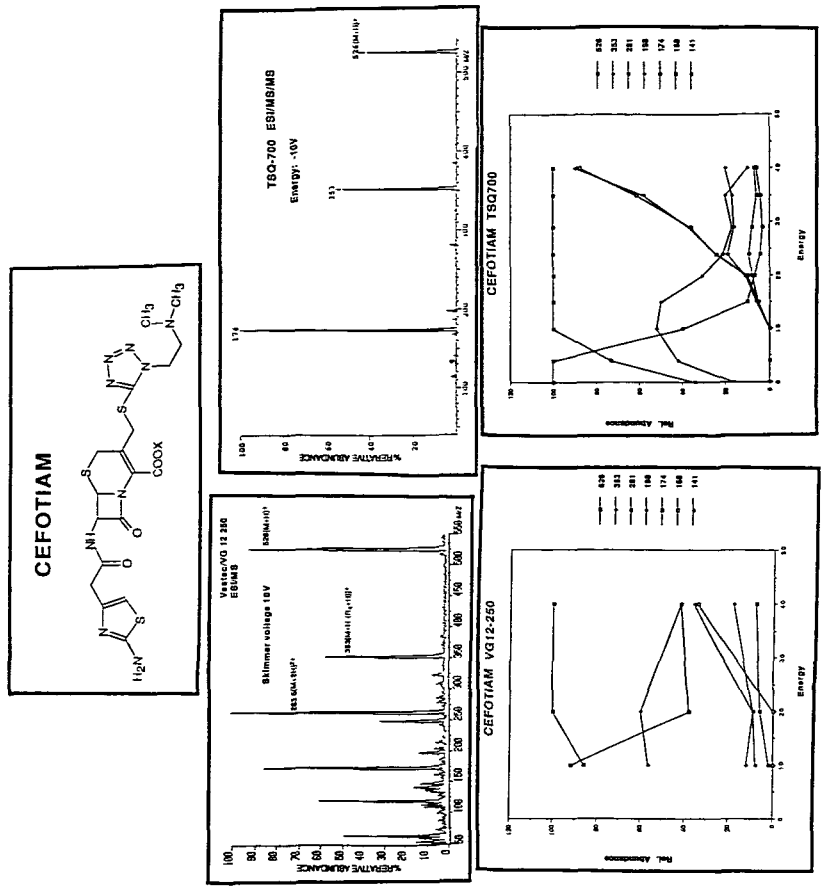

Figure. 1

TYROSINASE-CATALYZED HYDROXYLATION OF LEUCINE ENKEPHALIN: ELECTROSPRAY IONIZATION MASS SPECTROMETRIC IDENTIFICATION OF THE REACTION PRODUCTS

Véronique Larsimont, Günther Hochhaus and Laszlo Prokai,
Department of Pharmaceutics and Center for Drug Discovery,
University of Florida, Gainesville FL 32610

The enzyme tyrosinase catalyses the ortho-hydroxylation of phenols and the subsequent oxidation of the resulting catechols to o-quinones It is common throughout nature and plays a central role in the biosynthesis of both norepinephrine and melanin. In addition, our group and others have shown that tyrosinase will react with tyrosine-containing peptides, including enkephalins, to give hydroxylated products [1-4]. It is known that enkephalins are deactivated and metabolised in vivo by aminopeptidases, carboxy-peptidases and enkephalinases [5]. However, since enkephalins and tyrosinase have been found in the same brain regions in some species [6, 7], our goal was to determine the exact nature of the products formed when tyrosinase reacted with leucine enkephalin (LE). Subsequently, as it is known that the integrity of the Tyr[1] residue in enkephalins is essential for interaction with opioid receptors [8, 9], we wished to compare the affinity of these products and leucine enkephalin itself to opioid receptors in rat brain homogenate.

The reaction between LE and mushroom tyrosinase was carried out under the following conditions: 1 mM LE, 50 mM ascorbic acid, 0.1 M potassium phosphate buffer (pH 7), 32 mg/ml mushroom tyrosinase at room temperature with constant shaking. The reaction was stopped after 1 hour by adding 66 ml of 1 M HCl per ml of incubation solution.

Chromatograpic separation of LE and the reaction products was realized using a Partisil 5 ODS-3 125 x 4.6 mm column (Whatman), a mobile phase of 12 5% acetonitrile (v/v) in citrate/dipotassium phosphate buffer (pH 5) at a flow rate of 1ml/min, and UV detection at 254 nm. In a control run, ascorbic acid was seen to elute in a large solvent front at 1 4 minutes and LE eluted with a retention time of 9 5 minutes. When the incubation mixture was applied to the system, two distinct additional peaks were seen on the chromatogram with retention times of 5 7 minutes and 7 3 minutes respectively.

For the isolation of the reaction products, aliquots of the incubation solution described above were applied to the HPLC system and the product peaks were collected and pooled according to their retention times The collected peaks were concentrated under a stream of nitrogen and purified using a Sep-Pak C_{18} cartridge prior to mass spectrometric analysis

A Vestec 200ES instrument (single quadrupole, 2000 Da mass range, Technivent VECTOR/ONE Data System) was used to obtain ESI mass spectra under the following conditions: Flat-tipped hypodermic needle (0 005 in i.d. x 0.010 in o d. x 0 75 in long) at 2.4 kV potential, spraying solvent of 3% AcOH in MeOH/H_2O (7/3 v/v), source block temperature of 250°C, spray chamber temperature of 50-65°C and repeller voltage at 18V for normal ESI and 50V for CID [10]. Electrospray ionization mass spectrometry provided intact molecular ions of LE and the products of the enzyme reaction and selective fragments were obtained by collision induced dissociation. The identification of the hydroxylated products of LE was achieved by comparing the ESI mass spectra obtained to those of the parent peptide The mono-hydroxylated enkephalin ([HO-Tyr[1]]-LE) gave molecular ions at *m/z* 572 and 594 for

$[M+H]^+$ and $[M+Na]^+$, respectively (Fig 1) compared to *m/z* 556 and 578 for the corresponding molecular ions in the parent enkephalin Under CID conditions (Fig 2), a 16 Da increase was also observed in the *m/z* value of the a and b sequence ions, starting with the a_1 ion of the series (*m/z* 152). On the other hand, the internal fragments *m/z* 120 and 177 are not affected. This is evidence that the phenylalanine moiety has not been modified. Therefore, the oxygen was incorporated, as expected, into the [Tyr[1]] residue. The ESI mass spectra recorded from the second product of the enzymatic reaction ([$(HO)_2$-Tyr[1]]-LE) have indicated, based on the 32 Da increment in *m/z* of the molecular ions as well as the a and b sequence ions when compared to the parent enkephalin, that additional hydroxylation also took place at the N-terminal tyrosine. The relative intensity of the peaks obtained from mass spectrometric analysis showed that [$(HO)_2$-Tyr[1]]-LE was a minor product and therefore, sufficient quantities could not be collected for use in receptor binding studies. The results of the binding studies indicated that the hydroxylation of LE by tyrosinase reduces its affinity to receptors in rat brain homogenate by a factor of 17.

REFERENCES

1 Tellier, M , et al (1991). J Pharm Biomed Anal **9**(7): 557-563
2 Marumo, K and J. H Waite, (1986), Biochim Biophys Acta. **872**. 98-103.
3. Rosei, M. A , et al, (1989), Biochem Int. **19**(6) 1183-93
4. Rosei, M. A., et al, (1991), Physiol Chem Phys & Med NMR. **23**. 59-65.
5 Venturelli, F., et al, (1985), Neurochem Res. **10**(3): 333-341.
6. Zhuo, H , et al, (1992), J Chem Neuroanatomy. **5**: 1-10.
7. Sesack, S. R. and V. M. Pickel, (1992), J Neurosci **12**(4): 1335-1350.
8. Morley, J. S., (1983), Br Med Bull. **39**(1) 5-10
9 Hansen, P. E. and B A. Morgan, (1984), in "Opioid Peptides: Biology, Chemistry and Genetics", (Udenfriend and Meienhofer, Eds) Vol 6, Academic Press Inc, Orlando
10. Allen, M H and M. L. Vestal, (1992), J Am Soc Mass Spectrom 3 18-26

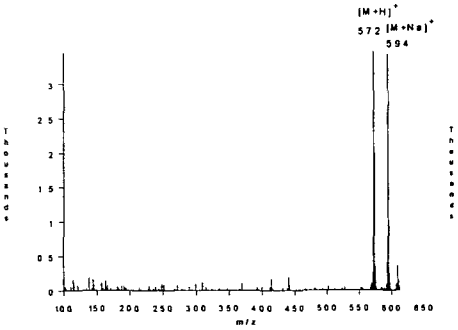

Fig. 1. ESI mass spectrum of [HO-Tyr[1]LE at 18V repeller voltage (soft ionization)

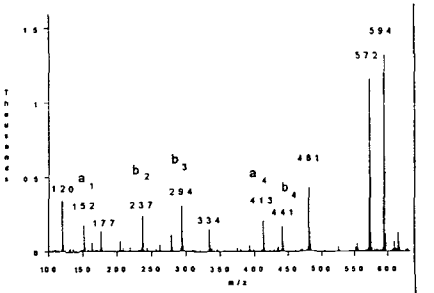

Fig. 2. ESI mass spectrum of [HO-Tyr1]-LE at 50V repeller voltage (collision induced dissociation)

Analysis of Mureidomycin Antibiotics by Ionspray Mass Spectrometry.

Duncan K. Bryant (1), Catherine S.V. Frydrych (2), and Gerald Risbridger (2).
SmithKline Beecham Pharmaceuticals, (1) Old Powder Mills, Tonbridge, Kent TN11 9AN, United Kingdom, (2)Brockham Park, Betchworth, Surrey RH3 7AJ, United Kingdom.

Atmospheric Pressure Ionisation Mass Spectrometry (API/MS) is proving to be a versatile ionisation technique for the analysis of a wide range of pharmaceutical compounds[1]. API/MS has been successfully applied here to the study of a class of antibiotic compounds called mureidomycins (1). These compounds, isolated as metabolites from a culture and purified by HPLC, were found to give a positive response to a translocase inhibitor screen. The structure contains m-tyrosine residues at both the N- and C-termini in addition two highly modified residues in-between. Firstly there is an unusual N-methylated diamino acid with an enamine-sugar uracil or dihydrouracil group as the side chain. Then moving towards the C-terminus there is a methionine residue that is reversed with its nitrogen linked to the C-terminal tyrosine residue via a ureido bond.

Ionspray proves ideal for providing rapid and unambiguous molecular weight data for challenging samples. The high sensitivity of the technique is also important for the analysis of culture metabolites that are often only available on the nanomole scale. Fast atom bombardment (FAB) can also be used to obtain spectra[1] although the sensitivity is considerably lower.

Ionspray Mass Spectrometry was performed on a Sciex API-III triple quadrupole mass spectrometer (Toronto, Canada). About 10-100pmol of sample was used for analysis. The eluant used for both positive and negative ion modes was generally 50% MeCN/50% 1%HOAc(aq) flowing at 20mL min^{-1}. In positive ion mode the ionspray voltage was 5kV and the orifice voltage was set at 70V. In negative ion mode the ionspray voltage was -4.5kV and the orifice voltage was varied between -70 and -120V. CID MS/MS was performed using argon as the collision gas at a thickness of $6x10^{14}$ atoms cm^{-2}.

The positive ion mode MS/MS ionspray spectrum of mureidomycin B is shown in Figure 1. A protonated molecule is observed at 843Da indicating a molecular weight of 842Da. It can be seen that there is extensive fragmentation of the backbone of the molecule that is analogous to the behaviour observed with peptides when subjected to low energy CID in triple quadrupoles[2]. However, unlike peptides, mureidomycins appear to exhibit sidechain fragmentation. The enamine-sugar-dihydrouracil moiety undergoes considerable fragmentation upon collision induced dissociation. Similar fragmentation patterns are observed for other members of the mureidomycin family. In negative ion mode ionspray of mureidomycin B a deprotonated molecule of 841Da is observed giving an unambiguous molecular weight assignment of 842Da.

The fragmentation of mureidomycins observed in both positive and negative ion modes is, as stated previously, analogous to that of peptides. Table 1 summarises the wide variety of fragment ion types observed in positive ion mode MS/MS including a, b, c, x, and y ions along with imminium ions and sidechain fragment ions. With acidic residues at both termini there is no preference for N- or C-terminal ions.

Fragmentation can also be induced by in-source CID, performed by increasing the orifice voltage. The optimum voltage for in-source CID can be found by ramping the orifice voltage from 20-250V. The optimum value for mureidomycins appears to about 150V that is much higher than the value observed for organic molecules[3] (80-120V).

Extracted ion chromatograms can also be used to observe the onset of CID in the tandem MS/MS experiment. By varying the argon collision gas thickness, one can observe the onset of decomposition of the pseudo-molecular ion. It was found that optimal fragment ion formation occurs at a gas thickness of about $4.5x10^{14}$ atoms cm^{-2}. This is somewhat higher than that observed for organic molecules[3].

References:
1. F.Isono, M.Inukai, S.Takahashi, and T.Haneishi, *J. Antibiotics*, 1989, **42**, 667-673.
2. D.F.Hunt, J.R.Yates III, J.Shabanowitz, S.Winston, C.R.Hauer, *Proc. Natl. Acad. Sci. U.S.A.* 1986, **83**, 6233.
3. D.K.Bryant, B.M.Stockton, F.Cottee, *Proceedings of the 40th ASMS Conference on Mass Spectrometry and Allied Topics*. May 31-June 5 1992, Washington, DC, p606-607.

Table 1. Positive Ion Fragmentation of Mureidomycin B; Ion Types.

m/z	Ion Type
104	Imminium
136	Imminium
193	c
285	Internal fragment ion
311	a
339	b
396	-
409	sidechain
422	sidechain
504	y
530	x
548	y+sidechain
616	sidechain
636	y
662	b
680	y
711	sidechain
729	sidechain

MUREIDOMYCIN B

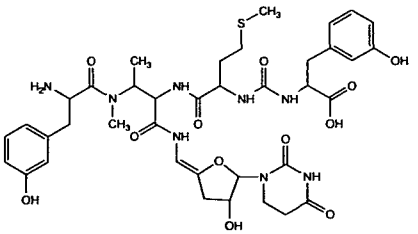

$C_{38}H_{60}N_8O_{12}S$ MW=842Da

Figure 1. Positive Ion MS/MS Spectrum of Mureidomycin B

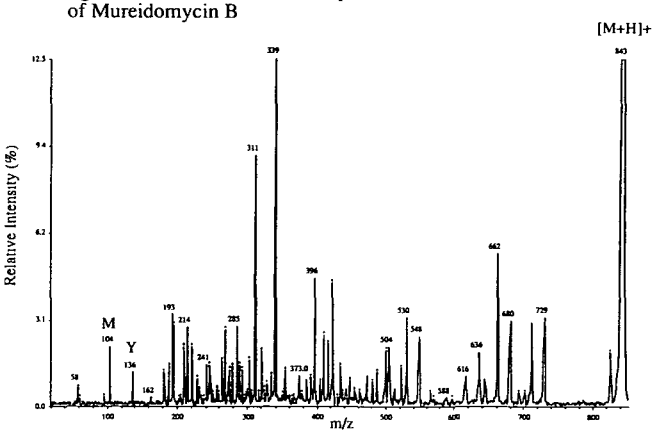

The Use of Electrospary-Mass Spectrometry for the Analysis of Pharmaceuticals, Proteins and Peptides

Paul C. Goodley and Steve Fischer, The Hewlett-Packard Co., Scientific Instruments, Palo Alto, CA, 94304

Electrospray ionization (ES) has not only expanded the mass range of conventional mass spectrometers (ms) by a factor of 40 It has also increased the applicability and sensitivity by the same factor For compounds which were either difficult or nearly impossible to analyze by ms a short year ago, can now be easily analyzed in a few minutes by ES-MS Experimental drugs and pharmaceuticals such as antibiotics and anticancer or tumor treating drugs can be analyzed directly using ES-MS

Compounds such as Taxol, Taxol metabolites, Vinblastine, and antitumor alkaloids and metabolites can be analyzed by ES-MS within minutes of collection or purification. Antibiotics such as Lincomycin, Erythromycin, Tobramycin, Penicillin G, Hydrogromycin B and Tetracycline can easily be analyzed from crude extracts by ES-MS The data from these compounds may be quantified using internal standards as references to less than five percent (5%) relative standard deviations (RSDs) For small proteins and peptides, be they natural or synthetic, and having mass less than 10,000 Daltons (DA), the same techniques may be applied to yield excellent quantitative data having RSDs less than eight percent without using internal standards When internal standards are used, the RSDs will drop below five percent

The low RSDs are a result of the ion source design where-by the electrospray chamber, which is at atmosphere pressure, is isolated from the high vacuum system and the ion lens system The pressure of the exiting gases and ions is held very stable. Figure 1 shows the detailed ion source The ions are generated in the Electrospray Chamber and transfered to the Capillary Exit region near the CID Supersonic Zone of Silence as shown in Figure 1 below.

Fig. 1

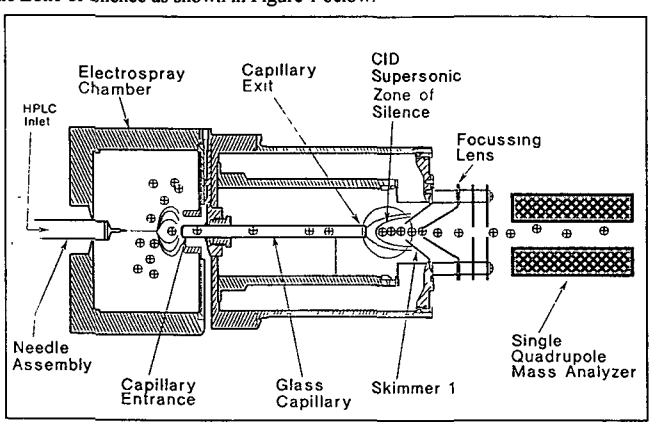

Figure 2 below shows three examples of using ES-MS with an untrasound droplet generator using the antibiotic, Lincomycin. Three sets of examples are shown. The top example set shows the extracted parent molecular adduct ion of Lincomycin at m/z 408, followed by its' full scan mass spectrum. The top trace in each set is a flow injection in which the peak elutes in 10 seconds or less. Each subsequent sets of data are similar, but the concentrations decrease from 100 nanograms per injection to 100 picograms for the last set of data. Detection levels are obvious for the full scan mode at ca 100pg.

Fig. 2

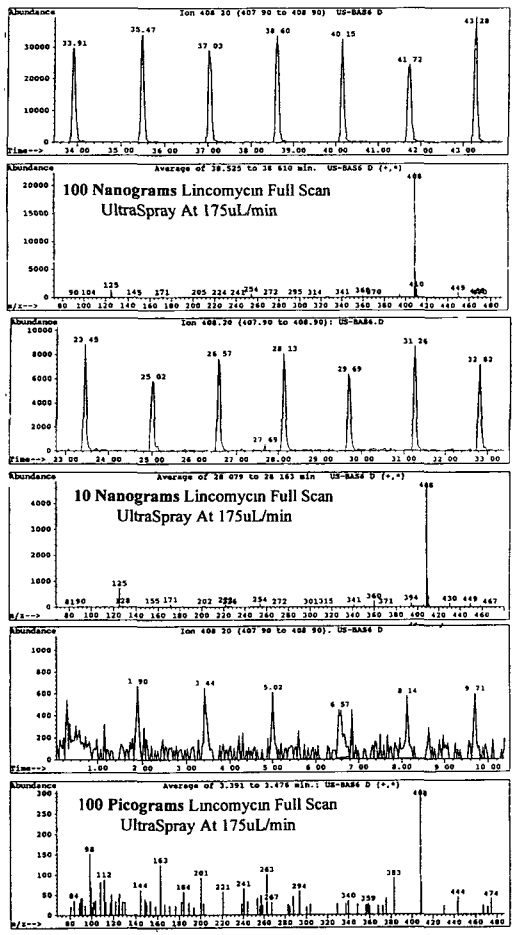

USE OF AN ON-LINE LIQUID CHROMATOGRAPHY TRAPPING COLUMN FOR ELECTROSPRAY MASS SPECTROMETRIC ANALYSIS OF CYTOKINE MEDIATORS INVOLVED IN INFLAMMATORY SKIN DISORDERS.

*I. Kay, M. Judge, A.I. Mallet and M.W. Greaves, St John's Institute of Dermatology, UMDS, University of London, St Thomas' Hospital, London SE1 7EH, England.

INTRODUCTION

We are currently investigating the use of ESI-MS for the identification, at the molecular level, of a family (chemokine) of cytokines with pro-inflammatory activities. These cytokines are characteristically basic, heparin binding, range from 8-10 kDa in molecular weight and have been implicated as mediators involved in inflammatory skin disorders.

The isolation procedures used in the extraction of cytokines, from biological matrices, give rise to samples which can contain a number of non-peptide components such as salts, ion-pairing reagents, detergents or preservatives. It is accepted that the efficiency of electrospray ionisation is affected by these substances. We describe here a method which circumvents this problem.

METHODS

Electrospray Mass Spectrometry

ESI-MS analysis was performed on a VG Masslab Trio 2, fitted with a VG Biotech ESI source (Fisons Instruments, UK). Peptide samples were introduced into the ESI-MS source in 50:49:1 acetonitrile/water/acetic acid v/v/v, containing 1 pmol/µl gramicidin S (ESI running solvent). An Isco model SFC-500 micro flow pump (Jones Chromatography, UK) was used to deliver the solvent at a flow rate of 7.5 µl/min. Gramicidin S was used to tune the instrument. The electrospray needle was held at 4 kV relative to the source and a cone voltage of 65 was applied. Ubiquitin was used as a calibrant. Unless otherwise stated ubiquitin, cytochrome C, and myoglobin were monitored using selected ion recording (SIR) at m/z 857, 824, and 893 respectively.

LC Trapping Column

The trapping column system (Figure 1) comprised a Rheodyne (model 8125) injection valve with 500 µl loop, a Rheodyne (model 7000) 6-way switching valve, and a microbore column (1 x 50 mm) packed (in house) with porous poly(styrene/divinylbenzene) PLRP-S (8 µm particle size, 300 °A pore size). Samples, diluted with water, if necessary, were loaded onto the column via the 500 µl injection loop. The column was washed for 3 minutes with acetonitrile/water/acetic acid 15:84:1 (v/v/v) using a Waters model 501 pump (500 µl/min). The 6-way valve was then switched and bound material was eluted off the column with ESI running solvent.

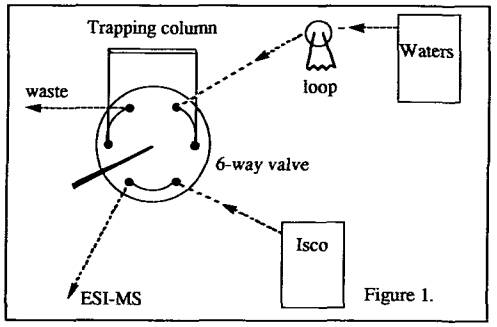

Figure 1.

Reagents Studied

The effects of various reagents (Table 1) on the efficiency of electrospray ionisation of three model peptides, ubiquitin, cytochrome C, and myoglobin were assessed directly and in conjunction with the on-line trapping column.

Extraction of chemokine peptides

Stratum corneum samples from healthy individuals and skin scale samples from Psoriatic patients were homogenised in 0.1 % TFA in a glass homogeniser, and centrifuged at 12,000 x g for 15 min. Supernatants from skin extracts were filtered (0.45 µm), concentrated, and applied to heparin affinity columns in 50 mM tris buffer (pH 8). The column was washed in buffer and bound material was eluted in buffer suplemented with 0.65 M NaCl. This material was chromatographed on Aquapore RP-8 and resultant HPLC fractions were analysed using the trapping column.

RESULTS

The effect of reagents (Table 1) on the efficiency of electrospray ionisation of ubiquitin, cytochrome C and myoglobin was determined using duplicate injections (10µl) for each peptide in the absence and in the presence of reagent. The results, presented in Table 1, are expressed as the % decrease in ESI signal intensity observed when peptides were analysed in the presence of reagent. The ability of the trapping column to remove ionisation suppressing reagents from ubiquitin (20 pmol) samples prior to ESI-MS is shown in Figure 2. A, Blank; B, Pure peptide; C, 0.1% TFA; D, 100mM phosphate; E, 0.2% Na azide containing samples. Similar results (not shown) were obtained with cytochrome C and myoglobin. The trapping column system has been used in the analysis of HPLC fractions derived from psoriatic scale extractions. An example is shown in Figure 3.

Table 1

Reagent	Conc. (%)	Peptide	Reduction(%)
TFA	0.01	Ubiquitin	93
		Cyto. C	90
		Myoglobin	62
Phosphate	10 mM	Ubiquitin	76
		Cyto. C	71
		Myoglobin	73
Na azide	0.02	Ubiquitin	58
		Cyto. C	68
PEG	0.005	Ubiquitin	66
SDS	0.01	Cyto. C	54

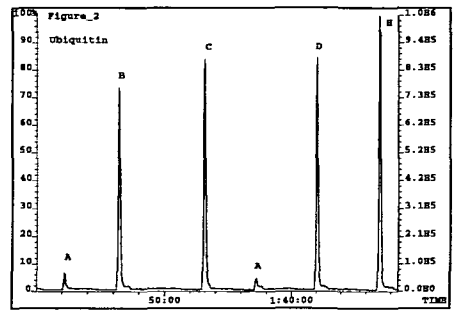

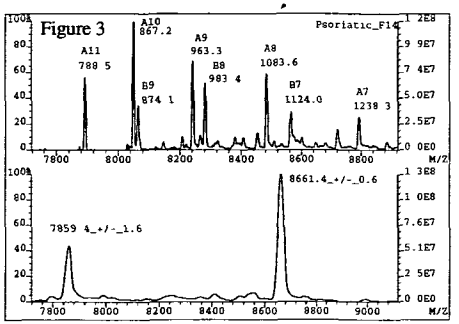

DISCUSSION AND CONCLUSIONS

We have demonstrated that the presence of salts, ion-pairing reagents, preservatives, or detergents can be detrimental to the efficiency of electrospray ionisation of peptides. This confirms the work of several other groups of workers. We have successfully circumvented this problem by using a trapping column which allows the removal of ionisation suppressing reagents from peptide samples prior to their analysis. Furthermore cytokines have a propensity to adsorb onto surfaces, particularly when taken to dryness. The trapping column system eliminates the requirement for samples to be taken to dryness as repeated injections onto the column enable peptides to be concentrated prior to ESI-MS. We are currently attempting to identify chemokine peptides in biological matrices with on-line LC trapping ESI-MS.

Analysis of Synthetic Peptide Impurities Using Capillary Electrophoresis/Electrospray Mass Spectrometry

Kenneth J. Rosnack, Justin G. Stroh
Glenn C. Andrews and David H. Singleton
Pfizer Inc, Groton CT 06340

We have constructed a CE/MS system based on experimental designs found in the literature.[1-3] We present several examples where so called single components were isolated by HPLC but were confirmed as mixtures by CE and CE/MS.

A mixture of Bradykinin and Magainin Spacer Peptide was run to test the performance & reliability of our CE/MS system. The CE/UV, reconstructed total ion electropherogram, and the averaged mass spectra for each component confirmed a working system. The HPLC/UV chromatogram of an isolated synthetic peptide Ac-C(Acm)PNEFTGDRC(Acm)QNYVM-NH_2 indicated a single component sample (99.3% by UV area). Direct infusion ESI/MS analysis of the sample indicated a mixture of desired peptide and a dehydration product. One could question whether the dehydration product is due to fragmentation of the peptide or whether it is indeed an impurity in the sample. The CE/UV and reconstructed total ion electropherograms of the Ac-C(Acm)PNEFTGDRC(Acm)QNYVM-NH_2 peptide sample are presented in Figure 1. The averaged mass spectrum of peak 1 indicated a doubly charged ion *m/z* 971.1 Da. Assuming that the peak is related to the synthesized peptide, the experimental mass of the component is 1941.6 Da, corresponding to dehydration of the intact peptide. The mass spectrum of peak 2 indicated the intact peptide. See Figure 2.

While analyzing a synthetic peptide MVII-C, we observed severe adsorption of the sample to the untreated fused silica. By analyzing the sample on a linear polyacrylamide coated column[4-5], we had virtually eliminated adsorption of this peptide. Coated columns were therefore used in all future experiments.

An HPLC/UV chromatogram of an isolated synthetic peptide, Heregulin-α, indicated a single peptide component at approximately 16 minutes. A CE/UV electropherogram, using a citrate buffer, of Heregulin-α (pI 9.3) also indicated a fairly clean sample. Because the pH of the citrate buffer was much lower than the pI of Heregulin-α and that sodium citrate was not compatible with ESI/MS, a buffer of 20mM ε-amino-n-caproic acid[6] (EACA) pH 4.6 was used. The averaged mass spectra of peaks 1 and 2 gave the same mass indicating the presence of isomers or perhaps, within mass accuracy, a deamidation product. Further analysis with isolation of the components would be required to evaluate the mixture.

We have demonstrated that CE and CE/MS are techniques that can solve practical problems encountered in the daily operations of a peptide synthesis laboratory. We have also found that the purity of HPLC isolated peptide samples can be confirmed through the use of CE and CE/MS. Coated fused silica capillary columns virtually eliminated compound adsorption resulting in better resolution and increased sensitivity as determined in our experiments.

References

[1]Smith, R.D.; Udseth, H.R., Barinaga, C.J.;, and Edmonds, C.J.; *J. Chromatogr.* **559**, (1991), 197-208.
[2]Johansson, I.A.; Pavelka, R.; and Henion, J.D.; *J. Chromatogr.* **559**, (1991), 515-528.
[3]Suter, M.J.-F.; DaGue, B.B.; Moore, W.T.; Lin, S.-H ; and Caprioli, R. M.; *J. Chromatogr.* **559**, (1991) 101-116.
[4]Hjerten, S.; *J. Chromatogr.* **347**, (1985), 191-197.
[5]We greatly appreciate and acknowledge the assistance on CE capillary coating technology provided by Dr. Paul Vouros *et al*, Department of Chemistry, Northeastern University, Boston, MA.
[6]Foret, F ; Szoko, E.; and Karger, B.L.; *J. Chromatogr.* **608**, (1992), 3-12.

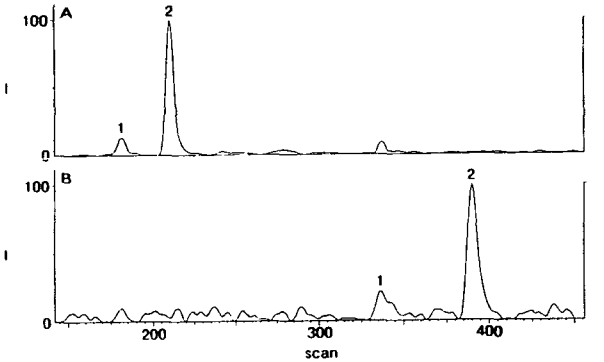

Figure 1: Top--CEUV Electropherogram of Ac-C(Acm)PNEFTGDRC(Acm)QNYVM-NH_2
Bottom--Total Ion Electropherogram of Ac-C(Acm)PNEFTGDRC(Acm)QNYVM-NH_2

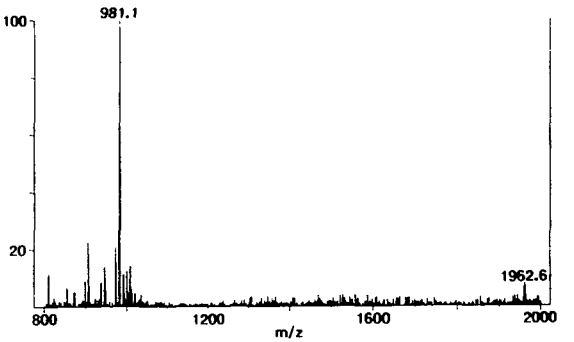

Figure 2: Mass Spectrum of Intact Ac-C(Acm)PNEFTGDRC(Acm)QNYVM-NH_2 From the CEMS Analysis.

Practical Considerations in the Capillary Electrophoresis - Electrospray Mass Spectrometry of Proteins

by Toni J. Thompson, Frantisek Foret, Daniel P. Kirby, Paul Vouros, and Barry L. Karger, Barnett Institute, Department of Chemistry, Northeastern University, Boston, MA 02115.

Capillary zone electrophoresis (CZE) -- electrospray ionization (ESI) mass spectrometry (MS) is a potentially powerful tool for the separation and identification of biomolecules. The CZE separation is affected by the properties of the background electrolyte (BGE), such as pH, concentration, and chemical composition. At the same time, the background noise level in the MS is, in part, determined by the species and concentration of the ions that are detected. This study systematically compares the CZE separation and ESI/MS detection of a protein mixture in several different BGE systems and liquid sheath compositions to develop a more complete understanding of the flexibility of the CZE-ESI/MS combination.

The mass spectrometer in this study was a Finnigan TSQ700 equipped with an electrospray ionization source. Mass spectra were obtained at a rate of one second/scan from *m/z* 600 - *m/z* 2000. The electrospray conditions included the 170°C drying gas (N_2) flowing at ~3000mL/min, and the gas sheath (O_2) flow rate was 190mL/min. The liquid sheath was of varying composition and flowed at 2.5 µL/min. The electrospray voltage was varied to obtain the most stable electrospray. The capillary electrophoresis power supply (Spellman CZE1000R) was operated at 20kV The separation column was 80 cm long X 75 µm i.d. and was coated in house with linear polyacrylamide. Sixty nL of the same sample, which consisted of cytochrome c, myoglobin, α-chymotrypsinogen A, β-lactoglobulin A, ribonuclease A, and β-lactoglobulin B, were introduced into the column by siphon injection for all analyses.

The figures on the following page illustrate some of the effects of the BGE and LS compositions on the separation and S/N. Figure 1 illustrates the separation with 6-aminohexanoic acid adjusted to pH of 4.4 with acetic acid as the BGE and the liquid sheath containing acetic acid. Figure 2 illustrates the effect on the separation when HCl is substituted for acetic acid in the liquid sheath.

A variety of BGE and LS conditions appears to be compatible with CZE-ESI/MS. Successful operation with this combination requires integration of LS, BGE, and ESI/MS. In no case have we seen that the spectra are compromised by these variations. The BGE composition determines the selectivity and CZE separation efficiency. When high selectivity is required, volatile or some non -volatile BGE constituents can be used,such as β-alanine or 6-aminohexanoic acid. Typical non-buffered solutions may be employed in cases where selectivity is sufficient. The liquid sheath composition can also affect the migration of the analytes, due to migration of anions from the LS toward the anode, forming an moving ionic boundary inside the capillary. This may result in a change in pH of the BGE and affect the effective charge on the proteins which can result in a change in their migration order and/or times. The BGE and LS compositions affect not only the migration but also the S/N and electrospray stability. Successful analyses can be obtained with BGE containing some non-volatile constituents and cations other than protons. One may choose to trade better S/N for separation selectivity.

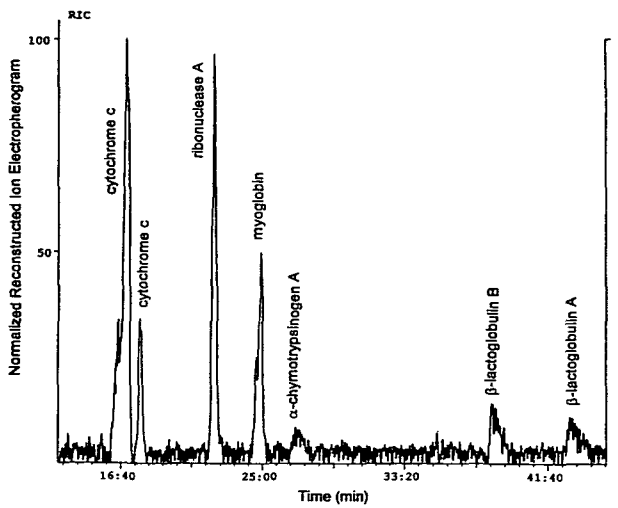

Figure 1:
CZE-ESI/MS
(600u-2000u)
BGE: 20mM EACA,
pH 4.4
LS: 1% HAc in
50% MeOH/H_2O

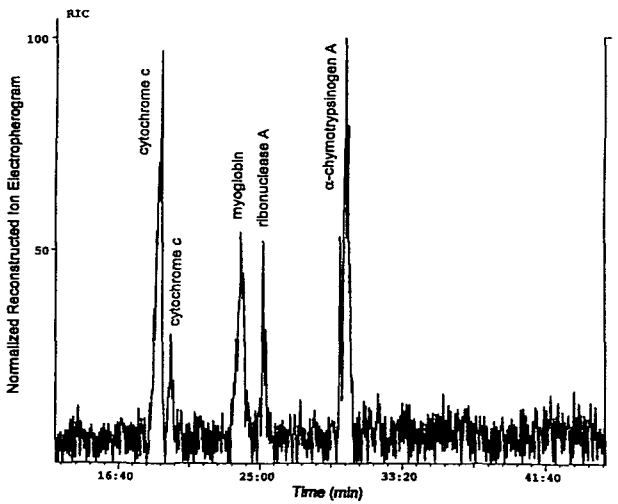

Figure 2:
CZE-ESI/MS
(600u-2000u)
BGE: 20mM EACA,
pH 4.4
LS: 10mM HCl in
50% MeOH/H_2O

Effect of Gas-Phase Acid Addition on the Electrospray Mass Spectrum of Myoglobin

*Baiwei Lin[a] and Jan Sunner[b]
[a]Lederle Laboratories, American Cyanamide, Pearl River, NY 10965
[b]Department of Chemistry, Montana State University, Bozeman,MT 59717

INTRODUCTION

Addition of acids to the electrospray solution tends to shift the charge distribution of a protein towards lower m/z. At the same time, the protein tends to denatured. Such denaturation will, in general, result in the dissociation of specific non-covalently bonded complexes.

In the case of myoglobin, denaturation is revealed by the accompanying dissociation of heme. The native myoglobin, with the heme, has a molecular weight of 17,566 Da. After the denaturation and the heme loss, the molecular weight is 16,951 Da. We studied the effect of adding acids, not to the ESI solution, but to the gas-phase in the electrospray source. Results from gas-phase are compared with those from addition of acids to the ESI solution. The effect of several different acids added to the gas-phase was also investigated.

EXPERIMENTAL

Figure 1 shows the instrumental set up for electrospray/quadruple mass spectrometer. A home-built electrospray ion source, shown in Figure 2, is interfaced to a quadruple MS (VG-TRIO2). A stainless steel transport capillary (i.d.=0.5mm) connects the electrospray at 1 atmosphere with the intermediate pressure chamber. A wound heater wire was used to control the capillary temperature. Optimum temperatures ranged from 75°C to 85°C.

RESULTS AND DISCUSSIONS

(A) Acidic Addition To Gas-Phase Versus ES Solution. When myoglobin was electrosprayed in pure water, only the native heme-globin complex was detected, as shown in Figure 3(a). The complex had few charges, $<10^+$, and the complex ions had low intensity. With only a small amount of acetic acid added to the protein solution, where pH was 5, an envelope of peaks for the denatured myoglobin appeared, Figure 3(b). In contrast, gas-phase acid addition gave a very different result, Figure 3(c). Only the native heme-globin complex was obtained. The appearance of HOAc in gas-phase significantly increased the charges on the native myoglobin, up to 12^+. More importantly, there was a fifty-fold increase in the signal intensity.

(B) The Effect Of Different Acids In The Gas-Phase. Addition of organic acids into the gas-phase, such as HOAc in Figure 4(a) and p-tolunesulfonic acid in Figure 4(b), gave very similar results. Both spectra show only heme-globin complex with relatively high ion intensities. Therefore no heme dissociation and presumably no denaturation occurred. The increase in the charge state may indicate that the protein conformation loosened with the presence of acid in the gas-phase.

Addition of HCl into the gas-phase had very different effects on the protein spectra. As shown in Figure 4(c), extensive heme dissociation was observed. Further, the signal-to-noise level was seen to be low. At a higher HCl flow rate, no spectra at all could be obtained. Addition of HCl into the gas-phase is seen to suppress the native myoglobin ions.

CONCLUTIONS

Acid addition into the gas-phase of ESI source can enhance the intensities of the native myoglobin ions in the electrospray spectrum since the addition of acetic acid into the gas-phase can only obtain heme-globin complex ions and therefore no heme dissociation occurred. The complex ion intensity was also greatly increased. However, the addition of the same acid into ESI solution resulted in a great denaturation of the myoglobin. The effect of gas-phase acid addition varied considerably between different acids. Some acids, such as HCl, resulted in the extensive denaturation of the protein with no signal improvements. Other acids, such as acetic acids and p-tolunesulfonic acid, provided a good environment for heme-globin complex and promoted native ion intensities.

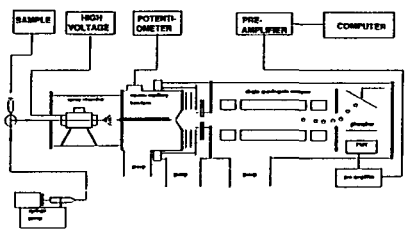

Figure 1. Schematic drawing of electrospray/quadruple MS.

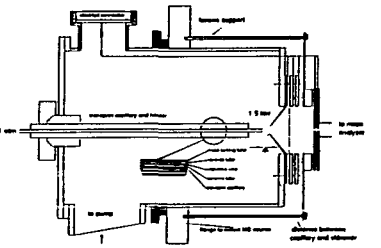

Figure 2. Electrospray ion source.

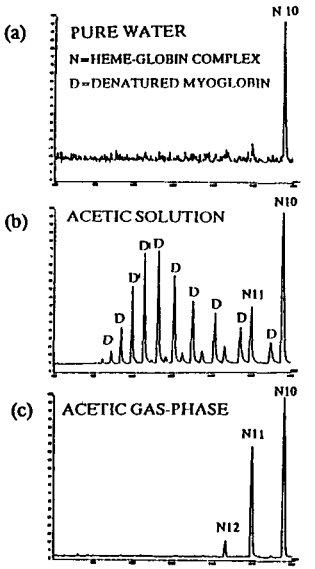

Figure 3. Acidic gas-phase versus acidic solution.

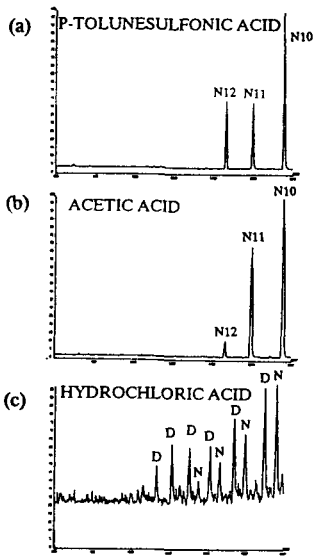

Figure 4. Different acids in the gas-phase.

Probing Ketone-Protein Adducts by Means of Electrospray Mass Spectrometry.

J.C.Y. Le Blanc*, K.W.M. Siu and R. Guevremont, Institute for Environmental Chemistry, National Research Council of Canada, Montreal Road, Ottawa (Ontario) Canada K1A 0R6.

In previous work we have shown that multiply charged ion distributions observed in the electrospray (ES) mass spectrum of proteins originate from pre-formed multiply charged protein ions in aqueous solution. An aqueous solution equilibrium model based on the pK_a's of acidic and basic sites on proteins was used to compare the distribution of ions in solution to the shape of the ion abundance profile in the electrospray mass spectrum [1-3]. Since the aqueous solution chemistry of proteins is reflected in their ES mass spectra, aside from the acid/base equilibrium, other types of equilibria taking place in solution may be monitored by ES-MS as well. Aldehydes and ketones are known to react with free amine in proteins to form a Schiff base (reaction 1). This reaction is quite simple and has the advantages of being site specific and with minimal alteration to the charge state.

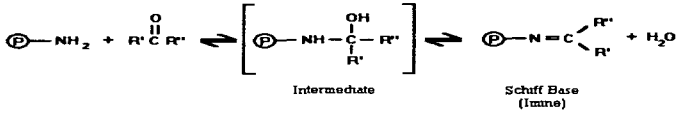

Reaction 1

When proteins are electrosprayed from solutions containing ketones or aldehydes, two types of distribution are observed: 1) the overall distribution describing the various multiply charged ions present in solution, and 2) for each given charge state, a series of peaks representing the equilibria of successive additions of ketones (or aldehydes) to free amino sites on the protein. Ubiquitin was electrosprayed from a solution containing water:methanol:acetone:piperidine (37:50:10:3 (v:v:v:v)); Figure 1 shows the overall charge distribution of the multiply charged ions, and the clusters of peaks representing the addition of acetone to each charge state. Since acetone can react at more than one site, the addition of acetone may be represented by successive addition steps as represented by the following scheme:

$$Ubiquitin^{-z} + Acetone \rightleftharpoons [Ubiquitin\text{-}Acetone]^{-z} + H_2O$$
$$[Ubiquitin\text{-}Acetone]^{-z} + Acetone \rightleftharpoons [Ubiquitin\text{-}Acetone_2]^{-z} + H_2O$$
$$\ldots\ldots\ldots + \ldots\ldots\ldots \rightleftharpoons \ldots\ldots\ldots + \ldots\ldots\ldots$$
$$[Ubiquitin\text{-}Acetone_{(x-1)}]^{-z} + Acetone \rightleftharpoons [Ubiquitin\text{-}Acetone_x]^{-z} + H_2O$$

The subscript **x** represents the maximum number of acetone that can react with the protein and **z** denotes the charge state of the protein. From the relative intensities of the ions in an ES mass spectrum, the equilibrium constant for each successive addition may be calculated for a given solution condition. Figure 2 shows the calculated equilibrium constant as a function of the number of ketone groups added to ubiquitin based on the results shown in Figure 1.

When water in the solution is gradually replaced with methanol or acetonitrile in the presence of acetone, a gradual increase in the number of imine formed is observed. In other words, the cluster of peaks for a given charge state will shift towards higher m/z values (e.g. see the ubiquitin-acetone ions with z=-7 in Figure 3). The formation of the imine results from the nucleophilic addition of free amine to acetone; in proteins only lysine residues and the N-terminal (if not blocked) may have free amine to react with acetone. By electrospraying two solutions, information on the composition of a protein may be

obtained as follows. The protein is first electrosprayed under regular conditions (water:methanol) to determine its molecular mass. A second protein solution containing acetone and in which the water has been replaced with another solvent (methanol or acetonitrile) is electrosprayed to determine the molecular mass of the protein with all the amino sites modified. From these two mass spectra, the number of lysines and N-terminal groups may be calculated:

$$Total\ Number_{(Lysine\ +\ N\text{-}Terminal)} = \frac{(\ Protein\ Mass_{(Acetone,\ DDW\ free)} - Protein\ Mass_{(Acetone\ free)}\ )}{40.06}$$

The numbers of lysines and N-terminal groups in several proteins were calculated as above and compared with values based on sequence information (Figure 4). The straight line represents a one to one correlation between experimental and expected values; the triangles indicate the experimental values. For all but one protein (β-lactoglobulin) the calculated number of lysines and N-terminal is statistically identical to the expected value. β-Lactoglobulin has one free cysteine group that can act as a nucleophile towards acetone addition thus resulting in too high a total amino number.

* Postgraduate student, Department of Chemistry, Queen's University, Kingston (Ontario) Canada K7L 3N6.

[1] R.Guevremont, K.W.M. Siu, J.C.Y. Le Blanc and S.S. Berman, *J. Am. Soc. Mass Spectrom.*, **3**, 216 (1992)
[2] J.C.Y. Le Blanc, K.W.M. Siu, R. Guevremont and S.S. Berman, *Org. Mass Spectrom.*, **26**, 831 (1991)
[3] J.C.Y. Le Blanc, K.M.W. Siu and R. Guevremont, *Int. J. Ion Process and Mass Spectrom.*, In press.

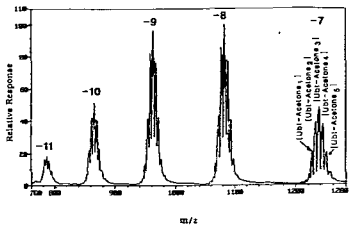

Fig.1 ES mass spectrum of bovine ubiquitin in DDW:MeOH:acetone:piper.(37:50:10:3(v:v:v:v)).

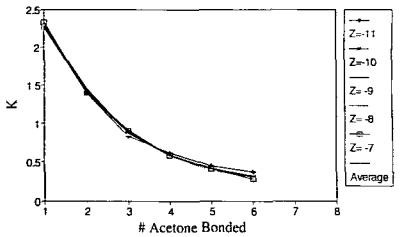

Fig.2 Equilibrium constants for the ubiquitin/acetone system under the conditions describe in Figure 1.

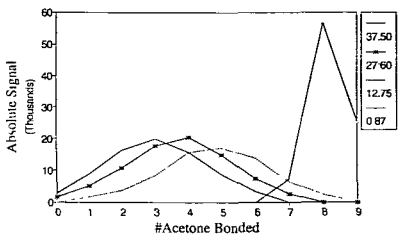

Fig. 3 Displacement of the cluster profile when the methanol/water ratio increases for Z=-7. All the solutions contained 10% (v/v) of acetone.

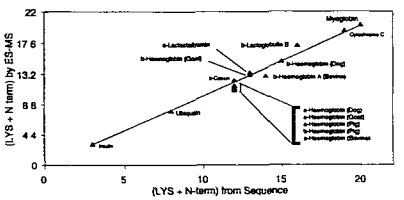

Fig. 4 Determination of the total number of lysine resisues and N-terminal by ES-MS and comparison with values obtained from sequence information.

Structural Analysis of Lipids by Negative ESI/MS/MS

Stephen Chan and Vernon Reinhold
Department of Nutrition, Harvard University School of Public Health, Boston, MA 02115

The introduction of electrospray ionization (ESI) offers an alterative approach for sensitive analysis of many biomolecules. Thus far, the majority of ESI applications are based on the detection of cations derived from proton or alkaline ion adductions. However, for biomolecules containing strong acidic residues, the formation of anions (through deprotonation) may be more abundant under negative ESI conditions. The formation of anions is especially important for lipophilic molecules such as endotoxic Lipid A and phospholipids because of the acidity of their phosphate groups.

Lipid A serves as the lipophilic membrane anchor for the outer polysaccharide coat of Gram-negative bacteria. It has been linked to many of the pathophysiological effects of the bacteria. The structural information of this class of compounds is extremely important because the toxicity levels of Lipid A different dramatically from structure to structure. For those structures associated with an extreme toxicity, a sensitive technique is needed in order to handle the small biological amount frequently available. Monophosphoryl Lipid A (MLA) moiety obtained from *Salmonella minnesota* Re595 along with several different phosphatidylethanolamines were chosen as models for our structural studies using negative ESI/MS/MS.

All the experiments were performed on a Finnigan TSQ-700 triple stage quadruple mass spectrometer equipped with an Analytica (Bradford, CT) electrospray ionization source. Oxygen is used as a shealth gas for electron scavenging during sample infusions. All the lipid samples were dissolved in a buffer containing a mixture of chloroform and methanol in a ratio of 2:1 (by volume). The pH was maintained at about 10 buffered by NH_4OH. Typically, the infused samples contain 40 μg of lipids in a 100 μl of buffer. The sample infusion rate is 0.75 μl/min and the mass spectrometer is operated at 10 sec/scan. The instrument tuning and calibration are based on a solution containing a mixture of insulin A and a tetra-peptide (MRFA). The solution is made of a mixture of methanol and water in a 7:3 ratio (by volume). Again NH_4OH was used to maintain the pH at 10.5.

The ESI mass spectrum shows the heterogeneity of the Lipid A sample (Figure 1) as was previously reported [1]. The very low noise level detected in the mass spectrum indicates the high sensitivity of the technique. Only singly charged species are observed for the MLA structure identified. In this particular sample, the hexaacyl MLA (m/z = 1716) is the predominant species. Our collision studies reveal that the predominant fragment ions are the loss of the fatty acid acyl groups at different sites. This information allows the acyl groups on MLA to be identified. The mass spectrum of phosphatidylethanolamine shows primarily the $[M-1]^-$ and $[2M-1]^-$ species (Figure 2). The same species were also observed for the phosphatidylethanolamines with mono- and di-methyl amine groups. The collision spectra derived from the $[M-1]^-$ indicate that the main fragment ions are the loss fatty acid acyl chains.

In summary, sensitive detection of lipids have been achieved using negative ESI/MS. Structural information about the acyl residues on the lipids can be revealed by MS/MS.

This studies can certainly be extended to other compound types containing phosphate residues similar to our lipid samples.

Reference

1. R. S. Johnson, G-R Her, J. Grabarek, J. Hawier and V. N. Reinhold; J. Bio. Chem., 265 (14), 8108, 1990.

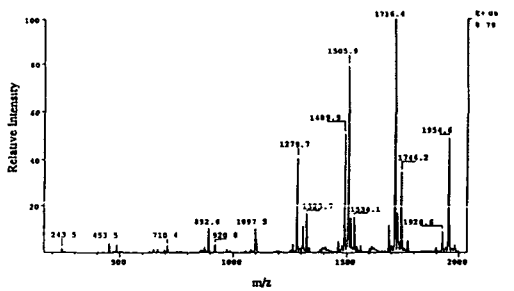

Figure 1. Negative ESI mass spectrum of monophosphoryl Lipid A moiety derived from *Salmonella minnesota Re595*. The different peaks represent the heterogeneity of the sample.

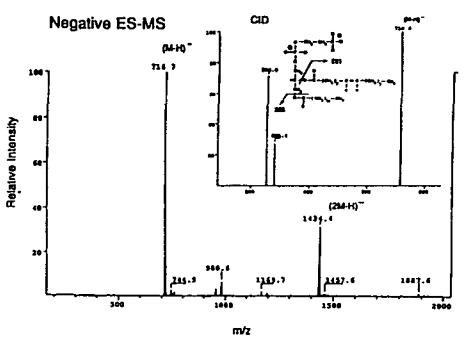

Figure 2. Negative ESI mass spectrum of L-α-phosphatidylethanolamine, β-oleoyl α-palmitoyl. The inserted spectrum is obtained from collision studies of the $[M-1]^-$ anions.

Chemical Properties of Diaryldiazomethane: An Electrospray Ionization Mass Spectrometric Study

Yunhui Wu* and Stephen R. Wilson
Department of Chemistry, New York University
Washington Square, New York, NY 10003

The discovery of the chemistry of diazo compounds was made a century ago. The first synthesis of ethyl diazoacetate in 1883 opened the wide field of diazo chemistry, which even today has not yet been exhausted. Recently, several mono-adducts of C_{60} have been prepared via cycloaddition of diazo compounds with fullerene molecules.[1,2] During this study, we have observed that ESI-MS is very efficient for investigating the chemical properties of diazo compounds. Although chemistry of diazo compounds is well known, direct detection of their adducts and dimers by mass spectrometer is usually not easy.

We have synthesized a crown ether tagged diaryldiazomethane (**1**).[2] With the use of electrospray ionization mass spectrometry, we are able to study the chemical properties of unstable diaryldiazomethane compounds. The reactions of diaryldiazomethane with O2, methanol, carboxylic acids (such as fatty acids and amino acids) and fullerenes are easily followed by this approach.

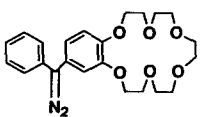

1

Figure 1 showed the ESI mass spectrum of products formed by mixing **1** with pure methanol at r.t. for 2 hours. Strong signals from the potassium complexes of the dimerized products were seen. In 5% AcOH methanol, however, the major product was the methyl ether derived from acid catalyzed addition of methanol to the diazo molecule (Figure 2). Oxidation products were also observed in both cases.

As an alternative, carboxylic acids can be derivatized and detected in the positive ion mode. Figure 3 is the ESI mass spectrum of the product formed by mixing **1** with N-Boc-l-Trp-OH, and only the corresponding ester was seen. Besides,

compound **1** also reacted with dipolarophile such as fullerenes.

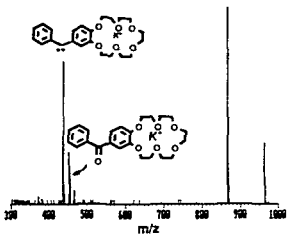

Figure 1 ESI mass spectrum of a solution of **1** in methanol (KOAc was added prior to the analysis The same procedure was used for the whole study)

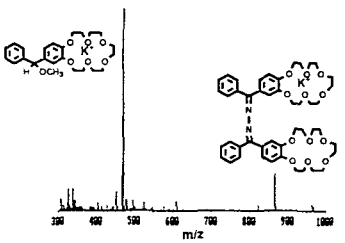

Figure 2 ESI mass spectrum of a solution of **1** in 5%AcOH methanol

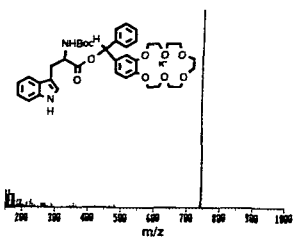

Figure 3 ESI mass spectrum (in KOAc/C_6H_6-MeOH) of the products from the reaction of **1** and Boc-l-Trp-OH

The results shown above have demonstrated that ESI-MS can be used for studying chemical properties of certain type of compounds. ESI-MS has proved itself that it is not only important to the measurement of biopolymers but also useful for the analysis of small organic molecules.

References:

1. Suzuki, T., Li, Q., Khemani, K. C., Wudl, F., Almarsson, Ö., *Science*, **1992**, 254, 1186
2. Wilson, S. R., Wu, Y., *J. Chem. Soc., Chem. Commun.*, in press

Quantification of a New Aryl Amidine

LTB_4 Antagonist (CGS 25019C) in Human Plasma Using Electrospray LC/MS

*M. J. Hayes, M. Leal and M. L. Powell,

Clinical Pharmacokinetics and Disposition, Pharmaceutical Div., Ciba-Geigy Corp., Ardsley NY, 10502

An analytical method has been developed for the determination of CGS 25019C (4-[5-[4-(aminoiminomethyl) phenoxy]pentoxy]3-methyoxy)-N,N-bis(1-metylethyl)benzamide (z)-2-Butenedioate (1:1). This compound has been shown to selectively antagonize the human LTB_4 receptor. Elevated LTB_4 levels have been found in psoriatic lesions, in the synovial fluids of patients with rheumatoid arthritis and gout, in arterial blood of asthmatic patients during wheezing attacks, and in rectal dialysate from ulcerative colitis patients.

The method is based on LC/MS and utilizes a structural analog as the internal standard. Samples (1 ml) were extracted with methylene chloride: hexane (60:40) under basic conditions, back extracted into sulfuric acid, and reextracted into methylene chloride:hexane. Separation was accomplished on a 0.32 mm x 5 cm C-18 column. Solvent A was 0.04% formic acid, solvent B was 0.04% formic acid in acetonitrile. A gradient was done from 5-95% B in 5 minutes. The flow rate was 5 ul/min. Mass spectrometry was carried out under positive ion electrospray conditions with selected ion monitoring at m/z 456 and 329 for drug and internal standard, respectively. The limit of quantification (LOQ) is 0.5 ng/ml.

Specificity was demonstrated by the lack of interfering peaks at the retention time of the drug and internal standard. Recovery and reproducibility assessments indiate good accuracy, precision and linearity over the validated concentration range of 0.25 to 50 ng/ml.

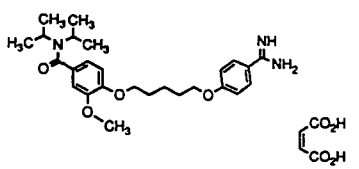

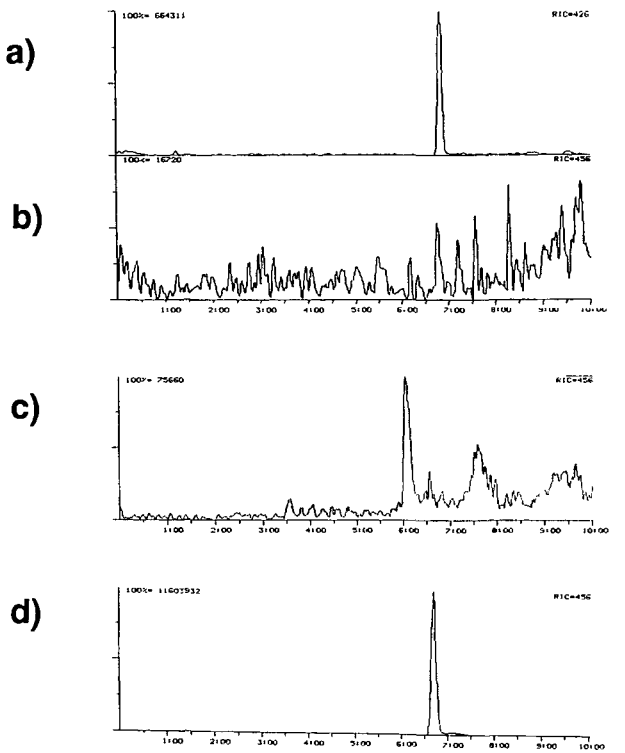

Figure 1 ESI - LC/MS chromatograms of human plasma spiked with internal standard and CGS 25019C: a) internal standard at 10 ng/ml (m/z 426), b) blank plasma, c) 0.25 ng/ml drug, d) 50 ng/ml drug.

Evaluation of Tandem MS vs. API Interface Voltage using Ionspray to Distinguish Isomers of Diarrhetic Shellfish Poisoning Toxins

J.C. Marr[1], and S. Pleasance[2] [1]Fenwick Laboratories Limited, Halifax, N.S., Canada, B3H 4M2, [2]Institute for Marine Biosciences, NRC, Halifax, N.S., Canada, B3H 3Z1 (present address: The Wellcome Foundation Ltd., Beckenham, Kent, U.K.)

The toxins okadaic acid (OA), dinophysistoxin-1 (DTX-1), and dinophysistoxin-2 (DTX-2) belong to a class of polyether compounds that are known to cause diarrhetic shellfish poisoning (DSP). Very little mass spectral data is available for these compounds, although a detailed study of EI and CI mass spectra of OA was been done by Benscath *et al.* (1). Ionspray mass spectrometry (ISP-MS) is a proven method for the detection of DSP toxins in complex samples (2). However, the mass spectra are very simple, the most abundant ions being the protonated molecule, little structural information is provided and the spectra produced by the isomers are identical. To aid in structural elucidation, and/or isomeric characterization, two methods were used to obtain additional fragmentation of the analyte ions. Conventional collision-induced dissociation (CID) using tandem mass spectrometry was compared with CID induced by increasing the API sampling orifice voltage from 40V to 100V. An orifice voltage of 80V produced sufficient fragment ions for characterization.

OA and DTX-2, and DTX-1 and the methylester of OA are isomeric pairs. The OA alcohol was also investigated to help define the nature of the fragment ions. The mass spectra from the five compounds were evaluated and compared to identify characteristic fragment ions that could be used to differentiate the isomers (Figure 1). For OA, DTX-1 and DTX-2, fragment ions which contain the CO_2H group were identified. Confirmation was possible by comparison with the OA methylester spectra (via a corresponding fragment ion 14 amu higher) and the OA alcohol (via a corresponding fragment ion 14 amu lower) (Table 1). Fragment ions that were unique to DTX-1, which contains an additional methyl group at C-35, were also identified (Table 1). The subtle difference between OA and DTX-2 (a methyl group at either C31 or C35) could not be determined, but DTX-1 and its biologically inactive isomer OA methylester can be distinguished.

The protonated molecule of OA was also subjected to conventional MS/MS and the resulting fragment spectrum was compared with mass spectra obtained using MS at increased orifice voltages. Inducing CID via increasing orifice voltage yielded informative fragmentation, with fewer rearrangements than tandem MS, making the spectra easier to interpret, with the disadvantage that the precursor ions were not mass selected. These diagnostic fragment ions will be used in future experiments on DSP toxins using SIM and MRM MS.

References

1. A. Benscath *et al. Rapid Commun. Mass Spectrom.* **5**, 283-290 (1991).
2. S. Pleasance *et al. Rapid Commun. Mass Spectrom.* **6**, 121-127 (1992).

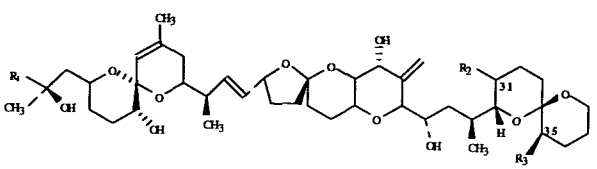

COMPOUND	R_1	R_2	R_3
OA	COOH	CH_3	H
DTX-2	COOH	H	CH_3
DTX-1	COOH	CH_3	CH_3
OA methylester	CO_2CH_3	CH_3	H
OA alcohol	CH_2OH	CH_3	H

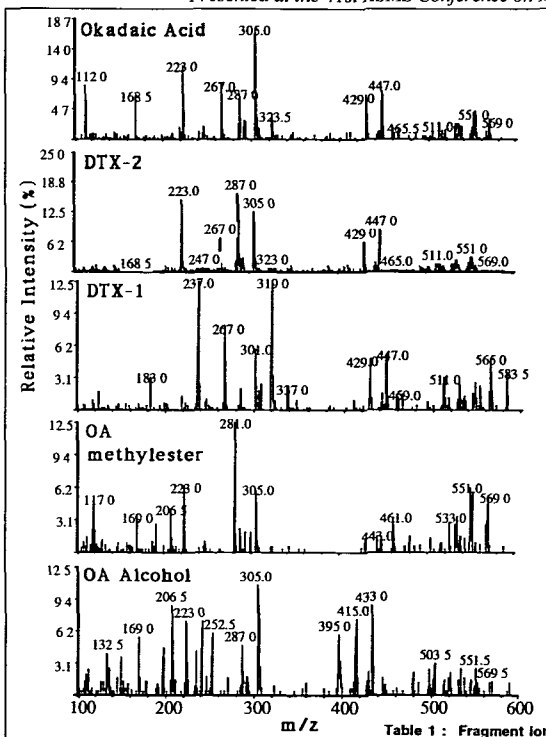

Figure 1: Background-subtracted FIA spectra over the region containing diagnostic fragment ions (100 to 600 amu) of okadaic acid, DTX-2, DTX-1, OA methylester and OA alcohol obtained by ion spray API mass spectrometry at an orifice voltage of 80V. Conditions: 30µL/min of 80% aqueous acetonitrile with 0.1% TFA.

Table 1 : Fragment ions observed for the DSP toxins and related compounds at a sampling orifice voltage of 80V.

	OA	DTX-2	DTX-1	OA methyl-ester	OA alcohol
$[M+H]^+$	805	805	819	819	791
$[M+H-H_2O]^+$	787	787	801	801	773
$[M+H-2H_2O]^+$	769	769	783	783	755
$[M+H-3H_2O]^+$	751	751	765	765	737
Fragment ions containing CO_2H group (unique to toxins)					
	267	267	267	**281**	**253**
	447	447	447	**461**	**433**
m/z 447-H_2O	429	429	429	**443**	**415**
Fragment ions unique to DTX-1					
	169	169	**183**	169	169
	223	223	**237**	223	223
	305	305	**319**	305	305
	569	569	**583**	569	569
m/z 569-H_2O	551	551	**565**	551	551

Characterization of Case-Associated Compounds in Oils Implicated in the Spanish Toxic Oil Syndrome Using Atmospheric Pressure Ionization Mass Spectrometry

Helen H. Schurz, Robert H. Hill, Rossanne M. Philen, Manuel Posada de la Paz*, Ignacio Abitua Borda*, Sandra Bailey, Larry L. Needham
Centers for Disease Control and Prevention, 4770 Buford Hwy, NE, Mailstop F17, Atlanta, GA 30341-3724
*Fondo de Investigacion Sanitaria, Instituto Nacional de la Salud, Madrid, Spain.

INTRODUCTION

In 1981, an epidemic that would later become known as the toxic oil syndrome (TOS), broke out in Spain affecting approximately 20,000 individuals, several hundred of whom have died. The disease was initially termed "atypical pneumonia", and was characterized in its acute phase by fever, eosinophilia and respiratory insufficiency. It later developed into a chronic phase that included neuropathy, scleroderma, hepatitis and pulmonary hypertension. Many victims of TOS still suffer the chronic effects of the disease. Through epidemiologic studies, the disease was linked to the consumption of food oils that were sold as olive oil in Madrid and its surrounding areas. Investigations showed that the oils actually contained rapeseed oil that had been denatured with aniline.

Even though a great deal of work has been performed on the oil samples since 1981, the etiological agent(s) of the disease have not been identified. Case-associated compounds (fatty acid anilides and aniline) have been detected in case oils. Hampering identification of the causative agent(s) of the disease, however, has been the uncertain history of some of the oils that were collected, and the lack of an animal model for the disease.

As if to magnify the importance of identifying the agent of TOS, in 1989, an epidemic clinically similar to TOS occurred in the United States. That disease, termed eosinophilia myalgia syndrome (EMS), was traced to the ingestion of L-tryptophan. The outbreak resulted in several thousand cases of EMS, and 36 deaths. The failure to identify etiological agents of TOS and EMS suggests that similar outbreaks of this type of disease are possible in the future.

Since the initial studies of TOS and EMS, new and more powerful analytical techniques like electrospray and atmospheric pressure chemical ionization (APCI) have become available as interfaces for liquid chromatography/mass spectrometry. Using a SCIEX API III mass spectrometer, we are designing experiments to quantitate case-associated compounds in the oils (anilino-propane diol and its esters, and fatty acid anilides), and screen for other aniline derived compounds. Presented here are the experiments designed to accomplish that task.

EXPERIMENTAL - Quantitation of Case-Associated Compounds

The compounds we are initially investigating are shown in the following figures. Previous analyses by capillary gas-liquid chromatography and high performance liquid chromatography (HPLC) with confirmation by mass spectrometry determined the fatty acid profiles of the oils. Further investigation using HPLC indicated that linolenyl anilide, linoleoyl anilide, palmityl anilide, oleoyl anilide, and stearyl anilide were present in concentrations ranging from 30 ppm to 2,000 ppm. Using HPLC and MS/MS analysis, the above anilides, as well as behenyl anilide, erucyl anilide, 8Z-eicosenyl anilide, 11Z-eicosenyl anilide, 13Z-eicosenyl anilide, bis-anilinopropanol, 3-amino-1,2-propane diol and its esters will be quantitated.

EXPERIMENTAL - Parent Scan Screening for Aniline Derived Compounds

Since the identity of the etiological agent of TOS has not been found, it is wise to assume that not all of the aniline derivatives have been discovered. To this end, we are screening the oils for other possible aniline containing compounds. Those so far studied consistently lose m/z 94, the anilide group. Assuming that other anilide compounds would dissociate under MS/MS conditions in a similar manner, parent scans examining for the loss of aniline could prove to be valuable in identifying other possible compounds to investigate as promoters of disease.

DISCUSSION AND CONCLUSION

The oils present many challenges to the analytical chemist, the primary of these being their age and their complex composition. Significant peroxidation of the oils has occurred since their collection in 1981. It is also likely that alteration or decomposition of many compounds has occurred. Our principle task is to account for all aniline-containing compounds and identify as many of these compounds as possible. Some aniline-containing compounds have shown themselves to be relatively stable, however the stability of the anilino-propane diol and its esters is unknown.

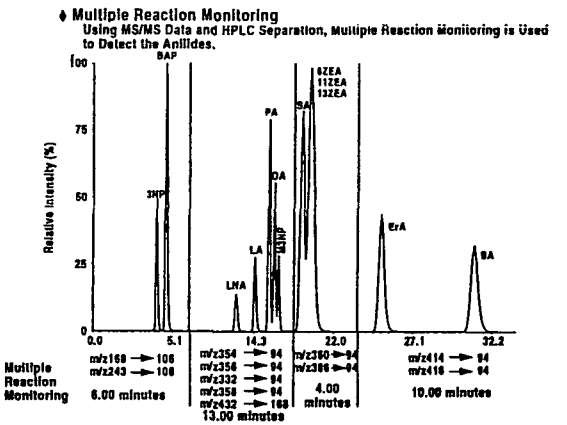

ACKNOWLEDGEMENTS

This work is part of a cooperative agreement to study the Toxic Oil Syndrome between the Centers for Disease Control and Pevention, Atlanta, GA, and Fondo de Investigacion Sanitaria, Instituto Nacional de la Salud, Madrid, Spain.

SELECTED REFERENCES

1. **Toxic Oil Syndrome: Current Knowledge and Future Perspectives.** 1992 WHO Regional Publications, European Series No. 42, World Health Organization, Copenhagen, Denmark.
2. **The toxic oil syndrome (TOS, 1981): from the disease toward a toxicological understanding of its chemical aetiology and mechanism** W.N. Aldridge *Toxicology Letters* **Vol. 64/65**, 59-70 **1992.**

Use of Crown Ethers to Enhance Electrospray Ionization Mass Spectra of Samples Containing Alkali Metal Salts

Anne B. Giordani, Parke-Davis Pharmaceutical Research, Division of Warner Lambert Company, 2800 Plymouth Road, Ann Arbor MI 48105

Introduction Alkali-metal-salt contaminants from synthesis or isolation steps and samples in alkali-metal-salt form often present analysis problems in electrospray ionization mass spectrometry (ES-MS). For instance, unresolved adducted species cause error in molecular weight determination. At a resolving power of 1000, this puts upper limits on exact molecular weight determinations of 6k, 22k and 38k for lithium, sodium and potassium-contaminated species, respectively. Interpretation of ES spectra is more complicated when the adducted species are formed from more than just a single type of charge carrier. The presence of alkali metal salts in samples analyzed by ES-MS causes a decrease in sensitivity due to dilution of the sample ion current when a multiplicity of adducted species is formed (e.g. $[M + 2H]^{+2}$, $[M + H + Na]^{+2}$ and $[M + 2Na]^{+2}$). In worse cases, no peaks representative of the sample are observed due to ion suppression or because the conductivity of the sample solution disrupts the stability of the electrospray. In addition, sensitivity is poor for alkali-metal-salt forms of acidic organic compounds which only weakly dissociate in solution.

An effective strategy for dealing with alkali-metal-salt contamination is chromatographic removal. Chromatographic "clean up" can be achieved by HPLC/MS, by HPLC-fraction collection or by solid-phase extraction using some of the disposable products which are on the market. Similarly, prior to analysis, alkali-metal-salt forms of acidic organic compounds can be converted to their free acid form by ion exchange chromatography.

Chromatographic approaches are time consuming, can be technically challenging and can result in sample losses due to sample handling, incomplete recovery of sample from the column, etc. Very few simple, non-chromatographic, strategies for dealing with alkali-metal-salt contamination have been reported. Precipitation from ammonium acetate solution has been shown to enhance ES mass spectra by removal of sodium counter ions from synthetic oligodeoxy-nucleotides.[1] Addition of small amounts of crown ethers to peptide samples before fast atom bombardment (FAB) analysis was demonstrated to be a simple and rapid way to remove interferences in FAB mass spectra caused by salt contamination.[2]

Crown ethers are synthetic macrocyclic compounds capable of binding cations.[3] The polyether ring size of 18-crown-6 ether makes it particularly selective for sodium and potassium ion binding in 1:1 complexes.[4] Reported here is the use of 18-crown-6 ether addition to direct infusion solutions prior to ES-MS analysis.

Results and Discussion One to one complexes of 18-crown-6 ether with H^+ (m/z 265), H_3O^+ (m/z 283), Li^+ (m/z 271), Na^+ (m/z 287) and K^+ (m/z 303) were observed by manual (20 µL) loop injection of 18-crown-6 ether in one to one (v:v) acetonitrile/ water, 0.01 M lithium acetate, 0.01 M sodium acetate and 0.01M potassium acetate/acetic acid (pH 2.4) solutions. The base peaks in the respective spectra were from the complexes of 18-crown-6 ether with Li^+, Na^+ and K^+. The proton and hydronium ion complexes of 18-crown-6 ether have relative intensities of less

than 20% in the Na^+ and K^+ spectra, whereas, in the Li^+ spectra their relative intensities are greater than 50%. This observation may be a reflection of the particularly favorable binding of 18-crown-6 ether with sodium and potassium cations compared to lithium cations.

The ES spectra of two synthetic peptide samples which contained significant, but unknown, amounts of sodium had improved signal to noise ratios, and no longer contained Na^+ adducted ions following dilution with a water/1% 18-crown-6 ether in methanol/acetic acid solution (final concentration of the synthetic peptides was approximately half, 18-crown-6 ether ≈ 0.02 M).

The effective removal of sodium adducts from the ES spectra of sodium-contaminated insulin solutions by the addition of 18-crown-6 ether to the analyte solution was demonstrated. The spectra from the solutions containing 18-crown-6 ether had significantly improved signal to noise ratios and prominent peaks representative of 18-crown-6 ether binding to the proton-adducted insulin ions. Sodium adduction seemed to be more favored in lower-charge-state ions compared to higher-charge-state-ions of insulin, whereas, 18-crown-6 ether binding seemed to be more favored in higher-charge-state proton-adducted ions compared to lower-charge-state proton-adducted ions of insulin.

The total ion current and the ion current of the $[M + H]^+$ peak in the ES-MS spectra of leucine enkephalin versus sodium chloride concentration was studied. Sodium chloride caused an erosion in both signal intensity and signal to noise ratio at increasing concentrations. The spectra of solutions containing 18-crown-6 ether had significantly better signal to noise ratios, including that of the $[M + H]^+$ ion. The total ion current of the crown ether-containing solutions increased with the sodium chloride concentration. However there was no concomitant increase in the ion current of the $[M + H]^+$ peak, the increase in total ion current was due to the increase in $[18\text{-crown-6 ether} + Na]^+$ and other crown-ether/sodium chloride related ions.

In the ES spectra of sodium suramin, a compound containing six sodium sulfonic acid groups, peaks representing multiple sodium losses carried more of the total ion current in the spectrum from crown ether solution than in the spectrum from acetonitrile/water solution.

Conclusions 18-Crown-6 ether addition is a simple, nonchromatographic strategy for dealing with alkali-metal contamination of solutions for ES-MS analysis. Addition of 18-crown-6 ether to the electrospray infusion solutions of sodium chloride-containing samples decreases formation of sodium-cationated species, and improves the sensitivity through major increases in the signal-to-noise ratios in ES-MS spectra. This is potentially a useful technique for molecular weight measurement of alkali-metal-contaminated samples by ES-MS. Crown ether binding to alkali-metal ions and to proton-adducted analytes is observable in the ES-MS spectra. The pairs of peaks representing the proton-adducted and the crown ether-proton-adducted ions carry complete molecular weight and charge state information about the analyte.

[1]J.T. Stults and J.C. Marsters, *Rapid Commun. Mass Spectrom.*, **5**, 359-363 (1991).
[2]R. Orlando, *Anal. Chem.*, **64(3)**, 332-334 (1992).
[3]J.J. Christensen, D.J. Ealough and R.M. Izatt, *Chemical Reviews*, **74(3)**, 351-384 (1974).
[4]C.J.Pedersen, *Science*, **241**, 536-540 (1988).

On-line Accurate Mass Analysis of a Pesticide Mixture by APCI LCMS on a Magnetic Sector Instrument

R.H. Bateman, *P.A. Bott and A.R. Woolfitt
Fisons Plc, VG Analytical, Floats Road, Wythenshawe, Manchester, M23 9LE, England.

Atmospheric Pressure Chemical Ionisation is a powerful technique when coupled to an LC system for the analysis of a wide range of compounds. Although APCI has been utilised as an LCMS interface on quadrupole mass spectrometers for a number of years, it is only recently that this technique has been transferred to magnetic sector mass spectrometers [1]. The obvious application for this is to obtain accurate mass measurements at higher resolving powers, which will assist in obtaining elemental compositions of unknown compounds.

The aim of this work was to investigate the factors which are important for the successful operation of an LCMS interface at high resolution. These include basic sensitivity checks, reproducibility of sample injections, chromatographic integrity and investigation of internal references for calibrating and mass measuring the sample.

Figure 1 shows the UV detector trace and full magnet scanning TIC trace of a mixture of n-methyl carbamate pesticides, chromatographic resolution is maintained through the LCMS interface.

Figure 2 shows the limits of detection for one carbamate pesticide, carbofuran. A detection limit of 150pg compares favourably with the sensitivity obtained on quadrupole instrumentation [2].

Figure 3 shows a spectrum of methanol clusters from a 50% methanol water solvent system, demonstrating a useful internal reference.

Figure 4 shows the accurate mass measurement for carbofuran by a narrow voltage scanning experiment at 3000 resolving power. Utilising the methanol cluster ions as calibrant, good mass measurements can be obtained.

APCI coupled to a magnetic sector mass spectrometer has the potential, in terms of sensitivity and chromatographic reproducibility, of being a useful technique for accurate mass determinations.

1. Woolfitt, A.R., Bateman, R.H., and Major, H.J., Proc. 40th ASMS Conf. p201-202.
2. Pleasance, S., Anacleto, J.F., Bailey, R.M., and North, D.H., J.Am. Soc. Mass Spectrom. 1992,3, p378-397.

Presented at the 41st ASMS Conference on Mass Spectrometry

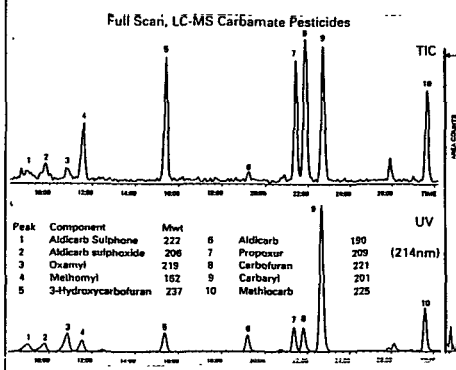

Figure 1.

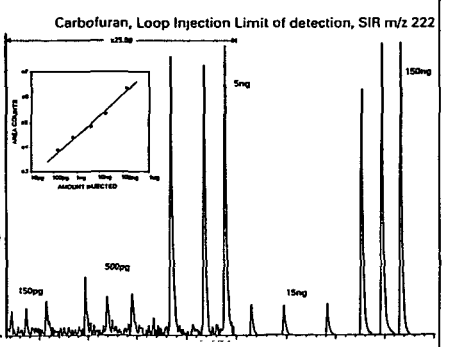

Figure 2.

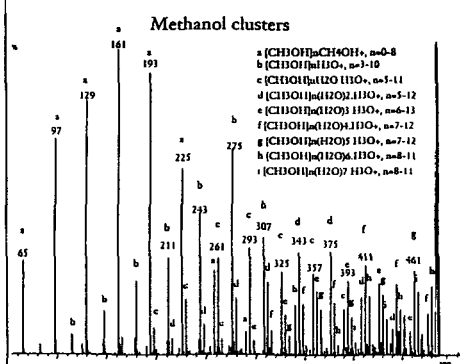

Figure 3.

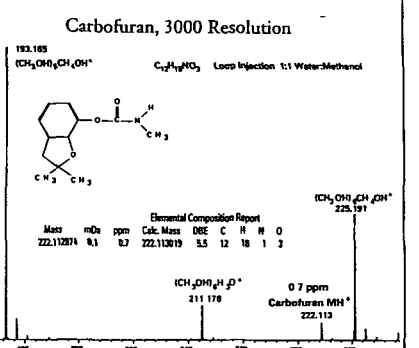

Figure 4.

Analysis of Venoms Used in Pesticide Research by Electrospray Ionization Mass Spectrometry

Ronald E. Shomo, II* and Charles Webster
FMC Corporation, Agricultural Chemical Group, Analytical Department
Princeton, New Jersey 08543

The use of venoms as pesticides is a novel approach in the agrichemical industry. The concept is simple, identifying a specific agent in a complex venom that is toxic to a particular insect pest and producing this agent on a commercial scale.

The analysis is difficult because of the complexity of these venoms coupled with limited quantities of sample (typically sub nanomoles). Electrospray ionization has the sensitivity to determine the identity of the desired agents in these venoms without consuming large quantities of material.

Figure 1 shows the electrospray results of a HPLC fraction of 62 pmoles of a native spider venom. The molecular weight was determined to be 6371.73 ± 0.9 u. The spectrum clearly indicates that two species are present. These species co-elute by HPLC, but are clearly distinguished by electrospray mass spectrometry. The second species molecular weight was measured at 6398.39 ± 0.4 u.

Figure 2 shows the electrospray data of 3 pmoles of a recombinant spider venom isolated by HPLC. The venom was mass measured at 6372.07 ± 0.9 u with a second component mass measured at 6397.14 ± 2.9 u.

The recombinant and the native spider venoms were thought to be identical in composition; however the HPLC retention times were dramatically different. This phenomenon was attributed to a difference in the way the protein folded.

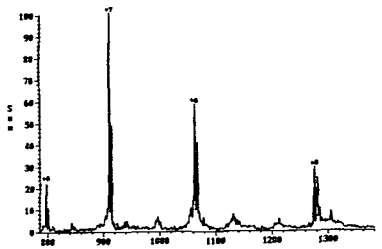

Figure 1
62 pmoles Native Spider Venom Molecular Weight 6371.73 ± 0.9 u

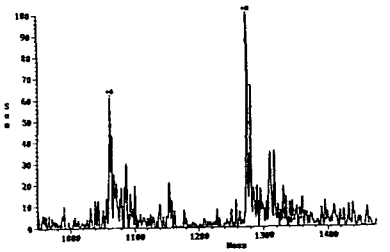

Figure 2
3 pmoles Recombinant Spider Venom Molecular Weight 6372.07 ± 0.9 u

IONIZATION OF AROMATIC HYDROCARBONS IN SOLUTION FOR ANALYSIS BY ELECTROSPRAY IONIZATION-MASS SPECTROMETRY

Keiji G. Asano and Gary J. Van Berkel
Analytical Chemistry Division, Oak Ridge National Laboratory, Oak Ridge TN 37831-6365

The applicability of electrospray ionization-mass spectrometry (ES-MS) is generally limited to analytes that are ionic in solution or that can be ionized in solution by acid/base chemistry. Neutral, nonpolar analytes such as polycyclic aromatic hydrocarbons (PAH's) are not typically amenable to ES-MS analysis. Furthermore, chemical derivatization aimed at adding an ionic moiety to these molecules is problematic due to the large variation in reactivity with molecule structure and the potential for multiple reaction products. This work presents our investigation of solution-phase electrochemical, chemical, and photochemical means to form cations of these compound types for analysis by ES-MS. The mass spectrometer employed was a modified version of a Finnigan-MAT ion trap mass spectrometer (ITMS) adapted to sample ambient air.[1]

We have previously shown[2] that radical cations of certain analytes may be formed via an electrochemical oxidation inherent in the ES process that occurs at the metal/solution interface in the ES needle. Formation and observation of these electrochemically generated radical cations required the "appropriate" analyte (i.e., easy to oxidize and stable as M^+ in solution) and the "appropriate" solvent system (i.e., inert to reaction with M^+). Radical cations can also be generated electrochemically by placing an electrochemical amperometric flow cell in-line with the ES. For the appropriate analytes, when the voltage difference between the two electrodes in the cell is zero, no ion signal is observed. When the potential between the two electrodes is increased to the proper level to oxidize that compound, the radical cation of the analyte can be observed. Therefore, as demonstrated by the data in Figure 1, variation of the cell potentials allows for selective ionization.

Chemical oxidants, including Brønsted acids, charge-transfer reagents, and Lewis acids can also be used to form cations of highly conjugated and aromatic systems.[3] As an example, the ES mass spectrum of β-carotene ionized in solution by dissolution in TFA is shown in Figure 2. Ionization selectivity is afforded by the use of different chemical oxidants. This is demonstrated in Figure 3 for the simulated elution of PAH's with post-column ionization in solution using a chemical oxidant. The strongest oxidant (SbF_5) affords the least selectivity, but affords the best detectability. The best selectivity is achieved using a weaker oxidant (DDQ/TFA). In such a case detectability for the easily oxidized compounds is still high, but is dramatically reduced for harder to oxidize compounds.

Light can also be used to ionize analytes in solution for analysis by ES-MS. This work made use of a 150 Watt xenon arc lamp that irradiated the solution just entering the ES needle. We found that irradiating the analyte solution with light may ionize a compound directly (or promote the compound to an excited state from which it can transfer an electron to another species in solution) or may ionize the analyte and/or promote reactions between the analyte neutral or ion in solution and other species originally in the solution or created by irradiation (Figure 4). Although not investigated, it is anticipated that various spectral filters or discrete wavelengths might be used to afford ionization selectivity as demonstrated above for electrochemical and chemical oxidation.

In summary electrochemical, chemical, and photochemical means can be used to form cations from analytes in solution for analysis by ES-MS. Variation of voltage gradients in solution, different chemical oxidants, and tunable light may each be used to afford ionization selectively. And finally, these results indicate that ES-MS might be used to probe the ionic products formed in solution during electrochemical, chemical, and photochemical experiments.

1. Van Berkel, et al. *Anal. Chem.* 1990, *62*, 1284. 2. Van Berkel, et al. *Anal. Chem.* 1992, *64*, 1586. 3. Van Berkel, et al. *Anal. Chem.* 1991, *63*, 2064

Research sponsored by the United States Department of Energy, Office of Basic Energy Sciences under contract DE-AC05-84OR21400 with Martin Marietta Energy Systems, Inc.

Figure 1

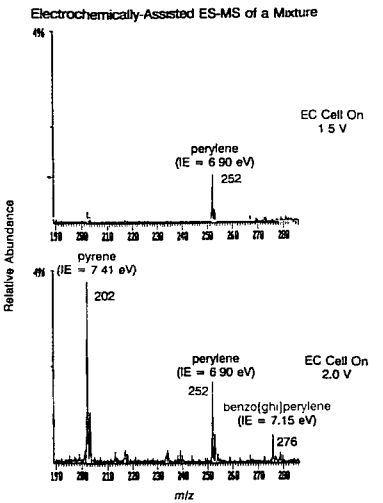

Figure 2

Cation Formation via Chemical Oxidation using a Brønsted Acid

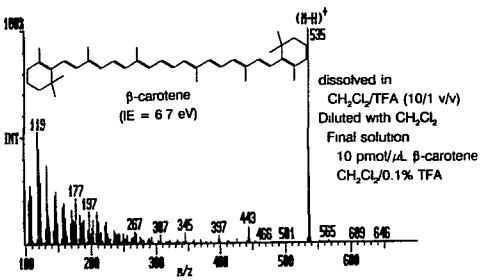

Selective Post-Column Ionization using Chemical Oxidants
Simulated Elution of PAH's using Flow Injection

Figure 3

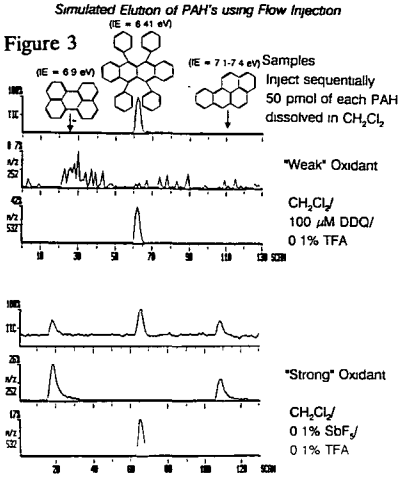

Figure 4 *Photoinduced Reaction Product*

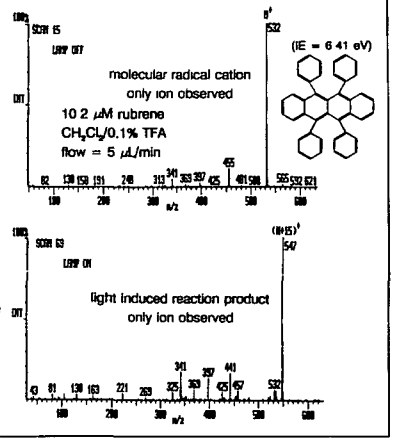

Studies of 1,3-Cycloaddition of Fullerene by Electrospray Ionization Mass Spectrometry

Yunhui Wu* and Stephen R. Wilson
Department of Chemistry, New York University
Washington Square, New York, NY 10003

Recently a burst of scientific investigations on fullerenes has occurred due to their unique structures and properties. Among the studies, cycloadditions of fullerenes with dienes and 1,3-dipoles have attracted much attention. Several mono-adducts have been isolated and characterized.[1]

During our studies on the application of electrospray ionization mass spectrometry (ESI-MS) to organic chemistry,[2] we have found that ESI-MS was very useful for studying cycloadditions of fullerenes. Our study started with the known reaction which involved C_{60} and diaryldiazomethane. When a mixture of C_{60} and C_{70} (9 : 1) was reacted with excess crown ether diaryldiazomethane (**1**) for 1 hr at 5-10 °C, up to hexa-adducts were detected by ESI-MS. Figure 1 shows the ESI mass spectrum of the products of this reaction after 3 days. Nitrones such as compound **2** showed similar reactivities under the same conditions.

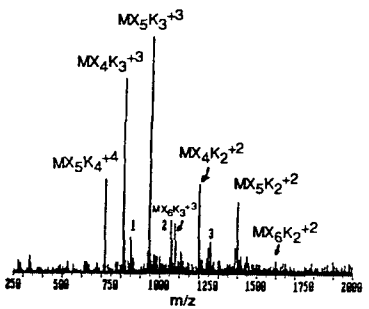

Figure 1. ESI mass spectrum of the products from the reaction of **1** and C_{60}/C_{70} (9 : 1) in benzene-methanol (1 : 1) containing KOAc M = C_{60}, X =

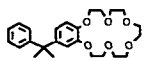

Peaks: 1, $C_{70}X_2K_2^{+2}$; 2, $C_{70}X_3K_2^{+2}$, 3, $C_{70}X_4K_2^{+2}$.

When ethyl diazoacetate (**3**) and α-methylbenzyl azide (**4**) were used, the addition reactions proceeded much slower and more than one type of product formed. The reaction of **3** with C_{60} at r.t. formed five-membered rings as major products. With

increasing temperature, more loss of nitrogen occurred. The least reactive dipole **4** only reacted with C_{60} at higher temperature. Products with losses of nitrogen molecules started to appear at about 100 °C.

Clearly, the nature of the products of 1,3-cycloadditions of C_{60} is both substrate and temperature dependent. Our studies have shown that the relative reactivities of the 1,3-dipoles used are as following:

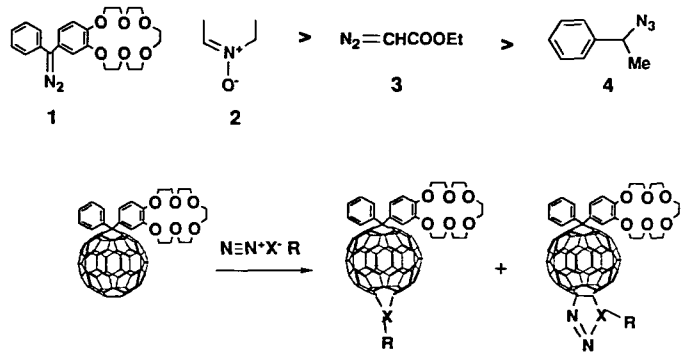

5-10 °C	X = CPh, R = Ar	Only	
25 °C	X = CH, R = COOEt	Minor	Major
65 °C	X = N, R = CHMePh	Minor	Major

Our results have shown that ESI-MS can be used not only for detection of products, but also for studying relative reactivities and mechanism. Since ESI-MS mainly reflects solution chemistry, we think its future in organic chemistry is bright.

References:

1. Prato, M., Suzuki, T., Foroudian, H., Li, Q., Khemani, K., Wudl, F., Leonetti, J., Little, R. D., White, T., Rickborn, B., Yamago, S , Nakamura, E., *J. Am. Chem. Soc*, **1993**, 115, 1594
2. (a) Wilson, S. R., Yasmin, A., Wu, Y., *J. Org. Chem.*, **1992**, 57, 6941 (b). Wilson, S R., Wu, Y., *J. Am. Soc. Mass Spectrom.*, in press.

Electrospray Ionization Mass Spectrometry Is a Useful Tool for Studying Fullerene Chemistry

Yunhui Wu* and Stephen R. Wilson
Department of Chemistry, New York University
Washington Square, New York, NY 10003

Mass spectrometry has played a critical role in C_{60} chemistry and indeed in its discovery. While MS is very sensitive, C_{60} derivatives are often fragile and non-volatile, so that great difficulties have been reported with even the mildest ionization methods. FAB-MS and LD-MS are often used for characterizing products from reactions of fullerenes, however, electrospray ionization mass spectrometry (ESI-MS) has been employed only in few cases.[1]

We have recently been exploring of the application of ESI-MS to organic chemistry and have found that ESI-MS is useful for the direct observation of fullerene reactions in solution. Our first observation was that oxyamination products of C_{60} could be detected. For example, the addition of iso-butyl amine and oxygen could be followed by ESI-MS in the positive ion mode (Figure 1). In addition, we have also detected methoxylated fullerene ions in the negative ion mode when fullerenes were treated with NaOMe methanol-toluene solution. Interestingly, only ions with additions of odd numbered methoxyl groups were seen. Deuterated reagents were used for the identification of the ions.

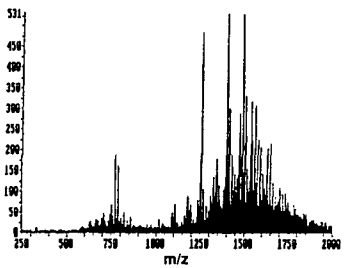

Figure 1. ESI mass spectrum (in 2.5%AcOH/MeOH-PhMe) of the products from the reaction of C_{60} and i-$BuNH_2$ in air at 24 hr

To facilitate the analysis of fullerene derivatives, we have synthesized a crown ether tagged C_{60} (**1**).[2] Based on the fact that this molecule has very similar chemical properties to C_{60} itself, we conducted a search of reactions of C_{60} and utilized ESI-

MS for the analysis of the products. By using this tagged molecule, we have directly observed the products from oxidation, oxyamination, methoxylation (in both positive and negative modes), bromination, hydroboration, Diels-Alder reaction, [2 + 3] cycloaddition and [2 + 2] photocycloaddition. Figure 2 shows ESI mass spectra of photochemical reaction mixtures of **1** and varied concentrations of 3-methyl-2-cyclohexen-1-one. As the concentration of enone increased, more multiple addition products formed.

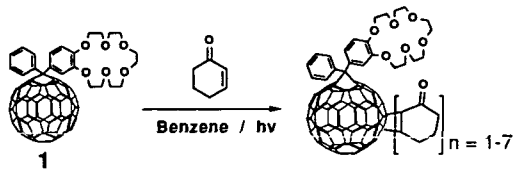

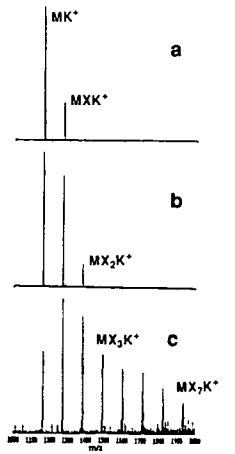

Figure 2 ESI mass spectrum of the products from the reaction of **1** and 3-methyl-2-cyclohexen-1-one in $KOAc/C_6H_6$-MeOH The concentration of the enone was increased by 10 and 100 fold from a to b, c M = compound **1**, X = 3-methyl-2-cyclohexe-1-one

Based on the study with the crown ether tagged C_{60}, we have successfully repeated the same photochemical reaction on C_{60} itself. The mono-adduct was isolated and fully characterized.

We hope that we have shown the great potential of ESI-MS in the field of fullerene chemistry. Although ESI-MS has limitations with regard to type of analyte, it is possible to be used efficiently with suitable strategies.

References:

1. Hiraoka, K., Kudaka, I., Fujimaki, S., *Rapid Commun. Mass Spectrom.*, **1992**, 6, 254
2. Wilson, S. R., Wu, Y., *J. Chem. Soc., Chem. Commun.*, in press

The Characterisation of Novel Ionic Platinum Complexes by Electrospray Ionisation Mass Spectrometry

R T Aplin, C V Robinson, V C M Smith The Dyson Perrins Laboratory, Oxford University, Oxford, U K OX1 3QY and S Lowes VG Biotech, Altrincham, Cheshire, U K. WA14 5RZ

C-S Activation of thiazolium salts and related compounds has been achieved by the reaction of (dppf)PtC_2H_4 and a series of thiazolium and benzothiazolium salts -

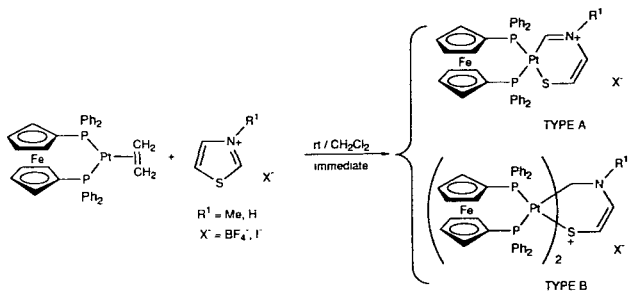

These ionic products are readily characterised by ESI MS where the molecular cation is the only intense peak in the spectrum -

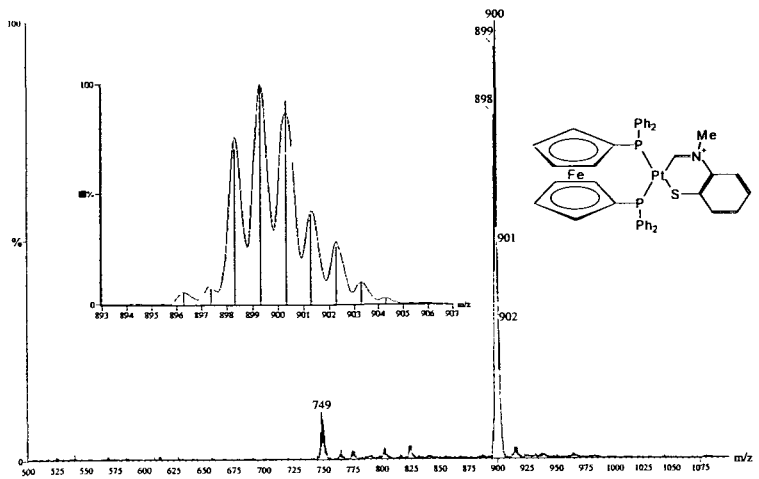

This is in marked contrast to their FAB spectra which are dominated by fragment ions and show evidence for ligand displacement by the FAB matrix N-methylthiazolium and N-methylbenzothiazolium salts afford 1 1 and 2 1 type A and B products -

N-methyl-2-methylthiazolium and N-methyl-2-methylbenzothiazolium salts afford type A products with the opposite regiochemistry -

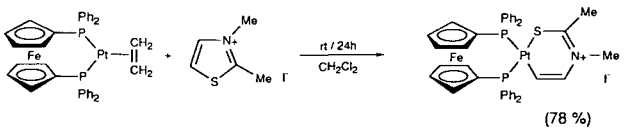

The acyclic analogue S,N,N-trimethylformamidinium tetrafluoroborate similarly affords type A product -

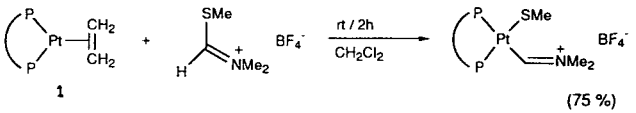

Cationic carbene products were obtained from the reaction of N-methyl-2-chlorobenzothiazolium tetrafluoroborate -

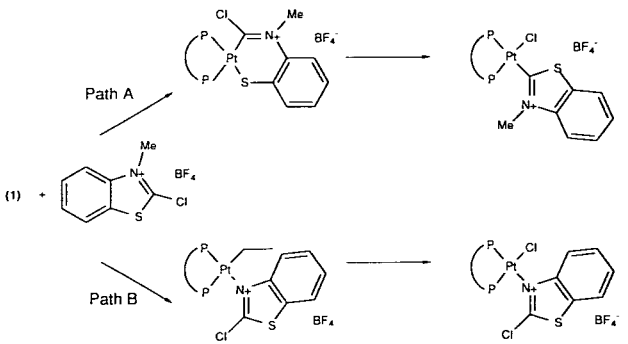

The ESI MS of this product, where the platinum is not part of a metallocycle, shows a low abundance molecular cation Loss of the heterocycle affords the base peak in the spectrum. In all the spectra the observed isotope pattern is in very good agreement with the theoretical pattern

ELECTROSPRAY MASS SPECTROMETRY OF METALLOCENES AND ORGANOMETALLIC SALTS

Xiaoming Xu, Steven P. Nolan, Mark L. Trudell, and Richard B. Cole*

Department of Chemistry, University of New Orleans, Lakefront Campus, New Orleans, LA 70148

An electrospray (ES) mass spectrometer (Vestec 201, Houston, TX) was used to analyze metallocenes $(C_5H_5)_2Fe$, $(C_5H_5)_2Ru$, & $(C_5H_5)_2Os$, and newly synthesized organometallic salts $[(CH_3)_5C_5RuC_6H_6]^+[CF_3SO_3]^-$ & $[(CH_3)_5C_5RuC_8H_7N]^+[CF_3SO_3]^-$. Each of these compound types contains metal-carbon bonds. Under normal ES ionization conditions, the organometallic salts exhibited very stable ionization and high sensitivity for molecular cations (Fig. 1). The isotope distribution patterns for the intact cations were in excellent agreement with those predicted by natural abundances.

The mass spectra of metallocenes (Fig. 2), on the other hand, showed molecular ions corresponding to oxidized forms of the neutral molecules, $[(C_5H_5)_2M]^+$ (M=Fe, Ru, Os). According to the generated isotope distribution patterns, protonated molecules were present in negligible quantities, and no doubly charged species were observed. Ferrocene, which can be ionized under normal ES operating conditions, showed very stable electrospray characteristics and high sensitivity. Ruthenocene and osmocene, however, were far more difficult to ionize. Their molecular ions could only be obtained at higher needle voltages, i.e., very near to corona discharge conditions. This result was attributed to higher $E_{1/2}$ (ox) values and higher ionization energies of ruthenocene and osmocene relative to those of ferrocene. For osmocene, conditions were established whereby protonation was competitive with oxidation, thus creating two pathways of ion formation. The obtained mass spectra demonstrate a clear example of the use of the electrospray instrument as an electrolytic cell [1,2]. Also observed were fragment ions $C_5H_5M^+$ (M = Fe, Ru) generated by collision-induced dissociation of the respective molecular ions.

Solution-phase reaction products of unstable forms of metallicinium ions were also observed in the ES mass spectrum. These products were present in particularly high abundances if the singly charged ion satisfied the 18-electron rule. In methylene chloride solvent, chloride ion was incorporated into the inner sphere of the metallocenes forming Cp_2RuCl^+ and Cp_2OsCl^+ (Fig. 2c) complexes via nucleophilic addition. Other products of nucleophilic addition to Ru(IV) and Os(IV) species (i.e., hydroxide and trifluoroacetate addition) were also produced. No analogous species were observed for ferrocene.

References

1. Blades, A.T.; M.G. Ikonomou; P. Kebarle, *Anal. Chem.* (1991) 63, 2109.
2. Van Berkel, G J.; S.A. McLuckey; G.L. Glish, *Anal Chem.* (1992) 64, 1586.

Figure 2. Electrospray mass spectra of metallocenes: (a) ferrocene in CH_3CN, skimmer-collimator voltage difference (ΔV) = 40 V; (b) ruthenocene in CH_3CN, ΔV = 17 V; (c) osmocene in CH_2Cl_2, ΔV = 2 V.

Figure 1. Electrospray mass spectra of organometallic salts in CH_3OH: (a) $[Cp^*RuC_6H_6]^+[CF_3SO_3]^-$ (1 mM); (b) $[Cp^*RuC_8H_7N]^+[CF_3SO_3]^-$ (1 mM).

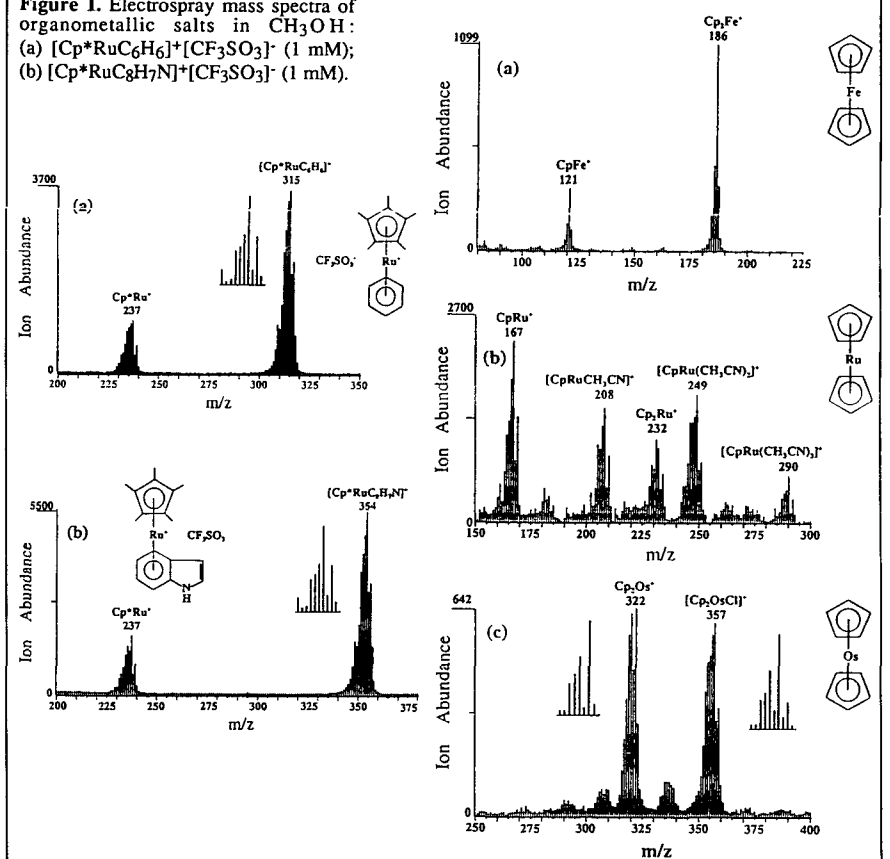

Electrospray vs. FAB for Organometallic Analyses

Deborah A. Grimm,[1] Aaron I. Baba,[2] and Russell H. Schmehl[2]
[1]604 Lindy Boggs, Coordinated Instrumentation Facility
[2]2015 Percival Stern, Department of Chemistry
Tulane University, New Orleans, LA 70118

Previously, organometallic species have been characterized using FAB-MS.[1-6] The FAB technique, however, is hindered by secondary processes; such as oxidation and/or reduction of the analyte, adduct formation and other reactions between the analyte and matrix. While ESI-MS has been used extensively for the analysis of peptides and other compounds of biological interest, it has not been routinely used for the analysis of organometallic species.[7] The purpose of this study is to qualitatively compare the FAB-MS and ESI-MS of a series of Ru-, Re- and di-metallic compounds.

All experiments were performed on a Kratos Concept 1H mass spectrometer. For the FAB experiments, the LSIMS source was used, and 3-nitrobenzyl alcohol was the matrix. For the ESI experiments, the buffer solution was 50/50 H_20/MeOH, 1% acetic acid; and the analytes were dissolved in pure MeOH. The acceleration potential was 8kV for FAB and 4kV for ESI. Data were collected in the raw data mode. Each spectrum is the average of 20-50 scans. The organometallic compounds were synthesized, and all other chemicals were acquired from commercial sources.

The compounds studied are outlined in Table 1. An example of the type of spectra obtained is shown in Figure 1. For this discussion, the compounds are grouped by charge states. **A** and **G** did not give any results or expected results and thus are not discussed here. **D, E, G** and **I** have a +2 charge state. **D, E** and **I** show loss of 2 PF_6's with reduction in FAB. Doubly charged ions are also observed at very weak intensities. By ESI, **D, E** and **I** give ions corresponding to loss of PF_6's with no reduction. **B, C** and **F** have a +3 charge state. For all three compounds, loss of 2 PF_6's with reduction is the major peak in the FAB spectra. However, weak doubly charged ions are also observed. These compounds by ESI do not show any reduction and do show a charge distribution that relates to successive loss of PF_6's. **H** and **J** have a charge state of +4. **H** gives no information under our FAB conditions, and **J** gives a very small ion which corresponds to loss of 2 PF_6's and reduction. Both compounds give much more information via ESI, but some reduction is observed with the loss of 3 and 4 PF_6's.

An important feature of FAB spectra is that fragmentation is observed for some compounds. For example, **I** (Fig. 1), shows loss of the ligand. Another feature of the FAB spectra, is that oxidation is observed for some of the compounds. These processes are not observed in ESI.

In conclusion:

1. FAB-MS gives information on organometallic species, but secondary processes such as reduction can complicate the spectrum.
2. ESI-MS is a viable tool for the analysis of organometallic species. It does not appear to be as susceptible to the above secondary processes.
3. FAB-MS loses its effectiveness at higher mass and higher charge state.
4. ESI-MS does not appear to be hindered by higher mass and higher charge state.
5. FAB-MS produces informative fragmentation.
6. ESI-MS does not produce informative fragmentation.

TABLE 1. COMPOUNDS STUDIED

SMP	STRUCTURE*
A	$[(CO)_3ClRe(b\text{-}b)Ru(tpy)Cl](PF_6)$
B	$[(dmb)_2Ru(b\text{-}b)Ru(tpy)CN](PF_6)_3$
C	$[(dmb)_2Ru(b\text{-}b)Ru(tpy)Cl](PF_6)_3$
D	$[Ru(dmb)_2bbdb](PF_6)_2$
E	$[Ru(dmb)_2bphb](PF_6)_2$
F	$[(dmb)_2RubphbRu(tpy)Cl](PF_6)_3$
G	$[Ru(dmb)_2(b\text{-}b)](PF_6)_2$
H	[[Ru(dmb)2]2bphb](PF6)4
I	$[Ru(bpy)_3](PF_6)_2$
J	$[[Ru(dmb)_2]_2bbdb](PF_6)_4$

*LIGAND STRUCTURES

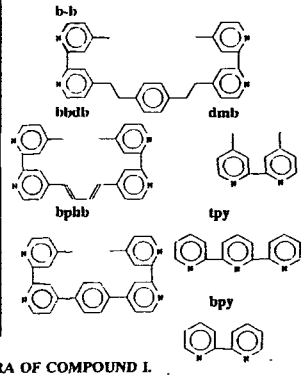

FIGURE 1. FAB-MS AND ESI-MS SPECTRA OF COMPOUND I.

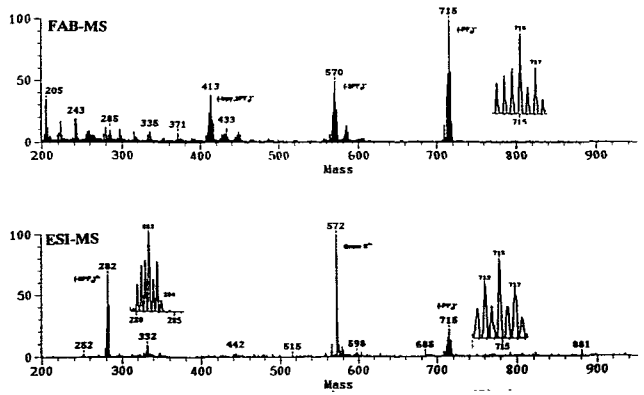

[1]G. Denti, S. Serroni, G. Sindona and N. Uccella, *J. Amer. Soc. Mass Spectrom.*, **1993**, 4, 306.
[2]P. Didier, L. Jacquet, A.K. Mesmachker, R. Hueber and A. van Dorsselaer, *Inorg. Chem.*, **1992**, 31, 4803.
[3]X. Liang, S. Suwanrumpha and R. Freas, *Inorg. Chem.*, **1991**, 30, 652.
[4]J. Miller, K. Balasammugam, J. Nye, G. Deacon and N. Thomas, *Inorg. Chem.*, **1987**, 26, 560.
[5]R. Cerny, B. Sullivan, M. Bursey and T. Meyer, *Inorg. Chem.*, **1985**, 24, 397.
[6]R. Cerny, B. Sullivan, M. Bursey and T. Meyer, *Inorg. Chem.*, **1983**, 55, 1954.
[7]F. Bitsch, C. Dietrich-Buchecker, A-K. Khemiss, J-P. Sauvage and A. Dorsselaer, *J. Amer. Chem. Soc.*, **1991**, 113, 4023.

D. Grimm acknowledges Tulane University and the CIF for financial support. A. Baba and R. Schmehl acknowledge the Petroleum Research Fund for support of the morganic synthesis. The Keck Foundation is gratefully acknowledged for purchase of the Kratos Concept.

A HEATED CAPILLARY ATMOSPHERIC PRESSURE IONIZATION SOURCE WITH AN ATMOSPHERIC PRESSURE CHEMICAL IONIZATION INTERFACE.

IAIN MYLCHREEST AND MARK HAIL, FINNIGAN MAT, SAN JOSE, CA 95134.

The recent explosion of interest in performing LC/MS analysis with atmospheric ionization techniques has led to the development of a number of ionization sources for both electrospray (ESI) and atmospheric pressure chemical ionization (APCI). A new atmospheric ion source has been developed based upon a heated metal capillary design (1), which allows APCI operation (Fig 1) and high flow ESI, at 1.0 to 1000 ul/ min of LC eluent.

The heated capillary provides a means of efficiently desolvating and transporting ions from ionization techniques such as APCI into a mass analyzer. For APCI operation the heated capillary is typically operated at 150 to 200 C, this provides enough energy to desolvate ions previously formed in the corona discharge region without thermally degrading them, and also assists in the desolvation of larger droplets formed in the APCI nebulizer and vaporizer probe. Liquid flow rates of up 2 ml/min in both normal and reverse phase LC are able to enter the source in APCI operation due to the desolvating ability of the heated capillary, although only a fraction of this flow actually passes through the capillary. The heated capillary allows high LC flow operation, but other features of the source contribute to improved sensitivity and detection limits of a wide range of compounds. The heated capillary in this source is off axis with respect to the the skimmer orifice, this is believed to prevent undesolvated droplets and particulates entering the mass analyzer, this significantly reduces the high background noise commonly seen in these high flow ESI and APCI techniques. This off axis arrangement typically increases the signal to noise by a factor of three to five (Fig 2). The desolvated ions in this off axis region are focussed towards the skimmer orifice axis using a tube lens (2) which enhances the detected ion signal by a factor of five. After passing through the skimmer the ions are focussed using an RF only octapole which efficiently passes the ions in to the mass analyzer. It is this RF only octapole that contributes significantly to the improved sensitivity of this source, providing factors of ten to one hundred fold increase in sensitivity over the same source utilizing a conventional lens system in this area.

APCI typically produces protonated molecular species or adducted molecular ions with little or no structural information. However it is possible to induce fragmentation of ions at different points in the source and create structurally useful information. Controlled thermal fragmentation is possible by raising the heated capillary above 200 C in APCI operation. Fragmentation can also be produced in the capillary-skimmer region by applying an accelerating potential to the capillary exit. The RF only octapole is primarily a focussing device but the application of an offset voltage accelerates ions in this region and allows them to collide with resident gas molecules and induces fragmentation ions identical to those produced in a conventional collision cell, although lacking the specificity of traditional MS/MS.

The analytical performance of this APCI source is demonstrated with the low picogram detection of steroids such as prednimustine (fig 3), boldenone, and testosterone. The potential for qualitative and quantitative analysis in the low picogram range is demonstrated in the selected reaction monitoring and single ion monitoring modes for these types of molecules. The analysis of ethoxylated polymers is shown using this APCI interface, producing molecular ion species of the individual polymer units up to molecular weights of 2000 Daltons. APCI operating in the negative ion mode is also demonstrated for the analysis of phenoxy acid herbicides and prostaglandins.

1. S.K. Chowdhury, V. Katta and B.T. Chait, Rapid commun. Mass Spectrom., 1990, 4, 81-87
2. I. Mylchreest and M. Hail, Proceedings of the 39th ASMS Conference on Mass Spectrometry and Allied Topics, Nashville, TN, 1991, 316

Atmospheric Pressure Chemical Ionization (APCI)

fig 1

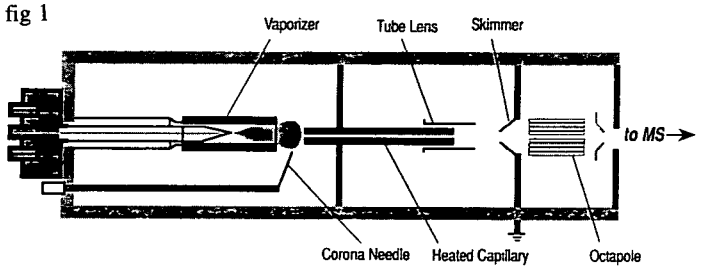

fig 2

EFFECT OF OFF AXIS HEATED CAPILLARY ON SIGNAL TO NOISE FOR APCI OPERATION

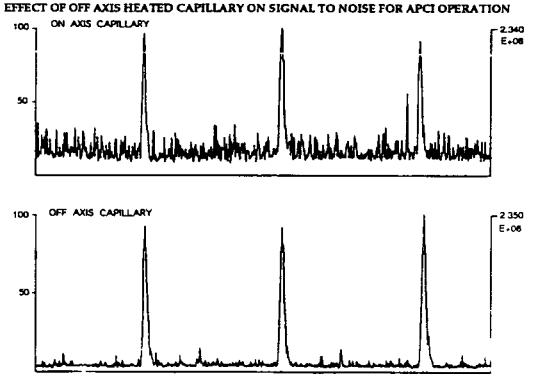

fig 3

APCI POSITIVE ION SELECTED REACTION MONITORING SENSITIVITY

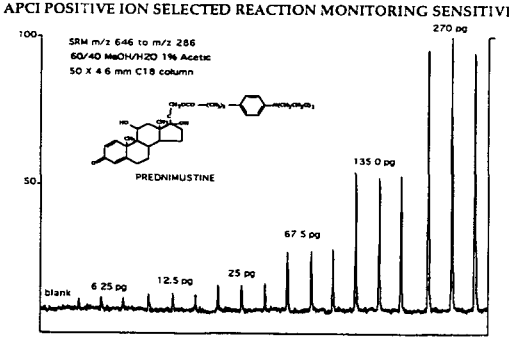

Development of High Sensitivity Detectors for Mass Spectrometry

*Anthony Bauco and Alan Then,
Galileo Electro-Optics Corporation, Sturbridge, MA 01566

Recent efforts to improve the sensitivity of mass spectrometry systems have begun to focus on the ion detector as the major opportunity for advancement. Until recently, current detectors were more than adequate for the systems since other components, such as the chromatograph, inlet, ion source, and mass analyzer, were the limiting factor in system sensitivity. Now that system sensitivity is pushing the limits of the current detector designs we are able to see the effects of new detector design concepts and technologies.

Most of the improvements have been in the areas of ion optics, electron multiplier material science, and electron multiplier geometry. Improved ion optics have resulted in better collection efficiency through improved coupling between the mass analyzer and electron multiplier. All of our testing was done on a HP5971 MSD which has a quadrupole mass filter. Each quadrupole provides a distinct beam profile and divergence that varies with the physical geometry and operating conditions. A unique detector must be designed for each quadrupole since the optimal ion optics are dependent on the beam profile and divergence. The ion optics of the detector should efficiently couple the mass filter output to the electron multiplier while blocking or avoiding the noise components exiting the mass filter such as photons and neutrals. Ion optics modeling and experimentation enables us to optimize the coupling between the detector and the various types of mass analyzers being used today. Improved material selection has also resulted in lower background noise by filtering or absorbing photons and neutrals. Improvements in multiplier geometry have resulted in lower dark noise generated by ion feedback and improved collection efficiency, defined as the percentage of available ions that are collected by the cone of the Electron Multiplier. Improvements in electron multiplier material science have resulted in greater linear output currents, extended life, and higher conversion efficiency, defined as the number of secondary electrons generated by an ion striking the cone of the Electron Multiplier. By combining greater linear output currents, higher gain, and lower noise we are able to extend the dynamic range of the detector, defined as the maximum linear input divided by the minimum detectable input.

The testing was done on Galileo's standard 4778 detector, supplied as original equipment on the HP5971 MSD, and Galileo's new high sensitivity plug in detector. Our software was HP's DOS chemstation REV A. We used a HP 5890 GC with a HP 7673 Autoinjector. A Deactivated injection port liner (HP5181-3587), 12M X .2mM X .33uM HP Ultra-1 column, and Merlin Microseal septum were used in the GC. All detectors were given a 12 hour test period with equal pumping times. The sample used was 100pg/ul of Methyl Stearate in Methanol with a 1ul injection. The EM voltage was set to Autotune plus 400V. The injection port and MSD interface temperatures were set to 280C. The oven program started at 100C with a 30C/min ramp to 280C, holding for 1min. The purge on time was set to 1 min. The MSD scan range was 45-370 amu, the A/D samples were 2^2, and the threshold was set to zero. We were able to see a decease in background noise by a factor of two to four. It was measured by sitting on mass 400, where there is very little real signal, and calculating the input current to the Electron Multiplier. This noise is not to be confused with the background created by a chromatograph where real signal is received at times it should not be. The following graphs are a plot of mass 298 versus time. The peak abundance, total RMS background noise, and resulting signal

to noise is provided. We were able to see a sensitivity increase of three to five times over the standard product with as much as a factor of ten at higher voltages. The maximum linear output current was well above 20 uA and separate experiments at Galileo have provided linear output currents as high as 100uA and promise even more. The techniques used here can be applied to other quadrupoles as well as other types of mass filters.

STANDARD 4778

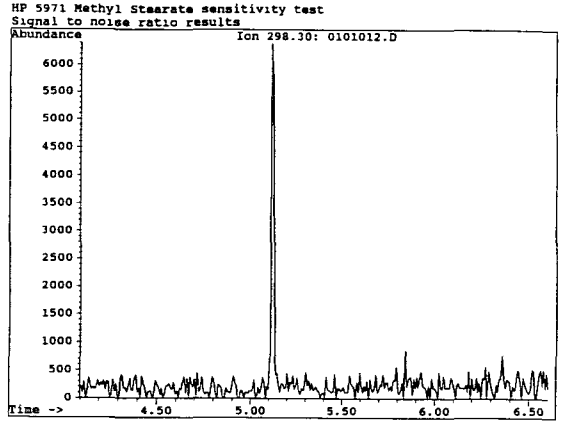

Maximum signal : 6229
RMS noise (4.513 to 4.913 min): 125
RMS signal/noise ratio: 50

NEW DETECTOR

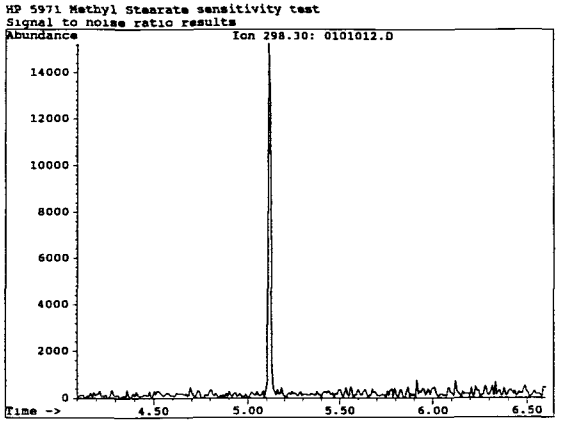

Maximum signal : 15172
RMS noise (4.513 to 4.913 min): 103
RMS signal/noise ratio: 147

Identification of Disease State Associated Antigens Presented to the Immune System by Class I MHC Molecules; Prospects for the Development of Synthetic Vaccines Against Viral Infection and Cancer.

*Wanda M. Bodnar, Donald F. Hunt, Andrea L. Cox, Theresa A. Davis, Hanspeter Michel, and Jeffrey Shabanowitz, Dept. of Chemistry, University of Virginia, Charlottesville, VA 22901; Robert A. Henderson, Craig Slingluff, and Victor H. Engelhard, Dept. of Microbiology and Beirne Carter Center for Immunological Research, University of Virginia School of Medicine, Charlottesville, VA 22901.

Cellular proteins are continually being degraded to nine and ten residue peptides in the cytosol. These fragments become associated with class I glycoprotein molecules that transport them to the cell surface for presentation to cells of the immune system (1). Cytotoxic T lymphocytes (CTL) bind to the class I molecules and check the nature of the peptides being presented. If they are derived from foreign proteins (viruses or tumors), the CTL become activated, multiply, and lyse the diseased cell. If only self peptides are presented, the CTL remain dormant and continue their surveillance of other cells in the neighborhood. Although the above description is somewhat oversimplified, it is clear that presentation of peptides derived from disease state associated proteins plays a critical role in activating an immune response. Sequence analysis of these peptides is a necessary first step in developing vaccines or other agents that modulate the immune response to particular diseases. The task is a challenging one because the peptide fragments characteristic of the disease state will be present in a complex mixture of several thousand peptides derived from normal cellular proteins. The concentration of any individual peptide in the mixture is usually in the range of 10-1,000 fmol/10^8 cells.

We have demonstrated previously that microcapillary HPLC electrospray ionization tandem mass spectrometry is a powerful tool for the sequence analysis of individual peptides present in fmol concentrations within extremely complex mixtures (2-4). Improvements in chromatographic separation should facilitate the identification of antigens from highly complex (>80 peptides) fractions which activate alloreactive, tumor specific, or autoimmune CTL. By subjecting biologically active fractions to a second dimension of chromatography, we effect a different separation of the peptides within the original fraction. Comparison of the peptide signals of biologically active fractions from the first and second dimension separations allows us to pinpoint likely candidates for epitope reconstitution. This methodology has enabled us to characterize a single HLA-A2.1 restricted peptide recognized by the CTL clone AHIII12.2. Characterization of this peptide represents a major analytical breakthrough, as it is only the second such antigen characterized directly from a complex mixture of self peptides (5).

Of particular interest, is the characterization of peptides which specifically activate CTL to kill human melanoma cells. Melanoma tumor

is the most serious form of skin cancer, leading to 6,500 deaths each year. In the U.S. alone, there are over 32,000 new cases reported yearly, with males ages 25-65 at highest risk. The main obstacle we face is the identification of a single activating peptide from within an HPLC fraction containing 50-300 peptides. To address this problem, we have employed the multistage chromatographic separation described above. The major limitation encountered with this protocol, however, was the loss of sample due to adsorption of peptides on the column and container walls. To overcome this problem we have constructed an apparatus that allows multidimension chromatography and both mass analysis and the cytotoxicity assay to be performed on a small fraction (3%) of the material isolated from $3x10^9$ cells. In figure 1, effluent from the microcapillary column is split, and a predetermined amount directed into the electrospray ionization source of the mass spectrometer. The complementary effluent is allowed to flow into individual wells of of a microtiter plate containing medium for biological assay. The end result is a record of the masses of the peptides deposited in each well. By increasing our chromatographic resolution, we are thus better able to pinpoint candidates which activate tumor specific CTL at trace levels.

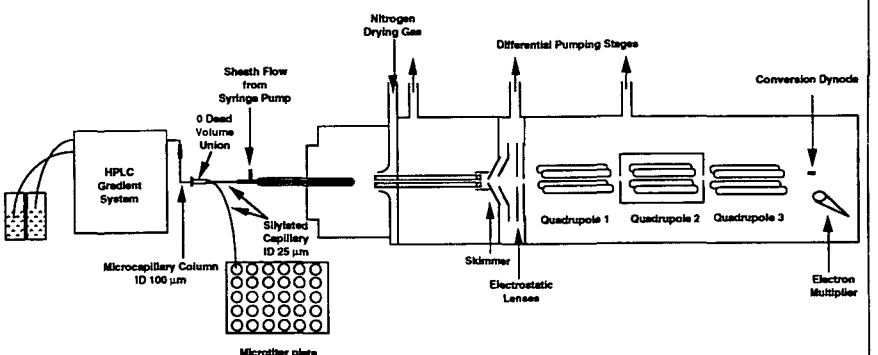

Figure 1. Microcapillary HPLC ESI MS/MS system with splitter to direct the effluent simultaneously to the mass spectrometer and to wells of a microtiter plate

References

1. Yewdell,J.W. et al., 1992, *Adv. Immunol.* 52, 1-123.
2. Hunt,D.F. et al., 1992, *Science* 255, 1261-1263.
3. Henderson,R.A. et al., 1992, *Science* 255, 1264-1266.
4. Huczko,E.L. et al., 1993, accepted *J. Immunol.*
5. Henderson,R.A. et al., 1993, submitted for publication.

Electrospray/capillary liquid chromatography (ESI/LC) and matrix assisted laser desorption (MALD) mass spectrometry for the analysis of expressed domains of carcinoembryonic antigen (CEA) and anti-CEA antibodies.

John E. Shively, Kristine Swiderek, Stanley Hefta, and Terry D. Lee. Beckman Research Institute of the City of Hope, Duarte, CA 91010.

CEA is a 180 kDa cell surface glycoprotein expressed in a variety of tumors of epithelial cell origin. Antibodies specific to CEA can be used as a serum test in vitro to monitor the recurrence of colon and other cancers, and in vivo for diagnosis and therapy of cancers of the colon, breast, and lung. CEA crossreactive antigens such as NCA (nonspecific crossreacting antigen) and BGP (biliary glycoprotein, also known as NCA-160) may interfere in tumor specific applications since they occur in a variety of normal tissues, including granulocytes. We have used several mass spectrometric techniques to study the structure of CEA, its crossreactive antigens, and engineered antibodies specific to CEA. Measurements of the molecular mass of CEA and NCA by mass spectrometry has been difficult since carbohydrate may comprise 50% of their molecular masses, and their glycosyl moieties, like most glycoproteins is notoriously heterogeneous. However, with the use of MALD/TOF/MS (on a Shimadzu instrument using a neodymium-YAG laser and sinapinic acid as a matrix) as an analytical tool, we have been able to show that CEA and NCA-55 (one of several glycoforms of NCA) have molecular masses of 135,000 and 55,000 (calculated at the maximum peak height). In the case of CEA this mass is substantially lower than that calculated by SDS-gel electrophoresis (180,000 Da), and for NCA agrees well. We have performed a variety of enzymatic and chemical deglycosylation studies on NCA-55 and shown that the loss in mass as analyzed by MALD/TOF/MS agrees well with masses predicted by other studies (**1**). When NCA or mutants lacking one, two, or three of the glycosylation sites in the N-domain (108 amino acids, three glycosylation sites) are expressed in HeLa cells and analyzed by MALD/TOF/MS the masses observed agree well with the calculated masses. The glycosyl deletion mutant studies of NCA demonstrate that the bacterial-lectin binding properties of this glycoprotein are contained within the first two glycosylation sites and probably involve protein as well as carbohydrate determinants. In addition, we have expressed a number of CEA domains and shown that their calculated and observed masses closely agree (**2**). Thus, this approach has been an accurate and sensitive (1-10 picomoles analyzed) method to analyze complex glycoproteins.

In order to study the site-specific structures of the glycosyl moieties of CEA and NCA, the reduced and alkylated forms were digested either with a combination of trypsin and chymotrypsin or pepsin and the glycopeptides purified by a combination of reversed phased and "hydrophilic" phase (polyhydroxylethylaspartamide) HPLC. Since the rather hydrophilic and heterogeneous glycopeptides do not resolve well on reverse phase HPLC, and give hard to interpret mass spectra results unless highly purified, it was necessary to use secondary chromatography approaches. In our hands, the best analytical tool for glycopeptide analysis was SIMS analysis (a Phrasor Instruments cesium ion gun) on a triple quadrupole mass spectrometer (Finnigan TSQ700). CEA has 28 N-glycosylation sites and a C-terminal glycosylphosphatidyl inositol moiety. A glycopeptide isolated from glycosyl site number 1 has the sequence SGREIIYPN*ASLLIQ, where the glycopeptide has a mass of 3738, 1675 of which is due to the peptide moiety (**3**). The SIMS spectrum shows sequential losses of Gal, Gal-GalNAc-Fuc, Gal-GlcNAc(-Fuc)-Man, etc., all the way down to the intact peptide at 1675 (no glycosyl moiety). Although the mass spectra cannot distinguish the structural nature of the sugar moieties, they can be logical assigned based on consensus

structures published for glycoproteins. When the same glycopeptide is analyzed by ESI, a hard to interpret mass spectrum is obtained. We attribute this difficulty to the occurrence of multiply charged fragments ions which include peptide and glycosyl fragments exhibiting no obvious pattern of fragmentation or charging. In comparison to CEA, NCA has 12 glycosylation sites of which a peptide from glycosyl site 1 has the sequence $(Man)_3(GlcNAc)_2Fuc$ as determined by MS/MS SIMS analysis. An indication of the sensitivity of the approach is given by the isolation of NCA-160 (BGP) from granulocytes and digestion with trypsin at the 50 picomole level on a nitrocellulose membrane and isolation of the resulting glycopeptides from capillary liquid chromatography (160 micron ID column). Analysis of 25% of the recovered glycopeptides (about 6 pmoles) by SIMS gave 30% of the sequence of the protein, including significant information about the location and nature of glycosyl residues. One example shown (**4**) predicts an M_7GN_2 glycosyl moiety.

The analysis of engineered antibodies to CEA has also benefited from mass spectral analysis. For the large fragments, including intact immunoglobulin (150,000 Da), we have routinely used MALD/TOF/MS. For the smaller fragments, including single chain antibodies (SCA) (28,000 Da), we have used ESI combined with LC/MS. We have found LC/MS a requirement for these analyses, since the samples are always isolated in bio-compatible buffers which severely interfere with direct infusion ESI. In one example, we have observed a mass of 28,133 for a SCA with a predicted mass of 24,146. Further structural analysis revealed that the SCA had the correct N- and C-terminal amino acid sequence. The SCA gave broad peaks on conventional wide pore C8 reversed phase packings in a capillary column. When the SCA is reduced and S-alkylated (by iodoacetic acid in 6 M guanidinium HCl and 10 mM DTT) the problem becomes so severe as to make analysis by ESI impossible. This problem was solved by using less absorptive polymer resins such as Polymer Labs **PR** packing. In this case, a single sharp peak was observed with a deconvoluted mass agreeing to within 10 mass units of that predicted. The polystyrene packing has other applications, including use in high pH solvent systems such as TEA/TFA. The high pH systems may have applications in negative ion ESI. Recently, we have analyzed strongly anionic macromolecules (carboranyl oligophosphates) and shown that they give excellent negative ion spectra on ESI LC/MS, but otherwise have been difficult to analyze by negative ion SIMS or MALD. We attribute the latter difficulties to the presence of strongly complexed cations which interfere in SIMS or MALD, but are removed during LC/MS, a technique ideally suited to ESI.

We conclude that multiple MS approaches are required to solve the diverse problems encountered in the analysis of protein conjugates of immunological interest.

References

1. Sauter, S.L., Rutherfurd, S.M., Wagener, C., Shively, J.E., and Hefta, S.A. Identification of the specific oligosaccharide sites recognized by type 1 fimbriae from E. coli on nonspecific cross reacting antigen, a CD66 cluster granulocyte glycoprotein. **J. Biol. Chem.**, in press.
2. Hefta, L.J.F., Chen, F.-S., Ronk, M., Sauter, S.L., Sarin, V., Oikawa, S., Nakazato, H., Hefta, S.A., and Shively, J.E. Expression of carcinoembryonic antigen and its predicted immunoglobulin-like domains in HeLa cells for epitope analysis. **Cancer Res. 52**, 5647-5655, 1992.
3. Swiderek, K.M., Lee, T.D., and Shively, J.E. Trace structural analysis of proteins. **Methods in Enzymol.**, in press.
4. Mahrenholz, A.M., Yeh, C.H., Shively, J.E., and Hefta, S.A. Microsequence and mass spectral analysis of nonspecific cross reacting antigen 160, a CD-15 positive neutrophil membrane glycoprotein. **J. Biol. Chem. 268**, 13015-13018, 1993.

Structural and Mechanistic Studies of Human Neutrophil Elastase by Mass Spectrometry

P. R. Griffin, T. A. Dickinson, B. G. Green, W. B. Knight, J. Doherty, and R. A. Mumford, Merck Research Laboratories, Rahway, N. J. and Glaxo, Inc. N.C.

Human Neutrophil elastase (HNE; EC 3.4.21.37) is a 220 amino acid serine protease that is present in mM concentrations in the azurophilic granules of polymorphic nuclear monocytes (PMN). HNE has been implicated in a number of inflammatory diseases (cystic fibrosis, bronchitis, emphysema, inflammatory bowel disease and perhaps rheumatoid arthritis). A series of β-lactams have been described by Merck Research Laboratories as mechanism-based inhibitors of elastase. Knowledge of the molecular nature of enzyme-inhibitor (E-I) complexes formed by reaction of HNE with β-lactams can lead to the proposal of a mechanism of inhibition consistent with both chemical and kinetic data. We have utilized capillary-HPLC-ESI-MS and matrix-assisted laser desorption ionization time-of-flight mass spectrometry (MALDI-TOF-MS) for probing the interaction between HNE and a β-lactam (1) and between HNE and α1-proteinase inhibitor (α1-PI).

Reaction of β-lactams with HNE produces very stable E-I complexes and the stability of these complexes was postulated by Firestone and co-workers (2) to be attributed to a "double hit" mechanism involving both acylation and alkylation of active-site serine and histidine, respectively. This "double hit" mechanism for b-lactams was derived from X-Ray crystallography experiments on cephalosporin inhibitors complexed with elastase. To probe this mechanism of inhibition HNE (25,199 Da as determined by HPLC-MS; see Figure 1) was reacted with L-680,833 (Figure 2) (k_{obs}/k_i = 680,000 $M^{-1}s^{-1}$; M.W. = 467). This reaction yielded an E-I complex with a mass of 25,523 Da (a mass shift of +324 Da; see Figure 2). The observed mass shift is consistant with the β-lactam ring opening followed by the loss of the phenoxy group at C4 and the incorporation of a molecule of water to the complex. The role of histidine in this complex is unclear. However, these results suggests that a "double hit" of active site serine and histidine may not be required to produce a stable E-I complex.

It is interesting to note that only irreversible E-I complexes were observed by HPLC-ESI-MS, ESI-MS using direct infusion in aqueous solutions, and by MALDI-TOF-MS. Reversible tight-binding complexes between HNE and secretory leucoprotease inhibitor (SLPI) were not observed yielding both intact HNE and intact SLPI. In addition, complexes between porcine pancreatic elastase (PPE) and β-lactams were analyzed affording identical results as obtained on HNE. Finally, complexes between HNE and α1-PI were analyzed by MALDI-TOF-MS. As expected, a 70 kDa complex of HLE-α1-PI was present as well as the 4.1 kDa peptide that is cleaved from α1-PI. These results demonstrate that mass spectrometry is a powerful tool to probe the mechanism of inhibition of enzymes by mechanism-based inhibitors.

1. W.B. Knight, K.M. Swiderek, T. Sakuma, J. Calaycay, J.E. Shively, T.D. Lee, T.R. Covey, B. Shushan, B.G. Green, R. Chabin, S. Shah, R.A. Mumford, T.A. Dickinson, and P.R. Griffin, *Biochemistry* 32, 2031-2035 (1993).
2. R.A. Firestone, P.L. Barker, J.M. Pisano, B.M. Ashe, and M.E. Dahlgren, *Tetrahedron* 46, 2255-2262 (1990).

Figure 1.

MASS SPECTRUM OF HUMAN PMN ELASTASE ISOZYME-4

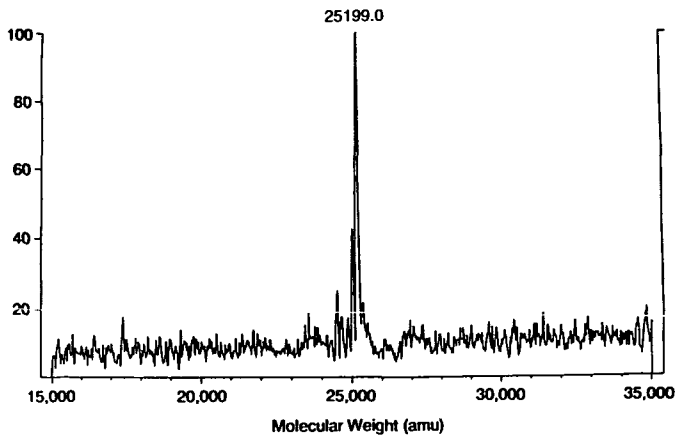

Figure 2.

MASS SPECTRUM OF THE L-680,833 DERIVED PMN ELASTASE-INHIBITOR COMPLEX

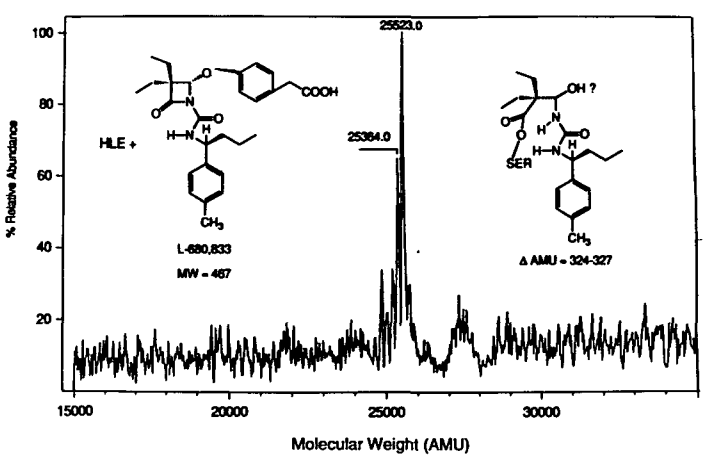

Separation and Characterization of Lipopolysaccharides from *B. catarrhalis* and *H. influenzae* Type B by CE-MS and MS-MS.*

J.F. Kelly[1], P. Thibault[2], H. Masoud[3], M.B. Perry[3], J.C. Richards[3]

[1]Dept. of Chemistry, Dalhousie University, Halifax, Canada, B3H 4J3, [2]Institute for Marine Biosciences, NRC, Halifax, Canada,B3H 3Z1, [3]Institute for Biological Sciences, NRC, Ottawa, Canada, K1A 0R6.

Lipopolysaccharides (LPS) are a unique group of biomolecules found on the outer surface of the cell walls of gram negative bacteria (1). LPS typically have endotoxic and O-antigenic properties and have been the subject of much scientific and medical interest. These complex oligosaccharides usually consist of three distinct regions: the O-specific chain, the Core, and the Lipid A. The latter region normally consists of fatty acids and phosphate groups bonded to a disaccharide of two D-glucosamine units, whereas the O-specific chain and the Core are almost exclusively carbohydrate.

Branhamella catarrhalis (*B.cat.*) has recently been recognised as an opportunistic pathogen and is often the sole causative agent of a number of respiratory diseases and acute otitis media (2,3). *Hemophilus influenzae* type b (*Hib*) infection can lead to meningitis in young children (4). In both cases, it is believed that LPS plays an important role in the expression of their virulence. Furthermore, the LPS isolated from these bacteria are unusual in that they lack an O-specific chain.

The separation and characterization of such complex biomolecules by conventional methods is difficult as they are large, polar, labile, and lack a significant UV chromophore. Furthermore, LPS isolated from a given species are typically heterogenous owing to varying degrees of substitution of the basic LPS structure. However, these compounds usually possess ionic functionalities which facilitate their analysis by techniques such as capillary electrophoresis. Successful separation and detection of the O- and N,O-deacylated LPS has been accomplished using capillary electrophoresis coupled with ionspray mass spectrometry (CE-ISP-MS).

The O-deacylated LPS were found to be amenable only to negative ion MS, which is consistent with the fact that these molecules contain acidic moieties but no protonation sites. CE-ISP-MS of O-deacylated LPS from *B.cat* revealed its natural heterogeneity (Fig. 1), which is due mainly to the number of phosphate or phosphoethanolamine groups attached to the principal LPS structure. The N,O-deacylated LPS were amenable to both positive and negative CE-ISP-MS. These two modes of detection permitted identification of the same compounds. Moreover, the principal analytes observed differ only in the number of hexose units they contain. Full mass scan acquisition for the N,O-deacylated LPS was typically carried out on picomole quantities of material. However, the limit of detection in selected ion monitoring mode was in the low femtomole range.

Structural characterization of the O- and N,O- deacylated LPS was achieved using tandem mass spectrometry with low energy CID. The principal fragmentation pathways observed arise from cleavage of the glycosidic bonds leading to sequential loss of the monosaccharide units (Fig. 2). Positive and negative MS-MS spectra of the doubly-charged O- and N,O-deacylated LPS were characterized by intense fragmentations corresponding to the lipid A moiety and its complementary fragment.

References:

1. O. Luderitz *et al.*, Current Topics in Membranes and Transport, **17**, 79, 1982.
2. M. Leinonen *et al.*, J. Infectious Diseases, **144**, 570, 1981.
3. M. Vaneechoute *et al.*, J. Clinical Microbiology, **28**, 182, 1990.
4. A. Kimura *et al.*, Infection and Immunity, **51**, 69, 1986.

*NRCC # 34861

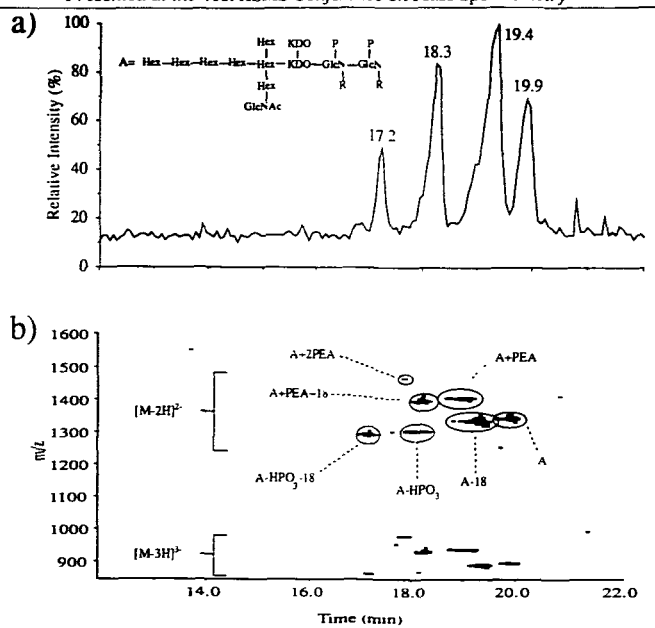

Figure 1: CE-MS (negative ion) analysis of O-deacylated LPS from *B. Catarrhalis*; (a) Full Scan (m/z 850-1600), Conditions: 50 mM NH_4COOH (pH 8.5), 30 ng inj. (total), 1.1 m x 50 µm i.d. capillary column, 25 kV; (b) Contour Profile.

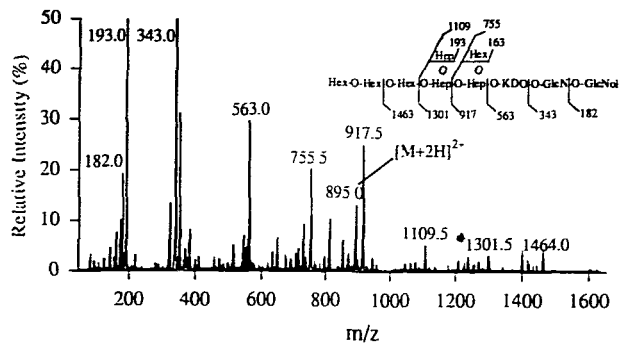

Figure 2: MS-MS (positive ion) spectrum of N,O-deacylated and dephosphorylated LPS from *H. Influenzae* type b.

STRUCTURAL CHARACTERIZATION OF THE ADJUVANT ACTIVE COMPOUNDS IN *QUILLAJA SAPONARIA* MOLINA EXTRACTS

C. E. Costello[1], K. E. Vogele[2], J. Thurin[2] and B. Morein[3]
[1]Department of Chemistry, Mass. Inst. of Technology, Cambridge, MA 02139
[2]The Wistar Inst., Philadelphia, PA 19104
[3]Royal Veterinary College, Stockholm, Sweden.

The ISCOM adjuvant, Immune Stimulatory Complex, is a 35-nm particle which is formed by mixing a saponin glycoside mixture, Quil-A, with cholesterol and antigen. Quil-A contains a multitude of different compounds, many of which are toxic. Before the adjuvant properties of these extracts can be exploited for human use in vaccines, it is necessary to establish structure-function relationships of the various components. In this study, the adjuvant active compounds in Quil-A have been purified through a series of chromatographic procedures and the active fractions followed by bioassay throughout the isolation procedure. Two compounds have been found to be responsible for most of the adjuvant activity and one is responsible for the formation of the ISCOM particle. Our preliminary data indicate that the isolated compounds are not identical to those previously published which were isolated from the same material (1-3). The The structures of the components of the most abundant adjuvant-active fraction and the core compound(s) obtained from it upon base hydrolysis are presently being determined, using a combination of mass spectrometry and multidimensional NMR. Positive- and negative-ion LSIMS and MS/MS and matrix-assisted laser desorption mass spectrometry have each contributed to the results.

Experimental. LSIMS and MS/MS mass spectra were obtained with a JEOL HX11/HX110 (E_1B_1-E_2B_2) tandem mass spectrometer, operated at +/- 10 kV acceleration. CID took place in a cell located between MS-1 and MS-2, floated at 3 kV *vs.* ground. MALDI mass spectra were obtained on a Vestec VT2000 linear time-of-flight instrument, using an LSI nitrogen laser (337 nm), +30 kV or -25 kV acceleration, and a LeCroy transient digitizer for data acquistion.

Results. LSIMS and MALDI mass spectra have been obtained for the fractions containing the intact saponins and for all of the components obtained by hydrolysis of the active fraction followed by chromatographic separations. The initial mixture was quite heterogeneous, and, indeed, some minor heterogeneity remained in all fractions even after extensive purification. Results from an earlier MS/MS investigation of simpler saponins (4) were helpful in assigning the product ion structures. The availability of hydrolysis products as well as intact saponins in this study helped with elucidation of new pathways. The most abundant components of the intact adjuvant have the apparent molecular weights 2019.2 and 2151.2, and the major hydrolysis product has molecular weight 1674.8. Minor but potentially important components vary in carbohydrate content and in the substitution of the triterpene. Evidence from the MS/MS data indicates that there is variation in all three carbohydrate regions of the structure. CID of fragment ions as well as the molecular species was needed to unravel the heterogeneity in each

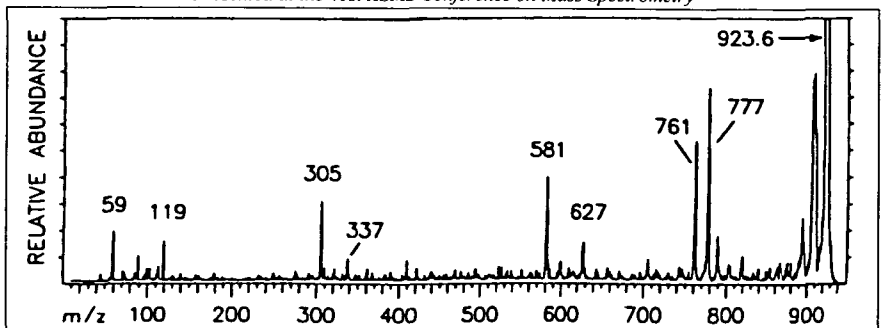

Fig. 1. CID mass spectrum of *m/z* 923.6 in the LSIMS of an active intact saponin fraction.

of these regions. Figure 1 shows the CID mass spectrum obtained for a fragment in the negative-ion LSIMS spectrum of intact acylated saponin that contains, among others, a pair of components differing in mass by 14 u. Scheme 1 shows assignments of the product ions from *m/z* 923. On the basis of the spectra obtained for *m/z* 909 and *m/z* 923, it could be determined that the mass shift occurred at the rhamnose residue. MS/MS was thus very useful to differentiate among the isomers that varied in carbohydrate chain size and branching patterns, whereas NMR was particularly good for distinguishing among the isomeric carbohydrate residues and for establishing linkage positions. MALDI was the fastest, most sensitive and most reliable method for determination of molecular weight heterogeneity.

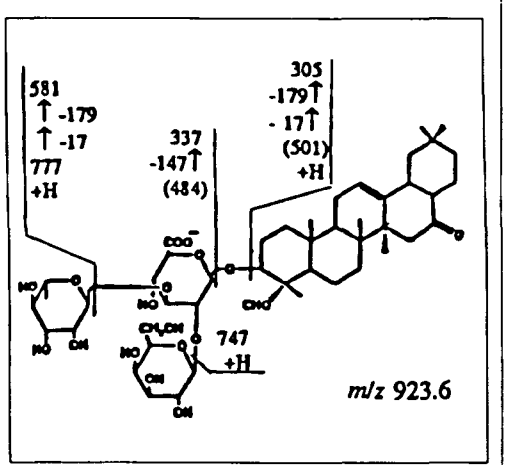

Scheme 1

References
1. R. Higuchi, Y. Tokimitsu and T. Komori, *Phytochemistry*, 1988, *27*, 1165-1168.
2. R. Higuchi, *et al.*, *Phytochemistry*, 1987, *26*, 229-235.
3. R. Higuchi and T. Komori, *Phytochemistry*, 1987, *26*, 2357-2360.
3. C. E. Costello, *et al.*, *Abstr. of 35th ASMS Conf.*, Denver, CO, May, 1987, p. 1-2.
Acknowledgements. These studies were supported by NIH grants from Nat'l Ctr for Res. Resources, RR00317 to K. Biemann, and the National Cancer Inst., CA09171 to H. Koprowski.

THE ROLE OF MASS SPECTROMETRY IN THE STRUCTURE DETERMINATION OF MUCINS EXPRESSED BY CARCINOMAS

R. L. Cerny and M. L. Gross, Department of Chemistry, University of Nebraska-Lincoln, Lincoln, NE 68588 and M. A. Hollingsworth, Eppley Institute for Research in Cancer, University of Nebraska Medical Center, Omaha, NE 68198

The basic cellular processes that regulate O-linked glycosylation of proteins are poorly understood. There is evidence that epithelial cells from different tissues glycosylate different serine and theonine residues on the same core of heavily O-glycosylated proteins such as mucins. Truncated oligosaccharides on mucins produced by tumors in epithelial tissues have been identified as tumor-associated antigens. It has also been postulated that the points of attachment of the oligosaccharides are altered by these tumors, thus exposing tumor associated epitopes on the mucin core regions. These epitopes are currently being evaluated as target antigens for diagnostic reagents and tumor vaccines.

MUC 1 is glycoprotein expressed by a wide variety of human adenocarcinomas and their normal epithelial counterparts. MUC 1 has a core protein consisting of 1272 residues. The central two thirds of the protein sequence consists of identical 20 amino acid tandem repeats. Synthetic peptides (30 residues and 20 residues) corresponding to the tandem repeat sequence were glycosylated *in vitro* using UDP-[^{3}H]GalNAc and N-acetylgalactosaminoyltransferase from pancreatic and breast tumor cell lines, HPAF and MCF7 respectively. The glycopeptides were purified by chromatography on Dowex 1 and P-10 columns, and then reverse phase HPLC on a C-18 column. Analysis of the resulting glycopeptides by mass spectrometry showed that up to three molecules of GalNAc linked to each repeat unit in the peptides (see Figure 1). The protonated 30 residue peptide has an average mass of 2869.6 daltons. Addition of a GalNAc subunit increases the molecular weight by 203 daltons. Fraction A contains glycopeptides incorporating principally 2 GalNAc subunits (but also 1 and 3), fraction B contains a glycopeptide with only one GalNAc subunit, and Fraction C contains the unmodified peptide. Purified glycopeptides were sequenced on a gas phase sequencer and glycosylated positions were determined by measuring the incorporated radioactivity in fractions collected flowing each round of Edman degradation. The results showed that two of three threonine resides and none of two serine residues on the MUC 1 tandem repeat peptides were glycosylated by both HPAF or MCF7 lysates at the following positions: GVTSAPDTRPAPGSTAPPAH (underlined T indicates GalNAc attachment).

Efforts are underway to improve the sensitivity of tandem mass spectrometry for the use in the analysis of clinical specimens, which cannot be studied by the modified Edman assay. Shown in Figure 2 is the CAD spectrum of 1 nanomole of a synthetic glycopeptide that incorporates one GalNAc unit. The spectrum was obtained using a ZAB-T, four sector mass spectrometer with array detection with a mass ratio of 1.21:1. Although the spectrum contains several abundant sequence ions, information on the position of the GalNAc moiety is absent. In fact, elimination of GalNAc is one of the most abundant fragments. Further work must be done to enhance the information obtained from the CAD spectrum.

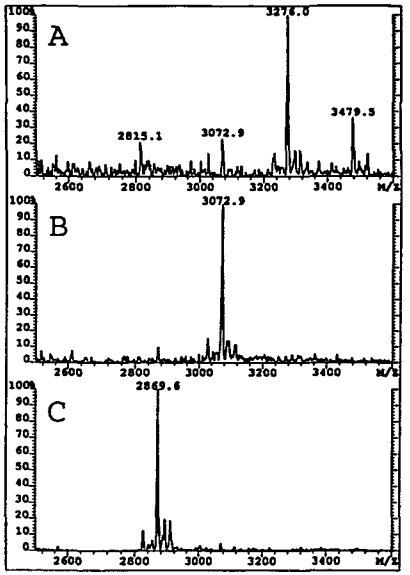

Figure 1.FAB mass spectra of fractions collected from reverse phase HPLC of MCF7: A) 24.2 min.; B) 25.0 min.; C) 26.2 min.

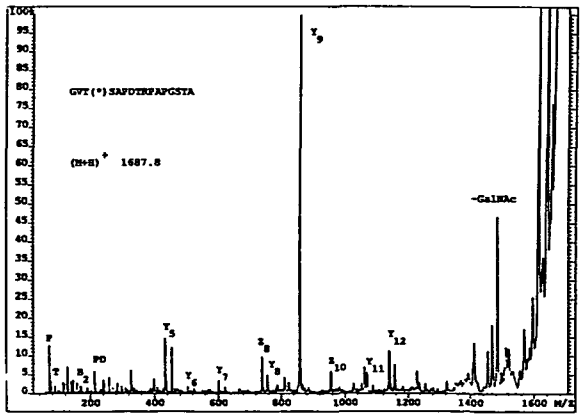

Figure 2. CAD spectrum of 1 nmole of synthetic glycopeptide obtained using array detector.

CHARACTERIZATION OF NATURALLY-OCCURRING AND MODIFIED FULLERENES BY FOURIER TRANSFORM MASS SPECTROMETRY *

Robert L. Hettich, Changming Jin, Rhys Thomas, and Robert N. Compton
Oak Ridge National Laboratory, Oak Ridge, TN 37831-6120
and
Peter R. Buseck and Semeon J. Tsipursky
Department of Geology, Arizona State University, Tempe, AZ 85287

Based on the remarkable stability and properties of fullerenes, it was thought that these species may have formed under natural conditions outside the laboratory and may be found in geological samples. Collaborative research between Peter Buseck, Semeon Tsipursky and Robert Hettich resulted in the first evidence of naturally-occurring fullerenes in a carbon-rich terrestrial rock sample from Russia. The natural source of fullerenes in this case was a carbon-rich rock (shungite) from Shunga, Russia. Buseck and Tsipursky noted that, under high resolution transmission electron microscope investigations, certain portions of this rock appeared to be identical to images of synthetic fullerenes. Examination of a few micrograms of this sample by laser desorption (266 Nd:YAG laser) Fourier transform mass spectrometry at ORNL revealed the presence of C_{60} and C_{70}, as shown in Figure 1 laser desorption spectrum. While these initial results were quite encouraging, the experimental parameters for this technique must be carefully controlled to insure that the fullerenes detected were present in the sample and were not created in the mass spectrometer by the laser desorption event. Examination of pure graphite samples indicated that fullerenes were not generated from pure graphite under these low energy laser desorption conditions (10^6 - 10^7 W/cm^2). In addition, thermal desorption of the sample (350 °C) followed by low energy electron capture also indicated the presence of C_{60} in this sample, shown in Figure 1 thermal desorption spectrum (a higher temperature is needed to thermally desorb C_{70} from the probe tip). These experiments were the final proof needed to verify the presence of fullerenes in the sample, because thermal desorption will not generate fullerenes from graphitic material. The origin of the shungite rock is a subject of debate at this time; it may be a product of either a volcanic or organic process. This shungite sample is similar in composition to meta-anthracite rank coals and is jet-black in appearance.

FTMS is useful for examination of the structures and properties of fullerene derivatives as well. For example, hydrogenated fullerenes were generated by exposing solid films of C_{60} to a high pressure of H_2 at elevated temperatures. Experimentally, C_{60} powder was placed in metal capsules (Pd and Au) and exposed to 1000 Bar of H_2 at 700 K for times ranging from 24-96 hours. Figure 2 shows the positive ion mass spectrum of a sample which was contained inside a Pd capsule for 90 hours during the hydrogenation process. Besides the typical pure C_{60} isotopic mass distribution at 720, 721, 722 amu, there is evidence of $C_{60}H_x$ for x up to 24. Identical results were obtained for both Pd and Au capsules, indicating that the metal capsule did not serve as a catalyst for these hydrogenation reactions. To examine whether the protons might be inside or outside the fullerene cage, the following charge exchange reaction was used (pyridine is known to be a stronger base than C_{60}).

$$\text{Pyridine} + C_{60}H_x^+ \text{ ------ } (\text{Pyridine}+H)^+ + C_{60}H_{x-1} \qquad (1)$$

The resulting mass spectrum revealed that the $C_{60}H_x^+$ containing an odd-number of hydrogens would undergo faster proton transfer to the pyridine than the even-numbered hydrogenated species. Further research is in progress to examine these hydrogenated fullerenes with other reagent gases.

Figure 1.

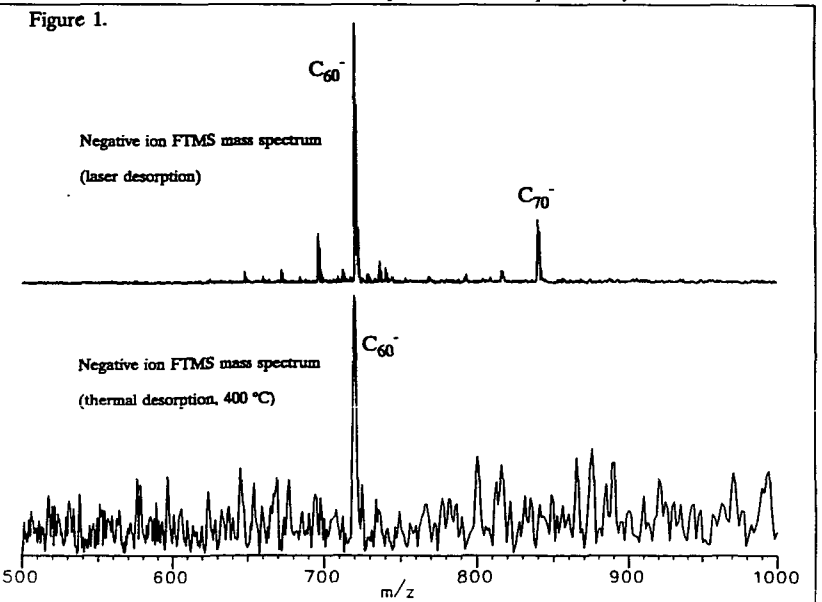

Figure 2.

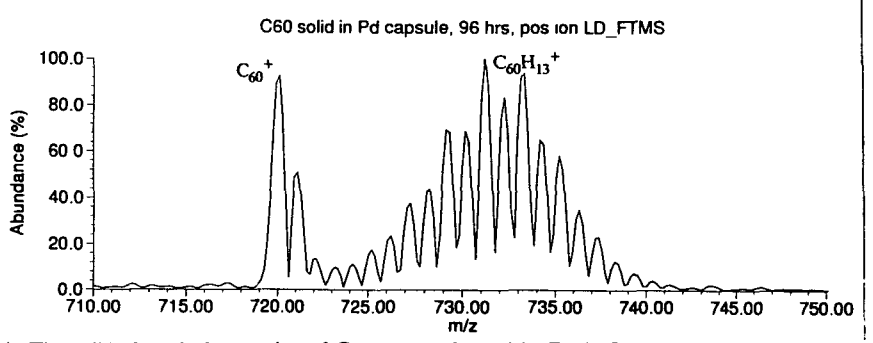

* The solid phase hydrogenation of C_{60} were performed by David Joyce and James Blencoe of ORNL Chemistry Division. This research was sponsored by the Oak Ridge National Laboratory Director's R&D Program and the Office of Health and Environment Research, U.S. Department of Energy under contract DE-AC05-84OR21400 with Martin Marietta Energy System, Inc.

Analysis of Fullerene Soot Extracts by Liquid Chromatography-Mass Spectrometry Using Atmospheric Pressure Ionization†

J.F. Anacleto,* Department of Chemistry, Dalhousie University, Halifax, N.S. Canada
M.A. Quilliam and **R.K. Boyd**, Institute for Marine Biosciences, NRCC, Halifax, N.S. Canada

Techniques have been developed for the analysis of fullerenes and related compounds present in materials such as soots produced by resistive heating of graphite in an inert atmosphere and condensates from benzene flames. The minor constituents of three fullerene-rich materials have been characterized by on-line LC-MS techniques using both positive and negative ion mass spectra obtained by atmospheric pressure chemical ionization (APCI). Two of the materials were soots, produced by resistive heating of graphite, from different commercial suppliers: one contained monoxides of the carbon clusters as the principal minor components (e.g., $C_{60}O$ and $C_{70}O$), while the other contained hydrogenated species including $C_{60}H_2$, $C_{60}H_4$, and $C_{70}H_2$ (1). The third material, a condensate from a controlled benzene flame, was shown to contain all of the minor constituents mentioned above as well as significant quantities of compounds that behaved under the APCI/MS conditions as isomers of the C_{60} and C_{70} fullerenes, and which reverted to the latter upon heating (2).

Further characterization of the flame soot extract was performed by LC coupled on-line to ionspray mass spectrometry (3). Charge-transfer complexation, using a post-column addition of either an electron donor or acceptor, was utilized as a pre-ionization technique. The negative ion mode experiments, using TMPD as the electron donor, produced intense $M^{-\cdot}$ ions corresponding to the C_{60} and C_{70} fullerenes, but failed to provide any information regarding the identity of the metastable constituents. Analyses in positive ion mode, using DDQ as the electron acceptor, showed that the metastable compounds yielded mass spectra consistent with their identification as fullerene adducts with highly unsaturated moieties C_nH_{2n-4} with n=5, 6, and 7 (Figure 1). The molecular radical cations of these adduct species were susceptible to facile fragmentation yielding the molecular ions of the corresponding fullerenes. Based on this information, the Diels-Alder adduct of C_{60} and cyclopentadiene has been synthesized and shown to be identical (based on ^{13}C and proton NMR) to the $C_{60}C_5H_6$ adduct (n=5) generated in the benzene flame (4).

The separation of fullerenes on four commercially available reversed-phase columns was also investigated using LC-APCI/MS (5). Three of the octadecylsilica (C_{18}) phases were incapable of adequately separating the fullerenes, present in a trichlorobenzene soot extract, according to carbon number. However, baseline resolution of nearly all the fullerenes (up to at least C_{96}) was achieved with a 2-(1-pyrenyl)ethylsilica phase. This was probably the result of increased π-bond interactions between the stationary phase and the fullerenes.

The resolution of individual fullerene isomers was best accomplished with a polymeric octadecylsilica bonded phase (Figure 2). All of the other stationary phases, monomeric C_{18} and pyrenyl, were very poor in this respect. A proposed mechanism for this unique ability combines the shape selectivity of polymeric phases, previously recognized for planar polycyclic aromatic hydrocarbons, and the "molecular footprints" of the fullerene isomers.

(1) J.F. Anacleto *et al.*, *Can. J. Chem.*, **70**, 2558-2568 (1992).
(2) J.F. Anacleto *et al.*, *Rapid Commun. Mass Spectrom.*, **6**, 214-220 (1992).
(3) J.F. Anacleto *et al.*, *Rapid Commun. Mass Spectrom.*, **7**, 229-234 (1993).

(4) V.M. Rotello *et al.*, *Tetrahedron Letters*, **34**, 1561-1562 (1993).
(5) J.F. Anacleto and M.A. Quilliam, *Analytical Chemistry*, accepted for publication.

†NRCC # 34862

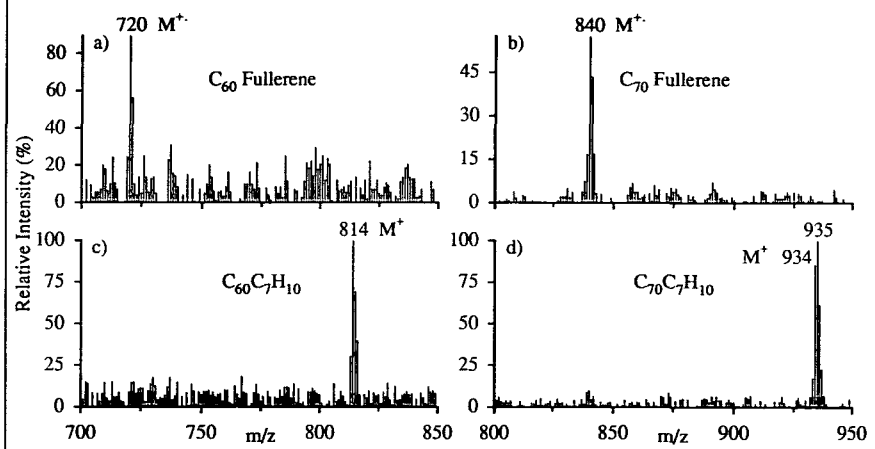

Figure 1: Charge-transfer ionspray mass spectra obtained during the LC-MS analysis of the flame-generated fullerenes. Spectra were obtained at the crests of the following chromatographic peaks: (a) C_{60}; (b) C_{70}; (c) and (d) thermally metastable components.

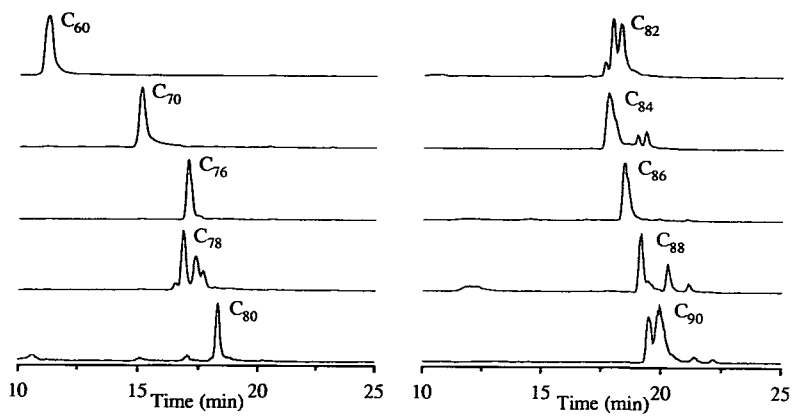

Figure 2: LC-APCI/MS selected ion chromatograms (monitoring molecular ions) from the analysis of a trichlorobenzene extract of graphite soot using a Vydac 201TP column (polymeric octadecylsilica phase).

Carbon Cluster Anions: C_5^- to C_{60}^-

Nigel G. Gotts, Gert von Helden, Michael T. Bowers
Department of Chemistry, University of California, Santa Barbara

Introduction:

Ever since the discovery of Buckminsterfullerene, carbon cluster ions have been at the forefront of many research efforts. In particular, the structures adopted by the carbon cluster ions have represented a major field of interest, as manifested by the question "Where do fullerenes come from"?

We recently introduced a novel experimental technique, dubbed "Ion Chromatography"[1], which enables structural analysis to be performed for a mass selected species. The procedure utilizes a high pressure drift cell. Ions passing through the cell are separated according to their collision cross section, and hence their structure. When applied to carbon cations, several structural families are observed. These sequentially manifest themselves in the order, Linear chains, Monocyclic rings, Bicyclic rings, Tricyclic rings, 3-D rings, Fullerenes/Cages, as cluster size increases[2].

Here we report on an extension of the study to include carbon anions. The object, to discern any differences in structural behaviour between the two ion forms.

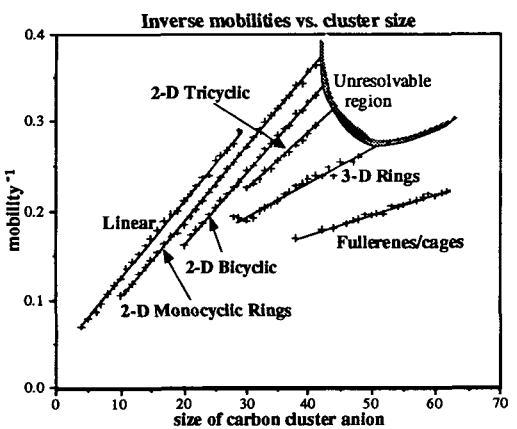

Figure 1

Experimental:

Carbon clusters, ions and neutrals alike, are produced in a typical laser vaporization source. Following supersonic expansion, the chosen ion species are accelerated to 5kV, and subsequently mass selected via a reverse geometry double focussing mass spectrometer. A 5-10 ms packet of the cluster ion of interest is then decelerated and injected into a high pressure drift cell, containing up to 5 Torr of helium. Ions drift through the cell under the action of a weak electric field. Collisions with the helium serve to spatially, and by analogy temporally, separate the different isomers present. Upon exiting the cell the ions are quadrupole mass analysed and detected. Data obtained in this manner is termed an Arrival Time Distribution (ATD). Fitting the

ATD's to obtain the mobilities of the isomers present is routinely performed via a computer peak matching program. Semi-empirical computer modelling procedures are adopted to match an observed mobility with a possible structure. The accuracy in this approach is typically to within a few percent.

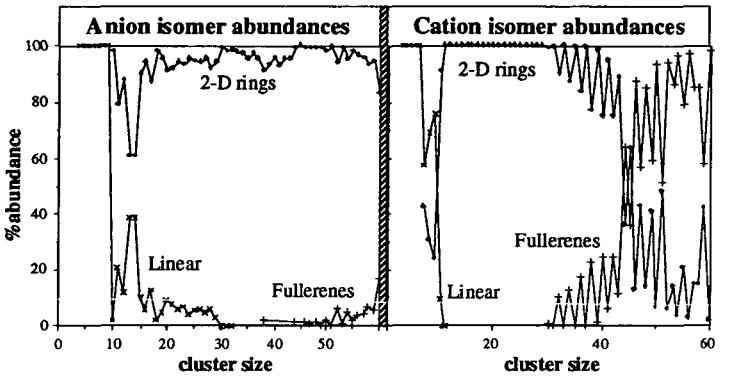

Figure 2

Results and Conclusions:

Figure 1 graphically depicts the observed structures for cluster anions in the range C_5^- to C_{62}^-; plotted as a function of inverse mobility. Note that ions of the same structure fall along a common gradient, and also that the 2-D tricyclic, bicyclic, and monocyclic rings possess similar slopes. Qualitatively these results are identical to those obtained for the cations.

Two notable exceptions occur in the linear and fullerene forms of the anions. In figure 2 we depict the percentage abundances observed for the linear, total 2-D ring (monocyclic+bicyclic+tricyclic), and fullerene systems. It is immediately apparent the linear cations vanish at a cluster size of ten units, while linear anions are still observed at C_{28}^-. Since the anions are probably formed via electron attachment to neutrals, it appears neutral linears may exist to quite large sizes.

For fullerenes an even/odd oscillation in relative abundance is apparent with even being favored. These structures dominate the ATD's of the cations above C_{44}^+, with C_{60}^+ more than 95% fullerene. On the other hand for anions fullerene abundances remain minor components up to and beyond C_{60}^-. For example only 20% of the C_{60}^- species possess the fullerene form, the remainder being planar rings.

What these results suggest is; a) since the same structural families are present for both the anions and cations, the neutrals almost certainly have these families also; linears, planar rings, fullerenes; b) the late development of the fullerene family in the anions probably reflects the rather larger electron affinity of planar ring systems over fullerenes, rather than an inherently greater stability of neutral planar rings over fullerenes.

References:

1. G. von Helden, N.G. Gotts and M.T. Bowers, *Nature*, **363**, 60 (1993).
2. G. von Helden et al., *The SPIE Conference on Applied Spectroscopy in Materials Science 2*, Los Angeles, CA, Jan 1992, **vol 1636**, pp 182-189 (1992).

MASS SPECTROMETRY OF UNUSUAL FULLERENE COALESCENCE PRODUCTS

J.H. Callahan, M.M. Ross and S.W. McElvany
Chemistry Division/Code 6113, Naval Research Laboratory, Washington, DC 20375-5000

L.D. Lamb and D.R. Huffman
Physics Department, University of Arizona, Tucson, AZ 85721

One of the unusual chemical characteristics of fullerenes is their ability to undergo reactions that apparently involve coalescence of smaller fullerenes resulting in larger clusters. Recent studies of this phenomenon have consisted of laser vaporization of pure fullerenes and mass spectrometric analysis of larger all-carbon ions (1,2). The speculation is that following photon-induced damage of the fullerenes, the species formed react to yield the larger clusters, which in all cases to date have been measured to have an even number of carbon atoms.

In a recent study, we detected the large, odd-numbered, pure-carbon clusters C_{119}, C_{129} and C_{139} in toluene extracts of soot produced in a graphite arc (3). Figure 1a shows a narrow-range mass spectrum from the methane negative ion/desorption chemical ionization (NI/DCI) analysis (4) of a soot toluene extract. Between m/z 1350 and 1600 essentially only C_{119}^- and C_{129}^- are observed. However, Figure 1b shows that when positive ion/desorption electron ionization is used extensive fragmentation results. Specifically, lower-mass ions corresponding to C loss, C_{118}^+ and C_{128}^+, and subsequent C_2 losses, C_{116}^+, C_{114}^+ and C_{126}^+, C_{124}^+, from C_{119}^+ and C_{129}^+, respectively, are observed. Collision-induced dissociation experiments proved unsuccessful in fragmenting either C_{119}^- or C_{119}^+ using 200-eV (lab) multiple collisions with xenon in the triple quadrupole instrument.

While it is evident that C_{119}, C_{129} and C_{139} correspond to "dimers" of C_{60}, C_{60}/C_{70} and C_{70} less one carbon atom, respectively; it is not obvious how this reaction might proceed. One possibility would involve oxygen whereby a CO or CO_2 loss could drive the process. To test this idea ozone was bubbled through toluene solutions of pure C_{60}, pure C_{70} and a 1/1 mixture of C_{60} and C_{70}. The NI/DCI analyses of these three samples are shown in Figures 2a, b and c, respectively. The O_3/C_{60} reactions yields predominately C_{119}, O_3/C_{70} yields mostly C_{139} and ozonolysis of the mixture yields C_{119}, C_{139} and C_{129} as the most abundant products.

These results indicate that ozone/fullerene reactions can result in opening of the cage followed by reaction with another fullerene to yield a larger carbon cluster. It appears that similar products can be formed in the graphite arc, also. Although the gas-phase behavior of the odd-numbered clusters is similar to that of fullerenes, the structures of these unusual species are unknown. However, these observations are consistent with reported oxidation-induced opening to fullerene tubes (5).

1. S.W. McElvany, J. Phys. Chem., **96**, 4935 (1992).
2. C. Yeretzian, K. Hansen, F. Diederich and R.L. Whetten, Nature, **359**, 44 (1992).
3. S.W. McElvany, J.H. Callahan, M.M. Ross, L.D. Lamb, D.R. Huffman, Science, in press.
4. M.M. Ross, H.H. Nelson, J.H. Callahan, S.W. McElvany, J. Phys. Chem., **96**, 5231 (1992).
5. P.M. Ajayan, S. Iijima, Nature, **361**, 333 (1993).

FIGURE 1.

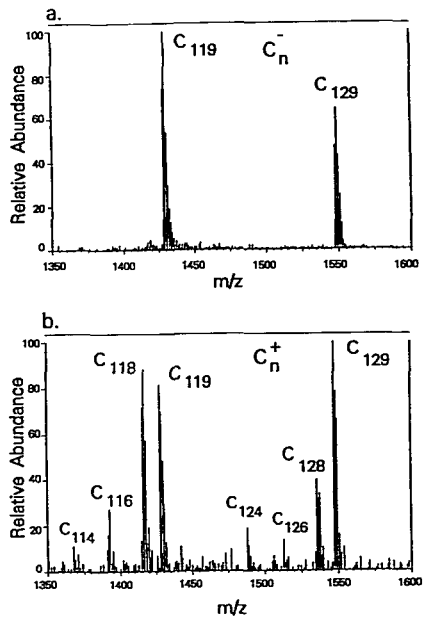

FIGURE 2.

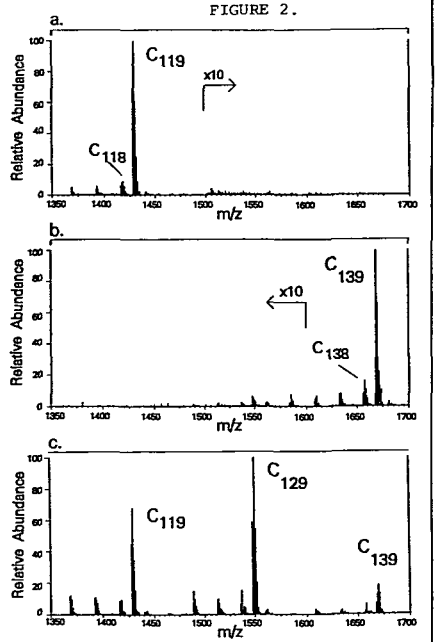

LASER DESORPTION MASS SPECTROMETRY OF PHOTOPOLYMERIZED C_{60} FILMS

D. S. Cornett*, M. A. Duncan, I. J. Amster
Department of Chemistry, University of Georgia, Athens, Georgia, 30602

A. M. Rao and P. C. Eklund
Center for Applied Energy Research, University of Kentucky, Lexington, Kentucky, 40511

Irradiation of thin films of C_{60} with intense visible or ultraviolet light initiates chemical reactions within the films. The phototransformation process produces films which are no longer soluble in toluene, whereas unirradiated, or pristine, films are readily soluble in this solvent. Based on evidence collected using numerous techniques, we recently proposed that the phototransformed films consisted of polymerized C_{60} molecules.[1] For example, several Raman bands observed for the C_{60} films shift significantly upon phototransformation, and X-ray diffraction shows that the spacing between adjacent cages is smaller after transformation. Laser desorption mass spectrometry provides direct evidence as to the composition of the films, and clearly demonstrates that phototransformed films are composed of cross-linked fullerene molecules.

Experiments are conducted in a linear time-of-flight mass spectrometer operated at 25 kV Laser desorption is accomplished using 337 nm (N_2 laser) light at a fluence of 5-30 mJ cm^{-2}. The restriction on the upper limit for the fluence is dictated by the fact that higher fluences produced a visible plasma at the surface, a condition which has been shown to produce higher fullerenes from C_{60}.[2,3] Also, desorbed ions are sampled directly into the mass spectrometer without the addition of any thermalizing gas which could promote the formation of clusters by condensation. 200 nm thick fullerene films are prepared by vacuum vapor deposition of 99% pure C_{60} directly onto stainless steel mass spectrometry probes. Phototransformation of the films is accomplished by exposure to either a 300 W Hg arc lamp or the 5 W output of an Ar^+ laser (all lines) for 1 to 12 hours. All sample handling is conducted in an inert atmosphere to minimize exposure to O_2. Pristine films are stored and transported in a dark environment to prevent any possible transformation by ambient light.

Because the wavelength of the laser light used for desorption is within the range which can cause transformation, pristine films have been analyzed under the same conditions as the transformed samples, to evaluate the possibility that the desorption laser causes transformation during the desorption process. Figure 1 shows mass spectra of transformed (1a) and pristine (1b) films, desorbed using a laser fluence of approximately 30 mJ cm^{-2}. As seen in Fig. 1a, laser desorption of a transformed film produces a broad distribution of ions extending to 15 kDa which we identify with clusters of cross-linked fullerene molecules, $(C_{60})_N$. The mass spectrum obtained from the pristine film, Fig. 1b, also exhibits a distribution of cluster ions. However, the mass range of this distribution terminates at a much smaller value of N than does the ion distribution shown in Fig. 1a. The insets of the two figures show an expanded view of the mass range encompassing the dimer and trimer ions of C_{60}. Clearly evident is the fact that each cluster peak is composed of a series of ion peaks, each separated by 24 Da. The similar nature of the two insets suggest that

the desorption laser does initiate a small degree of phototransformation. At a laser fluence of ca. 10 mJ cm^{-2}, mass spectra obtained from a transformed film exhibit a cluster distribution extending up to $(C_{60})_{10}$, while a pristine film produces less than 1% of $(C_{60})_2$ relative to C_{60} molecular ion. This data suggests that the cluster ions observed in the phototransformed mass spectrum are indeed being directly sampled from a polymerized film. Higher mass distributions observed at higher fluences indicates that more energy must be deposited into the film in order to disrupt the bonding of larger particles.

REFERENCES:

1. Rao, A.M.; Zhou, P.; Wang, K.-A.; Hager, G.T.; Holden, J.M.; Wang, Y., Lee, W.-T.; Bi, X.-X.; Eklund, P.C.; Cornett, D.S.; Duncan, M.A.; Amster, I.J. *Science, 1992, 259,* 955.
2. Yeretzian, C.; Hansen, K.; Diedrich, F.; Whetten, R.L. *Nature* **1992,** *359,* 44.
3. Wood, T.D.; Van Cleef, G.W.; Mearini, M.A.; Coe, J.V.; Marshall, A.G. *Rapid Commun. Mass Spectrom.* **1993,** *7,* 304.

Figure 1.

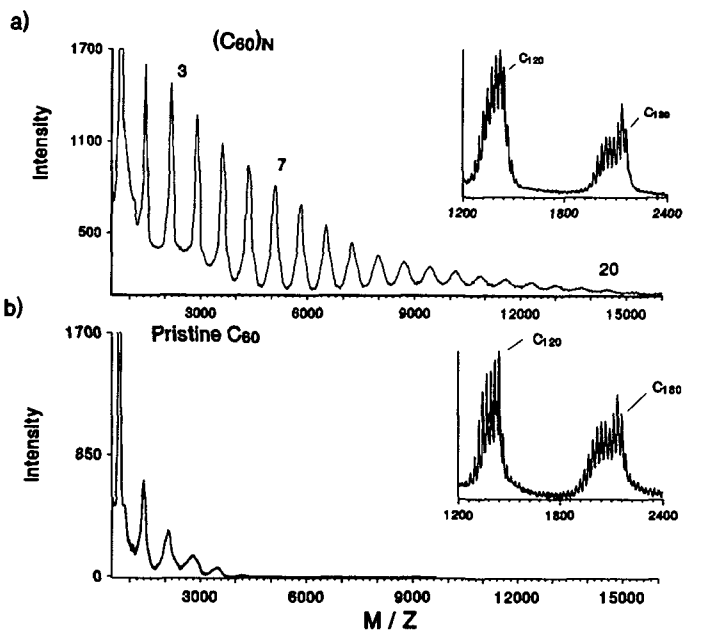

DYNAMIC SIMS

R.G. Wilson, Hughes Research Laboratories, Malibu, CA 90265

This review of dynamic SIMS includes discussions of fundamentals, including enhancement of positive secondary ions by using O_2 primary ions, and the enhancement of negative secondary ions by using Cs primary ions, the measurement of RSFs (relative sensitivity factors) for quantification of dynamic SIMS for both positive and negative secondary ions, and the observation of systematics in these RSFs[1-4] for many materials including semiconductors,[1,3,4] insulators,[5] polymers,[6] and metals[7-9], and quantification issues. Ionization efficiencies from 1 to 100% can be achieved for many elements, and, for a sector magnet instrument with about 10% transmission, corresponding useful yields of 10^{-1} to 10^{-3} are achieved for many elements (with low ionization potential or high electron affinity). Exceptions are elements with high ionization potential and low electron affinity. RSFs and quantification can be accurate to within 10 or 20% for limited elements and controlled conditions within one laboratory[10] and within 30% among many laboratories,[11-14] and within 60% for many elements, many analysts, many instruments, and over many years.[4] RFSs (systems) can be determined for many materials within a factor of 5 by preparing and measuring only two standards.[2] The dependence of RSFs on instrument and analysis conditions is considered.[15] Only the position of the analysis spot within the target holder window for sector magnet instruments causes significant error. Approximate detection limits for dynamic SIMS are discussed. Charge compensation using sector magnet instruments is demonstrated, as are high mass resolution, dynamic range, and the use of isotopes and molecular species to enhance dynamic range/detection sensitivity.[4] General applications to depth profiling, bulk analysis, and imaging are distinguished, but imaging is not dealt with here. Specific practical applications to materials growth and device structures are illustrated, including 1% change in stoichiometry, Be- and Si-doped HBTs, stacked multilayer III-V devices, spreading of annealed delta doped layers, nipi structures, quantum wells, In- and As-doped II-VI devices, II-VI superlattices, deep implantation-channeled profiles, and the profiling of Na in insulators. Details of many of these issues can be found in references 4 and 16.

1. R.G. Wilson, "Secondary ion mass spectrometry sensitivity factors versus ionization potential and electron affinity for many elements in HgCdTe and CdTe using oxygen and cesium ion beams," J. Appl. Phys. 63, 5121 (1988)
2. R.G. Wilson and S.W Novak, "Systematics of secondary ion mass spectrometry relative sensitivity factors versus ionization potential and electron affinity for semiconductors and insulators," J. Appl. Phys. 69, 466-74 (1991).
3. F.A. Stevie and R.G. Wilson, "Relative sensitivity factors for positive molecular ions sputtered from Si and GaAs," J. Vac. Sci. Technol. A9, 3064-70 (1991)
4. R.G. Wilson, F.A. Stevie, and C.W. Magee, Secondary Ion Mass Spectrometry, [Wiley, New York, 1989]
5. R.G. Wilson, C.L. Kirshbaum, G.E. Lux, S.P. Smith, and C. Hitzman, "SIMS depth profiling and relative sensitivity factors and systematics for more than 50 elements from H to U implanted in insulators (SiO_2, Si_3N_4, Al_2O_3, UO_2, ZnS, ZnSe, and diamond," Secondary Ion Mass Spectrometry SIMS VIII, A. Benninghoven, K.T.F. Janssen, J Tumpner, and H.W. Werner, Eds. [Wiley, NY, 1992] pp. 151-154

6. R.G. Wilson, G.E. Lux, and C.L Kirschbaum, "Depth profiling and secondary ion mass spectrometry relative sensitivity factors and systematics for organic polymers," J. Appl. Phys. 73, 2524-29 (1993)
7. R.G. Wilson, F.A. Stevie, G. Lux, C.L. Kirschbaum, S. Frank, and J. Pallix, "Depth profiles, projected ranges, and secondary ion mass spectrometry relative sensitivity factors and for more than 50 elements from hydrogen to uranium implanted into metals," Surface and Coatings Technology 51, 358-363 (1992)
8. R.G Wilson and F.A. Stevie, "SIMS depth profiling and relative sensitivity factors and systematics for elements from hydrogen to uranium implanted in metal matrices (Be, Al, Ti, Ni, W, and Au) submitted to J. Appl. Phys.
9. G.E. Lux, F.A, Stevie, P.M. Kahora, R.G. Wilson, and G.W. Cochran, "Secondary ion mass spectrometry quantification of elements in $TiSi_2$, TiN, and TiW matrices," to be published in J. Vac. Sci. Technol.,1993
10. G.D.T. Spiller and T. Ambridge, Secondary Ion Mass Spectrometry SIMS V, A. Benninghoven, et al., Eds. [Springer, Berlin, 1986] pp. 127-129
11. S.M. Hughes and R.J. Colton, "Results of a SIMS round robin sponsored by ASTM committee E-42 on surface analysis," Surf. Interface Analysis 14, 101 (1989)
12. D.S. Simons, P.H. Chi, P.M. Kahora, G.E. Lux, J.L. Moore, S.W. Novak, C. Schwartz, S.A. Schwarz, F.A. Stevie, and R.G. Wilson, "Are relative sensitivity factors transferrable among SIMS instruments?," Secondary Ion Mass Spectrometry SIMS VII, A. Benninghoven, C.A. Evans, K.D. McKeegan, H.A. Storms, and H.W. Werner, Eds. [Wiley, NY, 1990], pp. 111-114
13. P. Roitman, D.S. Simons, P.H Chi, R.M. Lindstrom, G.E. Lux, S. Baumann, S.W. Novak, R.G. Wilson, D. Farrington, J. Keenan, F.A. Stevie, J.L. Moore, R.B. Irwin, A.J. Filo, C.W. Magee, R. Alcorn, and D. File, "Round-robin study of implants in Si and SiO_2 using SIMS, RBS, and NAA," Secondary Ion Mass Spectrometry SIMS VII, A. Benninghoven, C.A. Evans, K.D. McKeegan, H.A. Storms, and H.W. Werner, Eds. [Wiley, NY, 1990], pp. 115-117
14. Y. Homma, S. Kurosawa, Y. Kubota, Y. Nakamura, K. Nomura, M. Shibata, H. Shichi, J. Takahashi, Y. Yoshikioka, and T. Ogawa, "Ion yield data of impurities in GaAs obtained from round robin study," Secondary Ion Mass Spectrometry SIMS VII, A. Benninghoven, C.A. Evans, K.D. McKeegan, H.A. Storms, and H.W. Werner, Eds. [Wiley, NY, 1990], pp. 119-123
15. G.E. Lux, S.P. Smith, and R.G. Wilson, "Dependence of SIMS relative sensitivity factors (RSF) on instrument conditions/parameters: Accuracy of RSF determinations," Secondary Ion Mass Spectrometry SIMS VIII, Amsterdam, Neth. Sept 1991
16. A. Benninghoven, F.G. Rudenauer, and H.W. Werner, Secondary Ion Mass Spectrometry, [Wiley, New York, 1987]

Static SIMS Studies of Alkylmethylphosphonic Acids Adsorbed on Substrates of Environmental Interest

J. C. Ingram, G. S. Groenewold, A. D. Appelhans, and J. E. Delmore, Idaho National Engineering Laboratory, P. O. Box 1625, Idaho Falls, ID 83415-2208

Alkylmethylphosphonic acids (AMPAs) may be detected rapidly and sensitively on environmental and industrial surfaces using static SIMS. The analysis of these compounds is important as they are degradation products of chemical weapons agents. Further, AMPAs are non-volatile and adsorb strongly to some substrates which make them difficult to extract and analyze by standard chromatographic methods.

Detection is achieved using a SIMS instrument equipped with two unique features: a) perrhenate (ReO_4^-) primary ion beam and b) pulsed secondary ion extraction for sample-charge neutralization. The perrhenate ion gun produces a large molecular anion and is operated at ca. 10 keV and 100 picoamps; it is highly efficient for sputtering molecular ions from a sample surface, giving improved sensitivity over conventional atomic ion guns. These features result in abundant secondary ions originating from the top few monolayers of the sample. Pulsed extraction alternately samples positive, then negative ions. By varying the positive/negative ratio, sample surface charging can be minimized. These features allow analysis of insulating samples such as leaves, which are not readily analyzed using conventional SIMS. Moreover, anion and cation spectra are acquired simultaneously. No sample preparation is required.

The AMPAs investigated in this study are listed in Table 1 along with their structures and molecular weights. Nanogram quantities of AMPAs are readily detected on plant leaves, steel, and some polymers.

Table 1. AMPAs

Alkylmethylphosphonic Acids	Structure	Acronym	MW (amu)
Ethyl methylphosphonic acid	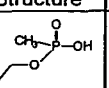	EMPA	124
Isopropyl methylphosphonic acid	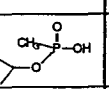	IMPA	138
Pinacolyl methylphosphonic acid	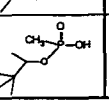	PMPA	180

In these studies, it was found that the anion spectra were more useful than the cation spectra for identification of AMPAs on various substrates. The methylphosphonic acid moiety present in the three molecules studied, shown in

Table 1, is responsible for similar fragmentation chemistries observed in the anion SIM spectra of these molecules. The anion spectrum of PMPA shown in Figure 1 is typical of spectra collected for other AMPAs.

Figure 1. SIM anion spectra of PMPA on a plant leaf and the blank leaf background.

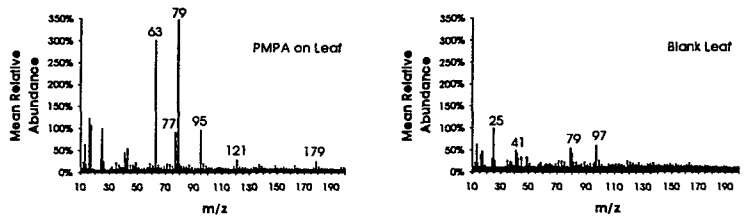

The fragment ions at 179^-, 121^-, 95^-, 79^-, 77^-, and 63^- marked on the PMPA spectra in Figure 1 are identified in Figure 2. The 79^- and 63^- ions are the most abundant ions observed in the anion spectrum and are attributed to PO_3^- and PO_2^-. The 95^- ion is interpreted as the methyl phosphonate ion which would arise from cleavage of the large alkyl groups from the parent molecule. Another fragment ion indicative of the methyl phosphonate moiety is observed at m/z 77^-, which is believed to have the structure presented in Figure 2. It is speculated that 77^- ion is formed by dehydration of the 95^- ion. The ion observed at m/z 121^- in the spectra is the most difficult ion to interpret. This ion would correspond to the loss of C_4H_{10} from $[PMPA - H]^-$. At the present time, the driving force for these eliminations has not been identified other than to surmise that the 121^- ion possesses unusual stability; two structures are proposed in Figure 2. The 179^- ion is identified at $[PMPA - H]^-$.

Figure 2. Fragment ions from PMPA on plant leaf.

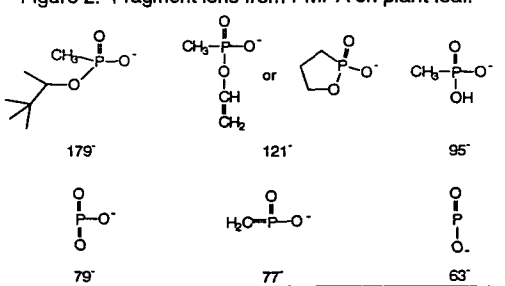

Anion spectra of IMPA and EMPA on leaves are similar to the spectrum shown in Figure 1 with the only difference being the m/z of the $[M-H]^-$ peaks.

Funding support by the U.S. Department of Energy, Office of Arms Control, is gratefully acknowledged.

Biological Sample Preparation for Imaging Organic SIMS

P. J. Todd, R. T. Short, J. M. McMahon,
J. T. Brenna, S. P. Markey
Analytical Chemistry Division
Oak Ridge National Laboratory
P.O. Box 2008, Oak Ridge, TN 37831-6365

Use of static SIMS and MS/MS to determine the distribution of biologically important compounds in tissue samples requires development in two areas. First has been development of instrumentation suitable for this purpose; the transmission characteristics of the instrument we have developed approach theoretical limits. Although further improvements in sensitivity through instrumental development are expected, for example, increased secondary ion yield, it is necessary that samples be prepared in such a way that they are amenable to analysis by SIMS. In short, improvements in sample preparation and handling will be crucial for further development and eventual use of the method. In this paper, we report on results obtained from various tissue samples, mainly with the goal of determining what must be done. The areas of consideration include fixing the sample, solving the problems of sample charging, distinguishing analyte-specific ions from the milieu of other secondary ions that are emitted from the sample, and enhancing the images that are created.

Biological tissue samples all contain water at preparation. Static SIMS is a surface analysis method, so that if the samples melt before analysis, surface spreading of analytes destroys their heterogeneity. Consequently, we have found the samples must be prepared frozen and dried under vacuum without ever thawing. Samples prepared in this way tend to be insulators. A charge compensation scheme that employs an electron flood gun and pulsed extraction has been used to solve the problem of sample charging.

Figure 1 shows secondary ion images obtained from two different dried tissue samples. In Fig.1A, a 1 μL spot of acetylcholine solution was deposited onto a liver sample that had been dried previously in vacuum. The localization of the acetylcholine secondary ion emission is the mark of a dried sample. If the surface of the sample is wetted, the analyte is spread rapidly and emission is diffuse. However, preparation of dry samples is problematic. In Fig. 1B, samples were prepared by cryosection of mouse brain, obtained from nude mice that had been plunged into liquid nitrogen. The mottled appearance of Fig. 1B arises because the sample surface is heterogeneous, and tends to peel from the target. The virtually uniform distribution attests to the fact that the samples were kept dry. When samples melt, soluble analytes migrate to the periphery of the sample.

Figure 2A-C, obtained from the liver sample shown in Figure 1A, show the utility, and loss of secondary ion current from using MS/MS for imaging. Fig. 2A shows the same data as Fig. 1A, but in a different presentation format, i.e., the image of m/z 146. The spike of acetylcholine is clearly visible. However, to the right, intense emission of secondary m/z 146 is also evident, where there is no acetylcholine. Fig 2B shows one image based on the intensity of the MS/MS 146->87 transition, characteristic of acetylcholine. Fig. 2C shows the sum of 12 such images, all taken from the same sample under static SIMS conditions. The vast suppression of chemical noise by MS/MS and reduction of electronic noise by signal averaging make it possible to clearly identify the location of the acetylcholine spike.

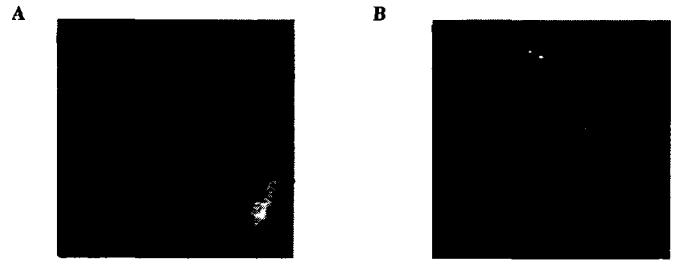

Figure 1. Secondary ion images obtained from dry tissue. In (A), 1 μL of acetylcholine was injected onto the previously dried sample. Because the sample was never wetted after the application, emission of m/z 146 from the acetylcholine is confined to the white spot. The rigorously prepared mouse brain section shown in (B) is an insulator, and tends to "peel".

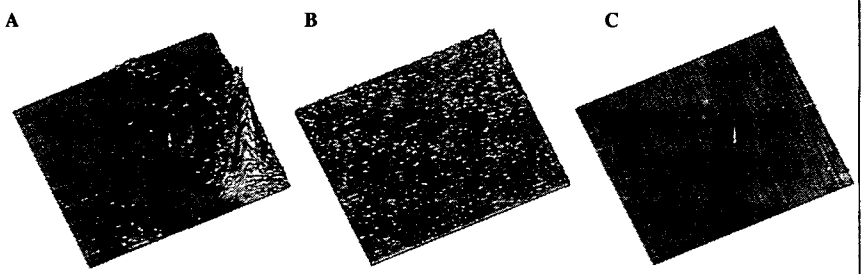

Figure 2. Reduction of Chemical and Electronic Noise. For reference, (A) has been generated from the same data as Fig. 1A., a secondary ion image. In (B), the image based on the intensity of the MS/MS transition m/z 146->87, and shows how electronic noise can replace chemical noise in the image. Electronic noise can be reduced by summing separate images, as shown in (C), which is the summed image of 12 separate MS/MS imaging scans of the sample.

This work was funded by Grant GM-RO1-41617 from the National Institutes of Health and by DOE Office of Basic Energy Sciences under contract DE-AC05-84OR21400 with Martin Marietta Energy Systems, Inc.

"The submitted manuscript has been authored by a contractor of the U.S. Government under contract No. DE-AC05-84OR21400. Accordingly, the U.S. Government retains a nonexclusive, royalty-free license to publish or reproduce the published form of this contribution, or allow others to do so, for U.S. Government purposes."

Surface Characterization by Reactive Collisions of Halide Ions with Self-Assembled Monolayer Surfaces

*Donald E. Riederer, Jr., Scott A. Miller, Mike Morris, Teodor Ast, T. Pradeep and R. Graham Cooks, Department of Chemistry, Purdue University, West Lafayette, IN 47907-1393
Matt Linford and Christopher E.D. Chidsey, Department of Chemistry, Stanford University, Stanford, CA 94305-5080

Ion/surface collisions in which atoms or groups are abstracted from the surface is a developing area in mass spectrometry. Self-assembled monolayers provide well-defined surfaces [1] for the study of these reactions which are (i) of fundamental interest, (ii) have the potential for providing a new method for surface chemical analysis, and (iii) have potential utility for the development of novel materials and chemically modified surfaces.

Detailed studies have been performed in which iodine ions (I^+) and iodine containing molecular ions ($CH_3I^{+\cdot}$, I_2^+) collide with fluorinated self-assembled alkyl surfaces [$CF_3(CF_2)_{11}(CH_2)_2$-Au] at collision energies ranging from 20 to 70 eV. These iodine containing ions are extremely reactive and produce several ion/surface reaction products in good abundance. Bromine and chlorine containing ions produce analogous products but of somewhat lower abundance. This is in sharp contrast to the behavior of hydrocarbon ions which yield few reactive products upon collisions with the fluorinated surface [2,3].

At a kinetic energy of 60 eV, collisions of I^+ with this surface yield as major products IF^+, CFI^+, IF_2^+, ICF_2^+ and $IC_2F_3^+$ (Figure 1) These endothermic reactions require C-C or C-F bond cleavage and are driven by the translational energy of the projectile. For example, collisions of I^+ with the fluorinated surface resulting in the production of IF^+ is estimated to be ≈58 kcal/mol (2.5 eV) endothermic [4] These reactions are distinctive in that they do not occur when the collision partner is a gas phase (rather than surface bound) species. This emphasizes the unique conditions that prevail during ion/surface collisions which allow cleavage of strong covalent bonds and incorporation of groups into the ionic projectile.

Many of the products formed when CH_3I^+ and I_2^+ are used as projectiles (Table 1) are the same as those produced by the I^+ projectile. Furthermore, the abundances of these products with respect to the scattered I^+ ion remain constant as the projectile is changed. This suggests that the iodine containing projectiles react first by fragmenting to yield I^+, followed by abstraction of groups from the surface.

Another process observed is the deposition ("soft-landing") of the primary projectile onto the target surface. These species can be detected by subsequent ion/surface reactions. For example, the ion at m/z 254 in Figure 1 and Table 1 corresponds to I_2^+ resulting from deposition of I atoms onto the fluorinated surface which then react with the primary beam to form I_2^+. Another example of deposition followed by abstraction is shown in Figure 2. The upper portion (Figure 2a) displays ions resulting from collisions of CH_3I^+ with a stainless steel surface. Products include CH_3I^+, $C_2H_4I^+$, and $CH_3ICH_3^+$ which arise from reaction of the primary ion with adventitious hydrocarbons present on the surface. The same projectile and surface are used in Figure 2b, however in this case, the surface was pretreated by exposure to a 5nA/cm^2 beam of $C_3F_6^+$ for a period of 40 min. In addition to the hydrocarbon products, the fluorine containing products IF^+, HIF^+, and CH_3IF^+ are observed as the result of fluorine or fluorocarbon deposition from the $C_3F_6^+$ beam and subsequent reaction with the $CH_3I^{+\cdot}$ projectile. Finally, recent observations indicate that metal ions such as W^+, Cr^+, Mo^+, and Fe^+ can undergo reactions in which several surface atoms are abstracted by a single projectile (Figure 3). Such reactions have potential application for surface analysis and controlled surface

modification for the production of microdevices.

1. C.E.D Chidsey, G.-Y. Liu, P. Rowntree, G. Scoles, *J. Chem Phys.*, 91 (1989) 4421.
2. M.R. Morris, D.E. Riederer, Jr., B.E. Winger, R.G. Cooks, T. Ast, and C.E D. Chidsey, *Int. J. Mass Spectrom. Ion Processes*, 122 (1992) 181.
3. A. Somogyi, T.E Kane, V.H. Wysocki, *Org. Mass Spectrom.*, 28 (1993) 283
4. ΔH_{rxn} was estimated using available data for gas phase species for the reaction $I^+ + C_3F_8 \rightarrow IF^+ + C_3F_7$. S.G. Lias, J.E. Bartmess, J.F. Liebman, J.L. Holmes, R.D. Levin, and W.G. Mallard, *J. Phys Chem. Ref. Data*, 17 (1988) Suppl. No 1.

Figure 1

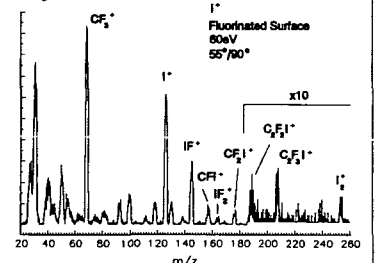

Table 1 Numbers indicate ion abundance with respect to I^+ + indicates ion abundance < 1%.

Product Ion	Projectile Ion I^+	CH_3I^+	I_2^+
CH_2F^+		20	
$C_2H_2F^+$		7	
CHF_2^+		14	
I^+	100	100	100
CH_3I^+		138	
IF^+	45	34	35
CFI^+	15	4	6
$CHFI^+$		2	
CH_3IF^+		8	
IF_2^+	5	3	2
CF_2I^+	8	9	13
$C_2F_2I^+$	2	1	1
$C_2F_3I^+$	4	1	2
$C_2F_4I^+$	+	+	+
$C_3F_4I^+$	+	+	+
I_2^+	-	-	30
I_2F^+			4

Figure 2

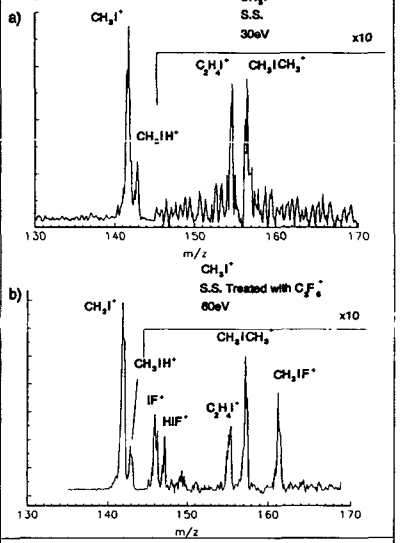

Figure 3

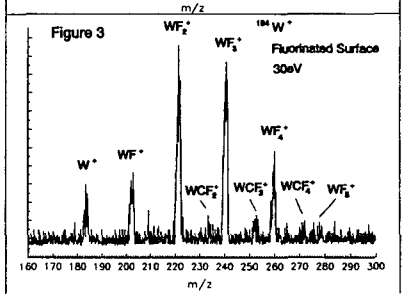

Organic Thin Films on Pd(111) and Ti Foils by TDS, LITD/FTMS, and AES

Ihab M. Abdelrehim, Nick A. Thornburg, Steve Pullins, Johari Sloan, Erika Cleaver, and *Donald P. Land, Department of Chemistry, University of California, Davis, CA 95616.

Transition metals are known to play a role in catalytic processes of organic adsorbates. Both Pd and Ti are of interest as catalysts. Also, the surface composition of Ti biomedical implants is thought to play a major role in the infectious rejection of implants. Molecular identification of species on Ti and TiO surfaces has proven difficult, however. In this study numerous organic species are adsorbed on Ti foils and a Pd(111) single crystal and surface analysis is performed by Auger electron spectroscopy (AES), thermal desorption spectroscopy with FT mass spectrometry (FTTDS), and laser-induced thermal desorption with post-ionization and FT mass spectrometry (LITD/FTMS). Direct comparison is made for the characteristics of desorption for benzene, propene, acetylene, and isopropanol. This is accomplished using a new instrument designed and constructed at UC Davis combining these three technologies.

These studies utilize laser power densities such that organics are desorbed as neutrals and the substrate is not ablated (1064 nm, 5ns, $<10^7$-10^8 W/cm^2). Post-ionization of neutrals is accomplished with a 70 V electron beam. LITD mass spectra were compared with gas-phase electron impact FT mass spectra for all four compounds and both types of spectra were identical in each case. This indicates that LITD, even from catalytic surfaces does not induce decomposition of the adsorbed species.

LITD/FTMS often yields the desorption of intact intermediates. Acetylene on Pd, when heated, can desorb or cyclotrimerize to form benzene. In the presence of sulfur, thiophene may be produced. During TDS, the benzene and thiophene thus formed primarily decompose. However, using LITD/FTMS these species are observed in abundance. In addition, we obtained low temperature desorption (100 K) of $C_3H_3^+$ which may be a fragment of a tightly bound C_4H_4 surface species proposed in this system, but as yet unobserved. This peak was not observed using FTTDS. Also, thiophene which appeared to be substantial in the LITD (30% of the base peak) was almost insignificant (<1%) in the TDS profile.

The TDS profile of benzene (Fig. 1) illustrates a true multiplex thermal desorption experiment. A complete mass spectrum is obtained in which different species and fragments can be monitored. Also, for the TDS of acetylene we observed the desorption of thiophene due to trace amounts of sulfur on the surface. This might have been missed if masses to be monitored needed to have been preselected. This demonstrates the importance of having a true multiplex TDS experiment.

The presence of alkali metals lead to direct ionization, flooding the cell, and not allowing the desorbed organics to fill the cell. The use of deflection plates allows us to deflect the alkali metals and facilitate the detection of the organic species. This information is presented by a colleague at the conference.

The use of these surface analysis techniques complement each other and allow for complete analysis of organic adsorbates. In addition to these techniques a FT reflection infrared spectrometer will be coupled to the instrument for vibrational studies.

Figure 1

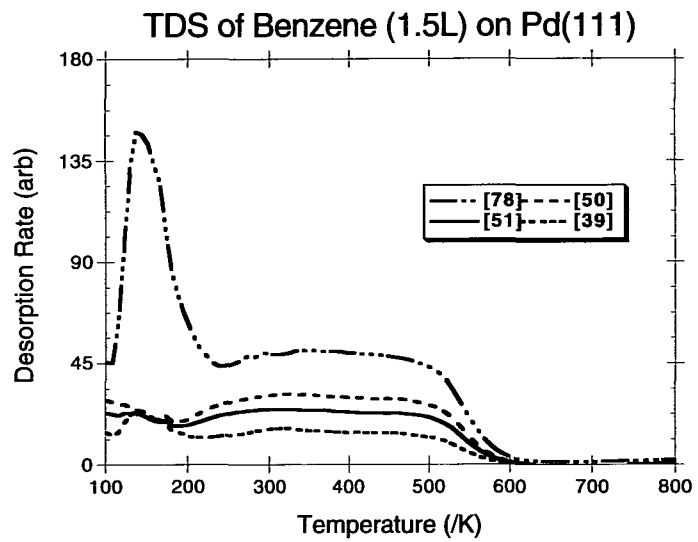

Shown above is a profile plot of a TDS experiment of benzene. The plot shows benzene (mass 78), and fragments of benzene (mass 39, 50 and 51).

Modern Analysis as the Catalyst for Today's Evolving Polymer Science

R.R.Matheson, Jr.
Marshall Research Laboratory
E.I. Du Pont de Nemours and Co.

Polymer science is concerned with structures on many length scales. The important properties of macromolecular materials can only be understood by reference to structural details that may encompass the local stereochemistry of particular atoms, preferred bond orientations over volumes of many cubic microns, and even the macroscopic proportions of entire articles. Polymer science has achieved considerable success in elucidating the functional consequences of molecular structure in three important limits: the so-called theta condition (1), the perfect crystal (2), and the state of equilibrium orientational order of rodlike molecules (3). Much of modern interpretation proceeds from comparison to one or more of these ideals.

However, several forces are acting to drive macromolecular materials far from these comfortable limits. Molecules of smaller average size dominate many of today's technologies. Mixtures of ever greater complexity appear. Many convenient solvents must be avoided in order to obviate environmental concerns (4). The history of handling and environmental exposure can change polymeric structures and performance in surprising ways that need elucidation (5). Increasingly subtle property differences among macromolecular systems assume economic or intellectual significance. Contemporary polymer science faces a rich array of important phenomena that cannot be readily understood as consequences of large, linear homopolymers in orientationally perfect, crystalline or theta conditions. Biological macromolecules generate much of this phenomenology.

Polymer science is evolving in response. Modern analytical techniques are key to this evolution. For polymer molecules far from one of the three limiting conditions structural details assume greater significance. Indeed, some structural features can determine how rapidly or even how closely macromolecules may approach those limits. End groups obviously make a greater contribution to properties as molecular weights decrease. The exact distribution of functionality (rather than an average amount) dominates configuration and properties under non-theta conditions. Branch points and stereochemical irregularities distort and constrain crystallization. The extremes of either side of a distribution of molecular weights dominate the phase equilibria that depend on orientational order (6). Only with precise and often sophisticated analytical tools can the consequences and interactions of such structural details be understood.

It is convenient to use mass spectrometry as a paradigm for the catalytic role that analyses assume in modern polymer science. One can find it applied to problems of mixtures (characterizing additives, solvents, etc.), of nonlinear structures (7), of new synthetic routes (characterizing end groups, monomer sequences, etc.) and complete molecular weight distributions (8). This is the kind of information that is required for polymer science to advance towards a more complete elucidation of the important properties of macromolecular materials.

Presented at the 41st ASMS Conference on Mass Spectrometry

REFERENCES

1. P.J.Flory (1949) J.Chem.Phys., 17, 303.
2. A.Keller (1957) Phil.Mag., 2, 1171.
3. P.J.Flory (1956) Proc.Roy.Soc., A234, 73.
4. Super. of Documents (1992) Federal Register, 57 (137), 31473.
5. Y.T.Chia, et al (1988) Polymer Preprints, 29, 468.
6. L.Prokai and W.J.Simonsick, Jr. (1992) Macromolecules, 25, 6532.
7. M.S.Kahr and C.L.Wilkins (1993) J.Am.Soc.Mass Spectrom., 4, 453.

1092a

POLYMER ANALYSIS BY MATRIX-ASSISTED LASER DESORPTION/IONIZATION TIME-OF-FLIGHT MASS SPECTROMETRY

PAUL O. DANIS AND DANE E. KARR
Rohm and Haas Research Laboratories
Spring House, PA 19477 USA

ARMIN HOLLE AND FRANZ MAYER-POSNER
Bruker-Franzen Analytik GmbH
2800 Bremen 33, Germany

CLIFF WATSON
Bruker Instruments, Inc.
Billerica, MA 01821 USA

Matrix-Assisted Laser Desorption/Ionization Time-of-Flight Mass Spectrometry (MALDI/TOF) has been a technique which has primarily focused on biomolecule analysis. However, the technique has the potential to make significant contributions in the area of polymer analysis. Previous work has shown that water soluble polymers can be analyzed using conditions similar to those of biopolymers.[1] Additionally, MALDI on polyglycols,[2-5] polystyrene,[4] and poly(methyl methacrylate)[4,6,7] have been shown using solvent mixtures and salt addition in the preparation.

We have further refined the technique of MALDI/TOF for polymers. This includes extending the mass range for poly(styrene sulfonic acid) to 400,000 amu as shown in Figure 1. In addition we have developed a simple method for the analysis of non-aqueous polymers. This method utilizes matrices such as sinapinic acid and dihydroxybenzoic acid. We dissolve the polymer of interest and a suitable matrix in an organic solvent and apply this mixture to the probe. We have found the matrices to be completely soluble in organic solvents such as acetone, methanol, and tetrahydrofuran which are common solvents for polymer systems.

Using the above approach to non-polar systems, we have obtained results for such polymers as poly(methyl methacrylate), poly(vinyl acetate), poly(vinyl chloride), poly(carbonate), poly(12-hydroxystearic acid), and poly(N-vinylpyrolidone/vinyl acetate). Figure 2 displays the result we have obtained for a poly(methyl methacrylate) of 59,000 molecular weight. The spectrum shows a singular distribution centered around 60,000 amu.

In addition, the double and triply charged distributions are observed as well as clusters corresponding to the dimer and trimer.

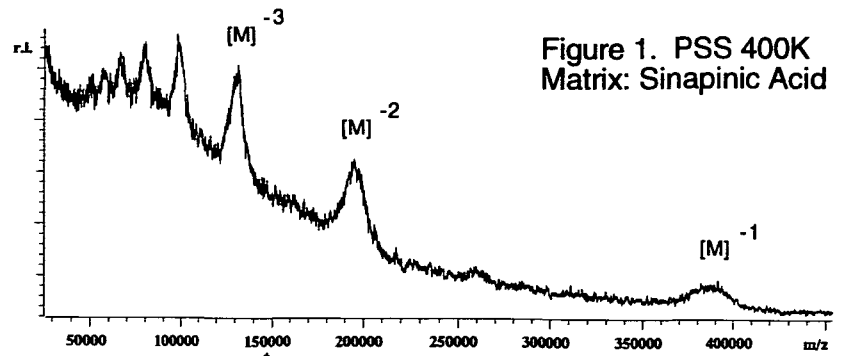

Figure 1. PSS 400K
Matrix: Sinapinic Acid

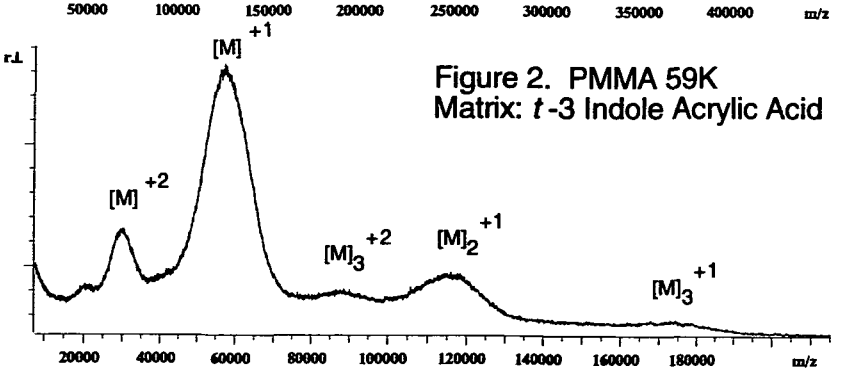

Figure 2. PMMA 59K
Matrix: *t*-3 Indole Acrylic Acid

1. P.O. Danis, D.E. Karr, F. Mayer, A. Holle, C.H. Watson, *Org. Mass Spectrom.* **27**, 843 (1992).
2. K. Tanaka, H. Waki, Y. Ido, S. Akita, Y. Yoshida, and T. Yoshida, *Rapid Commun. Mass Spectrom.* **2**, 151 (1988).
3. J.A. Castro, C. Koester, and C. Wilkins, *Rapid Commun. Mass Spectrom.* **6**, 239 (1992).
4. U. Bahr, A. Deppe, M. Karas, and F. Hillenkamp, *Anal. Chem.* **64**, 2866 (1992).
5. P. Juhasz, C.E. Costello, and K. Bieman, *J. Am. Soc. Mass Spectrom.* **4**, 399 (1993).
6. P.O. Danis, D.E. Karr, D.G. Westmoreland, M.C. Piton, D.I. Christie, P.A. Clay, S.H. Kable, and R.G. Gilbert, *Macromolecules*, submitted.
7. P.O. Danis, D.E. Karr, *Organic Mass Spectrom.*, submitted

ToF SIMS STUDY OF ADDITIVE MIGRATION ON POLYMER SURFACES

L. Lianos, Tran Minh Duc, CENATS, Claude Bernard University, 43 Bd 11 Novembre 1918, F69622 Villeurbanne, France

S. Reichlmaier, J. Hammond, Physical Electronics Division, Analytical Laboratory, 6509 Flying Cloud Drive, Eden Prairie, MN 55344 USA

Surface migration of additives is an important issue in the polymer industry. Additive "blowout" could modify surface properties and thus induce problems when improved wettability, adhesion, transparency or chemical inertness is needed. The essential capabilities for solving this kind of problems are high surface sensitivity, high mass and spatial resolution, all combined in the ToF Static SIMS method (Figure 1) as well as the possibility of analysing insulating materials "in situ".

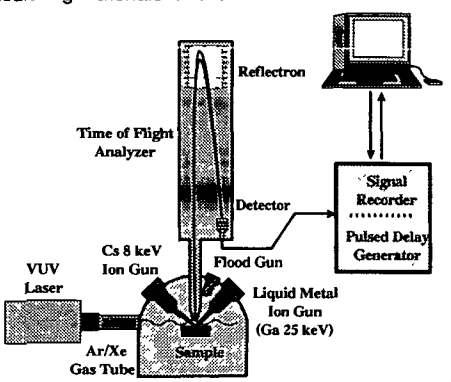

Figure 1. : The ToF SIMS instrument

Our ToF analyser combines high mass resolution and high mass accuracy with an exceptional sensitivity thanks to a parallel and multi ion detection and the absence of dispersion optics. In the performances of the method we could also include the great mass range (up to 15000 D) with a constant high transmission and high signal/noise ratio.

Working with a Cs (t_{pulse} < 1 ns) source allow us to obtain a high mass resolution (10000 M/ΔM at 28 D) in order to separate and unambiguously identify fragments appearing at the same nominal mass. High lateral resolution can also be achieved by employing a micro-focused Ga^+ gun as the primary ion beam. This configuration can provide chemical maps of the surface with a lateral resolution of 200 nm.

Static SIMS spectra were acquired in both positive and negative ion mode for additives belonging to different families : Antioxidants (Irganox 1010, Irganox 1076, Irganox 3114, Ionox 330, Irgafos 168), Acid acceptors (Calcium stearate), Anti-UV (Tinuvin 622), Flame Retardants (Adine 505, Dechlorane 505) and Lubricants (Erucamide).

The high transmission of the ToF analyser permits the detection of the parent ion peaks with a high mass accuracy, of most of the additives analysed here (Figure 2). The fragmentation

pathways of these materials are also investigated. Both the parent ion peak and the fragmentation pattern serve as a fingerprint for the additive and can be used for its identification and further on to the study of its spatial distribution on a polymer surface.

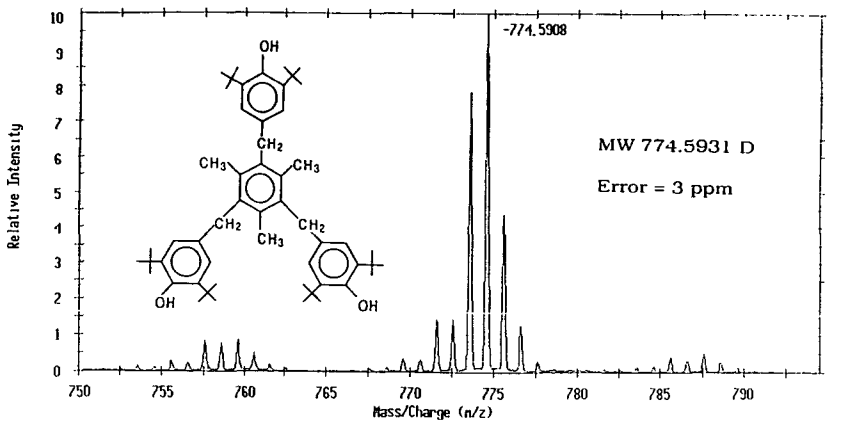

Figure 2. : Static SIMS spectrum of IONOX 330 (Positive Ions, 750 to 800 D)

Studies of additive migration on a polypropylene (PP) pellet surface show that non-organic additives could be detected even at bulk concentrations of the order of 200 ppm. Organic additives could also be identified even through their parent molecule peak but in higher bulk concentrations. Some cases of additive migration on the surface of the polymer are examined by imaging static ToF-SIMS (Erucamide in PP, Glyceryl MonoStearate (GMS) in PP and GMS in PolyEthyleneTerephthalate).

References

1. A. Benninghoven, F.G. Rudenauer and H.W. Werner, in *Secondary Ion Mass Spectrometry*, ed. by P.J. Elving and J.D. Winefordner, John Wiley, Chichester (1987).

2. M.P. Mawn, R.W. Linton, S.R. Bryan, B. Haggenhoff, U. Jurgens and A. Benninghoven, J. Vac. Sci. Technol. **A 9 (3)**, 1307 (1991).

Acknowledgment

The GMS/PET sample for imaging was supplied by M.J. Hearn and D. Briggs of ICI, Wilton, U.K.

MICROSTRUCTURE OF COPOLYMERS BY STATISTICAL MODELLING OF THEIR MASS SPECTRA

GIORGIO MONTAUDO
Dipartimento di Scienze Chimiche, Universita' di Catania,
Viale Andrea Doria, 6 95125 Catania (Italy)

A novel method for the determination of the microstructure of copolymers is presented. Statistical modeling of the mass spectral intensities of copolymers has been used here to derive information on the distribution of monomers along the copolymer chain, and a procedure to find the composition and the sequence of the copolymers analyzed has been developed. Although polymers often possess molecular dimensions too elevate to be revealed by conventional high resolution mass spectrometers, MS has been successfully used to identify the mixtures of oligomers formed in the partial degradation of synthetic and biological copolymers, or of the oligomers contained in low molecular weight copolymers[1-13]. We have recently found that opportune decoding of the information contained in the mass spectral intensities leads to the determination of composition and microstructure in copolymers, and this represented a significant progress with respect to the past, since only the mass numbers corresponding to MS peaks had been used in previous work on the structural delucidation of copolymers by MS[5-9]. Mass Spectrometry is a powerful and rapid analytical method and, being able to look at the mass of individual molecules in a mixture of homologues, is particularly suitable for the detection of a series of oligomers. However, mass spectra had not been exploited to estimate oligomers distributions, due to the diffuse notion[1,2] that a lack of correlation existed between EI (electron impact) peak intensities and concentration of the oligomers in the mixture. The introduction of soft-ionization techniques, as chemical ionization (CI), fast atom bombardment (FAB), secondary ions mass spectrometry (SIMS), laser desorption (LD, MALDI), field desorption and field ionization (FD and FI), etc., has largely eliminated this problem, and sizeable evidence has been now accumulated showing that, in many cases, peak intensities of molecular ions appearing in mass spectra reflect the relative amounts of oligomers present in the mixture[1-9]. In order to extract quantitative information about the composition and sequence of copolymers, one has to learn how to exploit MS peak intensities, which depend from the relative abundances of the oligomers present in the spectrum and are directly related to the microstucture of the copolymers. The statistical analysis of copolymers makes use of Bernoullian and Markovian models in order to characterize the microstructure of copolymer samples[5-6], and assuming a theoretical distribution and then fitting the calculated oligomer abundances with the experimental MS peak intensities, the copolymer composition can be determined. In our first approach to the problem, we analyzed by FAB-MS some microbial copolyesters having Bernoullian distributions, which were subjected to partial methanolysis in order to reduce their molecular weights, and it was assumed that the chain cleavage agent was producing a non-selective process. This introduced a limitation in our approach, since the intensity of mass peaks actually depends both on the distribution of comonomers along the chain, and on the cleavage process. Furthering our studies we have found that, from the analysis of the mass spectra, it is possible to ascertain if the cleavage of a copolymer chain occurred by a selective or a non-selective process, therefore removing the above ambiguity. Furthermore, we have extended our computations to determine the composition and the microstructure of several copolymers whose mass spectra have been recently reported in the literature[6]. These spectra have been recorded using different ionization techniques as: LD, FAB, FI, EI, and refer both to low molecular weight copolymers (that can analyzed directly without subjecting the copolymer to partial cleavage to reduce their molecular weight), and to high copolymers. The copolymers analyzed are both of the addition and condensation type.

Mass spectra may provide direct composition estimates and we have now derived simple mathematical formulas that allow to estimate the copolymer composition, independent from the statistical calculations, by direct analysis of the mass spectra. This analysis allows also to ascertain if the process used to cleave the copolymer chain has been a selective or an unselective one. Statistical modeling of mass spectra of copolymers has thus reached a certain level of generalization, and it can be used to complement NMR analysis, which has been so far the only technique available for sequencing copolymers. In order to perform numerical calculations, all the formulas have been implemented in a computer program, MACO, written in Standard ANSI Fortran that runs on a Microwax computer. All the mass spectra of copolymers studied have been analyzed employing this program. The present version of the computer program (MACO 4) has proved able to deal with all the cases considered here (both addition and condensation copolymers), independent from the MS ionization technique and from the method by which the partial degradation was performed (methanolysis, aminolysis, ozonolysis photolysis, pyrolysis), and also in the case of low molecular weight copolymers (preformed oligomers).

REFERENCES

1. Schulten, H.-R.; Lattimer, R. P. **Mass Spectrom. Rev. 1984,** 3,231.
2. Montaudo G. **Rapid Comm. Mass Spec. 1991,** 5, 95; Montaudo, G., Puglisi, C. in **Comprehensive Polymer Science** - First Suppl. Pergamon Press: London 1992 p. 227.Montaudo, G., Puglisi,C. in **Developments in Polymer Degradation, Vol.7,** Grassie, N. Ed.; Elsevier: London **1987**; p.35. Foti, S.; Montaudo, G. in **Analysis of Polymer Systems** Bark, L.S.; Allen, N.S.; Eds.; Elsevier: London **1982**, p.103.
3. Garozzo D.; Giuffrida M.; Montaudo G. **Macromolecules 1986,** 19, 1643. Ballistreri A.; Garozzo D.; Giuffrida M.; Montaudo G. **Anal.Chem. 1987**, 59, 2024; **Macromolecules 1986**, 19, 2693. Ballistreri, A.; Garozzo,D.; Giuffrida,M.; Impallomeni,G,; Montaudo,G. **Polym. Deg. & Stab. 1988,** 23, 25. Montaudo, G.; Puglisi, C.; Scamporrino, E.; Vitalini, D. **Macromolecules 1986,** 19, 2157. Montaudo, G.; Puglisi, C.; Samperi,F.; **Polym. Deg.& Stab. 1989,** 26, 285. Montaudo, G., Puglisi, C., Rapisardi, R., Samperi, F. **Polym. Deg.& Stab. 1991,** 31, 229, 291. Montaudo, G.; Scamporrino, E.; Vitalini, D. **Makromol. Chem. Rapid. Comm. 1989,** 10, 431.
4. Maravigna,P.; Montaudo, G. in **Comprehensive Polymer Science - Vol. 5,** Pergamon Press: London **1989** p. 63. Mandolini, L.; Montaudo, G.; Roelens, S.; Scamporrino, E.; Vitalini, D. **Macromolecules, 1989,** 22, 3275. Montaudo, G.; Puglisi, C.; Scamporrino, E.; Vitalini, D. **Macromolecules, 21,** 1594 (1988). Ballistreri, A.; Garozzo, D.; Giuffrida, M.;Impallomeni, G.; Montaudo, G. **Anal. Chem. 1990,** 62, 279; **Macromolecules 1987,** 20, 1029.
5. Montaudo, M.S.;Ballistreri, A.;Montaudo,G. **Macromolecules 1991**, 25, 5051.
6. Montaudo, M.S.;Montaudo,G. **Macromolecules 1992**, 25, 4264
7. Montaudo, G.;Montaudo, M.S.; Scamporrino, E.; Vitalini, D. **Macomolecules 1992,** 25, 5100,
8. Ballistreri A.; Garozzo D.; Giuffrida M.; Montaudo G.;Montaudo M.S. **Macromolecules 1991**, 24, 1231.
9. Ballistreri A.; Garozzo D.; Giuffrida M.; Impallomeni G.; Montaudo G. **Macromolecules 1989,** 22, 2107.
10. Ballistreri A.; Impallomeni G.; Montaudo G.; Lenz R.; Kim B.;Fuller R.C.**Macromolecules 1990,** 23,5059; **1992**, 25, 1845.
11. Montaudo, G.; Scamporrino, E.; Vitalini, D. **Macomolecules 1989,** 22, 623; **J. Polym. Sci.Part A. Polym. Chem. 1992** 30, 525.
12. Montaudo G.; Puglisi C.; Samperi F. **Polym. Bullettin 1989,** 21, 483.
13. Montaudo, G.; Scamporrino, E.; Vitalini, D. **Macomolecules 1989,** 22, 627; **1991**, 24,376.

Direct and Matrix-Assisted Laser Desorption Fourier Transform Mass Spectrometry of Polymers

Charles L. Wilkins, John A. Castoro, and Michael S. Kahr, Department of Chemistry, University of California, Riverside, CA 92521

Characterization of polymers by laser-assisted mass spectrometric methods is of interest for a number of reasons. In the context of high performance ion cyclotron resonance mass spectrometry (FTMS), its demonstrated high mass resolution, excellent mass measurement accuracy, and applicability to highly non-volatile samples are the primary analytical advantages. During the past several years, direct laser desorption FTMS using high power pulsed carbon dioxide (IR) or Nd-YAG (UV) lasers has been shown to be a powerful tool for analysis of polar polymers and polymer additives. In the very recent past, the newer technique of matrix-assisted laser desorption has also been adapted to FTMS for this purpose. Recent results using both methods are discussed in this paper.

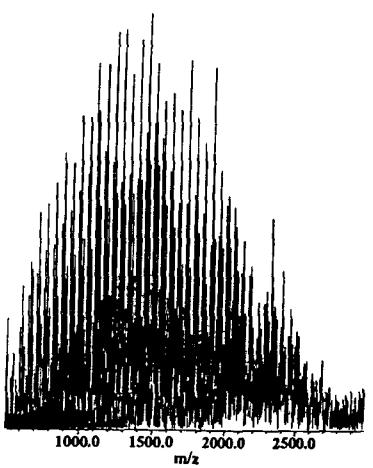

Figure 1 - Laser desorption-silver CI FTMS spectrum of an isobutylene sample.

Experience has shown [1-3] that it is relatively easy to obtain high resolution FTMS spectra of heteroatom-containing polymers with average molecular weights up to about 8,000-10,000 daltons using direct carbon dioxide laser desorption with FTMS detection. In fact, because oligomer ions produced in this way are so abundant, in favorable cases, it is possible to obtain ultrahigh mass resolution [3]. However, for higher mass polar polymers and hydrocarbon polymers, direct carbon dioxide laser desorption FTMS generally fails to produce mass spectra revealing oligomer distributions. Instead, spectra showing predominantly fragment ions are observed.

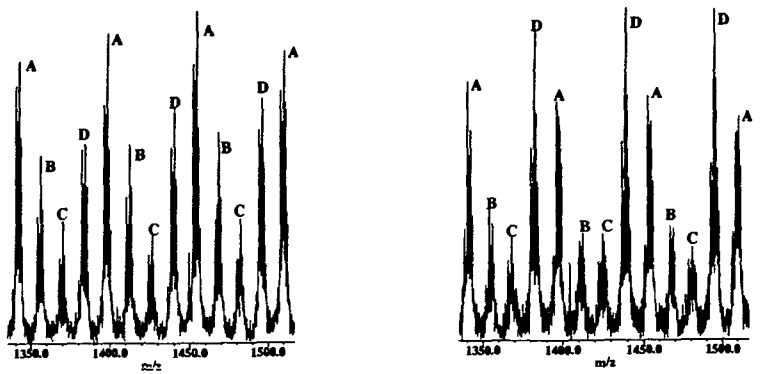

Figure 2 - Partial silver-CI LD-FTMS spectra of two different commercial isobutylene samples.

In this presentation the advantages and disadvantages of laser-assisted FTMS methods for polymer analysis are reviewed, with examples drawn from both polar and non-polar polymer classes. In the latter case, it has recently been shown that a combination of direct carbon dioxide laser desorption combined with chemical ionization methods is efficacious[4]. Figures 1 and 2 show some recent results for polyisobutylene samples. In addition, recent results show that matrix-assisted laser desorption/ionization (MALDI) Fourier transform mass spectrometry has some distinct advantages for high mass polar polymer analysis.

Finally, a number of examples of ultrahigh resolution polymer mass spectra will demonstrate the significantly enhanced analytical performance that is possible with FTMS-MALDI, as compared with more common TOF-MALDI measurements.

References

1. R.S. Brown, D.A. Weil, and C.L. Wilkins, *Macromol.*, **1986**, *19*, 1255-1260.
2. L.M. Nuwaysir and C.L. Wilkins, *Anal. Chem.*, **1988**, *60*, 279-282.
3. C.F. Ijames and C.L. Wilkins, *J. Am. Chem. Soc.*, **1988**, *110*, 2687-2688.
4. M.S. Kahr and C.L. Wilkins, *J. Am. Soc. Mass Spectrom.*, **1993**, 4 (in press).

Acknowledgement

Support of this research by the National Science Foundation, grant CHE-92-01277 is greatfully acknowledged.

Pyrolysis Field Ionization Mass Spectrometry (Py-FI-MS) of Polyolefins.

Robert P. Lattimer, The BFGoodrich Research and Development Center, Brecksville, Ohio 44141.

Five high molecular weight polyolefins (saturated hydrocarbon polymers) were examined: Polyethylene (PE), poly(isobutylene) (PIB), polypropylene (PP), poly(1-butene) (P1B), and poly(4-methyl-1-pentene) (P4M1P). Pyrolysis (Py) was carried out by heating the polymers in the direct probe of a Finnigan MAT 95Q mass spectrometer. Volatile hydrocarbons produced at the onset of pyrolysis ($\approx$350-400°C) were examined by field ionization (FI-MS), using standard carbon dendrite emitters. Volatile products were typically observed at every carbon number to masses well above 1000 Da. The distributions of pyrolyzates showed some similarities among the various polymers. For all of the materials, *alkene* oligomers (MW = $x\,n$, where x is the mass of the olefin monomer and n is the oligomer number) were dominant at lower masses. For most of the polymers, *dialkene* oligomers tended to be the most prominent pyrolyzates at higher masses. As an example, a Py-FI mass spectrum for PP is attached. The **A** series oligomers (alkenes) and **E** series oligomers (dienes) are marked.

Degradation mechanisms have been proposed to explain the observed patterns of volatile pyrolyzates. As an example, the dominant mechanism for formation of **A** series oligomers from the alkyl ethylene polymers (PP, P1B, P4M1P) is shown below. The first step is a homolytic main chain cleavage, which produces two free radicals. These may be primary, secondary or tertiary radicals, depending on the polymer structure. The chain-end radicals then undergo "backbiting" processes in which the radical site is transferred along the chain, with concurrent rearrangement of hydrogen atoms. When the formation of both secondary and tertiary internal radicals is possible, the tertiary radicals are strongly preferred. These internal radicals then undergo ß-scission and hydrogen abstraction reactions to yield both volatile and nonvolatile (high polymer) products. The nonvolatile products are terminally unsaturated; these intermediates can undergo further decomposition to yield the diene oligomers that are the dominant higher mass pyrolyzates observed via FI-MS.

Py-FI-MS is perhaps unique in its ability to detect pyrolysis products over such a wide mass range (> 1000 Da). The in-source pyrolysis (with its short transfer distance to the field emitter) and the inherent soft ionization capability of FI-MS combine to make the detection of these higher mass products possible.

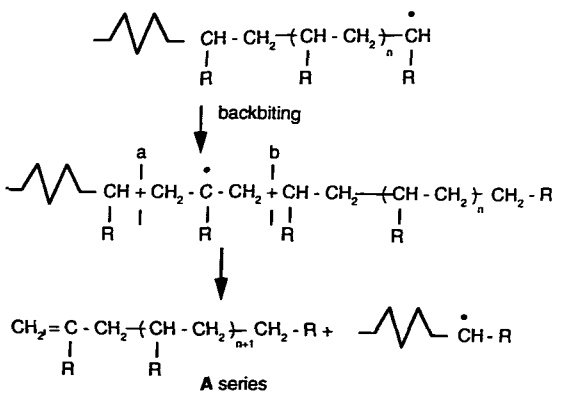

Pyrolysis Field Ionization Mass Spectrum (Py-FI-MS) of Polypropylene (isotactic PP).

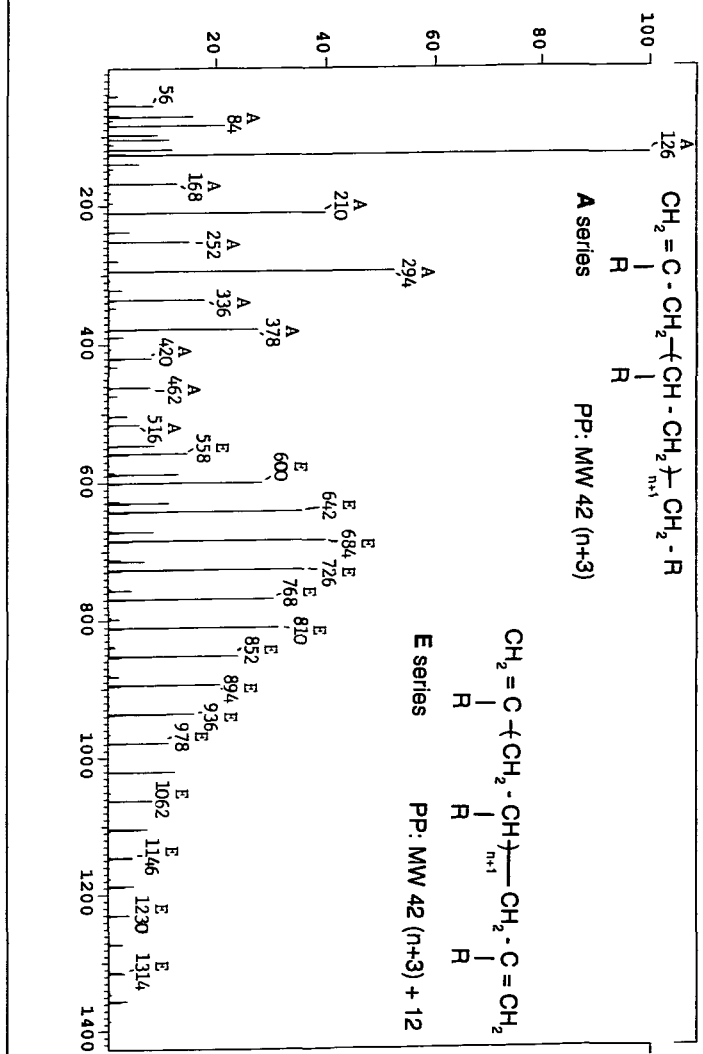

Characterisation of Polyester-based Surface Coatings by Pyrolysis GC/MS and Electrospray MS.

Susan M. Hunt, Malcolm R. Binns and Margaret M. Sheil
Dept. Chemistry, University of Wollongong, Northfields Ave, Wollongong NSW 2522 AUSTRALIA

Polyester resins are used extensively in paints which serve as protective and decorative surface coatings for a range of products including building materials and metal appliances. Polyesters are synthetic polymers that generally contain di-acid and diol monomers formed into polyester chains by a condensation reaction. In paint formulations, the polyester chains are joined together by "cross-linking" agents in a high-temperature reaction process known as "curing" which produces a solid, high molecular weight coating. Chemical characterisation of polyesters is important for the analysis of structural anomolies and degradation products of coatings to aid in the development of coatings with improved durability and performance. Thus we report here the results of an evaluation of several different mass spectrometric techniques for the characterisation of polyesters resins used in surface coatings.

The first method evaluated was a simultaneous-pyrolysis methylation (SPM) technique developed by Challinor[1] in which the polyester is mixed with a methylating reagent, tetramethyl ammonium hydroxide (TMAH) and pyrolysed in the injection port of the GC. On reaching the pyrolysis temperature (770°C), the polyester undergoes the hydrolytic methylation reaction shown below:

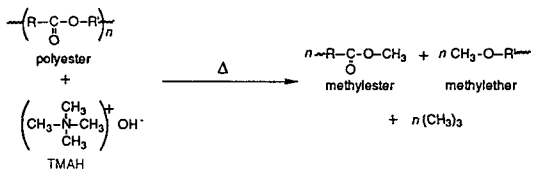

Pyrolysis and derivatisation occur simultaneously and the methylated pyrolysis products are analysed immediately by GC/MS. Methylation encourages the formation of larger and less polar fragments compared with direct pyrolysis. Figure 1, shows a typical pyrogram for a polyester and its monomeric components illustrating that the monomers can be readily identified.

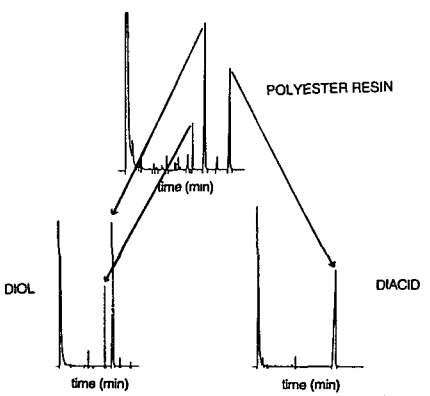

Figure 1: SPM pyrograms for polyester 1 and its component diacid and diol.

Further, the SPM method is extremely versatile, being applicable to a range of different samples including the polyester resins, liquid paints (comprising resin, pigment and crosslinker) and solid (cured) paint coatings.

Secondly, in a novel application of the technique, fourteen polyesters were analysed by electrospray ionisation (ESI). Singly-charged species are produced, as shown in a typical spectrum given in figure 2, so molecular weight distributions of the polyesters can be clearly identified.

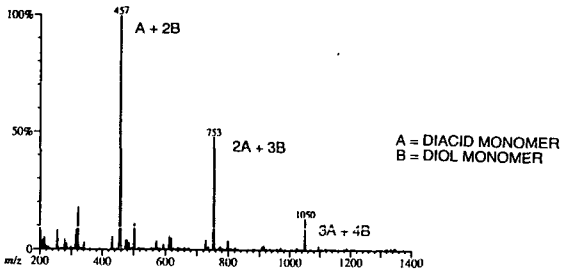

Figure 2. ESI spectrum of polyester 1
(50% CH_3CN, 1% formic acid, 5 µL/min, 2.5 µg/mL polyester)

The ESI spectra enabled indentification of: the range of chemical structures present in each sample; the distribution of acid versus alcohol "end groups" (important in the stability of cross-linked resins) and; any structural anomalies such as those caused by fragmentation of the monomer prior to polymerisation. The identities of the peaks in the ESI spectra were confirmed by ES/MS/MS experiments.

Finally, table 1 shows the number average molecular weights (M_n) determined from ESI compared to the results from other techniques including gel permeation chromatography(GPC), osmometry (VPO) and matrix-assisted laser desorption (MALDI). These data, especially the MALDI, suggest that the M_n's determined by ESI are lower than the true molecular weights of the samples. This is possibly a consequence of the poor solubility of the polyesters in the aqueous acetonitrile solutions used for these analyses being more significant in the case of ESI. We are currently investigating this further by comparing a range of electrospray solvents for the polyesters and water soluble polymers.

Comparison of M_n determined for four polyesters by a range of techniques.

Polyester	ESI	GPC	VPO	MALDI
1	510	773	1400	1356
2	537	842	2050	
3	618	1140	2247	1471
4	610	1419	1933	

Thus SPM and ESI appear to be complimentary techniques for the analysis of polyesters with the former useful for monomer identification and the latter enabling structural characterisation of oligomeric species.

We are grateful to Paul Humphries and Stephen Davis of Kratos Analytical for MALDI spectra.

1. J.C. Challinor *J. Anal. Appl. Pyrol.* 18 (1991) 233-244

The Mass-Changing Reaction Between MS and MS

Christie G. Enke
Michigan State University
and
Richard A. Yost
University of Florida

Tandem mass spectrometry (MS/MS) has achieved a very high level of importance in the field of mass spectrometry. In the analysis of targeted compounds in complex mixtures, the first mass analyzer is used to select ions of the targeted compound's mass and the second mass analyzer provides the targeted compound's mass spectrum or detects an m/z value in that spectrum. Much more information concerning the structure of pure compounds is provided by obtaining, with the second mass analyzer, the mass spectrum of each of the m/z values appearing in the mass spectrum from the first mass analyzer. These common conceptualizations and applications of tandem mass spectrometry, and indeed the nomenclature of MS/MS instrumentation itself (BE, QQ, etc.), tends to concentrate on the types of mass analyzers employed and appears to take for granted the essential process occurring between the mass analyzers. It is clear that without some mass changing (or, more rigorously, mass-to-charg-changing) reaction after the first mass analyzer, the MS in the second mass analyzer stands for "more of the same". This presentation reflects on the historical significance of the recognition of low-energy collision-induced dissociation (CID) in the development of the triple-quadrupole mass spectrometer and on the importance and variety of mass-changing reactions in the overall field of tandem mass spectrometry.

Our own entry into mass spectrometry was in pursuit of the goal of creating a computer-controlled analytical instrument which would incorporate both separation and identification stages, and, in which the computer could randomly select the sample components to be identified. In the consideration of quadrupole mass analyzers for each stage of such an instrument, the immediate problem was how to energize the ions selected by the first quadrupole mass analyzer so that the second quadrupole would have a spectrum of m/z values to obtain for compound characterization. In a private conversation, Graham Cooks, who had already recognized the separation and identification processes inherent in mass-analyzed ion kinetic energy spectrometry (MIKES)[1], encouraged us in this work and suggested that high-energy collision-induced dissociation (CID) might be easier than the electron-impact excitation that we were considering. High kinetic energy was considered necessary because, in the MIKES instruments, ion

[1]Cooks, R. Graham, "Collision Spectroscopy," R. Graham Cooks, Editor, Plenum Press, 1978, page 426

fragmentation efficiency was known to fall off dramatically below a few thousand electron volts of ion kinetic energy. In his later angle-resolved MIKES studies, Graham showed the fragmentation losses at lower energy to be due to the larger scattering angle of the products[2].

The Office of Naval Research funded the tandem quadrupole project at Michigan State University (more for the novelty of the data system approach than the soundness of the mass spectrometry). The question of the method of interquadrupole ion excitation remained open at the time of the 1977 ASMS meeting (Washington, DC) when, in a serendipitous meeting with Jim Morrison of La Trobe University, Australia, we mutually recognized that the process that produced the background fragment ions interfering with his tandem quadrupole photon-induced fragmentation studies was exactly the process we needed for our proposed analytical instrument. Experiments performed by Yost on Morrison's instrument resulted in a publication demonstrating the feasibility of an analytical triple-quadrupole mass spectrometer[3] and in a patent on low-energy CID in an rf-only quadrupole on which Morrison is a coinventor. Simulations performed with the now-familiar (but then as yet unpublished) SIMION, developed by Morrison and McGilvery at LaTrobe, proved invaluable in these studies. Our results were confirmed by Hunt and Shabanowitz[4] on a triple quadrupole mass spectrometer they constructed in an incredibly short time, and by Cooks[5] on an equally spontaneous double-quadrupole mass spectrometer while the triple quadrupole in our laboratory was still under construction. Only a little later, our instrument produced data[6] and several studies on the energetics and utility of low-energy CID were performed in our lab and others[7,8]. Computer control and data acquisition for all the MS/MS scans were developed and one of the first instrument command languages for user programming of automated experimental sequences was developed[9,10].

As a mass-changing reaction between mass analyzers, both high-energy and low-energy CID have great and undisputed power and usefullness. MS/MS with CID has been employed in a substantial fraction of the papers presented at this meeting. However, the field is far from mature. We are only approaching the adoption of a common format for MS/MS data and

[2]Laramee, J.A., P.H. Hemberger, and R.G. Cooks, Int J. Mass Spectrom & Ion Proc, **33** 231 (1980)
[3]Yost, R.A. and C.G. Enke, J. Am Chem Soc, **100**, 2274-2275 (1978)
[4]Hunt, D.F., J. Shabanowitz, and A. Giordani, Anal Chem **52**, 386 (1980)
[5]Zakett, D., R.G. Cooks, W.J. Fies, Anal Chim Acta **119**, 129 (1980)
[6]Yost, R.A. and C.G. Enke, Anal Chem **51**, 1251A (1979).
[7]Yost, R.A., D.C.McGilvery, D. Smith, J.D. Morrison, and C.G. Enke, Int. J of Mass Spectrom & Ion Proc **30**, 127 (1979)
[8]Douglas, D.J., J.Phys Chem, **86**, 185 (1982)
[9]Newcome, B.H. and C.G. Enke Rev Sci Inst. **55**, 2017-22 (1984)
[10]Myerholtz, C.A., A.J. Shubert, M.J. Kristo, and C.G. Enke Instruments and Computers, **3** 13-14 (1985)

agreement on a universally useful experimental protocol still seems a long way off. There are few available libraries of MS/MS data and general rules for the structural interpretation of the full MS/MS data set (the product spectra of all significant precursors) are few. What is needed is the development of an expert system despite the lack of codified human expertise to implement. We have worked on a system to discover correlations between chemical substructures and patterns in the MS/MS spectra[11], but a generally useful system has not yet been achieved. All these are areas where further development is needed to bring the applicability of MS/MS to the mature level enjoyed by practitioners of single-stage mass spectrometry.

The inherently low kinetic energy of ions in the triple quadrupole mass spectrometer makes it a natural environment for the observation of ion-molecule reactions. This is a form of mass-changing reaction in which the selected ion reacts with a neutral reactant gas introduced into the center quadrupole collision chamber. This can be called a collisionally-activated reaction (CAR) even though, in practice, the ion-molecule products are favored over the CID products at near-thermal kinetic energies. With our initial triple quadrupole instrument, we observed many interesting products, even with argon as the collision gas. With a deuterated selected ion or reactant molecule, a variety of H-D exchange products were observed. In 1981, Porter, Beynon and Ast[12] called the MS/MS instrument, "a complete chemical laboratory," in which synthesis, purification, reaction, and analysis occur in the source, MS1, collision cell, and MS2 respectively. This concept is still to be fully explored.

The CAR process can provide greater specificity than direct ion fragmentation. In Yost's lab, the cyclopentadiene molecular ion was readily distinguished from the linear 1-pentene-3-yne molecular ion (same m/z and composition) by CAR with isobutane while the CID products of these two ions differed only slightly in their relative ion abundances[13]. Yost's group also developed a "reverse" CAR system in which the effluent from a GC served as the collision gas. When piperidine molecular ion was selected by the first mass analyzer, the formation of product ions is selective for electrophiles (potential carcinogens)[14]. Orlando, Fenselau, and Cotter have demonstrated the efficient production of sequence ions of polypeptides by endothermic proton transfer reactions[15]. A scheme developed in Enke's lab for GC/MS/MS analysis of PCB's depends on the reaction of the selected molecular anion with O_2 reagent in the center quadrupole to produce the oxygen-chlorine

[11]for the most recent paper, see, Hart, K.J., P.T. Palmer, D.L. Diedrich, and C.G. Enke, J. Am Soc Mass Spectrom. 3, 159 (1992)
[12]Porter, C.J., J.H. Beynon, and T. Ast, , Organic Mass Spectrom., 16, 101 (1981)
[13]Fetterolf, D.D., and R.A. Yost, Int. J. Mass Spectrom & Ion Proc., 62, 33 (1984)
[14]Freeman, J.A., J.V. Johnson, M.E. Hail, R.A. Yost and D.W. Kuehl, J. Am Soc Mass Spectrom, 1, 110 (1990)
[15]Orlando, R., C. Fenselau, and R.J. Cotter, J. Am. Soc. Mass Spectrom. 2, 189 (1991)

exchange product ion[16]. By cycling through the appropriate precursor/product mass pairs as the chromatogram develops, a separate ion chromatogram can be obtained for each degree of PCB chlorination from 4 through 7. For the study of ion-molecule reactions, the ion trap and Fourier transform mass spectrometers have the advantages that the ion kinetic energy is inherently near-thermal and long and controlled reaction times are readily achieved. For incorporation into an analytical scheme, particularly for chromatographic detection, the triple quadrupole has the advantage that the process in each stage is continuous.

Even though mass-changing reactions have been stressed in this talk, charge-changing reactions between the mass analyzers are also effective. Charge-changing processes that have been used with MS/MS include charge stripping, charge inversion (Cooks), and neutralization-reionization (McLafferty).

Ion fragmentation has also been achieved by processes other than CID. Collision with a surface (SID) introduced in Graham Cooks' lab has been observed, extended, and applied by several others[17]. Another technique of growing significance is photon-induced dissociation (PID). Following early studies by Morrison and Vestal, many others have explored this technique[18]. High-efficiency PID in an interaction region between two time-of-flight mass analyzers has recently been demonstrated in Enke's lab[19]. Fragmentation efficiencies of 10% to 70% have been achieved in an instrument designed to produce ten or more PID product ion spectra per second so that MS/MS data sets can be obtained from chromatographically delivered sample.

The mass-changing reaction has quietly become the main thrust of MS/MS research following an early preoccupation with the hardware of mass analysis. From the examples cited, we can see that it is this process that is at the very heart of the ability of MS/MS to extend the characterizing power of single-stage mass spectrometry. The mass-changing reaction part of the MS/MS story is far from finished. For each of the techniques currently employed, still more work is needed to understand and characterize the fundamentals of the processes and thus apply them more effectively. Techniques for the improvement of the process efficiencies will be very welcome, and much work remains to be done in the development of more techniques that are selective for particular chemical structures or reactivity.

[16]Lopshire, R. J. Lee, T. Victorine, J. Bradford, and C. Enke, in preparation.
[17]For example, see works of Aberth, Mabud, Schey, and Wysocki
[18]For example, see works of Duncan, Reilly, Russell, Shlag, and Biemann
[19]Seeterlin, M., P. Vlasak, D. Beussman, R. McLane, and C. Enke, J. Am Soc Mass Spectrom. In press.

Young Mass Spectrometrists Interest Group
Workshop: Perspectives on Publication from the Inside Sunday, May 30, 7:30-9:00 p.m.

A panel of seven editors representing eight journals addressed several issues related to publication. The editors and their journals were Michael Bowers (J. Am. Chem. Soc., Int. J. Mass Spectrom. Ion Processes), Richard Caprioli (Biol. Mass Spectrom.), Catherine Fenselau (Anal. Chem.), Michael Gross (J. Am. Soc. Mass Spectrom.), Doug Ridge (Org. Mass Spectrom.), Alan Marshall (Rapid Commun. Mass Spectrom.), and Fred McLafferty (Accts. Chem. Res.). During the first hour of the workshop, each panel member presented their thoughts on a single publication related issue. During the last half hour of the workshop, the audience questioned the panel members on a broad range of topics. Approximately 150 people were in attendance, and their participation in the question-and-answer session made this a lively and informative workshop.

Michael Bowers discussed the factors authors should consider in selecting a journal for publishing their work. He divided the journals represented in the workshop into ACS versus non-ACS publications, and pointed out that ACS journals are broader in scope than the non-ACS journals. To decide which category of journal is most appropriate for a paper, the author should consider whether the work in question is technique driven, and therefore better matched with the more narrowly focused non-ACS journals, or directed toward a chemical problem, and therefore suitable for the broader audience of an ACS journal. Bowers also presented his thoughts on the reviewing process, and pointed out that reviewers may miss the point of a paper. In such a case, the editor will usually side with the reviewer, and under these circumstances, it is appropriate and necessary for the author to fight back.

Richard Caprioli advised the audience on the appropriate way to respond to reviewers. Reviews are intended to inform not only the editor, but also the authors. Although reviewers are people, and therefore capable of making mistakes, in his experience, Caprioli finds that papers are improved by the review process. Authors should not take reviews personally, but rather consider them as unbiased, outside evaluations of their work. When rebuttal of a reviewer's comments is required, the author needs to document his arguments with references to published work. Editors are not adversaries in the publication process, and in fact, wish to publish quality science in their journals.

Catherine Fenselau described the manner in which reviewers are selected and their reports interpreted. Editors look for people with a record of objectivity, and who provide informative reviews. Editors try to avoid reviewers that have a conflict-of-interest or that are strong adversaries of the author. A good review will tell the editor if the experiments are well planned, if the interpretation is reasonable, and if there are similar papers in press or that have been published. Fenselau discourages reviewers from focusing on editorial changes, although some may be suggested where minor revision is needed. Major revision of a manuscript is necessary if the structure of the paper needs to be changed, or if additional experiments are required before publication. Although reviewers may suggest additional experiments, the editor must make the difficult decision regarding the necessity of this exercise. Often, the suggested additional experiments are more appropriately the subject of further work and additional papers. Some advice was offered for contributors in interpreting reviews of their papers: if the reviewer misses the point, then it probably needs to be better written! This advice was echoed by several of the panel members.

Michael Gross reminded the audience that as the society's journal, *JASMS* has the broadest scope of all the mass spectrometry journals. In his experience as an editor, the slowest step in the publication process is manuscript revision, which is entirely under an author's control. He then

described the information that should be provided in a cover letter that accompanies a submission. It is not particularly useful to tell the editor why the work is important, as the reviewers will provide this information. It is important for the author to suggest reviewers and to veto reviewers in the cover letter. When submitting a revised manuscript, the cover letter needs to be far more detailed than the letter that accompanied the original submission. Revisions should be itemized, and editors find it useful if the manuscript is "yellow lined" to show the changes that have been made. Gross advised reviewers to ask themselves if they are being overzealous in their critique, and cautions against being overly picky in suggesting changes.

Doug Ridge proposed that mass spectrometry is of wider interest than often credited. He recommended as a general rule for authors to address the widest possible audience, that is, to publish in ACS journals when appropriate. As for selecting a non-ACS journal for publication, he reminded the audience that *Organic Mass Spectrometry* and *International Journal of Mass Spectrometry and Ion Processes* are international journals with wide readerships. *OMS* traditionally publishes chemically oriented papers, while *IJMSIP* is more physically oriented.

Alan Marshall discussed the purpose of publishing work as a communication. This type of publication allows one to stake out a new territory. However, Marshall warned against publishing all work as communications. A communication can be used to publish preliminary results, but a full paper should follow after the completion of more detailed studies. It is generally a bad idea to split up a large piece of work into several smaller pieces. Marshall pointed out that the National Science Foundation was aware of this practice, and has changed their rules for reporting prior work in a proposal by limiting principal investigators to listing only five relevant publications.

Fred McLafferty summarized the ideas that had been presented, and put them into a broader perspective. He divided journals into two categories - primary and review. He implored the audience to learn about the journals in their field by reading them. In preparing a paper, it is important for the author to know the impact of his work. Authors need to make clear in the first paragraph why the reader should go on. It is also important to have a good title and abstract to attract a reader's interest. His advice is to first pick the audience, pick the journal, and then to sell the idea. With regards to the role of the editor, McLafferty pointed out that as the buck stops with the editors, they must make the final decision about the publication of a paper, and that a reviewer's comments are only advisory. Finally, he reminded the audience that it is their duty to provide good reviews, as this keeps up the quality of a journal.

At this point, questions were entertained from the floor. One of the better established young mass spectrometrists, Klaus Biemann, stated that he was aware of a practice by some authors of publishing the same data in more than one journal. The panel agreed that this is an unethical practice, and should be discouraged. The question was raised that good papers are frequently rejected from *Journal of the American Chemical Society* because they do not meet the criterion of "being suitable for publication in *JACS*". Fred McLafferty pointed out that most journals have a page budget which cannot be exceeded, and therefore must at times reject worthy papers. Mike Bowers said that this being the case, he often rejects papers when there is a lack of consensus among the reviewers regarding suitability for the journal. Several other questions were addressed to the panel, and discussed at length. The workshop concluded at 9:00 p.m.

Submitted by,
Jon Amster
Jon Amster
Organizer for the Young Mass Spectrometrists Interest Group

Summary of Workshop on Field/Portable Mass Spectrometry

Organized by John F. Wacker[1] and M.Judith Charles[2]

[1]Pacific Northwest Laboratory, P.O. Box 999, Richland, WA 99352)
[2]Department of Environmental Sciences and Engineering, University of North Carolina, Chapel Hill, NC 27599-7400

The objective of the workshop was to provide information about developments in field/portable mass spectrometry and to stimulate discussion among the speakers and the audience. The following are highlights of the workshop.

Presentations

1. Mitchell D. Erickson, Argonne National Laboratory, Environmental Research Division, "Field Analysis: What do We Need and Why?"

Generic types of fieldable mass spectrometers, ranging from large mobile laboratories to portable instruments capable of *in-situ* measurements were described. Future needs and requirements (*e.g.*, better sample/instrument interfacing, routine implementation, on-the-fly decision making), including the need for regulators to accept field/portable mass spectrometry methods, were discussed.

2. David Koppenaal, Pacific Northwest Laboratory, Atomic and Molecular Chemistry Section, "Needs for Inorganic Mass Spectrometry."

Major application areas for *in-situ* inorganic and isotopic mass spectrometry, such as environmental cleanup, national security, and atmospheric chemistry, were discussed. Target species include toxic metals (As, Cd, Hg, etc.), isotopics of actinides, fission products (*e.g.*, ^{129}I and ^{99}Tc), and atmospheric trace constituents (noble gases, Cl-N-O-H_2O species, etc.). A variety of methods were described, including the use of laser ablation—inductively-coupled plasma mass spectrometry for analyzing radioactive samples.

3. J. Michael Ramsey, Oak Ridge National Laboratory, "Microminiaturized Instrumentation for Chemical Separations."

Described the development of "LC-on-a-chip." Capillary-zone-electrophoresis separation of Sr from Rb (40,000 theoretical plates), using a column (10-μm ID by 10-cm long) etched onto a 0.1 cm^2 area on a glass slide, was demonstrated.

4. Brian Andresen, Lawrence Livermore National Laboratory, Applied Technology Program, "Lawrence Livermore Experiments with Small Mass Spectrometer Systems."

Described the coupling of a microbore gas chromatograph column to an HP 5971A quadrupole mass spectrometer. The system, complete with vacuum pumps and

electronics, weighs 60 lbs, consumes 350 W, fits into a large suitcase, and is capable of achieving ppb sensitivity for many volatile organic compounds.

5. Phil Hemberger, Los Alamos National Laboratory, "Evolution of Transportable Ion Trap Mass Spectrometers at Los Alamos: Macro to Micro."

Described small ion trap mass spectrometers under development, including a gas chromatograph/mass spectrometer that can be used on a truck and an ion trap that fits in a beer can.

6. Neil S. Arnold, Center for Micro Analysis and Reaction Chemistry, The University of Utah, "Man Portable GC/MS for In Situ Field Applications."

The evolution of the instrument developed at the University of Utah was described. The current version is a 60-lb instrument that can easily be carried in a back-pack and can detect 100 ppb of toluene and benzene. Work is underway to produce an instrument that weighs 25 lbs and uses <75 W.

7. Albert Robbat, Trace Measurements Analytical Laboratory, Department of Chemistry, Tufts University, "GC/MS: A cost effective means for conducting site characterization."

The presentation emphasized the poor reproducibility of laboratory measurements for characterizing VOCs at contaminated site, the cost of the analyses, and the inability to characterize a site despite analyzing a large number of samples. A site can be more effectively characterized by analyzing samples in the field, while being faster and less expensive than laboratory analysis.

8. Marc Wise, Oak Ridge National Laboratory, "Field Transportable Ion Trap Mass Spectrometer for Real-Time Environmental Monitoring."

Development of an ion trap mass spectrometer that weighs 120 lbs, consumes 550 W, and can perform analyses by electron or chemical ionization (positive and negative ion detection) was described. The mass spectrometer is capable of detecting ppb- to ppt-levels of VOCs in air and water.

Discussion

The potential commercialization of field/portable mass spectrometers was discussed. Concerns were raised about the cost of the instrumentation and the need to alter regulations to accept methods based on field/portable mass spectrometry. The need for performance-based methods and the willingness for regulatory agencies to accept these methods was discussed.

Isotopic Applications Interest Group Workshop

"Signals and Noise: Measurement Limits in Mass Spectrometry"

The workshop on the final evening of the conference drew an attendance of about fifty persons. The workshop was a tutorial session covering four topics:

- General aspects of measurement and limits
  Dr. John Stein, GE-Vallecitos Nuclear Center
- Faraday cup measurements
  Dr. Karleugen Habfast, Finnigan MAT
- Pulse counting measurements
  Prof. John Hayes, Indiana University
- Data rejection criteria
  Dr. David Smith, Oak Ridge National Laboratory

Dr. Stein's overview answered three questions:

"What is the signal?" Singly charged ions of the sample of interest that give a usable current or pulse from the detector.

"What is the noise?" Unwanted ions (molecular, memory, multiply charged, or metastable) from the source; scattered ions or neutrals from the analyzer; ions from ion pumps and vacuum gauges; detector noise due to cosmic rays, dark current, and electronics.

"What is the detector?" Faraday cup, electron multiplier, Daly detector, or P-N junction and its associated electronics.

Dr. Habfast asserted that a Faraday cup is the most accurate device to measure singly charged ions. It cannot distinguish one multiply charged ion from multiple singly charged ions. It is bias free but does have limited precision. Limitations are due to 1) RC time constant of the electrometer amplifier, 2) linearity of the high-ohm resistor (negligible with today's high quality resistors), 3) electrometer noise, and 4) secondary electron emission from the Faraday cup itself. The latter effect is minimized by making the cup deep (at least 20x the aperture size), by using special coatings and shapes to reduce secondary emission, and by preventing the escape of secondaries with magnetic or electrostatic fields.

Prof. Hayes described the statistical nature of ion arrival at the detector and the effect of counting system deadtime on count losses. The conventional approach to count loss corrects only for first-order coincidences. More accurate approaches consider higher orders of ion coincidence. The optimal approach is to measure an effective deadtime experimentally. Uncertainty in the deadtime places upper limits on the usable count rate as well as the attainable precision. Hence, it is more important to minimize the uncertainty in the deadtime than it is to minimize the deadtime itself.

Pulse counting gives better signal-to-noise at low signal levels, but analog measurement gives higher precision at high signal levels.

Dr. Smith related pulse-counting statistics to the rejection of outliers. Although count data follow a Poisson probability distribution, the ratios of count data do not follow any well-defined probability distribution. The use of normal distribution statistics to reject ratio data and assign confidence intervals is inaccurate, but the inaccuracy becomes negligible for large counts. Quality control can be improved by the use of a two-dimensional control chart instead of a one-dimensional chart. A plot of two parameters, such as concentration vs. isotopic ratio, yields more information and can frequently point to the cause of a problem when one arises.

General discussion followed the presentations.

A brief business meeting followed the workshop. Announcement was made of the second A. O. Nier Symposium on Inorganic Mass Spectrometry to be held in Durango, Colorado, on 10-12 May 1994. The conference will feature invited oral papers and contributed posters on high-sensitivity measurements in isotope geochemistry, nuclear energy, environmental assessment, accelerator mass spectrometry, other areas of inorganic mass spectrometry, and current advances in instrumentation development. Symposium sponsors are the Isotope Science Group of Los Alamos National Laboratory, the Chalk River Nuclear Laboratory of Atomic Energy of Canada, and the Idaho National Engineering Laboratory.

Discussion ensued regarding the competition for attendance between the A. O. Nier Symposium and the 1994 ASMS Conference which will follow only three weeks later. Those present, representing both the Isotopic Applications and Elemental Analysis Interest Groups, expressed a strong preference for the Nier Symposium because of its greater concentration of papers of interest. A few indicated that they would probably attend both the Nier Symposium and the ASMS Conference.

A discussion of topics for workshops or symposia at future ASMS Conferences centered on isotope ratio measurements in biological samples. The use of stable isotopes is increasing in biological studies because of the difficulty of getting approval for the use of radionuclides. The advantages and disadvantages of various ionization methods applied to the elements of interest in these studies would be valuable. A related instrumentation issue is that "many" in the biological field are using mass spectrometers not designed for ratio work to do ratio measurements.

The linking of Elemental Analysis and Isotopic Applications papers in both the oral and poster sessions this year was regarded as a good move.

Jim Stoffel(s)

Submitted by Jim Stoffel(s)
Interest Group Coordinator

LABORATORY MANAGERS INTEREST GROUP

WORKSHOP ON AUTOMATION IN THE MASS SPECTROMETRY LABORATORY

The topic of this year's workshop was "Automation in the Mass Spectrometry Laboratory". With the current slow economic growth, many laboratory managers are faced with the not uncommon task of being asked to "do more with less" - less personnel, less financial resources, less capital budget. Automation offers a means of increasing productivity while providing benefits for the end-user.

Mark Bean of SmithKline Beecham discussed automated molecular weight determinations using electrospray on a Sciex API III LC/MS system. Mark reported good results for the analysis of most compounds containing heteroatoms, from the very small up to medium-sized proteins. Either MW or MW plus fragmentation information (via manipulation of orifice potential) was readily obtainable. Other benefits of ESI analysis include the production of simple spectra, which lends itself to automated spectral processing. Automation also allows more time for challenging samples and speeds up the turn-around time for routine analyses.

Chemists submit a predetermined amount of dry sample in an autosampler vial attached to a submission form. The sample is dissolved in the chemists' solvent of choice; however, no acidic solvents are used. DMF and DMSO are generally avoided due to the production of multimeric species in the electrospray spectra. The samples are then sorted into two groups according to elution solvent requirements. Solvent A is used for those samples that elute in acidic aqueous methanol, while solvent B is used for those that will elute in acidic MeCN/MeOH. Each sample is injected twice; once for positive ion mode, and once again for negative ion mode. Solvent blanks and standards are injected for each of the solvent runs, and the solvent lines are washed prior to shutdown.

A translation program resident on the in-house VAX generates the Sciex acquisition batch file from the logged-in samples. The file is then transferred from the VAX to the Sciex MacIntosh computer. A sample tracking sheet is also generated at the same time. The instrument is tuned and calibrated daily, and the new calibration files are read into the acquisition method. Using the scripting feature of MacSpec, spectra are printed, having been adjusted for mass range, number of plot boxes, normalization, etc. The spectra are then distributed to the MS analysts (noted on the tracking sheet) for interpretation.

Ken Matuszak of Abbot Laboratories described an integrated robotics/MS system which utilizes ammonia desorption chemical ionization (DCI) for molecular weight confirmation.

Chemists enter sample information such as ID, solvent, and expected molecular weight, into a microVax oracle data base. Sample and solvent information are transferred to the DECstation. Samples are barcoded, which is then read and sent to the DECstation. A separate program matches the barcode and sample information, and send sample information to a Finnigan SSQ 700, and solvent information to a Zymark robot. The robot then prepares the sample and places it on the probe. The TSQ sets up the appropriate scan range based upon expected molecular weight, performs the analysis, processes the data and prints a hardcopy.

Approximately 8,000 samples are run on an annual basis. The system runs virtually unattended. Maintanance includes replacing the ion source and DCI filaments, recalibration (every three months), ion volume changes and source cleanings, and quadrupole maintenance. The number one problem has been the submission by the chemist of too much sample, which results in a saturated spectrum. Sample overload can also lead to source contamination and carry-over. Sample requirements are for between 0.5 and 1.0 mg. To avoid this problem, samples are reviewed before they are placed in the robot rack. Other minor problems include computer hang up and an occasional mishap from the robot.

Jane Gale of Bristol-Myers Squibb covered the topic of automated analysis of clinical samples for pharmacokinetic and bioavailability studies. Jane reviewed the benefits of automation, including increased productivity, a reduction on the reliance on contract labs (with concomitant cost reduction), maximization of instrument utilization, and improvement in analyst safety (less contact with potentially harmful biological fluids). Automation also helps in the tracking of samples, and can greatly accelerate the drug development process, which relies heavily on clinical studies.

Sample types include drugs, metabolites, and endogenous materials in matrices such as blood, urine, milk, and cerebrospinal fluid. Analytical techniques include GC/MS, LC/MS, and HPLC. Automation currently implemented includes robot-operated extractions, autosampler injections, data acquisition into batch files without operator intervention, and transfer of raw data to spreadsheets or mainframe programs for linear regression and calculation of predicted concentrations.

Jane outlined plans for further development of automation, from sample receipt to sample re-storage. A robot would take clinical sample tubes from an automatic feeder, move the sample across a barcode reader, place the sample in a storage rack and decontaminate in a bleach bath. Robots would then transfer samples to a freezer. Autosampler racks would be prepared robotically and would include standards and QC samples, as well as the study samples. This would be followed by transfer to the various workstations (GC/MS, LC/MS) for analysis. Samples would be subsequently returned to the freezer for storage. Up to 400,000 clinical samples could be analyzed per annum.

Jeff Kiplinger of Pfizer, Inc. concluded the workshop with a slightly different spin by reporting Pfizer's efforts in both the US and UK to establish hands-on mass spectrometry for molecular weight confirmation. Jeff outlined requirements for the system, including liquid introduction, soft ionization to produce MW information, ease of use (idiot proof), and low maintenance. Jeff reminded the workshop audience that users of such a service would have little or not instrumental experience, and that the system would have to be as simple as possible. Use by unsophisticated users means many unanticipated problems!!

Following evaluation of various ionization techniques for MW determinations, including thermospray, electrospray, particle beam/CI, particle beam/EI, and CF-FAB, it was found that particle beam/CI and thermospray produced reliable data in 75-90% of samples. Pfizer-UK installed a Fisons Trio-100 with TSP and PB on two systems, while an HP MS-Engine with ammonia CI PB was installed in the US, where throughput is currently 12,000 samples/quarter. Throughput in the UK lab is at 8,000 samples/quarter.

Jeff discussed the fact that the design and implementation of such a system requires the integration of several non-compatible parts. Vendors have been slow to design hardware/firmware/software with compatibility. Jeff suggested a long-term commitment with one manufacturer may be the best way to approach this problem.

Jeff offered other tips as well, suggesting that the system shouldn't be located too far away from the spectroscopists responsible for it. Sufficient training must be given including both spectral interpretation and instrument operation. Be prepared for user dependency. Finally, automation tends to spur growth in sample submission.

The workshop was well received and generated good discussion and interchange of ideas. Some of the approximately 80 attendees suggested a follow up in a few years, and perhaps having an oral or poster session devoted to laboratory automation.

Respectfully submitted,

Gerry Di Donato

Gerry DiDonato
Workshop Organizer

Workshop: Matching LC with MS; Current and Future Options

The LC/MS Interest Group conducted a spirited workshop on Thursday evening, June 3rd, with ca. 150-200 people attending. The workshop was structured in response to feedback from prior workshops. It was felt that these workshops had been too structured, time being filled with formal presentations and discussion from "gurus". Too few "real questions" were addressed and audience involvement was perceived as minimal. To address these concerns, we had **no structure** to this years workshop. I served only as a facilitator for questions that were posed by the audience. The role of the facilitator was to engage, challenge, and even intimidate the audience in an effort to provoke their involvement. The risk of chaos was well worth it as many excellent topics were discussed. The most encouraging part of the workshop was that almost all attendees got involved in the workshop by either asking, or answering questions.

The following is a summary of some of the questions posed. The audience submitted written questions at the beginning of the workshop. The availability of space prohibits a complete summary of the answers. Hopefully, these will give the flavor of the workshop.

How can LC/MS become as simple to use as traditional HPLC detectors (UV,etc)?
What is the optimal liquid flow rate for electrospray?
Where will Particle Beam LC/MS be in two years?
Where will Thermospray LC/MS be in two years?
Is there a need for a standard reference compound and standard reference spectrum for LC/MS?
Will there ever be a universal LC/MS interface?
What can be done to significantly increase the sensitivity of PB/LC/MS?
Will standard LC equipment meet the needs of present MS inlets or will there be a new generation of LC equipment?
What is the best LC column size for API/LC/MS?
Is it important to confine or restrict LC flow rates for the sake of the MS?
Can ultrasonic assisted electrospray really work at high flow rates, and if so, why is all the work shown at 50 uL?
Is anyone routinely doing accurate mass work with API LC/MS; and if so, what resolution and accuracy are they achieviing?

Based on feedback since this workshop, attendees would prefer this less structured, more interactive format. We will try this again in the future. I would like to thank all the participants for getting involved and contributing to a productive workshop.

Respectfully,

Ross Willoughby

FROM: David D. Stranz, Fisons Instruments

SUBJECT: Summary of discussions at the ASMS meeting

The Computer Interest Group workshop was held on Monday evening, 31 May 1993, at the ASMS annual meeting in San Francisco. The sole topic of that meeting was the status of the AIA Mass Spectrometry Data Interchange effort. Following the workshop, a meeting of vendors participating in the effort was held to develop plans for testing and final release of products implementing the interchange specification. I am pleased to furnish this summary of the workshop and vendors' discussion.

There were approximately 50 attendees present during the workshop, both end users and vendors. Dave Smith (PE-Sciex) welcomed the participants, explained the purpose of the workshop, then introduced me. I gave an overview of the AIA/MS effort and presented the current status and projected testing and release schedule. In brief, the status is that a second release of beta-level documentation and software was made in March 1993, and was distributed to vendors and other implementors at Pittcon. Several vendors have implemented applications using the tool kit, and have begun producing test files in netCDF format.

Following my talk, Don Zakett (Dow Chemical Company) presented his perspective as an end user, and gave some observations as a beta tester of several vendors' preliminary implementations. Slow conversion of large data sets (tens of megabytes) was identified as a potential usage problem. David McLaughlin (Eastman Kodak Company) gave some further views with respect to his use of the MS tool kit in exporting data from Kodak's corporate spectral database into netCDF format for import into a commercial MS data system. Performance on large files and some inadequacies in the implementation for spectral libraries were noted as problems.

During the discussion period, several concerns were raised. First, there was strong interest in using the AIA/MS netCDF files for long-term archival storage of mass spectral data. My answer was that we are also very interested in providing an archival storage mechanism, but the current state of the specification and implementation is too unstable to permit that. It will likely be several years before the specification stabilizes sufficiently. We did agree, however, to provide "version translators" which would update an AIA/MS file from the preceding version to the new in the event we release a new version. This would permit users who do archive data to keep their archives current.

Second, several users expressed concern about our validation of the software. There are three aspects to this: validation of the applications provided by vendors, validation of the AIA/MS tool kit, and validation of the underlying Unidata netCDF tool kit. Vendors are obviously responsible for certifying their own software. Round-robin testing will serve both to validate the files produced by vendors' implementations and the AIA/MS tool kit. I have suggested to the AIA that they become involved in the validation process for the netCDF tool kit, since it has been recommended and is presently serving as the underlying protocol for all AIA data interchange

implementations. The Laboratory Automation Standards Foundation (a non-profit organization assisting in standards development) might be an appropriate body to provide such validation.

Third, we discussed future directions for the MS effort. Three avenues were presented: full integration of the chromatography and mass spectrometry specifications; extension of the MS specification to cover MS/MS, FT/MS, and time-of-flight MS; and extension to cover quantitative and qualitative results and GALP information. By a show of hands, integration of chromatographic information was chosen as most important. Very little interest, other than by vendors themselves, was shown for other MS techniques. There was also some discussion of splitting the MS specification at some point into two parts, one describing experimental data sets, and another specifically tailored for spectral libraries. The current specification enforces a somewhat awkward marriage of these two topics into one.

After the workshop, vendors and interested parties held a brief meeting to discuss status and forward directions. Three issues were discussed: required enhancements and modifications to the beta release before final testing and public release, a formal round-robin testing plan, and projected release dates for products containing the AIA/MS specification.

With respect to modifications: Several individuals expressed interest in incorporating additional information, most of which was within the scope of the existing specification and will be added. In particular, explicit description of selected ion monitoring data (*i.e.* mass groups and monitoring times) was considered important in reconstructing SIM/SIR/MID data sets. There was also a request for some convenience functions to be added to the programming tool kit to make retrieval of TIC and certain other data easier. I agreed to incorporate these changes, and will make a final version of the documents and tool kit available by the end of June.

The vendors agreed that following receipt of the final beta distribution, they would develop applications to both read and write interchange files, and conduct round-robin testing of all major parts of the specification. This testing will be completed by the end of September, at which time we will submit the results to the AIA board for acceptance. I stressed the importance of AIA certification, and set a goal of at least 50% compliance before I could submit the results. Testing will be conducted by exchange of data files among the various vendors and end user beta testers. I will serve as recipient for all files on PC diskette; Jim Watt (PE Nelson) will make these files available via anonymous FTP, and I will furnish diskette copies to testers without network access. I will correlate testing results and notify participants of required changes.

Once testing is complete, I will submit the results to AIA for acceptance. We expect that the AIA will act on the request in time to allow us to make the specification fully public and begin distributing products which contain it by the end of this calendar year.

I will provide full details of the logistics of the round-robin testing plan with the revised distribution at the end of June. In the meantime, if you have not received a copy of the March 1993 beta distribution, please contact me.

The AIA/MS interchange effort is much anticipated by the end user community. Several individuals expressed their pleasure with the progress made to date, and are eagerly anticipating release of products. I would like to thank all of the participants in this long effort for their assistance and cooperation. We are nearing the end of the tunnel, and I am confident we will emerge successful.

INDEX OF AUTHORS PAGE NO

Abadia, J. 33a
Abbas, N. M. 495a
Abbott, F. 562a
Abbott, F S 559a
Abdelrehim, I 1091a
Abedelrehim, I. 684a
Abian, J. 33a, 985a
Abrams, G. D. 72a
Abramson, F. P. 554a, 555a, 558a
Acheampong, A. 48a
Ackermann, B. L. 873a
Adams, W. J. 37a
Adams, J. 1016a, 1017a, 489a, 512a
Aebersold, R. 415a
Aggarwal, S. K. 736a, 815a
Agnes, G. R. 772a
Agren, H. 482a
Ahluwalia, R. 586a
Ahmed, M. S. 487a
Aicher, K. P. 1037a
Alameddin, N. G. 174a
Albrecht, A. M. 869a
Aldridge, J. C. 121a
Alexander, A. J. 420a
Alexander, L. R. 273a
Alexander, M. L. 709a
Allard, M. 219a, 220a
Allen M 748a
Alley, G. T. 438a
Allison, J. 14a, 255a, 436a, 583a
602a, 667a
Allmaier, G. 111a, 233a
Allman, S. L. 657a
Alluri, M. R. 32a
Alvarez, E. J. 991a
Amano, M. 807a
Amatayakul-Chantler, S. 605a
Amirav, A. 20a, 665a
Amster, I. J. 170a, 175a, 196a
197a, 798a, 1086a
Anacleto, J. F. 1083a
Anderegg, R. J. 387a, 592a
Andersen, J. S. 609a, 713a, 906a
Andersen, J. 600a
Anderson, G. A. 454a
Anderson, V. E 336a
Andren, P. E. 41a
Andresen, B. D. 934a
Andrews, G. C. 1056a
Andrews, P. C. 581a, 602a, 610a
Andrews, S. R. 484a
Andrzejewski, D. 137a
Anex, D. S. 782a
Anheuser, K. 216a
Annan, R. S. 874a

INDEX OF AUTHORS PAGE NO

Annan, R. 263a, 867a
Anthony, D. C. 870a
Antonino, L. C. 350a
Aplin, R. T 614a, 1071a
Appelhans, A D. 634a, 643a, 1088a
Arakawa, T. 89a
Arbogast, B. 891a
Arbon, R. E 128a
Armentrout, P B 298a
Arnold, N S. 51a, 439a, 800a
Arnott, D. 377a
Arrowsmith, P. 817a
Asano, K. G. 700a, 749a, 930a
1068a
Asgharian, N. 968a
Ashe, T. R. 202a
Ashraf, J. 44a
Ast, T. 1024a, 1090a
Audier, H. E. 477a, 513a, 977a
978a, 979a
Auriola, S. 866a
Ausloos, P. J. 153a
Avery, M. 49a
Axelson, J. E 559a
Axelsson, J. 757a, 915a
Ayre, C. R. 662a
Baba, A. J. 1073a
Babcock, L. M. 169a
Bacon, J. P. 368a
Baczynskyj, L. 37a, 347a, 348a
Bade, E G. 353a
Bagnati, R. 61a
Bahr, U. 529a
Bailey, J. M. 588a
Bailey, M. R. 837a
Bailey, S 396a
Bailey, S. L. 1064a
Baillie, T. A. 43a, 317a, 831a
863a
Baird, G. S. 736a
Bajic, S. 576a
Baker, C. W 210a
Baker, T. R. 64a, 679a, 763a
Bakhitiar, R. 172a, 173a, 963a
999a
Baldo, L. 385a
Ballard, K. D. 920a
Ballevre, O. 332a
Banks, J. 16a
Banks, J. F. 287a
Barcelo, D 985a
Barinaga, C J. 458a
Barnard, D. R. 113a
Barofsky, D. F. 227a, 266a
Barr, J. R 273a

INDEX OF AUTHORS PAGE NO

Barry, J. P. 252a
Barshick, C. M. 722a, 727a, 728a
823a, 825a
Barshick, S. A. 125a
Bartlett, M. G. 119a, 584a
Bartmess, J. E. 440a, 506a, 958a
Bartner, P. 267a
Barton, D. 72a
Barton, R. D. 327a
Basic, C 588a
Bateman, R. H. 422a, 754a, 928a
1066a
Bates, P. S. 74a
Batey, D. W. 599a
Bauco, A. 1075a
Bauer, E. 349a, 351a
Bauer, M D. 354a
Bauer, S. 806a
Bauhofer, A. 353a
Baumeister, K. 349a, 351a
Baykut, G 644a, 645a
Bayne, C. K. 126a
Bazdikian, J. 989a
Beals, D M. 734a
Bean, M. 263a, 867a
Bean, M. F. 1050a
Beavis, R. C. 427a, 658a, 900a
Becchi, M. 835a
Becker, B. L. 681a
Becker, C. H. 437a, 662a, 676a
Beebe, D A. 574a
Behymer, T. D. 289a
Bekken, B. M. 826a
Beland, F. A. 243a
Belas, F. J. 333a
Bell, D. J. 379a
Bellar, T. A. 289a
Belley, M. 570a
Benavides, R. 557a
Bencsath, F. A. 856a
Benjamin, D. 376a
Benoit, F. M. 533a
Benson, L. M. 399a, 580a, 833a
843a
Bentz, B. L. 231a
Beranova, S. 29a, 280a, 499a
1011a
Berberich, D. W 629a
Berger, P. 544a
Berger, S. L 599a
Berman, J. 908a
Bernier, U. R. 113a, 527a
Berthomieu, D. 477a, 977a, 979a
Bertrand, M. J. 217a, 219a, 220a
221a, 237a, 997a, 1047a
Betowski, L. D. 397a

INDEX OF AUTHORS PAGE NO

Beu, S. C. 591a, 686a, 720a, 797a
Beuhler, R J. 5a
Beussman, D. J 938a
Beylot, M. 336a
Bhide, A. 84a, 86a
Biellmann, J.-F. 869a
Biemann, K. 265a, 358a, 360a
409a, 435a, 660a, 887a
Bier, M E. 456a
Bier, D. M 68a
Bierbaum, V. M. 189a
Billeci, T. M. 421a
Biller, J. E 435a
Binns, M. R. 1098a
Birchenough, A. D. 422a
Birken, S. 883a
Bitensky, I 238a
Bitsch, F. 40a, 578a
Bjork, H. 136a, 969a
Blackburn, R. K. 345a
Blackstock, W. P. 107a
Blair, I A 240a, 333a, 363a
556a, 844a, 851a, 853a, 924a
Blanchard, W C. 950a
Blay, P. 1033a
Bleasby, A. J. 596a
Blewett, C. W. 528a
Block, E 314a
Blum, S. C. 144a
Boaretto, E. 23a
Bodnar, W. M. 376a
Boekelmann, V. 680a
Bogart, K H. A. 949a
Bogen, K. T. 22a
Boggess, B 223a
Bognar, J A. 188a
Bohme, D. K 392a
Bokens, H. 329a
Boleda, M R. 112a
Bollag, J.-M. 390a
Bollen, B. 318a, 474a, 459a
688a
Bolton, J L. 134a
Bonaventura, C. J. 870a
Bonaventura, J. 870a
Bonham, C. C. 234a, 235a
Boni, R. L 320a
Boon, J. 433a
Boone, C. 805a
Booth, M. M. 445a, 712a, 716a
Borchers, C. 597a
Borda, I. A. 1064a
Bordeaux, K 544a
Borders, D. B. 32a
Bordoli, R. S 218a, 422a, 928a
Born, M. 962a

INDEX OF AUTHORS PAGE NO

Bornsen, K. O 775a
Bortolini, O. 187a, 795a
Borum, P. R. 444a
Bott, P. A. 1066a
Bott, G. 932a
Bott, P. A. 754a
Bouley, W. 213a
Bourhis, K. 190a
Bowers, M. T. 300a, 301a, 489a
508a, 1084a
Bowie, J. H. 1018a
Boyd, R K. 398a, 608a, 766a
1014a, 1083a
Boyle, J. G. 16a, 746a
Bradford, J. 812a
Bradley, C. D. 236a
Bradshaw, S. 453a
Bradshaw, S. C. 152a
Braggins, T. J. 626a
Branco, P. S. 243a, 261a
Brand, W A 829a
Brandt, K. M. 43a, 317a
Braybrook, C. 928a, 932a
Breau, A. P. 319a, 507a
Brekenfeld, A. 645a
Brenna, J. T. 147a, 738a, 828a
Brennan, P. J. 366a
Brenner, V 979a
Brenton, A. G. 256a
Brewer, C. F. 611a
Briggs, D. 538a
Bright, D. S. 827a
Brinded, K. 551a
Brinkmalm, G. 232a, 238a
Briscoe, J. L. 629a
Bristow, A 598a
Brittain, R. D. 459a, 638a, 639a
Brodbelt, J 860a, 861a, 968a
Brodbelt, J. S. 162a, 163a, 192a
964a, 965a, 966a, 967a, 991a
Brodbelt, J. A. 151a
Bronson, G E. 37a, 347a, 348a
Brooks, J. M. 122a
Brooks, P. J. 516a
Brooks, P. W. 636a
Brown, R. S. 668a, 949a
Brown, D. W. 133a, 134a
Browner, R. F. 119a, 663a, 762a
Brownsill, R 318a
Brubaker, G. 213a
Bruce, J. E. 3a, 454a, 768a
Brudny-Kloppel, M. M. 552a
Brueggemann, E. E 546a
Bruenner, B. A. 367a
Bruins, A. P. 741a, 744a
Brunengraber, H 336a
Bruner, F. 637a

Brunet, J. 322a
Bryant, D. K. 1053a
Buchanan, M V. 125a, 126a, 249a
438a, 740a, 764a, 822a
Buchannon, W. D. 1012a
Buckner, S. W 182a, 476a 1003a
Budde, W. L. 289a
Bunn, T. L. 623a
Burford, N 1033a
Burgers, P C. 282a
Burgoyne, T W. 729a
Burka, L T. 50a, 543a
Burlet, O. 365a
Burlingame, A. L. 94a, 886a, 890a
937a
Burroughs, J. A. 441a
Burrows, D. G. 133a, 134a
Bursey, M. M. 590a
Busch, K I 117a, 119a, 584a
911a, 995a, 996a
Buseck, P R. 428a
Bushnell, J. E. 301a
Butler, I. J. 344a
Buttrill Jr., S. E. 468a, 802a
Byrd, G. D. 56a
Cable, P. R. 467a
Cadre, B. M. 441a
Caesar, J 91a
Cai, Z. 131a, 404a, 624a
Cai, J 280a, 499a
Caimi, R. 828a
Calaycay, J. 1078a
Calaycay, J. R. 378a
Caldas, E D 313a
Caldwell, K. 331a
Caldwell, G W 832a
Callahan, J. H. 912a, 1006a, 1085a
Calvey, E M. 314a
Camp II, D. G 272a
Campana, J. E 432a, 433a, 651a
681a, 719a
Campbell, J. A 393a
Campbell, V. L 443a, 796a
Campbell, V. 751a
Canova-Davis, E. 868a
Cantle, J. 818a
Cantone, J. 500a
Cao, Y 995a
Caparros, M 111a
Caple, R. 80a
Cappellini, L. 646a
Cappiello, A. 637a
Caprioli, R 424a
Caprioli, R. M. 41a, 47a, 344a
894a
Cardin, J 1075a
Carlsen, L 993a

Carlson, J. B. 737a
Carlson, R. E 119a, 911a
Carlson, J. E 81a
Carlson, R. 80a
Carlson, R. M 973a
Carr, S. 263a, 867a
Carr, S. A. 874a, 1050a
Carrier, A. 1047a
Carroll, J. A. 696a
Carson, P. G. 804a, 944a
Carter, G. T. 32a
Caruso, J. A. 388a, 628a
Cassady, C. J 198a, 199a
Castoro, J. A. 413a, 359a, 1096a
Catinella, S. 385a, 446a, 795a
Cerniglia, C. E. 141a
Cerny, R. L. 242a, 916a, 1081a
Chace, D. H. 337a, 842a
Chace, M 535a
Chai, W. 85a, 90a, 95a
Chait, B 380a
Chait, B. T. 352a, 414a, 415a
616a, 621a, 658a, 787a, 883a
836a, 900a, 945a, 1008a
Chakel, J A. 669a
Chambers, David M. 934a
Chan, K. 75a, 500a, 545a
Chan, S 91a, 102a, 1060a
Chan, S. Y. 93a
Chang, T. T. 531a
Chang, Y.-S 343a
Chang, C 498a
Chang, D. P. Y 114a, 116a
Charles, M J 630a
Chaudhary, A K 240a
Chaudhary, T. 615a
Chauret, N. 341a, 570a
Chen, H 181a
Chen, Q. 165a
Chen, R. 448a, 462a
Chen, S 99a, 361a, 521a, 921a
Chen, C H. 657a
Chen, C. J. 840a
Chen, Q. 167a
Chen, S. L. 872a
Chen, Y. 1021a
Chen, Y.-C. 215a
Cheng, X. 194a
Cheng, Z. L. 742a
Chenna, A. 254a
Chevrier, M R. 108a
Chi, P. H. 229a
Chiarelli, M. P. 241a, 243a, 261a
Chidsey, C. E D. 1090a
Chien, M 295a, 942a
Choi, Y. 536a
Choi, S -S 992a

Chorush, R. A. 277a, 492a
Chou, J. Z. 836a
Chou, C.-W. 664a
Chou, P. K. 307a
Choudhury, T 806a
Chow, D. 88a
Christou, G. 1013a
Chu, I.-H. 164a, 166a
Chui, Y. C. 37c
Chung, H. L. 121a
Chyall, L. J. 31a
Ci, X. 1035a
Cinque, T. 500a
Cisper, M. E. 449a, 455a, 709a
Clare, R. A. 769a
Clay, K. L. 514a
Clayton, E. 928a
Clemett, S. J. 428a, 429a
Cleven, C. D. 472a, 473a
Coast, G. M. 368a
Cochran, D. 545a
Cody, R. B. 426a
Cohen, S. L. 414a
Cohen, A. I. 323a
Colby, B. N. 813a
Cole, M. J 53a, 547a, 548a
838a, 1032a
Cole, R. B. 771a, 1041a, 1072a
Cole, P A. 439a
Coles, J. 17a
Collette, T. W. 127a
Colorado, A 860a
Comisarow, M. B 176a
Compton, R 1007a, 1082a
Conboy, J. J. 1050a
Conboy, J. 263a
Cook, D. K. 764a
Cook, K 223a
Cook, K. D. 740a
Cooks, R. G 187a, 383a, 472a,
473a, 498a, 697a, 708a, 709a,
789a, 806a, 1023a, 1024a, 1090a,
Cooper, B. T. 1003a
Cooper, G. R. 273a
Coopersmith, B. I 982a, 983a
Cordero, M. M. 280a, 496a, 499a
503a
Corley, D G. 288a
Cornett, D. S. 1086a
Cornish, t. J. 948a
Corr, J. 732a
Correia, N. 482a
Costello, C. E. 79a. 81a 360a
1080a
Cosulich, D 44a, 862a
Cotter, R. J 108a, 359a, 431a
604a, 714a

Cotter, R. 948a
Cottrell, J. S. 78a, 596a, 952a
Cottrell, J. C 146a
Coutant, J. E. 873a
Covey, J. P. 432a, 433a, 651a
Covey, T. 101a, 319a, 748a
905a
Covey, T. R. 292a
Cowgill, C. 891a
Cox, K A. 383a
Cox, A. L. 1076a
Cox, K. A 697a
Craig, A. G. 594a, 882a
Craik, C. S 886a
Cramers, C. A 13a
Crandall, J. K. 981a
Creaser, C. S 470a
Cristini, A 131a
Cromwell, E. F. 817a
Crouch, R. K. 620a
Crutcher, R. I. 438a
Cudny, H. 615a
Culbertson, J A. 986a
Culea, M. 855a
Cullen, W. R. 394a
Curtis, J M. 921a, 1033a
Cusworth III, W. H. 756a
Cyr, T. D. 573a
D'Agostino, P A. 627a
D'Antiono, J. A. 206a, 211a
D'Arcy, P. H. 813a
D'Arienzo, C. 323a
Dagan, S. 20a, 665a
Dahl, D. A. 634a, 643a, 1088a
Dahlke, G. 505a
Dales, L. N. 581a
Dalleska, N. 298a
Dang, T. T. 189a, 923a
Danis, P. O. 1093a
Danon, A. 665a
Das, B. C. 160a
Das, P. 267a
Dass, C 382a, 510a, 619a
Davey, S. N. 110a, 913a
David, F. 336a
Davis, M. R. 43a, 317a, 831a
Davis, S. C. 649a
Davis, A. 807a
Davis, B. A. 850a
Davis, S. 888a
Davis, T. A. 1076a
Davoli, E. 61a, 646a
Dawson, B. 573a
Day, R. A. 586a
De Hoffman, E. 858a, 961a
De Jong, A. P. J. M. 257a
De La Rosa, A. 599a

De Vries, M. P. 849a
Dearden, D. V. 164a, 165a, 166a
167a
Dearth, M. A 120a
Dechert, G. J. 212a
Deffense, E. 858a
Degenhardt, C. 354a
Deinzer, M. L. 811a, 891a
Dejarme, L. 806a
Delmore, J E. 634a, 643a, 1088a
DeLong, A. 36a
DeLong, S E 464a, 799a
Delprato, U. 646a
DeMaio, W. 44a, 862a
Demirev, P. 232a, 238a, 757a
915a
Deng, Y. 971a
Denhez, J. P 979a
Deppe, A. 529a
DePrince, R. 898a
DePuy, C. H. 189a, 960a
Derrick, P. J. 99a, 361a, 521a
921a
DeSantolo, A. M. 718a
Desiderio, D. M. 364a, 382a
DesJardin, M. 209a
DesJardin, M. A 208a
Deterding, L. J. 50a
DeVries, M. S. 782a
Dey, M. 1036a
Dhahir, P. M. 319a
Dharmasiri, K. A. N. 541a
Dick, D. L. 949a
Dickinson, T. A. 378a
Dickinson, T 1078a
Diekema, K. A. 873a
Dietrich, A. 398a
Dilliplane, R. L. 539a
Dilts, M. J. 537a, 834a
Dimitrou, E. 1013a
Dinerstein, R. J. 873a
Ding, J.-M. 747a
Dive, G. 961a
Dix, K. 50a
Dixon, R. A. 312a
Dobberstein, P. 12a
Dobson, R. L. M. 679a, 763a
Doerge, D. R. 576a
Dogruel, D. 659a, 664a
Doherty, S. 19a, 209a
Doherty, J. B. 1078a
Doherty, S. J. 208a
Dolzine, T. W. 857a
Dongre, A. R. 1019a, 1025a
Donnelly, B. 859a
Doom, J. P. 288a
Doroshenko, V. M. 714a

Doster, D. E. 534a, 739a
Douglas, D. 732a, 905a
Downard, K. M. 360a
Downey, B. P 330a
Downey, S W. 640a
Doyle Jr., R. J. 1010a
Drazen, J. M. 100a
Dressler, R A 191a
Drinkwater, D. E 206a, 524a
Driskell, W. J. 396a
Du, Y. 586a
Duan, J. 991a
Duc, T. M. 1094a
Ducharme, Y. 341a
Duckworth, D. C. 728a, 822a, 824a
Duffin, K. L. 288a
Duhr, A. 929a
Duker, J. M. 97a, 834a
Dulcks, T. 1a
Duncan, M. A. 1086a
Dupont, A. 104a
Durden, D. A. 850a
Dwek, R. A. 605a
Dyck, L. E. 850a
Dzidic, I. 642a
Eades, D. M. 693a, 801a
Eakin, A. E. 886a
Earl, W. L. 449a
Eberlin, M. N 974a, 975a
Eckart, K. 218a, 384a
Eckerskorn, C. 784a
Edmonds, C. G. 260a, 272a, 1040a
Edmondson, R. D. 935a, 940a
Edsall, L. 342a
Egsgaard, H. 993a
Eiceman, G. A. 988a
Eichmann, E. 163a, 966a
Eichmann, E. S. 965a
Eickhoff, D. 354a
Eiden, G. C. 449a, 455a
Eigendorf, G. 562a
Eigendorf, G. K. 394a, 994a
Eitzer, B. D. 132a, 633a
Eklund, P. C. 1086a
Emerson, B. 640a
Emery, M. L. 438a
Emmett, M. R. 47a
Emmett, M. E. 41a
Eng, M. L. 868a
Engelhard, V. H. 376a, 1076a
Engstrom, J. 109a, 276a
Enke, C. G 14a, 812a, 938a
Ens, W. 4a, 434a, 677a
776a, 955a
Erickson, B. W. 387a
Ericson, J. F. 547a

Eriksson, J. 238a, 915a
Ervin, K. M. 306a
Essalouh, L. 906a
Evans, A M. 256a
Evans, J. E. 572a
Evans, R. A. 857a
Evans, S. 901a
Eyler, J. R. 174a, 299a, 445a
722a, 752a, 823a,825a, 1030a
1031a
Eyring, H. 674a
Fabris, D. 753a
Fales, H M. 87a, 599a, 612a
701a
Falick, A. M. 381a, 917a
Famiglini, G. 637a
Fanelli, R. 61a, 646a
Fang, L. 755a
Farmer, T. B. 894a
Farnsworth, P B. 731a, 816a
Faubert, D 997a
Faull, K. F. 610a
Fay, L. B. 332a
Fedele, D. 385a
Fedora, J. W. 202a, 205a
Feistner, G. J. 294a, 370a, 610a
Feizi, T. 90a
Feng, R. 37c, 237a, 356a, 1020a
Fenn, J. 16a
Fenn, J. B. 1028a
Fennessey, P. V. 830a
Fenselau, C. 194a, 410a, 753a
779a, 879a, 1042a
Fenselau, C. C. 355a
Fenyo, D. 232a, 945a
Fetterolf, D. D. 808a
Fiedler, W. 597a
Figueroa, I. 123a
Finch, J. W. 287a, 426a, 654a
775a
Fischer, S. 1054a
Fischer, W. H. 882a
Fisher, D. L. 60a
Fitzgerald, M. C. 673a, 788a
Fitzgerald, R. L. 568a, 569a, 736a
815a
Fitzgerald, W. P. 205a
Flament, M.-M. 835a
Fleet, I. A. 810a
Fleming, R. H. 826a
Flory, D. R. 830a
Flurer, R. A. 311a
Fogerson, K. 65a
Forest, E. 875a
Foret, F. 1057a
Forte, J. G. 88a

Fouda, H. G. 49a, 53a, 326a
547a, 548a, 838a
Fountain, S. T. 536a, 773a
Fournier, F. 190a
Fournier, J. 483a
Fournier, P. G. 483a
Francis, E. S. 15a
Franklin, A. M. 925a
Franklin, R. L. 1026a
Franklin, J. C. 721a
Frantz, C. 251a
Frantz, C. E. 22a
Franzen, J. 447a, 645a, 690a
Fraser, I. J. 769a
Freedman, P. A. 818a
Freeman, C. G. 185a
Freiser, B. 305a
Freiser, B. S. 171a, 180a
Fridland, G. 364a
Friedman, L. 5a
Frydrych, K. 1053a
Fuerstenau, S. D 1028a
Fukada, Y. 375a
Fukuda, E. K. 511a, 839a
Fukushima, K. 371a
Fultz, E. 251a
Fultz, E. D. 22a
Fura, A. 96a, 275a
Futrell, J. 304a, 491a, 1021a
Gage, D. 408a
Gage, D. A. 105a, 255a, 343a
436a, 585a, 602a, 889a
Gaillimore, R. 605a
Gale, D. C. 1040a
Gale, P. J. 323a
Gallagher, R T 888a
Galliani, G. 61a
Gallimore, J. R. 598a
Gallon, A A. 532a
Ganem, B. 262a
Ganem B. 877a
Ganguly, A. K. 357a
Gard, E. 1001a
Garozzo, D. 82a
Garst, M. 48a
Gaskell, S. J. 39a, 365a, 920a
Gauthier, A D. 845a
Geddes, M. M. 1038a
Geisow, M. 907a
Gelbart, Z. 23a
Gellene, G. I. 278a, 303a
Gelpi, E. 33a
Geno, P. W. 312a
George, M. 242a, 972a
Gerhardinger, C 385a
German, J B. 367a

Getek, T. A. 59a
Ghosh, A. 572a
Ghosh, D. K. 374a
Giam, C. S. 480a, 487a
Giblin, D. 972a
Giblin, D. E. 624a
Gibson, B. W. 109a 276a, 872a
Gibson, B. 579a
Gibson, G. W. 917a
Giese, R. W. 566a
Giessmann, U. 1a, 529a
Giglio, J. J. 388a
Gijbels, R. 678a
Gilbert, J. R. 208a
Gilchrist, D. G. 313a
Giles, K. 400a, 896a
Gillen, G. 827a
Gillespie, T. A. 36a, 327a
Gilliam, J. H 571a
Gimbert, Y. 961a
Gimon, M E 412a, 935a
Giordani, A. B. 1065a
Giraud, D 160a
Girijavallabhan, V. 357a
Glish, G. L. 630a, 803a
Glocker, M. O. 597a, 891a
Goeinger, D. E 438a, 700a, 749a
930a, 931a
Goff, M. L. 859a
Goldschmidt, R. 778a
Goldthwaite Jr., C. A. 556a
Goodings, J. M. 392a
Goodlett, D. R. 258a
Goodley, P. C. 1054a
Goodman, J. J. 147a
Goodman, K. J 738a
Goodwin, R. M. 36a, 327a
Gordon, B. M. 567a
Gordon, D. G. 57a
Gorman, G. S. 170a, 197a, 798a
Gorshkov, M. V. 442a
Gotkis, Y. 509a
Gotts, N. 508a. 1084a
Gozzo, F. C 974a
Grabowski, J. J 161a, 307a, 959a
Graham, E. 44a
Graham, D. G. 870a
Grant, K. E. 393a
Grantham, V. M. 725a
Graul, S. T. 191a, 489a
Gray, J. 1075a
Gray, W. R. 882a
Greathead, R. J. 649a, 901a
Greaves, J. 225a
Greaves, M. W. 1055a
Green, B N 74a, 85a, 146a

Green, B. 907a
Green, B. G. 1078a
Green, J. G. 532a
Green, M. D. 908a
Greene, H. L. 924a
Greer, J. B. 339a
Gregg, H. R. 934a
Gregg, M. 396a
Gregor, I. K. 179a
Gregson, J. M 259a
Grey, H. M. 377a
Griffin, P. R. 378a, 1078a
Griffin, T. P. 444a, 715a
Griffith, K. S. 278a, 303a
Griffith, W. J. 482a, 484a, 846a
847a
Grigsby, R. D. 204a
Grillo, M. P. 831a, 863a
Grimley, C 421a
Grimm, C. C. 626a
Grimm, D. A. 1073a
Grimsrud, E. P. 188a, 986a
Groenewold, G. S 634a, 643a, 1088a
Gronert, S. 960a
Gross, D. S. 457a
Gross, M. L. 30a, 131a, 178a
242a, 404a, 450a, 488a, 624a
691a, 880a, 916a, 972a, 1081a
Grossman, S. J. 570a
Grotemeyer, J. 941a, 1036a, 1037a
Grundwurmer, J. 941a
Gu, M. 279a, 625a
Guadliana, M. A. 54a
Guan, S. 442a, 451a, 462a
471a, 475a, 650a, 687a, 689a
Guan, Z. 430a, 443a, 751a, 796a
Guarino, A. M. 856a
Guckert, R. 929a
Guerin, M. R. 125a, 126a
Guettler, R D 186a
Guevremont, R 2a, 742a, 990a
1059a
Guido, D. M. 865a
Guilhaus, M. 17a, 150a
Gulcicek, E. E. 746a
Gulcicek, E. 16a
Gunsalus, I. C. 374a
Gupta, S. 362a
Ha, J. 497a
Haas, J. 651a
Haas, J. A. 681a
Habibi-Goudarzi, S. 271a, 245a
683a, 685a, 1029a
Hachey, D. L. 855a
Hadjarab, F 692a, 796a
Haegele, K. 351a
Hagen, A P. 204a

Haigh, B. 655a
Hail, M. 291a, 386a, 745a
1074a
Hakansson, P. 232a, 238a, 757a
915a
Hall, C. 559a
Hall, S. C. 937a
Halm, K. A. 52a, 542a, 603a
Halsall, H. B. 81a
Halverson, J E. 635a
Hammerstedt, R. H. 518a
Hammerum, S. 978a
Hammond, J. 538a, 1094a
Hanash, S. 408a
Hancock, A. B. 240a
Haney, C. A. 406a
Hanley, L. 441a, 1022a
Hannappel, E. 349a, 351a
Hanspeter, M. 1076a
Haran, M. 379a
Harcourt, D 48a
Harden, C. S. 988a
Hardin, C. C. 258a
Harnish, D. 479a
Haroldsen, P. 324a, 334a
Harper, C. J. 692a
Harrata, A. K. 771a
Harris, F M 256a, 482a, 483a
484a
Harris, A 264a, 881a
Harrison, A. G. 490a
Harrison, W. W. 723a
Hars, G. 800a
Hart, J R 129a
Hart, K. J. 245a, 685a, 749a
1029a
Hartman, T. G. 839a
Hartmann, S. 73a
Harvey, D. J. 98a, 422a, 522a
523a
Haseltine, J. N. 995a
Hashimoto, S. 617a
Hasselfield, J. A. 679a, 763a
Hatcher, J. A. 440a
Hauer, M. J. 560a
Hawes, E M. 62a
Hawthorne, D. 323a
Haydock, F. J 957a
Hayes, M. J 553a, 1062a
Headley, J. V. 636a
Hearn, B. A. 464a, 799a
Hearn, M. J. 538a
Hefta, S. 1077a
Heimark, L. 267a
Hein, R. E 681a
Heine, C. E. 1038a
Heinen, G 645a

INDEX OF AUTHORS PAGE NO

Heinze, T. M. 59a
Hellerstein, M. 331a
Hemberger, P. H. 449a, 455a, 709a
Hemling, M 263a
Hemling, M. E. 1050a
Henderson, L. O. 273a
Henderson, R A 1076a
Hendren, W. 898a
Hendrickson, C. L 702a, 703a, 796a
Henion, J. 262a, 469a, 794a
877a
Henion, J. D. 45a, 51a, 75a, 871a
Henzel, W. J 421a
Hercules, D. M 228a
Hermsen, S. S. 668a
Herold, D. A. 568a, 569a, 736a
815a
Herold, E. G. 570a
Hess, D. 415a
Hesselberth, P. E. 679a, 763a
Hesso, A. 136a, 969a
Hettich, R. 250a, 1007a, 1082a
Hettich, R. L. 249a
Heyes, M. P. 555a
Hieftje, G. M. 729a, 954a
Hieshima, G. 144a
Higashi, R. M. 403a
Hileman, F. D. 288a
Hileman, M. S. 438a
Hilkert, A. 829a
Hill, S. E. 296a, 310a
Hill, J. A. 435a
Hill, R. H. 1064a
Hill Jr., R. H. 396a
Hillenkamp, F. 246a, 529a, 674a
784a
Hillman, S. L. 842a
Hines, H. B. 546a
Hines, W. M. 872a, 917a
Hintz, P. A. 306a
Hinz, K.-P 946a
Hiserodt, R. 839a
Hites, R. A. 729a
Hittle, L. R. 228a
Ho, J. S. 289a
Hochhaus, G. 1052a
Hodge, V. 807a
Hoeger, C. 594a
Hoekman, D. 453a, 700a, 930a
Hoffman, A. D. 888a
Hofstadler, S. A. 3a, 454a, 768a
Hogan, J. D. 139a, 631a
Hogge, L. R. 72a, 516a
Hojrup, P. 159a, 268a, 600a
Hoke, S. H. 498a
Holcomb, M. 141a

INDEX OF AUTHORS PAGE NO

Holland, J F. 14a
Holland, W. B. 253a
Holle, A 526a, 1093a
Holliman, C L 30a, 691a
Hollingsworth, M. A. 1081a
Hollingsworth, R. I. 105a
Hollis, J S. 142a
Hollos, G. 23a
Holman, R. L. 958a
Holmes, J. L. 26a, 281a, 285a
479a, 493a
Honing, M. 985a
Honovich, J. P. 183a
Hoover, R. 851a
Hop, C E. C A 284a, 501a
Horlick, G. 772a
Hornedo, A 123a
Howald, W. N. 565a
Howard, A. 378a
Howell, S. 545a
Hoyes, J. 107a
Hronowski, X 431a
Hsieh, F.-Y. 924a
Hsieh, Y. L. 262a, 871a, 877a
Hsu, C. S. 144a, 212a, 297a
Hsu, F.-F. 68a
Hu, P 880a
Hu, Z. 876a
Hu, D. W. 439a
Hua, S. 355a
Huang, C.-H. 841a
Huang, E. C. 267a, 357a
Huang, J J. Z. 363a
Huang, L. Q 655a
Huang, R. 374a
Huang, 171a, 305a
Huang, Z.-H. 105a, 255a, 541a
585a
Huang, E. 101a
Huang, J. 909a
Hubert, M. 154a
Huberty, M. 425a, 881a
Huczko, E. L. 376a
Huddleston, M. 263a, 867a
Hudson, C. E. 480a
Huels, W. 647a
Hughes, R. J. 389a, 392a
Hughes, B. M. 629a
Hughes, D. E. 420a
Hughes, K. D. 911a
Humber, L. 545a
Hunt, D. F. 376a, 377a, 1076a
Hunt, J. E. 524a
Hunt, S. M. 1098a
Hunziker, H. E. 782a
Hur, H. Y. 641a

INDEX OF AUTHORS PAGE NO

Hurst, G B. 249a
Huston, C. 688a
Huston, C K. 639a
Hutchens, T. W. 416a, 417a, 418a
781a
Hutchens, B 733a
Hutton, T. 598a, 605a, 907a
Hutton, R. C. 818a
Iannucci, R. M. 553a
Ichikawa, Y. 106a
Iden, C. R. 244a, 247a, 254a
Ideo, H. 371a
Ijames, C F. 460a
Illies, A. 971a
Impallomeni, G. 82a
Ingemann, S 179a, 478a, 962a
Ingram, J C. 634a, 643a, 1088a
Ingram Jr., L. L. 138a
Inoue, T. 130a
Ireland, P. 130a, 901a
Isaksen, G. H. 144a
Isbell, J. J. 967a
Ishihara, M. 158a, 933a
Issakova, O. L. 145a
Itani, M. 566a
Ito, H. 1004a, 1005a
Jackett, S. 1048a
Jackson, T. J. 122a
Jackson, P. 318a
Jackson, P. J. 484a
Jacobs, P. L. 849a
Jacobson, D. B. 172a, 173a, 963a
999a
Jaeschke, H. 39a
Jajoo, H. K. 240a
Jakubowski, E. M. 857a
James, M. 971a
Janota, K. 316a
Jaquinod, M. 578a, 869a
Jardine, I. 291a, 386a
Jarman, M. 37c
Jarrell, A. 765a
Jarvis, S. A. 400a, 896a
Jayasimhulu, K. 586a
Jemal, M. 323a
Jennings, R. J. K. 939a
Jensen, O. N. 266a
Jensen, J. 481a, 926a
Jensen, N. J. 922a
Jenson, D. D. 735a
Jesaitis, A. 373a
Jester, E. L. 856a
Jiang, L. 1048a
Jin, C. 1007a, 1082a
Jin, L. 831a
Jochheim, C. M. 317a

INDEX OF AUTHORS PAGE NO

Johansen, K. 324a
John, C M. 224a
Johnson, J. V. 527a, 693a, 711a
712a
Johnson, R. S. 885a
Johnson, C A. 514a
Johnson, K. L. 399a, 580a, 833a
843a
Johnson, P. J 457a
Johnson, R R. 23a
Johnston, M V. 407a, 804a, 944a
Jones, D. 901a
Jones, D S. 888a, 57a
Jones, J. A. 622a
Jones, J. L. 27a, 1019a
Jones, T. L 397a
Jones, A. D. 114a, 115a, 116a
313a, 367a, 403a, 587a
Jones, P. R. 886a
Jones, R. B 657a
Jones, W J. 210a, 832a
Jones Jr , G. C. 186a
Jonscher, K. R. 695a
Judge, M. 1055a
Juhasz, P. 409a
Julian Jr., R. K 708a
Junker, E 216a
Jursberg, D. C. 430a
Justesen, U. 39a
Kadtke, B. V. 212a
Kahr, M. S. 783a, 1096a
Kaltashov, I. A. 1042a
Kalyuzhny, M. 419a
Kamel, A. 333a
Kamienski, C. 626a
Kammer, H.-F. 232a
Kan, Z. 176a
Kanai, M. 371a
Kanda, P. 343a
Kane, T. E. 914a, 1027a
Kaneda, T. 168a
Kang, H. 1023a
Kannuck, R. M. 809a
Kapiloff, E. G. 306a
Kaplan, D. L. 369a
Karagozler, A. A. 586a
Karas, M. 246a, 529a, 674a
784a
Karger, B. L. 1057a
Karlsson, B. 232a
Karnicky, J. 468a, 802a
Karr, D. E. 1093a
Kass, S. 308a, 505a
Kassahun, K. 317a, 831a
Kassel, D. B. 10a, 747a, 908a
Katakuse, I. 1004a

INDEX OF AUTHORS PAGE NO

Kato, I. 46a
Kaufmann, R. 670a, 680a, 774a, 946a
Kay, I. 1055a
Kayganich, K. A. 519a
Keating, G. 22a
Kelley, P. 453a
Kelly, M. A. 355a
Kelly, J. F. 1079a
Kelly, M. 7a, 753a
Kelly, P. B. 114a, 115a, 116a
Kelm, G. R. 64a
Kemper, P. R. 300a, 301a
Keniom G B. 534a, 739a
Kennady, J. M. 309a, 719a
Kennedy, C. D. 292a
Kennedy, I. M. 114a, 116a
Kennerley, S. 759a
Kenney, W. C. 84a, 89a
Kent, S B. H. 658a
Kenttamaa, H. I. 28a, 31a, 309a, 719a, 970a, 1000a
Kenyon, G 872a
Keough, T. 354a, 675a, 679a, 763a, 897a
Kerns, E. H. 42a, 66a, 69a, 296a, 310a, 895a
Khan, I 299a
Kilby, G. W. 918a
Kilius, L. R. 25a
Kim, H. S. 448a
Kim, H.-Y. 342a, 520a
Kim, J 40a, 381a
Kim, K. S. 840a
Kimber, M. 759a, 779a
King, D 331a
King, F. L. 820a, 998a
King, R. C. 951a
King, T. 785a
Kinsel, G. R. 412a, 935a, 940a
Kinser, R. D. 195a
Kiplinger, J. P. 54a, 506a, 574a, 910a
Kirby, D. P. 1057a
Kirpekar, F. 246a
Kirsch, D. 670a
Kirtley, K. E. 241a
Klassen, R. 648a
Kleman, K. M 381a
Klitus, N. A 395a
Klohr, S. E. 42a, 66a, 69a
Klohr, S. 895a
Kloppel, K. D. 552a, 892a
Kluge, H.-J. 694a
Klunk, L J. 333a, 556a
Knapp, D R 589a, 595a, 620a

INDEX OF AUTHORS PAGE NO

Knepper, T. 890a
Knight, D. 689a
Knight, W. B. 1078a
Knighton, W. B. 128a, 188a
Knobeler, M. 750a
Knobler, M. 899a
Knowles, B. 655a
Kochling, H. J. 435a
Koenig, S. 682a
Koerber, S C 594a
Koester, C. 526a
Kofel, P. 682a, 976a
Kohler, B. E. 1034a, 1035a
Kokame, K. 375a
Konishi, Y. 356a, 1020a
Koppenaal, D. W. 458a
Kornas, T 213a
Kornishki, T. 120a
Kostanovsky, R G. 183a
Kostiainen, R. 741a, 744a
Kostura, M. 378a
Koumenis, I. L. 733a
Kowalak, J. A. 270a
Kramer, R. 878a
Kravetz, L. 642a
Kreek, M. J 836a
Kristiansen, K. 246a, 600a
Krock, K A 148a
Kroeker, R. 308a
Krueger, U. 349a, 351a
Kruger, T. 904a
Kruppa, G. 750a
Kruppa, G. H. 899a
Kubiak, C P 235a
Kubiak, T. M 347a, 348a
Kubo, R 377a
Kubota, E. 730a
Kucharczyk, N. 549a, 550a
Kuehl, D. 80a
Kuehl, D. W. 622a, 973a, 983a
Kuhara, T 279a, 927a
Kuhnz, W. 552a
Kunihiro, F 933a
Kunkel, G J 119a, 996a
Kunze, K. L. 565a
Kurys, G L. 599a
Kusmierz, J J. 558a
Kussmann, M. 890a
Kutal, C. R. 175a
Kwan, E. 559a
Labdon, J. E. 615a
Labelle, M. 570a
Lacey, M. P. 675a, 679a, 897a
Lam, Z. 473a
Lammert, S. A 472a
Lamoree, M 1046a

INDEX OF AUTHORS PAGE NO

Land, D. P. 684a, 1091a
Lane, S. J. 551a
Lane, K. R. 180a
Langford, M. L. 482a, 483a, 704a, 705a
Lanyon, V. 214a
Lapolla, A. 385a
Laprevote, O. 160a
Laramee, J. A. 811a
Larick, D. 406a
Larsen, B. 83a
Larsimont, V. 1052a
Laskin, J. 509a
Lattimer, R. P. 530a, 1097a
Lattimer, R. S. 503a
Lau, B. P.-Y. 648a
Lau, B 381a
Laude Jr , D. A. 430a, 443a, 452a, 497a, 692a, 702a, 703a, 713a, 751a, 796a
Laukien, F. H 825a
Lawrence, R. F. 565a
Lawson, A. M. 85a, 90a, 95a
Lay Jr., J. O. 141a, 241a, 243a, 261a
Laycock, J. D. 55a
Le Blanc, J C. Y. 2a. 1059a
Leal, M 1062a
Leary, J. 92a, 275a
Leary, J. A. 96a, 486a, 923a, 932a
Lebl, M. 145a
LeBlanc, M D 398a, 837a
LeBlanc, J C Y 742a
Leblanc, D. 978a
Lebrilla, C. B 200a, 696a, 1001a
Lecchi, P. 424a
Lech, J. 839a
Leclercq, P. A. 13a
Lee, E. D. 956a
Lee, J. 161a
Lee, M. L 15a
Lee, E. D. 15a, 731a, 816a, 957a
Lee, H 536a
Lee, H G. 956a
Lee, J. 307a, 812a, 959a
Lee, M. L 731a, 816a
Lee, M S. 42a, 66a, 69a, 296a, 310a, 895a
Lee, M.-K. 525a
Lee, T. D 145a, 226a, 378a, 588a, 610a, 1077a
Lee, T.-H. 91a, 306a
Lee, W D. 204a
Leeck, D. T. 719a
Lehmann, W D 893a

INDEX OF AUTHORS PAGE NO

Lehn, J. M. 878a
Leigh, D. A. 110a, 913a
Leiker, T. J. 135a
Leize, E. 104a, 869a, 878a
Lennon, J. J. 668a
Lepine, F. 494a, 854a
LeTavernier, J. F 104a
Levis, R. J. 786a
Levy, M. 350a
Lewis, T. M. 1009a
Lewis, J. 939a
Leykam, J. 889a
Li, L. 18a, 344a, 671a. 672a
Li, Y. T 262a, 877a
Li, C. 341a
Li, C. S. 340a, 346a
Li, G. 954a
Lianos, L. 1094a
Liao, P.-C. 408a, 602a, 667a
Lias, S G. 153a
Liberles, S. 357a
Liegener, C. M. 482a
Lifshitz, C. 509a
Light-Wahl, K. J. 8a
Lim, H K. 51a, 75a, 262a, 871a
Limbach, P. A 471a, 710a, 822a
Limbird, L E. 363a
Lin, B 1058a
Lin, B.-W. 373a
Lin, S.-N. 344a
Lin, Y. 809a
Lin, Y. Y. 840a
Lin, G. 62a
Lin, H.-Y. 290a, 461a
Lin, L A 311a
Linberg, L F 339a
Lindinger, M 694a
Linford, M 1090a
Ling, V. T. 868a
Ling, Y.-C. 525a
Ling, Y -P. 525a
Linscheid, M. 401a
Liou, J. 162a, 163a
Lious, J. 967a
Lipniunas, P. H. 88a
Litorja, L. 495a
Little, D 759a
Little, D. P. 591a
Liu, Y. 607a
Liu, D. 855a
Liu, J. 895a
Liu, J.-H. 335a
Liukkonen, R. J. 973a
Lloret, R 112a
Loffelhardt, W 111a
Logan Jr., T P 857a

INDEX OF AUTHORS PAGE NO

Londry, F. A. 446a, 790a
Long, J. M. 391a
Long, C. 631a
Lonning, P. E. 37c
Loo, J. A. 6a, 919a
Loo, R. R. O. 581a
Lopshire, R. A 812a
Loraine, G. A 630a
Lorber, A. 144a
Lord, G. A. 57a
Lord, W D. 859a
Lowes, S. 540a, 576a, 598a
605a, 1071a
Lubman, D. M. 295a, 408a, 536a
773a, 903a, 942a
Lucas, P. N. 845a
Lucke, R. B. 393a
Ludicky, R. A. 534a, 739a
Lukaszewicz, J 548a
Lukic, D. 553a
Luo, C. 661a
Lustig, D. A. 239a
Luther, E. 326a
Luttgens, U. 1a
Lykins Jrs., B. W. 127a
Lynch, D. W. 721a
Lynch, M. J. 547a
Ma, Y.-C. 520a
Ma, W. 40a
Maas, J. W. 557a
Macfarlane, R. D. 876a
MacKenzie, S. L. 516a
MacMahon, T. 535a
MacMillan, D. K. 366a
Madilao, L. L. 994a
Maechling, C. R. 428a, 429a
Maeder, M. 150a
Maggio, V. L. 273a
Mahalakshmi, P. 619a
Mahoney, J. F. 140a, 226a, 230a
Mahr, E. 882a
Maier, C. 349a, 351a
Maio, S. M. 321a
Maisey, E. A. 107a
Maisonneuve, I. M 836a
Makarov, a. a. 649a
Malat, J. 490a
Malek, R. 707a
Maleknia, S. D. 81a
Mallet, A. I. 73a, 203a, 368a
1055a
Malspeis, L. 58a
Mamer, O A. 340a, 494a, 854a
Mamer, C. S. 247a, 598a, 605a
Mamer, O. 346a
Mandal, D. K. 611a

INDEX OF AUTHORS PAGE NO

Mandich, M. L. 718a
Mandrell, R 579a
Mann, M. 7a 159a, 268a, 706a
774a, 884a, 899a, 947a
Manrow, R. E. 599a
Mansoori, B. A. 804a
Manura, J. J. 405a
March, R. E 389a, 392a, 446a
790a, 925a, 989a, 1039a
Marcus, R. K. 725a, 821a, 467a
724a, 726a
Marecic, T. C. 1049a
Marecic, T. 765a
Marggraf, U. 401a
Markey, S P 320a, 338a, 460a
555a
Markides, K. E. 15a, 957a
Marnett, L. J. 240a
Marquette, E. 698a
Marquez, C. D. 335a
Marquez, C 557a
Marr, J. C. 1063a
Marschall, H-U. 846a
Marsh, E. P. 669a
Marshall, A. G. 442a, 448a, 451a
462a, 471a, 475a, 650a
687a, 698a, 699a, 710a
791a, 822a
Martin, L. B. 247a
Martin, L. L. 339a
Martin, S. 264a, 425a, 881a
Marto, J. A. 471a, 822a
Martyn, J. A. J. 34a
Masatsugu, Y. 375a
Mason, S. 1033a
Masoud, H. 1079a
Massey, I. 324a, 334a
Massiot, G. 87a
Masucci, J. A. 210a, 832a, 845a
Matheson Jr., R. R. 1092a
Mathews, W. R. 865a
Matsumoto, I. 46a
Matsuo, T. 158a, 1004a, 1005a
Matsuura, K. 1005a
Mattina, M. J. I. 132a
Matusik, J. E. 314a, 315a
May, M. A. 710a
Mayer, F. 1093a
Mayer-Posner, F. J. 526a, 892a
893a
Mayol, R. 333a
Mayol, R. F. 556a
McAdoo, D. J. 480a, 487a
McCague, R. 37c
McCarley, T. D. 861a, 964a
McCauley, H. 864a

INDEX OF AUTHORS PAGE NO

McClennen, H. 51a
McCloskey, J. A. 259a, 270a
McCullough-Catalano, S. 226a
McDevitt, J. T. 430a
McDonald, T J. 122a
McDowall, M. 318a
McDowall, M. A. 400a, 540a, 896a
McElvany, S. W. 1085a
McEwan, M. J. 185a
McGibbon, G. A. 282a
McGuire, J. M. 127a, 577a
McIntosh, A. 151a, 991a
McIver, R T. 511a
McKay, G. 62a
McKenna, R. 865a
McLafferty, F. W 277a, 492a
591a, 686a, 720a, 797a
McLane, R. D 14a, 938a
McLean, M. A. 416a, 418a, 781a
McLuckey, S A. 245a, 271a, 438a
683a, 685a, 700a
749a, 930a, 793a, 1029a
McMahon, J. M. 222a, 253a, 1089a
McMahon, T. B 184a, 977a, 1002a
McNeal, T. L. 169a
Meadows, L. R. 998a
Medzihradsky, D. 579a, 872a
Medzihradszky, K. 917a, 937a
Mei, Y. 726a
Meijvogel, C. 10a
Meikrantz, D. H. 128a
Meirav, O 23a
Meisels, G. G. 155a
Melaugh, W. 109a, 276a
Mello, C. M. 369a
Mellon, F. A. 99a
Melton, L. 387a
Mendez, A. 989a
Meng, A. 11a
Menzies, A. 573a
Merke, J. 406a
Merriweather, R. 126a
Mesmer, M. Z. 311a
Metral, C. J. 586a, 760a
Meuzdaar, M. L. C. 51a
Meuzelaar, H. L C. 439a, 800a
Meyer, J. 875a
Michael, S. M. 295a, 942a
Michaelis, K. 329a
Midha, K. K. 62a
Miesbauer, L. 606a
Mikaya, A. 153a
Miketova, P. 70a
Miller, M. L. 859a
Miller, S. A. 1023a, 1024a, 1090a
Miller, D. 378a
Miller, L. V. 830a

INDEX OF AUTHORS PAGE NO

Miller, W. T. 874a
Millie, P. 979a
Milliken, J A 1006a
Millington, D. S 337a, 842a, 870a
Mills, P., D. 457a
Milot, S 494a
Milton, R 380a
Milton, S. 380a
Minard, R. 390a
Minard, B. 518a
Mincher, B. J. 128a
Minnikin, D E 73a
Mirza, U. A. 352a, 616a
Mitchell, D. W. 464a, 799a
Mitrovich Jr., S. 902a
Mock, K. 291a, 386a, 582a
Mohendano, L. 112a
Moini, M. 124a, 1048a
Molinaro, N. 500a
Molineaux, S. 378a
Mollova, N. N. 70a
Monaghan, J J 810a
Moncur, J. G. 201a
Monson, S. J. 404a
Montaudo, G. 1095a
Montgomery, Jane A 322a
Montgomery, J. A. 854a
Moody, A. E. 913a
Moore, C 130a, 579a, 759a
779a
Moore, I. M. 70a
Mora, R. 100a
Moradpour, A. 961a
Morand, K. 7a, 706a, 884a, 947a
Mordehai, A. 51a, 469a, 794a
Morehouse, L. A. 574a
Morein, B. 1080a
Morgan, D. G. 590a
Morgenstern, D. A. 235a
Moro, L. 662a
Morre, J. 124a
Morris, M. 608a, 1024a, 1090a
Morris, B. J. 272a
Morrison, M. 185a
Morrow, J. D. 865a
Mort, J. S. 356a
Morton, G. 44a, 862a
Morton, T. H. 479a, 485a, 513a
1034a
Mortz, E. 268a
Moseley, M. A. 52a, 60a, 542a
603a
Moulis, J. M. 875a
Mourgues, P. 978a
Mowdy, D. 856a
Mroz, E. J. 819a
Muenster, H. 758a, 936a

INDEX OF AUTHORS PAGE NO

Muir, D. C. G. 143a
Mujsce, A. M. 640a
Mullen, S. L. 157a
Muller, A. J. 640a
Mulligan, K. J. 864a
Mullis, J. O. 60a
Mulvana, D. E. 71a, 325a
Mumford, R. 1078a
Mumford, R. A. 378a
Munson, B 984a
Murad, E. 191a
Murakami, S. 324a
Murphy, A. T. 507a
Murphy, C. M. 410a
Murphy, D. M. 419a, 943a
Murphy, C. 753a
Murphy, R. C. 366a, 515a, 519a
575a
Murray, K. K. 652a, 780a 940a
Murrell, J. 704a
Murugesan, V 959a
Musselman, B. 933a
Musselman, B D. 287a, 426a, 730a
775a
Musser, S M. 315a, 1043a
Mwakapumba, J. 306a
Myers, D. P. 954a
Mylchreest, I 291a, 386a, 745a
1074a
Naclerio, R. M 339a
Nadella, R. K. 229a
Nagarajan, K. 701a
Nagra, D. 671a, 672a
Nanayakkara, V. 309a
Naritsin, D. B. 320a
Natowicz, M. R 572a
Nave, R. 349a, 351a
Naves de Brito, A. 482a
Navetta, K. 49a, 326a
Naylor, S 399a, 580a, 833a
843a
Nazrul, M. 299a
Neal, J. M. 565a
Needham, L. L. 273a, 1064a
Neese, R. A. 331a
Nelson, C. C. 65a
Nelson, R. W. 418a, 656a
Nelson, H H. 1085a
Nelson, R. W. 416a, 781a
Nelson, S. D. 563a
Nero, V. P. 206a, 211a
Neubauer, K. R. 804a, 944a
Neville, W. A. 379a
Newton, R. P 256a
Ng, K. 423a, 840a
Ng, J 305a
Ng, K T 402a

INDEX OF AUTHORS PAGE NO

Nguyen, V. 479a
Nguyen, H. 48a
Nibbering, N. M. M. 179a, 478a
962a
Nickbarg, E. 264a, 881a
Nicol, G. R. 195a
Nicol, G 984a
Nicolaou, K. C. 106a
Nicoll-Griffith, D. 341a, 570a
Nieder, M. 40a
Niessen, W. M. A 77a, 761a, 1046a
Nieves, E. 611a
Nigam, S. 615a
Nigge, W. 401a
Nikolaev, E. N 183a, 442a
Nishimoto, M 134a
Nobes, B. 556a, 844a
Nobes, B J. 924a
Noble, G. 605a
Nocerini, M. R. 838a
Nogar, N S. 449a, 455a, 709a
Nojima, K. 1005a
Nolan, J. 518a
Nolan, S. P. 1072a
Nold, M. J. 280a
Noon, K. 255a
Norbash, K. 1021a
Nordhoff, E 246a
North, D. H. 837a
Norwood, D L. 60a, 330a
Nowakowski, M A 548a
Nowlin, J. G. 642a
Noyes, R. A 115a, 116a
Nuwaysir, L M 601a
O'Brien, R 990a
O'Connor, P B 686a, 720a, 797a
O'Connor, P. M. 188a
O'Hair, R. A. J. 960a
O'Hara, K. 1051a
O'Neil, J 955a
O'Neill, J. A. 78a
Oatis Jr., J. E. 589a, 620a
Obermeyer Jr., W. R 315a
Oberth, C. 587a
Occolowitz, J. L. 571a
Odom, R. W. 224a, 669a
Ogawa, Y 46a
Ohanessian, G 979a
Ohkura, T. 371a
Ohorodnik, S. K 723a
Ohyama, Y. 853a
Oishi, S. 37a
Okumura, Y. 168a
Olivares, J. A. 819a, 830a
Olson, D J. 72a, 516a
Onigbinde, A 984a
Oppenheimer, J R 641a

INDEX OF AUTHORS PAGE NO

Oriedo, V. J. B. 302a, 411a
Orkiszewski, R. 39a
Orr, G. A. 611a
Ortegon, M. E. 832a
Orth, R. G. 629a
Osei-Twum, E. Y. 495a, 854a
Otsuka, K. 730a
Otsuki, A. 617a
Overberg, A. 529a
Overly, C. M. 819a
Overton, S. V. 405a
Owens, K. 778a
Owens, K. G. 951a
Ownby, D. W. 900a
Paiva, N. L. 312a
Pakarinen, J. M H. 1000a
Pakkanen, T. A. 1000a
Palm, L. 600a
Palma, P. 637a
Palmer, P. T 814a
Pamidi, A. 339a
Pan, C. 820a
Pannell, L. K. 87a, 599a, 701a
Papac, D. I 589a, 620a
Papageorgopoulos, C. 331a
Papaleo, R. 232a, 238a
Papayannopoulos, I. A. 265a, 360a
Papov, V 887a
Pappin, D. J C 596a
Parello, J. 906a
Parent, D. C 1003a
Park, M. A. 912a, 953a, 1006a
Parker, C. E. 543a, 743a, 1051a
Parker, D 74a
Parks, T. M. 1033a
Parnis, J M. 1039a
Parr, G R 673a, 788a
Parry, S M. 203a
Parry, D. E. 484a
Patrick, J. 806a
Patterson, D G. 273a
Patterson, K S 127a
Patterson Jr., D G. 129a
Paul, G. J. C 217a, 237a, 997a
Paul, M. 23a, 707a
Pauly, G. G. 842a
Pavlovich, J. G. 227a
Pawlosky, R. J 561a
Payne, A. W. 149a, 236a
Peake, D. 754a
Pearson, P. G. 563a, 564a
Pedder, R. E. 711a, 717a
Peder, R 765a
Pedro, M. 111a
Peiris, D. M 1030a, 1031a
Penn, S M 1049a
Pepys, M B 598a, 605a

INDEX OF AUTHORS PAGE NO

Pereillo, J. M 852a
Perel, J. 140a, 230a
Pergantis, S A. 394a, 994a
Perkins, J. R. 9a
Perkins, J. r. 888a
Perlat, M. C. 190a
Perreault, H. 79a
Perry, M. B. 1079a
Pesch, R. 12a, 647a, 758a
936a
Peschke, M. 971a
Petillot, Y. 875a
Pfaff, H. 647a
Philen, R. M. 1064a
Philips, D. 618a
Phillips, D. R. 674a
Phillips, F. M. 24a
Phillips, J. B. 805a
Phillips, L. R. 58a
Phillips, A 636a
Phillips, A. M. 422a, 754a
Phillips, K M. 567a
Phillips, N. 109a, 276a
Phinney, C. S. 632a
Piatek, B. 423a
Picard, C. 852a
Pinkston, J. D. 293a
Pitsenberger, C. C. 170a, 798a
Pittenauer, E 111a, 233a
Plaggenborg, L. 1012a
Pleasance, S. 766a, 769a, 1063a
Pleva, S. G. 118a
Pochkowski, J. M 467a, 734a
Polce, M. J. 29a, 283a, 499a
Ponthus, C 852a
Poon, G K. 37c
Pope, M 182a, 476a
Poppe,Schriemer, N. 677a, 955a
Porter, J. 594a
Posada de la Paz, M. 1064a
Powell, M. L. 553a, 1062a
Prakash, C. 851a
Pramanik, B N. 101a, 267a, 357a
Pratt, D. A 361a
Preece, S. 576a
Preston, L. M 652a
Price, K R. 99a
Prior, J 23a
Profilet, R. 305a
Prokai, L. 1052a
Provost, L. R. 627a
Przbylski, M 349a, 351a, 353a
597a, 743a, 890a
Pu, Y. M. 338a
Puckrin, E. 389a
Pullins, S 684a, 1091a
Purdon, M P 328a

INDEX OF AUTHORS PAGE NO

Purdy, A 1006a
Puzycki, M. A 938a
Qian, K. 297a
Qin, J. 755a
Quilliam, M. A 766a, 837a, 1083a
Quinn, J. P. 720a
Quinn, M. 373a
Quinones, M. A. 207a
Quirke, J. M. 55a, 207a, 767a
Qureshi, N. 431a
Rademacher, T W. 605a
Ragunathan, N. 148a
Rahbek-Nielsen, H 600a
Ramaley, L. 398a
Ramanathan, R. 752a
Ramanujam, V M S 404a, 624a
Ramanujam, W. M. S. 131a
Rambo, E. 981a
Ramos, L. S. 133a
Ramsey, R S. 749a
Ranasinghe, Y. A. 630a
Ranatunga, T D. 309a, 970a
Rao, A. M. 1086a
Rao, M. V. 229a
Rapp, U. 892a, 893a
Rashed, M. 862a
Rasmussen, H. H. 268a
Rayne, R. C 368a
Reddy, D. M. 244a
Reddy, G. S. 67a
Reed, N. M. 818a
Reents Jr., W. D. 640a, 718a
Regg, B. T. 873a
Reiche, P. A. 574a
Reichert, P. 267a
Reichlmaier, S. 538a, 1094a
Reid, C. J. 482a
Reider, M. W. 336a
Reilly, J. P. 785a
Reilly, P. T. A. 785a
Reimann, C. 232a, 915a
Reimann, C. T. 757a
Reimer, M. L. J. 494a, 854a
Reinhard, H. 682a
Reinhold, V. N. 93a, 100a, 102a
274a
Reinhold, B. 91a, 93a, 102a
Reinhold, V. 91a, 1060a
Reinhoud, N. J. 1046a
Reiser, H. P. 708a
Reiter, A. 1017a
Rempel, D. L. 30a, 450a, 488a
691a
Ren, X. 816a
Rendon, T. 217a
Requejo, A. G. 144a
Rhodes, D. 234a

INDEX OF AUTHORS PAGE NO

Rhodes, J. C. 119a, 234a, 663a
762a, 1079a
Richardson, D. E. 299a
Richardson, S. D. 127a
Richardson, D. E 174a
Riciputi, L, R. 728a, 824a
Ricketts, J. P. 952a
Ridell, M. 73a
Ridge, D. P. 177a, 181a, 195a
Riederer, D. E 1023a, 1024a
1090a
Rieger, R 244a
Rieger, R A 247a
Riegner, D 692a
Riggs, A. F. 900a
Riley, D. 430a
Riley, T. A. 679a, 763a
Rimmer, D. A. 400a
Rindgen, D. 34a
Rinehart, K. L. 316a, 374a, 577a
Risbridger, G. 1053a
Rivera, J 112a
Rivers, J. M. 121a
Rivier, J. E. 594a, 882a
Roach, L. 150a
Roach, P. L. 614a
Robbins, R. C. 481a, 926a
Robbins, D. K. 507a
Robbins, W. K. 297a
Roberts, L J. 865a
Roberts, M. A. 586a
Robertson, V. 775a
Robins, S. P. 361a
Robinson, C. V 614a, 1071a
Roboz, J 11a, 611a
Rockwood, A. L. 3a
Roe, D. S. 337a
Roepstorff, P. 159a, 246a, 268a
609a, 610a, 621a, 906a
Roher, A. E. 604a
Rohm, I. 892a
Rohrbaugh, D. K. 118a
Roitman, E. 381a
Rollgen, F. W. 1a, 216a
Rollins, K. 939a
Romanyshyn, L. A. 549a
Romero, J. 112a
Ronkko, K. M. 866a
Rontree, J. 318a, 329a
Rosankiewicz, J. 95a
Rosario, O. 123a
Rose, M. E. 400a, 896a
Rosen, R. T. 839a
Rosnack, K. J. 618a, 1056a
Ross, M. M. 1085a
Ross, P. L. 407a
Ross III, C. W. 475a

INDEX OF AUTHORS PAGE NO

Rossi, O. 646a
Rostad, C. E. 135a
Rothwell, A P. 235a
Rothwell, I. 305a
Roussis, S. G 202a, 205a
Rowan, A. D. 356a
Rowlands, M. G. 37c
Rozenberg, R. 858a
Rozynov, B. V. 80a, 973a
Rozzelle Jr , J E 387a
Ruatta, S. A. 140a, 230a
Rudewicz, P J. 292a
Rurak, D. W. 559a
Russell, D. H. 302a, 411a, 412a
652a, 653a, 780a
935a, 940a, 1009a
Ryan, M. F. 174a, 299a
Sabesan, S. 83a
Saccomano, N. A. 618a
Sadagopa Ramanujam 242a
Saegesser, M. 682a
Saito, K. 320a, 555a
Saito, Y. 1005a
Sakuma, T. 292a, 545a, 748a
Sakurai, T. 1004a
Salama, Z. B. 329a
Salem Jr., N 561a
Sallans, L. 180a, 528a
Salter, R. H. 191a
Salzmann, J.-P. 10a
Samaras, Y. 234a
Sanchez-Baeza, F. 33a
Sanders, M. 291a, 386a, 582a
Sanders, P. E. 321a, 560a
Saraste, M. 7a
Satzger, R. D. 311a
Sautiere, P. 578a
Sawada, M. 168a
Sburlati, A. R. 599a
Scanlan, G. F. 399a, 580a, 833a
843a
Scarberry, R. E. 595a
Scatina, J. 545a
Schachterle, S. 638a
Schaefer, J. P. 351a
Schafer, K. P. 349a
Schantzer, A. 869a
Schey, K. L. 269a, 654a
Schieltz, D. M. 659a, 664a
Schilling, A. B. 35a, 142a, 214a
Schindler, P. 578a
Schlunegger, U. P. 682a, 976a
Schmehl, R. H. 1073a
Schmeits, G. J. H. 849a
Schmid, E. R. 111a, 233a
Schmidt, E. 713a

INDEX OF AUTHORS PAGE NO

Schneider, K 787a, 900a
Schneider, R. P. 53a, 326a, 838a
Schneider, R. E. 328a, 897a
Schofield, C. J. 614a
Schols, H. A. 77a
Schram, K. H. 70a
Schreck, C. E. 113a
Schroeder, E 12a, 758a, 936a
Schubert, R. 647a
Schultz, R H 298a
Schurz, H H. 1064a
Schwartz, S. J. 517a, 841a
Schweikert, E. A. 953a
Schweikhard, L. 694a, 699a, 792a
Schweizer, J. 893a
Scoble, H. 264a, 425a, 881a
Scrivens, J. H. 939a
Seabrook, G. 103a
Sears, J. 373a
Sears, L. J. 128a, 391a
Seifried, S. E. 266a
Selby, T. L. 280a, 503a
Self, R. 361a
Seneca, C. 615a
Senko, M. W. 720a, 797a
Sepetov, N. F 145a
Sequeira, A J. 567a
Seraglia, R. 385a
Sericano, J L. 122a
Sette, A. 377a
Settineri, C. A. 94a
Shabanowitz, J. 376a, 377a, 1076a
Shackleton, C. H. L. 40a, 381a
Shaffer, B. A. 468a, 802a
Shaffer, S. A. 279a, 502a, 927a
Shah, B. 84a, 898a
Shahgholi, M. 740a, 764a
Shaler, T. A 485a, 1034a, 1035a
Shalosky, J. 752a
Shalosky, J. A. 445a
Shank, R. P. 832a
Sharp, T. R. 848a
Sharpe, P. 299a
Shea, K. J. 225a
Sheeha, E. 765a
Sheehan, E. W. 97a, 770a, 834a
Sheeley, D. M. 87a, 599a, 612a
Sheffels, P. R. 863a
Sheil, M. M. 918a, 1098a
Sheng, L.-S. 432a, 433a, 651a
Shick, C. R. 821a
Shick Jr., C. R. 724a, 725a
Shida, Y. 1051a
Shiea, J. 215a
Shimanskas, C. 423a
Shimonishi, Y. 375a

INDEX OF AUTHORS PAGE NO

Shin, T. K. 1034a
Shinohara, H. 1005a
Shively, J. E. 378a, 588a, 1077a
Shoemaker, J. D. 63a
Shoff, D. B. 988a
Shomo II, R. E. 395a, 1067a
Short, R. T. 222a, 253a, 1089a
Shukla, A. 304a, 491a, 1021a
Shushan, B. 748a
Shyong, B. J. 105a, 255a
Siconolfi, D. J. 640a
Siegel, M. M. 213a, 909a
Siegmund, R. F. 402a
Simmons, T. A. 76a
Simons, D. S 229a
Simpson, J. T. 338a
Simpson, C. F. 203a
Sin, C. H. 15a, 731a, 816a
957a
Sinclair, J. D. 640a
Singh, H. N. 339a
Singleton, D. H. 1056a
Sinha, A. J. W. 560a
Sisenwine, S. 545a
Siu, K. W. M. 2a, 742a, 990a
1059a
Siuzdak, G. 106a
Sjovall, J 846a, 847a
Skilling, J. 146a
Slingluff, C. 1076a
Sloan, J. 684a, 1091a
Slopis, J. M. 344a
Small, J. H. 225a
Smit, W. A. 80a
Smith, C. H. 114a, 115a, 116a
Smith, D. H 727a, 728a, 824a
Smith, D. L. 593a, 606a, 607a
Smith, P. B. 76a
Smith, C. A. 293a
Smith, J. B. 606a
Smith, J. P. 110a
Smith, J. R. 857a
Smith, L. M. 673a, 788a
Smith, P. B. W. 988a
Smith, P. C. 335a
Smith, R. D. 3a, 8a,258a, 454a
768a, 919, 1040a, 1045a
Smith, R. L. 28a, 31a
Smith, R. W. 282a
Smith, V. C. M. 1071a
Smithwick III, R W. 721a
Smoliakova, I. P. 80a
Snyder, A. P. 76a, 988a
Snyder D. F. 284a
So, H -Y 992a

INDEX OF AUTHORS PAGE NO

Sofia, R. D. 549a, 550a
Sogaard, M. 609a
Solouki, T. 302a, 411a, 940a
Somogyi, A. 27a, 914a, 1019a
1026a, 1025a, 1027a
Song, H. 554a
Sonnen, S. 811a
Sorensen, C. 880a
Sossi, V. 23a
Southern, L. 689a
Spangler, G. E. 987a
Spanos, g. 517a
Sparadoski, R. E. 549a, 550a
Speir, J. P 170a, 196a, 798a
Speltz, D. 459a
Spengler, B. 670a, 680a, 774a
946a
Sphon, J. A. 314a, 315a, 1043a
Spicer, V 776a, 955a
Spiess, J. 218a, 384a
Spina, E 82a
Spino, L. A. 642a
Springer, D. L. 260a, 272a
Sproch, N. 904a
Squires, R. R. 180a
Stack, R. F. 292a
Staempfli, A. A. 332a
Stafford, R G 546a
Stahl, D. C. 145a
Stahle, P. L. 845a
Standing, K. G. 4a, 434a, 677a
776a, 955a
Starvic, B. 648a
Ste. Marie, L 322a
Steding, A. 676a
Stein, S E. 153a
Stemmler, E. A. 249a
Stephenson, J. L. 712a, 716a
Stephenson Jr., J. L. 445a
Stern, G. A. 143a
Stetzenbach, K. 807a
Stevens, R. D. 870a
Stiller, S. W. 700a, 930a
Stirk, K 1000a
Stirk, K. M. 28a, 31a
Stoeckli, M. 682a, 976a
Stone, J. A. 193a
Stoney, K 582a
Strahler, J. 408a
Strahler, J R. 602a, 903a
Straub, J. 156a
Straub, K. 350a
Straub, R. 38a, 290a, 1044a
Street, J. M. 572a
Streeter, A. J 845a

INDEX OF AUTHORS PAGE NO

Stroh, J. G. 618a, 1056a
Stroh, J. 390a
Stroobant, V. 858a
Strupat, K. 784a
Stults, J. T. 421a, 601a
Sturm, E. 351a
Stygall, J. W. 470a
Suckau, D. 591a
Sumner, L. W. 312a
Sumpter, T. 922a
Sumpter, T. L. 958a
Sun, Y. 354a
Sun, F. 577a
Sundquist, B. U. R. 232a, 238a
757a, 915a
Sunner, J. 373a, 1058a
Supko, J. G. 58a
Susin, S. 33a
Sutherland, J. B. 141a
Sutton, C. W. 78a, 596a, 952a
Svensson, B. 609a
Svensson, S. 482a
Svoboda, M. 353a
Swan, P. d. 429a
Swanson, A. 640a
Swanson, S. 36a
Swanstrom, R. 908a
Sweeley, C. C. 105a
Sweeney, M. J. 362a
Swenson, S. 266a
Swiderek, K. 1077a
Syka, J. E. P. 709a
Szente, L. 678a
Szulejko, J. E. 184a
Taaghol, A. 402a
Tabet, J. C. 190a, 961a
Takahashi, S. 168a
Takai, Y. 168a
Takao, T. 375a
Takasuga, T 130a
Takayama, K. 431a
Takigiku, R. 328a, 897a
Talbo, G. 7a, 884a, 947a
Tamura, J. 426a
Tang, K. 657a
Tang, W 562a
Tang, X. 666, 678, 1015a
Tang, X.-J. 1014a
Tang, D. 579a
Tang, S.-Y. 544a
Tang-Liu, D. 48a
Tangarone, B. 264a
Tanida, K. 375a
Tarr, M. A. 762a
Taylor, W.'S. 169a
Taylor, A. 318a

INDEX OF AUTHORS PAGE NO

Taylor, N. L. 551a
Teffera, Y 555a
Teixeira, A. J. R. 257a
Teklehaimanot, B. 155a
Tenaschuk, D. M 516a
Terlouw, J. K. 282a
Testino Jr., S. A. 117a
Tetler, L. W. 57a, 110a, 810a
913a
Theberge, R. 221a
Then, A. 1075a
Thibault, P. 613a, 921a, 1014a
1015a, 1079a
Tholmann, D. 1002a
Thomas, R. 1082a
Thompson, A. G. 374a, 577a
Thompson, T. J 1057a
Thompson, C. V. 438a
Thompson Jr., H. C. 141a
Thomson, B. 748a
Thomson, B. A. 921a
Thomson, D. S. 419a
Thornburg, N. A. 684a, 1091a
Thornburg, K. R. 269a, 595a
Thornburgh, B. A. 560a
Thrall, B 258a
Thrall, B. D. 272a
Thruston Jr., A. D 127a
Thurin, J 1080a
Tien, L. T. 457a
Tighe, T. 518a
Tilton, R. 655a
Tinke, A. P 761a, 1046a
Tjaden, U. R 761a, 1046a
Tobkes, N. 615a
Todd, J. F. J. 704a, 705a, 925a
Todd, P. J. 222a, 253a, 1089a
Tomassian, A. D. 623a
Tomer, K. B. 9a, 50a, 543a
743a, 888a, 1051a
Tomlinson, A. J. 399a, 580a, 833a
843a
Tomlinson, M. 628a
Tomy, G T. 143a
Tonn, G. R. 559a
Tornaeus, J. 136a, 969a
Tortajada, J. 477a
Tosh, R. 1021a
Toto, J. 489a
Townsend, R. R. 88a
Trager, W. F. 565a
Traldi, P. 385a, 446a, 795a
Tran, T. B. 279a, 502a
Trang, C. K. 629a
Treuheit, M. J. 81a
Trimble, L. 341a

INDEX OF AUTHORS PAGE NO

Trudell, M. L. 1072a
Truscello, A. M. 110a
Tsao, R 213a, 909a
Tsarbopoulos, A. 101a, 267a, 357a
Tseng, J.-L 364a, 382a
Tuinman, A. A 506a
Tulich, L J. 64a
Tullius, M. 109a, 276a
Turecek, F. 279a, 502a, 625a
756a, 927a
Turner, C. A. 175a, 798a
Turteltaub, K. 251a
Turteltaub, K W. 22a
Tyagarajan, K. 88a
Udseth, H. R. 1045a
Uhrich, M. 291a, 386a
Uhrig, M. S. 567a
Uliana, P. 862a
Umeda, Y. 46a
Unger, S E. 52a, 542a, 603a
Urban, D. T. 439a
Urtti, A 866a
Vainiotalo, P. 1000a
Vairamania, M. 484a
Vaisar, T 980a
Van Amsterdam, M. W. 478a
Van Berkel, G. 207a, 749a, 767a
931a, 1068a
Van Breemen, R. B 345a, 517a
841a
Van de Werken, G. 257a
Van Den Berg, K. J 179a
Van Der Greef, J. 77a, 286a, 761a
1046a
Van Der Hoeven, R. A. M. 77a, 761a
Van Dorsselaer, A. 104a, 578a
869a, 878a
Van Halbeek, H. 84a, 86a, 89a
Van Koppen, P. A. M. 300a
Van Soest, R. 11a
Vanslyke, S. J. 766a
Vargas, R. R. 712a
Varghese, J. 1041a
Vartanian, V. H. 452a, 713a
Vath, J. 264a, 425a, 881a
Vega, O. 389a
Vela, N. P. 388a
Vellanki, J. 229a
Venczel, E. 23a
Venkatramani, C. J. 805a
Ventura, F. 112a
Verentchikov, A. 4a, 434a
Verner, P. 95a
Vertes, A. 666a, 678a, 777a
Vestal, M. L. 656a
Vestal, M. V. 733a
Vestling, M. M. 76a, 779a

INDEX OF AUTHORS PAGE NO

Vetters, H.-P. 645a
Victorine, T. 812a
Vidavsky, I 492a
Visentini, J. 219a, 220a
Visor, J 65a
Vlasak, P. R. 938a
Vogel, J S 22a
Vogel, J. 251a
Vogele, K. E. 1080a
Volk, K. J. 42a, 66a, 69a
296a, 310a, 895a
Volkmann, R. A. 618a
Vollmer, D L 178a, 488a
Von Helden, G. 301a, 508a, 1084a
Von Hippel, P. G. 266a
Voorman, R. L. 321a
Voragen, A. G J. 77a
Vorm, O. 621a
Vouros, P. 34a, 67a, 248a, 252a
369a, 737a, 1057a
Voyksner, R. D 38a, 290a, 461a
1044a
Vrbanac, J. J. 560a
Wachs, T. 45a
Wada, Y 372a
Wade, T. L. 122a
Wagenmann, M. 339a
Wagner, D. S. 387a, 592a
Wahl, J H 1045a
Wahl, M. C. 471a, 650a
Walder, A J. 818a
Walder, R. M. 429a
Walker, S. 380a, 658a
Walla, C. A. 152a
Wallace, S. K. 119a
Walls, F. C. 937a
Walsh, M T. 138a
Walsh, J. S. 52a
Walsh, K. A. 885a
Walter, B. 553a
Walther, B. 318a
Walton, T. J. 256a
Wampler III, F. M. 591a
Wanczek, K. P. 465a, 466a, 644a
707a, 750a
Wang, B H. 660a
Wang, C. R. C 718a
Wang, J. 585a, 628a, 844a
Wang, J.-S. 504a
Wang, M. 463a
Wang, Y. 466a, 690a
465a, 707a
Wang, Y. K. 408a, 903a
Wang, J.-P. 525a
Wang, K. 602a
Wang, L. 68a
Wang, M. 474a, 688a, 698a

INDEX OF AUTHORS PAGE NO

Wang, P. 545a
Wang, P. P. 170a, 798a
Wang, R. 380a, 658a, 883a
Wang, Y. 465a, 707a
Ward, B. 313a
Ward, E. E. 169a
Watanabe, C. 421a, 750a
Watson, C. 899a
Watson, E. 84a, 86a, 89a, 898a
Watson, C. H. 722a, 823a, 825a
1093a
Watson, D. C. 613a
Watson, J. T. 14a, 436a, 541a
585a, 889a
Watteyne, B. 439a
Watts, P. 704a
Waugh, R. J. 1018a
Webb, C 807a
Weber, G. L. 563a, 564a
Webster, C. 1067a
Wehmeyer, K. R 64a
Weigt, D. 651a
Weinberger, S. R. 775a
Weinmann, W. 743a
Weintraub, S. T. 335a, 557a
Weir, M R. 260a, 446a
Weiss, G. 645a
Weisz, A. 137a
Wellemans, J. M. Y. 916a
Weller, R. R. 467a
Wells, G. 463a, 474a, 688a
Wells, G. J. 790a
Wenclawiak, B. W. 1012a
Wendt, H. R. 782a
Wentland, J. 838a
Wentzell, P. D. 766a
Werner, J. A. 507a
Wesdemiotis, C. 29a, 280a, 283a
496a, 499a, 503a, 1011a,
West, A. 379a
Westmacott, G. 434a
Westmore, J. B. 143a, 677a, 955a
1012a
Westra, J G. 257a
Wetherold, J. 430a
Wexler, A. S. 804a, 944a
Wheelan, P. 575a
White, M. A. 653a
Whitehill, A. B. 972a
Whitehouse, C. 16a
Whitehouse, C. M. 287a, 746a
Whitehouse, L. W. 573a
Whiteley, L. O. 328a
Whitney, J. L. 69a
Whittal, R. 672a
Wichmann, J. K. 549a, 550a
Wiedmann, F. A. 29a, 283a, 499a

INDEX OF AUTHORS PAGE NO

Wiehr, D 890a
Wiezorek, B 644a
Wight, H. 759a
Wilkins, C. L. 148a, 359a, 413a
783a, 1096a
Williams, J. C. 697a
Williams, T. D. 932a
Williams, E. R. 457a
Williams, J. D. 498a, 709a
Williams, P. 659a, 661a
664a
Williams, S 191a
Williams, T. L. 692a
Willoughby, R. C. 765a, 770a
1049a
Wilson, R. G. 1087a
Wilson, S. R. 1061a, 1069a, 1070a
Wiltshire, N. 857a
Winans, R. E. 524a
Windig, W. 149a
Winger, B. E. 3a, 8a, 681a, 768a
Winniford, B. 19a
Winter, C. K. 313a
Wise, M. B. 126a, 438a
Witkop, G. 156a
Witkowska, H. E. 381a
Witter, A. E. 403a
Wolf, S. 248a
Wollnik, H. 929a
Wong, C. M. 814a
Wong, C.-H. 106a
Wong, S. C. 421a
Wood, J. M 527a
Wood, T. D. 650a, 699a
Wood, A. J. 234a
Wood, K. V. 234a, 235a
Wood, S. 354a
Woodard, C. L. 857a
Woods, A. S. 359a, 604a
Woolfitt, A. R. 218a, 422a, 754a
1066a
Wouters-Tyrou, D. 578a
Wronka, J. 750a, 825a, 899a
Wu, H. 583a
Wu, H.-F 162a, 163a, 192a
Wu, J. 200a
Wu, K. J. 437a, 676a
Wu, M. 731a, 816a
Wu, W. N. 51a, 845a
Wu, Y. 1061a, 1069a, 1070a
Wu, Q. 1022a
Wu, Z. 753a, 879a
Wycherley, D. 400a, 896a
Wysocki, V. H. 27a, 912a, 914a
1019a, 1026a, 1027a
Wysocki, V. 1025a
Xiang, X. 689a

INDEX OF AUTHORS	PAGE NO
Xu, X.	1072a
Xu, Y.	1072a
Yamada, H.	168a
Yamashita, K.	371a
Yan, L.	364a
Yan, Y.	387a
Yang, S. S.	187a
Yang, Y. J.	1030a
Yang, C.-Y.	365a
Yang, W.-J.	234a
Yates, N. A.	444a, 715a
Yates, H	939a
Yates III, J R	695a
Yee, A.	955a
Yergey, J. A.	340a, 341a, 346a
	570a
Yeung, B.	67a, 369a
Yip, T -T	416a, 417a, 418a
	781a
Yong, M S	636a
Yoshida, H.	250a
Yoshizawa, T	375a
Yost, R A.	55a, 113a, 444a, 445a
	527a, 622a, 693a, 711a, 712a
	715a, 716a, 801a, 982a, 983a
Young, M.	266a
Young, N M	613a
Young, R.	340a, 346a
Yu, C.-P.	981a, 1013a
Yu, X	167a, 879a
Yu, Z.	886a
Yu, Q.	11a, 611a
Yu, W.	264a, 425a, 881a
Yuen, C. T.	90a
Yungwirth, T	415a
Zagloul, E.	44a
Zagorevskii, D. V.	285a, 493a
Zaia, J.	358a
Zaluzec, E. J	436a, 889a
Zamboni, R.	570a
Zamecnik, J.	103a
Zare, R. N.	186a, 428a, 429a
	755a
Zeller, L. C.	719a
Zha, Q.	641a
Zhang, J. Y	844a, 851a, 853a
Zhang, T.	177a
Zhang, W.	415a, 1008a
Zhang, X.	1039a
Zhang, J.	846a, 847a
Zhang, L.	805a
Zhang, M. Y.	75a, 500a
Zhang, Z.	593a, 595a
Zhao, H	512a, 1016a, 1017a
Zhao, R.	491a

INDEX OF AUTHORS	PAGE NO
Zheng, Y.-J.	486a
Zhou, J.	677a, 776a
Zhou, Z.	92a, 321a
Zhu, H.	900a
Zidarov, D.	219a, 220a
Ziffer, H	338a
Zirrolli, J. A	515a, 575a
Zollinger, M.	233a
Zou, G.	390a
Zoubarev, R.	232a, 915a
Zuccato, E.	61a

INDEX OF KEYWORDS PAGE NO

2 groups
2,3,6-Tribromoaniline 137a
252 Cf-PDmS 876a
5-Lipoxygenase 341a
AB Initio 308a
APCI 12a, 15a, 49a, 120a,190a
291a, 295a, 319a, 326a, 389a, 576a
648a, 769a, 987a, 1066a, 1074a
APCI-MS/MS 988a
API 794a, 1083a
API/APCI 392a
API/Ionspray 1063a
Ab Initio Calculations 974a
Abecarnil 552a
Abstraction, Hydrogen 1038a
Accelerator M/S 23a
Accurate Mass 750a, 1066a
Acid 393a, 1010a
Acid Bile 846a
Acid-Base (Aqueous) 742a
Acids 1058a
Acids, Amino 63a, 195a, 384a, 558a
588a, 674a, 842a, 850a
855a, 1061a
Acids, Bile 328a, 572a, 847a
Acids, Fatty 492a, 496a, 517a
528a
Acids, Nucleic 244a, 270a
Acids, Organic 63a, 72a, 336a
854a, 1009a
Acycarnitines 444a
Acyl Glucuronide 335a
Acylated Peptides 590a
Acylcarnitines 540a, 842a
Addition 976a
Additives 402a, 538a
Additives Polymers 1094a
Adduct Ions 701a, 969a
Adduct 22a, 244a, 247a, 248a
251a, 252a, 254a, 916a
965a, 995a
Adducts, Protein 367a, 870a, 1058a
1059a
Adducts, Radical 322a
Aerosols 419a, 640a, 765a, 770a
780a, 800a, 804a, 944a, 946a
Affinity 184a
Affinity, Binding 167a
Affinity, Cation 164a, 165a, 995a
Affinity, Electron 299a
Affinity, Proton 185a, 199a, 200a
674a, 1009a
Air Sensitive Compounds 1033a
Alcohols 58a, 970a
Alcohols-Chlorophenols 988a
Aldehydes 367a, 392a
Aldose-ketose 486a

INDEX OF KEYWORDS PAGE NO

Alkali Adducts 1015a
Alkali Metals 684a
Alkaloids 311a, 316a, 396a
965a
Alkanes 307a, 1038a
Alkylation 1006a
Alkylbis(trifluoromethyl) 136a
Allergy 339a
Allyl halide 973a
Amines 206a, 211a, 293a, 311a
513a, 740a, 850a
Amino Acid 110a
Aminoglycoside 38a, 59a
Amylin 603a
Analysis 62a, 139a, 546a
568a, 569a, 631a
Analysis - Environmental 126a, 389a
Analysis - Pollutants 126a
Analysis Exhaust 389a
Analysis Mixture 406a
Analysis Protein 903a
Analysis Quant. 647a
Analysis Trace 957a
Analysis, Drug 53a, 61a, 64a, 287a
292a, 319a, 326a, 394a, 541a
542a, 545a, 553a, 554a, 559a
562a 563a, 564a, 576a, 769a
808a, 838a, 859a, 1062a
Analysis, Elemental 635a, 721a
722a, 723a, 727a, 730a, 731a
732a, 816a, 817a, 819a, 822a
823a, 825a
Analysis, Environmental 115a, 116a
117a, 119a, 129a, 131a, 133a
134a, 143a, 398a, 401a, 403a
404a, 419a, 455a, 624a, 629a
630a, 634a, 635a, 636a, 640a
643a, 646a, 730a, 734a, 803a
804a, 805a, 807a, 809a, 813a
1088a
Analysis, Essential Oils 148a, 406a
Analysis, Exhaust 120a
Analysis, Explosives 808a
Analysis, Fuel 206a, 524a
Analysis, Microparticle 419a, 429a
640a, 804a, 944a, 800a
Analysis, Mixture 19a, 143a, 151a
202a, 268a, 674a, 805a, 906a
922a
Analysis, Multielement 729a, 807a
954a
Analysis, Nonvolatiles 222a, 441a
Analysis, On-Line 208a, 209a, 294a
582a, 749a, 804a, 944a
Analysis, Organic 231a, 634a, 643a
854a, 991a, 1009a, 1088a

INDEX OF KEYWORDS PAGE NO

Analysis, Pharmaceutical 34a, 54a
64a, 71a, 319a, 325a, 327a
507a, 554a, 848a
Analysis, Pollutants 114a, 115a
116a, 135a, 143a, 403a
449a, 988a
Analysis, Protein 9a, 159a, 408a
611a, 654a, 894a, 899a, 1057a
Analysis, Quantitative 34a, 103a
273a, 322a, 327a, 328a, 332a
565a, 769a
Analysis, Surface 231a, 634a
643a, 806a, 1088a, 1090a
Analysis, Tissue 131a, 251a
566a, 893a
Analysis, Trace 566a, 733a, 807a
808a, 857a
Analysis, Ultratrace 23a, 24a
129a, 647a, 700a, 734a
Analysis, Ultratrace anal 404a
Analysis, Volatile Organ. 19a, 113a
125a, 395a, 629a, 646a, 864a
Analysis-Drug Metabolism 833a
Anions 180a, 245a, 500a, 616a
958a, 962a, 986a, 990a, 1084a
Antiaromaticity 308a
Antibiotics 239a, 420a, 576a
608a, 614a, 860a, 871a, 964a
1051a, 1053a, 1054a
Antibodies 308a, 1077a
Antiviral Activity 840a
Anxiolytic 44a
Aquatic Environmental 809a
Aqueous Solution 742a
Arachidonic Acid 561a
Aromatics 193a, 206a, 500a
968a, 1038a
Aromatics Polycyclic 112a, 133a
428a, 429a, 476a, 989a, 995a
Array Detector 422a
Arrival-time Distribut. 300a
Arsenium cations 1033a
Asp-Pro 425a
Asphalt 204a
Automation 149a, 647a, 842a
952a
Azo-dyes 117a
Bacitracin 909a
Bases 1059a
Bees 405a
Benzene 125a
Benzodiazepines 569a, 861a
Biliprotein 617a
Binding energy 300a
Biological MS 312a, 617a
Biological Matrix 323a

INDEX OF KEYWORDS PAGE NO

Biomarkers 22a, 144a, 322a
367a, 418a, 870a
Biomaterials 16a, 224a, 258a
332a, 334a, 360a, 366a, 413a
426a, 654a, 673a, 681a, 793a
893a, 1080a, 1091a
Biopolymers 81a, 418a, 433a
Bitumen 207a
Blots 415a
Bond Strengths 298a, 301a, 971a
Bond, Peptide 195a, 383a
Borocations 309a
Breast Implants 533a
Bridge, Disulfide 349a, 677a, 881a
889a
Brimonidine 48a
Buspirone 556a
C-Glucosides 80a
C2H4 2+ 483a
CAD 1028a
CAE 762a
CE 9a, 399a, 400a, 743a, 749a
833a, 895a, 896a, 952a, 1046a
1057a, 1079a
CE-MS 398a
CE/CZE 1056a
CF-LSIMS 341a
CI 126a, 170a, 196a, 210a
477a, 513a, 516a, 569a, 630a
639a, 688a, 736a, 845a, 854a
859a, 897a, 965a, 972a, 984a
989a, 991a, 994a
CID 65a, 96a, 97a, 178a, 180a
243a, 259a, 261a, 271a, 283a
294a, 304a, 317a, 369a, 400a
446a, 463a, 474a, 491a, 493a
497a, 516a, 518a, 519a, 580a
719a, 756a, 844a, 846a, 847a
853a, 858a, 860a, 879a, 919a
925a, 928a, 929a, 931a, 932a
933a, 960a, 970a, 980a, 989a
1006a, 1021a, 1029a, 1051a
1052a, 1081a
CID, High Energy 410a, 496a, 503a
620a, 753a, 886a, 1017a
CID, Ion Fragmentation 515a
CID, Low Energy 39a, 49a, 298a
366a, 685a 711a, 717a, 838a
918a, 969a, 1014a
CID, High Energy 358a, 512a, 917a
920a, 969a, 1016a
CRIMS 124a, 337a, 554a, 556a
558a
CZE 52a, 248a, 252a, 420a
457a, 546a, 755a, 916a
Calcul'ns, Ion Trajector 158a, 462a
464a, 689a, 710a, 799a, 951a

INDEX OF KEYWORDS PAGE NO

Calculations, Theoretical 28a, 464a
489a, 777a, 799a
Calculations 979a
Calculations, Ab Initio 199a, 502a
961a 1025a, 1026a, 1027
Calculations, MO 282a, 696a, 1000a
Calixarene 167a
Calmodulin 265a
Cancer Treatment 70a
Capillary 1047a
Capillary Electrophoresis 203a
1041a, 1045a
Capillary HPLC 378a, 618a, 1078a
Carbamates 391a, 985a
Carbohydrates 63a, 78a, 81a, 82a
87a, 88a, 91a, 92a, 93a, 94a
96a, 97a, 98a, 100a, 102a, 104a
106a, 109a, 198a, 274a, 275a
276a, 612a, 1060a, 1079a
Carbonyls 180a
Carboxylic Acids 203a, 967a
Carboxypeptidase 903a
Carcinogens 206a, 248a, 251a
252a
Carotenoids 841a
Catalysis 174a, 1091a
Catecholamine Metabolites 35a
557a
Cathepsin B 356a
Cation Attachment 166a
Cations 512a, 849a, 970a, 1065a
Cerebrosphinal Fluids 70a
Charge Exchange 192a, 484a
914a, 1007a
Charge Remote 358a
Charge-Trans.Complexation 1068a
Charge Transfer 177a, 299a
484a, 1020a
Charge State 750a
Charge, Multiple 271a, 743a
921a, 936a, 1029a
Chelates 736a, 1012a
Chemical Ionization 321a
Chemical Reactions 66a
Chemometrics 133a, 144a, 150a
Chiral Recognition 164a, 168a
923a
Chlorine dioxide by-prod. 127a
Chloroflexus thioredoxin 265a
Chloroformates 585a
Chlorosulfonated 532a
Choline 234a, 924a
Chromatography 16a, 119a, 147a
606a, 734a, 816a, 738a,
Chromatography, Affinity 601a
Chromophores 653a
Cichloromethane 1039a

INDEX OF KEYWORDS PAGE NO

Cl 17a
Clincial Chemistry 418a
Clinical 381a
Clinical Urine Sample 549a
Cluster Formation 996a, 1036a
Cluster, Proton Bound 1009a
Clusters 455a, 508a, 509a, 718a
752a, 940a, 1003a, 1004a
1013a, 1028a, 1036a, 1084a, 1085a
Clusters, Ionic 226a, 306a, 971a
1002a, 1011a
Coal 441a
Coal Fly Ash 628a
Cobalt 275a
Collision 482a
Collision Cell 812a, 905a
Collision Induced Dis. 501a
Collision, High Energy 360a, 502a
Collision, Low Energy 193a, 365a
748a
Collision, Surface 1023a, 1090a
Collision-Induced Dis. 194a, 263a
284a
Collisional Activation 1020a
Collisional Stabilization 443a
796a
Collisions, Reactive 27a, 183a
193a
Collisions, Surface 27a, 492a
1022a
Combustion 623a
Complex 487a, 880a
Complex, Ion-Neutral 168a, 477a
478a, 479a, 485a, 1000a, 1034a
Complex, Ionic 409a
Complex, Non-covalent 6a, 106a
164a, 904a
Complexation 106a, 162a, 168a
Complexes 869a
Composting 633a
Compound-type Dist. 212a
Compressed Chromatography 14a
Computational Methods 150a, 480a
813a
Computer 148a, 156a, 956a
Computer Database 153a
Computer Library 641a
Computer Modeling 376a, 481a, 692a
777a, 710a
Computer Program 145a,149a, 156a
157a, 159a, 245a, 594a, 595a, 907a
917a, 421a
Computer Simulation 447a, 448a
689a, 925a, 951a, 710a
Condensed Phase 217a, 237a
Cone-Nozzle Dissociation 909a

INDEX OF KEYWORDS PAGE NO

Conformation 83a, 592a, 615a
1020a
Conformation, Protein 6a, 7a, 593a
607a, 751a
Conformations 352a
Conjugates 312a
Conjugation 43a, 317a, 334a, 543a
655a
Contaminants 122a
Continuous 539a
Continuous Flow FAB 95a, 316a
Continuous-Flow MALD 18a, 671a
672a
Continuous-flow LSIMS 312a
Contour Plots 623a
Cortisol 68a
Coulomb Effect 442a
Covalent Adduct 335a
Cross Sections 191a, 905a
Cross-linking 414a, 894a
Crown Ether 167a
Cruzain 886a
Cryptands 165a
Curtain Gas 1050a
Curve Fitting 147a
Curves, Breakdown 627a
Cyclic Peptides 316a
Cyclization 481a, 966a
Cycloaddition 476a, 1069a
Cycloalkanes 1038a
Cyclodextrin 74a, 110a, 329a
Cystine 885a
Cytokines 1055a
D5-Glycerol 510a
DCI 210a, 528a, 552a, 994a
1085a
DNA 246a, 248a, 251a, 252a, 253a
272a, 657a, 660a, 786a, 787a
DNA-Adducts 240a
DNA-Protein Crosslinking 260a
DSP Toxins 1063a
Data Analysis 155a, 656a, 907a
956a
Data Base 156a, 596a, 852a, 899a
Data System 154a, 156a, 956a
Database 153a, 159a
Debrominated 48a
Dechlorination 128a, 221a, 494a
Decomposition 857a, 1097a
Deconvolution 14a, 17a, 122a
150a, 155a, 813a
Degradation 118a, 239a, 622a
666a
Degradation (Thermal) 293a
Degradation, Edman 588a
Deoxyadenosylcobalamin 46a
Deoxynucleotides 248a, 788a

INDEX OF KEYWORDS PAGE NO

Depth Profile 1087a
Derivation 392a
Derivatives 1006a
Derivatization 58a, 71a, 95a
117a, 118a, 128a, 313a, 325a
338a, 343a, 350a, 358a, 541a
562a, 583a, 584a, 585a, 767a
846a, 903a
Des-Methyl Danofloxacin 547a
Desorption 98a, 226a, 428a
429a, 434a, 522a, 523a, 653a
760a, 914a, 953a, 1010a
Desorption, Thermal 204a, 210a
Detection Limit 1046a
Detection, High Mass 230a, 434a
650a, 949a
Detector, Array 13a, 729a
Detector, Focal Plane 13a, 758a
Detector, Tim-Array 943a
Detector, array 916a, 937a
Detergents 581a
Deuterium Labelling 478a
Diamines 856a
Diarrh.Shellfish Poison. 1063a
Diazo Compounds 1061a
Dications 482a, 483a
Digest Proteolytic 581a, 599a
779a
Digest Tryptic 373a
Digests 355a
Digests Enzymatic 379a, 408a
415a, 602a, 606a, 607a, 903a
Digests, Proteolytic 345a
Digests, Tryptic 779a, 921a
Dimers 8a, 349a, 757a
1033a
Dimer, Noncovalent 351a
Dimer/Trimer 528a
Dimethylaminomethylene 495a
Dinitrotoluene 705a
Diols 923a
Dioxins 129a, 132a, 811a
Dipole Stabilized Ion 505a
Diradicals 29a, 283a, 307a
Disaccharides 198a, 696a
Discharge, Corona 120a
Disease, Metabolic 572a
Dissociation 177a, 425a, 487a
919a, 1028a
Dissociation CID 106a
Dissociation Kinetics 511a
Dissociation Unimolecular 489a
493a, 677a, 955a, 1002a
Dissociation, Ion-Induced 699a
Dissociation, Surface-Ind 912a
Distonic Ions 26a, 30a, 975a
978a

Distribution Function 122a
Distribution, Velocity 191a, 1008a
Distribution,Charge Stat 592a
742a, 1058a, 1059a
Disulfide Bridge 354a, 882a
Disulfides 618a, 885a
Diuretic Hormone 368a
Doramectin 548a
Double Charge Transfer 483a
Drinking water 127a
Droplet Formation 765a, 770a
Drug Analysis 343a
Drugs 62a, 566a
Dyes 137a, 220a, 223a, 398a
504a, 756a, 911a 1008a
Dynorphin Peptides 836a
ECNCI 240a, 257a, 320a, 338a
568a, 569a, 851a, 990a
EI 17a, 58a, 126a, 201a, 328a
473a, 507a, 537a, 569a, 587a
627a, 637a, 736a, 845a, 857a
980a, 981a, 992a, 995a
ESI 1a, 2a, 3a, 4a, 5a, 6a, 7a, 8a
9a, 11a, 12a, 16a, 34a, 35a 36a
38a, 39a, 41a, 47a, 52a, 76a, 77a
85a, 88a, 91a, 96a, 97a, 100a
109a, 111a, 146a, 207a, 237a
245a, 247a, 252a, 254a, 260a
272a, 276a, 290a, 291a, 294a
318a, 343a, 347a, 348a, 349a
350a, 353a, 360a, 366a, 370a
371a, 372a, 373a, 376a, 377a
378a, 382a, 386a, 387a, 391a
397a, 399a, 400a, 401a, 422a
443a, 454a, 457a, 461a, 469a
540a, 541a, 542a, 543a, 546a
547a, 548a, 552a, 553a, 580a
581a, 588a, 592a, 598a, 599a
601a, 603a, 605a, 609a, 610a
611a, 612a, 614a, 615a, 616a
618a, 636a, 648a, 720a, 732a
740a, 742a, 743a, 744a, 745a
749a, 750a, 751a, 752a, 753a
754a, 755a, 756a, 758a, 763a
764a, 765a, 770a, 796a, 834a
835a, 867a, 870a, 873a, 875a
879a, 884a, 896a, 897a, 899a
902a, 903a, 904a, 905a, 906a
907a, 909a, 918a, 919a, 921a
936a, 1014a, 1015a, 1019a, 1030a
1032a, 1033a, 1040a, 1042a, 1043a
1044a, 1046a, 1050a, 1051a, 1052a
1056a, 1057a, 1058a, 1061a, 1062a
1064a, 1065a, 1067a, 1068a, 1069a
1070a, 1071a, 1073a, 1077a, 1078a
ESI Ion Formation 742a
ESI MS 368a

ESI source 1040a
ESI, Negative 82a, 244a, 270a
867a, 1044a, 1059a, 1065a
ESI-MS 37a, 203a, 351a, 596a
600a, 746a, 1055a
ESMS 104a, 578a, 869a, 878a
Education 157a
Eicosanoids 346a, 844a, 851a
853a
Elastase 1078a
Electrochemical Ion. 1068a
Electrochromatography 57a
Electrodeposition 725a
Electron Affinity 181a
Electron Beam Ion Trap 703a
Electron Capture 482a, 557a, 856a
986a
Electron Detachment 704a
Electron Monochromator 811a
Electron Multiplier 1075a
Electronic States 300a, 302a
Electrophile 983a
Electrophoresis 408a, 421a, 436a
784a, 415a
Electrospray 32a, 33a, 37c, 40a
45a, 59a, 93a, 101a, 102a, 258a
267a, 271a, 274a, 275a, 329a
335a, 352a, 355a, 356a, 357a
364a, 381a, 591a, 617a, 741a
747a, 771a, 793a, 794a, 831a
839a, 868a, 874a, 895a, 1020a
1028a, 1029a, 1041a, 1045a 1048a
1053a, 1054a, 1060a, 1072a
Electrospray Ionization 10a, 767a
768a, 908a
Elemental 724a, 725a, 821
Elemental Analysis 458a, 726a
Emission, Second. Electr.230a, 757a
Emission, secondary ion 226a, 949a
Enantiomers 83a, 110a, 851a, 923a
Enantioselec. Glucuronid. 333a
Endothermic Reaction 192a
Energy Deposition 1024a
Energy Transfer 304a, 491a, 912a
997a, 1021a
Energy resolved MS 969a
Energy, Activation 204a
Energy, Dissociation 298a, 301a
685a
Energy, Excess 487a
Energy, Internal 196a
Enkephalins 382a
Environmental 123a, 124a, 289a
641a, 806a, 985a
Environmental Analysis 814a
Environmental Monitoring 136a
Enzymatic digests 618a

Enzymes 42a, 78a, 356a, 586a
596a, 614a, 872a, 892a, 897a
Enzyme Digests 10a
Enzyme-Inhibitor Complex 1078a
Epoxide 851a
Erythrocytes 887a
Essential Fatty Acids 561a
Ester, Fatty Acids 351a, 515a
1061a
Esters 490a, 958a
Etector, Array 817a
Ethers 984a
Ethylene Glycol 2a
Excitation 451a, 1024a
Excited State 302a, 483a, 652a
Experimental Design 406a
Explosives 700a, 705a, 808a, 811a
External Ion Source 681a
Extraction 123a, 327a, 328a
406a, 628a, 859a
FAB 69a, 82a, 84a, 86a, 87a, 89a
105a, 111a, 141a, 168a, 213a
214a, 215a, 219a, 220a, 223a
235a, 241a, 242a, 243a, 254a
255a, 256a, 261a, 313a, 340a
364a, 365a, 366a, 374a, 379a
404a, 410a, 486a, 518a, 519a
525a, 539a, 540a, 563a, 571a
577a, 584a, 585a, 586a, 590a
636a, 642a, 718a, 737a, 830a
844a, 845a, 846a, 847a, 849a
853a, 881a, 911a, 1012a, 1013a
1018a, 1073a
FAB Continuous Flow 50a, 61a, 67a
72a, 236a, 340a, 345a, 369a
572a, 593a, 607a, 760a, 841a
916a
FAB Dynamic 216a, 218a
FAB Desorption 160a
FAB,Continuous Flow 873a
FAB-MS 890a, 891a
FAB-MS-MS 73a, 375a
FAB/LSIMS 217a, 237a
FABMS 70a
FD 423a
FIMS 359a
FT-ICR 694a, 978a
FT-MS 28a
FTICR 302a, 454a, 768a, 977a
FTIR 148a
FTMS 3a, 30a, 31a, 164a, 165a
166a, 167a, 170a, 171a, 174a
175a, 176a, 177a, 179a, 181a
182a, 195a, 196a, 197a, 198a
199a, 249a, 250a, 305a, 309a
413a, 430a, 432a, 433a, 440a
442a, 443a, 448a, 450a, 452a

FTMS 457a, 460a, 462a, 464a, 466a
467a, 471a, 475a, 481a, 487a
488a, 497a, 511a, 591a, 650a
651a, 681a, 686a, 689a, 691a
692a, 699a, 702a, 703a, 707a
710a, 713a, 718a, 719a, 720a
722a, 750a, 751a, 752a, 783a
791a, 796a, 798a, 799a, 822a
823a, 825a, 899a, 958a, 962a
972a, 992a, 1000a, 1002a, 1003a
1007a, 1030a, 1031a, 1082a, 1096a
FTMS/LD 809a
FTiR 389a
Factor Analysis 150a, 151a
Factors, Response 721a
Fast GC-MS 14a, 20a
Fatty Acids 844a
Favonoids 312a
Fermentation 288a
Ferrocene 1023a
Field Desorption 212a, 1038a
Fingerprints 231a
Flavor compounds 922a
Flow 539a
Flow Injection Analysis 317a, 837a
Flowing Afterglow 161a, 169a, 189a
306a, 307a, 308a, 505a, 959a, 960a
Fluid 123a
Fluorescence 652a
Flux 223a
Foods 648a
Four-Sector MS/MS 511a
Fourier Trans. Ion Cyclo. 970a
Fragmentation 83a, 246a, 368a
388a, 431a, 446a, 507a, 632a
653a, 662a, 686a, 788a, 847a
848a, 858a, 863a, 872a, 876a
992a, 997a, 1028a, 1037a
Fragmentation Mechanism 92a, 478a
503a, 512a, 583a, 920a, 926a
981a, 1014a, 1015a
Fragmentation Pathway 29a, 69a
92a, 259a, 284a, 446a, 490a, 496a
499a, 501a, 503a, 504a, 515a
696a, 705a, 926a, 1011a, 1012a
Fragmentation Peptide 269a
580a, 589a, 595a, 599a, 918a
921a, 955a, 1014a, 1015a
Fragmentation, Thermal 855a
Fragmentation,chrg.remote 496a
Fullerenes 238a, 430a, 508a, 509a
912a, 913a, 1005a, 1006a, 1007a
1070a, 1082a, 1083a, 1084a, 1085a
1086a

INDEX OF KEYWORDS PAGE NO

Function Groups 69a, 187a, 220a 767a
Fundamentals 183a, 442a, 448a 465a, 650a, 687a, 791a
Furans 132a, 524a
GC 56a, 134a, 337a, 339a, 540a 557a, 564a, 738a, 805a, 829a 938a, 984a
GC transfer line 19a, 201a, 439a
GC-EIMS 863a
GC-MS/MS 627a
GC/EM/MS 811a
GC/MS 17a, 19a, 63a, 64a, 68a, 71a 112a, 117a, 118a, 121a, 125a 132a, 134a, 137a, 139a, 144a 148a, 150a, 201a, 206a, 257a 313a, 322a, 324a, 325a, 327a 328a, 332a, 336a, 338a, 344a 389a, 395a, 406a, 439a, 444a 459a, 468a, 474a, 507a, 514a 532a, 535a, 536a, 553a, 559a 560a, 561a, 562a, 565a, 566a 587a, 624a, 626a, 630a, 631a 633a, 638a, 639a, 641a, 647a 688a, 698a, 715a, 716a, 739a 813a, 839a, 850a, 851a, 854a 856a, 857a, 859a, 864a, 991a
GC/MS RI-Standard 136a
GC/MS/MS 931a
GC/MS/MS RI-Standard 136a
GC/MS/SIM 131a
GC/NCI-MC 323a
GC/NCIMS 342a
GCIMS 384a
GI (chemical ionization) 993a
GID (High energy) 993a
GSH Conjugates 831a
Ganefromycins 32a
Gas Chromatography 405a, 567a
Gas Phase 83a, 165a, 184a 411a, 905a, 960a, 981a, 1034a
Gas Sampling 623a
Gel Electrophoresis 937a
Gentamicin 59a
Geochemistry 144a
Geology 24a, 1082a
Glow Discharge 683a, 700a, 705a 721a, 722a, 723a, 724a, 725a 726a, 727a, 728a, 820a, 821a 822a, 823a, 824a, 825a, 930a 998a
Glucose 103a
Glucuronides 36a, 543a, 847a 853a, 1042a
Glutaredoxin 887a
Glutathione Conjugate 37a
Glutathiones 543a

INDEX OF KEYWORDS PAGE NO

Glycans 85a, 102a
Glycerol 510a
Glycinebetaine 234a
Glycines 199a
Glycoalkaloids 99a
Glycoconjugates 90a, 98a, 907a 1080a
Glycolipds 73a, 79a, 95a, 274a 522a
Glycols 76a, 78a, 81a, 84a, 86a 88a, 89a, 91a, 94a, 101a, 264a 274a, 370a, 371a, 372a, 386a 598a, 605a, 613a, 895a, 984a 1077a, 1081a,
Glycosidases 94a
Glycoside 87a
Glycosides 835a
Glycosylation 78a, 88a, 91a, 94a 108a, 263a, 372a, 385a, 609a
Growth Promoters 32a
Guadrupole MS 623a
Guanine 259a
H/D Exchange 583a
HFIP 323a
HIV 321a
HPLC 49a, 53a, 61a, 326a, 330a 401a, 556a, 793a, 838a, 886a 902a, 1066a
HPLC - capillary 11a, 67a, 72a 100a, 345a, 346a, 570a, 748a 834a, 841a, 922a, 1076a
HPLC, microbore 207a, 1042a
HPLC/MS 59a
Halocarbons 482a, 962a
Halogens 124a
Hemoglobin 381a
Heparin 85a
Herbicides 142a
Heteroatomic ions 973a
Heterocyclic 293a
Heterocyclic Aromatic Am. 648a
High Mass Ions 5a
High Purity Gas 957a
High Resolution 3a, 454a, 750a 768a
High Speed Data Process. 15a
High energy collision 233a
High-resolution 129a, 1048a
Highly Charged Ions 5a
Histones 260a, 578a, 906a
Honey 405a
Host-guest complexes 75a
Human 70a
Human Plasma 103a, 836a
Human Urine 329a
Hybrid 365a, 932a
Hybride Abstration 237a

INDEX OF KEYWORDS PAGE NO

Hydrazinolysis 100a
Hydroboration 1006a
Hydrocarbons 169a, 201a, 632a 783a, 989a
Hydrogen-bonding 163a
Hydrogen/Denterium Ex. 145a, 387a 414a, 592a, 593a, 607a, 1050a
Hydrolysis 119a, 256a, 374a
Hydroxyatrazine 404a
Hyperthermal 665a
Hypervalence 225a
ICP 731a, 818a
ICP/MS 458a, 628a, 807a
ICPMS 635a
ICR 792a
IMINOLS 282a
IR 1031a
IRMPD 1031a
Identification 868a
Image Processing 827a
Imaging, Microbeam 428a
Imaging, Secondary 224a
Imaging, Secondary Ion 222a, 1089a
Immobolization 436a
Immonium Ions 917a
Immun. Cromatography
Immunoaffinity Chrom. 65a
Immunoassay 65a, 892a
Immunology 377a
Impurity Profiling 310a
In Vivo 41a, 47a, 50a, 331a
Infrared Pyrolysis 644a
Infrared Spectroscopy 1039a
Inhibition 344a, 886a
Inhibitor 341a
Inorganic 1087a
Insecticide 810a
Insects 113a
Instrumentation 9a, 13a, 16a 140a, 208a, 209a, 210a, 230a 269a, 400a, 438a, 443a, 444a 448a, 452a, 461a, 462a, 466a 468a, 474a, 475a, 571a, 632a 668a, 690a, 706a, 707a, 713a 724a, 726a, 729a, 745a, 791a 796a, 802a, 821a, 828a, 896a 927a, 934a, 942a, 943a, 951a 954a, 1074a
Insulin 335a
Interface 388a, 556a, 1047a
Interface Voltage 1063a
Interface, Moving Belt 577a, 828a
Interferences 11a
Interleukin -12 264a
Intermediate, Reactive 960a
Intermediates 970a
Intramolecular interact 966a

INDEX OF KEYWORDS PAGE NO

Ion Chemistry 302a
Ion Clouds 472a
Ion Cooling 650a, 702a, 708a, 1003a
Ion Counting 758a, 830a
Ion Cyclotron Reson. MS 467a
Ion Deceleration 933a
Ion Deflection 684a
Ion Desorption 2a, 228a, 662a 670a, 680a, 765a, 770a, 775a
Ion Detection 230a, 440a, 526a 691a, 949a, 1075a
Ion Ejection 447a, 451a, 473a 639a, 688a, 689a, 692a, 697a 698a, 802a, 1008a
Ion Energetics 463a, 711a, 717a 776a
Ion Energies 704a
Ion Focusing 934a
Ion Formation 985a
Ion Fragmentation 1039a
Ion Imaging 224a
Ion Implantation 229a
Ion Injection 452a, 460a, 461a 471a, 683a, 700a, 710a, 714a 716a, 718a, 822a, 930a, 976a
Ion Isolation 446a, 451a, 453a 468a, 474a, 693a, 802a
Ion Loss 473a, 801a
Ion Mirror 4a, 776a
Ion Mobility 188a, 808a, 988a
Ion-Molecule 300a
Ion Molecule Chemistry 160a, 505a
Ion Molecule Reaction 175a, 194a 308a, 309a, 456a, 726a, 973a 974a, 975a, 976a, 978a 979a 981a, 1020a
Ion Pairing 849a
Ion Reactivity 176a, 179a, 190a 487a, 961a, 972a, 980a
Ion Remeasurement 798a
Ion Solvation 740a, 1010a, 1033
Ion Source 158a, 427a, 741a
Ion Spray 45a, 51a, 75a 794a, 871a
Ion Sputtering 1010a, 1024a
Ion Storage 440a, 460a, 461a 469a, 708a, 801a
Ion Structure 26a, 505a
Ion Suppression 1065a
Ion Trajectories 472a, 708a, 789a
Ion Trajectory Calc. 467a
Ion Transport 5a, 469a, 1043a

Ion Trap 271a, 322a, 444a, 447a
448a, 453a, 458a, 459a, 463a
469a, 474a, 630a, 632a, 682a
688a, 690a, 692a, 693a, 698a
700a, 701a, 702a, 703a, 711a
715a, 716a, 717a, 719a, 790a
793a, 794a, 795a, 801a, 926a
930a, 976a,
Ion Trap Electrodynamic 795a, 800a
Ion Trap MS 455a, 466a, 814a
Ion Trap Quadrupole 126a, 151a
192a, 383a, 438a 441a, 445a
446a, 451a, 453a, 461a, 468a
470a, 472a, 473a, 683a, 685a
687a, 697a, 706a, 708a, 709a
711a, 714a, 717a, 749a, 789a
791a, 800a, 802a, 803a, 806a
860a, 861a, 931a, 964a, 966a
967a, 968a, 982a, 983a, 991a
1029a
Ion Trap, el 465a
Ion Trapping 792a
Ion Velocity 232a, 670a, 680a
746a, 751a
Ion Yield 427a, 721a
Ion Enthalpies 26a
Ion Neutral Complexes 979a
Ion-Molecule Reactivity 174a
Ion-pairing 227a, 311a
Ionization 279a, 653a, 699a, 1049a
Ionization Efficiency 412a, 741a
761a
Ionization Energy 299a, 482a, 483a
484a
Ionization Mechanism 237a, 652a
667a, 668a, 699a, 740a, 764a
778a, 820a, 998a, 1037a
Ionization Multiphoton 1034a
Ionization Potential 997a
Ionization Process 663a, 740a
760a, 764a, 778a
Ionization Efficiency 1044a
Ionization, Chemical 476a, 639a
Ionization, Electrospray 942a
Ionization, Field 204a, 1097a
Ionization, High Pressure 722a
Ionization, Multiphoton 114a, 186a
773a,782a, 942a, 1035a
Ionization, Penning 820a, 997a
Ionization, Pulsed 419a, 987a
Ionization, Thermal 735a
Ionization, Field 530a
Ionization/single photon 437a
Ionophore 74a, 168a, 239a, 577a
Ions, Adduct 30a, 187a, 348a
397a, 498a, 967a, 991a, 996a

Ions, Distonic 27a, 28a, 29a, 31a
283a, 1000a
Ions, High Mass 4a, 691a, 720a
800a
Ions, Isomeric 185a, 241a
Ions, Metastable 479a, 489a, 515a
773a, 1011a
Ions, Molecular 411a, 459a, 480a
632a, 977a, 1027a
Ions, Product 475a, 955a
Ions, adduct 861a, 964a
Ionspray 42a, 43a, 49a, 53a, 106a
292a, 317a, 354a, 398a, 545a
608a, 613a, 732a, 741a, 748a
766a, 838a, 877a, 885a, 1043a
1079a
Ionspray MS 46a
Isolated State 1024a
Isomeric Ions 284a, 974a, 1026a
Isomerization 486a, 506a, 1039a
Isomers 102a, 151a, 166a, 185a
275a, 283a, 611a, 835a, 967a
968a, 980a, 982a
Isotachophoresis 203a, 1046a
Isotope 561a
Isotope Dilution 273a, 320a, 324a
330a, 565a, 646a, 727a, 734a
832a
Isotope Effects 189a, 383a, 479a
Isotope Enrichments 337a
Isotope Exchange 193a, 1001a
Isotope Ratio 24a, 735a, 818a
826a, 827a
Isotope Ratio MS 22a, 147a, 727a
728a, 733a, 734a, 738a, 825a
828a, 829a, 830a
Isotope Effects 303a
Isotope, Stable 332a, 553a, 554a
558a, 559a, 727a, 843a, 910a
Isotopes 977a
Isotope, Stable 926a
K+IDS 583a
KIDS 1092a
Keratines 893a
Keratinocytes 575a
Ketoconazole 573a
Ketones 987a, 1059a
Kinetic Energy 192a, 668a, 670a
680a, 751a
Kinetic Energy Release 155a, 489a
490a, 923a
Kinetics 138a, 174a, 183a, 184a
189a, 197a, 704a, 925a, 927a
958a, 968a, 1001a, 1002a
L-SIMS, Dynamic 1081a

LC 18a, 35a, 36a, 45a, 56a, 62a
97a, 141a, 142a, 214a, 247a
287a, 288a, 291a, 295a, 297a
311a, 314a, 315a, 319a, 320a
338a, 369a, 386a, 388a, 396a
470a, 542a, 547a, 548a, 576a
663a, 671a, 672a, 745a, 758a
762a, 769a, 828a, 840a, 866a
867a, 898a, 907a, 952a, 1043a
1047a, 1049a, 1062a, 1074a
LC, Anion Exchange 77a, 86a, 89a
LC, Capillary 38a, 52a, 91a, 143a
236a, 394a, 551a, 582a, 873a
874a, 1077a
LC, Microcapillary 294a, 370a
376a, 377a, 572a, 610a, 637a
762a, 841a
LC, Nanoscale Capillary 41a, 47a
LC, microcolumn 95a
LC,Anion-exchange 84a
LC-CRIMS 555a
LC-MS optimization 766a
LC-MS-MS 317a, 837a
LC-TSP-MS 985a
LC-MS sensitivity 766a
LC/ESI 94a
LC/MS 10a, 32a, 40a, 48a, 101a
290a, 296a, 310a, 312a, 314a
315a, 321a, 329a, 381a, 394a
535a, 540a, 544a, 545a, 582a
612a, 608a, 648a, 754a, 794a
839a, 1083a
LC/MS/MS 310a, 318a, 544a, 549a
550a
LD 162a, 170a, 196a, 197a, 430a
437a, 441a, 449a, 497a, 650a
657a, 676a, 733a, 783a, 798a
782a, 1086a, 1096a,
LDMS 600a
LIPID 1089a
LITD/FTMS 684a
LSI/MS/MS 924a
LSIMS 219a, 510a, 580a
LSIMS - continuous flow 346a
Label-stable 44a
Labeling 373a, 889a
Labeling, (41Ca) 23a
Labeling, Deuterium 279a, 305a
479a, 563a, 863a
Labeling, Isotope 22a, 332a, 492a
829a, 862a
Labeling, Stable Isotope 208a, 259a
273a, 336a, 379a, 854a, 993a
Lactams 62a
Lactram 964a
Large Molecule Ionization 272a

Laser 98a, 107a, 407a, 522a
523a, 671a, 672a, 778a, 785a
1096a
Laser Ablation 427a, 536a, 640a
817a, 944a, 1008a
Laser CO2 651a
Laser Desorption 154a, 455a, 663a
684a, 712a, 773a, 787a, 900a
948a, 1091a
Laser Desorption MS 836a
Laser Dye 1041a
Laser Ionization 786a
Laser N2 651a
Laser Vaporization 786a
Laser, CO2 114a, 432a, 433a
Laser, Microprobe 419a, 428a, 429a
Laser, Nd YAG 651a
Lead 736a, 815a
Leukotrienes 39a, 339a, 340a
346a
Leukotriene B4 575a
Lewisite 857a
Li-attachment 1032a
Library Searching 152a, 813a
Linked Scan 54a, 82a, 236a, 495a
518a, 572a, 910a, 936a
Linoleic Acid 561a
Lipid 39a, 276a, 324a, 346a
367a, 515a, 517a, 523a, 738a
844a, 858a, 865a, 1060a
Lipid A 431a
Lipid Modification 375a
Lipophilic 74a
Lipopolysaccharides 109a, 276a
431a, 1079a
Lipoxygenation 342a
Liquid Chromatography 613a, 937a
Liquid SIMS 60a, 79a, 218a
220a, 221a, 223a, 225a, 239a
334a, 528a, 551a, 573a, 619a
760a, 872a, 880a, 939a, 1005a
1019a
Liquid SIMS-Contin.Flow 570a
Liquid chromatography 289a
Lithium 54a, 910a
Locust 368a
Low energy collision 111a, 233a
Low-resolution 1048a
Lung Surfactant Proteins 351a

INDEX OF KEYWORDS PAGE NO

MALDI 18a, 78a, 79a, 81a, 107a
108a, 154a, 246a, 249a, 250a
264a, 268a, 343a, 359a, 370a
379a, 380a, 385a, 408a, 409a
410a, 411a, 412a, 413a, 414a
416a, 417a, 418a, 420a, 421a
422a, 423a, 424a, 431a, 432a
434a, 435a, 436a, 441a, 425a
426a, 437a, 526a, 529a, 596a
602a, 604a, 615a, 621a, 651a
652a, 654a, 655a, 656a, 657a
658a, 660a, 666a, 667a, 668a
669a, 670a, 671a, 672a, 673a
674a, 675a, 676a, 677a, 678a
679a, 680a, 695a, 713a, 714a
774a, 775a, 776a, 777a, 779a
780a, 781a, 784a, 788a, 793a
879a, 881a, 887a, 889a, 892a
893a, 894a, 897a, 898a, 899a
903a, 935a, 940a, 941a, 945a
947a, 949a, 952a, 1077a, 1080a
1093a, 1096a
MALDI MS 266a
MIP 124a
MNDO 486a
MO Calculations 975a
MS 56a, 97a, 141a, 291a, 339a
388a, 396a, 399a, 402a, 721a
757a, 765a, 770a, 834a, 835a
866a, 900a, 953a, 1047a, 1049a
1070a
MS High Resolution 58a
MS Ion Trap 704a
MS Magnetic Sector 9a, 12a, 218a
287a, 360a, 384a, 426a, 470a
551a, 933a, 934a, 939a
MS Peptide Mapping 266a
MS Quadrupole 209a, 241a, 261a
582a, 588a, 637a, 812a, 1051a
MS Time-of-Flight 4a, 16a, 17a
98a, 107a, 114a, 115a, 116a
154a, 155a, 295a, 423a, 431a
434a, 522a, 523a, 640a, 655a
657a, 677a 733a, 746a, 755a
776a, 778a, 780a, 782a, 915a
938a, 940a, 941a, 942a, 943a
946a, 947a, 949a, 950a, 954a
955a
MS Double Focusing 13a, 435a
729a, 817a, 934a, 989a
MS Energy-Resolved 484a
MS High Resolution 297a, 442a
562a, 720a, 730a, 852a, 996a
MS ICR 411a, 464a, 686a, 699a
799a, 822a, 825a

INDEX OF KEYWORDS PAGE NO

MS Ion Trap 51a, 125a, 290a, 295a
447a, 449a, 453a, 459a, 463a
509a, 638a, 690a, 698a, 712a
843a, 925a, 950a
MS/MS 28a, 33a, 36a, 39a, 40a, 42a
43a, 50a, 52a, 54a, 60a, 64a, 65a
66a, 67a, 72a, 76a, 79a, 85a, 87a
93a, 99a, 102a, 109a, 113a, 120a
135a, 141a, 144a, 187a, 239a
241a, 243a, 245a, 261a, 269a
288a, 292a, 296a, 304a, 314a
315a, 333a, 354a, 361a, 365a
374a, 376a, 377a, 433a, 438a
444a, 457a, 463a, 471a, 475a
491a, 500a, 506a, 510a, 516a
517a, 518a, 521a, 530a, 539a
545a, 547a, 548a, 563a, 564a
573a, 577a, 579a 580a 589a
590a, 595a, 599a, 603a, 610a
613a, 619a, 620a, 622a, 627a
636a, 638a, 682a, 685a, 715a
748a, 753a, 763a, 769a, 789a
803a, 812a, 814a, 833a, 840a
842a, 852a, 880a, 885a, 887a
909a, 910a, 911a, 913a, 915a
916a, 918a, 919a, 922a, 925a
928a, 929a, 930a, 932a, 933a
935a, 936a, 938a, 939a, 945a
955a, 961a, 974a, 993a, 998a
1009a, 1015a, 1021a, 1032a
1051a, 1053a, 1060a, 1063a
1064a, 1076a, 1080a, 1081a
MS3 (or MSn) 974a, 975a
MSIMS 190a, 282a, 383a, 445a, 498a
701a, 803a, 843a, 920a, 930a
Macrocycles 163a
Macrolide 348a, 545a, 577a, 1032a
Macrolides Antibiotics 837a
Maillard Chemistry 399a
Malondialdehyde 240a
Man Portable MS 439a
Marine Oil 924a
Mass Accuracy 159a, 426a, 442a
538a, 669a, 697a, 706a, 722a
947a, 994a
Mass Calibration 462a, 469a, 538a
706a, 712a, 940a, 941a, 947a
Mass Discrimination 450a, 691a
692a, 757a
Mass Exact 586a
Mass Profile Monitoring 131a
Mass Profile in SIM 624a
Mass Range 413a, 434a, 706a
712a, 719a
Mass Resolution 4a, 413a, 669a
714a, 719a, 790a, 823a, 934a
936a, 943a, 950a

INDEX OF KEYWORDS PAGE NO

Mass Spectrom 694a, 792
Mass Spectrometry 57a, 80a, 537a
Matrix Effect 217a, 222a, 421a
456a, 775a, 221a, 1089a
Matrix Reactions 519a
Matrix Structure 652a
Matrix Effects 105a, 849a
Matrix-Isolation 1039a
Maxam-Gilbert 660a
Maximum Entrophy 146a
Mechanism 308a, 771a, 963a
1097a
Mechanism Inhibition 221a, 1078a
Melanoidins 399a
Membrane Protein 363a
Membrane Unit 645a
Mercapturic acids 233a
Mercury 635a, 815a
Metabolic Disorder 46a
Metabolism 331a, 335a, 341a, 361a
567a, 831a, 840a, 843a, 846a
863a
Metabolites 36a, 43a, 44a, 48a
49a, 52a, 56a, 62a, 63a, 65a
72a, 134a, 292a, 294a, 318a
320a, 337a, 344a, 345a, 544a
546a, 553a, 549a, 550a, 554a
555a, 558a, 562a, 563a, 564a
570a, 573a, 574a, 575a, 603a
834a, 838a, 845a, 849a, 850a
852a, 853a, 862a
Metabolites LC/MS/MS 37c
Metal Complex Ions 175a
Metal Ion Chemistry 160a, 170a
Metal Ion binding 876a
Metal/Ligand Complex 160a
Metalloporphyrins 181a, 497a, 737a
Metalloprotein 7a, 877a
Metallothioneim 877a, 879a
Metals 96a, 116a, 162a, 169a
180a, 298a, 301a, 306a, 417a
723a, 733a, 815a, 877a, 880a
923a, 1016a, 1017a
Metastable 977a
Metastable Ions 284a, 478a, 501a
776a, 979a
Metastable atoms 997a
Methane CI 118a
Methylcobalamin 46a
Methylmalonic Acidemia 46a
Micorsomes 556a
Microanalysis 582a
Microcolumn Chromatog. 15a
Microdialysis 41a, 42a, 47a, 50a
344a, 832a, 836a
Microprobe, Organic 253a, 428a
429a

INDEX OF KEYWORDS PAGE NO

Microwave Plasma 124a, 337a, 388a
Milk 132a
Milk fat 517a
Miniaturized GC 645a
Mirror, Ion 773a
Mixed glyc.-D5-glyc.clus. 510a
Mixture Analysis 205a, 316a
Mixtures 207a, 843a
Mobile GC/MS 645a
Modeling Molecular 166a, 412a
1016a, 1017a
Models, Reactivity 477a, 513a
965a
Modified Cyclodextrin 75a
Modified Peptides 266a
Modular Sampling Systems 645a
Molecular Beams 20a, 665a, 761a
782a
Molecular Dynamic 186a, 191a, 304a
491a 1021a
Molecular Imaging 1094a
Molecular Recognition 60a, 162a
164a, 871a
Molecular Weight 60a, 527a
Molecular Weight Dist. 212a
Molecular Recognition 163a
Momentum Separator 761a
Monitoring - Air 438a, 439a
805a, 946a
Monitoring - Real Time 804a
Monitoring, Environmental 629a
803a
Monitoring, Real Time 19a, 208a
209a, 439a, 944a
Monlayer, Self Assembled 27a, 914a
1023a, 1025a, 1026a, 1027a, 1090a
Monolayer, Self-addressed 1019a
Monomers 1095a
Mosquitoes 113a
Mucin 100a
Mucopeptide Precursor 871a
Multiphoton Ionization 18a, 115a
116a, 662a, 785a, 1036a, 1037a
Multiple Charged Ions 382a
Multiple Collector MS 818a
Multiple Sample 213a
Multiply charge 906a
Multipoles 186a, 191a, 447a
698a, 932a
Multispectral id. 127a
Mycobacteria 73a
Mycocerosic Acids 73a
Myristate 375a
N-acetyl-cysteine conjug. 37a
N-Acetyl-P-Benzoquinone. 37a

NCI 71a, 103a, 135a, 307a, 325a
327a, 336a, 494a, 500a, 535a
550a, 565a, 736a, 815a, 855a
858a, 865a, 959a, 961a,
NMR 504a
NRMS 29a, 279a, 280a, 281a, 282a
283a, 284a, 285a, 492a, 493a
496a, 499a, 501a, 502a, 503a
625a, 927a, 1011a
Natural Products 51a, 66a, 296a
314a, 315a, 316a, 498a, 551a
835a, 840a, 994a, 1050a, 1080a
Nebulization 287a
Nebulizer 663a, 762a, 780a, 1050a
Negative Ion Chem. Ioniz 514a
Negative Ions 77a, 105a, 705a
767a, 771a, 1018a
Neuropeptide 41a, 344a, 382a, 619a
Neurotransmitters 850a
Neutral Fragmentation 407a
Neutralization 616a
Nicotine 56a
Nitric Oxide 120a
Nitrogen Compounds 297a
Non-Covalent Complex 347a, 348a
Non-Linear Resonance 801a
Non-covalent Complex 258a
Non-covalent Interaction 7a, 267a
357a
Non-volatile Compounds 289a
Nucleic Acids 673a
Nucleobases 241a, 243a, 261a
Nucleophiles 976a, 983a
Nucleoproteins 256a
Nucleotides 214a, 227a, 240a
243a, 254a, 255a, 257a
259a, 319a, 495a, 679a, 1044a
Nucleotide-Protein Cross. 266a
Nylon 436a
Oligoculeotides 660a
Oligomers 8a, 247a, 984a
Oligonucleotides 3a, 244a, 245a
246a, 247a, 249a, 250a, 270a
271a, 280a, 657a, 676a, 763a
787a, 788a, 1029a
Oligosaccharide 77a, 83a, 84a
85a, 86a, 88a, 89a, 90a, 92a
95a, 107a, 274a, 372a, 422a
605a, 696a,
On-Line LC-MS/ESI 809a
On-line Analysis 1056a
Opioid Peptide Precursor 364a
Optical Microspray 412a
Optics, Ion 933a
Optics, Laser 427a
Organic Guest 167a
Organo Metallics 401a

Organometallic 1072a
Organometallic 488a
Organometallics 176a, 179a, 182a
235a, 285a, 299a, 300a, 301a
394a, 397a, 476a, 488a, 626a
752a, 1071a, 1072a, 1073a
Organophosphate 627a
Organophosphorus 969a
Organosilanes 1025a
Orifice Potential 747a
Orthogonal Acceleration 15a, 731a
816a, 957a
Oxidation 219a, 367a, 430a
587a, 883a, 884a
Oxide Formation 735a
Oxidized Phospholipids 519a
PAHs 122a
PCB's 122a, 128a, 494a, 811a
812a, 990a
PCDD/Fs 131a
PCDTs 624a
PD 232a, 234a, 238a, 268a
353a, 604a, 621a
PDMS 597a, 600a
PFAI 323a
PFB 257a
PFB Derivatives 240a, 336a, 528a
557a
P-Benzo-Quinone 37a
P-Phenylenediamine 809a
Pancreatic Lipase 567a
Partical-Beam 402a
Particle - Beam 362a
Particle Beam 211a, 214a, 289a
320a, 321a, 330a, 338a, 362a
402a, 470a, 527a, 534a, 535a
537a, 622a, 637a, 663a, 739a
761a, 762a, 946a, 1049a
Peak Match 624a
Penicillins 38a
Penning Traps 792a
Peptides 6a, 145a, 159a, 170a, 194a
196a, 197a, 200a, 214a, 219a
226a, 263a, 268a, 269a, 273a
280a, 302a, 345a, 347a, 350a
352a, 355a, 359a, 361a, 363a
368a, 369a, 377a, 383a, 384a
386a, 409a, 411a, 422a, 424a
435a, 512a, 579a, 581a, 583a
585a, 586a, 590a, 595a, 596a
603a, 604a, 616a, 618a, 621a
653a, 658a, 667a, 674a, 743a
748a, 749a, 754a, 758a, 773a
779a, 873a, 876a, 880a, 884a
896a, 902a, 908a, 917a, 918a
919a, 920a, 928a, 932a, 937a
947a, 1001a, 1016a, 1017a, 1018a

Peptides 1019a, 1042a, 1041a
1056a, 1057a, 1076a
Peptide Sequencing 265a, 363a
Peptide Synthesis 375a
Peptide Pituitary 370a, 610a
Peptide, Cyclic 354a, 362a, 437a
678a, 882a
Peptides Modified 358a, 587a
594a, 601a, 872a, 891a, 1052a
1053a
Peptides Synthetic 432a, 589a
594a
Peptides, Opioid 1052a
Peptidoglycans 111a
Peptiduria 896a
Perfusion Chromatography 10a
Permethylation 242a
Peroctyl 74a
Peroxidation 293a, 865a
Peroxides 959a
Pesticides 135a, 400a, 468a, 630a
636a, 637a, 638a, 639a, 1066a
Petroleum 201a, 202a, 205a
403a
Petroleum Residua 212a
Petroleum, Polars 297a
Pharmaceuticals 290a, 291a, 330a
470a, 549a, 550a, 570a, 574a
832a, 845a, 848a, 861a, 862a
864a, 996a, 1044a, 1054a, 1089a
Pharmacokinetics 22a, 34a, 50a
329a, 559a, 837a
Pharmacology 363a
Phase I 318a
Phase II 318a
Phenobarbital 333a
Phenolic Lipids 73a
Phosphates 90a, 255a, 625a, 634a
Phosphine Sulphide 136a
Phospholipids 70a, 471a, 514a
518a, 519a, 520a, 521a, 523a
865a, 924a, 1060a
Phosphorylation 263a, 416a, 578a
600a, 612a, 619a, 620a, 747a
Phosphorylation Protein 408a, 415a
417a, 589a, 599a, 601a, 602a
867a, 874a
Photochemical Ionization 1068a
Photochemistry 138a, 182a, 407a
437a, 445a, 987a
Photodissociation 407a, 445a, 472a
662a, 935a, 938a, 1003a, 1030a
1031
Photoelectron Spec. 505a
Photolysis 55a, 138a
Phycocyanin 617a
Phycoerythrin 617a

Physiology 113a, 331a
Pineal 342a
Pituitary 364a
Plants 33a, 99a
Plasma 45a, 53a, 998a
Plasma Desorption 111a, 233a, 235a
Plasma Source 295a, 723a, 729a
730a, 817a, 819a, 820a
Plasma, Human 71a, 325a, 326a
605a
Platelet Activat. Factor 862a
Polyamic acid 525a
Polyaromatic Hydrocarbons 114a
133a, 134a, 805a, 1068a
Polycyclic Aromatics 115a
Polyethers 162a, 163a
Polyethylene 532a
Polyethylene Glycols 503a, 866a
966a
Polyglycine 590a
Polymers 426a, 524a, 525a, 526a
527a, 529a, 530a, 531a, 532a
534a, 535a, 536a, 537a, 538a
539a, 644a, 675a, 782a, 783a
1086a, 1092a, 1093a, 1095a, 1096a
1097a
Polymer, Additives 423a, 530a
537a, 739a
Polymer, nonpolar 783a
Polymide 525a
Polynucleotides 753a
Polyols 228a, 527a
Polypeptides 753a, 935a
Polystyrenes 526a
Polyunsaturates 342a
Polyurethane Foam 533a
Porphyrins 55a, 207a, 497a, 737a
Positive Ions 767a
Post Trans. Modificatio 260a, 609a
Postsource decay 774a
Primary Sequence 378a
Principal Component Anal 133a, 149a
Probe 213a
Probe, Microdistillation 204a
Probe, Solids 149a, 210a
Processing 836a
Processing mechanism 356a
Proenkephalin A. 619a
Proline 1018a
Prostaglandins 865a
Protamine 578a
Protease Digest 424a
Protein Adducts 266a
Protein Aggregates 768a
Protein Dimer 267a
Protein Inhomogeneities 265a
Protein Ladder Sequencing 658a

INDEX OF KEYWORDS PAGE NO

Protein Phosphorylation 695a
Protein Refolding 891a
Protein Structure 387a, 781a
Protein Modific. Analysis 415a
Protein/Peptides 10a
Proteins 3a, 6a, 8a, 11a, 101a
146a, 263a, 273a, 331a, 347a
349a, 350a, 351a, 352a, 355a
357a, 359a, 365a, 374a, 385a
409a, 410a, 416a, 417a, 418a
421a, 427a, 435a, 436a, 578a
581a, 584a, 591a, 596a, 597a
604a, 606a, 607a, 611a, 613a
615a, 616a, 621a, 658a, 666a
673a, 747a, 775a, 779a, 781a
784a, 867a, 868a, 869a, 872a
874a, 875a, 879a, 883a, 886a
887a, 889a, 890a, 892a, 893a
894a, 895a, 900a, 904a, 905a
Proteins Recombinant 84a, 86a, 89a
264a, 353a, 379a, 609a, 881a
891a, 898a
Proteins, Identification 268a
Proteins, membrane bound 373a, 654a
Proton 184a
Proton Affinities 198a, 392a, 978a
985a
Proton Transfer 183a, 192a, 195a
780a, 962a, 993a
Protonation 198a, 280a, 477a
513a, 667a, 743a, 981a
Protons, Exchangeable 193a, 507a
Psychoactive Drug 333a
Pyrethroid 810a
Pyrolysis 524a, 530a, 532a, 1097a
Quadrupole MS 884a
Quadrupolar Excitation 175a, 798a
Quadrupole, Ion Trap 456a
Quality assurance 647a
Quality control 153a
Quantification 137a, 146a
Quantitation 868a, 1049a, 1087a
Quantitative Analysis 234a
Quantization 104a
Quaternary Isoquinolines 51a
Quinolinic Acid 555a
Quinolones 860a
RESERPINE 45a
RFGD 467a, 820a, 824a, 998a
RGA 139a, 140a, 631a, 646
RNA 246a, 270a, 660a
RRKM 509a
Raction, Monitoring 883a
Radiation 119a
Radiation Damage 250a
Radicals 31a, 279a, 499a, 502a
587a, 962a, 990a

INDEX OF KEYWORDS PAGE NO

Radio Freq. Plasma Ioniz. 816a
Radio Frequency 467a, 724a, 821a
Rapid Characterization 69a
Rare Earths 807a
Rat liver Microsomes 333a
Rate Constants 174a
Reaction 172a
Reaction Charge Exchange 704a, 757a
Reaction Monitoring 288a
Reaction Products 898a
Reaction SN2 188a
Reaction Association 971a
Reaction Biomolecular 655a
Reaction Gas Phase 161a, 171a
200a, 305a, 307a, 498a, 682a
959a, 987a, 992a
Reaction Ion Molecule 28a, 30a, 31a
161a, 163a, 165a, 166a, 169a
176a, 179a, 180a, 183a, 185a
186a, 187a, 191a, 298a, 299a
301a, 306a, 475a, 506a, 682a
716a, 718a, 823a, 860a, 861a
959a, 960a, 961a, 964a, 966a
967a, 968a, 971a, 972a, 980a
982a, 983a, 988a, 990a, 992a
1000a, 1002a
Reaction Ion Surface 27a, 914a
1025a, 1026a, 1027a, 1090a
Reaction, Ion-Ion 986a
Reaction Mechanism 31a, 161a
169a, 171a, 179a, 187a, 217a
282a, 300a, 305a, 309a 489a
493a, 494a, 883a
Reaction Molecular 182a
Reaction Monitoring 208a, 655a
812a, 1069a, 1070a
Reaction Products 1061a, 1069a
1070a
Reaction Surface 1022a
Reaction Gas-phase 300a, 996a
Reactions SN2 189a
Rearrangement 29a, 161a, 178a
285a, 477a, 479a, 493a, 513a
485a, 499a, 999a, 1010a, 1014
Receptors 348a, 363a
Recombinant 615a
Redistribution 229a
Reduction 219a, 220a, 221a, 223a
339a, 566a, 882a, 885a, 889a
Reference Spectra 153a
Relaxation Radiative 509a, 1003a
Remeasurement 796a
Resonance 690a, 711a
Resonance Excitation 693a
Retinoic Acid 323a
Reversibility 352a
Rhodopsin 620a

INDEX OF KEYWORDS PAGE NO

Riboflavins 33a
Rutin 121a
SCRAMJET 623a
SD 953a
SDS 215a
SFC 293a
SFE 626a
SID 269a, 457a, 912a, 914a, 929a
938a, 945a, 1019a, 1022a, 1023a
1025a, 1026a, 1027a, 1090a
SIM 129a, 313a, 324a, 520a, 542a
559a, 873a, 1062a
SIMS 227a, 228a, 471a, 525a, 830a
842a, 891a, 995a, 1087a
SIMS, Organic 224a
SIMS, Static 224a, 231a, 253a
634a, 643a, 1088a, 1089a
SIN 492a
SPPS 390a
SRM 34a, 53a, 64a, 326a, 542a
SS-Agonists 1046a
SS-Carboline 552a
SS-Lactams 586a, 614a
SWIFT 451a
Saccharides 486a, 922a
Said adducts 69a
Salts 1065a
Sampling 11a, 42a, 139a, 140a
438a, 449a, 631a, 775a
Sampling Small Volume 1040a
Saponin 87a
Scans Precursor 939a
Scans Product 939a
Scans Precursor Ion 625a
Scans Reaction Intermed. 920a
Seafood 856a
Sec. Electron Emission 5a
Secondary Ion 953a
Secondary Ion Imaging 826a
Secondary Ion Mass Spec 827a
Secular Frequency 693a
Selected Ion Flow Tube 185a
Selective Ion Monitoring 810a
Selenium-methionine 883a
Self-CI 701a
Semiconductors 140a, 730a, 819a
Seondary Ion Mass Spect. 229a
Separations 79a, 148a, 297a, 833a
Sequencing 145a, 353a, 355a, 366a
369a, 374a, 380a, 382a, 410a
579a, 588a, 589a, 595a, 610a
620a, 658a, 676a, 679a, 747a
763a, 774a, 884a, 909a, 917a
921a, 928a, 937a, 1076a
Sertraline 848a
SiD 1024a
Silanes 172a, 999a

INDEX OF KEYWORDS PAGE NO

Siliconates 225a
Single Crystal 1023a
Single Photon Ionization 407a
Skin 1055a
Solutions 725a
Solvation 1030a, 1031a
Solvents 2a, 741a
Space Charge 453a, 462a, 686a
687a, 689a, 697a, 701a, 703a
708a
Speciation 815a
Specificity 190a
Spectra Peak Shape 450a
Sphingolipids 522a
Spontaneous 953a
Sputtering 216a, 232a, 238a, 915a
1022a
Stability Constants 160a
Stability Diagram 683a
Stable Isotope 331a
Stable Label 560a
State Transition 476a, 958a
State-selected 186a
States Electronic 480a, 1035a
States Excited 279a, 927a
Static Headspace 864a
Statis TOF-SIMS 1094a
Stereochemistry 305a
Steroids 57a, 541a, 568a, 834a
Steroids, Anabolics 541a
Streptomyces ssp. 32a
Structural Determinations 81a
Structure 172a, 963a
Structure Determination 54a, 58a
76a, 138a, 199a, 280a, 296a
398a, 499a, 504a, 506a, 574a
575a, 594a, 600a, 841a, 852a
882a, 926a, 982a, 1013a, 1079a
Structure Peptide 362a, 376a, 380a
594a, 774a, 903a, 935a, 1081a
Structure Elucidation 66a
Structure Protein 264a, 353a, 372a
414a, 416a, 417a, 598a
Substrate Optimization 908a
Substructure Analysis 66a
Sulfate Conjugates 543a
Sulfur Types 205a
Sulphates 90a
Supercritical 123a
Supersonic 20a, 665a
Surface Activity 215a
Surface Analysi 684a, 1091a, 1094a
Surface Effects 778a
Surface Ionization 665a, 761a
Surface Topology 597a, 890a
Surfactants 105a, 215a, 227a
255a, 621a, 642a, 764a

INDEX OF KEYWORDS	PAGE NO
Surfactant Protein B	349a
Synthetic Peptides	343a, 380a, 1056a
TD-GC-MS	531a
TLC-liquid SIMS	90a
TOF	15a, 669a, 731a, 816a, 928a, 945a, 956a, 957a, 1086a
TOF-MS	14a
TOF-SIMS	538a
TOS (Toxic Oil Syndrome)	1064a
TPEPICO	155a
TSP	552a
TSQ-70	973a, 1048a
Tamoxifen	37c
Tandem MS	265a, 810a, 948a
Target capture	194a
Taxane Database	310a
Taxanes	412a, 498a
Taxol	40a, 296a, 310a, 1054a
Terminal Olefins	863a
Tertiary Structure	597a, 890a
Testosterone	568a
Tetraalkylammonium cation	1011a
Theoretical Calculations	501a
Thermal Analysis	531a
Thermal Annealing	229a
Thermal Degradation	121a
Thermal Desorption	395a, 405a, 633a, 662a
Thermal Desorption GC/MS	644a
Thermal Extraction	202a
Thermally Stable	229a
Thermogravimetry	121a
Thermospray	1047a
Thermospray	33a, 44a, 55a, 59a, 60a, 77a, 142a, 143a, 212a, 233a, 289a, 292a, 311a, 314a, 315a, 330a, 362a, 393a, 394a, 396a, 401a, 549a, 550a, 622a, 832a, 839a, 862a, 866a
Thermospray LC/MS	520a
Thermospray MS	48a
Thermospray, LC/MS/MS	342a
Thin Films	1091a
Thio-containing Sugar	80a
Thioethers	478a
Time Dependence	217a
Time-of-Flight	18a, 671a, 672a, 948a, 951a
Tobacco Flavor	121a
Toluene Diamine	533a
Toluene Diisocyanate	533a
Toxins	313a, 362a, 546a, 678a, 859a, 882a
Trace Analysis	536a
Trace Elements	628a
Trajectories Ion	686a, 709a, 798a

INDEX OF KEYWORDS	PAGE NO
Transducin-subunit	375a
Transient Recorder	14a
Transition Metal	172a, 963a
Trap Design	694a
Trapped Ion Cell	452a
Trapping Column	1055a
Triacylglycerides	516a
Trialkylsilyl	495a
Triglyceride	517a, 858a, 924a
Trypetc Digest	902a
Trypsin	364a, 424a
Tryptophan	555a
Ultra High Vacuum	1022a
Ultrasound	38a, 290a
Ultraspray	287a
Unimolecular	977a
VG-ZAB	1048a
VOC	633a
Vancomycin Family	871a
Vaporization	2a
Variant	868a
Venoms	1067a
Vitamins	67a
Volatiles	405a
Water Analysis	112a
Wax Fractions	202a
Weak Interaction	878a
Work Function	230a
Xenobiotics	43a, 358a, 403a, 564a